72
dex
10

Physics Abstracts

Science Abstracts Series A
January–June 1972

Subject Index part B

U. of ILL. LIBRARY
DEC 8 1972
CHICAGO CIRCLE

inspec
The Institution of Electrical Engineers

Physics Abstracts

Volume 75, part I January–June 1972

Subject Index part B

inspec
The Institution of Electrical Engineers

Physics Abstracts is published every two weeks by the Institution of Electrical Engineers in association with the American Institute of Physics. Twice-yearly subject and author indexes covering the period January–June and July–December are included in the subscription. Printed by Unwin Brothers Limited, Woking and London, England. Second class postage paid in New York, NY 10001, USA.

© 1972: THE INSTITUTION OF ELECTRICAL ENGINEERS

CONTENTS

Title page i
Contents list and explanation ii
Subject index S 353
Yellow pages LSH 1

Six-monthly indexes

Cumulative indexes to Science Abstracts are published twice a year covering the period January-June and July-December. They comprise Author and Subject indexes and some specialised or 'small' indexes.

Author indexes

This lists in alphabetical order all authors of papers abstracted in the abstracts journal during the six months covered by the index together with the title of the paper. Where there are co-authors of a paper the title of the paper is given only under the name of the first author. The serial number of the paper in the abstracts journal is in the form 2-12345, ie 1972—abstract no. 12345.

'Small' indexes

These are specialised indexes which allow the user to find quickly particular types of information which might be difficult to find using the subject or author indexes.

Bibliography index

In this index reference is made to articles which contain a significant list of references or bibliography on the subjects listed.

Book index

This gives details of books received and abstracted by the abstracts journal.

Patent and Report indexes

These give details of those reports or patents which have been abstracted in the abstracts journal during the past six months.

Conference index

This index lists conferences for which published proceedings have been received and abstracted. Reference is given to the individual papers and their serial numbers in the abstracts journal.

Subject index

The subject index provides an alphabetical subject key to the articles included in the abstracts journal. Some general guidance on its use is given below:

1. Look in the index for the name of the specific subject in which you are interested. In most cases this name will be a heading in the index and you will find relevant articles listed under it.

2. Occasionally you will be directed from the subject heading chosen to a different heading under which the relevant or additional articles are listed.

3. If you do not find the subject heading you first choose, try a more general heading.

4. If you have difficulty at any stage in determining the appropriate heading, consult the Classified List of Headings on the yellow pages at the end of the index. This gives for each broad subject area the headings used in the subject index. Choose the most appropriate and look them up in the index.

5. Each entry under the heading relates to an article appearing in the abstracts journal and gives the serial number of that article in the journal preceded by the last digit of the current year, eg 2—12345: ie Abstract number 12345 in the abstracts journal for 1972.

Mechanical strength continued
plastics, durability, freq. depend. of fatigue limit, relax. phenomena effects 2—32630
plastics 2—15885
poly(piperazine amides) films 2—9293
polycaproamide, static and fatigue strength, liquid immersion effect 2—29289
polycarbonate, injection moulded, molec. orientation and weight effects on Izod impact strength 2—22280
polyethylene, rel. to surface active media, stress, electron irrad. 2—39811
polyethylene terephthalate, amorphous and cryst., brittle strength 2—39845
polymer, failure surface in principle stress space 2—15815
polymer, rupture processes 2—1746
polymer fibre, plastic deformation, charm scission 2—15845
polymer fibre, rel. to mol. wt. and struct. 2—15643
polymeric materials, testing apparatus, extension, creep, relax., in ionizing rad. 2—39880
polypropylene film, metallic filler, mag. field effect 2—29406
proof stress, computer aided analysis of high temp. data 2—32612
Pyromet 860, precip. strengthening, effect of Ti and Al content 2—29394
quartz, temperature dependence of ultimate strength 2—39879
rock, stamp-load bearing strength, fracture mechanism 2—30233
rocks, reduction by 10.6μ laser irradiation 2—29280
rupture, crack critical opening, slow and dynamic bending test 2—9706
sandstone, effect of size and stress concentration on dilatancy and fracture 2—29320
sealing materials, laboratory testing device 2—22313
shock acceleration reproducibility 2—22318
solid, theory, review 2—22277
stainless steel, containing Ti oxides, influence of precipitate morphology on creep at rupture 2—9674
steel, after thermomechanical treatment and creep 2—9731
steel, alternating fatigue strength change by surface machining 2—29301
steel, austenite, thermomechanical strengthening 2—9728
steel, austenitic, effect of thermomechanical treatment on cyclic strength 2—9688
steel, austenitic, hot working struct. 2—9729
steel, austenitic, precipitation-hardening, fatigue limit and durability 2—36152
steel, borated, fatigue strength, residual stresses 2—39808
steel, brazed joints, effect of bond zones on mech. strength 2—19253
steel, carburized, effect of mean stress on fatigue strength 2—32626
steel, Cr-Mo-V, creep strength, effect of enhanced purity 2—32617
steel, Cr-Ni-Mn, variation with carbon vanadium content 2—1318
steel, Cr-Ni-Mn type, effect of nitrogen 2—9654
steel, cyclic heating effects 2—25516
steel, cyclical strength during variations of local stress 2—19190
steel, ductile fracture 2—29276
steel, effect of ageing conditions 2—36118
steel, effect of Ge content 2—36203
steel, effect of nonmetallic inclusions 2—36139
steel, failure in shock loading 2—39813
steel, fatigue strength, effect of heat treatment 2—36151
steel, fatigue strength, notch dependency under superimposed h.f. stress 2—32631
steel, forge-quenched, effect of tempering temp. 2—12898
steel, fracture strength of cementite particles 2—39839
steel, fracture toughness, effect of crack angle 2—3906
steel, fracture toughness, effect of fluidized bed heating 2—36216
steel, heat treatment, toughness rel. to serrated grain boundaries 2—19204
steel, heat-resistant, effect of alloying additions on creep rupture strength 2—9687
steel, high strength, tending to brittle rupture 2—39809
steel, high temperature conditions, obs. 2—29333
steel, high-Cr, fracture toughness, O content effects 2—36155
steel, high-Mn, resistance rel. to valve mat. development 2—3958
steel, low alloy, brittle fracture tendency, effect of alloying with molybdenum 2—1301
steel, low alloy, brittle fracture tendency at liq. n temp., tests using notch fracture technique 2—1300
steel, low alloy, brittle fracture tendency at low temperatures, effect of titanium additives 2—9680
steel, low alloy, relation to concentration and testing temperature 2—1305
steel, low C, annealed, through-thickness strength 2—39892
steel, low C, grain size depend. of fatigue strength 2—12855
steel, low C, strain hardening, effect of type of stress 2—36212
steel, low-cycle fatigue strength, thermal effect 2—39827
steel, maraging, strengthening with alloying elements 2—36218
steel, maraging strainless, fracture toughness 2—36243
steel, martensite, impact deformation strengthening 2—39901
steel, martensitic stainless, effect of thermomagnetic treatment 2—36280
steel, mild, biaxial strength criterion at low endurance 2—15867
steel, notched fatigue strength, application of finite element elastic-plastic stress analysis 2—15819
steel, quenched, aged, rel. to alloy additions, heat treatment conditions 2—19239
steel, relation to brittle fracture, effect of V and N impurities 2—6517
steel, stainless, rupture, He environmental effects 2—12871
steel, stainless, type 304, creep rupture specimens, metallography 2—39800
steel, static and dynamic loading, reproducible procedures 2—1303
steel, strengthening using hydroextrusion 2—9745
steel, structural, effect of preliminary heat treatment 2—36206
steel, tempering, fracture toughness, temp. depend. 2—3891
steel, wear-resistant, effect of C and V content 2—36237
steel, with Nb additive, effect of precipitates 2—9738
steel, XC 38, ductility, inclusions effects 2—15853
strains, diffr. meas., by surface impressed diffr. grating 2—36182
tubular specimen testing at high temp. under combined action of internal pressure and axial load 2—19225
turbine blade fastenings 2—5180
wear resist. testing machine 2—22312
wire, apparatus for fatigue tests 2—29353
Zircaloy tubing, rupture ductility, hydride platelets orientation effect 2—15842
Al-Fe-Ni:(Mg,Cr,Mn) alloy, nuclear reactor material, resistance to water corrosion, 220°-31°C, comp. depend. 2—13581
Al-Mg alloy, influence of alloying additions 2—12846
Al, electron microscope study of ductile rupture surface 2—39812

Mechanical strength continued
Al, failure, rupture, influence of surface lubrication and u.s. sound 2—39807
2024 Al, Rehbinder effect, effect of anodic oxide coating 2—1286
Al, yield strength, u.s. strain effects 2—39818
Al alloy, fracture toughness, effect of crack angle 2—3906
Al alloy 2024, thermomechanical treatment, yield strength, microstructure 2—32701
Al alloy 7075 T6, influence of thickness on fracture toughness parameter 2—15861
Al_2O_3, alumina, fracture at surface flaws, thermal expansion anisotropy effect 2—12886
Al_2O_3, films evaporated onto a steel substrate by electron bombardment heating 2—35886
Al_2O_3, sintered with vitrifying additives 2—36199
Al_2O_3, sodium borosilicate glass, dispersed composite system, fracture energy, strength 2—32624
Be-1%Fe, rupture, Mossbauer obs.32722 2—32722
C fibre, composites, flexure and shear strength, oxidation effects 2—36266
C fibre, neutron irradiation, fracture, Young's modulus, struct. 2—19193
C fibre, polyacrylonitrile-based 2—3852
C fibre, pyrolytic graphite coating effects 2—25610
Co-Fe-Ni/NbC(TaC) fibre reinforced eutectic systems, directional solidification, sogt magnet 2—3438
Co-Ni-Cr-Mo alloy, precip. hardening and phase transformation 2—19296
Cr-Ni-Ti, austenitic steel, intercryst. rupture rel. to creep resist. 2—9675
Cr-V steels, effect of Mo content and yield point on creep rupture strength 2—29286
Cr-Zr-Nb-C alloy, stress rupture and ductility control by microstruct. modification 2—9692
Cu-Al, effect of thermomechanical treatment 2—36202
Cu-Al alloy, effect of deform. and annealing temp. 2—12888
Cu-Al alloy, internally oxidized 2—39887
Cu-Be-Co alloy, fatigue strength, effect of heat treatment conditions 2—29299
59wt.%Cu-12wt.%Ni29wt.%Zn alloy, superposition of strengthening mech. by thermomech. treatment 2—32688
Cu-Ti alloy, decomposition and strengthening effects 2—39922
Cu, Al_2O_3 and ZrO_2 dispersion reinforced 2—1341
Cu, alloy, yield strength, age hardening, heat treatment, rel. to cold working 2—19241
Cu, electron microscope study of ductile rupture surface 2—39812
Cu, fatigue, freq. effect, high temp. 2—36147
Cu, polycrystalline sample, effect of Hg on breaking strength, under effect of u.s. vibration 2—6557
Cu, single crysts., fatigue life, fatigue hardening, work hardening, cyclic deform., fracture 2—6568
Cu and Kovar cold-welded joints, strength of small thickness sheets 2—6603
Cu solid solutions, low temp. intergranular brittleness 2—19203
Fe-Al-Cr alloy, creep rupture strength, effect of Ti and Mo 2—29430
Fe-Co alloy, phase transformation, struct., comp. depend. 2—19268
$Fe\text{-}Cr_7C_3$ eutectic, oriented crystallization, struct. 2—3436
Fe-Ni-Cr-Ti alloy, γ-hardened, strengthening mech., precip., γ_{apb} calcs. 2—32733
Fe-Ni martensite, rel. to transform. induced substructs. 2—22358
Fe-Si, effect of nonmetallic inclusions 2—36139
Fe, cast, electron microscope study of ductile rupture surface 2—39812
α-Fe, fatigue failure, intergranular fatigue cavitation at elevated temps. 2—25515
Fe, grain size dependence of plane strain fracture toughness, K_{Ic} 2—15864
Fe alloy, ageing effect 2—1353
Ge-As solid solution, pseudodislocational interactions, dispersion strengthening 2—39697
$Li_2O\text{-}SiO_2$ glass-ceramic, mech. props. rel. to crystallization 2—36140
Mg-Zn alloy, strength in various ageing states, mechanism of precipitation hardening 2—6599
MgO:Ni,Fe,Co, and fibre reinforced, strength, fracture toughness 2—39814
Mn-Cu-Fe, alloy, elinvar-type, nonmag., cold worked, heat treated, rigidity modulus meas. 2—29233
MnZn alloy, Hall-Petch relation and strengthening mechanism 2—6546
Nb-N alloy, yield stress, solution hardening 2—9661
Nb-O alloy, yield stress, solution hardening 2—9661
Ni-Al alloy, precipitation-hardened 2—29404
Ni-Cr elec. resist. heating alloys, rel. to lifecycle, added elements effects 2—32732
Ni, dispersion hardened, ThO_2 particles 2—9690
Ni, ZrO_2 dispersioning strengthening 2—39902
Ni alloy, alternating fatigue strength change by surface machining 2—29301
Ni alloy, Mar-M200, Hf doped, rupture life and ductility enhancement 2—15865
Ni alloys, development as high performance, high temp. mats., review 2—12973
Ni and alloys, dispersion hardened, role of microstruct. in strengthening 2—39936
Ni_3Ga, yield stress, anomalous temp. depend. 2—3870
PbTe, containing impurities, homogeneity study 2—36035
Pu-Ga alloy, plastic deformation, mech. props. rel. to temp. and homogeneity 2—15839
SiC, self-bonded, factors affecting fracture strength 2—29329
SiO_2 glass, strengthening by high pressure Ar impregnation 2—12892
Ti-Al-Cr and Ti-Al-Cr-Mo alloy, after annealing 2—36142
Ti-V and Ti-V-Al alloys, after quenching, comp. depend. 2—36141
Ti alloy, cold working and heat treatment, structural hardness, breaking stress 2—12949
α-Ti and alloys, effect of B-stabilizer 2—36143
V-Ti alloy, solid soln. strengthening and weakening 2—29441
W, dispersion strengthening, by chemical covapour deposition of W and HfN 2—22351
W alloy, for incandescent lamp filaments 2—39914
W composite, heat resist. alloy coated, creep rupture strength 2—12885
Zn, hydrostatic extrusion, struct. and plasticity 2—19184
Zr-(2.5 wt.%)Nb alloy, age-hardened 2—12952
Zr-Sn solid soln., substruct. strengthening 2—12953
α-Zr, substruct. strengthening 2—12953
Zr alloy, high-strength, for reactor press. tube appl. 2—39945

Mechanical strength continued
compressive
β- brass, single crystals, dynamic compressive behaviour, yield stresses 2—3853
brittle material, complexed stressed state, static friction effect 2—19202
brittle nonmetallic materials, impact testing 2—25540
concrete, strain and ultimate strength, triaxial stress 2—15859
concrete, under repeated compressive loads, effect of understressing 2—22345
foam plastic, meas. method and apparatus 2—25542
lattice strain in shocked stressed metals by impact test 2—19191
nuclear reactor pressure vessels, concrete 2—15066
pre-fractured rocks, Westerly granite and Cedar City tonalite 2—33429
rapid loading testing machines, electrical correction of dynamometric systems 2—29364
rigid-plastic body, breaking stresses and deformation speeds along rupture 2—5201
second order standard force measuring machine with double acting lever for obs. 2—19231
short cylindrical shells, Koiter's buckling mode, critical stress determ. 2—27137
steel at sub-zero temperatures 2—1406
Al_2O_3, Mo-dispersed, grain size depend. 2—15862
Al_2O_3, Mo-dispersed, grain size depend. 2—15863
MgO, precip. strengthening by $MgFe_2O_4$ 2—29402
MgO microcryst., electron microscope obs. 2—9689
SiO_2 film thermally grown on Si, buckling rel. to thickness/window width ratio 2—9283
shear
composite, fibre-reinforced, pull-out test 2—15943
crack nucleation, critical shear stress, conformed mapping 2—29313
double shear tests, improved device reduces additional stresses 2—29366
glass-fibre-epoxy resin specimens, short beam 2—3890
keyed and shrink-fit assemblies, high tensile steel keys 2—19197
macromolecular solutions, computerized measurement, of complex shear modulus 2—25015
poly2-hydroxyethyl methacrylate, temp. dependence of storage and loss shear modulus 2—25514
pure shear testing, procedure, device 2—36188
rocks, building materials, shear testing procedure 2—39869
water, liquid, limiting, dependence of rate of motion of float on temp. 2—21939
Al-Ga alloy, rel. to Ga additions 2—32702
Al, shear modulus, effect of neutron irradiation at 4K, variation with Frenkel defects concentration 2—22278
C fibre-epoxy resin, rel. to electrolyte wetted fibre obs. 2—12644
Cu-Cd, base alloy, increase in critical resolved shear stress in temp. independent region 2—9766
Cu-In, base alloy, increase in critical resolved shear stress in temp. independent region 2—9766
Cu, OFHC, pressure derivative, pressure and strain sensitivity 2—22279
Cu, shear modulus, effect of neutron irradiation at 4K, variation with Frenkel defects concentration 2—22278
MgO, precip. strengthening by $MgFe_2O_4$ 2—29402
Pt, shear modulus, effect of neutron irradiation at 4K, variation with Frenkel defects concentration 2—22278
tensile
amorphous polymer, internal friction correlation 2—36145
anelastic material in simple tension, failure 2—140
brass, fracture toughness, struct. damage effects 2—15837
brittle materials, test apparatus 2—19227
cartilage, tensile properties, effect of strain rate 2—41283
ceramic joint, temp. depend. testing 2—25543
composite, fibre reinforced, bounding approach 2—36133
composite, filamentary, ultimate strength degradation 2—36135
composite, notched, crack size depend. 2—36134
composite with random discontinuous reinforcing fibres and brittle matrices 2—15858
creep of thermoplastics in tension, measurement at high pressure in petroleum-vapour atmospheres 2—39970
creep testing apparatus 2—19219
dacite, relationship with percentage void fracture 2—29319
double cantilever beam test for fracture toughness 2—25565
fibre reinforced plastics, NDT using u.s. reson. method 2—32658
fibreglass rod, effect of surface softening 2—39804
fracture mechanics, stress conc. approach 2—25523
fracture toughness measurement effect of specimen type and prep. 2—39864
glass fibre reinforced composite, effect of gauge length and strain rate 2—39805
glass-fibre-epoxy resin specimens, modulus and stess-strain curve 2—3890
glassy plastics, mechanism of molec. wt. dependence of brittle strength 2—39830
glued metal joints, effect of preliminary impact 2—29347
glycerol, dynamic tensile failure 2—12525
graphite, polycryst., temp. and stress effects 2—32615
n-hexane, superheated, measurement by ultrasonic cavitation 2—9066
hot hardness testing 2—25550
keyed and shrink-fit assemblies, comparison of torsional strengths using high tensile steel keys 2—19197
metal, cubic, anisotropy in sheet forming operations 2—25582
metal, fracture toughness parameters 2—29321
metal, treatment to raise yield point 2—12923
notched bar impact test for fracture toughness determ. 2—25564
nuclear reactor fuel cladding, under combined effect of creep and plasticity 2—21465
nuclear reactor pressure vessel connecting pipes, analysis 2—15055
plastics, testing at a constant rate of stress change 2—29355
poly(2-hydroxethyl methacrylate), water swollen gel, crosslinking effect 2—35807
polycarbonate, effects of cold rolling 2—1308
polyethylene, high density, after cold rolling 2—39792
polyethylene, low press., rel. to molecular struct. 2—28978
polyformaldehyde, mullite filler, deformation, rupture, microstructure 2—29293
polymers, crystalline, molecular mechanism of chain rupture 2—29292
polystyrene 2—15888
polyvinyl alcohol fibres, effects of stretching 2—15649
polyvinyl chloride film, electric discharge effect 2—16269
reactor fuel, post-irrad. exam. techniques 2—38755

Mechanical strength continued
tensile continued
reactor pressure vessels, overstressing technique for securing brittle failure 2—24291
rubber cross linked by dicumyl peroxide, effects 2—25508
sapphire, 0° filament tensile behaviour, 25-1325°C 2—39806
second order standard force measuring machine with double acting lever for obs. 2—19231
steel, austenitic, and yield and creep strength, C effects in types 304 and 316 2—1304
steel, austenitic stainless, crack propagation, relationship of nitrogen to stress corrosion 2—1326
steel, bainitic, rel. to microstructure 2—9686
steel, blue brittleness, tensile testing study 2—36115
steel, brittle fracture strength 2—25526
steel, casehardened, B addition effect 2—12891
steel, correl. with errosion resist. 2—39853
steel, Cr-Mo martensitic, fracture toughness, heat treatment depend. 2—12908
steel, dynamic fracture strength, shock precompression effect 2—12889
steel, effect on fatigue limit 2—36149
steel, fatigue strength under axial load, effect of surface hardening 2—36150
steel, fracture toughness, struct. damage effects 2—15837
steel, fracture toughness and Charpy impact data 2—25533
steel, fracture toughness variation prediction from small specimen tests 2—25524
steel, high-Cr, fracture toughness, effect of N content 2—36156
steel, high-strength KhGR, rel. to mech. characterization tests 2—39877
steel, low temp. 2—36113
steel, mild, grain size effect on fracture initiation 2—29327
steel, neutron irrad., rel. to defect struct. obs. 2—1232
steel, notched, stressed, yield stress, area reduction, elongation at rupture 2—12890
steel, pre-strained, stressed, yield strength, ductility, permanent strain, cracks 2—12854
steel, stainless, carburization in Na influence 2—13569
steel, stainless, creep rupture rel. to cold-drawing, temp.-depend., type 316 2—1292
steel, stainless, creep-rupture testing 2—3880
steel, strength drop at cryogenic temps. 2—36138
steel, structural, relaxation after welding, heat treatment and residual stress 2—12944
steel, super-high-density sintered, props. 2—6561
steel, TRIP-type, fracture toughness 2—36172
steel, X 15 N 9 Yu, dynamic and static strength effect of heat treatment 2—6554
superalloy, controlled by use of precip. phases 2—29387
superelastic thin-walled tube and spherical shell, rupture 2—2216
tensile tests, determ. of stress- strain flow curve 2—36189
test structure in hydrostatic pressure environment 2—17136
testing, 'machine hardness' concept 2—29379
testing device, usable at 123 K for electron microscope obs. 2—22315
thermoplastic, C-fibre reinforced 2—1336
Viton A-HV vulcanizates, effect of crosslink density on time-temp. dependence 2—25512
water, dependence on volume 2—21937
welded joints in biaxial tension 2—6533
welded metal joint testing 2—29354
Al/C fibre composite, continuously cast 2—29282
Al-Cu alloy, plane strain fracture toughness 2—29322
Al-Mg, alloy, effect of deposited metals in rapidly solidified structures 2—3888
Al-Zn-Mg, alloy, effect of deposited metals in rapidly solidified structures 2—3888
Al, alloy, creep rupture props. 2—19187
Al, commercially pure, effect of deposited metals in rapidly solidified structures 2—3888
Al, dynamic fracture strength, shock precompression effect 2—12889
Al alloy, effect on erosion rate 2—29339
Al alloy cylinders under internal press. 2—39837
Al alloys, fracture extension resist. determ. 2—29323
Al alloys, fracture toughness, struct. damage effects 2—15837
Al alloys, obs. 2—29417
Al alloys, plane strain fracture toughness, effects of specimen size 2—36166
Al_2O_3, filament-reinforced plasma-sprayed 2—36264
Al_2O_3 filaments, surface damage effect 2—19192
Be, fracture toughness, review 2—29324
Be, hot pressed, temp. and strain rate depend. 2—29283
C, fibres, effect of fast neutron irrad. 2—9683
C fibre, 'Grafil A', rel. to dia. 2—36137
C fibre, obtained by thermal decomp. of vaporized hydrocarbon 2—36265
Co-Ni-Cr alloy, ThO_2 dispersion strengthened, rupture and corrosion resistance 2—19266
Co-base alloy, Haynes No. 188, rel. to appl. 2—39920
Cr-V steels, effect of Mo content and yield point on creep rupture strength 2—29286
Cu-Al_2O_3, microstructure, obs. 2—39913
Cu-Be-Co alloy, effect of heat treatment conditions 2—29299
Cu-Be alloy, changes in tensile properties during irradiation and post-irradiation ageing 2—29284
Cu-(1.9 wt.%)Be alloy, precip. substruct. depend., rel. to fatigue strength 2—22283
Cu-Ni-Si-Mg(Cr) alloy, cold working rel. to age hardening behaviour 2—32706
Cu, dispersion strengthened, temp. depend. 2—9684
Cu alloy, effect on erosion rate 2—29339
Cu rods, hydrostatically extruded, residual stress distribution 2—3883
Fe-Al-Cr alloy, effect of Ti and Mo additives 2—29430
Fe-Mn alloy, rel. to microstruct. 2—32767
Fe-1.1at%Nb, substitutional dynamic strain ageing effects 2—3866
Fe, cast, ductile-brittle transition temp, heat treatment depend. 2—39832
Fe, deformation and rupture, Al particles effect 2—9693
Ge, ductility and brittleness rel. to molten metal contact 2—29310
Na_2O-B_2O_3-SiO_2 glass fibre, quick loading, comp. depend. 2—19194
Ni-Al_2O_3, alloy, electrolytically deposited, dispersion hardening, tensile tests 2—19236
Ni-Cr-Fe alloys, neutron irradiation, extension rate, grain size, ductility 2—25513

Mechanical strength continued
tensile continued
Ni-SiO, composite film, and microhardness 2—15666
Ni, neutron irradiation, extension rate, grain size, ductility 2—25513
Ni alloy, effect on erosion rate 2—29339
Pb-Cd-Sb alloy, rel. to microstruct. and alloy comp. 2—19269
SiC, whiskers, ribbon- like, surface defects, etching 2—12673
Ti-Al-Sn-Zr-Mo alloy, fracture toughness rel. to microstruct. 2—39942
Ti-V-O and Ti-V-Al-O alloys, fracture toughness, effect of O content 2—36144
Ti, dynamic strain ageing, tensile tests, 77-1026K 2—25581
Ti alloy, effect on erosion rate 2—29339
Ti alloy, fracture toughness 2—36174
V-Ti, V-Ti-Nb, Si/Ge alloying effects on creep strength 2—1295
W-Re alloy, high temp. strength, comp. depend. 2—1290
W, dislocation interaction with C atoms, tensile tests, internal friction meas. 2—29184
Zn-Al, alloy, eutectoid, superplastic, extrusion speed and temp. rel. to extrusion stress and mech. props. 2—19255

Mechanics
see also Dynamics
adaptation of tensile testing machine 2—29361
analogues for time dependent Josephson phenomena 2—2049
angular momentum and spin, relation between classical and quantal theorem 2—14110
automobile wheels, static vs spin balancing 2—17279
bar structure, matrix equation 2—37665
book on theoretical mechanics 2—37668
brachistochrone problem generalization introducing slide friction 2—17291
Canonical formalism, definitions of symmetry and invariance 2—27114
Cauchy-Green deformation tensor, inequality sets among principal invariants 2—27188
centre of mass of system of particles, Lagrange's theorem 2—17280
classical, derivation from quantum mechanics 2—17223
classical, formulation in auxiliary algebras 2—20841
classical, on Lie groups 2—23241
classical, solutions to relativistic two-body problems 2—33889
classical states, existence as distributions with extended supports 2—20883
conference on theoretical and applied mechanics, Haifa, Israel (1971) 2—115
Coulomb potential, noncalculus derivation, nonscience students 2—27007
cylinder falling under gravity in contact with larger fixed cylinder 2—27125
elastic mechanisms, optimal adjustment 2—27118
generalized many-body problem 2—33591
generalized restricted three body problem, one body exerts no influence on others 2—17278
half-plane structures for simply supported uniform loading, optimum soln. 2—5173
hereditary media, linear theory 2—33987
holography applications, conference (Los Angeles, August 1971) 2—14147
holonomic mechanical system with n degrees of freedom, classification of linear integrals 2—37666
ideal resonance problem, second-order solution by Lie-series 2—27116
intermediate, computer assisted course 2—17149
invariant, general results 2—11319
Lagrangians with higher order derivatives 2—17275
Lenz vector, generalization 2—14156
Lorentz transformation, derivation based on Newtonian mechanics 2—27123
mass centre motion of system, demonstration 2—23316
momentum and angular momentum in relativistic classical particle mechanics 2—30769
motion of rigid body, Weierstrass p-function, half-periods evaluation 2—117
motion of rigid body, Weierstrass p-function 2—116
non-spherical globule, pressure distribution on the surface 2—37667
nonlinear static structural, self-correcting initial value formulations 2—20893
nonlocal variational, constructive approach 2—23315
one-dimensional three-body problem, solution 2—17277
orthotropic multilayered plates, simplified treatment 2—23324
orthotropic plates, laminated, and shallow shells, finite element computer program 2—2212
point particles, interacting, relativistic and realistic classical mechanics 2—7733
polygenic systems, one dimensional continuous, stability 2—27212
potential well, escape model 2—30830
relativistic classical particle mechanics, example construction 2—33894
rigid body, two important questions clarified 2—17283
rolling of cylinder on rigid/perfectly plastic half-space 2—37671
shell buckling eigenproblem, application of gradient minimization methods and higher order discrete elements 2—2211
simple structure, consistent equations for large scale deflections 2—27115
singular perturbation problems, degenerate forms having many solns. 2—33966
spinning particle, relativistic classical mechanics 2—27117
stability problems, nonconservative, adjoint variational methods 2—5171
structural, of nuclar reactors application of similitude 2—15085
structural, self correcting incremental approach 2—27136
structural analysis using NASTRAN computer program 2—2210
two-dimensional particle mechanics, use of method of complex potentials 2—17276
Universe mechanics, macro-objects, fundamental elements 2—30404
variable mass systems in Newton's second law, example 2—14155
variational principles and generalized potentials 2—118
whirling of three dimensional elastic shaft-disc system, stability theorem 2—125

Mechanics of gases *see Aerodynamics*

Mechanics of liquids *see Hydrodynamics*

Medical science
see also Physiology; Radiation protection
alpha e.e.g. fields multichannel topography 2—11205
bone scanning with ^{18}F, review of 10 years experience 2—30676
bone turnover assessment by micro- and auto-radiography 2—30674
bradykinin and autonomic nervous system inhibition on systematic and regional hemodynamics in unanesthetized rhesus monkeys 2—37438

Medical science continued
chromosome rupture by X-rays, γ, α, p, n 2—2021
circulation physiology, averaging computer analysis of displacement ballistocardiograms 2—23142
collimators, focused, method for reduction of energy dependence of resolution 2—23147
dynamic radioisotope recording, sequential input output model 2—20739
e.e.g. analysis by computer 2—14038
electron microscope imaging of neurons laboratory processing and handling 2—17759
e.m.g. jitter in normal human muscles 2—11204
engineering in medicine and biology, proceedings of 24th annual conference, Las Vegas, 1971 2—41292
Farmer Dosemeter Mk. II, calibration and equilibration times, errors 2—33792
Farmer Dosemeter Mk. II, pressure time-constants and correction factors 2—33791
filter for phase-frequency analysis of electrical signals from brain 2—20729
focused, ultrasound, for local treatment of biological tissue 2—30666
hearing disorder diagnosis, impedance bridge performance 2—33805
heart disease, diagnosis, treatment, electronic tools 2—2032
heart-lung machines, hydrodynamic indexes of polymer tubes for 2—20722
human electroencephalogram, separation of sinusoidal components of alpha rhythm 2—33789
image analysing computer, pharmaceutical and clinical applications 2—7589
intra-uterine transfusion, radiation doses given to mothers and foetuses 2—37450
low temp. treatment of bone for joint surface allografts 2—41285
lung ultrastructure, effects of hyperoxia 2—11197
marrow scanning with radiocolloids 2—30678
microneurosurgery, colour TV applic. 2—20733
muscular dystrophy, H-reflex 2—41286
nuclear medicine measuring apparatus kit 2—5033
particle accelerator use 2—14786
particle counter 2—23152
patient monitoring, electronic, intensive care, computer information handling 2—2019
powder toxicology, automated gravimetric system for characterization by adsorption 2—22079
Quantimet Cytoscreen for scanning for malignant cells 2—7603
Quantimet Cytoscreen pattern recognition system for screening cervical smears 2—7602
radiography, electron beam depth dose curves, surface ionization ratio for 3 to 11 MeV 2—37451
radiography electron beam depth dose curves, theoretical and experimental curves for 3 to 11 MeV 2—33790
regional blood volume in lung, radioisotope technique 2—30673
separation of lung-liver scintiphotos due to ascites, subdiaphragmatic abcess 2—41289
serial pulmonary perfusion scanning in radiation therapy for bronchogenic carcinoma 2—20740
skeletal imaging agents 2—30677
skin burns due to short duration heat flux, cond. model 2—20738
tomography, detection of small intrarenal calcifications 2—33787
ultrasonic contrast increasing in human tissue 2—23145
ultrasonic tomographic examination of blunt abdominal injuries 2—20723
u.s. diagnosis, data preparation and processing 2—37445
u.s. diagnosis, pulse echo method, sound head sensitivity 2—37446
u.s. Doppler vel. meter for cardiography 2—30679
Ca, whole body content det. by in vivo neutron activation analysis 2—26956
^{111}In, cyclotron production from ^{111}Cd, for nuclear medicine applications 2—28239
^{220}Rn decay produces in air, coagulation rates 2—22018
^{85}Sr bone scan in neoplastic disease 2—30675

Meissner effect *see Superconductivity*

Melting
see also Zone melting and refining
ablating-slab problem, total melting time 2—9206
actinide metals, volume contraction 2—35825
$CsHF_2$, rel. to polymorphism at high pressures 2—36282
cubic crystal, Lindemann criterion, rel. to characteristic temp. 2—35820
disperse system, rel. to solid surface energy determ. 2—6318
dissolution of crystals in its own melt 2—35822
earth's core 2—26407
finely divided solids, characts. determ. by n.m.r. 2—9208
flat surface, heat transfer under conditions of forced convection and laminar boundary layer 2—1137
fusion temp. at high pressure for rocks and metals, equation for det. 2—28941
glass, K, OK, LF, TBF and OF types in graphite crucibles in vacuum and inert gases 2—35821
hard sphere Bose gas, phase changes, computer simulation 2—15626
ice electrification depend. on earlier freezing rate 2—7292
lanthanide metals, volume contraction 2—35825
lunar rock samples, differential thermal analysis and gas release studies 2—7509
melting curve anomaly, high pressures, model 2—39419
metal, change of volume, rel. to rare gas 2—25140
metal, non-ferrous, impurity removal 2—18875
metal, shock induced melting 2—39420
metal, theory 2—9207
metal, under controlled conditions, rel. to thermometer calibration 2—17453
metals 'ideal three phase model' thermodynamic properties 2—32306
methane, melting pressure meas., Simon eqn. representation 2—25142
molecular crystal, liquid crystalline transition, short range orientational order effect 2—15187
molecular crystals, 'ideal three phase model', thermodynamic properties 2—32306
molecular crystals, nematic liquid crystalline phase, theory 2—28790
monovalent metal nitrates, mechanism of fusion 2—3771
naphthalene, equilibrium form near m.p., nonsingular surfaces 2—18925
nylon-6,6 and nylon-6,10 copolymers with nylon-6T, melting and crystallization 2—9210
n-paraffins, high press. phase relations 2—15629
poly(2,6-dimethyl-1,4-phenylene oxide) in ternary mixtures with toluene and polystyrene, crystallization and melting 2—32319

Melting continued

poly(ethylene oxide) of low molecular weight, determ. of melting transitions, and interfacial free energy 2—39422
polymers, homo-and co-, partial metlting, small angle X-ray scattering 2—18907
polyoxymethylene cryst., morphological changes 2—3476
porous body, liquid phase capillarity 2—3434
positron annihilation applic. 2—18876
premelting phenomena in crystals of chain molecules, small angle X-ray scattering 2—18907
rare gas, change of volume, rel. to metals 2—25140
reactor rods and plates under internal heat generation 2—14293
refractory metals, floating zone furnace 2—23187
relaxion model for correl. with diffusion 2—36071
semiconductors, binary, cubic, Debye temp. from Lindemann's melting law 2—40048
statistical mechanical mechanism, lattice theory 2—39418
steel, austenitic stainless, 20%Cr-25%Ni, localized melting 2—36301
steel, casting, working, heat treatment, defect origin 2—32690
two-dimensional crystal, molecular dynamics study 2—28942
water, periodic freezing and melting, theoretical study 2—1135
Al, effect on electronic struct., n.m.r. obs. 2—7136
$AlCl_3$, vol. change on fusion 2—18873
Bi-Cd alloy, change in ultrasonic velocity 2—39421
Bi-Sb alloy, change in ultrasonic velocity 2—39421
Cu, effect on electronic struct., n.m.r. obs. 2—7136
Fe, cast, laboratory scale melting and solidification method 2—35818
$FeCl_2$ frozen aqueous soln., D.T.A., unusual crystallization phenomena 2—35824
Ge-S system, fusibility diagram 2—1138
Ge surface, laser irrad. 2—12647
He, P-T melting curves, exptl. determination 2—9209
Hg, thermograms 2—12612
In-Sn alloy, change in ultrasonic velocity 2—39421
KHF_2, rel. to polymorphism at high pressures 2—36282
Kr, model cryst., mol. dynamical calcs., computer simulation 2—16015
Kr, P-T melting curves, exptl. determination 2—9209
Na, theory 2—9207
Ne, P-T melting curves, exptl. determination 2—9209
Pb-Bi system, contact, press. depend. 2—18879
Pb layer on Cu substrate, LEED obs. 2—29037
$RbHF_2$, rel. to polymorphism at high pressures 2—36282
Sn-Cd alloy, Cd segregation, neutron radiography obs. 2—15633
UO_2-PuO_2 fuels, heat rating 2—2860

Melting point

alkali metal molybdates and tungstates, rel. to oxygen ion effective charge 2—28945
alloy, Cu_3As, prep. and props. 2—1409
group III-V systems, ternary, phase diag. calcs. 2—22354
high temp. mat., technique for meas., applic. to liquidus area exam. 2—9793
ionic cryst., empirical formula 2—25139
ionic crysts., rel. to press., Ida theory 2—35823
metal particle, surface diffusion and sintering enhancement by addition of impurities decreasing surface m.p. 2—22326
organic substances, rel. to appl. as temp. standards 2—34224
Pt metals, lattice parameters, -189 to 1709°C, solid equation of state 2—19304
rare earth zirconium oxides, $Ln_2O_3.2ZrO_2$ 2—36284
rare-earth borides, B-rich, limiting values 2—9337
thermophysical high temp. prop., high speed meas. 2—19410
Al, γ-irradiation effects 2—6281
$Ca_{10}(PO_4)_6F_2$-$Ca_4Y_6(SiO_4)_6F_2$ solid solution, comp. depend. 2—36275
CeN, in N_2 between 10^{-2} and 21 atmos. 2—18878
Cu_3As, prep. and props. 2—1409
CuBr characterization 2—39581
CuP_2, chemically deposited 2—29094
Dy_2O_3 X-ray diffraction study of crystal structure near melting point 2—6451
InI, determ. from high temp. spectroscopy and tensimetry meas. 2—28944
Mn_2PO_4Cl, flux grown crysts. 2—22111
NH_4HF_2, melting curve, high press. polymorphism 2—25141
Na, vol. expansion, thernal cond. and elec. resist. behaviour 2—16070
Rh_7B_3 and $RhB_{1.1}$ 2—1404
Tb_2O_3, X-ray diffraction study of crystal structure near melting point 2—6451

Membranes

axisymmetric circular, large diflection response, solution by nonlinear relaxation method 2—2203
biological, struct. and function rel. to mesomorphic phases in phospholipids 2—9097
biological, use of lipid spin labels in e.s.r. studies 2—20717
biological-membrane ion transport 2—11198
cell surface liquid crystalline behaviour 2—9098
circular, transducer for monitoring oscillations 2—17358
circular and annular damped, forced sinusoidal vibration impedance and transmissibility frequency dependence 2—34066
cylindrical, dynamic behaviour 2—30846
dynamic current voltage characteristics, measurement apparatus 2—37871
electrodiffusion equation, analogue computer solution 2—17271
electrolyte transfer in steady elec. and mag. fields, capillary model 2—39356
Foppl Hencky eqn., variational principles for boundary value problem 2—2063
hydroxyapatite, compacted powder, flow and sorption of Ar, N_2, CO_2, He, H_2, Ne, 77-303K 2—39554
interpolymer, investigation of water permeability and selectivity 2—12557
ion-exchange membranes, electroosmosis, hydrodynamic model 2—28829
lipids, bimolecular, semiconductive and photoconductive properties 2—26941
nonlinear viscoelastic, axially symmetric stretching 2—37710
optimal perforation spacing in reverse osmosis support tubes 2—12555
plane stress waves in membranes caused by arbitrary pressure wave 2—17375
polyethylene, effect of pressure on gas permeability coefficients of 1,1-difluoroethylene and fluoroform, free volume theory application 2—35691
polyethylene, permeability and diffusion coefficients of dimethyl sulphoxide 2—35752
polyethylene permeation of gas and liq. propane and propylene 2—25066

Membranes continued

reflection coefficient for dilute non-electrolyte solutions 2—28830
simulation of diffusion, lumped RC network as analogue model 2—2326
tubular reverse osmosis, concentraton polarization at phase boundary 2—12556
ultrafiltration mass transport, enhancement due to u.s. waves 2—30044
unsymmetric trapezoidal plates, simple supported 2—23342
Ag, O_2 permeation through 2—25461
C, surface props., adsorption of Kr 2—3494

Memory devices *see Calculating apparatus; Magnetic devices; Storage devices; Superconducting devices*

Mendelevium

No entries

Mendelevium compounds

No entries

Mercury

a.c. arc lamps, modulated spectra 2—38163
arc, low pressure, efflux of atoms from cathode spot 2—24942
arc, low pressure, stability of strongly ionized positive column 2—24877
arc, l.p., efflux of atoms from cathode spots 2—12479
arc, modulated, as excitation sources in luminescence spectroscopy 2—2470
arc discharge, gas density pulse obs. 2—24941
arc plasma electrical conductivity and optical reduction of ionization potential, correlation of peculiarities 2—39120
astronomical constants from Earth-Mercury radar data 2—33748
atm., collision with Ar*, Penning ionization electron energy spectra 2—12055
atom, absolute oscillator strengths of 3 transitions 2—8446
atom, collisional quenching and depolarization of resonance radiation 2—5841
atom, effect of interatomic resonant collisions on lifetime of 6^3P_1 state 2—21509
atom, electron impact excited resonance transitions, minima in generalized oscillator strengths 2—5816
atom, electron scattering, high energy scattering factors 2—31688
atom, electron scattering effect of virtual transitions, channel coupling and polarization 2—31687
atom, excitation functions of the 6^3P_1 and 6^3P_0 levels in a Na-Hg vapour mixture 2—28193
atom, finite continuous emission spectrum press. depend. 2—35137
atom, Lande factors of 6s7s $^3S_1$ levels 2—24341
atom, photoelectron ang. distrib., variation with energy obs. 2—38825
atom, radiative level shifts and Raman effect under laser irrad. 2—24342
atom 6^3P_1 state, coherent diffusion of radiation in modulation resonance expt. 2—31646
atomic spectra, Stark shift in $6s6p^3P_1$ state 2—38811
atoms, $5d^{10}6s6p+5d^96s^26p$ configurations, energy level calc. 2—2938
atoms, collisions with Cs and K, differential scattering cross sections and intermolecular potential energy curves 2—888
atoms, collisions with superthermal K atoms, ang. scattering cross sections 2—682
atoms, concentration measurement behind a shock front using continuous recording of interference fringe shift 2—28596
atoms, electron impact excitation, differential cross section meas. 2—621
atoms, electron impact excitation of 6^1P_1 state, distorted wave calc. of electron spin polarization 2—622
atoms, photoionization calc., inclusion of intrachannel interactions 2—601
atoms, spectral emission from Hg-Ar discharge, influence of N_2 and CO impurities 2—2939
autoionization of high-temperature monatomic vapour 2—28201
capacitive discharge, breakdown phenomena 2—21887
cathode in He-Ne laser 2—27482
chemical composition and origin 2—20640
in chrysotile asbestos, supercond. and semicond. transition 2—29634
compressibility beyond critical region, p-v-t relations 2—28935
compressibility measurement, isothermal 2—12515
cyclotron reson., effective masses 2—4145
dielectric breakdown of low density vapour 2—3268
diffusion coefficient meas., effect of cell dimens. 2—35748
discharge, afterglow of self absorbed Hg 2537 Å radiation, effect of Ar on decay time 2—32124
discharge, hollow cathode, low pressure, beam- plasma interaction 2—24861
discharge lamps, electrodeless, high stability, construction 2—2460
discharge tube, low pressure, ionization degree meas. on anode side of electrical double sheath 2—8924
effective cross sections of excited ion formation in electronic collisions, calc. by meas. line intensities 2—5800
Fermi surface, pseudopotentials cryst. phase 2—1464
flow velocity meas. in transverse mag. field comparison of hot wire and conduction methods 2—1048
Hall coeff., near metal insulator transition, elec. cond. 2—39385
Hall effect, information on pseudogap formation 2—15609
Hall effect measurement by Corbino method 2—1113
Hall effect near metal-insulator transition 2—19623
hollow cathode glow discharge, breakdown, resonant beam- plasma interaction mechanism 2—15513
ion implantation, InSb and CdTe, lattice disorder and outdiffusion 2—25370
isotopic abundances in Hg stars 2—4830
liquid, contact angle with graphite flakes 2—3489
liquid, electronic structure from nonlocal energy dependent model potentials 2—39328
liquid, metastable struct. near melting point, X-ray diffr. obs. 2—21959
liquid-vapour interface transport obs. using radioactive tracer 2—25004
liquid/saturated vapour equilib., crit. constants effects 2—28950
luminescence of thionaphthene, acenaphthene, and coronene with Hg added 2—3125
melting and freezing, thermograms 2—12612
MHD flow in travelling magnetic field, transitory reversed and turbulent motion 2—28493
natural convection at low Grashof numbers, exptl. determ. 2—30888
odd isotopes, relaxation time of optically oriented atoms 2—18287
permeability in channels of zeolites 2—1384
photoionization and cross sections for ion production, meas. by photoelectron spectroscopy 2—2947
plasma, dense, nonideal, electrical conductivity obs. at high temp. 2—28517

Mercury continued
plasma, diffusion velocity 2—1009
plasma, feedback control of self-excited electrostatic waves 2—18652
plasma, parametric excitation of oscill. 2—32056
positive column, axial electron density gradients 2—15508
positive column, high pressure, electron mobility 2—35589
solid at 4.2K, high-magnetic-field effect on electron- dislocation interaction 2—25674
solidification rate determ. by acoustic method 2—39423
specific heat, spline correl. function 2—18812
spreading, on solid in electrolytic soln., elec. field effects 2—6220
structure, elec. resist., X-ray obs. 2—35727
superconducting, electron-phonon mass enhancement, temp. depend. 2—25785
superconducting, electronic thermal cond. 2—22507
supercritical fluid, thermopower 2—25149
surface tension on glass, W and Mo substrates, sessile drop technique 2—21970
surface wave parameters, influence of spatially dependent electric fields 2—9062
thermal diffusivity, heat pulse technique applic. 2—18818
thermopower and resistivity, temp. depend., calc. 2—3404
trace analysis in environmental samples, semiconductor detector optimization 2—30127
vapour, condensation, dropwise, 70-185°C 2—18889
vapour, electrical and optical properties, measurement apparatus for transition metal to insulator density range 2—9036
vapour, Faraday effect obs. in optically, oriented ^{199}Hg and ^{201}Hg 2—24985
vapour, long capillary positive column, basic props. 2—24876
vapour, resonance radiation, forward scattering 2—8448
vapour, thermodynamic props. 2—18756
vapour Ar arc discharge, cathode fall depend. on cathode qualities 2—39228
vapour pressure obs. using boiling point method 2—28962
vapour-H_2 mixtures, discharges, ignition potential 2—3264
water pollutant, nonflame atomic absorption analysis 2—22892
CdSb:Te, Hg, influence of double doping on elec. props. and band struct. 2—36499
Cs-Hg, high resolution meas. of differential scattering cross section, intermolecular potential determ. by inversion of data 2—28427
H-Hg, scattering at theral energies, determ. energy dependence of integral cross section 2—2992
Hg-Ar, Hg-Kr, Hg-He gas mixtures, optical breakdown threshold 2—35626
Hg-Ar discharge, low pressure a.c., supply freq. effects on positive column 2—21884
Hg-Ar discharge, spectral emission, influence of N_2 and CO impurities 2—2939
Hg-Ar(Ne) afterglow, electron temp. and Hg(6^3P) density decay 2—32129
Hg-Cd, mixture, sensitized fluorescence, width of 3261 Å spectral line 2—8447
Hg-Cu_2O contact, barrier capacitance anomaly at Hg melting pt. 2—25885
Hg-Ga system, shape of coexistence curve near T_c 2—15578
Hg-rare gas discharge, strongly modulated, nonlinear effects 2—15507
Hg II line in Hr 465 peculiar A star, shape changes (from 1961-1969) 2—10879
Hg inert gas intermolecular potentials molec. beam determination 2—24572
Hg traces in host material detected by new atomic absorption spectrometer from hyperfine structure lines in mag. field 2—8038
Hg^0, in alkali halide, optical absorp. 2—3801
$^{198}Hg+^{202}Hg$ collisions, population, orientation and alignment transfer 2—24356
^{199}Hg, 6^3P_2 state, collisions with Hg in ground state, relaxation phenomena 2—28222
^{199}Hg, hyperfine struct., Fourier spectroscopy obs. 2—588
^{199}Hg spin, relaxation rate dependence on magnetic field 2—630
Hg($6^3P_{1\to 0}$) spin-orbit relaxation in vibrational excitation of CO 2—15292
Hg(6^3P_2)$\to$Hg(6^3P_1) transition, relative intramultiplet quenching cross sections 2—28192
in In, effect on Fermi surface topology 2—6724
K-Hg, high resolution meas. of differential scattering cross section, intermolecular potential determ. by inversion of data 2—28427
Os-Pt-Hg abundance peak in Ap stars and very heavy cosmic rays 2—33624
Tl:Hg, supercond transition temp., impurity effects 2—36473

Mercury, planet
ice caps, refuting evidence for existence 2—37367
imaging from a flyby 2—7524
intensity obs. during transit, correction for scattered light 2—4977
isophotometric meas. in white light, comparison with intensity or sunspot's umbra 2—11010
mass, from anal. of optical, radar and radio tracking data 2—13994
microwave continuum brightness temperature 2—30556
passage across disk of Sun 2—30578
passage along disk of Sun, position angles and contact instants 2—7534
perihelion motion, dependence on 4th order potential in quantum field theory 2—7649
perihelion motion, discussion within framework of quantum theory of gravity 2—7650
position, meridian obs. for 1963-67 2—1989
radar scattering properties, backscattering properties, rotation period 2—14000
topography and scattering characteristics at 3.8 cm radar wavelength 2—33746
transit, photographic obs. 2—26912

Mercury compounds
chalcogenides, core electron level obs. x-ray induced electron emission obs. 2—19811
chalcogenides, energy band structure 2—4121
Raman spectra of organic and inorganic substances in water pollution 2—12150
sulphides and sulphates, X-ray L_{23} spectra of quantum efficiency of S photoemission 2—26204
$Cd_{0.1}Hg_{0.9}Te$, film, Hall coeff. and mobility thickness depend. 2—10012
$Cd_xHg_{1-x}Se(Te)$, interband Faraday effect 2—13436
$Cd_xHg_{1-x}Se(Te)$, interband Faraday rot. 2—13435

Mercury compounds continued
$Cd_xHg_{1-x}Te$, Shubnikov-de Haas oscillation, Landau level splitting 2—32998
$Cd_xHg_{1-x}Te$ alloys, relativistic effects on energies of optical transitions 2—29684
$Cd_xHg_{1-x}Te$ alloys, Hall mobilities, press. and temp. depend. 2—4209
$Cd_xHg_{1-x}Te$ mixed cryst., e.p.r. of Mn^{2+} 2—13537
$Cd_xHg_{(1-x)}Te$ fundamental features of energy band structure 2—4121
CdTe-HgTe, heterostruct. with built-in homojunction, photovoltaic effect 2—13350
Hg-Bi system, liq., electronic struct. 2—9078
Hg-In alloy, powdery, grain model 2—12983
Hg-In system, liq., electronic struct. 2—9078
Hg complex, $[(NH_2)_2CS]_2.Hg(CN)_2$, X-ray analysis of room temp. cryst. structure 2—32458
Hg complex, cis-dithiocyanotobis(1,10-phenanthroline)merucry(II), crystal structure 2—12725
Hg complexes, bis(perfluorovinyl)mercury and methyl(perfluorovinyl)mercury n.m.r., magnetic nonequivalence 2—15310
$Hg_{1-x}Cd_xTe$ alloy, compositional dependence of energy bands and optical gap 2—9933
$Hg_{1-x}Cd_xCr_2S_4$, B-site spinel, exchange integrals detn., Weiss molecular field theory 2—36679
HgCdTe, photocond., minority carrier sweepout, high field obs. 2—22645
HgCdTe i.r. detectors at 4 to 6 μm and room temperature 2—7774
p-$Hg_{1-x}Cd_xTe$, carrier conc. press. depend., 4.2 and 77K 2—32983
$Hg_{1-x}Cd_xTe$, epitaxial vapour growth 2—29036
$Hg_{1-x}Cd_xTe$, cryst. growth, homogeneous, Bridgman method, comp. distrib. rel. to growth interface 2—25275
$Hg_{1-x}Cd_xTe$, electron mobility 2—25823
$Hg_{1-x}Cd_xTe$, galvanothermomagnetic obs. det. of nonuniform thermal gradients using liquid crystals 2—34225
$Hg_{1-x}Cd_xTe$, i.r. detector, epitaxial growth and spectral response 2—17412
$Hg_{1-x}Cd_xTe$, solid soln., thermal cond. 65-300 K 2—22433
$Hg_{(1-x)}Cd_{(x)}Te$ reflectivity at room temp. from 200-400 cm^{-1} using far i.r. reflection interferometer 2—34480
$Hg_xCd_{1-x}Te$, dislocations, etching study 2—9558
$HgCl_2$, powder sample, n.q.r. obs. 2—7156
$HgCl_2$, shock wave induced luminesc. 2—10417
$HgCo(CNS)_4$, mag. susceptibility temp. depend. 2—1600
$HgCr_2Se_4$, semiconducting spinel, lattice vibrations, i.r. reflection and transmission spectra 2—19374
HgH, potential energy curves from extension of RKR method 2—18374
HgI, single crystals, used as γ-ray spectrometer 2—2620
HgI_2, feasibility for gamma ray spectrometer use 2—34820
HgI_2, optical spectra, 2-6 eV region, 4.2K and 79K 2—33265
HgI_2, phase transition, Raman scatt. and i.r. absorp. obs. 2—16543
HgI_2, Raman spectra obs. at quadratic-orthorhombic transition pt. 2—29934
HgI_2, spectral distrib. of photopolarization current 2—19786
HgIn, cryst. struct. 2—19053
$Hg(NH_3)_m$, emission profiles, dissoc. constants 2—30084
HgO, surface photoconductivity, spectral response 2—4304
HgO cinnabar, lattice vibrations studied with Raman laser and far i.r. techniques 2—32810
HgS-HgI_2 system, phase diagram, rel. to electrooptic modulator prod. 2—35936
HgS, cinnabar, lattice dynamics 2—16011
α-HgS, cinnabar acousto-optical props. 2—19973
HgS, cryst. growth from soln., technique and apparatus 2—15687
α-HgS, film, vac. deposition and heat treatment 2—3535
HgS, for electrooptic modulator, cryst. growth 2—35936
HgS, thermomodulation of edge absorpt. 2—40666
HgS, X-ray $L_{II,III}$ photoemission spectra fine structure study 2—36909
HgS, X-ray $L_{II,III}$ emission spectra, ESCA technique 2—36919
$HgS_zSe_{1-z}:Mn^{2+}$, $HgS_uTe_{1-u}:Mn^{2+}$, e.p.r. rel. to bonding 2—26280
HgS_xSe_{1-x}, transport props., temp. depend. 2—13233
$HgSe:Mn^{2+}$, $HgSe_xTe_{1-y}:Mn^{2+}$, e.p.r. rel. to bonding 2—26280
HgSe, annealing in Se, effect on resist. and stoichiometry 2—25442
HgSe, Debye-Waller factors calc. 2—36333
HgSe fundamental features of energy band structure 2—4121
HgSe(Te), d-levels location from u.v. photoemission obs. 2—22658
HgSe(Te), u.v. photoemission obs. of upper d levels 2—25979
$HgTe:Mn^{2+}$, e.p.r. rel. to bonding 2—26280
HgTe, band struct. determ. 2—40279
p-HgTe, lattice thermal cond., thermopower 2—32855
HgTe, mean-square atomic displacements, temp. depend. 2—36317
HgTe, reflectivity and band struct. 2—33303
HgTe, termal cond., 65-300 K 2—22433
HgTe fundamental features of energy band structure 2—4121
HgTe thin films investigation of chemical composition by electron microprobe analysis 2—4619
In-Hg amalgam on semicond., ohmic contacts 2—13276
In_2Te_3-Hg_3Te_3 alloy, photocond. and photovolt. effect, 2-12 μm 2—33071
(Zn,Cd,Hg)S:Cu,In electroluminor, electrolum., radiation enhancement 2—36968

Mesic atoms *see Atoms, mesic and muonic*

Mesic molecules *see Molecules, mesic and muonic*

Mesomorphic state *see Liquid crystals*

Meson field theory *see Field theory, quantum/meson field*

Mesons
see also Atoms, mesic and muonic; Cosmic rays/mesons; Hyperons; Kaons; Molecules, mesic and muonic; Pions
dynamical quark model based on principle of temperate interaction 2—403
electromagnetic form factors investigated in ur-citon scheme 2—23880
fundamental particle concept 2—38281
hard and soft limits, dispersion relations 2—14621
high energy exchange reactions, dips and spikes in differential cross sections 2—14533
inner structure, rel. to O(3,1) model of hadrons 2—38247
model as bound state of heavy quarks considered 2—17842
ninth pseudoscalar meson, asymptotic SU(3) symmetry 2—363
pole dominance principles relationship with current algebra 2—31177
pseudoscalar, chiral symmetry breaking, nonlinear realizations and effective Lagrangian 2—2541
pseudoscalar, coupling to spin-$^1/_2$ baryon, study of resonance dominance of form factors 2—14549

Mesons continued
pseudoscalar, electromag. mass differences, study using inclusion of electromag. into perturbation theoretic approach to PCAC 2—14525
pseudoscalar, nonlinear realizations of broken SU(3)×SU(3) 2—21280
pseudoscalar, problems with Kemmer-Duffin formalism 2—31257
scalar, in Gell-Mann-Oakes-Renner model 2—17841
soft meson exchange, summing using relativistic eikonal approx. 2—2543
soft mesons theorems corrections, weak PCAC point of view 2—5519
SU(3)×SU(3) symmetry breaking, emphasis of Nambu Goldstone realization 2—38309
SU(3) orbits in E_8, parametrization 2—31221
unified classification, using meson ladder of U(6,6) symmetry 2—38280
η, problems investigated using concept of axial quark number in framework of chiral Lagrangians 2—14625
$\eta\pi$, mixing study using inclusion of electromag. into perturbation theoretic approach to PCAC 2—14525
absorption
No entries
capture
see also Nuclear reactions and scattering due to/mesons
No entries
decay
diffractive dissociation into three particles 2—364
meson→$\gamma l\bar{l}$ as test of $K_L\to\mu^+\mu^-$ puzzle 2—23830
nonleptonic slow decay in quark models 2—38282
resonances, centrifugal barrier effects in partial decay widths 2—27762
resonances, scaling behaviour of produced particles 2—2569
three-body decay amplitudes, relativistic two-variable expansions 2—17808
vector mesons, electromag. decay calc. using relativistic quark model 2—23869
vector mesons, e.m. decays, comparison of experiment and theory 2—21294
A_1, hard pion current algebra predictions 2—17952
$A_1\to\rho\pi$, consequences of pure D-wave decay 2—21298
$A_2^-\to\pi^-$+neutrals, near threshold, evidence for structure in resonance 2—5548
$A_2\to\eta\pi^\pm$, comparison to other decay modes obs. in $\bar{p}p$ annihilation at rest 2—11634
$\varepsilon\to\gamma\gamma$, calculation of decay widths 2—34600
η, radiative decay, quark loop model 2—31259
$\eta\to3\pi$, study using three triplet model 2—17810
$\eta\to3\pi$ calc. by Lovelace-Veneziano pole model, systematics provided by electromagnetic tadpole 2—38284
$\eta\to\mu^+\mu^-$, test of validity of neglecting $K_l^0\to\pi^+\pi^-\gamma\to\mu^+\mu^-$ in establishing unitary bound for $K_l^0\to\mu^+\mu^-$ 2—14630
$\eta\to\pi^+\pi^-\pi^0$ study using inclusion of electromag. into perturbation theoretic approach PCAC 2—14525
$\eta\to\pi^0\gamma\gamma$, subtraction constant calc., applic. of duality finite energy sum rule method 2—2544
$\eta\to\pi\pi\pi$, khuri-Treiman model 2—17889
$f\to\gamma\gamma$, calculation of decay widths 2—34600
$f'\to\pi\pi$, decay modes, strange spin 2—38341
$\gamma\to\omega\gamma$, radiative decay, calc. using Veneziano model 2—17951
$K^*\to K\gamma$, decay mode study using SU(3) and vector meson dominance 2—27767
$K^*\to K\pi\pi$, decay mode study using SU(3) and vector meson dominance 2—27767
$\omega\to2\pi$, branching ratio, in $\pi^-p\to\pi^+\pi^-n$ reaction at 15 GeV/c 2—27756
$\omega\to2\pi^0\gamma$, radiative decay in pole model, photon energy spectrum expressions 2—34701
$\varphi\to K^+K^-$, obs. in photoprod. of φ from ρ and C at 5.2 GeV 2—14678
$\varphi\to\eta\gamma$, obs. in $\pi^-p\to n\varphi$, branching ratio 2—17953
$\varphi\to\pi^+\pi^-$, G-parity nonconserving decay search 2—14678
$\varphi\to\rho\pi$, decay modes, strange spin 2—38341
$X^0(960)\to\rho e^+e^-$, radiation decays, spin-parity determ. 2—31309
$X^0(960)\to\rho\gamma$, radiation decays, spin-parity determ. 2—31309
X_o, radiative decay, quark loop model 2—31259
detection, measurement
wire chamber spectrometer, h.v. pulsing system, readout and data acquisition systems 2—14750
effects
No entries
interactions
see also Nuclear reactions and scattering due to/mesons
boson spectroscopy and natural and unnatural spin parity systems 2—21253
meson-baryon reactions in Regge models, hyperon polarization 2—38283
meson-nucleon, produced pion spectra in diffractive model 2—31284
photon- meson- meson, bootstrap conditions, success of vector dominance model 2—17820
strong interactions, generalised theory, group theoretical approach 2—27768
SU(n) Lie algebras, special bootstrapping property 2—31235
vector meson couplings, relativistic quark model, electromagnetic decay 2—23869
magnetic moment
No entries
mass
spectrum near $X^0(958)$ studied in $\pi^-+p\to$missing mass+n reaction near threshold 2—38308
$\eta\to3\pi$ decay description, e.m. mass difference systematics provided by e.m. tadpoles 2—38284
production
C-even, by high energy electron colliding beams, measurement of mass, spin and width 2—8129
exotic mesons produced by baryon exchange and $\bar{B}B$ coupling to exotic channels 2—23867
fireballs, properties in different energy regions 2—23900
multiple, model, cosmic ray propagation in atmosphere 2—5566
multiple, two-fireball and H-quantum models 2—5567
multiple production models, rel. to cosmic ray propagation in atmosphere, extensive Monte Carlo calculation 2—26552
photoproduction, conference 2—31258
photoproduction of vector neutral mesons on nucleons, Glauber model, quark model 2—14673
pseudoscalar, consequences of SU_3 invariance, absence of exotic resonances and duality for photoproduction 2—23832
pseudoscalar meson, photoprod., 0.5 to 2.5 GeV 2—34653

Mesons continued
production continued
pseudoscalar meson prod., application of Chew Pignotti duality 2—11590
resonances, centrifugal barrier effects in prod. amplitudes 2—27762
resonances, photoproduction with positron annihilation radiation 3 prong events 2—17821
two-meson production in $\bar{p}p$ annihilations at rest, gauge-invariant chiral Lagrangian model 2—31326
vector meson, new, diffractive photoprod. on nuclei, interference effect 2—31305
vector meson photoprod. on nuclei at large momentum transfer 2—21421
vector meson photoprod. on nuclei in ρ-ω interference region 2—31304
vector mesons, photoproduction, comparison of experiment and theory 2—21294
yield from 70 GeV p interaction obs. 2—5555
A, coherent production in high energy elon nucleus scattering 2—28014
A_2^-, in channel π^-+neutrals, near threshold 2—5548
A_2^+, production in 5.45 GeV/c π^+p interactions 2—17955
A_3^+ production in π^+d, π^+p interactions, non-conservation of s-channel helicity 2—2554
$d\bar{p}\to N$+meson, spin effects 2—14627
ε, geometrical approach, comparison of dual predictions with expt. 2—34698
η, determ. cross sections for production in six prong π^+p interactions at 8 GeV/c 2—17934
η, forward behaviour of differential cross section rel. to dip mechanism tests 2—8134
η, forward behaviour of differential cross section, rel. to decisive tests for dip mechanisms 2—2508
η, forward photoproduction off nucleons, Regge models 2—17925
η, in 4 and 6 prong events from π^+p interactions at 5.45 GeV/c 2—31290
η, photoproduction on hydrogen, 4 and 8 GeV, differential cross section measured 2—8153
η photoproduction, apparent anomaly and stray baryonic states 2—21281
η production by pseudoscalar mesons, high energies 2—14626
η' production by pseudoscalar measons, high energies 2—14626
f^0, cross section in $\pi^-p\to\pi^-\pi^+n$ reaction at 4.45 GeV/c 2—23855
$\gamma N\to(1/2)^++2^+$, SU(6) symmetry study 2—5522
$\gamma N\to(3/2)^++2^+$, SU(6) symmetry 2—5522
$K^{*0 or -}(890, 1420)$ prod. in K^-p reactions at 14.3 GeV/c 2—23840
K(890) comparison with φ production using SU(3) invariance 2—23877
NN collisions, 250 GeV, multiple production 2—2604
ω, photoprod. on nuclei, cross section 2—31313
ω electroproduction, model test of $\rho\omega\pi$ vertex 2—8185
ω photoproduction, effect of natural parity exchange 2—34700
φ, comparison with K(890) production using SU(3) invariance 2—23877
φ, photoprod. at 5.2GeV from ρ and C, study of forbidden decay of $\varphi\to\pi^+\pi^-$ 2—14678
Q, cross over obs. in production differential cross sections 2—31302
Q, density matrices analysed to give helicity structure and relative magnitude of coupling to A_1 production 2—14680
ρ, coherent production in high energy elon nucleus scattering 2—28014
ρ, photoproduction, existence of fixed pole 2—424
ρ^0, cross section in $\pi^-p\to\pi^-\pi^+n$ reaction at 4.45 GeV/c 2—23855
ρ^0, ω, backward production in inelastic ep scattering 2—34702
ρ^0, photoprod. on nuclei, cross section 2—31313
ρ^0, photoprod. on protons, cross sections 2—27707
ρ^0 photoprod., Regge pole model analysis 2—27766
ρ^0 photoproduction, closure approx. in deuterium and non-diffractive amplitudes 2—425
ρ^0 photoproduction, effect of natural parity exchange 2—34700
$X^0(960)$, electromag. prod. processes, spin parity determ. 2—31309
x^0, in 4 and 6 prong events from π^+p interactions at 5.45 GeV/c 2—31290
A_1, density matrices analysed to give helicity structure and relative magnitude of coupling to Q production 2—14680
ρ, photo- and electroprod. in deep inelastic region, Regge pole analysis 2—14681
ρ^0 photoproduction scattering on nucleons, high energy role played by mediating pion pairs 2—31195
resonances
$A\sigma\pi$ vertices, hard meson calc. 2—31308
centrifugal barrier effects in partial decay widths, shapes and production amplitude 2—27762
charged vector meson, scattering in static field at high energies 2—21296
chiral and gauge field theories, Regge pole content 2—17790
coincidence electroproduction, $ep\to epx^0$ scattering with missing mass in ρ meson region 2—23876
decay, scaling behaviour of produced particles 2—2569
decay widths based on harmonic oscillator quark model 2—21293
diffractive resonance production, helicity conservation and longitudinal phase space 2—31301
electron-meson deep inelastic scattering, scale invariance of structure function and generalized vector dominance model 2—31201
excitation levels of rotational bands deduced using principles of nuclear physics, definition of hadron basis set 2—31210
exotic mesons produced by baron exchange and $\bar{B}B$ coupling to exotic channels 2—23867
final vector mesons, Veneziano model predictions of density matrices 2—422
isolation in high multiplicity processes 2—5514
isoscalar vector mesons, coupling constants to nucleon and dispersion-theoretic sum rules 2—31311
isovector form factors and rho-prime, pole model description 2—38307
narrow neutral mesons, obs. near 950 MeV in $\pi^-p\to M^0n$ reaction 2—23870
narrow peaks, near $\eta'(958)$, rel. to hadronic state classification 2—11625
neutral vector meson photoproduction, quark model 2—5546
nucleon-nucleon scattering, pseudoscalar and vector meson models for processes outside phenomenological core 2—8192
photoproduction, conference 2—31258
photoproduction of vector neutral mesons on nucleons, Glauber model, quark model 2—14673
photoproduction with positron annihilation radiation 3 prong events 2—17821
production, in $K^+p\to KN\pi$ reactions in intermediate energy range 2—17907
production and decay of two interfering resonances on nuclei 2—34697
production cross section for ρ, ω^0, X^0 and D^0 in six prong π^+p interactions at 8 GeV/c 2—17934
production cross section meas. in K^-n reactions at 4.91 GeV/c 2—34667

Mesons continued
resonances continued
pseudoscalar and vector mesons, recoil effects in model of higher baryon couplings 2—8183
renormalizable massive vector meson theory, perturbation theory of the Higgs phenomenon 2—31303
resonance splitting, pole insertion in generalized phase space factor 2—8181
spinless meson and kaon resonances, rel. to derivation baryon resonances 2—23894
towers, direct channel interference in $\bar{N}N \to K\bar{K}$ interactions 2—27770
V-particle, composite nature, Lee model with additional Fermi interaction 2—8061
vector meson, new, diffractive photoprod. on nuclei, interference effect 2—31305
vector meson couplings, relativistic quark model, electromagnetic decay 2—23869
vector meson dominance, gauge invariance 2—17853
vector meson dominance, study using storage rings 2—14783
vector meson dominance analysis of single pion electroproduction 2—11629
vector meson dominance and Lorentz contraction for nucleon electromagnetic form factors 2—14687
vector meson dominance breaking, rel. to photoreactions on nuclei 2—18172
vector meson dominance in high energy photoreactions 2—14575
vector meson dominance model, rel. to single π^+ electroproduction 2—17928
vector meson photoprod. on nuclei at large momentum transfer 2—21421
vector meson photoprod. on nuclei in ρ-ω interference region 2—31304
vector meson production, from pion photoproduction, vector meson dominance model 2—8184
vector mesons, ρ, ω and φ, consequences of e^-e^+ colliding beam expts. 2—23802
vector mesons, contribution to nucleon-nucleon OBEP potentials 2—8190
vector mesons, e.m. decays and photoproduction, comparison of experiment and theory 2—21294
vector mesons, neutral, role in photoprod. of $e^+ e^-$ nucleon lepton pairs 2—28018
vector-dominance model, partial conservation of axial-vector current and decoupling of $\pi\rho\omega$ 2—14643
vector-meson dominance for electromagnetic form factors, implications of Veneziano model 2—14619
vector-meson dominance form factor, modification by bound state wave functions calc. 2—17842
A_1-A_2 interference, comparison for $\pi^\pm\rho$ reactions at 5 GeV/c 2—17932
A, coherent production in high energy elon nucleus scattering 2—28014
$a^\pm$ particle model, status in terms of data on CP non conservation 2—11623
A_1, mechanism of production, density matrices analysed to give helicity structure and relative magnitude of coupling to Q production 2—14680
A_1 decays, hard pion current algebra predictions 2—17952
A_1 dominance, deviation in N axial vector form factor 2—31315
A_1 production, t-channel helicity conservation and Deck effect 2—5549
$A_1 \to \rho\pi$ decay, consequences of pure D-wave decay 2—21298
A_2, double peaking as self-absorption of single peak in $\pi + p \to p + A_2$ production process 2—8186
A_2, splitting, rel. to strong destructive interf. between reson. and background 2—11630
A_2 split resonances, multichannel formalism for two overlapping resonances, phenomenological analysis 2—14679
A_2^-, mass spectrum study in reaction $\pi^- p \to A_2^- p$, $A_2^- \to \pi^-$+neutrals, near threshold 2—5548
A_2^+, production in 5.45 GeV/c $\pi^+ p$ interactions 2—17955
$A_2 \to \eta\pi^\pm$, decay, comparison to other decay modes obs. in $\bar{p}p$ annihilation at rest 2—11634
A_3^+ production in $\pi^+ d$, $\pi^+ p$ interactions, non-conservation of s-channel helicity 2—2554
$A_3 \to f\pi$, J^{P3} quantum numbers determ. from spin and parity analysis of charged 3π system 2—14682
A3 region of the three-pion mass spectrum in the $\pi^- p \to p\pi^+\pi^-\pi^-$ reaction 2—31314
Δ, Regge trajectory calc. using N/D formalism 2—17954
$\Delta^{++}\omega^0$, final states prod. in $\pi^+ p$ reactions at 5.45 GeV/c 2—5542
$\Delta^{++}\rho^0$, final states prod. in $\pi^+ p$ reactions at 5.45 GeV/c 2—5542
e, A_2 Regge trajectory exchange degeneracy, evidence from KN charge exchange reactions 2—17908
ε, coupling constants, scale invariance breaking 2—31300
ε meson couplings, rel. to backward scattering duality constraints 2—21271
ε production, geometrical approach, comparison of dual predictions with expt. 2—34698
$\varepsilon \to \gamma\gamma$, calculation of decay widths 2—34600
f-, electromagnetic couplings estimates 2—34699
f^0, decay angular distributions, prod. in 1 π exchange, explanation in terms of kinematical reflection of N* 2—2557
f^0, production and decay in $\pi^+ d$ interactions at 5.1 and 9 GeV/c 2—31312
f^0, structure observed in $\pi^+ d \to p_s p\pi^+\pi^-$ 2—21297
f^0, structure observed in $\pi^+ d$ interactions, Breit-Wigner and dipole descriptions 2—23872
f^0 dominated Pomeron, consequences for inclusive reactions 2—423
f^0 exchange in S-wave $\pi\pi$ scattering 2—14669
f^0 mass region, evidence for structure in $\pi^+ n \to p\pi^+\pi^-$ 2—31307
f^0 production cross section in $\pi^- p \to \pi^-\pi^+ n$ reaction at 4.45 GeV/c 2—23855
$f \to \gamma\gamma$, calculation of decay widths 2—34600
f′ trajectory, scale invariance and Goldstone bosons 2—23873
$f' \to \pi\pi$, decay modes, strange spin 2—38341
$\gamma \to \omega\gamma$, radiative decay, calc. using Veneziano model 2—17951
$\gamma\omega\omega$, coupling constants from Veneziano model 2—17951
K^*, ρ, ω, production in $K^+K^-\pi^+\pi^-$ and $K^+K^-\pi^+\pi^-\pi^0$ final states of $\bar{p}p$ annihilations at 2.2 GeV/c 2—34727
$K^* \to K\gamma$, decay mode study using SU(3) and vector meson dominance 2—27767
$K^* \to K\pi$, vertex, calc. of sum rule based on techniques of current algebra and dispersion relations 2—2570
$K^* \to K\pi\pi$, decay mode study using SU(3) and vector meson dominance 2—27767
K**(1420) trajectory, absorption corrections, hyperon polarization in Regge models 2—38283

Mesons continued
resonances continued
K*(1420) production and decay properties in K-p interactions at 3.9 and 4.6 GeV/c 2—14686
$K^{*0 or -}$(890, 1420) prod. in $K^- p$ reactions at 14.3 GeV/c 2—23840
K*(890), charge-exchange production mechanism 2—17956
K*(890), production and decay properties in K-p interactions at 3.9 and 4.6 GeV/c 2—14686
K*(890) and (1420) production in quasi two-body K-p reactions at 10 GeV/c 2—14685
K*(890) production in $K^+ n \to K^+\pi$-p charge exchange reaction, 9 GeV/c 2—11631
K*(890) trajectory, absorption corrections, hyperon polarization in Regge models 2—38283
K(890) production, comparison with φ production using SU(3) invariance 2—23877
κ^+-κ^0 mass difference, estimates using broken chiral symmetry 2—34659
κ, symmetry-breaking role 2—426
κ resonance, in sum rules for K_{l3} form factors 2—38286
ω-ρ mixing, effect on strong interactions 2—31306
ω-ρ mixing effect in $e^+e^- \to \pi(\eta)\gamma$ reactions 2—31207
ω, photoprod. on nuclei, cross section 2—31313
ω, photoprod. on protons, comparison of data with VDM predictions 2—34703
ω complex Regge poles, in π^0 photoproduction on nucleons 2—27752
ω electroproduction, model test of $\rho\omega\pi$ vertex 2—8185
ω exchange isolated in reactions $\pi p \to \rho N$ at 6 GeV/c 2—14677
ω exchanges, coupling constants of isosclar vector mesons to nucleon 2—31311
ω photoproduction, effect of natural parity exchange 2—34700
ω universality relation shown to agree with expt. at Serpukhov energies up to 50 GeV 2—31310
ω^0, spin density matrix elements determ. in reaction $\pi^- p \to \omega^0 n$ 2—14676
$\omega \to 2\pi$, branching ratio, in $\pi^- p \to \pi^+\pi^- n$ reaction at 15 GeV/c 2—27756
$\omega \to 2\pi^0\gamma$, radiative decay in pole model, photon energy spectrum expressions 2—34701
$\omega\varphi$ mixing angles, determination from Weinberg sum rules 2—23871
P_{11}(1470), formation in γn interactions 2—8182
φ, photoprod. at 5.2GeV from ρ and C, study of forbidden decay of $\varphi \to \pi^+\pi^-$ 2—14678
φ, photoprod. on protons, comparison of data with VDM predictions 2—34703
φ exchanges, coupling constants of isoscalar vector mesons to nucleon 2—31311
φ production, comparison with K(890) production using SU(3) invariance 2—23877
$\varphi \to \eta\gamma$, decay, obs. in $\pi^- p \to n\varphi$, branching ratio 2—17953
$\varphi \to \rho\pi$, decay modes, strange spin 2—38341
$\pi^-\gamma$ resonance, possible existence at 270 MeV indicated by the reaction π-$p \to p + (\pi$-$\gamma) + m\pi^0$ 2—11627
$\pi\mu$ resonance, limits on width 2—23868
Q, cross over obs. in production differential cross sections 2—31302
Q, mechanism of production, density matrices analysed to give helicity structure and relative magnitude of coupling to A_1 production 2—14680
Q production, t-channel helicity conservation and Deck effect 2—5549
ρ/ω interference in $\bar{p}p$ annihilation at 2.3 GeV/c, absence of discrete s-channel resonances 2—8202
ρ-ω interference in $\pi^- p \to \pi^+\pi^- n$ reaction at 15 GeV/c 2—27756
ρ, application of improved relativistic generalization of Breit-Wigner formula 2—5547
ρ, causality test using e.m. corrections to $\pi^- p \to \pi^+\pi^- n$ reaction 2—34704
ρ, coherent production in high energy elon nucleus scattering 2—28014
ρ, photoproduction, existence of fixed pole 2—424
ρ, photoproduction in $\gamma p \to \rho^0 p$ reaction at 5.5-18 GeV 2—14552
ρ, Regge trajectory calc. using N/D formalism 2—17954
ρ and A_1 widths, relationship by Weinberg sum rules 2—23874
ρ complex Regge poles, in π^0 photoproduction on nucleons 2—27752
ρ dominance electromagnetic pion form factor with vacuum polarization insertions 2—27764
ρ exchange, factorization test 2—8187
ρ exchange, non-flip, in πN scattering, cut correction generation 2—27758
ρ exchange in S-wave $\pi\pi$ scattering 2—14669
ρ production, prediction from pion photoproduction and vector meson dominance model 2—8188
ρ resonance parameters determ. in $\pi^+\pi^-$ production by e^+e^- annihilation in ρ energy range 2—38241
ρ trajectory and wide-angle $\pi^- p \to \pi^0 n$ data 2—17942
ρ^0, decay angular distributions, prod. in 1 π exchange, explanation in terms of kinematical reflection of N* 2—2557
ρ^0, ω, backward production in inelastic ep scattering 2—34702
ρ^0, photoprod. on nuclei, cross section 2—31313
ρ^0, photoprod. on protons, comparison of data with VDM predictions 2—34703
ρ^0, photoprod. on protons, cross sections 2—27707
ρ^0, photoproduction in Compton scattering on nucleons at high energies 2—8110
ρ^0 electroprod. on protons, differential cross sections 2—27765
ρ^0 photoprod., Regge pole model analysis 2—27766
ρ^0 photoproduction, closure approx. in deuterium and non-diffractive amplitudes 2—425
ρ^0 photoproduction and scattering on nucleons, high energy role played by mediating pion pairs 2—31195
ρ^0 photoproduction from H, D and complex nuclei, 4-9 GeV, determ. detailed dipion mass-spectrum fits 2—14684
ρ^0 production cross section in $\pi^- p \to \pi^-\pi^+ n$ reaction at 4.45 GeV/c 2—23855
ρ° photoproduction, effect of natural parity exchange 2—34700
ρ', rel. to analysis of $e^+e^- \to \pi^+\pi^-\pi^+\pi^-$ reaction 2—38244
ρ—ω, interference and exchange degeneracy in $\pi^+ p$ interactions at 5.45 GeV/c 2—5540
$\rho^0 N$ cross section determ. from elastic photoproduction on deuterium 2—14683
$\rho\omega$ interference model, for coherent nuclear 3π production in A_1 region 2—38623
$\rho\omega\pi$, vertex, test using electroprod. of ω-meson 2—8185
σ-exchange potential for nucleon-nucleon scattering 2—34712
σ, electromagnetic couplings estimates 2—34699
σ, prediction from application of axiomatic field theory to $\pi\pi$ scattering 2—11622
σAA vertices, hard meson calc. 2—31308

Mesons continued
resonances continued
$\sigma\pi\pi$ vertices, hard meson calc. 2—31308
V^0N scattering, slope parameter in differential elastic cross section 2-21421
$V^0\pi$ elastic-scattering amplitudes, method for experimental study of energy dependence in vector-dominance model 2—17935
W, in weak interactions, Feynman rules for production and calculations 2—421
$W^\pm$, in chimeron model, identification with $a^\pm$ particle, relevance to CP problem 2—11623
$W^\pm$ prod., near forward neutrino, gross CP effects, prediction from Gell-Mann model of CP violation 2—362
X^0 (960), spin-parity determin. electromag. production processes and radiation decays 2—31309
x^0 production in 4 and 6 prong events from π^+p interactions at 5.45 GeV/c 2—31290
X^0(958) meson mass spectrum near resonance studied in $\pi^-+p\rightarrow$missing mass+n reaction near threshold 2—38308
ρ, photo- and electroprod. in deep inelastic region, Regge pole analysis 2—14681
ρ photoproduction, high energy, comparison of diffraction-dissociation model with empirical data 2—23875
ρ', introduced to interpret the stopping process $\bar{p}p\rightarrow\pi^+\pi^-\pi^0$ 2—31325
X_o, radiative decay, quark loop model 2—31259

scattering
ABFST multiperipheral model, pseudoscalar meson octet inclusion 2—21269
charged vector meson, scattering in static field at high energies 2—21296
dual N-meson amplitudes, algorithm for construction 2—5521
electron-meson deep inelastic scattering, scale invariance of structure function and generalized vector dominance model 2—31201
meson-baryon, isospin bounds on polarization 2—14622
meson-baryon, S-channel helicity amplitudes with $n\geqslant2$ 2—34654
meson-baryon, unitary symmetry and duality 2—8152
meson-baryon, without parity doublets dual model 2—5520
meson-baryon coupling constants, strong coupling model with isospin hypercharge symmetry 2—38310
meson-meson, pseudoscalar, multiperipheral model with Veneziano type production amplitudes, exchange degenerate and exotic trajectories 2—38279
meson-meson, review 2—14624
meson-nucleon, resonance generation, inverse problem study, partial waves 2—23831
meson-nucleon scattering, Feynman-diagram models of Fermion Regge-pole conspiracies 2—34655
pseudoscalar meson-baryon high energy forward scatt., total cross sect. from multiperipheral model 2—14623
pseudoscalar meson-pseudoscalar meson, derivation of SU3 couplings, canonical mixing, angles and absence of exotics 2—17888
$\eta^0\eta^0$, finite-energy sum rules in Virasoro model 2—21282
$\rho^0N\rightarrow\rho^0N$ elastic scattering, high energy role played by charged pion pairs mediating 2—31195

spin and parity
diffractive prediction of mesonic systems, natural parity exchange of Gribov- Morrison parity rule 2—404
ω photoproduction, effect of natural parity exchange 2—34700
ρ° photoproduction, effect of natural parity exchange 2—34700

Mesosphere *see Atmosphere*

Metal-insulator-metal structures and devices
see also Tunnelling
cadmium arachidate, organic monomolecular layers, neg. resistance obs. 2—36568
current filament detect., a.c. detect. scheme, electron microscope obs. 2—40311
d.c. conduction mechanisms, book 2—29732
electron injection, arbitrary band structure 2—4256
fatty acid salt monolayers between metal electrodes, tunnelling 2—1547
field emitters, breakdown mechanism 2—13289
high-field cond. laws in prescence of trapping 2—25904
interface barrier energies from photoresponse, electron scatt. effect 2—33039
Langmuir film, elec. properties 2—4273
m.i.m. structure, defects 2—3506
m.i.m.i.m., hot electron transport through metal films 2—36566
m.i.s.m., with CdS layer, electron emission 2—10098
m.o.s.f.e.t., X-irrad. effects 2—13296
polymer, bistable electrical switching 2—6873
Poole-Frenkel emission centres obs. by e.p.r. in reactively sputtered SiO_x 2—1726
sandwich cathode, height and half widths of ang. distrib. of electrons emitted from traps 2—10150
secondary electron emission produced by 50 MeV electrons in metal-low density dielectric film-metal sandwich 2—25983
silico-organic polymer film in glow discharge, threshold breakdown potentials 2—4258
space-charge-limited and contact-limited transient photoinjection currents 2—13288
tunnel junction, current response time limit 2—1545
tunnel junction, temp. depend. of tunnel current, insulator prop. effects 2—40308
tunnelling, film thickness depend. 2—13081
tunnelling, low energy barrier detn. 2—22597
tunnelling current calc., electron-phonon interaction effects 2—19722
tunnelling current calc., free electron description 2—6870
tunnelling current calc., localized impurity states influence 2—6871
voltage and resistance rise at high temp., as function of temp. 2—1546
zero bias anomalies due to paramag. impurities 2—13070
Zircaloy-2/anodic oxide/Au structure, elec. breakdown 2—10113
Al-Al_2O_3-Al, energy-momentum relation in tunnelling barrier 2—19724
Al-Al_2O_3-Al, photoemissive detn. of barrier profile 2—4257
Al-Al_2O_3-Al, source of voltage and large resistance at high temp. 2—1546
Al-Al_2O_3-Al, space charge effect on elec. strength depend. on insulator thickness 2—29734
Al-Al_2O_3-Al junctions, tunnel thickness 2—40309
Al-Al_2O_3-Au, electroluminesc., electron emission, and negative resistance 2—19725
Al-Al_2O_3-Au, ionic conduction and time dependent polarization 2—36584

Metal-insulator-metal structures and devices continued
Al-Al_2O_3-Au structure, electron emission, elec. cond., electroluminescence 2—13290
Al-SiO_x-Ag cold cathode, electron emission, attenuation length 2—25971
Al-SiO_x-Ag thin film cathode, elec. props. 2—19723
Al-SiO-Al condenser, temp. depend. of SiO film breakdown 2—13308
Al-borosilicate glass-Al, space charge effect on elec. strength depend. on insulator thickness 2—29734
Au-LiF-Au and Au-LiF-Al, preparation by vacuum evaporation 2—39494
CdSe-SiO_x, conduction mechanism, interface phenomena 2—13291
Nb-NbO_2-NiCr, current filament detect., a.c. detect. scheme, electron microscope obs. 2—40311
Nb_2O_5, dielec. relax. and tunnelling rel. to metallic impurities 2—10099
Si metal-p^+-p-p^+- metal dielec. devices, space-charge-limited current flow 2—13292
Ta-Ta_2O_5-Au, electroluminesc., electron emission, and negative resistance 2—19725
Ta_2O_5, current transport, effective dielectronic constant 2—6872
V_2O_5-P_2O_5 glass, high resistance, negative resistance and high- conductivity obs. 2—40314
WO_3, voltage controlled rsistance characs., a.c. and d.c. conductivity 2—36567

Metal-insulator-semiconductor structures and devices
see also Tunnelling
capacitor, Cole-Cole plotting of surface state admittance 2—10100
charge coupled devices, fast interface state losses, simple model 2—33041
charge pumping and low frequency noise 2—10104
CMNOS structures, radiation effects, electronic recovery 2—19735
d.c. conduction mechanisms, book 2—29732
electrolyte-insulator-semiconductor structure, differential capacitance, flat band voltage 2—4255
ferroelectric field effect for oxygen depleted $Pb(Zr_{0.65}Ti_{0.35})O_3+Nb_2O_5$ surface layers 2—40357
field-effect meas. during deposition of semiconductor on ferroelectric, film characterization 2—40231
flat band shift, controlled charge injection 2—4260
general study within large frequency range 2—25906
high-field cond. laws in prescence of trapping 2—25904
ideal, capacitance-voltage characteristics calc. 2—25905
interface elec. props., irrad. effects, insulating film props. rel. to rad. sensitivity 2—40315
interface phenomena, diffusion of ions in oxide layer 2—18919
interface state density measurement, capacitance derivative method 2—29735
inversion layer mobility, theory 2—22553
LSI/m.o.s. logic system, modelling and radiation effects 2—17520
m.a.o.s diode, two carrier charge transport and storage model 2—36571
m.a.s., m.a.o.s., electrode effects on CV hysteresis behaviour 2—33042
memory transistor, charge transport time depend., direct tunnelling model 2—22598
m.n.o.s. diode, two carrier charge transport and storage model 2—36570
m.n.o.s. memory device, influence of charge storage mechanisms 2—36572
model, G/U charact. 2—19726
m.o.s., surface potential fluctuations generated by interface charge inhomogeneities 2—40318
m.o.s., surface states response, influence of recomb. dynamics 2—33043
m.o.s. circuits, characteristics for radiation hardened aerospace systems 2—19742
m.o.s. memory, non-volatile, preprogrammed by use of ionizing radiations 2—19736
M.O.S. struct., direct meas. of built-in voltage, method 2—13295
m.o.s. structs., dielec. loss, electrode deterioration, Na problem 2—22600
m.o.s. structure, tunnelling into amorphous InSb or GaSb films 2—19647
m.o.s. structures effect of crystallographic orientation of Si substrates on the effective surface state charge density 2—25909
m.o.s. technology, advances in ion implantation 2—25878
m.o.s. X-ray detector with integrated detection, memory and readout 2—27887
m.o.s./LSI, transient ionizing radiation effects 2—19737
m.o.s.f.e.t.s. in nuclear instrumentation amplifiers 2—31377
m.o.s.t., radiation hardening 2—19738
m.o.s.t., Si inversion layer, electron conductivity-mass anisotropy calc. 2—36569
m.o.s.t. inversion layer, hole mobility, low temp. Hall effect obs. 2—16254
negative conductance in interdigital electrode struct. on oxidized surface 2—25910
oxide charge distrib., photoinjection studies 2—1550
p-channel, radiation hardening by optimization of thermal SiO_2 gate insulator 2—19734
phosphosilicate glass stabilization 2—1549
piezoelectric field effect transducer, acoustic wave detection 2—20934
radiation and oxide metal interactions in m.o.s. 2—19731
radiation induced perturbations in electrical propertes 2—6874
radiation response at dose rates from 10^9 to 10^{12} Rad (Si)/s 2—22599
shift register, charge-transfer, surface transport obs. 2—40317
surface barrier m.o.s. diodes, optical energy gaps determ. from photovoltage meas. 2—40381
surface states, fast spectrum, obs. by differential C-U method 2—33040
traps, volume and interface, simultaneous detn. from C-V characteristics 2—4259
tunnelling probability, influence of band bending 2—19727
Al-Al_2O_3-Si, oxide prep. and nitrous oxide and aluminium trimethyl 2—1557
Al-Al_2O_3-Si, oxide prepared by glow discharge technique 2—1556
Al-Al_2O_3-Si system, internal photoemission, energy band diagram 2—13358
Al-P_2O_5.SiO_2-SiO_2-Si, multiple dielectric, charge distribution 2—10102
Al-SiO_2-Si structure, I-V characts., effect of dislocations in Si 2—36573
Al_2O_3- SiO_2-Si, m.a.o.s. struct., charge storage 2—13293
Al_2O_3-Si; Al_2O_3-SiO_2-Si, struct., C-V shift characts. 2—13294
Al_2O_3 m.o.s. devices, radiation-induced trapped charge, relaxation phenomena 2—19739
Au-InSb, oxide-InSb struct., charge exchange between traps 2—13297
CdSe-SiO_x system investigation by m.i.s. structure capacitance meas. method 2—25907
GaAs-Al_2O_3-Al photoexcited electron transport, photoelec. studies 2—40379
GaAs-Si_3N_4, deposition of Si_3N_4 and flat-band parameters 2—15665
Ge, amorphous, tunnelling into m.o.s. struct. 2—13298

Metal-insulator-semiconductor structures and devices continued
Ge_3N_4-Ge, trap levels and barrier height, C-V characteristics and photoemission 2—10101
InAs-oxide-Pb, electron tunelling, surface accumulation layer obs. 2—13265
InSb devices, magnetoresist. 2—19728
M-Al_2O_3-SiO_2-Si, m.a.o.s., charge injection 2—1548
Si-Al_2O_3, effects of heat treatment on Si surface potential 2—29736
Si-Al_2O_3Al, photoexcited electron transport, photoelec. studies 2—40379
Si-SiO_2-Al, surface effects of gamma irradiation 2—10105
Si-SiO_2-Al gamma radiation damage studies by internal photoemission 2—19730
Si-SiO_2-Al_2O_3, effects of heat treatment on Si surface potential 2—29736
Si-SiO_2-Cr gamma radiation damage studies by internal photoemission 2—19730
Si-SiO_2, interface density and pot., v.l.f. m.o.s. capacitance meas. 2—6833
Si-SiO_2, interface state parameters detn., conductance and capacitance obs. 2—40320
Si-SiO_2, surface electron transport in m.o.s.f.e.t. and m.o.s. devices, paramag. centre effects, e.p.r. obs. 2—10095
Si-SiO_2 interface, nonuniform lateral ionic impurity distribs. 2—40313
Si-SiO_2 interface, surface state annealing parallel to B_2 centre annealing in irrad. SiO_2 2—40312
Si-SiO_2 interface states, generation and distrib. obs. using bias temp. treatment 2—29737
Si, amorphous, tunneling into m.o.s. struct. 2—13298
n- Si, tunnelling characteristics, phonon structure 2—16255
Si (110) surface n-channel m.o.s.f.e.t., conductivity anisotropy obs. 2—16239
Si f.e.t., differential negative resistance of n-type inversion layer 2—19740
Si film, epitaxial on sapphire, carrier transport mechanisms, m.i.s. deep depletion Hall effect struct. obs. 2—40293
Si film, on sapphire, elec. props. depth variation, m.o.s. Hall technique 2—19688
Si film, on sapphire, elec. props. depth variation, m.o.s. Hall technique 2—19688
Si m.i.s. strucrure, anomalous recombination 2—25908
Si m.o.s. inversion layer, transport phenomena, effective mass approach 2—19744
Si m.o.s.t., interface-state density and mobility ratio obs. 2—16240
Si m.o.s.t., inversion layer, hole drift vel. 2—19743
Si negative resistance diode, m.i.(n-p). struct. 2—40316
SiO_x-CdSe, volume and interface traps, simultaneous detn. from C-V characteristics 2—4259
SiO_2-Si, 20-40 Å oxide film on nondegenerate Si, interface states 2—22601
SiO_2-Si, deep electronic traps, photocond. and CV characts. obs. 2—36574
SiO_2-Si, dielectric breakdown 2—10103
SiO_2-Si, surface state characterization, quasi-static technique 2—16253
SiO_2 electron injection, scatt. in image pot. well 2—40319
SiO_2 electron irradiated, short term charge annealing 2—19732
SiO_2 layer, defects, activation energy of charge carrier diffusion 2—25911
SiO_2 layer in m.o.s. system, relaxation polarization, surface potential stability 2—4269
SiO_2 noncrystalline, defect structure and irradiation behaviour 2—19733
SiO_2 v.u.v. radiation charging 2—19741
SiO_x film in MNOS, oxidation growth using nitric acid 2—12666
Te-TeO_2-Pb, tunnelling junction, phonon assisted tunnelling effect 2—29688
Te film, on TGS substrate, ferroelec. field effect temp. dependence 2—36517
ZnSe electroluminescent device, exhibiting switching and memory 2—33327

Metal-semiconductor boundaries *see Semiconductor-metal boundaries*

Metallo-organic compounds *see Organic compounds*

Metallography
alpha autoradiography, use of cellulose nitrate detector films 2—36191
apparatus for 4.2-300 K studies 2—39854
conference, Aalen, Germany, Sept. (1971) 2—32680
crystal growth and grain boundary migration, optical obs. method 2—39590
defect observation, optical and scanning electron microscopy 2—32498
electron microscope methods 2—32428
electron microscope methods 2—32429
fractographic head, measurement of microhardness 2—29368
fractography, improvement in specimen preparation 2—19221
instrumentation for qualitative picture analysis 2—32682
metallographic chart construction, statistical method 2—6642
metallographic struct. evaluation by computer 2—32437
microarea electron diffraction technique in high voltage electron microscopy, applications 2—3657
microprobe analysis and colour etching, combined technique 2—36227
Mischmetal-Mg alloys, metallographic prep. 2—12974
physical metallurgy, tools and techniques, book 2—25560
polishing powder, Al_2O_3, scanning electron microscope evaluation 2—36192
polymers, techniques 2—35854
quantitative, principles and practical methods 2—25561
reactor fuel, post-irrad. exam., sampling methods 2—38756
reactor fuel elements, post-irrad. exam. 2—38760
reactor fuel post-irrad. exam. facilities 2—38751
replica preparation, single-stage C extraction, for obs. near edge of sectioned specimen 2—36228
scanning electron microscopy 2—29127
specimen preparation and examination techniques 2—25562
steel, microstructure exam. using electron microscope 2—39642
steel, nonmetallic inclusions, examination and determination techniques 2—1257
steel, pressure melted, high N content 2—32686
steel, quenched, recrystn. during rapid heating, metallographic obs. 2—29389
steel, recrystallisation, struct., during slow heating 2—15906
stereology, basic integral formulae, procedure for counting figures of polished sections 2—39627
stereology of cubic particles, obs. of simulated microstruct. 2—12702
uniformly distributed finite particles average nearest-neighbour distance calc. 2—36226
Ag single crystal, strain free prep. 2—22126
Al, 99.5%, coarse grained cast, orientation detn. by anodic etching and optical obs. 2—19264

Metallography continued
Al, thermal pits, condensation cavities, obs. using liquid Ga embrittlement 2—9253
Al single crystal, strain free prep. 2—22126
Be, microcracks, microscale plastic flow, grain boundaries, fracture surfaces 2—12906
γ'-Cu-Al-Ni, alloy, martensitic, elastic twinning, stress effects 2—15769
γ'-Cu-Al, alloy, martensitic, elastic twinning, stress effects 2—15769
Cu single crystal, strain free prep. 2—22126
Fe-C-Cr, alloy, austenite-proeutectoid ferrite transform., metallographic obs. 2—22359
Fe-Ni-Mn alloy, isothermally treated, martensitic transform. characts., metallographic obs. 2—32765
Fe, grey cast, specimen prep. for graphite distrib. assessment 2—19051
Mg alloy, cavity growth caused by flow, obs. 2—39788
Mo, plastic deform., fine struct. changes during rolling 2—32508
Nb single crystal, strain free prep. 2—22126
Ru, electromech. polishing, etching, prep. for optical metallography 2—12650
Ti-Al-V alloy, etching, O_2 effect 2—32735
Ti-(6wt%)Al-(4wt%)V, alloy, texture analysis, colour metallography, colour anodizing technique 2—12735
W vortex plate, cracking, gas combustion, defects 2—32641
$ZrCr_2$, wave dispersive electron beam microanalysis and energy dispersive scanning microscopy 2—22167

Metallurgy
see also Ageing; Metallography; Zone melting and refining
5th international vacuum conference, Boston, Mass., USA, Oct. (1971) 2—41374
actinides, metallurgical properties, relationship with atomic spectra 2—21502
ageing, duraluminium-D16T, effect of uniform compression at 77K 2—12965
alloy steels, critical points, influence of original structure 2—29469
conference, French Soc. autumn meeting, Paris, 1971 2—9727
conical turning, lubrication and rate of rotation, plastic deformation characts. 2—12844
decarburization in a converter during refinement, potential theory 2—40799
electro-slag remelting 2—35978
electron probe microanalysis 2—30124
electrospark alloying process, regularities in formation of hardened layer 2—6608
equilibrium diagrams and their importance in non-destructive testing theory 2—6643
extraction, properties and applications of special metals 2—3925
field ion microscopy 2—29130
flaw characterisation using interference effect in multifrequency pulse echo 2—34139
glued metal joints, effect of preliminary impact on strength 2—29347
heat pipe oven, heater with homogeneous temperature distribution 2—20764
hot sample, electronic microanalysis 2—12925
inclusion flotation, wettability effects, simulation expt. 2—3414
levitation melting, stability considerations 2—12922
light-figure microscope 2—29132
liquisol quenching apparatus 2—3930
lunar spinels, subsolidus reduction 2—10995
materials standards 2—19234
mechanically nonhomogeneous bodies, strain investigation using photosensitive coatings 2—29346
metallographic chart construction, statistical method 2—6642
non-destructive testing of adhesive bonded metal-to- metal joints 2—32676
physical, book 2—25560
physical tools and techniques, book 2—29372
powder, applic. to nuclear industry 2—8408
powder, conf., London, England, Nov. (1971) 2—9726
powder, material and process improvements 2—3969
rapid quenching apparatus for small specimens 2—23186
scanning electron microscopy 2—29127
steel, carburisation process 2—1366
steel, case-hardening process, standardisation 2—3814
steel, continuous casting plants, operating techniques and utilization times 2—3944
steel, equilibrium considerations for non-destructive testing 2—29492
steel, processing effects on two-layered corrosion resistant structure 2—1365
steel ingot, solidification process, differential mathematical model 2—3442
steel smelting and hot working 2—1345
superconducting alloys, high-field, rel. to pulsed-field meas. 2—25790
thermodynamic potential variation during process, calc. method 2—40799
transient processes in welding arc, mathematical model 2—20770
ultrasonic testing, half-value depth of reflecting zones 2—11356
vacuum metallurgy, conf, New York (1971) 2—33836
vacuum metallurgy, review, book 2—19238
vacuum treatments, maximum rate obtainable in sorption and degassing processes 2—41415
welds, temporary stresses during tempering 2—6534
of welds produced in friction welding 2—1354
Al-killed steel, continuous casting strand 2—1368
Am, metallurgical properties 2—22323
Bk, metallurgical properties 2—22323
C-Mn killed steel, continuous casting strand 2—1368
Cm, metallurgical properties 2—22323
Cu, spiral elongation test, annealability, impurities, heat treatment, quality factors 2—3932
Fe-Si crystalographic observation, deformed layers, cutting process 2—36223
Ni alloys, development as high performance, high temp. mats., review 2—12973
U recovery, precipitation of UN from liquid U-Sn alloy 2—8405

Metals
see also Alloys; Metallography; Semiconductors; Semimetals
abundance in M67 galactic cluster stars 2—20539
abundance indices for F-type disk population stars 2—20553
abundances in Groombridge 1830 subdwarf 2—41090
acoustic emission study, review 2—22314
adhesion and friction, cryst. struct. and defect effects 2—3921
adsorbate on metals, u.v. photoemission spectroscopy 2—36625
adsorbed layers, i.r. spectroscopy, sensitivity improvements 2—15673

Metals continued
adsorption of He, Ne, Ar, atom probe field ion microscope obs. 2—9427
adsorption of nonpolar gases, adsorption isotherms, isosteric heat data 2—6377
aerosols, generation direct from surface for spectrochem. anal. 2—20215
antiferromagnetic, electromagnetic fluctuations in a mag. field 2—6989
atom formation in flames, absorption and emission data 2—5279
atoms, collisions of second kind, spectral study 2—2960
backscattering of high energy heavy ions, Monte Carlo calc. 2—40101
b.c.c., crystallization, electronic struct. influence 2—18974
b.c.c., microstrain and dislocation relax. 2—12826
b.c.c., ultimate tensile stress, structure sensitivity 2—25492
bulk modulus, press. depend., calc. from shock wave data 2—32573
cavitating effect of cryogenic liqs. 2—39915
cermet, surface polishing, diamond pastes evaluation 2—22064
coating with polymers by electrophoretic deposition 2—1760
compatibility determ. by static friction tests 2—29458
compatibility effects on tribological characts. 2—29343
component failure, heat treatment effect 2—32627
condensed matter conference, Geneva, Switzerland, Sep. (1971) 2—12624
core annihilation rates, calc. 2—36431
corrosion, He environmental effects in high temp. reactors 2—11913
crack trajectory, effect of direction of application of tensile stress 2—3901
creep, low temp., exhaustion theory 2—39795
creep, testing in ultrasonic field over wide temp. range 2—29363
creep and low cycle fatigue, anomalies 2—39797
creep investigation, temp. differential method 2—36126
creep monitoring in tubular specimens, eddy current diametral extensometer appl. 2—39862
cryogenic props., used in low temp. normal and superconducting magnets 2—14371
crystal growth, suppression of striations 2—25268
cubic, anisotropy in sheet forming operations 2—25582
cubic, Debye charact. temp. 2—32791
cubic, elastic consts., failure of Cauchy relation 2—9631
cubic, straight dislocation, elastic energy 2—1253
cubic, vacancy form. entropy 2—36016
cyclic loading, dissipation and damage, theory 2—15828
cyclic stressing, by 20 kHz u.s. waves, for testing and quality control 2—19233
cyclotron resonance, h.f. study of electron- phonon interaction 2—16126
Debye temperature, calc. using Morse potential function 2—4062
defect clustering, anomalous X-ray transmission, theory 2—15746
defect indications detection before, during and after load applic. 2—32664
deformation parameters, computer estimation 2—32601
deformation texture, theory 2—39916
dendrite morphology, holographic obs. on transparent org. cpds., simulation expt. 2—15669
diamagnetism, giant impurity, calc. using bound impurity orbitals 2—1602
diffusion, molten Sn bath for activation vol. determ. 2—9606
diffusion, penetrability and solubility coefficients of H and D 2—29229
diffusion, relation between melting heat and activation energy 2—39726
diffusion of gas, det. of activation energy 2—39717
diffusion of H_2, effect of microvoids 2—39723
diffusion of noncond. inclusions, pores, in elec. field 2—29208
diffusion under influence of ultrasound, phase growth 2—25460
diffusional kinetics of intermetallic phase growth at metal/metal interface 2—36074
diffusional motion of nonspherical inclusions 2—39718
dislocation damping, strain amplitude 2—3775
dislocation vel. and density determ. from deform. waves of continuous yielding 2—36108
dispersion hardening, strain hardening due to dispersed second phase 2—25574
ductile, critical plane-strain stress intensity factor 2—19208
ductile, erosion 2—9719
dynamic stress/strain curve of uniaxial compression 2—32594
elasticity, from dynamic matrix, microscopic theory 2—15795
electric fields induced by gravity, electrochemical systems in thermodynamic equilibrium 2—6070
electrical resistivity determination at high temperatures and pressures, phase transformations 2—37528
at electrolyte interface, opt. props., double-layer structure models 2—9235
electron and positron absorpt., empirical relations 2—29570
electron emission induced by laser radiation, instrument 2—40390
electron microscopy, replica technique for simultaneous obs. of interior and surface 2—19029
electronic structure, fully automated device for investigation by positron annihilation 2—6705
electronic structure obs. by n.m.r., effects of melting 2—7136
e.m. and critical phenomena 2—19482
e.p.r. lineshape on localized spins 2—10477
e.p.r. obs., rare earth impurities in metals, cond. electron coupling, review 2—4536
fatigue failure prediction, complicated stress-strain history 2—39817
fatigue failure study by resistance strain gauge 2—29350
f.c.c., cryst. growth from melt, vacancy condensation and dislocation form. 2—9534
f.c.c., LEED spectra, layer-KKR method calcs. 2—35864
f.c.c., solubility of H/D, isotope effect, calc. 2—19260
f.c.c., twin boundary energy, temp. coeff., stacking fault energy 2—32533
f.c.c., twinning- gliding dislocations interactions, deform. twins growth and struct. 2—15766
f.c.c., X-ray and neutron scatt. by dumbbell interstitials 2—9540
f.c.c. and h.c.p., stacking fault energy rel. to impurity conc. 2—22212
ferromagnetic, dynamical susceptibilities 2—19853
ferromagnetic, electronic contrib. to Faraday effect, obs. using 230 and 330 keV photons 2—7030
ferromagnetic, heat conductivity mechanism 2—13056
ferromagnetic, polycryst., temp. depend. of neg. Barkhausen jumps in magnetiz. process 2—29815
fibre, porous, pressing and sintering, deformation, residual stress relaxation 2—29257
fibre composites, elevated temperate morphological stability, coarsening behaviour 2—1383
field ion microscopy 2—29130
film, θ cutoff model of size effect in conductivity 2—36436
film, chemisorption of gases, elec. resist. changes 2—32915
film, diffusion, review 2—19137

Metals continued
film, diffusion of disparate metal, electron microscopy techniques 2—39732
film, discontinuous, electrical cond. and electron emission 2—19540
film, elec. field effect on formation 2—9254
film, electrolytic nucleation 2—39592
film, gas adsorp., sticking probability measurement 2—39546
film, initial stage of deposition, electrostatic field effects 2—29021
film, nucleation on nonmetallic substrate surface defects 2—39486
film, reactively sputtered, influence of surface adsorp. characts. 2—22068
film, single crystal, vacuum depositing technique 2—9259
film, size-depend. elec. cond. 2—19541
film, thickness meas., Leonard-Ramey method 2—3508
film, transport props., size effect 2—29612
film, uneven vacuum deposition 2—3513
film, void form. and growth during electromigration 2—9608
film adhesion to glass and MgO, tangential shear meas. 2—3977
film reactively sputtered, surface absorpt. characs. effect on compound form. or gas incorp. 2—39481
films, ion beam sputter deposited, nucleation, growth 2—6343
films, isotropic thin, electron transport 2—4098
films, with ellipsoidal Fermi surfaces, conductivity 2—4154
fine particles produced by gas evaporation, mean size and size distrib. 2—25605
flaw characterisation using interference effect in multifrequency pulse echo 2—34139
fluids, properties in critical region 2—8876
forming, f.c.c. and b.c.c. metals in conical flow 2—36211
fracture, semifragile tears and progressive fissuraction 2—22281
fracture toughness parameters 2—29321
freezing and melting under controlled conditions, rel. to thermometer calibration 2—17453
friction, static and dynamic rel. to hardness 2—9723
friction process with polymers, in s.h. vacuum, 300-10K 2—36179
friction stress, during high temp. creep, theory 2—12866
fusion temp. at high pressure, equation for det. 2—28941
gaseous impurity, detection by mass spectrometry, isotope dilution method 2—10656
glass forming tendency, theory 2—9224
glassy alloy, structural model 2—32713
grain boundary, bubble raft model, order struct. and dislocations 2—15770
graphite based synthetic metals, electrical anisotropy 2—40171
hard, fracture structs., electron microscope obs. 2—32651
hardening by ordered coherent precipitates 2—19259
h.c.p., lattice dynamics 2—6647
h.c.p., X-ray diffraction peak broadening analysis, computer program 2—35974
heat resistance diagrams, parametric construction 2—4593
hexagonal, electrostatic contribs. to first, second and third order elastic consts. 2—19154
inert gas solid, compressive metallization 2—19498
interface with anthracene crystal, exciton dissoc. rate const., charge transfer 2—3490
interface with liq. He, Kapitza resist. 2—36361
internal friction, dislocation components 2—29240
internal friction and shear modulus, measurement by method of forced vibrations 2—29362
ion implantation damage, effects on hyperfine interaction meas. 2—19946
irradiation, void nucleation defect co-precipitation 2—32490
laser absorpt. characts. 2—25568
lattice dynamics, mol. rot., n.m.r. obs. 2—37000
line-blanketed stellar atmospheres, artificial absorption edges 2—30446
mag. and metallurgical properties, correlation, apparatus 2—16352
magnetic, emission and absorption spectra 2—26150
magnetic-after effect, defects and domains 2—19860
mechanical anisotropy due to non-random distrib. of crystal orientations 2—29255
mechanical strength, method of comparison at different temps. 2—29278
medium melting point, single cryst. tubes, growth, from the melt, Bridgman method 2—6402
melting, change of volume, rel. to rare gas 2—25140
metal-ceramic contact junction heat transfer at pressures of 5.10^5-200.10^5 N/m^2 and temps. of 583 to 873K 2—29565
metal-graphite contact junction heat transfer at pressures of 5.10^5-200.10^5 N/m^2 and temps. of 583 to 873K 2—29565
metal-H_2O interfaces, point charge and dipole image potentials 2—34278
metal/polymer composite, elec. resist. 2—40160
monolayer energy calc. for like ions 2—29067
neutron irradiated, void nucleation, computer evaluation 2—29163
n.m.r., spin-lattice relax. time due to nuclear quadrupole interaction, calc. 2—19931
n.m.r., temp.-independ. spin-lattice relax. time 2—29843
noble, cond. electron scatt. obs. using de Haas-van Alphen effect 2—16087
noble, lattice dynamics 2—32803
noble, lattice dynamics 2—32800
noble, phonon dispersion relations 2—4030
non flangible, fracture extension resistance in fracture safe design of nuclear reactors 2—15061
non-ferrous, melting 2—18875
nondestructive testing, by pulsed eddy currents 2—29380
nuclear acoustic resonance dispersion 2—7128
nuclear radiation effects on fast fracture behaviour and critical crack size 2—15877
nuclear spin phonon coupling, acoustic mag. reson. 2—40787
optical absorption, calorimetric method for scanning obs. 2—4431
optical props., review 2—19956
optically-induced r.f. field in static mag. field 2—33188
oxidation, adsorption of O_2 2—3521
oxidation, statical method of secondary ion mass spectroscopy 2—13594
oxidation resistance, Y addition effects, void formation suppression mechanism 2—22877
oxide-metal, carbide-metal, liq.-solid systems, wetting, rel. to sintering 2—6316
paramagnetic, spin susceptibility, surface effects 2—40414
particles, submicron size, plasma resonance description of white light scattering characteristics 2—13471
photodesorption and electron impact desorption from metals, threshold energy and mechanisms 2—6361
photoemission, review 2—19800
photoemission from thin films, boundary scattering effects 2—33087

Metals continued
photoerosion products studied using laser, method of meas. vapour contents 2—16074
plastic deform., review 2—12845
plastic deformation, energy relations, method of temp. meas. 2—19178
plastic deformation, high voltage electron microscopy 2—3863
plastic deformation by cold working, reduction of latent energy in heat cond. equation 2—39883
plastic flow, phenomenological theory, static recovery effects 2—39794
plasticity, dislocation movement, internal variable thermodynamic theory 2—12843
plasticity, statistical interpretation 2—3875
plate, mech. props. rel. to standard forming tests 2—9681
point defect prod. on irrad., recovery, b.c.c. and h.c.p. 2—15745
point dipole near metal surface, Thomas-Fermi response, effective polarizability 2—15652
polycrystal, plastically deformed, internal friction, Granato-Lucke theory, Rogers and Gelli modifications 2—12827
polycrystalline anisotropic, deformation effect of stress strain properties 2—36102
polymorphism, Debye temp. effect analysed 2—25323
in population II stars, contribution of cosmic ray nuclei 2—10852
porous, eqn. of state under strong shock compression 2—3847
positron annihilation in single crysts., temp. effects 2—25714
positron interaction, with defects 2—3778
powder, energy absorption during compaction 2—39955
powder, sintering, shrinkage equation 2—6620
powder, stressed state diagram, anal. 2—1377
pulsed-arc welding, tungsten electrode, influence of metal solidification pattern on hot cracking 2—12957
purity characterisation by eddy current decay method of meas. by residual resistivity 2—29344
quench hardening and point defects, book 2—12930
quenched, irradiated, secondary defects, nucleation, growth, annihilation 2—3766
radiation damage, computer simulation 2—15737
Raman scatt. line broadening, rel. to electron- phonon interaction 2—16514
rare, processing and applications 2—3925
recrystallization in emission electron microscope 2—39882
refractory, cryst. growth, cold metal crucible system 2—25267
refractory, dispersion hardening, review 2—32747
refractory, film, electron beam deposited, ion effects 2—39476
refractory, latent heat of fusion obs. at high current densities 2—28943
refractory, melting, floating zone furnace 2—23187
refractory, thermocouples, parameters needed for high performance 2—27334
resistivity, Bloch-Grueneisen parameters evaluation, program 2—32923
resistivity, fast neutron irradiation induced, recombination volumes 2—25763
secondary electron emission, by medium energy ion bombardment, comparison of exptl. results with theoret. predictions 2—19814
secondary ion emission from thin targets 2—10164
secondary ion emission on Ar bombardment, mass spectra 2—4330
self diffusion, curved Arrhenius plots 2—19133
self-diffusion, pseudopot. applic. 2—12791
shock compression, effects of electronic struct. 2—39769
shock melting and vaporization 2—39420
shock vaporization, rel. to equation of state determ. above 200 kbar 2—22044
sintering enhancement by impurity addition, prediction and control 2—22326
solid phase dissolution in liq. phase 2—32242
specific heat electronic and Debye temp., determ. method 2—16032
spectrochemical analysis using laser light sources 2—37065
sputtered atoms energy meas. 2—36370
sputtering, photon emission during ion bombardment 2—10357
stars, F and early G dwarfs, abundances from colours 2—4877
stellar blanketed model atmospheres, photometric observations 2—26697
strain hardening, plastic deformation, strengthening coeff. 2—12951
strength testing apparatus, at high temp. and ultrahigh vacuum 2—3924
stress corrosion cracking, capillary model 2—19205
stress corrosion cracking mechanisms 2—32635
stress-corrosion cracking, electrode kinetics 2—20189
stress-strain-temperature-time relationship, characterization in metals and alloys 2—15817
superplasticity, heat resist. 2—36110
superplasticity, origin of quasiliquid state 2—32614
superplasticity 2—29256
surface, acoustic phonons, Brillouin scatt. 2—16453
surface, Auger spectroscopy 2—1503
surface, H ion trapping, reflection and re-emission 2—39551
surface, intensities of Auger lines excited by electron and X-ray irrad. 2—12638
surface, residual polishing agent rel. to hardness, nucl. reaction reson. obs. 2—12634
surface, vacancy condensation pits, on quench annealing 2—6320
surface crack, mag. field of eddy currents excited by contact inductor 2—29376
surface emission properties, effect of bombarding ions energy above and below sputtering 2—36371
surface hardening, u.s. and vibromagnetic methods 2—36196
surface interaction of ion, dynamics inclusion 2—6308
surface layers, plastic flow analysis for tools and dies 2—34000
surface monolayer props. 2—29068
surface plasmon excitation, field ion spectroscopy applic. 2—16123
surface plasmon spectrum, field ion microscopy applic. 2—16122
surface scatt. of He atoms, Debye-Waller factor 2—12635
surface self-diffusion, book 2—28989
surface self-diffusion, electrostatic field effects 2—1162
surfaces, review 2—12637
thermal conductivity, rel. to lattice struct. and defect distrib. 2—1439
thermal contact conductance, nomograms 2—17428
thermal diffusivity, temp. depend., apparatus for solid and liquid phases 2—19443
thermal diffusivity, temp. dependence, and true specific heat, apparatus 2—29553
thermal fatigue under multiaxial thermal stresses 2—39820
thermodynamics, statistical, of electron transport, undergraduate book 2—13068

Metals continued
thermopower, diffusion term calc. without approximation 2—4289
thin films, reflectance and transmittance from oblique incidence measurements 2—31088
transmission electron microscopy, modified double-jet electrolytic thinning technique 2—15708
tunnelling conduction, voltage induced, granular metals 2—16133
u.s. fatigue 2—39818
vacancies, positron trapping, angular correlation data analysis 2—25386
vacancy conc., atom arrangements, stat. thermodynamic eqns. 2—6480
vacancy formation energies from positron annihilation 2—19086
vacancy thermal expansion effect on press. variation of activation enthalpy 2—39722
for vacuum systems, electron impact desorption obs. 2—39544
vapour, autoionizing spectra, vac. u.v. obs. 2—18308
vapour, photoionization cross-section meas. 2—18297
viscoplastic props. of metal crystals 2—6492
volume change meas. and characts. 2—3862
weld strain in brittle temperature range 2—12956
welding, crystal structure of metals deposited by pulsed-arc process 2—12958
welding, effect of metal thickness on nature of stressed and strained states 2—19249
welding, strain behaviour during solidification 2—15917
welding, technical strength criteria and tests during solidification 2—15918
welding, temporary strength during solidification 2—15916
whisker diodes, thermal field emission as i.r. light rectification mechanism 2—16323
wire, size-depend. elec. cond. 2—19541
wire specimens, saturation with ionized media in glow discharge 2—6508
work function determ., charge accumulation method, meas. apparatus 2—36621
X-ray spectra, absorpt. in X-u.v. range 2—1702
yield point raising treatments 2—12923
Ba_2FeReO_6, ordered perovskite, metallic conduction 2—22691
$Bi_2Ru_2O_7$, $Bi_2Ir_2O_7$ electronic characterization, cryst. chem. considerations, elec. and mag. meas. 2—10076
$Ti_{1-x}V(Cr)_xS_2$, electronic characterization 2—9350
$Tl_2Ir_2O_7$, $Tl_2Os_2O_7$, electronic characterization, cryst. chem. considerations, elec. and mag. meas. 2—10076

liquid *see Liquid metals*

theory
acoustic cyclotron reson., phase shift 2—32907
adsorption, quantum theory, book 2—15672
adsorption, quantum theory, review 2—15676
alkali, Li, Resist. and electron-phonon interaction 2—1455
alkali, mag. susceptibility change due to pseudopot. mag. field depend. 2—1604
alkali, pseudopotentials from variable phase approach to scatt. theory 2—29592
alkali metal, liq., ionic potential 2—21955
alloy, binary, dilute, resist. calc. from Ashcroft model pot. 2—40166
alloy, dil. nonmagnetic, cond. electron scatt., kinetic equation 2—13069
alloy, screened form factors of model potentials 2—40140
alloy, structure, algebraic model, based on Boolean functions 2—9436
amorphous and disordered, phonon enhanced cyclotron mass and electronic sp. ht. 2—16101
angular size effect in inclined mag. field 2—13099
b.c.c., phonon dispersion, two parameter model potential method 2—19365
binding energy and lattice constants, pseudopotential calc. 2—40139
collective behaviour of electron system, self-consistent pot. 2—40150
conduction e.s.r. in plates 2—26270
crystal potential, electron spectra calc. 2—9919
crystallization, electronic theory 2—18974
cubic, de Launay formulae for elastic constants 2—29232
cubic, lattice dynamics, extended De Launay's model 2—19335
cubic, pressure-volume relation anharmonicity, Morse function description 2—9851
cubic metals, Debye-Waller factors, temp. dependence 2—6649
cyclotron reson., Azbel'-Kaner theory, retardation effects 2—13104
d-band, pseudo Green's functions and pseudopot. theory 2—25723
de Haas-van Alphen effect, SCF approach in irreversible statistical mechanics framework 2—29609
density of states determ. from tunnelling conductance meas. 2—1459
dielectric function and effective band edge theory 2—29596
dislocations and plastic deformation, review 2—39778
effective ion-ion interactions 2—22091
electrical conduction, localized electrons and interactions with local modes 2—19537
electrical conductivity and phonon drag at low temperature 2—22486
electrical resist. at antiferromag. transitions 2—25760
electromechanical effects 2—25762
electron correlations, band structure effects 2—36394
electron correlations, set of coupled equations derived 2—36393
electron distrib. around mobile and fixed point charges 2—25747
electron exchange and correl. energies, elastic const. relationships applic. 2—1275
electron Fwrmi liquid, parametric instability of magnetiz. 2—25990
electron gas, dielec. function, numerical calc. scheme 2—9945
electron gas, displacement and collective variables method, numerical calc. 2—40155
electron gas, nonuniform, correl. potentials 2—32901
electron gas, screening of single positive charges, Hartree-Fock approx. 2—19525
electron gas, square well pot., impurity calc. and Schrodinger eqn. 2—16091
electron problems, Schrodinger eqn. separation 2—13066
electron valence band struct., soft X-ray band emission 2—4465
electron work function, relation to electronic structure 2—6914
electron-phonon interactions, influence on phonons damping 2—1454
electron-phonon system, damping of h.f. sound waves 2—19406
electronic density of states, core electron effect, electron-phonon interactions 2—4095
electronic structure rel. to props. 2—40121
e.m. absorption, quantum size effects in thin films 2—40135
e.p.r. width, temp. depend. 2—22822
excitonic states, spin susceptibility and impurity effects 2—40147
f.c.c., pair pot. calc. for stacking fault, twin and point defect energies 2—15747

Metals continued
theory continued
Fermi surface, relax.-time represent. and Dingle- Robinson temp. inversion 2—36401
Fermi surface of d- and f-block metals 2—16088
ferromagnet, side-jump model applic. to Hall and Nernst effects 2—22484
ferromagnetic electron gas, effect of exchange interactions on the dielectric response 2—19847
ferromagnetic resonance linewidth anomalous contrib., analogy to anomalous skin effect 2—10465
film, discontinuous, charge activation theory of cond. 2—40162
film, electron energy loss spectra, phonon effects 2—6699
film, longit. magnetoresist. and partially specular boundary scatt. 2—25756
film, quantum magnetoacoustic oscillations 2—6722
film, quantum size effect, direct verification 2—40125
film, thickness effects, piezoresist., resist. strain coeffs. 2—40163
film on dielec. substrate, pot. barrier height and tunnelling electron mass 2—1452
gravity induced electric fields calc. from periodicity deviations of the lattice 2—9914
Hall waves, dispersion law 2—1479
h.c.p., lattice dynamics, Sharma-Joshi modified model, tensor force model 2—40022
h.c.p., pair pot. calc. for stacking fault, twin and point defect energies 2—15747
h.c.p., phonon dispersion relation, Debye temp., modified axially symm. model 2—40049
heavy rare earth metals, electric field gradient estimated from exptl. hyperfine interaction data 2—26091
Herzfeld theory of metallic conductivity 2—36437
impure, anomalous electron-phonon props. 2—6755
intergranular force from free electron energy variation 2—29014
internal elec. fields, induced by Earth's gravitational field 2—22449
interpolation schemes based on phase shifts, choice of muffin tin zero 2—4111
ion-ion potential, pseudopotential calc., simple metals 2—22095
Knight shift oscillations and nucl. relax. times in crossed elec. and mag. fields 2—40768
Kubo-Mott formula, high-field magnetoresistance 2—32912
lattice dynamics, modified shell model treatment 2—19322
liquid alloy, electrotransport theory 2—21999
liquid state, absolute thermoelectric forces 2—21998
logarithmic central potential between atom pairs 2—15680
magnetic system, cond. electron scatt. by critical fluctuations 2—40122
magnetic system, impurity resist., nonlinear conc. depend. 2—4155
magneto surface impedance and surface scattering effects 2—40165
magnetoacoustic attenuation by Bragg-reflected electrons, jellium model 2—4052
magnetoconductivity, theorem 2—36438
magnetoresistance, anomalous longit. 2—13108
magnetoresistance, transverse, onset of linear field dependence, polycrystalline open Fermi surface metal 2—4156
melting curves calc. 2—9207
monovalent metals under uniaxial tension, elastic moduli calc. 2—9634
muffin tin zero, phase shifts and logarithmic derivatives 2—16098
negative work function, of thermal positrons 2—25969
noble, Fermi surface data inversion 2—36404
noble, Fermi surface interpolation schemes, muffin tin zero 2—16099
noble, phonons, modified shell model treatment 2—19347
noble, small angle scatt. and Kapitza law rel. to magnetoresist. 2—9950
noble, spin and spin-orbit interaction dependent mag. pseudopot. 2—36659
noble metal alloy, electron-phonon interaction, rel. to rigid band model 2—32878
optical properties, nonlocal effects, specular and diffuse electron scatt. 2—16413
orbital mag. susceptibility in tight-binding approx. 2—16345
orbital susceptibility of electrons, theory 2—40411
oxidation, parabolic, thin film parabolic growth low, elec. field effects 2—15660
paramagnetic system, local moments, Hubbard model 2—36665
particle, in transparent medium, surface plasmon energy calc. 2—40152
phase stability, electronic energy considerations 2—25237
phonon damping of dirty normal metal, thermal Green function 2—13067
phonon induced self energy and mass enhancement of electrons 2—4107
phonon limited mean free path, r.f. size effect 2—16085
polarisability of small particles in quasistatic elec. field 2—36434
positron annihilation in nearly-free electron band systems 2—22481
positrons, core annihilation 2—22482
pseudopotential approach to magnetic energy bandstructure and magnetic breakdown 2—32913
pseudopotential calc. of binding energies, struct. and lattice consts. 2—9317
quasiparticle damping, electron- phonon effects 2—16084
reflectivity, high temp. interpret. 2—40605
residual resist., calc. by Srivastava-Sharma pseudopot. and Ashcroft pseudopot. 2—40177
residual resistivity, Lorentz corrections 2—19538
resonant density oscillation around transition metal impurity 2—30021
skin effect, equation for plane-parallel plate and ferromag. cylinder 2—36435
sound propagation, generalized transport equations for coupled electron-phonon system 2—40059
spin polarization and spin fluctuation interactions 2—40440
spin relaxation of cond. electrons 2—6999
spin wave correls. in many-band model 2—10176
spin wave theory, weakly attenuating, in electron liq. 2—26007
spin-lattice relaxation, electron transition, non-mag. impurity effect 2—22716
stacking order stability in c.p. alloys, Fermi sphere deform. effects 2—12713
static screening, around fixed foreign charge 2—40119
surface, electronic wave functions, phase rule 2—32889
surface, rough, photon interactions 2—4427
surface, screening of external fields and excess charge distrib., jellium model 2—25737
surface, second harmonic radiation 2—4422
surface impedance of thin slabs, harmonic oscillations 2—16118
surface magnetic susceptibility in plates, role of tangential electrons 2—25989

Metals continued
theory continued
surface plasmon, variational calculation of dispersion relation 2—36425
surface plasmon coherent excitation by charged particle scatt. 2—32899
surface plasmons and image potential 2—22476
surface state energies and density of states 2—32890
thermodynamic properties, of electron gas at metallic densities 2—19423
thermopower, low temp., oscill. temp. depend. explained 2—16135
tight binding integrals, calculation and parametrisation, simplified procedure 2—22468
transition metal liquid alloys, resist., Faber-Ziman model 2—18847
transport processes, nearly free electron model, point defect scattering 2—25717
two electron correlations applied to beta brass type structures, vacancy variants 2—3768
valence electrons, energy operator, approx. diagonalization 2—19486
work function, changes due to alkali adsorption. jellium model 2—4313
work function, surface dipole contribution 2—16324
work function and surface structure, calc. for simple metals 2—39455
X-ray emission spectrum, electron interaction effects 2—26205
x-ray spectra, electron gas correls. and core hole effects 2—1701
X-ray spectra, i.r. catastrophy and excitons 2—33291
X-ray spectra, many-electron effects 2—29942
X-ray threshold absorpt. 2—29940
Ag, electron irrad., radiation emission 2—4085
Al, surface plasmon excitation by photons, effects of surface roughness 2—16464
Al, surface state energies, band struct. matching method determ., Forstmann-Heine method 2—6732
Al energy band determ. via model-pseudopotential approach 2—29616
Al films, surface plasmons, photoemission obs. 2—4131
Al films, surface plasmons and roughness-induced light scatt. 2—4130
Be, calc. of soft X-ray photoelectron spectra using band theory of metals 2—36631
Cd, elastic anisotropy in model for electron mean free path meas. on lens part of Fermi surface 2—13086
Cr, density of states calc. by combination of plane waves method 2—36414
Cr zone structure, electron energies density of states X-ray spectra, Green's function method 2—36415
Cu, Fermi surface topology rel. to linear field dependence of transverse magnetoresistance 2—4156
$CuGe_{0.5}Sb_{0.5}$, struct. phenomena, 2-electron correlation model 2—29466
$Cu_{10}Sn_3$, struct. phenomena, 2-electron correlation model 2—29466
Ga, effective masses and electronic orbits from ACR obs. 2—16127
Mg, anisotropy in Compton profile 2—4468
Na optical conductivity, exponential dependence of Drude tail anomaly 2—10349
Pb, radial electronic charge density distrib. 2—36395
Pd, conduction electron propag., electron-ion matrix element determ. 2—1460
Pd, dielec. screening function 2—16111
Pd, mag. polarization of cond. electrons due to mag. moment 2—1632
PdH_x, electron-ion potential approx. model, muffin-tin potentials 2—1460
V_3Ga, tight binding integrals, calculation and parametrisation, simplified procedure 2—22468

Metamagnetism
anisotropic antiferromagnet, stress effects on metamag. transitions 2—33162
neptunium (V) oxalate, properties studied from 2.4-37.5K, metamagnetic phase transition at 11.6K 2—19888
tricritical pts., droplet model 2—10234
Co antigorites and talcs 2—36761
$CoCl_22H_2O$, antiferromag., p.m.r. 4.2 K, high field, metamagnetic transitions 2—20157
$CoCl_2.2H_2O$, phase transitions, temp. depend. 2—10241
$CsCoCl_3.2H_2O$, transition obs., 1.1K 2—40548
$Cu(OH)_2$, Neel temp. phenomena 2—26061
$DyAlO_3$, absorpt. spectra, magnetic ordering effects 2—33259
$DyAlO_3$, critical fields 2—10245
$DyAlO_3$, critical fields 2—10246
DyOOH, in high fields, mag. prop. obs. 2.4-273 K 2—19926
Er-Mn-Al system, $ErMn_2$-$ErAl_2$ alloy 2—40553
ErOOH, in high fields. mag. prop. obs. 2.4-273 K 2—19926
$ErVO_4$, phase transition, magnetothermal resist. obs. 2—22707
Eu_3As_2 film, mag. ordering, photocond. and optical absorpt. study 2—36722
$FeCl_2.2H_2O$, Mag. phase diagram, metamag. transitions 2—36767
$Mn_{1-x}Cr_xAu_2$, helical to ferromag. transition 2—33135
Ni antigorites and talcs 2—36761
TbOOH, in high fields, mag. props. obs. 2.4-273 K 2—19926

Meteorites
see also Meteors
Angra dos Reis, fission origin of fossil tracks 2—14006
angra dos Reis, isotopic composition of ^{244}Pu fission Xe, reevaluation using lunar spallation Xe systematics 2—1997
Assam, gas rich hypersthene chondrite 2—1998
black hypersthene chondrites, Rb/Sr studies, effects of shock and reheating 2—23119
Carbo Fe meteorites, spallogenic He, Ne and Ar, thermal release characteristics 2—33755
chemical links with lunar surface 2—1971
chemistry, giving evidence for conditions in early solar system 2—41168
chondrites, mass fractionation and isotopic anomalies of Xe and Kr 2—17042
chondritic, synthesis of majorite and other high pressure garnets and perovskites 2—17041
chondrules in Apollo 14 samples, implications for origin of chondritic meteorites 2—37351
cooling rates, Fe, equation for det. from Goldstein Short graph 2—11016
Crater 9, possible masses, entry trajectory and orbital calculations 2—23118
cratering formulas and scaling methods 2—22943
formation of parent bodies, accretion processes 2—41215
Kapoeta, isotopic composition of ^{244}Pu fission Xe, reevaluation using lunar spallation Xe systematics 2—1997
Lost City, det. of temp. gradient induced by atmospheric friction using thermoluminescence 2—11021
Luna 16 samples, trace element concs. 2—20666
lunar bombardment, crater population development 2—1975

Meteorites continued

- magnetic and elastic props. and density obs. 2—30598
- microtectites, origin as result of cometary impacts with Earth 2—23120
- Moon, Imbrian basin, nature of body causing formation from composition of Apollo 14 samples 2—37350
- multicomponent composition effects on radio reflections from meteor trails 2—33753
- Muong Nong glass and Libyan Desert glass, gas inclusions, mass spectrometric analysis 2—37374
- natural remanent magnetization, early interplanetary magnetic fields 2—4987
- Orgueil meteorite, magnetite composition analysis using a scanning electron microscope 2—7542
- origin of metallic ions in ionosphere E-region 2—41006
- particles in atmosphere, electron microscope photographs 2—1839
- pasamonte, isotopic composition of ^{244}Pu fission Xe, reevaluation using lunar spallation Xe systematics 2—1997
- Pultusk shower, number and mass of fragments det. 2—11017
- Raco, K-Ar age 2—11018
- Sikhote-Alin shower, mass distribution of individual specimens 2—30593
- St, Severin, isotopic composition of ^{244}Pu fission Xe, reevaluation using lunar spallation Xe systematics 2—1997
- stony, struct. determ., electron petrography obs. 2—7543
- Stopfenheim Kuppel, Ries Kessel, and Stenheim Basin, a triplet cratering event 2—14005
- terrestrial age of stony meteorites from radiocarbon content 2—26869
- Tunguska, propagation of air waves rel. to atmos. inhomogeneity 2—30269
- CrN, discovery in Fe meteorites, carlsbergite 2—11022
- Fe, chemical analysis of Ni, Co, P and C content 2—11020
- Fe, cooling rates, equation for det. from Goldstein Short graph 2—11016
- Fe, formation, model 2—1999
- Fe, Iron River, identification 2—11019
- Fe, Sikhote-Alin shower 2—11015
- Fe, unshocked and shock loaded, defect struct., electron microscope obs. 2—3709
- He isotopic composition in carbonaceous chondrites 2—7541
- ^{129}I, ^{244}Pu and superheavy elements, extinct, and solar system history 2—1996
- Ne isotopic composition in carbonaceous chondrites 2—7541

Meteoroids *see Meteorites*

Meteorological instruments

see also Anemometers; Hygrometers; Ionosphere measuring apparatus

- airborne remote clear air turbulence detection equipment, development 2—40917
- atmospheric electricity and lightning detector 2—16848
- balloon, tethered, temp. and humidity probing 2—1830
- data stations, unattended environmental oceanographic and meteorological monitoring equipment 2—40903
- electronic equipment, conference, (Washington D.C., August 1971) 2—16723
- energy balance methods for estimating atmospheric thermal radiation 2—30266
- experimental continuous recording sonde, vertical temperature structure at mesoscale 2—16804
- fine thermocouples for obs. of vapour pressure and temp. 2—20309
- hot wire anemometers, constant temperature, feedback control theory 2—40915
- humidity monitor, sorption type, lag obs. 2—20315
- humidity sensors, direct obs., merits and limitations 2—1843
- Jimsonde, high resolution temperature sensor, comparative test results 2—16803
- laser velocimeter for remote wind sensing 2—37126
- miniature Mattauch-Herzog mass spectrometer for investigating upper atmosphere 2—566
- Nimbus satellite, Fourier spectroscopy 2—22953
- photographs recuperation, transmitted by satellite 2—37127
- psychrometer, heated air adiabatic saturation, construction and testing 2—30270
- PTU probe and FM magnetic recorder for aircraft 2—1832
- radar, 10 cm, as clear air turbulence detector 2—40939
- radar, FM-CW, data interpretation 2—1819
- radar altimeter for balloon payloads, design 2—16800
- radar-acoustic atmospheric sounding system for temp., and weather forecasts 2—26482
- radiometer sonde, for obs. of stratospheric emission due to water vapour in its rotational band 2—20308
- raindrop analyzer for automatic counting and sizing 2—33464
- raingauges, ground-level 2—1823
- remote sensing techniques 2—33446
- spaced sensors, use for wind, temp. and refractive index gradients 2—1835
- telemetering system with central monitoring and control of land and buoy telemeters 2—16802
- transponder rocketsonde, miniaturized, for trip. and wind data 2—16801
- turbulence, vertical scan technique in infrared radiometric detection 2—15530
- wind and air density sensor for rockets to operate 75 to 95 km up 2—26511
- for wind and temp. obs., problems and assessment 2—1831
- for wind shear and temp. probing 2—1833
- O_3, atmospheric, ground level density measurement 2—30276

Meteorology

- ageostrophic wind determ. from satellite data for cloudiness 2—7276
- air pollution, effects of various conditions 2—30275
- air pollution problems 2—4661
- Antarctica, extreme winds, measurements and recordings 2—40951
- atmosphere interaction with ocean, fog and cloud formation 2—30288
- balloons, new testing technique 2—16797
- boundary-layer analysis, correlation of surface and radiosonde observations 2—13677
- clear air turbulence associated with large temperature change 2—30278
- cloud form. and weather development, TV pictures and i.r. images comparison 2—7250
- convective storms, Doppler radar identification by plan shear indicator 2—13704
- cyclones, extratropical, two types of development 2—1858
- data analysis, dynamical, assimilation of past data, error reduction 2—13674
- data assimilation in dynamical analysis, continuous system 2—13671
- data assimilation systems, continuous 2—13675

Meteorology continued

- data collection, satellite system 2—30262
- day-of-the-week variation in weather 2—1824
- digital rain measuring unit 2—7248
- dynamic, equation of wind satisfying balance equation 2—20334
- dynamic modelling for GARP, global modelling at Meteorological Office 2—40913
- dynamic modelling for GARP, global modelling at UK Universities 2—40914
- earth surface and atmosphere characteristics determination by microwave technique 2—16798
- equivalent potential temperature during severe weather situation 2—13691
- extraterrestrial particles, magnetic spheroids, global deposition, association with rainfall 2—22969
- fields, adapting, use of variable weight functions 2—20307
- fields, statistical methods in obs. of structure 2—1827
- forecasting, rel. between convective clouds and thunderstorms and synoptic scale systems 2—13709
- forecasting heavy rainfall along Gujarat coast in association with Bay depressions 2—20338
- forecasts, visibility, surface wind and low cloud, scoring system 2—4659
- global atmospheric research programme, GARP, and UK participation, discussion meeting (London, November 1971) 2—40910
- hail-producing thunderstorms, location and investigation by infrasound 2—13717
- hailstorm, multicellular, radar reflectivity profiles of individual cells 2—13716
- haloes, graphical guide 2—1825
- humidity field prediction problems 2—13678
- hurricane Celia, August 1970, information received from NOMAD weather buoy 2—16830
- hurricanes, forecasting, tracking, weather radar for Caribbean Sea area 2—37125
- ice nucleation on organic substances, observed in cloud chamber 2—4660
- IEEE Region 8 Convention, Lausanne, (1971) 2—7251
- information processing by space systems 2—7253
- initialization and non-synoptic data assimilation 2—1822
- instability criterion for top heavy fluid layers 2—39292
- i.r. radiometry, mapping of hailswaths 2—13718
- Lagrangian description applic. 2—4658
- lee waves, obs. using high power radar 2—20326
- lidar system applic. 2—7245
- Mediterranean summer storm of Sept. 1969, rapid cyclonic developments 2—33460
- meridian circulation, subsidence wells, stormy depressions and melting fronts 2—20306
- mesoscale vertical motions, radar method of obs. 2—20325
- meteorology, finite difference estimates of derivatives for an irregular pattern of points 2—5168
- numerical prediction, minimum size of mountain regions and convective areas 2—20305
- oscillations, long period, of various elements, spectra 2—13672
- palaeoclimatological data from isotope studies 2—10727
- palaeoclimatology of polar ice sheets, atmospheric turbidity rel. to surface temperature 2—30263
- precipitation forecasting, quantitative, numerical model 2—37148
- precipitation intensity variation with synoptic type over Midlands 2—40958
- probing using tethered balloon 2—1830
- proximity soundings for thunderstorms with snow 2—13710
- radiation, global, dependence on turbidity and cloud cover, calc. 2—37076
- radio, effects of additive noise on calculated statistics of input signals 2—1826
- radio, radar and lidar 2—7244
- radio interferometer noise, missile-tracking 2—33482
- radiosondes for radio refractive index obs. as function of height 2—1834
- rain density quantitative determ. using digital meas. values input and processing 2—7246
- rain intensity, droplet spectra and radar reflectivity, comparative study 2—7247
- rainfall forecasting over small catchment areas by synoptic typing 2—20339
- rainfall meas. by radar as specific identification task 2—22970
- remote rel. to in situ obs. of parameters 2—1836
- remote rel. to in situ obs. of parameters and processes 2—1829
- remote sensing applications to world weather watch 2—20310
- satellite communication under unfavourable conditions 2—7314
- Scotland, spring and autumn reversals of stratospheric winds 2—33459
- severe local storms, detection, prediction, economics and structure, conference (Boston, USA, 1971) 2—13695
- severe storm identification with quantitative echo intensity data 2—13692
- severe storm prediction by screening regression using forecast predictors 2—13701
- severe thunderstorms and tornadoes forecasting, screening regression techniques 2—13702
- severe weather forecasting, use of computers, SWEAT index 2—13696
- shear induced clear air turbulence 2—40939
- snowstorms of 1970, March 4 in central and south-east England 2—40916
- sound propagation through model cylindrical vortex, with viscous core, synoptic weather conditions 2—17381
- state variable determination by Raman components of laser atmospheric backscatter 2—16808
- stratification depend. of ground-surface parameters 2—4662
- streamflow estimation using Thornthwaite's climatic water-balance 2—40959
- strong turbulent pycnoclines, approximate model 2—30238
- temperature, wind, pressure and density obs. in mesosphere 2—7258
- thunderstorm and tornado forecasting, stability indices 2—13708
- thunderstorm forecast technique from modelling considerations, severe storm development 2—13697
- thunderstorm gust fronts, characteristics 2—40953
- thunderstorm prediction using instability energy index in combination with standard significators 2—13699
- thunderstorms, lee slope study, forecasting along front range of Rocky Mountains 2—13700
- thunderstorms, Oklahoma compared with Malaysia, aircraft obs. of turbulence, temp. variation and cloud top heights 2—40952
- thunderstorms and severe weather, obs. of infrasound and subsonic disturbances 2—37124

Meteorology continued
tornado forecasting, statistics of surface conditions after meso low of thunderstorm 2—13698
tornado-producing thunderstorms, prediction by aerial photography 2—13703
tornadoes, prediction from h.f. radio noise from thunderstorms 2—13705
tornadoes and water spouts, theoretical model 2—12488
tower rel. to tethered balloon obs. 2—1837
tropical cyclone behaviour, cloud seeding and variations of sea surface temperature 2—37146
turbulence, clear air, development by synoptic scale processes 2—40940
turbulence, clear air, operational forecasting for aircraft safety 2—40942
turbulence, clear air, stable layers associated with 2—40945
urbanisation effects on monthly mean air temperature 2—40920
variables, representation by empirical orthogonal functions 2—1828
vertical coupling between upper and lower tropospheres in Indian monsoon 2—7278
weather modification field program, in Lake Tahoe region 2—7254
weather predictability and forecasting, discussion 2—40912
weather radar data processing system 2—7252
weather research, findings of Meteor series satellites 2—30261
S,Cl- in precipitation samples, interpretation 2—1821

Meteors
see also Meteorites
charged micrometeors, surface of zero relative velocity in limited circular three body problem with magnetic dipole 2—26866
cometary meteoroids, review 2—41212
deceleration in visible section of trajectory 2—30588
double station, 38421, spectral data on terminal flare and wake 2—4984
element abundances, TV recording of faint meteors 2—4983
extraterrestrial particles, magnetic spheroids, global deposition, association with rainfall 2—22969
faint spectra analysis, NASA Faint Meteor Spectra Patrol 2—14004
formation of parent bodies, accretion processes 2—41215
Geminid shower, effect of geomagnetic field on radar echoes 2—4985
head echoes rate variation with diurnal motion of radiant 2—30594
i.r. spectrum of bright meteor observed in Japan, 1968 Quadrantids 2—30597
Leonid and Geminid showers, effect on ionosphere, sporadic E 2—4730
meteoritic complex in solar system, review 2—41214
micrometeoroid distributions, search for inhomogeneities and possible relation to cometary matter 2—4988
optical methods obs., review 2—7301
Perseids, obs. of main radiants 2—30590
Perseids, observation by two-channel photoelectric method 2—7540
photographic and radar obs. determ. of electron attachment rates 2—11014
Quadrantid shower, radar det. of right ascension and declination 2—26867
Quadrantid shower, radio echo obs. 2—33754
Quadsantid shower contamination of upper atmosphere 2—4986
radar detection of meteor trails, effect of antenna radiation pattern and wind velocity 2—22964
radar echoes, effect of geomagnetic field 2—4985
radar observations of trails, winds and turbulence in upper atmosphere 2—33497
radio, rate rel. to Na abundance in upper atmos. 2—17040
radio meteor echoes, effect of small scale wind shears 2—30596
radio reflection from trails, effects of multicomponent composition of meteorites 2—33753
radio signals scattered from trails to study ionosphere 2—13775
secular perturbations of streams, conditions of meeting Earth 2—30595
shower structure in sporadic background 2—41053
sporadic, diurnal variation in mass distribution 2—26868
sporadic background, contribution of lunar particles 2—30589
streams, orbital dispersion, review 2—41213
trail drifting, vertical velocity component of regular wind in meteor zone 2—22985
trail observations of meridional mesospheric wind field, semiannual redistribution of neutral oxygen 2—30309
trail speed observations with an optical wedge shutter 2—7538
visual observations, luminosity functions and distribution steepness 2—7539
$Fe+N_2$, O_2 reactions, ionization and spectral emission at simulated meteor conditions 2—33752
K I emission cross-section by ion-beam technique, radiative efficiency 2—26865

Metrology *see Measurement; Mechanical measurement*

Mica
brittleness, determ. by shock figure method 2—1317
electron bombard., charge accumulation, path length 2—36587
film, effect of electron bombardment, radiation damage, elec. and mech. stability 2—9258
i.r. spectra of Siberian deposits, 0.75-15 μm 2—1685
mica-paper-tape insulation, dielectric props., effects of manufacturing parameters 2—4261
muscovite, crystal struct., symmetry of electron diffr. diagrams 2—9442
muscovite, i.r. spectra of deformation vibration of H_2O 2—15304
muscovite, secondary cleavage 2—6396
muscovites, i.r. spectroscopic study of isomorphic changes 2—29919
optical props., vacuum u.v. 2—40648
particle track length obs. for heavy ions 2—38391
phlogopite, crystal struct., symmetry of electron diffr. diagrams 2—9442
phlogopite, i.r. spectra of deformation vibration of H_2O 2—15304
quantitative determ. of H_2O using i.r. spectroscopy 2—30114
solid solution, formation between $k_2Mg_6Al_2Si_6O_{20}F_4$ and Al-free mica 2—36302
surface, spreading kinetics of polydimethylsiloxane 2—25177
surface composition analysis by ion scatt. spectrometry 2—39454
ultracold neutron absorption, total cross section 2—18250
K/Ca dates from pegmatitic 2—16767
$KMg_3FeSi_3O_{10}(OH)_2$, synthetic ferriphlogopite, tetrahedral Fe^{3+} Mossbauer parameters 2—10327

Micelle systems *see Colloids*

Microanalysis *see Chemical analysis*

Microhardness *see Hardness*

Micrometeorites *see Meteorites*

Micrometry
see also Interferometry; Strain gauges; Thickness measurement
No entries

Microphones
see also Transducers
air attenuation values for free-field calibration 2—7754
calibration, absolute, by Rayleigh disc method 2—30870
condenser, calibration under increased atmospheric pressures 2—11358
directional, dynamic, studio type 2—168
electret principle applic. 2—23372
gas diode, plasma acoustics 2—35548
hydrophone, particle velocity, calibration 2—37767
outdoor station reliability 2—23363
rotating, measurement of sound pressure levels and reverberation decays 2—2246
solid-state, using strain-type transducer 2—27268
STL-Ionophone design, props. and applics. 2—23362
thermal agitation noise detection using ribbon velocity microphone 2—20935
windnoise protection 2—23361

Microphotometers *see Densitometry*

Microprobe analysis *see Electron probe analysis*

Micropulsations
broad band activity, rel. to magnetospheric, interplanetary and solar phenomena 2—16923
damped type, interpretation as interaction between hydromagnetic oscillations and magnetospheric motions, model 2—16924
decreasing period pulsation intervals and development of asymmetry in the ring current 2—10775
pc, comparison of occurrences with ionosphere sporadic echoes of type h 2—20424
Pc 1-2 and IPDP at the auroral zone 2—13798
Pc-1, scattering of energetic outer radiation belt protons 2—33513
periods, latitude dependence and origin studies 2—41013
Pi 2, association with Bay occurrence at Lerwick and Halley Bay 2—41014
Pi 2, impulsive, association with bays 2—41015
Pi 2 events, effect of coastline on electric fields 2—4751
plasmapause positions of OGO-V satellite crossings, comparison with Pi micropulsation events 2—30313

Microscopes
see also Electron microscopes; Ion microscopes
acoustic, laser, scanning, operating characteristics 2—283
double perflectometer for measuring diameters of small holes 2—5438
durability of optical components under tropical conditions 2—38093
granite stage and measuring, with computer control 2—2450
hole inspection, optical system and applications 2—5436
hologram, portable, design, construction and testing 2—21119
hologram portable, high resolution, using pulsed ruby laser light source 2—23713
incident light, Tolansky interferometer as accessory 2—5413
interference, a.c. differential, based on principle of Nomarski microscope 2—34491
interference for meas. of surface roughness, comparison 2—23709
light refraction coefficients from phase analysis of mixtures of solids 2—4428
light-figure, design and applic. to metal specimens 2—29132
photoelectric scanning, theoretical and experimental studies 2—5435
photometric analysis of immunofluorescence in biology, potentiometric recording 2—5053
polarizing, examination of retinal rods of frogs, linear dichroism 2—11219
polarizing, large aperture number, behaviour between opposed polarizers 2—23718
stereomicroscopes, hints for increased effectiveness 2—2447
surgical contact, diagnostic investigation of microstructure of human organs 2—5437
thermal microscope for temperature measurement of small areas 2—7764
TV laser microscope, magnification of 30 to 3000 on videocontroller 2—27616
twin microscope for thickness measurement of opaque and transparent objects, thickness profiles of semiconductor counters 2—14063
u.v., use of Vidicon-type TV camera tube for remote observation 2—38094

Microscopy
see also Electron microscopy; Field ion microscopy
for biological research, computerized system 2—2018
coke structure study 2—1385
contact fluorescence microscopy, microstructure of thick biological specimens and organs 2—33783
contrasting, projection and photography of microscopic objects 2—31116
dark ground, diffraction images of partially coherent phase discs 2—21161
defect metallography 2—32498
dislocation, contrast due to stress birefr., i.r. obs. 2—15763
field emission, use of equidensitometry 2—29124
filamentary crystals, det. of physical dimensions 2—19282
glass, crystals in bubbles, method for analysis 2—32315
holographic, high magnification, depth of imaged volume 2—23655
holographic, Lippmann-Bragg holograms for medical microscopic analysis 2—14459
metallography, conference, Aalen, Germany, Sept. (1971) 2—32680
metallography, high and low temp. methods 2—25562
modular electronic system for quantitative light microscopy 2—2451
non-Airy pupil fns., influence of partially coherent illumination 2—27613
nondestructive exam. of irrad. fuel pins 2—38753
optical, obs. of cryst. growth and grain boundaries in metals 2—39590
optical, operator error 2—17708
particle size and pore size, distrib. determ. by photomicrographic method 2—25608
particle size and shape, absolute meas., primary standard 2—5113
particle size density distribution, f(x), eqns. relating radii F(R) to f(x) 2—38086
particle track visualization in solids, use of interference-contrast microscopy 2—5597
phase analysis of mixtures of solids, light refraction coefficients 2—4428
polarization, obs. of anisotropy effects on (010) axis of stibnite 2—19965
polyethylene, supermolecular struct., opt. microscope obs. 2—35854
polyethylene, superstructure, optical reflection obs. 2—32684
quantitative, image formation 2—5406
quasielastic light scattering, dynamic properties of macromolecules 2—34514
reactor fuel, post-irrad. exam. techniques 2—38755
reactor fuel elements, post-irrad. exam. 2—38760
reflected light measurements 2—32681

Microscopy continued
secondary and trace ingredients in mixtures of solids, techniques of identification 2—3604
stereology of cubic particles, obs. of simulated microstruct. 2—12702
surface thin layer, relief, diffusion zones 2—32327
thermomicrography 2—37802
white light, three dimensional, using multipole image storage and decoding 2—34529
Al coating, porosity 2—25612
Ni, electroless deposits on glass, interfacial props. 2—32372
SiC, polar surface identification, phase contrast method 2—18923

Microstructure of crystals *see Crystal structure/microstructure; X-ray examination of materials/microstructure*

Microtomes *see Biological technique and instruments; Laboratory apparatus and technique; Microscopy*

Microtrons *see Particle accelerators*

Microwave spectra *see Spectra*

Microwave spectrometers *see Spectrometers, radiofrequency*

Microwave techniques and devices
altimeter experiment on Skylab S-193, objectives and capabilities 2—20225
antenna monitoring with multiple channel interferometer 2—5411
BARITT diodes, transit-time oscillations 2—36556
beamguides, confocal lensed and irised 2—34260
biological safety standards 2—5039
biological systems, effects of radiation 2—7595
biomacromolecular system, microwave dielectric and Hall effect measurement 2—34286
cavities, low temperature, circularly polarized, designs 2—4144
cavity perturbation meas. of temp. dependent dielectric constant, method for minimizing airgap contact impedances, application to GaAs and Si 2—25850
circular magnetron, pre-oscillation charge distribution, diffusion equation 2—31011
circular resonator, excitation of travelling wave regime 2—23430
conductivity measurement of semiconductor slabs, transmission of TE$_{11}$ microwaves in circular waveguide 2—19679
conductivity of small crystals at 10^{10} Hz 2—17487
detection by reflex klystrons, mechanism 2—27350
diagnostics of semiconductor crystals, review of methods 2—22555
dielectric constant and tan δ meas. in low loss liqs. using liq.-filled wave guide 2—28880
dielectric loss angle tangent meas. by waveguide resonance method, errors associated with coupling with transmission line 2—21004
dielectric parameters of liquids at mm wavelengths, det. using method of variable thicknesses and waveguides 2—35775
diodes, backward and point contact, signal-to-noise ratios as function of incident amplitude modulated microwave power 2—27367
discharge lamps, low-pressure rare gas, visible and near u.v. spectra 2—2469
electric gas discharges in microwave food processing techniques 2—7596
electro-optical modulator in modulation method of phase detection, errors 2—31112
electron spin induction cavities, decoupling perpendicular modes 2—17500
emission from snow, temp. measurement 2—16770
exposure system for biological specimens 2—20716
Fabry-Perot resonator, e.m. fields investigated 2—23433
ferrites, Li, fabrication and properties 2—23432
ferrites, susceptibility down to 10^{-5}, ultrasensitive technique 2—23469
ferroelectrics applics., review of developments in Europe 2—40340
field configuration display utilizing semiconductor excess charge carriers 2—27348
focusing of 52-GH$_z$ beams by cylindrical mirrors 2—23438
focussing action on electron beam during capture in acceleration mode of cyclic accelerator 2—31392
Gunn devices, GaAs epitaxial layers, growth by vapour, liquid phase methods 2—32401
Gunn oscillators, ionizing radiation effects 2—22596
harmonic mixing of microwave and i.r. laser radiation using Josephson junction and maser 2—38027
holography, applic. of e.m. field mapping by photochromics 2—11387
holography, applic. to plasma diagnostics 2—17650
holography, application to e.m. phenomena obs. 2—18640
interferometer, superheterodyne, stabilized, with high resolution 2—17494
interferometry as a method of measuring dynamic clearances 2—11393
Josephson junction as freq. analyzer and mixer of submm. radiation sources 2—13185
Josephson parametric amplifier, at 30 MHz, self-pumped 2—19604
klystron type bunchers, radiation intensity calc. 2—34326
liquids, dielectric properties, investigation over a wide temperature range 2—18844
magnetic susceptibility meas., diagonal and non-diagonal, applic. to EuO 2—1628
magnetic susceptibility meas., frequency-dependent, pulse-resonance method 2—2335
magnetodielectrics, magnetic permeability and magnetic loss angle 2—17527
magnetron, smooth-bore, turbulent diffusion 2—23546
Mars, continuum brightness temp. 2—30556
Mercury, continuum brightness temp. 2—30556
meteorological characteristic determination from airborne passive microwave measurements 2—16798
microstrip, magnetic substrates, design theory 2—23455
microstrip on ferrite, garnet substrates, e.m. propagation 2—27358
microwave 2-port, efficiencies from reflection coefficient measurements 2—23457
mixer, n-GaAs, gain and frequency conversion efficiency, effect of charge carrier mobility 2—25819
nuclear states, excited, lifetime meas. 2—8274
ocean surface wind fields det. by remote passive microwave technique 2—16786
open-ended cavity for H$_2$ density obs., liquid and two-phase systems 2—27346
operating in transverse, radial TM modes, mode chart, unloaded Q-factor 2—23431
oscillators, Gunn effect, physical principles, material assessment, book 2 -29731
p-i-n diode switches, neutron damage 2—22583
Peake's emission model for temp. meas. 2—2282

Microwave techniques and devices continued
permittivity meas. at microwave frequencies using open resonator 2—2323
permittivity measurement, applic. to strongly polar liquids 2—21994
phase distribution of field in open quasioptical systems, measuring unit 2—17469
phase measurements, associated with Goos-Hanchen shift 2—20974
plasma column, nonlinear scattering 2—18614
plasma diagnostics, discharge under external h.f. field 2—28600
plasma electron density meas. set-up 2—24768
plasma generation, in crossed and parallel fields 2—24781
plasma klystron, nonlinear bunching 2—251
plasma radiation, microwave spectra in toroidal apparatus with turbulent heating 2—3211
plasma stochastic heating by random microwave noise 2—32004
plasma-beam discharge microwave signal attenuation, effects of l.f. oscillations 2—24798
propagation, multipath, theory and expts. 2—16857
radiodefectoscope, scanning of plastic tubing, 4 to 8 mm. microwave band 2—2250
radiometer, superheterodyne, for millimeter and submillimeter bands, 2—27349
radiometry, sea surface roughness mapping 2—16783
radiowave attenuation above 10 GHz, equivalent precipitation model 2—10736
radiowave attenuation due to rain for frequencies above 10 GHz, calc. 2—10735
rectangular aperture antenna with lateral diffusion, microwave breakdown predictions 2—11401
refractometer having single cavity frequency and bandwidth stabilized, patent 2—216
resistivity measurement of semiconductors 2—19681
resonance BWT in autodyne radiospectrometer 2—2314
resonator method for dielectric props. at 10^{10}Hz, applic. to polymers in γ-irrad. field 2—29740
Rozhdestevenskii interferometer, quasioptical analog, for obs. of refractive index of dielectrics 2—34238
scattering by surface charge waves, excited on plasma column 2—35481
semiconductor, elec. props. meas. 2—16233
semiconductor, process control, thermal and elec. meas. 2—29694
semiconductor electric and photoelectric prop. det., apparatus 2—34239
signal processing, applic. of nonlinear interactions in ferroelec. ceramics 2—40342
simple stabilized microwave source, Gunn oscillator 2—20975
smooth-bore magnetron, turbulent diffusion, Brownian motion theory applied 2—37925
soil, characteristic det. remotely from radiation 2—16774
solar burst spectrographic radiometer 2—26893
spectrograph construction and application at La Plata University 2—14342
spectrometer, Camspek 2—2312
spectroscopy, Stark modulator, simple and versatile 2—2313
superconducting point contact junction arrays, radiation generation and detection 2—13194
techniques, book 2—2295
temperature measurements of controlled terrain 2—16734
thermal emission from sea, limiting factors of microwave meas. 2—16787
transistor, fabrication by ion implantation 2—25900
TWT amplifier, rel. to noise in relativistic electron beam 2—2349
u.h.f. noise reference, stable low temp., coaxial termination for immersion in liquid N$_2$ 2—20976
undergraduate experiments yielding unexpected results 2—27004
underwater sound sources detection, radiation reflection from water surface 2—14274
unit for investigating solid dielectrics and magnetic materials, refractive index and absorption coeff. obs. 2—34237
v.u.v. atomic line source, 35 GHz microwave excitation of gas discharge in tapered waveguide 2—27661
wave attenuation, rainfall effect 2—26507
wave attenuation, rainfall effect 2—26506
waveguides, ferrite-filled, curved, application of decoupled vector wave equation in orthogonal curvilinear coordinates 2—23421
waveguides, square, rectangular with rounded corners, attenuation constants, eigenfunctions, eigenvalues 2—23456
X-band, resonance curve and Q-factor meas. 2—11390
GaAs, high voltage microwave e.m.f. 2—29668
n-GaAs, velocity/field characteristics obs., comparison with n-InP 2—6811
n-InP, velocity/field characteristics obs., comparison with n-GaAs 2—6811
InSb, plasma pinch channel, effective cross-section, microwave measurement 2—25750
n-InSb low-inertia radiation detector, millimetric 2—17496
Nb cavity, Q-value, X-band 2—4181
Nb superconducting cavity, resistance ratio meas. for material evaluation 2—25800
SmCO$_5$ permanent magnet, lightweight for electron beam focusing 2—21032
ZnO acoustic transducers, r.f. diode sputtered 2—14269

Mie theory *see Scattering*

Milky way *see Galaxies/the Galaxy*

Mineralogy *see Minerals*

Minerals
see also Mica; Quartz; Ruby
actinolite, struct. and bonding 2—9440
adamite:Cu^{2+}, spin Hamiltonian parameters detn., e.p.r. obs. 2—36994
alkali feldspar, exsolution, elastic stresses, perioidic twins, electron microscopy 2—25414
anisotropic rocks, brittle fracture initiation in and ultimate failure, theory 2—29296
anorthite, domain texture, electron microscopy 2—32449
anorthite, struct. refinement, bond lengths and angles 2—9464
apatite, e.p.r. of Mn^{2+}, impurity distrib. regularities 2—10498
apatite, i.r. spectral investigation of structural changes during hydrothermal treatment 2—39635
Apollo 11 sample 10071, petrology of differentiated mini-igneous complex 2—13981
Apollo 14 crystalline rocks, geochemistry of opaque samples 2—13987
Apollo 15, anorthosite crystallization age determination 2—41184

Minerals continued
- Apollo 15 anorthosite 15415 sample, texture, mineralogy and metamorphic history 2—41186
- Apollo 15 anorthosite slide 15415,18 sample, mineralogic and petrologic study 2—41185
- Apollo 15 basalt 15555, geochemistry 2—41183
- Apollo 15 geochemical x-ray fluorescence experiment 2—41187
- Apollo 15 lunar samples, description of finds 2—41176
- Apollo 15 rock 15555, cosmic ray exposure and gas-retention ages 2—41182
- Apollo 15 rock 15555 chip, rare gas retention ages 2—41181
- Apollo 15 sample 15555, chemistry geochronology and petrogenesis 2—41178
- Apollo 15 samples, geologic setting 2—41177
- Apollo 15 samples, primordial radioelements and cosmogenic radionuclides 2—41188
- Apollo sample 15555, ^{40}Ar- ^{39}Ar dating 2—41179
- Apollo sample 15555, Rb-Sr and K-Ar dating 2—41180
- azurite, cryst. struct., neutron diffr. obs. 2—29140
- basalt lavas, regional hydrothermal alteration, magnetic and opaque petrological response 2—4640
- basalts, Apollo 11, petrogenesis and implications of lunar origin 2—23106
- basalts, magnetic hysteresis obs. and Curie point det. 2—37100
- basic magmatism and continental drift in Guiana 2—7240
- beryl, i.r. refl. spectrum, anharmonicity 2—26143
- beryl, transmission and reflection spectra measured in the i.r. with polarized light 2—10365
- bone, determination of mineral content using a densitometric method 2—37444
- boracites, atomic displacements due to polarity changes 2—32465
- brucite, decomposition, solid state reaction kinetics appl. 2—36253
- calcite, replacement in radiaxial fibrous form after syn-sedimentary cement 2—7234
- cassiterite, electrical properties, prospecting 2—26439
- chondrules in Apollo 14 samples, implications for origin of chondritic meteorites 2—37351
- chrysotile asbestos, microstruct., high resolution electron microscope obs. 2—3716
- clay, e.p.r. signals, rel. to radicals in lattice 2—10474
- in clay deposits of N.W. Quebec 2—26452
- clinamphiboles, lattice consts. 2—9441
- coesite, solid state isotherms 2—4642
- colemanite, ferroelectric., internal bias fields 2—13317
- cordierite, low temperature form, ^{1}H and ^{27}Al n.m.r. investigations 2—30019
- cordierite sinters, radiative emission meas. by cooling of specimens 2—27309
- α-corundum in lunar dust 2—13996
- cummingtonites, Mossbauer spectra, ^{57}Fe quadrupole spectra 2—10324
- dacite, effect of moisture and temp. on fracture morphology 2—29319
- dating techniques from retention of radiogenic gases 2—7229
- datolite, positions of hydrogen atoms 2—19044
- datolite, transmission and reflection spectra measured in the i.r. with polarized light 2—10365
- deep sea basalt, U/He ages as indicators of excess Ar 2—33434
- emerald, spin Hamiltonian Cr^{3+} ions in trigonal field 2—10494
- ferrimagnetic, obs. using resonance of spin precision of electrons causing ferromagnetism 2—1908
- ferromagnetic, effect of high pressure and temp. on changes in isothermal residual magnetization and coercive force 2—33561
- fluorapatite, natural cryst., surface energy 2—6328
- fluorapatite single crystals, pulsed n.m.r. investigation of ^{19}F chemical shift anisotropy 2—22841
- fluorite, thermolum. response to γ-ray irrad. 2—27902
- forsterite, natural, olivine-spinel transformation, 98-130 kb and 700-1100°C 2—9786
- fossil track and thermoluminescence studies of luna 16 material 2—20660
- gamma irradiated, K-Ar dating 2—26462
- gamma-gamma logging for density measurement, reliability improvement 2—30205
- garnets and perovskites, high-pressure synthesis 2—17041
- geological processes, temperature changes associated with adiabatic decompression 2—13622
- goetzenite, cryst. struct. 2—9463
- granite, Westerly, shock wave attenuation, Q values, intra- grain dislocation kinks 2—3841
- graphites, nuclear, impurities determ. by instrumental activation analysis 2—7201
- greenschist facies meta-volcanic rocks, X-ray powder diffraction obs. 2—30129
- heterosite, crystal structure 2—25332
- ilmenite, hyperfine interactions of Fe^{2+} 2—19986
- Indian biotites, fission track ages 2—4645
- interplanetary grain aggregates, ordinary chondrites, irradiation history 2—41217
- iron ore, analysis by X-ray fluorescence spectrometry 2—10675
- isotropic rock, brittle fracture initiation in and ultimate failure 2—29295
- Jurassic Chon Aike formation, paleomagnetism and radiometric 2—26564
- kaolinite, decomposition, solid state reaction kinetics appl. 2—36253
- keatite, significance of bridging oxygens in thermal expansion 2—16062
- legrandite, cryst. struct. 2—19061
- limestone, Solenhofen, shock wave attenuation, Q values, intra-grain dislocation kinks 2—3841
- luminescence petrography review 2—1795
- Luna 16, G-2 soil, neutron capture on Gd and Sm 2—20655
- Luna 16, Li, K, Rb, Sr, Ba, rare-earth, Zr and Hf concs. in fines 2—20662
- Luna 16 regolith samples, chemical features 2—20661
- Luna 16 soil, conc. of rare earths and trace elements 2—20664
- Luna-16-G-7 fines, rare gas studies by stepwise heating technique, a low fission solar wind Xe 2—20656
- lunar, Apollo ii samples 2—4956
- lunar, petrology of Mare Fecunditatis regolith 2—20644
- lunar, terrestrial analogs, optical constants, lunar origin det. 2—26813
- Lunar 16 dust samples, inert gas meas. 2—20657
- lunar anorthosites, chemical composition and parent liquids 2—13982
- lunar Apollo 14 inverted pigeonites as samples of lunar plutonic rocks 2—37343
- lunar Apollo 15 anorthosite 15415, ^{40}Ar-^{39}Ar age and cosmic irradiation history 2—37342
- lunar basalt genesis, Eu anomaly 2—13985

Minerals continued
- lunar basalts, Mare Fecunditatis, gas retention and cosmic ray exposure ages 2—20654
- lunar basalts, microprobe obs. 2—20642
- lunar basalts, petrological and chemical obs. 2—20652
- lunar fines, electron microprobe obs. 2—20643
- lunar mare basalt age, crust and mantle evolution 2—13984
- lunar materials, U, Th, Pb and rare earth element abundances and ^{207}Pb/^{206}Pb ages 2—37344
- Lunar regolith, rare gas adsorption 2—37347
- lunar rocks, neutron capture effects in Gd and the irradiation histories 2—13978
- lunar samples, bulk composition obs. 2—20650
- lunar samples, h.v. transmission electron microscopy 2—10999
- lunar samples, luminescence and thermoluminescence 2—13986
- lunar samples, Mare Fecunditatis, obs. of opaque minerals and spinels 2—20651
- lunar samples, petrology of Apollo 12 basalts 2—13983
- lunar soil, Luna 16 sample, microbasalt, extremely mafic magma 2—20648
- lunar soil, Mare Fecunditatis, relative proportions and petrological signficance of particles 2—20646
- lunar soil, Sea of Fertility, petrology 2—20647
- lunar soil fragments, electron microprobe obs. 2—20645
- lunar spinels, compositional variations 2—7515
- magnetic silicate liquids, SiO$_2$ concentrations rel. to viscosity, model for calculation 2—40889
- magnetite, magnetoresistance, 77-300K, phase transition 2—25816
- magnetite and haematite, thermoremanent magnetization, effect of thermal fluctuations during a.c. field treatment 2—30380
- Mare Fecunditatis, extreme radiation damage in soil 2—20659
- Martian surface materials and infrared absorptions from Mariner 7 recordings 2—30561
- meteoritic and non-meteoritic trace elements in Luna 16 samples 2—20666
- molybdenite, crystal struct., symmetry of electron diffr. diagrams 2—9442
- molybdenite, isotropic abundance of Mo 2—40902
- molybdenite, MoS$_2$ crystal, cold working, microstructure, X-ray line broadening 2—25409
- monetite, CaHPO$_4$, cryst. struct., H position, neutron diffr. 2—12719
- Moon, ilmenite basalts, Apollo 11, petrology 2—13989
- Moon, Imbrian basin, nature of body causing formation from composition of Apollo 14 samples 2—37350
- mordenite, sorption of N$_2$, O$_2$, and Ar 2—22082
- mullite decomp. under h.p. 2—33821
- muscovites, Indian, fission track technique dating and fossil radiation damage 2—7227
- muscovites, i.r. spectroscopic study of isomorphic changes 2—29919
- neutron activation analysis of 29 elements in Luna 16 soil 2—20663
- newberyite, e.s.r. of Mn^{2+} impurities, mag. complexes 2—26282
- below ocean floor, prospecting 2—30222
- oligoclase, low and high albite, cryst. struct. 2—9439
- olivine-spinel phase boundary in descending lithosphere 2—22932
- olivines, elasticity and equations of state in Mg$_2$SiO$_4$-Fe$_2$SiO$_4$ system 2—30213
- organo-montmorillonities, interstratified layer struct. 2—29081
- parammelsbergite, cryst. struct., X-ray obs. 2—25342
- periclase, dielectric props., effects of additives and densification 2—16260
- phenakite, cryst. struct. 2—9456
- plagioclase satellite refls. origin 2—6420
- plate tectonic emplacement of upper mantle peridotites along continental edges 2—22933
- preobazhenskite, Mg$_3$[B$_{11}$O$_{14}$(OH)$_8$Ho$_2$], cryst. struct. 2—19055
- prospecting, measurement of horizontal gradient of g 2—30143
- proustite, frequency dependence of acoustic absorption use of single crystals in acousto-optic devices 2—6664
- proustite, second harmonic generation in CW CO$_2$ laser 2—22722
- proustite crystal, frequency mixing of outputs of ruby laser and tunable dye laser 2—27488
- pyrite, low temp. photoconduction phenomenon 2—4300
- pyrrhotite, defect struct., Electron microscope obs. 2—22201
- rare earth and bulk abundances in Luna 16 soil levels A and D 2—20665
- remote sensing for use in mineral exploration 2—4625
- remote sensing technology 2—13612
- resource inventory of Californian desert, remote sensing methods 2—20277
- rhodochrosite, complex refractive index in range 0.33 to 2.5 μm 2—7040
- Rochechouart impact structure, paleomagnetic age determination 2—37229
- rock powders, determ. of average atomic number by X-ray scattering 2—33838
- rocks, mechanical strength reduction by 10.6 μ laser irradiation 2—29280
- rocks, shear testing procedure 2—39869
- rocks, thermal conductivity det. by steady state method 2—16732
- samples, geochemistry of three cores from the East Pacific Rise 2—16751
- sandstone, effect of size and stress concentration on dilatancy and fracture 2—29320
- scholzite, dehydration and transform. phases 2—19294
- schroeckingerite, ^{236}U/^{238}U measurements 2—40900
- Sea of Fertility, U-Th-Pb soil analysis 2—20668
- Sea of Plenty, particle track record of soil 2—20658
- seafloor exploration using system utilizing neutron activation analysis 2—30210
- siltstone, anisotropic, brittle fracture initiation in and ultimate failure of 2—29297
- sodalite, cathodochromic props. 2—13590
- spinel-type, spin pairing of Fe(II), and corresponding phases 2—40584
- β-spodumen, ferroelec. props. 2—29756
- β-spodumene, significance of bridging oxygen in thermal expansion 2—16062
- stishovite, solid state isotherms 2—4642
- submarine basalts, characteristic thermomagnetic curve 2—23042
- sulphide, desorption of xanthate, u.s. wave effects 2—29069
- sulphides and sulphates, and rocks, visible and near i.r. spectra 2—20010
- terrestrial, transmission electron microscope examination 2—10704
- tetrahedrite, transgrowth twins form. 2—9354
- thermoluminescence, abnormal fading characts. 2—29985
- thucholite, ^{236}U/^{238}U measurements 2—40900
- tinaxite, NaK$_2$Ca$_2$TiSi$_7$O$_{19}$(OH), cryst. struct. 2—1229
- titano-magnetite, magnetic processes in oceanic ridge 2—13802

Minerals continued
titano-magnetite ores, spectral analysis in spark discharge of blast formed disperse particles 2—4616
titanomaghemite, saturation magnetization reversal on heating 2—16932
titanomagnetites, exchange anisotropy 2—41017
titanomagnetites, natural intermediate, single-multidomain transition 2—1592
titanomagnetites, oxidised synthetic and natural, rotational hysteresis obs. 2—1599
topaz, transmission and reflection spectra measured in the i.r. with polarized light 2—10365
tridymite, phase transition shift, heat of transformation 2—9824
ultrasonic wave velocity obs., electronic computing method of obs. 2—33427
uraninite, ^{236}U/^{238}U measurements 2—40900
velocity of sound, dependence on hydrostatic pressure 2—26391
vermiculite, exfoliated, heat transmission factor meas., cryogenic temp. 2—17433
wulfenite, isotopic abundance of Mo 2—40902
zeolite, simple theoretical absorption isotherms for sorption of gases 2—6368
zeolite, synthetic, sp. ht., heat of fusion of absorbed water 2—19424
zeolite lattices with Hg filled channels, struct. behaviour 2—6444
zeolite Y, heats of adsorpt. of Ar, N_2, CO, CO_2, ethene and ethane 2—35927
zeolites, e.p.r. linewidth temp. depend. 2—10478
zeolites, liquid metal filling of marrow channels 2—1384
zeolites, n.m.r. pulsed field gradient obs. of diffusion processes 2—10592
zeolites, synthetic, dielectric investigation between 30 Hz and 12 MHz 2—1551
zoisite, transmission and reflection spectra measured in the i.r. with polarized light 2—10365
^{40}Ar/^{39}Ar age spectrum technique, test on biotite, feldspar, hornblende, muscovite, granodiorite, microcline and albite 2—16766
B, Li, N_2, Th, U determination using nuclear track technique 2—7200
$CaCO_3$, calcite, sorption of water vapour and N_2, effect of ball-milling 2—35911
$Ca_4Nd_6(SiO_4)_6.F_2$, britholite, synthetic, i.r. absorption spectra, effect of replacing Ca by Mg, Sr, or Ba 2—33258
$Cd_5[SiO_4]_2(OH)_2$, cryst. struct. 2—9466
Co antigorites and talcs, antiferromagnetism 2—36761
Cu_2S, low chalcocite and relation to monoclinic system 2—6432
Fe-Mn nodules, dredged from Pacific Ocean, Mossbauer effect analysis 2—33424
Fe, $K_{\alpha 1,\alpha 2}$-and $K_{\beta 1},\beta'$ spectra 2—33296
$FePO_4.2H_2O$, solubility equilibrium constant and saturation curve for synthetic strengite in dilute phosphoric acid solutions 2—40890
Ni antigorites and talcs, antiferromagnetism 2—36761
^{18}O/^{16}O isotopic analysis of Luna 16 soil 2—20667
Si-containing, X-fluorescence, K-spectrum of Si 2—33312
Th and U content, nondestructive determ. by gamma ray spectrometry 2—4608
U and Th content, nondestructive determ. by gamma ray spectrometry 2—4608
^{236}U/^{238}U measurements in terrestrial minerals and processed ore 2—40900
Minor planets *see Planets*
Mirages *see Atmospheric optics*
Mirrors
see also Telescopes/astronomical
aspherical, Hartman Null test 2—23670
aspherical, testing by interferometry 2—34485
ball, for use in holography 2—17654
catadioptric imaging systems, meniscus aberration correctors, book 2—27626
Cer-Vit, lightweight, centre-mounted, for Lunar laser ranging pulses 2—21140
combined cylindrical electron mirrors, dispersion and aberrations 2—30997
compound mirror open resonators obs. of losses and field patterns 2—34377
cylindrical, focusing of 52 GH_z beams 2—23438
elastic deformations of Steward Observatory 230-cm. and Optical Sciences Center 154-cm. mirrors 2—27610
electron, cylindrical, combined, of electric and mag. fields, paraxial properties 2—2354
electrostatic, fringing field 2—34318
electrostatically scanned film reflectors for interferometer and laser applications 2—23671
high reflector power, near i.r. and u.v., prep. 2—31126
lasers, gaseous, reflector loss 2—34384
metal film, for CO_2 laser, minization of damage susceptibility 2—27638
mount for long wavelength lasers 2—27457
multilayer dielectric for He-Ne lasers, laboratory construction 2—14416
nonabsorbing, produced by precipitation of oxides, for u.v. Fabry-Perot interferometers 2—38062
parabolic, off-axis, anal. of He-Ne laser surface reflections 2—34435
parabolic solar concentrators, estimation of accuracy of reflecting surfaces 2—34432
paraboloid, correction by pairs of spherical mirrors 2—7579
plane, horizontally oriented, elastic deflections 2—14441
primary, paraboloidal, synthesis by spherical mirrors 2—34436
quality control, use of interferometers 2—34518
reflectometry, properties of specular and near-specular surfaces, theory and applications, measurement of reflectance, book 2—2420
resonator, with saturable gain medium, modal field distributions det. 2—5350
semitransparent dielectric wide-band mirrors consisting of nonuniformly thick interference layers, design and preparation 2—27633
solar concentrator, radiant flux density distribution meas. by calorimetry 2—23412
solar concentrator with stationary plane mirrors 2—23674
solar concentrators, application of theory at similarity 2—34433
solar concentrators, construction and power characteristics of paraboloidal concentrators composed of doubly curved facets 2—23675
solar energy concentration, review 2—34437
solar reflectors, energy transport and distribution characteristics in reflection field as whole 2—23672
spherical, 27.5 m, calc. of optical effects 2—7966
spherical, 27.5 metres, photographic recording of optical effects 2—7965
Mirrors continued
spherical concave, errors in approximating radius of curvature with He-Ne laser 2—34431
telescope, with random surface undulations, illumination distrib. in diffraction image 2—17677
triple reflection rectangular prism for use as a triple mirror 2—7967
tunnel, zoomable kaleidoscopic 2—5432
u.v. wide-band reflectors, chemical deposition from Th and Si oxides 2—34515
X-ray tubes, anodes made of low-alloy Cr 2—30743
Al, with MgF_2 and LiF overcoating, effect of deposition rate, substrate temp. and aging on v.u.v. reflectance 2—34434
Co, thin flat, for polarization of thermal neutrons fabrication 2—17995
Mixing *see Heat of solution; Solubility; Solutions*
Moderation *see Neutrons and antineutrons/moderation*
Moderators *see Nuclear reactors, fission/materials*
Modulation of light *see Light/modulation*
Modulation spectroscopy
see also Electroreflectance; Magnetoreflectance; Piezoreflectance; Thermoreflectance
gating technique for selective modulation of resonance lines from hollow cathode lamps 2—34556
linearized thire-derivative, with depletion-barrier modulation 2—33240
metal, thermomodulation spectra 2—36855
non-dispersive system for atomic absorption spectroscopy 2—8041
self-correlation detection applic. 2—8027
spectrometer, for semiconductor studies 2—1692
Moire fringes *see Interference/light*
Moisture
see also Atmosphere/humidity; Humidity; Permeability, mechanical
atmosphere, effects on propagation of internal and acoustic gravity waves 2—33449
digital electronic moisture meter and regulator 2—28685
field neutron moisture meter, vertical resolving power improvements 2—13629
meter, u.h.f. for solid and friable materials 2—19230
strain gauge sensitivity, effect of moistureproof coatings 2—29253
in $BaTiO_3$ environment, effect on conductivity 2—16286
in $BaTiO_3$ environment, effects on surface pot. 2—16285
Molar volume *see Density*
Molecular beams
see also Particle velocity analysis
adiabatic transition by irrad. freq. variation 2—28265
bombardment of pure or mixed gas, obs. 2—38880
n-butane free jets relaxation study from mass spectra temp. dependence 2—24518
differential scattering apparatus with low temperature bolometer detector 2—18398
ethane, supersonic, absolute intensities, velocity distrib., crystal target 2—21585
extraction from equilibrium gas flows, shock beam model 2—21584
formaldehyde, multiphoton transition, 106 kHz 2—31855
halogen molecule-deuterium atom beam collision study 2—13564
high energy, converging, ioniz. method 2—12096
Kepler, inclined-beams instrument for study of two particle collisions 2—11998
methane, supersonic, absolute intensities, velocity distrib., crystal target 2—21585
nozzle beams, scattered gas density determination 2—38882
O_2 supersonic beams interacting with surface of Si crystal 2—6314
radiative shift of spatiotemporal modulation lines in r.f. field 2—31772
scattering, application of deconvolution techniques 2—24571
scattering apparatus with perfect focussing mass spectrometer 2—2913
supersonic, absolute intensities, vel. distrib., single crystal technique 2—21585
supersonic, calibration of slotted disc velocity selector 2—769
supersonic jets, expanding, cluster formation, effect of press., temp., nozzle size and test gas 2—21904
system combining nozzle source with low temp. pumping for gas-surface scattering obs. 2—32324
Zeeman-Stark effect due to translational motion 2—28264
Ar, supersonic, absolute intensities, velocity distrib., crystal target 2—21585
C_3O_2 electric field deflection behaviour 2—31783
C_3S_2, electric field deflection behaviour 2—31783
CsF, r.f. spectra, electric dipole moment and quadrupole coupling const. up to v=8 2—5926
GaAs:Sn, Ge, Mg epitaxial film growth, observation of surface structure 2—3553
HNCO and DNCO, molecular-beam microwave spectra 2—31795
He, exam. of O_2 chemisorbed layer on Re 2—35919
KNa, molecular beam resonance study 2—38920
KNa, molecular beam resonance study 2—38920
^{39}K ^{19}F, molec. beam resonance investigation of Stark effect 2—21646
LiNa, molecular beam resonance study 2—38920
LiOH(D), molecular beam electric resonance spectra, vibrational states 2—8663
N_2, supersonic, absolute intensities, velocity distrib., crystal target 2—21585
NO beam, state-selected, method of production 2—8864
NO mass spectrometric identification of paramagnetic component 2—18397
NO_2 mass spectrometric identification of paramagnetic component 2—18397
O_2 mass spectrometric identification of paramagnetic component 2—18397
^{87}RbF, molec. beam resonance meas. of h.f.s., Stark and Zeeman effect 2—21641
TlCl isotopes, molec. beam resonance meas. of h.f.s. and Zeeman and Stark effects in different vibrational states 2—21645
^{205}Tl^{19}F, molec. beam resonance investigation of Stark effect 2—21646
Molecular orbitals *see Molecules/electronic structure; Orbital calculation methods*
Molecular relaxation *see Molecules/relaxation*
Molecular spectra *see Spectra/inorganic molecules; Spectra/molecules; Spectra/organic molecules and substances*
Molecular structure *see Molecules/configuration and dimensions*

Molecular weight
n-alkanes in 1-chloronaphthalene solvent, effect on refractive index increment 2—6235
glassy plastics, effect on brittle strength 2—39830
hydrocarbons, regularity in diffusion coefficients of homologous series 2—32188
nylon-6, effect on isothermal crystallization kinetics 2—3471
poly(ethylene oxide) of low molecular weight, study of melting behaviour 2—39422
polycarbonate, effect on Izod impact strength of injection moulded specimen 2—22280
polydimethylsiloxane, rel. to viscosity of melts under high pressure 2—25059
polyethylene, branched, determination from combined gel permeation chromatography and gradient elution fractonation rel. to structural evaluation 2—28424
polyethylene, distribution effects on capillary flow of high density melts 2—21944
polyethylene, distribution effects on rheological properties of high density melts 2—21929
polyethylene, low press., mech. props. rel. to molecular struct. 2—28978
polyethylene, low-density, molecular weight distribution and long-chain branching 2—8848
polyethylene in 1-chloronaphthalene solvent, effect on refractive index increment 2—6235
polystyrene solution, X-ray obs. 2—3370

Molecular weight determination
automatic meas. app. based on mol.-flow networks 2—39241
by light scattering measurements on liquids at small angles 2—3391
polylysine in solution, reliability of diffusion coeffs. determ from spectrum of scattered light checked by mol. weight meas. 2—39403

Molecules
see also Kinetic theory, Polarisability; Spectra
adsorbed on homogeneous surface, adsorbate-adsorbate association 2—35902
alkali metal atom interactions in rare gas matrix, stable molecular state formation 2—24387
anisotropic scattering of light, many-molecular correlation, in simple fluids 2—6231
anthracene excimer, i.r. absorpt. study during pulse radiolysis of solns. in benzene 2—20203
anthraquinone, adsorbed on W, energy distrib. of field emitted electrons 2—29075
aromatic. orientation distrib. function in frozen liquid crystals from triplet e.s.r. spectra 2—38950
coherence, in quantum electronics, review 2—27445
coherence effect in electron pair production, Born approx. 2—31738
collision complex in H^++F scattering, theory of fine structure transitions 2—5838
conditionally convergent integrals, evaluation 2—28242
configuration of spherical, non-polar dense gases and liquids 2—6194
Coulomb Green function, equivalence of expressions 2—2905
Coulomb potential, screened, properties 2—5774
Coulomb T-matrix, on-shell 2—2906
cyclic organic molecules, strobilism 2—28356
diatomic gas, loaded sphere model for computer simulation for shock wave studies 2—18743
dielectric polarization and alignment, classical statistical mechanics 2—1106
electron affinity, evaluation of current values 2—15278
ellipsoid model, gas scattering function 2—1031
exclusion principle violating diagrams, generalization of many body-theory 2—28163
formaldehyde, proton affinities of O and N, electrostatic molecular potential study 2—18505
formation in triple collisions of 3 alkali metal atoms 2—11991
formation on interstellar grains in H I regions 2—37315
hamiltonian theory of molecule-electromagnetic field system 2—21574
harmonic oscillator, forced, correspondence principle methods 2—5773
harmonic oscillator two-centre integrals, application 2—27068
hydrides, photoejection of proton 2—24472
hydrogen-bonded complexes, proton transfer, environment effects, dielectric obs. 2—8555
interstellar, formation mechanisms 2—13926
ionization potentials, evaluation of current values 2—15278
kinetic energy quantum transcription of nuclei in body-fixed axis system 2—18373
many electron systems of interacting particles, calc. of second order physical props by Green's functions 2—8415
many-body methods, applic. to calculations 2—562
mixtures; quantum and classical, density expansion of distribution functions 2—2166
photoconductivity of matrix-isolated molecules at low temperature 2—25951
photosensitized ionization, by Ar 2—8551
photosensitized ionization, by Ar 2—8551
physico-chemical properties, calc. using difference interpolation method 2—24414
Rayleigh and Raman scattering in magnetic fields, polarization dependence of intensity 2—31745
rotatory strength, upper and lower bounds for perturbed anisotropic harmonic oscillator one-electron model 2—31735
slowly reorienting systems, magnetic resonance spectra, density matrix formulation 2—18393
of three identical particles interacting via three mutual morse potentials, ground state binding energy 2—11306
transplutonium, thermodynamic principles of systematics, extrapolation from rare earth and actinide series 2—22851
CH, energy calc. by many-body perturbation theory 2—35239
CO_2-N_2-He laser passive Q-switching by saturable filter containing OsO_4 vapour 2—27494
$CaSO_4$-1/2H_2O, infrared spectra of supposed α and β forms 2—5923
Cs molecular component in multiphoton ionization of Ce atomic beam by Q-switched Nd-glass laser at 1.06 μm 2—12019
D_3 existence and lifetime 2—28287
K_2 form. in metal vapour, atomic orientation effect 2—18324
Rb inert gas molecules, exptl. evidence for existence from relaxation of polarized Rb atoms in inert gas 2—28224

Molecules continued
configuration and dimensions
see also Chemical structure; Crystal structure, atomic
π-conformers, core repulsion and prediction of energy levels 2—38877
adiabatic internuclear distance, calc. allowing for breakdown of Born-Oppenheimer approx. 2—12078
carboxylic acid salts, H atom position in A-type H-bands 2—8747
complex, use of mathematical logic to determ. structure from i.r. vibration spectra 2—28246
complex molecules, formed by field ionization of aniline-nitrobenzene mixtures, structure 2—15351
computer perception of significant structural features in complex molecules 2—38947
computer-assisted synthetic analysis by interactive computer graphics 2—38946
computer-assisted synthetic analysis of complex molecules, generation of synthetic intermediates 2—38948
core electron effects, pseudopotential method calc. 2—21578
cyclobutane carboxylate ion, determ. from vibrational spectra 2—5969
D_{4h} symmetry, covalency reduction factors and estimation of bonding parameters 2—3025
diameter meas. using acoustic method 2—35217
diatomic molecules, internuclear distance from estimated spectroscopic intensities 2—8531
1,2-dibromoperfluoropropane, ^{19}F n.m.r. spectra, conformational energy difference between gauche and trans isomers 2—28359
emitting atom symmetry, effect on X-ray line shape and position 2—35192
equilibrium distances of diatomic molecules by CNDO method 2—771
formaldehyde oxime, Raman spectra discussed with regard to molecular structure 2—8777
gaseous electron-diffraction data, least-squares det. slop and curvature criteria for background 2—18391
hydrocarbon-type chain, matrix formalism 2—15416
mean-square amplitude matrix, new formula for calc. element, of large matrices 2—24426
n.m.r. study using chemical shift reagents 2—5304
non-rigid molecules, internal symmetry groups 2—35215
nonlinear triatomic molecules, structural parameters and valence force consts. 2—8538
overlap, identification with subgroup of group permutations 2—31765
oxygen containing molecules ab initio calcs. 2—28255
pair of linear molecules, equilibrium configurations for mutual orientation 2—39023
point group symmetries, tensor elements of electric multipole moments 2—8549
point groups, application of Racah algebra to classification of states and interaction operators 2—12065
pyramidal inversion barriers for first and second row elements, CNDO/2 calc. 2—24427
spectroscopic study 2—583
structural parameters and potential constants, group theoretical evaluation of their numbers 2—21569
Urey-Bradley calculations using 4- and 5-atom configurations 2—12087
XY_2 type nonlinear mol., invariable distortion coeffs. for isotopic substitutions 2—758
N free radicals, steric effects on stability 2—26374

configuration and dimensions, inorganic
AH_n and AH_n^+ (A=C,N,O, or F), geometries, ab initio MO calc. 2—24425
hexafluorides, analysis of structural data 2—823
neutron diffraction, review 2—29133
nitrosyl compound, bonding, increased valence theory 2—8679
$AlCl_3$, Al_2Cl_6, matrix isolated, structure investigations using i.r. spectrum 2—31775
$AlCl_3$, matrix isolated, i.r. spectrum indicating pyramidal structure 2—12101
Ar, liquid, structure effects on free ion yields and reaction kinetics in radiolysis 2—22886
B_2Br_4, vibrational spectra study 2—15284
BF_2OH, structure and dipole moment from microwave spectrum 2—35230
BH_3NH_3, change in equilibrium geometry, with rotation 2—12106
$B(OH)_3$ 2—29909
$B_2O_3H_2$, conformation, CNDO and INDO calculations 2—38887
Bi, complex, $Bi(S_2C_2H_4)X$, i.r. spectra, ligand configuration, vibr. assignment 2—8769
$BiCl_3$, X-ray diffr. obs. 2—9457
BrCn, dimer structure, matrix-isolated i.r. spectral study at 20K 2—8588
BrF_5, symmetry 2—5912
CF_6^{2-}, possible existence, theoretical study 2—38892
C_2N_4, symmetry 2—38895
CO_3, ab inito LCGO MO SCF calc. 2—8589
C_3O_2, LCGO MO SCF calc. 2—21591
ClCN, dimer structure, matrix-isolated i.r. spectral study at 20K 2—8588
ClNCO, electron diffraction determination of structure 2—28281
Cr complex, $Cr_2O_7Mg.2[(CH_2)_6N_4]6H_2O$, X-ray study of structure 2—781
CrF_4, bonding nature, from mol. rotational spectrum 2—8606
Cu^{2+}, complexes with diethyldithiocarbamate and diethyldithiophosphate, ligand props., e.s.r. obs. 2—24450
$Cu(NH_3)_4(NO_3)_2$ in soln., e.p.r. study 2—21599
DOF, microwave spectra, rotational constants and structural parameters 2—8626
Eu complex, dibenzoylmethane, symmetry around central ion in crystn. forms 2—40663
$EuCl_2$, in Ar, Kr or N_2 matrix, i.r. absorpt. study 2—28327
FD_2^+, i.r. spectrum, determ. of structure and force constants 2—8612
FH_2^+, i.r. spectrum, determ. of structure and force constants 2—8612
FHD^+, i.r. spectrum, determ. of structure and force constants 2—8612
F_3NO, CNDO and INDO approxs. 2—15299
Fe complexes, derivatives of $[SCH_3Fe(CO)_3]_2$ 2—785
$GeCl_4$, symmetry forbidden bands from ν_2(e) mode in i.r. spectrum 2—35248
GeH_3Be, Ge-Br bond length determ. from rotational spectra 2—18421
GeH_2Br, radical, shape, structure and bonding 2—12127
GeH_2Cl, radical, shape, structure and bonding 2—12127
GeH_3I, Ge-I bond length determ. from rotational spectra 2—18421
H_5^+, ab initio quantum mechanical variational calc. 2—8629
HCN isotopes in Ar matrices, i.r. spectra 2—8643
HCl, self-consistent field study of bonding. geometry and physical props. 2—8630

Molecules continued
configuration and dimensions, inorganic continued
HNO_2, cis and trans, structural parameters rel. to cis interaction 2—788
HO_2 radical, geometry, SCF CI calculation 2—31794
H_2O, meas. of H-O-H bond angle in $CuF_2.2H_2O$ by neutron diffraction 2—35985
H_2O, molecular model for prenucleation clusters 2—35378
H_2O, theoretical study of hydrated electrons using SCF MO calculations on small clusters of molecules 2—12153
H_2O_2, in solids, O-O bond shortening 2—39662
HOF, microwave spectra, rotational constants and structural parameters 2—8626
$H_3O^+(H_2O)_n$, n=0-4, geometry 2—24456
H_2PPF_2, conformation from analysis of Stark effect in microwave spectrum 2—15305
H_2S^+ vibrational envelope and bond angle in first excited state , calc. from photoelectron spectrum of H_2S 2—28303
HSiI bond angles of upper and low electronic states determ. from absorption spectrum 2—35260
Hg, complex, cis- dithiocyanotobis(1,10-phenanthroline)mercury(II), and crystal structure 2—12725
IO_2F^- radical 2—20142
$(KOH)_2$, stabilized in Ar matrix at 4.2 K, i.r. absorption spectra, frequencies of OH vibrations and configuration determ. 2—28304
Li_2, mole., bond formation study as function of internuclear distance 2—798
LiOH(D), molecular beam electric resonance spectra 2—8663
Mg complex, $Cr_2O_7Mg.2[(CH_2)_6N_4].6H_2O$, X-ray study of structure 2—781
MgO, iterative calc. by perturbation of configuration interaction for fundamental and first excited states 2—35263
Mn, complex, $Mn(CO)_3C_5H_5$, in nematic solvent, n.m.r. spectra, geometry of C_5H_5 ring 2—8666
Mn complex π-methylcyclopentadienyl manganese tricarbonyl, structure determ. from p.m.r. studies in nematic phase 2—21622
N_4^-, comparison of molecular orbital calc. of contact hyperfine interaction and e.p.r. spectra to determ. geometry 2—21629
NCl, bond length and angle, mean amplitude of vibration, electron diffraction study 2—8676
N_2F_2, cis and trans isomers, CNDO/2 calc. 2—18473
N_2F_4, gaseous electron diffraction study 2—15320
NH_3, rotational spectra, analysis, determ. of structural parameters 2—802
NH_3^+, structure in $^2A_1''$ state 2—8671
N_2H_4 cation radicals, geoemetry 2—31810
$(NO)_2$, ab initio SCF MO calcs. of configuration and dissoc. energy 2—35268
NO_2, N_2O and N_2O_4, CNDO/2 study 2—5936
N_2O_4, shape and size investigation by gaseous electron diffraction 2—38922
Ni, complex, of dimercaptodiethyl sulphide, from i.r. spectrum 2—8769
$OH^-(H_2O)_n$, n=0-4, geometry 2—24456
PF_2CN gas phase, electron diffraction det., sector-microphotometer method 2—18466
PF_2NH_2 2—31820
PH_3, P pyramidal inversion process, ab initio SCF-LCAO-MO study 2—31822
$(PNF_2)_3$, gas phase, electron diffraction study 2—5946
P_4O_{10}, normal coordinates and force field 2—28318
$POCl_{3\odot}^-$, radical anion, e.s.r. study of structure 2—821
PbO, matrix isolation i.r. spectroscopic study 2—15330
Pb_2O_2, matrix isolation i.r. spectroscopic study 2—15330
Pb_4O_4, matrix isolation i.r. spectroscopic study 2—15330
Pt complex, bis(triphenylphosphine) platinum dioxide chloroform adduct 2—29149
SF_6, soft X-ray spectrum, effect of symmetry, photoionization of atoms 2—35285
SO_2, rot. anal. of O-O band, excited state consts., excited state r_0 structure 2—15333
$Se(GeHp3)_2$ gas, molecular structure, sector- microphotometer method of electron diffraction 2—18468
SeO_2 and $(SeO_2)_2$, stereochemical assignments 2—28326
SiF_4, soft X-ray spectrum, effect of symmetry, photoionization of atoms 2—35285
SiH_4 force constants and dipole moment derivatives calc. for symmetric and antisymmetric stretching and bending vibr. modes 2—12193
$SmCl_2$, in Ar, Kr or N_2 matrix, i.r. absorpt. study 2—28327
$SnCl_4$, symmetry forbidden bands from ν_2(e) mode in i.r. spectrum 2—35248
$TeCl_2Br_2$, vapour phase, study using data from $TeCl_4$ and $TeBr_4$ 2—24488
TiO_2, bond angle 2—24489
UO_2 ion, coordination geometry, correlation with vibronic spectra 2—15341
VO_2^{2+} complexes with diethyldithiocarbamate and diethyldithiophosphate, ligand props., e.s.r. obs. 2—24450
$YbCl_2$, in Ar, Kr or N_2 matrix, i.r. absorpt. study 2—28327
Zn complex, dichlorobis(4-methylpyridine)zinc(II) and cryst. structure 2—12738

configuration and dimensions, macromolecules
A-B block copolymer, isolated molecule, block segregation study 2—24560
amylose tricarbanilate, chain length depend. of mean square radius of gyration 2—862
cellulose tricarbanilate, chain length depend. of mean square radius of gyration 2—862
chain, configuration-dependent properties, mathematical methods 2—15409
chain dynamics, local jump models 2—15410
chain molecule, asymptotic behaviour of distribution functions 2—8844
end-to-end distance of two-dimensions excluded vol. chains, limiting distrib. 2—860
ethylene propylene terpolymer stress optical coeffs. of rubbery state, temp. dependence, chain length 2—25507
light optical diffraction patterns produced by electron micrographs 2—8835
molecular shape determ., X-ray scatt. in two dimens. from shapes with inclusions 2—35361
α-olefin isotactic copolymers, conformational equilibria 2—35364
paraffin chains, CNDO calc. of side chain main chain ang. dependence 2—24562

Molecules continued
configuration and dimensions, macromolecules continued
peptide chains, CNDO calc. of side chain main chain ang. dependence 2—24562
poly(L-alanine) 2—38982
poly-β-benzyl-L-aspartate, helix coil transition region of dielectric relaxation due to dipolar orientation 2—8846
poly-DL-alanine, poly-L-alanine, chain conformation from neutron scattering study 2—35368
polybutadiene, stress optical coeffs. of rubbery state, temp. dependence, chain length 2—25507
polyethylene, branched, structural evaluation by combined gel-permeation chromatography and gradient electron fractionation 2—28424
polyethylene, configurational statistics on chain placed on rigid lattice 2—21710
polyethylene, low-density, molecular weight distribution and long-chain branching 2—8848
polyethylene light-microscopic investigation 2—3132
polyisobutylene, dil. soln., statistical radii of gyration, excluded volume effects 2—25033
polyisoprene, stress optical coeffs. of rubbery state, temp. dependence, chain length 2—25507
polymer, molecular rheology 2—18538
poly-N-methyl-l-alanine, Monte Carlo calculations of average dimensions using hard-sphere models 2—24564
polymethylene, short model chains, configurational statistics 2—24561
polyphenoxy radicals, conformation, e.s.r. determ. 2—35369
polysarcosine, randomly coiling, Monte Carlo calculations of average dimensions using hard-sphere models 2—24564
polystyrene, conformational transpositions in vitreous solidification process 2—12625
polyvinyl alcohol films, optical study of chain orientation 2—6004
polyvinylidene chloride-co-methacrylonitrile, monomer sequence distributions by p.m.r. spectroscopy 2—28425
propylene-butadiene alternating copolymers, 220 MHz n.m.r. evidence of alternating sequences 2—35370
protein, freedom of dihedral angles and energy calc. 2—39017
protein, representation and computation of conformations 2—39016
tRNA, high resolution scanning electron microscopy 2—8834
semiflexible helices, mean square raius of gyration and end-to-end distance rel. to degree of polymerization 2—861
structure from light scattering obs. 2—18537
styrene-α-methylstyrene block copolymers, conformations in dilute solution 2—35371
styrene-butadiene copolymer stress optical coeffs. of rubbery state, temp. dependence, chain length 2—25507
Treloar's distribution for length of freely connected chain, derivation and numerical implications 2—8843
U.S. absorpt. meas. of config. and conform. changes 2—28422
virus structures, X-ray diffraction examination 2—15412

configuration and dimensions, organic
bis-(bromomethyl)-mercury, structure from vibrational assignment of i.r. and Raman spectra 2—21669
1,8-bis(dimethylamino)naphthalene radical anion, hyperfine coupling consts., steric hindrance 2—21667
bis-(iodomethyl)-mercury, structure from vibrational assignment of i.r. and Raman spectra 2—21669
N,N′-diethyl-pseudoisocyaninchloride 2—9506
acetamide, monomeric, structure determination from i.r. data 2—8722
acetic anhydride, conformation 2—28338
acetylacetone, structure of enol and keto tautomers determ. by electron diffraction 2—24498
acrolein and singly substituted methyl derivatives, excited singlet-state geometries 2—35337
acylfuranes, preferred conformation in benzene solution, determination from elec. moments 2—38956
adamantane, isotopic, application of new formula for large mean-square amplitude matrices 2—24426
adenosine triphosphate, hydrated disodium salt, and cryst. structure 2—3744
alkanecarbodithoic acids, s-cis conformation 2—24500
n-alkanes, computer simulation, Monte Carlo method 2—8727
alkyl radicals, e.s.r. study of conformations 2—18480
peri-alkylnaphthalene anions, chain-boat interconversion 2—35303
amide, in water, n.m.r. obs. 2—6255
amino acid radicals in X-irrad. N-benzoylalanine single crysts., e.p.r. obs. 2—8735
γ-aminobutyric acid, n.m.r. study 2—8730
α- aminophosphinic acids, i.r. spectra and switterionic structure 2—18523
3-aminopropyl dibutylboron with bases, vibrational spectra, hydrogen bonds and fermi resonance 2—31837
[10]annulenes 2—3070
anti-tricyclo $[4.2.2.0^{2.5}]$-deca-3,9-diene-7,8-endo- dicarboxylic anhydride, X-ray diffraction investigation 2—833
azobenzene, Raman spectra, meas. standard intensities, polarization ratios, determ. structure 2—24505
p-azoxydianisole, equilibrium geometry, Raman spectrum and quantum chemical study 2—8733
benzonitrile, geometric distortion studied by high-resolution n.m.r. in the nematic phase 2—31840
benzonitrile in polycryst. matrices, vibr. anal. of luminescence in terms of excited state geometries 2—31839
2,1,3-benzothiadiazole, in liq. cryst. phase, proton skeleton geometry, HCC angles, n.m.r. obs. 2—8566
benzyl compounds, i.r. and Raman spectra, vibr. assignments, asymmetric structure 2—8742
benzyl derivatives, para substit., i.r. and Raman spectra, vibr. assignment, asymmetric structure 2—8743
benzyl radical configuration calc. by π-SCF-MO and MINDO/1SCF-MO methods 2—38963
N-benzylidenemethylamines, para-substit. electronic absorption spectra, non-planar conformation 2—8740
benzylidine aniline, geometry, ASMO-CI calc. 2—28350
1,1′-biaziridine, conformation from vibrational spectra data 2—38968
bicyclo [3.1.0] hexane substituted with O or CH_2, confirmation investigated 2—12215
bicyclo[2.1.0]pentane, band lengths and dihedral angle from microwave spectra 2—31841
bicyclo[2.1.1]hexane 2—24514
biphenyl, vibrational spectra and dihedral angles 2—38967

Molecules continued
- **configuration and dimensions, organic** continued
  - bis(acetic acid)-BF_3 complex, i.r. spectra study 2—24546
  - bis(methanol)-BF_3 complex, i.r. spectra study 2—24546
  - bis(trifluoromethyl) diselenide, electron diffraction determ. 2—24516
  - bis(trifluoromethyl) monoselenide, electron diffraction study 2—24515
  - 2,2′-bis(6-methyl-3-pyridinol) 2—29157
  - 7-bromo-2,3-dihydro-1-methyl-5-phenyl-1,4-benzodiazepin-2- one, 1:1 complex with chloral hydrate, determ. by heavy atom method 2—9505
  - bromopropene, rotational isomerism 2—28381
  - butoxides of Na and K, vibrational spectra study 2—5964
  - t-butyl chloride, comparison of electron diffraction and microwave spectroscopic structures 2—15359
  - calcium hydrazinecarboxylate, anhydrous 2—9504
  - carbonyl compounds, conformation from obs. of $n\rightarrow\pi^*$ transition sensitivity to solvent effects, importance of hindered carbonyl bisection 2—24521
  - chloral hydrate, 1:1 complexes with 7-bromo-2,3-dihydro-1-methyl-5-phenyl-1,4- benzodiazepin-2-one, and 7-chloro-2,3-dihydro-1- methyl-5-phenyl-1,4-benzodiazepin-2-one, determ. by heavy atom method 2—9505
  - 7-chloro-2,3-dihydro-1-methyl-5-phenyl-1,4-benzodiazepin-2-one, 1:1 complex with chloral hydrate, determ. by heavy atom method 2—9505
  - 3-chloro-2-chloro-methyl-1-propene, rotational isomerism 2—28382
  - chloro- and bromocyclopentane, vibrational spectra, conformational analysis 2—18495
  - chloroaniline+n- dinitrobenzene complex, molecular orbital calc. 2—35318
  - p-chlorobenzotrichloride, n.q.r. obs. 2—5966
  - chlorofluoroacetamide radical, structure from e.s.r. study and MO calc. on X-irradiated dichlorofluoroacetamide crystals 2—26267
  - bis-chloromethyl)-mercury, structure from vibrational assignment of i.r. and Raman spectra 2—21669
  - chloromethyl radical, e.s.r. study in CH_3Cl single crystal 2—8792
  - chloropropene, rotational isomerism 2—28381
  - 2-chloropropenes, deuterium substituted, microwave spectra, CH_3gp conformation 2—31844
  - p-chlorostyrene chains, dipole moments and random coil dimensions 2—8753
  - cinnamaldehyde-imines, n.m.r. study 2—5967
  - computer perception of significant rings in complex cyclic structures, algorithm 2—38949
  - conjugated systems, failure of CNDO/2 method to predict barriers and conformations 2—3099
  - copper(II) acetates, bridging bidentate acetate groups 2—35320
  - copper (II) carboxylates, symmetry, e.p.r. obs. 2—28362
  - copper hexadecachlorophthalocyanine, in epitaxial films 2—9292
  - in crystal, effects of intermolecular forces 2—3742
  - cyanamide, nonplanarity, CNDO/2 calculations 2—28364
  - cyanuric fluoride, C-F bond length det. from Raman spectra 2—35357
  - cyclic phosphonium iodide, X-ray obs. 2—6465
  - cyclobutane, i.r. and Raman spectra, vibrational assignments for D_{2d} symmetry 2—28365
  - cyclobutane, valence orbitals consequences on conformations 2—28363
  - cyclohexane, gaseous, electron diffraction study 2—5970
  - trans-cyclohexane-1,4-dicarboxylic acid, K salt, struct., bond lengths 2—36000
  - cyclononane, n.m.r. evidence 2—24522
  - cyclopentane, barrier to planarity, Raman spectroscopic determination 2—15365
  - cyclopentane, halogen derivatives, conformation 2—35323
  - cyclopentanone, far i.r. spectra and conformational energy 2—35322
  - cyclopropyl methyl ketone, microwave spectrum, barrier to internal rotation, dipole moment, conformation 2—21673
  - cyclopropylacetylene, bond lengths determ. from microwave spectrum 2—35321
  - deoxycytidine-3′-monophosphate, energy calcs. for isomeric structure using extended Huckel theory 2—12234
  - deoxycytidine-3’-monophosphate, semi-empirical MO calculations for isomeric structures 2—12235
  - dialkylamino radicals 2—18525
  - 1,2- diazadiene-1,3 compounds, config. from electronic spectra 2—18483
  - diazaphosphetidines, ^{19}F NMR spectra discussed in terms of molecular conformation 2—28366
  - 1,2-dichloroperfluoropropane, ^{19}F n.m.r. spectra, conformational energy difference between gauche and trans isomers 2—28359
  - 4,11-dichloroquinacridone, X-ray determ. 2—6466
  - dichlorosilicon, phthalocyanine, structure from i.r. spectrum 2—38972
  - difunctional derivatives, X-CHR-CHR′-Y, n.m.r. study 2—8572
  - 4,4′dihalogenobiphenyls, vibrational spectra and dihedral angles 2—38967
  - 5,6-dihydrouracil-6-yl radical, conformation studies in mol. crysts. 2—15372
  - dimercaptodiethyl sulphide, from i.r. spectrum 2—8769
  - N,N-dimethyl-thiourea S-trioxide, study by heavy atom method 2—5996
  - dimethylallene, microwave spectrum, barrier to internal rot., rot. consts. dipole moment, r_0-type structural data 2—18499
  - p-dimethylaminobenzaldehyde hydrobromide, x-ray determination 2—39660
  - dimethylaminodichloroarsine, Raman spectra study 2—24528
  - dimethylaminodichlorophosphine, gauche conformation 2—28369
  - dimethylcadmium, structure study, normal coordinate analysis 2—21680
  - dimethyldisulphide, electron diffraction study 2—24529
  - 1,2- and 1,3-dimethylenecyclobatane, symmetrics determ. from vibrational spectra 2—12238
  - dimethylmercury, structure study, normal coordinate analysis 2—21680
  - dimethylzinc, structure study, normal coordinate analysis 2—21680
  - p-dinitrobenzene, geometric distortion studied by high-resolution n.m.r. in the nematic phase 2—31840
  - 1,4- dioxadiene, conformation, ab initio study 2—18498
  - 1,4-dioxane ring inversion barrier 2—28367
  - dioxyphosphorane, bicyclic 2—25361
  - p-dithiin p.m.r. study of orientation in lyotropic liq. cryst. 2—18500
  - ethanediol, configuration in solid and liquid from i.r. spectrum 2—8769
  - ethanes, disubstituted, Karplus equation failure to predict ang. depend. of J_{vic} 2—763
  - ethyl nitrate, microwave spectrum, rotational constants of trans and gauche rotamers 2—12241
  - ethyl thiocyanate 2—35327
  - ethylene, equilibrium geometry from ab initio calc. by force relaxation method 2—8767
  - ethylenediamine, conformations, extended Huckel theory study, minimal energy forms 2—28375

Molecules continued
- **configuration and dimensions, organic** continued
  - ethyleneimine substitution structure from microwave gas spectra 2—24534
  - etioporphyrins, photoreduction products, n.m.r. spectra 2—28374
  - flexible polymer, unperturbed dimensions from viscosity relations 2—25057
  - fluorocarbonium ions, $(FCH_2)^+$ and $(F_2CH)^+$, ab initio MO study 2—21684
  - fluorochloroacetones, ^{19}F n.m.r. and ^{13}C satellite spectra, conformational preferences, C-F coupling const. 2—28377
  - formamide 2—38982
  - formic acetic anhydride, sector-microphotometer method of electrodiffraction 2—18506
  - formic acid, rot. spectrum and isotopic substitutions 2—18509
  - formyl formide, conformation and electronic structure, valence shell calc. 2—18507
  - fulvenallene 2—28378
  - fumarofine, structure 2—3096
  - α-glycine, conformation of $H_3NCH_2OO^-$ ion 2—28379
  - glyoxal, cis-, perpendicular and trans-, conformation 2—18510
  - halogenated methyl radicals, substituent affects on geometry 2—31863
  - 2-halomethyl-1,3-dioxans, double ultrasonic relaxation, ring inversion and internal rotation 2—24530
  - heterocyclics, 5 membered, unsaturated, chem. shifts, H-H coupling consts., proton mag. reson. spectra 2—12256
  - hexafluorobenzene, C-F bond length det. from Raman spectra 2—35357
  - hexafluoropropene, C=C bond twisting, investigation using microwave spectrum 2—15380
  - hexahydro-1,3,5-trichloro and trinitroso s-triazine, geometry 2—31859
  - hydrocarbons, C_3 molecules, MO calc. of polarities 2—28383
  - 8-hydroxyquinoline-N-oxide 2—9508
  - iminoxy radical, formed from γ-radiation of 5-nitrouracil, e.s.r. structure study 2—10651
  - indenyl carbanion-alkali metal ion pairs, n.m.r. study 2—18512
  - isodiazomethane, CH_2N_2 isomer, theoretical investigation 2—8751
  - ketyls, nonplanarity of carbonyl carbons from INDO approx. SCF MO theory 2—8786
  - liquid crystal, effects on transitions 2—9090
  - liquid crystals, effects on smectic phase formation 2—9091
  - macromolecules, quasielastic light scattering under optical microscope 2—34514
  - malic acid free radical, conformational anal. using PCILO method, conformation by INDO calc. of coupling consts. 2—8789
  - mesitylene, electron-irradiated, consequent radical, CNDO/2 calc. 2—5980
  - methane, interpretation of mol. beam radiofrequency, ortho-para transitions 2—12266
  - methane radical cation, tetracoordinated three-centre bound config. 2—8791
  - methoxydifluorophosphine, molec. structure from microwave spectrum 2—15387
  - 2-methoxyethanol, confirmation determination from meas. in microwave spectrum 2—12262
  - methyl cyclopropanols, structure and isomerism of rotation about C-O determ. by solvent effect of pyridine on n.m.r. 2—5968
  - methyl iodide, ground state geometry determ. from i.r. spectrum study of dideutero methyl iodide 2—12221
  - methyl nitrate 2—18514
  - methylcyclohexane, gaseous, electron diffraction study 2—5970
  - methylene groups, dihedral angle assignment by n.m.r. coupling constants 2—3066
  - methylpropenals, singly substituted, excited-state geometries 2—35337
  - methylpropenals, singly substituted, excited-state geometries 2—35336
  - monodeuterobenzonitriles, in polycryst. matrices, vibr. anal. of luminescence in terms of excited state geometries 2—31839
  - monofluoroacetic acid 2—38996
  - monofluorobenzaldehydes and derivatives, conformations 2—5982
  - N-halogen secondary amides, i.r. spectra, cis-trans isomerism 2—28344
  - 1- and 2- naphthaldehyde, possible hydrogen bonding from dielectric relaxation meas. 2—15601
  - nitriles, complexes formed with proton donors, structure from dipole moment measurements 2—28391
  - nitrobenzene, structure relaxation during internal rotation of the nitro group 2—38997
  - p-nitrobenzonitrile, geometric distortion studied by high-resolution n.m.r. in the nematic phase 2—31840
  - 2-nitroethanol, rotational isomerism 2—28389
  - organometallic β vinyl chloride (Hg, Sh, Tl, Sb), cis and trans config., i.r. absorp. obs. 2—31872
  - oriented molecules, n.m.r. obs. 2—5956
  - 3-oxetanone, partial structure from microwave spectrum data 2—15389
  - oxyphosphorane, four-membered cyclic ring with pentavalent phosphorous 2—25360
  - palladium n-propyl mercaptide, bond lengths and angles 2—6464
  - pepper acids, n.m.r. and INDOR study 2—8812
  - perdeuterobenzonitrile, in polycryst. matrices, vibr. anal. of luminescence in terms of excited state geometries 2—31839
  - perfluoroethyl iodide, electron diffraction structure study r_g parameters 2—31868
  - perfluoroisopropyl iodide, electron diffraction structure study r_g parameters 2—31868
  - perfluoromethyl iodide, electron diffraction structure study r_g parameters 2—31868
  - phenothiazine and N-substituted derivatives, configuration determination by n.m.r. 2—12271
  - phenothiazines, substituted dipole moments meas., bending of nucleus 2—38999
  - phenyl substituted imidazyl and pyrryl radicals, spin density distrib. determ. from e.s.r. spectra 2—8807
  - phenylacetylenes, D-substituted, first excited singlet state geometry, fluoresc. study 2—35345
  - phosphadiazetidinones, ^{19}F NMR spectra discussed in terms of molecular conformation 2—28366
  - piperidine hydrochloride, heavy atom technique 2—25362
  - pivalonitrile-N-oxide, microwave spectrum, bending mode estimate, symmetric top molecule 2—5989
  - polystyrene-polybutadiene- polystyrene macroscopic ‘single crystal’, from i.r. spectra 2—15417
  - propanes, methyl substituted, structure effects on free ion yields and reaction kinetics in radiolysis 2—22886

Molecules continued
configuration and dimensions, organic continued
propyl cations, geometries and energies, ab initio MO calculations 2—39001
propylene-vinlcyclohexane copolymers, structure study from i.r. spectra 2—24563
propynyl boron difluoride, i.r. spectrum, fundamental assignment, G_{12} symmetry group 2—8813
pyreno-(1′,2′:1,2)-pyrene, mol. struct. and cryst. struct. 2—32480
quinacridone, X-ray determ. 2—6466
quinoxaline, oriented in nematic phase, proton skeleton, spin spin coupling consts., n.m.r. obs. 2—9183
radicals, configuration study using MINDO method 2—827
retro-β-ionylidene acetic acid, conformational energy calc. by PCILO method 2—12293
s-triazine, geometry in excited state determ. from rotational analysis of J-structure of band in 3100 Å system 2—12288
selection rules of molecules having one, two and three CH_3 tops evaluated using PE-group 2—8511
selenophene, oriented in lyotropic mesophase, n.m.r., direct couplings and interproton distance 2—28409
semidiones, planarity of carbonyl carbons from INDO approx. SCF MO theory 2—8786
semiquinones, planarity of carbonyl carbons from INDO approx. SCF MO theory 2—8786
silyl radicals, trimethylsilyl substituted, substituent effects on geometry 2—31863
N-silylpyrrole, electron diffraction investigation 2—5994
tert-butyl-1,3-dioxanes, conformation, ^{13}C mag. reson. study 2—3074
tetrabenzopentafulvalene derivatives, geometrical isomerism, n.m.r. obs. 2—12281
3,4,5,6-tetrachloro-2,7-dihydrothiepin, n.m.r. study of ring inversion 2—28413
tetracyanoethylene oxide, X-ray and neutron diffraction data 2—28411
tetracyanomethanes, structure determination by electron diffraction 2—21702
4-tetrahydrothiapyranols, substituted, elec. dipole moments rel. to conformational studies 2—28410
4-tetrahydrothiapyranones, substituted, elec. dipole moments rel. to conformational studies 2—28410
3,3,6,6,-tetramethyl-1-thiacycloheptine molecular structure 2—39010
tetramethylene cyclobutane-d_o and -d_s, vibrational spectra measured, symmetry determ. 2—12282
thallium(I) nitroparaffins, structure determination from i.r. and n.m.r. studies 2—12287
thiazyl compounds, bonding, increased valence theory 2—8679
thoacetamide-S-oxide, crystal and molecular structure by heavy atom method 2—18529
tolane, Raman spectra, meas. standard intensities, polarization ratios, determ. structure 2—24505
1,1-di-p-tolylethylene, conformational analysis 2—28415
transient free radicals, e.s.r. study of conformations 2—18480
trichloromethyl group contribution to dipole moment of cyclic molecules 2—38952
trifluorobenzene, C-F bond length det. from Raman spectra 2—35357
trifluoromethyl selenium cyanide, electron diffraction determ. 2—24555
1,1,4-trimethyl-5-carboxy-cyclopentene-4, conformational energy calc. by PCILO method 2—12293
trimethylarsenic dibromide and dichloride, interpretation of vibr. spectra on basis of symmetry 2—18536
trimethylene oxide in nematic liquid crystal, geometry determ. from NMR spectrum 2—35354
1,2,4-trioxacyclopentane, structure determination from microwave spectrum 2—15400
1, 2, 5- trioxan, gaseous, electron diffraction investigation 2—18532
triphenyltin carboxylates, Mossbauer study of effect of helical chain 2—5954
tris-(1,2-dimethylhydrazino)-diphosphine, X-ray obs. 2—6467
urea, urea-d_4, structure determination from i.r. data 2—8722
urea clathrate structure, ordering of 1,5-dichloropentane molecules 2—3751
vinyl chloride chains, random coil dimensions and dipole moments, effect of isotacticity 2—8840
zinc uranyl acetate, U—O bond distance 2—3128
Co complexes, stereochemistry, X-ray obs. 2—32452
$H_3NCH_2COO^-$ ion, conformation 2—28379
He_3^+, SCF and CI calc. of geometry 2—35258
SnH_3Br, Sn-Br bond length from microwave spectrum 2—15337

dissociation
see also Heat of dissociation
acetone, reaction pathway for photodissociation calc. using CNDO/2 approx. molecular orbital method 2—31835
Auger dissociation, in collisions with multiply charged ions 2—868
benzene mol. ion, prod. by charge exchange, dissoc. lifetime 2—24513
benzonitrile mol. ion, prod. by charge exchange dissoc. lifetime 2—24513
n-butane free jets expansion, fragment ions rel. to mass spectra 2—24518
in cascade arcs, vacuum u.v. spectroscopy 2—21593
collision-induced, simplistic optical model analysis 2—8503
diatomic molecule, disintegration cross section on collision with atom 2—11991
diatomic molecules, incubation time prediction 2—21587
dissociative attachment, and resonance near excitation threshold, non adiabatic effects 2—31737
dissociative electron attachment, theory 2—12067
dissociative recombination, lower vibrational state and ground vibrational state models 2—12068
electron impact, dissociative excitation processes for simple molecules 2—5893
equilibrium constant, for gas system 2—39266
formaldehyde, photodissociation, potential energy surfaces 2—20201
four-atomic molecules, collisional dissociation into diatomic species, initial vibrational and rotational population distributions predicted by statistical model 2—866
gases, by electron bombardment 2—18392
hot molecules, resonance dissociative attachment 2—24428
hydrocarbon ions, Ch_n^+m ub collisions with N_2 at 40 to 140 keV 2—900
hydrocarbons, residual, laser produced dissoc. 2—28386
ionic fragmentation, quasi- equilibrium theory 2—38864
methane, thermal dissociation on hot W emitter tips, field emission microscopy 2—30059

Molecules continued
dissociation continued
methylamine and deuterated derivatives, mass spectrometric study of negative ions formation by electron impact 2—3898[illegible]
photodissociation of excited molecules following pumping by monochromatic laser radiation, method of selective breaking of bonds 2—31759
polyatomic, general formulae for Hertzlberg type I predissociation 2—38867
predissociation by continuum of bound state without curve crossing 2—18462
thiophene mol. ion, prod. by charge exchange, dissoc. lifetime 2—24513
unimolecular breakdown processes, exact calculation 2—26326
AlO emitted from H flame at atmospheric pressure, 2300-2700 K, second-law calc. of bond association energy 2—10617
$ArHg^+$ ions, dissociation energy estimated following collision processes 2—18337
$2AsI_2 \rightleftharpoons 2AsI + I_2$, temp. depend. of equilib. const. 2—28934
Br_2, in shock waves, dissociation rate meas. at 1500 to 2700K 2—24459
Br_2 dissociation in Ar, incubation time prediction 2—21587
CO, by electron impact at 10 keV 2—12170
CO, by He(2^3S), dissociative excitation rate constants 2—12305
CO, in collisions with H, $H^\pm$, slow negative ion formation processes 2—874
CO, mechanisms producing $C_2{}^*(A_3\Pi_g)$ molecules in afterglow 2—35615
CO_2, by 30, 50, 100 eV election impact, temperature dependence of total ionization cross section in 300-2100 K range 2—3037
CO_2, by electron-impact, translational spectroscopy of metastable and long-lived Rydberg fragments 2—3058
CO_2, dissociative charge exchange collision with He^+, differential cross section measurements 2—873
CO_2, electron impact dissociative excitation, nonthermal rotational population of $CO(A^1\Pi)$ state 2—5920
CO_2, photodissociation, yield meas. for $CO(a^3\Pi)$ fragments 2—3033
CO_2, photodissociative excitation, meas. of CO fourth positive system 2—778
CO_2 photodissociation obs. of phosphorescence from $CO(a^3\Pi\text{-}X^1\Sigma)$ Cameron bounds 2—28276
CO_2 pulsed laser, dissociation effect on inversion 2—2396
$CO_2 \rightarrow O(^1S)+CO(X^1\Sigma)$, vacuum u.v. photodissociation, time of flight spectroscopy of metastable fragments 2—777
$CS_2 \rightarrow CS(A^1\Pi)+S(^3P_2)$, photodissociation in vacuum u.v., determ. of $D_0{}^0$(SC-S) 2—37053
Cl_2 dissociation in Ar, incubation time prediction 2—21587
ClNO→Cl+NO photodissociation, comparison of quasidiatomic model predictions with photofragment spectrum meas. 2—780
D_2 metastable ions, dissociation mechanism 2—35254
D_2^+, collision induced, threshold-2 keV with gaseous targets, excitation energies determ. 2—12308
D_2^+, photodissociation from 2472 to 13613 Å, cross sections 2—31801
D_2S, dissociative attachment, formation of DS- 2—24458
D_2S, dissociative electron attachment, cross section for DS^- formation 2—12137
$H^+{}_2 \rightarrow H^+ + H$, collision-induced, kinetic energy release 2—28296
$H^+{}_3 \rightarrow H^+ + H_2$ and $H^+{}_3 \rightarrow H^+{}_2 + H$, collision-induced, kinetic energy release 2—28296
H_2, by collision with Li^+, expt. evidence for spectator mechanism 2—18422
H_2, by collision with Na^+ at 5 to 42 keV 2—883
H_2, by double electron excitation, photoelectron spectroscopy obs. 2—18423
H_2, by electron impact, angular intensity dist. of product metastable atoms meas., deduced final states involved 2—3048
H_2, by Li^+ and Na^+ impact 2—882
H_2, collisions with H^+, H, 1-30keV, cross section for emission of Lyman-alpha radiation 2—5872
H_2, direct and dissociative ioniz. 2—24457
H_2, in electric discharge, model 2—3046
H_2, predissociation, u.v. Ly_α-fluorescence obs. 2—18432
H_2, spontaneous, radiative calc. 2—38912
H_2 and D_2, D $^1\Pi_u$–X $^1\Sigma_g^+$ system, predissociation, effect of rotation on lifetime 2—21608
H_2 by He, studied at 5500K using quasiclassical approx. determ. rate constant for reaction 2—21714
H_2 metastable ions, dissociation mechanism 2—35254
H_2^+, by electron impact, application of Born theory to angular and energy distribution of protons 2—3047
H_2^+, collision induced, threshold 2 keV with gaseous targets, excitation energies determ. 2—12308
H_2^+, collisional dissociation on He, formation of fast excited H atoms 2—31718
H_2^+, dissoc. recomb. as cause of axial density decay in long diffused plasma column 2—28569
H_2^+, H_3^+, neutral atom form. 2—8484
H_2^+, H(2p) and H(2s) formation in collisions with He, ang. dependence 2—885
H_2^+, photodissociation from 2472 to 13613 Å, cross sections 2—31801
H_2^+, x=1-3, collisions with He, Ar, N_2, H_2 targets, 75-1000keV formation of excited H atoms 2—5853
H_2^+ ions, by electrons, cross sections for interaction energies between 25.4 and 715 eV 2—31797
H_3^+, collisional dissociation on He, formation of fast excited H atoms 2—31718
H_3^+, in collisions with H_2 and N_2 at 410 to 1800 keV, cross section meas. 2—884
HBr, in shock waves, dissociation rate meas. at 1500 to 2700K 2—24459
HCl, photodissociation using laser radiation 2—21524
HD metastable ions, dissociation mechanism 2—35254
HD^+, electron impact dissociation, asymmetry in ang. distribution of fragments 2—3042
HDS, dissociative attachment, formation of HS- and DS- 2—24458
HDS, dissociative electron attachment, cross section for HS^- and DS^- formation 2—12137
H_2O, electron attachment studies 2—21870
H_2S, dissociative attachment, formation of HS- 2—24458
H_2S, dissociative electron attachment, cross section for HS^- formation 2—12137
H_2S, negative ion formation by dissociative attachment 2—32114
He_2^+, dissociative recombination of electrons 2—35259
He_2^+, photodissociation from $^2\Sigma_u^+$ state into $^2\Sigma_g^+$ and $^2\pi_g$ states, cross section calculation 2—795

Molecules continued
dissociation continued
HeH^+, in collisions with H_2 and N_2 at 520 fo 1025 keV, cross section meas. 2—886
HeH^+, isotopic, collision induced unimolecular dissociation 2—887
$He^+ + CO_2$, dissociative charge exchange, differential meas. 2—31730
I_2, quantum yield for unimolecular dissociation in visible absorption 2—31803
Li^+-He colliding systems, products of π' and Δ' states 2—735
N_2, by collision with Na^+ at 5 to 42 keV 2—883
N_2, by electron impact, detection of high-Rydberg levels of atomic N by Auger ejection of electrons 2—2950
N_2, by electron impact at 10 keV 2—12170
N_2, dissociative excitation by electron impact, vacuum u.v. emission features 2—8669
N_2, induction time, exptl. obs. 2—24479
N_2, multiphoton ioniz. and dissoc. at $\lambda = 0.53\ \mu$ 2—35272
N_2, with $He(2^3S)$, dissociative excitation rate constants 2—12305
N_2 ($B^3\pi_g$, v=13), formation by inverse predissociation from $N(^4S_o)$ atoms 2—803
N_2^+, collision induced, threshold-2 keV gaseous targets, excitation energies determ. 2—12308
N_2^+, predissociation, monomolecular and collision induced in mass spectrum 2—12162
N_2^+, predissociation of collisionally excited states 2—896
N_2F_4, laser induced dissoc., rate 2—31808
NH_3, electron attachment studies 2—21870
NH_3, on electron collision, vac. u.v. spectral obs. 2—18454
NO, electron impact dissociative excitation in vacuum u.v. 2—3054
NO^+, in collisions with He at 2 to 5 keV 2—895
$NO^+ \rightarrow O^+ + N$ unimolecules dissociation, translational spectroscopy 2—21624
NO_2 photodissociation, angular distribution of recoil O atoms 2—30086
NO_2 photodissociation, energy partitioning 2—30085
N_2O, on electron collision, vac. u.v. spectral obs. 2—18454
$N_2O \rightarrow O(^1S) + N_2(X^1\Sigma) \rightarrow O(^2P) + N_2(A^3\Sigma)$, vacuum u.v. photodissociation, time of flight spectroscopy of metastable fragments 2—777
NOCl photodissociation, energy partition and recoil photofragment angular distributions 2—30087
Na-O species, dissociation enthalpy, deduction from Hartree-Fock molec. orbital studies of neutral molecule and ions 2—37032
NaI photodissociation fluorescence of $Na^*(3p^2P)$ D lines obs. 2—12180
O_2, by 35 eV electron impact, energy spectrum of O^+ fragments meas., compared with similar spectra 2—3059
O_2, by collision with Na^+ at 5 to 42 keV 2—883
O_2, by electron impact, translational spectroscopy of metastable and long-lived Rydberg fragments 2—3058
O_2, electron impact dissoc., absolute prod. cross sect. of $O(^5S^0)$ 2—21520
O_2, interaction with O and He atoms in shock tube, u.v. absorpt. spectra 2—18461
O_2, photodissociation continuum of Schumann-Runge system, theoretical calc. 2—818
O_2 dissociation in Ar, incubation time prediction 2—21587
$O_2 \rightarrow O(^3P) + O(^1S)$, vacuum u.v. photodissociation, time of flight spectroscopy of metastable fragments 2—777
OH, formation through inverse predissociation 2—816
OH, possible formation through inverse predissociation 2—12186
OH, predissociation by continuum of bound state without curve crossing 2—18462
$OSCl_2$, photodissociation in vacuum u.v., heat of formation of SO 2—33385
Rb_2, under laser pulse irradiation, rel. to absorpt. spectra 2—24485
SO_2, fluorescence and predissociation 2—35286
SO_2, in d.c. He-SO_2 discharges, positive ion sampling 2—15506
TiO, gaseous, dissociation energy derived from titanium-oxygen reactions studied with Knudsen effusion-mass spectrometer 2—28329
TiO_2, gaseous, dissociation energy derived from titanium-oxygen reactions studied with Knudsen effusion-mass spectrometer 2—28329

dissociation energies
diatomics, ground states, comparison of actual and linearly extrapolated values 2—18372
epoxy resins, ionic dissoc. energy in elect. cond. behaviour 2—25912
metal compounds, spectrophotometric det. 2—12197
siloxanes, bond energies 2—15414
1,1,1-trifluoroethane, bond energies 2—15403
BO_3, ionic dissoc. energy in elect. cond. behaviour 2—25912
BP, measurement 2—31777
CO, ion-pair processes, by electron impact, mass spectrometric study 2—8623
CaF, $X^2\Sigma$, $A^2\Pi$ and $B^2\Sigma$ states, dissociation products 2—3034
Cr complex, $Cr(CO)_6$, ab initio SCF-MO calcs. comparison with exptl. results 2—21634
CsO, ion model calc. and ground state 2—28266
EuC_2, mass spectrometric determination 2—15298
FO, ground state radicals, from appearance potential of FO^+ 2—22875
H_2, ion- pair processes, by electron impact, mass spectrometric study 2—8623
He_2, excited state dissociation energy determ. from potential curves from continuous spectra 2—38917
He_2, of $A^1\Sigma_u^+$ state 2—8655
He_2 calc. of potential of lowest excited singlet state, comparison with expt. 2—21612
He_2^+, of $X^2\Sigma_u^+$ state 2—8655
He_3^+, SCF and CI calc. 2—35258
HoAg 2—24473
HoAu 2—24473
$HoAu_2$, atomization energies by high temp. mass spectrometry 2—28302
Ho_2 2—24473
IO, estimate from R-K-R curve 2—24475
KO, ion model calc. and ground state 2—28266
LiO, ion model calc. and ground state 2—28266
$LuAu_2$, atomization energies by high temp. mass spectrometry 2—28302
MnO_4 estimated from study of Resonance Raman effect in $KMnO_4$ 2—12565
NO, ion-pair processes, by electron impact, mass spectrometric study 2—8623
NO, $X^2\Pi$ and $A^2\Sigma^+$ states, restricted Hartree Fock calculations 2—35266
$(NO)_2$, ab initio SCF MO calcs. of configuration and dissoc. energy 2—35268
NaO, ion model calc. and ground state 2—28266

Molecules continued
dissociation energies continued
Ni complex, $Ni(CO)_4$, ab initio SCF-MO calcs. comparison with exptl. results 2—21634
O_2, ion-pair processes, by electron impact, mass spectrometric study 2—8623
P_2, from predissoc. at $\nu'=10$ and 19 of $C^1\Sigma^+_u$ state 2—31819
PdGe, mass spectrometric Knudsen cell method 2—28321
PtP, upper limit 2—5948
RbO, ion model calc. and ground state 2—28266
RhP, and identification 2—5948
SF_3-F bond 2—31826
$SrCl_2$, spectrophotometric det. 2—38942
SrOHCl, spectrophotometric det. 2—38942
$TbAu_2$, atomization energies by high temp. mass spectrometry 2—28302
TlAs, exptl. investigation 2—15339
TlBi, gaseous, determ. from thermodynamic treatment of Knudsen cell-mass spectrometric data 2—21644

electron scattering
benzene, radiation emission for 0 to 500 eV incident energies 2—5961
diatomic, application of adiabatic-nuclei theory to vibrational excitation by electron impact 2—18384
diatomic, selection rule for parity unfavoured transitions 2—12090
diatomic molecule, resonance effects 2—18375
diatomic molecule, vibrational excitation, parametric resonance effect 2—751
diatomic molecule-slow electron, resonance effects 2—18375
diffraction patterns, single beam densitometer for precise obs. 2—38878
dipolar charges, fixed, model 2—754
dissociative excitation, mechanisms, for simple molecules 2—5893
effective long range potential derived, symmetry properties discussed 2—28207
eikonal approx. application to elastic scatt. from spherically symmetric potential 2—31686
elastic and inelastic cross sections 2—24834
electron impact spectra, direct method for obtaining from ICR mass spectrometer 2—35110
electron impact spectroscopy, group theoretical selection rules 2—2952
ethane, ion molecule reaction chemistry, low electron energy, study by ICR spectroscopy 2—33373
formaldehyde, rot. transition by electron collision 2—18437
formaldehyde, valence and Rydberg transitions, dependence of generalized oscillator strength on momentum transfer 2—15376
frame transformation theory, rotational and vibrational excitation formulae 2—12069
gas, differential cross sections for low energy elastic scatt., elec. diffractometer design 2—38881
gas, optical breakdown threshold 2—39217
inelastic, Renner effect in energy loss spectra 2—12070
intramolecular multiple scattering in gas phase electron diffraction, model calcs. 2—21560
many-particle scattering, effects of approximate cluster functions on parameters and improved pseudostate expansion 2—11995
methane, formation of energetic protons by electron impact 2—3154
methanol, triplet excitation by low energy electron impact spectra 2—24453
methylamine and deuterated derivatives, mass spectrometric study of negative ions formation by electron impact 2—38988
optical oscillator strengths by electron impact spectroscopy 2—8515
porphyrins, chlorines, electron excitation spectra, interpretation 2—39000
resonance energy det. from broadened profiles 2—21525
resonant, angular distribution theory 2—750
resonant collisions, determ. branch structure in rotational excitation 2—18382
transmission of energy monochromated electrons, energy loss spectra, excitation of vibr. levels 2—12099
triatomic linear molecule, with Renner effect, inelastic scatt. 2—5909
water, triplet excitation by low energy electron impact spectra 2—24453
CO, electron impact excited emission cross sections, meas. from 1260 to 5000Å 2—5919
CO, electron impact spectrum, abs. generalized oscillator strengths for $B^1\Sigma^+ \leftarrow X^1\Sigma^+$ and $C^1\Sigma^+ \leftarrow X^1\Sigma^+$ transitions 2—12115
CO, energy losses of 10 keV electrons, ionization and fragmentation 2—12170
CO, excitation of electronic states, cross section determination from energy loss spectrum 2—15293
CO, inner shell electrons, ionization by 10 keV electron as function of energy loss 2—39195
CO, near-thermal energies, effect of molecular wavefunction 2—18405
CO, negative ion formation, discrepancy between single collision and electron swarm methods of obs. 2—24832
CO, resonance obs. at 10.04 eV 2—772
CO, resonance obs. at 10.05 eV 2—807
CO, resonance scatt. 2—5916
CO, vibrational excitation by electrons at 10 to 100 eV 2—12171
CO N_2 mixtures with inert gases, determ. dependence of annihilation rates of slow positron on molecular concentration 2—24467
CO resonance excitation 2—808
CO_2, dissociation, translational spectroscopy of metastable and long-lived high Rydberg fragments 2—3058
CO_2, dissociation by 30, 50, 100 eV electron impact temperature dependence of total ionization cross section in 300-2100 K range 2—3037
CO_2, dissociative excitation, nonthermal rotational population of $CO(A^1\Pi)$ state 2—5920
CO_2, elastic scattering of low energy electrons at 180° 2—18408
CO_2, electron impact excited emission cross sections, meas. from 1260 to 5000Å 2—5919
CO_2, threshold electron impact excitation spectra studied by SF_6 scavenger technique 2—28313
COS, threshold electron impact excitation spectra studied by SF_6 scavenger technique 2—28313
CS_2, threshold electron impact excitation spectra studied by SF_6 scavenger technique 2—28313
Co, valence electrons, ionization by 10 keV electrons as function of energy loss 2—39194
H_2, 1-10eV, differential and integrated cross sections for vibrational and vibrational-rotational excitation 2—12136
H_2, cross sections for rotational excitation by slow positron impact calc. in distorted wave approx. 2—24466
H_2, electron-impact cross sections and energy deposition 2—24457

Molecules continued
electron scattering continued
H_2, electron impact excitation of Lyman and Werner bands 2—5931
H_2, excitation of Werner bands by electron impact (300 eV) 2—35253
H_2, G(3d $^1\Sigma_g^+$) state excitation, microwave optical magnetic resonance 2—21605
H_2, inelastic excitation, total cross sections 2—794
H_2, low energy positron scattering, rotational excitation 2—5932
H_2, parity forbidden transitions, excitation by energetic electronics 2—12141
H_2, resonant excitation of $B^1\Sigma^+_u$ state, close coupling calc. 2—793
H_2, simultaneous vibrational-rotational excitation by low energy electrons 2—12140
H_2, vacuum u.v. laser, electron beam excitation 2—17601
H_2, vibrational and rotational excitation, by slow electron impact, 0.3-15 eV 2—790
H_2^+, proton production cross section meas. 2—3144
H_2^+, survey of exptl. and theoretical determ. of cross section for proton production 2—31798
H_2^+ dissociative collisions, application of Born theory to angular and energy distribution of protons 2—3047
H_2^+ ions, dissociative excitation, cross sections for interaction energies between 25.4 and 715 eV 2—31797
HD^+, electron impact dissociation, asymmetry in ang. distribution of fragments 2—3042
H_2O, electron impact excitation, 3 to 6 eV 2—8617
H_2O, electron scatt. spectra, theoretical interpretation 2—12138
H_2O rot. transition by electron collision 2—18437
$H_2+e\rightarrow H(2S)+H+e$, dissociative excitation process, meas. angular intensity dist. of metastable atoms, deduced final states involved 2—3048
N_2, 500eV incident electrons, energy loss cross sections, study of inelastic continuum 2—8670
N_2, C $^3\Pi_u$ state, electron impact excitation of v'=3 and 4 levels, electron emission band obs. 2—5938
N_2, cross sections for rotational excitation by slow positron impact calc. in distorted wave approx. 2—24466
N_2, dissociative excitation by electron impact, vacuum u.v. emission features 2—8669
N_2, energy losses of 10 keV electrons, ionization and fragmentation 2—12170
N_2, excitation of metastable $E^3\Sigma_g^+$ state 2—31814
N_2, inner shell electrons, ionization by 10 keV electron as function of energy loss 2—39195
N_2, metastable states excitation 2—18452
N_2, N_2^+, decay of electron impact excited states, time resolved studies 2—5939
N_2, resonance excitation 2—808
N_2, resonance obs., derivation of N_2^- potential curve and width of 11.48 eV state 2—807
N_2, valence electrons, ionization by 10 keV electrons as function of energy loss 2—39194
N_2, vibrational excitation by electrons at 10 to 100 eV 2—12171
N_2 mixtures with inert gases, determ. dependence of annihilation rates of slow positrons on molecular concentration 2—24467
N_2^+, impact excitation of O-O band 2—18450
NH_3, vacuum u.v. spectra 2—18454
NO, electron-impact excitation, absolute cross sections 2—24478
NO, electron impact dissociative excitation in vacuum u.v. 2—3054
NO, resonances, vibrational progression rel. to Rydberg states 2—812
NO vacuum-u.v. excitation cross sections determ. 2—21627
N_2O, threshold electron impact excitation spectra studied by SF_6 scavenger technique 2—28313
N_2O, vacuum u.v. spectra 2—18454
O_2, angular dependence of electron impact excitation cross sections 2—31817
O_2, cross sections for rotational excitation by slow positron impact calc. in distorted wave approx. 2—24466
O_2, cross sections meas. from 0 to 4eV rel. to negative molec. ion spectroscopy 2—819
O_2, differential and integral cross sections determ. for impact energies 4-45 eV, scattering angles 0°-90° 2—15328
O_2, dissociation, translational spectroscopy of metastable and long-lived high Rydberg fragments 2—3058
O_2, dissociative ionization by 35 eV electron impact, energy spectrum of O^+ fragments meas. 2—3059
O_2, electron impact dissoc., absolute prod. cross sect. of $O(^5S^0)$ 2—21520
O_2, emission cross sections for O I and O II 2—2946
O_2, resonance electron spectrometric obs. of electronic collisions 2—5902
O_2, resonance structure interpretation in 0 to 1.2 eV energy range 2—820
O_2, selection rule for parity unfavoured transitions 2—12090
O_2, vibrational and electronic excitation due to low energy electron collisions 2—814
O_2, vibrational excitation by electrons at 10 to 100 eV 2—12171
O_2, vibrational structure from formation of $O_2^-X^2\Pi_g$ 2—24483
O_2 resonances, vibratioal progression rel. to Rydberg states 2—812
OH, quantum state dependence 2—3152
ReF_6, multiple intramolec. scattering effects on electron diffraction patterns 2—38937
electronic structure
see also LCAO calculations
π-conformers, core repulsion and prediction of energy levels 2—38877
AH_n and AH_n^+ (A=C,N,O,or F), ab initio MO calc. of geometries and energies 2—24425
benzonitrile in polycryst. matrices, vibr. anal. of luminescence in terms of excited state geometries 2—31839
bonds, covalent, hybridization in context of separability of bond functions 2—28256
calculation methods for complexes and impurity molecules in crystals 2—3022
charge distribution, calculation method 2—35207
charge distribution, virial field relationship, spatial partitioning of molec. properties 2—28258
cluster model, self-consistent-field 2—19505
Compton scattering and electron momentum distribution 2—1676
conjugated, vibrational spectra of excited electronic states calc., evaluation of vibronic transition intensities 2—12083
conjugated molecules, π-electron polarizability, multiconfiguration approx. 2—12089
core electron effects, pseudopotential method calc. 2—21578

Molecules continued
electronic structure continued
core resonance integral used in semi-empirical π-electron calculations 2—35216
core-electron binding-energy shifts, estimation using equivalence of equally charged cores 2—35223
cyclobuta[b]quinoxalines, spectra measured calculated values of transition energies and oscillator strengths 2—12229
density localization of orbitals 2—35124
deuteron quadrupole coupling strength meas. 2—8647
diamagnetic susceptibilities and shielding in large molecules, LCAO calcs. 2—12085
diatomic molecular orbitals, bonding properties 2—770
diatomic molecule, d/dR operator between exact electronic states, simple expressions for off-diagonal matrix elements 2—8558
diatomic molecules, new potential function 2—24420
diatomic molecules, validity of Fogarassy-Ne'meth potential function 2—35212
diatomic oscillator, rotating, vibrating calc. of rotational and vibrational transitions in collisions with atoms 2—8854
diatomics, absorption and excitation cross sections averaged over vibr. structure 2—8563
diatomics, single bond properties semi- empirical calc. 2—31760
electron attachment, hydrated electron reaction rates predicted from data on attachment processes in gases 2—12088
electron repulsion integrals, four-centre, evaluation between 1s Slater atomic orbitals 2—3023
electron repulsion integrals 2—35108
electronic correlation effects, computer prog. for generalized Bethe Goldstone calcs. 2—35211
ESCA, correlation between K-electron chemical shifts and valence electron density 2—35210
ESCA chemical shifts of C and N by MINDDO/1 valence electron SCF MO method 2—35209
e.s.r. spectroscopy conference 2—17499
excited states, description by configuration interaction theory 2—12086
exciton states, influence of high ageing states, dipole theory study 2—8560
ferric dithiocarbamate, n.m.r. obs. 2—5965
Franck-Condon factor for a Morse oscillator when z is small, contribution to theory of radiationless transitions 2—28259
free radicals, hyperfine coupling, augmented basis functions 2—21579
gas, induced transparency due to electronic vibrational transitions 2—743
Gaussian type orbitals, field and field gradient integrals, computer programs 2—35206
Green's function method for calc. of energy levels of molecules with non-muffin-tin potential 2—18543
ground and excited states, LCOAO Ruedenberg expansion method 2—8545
ground state vibrational temp. determ. by reversal of spectral lines in i.r. region of CO_2 laser 2—15256
hyperfine, application or theory or irreducible tensor operators 2—757
isolated large molecule, sequence congestion effects in optical selection studies of electronic relaxation 2—31762
isolated molecule, energy level scheme, excitation of vibr. broadened by monochromatic e.m. field 2—31763
large molecules, intermediate level structure in highly excited electronic states 2—35214
ligand field theory calculations, effective perturbation method 2—38874
light diatomic, centrifugal distortion in spin-orbit coupling of triplet states 2—38883
linear polyatomic in vibrationally degenerate levels of electronic $^2\Sigma$ and $^3\Sigma$ states, rotational energies calc. 2—8526
manganic dithiocarbamate, n.m.r. obs. 2—5965
MC-SCF theory, method of one-electron Hamiltonian 2—35106
molecular symmetry adapted linear combinations of atomic orbitals, computer generation 2—31756
monodeuterobenzonitriles, in polycryst. matrices, vibr. anal. of luminescence in terms of excited state geometries 2—31839
multicentre integral evaluation, group-theoretical method 2—31764
multielectron systems, two-particle approximation for Brenig formalism 2—561
multiplet theory for single configuration for symmetric wave functions 2—3014
n-π^* transition energies in small molecules, SCF-CI calculations 2—38875
natural orbitals of Lowdin, approximation using Green's function method 2—38873
nitro compounds, increased valence- formulae generated from electronic structure studies of N_2O_4 2—12168
nitroso compounds, increased valence-formulae generated from electronic structure studies of N_2O_4 2—12168
non-crossing rule in quantum mechanics 2—35202
one- and two-electron diatomic molecules, ground state energy calc. by double perturbation theory with screening const. 2—8635
open shell molecules, theory for band intensities of photoelectron spectra 2—31741
oriented molecule, ellipticity and rotatory strength of electronic transition 2—31761
oxygen containing molecules ab initio calcs. 2—28255
perdeuterobenzonitrile, in polycryst. matrices. vibr. anal. of luminescence in terms of excited state geometries 2—31839
perturbation theory for excited states, electric polarizabilities 2—38986
photoelectron spectroscopy, X-ray and u.v. sources 2—8564
photoelectronic spectroscopy and Mo structure elucidation 2—35218
pi electron Hamiltonian, exact derivation 2—24424
polyatomic and complexes, permitted terms in MO and HL schemes, group-theoretical methods 2—15276
polyatomic molecules, Gaussian expansion of Slater-type atomic orbitals 2—21575
polyatomic systems, construction of localized orbitals, case of several partially filled bands 2—8540
polyatomic systems, localized HF orbitals for open shell case 2—8556
polyatomic systems, localized orbitals, open shell extended Huckel approximation 2—8557
polyatomics, relative nonradiative decay rates of initially selected vibronic levels 2—21558
polycentric systems, hybrid orbital construction by maximum overlap method 2—35201
polytetrafluoroethylene, core and valence energy levels by electron spectroscopy 2—6003

Molecules continued
electronic structure continued
predissociation by continuum of bound state without curve crossing 2—18462
RKR potential curves obtained directly from single resonance fluorescence doublet series 2—21562
semiclassical vibr.-rot. transition probabilities, collision induced for rotational state averaged potentials 2—8574
spectroscopic study 2—583
stabilization energy of electronic levels rel. to universal interactions in binary solvent 2—24574
Stark effect rotational level splitting, double resonance expt. 2—38879
term values of Rydberg transitions, dependence of molecular composition for wide range of compounds 2—8522
three centre nuclear attraction integrals with Slater type atomic orbitals, analytic evaluation 2—8541
transition moment dependence on nuclear configuration, effect on vibronic interactions in adiabatic approx. 2—15262
triatomic molecules, rotation bending energy levels calc. 2—31754
triatomics, study of nonadiabatic coupling and transitions between electronic states 2—8559
valence electron calculation, for molecules containing second row atoms 2—8544
valence region, from multiplet splittings in photoelectron spectra 2—35226
valence region from X-ray photoelectron spectroscopy 2—35225
Van Vleck effective Hamiltonian, extension to include effect of vibr. ang. momentum 2—8562
vibrating rotating molecule, expansion of Hamiltonian in terms of S-vector formalism 2—8561
vibration levels excitation due to electron transmission 2—12099
X-ray absorption spectra, semiquantitative interpretation 2—31766
$AlCl_3$, pyramidal 2—12101
C_2 opacity probability distribution functions inc. stellar isotopic forms 2—5913
CN opacity probability distribution functions inc. stellar isotopic forms 2—5913
CS_2, charge distribution determ. by Hartree-Fock-Roothaan molecular orbital calc. 2—21598
N free radicals, effects on stability 2—26374
N_2 beam, energy of long-lived excited states detected and meas. 2—18337
PH_2, electron affinity determ. from cross section for photodetachment of electrons from PH_2- 2—15331
Si_2, absorption spectrum between 4800 and 3000 Å, yielding new data on first excited state 2—8706

electronic structure, inorganic
carbon tetrachloride polarity in vibrational state obs., due to vibrationally induced dipole moment 2—12218
carbon tetrafluoride polarity in vibrational state obs., due to vibrationally induced dipole moment 2—12218
core-level binding-energy shifts calcs. from MO theories 2—35195
dihalocompounds, molecular orbital assignment from photoelectron spectra 2—35242
hydrides, analogues to ionized inert gases, mol. orbitals from vac. u.v. and photoelectron spectra 2—18409
hydrides, groups IV to VII, quantum mechanical calc. of molecular radii 2—35227
inconsistency of assignment of vibrational levels to O_g^+ state with long range behaviour 2—8661
metal complexes, acetylacetonates, INDO calc. of spin densities 2—811
metal tetrachlorides, electronic spectra, assignment of electronic transitions 2—12100
molecule, and isotopic species, submillimeter wave spectra, rotational transition assignment 2—12146
orbital calculation, simplified UHFMCZDO matrix element formalism 2—8577
point charge-point dipole model for vibrating triatomic molecules 2—35213
rare earth trifluorides, valence band obs. from multiplet splitting, 2-electron excitation 2—35282
small diatomic molecules, floating spherical Gaussian orbital calc. 2—21633
transition metal aquo complexes, first series spin density distrib., SCCC-DODS calcs. 2—12097
transition metal salts, bonding from multiplet splitting in X-ray photoelectron spectra 2—35291
water, electronic correlation effects, computer prog. for generalized Bethe Goldstone calcs. 2—35211
water, triplet excitation by low energy electron impact spectra 2—24453
X-ray absorption spectra, evidence of effective potential barrier 2—35193
$[Ru^{II}(CN)_5NO]^{2-}$, electronic absorption spectrum calc. and obs. 2—5949
$[NiCl_6]^{4-}$ semiempirical MO calc. 2—18459
AlO, ab initio calc of $B^2\Sigma^+$-$X^2\Sigma^+$ oscillator strengths 2—8581
AlO, laser excited fluorescence and radiative lifetimes of levels of $B^2\Sigma$ state 2—8580
As_2, new systems 2—18402
AsF, emission spectrum, 7320-7400 Å, obs. of new $^1\Pi$ state, rotational constants 2—18403
AsF absoprtion spectrum analysed, 2 new singlet systems 2—773
B, extended Gaussian-type basis, SCF MO method 2—31776
BH, electronic correlation effects, computer prog. for generalized Bethe Goldstone calcs. 2—35211
BH_2, ground and excited states, Hartree Fock method using Slater basis set 2—8579
BH_3, application of extended coupled-pair, many-electron theory 2—12105
B_2H_6, generalized valence bond orbitals 2—8583
$B_2O_3H_2$, CNDO and INDO calculations 2—38887
BaO, $A^1\Sigma-X^1\Sigma$ system, Franck-Condon factors, r-centroids and oscillator strength 2—15286
BaO, radiative lifetimes and quenching cross sections of $A^1\Sigma$ state from fluorescence decay 2—8584
BeCl, rotational analysis of $A^2\Pi$-$X^2\Sigma^+$ band system, determ. of principle molecular constants 2—28271
BeH, Λ doubling in $^2\Pi$ states calc. from HF wavefunctions to test validity of Van Vleck's hypothesis 2—21637
BeH_2, valence bond calc., comparison with MO calc. 2—8587
BeO, role of electron correlations in predictions of electronic ground state 2—31778
Br_2, vibrational structures of $E \rightleftharpoons B$ emission systems 2—21618
BrHBr- bihalide ion, proton shielding studied, simple electrostatic model description 2—31792

Molecules continued
electronic structure, inorganic continued
C_2^-, two photon photodetachment of electrons, confirmation of $^2\Sigma_g^+$ ground state 2—24444
CCO $A^3\Pi_r$-$X^3\Sigma^-$ band system studied in transient absorption spectrum in flash photolysis of C_3O_2 2—8603
CF, LCAO-MO SCF calcs. of ground and excited spectroscopic states, determ. of spin-orbit coupling 2—38897
CF, multiconfiguration HF calcs. of potential curves of ground and some excited states 2—8597
CH, Λ doubling in $^2\Pi$ states calc. from HF wavefunctions to test validity of Van Vleck's hypothesis 2—21637
CN, radical, quenching of $B^2\Sigma^+$ fluorescence 2—8593
C_2N_2, rotational structure in $^1\Sigma_u \leftarrow {}^1\Sigma_g^+$ transition at 2200A, vibrational anal. 2—21592
CNBr, geometries of various states from vibrational band intensities in photoelectron spectra 2—774
$CNCl^+$, geometries of various states from vibrational band intensities in photoelectron spectra 2—774
CNI, geometries of various states from vibrational band intensities in photoelectron spectra 2—774
CO, absorption spectrum in Hopfield helium continuum region, obs. of Rydberg series 2—31785
CO, analysis of new absorption bands 2—28277
CO, bands of fourth positive system, obs. fluorescence excited by 1306 Å oxygen resonance line 2—18416
CO, energies and properties of excited states, ab initio calcs. 2—8640
CO, generalized separated electron pair model calculations 2—35234
CO, open-shell states, SCF theory applic. 2—8591
CO, photoelectron spectra, study of autoionization, vibrational structure 2—8674
CO, RKR potential for $X^1\Sigma^+$ state 2—18411
CO, r.f. spectroscopy of perturbed excited states 2—8599
CO, vibr. excitation rates in $O+CS \rightarrow CO+S$ reaction 2—15289
CO rotational dependence of lifetime of a^3II metastable state, exptl. and theoretical decay plots compared 2—15295
CO study of vibrational and rotational levels of metastable $a^3\Pi$ state 2—8598
CO^-, Feshbach resonance, decay characts. 2—35238
CO^+ comet-tail band system, calc. of Einstein A coefficients, band oscillator strengths and absolute band strengths 2—18417
CO_2, discharge, excitation and relaxation of upper laser level 2—35233
CO_2, effect of Fermi resonance on temp. dependence on rotational vibrational transitions 2—776
CO_2, i.r. luminescence spectra, rot. consts. of vibr. levels 2—12112
CO_2, measurement of population of upper and lower levels in activated system CO_2+air+He 2—28284
CO_2, near i.r. absorption spectra, vibr. energy levels and rot. const. determ. 2—12111
CO_2, potential energy function, 4th order approx., vibr. energy levels, spectroscopic constants 2—12110
CO_3, ab inito LCGO MO SCF calc. 2—8589
C_3O_2, LCGO MO SCF calc. 2—21591
C_3O_2, orbital determ., ESCA line intensities obs. 2—35219
COS, upper state in continuum spectrum 2—15291
CSClF, u.v. band spectra, identification of electronic transitions, vibronic assignments 2—12120
CaO, investigation of ground state, matrix spectra of Ca and CaO 2—35241
Cl_2, photoionization cross sections of valence mol. orbitals, valence electron approx. 2—8621
Cl_2, vibrational structures of $E \rightleftharpoons B$ emission systems 2—21618
ClF, BrF, ClCN, BrCN, ICN, Zeeman effect study 2—12123
ClF, SCF LCAO MO calculations, polarization effect of 3d orbitals 2—5924
ClHCl-, bihalide ion, proton shielding studied, simple electrostatic model description 2—31792
ClO_4^-, SCF LCAO MO calculations, influence of Cl 3d orbitals 2—5924
Co, $(a^3\Pi)$ metastable state prod. by recombination of Co_2^+ in He afterglow, lifetime and quenching 2—8594
Cr complex, $Cr(CO)_6$, all ab initio SCF-MO calcs. in better-than-minimal basis presented 2—21634
$Cr(CN)_5No^{n\pm}$, MO description, electronic transition assignment 2—3038
$Cr(CO)_6$ complex, electronic spectra interpreted using non-empirical molecular orbital calcs. 2—12124
$Cr(CO)_5NH_3$ complex, electronic spectra interpreted using non-empirical molecular orbital calcs. 2—12124
CrIII complexes, tris chromium sulphur chelates, absorption and emission spectra, vibr. structure, energy forbidden transitions 2—21596
$Cr(NH_3)_5NO^{n\pm}$, MO description, electronic transition assignment 2—3038
CsO $^2\pi$ ground state calc. by ion model 2—28266
CuBr, rotational analysis of D-X band system 2—8608
DBr, hyperfine structure and Stark effect of $J=O \rightarrow$ rotational transition 2—8648
D_2S, nuclear hyperfine structure and mol. constants from mol. beam expt. 2—8611
F cpds., X-ray photoelectron spectroscopy of F k level 2—35245
F_2, electronic states, absorption and emission spectra 2—38907
F_2, photoionization cross sections of valence mol. orbitals, valence electron approx. 2—8621
F_2, potential curve of ground state, method of optimized valence configurations 2—28289
F_2^+, 13 lowest electronic states, calculated potential energy curves 2—8613
FHF-, bihalide ion, proton shielding studied, simple electrostatic model description 2—31792
F_3NO, CNDO and INDO approxs. 2—15299
Fe complex, ferric β-diketones, effect of pressure, Mossbauer and optical absorption study 2—28291
Fe(III) cpds. in ethylene glycol, liq. and frozen, e.p.r. obs. 2—12582
Fe(III) phenyl substituted complexes, n.m.r. study of changes in electronic structure due to aromatic substitution 2—31791
$Fe(NH_4)_2$ $(SO_4)_2.6H_2O$, meas. of magnetic anisotropies and principal susceptibilities to determ. sign of molecular anisotropy structure 2—28290
GeD anomalous doublet splitting in $^2\Delta$ states 2—3063
GeH anomalous doublet splitting in $^2\Delta$ states 2—3063
GeH_3X and GeH_2X_2 (X=F, Cl, Br, or I), valence-shell energy levels 2—21643

Molecules continued
electronic structure, inorganic continued
H_2, $^3\Sigma_u^+$ state, variational calc. of additivity of 2nd order contribs. to intermol. potentials 2—8866
H_2, ab initio LCAO MO calc. with efficient GTO basis sets 2—21577
H_2, autoionization rates for $\Delta_v=1$ vibrational transitions calc. by internal conversion theory 2—12139
H_2, Compton profile of ground state, discrepancy between theory and experiment 2—12135
o-H_2, hyperfine structure of N=1 rotational level of single vibrational state 2—787
H_2, metastable $c^3\Pi_u$ state, magnetic hyperfine and Zeeman interactions 2—38914
H_2 wavefunction determ. from H_2^+ molecular orbitals 2—21606
H_2^+, hyperfine struct. 2—31800
H_2^+, James wavefunction for ground state 2—21602
H_2^+, number of bound vibr. states, scattering lengths of lowest potentials 2—12130
H_2^+, variational wavefunctions, exact radial elliptic coordinate dependence 2—31796
H_2^+, vibration rotation eigenenergies of $2p\pi_u$ and $3d\sigma_g$ states 2—18434
H_3, calc. of 3-body energy term in $^4A_2$ quartet state 2—8622
H_3^+, ground- state, analytical SCF energy expression 2—24463
H_3^{2+}, four-centre expansion 2—15301
HBr^+, v=0 level of $A^2\Sigma$ state prod. in He^++HBr collisions 2—31883
HCP and HCN, CNDO/2 calc., comparison of results 2—18426
HCl, photoionization, cross sections of valence mol. orbitals, valence electron approx. 2—8621
HCl, relaxation rate from $v''=3$ vibr. state excited by dye laser radiation 2—24454
HCl, SCF LCAO MO calculations, polarization effect of 3d orbitals 2—5924
HCl^+, v=0 level of $A^2\Sigma$ state prod. in He^++HCl collisions 2—31883
$HD^{80}Se$, hyperfine structure of $4_2 \rightarrow 4_1$ rotational transition by beam maser spectroscopy 2—24455
HF, comparison of one centre and polycentre wavefunctions in HF formulation 2—35204
HF, electronic states, absorption and emission spectra 2—38907
HF, photoionization cross sections of valence mol. orbitals, valence electron approx. 2—8621
HF dimer, vibrational and rotational levels determ. 2—8646
HF^+, ab initio SCF calc. of potential energy curves 2—24465
HF_2, i.r. spectrum, null gap region, rotational structure 2—12133
HNCO and DNCO, hyperfine splittings 2—31795
HNO, oscillator strength of far u.v. system 2—18430
HO_2 radical, SCF CI calculation 2—31794
H_2O, energies and properties of excited states, ab initio calcs. 2—8640
H_2O, rel. to band struct. of cubic ice 2—16106
H_2O, study of noadiabatic coupling and transitions between electronic states 2—8559
H_2O, triplet excitation by low energy electron impact spectroscopy, cross section determ. 2—15311
H_2O dimer, hydrogen bond, effect of electron correl. 2—5930
H_2O vapour, energy levels of some states determ. from near i.r. spectra 2—8659
$H_2{}^{16}O$, submillimeter microwave spectrum. rotational transition meas. 2—18400
$H_2{}^{18}O$, i.r. spectra of vapour, rotational structure of ν_2 band, vals. of energy levels of 1st excited state 2—12132
H_2O_2, calculation of ground state in two-centre approximation 2—789
$H_3O^+(H_2O)_n$, n=0-4, structures and energetics, ab initio MO calc. 2—24456
H_2S, and isotopic species, submillimeter wave spectra, rotational transition assignment 2—12146
H_2S photoelectron spectrum, calc. of vibrational envelope and bond angle in first excited state of H_2S^+ 2—28303
HSiBr, Hamiltonian for large amplitude bending and K-type rotation, effect on higher rot. energy levels 2—12131
He_2, description of $3p\pi$, $^{1,3}\Pi_g \rightarrow 2s\,^{1,3}\Sigma_u^+$ band system, characterization of 2s, $a^3\Sigma_u^+$, $A^1\Sigma_u^+$ $3p\pi$, $e^3\Pi_g$ and $E^1\Pi_g$ states 2—12149
He_2, dissoc. energy of $A^1\Sigma_u^+$ state 2—8655
He_2, dissoc. energy of $X^2\Sigma_u^+$ state 2—8655
He_2, selected states and vibrational numbering of Tanaka-Yoshino bands 2—21613
He_2, spin optimized SCF calc. of $^1\Sigma_g^+$ ground state 2—15308
He_2 calc. of potential of lowest excited singlet state, determ. rotational and vibrational const., dissociation energy 2—21612
He_3, He_4 potential energy surface calc., SCF-LCAO-MO method 2—12309
HeH, interaction potential and hyperfine shift as function of internuclear distance 2—21611
HeH^+, Franck Condon factors for bound state-continuum transitions 2—8656
HeH^{2+}, $1s\sigma$ state, geometric-mean wave function 2—35257
HfI, obs. of new band spectrum in emission from radiofrequency discharge 2—8657
I_2 vibrational structures of E→B and F→X emission systems 2—21618
IHI- bihalide ion, proton shielding studied, simple electrostatic model description 2—31792
IO_2F^- radical 2—20142
$^{127}I_2$, nuclear hyperfine structure in electronic spectrum obs. by saturated absorption spectroscopy 2—12156
Ir (III) compleses, modulation of $(dl\pi^*)$-$(\pi$-$\pi z2u)$ configuration interaction, by solvent effects, luminescent state prod. 2—12157
KO $^2\pi$ ground state calc. by ion model 2—28266
LaO, $C^2\pi \rightarrow A'\ ^2\Delta$ and $C^2\pi \rightarrow X^2\Sigma^+$ transitions, high resolution analysis 2—12192
LaO, low-lying electronic states, interpretation 2—5950
LaO, rotational analysis of O-O band of $C^2\Pi \rightarrow X^2\Sigma^+$ transition 2—3049
LaO, vibr. consts. of $C^2\Pi$, $A'^2\Delta$ and $X^2\Sigma^+$ states, band heads of $C^2\Pi_r \rightarrow A^2\Delta_r$ and $C^2\Pi_r \rightarrow X^2\Sigma^+$ electronic transitions 2—18440
Li_2, ab initio LCAO MO calc. with efficient GTO basis sets 2—21577
Li_2, potential curve of lowest triplet state calc. by multiconfigurational approach 2—35261
Li_2, use of Hartree Fock wavefunctions in band formation study 2—798
LiH, ab initio G1 effective potentials for calc. of excited states 2—28306
LiH, ab initio LCAO MO calc. with efficient GTO basis sets 2—21577
LiH, MC-SCF study of $X^1\Sigma^+$, $A^1\Sigma^+$, $^3\Sigma^+$ and $^{1,3}II$ states, potential curves, spectra, transition probabilities 2—15314
LiH, orbital description of excited states 2—28307

Molecules continued
electronic structure, inorganic continued
LiO, $^2\pi$ ground state calc. by ion model 2—28266
Li_2O, separated electron pair calculation 2—35262
$^7Li,^{79,81}Br$, hyperfine structure investigated by molecular beam electric resonance 2—8662
Mg_2, in solid rare gas matrices, absorption spectrum, correlation of bands to $A^1\Sigma \leftarrow X^1\Sigma$ transition 2—8665
MgO, LCAO MO SCF calculation of electronic states obs. in spectrum 2—8664
Mn complex, magnesium phthalocyanine in α-chloronaphthalene, obs. of fluorescence from high vibr. levels of electronic excited states 2—18385
MnO_4^-, two-electron integral evaluation by orbital-product expansion method 2—3050
N_2, collisional excitation by N atoms of first positive and first negative radiation in 6000-14000K range 2—15319
N_2, excitation mechanism for population of vibr. levels of $C^3\Pi_u$ state 2—21630
N_2, molecular constants of $B^3\Pi$ and $A^3\Sigma$ states calculated 2—12166
N_2, open-shell states, SCF theory applic. 2—8591
N_2, orbital determ., ESCA line intensities obs. 2—35219
N_2, photoelectron spectra, study of autoionization, vibrational structure 2—8674
N_2, relative population of vibr. levels of $B^3\Pi_g$ state in glow discharge 2—35267
N_2, rot. structure of 0,0 band, basis of temp. determ. in CO_2+N_2+He mixtures 2—1008
N_2, vacuum u.v. absorption spectrum, o-X system, rot. consts. of vibr. levels 2—15325
N_2, vibr. temp. of $B^3\Pi_g$ state from relative intensity of first positive band system 2—31813
N_2^+, collisional excitation by N_2 of first positive and first negative radiation in 6000-14000K range 2—15319
N_3^-, NO_2^-, NO_3^-, valence shell electronic structure photoelectronic spectroscopy obs. 2—35276
N_3^-, valence region from X-ray photoelectron spectroscopy 2—35225
NF_2, LCAO-SCF-MO calc., Slater and Gaussian basis functions 2—8684
NF_3, high resolution study of l-type resonance in ν_4 band 2—8673
NH, fine structure $^3\Pi$ and $^3\Sigma^-$ states 2—21586
NH_2, $^2B_1$, $^2A_1$ and $^2B_2$ states, Hartree Fock method using Slater basis set 2—8579
NH_2, geometries of Renner Teller states, ab initio calcs. 2—12173
NH_2, isotropic hyperfine coupling constants 2—31812
NH_3, collision induced rotational transition, microwave double resonance study 2—12177
NH_3, configuration interaction wavefunctions and computed inversion barriers 2—35277
NH_3, ionization, Franck Condon factors for transition from ground to ionic state 2—18455
NH_3^+, structure in $^2A_1''$ state 2—8671
N_2H_4, calculation of ground state in two-centre approximation 2—789
NNO^+, intermediate product of $O^+ + N_2$ reaction, configuration interaction calculation 2—12014
NO-, vibrational progressions of resonances, association with Rydberg states 2—812
NO, $A^2\Sigma^+$ state, lifetimes of $v'=0,1,2$, levels 2—12164
NO, electronic states determ. from mass spectrometric identification of paramagnetic component of molecular beam 2—18397
NO, γ, ε and δ system, fluorescence spectrum polarization of rotational lines, vibr. band intensities 2—8675
NO, laser magnetic resonance obs., magnetic and electrical dipole transitions obs., g factor and hyperfine structure separation calc. 2—38928
NO, Λ doubling in $^2\Pi$ states calc. from HF wavefunctions to test validity of Van Vleck's hypothesis 2—21637
NO, magnitude of multiplet splitting in X-ray photoelectron spectra, spin density implications 2—8672
NO, photoelectron spectra, study of autoionization, vibrational structure 2—8674
NO, $X^2\Pi$ and $A^2\Sigma^+$ states, hyperfine constants and spin densities 2—35266
NO^+, obs. by He and Ar resonance lines photoelectron spectrometry 2—15316
NO_2, electronic states determ. from mass spectrometric identification of paramagnetic component of molecular beam 2—18397
NO_2, N_2O and N_2O_4, CNDO/2 study 2—5936
NO_2, vibronic effects in decay of fluorescence excited in first excited singlet state, lifetime 2—35284
N_2O, 00°1-10°0 laser band study by frequency mixing in i.r. metal-metal oxide-metal point contact diode 2—31041
N_2O, line strengths of bands in 2.9 micron region, dipole moment matrix element 2—18448
N_2O, relative rotational line intensities of various transitions, 250 and 300 K 2—24480
N_2O^+, photoionization and photoelectron spectroscopy, validity range of selection rule 2—12163
N_2O_3, gaseous, i.r. spectrum, −120°C, assignment of vibration rotation bands 2—12178
N_2O_4, molecular orbital studies, increased valence formulae described 2—12168
NOF and FNO, ab initio MO calculations 2—24477
NOH and HNO, ab initio MO calculations 2—24477
NOLi and LiNO, ab initio MO calculations 2—24477
$(NPX_2)_n$, X=halogen, with D_{nh} symmetry, CNDO/2 approx. 2—24481
NS, vibr. and rot. analysis of $^2\Pi_r$-$X^2\Pi_r$ band system 2—18447
NSe, electronic spectrum, 2800-3200Å, vibr. and rot. analysis of 12 red degraded bands 2—18456
$^{14}NH_3$, quadrupole tensor evaluated first and second order Zeeman effects obs. 2—8682
N_2^{*+}, product of N_2 rare gas ion collisions, vibrational and rotational distributions 2—10600
NaO, $^2\pi$ ground state calc. by ion model 2—28266
NaO, NaO^+, NaO^-, Hartree-Fock molec. orbital studies, deduction of Na-O species properties 2—37032
Nd, fine structure of $^3\Pi$ and $^3\Sigma^-$ states 2—21586
Ni, complex, bis-(π-allyl), orbital assignment from photoelectron spectra obs. 2—35280
Ni complex, $Ni(CO)_4$, all ab initio SCF-MO calcs. in better-than-minimal basis presented 2—21634
Ni complex, tris(o-phenanthroline)Ni II ions, SCF calc. rel. to electron delocalisation 2—3056

Molecules continued
  electronic structure, inorganic continued
    Ni II complexes, INDO calc. of spin densities 2—811
    O_2^-, vibrational progressions of resonances, association with Rydberg states 2—812
    O_2, annihilation of $^1\Delta_g$ state by excited state triplet sensitizers 2—22856
    O_2, electronic states determ. from mass spectrometric identification of paramagnetic component of molecular beam 2—18397
    O_2, energies and properties of excited states, ab initio calcs. 2—8640
    O_2, open-shell states, SCF theory applic. 2—8591
    O_2, photoelectron spectra of some autoionizing resonance states 2—8692
    O_2, quality of mol. wavefunction, charge distrib. around O atom 2—5944
    O_2, vibrational structure from formation of $O_2^-X^2\Pi_g$ in electron scattering 2—24483
    O_2^+, molecular ion, localized and delocalized 1s hole states 2—8689
    O_3, energies and properties of excited states, ab initio calcs. 2—8640
    O_4, cooperative optical transitions, dipole intensity computation, symmetry of dimeric and exciton states 2—24484
    OF, $^2\Pi$ state, ab initio calc. of Hartree Fock wave function 2—31818
    OH, $C^2\Sigma^+$ state in emission spectrum 2—28316
    OH, isotropic hyperfine coupling constants 2—31812
    OH, Λ doubling in $^2\Pi$ states calc. from HF wavefunctions to test validity of Van Vleck's hypothesis 2—21637
    OH, predissociation by continuum of bound state without curve crossing 2—18462
    OH, theoretical determ. of rotational and vibrational levels, spin-orbit coupling and magnetic g factors 2—12188
    OH^+, fine structure of $^3\Pi$ and $^3\Sigma^-$ states 2—21586
    $OH^-(H_2O)_n$, n=0-4, structures and energetics, ab initio MO calc. 2—24456
    PH_3, rel. to P pyramidal inversion process, ab initio SCF-LCAO-MO study 2—31822
    PO, emission spectrum attributed to $^2\Sigma$-$^2\Sigma$ transitions, rotational structure of bands 2—18465
    Pb^{4+}, ($Xe4f^{14}5d^{10}$), numerical HF SCF wavefunctions 2—31823
    Pd, complex, bis-(π-allyl), orbital assignment from photoelectron spectra obs. 2—35280
    PdH(D), e.s.r. spectra of $^2\Sigma^+$ ground state, bonding nature, hyperfine coupling and g tensor components 2—12189
    Pt complexes of types K_2PtX_4, K_2PtX_6 and $(PPh_3)_2PtX_2$, X-ray investigation 2—33300
    Pt coord. cpds., core-level region, photoelectron spectroscopy 2—35281
    Pt cpds., X-ray photoelectric spectroscopy 2—31824
    RbO $^2\pi$ ground state calc. by ion model 2—28266
    SF_6, orbital determ., ESCA line intensities obs. 2—35219
    SH, isotropic hyperfine coupling constants 2—31812
    SO_2, rot. anal. of O-O band, excited state consts., excited state r_0 structure 2—15333
    SO_2, single vibronic level lifetimes of first excited singlet state 2—8703
    SO_2, vibronic effects in decay of fluorescence excited in first excited singlet state, lifetime 2—35284
    Sb_2, new systems 2—18402
    ScO, energy of $^2\Delta$ state, high resolution analysis 2—12192
    ScO, low-lying electronic states, interpretation 2—5950
    $SiCl_4$ polarity in vibrational state obs. due to vibrationally induced dipole moment 2—12218
    SiH_3X and SiH_2X_2 (X=F, Cl, Br, or I), valence-shell energy levels 2—21643
    SiO, orange system, $^2\Pi$ to $^2\Sigma$ transition, rotational analysis of band (0,0) 2—31827
    SiO, potential curves for valence-excited states 2—8702
    SnD anomalous doublet splitting in $^2\Delta$ states 2—3063
    SnH anomalous doublet splitting in $^2\Delta$ states 2—3063
    TcO_4^-, SCCC-MO calc. 2—18474
    TiO, $^1\Delta$ to $a^1\Delta$ transition, rotational analysis 2—31832
    TiO, spectroscopic observations in inert matrices at 4°K 2—24489
    TiO_2, spectroscopic observations in inert matrices at 4°K 2—24489
    TlBr, derivation of electric dipole moments from Stark effect meas. on pure rotational transitions 2—8711
    TlI, derivation of electric dipole moments from Stark effect meas. on pure rotational transitions 2—8711
    UO_2^{2+}, new absorption bands, assignment rel. to vibr. levels of ground state 2—35294
    $VOCl_25NH_3$ proposed on the basis of obs. absorption spectra 2—15342
    YO, energy of $^2\Delta$ state, high resolution analysis 2—12192
    YO, low-lying electronic states, interpretation 2—5950

  electronic structure, organic
    α-substituted vinyl radicals, determ. from obs. e.s.r. spectra and INDO calcs. 2—8712
    π-electron free radicals, spin-restricted SCF-CI theory of contact hyperfine splittings 2—18389
    π-electron polarizability, rel. to orbital calc. 2—18475
    acepleiadylene, and electronic transitions 2—28340
    acetanalide, CNDO computations 2—829
    acetanilides, disubstituted, ortho-effects in mass spectra, removal of excitation probability for low lying energy states of ion 2—38954
    acetonitrile, $2\nu_8$ state, effects of accidentally strong resonance in rot. spectrum, mol. consts. level separation 2—12203
    acetonitrile, doubling excited degenerate vibr. state, rot. spectrum, anharmonicity const., transition study 2—12202
    acetonitrile-d_3 and water, H bonded complexes obs. i.r. transitions involving vibrations 2—8754
    acetophenone, single crystal e.p.r. studies of photoexcited states 2—26360
    acetylene, assignment of bands at 2.1 to 2.2μ 2—21654
    acetylene, bond orders and elec. quadrupole moments from point-charge model 2—28372
    acetylene and d_1 and d_2 deuterated species, rotational structure of vibrational bands 2—21653
    acetylenic organotin compounds, π-electron molecular interactions 2—15347
    acrolein, cis and trans isomers, mag. rotation spectrum, band assignment, energy level diagram 2—12204
    acrolein and singly substituted methyl derivatives, bond order reversal and substituent interaction in $S_1(n,\pi^*)$ 2—35337
    adenine, charge distributions, comparison of extended Huckel and CNDO calculations 2—38957
    adenine, electron density and dipole moment analysis of valence electron wavefunctions 2—35302
    allene, MO calc. of geometry, energy and polarity 2—28383
    amide, in water, n.m.r. obs. 2—6255

Molecules continued
  electronic structure, organic continued
    amino acid radicals in X-irrad. N-benzoylalanine single crysts., e.p.r. obs. 2—8735
    amino anthracenes, nonsymmetrical, moment directions of electronic transitions 2—21657
    2-aminonaphthalene-6- sulphonate and derivatives, intramolecular charge transfer 2—28343
    anhydrides, electronic absorption spectra, obs. bathochromic shift of $\pi\pi^*$-band of PA 2—28345
    aniline, $^1B_2\leftarrow{}^1A_1$ transition, electric field induced perturbations 2—21658
    aniline and haloaniline complexes with 2, 4, 6-trihalophenols, crystalline, i.r. and n.q.r. spectra 2—10340
    anthracene, 9-carbonyl derivs., temp. effect on fluorescence intensity due to intersystem crossing 2—24503
    anthracene, e.p.r. studies of deuteration effect on intersystem crossing 2—12208
    anthraquinone in solutions, delayed thermal fluorescence, steady-state model 2—28874
    aromatic σ-type radicals, e.s.r. 2—18482
    aromatic hydrocarbon radicals, proton hyperfine splitting and electron density relationships 2—18490
    aromatic hydrocarbons, derivation and evaluation of electronic matrix elements governing intersystem crossing 2—31834
    aromatic hydrocarbons, intermediate level structure in highly excited electronic states 2—35214
    aromatic hydrocarbons and perfluoro analogues, charge distributions as determ. by ESCA 2—31860
    aromatic nitriles, anion radicals, i.r. study of intramol. electron interaction 2—8732
    aromatic nitro-substituted anion radicals, electronic spectra and molecular orbital interpretation 2—834
    aryl cations, substituted, INDO calculations 2—28346
    2,6-bis(4-azidobenzylidene) cyclohexanone, stereoisomers, electronic structure and spectra, dipole moments, SCF MO LCAO methods 2—12233
    azines, substituted by amine groups, amine-imine tautomerism 2—21659
    azobenzene, p-monosubstituted derivs., polarization absorption spectra, electronic transitions 2—836
    azonaphthalenes, basicity and electronic spectra, spectrophotometric study 2—28347
    azulene, linewidths for $S_1\leftarrow S_0$ and $S_2\leftarrow S_0$ nonradiative processes 2—31838
    azulene, perturbation treatment of spin-orbit coupling using CNDO/s wavefunctions 2—12091
    barbituric acid and its 2-thio derivative, comparison between radicals formed by radiation, e.s.r. study 2—21662
    benzaldehyde, zero field splitting, phosphorescence rate consts. and vibronic activity in lowest triplet state by p.m.d.r. 2—28353
    benzanthracene, zero field splitting coeffs. of e.s.r. of lowest triplet level, calc. using Huckel approx. 2—12275
    benzene, anal. of antiresonances in Rydberg spectrum in terms of theoretical line shape parameters 2—8802
    benzene, excimer intrinsic fluorescence yield and lifetime, temp. dependence 2—28352
    benzene, non radiative relaxation of excited A^1B_{2u} state 2—24511
    benzene, orbital determ., ESCA line intensities obs. 2—35219
    benzene, S_1 state, fluorescence and intersystem crossing as function of rotational energy 2—24510
    benzene $^3B_{1u}$ state, obs. of Zeeman effect, evidence for dynamic pseudo Jahn Teller distortion 2—20109
    benzene vapour, optical absorption spectrum, photon energies 6-35 eV, electronic structure assignment 2—15358
    benzenes, fluorinated, K electron binding energy shifts, CNDO potential model calc. 2—8771
    benzenes, monosubstituted, variable electronegativity SCF-MO calc. 2—15353
    benzenes, substituted, use as photographic developing agents 2—14494
    1:2 benznaphthacene, zero field splitting coeffs. of e.s.r. of lowest triplet level, calc. using Huckel approx. 2—12275
    benznitrile, single crystal, e.p.r. studies of photoexcited states 2—26360
    benzoic acid, effect of dimer formation on emission spectrum, position of (n,π^+) triplet state 2—35310
    benzophenone, energy resolved decay, strong coupling between S_1 and T_1 vibronic levels 2—8737
    benzophenone, radiative decay of lowest excited singlet state 2—3073
    p-benzoquinone, effect of methyl and hydroxyl substituents, π-electron calculations 2—35307
    p-benzoquinone and methyl derivatives CNDO-CI study of effects of substitutions on electronic spectrum 2—12210
    benzyl, symmetry of first excited state determ. by rotational contour analysis of vibronic bands of emission spectra 2—15355
    benzyl radical, valence bond calculations of spin density distribution 2—38959
    benzylidine aniline, ASMO- CI calc. 2—28350
    bicyclobutane, charge distribution 2—35313
    bicyclobutane, LCAO calculations 2—38965
    bicyclo[1.1.1]pentane, ab initio MO calculations 2—39011
    biphenyl based series, phenanthrene-carbazole-dibenzothiopene-dibenzofuran, polarization of electronic transitions 2—28355
    bis(pyridine)halogen(I) cations, CNDO/2 calculations 2—38966
    bond order in π-electron theory 2—18390
    s-trans-1,3- butadiene, ab initio investigations of $\sigma-\pi$ interactions in electronic states 2—24517
    butadiene, CI calcs. on pi-electron states 2—8746
    1,3-butadiene, electronic spectrum application of molecule within a molecule method to transitions 2—35298
    trans butadiene, with four π-electrons, solution of molecular Bethe-Goldstone equation 2—35205
    butene, cis and trans, and their ions, ab initio MO calcs. 2—24520
    carbenes, spin dipole spin dipole contrib. to zero field splitting parameters 2—12220
    carbomethoxycyanobenzyl radicals, e.s.r. spectra in 40°-200°C range, obs. of π- and σ- spin delocalization into the phenyl ring 2—31842
    carbonium ions, LCAO calculations 2—31843
    4-chloroacetophenone, single crystal e.p.r. studies of photoexcited states 2—26360
    chloroethylenes, π characteristics, SCF-LCAO theory 2—15364
    chlorofluorobenzene, transition moments, band contour anal., changes in rot. const. on excitation 2—12213
    chlorofluoroethylenes, far u.v. spectra, band assignment 2—12242

Molecules continued
electronic structure, organic continued
chloroform and proton acceptor complexes, H bonded, obs. i.r. transitions involving vibrations 2—8754
chromocene, photoelectron spectra, band intensities from theory for open shell molecules 2—31741
chromone, u.v. absorption spectra, band assignment, solvent and substituent effects 2—28360
chromones, 2-substituted, u.v. absorption spectra, band assignment, solvent and substituent effects 2—28360
core-electron (photoelectron) spectroscopy, rel. to n.m.r chem. shift contribs. 2—35297
coumarin and related molecules, triplet-triplet absorption studies on 11000-27000 region 2—12225
coumarins, assignment of lowest excited singlet and triplet states on basis of luminescence measurements 2—12226
coumarins, u.v. spectra, description of $\pi-\pi^*$ transitions 2—8755
crotonaldehyde, vibrational- electronic analysis of $S_1(n,\pi^*)$ 2—35336
cyanamide, CNDO/2 calculations 2—28364
cyanamide groups 2—28393
cyanopyridine vapour, isomers, absorption spectra, ${}^1n\rightarrow{}^1\pi$ transition 2—31846
cyclic polyenes, energy, Theta-function overlap approximation 2—15392
cyclobutane, valence orbitals, symmetry properties 2—28363
cyclooctatetraene and related systems, ab initio SCF LCAO MO calc. 2—3078
cyclopropane, analysis of $\nu_5+\nu_{10}$ band, l-type resonance effects 2—8757
cyclopropane, generalized valence bond orbitals 2—8758
cyclopropane, MO calc. of geometry, energy and polarity 2—28383
cyclopropane, study of l-type resonance effects in $\nu_5+\nu_{10}$ band 2—21674
cyclopropanone, closed- and open-ring structures investigated in LCAO-MO-SCF, calculation 2—12228
cyclopropene, MO calc. of geometry, energy and polarity 2—28383
di-t-butyl nitroxide, magnitude of multiplet splitting in X-ray photoelectron spectra, spin density implications 2—8672
dialkylamino radicals 2—18525
diaminodiphenylmethane isomers and the diisocyanates, phenyl π-electrons interaction, u.v. study 2—28371
diarylethanes, meas. by electron impact mass spectrometry, search for ring orbital interaction 2—35325
diarylmethanes, meas. by electron impact mass spectrometry, search for ring orbital interaction 2—35325
diazanaphthalenes, photoelectron spectra, ordering of π and nitrogen lone pair orbitals 2—15371
diazaphenanthrenes, linear correlation between ${}^1H$ chem. shift and electron density 2—24551
p-dichlorobenzene, first ${}^3\pi\pi^*$ state, optically detected mag. resonance 2—8763
dichloroethylene, mol. orbital interpret. photoelectron and X-ray emission spectra 2—35328
trans-15,16-diethyl dihydrogen, π-electron loop separation calc. 2—38979
difluorobenzene, transition moments, band contour anal., changes in rot. const. on excitation 2—12213
diimide, ab initio CI treatment of ground and excited states 2—12086
trans-15,16-dimethyl dihydropyrene, π-electron loop separation calc. 2—38979
2,2-dimethyl-4-cyclopentene-3,5-dione, soln. and vapour, electronic spectra, absorption band assignment 2—8788
3,3′-dimethyldiazirine, electronic absorption spectra 2—24526
dinaphtho[2,1-2′,3′]furan-8,13-dione and dinaphtho[1,2-2′,3′]furan-7,12-dione 2—24538
ethane, bond orders and elec. quadrupole moments from point-charge model 2—28372
ethane, localized molecular orbitals and comparison with C-H bond in methane 2—35338
ether groups 2—28393
ethyl cations, LCAO calculations 2—31843
ethyl nitrate, assignment of torsionally excited states of rotamers 2—12241
ethylene, ab initio CI treatment of ground and excited states 2—12086
ethylene, bond orders and elec. quadrupole moments from point- charge model 2—28372
ethylene, electronic transitions with large generalized oscillator strengths 2—8768
ethylene, orbital symmetries, ang.distribs. of photoelectronic π- and σ-bonding 2—35329
ethylene-Ag^+ complex, calc. using nonempirical SCF theory 2—8766
9-ethylguanine, polarization of electronic transitions 2—24533
ferrocene, electron levels, collective motion model 2—28376
9-fluorenone, obs. of low lying excited states in absorption spectrum 2—18504
p-fluoro-α-methylstyrene radical anions, spin density distributions, unrestricted Hartree-Fock calculation 2—28388
fluorobenzenes, Rydberg states 2—21685
fluorobenzenes, valence-shell transitions in vacuum u.v. 2—38981
fluorocarbonium ions, $(FCH_2)^+$ and $(F_2CH)^+$, ab initio MO study 2—21684
formaldehyde, ab initio CI treatment of ground and excited states 2—12086
formaldehyde, perturbation treatment of spin-orbit coupling using CNDO/S wavefunctions 2—12091
formaldehyde, singlet-triplet resonance interaction in A_2 states 2—31856
formaldehyde isotopes, spin-rotation spin-spin and quadrupole coupling constants 2—12247
formic acid, various conformations, semiempirical CNDO and INDO calcs. 2—24537
formyl formide, conformation and electronic structure, valence shell calc. 2—18507
fulminic acid, assignment of vibr. satellites obs. in rot. transition, vibr.-rot. interaction const. microwave and millimeter wave spectra 2—12268
fulminic acid, rotational spectrum 40-300 GHz, transitions of vibrationally excited states 2—21686
fulvene, microwave spectra, dipole moment 2—8779
fulvene, vapour and mixed crystal spectra, lowest energy electronic transition 2—8780
furan, orbital determ., ESCA line intensities obs. 2—35219
furan, valence charge distrib. calc. by charge iterative extended Huckel approach 2—5992
furanquinones 2—24538
furocoumarins, assignment of lowest excited singlet and triplet states on basis of luminescence measurements 2—12226

Molecules continued
electronic structure, organic continued
glyoxal, cis-, perpendicular and trans-, ab initio calculations 2—18510
glyoxal vapour, fluorescence and phosphorescence from laser excited first singlet excited state 2—12249
hemin, calculation of spin-spin and spin-orbit contribution to zero-field splitting 2—31858
hydrocarbons, C_3 molecules, MO calc. of geometries, energies and polarities 2—28383
hydrocarbons, closed shell alternant, PPP model, consequences of non-linearity of Hartree-Fock approach 2—35203
hydrocarbons, conjugated, perturbation theory for excited states, electric polarizabilities 2—38986
hydrocarbons, floating spherical Gaussian orbital model for ESCA chemical shifts for inner shells electrons 2—35335
hydrocarbons, generalized valence bond orbitals 2—8758
hydrocarbons, MIM calculations of electronic bands involving triplet states 2—38987
hydrocarbons, nonalternant, calc. of electronic absorption spectra 2—12252
hydrocarbons, saturated, magnetic susceptibility calc. 2—28384
hydrocarbons, second moment of charge distribution rel. to diamagnetic susceptibility 2—35334
hydroxyphenazines, PPPMO calcs., charge density, bond order, oscillator strength and electronic transition energy 2—8785
hydroxyphenazines, PPPMO calcs., transition energies and oscillator strengths, electronic spectra 2—12251
hyperfine splittings, spin-restricted SCF-CI theory 2—18389
1-indanone, in divene host, optically detected e.s.r. study of lowest n-π^* triplet states 2—24542
iodo-e naphthaquinone-1, 4, structure obs. 2—6462
ion-radicals, electronic spectra and molecular orbital interpretation 2—834
ionone, α and β systems, nonplanarity in π radical 2—31861
isobutene, vibronic structure of 1790 Å transition 2—12254
N-isopropylcarbazole, and radicals spectra, energy levels, splitting parameters 2—18513
isoxazde, improved LCAO method 2—18518
ketones, aliphatic, $n\rightarrow\pi^*$ transition shifts, contribs. from intermol. interactions and H bonds 2—3104
macromolecules with conjugated C=C bonds, paramagnetism 2—35362
maleic anhydride, soln. and vapour, electronic spectra, absorption band assignment 2—8788
metal phthalocyanines, molecular electronic structure, molecular orbital treatment 2—15390
methacrolein, vibrational analysis of $S_1(n,\pi^*)$ 2—35336
methane, bonds covalent, hybridization in context of separability of bond functions 2—28256
methane, comparison of one centre and polycentre wavefunctions in HFR formulation 2—35204
methane, localized molecular orbitals and comparison with C-H bond in ethane 2—35338
methanes, fluorinated, K electron binding energy shifts, CNDO potential model calc. 2—8771
methanol, triplet excitation by low energy electron impact spectra 2—24453
methanol, triplet excitation by low energy electron impact spectroscopy, cross section determ. 2—15311
methyl cations, LCAO calculations 2—31843
methyl cyanide and isocyanide, ab initio SCF calculations 2—38993
methyl radical, configuration interaction wavefunctions and computed inversion barriers 2—35277
methyl vinyl ketone, vibrational analysis of $S_1(n\pi^*)$ 2—35336
methylcyanide, core binding energy shift determ., ab initio mol. wave functions 2—35341
methylene, generalized valence bond wavefunctions for low lying states 2—21694
methylenecyclopropane, INDO calculations on lowest energy singlet and triplet states, ring opening studied 2—8794
methylisocyanide, core binding energy shift determ., ab initio mol. wave functions 2—35341
α-methylstyrene radical anions, spin density distributions, unrestricted Hartree-Fock calculation 2—28388
methylthiocyanate, core binding energy shift determ., ab initio mol. wave functions 2—35341
monocyclic molecules, diamag. susceptibility, small radius potential model, ring π-electron contrib. 2—38945
monofluorobenzaldehydes and derivatives, INDO calculations 2—5982
monofluorobenzene, lifetimes and quantum yields of fluoresence from vibronic states 2—21697
monomethyldiazirine, u.v. obs. spectrum, rotational fine structure of 0-0 band at 3424 Å 2—12267
monomethylphosphine, ab initio LCAO-MO-SCF calculations 2—18515
N-acetyl-methionyl-dimethylamide, molecular struct. determ. 2—6457
naphthalene, anal. of antiresonances in Rydberg spectrum in terms of theoretical line shape parameters 2—8802
naphthalene, gas phase triplet absorption spectrum, obs. of 4 electronic transitions 2—8803
naphthalene, vapour, fluorescence lifetimes of vibronic levels 2—3111
nitramines, conjugated, electronic absorpt. spectra 2—8804
nucleic acid bases, in region of inner shell excitation 2—22446
nucleic acid bases, in region of outer shell excitation 2—22445
oxadiazole, improved LCAO method 2—18518
oxazole, improved LCAO method 2—18518
oxo-2 dioxaphosphorinane-1,3,2 derivatives, basicity of phosphoryl group 2—18517
parabenzoquinone π-complexes, degree of delocalization of n-orbitals, calc. 2—18519
pentaphenylcyclopentadienyl, methyl substituents effects on orbital degeneracy 2—24525
peptide group 2—28393
perdeuterobenzene, lifetimes and quantum yields of fluorescence from vibronic states 2—21697
perylene, electrochromic spectra in polystyrene matrix, change in polarizability and dipole moment between ground and excited states 2—13488
phenanthrene, zero field splitting coeffs. of e.s.r. of lowest triplet level, calc. using Huckel approx. 2—12275
phenols, substituted, electron density distrib. calc. by semiempirical MO methods 2—24549
phenols, substituted, solns., electronic absorption spectra, waveband shifts obs. 2—12274

Molecules continued
  electronic structure, organic continued
    phenyl substituted imidazyl and pyrryl radicals, spin density distrib. determ. from e.s.r. spectra 2—8807
    5-phenyl-2-(4- dimethylaminophenyl)-oxazole-1,3 2—3116
    5-phenyl-2- (4-dimethylaminophenyl)-oxadiazole-1,3,4 2—3116
    phenylacetylene, single crystal e.p.r. studies of photoexcited states 2—26360
    phosphorescent triplet states, optically detected adiabatic inversion 2—21581
    phthalazine, dipole moment changes for excitation to different levels, $n\rightarrow\pi^*$ transition 2—8811
    phthalocyanines 2—855
    pivalonitrile oxide, assignment of vibr. satellites obs. in rot. transition, vibr.-rot. interaction const. microwave and millimeter wave speectra 2—12268
    polyacenes, $\pi\pi^*$ triplet-triplet energy calc. 2—12201
    polyacenes, zero field splitting coeffs. of e.s.r. of lowest triplet level, calc. using Huckel approx. 2—12275
    polyacenes, zero field splitting coeffs. of e.s.r. of lowest triplet level, calc, uing Huckel approx. 2—12275
    polyenes, electronic spectra, SCFMO calc. with configuration interaction 2—8847
    polymers, comparison of coupling formalisms from calc. of DNA hypochromism 2—8839
    polymers, linear, Fourier representation methods 2—35367
    polymers, substituted, electronically excited state, properties 2—864
    polystyrene, transitions in π system rel. to opt. props. in vac. u.v. 2—20009
    potential surface calculations, INDO and CNDO, rel. to isomer stability 2—8718
    propane, MO calc. of geometry, energy and polarity 2—28383
    propene, MO calc. of geometry, energy and polarity 2—28383
    propyl cations, geometries and energies, ab initio MO calculations 2—39001
    propyne, MO calc. of geometry, energy and polarity 2—28383
    protein, non-heme iron, X-ray photoelectron spectroscopy 2—31873
    psoralens, u.v. spectra, description of π—π^* transitions 2—8755
    pyrazine, ab initio CI treatment of ground and excited states 2—12086
    pyrazine, from photoelectron, u.v., mass and electron impact spectra 2—28403
    pyrazine, photoelectron spectrum, correlation between ionization bands and electronic levels 2—28402
    pyrazole, implications of quadrupole coupling constants 2—5993
    pyrene, laser excited fluorescence S_2 emissions, intermediate strong coupling and vibr. redistrib. effects 2—15393
    pyridazine, from photoelectron, u.v., mass and electron impact spectra 2—28405
    pyridines, lactam and thione forms 2—28406
    pyrimidine, from photoelectron, u.v., mass and electron impact spectra 2—28404
    pyrimidines, lactam and thione forms 2—28406
    pyrrole, valence charge distrib. calc. by charge iterative extended Huckel approach 2—5992
    quinones, PPPMO calcs., charge density, bond order, oscillator strength and electronic transition energy 2—8785
    quinones, PPPMO calcs., transition energies and oscillator strengths, electronic spectra 2—12251
    quinosialine and d_0 deriv., electronic vapour absorption ($\pi^*\leftarrow n$) spectra study 2—12279
    rhodamine 6G, electrochromic spectra in polystyrene matrix, change in polarizability and dipole moment between ground and exicted states 2—13488
    self-consistent MO methods, Gaussian-type basis sets 2—21648
    styrene, band contour anal., transition moments 2—12213
    styrene-MMA, transitions in π system rel. to opt. props. in vac. u.v. 2—20009
    styryldiazines, linear correlation between ^{1}H chem. shift and electron density 2—24551
    substituted benzenes, uncoupled Hartree-Fock calc. of ring currents 2—21664
    sydnones, valence electron density calculated in the IEH approach, presented as contour diagrams 2—8820
    testosterone acetate, ODMR determination of zero field splitting parameters 2—35352
    tetracene, polarization data for triplet triplet absorption spectrum, band assignment 2—8823
    s-tetracyanobenzene-toluene complex, structure of fluorescent and phosphorescent states from absorption and emission spectra 2—15397
    tetracyanoethylene oxide, aspherical electron charge density 2—28412
    tetracyanoethylene oxide, electron density 2—28411
    tetracyanoethylene-trans- stilbene mol. complex, effect of external elec. field on charge transfer excited state 2—31870
    tetrafluoromethane, orbital determ., ESCA line intensities obs. 2—35219
    α-tetralone, in divene host, optically detected e.s.r. study of lowest n-π^* triplet states 2—24542
    thioformaldehyde, ground state constants obtained from analysis of i.r. spectrum near 3μ 2—12286
    thionine, protonation rate const. of triplet state by laser flash photolysis 2—37056
    thiophene, orbital determ., ESCA line intensities obs. 2—35219
    thiophene and bromo-derivs., from high-resolution photoelectron spectra 2—35340
    s- triazine, mixed mag. and electric dipole transition for absorption to lowest energy excited singlet state 2—8827
    s-triazine, Rydberg transitions, from photoelectron, u.v., mass and electron impact spectra 2—28416
    tricyclo[1.1.1.0^{1,3}]pentane, ab initio MO calculations 2—39011
    trifluoroacetonitrile, microwave spectrum of excited vibr. states, obs. of J→J+1 transitions 2—12292
    β-trihalogeno borazines of symmetry D_{3h} 2—28356
    trimethylamine borane, vacuum u.v. spectra, obs. of 2 electronic transitions 2—3127
    trimethylamine complexes with I_2, Br_2, IBr and ICl, Raman and i.r. spectra band assignment to vibrations, force constants 2—12294
    2,4,5-trimethylbenzaldehyde in durene, assignment and location of 2nd triplet state 2—15402
    1,3,5-triphenylbenzene anion radical, orbital degeneracy obs., e.p.r., p.m.r. and d.m.r. 2—8808
    triphenylenes, 2-substituted, lowest excited triplet state, optical and e.s.r study 2—35356

Molecules continued
  electronic structure, organic continued
    1,3,5- triphenylpyrazole, calculation of π-electron states by LACO MO method with Huckel approximation 2—3115
    two-quanta photoprocesses, aromatic molecules 2—20198
    vinyl cyanide, valence shell calculations 2—18534
    vinyltrifluorosilane microwave spectrum, dipole moment from Stark shifts of rotational transitions 2—21706
    xanthone 2—24557
    zinc tetrabenzporphin, fluorescence of second excited singlet and quasiline structure studied 2—12295
    CH_2^+, ground and excited states, Hartree-Fock method using Slater basis set 2—8579
    CO, band strength of 0,0 band of $a^3\Pi$-$X'\Sigma$ transition, radiative lifetime of $a^3\Pi$ state 2—18407
    DCl, electronic absorption spectra, states assoc. with $(\sigma^2\pi^3)c\pi$ and $(\sigma^2\pi^3)c\sigma$ configuration 2—18424
    HCl, electronic absorption spectra, states assoc. with $(\sigma^2\pi^3)c\pi$ and $(\sigma^2\pi^3)c\sigma$ configuration 2—18424
    N_2, ground state calc. using perturbation procedure for constrained SCF LCAO MO eqns. 2—31758
    S orbital electronegativity and ^{35}Cl n.q.r. in molecules containing S-Cl bond 2—21650
  excitation
    acridine orange, e.s.r. triplet exciton spectrum 2—21651
    adiabatic transition by irrad. freq. variation 2—28265
    aromatic hydrocarbons, decay spectrum of highly excited state of large molecules 2—35214
    aromatic hydrocarbons in soln., triplet monomers and excimers, lifetimes 2—9143
    azulene, vapour, single vibronic level lifetimes 2—8736
    benzene, S_1 state, effect of rotational excitation on electronic relaxation 2—24510
    benzene vapour, single vibronic level lifetimes 2—8736
    chlorofluorobenzene, transition moments, band contour anal., changes in rot. const. on excitation 2—12213
    collisional deactivation rates of electronically excited molecular ions 2—31877
    collisional rotational excitation, generalized phase shift treatment, classical limit 2—6008
    collisions, meas. of excited state lifetimes on function of particle density in nanosecond region 2—11999
    diatomic, application of adiabatic-nuclei theory to vibrational excitation by electron impact 2—18384
    diatomic, autoionizing states, mol. consts., photoelectron spectroscopy 2—8565
    diatomic, electron impact excitation, selection rule for parity unfavoured transitions 2—12090
    diatomic, vibrational excitation by atom, quantum mechanical impulse approx. 2—3134
    diatomic molecule, electeon impact vibrational excitation, parametric resonance effect 2—751
    diatomic molecule-slow electron collisions, resonance effects 2—18375
    diatomics, absorption and excitation cross sections averaged over vibr. structure 2—8563
    4,10-diazachryzene, in lowest triplet state, acid-base equilibria 2—18497
    diazomethane, comparative study of random phase approx. Hartree Fock of single excited configuration interaction methods of computing excitation energies 2—15277
    difluorobenzene, transition moments, band contour anal., changes in rot. const. on excitation 2—12213
    electron impact, dissociative excitation processes for simple molecules 2—5893
    electron impact, vibrational and rotational excitation, frame transformation theory applic. 2—12069
    endoergic collision processes, vibrational excitation 2—21712
    ethylene, nonlinear i.r. absorption, excited state effects 2—18501
    evanescent photons, absorption and emission in fluorescence 2—31736
    exciton states, influence of high ageing states, dipole theory study 2—8560
    above first ionization potential, isotope effects on ionization yields 2—759
    fluorescence polarization, conc. quenching by excitation transfer, anisotropy and 2nd nearest neighbour considerations 2—8552
    formaldehyde, comparative study of random phase approx. Hartree Fock of single excited configuration interaction methods of computing excitation energies 2—15277
    formaldehyde, interstellar, photochemistry and lifetimes 2—4898
    formaldehyde, singlet-triplet resonance interaction in A_2 states 2—31856
    formaldehyde and ^{13}C and ^{18}O species, hyperfine components of 2_{11}-2_{12} transitions 2—35331
    formaldehyde and ^{13}C species, at mm wavelengths, transition obs. 2—35332
    formic acid, comparative study of random phase approx. Hartree Fock of single excited configuration interaction methods of computing excitation energies 2—15277
    gas, nonlinear level crossing in the standing wave field 2—31744
    gas, optical breakdown threshold 2—39217
    glyoxal vapour, fluorescence and phosphorescence from laser excited first singlet excited state 2—12249
    inert gas liquids, rel. to vac. u.v. αnduced luminesc. 2—20113
    ionization via metastable species, and production and destruction of excited states 2—21863
    isolated molecule by monochromatic e.m. field, of vibrationally broadened band, energy level scheme 2—31763
    isoquinoline, threshold electron excitation spectra, obs. of compound negative ion resonances and electronic transitions 2—35350
    large molecules, highly excited singlet state, internal conversion 2—5897
    lasers, wavelength tunable, vibration- rotation absorption and excitation spectra 2—749
    methane, excited in cavity, stimulated Raman scattering, threshold characteristics 2—850
    methane, interstellar, photochemistry and lifetimes 2—4898
    methane, photoionization total and differential cross sections, X- and u.v. excitation, calcs. 2—18458
    methanol, triplet excitation by low energy electron impact spectra 2—24453
    methanol, triplet excitation by low energy electron impact spectroscopy, cross section determ. 2—15311
    methyl bromide excited above first ionization potential isotope effects on ionization yields 2—759

Molecules continued
  excitation continued
    N_2 ($B^3\pi_g$, v=13), formation by inverse predissociation from N(^4S_o) atoms 2—803
    naphthalene, threshold electron excitation spectra, obs. of compound negative ion resonances 2—35350
    naphthalene, vapour, single vibronic level lifetimes 2—8736
    nucleic acid bases, inner shell excitation 2—22446
    nucleic acid bases, thin films, energy loss functions for 25 keV electrons, outer shell excitation 2—22445
    in organic dye lasers, absorption of pumping radiation, effect on efficiency 2—37970
    organic molecules, triplet states, optically detectable double resonance 2—12198
    conjugated phenylacetylenes in glasses at 77K, photoexcited triplet state, e.p.r. detection 2—16690
    phthalazine, dipole moment changes for excitation to different levels, $n\rightarrow\pi^*$ transition 2—8811
    poly 2-vinyl naphthalene, in fluid and glassy solvents, obs. of temp. dependent excimer emission in fluorescence spectra 2—8849
    polyethylene, vibrational excitation rel. to photochemical decomp. 2—33389
    polymers, substituted, electronically excited state, properties 2—864
    pyrene soln. in toluene, excimer fluorescence, pressure dependence up to 10 kbar 2—15596
    pyridine, gas obs. of singlet-triplet transition by ion and electron impact 2—21699
    quinoline, threshold electron excitation spectra, obs. of compound negative ion resonances and electronic transitions 2—35350
    radiationless transitions, chem. reactions, relaxation phenomena in excited mols. 2—35200
    radiationless transitions, electronic relax. processes 2—35196
    relaxation processes 2—8520
    resonance Raman effect due to excitation in absorpt. continuum 2—745
    rotational by resonant electron molecule collision, determ. branch structure 2—18382
    tetrahedral molecules, pure rotational transitions from ground vibronic states 2—12081
    transfer of electronic excitation energy between separated chromophores 2—21711
    triatomic linear molecule, with Renner effect, inelastic electron scatt. 2—5909
    triphenylenes, 2-substituted, lowest excited triplet state, optical and e.s.r study 2—35356
    two-photon, fluorescence polarization 2—31748
    vertical excitation as transient phenomenon 2—38876
    vibration levels excitation due to electron transmission 2—12099
    vibrational deexcitation of highly excited polyatomic mols., collisional energy transfer 2—24573
    vibrational on collision, dependence of transition probability on impact parameter 2—6006
    water, triplet excitation by low energy electron impact spectra 2—24453
    weak vibrational excitation during molecular collisions, semiclassical theory 2—39022
    zinc porphin, lowest triplet state, dynamics by microwave induced delayed phosphorescence 2—18535
    zinc porphin, lowest triplet state, phosphorescence modulation by microwaves 2—21707
    AlO, laser excited fluorescence and radiative lifetimes of levels of $B^2\Sigma$ state 2—8580
    AsO, chemical excitation obs. in flame emission spectra 2—38886
    BCl_3, electron impact excitation in electron attachment processes 2—32113
    BF_3, electron impact excitation in electron attachment processes 2—32113
    Br_2, $B^3\Pi(0_u^+)$ state excitation in recombination of ground state $^2P_{3/2}$ Br atoms 2—24441
    Br_2, charge exchange with alkali atoms, adiabatic electron affinities 2—38898
    C_2^-, matrix isolated, laser excited fluorescence study 2—35236
    CD^+, produced in C^++D_2 reactive scattering, energy and angular distribution studied in 3.47-8.48 eV range 2—12008
    CO_2-N_2-He mixtures, vibrational population inversions behind normal shock waves 2—24442
    CO, by electron impact, resonance obs. at 10.04 eV 2—772
    CO, by He(2^3S), dissociative excitation rate constants 2—12305
    CO, electron impact excitation of electronic states, cross section determination from energy loss spectrum 2—15293
    CO, electron impact excited emission cross sections, meas. from 1260 to 5000Å 2—5919
    CO, electron impact resonance obs. at 10.05 eV 2—807
    CO, from photodissociation of CO_2, meas. of fourth positive system 2—778
    CO, photoionization fluoresc. band intensities 2—21593
    CO, r.f. spectroscopy of perturbed excited states 2—8599
    CO, resonance excitation by electron impact 2—808
    CO, stimulated emission observation in 1800-2000 Å range following discharge in gas at 60 torr 2—267
    CO, vibr. excitation rates in $O+CS\rightarrow CO+S$ reaction 2—15289
    CO, vibrational excitation by collisions with He 2—871
    CO, vibrational excitation in the spin-orbit relaxation Hg($6^3P_{1\rightarrow 0}$) 2—15292
    CO, vibrational excitation by electrons at 10 to 100 eV 2—12171
    CO interstellar, photochemistry and lifetimes 2—4898
    CO_2, electron impact dissociative excitation, nonthermal rotational population of CO($A^1\Pi$) state 2—5920
    CO_2, electron impact excited emission cross sections, meas. from 1260 to 5000Å 2—5919
    CO_2, measurement of population of upper and lower levels in activated system CO_2+air+He 2—28284
    CO_2, threshold electron impact excitation spectra studied by SF_6 scavenger technique 2—28313
    CO_2, vibr. thermalization, temp. depend. 2—28274
    CO_2 discharge, of upper laser level 2—35233
    CO_2^+, electronically excited, collisional deactivation rates 2—31877
    COS, threshold electron impact excitation spectra studied by SF_6 scavenger technique 2—28313
    COS, via effective energy transfer from CO 2—28428
    CS_2, afterglow emission studied following excitation in microwave or Ar discharges, 360-640 nm 2—24448

Molecules continued
  excitation continued
    CS_2, threshold electron impact excitation spectra studied by SF_6 scavenger technique 2—28313
    CS_2 vapour, laser excited fluorescence, double exponential decay 2—12108
    Cl_2, charge exchange with alkali atoms, adiabatic electron affinities 2—38898
    D_2, vibrational excitation and transfer, distorted wave calculation 2—38906
    D_2, vibrational excitation in collisions with H^+ 2—881
    D_2 highly excited states formed by electron capture collisions of H_2^+ in H_2 gas, population determ. 2—38915
    H_2, 1-10 eV electron scattering, differential and integrated cross sections for vibrational and vibrational-rotational excitation 2—12136
    H_2, collisional excitation with Ar*, near resonant electronic energy transfer, fluorescence obs. 2—28432
    H_2, cross sections for rotational excitation by slow positron impact calc. in distorted wave approx. 2—24466
    H_2, electron-impact cross sections and energy deposition 2—24457
    H_2, electron impact excitation of Lyman and Werner bands 2—5931
    H_2, electron impact resonant excitation of $B^1\Sigma^+_u$ state, close coupling calc. 2—793
    H_2, excitation of Werner bands by electron impact (300 eV) 2—35253
    H_2, G(3d $^1\Sigma_g^+$) state excitation, microwave optical magnetic resonance 2—21605
    H_2, in collisions with H and He, cross section calc. using dose coupling equations in quasiclassical approx. 2—877
    H_2, inelastic excitation by electron impact, total cross sections 2—794
    H_2, parity forbidden transitions, excitation by energetic electronics 2—12141
    H_2, production of 1 to 42 keV/nucleon X $^1\Sigma_g^+$ and c $^3\Pi_u$ states in H_2-Mg collisions 2—31880
    H_2, rotational excitation by low energy positron scattering 2—5932
    H_2, rotational excitation by collisions with Li^+, classical study 2—8859
    H_2, simultaneous excitation and photoionization, obs. from photoelectron spectra at 247 Å 2—35256
    H_2, simultaneous vibrational-rotational excitation by low energy electrons 2—12140
    H_2, transitions between excited states, possible origin of diffuse interstellar absorption lines 2—12142
    H_2, vacuum u.v. laser, electron beam excitation 2—17601
    H_2, vibrational and rotational excitation, by slow electron impact, 0.3-15 eV 2—790
    H_2, vibrational excitation and transfer, distorted wave calculation 2—38906
    H_2, vibrational excitation by collisions with He atoms, ang. distributions in eV region 2—876
    H_2, vibrational excitation by H^+ impact 2—15427
    H_2, vibrational excitation in collisions with H^+ 2—881
    H_2, zero field level crossing in excited rotational levels, radiative lifetime meas. 2—35250
    H_2 highly excited states formed by electron capture collisions of H_2^+ in H_2 gas population determ. 2—38915
    H_2 vibrational excitation by He, collision energy dependence of ang. distrib. 2—28292
    H_2^+, vibrational excitation, rel. to reaction cross section enhancement of statistical phase space theory 2—16679
    H_3 highly excited principle quantum states formed by electron capture collision of H_3^+ in H_2 gas 2—38916
    HBr, vibrational and rotational excitation in He(2^3S_1) Penning ionization 2—21716
    HCl, relaxation rate from $v''=3$ vibr. state excited by dye laser radiation 2—24454
    HCl, vibrational and rotational excitataion in He(2^3S_1) Penning ionization 2—21716
    HD-Li^+, interaction potential, rot. excitation cross sections region 2—3148
    HD, ionization energies of Rydberg series, 700-1000 Å absorpt. spectrum 2—18435
    HD highly excited states formed by electron capture collisions of H_2^+ in H_2 gas, population determ. 2—38915
    HD($B^1\Sigma_u^+$), excitation process by absorption of Ar resonance lines 2—12129
    HNCO, in interstellar medium, 1_{01}-0_{00} transitions 2—26759
    HNCO, microwave spectra, rotational transitions 2—38902
    $(H_2O)_2^-$, hydrated electrons, theoretical calc. of excitation energy 2—12153
    H_2O, comparative study of random phase approx. Hartree Fock of single excited configuration interaction methods of computing excitation energies 2—15277
    H_2O, electron impact excitation, 3 to 6 eV 2—8617
    H_2O, interstellar, photochemistry and lifetimes 2—4898
    H_2O, photoionization total and differential cross sections, X- and u.v. excitation, calcs. 2—18458
    H_2O, triplet excitation by low energy electron impact spectroscopy, cross section determ. 2—15311
    H_2O vapour, in laser, direct electron impact 2—17598
    H_2S, photoionization total and differential cross sections, X- and u.v. excitation, calcs. 2—18458
    $H+H_2$, collinear exchange reactions, with vibr. excitation reaction probabilities and thermal rate consts. 2—10608
    He_2, metastable states produced in electron-bombarded superfluid He, dynamics 2—32299
    He_2^+, vibrational and rotational excitation of ions formed by associative ionization in a recombining plasma 2—24672
    HeH^+ produced in chemiionization reaction of metastable He with H_2, energy distribution measured 2—12054
    I ions, $2p_{3/2}$ and $2p_{1/2}$ vacancy production by collisions at 15 to 60 MeV, differentiation 2—667
    I_2, 213 cm^{-1} line, exciting freq. depend., relative scattering cross section, by resonant Raman effect 2—5933
    I_2, charge exchange with alkali atoms, adiabatic electron affinities 2—38898
    I_2, collisional depolarization of laser excited fluorescence 2—38919
    I_2 bands, excitation functions 2—31804
    IBr, charge exchange with alkali atoms, adiabatic electron affinities 2—38898
    N_2, C $^3\Pi_u$ state, electron impact excitation of $v'=3$ and 4 levels, electron emission band obs. 2—5938
    N_2, collisional excitation by N atoms of first positive and first negative radiation in 6000 to 14000K range 2—15319

Molecules continued
excitation continued
N_2, cross sections for rotational excitation by slow positron impact calc. in distorted wave approx. 2—24466
N_2, dissociative excitation by electron impact, vacuum u.v. emission features 2—8669
N_2, $E^3\Sigma_g^+$ state, cascade contrib. to day glow 2—16880
N_2, electron impact excitation of metastable $E^3\Sigma_g^+$ state 2—31814
N_2, electron impact resonance obs., derivation of N_2^- potential curve and width of 11.48 eV state 2—807
N_2, excitation mechanism for population of vibr. levels of $C^3\Pi_u$ state 2—21630
N_2, H-atom impact, 20 to 120 keV, Lyman-α radiation prod. 2—18311
N_2, N_2^+, decay of electron impact excited states, time resolved studies 2—5939
N_2, population inversion, pulsed discharge 2—5367
N_2, pure and mixtures with Ar, influence of metastable N_2 molecules on excitation 2—15509
N_2, relative populations of C^3II_u and $B^2\Sigma_u^+$ states 2—31806
N_2, resonance excitation by electron impact 2—808
N_2, rotational excitation by collisions with Na^+ and Li^+ 2—894
N_2, vibrational excitation by electrons at 10 to 100 eV 2—12171
N_2, with $He(2^3S)$, dissociative excitation rate constants 2—12305
N_2 metastable states excitation by electron impact 2—18452
N_2^+, charge transfer excitation of first negative 3914 Å band by protons, photon-particle coincidence meas. 2—809
N_2^+, collisional excitation and predissociation of excited states 2—896
N_2^+, collisional excitation by N_2 of first positive and first negative radiation in 6000-14000K range 2—15319
N_2^+, electron impact, 3914 Å 2—18450
N_2^+, electronically excited, collisional deactivation rates 2—31877
N_2^+, excitation of $C\ ^2\Sigma_u^+$ state by collisions with He^+ and Ne^+ 2—893
NH_3, interstellar, photochemistry and lifetimes 2—4898
NH_3, on electron collision, vac. u.v. spectral obs. 2—18454
NO, electron-impact excitation, absolute cross sections 2—24478
NO, electron impact dissociative excitation in vacuum u.v. 2—3054
NO, monochromatic excitation of rotational levels in vibrational levels of $A^2\Sigma^+$ state 2—12175
NO, Penning ionization and photoionization to $X^1\Sigma^+$ state of NO^+, comparison of vibrational transition probabilities 2—21625
NO, vibr. thermalization, temp. depend. 2—28274
NO vacuum-u.v. excitation cross sections, electron impact determ. 2—21627
NO_2, charge exchange with alkali atoms, adiabatic electron affinities 2—38898
NO_2, electronic excitation in collisions with Na at 1 to 30 eV 2—687
N_2O, on electron collision, vac. u.v. spectral obs. 2—18454
N_2O, threshold electron impact excitation spectra studied by SF_6 scavenger technique 2—28313
N_2O^+, photoionization and photoelectron spectroscopy, validity range of selection rule 2—12163
NaO^-, excitation energies, Hartree-Fock molec. orbital calc. 2—37032
O_2, absorption in Schumann Runge continuum 2—3057
O_2, angular dependence of electron impact excitation cross sections 2—31817
O_2, by electron impact, resonance structure interpretation in 0 to 1.2 eV energy range 2—820
O_2, charge exchange with alkali atoms, adiabatic electron affinities 2—38898
O_2, electron impact, 4-45 eV, differential and integral cross sections determ. 2—15328
O_2, electron impact excitation selection rule for parity unfavoured transitions 2—12090
O_2, electronic collisions, resonance electron spectrometry obs. 2—5902
O_2, vibrational and electronic excitation due to low energy electron collisions 2—814
O_2, vibrational excitation by electrons at 10 to 100 eV 2—12171
O_2 cross sections for rotational excitation by slow positron impact calc. in distorted wave approx. 2—24466
O_2 Herzberg Bands, in nightglow 2—20382
O_2 soln. in methanol, $^1\Delta$ lifetime direct meas. by laser pulse technique 2—8688
O_2^- spectra in alkali halide crystals, vibrational structure 2—813
O_2^+, vibrational and rotational excitation in $He(2^3S_1)$ Penning ionization 2—21716
$O_2(^1\Delta_g)+SO(^3\Sigma^-)\rightarrow SO(^1\Delta)+O_2(^3\Sigma_g^-)$, kinetic study by e.p.r., absolute rate constant 2—10612
$O_2(^3\Sigma\text{-}_g)$, vibrationally excited, formation in reactions of $O(^1D)$ atoms with O_2 and O_3 2—12183
Op_2 vibrationally excited, equilibrium densities for day and night, in upper atmosphere 2—22984
S_2^- spectra in alkali halide crystals, vibrational structure 2—813
SO_2, electronic excitation in collisions with Na at 1 to 30 eV 2—687
SO_2, single vibronic level lifetimes of first excited singlet state 2—8703
$SO(^1\Delta)\rightarrow SO(^3\Sigma^-)$, e.p.r. study of decay mechanism at reaction vessel walls 2—10612
ScO, excitation energies of unobserved $A'^2\Delta$ states 2—5950
TlI, mechanism of pulsed lasing of green line in a vapour discharge 2—27486
Xe_2, decay in afterglow 2—24359
YO, excitation energies of unobserved $A'^2\Delta$ states 2—5950

intermolecular mechanics
see also Association; Collision processes/molecules; Kinetic theory/gases; Liquids/structure; Liquids/theory; Solids/theory
benzyl fluorides, inter and intramolecular movements studied by distortion in n.m.r. signals from ^{19}F 2—24512
Born-Green-Yvon theory, graph- theoretic analysis appl. to 4th virial coeff. for 12-6 potential 2—6016
borosilicate glass, van der Waals forces, dynamic technique for obs. 2—39028
Casimir-Polder interactions, long-range, moment theory bounds 2—21529
in chemical reactions, X-ray obs. 2—35933
cholesterol esters liquid crystals, intermol. interactions in three phases 2—28869
closed-shell molecules, model for calculating intermolecular forces 2—24367
conformation of mol. in cryst., rel. to intermol. forces 2—3742
diatomic oscillator, rotating, vibrating calc. of rotational and vibrational transitions in collisions with atoms 2—8854

Molecules continued
intermolecular mechanics continued
diatomics in soln., effect on determ. of dopole moment and polarizability function 2—18377
dipolar interaction effects in flow birefringence in isomeric liquids 2—6013
DNA polymer type, intercalation interaction of small molecules 2—8842
excitation transfer and internal conversion 2—21711
first order perturbative terms in interaction between molecules, calc. using POLYATOM 2—3137
fluid with a soft core, perturbation theory for expansion of radial distribution function 2—21724
force triangle for representing structure of multipole treatment of intermolecular forces 2—15419
Helmholtz free energy for system of particles acting through Lennard-Jones 12-6 potential 2—32222
hydrocarbon-fluorocarbon mixtures, interaction virial coefficients 2—28734
interaction energies between non-bonded H atoms, perturbation calc. 2—15269
interaction potential between polar molecules studied, solution using weighted Boltzmann factor proposed 2—9125
interactions, effect on coherent electric quadrupole radiation processes 2—12299
interactions in region of small overlap, Rayleigh-Schrodinger perturbation theory 2—15420
ketones, aliphatic, $n\rightarrow\pi^*$ transition shifts, contribs. from intermol. interactions and H bonds 2—3104
Landau-Teller interaction, exact quantum-mechanical transition probabilities 2—21713
liquid-solid transition simulation, response function model 2—18880
in liquids, analytic effective potential compared with computer calc. of many-body effects 2—35725
long range interaction energies using Gaussian basis sets and one centre method 2—35170
long range interactions in an extended van der Waals equation of state 2—18540
m-6-8 potential function for fluids, third virial coeff. determ. 2—35389
methane+H system, UHF LCAO MO GTO study of hydrogen exchange and abstraction 2—26336
monatomic gas mixtures, determ. of potential parameters for Buckingham's modified potential 2—35373
monolayer assemblies, chromophore interactions 2—35374
monosubstituted benzenes, anisotropy of intermolecular potential energy, pressure dependence 2—39392
naphthalene in durene crystals, phosphorescence discussion in terms of phonons resonance pair interactions and intermol. energy transfer 2—20111
nematic liquid crystal, calc. of spectrum of elementary excitation 2—15568
nitromethane, nitromethane-d_3, matrix-isolated, intermolec. potentials, calc. from force constants 2—24547
non-additive interactions, effects 2—98
non-muffin-tin potential, generalization of Green's function methods 2—18543
nonpolar molecules represented as dipoles, exact energy of interaction 2—35376
nonretarded van der Waals interaction between anisotropic long thin rods at all angles 2—35386
nuclear relaxation, and mol. pair distrib., in liquid mixtures 2—6251
pair of linear molecules, equilibrium configurations for mutual orientation 2—39023
pair potentials, equivalence of Mie (n,6) and exponential-6 in reproducing second virial coefficients of gases 2—21913
pairwise interactions between oppositely charged nonspherical ions, calc. potential energy function 2—18541
phenol vapour, intermolec. interactions, investigation using second virial coefficients and Stockmayer model 2—39027
phenol-methylpyridinoxide complex, H bond system, obs. of intra and inter-mol. vibrations 2—24548
phenols, chlorine substituted, complexes with acetonitrile, i.r. study of intermol. H bonds 2—856
phosphine oxides, spectroscopic study of intermolecular interactions 2—28434
phthalocyanine, crystalline metal-free, interactions between molecules calc. using π-electron theory 2—39003
polar gases, potential functions and virial coeffs. 2—15537
polar gases, potential functions and virial coeffs. 2—15536
polarised medium, nonadiabatic transition probability, WKB approximation 2—865
polyoxymethylene, orthorhombic crystals, intermolecular potential evaluated 2—16576
polystyrene, motion of molecular groups at low temperature investigated by studying dynamic mechanical properties 2—6518
potential, hard and soft functions in approximate equation of state 2—31889
potential energy function for interaction between oppositely charged nonspherical ions 2—18541
potential-energy surface variations, influence on exchange-reaction probabilities 2—22858
potentials tested by molecular dynamics method, calc. of pressure and total energy 2—35375
quinoline, liq. and solid states, vibr. spectra study 2—35377
radiationless transitions, chem. reactions, relaxation phenomena in excited mols. 2—35200
repulsive inverse power potential, classical deflection angle, exact series solution 2—24569
repulsive potential between molecules, atomic distortion and combining rule 2—31700
retarded resonance interactions between optically active molecules 2—8850
rhodamine 6G, soln., intermol. energy transfer and conc. depolarization of luminescence 2—6237
rhodamine dye solutions, associated molecule formation, study using electronic absorption spectra 2—39372
second virial coefficients of line-core molecules 2—22031
second virial coefficients of line-core molecules 2—22030
semiclassical scatt. theory and total cross sections, systems with many crossing points 2—7686
short range forces, convergence of multibody expansions 2—12309
singlet-triplet transitions induced by exchange with paramagnetic molecules and coupling of spin angular momenta 2—39021

Molecules continued
  intermolecular mechanics continued
    square well fluid, augmented van der Waals theory, corrections 2—24584
    Stockmayer (m,6,3) potential function, tables of second virial coeffs. and derivatives 2—24977
    tetracyanoethylene solution in mesitylene, π-π charge transfer complex, obs. of intermolecular vibrations in spectra 2—28426
    thermodynamic perturbation theory for fluid of molecules interacting via Stockmayer potential 2—39024
    three-body nonadditive free energy of gases adsorbed on solids of arbitrary electron delocalization 2—35372
    time correlation function computation, statistical analysis of error 2—32220
    toluene, liq. and solid states, vibr. spectra study 2—35377
    toluene, singlet excitations, interaction with triplet molecules of naphthalene-d_8 2—9140
    two-dimensional gases, molecular dynamics and formation of bound states 2—15533
    universal interactions in soln. rel. to stabilization energy of molecular electronic levels 2—24574
    uranyl compounds, frozen solns., energy transfer distances 2—3153
    Van der Waals effects on n.m.r. chemical shifts 2—12094
    van der Waals force constants, upper and lower bounds from half-integer strength sums 2—24580
    van der Waals forces between two spheres, extension of van Kampen's method 2—18547
    Van der Waals interactions, effect on i.r. spectra of hydrogen bonded complexes 2—24575
    van der Waals potentials, long-range, sum-rule moment bounds 2—21528
    water, adsorbed molecules, intermol. interactions 2—10618
    Ar-Ar intermolecular potential determ. from crossed beam differential elastic scattering meas. 2—15422
    Ar-H_2 system, intermol. pot. parameters, effective cross sections 2—15426
    Ar, formed in Ar-Ar collisions, quantum undulations in intermolecular potentials 2—870
    Ar, intermolecular pair potential 2—18544
    Ar, pressure and total energy calc. by molecular dynamics method to test intermolecular potentials 2—35375
    Ar liquid, mean Laplacian of intermolec. potential from liquid-vapour fractionation from triple point to critical point 2—39432
    CO, molec. dynamic study in liquid Ar 2—3141
    CO_2, shock tube meas. of rate of vibrational energy transfer to CO, 730-2325K 2—8858
    CO_2+H_2 mixtures, vibrational-rotational energy exchange, 344 to 742 K 2—3140
    Cs-Hg, high resolution meas. of differential scattering cross section, intermolecular potential determ. by inversion of data 2—28427
    Cs-Hg system, intermolec. potential energy curves 2—888
    H_2-H_2 dispersion energy, variational calculation of dipole-dipole contribution 2—21717
    H ($B^1\Sigma_u^+$)+He(1S), interaction potential determ. by ab initio calcs. to interpret energy transfer expts. 2—18546
    H_2, $^3\Sigma_u^+$ state, variational calc. of additivity of 2nd order contribs. to intermol. potentials 2—8866
    H_2, intermolecular forces, nonsphericity meas. using anisotropy in Dicke narrowing of rotational Raman lines 2—38903
    H_3 model, non additivity in intermol. forces, comparison of different calculation methods 2—3143
    HCl, perturbed by Ar, vibr. depend. of intermol. pot. 2—8618
    H_2O, molecular model for prenucleation clusters 2—35378
    $H+H_2 \rightarrow H_2+H$ reaction probabilities, influence of variations of potential-energy surface 2—22858
    He-H_2 collisions, spherical potential for atom molecule separation of 2.7-3.3Å determ. from cross section 2—28430
    He_2, LCAO MO SCF calc. of first order perturbation internal energy terms 2—3135
    He_3 model, non additivity in intermol. forces, comparison of different calculation methods 2—3143
    HeH_3^+ potential energy surface, ab initio calculation 2—18436
    He+He system, intermolec. potentials from crossed beam differential elastic scatt. meas. 2—8861
    He*-H potential, well depth estimated from study of Penning ionization processes 2—18365
    Hg inert gas intermolecular potentials molec. beam determination 2—24572
    I complexes, electronic, spectra, effect of intermolecular interactions 2—8578
    K-Hg, high resolution meas. of differential scattering cross section, intermolecular potential determ. by inversion of data 2—28427
    K-Hg system, intermolec. potential energy curves 2—888
    KrKr system, multiparameter intermolec. potential, derivation from low energy differential cross section meas. 2—891
    Li-Kr, system, intermolec. potnetial 2—892
    Li-Xe system, intermolec. potential 2—892
    N_2, intermolec. potential, investigation via collision induced i.r. absorption from 77 to 297K 2—8668
    Ne+Ne system, intermolec. potentials from crossed beam differential elastic scatt. meas. 2—8861
    O_2, shape of intermolecular interaction potential from Senftleben effect study 2—15538
    O_2 microwave spectrum, pressure broadening calc., strong-collision model 2—18460
    PCl_3, liq. and solid states, vibr. spectra study 2—35377
  internal mechanics
    F- and Cl-substitutedacetaldehyde, normal coordinate analysis, force consts. determ. 2—8724
    alkyl anthracene, fluorescence study of intramol. energy transfer 2—18481
    alkyl fluorenole, fluorescence study of intramol. energy transfer 2—18481
    aromatic nitriles, anion radicals, i.r. study of intramol. electron interaction 2—8732
    7-azaindole dimer, potential energy curves of protons in H bonds in ground and excited states 2—5958
    benzyl fluorides, inter and intramolecular movements studied by distortion in n.m.r. signals from ^{19}F 2—24512
    bonding described with hybrid orbitals 2—756
    1,3-butadiene, internal rotation, study via ab initio calcs. 2—28357
    p-chlorobenzotrichloride, n.q.r. obs. 2—5966
    clathrate-type double hydrates, n.m.r. study of molecular movement 2—847

Molecules continued
  internal mechanics continued
    conjugated systems, failure of CNDO/2 method to predict barriers and conformations 2—3099
    coronene, internal conversion meas. of fluorescence yields and triplet state prod. 2—3121
    cyclopropyl methyl ketone, microwave spectrum, barrier to internal rotation, dipole moment, conformation 2—21673
    diatomic, r-centroid, calc. from potential energy curves 2—3024
    diatomic molecules, internuclear distance from estimated spectroscopic intensities 2—8531
    diatomic molecules, new potential function 2—24420
    diatomic molecules, validity of Tietz potential functions 2—31734
    diatomic potential energy curves, extension of RKR method 2—18374
    diatomic vibrational potential functions, determination from integration of Poisson equation 2—8527
    diatomics, formula for potential energy curves 2—15254
    dimethylallene, microwave spectrum, barrier to internal rot., rot. consts. dipole moment, r_0-type structural data 2—18499
    diphenyl ethers, highly substituted, energy barriers to rotation about Ar-O bond determ. from n.m.r. spectra 2—38975
    diphenylamine in CCl_4 solution, dipole-dipole interactions and solvent effects 2—15373
    excitation transfer and internal conversion 2—21711
    formaldehyde, photodissociation, potential energy surfaces 2—20201
    formic acid dimer, nonempirical calc. of intramolecular rearrangement 2—3092
    gas molecules contribution of intramol. multiple scattering to electron diffraction patterns 2—21559
    2-halocyclohexanols, OH-halogen intramolec, H-bond, potential function model 2—21687
    2-haloethanols, OH-halogen intramolec. H-bond, potential function model 2—21687
    o-halophenols, OH-halogen intramolec. H-bond, potential function model 2—21687
    harmonic potential constants, determination using Monte Carlo method 2—31739
    1,2,3,6,7,8-hexahydropyrene, monovalent positive and negative ions, conformational interconversion 2—18511
    hydrogen bond, adjustment of double-minimum potentials by sum of Hulburt-Hirschfelder potentials 2—5901
    interaction energies between non-bonded H atoms, perturbation calc. 2—15269
    internal rotation, motion description using whirling type internal coordinate 2—15266
    intramolecular coupling in large molecules, nature, internal conversion 2—3017
    intramolecular multiple scattering in gas phase electron diffraction, model calcs. 2—21560
    Kassel relaxation process, exact soln. 2—8851
    macromolecular solns., intramol. pot. barrier determ. 2—28800
    methacrylonitrile, barrier to internal rotation of CH_3 gp 2—8799
    methanol, liquid proton motions studied by cold neutron scattering 2—25035
    methyl isocyanide, isomerization, failure of RRKM theory 2—3109
    methylcyanide, intramolecular core level shifts, ab initio mol. wave functions 2—35341
    methyliocyanate, intramolecular core level shifts, ab initio mol. wave functions 2—35341
    methylisocyanide, intramolecular core level shifts, ab initio mol. wave functions 2—35341
    methylsilane, barrier to internal rotation and its derivatives w.r.t. vibrational coordinates 2—12264
    non-crossing rule in molecular quantum mechanics 2—35202
    non-rigid molecules, internal symmetry groups 2—35215
    oriented molecules, n.m.r. obs. 2—5956
    pentahalogenotoluenes, i.r. study of barriers to internal rotation form vibr. band width meas. 2—8806
    polyatomic vibrational potential functions, multiple perturbation expansion 2—21567
    potential energy curves, discontinuities in single config. theory calc. 2—3018
    potential energy surface construction, for processes with change in electron config. 2—18387
    1,3propidactone, ring puckering potential function 2—21698
    pyrene, laser excited fluorescence S_2 emissions, intermediate strong coupling and vibr. redistrib. effects 2—15393
    pyrene, vapour, effects of intramol. vibr. redistrib. in S_1 fluorescence 2—3117
    relaxation, derivation of master equation using projector operator techniques in Liouville space 2—33933
    siloxanes, appearance potentials 2—15414
    ten-electron hydrides, ground state energies, variational perturbation theory calc. 2—15273
    tetracene, internal conversion meas. of fluorescence yields and triplet state prod. 2—3121
    1,1,1-trifluoroethane, appearance potentials 2—15403
    trimers, weakly bound by three mutual Morse potentials, calc. of J=0 binding energies 2—744
    Urey-Bradley calculations using 4- and 5-atom configurations 2—12087
    vibration-rotation interaction const. and mean square amplitude of vibration, transformation under rotation of coordinate axes 2—752
    water, intramolecular vibrations in liquid state 2—39330
    o-xylene, exchange contribs. to internal rotation barrier 2—859
    $AlBr_4^{2-}$, intramol. force field, force consts., Coriolis coupling consts., vibr. amplitudes and potential energy distrib. 2—31774
    ArO^+, potential energy surfaces for low lying electronic states, molecular orbital calcs. 2—15307
    BH, r-centroids of A-X band systems 2—3028
    BH_3NH_3, SCF calc. of barrier to internal rotation, w.r.t. vibrational coords. 2—12106
    BiCl, A-X system, transition moment as function of internuclear separation 2—3029
    CF, multiconfiguration HF calcs. of potential curves of ground and some excited states 2—8597
    CH, potential curve for $^2\Pi$ ground state 2—35239
    CH^+, potential energy curves, ab initio calc. 2—31786
    CN, r-centroid, calc. from potential energy curves 2—3024
    CO_2, anisotropic potential energy surfaces, determination from inert gas atom collision data 2—6012

Molecules continued
internal mechanics continued
CO_2, potential energy function, 4th order approx., vibr. energy levels, spectroscopic constants 2—12110
CO_2, simple potential energy function 2—31784
$CO_2(xyo)+CO_2 \rightarrow CO_2(001)+CO_2$ shock tube meas. of vibrational relaxation, reaction rate obtained 2—35235
$Co_4(CO)_{12}$, forces between metallic atoms, derivation from i.r. spectra 2—38900
Cr(III) complexes with intramolecular exchange, e.p.r. obs. 2—8609
CsF, prod. by reactive beam scattering of Cs by SF_6 and SF_4, vibr. energy distrib. 2—21597
CsH, potential energy curves, applicability of Morse potential, rot. consts., r-centroids, Franck Condon factors 2—18457
Cu(II) complexes with intramolecular exchange, e.p.r. obs. 2—8609
DI, repulsive potential curve, semi-experimental determ. 2—3043
DI, repulsive potentials from electronic absorption spectra 2—12144
F_2, potential curve of ground state, method of optimized valence configurations 2—28289
F_2^+, 13 lowest electronic states, calculated potential energy curves 2—8613
Fe(III) complexes with intramolecular exchange, e.p.r. obs. 2—8609
GaH, r-centroids of A-X band systems 2—3028
H_2^-, potential energy curve calc. using separable potential model 2—3044
H_3, calc. of 3-body energy term in $^4A_2$ quartet state 2—8622
HF^+, ab initio SCF calc. of potential energy curves 2—24465
HI, repulsive potential curve, semi-experimental determ. 2—3043
HI, repulsive potentials from electronic absorption spectra 2—12144
HI, repulsive potentials from electronic absorption spectra 2—12144
HI_2 radical, vibrational potential function 2—21604
HNCS, intramol. interaction, temp. depend. of vibr. band intensities of i.r. spectra 2—12567
H_2O_2, barrier to internal rotation, investigation using H-F approx. 2—8641
He_2, potential curve for $2s\sigma^3\Sigma_u^+$ state 2—31802
He_2, potential energy curve prediction from interatomic correlation energy and van der Waals attraction 2—21552
HeH, interaction potential and hyperfine shift as function of internuclear distance 2—21611
HeH, potential curve determination rel. to translational absorption line shape calc. 2—796
HeO^+, potential energy surfaces for low lying electronic states, molecular orbital calcs. 2—15307
$He+H_2$, system, intermolec. potential parameters from abs. cross section meas. in energy range 0.1 to 2.8 eV 2—3147
He+He system, intermolec. potential parameters from abs. integral cross section meas. in energy range 0.1 to 2.8 eV 2—3147
HgH, potential energy curves from extension of RKR method 2—18374
InH, r-centroids of A-X band systems 2—3028
KH, potential energy curves, applicability of Morse potential, rot. consts., r-centroids, Franck Condon factors 2—18457
Li_2, potential curve of lowest triplet state calc. by multiconfigurational approach 2—35261
LiCs, singlet potential determination from LiCs system total scatt. cross section 2—21621
LiH, MC-SCF study of $X^1\Sigma^+$, $A^1\Sigma^+$, $^3\Sigma^+$ and $^{1,3}\Pi$ states, potential curves, spectra, transition probabilities 2—15314
$^7Li^{79,81}Br$, electric quadrupole interaction constants, spin-rotation and spin-spin interaction constants 2—8662
β-N_2, barrier to rotation, determ. from heat capacity data 2—4067
N_2, r-centroid, calc. from potential energy curves 2—3024
N_2^-, potential curves, derivation from N_2 electron scattering data 2—807
N_2O, anisotropic potential energy surfaces, determination from inert gas atom collision data 2—6012
Na_2^+, potential curve calc., Na^++Na resonance charge transfer cross sections 2—3055
NaH, potential energy curves, applicability of Morse potential, rot. consts., r-centroids, Franck Condon factors 2—18457
NeN^+, potential energy surfaces for low lying electronic states, molecular orbital calcs. 2—15307
O_2^-, ground and excited states, potential energy calc. 2—15297
$O+O^-$, adiabatic potential curves, ab initio calc. 2—12185
P_2, potential curves of all low lying states 2—31819
RbH, potential energy curves, applicability of Morse potential, rot. consts., r-centroids, Franck Condon factors 2—18457
$Rh_4(CO)_{12}$, forces between metallic atoms, derivation from i.r. spectra 2—38900
SeO_2, microwave spectrum, 3rd order potential constants and dipole moment 2—31828
SiH, Franck-Condon factor and true potential energy curves 2—5951
SiH^+, Franck-Condon factor and true potential energy curves 2—5951
SiO, potential curves for valence-excited states 2—8702

moments
acetylene, electrical quadrupole moment from point-charge model 2—28372
acyl-pyrroles, electric dipole moments in solution 2—39380
acylfuranes, elec. moment rel. to determination of preferred conformation in benzene solution 2—38956
adenine, electron density and dipole moment analysis of valence electron wavefunctions 2—35302
alkanecarbodithoic acids, dipolar moment 2—24500
amino anthracenes, nonsymmetrical, moment directions of electronic transitions 2—21657
aromatic hydrocarbon radicals, degenerate, g- factor deviations 2—18489
aromatic molecules, magnetic anisotropies determ. using Cotton-Mouton effect 2—24495
asymmetric rotors, Stark effect, dipole moment determ., new approach 2—8547
asymmetric top moments, rel. to traces of products of angular momentum operators 2—17219
2,6-bis(4-azidobenzylidene) cyclohexanone, stereoisomers, electronic structure and spectra, dipole moments, SCF MO LCAO methods 2—12233
azo group, α,β-unsaturated, u.v electronic spectra, dipole moments, config. study 2—18483
benzene, mag. susceptibility anisotropy, from Cotton-Mouton effect meas. 2—18486
benzonitrile, lowest-lying singlet $\pi^* \leftarrow \pi$ transition, rotational analyses, dipole moment changes 2—35343
4H-benzo[def]carbazole, first excited state dipole moment from solvent shifts of absorption and fluorescence bands 2—24508
bicyclobutane, quadrupole 2—35313

Molecules continued
moments continued
bicyclo[2.1.0]pentane, dipole moment 2—31841
bicyclo[2.1.1]hexan-2-one, dipole moment from analysis of microwave spectrum 2—8744
bromoform autocorrelation functions of dipole moment theoretical and experimental values compared 2—38985
calculation of electric dipole and quadrupole moments 2—35207
carbon tetrachloride polarity in vibrational state obs., due to vibrationally induced dipole moment 2—12218
carbon tetrafluoride polarity in vibrational state obs., due to vibrationally induced dipole moment 2—12218
chloroform autocorrelation functions of dipole moment theoretical and experimental values compared 2—38985
chloromethyl radical, e.s.r. study in CH_3Cl single crystal 2—8792
p-chlorostyrene chains, dipole moments and random coil dimensions 2—8753
cyclic molecules, contribution of trichloromethyl group to dipole moments 2—38952
cyclopentane, CNDO calc. of dipole moments 2—8546
cyclopropane and derivatives, anisotropy of polarizability 2—839
cyclopropyl methyl ether, microwave spectrum, dipole moment component determination from quantitative Stark effect meas. 2—12230
cyclopropyl methyl ketone, microwave spectrum, barrier to internal rotation, dipole moment, conformation 2—21673
cyclopropylacetylene, dipole, moment determ. from microwave spectrum 2—35321
diatomic, inclusion of nuclear motion in calcs. of magnetic properties 2—24435
diatomics, dipole moments, semi-empirical calc. 2—31760
diatomics in soln., spectroscopic method for determ. dipole moment and polarizability function 2—18377
diketene, determ. electric moments and magnetic properties from Zeeman effect studies 2—21675
dimethylallene, microwave spectrum, barrier to internal rot., rot. consts. dipole moment, r_0-type structural data 2—18499
diphenylamine in CCl_4 solution, dipole-dipole interactions and solvent effects 2—15373
dipolar interaction effects in flow birefringence in isomeric liquids 2—6013
dipole dipole interaction rel. to vibrational spectra, influence of solvents 2—25090
dipole moment of electronically excited molecules, absorption and fluorescence spectra 2—8554
dipole moments in ground and excited equilibrium electronic states 2—24574
dipole moments in liquid state, calculation method 2—39376
dipoles, microwave radiation, resonance interaction calculation 2—24419
electric multipole moments, tensor elements for all pt. gp. symmetries 2—8549
electric quadrupole moments, role of N-mixing in Nilsson model calc. 2—38437
ethane, electrical quadrupole moment from point-charge model 2—28372
ethyl thiocyanate, dipole 2—35327
ethylene, electrical quadrupole moment from point-charge model 2—28372
9-ethylguanine, electric dipole transition moments 2—24533
ethynylbenzene, lowest-lying singlet $\pi^* \leftarrow \pi$ transition, rotational analyses, dipole moment changes 2—35343
five-membered rings, CNDO calc. of dipole moments 2—8546
fluoroform autocorrelation functions of dipole moment theoretical and experimental values compared 2—38985
formamide, quadrupole 2—38982
^{15}N formamide, Zeeman effect, molecular quadrupole moments determ. 2—12246
fulvene, microwave spectra, struct., dipole moment 2—8779
glyoxal, dipole moments, of trans. perpendicular and cis forms 2—18510
hexafluorobenzene, mag. susceptibility anisotropy, from Cotton-Mouton effect meas. 2—18486
hydrocarbons, C_3 molecules, MO calc. of polarities 2—28383
hydrogen-bonded complexes, dipole moment of hydrogen bond depend. on permittivity of solvent 2—8555
ice, dipole moment derivative of H bond, calc. assuming molecules are non-overlapping polarizable charge distrib. 2—39569
ion-quadrupole effects in ion-molecule collision 2—12300
magnetic and electric moment, dipole moment derivatives calc. using expressions for derivatives of eigenvalues of hamiltonian 2—37616
methane, dipole moment derivatives 2—21692
methane, ground state elec. dipole moment 2—849
2-methoxyethanol, total dipole moment determination from Stark effect meas. in microwave spectrum 2—12262
methyl nitrate, dipole 2—18514
methyldifluorophosphine, dipole moment calc. from Stark effect meas. in microwave spectrum 2—15386
methylene fluoride, high-resolution Zeeman measurements of quadrupole moments 2—35339
methylenecyclopropane, INDO calculations on lowest energy singlet and triplet states, ring opening studied 2—8794
nitriles, complexes formed with proton donors, structure from dipole moment measurements 2—28391
nitrobenzal anils, relaxation times and dipole moments, dil. solution method 2—31867
3-oxetanone, dipole moment for ground vibrational state from microwave spectrum data 2—15389
paramagnetic, proton spin lattice relaxation, collision time correlation 2—5905
1-penten-3-yne, microwave spectrum, electric dipole moment, rotational constants 2—12270
perylene, electrochromic spectra in polystyrene matrix, change in polarizability and dipole moment between ground and excited states 2—13488
phenothiazines, substituted dipole moments meas., bending of nucleus 2—38999
phenyl isocyanide, lowest-lying single $\pi^* \leftarrow \pi$ transition, rotational analyses, dipole moment changes 2—35343
5-phenyl-2-(4-dimethylaminophenyl)-oxadiazole- 1,3,4, excited singlet state, dipole moment 2—3116
5-phenyl-2-(4-dimethylaminophenyl)-oxazole-1,3, excited singlet state, dipole moment 2—3116
phthalazine, dipole moment changes for excitation to different levels, $n \rightarrow \pi^*$ transition 2—8811
polymers, contributions to optical rotation from moments of monomers 2—8841

Molecules continued
moments continued
β-propiolactone. determ. electric moments and magnetic properties from Zeeman effect studies 2—21675
1-D- and 4-D-pyrazole, microwave spectra, quadrupole coupling theory of hyperfine structure 2—5993
pyridine, electric dipole moment of lowest excited singlet state 2—12278
pyridine bromine charge transfer complexes in C_6H_6, far i.r. spectra, force consts., dipole moment 2—8816
pyridine-halogen complexes, far i.r. intensity and normal coordinate studies, force consts., dipole moments 2—8817
quadrupolar, n.m.r. obs. 2—12095
quadrupole, comparison with nuclear quadrupole moments 2—34275
quadrupole, moments, molecules including 2nd row elements, all valence electron calcs. 2—21576
quadrupole moments meas. from Zeeman effect 2—8510
rhodamine 6G, electrochromic spectra in polystyrene matrix, change in polarizability and dipole moment between ground and exicted states 2—13488
rotational line strengths calc. for $^3\Sigma^\pm$—$^3\Sigma^\pm$ electric dipole transitions with intermediate coupling 2—3015
silyl methyl ether, dipole moment calc. from Stark splitting in microwave spectrum in 8 to 40 GHz region 2—15394
tetracyanoethylene-trans-stilbene mol. complex, effect of external elec. field on abs. spectrum and electric dipole moment 2—31870
4-tetrahydrothiapyranols, substituted, elec. dipole moments rel. to conformational studies 2—28410
4-tetrahydrothiapyranones, substituted, elec. dipole moments rel. to conformational studies 2—28410
1,3,5-trifluorobenzene, mag. susceptibility anisotropy, from Cotton-Mouton effect meas. 2—18486
2,2,2-trifluoroethylamine, dipole moment components from microwave spectrum 2—12290
trifluoroethylamine, normal and deuterated, dipole moment rel. to intramolecular H-bonding 2—21703
vinyl chloride chains, random coil dimensions and dipole moments, effect of isotacticity 2—8840
vinyl germane, dipole moment calc. from Stark effect meas. in microwave spectrum at 12.4 to 40.0 GHz 2—15406
vinyltrifluorosilane microwave spectrum, dipole moment from Stark shifts of rotational transitions 2—21706
2,4-xylenol u.v. absorption spectrum, small migration moment 2—15407
^{210}At, det. using ^{209}Bi(α,3n)^{210}At reaction and melted Bi target 2—21315
^{210}At, det. using ^{209}Bi(α,3n)^{210}At reaction and melted Bi target 2—31346
BBr_3, B-Br bond moment 2—38888
BF, elec. dipole moment for ground vibrational state determination from microwave spectrum 2—15285
BF_2OH, structure and dipole moment from microwave spectrum 2—35230
BH_3NH_3, change in dipole moment with rotation 2—12106
$B_2O_3H_2$, dipole, CNDO and INDO calculations 2—38887
BrCN, electric quadrupole moments, g values magnetic-susceptibility anisotropies determ. from Zeeman effect studies 2—24437
BrF, electric quadrupole moments, g values magnetic-susceptibility anisotropies determ. from Zeeman effect studies 2—24437
CO $a^3\pi$, electric dipole moment calc., using configuration interaction technique 2—8595
CO_3, dipole moment derivatives, ab initio LCGO MO SCF calc. 2—8589
CS $A^1\pi$, electric dipole moment calc., using configuration interaction technique 2—8595
CS_2, quadrupole moment sign determ. by Hartree-Fock-Roothaan molecular orbital calc. 2—21598
ClCN, elastic quadrupole moments, g values magnetic-susceptibility anisotropies determ. from Zeeman effect studies 2—24437
ClF, BrF, ClCN, BrCN, ICN, Zeeman effect, quadrupole moments determ. 2—12123
ClF, electric quadrupole moment, g values, magnetic-susceptibility anisotropies determ. from Zeeman effect studies 2—24437
CsF, molecular beam, r.f. spectra, electric dipole moment and quadrupole coupling const. up to v=8 2—5926
D_2, dipole transition moment, emission continuum 2—12143
FCl, radio frequency, spectrum obs., hyperfine parameters and dipole moment 2—8614
GeH_3Br, Br quadrupole coupling const. determ. from rotational spectra 2—18421
GeH_3I, I quadrupole coupling const. determ. from rotational spectra 2—18421
H halides, gas phase absolute intensities of i.r. vibrational bands, influence of bond and lone pair moments on total dipole moment 2—28298
H halides, in CCl_4 soln., absolute intensity of i.r. bands, signs of M_t quantities in dipole moment 2—28299
H_2, dipole transition moment, emission continuum 2—12143
HBr, absolute i.r. intensity meas., value of terms Mi of dipole moment function 2—28297
HCL, spectroscopic method for determ. dipole moment and polarizability function 2—18377
HCl, absolute i.r. intensity meas., values of terms Mi of dipole moment function 2—28297
HCl, quadrupole moment obs. 2—12145
$(HCl)_2$ dipole moment obs. 2—8645
HF, elec. dipole moment, evaluation of higher terms for vibration-rotation bands 2—21609
HF, quadrupole moment obs. 2—12145
$(HF)_2$ dipole moment obs. 2—8645
$(HF)_2$ electric dipole moments determ. from r.f. and microwave spectra 2—21614
HI, absolute i.r. intensity meas., values of terms Mi of dipole moment function 2—28297
HNO_2, cis and trans, electric dipole moments 2—788
HeH, dipole moment 2—796
ICN, electric quadrupole moments, g values magnetic-susceptibility anisotropies determ. from Zeeman effect studies 2—24437
N_2, quadrupole moments, best fit values 2—15324
N_2, quadrupole moments best fit values 2—18449
NH_3, diamagnetic shielding and susceptibility constants and dipole moment calc. using near HF wavefunctions 2—21626
NO, laser magnetic resonance obs., magnetic and electrical dipole transitions obs., g factor and hyperfine structure separation calc. 2—38928
NO, magnetic dipole transitions in far infra-red spectrum 2—38931
NO, $X^2\Pi$ and $A^2\Sigma^+$ states, elec. dipole and quadrupole moments, restricted Hartree Fock calculations 2—35266

Molecules continued
moments continued
N_2O, line strengths of bands in 2.9 micron region, dipole moment matrix element 2—18448
N_2O, quadrupole moments best fit values 2—18449
N_2O, self broadened and N_2 broadened half widths, 297K, quadrupole moments 2—15324
NaO, NaO^+, NaO^-, dipole and quadrupole moments from Hartree-Fock molec. orbital studies, deduction of Na-O species properties 2—37032
O_3, dipole moment determ. from Stark effect in millimetre wave spectrum 2—8691
OF, $^2\Pi$ state, ab initio calc. of dipole and quadrupole moments 2—31818
OH radical, dipole moments determ. from high-field Stark effects on near u.v. spectrum 2—8698
O^-...H-N^+ ion pair, rel. to hydrogen bond model 2—8555
P-S, dipole, rel. to struct. determ. 2—3021
PF_2NH_2 2—31820
PH_3, dipole moment rel. to P pyramidal inversion process, ab initio SCF-LCAO-MO study 2—31822
PN electric dipole moment calc. 2—38936
^{87}RbF, elec. dipole and rotational magnetic dipole moments, molec. beam resonance meas. 2—21641
SeO_2, microwave spectrum, 3rd order potential constants and dipole moment 2—31828
Si halide, matrix element of dipole moment of transition, depend. on r-centroid intensities 2—18469
$SiCl_4$ polarity in vibrational state obs. due to vibrationally induced dipole moment 2—12218
SiH_4 force constants and dipole moment derivatives calc. for symmetric and antisymmetric stretching and bending vibr. modes 2—12193
TlBr, derivation of electric dipole moments from Stark effect meas. on pure rotational transitions 2—8711
TlCl isotopes, elec. dipole and mag. rotational dipole moments, from molec. beam resonance meas. in different vibrational states 2—21645
TlI, derivation of electric dipole moments from Stark effect meas. on pure rotatioal transitions 2—8711
XeHCl, dipole moment obs. 2—8645

nuclear coupling
1,8-bis(dimethylamino)naphthalene radical anion, hyperfine coupling consts., steric hindrance 2—21667
acetone, MO studies of $^4J_{hh}$, comparison with oriented p.m.r. spectra 2—28339
benzenes, trisubstituted, additivity relation for proton-proton coupling consts. 2—38961
3,4-benzophenanthrene, p.m.r. spectra, determ. chemical shifts, coupling constants at infinite dilution in CCl_4 2—24507
N-t-butylstyrenimine, solvent effects on proton-proton coupling consts. 2—35793
chloroacetaldehyde, quadrupole coupling constant, meas. in microwave spectrum at 8 to 40 GHz 2—8752
2-chloroaniline-^{15}N, long-range coupling constants to amino protons from ring protons 2—21670
2-chloropropenes, deuterium substituted, quadrupole coupling constants 2—31844
cinnamaldehyde-imines, n.m.r. and INDOR 2—5967
complex spin systems, homonuclear spin coupling effects on transverse relaxation rates of n.m.r. lines 2—24431
cyanamide, CH_2N_2 isomer, N quadrupole coupling const. calc. 2—8751
cyclopropane, valence bond calcs. of vicinal proton coupling consts. 2—38974
diatomics, spin spin coupling const., ab initio calc. 2—8502
diazirine, CH_2N_2 isomer, N quadrupole coupling const. calc. 2—8751
diazomethane, CH_2N_2 isomer, N quadrupole coupling const. calc. 2—8751
difluoroethylenes, solvent and temp. dependence of H—H, H—F and F—F coupling consts. 2—31851
1,2-dihaloalkanes, vicinal proton coupling constant effect of solvent 2—12240
dimethyl sulphoxide MO studies of $^4J_{hh}$, comparison with oriented p.m.r. spectra 2—28339
dimethylsulphoxide, long range ^{13}C-H coupling 2—28300
ethane, valence bond calcs. of vicinal proton coupling consts. 2—38974
ethyl compounds, ^{13}C-^{13}C coupling constants 2—842
ethyl fluorides isotopically substituted, N.M.R. studies of spin-spin coupling constant 2—24535
ethyl formate, formyl J_{ch}, solvent and temp. depend. 2—5976
ethylene, Fermi contact contrib. to coupling consts., SCF LCGO MO calc. 2—8620
ethylenes, alkyl substituted, coupling consts., chem. shifts, n.m.r. obs. 2—12261
fluorinated heterocyclic compound, long range coupling consts. 2—5974
fluorochloroacetones, ^{19}F n.m.r. and ^{13}C satellite spectra, conformational preferences, C-F coupling const. 2—28377
fluoroethylene, Fermi contact contrib. to coupling consts., SCF LCGO MO calc. 2—8620
formamide, N quadrupole spin coupling tensor calc. from rotational spectra 2—3093
heteroaromatic phosphine derivatives, ^{1}H- ^{31}P long range coupling consts., INDOR spectra 2—12250
heterocyclics, 5 membered, unsaturated, H-H coupling consts., proton mag. reson. spectra, $223\leqslant T\leqslant 383K$ 2—12256
β-1,2,3,4,5,6-hexachlorocyclohexane, ^{13}C-H constants, Fourier transform spectra 2—15356
hexahelicene, p.m.r. spectra, determ. chemical shifts, coupling constants at infinite dilution in CCl_4 2—24507
hexamethylphosphoramide, long range ^{13}C-H coupling 2—28300
indirect spin-spin coupling const. calc. by NEMO wavefunction 2—8573
inter-ring proton couplings, INDO-MO calculations 2—21583
interproton spin-spin coupling across dual path in five-membered rings 2—28331
light diatomic, centrifugal distortion in spin-orbit coupling of triplet states 2—38883
malic acid free radical, conformational anal. using PCILO method, conformation by INDO calc. of coupling consts. 2—8789
methacrylonitrile, ^{14}N quadrupole coupling const. from microwave spectrum 2—8799
methyl pyridine, INDOR study 2—5981
3-methyl-pyrrole, assignments made in analysis of NMR spectrum 2—12260
methylamine, vicinal H-H coupling, dihedral angle dependence, lone-pair orientation effect 2—5986

Molecules continued
nuclear coupling continued
methylene groups, dihedral angle assignment by n.m.r. coupling constants 2—3066
1-methylpentaborane(9), B-C coupling constants 2—24543
monofluorobenzaldehydes and derivatives, spin coupling mechanisms 2—5982
nematic liquid crystals, determ. of deuterium quadrupole coupling consts. by n.m.r. 2—28263
nitroxide free radicals, e.p.r. 2—5984
organic systems, $^1H—^{19}F$ spin coupling, calc. by finite perturbation method 2—8571
oximes, NH and CH spin couplings, effect of lone pair orientation 2—5986
pentahelicene, p.m.r. spectra, determ. chemical shifts, coupling constants at infinite dilution in CCl_4 2—24507
phenoxy radicals, partially fluorinated, hyperfine coupling consts. 2—18522
phenoxy radicals, proton hyperfine coupling constants 2—5987
phenylacetic acid and derivatives 2—35344
phosphonic acid esters, angular dependence of β-P hyperfine couplings 2—15391
polyphenoxy radicals, hyperfine coupling of ring protons 2—35369
proton-proton coupling, medium and association effects in solvents 2—35793
pyrazole, microwave spectra, nuclear quadrupole coupling constants 2—8815
pyrazole, microwave spectrum, hyperfine structure, ^{14}N coupling consts., rotational constants 2—18526
pyridine-^{15}N, ^{15}N-H and ^{15}N-^{13}C coupling consts. 2—24550
quinoxaline, oriented in nematic phase, proton skeleton, spin spin coupling consts., n.m.r. obs. 2—9183
radicals, unrestricted Hartree-Fock description 2—3026
selenophene, oriented in lyotropic mesophase, n.m.r., direct couplings and interproton distance 2—28409
singlet-triplet transitions induced by exchange with paramagnetic molecules and coupling of spin angular momenta 2—39021
spin-spin coupling constants, effect of solvent molecular motion 2—18395
styrenimine, solvent effects on proton-proton coupling consts. 2—35793
tri-2-thienylphosphine, tri-3-thienylphosphine assignments and signs of ^{13}C-^{31}P coupling constants from off-resonance proton decoupled $_{13}C$ spectra 2—31871
transition metal phosphine complexes, P-P coupling constants 2—12098
1,3,5- trichlorobenzene, oriented, natural abund. of ^{13}C mag. resonances 2—28361
trifluoromethylquinoxalines, long-range H-F spin-spin coupling 2—24554
trimethylene oxide in nematic liquid crystal, direct coupling consts. determ. from NMR spectrum 2—35354
trithienylphosphines, methyls substit., signs and magnitudes of long range $^1H-^{31}P$ spin coupling consts. 2—12291
AgCl, AgBr, AgI, quadrupole coupling constants from microwave rotation spectrum 2—28270.
AlBr, AlI, quadrupole coupling from millimetre wave rotational spectra rel. to bond investigation 2—21588
B-C coupling constants 2—24543
BF, elec. quadrupole constants for ground vibrational state, determination from microwave spectrum 2—15285
BrF_5, quadrupole coupling constants 2—5912
CF, LCAO-MO SCF calcs. of ground and excited spectroscopic states, determ. of spin-orbit coupling 2—38897
$^{59}Co(III)$ sow spin octahedral complexes, effect of symmetry-breaking perturbations on interpretation of quadrupole coupling data 2—28262
CsF, molecular beam, r.f. spectra, electric dipole moment and quadrupole coupling const. up to v=8 2—5926
D_2S, quadrupole coupling constants 2—8611
H-F long-range spin-spin coupling, support for through-space mechanism 2—24554
H_2, Fermi contact contrib. to coupling consts., SCF LCGO MO calc. 2—8620
HD, Fermi contact nuclear spin-spin coupling, molecular orbital sum-over-states method 2—8636
HD, spin spin coupling const., ab initio calc. 2—8502
$HD^{80}Se$, quadrupole, spin and spin rotation coupling constants 2—24455
HNCO and DNCO, quadrupole coupling constants 2—31795
HNO_2, cis and trans, quadrupole coupling constants 2—788
H_2O, Fermi contact contrib. to coupling consts., SCF LCGO MO calc. 2—8620
$^{127}I_2$, nuclear hyperfine structure in electronic spectrum obs. by saturated absorption spectroscopy 2—12156
LiOH(D), molecular beam electric resonance spectra 2—8663
NF_2 radical, microwave Zeeman spectra, electron spin-rotation interaction 2—8678
NH_3, quadrupole coupling constants calc. using near HF wavefunctions 2—21626
NH_3^+ radical, hyperfine coupling constant, perturbation approach to evaluation of vibrational effects 2—21623
O_2, quadrupole coupling const. of ^{17}O 2—5944
P-P constants in phenyl substituted phosphonitrilic fluoride trimers 2—15329
PF_2NH_2, quadrupole coupling constants 2—31820
^{31}P-^{77}Se, coupling, ^{31}P n.m.r. study to characterize P=Se bond 2—5903
Pb complex, bis acetylacetonato dimethyllead, p.m.r. spectra ^{13}C-H and ^{207}Pb-C-H coupling consts. 2—28320
PdH(D), e.s.r. spectra of $^2\Sigma^+$ ground state, bonding nature, hyperfine coupling and g tensor components 2—12189
^{87}RbF, molec. beam resonance meas. 2—21641
SF_5Cl, quadrupole hyperfine effects in microwave spectrum 2—38939
SnH_3Br, quadrupole hyperfine coupling constants from microwave spectrum 2—15337
SnH_3I, quadrupole hyperfine coupling constants from microwave spectrum 2—15337
TlCl isotopes, quadrupole coupling const. of Cl nucleus, from molec. beam resonance meas. in different vibrational states 2—21645

relaxation
see also Acoustic wave propagation; Dielectric phenomena; Liquids/theory; Nuclear magnetic resonance and relaxation; Paramagnetic resonance and relaxation
acetone-^{18}O, isotope effect on nonradiative relaxation 2—35301
anharmonic oscillators, classical theory of vibrational relaxation 2—28251
anharmonic oscillators, vibr. relaxation 2—12075
azulene vapour, single vibronic level lifetimes 2—8736

Molecules continued
relaxation continued
benzene, influence of final-state spectrum in radiationless transitions studied by Laplace transform method 2—38962
benzene, lifetimes of individual vibronic states 2—8734
benzene, non radiative relaxation of excited A^1B_{2u} state 2—24511
benzene, S_1 state, effect of rotational excitation 2—24510
benzene vapour, single vibronic level lifetimes 2—8736
benzenes, methyl substituted, nonradiative transitions from first excited singlet state, rate constant meas. 2—12209
butyric acid, u.s. absorption at 20 to 90°C 2—18819
collisional, microwave absorption spectra, rel. to rotational energy transfer investigation 2—12297
coronene, reorientation of molecule in solid state, n.m.r. investigation 2—10567
α,ω-dibromoalkanes in benzene solutions, intramolec. cooperative relaxation 2—1109
α,ω-dibromoalkanes in benzene solutions 2—1109
dielectric, of rigid molecules in supercooled decalin, 50 Hz-100 kHz 2—35776
DNA, radiationless transition for a proton from H-bond 2—39015
electronic relaxation processes in large molecules, specification of proper basis set 2—3017
excited systems 2—8520
formaldehyde, radiationless transition probability, non-empirical study 2—8513
Franck-Condon factor for a Morse oscillator when z is small, contribution to theory of radiationless transitions 2—28259
gas, U.S. absorpt. meas. of rot. relax. 2—28254
2-halomethyl-1,3-dioxans, double ultrasonic relaxation, ring inversion and internal rotation 2—24530
intersystem crossing relative rates, determination from pulsed excitation microwave double resonance 2—8567
intersystems crossing, communicating states model for isolated molecules 2—8505
intramolecular, derivation of master equation using projector operator techniques in Liouville space 2—33933
intramolecular nonradiative transitions, non Condon scheme 2—28241
isolated large molecule, radiationless decay, role of frequency changes on optical selection 2—21566
isolated large molecule, sequence congestion effects in optical selection studies of electronic relaxation 2—31762
luminescence, stochastic model solved for different rates of vibrational and electronic relaxation 2—31742
metalloporphyrins, probabilities of intercombination transitions 2—35347
methyl isocyanide, isomerization, failure of RRKM theory 2—3109
naphthalene, nonradiative decay, excitation energy and deuteration dependence 2—28390
naphthalene vapour, single vibronic level lifetimes 2—8736
nitrobenzene, structure relaxation during internal rotation of the nitro group 2—38997
orientational investigation using hydrodynamic theory of angular velocity autocorrelation function 2—21722
1,4-paradioxane in soln., rot. relax., nucl. spin-lattice relax. obs. 2—9172
perylene, possible reorientation of molecule in solid state, n.m.r. investigation 2—10567
phthalimide gaseous derivatives, radiationless transitions, activation energy and excited state lifetimes 2—28395
polyatomic, anharmonicities in nonradiative transition theory 2—8504
polyatomic molecules, Franck- Condon factors and method of steepest descent 2—8507
polyatomic molecules, Franck-Condon factors for radiationless transitions 2—8506
polyatomics, relative nonradiative decay rates of initially selected vibronic levels 2—21558
polymethyl acrylate, Brillouin spectra obs. 2—26202
porphyrins, probabilities of intercombination transitions 2—35347
radiationless decay and interstate energy equilibrium, its own heat bath 2—38865
radiationless transition probability, multi- phonon transition, Franck-Condon factor 2—24415
radiationless transition probability, non-empirical study 2—8513
radiationless transitions, chem. reactions, theoret. framework 2—35200
radiationless transitions, electronic relax. processes 2—35196
radiationless transitions, influence of final-state spectrum studied by method based on Laplace transform 2—38868
radiationless transitions, molecule as own heat bath 2—38863
radiationless transitions, temperature effect 2—24413
rhodamine 6G, H-bonding effect on orientational relaxation in solutions, investigation using psec light pulses 2—3394
rotational, model for mechanism of relaxation 2—15423
spherical gas molecules, rotational relaxation 2—18379
triphenylene, possible reorientation of molecule in solid state, n.m.r. investigation 2—10567
weak interaction model to describe rotational relaxation of a system 2—38870
$AsH_3(D_3)$, liq., from pulsed n.m.r. relax. obs. 2—35792
Br_2, rel. to nonequilibrium effects in atomic recombination reactions in Ar 2—37027
$CN(B^2\Sigma^+)$, formed by interaction of metastable Ar with CNBr, collision induced rotational relaxation 2—35243
CO_2-N_2-M mixture, vibr. energy transfer consts. 2—31780
CO, vibrational relaxation, shock tube study using pressure meas. 2—28273
CO_2, 2.7μ and 4.3μ bands, atmospheric 2—7300
CO_2, collisions with N_2 and inert gases, rate equations for vibrational relaxation, applic. to spectrophone data 2—8857
CO_2, i.r. vibrational relaxation times, using spectrophone 2—18415
CO_2, laser, cross relaxation 2—23584
CO_2, shock-heated, vibrational relaxation of 10^00 and 02^00 states 2—8600
CO_2, shock-heated, vibrational relaxation of 10^00 and 02^00 states 2—8602
CO_2, vibrational, statistical model 2—5915
CO_2 discharge, of upper laser level 2—35233
CO_2+N_2, reacting u.s. stream, mechanism of chemical and vibrational relaxation, numerical study 2—40804
$CO_2(xyo)+CO_2 \rightarrow CO_2(001)+CO_2$ shock tube meas. of vibrational relaxation, reaction rate obtained 2—35235
CS, vibrational relaxation 2—5917
D_2, vibrational relaxation after collisions with He 2—35381

Molecules continued
relaxation continued
H complexes, H_2 phthalocyanines, relaxation mechanisms from excited singlet states, spin-orbit coupling effects 2—35279
H_2, Ar, system, rotational relaxation time, Monte Carlo trajectory calc. 2—3040
H_2, lifetime of $(1s3p)^3\Pi_u$ level 2—18428
H_2, rotational relaxation times meas. in cryogenic shock tube, 140-450K 2—24464
H_2 isotopes, collision cross sections governing relaxation of angular momentum polarizations 2—39026
HBr, mixtures, vibration-to-vibration energy transfer 2—8625
HBr, vibrational relaxation in H halides 2—8624
HCl, relaxation rate from $v''=3$ vibr. state excited by dye laser radiation 2—24454
HF, room temperature rates of vibrational relaxation by HF, Ar, N_2, D_2, H_2, CO_2 determ. from laser- induced fluorescence 2—21615
methane, vibrational relaxation times meas. with spectrophone, use of NH_3 on C_2H_6 as calibration gas studied 2—12257
Mg complexes, Mg phthalocyanines, relaxation mechanisms from excited singlet states, spin-orbit coupling effects 2—35279
N_2-water vapour mixture, vibrational relaxation times 2—15318
N_2, vibrational relaxation rates, by H_2O, shock tube meas. 2—28311
N_2 discharge, Raman spectral obs. 2—38930
NH_3, cross relaxation in rotational inversion doublets 2—38923
NH_3, vibrational and rotational relaxation data from u.s. absorption meas. 2—31811
NO, collision induced vibration- translation relaxation, mechanisms for resonance production 2—35382
N_2O pure, rate of relaxation determ. from collision meas. with CO_2 2—18542
O_2 and mixtures with H_2, He_3, He_4, vibrational relaxation times determ. from sound absorption measurements 2—38932
Pd complexes, Pd phthalocyanines, relaxation mechanisms from excited singlet states, spin-orbit coupling effects 2—35279
Rh complexes, Rh phthalocyanines, relaxation mechanisms from excited singlet states, spin-orbit coupling effects 2—35279
SO_2/O_2 mixtures, meas. of sound absorption due to vibrational relaxation, existence of vib.-vib. coupling 2—15338
SO_2, $^3B_1$ state, nonradiative lifetimes 2—8704
SO_2, single vibronic level lifetimes of first excited singlet state 2—8703

rotation
absorbed molecules in mordenite 2—22082
acetonitrile, $2\nu_8$ state, effects of accidentally strong resonance in rot. spectrum, mol. consts. level separation 2—12203
acetonitrile, doubling excited degenerate vibr. state, rot. spectrum, anharmonicity const., transition study 2—12202
acetophenone anion radicals, restricted internal rotation influence on e.s.r. spectra 2—828
N-acetyl-phenylhydroxylamine and its methyl ether, n.m.r. study of hindered internal rotation 2—38955
acetylene, in compressed gaseous mixture, i.r. rotational correlation functions of bending vibr. 2—15315
acetylene, rotation-vibration coupling constants from spectra in 5μm region 2—12200
acetylene and d_1 and d_2 deuterated species, rotational structure of vibrational bands 2—21653
acrolein, magnetic rotation and absorption spectra cis and trans isomer transitions 2—3069
alkyl radicals, e.s.r. study of hindered internal rotation 2—18480
alkylalkoxynitroxide radicals, e.s.r. study of decay processes and rotation 2—8728
amine, in soln., molecular dynamics, n.m.r. obs. 2—6256
2-aminoacetophenone, free energy barrier to rotation of amino group around N-aryl bond 2—12206
ammonium salts, spin symmetry sites, p.m.r. obs. 2—40776
angular velocity autocorrelation function, hydrodynamic theory 2—21722
aromatic molecules, in nematic liq. cryst. relat. between orientation and principal polarizabilities 2—15352
asymmetric rotors, Stark effect, dipole moment determ., new approach 2—8547
band contour method, validity for determ. consts. from unresolved bands 2—15267
benzaldehyde, conjugated system, pot. function for rotation about CC single bonds, CNDO/2 calc., inaccuracy of method 2—3099
benzaldehyde anion radicals, restricted internal rotation influence on e.s.r. spectra 2—828
benzene, effect on radiative decay and intersystem crossing to triplet state 2—24510
benzene, meas. of rotational diffusion tensor by Raman scattering 2—9135
benzonitrile, lowest-lying singlet $\pi^*\leftarrow\pi$ transition, rotational analyses, dipole moment changes 2—35343
benzoyl fluoride, rotational assignment of microwave spectrum from 26.5 to 40.0 GHz 2—15357
benzoyl fluoride microwave spectrum, rotational and vibrational assignments to ground and excited torsional states 2—15354
benzyl, symmetry of first excited state determ. by rotational contour analysis of vibronic bands of emission spectra 2—15355
bicyclo[2.1.1]hexan-2-one, constants for various states of low frequency vibr. mode 2—8744
biphenyl, conjugated system, pot. function for rotation about CC single bonds, CNDO/2 calc., inaccuracy of method 2—3099
bis(pyridine)halogen(I) cations, barrier to internal rotation, CNDO/2 calculation 2—38966
5,5'-bisisoxazole in liquid crystals, CNDO calc. of potential energy for the internal rotation of two rings 2—18493
borazole, Raman spectra 2—17731
2-bromo-1-butene, i.r. spectra and rotational isomerism 2—24519
bromobenzene quadrupole hyperfine structure in rotational spectrum analysed 2—12216
2-bromobutane, rotational isomerism from i.r. spectra in crystalline and glassy states 2—40685
1,3-butadiene, ab initio SCF and CI calculations of barrier to internal rotation 2—38971
1,3-butadiene, conjugated system, pot. function for rotation about CC single bonds, CNDO/2 calc., inaccuracy of method 2—3099
1,3-butadiene, internal rotation, study via ab initio calcs. 2—28357
t butyl chloride, comparison of electron diffraction and microwave spectroscopic structures 2—15359
butyric acid, u.s. absorption at 20 to 90°C 2—18819

Molecules continued
rotation continued
carbamyl fluoride, centrifugal distortion constants from microwave spectrum 2—35314
carbon tetrafluoride, Raman spectra 2—17731
carbonyl fluoride, calc. of inertia defects, vibrational-rotational interaction constants and force constants 2—8749
centrifugal distortion analysis, numerical stability 2—755
centrifugal distortion constants, derivation of Jacobian elements 2—12092
centrifugal distortion constants, relationship with force field, XYZ type molecules 2—35198
centrifugal distortion effects, expression using S-vector formalism for vibr.-rot molecule 2—8561
1-chlor-3-fluor-propyne, numerical stability of centrifugal distortion analysis 2—755
2-chloro-1-butene, i.r. spectra and rotational isomerism 2—24519
1-chloro-2-bromoethane, energy differences between rotational isomers from i.r. band intensity calc. 2—21677
chlorobenzene, far i.r. absorption interpreted by correlation function for rotational velocities 2—39368
chlorobenzene, quadrupole hyperfine structure in rotational spectrum analysed 2—12216
2-chlorobutane, rotational isomerism from i.r. spectra in crystalline and glassy states 2—40685
chlorofluorobenzene, transition moments, band contour anal., changes in rot. const. on excitation 2—12213
chloroform, far i.r. absorption interpreted by correlation function for rotational velocities 2—39368
2-chloropropenes, deuterium substituted, rotational consts. and moment of inertia 2—31844
collision-induced rotational transitions, Born approximation treatment 2—18380
collisional rotational excitation, generalized phase shift treatment, classical limit 2—6008
conjugated systems, failure of CNDO/2 method to predict barriers and conformations 2—3099
coupling between states formed in He^+-He collisions, effect on differential elastic and inelastic cross sections 2—733
crystal, reorientation calc. from interatomic pot. anharmonicity 2—9842
cumulenes, rotating barrier end groups 2—837
cyclohexane, solid, rot. transitions, obs. and theory 2—15977
cyclopentane, CNDO calculation of pseudorotational potential energy 2—8546
cyclopentanone, far i.r. spectra and hindered pseudorotation 2—35322
cyclopropane, solid, rot. transitions, obs. and theory 2—15977
cyclopropyl carbinyl chloride, microwave spectrum and rotational isomerism 2—15367
cyclopropyl carbinyl fluoride, microwave spectrum and rotational isomerism 2—15367
cyclopropyl methyl ether, microwave spectrum, determination of methyl barrier to internal rotation 2—12230
cyclopropyl methyl ketone, microwave spectrum, barrier to internal rotation, dipole moment, conformation 2—21673
diatomic, from collisional dissociation of four-atomic molecules, initial rotational distributions predicted by statistical model 2—866
diatomic, rare gas perturbed, vibr.-rot. line broadening 2—8575
diatomic mol., rot. and vibr. consts. determ. from spectrum with unresolved rot. struct. 2—24434
diatomic molecules, determ. of J_{max}, approx. relation 2—8530
diatomic molecules, rotational structure of $^4\Sigma$ states, general theory 2—5895
1,2-dibromoethane, energy differences between rotational isomers from i.r. band intensity calc. 2—21677
dichlorodurene, solid, molecular reorientation studied by meas. of nuclear magnetic relaxation times 2—20167
1,2-dichloroethane, energy differences between rotational isomers from i.r. band intensity calc. 2—21677
1,2-dichloroethane, equil. const. and pot. barrier for rot. isomers 2—21676
1,2-dichloroethane, proton spin-lattice relaxation in carbon tetrachloride solutions 2—18857
dicyclohexane, proton spin-lattice relax. and C-C bond pot. barrier 2—8760
diethyl amine, rotational isomerism rel. to vibrational spectra 2—3082
difluoro diazirine, centrifugal distortion constants 2—3081
difluorobenzene, transition moments, band contour anal., changes in rot. const. on excitation 2—12213
2,2'-difluorobiphenyl conjugated system, pot. function for rotation about CC single bonds, CNDO/2 calc., inaccuracy of method 2—3099
2,5-dihydropyrrole, rotation constants from microwave spectrum, centrifugal distortion corrections 2—18496
dimethyl benzamide, hindered rotation, applic. of multi-site exchange theory 2—22853
N,N-dimethyl carbamyl fluoride, hindered rotation, n.m.r. study 2—22852
dimethyl trifluoroacetamide, hindered rotation, applic. of multi-site exchange theory 2—22853
N,N-dimethylacetamide, hindered internal, activation parameters, solvent effects, n.m.r. obs. 2—12255
dimethylacetamide, hindered rotation, applic. of multi-site exchange theory 2—22853
dimethylallene, microwave spectrum, barrier to internal rot., rot. consts. dipole moment, r_0-type structural data 2—18499
N,N-dimethylformamide, hindered internal, activation parameters, solvent effects, n.m.r. obs. 2—12255
dimethylketene, rotational Zeeman effect in microwave spectrum, determ. of molecular g-tensor 2—38978
unsym-dimethylselenourea and similar compounds, hindered rotation barrier 2—24527
dimethylsulphoxide, numerical stability of centrifugal distortion analysis 2—755
1,3-dioxolane, microwave spectra, pseudorotation 2—8761
diphenyl ethers, highly substituted, energy barriers to rotation about Ar-O bond determ. from n.m.r. spectra 2—38975
dipolar molecules constrained by electric field, rotatory diffusion 2—21564
dipoles, microwave radiation, resonance interaction calculation 2—24419
distortion and rotation consts. of parallel fundamental bands perturbed by Coriolis resonance 2—31753
electron impact excitation, frame transformation theory applic. 2—12069
electron-ion recombination coeff. during triple collisions in molecular gas 2—21873
electronic spectra, determ. of vibr. and rot. consts. 2—18386

Molecules continued
rotation continued
epichlorohydrin, microwave spectrum and rotational isomerism 2—15367
epifluorohydrin, microwave spectrum and rotational isomerism 2—15367
ethane, internal rotation barrier, determination by SCF-Xα scattered wave method 2—35326
ethane, internal rotation barrier, rel. to energy partitioning 2—3086
ethane, solid, rot. transitions, obs. and theory 2—15977
ethane, theory of internal rotation barriers 2—24532
ethanol, barriers to internal rotation 2—28373
ethyl alcohol, influence of H-bond cold neutron transmission obs. 2—15349
ethyl fluoride, theory of internal rotation barriers 2—24532
trans ethyl methyl ether-type molecules, skeletal torsional frequencies 2—31852
ethyl nitrate, microwave spectrum, rotational constants of trans and gauche rotamers 2—12241
ethyl thiocyanate, rotational constants 2—35327
ethylene glycol, study of rotational isomers with i.r. absorption band spectra 2—38980
ethylgermanes, barriers to internal rotation 2—28373
ethylsilanes, barriers to internal rotation 2—28373
ethynylbenzene, lowest-lying singlet $\pi^*\leftarrow\pi$ transition, rotational analyses, dipole moment changes 2—35343
excitation by resonant electron molecule collision, determ. branch structure in rotational transition 2—18382
ferroelectric crysts., hindered, n.m.r. obs. 2—37000
five-membered rings, CNDO calculation of pseudorotational potential energy 2—8546
five-membered rings, far i.r. spectra, effect of finite central barrier on pseudorotation 2—15343
fluorobenzene, far i.r. absorption interpreted by correlation function for rotational velocities 2—39368
fluoroform, fluoroform-d, rotational hyperfine spectrum 2—12244
formaldehyde, rot. transition by electron collision 2—18437
formaldehyde-d_2, Coriolis perturbed absorpt. bands 2—8776
formamide, high resolution rotational spectra 2—3093
formic acid, rot. constants and structure using isotopic substitutions 2—18509
formic acid, rotational spectrum of vibrational ground state 8 to 300 GHz 2—18508
fulminic acid, assignment of vibr. satellites obs. in rot. transition, vibr.-rot. interaction const. microwave and millimeter wave spectra 2—12268
fulminic acid, rotational spectrum 40-300 GHz, transitions of vibrationally excited states 2—21686
furan, [2,5-D_2], Zeeman effect in ground vibrational state 2—38984
gas, U.S. absorpt. meas. of rot. relax. 2—28254
glycol alcohol, influence of H-bond, cold neutron transmission obs. 2—15349
glyoxal, $^{13}C_2$ substituted, visible electronic band 2—8781
glyoxal, conjugated system, pot. function for rotation about CC single bonds, CNDO/2 calc., inaccuracy of method 2—3099
3-1 halogeno-2-halogenomethyl- propene, vibrational spectra, rotational isomers 2—18524
2-halomethyl-1,3-dioxans, double ultrasonic relaxation, ring inversion and internal rotation 2—24530
heavy diatomic, consts. determ. from spectra with unresolved rot. struct. 2—18399
hexafluorobenzene, Raman spectra 2—17731
hexafluoropropene, C=C bond twisting, investigation using microwave spectrum 2—15380
hexamethylethane cryst., n.m.r. obs. 2—13556
hydrogen-bonded ferroelectric cryst., dipolar relax. study of l.f. motion 2—10259
inertia tensor and centrifugal stretching constants, calculation of derivatives 2—28249
internal rotation, motion description using whirling type internal coordinate 2—15266
2-iodubutane, rotational isomerism from i.r. spectra in crystalline and glassy states 2—40685
i.r. emission by nonisothermic gaseous layers 2—3329
isopropylalcohol in liquid state, i.r. study 2—15593
isorhodamine, i.r. absorp., spectra obs. 2—39005
$K_2MFe(NO_2)_6$, (M=Ca, Sr, Ba, Pb), hindered rot. of NO_2^- group from Mossbauer obs. 2—36836
lead dicalcium propionate, p.m.r. obs. of hindered CH_3-rotation 2—10574
light diatomic, centrifugal distortion in spin-orbit coupling of triplet states 2—38883
linear molecular gas, susceptibility echos, short optical pulse 2—5908
linear polyatomic in vibrationally degenerate levels of electronic $^2\Sigma$ and $^3\Sigma$ states, rotational energies calc. 2—8526
liquid, intra- and intermol. contrib. 2—9173
liquid, rot. motion of axially symmetric mol. 2—15562
liquid, sub-mm. spectral obs. 2—15563
liquids, hindered molecular rotation, correlation time 2—25034
liquids, rotational correlation times determ. from Raman bandshapes 2—25089
long chain alcohols, hindered rotation rel. to Kirkwood correlation factor and dielec. properties 2—39388
magneto optical activity associated with symmetry-forbidden transition 2—18381
metal, hindered, n.m.r. obs. 2—37000
methacrylonitrile, barrier to internal rotation of CH_3 gp, rotational consts. 2—8799
methane, ν_3 band analysis 2—12258
methane, deuterated, calculation of i.r. spectra of ν_3 and ν_4 modes in Kr and Xe matrices 2—40668
methane, influence of centrifugal distortion of molecule on spin lattice relaxation in gas 2—35316
methane, meas. and analysis of ν_3 band 2—38991
methane, rot. analysis of ν_4 band 2—31862
methane, solid, proton spin-lattice relax. obs. 2—10279
methanols, isotopic, analysis of torsion-rotation spectrum, determ. molecular constants 2—8798
methoxydifluorophosphine, rotational constants from microwave spectrum 2—15387
2-methoxyethanol, rotational constant determination from microwave spectrum 2—12262
methyl alcohol, influence of H-bond, cold neutron transmission obs. 2—15349

Molecules continued
rotation continued
methyl azidoformate, methyl azidoformate-d_3, microwave spectrum at 26.5 to 40.0 GHz, ground state rotational constants 2—15388
methyl chloride and fluoride, rot. collisional number determ. from thermal transpiration meas. 2—18767
methyl group, in crystalline methyl derivatives of naphthalene, proton spin relaxation investigation 2—22844
methyl groups in methyl naphthalene crystals, description of proton spin relaxation data 2—40786
methyl iodide, ground state geometry determ. from rotational constants of this and deuterated molecules 2—12221
methyl isocyanide, rot. spectrum for ν_8=1 and ν_8=2 excited vibr. states 2—24544
methyl malonic acid cryst., γ-irrad., methyl group tunnelling rot. freq. 2—22848
methyl naphthalene, cryst., rot., barriers of CH_3 groups 2—10573
methyl torsional modes in molecular solids 2—12265
methylamine-d, inversion coordinate and barrier height for asymmetric amino group NHD determ. 2—12259
methyldifluorophosphine, rotational constant determination from microwave spectrum 2—15386
methylene fluoride high-resolution Zeeman measurements 2—35339
methylene halides, distortion constants 2—3108
methylhydrazine, cis and trans barrier heights 2—38990
5-methylrhodamine, far i.r. spectra rotatory oscill. effects 2—39006
methylsilane, barrier to internal rotation and its derivatives w.r.t. vibrational coordinates 2—12264
molecular cryst., ^{35}Cl quadrupole relax., CCl_3-reorientation 2—10276
molecular cryst., internal mobility, n.m.r. obs. 2—10538
molecular crysts., hindered, n.m.r. obs. 2—37000
molecule, and isotopic species, submillimeter wave spectra, rotational transition assignment 2—12146
monofluoroacetic acid, rotational transitions 2—38996
monofluoroacetylene, rotational structure of ν, and 2ν, i.r. bands, centrifugal distortion const. 2—5983
monomethyldiazirine, u.v. obs. spectrum, rotational fine structure of 0-0 band at 3424 Å 2—12267
monomethylphosphine, ab initio LCAO-MO-SCF calculations, effect of rotational barrier on electronic structure 2—18515
monosubsituted benzenes, coupling between rotational and translational motions, pressure dependence 2—39392
near symmetric rotor, determ. reduced Hamiltonian in context of perturbation theory 2—21565
nitrobenzene, structure relaxation during internal rotation of the nitro group 2—38997
nitrorhodamine, far i.r. spectra, rotatory oscill. effects 2—39006
non-interacting spherical, rotational correlation function, inelastic neutron scattering 2—14117
nonpolar, purely rot. spectra from vib. ground states 2—21570
orientational broadening of Raman line shapes, in liquids, analysis 2—8514
3-oxetanone, rotational constants from microwave spectrum, rel. to ring-bending potential function 2—15389
oxyhaemoglobin, nitroxide radical spin labelled, effect of slow rotational motion on p.m.r. 2—25106
1,4-paradioxane in soln., rot. relax., nucl. spin-lattice relax. obs. 2—9172
pentahalogenotoluenes, i.r. study of barriers to internal rotation form vibr. band width meas. 2—8806
1-penten-3-yne, microwave spectrum, electric dipole moment, rotational constants 2—12270
1-pentyne, rotational isomerism from microwave spectrum 2—8805
permutations group, connection, overlap group study 2—31765
peroxylamine disulphonate radical in liquid and frozen media, anisotropic rotational reorientation, e.s.r. study 2—16644
phenyl isocyanide, lowest-lying singlet $\pi^*\leftarrow\pi$ transition, rotational analyses, dipole moment changes 2—35343
pivalonitrile oxide, assignment of vibr. satellites obs. in rot. transition, vibr.-rot. interaction const. microwave and millimeter wave speectra 2—12268
pivalonitrile solns., reorientation models 2—9154
Placzek-Teller coefficients for intensity of Raman rotation-vibration line of symmetric top derived for $-\Delta J$ 2—12071
plastic crystal, nitroxide radical doped cyclohexane, e.p.r., ENDOR 2—26292
polar liquids, restrictions to rot. 2—9182
polyatomic molecules, calc. of centrifugal stretching constants 2—35199
polyatomic vibration-rotation interactions, choice of rotating axes 2—15264
polyatomics, forbidden rotational spectra, intensity acquirement by centrifugal distortion mech. 2—18383
polyisobutylene, dil. soln., statistical radii of gyration, excluded volume effects 2—25033
propenes, chlorinated, rotational isomerism, steric effects, n.m.r. obs. 2—12227
pyrazole, microwave spectrum, hyperfine structure, ^{14}N coupling consts., rotational constants 2—18526
2- pyrone, microwave spectra assignment and rotational consts. determ. 2—12231
Raman spectroscopy, high-resolution rotation-vibrational, with laser excitation 2—24417
relaxation mechanism, model based on probability of collision induced transfer 2—15423
reorientational motions about different axes, liquids, Raman scattering study 2—9135
rotational energy transfer, investigation using collisional relaxation of microwave absorption spectra 2—12297
rotational line strengths calc. for $^3\Sigma^\pm$—$^3\Sigma^\pm$ electric dipole transitions with intermediate coupling 2—3015
rotational spectra, systematic interpretation based on Stark effect 2—38871
s-triazine, analysis of J-structure of band in 3100 Å system 2—12288
selection rules of molecules have one, two and three CH_3 tops, rotation-internal-rotation considered 2—8511
semiclassical vibr.-rot. transition probabilities, collision induced for rotational state averaged potentials 2—8574
in solid, n.m.r., model formulae 2—40794
spherical gas molecules, rotational relaxation 2—18379
spherical top molecules contribution of Coriolis coupling to rotational energy of degenerate vibronic states 2—21571

Molecules continued
rotation continued
spherical tops, gas phase Raman spectra, rotational profiles of vibrational bands 2—28250
spherical-top molecules, collision-induced far i.r. rotation-translation spectrum, quantum theory 2—5896
Stark effect rotational level splitting, double resonance expt. 2—38879
strontium dicalcium propionate, p.m.r. obs. of hindered CH_3- rotation 2—10574
succinonitrile, plastic cryst. state, light scatt. obs. 2—26203
succinonitrile, plastic phase, light scattering obs. 2—16589
symmetric top molecules, determ. of axial rotation const. from vibr. rot. spectra 2—8534
symmetric-top molecules, $(D_k)_0$ values obtained from perpendicular fundamental rotation vibration bands 2—12076
temperature meas. using electron probe 2—31751
2,3,4,5-tetrachloro-trans-hexatriene, obs. of conformational isomerism by rotation about single C-C bond 2—8825
tetrachloroparaxylene, solid, molecular reorientation studied by meas. of nuclear magnetic relaxation times 2—20167
1,2-disubstituted tetrafluoroethanes, n.m.r. spectra, rot. isomerism, coupling consts. 2—12283
tetrahedral molecules, pure rotational transitions from ground vibronic states 2—12081
tetrahedral molecules, vibration-rotation interaction, extension of Hecht's theory 2—12080
tetramethylammonium halide crystals, molec. motion investigations using proton spin-lattice relaxation time meas. 2—29849
s-tetrazine, vapour, rotational fine structure of 5500 Å band, moment of inertia 2—8824
1,3,4- thiadiazole, microwave spectrum, centrifugal distortion 2—18530
thioformaldehyde, i.r. spectrum observed in C-H stretching region, rotational analyses of bands 2—12284
toluene, toluene-d_5, rotational isomerism of methyl groups rel. to interpretation of i.r. spectra 2—15398
transient free radicals, e.s.r. study of hindered internal rotation 2—18480
triatomic molecules, rotation bending energy levels calc. 2—31754
2,3,4-tricarbahexaborane(7), rotational constants from microwave spectrum at 8 to 38 GHz 2—15399
1,2,3-trichlorotrimethylbenzene, solid, molecular reorientation studied by meas. of nuclear magnetic relaxation times 2—20167
trifluoroacetonitrile, force field, Coriolis consts., mean amplitudes, centrifugal distortion consts. 2—8828
trifluoromethylhypofluorite, ground state rotational constants from microwave spectrum at 8 to 40 GHz 2—8826
triglycine sulphates, ENDOR on radicals of glycine II and III 2—10583
tripropargyl amine, i.r. and Raman spectra, vibr. assignments, rotational isomerism 2—18533
tunnelling methyl groups in crysts., proton relax. and h.f.s. 2—26291
vibration rotation bands, meas. in high resolution spectra in 8 to 20 μm region 2—12079
vibration rotation Hamiltonian, 4th order of bent XYX type molecule 2—15275
vibration-rotation and vibration spin interactions in multiplet states 2—8562
vibration-rotation energies, remarks on two-step procedure for calculation 2—8536
vibration-rotation interaction const. and mean square amplitude of vibration, transformation under rotation of coordinate axes 2—752
vibration-rotation interaction theory, choice of molecule-fixed axes examined 2—8535
vibrational rotational spectra, line intensity eqns. taking into account accidental Coriolis resonance 2—746
vibrational-rotational interactions, contact transformations, closed form 2—8537
vinyl germane, rotational constant determination from microwave spectrum 2—15406
vinyl trifluorosilane, rotational constants from microwave spectrum 2—15405
l- vinyl-o-carborane, plastic crystalline behaviour, n.m.r. obs. 2—33358
vinyltrifluorosilane microwave spectrum, dipole moment from Stark shifts of rotational transitions 2—21706
weak interaction model to describe rotational relaxation of a system 2—38870
o-xylene, exchange contribs. to internal rotation barrier 2—859
xylenes, liq., rot. correl. times, spin- lattice relax. obs. 2—9185
XYZ type, bent, constants determ. by Green's function analysis 2—24432
AgBi, consts. determ. from spectra with unresolved rot. struct. 2—18399
AgBi, rot. and vibr. consts. determ. from spectrum with unresolved rot. struct. 2—24434
AgCl, AgBr, AgI, microwave rotation spectrum 2—28270
AlCl, AlBr, AlI, millimetre wave rotational spectra, determination of rotation-vibration interaction 2—21588
AsF, emission spectrum, 7320-7400 Å, obs. of new $^1\Pi$ state, rotational constants 2—18403
$AsH_3(D_3)$, liq., from pulsed n.m.r. relax. obs. 2—35792
BF, rotational constants for ground vibrational state, determination from microwave spectrum 2—15285
BH_3NH_3, SCF calc. of barrier to internal rotation, w.r.t. vibrational coords. 2—12106
BaO, $A^1\Sigma$—$X^1\Sigma$ system, Franck-Condon factors, r-centroids and oscillator strength 2—15286
BeCl, rotational analysis of $A^2\Pi$-$X^2\Sigma^+$ band system, determ. of principle molecular constants 2—28271
Br_2, extreme red absorption spectrum $A^3\pi(1_u)\leftarrow X^1\Sigma_g^+$, vibrational and rotational assignment 2—38889
Br_2, rel. to nonequilibrium effects in atomic recombination reactions in Ar 2—37027
BrF_5, rotational consts., centrifugal distortion consts. 2—5912
$^{79}Br^{81}Br$, $A^3\pi(1)$—$X^1\Sigma^+$ system, Franck-Condon factors and r-centroids 2—38890
CCO, rotational analysis of $A^3\Pi_i$-$X^3\Sigma$- band system 2—8603
CN vibration-rotation interaction effects on Franck-Condon factors for $B^2\Sigma^+$-$X^2\Sigma^+$ transition by asymptotic expansion method 2—28282
C_2N_2, rotational structure in $^1\Sigma_u\leftarrow{}^1\Sigma_g^+$ transition at 2200A, vibrational anal. 2—21592
C_2N_2, structure of 2500 Å system analysed by band contour method 2—12109
$CN(B^2\Sigma^+)$, formed by interaction of metastable Ar with CNBr, collision induced rotational relaxation 2—35243

Molecules continued
rotation continued
CNBr, vibr.-rot. spectrum, Fermi reson. 2—15288
CO-gas mixtures, rot. correl. functions 2—18404
CO, analysis of new absorption bands 2—28277
CO, nonthermal rotational population of $A^1\Pi$ state, obs. in electron impact dissociative excitation of CO_2 2—5920
CO, profiles of i.r. absorption bands in liquids, rotational motion 2—775
CO,absolute oscillator strengths of transitions of vibration-rotation spectra 2—12113
CO rotational dependence of lifetime of $a^3\Pi$ metastable state, exptl. and theoretical decay plots compared 2—15295
CO study of vibrational and rotational levels of metastable $a^3\Pi$ state 2—8598
CO^+ collisions with Ar, conditions for rotational excitment considered 2—12304
CO_2, 10.4 μm band, N_2 broadened collisional width, variation with rot. quantum no. 2—38899
CO_2, effect of Fermi resonance on temp. dependence on rotational vibrational transitions 2—776
CO_2, i.r. luminescence spectra, rot. consts. of vibr. levels 2—12112
CO_2, near i.r. absorption spectra, vibr. energy levels and rot. const. determ. 2—12111
CO_2 dimers in 'locked' configuration, i.r. spectrum studied 2—8605
COF_2, liquid, degrees of freedom assignment from significant structure theory 2—28785
CO_2+H_2 mixtures, vibrational-rotational energy exchange, 344-742 K 2—3140
$C^{34}S$, structure in $^1\Pi$-$^1\Sigma^+$ transition 2—8590
Ca_2 vapour, $^1\Sigma$-$^1\Sigma$ transition, rotational structure of spectrum 2—8601
Cl_2, computer simulation of rotational structure of Raman bands 2—21594
Co(III) complex, NN′-dialkyldithiocarbamates, anomalous p.m.r. spectra, hindered rotation about C-N bond 2—21595
$Co(NH_3)_6I_2$, internal rot. of NH_3 groups, i.r. spectra obs. 2—10375
CrF_4, spectra rel. to bond nature 2—8606
CsBr, quadrupole hyperfine structure 2—38901
CsH, potential energy curves, applicability of Morse potential, rot. consts., r-centroids, Franck Condon factors 2—18457
CuBr, analysis of D-X band system 2—8608
$^{63}Cu_2$, rot. analysis of A-X system bands 2—783
D_2, vacuum u.v. emission spectrum, vibr. and rot. consts. of ground and excited states 2—18419
D_2 liquid, n.m.r., longitudinal relaxation 2—6249
DBr, hyperfine structure and Stark effect of J=O→rotational transition 2—8648
DCl, far i.r. rotational spectra, line shape parameters, interferometric meas. 2—15302
D_2O, high resolution photoelectron spectrum meas. rotational structure partially resolved 2—12151
DOF, microwave spectra, rotational constants and structural parameters 2—8626
D_2S, millimeter and submillimeter wave rotational spectrum, rotational constants and centrifugal distortion effects 2—21600
DSSD, millimeter wave rotational spectrum, anomalous K doubling by centrifugal distortion 2—24461
DSSD millimetre wave rotational spectrum, Q branches 2—24451
F_3SiSiH_3, rotational constants from microwave spectrum at 8 to 38 GHz 2—15300
FeO vibration-rotation radiative band intensity meas. 2—35247
$FeSiF_6.6H_2O$ crystal, investigation of pressure dependence of internal reorientation of SiF_6^{--} group 2—37006
GeH_4 and GeD_4, solid, n.m.r. obs. 2—10265
GeH_3I, four isotopic species, microwave spectra 2—18421
GeH_3r, six isotopic species, microwave spectra 2—18421
GeTe, rotational transition J=2→3, hyperfine structure meas. 2—8615
H_2, 1-10eV electron scattering, differential and integrated cross sections for vibrational-rotational excitation 2—12136
H_2, 21.22 eV photoelectron spectrum, rotation structure 2—18431
H_2, ang. distribution of photoelectrons, rot. ionization range 2—35255
H_2, Ar, system, rotational relaxation time, Monte Carlo trajectory calc. 2—3040
H_2, frequency shifts of rotational lines, collision induced 2—8651
H_2, rotational excitation by low energy positron scattering 2—5932
H_2, rotational excitation by collisions with Li^+, classical study 2—8859
H_2, rotational Raman lines, anisotropy in Dicke narrowing rel. to measure of nonsphericity of intermolecular forces 2—38903
H_2, rotational relaxation times meas. in cryogenic shock tube, 140-450K 2—24464
H_2, simultaneous vibrational-rotational excitation by low energy electrons 2—12140
H_2, zero field level crossing in excited rotational levels, radiative lifetime meas. 2—35250
H_2 and D_2, D $^1\Pi_u$—X $^1\Sigma_g^+$ system, predissociation, effect of rotation on lifetime 2—21608
H_2 rotational line narrowing in inert gas mixtures due to pressure 2—8649
H_2^+, vibration rotation eigenenergies of $2p\pi_u$ and $3d\sigma_g$ states 2—18434
HBr-DBr collisions, vibration to rotation energy transfer 2—31881
HCN, rovibrational energy levels, calc. using rigidly bending rigid-rotor Hamiltonian 2—15306
HCO radical, e.p.r. microwave absorpt. spectra, rotational transition 2—8720
HCl, far i.r. rotational spectra, line shape parameters, interferometric meas. 2—15302
HCl, perturbed by Ar, vibr.-rot. spectrum, line widths and shifts 2—8618
HCl, profiles of i.r. absorption bands in liquids, rotational motion 2—775
HCl, rot. collisional number determ. from thermal transpiration meas. 2—18767
HCl, rotational Raman lines, meas. of pressure broadening 2—3039
HD-Li^+, interaction potential, rot. excitation cross sections region 2—3148
HDS, microwave rotational spectrum, centrifugal distortion analysis and rotational constants 2—8631
HF, in H_2-F_2 chemical laser, time resolved spectroscopy, vib.-rot. transitions 2—5364
HF, vibration-rotation interaction term, contribution to potential 2—791
HF, vibration rotation bands, evaluation of r-centroids and higher terms of elec. dipole moment 2—21609
HF, vibrational-rotational stimulated emission from flash photolysis of N_2F_4+RH systems 2—270
HF dimer spectrum, rotational structure 2—8639

Molecules continued
rotation continued
HF_2, i.r. spectrum, null gap region, rotational structure 2—12133
$(HF)_2$, splitting of rotational energy levels due to H tunnelling motion obs. in r.f. and mcirowave spectra 2—21614
HN_3, rotation-vibration spectrum in near i.r. and visible 2—15303
H_2O, high resolution photoelectron spectrum meas. rotational structure partially resolved 2—12151
H_2O, rot. transition by electron collision 2—18437
H_2O, rotational analysis of the emission spectrum of an oxy-hydrogen flame 2—12152
H_2O, rovibrational energy levels, calc. using rigidly bending rigid-rotor Hamiltonian 2—15306
$H_2{}^{16}O$, submillimeter microwave spectrum, rotational transition meas. 2—18400
$H_2{}^{18}O$, i.r. spectra of vapour, rotational structure of ν_2 band, vals. of energy levels of 1st excited state 2—12132
H_2O_2, barrier to internal rotation, investigation using H-F approx. 2—8641
HOF, microwave spectra, rotational constants and structural parameters 2—8626
H_2S, and isotopic species, submillimeter wave spectra, rotational transition assignment 2—12146
H_2S, microwave spectrum and centrifugal distortion effects 2—38904
H_2S, structure of $^2A_1$ band in photoelectron spectrum correlated with transitions to vibrational-rotational levels 2—24474
HSSD, millimetre wave rotational spectrum, $^rQ_0$ branch 2—38909
HSSH millimetre wave rotational spectrum, P,Q and R branches 2—28294
HSiBr, Hamiltonian for large amplitude bending and K-type rotation, effect on higher rot. energy levels 2—12131
H_2+H, rotationally inelastic scattering, quantum mechanical treatment 2—39025
He_2, vibrational and rotational constants from potential curve for $2s\sigma{}^3\Sigma_u^+$ state 2—31802
He_2 calc. of potential of lowest excited singlet state, determ. rotational and vibrational consts., dissociation energy 2—21612
$^{127}I_2$, excited by 632.8 nm He/Ne laser, lifetime meas. 2—12155
KH, potential energy curves, applicability of Morse potential, rot. consts., r-centroids, Franck Condon factors 2—18457
$K_2MFe(NO_2)_6$, (M=Ca, Sr, Ba, Pb) quadrupole splitting, hindered rot. of NO_2^- group, rel. to π-bonding 2—36836
$^{39}K\,^{19}F$, rel to Stark effect, molec. beam resonance meas. 2—21646
LaO, band spectrum, rotational constants 2—12159
LaO, rotational analysis of O-O band of $C^2\Pi \rightarrow X^2\Sigma^+$ transition 2—3049
LiOH(D), molecular beam electric resonance spectra 2—8663
LuO, β-system analysis 2—799
β-N_2, barrier to rotation, determ. from heat capacity data 2—4067
N_2, population distribution det. by electron beam fluorescence to probe hypersonic shock wave 2—39265
N_2, rotational excitation by collisions with Na^+ and Li^+ 2—894
N_2, rotational inelasticity of collisions with Ar, comparison of generalized phase shift and classical trajectory calc. 2—8862
N_2, vacuum u.v. absorption spectrum, o-X system, rot. consts. of vibr. levels 2—15325
NF_2 free radical, microwave rotational spectrum 2—12179
NF_2 radical, microwave Zeeman spectra, electron spin-rotation interaction 2—8678
NH_3-Ar(N_2) systems, i.r. spectra, temp. and conc. effects 2—10391
NH_3, collision induced rotational transition, microwave double resonance study 2—12177
NH_3, cross relaxation in rotational inversion doublets in far infra-red 2—38923
NH_3, hydrogen spin-rotation determ. from application of Racah algebra to point groups 2—12065
NH_3, liquid, mol. motions from neutron scatt. obs. 2—35726
NH_3, Stark effect on vibr.-rot. transition, h.f.s. 2—24476
NH_3, vibr.-rot. transition, absortion saturation 2—5934
NH_3, vibration-rotation spectrum, rotational analysis of 6450 A band 2—28312
NH_3, vibration-rotation spectrum 2—21631
NH_3, vibrational and rotational relaxation data from u.s. absorption meas. 2—31811
NH_4^+ ion, rotational freedom in NH_4ClO_4 2—40675
NH_4BF_4, polycryst., NH_4^+ reorientation, n.m.r. obs. 2—10559
NH_4ClO_4, polycryst., NH_4^+ reorientation, n.m.r. obs. 2—10559
$(NH_4)_2SiF_6$, NH_4^+ reorientation, p.m.r. study 2—37011
$(NH_4)_2SnBr_6(Cl_6)$, NH_4^+ reorientation, p.m.r. study 2—37011
N_2O-gas mixtures, rot. correl. functions 2—18404
NO, γ, ε and δ system, fluorescence spectrum polarization of rotational lines, vibr. band intensities 2—8675
NO, monochromatic excitation of rotational levels in vibrational levels of $A^2\Sigma^+$ state 2—12175
NO, rotational lines in far i.r. spectrum 2—38931
NO, spectra, $^2\pi_{3/2}$-$^2\pi_{1/2}$ transition 2—8687
NO radicals, viscous medium, rotational correlation time calc. from e.s.r. calcs. 2—8686
NO_2 impurity in KCl, hindered rotation at 2°K, e.s.r. obs. 2—15322
N_2O, 00°1 qnd 10°0 levels, rotational consts. 2—31041
N_2O, in compressed gaseous mixture, i.r. rotational correlation functions of bending vibr. 2—15315
N_2O_3, gaseous, i.r. spectrum, −120°C, assignment of vibration rotation bands 2—12178
N_xO_y, distortion const., Green's function analysis 2—18443
NS, vibr. and rot. analysis of $^2\Pi_r$-$X^2\Pi_r$ band system 2—18447
NSF, triplet state at 5360 Å, Zeeman study and preliminary rotational analysis 2—3051
$N(SO_3)_2^{2-}$, e.s.r. study 2—22826
NSe, electronic spectrum, 2800-3200Å, vibr. and rot. analysis of 12 red degraded bands 2—18456
Na_2, collision-induced rotational transitions, asymmetries, Born approximation treatment 2—18380
NaH, potential energy curves, applicability of Morse potential, rot. consts., r-centroids, Franck Condon factors 2—18457
$NaH_3(SeO_3)_2$, e.p.r., external stress effects on unstable orientation 2—10514
$Na_2(b^1\pi_u)$ state, collision induced energy transfer 2—3151
$Ni(NH_3)_6I_2$, internal rot. of NH_3 groups, i.r. spectra obs. 2—10375
O_2, cross sections for rotational excitation by slow positron impact calc. in distorted wave approx. 2—24466

Molecules continued
rotation continued
O_2, Raman spectrum, meas. of intensities of spin satellites of S(3) and S(5) lines 2—8695
O_2 vibrational-rotational lines, pressure broadening, strong-collision model 2—18460
O_3, high resolution meas. of $\nu_1 + \nu_2 + \nu_3$ absorption band in 3.59 μm region, rigid rotator analysis 2—8696
O_3, recalc. of new rot. constants from millimetre wave spectrum 2—8691
OCS in solution, determ. of band width and profile of ν_3 mode, separation of rotational and vibrational effects 2—38934
OH, temperature in l.v. luminescent discharge and d.c. arc in Ar containing water vapour 2—24936
OH ground state vibr.-rot. bands, obs. in chemiluminescent O_3-olefin gas phase reactions 2—22868
OH levels, spin orbit coupling constant and Λ-doublet constants obtained 2—12188
PBr_3 rotational diffusion tensors obtained from viscosity and halogen NMR relaxation time data 2—15281
PCl_3, rotational diffusion tensors obtained from viscosity and halogen NMR relaxation time data 2—15281
PF_3, liquid, degrees of freedom assignment from significant structure theory 2—28785
PN, rotation spectrum, new constants 2—38936
PO, emission spectrum attributed to $^2\Sigma$-$^2\Sigma$ transitions, rotational structure of bands 2—18465
$POCl_3$, rotational diffusion tensors obtained from viscosity and halogen NMR relaxation time data 2—15281
^{31}P compounds, spin rotation interaction constants derived from chemical shift data, and from NMR relaxation and viscosity data 2—15281
RbH, potential energy curves, applicability of Morse potential, rot. consts., r-centroids, Franck Condon factors 2—18457
Rh(III) complex, NN′-dialkyldithiocarbamates, anomalous p.m.r. spectra, hindered rotation about C-N bond 2—21595
SF_5Cl, quadrupole hyperfine effects in microwave spectrum 2—38939
SO_2, rot. anal. of O-O band, excited state consts., excited state r_0 structure 2—15333
SO_2, rotational analysis of $^3\beta_1 \leftarrow {}^1A_1$ bands 2—12191
$SO_2{}^{35}Cl^{35}Cl$, A, B and C consts. determ. 2—24486
SbF, rotational analysis of C_2 system 2—824
SeN, analysis of electronic spectra 2—35288
SiD, rotational analysis of 3250Å bands 2—5952
SiH, rotational analysis of 3250Å bands 2—5952
SiO, orange system, $^2\Pi$ to $^2\Sigma$ transition, rotational analysis of band (0,0) 2—31827
SiO, vibl. and rotl. analysis of $^3\Pi_r$-$a^3\Pi_r$ transition 2—35289
SnCl, rotational analysis of visible band systems 2—31831
SnH_3Br, centrifugal distortion constant from microwave spectrum 2—15337
SnH_3I, centrifugal distortion constant from microwave spectrum 2—15337
SnI_4, liq., sub-mm. spectral obs. 2—15563
Te_2 gas, $A0_u^+$, $B0_u^+$—$X0_g^+$ systems, rotational analysis 2—35292
TiO, $^1\Delta$ to $a^1\Delta$ transition 2—31832
$^{205}Tl^{19}F$, rel. to Stark effect, molec. beam resonance meas. 2—21646

vibration
bis-(bromomethyl)-mercury, vibrational assignment of i.r. and Raman spectra rel. to structure determination 2—21669
bis-(chloromethyl)-mercury, vibrational assignment of i.r. and Raman spectra rel. to structure determination 2—21669
bis-(iodomethyl)-mercury, vibrational assignment of i.r. and Raman spectra rel. to structure determination 2—21669
1,2-dichloroethane, vibrational i.r. and Raman spectra studied 2—8759
acenaphthene-d_{10}, i.r. and Raman spectra, fundamental assignment 2—28341
F- and Cl-substitutedacetaldehyde, force consts. determ. from normal coordinate analysis 2—8724
acetic acid, hydrogen bonded cyclic dimer, near i.r. spectra, vibrational analysis 2—21652
acetic anhydride, normal coordinate analysis 2—28338
acetone, valence force field, Raman spectra obs. 2—18479
acetonitrile, correl. functions determ. from i.r. spectra and r.f. data 2—31752
acetonitrile, doubling excited degenerate vibr. state, rot. spectrum, anharmonicity const., transition study 2—12202
acetonitrile N-oxide, force field, mean square amplitudes of vibration, shrinkage effect, Coriolis coupling coeffs. 2—38958
acetonitrile-d_3 and water, H bonded complexes, obs. i.r. transitions involving vibrations 2—8754
acetonitrile-water complexes, OH group stretching vibrations, i.r. spectrum 2—25092
acetophenone in variety of matrices, phosphorescence, pseudo-Jahn-Teller distortion 2—29966
N-acetyl-2-thiohydantoine, i.r. spectra 2—5957
acetylene, assignment of bands at 2.1 to 2.2μ 2—21654
acetylene, in compressed gaseous mixture, i.r. rotational correlation functions of bending vibr. 2—15315
acetylene, rotation-vibration coupling constants from spectra in 5μm region 2—12200
acetylene and d_1 and d_2 deuterated species, rotational structure of vibrational bands 2—21653
acetylene in soln., Fermi reson. 2—18478
adamantane, excited electrnic states, sharp vibronic structure 2—12205
adsorbed molecules in mordenite 2—22082
aldehyde-BF_3 complexes, i.r. spectra 2—24501
aldehydes, fund. and harmonic vibrs., Fermi reson. 2—24499
aldehydes, saturated aliphatic, modulation of $n \rightarrow \pi^*$ absorption band 2—21689
2- alkyl-iminobenzoxazolones, azomethine group spectra, influence of alkyl radical, on characteristic frequency 2—835
amino phosphines and arsines, i.r. and Raman spectra, vibrational spectra 2—12207
aminophenetoles, i.r. absorption spectra, vibrational analysis 2—3113
o-, m- and p-aminophenol, thermodynamic functions calc. from vibrational spectroscopy data 2—15350
p-aminophenol derivatives, hydrohalides, solid state ion exchange with matrix, i.r. spectra 2—10594
3-aminopropyl dibutylboron with bases, vibrational spectra, hydrogen bonds and fermi resonance 2—31837
anharmonic oscillators, classical theory of vibrational relaxation 2—28251
anharmonic oscillators, vibr. relaxation 2—12075

Molecules continued
  vibration continued
    aniline, hydrogen bonded complex, i.r. spectrum determ. free force constant of stretching vibration of H bond 2—12277
    aziridines, i.r. and Raman spectra, vibrational analysis 2—12219
    trans-azobenzene and isotopic derivatives, vibrational spectra 2—35304
    azulene vapour, single vibronic level lifetimes 2—8736
    benzaldehyde, vibronic intensification of $^1U(n\pi^*)\leftarrow S_0$ absorption spectra 2—12211
    benzaldehyde, vibronic interactions in $^3U(n\pi^*)\rightarrow S_0$ phosphorescence 2—12212
    benzaldehyde, zero field splitting, phosphorescence rate consts. and vibronic activity in lowest triplet state by p.m.d.r. 2—28353
    benzene, 'Kekule' vibration assignment, CNDO/2 study 2—21666
    benzene, lifetimes of individual vibronic states 2—8734
    benzene, methyl substituted derivatives, vibrational spectra 2—35309
    benzene, temperature dependence of widths and integrated intensities of polarized Raman lines 2—28351
    benzene cryst., far-i.r. absorpt. external vibr. lines broadening at melting pt. 2—20053
    benzene derivatives, substituted, role of symmetry of a vibration in temperature dependence of i.r. band intensity 2—24509
    benzene vapour, single vibronic level lifetimes 2—8736
    benzene-chromium-tricarbonyl, Raman spectra, frequency assignment 2—28354
    benzonitrile and d_5 analogue, i.r. spectra, theoretical study of vibrational assignments 2—35312
    benzonitrile in polycryst. matrices, vibr. anal. of luminescence in terms of excited state geometries 2—31839
    benzophenone, crystalline and in soln., vibrational spectra, effect of u.v. illumination 2—26363
    p- benzoquinone and derivatives phosphoresc. spectra 2—5959
    benzoxazole, vibr. spectra 2—28348
    benzoyl fluoride, vibrational assignment of microwave spectrum from 26.5 to 40.0 GHz 2—15357
    benzoyl fluoride microwave spectrum, rotational and vibrational assignments to ground and excited torsional states 2—15354
    benzyl, symmetry of first excited state determ. by rotational contour analysis of vibronic bands of emission spectra 2—15355
    benzyl compounds, i.r. and Raman spectra, vibr. assignments, asymmetric structure 2—8742
    benzyl derivatives, para substit., i.r. and Raman spectra, vibr. assignment, asymmetric structure 2—8743
    benzyltin derivatives, for i.r. and Raman spectra, vibrational assignment 2—21665
    1,1′-biaziridine, conformation from vibrational spectra data 2—38968
    bicyanine dimer, electron- vibrational spectra, strong coupling case 2—12214
    bicyclo [3.1.0] hexane substituted with O or CH_2, ring-puckering vibration investigated 2—12215
    bicyclo-[2,2,2]-octane, excited electronic states, sharp vibronic structure 2—12205
    bicyclo[2.1.1]hexan-2-one, low frequency vibration 2—8744
    biphenyl, vibrational spectra and dihedral angles 2—38967
    biphenyl based series, phenanthrene-carbazole-dibenzothiopene-dibenzofuran, polarization of electronic transitions 2—28355
    biphenyl cryst., far-i.r. absorpt., external vibr. lines broaden at melting pt. 2—20053
    bis(acetic acid)-BF_3 complex, vibrational spectra 2—24546
    bis(methanol)-BF_3 complex, vibrational spectra 2—24546
    bis(pyridine)halogen(I) cations, force constants, CNDO/2 calculation 2—38966
    borine carbonyl, high resolution spectrum of ν_5 perpendicular band 2—8582
    2-bromo-1-butene, i.r. spectra and vibrational assignments 2—24519
    bromocyclobutane, ring-puckering vibration, far i.r. study 2—15366
    bromoform, approx. force field 2—3076
    bromoform-D_1, approx. force field 2—3076
    bromoiodoacetylene, vibrational assignment rel. to force constant determination for dihaloacetylenes 2—38970
    n-butane free jets relaxation study from mass spectra temp. dependence 2—24518
    butoxides of Na and K, vibrational spectra study of structure 2—5964
    t-butyl cyanide, i.r. and Raman spectra, vibrational assignment 2—5963
    carbon tetrachloride, matrix isolated in Ar, Raman spectra, intramolecular force field obs. 2—35315
    carbon tetrachloride polarity in vibrational state obs., due to vibrationally induced dipole moment 2—12218
    carbon tetrafluoride polarity in vibrational state obs., due to vibrationally induced dipole moment 2—12218
    carbonyl fluoride, calc. of inertia defects, vibrational-rotational interaction constants and force constants 2—8749
    carbonyl group containing molecules, i.r. spectra, stretching and torsional modes obs. 2—8750
    carboxylic acid dimers, saturated, simulation of abnormal i.r. spectra due to H-band proton stretching vibrations 2—15360
    carboxylic acid hydracides, N-H vibration intensities calc. 2—8748
    chloro maleic anhydride, vibrational spectra, assignment and force constant calc. 2—12223
    2-chloro-1-butene, i.r. spectra and vibrational assignments 2—24519
    chloro-2-butyne, force constants determ. from normal coordinate calculations 2—21668
    p- chloroaniline, lowest singlet state in pure and mixed crystals 2—40684
    chlorobenzene, temperature depencence of widths and integrated intensities of polarized Raman lines 2—28351
    chlorobenzene-D_5, near u.v. absorption spectrum vibrational analysis 2—3075
    chlorocyclobutane, ring-puckering vibration, far i.r. study 2—15366
    chloroform, approx. force field 2—3076
    chloroform, temperature dependence of widths and integrated intensities of polarized Raman lines 2—28351
    chloroform and proton acceptor complexes, H bonded obs. i.r. transitions involving vibrations 2—8754
    chloroform-D_1, approx. force field 2—3076
    3-chloropropyne, force constants determ. from normal coordinate calculations 2—21668
    cholesterol esters liquid crystals, vibrational spectra in crystal, cholesteric and isotropic phases 2—28869
    N,N-cinnamamides, para- and meta-substituted, substituent effect on i.r. carbonyl stretching vibrations and hydroxyl frequency shifts 2—38977

Molecules continued
  vibration continued
    collision-induced transition probabilities calculated from three-dimensional model 2—35379
    collisions, vibrational-translational energy transfer, semiclassical transition probabilities (S-matrix) 2—8853
    complex, far i.r. spectra, band shape anharmonicity 2—8533
    complex, use of mathematical logic to determ. structure from i.r. vibration spectra 2—28246
    conjugated, vibrational spectra of excited electronic states calc., evaluation of vibronic transition intensities 2—12083
    copper(II) acetates, fundamental modes 2—35320
    copper formate tetrahydrate and deutero derivative, spectral obs. 2—10341
    Coriolis coupling coeff., expression using S-vector formalism for vibr.-rot molecule 2—8561
    Coriolis coupling constants, for molecules XY^2 and X^3, symmetry C_{2v}, parametric study 2—38872
    correlation functions determ. from i.r. spectra and r.f. data 2—31752
    crotonaldehyde, vibrational analysis of $S_1(n,\pi^*)$ 2—35336
    cyanocyclobutane, ring-puckering vibration, far i.r. study 2—15366
    cyclic alkanes, excited electronic states, sharp vibronic structure 2—12205
    cyclobutane, i.r. and Raman spectra, vibrational assignments for D_{2d} symmetry 2—28365
    cyclobutane carboxylate ion, aqueous, determ. of fundamental characteristic vibrations 2—5969
    cyclobutane-carboxylic acid vibrational spectra 2—24523
    cyclohexane, excited electronic states, sharp vibronic structure 2—12205
    cyclohexane cryst., far-i.r. absorpt., external vibr. lines broadening at melting pt. 2—20053
    cyclopentadiene, vibrational analysis of photoelectron spectra 2—3097
    cyclopentadienyl thallium, Coriolis consts. from microwave spectrum 2—15268
    cyclopentane, halogen derivatives, vibrational spectra and analysis 2—35323
    cyclopentanone, bending and twisting co-ordinates and far i.r. spectra 2—35322
    cyclopentanone, gas phase and in solution, i.r. spectra study of Fermi resonance in $\nu_{c=o}$ region 2—24524
    cyclopentanone in hexane soln., conc. depend. of absorpt. band 2—25096
    cyclopropane, analysis of $\nu_5+\nu_{10}$ band, l-type resonance effects 2—8757
    cyclopropane, i.r. absorpt. and Raman scatt., vibr. transitions 2—33278
    cyclopropane, study of l-type resonance effects in $\nu_5+\nu_{10}$ band 2—21674
    cyclopropyl carbinyl chloride, vibrational satellites in microwave spectra 2—15367
    cyclopropyl carbinyl fluoride, vibrational satellites in microwave spectra 2—15367
    deexcitation of highly excited polyatomic molecules, collisional energy transfer 2—24573
    diarylthallium (III) derivatives, aromatic ring vibrations 2—21679
    diatomic, application of adiabatic-nuclei theory to vibrational excitation by electron impact 2—18384
    diatomic, from collisional dissociation of four-atomic molecules, initial vibrational population distributions predicted by statistical model 2—866
    diatomic, rare gas perturbed, vibr.-rot. line broadening 2—8575
    diatomic, vibrational distribution change on transition between electron states in collisions with electrons 2—3138
    diatomic, vibrational excitation by atom, quantum mechanical impulse approx. 2—3134
    diatomic gas, effect of spacing of vibrational energy levels on dissociation 2—30038
    diatomic mol., rot. and vibr. consts. determ. from spectrum with unresolved rot. struct. 2—24434
    diatomic molecule, electeon impact vibrational excitation, parametric resonance effect 2—751
    diatomic molecules, vibrational transition probabilities theoretical determ. 2—24418
    diatomic vibrational potential functions, determination from integration of Poisson equation 2—8527
    diatomics, absorption and excitation cross sections averaged over vibr. structure 2—8563
    diatomics, bond stretching force constants 2—31760
    dibenzyl mercury, far i.r. and Raman spectra, vibrational assignment 2—21665
    dibromo maleic anhydride, vibrational spectra, assignment and force field derivation 2—12222
    dichloro maleic anhydride, vibrational spectra, assignment and force field derivation 2—12222
    1,1-dichloroethylene, crystal structure study using vibrational spectra 2—6460
    2,3dichloronaphthoquinone, i.r. and Raman spectra, vibr. assignment of obs. bands 2—31849
    3,5-dichlorophenol, temp. dependence of Cl.n.q.r. frequencies, torsional frequencies 2—28419
    dichlorophenols, and deuterated analogues, vibrational analysis of i.r. spectra 2—3080
    dichlorophenols, electronic absorption spectra in vapour phase, vibrational assignment 2—35319
    dichlorophenols, i.r. and Raman spectra, fundamental assignment 2—8764
    diethyl amine, vibrational spectra and rotational isomerism 2—3082
    difluorobenzenes, isomeric, electronic emission spectra, vibrational assignment 2—35330
    2,2-difluoropropane, vibrational assignment of Raman and i.r. spectra 2—3083
    digermane, bond flexibility force constants 2—31853
    4,4′dihalogenobiphenyls, vibrational spectra and dihedral angles 2—38967
    2,3-dihydrofuran, microwave spectra for vibrational states of ring bending mode, Stark effect meas. 2—12237
    diiodomethyl radical, matrix i.r. spectrum, vibrational assignment 2—8800
    dimethyl oxalate, valence field force constants obtained by normal coordinate analysis 2—8793
    dimethyl pyridine, vibratory spectra, interpretation and freq. calc. 2—38998
    dimethyl sulphide, vibrational spectra 2—38994
    dimethyl sulphone, vibrational spectra 2—38994
    dimethyl sulphoxide, vibrational spectra 2—38994
    N,N-dimethylacetamide, valence force field and A′ symmetry vibrations 2—841
    dimethylamine in solution 22-190°C, i.r. study of association and NH stretching vibration modes 2—28368

Molecules continued
vibration continued
dimethylaminodichloroarsine, i.r. and Raman spectra and assignment 2—24528
dimethylaminodichlorophosphine, vibrational assignment 2—28369
N,N-dimethylbenzamides, para- and meta-substituted, substituent effect on i.r. carbonyl stretching vibrations and hydroxyl frequency shifts 2—38977
dimethylcadmium, structure study, normal coordinate analysis 2—21680
1,2-and 1,3- dimethylenecyclobutane, vibrational spectra measured, determ. symmetry 2—12238
dimethylmercury, structure study, normal coordinate analysis 2—21680
dimethylmercury, valence force field determ. from vibrational freqs. of d_0 and d_6 species 2—5972
dimethylphenols, i.r. and Raman spectra, fundamental assignment 2—8764
dimethylselenium difluoride and deuterium analogue, vibrational spectrum 2—12239
N,N-dimethylthiopropionamide, normal coordinate analysis 2—5973
dimethylzinc, structure study, normal coordinate analysis 2—21680
dioxane cryst., far-i.r. absorpt., external vibr. lines broadening at melting pt. 2—20053
1,3-dioxolane, microwave spectra, pseudorotation 2—8761
diphenyl monocrystal, low temps., far i.r. absorption spectra 2—16504
1,4-diselenan, vibrational spectra, assignments and force constant calc. 2—12236
disilane, bond flexibility force constants 2—31853
1,4-dithian, Raman spectra, force constant calc. and vibrational assignments 2—12285
DNA, Fermi resonance of i.r. vibrations in NH_2 groups 2—28423
Dunham coeff., expressions allowing for breakdown of Born-Oppenheimer approx. 2—12078
electron impact excitation, frame transformation theory applic. 2—12069
electron-ion recombination coeff. during triple collisions in molecular gas 2—21873
electronic spectra, determ. of vibr. and rot. consts. 2—18386
electronic transitions, vibronically-induced symmetry-forbidden, theoretical formalism 2—12084
endoergic collision processes, vibrational excitation 2—21712
energy flow from terminal bond into molecule, coupled oscillator model 2—8501
energy transfer, coupled oscillator model considered 2—8525
epichlorohydrin, vibrational satellites in microwave spectra 2—15367
epifluorohydrin, vibrational satellites in microwave spectra 2—15367
ethane, bond flexibility force constants 2—31853
ethane, ionization, ab initio MO calcs. of force constants and vibrational frequencies 2—21683
ethane-d_3, i.r. spectrum, vibr. frequencies, force consts., Coriolis zetas 2—12243
ethanol, torsional modes 2—28373
ethers, divinyl, spectral evidence of vibrational coupling of double bonds 2—8770
trans ethyl methyl ether-type molecules, skeletal torsional frequencies 2—31852
ethylene, ethylene-d_4, vibrational structure in photoelectron spectra rel. to vibrational spectrum of $K[PtCl_3(C_2H_4)].H_2O$ 2—3087
ethylene, force field and constants, determ. from SCF MO wavefunctions 2—8767
ethylene and ethylene-d_4, N→V transition calc. and vibrational structure of V band reproduced 2—12083
ethylenediamine salts, vibrational spectra 2—3089
ethylgermanes, torsional modes 2—28373
ethylsilanes, torsional modes 2—28373
excitation on collision, dependence of transition probability on impact parameter 2—6006
nfatty acid amides, i.r. spectra, vibrational analysis 2—15374
fluoroform, approx. force field 2—3076
fluoroform-D_1, approx. force field 2—3076
2-fluoropropene, i.r. and Raman spectra, normal coordinate analysis 2—8773
force const. solutions with singular jacobian, external nature 2—15261
force constant, calc. using expressions for derivatives of eigenvalues of hamiltonian 2—37616
force constant calc., extended L-matrix approx., empirical constraint on ratio L_{12}/L_{21} for n=2 eigenvalue problems 2—21572
force constant matrices, diagonal and non-diagonal, iterative method of calculation 2—12077
force constants of diatomic molecules by CNDO method 2—771
force field of XYZ type molecules, relationship with centrifugal distortion consts. 2—35198
formaldehyde, spin-vibronic perturbations in $^1A_2$ state 2—15377
formaldoxime, vibrational analysis of i.r. spectra, normal vibrations and torsional barrier 2—3094
formic acetic anhydride, i.r. and Raman spectra, normal coord. anal. 2—8778
formic acid, hydrogen bonded cyclic dimer, near i.r. spectra, vibrational analysis 2—21652
Franck-Condon factor, quantum-mechanical approach 2—15263
fulminic acid, absorption spectrum from 200 to 450 cm^{-1} assignment 2—12248
fulminic acid, assignment of vibr. satellites obs. in rot. transition, vibr.-rot. interaction const. microwave and millimeter wave spectra 2—12268
fulminic acid, rotational spectrum 40-300 GHz, transitions of vibrationally excited states 2—21686
fulvene, vapour and mixed crystal spectra, lowest energy electronic transition 2—8780
furan, vibrational analysis of photoelectron spectra 2—3097
furan, [2,5-D_2], rotational Zeeman effect in ground vibrational state 2—38984
gas, induced transparency due to electronic vibrational transitions 2—743
gas, optical breakdown threshold 2—39217
α-glycine, valence force field and conformation of $H_3NCH_2COO^-$ ion 2—28379
glycine isotopic species in Ar and N_2 matrices, i.r. spectra, band assignment 2—31857
glyoxal, glyoxal-d, vibrational assignment of i.r. spectra 2—3098
glyoxylic acid, i.r. and Raman spectra and assignment, 4000 to 300 cm^{-1} 2—24539
gromo maleic anhydride, vibrational spectra, assignment and force constant calc. 2—12223

Molecules continued
vibration continued
ground state vibrational temp. determ. by reversal of spectral lines in i.r. region of CO_2 laser 2—15256
group IVa dihalides isolated in solid Ar, N_2 matrices, vibrational Raman spectra depolarization meas. 2—38884
group V and VI hydrides, valence shell orbital structures 2—8576
group V hydrides, partially deuterated and tritiated, harmonic wavenumbers and normal coords. calc. 2—18444
halobenzenes, assignment to nu_{19b} fundamental 2—35333
halogenoethylenes and halogenogermanes, sum rules 2—8782
halogenomethanes, resonance Raman spectra excited by u.v. N_2 pulsed laser 2—28380
halomethyl radicals, anharmonic potential functions for out-of-plane modes 2—21688
Hamiltonian for coupled diatomic molecules 2—8646
harmonic force constants, evaluation from Hartree-Fock-Roothaan wave functions 2—12074
Herzberg-Teller theory, assumption that Duschinsky effect may be neglected examined 2—12082
hexahydro-1,3,5-trichloro and trinitroso s-triazine, analysis of vibrational spectra 2—31859
hexahydro-1,3,5-trinitro s-triazine, monocrystal spectra, 10 to 200 cm^{-1} 2—15379
hexamethyldisiloxane, antisymmetric valence vibrs. of Si-O-Si bridge 2—3101
hexamethyltrisiloxane, antisymmetric valence vibrs. of Si-O-Si bridge 2—3101
hydantoine, Raman spectra 2—5979
hydrates of various salts, stretching frequencies of H_2O molecules 2—20016
hydrocarbons, halogen substit., gas phase Raman intensities, vibrational study 2—12253
2-hydroxycarboxylic acids, OH stretching vibrations 2—28385
hydroxyl group containing molecules, i.r. spectra, stretching and torsional modes obs. 2—8750
inertia tensor and centrifugal stretching constants, calculation of derivatives 2—28249
interaction energies between non-bonded H atoms, perturbation calc. 2—15269
internal coordinate basis for numbering vibrs. 2—35197
inverse vibrational problem, the extended vibrational Jacobian $\partial \Lambda_{ij}/\partial F_{kl}$ 2—12072
iodo(methyl)germanes 2—845
isobutene, vibronic structure of 1790 Å transition 2—12254
isobutene-d_0, -d_6, -d_8, Raman spectra of polycrystalline samples meas. assignments to fundamental modes made 2—13492
isolating frequencies of functional groups 2—15270
ketones, interaction with compounds containing —OH, C=O valence oscillation line shift 2—8787
ketones, saturated aliphatic, modulation of $n\rightarrow\pi^*$ absorption band 2—21689
ketones, substituent constant derived from carbonyl stretching frequencies 2—15382
ketones, torsional vibrations, calc. using Green's function method 2—28387
linear polyatomic in vibrationally degenerate levels of electronic $^2\Sigma$ and $^3\Sigma$ states, rotational energies calc. 2—8526
luminescence, stochastic model solved for different rates of vibrational and electronic relaxation 2—31742
methacrolein, vibrational analysis of $S_1(n,\pi^*)$ 2—35336
methane, assignment of transitions in $\nu_3+\nu_4$ band 2—8790
methane, force constants, near Hartree-Fock calc. 2—21692
methane, harmonic spectra of dense phases 2—36892
methane, i.r. absorption study of ν_4 band, 1225-1400 cm^{-1} 2—21696
methane, meas. and analysis of ν_3 band 2—38991
methane, rel. to Jahn-Teller splitting, high-resolution photoelectron spectra obs. 2—35340
methane, rot. analysis of ν_3 band 2—12258
methane, rot. analysis of ν_4 band 2—31862
methyl(methylthio) mercury, vibrational assignment of i.r. and Raman spectra 2—21693
methyl acetate, valence field force constants obtained by normal coordinate analysis 2—8793
methyl bromide -d_3, i.r. spectrum, analysis of ν_4, P and R structure 2—21695
methyl cyanide, vibrational analysis using empirical force field 2—21691
methyl cyanide mean vibration amplitudes calc. 2—24545
methyl cyanide-d_3, vibrational assignment of near i.r. spectra, derivation of Coriolis coupling const. and anharmonicity coeff. 2—38992
methyl formate, valence field force constants obtained by normal coordinate analysis 2—8793
methyl group, assignment of CH stretching modes 2—831
methyl halides, vibrational analysis using empirical force field 2—21691
methyl isocyanide, rot. spectrum for $\nu_8=1$ and $\nu_8=2$ excited vibr. states 2—24544
methyl silyl acetylene, mean amplitudes and Coriolis coupling constants 2—15385
methyl vinyl ketone, vibrational analysis of $S_1(n,\pi^*)$ 2—35336
methylamine-d, inversion coordinate and barrier height for asymmetric amino group NHD determ. 2—12259
methylene, singlet, vibrational deactivation by collision induced integration crossing 2—12311
methylenecyclopentane, liq. and vap. i.r. and Raman spectra, fundamental frequency assignment 2—12263
methylhydrazine, N-N torsional potential function 2—38990
methylsilane, barrier to internal rotation and its derivatives w.r.t. vibrational coordinates 2—12264
o- and m-methylstyrenes, i.r. spectra, band assignment 2—3107
N-methylthioacetamide, i.r. spectra, normal coordinate anal., functional gp. frequencies 2—31864
monodeuterobenzonitriles, in polycryst. matrices, vibr. anal. of luminescence in terms of excited state geometries 2—31839
monodeuteromethane, Coriolis resonance between ν_3, ν_6 and ν_5 bands 2—31753
monoiodomethyl radical, matrix i.r. spectrum, vibrational assignment 2—8800
MX_6 type ions and molecule, X=CL, Br, force constants evaluated using three models for pot. field 2—35229
naphthalene, vapour, fluorescence lifetimes of vibronic levels 2—3111

Molecules continued
  vibration continued
    naphthalene vapour, single vibronic level lifetimes 2—8736
    neopentane and d_{12} analogue, normal coordinate anal. mean amplitudes of vibration 2—31865
    nitroanesoles, i.r. absorption spectra, vibrational analysis 2—3113
    p-nitroaniline, near i.r. spectra, anharmonic consts. determ. 2—4461
    nitromethane, nitromethane-d_3, matrix-isolated, force constants, calc. of intermolec. potentials 2—24547
    o- and p-nitrophenetoles, vibrational assignment of i.r. spectra 2—31866
    nonlinear triatomic molecules, structural parameters and valence force consts. 2—8538
    nonpolar, purely rot. spectra from vib. ground states 2—21570
    normal modes, drawing by computer 2—8523
    octahedral haloanions of IV B group elements, force constants and mean amplitudes 2—3035
    octamethylcyclotetrasiloxane, antisymmetric valence vibrs. of Si-O-Si bridge 2—3101
    organometallic acetylides, i.r. and Raman spectra, vibrational assignment 2—15345
    3-oxetanone, ring-bending vibration rel. to microwave spectrum 2—15389
    n-paraffins, vibrational modes of Raman bands 2—28392
    2,4,α,α,α-pentachloro toluene, temp. dependence of Cl n.q.r. frequencies, torsional frequencies 2—28419
    pentaerythritol-d_0 and -d_4, crystal spectra, vibrational assignments and force constant 2—18521
    pentahalogenotoluenes, i.r. study of barriers to internal rotation form vibr. band width meas. 2—8806
    perdeuterobenzonitrile, in polycryst. matrices, vibr. anal. of luminescence in terms of excited state geometries 2—31839
    phenacyl chloride, temp. dependence of Cl n.q.r. frequencies, torsional frequencies 2—28419
    phenanthrene in durene crystal system, absorption spectra, vibronic coupling 2—9322
    phenazine, i.r. and Raman spectra, vibrational assignments 2—8809
    phenazine, Raman spectra measured, fundamental frequency assignments mode 2—12273
    phenol-methylpyridinoxide complex, H bond system, obs. of intra and inter-mol. vibrations 2—24548
    phenolate ions, hydrated, isotopic, C-O stretching i.r. band frequency 2—28396
    phenolic methacrylate anhydrides, i.r. bands assignment 2—28334
    phenolic methacrylates, i.r. bands assignment 2—28334
    phenyl compounds, monosubstituted, Gordy's rule applied to X bond 2—8810
    phenylacetylene, i.r. spectra, theoretical study of vibrational assignments 2—35312
    phenylacetylenes, D-substituted, anal. of fluoresc. 2—35345
    phthalaldehyde, vibrational assignment of i.r. spectrum 2—35342
    picolines, spectra, rel. to methyl substitution effects in pyridine 2—35346
    pivalonitrile oxide, assignment of vibr. satellites obs. in rot. transition, vibr.-rot. interaction const. microwave and millimeter wave speectra 2—12268
    pivalonitrile-N-oxide, microwave spectrum, bending mode estimate, symmetric top molecule 2—5989
    Placzek-Teller coefficients for intensity of Raman rotation-vibration line of symmetric top derived for $-\Delta J$ 2—12071
    point charge-point dipole model for vibrating triatomic molecules 2—35213
    polyatomic, force fields, least squares criterion 2—8532
    polyatomic vibration-rotation interactions, choice of rotating axes 2—15264
    polyatomic vibrational potential functions, multiple perturbation expansion 2—21567
    polyethylene, vibrational excitation rel. to photochemical decomp. 2—33389
    polymers, skeletal vibration bands, effect of anharmonicity on half widths 2—31874
    polymers, vibronic interaction theory 2—6000
    polynucleotides, Fermi resonance of i.r. vibrations in NH_2 groups 2—28423
    potential constants and structural parameters, group theoretical evaluation of their numbers 2—21569
    potential energy distribution, alternative calculation 2—28248
    predissociation by continuum of bound state without curve crossing 2—18462
    propane-d_6, vibrational assignment of i.r. and Raman spectra, symmetric valence of vibrational frequencies of methylene and methyl groups 2—39002
    propargyl alcohol and deuterium analogues, vibrational assignment of i.r. and Raman spectra 2—5990
    1,3propidactone, ring puckering potential function 2—21698
    propionic acid, vibrational spectra 2—28399
    propyne, vibrational analysis using empirical force field 2—21691
    propynyl boron difluoride, i.r. spectrum, fundamental assignment, G_{12} symmetry group 2—8813
    purine sodium salt, i.r. spectra, freq. variations due to proton loss 2—10342
    pyramidal inversion barriers for first and second row elements, CNDO/2 calc. 2—24427
    pyrazine photoelectron spectrum, transitions identified by method based on analysis of vibrational fine structure of ionization bands 2—28402
    pyrene, laser excited fluorescence S_2 emissions, intermediate strong coupling and vibr. redistrib. effects 2—15393
    pyrene, vapour, effects of intramol. vibr. redistrib. in S_1 fluorescence 2—3117
    pyridazine-d_0 and pyridazine-d_4, vibrational spectra 2—35349
    pyridine, hydrogen bonded complex, i.r. spectrum determ. force constant of stretching vibration of H bond 2—12277
    pyridine bromine charge transfer complexes in C_6H_6, far i.r. spectra, force consts., dipole moment 2—8816
    pyridine-halogen complexes, far i.r. intensity and normal coordinate studies, force consts., dipole moments 2—8817
    pyrrole, vibrational analysis of photoelectron spectra 2—3097
    pyrylium cation and deuterated analogues, i.r. spectra, vibrational assignment 2—39004
    quinoline, liq. and solid states, intermolecular dynamics, vibr. spectra study 2—35377
    quinoxaline, vapour and mixed crystal spectra, $\pi^*\leftarrow$n transition 2—10400

Molecules continued
  vibration continued
    Raman spectroscopy, high-resolution rotation-vibrational, with laser excitation 2—24417
    rare earth β-diketonates, stretching force constants for metal oxygen bonds, determination from i.r. absorption spectra 2—21620
    redundant forces and compliance constants 2—21568
    rhodanine, vibr. spectra 2—8819
    ruthenocene, mean amplitudes of vibration and perpendicular amplitude correction coeff. 2—28407
    second-order case, compliances and vibration amplitudes, parametric form 2—15265
    selection rules of molecules having one, two and three CH_3 tops, torsional-vibration considered 2—8511
    semiclassical vibr.-rot. transition probabilities, collision induced for rotational state averaged potentials 2—8574
    silacyclobutane, normal co-ordinate analysis, mean amplitudes detn. 2—18527
    spectra, i.r. and Raman, book on the foundations of the subject 2—5899
    spectral characteristics rel. to dipole- dipole interaction, influence of solvents 2—25090
    spectroscopy, its interpretation, undergraduate booklet 2—5898
    spectrum of vibronic manifold, influence on radiationless transitions 2—38868
    spherical top molecules, Coriolis coupling in degenerate vibronic states 2—21571
    spherical tops, gas phase Raman spectra, rotational profiles of vibrational bands 2—28250
    succinonitrile, liquid and plastic phases, Raman spectra, vibrs. assignment 2—33288
    sulfoxide complexes, quasi-octahedral, coordinate bond, vibrational model 2—12280
    symmetric top molecules, matrix elements of powers of P and Q operators for isotropic two dimensional oscillator 2—37619
    symmetric tops, matrix elements of 1st and 2nd order Coriolis interactions 2—15268
    symmetric-top molecules, $(D_k)_0$ values obtained from perpendicular fundamental rotation vibration bands 2—12076
    symmetry group for classification of vibrational modes where ethyl group rotates freely 2—18503
    tetrabenzyl germanium, far i.r. and Raman spectra, vibration assignment 2—21665
    1,2,4,5-tetrachlorobenzene, temp. dependence of Cl n.q.r. frequencies, torsional frequencies 2—28419
    tetracyanoethylene solution in mesitylene, π-π charge transfer complex, obs. of intermolecular vibrations in spectra 2—28426
    tetracyanomethanes, Bastansen-Morino shrinkage effects, determination for unbound atomic distances 2—21702
    tetraethyllead, mol. vibr. analysis of obs. C-Pb-C bending funds 2—24553
    tetrahedral molecules, pure rotational transitions from ground vibronic states 2—12081
    tetrahedral molecules, vibration-rotation interaction, extension of Hecht's theory 2—12080
    tetramethyl phosphorus nitride, i.r. and Raman spectra, vibrational assignment 2—8822
    tetramethylene cyclobutane-d_o and -d_s, vibrational spectra measured, symmetry determ. 2—12282
    s- tetrazine, resonance fluorescence and its quenching 2—39009
    thiazolidindione-2,4, vibr. spectra 2—8819
    thioketones, aliphatic, i.r. and Raman spectra, intensity and position of thiocarbonyl $\nu_{c=s}$ band 2—28414
    thiophene, vibrational analysis of photoelectron spectra 2—3097
    thiourea, inter- and intra-molecular force consts., i.r. and Raman active vibrations 2—29513
    thiourea, temp. dependence of i.r. and Raman spectra, mol. and lattice vibrations phase transition 2—29923
    1,4-thioxan, vibrational spectra, force constant calc. and vibrational assignments 2—12285
    tolane, Raman spectra meas. normal coordinate analysis and vibrational assignment attempted 2—24505
    toluene, liq. and solid states, intermolecular dynamics, vibr. spectra study 2—35377
    toluene, temperature dependence of widths and integrated intensities of polarized Raman lines 2—28351
    trans CH groups, molecules with atoms having lone pair, influence of rotamer forms on stretching vibration 2—21563
    triatomic C_{2v} type, mech. anharmonicity contrib. to i.r. band intensities 2—35228
    triatomic linear molecule, with Renner effect, inelastic electron scatt. 2—5909
    triatomic molecules, rotation bending energy levels calc. 2—31754
    2,3,5-trichloro-p-benzoquinone, vibrational assignment of i.r. spectrum 2—35353
    trifluoroacetic acid, i.r. spectra, vibrational assignment 2—3126
    trifluoroacetic anhydride, i.r. spectra, vibrational assignment 2—3126
    trifluoroacetonitrile, force field, Coriolis consts., mean amplitudes, centrifugal distortion consts. 2—8828
    1htrifluorocyclopropene, i.r. spectra, vibrational assignment 2—12289
    trimethyl acetonitrile, i.r. and Raman spectral, vibrational assignment 2—21704
    trimethyl germanium fluoride, i.r. and Raman spectra, normal coordinate anal. 2—24556
    trimethylamine complexes with I_2, Br_2, IBr and ICl, Raman and i.r. spectra band assignment to vibrations, force constants 2—12294
    trimethylarsenic dibromide and dichloride, i.r. and Raman spectra, vibr. assignments and force field calcs. 2—18536
    2,4,5-trimethylbenzaldehyde temp. dependence of vibr. structure of phosphorescence spectrum 2—15402
    trimethylene oxide, ring puckering vibr., vapour phase Raman spectrum 2—18531
    trimethylene oxide in nematic liquid crystal, vibrational motion determ. from NMR spectrum 2—35354
    triphenylverdasile, corresponding ions and the leucocompound, comparative study of i.r. spectra of radicals 2—39012
    triplet ketones, applicability of electronic-vibrational energy transfer to H abstraction 2—30080
    tripropargyl amine, i.r. and Raman spectra, vibr. assignments, rotational isomerism 2—18533
    1,3,5-triselenan, vibrational spectra, assignments and force constant calc. 2—12236

- **Molecules** continued
  - **vibration** continued
    - 1,3,5-trithian, force constant calc. and vibrational assignment 2–12236
    - uranyl compounds, mechanism for appearance of internal vibrations of the ligands in luminescence spectra 2–24491
    - urea, assignment of i.r. vibrations 2–28418
    - vibration rotation bands, meas. in high resolution spectra in 8 to 20 μm region 2–12079
    - vibration rotation Hamiltonian, 4th order of bent XYX type molecule 2–15275
    - vibration-rotation energies, remarks on two-step procedure for calculation 2–8536
    - vibration-rotation interaction const. and mean square amplitude of vibration, transformation under rotation of coordinate axes 2–752
    - vibration-rotation interaction theory, choice of molecule-fixed axes examined 2–8535
    - vibrational ang. momentum effect, vibr. rot. and vibr. spin interactions 2–8562
    - vibrational rotational spectra, line intensity eqns. taking into account accidental Coriolis resonance 2–746
    - vibrational-electronic circular dichroism spectra, low resolution analysis 2–8528
    - vibrational-rotational interactions, contact transformations, closed form 2–8537
    - vibronic interactions considered in terms of adiabatic approx. 2–15262
    - vinyl bromide, i.r. vibration-rotation spectra, Coriolis interaction 2–8829
    - vinyl chloride, i.r. vibration-rotation spectra, Coriolis interaction 2–8829
    - vinyl fluoride, vacuum u.v. photolysis prods., assignment and force field, bonding 2–8830
    - vinyl iodide, i.r. vibration-rotation spectra, Coriolis interaction 2–8829
    - vinylidene halides, normal and deuterated, generalised mean square vibration amplitudes 2–21705
    - water, intermolecular motions in liquid state, normal coordinate analysis 2–39331
    - water, intramolecular vibrations in liquid state 2–39330
    - water, zero pt. vibr. motion, near Hartree Fock limit, one-electron props., force constants 2–8642
    - weak vibrational excitation during molecular collisions, semiclassical theory 2–39022
    - whirling type internal coordinate definition, internal rotation study 2–15266
    - $X(YZ_3)_4$ molecular model, symmetry coordinates of vibrations 2–31865
    - XY_5Z_2 molecules of D_{5h} symmetry, G, F, and Σ matrices 2–28252
    - XYZ type, bent, constants determ. by Green's function analysis 2–24432
    - zinc uranyl acetate, U–O force constant 2–3128
    - ^{a} BD_3CO, A=10, 11, molecular vibrational constants calculated from standardized set of symmetry coordinates 2–12104
    - $^{a}BH_3CO$, A=10, 11, molecular vibrational constants calculated from standardized set of symmetry coordinates 2–12104
    - Ag olefin complexes, νC=C stretching frequencies rel. to i.r. and Raman spectra 2–15282
    - AgBi, rot. and vibr. consts. determ. from spectrum with unresolved rot. struct. 2–24434
    - $AlBr_4^{2-}$, intramol. force field, force consts., Coriolis coupling consts., vibr. amplitudes and potential energy distrib. 2–31774
    - AlCl, AlBr, AlI, millimetre wave rotational spectra, determination of rotation-vibration interaction 2–21588
    - Ar-Ar intermolecular potential, vibrational energy levels and second virial coefficient 2–15422
    - Ar, interatomic pair potential determ. from scattering and spectroscopic data 2–3027
    - As_4 vapour at elevated temp. vibrational Raman spectra excited by in-cavity laser radiation 2–24438
    - AsH_3, Coriolis resonance between ν_2 and ν_4 bands 2–31753
    - As_4O_6 vapour at elevated temp. vibrational Raman spectra excited by in-cavity laser radiation 2–24438
    - BBr_3, out-of-plane bending force constant 2–38888
    - B_2Br_4, crystalline and fluid, vibrational spectra and molecular symmetry 2–15284
    - BF, microwave spectrum, molecular constant determination for vibrational ground state 2–15285
    - BF_4^-, calculation of valence force field, force constants of F_2 matrix presented 2–12107
    - BH, Franck-Condon factors and r- centroids of A-X band systems 2–3028
    - BH_3NH_3 SCF calc. of barrier to internal rotation, w.r.t. vibrational coords. and force constants 2–12106
    - $BaCl_22(ONH_3)$ i.r. absorption spectra, vibrational analysis 2–15294
    - BaO, $A^1\Sigma-X^1\Sigma$ system, Franck-Condon factors, r-centroids and oscillator strength 2–15286
    - Bi, complex, $Bi(S_2C_2H_4)X$, i.r. spectra, ligand configuration, vibr. assignment 2–8769
    - Br, vibrational structures of $E\rightleftharpoons B$ emission systems 2–21618
    - Br_2, extreme red absorption spectrum $A^3\pi(1_u)\leftarrow X^1\Sigma_g^+$, vibrational and rotational assignment 2–38889
    - Br_2 Raman, reson. effect in absorpt. continuum, degree of depolarization of vibr. bands 2–24440
    - BrCN, Fermi resonance, matrix-isolated i.r. spectral study at 20K 2–8588
    - BrCN, matrix isolation, i.r. spectra, Fermi resonance 2–12122
    - BrF_3, force fields 2–18412
    - $^{79}Br^{81}Br$, $A^3\pi(1)-X^1\Sigma^+$ system, Franck-Condon factors and r-centroids 2–38890
    - $^{79}Br^{81}Br$, Franck-Condon factors and r-centroids for $B^3\Pi(0_u^+)-X^1\Sigma_g^+$ system 2–38891
    - C_3, bending frequency 2–38894
    - C_4, C_5 and C_6, pure and mixed-isotope, Σ_u^+ freqs. and stretching force consts. 2–3031
    - CCO stretching vibrations and Fermi resonance observed in $A^3\Pi_i$-$X^3\Sigma$-band system 2–8603
    - CN vibration-rotation interaction effects on Franck-Condon factors for $B^2\Sigma^+$-$X^2\Sigma^+$ transition by asymptotic expansion method 2–28282
    - C_2N_2, rotational structure in $^1\Sigma_u\leftarrow{}^1\Sigma_g^+$ transition at 2200A, vibrational anal. 2–21592
    - C_2N_2 analysis of structure of 2500 Å system 2–12109
    - C_2N_4, cis and trans symmetry 2–38895
    - CNBr, vibr.-rot. spectrum, Fermi reson. 2–15288
    - CO_2-N_2-He mixtures, vibrational population inversions behind normal shock waves 2–24442
    - CO_2-N_2-He plasma, electrically excited spectrum from 4.2 to 5.5 μm 2–12118
    - CO_2-N_2-M mixture, vibr. energy transfer consts. 2–31780
    - CO-N_2 vibrational exchange, shock tube meas. 2–28311
    - CO_2-N_2 mixture, kinetic cooling, by CO_2 laser radiation absorp., vibrational energy transfer 2–18757
    - CO_2-N_2^* flowing mixtures, vibrational energy exchange, i.r. emission at 2.7 μm 2–21590
    - CO-gas mixtures, rot. correl. functions 2–18404
    - CO, A $^1\Pi$ state, measured lifetimes of first seven vibrational levels 2–3030
    - CO, analysis of new absorption bands 2–28277
    - CO, electrical laser, pumping mechanism, vibrational energy exchange 2–269
    - CO, i.r. emission, vibr. transitions 2–28275
    - CO, lifetimes of two vibronic levels of $B^1\Sigma^+$ state and transition moment of $B^1\Sigma^+-X^1\Sigma^+$ transition 2–35244
    - CO, photoelectron spectra, study of autoionization, vibrational structure 2–8674
    - CO, vibr. excitation rates in $O+CS\rightarrow CO+S$ reaction 2–15289
    - CO, vibrational excitation by collisions with He 2–871
    - CO, vibrational excitation in the spin-orbit relaxation $Hg(6^3P_{1\rightarrow 0})$ 2–15292
    - CO, vibrational excitation by electrons at 10 to 100 eV 2–12171
    - CO, vibrational relaxation, shock tube study using pressure meas. 2–28273
    - CO,absolute oscillator strengths of transitions of vibration-rotation spectra 2–12113
    - CO adsorbed on W, vibr. props. 2–32396
    - CO study of vibrational and rotational levels of metastable $a^3\Pi$ state 2–8598
    - CO^+, enhancement of vibrational level population by photoelectron spectrometry 2–35265
    - CO^+ collisions with Ar, probability of multiquantum vibrational transitions determ. 2–12304
    - CO_2, asymmetrical mode, vibrational temp. obs. 2–24447
    - CO_2, collision broadened line widths, effects of Coriolis interaction on line strengths of 3339 cm^{-1} band 2–18410
    - CO_2, collisions with N_2 and inert gases, rate equations for vibrational relaxation, applic. to spectrophone data 2–8857
    - CO_2, effect of Fermi resonance on temp. dependence on rotational vibrational transitions 2–776
    - CO_2, i.r. vibrational relaxation times, using spectrophone 2–18415
    - CO_2, pure and N_2 perturbed, linewidths of ν_3-ν_1 transition 2–31781
    - CO_2, shock-heated, vibrational relaxation of 10^00 and 02^00 states 2–8602
    - CO_2, shock-heated, vibrational relaxation of 10^00 and 02^00 states 2–8600
    - CO_2, vibr. thermalization, temp. depend. 2–28274
    - CO_2, vibrational deactivation by collisions with HF and DF at 75 and 100C 2–15425
    - CO_2 adsorbed on NaCl film vibrational frequency shifts and splittings 2–5914
    - CO_2 collisions with N_2O, CO, $^{13}CO_2$, $^{15}N_2$, D_2, ^{13}CO determ. temperature dependence of nearly resonant vibrational energy transfer 2–18542
    - CO_2 dimers in 'locked' configuration, i.r. spectrum studied 2–8605
    - CO_2 photodissociation, determ. of approximate vibrational distribs. of Cameron bonds 2–28276
    - CO_2 vibrational states lifetimes, spectrophone measurements interpretation 2–24436
    - CO_3, valence force field constants, ab initio LCGO MO SCF calc. 2–8589
    - C_3O, force constants and stretching frequencies 2–31782
    - C_3O_2, high-resolution photoelectron spectra, vib. analysis 2–35240
    - $CO(CN)_2$, vacuum u.v. absorption spectrum, vibrational assignments 2–3032
    - COF_2, Fermi resonant 1943 cm^{-1} band, temp. dependence of spectral intensity 2–8592
    - $(CO)Fe(PF_3)_4$, C_{3v} and C_{2v} isomers, i.r. and Raman spectra, assignments 2–24446
    - CO_2+H_2 mixtures, vibrational-rotational energy exchange, 344-742 K 2–3140
    - CO_2+N_2, reacting u.s. stream, mechanism of chemical and vibrational relaxation, numerical study 2–40804
    - $CO_2(xyo)+CO_2\rightarrow CO_2(001)+CO_2$ shock tube meas. of vibrational relaxation, reaction rate obtained 2–35235
    - CS, vacuum u.v. photoelectron spectrum, vibrational fine structure studied for information on ionization potentials 2–28285
    - CS, vibrational relaxation 2–5917
    - CSClBr, i.r. and Raman spectra, vibrational analysis 2–38896
    - CSClF, u.v. band spectra, identification of electronic transitions, vibronic assignments 2–12120
    - Ca_2 vapour, $^1\Sigma$-$^1\Sigma$ transition, vibrational structure of spectrum 2–8601
    - $CaCl_22(ONH_3)$ i.r absorption spectra, vibrational analysis 2–15294
    - Cd trihaloanions, force fields and mean vibration amplitudes 2–28280
    - $CdCl_22(ONH_3)$ i.r. absorption spectra, vibrational analysis 2–15294
    - Cl_2, vibrational structures of $E\rightleftharpoons B$ emission systems 2–21618
    - ClCN, Fermi resonance, matrix-isolated i.r. spectral study at 20K 2–8588
    - ClCN, matrix isolation, i.r. spectra, Fermi resonance 2–12122
    - ClF photoelectron spectrum meas. spin-orbit splitting in first vibrational band observed 2–12121
    - ClF_3, force fields 2–18412
    - $Co_4(CO)_{12}$, stretching frequency from i.r. spectra 2–38900
    - CoF_2, liquid, degrees of freedom assignment from significant structure theory 2–28785
    - Cr complex, $Cr(CO)_6$, ab initio SCF-MO calcs. of force constants, comparison with exptl. results 2–21634
    - $Cr(CO)_6$, liquid, Raman spectra, automatic assignment of observed frequencies and combinations 2–39369
    - CrIII complexes, tris chromium sulphur chelates, absorption and emission spectra, vibr. structure, energy forbidden transitions 2–21596
    - CrO_4^{2-}, r.m.s. amplitude 2–3064
    - CsBr, quadrupole hyperfine structure 2–38901
    - CsF, prod. by reactive beam scattering of Cs by SF_6 and SF_4, vibr. energy distrib. 2–21597
    - CsF, produced by reactive beam scatt., vibrational energy distribution 2–782
    - Cs_2SO_4 in inert gas matrices, 4.2 K, i.r. absorption spectra, vibr. assignment 2–31790
    - D_2-He collisions, vibrational energy transfer 2–35381
    - D_2, excitation and transfer, distorted wave calculation 2–38906

Molecules continued
vibration continued
D_2, vacuum u.v. emission spectrum, vibr. and rot. consts. of ground and excited states 2—18419
D_2, vibrational excitation in collisions with H^+ 2—881
2,3-difluoroaniline, i.r. spectrum, vibr. assignment of fundamental frequencies 2—31850
$EuF_2(Cl_2)$, in Ar, Kr or N_2 matrix, i.r. absorpt. study 2—28327
FD_2^+, i.r. spectrum, determ. of structure and force constants 2—8612
FHD^+, i.r. spectrum, determ. of structure and force constants 2—8612
FeO vibration-rotation radiative band intensity meas. 2—35247
Fh_2^+, i.r. spectrum, determ. of structure and force constants 2—8612
GaH, Franck-Condon factors and r-centroids of A-X band systems 2—3028
$GeBr_4$, i.r. spectra, frequency assignment 2—35248
$GeCl_4$, i.r. spectra, frequency assignment, symmetry forbidden bands from $\nu_2(e)$ mode 2—35248
GeH_2, prod. in vacuum u.v. photolysis of GeH_4, i.r. spectrum, frequency assignment 2—8616
GeH_3, prod. in vacuum u.v. photolysis of GeH_4, i.r. spectrum, frequency assignment 2—8616
GeH_4, absorption spectra, 2-17 μ region, vibrational band analysis 2—21601
GeH_2Br, prod. in vacuum u.v. photolysis of GeH_3Br, i.r. spectrum, normal coordinate anal. 2—12127
GeH_2Cl, prod. in vacuum u.v. photolysis of GeH_3Cl, i.r. spectrum, normal coordinate anal. 2—12127
H complexes, H_2 phthalocyanines, relaxation mechanisms from excited singlet states, spin-orbit coupling effects 2—35279
H^- stretching vibration, anharmonicity in H-bonds 2—28247
H_2, 1-10 eV electron scattering, differential and integrated cross sections for vibrational and vibrational-rotational excitation 2—12136
H_2, autoionization rates for $\Delta_v=1$ vibrational transitions calc. by internal conversion theory 2—12139
H_2, Compton profile calc., vibrational correction 2—21603
H_2, excitation and transfer, distorted wave calculation 2—38906
H_2, frequency shifts of quadrupolar components of collision induced fundamental i.r. band 2—31799
H_2, simultaneous vibrational-rotational excitation by low energy electrons 2—12140
H_2, vibrational excitation by collisions with He atoms, ang. distributions in eV region 2—876
H_2, vibrational excitation by electron impact, application of adiabatic-nuclei theory 2—18384
H_2, vibrational excitation by H^+ impact 2—15427
H_2, vibrational excitation in collisions with H^+ 2—881
H_2, vibrational force const., accurate calc. by variation perturbation method 2—8627
H_2, vibrational radiative lifetimes 2—38912
H_2^+, vibration rotation eigenenergies of $2p\pi_u$ and $3d\sigma_g$ states 2—18434
H_2^+, vibrational excitation, rel. to reaction cross section enhancement of statistical phase space theory 2—16679
H_2^+ inclusion of nuclear motion in calcs. of vibrational Raman scattering 2—24435
HBr-DBr collisions, vibration to rotation energy transfer 2—31881
HBr, mixtures, vibration-to-vibration energy transfer 2—8625
HBr, vibrational and rotational excitation in $He(2^3S_1)$ Penning ionization 2—21716
HBr, vibrational relaxation in H halides 2—8624
HCN, rovibrational energy levels, calc. using rigidly bending rigid-rotor Hamiltonian 2—15306
HCN isotopes in Ar matrices, i.r. spectra 2—8643
HCl, HBr, and HI, reactions with atomic Fl, initial vibrational energy level distrib. determ. by i.r. chemiluminescence 2—10607
HCl, perturbed by Ar, vibr.-rot. spectrum, line widths and shifts 2—8618
HCl, vibrational and rotational excitation in $He(2^3S_1)$ Penning ionization 2—21716
HCl ground vibrational state quadrupole moment 2—12145
HD, Rydberg obs., 700-1000 Å Absorpt. spectrum 2—18435
HD, vibrational radiative lifetimes 2—38912
HF, ground vibrational state quadrupole moment 2—12145
HF, in H_3-F_2 chemical laser, time resolved spectroscopy, vib.-rot. transitions 2—5364
HF, photoelectron spectra obs., use of cylindrical-mirror analyzer 2—35293
HF, room temperature rates of vibrational relaxation by HF, Ar, N_2, D_2, H_2, CO_2 determ. from laser- induced fluorescence 2—21615
HF, vibration-rotation interaction term, contribution to potential 2—791
HF, vibration rotation bands, evaluation of r-centroids and higher terms of elec. dipole moment 2—21609
HF, vibrational-rotational stimulated emission from flash photolysis of N_2F_4+RH systems 2—270
HF first order effect of vibrational quantum number on half-width 2—38910
HF model of large amplitude vibrational motion of coupled rods 2—8646
HI_2 radical, vibrational potential function and force constant 2—21604
HN_3, rotation-vibration spectrum in near i.r. and visible 2—15303
H_3NCH_2COO ion, valence force field and conformation 2—28379
HNCS, liquid, temp. dependence of vibr. band intensities in i.r. spectra 2—12567
H_2O, anharmonic force constants, calc. in general quartic force field 2—21607
H_2O, in organic solvents, possible motional effects on vibrational spectrum in fundamental stretching region 2—39370
H_2O, rovibrational energy levels, calc. using rigidly bending rigid-rotor Hamiltonian 2—15306
H_2O i.r. spectra of deformation vibration in micas 2—15304
HOCl, i.r. spectrum, gas phase, ν_2 band study 2—18425
HOF, in dil. N_2 matrix, i.r. spectrum, obs. of fundamental frequencies 2—8638
H_2S, structure of $^2A_1$ band in photoelectron spectrum correlated with transitions to vibrational-rotational levels 2—24474
H_2S^+ radical ion, vibronic patterns of photoelectron and optical spectra 2—21616
H_2S^+ vibrational envelope and bond angle in first excited state , calc. from photoelectron spectrum of H_2S 2—28303
HSiBr, Hamiltonian for large amplitude bending and K-type rotation, effect on higher rot. energy levels 2—12131
$HSiBr_{3-n}I_n$, ground vibrations determ. from Raman spectra, identification from p.m.r. spectra 2—24487

Molecules continued
vibration continued
$HSiCl_{3-n}I_n$, ground vibrations determ. from Raman spectra, identification from p.m.r. spectra 2—24487
$HSiI_3$, ground vibrations determ. from Raman spectra 2—24487
HTO in H_2O, laser Raman spectra, contributions of OT and OH stretching vibrations 2—32268
H_2+H, collinear exchange reactions, with vibr. excitation, reaction probabilities, thermal rate consts. 2—10608
H_2+He, vibrational energy transfer 2—28433
$Hd(B^1\Sigma_u^+)$, vibrational energy transfer 2—12129
He_2, numbering of Tanaka-Yoshino bands 2—21613
He_2, vibrational and rotational constants from potential curve for $2s\sigma^3\Sigma_u^+$ state 2—31802
He_2 calc. of potential of lowest excited singlet state, determ. rotational and vibrational consts., dissociation energy 2—21612
He_3^+, vibrational constants, SCF and CI calc. 2—35258
HgI_2, l.f. Raman line assignment to external vibr. mode 2—29934
I vapour resonant Raman effect, time ordered diagrams for creation of higher vibrational levels 2—12073
I_2, monochromatically excited, quenching and vibrational relaxation in $v'=6$ 2—18438
I_2, reson. Raman effect in absorpt. continuum, degree of depolarization of vibr. bands 2—24440
I_2, vibrational structures of E→B and F→X emission systems 2—21618
$^{127}I_2$, excited by 632.8 nm He/Ne laser, lifetime meas. 2—12155
InH, Franck-Condon factors and r-centroids of A-X band systems 2—3028
KBH_4 and KBD_4, i.r. and Raman low temp. vibrational spectra 2—10384
$K_4Cr(CN)_5NO$, i.r. spectra obs. 2—22770
KHF_2, i.r. and Raman spectral studies 2—26169
K_2O, prod. in matrix reaction, i.r. spectrum, force constants 2—12158
KOH, stabilized in Ar matrix at 4.2 K, i.r. absorption spectra, force field calc. 2—28304
$(KOH)_2$, stabilized in Ar matrix at 4.2 K, i.r. absorption spectra, frequencies of OH vibrations and configurations determ. 2—28304
$^{39}K\,^{19}F$, rel. to Stark effect, molec. beam resonance meas. 2—21646
$K[PtCl_3(C_2H_4)].H_2O$, vibrational spectrum, relationship with vibrational structure in photoelectron spectra of ethylene and ethylene-d_4 2—3087
LaO, vibr. consts. of $C^2\Pi$, $A'^2\Delta$ and $X^2\Sigma^+$ states, band heads of $C^2\Pi_r \rightarrow A^2\Delta_r$ and $C^2\Pi_r \rightarrow X^2\Sigma^+$ electronic transitions 2—18440
$LiAlF_4$, mean amplitudes, i.r. spectra of matrix isolated vapours 2—797
$LiBH_4$ and $LiBD_4$, polycrystalline, i.r. and Raman vibrational spectra, 80K 2—10389
LiO_2, from Li+O_2 cocondensation reaction, matrix laser Raman spectra 2—38921
LiO_2 in oxygen matrices, assignment of vibrational modes in i.r. and Raman spectra 2—28308
LiOH(D), molecular beam electric resonance spectra 2—8663
^{7}LiCN and ^{6}LiCN, matrix isolated, i.r. spectra, vibrational modes band assignment 2—12160
LuO, β-system analysis 2—799
MN (II) complex, $MnX_4(C_5H_5NH)_2$ 2—25338
methane, vibrational relaxation times meas. with spectrophone, use of NH_3 on C_2H_6 as calibration gas studied 2—12257
Mg complexes, Mg phthalocyanines, relaxation mechanisms from excited singlet states, spin-orbit coupling effects 2—35279
$MnCl_22(ONH_3)$ i.r. absorption spectra, vibrational analysis 2—15294
MnO_4 ions, r.m.s. amplitude 2—3064
$Mo(CO)_6$, liquid, Raman spectra, automatic assignment of observed frequencies and combinations 2—39369
MoO_4^{2-}, r.m.s. amplitude 2—3064
MoO_4^{2-}, vibrational spectra and force constants 2—35264
MoS_4^{2-}, vibrational spectra and force constants 2—35264
N_2-O collisions with nonpairwise interaction, calc. of vibrational transition probabilities 2—15238
N_2-water vapour mixture, relaxation times 2—15318
N_2, excitation, observation of photoionization spectrum in 79.5-84.0 nm region 2—3053
N_2, in solid Ar matrix, induced fundamental i.r. band 2—18472
N_2, liquid and dense gas, injected hot electron thermalization 2—12577
N_2, photoelectron spectra, study of autoionization, vibrational structure 2—8674
N_2, relative population of vibr. levels of $B^3\Pi_g$ state in glow discharge 2—35267
N_2, vacuum u.v. absorption spectrum, o-X system, rot. consts. of vibr. levels 2—15325
N_2, vacuum u.v. emission from Lewis Rayleigh afterglow, rel. to recombination of N atoms via $N_2(a'\pi_g)$ and $N_2(a'1\Sigma_u^-)$ states 2—804
N_2, vibr. temp. of $B^3\Pi_g$ state from relative intensity of first positive band system 2—31813
N_2, vibrational excitation by electrons at 10 to 100 eV 2—12171
N_2, vibrational relaxation rates, by H_2O, shock tube meas. 2—28311
N_2, vibrationally excited photoionization spectrum meas. in 79.58-84.20 nm region 2—18446
N_2^+, enhancement of vibrational level population by photoelectron spectrometry 2—35265
NCl, bond length and angle, mean amplitude of vibration, electron diffraction study 2—8676
NCl_3, isotopic species, atomic, bond, and mol. polarizabilities, root mean square amplitudes statistical thermodynamics 2—5937
NF_3, high resolution study of l-type resonance in ν_4 band 2—8673
NH_3, force const. calc. in valence force system of coordinates using Gell-Mann and Feynman theory 2—800
NH_3, one-electron properties, effects of vibl. distortions due to inversion motion 2—21626
NH_3, Stark effect on vibr.-rot. transition, h.f.s. 2—24476
NH_3, vibr.-rot. transition, absortion saturation 2—5934
NH_3, vibration-rotation spectrum, rotational analysis of 6450 A band 2—28312
NH_3, vibrational and rotational relaxation data from u.s. absorption meas. 2—31811
NH_3 gas, vibration- rotation spectrum, vibr. assignments 2—21631
NH_3 radical, vibrational effects on hyperfine coupling constants, perturbation approach to evaluation 2—21623
NH_3^+, excitation stretching vibrations in ionization of NH_3 2—18455
NH_4^+, motion and correlation functions 2—8677
NH_4BF_4 vibrational spectra, 17 to 300K 2—24482
NO-H_2 mixtures adsorbed on W, vibr. props. 2—32396
N_2O-gas mixtures, rot. correl. functions 2—18404

Molecules continued
vibration continued
NO-, vibrational progressions of resonances, association with Rydberg states 2—812
NO, absolute oscillator strength measurements of γ-system 2—38925
NO, collision induced vibration- translation relaxation, mechanisms for resonance production 2—35382
NO, γ, ε and δ system, fluorescence spectrum polarization of rotational lines, vibr. band intensities 2—8675
NO, monochromatic excitation of rotational levels in vibrational levels of $A^2\Sigma^+$ state 2—12175
NO, Penning ionization and photoionization to $X^1\Sigma^+$ state of NO^+, comparison of vibrational transition probabilities 2—21625
NO, photoelectron spectra, study of autoionization, vibrational structure 2—8674
NO, spectra, $^2\pi_{3/2}$-$^2\pi_{1/2}$ transition 2—8687
NO, vibr. thermalization, temp. depend. 2—28274
NO abs. oscillator strength estimates for some bands of β system 2—35271
NO vibronic states, population and predissociation 2—18445
NO_2, vibronic effects in decay of fluorescence excited in first excited singlet state, lifetime 2—35284
N_2O, in compressed gaseous mixture, i.r. rotational correlation functions of bending vibr. 2—15315
N_2O, in solid N_2 matrix, i.r. spectra, anharmonic force constants 2—12169
$N_2O_2^{2+}$ vibr. assignment, alternative force fields, least squares study 2—31815
N_2O_3, gaseous, i.r. spectrum, —120°C, assignment of vibration rotation bands 2—12178
N_xO_y, molecular consts., Green's function analysis 2—18443
NS, vibr. and rot. analysis of $^2\Pi_r$-$X^2\Pi_r$ band system 2—18447
NSe, electronic spectrum, 2800-3200Å, vibr. and rot. analysis of 12 red degraded bands 2—18456
$NaAlF_4$, mean amplitudes 2—797
$NaBH_4$ and $NaBD_4$, i.r. and Raman low temp. vibrational spectra 2—10384
$NaBO_2$, ^{18}O-labelled, B-O stretching vibrations 2—21589
$NaHF_2$, i.r. and Raman spectral studies 2—26169
$Na_2(b^1\pi_u)$ state, collision induced energy transfer 2—3151
Ni complex, $Ni(CO)_4$, ab initio SCF-MO calcs. of force constants, comparison with exptl. results 2—21634
O_2-, vibrational progressions of resonances, association with Rydberg states 2—812
O_2, collision induced vibrational and electronic spectra from 90 to 115 K 2—21635
O_2, i.r. fundamental vibration band obs., collision-induced 2—8697
O_2, photoelectron spectra of some autoionizing resonance states 2—8692
O_2, vibrational and rotational excitation in $He(2^3S_1)$ Penning ionization 2—21716
O_2, vibrational excitation by electrons at 10 to 100 eV 2—12171
O_2, vibrational structure from formation of $O_2^-X^2\Pi_g$ in electron scattering 2—24483
O_2 and mixtures with H_2, He_3, He_4, vibrational relaxation times determ. from sound absorption measurements 2—38932
O_2 vibrational-rotational lines, pressure broadening, strong-collision model 2—18460
O_3, high resolution meas. of $\nu_1 + \nu_2 + \nu_3$ absorption band in 3.59 μm region, rigid rotator analysis 2—8696
O_3, i.r. absorpt. bands, anharmonicity coeffs. 2—31816
OCS, i.r. emission, rot.-vibr. struct. of transitions 2—28275
OCS in solution, determ. of band width and profile of ν_3 mode, separation of rotational and vibrational effects 2—38934
OH, predissociation by continuum of bound state without curve crossing 2—18462
OH ground state vibr.-rot. bands, obs. in chemiluminescent O_3-olefin gas phase reactions 2—22868
OH levels, spin orbit coupling constant and Λ-doublet constants obtained 2—12188
OH radical, transition probability for pure vibrational transition determ. from high-field Stark effect on near u.v. spectrum 2—8698
$O_2(^3\Sigma^-_g)$, vibrationally excited, formation in reactions of $O(^1D)$ atoms with O_2 and O_3 2—12183
PCl_3, i.r. spectra, symmetric top force constants 2—38935
PCl_3, liq. and solid states, intermolecular dynamics, vibr. spectra study 2—35377
PF_3, liquid, degrees of freedom assignment from significant structure theory 2—28785
PH_3, effects of Coriolis resonance in ν_2 and ν_4 bands, spectral determ. 2—8700
PH_3, force constants rel. to P pyramidal inversion process, ab initio SCF-LCAO-MO study 2—31822
$(PNCl_2)_3$, ^{15}N-labelled, vibrational assignment of i.r. spectra 2—28319
P_4O_{10}, fundamental frequencies 2—28318
P_4O_{10}, normal coordinate analysis, force consts., mean amplitudes of vibration from spectral study 2—18467
P_4O_6, normal coordinate analysis, force consts., mean amplitudes of vibration from spectral study 2—18467
$PbCl_4$, fundamental values determ. from Raman spectra of neat liquid and n-pentane solution 2—12568
Pd complex, $[Pd(NH_3)_4]Cl_2.H_2O$, vibr. spectra 2—33270
Pd complex, $[Pd(NH_3)_4]Cl_2.H_2O$, vibr. spectra 2—33270
Pd complexes, Pd phthalocyanines, relaxation mechanisms from excited singlet states, spin-orbit coupling effects 2—35279
Pt olefin complexes, $\nu C{=}C$ stretching frequencies rel. to i.r. and Raman spectra 2—15282
Pt(II) complex, PtX_2L_2, X=Cl, Br and I, L=dialkyl sulphide, i.r. and Raman spectra, fundamental assignment 2—28322
Rb_2O, prod. in matrix reaction, i.r. spectrum, force constants 2—12158
RbOK, prod. in matrix reaction, i.r. spectrum, force constants 2—12158
ReF_6, i.r. spectra, Jahn Teller vibrations, zeta const. 2—31825
ReF_6, vibronic structure of 5000 cm^{-1} transition 2—3060
ReO_4^-, r.m.s. amplitude 2—3064
Rh complexes, Rh phthalocyanines, relaxation mechanisms from excited singlet states, spin-orbit coupling effects 2—35279
$Rh_4(CO)_{12}$, stretching frequency from i.r. spectra 2—38900
RuO_4, i.r. and Raman spectra, coriolis consts., quadratic force constants 2—12190
S_3, S_4, vibrational band heads in unsaturated S spectrum at 300 to 650 C 2—15334
$SBr_2(Cl_2)(F_2)(H_2)$, mol. force field 2—8701
SO_2/O_2 mixtures, meas. of sound absorption due to vibrational relaxation, existence of vib.-vib. coupling 2—15338
SO radical vibr. temp. in H_2S-O_2 flame 2—22874
SO_2, mean square parallel and perpendicular amplitudes, electron diffraction study 2—822
SO_2, single vibronic level lifetimes of first excited singlet state 2—8703
SO_2, vibrational structure of 2348 Å system 2—15335
SO_2, vibronic effects in decay of fluorescence excited in first excited singlet state, lifetime 2—35284
SO_3, mean square parallel and perpendicular amplitudes, electron diffraction study 2—822
SO_2BrF and SO_2ClF, force field calculation 2—28324
$SO_2{}^{35}Cl^{35}Cl$, centrifugal distortion coeffs. 2—24486
SbF, effective vibrational temperature in A_2 system 2—3061
$SeBr_2(Cl_2)$, mol. force field 2—8701
SeN, analysis of electronic spectra 2—35288
SeO_2, matrix isolated, i.r. study rel. to thermodynamic function calc. 2—8705
SeO_2 and $(SeO_2)_2$, vibrational analysis 2—28326
$SiBr_4$, force constant relationships, derivative 2—18470
$SiBr_4$, i.r. spectra, frequency assignment 2—35248
$SiBr_{4-n}I_n$, ground vibrations determ. from Raman spectra 2—24487
$SiCl_4$, i.r. spectra, frequency assignment, symmetry forbidden bands from $\nu_2(e)$ mode 2—35248
$SiCl_4$ polarity in vibrational state obs. due to vibrationally induced dipole moment 2—12218
$SiCl_nBr_{4-n}$, force constants and ground oscillations 2—18470
SiD_3NCO, mean amplitudes and shrinkages from spectroscopic data 2—3062
SiD_3NCS, mean amplitudes and shrinkages from spectroscopic data 2—3062
Si_2F_6, i.r. and Raman vibr. spectra, normal coordinate anal., stretching force constants 2—8709
SiH_4 force constants and dipole moment derivatives calc. for symmetric and antisymmetric stretching and bending vibr. modes 2—12193
SiH_3D, high resolution i.r. spectrum of Si-H stretching region 2—8710
SiH_3NCO, mean amplitudes and shrinkages from spectroscopic data 2—3062
SiH_3NCS, mean amplitudes and shrinkages from spectroscopic data 2—3062
SiI_4, force constant relationships, derivative 2—18470
SiO, vibl. and rotl. analysis of $^3\Pi_r$-$a^3\Pi_r$ transition 2—35289
Sm complexes, ethyl 1-methyl acetoacetates and ethylbenzoylacetates, force constant determination from i.r. absorption spectra 2—28328
$SmF_2(Cl_2)$, in Ar, Kr or N_2 matrix, i.r. absorpt. study 2—28327
TcO_4^-, r.m.s. amplitude 2—3064
$TiCl_nBr_{4-n}$, i.r. and Raman spectra, force constants 2—18471
TiO, spectroscopic observations in inert matrices at 4°K 2—24489
TiO_2, spectroscopic observations in inert matrices at 4°K 2—24489
TlCl isotopes, h.f.s. and Zeeman and Stark effects, molec. beam resonance meas. in different vibrational states 2—21645
$^{205}Tl^{19}F$, rel. to Stark effect, molec. beam resonance meas. 2—21646
U-ligand vibrations frequencies and intensities in mono- and trifluoro-oxalate 2—28330
UF_6, force fields 2—38943
UO, frequency and force constant 2—825
UO_2, stretching mode 2—825
UO_2^{2+}, characteristic freq. of valency oscillations 2—35295
UO_2^{2+}, new absorption bands, assignment rel. to vibr. levels of ground state 2—35294
VO_4^{3-}, r.m.s. amplitude 2—3064
$VOCl_25NH_3$ absorption spectra corresponding to deformation oscillations of coordinated molecule 2—15342
$W(CO)_6$, liquid, Raman spectra, automatic assignment of observed frequencies and combinations 2—39369
WF_6, force fields 2—38943
WO_4^{2-}, r.m.s. amplitude 2—3064
$YbF_2(Cl_2)$, in Ar, Kr or N_2 matrix, i.r. absorpt. study 2—28327

Molecules, mesic and muonic
No entries

Mollier diagrams *see Thermodynamic properties*

Molybdenum
activator of thermolum. $Li_2B_4O_7$ 2—27900
adsorbed oxygen, effect on emission electron microscope image 2—18960
adsorption of CO, on (100) face 2—29065
adsorption of Rb, Auger electron spectroscopy 2—12684
atom, A=95,97, hyperfine structure intervals of $4d^55s$ $^7S_3$ ground state, nuclear quadrupole moment 2—21513
atom, ESCA study of $2p^43d^{10}$ to $2p^33d^9$ transition, L-series 2—31641
b.c.c., point defect prod. on irrad., recovery 2—15745
casting, struct. rel. to carbon content 2—19237
cathode fall of glow discharge for inert gases 2—6120
channelling of low-energy alkali ions 2—36391
crystal, plastic deform. rel. to paramag. susceptibility 2—16347
crystal X-ray anal., effect of energy of exciting protons on ratio of intensities of characteristic and scattered radiation 2—40854
depth distribution for Kr ions, radiochemical technique 2—25712
desorption kinetics, surface lifetimes of adsorbed F_2, Cl_2, Br_2, I_2 2—35915
desorption of BaO films, temp. and degree of coverage depend. 2—6383
diffusion of U, rate and temp. meas. 2—12795
dislocation relation peaks, investigations in principal directions at 10, 20, 50 MHz 2—29251
dispersed phase in Al_2O_3, mech. props. 2—15862
dispersed phase in Al_2O_3, Mech. props. 2—15863
dispersion hardening by ZrO_2, ThO_2, HfO_2 2—32747
elastic limit, anomalous grain size depend. 2—12860
electrical resistivity, at high temps. single crystal 2—6750
electrode, effect of purity and high temp. on thermoelectric characteristics 2—29763
emissivity meas., 1200-2400K 2—4083
emitters of in-core thermionic reactor, W layer diffusion 2—14363
enthalpy, 1962-2869K, meas. by drop calorimetry, heat of fusion calcs. 2—35819
extraction, properties and applications 2—3925
fatigue, coaxing phenomenon, grain size effects 2—39829
Fermi surface, r.f. size effect study 2—6725
film, chemical vapour-deposition, FIM study 2—22073

Molybdenum continued
  - film, discontinuous, r.f. cond., oxidation and chemisorpt. of O_2 effects 2—40178
  - film, on thermally oxidized Si, characterization 2—12660
  - film, sputter deposition and removal from metal surfaces, Auger analysis 2—39514
  - high purity, research survey 2—12924
  - in Inco 718, content change effect on precip. hardening9820 2—9820
  - isotopic abundance in terrestrial minerals 2—40902
  - lattice dynamics 2—29234
  - lattice parameters and thermal expansion coeff. determ., 30-180K, X-ray method 2—3694
  - liquid, enthalpy, 2890-2925K, meas. by drop calorimetry 2—35819
  - neutron irrad. damage, dislocation loop contrast 2—19079
  - neutron irrad. damage and annealing 2—19077
  - neutron irrad. damage and annealing 2—19078
  - orientated bicrystal, intergranular fragility 2—12896
  - permeability of H, surface effects 2—29220
  - plastic deform., fine struct. changes during rolling 2—32508
  - plastic deformation, strain-rate and temp. depend. of yield and flow 2—39790
  - plastically deformed, subgrain growth during annealing 2—12946
  - polycrystal, pure, hydrostatic pressure effects on flow stress 2—39801
  - purification from C impurities by heating in H_2 atmos. 2—22861
  - recovery after neutron irrad. and cold work 2—15743
  - slip bands, observation by X-ray diffr. 2—15726
  - in steel, austenitic, interaction with C 2—32787
  - steel, low alloy, brittle fracture tendency, effect of alloying with molybdenum 2—1301
  - steel, quenched, aged, alloy addition, effect on mech. props., weldability 2—19239
  - steel impurity, rel. to stress corrosion cracking, electron microscope obs. 2—19212
  - superconducting, hypersound attenuation 2—16181
  - superconducting T_c, grain size effect 2—19599
  - surface, charact. electron energy loss spectra during oxidation 2—9250
  - surface, low energy noble gas ion bombardment, energetic neutrals scatt. 2—6332
  - surface diffusion of Cu 2—28999
  - surface electron structure, positron annihilation obs. 2—36419
  - thermal diffusivity, 20 to 2000°C 2—19462
  - transition probabilities, absolute, 450-510 nm 2—2944
  - u.s. attenuation in single crystals, dislocational internal friction 2—6497
  - void lattice and regular arrays 2—1231
  - wire, ductility, effect of grain size and C content 2—12884
  - X-ray spectra, relations between L_{III} absorp. limit and $L\beta_{2,15}$ lines 2—26206
  - CaF_2-BaF_2 eutectic-impregnated, friction and wear obs. 2—12917
  - in Cr, effect on Neel temp. 2—19923
  - inFe-Al-Cr alloy, effect on oxidation resist. and mech. props. 2—29430
  - Mo:C, C distrib. and diffusional mobility 2—36052
  - Mo VII, Rydberg series, quantum defect 2—15219
  - Mo VII resonance-line spectrum in the vacuum u.v. 2—18312
  - Mo wire, recrystallized, grain size and carbon content effects on ductility 2—29262
  - Mo^{5+}, e.p.r. in Cs_2ZrCl_6, 4.2-77 K 2—4539
  - Mo^{5+} e.p.r. in GeO_2 2—33339
  - W-Mo thermocouple, calibration curve in 0-2000°C temp. range 2—17455

Molybdenum compounds
  - alloy, TZM, thermal cond., 90 to 1200 K 2—19442
  - Hastelloy X, cyclic oxidation kinetics, 760-1200°C 2—40814
  - molybdates, alkalimetal, single cryst. struct. determ. 2—9480
  - molybdates, normal I-VI spinels, i.r. spectrum, vibrational assignment 2—10382
  - molybdates, trivalent metal, struct. and phase relns. 2—9340
  - molybdenite, crystal struct., symmetry of electron diffr. diagrams 2—9442
  - molybdenite, isotropic abundance of Mo 2—40902
  - MoO_3, O_2 self-diffusion, ionic cond. obs. 2—19148
  - MoS_2:Nb, e.p.r. investigation of band structure 2—32883
  - sulphur phase ternaries, $M_2\ Mo_nS_{n\|1}$ M=alkali metal, n=2, 5, struct., prep. 2—9478
  - sulphur phase ternaries, $M\ Mo_nS_{n\|1}$, M=Ag, Sn, Ca, Sr, Pb, Ba, Ni, Co, Fe, Cr, Mn, Cu, Mg, Zn, Cd, struct., prep. 2—9478
  - Al-Mo system, phase equilibria 2—4015
  - Co-Mo, alloy, liquid state, density meas. 2—3374
  - Co-25wt.%Mo alloy, CaF_2-BaF_2 eutectic-impregnated, friction and wear obs. 2—12917
  - Co-Ni-Cr-Mo alloy, precip. hardening and phase transformation 2—19296
  - Cr-Mo alloy, Seebeck coeff. rel. to para-antiferromag. transition 2—13415
  - Cr-V steel, effect of Mo content and yield pt. on creep rupture strength 2—29286
  - CrNi-Mo film, struct. and elec. props. 2—39505
  - Fe-Mo-Co system, phase diagram 2—40004
  - Fe-Mo-O system, phase equilib. and thermodynamics 2—40008
  - Fe-Mo alloy, nitrided, FIM determ. of precipitate comp. 2—12969
  - Fe-Mo dilute alloy, hyperfine field at Fe atoms, temp. depend. 2—16436
  - Fe-Mo dilute alloy, spin-lattice relax. time 2—19932
  - Fe-3at.%Mo, steel phase transform. rel. to double Bragg scatt. 2—36279
  - Fe-Ni-Co/SiO_2/Fe-Ni-Mo layer system, domain boundaries and coercive force 2—13407
  - Fe-Ni-Co-Mo, steel, pre-precipitation and reversion 2—9809
  - Fe-Ni-Co-Mo alloy, martensitic, ageing, formation of metastable ω phase 2—36299
  - Fe-Ni-Mo-Co, martensitic alloy, temper hardening, X-ray diffr., electron microscopy 2—9740
  - Fe-Ni-Mo, alloy, lattice distortion due to deformation 2—15721
  - Fe-Ni-Mo, martensitic alloy, temper hardening 2—9739
  - Fe—Ni—Mo—C alloy, martensite transform. twinning 2—9807
  - Mo-C-O alloy, C and O surface migration, rel. to chemisorption and precipitation 2—9252
  - Mo-Co-Fe, alloy, quenched from $\alpha+\gamma$ field, transform. microstructs. 2—12998
  - Mo-Co dil. alloys, mag. susceptibility and low temp. sp. ht. 2—19827
  - Mo-Fe, powders, coarse and fine, isothermal sintering, exponential law, logarithmic time law 2—12982
  - Mo-Fe dil. alloys, mag. interactions 2—40408
  - Mo-Fe dil. alloys, mag. susceptibility and low temp. sp. ht. 2—19827
  - Mo-Fe dilute alloy, relaxation phenomena due to s-d exchange interaction 2—19978

Molybdenum compounds continued
  - Mo-Fe dilute system, Mossbauer spectra, relax. due to s-d exchange interaction of ^{57}Fe 2—40631
  - Mo-Ir(Rh) alloys, spin fluctuation effects on supercond. 2—19600
  - Mo-Mn-C system, phase equilib., X-ray study 2—13013
  - Mo-N, solid soln., supersaturated, isochronic ageing 200-550°C, soln. clusters, precip. growth 2—25599
  - Mo-Nb-Hf alloy, phase diagram, hardness, metallography, X-ray analysis 2—4019
  - Mo-Nb monocrystalline alloys, work function, additive character of variation, anisotropy 2—13352
  - Mo-Ni-Fe alloy, martensitic transform., rel to cooling rate, plastic deform., hardening 2—29467
  - Mo-O system, absorpt. spectra 2—26174
  - Mo-Pd system, diffusion, electron probe microanal. study 2—36078
  - Mo-Re-C alloy, C distrib. and diffusional mobility 2—36052
  - Mo-Re alloys, supercond., u.s. attenuation, energy gap anisotropy 2—16180
  - Mo-Re dil. alloys, elastic consts. 2—29234
  - Mo-(35 at. %)Re alloy, slip patterns and deform. twins correl. 2—15765
  - Mo-Ti-C alloy, deformed, subgrain growth during annealing 2—12946
  - Mo-Ti, alloy, microsegregation, rel. to cooling rate, comp., electron probe analysis 2—29439
  - Mo-V, alloy, dilate, mag. susceptibility, Knight shift 2—19836
  - Mo-W-O system, ternary phase formation 2—22378
  - Mo-Zr-Ti, alloy, forming process behaviour, corrosion and oxidation resist. rel. to Al content 2—29411
  - Mo alloy, grain size rel. to B content 2—12729
  - Mo^{5+} cpds., ions effective mag. moment, derivation from cryst. elec. field 2—40587
  - $MoAs_2$, supercond. props. 2—32927
  - Mo_2C-Re solid solution, comp. depend. of supercond. crit. temp. 2—22498
  - Mo_2C layer build up on steel by open arc 2—32739
  - $Mo(CO)_6$, liquid, Raman spectra, automatic assignment of observed frequencies and combinations 2—39369
  - $Mo(CO)_6$+X flames (X=H,N,O), chemiluminescence band system 2—22865
  - Mo(II) complex, structure study using X-ray crystallography, determ. of MoCl bond lengths 2—39647
  - Mo(II) complex, X-ray determ. of structure and comparison with related compounds 2—35992
  - MoMn-Al_2O_3 bond strengths, sintering conditions effect 2—32753
  - MoO_3:Ni, defect struct. and elec. cond. 2—10026
  - MoO_3, elec. resist. response to hydrogen in air 2—26380
  - MoO_4^{2-}, vibr. spectra, r.m.s. amplitude 2—3064
  - MoO_4^{2-}, vibrational spectra and force constants 2—35264
  - Mo_xO_{3x-2} series, (x=19, 20, 21, 22), cryst. struct. 2—25339
  - MoS_2, anisotropic layer structures, electrical contacts and conductivity 2—1477
  - MoS_2, u.v. spectra, interband transitions, plasma reson. 2—13463
  - MoS_2 + Cu or Sn covering, self lubricating antifriction coating 2—6335
  - MoS_2 crysts., compressibility 2—25497
  - MoS_2 in epoxy resin, wear life coeffs. 2—22294
  - MoS_2 intercalation cpds., supercond. 2—32939
  - MoS_2 layer material, lubricating mechanism 2—22300
  - MoS_2 molybdenite, mag., elec., thermoelec. props. and Hall effect 2—36513
  - MoS_2 surface, etch pits struct. and growth 2—32341
  - MoS_2 type bonded solid film lubricant, humidity effects on frictional props. 2—22301
  - MoS_4^{2-}, vibrational spectra and force constants 2—35264
  - $MoS_2(Se_2)(Te_2)$, band struct. 2—32886
  - $MoSe_2$, exciton-exciton interaction during laser irrad. 2—19788
  - $MoSi_2$ powder, supersonic grinding kinetics 2—15939
  - $MoTe_2$, lattice parameters 2—25340
  - Nb-Mo-N system, equilib. conc. and solubility of N_2 2—4020
  - Nb-Mo-N system, phase diagram 2—19314
  - Nb-Mo-N system, thermodynamics of α solid soln. 2—19313
  - Nb-Mo alloy, flux-flow resist., Ettingshausen effect, thermal and mag. props. 2—13167
  - Nb-Mo alloy, with Fe impurity, localized mag. moment, Mossbauer obs. 2—36847
  - Nb-Mo alloys, supercond., transport entropy of vortices 2—13161
  - Ni-Al-W-Mo-Co alloy, dispersion-hardened, thermomechanical treatment 2—9733
  - Ni-Co-Cr-Mo alloy, heat resistant, σ-phase precip. mechanics 2—9821
  - Ni-Cr-Mo alloys, corrosion, electrochemical behaviour 2—1754
  - Ni-Cr-Mo powder alloy, heat treatment effect on elec. cond., mech. and corrosion props. 2—19280
  - Ni-Mn-Fe-Mo alloy, mag. props. 2—13400
  - Ni-Mo, high quality, production of very thin strips by cold working 2—1352
  - Ni-Mo alloy, order-disorder process 2—39996
  - Ni-Mo alloy, solidified at fast cooling rates, metastable phases 2—36305
  - Ni-Mo alloys, ordering kinetics, X-ray and electron microscope obs. 2—36293
  - Ni-Mo powder alloy, heat treatment effect on elec. cond., mech. and corrosion props. 2—19280
  - Ni_3Mo alloy, dissociated antiphase boundaries 2—9548
  - Ni_4Mo alloy, ordering process during isothermal annealing, field-ion microscope obs. 2—36294
  - Ti-(8 wt.%)Al-(1 wt.%)Mo-(1 wt.%)V alloy, sustained loud environmental crack growth 2—29330
  - Ti-Al-Cr-Mo alloys, strength and plasticity 2—36142
  - Ti-Al-Sn-Zr-Mo alloy, tensile props. rel. to microstruct. 2—39942
  - Ti-Mo-Ni system, polythermal section, microstructure, resistivity, dilatometry, X-ray analysis 2—32788
  - Ti-Mo alloy, continuous cooling transform., rel. to ω phase precipitation 2—29481
  - Ti-Mo alloy, fluctuation supercond. 2—13181
  - β-Ti-Mo alloy, isothermal phase transform. 2—12979
  - Ti-Mo alloys, supercond. T_c enhancement on mech. deform. 2—6781
  - Ti-Mo alloys, supercond. transition temp., lattice instability, electron/atom ratio 2—40214
  - U-Mo-Nb-Zr alloys, phase transformations, carbide inclusions effect 2—13004
  - U-Mo alloy, stress corrosion cracking 2—12911
  - U-Nb-Mo system, kinetics of transform. of γ phase 2—36309
  - Zr-(3 wt.%)Mo-(1 wt.%)Al alloy, thermal decomposition, Al effect 2—25640

- **Molybdenum compounds** continued
  - Zr–Cu–Mo alloys, struct. transforms. on continuous cooling 2–1391
  - Zr–(3 wt.%)Mo–(1 wt.%)Al, tempering of strain induced martensitic phase, struct. and morphology 2–25639
- **Monitoring** *see Radiation monitoring*
- **Monochromators**
  - *see also Filters, optical; Light sources; X-ray monochromators*
  - computer analysis of instrument function 2–27656
  - double, Heath EU-700 in tandem, low cost monochromator 2–21178
  - double grazing incidence, for vacuum u.v., construction 2–14468
  - Fabry-Perot, nebular two-etalon, propane scanned photoelectric for astronomical applic. 2–30647
  - gratings, u.v., solar spectra, results from three balloon flights 2–11059
  - intensity distribution in exit slip plane calc. for spatially coherent illumination 2–38153
  - for i.r. spectrometers, efficiency factor 2–38158
  - neutron, high resolution, focusing 2–32432
  - neutron, using bent focusing Cu cryst. 2–25313
  - plane grating, elimination of aberrations 2–27570
  - stigmatic, grazing incidence, for synchrotrons 2–34867
  - for synchrotron orbital radiation source, design, construction and performance testing 2–14468
  - trochoidal, monoenergetic electron source, characteristics det. by calc. by electron energy distrib. 2–34316
  - vacuum u.v., developments at Univ. Wisconsin 2–14468
  - vacuum u.v. corrected, design 2–14467
  - vacuum u.v. focusing and concave grating aberration calcs. 2–14451
  - vacuum u.v. plane polarized monochromatic collimated beam production 2–17702
  - v.u.v., grazing incidence, with fixed exit slit 2–31141
  - X-ray premonochromator for Picker vertical axis diffractometer 2–32417
- **Monolayers** *see Adsorbed layers*
- **Monomers** *see Molecules*
- **Monomolecular layers** *see Adsorbed layers*
- **Monopoles, magnetic** *see Magnetic monopoles*
- **Monte Carlo method** *see Statistical analysis*
- **Moon**
  - American and Soviet space research studies, review 2–17028
  - anorthosite analysis 2–7511
  - anorthosites, chemical composition and parent liquids 2–13982
  - Apennine-Hadley region, geological implications of earth-based radar and i.r. measurements 2–1985
  - Apollo 11, 12 and 14 data review 2–1981
  - Apollo 11 lunar dust, single domain Fe grains distribution 2–4339
  - Apollo 11 rock samples, differential thermal analysis and gas release studies 2–7509
  - Apollo 11 sample 10071, petrology of differentiated mini-igneous complex 2–13981
  - Apollo 12, petrology of basalts 2–13983
  - Apollo 12 samples, measurement of S concentrations and isotope ratios $^{33}S/^{32}S$, $^{34}S/^{32}S$, $^{36}S/^{32}S$ 2–17027
  - Apollo 14 crystalline rocks, geochemistry of opaque samples 2–13987
  - Apollo 14 inverted pigeonites as samples of lunar plutonic rocks 2–37343
  - Apollo 15, anorthosite crystallization age determination 2–41184
  - Apollo 15 anorthosite 15415, ^{40}Ar-^{39}Ar age and cosmic irradiation history 2–37342
  - Apollo 15 anorthosite 15415 sample, texture, mineralogy and metamorphic history 2–41186
  - Apollo 15 anorthosite slide 15415,18 sample, mineralogic and petrologic study 2–41185
  - Apollo 15 basalt 15555 and soil 15531 geochemistry 2–41183
  - Apollo 15 geochemical x-ray fluorescence experiment 2–41187
  - Apollo 15 lunar samples, description of finds 2–41176
  - Apollo 15 mare basalt age, crust and mantle evolution 2–13984
  - Apollo 15 mission 2–20672
  - Apollo 15 rock 15555, cosmic ray exposure and gas-retention ages 2–41182
  - Apollo 15 rock 15555 chip, rare gas retention ages 2–41181
  - Apollo 15 sample 15555, chemistry geochronology and petrogenesis 2 41178
  - Apollo 15 samples, geologic setting 2–41177
  - Apollo 15 samples, primordial radioelements and cosmogenic radionuclides 2–41188
  - Apollo sample 15555, ^{40}Ar- ^{39}Ar dating 2–41179
  - Apollo sample 15555, Rb-Sr and K-Ar dating 2–41180
  - ash flow, fundamental eqns. from kinetic theory 2–35803
  - atmosphere from solar wind, meteoric volatilization and internal degassing contributions 2–1982
  - automatic vehicle studies for information on evolution of solar system 2–41169
  - basaltic fragment, minerology, petrology and chemistry 2–20652
  - basalts, Apollo 11, petrogenesis and implications of lunar origin 2–23106
  - basalts, crystallization of plagioclase and significance 2–26814
  - boulder distribution near small craters and crater shapes 2–1977
  - Brown's lunar theory, analysis of approximations, lunar ephemerides 2–1937
  - chemical composition and origin 2–20640
  - chemical links with stony meteorites 2–1971
  - chondrules in Apollo 14 samples, implications for origin of chondritic meteorites 2–37351
  - Copernicus crater, large scale surface pattern associated with ejecta blanket and rays 2–23110
  - α-corundum in lunar dust 2–13996
  - crater population, development with time under bombardment by meteoroids and solar wind 2–1975
  - crater shape, genetic implications 2–26822
  - craters, maria, origin deduced from Orbiter photographs 2–10996
  - craters, morphological maturity as function of age and dimensions 2 30538
  - density function determination 2–13992
  - differentiation model 2–7513
  - dual frequency bistatic-radar obs. with Apollo 14 2–33731
  - Earth-Moon system, evolution rel. to tides 2–41190
  - elastic properties of interior 2–41219
  - electrical conductivity model, interpretation of dayside and nightside e.m. response 2–17030
  - electrical props., Apollo 17 expt. 2–33733
  - e.m. ground-wave propagation for two mathematical models 2–30913
- **Moon** continued
  - exosphere, lateral transport of particles, applicability of diffusion model 2–20376
  - figure and relief from reduction of photographs 2–30537
  - fines, Apollo 11, density, pressure and temperature effects on heat transfer 2–20639
  - force on Earth causing nutations in motion 2–10812
  - fossil track and thermoluminescence studies of luna 16 material 2–20660
  - Fra Mauro formation, age 2–1972
  - Fra Mauro formation, Rb-Sr age 2–1974
  - Fra Mauro formation, rock types, nature and origin 2–1973
  - gas accumulation in surface layers 2–1979
  - geomagnetic field variations, Chapman-Miller computations 2–17032
  - gravimeter for surface 2–20669
  - gravitational field for injection of space vehicles into stationary Earth-satellite orbit 2–30393
  - gravity, Apollo 14 Doppler radio tracking meas. 2–37352
  - gravity, at Apollo 14 landing site 2–26821
  - gravity analysis from long-term effects 2–26820
  - gravity estimate from high altitude spacecraft Doppler data 2–17029
  - gravity profile, semiautomatic, self-levelling gravimeter 2–17034
  - grazing occultation of α Scorpii (Antares) 2–41091
  - grazing occultations over Canada in (1972) 2–37346
  - heat conduction, calculation for model surface 2–4952
  - highlands, differentiation and volcanism, photogeologic evidence 2–37345
  - ilmenite basalts, Apollo 11, petrology 2–13989
  - Imbrian basin, nature of body causing formation from composition of Apollo 14 samples 2–37350
  - Improved Lunar Ephemeris and Newcomb's Tables of the Sun, reference systems comparison 2–41189
  - inert gases in Luna 16 dust samples 2–20657
  - interior structure, seismic studies 2–7510
  - interior temperature profile, rel. to radioactive heat sources 2–20671
  - internal friction, dislocation mechanism, lunar rock quality factor from mechanical vibrations and moonquakes 2–13993
  - internal structure, comparison with Earth 2–4641
  - internal structure, gravitational anomalies and relief 2–7505
  - interplanetary dust concentration on surface 2–20670
  - i.r. radiation directional characteristics 2–1978
  - landscape, chemistry and history of formation 2–7517
  - low energy protons, action on lunar Ba isotopes to produce Xe 2–10994
  - luminescence and thermoluminescence of Apollo 12 lunar samples 2–13986
  - Luna 16, Li, K, Rb, Sr, Ba, rare-earth, Zr and Hf concs. in fines 2–20662
  - Luna 16 basalt fragments, microprobe obs. 2–20642
  - Luna 16 fines, lithic fragments, glasses and chondrules 2–20643
  - Luna 16 landing site, geologic setting 2–20641
  - Luna 16 regolith samples, chemical features 2–20661
  - Luna 16 sample, microbasalt, extremely mafic magma 2–20648
  - Luna 16 soil, conc. of rare earths and trace elements 2–20664
  - Lunar regolith, rare gas adsorption 2–37347
  - magnetic field, amplification of variations at surface 2–17031
  - magnetic field, interaction with solar wind 2–37348
  - magnetic monopoles in lunar material 2–14528
  - magnetic variations, dynamo theory 2–13791
  - Mare Fecunditatis, basalt fragment, gas retention and cosmic ray exposure ages 2–20654
  - Mare Fecunditatis, extreme radiation damage in soil 2–20659
  - Mare Fecunditatis, obs. of opaque minerals and spinels 2–20651
  - Mare Fecunditatis, relative proportions and petrological significance of particles in soil 2–20646
  - Mare Fecunditatis, shock metamorphic effects in soil sample 2–20649
  - Mare Fecunditatis regolith, petrology 2–20644
  - mare soil, cracking and formation of clods 2–13990
  - maria, formation in a convective cell theory 2–7205
  - Marius Hills, lava tubes and channels 2–26818
  - mascon free, gravity field computation 2–7516
  - meteoritic and non-meteoritic trace elements in Luna 16 samples 2–20666
  - microbreccia, dunite-norite, identification and analysis, from Fra Mauro 2–10991
  - mineral and bulk composition of Luna 16 fragments 2–20650
  - minerals, American Astronomical Society, Amherst, USA 1971, conference 2–26623
  - minerals, U, Th, Pb and rare earth element abundances and $^{207}Pb/^{206}Pb$ ages 2–37344
  - Montes Apenninus LAC 14, radar and i.r. response comparison 2–33732
  - near side, systematic geologic mapping, appearance 3.3 and 4.0 billion years ago 2–26816
  - near side, systematic geologic mapping 2–26815
  - neutron activation analysis of 29 elements in Luna 16 soil 2–20663
  - neutron capture on Gd and Sm in Luna 16, G-2 soil 2–20655
  - occultation of stars, 1968-69 Gorky obs. 2–30437
  - occultations, multiple systems, photoelectric measurements 2–13976
  - occultations, photoelectric observations 2–13975
  - occultations of stars, prediction of series and periodicity 2–7372
  - occultations of stars 2–1952
  - occultations of stars is the year 1970 at Cracow Astronomical Observatory 2–26649
  - orbital mass spectrometer, Apollo 15 flight 2–41174
  - origin, geochemical evidence, element deficiencies 2–33724
  - origin, optical constants of terrestrial analogs of minerals 2–26813
  - origin, plasma to planets, conference (Saltsjobaden, Sweden, Sept 1971) 2–41164
  - origin, Th-content of moon rock and terrestrial basalt obs. 2–30547
  - origin and physiography 2–23112
  - origin of Earth Moon system in terms of a convective cell theory, and formation of the lunar maria 2–7205
  - particles, contribution to meteoric sporadic background 2–30589
  - phase curves, model for non-atmospheric bodies 2–20637
  - photographic obs. for det. of ephemeris time 2–41172
  - plasma sheet ions at surface preceding substorm onset 2–4955
  - Posidonius crater, transient phenomena, polarization charge 2–30535
  - position rel. to stellar background, instrumentation 2–41173
  - potential model, L1, mass distribution 2–23109
  - radiation, visible scanning photoelectric polarimeter for Stokes parameter 2–11175
  - radio source, 15.5 and 31.6 GHz, propagation test for satellite communications 2–16864
  - radio wave refraction, properties of the lunar surface 2–4953
  - rare earth and bulk abundances in Luna 16 soil levels A and D 2–20665

Moon continued
- rare gas studies in Luna-16-G-7 fines by stepwise heating technique, a low fission solar wind Xe 2—20656
- regolith, mech. props. 2—33728
- remanent magnetization of rock samples 2—13979
- rille Rima Goclenius II 2—23107
- rock, breccia and soil samples, ^{40}Ar-^{39}Ar ages and cosmic ray exposure ages 2—4951
- rock types, nature and origin, Fra Mauro formation 2—1973
- rocks, crystalline, petrology and minerology 2—4950
- rocks, igneous, Rb-Sr ages 2—1972
- rocks, simulated, for space mission mineral resources 2—17033
- rocks, surface orientation det. from obs. of distrib. of microcraters, soil covers and glass coatings 2—30542
- rocks, X-γ emitter obs. using liquid scintillation NaI(Tl) coincidence detector 2—27869
- rocks and minerals on the surface, Apollo ii, description 2—4956
- Rover exploration, unmanned, objectives and requirements 2—1980
- samples, Apollo 12, crystalline rock and fines 2—4954
- samples, Apollo 12, magnetic properties of crystalline rock and fines 2—4954
- samples, Apollo 14, geologic setting 2—1984
- samples, Apollo 14, preliminary examination 2—1983
- samples, characterization of hyper-velocity particle impact craters 2—10997
- samples, electron microprobe analysis 2—4958
- samples, h.v. transmission electron microscopy 2—10999
- samples, microcraters, scanning electron microscope characterization 2—10998
- samples, morphology and search for biogenic forms 2—4957
- satellites orbiting earth, effect on motion 2—20442
- Sea of Fertility, petrology of basaltic and monomineralic soil fragments 2—20647
- Sea of Fertility, U-Th-Pb soil analysis 2—20668
- Sea of Plenty, particle tracks record of soil 2—20658
- seismic and other experiments left on lunar surface by Apollo missions 2—33729
- seismic energy release, recording by stations installed by Apollo 12 and 14 2—37349
- seismograms for LM and S-IVB impacts, modulation mirage interpretation 2—13977
- selenographic zero-point position in geocentric frame of reference 2—33723
- silicate materials, angular azimuthal distributions of high energy cosmic rays 2—10801
- soil, and analogues, relative permittivity, dielec. loss tangents, elec. resist. 2—33727
- soil, bearing strength and mechanical props. 2—26819
- soil, friction and abrasion props. 2—33726
- soil, lithic and vitreous fragments, petrology, from Mare Fecunditatis 2—10992
- soil, model age and Rb-Sr age of basalt fragments 2—20653
- soil, noble gas analysis of KREEP fragments 2—7507
- soil, thermal props, rel. to terrestrial analogs 2—33725
- soil fragments, silicate melt inclusions and glasses 2—20645
- soils, mixing models and recognition of end member groups 2—1976
- Soviet robots, summary of scientific results 2—7518
- spin-stabilized lunar satellite, attitude determination using Kalman filter 2—20453
- spinels, compositional variations 2—7515
- spinels, subsolidus reduction 2—10995
- influence on sporadic-E region, altitude, density variations 2—37222
- stereoscopic pictures, (1840-1864) process 2—30534
- surface, impact crater ejecta thickness 2—30541
- surface, meteorite flux as function of Earth-Moon distance, crater counting 2—26817
- surface, reflection and scattering of radio waves 2—30536
- surface, selection of points for development of fundamental control system 2—23108
- surface features, evidence of vulcanism 2—20673
- surface fines, thermal cond. and diffusivity under landing site conditions 2—20674
- surface mechanical properties, computer simulation of Surveyor data 2—23105
- surface temp. at Tranquillity Base 2—23104
- surface temps. from Apollo 12, diurnal variation 2—23111
- surface topography, study by Luhokhod-1 in vicinity of Heraklidus mountains 2—17035
- surface volatilization evidence from Apollo 14 feldspar- phyric basalts 2—7512
- topography meas. by radar interferometry 2—33730
- transient lunar phenomena, modified theory 2—30540
- transient lunar pheomena, albedo of lunar rock dust, changes during fluidization 2—13991
- vacuum meas. on lunar surface 2—41175
- western hemisphere, surface structure and limbus coordinates, Zond-6 study 2—30539
- B abundance in fines from Apollo and Luna missions 2—7508
- Be abundance in fines from Apollo and Luna missions 2—7508
- Eu anomaly, lunar basalt genesis 2—13985
- ^{158}GdO/^{157}GdO enrichments due to neutron capture, irradiation histories 2—13978
- Li, abundance in fines from Apollo and Luna missions 2—7508
- Nd:glass laser and coude system as transportable lunar ranging system 2—23045
- ^{18}O/^{16}O isotopic analysis of Luna 16 soil 2—20667
- Rb-Sr ages on density and size fractions of Apollo 11 fine soil sample 2—13988
- ^{222}Rn, distribution on surface 2—7514
- ^{149}Sm/^{154}Sm rocks, isotope ratio change due to neutron capture 2—13980
- Xe, induced by low energy solar flare protons on Ba isotopes 2—10994
- ^{131}Xe excess in rocks due to neutron resonant capture by ^{130}Ba 2—7506

Morphology, crystal *see Crystal morphology*

Morse potential *see Kinetic theory; Molecules/intermolecular mechanics*

Mosaic structure *see Crystal structure/microstructure*

Mossbauer effect
- *see also Gamma-rays/absorption; Nuclear excitation*
- γ-ray diffraction theory, kinematic approx. 2—29881

Mossbauer effect continued
- absorption spectra of E2 and E2/M1 transitions, observation of interference effects 2—24136
- actinides, nuclear transitions 2—21402
- antiferromagnet, electron spin relaxation above Neel point 2—22714
- arbitrary polarizations, transmission and scattering 2—38467
- bis-(N,N-diethyldithiocarbamato)iron(III) chloride, investigation of ferromagnetic transition at 2.43K by intermolec. exchange 2—10209
- crystal zero point velocity determination 2—36324
- diffractometer for crystal spectra obs. 2—26120
- disordered lattice, resonanant absorption energy shift calc. 2—19976
- electric field gradient in very small crystalline particles 2—26122
- electronic structure of point defects, Mossbauer and spin resonance obs., book 2—32876
- ferri-diopside, absorption spectra of synthetic samples 2—7054
- ferric dithiocarbamate, paramagnetic molecule 2—5965
- force constants, calc. from temp. shift and recoil-free fraction 2—40618
- frozen aqueous solutions for study of spectra of complexed ions, cooling rate criterion for glass formation 2—35827
- furnace for high field experiments 2—22733
- GdIG, hyperfine struct. of Gd isotopes 2—7140
- glass, Fe$_2$O$_3$-rich, anomalous mag. behaviour 2—33132
- glass, Sn containing, temperature dependence of Mossbauer coeff. 2—10317
- group II-IV-V compound, ABC$_2$ type, of ^{57}Fe 2—1669
- Heusler alloys, hyperfine fields at Ni sites 2—40632
- Heusler alloys, hyperfine fields at Sb sites 2—40633
- high field technique using strong field produced by supercond. magnet 2—40617
- hyperfine structure, effect of e.s.r. transitions 2—16429
- impurity atom diffusion, effect on width and intensity of Mossbauer line 2—13441
- impurity diffusion rel. to linewidth, line position of fine struct. Mossbauer spectra 2—19980
- invar, antiferromag. phase obs. 2—33168
- Invar alloy, anomalous props. 2—33221
- iron chelates irradiated with electrons, absorption spectra 2—19975
- isomer shift calc. 2—36830
- Kapton film, Sn(II) sensitizer deposit obs. 2—13588
- Laves iron earth compounds, crystalline interaction anisotropy 2—4441
- line shape theory, thick absorber, expression of integrals as polynomials 2—24137
- local field parameters determ. 2—1667
- magnetic materials, characterisation, review 2—16428
- magnetic materials, zero and multiphonon line shape calc. 2—36323
- magnetic system, time dependent hyperfine interactions, crystal field effects 2—26090
- manganic dithiocarbamate, paramagnetic molecule 2—5965
- manganite spinel, Jahn-Teller distortion obs. 2—36829
- Mn$_{5-x}$Fe$_x$Si$_3$, bonding, crystal chemistry, paramag. moment 2—25245
- myoglobin, vibration and defect contribs. to temp. factors, Mossbauer and X-ray obs. 2—4041
- neptunium (V) oxalate, spectra of 59.54 keV γ ray in ^{237}Np taken from 4.2-80K, magnetic hyperfine splitting 2—19888
- n.m.r. radiative detection applic. 2—26301
- nuclear transitions, tests for T-invariance 2—11717
- polyacrylonitrile, ^{57}Fe spectra, study of polymer dynamics in glass transition region 2—22736
- quadrupole splitting meas., absorber thickness effect 2—14926
- quartz, grinding, mech. activation, ^{57}Fe Mossbauer obs. 2—32712
- quartz-Fe dispersion, mechano-chemical reactions 2—19988
- rare earth cobaltates, high spin-low spin equilib. study 2—36656
- rare earth ferrites, Ln$_{1-x}$Ca$_x$Fe$_{1-x}$Sn$_x$O$_3$, hyperfine interactions of Sn atoms 2—7059
- rare earth iron garnet, hyperfine field on ^{119}Sn, rare earth contrib. 2—22741
- rare earths, Mossbauer isomer shift re-evaluation 2—18130
- rare gas solids, hyperfine interactions of ^{119}Sn, 4.2 K 2—19981
- refrigeration of apparatus for high pressure Mossbauer studies 2—30724
- relative γ-transition probabilities, formulas for the most usual Mossbauer isotopes 2—5641
- r.f. effects on Mossbauer spectra, pulsed method for detection 2—19977
- second order Doppler shift elimination 2—36831
- spectra, background interference, det. using filtering with Fe-transition metal alloys 2—26121
- spectra evaluation, ALGOL 60 programs 2—30105
- spectra from hyperfine split absorbers, level separation det. 2—13442
- spectrometer, 'simultaneous' accumulation of standard and unknown spectra 2—17156
- spectrometer, automatic constant velocity 2—38355
- spectrometer, design and performance 2—21321
- spectrometer doppler drive design 2—14743
- spectroscopy, conference, Clayton, Australia (1971) 2—8509
- spectroscopy, real shape of spectral lines, effect of exptal. geometry on shape 2—34904
- spectroscopy, resolution improvement, Fourier transform. method 2—29889
- spectroscopy applications to chemical engineering 2—1666
- spectroscopy in biomedicine 2—17122
- spectroscopy technique for surface analysis and Fe bearing material 2—16430
- steel, stainless foil, deformed, quadrupole splitting obs. 2—36840
- temperature measurement 10-^{3}K region 2—41363
- transition metal alloy, topologically close packed phases, band struct., elec. and mag. props. 2—35977
- transition metal phosphides containing iron obs. 2—4444
- triphenyltin carboxylates, spectroscopic study of effect of helical chain 2—5954
- for velocity meas. of structures in ear 2—7608
- vibrational resonance states lifetime determination 2—29880
- YIG:Sn, meas. of temp. dependence of hyperfine field acting on ^{119}Sn 2—4354
- YIG, h.p. phase, mag. struct. 2—10330
- Al, thermal diffuse scatt. at Bragg refls. 2—19402
- Am compounds, chemical characterisation by ^{243}Am Mossbauer spectroscopy 2—22734
- As$_2$Te$_3$ and As$_2$Se$_3$.As$_2$Te$_3$, glass-cryst. transition influence on local symmetry 2—1670
- Au-Fe solid soln., of ^{57}Fe, hyperfine splitting 2—19828
- BaFe$_{12}$O$_{19}$, mag. sublattices 2—29882

Mossbauer effect continued
Ba_2FeReO_6, ordered perovskite, Fe valence and spin state 2—22691
$BaFe_{12-2x}Zn_xTi_xO_{19}$, mag. hyperfine fields, Zeeman patterns 2—33216
$BaTiO_3$, of ^{119}Sn, study of lower phase transitions 2—29463
$Ba_2Zn_2Fe_{12}O_{22}$, Mossbauer spectra, obs. of large amplitude oscillation of magnetic moments at 96 MHz rel. to hyperfine field collapse 2—10226
Be-1%Fe, effects of mechanical strain obs. 2—32722
Bi-Sn alloy, metastable phase BiSn formation under pressure, kinetics 2—9794
$Bi_{3-x}Ca_{2x}Fe_{5-x}V_xO_{12}$, room temp. 2—13445
$Bi_2Fe_4O_9$ parameters, spectra, pure, chromium doped, above and below magnetic ordering temperature 2—4442
CaF_2:Eu^{2+}, ^{151}Eu isomer shift, temp. depend. 2—19982
$Cd_{0.98}Fe_{0.02}Cr_2S_4$, of ^{57}Fe, quadrupole interaction below Curie pt. 2—26124
$CdFe_2O_4$, spectra meas. in applied magnetic field, deduced electric field gradients at ^{57}Fe 2—1671
Ce_2Fe_{17}, ferro-helimag. transition, Fe electronic config. 2—26034
Co-Fe-Ge alloy, mag. hyperfine spectra, Mossbauer obs. 2—40620
Co-Te system, stoichiometry obs. 2—16433
β-Co fine particles, mag. transition associated relax. behaviour 2—1626
Co_xTe, x=0.54, 0.67, 0.85, isomer shift, quadrupole splitting 2—26132
Co_3O_4:Eu, α-irrad., colour centres 2—36064
CoS_2, of ^{57}Fe, transferred hyperfine mag. field 2—40617
Co_9S_8, metallic charact., Pauli paramag., thermoelec. power 2—25766
$CoSO_4.7H_2O$, obs. of time-dependent recoilless fraction at Fe^{3+} site 2—33217
$Co_xZn_{1-x}Fe_2O_4$ ferrite, mixed, spin relax., relax. times rel. to Zn^{2+} conc. 2—40577
Cr-Fe, dilute alloy, exchange field 2—10321
Cr-Mn alloys, temp. depend. of mag. hyperfine field at ^{57}Fe 2—40621
$Cr_{0.8}Fe_{0.2}OOH$, thermal conversion to sesquioxide, paramag. to paramag. transform., Mossbauer obs., 400-900K 2—40628
CrTe, Cr_2Te, Cr_2Te_3, ionicity obs. 2—4446
Cs_3FeCl_6, consistent difference in parameters of spectra indicate that compound can exist in two forms 2—36832
$CsSb_2F_{11}$, ^{121}Sb Mossbauer data rel. to structural parameters 2—1668
Cu-Fe alloys, mag. and struct. transforms. of Fe precipitates 2—39981
Cu-Ni alloys, Fe-doped, critical mag. ordering temps. 2—40468
Cu-Zn alloys, Fe local moment behaviour 2—40416
$CuCr_2Te_3I$, ionicity obs. 2—4446
$Cu_4Fe_4S_8$, $Cu_{18}Fe_{16}S_{32}$ and $Cu_9Fe_9S_{16}$, cryst. and mag struct. 2—32454
Cu_2MnSn, study of hyperfine fields at Sn sites 2—36833
$DyFe_2$, quadrupole shift at ^{57}Fe site 2—10318
DyH_2, low temp., Dy^{3+} level obs., mag. moments 2—7055
DyM, M=Cu, Ag, Zn, Zn, Rh, relax. effects on hyperfine interaction 2—26125
$Dy_xR_{1-x}Fe_2$, R=Tb, Er, Tm, mag. anisotropy, spin rotations and crystalline field detn. 2—26123
^{161}Dy, 26 keV Mossbauer transition, determ. of L-shell conversion coefficient 2—2728
^{161}Dy, interference of photoelectric and nuclear resonance absorption of 26 keV E1 γ rays studied by transmission and scattering Mossbauer expts. 2—2727
^{161}Dy Mossbauer thermometer, low temp. calibration 2—37828
ErI_3, interpretation of unresolved quadrupole splitting in ^{129}I spectra 2—40629
EuF_2, ^{151}Eu isomer shift, temp. depend. 2—19982
EuSe:Gd(La), hyperfine interactions 2—13444
Eu_2SiO_4, nuclear gamma resonance study of ferromag. transition temp., quadrupole interaction, hyperfine field and isomer shift 2—19855
Eu_3SiO_5, nuclear gamma resonance study of ferromag. transition temp., quadrupole interaction, hyperfine field and isomer shift 2—19855
Eu_2TiO_4, of ^{151}Eu, h.f.s. 2—33218
Fe-Al, Fe-Ga, temp. depend. of hyperfine field at Fe atom 2—33222
Fe-Al dilute alloy, hyperfine field at Fe atoms, temp. depend. 2—16437
Fe-Al(Mo) dilute alloy, spectrum resolution improvement, Fourier transform. method 2—29889
Fe-Co dilute alloy, hyperfine field distrib. 2—13448
Fe-Ga alloys, metastable, BiF_3-type ordering 2—13446
Fe-Ga dilute alloy, hyperfine field at Fe atoms, temp. depend. 2—16437
Fe-Ga metastable alloy, BiF_3-type ordering obs. 2—33225
Fe-Ga solid solution, hyperfine interactions 2—33224
Fe-M dilute alloy, (M=Ti, V, Cr, Mn, Co, Ni), hyperfine field at Fe atoms 2—13449
Fe-M dilute alloys, (M=Mo, Ru, Rh, Pd, W, Re, Os, Ir, Pt), hyperfine field 2—16436
Fe-Mn nodule, high temp. decomposition, quadrupole splitting 2—26131
Fe Mn nodules, dredged from Pacific Ocean, Mossbauer effect analysis 2—33424
Fe-N, martensite, interstitial ordering, precip., microhardness, internal friction, Mossbauer obs., 293-353K 2—9543
Fe-Pd-P alloys, amorphous, mag. prop. obs. 2—19877
Fe-Pd-Si, amorphous alloy, spectral study, magnetism model based on local ferromag. order 2—4375
Fe-Pt alloy, of ^{195}Pt, isomer shifts 2—10322
Fe-Si alloy, detection of ordered solid soln. struct. 2—19987
Fe-Sn alloy, hyperfine field distrib. determ. 2—40627
Fe-Sn dilute alloy, hyperfine field at Fe atoms, temp. depend. 2—16435
Fe-Te system, stoichiometric or nearly stoichiometric compositions, quadrupole splitting and isomer shift 2—36841
Fe-transition metal dil. alloys, h.f.s., anomalous temp. depend. of impurity moment 2—22739
$(Fe,Mg)_7Si_8O_{22}(OH)_2$, cummingtonites, ^{57}Fe quadrupole splitting 2—10324
$(Fe,Ni)_9S_8$, metallic charact., Pauli paramag., thermelec. power 2—25766
Fe, anharmonic and mag. ordering contrib. 2—40625
Fe, charge and spin perturbation around nonmag. impurities 2—22740
Fe, domain and wall hyperfine fields 2—19985
Fe, energy shift temp. and pressure depend. for ^{57}Fe 2—36325
Fe, interference between nucl. resonant and Rayleigh Thomson scatt. 2—29883
Fe, oxidation process, Mossbauer obs. 2—40813
Fe (II) complex, bis(2,2′-bipyridyl) series, spin free spin paired solids 2—19984
Fe alloy, spectrum of carbide particles rel. to martensite recovery 2—10320
Fe alloys, temp. dependence of hyperfine field near 3d impurities 2—13443
Fe complex, (Fe Salen Cl)$_2$, mag. hyperfine field, exchange const. 2—40624

Mossbauer effect continued
Fe complex, eight-coordinated tetrakis-(1,8- naphthyridine) Fe(II) perchlorate, obs. of extremely large quadrupole splitting 2—22735
Fe complex, $FeSo_4.(CH_2NH_3)_2SO_4.4H_2$, ethylenediammonium cation contrib. to Mossbauer parameters 2—13447
Fe complex, ferric β-diketones, effect of pressure on electronic structure 2—28291
Fe complexes, derivatives of $[SCH_3Fe(CO)_3]_2$ 2—785
Fe complexes, $Fe(py)_2Cl_2$ and $Fe(py)_4Cl_2$, electronic and Mossbauer spectra and mag. moment 2—16431
Fe film, spectra, analysis, thickness 1-42 Å, 15-350 K 2—40626
Fe in atmospheric air, content det. from spectra 2—1842
$Fe_{0.67}Te$, isomer shift, quadrupole splitting 2—26132
Fe^{2+} compounds, pseudotetrahedral, crystal field interpretation 2—36789
Fe_3Al, of ^{119}Sn impurity, mag. hyperfine field determ. 2—7058
$FeBr_2$, di- and tetra-hydrates, line splitting and elec. field gradient 2—19983
Fe_3C, ferromag., spin orientation detn. from Mossbauer line intensity and X-ray textures 2—36702
$FeCO_3$, origin of asymmetric quadrupole doublets 2—33223
$FeCl_2$, matrix- isolated, nuclear gamma resonance studies at 4.2°K 2—35246
$FeCl_2$, temp.-depend. cryst. field and electronic charge density 2—10323
$FeCl_2$ frozen soln., meas. from −180°C to melting point 2—10316
$Fe_{1-x}Co_xSi$, of ^{57}Fe, temp. and comp. depend. 2—26127
FeF_2, quadrupole splitting of ^{57}Fe generated by 3d electron 2—7057
$FeF_{2(3)}$, temp.-depend. cryst. field and electronic charge density 2—10323
Fe(II) and (III), complexes with 1,10 phenanthroline and 2,2′-bipyridyl, study of structure and bonding 2—7056
Fe(II) complex, phenanthroline, ^{57}Fe spectra and mag. susceptibilities down to 1.2K 2—16432
Fe(II) complexes, study of slow electronic relaxation in $^5T_2$-$^1A_1$ spin equilibria 2—26126
$Fe_2Mo_3O_8$ and $FeZnMo_3O_8$, mag. ordering and trigonal symmetry obs. 2—33220
$Fe(NH_4SO_4)_2.6H_2O$:Cu^{2+}, quadrupole hyperfine anisotropy obs. and mag. susceptibility 2—36843
$FeNi_3$, of ^{119}Sn and ^{57}Fe, hyperfine field, spin polarization 2—40623
$Fe_{1-x}Ni_xSi$, of ^{57}Fe, temp. and comp. depend. 2—26127
Fe_2O_3-Al_2O_3, spin relax. time of Fe^{3+}, impurity ions effects, Mossbauer obs. 2—40574
(1-x)Fe_2O_3-x Al_2O_3, hematite, mag. dilution effects on Morin phase transition 2—19915
$Fe_{1-x}O$, non-stoichiometry, quadrupole and Zeeman splitting 2—26129
$Fe_{1-x}O$, wustite, spectrum compared with $Fe_{1.0}O$ spectrum 2—26128
δ-Fe_2O_3, identified as dehydration product of FeOOH 2—1745
α-Fe_2O_3, r.f. magnetostrictively-induced Mossbauer sidebands, particle size depend. 2—33219
Fe_3O_4, elec. quadrupole interaction and hopping model interpret. 2—36839
Fe_3O_4, low temp. phase transition and multiple ordering 2—36278
Fe_3O_4, magnetite, Al^{3+}, Ga^{3+} or In^{3+} substituted, cation distributions, X-ray obs. 2—19049
Fe_3O_4, magnetite, low temp. spectra rel. to structural vacancies 2—26130
Fe_3O_4, magnetite, vacancy distrib., Verwey transition 2—9538
FeOCl, temp. range 1.96-298K, isomer shift, quadrupole splitting, parameters 2—4443
$Fe(OH)_2$, dehydration, haematite transformation, magnetic props., i.r. spectra 2—22862
$FeOHSO_4$, antiferromag., hyperfine field orientation, electric field gradient, ^{57}Fe energy levels 2—10325
FeOOH, thermal conversion to sesquioxide, paramag. to antiferromag. transform., Mossbauer obs., 400-900K 2—40628
$Fe_3(PO_4)_2.8H_2O$, spin flip obs. 2—40617
Fe_3Pt, of ^{57}Fe, temp. depend. of hyperfine field 2—22737
FeS, $Fe_{0.94}S$, defect structure obs. 2—35989
$FeS_{1\|x}$, phase transition obs. 2—15965
$FeSO_4$, quadrupole splittings, elec. field gradient 2—1672
$FeSO_4.7H(D)_2O$, quadrupole splitting, effect of H_2O and D_2O ligands 2—36844
$FeSO_4.7H_2O$, trimethylene glycol solution, molecular motion, diffusion 2—22738
Fe_3Si, of ^{119}Sn impurity, mag. hyperfine field determ. 2—7058
$FeSiF_6$:$6H_2O$, single cryst., principle axis location, EFG sign and mag. struct. 2—29885
$FeSiF_6.6H_2O$, quadrupole hyperfine anisotropy obs. 2—36842
FeSn, antiferromag. and paramag. states, hyperfine parameters 2—29884
FeSn, hyperfine field temp. depend. at Fe atoms 2—16434
Fe_2TeO_6, hyperfine field at Te^{6+} sites 2—40557
$FeTiO_3$, ilmenite, hyperfine interactions of Fe^{2+} 2—19986
$FeVO_4$, and cryst. struct. 2—19050
$FeWO_4$, ^{182}W spectra 2—13452
$^{56}Fe(d,p)^{57}Fe^*$, magnetic sublevel populations, polarization transfer to residual nucleus 2—18236
^{57}Fe, amplitude modulation of 14.4 keV gamma rays 2—24161
^{57}Fe, resonant absorpt., and scatt. 2—14938
^{57}Fe Mossbauer spectroscopy, 3d wave functions 2—36835
^{57}Fe Mossbauer spectroscopy, quadrupole splitting due to single 3d electron 2—36834
^{57}Fe source, prep. and isomer shift 2—38492
Gd-Sn alloy, nuclear Zeeman effect, mag. props. 2—13453
Gd compounds, ^{155}Gd, isomer shift, quadrupole splitting hyperfine interaction 2—10326
GdFe garnet, hyperfine field on ^{119}Sn, rare earth contrib. 2—22741
GdI_3, interpretation of unresolved quadrupole splitting in ^{129}I spectra 2—40629
^{157}Gd, isomer shift and g-factors 2—31488
Ge-Sn solid soln., of ^{119}Sn, quenching effect 2—29886
GeTe, of ^{129}I, isomer shift and effective charge 2—1673
He, liq., excitation spectrum near λ transition 2—12608
^{180}Hf, magnetic moment and structure of 1142 keV 8- two-quasiparticle state 2—8309
$HoFe_2$, quadrupole shift at ^{57}Fe site 2—10318
$Ho_xR_{1-x}Fe_2$, R=Tb, Er, Tm, mag. anisotropy, spin rotations and crystalline field detn. 2—26123
$Ho_xTb_{1-x}Fe_2$ cubic Laves compounds, directions of easy magnetization determ. by Mossbauer effect in ^{57}Fe 2—19916
Ir-Fe alloy, nuclear gamma resonance study, hyperfine field measurements, conc. effects 2—19979
Ir-Ni alloy, nuclear gamma resonance study, hyperfine field measurements, conc. effects 2—19979

Mossbauer effect continued
K complex, $K_2MFe(NO_2)_6$, (M=Ca, Sr, Ba, Pb), isomer shift and quadrupole splitting 2—36846
KCl, of ^{129}Te, local environment of impurity 2—10319
$K_3Fe(CN)_6$, quadrupole interaction and paramagnetic anisotropy temp. depend. 2—36845
$K_4Fe(CN)_6.3H_2O$, ferroelec. phase transition investigated 2—29888
$KFeF_4$, 2-dimens. antiferromagnet 2—26067
$KFeF_4$, hyperfine spectra, sublattice magnetiz. 2—40564
$K_2MFe(NO_2)_6$, (M=Ca, Sr, Ba, Pb), quadrupole splitting, hindered rot. of NO_2^- group, rel. to π-bonding 2—36836
$KMgF_3$, of ^{57}Fe, h.f.s., Fe^{2+} electronic props. 2—29887
$KMg_3FeSi_3O_{10}(OH)_2$, synthetic ferriphlogopite, tetrahedral Fe^{3+} parameters 2—10327
$KSbF_x$ (x=4,5,6) and KSb_2F_7, ^{121}Sb Mossbauer data rel. to structural parameters 2—1668
$K_3[Fe(CN_6)]$, proton irradiation effects obs. 2—16438
$K_4[Fe(CN_6)].3H_2O$, proton irradiation effects obs. 2—16438
$KfEf_3$, temp.-depend, cryst. field and electronic charge density 2—10323
Kr, solid, interpretation of recoil fractions of ^{83}Kr 9.3 keV transition 2—33226
$LaCoO_3$, localized to itinerant electron transitions 2—36837
LaI_3, interpretation of unresolved quadrupole splitting in ^{129}I spectra 2—40629
$LiAl_5O_8$, of $^{57}Fe^{3+}$, mag. field effects 2—40630
LiCl, of ^{129}Te, local environment of impurity 2—10319
$LiCr_{1-x}Fe_xO_2$, antiferromagnetic ordering obs. 2—19924
$Li_{0.5}Fe_{2.5-x}Al_x(Ga_x)O_4$, elec. field gradient 2—10328
$Li_3Fe(CN)_6.nH_2O$, hydration phenomena study 2—33215
Lu_2Fe_{17}, ferro-helimag. transition, Fe electronic config. 2—26034
MFe_2Se_4 (M=Ti, V, Cr, Fe, Co, Ni), mag. struct. meas. 2—19908
γ-Mn, of ^{57}Fe, moment obs. 2—40617
$Mn_{5-x}Fe_xGe_3$, (x=0.5, 1.0 and 1.5), effects of Fe substitution in $Mn_5Ge_3D8_8$ struct. 2—19867
$MnFe_2O_4$, distrib., spin arrangement 2—40617
MnO, of ^{119}Sn, Neel pt. phenomena, Zeeman splitting 2—13450
Mo-Fe dilute alloy, relaxation phenomena in Mossbauer spectra due to s-d exchange interaction 2—19978
Mo-Fe dilute system, of ^{57}Fe, relax. due to s-d exchange interaction 2—40631
$NH_4Fe(SO_4)_2$, ferroelec., spectral dip rel. to spontaneous polarization 2—6885
$(NH_4)_2SbCl_5$, ^{121}Sb Mossbauer data rel. to structural parameters 2—1668
NaCl, of ^{129}Te, local environment of impurity 2—10319
$Na_2Fe(CN)_5NO,2H_2O$, diffr. of reson. γ-rays due to quadrupole interaction 2—16439
$Na_3Fe(CN)_6.nH_2O$, hydration phenomena study 2—33215
$NaSbF_4$, ^{121}Sb Mossbauer data rel. to structural parameters 2—1668
Na_2WO_4, ^{182}W spectra 2—13452
$Na_2[Fe(CN)_5NO].2H_2O$, trimethylene glycol solution molecular motion, diffusion 2—22738
Nb-Mo alloy, with Fe impurity, localized mag. moment 2—36847
Ni-Al alloy, surface layer of diffused ^{57}Co 2—40619
Ni-Co ferrite, rel. to thermomagnetic processing 2—40528
Ni-Fe, solid soln., of ^{57}Fe, and positron annihilation 2—4445
Ni, near-paramag. region, induced magnetiz. obs. 2—40634
Ni ferrite, Co-containing, thermomagnetic effects on spectra 2—36917
$Ni_{0.67}Te$, isomer shift, quadrupole splitting 2—26132
$NiFe_{2-x}Cr_xO_4$, Mossbauer spectral investigation of crystal and band structure 2—35996
$NiFe_xCr_{2-x}O_4$, ferrite, chem. shift, mag. field on nuclei, quadrupole splitting 2—40635
Ni_3Ga:Fe very dilute alloys, meas of giant magnetic moments 2—19868
Ni_2MnSn, study of hyperfine fields at Sn sites 2—36833
Ni_2Te_3, ionicity obs. 2—4446
$Ni_xZn_{1-x}Fe_2O_4$ ferrite, mixed, spin relax., relax. times rel. to Zn^{2+} conc. 2—40577
^{61}Ni in $NiCr_2O_4$, study of electric quadrupole and mag. dipole moments of 67.4 keV level 2—5656
PbTe, of ^{129}I, isomer shift and effective charge 2—1673
$PbTiO_3$, ferroelec. transition, soft modes 2—36848
$PbZrO_3$ and $PbTi_{0.2}Zr_{0.8}O_3$, phase transitions 2—4001
Pd-Fe, solid soln., of ^{57}Fe, and positron annihilation 2—4445
Pd_2MnSb Heusler alloy, giant hyperfine field at ^{121}Sb 2—33227
Pd_2MnSn study of hyperfine fields at Sn sites 2—36833
^{141}Pr, scattering of 145.4 keV γ-rays, isomer shifts, charge radius, mag. moment 2—18124
Pt-Fe, solid soln., of ^{57}Fe, and positron annihilation 2—4445
Pt-Ir alloy, ^{195}Pt n.m.r. 2—26306
^{195}Pt, 130 keV state g-factor meas. by Mossbauer effect 2—18145
$RbFeCl_3$, one-dimens. mag. ordering obs. 2—40563
α-$RbFeF_4$, hyperfine spectra, sublattice magnetiz. 2—40564
Re, quadrupole splitting of 6.2 keV γ rays of ^{181}Ta 2—36838
Sb-Bi alloys, isomer shift and linewidth 2—16441
Sb, anisotropy in single crystal, 77 K 2—16440
Sb_xSe_y, amorphous and crystalline phase obs. 2—13451
Si, of ^{57}Fe, interstitial and cobalt-vacancy complex obs. 2—1675
Si, thermal diffuse scatt. at Bragg refls. 2—19402
Sn-S system, phase equilib. 2—1674
Sn-Se system, phase equilib. 2—1674
Sn, quantitative analysis in NBS SRM Cu-base alloys and ore concentrates by Mossbauer spectroscopy 2—16710
β-Sn, recoilless fraction temp. variation 2—36326
Sn chalcohalides, chem. shift compared with chemical shift in $K_{\alpha 1}$ line 2—10329
SnTe, of ^{129}I, isomer shift and effective charge 2—1673
SnX_2, X=halide, study of electronic config. of α-Sn 2—4097
^{119}Sn thin film, backscatter Mossbauer spectra obtained with internal conversion electrons 2—35895
^{119m}Sn, maximum resonance cross-section and f factors using solid state detector 2—11760
$SrFe_xMn_{1-x}O_{3-y}$, Fe valence state determ. 2—9492
$Sr_4Fe_6O_{13}$, rel. to antiferromag. props. 2—39652
$ThCo_{5-5x}(Ni_{5-5x})Fe_{5x}$, cryst. struct., conc. depend. 2—25348
V-Fe alloy, 80-1100 K 2—39943
W, temp. variation of recoilless fraction and thermal shift for ^{183}W 2—36327
$W(CO)_6$, ^{182}W spectra 2—13452
WO_3, ^{182}W spectra 2—13452
^{182}W spectra in W compounds 2—13452
^{183}W, linewidths and half-lives of 46.5 and 99.1 keV levels observed 2—11774
YIG, application of theory of γ-ray diffraction 2—29881
$YbCl_3.6H_2O$, paramag. relax. temp. depend. ^{170}Yb and ^{171}Yb obs. 2—10273
$Yb_2O_2S(Se)$, of ^{170}Yb, Neel pt. phenomena, mag. moments, h.f.s. 2—26133
$Yb_2(SO_4)_3.8H_2O$, paramag. relax. temp. depend. ^{170}Yb and ^{171}Yb obs. 2—10273
$ZnFe_2O_4$, spectra meas. in applied magnetic field, deduced electric field gradients at ^{57}Fe 2—1671

Motors *see Electrical machines*

Multiple stars
ADS 8197, visual binary, astrometric study 2—33621
ADS 9090, nearby long-period visual binary, parallax, orbital motion 2—33679
ADS 9094, visual binary, masses, mass ratio and parallax determinations 2—41121
ADS 9716, visual binary, masses, mass ratio and parallax determinations 2—41121
ST Aquarii, colour change of eclipsing binary30501 2—30501
β Ari, spectroscopic binary, orbital element obs. 17011 2—17011
LY Aur, O-type eclipsing binary, photoelectric obs. 30498 2—30498
LY Aurigae, eclipsing binary, differential UBV photometry 41124 2—41124
BD+16°516, Hyades member, eclipsing binary, mass loss obs. 2—37290
BD+16°516, white dwarf elipsing binary 2—37309
BD+16°516B, eclipsing binary, of white dwarf 2—1964
BD+75°403, visual binary, masses, mass ratio and parallax determinations 2—41121
binaries, Bernoulli's theorem pertaining to gas flow in close systems 2—10901
binaries, close, mass distribution 2—7449
binaries, criteria for detection amongst Wolf-Rayet stars 2—13918
binaries, dynamically formed evolution 2—20581
binaries, method for calc. of orbital eccentricity for eclipsing system, application to V526 Sagittarii 2—33681
binaries, spectroscopic, in IC 4665 open cluster, orbital elements and radial velocities 2—10895
binaries, ultra short-period, gravitational radiation and mass transfer 2—26741
binaries exhibiting a single spectrum, mass ratio rederived 2—13893
binary, β Lyr, secondary component, collapsar 2—33658
binary, BD+16°516 B component, limb darkening obs. 2—4895
binary, visual, C star and M star combined 2—26736
binary CW Cephei, u.v. observations 2—7451
binary encounters, regularization method 2—41135
binary evolution, cluster models 2—10865
binary systems, close, comparison of consequences of theories of evolution 2—4836
binary systems, dissolution time by passing field stars 2—41131
binary systems, dissolution time theory tests, evolution of energies and excentricities 2—10904
binary systems, evidence for collapsed objects in 2—10909
binary systems, evolution theories 2—7419
binary systems, period-rotational velocity relation 2—4896
binary systems, spectroscopic observations of orbital elements 2—17011
binary systems containing black holes 2—10908
44i Bootis, eclipsing contact binary, sudden period changes37310 2—37310
TY Bootis eclipsing variable, orbital solution from UBV photometry33678 2—33678
Z Camelopardalis, binary, gravitational radiation and mass transfer 2—4885
AR Cas, spectroscopic binary, orbital element obs. 2—17011
Cent X-3, X-ray pulsations due to occulting binary system 2—26799
Centaurus X-3, limiting mass 2—41156
Centaurus X-3, neutron star component 2—41157
U Cephei, close binary, emission lines and evolution 2—7455
U Cephei, eclipsing binary, rotation and evolution7456 2—7456
VV Cephei, rotationally extended Be envelope17008 2—17008
close binaries, gaseous ring envelopes, spectral absorption lines 2—26742
close binary, AW UMa, model for totally eclipsing system 2—26743
close binary, photometric behaviour 2—41123
close binary star, convective-unstable layer in periodic gravitational field 2—26745
cluster evolution, collisionless phase 2—41138
clusters, collapsing, forming run-away stars, reproducibility 2—10905
contact binaries, relative luminosity and surface brightness 2—41097
contact binary systems, energy transfer in superdiabatic part of convective envelope 2—26744
RW Coronae Borealis, eclipsing binary, light curve and orbital elements 41118 2—41118
θ CrB, binary system, near i.r. photometry 2—23080
W Crucis, long period eclipsing binary, photometric observations 2—41120
CV Serpentis, eclipse puzzle 2—7452
31 Cygni, binary of K416 and B4V spectral types, analysis of photoelectric light curve 2—7450
V 453 Cygni, minima and light elements4879 2—4879
double, astrometric obs. with Lallemand's electronic camera 2—7448
double, micrometer measures 2—20589
double, rotational coupling, correlation between true velocities 2—20580
double, statistics of obs. 2—7454
double stars, visual observations of position angle and distances of 168 objects 2—41122
double systems, UBV magnitudes and colour indices 2—4892
eclipsing, determination of period 2—7443
eclipsing binaries, instructional uses of computer 2—33846
eclipsing binaries in other galaxies 2—41125
eclipsing binary KZ Pavonis as member of visual multiple h5231 2—7453
formation, numerical expts. on escape from nonisolated clusters 2—13914
formation and escape from non-isolated clusters 2—41129
U Geminorum, binary, gravitational radiation and mass transfer4885 2—4885
γ Germinorum, spectroscopic binary, parallax and astrometric orbit26731 2—26731
gravitational N-body systems, fourth-order polynomial method for direct integration 2—41050

Multiple stars continued
Groombridge 34, nearby long-period visual binary, parallax, orbital motion 2—33679
HD 128661, spectroscopic binary, orbital element obs. 2—17011
HD 176318, binary, spectroscopic orbit 2—17007
HD 201359, spectroscopic binary, orbital elements 2—7446
HD 209813, spectroscopic binary, orbital element obs. 2—17011
HD 59543, runaway binary system, B5 star with possible collapsed companion 2—26710
HD 91948, binary, spectroscopic orbit 2—17007
θHerculis, radial velocity measurements rel. to possible binary properties 2—41104
99 Herculis, visual binary, astrometric study 2—33621
HR6773, possible eclipsing binary 2—20585
HR 2902, VV Cephei-type binary, spectral features in 1971, far u.v. observations, shell spectra 2—30461
HZ 22, old evolved binary, period velocity curve and structure det. 2—33677
UZ Leonis, eclipsing binary, photoelectric observations, light curve 41119 2—41119
lunar occultations, photoelectric measurements 2—13976
β Lyrae, eclipsing binary, radio emission obs.23091 2—23091
β Lyrae binary system new evidence of a black hole as the secondary from u.v. photometry 2—13827
TU Muscae, binary, light curve and minima20592 2—20592
one-dimensional stellar system, collisionless, multiple-phase space density, evolution 2—30453
VV Ori, eclipsing binary, UBV ground based obs., and u.v. OAO obs. 33683 2—33683
ER Orionis, binary minimum 2—20591
β Persei, eclipsing binary, radio emission obs. 2—23091
o Persei, spectroscopic binary, rel. to β Cephei stars and the II Perseus association 30493 2—30493
ζ Phoenicis, eclipsing binary, photoelectric calculation of primary minimum 2—30500
photometric proximity effects in close binary systems, average brightness weighted values of gravity and effective temperature for stars filling Roche Lobes 2—26732
AU Puppis, eclipsing binary, orbital elements det. 2—37312
vv Puppis, eruptive binary, slow variations in brightness 2—26733
VV Puppis rapid blue variable, binary, eclipses and qualitative model41108 2—41108
WZ Sagittae, binary, gravitational radiation and mass transfer 2—4885
β Sco, faint companion from occultation by Io26835 2—26835
β Sco, occultation by Jupiter, obs. H/He ratio in Jovian atmosphere 2—7523
β Scorpii, occultation by Jupiter, information on Jovian atmosphere 4963 2—4963
β Scorpii, occultation by Jupiter, u.v. photometry, interpretation of Jovian atmosphere 4964 2—4964
βScorpii, occultation by Jupiter (May 13, 1971) 2—33736
β Scorpii, occultations, solar-composition Jovian atmosphere 4966 2—4966
β Scorpii system, A-component absolute position 2—4890
β Scorpii system, occultation of individual components by Jupiter and Io30497 2—30497
semidetached binary systems, time-dependent studies of dynamical instabilities 2—26727
WZ Sge rapid blue variable, binary, light curves, flickering and bright spot 41107 2—41107
spectroscopic binaries, small amplitude, search among main sequence F-type stars 2—20579
spectroscopic binaries in Cepheus OB 3, orbital elements 2—26729
spectroscopic binaries in open cluster NGC 2516 2—17004
spectroscopic binary with a heavy companion, HD 226868, possible connection with Cygnus X-1 2—13890
stellar ring 274, bright stars distance 2—30495
triple system, velocity effects and disintegration times 2—33680
U Gem cataclysmic variables, ultra short-period binary, gravitation radiation and mass transfer 2—26741
W UMa binary systems, zero age models for contact binaries 2—30492
W Ursa Majoris, relative luminosity and surface brightness 2—41097
W Ursae Majoris, eclipsing binary, photoelectric observations, variations in light curve 41117 2—41117
4 Ursae Minoris, binary, revised orbit from spectrographic data 2—20586
V642 Orionis, eclipsing binary system, UBVRI photometry 2—20588
γ^2Vel, binary absolute magnitudes and spectral types of compounds 2—20578
BU Velorum, eclipsing binary, light curve20590 2—20590
W Ursae Majoris systems, common envelope models for V566 Ophiuchi, RR Centauri, RZ Tauri, FG Hydrae and DK Cygni 2—33684
Wolf 424, visual binary, astrometric study 2—33621
kpr 112, visual binary, astrometric study 2—33621
W UMa eclipsing binaries, structure obs., rectifiable 2—30496

Muonic atoms *see Atoms, mesic and muonic*

Muonic molecules *see Molecules, mesic and muonic*

Muonium
electronic gyromagnetic ratio, Kr-induced pressure shift 2—18369
h.f.s. pressure shifts, quadratic, in Ar and Kr 2—3012
hyperfine interval, precision meas. using Ramsey resonance in zero field 2—3011
polar media, muonium scatt. rel. to permittivity dispersion 2—22605
μ^+ depolarization, charge exchange, transverse mag. field 2—21250

Muons
see also Cosmic rays/muons; Nuclear reactions and scattering due to/muons
anomalous magnetic moment, bound for hadronic contributions 2—8123
in Fe, with momentum 30 GeV/c, focusing properties and transport with energy decrease21023 2—21023
flux calculation program in radiation shields 2—2873
magnetic moment, anomalous, order of magnitude of 8th order corrections 2—31208
magnetic moment, hadronic contribution 2—17835
magnetic moment corrections due to hadron vacuum polarization 2—5483
magnetic moment influence of heavy lepton decaying into muon and photon 2—8115
polarization vector in $K_{\mu 3}{}^{\pm}$ decays, radiative corrections 2—14635
shielding calculations, heterogeneous active and passive shields 2—2871

Muons continued
stopping muon expt., verification of existence of intermediate W-boson 2—14672
tracks and energy loss calcs. in various adsorbants, 2-600 GeV 2—5600
transport, shielding of high energy proton accelerators 2—2870
eμ mass doublet, derivation from general relativity 2—20827
μ^+ energy meas. in $\pi^+ \rightarrow \mu^+ \nu_\mu$ decay 2—379
CsI energy loss and range-energy relation 2—4091
MnCl$_2$ solution, decay of coherent spin precession of polarized positive muons 2—18851
capture
$\mu^- p \rightarrow n \nu_\mu$, radiative corrections 2—34621
^{12}C, transition rate for ground state to ground state in capture of negative muons 2—11821
decay
Fitch-Cronin effect, prediction from Gell-Mann model of CP violation 2—362
$\mu^+ \rightarrow e^- \nu_e \bar{\nu}_\mu e^+ e^-$, calc. in lowest order of weak and electromagnetic interactions 2—23803
$\mu \rightarrow e \nu \underline{\nu}$, electron spectrum analysis 2—21249
$\mu \rightarrow e \nu \nu$, mass restrictions of neutrino, W-boson and variants of weak interaction 2—14579
detection, measurement
magnetic spectrometer obs. of flux and charge ratio 2—8225
muon-spectrum charge ratio meas. at large zenith angle and high energies, survey of data 2—436
TeV energy spectrometer, sea level spectra 2—31336
interactions
anomalous interaction with hadrons studied 2—11578
beam guide, made of units of magnetised Fe, identification of intermediate bosons 2—14883
fast, cross section for electron pair production 2—24059
production and detection of spinless W boson 2—27763
$\mu(Z) \rightarrow \mu \nu \nu(Z)$, self-coupling of weak lepton currents 2—2517
W boson, spin-1, production via muon beams 2—17947
production
in cosmic radiation neutral components at sea level 2—27781
large angle pair prod., high energy collision of electron and positron beams 2—14573
massive pair prod., triple Regge and annihilation contribs. 2—17865
massive pairs, photoproduction of protons at high energies, field theoretical parton model 2—11577
pair prod. in e+e$^-$ annihilation in energy range 1.5 to 2.1 GeV 2—17837
pair production, total cross sections, Sandakov technique calc. 2—38243
multi-photon beam in nuclear Coulomb field 2—8114
sea level, via long-lived secondary particles, explanation of results on muon spectrum charge ratio meas. 2—436
$e^+e^- \rightarrow \mu^+\mu^-$ dispersion relations, (Gs)^3 terms 2—14577
$K_l{}^o \rightarrow \mu^+\mu^-$, nonlocal weak current-current coupling 2—14632
scattering
μN, high energy inelastic scatt., secondary particle production and hypothesis of banking fragmentation 2—11579
μp, high energy, weak neutral currents and polarization effects 2—34622
μp, question of anomalous interaction discussed 2—11578
$\nu\mu$ inelastic scatt., effect of lepton polarization props. on spectra and electrons and photons prod. 2—27710

Music *see Acoustics/musical*

Musical instruments
electropiano, educational, acoustical output 2—34132
flute mouthpiece, continuous displacement of lateral hole 2—34137
kettledrum, vibrating, effect on frequency of applic. of mass load at point 2—20913
orchestra music spectrum amplitude distribution 2—170
SHAKUHACHI, moisture effect on timbre 2—34134
sound loudness, difference limen 2—33798
violin, body made entirely of brass sheet, high tonal quality 2—27273
violin, vibr. modes obs. by hologram interferometry and electroacoustical meas. 2—30872
violin body vibrs. at eigenfreqs. 2—34136
violin plates, vibr. mode obs. by hologram interferometry 2—34135
violin string sounds, transient shapes 2—34133
wind instruments, pitch problem, tuning improvement method 2—34138

Navier-Stokes equations *see Flow; Hydrodynamics*

Nebulae
see also Planetary nebulae
Balmer lines, effect of flue of relativistic electrons on relative intensity 2—30434
4c51.12, radio nebula, centimetre wavelength observations 2—41148
VY C Ma, H$_2$O line emission 2—4807
Carina, OH optical depth map 2—26643
Crab, 10μm flux obs. 2—7394
Crab, γ-ray obs. 2—4948
Crab, Compton synchrotron spectrum of γ-rays calc. 2—26645
Crab, critical energy for gamma ray absorption by photons 2—10925
Crab, historical survey 2—4805
Crab, interstellar absorption of X-rays 2—37270
Crab, search for polarized X-rays using focusing graphite crystal polarimeter 2—7388
Crab, search for polarized X-rays using incoherent scattering polarimeter 2—7389
Crab γ source search at 10^{11}-10^{12} eV, lower limit to magnetic field 2—33722
Crab Nebula, balloon-borne X-ray observations, 30-100 keV 2—7482
Crab Nebula, graphite grains as explanation of 10 μm flux excess 2—7395
Crab Nebula, pulsed gamma radiation, balloon observations, 50 MeV 2—10952
Crab Nebula, X-ray polarization det. 2—41155
Crab Nebula region, obs. of γ-quanta of energy >100 MeV 2—16968
Crab pulsar, interstellar scattering two-region model 2—4934
Cygnus Loop, filamentary, obs. at 408 MHz, rel. between optical and radio structure 2—13878
dark galactic clouds, formaldehyde absorbtion at 4.83 GHz 2—7396
diffuse, image tube photography in [S III] λ9532 2—20505
diffuse, with unusual emission filaments, evidence for collisional excitation 2—10839
30 Doradus, in Large Magellanic Cloud, internal kinematics 2—16965
30 Doradus region, red stars 2—7392
DR 21, Orion, radio recombination lines 2—33614
emission models for gaseous nebulae, recombination coefficients 2—20506

Nebulae continued
filamentary, Hα, in Cygnus, distance and excitation 2—7390
galactic, radio emission, spectra characteristic of HII region 2—33618
galactic nebulosities, in southern hemisphere, positions, finding charts and descriptions 2—1944
gaseous, diffuse cosmic X-rays, characteristic line spectra, mode of excitation 2—7370
gaseous, recombination spectra, H and He lines at optical wavelengths 2—13879
gravitational wave sources, upper limit using radiometers directed at galactic centre and Crab Nebula 2—33576
Great Andromeda, most probable precise modulus 2—7393
Gum, extent and nature 2—23066
Gum, ionization and heating by energetic particles from the Vela X supernova 2—20507
Gum, model, from obs. of Lyman α photons scattered from interstellar H streaming into solar system 2—7391
Gum Nebula, low resolution radio maps in southern Milky Way 2—33619
H I region towards K3-50, soft X-rays ruled out as interstellar ionizing mechanism 2—10841
IC 418, radio recombination lines 2—33614
IC 443, supernova remnant obs. at 408 MHz 2—16967
M17, image tube photography in [S III] λ9532 2—20505
M17, obs. at 345μ 2—10969
M8, image tube photography in [S III] λ9532 2—20505
M8 and M42, Hα and [NII] profiles and brightness ratios 2—37272
NGC 2264 Bok globule, obs. of CS, HCN, X-ogen and HNC, new notation for unknowns 2—30435
NGC 2392, half angstrom filtergrams 2—4808
NGC 6210, radio recombination lines 2—33614
NGC 6888, Rosette, radio recombination lines 2—33614
NGC 7027, radio recombination lines 2—33614
Nova Delphini 1967, spectral observations between 5600 and 8800 Å (in 1970) 2—13911
NRAO 588/589, radio nebula, centimetre wavelength observations 2—41148
NRAO 589A and 4C51.12, radio nebulae, distance estimates 2—41149
Orion, Balmer line intensities near series limit 2—4804
Orion, flux density obs. at cm. wavelengths 2—4920
Orion, internal motions, OIII 5007 Å line profile and small components with radial velocities, obs. 2—13880
Orion A, H_2O line emission 2—4807
Orion A, H_2O line emission regions, study by very long baseline interferometry 2—41154
Orion A, microwave emission from nonmetastable levels of NH_3 2—10933
Orion A, W3, W49, W51, H recombination lines at 16.5 GHz 2—33617
Orion Nebula, θ^1 Orionis C, accretion of infalling ionized material 2—41087
Orion Nebula, attempt to detect interstellar molecular hydrogen 2—20599
in PHL 5200 quasar, indirect evidence for presence of dust 2—33704
photoionization of gas clouds by non-thermal radiation spectra 2—10842
photoionized, time dependence of emission line strengths 2—10840
photometry with echelle spectrograph, temperature determinations 2—26937
planetary, 37-5°1, peculiar slow nova V605 Aquilae occurring close to centre 2—20573
RSPuppis galactic cepheid, spatial and time variations in structure and light intensity 2—23078
radiation, American Astronomical Society, Amherst, USA 1971, conference 2—26623
radiative recombination of hydrogenic ions in high temp. plasmas 2—16964
radio emission at 606 MHz from small galactic nebulae, identification with optical objects 2—33616
reflection, spectrophotometric studies 2—7387
resonance line radiation escape, numerical solutions and scaling law 2—37271
solar, evolution, models, role of early interplanetary mag. field 2—4987
solar physics and gaseous nebulae, conference (Cambridge, USA, April 1971) 2—23122
solar system, mass distrib., origin from single contracting nebula 2—10990
spectrum line excitation, temperature of central star 2—33615
surrounding VY CMa, polarization and structure 2—16966
velocity-longitude plot of objects at the Galactic centre, solid rotation within 0.32 kpc 2—4792
W49, H_2O line emission 2—4807
H II and N II, interference-filter, image-tube photography 2—26646
Hα filamentary, in Cygnus, distance and excitation 2—7390
HeI singlet spectrum, calc. of recombination coeffs. and intensity ratios 2—26644
S II and O I line intensity ratios in gaseous nebulae and nuclei of galaxies 2—37266

Neel temperature *see Magnetic properties of substances*

Negatons *see Electrons*

Negatrons *see Electrons*

Nematic phase *see Liquid crystals*

Neodymium
activator in glass fluorescence of divalent manganese 2—4493
adsorbed layer, on W(111) face, elec. field influence on coverage 2—9314
aprotic laser solns., Brillouin and Rayleigh scatt. 2—32269
Arcturus, identification of Nd II in emission 2—16995
glass laser, effect of induced birefringence of active material on operation 2—11483
glass laser, kinetic operation regime, long resonator lengths 2—27511
glasses, absorption of emission from impulse lamps 2—27662
laser, frequency tuning and extraction of second harmonic radiation from prism dispersion resonator 2—37988
laser, Q-switched, radiation statistics 2—21084
laser, quasicontinuously operating under spike free conditions 2—27509
laser, with narrow spectral lines, method of generation and increasing emission 2—27512
laser radiation, third harmonic, optical initiation of directional electric breakdown in air 2—39218
lasers, numerical evaluation of amplifying media 2—7935
Nd:$SnCl_4POCl_3$ laser, circulation type, spatial and energy characteristics 2—273
$Ba_2MgGe_2O_7$:Nd, luminescence properties, exp. data 2—16617
$Bi_4Ge_3O_{12}$:Nd, Czochralski synthesis and properties 2—32405
Ge:Nd,Eu, magnetoresist., paramag. susceptibility 2—13270

Neodymium continued
HfO_2:Nd^{3+}, absorpt. spectra and emission of Nd^{3+} 2—33269
$LiTmF_4$:Nd^{3+}, fluorescence and absorption spectra, possible use as laser material 2—36944
Nd: glass, laser ring cavity, mode locking 2—5373
Nd: glass laser, high power, design of active elements 2—37986
Nd^{3+}:$CaWO_4$, polarized Zeeman fluorescence spectra, energy and polariza tion meas. 2—16615
Nd:glass fibre laser, regular pulsations of intensity of stimulated radiation 2—37987
Nd:glass laser, breakdown in gases, used in pulses or mode-locked trains of pulses 2—24895
Nd:glass laser, effect of Nd absorption bands on generation energy 2—280
Nd:glass laser, effects of u.v. on performance characteristics, need to eliminate wavelengths corresponding to inactive absorption region 2—27501
Nd:glass laser, improved material, efficiency and damage threshold obs. 2—27513
Nd:glass laser, measurements of coherence 2—37938
Nd:glass laser, multichannel, single pulse, construction 2—27510
Nd:glass laser, wavelength tuned by mixing acridine red and rhodamine 6 G in dye cell 2—5374
Nd:glass laser, with high spatial coherence of radiation 2—27507
Nd:glass laser and coude system as transportable lunar ranging system 2—23045
Nd:glass laser generation of monoimpulsive radiation on non-instantaneous inclusion of resonator 2—31048
Nd:glass laser with periodic Q-switching as source of discrete train of light pulse for high speed cinematography 2—27499
Nd:glass mode-locked laser, single picosecond light pulses 2—21113
Nd^{3+}:glass, emission spectra asymmetry 2—1711
Nd^{3+}:glass, laser, giant pulse prod. 2—23611
Nd^{3+}:$KY(WO_4)_2$, stimulated emission and laser props. 2—27508
Nd:PO_4 glass, Nd:$SeOCl_2$, Nd:$POCl_3$ lasers, narrow band oscillation, spectral line characteristics 2—17627
Nd^{3+}:$POCl_3$:$ZrCl_4$ liq. laser, *Q*-switched, output characts. 2—7928
Nd:$POCl_3$ liquid laser, spectral output props. 2—34399
Nd^{3+}:$POCl_3$ liquid laser systems, properties 2—17610
Nd:YAG, c.w. Kr arc pumped, characteristics at 20 kW 2—21088
Nd:YAG laser, applic. in optical communication system 2—21091
Nd:YAG laser, CW, second harmonic generation in $LiNbO_3$ crystals 2—37989
Nd:YAG laser, mode locked states obs. 2—21092
Nd:YAG laser, single longitudinal mode, elimination of multilongitudinal mode oscillation 2—17628
Nd:YAG laser, solar pumping 2—21090
Nd:YAG laser, time characteristics of radiation 2—17630
Nd:YAG laser, u.v. light generation by frequency doubling twice 2—11480
Nd:YAG laser optical pumping by vortex discharge as pumping source, comparative study of Ar, Xe, and Kr 2—27448
Nd^{3+}:YAG pulsed laser, influence of lamp filling on pumping conditions 2—27500
Nd:YAl garnet-$Ba_2NaNb_5O_{15}$ harmonic source 2—281
Nd^{3+}:$YAlO_3$, continuous laser action, losses 2—14427
Nd^{3+}:$Y_3Al_5O_{12}$, Nd^{3+}:$CaWO_3$ crystal laser, pyrolamp illuminator 2—27514
Nd^{3+}, amplification cross-section in $POCl_3$-$SnCl_4$-(H_2O) system 2—21081
Nd^{3+}, in crysts. and glasses, simultaneous lasing at 1.06 and 1.3 μm 2—34402
Nd^{3+}, in Czochralski grown $Y_3Al_5O_{12}$, distrib. coeff. 2—19118
Nd^{3+}, in $GdAlO_3$:Nd^{3+}, optical absorpt., luminesc. and stimulated emission spectra 2—20097
Nd^{3+}, in germanate glass, spectral and laser props. 2—20102
Nd^{3+}, in $LiYF_4$, ground term energy states, absorp. spectra obs. 2—20043
Nd^{3+}, in $POCl_3$-$ZrCl_4$, liquid laser system 2—27497
Nd^{3+}, mecanism of solubilization of Nd by Gd or Lu 2—29092
Nd^{3+}, paramagnetic impurity in yttrium ethyl sulphate, obs. from n.m.r. of proximate nuclei 2—37015
Nd^{3+} e.p.r. in SrF_2, stress-induced g-shifts 2—10524
Nd^{3+} in $Ba_{0.25}Mg_{2.75}Y_2Ge_3O_{12}$, optical spectra and laser action 2—16616
Nd^{3+} in lanthanide fluorides, far-i.r. Stark and Zeeman splitting 2—40669
Nd^{3+} in $YAlO_3$, optical spectra and intensities 2—4496
Nd^{3+} lasers, stimulated emission cross section 2—37985
$POCl_3$:Nd^{3+} laser amplifier, performance 2—23605
ZnO_2:Nd^{3+}, absorpt. spectra and emission of Nd^{3+} 2—33269

Neodymium compounds
ethyl sulphate, spin-lattice relax., mag. field depend. 2—22719
$KY(WO_4)_2$:Nd^{3+}, laser, transition cross sections, fluorescent line width and branching ratios 2—31051
La-Nd dil. alloys, spin-lattice relax. of ^{139}La 2—36786
$NaNi_2$, sp. ht., 1.6-4K 2—16038
Nd:YAG lasers, TEM_{00} output power, obs. 2—21094
Nd^{3+}:YAG laser, carrier frequency controlled gigabit pulse generation 2—7934
Nd:YAlG laser, applic. in pulse optical communications 2—21093
Nd-Bi alloy, phase diagram and elec. props. 2—1413
Nd-Dy alloys, mag. and struct. props. 2—19834
Nd-Ln-Co ternaries, Ln=Dy, Gd magnetic characteristics 2—10213
Nd-Rh alloys, Nd_3Rh, Nd_7Rh_3 and $NdRh_3$ phases, cryst. struct. 2—22161
Nd complex, neodymium tris-2,2,6,6-tetramethyl-3,5-heptanedione 2—18441
Nd^{3+} complex, energy levels, spectroscopic parameter, diffuse refl. spectra 2—26147
$NdAlO_3$, trigonal, cryst. struct. refinement from single cryst. X-ray data 2—19058
NdC_2, vaporization and surface ionization 2—35840
$NdCl_3$, magnetostriction model, second order phase transition 2—6985
$NdCo_2$, heat capacity obs. 8-300 K, rel. to mag. transitions 2—19869
$NdCo_2$, mag. ordering temp., press. depend. 2—33142
$NdCo_2$, strong field magnetiz. 2—33159
$NdCo_2$, thermal variation of lattice parameters, mag. transition 2—26054
$NdCo_3$, e.p.r., mag. behaviour 2—10518
$NdCo_3$, mag. structure, neutron diffr. obs. 2—36703
$NdCrSe_3$, elec. props., semicond. behaviour 2—10029
$NdFe_2$, Laves phase compound, synthesis method 2—22343
$NdFeO_3$, mag. struct. 2—40565
$Nd_3Ga_5O_{12}$ and $Nd_3Ga_5O_{12}$-$Ln_3Ga_5O_{12}$ solid soln., Czochralski growth 2—19003
NdH_2-NdH_3 system, dissoc. press., thermodynamic props., and soln. parameters 2—22379

- **Neodymium compounds** continued
  - Nd$_x$La$_{1-x}$OCl, phosphor, concentration quenching of luminescence by dipole quadrupole mechanism 2–36927
  - Nd$_2$(MoO$_4$)$_3$, precision lattice parameters, ferroelectric-paraelectric structural transition 2–9486
  - NdNi$_5$, sp. ht. obs., 1.6-4K 2–16037
  - Nd$_2$O$_3$-ZrO$_2$ system, solid soln. and compound formation 2–29495
  - Nd$_2$O$_3$, monoclinic to hexagonal transformation, martensitic character, electron microscope and diffr. exam. 2–4000
  - Nd$_2$O$_3$ film, breakdown strength, thickness depend. 2–13306
  - Nd(O$_2$PCl$_2$)$_3$/POCl$_3$/ZrCl$_4$, liq. laser soln. i.r. spectrum, relative intensities and frequency assignment 2–35769
  - NdPb$_3$, magnetic props., temp. range 2.8-300K 2–4346
  - NdPd$_3$, mag. props. 2–19829
  - Nd$_2$S$_3$, lattice oscillations, dielec. permittivity, molar heat capacity, i.r. spectra 2–40670
  - Nd$_2$S$_3$, struct., density, reflection spectra 2–40671
  - Nd$_2$S$_3$(Se$_3$)(Te$_3$), sp. ht. electronic component 2–1433
  - Nd$_3$Sc$_{1.35}$Fe$_{3.65}$O$_{12}$ garnet, anisotropy of magnetization at low temperatures 2–10201
  - Nd$_2$SiO$_5$-MeSiO$_3$ (Me=Ca, Ba or Sr), amorphous system, apatite phase, i.r. spectra, comp. depend. 2–18894
  - U-Co-Nd, lattice parameters, solubility limits, phase diagrams 2–9838
- **Neon**
  - absorption in solid Xe, quantum mechanical states 2–25228
  - adsorption by metals, atom probe field ion microscope obs. 2–9427
  - arcs, low voltage, fire ball mode, obs. of concn. of excited atoms 2–9014
  - atom, 3P$_0$ and 3P$_2$ metastable states, Penning ionization cross sections 2–12044
  - atom, 3P$_{2,0}$ state, impact Penning and associative ionization of Ar, Kr, Xe, two state semiclassical model 2–11974
  - atom, ^{3}P$_1$ resonance level, lifetime estimate using interference phenomena 2 31670
  - atom, collision with K$^+$ ion, excitation section structure, applicability of three term model 2–38841
  - atom, collisions with H$^+$, H(2p) and H(2s) formation, differential charge transfer meas. 2–2993
  - atom, collisions with K$^+$, determination of repulsive potentials from total scattering cross sections 2–12010
  - atom, collisions with O$^+$ at 50 to 200 keV, natural widths of kinetic energy loss distributions 2–15239
  - atom, correlation energy calc. of 1s hole state 2–21515
  - atom, electron impact ionization, total and differential cross section meas. 2–5861
  - atom, electron impact L-shell ionization calc., occurrence of delayed maxima 2–8467
  - atom, energy spectra of ejected electrons from autoionizing states excited by electron bombardment 2–15248
  - atom, hyperpolarizability calc. by Hartree-Fock method 2–11955
  - atom, ionization by ejection of outer shell s electron following electron impact, cross section for electrons up to 20 keV 2–5821
  - atom, metastable ^{3}P$_0$ and ^{3}P$_2$ states, lower lifetime limits 2–21518
  - atom, optical excitation functions 2–18362
  - atom, photoionization cross sections partition, exptl. obs. in soft-X-ray region 2–35166
  - atom, photoionization total and differential cross sections, X- and u.v. excitation, calcs. 2–18458
  - atom, polarizability, correlation corrections, error due to use of commuting potential 2–21516
  - atom, pressure broadening and shift of 1.15 μm line, constants in Lennard Jones interatomic potential determ. 2–21517
  - atom, shape of absorbed spectral line at λ=743 Å, Doppler and Lorentz broadening 2–15221
  - atom, simultaneous ionization and excitation by electron collision, cross section for 3p states of Ne II meas. 2–5804
  - atom, single charge transfer collisions with H^{++}, observed selection rule for exit channels 2–24409
  - atom, slow positron elastic scatt., energy dependence of cross section 2–5887
  - atom, spectra, metastable levels and isotopic effects 2–8453
  - atom, spectra and mean lives using beam-foil technique, 350 to 920Å 2–15222
  - atom, structure obs. in total electron impact cross section using transmission spectroscopy 2–31689
  - atom, van der Waals constants and nonadditive triple-dipole force constants calc. by coupled H.F. approximation 2–28232
  - atom ^{3}P$_{2,0}$ state, impact ionization of Ar, Kr, ^{2,0}Xe, velocity dependence of cross section 2–11966
  - atom-electron collision, vac. u.v. spectral obs. 2–18454
  - atomic spectra, isotope shifts, gain method of measurement 2–21514
  - atoms, collision with C^{2+}, N^{2+}, O^{2+}. meas. of diff. scattering with one electron capture, 0.7-3.0 keV interp. of curve crossing 2–672
  - atoms, collisions with Ar, excitation of inner and outer shells, inelastic energy losses and ionization 2–2965
  - atoms, collisions with C$^+$, N$^+$, O$^+$, Ne$^+$ at keV energies, KLL Auger electron emission 2–663
  - atoms, collisions with C$^+$, O$^+$, N$^+$, Ne$^+$, Na$^+$ K-shell excitations, differential investigation of velocity dependence 2–2967
  - atoms, differential inelastic scatt by He^{2+}, cross section meas. and single charge exchange investigation 2–730
  - atoms, elastic scatt. of H$^+$, inversion problem 2–706
  - atoms, excited, drift in d.c. discharge tube, model 2–8995
  - atoms, large angle collisions with H$^+$, differential cross section meas. and interaction potential determination 2–710
  - atoms, low energy electron scatt., ang. distribution meas. 2–725
  - atoms, low energy electron scattering, drift velocities, momentum transfer cross section 2–28208
  - atoms, slow electron scatt., phase shift analysis 2–628
  - atoms, slow electron scatt., phase shift analysis 2–5820
  - Compton profile meas. using Ag and Mo X-rays 2–18451
  - Compton scattering of X-rays from gas, comparison of exptl. and theoretical profiles 2–15234
  - contracted positive column, energy dissipation mechanism 2–24880
  - diffraction and scattering from WC surface 2–25174
  - diffusion cross sections and resonant charge transfer in 195 to 690 degrees K 2–39290
  - diffusion in B$_2$O$_3$, desorption rates, diffusion coeffs., activation energies 2–3819
  - discharge, investigation into the positive column 2–1004
- **Neon** continued
  - discharge, radiation temp., comparison with meas. from electron energy distrib. and radiometers 2–24862
  - discharge, r.f. sputtering, Penning ionization 2–4087
  - discharge, sparking voltage reduction due to mag. field parallel to electrode axis 2–9006
  - discharge radiation temperatures, comparison of those calculated from electron energy distributions with radiometer meas. 2–35609
  - electron mobility near critical point 2–35817
  - flash tubes, applic. to cosmic ray studies 2–38336
  - flash tubes, high pressure small diameter, digitisation 2–27798
  - flash tubes, use at high repetition rates 2–38379
  - flow, sorption, through hydroxyapatite compacted powder membrane, 77-303K 2–39554
  - gas, dc-induced second harmonic coefficients, calc. of absolute values 2–24984
  - gas discharge, magnetized, plasma oscillations, obs. 2–32055
  - ground term resonance line, 743 Å, accurate measurement to fifth order, calculation of other lines in vacuum u.v. 2–8427
  - ion bombardment of Ag single crystal, sputtering yields for temps. from 200-600°C 2–32859
  - ions in stellar atmospheres, continuous absorption 2–15202
  - isotopic composition in carbonaceous chondrites 2–7541
  - jet, high-energy, gas flow obs. 2–8915
  - laser, u.v., electron beam pumping 2–34381
  - leak rate through thin polycarbonate films 2–3816
  - liquid structure factor, second derivative w.r.t. pressure, quadruplet correlation function 2–35729
  - low pressure discharge, dependence of electron distrib. function on discharge current 2–15444
  - magnetoplasma, resonances in microwave emission 2–15484
  - mean life of 2p$_9$ and 2s$_5$ levels, method of incorporating cascade decay curves into atomic transition probability measurements 2–591
  - metastable atoms, high kinetic energy, rearrangement ionization reactions with D$_1$ and HD 2–12013
  - in meteorite, Assam, rel. abundance 2–1998
  - multiply charged ions, by hot cathode source 2–34860
  - optical pumping, of $J=1$-$J=1$ transition by laser line, nonlinear effects 2–24358
  - plasma, electrical conductivity det. in cascaded arcs, effect of deviations from LTE 2–28522
  - plasma, externally excited ionization waves in the weak current column 2–6092
  - plasma, metastable densities 2–8922
  - plasma, partially ionized, low temp., conductivity tensor 2–24671
  - plasma, time resolved meas. of electron distribution function in low-pressure arc 2–39096
  - plasma afterglow, highly ionized, decay and electron density obs. 2–24676
  - plasma arcs, l.v., ionisation mechanism 2–12372
  - plasma with ionization waves, time resolved obs. of electron energy distribution function 2–32073
  - positive column, oscillation in longitudinal mag. field, effect of H$_2$ on current convective instability 2–6117
  - pulsed gas laser, spatial and temporal coherence of superradiance 2–14420
  - pulsed subnanosecond laser, amplified spontaneous emission 2–31042
  - single crystal, elastic constants, Brillouin spectra obs. 2–16586
  - solar corona abundance, det. from e.u.v. spectra 2–20692
  - solid, determ. of thermal expansion at pressures to 20 kbar 2–16057
  - solid, eqn. of state, harmonic approx. 2–40032
  - solid, extreme u.v. reflection spectra 2–19995
  - solid, Hartree-Fock band struct. and optical gap 2–16104
  - solid, lattice dynamics 2–6653
  - solid, modified Morse pot., pot. energy curves, phonon dispersion curves 2–40047
  - solid P-T melting curves, exptl. determination 2–9209
  - superradiation, interaction with resonantly absorbing surface, nonlinear absorption 2–11505
  - thermal diffusion factors, isotopic, determ. 584-803 K 2–9047
  - thermal expansivity data, rel. to thermal vacancies 2–16042
  - third virial coefficients, contributions from three-body dipole and quadrupole interactions 2–22029
  - vapour pressure measurement of natural and isotopes ^{20}Ne, ^{22}Ne, from triple point to normal boiling point 2–30750
  - viscosity and thermal cond., high temp. calc. 2–18770
  - Ar-Ne mixture, thermal diffusion factor meas. 2–3333
  - D, u.v. lamps, design and emission characteristics 2–31131
  - H-Ne collisions at 10 to 35 keV, excitation of n=3 states in H 2–38849
  - H-atom impact, 20 to 120 keV, Lyman-α radiation prod. 2–18311
  - He-Ne, laser, cw at 88 THz, absolute frequency measurement 2–17174
  - He-Ne, laser, mechanical vibration noise 2–27473
  - He-Ne gas laser, oscillation frequency stabilization, by comparison with r.f. standard 2–17604
  - He-Ne laser, alignment system 2–14409
  - He-Ne laser, contrast power resonances using methane absorption cell 2–27470
  - He-Ne laser, dispersion characteristics at 3.39 μm 2–23598
  - He-Ne laser, effect of the method of introducing losses on the competition of the two modes 2–14407
  - He-Ne laser, freq. fluctuations due to acoustic noise 2–23596
  - He-Ne laser, frequency stabilisation of unmodulated output 2–11461
  - He-Ne laser, in strong magnetic field, plasma generation 2–2386
  - He-Ne laser, interaction of Ne 3s$_2$$\rightarrow$2p$_4$ and 3s$_2$$\rightarrow$3p$_4$ transitions in travelling wave regime 2–23597
  - He-Ne laser, intercavity metastable meas. 2–5353
  - He-Ne laser, internal mirror, two-mode frequency stabilization 2–31034
  - He-Ne laser, laboratory construction of multilayer dielectric mirrors 2–14416
  - He-Ne laser, limits of one frequency mode 2–31037
  - He-Ne laser, methane-stabilized, freq. stability 2–14417
  - He-Ne laser, method for stabilizing frequency using Lorentzian absorption profile in an external gas cell 2–14418
  - He-Ne laser, steady state amplitude fluctuations, natural spectral line width 2–31036
  - He-Ne laser, temp. effects 2–27485
  - He-Ne laser discharge, excitation transfer between excited He atoms and Ne 2–17603
  - He-Ne laser emission, 100% modulation 2–2419
  - He-Ne laser with Hg cathode 2–27482

Neon continued
He-Ne laser with homogeneously broadened line, competition between two axial modes 2—27483
He-Ne lasers, frequency stabilisation and instability meas. 2—14419
He-Ne mixture, laser transition $3s_2$-$3p_1$ 2—38814
He-Ne plasma, metastable densities 2—8922
He-Ne ring laser, single isotope 2—21073
He-Ne system, compressibility and virial coefficient 2—39274
He-Ne system, diffusion coeff., conc. depend. 2—24987
HeNe laser, mode coupling, obs. 2—14410
^{4}He-Ne, quasiresonant collisions, depolarization of metastable level 2—31727
Hg-Ne afterglow, electron temp. and $Hg(6^3P)$ density decay 2—32129
Na^++Ne, low energy collisions, phase interference effects obs. in total cross section 2—2979
Ne:Cs solid, optical absorpt. spectra, dynamical Jahn-Teller effect 2—10392
Ne/H abundance ratio in dwarf blue galaxies 2—26625
Ne/He streamer chamber, Lichtenberg figure ringing 2—21336
Ne-Ar, dilute solutions, far. i.r. absorption spectrum arising from collision induced dipole moments 2—9136
Ne-Ar antisymmetric system, orbital energy internuclear separation curves determ. using ab initio HF molecular orbital method 2—28214
Ne-Ar gas mixture, translational absorption spectra computed 2—5791
Ne-H mixture in bubble chamber, homogeneity and stopping power 2—2644
Ne-H^+ differential elastic scattering, inversion problem 2—666
Ne-He, internal-mirror lasers, polarization props. at 6328 Å 2—23595
Ne-He, low pressure discharge, dependence of electron distrib. function on discharge current 2—15444
Ne-He, mixture, field ionization, field adsorption 2—6382
Ne-He afterglow, electron density decay after cataphoresis 2—24677
Ne-He laser, mode selection method, saturation effects 2—17605
Ne-Kr binary mixtures and pure gas, viscosity meas. determ. of thermal conductivity and binary diffusion coeff. 2—35688
Ne-Ne symmetric system, orbital internuclear separation curves determ. using ab initio HF molecular orbital method 2—28214
Ne^+-Ne collisions, cross section for production of K shell vacancies calc. using electron-promotion model 2—24376
Ne^+-Ne collisions, inelastic, MO calculations for internuclear separation between 0 and 2.00 a.u. 2—689
Ne^+-Ne collisions, inelastic energy losses on electron transitions in outer and inner shells 2—24389
Ne gas, temp. dependence of positron annihilation rate determ. by solving Boltzmann diffusion equation 2—28229
Ne II, detectability at galactic centre, i.r. obs. 2—26619
Ne IX line emission from coronal features and electron density 2—11146
Ne IX X-ray line emission, with rocket-borne spectrometer/monochromator for solar corona mapping 2—11157
Ne VIII, 2s→nf transitions, Coulomb-Born I cross sections 2—35151
Ne VIII transitions between levels of principle quantum numbers 3, 4 and 5, identification and transition probabilities 2—31656
Ne^+, channelling in Cu, critical angle determ. using charact. X-ray generation 2—29575
Ne^+, collisional excitation of C $^2\Sigma_u^+$ state of N_2^+ 2—893
Ne^+, collisions with Ar, excitation of inner and outer shells, inelastic energy losses and ionization 2—2965
Ne^+, collisions with C foil, equilibrium charge distributions 2—5833
Ne^+, collisions with N_2 and Ne, at keV energies, KLL Auger electron emission 2—663
Ne^+, collisions with Ne, K-shell excitations, differential investigation of velocity dependence 2—2967
Ne^+, scattered through angles <2° by Ne gas atoms, 3.5 to 90 keV, meas. of inelastic energy loss spectra 2—670
Ne^+, transition probabilities for f-d transitions 2—24347
Ne^{3+}, outer shell multi configuration approx., energy matrix elements 2—28196
^{20}Ne, $3S_2$-$3p_4$ transition 2—8454
^{20}Ne, $3s_2$-$3p_4$ laser transition, pressure dependence of radiation width, broadening and frequency 2—8455
^{20}Ne, abundance on surface of magnetic neutron stars 2—30477
^{20}Ne atoms, excitation for X-ray spectroscopy 2—15216
^{21}Ne, excited levels orientation by optical pumping 2—18331
^{21}Ne, hyperfine structure of excited states and quadrupole moment, using laser-induced line-narrowing technique 2—24346
Ne+Ne, low energy collisions, phase interference effects obs. in total cross section 2—2979
Ne+Ne system, intermolec. potentials from crossed beam differential elastic scatt. meas. 2—8861
Ne^*-Xe collision, Penning ionization electron energy spectra 2—12055
$Ne^*+H_2 \rightarrow NeH^++H+e^-$, rearrangement ionization, study at high collision energies 2—10610
$Ne^*(2p^53s^3P)$+Ar, ionization total cross sections calc. semiclassically in the energy range 0.001 to 1000 eV 2—28212
Si:Ne ion implanted, crystal damage and elec. props. 2—25380

Neon compounds
NeN^+, potential energy surfaces for low lying electronic states, molecular orbital calcs. 2—15307

Neptune
atmosphere, thermal opacity due to methane-H_2 collisions 2—26823
mass determination from obs. of 5 outer planets and 7 minor planets 2—11002
position, meridian obs. for 1963-67 2—1989
satellites, physical and chemical nature 2—7535

Neptunium
spin fluctuations and anomalous resist. 2—40409
superconductivity, review 2—13147
^{238}Np fission, competition with β decay 2—2789
^{238}Np growth, neutron irradiation of ^{235}U and ^{237}Np 2—2789

Neptunium compounds
NpN, mag. props. 2—33140
NpSb, mag. props. 2—33140
$UO_{2\|x}$-NpO_2 system, phase relations 2—1405

Nernst effect *see Magnetothermal effects*

Nernst-Ettinghausen effect *see Magnetothermal effects*

Neumann algebra *see Algebra; Elementary particles; Field theory, quantum*

Neutrettos *see Neutrinos and antineutrinos*

Neutrinos and antineutrinos
see also Cosmic rays/neutrinos; Nuclear reactions and scattering due to/neutrinos
Adler's sum rules for scattering rederived using light cone commutators 2—34612
distinction between ν and $\bar{\nu}$ w.r.t. weak interactions and lepton conservation laws 2—21234
emission, rel. to angular momentum changes in astrophysical processes 2—37286
Fermi statistics of order 2, neutrino theory of light 2—38229
heavy lepton production in inclusive neutrino reactions 2—34605
heavy leptons and associated neutrinos, possible existence and astrophysical consequences 2—2516
heavy neutral lepton production 2—17825
helicity, existence of right hand spin type considered 2—34610
high energy experiments, new proposals 2—23791
high energy neutrino processes, apparent violation of $\Sigma S=\Delta Q$ rule 2—31198
high energy scattering, sum rule and light-cone commutators 2—21242
induced production reactions on p and d, isostructure of weak currents 2—34588
interactions, weak leptonic currents and form factors 2—21237
mass, upper limit, from $\mu \rightarrow e\nu\nu$ decay 2—21249
mass and degeneracy in end point behaviour of tritium β-spectrum 2—34609
mass bounds considered from spacelike side 2—34608
mass considerations and the decay $K_l^0 \rightarrow \nu\bar{\nu}_l$ 2—34611
neutrino production of charged lepton pairs, angular correlations of leptons 2—14561
pair exchange, upper bounds on possible asymptotic growth of cross section 2—8102
photon composite, statistics of two fermion system 2—38223
production and detection of spinless W boson in neutrino interactions 2—27763
production in processes of astrophysical significance, application of IVB theory 2—21239
in Rainich geometry2115 2—2115
relativistic wave equations, analysis 2—23792
scattering, chiral symmetry breaking effects 2—14564
scattering, deep inelastic, chiral symmetry breaking 2—380
scattering, deep inelastic, investigation using direct channel resonance model 2—17829
scattering, with nucleons, current algebra sum rules and duality 2—377
semi-inclusive reactions, isospin constraints 2—31199
spin-1 resonance formation in high-energy neutrino scattering, non-local effects 2—14563
stability of neutrinos with finite mass, consequences for solar-neutrino expts. 2—17827
in unified spinor field theory of relativity 2—17215
weak interactions, neutrino-lepton, rel. to lepton charge 2—17828
weakly interacting, impossibility as means of meas. black hole lepton number 2—23249
pre-white dwarf stars, effect of emission on evolution 2—20560
$e^+e^- \rightarrow \nu\nu$, dispersion relations, $(Gs)^3$ terms 2—14577
$e^-\nu \rightarrow$ hadrons, test of Weinberg sum rules for chiral $SU_2 \times SU_2$ current algebra 2—23794
$\mu \rightarrow e\nu\nu$, muon decay, mass restrictions of neutrinos, W-boson, and variants of weak interaction 2—14579
ν_μ, mass upper limit determ. from $\pi^+ \rightarrow \mu^+ + \nu_\mu$ decay 2—379
$\nu(Z) \rightarrow \nu\mu\mu(Z)$, self-coupling of weak lepton currents 2—2517
$\nu d \rightarrow \mu$-pp, elastic scattering studied at moderate energies, effect of final state interactions and deuteron binding 2—14562
νe, elastic scatt., differential cross-sections, electron polarization depend. 2—5498
νe, scattering, exptl. investigation rel. to weak interaction theory 2—38216
νe, scattering, prediction for cross sections in Weinberg's model of weak interactions 2—2518
νe, weak interaction, high energy, cross sections 2—17812
$\nu_e e^- \rightarrow \nu_e e^-$, cross sect. calc. for elastic scattering by fission antineutrinos 2—5500
$\bar{\nu}_e e^- \rightarrow \bar{\nu}_e e^-$, search for, status 2—21243
$\nu\mu$ inelastic scatt., effect of lepton polarization props. on spectra and electrons and photons prod. 2—27710
νN, deep inelastic scatt., inequalities for structure functions, algebraic structures, tests 2—27711
νN inelastic interactions, determ. of threshold relations following from scaling and duality 2—34613
νN interactions, deep inelastic, study using conserved axial vector currents and current commutation relations 2—21241
νN interactions, quark model of resonance excitation 2—31332
νn scattering, deep inelastic relations among structure functions derived using light cone commutators 2—38231
νN scattering, Low Energy Theorems use to obtain sum rules for critical cross sections at $Q^2=0$ 2—21240
$\nu_\mu \nu_e \rightarrow \mu^- e^+$, high-energy limit of lowest-order weak amplitudes with e.m. radiative corrections in ladder approximation 2—38230
νp interactions, at CERN synchrotron, cross sections, status report 2—23793

Neutron diffraction
fluids, eqns. in terms of invariant expansion of 2-body statistical correlation function 2—7700
index of refraction formalism, spin orbit effects, study of asymmetrics in neutron guides 2—25316
polarized, energy selectrion by pseudorandom modulation 2—31328

Neutron diffraction crystallography
see also Crystal structure, atomic
conference, Karlsruhe, Germany, Sept. 1971 2—25279
cryostat, for single cryst. studies, construction and operation 2—25284
cryostate, facile cond. type, for neutron diffr. expts., 4.2-300 K 2—11231
crystal impurities, inelastic incoherent neutron scatt., mass and central force const. changes 2—32793
diffractometer three-cryst., focusing effects 2—9428
finite linear chain, lattice mechanics 2—15986
Fourier transformation of intensity data, limitations for polyatomic glasses 2—22055
glass structure, quasicrystalline model 2—18897
impurity crysts., inelastic scatt. by localised vibrs., scatt. cross section 2—15710
index of refraction formalism, spin orbit effects, study of asymmetrics in neutron guides 2—25316

Neutron diffraction crystallography continued
interatomic force constants derivation from phonon frequencies 2—4027
Laue method, modified 2—25314
line width calc., integral intensity meas., neutron diffractometer with equatorial survey circuit 2—6416
magnon studies at pulsed neutron source 2—29808
monochromator, bent focusing Cu cryst. 2—25313
monochromator, high resolution, focusing 2—32432
moving lattices, modified Ewald construct. for reflected neutrons 2—22145
multiple diffr. effects in single cryst. diffractometry 2—25312
multiple-diffraction effects in intensity obs. on single crysts. 2—3609
multivariate correl. techniques for inelastic scatt. 2—19040
Pendellosung fringes, double crystal arrangement 2—9429
phonon frequency distribution function derivation, neutron inelastic coherent scatt. 2—25655
piezoelectric vibrations 2—25317
pyrolytic graphite filters 2—6417
scanning mode selection 2—3681
scanning with optimum detector/crystal motion coupling 2—3684
small angle scattering, correlation method 2—3682
small angle scattering, rel. to permittivity dispersion in polar media 2—22605
small angle scattering apparatus with multidetector 2—3683
spectrometer, triple axis, focusing conditions 2—15711
spectrometer, with improved energy resolution 2—29131
symbolic addition method for phase determ. 2—22134
topography, crystals ~1 cm thick 2—3710
transmission measurement of cross sections of Bi, Pb, Si and C, 130 eV 2—19478
triple-axis spectrometer, (Q,ω) transmission function 2—3680
vibrating cryst., neutron time spectrum 2—9430
white radiation neutron beam technique 2—32431

Neutron diffraction examination of materials
55.9% deuterated, study of H atom positions 2—29141
alloy, binary static displacement of atoms, determ. using anomalous scattering 2—3691
alloy, disordered, multi-atom interaction energies 2—15931
amorphous system, partial struct. factors separation using anomalous scatt. 2—12536
antiferromagnet, fluctuations and scattering processes near crit. mag. field 2—6988
antiferromagnetic transition metal fluorides, study of mixed crystals 2—40543
aromatic hydrocarbon cryst., phonon density of states 2—19400
aromatic molecular polycrystals, excitations and anharmonic effects, neutron scattering study 2—25667
p-azoxyanisole, nematic, self-diffusion tensor, temp. depend. 2—25045
p-azoxyanisole liq. cryst., self-diffusion anisotropy, coeffs. 2—6225
Bloch walls, elastic scatt. of cold neutrons, domain structure 2—29811
α-brass, texture transition, orientations, neutron diffr. 2—19047
carboxylic acid salts, H atom position in A-type H-bands 2—8747
clycol alcohol, mol. rot., influence of H-bond, cold neutron transmission obs. 2—15349
dynamic critical phenomena, inelastic state rel. to time depend. fluctuations above order-disorder T_c 2—19818
ethyl alcohol, mol. rot. influence of H-bond cold neutron transmission obs. 2—15349
ferromagnet, near antiferromag. transition point 2—1615
ferromagnet, scatt. from impurity pairs 2—22669
ferromagnet, spin diffusion parameter, critical scatt. 2—4358
ferromagnetic domains, single-multitransition of precipitates in Cu-1%Co 2—4361
ferromagnetic single domain, precipitates in Cu-1%Co 2—4360
glass, polyatomic, limitations of Fourier calc. 2—22055
graphite, lattice consts. variation and Debye-Waller factors 2—9865
Heisenberg antiferromagnet, magnon-magnon interaction effects 2—16391
ice I, incoherent neutron inelastic scattering data, anal. using lattice dynamical model 2—29510
inorganic materials, review 2—29133
ionic mixed crystal, magnetization 2—33103
lattice distortion around point defects, effect on scatt. cross section 2—32502
lattice vibration amplitude, evaluation from anomalous neutron scatt. 2—1420
lattice vibrs., freq. distrib. function determ. 2—32817
liquid, atomic transport coeff., rel. to neutron scatt. function 2—3360
liquid, partial struct. factors separation using anomalous scatt. 2—12536
liquid metals, in elastic scatter, correction, X-ray test 2—3362
liquids, by equal path time of flight diffractometer 2—32227
liquids, radial density function, data scaling by Krogh Moe-Norman-Vainshtain method 2—35731
liquids, scattering amplitude meas. using Christiansen filter technique 2—19038
magnetic scatt. by unfilled shells config. 2—13367
magnetic scattering of ultracold neutrons, cross sections 2—19039
magnetic structure factors, Fourier techniques 2—13365
magnetic structures, review 2—25988
metal, f.c.c., scatt. by dumbbell interstitials 2—9540
methane, liq., multiple scatt. effects, atomic motions 2—9080
methyl alcohol, mol. rot., influence of H-bond, cold neutron transmission obs. 2—15349
monosodium acetylide, crystal parameters at 293 and 5K 2—39661
non-crystalline solids, by equal path time of flight diffractometer 2—32227
orthoferrites and orthochromites, nonaxial antiferromag. axes 2—26064
paramagnet, with short range order, modified convolution approx. model 2—33112
polarized thermal neutrons, applications and techniques 2—1220
poly-DL-alanine, poly-L-alanine, chain conformation from neutron scattering study 2—35368
polytetrafluoroethylene, interchain force field and elastic constants from phonon dispersion curve 2—40039
powders, scattering amplitude meas. using Christiansen filter technique 2—19038
rare earth, scatt. theory 2—36698
rare earth metals, mag. interactions from scatt. obs. 2—16341
rare earth perovskites, ordering 2—1645
superconductor, hysteretic low-k type II, flux line arrangement obs. from depolarization expt. 2—19570
superconductor, phonon spectra obs. 2—19395
superconductor, type II, small-angle scatt. obs. of vortices 2—19591

Neutron diffraction examination of materials continued
TMMC, spin dynamics 2—22713
TMMC, spin waves 2—22697
transition metal carbides, phonon spectra, physical and chemical props. 2—6655
transition metal sulphides, $Me_xNb(Ta)S_2$ Me=Mn, Cr, Fe, Co, Ni, V 2—3722
transition metals, ferromag. density of states of majority spin bands 2—40443
transition metals, lattice dynamics 2—32814
trichloroacetic acid dimer, hydrogen bond study 2—36006
Al-V alloy, disorder-order transform. obs. 2—39994
Al-Zn alloy, pre-precipitation, small-angle scatt. obs. 2—3939
Ar, liq., struct. factor determ., 84.5K 2—39332
Ar, pair potential meas. at low density 2—9028
Ar h.c.p. single cryst. doped with 2% O_2 structure confirmation 2—18976
$BaCeO_3$, cryst. struct., lattice parameter relations, ionic radii effects 2—32443
$BaMnO_3$(2H), magnetic and cryst. struct. obs. 2—19918
$BaPrO_3$, cryst. struct., lattice parameter relations, ionic radii effects 2—32443
$BaTbO_3$, cryst. struct., lattice parameter relations, ionic radii effects 2—32443
Be phonon dispersion curves 2—19356
BeF_2, vitreous, struct. determ. 2—25160
Bi-Ca-V ferrite garnet, indirect exchange interaction, V participation 2—36739
Bi_3TiNbO_9, ferroelec., crystal structure 2—32445
$Bi_4Ti_3O_{12}$, crystal struct. 2—32446
β-brass, Ising ferromagnet, phase changes obs. 2—26029
CaF_2, data analysis in terms of thermal vibs. of atoms 2—4043
CaF_2 with excess anions, Bragg scatt. obs. of defect struct. 2—12758
$Ca_3F_2(GeO_4)_3$, mag. struct. and space group 2—33169
$Ca_3Fe_2Ge_3O_{12}$, antiferromag. struct., super-superexchange interaction 2—26059
$CaHPO_4$, monetite, H positions 2—12719
Ca_2IrH_5, crystal structure 2—3703
$Ca_3Mn_2Ge_3O_{12}$, garnet, atomic struct. 2—19045
CaO, dispersion relations curves, explained on basis of three body force model 2—36330
CaO, freq. wave vector rel. meas., combined density of states calcs. 2—36329
CaO, lattice dynamics 2—19359
CaO, phonon dispersion relations 2—19396
$Ca(OH)_2$, lattice vibrations, obs. 2—4033
Ca_2RhH_5, crystal structure 2—3703
Ca_2RuH_6, crystal structure 2—3703
CdTe:Cu(Ga)(In), detector mat. evaluation 2—36539
CeD_x, nonstoichiometric, interstitial and vaçancy obs., order-disorder transition 2—25387
Ce_2Fe_{17}, ferro-helimag. transition 2—26034
Co-Fe alloy, neutron scattering by spin waves, effect of phonon scattering 2—29808
Co, mag. form factor, high temp. f.c.c. phase 2—36708
CoF_2, two-magnon scatt. 2—40545
CoMnSb, Heuster alloy, mag. struct. determ. 2—19862
CoO, short range mag. order 2—26060
$Co_xZn_{1-x}Fe_2O_4$ ferrite, x=0.25, 0.5, 0.75, mag. struct. 2—40521
Cr-Mn, itinerant electron ferromagnet, phase changes obs. 2—26029
CrAs, mag. transition, specific heat, latent heat of transformation 2—10242
Cr_2As, antiferromag., magnetic struct. 2—33170
$Cr_xTi_{2-x}O_3$ solid solution, weak ferromag., 77-300K 2—19875
CsBr, lattice dynamics 2—6654
$CsMnCl_3$, mag. struct. 2—4409
$CsMnCl_3.2H_2O$, proton distrib., mag. struct. 2—33172
Cu-Fe dil. alloys, Kondo effect 2—19826
Cu-Mn, alloys, short range order 2—39640
Cu-Mn alloys, atomic and mag. short range ordering 2—1228
Cu-1%Co, single-multi domain transition of ferromag. precipitates 2—4361
Cu-1%Co, single ferromag. domain precipitates 2—4360
CuCl, molten, partial struct. factors 2—12538
$CuF_2.2H_2O$ crystal structure, meas. of H-O-H bond angle in water molecule at 298K 2—35985
$Cu_3(OH)_2(CO_3)_2$, azurite, struct. determ. 2—29140
D_2O-ice, phonon dispersion curves 2—19367
$DyAsO_4$, mag. struct. 2—13417
DyCu, magnetic structure 2—10238
$DyPO_4$, antiferromag. struct. determ. 2—26063
$DyPO_4$, spin structure, confirmation as ideal 3D Ising system 2—4404
DyRh, mag. struct. 2—40554
Er-Dy(Ho)(Tb)(Gd) alloys., mag. struct., anisotropy, exchange interactions, 4.2-293k 2—26024
Er-Mn-Al alloy, mag. ordering 2—40553
Er, at 4.6K in magnetic cone phase, scattering by spin waves studied 2—10189
Er, field depend. spin struct. 2—40470
$ErAl_3$, antiferromag. struct. and Neel temp. determ. 2—26065
$ErCo_3$, magnetic structure 2—36703
$ErFeO_3$, spin reorientation 2—4411
ErRh, mag. struct. 2—40554
EuO, Heisenberg ferromagnet, critical neutron scattering 2—10190
EuO, Heisenberg ferromagnet, phase changes obs. 2—26029
EuO, spin wave dispersion curves, exchange interactions 2—40472
EuS, Heisenberg ferromagnet, critical neutron scattering 2—10190
EuS, Heisenberg ferromagnet, phase changes obs. 2—26029
EuS, spin wave dispersion curves, exchange interactions 2—40472
Fe_3Al, ordered and disordered, lattice dynamics 2—16016
$FeCl_2$, mag. props. in zero field, excitations 2—26066
FeF_2, critical mag. scatt. 2—10248
(FeNi)-Au system, mag. moment props. 2—36712
Fe_3O_4, magnon dispersion relations 2—36748
FeRh alloy, ordered, diffuse scatt., mag. moment obs. 2—10247
Ga, liquid at 20°C, determ. structure functions, comparison with X-ray diffraction data 2—15565
Ga, supercooled, quasi-electric scatt., struct. factor 2—15566
GaAs, and X-ray scattering, by non-thermal phonon groups 2—4034
Gd, mag. moment distrib. 2—19879
Ge, diffr. topographs 2—3710

Neutron diffraction examination of materials continued
- Ge, phonon density of states, 80K 2—32809
- GeO_2, vitreous, struct. 2—22056
- H_2, h.c.p. and f.c.c., phonon density, libron states density 2—19397
- HCl single crystal, structure and phase transition 2—32457
- He, h.c.p., Bragg refls., anharmonicity 2—16017
- He, liquid, investigation of excited state above phonon-roton spectrum 2—15620
- ^{4}He, b.c.c. single crystal, inelastic scattering, determ. dispersion relations, elastic constants 2—25135
- ^{4}He, b.c.c. solid, inelastic scattering, Debye-Waller factor, phonon interaction processes 2—35815
- Ho-Dy alloy, mag. struct., anisotropy, exchange interactions, 4.2-293k 2—26024
- $HoCo_3$, magnetic structure 2—36703
- HoRh, mag. struct. 2—40554
- $KCl:NH_4Cl$, local torsional and translational modes 2—19399
- $KFeF_4$, 2-dimens. antiferromagnet 2—26067
- $KFeF_4$, mag. struct. 2—40564
- KHF_2, rel. to crystal and molec. dynamics 2—26169
- KH_2PO_4, ferroelec. phase transform., lattice modes 2—19398
- KN_3, lattice dynamics 2—4035
- $KNbO_3$, cubic ferroelectric, phase transition, diffuse mode scatt. 2—13318
- $KTa_{0.63}Nb_{0.37}O_3$, cubic ferroelectric, soft phonon dispersion modes 2—13029
- $KTaO_3$, linear- displacement correls. 2—22408
- $La_{1-x}Ba_xMn_{1-x}M_xO_3$, M=Mn, Ti, cryst. and mag. struct. 2—4362
- $LiCrS_2$, mag. struct. 2—3713
- $LiH_3(SeO_3)_2$, ferroelectric, hydrogen bonding 2—25335
- $LiVs_2$, mag. struct. 2—3713
- Lu_2Fe_{17}, ferro-helimag. transition 2—26034
- MFe_2Se_4 (M=Ti, V, Cr, Fe, Co, Ni), mag. struct. meas. 2—19908
- Mg, normal-mode frequencies at 290K, meas. by slow neutron inelastic scatt. 2—6656
- Mg_2Pb, lattice dynamics 2—25664
- $MgZn_2$, inelastic scatt. cross section, group theoretical calc. 2—22402
- Mn_3B_4, mag. struct. determ. 2—22709
- $MnCO_3$, spin-wave excitations and dispersion curves 2—36760
- $MnFe_2O_4$, magnon dispersion relations 2—36748
- Mn_3NiN, magnetic structure and spin rotation 2—1644
- MnO, paramagnet, modified convolution approx. model applied 2—33112
- MnO, spin wave spectrum, 4.2K 2—36775
- $Mn(OH)_2$, mag. and cryst. struct. 2—36776
- $x\ Mn_3O_4+(1-x)Cu(Fe,Cr)_2O_4$, cation distrib. rel. to lattice distortion, X-ray and neutron scatt. obs. 2—22720
- MnP, helical, magnetiz. process 2—40497
- $MnPd_2$ antiferromagnet, cryst. and mag. struct. determ. 2—16398
- $MnPt_3$, ferromag., spin-wave dispersion, phonons, neutron scatt. obs. 2—22676
- $MnPt_3$ alloy, antiferromag. coupling of nearest-neighbour Mn atoms 2—19925
- NH_3, liquid, mol. motions 2—35726
- NH_3, solid, neutron scatt. kernel 2—40038
- NH_4Br, use of different procedures 2—25341
- Na, phonon meas., resolution effects 2—4036
- $NaCa_2Ni_2V_3O_{12}$, garnet, with one sub-lattice, disposition parameters of O atoms 2—6445
- $NaHF_2$, rel. to crystal and molec. dynamics 2—26169
- $NaNO_3$, lattice dynamics 2—19381
- $Na_2O.SiO_2.6H_2O$, location of hydrogen atoms 2—6442
- Nb, supercond., flux line lattice obs. 2—9967
- Nb single crystals, quasielastic scattering expts., hydrogen diffusion study 2—9611
- Nb_3Sb, observation of softening of acoustic shear modes near phase transition at 45 K 2—9864
- $Nb_{0.73}Ta_{0.27}$, supercond., flux line lattice obs. 2—9967
- $NdCo_3$, magnetic structure 2—36703
- $NdFeO_3$, mag. struct. 2—40565
- Ni-Fe-V system, ordering 2—39938
- Ni-22.7-38 at.%Mn alloy, phase transform., 673-908 K 2—25635
- Ni, domain size and stability, scaling laws, Curie pt. region, neutron depolarization obs. 2—16365
- β-$Ni(IO_3)_2.2D_2O$, atomic crystal structure and magnetic structure 2—9484
- Ni_3Mn, phase transitions, small angle scatt. obs. 2—19303
- NiMnSb, Heusler alloy, mag. struct. determ. 2—19862
- NiS, metal-insulator paramag.-antiferromag. transition 2—16349
- α-O_2, solid, mag. form factor determ. 2—29839
- $PrCo_3$, magnetic structure 2—36703
- $Pr_{0.333}Cu_{0.1}Al_{0.566}$, crystal field effects in magnetiz. temp. dependence 2—10216
- $PrFeO_3$, mag. struct. 2—40565
- $RbFeCl_3$, one-dimens. mag. ordering obs. 2—40563
- α-$RbFeF_4$, mag. struct. 2—40564
- $RbMnF_3$, Heisenberg ferromagnet, phase changes obs. 2—26029
- S, liquid, coherent scattering amplitude and total effective cross section to subthermal neutrons 2—18791
- Se, hexagonal, compressibility 2—32600
- Se, hexagonal, determ. of anisotropic compressibility and thermal expansion 2—15731
- Se, phonon dispersion curves, acoustic mode meas. 77 K and 298 K, optical mode meas. 77 K 2—4042
- Si, wedge shaped crystal, Pendellosung fringes, double crystal. arrangement 2—9429
- SiO_2, amorphous, total small angle scatt. cross-section 2—22051
- SiO_2, quartz, rel. to diffuse X-ray scatt., near α-β transition 2—4038
- Sm, mag. struct. 2—40494
- SrF_2, data analysis in terms of thermal vibs. of atoms 2—4043
- Sr_2IrH_5, crystal structure 2—3703
- Sr_2RhH_5, crystal structure 2—3703
- Sr_2RuH_6, crystal structure 2—3703
- $SrTiO_3$, critical behaviour near 105K 2—15974
- $SrTiO_3$, displacive type transition, phonon freqs. 2—19305
- Tb-Mn-Al alloy, mag. ordering 2—40553
- Tb, magneto-elastic coupling, acoustic wave vel., magnon-phonon interactions 2—13393
- $TbCo_3$, magnetic structure 2—36703
- Te, liq., struct. evolution, temp. depend. 2—12539
- UAs-USe system, mag. phase transitions 2—4380
- UC-ZrC solid solns. cubic lattice parameter var. with temperature and composition 2—15733
- U_4O_9, superlattice struct. 2—32475
- α-VH_x (x=0.198, 0.57), quasielastic thermal neutron scatt. investigation of H diffusion 2—36073
- Yb_2O_2S, magnetiz. process obs. rel. to Yb^{3+} crystalline field 2—19928
- Zn, phonon freqs., 80K 2—1423
- $ZnCr_2O_4$ exchange integral determ. from paramag. neutron scatt. obs. 2—22666
- $Zn_{0.87}Mn_{0.13}Fe_2O_4$, mag. struct. obs. 2—36784

Neutron radiography *see Radiography*

Neutron sources *see Neutrons and antineutrons/production*

Neutron spectra
- accelerator, fission yields 2—511
- activation integrals of threshold detectors used for fast neutron spectrum investigations 2—34822
- in alumina spherical pile, meas. by time-of-flight method, eV-MeV range 2—28102
- in barytes concrete pile, meas. by time-of-flight method in MeV-300 keV range 2—28103
- collimated fast neutron energy spectra for variety of Pu-Be sources 2—11790
- cosmic origin, flux variation of fast neutrons meas. as function of geomagnetic latitude and altitude 2—41016
- delayed nuclear fission products 2—2827
- Doppler effect measurements on small fuel samples, interpretation for fast reactor 2—28137
- energy spectra from different size ^{239}Pu-Be(α,n) sources 2—28010
- fast reactor spectra, threshold detector evaluation 2—38351
- fast subcritical assembly, STSF-1A, containing ^{238}U, ^{235}U and BeO, 50 eV-8 MeV 2—38732
- ice, steady-state spectra, 268 to 4K 2—8378
- nuclear reactor, critically built VVR-M type, integrated characteristics 2—28156
- p-wave capture 2—38611
- scattering of fast neutrons from natural lead targets, 2.2-2.4 MeV, angles >175°, obs. of resonance 2—24225
- shield-leakage from synchrocyclotron 2—2885
- single event spectra, Monte Carlo analysis 2—28106
- thermal, discrete energy represen., scatt. matrix constr. 2—38673
- time-of-flight, quasi-elastic and inelastic cold neutron scattering separation using fast Fourier transforms 2—11836
- time-of-flight det., anal. of efficiency of detection of captured γ-rays 2—27892
- (^{3}He,n) reaction up to the continuum near A=50 2—31582
- $^{87,\ 88}$Br as precursors for delayed neutrons, low energy spectrum 2—5728
- ^{87}Br, β decay, γ ray emission in competition with neutron emission 2—18160
- ^{12}C, in Po-Be source, spectrum from 4.43 MeV level 2—21374
- ^{40}Ca, spectrum and asymmetry of neutrons emitted after polarized muon capture 2—35059
- ^{48}Ca intermediate structure, S- and P-wave neutron spectroscopy 2—24160
- ^{49}Ca, S- and P-wave, doorway-state theory of intermediate structure applied to neutron doorway escape widths for 2p-1h states 2—24159
- Er, A=164, 166, 167, 168, 170, neutron resonance spectroscopy, level spacings, Dyson's theory 2—34967
- ^{137}I, β-delayed neutron energy spectrum meas. with high resolution neutron spectrometer 2—24185
- Na_2CO_3 anhydrous pile, meas. at energy of Na_2 resonance with time-of-flight method by an electron linac 2—28101
- ^{16}O, spectrum and asymmetry of neutrons emitted after polarized muon capture 2—35059
- ^{207}Pb intermediate structure, S- and P-wave neutron spectroscopy 2—24160
- Pu fast reactor, compared with fundamental mode calculated values 2—536
- $Pu(NO_3)_4$, scattering kernels of ^{239}Pu and H compared with theoretical calculations in three different solutions 2—520
- ^{89}Sr, S- and P-wave, doorway-state theory of intermediate structure applied to neutron doorway escape widths for 2p-1h states 2—24159
- U fast reactor, compared with fundamental mode calculated values 2—536
- ^{235}U unreflected critical assembly, fission spectrum 2—38710
- ^{91}Zr, S- and P-wave, doorway-state theory of intermediate structure applied to neutron doorway escape widths for 2p-1h states 2—24159

Neutron spectrometers
- calibration of low intensity neutron sources 2—8227
- crystal system, with improved energy resolution 2—29131
- direct-charge detectors for beams 2—27852
- double chopper facility for wavelength range 4 to 16 A 2—14751
- fabrication of thin flat Co mirrors for polarization of thermal neutrons 2—17995
- fast neutron time-of-flight spectrometer, extension to two-detector system 2—27854
- organic scintillators, for fast neutron spectroscopy, influence of neutron induced alpha particles on pulse height 2—31361
- proton-recoil, simultaneous det. of fast-neutron spectra by time-of-flight and pulse height unfolding 2—8228
- proton-recoil proportional counter spectrometer, response functions 2—24076
- using proton-recoil proportional counters, in energy range up to 10 MeV 2—27864
- shelled activation detectors, measurement at kV energies 2—5580
- slow rotating crystal time of flight spectrometer, general freq. spectra meas. 2—31353
- spin-flip-chopper with high repetition rates 2—11656
- time of flight, for meas. of scattered neutrons from 150 cm cyclotron 2—18001
- time of flight, operation 2—27836
- time of flight fast, design and fabrication 2—21325
- time of flight system for ^{2}H(d,n)^{3}He reaction 2—34825
- time-of-flight, for neutron-gamma coincidence expts. 2—38359
- time-of-flight, STEK 2—18005
- time-of-flight facility, detector efficiency 2—27839
- triple axis, focusing conditions 2—15711
- triple-axis, (Q,ω) transmission function 2—3680
- tripleaxis, high resolution, design 2—27837
- two crystal diffractometer, for IRT-m pulsed reactor applications 2—18006
- In foil neutron detector, Cd ratio for atmospheric neutrons 2—21331

Neutron transport theory
see also Neutrons and antineutrons/diffusion; Neutrons and antineutrons/moderation
absorbing multipoles, doubly-periodic array 2—28109
accelerators, high eneergy protons, access tunnels 2—2876
anisotropic collision probabilities in cell problems 2—38676
anisotropic diffusion coefficient in generalized x,y geometry 2—8383
anisotropy, use of Au resonance foils 2—28107
asymptotic spectra det. and false absorption effect 2—38674
atmospheric neutrons, effects of ground on steady state and time dependent transport 2—7318
i-group bidimensional finite medium convolution fluxes 2—2837
Boltzmann equation, boundedness, continuity, positivity and dominance of the soln. 2—28110
CIRENE reactor, program for calc. nuclear coeffs. of axial reflector 2—2849
constant collision density assumption in intermediate region 2—514
cylindrical duct with helical iron plug, spatial distributions of neutrons and photons 2—5765
difference schemes for solving neutron transport equation 2—521
diffusion, coeff. det. in XY geometry, TRUD anisotropic diffusion code for computation 2—38675
diffusion, few-group theory, adequacy for calcs. for loosely coupled cores 2—516
extrapolation distance calc. for one-group transport with anisotropic scattering 2—23308
fast multiplying syst., eigenvalue spectrum of transport operator 2—38679
fast reactor flux and importance spectra, model 2—8382
fermi-age equation, approx. solution, modal analysis 2—18251
finite reactor lattice, flux, disadvantage factors and diffusion in square cells and slabs 2—38680
first flight collision probabilities in annular system and its application to cluster geometry 2—5733
first-flight probabilities, linear anisotropic, for cylindricalized Wigner-Seitz cells 2—512
flux distribution control in nuclear reactors, performance simulation on hybrid computer 2—8401
flux perturbations due to absorbing foils, variational method accuracy 2—8379
fuel lattices, cluster type, calc. of collision probabilities 2—513
fusion reactor blankets, neutron physics 2—31618
Green's functions and interpretation of Poincare-Bertrand formulae 2—2836
high temperature lattice test reactor, neutron multiplication factors as function of temp. 2—8391
hybrid method for solving reactor space-time-dependent equations 2—28123
information flow for the treatment of discontinuities in synthesis techniques 2—28114
integral versions of area ratio method of pulsed neutron reactivity meas. 2—24252
inverse neutron kinetics technique, reactivity calibrations, error sources 2—24254
Milne problem, thermal neutron, applic. of normal mode expansion method 2—515
moderator correction for wide resonance using Greuling-Goertzel approximation 2—38669
monoenergetic Boltzmann equation, solution for finite parallelepiped 2—24255
monoenergetic Boltzmann equation, solution in cylindrical geometry 2—24256
multigroup, particular solutions 2—2835
multigroup criticality problem, solution using eigenfunction expansion method 2—31617
multigroup criticality problems, eigenfunction expansion method of solution, treatment of sloping plane boundary interfaces 2—31612
multigroup cross sections, rigorous collapse procedure 2—38683
multigroup diffusion theory, variational flux synthesis methods 2—38682
multigroup diffusion theory perturbation program JINX 2—5737
multigroup transport equation, degenerate kernel 2—21460
nuclear reactor neutron dynamics in space-time, analysis on hybrid computer 2—8402
operator, eigenvalue spectrum for fast multiplying syst. 2—38679
optimum flux bounds for space-time reactor problems, using linear programming 2—8390
penetration in infinite homogeneous media, bounds to truncation errors in biorthogonal polynomial approx. 2—27105
perturbation theory, generalized, reactor integral characteristics 2—75
point kinetics equation soln. 2—5734
reactor kinetics, formulation and application of transfer and scattering matrix techniques 2—28122
reactor problems, evolution operator method 2—31616
reactors two-dimensional shielding calculations using combination of diffusion theory and line-of-sight method 2—38771
scattering method order in plane geometry, one-velocity problems 2—38681
slowing down equation, infinite medium Green function with energy dependence 2—31614
slowing down equations, Goertzel-Greuling form 2—38677
space-energy-time iterative synthesis in diffusion theory 2—35100
spectral codes, positive difference scheme based on Greuling Goertzel approximation 2—522
stochastic model, dilute neutron gas 2—38686
thermal neutrons, near moderator discontinuity, Boltzmann eqn. 2—35099
thermal scattering kernels, Cadilhac models 2—15032
thermal-neutron spectra, discrete energy represen., scatt. matrix constr. 2—38673
three dimensional problems, synthesis using two dimensional trial functions 2—38685
transmission and reflection coefficient with anisotropic scattering 2—15031
transport equation, applic. of Noether's theorem 2—21461
two-group with anisotropic scattering 2—11889
Usachev-Gandini perturbation theory, formal functional treatment and variational principle 2—38684
variational synthesis with discontinuous trial functions 2—27036
CeH$_x$, neutron thermalization rel. to moderator applic. 2—31613
Fe bulk assemblies, experimental and analytical studies 2—28112
YH$_x$, neutron thermalization rel. to moderator applic. 2—31613

Neutrons and antineutrons
see also Cosmic rays/neutrons; Nucleons and antinucleons
abundance in synthesis of light elements 2—8206
in atmosphere, effects of ground on steady state and time dependent transport, and secondary γ rays 2—7318
beta decay, T-violating effects, generalisation of Kim-Primakoff theorem 2—31327
charge, investigation using ultra-cold neutron beam in intense elec. field 2 431
in chemical analysis, resonance method for determ. high B concs. 2—30128
dose distrib. of fast neutrons, in concrete labyrinth 2—2875
electric dipole moment, limit imposed on nuclear time-reversal-invariance violation 2—34901
flux distrib., radial and axial, in Gentilly BLW reactor 2—5740
form factors, charge, from threshold π electroprod. 2—27750
leakage through personnel penetrations in hadron shields 2—2874
mass difference between proton and neutron 2—17971
neutron gas, symmetry energy and single particle potential, rearrangement contribution 2—11713
properties and applications, educational article 2—8205
proton-neutron mass difference, finite difference in structure functions, scale invariance 2—17959
scattering by lattice site, model for blocking effect 2—9904
structure function, sum rule for difference from proton structure function 2—27774
structure functions, ratio with proton functions effect of t-channel descript. of electroprod. 2—17832
transmission measurement of cross sections of Bi, Pb, Si and C, 130 eV 2—19478
np, mass difference, calc. taking into account i.r divergent contributions to mass shift 2—5142
p-n e.m. mass difference and inelastic electron scattering 2—38312
p-n mass difference, computation in Sudarshan theory of universal primary interactions 2—17960
p-Si, calc. of reverse annealing 2—19690

absorption
see also Nuclear excitation; Nuclear reactions and scattering due to/neutrons
air, total cross section for ultracold neutrons 2—18250
attenuation in shielding materials 2—38769
diffusion in aqueous absorbing solns. from fast point source 2—5735
field neutron moisture meter, vertical resolving power improvements 2—13629
glass, total cross section for ultracold neutrons 2—18250
mica, total cross section for ultracold neutrons 2—18250
pyrolytic graphite filters 2—6417
regular absorption systems, analysis 2—28098
sources in moderating solutions, cavity-wall and self-absorption correction factors 2—28104
Al, total cross section for ultracold neutrons 2—18250
Au, total cross section for ultracold neutrons 2—18250
B filter, calc. of neutron transmission function, 1/E spectrum in graphite moderator 2—544
BeO, attenuation const., derivation from amplitude and phase shift meas. of thermal neutron waves 2—28108
Cd filter, calc. of neutron transmission function, 1/E spectrum in graphite moderator 2—544
Cu, total cross section for ultracold neutrons 2—18250

angular distributions
air-ground interface effect, last-collision model 2—28115
earth albedo neutrons from 10 to 100 MeV 2—37198
fission neutrons emitted from individual fragments of spontaneous fission of ^{252}Cf 2—8375
prompt neutrons, from fast neutron induced fission, fission fragment anisotropy effects 2—35090
(p,n) reactions in ^{18}O, ^{37}Cl, ^{41}K, ^{53}Cr, ^{59}Co, reaction cross sections 2—14985
^{12}C, energy levels between 1.7 and 6.4 MeV using ^{9}Be(α,n)^{12}C reaction 2—31573
^{12}C(d,n)^{13}N*(p)^{12}C, measurement of neutron-proton correlations 2—31578
^{2}H(d n)^{3}He ang. distrib. of vector analysing power 2—18224
Pb target, A=206 to 208, inelastic scattering of neutrons at 13.7 MeV 2—38617
Pb(n,n), A=206 to 208, study at 13.7 MeV 2—38606

capture *see Nuclear reactions and scattering due to/neutrons*

detection, measurement
see also Dosimetry; Neutron spectrometers
activation integrals of threshold detectors used for fast neutron spectrum investigations 2—34822
by associated particle counting, discrimination technique 2—11669
corona counters for slow neutrons 2—2639
cosmic ray ionisation detector, patent 2—21327
density fluctuations in nuclear reactors, model kinetic equations 2—5730
detector sensitive to spot at which neutrons have been transmitted using proportional counter 2—31357
flux density distrib. around neutron generator target 2—28105
flux density meas., using fission chamber as secondary standard 2—11650
flux density standard, correction factor for perturbations caused by activation probe 2—5731
flux monitoring in activation analysis, use of Fe foils 2—28157
gamma quanta separation using two-dimensional analysis mode 2—24082
gaseous chemical dosimeters, mixed reactor radiations 2—559
hodoscope using multiwire proportional counters 2—24096
in-core self-powered neutron detectors, high- temp. performance 2—15172
integral flux in range 10^{14}-10^{16} thermal neutrons per cm^2 determ. by gold foil activation 2—11887
intensity of high energy neutron beam for biological and medical applications 2—5042
low energy spectrum of delayed neutrons from ^{87}Br and ^{88}Br precursors 2—5728
nuclear reactor safety instruments neutron burst signals, detection using multiplication 2—38763
organic scintillators, measurements and calculations of efficiencies 2—2633
PENA flux measuring system with fast-response 2—5595
plastic scintillator, absolute efficiency in 1-200 MeV range 2—34790
polarization studies using spin-precession method with continuous energy spectrum 2—23891

Neutrons and antineutrons continued
detection, measurement continued
polycarbonate detector sandwiched between U fission foils, track obs. 2—38390
proton-recoil proportional counter for obs. in energy range up to 10 MeV 2—27864
pulse shape analyzer for fast neutron- gamma discrimination in liquid scintillator 2—14774
radiographic imaging, multiwire proportional chambers adaption with delay line readouts 2—27863
radiography, position-sensitive proportional counter 2—27862
scintillators, computer simulation of detection process 2—24083
sensor, self powered for flux obs. in high temp. nuclear reactor 2—11914
spectrometer, time of flight, fast, design and fabrication 2—21325
spectrometer, two crystal diffractometer, for IRT-m pulsed reactor applications 2—18006
thermal neutron flux densities, unit of measurements 2—35098
threshold detectors of fast neutron spectra, evaluation 2—38351
threshold detectors using principle of neutron fission reaction 2—27853
threshold miniature counters operating in corona region 2—31358
time of flight spectrometer for meas. of scattered neutrons from 150 cm. cyclotron 2—18001
velocity selector for cold neutrons using two rotor phased chopper system 2—27893
B lined chamber working under current collection and no multiplication conditions, for whole dynamic range of reactor 2—31375
BF_3 proportional counter immersed in water moderator, for study of photonuclear reactions 2—18009
$Cd(NO_3)_2$ and NaCl solutions as detector for recording of neutrons 2—38365
^{235}U unreflected critical assembly, time-of-flight and multiple foil meas. 2—38710
W, thermal flux monitor at v. high temps. 2—8239
diffusion
see also Neutron transport theory
absorbing aqueous solns. from fast point source 2—5735
anisotropic diffusion coefficient in generalized x,y geometry 2—8383
asymptotic theory, extension to reflected syst. 2—38672
coeff. det. in XY geometry, TRUD anisotropic diffusion code for computation 2—38675
in crystalline moderator assemblies, diffusion length, effect of transverse dimensions 2—517
few-group theory, adequacy for calcs. for loosely coupled cores 2—516
finite element method, applic. to reactor physics problems 2—38678
finite element method, application to multigroup diffusion equation 2—28111
first flight collision prohbabilities for neutrons in annular system and its application to cluster geometry 2—5733
ice, pulsed-neutron diffusion parameters, at −20°C 2—518
multigroup diffusion theory, variational flux synthesis methods 2—38682
perturbation theory, generalized, reactor integral characteristics 2—75
space energy factorization evaluation for two dimensional problems in liquid metal fast breeder reactor 2—5736
space-energy-time iterative synthesis in diffusion theory 2—35100
theory for media consisting of lattices of large cross section cavities 2—38668
thermal neutrons, comparison of pulsed neutron technique and stationary method 2—28153
Usachev-Gandini perturbation theory, formal functional treatment and variational principle 2—38684
BeO, amplitudes and phase shifts of thermal neutron waves meas., attenuation and phase shift constants derivation 2—28108
H_2O-D_2O mixtures, pulsed-neutron diffusion parameters, near freezing point 2—518
effects
see also Nuclear reactions and scattering due to/neutrons
asbestos, composition of blended samples by neutron activation analysis 2—7199
atomic displacement model for crystals 2—12744
boronated graphites heated to 1400°C and 2000°C, exptl. study of radiation effects on mechanical properties 2—32570
chromosome rupture 2—2021
creep deflection of pressure tubes in horizontal reactors 2—15167
creep mechanism and dislocation climb in irradiated materials 2—22273
damage and annealing in high purity Ge radiation detectors 2—24091
depleted zone formation and recovery, during neutron irrad., theory 2—6471
diamond, heavy irrad. effect on elec. resist. 2—36496
diamond, neutron-irradiated, e.s.r. spectra 2—40755
diode frequency mutlipliers, step-recovery 2—22582
dose distributions in wet tissue as a function of LET_∞ 2—5060
embrittlement by irradiation, f.c.c. alloys 2—1319
embrittlement of reactor pressure vessel steels, high temp. damage functions 2—11905
fast neutrons, biological effects, obs. 2—30669
f.c.c. crystal, irradiation strengthening 2—15895
glass, Ge-Te(Se), fast neutron damage threshold 2—1516
graphite, dimensional changes under irradiation 2—12747
graphite, fast neutron dose effect on struct. 2—11911
graphite, irrad., dimens. and phys. prop. changes 2—21471
graphite, irrad., dimensions, elec. resist. and Young's modulus meas. 2—39873
graphite, irrad., dimensions, thermal expansion, porosity and microstructure 2—3756
graphite, irrad., dimensions, thermal expansion and microstructure 2—3759
graphite, irrad., effect of pitch-binder coke content on props. 2—22175
graphite, irrad., elec. resist. rel. to thermal cond. 2—13220
graphite, irrad., negative magnetoresist. 2—22528
graphite, irrad., submicroporosity temp. and dose depend. 2—29165
graphite, irrad. damage, effect on interlayer props., model 2—3758
graphite, low temp. irrad., Young's modulus and internal friction 2—22259
graphite, nuclear, neutron irrad. above 1200°C, increased mech. lifetime, radiation damage 2—19152
graphite, pyrolytic, irrad. 250-470°C, change in dimens. density, thermal cond., thermal expansion coeffs. 2—19432
intermetallic compounds, irrad., struct. and props. 2—9518
on logic circuits, TTL, radiation hardened, response 2—18019
on LSI/m.o.s. logic system 2—17520
metal, b.c.c. and f.c.c., point defect prod. and recovery 2—15745

Neutrons and antineutrons continued
effects continued
metal, irrad., void nucleation, computer evaluation 2—29163
metal, resistivity, recombination volumes 2—25763
p-i-n microwave diode switches, permanent damage 2—22583
miniature pig performance, compared to gamma irradiated pig performance 2—20721
nuclear fuel compacts, coated particle matrix type, irrad., dimens. and phys. prop. changes 2—21471
nuclear fuel elements, irradiation analysis 2—14169
nuclear materials, irrad., swelling, quasi-chemical model 2—32489
nuclear reactors, damage surveillance, interpretation of structural significance 2—15150
p-n junction formation by in-pile irradiation doping of Si^{30} 2—13280
piezoelectric quartz vibrators, resonance frequency and elastic properties 2—25934
ratchetting growth of materials due to thermal cycling 2—15825
reactor fuel, post-irrad. exam., sampling methods 2—38756
reactor fuel, post-irrad. exam. techniques 2—38755
reactor fuel, post-irrad. exam. techniques at Studsvik 2—38750
reactor fuel elements, fission gas annealing test in post-irrad. exam. 2—38757
reactor fuel elements, post-irrad. exam. 2—38760
reactor fuel elements, spherical, gamma spectrometry applic. 2—38759
reactor fuel pins, irrad., NDT, optical viewing devices 2—38753
reactor fuel pins, post-irrad. exam. techniques 2—38754
reactor fuel post-irrad. exam. by hot cell techniques 2—38752
reactor fuel post-irrad. exam. facilities 2—38751
semiconductor, Ge-Te(Se) glass, fast neutron damage threshold 2—1516
semiconductor junctions, n^+pp^+ and p^+nn^+, C-V characts. 2—22579
semiconductors, displacement energy effects, requirements for standardiza tion of damage curves 2—19692
silicate glazes for vitroceramic fuel, irrad. effects on vol. and viscosity 2—11901
solar coronal heating theory, observational test 2—11147
solid solution, substitution type disorder, computer simulation 2—3753
steel, 9Ni-4Co-0.20C weldment, post-irrad., notch ductility 2—15834
steel, irrad. effects on bulk and micro-flow fracture behaviour 2—25525
steel, stainless, fast neutron damage, simulation by ion implantation 2—6475
steel, stainless, He generation on irrad. 2—12748
steel, stainless, types 304 and 316, defect prod., electron microscope obs. 2—1236
steel, stainless, void formation, thermo-mechanical treatment effect 2—6469
steel, stainless, void formation rel. to neutron irrad. temp., 400-600 °C 2—19073
steel, structure, tensile properties, function of fast reactor irradiation temperature 2—1232
steel reactor casing, oxidation by neutron activated UPu oxide fuel 2—13577
therapy, relation between RBE and dose 2—17124
transistors, bipolar, gain degradation mechanism 2—22591
transistors, current gain response in gamma-ray and neutron environment 2—22590
transistors, short term annealing in biased off mode 2—19711
void formation during irradiation, theory 2—25365
zircaloy-2, cold worked, 300-450°C, creep accel. mechanism 2—25510
Zircaloy-2, radiation enhancement of oxidation 2—13580
Al-2.8 at%Zn-1.4 at%Mg, alloy, neutron irrad. rel. to precip. and G.P.zones 2—29418
Al-5.0 at%Ag-5.0 at%Zn, alloy, neutron irrad. rel. to precip. and G.P.zones 2—29418
Al, grain boundary internal friction peak 2—22217
Al, hardening, vacancy precipitation 2—19072
Al, shear modulus, effect of neutron irradiation at 4K, variation with Frenkel defects concentration 2—22278
Al pure, neutron irradiation at 20 K, electron microscope examination of defects 2—29164
Al_2O_3 and impurity effects on radiation induced swelling 2—12745
B_4C, thermal neutron irrad., He bubble formation 2—3755
C-Si, fuel coating, irrad. induced dimens. change 2—22176
C, fibres, tensile strength, effect of fast neutron irrad. 2—9683
C, pyrolitic, irrad. damage annealing, phys. props. 2—3757
C, pyrolytic, irrad., dimens. and phys. prop. changes 2—21471
C, stress-graphitized pyrolytic nuclear irrad., internal friction and elastic modulus 2—32587
C fibre, strength, Young's modulus, struct. 2—19193
CaF_2 pure crystals, absorption bands meas. after neutron irradiation at low temperatures 2—33254
$CaWO_4$, point effects due to neutron irradiation, e.p.r. obs. 2—6478
$CaWO_4$, radiation damage, e.p.r. obs. of S=3/2 defect 2—20133
CdSe, laser action 2—17638
Cu-Au alloy, Frenkel defect prod. rel. to deviation of longit. magnetoresist. from Kohler's Rule 2—16143
Cu-Au alloy, resistivity changes, deviations from Matthiessen's rule 2—16144
Cu-Be alloys, changes in resistivity during high temperature neutron irradiation 2—29166
Cu-Be alloys, zone formation and precipitation, 100-160°C 2—39905
Cu, defect cluster visibility, electron microscopy 2—9520
Cu, elastoresistivity, thermal recovery 2—25371
Cu, irrad. effects on internal friction, radiation damage 2—15805
Cu, shear modulus, effect of neutron irradiation at 4K, variation with Frenkel defects concentration 2—22278
Fe-Cr-Ni alloy, embrittlement 2—1319
Fe, irrad., vacancy prod. rate 2—12744
GAAs laser diodes, irradiation effects 2—21098
GaAs, optical props., band edge density of states detn. 2—29916
GaAs metallic spike zones, effects on electrical properties 2—19621
GaP light emitting diode, radiation damage 2—20094
Ge, irrad.-induced defect form., light sensitivity 2—12749
p-Ge, neutron irradiation damage at 70 K, meas. isochronal annealing curves 2—29168
Ge(Li) diodes in γ-ray detector fast neutron damage 2—24092
Ge_xSe_{1-x} glass, fast neutron damage threshold 2—1516
Ge_xTe_{1-x} glass, fast neutron damage threshold 2—1516
LiF, irrad. defects, e.p.r. obs., 77 K 2—13540
LiF, neutron irrad., defects, struct., effect of annealing 2—32487
LiF, reactor irrad., macropore formation 2—19075

- **Neutrons and antineutrons** continued
  - **effects** continued
    - Mg, hardening, vacancy precipitation 2—19072
    - Mg, yield stress obs. 2—36119
    - MgO, irrad., low temp. thermal cond. 2—29566
    - Mo, Irrad., high temp. recovery 2—15743
    - Mo, irrad. damage, dislocation loop contrast 2—19079
    - Mo, irrad. damage and annealing 2—19077
    - Mo, irrad. damage and annealing 2—19078
    - NaF, point defect formation 2—1245
    - Nb-50%Ti, type II supercond., crit. current density29631 2—29631
    - Nb-25%Zr, type II supercond., crit. current density 2—29631
    - Ni-0.3wt.%C, alloy, decomposition, metastable carbide formation 2—6618
    - Ni-Cr-Fe alloy, extension rate, tensile strength, grain size 2—25513
    - Ni, extension rate, tensile strength, grain size 2—25513
    - Ni, He generation on irrad. 2—12748
    - Ni, void growth and nucleation 2—9526
    - $PbCl_2$ single crystals, effect of low temp. neutron irradiation investigated based on optical absorption methods 2—29195
    - $PbTiO_3$ pyroelectric i.r. detector 2—17414
    - Pt, shear modulus, effect of neutron irradiation at 4K, variation with Frenkel defects concentration 2—22278
    - ^{239}Pu fueled lattice, evaluation of spectral effects by foil activation 2—5732
    - Re, irrad., low temp. recovery spectrum 2—15744
    - Se, irrad. effects on resist. and thermopower 2—6823
    - Si:Li, carrier removal 2—19652
    - Si:Li solar cell, irradiation damage, annealing and doping effect 2—22179
    - Si:O, neutron irrad., i.r. absorpt. spectra before and after 2—22223
    - Si, defect annealing obs. by space-charge-limited current 2—33020
    - Si, divacancy associated i.v. absorp. bands 2—22777
    - n-Si, reactor irrad. enhanced hetero-diffusion of Au and Zn 2—29193
    - Si detectors, surface stability to neutron bombardment 2—38376
    - Si junction f.e.t., defect formation in space-charge region, effect on characts. 2—10093
    - Si junction f.e.t., radiation responses 2—22593
    - Si junction f.e.t., trapping centre production 2—19712
    - Si surface barrier detectors, effects of irradiation on meas. of fission fragment properties 2—27873
    - SiC, irrad., e.p.r., defects obs. 2—1729
    - SiC light emitting diode, radiation damage 2—19708
    - SiC light emitting diodes, review 2—20116
    - SiC whiskers, irrad. damage 2—39674
    - SiO_2, fused, optical absorpt., irrad. effects 2—15785
    - ThO_2-15% UO_2 pellets, possible fuel for homogeneous aqueous suspension reactor, neutron irradiation studies 2—5754
    - (U, Pu)O_2 fuel, creep, irrad. effect 2—11902
    - UC, irrad., creep behaviour 2—29274
    - UN, irrad., creep behaviour 2—29274
    - UO_2, helix fabrication for irrad. creep meas. 2—36254
    - UO_2, irrad., creep behaviour 2—29274
    - UO_2 epitaxial film, irrad., electron microscope obs. 2—29045
    - V, radiation prod. defects, annealing, effect of interstitial impurities, 375-575K 2—25443
    - W, irrad. under stress., induced growth 2—32492
    - W, radiation damage annealing, electron microscopy 2—9758
    - Zr, neutron irrad. obs. rel. to void formation 2—32494
    - Zr alloy, radiation enhancement of oxidation 2—13580
    - ZrH_x, fast neutron irrad. induced swelling 2—36014
  - **interactions**
    - with medium in magnetic field, induced radiation 2—17972
    - neutron-electron bound state, possibility for free existence 2—27938
    - en, electroprod. cross section, upper limit of isotensor contrib. in $\Delta(1236)$ region 2—23797
    - $en\to e'p\pi^-$, threshold region, low energy 2—5536
    - γn, formation of $P_{11}(1470)$ resonance 2—8182
    - $\gamma n\to\pi^-p$ polarization parameters, target asymmetry 2—34675
    - $\gamma n\to\pi^+p$, 0.5 to 2.5 GeV, differential cross section polarization and asymmetry ratio 2—34653
    - $K^-+n\to K^0p$, phenomenological study of amplitude 2—34663
    - $K^+\to K^0p$, 10 GeV/c, cross sections determ. 2—14638
    - $K\text{-}n\to p\text{-}\pi\text{-}p\bar{K}^o$, study at 4.91 GeV 2—34668
    - $K\text{-}n\to\pi\text{-}\pi\text{-}p\bar{K}^on$, study at 4.91 GeV 2—34668
    - $K\text{-}n\to\pi\text{-}\pi\text{-}p\bar{K}^o\pi^o$, study at 4.91 GeV 2—34668
    - K^-n, at 4.5 GeV/c, final states with three charged particles and visible $\bar{K}^0$ production 2—8159
    - $K^-n\to\Sigma^{\mp}$+mesons, 4.93 GeV/c, cross sections, four momentum transfer distributions, density matrix elements 2—5528
    - $K^-n\to\pi^-\Lambda$, differential cross section and polarization, model with exchange degeneracy and duality, failure of Regge cut models 2—17911
    - $K^-n\to\pi^-\Lambda^0$, 3 GeV/c, angular distribution and polarization in new interference model 2—14639
    - $K^-n\to\pi^-\pi^-\pi^+\Delta^0$, 4.91 GeV/c, meas. of reaction cross section and cross section for resonance production 2—34667
    - $K^-n\to\pi^-\pi^-\pi^+\Lambda^0$, 4.91 GeV/c, meas. of reaction cross section and cross section for resonance production 2—34667
    - $K^-n\to\pi^-\pi^-\pi^+\Lambda^0\pi^0$, 4.91 GeV/c, meas. of reaction cross section and cross section for resonance production 2—34667
    - $K^+n\to k^+\pi$-p, 9 GeV/c, $K^*(890)$ production 2—11631
    - $Kn\to K^0p$, differential cross section, Pomeranchuk theorem violation 2—8151
    - nn, in ^3H and ^3He, ^1S scattering length rel. to binding energy difference 2—2687
    - $np\to d\gamma$, study of meson exchange effects 2—23890
    - $np\to pp\pi^-$, 2-30 GeV, theoretical analysis in framework of Reggeized OPE model 2—27772
    - pn, isospin analysis of single pion production at 7.0 GeV/c 2—27748
    - pn interactions in flight, odd-even ratio for pionic annihilation 2—5559
    - $pn\to3\pi$, at rest, resonance structure of Veneziano model 2—17970
    - $pn\to pp\pi$-, isobar production and diffraction dissociation at 7.0 GeV/c 2—34731
    - $pn\to\pi^+\pi$-π-, comparison of analyses by rising-shift model and Veneziano model 2—34730
    - $pn\to\pi^+\pi^-\pi^-$, exptl. investigations 2—38326
    - $pn\to\pi^+\pi^-\pi^-$ at rest, duality and final-state interaction 2—23888
    - $\pi^+n\to K^+\Lambda$, differential cross section and polarization, model with exchange degeneracy and duality failure of Regge cut models 2—17911
    - $\pi^+n\to\omega p$, density matrix element meas. rel. to dip mechanism tests 2—8134
    - $\pi^+n\to p\pi^+\to\omega\Delta^{++}$, rel. to decisive tests for dip mechanisms 2—2508

- **Neutrons and antineutrons** continued
  - **interactions** continued
    - $\pi^+n\to p\pi^+\pi^-$, 7 GeV/c, $\pi\pi$ scattering studied, obs. of S-wave resonance in the f^0 mass region 2—17950
    - $\pi^+n\to p\pi^+\pi^-$, f^0 mass region, evidence for structure 2—31307
    - HeLa cells, irradiated in 14 MeV neutron beam, measurement at RBE, OER and recovery from sub lethal damage 2—26965
  - **moderation**
    - *see also Neutron transport theory*
    - fast neutrons, generalized model for elastic and inelastic slowing down 2—38671
    - fast reactor flux and importance spectra, model 2—8382
    - fast reactors, improvements on continuous neutron slowing down theory 2—8381
    - graphite moderator, determ. of 1/E spectrum 2—544
    - in graphite-H_2O system, space energy distribution 2—11888
    - in ice, at 77°K, thermalization 2—28099
    - moderator correction for wide resonance using Greuling-Goertzel approximation 2—38669
    - Placzek functions calc. with synthetic kernel approximation 2—5729
    - reactor neutrons, using cold source 2—24253
    - slowing down equations, Goertzel-Greuling form 2—38677
    - slowing down theory, improvemets for fast reactors 2—8381
    - in water, at 318°K, thermalization 2—28099
    - water, light and heavy, slowing down times 2—2838
    - light water thermalization parameters, meas. using pulsed neutron technique 2—2854
    - MgO, SiO_2, Bi single crystals, suitability as filters for high intensity neutron beams 2—15029
    - Sb-Be source production, meas. of neutron age in water by infinite plane detector method 2—28100
  - **polarization**
    - angular variation, 2.6 MeV from $^{12}C(d,n_0)^{13}N$ reaction 2—18232
    - capture of polarized neutrons by oriented nuclei, use in expts. on spins of compound nuclear states 2—34770
    - continuous energy spectrum of neutrons, neutron spin-precession method 2—23891
    - using mirror, thin flat Co., fabrication 2—17995
    - in muon capture, by nuclei of emitted neutrons 2—38584
    - production using polarized ion source 2—34363
    - reflection, total and asymmetric method of meas. surface dipole 2—38347
    - (d,n) reactions on ^{10}B, ^{11}B, ^{12}C, 2.7 - 3.9 MeV, meas. angular distributions 2—28074
    - (n,γ) polarization experiments, interference of the two capturing states of oriented nuclei 2—31551
    - np scatt., n polarization meas., n energy=16.2 MeV 2—38327
    - $^{12}C(n,n)^{12}C$ 1.9-5.2 MeV, polarization and differential cross-section 2—18200
    - $^{40}Ca(d,n)$, neutron polarization meas., comparison with DWBA calc. 2—38614
    - $^2H(d,n)^3He$, 0.87 to 5.00 MeV, polarization meas. 2—38636
    - $^2H(d,n)^3He$, at 10.8 MeV, polarization obs. at 6 lab. angles 2—8357
    - $^3H(p,n)^3He$, 1.5 to 5.0 MeV, polarization meas. 2—38588
    - $^3He(d,n)^4He$ reaction and np scatt., meas. at 32 MeV 2—15008
    - ^4He, polarization measurements and analysis of neutron scattering from 11.0 to 30.3 MeV 2—31554
    - $^{24}Mg(d,n)$, neutron polarization meas., comparison with DWBA calc. 2—38614
    - $^{28}Si(d,n)$ neutron polarization meas., comparison with DWBA calc. 2—38614
  - **production**
    - booster, repetitively pulsed, static and dynamic experiments 2—31615
    - cold source at reactor FRJ-2, instrumentation 2—24264
    - cold source at reactor FRJ-2, planning and development 2—24261
    - cold source at reactor FRJ-2, temperature meas. 2—24288
    - cold source at reactor FRJ-2, thermodynamic design 2—24262
    - cold source at reactor FRJ-2 2—24263
    - delayed fission, energy spectrum 2—2827
    - delayed fission products, quantitative assay of fissionable materials 2—28097
    - delayed neutron probabilities and calculated cumulative fission yields 2—28096
    - directional emitter of thermal neutrons using paraffin block as moderator and reflector 2—38346
    - electronuclear generation, accelerator physics research at AECL 2—11691
    - isotropic source, use of linear accelerator 2—38417
    - monoenergetic, eV-keV range, using resonance scatterers in tangential beam tube of reactor 2—34752
    - neutron, based on ^{241}Am and ^9Be 2—17974
    - neutron energy spectra and flux distributions for D-D reactions in plasma focus type z-pinch discharges 2—24718
    - neutrons, from cold source 2—27830
    - plasma emission, laser produced plasma 2—21814
    - plasma focus, velocity distribution of ions 2—12393
    - on plasma heating with very short laser pulses 2—24651
    - polarized n production using polarized ion source 2—34363
    - seafloor mineral exploration using system utilizing neutron activation analysis 2—30210
    - source of 14 MeV neutrons, rotating ^3H target 2—24065
    - sources, low intensity, calibration method 2—8227
    - sources based on ^{241}Am and ^9Be 2—17974
    - sources in moderating solutions, cavity-wall and self-absorption correction factors 2—28104
    - spin-flip-chopper with high repetition rates 2—11656
    - tube generators, high voltage multiplier as accel. voltage source 2—18051
    - very cold, current calc. 2—18249
    - $\pi^-p\to\eta n$, total cross sections constancy 2—17931
    - $^9Be(d,n)$ neutron spectra and application to transmission of C and polyethylene samples 2—5711
    - $^9Be(\gamma,n)$, monoenergetic beam at KeV energies 2—5560
    - ^2H, ^3H targets, for therapy and activation analysis 2—34755
    - ^2H_2O thermal column, for thermal flux generation in nuclear reactor 2—38716
    - Pu-Be sources, collimated fast neutron energy spectra 2—11790
    - ^{239}Pu-$Be(\alpha,n)$ sources of different sizes, neutron energy spectra 2—28010
    - Sb-Be source of plane type, meas. of neutron age in water 2—28100
  - **reflection**
    - polarized, asymmetric total reflector, method of meas. surface dipole 2—38347

Neutrons and antineutrons continued
 scattering
  acetonitrile, liquid, comparative study of quasielastic scattering and nmr relaxation 2—1073
  anisotropic, effect in square cell with thin moderator 2—38670
  anisotropic, transmission and reflection coefficient 2—15031
  chopped neutrons, influence of nuclear surface and Coulomb interaction on diffraction 2—18197
  cold neutron time-of-flight spectra analysis using direct fast Fourier transformation 2—11836
  diffraction theory, interference 2—17973
  extrapolation distance calc. for one-group transport with anisotropic scattering 2—23308
  fluid, classical, effective-field approx. for coherent scatt. 2—8871
  inelastic, liquid metals, data correction, X-ray test 2—3362
  inelastic scattering in gas of spherical molecules 2—14117
  lattice mechanics and rotational diffusion study 2—19401
  liquids, simple classical, incoherent scatt. for large momentum transfer 2—12537
  methanol, liquid, cold neutron scattering, study of proton notions 2—25035
  neutron detection using resonant scattering from ^{7}Li to identify levels following neutron producing reactions 2—27890
  neutrons, diffuse, spectrometric meas. 2—27838
  reactor neutrons, slowing using cold source 2—24253
  rigid, and false absorption effect 2—38674
  rotons, in liquid He 2—28925
  slow neutrons, cross section, rel. to classical mean-square displacement function 2—2834
  in square cell with thin moderator, effect of anisotropic scatt. 2—38670
  thermal kernels, Cadilhac model 2—15032
  en deep inelastic scattering, structure functions 2—31200
  n-n, forced reflection neutron collimator 2—14738
  nn scattering length from 13.95 MeV ^{3}H(n,2n)^{2}H reaction 2—2786
  np, calcs. using finite difference soln. of partial wave Schrodinger eqn. 2—7672
  np charge exchange scatt., comparison of Michigan and mixed model 2—8207
  νn, deep inelastic, relations among structure functions derived using light cone commutators 2—38231
  pn, elastic scatt., cross section estimates from pd scattering data at 24.0 GeV/c 2—34721
  π^-n→nπ^-, elastic backward scatt., 23 and 40 GeV/c, differential cross sections 2—27753
  Ar fluid, 5-80 MeV, studied over wide range of conditions including triple point and critical point 2—31892
  D_2, mols., cold and thermal scatt. cross sections, 173-373K 2—15327
  D_2O, cross section computation program 2—15030
  from H_2O, inelastic scattering, temperature dependence 2—519
  He II superfluid, large momentum transfer and condensate fraction 2—1133
  He liquid, high-energy neutrons, application of correction terms to impulse approximation 2—25125
  $K^+n \to K^0p$, charge exchange scattering 2—17915
  O_2, mols., cold and thermal scatt. cross sections, 173-373K 2—15327
  UC, low energy scattering 2—28113
 scattering, neutron-proton
  elastic, 4.8 GeV/c, small angle differential cross section over four momentum transfer range 2—11641
  polarisation of scattered neutrons meas., n energy=16.2 MeV 2—38327
  pn, elastic, near 1.8 GeV/c, differential cross sections 2—31324
Newtonian fluids *see Fluids*
Nickel
  absorption spectra, band struct., 4K 2—16496
  adsorption and desorption of oxygen on Ni by electron impact 2—6373
  adsorption for H, and desorption, kinetics studied 2—6371
  adsorption of acetylene and ethane, fiel-emission studies 2—1196
  adsorption of Ag, H, O oxides, specular reflection spectra, monolayer thickness range 2—9310
  adsorption of CO, at 44K, i.r. spectra obs. 2—22086
  adsorption of S, struct. study using LEED 2—6359
  adsorption of sulphur and sulphides, distinction by Auger spectroscopy 2—39557
  atom, Lα line shapes near threshold of excitation 2—21506
  atom, X-ray K-fluoresc. yields 2—8443
  atom excitation from shakeup photoelectron spectra of solid NiO 2—36636
  atoms, soft X-ray spectra, classification 2—5786
  Auger spectra of C 2—3500
  in brine, atomic absorption spectroscopy obs. 2—10661
  casting, crystal lattice defects, secondary boundary structures 2—15772
  cavitating effect of cryogenic liqs. 2—39915
  chemisorption of CO and O, photoemission energy level measurements 2—4325
  chemisorption of H_2, MO models 2—26345
  Compton profile due to 1s electrons 2—24340
  corrosion, in liq. Na, rel. to temp. and Na vel. 2—37046
  creep, high temp., substruct. changes, porosity, dislocation density, shear modulus obs. 2—12730
  creep, steady state rate, screw dislocation motion with jogs 2—9676
  critical fluctuations, ^{100}Rh time differential perturbed ang. correl. obs. 2—40487
  crystal, electropolishing, heat cycling, substruction disorientation, x-ray exam. 2—12778
  crystal, grown by Czochralski method, substruct. 2—25343
  crystal growth, suppression of striations 2—25268
  deformed, coercive force and remanence, Bi films influence 2—6976
  deformed at high press., dislocation struct., flow stress 2—22210
  desorption of D_2 speed distributions 2—6369
  desorption of H_2, spatial distrib., comp. and orientation effect 2—25231
  in diamond, struct. impurity, e.p.r. obs. 2—13535
  diffusion, in MgO, up to 2500°C, enthalpy of motion detn. 2—25469
  diffusion, in Ni_3Al, $Ni_3(AlTi)$ 2—3811
  diffusion, of Ag, lattice coeff. 2—12811
  diffusion, quantum, of H, freq. factor, tunnelling effect, transfer mechanism, migration energy 2—12813
  diffusion in bimetal structures 2—1270
  diffusion in molten $LiF-BeF_2-ZrF_4$, coeff. determ. by linear sweep voltammetry and chronopotentiometry 2—18810
  diffusion in NiO, correlation factor and effect of Co addition 2—36079
Nickel continued
  diffusion in Zircaloy-2 2—12817
  diffusion of H_2, coeff. determ. 2—36080
  diffusion of oxygen, determ. from internal oxidation kinetics of Ni-Be alloy 2—29221
  diffusion of S on (110) face, Auger spectroscopy 2—3499
  dislocations and low angle boundaries, electrolytic decoration with Cu 2—39701
  dispersion hardened, role of microstruct. in strengthening 2—39936
  dispersion hardened, ThO_2 particles, high temp. strength 2—9690
  dispersion strengthening by ZrO_2 2—39902
  elastic consts., second- and third-order lattice theory 2—9632
  electrodeposit, struct. and cryst. growth on polished Cu 2—3539
  electroless deposit on glass, interfacial props. 2—32372
  electrolytic, magnetoelastic damping, anisotropy, hysteresis in magnetic field 2—4379
  electron density of states, Brillouin zone integration by combined linear and quadratic interpolation 2—19501
  electron energy loss spectra, low energy peaks, oxide effects 2—29583
  electron radiation damage, in h.v. elec. microscope, point defect cluster formation 2—19069
  electronic stopping power of 21 keV Ne ions 2—9913
  electronic struct. of virtual bound state 2—16110
  energy gap, spectra obs. 2—25735
  epitaxial film, domain struct. from galvanomagnetic meas. 2—13410
  fast neutron irradiation, resist. recombination volume 2—25763
  fatigue cycled, surface layer dislocation substruct. 2—12887
  ferrites, form., influence of mixing 2—32711
  ferromagnet, domain size and stability, scaling laws, Curie pt. region, neutron depolarization obs. 2—16365
  ferromagnetic, energy bands 2—9935
  ferromagnetic, Hall resist. rel. to conduction, influence of $\Delta\rho/\rho$ effect 2—19548
  ferromagnetic electronic struct., d-band photoelectron energy distrib. near Curie temp., exchange splitting 2—33091
  ferromagnetic resonance, in plastically deformed single cryst. 2—36972
  film, adsorbed layer of Co, calorimetric i.r. spectroscopy 2—18955
  film, adsorption of H and deuterium study 2—6372
  film, amorphous, spin wave reson. and stress effects 2—20129
  film, condensed, substrate influence on nucleation nature 2—6345
  film, critical grain size for ferromag. 2—40510
  film, discontinuous, on dielec. substrate, electron cond., resist. coeff., 130-300K 2—40180
  film, electrodeposited, magnetization, substrate influence 2—4392
  film, electrodeposited, stripping of large areas 2—12662
  film, electrolytic, coercive force, tensile and torsional stress effects 2—4394
  film, electron energy losses 2—6704
  film, epitaxial, plane galvanomag. effect anisotropy 2—33152
  film, Faraday effect and ellipticity 2—10311
  film, granular, mag. props. 2—36727
  film, noncryst., structure, elec. diffraction obs. 2—6429
  film, plated, on Fe substrate, electrolytic stripping process 2—37049
  film, polycryst., annealing behaviour of magnetostrictively induced anisotropy 2—16381
  film, reactively sputtered, influence of surface adsorp. characts. 2—22068
  film, resist., spontaneous evolution 2—9958
  film, transverse magnetoresist. anisotropy and geometrical size effect 2—32921
  film, vacuum deposited, internal friction, 4.2-77 K 2—29245
  film, vacuum-deposited, mechanism of internal stress form. 2—39516
  film microwave helicon-magnon interaction 2—16382
  film on Fe-Si alloy, magnetostriction dependent on thickness 2—1635
  film thickness dependence of thermopower and temperature resistance coefficient 2—6892
  film with alternating Al, deposition apparatus 2—18932
  films, refractive index and extinction coeff., polarimetric obs. 2—33199
  foil, 20 MeV C^{2+} bombardment, void formation, swelling rel. to dose 2—6476
  foil, bulk diffusion of ^{14}C, 350 to 700C 2—12812
  foil, effect of H_2 on crystalline struct. imperfection 2—15941
  form factors, local pseudopot., band gap 2—6723
  Hall coefficient and resistivity, effect of plastic deform. 2—22492
  heat of adsorption, neutral mixed layers and surface reconstruction 2—29068
  heat of sublimation, mass spectrometric obs. 2—36351
  high-temperature stable thin-film thermocouples, oxidation and diffusion problems 2—30900
  hyperfine fields of ^{75}As 2—36806
  hyperfine fields of As 2—36805
  impurity mode energy, in antiferromag. $RbMnF_3$ and MnF_2 2—16562
  interfacial energy ratio, grain-twin boundary 2—9573
  i.r. absorptivities at room and liquid He temperatures, derived from reflectivity measurements 2—26106
  laser beam irradiated, elec. resist., and point defect. form. 2—9533
  LEED, from (100) surface, beam threshold and surface reson. effects 2—32342
  light cond., interband transitions 2—26171
  linear compressive strain, press. depend. to 20 kbar, phase transformations 2—9818
  liquid, solubility of N and C, scaled particle theory 2—21965
  liquid, viscosity and density 2—28805
  magnetic anisotropy energy press. depend. 2—6971
  magnetic hyperfine fields at ^{204}Bi 2—29858
  magnetic internal energy, temp. depend. 2—40457
  magnetic ordering, intermediate stage 2—13371
  magnetic props. anisotropy after plastic deform. 2—40450
  magnetization, pressure depend., itinerant electron model 2—16378
  magnetization press. depend. 2—19845
  magneto-optical anisotropy, spin-orbit coupling effects 2—16425
  magneto-plastic effects, in single cryst. 2—33144
  magnetomechanical damping, applied stress effect 2—33149
  magnetomechanical damping, plastic deform. effect 2—19890
  magnetostriction coefficients 2—6978
  magnetostriction constants 2—6977
  mechanical twinning, in single cryst. by compression 2—9665
  meteorite content, chemical analysis 2—11020
  microeddy current mag. damping 2—10215
  microhardness, rel. to proton and α-particle irrad. 2—39847
  microhardness increase under action of u.s. waves 2—9663
  near-paramagnetic region, induced magnetiz., Mossbauer obs. 2—40634

Nickel continued
neutron irrad. induced He generation 2—12748
neutron irradiation, extension rate, tensile strength, granular struct. 2—25513
neutron irradiation, void growth and nucleation 2—9526
nuclear relax. of ^{195}Pt, high-field obs. 2—40579
optical constants, band struct. 2—10299
oxidation, growth kinetics of absorbant layer and optical indices determ. 2—25204
phonon freq. distrib. functions determ. 2—13023
photoelectrons, spin polarization 2—1588
piezo soft X-ray effect, band struct. 2—22792
plastically deformed, recovery, elec. cond. study 2—36120
polycrystalline layer, on NaCl, transmission of struct. information 2—6333
porosity effect on elec. and thermal cond. 2—19464
powder, active, sintering mech., mass transport mech. 2—36259
powder, aerosol, partial hysteresis cycles at various degrees of oxidation 2—16376
powder, effect of H_2 on crystalline struct. imperfection 2—15941
powder, mag. props., particle size depend. 2—40513
powder, vacuum hot pressing, effect of u.s. waves 2—1347
powder compacts, verification of existence of oriented microstresses by X-ray examination 2—39960
powder in two- and three-phase mixtures, determ. thermal conductivity by line source method 2—22432
powder pressing, effect of press. and temp. 2—3972
proton energy loss distribution in foils 2—6703
proton irradiation, void formation by flash heating 2—22177
pure, porous-homogeneous couple, vacancy migration, pore redistrib. 2—12986
radiation damage in 500 kV electron microscope, dislocation loops 2—1238
Raney, oxidation and reduction mechanism obs. by sorption expts. 2—13575
recovery, recrystallization and polygonisation after high strain rate deformation 2—9748
recrystallisation during hot deform., strain rate torsion tests, torque-twist curves 2—32699
recrystallization pt. on microhardness curve, relationship with degree of formation before annealing 2—9718
saturation magnetization, decrease due to non transition element impurity atoms, mechanism 2—6726
single crystal films, heteroepitaxial growth by vacuum evaporation 2—3538
single crystal growth by floating zone technique using induction heating 2—3585
sintering kinetics of Ni activated W 2—6625
solar curves of growth, revised gf scale 2—33761
spin polarization and spin fluctuation interactions 2—40440
sputtering, reactive, in Ar-O_2 mixtures, molecular sputtering mode obs. 2—1012
stacking fault energy, twin boundary energy temp. coeff. 2—32533
in steel, austenitic, effect on NbN solubility and precip. 2—12968
in steel, austenitic stainless, effect on hot ductility 2—9672
steel, quenched, aged, alloy addition, effect on mech. props, weldability 2—19239
steel impurity, effect on plastic properties 2—6538
surface, soft X-ray appearance pot. spectra, effect of oxygen 2—35872
surface microstruct., scanning electron microscope obs. 2—39464
surface reactions, O_2-H_2 radicals, low pressure discharges 2—35620
tensional deformation, secondary recrystallisation structure 2—12947
tensional deformation, twinning struct. growth, X-ray obs. 2—12862
texture of electrolytic deposits, contrib. of twinned crystallites 2—1179
thermal emissivity near Curie temperature 2—1440
thin film, electrodeposited, internal stresses meas. device 2—39508
thin target, electron beam transmission from vacuum to air 2—1443
three layered strip, nickel-steel-nickel, strength characteristics, bonding 2—9759
two dimensional Hall effect 2—16136
valence band struct. from u.v. photoelectron spectra 2—36650
Vickers microhardness indentation, plastic deformation inhomogeneity, emission electron microscopy 2—19174
volumetric effects during heating after u.s. vibrs. 2—39894
X-ray emission spectra, Lorentzian representation of line shape 2—40699
CdS:Ni^+, e.p.r., g-factor and hyperfine struct. 2—30016
Cu-Ni-Cr coating, testing at marine microclimate 2—1751
Fe-Ni magnetic films, vacuum deposited on glass, photography using i.r. laser pulses 2—27683
Ge:Ni, excited by laser rad., electron-hole recomb. at deep impurity centres 2—22558
n-Ge:Ni, hot electron lifetime temp. depend., photocurrent decay obs., carrier scatt. by impurities 2—29702
MgO:Ni, mag. circular dichroism, vibr. induced d→d transitions 2—22773
MgO:Ni, paramag. cryst., phonon avalanche, Brillouin scatt. 2—16018
MgO:Ni^{2+}, Raman relax. rates of Ni^{2+}, Debye model of phonons 2—40044
MoO_3:Ni, defect struct. and elec. cond. 2—10026
Ni:Ar implanted, hyperfine mag. field 2—10292
Ni:Re, hyperfine field at ^{187}Re nuclei, time differential perturbed angular correl. obs. 2—36798
Ni:ThO_2, rapid quenching effects, internal stresses, rel. to mech. props. 2—32599
Ni/GaAs, surface-barrier structures by chemical deposition 2—25892
Ni/Na overlayer system, surface struct. 2—28985
Ni-SiO_2, composite film, tensile strength, microhardness 2—15666
Ni-ThO_2, dispersion strengthened, annealing, ThO_2 praticle growth, electron microscopy 2—9734
Ni-air porous cathodes, Pd catalyzed, performance in secondary Zn-air cell 2—11418
Ni (111), characteristic energy loss of slow electrons scattered from surface, temperature dependence in Curie point region 2—28991
Ni I, lifetime obs. of optical levels using phase shift method 2—31680
Ni II, odd configurations, theoretical investigation 2—2945
Ni XI-XVII, classification of emission lines from $3s^2 3p^n$—$3s3p^{n+1}$ and $3p^n$—$3p^{n-1}3d$ transitions 2—21519
Ni XV emission line data, enhanced solar coronal region 2—17094
Ni XVII, XVIII, identifications in the extreme u.v. in a solar flare 2—26915
Ni XVIII, relativistic corrections to ionization energies and dipole oscillator strengths 2—8445
Ni^+, 4 MeV ions bombardment of C foils, lifetime 2—34361
Ni^+ at tetrahedral sites, field models modification, Jahn-Teller interaction 2—7013
Ni^{2+}, ferrimag. resonance in BiCaVI garnet 2—4534
Ni^{2+}, hydrated, e.p.r. in $ZnSeO_4.6H_2O$ 2—10525
Ni^{2+}, ion absorpt. transition temp. depend. in mag. host materials 2—33267
Ni^{2+}, Ni^{3+}, e.p.r. in $2MgO.2Al_2O_3.5SiO_2$ glass 2—30013
Ni^{2+}, octahedral complex in ionic cryst., overlapping and covalency effects on optical spectra 2—19990
Ni^{2+} e.p.r. in CaO, linewidth ang. variation 2—7116
Ni^{2+} in $KMnF_3$, e.s.r./ENDOR, hyperfine interactions 2—20144
Ni^{2+} spin-lattice relax. in $La_2Mg_3(NO_3)_{12}$ 2—10267
Ni^{3+} mag. props. in $Sr_2Ni_xAl_{1-x}SbO_6$, solid solns. 2—13378
NiXV Nova Delphini 1967 nebula, forbidden transition increased stability or intensity in spectral range 5600 to 8800 Angstroms 2—13911
$^{58}Ni^{6+}$, metal ion production, for Harwell variable energy cyclotron 2—34778
^{63}Ni, standardization, half-life and neutron-capture cross-section 2—5679
Ni(100), absorption of CO, structural influences on adsorption energy 2—25227
Ni(110) surface, photodesorption of adsorbed CO 2—29066
Si:Ni diode, current-voltage characts., turnover voltage, photocond., diode parameters 2—22586
inSi, homogeneity breakdown, during joint diffusion of Ni and P 2—36058
$Zn_xCd_{1-x}S$:Ag,Ni, photoluminescence mechanism, energy band model 2—4480
ZnS:Ni^+, e.p.r., g-factor and hyperfine struct. 2—30016
ZnSe:Ni, two-stage excitation of anti-Stokes luminesc. 2—33311
$ZnSeO_4.6H_2O$:Ni^{2+}, optical activity 2—16420

Nickel alloys
see also Nickel compounds
Alnico, domain struct. change during partial hysteresis cycle 2—13388
Alnico, ferromagnetic phases, indirect evaluation of individual props. using electrochem. means 2—26031
alnico, superstruct. defects, thermal antiphase domains, superdislocations 2—29175
Alnico crystal, mag. struct., remagnetization 2—1621
Alnico-V alloy, 0.5%Ti, metallurgical and mag. props. 2—4368
c.p., stacking order stability 2—12713
development as high performance, high temp. mats., review 2—12973
dilute, extraordinary Hall effect, transition metal impurity effects 2—19549
dilute, interaction energy between two impurities 2—1458
dilute, nucl. relax. of ^{55}Mn and ^{59}Co, high-field obs. 2—40579
dispersion hardened, diffusional creep 2—1293
dispersion hardened, role of microstruct. in strengthening 2—39936
Elinvar, Young's modulus, effect of tempering 2—12823
Elinvar film, domain struct. and remagnetization process 2—13406
erosion rate, rel. to mech. props. 2—29339
fatigue strength rel. to surface machining 2—29301
Fe-Ni films, exchange stiffness const. 2—19897
Hastelloy X, cyclic oxidation kinetics, 760-1200°C 2—40814
Hastelloy X, thermal conductivity, elec. resistivity and thermopower, 4-300K 2—25692
Heusler, hyperfine fields at Ni sites 2—40632
Heusler, hyperfine fields at Sb sites 2—40633
high temperature, effect of aluminide coating on high cycle fatigue behaviour 2—25600
Inco 718, precip. hardening, effect of Ti, Al, Nb and Mo content changes 2—9820
incoherent annealing twin boundary, elec. microscope obs. 2—9572
Inconel 600, explosive shock deformation, thermal recovery 2—9656
Inconel 600 heat exchanger tubing, stress assisted corrosion in high temp. water 2—11909
Inconel 700 alloy, γ' precip. growth on ageing 2—39986
Inconel 706, heat treatment, props. and fabricability 2—29395
Inconel 713 C, weldability, hot cracking sensitivity and mech. props. 2—29291
Inconel 718, thermal cond., 90 to 1200 K 2—19442
Inconel 718, thermal conductivity, elec. resistivity and thermopower, 4-300K 2—25692
Inconel X750, intergranular stress corrosion cracking in pressurized water 2—11910
Incramet, elec. and thermal cond. 2—19456
Invar, γ-phase stability, effect of alloying additions 2—36281
invar, ΔE effect, E=Young's modulus, variation with temp. 2—33145
invar, ΔE magnetovolume effect, Weiss two γ-states treatment 2—33146
Invar, anomalous props., Mossbauer obs. 2—33221
Invar, antiferromag., susceptibility, temp. depend. 2—16397
Invar, high field susceptibility, temp. and conc. depend. 2—4371
Invar, internal friction in alternating mag. field 2—12834
Invar, mag. internal friction peak, -20°C 2—12833
Invar, thermal expansion, 4.2-300K effect of heat treatment conditions 2—36355
Invar films, spin wave reson., dispersion coeff. obs. 2—40744
magnetic anisotropy energy; temp. and impurities effect 2—19872
Mar-M200, Hf doped, rupture life and ductility enhancement 2—15865
mechanical properties of pulsed-arc welded joints, thin-walled components 2—1274
molten, solubility of nitrogen 2—9767
Nimalloy, mag. props., effect of Fe and Mo additions 2—13400
Nimonic 75, friction and wear props. 2—22297
nimonic 75, wear characts., rel. to surface temp. 2—39849
permalloy, film, electro-deposited, time instability 2—10222
permalloy, film, plated NDRO wire, structure detn. 2—19899
Permalloy, thermomag. treated, magnetostriction, field depend., plane anisotropy 2—16377
Permalloy cct. elements, magnetiz. 2—36713
Permalloy film, ferromag. reson. linewidth, temp. depend. 2—40743
Permalloy film, intrinsic ferromag. reson. linewidth 2—20126
permalloy film, magnetization reversal, stray field blocking, rotational hysteresis 2—4393
permalloy film, spin-wave resonance fields, linewidths and intensities 2—13527
Permalloy film, vacuum-deposited, mechanism of internal stress form. 2—39516
Permalloy films, mag. domain patterns after plastic deform. 2—40508

Nickel alloys continued
- Permalloy films, magnetostatic interaction of mosaic struct. elements 2—40505
- Permalloy films, recrystallization 2—1349
- Permalloy films, spin wave reson. linewidth depend. on thickness 2—7111
- Permalloy interdiffusion with Cu in plated-wire memory annealing 2—1348
- permanent magnet materials characterization 2—40514
- precipitation hardened, creep induced twinning 2—9574
- Pyromet 860, precip. strengthening, effect of Ti and Al content 2—29394
- solid solns., non-equil., short-range order estab. 2—9772
- spectral analysis of H 2—16700
- super-refractory, dynamic recrystallization 2—12948
- superalloy, precip. of intermetallic cpds. and carbides, electron microscope obs. 2—32731
- superalloy, soln. treated, aged, intergranular films 2—25344
- superrefractory, creep, high-temp. fatigue 2—29271
- surface struct., effect of low energy He^+ ion injection, electron microscope obs. 2—3498
- Ticonal, conjugation of metastable phases 2—12976
- Ag-Ni two-phase targets, reduced sputtering yields 2—32864
- Al-Fe-Ni:(Mg,Cr,Mn) nuclear reactor material, resistance to water corrosion, 220°-315°C, comp. depend. 2—13581
- Al-Ni dil. alloys, virtual bound state obs. from A $L_{2,3}$-absorpt. spectra 2—20022
- Al_3Ni-Al eutectic rod, thermal stability rel. to growth 2—22336
- β-AlNi, stacking fault broadening and separation of strain and fault effects 2—32535
- AlNiCo 5 cylindrical magnets, external axial field graph 2—238
- Au-Ge-Ni, ohmic contact on n-GaAs, specific resistance 2—29715
- Au-Ni, discussion of spinodal hypotheses and precipitation 2—29425
- Co-Fe-Ni/NbC(TaC) fibre reinforced eutectic systems, directional solidification, sogt magnet 2—3438
- Co-Fe-No-Nb, semihard mag., for remanent reed switch applics. 2—40463
- Co-Ni-Cr-Mo, precip. hardening and phase transformations 2—19296
- Co-Ni-Cr, precipitation by internal oxidation 2—9796
- Co-Ni-Cr, ThO_2 dispersion strengthened, strength and corrosion resistance 2—19266
- Co-Ni-Ti, decomposition, modulated structure 2—9467
- Co-Ni, liquid state, density meas., structure 2—3374
- Co-Ni, martensite transform., shape memory effect 2—9789
- Co-Ni, thin film, Hall effect and magnetoresist. 2—13403
- Co-Ti-Ni precip of γ'-Co_3Ti 2—9797
- Cr-Fe-Ni particles, lattice parameters 2—12721
- Cr-Ni, dilatrometic investigation of transformations and determination of coefficient of linear expansion 2—9892
- Cr-Ni, high temp. self-diffusion of ^{51}Cr 2—12802
- Cr_xM_{1-x}—M_x—$Cr_{1-x}C_3$, (M=Fe, Co, Ni), eutectic, directional solidification, feathered morphology 2—3441
- CrNi film, sputtered, struct. and elec. props 2—39505
- Cu-Al-Ni, γ'-phase morphology, electron microscope obs. 2—36042
- Cu-Al-Ni, martensitic transformation, internal friction obs. 2—3842
- Cu-Ni/BN composite plasmic coating, prep., struct., and props. 2—12985
- Cu-Ni-Fe, spinodal, microstruct. changes on fracture 2—9685
- Cu-Ni-Mn, dil., resist. and magnetoresist., Kondo effect 2—1484
- Cu-Ni-Mn, order-disorder transform. 2—15981
- Cu-Ni-Pd system, struct., 400-700°C, X-ray obs. 2—3705
- Cu-Ni-Sn system, Cu corner, binary and ternary diffusion 2—19143
- Cu-Ni-Zn, phase regions, elec. resist. study 2—25641
- Cu-Ni-Zn, thermopower, 3d band filling 2—16304
- Cu-Ni, Auger spectra, comp. depend. 2—12646
- Cu-Ni, Debye temperature, effect of lattice defects 2—19383
- Cu-Ni, density of states, X-ray photoemission spectroscopy meas. of valence band 2—25731
- Cu-Ni, dil., low field magnetoresistance 2—1474
- Cu-Ni, dil. Fe effect on low temp. sp. ht. 2—40071
- Cu-Ni, disordered binary substitutional Debye charact. temp. 2—22422
- Cu-Ni, Fe-doped, critical mag. ordering temps. 2—40468
- Cu-Ni, Fermi surface, positron annihilation 2—16129
- Cu-Ni, Fermi surface, positron annihilation obs. 2—32879
- Cu-Ni, Kirkendall effect and diffusion coeff. 2—39740
- Cu-Ni, ordered, band struct. 2—16105
- Cu-Ni, random, density of states 2—4119
- Cu-Ni, resistivity changes arising from cyclic deformation 2—15905
- Cu-Ni, solidification, chem. comp., constitutional diag., diffusion constant 2—28936
- Cu-Ni, solidification, rate effects on comp. at liquid-solid interface 2—28937
- Cu-Ni, solidification, sudden rate changes, initial transient and solute-distrib. profiles 2—28938
- Cu-Ni, vacuum u.v. spectra, comparison with sandwich structures 2—20021
- Cu-Ni films, thermopower, thickness depend. 2—6893
- CuNi, quenching temp. influence on high temp. phase retention 2—25570
- Fe-Cr-Ni-C-Si-Mn-P-Si-Nb, chill cast roll iron, isothermal austenite decomposition 2—3996
- Fe-Cr-Ni, austenitic, volume and intergranular diffusion, grain boundary energy, comp. depend. 2—12808
- Fe-Cr-Ni, austenitic steel, magnetism and structural stability 2—26038
- Fe-Cr-Ni, neutron irrad., embrittlement 2—1319
- Fe-Cr-Ni, transitional ferrite phase form. 2—29435
- Fe-Cr-Ni, transitional ferrite phase form. 2—29434
- Fe-Cr-Ni alloys, austenitic, charging in H, effect on crack formation 2—6577
- Fe-Cr-Ni steel, austenitic, H embrittlement 2—29308
- Fe-Mn-Ni, Invar anomaly 2—13051
- Fe-Ni-Al-Co, thermomag. treatment quality, mag. texture study 2—36239
- Fe-Ni-C, martensites, elastic props. from sound velocity and mass density obs. 2—3829
- Fe-Ni-C, martensites, morphology rel. to formation temp. 2—12775
- Fe-Ni-C, martensitic, H_2 embrittlement 2—12910
- Fe-Ni-C, peak of internal friction in newly heat-treated martensite 2—39765
- Fe-Ni-Co/SiO_2/Fe-Ni-Mo layer system, domain boundaries and coercive force 2—13407
- Fe-Ni-Co-Mo, martensitic, ageing, formation of metastable ω phase 2—36299
- Fe-Ni-Co-Mo, steel, pre-precipitation and reversion 2—9809
- Fe-Ni-Co, thermal expansion, low temp. invar anomalies, magnetic field dependence 2—16052

Nickel alloys continued
- Fe-Ni-Co, thermal expansivity, effect of Co on invar characteristics 2—16051
- Fe-Ni-Cr-C system, austenite phase, equilib. C content determ. 2—40007
- Fe-Ni-Cr-Ti, austenitic, plastic deform. rel. to σ- phase form. 2—29471
- Fe-Ni-Cr, effect of austenitizing conditions on martensite formation 2—32768
- Fe-Ni-Cr, martensitic transform. kinetics and martensite morphology 2—36277
- Fe-Ni-Cr, steel, austenitic, B solubility 2—22339
- Fe-Ni-Cr alloy, inoxidizable, austenitic, metastable, level in elastic limit 2—25478
- Fe-Ni-Cr austenitic matrix, carbide nucleation and precipitation, B effect 2—9810
- Fe-Ni-Cr steel, austenitic, stainless, B solubility, solubility curve, solubility boundary 2—22340
- Fe-Ni-Mn, Co-substituted, Invar theory 2—40499
- Fe-Ni-Mn, isothermal martensitic transform., kinetics 2—9804
- Fe-Ni-Mn, martensitic transformations nucleation model 2—22357
- Fe-Ni-Mo-Co, martensitic, temper hardening, X-ray diffr. electron microscopy 2—9740
- Fe-Ni-Mo, lattice distortion due to deformation 2—15721
- Fe-Ni-Nb(Mo), martensitic, temper hardening 2—9739
- Fe-Ni-P film, mag. field induced anisotropy 2—36725
- Fe-Ni-graphite, sintering, struct., and phase comp. 2—12938
- Fe-Ni, coercive field, Neel theory 2—33136
- Fe-Ni, Curie pt. shift under hydrostatic press. 2—40478
- Fe-Ni, diffusion coeff. of hydrogen 2—36080
- Fe-Ni, diffusion of C, activation volumes 2—19144
- Fe-Ni, dil., hyperfine field at Fe atoms, temp. depend. 2—13449
- Fe-Ni, Fe-Ni-Co austenitic phase stabilization, thermal cycling 2—15909
- Fe-Ni, Hall coeff. and resist., effect of plastic deform. 2—22492
- Fe-Ni, initial magnetiz. by wall displacement 2—26027
- Fe-Ni, liquid state, density meas., structure 2—3374
- Fe-Ni, mag. props., electron irrad. effects 2—29818
- Fe-Ni, magnet design 2—6960
- Fe-Ni, magnetovol. effects 2—13402
- Fe-Ni, martensite transform., shape memory effect 2—9789
- Fe-Ni, martensitic transform. kinetics and martensite morphology 2—36277
- Fe-Ni, quenched-in vacancies, influence of hydrogen 2—39679
- Fe-Ni, shock loading, microstructure, α-γ transformation 2—3867
- Fe-Ni, stress corrosion cracking mechanism 2—6574
- Fe-Ni, thermal expansion, invar anomalies, new model from expt. obs. of coarsening by electron diffr. 2—16053
- Fe-Ni, thermodynamic activity, entropy, heat of mixing 750-1150°C 2—39929
- Fe-Ni film, domain boundary creep, temp. depend., 20 to −190°C 2—9644
- Fe-Ni film, electrodeposited cylindrical, internal macrostresses 2—35889
- Fe-Ni film, electrodeposited cylindrical internal macrostresses 2—35890
- Fe-Ni film, electrodeposited on cylindrical substrate, hysteresis loops 2—40507
- Fe-Ni film, electrodeposited on cylindrical substrate, internal stresses, disloc. theory 2—40506
- Fe-Ni film, electrodeposited, perpendicular anisotropy 2—36723
- Fe-Ni films, exchange const. determ. from standing spin wave reson. 2—10467
- Fe-Ni Invars, Mn-substituted, Curie temp. press. depend. 2—40483
- Fe-Ni martensite, transform. induced substructs., X-ray and elec. microscope obs. 2—22358
- Fe-Ni system, explosively loaded, hardening, recrystallization, grain boundaries 2—9575
- Fe-Ni system, metastable equilib., T_0-p-c diagram 2—13009
- Fe-Ni whiskers, growth and structure 2—18950
- (Fe,Co,Ni)-NbC, magnetically soft eutectic composite 2—22687
- (FeNi)-Au system, mag. moment props., magnetiz. and neutron scatt. obs. 2—36712
- $FeNi_3$, Mossbauer spectra of ^{119}Sn and ^{57}Fe, hyperfine field, spin polarization 2—40623
- $Fe_{0.70}Ni_{0.30}$, antiferromagnetism at high pressures 2—33168
- $Fe_{1-x}Ni_xAl$ solid solns., struct., density, mag. props. 2—39641
- $Fe_{65}(Ni_{1-x}Mn_x)_{35}$, low temp. sp. ht., rel. to mag. props. 2—33133
- FeNiMo films, magnetization reversal 2—19891
- Fe—Ni, martensite transform. twinning 2—9807
- Fe—Ni—C, activity coeff. of C, comp. depend. 2—9768
- Fe—Ni—Mo(V)—C, martensite transform. twinning 2—9807
- Ir-Ni, nuclear gamma resonance study, hyperfine field meas., conc. dependence 2—19979
- Mg-Co-Ni 9-layer Laves phase, composition and lattice constants determ. by single crystal and powder X-ray diffraction 2—39645
- Ni/Cu, adsorption of gases on single crystal surfaces, role of interaction energies 2—15675
- Ni/ZrO_2 composite, dispersion strengthening 2—12874
- Ni-Ag alloy, spring characteristics of thin leaf springs 2—25476
- Ni-Al-Cr, electrochemical seperation of intermetallic γ'-phase 2—30078
- Ni-Al-Cu, single crysts., internal friction temp. depend., 173-373 K 2—32589
- Ni-Al-Cu film, martensitic transform., growth of γ'-phase 2—29464
- Ni-Al-Nb, precipitation characteristics 2—19302
- Ni-Al-W-Mo-Co, dispersion- hardened, thermomechanical treatment 2—9733
- Ni-Al, dilute, quenched, solute dispersion, X-ray diffr. obs. 2—25587
- Ni-Al, γ' phase precip., FIM obs. 2—39907
- Ni-Al, light cond., interband transitions 2—26171
- Ni-Al, Mossbauer effect in surface layer of diffused ^{57}Co 2—40619
- Ni-Al, precip. morphology and effect on mech. props. 2—29404
- Ni-Al_2O_3-Mg Al_2O_3 particle coarsening 2—32743
- Ni-Al_2O_3, electrolytically deposited, dispersion hardening, tensile tests 2—19236
- Ni-Be, internal oxidation, diffusivity determ. for oxygen in Ni 2—29221
- Ni-0.3wt.%C, neutron irradiated, decomposition, metastable carbide formation 6618 2—6618
- Ni-Co-Cr-Mo, heat resistant, σ-phase precip. mechanics 2—9821
- Ni-Co, effect of mag. transform. on creep 2—12873
- Ni-Co, electron probe microanalysis corrections 2—16711
- Ni-Co, f.c.c., electronic sp. ht., interstitial carbon influence 2—16114
- Ni-Co, mag. props., influence of applied mag. field during electrolysis 2—19882
- Ni-Co films, exchange stiffness const. 2—19897
- Ni-Co layers electroplated on Cu wires, remagnetization 2—13411

Nickel alloys continued
Ni-Co Nernst-Ettingshausen effect rel. to Hall effect 2—32920
Ni-Co single crystal, magneto-plastic effects 2—33144
Ni-Co(Cu)(Fe), dil., mag. anisotropy energy 2—16369
Ni-Cr-Al, oxidation, 1000-1200°C 2—10624
Ni-Cr-Al, struct. imperfections in thin oxide surface film 2—6490
Ni-Cr-Fe, defects rel. to heat treatment 2—32499
Ni-Cr-Fe, neutron irradiation, extension rate, tensile strength, granular struct. 2—25513
Ni-Cr-Mo, corrosion, electrochemical behaviour 2—1754
Ni-Cr-Mo powder, heat treatment effect on elec. cond., mech. and corrosion props. 2—19280
Ni-Cr-Nb-Co, alloy quenched and reheated, study of cell precipitation 2—25563
Ni-(20 wt.%)Cr, recrystallization, effects of Al+Ti complex additions 25573 2—25573
2—19247
Ni-Cr, 1000-1350°C, degree of ionization and electrotransport phenomena 2—40179
Ni-Cr, comp. depend. of mag. moment 2—22688
Ni-22.7-38 at.%Mn, phase transform., neutron diffr. and X-ray scatt. obs., 673-908 K 2—25635
Ni-Cr, creep, effect of grain size and precip. parameters 2—12872
Ni-Cr, dil., electronic struct. of virtual bound state 2—16110
Ni-Cr, dil., two-current cond. processes and spin mixing 2—1486
Ni-Cr, elec. resist. heating, lifecycle, added elements effects 2—32732
Ni-Cr, interfacial energy ratio, grain-twin boundary 2—9573
Ni-Cr, plastically deformed, recovery, elec. cond. study 2—36120
Ni-Cr alloy, influence of diffusion creep on precipitate-free zone form 2—29270
Ni-Cr eutectic, oxidation, Cr_2O_3 layer formation and microstructure 2—4587
Ni-Cr steel, effect of Si on joints in austenitic steel 2—3957
Ni-Cr thick films, sputtered, deposition temp. effect on condensed phases 2—32371
Ni-Cr thin film, struct. and resist. 2—32373
Ni-(25 wt.%)Cr, ^{51}Cr electrotransport, diffusion coeff. 2—1272
γ'-Ni-Cu-Al, martensitic, elastic twinning, stress effects 2—15769
Ni-Cu-Au(Si)(Zn), ternary solid solutions, reciprocal mag. susceptibility, antiparallel coupling 2—4347
Ni-Cu-1 wt.%Si, ageing behaviour, precip., GP zone form., struct. 2—25578
Ni-Cu-Fe-graphite, sintering, phase and struct. changes 2—1401
Ni-Cu-Si-Mg(Cr) age hardening behaviour rel. to cold working 2—32706
Ni-Cu-Si, mag. and struct. props. 2—33116
Ni-Cu, differential sputtering yield 2—19477
Ni-Cu, dilute, charge density oscill. around impurities n.q.r. obs. 2—16666
Ni-Cu, ferromag. alloy, n.m.r. study, localization of excess electrons around solute atoms 2—4558
Ni-Cu, high field susceptibility, density of superparamag. clusters 2—26041
Ni-Cu, interdiffusion, void form., marker movement, press. effects 2—39738
Ni-Cu, interdiffusion coeff., conc. depend., diffusion coeff. at infinite dilution. 2—19146
Ni-Cu, light cond., interband transitions 2—26171
Ni-Cu, liquidus and solidus curves, electron probe microanalysis, point counting obs. 2—3433
Ni-Cu, melt, dissolution of O_2, enthalpies of reaction, e.m.f. obs., activation parameters 2—3956
Ni-Cu, Ni-Cu-C, mechanical properties, at temperatures between 78 and 523 K 2—1278
Ni-Cu, radiation damage in 500 kV electron microscope, dislocation loops 2—1238
Ni-(33 at.% Cu clustering kinetics 2—15934
Ni-Cu_9Al_4, powder, ternary mixed compact, sintering behavior, expansion, Kirkendall diffusion 2—19279
12wt.%Ni-59wt.%Cu29wt.%Zn, thermomech. treated., strengthening mech. superposition32688 2—32688
Ni-Fe-Cr-Ti, γ' hardened, strengthening mach., precip., γ_{apb} calcs. 2—32733
Ni-Fe-Mn, isothermally treated, martensitic transform. characts. 2—32765
Ni-Fe-Mo, martensitic transform., rel. to cooling rate, plastic deform., hardening 2—29467
Ni-Fe-Nb alloys, magnetic properties, electrical resistivity and hardness 2—4372
Ni-Fe-Ta, mag. props., elec. resist., hardness 2—29812
Ni-Fe-V system, ordering 2—39938
Ni-Fe-W system, atom ordering 2—39650
Ni-(50 wt.%)Fe, secondary recrystn. mechanism39937 2—39937
Ni-Fe, cryst. growth, suppression of striations 2—25268
Ni-Fe, current flow effect on hysteresis and domain wall motion 2—33148
Ni-Fe, deformability, initial permeability, de-oxidation elements addition effect 2—4367
Ni-Fe, diffusion of C, effect of annealing struct. defects 2—32561
Ni-Fe, dil., two-current cond. processes and spin mixing 2—1486
Ni-Fe, f.c.c. lattice, para-process susceptibility rel. to comp. 2—29478
Ni-Fe, ferromag., conc. depend. of av. mag. moment, Ising model calc. 2—16351
Ni-Fe, light cond., interband transitions 2—26171
Ni-Fe, oxidation kinetics, and development of oxide scale 2—16683
Ni-Fe, shielding against current in coaxial config. 2—40488
Ni-Fe, solid soln., positron annihilation and Mossbauer effect 2—4445
Ni-Fe, thermodynamic functions, activities, mass spectrometric obs. 2—36351
Ni-Fe film, electrodeposited, critical curves for mag. fields 2—19898
Ni-Fe film, high temp. domain struct. determ. 2—10223
Ni-Fe film, induced uniaxial mag. texture 2—26050
Ni-Fe film, magnetization state, thickness and eddy current effects 2—36726
Ni-Fe film, trigger effect in constant mag. fields 2—40511
Ni-Fe films, mag. props., rel. to struct. 2—36728
Ni-Fe films, magnetoresist., ang. depend. 2—33153
Ni-Fe invar, resistivity and thermopower meas. in 1.5-125 K range, result, interpreted in weak ferromagnet band model 2—36440
Ni-Fe rectangular hystersis core, flux reversed 2—36716
Ni-Fe steel, austenitic phase stability, heat cycling effects 2—29436
Ni-Ga, ferromag. alloy, n.m.r. study, localization of excess electrons around solute atoms 2—4558

Nickel alloys continued
Ni-H system, crit. atomic ratio for disappearance of ferromagnetism 2—40490
Ni-H system, h.p. Hall effect 2—4378
Ni-H(D) solid solution, thermodynamic function, calc. 2—3961
Ni-Ir, dil. ferromag., nuclear electric quadrupole interaction of Ir nuclei, n.m.r. obs. 2—20160
Ni-M solid solutions, effect of solute (M=Al, Cr, Si, Sb, Ti) on mech. props. 2—25505
Ni-Mn-Cu, nonmag., Elinvar type, heat treated, cold worked, Youngs modulus, rigidity, thermal expansion, hardness 2—19161
Ni-Mn-Fe system, mag. anisotropy, magnetostriction, permeability 2—40455
Ni-Mn, ferromag., conc. depend. of av. mag. moment, Ising model calc. 2—16351
Ni-Mn, light cond., interband transitions 2—26171
Ni-Mn, magnetic anisotropy, magnetostriction 2—40454
Ni-Mn, nonmag., Elinvar, heat treated, cold woked, Youngs modulus, thermal expansion, rigidity, hardness, 123-673K 2—19162
Ni-Mn, order-disorder transform. 2—15981
Ni-(20.5wt.%)Mn, mag. permeability, elec. props., homogenizing treatment effect 2—13399
Ni-Mo, disorder-order process 2—39996
Ni-Mo, high quality, production of very thin strips by cold working 2—1352
Ni-Mo, ordering kinetics, X-ray and electron microscope obs. 2—36293
Ni-Mo, solidified at fast cooling rates, metastable phases 2—36305
Ni-Mo powder, heat treatment effect on elec. cond., mech. and corrosion props. 2—19280
Ni-Nb, nucleation of long range order, elec. resist. study 2—12972
Ni-Nb, solidified at fast cooling rates, metastable phases 2—36305
Ni-P film surfaces, ellipsometric study 2—32370
Ni-P films, struct. and elec. resist., annealing effects 2—15969
Ni-P layers, imperfectly crystallized quasi-amorphous, struct. 2—22074
Ni-Pd-P amorphous, elec. resist., temp. coeff., rel. to P content, 4.2-300 K 2—40182
Ni-Pt-P-Cr, amorphous, elec. resist. and mag. susceptibility 2—6761
Ni-Pt, ferromag.-paramag. transition 2—40489
Ni-Rh, elec. resist., giang mag. polarization clouds 2—22493
Ni-Rh, giant moments 2—40486
Ni-Rh, low temp. heat capacity anomaly, superparamag. behaviour 2—13045
Ni-Si, energy changes in magnetiz. 2—33139
Ni-Ta, hyperfine field at ^{181}Ta, temp. dependence 2—36799
Ni-Ta, Ni_8Ta nucleation 2—15970
Ni-Ta, solidified at fast cooling rates, metastable phases 2—36305
Ni-Th, particle size, interparticle spacing, influence on mech. behaviour 2—3963
Ni-Ti, fractional determ. of TiO, TiN, TiC 2—30110
55 at.%Ni-Ti, hardening, rel. to Ti_2Ni_3 precip. 2—39903
Ni-Ti, solidified at fast cooling rates, metastable phases 2—36305
Ni-Zn, ferromag. alloy, n.m.r. study, localization of excess electrons around solute atoms 2—4558
Ni-Zn ferrites, cryogenically crushed, prep. and props. 2—16384
Ni-Zn system, reactive diffusion, phase formation, press. depend. 2—12996
Ni-Zr, solidified at fast cooling rates, metastable phases 2—36305
Ni-(Cu, Sb, Ir), dilute ferromag., isotope pair struct. anomalies, n.m.r. 2—20159
Ni-(11.1, 13.8 at.%)Al, precip. reactions at 425°C, Curie temp. change, magnetization vs. temp., ageing 2—29403
Ni-transition metal, dil., electronic sp. ht. 2—16039
Ni bronze, supersaturated soln. transformation, kinetics 2—9819
Ni super-alloy, plastic deformation, microstructure 2—12863
βNiAl, dislocation reactions in high temp. creep 2—9677
NiAl, elec. resist., thermo-emf, Hall effect 2—6760
Ni_3Al, band model of ferromag. 2—40442
Ni_3Al, diffusion of Ni 2—3811
Ni_3Al, low temp. elec. and thermal resist. 2—40095
Ni_3Al, mech. props., anomalous temp. depend. 2—6548
Ni_3Al, mech. props., anomalous temp. depend. 2—6547
Ni_3Al, yield point and flow stress, temp. and strain depend. 2—12861
Ni_3(AlTi), diffusion of Ni 2—3811
Ni_2Cr, critical shear stresss, ordering effects 2—9662
Ni_3(Fe,Mn), antiphase domains 2—6446
NiFe, Barkhausen noise, autocorrelation function 2—22684
Ni_3Fe, critical order/disorder transformation temp., biphase domain 2—12780
Ni_3Fe, $Ni_3(Fe_{0.76}Al_{0.24})$, ordered domain formation, anti-phase walls 2—9581
Ni_3Fe, short range order correl. with phys. props. 2—25601
Ni_3Ga, nearly-ferromag., low temp. sp. ht. rel. to clustering and spin fluctuations 2—19856
Ni_3Ga, yield stress, anomalous temp. depend. 2—3870
Ni_3Mn, annealed, ordering during loading, elec. resist., yield point, elastic deform. 2—15971
Ni_3Mn, electron irrad. induced disorder 2—22373
Ni_3Mn ferromagnetic alloy, electronic structure 2—33123
NiMnSb, Heusler alloy, atomic and mag. struct. determ. 2—19862
Ni_2MnSn, Mossbauer effect study of hyperfine fields at Sn sites 2—36833
Ni_3Mo, dissociated antiphase boundaries 2—9548
Ni_4Mo, antiparallel twins, FIM study 2—22216
Ni_4Mo, ordering kinetics, model 2—9831
Ni_4Mo ordering process during isothermal annealing, field-ion microscope obs. 2—36294
NiTi martensite, stacking faults 2—15768
Ni_3Ti, oxidation kinetics 2—20188
Ni_8Ti single crystal, partially ordered, flow stress obs. 2—25504
Ni_4W, peritectoid growth 2—13006
Ni_8X, X=combinations of V, Nb, Ta, order-disorder reactions, electron diffr., elec. resist. obs. 2—13007
Ni—V—C, VC_x precip., electron microscope obs. 2—9769
Pd-Ni, disordered, spin fluctuations 2—10173
Pd-Ni, elec. resist., paramag.-ferromag. transition 2—1606
Pd-Ni, ferromagnet, electron transport props., 1.5-78 K 2—22494
Pd-Ni, X-ray spectra and band structure 2—36918
$(Pd_{60-x}—Pt_x—Ni_{40})_{75}—P_{25}$, elec. resist., 1.2-300 K 2—19550
Pt-Ni, mag. props. in ordered and disordered states 2—40419
PtFe-PtNi, order-disorder transformation, magnetization, coercive force, lattice parameters 2—1633

- **Nickel alloys** continued
  - Pu-Ga-Ni system, unit cell parameters, X-ray diffr. 2—15730
  - Rh/Fe-Ni, plated alloy, lattice parameters during heat treatment 2—9471
  - Ru-Ni, spin fluctuation effects on supercond. 2—19600
  - ThNiSn, atomic struct., Debye-Scherrer determ. 2—3736
  - Ti-Mo-Ni system, polythermal section, microstructure, resistivity, dilatometry, X-ray analysis 2—32788
  - TiC-Ni, sintered, wear resist. 2—9777
  - TiNi, martensite struct., rel. to premartensitic instability 2—9825
  - TiNi, resistivity peak on thermal cycling, shape memory effect 2—29479
  - Yb-Ni system, cpd. formation, X-ray diffr. study 2—25349
  - Zr—Cu—Ni, struct. transforms. on continuous cooling 2—1391
- **Nickel compounds**
  - *see also Nickel alloys*
  - antigorites and talcs, antiferromagnetism 2—36761
  - ferrites, polycrystalline, meas. of Young, rigidity and bulk moduli at room temp. 2—36097
  - nickelides, MNI_5, M=La, Ce, Pr, Nd, Gd, sp. ht. obs., 1.6-4K 2—16037
  - oxides, free and bound charge carriers 2—10028
  - Permalloy thin films, magnetic anisotropy in local regions, by Lorentz microscopy 2—13409
  - sulphides adsorbed on metal surfaces, distinction from sulphur by Auger spectroscopy 2—39557
  - $[NiCl_6]^{4-}$ semiempirical MO calc. 2—18459
  - Co-Ni-Cr-Mo alloy, precip. hardening and phase transformation 2—19296
  - Co_xWO_3, bronze, density rel. to structure 2—32451
  - $Cu_{0.75}Ni_{0.25}Fe_2O_4$, elec. cond. 2—1513
  - InSb-NiSb eutectic, measurement of heat flow, using Nernst effect 2—37810
  - K_2NiF_4, anisotropy, antiferromag. reson. study 2—36974
  - Ni-Co-Dy ternaries, magnetic characteristics 2—10213
  - Ni-Co-Mn-Cu ferrite, piezomag., impedance 2—29827
  - Ni-Co, alloy, single crystal growth by floating zone technique using induction heating 2—3585
  - Ni-Co ferrite, Mossbauer and X-ray spectra obs. 2—40528
  - Ni-Cu-Co-Fe ferrites, magnetostrictive, magnetomech. props., 233-373K 2—40529
  - Ni-Fe cylindrical film, transverse magnetiz. using modified Procopia effect 2—19881
  - Ni-Th, intermetallic compound, struct., disordered substitutions, X-ray obs. 2—6452
  - Ni-Y, intermetallic compound, struct., disordered substitutions, X-ray obs. 2—6452
  - Ni, complex, of dimercaptodiethyl sulphide, i.r. spectrum, configuration 2—8769
  - Ni complex, acetylacetonate alkylamine complex, p.m.r., contact and pseudocontact shift study 2—28283
  - Ni complex, bis-(π-allyl), orbital assignment from photoelectron spectra obs. 2—35280
  - Ni complex, Cu(II) doped α-bis(thiosemicarbazide) Ni(II) $SO_4.3H_2O$, e.p.r., covalent bonding 2—26286
  - Ni complex, n.m.r. of ^{14}N and ^{13}C 2—8685
  - Ni complex, $Ni(CO)_4$, all ab initio SCF-MO calcs. in better-than-minimal basis presented 2—21634
  - Ni complex, tetramethylammonium trichloronickelate(II), mag. props. 2—40550
  - Ni complex, tris(o-phenanthroline)Ni II ions, SCF calc. rel. to electron delocalisation 2—3056
  - Ni complex $[TMPD^+]_2$ $[Ni(mnt)_2]^{2-}$, triplet exciton e.p.r. and structure 2—30005
  - Ni complexes, cyclopentadienyl, ^{31}P chemical shifts 2—810
  - Ni complexes, $M_2[M'Ni](NO_2)_6$ type, cooperative Jahn-Teller effect 2—19943
  - Ni ferrite, Co-containing, thermomagnetic effects on X-ray and Mossbauer spectra 2—36917
  - Ni II complexes, INDO calc. of spin densities 2—811
  - $Ni_{0.67}Te$, Mossbauer effect, isomer shifts, quadrupole splittings 2—26132
  - Ni^{2+} complex, 'oxinate', u.v. and visible reflectance spectra 2—22751
  - Ni_3Al, electron bands and magnetic props. 2—4383
  - $Ni_3Al_xT_{1-x}$, x=0, 0.5, 1, lattice parameter mismatch, thermal expansion coeff. obs. 2—25345
  - $NiAs_2$, parammelsbergite, cryst. struct., X-ray obs. 2—25342
  - $Ni_3(BO_3)_2$, crystal structure study by least squares refinement method 2—32471
  - $Ni_3B_7O_{13}I$, ferroelastic-ferroelec. ferrimag cryst. 2—29756
  - $NiCO_3$-$MgCO_3$ system, stability relations 2—12999
  - $NiCO_3$, hydrothermal cryst. growth 2—25252
  - $Ni_xCd_{1-x}Fe_2O_4$, struct. and mag. props., comp. depend. 2—1639
  - $NiCl_2$, layer-like, adsorption of rare gases, first layer formation by 2D condensation 2—22087
  - $NiCl_2$, layer-type crystals, u.v. and soft X-ray absorpt. spectra 2—20033
  - $NiCl_2.2H_2O$, low temp. anomalous mag. sp. ht. 2—22712
  - $NiCl_2.6H_2O$, far-i.r. absorpt., deuteration effects, vibrs. obs. 2—22756
  - $NiCl_2.6H_2O$, mag. axes temp. depend., mag. anisotropy 2—22711
  - $Ni_{1-x}Co_xFe_2O_4$, coercive force and magnetostriction, effect of prep. method 2—29829
  - NiCr, amorphous thin film, occurrence of e minimum in the electrical resistance meas. between 42 K and room temp. 2—13107
  - $NiCr_2O_4$, cryst. distortion, temp. depend. 2—3988
  - $NiCr_2O_4$, Jahn-Teller phase transition, X-ray crit. scatt. obs. 2—32777
  - $Ni_xCu_{1-x}Fe_2O_4$, Curie temp., cation distrib. influence 2—33158
  - NiF_2, antiferromag., light scatt., mag. field effects 2—16537
  - NiF_2, critical behaviour, Neel pt. 2—10249
  - NiF_2, pressure induced polymorphism 2—15732
  - $NiF_2.5HF.6H_2O$, internal motions, n.m.r. obs., 90-400K 2—40779
  - $NiFe_{2-x}Cr_xO_4$, crystal and band structure, X-ray and Mossbauer spectral investigation 2—35996
  - $NiFe_xCr_{2-x}O_4$, ferrite, struct., internal fields, X-ray and Mossbauer obs. 2—40635
  - $NiFe_2O_4$ films, prep., microstruct., mag. props. 2—18941
  - $Ni_xFe_{3-x}O_4$, containing antiferromag. precip., rotational hysteresis 2—22693
  - $Ni_xFe_{3-x}O_{4\|y}$, mag. anisotropy, Fe^{2+}ion conc. depend 2—1601
  - $Ni_xFe_{3-x}O_4$, oxygen nonstoichiometry and defect struct. 2—29174
  - $NiFe_2Se_4$, mag. struct., neutron diffr., elec. cond., Mossbauer effect obs. 2—19908
  - $NiFe_2Se_4$, thermal cond., 100 to 500 K 2—19459
  - $NiFl_2O_4$ sputtering, reactive, in Ar-O_2 mixtures, molecular sputtering mode obs. 2—1012
- **Nickel compounds** continued
  - Ni_3Ga:Fe very dilute alloys, Mossbauer effect meas. of giant magnetic moments 2—19868
  - $Ni_3IB_7O_{13}$, opt. and chem. props. 2—15936
  - Ni(II) complex, $(Et_4N)_2NiCl_4$, lattice-ion interactions 2—36791
  - Ni(II) complex, isopropylsalicylaldimine, susceptibility and anisotropy 2—36661
  - β-$Ni(IO_3)_2.2D_2O$, crystallographic and magnetic structure, X-ray and neutron diffraction examination 2—9484
  - $NiIn_xFe_{2-x}O_4$, ^{115}In n.m.r. study 2—40778
  - $NiIn_2S_4$, $NiIn_2S_{4-x}Se_x$, prep., elec. resist., paramag., antiferromag. interactions 2—29800
  - NiMn ferrites, anomaly in resistivity-temperature characteristics in Curie-point region 2—19534
  - Ni_3Mn, phase transitions, small angle neutron scatt. obs. 2—19303
  - $Ni(NH_3)_6I_2$, internal rot. of NH_3 groups, i.r. spectra obs. 2—10375
  - $Ni(NO_3)_2.6H_2O$, sp. ht., low temp., antiferromag. interactions 2—1434
  - $NiNb_2O_6$, i.r. absorpt. spectra, cryst. chem. 2—10396
  - $Ni_xNb(Ta)S_2$ magnetic and crystal structure 2—3722
  - NiO:Li, current noise measurements 2—40278
  - NiO:Li, Hall effect anomaly calc. 2—22518
  - NiO-α-Fe_2O_3, fired mixtures, quantitative phase anal. 2—13014
  - NiO-MgO-Fe_2O_3 system, Curie point and cryst. struct. 2—1414
  - NiO-MgO, solid soln., thermodynamic properties 2—4061
  - NiO, adsorpt. of Ar, effect of chemisorbed species 2—35916
  - NiO, adsorption of Te from soln., rel. to defective reactor fuel location 2—12685
  - NiO, antiferromag, magnon excitation by electron tunnelling through Ni-NiO-Pb junctions 2—10240
  - NiO, antiferromag., surface magnetization, exchange interaction temp. depend. electron scatt., $T_n \leqslant T \leqslant 295K$ 2—6995
  - NiO, Co and Ni diffusion 2—36079
  - NiO, electronic struct. 2—13092
  - NiO, electronic struct. 2—13093
  - NiO, epitaxial, hole drift mobility, photoexcitation obs. 2—10027
  - p-NiO, free and bound charge carriers 2—10028
  - NiO, limit of solubility in ZnO, X-ray studies, magnetic investigation 2—3962
  - NiO, magnetostriction, strain temp. depend. 2—6994
  - NiO, photoelectron spectra, excited states of Ni in solid, satellite emission 2—4328
  - NiO, positron lifetime correlations 2—4150
  - NiO, powder, degassing temp. rel. to sp. surface area and heat of wetting 2—6623
  - NiO, pressure sintered, elastic moduli meas. by resonant sphere, three part composite oscillator, and pulse transmission methods 2—12825
  - NiO, Raman scatt. by four magnons 2—36903
  - NiO, refractory, cryst. growth by floating zone method 2—29098
  - NiO, shakeup photoelectron spectra 2—36636
  - NiO, single cryst., photocond. in visible and near u.v. region 2—10138
  - NiO, spectrum observed in low-pressure arc with Ni electrode 2—14485
  - NiO, stoichiometry limits 2—22099
  - NiO, two-magnon Raman scatt. 2—16509
  - NiO, valence band structure, X-ray photoemission spectroscopy 2—36639
  - NiO cathodes, pressed porous, for production of intense electron beams 2—21027
  - NiO in MgO, e.p.r. line shape evolution 2—1728
  - NiO layer on Ni alloy, use of 'shake-up' satellites in photoelectron spectra for analysis 2—7192
  - NiO Raman, scattering by phonons, magnons and phonon- magnon interactions from 10-650K 2—26195
  - NiO surface, clean, exchange scatt. effects on LEED 2—39463
  - $Ni_{85}P_{15}$, amorphous, temp. depend. of magnetization 2—22694
  - NiS, metal-insulator paramag.-antiferromag. transition 2—16349
  - NiS, metal-nonmetal transition 2—19515
  - NiS, press.-temp. phase diagram and cryst. struct. 2—26069
  - NiS_2, antiferromagnet, magnetization, susceptibiliyy, and weak ferromagnetism 2—33137
  - α-Ni_7S_6, cryst. struct., X-ray determ. 2—39649
  - $NiSF_6.6H_2O$ powder, e.s.r. spectrum at 6 katm. 2—27370
  - NiSb-InSb eutectic alloy, thermal cond., temp. depend. and anisotropy 2—19460
  - $NiSeO_4.6H_2O$, optical activity 2—16420
  - $NiSeO_4.6H_2O$, optical activity 2—19966
  - Ni_2Si, physical props. 10-350K, electron energy spectra discussed 2—40141
  - $NiSiF_6.6H_2O$, internal motions, n.m.r. obs., 90-400K 2—40780
  - NiTe, polycrystalline thin film, electrical and galvanomag. props. as function of thickness 2—1520
  - Ni_2Te_3, Mossbauer effect, ionicity 2—4446
  - Ni_3TeO_6, mag. props., ligand field treatment 2—16348
  - NiTiSb, para-mag. susceptibility detn. 2—13397
  - $Ni_{0.5}Zn_{0.5}Fe_2O_4$, anisotropy and mag. losses, effect of CoO addition 2—29830
  - $Ni_xZn_{1-x}Fe_2O_4$, ferrite mixed, spin relax., relax. times rel. to Zn^{2+} conc., Mossbauer obs. 2—40577
  - $Ni_xZn_yFe_2O_4$, optical consts., ellipsometric determ. 2—36816
  - $Ni^{II}U_2{}^{V}F_{12}.4H_2O$, optical absorption spectra and magnetic susceptibilities 2—33275
  - Nio, hole drift mobility at high temp. 2—13226
  - $ni(OH)_2$, adsorption of Te from soln., rel. to defective reactor fuel location 2—12685
  - $Zn_xNi_{1-x}Fe_2O_4$, effect of Dy substitution on props. 2—13413
- **Night sky** *see Airglow*
- **Nightglow** *see Airglow*
- **Nilsson's model** *see Nucleus/models*
- **Niobium**
  - *see also Superconducting materials/niobium*
  - band struct., reson. density of states, photoluminesc. obs. 2—16640
  - band structure, plane-wave-Gaussian energy bands 2—4125
  - bremsstrahlung photon emission, 1 BeV electron and positron interaction 2—13498
  - carburization kinetics, in acetylene atmosphere 2—26340
  - carburization kinetics, in methane atmosphere 2—26341
  - channelling of 300 keV deuterons, particle flux, energy peaking, computer simulation 2—36385
  - cold deformed, dislocation rearrangement rel. to time and temp., 1273-1473K 2—36034

Niobium continued
crystals, deform., flux line dislocation interaction, dislocation density rel. to annealing 2—25410
deformation twinning, pre-strain effects 2—32538
desorption of Na and K, activation energies, mean adsorption lifetimes 2—6384
desorption of oxygen, sticking probability interaction kinetics 2—9308
diffusion, of H and D, quantum theory 2—15790
diffusion of hydrogen in single crystals 2—9611
diffusion of U, rate and temp. meas. 2—12795
disintegration at high temp. and stresses, protection by vacuum diffused coatings 2—6595
dislocation damping by phonon viscosity 2—29183
dispersion hardening by ZrO_2, ThO_2, HfO_2 2—32747
electrotransport of C, above 1900°C 2—22251
extraction, properties and applications 2—3925
Fermi surface and scattering processes, magnetoresist. study 2—25734
film preparation by double-cathode sputtering system 2—29043
glide dislocation, elastic energy 2—1253
heat capacity, elec. resistivity, thermal radiation, subsecond meas., 1500-2700K 2—40076
in Inco 718, content change effect on precip. hardening9820 2—9820
interstitial diffusion in work hardened material, annealing temp. depend., resist. obs. 2—15910
interstitial solute pick-up, annealed sample, Hall-Petch plot 2—9544
lattice dynamics, frequency/wave vector dispersion relations for normal modes of vibration 2—22384
lattice vibration spectra, determination of specific heats and Debye temp. 2—22405
in Mn-Si steel with low C, influence on precipitate struct. 2—9812
oxidation, conc. variation with depth of absorbed oxygen 2—16682
phase analysis in low carbon steel 2—1741
plastic deformation, strain-rate and temp. depend. of yield and flow 2—39790
plastically deformed, recovery, supercond. crit. temp. 2—19559
polycrystalline, Hall Petch parameters, grain size and extrapolation methods 2—15820
proton dechannelling, min. yield 2—40109
recovery, stage III, deformation temp. effects 2—25575
single crystal, strain free prep. 2—22126
slip band propag., strain deformation, twinning, dislocation movements in single cryst. 2—3884
solid solution with dissolved O_2 and N_2, resist., hardness 2—3942
spin-lattice relaxation of ^2H, quadrupole coupling 2—7129
sputtering, by Nb, H, D and He ions, 10 to 80 keV 2—4086
in steel, austenitic stainless, effect on stress corrosion cracking 2—29326
in steel, influence of precip. on mech. props. 2—9738
steel, quenched, aged, alloy addition, effect on mech. props., weldability 2—19239
surface, control of morphology and purity during treatment, use in r.f. supercond. 2—39462
thermal negative ion emission from wire coated with Cs halides 2—22655
thermionic electron emission, polycrystalline and film specimens 2—4322
X-ray K-emission, ionicity and valence 2—20084
Li-Na binary metallic liquid, obs. of paraconductivity above critical point 2—12576
Nb VI, ionization pot. and Rydberg series 2—15219
Nb VI resonance-line spectrum in the vacuum u.v. 2—18312
^{95}Nb diffusion in γ-phase of U-Nb alloys 2—29206
Nb^{4+}. e.p.r. in Cs_2HfCl_6, 4.2-77 K 2—4539
inNi-Cr alloy, effect of grain size and precip. on creep 2—12872
oxidation reactions and resistance 2—30065
$SrTiO_3$:Nb, free carrier optical absorpt. 2—36887

Niobium compounds
alloy, deformed, annealing, cellular struct., ductility 2—9646
alloy, electron-beam welding to titanium alloys 2—19254
alloy, oxidation protection, by Al coating containing additions of various elements 2—9267
alloys, disintegration at high temp. and stresses, protection by vacuum diffused coatings 2—6595
Nb_3Al-Nb_3Ga-Nb_3Ge, alloy, pseudoternary system, investigation of certain sections 2—6617
X-ray K-emission, ionicity and valence 2—20084
Al-Nb, X-ray emission spectrum study of band structure 2—36911
CaO-Nb_2O_5-TiO_2-SiO_2, liquidus detn. in the 15% SiO_2 plane 2—9204
Co-Fe-Nb alloy, cold drawn, annealed, hardness, coercive force, magnetization 2—1625
Co-Fe-Ni-Nb alloys, semihard mag., for remanent reed switch applics. 2—40463
Cr-Zr-Nb-C alloy, stress rupture and ductility control by microstruct. modification 2—9692
Fe-Co-Nb alloy, Nb additions rel. to long range ordering 2—29487
Fe-Co-V-Nb alloy, Nb additions rel. to long range ordering 2—29487
Fe-Nb-C, steel, segregation mech., phase struct., annealing tests, electron refr. obs. 2—32729
Fe-Nb dilute alloy, spin-lattice relax. time 2—19932
Fe-1.1at%Nb, dynamic strain ageing effects on mechanical behaviour 2—3866
Fe-(1.1 at%)Nb alloy, substitutional strain ageing, serrated flow 2—6536
Fe-Ni-Cr:Nb, steel, Nb content rel. to B solubility, intermetallic form. 2—22339
Fe-Ni-Nb, martensitic alloy, temper hardening 2—9739
(Fe,Co,Ni)-NbC, magnetically soft eutectic composite 2—22687
Fe—V—Nb—C alloy, VC_x precip., electron microscope obs. 2—9769
K_2O-SrO-Nb_2O_5 system, ferroelec. characterization 2—40352
$LiNbO_3$ to Li_3NbO_4, nonstoichiometric crystals, ^{93}Nb linewidths 2—40777
Mo-Nb-Hf alloy, phase diagram, hardness, metallography, X-ray analysis 2—4019
Mo-Nb noncrystalline alloys, work function, additive character of variation, anisotropy 2—13352
Nb:H, Curie-Weiss temp. depend. of paraelasticity 2—22262
Nb-Al-Ce(La)(Y)(Pr) alloy, hardness rel. to comp. and annealing 2—4021
Nb-Al-Ge film, high vac. annealed, supercond. props. 2—40200
Nb-Al-Ge films supercond., critical parameters 2—32942
Nb-C-Re system, intermetallic cpd. structs. 2—36304
Nb-C solid soln., C solubility, 1500-2150°C 2—32718
Nb-Cu alloy, oxidation reactions and resistance, effect of Cu content 2—30065
Nb-Ge-Al alloy, low temp. cubic- tetragonal transform. 2—9817
Nb-H alloy, plastic deform., effect on elec. resistivity 2—39935

Niobium compounds continued
Nb-H system, ferroelasticity rel. to phase diagram determination 2—9694
Nb-H system, proton spin-lattice relax. times, conc. depend. 2—7008
Nb-Mo-N system, equilib. conc. and solubility of N_2 2—4020
Nb-Mo-N system, phase diagram 2—19314
Nb-Mo-N system, thermodynamics of α solid soln. 2—19313
Nb-Mo alloy, flux-flow resist., Ettingshausen effect, thermal and mag. props. 2—13167
Nb-Mo alloy, with Fe impurity, localized mag. moment, Mossbauer obs. 2—36847
Nb-Mo alloys, supercond., transport entropy of vortices 2—13161
Nb-N alloy, flow stress, soln. hardening 2—9661
Nb-NbO_2-NiCr m.i.m. struct., current filament detect., a.c. detect. scheme, electron microscope obs. 2—40311
Nb-O alloy, flow stress, soln. hardening 2—9661
Nb-Ta-Ti, Nb-V-Ti system, superconduct., T_c determ. from planned expt. method using simplex lattice concept 2—4175
Nb-Ta-W-Mo, Cb-132 alloy, oxidation behaviour 2—13578
Nb-Ta, type II superconductor, magnetic behaviour at small Ginzburg-Landau parameters (χ) 2—19569
Nb-Ta alloy, type II superconductor, critical current depend. on defect structure of flux line lattice 2—19556
Nb-Ta alloys, supercond. props. 2—19588
Nb-Te system, phase study Nb_3Te_7 to Fe 2—9841
Nb-(60 at.%)Ti alloy, critical supercurrents and pinning of vortices 2—19584
Nb-Ti alloy, peak effect, rigidly pinned vortex model 2—13168
Nb-Ti alloy, Young's modulus temp. depend. 2—36095
Nb-Ti system, supercond., electronic struct., heat capacity analysis 2—40195
Nb-50%Ti, type II supercond., crit. current density, neutron irrad. effects29631 2—29631
Nb-64%Ti alloy, hard superconductor, cylindrical sample, magnetiz. and size effect 2—36460
5wt.%Nb-U alloy, γ-quenched, stress corrosion cracking, ageing conditions effects 2—36175
Nb-W system, phase diagram 2—39968
Nb-(25 at.%)Zr, Joule-heating power dissipation in hollow tube 2—36461
Nb-Zr alloy, high-field superconductor, pulsed-field meas. rel. to metallurgical processes 2—25790
Nb-25%Zr, supercond., low field critical current density from magnetiz. data 22502 2—22502
Nb-25%Zr, type II supercond., crit. current density, neutron irrad. effects 2—29631
7.5 wt.%Nb-2.5 wt.%Zr-U alloy, elastic consts. rel. to press., 1 bar-18 kbar 2—32580
Nb alloy, diffusion layer oxidation, struct. obs. 2—4590
Nb alloy, grain size rel. to B content 2—12729
Nb_3Al-Ta_3Al system, annealing, solid solubility 2—9775
Nb_3(Al, Ge) films, vacuum deposited, supercond. props. 2—40208
Nb_3Al, upper critical fields 2—32940
Nb_3Al and $Nb_3Al_{0.75}Ge_{0.25}$ film prep., resist. ratio 2—29013
Nb_3Al supercond., high mag. field props. 2—19586
$Nb_{0.75}(Al_{0.75}Ge_{0.25})_{0.25}$, upper critical fields 2—32940
$Nb_3Al_xGe_{1-x}$, supercond. 2—40207
$NbAs_2$ and isomorphs, supercond. props. 2—32927
NbB_2, thermal expansion over temp. range 300-2500°K 2—6683
$NbBF_9^-$ chem. shift, spin coupling, mag. resonance obs. 2—5927
NbC-TiC, high porosity complex carbide prep. 2—39969
NbC, band structure, tight binding method 2—4124
NbC, diamond grinding, surface work hardening, microstructure 2—3871
NbC, phonon spectra, pseudopot. approach 2—19321
NbC, precip. in steel, effect of hardening conditions 2—36234
NbC, slip system determination by hardness anisotropy 2—9564
NbC, solubility and precipitation in Fe austenite, impurity addition effects 2—12962
NbC, X-ray spectra, energy band struct. 2—40706
NbC layer build up on steel by open arc 2—32739
NbC_x, shocked, microcrack form. and plastic deform. 2—29328
NbC_x, thermodynamic props., determ. from sp. ht. 2—13044
Nb_6C_5, ordering, superlattice and domain struct. obs. 2—9483
$Nb_2Co_4O_9$, magnetoelectric effect after parallel annealing treatment 2—4406
Nb_3Ga, supercond. transition temp., phase diagram 2—32941
Nb_3Ga, upper critical fields 2—32940
Nb_xGa_{1-x} alloy, upper critical fields 2—25789
NbN, band struct. 2—9934
NbN, s-band state density at Fermi energy 2—13089
NbN, solubility and precip. in steel, effect of Mn, Si, Cr or Ni 2—12968
NbN, stabilized, a.c. losses 2—9971
NbN film, reactively sputtered, supercond. props. rel. to substrate temp. and struct. 2—40199
NbN films, critical parameters 2—32942
NbN films, supercond. props., thickness depend. 2—19589
$NbNF_{11}$, N=P, As, Sb, Ta, chem. shift, spin coupling, mag. resonance obs. 2—5927
NbO_2-Nb_2O_5, Nb_2O_5-Nb_3O_7F systems, intergrowth phases, homogeneity 2—9336
Nb_2O_5-WO_3 Wadsley defects, effect of annealing 2—3792
Nb_2O_5-ZnO system, phase relations 2—25644
Nb_2O_5-ZrO_2 system α-PbO_2 type phases, cation deficiencies and superstructure 2—9482
NbO_2, cryst. growth by chem. transport reaction 2—25256
Nb_2O_5, anodized oxide film, thickness, dependence of final voltage and time at this voltage 2—3537
Nb_2O_5, candoluminesc. 2—7106
Nb_2O_5, defect struct., correl. between lattice fringes and atomic positions 2—19056
Nb_2O_5, film, gaseous anodization, elec. and optical props. 2—13301
Nb_2O_5, high pressure phase transitions 2—29477
Nb_2O_5, m.i.m. struct., dielec. relaxation and tunnelling rel. to metallic impurities 2—10099
Nb_2O_5, O_2 self-diffusion, ionic cond. obs. 2—19148
Nb_2O_5.CuO-CaO.SiO_2-TiO_2, plane in quaternary CaO-Nb_2O_5-TiO_2-SiO_2 system, liquidus temp. determ. 2—3431
Nb_3P, Knight shift, spin lattice relaxation, conduction process 2—4559
NbRhGe, cryst. chemistry 2—9349
NbRhGe struct. relns. with other transition metal germanides 2—18969
NbS_2 pyridine intercalation complex, elec. field gradient 2—19947

Niobium compounds continued
Nb_3Sb, acoustic-phonon instability and critical scattering near phase transition at 45 K 2—9864
$NbSe_2$, press. induced supercond. 2—16182
$NbSe_2$, reflectivity anisotropy band struct. 2—10350
$NbSe_2$, supercond. and magnetoresist. 2—19590
$NbSe_2$, superconducting, layer structure, energy gap meas., temp. dependence 2—4165
$NbSe_2$, u.v. spectra, interband transitions, plasma reson. 2—13463
$NbSe_2$, ultrathin layers, superconducting resistive transition 2—19560
$NbSe_2$ crysts., compressibility 2—25497
Nb_3Se_4, Nb_2Se crystal structure, imperfections, void channels 2—3723
Nb_4Si, Nb_5Si_3, enthalpy, 1200-2200 K 2—13039
Nb_3Sn, cubic phase, study of temp. dependence of optical modes, elastic constants 2—9863
Nb_3Sn, high-field superconuctor, pulsed-field meas. rel. to metallurgical processes 2—25790
Nb_3Sn, lattice transform., X-ray obs. 2—22364
Nb_3Sn, normal and supercond. props. rel. to density of states 2—29637
Nb_3Sn, uniaxial stress effect on supercond. T_c 2—19587
Nb_3Sn film, cylindrical metallic substrate, fast rotation deposition technique 2—39515
Nb_3Sn films on Nb, deposition and critical temp. props. 2—12661
Nb_3Sn layers as protective coverings for Nb surfaces 2—32943
Nb_3Sn ribbon, doped, prep., microstruct. and high field supercond. props. 2—32944
NbTa, type II superconductor, flux line arrangements in hysteretic low-k samples 2—19570
$Nb_{0.73}Ta_{0.27}$, supercond., flux line lattice, neutron diffr. obs. 2—9967
$Nb_{75}Ta_{25}$, type II superconductor, small-angle neutron scatt. obs. of vortices 2—19591
Nb_3Te_4 imperfections, void channels .2—3723
NbTi superconducting magnet, enhancement of quench fields on cooling below 4.2 K, method for maintaining 2.17 K with He at constant 1 atm. 2—27410
$Nb_{0.88}Ti_{0.12}N$ film, supercond. fluctuation rounding of resistive transition 2—13166
NbZrTi alloy-Cu wire, solenoid, production of strong impulsive mag. fields 2—23517
Ni-Al-Nb alloy, precipitation characteristics 2—19302
Ni-Cr-Nb-Co, alloy quenched and reheated, study of cell precipitation 2—25563
Ni-Fe-Nb alloys, magnetic properties, electrical resistivity and hardness 2—4372
Ni-Nb alloy, nucleation of long range order, elec. resist. study 2—12972
Ni-Nb alloy, solidified at fast cooling rates, metastable phases 2—36305
$TaCo_2(Fe_2)$, Laves phases, temp. depend of microhardness 2—22290
Ti-(25 at.%)Nb alloy, omega phase formation, mechanism and kinetics, small angle X-ray scatt. 2—4006
$Ti_2Nb_{10}O_{29}$, cryst. struct., high-resolution electron microscopy obs. 2—12734
$TiO-Nb_2O_5$, ceramic semiconductor, electrical properties, influence of Nb_2O_5 percentage 2—6793
U-Mo-Nb-Zr alloys, phase transformations, carbide inclusions effect 2—13004
U-Nb-Zr alloy, γ^0 phase domain struct. 2—9495
U-Nb-Zr alloy, oxidation and temp. cycling, flexure study 2—10627
U-Nb-Zr and U-Nb alloys, stress corrosion cracking, effect of Cl^- 2—29331
U-Nb-Zr(Mo) system, kinetics of transform. of γ phase 2—36309
U-Nb alloys ^{235}U and ^{95}Nb diffusion, in 930-1900°C temp. range 2—29206
V-Ti-Nb, Si alloying effects on creep and creep strength 2—1295
Zn-Nb alloy, $\beta \rightarrow \omega$ transform., u.s., elastic consts., and X-ray studies 2—40014
Zr-Nb alloy, hydrogenation and fatigue failure 2—29303
Zr-Nb alloy, martensitic transform. 2—9827
Zr-Nb carbides, nonstoichiometric, thermodynamic model allowing for comp. depend. of parameters 2—25603
Zr-(2.5 wt.%)Nb alloy, age hardening 2—12952
Zr-25%Nb fuel claddings and pressure tubes in water cooled reactors 2—18257
$ZrO-Nb_2O_5$, ceramic semiconductor, electrical properties, influence of Nb_2O_5 percentage 2—6793

Nitrogen
β-form, rotational heat capacity from heat capacity of N_2-Ar mixture, barrier to rotation 2—4067
absorption by porous ThO_2 2—35924
absorption spectra, 730-980 Å, high resolution 2—18453
absorption spectrum, high resolution study from 730 to 980 Å 2—35269
abundance gradients across spiral galaxies, planetary nebulae rel. to interstellar medium enrichment 2—37269
acoustic dispersion at frequencies to 5.10^4 MHz/atm. 2—6160
adsorption, on metal film, during reactive sputtering, influence of surface adsorp. characts. 2—22068
adsorption, on stainless steel, isotherm meas. at 77 to 90K and 10^{-9} to 10^{-4} torr 2—32390
adsorption, on Ti foil at low pressure, ultrahigh vac. microbalance obs. 2—39566
adsorption by silicas, adsorpt. isotherm analysis 2—35923
adsorption in zeolite Y, heat of adsorpt. 2—35927
adsorption on glassy pyrogenic silica, surface area determ. 2—39565
adsorption on graphite, physical 2—18957
adsorption on Ta, RHEED obs. 2—12686
adsorption on W, sticking probabilities, surface coverage, molecular beam technique 2—25234
Andromeda galaxy, relative line strengths and abundances in emission regions in the nucleus and disk 2—13851
arc, high pressure, in strong axial gas flow 2—24944
arcs, d.c. cascade, electrical time constants obs. 2—18718
arcs, radiative energy transport det. 2—24943
atmospheric, raman spectra, obs. using remote spectrometer 2—34553
atmospheric, relationship between conc. and solar activity in 130-200 km height range 2—22982
atom, outer shell multi configuration approx., energy matrix elements 2—28196
atom, radiative recombination to form stable molecule 2—18345
atom calc. of quadrupole coupling constants 2—24316
atomic, dissociative excitation of long-lived Rydberg states by electron impact on N_2 2—2950

Nitrogen continued
atomic, excitation in He afterglow with traces of N_2 2—28194
atomic spectra, beam foil excited, lifetimes of NII-NV energy levels 2—35142
atomic spectrum, meas. in long wavelength and vacuum u.v. region 2—5790
atoms, conc. dependence of thermal transport in Ta 2—6512
atoms, electron impact at 1 to 10 keV, secondary electron energy and angular distribution 2—5814
atoms, large angle collisions with H^+, differential cross section meas. and interaction potential determination 2—710
atoms, neutral and ionized, electronic structure and term energies 2—585
atoms, recombination on steel surface, effect of adsorbed gases 2—5802
atoms, recombination via $N_2(a'\pi_g)$ and $N_2(a'1\Sigma_u^-)$ states 2—804
auroral, vibrational distribution, theoretical 2—4707
body, total content det. by fast neutron activation analysis 2—20718
breakdown, Nd:glass laser induced, used in pulses or mode-locked trains of pulses 2—24895
bubble growth rate during boiling on metallic heating surfaces 2—28772
cascade arc, radiative energy transport 2—24913
charge transfer reactions with Ar^+, obs. using ion injection drift tube 2—24838
compressibility, equation of state 2—3323
Compton scattering using γ-rays, Compton profiles 2—35190
concentration on Mars, low level explained by nonthermal escape mechanism 2—26840
conductance decay calculations of cylindrical arcs in N_2, SF_6, Ar 2—24927
cosmic ray nuclei, interstellar propagation, differential kinetic energy/nucleon spectra 2—4764
in dayglow, resonance scattering of first positive system 2—40985
desorption, from powder, specific surface measurement 2—15938
detection in various matrices using nuclear track technique 2—7200
detector, quantitative, by detection of secondary electron emission from Cu or AgMg surfaces 2—27885
diffusion, competitive in β-Ta film 2—39531
diffusion in Si powder compacts 2—39961
diffusion in V, 60-1825°C 2—22252
diluent, in HF chemical laser 2—21076
discharge, measurements on the stratification at low pressure 2—1010
discharge, mixed with CO, CO_2 or N_2O, i.r. afterglow emission 2—39211
discharge, Raman spectra, relaxation rate and energy transfer 2—38930
discharge, sparking voltage reduction due to mag. field parallel to electrode axis 2—9006
discharges, streamer and Townsend, optical meas. of luminous fronts 2—21879
dissociation of molecule by electron collision in electrical discharges 2—35275
dissolved in Nb, resist. hardness 2—3942
effect on ductile-brittle transition in heat treated Fe 2—15836
electron avalanches, energy and electron energy distributions 2—35628
ESCA chemical shifts by MINDO/1 valence electron SCF MO method 2—35209
flames, temperature det. using Raman scattering 2—37824
flow, sorption, through hydroxyapatite compacted membrane, 77-303K 2—39554
flow parameters behind shock waves 2—28693
free radicals, stability, steric and electronic effects, coupling constants from e.s.r. 2—26374
gas, dense, hot electron injection, backscatt., thermalization, diffusion and drift 2—12577
gas, K_α emission spectrum 2—21628
gas, solubility in water temp. dependence 2—25052
gas at moderate and high densities, two potential model for equations of state 2—39273
gas mixtures with CHF_3, CH_3F and CH_3CN, heat conductivity in electric field 2—3326
gas target, ejection of secondary electrons in collisions with 200-500 keV protons 2—12057
high pressure, laser initiated multimegavolt switch closure 2—17649
hypersonic shock wave, electron beam fluorescence investigation and rotational states 2—39265
internal Penning source, for heavy ions 2—34861
ion beams, acceleration in Bevatron 2—14809
ion implantation, in n-CdS, p-type layer formation 2—25422
ion implantation, in Si, Si_3N_4 formation, i.r. absorp. obs. 2—26173
ion implantation into CdS 2—15774
ionospheric D-region, ionization process 2—7336
ions, electron impact excitation cross sections 2—5822
ions, emittance measurements from Penning type ion source 2—34335
i.r. absorption, collision induced, study in temp. range 77 to 297K 2—8668
jet, underexpanded, rotational temperature distribution analysis by rotational relaxation 2—6140
jets, freely expanding, perpendicular temp. and translational freezing studies by mol. beams 2—28686
laser, excitation mechanisms, pulsed discharge 2—5367
laser, pulse emission in first positive system with cooling of gas 2—37968
laser, u.v., electron beam pumping 2—34381
laser amplifier, 50 MW, 3371 Å 2—31039
laser pumping, oscillator-amplifier dye laser system 2—11475
leak rate through thin polycarbonate film 2—3816
liquid, cooled bath for ruby laser, frequency shifting by adding He gas to vapour phase 2—34400
liquid, hot electron injection, backscatt., thermalization diffusion and drift 2—12577
liquid, in cryostat, device for automatic control of level 2—20777
liquid, index of refraction and absorption index, submillimeter wave region 2—32266
liquid, level control with low-high regulation 2—30723
liquid, under saturated vapour pressure, sound velocity using law of corresponding states 2—35760
liquid, vibrational lifetimes 2—19360
liquid as fuel for micromotors in space vehicles, specific impulse calc. 2—30399
liquid/saturated vapour equilib., crit. constants effects 2—28950
low pressure discharge, study of positive column props. 2—6115
luminescence spectrum, 6500-11500 Å, excitation by 13 kev electrons of pure N_2 and N_2-He mixtures 2—31809
martian atmosphere evolution 2—41194
in metal, det. by mass spectrometry, isotope dilution method 2—10656

Nitrogen continued

- molecular collisions with neutral Cs, excitation transfer cross sections 2—35152
- molecular core-level binding-energy shifts calcs. from Mo theories 2—35195
- molecular solid, quadrupole forces, quantum lattice dynamics treatment 2—32789
- molecule, absorpt. cross sections and ionization efficiencies 300-1000 Å region 2—21639
- molecule, C $^3\Pi_u$ state, electron impact excitation of $v'=3$ and 4 levels, electron emission band obs. 2—5938
- molecule, collision with Ar, rotational inelasticity, comparison of generalized phase shift and classical trajectory calculations 2—8862
- molecule, collision with H_2, anisotropy of total collision cross section 2 3146
- molecule, collisions with 10 keV electrons, ionization, fragmentation and electron energy loss 2—12170
- molecule, collisions with He, low energy scattering cross sections 2—24408
- molecule, collisions with K atom, K ionization cross section 2—31706
- molecule, collisions with O_2, rate equations for vibrational relaxation, applic. to spectrophone data 2—8857
- molecule, decay of electron impact excited states, time resolved studies 2—5939
- molecule, dissociation, obs. of induction time 2—24479
- molecule, dissociative excitation by electron impact, vacuum u.v. emission features 2—8669
- molecule, dissociative excitation by He(2^3S), rate constants 2—12305
- molecule, electron impact excitation of metastable $E^3\Sigma_g^+$ state 2—31814
- molecule, electronic transition moment variation in first and second positive band systems 2—38927
- molecule, excitation mechanism for population of vibr. levels of $C^3\Pi_u$ state 2—21630
- molecule, ground state calc. using perturbation procedure for constrained SCF LCAO MO eqns. 2—31758
- molecule, in solid Ar matrix, induced fundamental i.r. band 2—18472
- molecule, intensity of first positive bands, study of region in which 2 and 3 body processes compete 2—18345
- molecule, internally excited, collisions with Na atoms, Na D-line radiation excitation 2—35161
- molecule, orbital determ., ESCA line intensities obs. 2—35219
- molecule, r-centroid, calc. from potential energy curves 2—3024
- molecule, reactive and charge transfer collisions with O^+, effects of metastable $O^+(^2D)$ 2—8482
- molecule, rot. structure of 0,0 band, basis of temp. determ. in CO_2+N_2+He mixtures 2—1008
- molecule, second positive bands in afterglow of N_2 and O_2 mixture 2—3052
- molecule, small angle charge exchange scatt. of He^+, meas. from 0.50 to 3.00 keV 2—5888
- molecule, vibr. temp. of $B^3\Pi_g$ state from relative intensity of first positive band system 2—31813
- molecule, vibrational excitation by electrons at 10 to 100 eV 2—12171
- molecule, vibrational relaxation rates, by m_2O, shock tube meas. 2—28311
- molecules, charge transfer excitation of first negative 3914Å band by protons, photon-particle coincidence meas. 2—809
- molecules, collisions with Al^+ and Er^+, total cross section for charge exchange 2—6011
- molecules, collisions with Ar and Kr, differential elastic scatt. cross section 2—898
- molecules, collisions with C^+, N^+, O^+, Ne^+ at keV energies, KLL Auger electron emission 2—663
- molecules, collisions with CH_n^+ at 40 to 140 keV, CH_n^+ dissociation 2—900
- molecules, collisions with H_3^+, H_3^+ dissociation cross section meas. at 410 to 1800 keV 2—884
- molecules, collisions with He, Ar, Kr, differential cross section, high resolution meas. 2—897
- molecules, collisions with HeH^+, HeH^+ dissociation cross section meas. at 520 to 1025 keV 2—886
- molecules, collisions with N^+, K-shell excitations, differential investigation of velocity dependence 2—2967
- molecules, elastic scatt. of H^+, investigation in 4 to 10 eV e.m. energy range 2—708
- molecules, elastic scatt. of H^+, quenching of quantum undulations in differential cross section 2—707
- molecules, electron impact resonance obs., derivation N_2^- potential curve and width of 11.48 eV state 2—807
- molecules, electronic structure of open shell states, SCF theory applic. 2—8591
- molecules, ionization and dissociation by collision with Na^+ at 5 to 42 keV 2—883
- molecules, resonance excitation by electron impact 2—808
- molecules rotational excitation by collisions with Na^+ and Li^+ 2—894
- multiply charged ion beam through celluloid film, determ. of electron loss and capture cross section 2—1447
- multiply charged ion source, variable energy cyclotron 2—34859
- N_2 ($B^3\pi_g$, v=13), formation by inverse predissociation from $N(^4S_0)$ atoms 2—803
- nonequilibrium dissociating flow over spheres and circular cylinders 2—39242
- photoionization yields for high and low solar activity using Monte Carlo simulation of model ionosphere 2—4713
- plasma, electron distribution function and mean energy 2—21769
- plasma, fields and pressure gradient during collapse of θ-pinch, ion azimuthal velocity calc. 2—18623
- plasma, quasistationary, production using rectangular current pulse 2—28606
- plasma, viscosity meas. 2—3228
- plasma arc, effect of curvature on thermal and dynamic props. 2—24692
- plasma jet, radial temp. distrib., emission spectra obs. 2—28510
- plasma jet, thermodynamic state calc. from dimensionless parameter 2—18590
- polyatomic gas, shear viscosity, room temp. mag. field effects 2—21925
- positive column, standing striations as solutions of Pekarek equation 2—32071
- pulsed laser with rhodamine 6G cavity, linewidth reduction technique 2—5366
- pumping, using orbitron getter-ion pump 2—33826
- quadrupole moments, best fit values 2—15324

Nitrogen continued

- quadrupole moments best fit values 2—18449
- rarefied gas, obs. of thermomag. slip 2—21918
- rotational Raman spectra 2—18464
- solar corona abundance, det. from e.u.v. spectra 2—20692
- solar energetic-particle events, composition, enrichment of very heavy nuclei 2—11082
- solid, extreme u.v. reflection spectra 2—19995
- solubility in liquid Fe, Co and Ni, scaled particle theory 2—21965
- solubility in molten heat-resistant alloys 2—9767
- solubility in molten steel, calc. 2—9771
- solubility in Nb-Mo-N system, equilib. conc. 2—4020
- solubility in Re, 2000-2700°C, 200-600 torr 2—32734
- sorption by ball-milled calcite 2—35911
- sorption in mordenite 2—22082
- stars spectra, CN red system, synthesis assuming Milne- Eddington model atmosphere 2—4849
- in steel, austenitic stainless, distrib. during solidification 2—9212
- in steel, austenitic stainless, effect on hot ductility 2—9672
- steel impurity, effect on strength to brittle fracture relation 2—6517
- streamer propagation, preioniz. control 2—21898
- supersonic molecular beam, crystal target, absolute intensity, vel. distrib. meas. 2—21585
- surface discharges, obs. 2—15510
- thermal cond. meas., column method eval. 2—18762
- thermal desorption from W, kinetics 2—29056
- transient species, atomic and molecular, photoelectron and chemielectron spectroscopy 2—35163
- vibrational relaxation time of N_2-water vapour mixture 2—15318
- viscosity, along saturation line in liquid and vapour phase and under pressure 2—39348
- viscosity, high temp. calc. 2—18770
- [NII] and $H\alpha$ 2—37272
- CO_2-N_2-He, Michelson laser interferometer, phase modulated Q-factor, relaxation processes 2—17688
- CO_2-N_2-He laser passive Q-switching by saturable filter containing OsO_4 vapour 2—27494
- CO_2-N_2-He mixtures, vibrational population inversions behind normal shock waves 2—24442
- CO_2-N_2-He plasma, electrically excited spectrum from 4.2 to 5.5 μm 2—12118
- CO_2-N_2-M mixture, vibr. energy transfer consts. 2—31780
- CO_2-N_2 gasdynamic laser gain, Na effect 2—23586
- CO_2-N_2 mixture, kinetic cooling by CO_2 laser radiation absorp. 2—18757
- CO_2, He, N_2 mixture gas lasers, modulation by GaAs, CdSe, CdS and CdTe crystals 2—17668
- CO_2+N_2+He, mixture, change of temp. with time determ. based on rot. structure of 0,0 band of N_2 2—1008
- $E^3\Sigma_g^+$ state, photoelectron impact excitation, cascade contrib. to day glow 2—16880
- in Fe, ductile brittle transition, effect of added nitrogen 2—25503
- Fe+N_2, O_2 reactions, ionization and spectral emission at simulated meteor conditions 2—33752
- GaP:N, epitaxial, efficient yellow luminesc. 2—7092
- H_2/H_2 mixture, adsorption on reduced Fe catalyst 2—30061
- H-N_2 collisions, 10, 25, 35 keV, cross section for destruction of 3s state in H 2—38854
- H-N_2 collisions at 10 to 35 keV, excitation of n=3 states in H 2—38849
- ^{17}H, in rare earth nitrate soln., n.m.r. exchange effects 2—6254
- He-N_2-CO_2 laser, molecular, electron beam controlled method of pumping at high pressure 2—34392
- He-N plasma time dependence of number densities of N^+, N_2^+, N_3^+, N_4^+, during decay period 2—24703
- He-N_2 mixture losses through ion- sampling orifice 2—39213
- He-N_2 mixtures, discharge, cataphoresis and nitrogen- removal processes 2—12466
- He-N_2 positive column, cataphoresis and N_2 removal processes 2—24878
- He-NH_3-N_2 system, immiscibility at 90 to 140°C and up to 3kb 2—12503
- I^{4+} to I^{18+} cross sections for electron capture and loss in N_2 and Ar 2—35580
- $In_{1-x}Ga_xP$:N, indirect and direct crystals, cw laser operation on A-line transition 2—17642
- N_2/CO,N_2/CO_2,N_2/ethylene, integral Joule-Thomson effect, check of predictive calculation methods 2—3325
- N_2-CO_2-He glow discharge, electron energy distribution and vibrational temperature obs. 2—24879
- N-CO_2, vibrational energy transfer time, laser meas. 2—2399
- N_2-CO, mixed gas adsorpt. on Pyrex glass at very low press. 2—39564
- N_2-CO, vibrational exchange, shock tube meas. 2—28311
- N_2-CO_2, supersonic transverse electrical discharges laser 2—23585
- N_2-CO_2 cross beam electric discharge convection laser 2—11471
- N_2-CO_2 gas dynamic laser, model for prediction of gain, saturation and pulse length 2—11460
- N_2-CO_2 laser, use for controlled thermonuclear fusion 2—24267
- N_2-Co liquid mixture, thermodynamic functions calc. 2—28840
- N_2-H_2-methane mixtures, Joule Thomson effects 2—24980
- N_2-H_2, determ. of binary diffusion coeffs. as function of temp., pressure and conc. 2—9045
- N_2-He-methane mixtures, Joule Thomson effects 2—24980
- N_2-He binary gas mixture, viscosity and diffusion coeff. 2—32185
- N_2-He mixtures, effective rate coeffs. for N_3^+ and N_4^+ form. 2—6010
- N_2-I_2 recombination of I atoms studied by flash photolysis 300-1173K 2—26356
- N_2-NH_3 gas mixture, heat conductivity, second order electric field effect 2—3327
- N_2-O collisions with nonpairwise interaction, calc. of vibrational transition probabilities 2—15238
- N_2-O_2 mixtures, decay of luminescence, irradiated by alpha particles, emission spectra 2—35274
- N_2^+-noble gas atoms, non-dissociative collisions, elastic scatt. and vibr. excitation 2—12310
- N_2-propane mixture, second virial coeffs., compressibility, 20-50°C 2—21915
- γ-N, n.q.r. obs., 4.2-35.1K 2—26315
- α-N, n.q.r. of ^{14}N and ^{15}N, temp. depend., isotope effects, T<35.6K 2—26316
- α-N, n.q.r. press. depend., lattice libration freq., elec. field gradient, 4.2-35.1K 2—26315
- α-N, solid, cryst. struct., mol. centre displacement, librations, at. separation 2—32467

Nitrogen continued
α-N, solid, cryst. struct., piezoelec. reson. 2—32466
N and N^+, capture and loss of electrons in air, N_2 and O_2, cross sections 2—32115
N II, fine structure transitions, proton induced, cross sections 2—35160
N II emission, interference-filter, image-tube photography, gaseous nebulae 2—26646
N III, electron impact ionization, cross section calc. for ground state config. 2—2953
N III, s-p and p-d oscillator strength calc. using frozen core version of Hartree Fock approx. 2—8441
N IV, u.v. spectrometry experiment on Mariner 9 for early type stars 2—37300
N IV emission lines in HD45166 2—7430
N VI, dielectric recombination satellite line intensities, meas. and interpretation 2—28171
N^-, in plasma, photodecay cross sect. meas. 2—18315
N^+, acceleration to 7.4 GeV in Princeton heavy ion accelerator, collisions with water vapour 2—38414
N^+, collisional excitation spectrum at 50 keV from He target 2—18344
N^+, collisions with Ar, excitation of inner and outer shells, inelastic energy losses and ionization 2—2965
N^+, collisions with C foil, equilibrium charge distributions 2—5833
N^+, collisions with N_2 and Ne, at keV energies, KLL Auger electron emission 2—663
N^+, ionization by electrons in merging beams 2—38822
N^+, K-shell excitations in collisions with Ne and N_2, differential investigation of velocity dependence 2—2967
N^+ acceleration in bevatron 2—38415
N^+ in iososphere F-region, height profile 2—41009
N^+ production in $N+Y^+ \rightarrow N^+ + Y^{(+)}$ reactions in 'Kepler', inclined-beam instrument, Y=He, Ne, Ar and N 2—11998
N_2, 2-10keV proton impact, cross section for excitation of 3p states of H by observing Balmer alpha and Lyman alpha photons 2—5854
N_2, 500eV incident electrons, energy loss cross sections, study of inelastic continuum 2—8670
N_2, collision with H and H^+ beams, Lyman-α emission cross sections 2—5868
N_2, collisional excitation by N atoms of first positive and first negative radiation in 6000-14000K range 2—15319
N_2, H-atom impact, 20 to 120 keV, Lyman-α radiation prod. 2—18311
N_2, H-atom impact, 20 to 120 keV, Lyman-α radiation prod. 2—18311
N_2, i.r. absorpt. spectrum, elec. field induced 2—31807
N_2, inner shell electrons, ionization by 10 keV electron as function of energy loss 2—39195
N_2, metastable $A^3\Sigma_u^+$ state, scattering and deactivation 2—15428
N_2, molecular constants of $B^3\Pi$ and $A^3\Sigma$ states calculated 2—12166
N_2, photoelectron spectra, study of autoionization, vibrational structure 2—8674
N_2, pulsed laser action 2—5365
N_2, pure and mixtures with Ar, influence of metastable N_2 molecules on excitation 2—15509
N_2, relative population of vibr. levels of $B^3\Pi_g$ state in glow discharge 2—35267
N_2, relative populations of C^3II_u and $B^2\Sigma_u^+$ states 2—31806
α-N_2, solid, dipolar spin-echo envelope modulation temp. depend. 2—7160
N_2, vacuum u.v. absorption spectrum, o-X system, rot. consts. of vibr. levels 2—15325
N_2, valence electrons, ionization by 10 keV electrons as function of energy loss 2—39194
N_2, vibrationally excited, photoionization spectrum in 79.5-84.0 nm region observed 2—3053
N_2, vibrationally excited, photoionization spectrum in flowing N_2 afterglows, application of technique to quenching by CO_2 and N_2O 2—806
N_2, vibrationally excited photoionization spectrum meas. in 79.58-84.20 nm region 2—18446
N_2, X-ray mol. scattering factors calc. 2—8865
N_2 9% and CO_2 91% mixture as Venusian atmosphere, spectral composition, emissivity and absorptivity 2—30584
N_2 adsorption structure on W obs. 2—6375
N_2 Compton profile meas. using Ag and Mo X-rays 2—18451
N_2 Compton scattering of X-rays from gas, comparison of exptl. and theoretical profiles 2—15234
N_2 concentration and temperature in thermosphere during 1970, March 7 solar eclipse 2—33522
N_2 crystal, polymorphic transformations, chemical potential and transition temperature 2—39989
N_2 gas, alpha particles $0.5 \leqslant E_\alpha \leqslant$ MeV, atomic stopping cross section determ. 2—21534
N_2 gas, collision with F ion, 4-54 MeV electron-transfer cross sections 2—28221
N_2 impulse discharges, emission studied in 1000-2000 Å region by photography 2—28667
N_2 laser, electron beam excited 2—23600
N_2 laser, pulsed, calc. of total power emitted at 3371 Å 2—31040
N_2 metastable states excitation by electron impact 2—18452
N_2 mixtures with inert gases, determ. dependence of annihilation rates of slow positrons on molecular concentration 2—24467
N_2 mol., multiphoton ioniz. and dissoc. at λ=0.53 μ 2—35272
N_2 photoionization, by soft X-rays at 0.28 and 1.49 keV, meas. of relative abundance of thermal energy ions 2—805
N_2 photoionization, effect of autoionization on angular distribution intensity of ejected photoelectrons 2—607
N_2 pink afterglow in dc field, quenching of optical emissions 2—18708
N_2 rotational excitation by slow positron, cross section calc. in distorted wave approx. 2—24466
N_2 solid, librational motion in the α phase studied in harmonic approximation 2—9861
N_2 thermal conductivity meas. under the influence of a magnetic field 2—12510
N_2 vibrational population of $A^3\Sigma_u^+$ and $B^3\Pi_g$ states 2—16888
N_2 vibrationally excited, total cross section for quenching of electronically excited alkali atoms at high temperatures 2—31692
N_2^-, molecular orbital calculation of contact hyperfine interaction, comparison with e.p.r. spectra 2—21629
N_2^+, collisional excitation by N_2 of first positive and first negative radiation in 6000-14000K range 2—15319
N_2^+, cross section meas. of collision induced dissociation and ion-molecular reactions 2—12308
N_2^+, decay of electron impact excited states, time resolved studies 2—5939

Nitrogen continued
N_2^+, electron-ion recombination, meas. in flowing afterglow 2—6108
N_2^+, electronically excited, collisional deactivation rates 2—31877
N_2^+, enhancement of vibrational level population by photoelectron spectrometry 2—35265
N_2^+, excitation of C $^2\Sigma_u^+$ state by collisions with He^+ and Ne^+ 2—893
N_2^+, luminescence, Franck-Condon factors and collisional deactivation 2—15323
N_2^+, predissociation in mass spectrum, monomolecular and collision induced 2—12162
N_2^+, predissociation of collisionally excited states 2—896
N_2^+, recombination coefficient meas. in flowing afterglow following electron-positive ion collisions 2—12000
N^{2+} collisions with He, Ne, Ar, meas. of differential scattering with single electron capture, 0.7-3.0 keV interp. of curve crossing 2—672
N_2^+ ion, electron impact excitation of O-O band 2—18450
N_2^+ merging beam studies of ion-molecule reactions with Ba 2—12006
N_2^+ u.v. auroral emissions, spectrographic recordings from rocket 2—30327
α-N_3, solid, k=0 librational spectrum, alternative description based on variational procedure 2—22403
N_4^-, molecular orbital calculation of contact hyperfine interaction, comparison with e.p.r. spectra 2—21629
N^{5+}, N^{6+} beams, acceleration to 7 GeV in synchrotron 2—14808
$N_2A^3\Sigma_u^+$ molecules, auroral, deactivation, atmospheric model 2—10747
$N(^2D)$ quenching reactions by O_2 and N_2O, temperature coefficients 2—16881
NI, 5199 angstrom doublet lines, daytime airglow 2—20379
NII Nova Delphini 1967 nebula, forbidden transition increased stability or intensity in spectral range 5600 to 8800 Angstroms 2—13911
NIV, emission spectra of WR stars 2—41102
$N_2^+(X^2\Sigma_g^+, v''=0)$, reactions with N_2 and other substances, study by kinetic absorption spectroscopy 2—22866
N_2—Ar^+ charge exchange collision, rate coeff. meas. 2—5832
N^+—O_2, charge exchange collision, rate coeff. meas. 2—5832
$N_2^+ + Ba \rightarrow BaN^+ + N$ merging-beam study, determ. cross sections and kinetic energy of products 2—12005
N_2+CO_2, collisions, vibrational energy exchange 2—3149
N_2+CO_2, reacting u.s. stream, mechanism of chemical and vibrational relaxation, numerical study 2—40804
$N+Mo(CO)_6$ flames, chemiluminescence band system 2—22865
$N^+ + N_2 \rightarrow N_2^+ + N$, apparent charge exchange reaction, cross section meas. 2—685
N_2+O^+ reaction, ab initio configuration interaction calculation of potential energy curves 2—12014
N_2+rare gas ions, interaction, products, rotational excitation, statistical phase space model 2—10600
N_2^*-CO_2 flowing mixtures, i.r. emission at 2.7 μm 2—21590
N_2^{*+}, product of N_2 rare gas ion collisions, vibrational and rotational distributions 2—10600
N_2^+4278 emission in SAR arc 2—20390
$N_2(a\ ^1\Pi_g)$, radiative lifetime and formation of metastable $N_2(a'\ ^1\Sigma_u^-)$ by intrasystem cascading 2—35270
inNb, interstitial solute pick-up, annealed sample, Hall-Petch plot 2—9544
O/N_2 ratio in atmosphere above 400 km during magnetic storm 2—16871
O/N_2 ratio in lower thermosphere, semiannual variations in the neutral composition of atmosphere 2—30309
O_2 mixtures, d.c. and h.f. discharges, T-layers in positive column 2—28669
p-Si:N ion implanted at cryogenic temps., elec. props. 2—25430
Si:N ion implanted buried layer, physical and elec. props. 2—25440
SiC:N, 6H polytype, Zeeman effect of the absorp. lines R_o and S_o 2—36885
SiC:N, e.p.r. lines, discrete saturation 2—7124
α-SiCiN, impurity adsorpt., electron transitions 2—7073

Nitrogen compounds
metal-B-N system, equilib. state, chemical bonding, crystal and electronic struct. 2—29489
molecular beam, mass spectrometric identification of paramagnetic component 2—18397
monovalent metal nitrates, defect mobility and density, elec. cond. obs. 2—3771
nitrate, alkali, molten, elec. cond. at high pressure 2—3403
nitride and carbide nuclear fuels, for fast breeder reactors 2—28148
nitride nuclear fuel irradiation capsule 2—35104
nitro, increased valence-formulae, generated from electronic structure studies of N_2O_4 2—12168
nitroso, increased valence-formulae, generated from electronic structure studies of N_2O_4 2—12168
nitrosyl, bonding, increased valence theory 2—8679
nitroxide radical, solid, Overhauser effect 2—26305
nitroxide radical complexes with transition metals, n.m.r. and e.p.r. obs. 2—26376
$2NO_2 \rightarrow 2NO + O_2$, thermal conductivity meas. made from 548-792K, deduced chemical kinetic constants 2—26321
rare earth nitrate, exchange effects, ^1H, ^{17}O and ^{14}N resonances 2—6254
Stark effect on vibr.-rot. transition, h.f.s. 2—24476
Cr-N system, partial and integral thermodynamic functions 2—22377
Fe-N alloy, vacancy trapping of interstitial solute atoms, internal friction obs. 2—32506
Fe-N solid solution, mag. field orienting of Fe_8N precipitate 2—3993
HNCO, in cometary spectra, detection 2—26863
Mo-N, solid soln., supersaturated, isochronic ageing 200-550°C, soln. clusters, precip. growth 2—25599
N_3^-, NO_2^-, NO_3^-, valence shell electronic structure photoelectronic spectroscopy obs. 2—35276
N_3^-, valence electronic struct. from X-ray photoelectron spectroscopy 2—35225
NCl, bond length and angle, mean amplitude of vibration, electron diffraction study 2—8676
NCl_3, isotopic species, atomic, bond, and mol. polarizabilities, root mean square amplitudes statistical thermodynamics 2—5937
ND molecule, fine structure of $^3\Pi$ and $^3\Sigma^-$ states 2—21586
N_2F_4-$NO(N_2)(CF)$ system, laser irradiation, photochemistry 2—20200
NF_2, molecule, electronic struct., LCAO-SCF-MO calc. 2—8684
NF_2 free radical, microwave rotational spectrum 2—12179
NF_2 radical, microwave Zeeman spectra, electron spin-rotation interaction 2—8678
NF_3, high resolution study of l-type resonance in ν_4 band 2—8673
N_2F_2, cis and trans isomers, CNDO/2 calc. 2—18473
N_2F_4, laser induced dissoc., rate 2—31808

Nitrogen compounds continued
N_2F_4 gaseous electron diffraction, structure study 2—15320
N_2F_4+RH systems, flash photolysis chemical HF lasers 2—270
N_2H_4-N_2O_4 impinging hypergolic streams, photographic study of sprays formed 2—7170
NH, enthalpy of formation in $NH_3/O_2/N_2$ flames 2—22872
NH molecule, fine structure of $^3\Pi$ and $^3\Sigma^-$ states 2—21586
NH_2, $^2B_1$, $^2A_1$ and $^2B_2$ states, Hartree-Fock method using Slater basis set 2—8579
NH_2, geometries of Renner Teller states, ab initio calcs. 2—12173
NH_2, isotropic hyperfine coupling constants 2—31812
NH_2 radical formation in γ-irradiated frozen aqueous azide soln. 2—10646
NH_2^-, photodetachment of electrons, electron affinity 2—35587
N_2H_4, calculation of ground state in two-centre approximation 2—789
N_2H_4 cation radicals, geoemetry 2—31810
N_2H_4 formation in liquid NH_3 under γ-radiolysis in presence of H 2—10648
NO-CCl_4 molecular beam collision, orientational anisotropy in total collision cross-section 2—8864
NO-H_2 mixtures adsorbed on W, vibr. props. 2—32396
NO_2-NO-O_2 nonequilib mixtures finite difference method for solution of turbulent tube flows 2—6128
N_2O_4-NO_2, equilib. mixture finite difference method for solution of turbulent tube flows 2—6128
N_2O-gas mixtures, rot. correl. functions 2—18404
NO-, vibrational progression of resonances, association with Rydberg states 2—812
NO, $^2\pi_{3/2}$, $j=m_j=3/2$ state, collisions with carbon tetrachloride, orientational anisotropy in total collision cross section 2—3150
NO, $A^2\Sigma^+$ state, lifetimes of $v'=0,1,2$, levels 2—12164
NO, absolute oscillator strength measurements of γ-system 2—38925
NO, adsorbed on evaporated alkali halide films, i.r. spectra 2—1195
NO, adsorption and disproportionation on copper exchanged Y zeolites 2—25226
NO, adsorption on amorphous C, e.s.r. obs. 2—6378
NO, atmospheric pollutant, tunable i.r. laser techniques for det. 2—40923
NO, charge transfer reactions with Ar^+, obs. using ion injection drift tube 2—24838
NO, collisions with Ar^+ and Kr^+, charge transfer cross sections in thermal and suprathermal range 2—658
NO, electron-impact excitation, absolute cross sections 2—24478
NO, electron impact dissociative excitation in vacuum u.v. 2—3054
NO, flame photometric determinations of diffusion coefficients 2—1041
NO, hyperfine structure states mixing in magnetic field 2—12174
NO, ion-pair processes, by electron impact, mass spectrometric study 2—8623
NO, γ, ε and δ system, fluorescence spectrum polarization of rotational lines, vibr. band intensities 2—8675
NO, laser magnetic resonance obs., magnetic and electrical dipole transitions obs., g factor and hyperfine structure separation calc. 2—38928
NO, magnetic dipole transitions in far infra-red spectrum 2—38931
NO, magnitude of multiplet splitting in X-ray photoelectron spectra, spin density implications 2—8672
NO, obs. absorption meas. of $\beta(B^2\Pi-X^2\Pi)$ band system 2—5935
NO, Penning ionization and photoionization to $X^1\Sigma^+$ state of NO^+, comparison of vibrational transition probabilities 2—21625
NO, photoelectron spectra, study of autoionization, vibrational structure 2—8674
NO, photoelectron spectra and partial photoionization cross sections 2—12167
NO, physical adsorption on graphite 2—18957
NO, Raman backscatt. cross sections 2—15542
NO, reaction with graphite, effect on graphite absorptive props. 2—35908
NO, role in obs. of electron densities of D-region 2—7338
NO, rotational Raman spectra 2—18464
NO, Senftleben-Beenakker effects and thermomag. torque in varying fields 2—9041
NO, spectra, $^2\pi_{3/2}$-$^2\pi_{1/2}$ transition 2—8687
NO, thermomagnetic torque, contributions from second derivative dyad of temperature and thermal creep 2—35686
NO, vibr. thermalization, temp. depend. 2—28274
NO, $X^2\Pi$ and $A^2\Sigma^+$ states, restricted Hartree Fock calculations of molecular properties 2—35266
NO $A^2\Sigma^+$, electronic quenching by O_2 $X^3\Sigma_g$ 2—28315
NO $A^2\Sigma^+$ state, radiative lifetime determ. from Hanle effect measurement 2—28314
NO abs. oscillator strength estimates for some bands of β system 2—35271
NO adsorbed on Li halides, i.r. spectra and dimerization 2—15677
NO anesthesia in cats, middle ear pressure changes 2—37503
NO collisions, mechanisms for resonance production postulated, temperature dependence of average transition probability 2—35382
NO flux through mesopause, source of odd N_2 in mesosphere and upper stratosphere 2—16872
NO from u.v. irradiation of alkali azides, e.s.r. 2—12182
NO gas, relative Raman cross section, rel. air pollution 2—35249
NO molecular beam, mass spectrometric identification of paramagnetic component 2—18397
NO molecule, Λ doubling in $^2\Pi$ states calc. from HF wavefunctions to test validity of Van Vleck's hypothesis 2—21637
NO radicals, viscous medium, rotational correlation time calc. from e.s.r. calcs. 2—8686
NO vacuum-u.v. excitation cross sections, electron impact determ. 2—21627
NO vibronic states, population and predissociation 2—18445
NO^+, dissociation in collision with He at 2 to 5 keV 2—895
NO^+, electron-ion recombination, meas. in flowing afterglow 2—6108
NO^+, ionospheric density, influence of neutral winds at night 2—23008
NO^+, merging beam studies of ion-molecule reactions with Ba 2—12006
NO^+, NO_2^-, NO_3^- ions in lower ionosphere during solar eclipses, rocket measurements 2—33533
NO^+, recombination coefficient meas. in flowing afterglow following electron-positive ion collisions 2—12000
NO^+ energy levels obs. by He and Ar resonance lines photoelectron spectrometry 2—15316
$NO^+ \rightarrow O^+ + N$ unimolecules dissociation, translational spectroscopy 2—21624
NO_2- in KCl, absorpt. and emission spectra, effect of impurities 2—16492
$(NO)_2$, ab initio SCF MO calcs. of configuration and dissoc. energy 2—35268

Nitrogen compounds continued
NO_2, CNDO/2 study of electronic structure and molecular geometry 2—5936
NO_2, charge exchange with alkali atoms, adiabatic electron affinities 2—38898
NO_2, collisions with Na atoms, 1 to 30 eV, electronic excitations 2—687
NO_2, electron affinity determ. from photoionization mass spectra of methyl and ethyl nitrate 2—12224
NO_2, electronically excited, short radiative lifetimes 2—8680
NO_2, nonequilibrium dissociating gas, turbulent flow in circular tube, heat transfer 2—12485
NO_2, Raman scattering, wavelength and pressure dependence obs. 2—38929
NO_2, rate const. for reaction with ReO_3^- and $(WO_3)_{n=1,2,3}$ 2—10613
NO_2, resnance fluorescence spectrum, interpretation 2—12172
NO_2, vibronic effects in decay of fluorescence excited in first excited singlet state, lifetime 2—35284
NO_2 concentration in $N_2O_4 \rightleftharpoons 2NO_2 \rightleftharpoons 2NO+O_2$ system, use of Beer-Lambert law 2—1769
NO_2 gas phase thermal reaction with ethylene at 25°C, mechanism for formation of products, rate constants 2—22867
NO_2 impurity in KCl, e.s.r., hindered rotation at 2°K 2—15322
NO_2 photodissociation, angular distribution of recoil O atoms 2—30086
NO_2 photodissociation, energy partitioning 2—30085
NO_2 photoionization by soft X-rays at 0.28 and 1.49 keV, meas. of relative abundance of thermal energy ions 2—805
NO_3, heat of formation and electron affinity determ from photoionization mass spectra of methyl and ethyl nitrate 2—12224
NO_3^-, in anisotropic $NaNO_3$ crystal, Einstein coefficient spectra, light wave fields differences 2—801
NO_3^- in powder state, diffuse reflectance spectra 2—29899
N_2O, 00°1-10°0 laser band study by frequency, mixing in i.r. metal-metal oxide-metal point contact diode 2—31041
N_2O, anisotropic potential energy surfaces, determination from inert gas atom collision data 2—6012
N_2O, atmospheric abundance deduced from rotational line intensities 2—22958
N_2O, CNDO/2 study of electronic structure and molecular geometry 2—5936
N_2O, collisions with Cs atoms, analysis of ion production 2—899
N_2O, emission feature at 11.7 cm^{-1}, assignment disputed 2—7302
N_2O, enhancement of turbulent diffusion in parallel wall duct 2—3312
N_2O, Franck Condon factors, harmonic oscillator, for ionization 2—15317
N_2O, i.r. absorption of fundamental bands, spectral mean parameters 2—15321
N_2O, in compressed gaseous mixture, i.r. rotational correlation functions of bending vibr. 2—15315
N_2O, in solid N_2 matrix, i.r. spectra, anharmonic force constants 2—12169
N_2O, intensity and half-width meas. of (00°2-00°0) band 2—38926
N_2O, line strengths of bands in 2.9 micron region, dipole moment matrix element 2—18448
N_2O, molecule-electron collision, dissociative excitation, vac. u.v. obs. 2—18454
N_2O, quenching of vibrationally excited N_2, study using photoionization technique 2—806
N_2O, refractive index of liquid in temp. range 130-260 K 2—18825
N_2O, relative rotational line intensities of various transitions, 250 and 300 K 2—24480
N_2O, self and N_2 broadened lines direct meas. quadrupole moments and hard sphere diameters 2—18449
N_2O, self broadened and N_2 broadened half widths, 297K, quadrupole moments 2—15324
N_2O, threshold electron impact excitation spectra studied by SF_6 scavenger technique 2—28313
N_2O absorption lines, foreign-gas broadening coefficients 2—28309
N_2O and N_2O-N_2 discharges, i.r. afterglow emission 2—39211
N_2O concentration in North Atlantic rel. to surface air 2—10722
N_2O gas, relative Raman cross section, rel. air pollution 2—35249
N_2O high resolution determ. of line intensities 2—12176
N_2O i.r. transmission 2—5925
N_2O photoelectron spectra and partial photoionization cross sections 2—12167
N_2O physically adsorbed on silica, i.r. spectra studied 2—9304
N_2O pulsed laser studies 2—272
N_2O^+, photoionization and photoelectron spectroscopy, validity range of selection rule 2—12163
$N_2O_2^{2+}$ vibr. assignment, alternative force fields, least squares study 2—31815
N_2O_3, gaseous, i.r. spectrum, —120°C, assignment of vibration rotation bands 2—12178
N_2O_4, CNDO/2 study of electronic structure and molecular geometry 2—5936
N_2O_4, molecular orbital studies, increased valence formulae described 2—12168
N_2O_4, molecular shape and size investigation by gaseous electron diffraction 2—38922
N_2O_4, partly dissociated into NO_2, heat transfer in condensation 2—6284
N_2O_4, Raman scattering cross section, Q-switched ruby laser excitation 2—5940
N_2O_4 dissociating, turbulent flow, heat transfer obs. 2—6127
$N_2O \rightarrow O(^1S)+N_2(X^1\Sigma) \rightarrow O(^3P)+N_2(A^3Z)$, vacuum u.v. photodissociation, time of flight spectroscopy of metastable fragments 2—777
N_xO_y, molecular consts., Green's function analysis 2—18443
NOCl photodissociation, energy partition and recoil photofragment angular distributions 2—30087
NOH, NOLi, and NOF, ab initio MO calculations 2—24477
NO—Ar^+ charge exchange collision, rate coeff. meas. 2—5832
$NO^++Ba \rightarrow BaN^++O, BaO^++N$ merging-beam study, determ. cross sections and kinetic energy of products 2—12005
NO_2+CS_2 flash photolysis, CO laser emission 2—2393
$NO+H_2$ mixtures, flash photolysis, far u.v. spectrum of HNO 2—18430
$NO+O+(M) \rightarrow NO_2^*+(M)$ airglow reaction, at low pressures, evidence for radiative recombination 2—7166
$N_2O+S(3D_2)$, prod. of NS radicals, contrib. of this reaction channel to total cross section 2—4569
NO-$+X \rightarrow NO+X+e$, rate constants for collisional detachment, 193-506K 2—21718
$NO^+.H_2O$ in equatorial D-region ionosphere, comparison of upleg ram with downleg wake 2—16908

Nitrogen compounds continued
$(NPX_2)_n$, X=halogen, with D_{nh} symmetry, electronic structure calc., CNDO/2 approx. 2–24481
NS, vibr. and rot. analysis of $^2\Pi_i$-$X^2\Pi_r$ band system 2–18447
NSF, triplet state at 5360 Å, Zeeman study and preliminary rotational analysis 2–3051
$N(SO_3)_2^{2-}$, reorientational motion, e.s.r. study 2–22826
NSe, electronic spectrum, 2800-3200Å, vibr. and rot. analysis of 12 red degraded bands 2–18456
$^{14}N^{16}O$, hyperfine Λ-doubling transitions obs. by molecular beam electric resonance method 2–8681
Nb-Mo-N system, equilib. conc. and solubility of N_2 2–4020
Nb-Mo-N system, phase diagram 2–19314
Nb-Mo-N system, thermodynamics of α solid soln. 2–19313
Nb-N alloy, flow stress, soln. hardening 2–9661
No, integrated intensity of fundamental band 2–21632
No_2, collisions with Cs atoms, analysis of ion production 2–899
SO_2, vibronic effects in decay of fluorescence excited in first excited singlet state, lifetime 2–35284
V-N alloy, phase transformation, banded microstructure 2–22367
ammonia
adsorption on SiC, room temp. 2–29070
atmospheric pollutant, tunable i.r. laser techniques for det. 2–40923
binary mixture, ethylene/ammonia, second virial coeff. 2–24976
collision induced rotational transition, microwave double resonance study 2–12177
dimers, presence deduced from spectra near 10 cm^{-1} 2–38924
electron attachment studies 2–21870
extra-galactic radiation, detection of inversion radiation from non-metastable states, new sources 2–26639
force const. calc. in valence force system of coordinates using Gell-Mann and Feynman theory 2–800
gas, Hg-photosensitized UV luminescence, evidence for cluster attachment 2–30084
gas, microwave spectrum, line shape study, low pressures 2–12165
gas, use as calibration for CH_4 spectrophone meas. 2–12257
gas, vibration-rotation spectrum, vibr. assignments 2–21631
ground state to $^2A_1''$ ionic state transition, Franck Condon factors 2–8671
interstellar, photochemistry and lifetimes 2–4898
i.r. spectra in the atmosphere 2–37138
Jupiter, spectrophotometry of 1.5 μm window 2–26832
liquid, electron pulse irradiation, elec. cond. 2–28890
liquid, mol. motions from neutron scatt. obs. 2–35726
microwave emission from nonmetastable levels of NH_3 in radiosources W3-OH, W43, W51, DR 21-OH, Orion A, and in direction of Sgr B2 2–10933
molecular collisions with H_2, observation of $\Delta k = \pm 3$ transitions 2–24579
molecular i.r. spectra, cross relaxation in rotational inversion doublets 2–38923
molecular rotation in inert gas matrixes, i.r. spectra 2–10391
molecule, analogue to ionized gas, mol. orbital determ. from vac. u.v. and photoelectron spectra 2–18409
molecule, analogue to ionized inert gas, mol. orbital determ. from vac. u.v. and photoelectron spectra 2–18409
molecule, collisions with H and H^+ at 1 to 25 keV, Lyman alpha emission cross sections 2–21544
molecule, configuration interaction wavefunctions and computed inversion barriers 2–35277
molecule, one-electron properties calc. using near-Hartree-Fock wavefunctions 2–21626
molecule, rotational spectra, analysis, determ. of structural parameters 2–802
molecule, vibr.-rot. transition, absorpt. saturation 2–5934
molecule, vibrational and rotational relaxation data from u.s. absorption meas. 2–31811
molecules, hydrogen spin-rotation determ. from application of Racah algebra to point groups 2–12065
partially deuterated and tritiated, harmonic wavenumbers and normal coords. calc. 2–18444
photoelectron spectra and partial photoionization cross sections 2–12167
refractive index of liquid in temp. range 130-260 K 2–18825
Saturn sub-cloud atmosphere, relative abundance, radio astronomical obs. 2–30580
solid, freq. distrib. func., neutron scatt. obs. 2–36321
solid, molecular and lattice vibrations, Raman obs. 2–19382
solid, neutron scattering kernel 2–40038
solid, neutron scattering kernel 2–40038
spectra, using far i.r. spectrometer 2–8634
supercritical, stability limits of solvated electrons 2–9158
vibration-rotation spectrum, rotational analysis of 6450 A band 2–28312
visible luminescence, irradiation by 10.6μ CO_2 laser pulses 2–35273
BCl_3, total electric polarization 2–15543
He-NH_3N_2 system, immiscibility at 90 to 140°C and up to 3kb 2–12503
ionization, Franck Condon factors for transition from ground to ionic state 2–18455
liquid, N_2H_4 formation under γ-radiolysis in presence of H 2–10648
molecule, electron collision, dissociative excitation, vac. u.v. spectral obs. 2–18454
NH_3-N_2 gas mixture, heat conductivity, second order electric field effect 2–3327
NH_3-NH_3^+ collisions, comparison of integrated capture cross sections with reaction cross sections 2–31882
NH_3 frozen aqueous soln., γ-irradiated for formation of NH_2 radical 2–10646
NH_3 radical, hyperfine coupling constant, perturbation approach to evaluation of vibrational effects 2–21623
NH_3^+, excitation stretching vibrations in ionization of NH_3 2–18455
NH_3^+, structure in $^2A_1''$ state 2–8671
$^{14}NH_3$, quadrupole tensor evaluated first and second order Zeeman effects obs. 2–8682
$^{15}NH_3$, i.r. microwave two-photon transitions 2–8683
ammonium compounds
chloranilates, hydrated, crystal data, X-ray diffr. 2–19062
chloranilates, hydrated, crystal data, X-ray diffr. 2–19062
explosives, oxidizer reactivity rel. to combustion 2–33374
halide solns., aqueous, sound vel. 2–28853
halides, effects of H bonding on i.r. spectra from vibr. study 2–10390
oxalate monoperhydrate, cryst. struct. 2–36003
spin symmetry sites, p.m.r. obs. 2–40776

Nitrogen compounds continued
ammonium compounds continued
KD_2PO_4, laser induced self focusing 2–22628
ND_4Cl, lattice dynamics 2–6651
$ND_4D_2AsO_4$, γ-irradiated single crystal, e.s.r. of free radicals 2–10122
ND_4ReO_4, far i.r. and laser-excited Raman spectra, librational mode obs. 2–10411
$(ND_4)_2SO_4$, n.m.r. powder spectra, 4.2K determ. of ^2H quadrupole coupling const. 2–10558
ND_4XO_4 (X=I,Re), i.r. and Raman spectra rel. to anomalous temp. dependence of n.q.r. 2–16556
NH and NH_2 radicals predictions for finding in interstellar space 2–17012
NH_3^+ radical, random motion and relax., e.p.r. obs. 2–26373
NH_4^+, motion and correlation functions 2–8677
$NH_4Ag_4I_5$, single crystal growth and crystal struct. 2–12698
$NH_4Al(SO_4)_2$:Fe, e.s.r. spectrum obs. 2–7115
NH_4BF_4, i.r. and Raman spectra, 17 to 300K 2–24482
NH_4BF_4, polycryst., NH_4^+ reorientation, n.m.r. obs. 2–10559
NH_4Br:Pb(Sn,Cu,In) phosphor, cryst. growth and spectra 2–1710
NH_4Br, crystn. habit in presence of wolframate, distrib. coeff. 2–25265
NH_4Br, disordered cubic phase, hypersound attenuation and dispersion, Brillouin scatt. obs. 2–26201
NH_4Br, neutron diffr. studies 2–25341
NH_4Br, proton spin- lattice relax., phase transition phenomena 2–10272
$NH_4Br(Cl)$, vacancy pair form. energies 2–22192
$(NH_3CH_3)^+$, in methylammonium alum, X-ray obs., scatt. curve, atomic scatt. factors 2–3690
$(NH_4)_2C_2O_4$ growth from aqueous solutions, dependence of growth velocity on supersaturation, temperature and viscosity 2–35941
$(NH_4)_2Cd_2(SO_4)_3$, ferroelec.-ferroelastic cryst., phase transformation mechanism 2–16291
$(NH_4)_2Cd_2(SO_4)_3$, mechanism of ferroelec. phase transformation 2–33057
$NH_4Cl:Cu^{2+}(2H_2O)$ effect of paramagnetic impurity on n.m.r. of proximate nuclei 2–37015
NH_4Cl:Pb(Sn,Cu,In) phosphor, cryst. growth and spectra 2–1710
NH_4Cl, critical temp. and pressure determination from vapour pressure curves 2–9216
NH_4Cl, disorder-order phase transition, Raman scattering study 2–22372
NH_4Cl, lattice dynamics 2–6651
NH_4Cl, meas. of variation of length of crystal at high pressure near order-disorder transition line 2–9830
NH_4Cl, mechanisms of charge transport 2–36586
NH_4Cl, order-disorder transform, effect on u.s. vel. 2–29528
NH_4Cl, powder sample, X-ray structure factors of first twenty reflections 2–29148
NH_4Cl, proton spin-lattice relax. times 2–7007
NH_4Cl, rayleigh scatt. as function of pressure and temperature in region of order-disorder transition 2–13456
NH_4Cl aqueous solns., NH_4^+ self-diffusion coeffs. 2–1092
NH_4ClO_4, polycryst., NH_4^+ reorientation, n.m.r. obs. 2–10559
NH_4ClO_4, vibrational spectra, phase changes, and rotational freedom of NH_4 ions 2–40675
NH_4ClO_4 dicarboxylic acid mixtures, burning velocity dependence on pressure 2–7172
NH_4ClO_4 flame, ionization processes, recombination coeff., press. depend. 2–28656
NH_4ClO_4 single crystals, gamma radiation induced dislocations 2–6441
NH_2D, Stark effect modulation of CO_2 laser 2–17589
NH_4F, e.s.r. of Cu^{2+}, tetrahedral site obs. 2–20149
NH_4F aqueous solution, solubility of quartz, temp. and conc. depend. 2–35739
$NH_4Fe(SO_4)_2$, Mossbauer spectral dip rel. to spontaneous polarization 2–6885
$NH_4H_2AsO_4$, γ-irradiated single crystal, e.s.r. of free radicals 2–10122
$NH_4H_2AsO_4$, n.q.r, of ^{75}As, elec. field gradient tensor in paraelec. phase 2–10589
$NH_4H_2AsO_4$, proton-lattice coupled motion 2–19376
NH_4HF_2, critical temp. and pressure determination from vapour pressure curves 2–9216
NH_4HF_2, melting curve, high press. polymorphism 2–25141
$(NH_4)_2H_3IO_6$, antiferroelectric, structure obs., using n.m.r. 2–1575
$NH_4H_2PO_4$-(5wt%)KH_2PO_4 crystal, γ-irrad., e.p.r. spectra, NH_3^+ hyperfine coupling 2–10511
$NH_4H_2PO_4$, far-i.r. absorpt. spectra in antiferroelec. and paraelec. phases 2–16494
$NH_4H_2PO_4$, ferroelectric modes Raman spectra, temp. depend. 2–16551
$NH_4H_2PO_4$, finely divided, permittivity 2–10121
$NH_4H_2PO_4$, laser induced self focusing 2–22628
$NH_4H_2PO_4$, $NH_4H_2AsO_4$, antiferroelectric, phase transitions, phonon spectra, Raman scatt. 2–16550
$NH_4H_2PO_4$, phonon modes and phase changes, Raman spectra 2–20062
$NH_4H_2PO_4$, potential distrib. and tertiary pyroelec. effect 2–6886
$NH_4H_2PO_4$, radiation effects on structure, phase transitions and dielectric props. 2–1442
$NH_4H_2PO_4$, second harmonic generation using fluorescein dye lasers 2–5368
$NH_4H_2PO_4$, second harmonic generation of polymethene dye laser, bright u.v. emission 2–27498
$NH_4H_2PO_4$, single crystal, electrooptical modulator 2–21133
$NH_4H_2PO_4$, tunable four photon parametric fluorescence 2–29866
$NH_4H_2PO_4$, used for doubling and summing of intracavity double dye laser 2–23604
$NH_4H_2PO_4$ crystals, det. of refractive index in i.r. region using parametric scattering of light 2–40607
$NH_4H_2PO_4$ crystals, double refraction, temp. dependence, spectrographic meas. over 20 to 65°C and λ=400 to 650 nm 2–7046
NH_4HSO_4 and ND_4DSO_4, i.r. spectra, temp. range 285 to 17°K 2–20046
NH_4I, cryst. growth from soln., on mica, substrate effects 2–35937
$NH_4NH_2SO_3$, cryst. struct. 2–22158
NH_4NO_3, phase IV, cryst. struct. 2–3718
NH_4NO_3IV, transformation twins, pseudosymmetry 2–9353
NH_4PF_6, spin exchange, spin-lattice relax. 2–10278
NH_4ReO_4, far i.r. and laser-excited Raman spectra, librational mode obs. 2–10411
$(NH_4)_2SO_4$, ferroelectric, anomalous spin-lattice relax. at 4 K 2–26082
$(NH_4)_2SO_4$, γ-irradiated, e.s.r. study of $N(SO_3)_2^{2-}$ reorientational motion 2–22826
$(NH_4)_2SO_4$ aqueous solns., NH_4^+ self-diffusion coeffs. 2–1092
$(NH_4)_2SO_4$ solutions, viscosity independence of half-width of $\nu_1(A_1)$ Raman line of SO_4 ion 2–1100

Nitrogen compounds continued
- **ammonium compounds** continued
  - $NH_4)_2SO_4.Ga_2(SO_4)_3.24H_2O$, of Cr^{3+}, satellite line obs. 2—10512
  - $(NH_4)_2SbCl_5$, ^{121}Sb Mossbauer data rel. to structural parameters 2—1668
  - $(NH_4)_2SiF_6$, ionic motion, p.m.r. study 2—37011
  - $(NH_4)_2SnBr_6(Cl_6)$, ionic motion, p.m.r. study 2—37011
  - $(NH_4)_2SnCl_6$, tunnelling- assisted proton spin-lattice relax. of NH_4^+, 20-125 K 2—26083
  - $(NH_4)_2U_2O_7 \rightarrow UO_2$ pellet, sintering/reduction 2—20187
  - NH_4XO_4 (X=I,Re) i.r. and Raman spectra rel. to anomalous temp. dependence of n.q.r. 2—16556
  - $NH_3+HF \rightarrow NH_4F$, molecular orbital studies 2—20178
  - Na-NH_3 solution, electron states, near metal-nonmetal transition 2—12573

Nobelium
- No entries

Nobelium compounds
- No entries

Noble gases *see Inert gases*

Noctilucent clouds *see Atmosphere/upper; Clouds*

Noise
- absolute temperature from the noise thermometer method, 292 to 635 K 2—27335
- bleached phase hologram, reduction method 2—27548
- bursts, duration discrimination 2—37467
- circular laser, disturbance effect on parametric resonance, exptl. and theoret. investigation 2—37945
- control, use of computer programs 2—20944
- control systems, buyer's guide 2—14278
- fibre optic plates, faceplates of CRT's, structure related noise 2—38109
- filtered, effect on intensity discrimination of pulsed sinusoids 2—37473
- j.g.f.e.t., thermal noise behaviour at 77 to 300K 2—1543
- microwaves and plasma stochastic heating 2—32004
- in multiplier of quadrupole mass spectrometer, reduction in ion counting mode 2—2918
- neutron, in reactors, produced by coolant temp. fluctuation and vibrations of control rod 2—15101
- neutron, probability distrib. by maximum likelihood method 2—15102
- nuclear emulsions, noise in photographic trace due to grain size 2—27917
- nuclear reactor, analysis, data extraction methods, review 2—24265
- nuclear reactor, analysis, data extraction methods 2—31620
- nuclear reactors spatial coherence function and cross power spectral density analysis by gamma radiation 2—24286
- nuclear track emulsion, relative scattering measurement, noise elimination 2—31391
- optical heterodyne detector, signal/noise ratio 2—38029
- photographic transparencies, subjective image quality, relative effects of gaussian and Poisson noise 2—5455
- photon counter, 10μ, due to laser pumping and internal upconversion 2 -37940
- pictorial evaluation using two dimensional optical Fourier approach for space imagery 2—34456
- plasma, det. from meas. of ion-acoustic resonances in cylindrical plasma 2—21843
- reactor, measurement of subcritical reactivity 2—28139
- relativistic electron beam rel. to TWT amplifier 2—2349
- S/N ratio in Fourier transforms spectrometry 2—38152
- seismic, source-generated 2—30166
- speckle elimination by stirring of sample in laser light scattering photometry 2—31056
- temperatures for Ar discharges at pressures 1 to 40 torr in tubes of 0.63 cm inner radius 2—12463
- causing temporary hearing loss 2—37471
- thermometer, temperature measurement in nuclear reactors 2—5761
- GaAs small-area diodes, shot-noise in output 2—22817
- He-Ne, laser, mech. vibration 2—27473
- NiFe, Barkhausen, autocorrelation function 2—22684
- ZnS:Ag, luminescence from donor-acceptor transitions, noise and modulation 2—22815
- Zn_2SiO_4:Mn, saturated cathodoluminescence, noise and modulation expts. 2—22816
- **acoustic**
  - acoustoelectric amplifier, reduced phonon noise 2—16028
  - aerodynamic, connection with turbulent fluctuating motion of fluid 2—3311
  - aerodynamic, diffraction theory 2—20931
  - aerodynamic sound due to source near half- plane in turbulent fluid 2—39259
  - aerofoil, aerodynamic noise 2—28722
  - aeronautical, units for nuisance measurement 2—17396
  - of aircraft, sound absorptive materials for control 2—14279
  - aircraft engine, reduction using acoustic lining 2—175
  - airplane interior, radiated by fuselage undergoing turbulent boundary layer excitation 2—174
  - atmospheric background noise reducers, identification of l.f. acoustic waves, active microbarograph array 2—37173
  - atmospheric infrasonic waves, detection by pipe arrays, coherent noise from turbulent boundary layers 2—37175
  - binaural summation of differently correlated noises 2—41319
  - biodynamic models of injury mechanisms 2—11191
  - boundary layer, controlled 2—28728
  - cavitation hydrodynamic noise, approx. theory 2—28760
  - composite sound loudness eval., optimal method 2—34147
  - compressor, axial, inlet sound power 2—34148
  - corona, meas. technique 2—24906
  - cylinder unstiffened, statistical analysis of radiation efficiency 2—2245
  - directivity of jet noise 2—27244
  - domestic appliances, reverberant and direct sound fields 2—37780
  - dosemeter, hearing loss assessment 2—37771
  - effect of duration on judged acceptability 2—20943
  - e.h.v. line corona, conference, New York (1972) 2—21890
  - emission monitoring, MTS modification to testing machine 2—37766
  - environmental effects on speech intelligibility and psychophysiological factors 2—30686
  - fan, characts. and determ. methods 2—34149
  - fan, sound power spectra similarity 2—37773
  - field sound transmission test 2—20945
  - flooring materials, impact noise reduction 2—34166
  - flow, in water filled tubes, effect of air bubbles at tube surfaces 2—17394

Noise continued
- **acoustic** continued
  - Gaussian noise generator, stationary high-level, smoothing m-sequence 2—20942
  - generation analysis in respect of supersonic jet 2—176
  - generation from supersonic shear layers, generalized convective wave theory 2—14276
  - hearing conservation, permissible noise criteria 2—37496
  - hearing damage hazards 2—7609
  - human factors, physical, sociological and psychological aspects 2—2255
  - human fatigue 2—17126
  - hyperbaric diving chamber, during dive to 100 ft 2—34144
  - impulse, live and tape recorded, temporary threshold shift studies 2—11361
  - impulse noise meas. and temporary threshold shifts, tape recording limitations 2—37484
  - industrial, effects on adolescents and standardization 2—26972
  - industrial control, conference, Cleveland (1971) 2—17398
  - infrasonic sound, mechanical and biological effects 2—23352
  - instability of tangential discontinuity in compressible medium 2—37772
  - interference by refl. at plane 2—30867
  - internal combustion engines, design of optimum expansion chambers 2—37775
  - isobar plotting of sound field by colour lights 2—23388
  - jet engine, noise reduction 2—7757
  - jet engine, simple-source theory 2—14275
  - John F. Kennedy Center for the Performing Arts, design problems 2—34155
  - lamp, reduction using reverse phase controlled dimmer 2—20946
  - loudness function, psychophysical correlates 2—27286
  - loudness level meas., recommended procedures 2—34145
  - loudness level of impulsive sounds 2—34146
  - masking pattern production technique 2—14044
  - measurement, effect on mental and physical output 2—37769
  - mechanical noise of deformation meas. for fault detection 2—29160
  - multiple pure tone, generation and evolution from non-uniformities in rotor geometry 2—14277
  - NORSAR theoretical model of seismic noise field 2—30172
  - nuclear reactor, coolant gas circuit components, acoustically induced stress 2—15145
  - in nuclear reactors, effects, velocity of sound in CO_2 2—3328
  - passive sonar processing, signals received by array of hydrophones 2—11360
  - perception level, det. by Mark VII and decibels 2—23166
  - physiological noise under supra-aural earcap, missing 6 dB effect 2—20378
  - pollution prevention 2—37770
  - power emitted by small noise sources in reverberant rooms 2—37779
  - practical aspects of control 2—17397
  - psychometric study of annoyance values of complex sounds 2—17395
  - pulsed industrial noise effects and standardization 2—23386
  - random amplitude distrib., statistical analysis 2—34152
  - reduction, in supersonic jet flows 2—28713
  - reduction in propeller fans using porous blades at free flow conditions 2—7758
  - sea, shallow water ambient noise, time variant characts. 2—30258
  - seismic noise obs. in Greece 2—13611
  - sonic boom in turbulence, statistics of random overpressure peaks 2—9023
  - sonic booms, animal responses 2—37500
  - sonic booms, conference, Acoustical Soc. America, (Houston Texas 1970) 2—34102
  - sonic booms, human response, in laboratory and community 2—37465
  - specification, turbon as discrete package of turbulent energy 2—20941
  - standards, policy of Acoustical Society of America 2—27285
  - standards for environmental pollution 2—30876
  - stochastic, relative evaluation of annoyance 2—17393
  - supersonic jet, three modes of sound radiation 2—176
  - supersonic jet generation 2—12492
  - thermal agitation in microphone, detection using ribbon velocity microphone 2—20935
  - traffic noise level, disturbance correlated to stat. fluctuations, meas. apparatus 2—23387
  - transmission line conductor corona 2—21892
  - undersea, and wind speed dependence 2—10716
  - underwater, radiated ambient and self noise, identification generation and measurement 2—37110
  - underwater l.f. ambient noise theory 2—30253
  - water supply systems, prediction method 2—34150
  - windnoise protection of microphones 2—23361
  - Windscale High Intensity Noise Rig for nuclear reactor pressure level and structural response determ. 2—38707
  - He-Ne laser, environment effects on frequency 2—23596
  - ZnO, photon counting distrib. of Brillouin scattered light from amplified vibr. noise 2—13494
- **electrical**
  - *see also Cosmic radiation, radiofrequency; Sun/radiation, radiofrequency*
  - cooled photodetector with wheel type modulator, analysis at internal noise 2—37806
  - corona, meas. technique 2—24906
  - dark current in photomultipliers, method of reduction at room temperature 2—34328
  - e.h.v. line corona, conference, New York (1972) 2—21890
  - electrochemical current source 2—30076
  - ferroelectric capacitor in d.c. field 2—33055
  - image dissector, statistical analysis of signal and noise pulses 2—27434
  - induced-noise discriminating circuit for nuclear radiation counting systems 2—38388
  - insulators, current flow, combined Poole-Frenkel and Schottky effects 2—40238
  - j.f.e.t., ceramic encapsulation, dielec. noise analysis 2—29726
  - Josephson junction, current fluctuations, power spectrum 2—13191
  - Josephson junctions, strongly coupled 2—13186
  - metal-semiconductor-metal diode, velocity fluctuations 2—36565
  - microplasma, in zener diode, investigation with scanning electron microscope 2—6863
  - microwave solar burst spectrographic radiometer, noise figure 2—26893
  - m.o.s. device, low freq. noise, rel. to charge pumping current 2—10104
  - nuclear reactor, polarity-correlation system 2—11916
  - p^+-n diode, junction noise at high injection 2—36558

Noise continued
electrical continued
photoconductor, band to band Auger processes 2—19781
photoconductor, two-dimensional transport processes, fluctuation theory 2—25953
photomultiplier, one electron, effects of prolonged operation on noise level 2—37928
photomultiplier, statistics 2—34327
photomultipliers, signal-to-noise ratio depend. on operating voltage 2—2370
radiation field, simulation of e.m. waves in plasmas 2—39128
radio interferometer, missile-tracking, meteorological data obs. 2—33482
radiowave propagation, multipath, on oversea line-of-sight path, noise meas. 2—16858
random walk model for 1/f noise 2—25806
random walk model for 1/f noise 2—25805
semiconductor electrolyte interface, impedance and noise in electron transfer 2—13585
superconducting In and Sn thin films, critical point fluctuations 2—40188
superconductor, type-I, dynamic intermediate state 2—13133
transistor, bipolar ^{60}Co γ-irrad. effects 2—22594
$CdCr_2Se_4$:Ga, current noise measurements 2—40278
CoO:Li, current noise measurements 2—40278
GaP p-n junctions, excess current- and luminescence-noise 2—22581
$GeSi_{1.2}As_3Te_{4.8}$ film, glass, switching noise 2—22530
NiO:Li, current noise measurements 2—40278
$PbTiO_3$ pyroelectric i.r. detector 2—17414
Si:Au, impedance and g-r noise under space-charge conditions 2—22567
Si f.e.t., noise temp. at 2 and 4 GHz, obs. 2—4253
Si junction transistors, effects of electron bombardment 2—13286
Si photodetector, for satellite appl., electron and X-ray effects 2—25967
TiO_2:Al, current noise measurements 2—40278

Noise abatement
see also Absorption/acoustic waves
attenuation spectra in acoustically treated rectangular duct 2—7750
camera running noise, blimps 2—173
concrete apartment house, sound reduction by wing wall 2—34170
control using computer programs 2—20944
ducts with sound absorbing Kapron fiber linings, frequency characteristics 2—27288
fan, axial, methods of fan noise reduction 2—37774
fan, axial flow, noise reduction 2—37776
lamps, applic. of reverse phase controlled dimmer 2—20946
measurement, effect on mental and physical output 2—37769
microphone station reliability under outdoor conditions 2—23363
pollution prevention 2—37770
radial diffuser configuration, performance of sound absorbing materials 2—14262
screen of arbitrary shape, diffr. methods 2—34151
sonic boom minimization, modification of aircraft configuration 2—35668
sound insulation of heavy wall, brick wall experiment 2—17402
transmission through thin walled spherical shell, ratios of sound pressures inside and out 2—27287
by vegetation and ground, scattering and attenuation 2—14265

Nomenclature and symbols
see also Units
acronyms and abbreviations in use at Kennedy Space Center 2—11237
organic chemistry, IUPAC rules, book 2—23211

Nomograms
see also Graphs
atmospheric vertical velocity standard deviation at 75.m and 225.m 2—7286
error calc. of energy of binary type nuclear reaction product and cross-section as function of emergence angle 2—27831
thermal contact conductance computation 2—17428
water evaporation from free surface 2—3449

Non-crystalline state *see Amorphous state; Vitreous state*

Non-Newtonian fluids
carboxymethylcellulose in water, free convection of heat from a vertical plate 2—37812
carboxypolymethylene in water, free convection of heat from a vertical plate 2—37812
dynamic properties under combined steady and oscillatory shearing flow 2—39298
elastic power law, steady flow, converging or diverging, with wall suction and injection, similarity solns. 2—911
film on withdrawn cylinder 2—28773
flow, shear unstable, conducting liquid with restricted rheological law in magnetic field 2—944
flow, slow, past droplet 2—912
flow, through circular tube, temp. distrib. 2—35406
flow-rate measurement orifice plate and Venturi meter 2—28473
helical flow of non-Newtonian liquids 2—1044
liquid, axial dispersion in packed bed 2—24989
oscillatory shear, comparison with steady state viscosity versus shear rate data 2—35397
improved parametric characterization of flow geometries 2—28454
plane Poiseulle flow, finite amplitude instability 2—28462
power law, in vertical tube, exptl. and theoretical study of combined free and forced laminar convection 2—37820
power law, pulsating flow in pipes, flow rates and power requirements 2—39037
Rayleigh's problem, unsteady state flow in semi infinite region 2—35407
saline solution, diffusion of O_2 2—35749
second order, separation in flow past circular cylinder 2—920
stability of particle motion near a wall 2—35399
stability of particle motion near a wall in Newtonian and non-Newtonian fluids 2—35399
turbulent mixing length formulation 2—24616
unsteady, laminar flows in pipes 2—35698
viscous liquids, flow, laminar motion 2—35700

Nonlinear optics
absorption during interaction of Ne superradiation with resonantly absorbing surface 2—11505
alkali metal vapour, phase matched with inert gas, third harmonic gen. 2—6161
anisotropic media, rotational contrib. to Brillouin scatt. and higher order photoelastic interactions 2—16423

Nonlinear optics continued
anisotropy induced by resonant absorption or amplification of radiation 2—2374
astronomical sources of maser action, review 2—30401
birefringence, electric and mag., quantum theory, variation-perturbation method 2—15540
bremsstrahlung, from electrons passing through ion field 2—31652
broadening of laser radiation spectrum due to increase in transmission of nonlinear filter 2—27530
carbon tetrachloride, nonlinear refractive index, due to nonlinear response of electronic currents 2—1096
cholesteric liquid crystals, phase-matched normal and umklapp third-harmonic-generation processes 2—32265
coherent, in two-level system, laser excited 2—27446
coherent excitation of polaritons and i.r. generation 2—4423
coherent magnetic vibrations generated by reflection of visible laser light on magnetic domain wall 2—31078
crystal, second harmonic generation by thermal interaction of waves 2—29867
crystals, equations for nonlinear susceptibility to harmonic generation rel. to microstructure 2—1653
damage in laser materials 2—33191
diffraction effects on self induced thermal distortion of laser beam in cross-wind 2—22962
e.m. waves, modulated in nonlinear dispersive medium, quasi particle concept 2—14305
ferroelectrics applics., review of developments in Europe 2—40340
filament form. by ultrashort pulses, relax. effect 2—37999
four photon parametric frequency selection in wide stimulated emission lines of dye laser 2—27487
geometrical, transition lines and singularities in the equations for nonlinear geometrical optics 2—31080
glass, nonlinear susceptibility 2—16418
glass, self-focussing of ultrashort and filamentary damage 2—13429
glasses and simple liquids, transparent, origins of Kerr effect 2—36812
group II-IV-V compounds, chalcopyrite semiconductors, nonlinear coefficient 2—26100
harmonic generation 2—22722
holographic recording materials, characterization 2—38007
image conversion, longitudinal and transverse resolution 2—11504
inhomogeneous media, nonlinear scatt. theory 2—16450
intensity fluctuations of beam after propagation in nonlinear medium 2—11506
interference effect in a field modulated by random Markoff process 2—24326
i.r. lasers, using proustite crystals, applic. 2—23570
laser damage of i.r. nonlinear materials 2—21047
laser glass, BSC-2, direct nondestructive measurement of self focusing 2—26099
laser light-frequency and amplitude conversion 2—23659
laser Q switch design, deuterated KDP, absorption data 2—36824
light trapping, electric control 2—4421
metal surface, second harmonic radiation 2—4422
microwave interaction in acentric crystals 2—23556
microwave susceptibilities of acentric cryst., absolute signs determ. 2—4424
modal fields distribution det. in open mirror resonators with saturable gain medium 2—5350
multi-focus structure of beam, Kerr medium 2—22723
nematic liquid crystal, deformation in electric field, electro-optic effect 2—6233
5-nitrouracil, susceptibility obs. 2—19954
non-monochromatic wave spectrum, propagation in nonlinear nondissipative medium 2—38052
nonenantiomorphous cryst., optical rectification effect 2—7034
parametric oscillation and second harmonic generation, simultaneous occurrence 2—10293
parametric oscillator, focussing effect 2—23569
perturbation approach to nonlinear response to pulse fields 2—7961
phase transitions, theory 2—14400
photochromic materials, phase holographic response function 2—34412
plane monochromatic waves on liquid surface, nonlinear attenuation 2—39366
plasma, self action of e.m. wave 2—12384
polar crystals, optical rectification by impurities 2—33210
polyvinylidene fluoride, film, second harmonic generation 2—19955
polyvinylidene fluoride, i.r. detectivity 2—13329
polyvinylidene fluoride films, poled 2—40367
pulse distortions in mismatched second harmonic generation 2—34408
Q-switched pulse stretching applications 2—14399
quartz, self-focussing of ultrashort and filamentary damage 2—13429
radiation modulation, effect of nonlinear characteristics on the error of the phase optical rangefinder 2—27564
Raman lasers and parametric amplifiers, review 2—5345
rare earth ion activated cryst., i.r.-visible conversion 2—26222
resonant susceptibility of solids 2—36823
resonator, second harmonic generation, pulse shortening, calc. 2—14402
saturable resonator characts. 2—31027
second harmonic aperture in nonlinear excitation by ultrashort light pulses 2—16414
second harmonic generation, non-stationary theory 2—21138
second harmonic generation in laser created plasma 2—31994
second harmonic generation inside Nd laser resonator 2—37988
second harmonic of laser generated in crystal, device for monitoring 2—17671
second harmonic power det. of nonlinear crystals 2—38031
second harmonic pulse shape under ultrashort pulse excitation 2—27563
self focusing channel, limiting value of diam. in medium with cubic nonlinearity 2—27360
self focusing in laser amplifier with large beam diameter 2—17646
self focusing medium, wave field struct. near foci 2—11503
self focusing of laser beams in inhomogeneous dielectric 2—31060
self focusing of particles in cyclic accelerator 2—14813
self focusing theory, rel. to laser beam damage in solids 2—29868
self-action of light arising from stimulated Raman scattering 2—23666
self-focusing, high density particle bunches, in periodic waveguide systems 2—14382
self-focusing and stimulated scattering in laser produced plasma 2—3212
self-focusing due to Kerr effect, rel. to stimulated Raman scatt. in liqs. and crysts. 2—28861

Nonlinear optics continued
self-focussing of TE_{01} and TM_{01} light beams, influence of longitudinal field components 2—31062
semiconductor, nonlinear optical phenomena, rel. to free carriers 2—36484
semiconductor, second harmonic generation, coherence lengths and susceptibilities near band edge 2—7036
semiconductor crysts. with variable effective mass, susceptibility 2—7033
semiconductor glass filter, absorption, transmission and luminescence spectra 2—22757
short light pulses, self focusing kinetics 2—34409
steady state self focusing in a medium with saturating nonlinearity 2—7787
step function light pulses, propagation in resonant medium 2—23665
sum-frequency generation rel. to exciton polaritons in noncentrosymmetric crystals 2—36865
third harmonic generation and intensity depend. refr. index 2—17670
triglycine sulphate, Curie temp., second harmonic scatt. 2—16294
tunable four photon parametric fluorescence, in nonlinear optical crystals 2—29866
wave-optics computer model, comparison with nonlinear laser-propagation experiments 2—14432
waveguide propagation of laser beams in dielectric media with saturating non-linearity 2—31061
Ag_3AsS_3, proustite, i.r. parametric oscillator 2—17578
Ag_3AsS_3, proustite, parametric image upconversion of 10.6 μm illuminated objects 2—21060
$AgGaS_2$ 2—9364
$AgGaS_2$, second harmonic generation meas. 2—1654
$AgGaS_2$, second harmonic generation coeffs. meas., possibility of laser application 2—1654
Al_2O_3, sapphire, high power laser beam scatt., nonlinear effects 2—16450
Ar gas, dc-induced second harmonic coefficients, calc. of absolute values 2—24984
Au film, laser modification of transmittance and reflectance, adherence and hardness 2—36813
$Ba_2NaNb_5O_{15}$, catastrophic surface damage during intracavity freq. doubling for Nd:YAG laser 2—29869
$Ba_2NaNb_5O_{15}$, second harmonic generation 2—13315
$BaTiO_3$, cubic phase, second optical harmonic generation 2—33192
$Bi_{12}GeO_{20}$, self-focussing and phonon scatt. of laser radiation 2—10295
CdS, hexagonal semiconductor, dispersion of nonlinear optical susceptibilities 2—4426
CdS, photodielec. lens effect 2—16415
CdSe, hexagonal semiconductor, dispersion of nonlinear optical susceptibilities 2—4426
CdSe, parametric mixing, phase matched nonlinear interaction 2—19950
CdTe, single crystal, continuous second harmonic generation 2—4425
$Cd[Hg(SCN)_4]$ tetragonal crystals with phase matching 2—7035
CsH_2AsO_4, efficient second harmonic generation of Nd^{3+}:glass picosec. laser pulses 2—37984
Cu^+ halides, photoelastic properties, phase matching of nonlinear optical processes 2—26119
$CuGa(In)S_2$ 2—9364
$CuGaS_2$, determ. of optical nonlinear coeffs. 2—1654
CuI, refr. index dispersion 2—1655
$CuInS_2$ second harmonic generation determ. 2—1654
GaP, nonlinear susceptibility, relative meas. and detn. of absolute value 2—40597
HIO_3 crystal, growth method and applications 2—29090
HIO_3 crystal, polarization and phase matching conditions 2—26101
He gas, dc-induced second harmonic coefficients, calc. of absolute values 2—24984
n-InSb, frequency conversion of e.m. radiation 2—10050
InSb, second harmonic generation, coherence lengths and susceptibilities near band edge 2—7036
KD_2PO_4, efficient second harmonic generation of Nd^{3+}:glass picosec. laser pulses 2—37984
KH_2PO_4, ordinary+extraordinary→extraordinary type interaction, vector synchronism conditions 2—10296
KH_2PO_4, relative nonlinear coefficients, cw ruby laser as pump source 2—36814
KH_2PO_4, self-focussing of ultrashort and filamentary damage 2—13429
Kr gas, dc-induced second harmonic coefficients, calc. of absolute values 2—24984
$LiIO_3$, beat generation, far i.r. 2—26102
$LiIO_3$, second harmonic generation, Nd:YAG laser, damage obs. 2—29864
α-$LiIO_3$, second harmonic generation, rel. to growth conditions 2—22724
$LiIO_3$, second harmonic generation coeff. 2—4447
$LiIO_3$ relative nonlinear coefficients, cw ruby laser as pump source 2—36814
$LiNbO_3$, far i.r. radiation generation by picosecond light pulses 2—7903
$LiNbO_3$, second harmonic generation, Nd:YAG laser, damage obs. 2—29864
$LiNbO_3$, second harmonic generation, phase matching angles and temps. 2—38037
$LiNbO_3$, self-focussing of ultrashort and filamentary damage 2—13429
$LiNbO_3$ applications 2—34367
$LiNbO_3$ crystal, influence of transverse inhomogeneity of refractive index on second harmonic generation 2—27562
$NH_4H_2PO_4$, second harmonic generation using fluorescein dye lasers 2—5368
Na vapour, obs. of amplitude modulated train pulse 2—23665
$NaBrO_3$, SHG, optical rotatory power 2—19952
$NaClO_3$, SHG, optical rotatory power 2—19952
$NaNO_2$, ferroelec., second harmonic coeffs., temp. depend. 2—19951
Nd:YAG laser, CW, second harmonic generation in $LiNbO_3$ crystals 2—37989
Ne-He, internal-mirror lasers, polarization props. at 6328 Å 2—23595
Ne gas, dc-induced second harmonic coefficients, calc. of absolute values 2—24984
$PbTiO_3$, single domain ferroelectric, optical transmission, refractive index and second harmonic generation coeffs. 2—19953
Rb, atomic, self-induced transparency 2—31671
Rb, vapour, 4-photon parametric processes following excitation by 2 lasers 2—606
Rb vapour, phase-matched, third harmonic generation 2—9037
RbH_2AsO_4 relative nonlinear coefficients, cw ruby laser as pump source 2—36814

Nonlinear optics continued
RbH_2PO_4 relative nonlinear coefficients, cw ruby laser as pump source 2—36814
SF_6, gaseous, obs. of amplitude modulated train pulse 2—23665
Te, laser beams mixing, turnable coherent radiation source 2—7931
TeO_2, paratellurite, second harmonic generation and Kleinman's symmetry relations 2—33193
TeO_2, second harmonic generation, Kleinman's symmetry condition violation 2—33194
TiO_2, rutile, antisymmetric suscept., Brillouin scatt. obs. 2—16423
$Zn[Hg(SCN)_4]$ tetragonal crystals with phase matching 2—7035

Novae
see also Stars
3C58, supernovae remnant, brightness and polarization structure, obs. at 2.8 cms 2—26791
3C 391 supernova remnant, effects of interstellar gas on continuum spectrum and cut off of low frequencies 2—37329
Aquilae 1970, spectrograms 2—20571
Cen XR-4, precursor to X-ray nova 2—26810
Cephei 1971, spectra 2—1962
Delphini 1967, monochromatic continuum magnitudes in spectra 2—7400
Delphini 1967, spectral observations of nebula between 5600 and 8800 Å (in 1970) 2—13911
G55.7+3.4, possible supernova remnant, mapping at 11 and 21 cm wavelengths, to investigate possible relationship with CP1919 2—10961
G55.7+3.4, possible supernova remnant, non-thermal shell source close to the direction of CP1919 2—10960
hydrodynamical processes 2—20563
IC443, supernova remnant, brightness and polarization structure, obs. at 2.8 cms 2—26791
IC 443, supernova remnant, obs. at 408 MHz 2—16967
identification novae and supernova in Palomar Sky atlas 2—30491
Mensae 1970b, in Large Magellanic Cloud, mean radial velocity of emission lines 2—26714
Monoceros Loop supernova remnant soft X-ray source of cooling neutron star 2—23096
N132D supernova remnant in Large Magellanic Cloud, obs. at 408 MHz 2—7490
N49 supernova remnant in Large Magellanic Cloud, obs. at 408 MHz 2—7490
N63A supernova remnant in Large Magellanic Cloud, obs. at 408 MHz 2—7490
NGC 4254, supernova spectrum type rel. to broad emission bands 2—41111
Nova Delphini 1967, radio variations 2—33666
Nova Serpentis 1970, radio variations 2—33666
nucleosynthesis in supernova models, exploding stars and neutron- proton ratio rel. to dense, high-temperature states 2—23070
r-process, nucleosynthesis of superheavy elements 2—23079
relativistic shock propagation and search for e.m. pulses from supernovae 2—37306
review of supernova remnants and their significance to astrophysics 2—7440
Serpentis 1970, spectroscopic obs. of early decline 2—20571
shock, axisymmetric, time development 2—23391
southern hemisphere search for supernovae 2—7441
spectra, type I, wavelength shifts of intensity minima of supernova 2—4878
supernova, type I, in NGC 5055, spectrum 2—4883
supernova, Type I of 1954 in NGC 4214, problems of intensity min. in spectrum and blue shifted He I absorption 2—23077
supernova 1970g, first epoch radio obs. identification with pointlike source 2—37303
supernova ejecta and production of ionizing u.v. radiation 2—37302
supernova flash effects on evolution of interstellar matter and thermal and ionization balance, time dependent model 2—37317
supernova in M63, magnitude on May 20 1971, revision 2—30485
supernova of 1006 A.D. radio obs. search 2—4874
supernova remnant Puppis A, radio map at 408 MHz 2—4875
supernova remnants, acceleration of galactic cosmic rays 2—30490
supernova remnants, polarization of 6 cm radio emission 2—20614
supernova remnants, relationship with H II regions from H I absorption measurements 2—16969
supernova remnants γ sources search at 10^{11}-10^{12} eV, null result 2—33722
supernova remnants in Aquila, high-sensitivity X- ray search 2—33719
supernova remnants in Maffei 1, radio luminosities 2—10894
and supernovae, American Astronomical Society, Amherst, USA 1971, conference 2—26623
supernovae, cooling effects on interstellar shock waves 2—26717
supernovae, critical energy for gamma ray absorption by photons 2—10925
supernovae, evolution theories 2—7419
supernovae, fluorescence pulses produced in upper atmosphere 2—40983
supernovae, ionizing interstellar gas, cooling and recombination 2—26754
supernovae, optically detected extragalactic upper limits of X-ray luminosities 2—26797
supernovae, rel. to r-process nuclides 2—37308
supernovae, type I, spectra, absorption bands, laboratory simulation 2—7438
supernovae, upper limits to X-ray luminosity 2—4947
supernovae envelopes, p-process in explosive nucleosynthesis 2—4833
supernovae explosion, explosive C-burning nucleosynthesis 2—16981
supernovae location in galaxies 2—20565
supernovae remnants, polarimetric obs. and magnetic field structure 2—26718
supernovae remnants, relative space positions with pulsars 2—23088
supernovae remnants, type II, mass 2—10892
supernovae remnants as new theory for giant loops 2—13913
supernovae remnants rel. to radio emission from normal spiral galaxies 2—13854
supernovae search with computer controlled telescope 2—26936
V605 Aquilae, peculiar slow nova, occurring within few seconds of arc of centre of planetary nebula 37-5°1 2—20573
Vela supernoval remnant, hard X-ray pulsations 2—26800
Vela X supernova, ionization and heating of Gum Nebula by energetic particles 2—20507
Vulpeculae 1968 (1)=LV Vul, photoelectric observations 2—41106
W28, supernova remnant, brightness and polarization structure, obs. at 2.8 cms 2—26791

Novae continued
W44, supernova remnant, brightness and polarization structure, obs. at 2.8 cms 2—26791
white dwarf evolution at 1.00 $M_\odot$ 2—17002
WY Sge, photometry 2—20572
X-ray nova Centaurus XR-4, X-ray burst before reported nova 2—13971
C detonation supernovae, critical core mass 2—33673
S II and O I line intensity ratios in a supernova remnant and nuclei of galaxies 2—37266

Novoids *see Novae*

Nuclear acoustic resonance
antiferromagnets, cubic, u.s. wave propag., reson. absorpt. linewidth 2—40789
double nucl.-nucl. acoustic mag. reson. 2—13558
metal, nuclear spin phonon coupling, acoustic mag. reson. 2—40787
metal, reson. dispersion 2—7128
saturation waves and spin- phonon coupling 2—6663
CsBr, single cryst., deformation, spin diffusion and anti-shielding factor 2—7157
LiF, Sternheimer antishielding factor of ^{7}Li 2—40775
MnTe, ^{55}Mn freq., mag. field depend. 2—20162
MnTe, of ^{55}Mn, rel. to u.s. attenuation around Neel temp. 2—1426
$NaClO_3$, double n.m.r., by acoustic excitation 2—33356
$RbMnF_3$, u.s. coupling to ^{19}F spins 2—37013

Nuclear alignment *see Nuclear polarization*

Nuclear bombardment targets
accelerator, coding system, calc. method for design 2—27932
accelerator assembly, isopropanol- solid CO_2 cooled 2—2656
butanol, polarization, effect of absorbed power 2—34774
butanol target for study of photoproduction reactions on polarized protons, construction and effects of radiation damage 2—34766
n-butanol-d_{10}, solid polarized, production by dynamic polarization of deuterons 2—36807
butanol-water-porphyrexide system, polarized proton target properties and performance 2—34779
1-butanol-water-porphyrexide system, proton polarization at 50kG and 1K 2—36808
clamp, fast mount, for use in scattering chambers 2—21316
clamp, fast mount, for use in scattering chambers 2—31347
Davis polarized proton target, computerized n.m.r. system 2—24064
deuteron, polarization in predeuterated 1-butamol and heavy water 2—14742
electron-nucleus scattering expt., method of increasing target thickness 2—28021
ethylene-glycol-Cr(V) system, polarized proton target properties and performance 2—34779
frozen, polarized proton, operation and performance 2—17992
gas, beam heating 2—24063
He^3 horizontal continuous flow cryostats for organic polarized proton targets 2—20775
heavy element impurities $Z \geqslant 20$, technique for determination 2—14740
large volume, physical arrangement for polarization measurement 2—34776
melted, for in-beam g-factor det. 2—21315
melted, for in-beam g-factor det. 2—31346
metallic hydride, behaviour of tritium in target on bombardment of deuteron beams 2—34780
oriented nuclei, expts. with (n,γ) reactions and neutron-induced fission 2—35049
oriented nuclei, neutron physics expts. for determ. spins of compound nuclear states 2—34770
1-pentanol-water-porphyrexide system, proton polarization at 50kG and 1K 2—36808
pinacone-Cr(V) system, polarized proton target properties and performance 2—34779
pion production by bombardment with protons for radiobiological and dosimetric studies 2—2888
polarization, measurement by nuclear magnetic resonance system 2—34773
polarization, non-resonant means of measurement, polarized ^{3}He targets considered 2—34777
polarization, on-line computer measurement using r.f. phase lock techniques 2—34775
polarization, target uniformity and radiation damage 2—34772
polarization experiments, choice of coordinate systems 2—35002
polarization measurement by e.p.r. line observation 2—27833
polarization measurement by means of the internal field 2—27834
polarized, ^{13}C dynamic polarization in 1-butanol: porphyrexide 2—36809
polarized, applic. of dilution refrigerator to dynamic and brute force polarization and spin freezing of protons 2—37527
polarized, calibration by polarized protons and deuterons 2—35021
polarized, conf., Springfield USA (1971) 2—34757
polarized, dynamic nuclear polarization and electronic spin-spin interactions 2—36997
polarized, dynamic polarization at $T<0.5K$ 2—34771
polarized, dynamic proton polarization in 1,8-octanediol-glycol mixtures 2—36811
polarized, large dynamic polarization of ^{19}F in CaF_2 2—36803
polarized, mechanisms of nuclear dynamic polarization by electron-nucleus dipolar coupling in solids 2—36800
polarized, proton polarization in hydrocarbons 2—36810
polarized, solid effect with inhomogeneous broadened e.s.r. line 2—36977
polarized, solid HD applic., p.m.r. obs. of spin lattice relaxation and nuclear polarization at $T<1K$ 2—37008
polarized, superconducting magnet applic. 2—34759
polarized ^{3}He-cooled, cryostat 2—34760
polarized butanol, meas. of polarization parameter in backward scattering in π^+p reactions 2—34694
polarized butanol target for meas. of π-N elastic scattering at high energy and low cross-sections 2—34691
polarized LMN crystal, scattering of polarized protons, spin correlation parameters 2—35020
polarized proton, rel. to elastic NN scattering studies at 300 to 3000 MeV 2—34715
polarized proton, used in test of time reversal invariance 2—34769
polarized target asymmetry for π^0 photoproduction at 4 GeV 2—34768
polarized target cryogenics, recent progress 2—34758
polarized target for polarization meas. of high energy charge exchange reactions, discussion of background due to bound protons 2—34765

Nuclear bombardment targets continued
polarized targets at electron accelerators, effects of beam and μ-wave heating, radiation damage and radiative corrections 2—34767
preparation of thin targets on thin graphite backing by molecular plating 2—31348
production from ^{238}Pu 2—27935
remote control of motion and position 2—31345
separated function frozen, present and future prospects 2—34763
separated junction frozen targets, present and future prospects 2—5575
shielding, heterogeneous active and passive shields, proton beams 2—2871
statically oriented nuclei, expts. with oriented radioactive nuclei 2—36801
thin absorbers, energy spread for a range of incident particles and targets 2—4089
As metal target preparation techniques, suitable for cyclotron irradiation 2—27835
Be, external, in intense intermediate energy proton beam, shielding requirements 2—34756
^{9}Be deuteron bombarded, neutron spectra 2—5711
^{209}Bi polarized target, production via low temp. polarization of Bi isotopes in ferromagnetic BiMn 2—36802
CaF_2 polarized, rel. to meas. of spin-dependent part of slow neutron scattering amplitude on ^{19}F 2—35053
H_2, liquid, 150 cm, construction 2—17994
H_2, liquid, 50 cm, with Mylar windows 2—17993
H_2, liquid, mylar with thin mylar sidewalls and vacuum housing 2—31344
HD, solid polarized, exptl. development 2—34764
H_2S preparation from atomic hydrogen and solid ^{34}S 2—14741
^{1}H, polarized, for low energy scattering expts. down to less than 10 MeV 2—11655
^{2}H, ^{3}H, neutron production for therapy and activation analysis 2—34755
^{3}H, 14 MeV neutron source 2—24065
^{3}He, compressed polarized gas 2—34762
^{3}He, polarized, construction for low energy scattering expts. 2—11654
^{3}He polarized target, device for studying reactions 2—27832
^{3}He polarized targets, possible production using adiabatic compression method 2—34761
^{3}He polarized targets, review of scattering experiments 2—35005
^{165}Ho, aligned, nuclear quadrupole moment meas. by proton scattering 2—34968
K, for recharging of protons to give H^- beams 2—7900
Li, for recharging of protons to give H^- beams 2—7900
Mg, for recharging of protons to give H^- beams 2—7900
NH_3, solid polarized, production by dynamic polarization of protons 2—36807
Na, for recharging of protons to give H^- beams 2—7900
$Tm^{2+}:CaF_2$, polarization of ^{19}F and ^{169}Tm by circularly polarized light 2—40596
W target, thick, scattering spectrum in terms of energy loss 2—8321

Nuclear decay schemes *see Radioactivity/decay schemes*

Nuclear decay theory
see also Beta decay theory; Nucleus/theory
alpha decay, approximation in calc. barrier penetration factor of R-matrix theory discussed, external problem investigated 2—8318
alpha decay, calc. of overlap integral 2—11785
half-life variations caused by chemical and physical means, review 2—24178
heavy nuclei, antianalogous states 2—18150
odd A nuclei, surface distributions of α-particles 2—34983
pre-equilibrium decay, nuclear density distribution 2—31496
recoil nuclei from α-decay, velocity measurement and mass determination 2—28003
sequential particle decay for aligned nuclei, angular correlations 2—21406
β- decay, e.m. final-state interaction contributions 2—2547

Nuclear emulsions *see Nuclear track emulsions*

Nuclear energy level lifetimes *see Nucleus/energy level transitions*

Nuclear excitation
see also Isobaric analog states; Mossbauer effect; Nucleus/energy levels
0^+ states excited in two-particle transfer reactions 2—24134
2^+ level, cross section, (n,n$'\gamma$) reactions 2—18208
A=8 system, excited states, investigation using ^{7}Li+n and ^{7}Li+p reactions 2—24141
actinides, $229 \leqslant A \leqslant 257$, quasiparticle and vibrational excitations, evidence from radioactive decay meas. 2—21401
closed-shell nuclei, coupling of particle-hole and surface excitations 2—2668
Coulomb, in heavy ion scatt., for excited level studies 2—31588
Coulomb, Sm nuclei recoiled by 4 MeV α-particles into different targets 2—2813
Coulomb excitation, electric quadrupole radial matrix elements, computer program 2—21365
Coulomb excitation, reaction list, 1956- June '71, Z=1 to Z=98 nuclei 2—35006
Coulomb excitation, recent developments 2—38455
deformation of excited nuclei and disappearance of shell effects with excitation energy, statistical description 2—24133
deformation vibrations, excitation by radiationless muonic transitions 2—18075
deformed even even nuclei, nonadiabatic theory of rotational-vibrational excitations 2—21370
deformed nuclei, $K^\pi=1$ excitation 2—11716
deformed nuclei, nuclear shape calculations 2—2676
E2 transition probabilities, even-even deformed nuclei, $2^+ \rightarrow 0^+$ ground state transitions 2—2672
electric quadrupole Coulomb excitation, differential cross sections, computer program 2—34998
electronic, high temp. gases, contribution to thermodynamic properties 2—21919
energy levels, investigation using γ-ray monochromator 2—2671
excitation energies, modified quasiparticle model 2—21364
fission fragments, dipole excitations at scission point studied in a classical model 2—18248
giant dipole and quadrupole resonances, cross section calc. using DWBA 2—2678
giant dipole resonance, evidence for isobaric spin splitting 2—38561
giant dipole resonances, effective interaction rel. to isospin splitting 2—18076
giant resonance excitation, resolution into isospin components, rel. to neutron and proton r.m.s. radii 2—31407

Nuclear excitation continued
heavy nuclei, shape isomer excitation energies 2—27968
highly deformed states, association with fission barrier 2—21353
inelastic excitation of unnatural parity states, by alpha-particles, one-step processes 2—14997
isospin centroid energy calc. 2—34903
isovector monopole strength 2—21366
light nuclei electro-excitation cross section depend. on coupling scheme 2—14977
medium and heavy nuclei, low-lying many particle-many hole states, quartet model 2—14919
medium heavy nuclei, lower excited state, new quasiparticle correlation 2—14920
nuclear matter, infinite, of interacting alpha- particles, excitation spectrum 2—38444
nucleon isobars, virtual excitation, form. by hadron-nuclei interaction 2—14921
rare-earth nuclei, equilibrium deformations of the ground and excited states 2—455
relativistic nuclear. model for dissociation in nuclear Coulomb field 2—21368
resonances, dynamical approach to S-matrix theory 2—18073
sd-shell nuclei, intrashell quartet excitations 2—31422
spectrum calcs. for nucl. matter 2—34898
spin-, isospin- and spin-isospin quadrupole modes in nuclei studied through modified surface delta interaction model 2—456
spontaneous fission isomers, excitation energies from threshold meas. 2 34894
transitions up to 10 MeV, E1 and M1 multipolarities, pair conversion coeffs. 2—8277
vibrating nucleus, collective states excitation by fast particles, semiclassical approximation 2—8319
$^{170, 172, 174, 176}$Yb, excitation functions of (p,p) scattering, IAR study 2—18136
^{27}Al, excitation energies of excited states, γ-ray energy meas. 2—11724
-^{7}Al(p,γ)$_{2}{}^{8}$Si, excitation functions, resonances 2—28036
^{243}Am, isomer states, spontaneously fissioning, excitation in inelastic scatt. of γ quanta 2—15026
^{36}Ar magnetic transitions excited by 180° electron scatt. 2—11738
^{205}At, three quasiparticle excitation in reaction ^{197}Au(^{12}C, 4n)^{205}At 2—18147
^{211}At, produced through ^{40}Ar+^{209}Bi transfer reactions, determ. excitation function and recoil ranges 2—11875
^{11}B, giant dipole resonance, evidence for isobaric spin splitting 2—38561
^{11}B, isospin splitting of giant dipole reson. 2—34907
^{7}Be, excitation energies of excited states, γ-ray energy meas. 2—11724
^{8}Be, ghost anomaly, ang. and reaction depend. 2—2688
^{12}C, low-energy neutrino excitation of giant resonance 2—34909
^{12}C, substate excitation of 2^{+} state by (p,p$'\gamma$) inelastic scatt. 2—34941
^{12}C deform. sign determ. from inelastic proton scatt. 2—27965
^{13}C, dipole resonance using intermediate coupling approximation 2—38475
^{13}C, electroexcitation of giant resonance 2—2767
^{112}Cd photoexcitation, study of energy levels 2—11758
^{37}Cl, excitation energies of excited states, γ-ray energy meas. 2—11724
^{248}Cm, population of 0^{+} states by (p,t) reaction 2—34920
^{158}Dy, moment of inertia by excitation of ground-state band to spin 22 2—34966
^{162}Dy, multiple Coulomb excitation of γ-vibrational bands using ^{16}O ions 2—14955
Er(A=166, 168, 170) multiple Coulomb excitation of γ-vibrational bands using ^{16}O ions 2—14955
^{19}F(α,γ), 3.5 to 4.7 MeV, excitation function for X-ray yields 2—35071
^{54}Fe, substate excitation of 2^{+} state by (p,p$'\gamma$) inelastic scatt. 2—34941
^{56}Fe, Coulomb excitation by ^{4}He and ^{16}O, static quadrupole moment determination from reorientation meas. 2—31472
^{57}Fe, doorway state effects in M1, radiative excitation of p-wave resonances 2—18108
^{68}Ge from ^{70}Ge(p,t), excited levels study 2—18110
^{69}Ge from ^{70}Ge(p,d), excited levels study 2—18110
^{70}Ge, initial state excitation by thermal neutron capture 2—11843
He ions directly scattered by heavy nuclei, possible explanation for gross structure observations 2—14998
^{115}In, by positron annhilation, cross section meas. 2—11759
^{41}K, excited states investigation from ^{40}Ar(p,γ)^{41}K reaction 2—5653
^{139}La, Coulomb excitation by proton scattering at 12 MeV 2—5664
^{6}Li, Coulomb breakup process in ^{208}Pb(^{6}Liαd) ^{208}Pb, ^{6}Li polarization effect 2—2816
^{6}Li excited states decay 2—8315
^{7}Li, Coulomb excitation of $^{1}/_{2}{}^{-}$ state, role of α+t channel 2—27962
^{7}Li, polarizability from Coulomb excitation 2—18087
Mg (A=24, 26), giant resonance formation in (γ,xn) reaction 2—38570
^{24}Mg, deformation from electron scattering 2—11783
^{24}Mg, excitation energies of low-lying states 2—31424
^{26}Mg, excitation energies of low-lying states 2—31424
^{97}Mo, Coulomb excitation using α-particle and ^{16}O projectiles, level structure investigation 2—34952
^{14}N, dipole excitations calc. 2—21376
^{15}N, dipole excitations calc. 2—21376
^{15}N(γ,p)^{17}C, 19.6—38.3 MeV, proton spectra obs. at giant resonance energies cross-sections 2—5684
^{93}Nb giant dipole states, photonuclear reaction study 2—2713
^{93}Nb lower levels Coulomb excitation with ^{16}O ions from 25 to 42 MeV 2—14948
Nd, A=141, 143, coupled particle-pairing vibrational states excited via (p,t) reactions, level assignments made 2—11765
^{58}Ni, substate excitation of 2^{+} state by (p,p$'\gamma$) inelastic scatt. 2—34941
^{58}Ni(^{16}O, ^{16}O$'$)^{58}Ni*, 34-58 MeV obs., interference between Coulomb and nuclear excitation 2—35083
^{16}O, many-particle excited states, calc. of energies, quadrupole moments and shapes 2—8283
^{18}O inelastic electron scattering cross sections for excitation of levels below 6.0 MeV measured 2—8326
Os, A=186,188,190,192, Coulomb excitation of 2^{+} states by ^{4}He, p and ^{16}O, B(E2) values 2—18142
^{208}Pb, and neighbouring nuclei, particle-oscillation coupling 2—14958
^{208}Pb, electron excitation of low-lying states 2—11778
Pd (A=104, 106), levels excited in (α,xn) reactions 2—24166
Pt, A=192,194,196,198, Coulomb excitation of 2^{+} states by ^{4}He, p and ^{16}O, B(E2) values 2—18142

Nuclear excitation continued
^{196}Pt, population of 0^{+} states by (p,t) reaction 2—34920
Pu (A=242, 244), population of 0^{+} states by (p,t) reaction 2—34920
^{239}Pu, isomer states, spontaneously fissioning, excitation in inelastic scatt. of γ quanta 2—15026
Rb, giant dipole states, photonuclear reaction study 2—2713
^{190}Re, excitation of 3 min activity using 14.8 MeV ^{190}Os (n,p) reaction 2—38616
^{103}Rh negative parity levels, Coulomb excitation with ^{4}He and ^{16}O ions 2—18117
^{32}S, excitation energies of low-lying states 2—31424
^{32}S, particle-hole excitation and surface excitation coupling 2—2668
^{34}S, excitation energies of excited states, γ-ray energy meas. 2—11724
Sc (A=48, 50), strongly excited 1^{+} states, obs. in ^{46}Ca(^{3}He,p)^{48}Sc and ^{48}Ca(^{3}He,p)^{50}Sc reactions 2—34937
Se, even isotopes, excitation cross sections of first 2^{+} levels in (n,n$'\gamma$) reactions 2—28043
^{80}Se, initial state excitation by thermal neutron capture 2—11843
^{25}Si, excited state obs. using reaction ^{28}Si(^{3}He, ^{6}He)^{25}Si at 70.4 MeV 2—34923
^{28}Si, deformation from electron scattering 2—11783
^{28}Si, shell model calculations of excitation spectrum 2—21384
^{30}Si, excitation energies of low-lying states 2—31424
^{151}Sm+^{35}Cl, Coulomb excitation by 50 MeV ^{35}Cl ions, B(E2) values of states populated 2—18126
^{124}Sn, excitation of particle-hole states by proton inelastic resonance scatt. 2—38513
Sr giant dipole states, photonuclear reaction study 2—2713
^{181}Ta, reactions induced with 40-110 MeV ^{11}B ions, excitation functions and recoil ranges determ. 2—11874
^{99}Tc, quantum characteristics of excited levels 2—11756
^{99}Tc Coulomb excitation with 52-64 keV ^{35}Cl ions, deduced level structure and lifetimes 2—18115
Th (A=230, 232), population of 0^{+} states by (p,t) reaction 2—34920
^{230}Th, deformation parameters and E4 transition probabilities from Coulomb excitation expt. 2—8313
^{205}Tl, excitation and resonance processes rel. to L and K X-ray emission from muonic ^{205}Tl 2—18371
U (A=234, 236, 238), population of 0^{+} states by (p,t) reaction 2—34920
^{238}U, deformation parameters and E4 transition probabilities from Coulomb excitation expt. 2—8313
^{49}V, study of excited states with ^{48}T,(p,γ)^{49}V reaction 2—27975
W, A=182,184,186, Coulomb excitation of 2^{+} states by ^{4}He, p and ^{16}O, B(E2) values 2—18142
W (A=182, 184, 186), population of 0^{+} states by (p,t) reaction 2—34920
^{130}Xe, energy level excitation during γ decay of ^{130}I, ^{130*}I 2—24184
^{89}Y, resolved states by 61.2 MeV protons, differential cross sections 2—21429
^{89}Y giant dipole states, photonuclear reaction study 2—2713
^{68}Zn, initial state excitation by thermal neutron capture 2—11843
^{90}Zr, giant dipole resonance, evidence for isobaric spin splitting 2—38561
^{90}Zr, resolved states by 61.2 MeV protons, differential cross sections 2—21429
^{90}Zr giant dipole states, photonuclear reaction study 2—2713

Nuclear explosions *see Explosions/nuclear*

Nuclear field theory *see Field theory, quantum*

Nuclear fission
see also Explosions/nuclear; Nuclear reactors, fission; Photofission
^{232}Th, independent yields of ^{133}I, ^{134}I and ^{135}I, reactor neutron induced 2—5727
^{232}Th neutron-induced fission, search for intermediate substructures in the fission cross section 2—31608
A=180-212, fission barriers calc. in two centre shell model using Strutinsky prescription 2—11876
A=200 nuclei, fragment shell influences calculated in improved two centre model 2—11877
A<226, influence of shells and pairing on the fission probabilities 2—31594
actinide nuclei, evidence for 2 shape isomers from fission studies in double humped barrier region 2—24149
actinide nuclei, fragment shell influences calculated in improved two centre model 2—11877
actinide region threshold energy, magic neutron number at 152 2—2819
asymmetric two centre shell model 2—31597
barrier, associated nuclear structure 2—21353
barriers, inclusion of axial asymmetry 2—24245
binary and ternary, distribution of initial fragment kinetic energy, statistical theory 2—8367
burn-up, nuclear data requirements for det. by chemical means 2—552
cross section, calculation method 2—15023
data analysis, using two part computer programme ISIS 2—5718
energy regain in laser heating of D-T plasma by mechanical magnetic accumulation 2—31983
heavy and superheavy, binary fission properties 2—38658
heavy ion scattering as tool for fission/fusion relationship 2—11697
heavy nuclei, fission barrier heights 2—27968
heavy nuclei, potential energy of deformation, fission barrier hts. 2—31595
intra-nuclear cascade calculations, inclusion of fission and charged-particle emission 2—34999
isomeric states in deformed nuclei, shell energies 2—14916
kinetic-energy operator, coordinate-dependent mass parameters 2—31591
low energy photofission of heavy elements, barrier heights 2—28091
mass asymmetry, interpretation based on deformation energy surfaces 2—31590
medium mass nuclei, search for spontaneous-fission isomerism 2—31600
meteorite Angar dos Reis origin of fossil tracks 2—14006
near barrier, induced by dipole and quadrupole photons 2—28090
neutron induced, as threshold detector for neutron spectra 2—27853
neutron induced, fission fragment anisotropy effect on measured prompt neutron energy and ang. distrib. 2—35090
oriented fissile nuclei, description of ^{3}H cryostat for use in research of fission phenomena 2—30720
proton- and γ-ray-induced 2—11879
quantum dynamic approach to asymmetry of process 2—31596
rate measurement, solid state track recorders 2—8411
ratio of fission to (n, 2n) in fast reactors 2—31606
resonance parameters of fissionable nuclei 2—8366
shape, surface, three parameter description 2—24243
spark chamber meas. of spatial velocity distrib. in critical assembly channel 2—5602

Nuclear fission continued
spherical and deformed nuclei, application of shell-correction approach to fission process 2 -34884
spontaneous, observed in a mercury source, superheavy element Z=112 2—2820
spontaneous fissioning isomers, review 2—21455
subthreshold neutron-induced, doorway parameters of resonances 2—38663
subthreshold reactions, interpretation by nuclear deformation theory 2—15022
superheavy elements formed by nucleosynthesis in universe 2—33578
superheavy nuclei, influence of octupole vibrations, potential energy surfaces 2—18244
superheavy nuclei, potential energy of deformation, fission barrier hts. 2—31595
superheavy nuclei, shell-model calculations of fission decay widths and probabilities 2—18245
superheavy nuclei, stability against spontaneous fission, potential energy surface calc. 2—21454
temperatures as function of average number of neutrons from fission 2—5716
ternary, scission point conditions, calc. for most probable fission mode 2—8369
track dating technique, fossil radiation damage, U concentration in muscovites 2—7227
trans bismuth nuclei, fission fross sections and spallation yields, >0.6 GeV 2—31593
two-mode mechanism, analysis of peak-to-trough ratios 2—510
Ag, proton induced fission, fragment energy spectra 2—2828
Ag binary fission cross- section induced by 29-GeV ^{14}N ions meas. 2—35093
Am, A=245, 246, spontaneously fissioning isomers identification 2—31602
^{232}Am, neutron-deficient nucleus, explanation of retarded fission 2—31601
^{234}Am, neutron-deficient nucleus, explanation of retarded fission 2—31601
^{242}Am from ^{241}Am fast neutron radiative capture, spontaneous fission cross-section 2—11847
^{243}Am, isomer states, spontaneously fissioning, excitation in inelastic scatt. of γ quanta 2—15026
^{244}Am from ^{243}Am fast neutron radiative capture, spontaneous fission cross section 2—11847
Au, binary fission cross-section induced by 29-GeV ^{14}N ions meas. 2—35093
^{197}Au, heavy-ion induced fission energetic balance 2—31610
^{8}Be$\rightarrow 2\alpha$, relevance of ^{8}Be structure in spherical shell, deformed shell and cluster models 2—14931
Bi, binary fission cross-section induced by 29-GeV ^{14}N ions meas. 2—35093
^{209}Bi, 77.3 MeV-^{4}He induced fission, mass and energy distribs., test of liquid drop model 2—24249
^{209}Bi, charged particle induced, determ. ^{134}Cs and ^{115}Cd isomer ratios 2—11884
^{209}Bi, heavy ion induced fission energetic balance 2—31610
Bk, A=242, 244, spontaneously fissioning isomers identification 2—31602
^{239}Cf, neutron induced, cross section 2—38662
^{249}Cf, induced by neutrons at 0.16 to 1.6 MeV, cross section 2—15025
^{249}Cf, neutron-induced, mass distribution of fission products 2—5723
^{249}Cf, thermal-neutron fission cross sections and resonance integrals meas. 2—28088
^{249}Cf, thermal neutron induced fission, fractional independent yield of ^{140}La, nuclear charge distrib. 2—35091
^{252}Cf, charge and mass distrib. determ. 2—2829
^{252}Cf, spontaneous, determ. total energy and angular distribution of emitted fission neutrons 2—8375
^{252}Cf, spontaneous fission, obs. of γ-rays from fission fragments 2—31611
^{252}Cf asymmetrical fission, potential energy of heavy nuclei 2—8376
^{252}Cf loaded fission ionization chamber, timing resolution 2—31373
^{254}Cf asymmetrical fission, potential energy of heavy nuclei 2—8376
Cm, A=243, 245, spontaneously fissioning isomers identification 2—31602
^{242}Cm, two-centre shell model, asymmetry in the fission process 2—15020
^{244}Cm, thermal-neutron fission cross sections, and resonance integrals meas. 2—28088
^{245}Cm, thermal-neutron fission cross sections and resonance integrals meas. 2—28088
^{246}Cm, thermal-neutron fission cross sections and resonance integrals meas. 2—28088
^{247}Cm, thermal-neutron fission cross sections and resonance integrals meas. 2—28088
^{248}Cm, thermal-neutron fission cross sections and resonance integrals meas. 2—28088
^{254}Es, thermal-neutron fission cross section and fission resonance integral meas. by plastic fission track recorders 2—35087
Fm isotopes, mass division symmetry 2—21453
^{254}Fm, two-centre shell model, asymmetry in the fission process 2—15020
^{227}Np, neutron-deficient nucleus, explanation of retarded fission 2—31601
^{228}Np, neutron-deficient nucleus, explanation of retarded fission 2—31601
^{237}Np, neutron induced fission of polarized nuclei, simultaneous determination of J and K quantum numbers 2—35089
^{237}Np, neutron induced through double humped fission barrier, analysis of resonances in 20-60 eV range 2—2824
^{237}Np aligned nucleus, neutron induced fission, determ. directional distrib. of fission fragments 2—35049
^{210}Po, two-centre shell model, asymmetry in the fission process 2—15020
Pu, A = 239-241, absorption to fission rate 2—498
Pu, A=238, 239, neutron induced fission, ang. distrib. and kinetic energies of fragments 2—28094
^{237}Pu, properties of two spontaneously fissioning isomers studied, half-lives of energy dist.meas. 2—2821
^{238}Pu, spontaneous fission half-life 2—31598
^{238}Pu nuclear characteristics and use as fuel in electric generators and heater units on spacecraft 2—8371
^{239}Pu, 0-1.6 MeV neutron induced, energy balance analysis of $\bar{\nu}$ values 2—38661
^{239}Pu, det. of ^{238}U capture rate in mixed oxide fast reactor lattices 2—35103
^{239}Pu, fragment yield, neutron induced fission 5.5 and 15 MeV 2—5721
^{239}Pu, isomer states, spontaneously fissioning, excitation in inelastic scatt. of γ quanta 2—15026

Nuclear fission continued
^{239}Pu, neutron induced fission, total delayed neutron yields as function of energy 2—31604
^{239}Pu, ratio of neutron cross sections of radiation capture and fission, $\lesssim 50$ keV 2—8347
^{239}Pu and ^{235}U cross sections ratio meas. at 30 keV and from 0.5 to 5.4 MeV 2—28089
^{239}Pu neutron number obs. in resonance neutron induced fission 2—5720
^{239}Pu(d,p), two-centre model, cross-section calc., evidence for intermediate structure 2—38653
^{240}Pu, total spontaneous and isomer fission half-lives 2—31599
^{241}Pu, evaluation of neutron cross-sections in unresolved resonance region 2—38620
^{242}Pu, neutron induced fission, total delayed neutron yields as function of energy 2—31604
^{226}Ra, charged particle induced, determ. ^{134}Cs and ^{115}Cd isomer ratios 2—11884
^{226}Ra asymmetrical fission, potential energy of heavy nuclei 2—8376
^{226}Ra neutron induced, 4—10 MeV, angular anisotropy of products 2—5722
^{181}Ta, 77.3 MeV-^{4}He induced fission mass and energy distribs., test of liquid drop model 2—24249
Th, production cross sections for ^{84}Rb, ^{86}Rb, ^{132}Cs and ^{136}Cs 2—2826
^{232}Th, 3 MeV neutron induced fission yield, mass distribution determ. 2—5719
^{232}Th, charged particle induced, determ. ^{134}Cs and ^{115}Cd isomer ratios 2—11884
^{232}Th, intermediate structure in photofission cross section, competition with photoneutron process 2—38575
^{232}Th 40-60 MeV proton induced fission, meas. of Rb and Cs isotopic cross sections 2—11880
^{232}Th asymmetrical fission, potential energy of heavy nuclei 2—8376
^{201}Tl, shell effects on saddle pt. deform. 2—34978
^{235}U and ^{239}PU cross sections ratio meas. at 30 keV and from 0.5 to 5.4 MeV 2—28089

products
alpha-particle accompanied fission, correlations 2—2832
angular correlations of fragments and prompt gamma-rays 2—2823
angular distrib. and kinetic energies of fragments from neutron induced ^{238,239}Pu fission 2—28094
charge and mass distrib. determ. for ^{252}Cf fission 2—2829
correlation of most probable kinetic energy with Coulomb energy and $\bar{\nu}_p$ 2—24246
delayed neutron probabilities and calculated cumulative fission yields 2—28096
delayed neutrons, quantitative assay of fissionable materials 2—28097
dipole excitations at scission point studied in a classical model 2—18248
even even fragments from ^{235}U, equilibrium deformation and quadrupole deformation parameter 2—28093
fragment anisotropy, effect on measured prompt neutron energy and ang. distrib. 2—35090
fragment energy degradation in elementary gases and solids, semi-empirical approach 2—8373
fragment energy spectra, for proton bombardment of Ag 2—2828
fragment mass, connection with number of radiated prompt fission neutrons 2—31607
fragments, excitation energies calc. from experimental kinetic energy data 2—28095
long range fragments search following thermal neutron induced fission of ^{235}U 2—24247
migration in fuel, post-irrad. exam. techniques at Studsvik 2—38750
neutrons, average number, rel. to fission temperatures 2—5716
neutrons, delayed, energy spectrum 2—2827
neutrons, delayed, total yields as function of energy of neutron inducing fission 2—31604
neutrons, emitted from individual fragments of ^{252}Cf spontaneous fission, total energy and ang. distribution determ. 2—8375
nuclear transformations, from isotopic dilution measurements of irradiated fuel using data processing code ISODIL 2—8409
nuclei with closed shells of 50 or 82, nuclear structure det. from γ-decay of products 2—38441
prompt neutron spectra, effect of centre of mass anisotropy, validity of Terrells relation 2—24250
radioactive waste disposal, review of management and handling 2—2858
ratio obs., track counting, automatic image analysis 2—5598
release performance of reactor fuel, post-irrad. exam. techniques 2—38761
reprocessing of thermal reactor fuels 2—2857
spontaneous fission fragments of ^{252}Cf, γ-transitions meas. 2—31611
spontaneous fission isomers, excitation energies from threshold meas. 2—34894
studies using position-sensitive semiconductor detectors 2—24086
track density, automatic image analysis obs. 2—5599
transport and release in fuel, post-irrad. exam. techniques 2—38755
transuranium nuclides, formation, production and uses 2—11695
yields in accelerator neutron spectra 2—511
^{41}Ar, system for reduction of release from research reactor facility 2—38715
^{213}At, fragment mass charge distrib. 2—35085
^{87}Br and ^{88}Br as precursors for delayed neutrons, low energy spectrum 2—5728
^{115}Cd, isomer ratio measured for charged particle induced fission of ^{238}U, ^{232}Th, ^{226}Ra, ^{209}Bi, deduced framgent angular momentum 2—11884
^{249}Cf fission by thermal neutrons, neutron yield and kinetic energy of fragments 2—15024
^{252}Cf, α-particle accompanied fission, ang. correlation 2—38659
^{252}Cf, energy loss in composite systs., expt. 2—38666
^{252}Cf, energy straggling through air using heavy ion surface barrier detector 2—8374
^{252}Cf, fragment γ-ray transitions, X-ray γ-ray coincidence study 2—2830
^{252}Cf, internal conversion cascades, X-ray coincidence study 2—2831
^{252}Cf, spontaneous fission, fragment K X-ray emission and nuclear charge distribution 2—11882
^{252}Cf, spontaneous fission, K X-ray studies 2—38660
^{252}Cf fragments, energy loss measurements in elementary gases and solids as compared with theory 2—8377
^{252}Cf fragments of specified atomic numbers, study of multiplicities of K X-rays 2—11883
^{252}Cf product trace analysis in plastic sheets using electron microscopy 2—21333
^{252}Cf spontaneous fission, neutron spectrum, fine structure 2—8370

Nuclear fission continued
products continued
^{244}Cm spontaneous fission, prompt neutrons and kinetic energy of fragments 2—15021
Cs from 40-60 MeV proton induced fission of ^{238}U, ^{235}U and ^{232}Th, isotopic cross sect. meas. 2—11880
^{132}Cs, form. cross section in proton interactions with U and Th 2—2826
^{134}Cs, isomer ratio measured for charged particle induced fission of ^{238}U, ^{232}Th, ^{226}Ra, ^{209}Bi, deduced fragment angular momentum 2—11884
^{134}Cs isomers produced in α fission of ^{238}U, e.m. mass separator rel. to radiochemical 2—11881
^{136}Cs, form. cross section in proton interactions with U and Th 2—2826
^{254}Fm, fragment mass and charge distrib. 2—35085
^{258}Fm, fragment mass and charge distrib. 2—35085
^{3}H, yields and energy distrib. from thermal neutron ternary fission of ^{235}U 2—24248
^{3}He yields and energy distrib. from thermal neutron ternary fission of ^{235}U 2—24248
^{4}He, yields and energy distrib. from thermal neutron ternary fission of ^{235}U 2—24248
I extruded, produces post shutdown surges in Xe activity due to a leak in fuel element 2—8393
I independent yields in reactor neutron induced ^{232}Th fission 2—5727
^{85}Kr, in atmosphere, activity meas. 2—40972
^{94}Kr, identification, half life and γ-ray spectra 2—11886
^{140}La, from thermal neutron induced fission of ^{249}Cf, fractional independent yield 2—35091
^{186}Os, fragment mass and charge distrib. 2—35085
^{213}Pb, fragment mass and charge distrib. 2—35085
^{239}Pu, thermal neutron fission, fragment K X-ray emission and nuclear charge distribution 2—11882
^{241}Pu, yield from freshly prepared specimen 2—28087
Rb, from 40-60 MeV proton induced fission of ^{238}U, ^{235}U and ^{232}Th, isotopic cross sect. meas. 2—11880
^{84}Rb, form. cross section in proton interactions with U and Th 2—2826
^{86}Rb, form, cross section in proton interactions with U and Th 2—2826
^{87}Se, ^{88}Se, ^{89}Se, neutron emission probabilities and fission yields 2—5726
Si surface barrier detectors effects of neutron irradiation on meas. of fission fragment properties 2—27873
^{232}Th, charge distrib. 2—11878
^{201}Tl, fragment mass and charge distrib. 2—35085
U, natural, cumulative fission yields of ^{66}Ni, ^{67}Cu, ^{172}Er, ^{175}Yb, ^{177}Lu 2—35097
^{233}U, thermal neutron fission, fragment K X-ray emission and nuclear charge distribution 2—11882
^{233}U and ^{235}U, thermal neutron induced, fractional cumulative yields 2—35086
^{235}U, fragment ang. distrib. obs., saddle point transition states 2—38667
^{235}U, neutron evaporation and energy distribution in individual fragments 2—35088
^{235}U, thermal fission, energy and ang. distrib. of long range charged particles 2—35096
^{235}U, thermal neutron fission, fragment K X-ray emission and nuclear charge distribution 2—11882
^{235}U, thermal neutron induced, mass distrib. of LRP fission products 2—21457
^{235}U thermal fission fragments, primary spins study from γ-emission 2—21459
^{235}U(n,f) investigation of conversion electrons from fragments and products, evidence for $J^{\pi}=0^{+}$ first excited state of ^{98}Zr 2—11755
^{236}U, prompt neutrons from fission fragments 2—18246
^{236}U fragments, study of average emission times of K X-rays 2—11883
^{238}U, by 16 and 42 MeV protons, α-particle emission 2—35095
^{238}U, fast neutron induced, mass distrib. of LRP fission products 2—21457
^{238}U, fragment energy distribution from neutron induced fission at 1.5 to 18.2 MeV 2—18247
^{143}Xe identification, half life and γ-ray spectra 2—11886
uranium
enrichment of isotopes, review of present trends and techniques 2—3010
fuel manufacture, review of economic problems 2—2856
natural, cumulative fission yields of ^{66}Ni, ^{67}Cu, ^{172}Er, ^{175}Yb, ^{177}Lu 2—35097
natural targets, effect of (α,n) reactions on ratio of induced to spontaneous fission 2—35084
production cross sections for ^{84}Rb, ^{86}Rb, ^{132}Cs and ^{136}Cs 2—2826
ternary fission, ^{235}U, slow neutron induced 2—2822
^{236*}U, following thermal neutron irradiation of ^{235}U, search for long range fission products 2—24247
^{239}Pu, absolute meas. of α for neutron energies of 10 keV to 1 MeV 2—31603
U, binary fission cross-section induced by 29 GeV ^{14}N ions meas. 2—35093
^{233}U, 0-1.6 MeV neutron induced, energy balance analysis of $\bar{\nu}$ values 2—38661
^{233}U, 77.3 MeV-^{4}He induced fission mass and energy distrib., test of liquid drop model 2—24249
^{233}U, neutron induced fission, total delayed neutron yields as function of energy 2—31604
^{233}U, thermal neutron fission, fragment K X-ray emission and nuclear charge distribution 2—11882
^{233}U aligned nucleus, neutron induced fission, determ. directional distrib. of fission fragments 2—35049
^{233}U fragment yield, neutron induced fission 5.5 and 15 MeV 2—5721
^{234}U, thermal neutron ternary fission, yields and energy distribs. of ^{3}H, ^{4}He, ^{3}He 2—24248
^{234}U, total spontaneous and isomer fission half-lives 2—31599
^{234}U and ^{235}U thermal neutron induced, nuclear charge distrib. comparison 2—35086
^{235}U, 40-60 MeV proton induced fission, meas. of Rb and Cs isotopic cross sections 2—11880
^{235}U, absolute meas. of α for neutron energies of 10 keV to 1 MeV 2—31603
^{235}U, by thermal neutron, calc. of dipole excitation of fission fragments at scission point 2—18248
^{235}U, fragment ang. distrib. obs., saddle point transition states 2—38667
^{235}U, neutron evaporation and energy distribution in individual fragments 2—35088
^{235}U, neutron induced, evaluation of direct meas. of no. of neutrons/fission ($\bar{\nu}$) 2—5724

Nuclear fission continued
uranium continued
^{235}U, neutron induced, total cross- section fluctuations inthe keV range 2—28052
^{235}U, neutron induced fission, total delayed neutron yields as function of energy 2—31604
^{235}U, neutron number obs. in resonance neutron induced fission 2—5720
^{235}U, photofission using variable energy beams of γ-rays determ. cross section from 5-8.3 MeV 2—21458
^{235}U, thermal fission, energy and ang. distrib. of long range charged particles 2—35096
^{235}U, thermal neutron cross section 2—15023
^{235}U, thermal neutron fission, fragment K X-ray emission and nuclear charge distribution 2—11882
^{235}U, thermal neutron induced, search for long range fission products 2—24247
^{235}U, thermal neutron induced, mass distrib. of LRP fission products 2—21457
^{235}U aligned nucleus, neutron induced fission, determ. directional distrib. of fission fragments 2—35049
^{235}U equilibrium deformation and quadrupole deformation parameter of even even fragments 2—28093
^{235}U fission fragments, yields and kinetic energies depend. on energy of bombarding neutrons 2—8372
^{235}U fragments transmission in solid media 2—1446
^{235}U thermal fission fragments, primary spins study from γ-emission 2—21459
^{235}U unreflected critical assembly, neutron spectra and reaction cross sections meas. 2—38710
^{235}U(n,f) investigation of conversion electrons from fragments and products, evidence for $J^{\pi}=0^{+}$ first excited state of ^{98}Zr 2—11755
^{236}U, detection of γ-rays preceding isomeric fission induced by neutron capture in ^{235}U 2—24244
^{236}U, neutron-induced fission, high-resolution cross section meas. 2—31605
^{236}U, prompt neutrons from fission fragments 2—18246
^{236}U, total spontaneous and isomer fission half-lives 2—31599
^{236}U, two-centre shell model, asymmetry in the fission process 2—15020
^{236}U neutron resonances, fission widths, 5.45-415 eV 2—21456
^{237}U, fission barrier parameters from fission widths of ^{236}U neutron resonances 2—21456
^{238}U, 40-60 MeV proton induced fission, meas. of Rb and Cs isotopic cross sections 2—11880
^{238}U, by 16 and 42 MeV protons, α-particle emission 2—35095
^{238}U, by 2.2 GeV protons, spectra of products 2—11885
^{238}U, charged particle induced, determ. ^{134}Cs and ^{115}Cd isomer ratios 2—11884
^{238}U, fast neutron induced, mass distrib. of LRP fission products 2—21457
^{238}U, fragment energy distribution from neutron induced fission at 1.5 to 18.2 MeV 2—18247
^{238}U, heavy ion induced fission, energetic balance 2—31610
^{238}U, induced by protons of 11.2 MeV and deuterons of 10.6 MeV, distribution of nuclear charge studied using Ge(Li) spectroscopy 2—35092
^{238}U, intermediate structure in photofission cross section, competition with photoneutron process 2—38575
^{238}U, neutron induced fission, total delayed neutron yields as function of energy 2—31604
^{238}U, photofission using variable energy beam of γ-rays determ. cross sections from 5-8.3 MeV 2—21458
^{238}U, yields of ^{131}Xe, ^{132}Xe, ^{134}Xe and ^{136}Xe obs. 2—5725
^{238}U α fission at medium energy, techniques for separation of ^{134}Cs isomers 2—11881
^{239}U, absorption to fission rate determ. 2—498
Nuclear fission reactors *see Nuclear reactors, fission*
Nuclear forces
see also Field theory, quantum/meson field
A=18 nuclei, diagrams with 4p-2h intermediate states, contrib. to effective interaction 2—21378
A=18 nuclei, effective interaction, contrib. of 2 particle ladder and RPA terms 2—31416
binding Λ_{00} and Λ_{10} calculations for realistic hard-core nucleon-nucleon potentials energy of nuclear matter, Λ_{00} and Λ_{10} calculations for realistic hard-core nucleon-nucleon potentials 2—31428
binding energies, shell corrections 2—21357
binding energy, sensitivity to nucleon-nucleon phase shift at high energies 2—21356
binding energy of Λ particle, calc. using separation method 2—454
binding energy sensitivity to high energy phase shifts, range of force depend. 2—34890
bond scheme, electrodisintegration cross sections 2—8328
center of mass potential energy used in checking procedure for energy and effective charge perturbation calcs. 2—14908
charge dependence, effect on binding of ^{3}H and n-d doublet scattering length 2—11721
charge symmetry from binding energy difference of ^{3}H and ^{3}He 2—2687
collective treatment of pairing Hamiltonian 2—2667
compression of nuclear matter, effect of increase of depth of potential wells and NN attraction 2—2814
deformation producing character of T=1 interactions 2—38436
deformed even even nuclei, potential energy expressions 2—21370
deuteron optical potential assuming effective interaction between nucleons 2—28061
effective two-body interaction in 1f-2p shell expressed in basis of SU$_3$ representation 2—18064
equivalent local potential in soluble model, full exchange effects, α-α scatt. 2—31414
equivalent two body interactions with specified bound state wave functions 2—31419
exchange currents and soft photon emission 2—2666
few-body problem formalism 2—14907
finity violating internucleon potential, pion exchange contributions 2—34877
G-matrix expansion of nuclear effective interaction, spectroscopic average of higher-order terms 2—34879
generator coordinate description of nucleus-nucleus scattering formulated 2—24194
Hamada-Johnston potential for quasi free peak for ^{2}H(p,2n)n reaction, off-shell spectator model 2—18189
harmonic oscillator relative coordinate transformation coeff. 2—38431
heavy nuclei, potential energy of deformation, fission barrier hts. 2—31595

Nuclear forces continued
heavy nuclei, single particle model calc. of total energy surfaces 2—27968
heavy-ion reactions, search for quasimolecules around Coulomb barrier 2—15016
internucleon potentials equivalence 2—34882
K-harmonic method, accuracy 2—14911
K-harmonics method in few nucleon problem 2—21358
local hard core potentials, unitary pole expansion of off shell t-matrix elements 2—14909
many body problems, difficulties in applying N-N interactions 2—11707
N-body cluster problem, Jastrow wave function 2—14918
neutron matter, magnetic properties 2—30482
neutron-proton $^1S_0$ interaction, separable potential model 2—18065
neutron-proton interaction, separable model potential 2—34880
non-central effective forces between nucleons 2—21355
nonstatic, nucleon-nucleon scattering, triplet state in momentum space 2—31415
nuclear matter, approximation to reaction matrix 2—31425
nucleon-nucleon correlations, short range in $^4He(\mu^-,n\nu)^3H$ 2—28024
nucleon-nucleon interaction, experimental study 2—8267
nucleon-nucleon interaction, optimal relativity effects 2—27943
nucleon-nucleon potential, momentum space calc. and helicity formalism 2—5631
nucleon-nucleon potential used to calculate p - ^{3}He scattering states 2—24210
nucleon-nucleon potentials from coupled partial waves using Marchenko theory 2—27942
nucleon-nucleon T-matrix factorization for realistic hard core potential 2—8269
nucleon-pair correlations effects on Monte Carlo intranuclear-cascade simulations 2—11708
nucleons behaviour inside nucleus 2—14903
optical potentials, nucleon-nucleus, $1/\gamma$ velocity dependence 2—24197
P-odd, CP violation in renormalizable weak interaction theory 2—38433
pairing correlations, simplified generator coordinate treatment 2—31417
pairing Hamiltonian, collective treatment, T=1 case 2—27941
phase shift equivalent momentum dependent potentials, off-shell effects 2—18063
pion-nucleon coupling const., allowed range 2—38434
potential, relation to nuclear matter in inelastic alpha-nucleus scattering 2—8355
range of force, phase shift, binding energy, relation 2—31427
reaction matrix, a method for fast convergence 2—31412
reaction matrix equation for nuclear matter, simple solution 2—18067
real potential well depth ambiguities in optical model analyses of elastic scattering 2—11856
realistic nucleon-nucleon potential formulation of Thomas-Fermi method for structure calcs. 2—31426
relativistic eikonal approximation in nucleon-nucleon scattering 2—31413
residual two-body interactions, pairing and quadrupole-pairing type 2—11699
saturation, asymptotic conditions 2—21354
separable single-particle Hamiltonian and its equivalent 2—27939
separation energies, analogue of Koopmans' theorem in renormalized Brueckner-Hartree- Fock theory 2—18062
spherical nuclei, Coulomb displacement energies 2—18066
spherical nuclei, Hartree Fock calcs. with Skyrme's interaction 2—27947
spin-spin interaction in nucleon-nucleus scattering investigated in optical model potential 2—14980
superheavy nuclei, potential energy of deformation, fission barrier hts. 2—31595
t-matrix for local potentials with hard-core, unitary pole expansion 2—34881
tensor correlations in nuclear matter evaluation of three body contributions to factor cluster expansion of energy expectation value 2—27949
tensor coupling, boundary condition model T matrix, derivation 2—11705
three body cluster energy using correlated wave function 2—14910
three body system, excited states calc. in local potential model 2—24132
three nucleon parameters, low energies, insensitivity to internucleon repulsion 2—2665
three-nucleon problem, nearly separable potentials 2—18068
three-nucleon system, matrix elements in K-harmonic method 2—38432
total binding energy of protons, impulse approximation and (p,2p) reaction considered 2—11714
two body pairing interactions, application of method for determ. ground state of Hamiltonian 2—11709
two phase shift equivalent potentials, 3 body correlation corrections to saturation curves 2—31418
two-body interaction, matrix elements and truncation in config. space 2—38435
two-nucleon interaction, off shell effects of high energy part 2—11710
two-nucleon potential, charge-dependent, with Yukawa radial dependence 2—27940
two-nucleon T matrix half off energy shell, expansion into power series 2—28025
two-pion-exchange nuclear potential calc. using dispersion theory 2—31411
N-N bound state problem in momentum space, helicity representation 2—34878
NN phase parameters, ambiguity near 330 MeV 2—452
NN scatt., low-energy, relativistic effects, soln. of Bethe-Salpeter eqn. 2—2573
nn scattering length from 13.95 MeV $^3H(n,2n)^2H$ reaction 2—2786
^{75}As, existence of parity non conserving nuclear potential confirmed in γ transition study 2—11776
^{12}C, Brueckner Hartree Fock calc. using density dependent effective interaction, binding energy estimate 2—11727
Ca, isotopes, phenomenological effective two body interaction 2—14943
^{44}Ca, structure from Hamada-Johnston and Tabakin interactions 2—31464
^{157}Ge, perturbation effect on K- absorpt. 2—38628
^{2}H, optical model potential derivation using Glauber theory 2—18216
^{3}H, binding energy, contribution of two-pion exchange three-body force 2—5643
^{3}H, binding energy, reference spectrum method 2—18085
^{3}H, binding energy from ^2H+n collisions in Faddeev formalism with local potential 2—21437
^{3}H, binding energy in unitary pole approx. using hard core pot. 2—34905
^{3}H, p-wave weight, role of LS and $(LS)^2$ forces 2—21358

Nuclear forces continued
^{3}He, Coulomb energy deduced by symmetry relation from charge form factors 2—14928
^{4}He, binding energy, calc. using method of 9-dimensional harmonics 2—461
^{4}He, binding energy, reference spectrum method 2—18085
^{4}He, p-wave weight, role of LS and $(LS)^2$ forces 2—21358
^{180}Hf, parity admixtures in nuclear forces γ transition study 2—31489
^{65}Ho, Coriolis coupling between [411 spin up] and [411 spin down] bands 2—21396
^{72}Kr and neighbouring isotopes, oblate groundstate deformation predicted by Strutinsky-type calcs. of potential energy 2—24163
$_\Lambda{}^9$Be, binding energy calc., variational principle, $\alpha-\alpha-\Lambda$ structure, Λ-N force 2—31452
^{20}Ne, Brueckner Hartree Fock calc. using density dependent effective interaction, binding energy estimate 2—11727
$^{16}O-^{16}O$ potential, dependence on ansatz prescribing density of compound system 2—11869
^{16}O, binding energy, third-order contribution 2—462
^{16}O, binding energy calculations and their dependence on the treatment of the Pauli operation in the G-matrix 2—31448
^{16}O, Brueckner Hartree Fock calcs., using density dependent effective interactions 2—11729
^{208}Pb, effective interaction between 2 phonon $J^\pi=O^+$ states, diagrammatic perturbation treatment 2—2739
^{154}Pm evidence for violation of Gallagher-Moskowski rules using Nilsson model 2—27986
Sm, 50.8 MeV proton scattering using simple optical model and reformulation DWBA and coupled channels 2—27985
^{181}Ta, parity admixtures in nuclear forces γ transition study 2—31489
^{159}Tb, parity admixtures in nuclear forces γ transitions study 2—31489
^{203}Tl, existence of parity non conserving nuclear potential confirmed in γ transition study 2—11776
^{203}Tl, parity admixtures in nuclear forces γ transition study 2—31489
^{182}W, parity admixtures in nuclear forces γ transition study 2—31489

Nuclear fusion
see also Explosions/nuclear; Nuclear reactors, fusion; Thermonuclear reactions
complete, induced by Kr^{23+} and Kr^{24+} ions, synthesis of superheavy nuclei 2—2825
configurational properties of fusioning plasma, confinement by fuel injection 2—32014
control of reaction and data collection by computer in plasma exps. 2—15019
controlled, application of laser produced dense plasmas 2—24783
controlled, reactor design 2—28129
controlled, use of high-powered N_2-CO_2 lasers 2—24267
controlled fusion power, future outlook 2—5738
electron beam accelerated ions, neutron output enhancement 2—35504
feasibility of steady state Tokamak operation 2—39147
fusion, induced by Kr^{23+} and Kr^{24+} ions, synthesis of superheavy nuclei 2—2825
heavy ion scattering as tool for fission/fusion relationship 2—11697
in high ion density artificial plasma, previously accelerated D ions, electrons 2—38665
ice, trigger criterion for steady fusion detonations 2—5717
laser beam production of fusion, review 2—2818
laser-produced plasma, heating mechanisms 2—8960
with lasers, sudden vaporization, heating of solid D-T pellet by very high power laser as yet unmade 2—24242
mirror containment problem, direct re-injection solution 2—8953
neutron yield from solid D_2 irrad. by laser beam 2—32052
plasma, fusion energy for a plane thermal wave during laser heating 2—39163
in plasma, laser focussing in conduction heating, spherical electron thermal wave 2—18592
in plasma, laser heating enhancement by addition of heavy impurities to target 2—18591
plasma physics, developments, fusion reactor technology problems 2—38703
plasma physics and controlled fusion research-conference (Vienna, 1971) 2—24644
radiological impact 2—24298
reactor blankets, neutron physics and thermodynamics 2—31618
reactors, environmental and economic advantages 2—28118
research apparatus use of Ti evaporation pump 2—41376
research in USSR, Tokamak systems 2—15018
superheavy element synthesis 2—31592
torus devices for thermonuclear fusion equipment 2—11915
^{116}Cd, ^{84}Kr induced fusion reactions, effective threshold and minimum distance of approach meas. 2—24241
D-T plasma, thermal explosion analogy 2—509
^{72}Ge, ^{84}Kr induced fusion reactions, effective threshold and minimum distance of approach meas. 2—24241
^2H-^3H laser triggered, maximum energy release calc. 2—6077
^2H-^3H plasma, microfusion during laser heating process, methods for raising the energy recovery 2—24653

Nuclear induction *see Nuclear magnetic resonance and relaxation*

Nuclear interactions *see Collision processes; Field theory, quantum/interactions; Elementary particles; Nuclear reactions and scattering*

Nuclear isomerism
see also Isomerism; Nucleus/energy levels
actinide nuclei, evidence for 2 shape isomers from fission studies in double humped barrier region 2—24149
ammonium salts, spin symmetry sites, p.m.r. obs. 2—40776
half-life measurement of short-lived isomers 2—27980
medium mass nuclei, search for spontaneous-fission isomerism 2—31600
spontaneous fission isomers, excitation energies from threshold meas. 2—34894
^{222}Ac, 66 sec isomer from bombardment of Pb with ^{18}O, decay with α emission 2—34994
Am, A=245, 246, spontaneously fissioning isomers identification 2—31602
^{130}Ba, isomeric transition $8\rightarrow6^+$, description using model 2—11762
Bk, A=242, 244, spontaneously fissionig isomers identification 2—31602
Cm, A=243, 245, spontaneously fissioning isomers identification 2—31602
^{190}Hg, 24.5 ns isomer, $^{181}Ta(^{14}N, 5n)$ study 2—38523
^{199}Hg, deday of $13/2^+$ obs. 2—5668

Nuclear isomerism continued
^{199m}Hg, hyperfine structure and isomeric shift 2—34977
^{55}Mn(γ,3n)^{52m,g}Mn, isomeric cross section ratios 2—24202
^{193}Os, investigation of β and γ ray spectra 2—18144
^{152}Pm, decay of isomers 2—31507
^{154}Pm, decay to levels of ^{154}Sm 2—18166
^{84}Rb isomer ratios, residual effects during ^{85}Rb de- excitation 2—31585
^{85}Rb(γ,n)^{84m,g}Rb, isomeric cross section ratios 2—24202
^{85}Rb(n,2n)^{84m,g}Rb, isomeric cross section ratios 2—24202
^{117}Sb, g-factor meas. of isomeric state 2—5662
^{45}Sc(γ,n)^{44m,g}Sc, isomeric cross section ratios 2—24202
^{45}Sc(n,2n)^{44m,g}Sc, isomeric cross section ratios 2—24202
^{115}Sn, g-factor meas. of isomeric state 2—5662
^{85}Sr isomer ratios, residual effects during ^{85}Rb de- excitation 2—31585
^{150}Tb, new 5.8 min isomer, β decay to ^{150}Gd excited states 2—31506
Te, separation into ground and metastable state isomers, γ-ray spectra 2—2719
^{236m}U, shape isomer, production in ^{235}(d,p) reaction via decay of class I states 2—11782
^{86}Y isomer ratios, residual effects during ^{85}Rb de- excitation 2—31585
^{87}Y isomer ratios, residual effects during ^{85}Rb de- excitation 2—31585

Nuclear magnetic resonance and relaxation
see also ENDOR; INDOR; Knight shift; Molecules/nuclear coupling Nuclear acoustic resonance; Proton magnetic resonance; Spin-lattice relaxation; Spin-spin relaxation
1,2-dichloroethane, liquid, p.m.r. obs., rel. to mol. motion 2—35794
AB-special type systems, with chemical exchange, root locus diagrams 2—14348
acetamide-^{15}N, solvent and temperature effects 2—15346
acetic acid single crystals, deuteron NMR spectra meas. determ. quadrupole coupling const. and asymmetry factors 2—20155
acetonitrile liquid, comparative study of quasielastic neutron scattering and relaxation 2—1073
N-acetyl- phenylhydroxylamine and its methyl ether, study of hindered internal rotation 2—38955
acetylene crystal, second moment, molecular motion 2—7147
acetylenes, linear, ^{13}C chem. shift 2—8723
actinide cpds., spin- lattice relax. in paramagnetic state, model 2—7009
alkali metal, ultra sound effect on Knight shift 2—16655
alkanecarbodithoic acids, partial assoc. in form of dimers by hydrogen bridges 2—24500
alloy, dil., cubic, elec. field gradients 2—10539
amide solution, in water, structure study 2—6255
amides, ^{15}N and ^{13}C Fourier spectra, coupling constants, shifts 2—6262
amine, in solution, molecular dynamics 2—6256
γ- aminobutyric acid, configuration 2—8730
amorphous and polycryst. solids, enhancement due to dynamic polarization produced by e.s.r. centre 2—40771
angular correlation of two gamma rays in asymmetric elec. field grad., effects of static and time depend quadrupole interactions 2—458
aniline, partially deuterated derivatives, incremental aromatic solvent induced shifts 2—18488
aniline solutions, molec. association investigation 2—22008
anthracene, proton relax. by excitons, low temp. 2—10277
antiferromagnetic transition metal fluorides, study of mixed crystals 2 40543
antiferromagnets nonmetallic type properties review 2—33346
apparatus for n.m.r. at low cost, use of earth's magnetic field and audio amplifiers 2—37863
aqueous solutions, ^{35}Cl, ^{37}Cl, ^{79}Br, ^{81}Br, determination of magnetic moments 2—22007
autobenzene, partially deuterated derivatives, incremental aromatic solvent induced shifts 2—18488
AX_2 system, proton cross relaxation effect 2—765
azidotriphenyl derivatives of group IV elements, bonding investigation 2—15395
p-azoxyanisole, phase transform., pressure effects, spectra 2—6206
benzene, ^{13}C n.m.r. chemical shift anisotropy 2—38964
benzene, r.f. irradiation effects on steady state Zeeman and dipolar energies 2—30032
benzene, spin echo in liquid phase 2—35790
benzene on NaY-zeolite, proton relax., −140 to 80°C 2—26086
benzenes, trisubstituted. additivity relation for proton-proton coupling consts. 2—38961
benzenoid hydrocarbons, non-planar condensed, p.m.r., theory of chemical shifts 2—24494
benzonitrile, geometric distortion studied by high-resolution n.m.r. in the nematc phase 2—31840
3,4 benzophenanthrene, p.m.r. spectra, determ. chemical shifts, coupling constants at infinite dilution in CCl_4 2—24507
3,4-benzophenanthrene, p.m.r. spectra, determ. chemical shifts, coupling constants at infinite dilution in CCl_4 2—24507
2,1,3-benzothiadiazole, in liq. cryst. phase, proton skeleton geometry, HCC angles 2—8566
benzyl fluorides, inter and intramolecular movements studied by distortion in n.m.r. signals from ^{19}F 2—24512
bihalide ions in solution, formation equilibria and proton shieldings studied by proton NMR 2—35789
biologically important aromatic acids 2—35344
biphenyl type crystal, anomalous dipolar relaxation due to slow motion 2—7000
4,4-bis(alkoxy)azobenzenes homologous series of nematic liquid crystals, relaxation 2—28898
5,5'-bisisoxazole in liquid crystals, NMR spectra study, interpretation based on conformational equilibrium 18493 2—18493
Bloch equations, matrix formulation, inclusion of indirect spin-spin coupling in first-order spectra 2—22852
bromobenzene, partially deuterated derivatives, incremental aromatic solvent induced shifts 2—18488
2-bromothiazole, double-quantum effects in p.m.r. spectrum 2—38969
butane-d_{10}, deuteron quadrupole coupling constant meas. 2—10568
1,3-butanediol, pressure and temp. studies of n.m.r. translational relaxation 2—35795
carbonyls of group VIb metals, ^{13}C n.m.r. 2—28268
chemical exchange, multi-site, nucl. spin transfer, rate meas. 2—13561
chemical exchange produced dependence of T_2 on Carr-Purcell separation 2—37023
chemical shift, diamag. and paramag. contribs., estimation from core-electron (photoelectron) spectroscopy 2—35297
chemical shift reagents, use in resolution of overlapping lines 2—5304

Nuclear magnetic resonance and relaxation continued
2-chloroacrylonitrile, inter- and intramolecular dipole relaxation effects in double resonance spectra 2—21671
chlorobenzene, partially deuterated derivatives, incremental aromatic solvent induced shifts 2—18488
cholesterol and thiocholesterol esters, transition temps., chemical shift obs. 2—15574
cinnamaldehyde-imines, coupling consts. 2—5967
circular mag. field effect on reson. lines 2—7812
clathrate-type double hydrates, n.m.r. study of molecular movement 2—847
completely deuterated organic compounds, ^{13}C-n.m.r., deuterium isotopic shift 2—8715
complex spin systems, transverse relaxation rates of each line, effects of homonuclear spin coupling 2—24431
coronene, reorientation of molecule in solid state, n.m.r. investigation 2—10567
crude oil, p.m.r. freq. and temp. depend. 2—9165
cyclohexane, cyclohexene on NaY-zeolite, proton relax., −140 to 80°C 2—26086
cyclohexane, spin echo in liquid phase 2—35790
cyclohexane diperoxide, chem. induced dynamic nucl. polarization, in biradical prods. 2—8756
cyclohexane-d_{11}, liquid crystalline solvent, partial deuterium substitution 2—6258
cyclononane, conformation, from ^{1}H and ^{13}C spectra 2—24522
cyclooctane, linewidth meas., self-diffusion, vacancy mechanism 2—15793
decalin, spin-lattice relax. time calc. 2—32280
dense fluid, high pressure study, intermol. forces and mol. motion 2—18789
diamagnetic crystal, magnetic impurity, relax. and n.m.r. saturation 2—10532
diazaphosphetidines, ^{19}F NMR spectra meas. and interpreted 2—28366
dibenzoylperoxide, chem. induced dynamic nucl. polarization, mag. field depend. 2—7182
1,2-dibromoperfluoropropane, ^{19}F n.m.r. spectra, conformational energy difference between gauche and trans isomers 2—28359
dichlorodi fluoromethane, interference effect in ^{19}F relax. 2—9180
dichlorodurene, relaxation times meas. interpreted in terms of molecular reorientation 2—20167
1,2-dichloroperfluoropropane, ^{19}F n.m.r. spectra, conformational energy difference between gauche and trans isomers 2—28359
diffusion mechanism in solids applic. 2—25458
difunctional derivatives, X-CHR-CHR′-Y, conformation 2—8572
1,2- dihaloalkanes in various solvents, effect of solvent on vicinal proton coupling constants 2—12240
dihalodiphenyl derivatives of group IV elements bonding investigation 2—15395
dilute spins in solids, high resolution n.m.r. by proton-enhanced nuclear induction spectroscopy 2—16653
dimethyl trichalcogenocarbonate, Se-containing, ^{1}H n.m.r. spectra, ^{77}Se-^{1}H coupling const. 2—21678
N,N-dimethylacetamide, hindered internal rot., activation parameters, line shape analysis 2—12255
N,N-dimethylformamide, hindered internal rot., activation parameters, line shape analysis 2—12255
dimethylformamide, proton, deuteron and nitrogen resonance in nematic polypeptide liquid crystals 2—31847
1,1′-dimethylmetallocenes, ^{13}C n.m.r. contact shift studies, spin delocalization 2—24531
unsym-dimethylselenourea and similar compounds, hindered rotation barrier 2—24527
p-dinitrobenzene, geometric distortion studied by high-resolution n.m.r. in the nematic phase 2—31840
diphenyl ethers, highly substituted, energy barriers to rotation about Ar-O bond determ. from n.m.r. spectra 2—38975
dipolar relax. in spin systems 2—10260
dipole-dipole system, temperature determ. 2—7028
direct method, applic. to n.m.d.r. 2—764
dispersion singularities, saturation, appl. to molecular triplet states 2—7002
double resonance, cross-relaxation 2—36999
double resonance of two 1/2 spin system, quantized field formalism 2—5302
double resonance spectrometer, synthesis of frequencies from one reference source 2—23472
dynamic critical phenomena, linewidths rel. to time depend. fluctuations above order- disorder T_c 2—19818
dynamic polarization of ^{1}H and ^{13}C at 21kG, obs. in radical solns. 2—25109
electronic structure of point defects, Mossbauer and spin resonance obs., book 2—32876
ethane-d_6, deuteron quadrupole coupling constant meas. 2—10568
ethanes, bromo-substituted, ^{13}C n.m.r. 2—21682
ethanes, disubstituted, Karplus equation failure to predict ang. depend. of J_{vic} 2—763
ethyl compounds, ^{13}C-^{13}C coupling constants 2—842
ethyl fluorides, isotopically substituted, exptl. and theoretical studies of coupling constants and chemical shifts 2—24535
ethylene- vinyl acetate copolymers, microstructure study 2—4563
ethylenes, alkyl substituted, chem. shifts, coupling consts. 2—12261
ethylenes, bromo-subsituted, ^{13}C n.m.r. 2—21682
etioporphyrins, photoreduction products, n.m.r. spectra 2—28374
ferric dithiocarbamate, paramagnetic molecule 2—5965
ferrites, microwave susceptibility down to 10^{-5}, ultrasensitive technique 2—23469
ferroelectric crysts., lattice dynamics, mol. rot. 2—37000
ferromagnet, dumped, effective spin spin interactions 2—33349
ferromagnets, nonmetallic type properties review 2—33346
finely divided solids, melting characts. determ. 2—9208
fluctuation spectra in interacting spin systems 2—37002
fluid systems, n.m.r. at critical points 2—9176
fluorinated heterocyclic compound, long range coupling consts. 2—5974
fluorobenzene, partially deuterated derivatives, incremental aromatic solvent induced shifts 2—18488
fluorochloroacetones, ^{19}F and ^{13}C satellite spectra, conformational preferences, C-F coupling const. 2—28377
fluorodichloromethane, ^{19}F rotating frame n.m.r. 2—9181
fluorotrichloromethane, ^{19}F rotating frame n.m.r. 2—9181

Nuclear magnetic resonance and relaxation continued
formaldehyde, absorption, emission and n.m.r. studies of form as function of solvent and temp. 2—35771
formic acid single crystals, deuteron NMR spectra meas. determ. quadrupole coupling const. and asymmetry factors 2—20155
free induction decay and spectrum, representation by means of pole zero diagram 2—766
free induction decay in magnetically modified solid 2—30020
free radicals, hyperfine coupling, augmented basis functions 2—21579
free-radicals, modulation effects in spin-echo signals 2—762
gas, spin-spin relax., quadrupole moments 2—12095
gas phase, relative magnitudes of second virial screening coeff. 2—9039
GdIG, hyperfine struct. of Gd isotopes 2—7140
glass, computer simulation of spectra, struct. inference 2—39435
glass, organic, relax. by non-paramag. impurities, low temp. 2—10275
glycerol, pressure and temp. studies of n.m.r. translational relaxation 2—35795
guanidinium aluminium sulphate hexahydrate, ferroelectric, molecular motion 2—7131
Hahn's echo in two-spin system solids 2—26296
halomethanes, ^{13}C relaxation, field-dependent contributions 2—28333
heptane, solid, line shape 2—30033
β-1,2,3,4,5,6-hexachlorocyclohexane, ^{1}H and ^{13}C Fourier transform spectra 2—15356
hexafluorobenzene, molecular reorientation between 77 to 270K, motional narrowing and spin-lattice relaxation time 2—26310
hexafluorobenzene, spin echo in liquid phase 2—35790
hexahelicene, p.m.r. spectra, determ. chemical shifts, coupling constants at infinite dilution in CCl_4 2—24507
hexamethylbenzene, solid, nuclear spin states associated with protons of CH_3 group 2—40783
hexamethyldisilane, solid, pulsed NMR studies of proton spin-lattice relaxation time in static and rotating frames 2—20168
hexamethylethane, linewidth meas., self-diffusion, vacancy mechanism 2—15793
hexamethylethane, solid, pulsed NMR studies of proton spin-lattice relaxation time in static and rotating frames 2—20168
hexamethylethane cryst., mol. motion obs. 2—13556
hexane-d_{14}, deuteron quadrupole coupling constant meas. 2—10568
h.f. voltages meas. 2—27386
high press. studies of liquids, probe 2—18854
high resolution spectra, analysis, book 2—18396
hydrogen bonded liquids, pressure and temp. studies of n.m.r. translational relaxation 2—35795
impure crystal, quantum mobility, spin echo damping study 2—40572
indenyl carbanion-alkali metal ion pairs, struct. determ. 2—18512
instruments, construction using modification of Fourier difference spectroscopy 2—14349
intermolecular relaxation, and mol. pair distrib., in liquid mixtures 2—6251
iodobenzene, partially deuterated derivatives, incremental aromatic solvent induced shifts 2—18488
iodoethane-d_2, quantum mechanical tunnelling effects in methyl group line shape 2—10569
Karplus equation, failure to predict ang. depend. of J_{vic} in disubstituted ethanes 2—763
lanthanide cpds., spin-lattice relax. in paramagnetic state, model 2—7009
line broadening, effect of macroscopic rot. of solid 2—26297
line broadening elimination by lowering temp., for care of N-F coupling in ^{19}F spectra 2—5306
line shape governed by time dependent Hamiltonian determ. by Green function method 2—12093
line shapes and moments for crystals and powders, numerical evaluation 2—33330
lineshape analysis using density-matrix perturbation theory for unlike-spin broadening 2—10534
lineshape theory for cryst. with paramag. impurities 2—10537
lineshift due to spin system interaction with nonresonant r.f. field 2—38833
liquid, fast passage with rotary resonance 2—9171
liquid, spin relax. by multipole interactions 2—32278
liquid, spin relax. times freq. depend., correl. time distrib. influence 2—35791
liquid cryst., Fourier spectroscopy applic. 2—9175
liquid crystal, orientational order and motion 2—15594
liquids, high pressure n.m.r. Fourier transform spectroscopy rel. to study of molec. motions and intermolec. interactions 2—9167
liquids, hindered molecular rotation, correlation time 2—25034
liquids, nuclear transverse cross relaxation, relevance to spin echo spectra 2—9168
liquids, spin rotational relaxation in one dimension, calc. of angular momentum correlation functions 2—18852
liquids, theory of symmetry, Liouville operator properties 2—8570
lithium stearate, second moments and local mag. field vals. from adiabatic rapid passage n.m.r. 2—10544
macromolecules, proton- decoupled ^{13}C n.m.r. spectra, theory of nuclear Overhauser enhancement and ^{13}C-^{1}H dipolar relaxation 2—35363
magic-angle in rot. frame, chem. shifts of solids 2—37001
magnetic space groups, n.m.r. techniques for investigating possible generation by crystallographic space groups 2—29792
magnetic surface, H_2 adsorption and ortho-para conversion 2—6365
magnetically ordered crysts., secodary nucl. spin echo effects 2—40770
manganic dithiocarbamate, paramagnetic molecule 2—5965
metal, lattice dynamics, mol. rot. 2—37000
metal, spin lattice relax. time due to nuclear quadrupole interaction, calc. 2—19931
metal, temp.-independ. spin-lattice relax. time 2—29843
methane, influence of centrifugal distortion of molecule on spin lattice relaxation in gas 2—35316
methane, solid, spin conversion obs. 2—10571
methyl cyclopropanols, structure and isomerism of rotation about C-O determ. by solvent effect of pyridine on n.m.r. 2—5968
methyl iodide, spin echo in liquid phase 2—35790
methyl naphthalene, cryst., rot., barriers of CH_3 groups 2—10573
methyl naphthalene, proton spin relaxation described by rotation of CH_3 groups 2—40786
methyl nitrate, solvent and temperature effects on ^{14}N nuclear spin relaxation 2—6259
methyl titanium halides 2—38989
2-methyl-2, 4-pentanediol, pressure and temp. studies of n.m.r. translational relaxation 2—35795

Nuclear magnetic resonance and relaxation continued
3-methyl-pyrrole, analysis of NMR spectrum, assignments of chemical shifts and coupling constants 2—12260
methylene groups, dihedral angle assignment by n.m.r. coupling constants 2—3066
1-methylpentaborane(9), determ. of B-C coupling consts. 2—24543
molecular cryst., internal mobility 2—10538
molecular crystals, optical nuclear spin polarization 2—16665
molecular crysts., lattice dynamics, mol. rot. 2—37000
molecular motion model formulae 2—40794
molecules, nuclear magnetic shielding calc. using expressions for derivatives of eigenvalues of hamiltonian 2—37616
monofluorobenzaldehydes and derivatives 2—5982
multi-site exchange theory, exptl. applic. to hindered rotation in amido-type systems 2—22853
multipole relax. in r.f. fields 2—40571
naphthalene, proton relax. by excitons, low temp. 2—10277
naphthalene type crystal, anomalous dipolar relaxation due to slow motion 2—7000
nematic liquid crystal, order parameter detn. 2—6261
nematic liquid crystal, T_1 angular dependence 2—6246
nematic liquid crystals, determ. of deuterium quadrupole coupling consts. 2—28263
nematic liquid crystals, relaxation in homologous series 2—28898
nematic solution, partially deuterated molecules, H-D dipolar coupling 2—9170
neutron induced by r.f. nucl. field, pseudo-mag. reson. 2—24138
p-nitrobenzonitrile, geometric distortion studied by high-resolution n.m.r. in the nematic phase 2—31840
nitroxide radical complexes with transition metals, and e.p.r. obs. 2—26376
n.m.r. obs. 2—6768
n.m.r. signal, analysis of form. 2—27372
nontransition element fluoride, ^{19}F diamagnetic screening, chemical shift 2—28288
nylon 66, doubly oriented, second moments of absorption spectra at 180°C compared with theoretical value 2—7148
nylon 66, investigations of chain mobilization and water mobility 2—22846
organic compounds, ^{13}C, Overhauser effect 2—15344
organic liquids, spin-lattice relaxation of ^{13}C nuclei 2—3408
organotin compounds, ^{119}Sn chemical shifts by double resonance 2—28332
oriented molecules, intramolecular motion obs. 2—5956
p-azoxyanisole, nematic, press. depend. of order parameter 2—15572
1,4-paradioxane in soln., mol. assoc. obs. 2—9172
paraffin, solidified in elec. and mag. fields, anisotropy, n.m.r. obs. 2—25939
paramagnetic molecule, isotropic n.m.r. shift, liquid and solid state 2—6250
pentahelicene, p.m.r. spectra, determ. chemical shifts, coupling constants at infinite dilution in CCl_4 2—24507
pentahelicene, p.m.r. spectra, determ. chemical shifts coupling constants at infinte dilution in CCl_4 2—24507
pepper acids, coupling constants 2—8812
perfluoromethylcyclohexane, solid, phase transitions 2—1380
perylene, possible reorientation of molecule in solid state, n.m.r. investigation 2—10567
phase transformation obs., review 2—6632
phenobarbital, N-H hydrogen bonding to electron donor, n.m.r. study 2—854
phenolic methacrylate anhydrides and i.r. and mass spectra, spectrometric data 2—28334
phenolic methacrylates and i.r. and mass spectra, spectrometric data 2—28334
phenothiazine and N-substituted derivatives, configuration determination 2—12271
phenoxy radicals, partially fluorinated, hyperfine coupling consts. and spin densities 2—18522
phenylacetic acid and derivatives 2—35344
pivalic acid, plastic crystalline phase, study of molecular motion 2—1737
pivalonitrile solns., rel. to mol. reorientation 2—9154
polar liquid, induced dielectric alignment 2—9149
polar solutes, proton chemical shifts in various solvents 2—28895
poly(*γ*-benzyl L-glutamate) in dichloromethane liquid cryst. solutions 2—28796
polyethylene, drawn, morphology and molecular motion, stress effects 2—15641
polyethylene terephthalate fibre, annealed chain folding, i.r. absorpt. spectra obs. 2—15642
polyethylenes, chlorinated, assignation of lines and analysis of Cl content 2—3130
polyformaldehyde, rigid partially deuterated, quantitative interpretation of B-n.m.r. spectra 2—6002
polymethylmethacrylate, drawn, meas. of molecular orientation by broad line n.m.r. 2—10576
polystyrene solutions in tetrachloroethylene ^{13}C Fourier transform n.m.r., effect of molecular weight on spin-lattice relaxation times 2—28901
polytypism in crysts., n.m.r. obs. 2—26298
potassium laurate-D_2O system, mesophases, mol. motion obs. 2—6212
propenes, chlorinated, rotational isomerism, steric effects, n.m.r. obs. 2—12227
N-propyl derivatives, n.m.r. spectra, study of general features by subspectral methods 2—28400
propylene-butadiene alternating copolymers, 220 MHz n.m.r. evidence of alternating sequences 2—35370
pulse technique with high sensitivity, for slowly relaxing systems 2—14347
pulsed, high resolution, new developments, review 2—7813
pulsed NMR spectroscopy, digital pulse programmer 2—37862
pulsed probe using water thermostat 2—17504
pyridine, ^{15}N and ^{13}C Fourier spectra, coupling constants, shifts 2—6262
pyridine-^{15}N 2—24550
pyrrole, ^{15}N and ^{13}C Fourier spectra, coupling constants, shifts 2—6262
quinoline, ^{15}N and ^{13}C Fourier spectra, coupling constants, shifts 2—6262
quinoline solutions, molec. association investigation 2—22008
quinolinium ion, ^{15}N and ^{13}C Fourier spectra, coupling constants, shifts 2—6262
quinoxaline, oriented in nematic phase, proton skeleton, spin spin coupling consts. 2—9183

Nuclear magnetic resonance and relaxation continued
radicals, spin coupling consts. rel. to e.s.r. hyperfine splitting consts. 2—3026
rare earth compounds, effects of high pressure on meas. 2—5100
rare earth nitrate, exchange effects, ^{1}H, ^{17}O and ^{14}N resonances 2—6254
relaxation, distinction between transverse and longitudinal relaxation times 2—24430
relaxation, role of spin symmetry conversion 2—16654
relaxation in magnetic resonance, book 2—1720
resonant density oscillation around transition metal impurity 2—30021
rotary spin echoes and line narrowing 2—20156
rotating frame relax. times calc. of weak-collision case 2—24429
ruby, of ^{27}Al and ^{17}O with dynamic polarization 2—13548
satellite lines, appl. in chemical studies 2—5906
selenophene, oriented in lyotropic mesophase, direct couplings and interproton distance 2—28409
self diffusion coefficient, from spin echo experiments 2—39721
semiconductor, group III-V cpds., lineshifts 2—10551
shielding tensor asymmetry, determ. components necessary to specify chemical shift of nucleus 2—21582
silica, adsorpt. of benzene, mobility and diffusion, n.m.r. spin echo obs. 2—35929
slow motions in solids, detection with wide-line n.m.r. 2—26295
sodium palmitate-H$_2$O system, mol. order, relax. times, self-diffusion obs. 2—35796
solid echo from spin 1/2 systems, quasiquadrupolar echoes 2—40769
solid struct., second moments method 2—26299
solids, effect of r.f. irradiation on lines, rates of dipolar and Zeeman energy creation 2—7127
spectra, motional narrowing, macroscopic and microscopic motions, rot. and concomitant motions 2—13552
spectroscopy, conference, Clayton, Australia (1971) 2—8509
spin echo, envelope modulation effect 2—26294
spin echo decay in ordered materials at low temp. 2—10535
spin echo for ^{13}C, ^{2}H, ^{1}H, and ^{19}F in small molecules in liquid phase 2—35790
spin echo techniques, terrestrial mag. field range 2—5307
spin echoes, inhomogeneous and magic sandwich, Loschmidt's paradox 2—13421
spin echoes, solids and liqs., nonexponential decay, Gaussian model, Lorentzian model 2—13420
spin echoes and their perturbations, experimental technique proposed 2—34274
spin lattice relaxation for case of anisotropic diffusion, longitudinal and transversal relaxation time determ. 2—26076
spin pair relaxation, hindered molecular rotation 2—15279
spin system in solid, Zeeman and dipole temps. in rot. frame, prolonged irrad. effects 2—33348
spin-coupling constants, inter-ring protons, calculation 2—21583
spin-echo, applic. of r.f. gate 2—20999
spin-lattice relax. in rot. frame, diffusion mechanism influence 2—10262
spin-spin coupling constants, effect of solvent molecular motion 2—18395
standardization method for ampere 2—5312
statically oriented nuclei in ferromagnetic lattices 2—36801
strain effects on coupling const. using dynamic nucl. polarization 2—10533
6-substituted purines, assignment of individual proton signals 2—5991
succinonitrile, line narrowing study of translational mol. motion 2—1738
superconductor, intermediate state, resonant u.s. absorpt. by nuclei 2—25782
surfactant+additive+water systems, mesomorphic phases 2—9096
symmetric molecules, spin Hamiltonian for twofold symmetry 2—15280
Teflon, ^{19}F line narrowing by rotary spin echoes 2—20156
teflon, proton and fluorine, spin lattice relax. time meas., CW-methods 2—7151
tert-butyl-1,3-dioxanes, ^{13}C magnetic resonance spectra 2—3074
tetrabenzopentafulvalene derivatives, geometrical isomerism, n.m.r. obs. 2—12281
3,4,5,6-tetrachloro-2,7-dihydrothiepin, ring inversion study 2—28413
tetrachloroparaxylene, relaxation times meas. interpreted in terms of molecular reorientation 2—20167
1,2-disubstituted tetrafluoroethanes, fluorine spectra, coupling consts. rot. isomerism 2—12283
tetramethylsuccinonitrile, line narrowing study of translational mol. motion 2—1738
tetraphenyl derivatives of group IV elements, bonding investigation 2—15395
thallium(I) nitroparaffins, n.m.r. studies rel. to molec. structure determination 2—12287
tri-2-thienylphosphine, tri-3-thienylphosphine assignments and signs of ^{13}C-^{31}P coupling constants from off-resonance proton decoupled ^{13}C spectra 2—31871
thiourea, ferroelec. phase, proton and deuteron reson. 2—10575
thiourea, ferroelectric, molecular motion 2—7131
three-spin system, interference effect in relax. 2—9174
tobacco mosaic virus solution, mol. order, relax. times, self-diffusion obs. 2—35796
toluene, spin echo in liquid phase 2—35790
transition metal layered dichalcogenide intercalation complex, elec. field gradient 2—19947
transition metal monoborides, determ. ^{11}B nuclear electric quadrupole interaction parameters 2—16652
transition metal phosphine complexes, P-P coupling constants 2—12098
1,3,5- trichlorobenzene, orientated, natural abund. of ^{13}C resonances 2—28361
1,2,3-trichlorotrimethylbenzene, relaxation times meas. interpreted in terms of molecular reorientation 2—20167
trimethylene oxide in nematic liquid crystal, determ. of molecular structure from spectrum 2—35354
1,3,5-triphenylbenzene anion radical, orbital degeneracy obs. using p.m.r. and d.m.r. 2—8808
triphenylene, possible reorientation of molecule in solid state, n.m.r. investigation 2—10567
triphenylmethylhydroperoxides, H-bond study using n.m.r. and i.r. spectroscopy 2—28417
turbulent flow in tube longitudinal turbulent diffusion studies by n.m.r. method 2—28455
u.s. saturation in line wings 2—10531
van der Waals effect in solutions, investigation by factor analysis 2—6247
Van der Waals effects on chemical shifts 2—12094

Nuclear magnetic resonance and relaxation continued
1- vinyl-o-carborane, plastic crystalline behaviour, linewidth as func. of temp. 2—33358
vinyltriphenyl derivatives of group IV elements, bonding investigation 2—15395
water eliminated Fourier transform technique, rel. to p.m.r. studies of biological macromolecules 2—23474
YIG, spin echo decay, low temp. 2—10535
Yttrium ethyl sulphate: Yb^{3+} and Nd^{3+}, effect of paramagnetic impurity on spectra 2—37015
zeolites, pulsed field gradient obs. of diffusion processes 2—10592
[Pt(NH$_3$)$_4$]Cl$_2$.2H$_2$O, anisotropy of chem. shift of ^{195}Pt nmr signal, position of Pt units in unit cell 2—26307
Al-Ga alloy, quadrupolar interaction, elec. field gradient 2—22839
Al-Ga(Ge)(Mg) dil. alloys, elec. field gradients 2—1732
Al-transition metal alloy, localized spin fluctuations 2—19822
Al, liq, and solid, electronic struct. obs. 2—7136
Al, self diffusion obs. 2—9615
Al, solid and liquid, Knight shift and spin-lattice relaxation, electronic structure 2—4112
Al films, Knight shift, supercond. T$_c$ phenomena 2—16174
Al$_2$SiO$_4$(f,OH)$_2$, topaz, determ. of ^{27}Al quadrupolar coupling constant and asymmetry parameter 2—10541
As-S-Sn system, rel. to glass and cpd. formation 2—37003
Au-V dil. alloys, of ^{51}V, spin and orbital contribs. 2—33114
Au-V dil. alloys, T^2 temp. depend. of ^{51}V Knight shift 2—33350
AuAl$_2$-AuGa$_2$-AuIn$_2$ pseudobinary alloys, satellite resons. 2—37004
Au$_4$Mn alloy, ordered, of ^{197}Au, h.f.s. 2—16656
B$_{10}$H$_{13}^-$, ^{11}B spectrum 2—5910
B$_2$O$_3$, crystalline, ^{11}B NMR meas. rel. to structure 2—22838
Ba$_3$Co$_2$Fe$_{24}$O$_{41}$ and Ba$_3$CoZnFe$_{24}$O$_{41}$, of ^{57}Fe, magnetic reversal, domain walls 2—30024
Ba$_2$Co$_2$(Ni$_2$)Fe$_{12}$O$_{22}$, of ^{57}Fe, cone mag. struct. 2—10543
Ba[Pt(CN)$_4$].4H$_2$O, anisotropy of chem. shift of ^{195}Pt nmr signal, position of Pt units in unit cell 2—26307
BeO, Stark shift of spin levels of ^{9}Be 2—22840
Bi:Te, hyperfine heat capacity and nucl. quadrupole interaction 2—16657
BrHBr- bihalide ion, proton shielding studied to elucidate electronic structure 2—31792
^{78}Br, γ-angular correlation of 120 μs state, time differential obs. of n.m.r. 2—5671
CH$_5^+$, theoretical ^{13}C chemical shifts 2—24497
C$_2$H$_5^+$, theoretical ^{13}C chemical shifts 2—24497
CS$_2$, ^{13}C relaxation, field-dependent contributions 2—28333
CS$_2$, spin echo in liquid phase 2—35790
^{13}C chemical shifts of tetramethylsilane determ. use of TMS as ^{13}C reference compound discussed 2—27376
^{13}C Fourier transform n.m.r. applied to conformation structure of cyclononane 2—24522
^{13}C n.m.r., applic. to investigation of adsorption 2—39550
^{13}C relaxation, field-dependent contributions 2—28333
^{13}C relaxation, small molecules, temperature dependence 2—38951
^{13}C satellite lines, rel. to isotope abundance ratio 2—5906
^{13}C spectroscopy, chemical applic. and instrumentation, review 2—27375
^{13}C undecoupled spectra, nuclear Overhauser effect 2—767
CaBSiO$_4$(OH), datolite, positions of hydrogen atoms 2—19044
CaF$_2$:Ce^{3+}, r.f. irradiation effects on steady state Zeeman and dipolar energies 2—30032
CaF$_2$:Eu^{2+}, effect of paramagnetic impurity on spectra 2—37015
CaF$_2$, of ^{19}F spins, nuclear mag. ordering 2—6991
CaF$_2$, second moments and local mag. field vals. from adiabatic rapid passage n.m.r. 2—10544
CaF$_2$, spin echoes, magic sandwich, line shape analysis of free induction decay 2—13422
Ca$_5$F(PO$_4$)$_3$ single crystal, pulsed n.m.r. investigation of ^{19}F chemical shift anisotropy 2—22841
CdS, chemical shift Cd^{113} 2—37005
CdSe, chemical shift Cd^{113} 2—37005
CdTe, chemical shift Cd^{113} 2—37005
CdTe, of ^{113}Cd, cond. electron g-factor 2—33351
^{111}Cd, method of realization of beat nuclear resonance 2—28211
CeAl$_x$, and susceptibility meas., paramagnetic behaviour, electronic contribs. 2—7134
CeSn$_3$, mag. ordering obs. 2—6941
Ce$_x$Y$_{1-x}$Al$_3$, temp. depend. of Knight shift and absorpt. lineshape 2—16658
Ce$_x$Y$_{1-x}$Al$_3$, temperature dependence of NMR line-width meas. between 100 and 1100 K 2—26300
ClHCl- bihalide ion, proton shielding studied to elucidate electronic structure 2—31792
ClO$_3$F, ^{35}Cl and ^{19}F spin-lattice relax. 2—8604
Co, spin echo of ^{59}Co, impurity effects 2—13549
Co (III) complexes, symmetric, ^{14}N and ^{59}Co relaxation studies 2—1119
CoCl$_2$.2H$_2$O, approx. Ising system, n.m.r. of ^{59}Co 2—33352
CoCl$_2$.6H$_2$O, of deuterons, quadrupolar coupling, hydrogen bonds 2—13550
CoF$_2$.5HF.6H$_2$O, internal motion determ., 90-400K 2—40779
CoMn(CO)$_9$, single- crystal broad-line ^{59}Co and ^{55}Mn n.m.r. 2—22842
CoSiF$_6$.6H$_2$O, internal motion determ., 90-400K 2—40780
^{57}Co, magnetic moments of oriented nucleus 2—38506
CrO$_2$, ferromag., of ^{53}Cr, hyperfine fields obs. 2—13551
Cr$_3$Te, rel. to magnetic props. in ferromag. region 2—26036
Cs atoms, Bloch- Siegart shifts 2—38833
CsCoCl$_3$.2H$_2$O, mag. struct., exchange interactions 2—40548
CsD$_2$AsO$_4$, ^{75}As quadrupole coupling const. 2—10554
CsMnF$_3$, antiferromag., ^{55}Mn spin echo obs. 2—16403
CsNiCl$_3$, of ^{35}Cl and ^{133}Cs, mag. props. 2—22703
Cs$_2$O-B$_2$O$_3$, glass and cryst. samples, struct. study 2—30026
Cs$_2$O-B$_2$O$_3$, glass and cryst. samples, effect of ionic motion 2—30025
Cu-Cr(Mn) dilute alloys, spin-lattice relax. times, obs. and analysis 2—7003
Cu-Fe dil. alloys, relax. rates temp. depend. above Kondo temp. 2—7004
Cu-Fe of ^{63}Cu, dil. alloys, rel. to Kondo effect 2—36657
Cu-Ge dil. alloys, elec. field gradients 2—10539
Cu, liq. and solid, electronic struct. obs. 2—7136
Cu, liq. and solid, electronic struct. temp. depend. 2—10545
Cu, Ruderman-Kittel interaction obs. 2—1733
Cu, spin-lattice relax. time, 1-10 mK 2—13553
Cu based dilute alloys, obs. of asymptotic behaviour of oscillation of charge density surrounding impurity 2—29608

Nuclear magnetic resonance and relaxation continued

- Cu dil. alloys, determ. of asymptotic region of charge density around impurities 2—20158
- Cu dil. alloys, elec. field gradients in single crysts. 2—16667
- Cu fine particles, size effect 2—40772
- CuBr, ^{63,} ^{65}Cu chemical shifts, precise meas. by high speed rotation method 2—4553
- CuCl, ^{63,65}Cu chemical shifts, precise meas. by high speed rotation method 2—4553
- CuCl, CuBr, magnetic screening of ^{35}Cl and ^{79}Br 2—28286
- CuI, ^{63,} ^{65}Cu chemical shifts, precise meas. by high speed rotation method 2—4553
- $CuSiF_6.6(4)H_2O$, internal motion determ., 90-400K 2—40780
- D_2, solid, h.c.p., spin-lattice and spin-spin relax. 2—10253
- D_2O, containing magnetic nuclei, obs. of enclathration as form of magnetic isolation 2—22843
- $DyPO_4$, of ^{31}P, antiferromagnetic transition obs. 2—6992
- Er, conically ordered ferromagnet, spin echo method, 1.4K 2—33353
- $Er_3Al_5O_{12}$, of ^{27}Al, quadrupole coupling const. detn. 2—10542
- EuFe garnet, of ^{151}Eu, hyperfine fields exchange anisotropy 2—36744
- EuSe, ordered state, of ^{151}Eu and ^{153}Eu, signals analysis 2—10546
- F_2, F_2-inert gas mixtures, spin relaxation 2—32180
- FHF- bihalide ion, proton shielding studied to elucidate electronic structure 2—31792
- FHF- ion and its homologues, high-resolution n.m.r. 2—784
- ^{19}F, attachment for recording on proton radiospectrometer 2—27377
- ^{19}F, in powders, single crysts., chem. shift anisotropies, shielding tensors, coherent averaging 2—13426
- Fe-Co dil. alloy, spin-lattice relax. of ^{59}Co 2—33180
- Fe-Co dilute alloy, hyperfine field distrib. 2—13448
- Fe-Ir, dil. ferromag. alloy, electric quadrupole interaction of Ir nuclei 2—20160
- Fe-M dilute alloy, (M=Ti, V, Cr, Mn, Co, Ni), hyperfine field at Fe atoms 2—13449
- Fe-Si alloys, ordered, cond. electron spin density oscillations 2—1611
- Fe-Si ordered alloys, enhancement factors and relax. times 2—1648
- Fe-(Cu, Sb, Ir), dil. ferromag. alloy, isotope pairs hyperfine struct. anomalies 2—20159
- Fe-transition metal dilute alloy, spin-lattice relax. time 2—19932
- Fe, charge and spin perturbation around nonmag. impurities 2—22740
- Fe, domain and wall hyperfine fields 2—19985
- Fe, high-field relax. times of ^{57}Fe 2—40579
- Fe, of ^{57}Co, radiative detection using Mossbauer effect 2—26301
- Fe, single and multiple passage studies of ^{60}Co 2—1734
- Fe alloys, temp. dependence of hyperfine field near 3d impurities 2—13443
- Fe complex, FeEDTA- in water, hydrolysis products 2—3409
- $FeBO_3$, of ^{57}Fe secondary spin echo, mag. props. 2—36768
- Fe(III) phenyl substituted complexes, n.m.r. study of changes in electronic structure due to aromatic substitution 2—31791
- α-Fe_2O_3, tightly pinned domain walls 2—36770
- Fe_3O_4, magnetite, ^{57}Fe hyperfine field spectra, conduction model 2—7137
- $FeSiF_6.6H_2O$, internal motion, press. depend. obs. 2—37006
- Ga halides in aqueous solutions, spin-lattice and spin-spin relaxation 2—1120
- $Ga_xFe_{3-x}O_4$, $GaNiFeO_4$, ferrimagnets, ^{57}Fe spin echo spectra, 4.2K 2—10547
- Gd-Lu(Y) alloys, of ^{165}Ho, hyperfine interactions rel. to noncollinear magnetic order 2—7138
- Gd intermetallic compounds, spin echo study 2—40773
- Gd_2Co_7, of ^{155}Gd, ^{157}Gd, and ^{59}Co, at 77K 2—4555
- $Gd_3Al_2(AlO_4)_3$ garnet, hyperfine interaction of ^{27}Al, 1.5-300 K quadrupole coupling 2—7139
- $Gd_3Al_5O_{12}$, of ^{27}Al, quadrupole coupling const. detn. 2—10542
- GdFe garnet, magnetized, spin-echo n.m.r. study of Gd quadrupole interactions 2—4554
- $GdPO_4$, of ^{31}P, antiferromagnetic transition obs. 2—6992
- H_2-He, mixtures test of linearity of spin lattice relaxation time as function of percentage of adulterant gas 2—8628
- H_2, solid, splitting, ortho content depend. 2—37007
- H_2 isotopes, collision cross sections, interrelationships with other transport and relaxation phenomena 2—39026
- H_2O, adsorbate in presence of paramag. impurities, mol. mobility determ. 2—25221
- H_2O and D_2O, spin echo in liquid phase 2—35790
- $H_5O_2^+AuCl_4^-.2H_2O$, ^{1}H and ^{2}H n.m.r., phase transitions and molec. motion 2—10548
- ^{3}He, solid, relax. rates, spectral density function 2—32301
- Hg complexes, bis(perfluorovinyl)mercury and methyl(perfluorovinyl)mercury, magnetic nonequivalence 2—15310
- Ho, low temp., ^{165}Ho spin echo interpret. 2—10550
- Ho alloys and intermetallics, ^{165}Ho spin echo, h.f.s. low temp. 2—10549
- IHI- bihalide ion, proton shielding studied to elucidate electronic structure 2—31792
- In-Pb dil. alloys, liq., ^{115}In Knight shifts 2—22006
- InP, of ^{31}P, nucl. spin dynamics 2—33355
- $KBrO_3$, quadripolar linewidth of ^{79}Br and ^{81}Br 2—7803
- KCl:Li$^+$, quadrupole line splitting in elec. field 2—37009
- K_2CoF_4, two-dimensional antiferromagnet, ^{19}F n.m.r. anomaly near critical temp. 2—30027
- K_2CuF_4, hyperfine interaction of ^{19}F, unpaired spin densities 2—10552
- KD_2AsO_4, ^{75}As quadrupole coupling const. 2—10554
- $K_4Fe(CN)_6.3H_2O$, para and ferroelectric, of ^{1}H 2—4556
- KH_2AsO_4, ferroelectric, long range correlation, n.m.r. and dielectric relax. obs. 2—10553
- KH_2PO_4, of ^{39}K, spin-lattice relax., ferroelec. transition phenomena 2—10581
- $KMnF_3$ and K_2MnF_4, critical phenomena 2—10555
- $KMn_{1-x}X_xF_3$, (X=Zn,Ni,Fe), of ^{19}F, local susceptibility obs. 2—40417
- $KNbO_3$, ferro-antiferroelec. phase transition obs. 2—16661
- $KNiF_3$, of ^{19}F, unpaired spins study 2—13554
- K_2NiF_4, family, two dimensional antiferromag., phase transition and critical phenomena 2—16392
- $K_2[Pt(CN)_4]Br_{0.3}.2,3H_2O$, anisotropy of ^{195}Pt shift, line broadening 2—10562
- $K_2[Pt(C_2O_4)_2].2H_2O$, anisotropy of chem. shift of ^{195}Pt nmr signal, position of Pt units in unit cell 2—26307
- $LaAlO_3$, transient study of phase transitions 2—9816
- $La_{1-x}Gd_xAl_2$, spin-lattice relax. of ^{139}La and ^{27}Al, impurity contrib. 2—33181
- $La_{3-x}Gd_xAl$, of ^{27}Al, rel. to gapless supercond. 2—6777

Nuclear magnetic resonance and relaxation continued

- $La_2Mg_3(NO_3)_{12}.24H_2O$, n.m.r. on oriented ^{57}Co, ^{58}Co and ^{60}Co 2—7141
- Li ions in water solutions in porous materials, relaxation times 2—1739
- Li spin-lattice relax. times, many-electron enhancement effects 2—16660
- LiF, ^{19}Fe and ^{7}Li spin-spin reservoir 2—7142
- LiF, proton and fluorine, spin lattice relax. time meas., CW-methods 2—7151
- $Li_{0.5}Fe_{2.5}O_4$, dipole and anisotropic hyperfine field effects, ^{57}Fe spectra 2—26304
- $Li_{0.5}Fe_{2.5-x}Al_xO_4$, spin echo, freq. temp. depend., mag. struct. 2—10556
- $LiFe_5O_8$, ordered, of ^{57}Fe, hyperfine fields 2—37010
- $LiN_2H_5SO_4$, dipolar relaxation of ^{7}Li, hindered rotation 2—7006
- $LiNbO_3$ to Li_3NbO_4, nonstoichiometric crystals, ^{93}Nb linewidths 2—40777
- $LiVO_2$, of ^{7}Li and ^{51}V, line shifts and broadening above and below transition temp. 2—7143
- $LiVo_3$, of ^{51}V, e.p.r. comparison 2—10565
- $Mg_2Al_4Si_5O_{18}.nH_2O$, low temperature form, ^{27}Al n.m.r. investigation of Al-Si order 2—30019
- MgCl, in aqueous phosphate solutions, ^{25}Mg n.m.r. 2—28897
- Mg_3P_2 powder, ^{31}P chemical shielding anisotropy at 99.4 MHz 2—10561
- $MgSiF_6.6H_2O$, ^{19}F nuclear spin lattice relaxation study and internal rotations 2—10577
- $MgSiF_6.6H_2O$, internal motion determ., 90-400K 2—40780
- Mn complex π-methylcyclopentadienyl manganese tricarbonyl, structure determ. from p.m.r. studies in nematic phase 2—21622
- Mn ferrite, multiple spin echoes for ^{55}Mn 2—4557
- Mn_3AlC, of ^{27}Al and ^{55}Mn 2—20161
- $MnCO_3$, antiferromag., ^{55}Mn spin echo obs. 2—16403
- $MnCr_2O_4$, of ^{55}Mn, cone angle obs. 2—20163
- MnF_2, of ^{19}F, lineshape analysis 2—10534
- Mn_3GaC, of ^{55}Mn, ^{69}Ga and ^{71}Ga 2—20161
- Mn_4N_x, of ^{55}Mn, mag. ordering 2—10557
- $MnSiF_6.6H_2O$, internal motion determ., 90-400K 2—40780
- ^{93m}Mo, magnetic moments of oriented nucleus 2—38506
- $(ND_4)_2SO_4$, powder spectra, 4.2K, determ of ^{2}H quadrupole coupling const. 2—10558
- $NH_4Cl:Cu^{2+}(2H_2O)$, effect of paramagnetic impurity on spectra 2—37015
- $(NH_4)_2SO_4$, ferroelectric, anomalous spin-lattice relax. and absorpt. lineshape at 4 K 2—26082
- Na, spin-lattice relax. times, many-electron enhancement effects 2—16660
- $NaBrO_3$, quadripolar linewidth of ^{79}Br and ^{81}Br 2—7803
- NaCl, ^{23}Na and ^{35}Cl spin-spin reservoir 2—7142
- NaCl, line broadening anisotropy due to plastic deform. 2—10560
- $NaClO_3$, double reson. by acoustic excitation 2—33356
- NaI, line broadening anisotropy due to plastic deform. 2—10560
- NaI, relax. via self-diffusion processes 2—9626
- Na_2MoO_4, hydrous and anhydrous, ^{23}Na n.m.r., meas. of quadrupole coupling constants, electric field gradient 2—37012
- $NaNO_3$, single crystal, nuclear quadrupole coupling constant of ^{23}Na, pressure and temp. dependence 2—16659
- $NaNbO_3$, ferro- antiferroelec. phase transition obs. 2—16661
- $NaVO_3$, of ^{51}V, e.p.r. comparison 2—10565
- Na_2WO_4, hydrous and anhydrous, ^{23}Na, n.m.r., meas of quadrupole coupling constants, electric field gradient 2—37012
- Na_xWO_3, transient study of phase transitions 2—9816
- Nb:^{2}H, spin- lattice relax. and quadrupole coupling 2—7129
- Ni-Cu, ferromagnetic alloy, analysis of structure of spectra, localization of excess electrons around solute atoms 2—4558
- Ni-Ga, ferromagnetic alloy, analysis of structure of spectra, localization of excess electrons around solute atoms 2—4558
- Ni-Ir, dil. ferromag. alloy, electric quadrupole interaction of Ir. nuclei 2—20160
- Ni-Zn ferromagnetic alloy, analysis of structure of spectra, localization of excess electrons around solute atoms 2—4558
- Ni-(Cu, Sb, Ir), dil. ferromag. alloy, isotope pairs hyperfine struct. anomalies 2—20159
- Ni, high-field relax. times of ^{195}Pt 2—40579
- Ni complex, of ^{14}N and ^{13}C 2—8685
- Ni complexes, cyclopentadienyl, ^{31}P chemical shifts 2—810
- Ni dil. alloys, high-field relax. times of ^{55}Mn and ^{59}Co 2—40579
- $NiF_2.5HF.6H_2O$, internal motion determ., 90-400K 2—40779
- $NiIn_xFe_{2-x}O_4$, hyperfine interactions of ^{115}In 2—40778
- $NiSiF_6.6H_2O$, internal motion determ., 90-400K 2—40780
- P-S(Se)-Sn system, rel. to glass and cpd. formation 2—37003
- P compounds, partially deuterated, chemical shift of ^{31}P 2—8716
- P gas, ^{31}P chemical shifts 2—32181
- PBr_3, relaxation data used to determ. ^{31}P spin rotation interaction constants 2—15281
- PCl_3-PBr_3, liq. mixture, ^{31}P and ^{35}Cl relaxation times meas. 2—9178
- PCl_3-$PBrCl_2$-PBr_2Cl-PBr_3, liq. mixture, ^{31}P relaxation times meas. 2—9178
- PCl_3, liq., ^{35}Cl relaxation times meas. 2—9178
- PCl_3, relaxation data used to determ. ^{31}P spin rotation interaction constants 2—15281
- $POCl_3$, relaxation data used to determ. ^{31}P spin rotation interaction constants 2—15281
- P_4S_3 single crystal, ^{31}P chemical shielding anisotropy at 99.4 MHz 2—10561
- P_4S_{10}powder, ^{31}P chemical shielding anisotropy at 99.4 MHz 2—10561
- ^{31}P, in aqueous H_3PO_4, effects of diamagnetic ions on relaxation 2—1121
- ^{31}P spin-lattice relaxation in liquid organic and inorganic compounds 2—32277
- P=Se, bond characterization by ^{31}P spectral study of ^{31}P-^{77}Se coupling 2—5903
- Pb-Bi(Tl) alloys, ^{207}Pb Knight shift in solid and liq. states 2—29796
- Pb, exchange consts. and Knight shift anisotropy 2—40781
- Pb single crystal, pseudodipolar coupling consts. detn. 2—33357
- Pd-Al dilute alloy, conc. depend. 2—40782
- Pd-V dilute alloy, conc. depend. 2—40782
- Pt-Ir alloy, Mossbauer effect, ^{193}Ir and ^{195}Pt 2—26306
- Pt complex, tetracyanoplatinates, anisotropy of ^{195}Pt shift 2—10562
- ^{195m}Pt, oriented in Fe, magnetic hyperfine splitting 2—27994
- Rb spin-lattice relax. times, many-electron enhancement effects 2—16660
- Rb_2CoF_4, two-dimensional antiferromagnet, ^{19}F n.m.r. anomaly near critical temp. 2—30027
- $RbFeF_3$, of ^{19}F, unpaired spin study 2—13554
- RbH_2AsO_4, proton and fluorine, spin lattice relax. time meas., CW-methods 2—7151
- $RbMnF_3$, antiferromag., ^{55}Mn spin echo, 4.2 K 2—16400
- Rh-Fe (Mn) dil. alloys, J_{sd} values determ. from linewidth obs. 2—10563

Nuclear magnetic resonance and relaxation continued
  SF_6/D_2O clathrate hydrate, powder, ^{19}F n.m.r. lineshapes, chemical shift and anisotropy, correlation times 2—28323
  SF_6, spin-lattice relax. in liq.-vapour critical region 2—39426
  Sc-rare earth dil. alloys, spin-lattice relax., localized moments influence 2—19934
  ScH_x, proton motion obs. 2—20164
  Si, adsorbed benzol, n.m.r. spin echo investigation 2—6374
  SmF_3, anomalous ^{19}F shift 2—7145
  Sn-Cu(Ag)(Au) alloys, liquid, Knight shift comp. depend. rel. to conduction electron density 2—9177
  Sn-In(Sb) dil. alloys, of ^{119}Sn, Knight shift anomalies 2—37014
  Sn (A=115, 117, 119), Larmor frequency meas. rel. to hyperfine structure anomalies 2—21527
  Tb, ferromag., of ^{153}Tb, spin echo technique 2—16662
  $TbPO_4$, of ^{31}P, antiferromagnetic transition obs. 2—6992
  Te, chem. shift tensors 2—29688
  $ThAl_2$, ^{27}Al n.m.r, dipolar doublet, quadrupole and anisotropic knight shift interactions 2—33347
  Ti-H system, spin-spin and spin-lattice relax., spin echo study 2—16401
  TiH_4, diffusion of H model, pulsed NMR technique 2—3813
  TlCl, spin-lattice relax. in rot. frame, diffusion mechanism influence 2—10262
  $TmFeO_3$, spin reorientation, ^{57}Fe absorpt., 75-114 K 2—16663
  UF_6, ^{19}F rotating frame spin-lattice relaxation, obs. via anisotropic chemical shift 2—4561
  V-Co alloys, of ^{51}V and ^{59}Co, mag. props. 2—10566
  V-N(O) dil. solid solns., ^{51}V quadrupolar effects 2—26308
  V-transition metal alloys, ^{51}V quadrupolar effects 2—26308
  $V_xCr_{1-x}B_2$, antiferromag. transition obs. 2—36781
  VF_3, mag. ordering obs. 2—36780
  VN_x, spectra, Knight shifts, influence of mag. fields. and composition 2—20166
  V_2O_3, antiferromag., of ^{51}V, h.f.s., quadrupolar broadening 2—10564
  V_2O_5, of ^{51}V. quadrupole coupling const. 2—10565
  ^{51}V in V_3Au, n.m.r. model proposed for normal and superconducting states 2—4564
  Xe, chemical shifts in ^{129}Xe n.m.r. induced by O_2 and NO admixtures 2—31833
  Y and dil. Y-Ce alloys, of ^{89}Y, h.f.s., Kondo effect role 2—13555
  $YFeO_3$, weak ferromag., ^{57}Fe hyperfine field, domain boundary oscillations 2—22681
  $ZnAl_2O_4$, natural Gahnite, of ^{27}Al, reson. lines, line shifts 2—26309
  Zn_3P_2 powder, ^{31}P chemical shielding anisotropy at 99.4 MHz 2—10561
  $ZnSiF_6.6H_2O$, internal motion determ., 90-400K 2—40780
  ZrH_n, n=1.0-1.9, spin-spin, spin-lattice relax. times temp. depend., spin-echo obs. 2—16402
 measurement
  application to blood flowmeter 2—6175
  calculation by analogue computer, response to pulsed irradiation, time sharing method 2—34271
  Carr-Purcell pulse separation, two-site solution for chemical exchange produced dependence of T_2 2—37023
  complex trace calculation, n.m.r. theory in solids 2—30023
  computerized system for Davis polarized proton target 2—24064
  conductor, bulk, using spin-helicon interaction 2—10540
  correlation time meas. from temp. depend. of coherent pulse averaging effects 2—14345
  dilute paramagnetic systems, discrete obs. near impurity, technique 2-37015
  f.m. spectrometer, for meas. of internal magnetic fields 2—17495
  Fourier transform n.m.r., driven equilibrium and spin-echo methods, signal-to-noise values 2—27379
  Fourier transform n.m.r., spin-lattice relaxation times 2—27380
  Fourier transform spectroscopy, repetitive pulses 2—27378
  IC detector operating over wide range 2—2320
  impulse method for automatic meas. of waterfoil ratio 2—10652
  line position determination, freq. modulated field and· double-lock spectrometer methods 2—7814
  line spread due to h.f. mag. field inhomogeneity 2—219
  liquids, spin lattice relaxation times, apparatus for obs at high pressures 2—37864
  multichannel analyzer for recording spin-echo signal 2—23475
  multispin p.m.r., digitization and computer processing of data 2—2316
  n.m.r. spectra, high resolution, selective relax. time meas., spin-echo signal 2—7150
  n.m.r. spectroscopy, nuclear spin relaxation, Fourier transform analysis 2—7149
  nuclear polarization in solids, ^{19}F and ^{169}Tm polarized in $Tm^{2+}:CaF_2$ by circularly polarized light 2—40596
  on-line computer calc. 2—23471
  phase quantization method 2—27381
  polarization of nuclear targets 2—34773
  polarizer for magnetization of the fluid in instruments 2—23473
  probe damper, single coil, for pulsed n.m.r. 2—2331
  pulse and Fourier transform NMR, book 2—2318
  pulse programmer for averaging of relax. meas. 2—7809
  pulsed applications of pulse generator system 2—2330
  pulsed single reson. spectra calc. by analog computer 2—7808
  pyridinium salts, fused, spectra 2—4562
  quadrupole spin echo obs. by two-freq. methods 2—7805
  R12B spectrometer, new variable temp. accessory 2—5305
  radioactive nuclei, radiative detection 2—37866
  review of today's techniques 2—14350
  sideband-oscillator stability 2—7810
  signal recording using mag. field intensity meter with improved signal-to-noise ratio 2—17503
  signal strength, effect of different types of modulation 2—2317
  spectral data indexing for fast accurate retrieval 2—21180
  spectrograph, helicoidal cavity 2—7803
  spectrometer, frequency modulated, with Robinson-type oscillator for internal mag. field meas. 2—2319
  spectrometer, pulsed, coherent, stabilization of resonance conditions 2—34270
  spectrometer, pulsed, with phase detection 2—34269
  spectrometer, super-regenerative, centre-shift elimination and lineshape response control 2—7807
  spectrometer, tunable, for v.h.f.-u.h.f. range 2—37865
  spectrometer, variable freq., double resonance probe 2—5303

Nuclear magnetic resonance and relaxation continued
 measurement continued
  spectrometer, Varian XL-100 modification for Fourier transform operation 2—34272
  spectrometer adaptation for ^{19}F obs. 2—7806
  spin echo, Carr- Purcell-Gill-Meiboom technique 2—35790
  spin echo equipment, broadband magnetic field stabilizer 2—17502
  spin echo in two spin systems, effects of chemical exchange and self-diffusion 2—768
  spin echoes, high resolution n.m.r. spectroscopy in solids 2—30022
  spin-lattice relaxation using triplet pulse sequences 2—34273
  strong field instrumentation and applics. 2—11406
  temperature regulation device, 95-475 K 2—14351
  time by pulse method, apparatus 2—34268
  time sharing spectra, analogue computer calc. 2—27382
  wide-line detection of slow motions in solids 2—26295
  ^{27}Al in $Y_3Al_5O_{12}$ garnet, temperature dependence of crystal field gradient 2—1735
  ^{13}C chemical shifts on TMS scale 2—31771
  ^{13}C spectroscopy, Fourier transform techniques 2—5907
  Hg, odd isotopes, relaxation time of optically oriented atoms 2—18287
  $MnFe_2O_4$, $MnCoFe_2O_4$, $MnFe_2O_4+0.16(Mn_3O_4)$, spin echo of ^{55}Mn nuclei in local fields 2—4532
  $(NH_4)_2H_3IO_6$, antiferroelectric, structure obs. 2—1575

Nuclear matter *see Nucleus/theory*

Nuclear orientation *see Nuclear polarization*

Nuclear photoeffect *see Gamma-rays/effects; Nuclear reactions and scattering due to/ photons*

Nuclear physics
  conference, nuclear and solid state physics, Bombay (1972) 2—34868
  conference, Sydney, Australia (1972) 2—38425
  conference on hyperfine interactions in crystals and nuclear props., Rehovot, Israel, 1970 2—5630
  explosives and desalination, peaceful uses 2—24251
  harmonic oscillator two-centre integrals, application 2—27068
  high energy, experimental, computer applications 2—5570
  instrument system, CAMAC, for work with computers 2—24062
  magnetic thin film recorder system for fact transients in nuclear diagnostics 2—30715
  measurements, role of Information Theory and Estimation Theory 2—27829
  measurements, using multi-channel analyzer and computer 2—439
  nuclear science symposium and nuclear power systems symposium, San Francisco (1971) 2—27934
  photonuclear expts. using combined energy and intensity sweeping 2—34751
  pure and applied research, 3 MeV Van de Graaff accelerator at Australian Inst. Nucl. Sci., review 2—38426
  synthesis of element 105 2—18058

Nuclear polarization
  amorphous and polycryst. solids, n.m.r. enhancement due to dynamic polarization produced by e.s.r. centre 2—40771
  aromatic molecules, optical nuclear polarization by selective population of nuclear sublevels 2—7027
  1-butanol: porphyrexide, ^{13}C dynamic polarization rel. to polarized target production 2—36809
  butanol, effect of absorbed power 2—34774
  n-butanol-d_{10}, solid dynamic polarization of deuterons rel. to polarized target production 2—36807
  1-butanol-water-porphyrexide system, proton polarization at 50kG and 1K, polarized target production 2—36808
  chemical, theory 2—26332
  collective virtual core excitation model description of core polarization exchange contribs. to inelastic nucleon scattering 2—31527
  core-polarization correction in energy spectrum 2—38466
  cyclohexane diperoxide, chem. induced dynamic nucl. polarization, in biradical prods. 2—8756
  dibenzoylperoxide, in binary solvent mixtures, chem. induced dynamic, mag. field depend. 2—7182
  dilute paramagnetic systems, from n.m.r. of nuclei near impurity, technique 2—37015
  DPPH in polystyrene, dynamic nuclear polarization rel. to localization of energy in organic molecules 2—15369
  dynamic, at $T<0.5K$, rel. to polarized target development 2—34771
  dynamic, by electron-nucleus dipolar coupling in solids, mechanisms 2—36800
  dynamic, enhancement of solid effect with inhomogeneous broadened e.s.r. line 2—36977
  dynamic, obs. of ^1H and ^{13}C at 21 kG in radical solns. 2—25109
  dynamic, of protons in polystyrene, cross relaxation due to electronic spin spin interactions 2—36997
  dynamic and brute force, spin freezing, possible applic. of dilution refrigerator 2—37527
  dynamic orientation, by saturating double flip transitions 2—16408
  dynamic polarization, related effect 2—29855
  e.p.r. line observation as method of determ. polarization of low-energy polarized target 2—27833
  ethylene glycol, Cr complex doped, dynamic polarization of protons 2—16669
  free-radical reaction products 2—20183
  highly polarized substances, measurement by nuclear magnetic resonance system 2—34773
  hydrocarbons, proton polarization rel. to polarized target production 2—36810
  internal field meas. for determ. of polarization in a low energy polarized target 2—27834
  large volume targets, physical arrangement for measurement 2—34776
  mesitylene, ^{13}C containing, study of multiplet effect in dynamic polarization 2—24496
  methyl group-containing solid, dynamic proton polarization due to temp. change 2—33361
  neutron physics expts. on oriented nuclei for determ. spins of compound nuclear states 2—34770
  nitroxide radical, solid, proton dynamic polarization rel. to Overhauser effect 2—26305
  nonstationary dynamic, theory 2—2685
  1,8-octanediol-glycol mixtures, dynamic proton polarization rel. to polarized target production 2—36811

Nuclear polarization continued
- oriented fissile nuclei, description of ^{3}H cryostat for use in research of fission phenomena 2—30720
- 1-pentanol-water-porphyrexide system, proton polarization at 50kG and 1K, polarized target production 2—36808
- porphyrexide in n-butanol and water, dynamic polarization and relax. meas. 2—25114
- radical solutions, of ^{1}H, ^{13}C and ^{19}F, 21 kG 2—6248
- reactions and scattering, theory in two particle reactions 2—28013
- recoil nuclei in muon capture 2—38583
- ruby:Cr^{3+}, acoustical dynamic polarization of ^{27}Al 2—29856
- ruby, n.m.r. of ^{27}Al and ^{17}O with dynamic polarization 2—13548
- sequential particle decay for aligned nuclei, angular correlations 2—21406
- solid effect, rel. to cryst. strain effects on e.s.r. and n.m.r. 2—10533
- solids, by optical pumping, ^{19}F and ^{169}Tm polarized in Tm^{2+}:CaF_2 by circularly polarized light 2—40596
- spin isospin core polarization, unique first forbidden β-decay, $A \approx 90$ 2—11788
- static orientation methods, expts. with oriented radioactive nuclei 2—36801
- targets, calibration by polarized proton and deuteron beams 2—35021
- targets, non-resonant means of measurement, polarized ^{3}He targets considered 2—34777
- targets, on-line computer measurement using r.f. phase lock techniques 2—34775
- targets, radiation damage and uniformity 2—34772
- tetrachlorosemiquinone in tetraethylene glycol dynamic effect 2—25111
- by u.s. waves 2—26097
- in viscous media, dynamic effect 2—25111
- viscous solution, paramag. impurities, Overhauser effect 2—25107
- viscous solution, paramagnetic impurities, Overhauser effect 2—25108
- xylols, ^{13}C containing, study of multiplet effect in dynamic polarization 2—24496
- yttrium ethyl sulphate, ytterbium doped, proton polarization 2—19948
- yttrium ethylsulphate: Dy(Yb), proton polarization by rot. cooling at $T<1K$ 2—29846
- (p,2p) reactions, theoretical expressions 2—31536
- ^{12}B recoil nuclei in muon capture 2—38583
- BiMn, ferromagnetic, low temp. polarization of Bi isotopes, production of polarized ^{209}Bi target 2—36802
- CaF_2:H, dynamic polarization temp. dependence 2—29857
- CaF_2, large dynamic polarization of ^{19}F by solid effect method, polarized target production 2—36803
- ^{57}Co, magnetic moment by n.m.r. of oriented nucleus 2—38506
- Fe, mag. hyperfine fields at ^{204}Bi 2—29858
- GaP:Te, of Ga and P nuclei at 27 K 2—36804
- HD, solid, p.m.r. obs. at $T<1K$ 2—37008
- ^{2}H(N,N) elastic scattering unitary model calcs. of nucleon polarization using realistic model for two-nucleon interaction 2—24208
- Hg, odd isotopes, relaxation time of optically oriented atoms 2—18287
- $La_2Mg_3(NO_3)_{12}$, dynamic polarization of protons 2—16669
- ^{6}Li, rel. to Coulomb breakup process in $^{208}Pb(^{6}Li\alpha d)^{208}Pb$ reaction 2—2816
- ^{7}Li, polarizability from Coulomb excitation 2—18087
- ^{93m}Mo, magnetic moment by n.m.r. of oriented nucleus 2—38506
- NH_3, solid, dynamic polarization of protons rel. to polarized target production 2—36807
- ^{21}Ne, excited levels orientation by optical pumping 2—18331
- Ni, mag. hyperfine fields at ^{204}Bi 2—29858

Nuclear power *see Nuclear reactors, fission*

Nuclear quadrupole resonance
- alkaline earth chlorates, temp. depend. of freq. 2—8585
- alum, elec. field gradient determ. 2—33360
- aniline and haloaniline complexes with 2, 4, 6-trihalophenols, crystalline, i.r. and n.q.r. spectra 2—10340
- 2-bromo-4-methyl acetanilide, of ^{79}Br, temp. variation, 77-302K 2—40793
- chlorinated methylbenzenes, ^{35}Cl spectra, influence of vibr. and reorientations of CCl_3 groups 2—10590
- p-chlorobenzotrichloride, structure and molecular motion 2—5966
- coupling consts., relativistic corrections, higher-order combinations 2—13547
- 2,4-dibromoaniline, of ^{79}Br, temp. variation, 77-302K 2—40793
- 2,4-dibromoanisole and 2,4,6- tribromoanisole, Zeeman effect in n.q.r. of ^{81}Br 2—8745
- p- dichlorobenzene, α-ray irrad., impurity form., cryst. struct. effect, n.q.r. obs. 2—26317
- 3,4-dichloronitrobenzene Zeeman spectra of ^{35}Cl 2—13560
- 3,5-dichlorophenol, temp. dependence of Cl.n.q.r. frequencies, torsional frequencies 2—28419
- electric field gradient tensor, parameters detn. for nuclei with half integral spin from Zeeman split n.q.r. spectra 2—33359
- ferroelectric near phase transition pt., kinetic eqns. 2—7155
- group theory approach 2—34275
- hexachloroethane, rel. to lattice vibr., molecular rot. and C-Cl_3 group internal. rot. 2—16668
- hydrazides, ^{14}N n.q.r. at 77K 2—24540
- hydrazines, ^{14}N nuclear qadrupole resonance spectra 2—8784
- 2,4,α,α,α-pentachloro toluene, temp. dependence of Cl n.q.r. frequencies, torsional frequencies 2—28419
- phase transformation obs., review 2—6632
- phenacyl chloride, temp. dependence of Cl n.q.r. frequencies, torsional frequencies 2—28419
- pyrimidine and purine nucleic acid bases, of ^{14}N, polycryst. powders, nuclear double resonance method 2—7159
- quinone powders, meas. of naturally abundant ^{17}O transition frequencies 2—37019
- spectrometer, super-regenerative, centre-shift elimination and lineshape response control 2—7807
- spectrometer, wide range, superregenerative, with varactor diode frequency modulation 2—17505
- survey, theory and exptl. techniques 2—27383
- 1,2,4,5-tetrachlorobenzene, temp. dependence of Cl n.q.r. frequencies, torsional frequencies 2—28419
- 1,3,4-thiadiazole, microwave spectrum, nuclear quadrupole coupling 2—18530
- Thiourea, ferroelec. phase, of ^{14}N, rel. to Stark effect 2—20171
- transition metal complexes with PCl_3, ^{35}Cl n.q.r. 2—28317
- xanthene powder, meas. of naturally abundant ^{17}O transition frequencies 2—37019

Nuclear quadrupole resonance continued
- Ag_2HgI_4, thermochromic, ^{127}I n.q.r. frequencies and critical broadening 2—10584
- Al-Ga dil. alloys, elec. field gradient, conc. depend. 2—10585
- $AsCl_3$ complex, binding, geometric config., relax., internal motions 2—26314
- $\alpha(\beta)$-As_4S_3, and far i.r. spectra, cryst. struct., point charge calcs. 2—10586
- $Ba(ClO_3)_2.H_2O$, elec. field gradient tensor parameters, from Zeeman split n.q.r. spectra 2—33359
- $Ba(ClO_3)_2.H_2O$, temp. dependence of n.q.r. frequencies from 77 to 350K 2—37018
- $BaCl_2.2H_2O$, Zeeman effect study 2—13559
- $BaI_2.2H_2O$, of ^{127}I, struct. relns. between iodide, bromide and chloride dihydrates 2—30035
- Be, nuclear quadrupole coupling of ^{12}B 2—36998
- ^{35}Cl, in powder sample, asymmetry parameter detn. 2—7156
- ^{35}Cl n.q.r. of 11 organic and 3 inorganic molecules, 77 K 2—24493
- ^{35}Cl n.q.r. of 59 organic molecules S-Cl bond 2—21650
- ^{35}Cl temp. depend. of nuclear quadrupole resonance and spin-lattice relaxation time in trichloroacetamide 2—10591
- Cu-M, alloys, dilute, M=Au, Zn, Ni, Pt, Pd, charge density distrib. around impurities 2—16666
- Cu_2HgI_4, thermochromic, ^{127}I n.q.r. frequencies and critical broadening 2—10584
- β-Ga in silicone oil dispersion, electric resonance 2—37017
- ^{71}Ga, in powder sample, asymmetry parameter detn. 2—7156
- HBr (Cl)(I) cryst., ferroelec., critical effects 2—10588
- H_5IO_6, powder samples, ^{127}I spectra, resonance frequencies of transitions, coupling constants 2—10587
- $H_5O_2^+AuCl_4^-.2H_2O$, ^{35}Cl n.q.r., phase transitions and molec. motion 2—10548
- $KBrO_3$, of ^{39}K 2—40790
- $KClO_3$, temp. dependence of n.q.r. frequencies from 77 to 350K 2—37018
- K_2SnCl_6, of ^{35}Cl, 77-320 K, phase transitions obs. 2—7158
- α-N, press. depend., lattice libration freq., elec. field gradient, 4.2-35.1K 2—26315
- α-N of ^{14}N and ^{15}N, temp. depend., isotope effects, $T<35.6K$ 2—26316
- α-N_2, solid, dipolar spin-echo envelope modulation temp. depend. 2—7160
- ND_4XO_4 (X=I,Re), anomalous temp. dependence, explanation using vibrational spectra investigation 2—16556
- $NH_4H_2AsO_4$, of ^{75}As, elec. field gradient tensor in paraelec. phase 2—10589
- NH_4XO_4 (X=I,Re), anomalous temp. dependence, explanation using vibrational spectra investigation 2—16556
- $NaBrO_3$, of ^{23}Na 2—40790
- $NaClO_3$, pure quadrupole reson. of ^{35}Cl, press. and vol. depend., press to 20 kbar 2—40791
- $NaClO_3$, temp. dependence of n.q.r. frequencies from 77 to 350K 2—37018
- Na_2MoO_4, hydrous and anhydrous, ^{23}Na n.m.r., meas. of quadrupole coupling constants, electric field gradient 2—37012
- $NaNO_3$, low temperature behaviour, 42-308K, of nuclear quadrupole coupling constant of ^{23}Na 2—30034
- $NaNO_3$, spin-lattice relax. of ^{23}Na, orientation depend. 2—19933
- Na_2WO_4, hydrous and anhydrous, ^{23}Na, n.m.r., meas of quadrupole coupling constants, electric field gradient 2—37012
- P-Cl compounds and complexes, ^{35}Cl n.q.r. 2—28317
- Pt complexes, Pt(II)-olefin, Br n.q.r. 2—5947
- $RbBrO_3$, of ^{85}Rb and ^{87}Rb 2—40790
- $SbCl_3$ complexes, temp. dependence of spin lattice relaxation of ^{121}Sb nuclei 2—19937
- $Sr(ClO_3)_2$, of ^{35}Cl, and r.f. absorpt., 77-300K 2—40792
- Ta_3Sn, type II supercond., spin lattice relax. 2—4173

Nuclear radius *see Nucleus/size*

Nuclear reactions and scattering
- *see also Chemical analysis/by nuclear reactions; Fallout; Nuclear bombardment targets; Nuclear excitation; Nuclear fission; Nuclear fusion; Nuclear spallation; Radioactivity; Stripping reactions; Thermonuclear reactions*
- actinide nuclei, sub Coulomb transfer reactions at low energy, cross section study 2—35066
- actinides, single nucleon transfer reactions rel. to nuclear structure studies 2—21420
- aligned nuclei, γ-ray direction correlation coefficients, graphical representation 2—11718
- analyticity of regularized integrals containing eigenfunctions with complex momentum, use in resonant states 2—7673
- centre of mass motion, discussion in framework of Glauber model 2—14971
- composite nuclei, high energy scattering, study based on Glauber's formalism 2—2760
- controlled fusion research, microwave electron density measuring systems 2—28592
- convergence problems arising in nuclear reaction theories 2—18170
- correlated basis functions method, role of dispersion effect 2—34888
- Coulomb functions in entire (η,ρ) plane, computer program 2—34997
- coupled channel calculations, using Feshbach projection technique, shell model aspects 2—486
- coupled channels model, existence of complex eigenvalues 2—24196
- deposition targets, identification of heavy element contaminants, $Z \geqslant 20$ 2—14740
- description by shell model conditions and particle correlations 2—31516
- direct reaction inelastic scattering for estimation of El strength functions 2—34892
- direct reaction theory using DWBA amplitudes extended to include transitions to many channel, many level final states 2—38653
- direct reactions, effects of non-orthogonality and virtual excitations 2—21419
- direct reactions, importance of second order processes 2—38558
- double and single, at medium energies 2—35004
- elastic scattering by nuclear Hartree Fock field, effects arising from truncation of harmonic oscillator basis 2—28011
- electric quadrupole Coulomb excitation, differential cross sections, computer program 2—34998
- elon scattering, optical formulation of high energy coherent production 2—28014
- energy deposition in plasma from elastic scattering 2—6067
- Faddeev eqns. in co-ordinate representation 2—8322
- Feynman graphs describing interactions in the final or initial states, study of singularities 2—18169

Nuclear reactions and scattering continued
four body break-up, kinematics phase-space and resonances, two particle coincidence meas. 2—14772
gamma-ray multiplicity in decay of residual nuclei from nuclear reactions 2—31519
generator coordinate description of nucleus-nucleus scattering formulated 2—24194
giant resonance excitation, resolution into isospin components, rel. to neutron and proton r.m.s. radii 2—31407
hadron scattering from light nuclei, Coulomb interference study by Glauber model 2—28015
heavy element, studies using position-sensitive semiconductor detectors 2—24086
heavy nuclei, production of, with A>250 2—11932
inelastic scattering, spin effects 2—38557
intra-nuclear cascade calculations, inclusion of fission and charged-particle emission 2—34999
isospin invariance and mirror symmetry in nuclear reactions, geometric consequences 2—14970
kinematical parameters, computer program 2—21416
at lattice site, model for blocking effect 2—9904
lepton scattering in nuclear matter in momentum transfer region 2—5686
light nuclei wave function verification, in nuclear reactions with clusters 2—28012
many particle reactions, Hauser-Feshbach method 2—21417
many-particle scattering equations, distortion potentials and reduction method 2—30797
multichannel scattering, bounds on reaction matrix 2—5680
multifermion interaction constants, limits from cosmic neutrino and muon data 2—27779
multiple scattering from fixed composite system, study of Glaubers theory 2—18171
neutron transfer reactions on light nuclei, comparison of spectroscopic information given by peripheral model and DWBA 2—8320
nuclei-hadron interaction, form. of nucleon isobars 2—14921
nucleon-nucleus optical potentials, $1/\gamma$ velocity dependence 2—24197
one-nucleon transfer reactions, configuration mixing effect on form factor, Hartree-Bogoliubov calc. 2—11814
overlapping resonances, correlations of resonance parameters 2—21418
partial widths and strong coupling of channels 2—31518
particle-resonance scattering, low energy, studied by N/D method, relation to three particle resonances 2—24198
phase shift equivalent momentum dependent potentials, off-shell effects 2—18063
photoemulsion nuclear reaction, DNEPR-1 computer simulation 2–38559
pickup reactions, soft-pion theorems rel. to direct processes 2—24199
polarization experiments, choice of coordinate systems 2—35002
polarization theory in two particle reactions 2—28013
polarization-transfer expts. with polarized spin-1 particle incoming, polarized spin-1 particle outgoing, parametrization 2—35063
polarized target and beam, spin correlation coefficients 2—35001
pre-equilibrium decay, nuclear density distribution 2—31496
R-matrix parameters, study of uniqueness when fitting cross section data using least-squares search routine MULTI 2—484
R-matrix theory, boundary condition parameter 2—38560
reaction list for charged particle induced reactions, July '70-June '71, Z=1 to Z=98 nuclei 2—35006
rearrangement processes, extension of Feshbach's method, two particle problem 2—11813
recoil from solids, knock out effects, emission probability 2—25702
resonance scattering on deformed nuclei and coupled channel approach 2—11811
resonance wave functions and parameters from coupled channel method 2—14972
self-nuclear reactions, R-matrix 2—35003
statistical processes, effect of generalization of Hauser Feshbach formalism to include isospin 2—11815
thin absorbers, energy spread for a range of incident particles and targets 2—4089
three-body collisions, separable expansions and perturbation theory 2—24195
three-body problem, application of method of Pade approximants, determ. binding energy 2—2122
three-body reactions, semiclassical Monte Carlo calc. of Coulomb effects in final state 2—35000
three-body systems, upper and lower bounds on phase shifts in variational formulation 2—28042
time-of-flight system for heavy particle identification in nuclear reactions 2–442
two-nucleon transfer, program for form factor calc. 2—35067
two-particle transfer reactions for studying excitation of 0^+ states 2—24134
two-step reaction processes, interference effects 2—34996
unified theory, classification of simple mechanism and compound nucleus states 2—31517
vibrating nucleus, collective states excitation by fast particles, semiclassical approximation 2—8319
d decay, isobaric analogue resonances in isospin-forbidden channels 2—31515
^{18}O(p,α)^{15}N, use in autodiffusion meas. of O in α-Zr 2—12818
^{3}He polarized target, device for studying reactions 2—27832
^{3}He polarized targets, review of scattering experiments 2—35005
^{14}N, stopped π^- capture, ^{8}B prod. 2—14996
Sm isotopes, two-neutron transfer reactions rel. to coexistence of spherical and deformed states 2—14973

chemical effects
see also Chemical effects of radiations/ionizing radiations
elemental analysis by elastic scattering of intermediate mass projectiles 2—10682
pre-ionization of MHD generator working medium 2—11426
steel reactor casing, oxidation by neutron activated UPu oxide fuel 2—13577
Ne^{21} production in nuclear reactions, rel. yields and efficiencies 2—11816

high energy $\geqslant$1 GeV
400 GeV cosmic ray hadron interaction cross-sections obs. 2—11812
antiproton-(emulsion) nuclei elastic scattering at 3GeV/c and matter density models 2—24213
EAS, increase of transverse momenta in nuclear interactions at energies $\geqslant 10^{12}$eV 2—38342

Nuclear reactions and scattering continued
high energy $\geqslant$1 GeV continued
hypernucleus production, in high energy reactions 2—21372
kaon and baryon- antibaryon production, at few TeV energy 2—38295
nucleon isobars, virtual excitation, form. by hadron-nuclei interaction 2—14921
pions, interactions with heavy emission nuclei, production of fast He and ^{3}H nuclei 2—38624
scattering, fine structure studies, applic. of optical model and Glauber approx. 2—2759
Z(ν_μ,μ^-e$^+\nu_e$)z, to 50 GeV, angular and energy distributions calc. 2—18178
Z($\nu\mu$,$\mu^-\mu^+\nu_\mu$)Z to 50 GeV, angular and energy distributions calc. 2—18178
p-Be collisions, 12.4 GeV/c, π^+ and π- production 2—11825
π(K)+A$\rightarrow\pi$(K)+A+l$^+$+l$^-$, $\geqslant$40 GeV, for meas. of e.m. form factors of π and K 2—14628
π>2 GeV, double charge exchange on nuclei, Glauber theory 2—14995
^{12}C cascade interactions with π^-, 5 GeV/c two-Λ^0 prod. 2—14707
^{56}Fe, photonuclear reaction yields at 1.5 GeV 2—2763
^{4}He, elastic pion scatt., differential cross section at 7.76 GeV/c 2—8352
^{4}He, spin and isospin in high energy proton elastic scattering and nuclear correlations 2—31529
Th, secondary effects produced by interaction with 28 GeV protons 2—35038
Tl, secondary effects produced by interaction with 28 GeV protons 2—35038
U, secondary effects produced by interaction with 28 GeV protons 2—35038
^{51}V, photonuclear reaction yields at 1.5 GeV 2—2763

Nuclear reactions and scattering due to
alpha-particles
2s-1d shell nuclei, elastic and inelastic scatt., 104 MeV, differential cross sections 2—21383
direct scattering of ions, possible explanation for gross structure observations 2—14998
elastic scattering, Frahn-Venter, Springer-Harvey and optical models, 25 MeV particles 2—8356
elastic scattering cross sections, back angle enhancements, determ. shell structure effect 2—24233
excitation of unnatural parity states by inelastic scattering, extension of Satchler's microscopic formulation to spin orbit force 2—35064
hybrid model, pre-equilibrium decay at moderate excitations 2—38634
inelastic α scattering, relation between nuclear matter and nuclear potential 2—8355
inelastic excitation of unnatural parity states, one-step processes 2—14997
light nuclei, structure factor for stripping mechanism 2—31575
potential model analysis 2—35065
Rutherford scattering in repulsive Coulomb field, derivation using hyperbola geometry 2—35060
scattering, effective alpha-nucleon interaction parametrization 2—501
scattering, evidence for existence of highly excited bands of intermediate resonances describing quasi-molecular rotations 2—28063
(α,xn) population of rotational levels in ^{158}Dy, ^{160}Dy, ^{162}Er, ^{168}Yb, nuclear moment of inertia at high rotational frequencies 2—27988
N^{4}He scatt. forward dispersion relations and ^{4}He ^{3}He n coupling const. 2—14982
^{89}(α,^{3}He), 65.7 MeV, cross sections, shell model structure of ^{90}Y, l=5 transitions data 2—34950
^{107}Ag, elastic scattering, method of resolving well depth ambiguities in optical model analysis 2—11856
^{27}Al(α,γ)^{31}P, investigation of ^{31}P energy levels 2—2703
^{27}Al(α,t), (α,α), 104 MeV, differential cross sections and normalization factors 2—21441
^{27}Al(α+pγ)^{30}Si, meas. of branching ratios and lifetimes of levels in ^{30}Si 2—34986
^{36}Ar(α,γ_0)^{40}Ca, giant resonance region 2—38642
^{40}Ar(α,nγ)^{43}Ca, 13.5 MeV, study of excited state properties of ^{43}Ca, spin values 2—24155
^{10}B, elastic scattering at energies 5 to 30 MeV 2—24235
^{10}B(α, ^{7}Li)^{7}Be, isospin invariance and mirror symmetry, geometric consequences 2—14970
^{10}B(α,d$_{1\gamma}$)^{12}C, study of angular correlation functions 2—31574
^{11}B(α,t,γ)^{13}C 2—31574
^{8}Be, asymptotic form of wave function for scattering from an incident α-particle 2—2794
^{9}Be(α,n)^{12}C, study of energy levels of ^{12}C between 1.7 and 6.4 MeV 2—31573
^{209}Bi(α,^{3}He)^{210}Bi, multiplet structure of ^{210}Bi 2—38529
^{209}Bi(α,3n)^{210}At, melted Bi target, det. of magnetic moment of ^{210}At 2—31346
^{209}Bi(α,3n)^{210}At, melted Bi target, det. of magnetic moment of ^{210}At 2—21315
C emulsion nucleus identification of medium energy α-particle induced reactions 2—24237
^{12}C (α,$\alpha_{4.43}$) ^{12}C*, 20-24 MeV, anal. using strong absorption model, ang distribs. 2—31565
^{12}C(α,^{3}He), (α,t), (α,α), 104 MeV, differential cross sections and normalization factors 2—21441
^{12}C(α,2α), intermediate energies, mechanism 2—31576
^{12}C(α,α_0), ^{12}C(α,$\alpha^1\gamma$), ^{12}C(α,^{8}Be), shell model and rotational calcs. for ^{16}O 2—38481
^{12}C(α,$\alpha_{1}\gamma$)^{12}C 2—31574
^{12}C(α,α), Regge-pole model for scattering 2—15000
^{12}C(α,α)^{12}C, angular distrib., phase shift anal. 2—2806
^{12}C(α,α) in 2$^+$ excited state, inelastic scattering, meas. of relative correlation function of α-γ angular correlations at 32.5 MeV 2—38630
^{12}C(α,$\alpha\gamma$), reaction-plane and spin-flip angular correlations 2—21446
^{12}C(α,γ)^{16}O, capture cross section, calc. at stellar energies 2—18231
^{16}C(α,α), Regge-pole model for scattering 2—15000
^{40}Ca(α,^{3}He), (α,t), (α,α), 104 MeV, differential cross sections and normalization factors 2—21441
^{40}Caα,pγ)^{43}Sc, 7-12 MeV, determ. lifetimes of levels populated in ^{43}Sc 2—18103
^{42}Ca, inelastic α scattering, relation between nuclear matter and nuclear potential 2—8355
^{46}Ca(α,d)^{48}Sc, study of levels of ^{48}Sc 2—31466
C(α,α), A=12, 13, 26.6 MeV., diff. cross sections and angular distributions 2—38631
^{116}Cd(α,t)^{117}In, study of In level scheme via proton transfer reactions 2—27983

Nuclear reactions and scattering due to continued
alpha-particles continued
^{140}Ce elastic scattering, method of resolving real well depth ambiguities in optical model analysis 2—11856
^{140}Ce(α,α')^{140}Ce, nuclear structure study 2—11764
^{35}Cl(α,pγ)^{38}Ar, 11.5 MeV, deduced lifetimes of levels in ^{38}Ar by Doppler shift method 2—27972
^{59}Co(α,α')^{59}Co, population of highly excited levels in ^{59}Co, energy spectra study 2—24162
^{59}Co(α,t)^{60}Ni, ang. distribution meas., DWBA analysis 2—2810
^{50}Cr(α,nγ)^{53}Fe, 5.6 to 10.0 MeV, study of low lying states in ^{53}Fe 2—11748
^{50}Cr(α,pγ)^{53}Mn, mean lives of low lying levels of ^{53}Mn measured by Doppler shift attenuation with p-γ coincidences 2—18106
^{65}Cu(α,αn), differential ranges of recoil product meas. over energy interval 24-42 MeV 2—35076
^{19}F(α,γ), 3.5 to 4.7 MeV, excitation function for X-ray yields 2—35071
^{19}F(α,nγ)^{22}Na, spin of 1984 keV level of ^{22}Na 2—38485
^{54}Fe(α,n)^{57}Ni, study of props. of levels at 2.443 and 3.003 MeV in ^{57}Ni 2—11749
^{56}Fe(α,p)^{59}Co, population of highly excited levels in ^{59}Co, energy spectra study 2—24162
^{160}Gd(α,3n)^{161}Dy, rotation-particle coupling in ground state band of ^{161}Dy 2—31490
^{70}Ge elastic scattering, method of resolving real well depth ambiguities in optical model analysis 2—11856
^{2}H(^{4}He,^{3}He)^{3}H, diffr. cross section presented at 82.1, 64.3, 49.9 MeV, study of charge asymmetry effects 2—28072
^{2}H(α,αn)p, 30-80 MeV, energy dependence of quasifree scattering 2—24234
^{2}H(α,αp)n, 30-80 MeV, energy dependence of quasifree scattering 2—24234
^{4}Hc (α-α), 0.35 MeV, bremsstrahlung cross section meas. 2—28066
^{26}Kg(α,n)^{29}Si reaction, study of principal decay modes and lifetimes of levels below 7.2 MeV in ^{29}Si 2—27971
^{139}La, scattering at 12 MeV, Coulomb excitation 2—5664
^{139}La(α,α')^{139}La, nuclear structure study 2—11764
^{6}Li(α,α_0), elastic scattering, 12.0-18.5 MeV, optical model analysis of angular distribution meas. 2—2793
^{6}Li(α,α), low-energy, nucleon exchange 2—18218
^{6}Li(α,αx)Y, 50 MeV, x=p, d, t, ^{3}He, α, determ. clustering characteristics of ^{6}Li 2—11723
^{6}Li(α,d)^{8}Be, excitation spectrum of ^{8}Be 2—2688
^{7}Li(α, n)^{10}B, differential cross section for α energies up to 8 MeV 2—15009
^{7}Li(α,α_0) elastic scattering, 12.0-18.5 MeV, optical model analysis of angular distribution meas. 2—2793
^{7}Li(α,α), low-energy, nucleon exchange 2—18218
^{7}Li(α,d), E_α=30 MeV, ang. distribs., DWBA and PWBAE analyses 2—31571
^{7}Li(α,p), E_α=30 MeV, ang. distribs., DWBA and PWBAE analyses 2—31571
^{7}Li(α,t), E_α=30 Mev, ang. distribs., DWBA and PWBAE analyses 2—31571
^{7}Li(α,t)^{8}Be, excitation spectrum of ^{8}Be, ghost anomaly 2—2688
^{175,176}Lu(α,xn), 24-48 MeV, study of decay of three-quasiparticle state in ^{177}Ta 2—11770
^{24}Mg(α,p), 28.8 MeV, study of J dependence for L=2 transfer 2—11863
^{26}Mg(α,n)^{29}Si, level scheme for ^{29}Si 2—2701
^{92}Mo(α,d)^{94}Tc, 50 MeV, high spin proton excited states population 2—31478
^{92}Mo(α,t)^{93}Tc, high spin proton states of ^{93}Tc 2—2696
^{97}Mo, Coulomb excitation meas. rel. to level structure investigation 2—34952
N, emulsion nucleus, identification of medium energy α-particle induced reactions 2—24237
^{14}N(α,α), 26.6 MeV, diff. cross sections and angular distributions 2—38631
^{14}N(α,γ)^{18}F, 0.5 to 1.2 MeV, total cross section measurement 2—2807
^{14}N(α,γ)^{18}F rate obs., w.r.t. stellar evolution 2—20530
^{14}N(α,n), excitation function 2—38641
^{15}N(α,γ)^{19}F, study of resonance at 850 keV, spin parity, lifetime, M1 transition strength determ. 2—35069
^{23}Na(α,nγ)^{26}Al, γ-ray distrib. meas., spin assignment of positive parity levels, evidence for ground state rot. band 2—2699
^{142}Nd, inelastic α scattering, relation between nuclear matter and nuclear potential 2—8355
^{20}Ne($\alpha,\alpha_{1.63}$)^{20}Ne*, 20-24 MeV, anal. using strong absorption model, ang. distrib. 2—31565
^{60}Ni(α,α'), influence on isospin decay of composite ^{64}Zn system formed, Bohr independence hypothesis 2—24181
^{62}Ni(α,α') influence of isospin on decay of composite ^{66}Zn system formed, Bohr independence hypothesis 2—24181
O, emulsion nucleus, identification of medium energy α-particle induced reactions 2—24237
^{16}O inelastic scattering, 40.5 MeV, excitation of 8.87 MeV 2- level, analysis including two-body spin-orbit force 2—35064
^{16}O(α,2α), intermediate energies, mechanism 2—31576
^{16}O(α,α), 26.6 MeV, diff. cross sections and angular distributions 2—38631
^{16}O(α,α), 5-11 MeV, ^{20}Ne high-spin states study 2—21382
^{16}O(α,γ)^{20}Ne, 4.65 MeV, 5^- resonance located 2—503
^{18}O(α,α')^{18}O, energy spectra, 20-23.4 MeV, spin and parity combinations 2—2694
^{190}Os(α,t)^{191}Ir, proton state population in ^{191}Ir 2—5666
^{192}Os(α,t)^{193}Ir, proton state population in ^{193}Ir 2—5666
^{208}Pb(α,2nγ), 43 MeV, study of high spin states in ^{210}Po 2—31495
^{208}Pb(α,α), E_α=166 MeV, neutron radius from optical potential anal. of data 2—11779
^{85}Rb, recoil ranges, isomer ratios and excitation functions 2—11864
^{85}Rb de-excitation, isomer ratios of ^{84}Rb, ^{85}Sr and ^{87,86,85}Y 2—31585
^{87}Rb(α,nγ)^{90}Y, γ-spectroscopic study of ^{90}Y levels 2—18112
^{104}Ru(α,2n)^{106}Pd, ^{104}Ru(α,4n)^{104}Pd, excitation of energy levels in ^{106}Pd and ^{104}Pd 2—24166
^{32}S(α,p), 28.8 MeV, study of J dependence of L=2 transfer 2—11863
^{28}Si(α,γ)^{32}S, investigation of ^{32}S energy levels 2—5649
^{29}Si(α,p)^{32}P, spins of ^{32}P levels determ. by angular-correlation studies 2—8292
Sm recoil, into different targets, integral angular distribution of radiation, measurement 2—2813
^{144}Sm, 50 MeV elastic and inelastic scattering to low lying states, cross section determ. 2—11857
^{144}Sm(α,2n)^{146}Gd, hindrance factor of E2 $6^+ \rightarrow 4^+$ transition in ^{146}Gd 2—2723

Nuclear reactions and scattering due to continued
alpha-particles continued
^{150}Sm, elastic and inelastic cross section meas. at 9 and 10 MeV, determ. reduced transition probability B(E2) of first 2^+ level 2—2724
^{152}Sm(α,2nγ)^{154}Gd, ^{154}Gd high-spin states γ-spectroscopic study 2—18128
^{152}Sm(α,2nγ)^{154}Gd, ^{154}Gd high-spin states γ- spectroscopic study 2—18128
^{152}Sm(α,3nγ)^{153}Gd, ^{153}Gd high-spin statesγ-spectroscopic study 2—18128
^{152}Sm(α,3nγ)^{153}Gd, ^{153}Gd high-spin states γ- spectroscopic study 2—18128
^{152}Sm(α,xn)$^{152,\ 153}$Gd, 32-43 MeV, population of high spin states 2—21395
^{46}Ti(αm nγ)^{49}Cr, 6-10 MeV, Doppler-shift attenuation method used in nγ coincidence meas. deduced levels of ^{49}r 2—18105
^{50}Ti(α,nγ)^{53}Cr, e.m. props. of ^{53}Cr. 2—34940
U(α,n), natural targets, effect of reactions on ratio of induced to spontaneous fission 2—35084
^{182}W(α,4n)^{182}Os, K-dependence of population of ^{182}Os levels 2—27991
^{89}Y(α,n)^{92}Nb, doubly isospin forbidden reaction, energies near I.A.Rs, cross section anomalies 2—31586
^{66}Zn, lifetimes of levels 2—27978
^{90}Zr, elastic scattering, method of resolving well depth ambiguities in optical model analysis 2—11856
^{90}Zr(α,t)^{91}Nb, high spin proton states of ^{91}Nb 2—2696
^{92}Zr(α,n)^{95}Mo, 12-43 MeV, study of high spin levels in ^{95}Mo 2—21391
^{94}Zr(α,n)^{97}Mo, 12-43 MeV, study of high spin levels in ^{97}Mo 2—21391
^{94}Zr(α3n)^{95}Mo, 12-43 MeV, study of high spin levels in ^{95}Mo 2—21391
Zr(α,d)Nb, 50 MeV, high spin proton excited states population 2—31478
Zr(α,t)Nb, 50 MeV, high spin proton excited states population 2—31478

cosmic rays
see also Cosmic rays/effects and interactions
400 GeV hadron interaction cross-section obs. 2—11812
Al, hadron interactions, multiple production of particles 2—5569

deuterons
absorption cross section of 25 GeV/c antideuterons on nuclei, analysis of CERN IHEP measurements using Glauber multiple scattering theory 2—5709
elastic scattering, data on deuteron optical potential 2—28061
light nuclei, structure factor for stripping mechanism 2—31575
nuclear emulsion, diffr. scatt. of 2.45 GeV/c deuterons 2—28064
optical model potential derivation using Glauber theory 2—18216
optical potential, relation to nucleon optical potential 2—28062
optical potential derivation 2—2796
polarized, calibration of polarized targets, cases of ^{3}He, ^{19}F and ^{15}N considered 2—35021
polarized beams, recent exptl. developments 2—35028
scattering, nonlocal optical potential 2—11851
scattering amplitude symmetry props. and spin dependence 2—2792
spin-dependent interactions due to coupling to stripping channels 2—2797
stripping, calculations based on soluble two-channel model 2—38635
stripping on doubly even nuclei, theory using method of quantum Green functions 2—2799
stripping reaction, singlet deuteron induced, normalization factor for zero and finite range DWBA calc. 2—15004
stripping reactions, Mitra's three body model reexamination, formulation of a DWBA 2—2798
with track emulsion, cross section determ. 2—14782
(d,n), 1.69 GeV/c, ang. distrib. of neutrons emitted in forward direction 2—15003
(d,p), E_d=12.3 MeV, tensor analyzing power, deuteron D-state effects 2—2803
(d,p), gamma-ray multiplicity in decay of residual nuclei from nuclear reactions 2—31519
(d,p) Coulomb stripping reaction, cross-section and proton polarization 2—5708
(d,p) direct reactions, effects of non-orthogonality and virtual excitations 2—21419
(d,p) reaction amplitude, DWBA 2—35068
(d,p) reaction anomaly at threshold of analogue channel, and p-wave neutron strength function 2—500
(d,p) stripping reaction to resonance state, peripheral model description, cross section calc. 2—21443
(d,t), rare-earth nuclei, angular distributions, two step model 2—38643
π^- production in interactions of relativistic deuterons with nuclei 2—21288
^{235}(d,p)^{236m}U, production of shape isomer via decay of class/states due to compound motion 2—11782
^{27}Al(d,p)^{28}Al, 23 MeV, low-lying states in ^{28}Al 2—34926
^{36}Ar(d,p)^{37}Ar, E_d=18.00 MeV, proton ang. distrib. 2—2779
^{38}Ar(d,p)$_{3}{}^{9}$Ar, 10.064 MeV, determ. of level structure of ^{39}Ar, orbital angular momentum transfer to target nucleus 2—34934
Au(d,np)Au, 12 MeV, deuteron break up under Coulomb interaction of nucleus 2—35079
^{10}B(d,α) isospin forbidden reaction, search for ^{12}C lowest T=2 state 2—38474
^{10}B(d,n), 2.7 - 3.9 MeV, determ. polarization angular distributions for neutrons 2—28074
^{11}B(d,3α)n, four body break up studied by simultaneous detection of α-α and α-n coincidences at 10.425 and 12.0 MeV 2—18230
^{11}B(d,n), 2.7 - 3.9 MeV, determ. polarization angular distributions for neutrons 2—28074
^{9}Be(d,d), 1 to 2.2 MeV, absolute differential cross section, angular distributions, optical model analysis 2—14999
^{9}Be(d,d), backward scattering, cross sections and angular distributions 2—38629
^{9}Be(d,γ)^{11}B, resonance struct. 2—2804
^{9}Be(d,n) neutron spectra and application to transmission of C and polyethylene samples 2—5711
^{9}Be(d,pγ)^{10}Be, spectroscopic and reaction mechanism information from ang. correlations at 0° 2—2808
^{9}Be(d,t)^{8}Be, excitation spectrum of ^{8}Be, ghost anomaly 2—2688
^{209}Bi, inelastic scatt., 13.1 MeV 2—18222
^{209}Bi(d,p)^{210}Bi, 17.0 MeV, shell model structure of ^{210}Bi 2—24176
^{209}Bi(d,p)^{210}Bi, multiplet structure of ^{210}Bi 2—38529
^{12}C(α,α')^{12}C, investigation of α-particle unstable states in ^{12}C 2—18089
^{12}C(d, ^{7}Li)^{7}Be, isospin invariance and mirror symmetry, geometric consequences 2—14970
^{12}C(d,^{7}Li)^{7}Be, asymmetries observed in cross section indicating violations of Barshay-Temmer isospin theorem 2—11861
^{12}C(d,α_2)^{10}B(1.74, T=1), isospin nonconservation, study of compound nucleus interpretation 2—8360
^{12}C(d,d), backward scattering, cross sections and angular distributions 2—38629

Nuclear reactions and scattering due to continued
deuterons continued
^{12}C(d,d)^{12}C, obs. of nonequilibrium instantaneous charge distribs. in the recoils 2–2795
^{12}C(d,d) elastic scattering, importance of two-step processes determ. from identification of resonances 2–38558
^{12}C(d,n_0)^{13}N, 3.6 to 12.0 MeV 2–15010
^{12}C(d,n_0)^{13}N, asymmetry of 2.6 MeV polarized neutrons 2–18232
^{12}C(d,n)^{13}N* (p)^{12}C, sequential reaction, mechanism and symmetry axes determ. 2–28081
^{12}C(d,n)^{13}N*(p)^{12}C, measurement of neutron-proton correlations 2–31578
^{12}C(d,p_o)^{13}C, differential cross section and p polarization from sudden approx. 2–31579
^{12}C(d,p) ^{13}C*, 2.6 and 2.8 MeV, importance of two-step processes determ. from identification of resonances 2–38558
^{12}C(d,p)^{13}C, 14.60 MeV, broad energy spectra of protons 2–2805
^{12}C(d,p)^{13}C, 3.9 to 5.8 MeV, polarization of protons 2–31577
^{13}C(d,n), 2.7 - 3.9 MeV, determ. polarization angular distributions for neutrons 2–28074
^{40}Ca, elastic scatt., coupled channel calc. 2–38632
^{40}Ca(d,$\alpha\gamma$)^{48}K, 4.42, 5.08 MeV, levels of ^{48}K determ. from α-γ angular correlations 2–35075
^{40}Ca(d,p)^{41}Ca, effects of 2-step processes in reactions leading to $^{3}/_{2}{}^{+}$2.02 MeV state 2–28077
^{43}Ca(d,p)^{44}Ca, spectroscopic strengths and transition rates 2–31464
^{46}Ca(d,^{3}He)^{45}K, angular distrib. and spectroscopic strength 2–2809
^{46}Ca(d,t)^{45}Ca, angular distrib. and spectroscopic strength 2–2809
^{37}Cl(d, pγ) ^{38}Cl, 3.1 MeV, study of levels below 2.75 MeV excitation energy in ^{38}Cl 2–24154
^{37}Cl(d,$\alpha\gamma$), ^{35}S, 4.25 MeV, study of states in ^{35}S 2–18100
Co, total reaction cross section for 13.6 MeV deuterons 2–28068
^{65}Cu total reaction cross section for 13.6 MeV deuterons 2–28068
Fe, total reaction cross section for 13.6 MeV deuterons 2–28068
^{54}Fe(d,α)^{52}Mn, 15 MeV, cross section meas., ^{52}Mn deduced levels and spectroscopic strengths 2–31471
^{56}Fe(d,p)^{57}Fe*, polarization transfer to residual nucleus, Mossbauer measurements 2–18236
^{57}Fe(d,^{4}He), new spin $^{1}/_{2}{}^{-}$ state observed in ^{55}Mn, shell model calculations 2–8287
^{58}Fe(d,α)^{56}Mn, 15 MeV, cross section meas., ^{52}Mn deduced levels and spectroscopic strengths 2–31471
^{1}H, elastic scatt., meas. of analysing powers iT_{11}, T_{20}, T_{21}, T_{22} 2–15006
^{1}H(d,pn)^{1}H, 27.5-19.2 three body break up spectra analysed to yield cross section for production of n-p pairs in singlet state 2–21431
^{2}H(d,d), phase shift anal., cross section and polarization data 2–11852
^{2}H(d,d)pn, 6-13 MeV, three-body break-up 2–28070
^{2}H(d,d)pn, angular distributions of quasi-free scattering 2–28071
^{2}H(d,dn)^{1}H, 27.5 MEV, deduced n-d quasi-free scattering from cross section, interpreted using modified simple impulse approximation 2–18223
^{2}H(d,dn)^{1}H, 6.0-13.0 MeV, meas, n-d and p-d coincidence spectra, nuclear-deuteron quasifree scattering discussed 2–11854
^{2}H(d,dn)p, coincidence spectra meas. with neutron detection at 200 degrees 2–24215
^{2}H(d,n)^{3}He, ^{2}H(d,p)^{3}H, difference in ang. distribution rel. to new ^{4}He levels 2–27960
^{2}H(d,n)^{3}He, 0.87 to 5.00 MeV, neutron polarization meas. 2–38636
^{2}H(d,n)^{3}He, 12 to 19 MeV, angular distributions and cross sections 2–31567
^{2}H(d,n)^{3}He, at 10.8 MeV, meas. of neutron polarization 2–8357
^{2}H(d,n)^{3}He, polarization differences from reaction D(d,p)T and charge symmetry 2–31568
^{2}H(d,n)pd, 11.3 MeV, search for spin-dependent effects in three body final state 2–21444
^{2}H(d,p)^{3}H, polarization transfer 2–38637
^{2}H(d,p)^{3}H, polarization differences from reaction D(d,n)^{3}He and charge symmetry 2–31568
^{2}H(d,p)^{3}H and ^{2}H(d,n)^{3}He, comparison of vector analysing powers 2–15007
^{2}H(d n)^{3}He ang. distrib. of vector analysing power 2–18224
^{3}H(d, ^{3}He)2n and ^{3}He(d, t)2p, charge symmetry in mirror reactions at 83 MeV 2–31569
^{3}H(d,^{3}Hen)n, neutron-neutron scattering length from kinematically complete measurement 2–5710
H(d,2p)n, Treiman-Yang criterion for quasifree scattering at dueteron energy 20 MeV 2–11853
^{3}He, polarized deuteron scattering, 4 to 11.5 MeV, analysing powers iT_{11}, T_{20}, T_{21} and T_{22} 2–35062
^{3}He(d, n)^{4}He, polarization of emitted neutrons, meas. at 32 MeV 2–15008
^{3}He(d, p^{3}He), at 10.92 MeV meas. yield of three-body break-up reaction 2–18226
^{3}He(d,p^{3}H), at 10.92 MeV meas. yield of three-body break- up reaction 2–18226
^{3}He(d,p)^{4}He, 13.6 MeV, meas. of asymmetry of proton emergence, polarization of target 2–27832
^{3}He(d,p)^{4}He, 2-6 MeV, angular distributions of proton polarization 2–38639
^{3}He(d,p)^{4}He, 2.8 to 11.5 MeV, differential cross-sections and analyzing powers iT_{11}, T_{20}, T_{21} and T_{22} 2–8358
^{3}He(d,p)^{4}He, $<$1 MeV, vector and tensor analyzing power 2–38638
^{3}He(d,t)2p and ^{3}H(d, ^{3}He)2n, charge symmetry in mirror reactions at 83 MeV 2–31569
^{3}He(d,tp)^{1}H, cross section determ. using DWBA treatment 2–18225
^{4}He(d,d′D)^{2}H, 52 MeV, ^{4}He T=0 excited states study 2–14930
^{4}He(d,d′t)^{1}H, 52 MeV, ^{4}He T=0 excited states study 2–14930
^{4}He(d,d), phase shift analysis 2–31570
^{4}He(d,d)^{4}He polarization-transfer expts. parametrization, constraints imposed by time reversal resonance 2–35063
^{86}Kr(d, ^{3}He(^{85}Br, ^{85}Br excited states, spins and parities assignment 2–11865
^{6}Li(d,pn), isospin selective reaction, obs. of spectral peaking characteristic of certain spin states 2–18227
^{7}Li(d,α)^{5}He, excited states in ^{5}He 2–24140
^{7}Li(d,α)^{5}He, search for high lying levels in ^{5}He 2–31445
^{7}Li(d,$\alpha\alpha$)n, 1.90-2.10 MeV, search for rescattering effects 2–18228
^{7}Li(d,γ)^{9}Be, 361 keV, analysis of γ ray spectra, deduced branching ratios to ^{9}Be 2–502
^{7}Li(d,nα)^{4}He, 2.07 and 2.09 MeV, study of n-α rescattering effects 2–2802
Li(d,n)^{8}Be, neutron yield curves, spin and parity of 4.8 MeV level of ^{8}Be 2–27963

Nuclear reactions and scattering due to continued
deuterons continued
^{24}Mg, deuteron stripping, coupled channel Born approx. description 2–15011
^{24}Mg, vector analysing power of (d,p) reactions at 12 MeV 2–35070
^{26}Mg(d,$\alpha\gamma$)^{24}Na, investigation of low-lying levels of ^{24}Na 2–2698
^{26}Mg(d,p)^{27}Mg, 2.0 to 3.0 MeV, angular distributions and excitation functions 2–35072
^{26}Mg(d,pγ)^{27}Mg, mean life and mixing coeff. meas. for ^{27}Mg 2–18099
^{55}Mn(d,p)^{56}Mn, 10.1 MeV, energy levels of ^{56}Mn 2–31587
^{92}Mo(d,n)^{93}Tc, DWBA calculations for reaction to unbound analog states, ang. distributions determ. 2–11867
^{92}Mo(d,n)^{93}Tc, E_d=12 MeV, neutron ang. distrib. 2–2717
^{92}Mo(d,pγ)^{93}Mo, coincidence meas. rel. to level structure and relative transition intensities in ^{93}Mo 2–34951
^{94}Mo(d,n)^{95}Tc, E_d=12 MeV, neutron ang. distrib. 2–2717
^{95}Mo(d,t)^{94}Mo, spectroscopic factors, comparison with partial decay strengths of ^{94}Mo(p,p′γ)^{94}Mo reaction 2–18195
^{96}Mo(d,n)^{97}Tc, E_d=12 MeV, neutron ang. distrib. 2–2717
^{14}N(d,α')^{12}C, investigation of α-particle unstable states in ^{12}C 2–18089
^{14}N(d,$\alpha'\alpha$)^{8}Be, investigation of α-particle unstable states in ^{12}C 2–18089
^{14}N(d,α)^{12}C, exptl. study at 1.7, 2.3, 2.9 MeV 2–31580
^{14}N(d,γ_0)^{16}O, resonance in giant-dipole region of ^{16}O, 2.1-2.9 MeV, determ. of location 2–28076
^{15}N(d, ^{3}He)^{14}C, 52 MeV, high-lying T=1 states in mass-14 nuclei, $1p_{1/2}{}^{2}$ and $1p_{1/2}1p_{3/2}$ diagonal matrix elements 2–18233
^{15}N(d,p), proton spectra from stripping reaction leading to unbound states of ^{16}N 2–8361
^{20}Ne(d,α)^{18}F, E_d<3.2MeV, ang. distribs. and absolute cross section 2–5712
^{20}Ne(d,p)^{21}Ne, ang. distributions and excitation functions in incident energy range 0.9 to 2.4 MeV 2–31581
^{22}Ne(d,α)^{20}F, E_d<3.2MeV, ang. distribs. and absolute cross section 2–5712
Ni, elastic and inelastic scatt., differential cross sections, on neutron excessive and deficient nuclei, 13.6 MeV 2–28065
Ni total reaction cross section for 13.6 MeV deuterons 2–28068
^{58}Ni, 11.8 MeV elastic scattering, derivation of optical potential for deuterons 2–2796
^{58}Ni(d,α)^{56}Co, levels of ^{56}Co 2–2709
^{58}Ni(d,p)^{59}Ni, Coulomb stripping, energy levels of residual nucleus 2–31584
^{60}Ni(d,α)^{58}Co, energy level scheme for ^{58}Co 2–21388
^{60}Ni(d,α)^{58}Co, high-resolution study of ^{58}Co energy levels 2–34943
^{62}Ni(d,α) two-particle transfer reaction, investigation of ^{60}Co 2–31474
^{62}Ni(d,p)^{63}Ni, Coulomb stripping, energy levels of residual nucleus 2–31584
^{64}Ni(d,α) two-particle transfer reaction investigation of ^{62}Co 2–31476
^{64}Ni(d,p)^{65}Ni, Coulomb stripping, energy levels of residual nucleus 2–31584
^{237}Np(d,2n)^{237m}Pu 8.5-14.5 MeV, production of spontaneously fissioning isomers, meas. excitation function and cross sections 2–2821
^{16}O, vector analysing power of (d,p) reactions at 12 MeV 2–35070
^{16}O(d,d), backward scattering, cross sections and angular distributions 2–38629
^{16}O(d,n), excitation function 2–38641
^{16}O(p,d)^{15}O, 31.8-45.4 MeV, distorted wave calcs. in adiabatic deuteron model 2–24218
^{17}O(d,n)^{18}F, DWBA analysis, E_d=4 MeV, ^{18}F level obs. 2–504
^{18}O(d,p)^{19}O, distorted wave calculation of spectroscopic factors for T=$^{3}/_{2}$ states in ^{19}O 2–11720
^{204}Pb, ^{206}Pb, ^{207}Pb and ^{208}Pb, inelastic scatt., 13.1 MeV 2–18222
^{208}Pb(d,t), neutron pick up reaction at sub Coulomb energies, neutron radius 2–2738
^{239}Pu(d,p) fission, two-centre model, cross-section calc., evidence for intermediate structure 2–38653
^{32}S(d,^{3}He)^{31}P, ^{32}S(d,t)^{31}S, charge-asymmetry meas., numerical estimate of isospin impurity in ^{32}S ground state 2–35073
^{32}S(d,n)^{33}Cl, 4.7 to 5.5 MeV, energy levels of ^{33}Cl 2–34930
^{32}S(d,p)^{33}S, E_d=18.00 MeV, proton ang. distrib. 2–2779
^{34}S(d,pγ)^{35}S, ang. correlations and decay of excited states 2–18100
^{34}S(d,pγ)^{35}S, lifetime of 1.99-MeV level of ^{35}S 2–2704
Si, low energy elastic scatt., tensor polarization and differential cross sections 2–18220
^{28}Si(d,p)^{29}Si, E_d=18.00 MeV, proton ang. distrib. 2–2779
^{28}Si(d,pγ)^{29}Si, spectroscopic and reaction mechanism information from ang. correlations at 0° 2–2808
^{151}Sm(d,d′), 5, 12 MeV, B(E2) values of states populated 2–18126
^{124}Sn(d,p)^{125}Sn, sub Coulomb stripping 2–18237
^{88}Sr(d,^{3}He)^{87}Rb 35 MeV single-proton transfer reaction, study of ^{88}Sr ground state, ^{87}Rb deduced levels 2–38645
^{46}Ti(d,τ)^{45}Sc, spins and parities of states in ^{45}Sc and evidence for single proton configurations in the ground state of ^{46}Ti 2–31465
^{48}Ti(d,p), 10 MeV, cross section meas., ^{49}Ti deduced levels 2–31468
^{203}Tl and ^{205}Tl, inelastic scatt., 13.1 MeV 2–18222
^{183}W(d,p), low lying levels of ^{184}W detn. 2–31492
^{89}Y(d,^{3}He)^{88}Sr, 30, 35.5, 40 MeV, single-proton transfer reaction, ^{88}Sr deduced levels 2–38645
^{89}Y(d,α)^{87}Sr, 12 MeV, study of ^{87}Sr levels 2–34949
^{89}Y(d,n)^{90}Zr stripping reaction, Coulomb effect 2–28078
^{89}Y(d,p), 33.3 MeV, cross sections, shell model structure of 90Y, l=5 transitions data 2–34950
^{89}Y(d,p)^{90}Y, 3 to 4.5 MeV and θ=150°, l_n-dependence of excitation functions 2–35078
^{89}Y(d,pγ)^{10}Y, γ-spectroscopic study of ^{90}Y levels 2–18112
^{173}Yb(d,t)^{172}Yb, empirical evidence for Coriolis coupling of octupole states of ^{172}Yb 2–24173
^{176}Yb, deuteron stripping, coupled channel Born approx. description 2–15011
Zn total reaction cross section for 13.6 MeV deuteron 2–28068
^{64}Zn(d,α)^{62}Cu, 15 MeV, DWBA calcs., ^{62}Cu deduced levels 2–31475
^{68}Zn(d,^{6}Li)^{64}Ni, differential cross section, 27.2 MeV 2–2812
^{90}Zn, 11.8 MeV elastic scattering, derivation of optical potential for detuerons 2–2796

electrons
angular distribution of slow radiation at energies from 12-22 MeV as function of target thickness and Z 2–28022
Compton scattering, theory of polarization phenomena 2–14978
elastic scattering, nuclear radii in high energy limit 2–8325
elastic scattering, short range correlations 2–35014

Nuclear reactions and scattering due to continued
electrons continued
electrodisintegration cross sections, nuclear bond scheme 2—8328
electron capture, inner bremsstrahlung theories 2—38580
energy resolution improvement and target thickness increasing in 180° expt. 2—28021
even-even nuclei, scattering from one- and two-phonon vibrational states 2—31526
Goldhaber-Teller oscillating liquid-drop model and inelastic electron scattering in light nuclei 2—27945
hypernucleus production, in high energy reactions 2—21372
inelastic scattering on finite nuclei, calc. of response function using perturbation theory 2—2765
light nuclei, disintegration, nucleon polarization 2—31525
light nuclei electro-excitation cross section depend. on coupling scheme 2—14977
low energy scattering by light nuclei nuclear dispersive contribs. 2—18176
odd-mass nuclei, scattering description using particle-core and particle-phonon coupling models 2—38578
proton structure from electron scattering using liquid H and D targets 2—2574
spectrum shape at high energies, application to proton and deuteron targets 2—2520
WKB method, generalized, second approx. 2—24203
Al, ratio of photodisintegration to electrodisintegration for 5.0 GeV bombardment 2—11822
^{36}Ar(e,e)^{36}Ar, 180°, magnetic transitions excitation 2—11738
^{138}Ba(e,e′p) reaction, isobaric analogs 2—2770
^{12}C(e,e′p), quasi free scattering using Saclay linear accelerator, information on shell structure of nuclei obtained 2—5687
^{12}C(e,e′p) at 600 MeV, analysis using Elton-Swift and PHF wave functions, comparison of predicted and exptl. cross section 2—2778
^{12}C(e,p), 100 to 250 MeV, excitation function for protons 2—35009
^{13}C, inelastic scatt., giant reson. study 2—2767
^{40}Ca, magnetic transition strength studied by 180° electron scattering 2—11737
^{40}Ca, quasi free scattering using Saclay linear accelerator, information on shell structure of nuclei obtained 2—5687
^{140}Ce(e,e′p) reaction, isobaric analogs 2—2770
^{63}Cu, scattering description using particle-core and particle-phonon coupling models 2—38578
Fe, ratio of photodisintegration to electrodisintegration for 5.0 GeV bombardment 2—11822
^{1}H, 1180 MeV, inelastic cross section 2—38581
^{2}H(e,e′), below 280 MeV, study of scattered electron spectra 2—18175
^{3}H, high energy inelastic scatt. form factors 2—38576
^{2}He(e,e), low energy scattering nuclear dispersive contribs. 2—18176
^{3}He, high energy inelastic scatt. form factors 2—38576
^{3}He(e,e′d(^{1}H, 16-27 MeV, search for structure in ^{3}He 2—31443
^{3}He(e,e), low energy scattering nuclear dispersive contribs. 2—18176
^{4}He (e,e), form factor in oscillator model including short range correlations 2—38577
^{4}He(e,e), elastic scattering, shell model analysis 2—2766
^{6}Li, 1180 MeV, inelastic cross section 2—38581
^{6}Li, nuclear structure investigation 2—27961
^{6}Li elastic scattering at low momentum transfer, determ. charge form factors, model dependent and independent rms radii 2—24204
^{7}Li elastic scattering at low momentum transfer, determ. charge form factors, model dependent and independent rms radii 2—24204
^{24}Mg, elastic and inelastic scatt. from 0$^+$, 2$^+$, 4$^+$ states, rotational model treatment 2—31454
^{24}Mg, high energy elastic scattering, analysed with phenomenological charge distribution and Woods-Saxon potential 2—8327
^{24}Mg, nuclear charge distributions from elastic electron scattering 2—34922
^{24}Mg, nuclear deformations detn. 2—11783
^{24}Mg(e,e′), form factors using shell-model wave functions 2—35012
^{25}Mg, nuclear charge distributions from elastic electron scattering 2—34922
^{26}Mg, nuclear charge distributions from elastic electron scattering 2—34922
^{92}Mo, elastic electron scattering, 200 and 300 MeV 2—18177
^{14}N(e,e)^{14}N, form factor calc. 2—2768
^{142}Nd(e,e′p) reaction, isobaric analogs 2—2770
^{20}Ne, elastic and inelastic scatt. from 0$^+$. 2$^+$, 4$^+$ states, rotational model treatment 2—31454
^{20}Ne, inelastic scattering, form factors of monopole transitions 2—31455
^{20}Ne(e,e′), form factors using shell-model wave functions 2—35012
^{16}O, inelastic scattering, calc. of response function using perturbation theory 2—2765
^{16}O(e,e), form factor in oscillator model including short range correlations 2—38577
^{18}O, inelastic scattering cross sections for excitation of levels below 6.0 MeV measured 2—8326
^{208}Pb, differential cross sections measured for scattering from ground and low-lying states 2—11778
^{208}Pb, inelastic scatt. rel. to nuclear structure investigations 2—18111
^{208}Pb(e,e), 124, 167 MeV, elastic cross sections at moderate momentum transfers, model-independent description of nuclear charge distrib. 2—28023
Pb(e,e), A=206 to 208, 30 to 90 MeV, cross sections, charge distribution parameters 2—38579
S, high energy elastic scattering, analysed with phenomenological charge distribution and Woods-Saxon potential 2—8327
^{32}S, inelastic electron scatt. through 180°, giant resonance structure 2—24205
^{32}S, magnetic transition strength studied by 180° electron scattering 2—11737
^{32}S(e,e′), form factors using shell-model wave functions 2—35012
^{28}Si, elastic and inelastic scatt. from 0$^+$, 2$^+$, 4$^+$ states, rotational model treatment 2—31454
^{28}Si, high energy elastic scattering, analysed with phenomenological charge distribution and Woods-Saxon potential 2—8327
^{28}Si, nuclear deformations detn. 2—11783
^{28}Si(e,e′), form factors using shell-model wave functions 2—35012
^{144}Sm(e,e′p) reaction, isobaric analogs 2—2770
Sn (A=116,118,124), 225.0 MeV, rel. to charge density distribution parameters 2—21393
^{88}Sr, inelastic scatt. rel. to nuclear structure investigations 2—18111

Nuclear reactions and scattering due to continued
electrons continued
Ta, ratio of photodisintegration to electrodisintegration for 5.0 GeV bombardment 2—11822
Zn e scatt., stable even-even isotopes, cross-section ratios and rms radius 2—11819
Zr, A=90-92, 94, 96, elastic scattering, diff. cross sections meas at 300 MeV, isotopic depend. of charge distributions 2—11820
^{90}Zr, elastic electron scattering, 200 and 300 MeV 2—18177
gamma-rays *see Nuclear reactions and scattering due to/photons*
heavy ions *see Nuclear reactions and scattering due to/nuclei of Z>2*
helium-3
^{116}Cd(^{3}He,d)^{117}In, study of In level scheme via proton transfer reactions 2—27983
elastic scatt. cross sections, complex ang. momentum methods 2—35061
optical interaction, absorptive potential description of underlying one body structure 2—28069
scattering, nonlocal optical potential 2—11851
stripping reaction, trinucleon induced, normalization factor for zero and finite range DWBA calc. 2—15004
(^{3}He, ^{7}Be), four nucleon pick up reaction, mechanism and strengths 2—15002
(^{3}He, Li), four nucleon pick up reaction , mechanism and strengths 2—15002
(^{3}He,^{6}Li) on A=10-27 nuclei. ang. distrib. and triton reduced widths 2—18229
(^{3}He,n) reaction up to the continuum near A=50 2—31582
(^{3}He,t) reactions, pickup-stripping mechanism 2—21442
^{a}Sb(^{3}He,d), A=121, 123, at 25 MeV, determ. energy levels of ^{122,123}Te 2—18119
^{27}Al(^{3}He,$\alpha\gamma$)^{26}Al, location of second $J^{\pi}=0^{+},T=1$ state in ^{26}Al 2—38488
^{40}Ar(^{3}He,α)^{39}Ar, single neutron hole states population below 11.4 MeV excitation energy 2—27973
^{10}B, ^{3}He reactions, ^{13}N compound nucleus from 25 to 36 MeV 2—38640
^{10}B(^{3}He,γ)^{13}N, 25-35 MeV, meas. differential cross section, include resonances not associated with ^{13}N giant dipole resonance 2—21445
^{10}B(^{3}He,pγ)^{12}C, 25-35 MeV, meas. differential cross sections, conclude resonances not associated with ^{13}N giant dipole resonances 2—21445
^{11}B(^{3}He,α) ^{10}B(α_0)^{6}Li, spin-parity determinations of ^{10}B levels 2—5645
^{9}Be(^{3}He, ^{6}Li), considered as direct reaction 2—31572
^{9}Be(^{3}He,^{3}He), 18 MeV, polarization of ^{3}He, cross sect. ang. distrib. 2—18219
^{9}Be(^{3}He, $\alpha\alpha$)^{4}He, 3 and 4 MeV, study of three α-particle final state, meas. angular correlations 2—24238
^{9}Be(^{3}He,n), 2.1 to 3.9 MeV, neutron polarization 2—8359
^{12}C(^{3}He,^{3}He), 20 MeV, 18 MeV, polarization of ^{3}He, cross sect. ang. distrib. 2—18219
^{12}C(^{3}He,^{3}Heγ), reaction-plane and spin-flip angular correlations 2—21446
^{13}C(^{3}He,n), 5.5 and 6.2 MeV, ^{15}O level study 2—18090
^{13}C(^{3}He,n)^{15}O, 6 MeV, cross section meas., ^{15}O deduced levels, spectroscopic factors, used to test coeffs. of fractional parentage 2—27966
^{14}C(^{3}He, ^{3}He), 2 to 7 MeV, angular distributions and excitation functions, levels of ^{17}O deduced 2—38476
^{14}C(^{3}He, α), 2 to 7 MeV, angular distributions and excitation functions, levels of ^{17}O deduced 2—38476
^{14}C(^{3}He, d), 2 to 7 MeV, angular distributions and excitation functions, levels of ^{17}O deduced 2—38476
^{14}C(^{3}He, p), 2 to 7 MeV, angular distributions and excitation functions, levels of ^{17}O deduced 2—38476
^{14}C(^{3}He,p)^{16}N, study of level scheme and spin and parity of ^{16}N 2—31449
Ca isotope targets, 29 MeV elastic scattering, determ., optical model parameters 2—18221
Ca(^{3}He, ^{4}He), 13.0 MeV, on even isotopes, ang. distrib. of transitions 2—15012
^{44}Ca nucleus, inelastic scattering to positive parity states at 29 MeV in microscopic model 2—15013
^{46}Ca(^{3}He,p)^{48}Sc, ^{48}Ca(^{3}He,p)^{50}Sc, obs. of strongly excited 1$^+$ states in Sc nuclei 2—34937
^{46}Ca(^{3}He,p)^{48}Sc, nuclear spectroscopy of ^{48}Sc 2—34938
^{48}Ca(^{3}He,t′)^{48}Sc, effect of two step process 2—21447
^{48}Ca(^{3}He,t)^{48}Sc, 23 MeV, study of levels of ^{48}Sc 2—31467
^{35}Cl(^{3}He,p)^{37}Ar, between 9 and 14 MeV, comparison with DWBA calc. 2—18235
^{59}Co(^{3}He,α)^{58}Co, high-resolution study of ^{58}Co energy levels 2—34943
Cr, isotope targets 29 MeV, elastic scattering, determ. optical model parameters 2—18221
^{50}Cr nucleus, inelastic scattering to positive parity states at 29 MeV in microscopic model 2—15013
^{50}Cr(^{3}He,t), 21.4 to 37.5 MeV, energy dependence of transitions to isobaric analogue ground states 2—31583
^{50}Cr(^{3}He,t)^{50}Mn, ^{50}Mn levels obs. 2—11744
^{50}Cr(^{3}He,t)^{50}Mn, 21.4-37.5 MeV, differential cross sect., deduced level scheme ^{50}Mn, energy dependent effects 2—11743
^{52}Cr nucleus, inelastic scattering to positive parity states at 29 MeV in microscopic model 2—15013
^{52}Cr(^{3}He,p), 15 and 16.5 MeV, ^{54}Mn level scheme study 2—21448
^{54}Cr(^{3}He,p)^{56}Mn, 15 MeV, meas. of proton angular distributions, ^{56}Mn deduced levels 2—505
Cu, A=63, 65, meas. of differential cross sections for 33 MeV elastic scattering, optical model analysis 2—28067
^{63}Cu(^{3}He,d)^{64}Zn, anal. of spectroscopic factors using intermediate coupling approach of unified model 2—2811
^{65}Cu(^{3}He,^{4}He), 32 MeV, differential ranges of ^{64}Cu recoils meas. by electrostatic collection technique 2—35077
^{65}Cu(^{3}He,d)^{66}Zn, anal. of spectroscopic factors using intermediate coupling approach of unified model 2—2811
^{162}Er, bombardment with 110 MeV ^{3}He particles, production of new α emitting isotopes ^{155,156}Tm 2—11801
^{19}F(^{3}He, ^{4}He)^{18}F(^{4}He)^{14}N, collinear particle-particle angular correlation meas. to determ. spins of 5.61 and 5.67 MeV levels of ^{18}F 2—11730
^{54}Fe(^{3}He,n)^{56}Ni, 14 MeV, meas. angular distributions, deduced ^{56}Ni energy levels 2—27977
^{54}Fe(^{3}He,p)^{56}Co, levels of ^{56}Co 2—2709
^{54}Fe(^{3}He,t), 21.4 to 37.5 MeV, energy dependence of transitions to isobaric analogue ground states 2—31583
^{54}Fe(^{3}he, dγ)^{55}Co, e.m. transitions in ^{55}Co 2—27976
^{56}Fe(^{3}He, t), charge exchange reaction to 0$^+$ and 2$^+$ analogue states, channel coupling effects 2—28035
^{56}Fe(^{3}He,p)^{58}Co, energy level scheme for ^{58}Co 2—21388
^{57}Fe(^{3}He,d)^{58}Co, high-resolution study of ^{58}Co energy levels 2—34943

Nuclear reactions and scattering due to continued
helium-3 continued
^{58}Fe(^{3}He,p) two-particle transfer reaction, investigation of ^{60}Co 2—31474
^{2}H(^{3}He,^{3}He), 7-18 MeV c.m. energy, meas. of cross section, no evidence of ^{5}Li excited states 2—28060
^{2}H(^{3}He,^{4}He)^{1}H, 7-18 MeV c.m. energy, meas. of cross section, no evidence of ^{5}Li excited states 2—28060
^{2}H(^{3}He,γ)^{5}Li, 2-26 MeV, transition intensities to levels in ^{5}Li, deduced levels 2—11860
(^{3}He,d), strength of reaction to unbound final states, correlation with penetrability for proton decay 2—15005
^{3}He,p) reactions with even targets in Ca-Fe range, search for 0^{+} antianalog states 2—11858
^{3}He(^{3}He,^{3}He), imaginary potential in resonance-group calculation 2—18217
^{3}He(^{3}He.2p)^{4}He, total cross section meas. below Coulomb barrier 2—2800
^{3}He(^{3}He,p^{4}He)p, kinematically complete expt., determ. of proton-proton scattering length 2—28073
^{4}He, elastic scatt., exchange reson., neutron-transfer model 2—2801
^{4}He, elastic scattering at 44.5 MeV studied in resonating group formalism, exchange effects 2—11855
^{6}Li(^{3}He,α)^{5}Li, search for high lying levels in ^{5}Li 2—31445
^{7}Li(^{3}He,α)^{6}Li, isospin and decay modes of ^{6}Li at E_{τ}=1.5 MeV 2—27969
^{7}Li(^{3}He,α)^{6}Li*(d)^{4}He, isospin and decay modes of ^{6}Li at E_{τ}=1.5 MeV 2—27969
^{7}Li(^{3}He,pn) used to study isospin forbidden particle decay of first T=3/2 states in ^{9}Be and ^{9}B 2—27964
^{24}Mg(^{3}He,pγ)^{26}Al, location of second J^{π}=0^{+}, T=1 state in ^{26}Al 2—38488
^{25}Mg(^{3}He.dγ)^{26}Al, location of second J^{π}=0^{+}, T=1 state in ^{26}Al 2—38488
^{26}Mg(^{3}He.t) charge exchange reaction to 0^{+} and 2^{+} analogue states, channel coupling effects 2—28035
^{92}Mo(^{3}He,d)^{93}Tc, levels up to a few MeV in ^{93}Tc 2—28079
^{92}Mo(^{3}He,dp)^{92}Mo, study of proton decay of six analogs of low-lying states in ^{93}Mo 2—28079
^{14}N(^{3}He.p)^{16}O, structure of states of ^{16}O 2—8285
^{15}N (^{3}He,p) ^{17}O double-stripping reaction at 18 MeV, study of 2p-1h structure of ^{17}O 2—24150
^{93}Nb(^{3}He,^{7}Be), 41 MeV. α pickup, reaction cross section 2—11868
^{20}Ne(^{3}He. ^{4}He)^{19}Ne, 18 MeV, study of excited states in ^{19}Ne, energy meas. 2—11862
^{22}Ne(^{3}He,d)^{23}Na, 15 MeV, excitation energies and angular distributions of levels in ^{23}Na below 10.2 MeV 2—11735
Ni, A=58, 60, 62, 64, meas. of differential cross sections for 33 MeV elastic scattering, optical model analysis 2—28067
^{58}Ni(^{3}He,n)^{60}Zn, 15 MeV, meas. angular distributions, deduced ^{56}Ni energy levels 2—27977
^{58}Ni(^{3}He.p)^{60}Cu, shell model calculation 2—38644
^{60}Ni(^{3}He,t')^{60}Cu*, quasi-inelastic scatt., effect of 2 step processes coupling potentials 2—31532
^{62}Ni, 37.7 MeV, global optical model analysis of elastic scatt. 2—38633
^{62}Ni(^{3}He.t), 21.4 to 37.5 MeV, energy dependence of transitions to isobaric analogue ground states 2—31583
^{16}O(^{3}He,^{3}He)^{16}O, study of levels of ^{19}Ne 2—27967
^{16}O(^{3}He,^{3}He) 18 MeV, 18 MeV, polarization of ^{3}He, cross sect. ang. distrib. 2—18219
^{16}O(^{3}He,α)^{15}O, study of levels of ^{19}Ne 2—27967
^{16}O(^{3}He,p)^{18}F, 2.95 MeV, parity of 3134 keV J=1 state in ^{18}F 2—14936
^{18}O(^{3}He,d)^{19}F, distorted wave calculation of spectroscopic factors for T=$^{3}/_{2}$ states in ^{19}F 2—11720
^{190}Os(^{3}He,d)^{191}Ir, proton state population in ^{191}Ir 2—5666
^{192}Os(^{3}He,d)^{193}Ir, proton state population in ^{193}Ir 2—5666
^{31}P(^{3}He,p)^{33}S, 6 to 14 MeV, angular distributions of four proton groups 2—8362
^{208}Pb(^{3}He,^{3}He'), ang. distrib. of levels excited in ^{208}Pb, 43.7 MeV 2—24236
^{208}Pb(^{3}He,n) two-nucleon transfer cross sections, effect of ground state correlations 2—38602
^{208}Pb(^{3}He,p) two-nucleon transfer cross sections, effect of ground state correlations 2—38602
^{32}S(^{3}He, ^{4}He)^{31}S, search for 1p neutron strength in ^{31}S, study of levels above E_{x}=4.5 MeV 2—14942
^{32}S(^{3}He,d) ^{33}Cl, 29.7 and 34.5 MeV, determ. single particle strengths for quasibound levels in ^{33}Cl 2—24153
^{28}Si(^{3}He,^{6}He)^{25}Si, 70.4 MeV, obs. of ^{25}Si excited states 2—34923
^{28}Si(^{3}He,α)^{27}Si, lifetimes of lower excited states in ^{27}Si 2—18098
^{28}Si(^{3}He,$\alpha\gamma$)^{27}Si, angular correlations and branching ratios of levels in ^{27}Si below 5MeV excitation 2—24152
^{29}Si(^{3}He,α)^{28}Si, 12 MeV, energy levels of ^{28}Si 2—34925
^{30}Si(^{3}He, pγ)^{32}p, γ-decays of lowest T=2 state of ^{32}p 2—8293
^{144}Sm(^{3}He,α)^{143}Sm, 18 MeV, spectroscopic factors, momentum mismatch 2—506
^{116}Sn(^{3}He,d)^{117}Sb*, strength of reaction to unbound final states 2—15005
^{88}Sr(^{3}He,d)^{89}Y 33.4 MeV, single-proton transfer reaction, study of ^{88}Sr ground state, ^{89}Y deduced levels 2—38645
Ti, isotope targets 29 MeV, elastic-scattering, determ. optical model parameters 2—18221
Ti (A=46; 50), 37.7 MeV, global optical model analysis of elastic scatt. 2—38633
^{46}Ti nucleus, inelastic scattering to positive parity states at 29 MeV in microscopic model 2—15013
^{48}Ti nucleus, inelastic scattering to positive parity states at 29 MeV in microscopic model 2—15013
^{48}Ti(^{3}He,t')^{48}V*, quasi-inelastic scatt., effect of 2 step processes coupling potentials 2—31532
^{50}Ti nucleus, inelastic scattering to positive parity states at 29 MeV in microscopic model 2—15013
^{51}V, 37.7 MeV, global optical model analysis of elastic scatt. 2—38633
^{51}V(^{3}He,d)^{52}Cr, 11.0 MeV, determ. of lifetimes of low-lying levels in ^{52}Cr 2—11746
^{89}Y(^{3}He,t)^{89}Zr to $T_{<}$ states, shapes of angular distributions determ. 2—11866
^{173}Yb(^{3}He,α)^{172}Yb, empirical evidence for Coriolis coupling of octupole states of ^{172}Yb 2—24173
Zn, A=64, 66, 68, meas. of differential cross sections for 33 MeV elastic scattering, optical model analysis 2—28067
^{64}Zn foils 22.2-43.4 MeV, determ. γ-ray spectra half lives of isotopes, cross section, excitation function, reaction mechanisms 2—24239
^{90}Zr(^{3}He,d)^{91}Nb isobaric energy splitting between $T_{>}$- and $T_{<}$-single particle states in ^{91}Nb 2—2716
^{90}Zr(^{3}He,t), 21.4 to 37.5 MeV, energy dependence of transitions to isobaric analogue ground states 2—31583

Nuclear reactions and scattering due to continued
helium-3 continued
^{91}Zr, 37.7 MeV, global optical model analysis of elastic scatt. 2—38633
^{92}Zr(^{3}He,^{7}Be), 41 MeV, α pickup, reaction cross section 2—11868

hyperons
No entries

mesons
see also Cosmic rays/effects and interactions
A=3+hypernucleus, production by K^{-} reaction at 1.5 GeV/c studied 2—38621
hypernuclei production in 1.5 GeV/c K^{-} interactions with light nuclei 2—38622
isobaric analogue states, excitation 2—2790
K capture in kaonic atoms, rel. to nuclear density distributions 2—15253
neutral vector meson photoproduction 2—5546
pion nucleus scattering, use of current algebra sum rules for determ. πN sigma term 2—14993
pion-nucleus charge exchange scattering at intermediate energies, calc. using Kisslinger optical potential 2—8350
pion-nucleus reaction, coherent 3π production in A_{1} region, model for $\rho\omega$ interference 2—38623
pions, high energy interactions with heavy emission nuclei, production of fast He and ^{3}H nuclei 2—38624
stopped negative pion interaction with C, obs. of emitted charged secondaries 2—35058
(π-, nn), 2pπ absorpt. comparison with 1sπ 2—38626
(π,$\pi l^{+}l^{-}$), π e.m. form factors meas. possibility 2—14644
^{4}He($\pi\pi$), amplitude calc. using Glauber model 2—14971
K--nucleus potential real part, 800 GeV/c 2—8348
K-, stopped in various target elements, calc. probability of formation of Σ hyperonic atoms 2—12062
K, K$l^{+}l^{-}$), K e.m. form factors meas. possibility 2—14644
K scattering above ~2 GeV/c, coherent prod. reactions 2—28055
K^{-} induced reactions, determ. of nuclear size from cross sections, for C, Al, Sn and Pb 2—11719
$K^{-}p\to\eta\Lambda$ cross section dip at $-t\sim0.4$ GeV^{2}, explanation 2—14626
L-, interaction with A$\doteq$20 nuclei, coherent prod. of K*- (890) at 10 and 12.7 GeV/c 2—8158
π-nucleus interaction in (3,3) resonance region, compaison of Kisslinger and Glauber models 2—24230
π-, 60 GeV/c interactions with light and heavy nuclei, investigation using standard and enriched emulsions 2—34685
π, nucleus scattering lengths analyzed in soft-pion theory and Fubini-Furlan mass dispersion relations 2—28054
π absorption, phenomenological model of p-wave absorption, coupling consts 2—28056
π elastic scattering on light nuclei, study in momentum space with Kisslinger's model 2—14994
π induced reactions, double charge exchange, nuclear structure studies 2—31564
π production on nuclei from Be to Pb, determ. of unstable boson-nucleon total cross sections 2—420
Π reaction on nucleus with A nucleons, production and decay of two interfering meson resonances 2—34697
π scattering, <100 MeV, s wave interaction, size resonance in partial amplitudes 2—31563
π scattering, energy region of resonance applicability of Glauber approx. 2—8349
π scattering, in nuclear matter in momentum transfer region 2—5686
π scattering above ~2 GeV/c, coherent prod. reactions 2—28055
π^{-} induced reactions, determ. of nuclear size from cross sections, for C, Al, Sn and Pb 2—11719
$\pi^{\pm}$ absorption cross sections, rel. to neutron distrib. in nuclei 2—2791
$\pi(K)+A\to\pi(K)+A+l^{+}+l^{-}$, $\geqslant$40 GeV, for meas. of e.m. form factors of π and K 2—14628
π>2 GeV, double charge exchange on nuclei, Glauber theory 2—14995
^{10}B(π^{+},P^{0})^{10}C near (3,3) resonance, impulse approx. 2—8353
^{11}B(π^{+},π^{0})^{11}C near (3,3) resonance, impulse approx. 2—8353
^{9}Be, pionic X-ray yields meas. using absolute efficiency technique, pion cascade calc. of 2p-level widths 2—28057
^{12}C, calculation of multiple scattering of pions 2—28058
^{12}C, K^{-}-capture, study of binding energy of product $_{\Lambda}{}^{10}$B 2—24146
^{12}C, pion-capture obs. 2—5707
^{12}C, pionic X-ray yields meas. using absolute efficiency technique, pion cascade calc. of 2p-level widths 2—28057
^{12}C, radiative π capture, neutron-photon angular correlations and energy spectrum of neutrons 2—11849
^{12}C cascade interactions with π^{-}, 5 GeV/c two-Λ^{0} prod. 2—14707
^{12}C(π,r), giant dipole resonance, transitions to odd parity states of ^{12}B 2—18214
^{12}C(π-, nn) 2Pπ absorpt., comparison with 1sπ 2—38626
^{12}C(π^{-},np), 100 MeV, energy and angle measurements 2—21440
^{13}C(π^{+},π^{0})^{13}N near (3,3) resonance, impulse approx. 2—8353
^{35}Cl, pion-capture obs. 2—5707
^{35}Cl and ^{37}Cl kaon capture, obs. of γ-rays emitted from ^{32}P first excited state 2—28059
Dy, K^{-} capture, effect of nuclear deformation on absorption rate 2—499
^{19}F pion-capture obs. 2—5707
^{157}Ge, perturbation effect on K- absorpt. 2—38628
^{3}H, pion absorption in (3,3) resonance region 2—35057
^{3}He, pion absorption in (3,3) resonance region 2—35057
^{3}He, π^{-} absorption, computation using Eckstein phenomenological model 2—8351
^{4}He, elastic pion scatt., differential cross section at 7.76 GeV/c 2—8352
^{4}He, $\pi^{\pm}$ elastic scattering at 97 MeV, meas. with high-pressure streamer chamber 2—24231
^{4}He, radiative pion capture rate from low lying Bohr orbits calculated 2—11848
^{6}Li, pionic X-ray yields meas. using absolute efficiency technique, pion cascade calc. of 2p-level widths 2—28057
^{6}Li(π-, nn) recoil momentum distrib., nucl. shape 2—38625
Ne, K^{-} absorption 2—8354
^{16}O, K^{-}-capture, study of binding energy of product $_{\Lambda}{}^{7}$Li 2—24146
^{16}O, K^{-} capture, study of deexcitation γ-rays, rates to proton or neutron single hole states in ^{15}O and ^{15}N 2—11850
^{16}O, pionic X-ray yields meas. using absolute efficiency technique, pion cascade calc. of 2p-level widths 2—28057
^{16}O, π-capture, nuclear deexcitation γ rays from ^{14}N, ^{15}N and ^{14}C 2—2691
^{16}O, π^{+} elastic and inelastic scattering, 385 MeV/c 2—24232
^{16}O target, disruption by capture of π^{-} in nuclear emulsion 2—38627

Nuclear reactions and scattering due to continued
- **mesons** continued
  - ^{208}Pb, K$^-$ capture, study of deexcitation γ-rays, rates to proton or neutron single hole states in ^{207}Pb and ^{207}Tl 2—11850
  - ^{32}S, kaon capture, obs of γ-rays emitted from levels in ^{32}P and ^{19}F 2—28059
  - ^{91}Zr(π^+,π^0)^{91}Nb, single charge exchange obs. by detecting decay proton from ^{91}Nb*, determ. cross section at 30 MeV 2—18215
- **muons**
  - capture, asymmetry of most energetic emitted neutrons, shell model calc. 2—21425
  - capture rate calc. in closure approx. independence of average ν energy adapted 2—31524
  - capture reaction, asymmetry of emitted neutrons 2—38582
  - capture reaction, polarization of emitted neutrons 2—38584
  - neutron multiplicity meas. for cosmic ray μ-capture in Fe, Cu, Zn, Sb, Pb, determ. dependence on A 2—24206
  - radiative capture, effect of finite size of p and π propagator on photon spectrum 2—2769
  - recoil nuclei polarization 2—38583
  - μ^- capture in heavy elements, emitted gamma ray spectra 2—5688
  - ^{12}B recoil nuclei polarization 2—38583
  - ^{12}C, asymmetry of emitted neutrons 2—38582
  - ^{12}C(μ^-,n$\nu\tau$)^{8}Li, reaction channels, angular correlation obs. 2—14979
  - ^{12}C(μ^-,ν)^{12}B, capture, ground state to ground state transition rate determ. 2—11821
  - ^{40}Ca, asymmetry of emitted neutrons 2—38582
  - ^{40}Ca, polarization of emitted neutrons in muon capture 2—38584
  - ^{40}Ca, spectrum and asymmetry of neutrons emitted after polarized muon capture 2—35059
  - ^{151}Eu, muon capture, populations of individual final levels 2—18180
  - ^{153}Eu, muon capture, populations of individual final levels 2—18180
  - Fe(μ,W$_0\nu$)Fe, 80-300 GeV, cross sections and differential distributions for W$_0$ prod. 2—27763
  - ^{4}He, muon capture, neutron spectrum and asymmetry of angular distribution 2—35015
  - ^{4}He, total muon capture rate calc. 2—18179
  - ^{4}He, total negative muon capture rate 2—35016
  - ^{4}He(μ^-,nν)^{3}H, neutron channel study, short range nucleon nucleon correlation effects 2—28024
  - ^{16}O, asymmetry of emitted neutrons 2—38582
  - ^{16}O, spectrum and asymmetry of neutrons emitted after polarized muon capture 2—35059
  - ^{32}S, asymmetry of emitted neutrons 2—38582
  - ^{32}S, polarization of emitted neutrons in muon capture 2—38584
  - ^{28}Si, polarization of emitted neutrons in muon capture 2—38584
  - ^{28}So, asymmetry of emitted neutrons 2—38582
- **neutrinos**
  - doubly-closed-shell nuclei, forward reaction-induced resolutions in limit of giant-resonance excitation 2—35013
  - lepton pair production, differential cross section 2—2764
  - Z(ν_μ,μ^-e$^+\nu_e$)z, to 50 GeV, angular and energy distributions calc. 2—18178
  - Z($\nu\mu$,$\mu^-\mu^+\nu_\mu$)Z to 50 GeV, angular and energy distributions calc. 2—18178
  - ^{12}C, low-energy neutrino excitation of giant resonance 2—34909
  - ^{37}Cl(μ_e,3-)^{37}Ar, cross section computation, detection of solar neutrinos 2—8329
  - Fe(ν,W$_0\mu$)Fe, 80-300 GeV, cross sections and differential distributions for W$_0$ prod. 2—27763
- **neutrons**
  - *see also Nuclear fission*
  - ^{22}Na, short-lived activities excited by 14.7 MeV neutrons 2—18093
  - A=18 to 40, kV capture in 2s-1d shell 2—38610
  - capture cross section in F, Mg, Al, Si, P and S from 20-80 keV, γ-ray spectra meas. 2—28047
  - capture cross sections, statistical theory of nuclear reactions tested in 200 to 800 keV range 2—38604
  - chopped neutrons, influence of nuclear surface and Coulomb interaction on diffraction 2—18197
  - cold neutron time-of-flight spectra analysis using direct fast Fourier transformation 2—11836
  - cross sections at 14 MeV, search for trends by statistical evaluation of available data, further expts. with various targets 2—2782
  - cross sections evaluated, consistency with critical mass data 2—2784
  - elastic scattering, 4.8 GeV/c, small angle differential cross section 2—11641
  - even-even nuclei, $80<A<160$, capture cross sections at 25 keV 2—21439
  - fast n studies, 100 keV<En, review 2—491
  - heavy nuclei (A$\geqslant$130), preformation of α particles by analysis of (n,α) reactions 2—21436
  - induced radioactivity in ground water system near proposed 300 GeV accelerator 2—5622
  - inelastic cross sections, formulae when spin of ground state $\neq$0 2—35041
  - Mn natural target, thermal neutron capture, lifetimes of 26 and 110 keV levels in ^{56}Mn determ. 2—8299
  - multigroup cross sections, effect of wide scattering resonances on group-averaged U and Pu resonance cross sections 2—8380
  - multiparticle reactions, correlation measurements in nuclear emulsions 2—35048
  - multiparticle reactions, correlation measurements in nuclear emulsions 2—35048
  - n-d doublet scattering length, effect of charge dependence of nuclear forces 2—11721
  - neutron induced multiparticle reactions, correlation measurement in nuclear emulsions 2—35048
  - neutron total cross sections in energy range 0.8 to 3.0 MeV 2—35040
  - nonelastic cross section, meas. at 14.2 MeV 2—35019
  - nuclear temps., stat. analysis 2—35042
  - optical, shell effects 2—38605
  - optical model pot., A-depend. 2—35022
  - p-wave capture spectra 2—38611
  - p-wave strength functions, comparison with optical model predictions 2—35043
  - radiative capture cross sections, 14 MeV neutrons, meas. by activation technique 2—2785
  - rare-earth isotopes, capture cross-sections determ. by mass spectrometer 2—496
  - reaction mechanism, study using fast n, review 2—491
  - resonance analysis code by least squares method 2—38607
  - resonance structure, examination by neutron spectroscopy 2—38445

Nuclear reactions and scattering due to continued
- **neutrons** continued
  - scattering of fast neutrons from natural lead targets, 2.2-2.4 MeV, angles >175°, obs. of resonance 2—24225
  - single event spectra, Monte Carlo analysis 2—28106
  - stellar element formation, capture exp. 2—41084
  - target thickness correction in polarized neutron-and-target expts. 2—14987
  - thermal neutron capture, $\gamma\gamma$ angular correlation meas., coincidence apparatus 2—24099
  - threshold reactions for fission neutrons, meas. of averaged neutron cross section 2—35046
  - total cross section meas. for incident neutron momenta 900-2600 MeV/c 2—2781
  - total cross sections for natural Be, C, N, O, Mg, Al and Si, 24-60 MeV 2—11841
  - transuranium nuclide production by neutron capture 2—11695
  - (n, 2n), collision integrals, approx. treatment 2—28040
  - (n, 2n) reaction, shell effect investigations at 14.8 MeV 2—35050
  - (n,2n), for heavy nuclei, cross section meas.. rel. to ^{27}Al(n,α)^{24}Na reaction 2—5700
  - (n,2n) reactions in medium-, heavy-meass region, 14-15 MeV, determ. activation cross sections, isomeric cross section ratios, systematics 2—35047
  - (n,α), for heavy nuclei, cross section meas., rel. to ^{27}Al(n,α)^{24}Na reaction 2—5700
  - (n,α) cross sections, 14 to 15 MeV, dependence on symmetry parameter 2—35051
  - (n,d), on light nuclei, exptl. investigation 2—2787
  - (n,γ), thermal neutron, in reactor, determ. of heat distrib. from γ spectra 2—38737
  - (n,γ) polarization experiments, interference of the two capturing states of oriented nuclei 2—31551
  - (n,γ) reaction study of ^{71}Ge, ^{73}Ge, ^{74}Ge and ^{75}Ge level schemes 2—27979
  - (n,n$'$,γ) reaction with very small scattering samples 2—8342
  - (n,n$'$), collision integrals, approx. treatment 2—28040
  - (n,n$'\gamma$), 14.4 MeV, in mass range A=46-88, cross sections 2—18208
  - (n,n$'\gamma$), multidimensional anal. of differential cross section involving pure isotopes 2—21435
  - (n,n$'\gamma$) reaction, in ^{27}Al, ^{51}V, ^{52}Cr, ^{55}Mn, ^{56}Fe, ^{93}Nb, ^{208}Pb and ^{209}Bi, gamma spectra and cross sections 2—11839
  - (n,n$'\gamma$) reaction on nuclei with A = 11-40, analysis of γ-ray spectra 2—35045
  - (n,nγ) reaction cross sections, use of statistical models for A=46-88 mass range 2—31556
  - (n,p), (n,α) reactions on light and medium nuclei, mechanism 2—38608
  - (n,p), for heavy nuclei, cross section meas., rel. to ^{27}Al(n,α)^{24}Na reaction 2—5700
  - (n,p), total cross section calc., Hauser-Feshbach method 2—21417
  - (n,pn), total cross section calc., Hauser-Feshbach method 2—21417
  - n, 2n) to fission ratios in fast reactors 2—31606
  - n,γ process, cross-sections, spin depend. meas. 2—24226
  - Al, total cross section between 23 and 45 MeV meas. by time-of- flight technique with transmission method 2—38609
  - ^{27}Al(n,γ)^{28}Al, circular polarization meas., levels of ^{28}Al 2—18206
  - ^{27}Al(n,p)^{27}Mg cross section meas. by β counting ^{27}Mg activity in Al foils, energies to 5.6 MeV 2—28049
  - Al(n,γ), 15 MeV, meas. of γ-ray spectra and differential 80° cross sections for discrete γ-ray line production 2—31555
  - Al(n,xγ), 5.3-9.0 MeV, cross sect. meas. spectra, ground state decay of levels 2—14989
  - ^{241}Am, absorption cross section meas. 2—498
  - ^{241}Am(n,γ)^{242}Am fast neutron radiative capture cross-sections 2—11847
  - ^{243}Am(n,γ)^{244}Am fast neutron radiative capture cross- sections 2—11847
  - ^{40}Ar(n,γ)^{41}Ar circular polarization meas., levels of ^{41}Ar 2—18206
  - ^{75}As(n,n$'\gamma$), inelastic scattering at 0.8-2.2 MeV, energy levels and transitions determined 2—11750
  - ^{195}Au(n,2n) cross sections to 12$^-$, 5$^+$ and 2$^-$ states of ^{196}Au 2—2731
  - ^{197}Au(n,γ) ^{198}Au cross-section at 22.8 keV, Monte Carlo calculation of neutron energy spectrum 2—5704
  - ^{198}Au(n,γ)^{199}Au, level scheme ^{199}Au below 1 MeV, examination, determ. of level energies 2—5669
  - ^{10}B(n,α)^{7}Li, 0.48 MeV, differential cross sect. for α- particles to ground and first excited states in ^{7}Li 2—11842
  - Ba (A=134, 135, 136, 137), neutron resonances 2—11844
  - ^{130}Ba(n,2p)^{131}Xe origin of excess ^{131}Xe in lunar rocks 2—7506
  - Be, total cross section between 23 and 45 MeV meas. by time-of-flight technique with transmission method 2—38609
  - ^{209}Bi, fast-neutron scattering, angular distributions 2—18202
  - Bi(n,n), elastic and inelastic scatt., 14.8 MeV, differential cross sect., collective state excitation 2—21434
  - C, total cross section between 23 and 45 MeV meas. by time-of- flight technique with transmission method 2—38609
  - ^{12}C, low energy scatt. cross sections, Hartree-Fock approx. 2—11837
  - ^{12}C(N,N), to 5 MeV, polarization of neutrons at 50° scattering 2—11838
  - ^{12}C(n,α)^{9}Be, 14 MeV, cross section, study by 1″×1″ stilbene scintillator 2—28046
  - ^{12}C(n,n$'$)3α, 14 MeV, cross section, study by 1″×1″ stilbene scintillator 2—28046
  - ^{12}C(n,n), backward scattering of 14.1 MeV particles, ang. distrib. meas. 2—18199
  - ^{12}C(n,n)^{12}C, comparison of Feshbach and R-matrix theories 2—38613
  - ^{12}C(n,n)^{12}C, comparison of Feshbach and R-matrix theories, particle-rotator model of ^{13}C 2—31549
  - ^{12}C(n,n)^{12}C, comparison of Feshbach and R-matrix reaction theories, shell model of ^{13}C 2—31548
  - ^{12}C(n,n)^{12}C 1.9-5.2 MeV, polarization and differential cross-section 2—18200
  - ^{40}Ca, elastic neutron scattering for energies up to 2 MeV 2—35054
  - ^{40}Ca, low energy scatt. cross sections, Hartree-Fock approx. 2—11837
  - ^{40}Ca(d,n), neutron polarization meas., comparison with DWBA calc. 2—38614
  - ^{40}Ca(n,$\alpha\gamma$)^{37}Ar, $4.85\leqslant E_n\leqslant 8.05$ MeV, meas. of γ spectra 2—38615
  - ^{40}Ca(n,γ)^{41}Ca circular polarization meas., levels of ^{41}Ca 2—18206
  - ^{40}Ca(n,n$'\gamma$)^{40}Ca, $4.85\leqslant E_n\leqslant 8.05$ MeV, meas. of γ spectra 2—38615
  - ^{40}Ca(n,pγ)^{40}K, $4.85\leqslant E_n\leqslant 8.05$ MeV, meas. of γ spectra, transitions in ^{40}K 2—38615
  - ^{43}Ca(n,γ)^{44}Ca γ-ray spectra, assignment of transitions to levels in ^{44}Ca 2—24158
  - Ca(n,γ) A=40, 42, 44, gamma-ray spectra 2—2788

Nuclear reactions and scattering due to continued
  neutrons continued
    Cd isotopes, total and scatt. cross-sections 2—24228
    ^{140}Ce, elastic scatt., local optical nuclear model 2—5698
    Ce(n,γ), 14 MeV, spectra of photons 2—8345
    ^{252}Cf synthesis in underground thermonuclear explosion 2—35094
    ^{250}Cm synthesis in underground thermonuclear explosion 2—35094
    ^{59}Co, elastic scatt., local optical nuclear model 2—5698
    ^{59}Co, meas. of spin-spin effect in neutron total cross section from 0.3 to 8.0 MeV 2—18210
    ^{59}Co(n,γ)^{60}Co. polarized thermal neutrons, γ-ray circular polarization 2—18211
    ^{133}Cs(n,γ), 14 MeV, spectra of photons 2—8345
    Cu, total cross-section between 23 and 45 MeV meas. by time-of-flight technique with transmission method 2—38609
    Cu(n$_{th}$,γ), natural copper, study of levels in ^{64}Cu up to 2300 keV 2—14939
    ^{161}Dy, neutron resonance, spin assignment 2—18131
    ^{163}Dy, neutron resonance, spin assignment, hyperfine coupling constants 2—18131
    Er, fast-neutron scattering, angular distributions 2—18202
    ^{18}F, short-lived activities excited by 14.7 MeV neutrons 2—18093
    ^{19}F, polarized thermal neutron scattering, spin-spin amplitude calc. 2—5697
    ^{19}F, spin-dependent part of scattering amplitude, meas. using polarized beam and polarized CaF$_2$ target 2—35053
    ^{19}F, spin-dependent part of slow neutron scatt. amplitude, meas. using polarized beam and polarized target 2—31550
    Fe, effective cross section in Doppler reson. region of large fast reactor 2—38726
    Fe, keV resonance neutron capture 2—18194
    Fe, natural, measurements of neutron cross-section minima 2—31558
    Fe. scatt. of 14 MeV neutrons, collective states excitation 2—14990
    ^{56}Fe, cross sections for inelastic interaction, $E_n \lesssim 20$ MeV 2—28048
    ^{56}Fe, total cross sections for (n,γ), (n,n′), (n,p) (n,2n) and (n,np), statistical model calcs. 2—494
    ^{56}Fe(n,p), threshold detector for fast neutron spectrum investigations, meas. of activation integral 2—34822
    ^{58}Fe(n,γ)^{59}Fe, γ-ray spectra obs. following thermal neutron capture 2—5702
    Fe(n,γ), use of Ge(Li) γ-ray detector 2—34806
    ^{257}Fm synthesis in underground thermonuclear explosion 2—35094
    ^{69}Ga, radiative capture cross section 2—8343
    ^{71}Ga, radiative capture cross section 2—8343
    Ga(n,γ), γ-ray circular polarization, spin assignments 2—18209
    ^{155}Gd(n,γ)^{156}Gd, gamma-ray transitions in ^{156}Gd 2—27987
    ^{158}GdO/^{157}GdO lunar rocks, enrichments due to neutron capture, irradiation histories 2—13978
    ^{70}Ge, thermal neutron capture, initial state excitation 2—11843
    ^{1}H, polarization of scattered neutrons, meas. at 32 MeV 2—15008
    ^{1}H, total cross section in MeV region 2—28045
    ^{1}H(n,γ)^{2}H, discrepancy between theory and expt. for total radiative thermal np capture cross section discussed, polarization effects 2—31552
    ^{2}H, elastic scatt. and polarization calc. with tensor force and p-wave interaction 2—28041
    ^{2}H, inelastic scatt., DWA calcs. 2—35044
    ^{2}H, total cross section in MeV region 2—28045
    ^{2}H scattering, upper and lower bounds on phase shifts in variational formulation 2—28042
    ^{2}H+n, scattering lengths and triton binding energy, Faddeev formalism with local potential 2—21437
    ^{2}H(n,n), elastic scattering at low energy, study of neutron observables, calc. differential cross section, depolarization factor 2—24224
    ^{2}H(n,n), phase parameters and differential cross section by Pade technique 2—14988
    ^{2}H(n,nnp), study of n-n interaction at 14.5 MeV 2—35052
    ^{2}H(n,p)2n, E_n=14.1 MeV, energy spectra of breakup protons 2—18203
    ^{2}H(n,p)2n, proton spectrum analysis 2—31553
    ^{2}H(n,p)nn, effect of quasifree scattering on shape of kinematically incomplete spectra at forward angles 2—38612
    ^{3}H(n,2n)^{2}H, 13.95 MeV, neutron-neutron scattering length 2—18204
    ^{3}H(n,2n)^{2}H, 13.95 MeV, rel. to neutron-neutron scatt. length 2—2786
    ^{3}He, neutron scattering, 5-matrix elements and phase shift analysis 2—28028
    ^{3}He, scattering of polarized 3 MeV neutrons, determ. resulting asymmetry in elastic scattering 2—24229
    ^{4}He, polarization measurements and analysis of neutron scattering from 11.0 to 30.3 MeV 2—31554
    ^{4}He(n,n), p-wave scattering considered as five body problem 2—492
    ^{178}Hf(n,γ)^{179}Hf, investigation of low energy excited state structure of ^{179}Hf 2—38510
    ^{199}Hg, slow neutron capture, meas. of conversion electron coeffs. and level scheme of ^{200}Hg 2—21397
    ^{165}Ho, cross section, parametric fit 2—497
    ^{113}In(n,n′)^{113m}In, reaction cross sections 2—31560
    ^{115}In (n,n′), threshold detector for fast neutron spectrum investigations, meas. of activation integral 2—34822
    ^{115}In(n,n′γ), energy levels in ^{115}In 2—27982
    ^{39}K, elastic scatt., local optical nuclear model 2—5698
    ^{39}K(n,γ)^{40}K, thermal neutron capture, meas. γ-ray spectra deduced Q-values, excitation energies of ^{40}K levels 2—18207
    ^{40}K, short-lived activities excited by 14.7 MeV neutrons 2—18093
    ^{41}K(n,γ)^{42}K thermal neutron capture, meas. γ-ray spectra deduced Q-values, excitation energies ^{42}K levels 2—18207
    ^{80}Kr(n,γ)^{81}Kr, thermal-neutron capture cross section and resonance capture integral 2—8344
    ^{85}Kr, 10.7 year, thermal neutron capture cross section and resonance integral 2—31559
    ^{139}La, fast-neutron scattering, angular distributions 2—18202
    ^{139}La, radiative capture cross section 2—8343
    ^{139}La(.nγ), 14 MeV, spectra of photons 2—8345
    ^{6}Li(n,α)T, neutron flux monitor, thin glass scintillation system 2—5588
    ^{6}Li(n,p)^{6}He, angular distribution meas. at 14 MeV 2—21438
    ^{7}Li resonant scattering, use as neutron detector in (p,nγ) reactions 2—38382
    ^{7}Li+n, excited states of A=8 system 2—24141
    ^{7}Li(n,^{3}n)^{5}Li, 19 MeV bombardment, search for bound trineutrons using helium-recoil scintillation, cross section meas. 2—493
    ^{7}Li(n,p)^{7}He, ^{7}He→^{3}n+^{4}He, 19 MeV bombardment, search for bound trineutrons using helium-recoil scintillator, cross section meas. 2—493
    ^{175}Lu(n,γ), investigation of ^{176}Lu level structure 2—34971

Nuclear reactions and scattering due to continued
  neutrons continued
    ^{24}Mg(d,n), neutron polarization meas., comparison with DWBA calc. 2—38614
    Mg(n,γ), 15 MeV, meas. of γ-ray spectra and differential 80° cross sections for discrete γ-ray line production 2—31555
    Mn(n,γ), γ-ray circular polarization, spin assignments 2—18209
    ^{92}Mo, excitation functions and isomer ratios for (n,2n), (n,α) and (n,p) reactions 2—35056
    ^{92}Mo, short-lived activities excited by 14.7 MeV neutrons 2—18093
    ^{95}Mo(n,γ)^{96}Mo, thermal, 2 keV and 25 keV neutrons, γ-spectra 2—14991
    ^{97}Mo(n,γ)^{98}Mo, thermal, 2 keV and 25 keV neutrons, γ- spectra 2—14991
    (n,γ) reactions on oriented nuclei 2—35049
    (n,n′γ) reaction, on Ni (A=58,60) and Zn (A=64,66,68), excitation cross section of first 2^{+} levels 2—11840
    N, resolution of nonelastic cross section discrepancy below 9 MeV 2—5696
    ^{14}N(n,p)^{14}C, 14 MeV, ang. distrib. and effective differential cross section meas. 2—5701
    ^{15}N, elastic and inelastic, cross sections and scattering amplitudes 2—31516
    ^{22}Na, slow neutron capture, charged particle emission 2—18205
    Na(n,n), elastic and inelastic scatt., 14.8 MeV, differential cross sect., collective state excitation 2—21434
    ^{93}Nb(n,2n)^{92}Nb, cross section at 14.0 MeV meas. and apparent discrepancy with theory, relevance to fusion reactor technology 2—24227
    ^{143}Nd(n,γ)^{144}Nd, obs. of new energy levels from gamma-ray spectra 2—34960
    Ni, 14 MeV neutron interactions, statistical emission of α-particles 2—35055
    ^{58}Ni(n,p), threshold detector for fast neutron spectrum investigations, meas. of activation integral 2—34822
    ^{59}Ni(n,α) cross sections for thermal neutrons, calc. 2—5703
    ^{62}Ni(n,γ)^{63}Ni, thermal, 2 keV and 25 keV neutrons, γ-spectra 2—14991
    ^{63}Ni, capture cross-section 2—5679
    ^{64}Ni(n,γ)^{65}Ni thermal neutron capture, γ-ray spectra meas., ^{65}Ni energy level deduced 2—28050
    Ni(n,γ), γ-ray circular polarization, spin assignments 2—18209
    N(n,γ), 15 MeV, meas. of γ-ray spectra and differential 80° cross sections for discrete γ-ray line production 2—31555
    ^{237}Np neutron irradiation, different energies, to produce ^{238}Np and ^{238}Pu 2—2789
    ^{238}Np growth, neutron irradiation of ^{235}U and ^{237}Np in different energy spectra 2—2789
    ^{16}O, low energy scatt. cross sections, Hartree-Fock approx. 2—11837
    ^{16}O, low energy scattering, origin of damping of wave functions in nuclear interior 2—11700
    ^{16}O(n,n), low energy S-wave scattering, Hartree-Fock and Perey-Buck non-local potentials, comparison 2—18201
    ^{16}O(n,p)^{16}N, use for oxygen content determ. in Fe powder 2—16716
    O(n,γ), 15 MeV, meas. of γ-ray spectra and differential 80° cross sections for decrete γ-ray line production 2—31555
    ^{190}Os(n,p)^{190}Re, 14.8 MeV, excitation of 3 min activity in ^{190}Re 2—38616
    Pb targets, A=206 to 208, inelastic scattering at 13.7 MeV, angular distributions of neutrons 2—38617
    ^{204}Pb(n,γ), 2 keV capture, absolute cross section determ. from prompt γ-ray spectrum 2—11845
    ^{207}Pb(n,γ), 2 keV capture, absolute cross sections determ. from prompt γ-ray spectrum 2—11845
    ^{207}Pb(n,γ)^{208}Pb thermal neutron capture, γ-spectrum 2—11846
    Pb(n,n), A=206 to 208, 13.7 MeV, angular distributions of neutrons 2—38606
    ^{141}Pr, fast-neutron scattering, angular distributions 2—18202
    ^{141}Pr, radiative capture cross section 2—8343
    Pu, A = 239-241, absorption to fission rate 2—498
    ^{238}Pu growth, neutron irradiation of ^{235}U and ^{237}Np in different energy spectra 2—2789
    ^{239}Pu, ratio of radiation capture and fission cross-sections, $\lesssim$50 keV 2—8347
    ^{239}Pu (n,γ), 0.5-5 MeV, relationship between level density and excitation energy in range 1-8 MeV 2—27999
    ^{239}Pu (n,n), 0.5-5 MeV, relationship between level density and excitation energy in range 1-8 MeV 2—27999
    ^{240}Pu, coherent scatt. amplitude 2—5706
    ^{240}Pu, fast neutron total, elastic and inelastic scattering cross sections 2—8341
    ^{241}Pu, evaluation of neutron cross-sections in unresolved resonance region 2—38620
    ^{242}Pu, coherent scatt. amplitude 2—5706
    ^{85}Rb, short-lived activities excited by 14.7 MeV neutrons 2—18093
    ^{85}Rb(n,2n)^{84m,g}Rb, isomeric cross section ratios 2—24202
    ^{103}Rh (n,n′), threshold detector for fast neutron spectrum investigations, meas. of activation integral 2—34822
    ^{103}Rh(n,n′)^{103m}In, reaction cross sections 2—31560
    Sb isotopes, reson. capture, spin assignment 2—31561
    ^{45}Sc(n,2n)^{44m,g}Sc, isomeric cross section ratios 2—24202
    ^{76}Se(n,γ)^{77}Se, structure of ^{77}Se 2—18212
    ^{77}Se(n,γ)^{78}Se, structure of ^{78}Se 2—18212
    ^{80}Se, thermal neutron capture, initial state excitation 2—11843
    ^{80}Se(n,γ)^{81}Se, captive mechanism, structure of ^{81}Se 2—18212
    Se(n,n′γ), excitation cross sections of first 2^{+} levels in even isotopes, energy dependence 2—28043
    ^{28}Si, cross sections for inelastic interaction, $E_n \lesssim 20$ MeV 2—28048
    ^{28}Si(d,n), neutron polarization meas., comparison with DWBA calc. 2—38614
    ^{28}Si(n,α)^{25}Mg cross-sections meas. to 5.6 MeV using Si semiconductor as target and detector 2—28049
    ^{28}Si(n,p)^{28}Al cross-sections meas. to 5.6 MeV using Si semiconductor as target and detector 2—28049
    ^{29}Si(n,α)^{25}Mg cross-sections meas. to 5.6 MeV using Si semiconductor 2—28049
    ^{30}Si(α,nγ), γ-ray angular distribution, ^{33}S deduced levels 2—18234
    ^{147}Sm, neutron resonances 2—31562
    ^{149}Sm/^{154}Sm lunar rocks, isotopic ratio change 2—13980
    ^{149}Sm, neutron resonances 2—31562
    ^{149}Sm(n,α), cross sections for α transitions using thermal neutrons 2—14992
    ^{115}Sn(n,γ)^{116}Sn, structure of low lying excited states of ^{116}SN 2—31484
    ^{86}Sr(n,γ)^{87}Sr, fluorescence after thermal neutrons capture and energy levels of ^{87}Sr 2—38503

Nuclear reactions and scattering due to continued
neutrons continued
Sr(n,n), elastic and inelastic scatt., 14.8 MeV, differential cross sect., collective state excitation 2—21434
Ta neutron capture γ-ray yields 2—28051
^{159}Tb, 14 MeV, spectra of photons 2—8345
^{232}Th (n,γ), 0.5-5 MeV, relationship between level density and excitation energy in range 1-8 MeV 2—27999
^{232}Th(n,n), 0.5-5 MeV, relationship between level density and excitation energy in range 1-8 MeV 2—27999
Ti, scatt. of 14 MeV neutrons, collective states excitation 2—14990
^{48}Ti(n,γ)^{49}Ti, thermal, 2 keV and 25 keV neutrons, γ-spectra 2—14991
^{48}Ti(n,γ)^{49}Ti, transitiions in ^{49}Ti 2—31557
^{50}Ti(n, γ)^{51}Ti thermal neutron capture, γ-ray spectra meas., ^{51}Ti energy levels deduced 2—28050
^{203}Tl(n,γ)^{204}Tl, γ-spectroscopic analysis of ^{204}Tl nuclear energy levels 2—2737
^{232}Tl(n,2n), average cross-section, neutrons of fission type reactor spectrum and γ-ray intensities of ^{231}Th 2—5705
^{235}U, new values of neutron nuclear data 2—28039
^{235}U, total cross-section fluctuations in the keV range 2—28052
^{235}U neutron irradiation, different energies, to produce ^{238}Np and ^{238}Pu 2—2789
^{238}U/^{235}U cross sections ratio for radiative capture det. and reduction of systematic errors 2—38618
^{238}U, radiative capture and transmission, resonance radiation widths 2—28053
^{238}U, relative capture rate, meas. by foil activation 2—38619
^{238}U, total and scattering cross sections 2—5699
^{238}U(n,γ), γ-ray energy spectra, calculated and measured 2—8346
^{239}U, absorption to fission rate determ. 2—498
^{51}V, cross sections for inelastic interaction, $E_n \lesssim 20$ MeV 2—28048
W neutron capture γ-ray yields 2—28051
W(n,γ), γ-ray circular polarization, spin assignments 2—18209
^{135}Xe, low energy cross section analysed using S-matrix and R-matrix theory, different energy dependence of resonance widths related to unitarity 2—28044
y, scatt. of 14 MeV neutrons, collective states excitation 2—14990
^{174}Yb (n, γ) ^{175}Yb, spectrum study, 26-1500 keV, level scheme of ^{175}Yb 2—18139
^{175}Yb, thermal neutron capture, ^{175}Yb energy level study 2—18138
^{176}Yb(n,γ)^{177}Yb, investigation of low energy excited state structure of ^{177}Yb 2—38510
Zn, total cross section between 23 and 45 MeV meas. by time-of-flight technique with transmission method 2—38609
^{64}Zn(n,p), threshold detector for fast neutron spectrum investigations, meas. of activation integral 2—34822
^{68}Zn, thermal neutron capture, initial state excitation 2—11843
Zr, scatt. of 14 MeV neutrons, collective states excitation 2—14990
^{90}Zr, excitation functions and isomer ratios for (n,2n), (n,α) and (n,p) reactions 2—35056
^{90}Zr, excited isobaric analogue states in ^{91}Zr 2—38504
^{90}Zr, inelastic scatt. cross section 2—2783
^{90}Zr(n,γ)^{91}Zr, fluorescence after thermal neutrons capture and energy levels of ^{87}Zr 2—38503
^{92}Zr(n,γ)^{93}Zr, fluorescence after thermal neutrons capture and energy levels of ^{93}Zr 2—38503
^{94}Zr, absorption cross sections, activation technique meas. 2—495
^{96}Zr, absorption cross sections, activation technique meas. 2—495

nuclei of Z>2
see also Ions/scattering
complex collisions, shell model 2—38649
Coulomb excitation in heavy ion scatt. 2—31588
Coulomb functions in entire (η,ρ) plane, computer program 2—34997
element 104 isotopes possible prod. in heavy-ion bombardment of transuranic nuclei 2—14902
heavy ion alpha transfer reactions 2—2815
heavy ion elastic scattering above Coulomb barrier, generalized Glauber approx. 2—8363
heavy ion reactions, Q-value dependence of cross section 2—38646
heavy ion scattering 2—11697
heavy ions, effective means of producing neutron surplus isotopes of light elements 2—2686
heavy-ion reactions, predominance of proton stripping over proton pickup statistical theory 2—28082
heavy-ion scattering, nuclear potential well depth calc. 2—2814
heavy-ion transfer reactions, Q-value dependence investigated with semi-classical theory 2—15015
kinetic-energy operator, coordinate-dependent mass parameters 2—31591
nucleon transfer reactions, systematics at low energies 2—5713
nucleus-nucleus interactions produced by heavy cosmic ray primaries in nuclear emulsions, 100-500 MeV/nucleon 2—31338
scattering of light fragments, pseudo-potentials coming from nuclear overlap and kinetic energy 2—507
sub-Coulomb heavy-ion neutron transfer reactions, differences between DWBA and Feynman-diagram approach 2—18238
subcoulomb collisions between nuclei of Ca-region, multiple transfer of T=1 pairs and quadruples 2—8364
super-heavy nuclei, production using heavy ion accelerator 2—11696
superheavy element synthesis, using Kr bombardment of compound nuclei 2—21451
transfer reactions between heavy ions 2—21449
transuranium nuclide production by heavy ion reactions 2—11695
^{a}Pt(^{16}O,^{16}O$'\gamma$), A=194-196, 198, 35 MeV, meas. of hyperfine interactions of Pt nuclei recoiling into He, vacuum, g-factors determ. 2—38648
^{a}Sm A=144, 147, bombardment with 103 MeV ^{14}N ions, production of new α emitting isotopes ^{155,156}Tm 2—11801
^{a}Sn, A=116, 120, elastic scattering of ^{16,18}O at energies near the Coulomb barrier 2—11870
^{27}Al(^{35}Cl,^{35}Cl)^{27}Al, lifetime of 843 keV level determ. using recoil distance method 2—8291
^{40}Ar+^{209}Bi transfer reactions, 190 to 270 MeV, determ. excitation function and recoil ranges of produced ^{211}At 2—11875
^{197}Au, elastic scatt. of 30 MeV ^{6}Li ions 2—18239
^{197}Au(^{12}C, 4n)^{205}At, three quasiparticle excitation of ^{205}At 2—18147
^{197}Au(^{24}Mg,5n)^{216}Pa as means of producing ^{216}Pa 2—8365
^{10}B, elastic scatt. of ^{7}Li, optical model analysis 2—38647
^{10}B(^{14}N,^{12}C)^{12}C, quasimolecule search around Coulomb barrier 2—15016
^{10}B(^{14}N,α)^{20}Ne, quasimolecule search around Coulomb barrier 2—15016

Nuclear reactions and scattering due to continued
nuclei of Z>2 continued
^{11}B, ^{16}O induced multi-nucleon transfer reactions rel. to nuclear structure of ^{15}N, ^{16}O, ^{20}Ne 2—38654
^{11}B(^{16}O, ^{15}N)^{12}C 27-60 MeV, meas. cross section, DWBA analysis deduced spectroscopic factors 2—18242
^{9}Be, elastic scatt. of ^{7}Li, optical model analysis 2—38647
^{249}Bk(^{16}O,4n)^{261}Ha, α-emitting isotope production 2—2740
^{249}Bk(^{18}O,5n)^{262}Ha, α-emitting isotope production 2—2740
^{12}C, ^{19}F induced multi-nucleon transfer reactions rel. to nuclear structure of ^{15}N, ^{16}O, ^{20}Ne 2—38654
^{12}C, elastic scatt. of ^{7}Li, optical model analysis 2—38647
^{12}C, elastic scatt. of 30 MeV ^{6}Li ions 2—18239
^{12}C, fragmentation of ^{14}N projectile nuclei at 29 GeV, inclusive isotope spectra at 0° 2—35081
^{12}C+^{12}C carbon-burning in stars, reaction rate 2—13892
^{12}C+^{12}C low energy reaction, phenomenological analysis suggesting α-particle model, calc. of astrophysical reaction rates 2—24240
^{12}C+^{16}O, elastic scattering, phase shift analysis using optical potential 2—38657
^{12}C+^{16}O, quasimolecular resonances 2—38656
^{12}C+^{18}O, excitation functions for the formation of ^{28}Al and ^{29}Al for ^{30}Si excitation energies of 30-40 MeV 2—28084
^{12}C(^{12}C, α)^{20}Ne, pole diagram, compound mechanism 2—11871
^{12}C(^{13}C,α)^{21}Ne, quasimolecule search around Coulomb barrier 2—15016
^{12}C(^{13}C,p)^{24}Na, quasimolecule search around Coulomb barrier 2—15016
^{12}C(^{14}N,α)^{22}Na, quasimolecules search around Coulomb barrier 2—15016
^{12}C(^{14}N,p)^{25}Mg, quasimolecule search around Coulomb barrier 2—15016
^{12}C(^{16}O,α)^{24}Mg, ^{12}C(^{16}O,p)^{27}Al and ^{12}C(^{16}O,d)^{26}Al excitation functions, high spin states of residual nuclei 2—38655
^{12}C(^{16}O,α)^{24}Mg, lifetime meas. of ^{24}Mg levels at 6.431 MeV (0^+) and 8.655 MeV (2^+) 2—38487
^{12}C(^{18}O, ^{18}O*)^{12}C, hyperfine interactions of first excited 2^+ state of ^{18}O in 7^+ and 6^+ ions 2—31451
^{12}C(^{19}F, ^{20}Ne)^{11}B 40-68.8 MeV, meas. cross section, DWBA analysis deduced spectroscopic factors 2—18242
^{12}C(^{19}F,$\alpha p\gamma$)^{26}Mg, lifetime of 1809 keV level determ. using recoil-distance method 2—8291
^{12}C(^{19}F,$n p\gamma$)^{29}Si, lifetime of 3626 keV level determ. using recoil-distance method 2—8291
^{12}C(^{6}Li, d)^{16}O, study of populated negative-parity states in ^{16}O 2—463
^{13}C on various targets, one neutron transfer reactions 2—38652
^{13}C(^{12}C, ^{12}C)^{13}C, 15 MeV and 19 MeV, molecular scattering states of neutron 2—15017
^{14}C+^{16}O, excitation functions for the formation of ^{28}Al and ^{29}Al for ^{30}Si excitation energies of 30-40 MeV 2—28084
^{14}C+^{18}O, excitation functions for formation of ^{30}Al, ^{29}Al and ^{27}Mg for ^{18}O energies of 13-41 MeV 2—28084
^{14}C(^{18}O, ^{16}O)^{16}C two-neutron transfer reaction, 13-41 MeV, determ. excitation functions, compared with attn. ^{18}O induced reactions 2—18243
Ca isotopes, elastic scatt. of ^{16}O, ang. momentum effects 2—35082
Ca(^{16}O,^{16}O), A=40, 42, 44, 48, real part of optical potential combined microscopic and phenomenological approach 2—508
^{40}Ca, elastic scatt. of 30 MeV ^{6}Li ions 2—18239
^{40}Ca(^{18}O, ^{14}C)^{44}Ti pick up reaction at 48 MeV, ang. distrib. to final states, cross sections 2—28086
^{40}Ca(^{6}Li,2n)^{44}V, 18.5 MeV, production of highly neutron deficient vanadium isotope with half-life 90±25 ns 2—11795
^{116}Cd, ^{84}Kr induced fusion reactions, effective threshold and minimum distance of approach meas. 2—24241
^{250}Cf(^{15}N,4n)^{261}Ha, α-emitting isotope production 2—2740
^{59}Co(^{20}Ne,2n)^{77}Rb, production of new neutron deficient isotope ^{77}Rb, half-life of γ ray spectra meas. 2—34989
^{50}Cr(^{35}Cl,^{35}Clγ), study of excited states of ^{50}Cr 2—34939
^{63}Cu(^{16}O,2n)^{77}Rb, production of new neutron deficient isotope ^{77}Rb, half-life and γ ray spectra meas. 2—34989
^{162}Dy, multiple Coulomb excitation of γ-vibrational bands using ^{16}O ions 2—14955
Er (A=166, 168, 170) multiple Coulomb excitation of γ-vibrational bands using ^{16}O ions 2—14955
^{54}Fe(^{18}O, ^{14}C)^{58}Ni, pick up reaction at 48 MeV, ang. distrib. to final states, cross sections 2—28086
^{56}Fe, Coulomb excitation by ^{4}He and ^{16}O, static quadrupole moment determination from reorientation meas. 2—31472
Gd (A=20, 22), reactions with ^{22}Ne and ^{20}Ne, production of W isotopes 2—11769
^{70}Ge(^{32}S, ^{32}S$'$), 75.7 MeV, Coulomb excitation, meas. of γ-ray yields, B(E2) transition to excited 0^+ state 2—38498
^{70}Ge(^{35}Cl, ^{35}Cl$'$) 60-83 MeV, Coulomb excitation, meas. of γ-ray yield, deduced B(E2) to excited 0^+ state 2—38498
^{72}Ge, ^{84}Kr induced fusion reactions, effective threshold and minimum distance of approach meas. 2—24241
^{1}H, fragmentation of ^{14}N projectile nuclei at 29 GeV, inclusive isotope spectra at 0° 2—35081
^{4}He(^{16}O,γ) capture reaction study of radiative width of ^{20}Ne 8^+ 11.948 MeV level 2—18096
^{4}He(^{35}Cl,p)^{38}Ar, mean lifetimes of 3.38 and 4.59 MeV levels prod. in ^{38}Ar 2—21386
Ho, reactions with ^{22}Ne and ^{20}Ne, production of Ir isotopes 2—11772
Ir(^{14}N,xnγ) reaction study of isomeric states in neutron-deficient Po isotopes 2—21379
^{191}Ir(^{14}N,xnγ) reaction study of isomeric states in neutron-deficient Po isotopes 2—21379
(^{6}Li,αd) reaction on heavy target, Coulomb disintegration of ^{6}Li 2—38650
^{7}Li(^{7}Li,p)^{13}B, 14 MeV, meas of excitation energies of levels in ^{13}B up to 8.7 MeV 2—34911
^{24}Mg(^{16}O,2nγ)^{38}Ca, product study, including proton rich nuclei, 22-33 MeV 2—21450
^{26}Mg(^{18}O, ^{16}O)^{28}Mg, two-neutron transfer reaction, 20-45MeV determ. excitation functions, angular distributions and differential ranges 2—18243
^{26}Mg(^{6}Li,^{6}He)^{26}Al, charge exchange reaction, meas. and DWBA analysis of ang. distributions 2—28085
^{26}Mg(^{7}Li, ^{7}Be)^{26}Na, 36 MeV, used to meas. mass of ^{26}Na 2—34924
Mo(^{18}O, ^{16}O) two-neutron transfer reactions, E>Coulomb barrier 2—31589
^{92}Mo(^{16}O, pn)^{106}In, obs. of β decaying state in ^{106}In 2—18162
^{97}Mo, ^{16}O scatt., Coulomb excitation meas. rel. to level structure investigation 2—34952
^{14}N, fragmentation at 2.1 GeV per nucleon 2—38651

Nuclear reactions and scattering due to continued
nuclei of Z>2 continued
^{14}N(^{14}N,^{4}He)^{24}Mg, 20.2 and 28.0 MeV, differential cross sections determ. search for transitions to high spin states 2—11873
^{14}N(^{6}Li,^{7}Be)^{13}C, one-nucleon transfer reaction at 32 MeV, isospin and fractional parentage studies 2—11872
^{14}N(^{6}Li,^{7}Li)^{13}N, one-nucleon transfer reaction at 32 MeV, isospin and fractional parentage studies 2—11872
^{58}Ni, elastic scatt. of 30 MeV ^{6}Li ions 2—18239
^{58}Ni(^{16}O, ^{16}O′)^{58}Ni* 34-58 MeV, excitation function obs. 2—35083
^{59}Ni(^{12}C,2n)^{68}Se, meas. of ^{68}Se half-life, separation of ^{68}As, assignment of γ ray transitions 2—38538
(^{16}O, ^{12}C) reactions, interpretation in terms of quartet states 2—15014
^{16}O-^{16}O elastic scattering, energy dependence of real part of optical potential due to nuclear rotation 2—18240
^{16}O-^{16}O potential, dependence on ansatz prescribing density of compound system 2—11869
^{16}O, elastic scatt. of 30 MeV ^{6}Li ions 2—18239
^{16}O + ^{16}O potential, shell model calc. 2—18241
^{16}O(^{6}Li,^{3}He)^{19}F, 24 MeV meas. of angular distrib. DWBA analysis comparison with ^{16}O(^{6}Li,t)^{19}Ne cross section 2—28083
^{16}O(^{6}Li,t)^{19}Ne, 24 MeV meas. of angular distrib. DWBA analysis comparison with ^{16}O(^{6}Li,^{3}He)^{19}F cross section 2—28083
^{18}O+^{18}O, excitation functions for formation of ^{34}P, ^{30}Al and ^{27}Mg for ^{18}O energies of 13-41 MeV 2—28084
^{18}O(^{18}O, ^{16}O)^{20}O two-neutron transfer reaction, 13-41 MeV, determ. excitation functions, compared with other ^{18}O induced reactions 2—18243
^{18}O(^{18}O, 2pn), 23-40 MeV, production of new isotope ^{33}Si, meas. of lifetime and decay scheme 2—38535
^{189}Os(^{31}P,4n)^{216}Pa as means of producing ^{216}Pa 2—8365
^{190}Os(^{31}P,5n)^{216}Pa as means of producing ^{216}Pa 2—8365
Pb bombardment with ^{18}O ions, formation of 66 sec isomeric state of ^{222}Ac 2—34994
^{208}Pb, elastic scatt. of 30 MeV ^{6}Li ions 2—18239
^{208}Pb(^{16}O,^{15}N)^{209}Bi, proton tunnelling, DWBA calc. of differential cross section 2—5714
^{208}Pb(^{16}O,^{17}O)^{207}Pb, neutron tunnelling, DWBA calc. of differential cross section 2—5714
^{208}Pb(^{6}Liαd)^{208}Pb,^{6}Li polarization effect on Coulomb breakup process 2—2816
Pt(^{12}C,xnγ) reaction study of isomeric states in neutron-deficient Po isotopes 2—21379
^{244}Pu(^{96}Zr,^{40}Ca)^{300}114, feasibility of producing superheavy nuclei of A≈300 2—471
^{32}S(^{16}O,2nγ)^{46}G, product study, including proton rich nuclei, 22-33 MeV 2—21450
^{28}Si, elastic scatt. of 30 MeV ^{6}Li ions 2—18239
^{28}Si(^{16}O,2nγ)^{42}Ti, product study, including proton rich nuclei, 22-33 MeV 2—21450
^{151}Sm+^{35}Cl, Coulomb excitation by 50 MeV ^{35}Cl ions, B(E2) values of states populated 2—18126
^{120}Sn, elastic scatt. of 30 MeV ^{6}Li ions 2—18239
^{181}Ta, reactions induced with 40-110 MeV ^{11}B ions, excitation functions and recoil ranges determ. 2—11874
^{181}Ta(^{14}N,5n)^{190}Hg, excited levels and 24.5 ns isomer 2—38523
^{99}Tc(^{35}Cl, ^{35}Cl′γ), 52-64 MeV, measured cross section, deduced ^{99}Tc level structure 2—18115
^{232}Th, bombardment with 290 MeV ^{40}Ar, production of new isotopes of Mg, Al, Si, P, Cl, S 2—5715
^{169}Tm(^{12}C,4n), 62-76 MeV, study of ^{177}Re energy levels 2—27989
U, bombardment with Kr, superheavy nucleus formation, detection by mass measurement of fission products 2—21452
^{172}Yb(^{11}B,4n), 52-60 MeV, study of ^{179}Re energy levels 2—27989
^{64}Zn(^{16}O,2n)^{78}Sr using 160 MeV oxygen ions 2—28005
nucleons
coherent production reactions from N and $\bar{\text{N}}$ scattering above ~2 GeV/c 2—28055
inelastic scattering, features of core polarization knock-out exchange contributions 2—31527
inelastic scattering from collective nuclei, comparison of formalisms based on deformed optical potential and deformed nuclear density 2—8331
multipole analysis of polarization, elastic and inelastic scatt. 2—21426
one-particle resonances 2—8332
optical model pot., real part calc. 2—35017
optical potential, off shell two-body t matrix 2—35018
optical potential, relation to deuteron optical potential 2—28062
radiative nucleon-deuteron capture below three-neutron break-up energy, wave function and dispersion theory analysis 2—31528
reactions, even-even and even-odd targets, potnetial model interpretation of isobaric analog resonances 2—28026
scattering, coupled channel calculations using Feshbach projection technique, shell model aspects 2—486
scattering, Perey-Buck effect 2—18198
triple scattering parameters, optical model analyses 2—18181
two-nucleon T matrix half off energy shell, expansion into power series 2—28025
^{2}H(N,N), cross sections, 11-23 MeV, nucleon polarization calc. 2—24207
N^{4}He scatt. forward dispersion relations and ^{4}He ^{3}He n coupling const. 2—14982
^{27}Al, pick up reaction from ^{28}Si, Coriolis bandmixing model calcs., agreement for oblate shape 2—31458
^{60}Ca, triple scattering parameters, optical model analyses 2—18181
^{2}H, break-up reaction, calc. of nucleon-nucleon correlation spectra of cross sections including final state interactions 2—38585
^{2}H, scattering calc., vector and tensor polarisations 2—21427
^{2}H(N,N), Faddeev-Mitra-Amado-Lovelace equations with separable tensor component, cross-sections and nucleon polarizations from 7.8 MeV to 31 MeV 2—14981
^{2}H(N,N) elastic scattering unitary model calcs. of nucleon polarization using realistic model for two-nucleon interaction 2—24208
^{92}Mo, 14.8 MeV (n,2n), (n,p), (n,α) cross sections 2—18213
(N,d), scattering, with S-, P- and D-wave forces, elastic differential cross sections and nucleon polarizations, 14.1 MeV 2—8330
^{82}Se, 14.8 MeV (n,2n), (n,p), (n,α) cross sections 2—18213
^{117}Sn, 14.8 MeV (n,2n), (n,p), (n,α) cross sections 2—18213
Te (A=128, 130), 14.8 MeV (n,2n), (n,p), (n,α) cross sections 2—18213
photons
bremsstrahlung, graphite filtering 2—23786
clustered nuclei, existence of fine structure in cross section, Feynman diagram theory 2—28017

Nuclear reactions and scattering due to continued
photons continued
complex nuclei, transparencies to photoproduced pions and recoil nucleons for high energy photons 2—5681
diffractive photoprod. of new vector meson, interference effect 2—31305
double positron-electron pair creation by 6.13 MeV photons incident of Ge(Li) detectors 2—28016
giant dipole resonance, evidence for isobaric spin splitting 2—38561
isospin sum rules, consequences for photonuclear reactions 2—31521
lepton pair production in nuclear field 2—8114
photoabsorption cross section, connection with response of system to weak external e.m. field 2—38448
photodisintegration integrated cross section, equivalence of two internucleon pots. 2—34882
photonuclear yield curve analysis 2—35007
photonuclear yield curves, analysis techniques 2—38566
photoproduction of $\pi^{\pm}$ from complex nuclei, 2 and 3 GeV 2—31283
photoproduction of e^{+}e^{-} nucleon lepton pairs, role of neutral vector mesons 2—28018
photoproduction of vector mesons in ρ-ω interference region 2—31304
photoproton experiments, method of energy loss correction for thick detectors 2—38352
resonant scattering, investigation of highly excited nuclear levels 2—2671
total cross sections, coupled-channel optical model calc., vector meson dominance breaking 2—18172
vector meson photoproduction at large momentum transfer, cross sections 2—21421
vector meson production, cross sections 2—31313
(γ,n), (γ,p), (γ,α), residual nuclei populated states 2—38563
(γ,n), photonuclear sum rules and systematics 2—38564
(γ,np) reactions, direct excitation of two nucleons, neutron-proton correlations 2—38565
(γ,p), (γ,n) reactions, calculations at photon energies between 40 and 100 MeV 2—38562
(γ,p), energies above pion production threshold, cross section calc. 2—21422
$\gamma\,^{3}$He→K$^{+}\,_{\Lambda}{}^{3}$H, current algebra study 2—18094
π photoproduction, 1160 MeV γ-quanta on C, Al, Cu, Ta, Pb 2—14974
π production at high energy, effect of two body correlations 2—31520
ρ^{0} photoproduction from H, D and complex nuclei, 4-9 GeV, determ. detailed dipion mass-spectrum fits 2—14684
^{27}Al (γ,p), energy states from proton energy spectra 2—31523
^{27}Al(γ,π^{+})^{27}Mg threshold to 120 MeV, π production cross-section meas. 2—5682
^{243}Am, isomer states, spontaneously fissioning, excitation in inelastic scatt. of γ quanta 2—15026
^{11}B(γ,π^{-})^{11}C threshold to 1200 MeV, π production cross-section meas. 2—5682
^{7}Be, photoproduction from C, B, Be and Li 2—5683
^{9}Be(gamma,t), 1200 MeV, tritium spectra and angular distributions 2—38567
^{9}Be(γ,n), high resolution cross section 2—38568
^{9}Be(γ,n) production of monoenergetic neutrons at KeV energies 2—5560
^{209}Bi, Raman scattering of 10.38 MeV photons 2—24200
^{12}C, giant dipole continuum, collective correlations 2—34908
^{12}C(γ,n), cross section calc. in giant resonance region, calc. in collective correlation model 2—18174
^{12}C(γ,p), 100 to 250 MeV, excitation function for protons 2—35009
^{12}C(γ,t), 1200 MeV, tritium spectra and angular distributions 2—38567
^{13}C(γ,p), cross section calc. in giant resonance region, calc. in collective correlation model 2—18174
^{40}Ca(γ,np), 19-30 MeV, cross section determ by counting residual γ-ray activity, comparison with calc. based on quasi-deuteron theory 2—485
^{40}Ca(γ,np), threshold-200 MeV, direct excitation of two nucleons, neutron-proton correlations 2—38565
^{112}Cd, elastic and inelastic scattering, study of energy levels 2—11758
^{35}Cl (γ,p) and (γ,n) reactions at 30 MeV, meas. of de-excitation γ-rays in residual nuclei 2—38569
^{37}Cl(γ,2p)^{35}P, half life and γ-ray energy meas. for new nuclide ^{35}P 2—5651
^{63}Cu(γ,n)^{62}Cu, threshold to 33 MeV cross sections, obs. of induced activity 2—21424
^{19}F (γ,p) and (γ,n) reactions at 30 MeV, meas. of de-excitation γ-rays in residual nuclei 2—38569
^{56}Fe, reaction yields at 1.5 GeV 2—2763
^{57}Fe(γ,n), doorway state effects in M1 radiative excitation of p-wave resonances 2—18108
^{3}He, photodisintegration cross sections calc. 2—11817
^{3}He, photodisintegration cross sections calc. 2—11817
^{3}He photodisintegration, E2 transition 2—21423
^{3}He(γ,p)d, with linearly polarized γ-rays, asymmetry parameters at 90° and energies from 180 to 300 MeV 2—18173
^{4}He(γ,d)^{2}H, influence of long-range clustering correlations in ^{4}He ground state on photoreaction studied 2—11818
^{4}He(γ,n$_{0}$)^{3}He, 90° differential cross section and evidence for isospin mixing in ^{4}He 2—27959
^{4}He(γ,p)^{3}H, photodisintegration, effect of tensor forces 2—35008
^{4}He(γ,p) and ^{4}He(γ,n) reactions, ratio of cross sections, 30.0-51.8 MeV 2—31522
^{115}In(γ,γ'), energy level study 2—8303
(γ,d) reactions, 620 and 1140 MeV on various nuclei, d and g. distrib. obs. 2—5685
^{6}Li(γ,p), ang. distribution of high energy photoprotons 2—28019
^{6}Li(γ,p)td, 35-80 MeV, quasi-α-particle photodisintegration 2—24201
^{7}Li(γ,t), 1200 MeV, tritium spectra and angular distributions 2—38567
^{24}Mg(γ,xn), ^{26}Mg(γ,xn), structure in photoneutron cross section and giant resonance formation 2—38570
^{25}Mg, photoneutron cross section determ. 2—2762
^{55}Mn(γ,3n)^{52m,g}Mn, isomeric cross section ratios 2—24202
^{15}N(γ,p)^{17}C, 19.6—38.3 MeV, proton spectra obs. at giant resonance energies cross-sections 2—5684
^{23}Na, photoneutron cross section determ. 2—2762
^{23}Na (γ,p) and (γ,n) reactions at 30 MeV, meas. of de-excitation γ-rays in residual nuclei 2—38569
O (γ,n), cross sections, analysis of irregularities, Feynman diagram theory 2—28017
^{16}O, photoprod. of π^{+}, ^{16}N giant reson. 2—35010
^{16}O, photoprod. of π^{+} 2—35011
^{16}O (γ,n), giant dipole resonance region, cross sections and scattering amplitudes 2—31516

Nuclear reactions and scattering due to continued
photons continued
^{141}Pr(γ,n)^{140}Pr, threshold to 33 MeV, cross sections, obs. of induced activity 2—21424
^{239}Pu, isomer states, spontaneously fissioning, excitation in inelastic scatt. of γ quanta 2—15026
^{85}Rb(γ,n)^{84m,g}Rb, isomeric cross section ratios 2—24202
^{32}S(γ,n)^{31}S*, 16.3-27.3 MeV, cross sections 2—38571
^{32}S(γ,np) 19-30 MeV, cross section determ. by counting residual γ-ray by activity, comparison with calc. based on quasi-deuteron theory 2—485
^{32}S(γ,p)^{31}P*, 16.3-27.3 MeV, cross sections 2—38571
^{45}Sc, total photoneutron cross section, threshold to 26 MeV, giant dipole states 2—38572
^{45}Sc(γ,n)^{44m,g}Sc, isomeric cross section ratios 2—24202
^{112}Sn(γ,p)^{111}In, cross section calc. from proton yield curve 2—8324
^{124}Sn(γ,p)^{123}In, cross section calc. from proton yield curve 2—8324
Sn(γ,n), A=114, 116, 117, 119 and 124, from threshold to 27 MeV, cross sections, neutron yield 2—28020
Ta, photofission and photofragmentation 600-1700 MeV photon 2—31609
^{232}Th, Raman scattering of 10.38 MeV photons 2—24200
^{232}Th(γ,n), intermediate structure in cross section, competition with photofission process 2—38575
^{238}U, Raman scattering of 10.38 MeV photons 2—24200
^{238}U(γ,n), intermediate structure in cross section, competition with photofission process 2—38575
^{51}V, reaction yields at 1.5 GeV 2—2763
Z(γ,e^{+}e-e^{+}e-), test of cross section of $\gamma\gamma \rightarrow$e^{+}e-e^{+}e- at high energy 2—11572
^{90}Zr, photoneutron cross section 2—38573
^{90}Zr(γ,p)^{89}Y, search for isobaric analogue states 2—38574

protons
deformed nuclei, importance of indirect transitions in (p,t) reactions 2—28031
double-analog state formation in heavy nuclei, role of pairing 2—18188
emulsion nuclei interaction with 76 GeV proton 2—31534
fragmentation due to 600 MeV bombardment, light isotope discrimination 2—24411
Hagedorn thermodynamic theory applic. 2—21430
hybrid model, pre-equilibrium decay at moderate excitations 2—38634
hypernucleus production, in high energy reactions 2—21372
inelastic scattering of 19.6 MeV protons, determ. differential cross section, spin-flip probability amplitude and asymmetry. 2—18182
inelastic scattering of polarized protons at analog resonances, analyzing power, polarization and spin flip 2—8333
isospin effects, generalized Hauser Feshbach formalism 2—11815
kinematic effective charges in photonuclear reactions 2—14975
light nuclei, spallation reactions, E$_{p}$=50, 100 and 153 MeV 2—8336
matter density models and antiproton-(emulsion) nuclei elastic scattering at 3GeV/c 2—24213
odd-odd nuclei, (p,n) reaction calc. rel-to investigation of regularity in multiplet properties 2—11715
optical model analysis of elastic scattering at 16 MeV 2—31546
optical model pot., A-depend. 2—35022
photodisintegration of light nuclei, influence of fractional parentage structure of ground state 2—21376
polarization during elastic scattering, energy dependence meas. 2—440
polarized, calibration of polarized targets, cases of ^{3}He, ^{19}F and ^{15}N considered 2—35021
polarized, scattering from polarized LMN crystal target, spin-correlation parameters at 47.5 MeV 2—35020
polarized beams, recent exptl. developments 2—35028
proton-proton bremsstrahlung cross section at 20 MeV 2—2775
quasielastic (p,n) reactions, differential cross sections meas. and optical model analysis 2—11832
recoil nuclei in heavy nuclide target, initiation of nuclear reactions 2—5691
resonance technique for analysis of metal surfaces 2—12634
Rutherford back scattering from metals at medium energies 2—35023
scattering at 20 and 50 MeV, existence of spin-spin interaction investigated 2—14980
target, thick, scattering spectrum in terms of energy loss 2—8321
(p,2p) reactions, polarization effects 2—31536
(p,α), pick-up form factors, computation method 2—2774
(p,α) reactions on light nuclei, E-$^{n}_{p}$(2$\leqslant$n$\leqslant$4) energy dependence of excitation functions explained by pre-equilibrium emmission model 2—31533
(p,d), around 20 MeV, differential cross sections and asymmetries 2—18193
(p,d), study of deeply bound neutron hole states 2—31421
(p,n) reactions in ^{18}O, ^{37}Cl, ^{41}K, ^{53}Cr, ^{59}Co, neutron angular distribs. 2—14985
(p,Nnπ) on photoemulsion nuclei, coherent diffraction π generation 2—23848
(p,p′), gamma-ray multiplicity in decay of residual nuclei from nuclear reactions 2—31519
(p,p) quasi free scattering, multiple scattering effects, differential cross section 2—24209
(p,t), excitation of low-lying 0^{+} states in actinides 2—14940
(p,t) reaction, population of 0^{+} states in actinide and A~190 nuclides 2—34920
(p,t) reaction on even even N=Z nuclei in 2s1d shell, energy level study 2—24214
K^{-}p$\rightarrow\eta\Lambda$ cross section dip at $-$t~0.4 GeV^{2}, explanation 2—14626
p, induced reactions, determ. of nuclear size from cross sections, for C, Al, Sn and Pb 2—11719
π photoproduction on nuclei with nucleon emission 2—8323
^{116} Cd, elastic and inelastic scattering at 12 MeV, determ. cross sections, deduced levels 2—18187
$^{170, 172, 174, 176}$Yb(p,p′), 10-15 MeV, excitation functions leading to 0^{+}, 2^{+}, 4^{+} and 6^{+} states of ground state rot. bands, IAR study 2—18136
16-18.2 MeV, search for nondirect effects in excitation functions 2—35026
^{70}(p,t)^{68}Ge 20 MeV, ^{68}Ge excited levels study 2—18110
^{a}Ca(p,d)^{b}Ca A=40, 42, 44, 48, b=39, 41, 43, 47, 40 MeV, spectroscopic factors derived from DWBA analysis, obs. of analogue states 2—35036
^{a}Te(p,t), A=124, 126, at 33 MeV, determ. energy levels of ^{122,124}Te 2—18119
^{27}Al(p,α,γ) 1.1-1.8 MeV, resonance levels in ^{28}Si observed, resonance strengths, partial proton widths, spectroscopic factors deduced 2—34915
^{27}Al(p,α,γ)^{24}Mg, 6.40 MeV, α-γ angular correlation 2—38594
^{27}Al(p,α)^{24}Mg, E$_{p}$=7.40 MeV, plastic detector study 2—14777
^{27}Al(p,α)^{24}Mg, low energy, rel. to investigation of states in ^{28}Si 2—31459
^{27}Al(p.α)^{24}Mg, meas. of reaction time at 633 and 1183 keV using blocking effect 2—24220

Nuclear reactions and scattering due to continued
protons continued
^{27}Al(p,γ) 1.1-1.8 MeV, resonance levels in ^{28}Si observed, resonance strengths, partial proton widths, spectroscopic factors deduced 2—34915
^{27}Al(p,γ)^{28}Si, excitation functions, resonances 2—28036
^{27}Al(p,γ)^{28}Si, investigation of ^{28}Si energy levels 2—34928
^{27}Al(p,γ)^{28}Si, yield curve obtained with implanted targets, determ. range of 50 keV Al^{+} ions in C, Cu, Mo and Ta 2—19479
^{27}Al(p,n) reaction mechanism at intermediate energies, ^{28}Si resonance 2—38595
^{27}Al(p,nγ)^{27}Si, 16 MeV, γ-spectrum 2—14986
^{27}Al(p,p′γ), 1.1-1.8 MeV, resonance levels in ^{28}Si observed, resonance strengths, partial proton widths, spectroscopic factors deduced 2—34915
^{27}Al(p,p), 1.1-1.8 MeV, resonance levels in ^{28}Si observed, resonance strengths, partial proton widths, spectroscopic factors deduced 2—34915
Al(p,x) reaction (X=p,d,t, ^{3}he, α), 19.8 GeV/c, energy distributions of light emission fragments 2—31545
^{36}Ar(p,^{3}He)^{34}Cl deuteron transfer reaction enhanced by neutron-proton pairing correlations 2—11831
^{36}Ar(p,n)^{36}K, half life determ. for ^{36}K 2—2744
^{40}Ar(p,γ)^{41}K, investigation of excited states of ^{41}K 2—5653
^{40}Ar(p,n)^{40}K, study of ^{40}K level lifetimes 2—38490
^{40}Ar(p,p′γ)^{40}Ar, obs. of isobaric analogues of ^{41}Ar levels 2—34935
^{40}Ar(p,p)^{40}Ar, study of ^{40}Ar level lifetimes 2—38490
^{75}As(p,nγ)^{75}Se, investigation of spins of low lying ^{75}Se levels 2—34947
^{197}Au(p,p), using polarized protons, differential cross sect. and polarization meas., 11-14 MeV 2—14984
^{11}B(p, γ) giant E1 resonances in ^{12}C 2—31446
^{11}B(p,3α), 163 keV, interference effects 2—38590
^{11}B(p,α)^{8}Be, 45 MeV, ang. distrib. and cross section meas. 2—11827
^{11}B(p,α)^{8}Be, DWBA anal. of ground state ang. distribs., finite range 2—11828
^{12}B(p, 2α)α, meas. cross section, deduced ^{12} C resonance at 17.23, 17.77 and 18.36 MeV 2—18192
Be target, 12.4 GeV/c, π^{+} and π- production 2—11825
^{9}Be(p,α)^{6}Li, 45 MeV, ang. distrib. and cross section meas. 2—11827
^{9}Be(p,α)^{6}Li, DWBA anal. of ground state ang. distribs., finite range 2—11828
^{9}Be(p,d$_{0}$)^{8}Be, BHMM theory of stripping reactions 2—31540
^{9}Be(p,d)^{8}Be, 46 and 100 MeV, deuteron optical potentials, spectroscopic factors 2—8338
^{9}Be(p,d)^{8}Be, excitation spectrum of ^{8}Be, ghost anomaly 2—2688
^{9}Be(p,p$_{1}$)9*Be, mechanism of excitation of 1.68 MeV $^{1}/_{2}{}^{+}$ level 2—11826
^{9}Be(p,pα)^{5}He, 26.0, 35.0 and 46.8 MeV, cross section meas. 2—21432
^{10}Be production from O, spallation cross section conflict with predictions 2—5692
Bi, scattering distributions for particles in 2 to 30 keV range 2—11824
^{209}Bi comparison of energy levels excited by nonresonant 16.10 MeV proton scattering of 14.95 MeV scattering from isobaric analogue states 2—24175
^{209}Bi(p,2p)^{208}Pb, obs. of IAR's in ^{210}Po, as enhancements in excitation function 2—14959
^{209}Bi(p,α), level densities of near doubly magic nuclei 2—38527
^{209}Bi(p,p′), 14-21 MeV, ^{210}Bi and ^{209}Bi deduced level structure from ^{210}Po IAR's 2—21400
^{209}Bi(p,p), using polarized protons, differential cross sect. and polarization meas., 11-14 MeV 2—14984
^{79}Br(p,n)^{79}Kr, conversion electron spectra, low lying states and transitions obs. 2—38501
^{81}Br(p,n)^{81}Kr, conversion electron spectra , low lying states and transitions obs. 2—38501
C, 660 MeV, long range α-particles, cluster structure of light nuclei 2—38468
C target, 10 to 28 GeV, inelasticities and inelastic cross section 2—31541
^{12}C, Coulomb interference in proton scattering at 144 MeV 2—31538
^{12}C deform. sign determ. from inelastic proton scatt. 2—27965
^{12}C elastic and inelastic scatt. of 30.4 MeV polarized protons 2—14983
^{12}C resonance states, determination from proton spin flip 2—31447
^{12}C(p,2p), at 460 MeV and 1 GeV analysis using Elton Swift and PHF wave functions and PWIA, comparison of predicted and exptl. cross section 2—2778
^{12}C(p,2p)^{11}B, angular correlations measured at 49.5 MeV, results compared with distorted wave impulse approx. 2—11830
^{12}C(p,2p)^{11}B, DWA calc. of low energy reactions in 1p shell 2—21433
^{12}C(p,2p)^{11}B, distorted wave t-matrix approx. analysis, E$_{p}$=75MeV 2—35032
^{12}C(p,α)^{9}B, high-spin assignments in the 1p-shell of ^{9}B 2—31544
^{12}C(p,d)^{11}C, E$_{p}$=185 MeV, DWBA analysis of differential cross sections for emitted deuterons, nondirect reaction mechanism indicated by ^{11}C levels 2—31542
^{12}C(p,p′), quasifree scattering at 1 GeV 2—31530
^{12}C(p,p′γ)^{12}C*, E$_{p}$=20 MeV substate excitation of 2^{+} state, transition from O^{+} state 2—34941
^{12}C(p,p), 1 GeV, cross section of quasi free scattering comparison with multiple scattering theory 2—24209
^{12}C(p,p), at energies around 4.81 MeV resonance, excitation function and polarization meas. 2—31531
^{12}C(p,p)^{12}C, obs. of lowest T=$^{3}/_{2}$ state in ^{13}N, 14 MeV resonance 2—21428
^{12}C(p,pd), 50 MeV, total cross sections, secondary p energy spectra, secondary nuclei momentum and angular distribs. 2—31535
^{12}C(p,pp)^{11}B, 385 MeV distorted wave analysis, determ. of radius and reduction factor 2—2777
^{13}C elastic and inelastic scatt. of 30.4 MeV polarized protons 2—14983
^{13}C(p,$\gamma_{1,2}$)^{14}N, 3-18 MeV cross-section obs., levels of ^{14}N determ. 2—2690
^{13}C(p,n)^{13}N$_{gs}$, microscopic analysis including core polarization exchange process 2—11829
^{13}C(p,p′γ)^{13}C, 3-18 MeV cross-section obs., levels of ^{14}N determ. 2—2690
^{14}C(p,γ_{o})^{15}N, 3.2 to 7.7 MeV, cross section and angular distribution 2—35033
Ca target, 5 to 6.4 MeV, elastic scattering, excitation functions 2—38586
^{40}Ca elastic scattering optical model description improved by addition of surface-peaked term to real-central potential 2—24211
^{40}Ca(γ,p) 15.2-24.6 MeV, determ. differential photoproton cross sections corresponding to different states of residual nucleus 2—14976
^{40}Ca(p,p′), quasifree scattering at 1 GeV 2—31530
^{40}Ca(p,p′γ)^{40}Ca, doorway state structure in ^{41}Si 2—38598
^{42}Ca, inelastic scatt. of 50 MeV protons to deformed states 2—11835
^{43}Ca(p,p′γ), 4.235 MeV, investigation of excited states with E$_{x}$<2.7 MeV 2—27974

Nuclear reactions and scattering due to continued
  protons continued
    ^{48}Ca(p,nγ)^{48}Sc, investigation of ^{48}Sc excited state properties 2—2705
    ^{49}Ca(p,γ), (p,p), (p,nγ), gamma ray decay from the analogue state of the ground state 2—31469
    Ca(p,p), energetic dependence of elastic scattering cross sections on thick targets 2—28033
    Ca(p,t), $J^{\pi}=0^{+}$ states, effective wave function calculation 2—14944
    Cd(p,p′), compound-nucleus contrib. 2—2771
    ^{140}Ce(p,p′), isobaric analogue resonance properties of ^{141}Ce in a unified model calculation 2—31547
    ^{140}Ce(p,p), obs of resonances in ^{141}Pr corresponding to IAR's of low lying ^{141}Ce levels 2—18123
    ^{35}Cl(p,p′)^{35}Cl*, determination of ^{35}Cl transition strengths 2—5650
    ^{35}Cl(p,p′γ)^{35}Cl, 5.47-5.61 MeV, Doppler shift attenuation meas., determ. lifetimes of first six excited states ^{35}Cl 2—31462
    ^{37}Cl(p,n)^{37}Ar, determination of ^{37}Ar transition strengths 2—5650
    ^{59}Co(p,p′)^{59}Co, population of highly excited levels in ^{59}Co, energy spectra study 2—24162
    ^{59}Co(p,p)^{59}Co 5.8-6.5 MeV, p polarization and ang. distrib. obs. 2—8334
    C(p,p), energetic dependence of elastic scattering cross sections on thick targets 2—28033
    Cr isotopes, elastic scattering, 2.8-6.3 MeV 2—489
    Cr(A=50,52,54), elastic and inelastic scatt. at incident energies of 6 MeV 2—11823
    ^{50}Cr(p,p′) ^{50}Cr*, using 12 MeV protons, ang. distrib. of absolute spin flip probability 2—18185
    ^{50}Cr(p,p′γ), study of excited states of ^{50}Cr 2—34939
    ^{50}Cr(p,t)^{48}Cr, 51 MeV, energy level study of ^{48}Cr, spin and parity assignments 2—2706
    ^{50}Cr(p,t)^{48}Cr, study of populated energy levels 2—467
    ^{52}Cr(p,p′)^{52}G*, using 12 MeV protons, ang. distrib. of absolute flip probability 2—18185
    ^{52}Cr(p,p)^{52}Cr 5.8-6.5 MeV, p polarization and ang. distrib. obs. 2—8334
    ^{52}Cr(p,p) elastic scattering, 2.4-4.1 MeV, obs. of IAR to excited 2.321 MeV level in ^{53}Cr 2—18186
    ^{52}Cr(p,t), study of excited states of ^{50}Cr and spin and parity assignments 2 -34939
    ^{53}Cr(p,n)^{53}Mn, 2.6 to 5.9 MeV, differential cross sections meas. determ. levels and transition rates in ^{53}Mn 2—11747
    ^{53}Cr(p,nγ)^{53}Mn, 4.9 MeV, differential cross sections meas. determ. levels and transition rates in ^{53}Mn 2—11747
    ^{53}Cr(p,p)^{53}Cr 5.8-6.5 MeV, p polarization and ang. distrib. obs. 2—8334
    ^{54}Cr(p,n), 1.8-2.9 MeV, isobaric analog states obs. in ^{55}Mn 2—2708
    ^{54}Cr(p,n)^{54}Mn, 2.6 to 3.1 MeV, energy levels of ^{54}Mn 2—38531
    cross sections for H, Be, C, Al, Fe, Cu, Ge, Sn, Pb, H_2O, B_4C, NaI in energy range 220-570 MeV 2—28032
    Cr(p,p)Cr A=50, 52, 54, 1.8-3.3 MeV, isobaric analogue states obs. in ^{51}Mn, ^{53}Mn, ^{55}Mn 2—2708
    ^{63}Cu(p,p′) influence on isospin decay of composite ^{64}Zn system formed, Bohr independence hypothesis 2—24181
    ^{64}Cu(p,p′), E_p=15.7 MeV, analysing power and spin dependence 2—28029
    ^{65}Cu, spallation, Monte Carlo simulation of nuclear cascade-evaporation 2—28037
    ^{65}Cu(p,n)^{65}Zn, isobaric analogue resonance in ^{66}Zn 2—8339
    ^{65}Cu(p,nγ)^{65}Zn, isobaric analogue resonance in ^{66}Zn 2—8339
    ^{65}Cu(p,p′) influence of isospin on decay of composite ^{66}Zn system formed, Bohr independence hypothesis 2—24181
    ^{65}Cu(p.p′), E_p=15.7 MeV, analysing power and spin dependence 2—28029
    ^{19}F(p,p′γ)^{19}F branching ratios obs. of states in ^{19}F 2—38482
    Fe, accelerator cave, nucleon and charged-pion albedo spectra 2—24222
    Fe, scattering distributions for particles in 2 to 30 keV range 2—11824
    Fe target, 10 to 28 GeV, inelasticities and inelastic cross section 2—31541
    ^{54}Fe elastic and inelastic scatt. of 30.4 MeV polarized protons 2—14983
    ^{54}Fe(p,γ), 1.7-3.0 MeV, ^{55}Co levels 2—38599
    ^{54}Fe(p,γ)^{55}Co, isobaric analogue states in ^{55}Co 2—21387
    ^{54}Fe(p,p′γ)^{54}Fe*, E_p=19.6 MeV, substate excitation of 2^{+} state, transition from O^{+} state 2—34941
    ^{56}Fe (p, nγ) ^{56}Co, coincidence expts. in 7.7-10 MeV range, meas. γ-ray spectra, deduced levels in ^{56}Co 2—24223
    ^{56}Fe(p,n′)^{56}Co*, quasi-inelastic scatt., effect of 2 step processes coupling potentials 2—31532
    ^{57}Fe(p,^{3}He), new spin $^{1}/_{2}{}^{-}$ state observed in ^{55}Mn, shell model calculations 2—8287
    ^{70}Ge(p,d)^{69}Ge, 20 MeV ^{69}Ge excited levels study 2—18110
    ^{72}Ge(p,p'e), 3.3 to 4.7 MeV, isobaric analogue states in ^{73}As 2—34946
    ^{1}H, ^{2}H, antiproton quasielastic and elastic scattering 2—38587
    ^{1}H(p, pπ^{0})^{1}H, at 600 MeV, differential cross section for π^{0} production 2—17923
    ^{2}H, Coulomb interference in proton scattering at 144 MeV 2—31538
    ^{2}H, proton scattering, 6-20 MeV, bremsstrahlung calc., Feshbach and Yennie model 2—28027
    ^{2}H(,pn)^{1}H, test of the impulse approximation validity in low energy deuteron break up 2—2772
    ^{2}H(p,2n)n theoretical analysis by a polar graph 2—31537
    ^{2}H(p,2p) at 600 MeV calc. of differential cross section using plane wave impulse approx. with corrections 2—31539
    ^{2}H(p,2p)n, 14.45 MeV, results compared with calculations using Amado model 2—8337
    ^{2}H(p,2p)n, p-p quasifree scattering, 21.5-56.4 MeV 2—2776
    ^{2}H(p,n)n, quasi free peak examined in off-shell spectator approx. for energies 14.4 MeV-100 MeV using Hamada Johnston potential 2—18189
    ^{2}H(p,p), 15-20 MeV, differential cross sections 2—2773
    ^{2}H(p,p), 7-9 MeV, bremsstrahlung cross sections 2—487
    ^{2}H(p,p)pn, 12.5 MeV, angular distributions of quasi-free scattering 2—28071
    ^{2}H(p,pn)^{1}H, 13.5 MeV three body break up spectra analysed to yield cross section for production of n-p pairs in singlet state 2—21431
    ^{2}H(p,pn)p, coincidence spectra meas. with neutron detection at 200 degrees 2—24215
    ^{2}H(p,pn)p, quasifree scattering effects 2—35031
    ^{2}H(p,pp)n, quasifree scattering effects 2—35031
    ^{2}H(p,pp)n, test of the impulse approximation validity in low energy deuteron break up 2—2772
    ^{2}H(p,π^{+})^{3}H, study of pion production 2—35030
    ^{3}H, proton scattering, 5-matrix elements and phase shift analysis 2—28028
    ^{3}H(p,n)^{3}He, 1.5 to 5.0 MeV, neutron polarization meas. 2—38588
    ^{3}He, elastic scattering, microscopic description starting from nucleon-nucleon potential 2—24210

Nuclear reactions and scattering due to continued
  protons continued
    ^{3}He(p,2p)^{2}H, 155 MeV, quasi free proton-proton scattering cross-sections 2—18190
    ^{3}He(p,π^{+})^{4}He, study of pion production 2—35030
    ^{4}He, Coulomb interference in proton scattering at 144 MeV 2—31538
    ^{4}He, inelastic scattering, 141 MeV 2—18183
    ^{4}He, proton scattering, 6-20 MeV, bremsstrahlung calc., Feshbach and Yennie model 2—28027
    ^{4}He, spin and isospin in high energy proton elastic scattering and nuclear correlations 2—31529
    ^{4}He(p,p), effects of intermediate N* state on forward scattering at 1 GeV 2—5689
    ^{4}He(p,p) elastic scattering, 20-45 MeV, angular distrib. of polarization and cross sections meas. across 23.4 MeV resonance 2—35024
    ^{4}He(p,p) elastic scattering, phase-shift analysis of cross section and polarization data, 20-40 MeV 2—35025
    ^{4}He(p,π^{+})^{5}He, study of pion production 2—35030
    ^{202}Hg(n,p), study of decay of ^{202}Au 2—31513
    ^{165}Ho, nuclear quadrupole moment meas. by proton scattering from aligned target 2—34968
    ^{41}K(p,γ)^{43}Ca, 1400-1750 keV, investigation of excited states in ^{43}Ca 2—14945
    ^{6}Li, Coulomb interference in proton scattering at 144 MeV 2—31538
    ^{6}Li (p,α), 45.0 MeV, α particle spectra measured, search for broad resonances 2—18084
    ^{6}Li(p,^{3}He), 45.0 MeV, ^{3}He spectra measured, search for broad resonances 2—18084
    ^{6}Li(p,pd)^{4}He, 100 MeV, angular correlations 2—18191
    ^{7}Li, Coulomb interference in proton scattering at 144 MeV 2—31538
    ^{7}Li+p, excited states of A=8 system 2—24141
    ^{7}Li(p,α)^{4}He cross section at low energies 2—24216
    ^{7}Li(p,n)^{7}Be, E_p=17.5 MeV, neutron spectra meas., differential cross sections 2—28034
    ^{7}Li(p,pt)^{4}He, cluster model wave function and DWIA analyses 2—38589
    ^{24}Mg(p,n)^{24}Al, 23 MeV, excitation energies of levels in ^{24}Al 2—18092
    ^{24}Mg(p,n)^{24}Al, half life determ. for ^{24}Al 2—2744
    ^{26}Mg(p,t)^{24}Mg, near 26 MeV, meas. of cross sections, angular distribs., excitation functions, DWBA calcs. 2—35035
    ^{204}Mg(n,p), study of new 40±3s activity of ^{204}Au 2—31513
    Mo(A=94, 98, 100), (p,d) reactions, evidence for neutron pick up from interior core 2—35037
    ^{94}Mo(p,p′γ)^{94}Mo, partial decay strengths, comparison with spectroscopic factors of ^{95}Mo(d,t)^{94}Mo reaction 2—18195
    ^{94}Mo(p,t)^{92}Mo, 40 MeV proton beam, spin and parity assessments 2—2780
    ^{94}Mo(p,t)^{92}Mo 40 MeV, deduced levels in ^{92}Mo 2—18114
    Mo(p,p), A=92,94,96,100, Ep=20,30,50 MeV, optical model analysis of cross sections and polarizations 2—28030
    Mo(p,p′), compound-nucleus contrib. 2—2771
    ^{14}N(p,2p)^{13}C, DWA calc. of low energy reaction in 1p shell 2—21433
    ^{14}N(p,γ) ^{15}O states in ^{15} O studied between 10.91 and 13.02 MeV excitation as resonances 2—27970
    ^{14}N(p,γ)^{15}O, determination of mass of ^{15}O 2—34913
    ^{14}N(p,p)^{14}N, rel. to investigations of double level at 8.92 MeV in ^{15}O 2—8284
    ^{14}N(p,pd), 50 MeV, total cross sections, secondary p energy spectra, secondary nuclei momentum and angular distribs. 2—31535
    ^{14}N(p,pγ) states in 15_{o} studied between 10.91 and 13.02 MeV excitation as resonances 2—27970
    ^{15}N(p,$\alpha\gamma$)^{12}C, shell model and rotational calcs. for ^{16}O 2—38481
    ^{15}N(p,n)^{15}O, threshold energy for reaction and mass of ^{15}O 2—31543
    ^{15}N(p,p′)^{15}N*, excitation function meas. level structure of ^{16}O, from 20-23 MeV 2—14933
    ^{23}Na(p,γ)^{24}Mg, accurate branching ratios 2—38593
    ^{23}Na(p,γ)^{24}Mg, resonance meas. 2—38592
    ^{23}Na(p,γ)^{24}Mg 0.3-1.9 MeV, meas. of proton energies and strengths of resonances, gamma decay, Q-value 2—38591
    ^{23}Na(p,p′)^{23}Na determ. of mean lifetimes and decay modes of levels populated in reaction 2—14941
    ^{143,145}Nd(p,t), coupled particle-pairing vibrational states in ^{141}Nd and ^{143}Nd excited, level assignments made 2—11765
    Nd(p,d), A=142-150, energy gap 2—18196
    Nd(p,t), A=142-150, pairing vibrations 2—18196
    ^{20}Ne, determination of deformation parameters by inelastic scattering of polarized protons 2—35034
    ^{20}Ne(p,n)^{20}Na, 23 MeV, excitation energies of levels in ^{20}Na 2—18092
    ^{20}Ne(p,n)^{20}Na, half life determ. for ^{20}Na 2—2744
    ^{22}Ne, determination of deformation parameters by inelastic scattering of polarized protons 2—35034
    ^{22}Ne(p,γ)^{23}Na, ang. distribution meas. of γ-rays 2—24219
    Ni, scattering distributions for particles in 2 to 30 keV range 2—11824
    ^{58}Ni(p,γ), $g_{9/2}$ analog resonances, with strong M1 transitions to antianalog states 2—18109
    ^{58}Ni(p,p′γ)^{58}Ni*, E_p=20 MeV, substate excitation of 2^{+} state, transition from O^{+} state 2—34941
    ^{58}Ni(p,p)^{58}Ni 5.8-6.5 MeV, p polarization and ang. distrib. obs. 2—8334
    ^{60}Ni(p,γ), $g_{9/2}$ analog resonances, with strong M1 transitions to antianalog states 2—18109
    ^{60}Ni(p,p)^{60}Ni 5.8-6.5 MeV, p polarization and ang. distrib. obs. 2—8334
    ^{62}Ni, scatt., E_p=2.43-2.63 MeV, rel. to isobaric analog states of ^{63}Ni 2—34945
    ^{62}Ni(p,α)^{59}Co, population of highly excited levels in ^{59}Co, energy spectra study 2—24162
    ^{62}Ni(p,γ), $g_{9/2}$ analog resonances, with strong M1 transitions to antianalog states 2—18109
    ^{64}Ni(p,nγ)^{64}Cu $\leqslant$3.1 MeV, excitation function, gamma-ray ang. distrib. and nγ correlations determ. 2—5693
    ^{64}Ni(p,p)^{64}Ni, 3.150 to 4.050 MeV, ang. distribution and obs. of isobaric analog states in ^{65}Cu compound nucleus 2—35027
    Ni(p,γ)Cu, M1 transition from $g_{9/2}$ analogue to anti-analogue state in Cu, A=59, 61, and 63 2—5655
    Ni(p,p′), compound-nucleus contrib. 2—2771
    ^{16}O (p,2p), distorted momentum distrib. calc. with complex pot. consistent with nucleon density distrib. 2—488
    ^{16}O elastic and inelastic scatt. of 30.4 MeV polarized protons 2—14983
    ^{16}O elastic scattering, optical model description improved by addition of surface-peaked term to real-central potential 2—24211
    ^{16}O(p,2p)^{15}N, angular correlations measured at 49.5 MeV, results compared with distorted wave impulse approx. 2—11830

Nuclear reactions and scattering due to continued
protons continued
^{16}O(p,2p)^{15}N, DWA calc. of low energy reaction in 1p shell 2—21433
^{16}O(p,α)^{13}N, high-spin assignments in the 1p-shell of ^{13}N 2—31544
^{16}O(p,α)^{13}N astrophysical importance of rate and cross section of reaction for nucleo-synthesis 2—24217
^{16}O(p,n)^{16}F, 23 MeV, excitation energies of levels in ^{16}F 2—18092
^{16}O(p,pd), 50 MeV, total cross sections, secondary p energy spectra, secondary nuclei momentum and angular distribs. 2—31535
^{18}O(p,p$'$), polarized protons, analysis of low lying positive parity states based on rotational model 2—8286
Os(p,p$'\gamma$) A=186,188,190,192, Coulomb excitation of 2^+ states, B(E2) values 2—18142
^{31}P(p,γ)^{32}S, 0.35-2.03 MeV, determ. proton energies and strengths of resonances, gamma decay, Q-value 2—38596
^{31}P(p,γ)^{32}S, resonance strengths 2—38597
^{231}Pa target, 35 to 63 MeV, yields of α-radioactive products, intra-nuclear cascade model analysis 2—35039
Pb target, 10 to 28 GeV, inelasticities and inelastic cross section 2—31541
^{207}Pb(p,p), using polarized protons, differential cross sect. and polarization meas., 11-14 MeV 2—14984
^{208}Pb(p,α), level densities of near doubly magic nuclei 2—38527
^{208}Pb(p,d), neutron pick up reaction at sub Coulomb energies, neutron radius 2—2738
^{208}Pb(p,γ)^{209}Bi, 8.8 to 18.0 MeV, interfering giant dipole and isobaric analogue resonances 2—490
^{208}Pb(p,n), optical model potential, energy dependence of isospin dependent part 2—38603
^{208}Pb(p,p), using polarized protons, dfferential cross sect. and polarization meas., 11-14 MeV 2—14984
^{208}Pb(p,t) two-nucleon transfer cross sections, effect of ground state correlations 2—38602
^{149}Pr(p,xn)$^{142-x}$Nd, 10.85 MeV, excitation function meas. 2—5695
^{185}Re(p,n)^{182}Os, K-dependence of population of ^{182}Os levels 2—27991
^{103}Rh(p,nγ)^{103}Pd, in-beam gamma-ray meas. of excited states in ^{103}Pd 2—11757
^{96}Ru(p,α)^{93}Tc, α particle spectrum obs. at 120°, new levels in ^{93}Tc reported 2—38545
^{32}S, collective states obs. by inelastic scatt. of polarized protons 2—31461
^{32}S(p,d)^{31}S, polarised protons at 24.5 MeV, asymmetry and differential cross sections 2—24221
^{32}S(p,γ)^{33}Cl, 3.36-5.41MeV, studies on analogue states in ^{33}Cl by isospin forbidden resonances 2—34931
^{32}S(p,γ)^{33}Cl, isospin forbidden resonances rel. to analog states in ^{33}Cl 2—34932
^{32}S(p,n)^{32}Cl, half life determ. for ^{32}Cl 2—2744
^{33}S(p,γ)^{34}Cl, 1058, 1098, 1121 keV, properties of levels in ^{34}Cl studied 2—11733
^{34}S, collective states obs. by inelastic scatt. of polarized protons 2—31461
^{34}S(p,d)^{33}S, polarised protons at 24.5 MeV, asymmetry and differential cross sections 2—24221
^{34}S(p,γ)^{35}Cl, γ ray transitions of ^{35}Cl 2—2704
^{45}Sc(p,p$'$), 49.75 MeV, differential cross sections of excited states 2—18184
Si, back-scattering of fast protons 2—22441
Si, scattering distributions for particles in 2 to 30 keV range 2—11824
^{28}Si(p,n)^{28}P, half life determ. for ^{28}P 2—2744
^{28}Si(p,nγ)^{28}P, 23 MeV, γ-spectrum 2—14986
^{29}Si(p,d)^{28}Si, investigation of energy levels in ^{28}Si 2—2700
^{29}Si(p,γ)^{30}P, E_p=2-3MeV, ^{30}P levels 2—31460
^{30}Si(p,t)^{28}Si investigation of energy levels in ^{28}Si 2—2700
Si(p,p), energetic dependence of elastic scattering cross sections on thick targets 2—28033
^{144}Sm, 30 MeV elastic and inelastic scattering to low lying states, cross section determ. 2—11857
^{144}Sm (p,p), (p,p$'$), 50.8 MeV, nuclear models' analysis 2—27985
^{148}Sm (p,p), (p,p$'$), 50.8 MeV, nuclear models' analysis 2—27985
^{148}Sm(p,p$'$)^{148}Sm, 24.5 MeV, asymmetry measurements of low lying states, coupled channel analysis 2—469
^{150}Sm (p,p), (p,p$'$), 50.8 MeV, nuclear models' analysis 2—27985
^{152}Sm (p,p), (p,p$'$), 50.8 MeV, nuclear models' analysis 2—27985
^{152}Sm(p,p$'$)^{152}Sm, 24.5 MeV, asymmetry measurements of low lying states, coupled channel analysis 2—469
^{154}Sm (p,p), (p,p$'$), 50.8 MeV, nuclear models' analysis 2—27985
Sn isotopes, sub-barrier (p,n) reactions in single particle resonance region 2—11833
^{116}Sn, inelastic proton scattering, transitions to collective and non-collective states, DWBA analysis 2—28080
^{117}Sn(p,n)^{117}Sb, 4.5 MeV, differential cross sections near 0^+ analogue states 2—8340
^{118}Sn, inelastic proton scattering, transitions to collective and non-collective states, DWBA analysis 2—28080
^{119}Sn(p,n)^{119}Sb, 4.5 MeV, differential cross-sections near 0^+ analogue states 2—8340
^{120}Sn, inelastic proton scattering, transitions to collective and non-collective states, DWBA analysis 2—28080
^{120}Sn(p,p$'\gamma$), proton spin flip probability in excitation of first 2^+ states, 30 MeV 2—24212
^{122}Sn(p,n)^{122}Sb, ^{122}Sb low-lying states study 2—11761
^{124}Sn, inelastic resonance scatt., excitation of particle-hole states 2—38513
^{124}Sn(p,p$'$), isobaric analog resonances of ^{124}Sn, inelastic decay with direct reaction background 2—2720
^{124}Sn(p,p$'\gamma$), proton spin flip probability in excitation of first 2^+ states, 30 MeV 2—24212
Sn(p,p$'$), compound-nucleus contrib. 2—2771
Sn(p,t), even isotopes, L=0 transitions analysis using pairing vibr. model, pairing and shell effects 2—31483
Ta target for 580 MeV and 19 GeV protons, excitation energy of residual lanthanide nuclei 2—35029
^{181}Ta(p,p), using polarized protons, differential cross sect. and polarization meas., 11-14 MeV 2—14984
Th, secodnary effects produced by interaction with 28 GeV protons 2—35038
^{232}Th target, 35 to 63 MeV, yields of α-radioactive products, intra-nuclear cascade model analysis 2—35039
^{46}Ti(p,t)^{44}Ti, 51 MeV, ang. distribs., level structure of ^{44}Ti 2—24157
^{48}Ti (p,γ) ^{49}V, study of excited states of ^{49}V 2—27975
^{49}Ti(p,p$'$), 12 MeV, cross section meas., ^{49}Ti deduced levels 2—31468
Tl, secondary effects produced by interaction with 28 GeV protons 2—35038

Nuclear reactions and scattering due to continued
protons continued
^{203}Tl(p,4n)^{200}Pb, ^{200}Pb lower levels obs. 2—18146
^{203}Tl(p,6n)^{198}Pb, ^{198}Pb lower levels obs. 2—18146
^{205}Tl(n,α), study of decay of ^{202}Au 2—31513
U, interaction with 28 GeV protons, charge and mass distribution of rare-earth products 2—11834
U, secondary effects produced by interaction with 28 GeV protons 2—35038
^{238}U(p,x)(x,y)^{254}Fm, search for ^{254}Fm production by secondary nuclear reaction of 11.5 GeV protons 2—28038
^{238}U(p,x)(x,y)^{256}Fm, search for ^{256}Fm production by secondary nuclear reactions of 11.5 GeV protons 2—28038
V isotopes, elastic scattering, 2.8-6.3 MeV 2—489
^{51}V(p,p)^{51}V, 5.8-6.5 MeV, p polarization and ang.-distrib. obs. 2—8334
W target, thick, scattering spectrum in terms of energy loss 2—8321
W(p,p$'\gamma$), A=182,184,186 Coulomb excitation of 2^+ states, B(E2) values 2—18142
^{89}Y(p,p$'$), excitation by 61.2 MeV protons of various states, differential cross sections 2—21429
Zn (A=64, 66, 68), elastic scatt. and polarization of 30.5 MeV protons, optical model analysis 2—5690
^{64}Zn(p,γ), $g_{9/2}$ analog resonances, with strong M1 transitions to antianalog states 2—18109
^{64}Zn(p,t)^{62}Zn, 27.5 MeV, angular distributions, ground state Q-value, levels of ^{62}Zn and spin-parity assignments 2—38495
^{66}Zn(p,γ), $g_{9/2}$ analog resonances, with strong M1 transitions to antianalog states 2—18109
^{67}Zn(p,nγ)^{67}Ga, low lying levels of ^{67}Ga 2—5658
^{68}Zn(p,p$_1'\gamma$)^{68}Zn*, study of ^{69}Zn low lying states 2—2712
Zn(p,γ)Ga, M1 transition from $g_{9/2}$ analogue to anti-analogue state in Ga, A=65, 67 2—5655
^{90}Zr, scattering, elastic and inelastic, of 185 MeV protons, differential cross sections and polarizations 2—8335
^{90}Zr(p,α)^{87}Y, computation of pick-up form factors 2—2774
^{90}Zr(p,p$'$), excitation by 61.2 MeV protons of various states, differential cross sections 2—21429
^{91}Zr(p,n), isobaric analogue resonances in ^{92}Nb 2—5694
^{91}Zr(p,nγ)^{91}Nb, excited states determ. for ^{91}Nb 2—2715
^{91}Zr(p,t)^{89}Zr, E_p=51.7 MeV 2—38600
^{91}Zr(p,t)^{89}Zr, zero range DWBA anal. 2—38601
^{92}Zr(p,α)^{89}Y, computation of pick-up form factors 2—2774
^{96}Zr(p,nγ)^{96}Nb, ^{96}Nb low-lying states study 2—11754
Zr(p,p$'$), compound-nucleus contrib. 2—2771
tritons
elastic scatt. cross sections, complex ang. momentum methods 2—35061
optical interaction, absorptive potential description of underlying one body structure 2—28069
stripping reaction, trinucleon induced, normalization factor for zero and finite range DWBA calc. 2—15004
(t,p) reaction study of neutron-rich isotopes near A=100 2—31479
(t,p) reactions, sum rules and two-particle units in the analysis of two-neutron transfer reactions 2—31566
(t,p) stripping reactions on deformed nuclei, finite range effects studied, cross- section determ. 2—11859
^{40}(alt,d$_0$)^{41}Ca meas. of angular distribs, near Coulomb barrier, DWBA analysis gives spectroscopic factor 2—35074
^{9}Be(t,α)^{8}Li, lifetime of first excited state of ^{8}Li 2—18088
^{12}C(t,p)^{14}C, differential cross section and polarization measurements at 16 and 20 MeV 2—28075
^{12}C(t,t)^{12}C, differential cross section and polarization measurements at 16 and 20 MeV 2—28075
^{40}Ca(t,d)^{41}Ca, effects of 2-step processes in reactions leading to $^{3}/_{2}{}^{+}$2.02 MeV 2—28077
Ca(t,p), J^π=0^+ states, effective wave function calculation 2—14944
^{3}H(t,n^{4}He)n, kinematically complete expt., determ. of neutron-neutron scattering length 2—28073
^{3}He(t,p^{4}He)n, kinematically complete expt., determ. of proton-neutron scattering length 2—28073
^{7}Li(t,p)^{9}Li, new states in ^{9}Li 2—2689
^{206}Pb(t,p)^{208}Pb, interpret. rel. to particle-core states in ^{208}Pb 2—35080
^{208}Pb(t,p) two-nucleon transfer cross sections, effect of ground state correlations 2—38602
^{116}Sn(t,p), transitions to collective and non-collective states, DWBA analysis 2—28080
^{118}Sn(t,p), transitions to collective and non-collective states, DWBA analysis 2—28080
Sn(t,p), even isotopes, L=0 transitions analysis using pairing vibr. model, pairing and shell effects 2—31483
^{47}Ti(t,p), 12 MeV, cross section meas., ^{49}Ti deduced levels 2—31468
X-rays *see Nuclear reactions and scattering due to/photons*
Nuclear reactors, fission
accident protection methods 2—38687
aqueous homogeneous suspension, hydrodynamic aspects 2—11892
biomedical applications, radionuclide production 2—41291
boiling water, finite element method for three dimensional stress and vibration analysis 2—15084
boiling water and spray cooled, heat transfer and slow burnout 2—1042
breeding ratio definition giving correct doubling time and fuel cycle reactivity variation 2—11890
buildings, aseismic design, stress analysis by finite element method 2—15081
Canada's nuclear power program 2—5741
CANDU-type PHW heavy water reactor fuel cycle costs, using Pu enriched UO$_2$ and natural U 2—11895
chamber design and manufacture, for secondary standards in meas. of neutron flux density 2—11650
circulation pump, stress analysis 2—15036
CIRENE, design and characteristics 2—15041
conference, nuclear and solid state physics, Bombay (1972) 2—34868
cooling, heat transfer to liquid metals flowing in-line through tube bundles at constant and exponential heat flux distribution 2—38723
core support structures, dynamic response subject to blowdown forces caused by loss of coolant accident 2—15093
corrosion in nuclear applications, book 2—38700
creep, nonlinear analysis at elevated temps. 2—14184
creep analysis of process tube 2—15168
critical assemblies and thermal research reactors, book 2—38701
critical nuclear reactor, formation of critical reactor by part of core 2—8384

Nuclear reactors, fission continued
  critically built VVR-M, integrated characteristics of slow neutron spectra 2—28156
  deposition rate of corrosion products, on surface of Zr alloy as function of coolant compos. temp. and irradiation 2—31625
  design, acoustic pressure level and structural response determ., Windscale High Intensity Noise Rig 2—38707
  design accuracy 2—38704
  design and construction of SNR 300 the German-Benelux fast breeder 2—31622
  design and stress analysis using BERSAFE finite element computer system 2—15083
  design criteria and how they are met 2—11893
  design optimization, nonlinear programming 2—35101
  diagnostic techniques, statistical 2—21474
  DIORIT. natural U, research reactor, D_2O cooled and moderated 2—11921
  earthquake analysis, structural dynamics in areas of low and average seismic activity 2—16742
  earthquake response analysis, nuclear reactor structures evaluated for damping efficiencies 2—15080
  EBR-II, post shutdown surges in Xe activity due to a leak in fuel element 2—8393
  elastic stress analysis of cylinder-to- cylinder shell models application to nozzles in cylindrical vessels 2—14178
  end plate behaviour prediction using triangular thick plate bending elements 2—14190
  engineering and development, Bulleid Memorial Lectures, Nottingham (1971) 2—526
  engineering development in Canada, conference, Chalk River, Ontario (1971) 2—11891
  engineering effects as sources of shochastic noise in neutron reaction rates 2—15043
  environmental pollution, comparison with conventional fuels 2—15028
  environmental radioactive purity near the IRT-2000 reactor 2—8413
  excursion, high energy, dynamic response of containment 2—15091
  excursion and accident analysis model, by computer 2—31623
  excursion radiation detection system 2—24289
  excursion radiation detection system using on-line computer 2—31630
  excursions, reliability of computer predictions of hydrodynamics 2—15090
  fast, explosive disassembly, theoret. anal. 2—38696
  fast, role in development of commercial power plants 2—24266
  fast breeder reactors, review 2—2846
  fast breeder type, Na cooled, radial core constraint, design 2—38706
  fast reactor, engineering, review 2—530
  fast reactor critical experiments, current status 2—21466
  fast reactor safety studies, role of water model experiments 2—540
  fast reactors, existence of voidage phenomenon 2—532
  fast-thermal BOR 60 core assembly, investigation of some characteristics 2—35102
  FRG-2, experiments and considerations for design and power increase 2—31621
  FRJ-2, cold neutron source 2—24261
  FRJ-2, cold neutron source instrumentation 2—24264
  FRJ-2, cold neutron source temperature meas. 2—24288
  FRJ-2, cold neutron source thermodynamic design 2—24262
  FRJ-2, n cold source 2—24263
  fuel element heat transfer, conductivity effects 2—184
  fuel failure propagation, pin to pin, importance of design-safety interactions on rate 2—15087
  fuel-element behaviour prediction, computer-aided analysis 2—21470
  gas cooled, heat exchanger, inhibition of catalytic decomp. of CO 2—4577
  gas cooled, high temp., heat transfer and fluid dynamics 2—525
  gas cooled, thermal, engineering, review 2—528
  gas cooled high temp. multi-purpose reactor design 2—531
  gas-cooled, review of performance and development of advanced designs 2—2852
  gas-cooled fast breeding, review 2—38698
  Gentilly BLW reactor, radial and axial neutron flux distrib. 2—5740
  Godiva, unreflected ^{235}U critical assembly, n spectra and reaction cross sections 2—38710
  heat conduction, thermoelastic and viscoelastic problems solved by method of orthogonal projection in Hilbert space 2—14286
  heat transfer to water, in tube flow at supercritical pressure 2—6169
  heavy water, ^{235}U, design 2—38714
  heavy water-moderated, heavy and light water and organic liquid cooled 2—2855
  HERALD, light water moderated and cooled reactor, operation and design 2—38718
  high temperature, gas-cooled, graphite fuel element 2—21468
  high temperature lattice test reactor, neutron multiplication factors as function of temp. 2—8391
  instrumentation, w.r.t. operation and design, review 2—21475
  instrumentation and control system for AGN- 201M reactor 2—38735
  IRT-TM reactor, reconstruction of dry experimental channels 2—28131
  light water, HTR-P core, power burst, effect of Doppler effect 2—38709
  light water, reviews of performance experience and control difficulties 2—2851
  low power reactor, use in neutron activation anal. and neutron radiography 2—38736
  MHD generator, induction with hollow nuclear reactor 2—11425
  neutron burst signals, detection using multiplication 2—38763
  neutron flux measuring self powered sensor 2—11914
  neutron generator target, neutron flux density distrib. 2—28105
  noise analysis, data extraction methods, review 2—24265
  noise analysis, data extraction methods, review 2—31620
  noise effects, velocity of sound in CO_2, temperatures $<100°C$ 2—3328
  nozzle-to-flat plate approach for stress concentration problem of nozzle to cylinder intersections 2—15056
  numerical calculation techniques 2—38691
  parallel flow through roughened rod cluster, forced convection heat transfer 2—31627
  parameters, estimation by optimal filtering method 2—533
  pebble bed core, AVR, THTR, mechanical problems 2—38712
  pipe nozzle junctions with curved transitions three dimensional finite-element analysis 2—15058
  piping system and stress analysis of intersecting cylindrical shells by finite element method 2—14177
  post burst accident models, heat transfer 2—15092
  power channels, vibrations induced by two phase coolant flow 2—14247

Nuclear reactors, fission continued
  power monitoring by measuring activities of ^{16}N and ^{17}N in primary cooling water 2—28116
  power reactors, development in U.K., review 2—527
  power station sites in India, atmospheric diffusion rel. to meteorological parameters 2—20321
  pressure tube type, loading due to channel rupture 2—15089
  pressure vessel, fracture control procedure 2—25566
  pressure vessel, in-service acoustic emission monitoring 2—28158
  pressure vessel connecting pipes, tensile strength analysis 2—15055
  pressure vessel flanges, elastic analysis of axially perforated cylinders 2—15060
  pressure vessel integrity, dynamic strain- ageing embrittlement effect 2—24294
  pressure vessel nozzles, three dimensional finite element analysis 2—15057
  pressure vessel technology, conf., London, England, May 1971 2—24293
  pressure vessels, application of stress analysis of rotating preforated shells 2—14176
  pressure vessels, current trends in control, surveillance of neutron irradiation effects 2—28126
  pressure vessels, cylindrical, plastic thermal stresses and strains 2—15054
  pressure vessels, equivalent energy procedure for fracture prediction 2—24290
  pressure vessels, heat affected zone fracture toughness 2—25528
  pressure vessels, safety analysis, elastic fracture mechanics applic. 2—24296
  pressure vessels, safety eval., fracture resist. 2—24292
  pressure vessels, simple finite method for stress concentration problems 2—15059
  pressure vessels, stress analysis using stress hybrid finite element model 2—14188
  pressure vessels, thick-walled, fracture mechanics technology applic. 2—24295
  pressurized water coolant system support structures, design 2—15053
  pulse, radiation detection system using on-line computer 2—15173
  PWR, core support structure design, analytical problems, techniques 2—38705
  radiation monitoring, thermoelec. obs. 2—8389
  radiation monitoring systems, review 2—38765
  rate measurement, solid state track recorders 2—8411
  reactivity, experimental absolute determination, new method 2—38688
  reactivity and power distribution meas., computer applic. 2—534
  reactivity det. by obs. of heat coefficient of reactivity and efficiency of compensating rods 2—28135
  reflected coupled-core reactor, core coupling meas., pulsed source experiments 2—38722
  reflected coupled-core reactor, reactivity meas., pulsed-source experiments 2—38721
  reliability of 2-out-of-3 system, consideration of number of spares and exchange time 2—38693
  resarch, use in neutron radiography 2—39872
  research and training, utilization, conference, Texas, February (1972) 2—38699
  research facility, system for reduction of ^{41}Ar release 2—38715
  research reactors, role in stimulating technology in underdeveloped countries 2—24258
  response of short cylindrical panels to random loads 2—14192
  safety anal., problems of explosions in interior 2—15088
  safety analysis, accident prevention, radiological consequences on environment 2—38725
  safety containment in case of coolant blow-down 2—15078
  safety of pressure vessels, industrial materials parameters 2—15062
  safety philosophy and experimental verification 2—28134
  shielding, computer graphic-aided design 2—38772
  signals, long time series, fast correlation and spectral anal., program system 2—14246
  similitude application to structural mechanics 2—15085
  simulation, real time, on hybrid computer or BWR and EFR 2—524
  stellarator and Tokamak types, model design studies, and economic feasibility 2—28141
  stress analysis of shells of revolution, application to primary vessels and containment shells 2—14174
  structure and stress and displacement velocity in plastic rotationally symmetric flow zones 2—14175
  subcritical assembly, thermal neutron pulse propagation, dependence on reactivity 2—38689
  synchrotron radiation to ionize wall originated impurities 2—18253
  technology, structural mechanics, conference (Berlin 1971) 2—15035
  temperature and mechanical strain cycling, comparison with isothermal fatigue 2—15037
  thermal biological irradiation facility, dosimetry 2—2886
  thermal insulation tests on prestressed concrete reactor vessels for water cooled power reactors 2—15094
  thermal neutron flux det. by activity ratio technique 2—38717
  thermionic diodes, in-core, disassembling machine 2—38758
  ventilation system, obs. of ^{131}I concentration 2—4698
  vibration tests on internals, rel. to calcs. 2—15174
  water cooled, full pressure containments, time dependent short-term pressure build-up 2—38690
  water cooled, thermal, engineering, review 2—529
  n spectra, fast, threshold detector evaluation 2—38351
  B neutron detector system for monitoring whole dynamic range 2—31375
  Na cooled, absorber material, europium applic. 2—38743
  Na cooled, sheathed thermoelements with boron nitride insulation 2—38742
  pressure vessels, overstressing technique for securing against brittle failure 2—24291
  ^{239}Pu fueled lattice, evaluation of neutron spectral effects by foil activation 2—5732

materials
  'Safe Dry Times' for irradiated NRU fuel assemblies 2—5756
  actinide-platinum metal-carbon system, ordered phase form. 2—29493
  active nondestructive assay techniques for nuclear materials 2—28159
  alloy stress corrosion and environmental effects 2—15116
  artificial graphite, rate- independent continuum theories, experimental verification 2—39779
  balance for weighing irradiated DFR experimental fuel pins 2—5762
  boiling water reactor containments, protection in case of accidents 2—15162

Nuclear reactors, fission continued
materials continued
bolted core support structure, prediction of stresses and fatigue strength 2—15175
burn-up, nuclear data requirements for det. by chemical means 2—552
Canadian Nuclear Power Demonstration Reactor, anal. of fuel pin bundles 2—5760
carbide and nitride fuels for fast breeder reactors 2—28148
carbide fuel irradiation capsule 2—35104
cell with thin moderator, monoenergetic disadvantage factor 2—28146
ceramic fuel:actinide compounds in pnictide and chalcogenide classes 2—18261
cermets, multiphase, obs. of orientation and distribution of dispersed phases 2—5753
clad fuel elements, cylindrical and spherical, thermal stresses 2—14225
clad pellet stacks, thermal stresses and interface stress states 2—14224
cladding, carburization obs. using single-stage extraction replicas 2—36228
cladding, non-bonded, wrinkling 2—14168
coated fuel particles for gas cooled fast reactor 2—28149
concrete containment structures in India, design and structural analysis 2—15097
concrete containments walls, thermal effects, elastic and inelastic behaviour 2—15096
concrete pressure vessel liners, prestressed, stress analysis 2—15154
concrete pressure vessel models, prestressed, mode of rupture under internal gas pressure 2—15152
concrete pressure vessels, prestressed, reduced-scale models, ultimate tests 2—15151
concrete pressure vessels, prestressed, stress-strain behaviour 2—15153
concrete pressure vessels of WYLFA nuclear power station, thermal insulation, structural behaviour 2—15156
concrete vessels, liners, pre- and post-buckling analysis, matrix displacement method 2—15155
containment vessels, steady state and transient thermoelastic behaviour, finite element analysis 2—15161
containment vibrations, determination of damping matrix in dynamic structural analysis 2—14249
coolant, velocity and temp. field, temp. distrib. in cladding and fuel 2—15120
core components, THTR, analysis of external loading stresses 2—15133
creep, thermal and irradiation induced, and swelling, application of finite element methods 2—15082
creep analysis of cylindrical shells under internal pressure 2—14185
creep deflection of pressure tubes in horizontal reactors 2—15167
deformation and melting in reactor rods and plates under internal heat generation 2—14293
dynamic fracture mechanics approach to vessel surveillance 2—15149
environmental effects, conf., London, England, July 1971 2—11906
fast breeder cores, parallel- flow-induced vibration of fuel rods, mathematical model 2—38733
fatigue crack propagation due to acoustically induced stress, fracture mechanics approach 2—15171
fracture toughness, prediction of radiation induced changes 2—15148
fuel, automatic control of recycling processes using spectrophotometry and condctivity obs. 2—28144
fuel, coated particle, stress and strain calcs. rel. to irradiation obs. 2—15119
fuel, defect studies by adsorption of fission products from soln. 2—12685
fuel, fission product release performance, post-irrad. exam. techniques 2—38761
fuel, post-irrad. exam. techniques 2—38755
fuel, post-irrad. exam. techniques at Studsvik 2—38750
fuel assembly, coupled tubular structures, lateral deformations 2—15137
fuel bundles, enthalpy imbalance in evaluating the dryout performance 2—5757
fuel bundles, multielement, thermocouples for meas. of surface temp. 2—5758
fuel cladding, electrokinetic method of measuring thickness, use of eddy currents 2—18263
fuel compacts, coated particle maxtrix type, neutron irrad., dimens. and phys. prop. changes 2—21471
fuel creep capsule, instrument equipped for in-pile measurement of fuel pin swelling and creep 2—11903
fuel cycle reactivity variation and doubling time calc. from definitions of breeding ratio 2—11890
fuel distribution, fuel cycles and materials 2—24276
fuel element, fluid flow, temp. field calc. 2—12316
fuel element, swage joint tightness, holographic determ. 2—25553
fuel element cladding, creep deformation, applic. of variational principles 2—14166
fuel element cladding, longitudinal stress distrib. 2—14167
fuel element corrosion and Th alloy compatibility with cladding materials 2—20190
fuel element frequency response, mechanical fuel-can interaction effects 2—15121
fuel elements, analysis of internal heating shock effects, expansions, stresses in specific element geometry 2—38745
fuel elements, behavior under delayed boiling conditions 2—15134
fuel elements, control rods and pressure vessels for pressurized water cooled reactors 2—5746
fuel elements, cylindrical, jacket, stability assuming initial ellipticity 2—28143
fuel elements, fission gas annealing test in post-irrad. exam. 2—38757
fuel elements, flash diffusivity in cylindrical coordinates 2—17444
fuel elements, HTGR, finite element analysis of stresses 2—15125
fuel elements, patent 2—554
fuel elements, porous, fission gas diffusion conditions 2—31628
fuel elements, post-irrad. exam. 2—38760
fuel elements, ratchetting growth of cladding 2—15825
fuel elements, spherical, gamma spectrometry applic. 2—38759
fuel elements, thermal, radiation and mechanical analysis 2—14169
fuel elements, tightly clustered bundle, response to initial thermal and mechanical loading condits. 2—15124
fuel elements, unirrad., thermal cond., 400 to 1400 K 2—19441
fuel elements and valve packings, irradiated, neutron radiography 2—18258
fuel fabrication, cost analysis, CANDU type 2—2861
fuel fabrication processes and costs 2—24277
fuel management, review of problems of utility and supply 2—2859

Nuclear reactors, fission continued
materials continued
fuel material swelling, models verification, use of microstructural data 2—21473
fuel materials, review of developments 2—24279
fuel particles, coated, mechanical behaviour calculation, using mathematical model 2—21472
fuel particles, conical fluidized beds for coating, model 2—18256
fuel pin, FTR type, loss-of- flow expt. in Mark II loop 2—38713
fuel pins, automated system for gamma scanning 2—38762
fuel pins, failed, fission gas release, effect of gas jet on surrounding pins integrity 2—15123
fuel pins, irrad., NDT, optical viewing devices 2—38753
fuel pins, parallel-flow induced vibrations 2—15136
fuel pins, post-irrad. exam. techniqes 2—38754
fuel post-irrad. exam. by hot cell techniques 2—38752
fuel post-irrad. exam. facilities 2—38751
fuel rod assemblies, finite, heat transfer, theory 2—38697
fuel rod bundles, mechanical stress due to temp. gradients 2—15120
fuel rod bundles, turbulent velocity distrib. and wall shear stress 2—15039
fuel rod vibrations induced by coolant flow 2—15135
fuel rods, anal. for creep buckling under external pressure 2—14165
fuel rods, enrichment det. by γ-ray spectrometry 2—38746
fuel rods, SATURN I modelling of mechanical and thermal behavior 2—15122
fuel-cladding mechanical interaction and resulting failure mechanism 2—11904
fuel-cladding mechanical interactions, parametric analysis 2—15826
fuelled graphite bricks, HTGR, stress and temperature distributions, finite element analysis 2—15127
fuelled spheres, post-irrad. exam., sampling methods 2—38756
fuels, analysis, conference (Berlin 1971) 2—15035
fuels, coated particle, bonding and compact, internal stresses, irradiation behaviour, models 2—15118
fuels, coated particle, stress analysis for consumption studies 2—15117
fuels, void movement along thermal gradient 2—25441
fuels and fuel cycles, isotope applications, Geneva 1971, conference 2—24257
gas circuit components, acoustically induced stress 2—15145
grain boundary, inert gas bubble growth, stress depend. 2—19067
graphite, effect of pitch-binder coke content and neutron irrad. on props. 2—22175
graphite, fast neutron dose and coolant gas impurities influence 2—11911
graphite, fracture surface, electron microscope obs. 2—3907
graphite, irrad., dimensions, elec. resist. and Young's modulus meas. 2—39873
graphite, irrad., elec. resist. rel. to thermal cond. 2—13220
graphite, mechanical resistance 2—17334
graphite, neutron field decay, exponential and non-exponential 2—5752
graphite, neutron irrad., dimens. and phys. prop. changes 2—21471
graphite, neutron irrad., dimensions, thermal expansion, porosity and microstructure 2—3756
graphite, neutron irrad., dimensions, thermal expansion and microstructure 2—3759
graphite, nuclear, neutron irrad. above 1200°C, increased mech. lifetime. radiation damage 2—19152
graphite, post-irrad. exam., sampling methods 2—38756
graphite, pyrolytic, neutron irrad. 250-470°C, change in dimens., density, thermal cond., thermal expansion coeffs. 2—19432
graphite, pyrolytic, thermal cond. and diffusivity, 300 to 2700K 2—19452
graphite, pyrolytic, thermal diffusivity anisotropy ratio, 300-1600 C 2—32852
graphite, thermal cond., effect of B or Br doping 2—22429
graphite components, strength and durability rel. to construction problems of a THTR 2—18265
graphite components, strength rel. to design problems 2—15129
graphite components, stress analysis, thermal and Wigner strain effects 2—15128
graphite components, THTR temperature and radiation induced stresses 2—15132
graphite fuel elements, helium-cooled HTR, operational stresses 2—15131
graphite fuel elements, HTGR stress analysis, finite element method 2—15126
graphite moderator, determ. of 1/E spectrum 2—544
graphite moderators, neutron diffusion length dependence on transverse dimensions 2—517
graphite prisms, with cold neutron source, pulse die-away expt. 2—38727
graphites, nuclear, impurities determ. by instrumental activation analysis 2—7201
heat exchanger tubesheets, plastic strain analysis 2—15141
heavy water, Canadian technology for producing and handling it 2—5759
high temperature reactors, Th cycle compared with low enriched U cycle 2—38741
ice as absorbent for gaseous fission products 2—543
IMFBR wire wrapped fuel assemblies, interchannel mixing 2—8406
Incoloy 800, rupture and creep, He environmental effects 2—12871
Inconel 600 heat exchanger tubing, stress assisted corrosion in high temp. water 2—11909
Inconel X750, intergranular stress corrosion cracking in pressurized water 2—11910
irradiated, γ-ray spectra obs. 2—8410
irradiated fuels, burn-up determination by heat output 2—38740
irradiation damage, review of problems of safety and economics 2—2844
irradiation swelling, model 2—32489
isotope enrichment techniques and economics of enrichment 2—24278
liquid metal coolants, arc emission spectroscopic obs. of Zr content 2—16703
mechanical supports for reactor equipment, dynamic analysis 2—15140
metal, He environmental effects in high temp. reactors 2—11913
metal, irradiated, void nucleation, defect co-precipitation 2—32490
mixed oxide fuel elements, radial temp. distribution calc. 2—38747
MTR type fuel elements, spent, ^{235}U content det. using delayed neutron yield technique 2—38748
neutron embrittlement high temp. damage functions for pressure vessel steels 2—11905
neutron radiation damage surveillance, interpretation of structural significance 2—15150
nitride fuel irradiation capsule 2—35104
non flangible metals, fracture extension resistance in fracture safe design 2—15061

Nuclear reactors, fission continued
materials continued
organic moderators and coolants, neutron properties of Santowax-R and Dowtherem-A 2—28153
oxide fuels, mixed, irrad., chem. effects of comp. changes 2—545
post-irradiation exam. techniques, conf., Reading, England (Mar 1972) 2—38749
pressure tube, connection with primary circuit, stress analysis 2—14170
pressure tubes, calandria tubes, new mechanical problems 2—15143
pressure tubes type reactor core, internal supporting structures, analytical model for static analysis 2—15047
pressure vessel, fatigue endurance, effect of prior and periodic overstressing 2—9695
pressure vessels, low cycle fatigue strength of nozzle end weldments 2—15170
pressure vessels, stress analysis 2—15146
pressure vessels analysis of thermal and mechanical stresses 2—15147
prestressed concrete containment structures, design procedures and test results 2—15164
prestressed concrete containment vessels, natural frequency and damping by dynamic analysis 2—15163
production using powder metallurgy 2—8408
radiation damage to internal and structural materials other than fuel assemblies 2—28145
radiation effect on fuels, fuel materials and assemblies 2—24282
rare earth metals as moderators 2—18260
rare earth-platinum metal-carbon system, ordered phase form. 2—29493
recovery, precipitation of UN from liquid U-Sn alloy 2—8405
reflection factor for γ- quanta in graphite cylinders 2—38738
reprocessing of thermal reactor fuels 2—2857
shells, initially stressed, stability and vibration 2—15159
sodium cooled fast breeder reactor, core design, elastic buckling of hexagonal fuel ducts 2—15138
solid, determ. of thermal expansion at pressures to 20 kbar 2—16057
stainless steel fuel cladding, effect of cold working on creep properties 2—3879
steam generator head under internal pressure, stress analysis 2—15144
steel, 316 stainless, 20 MeV C^{2+} irradiation, void swelling, dose depend. 2—6468
steel, austenitic, effect of carbon on high temperature properties, interaction with plutonium carbide 2—1304
steel, austenitic and ferritic, mass transfer and corrosion rate in liquid sodium 2—13583
steel, austenitic stainless, stress corrosion and design considerations for use in boiler plant 2—15115
steel, brittle fracture initiation in residual stress field 2—25522
steel, brittle fracture strength 2—25526
steel, bulk and micro-flow fracture behaviour, neutron irrad. effects 2—25525
steel, carburization in carbon monoxide and methane 2—16678
steel, ferritic, compatibility with liq. Na at high temp. 2—13570
steel, fracture toughness and Charpy impact data 2—25533
steel, protection in liq. Li by beams of metallic diffused layers 2—4592
steel, stainless, carburization in Na containing carbon impurities, effect on mech. props. 2—13569
steel, stainless, fast neutron damage, simulation by ion implantation 2—6475
steel, stainless, heavy ion bombardment, defect struct. 2—9517
steel, stainless, neutron irrad. induced He generation 2—12748
steel, stainless, neutron irradiation, void formation rel. to thermomechanical treatment 2—6469
steel, stainless, radiation-induced swelling 2—24283
steel, stainless, rupture and creep, He environmental effects 2—12871
steel, stainless, type 304, elastic-plastic constitutive equations 2—15823
steel, stainless, type 316, creep and creep rupture testing rel. to cold-drawing 2—1292
steel, stainless, types 304 and 316, fast reactor irrad. damage 2—1236
steel, stainless, void formation rel. to neutron irrad. temp., 400-600 °C 2—19073
steel, stainless stress corrosion cracking resist., comp. effects 2—15882
steel, stainless type 304, resistance to fatigue crack growth at high temps. due to cold working 2—15884
steel, stress corrosion cracking in water cooled reactors 2—11908
steel components, corrosion measurement using laser beam 2—21467
steel plates, brittle fracture 2—25567
steel stainless structural material, creep and creep-rupture tests 2—3880
structural components, branch-pipe tee connection, limit analysis and plastic collapse 2—15142
structural design rules from high temp. material properties 2—15110
structural systems, static and dynamic analysis, computer program 2—15139
thermal analysis of cylindrical shells under internal pressure 2—14185
thin shell pressure vessels, stress analysis, finite element methods 2—15157
thin shell structures, curved finite elements analysis 2—15158
time dependent creep in metallic nozzle entering spherical pressure vessel 2—15169
vitroceramic fuel, coating technique 2—11901
waste disposal in subsurface cavity, temp. increase 2—22916
light water thermalization parameters, meas. using pulsed neutron technique 2—2854
ZEEP rods heavy water moderated lattices, buckling 2—8407
Zircalloy-2, cold-rolled, microstruct. 2—29185
zircalloy-2 reactor pressure tubes, creep limit in design 2—5751
Zircaloy, fuel claddings and pressure tubes in water cooled reactors 2—18257
Zircaloy, stress corrosion cracking in iodine vapour 2—15114
Zircaloy tubing, hydride platelets orientation and effect on mech. props. 2—15842
Zircaloy tubing, in-pile corrosion and hydrogen pick-up 2—11907
Zircaloy tubing, influence of reduction values on texture formation 2—25569
zircaloy-2, cold worked, 300-450°C, creep accel. mechanism 2—25510
Zircaloy-2, corrosion and hydriding in BWRs 2—15113
Zircaloy-2, diffusion of Ni and Sn 2—12817
Zircaloy-2, hydrogen embrittlement, effect of plastic props. 2—29311
Zircaloy-2, radiation enhancement of oxidation 2—13580
Zircaloy-2-fuel casings, effect of neutron irradiation on tangential and axial elastic limits 2—11900
Ag-In-Cd plate type shim rods, MTR fuel elements, flux density and reactivity measurements 2—15040

Nuclear reactors, fission continued
materials continued
Al-Fe-Ni: (Mg,Cr,Mn) alloy, resistance to water corrosion, 220°-315°C, comp. depend. 2—13581
Al, irrad. swelling, expt. test of quasi-chemical model 2—32489
Al_2O_3, in H_2 atmosphere, thermal etch figure 2—28997
Al_2O_3, plasma arc sprayed, struct., electron microscope obs. 2—15663
Al_2O_3 impurity effects on radiation induced swelling 2—12745
B filter, calc. of neutron transmission function, 1/E spectrum in graphite moderator 2—544
B_4C, thermal neutron irrad., He bubble formation 2—3755
Be, hot pressed, tensile props., temp. strain rate depend. 2—29283
Be, neutron irradiated, He gas bubbles behaviour 2—28147
Be moderators, neutron diffusion length dependence on transverse dimensions 2—517
BeO spherical fuel elements, three dimensional transient thermoelastic stresses 2—15130
C-Si, fuel coating, neutron irrad. induced dimens. change 2—22176
C, pyrolytic, neutron irrad., annealing, phys. props. 2—3757
C, pyrolytic, neutron irrad., dimens. and phys. prop. changes 2—21471
C, stress-graphitized pyrolytic, internal friction and elastic modulus, nuclear irrad. effects 2—32587
Cd filter, calc. of neutron transmission function, 1/E spectrum in graphite moderator 2—544
CeH_x moderator, neutron thermalization 2—31613
^{252}Cf neutron source, neutron source, encapsulation efficiency of Zircaloy-2 compared to stainless steel 2—549
Cm_2O_3 products, emission spectrographic det. of Am content 2—30109
coated fuel particles (0.5-1 mm dia.), SiC and pyrocarbon coated UO_2 2—551
Cu, irrad. swelling, expt. test of quasi-chemical model 2—32489
Eu_2O_3, absorber, in fast reactors, characteristics 2—38743
HTR fuels, UO_2(5% enriched) with SiC and pyrocarbon coating 2—551
He and CO_2 as coolants, comparison 2—28151
Mg, irrad. swelling, expt. test of quasi-chemical model 2—32489
Mg, nitrogenation kinetics effect of N_2 purity 2—30050
Mg, nitrogenation with simultaneous metal sublimation 2—30051
Mk.3 reactor, coated particle fuels (0.5-1 mm dia. SiC and pyrocarbon coated UO_2) 2—551
$(NH_4)_2U_2O_7 \rightarrow UO_2$ pellet, sintering/reduction 2—20187
Na-Ar two-phase flow in verticle channel, void fraction and heat transfer coeff. 2—21932
Na-K eutectic alloy, critical heat flow during boiling in conditions of free convection 2—28954
Na-K liquid alloys, volume thermal expansion coefficients 2—25068
Na, liq., speed of sound, 1000 to 1500C 2—15588
Na_3PO_4, corrosion inhibitor in cooling water circuits 2—2847
$Na+H_2O$ reaction, research review 2—40801
Nb, sputtering, by Nb, H, D and He ions, 10 to 80 keV 2—4086
Ni, neutron irrad. induced He generation 2—12748
Ni, proton irradiation, void formation by flash heating 2—22177
Ni foil, 20 MeV C^{2+} bombardment, void formation, swelling rel. to dose 2—6476
α-Pu, extruded, elongation rel. to grain size 2—6550
β-Pu, length change due to self- irradiation damage, 4K 2—19080
Pu, neutron spectra compared with fundamental mode calculated values 2—536
PuO_2/UO_2, fluoridation method for reprocessing 2—15111
PuO_2-UO_2 fuel mixtures, neutron radiography testing with TiO_2, Eu_2O_3, RhO_2 mixtures as analogues 2—550
PuO_2-UO_2 fuels, det. of ^{238}U capture rates rel. to ^{239}Pu fission 2—35103
PuO_2-UO_2 microlattice, expts. in LWR for design of fuel elements 2—24270
PuO_2, thermal cond., high temp. 2—19465
PuO_2 and UC fuels, rel. to operating experience in fast exptl. reactors in USSR 2—15099
^{235}Pu production, irradiation of ^{237}Np, minimum ^{236}Pu contamination 2—8394
$^{238}PuO_2$ lattice parameters meas. by X-rays, effects of temp. and long exposure 2—39651
$^{239}PuO_2$ single cryst., high temp. soln. growth 2—25266
ScO_x-actinide oxide systems, phase relationships 2—12610
Th-N-O system, phase diagram 2—36307
Th, binary alloy systems, phase diagrams 2—18262
Th fuel cycle developments 2—24281
ThO_2-PaO_2-UO_2 solid soln. formation, exchange of Pa^{4+} in molten LiF-BeF_2-ThF_4 with U^{4+} and Th^{4+} 2—10593
ThO_2-15% UO_2 pellets, possible fuel for homogeneous aqueous suspension reactor, neutron irradiation studies 2—5754
U-C-O, Pu-C-O and U-Pu-C-O systems, phase diagrams 2—12611
U-Nb-Zr and U-Nb alloys, stress corrosion cracking, effect of Cl^- 2—29331
U-Nb-Zr(Mo) system, kinetics of transform. of γ phase 2—36309
U-Nb alloys, diffusion and thermodynamic γ-phase props. 2—29206
U-Pu fuel cycles for thermal and fast reactors 2—24280
U-Si-Be system, phase relations 2—13016
U-Si system, phase diagram 2—40012
U-V-C system, phase transform., C content effects 2—36310
$(U, Pu)O_2$ fuel, creep, irrad. effect 2—11902
$(U, Pu)O_2$ fuel, in-pile thermal cond. meas. 2—18266
$(U, Pu)O_2$ mixed oxides, thermal cond., high temp. 2—19465
$(U,Th)O_2$ mixed cryst., thermal diffusivity 2—19467
U, neutron spectra compared with fundamental mode calculated values 2—536
U, Pu fuel compositions, properties and irradiation behaviour 2—15112
U and Pu potentiometric determination in mixed oxides 2—30104
U enrichment, review of trends and techniques 2—3010
U fuel, highly enriched, depletion and isotopic composition relation, empirical expressions 2—28152
UAl_4, UAl_3, UAl_2, liquid solutions, thermodynamic props. obs. by e.m.f. method 2—38739
UC_2-C system, C thermal diffusion model 2—29226
UC-UC_2, UC-UN alloys, lattice dimensions, X-ray diffr., 760-2250°C 2—19307
UC-ZrC solid solns. cubic lattice parameter var. with temperature and composition 2—15733
UC, fuel, creep, neutron irrad. effects 2—29274
UC spheres preparation by carbothermic reduction of sol-gel UO_2-C spheres 2—7189

Nuclear reactors, fission continued
materials continued
UC_2, granulated, thermal decomp., reaction kinetics, grinding energy 2—4579
UF_6, mechanism of H_2 reduction 2—30063
$UMoC_2$, anisotropic thermal expansion, 20-1100°C 2—36359
UN-UC-Fe system, phase equil. 2—1416
UN, fuel, creep, neutron irrad. effects 2—29274
UN, heat capacity, 386.8-701.3K 2—19428
UN, high temp. thermodynamic props. 2—40796
UN, $UN_{1.572}$ and a sintered powder, chemical anal. 2—26381
U_2N_3, equilib. N_2 press., thermodynamic props. 2—7164
$UO_{2\|x}$-NpO_2 system, phase relations 2—1405
UO_2-PuO_2 fuel, O_2:metal ratio effects 2—2862
UO_2-PuO_2 fuels, melting heat rating 2—2860
UO_2-ThO_2, measurement of temp. dependence of K_∞ for a high temperature gas-cooled reactor lattice 2—38744
UO_2-$UO_{2.67}$-ThO_2 system, phase relations 2—1405
UO_2, fission induced creep, instrumented capsule for meas. 2—11917
UO_2, fuel, creep, neutron irrad. effects 2—29274
UO_2, fuel, in-pile thermal cond. meas. 2—18266
UO_2, helix fabrication for irrad. creep meas. 2—36254
UO_2, in H_2 atmosphere, thermal etch figure 2—28997
UO_2, molten, pressure of vaporizing U-bearing species 2—28150
UO_2, thermal conductivity 500°C to melting point, temperature dependence, mechanisms 2—32858
UO_2, Xe diffusion, effect of stoichiometry 2—29225
UO_2 and graphite components, stress analysis, finite element matrix displacement method 2—17307
UO_2 epitaxial film, growth and neutron irrad. effects 2—29045
UO_2 fuel elements for thermal water reactors 2—8404
UO_2 fuel rods, Zircaloy clad failure characteristics under loss-of-coolant condits. 2—15086
UO_2 fule pin, elongation under radiation 2—5750
UO_2 particles, SiC and pyrocarbon coated, composition and manufacture, HTR 2—551
UO_2 pellet, in-pile thermal gradient, out-of-pile simulation 2—28155
$UO_{2\|x}$, self-diffusion of oxygen 2—12815
$UO_{2\pm x}$, composition changes, 1950 K 2—25637
UPu mixed oxides, neutron activated oxidation of steel casing 2—13577
$(U_{0.8}Pu_{0.2})O_{1.97}$, enthalpy, 2350 to 3000K 2—13040
U_3Si fuel elements, burnup and swelling temp. depend. 2—546
U_3Si phase, X-ray diffr. pattern of U_3Si_2, rel. to microstruct. 2—32476
UWC_2, anisotropic thermal expansion, 20-1100°C 2—36359
^{235}U-Al fuel forms, static and pulsed reactivity measurements in water 2—548
^{235}U, design and development of packaging for low enriched bundles 2—5755
^{235}U minimum critical mass reflected by natural uranium in water 2—547
V, diffusion of C, nitrogen and oxygen, 60-1825°C 2—22252
V alloy cladding behaviour in helium cooled reactors 2—11912
V alloy development for sodium-cooled fast breeder 2—18259
W-Re clad oxide fuel, high temp. swelling due to fission gas bubbles 2—28154
Xe, fission product, diffusion in CaF_2, defect trapping, 750-1000°C 2—22245
YH_x moderator, neutron thermalization 2—31613
Zr-Cr alloy, corrosion in steam, 325-700°C, rate law 2—20191
Zr-Cr alloy, lattice strain, crystallite size and hardness 2—22291
Zr-(3 wt.%)Mo-(1 wt.%) Al, tempering of strain induced martensitic phase 2—25639
Zr-(3 wt.%)Mo-(1 wt.%)Al alloy, thermal decomposition, Al effect 2—25640
Zr-Nb alloy, martensitic transform. 2—9827
Zr-(2.5 wt.%)Nb alloy, age hardening 12952 2—12952
Zr-Pu dilute alloy, $\beta \rightarrow \alpha$ transform., crystallographic study 2—29483
Zr-Sn solid soln., substruct. strengthening 2—12953
Zr, hydrogen embrittlement, effect of plastic props. 2—29311
Zr alloy, high-strength, for press. tube appl. 2—39945
Zr alloy, high temp. diffusion, rel. to creep deform. 2—12875
Zr alloy, radiation enhancement of oxidation 2—13580
Zr and zircaloy-2, hydride precipitation rel. to heat treatment 2—22369
α-Zr substruct. strengthening 2—12953
ZrH_x, fast neutron irrad. induced swelling 2—36014
Zr-25%Nb fuel claddings and pressure tubes in water cooled reactors 2—18257
operation
absorber rod direct insertion into a spherical pile, THTR 2—15104
absorber rod system, THTR, core wall and floor loading 2—18255
accident precautions, ice as absorbent for I_2 and CH_3I 2—543
analysis of thermal nuclear reactions 2—2848
Argonne research reactor CP-5, safety problems in case of light water infiltration 2—8397
automatic image analysis for fission ratio measurements 2—24100
benchmark gas core reactor, critical equipment with spherical symmetry 2—8392
blowdown accident, hot or cold leg break, response of reactor internals 2—15108
boiling water reactor, simulated rupture of main steam pipe 2—15095
boron controlled reactor, optimal controls for Xe shutdown problems 2—5745
breeder reactors and advanced converters, review of international development 2—2843
burst cartridge detection in BR-5 reactor 2—8396
BWR, axial transients in xenon, calc., computer program 2—38724
BWR, hydrodynamic instability of two-phase flow system 2—35408
capacity optimization taking into account the thermal reliability of the core 2—8395
central control rod effectiveness, thermal simulation 2—11899
channel boiling, prospects in Leningrad atomic power station 2—15034
commercial production of radioisotopes 2—38862
computer simulation model for electricity generating system 2—2853
concrete, strain and ultimate strength under triaxial compressive stress 2—15859
concrete pressure vessels, creep analysis 2—15067
concrete pressure vessels, mechanical behaviour at operatonal temperature of 70°C 2—15066
core-cooling systems, critique of AEC's interim safety criteria 2—18254
coupled-core, stability analysis and criteria 2—21469

Nuclear reactors, fission continued
operation continued
distribution of products of nuclear activation of heat carrier, boiler design effects 2—38702
Doppler effect measurements on small fuel samples, interpretation in fast reactor spectra 2—28137
dosimetrical control of irradiation facilities 2—11898
dryout obs., combined photographic film thickness and temp. technique 2—24275
effects of earthquakes, mathematical model derived from experimental data 2—15098
excursion, uncontrolled, biological shield 2—15183
excursion and accident analysis model, by computer 2—31623
excursion propagation, Eulerian method of analysis 2—15106
fast, cladding strength analysis, under combined effect of creep and plasticity 2—21465
fast, operational and design experience in USSR 2—15099
fast breeder reactors, review 2—28125
fast subcritical assembly, STSF-1A, containing ^{238}U, ^{235}U and BeO, meas. of n spectra 2—38732
feedback behaviour of prompt moderator heating effect 2—539
forced convection burnout in water, Freon 12 modelling 2—18264
fuel, efficient utilization in fast reactors 2—15100
fuel reprocessing plants, improved techniques 2—24274
gamma ray monitor, use at perimeters and surroundings 2—5769
gas cooled, heat conduction in multiconnected composite regions with radiative boundary conditions 2—14285
gas-cooled fast breeder, assessment of different designs 2—8387
gas-cooled reactors, emergency cooling using dissociating coolant 2—5748
graphite moderated reactors, multiple control rod effect 2—28132
heat distribution in core, from meas. of thermal neutron capture γ spectra 2—38737
hot gas channels in the bottom of the core, THTR 2—15103
HTR pulse operation, detect. of boiling water with hydrophone 2—38728
HTR-P core, power burst, effect of Doppler effect 2—38709
in-core fuel management optimization in H_2O reactors, applic. of linear programming 2—541
in-core self-powered neutron detectors, high- temp. performance 2—15172
inelastic analysis in equipment design 2—14215
internals response under blowdown accident 2—15107
irradiated internals, verification of design load conditions 2—18252
kinetics, space-dependent, three-node model 2—535
linear extrapolation distances for centrally and eccentrically located control rods 2—8400
liquid metal fast breeder reactors, incipient boiling superheat of Na coolant 2—28136
loss-of-coolant accidents, thermodynamic problems 2—15160
methyl iodide trapping by charcoal at high temp. and press. 2—5763
multielement thermionic experimental assembly tests at the universal loop device of a light H_2O reactor 2—11894
multiregional analysis of temp. fields in finite rod bundles cooled by liquid metals 2—15166
natural convection water loop, temp. fluctuation meas. 2—538
neutron booster, repetitively pulsed, static and dynamic experiments 2—31615
neutron dynamics in space-time, analysis on hybrid computer 2—8402
neutron flux density control, dynamic performance simulation on hybrid computer 2—8401
neutron noise probability distrib. by maximum likelihood method 2—15102
neutron noise produced by coolant temp. fluctuation and vibrations of control rod 2—15101
neutron spectrometer, two-crystal, for horizontal channel of IRT-m pulsed reactor 2—18006
noise studies, polarity-correlation system for fast reactor 2—11916
optimal control of point model reactors, application of nonlinear programming 2—5747
optimal power change with internal feedback 2—2850
oxalic acid as a chemical dosimeter for mixed pile radiation in multimegarad range 2—5768
pebble bed reactor—once through then out, physical properties 2—8398
Phenix, Na cooled fast reactor, study of random vibrations of hydrodynamic origin 2—38711
pod boiler concrete pressure vessels design 2—15073
power burst shape, of HTR-P core, effect of Doppler effect 2—38709
power distribution from analysis of in-core detector readings 2—38729
pressure vessel, concrete, stress calculation experimental verification 2—15077
pressure vessel, failure analysis of concrete, uase of Monte Carlo methods in finite element calculations 2—15070
pressure vessel, prestressed concrete, stress analysis by the finite element method 2—15068
pressure vessel, stress analysis of prestressed concrete in Brazil 2—15074
pressure vessel models, fracture studies on nuclear grade steel 2—15063
pressure vessels, acoustic emission anal. of crack propagation up to fracture 2—15064
pressure vessels, acoustic emission as non-destructive testing method for incipient failures 2—15065
pressure vessels, calculation of creep of concrete by approximate method 2—15071
pressure vessels, design concept and analysis of concrete structure with axial ribs 2—15075
pressure vessels, experimental and theoretical mode of behaviour of concrete when pressurized to failure hydraulically and pneumatically 2—15076
pressure vessels, H_2O migration in concrete, action of temperature gradient and pore pressures 2—15948
pressure vessels, mechanical behaviour of concrete end slabs 2—15069
pressure vessels, prestressing and proof pressure testing of concrete 2—15072
pressure vessels, stress and strain distributions around cracks near nozzles 2—15177
pressure vessels, time-temp. extrapolation techniques as applied to concrete creep. strains 2—15849
pressure vessels, two-dimensional time-dependent analysis by the finite element method 2—15179
pressure vessels and piping acoustic emission as non-destructive testing method for cracks 2—15178
pulse die-away phenomena, in small graphite prisms, cold neutron source 2—38727

Nuclear reactors, fission continued
operation continued
pulsed fast reactor critical assembly with temp. feedback, kinetics and safety eval. 2—38720
quick closing valve for use in power chemicals cooled by evaporating water 2—15176
radiation detection monitors 2—38773
radiation effect on fuels, fuel materials and assemblies 2—24282
reactivity pulsing system, design, construction and optimization (IBR-2) 2—15038
reactor circuit components, instationary flow phenomena 2—15109
refuelling, quasi-optimal method solved by hybrid simulation 2—8403
research reactor core 2 MW, unperturbed thermal flux generation 2—38734
research uses and applications to energy conversion 2—24259
safety, structural considerations, Geneva 1971, conference 2—24257
safety systems, development in USSR 2—15182
shut down reactivity meas., integral versions of area ratio method 2—24252
shut-down, fuel element temp. as function of cooling conditions 2—11897
space-dependent transfer functions with temp. feedback 2—38730
steam generators, sodium heated, estimation of tube wall temperatures in the evaporator region 2—5749
steel, 10CrMoNiNb910 fracture behaviour of coolant pipes 2—19210
temperature measurement by noise thermometry 2—5761
thermal insulation systems for prestressed concrete vessels for high temp. gas cooled power reactors 2—15180
thermal neutron flux generation using D_2O thermal column 2—38716
time dependence of fission product cross sections in fast reactors 2—38731
torsional frequency, analysis of a rotor system, CDC 6600 computer code 2—5169
transient stages, jacket stability obs. 2—28143
vessel internal supporting flange, optimization of operation from structural stresses and deformations 2—15046
vibration, fluid flow induced in annular diffuser 2—39074
VIPER pulsed reactor, temperature measurement using intrinsic junctions 2 38764
viscous damping of rapidly heated fuel rods 2—15105
void fraction measurement by single type probe 2—553
water cooled and moderated design, construction and operation in USSR 2—15033
^{3}H effluent monitoring 2—11918
Na cooled fast, developments prospects and technical problems 2—28117
Xe shutdown, Pontryagin's optimum theory appl. to minimum loss of max. power 2—5744

theory
accident analysis for cooled breeder reactor, rectangular containment system design 2—15079
accident analysis for LMFBR 2—542
adiabatic fixed, bed, limiting conditions, thermal radiation consideration 2—537
Bethe-Tait method of analysis of hypothetical destructive reactor accidents 2—2840
CANDU-BLW, heat transfer and fluid dynamics research 2—11896
CANDU-PHW, heat transfer and fluid dynamics research 2—11896
CIRENE reactor, program for calc. nuclear coeffs. of axial reflector 2—2849
coarse group calcs. in fast reactor, comparison with fine group calc. 2—38695
coherence function measurements for reactor noise analysis, precision 2—24287
coolant, heat transfer with variable cond., linearization of Sparrow and Koopman's method 2—37811
core, eigenvalue separation using static flux tilt and two-detector noise methods 2—516
core structural design and core restraint configurations rel. to above-core functions 2—15048
critical buckling and flux distribution for cores by variational method to optimize core geometry 2—24269
critical heat fluxes of full flux shapes from partial flux shapes 2—5743
critical mass and breeding gain investigations in a model of a typical large sodium-cooled fast reactor 2—2845
design analysis for LMFBR core restraint and support 2—15045
design development of core support structures for gas cooled reactors 2—15044
dynamic analysis of internal structures with impact between components 2—38694
effective cross section in Doppler resonance region of large fast reactor 2—38726
eigenvalue sensitivity, reduction by state variable feedback 2—2839
energy optimal Xe shutdown 2—31624
explosive disassembly of fast react., following loss of coolant 2—38696
fast breeder reactors, sodium boiling accidents 2—523
fast high flux test reactor, design problems of loop pressure tubes 2—15050
fast reactor flux and importance spectra, model 2—8382
fast reactors, improvements on continuous neutron slowing down theory 2—8381
fermi-age equation, approx. solution, modal analysis 2—18251
fuel cladding tubes, strains due to cracked cylindrical fuel pellets expansion 2—21462
fuel elements, temperature and stresses, due to nonuniform surface heat transfer 2—21464
fuel elements deformation, long-term, probabilistic visco-elastic models 2—21463
fuel lattices, cluster type, calc. of collision probabilities 2—513
head plate design, internal energy absorption by a layer of crushable material 2—15049
heat transfer for finite fuel rod assemblies 2—38697
heat transfer in slug flow through closely packed rod bundles, multiregion analysis of effect of rod displacement 2—28140
hot box pressure dome and skirt, design and stress analysis 2—15052
hot channel factor as function of hot channels in core 2—8386
in-line flow through unbaffled rod bundles, turbulent flow heat transfer 2—185
inverse neutron kinetics technique, reactivity calibrations, error sources 2 24254
Keff calc. for bare cylinder and hexagonal geometries 2—38708
kinetic equations soln, roots and coeffs., for heavy water moderated reactor 2—5742

Nuclear reactors, fission continued
theory continued
kinetics, adjoint equations, with delayed neutron source 2—28127
kinetics of neutron transport, formulation and application of transfer and scattering matrix techniques 2—28122
liquid metal fast breeder, space energy factorization evaluation for two dimensional neutron diffusion theory 2—5736
liquid metal fast breeder reactor, hot channel analysis, statistical theory of extremes 2—28128
mathematical model for parameter fitting in the frequency domain with alternative forms of weighting function 2—5739
multigroup criticality problem, solution using eigenfunction expansion method 2—31617
multigroup criticality problems, eigenfunction expansion method of solution, treatment of sloping plane boundary interfaces 2—31612
neutron density fluctuations, model kinetic equations 2—5730
neutron diffusion, hybrid method for solving reactor space-time- dependent equations 2—28123
neutron scattering, anisotropic, effect in square cell with thin moderator 2—38670
neutron transport theory calc. of flux, disadvantage factors and diffusion in square cells and slabs 2—38680
noise, statial coherence function and cross power spectral density analysis 2—24286
nonlinear and transport problems, evolution operator method 2—31616
optimal core composition 2—8388
power reactor fuel element dynamic heat transfer analysis 2—15165
pressure tube, hot channels, design and operation criteria 2—15051
pressure vessel design, thermoviscoelastic axisymmetric stress analysis, finite element and finite difference computer techniques 2—17348
prompt jump approximation, error estimation 2—38692
reactivity, subcritical, use of reactor noise 2—28139
reactivity, temperature dependence 2—31619
reactivity change, long term, heterogeneous method for calculation in reactor with burnable poison rods 2—28138
reactivity perturbations calc., Monte Carlo method 2—28120
reflected slab reactor, analysis of pulsed source reactivity using one group diffusion model 2—24285
rod lattice, thermal diffusion area depend. on rod dipole response coefficient 2—38719
space-time reactor dynamics, appl. of semigroup theory 2—28121
space-time reactor problems, optimum bounds, using linear programming 2—8390
stochastic neutron population model with feedback 2—28119
stress analysis for complex structures in presence of creep, computer program 2—17306
temperature distributions and thermal stresses, simulation on computer using finite element techniques 2—17354
thermoelastic and thermoplastic behaviour of solids of revolution, analysis by finite element method 2—17355
zero power reactor, multiple-input zero power describing functions 2—8385
n diffusion theory, few-group model, adequacy tested 2—516
Fe bulk assemblies, experimental and analytical studies of fast neutron transport 2—28112

Nuclear reactors, fusion
advantages, environmental and economic 2—28118
blanket cooling and heat conversion cycles 2—24273
conference on plasma physics and controlled thermonuclear fusion, Madison, USA (1971) 2—21760
controlled, design 2—28129
controlling methods, magnetic confinement, international efforts 2—2842
cooling and radioactive waste disposal, safety 2—24284
fast neutral injection for plasma heating and reactor start-up 2—28142
feedback stabilisation of thermal plasma instabilities 2—24268
lasers, long-wavelength, applic. to controlled thermonuclear reactions 2—24267
mirror, efficient recirculation of power, model 2—28133
mirror machine with direct conversion, engineering and economics 2—28130
mirror with direct conversion, thermal efficiency 2—8399
model for technical problems evaluation, state of the art 2—28124
neutronic and thermal design of blankets 2—24272
plasma confinement, current outputs, control techniques 2—18647
plasma physics and controlled fusion research-conference (Vienna, 1971) 2—24644
plasma stability and reaction products, linear theory 2—24754
pulsed, heating system, laser beam applic. 2—2841
radiological impact 2—24298
steam-water mixture in sixteen rod bundle, heat transfer crisis data 2—31626
superconducting magnet system design for Tokamak reactor 2—24271
Nb as reactor blanket material, meas. of ^{93}Nb(n,2n)^{92}Nb cross section at 14.0 MeV, implication of apparent discrepancy with theory 2—24227

Nuclear relaxation *see Nuclear magnetic resonance and relaxation*

Nuclear scattering *see Nuclear reactions and scattering*

Nuclear-solid interactions *see Mossbauer effect; Solids*

Nuclear spallation
cross sections of ^{10}Be from O, conflict with predictions 2—5692
light nuclei, proton induced, E_p=50, 100 and 153 MeV 2—8336
trans bismuth nuclei, fission fross sections and spallation yields, >0.6 GeV 2—31593
in CsI crystal or satellite X-ray detector, contribution to background rate 2—17984
^{65}Cu, Monte Carlo simulation of nuclear cascade evaporation 2—28037

Nuclear structure
(f,p) shell nuclei, structure information, single particle model 2—34876
(j-1) states anomalous coupling, excitation energies calc. 2—8275
actinides, from single nucleon transfer reactions 2—21420
calculations, structure considering two body interactions 2—8263
compressibility effect on shell model pot. 2—11711
density distributions possible study from K capture in kaonic atoms 2—15253
double charge exchange of pions, tool for structure studies 2—31564
empirical determination from mass sum rule violation 2—34889
even even ^{235}U fission fragments, equilibrium deformation and quadrupole deformation parameter 2—28093
even-even nuclei, p-f shell, Hartree- Fock-Bogoliubov calcs. 2—11703
fast neutron studies, review 2—491

Nuclear structure continued
- generator coordinate method for many body problem 2—2660
- Hartree Fock contributions to the effective charge and interaction in the sd shell 2—2659
- j^n configuration states, calc. of structure as function of relative coupling strength 2—2674
- light 4N nuclei with density dependent forces, calc. of α-cluster configurations 2—24139
- light N=82 nuclei, shell-model predictions 2—8264
- light nuclei, α-particle clustering, saturation mechanisms 2—38440
- neutron and proton system, charge independent pairing interaction, generalized Bogolyubov-Valatin transformation 2—14904
- neutron bound S-states, Woods-Saxon potential calc. 2—2673
- neutron distribution, rel. to $\pi^{\pm}$ absorpt. cross section 2—2791
- neutron hole states, deeply bound, (p,d) reaction study 2—31421
- non-additive interactions, effects 2—98
- nuclei with closed shells of 50 or 82, det. by obs. of γ-decay of fission products and resonant scattering of neutron capture γ-rays 2—38441
- pairing interactions, number-conserving algebraic method 2—34870
- pre-equilibrium decay, nuclear density distribution 2—31496
- quartet states rel. to (^{16}O, ^{12}C) reactions 2—15014
- rare-earth nuclei, equilibrium deformations of the ground and excited states 2—455
- resonance structure, examination by neutron spectroscopy 2—38445
- review of structure studied from weak and related processes 2—31410
- rotational bands and SL(3,R) symmetry 2—34900
- sd-shell nuclei, light, α-cluster structure and weak coupling feature 2—38451
- shell effects. in nucl. temps. 2—35042
- shell model calculations for A=6-9 with Sussex matrix elements 2—11722
- shell model pot., compressibility effect 2—11711
- shell-structure effect on elastic α scattering 2—24233
- spherical and deformed nuclei, shell correction approach to nuclear shell effects 2—34884
- spherical nuclei, relativistic self consistent meson field theory 2—11704
- SU(3) fractional parentage in 1p-shell, computer program 2—21348
- surface delta interaction and spherical Hartree-Fock Bogoliubov calcs. 2—11702
- ^{107}Ag, single-particle density distributions in the extreme nuclear surface 2—14950
- ^{12}B, effects on β decay 2—11791
- ^{8}Be structure in spherical shell, deformed shell and cluster models, appl. to fission problem 2—14931
- ^{12}C, giant dipole continuum, collective correlations 2—34908
- ^{12}C, information on shell structure from quasi- free electron scattering expts. 2—5687
- ^{12}C resonance states, determination from proton spin flip 2—31447
- ^{40}Ca, information on shell structure from quasi-free electron scattering expts. 2—5687
- ^{140}Ce, α scatt. study 2—11764
- ^{19}F, α-cluster structure and weak coupling feature 2—38451
- ^{135}I shell-model predictions 2—8264
- ^{139}La, α scatt. study 2—11764
- ^{6}Li, charge form factor, determination from high energy electron scatt. 2—27961
- ^{6}Li, clustering characteristics studied by quasielastic scattering of 50 MeV α particles 2—11723
- ^{12}N, effects on β decay 2—11791
- ^{15}N, investigations using ^{16}O and ^{19}F induced multi-nucleon transfer reactions in ^{12}C and ^{11}B 2—38654
- ^{20}Ne, determination of deformation parameters by inelastic scattering of polarized protons 2—35034
- ^{20}Ne, investigations using ^{16}O and ^{19}F induced multi- nucleon transfer reactions in ^{12}C and ^{11}B 2—38654
- ^{22}Ne, determination of deformation parameters by inelastic scattering of polarized protons 2—35034
- ^{16}O, alpha-cluster ground state 2—31450
- ^{16}O, investigations using ^{16}O and ^{19}F induced multi- nucleon transfer reactions in ^{12}C and ^{11}B 2—38654
- ^{208}Pb, investigations using inelastic electron scattering 2—18111
- ^{148}Pm, structure of 1^- ground state 2—34963
- ^{133}Sb, shell-model predictions 2—8264
- ^{88}Sr, investigations using inelastic electron scattering 2—18111
- ^{134}Te shell-model predictions 2—8264
- ^{230}Th, deformation parameters and E4 transition probabilities from Coulomb excitation expt. 2—8313
- ^{238}U, deformation parameters and E4 transition probabilities from Coulomb excitation expt. 2—8313

Nuclear track emulsions
- acoustic treatment at 50 Hz of mounted layers, accelerated diffusion of developer 2—27918
- chamber, Chacaltaya expt. 2—8243
- chamber combined with ionization spectrometer for studying hadron interactions around 10 TeV 2—27793
- chamber for obs. of extremely high cosmic ray muon interactions 2—27818
- chamber for obs. of zenith angle distrib. of extremely high energy cosmic ray muons 2—27819
- charged particle track simulation, using δ-ray theory of track struct. 2—21337
- cosmic ray charge spectrum meas. Using Ilford K2 emulsion 2—34745
- dosimetry of protons, alpha particles and heavy ions of high energy 2—5063
- emulsion chambers, rel. to cosmic ray muon studies in TeV energy range 2—24044
- emulsion chambers, rel. to study of high energy cosmic rays 2—24049
- emulsion nuclei interaction with 76 GeV proton 2—31534
- grain counting efficiency in autohistoradiograms 2—11687
- grain densities along particle tracks primary and secondary 2—2651
- high-speed inspection of plates 2—24114
- neutron induced multiparticle reactions, correlation measurements 2—35048
- nitrocellulose and acetylcellulose, alpha particle energies 2—18030
- noise in photographic trace due to grain size 2—27917
- relative scattering measurement, noise elimination 2—31391
- sensitivity centres in microcrystals 2—24113
- sensitization by p-dimethylaminostyryl dyes, creation of unstable traps for conductivity electrons 2—27916
- track analysis techniques 2—27785
- d, m.f.p. and interaction cross section determ. 2—14782

Nuclear track emulsions continued
- π^- capture by ^{16}O in emulsion and disruption of nucleus 2—38627
- π^- interaction, 7.5, 17 and 60 GeV 2—11612
- ^{3}H, detection, determination of efficiency 2—5603

Nucleation
- calcium tartrate, in gels, effect of Fe^{3+} contamination 2—15685
- cluster density and size distribution, influence of crit. cluster size 2—39484
- condensation homogeneous, upon moderate supersaturation, nucleation theory 2—32309
- crystal, two dimensional, on structureless substrate 2—39575
- crystal growth, classical heterogeneous theory 2—19013
- diamond synthesis, liquid metal catalysis 2—19001
- electric field on nucleation kinetics 2—39417
- electrolyte crystal, from aqueous soln., interfacial tension data 2—18988
- eutectic crystallization, interfacial boundaries 2—1141
- film, shape stability of nucleus, role of interface kinetics 2—18927
- film growth, Monte Carlo study 2—9256
- film growth studies, low energy ion multiple refl. technique 2—32331
- gel, crystal nucleation mechanism 2—18999
- heterogeneous, influence of surface diffusion processes on the kinetics 2—1170
- heterogeneous theory, kinetics, critical impingement rates, nucleation barrier, critical nucleation 2—6342
- high vacuum deposition, cluster formation theory 2—39483
- ice, by AgI-AgBr solid solution 2—3693
- ice, observed in cloud chamber, organic substances used as artificial nuclii 2—4660
- kinetics, review 2—39592
- liquid drop model appl. to condensation of Zn vapour in supersonic carrier gas 2—32146
- melt crystallization, interfacial energies of suspended particles 2—19014
- metal film, on nonmetallic substrate surface defects 2—39486
- microcrystalline clusters in gas, thermodynamic properties calc. using single-configuration approximation 2—35683
- non-equilibrium factor calc. method 2—22115
- photographic imaging media, applications of nucleation technology 2—23731
- polypropylene, isotactic, on graphite fibres 2—9231
- polystyrene, isotactic stretched, crystal nucleation 2—22060
- seeding, growth process for crystallization operation 2—29102
- soda-baria-silica system 2—3457
- solid from pure melts, free energy of fusion 2—18881
- vapour pressure of small clusters 2—12621
- water drops, by Brownian contact with AgI and other aerosols 2—18859
- Ag, epitaxial deposition on molybdenite 2—29024
- Ag, on SiO$_2$, cluster density vs. deposition duration 2—12652
- Ag film, on graphite, size distrib. of nuclei 2—29023
- Ag film, on SiO$_2$, in ultra-high vac. 2—32355
- Ag film, on SiO$_2$, in ultra-high vac. 2—32356
- Ag film, on SiO 2—29041
- Ag film, preferential deposition induced by Au ion implantation of substrate 2—12784
- AgI-KI acetone soln., emitted smoke ice forming ability 2—22972
- AgI-PbI$_2$ solid mixture, emitted smoke ice forming ability 2—22971
- Al-Si, alloy, vacancy enhanced, Si atom nucleation 2—3953
- Al, on KCl, Brownian motion of crystallites on substrate surface 2—32359
- Al(OH)$_3$, in seetled caustic aluminate soln., electron microscope obs. 2—18990
- Au film, condensed, substrate influence on nucleation nature 2—6345
- Au films on NaCl at low temps., application of high resolution shadow casting 2—6347
- Au on NaCl, high-resolution shadow casting obs. 2—39495
- CaSO$_4$.2H$_2$O, homogeneous, crystn. from aq. soln. at 30°C 2—12697
- Cu-Cr, immiscible film, thermally activated, electron microscope obs. 2—6350
- Cu basic carbonates, study of amorphous-crystalline transformation, determ. nucleation activation energy 2—29103
- Fe-C-Cr, alloy, austenite-proeutectoid ferrite transform. 2—22359
- Fe-Mn alloy, α' martensitic transformation, elec. microscope obs. 2—19301
- Fe-Ni-Cr austenitic matrix, of carbides, kinetics of precipitation, B effect 2—9810
- Fe-Ni-Mn alloy, martensitic transformation, nucleation model 2—22357
- Fe, white cast, annealing, graphitization, module growth 2—15907
- GaAs, on W (111) face 2—29033
- H$_2$O, molecular model for prenucleation clusters 2—35378
- He, superfluid, stochastic theory of nucleation of quantized vortices 2—6272
- Li$_2$O.P$_2$O$_5$.SiO$_2$ glass, lithium disilicate crystn., electron microscope obs. 2—39440
- NaClO$_3$, collision process at supersaturation, followed by dilution 2—18991
- Ni film, condensed, substrate influence on nucleation nature 2—6345
- Ni$_8$Ta, in Ni-Ta alloy, structural processes 2—15970
- Ni$_4$W, peritectoid growth 2—13006
- SiC whiskers, from SiO$_2$-C-H system 2—18952

Nuclei with A$\leqslant$5
- 3 body problem, bound states and scattering processes, numerical study 2—38471
- ^{4}He(γ,d)^{2}H, influence of long-range clustering correlations in ^{4}He ground state on photoreaction studied 2—11818
- A=3+hypernucleus, production by K$^-$ reaction at 1.5 GeV/c studied 2—38621
- proton spin relaxation in methyl naphthalene crystals described by rotation of CH$_3$ groups 2—40786
- radiative nucleon-deuteron capture below three-neutron break-up energy, wave function and dispersion theory analysis 2—31528
- sum rule for M1 transitions, validity of SU(4) symmetry 2—38449
- ^{2}H(N,N), cross sections, 11-23 MeV, nucleon polarization calc. 2—24207
- ^{4}He($\pi\pi$), amplitude calc. using Glauber model 2—14971
- ^{1}/H spin-lattice relax. in liq. xylenes 2—9185
- 1H, n.m.r. spectra of bis acetylacetonato dimethyllead 2—28320
- H, spin lattice relaxation time of p-azoxyanisole nematic mesophase 2—18856
- H n.m.r. study of H$_2$S and H$_2$Se 2—26302
- H^1 magnetic resonance in 2-bromothiazole, double-quantum effects in spectrum 2—38969
- ^{1}H-^{19}F spin coupling in organic systems 2—8571
- ^{1}H, antiproton quasielastic and elastic scattering 2—38587
- ^{1}H, dynamic nuclear polarization at 21 kG 2—6248

Nuclei with A⩽5 continued

^{1}H, dynamic polarization at 21 kG in radical solns. 2—25109
^{1}H, dynamic polarization in solid nitroxide radicals 2—26305
^{1}H, dynamic polarization in 1,8-octanediol-glycol mixtures rel. to polarized target production 2—36811
^{1}H, dynamic polarization in solid NH_3 rel. to polarized target production 2—36807
^{1}H, elastic deuteron scatt., meas. of analysing powers iT_{11}, T_{20}, T_{21}, T_{22} 2—15006
^{1}H, electron scattering, 1180 MeV, inelastic cross section 2—38581
^{1}H, fragmentation of ^{14}N projectile nuclei at 29 GeV, inclusive isotope spectra at 0° 2—35081
^{1}H, in KH_2PO_4, chem. shift at 300K, rel. to C_6H_{12} 2—13427
^{1}H, in rare earth nitrate soln., n.m.r. exchange effects 2—6254
^{1}H, in rare earth nitrate soln., n.m.r. exchange effects 2—6254
^{1}H, n.m.r. in para and ferroelectric $K_4Fe(CN)_6.3H_2O$ 2—4556
^{1}H, n.m.r. in para and ferroelectric $K_4Fe(CN)_6.3H_2O$ 2—4556
^{1}H, n.m.r. spectra of Co(III) and Rh(III) NN′-dialkyldithiocarbamates 2—21595
^{1}H, n.m.r. spectrum of methyl substit. trithienylphosphines 2—12291
^{1}H, n.m.r. study of orientation of p-dithiin in lyotropic liq. cryst. 2—18500
^{1}H, nuclear spin lattice relaxation studying $MgSiF_6.6H_2O$ 2—10577
^{1}H, p.m.r. in crude oil, freq. and temp. depend. 2—9165
^{1}H, p.m.r. in Ta-H system, 77-300 K 2—20165
^{1}H, p.m.r. obs. of 1,3,5-triphenylbenzene anion radical 2—8808
^{1}H, polarization at 50kG and 1K in 1-butanol (1-pentanol)-water-porphyrexide systems, polarized target production 2—36808
^{1}H, polarization in hydrocarbons rel. to polarized target production 2—36810
^{1}H, polarization in organic materials rel. to polarized proton production 2—34779
^{1}H, polarization of scattered neutrons, meas. at 32 MeV 2—15008
^{1}H, spin-lattice relax. times in Nb-H system 2—7008
^{1}H, spin lattice relaxation in solids, calc. 2—1647
^{1}H, spin lattice relaxation times in liq. chloroform 2—9179
^{1}H, spin lattice relaxation in binary liquid mixtures 2—9169
^{1}H, spin lattice relaxation in nematic p-methoxybenzylidene p-n-butylaniline 2—25113
^{1}H, spin relaxation in liq. thiophene 2—9184
^{1}H chemical shift in styryldiazines and diazaphenanthrenes 2—24551
^{1}H magnetic resonance spectra, trans-15,16-dimethyl dihydropyrene and trans-15,16-diethyldihydropyrene, chemical shift calc. using π-electron ring current hypothesis 2—38979
^{1}H n.m.r., solid HD, spin lattice relaxation and nuclear polarization at $T<1K$ 2—37008
^{1}H n.m.r. in liq. 1,2-dichloroethane, mol. motion obs. 2—35794
^{1}H n.m.r. in lyotropic liquid crystals 2—35796
^{1}H n.m.r. spectra of benzene and —1—^{13}C derivative 2—5962
^{1}H n.m.r. spectral identification of $HSiCl_{3-n}I_n$ and $HSiBr_{3-n}I_n$ 2—24487
^{1}H p.m.r. in cryst. methyl naphthalene 2—10573
^{1}H p.m.r. in ferroelec. thiourea 2—10575
^{1}H p.m.r. in hexamethylethane cryst. 2—13556
^{1}H p.m.r. in lead and strontium dicalcium propionates 2—10574
^{1}H p.m.r. in olfactory nerve of garfish, water metabolism 2—7587
^{1}H p.m.r. in polymers 2—13557
^{1}H relax. by excitons in anthracene and naphthalene 2—10277
^{1}H relax. in benzene, cyclohexane, cyclohexene on NaY-zeolites 2—26086
^{1}H resonance shifts in Co and Ni acetylacetonate alkylamine complexes 2—28283
^{1}H spin-lattice relax. and dynamic polarization in ethylene glycol and $La_2Mg_3(NO_3)_{12}$ 2—16669
^{1}H spin-lattice relax. in polar liquids 2—9182
^{1}H spin-lattice relax. in dicyclohexane 2—8760
^{1}H spin-lattice relax. in Nd-doped $La_2Mg_3(NO_3)_{12}.24H_2O$ 2—10269
^{1}H spin-lattice relax. in solid methane 2—10279
^{1}H spin-lattice relax. in NH_4Br 2—10272
^{1}H spin-lattice relax. in irrad., polycarbonates 2—10280
^{1}H spin-lattice relaxation time and AS-p, spin-spin coupling constants in liquid AsH_3 2—35792
^{1}H spin-lattice relaxation, rel. to investigation of selective adsorption in polymer solutions 2—39393
^{1}H(d,pn)^{1}H, 27.5-19.2 three body break up spectra analysed to yield cross section for production of n-p pairs in singlet state 2—21431
^{1}H(n,γ)^{2}H, discrepancy between theory and expt. for total radiative thermal np capture cross section discussed, polarization effects 2—31552
^{1}H(p,pπ^0)^{1}H, at 600 MeV, differential cross section for π^0 production 2—17923
^{2}H, antiproton quasielastic and elastic scattering 2—38587
^{2}H, break-up reaction, calc. of nucleon-nucleon correlation spectra of cross sections including final state interactions 2—38585
^{2}H, Coulomb interference in proton scattering at 144 MeV 2—31538
^{2}H, d.m.r. obs. of 1,3,5-triphenylbenzene anion radical 2—8808
^{2}H, dynamic polarization in solid n-butanol-d_{10} rel. to polarized target production 2—36807
^{2}H, inelastic neutron scatt., DWA calcs. 2—35044
^{2}H, neutron elastic scatt. and polarization calc. with tensor force and p-wave interaction 2—28041
^{2}H, neutron scattering, upper and lower bounds on phase shifts in variational formulation 2—28042
^{2}H, nucleon scattering calc., vector and tensor polarisations 2—21427
^{2}H, optical model potential derivation using Glauber theory 2—18216
^{2}H, proton scattering, 6-20 MeV, bremsstrahlung calc., Feshbach and Yennie model 2—28027
^{2}H, singlet state, binding energy calculation 2—460
^{2}H, total neutron cross sections in MeV region 2—28045
^{2}H n.m.r. in ferroelec. thiourea 2—10575
^{2}H n.m.r. in lyotropic liquid crystals 2—35796
^{2}H spin-lattice relax. in Nb, quadrupole coupling 2—7129
^{2}H spin-lattice relax. in hydrogen- bonded ferroelectrics 2—10259
^{2}H spin-lattice relaxation time and As-d spin-spin coupling constants 2—35792
^{2}H+n, scattering lengths and triton binding energy Faddeev formalism with local potential 2—21437
^{2}H(^{3}He,^{3}He), 7-18 MeV c.m. energy, meas. of cross section, no evidence of ^{5}Li excited states 2—28060
^{2}H(^{3}He,^{4}He)^{1}H, 7-18 MeV c.m. energy, meas. of cross section, no evidence of ^{5}Li excited states 2—28060
^{2}H(^{3}He,γ)^{5}Li, 2-26 MeV, transition intensities to levels in ^{5}Li, deduced levels 2—11860

Nuclei with A⩽5 continued

^{2}H(^{4}He,^{3}He)^{3}H, diffr. cross section presented at 82.1, 64.3, 49.9 MeV, study of charge asymmetry effects 2—28072
^{2}H(N,N), Faddeev-Mitra-Amado-Lovelace equations with separable tensor component, cross-sections and nucleon polarizations from 7.8 MeV to 31 MeV 2—14981
^{2}H(N,N) elastic scattering unitary model calcs. of nucleon polarization using realistic model for two-nucleon interaction 2—24208
^{2}H(α,αn)p, 30-80 MeV, energy dependence of quasifree scattering 2—24234
^{2}H(α,αp)n, 30-80 MeV, energy dependence of quasifree scattering 2—24234
^{2}H(d,d), phase shift anal., cross section and polarization data 2—11852
^{2}H(d,d)pn, 6-13 MeV, three-body break-up 2—28070
^{2}H(d,d)pn, angular distributions of quasi-free scattering 2—28071
^{2}H(d,dn)^{1}H, 27.5 MEV, deduced n-d quasi-free scattering from cross section, interpreted using modified simple impulse approximation 2—18223
^{2}H(d,dn)^{1}H, 6.0-13.0 MeV, meas, n-d and p-d coincidence spectra, nuclear-deuteron quasifree scattering discussed 2—11854
^{2}H(d,dn)p, coincidence spectra meas. with neutron detection at 200 degrees 2—24215
^{2}H(d,n)^{3}He, ^{2}H(d,p)^{3}H, difference in ang. distribution rel. to new ^{4}He levels 2—27960
^{2}H(d,n)^{3}He, 0.87 to 5.00 MeV, neutron polarization meas. 2—38636
^{2}H(d,n)^{3}He, 12 to 19 MeV, angular distributions and cross sections 2—31567
^{2}H(d,n)^{3}He, at 10.8 MeV, meas. of neutron polarization 2—8357
^{2}H(d,n)^{3}He, polarization differences from reaction D(d,p)T and charge symmetry 2—31568
^{2}H(d,n)pd, 11.3 MeV, search for spin-dependent effects in three body final state 2—21444
^{2}H(d,p)^{3}H, polarization differences from reaction D(d,n)^{3}He and charge symmetry 2—31568
^{2}H(d,p)^{3}H, polarization transfer 2—38637
^{2}H(d,p)^{3}H and ^{2}H(d,n)^{3}He, comparison of vector analysing powers 2—15007
^{2}H(d n)^{3}He ang. distrib. of vector analysing power 2—18224
^{2}H(e,e′), below 280 MeV, study of scattered electron spectra 2—18175
^{2}H(e,e), low energy scattering by light nuclei nuclear dispersive contribs. 2—18176
^{2}H(n,n), elastic scattering at low energy, study of neutron observables, calc. differential cross section, depolarization factor 2—24224
^{2}H(n,n), phase parameters and differential cross section by Pade technique 2—14988
^{2}H(n,nnp), study of n-n interaction at 14.5 MeV 2—35052
^{2}H(n,p)2n, proton spectrum analysis 2—31553
^{2}H(n,p)nn, effect of quasifree scattering on shape of kinematically incomplete spectra at forward angles 2—38612
^{2}H(p,2n)n, theoretical analysis by a polar graph 2—31537
^{2}H(p,2p) at 600 MeV calc. of differential cross section using plane wave impulse approx. with corrections 2—31539
^{2}H(p,2p)n, 14.45 MeV, results compared with calculations using Amado model 2—8337
^{2}H(p,2p)n, p-p quasifree scattering, 21.5-56.4 MeV 2—2776
^{2}H(p,n)n, quasi free peak examined in off-shell spectator approx. for energies 14.4 MeV-100 MeV using Hamada Johnston potential 2—18189
^{2}H(p,p), 15-20 MeV, differential cross sections 2—2773
^{2}H(p,p), 7-9 MeV, bremsstrahlung cross sections 2—487
^{2}H(p,p)pn, 12.5 MeV, angular distributions of quasi-free scattering 2—28071
^{2}H(p,pn)^{1}H, 13.5 MeV, three body break up spectra analysed to yield cross section for production of n-p pairs in single state 2—21431
^{2}H(p,pn)^{1}H, test of the impulse approximation validitiy in low energy deuteron break up 2—2772
^{2}H(p,pn)p, coincidence spectra meas. with neutron detection at 200 degrees 2—24215
^{2}H(p,pn)p, quasifree scattering effects 2—35031
^{2}H(p,pp)n, quasifree scattering effects 2—35031
^{2}H(p,pp)n, test of the impulse approximation validity in low energy deuteron break up 2—2772
^{2}H(p,π^+)^{3}H, study of pion production 2—35030
^{3}H, atomic effects in β-spectrum 2—14963
^{3}H, binding energy, contribution of two-pion exchange three-body force 2—5643
^{3}H, binding energy, Faddeev eqn. in separable approx. formulation 2—27958
^{3}H, binding energy, reference spectrum method 2—18085
^{3}H, binding energy from ^{2}H+n collisions in Faddeev formalism with local potential 2—21437
^{3}H, binding energy in unitary pole approx. using hard core pot. 2—34905
^{3}H, effect of charge dependence of nuclear forces on ground state energy 2—11721
^{3}H, exchange magnetic form factor 2—5642
^{3}H, high energy inelastic scatt. form factors 2—38576
^{3}H, induced radioactivity in ground water system near proposed 300 GeV accelerator 2—5622
^{3}H, magnetic moment operator for three particle nucleus, calculated correction 2—31444
^{3}H, p-wave weight, role of LS and $(LS)^2$ forces 2—21358
^{3}H, pion absorption in (3,3) resonance region 2—35057
^{3}H, proton scattering, 5-matrix elements and phase shift analysis 2—28028
^{3}H, selection rule for K-harmonics 2—18086
^{3}H, yields and energy distrib. from thermal neutron ternary fission of ^{235}U 2—24248
^{3}H and ^{3}He, binding energy difference, appl. to study of charge symmetry of nuclear forces 2—2687
^{3}H Beta-ray spectra, high-luminosity, high- resolution study of the end-point behaviour 2—34587
^{3}H beta ray spectra, high-luminosity, high- resolution study of end-point behaviour 2—34609
^{3}H binding energy sensitivity to off-shell behaviour of the 2 body T-matrix 2—38472
^{3}H(d, ^{3}He)2n and ^{3}He(d, t)2p, charge symmetry in mirror reactions at 83 MeV 2—31569
^{3}H(d,^{3}Hen)n, neutron-neutron scattering length from kinematically complete measurement 2—5710
^{3}H(n,2n)^{2}H, 13.95 MeV, rel. to neutron-neutron scatt. length 2—2786
^{3}H(n,2n)^{2}H, 13.95 MeV, neutron-neutron scattering length 2—18204
^{3}H(p,n)^{3}He, 1.5 to 5.0 MeV, neutron polarization meas. 2—38588

Nuclei with A$\leqslant$5 continued
^{3}H(t,n^{4}He)n, kinematically complete expt., determ. of neutron-neutron scattering length 2—28073
^{3}H$\to$^{3}He+e-+υ-$_{e}$, calc. of meson exchange corrections using realistic nuclear wave functions 2—18155
^{4}H meson-less decay model 2—24145
^{7}H p.m.r. in Lu-H system 2—7144
^{4}Hc (α-α), 0.35 MeV, bremsstrahlung cross section meas. 2—28066
H(d,2p)n, Treiman-Yang criterion for quasifree scattering at dueteron energy 20 MeV 2—11853
^{3}He, ^{4}He, elastic scattering at 44.5 MeV studied in resonating group formalism, exchange effects 2—11855
^{3}He, binding energy, wave function, harmonic polynomial calc. 2—5644
^{3}He, charge form factor calc. 2—34906
^{3}He, Coulomb energy deduced by symmetry relation from charge form factors 2—14928
^{3}He, exchange magnetic form factor 2—5642
^{3}He, excitation energies up to 30 MeV examined in study of ^{6}Li(p,^{3}He) and ^{6}Li(p,α) reactions, search for broad resonances 2—18084
^{3}He, high energy inelastic scatt. form factors 2—38576
^{3}He, magnetic moment operator for three particle nucleus, calculated correction 2—31444
^{3}He, neutron scattering, 5-matrix elements and phase shift analysis 2—28028
^{3}He, photodisintegration cross sections calc. 2—11817
^{3}He, photodisintegration cross sections calc. 2—11817
^{3}He, pion absorption in (3,3) resonance region 2—35057
^{3}He, polarized, calibration by polarized protons and deuterons 2—35021
^{3}He, polarized deuteron scattering, 4 to 11.5 MeV, analysing powers iT_{11}, T_{20}, T_{21} and T_{22} 2—35062
^{3}He, π^{-} absorption, computation using Eckstein phenomenological model 2—8351
^{3}He, scattering of polarized 3 MeV neutrons, determ. resulting asymmetry in elastic scattering 2—24229
^{3}He, structure by reaction ^{3}He(e,e′d)^{1}H at 16 to 27 MeV 2—31443
^{3}He, study of three-body break-up in reactions with d at 10.92 MeV 2—18226
^{3}He, vector-meson effects in electric form factor 2—14929
^{3}He, yields and energy distrib. from thermal neutron ternary fission of ^{235}U 2—24248
^{3}He elastic scattering of protons, microscopic description starting from nucleon-nucleon potential 2—24210
^{3}He photodisintegration, E2 transition 2—21423
^{3}He polarized target, device for studying reactions 2—27832
^{3}He target, polarization, non-resonant means of measurement 2—34777
^{3}He(^{3}He,^{3}He), imaginary potential in resonance-group calculation 2—18217
^{3}He(^{3}He,2p)^{4}He, total cross section meas. below Coulomb barrier 2—2800
^{3}He(^{3}He,p^{4}He)p, kinematically complete expt., determ. of proton-proton scattering length 2—28073
^{3}He(d, n)^{4}He, polarization of emitted neutrons, meas. at 32 MeV 2—15008
^{3}He(d, t)2p and ^{3}H(d, ^{3}He)2n, charge symmetry in mirror reactions at 83 MeV 2—31569
^{3}He(d,p)^{4}He, 13.6 MeV, meas. of asymmetry of proton emergence, polarization of target 2—27832
^{3}He(d,p)^{4}He, 2-6 MeV, angular distributions of proton polarization 2—38639
^{3}He(d,p)^{4}He, 2.8 to 11.5 MeV, differential cross-sections and analyzing powers iT_{11}, T_{20}, T_{21} and T_{22} 2—8358
^{3}He(d,p)^{4}He, <1 MeV, vector and tensor analyzing power 2—38638
^{3}He(d,tp)^{1}H, cross section determ. using DWBA treatment 2—18225
^{3}He(e,e′d(^{1}H, 16-27 MeV, search for structure in ^{3}He 2—31443
^{3}He(e,e), low energy scattering nuclear dispersive contribs. 2—18176
^{3}He(γ,p)d, with linearly polarized γ-rays, asymmetry parameters at 90° and energies from 180 to 300 MeV 2—18173
^{3}He(p,2p)^{2}H, 155 MeV, quasi free proton-proton scattering cross-sections 2—18190
^{3}He(p,π^{+})^{4}He, study of pion production 2—35030
^{3}He(t,p^{4}He)n, kinematically complete expt., determ. of proton-neutron scattering length 2—28073
^{4}He, ^{3}He elastic scatt., exchange reson., neutron-transfer model 2—2801
^{4}He, binding energy, calc. using method of 9-dimensional harmonics 2—461
^{4}He, binding energy, reference spectrum method 2—18085
^{4}He, Coulomb excitation of ^{56}Fe rel. to static quadrupole moment determination from reorientation meas. 2—31472
^{4}He, Coulomb interference in proton scattering at 144 MeV 2—31538
^{4}He, elastic pion scatt., differential cross section at 7.76 GeV/c 2—8352
^{4}He, form factor in oscillator model including short range correlations, study by elastic electron scattering 2—38577
^{4}He, inelastic proton scattering, 141 MeV 2—18183
^{4}He, isospin mixing in dipole states, ^{4}He(γ,n$_{0}$) reaction study 2—27959
^{4}He, meson-less decay model 2—24145
^{4}He, muon capture, neutron spectrum and asymmetry of angular distribution 2—35015
^{4}He, N scatt., forward dispersion rels. and ^{4}He ^{3}He n coupling const. 2—14982
^{4}He, new levels rel. to difference in ang. distribution for reactions ^{2}H(d,n)^{3}He and ^{2}H(d,p)^{3}H 2—27960
^{4}He, nuclear backscattering on Si, random spectrum defined 2—25715
^{4}He, p-wave weight, role of LS and (LS)^{2} forces 2—21358
^{4}He, polarization measurements and analysis of neutron scattering from 11.0 to 30.3 MeV 2—31554
^{4}He, proton scattering, 6-20 MeV, bremsstrahlung calc., Feshbach and Yennie model 2—28027
^{4}He, $\pi^{\pm}$ elastic scattering at 97 MeV, meas. with high-pressure streamer chamber 2—24231
^{4}He, radiative pion capture rate from low lying Bohr orbits calculated 2—11848
^{4}He, selection rule for K-harmonics 2—18086
^{4}He, spin and isospin in high energy proton elastic scattering and nuclear correlations 2—31529
^{4}He, T=0 states study from ^{4}He(d,d′t)^{1}H and ^{4}He(d,d′d)^{2}H at 52 MeV 2—14930
^{4}He, three α-particle final state in ^{9}Be(^{3}He,$\alpha\alpha$)^{4}He studied at 3 and 4 MeV 2—24238
^{4}He, total muon capture rate calc. 2—18179
^{4}He, total negative muon capture rate 2—35016
^{4}He, yields and energy distrib. from thermal neutron ternary fission of ^{235}U 2—24248

Nuclei with A$\leqslant$5 continued
^{4}He(^{16}O,γ) capture reaction study of radiative width of ^{20}Ne 8^{+} 11.948 MeV level 2—18096
^{4}He(^{35}Cl,p)^{38}Ar, mean lifetimes of 3.38 and 4.59 MeV levels prod. in ^{38}Ar 2—21386
^{4}He(d,d), phase shift analysis 2—31570
^{4}He(d,d)^{4}He polarization-transfer expts. parametrization, constraints imposed by time reversal resonance 2—35063
^{4}He(e,e), elastic scattering, shell model analysis 2—2766
^{4}He(γ,p)^{3}H, photodisintegration, effect of tensor forces 2—35008
^{4}He(γ,p) and ^{4}He(γ,n) reactions, ratio of cross sections, 30.0-51.8 MeV 2—31522
^{4}He(μ^{-},nν)^{3}H, neutron channel study, short range nucleon nucleon correlation effects 2—28024
^{4}He(n,n), p-wave scattering considered as five body problem 2—492
^{4}He(p,p), effects of intermediate N* state on forward scattering at 1 GeV 2—5689
^{4}He(p,p) elastic scattering, phase-shift analysis of cross section and polarization data, 20-40 MeV 2—35025
^{4}He(p,p) elastic scattering, 20-45 MeV, angular distrib. of polarization and cross sections meas. across 23.4 MeV resonance 2—35024
^{4}He(p,π^{+})^{5}He, study of pion production 2—35030
^{5}He, excited states, study using ^{7}Li(d,α)^{5}He 2—24140
^{5}He, search for high lying levels using ^{7}Li(d,α)^{5}He reaction 2—31445
^{5}Li, deduced levels and transition intensities to ground and first excited state from ^{2}H(^{3}He,γ)^{5}Li reactions 2—11860
^{5}Li, energy dependence of phase shifts and spin and parity assignments from p-^{4}He elastic scattering data 2—35025
^{5}Li, search for high lying levels using ^{6}Li(^{3}He,α)^{5}Li reaction 2—31445

Nuclei with 6$\leqslant$A$\leqslant$19
A=14, calc. of levels using weak coupling approach 2—21375
A=16-19, γ-transitions and spectroscopic factor, weak coupling model 2—21377
A=18 nuclei, diagrams with 4p-2h intermediate states, contrib. to effective interaction 2—21378
A=18 nuclei, effective interaction, contrib. of 2 particle ladder and RPA terms 2—31416
A=6 to 9, struct. calcs., energy levels 2—38469
A=8 system, excited states, investigation using ^{7}Li+n and ^{7}Li+p reactions 2—24141
A = 11, 14, 19, (n, n′γ) reaction, analysis of γ-ray spectra 2—35045
cluster structure, study from reaction C(p,α) at 660 MeV 2—38468
neutron capture cross sections from 20-80 keV 2—28047
nuclear component of primary cosmic radiation, observations from Cosmos 136 satellite 2—8215
production in 1.5 GeV/c K^{-} interactions with light nuclei 2—38622
sum rule for M1 transitions, validity of SU(4) symmetry 2—38449
^{a}O, A=16, 18, elastic scattering by ^{116,120}Sn at energies near Coulomb barrier 2—11870
Al, determ. from anal. of reactions cross sections due to π^{-}, K^{-} and $\bar{\text{p}}$ in range 20-60 GeV/c 2—11719
^{8}B prod. in ^{14}N capture of stopped π^{-} 2—14996
^{9}B, high-spin assignments in the 1p-shell obtained with the J-dependent (p,α) reaction on ^{12}C 2—31544
^{9}B, isospin forbidden particle decay of first T=3/2 state studied by ^{7}Li(^{3}He,pn) reaction 2—27964
^{9}B, isospin mixing in J^{π}=$^{3}/_{2}{}^{-}$ state, first T=$^{3}/_{2}$ analogue states, Coulomb interaction contribution to width 2—14932
^{10}B, ^{3}He reactions, ^{13}N compound nucleus from 25 to 36 MeV 2—38640
^{10}B, elastic α-particle scattering at energies 5 to 30 MeV 2—24235
^{10}B, elastic scatt. of ^{7}Li, optical model analysis 2—38647
^{10}B, magnetic moment of 1^{+} first excited state 2—24142
^{10}B levels, spin-parity determinations by ^{11}B(^{3}He,α)^{10}B(α_{0})^{6}Li correlations 2—5645
^{10}B(^{14}N,^{12}C)^{12}C, quasimolecule search around Coulomb barrier 2—15016
^{10}B(^{14}N,α)^{20}Ne, quasimolecule search around Coulomb barrier 2—15016
^{10}B(^{3}He,γ)^{13}N, 25-35 MeV, meas. differential cross sections, include resonances not associated with ^{13}N giant dopole resonance 2—21445
^{10}B(^{3}He,pγ)^{12}C, 25-35 MeV, meas. differential cross sections, conclude resonances not associated with ^{13}N giant dipole resonances 2—21445
^{10}B(^{3}He,pγ)^{12}C, 25-35 MeV, meas. differential cross sections, include resonances not associated with ^{13}N giant dipole resonance 2—21445
^{10}B(α, ^{7}Li)^{7}Be, isospin invariance and mirror symmetry, geometric consequences 2—14970
^{10}B(α,d$_{1\gamma}$)^{12}C, study of angular correlation functions 2—31574
^{10}B(d,α) isospin forbidden reaction, search for ^{12}C lowest T=2 state 2—38474
^{10}B(d,n), 2.7 - 3.9 MeV, determ. polarization angular distributions for neutrons 2—28074
^{10}B(n, α)^{7}Li, autoradiographic method for B content. determ. 2—16713
^{10}B(n,α)^{7}Li, 0.48 MeV, differential cross sect. for α- particles to ground and first excited states in ^{7}Li 2—11842
^{10}B(π^{+},π^{0})^{10}C near (3,3) resonance, impulse approx. 2—8353
^{11}B, ^{16}O induced multi-nucleon transfer reactions rel. to nuclear structure of ^{15}N, ^{16}O, ^{20}Ne 2—38654
^{11}B, isospin splitting of giant dipole reson. 2—34907
^{11}B, n.m.r. in $B_{10}H_{13}^{-}$ 2—5910
^{11}B, n.m.r. in Cs_2O-B_2O_3 glasses and cryst. 2—30026
^{11}B, photonuclear giant dipole resonance, evidence for isobaric spin splitting 2—38561
^{11}B, resonance struct. in reaction ^{9}Be(d,γ)^{11}B 2—2804
^{11}B n.m.r. in crystalline B_2O_3 2—22838
^{11}B nuclear electric quadrupole interaction parameters determ. from n.m.r. study of transition metal monoborides 2—16652
^{11}B(^{16}O, ^{15}N)^{12}C 27-60 MeV, meas. cross section, DWBA analysis, deduced spectroscopic factors 2—18242
^{11}B(^{3}He,α)^{10}B(α_{0})^{6}Li, spin-parity determinations of ^{10}B levels 2—5645
^{11}B(α,t$_{1\gamma}$)^{12}C 2—31574
^{11}B(d,3α)n, four body break up studied by simultaneous detection of α-α and α-n coincidences at 10.425 and 12.0 MeV 2—18230
^{11}B(d,n), 2.7 - 3.9 MeV, determ. polarization angular distributions for neutrons 2—28074
^{11}B(γ,π^{-})^{11}C threshold to 1200 MeV, π production cross-section meas. 2—5682
^{11}B(p, γ) reaction study of giant E1 resonances in ^{14}C 2—31446
^{11}B(p,3α), 163 keV, interference effects 2—38590
^{11}B(p,α)^{8}Be, 45 MeV, ang. distrib. and cross section meas. 2—11827
^{11}B(p,α)^{8}Be, DWBA anal. of ground state ang. distribs., finite range 2—11828
^{11}B(π^{+},π^{0})^{11}C near (3,3) resonance, impulse approx. 2—8353

Nuclei with 6⩽A⩽19 continued
^{12}B, nuclear quadrupole coupling in Be crystal 2—36998
^{12}B recoil nuclei polarization in muon capture 2—38583
^{12}B(,2α)α, meas. cross section, deduced ^{12}C resonance at 17.23, 17.77 and 18.36 MeV 2—18192
^{13}B, excitation energies of levels up to 8.7 MeV meas. by ^{7}Li(^{7}Li,p)^{13}B reaction 2—34911
Be neutron, total cross section between 23 and 45 MeV meas. by time-of-flight technique with transmission method 2—38609
^{7}Be, cosmic ray produced, rel. to atmospheric exchanges 2—20324
^{7}Be, excitation energies of excited states, γ-ray energy meas. 2—11724
^{7}Be, photoproduction from C, B, Be and Li 2—5683
^{7}Be in the atmosphere, artificial production in thermonuclear explosions, abundance increases 2—30302
^{8}Be, asymptotic form of wave function for scattering from an incident α-particle 2—2794
^{8}Be, excitation spectrum, ghost anomaly, ang. and reaction depend. 2 2688
^{8}Be, spin and parity of 4.8 MeV level from Li(d,n) reaction 2—27963
^{8}Be structure in spherical shell, deformed shell and cluster models, appl. to fission problem 2—14931
^{9}Be, analysis of γ ray spectra from ^{7}Li(d,γ) at 361 keV deduced branching ratios to levels 2—502
^{9}Be, decay properties of excited states studied in four-body break up of ^{11}B(d,3α)n reaction 2—18230
^{9}Be. elastic scatt. of ^{7}Li, optical model analysis 2—38647
^{9}Be, isospin forbidden particle decay of first T=3/2 state studied by ^{7}Li(^{3}He,pn) reaction 2—27964
^{9}Be, isospin mixing in $J^{\pi}=3/2^{-}$ state, first $T=3/2$ analogue states, Coulomb interaction contribution to width 2—14932
^{9}Be, pionic X-ray yields meas. using absolute efficiency technique, pion cascade calc. of 2p-level widths 2—28057
^{9}Be, spin-lattice relax, in rare earth intermetallic 2—26078
^{9}Be n.m.r. in BeO, Stark effect 2—22840
^{9}Be(^{3}He, ^{6}Li), considered as direct reaction 2—31572
^{9}Be(^{3}He,^{3}He), 18 MeV, polarization of ^{3}He, cross sect. ang. distrib. 2—18219
^{9}Be(^{3}He, $\alpha\alpha$)^{4}He, 3 and 4 MeV, study of three α-particle final state, meas. angular correlations 2—24238
^{9}Be(^{3}He,n), 2.1 to 3.9 MeV, neutron polarization 2—8359
^{9}Be(α,n)^{12}C, study of energy levels of ^{12}C between 1.7 and 6.4 MeV 2—31573
^{9}Be(d,d), 1 to 2.2 MeV, absolute differential cross section, angular distributions, optical model analysis 2—14999
^{9}Be(d,d), backward scattering, cross sections and angular distributions 2—38629
^{9}Be(d,γ)^{11}B, resonance struct. 2—2804
^{9}Be(d,n) neutron spectra and application to transmission of C and polyethylene samples 2—5711
^{9}Be(d,pγ)^{10}Be, spectroscopic and reaction mechanism information from ang. correlations at 0° 2—2808
^{9}Be(d,t)^{8}Be, excitation spectrum of ^{8}Be ghost anomaly 2—2688
^{9}Be(γ,n), high resolution cross section 2—38568
^{9}Be(γ,n) production of monoenergetic neutrons at KeV energies 2—5560
^{9}Be(γ,t), 1200 MeV, tritium spectra and angular distributions 2—38567
^{9}Be(p,α)^{6}Li, 45 MeV, ang. distrib. and cross section meas. 2—11827
^{9}Be(p,α)^{6}Li DWBA anal. of ground state ang. distribs., finite range 2—11828
^{9}Be(p,d_0)^{8}Be, BHMM theory of stripping reactions 2—31540
^{9}Be(p,d)^{8}Be, 46 and 100 MeV, deuteron optical potentials, spectroscopic factors 2—8338
^{9}Be(p,d)^{8}Be, excitation spectrum of ^{8}Be, ghost anomaly 2—2688
^{9}Be(p,p_1)9*Be, mechanism of excitation of 1.68 MeV $1/2^{+}$ level 2—11826
^{9}Be(p,pα)^{5}He, 26.0, 35.0 and 46.8 MeV, cross section meas. 2—21432
^{10}Be production from O, spallation cross section conflict with predictions 2—5692
C, 660 MeV, long range α-particles, cluster structure of light nuclei 2—38468
C, emulsion nucleus, identification of medium energy α-particle induced reactions 2—24237
C, proton interactions, 10 to 28 GeV, inelasticities and inelastic cross section 2—31541
C, π^{-} meson reaction, 3 pion coherent prod. 2—11610
C, π photoproduction, 1160 MeV γ quanta 2—14974
C, size determ. from anal. of reaction cross sections due to π^{-}, K^{-} and $\bar{p}$ in range 20-60 GeV/c 2—11719
C, terrestrial age of stony meteorites from radiocarbon content 2—26869
C neutron total cross section between 23 and 45 MeV using time-of-flight technique with transmission method 2—38609
^{10}C, superallowed Fermi decay, branching ratio, significance for weak vector interaction 2—21411
^{11}C energy levels studied in ^{12}C(p,d) reaction at 185 MeV, evidence of nondirect reaction mechanism 2—31542
^{12}C/^{13}C abundance ratio and neutrino emission process in the Sun 2—11026
^{12}C, ^{19}F induced multi-nucleon transfer reactions rel. to nuclear structure of ^{15}N, ^{16}O, ^{20}Ne 2—38654
^{12}C, α-particle unstable states, investigation using nuclear reactions 2—18089
^{12}C, Brueckner Hartree Fock calc. using density dependent effective interaction, binding energy estimate 2—11727
^{12}C, calculation of multiple scattering of pions 2—28058
^{12}C, Coulomb interference in proton scattering at 144 MeV 2—31538
^{12}C, elastic scatt. of ^{7}Li, optical model analysis 2—38647
^{12}C, energy levels between 1.7 and 6.4 MeV using ^{9}Be(α,n)^{12}C reaction 2—31573
^{12}C, excited state stability and band cut-off 2—38473
^{12}C, fragmentation of ^{14}N projectile nuclei at 29 GeV, inclusive isotope spectra at 0° 2—35081
^{12}C, giant dipole continuum, collective correlations 2—34908
^{12}C, giant E1 resonances, study from ^{11}B(p, γ) reaction 2—31446
^{12}C, ground state binding energy calc. including repulsive core 2—8282
^{12}C, in Po-Be source, neutron spectrum from 4.43 MeV level 2—21374
^{12}C, K^{-}-capture, study of binding energy of product $_{\Lambda}{}^{10}$B 2—24146
^{12}C, low-energy neutrino excitation of giant resonance 2—34909
^{12}C, low energy scatt. cross sections, Hartree-Fock approx. 2—11837
^{12}C, low lying states structure study using cluster model with varying hinge angle 2—11725
^{12}C, lowest T=2 state, search for in isospin forbidden reactions 2—38474

Nuclei with 6⩽A⩽19 continued
^{12}C, many-particle excited states, calc. of energies. quadrupole moments and shapes 2—8283
^{12}C, muon capture, asymmetry of emitted neutrons 2—38582
^{12}C, particle vibration coupling, giant dipole resonance 2—18174
^{12}C, pion-capture obs. 2—5707
^{12}C, pionic X-ray yields meas. using absolute efficiency technique, pion cascade calc. of 2p-level widths 2—28057
^{12}C, radiative π capture, neutron-photon angular correlations and energy spectrum of neutrons 2—11849
^{12}C, spin and spin-isospin dipole oscillations 2—24143
^{12}C, substate excitation of 2^{+} state by (p,p′γ) inelastic scatt. 2—34941
^{12}C, three-alpha model 2—34910
^{12}C, variational calc. of quadrupole deformation energy and ground state energy 2—11726
^{12}C (α,$\alpha_{4.43}$) ^{12}C*, 20-24 MeV, anal. using strong absorption model. ang. distribs. 2—31565
^{12}C cascade interactions with π^{-}, 5 GeV/c two-Λ^{0} prod. 2—14707
^{12}C decay studied via ^{11}B(p,2α)α reaction 2—18192
^{12}C deform. sign determ. from inelastic proton scatt. 2—27965
^{12}C elastic and inelastic scatt. of 30.4 MeV polarized protons 2—14983
^{12}C γ-ray decay of 15.11 MeV t=1 state, determ. branching intensities 2—24144
^{12}C resonance states, determination from proton spin flip 2—31447
^{12}C+^{12}C carbon-burning in stars, reaction rate 2—13892
^{12}C+^{12}C low energy reaction, phenomenological analysis suggesting α-particle model, calc. of astrophysical reaction rates 2—24240
^{12}C+^{16}O, elastic scattering, phase shift analysis using optical potential 2—38657
^{12}C+^{16}O reaction, quasimolecular resonances 2—38656
^{12}C+^{18}O, excitation functions for the formation of ^{28}Al and ^{29}Al for ^{30}Si excitation energies of 30-40 MeV 2—28084
^{12}C(^{12}C, α)^{20}Ne, pole diagram, compound mechanism 2—11871
^{12}C(^{13}C,α)^{21}Ne, quasimolecule search around Coulomb barrier 2—15016
^{12}C(^{13}C,p)^{24}Na, quasimolecule search around Coulomb barrier 2—15016
^{12}C(^{14}N,α)^{22}Na, quasimolecule search around Coulomb barrier 2—15016
^{12}C(^{14}N,p)^{25}Mg, quasimolecule search around Coulomb barrier 2—15016
^{12}C(^{16}O,α)^{24}Mg, ^{12}C(^{16}O,p)^{27}Al and ^{12}C(^{16}O,d)^{26}Al excitation functions, high spin states of residual nuclei 2—38655
^{12}C(^{16}O,α)^{24}Mg, lifetime meas. of ^{24}Mg levels at 6.431 MeV (0^{+}) and 8.655 MeV (2^{+}) 2—38487
^{12}C(^{18}O, ^{18}O*)^{12}C, hyperfine interactions of first excited 2^{+} state of ^{18}O in 7^{+} and 6^{+} ions 2—31451
^{12}C(^{19}F, ^{20}Ne)^{11}B 40-68.8 MeC, meas. cross section, DWBA analysis deduced spectroscopic factors 2—18242
^{12}C(^{3}He, ^{3}Heγ), reaction-plane and spin-flip angular correlations 2—21446
^{12}C(^{3}He,^{3}He), 20 MeV, 18 MeV, polarization of ^{3}He, cross sect. ang. distrib. 2—18219
^{12}C(^{6}Li, d)^{16}O, study of populated negative-parity states in ^{16}O 2—463
^{12}C(N,N), to 5 MeV, polarization of neutrons at 50° scattering 2—11838
^{12}C(α,^{3}He), (α,t), (α,α), 104 MeV, differential cross sections and normalization factors 2—21441
^{12}C(α,2α), intermediate energies, mechanism 2—31576
^{12}C(α,α_0), ^{12}C(α,$\alpha^1\gamma$), ^{12}C(α,^{8}Be), shell model and rotational calcs. for ^{16}O 2—38481
^{12}C(α,$\alpha_1\gamma$)^{12}C 2—31574
^{12}C(α,α')^{12}C, investigation of α-particle unstable states in ^{12}C 2—18089
^{12}C(α,α), Regge-pole model for scattering 2—15000
^{12}C(α,α)^{12}C, angular distrib., phase shift anal. 2—2806
^{12}C(α,α) in 2^{+} excited state, inelastic scattering, meas. of relative correlation function of α-γ angular correlations at 32.5 MeV 2—38630
^{12}C(α,$\alpha\gamma$), reaction-plane and spin-flip angular correlations 2—21446
^{12}C(α,γ)^{16}O, capture cross section, calc. at stellar energies 2—18231
^{12}C(d, ^{7}Li)^{7}Be, isospin invariance and mirror symmetry, geometric consequences 2—14970
^{12}C(d,^{7}Li)^{7}Be, asymmetries observed in cross section indicating violations of Barshay-Temmer isospin theorem 2—11861
^{12}C(d,α_2)^{10}B(1.74, T=1), isospin nonconservation, study of compound nucleus interpretation 2—8360
^{12}C(d,d), backward scattering, cross sections and angular distributions 2—38629
^{12}C(d,d)^{12}C, obs. of nonequilibrium instantaneous charge distribs. in the recoils 2—2795
^{12}C(d,d) elastic scattering, importance of two-step processes determ. from identification of resonances 2—38558
^{12}C(d,n_0)^{13}N, 3.6 to 12.0 MeV 2—15010
^{12}C(d,n_0)^{13}N, asymmetry of 2.6 MeV polarized neutrons 2—18232
^{12}C(d,n)^{13}N* (p)^{12}C, sequential reaction, mechanism and symmetry axes determ. 2—28081
^{12}C(d,n)^{13}N*(p)^{12}C, measurement of neutron-proton correlations 2—31578
^{12}C(d,p_o)^{13}C, differential cross section and p polarization from sudden approx. 2—31579
^{12}C(d,p)^{13}C, 14.60 MeV, broad energy spectra of protons 2—2805
^{12}C(d,p)^{13}C, 3.9 to 5.8 MeV, polarization of protons 2—31577
^{12}C(e,e′p), quasi free scattering using Saclay linear accelerator, information on shell structure of nuclei obtained 2—5687
^{12}C(e,e′p) at 600 MeV, analysis using Elton-Swift and PHF wave functions, comparison of predicted and exptl. cross section 2—2778
^{12}C(e,p), 100 to 250 MeV, excitation function for protons 2—35009
^{12}C(γ,n), cross section calc. in giant resonance region, calc. in collective correlation model 2—18174
^{12}C(γ,p), 100 to 250 MeV, excitation function for protons 2—35009
^{12}C(γ,t), 1200 MeV, tritium spectra and angular distributions 2—38567
^{12}C(μ^{-},n$\nu\tau$)^{8}Li, reaction channels, angular correlation obs. 2—14979
^{12}C(μ^{-},ν)^{12}B, capture, ground state to ground state transition rate determ. 2—11821
^{12}C(n,α)^{9}Be, 14 MeV, cross section, study by 1″×1″ stilbene scintillator 2—28046
^{12}C(n,n′)3α, 14 MeV, cross section, study by 1″×1″ stilbene scintillator 2—28046
^{12}C(n,n), backward scattering of 14.1 MeV particles, ang. distrib. meas. 2—18199
^{12}C(n,n)^{12}C, comparison of Feshbach and R-matrix theories, particle-rotator model of ^{13}C 2—31549
^{12}C(n,n)^{12}C, comparison of Feshbach and R-matrix reaction theories, shell model of ^{13}C 2—31548
^{12}C(n,n)^{12}C, comparison of Feshbach and R-matrix theories 2—38613
^{12}C(n,n)^{12}C 1.9-5.2 MeV, polarization and differential cross section 2—18200

Nuclei with $6 \leqslant A \leqslant 19$ continued
^{12}C(p,2p), at 460 MeV and 1 GeV, analysis using Elton-Swift and PHF wave functions and PWIA, comparison of predicted and exptl. cross section 2—2778
^{12}C(p,2p)^{11}B, angular correlations measured at 49.5 MeV, results compared with distorted wave impulse approx. 2—11830
^{12}C(p,2p)^{11}B, DWA calc. of low energy reaction in 1p shell 2—21433
^{12}C(p,2p)^{11}B, distorted wave t-matrix approx. analysis, E_p=75MeV 2—35032
^{12}C(p,α)^{9}B, high-spin assignments in the 1p-shell of ^{9}B 2—31544
^{12}C(p,d)^{11}C, E_p=185 MeV, DWBA analysis of differential cross sections for emitted deuterons, nondirect reaction mechanism indicated by ^{11}C levels 2—31542
^{12}C(p,p′), quasifree scattering at 1 GeV 2—31530
^{12}C(p,p′γ)^{12}C*, E_p=20 MeV substate excitation of 2^+ state, transition from O^+ state 2—34941
^{12}C(p,p), 1 GeV, cross section of quasi free scattering comparison with multiple scattering theory 2—24209
^{12}C(p,p), at energies around 4.81 MeV resonance, excitation function and polarization meas. 2—31531
^{12}C(p,p)^{12}C, obs. of lowest T=$^3/_2$ state in ^{13}N, 14 MeV resonance 2—21428
^{12}C(p,pd), 50 MeV, total cross sections, secondary p energy spectra, secondary nuclei momentum and angular distribs. 2—31535
^{12}C(p,pp)^{11}B, 385 MeV distorted wave analysis, determ. of radius and reduction factor 2—2777
^{12}C(π,r), giant dipole resonance, transitions to odd parity states of ^{12}B 2—18214
^{12}C(π-, nn) 2Pπ absorpt., comparison with 1sπ 2—38626
^{12}C(π^-,np), 100 MeV, energy and angle measurements 2—21440
^{12}C(t,p)^{14}C, differential cross section and polarization measurements at 16 and 20 MeV 2—28075
^{12}C(t,t)^{12}C, differential cross section and polarization measurements at 16 and 20 MeV 2—28075
^{13}C-^{13}C coupling constants in ethyl compounds 2—842
^{13}C, dipole resonance using intermediate coupling approximation 2—38475
^{13}C, dynamic nuclear polarization at 21 kG 2—6248
^{13}C, dynamic polarisation at 21kG in radical solns. 2—25109
^{13}C, dynamic polarization in 1-butanol: porphyrexide rel. to polarized target production 2—36809
^{13}C, giant resonance, inelastic electron scatt. study 2—2767
^{13}C, isobaric analog states, calc. in multishell configuration space 2—34912
^{13}C, mag. resonance, natural abundance in orientated 1,3,5-trichlorobenzene 2—28361
^{13}C, n.m.r. Fourier spectra 2—6262
^{13}C, n.m.r. satellite lines, rel. to isotope abundance ratio 2—5906
^{13}C, n.m.r. spectroscopy, Fourier transform techniques 2—5907
^{13}C, particle-rotator model of positive-parity states, comparison of Feshbach and R-matrix theories for ^{12}C(n,n)^{12}C reaction 2—31549
^{13}C, spin-lattice relaxation in organic liquids 2—3408
^{13}C, spin-lattice relaxation in organic compounds, temp. depend. 2—35296
^{13}C, spin lattice relaxation in organic compounds 2—15344
^{13}C chemical shifts of tetramethylsilane determ. by NMR, use of TMS as ^{13}C reference compound discussed 2—27376
^{13}C dynamic polarization in xylols and mesitylene 2—24496
^{13}C elastic and inelastic scatt. of 30.4 MeV polarized protons 2—14983
^{13}C Fourier transform n.m.r. effect of molecular weight on spin-lattice relaxation times of polystyrene in solution 2—28901
^{13}C n.m.r., applic. to investigation of adsorption 2—39550
^{13}C n.m.r. chemical shift anisotropy in benzene 2—38964
^{13}C n.m.r. contact shift studies of 1,1′-dimethylmetallocenes 2—24531
^{13}C n.m.r. in linear acetylenes 2—8723
^{13}C n.m.r. in paramag. complexes 2—8685
^{13}C n.m.r. study of conformation of tert-butyl-1,3-dioxanes 2—3074
^{13}C on various targets, one neutron transfer reactions 2—38652
^{13}C positive parity states, comparison of Feshbach and R-matrix reaction theories for ^{12}C(n,n)^{12}C reaction 2—31548
^{13}C satellite spectra of ^{19}F n.m.r. spectra of fluorochloroacetones 2—28377
^{13}C spin-lattice relax. times and chem. polarization 2—8796
^{13}C spin-lattice relax. under proton decoupling conditions 2—10257
^{13}C undecoupled spectra, nuclear Overhauser effect 2—767
^{13}C(^{12}C, ^{12}C)^{13}C, 15 MeV and 19 MeV, molecular scattering states of neutron 2—15017
^{13}C(^{3}He,n), 5.5 and 6.2 MeV, ^{15}O level study 2—18090
^{13}C(^{3}He,n)^{15}O, 6 MeV, cross section meas., ^{15}O deduced levels, spectroscopic factors, used to test coeffs. of fractional parentage 2—27966
^{13}C(d,n), 2.7 - 3.9 MeV, determ. polarization angular distributions for neutrons 2—28074
^{13}C(γ,p), cross section calc. in giant resonance region, calc. in collective correlation model 2—18174
^{13}C(p,$\gamma_{1,2}$)^{14}N, 3-18 MeV cross-section obs., levels of ^{14}N determ. 2—2690
^{13}C(p,n)^{13}N$_{gs}$, microscopic analysis including core polarization exchange process 2—11829
^{13}C(p,p′γ)^{13}C, 3-18 MeV cross-section obs., levels of ^{14}N determ. 2—2690
^{13}C(π^+,π^0)^{13}N near (3,3) resonance, impulse approx. 2—8353
^{14}C, deexcitation γ-rays after π- capture on ^{16}O 2—2691
^{14}C in biological tissues, radioassay by modified plastic bag combustion technique 2—14040
^{14}C+^{16}O, excitation functions for the formation of ^{28}Al and ^{29}Al for ^{30}Si excitation energies of 30-40 MeV 2—28084
^{14}C+^{18}O, excitation functions for formation of ^{30}Al, ^{29}Al and ^{27}Mg for ^{18}O energies of 13-41 MeV 2—28084
^{14}C(^{18}O, ^{16}O)^{16}C two-neutron transfer reaction, 13-41 MeV, determ. excitation functions, compared with other ^{18}O induced reactions 2—18243
^{14}C(^{3}He,p)^{16}N, study of level scheme and spin and parity of ^{16}N 2—31449
^{14}C(p,γ_o)^{15}N, 3.2 to 7.7 MeV, cross section and angular distribution 2—35033
^{16}C(α,2α), intermediate energies, mechanism 2—31576
^{16}C(α,α), Regge-pole model for scattering 2—15000
C(α,α), A=12, 13, 26.6 MeV, diff. cross sections and angular distributions 2—38631
C(p,p), energetic dependence of elastic scattering cross sections on thick targets 2—28033
^{16}F, excitation energies of levels, study by ^{16}O(p,n)^{16}F at 23 MeV 2—18092
^{18}F, energies of lowest five T=1 states, Coulomb energy shifts 2—14935
^{18}F, energy levels, shell model calculation, and effective interaction in s-d shell 2—464
^{18}F, energy levels, spins and parities 2—504

Nuclei with $6 \leqslant A \leqslant 19$ continued
^{18}F, isospin mixed 5.61 and 5.67 MeV levels, spins determ. by angular correlation meas. 2—11730
^{18}F, low lying level using harmonic oscillator and Woods Saxon wave functions 2—5646
^{18}F, parity of 3134 keV J=1 state using reaction ^{16}O(^{3}He,p) at 2.95 MeV 2—14936
^{18}F, short lived activities excited by 14.7 MeV fast neutrons 2—18093
^{18}F for bone scanning, review of 10 years experience 2—30676
^{19}F-^{1}H Overhauser effect in KF aqueous solns. 2—28896
^{19}F, anomalous n.m.r. shift in SmF$_3$ 2—7145
^{19}F, branching from levels observed using proton scatt. reaction 2—38482
^{19}F, chemical shift in CF$_4$, SiF$_4$, and SF$_6$ 2—5953
^{19}F, core excited states, α-cluster structure and weak coupling feature 2—38451
^{19}F, dynamic nuclear polarization at 21 kG 2—6248
^{19}F, energy spectrum of non-normal-parity states produced using non-central particle- hole interaction 2—11732
^{19}F, in CaF$_2$, chem. shift at 300K, rel. to CF$_3$COOH 2—13427
^{19}F, isobaric analog states, calc. in multishell configuration space 2—34912
^{19}F, large dynamic polarization in CaF$_2$ by solid effect method, polarized target production 2—36803
^{19}F, n.m.r in K$_2$CuF$_4$, hyperfine interaction, unpaired spin densities 2—10552
^{19}F, n.m.r. distortion of signals used to study inter and intramolecular mechanics in benzyl fluorides 2—24512
^{19}F, n.m.r. in KNiF$_3$ and RbFeF$_3$ 2—13554
^{19}F, n.m.r. in LiF 2—7142
^{19}F, new high spin states forming part of K=$^3/_2{}^+$ rotational bands 2—2695
^{19}F, nuclear spin lattice relaxation study in MgSiF$_6$.6H$_2$O 2—10577
^{19}F, obs. γ-rays from 110 and 197 keV levels following kaon capture in ^{32}S 2—28059
^{19}F, pion-capture obs. 2—5707
^{19}F, polarization by pumping circularly polarized light in Tm^{2+}:CaF$_2$ 2—40596
^{19}F, polarized, calibration by polarized protons and deuterons 2—35021
^{19}F, polarized thermal neutron scattering, spin-spin amplitude calc. 2—5697
^{19}F, resonances and resonance parameters deduced from ^{14}N(α,γ)^{18}F cross section measurement 2—2807
^{19}F, spin-dependent part of slow neutron scatt. amplitude, meas. using polarized beam and polarized target 2—31550
^{19}F, spin-dependent part of slow neutron scattering amplitude, meas. using polarized beam and polarized CaF$_2$ target 2—35053
^{19}F, spin-lattice relax. in solid SF$_6$, 300-4.2 K 2—26085
^{19}F, spin ordering in CaF$_2$, n.m.r. and susceptibility obs. 2—6991
^{19}F, study of resonance at 850 keV in ^{15}N(α,γ) reaction spin, parity, lifetime and M1 transition strengths determ. 2—35069
^{19}F, T=$^3/_2$ states, calculation of spectroscopic factors from ^{18}O(^{3}He,d) reaction 2—11720
^{19}F (γ,p) and (γ,n) reactions at 30 MeV, meas. of de-excitation γ-rays in residual nuclei 2—38569
^{19}F chem. shift anisotropies in powders, single crysts., shielding tensors, from n.m.r. spectra 2—13426
^{19}F n.m.r., p.m.r. spectrometer adaptation 2—7806
^{19}F n.m.r. in ClO$_3$F, spin lattice relax. 2—8604
^{19}F n.m.r. in impure paramagnets 2—40417
^{19}F n.m.r. in MnF$_2$ 2—10534
^{19}F n.m.r. in nontransition element fluorides, chemical shift 2—28288
^{19}F n.m.r. line narrowing by rotary spin echoes in Teflon 2—20156
^{19}F n.m.r. lineshape for SF$_6$/ D$_2$O clathrate hydrate powder samples 2—28323
^{19}F n.m.r. spectra, elimination of line broadening due to N-F coupling by lowering temp. 2—5306
^{19}F n.m.r. spectra of 1,2-dihaloperfluoropropanes 2—28359
^{19}F n.m.r. spectra of fluorochloroacetones 2—28377
^{19}F n.m.r. studies of diazaphosphetidines and phosphadiazetidinones 2—28366
^{19}F nucl. acoustic reson. in RbMnF$_3$ 2—37013
^{19}F rotating frame n.m.r. in CHFCl$_2$ and CFCl$_3$ 2—9181
^{19}F spin-lattice relax. in dichlorodi fluoromethane, interference effect 2—9180
^{19}F—^{1}H, spin coupling in organic systems 2—8571
^{19}F(^{3}He, ^{4}He)^{18}F(^{4}He)^{14}N, collinear particle-particle angular correlation meas. to determ. spins of 5.61 and 5.67 MeV levels of ^{18}F 2—11730
^{19}F(α,γ), 3.5 to 4.7 MeV, excitation function for X-ray yields 2—35071
^{19}F(α,nγ)^{22}Na, spin of 1984 keV level of ^{22}Na 2—38485
^{2}H(n,p)2n, E_n=14.1 MeV, energy spectra of breakup protons 2—18203
^{6}Li, ^{7}Li NMR relaxation times in water solutions in porous materials 2—1739
^{6}Li, Coulomb disintegration in the field of heavy target 2—38650
^{6}Li, Coulomb interference in proton scattering at 144 MeV 2—31538
^{6}Li, electron elastic scattering at low momentum transfer, determ. charge form factors, model dependent and independent rms radii 2—24204
^{6}Li, electron scattering, 1180 MeV, inelastic cross section 2—38581
^{6}Li, isospin and decay modes from ^{7}Li(τ,α)^{6}Li and ^{7}Li(τ,α)^{6}Li*(d)^{4}He reactions at E_τ=1.5 MeV 2—27969
^{6}Li, nuclear structure investigation using high energy electron scatt. 2—27961
^{6}Li, pionic X-ray yields meas. using absolute efficiency technique, pion cascade calc. of 2p-level widths 2—28057
^{6}Li, polarization rel. to Coulomb breakup process in ^{208}Pb(^{6}Liαd)^{208}Pb reaction 2—2816
^{6}Li (p,α), 45.0 MeV, α particle spectra measured, search for broad resonances 2—18084
^{6}Li excited states decay 2—8315
^{6}Li ions, 30 MeV, elastic scatt. from ^{12}C, ^{16}O, ^{28}Si, ^{40}Ca, ^{58}Ni, ^{120}Sn, ^{197}Au, ^{208}Pb 2—18239
^{6}Li(^{3}He,α)^{5}Li, search for high lying levels in ^{5}Li 2—31445
^{6}Li(α,α_0), elastic scattering, 12.0-18.5 MeV, optical model analysis of angular distribution meas. 2—2793
^{6}Li(α,α), low-energy, nucleon exchange 2—18218
^{6}Li(α,αx)Y, 50 MeV, x=p, d, t, ^{3}He, α, determ. clustering characteristics of ^{6}Li 2—11723
^{6}Li(α,d)^{8}Be, excitation spectrum of ^{8}Be 2—2688
^{6}Li(d,pn), isospin selective reaction, obs. of spectral peaking characteristic of certain spin states 2—18227
^{6}Li(γ,p), ang. distribution of high energy photoprotons 2—28019
^{6}Li(γ,p)td, 35-80 MeV, quasi-α-particle photodisintegration 2—24201
^{6}Li(n,α)T, neutron flux monitor, thin glass scintillation system 2—5588

Nuclei with $6\leqslant A\leqslant 19$ continued
^{6}Li(n,p)^{6}He, angular distribution meas. at 14 MeV 2—21438
^{6}Li(p,^{3}He), 45.0 MeV, ^{3}He spectra measured, search for broad resonances 2—18084
^{6}Li(p,pd)^{4}He, 100 MeV, angular correlations 2—18191
^{6}Li(π-, nn) recoil momentum distrib., nucl. shape 2—38625
^{7}Li, Coulomb excitation of $^{1}/_{2}^{-}$ state, role of α+t channel 2—27962
^{7}Li, Coulomb interference in proton scattering at 144 MeV 2—31538
^{7}Li, dipolar relaxation in $LiN_2H_5SO_4$, hindered rotation, n.m.r. obs. 2—7006
^{7}Li, ground and first excited state formation in ^{10}B(n,α)^{7}Li reaction at 0.48 MeV 2—11842
^{7}Li. n.m.r. in LiF 2—7142
^{7}Li, n.m.r. in $LiVO_2$ above and below transition temp. 2—7143
^{7}Li, nuclear hyperfine parameters for LiOH(D) molecular beam electric resonance spectra 2—8663
^{7}Li, polarizability from Coulomb excitation 2—18087
^{7}Li, Sternheimer antishielding factor in LiF 2—40775
^{7}Li lifetime of 477 keV state determ. by meas. Doppler broadening of emitted γ rays 2—11240
^{7}Li neutron resonant scattering, use as neutron detector in (p,nγ) reactions 2—38382
^{7}Li+n, excited states of A=8 system 2—24141
^{7}Li+n reactions, cross section meas., search for bound trineutron using helium recoil scintillation 2—493
^{7}Li+p, excited states of A=8 system 2—24141
^{7}Li(^{3}He,α)^{6}Li, isospin and decay modes of ^{6}Li at E_{τ}=1.5 MeV 2—27969
^{7}Li(^{3}He,α)^{6}Li*(d)^{4}He, isospin and decay modes of ^{6}Li at E_{τ}=1.5 MeV 2—27969
^{7}Li(^{3}He,pn) used to study isospin forbidden particle decay of first T=3/2 states in ^{9}Be and ^{9}B 2—27964
^{7}Li(^{7}Li,p)^{13}B, 14 MeV, meas of excitation energies of levels in ^{13}B up to 8.7 MeV 2—34911
^{7}Li(α, n)^{10}B, differential cross section for α energies up to 8 MeV 2—15009
^{7}Li(α,α_0) elastic scattering, 12.0-18.5 MeV, optical model analysis of angular distribution meas. 2—2793
^{7}Li(α,α), low-energy, nucleon exchange 2—18218
^{7}Li(α,d), E_{α}=30 MeV, ang. distribs., DWBA and PWBAE analyses 2—31571
^{7}Li(α,p), E_{α}=30 MeV, ang. distribs., DWBA and PWBAE analyses 2—31571
^{7}Li(α,t), E_{α}=30 Mev, ang. distribs., DWBA and PWBAE analyses 2—31571
^{7}Li(α,t)^{8}Be, excitation spectrum of ^{8}Be, ghost anomaly 2—2688
^{7}Li(d,α)^{5}He, excited states in ^{5}He 2—24140
^{7}Li(d,α)^{5}He, search for high lying levels in ^{5}He 2—31445
^{7}Li(d,$\alpha\alpha$)n, 1.90-2.10 MeV, search for rescattering effects 2—18228
^{7}Li(d,γ)^{9}Be, 361 keV, analysis of γ ray spectra, deduced branching ratios to ^{9}Be 2—502
^{7}Li(d,nα)^{4}He, 2.07 and 2.09 MeV, study of n-α rescattering effects 2—2802
^{7}Li(γ,t), 1200 MeV, tritium spectra and angular distributions 2—38567
^{7}Li(p,α)^{4}He cross section at low energies 2—24216
^{7}Li(p,n)^{7}Be, E_{p}=17.5 MeV, neutron spectra meas., differential cross sections 2—28034
^{7}Li(p,pt)^{4}He, cluster model wave function and DWIA analyses 2—38589
^{7}Li(t,p)^{9}Li, new states in ^{9}Li 2—2689
^{9}Li, new states, determ. from ^{7}Li(t,p)^{9}Li study 2—2689
Li(d,n)^{8}Be, neutron yield curves, spin and parity of 4.8 MeV level of ^{8}Be 2—27963
$_{\Lambda}^{10}$B, binding energy calc. from K^--captive in ^{12}C 2—24146
$_{\Lambda}^{7}$Li, binding energy calc. from K^--captive in ^{16}O 2—24146
$_{\Lambda}^{7}$Li→^{4}He ^{3}He π^-, energy and angular distributions of decay products 2—38478
$_{\Lambda}^{7}$Li→pd$\alpha\pi^-$, energy and angular distributions of decay products 2—38478
$_{\Lambda}^{8}$He, existence established, Λ-hyperon separation energy 2—5648
$_{\Lambda}^{9}$Be, binding energy calc., variational principle, α—α—Λ structure, Λ-N force 2—31452
$_{\Lambda}^{9}$Be, ground state binding energy calc. including repulsive core 2—8282
N, A=16, 17, activities measured in primary cooling water of nuclear reactor for power monitoring 2—28116
N, emulsion nucleus, identification of medium energy α-particle induced reactions 2—24237
N, resolution of nonelastic cross section discrepancy below 9 MeV 2—5696
N (A=14, 15), charge radius differences 2—14937
^{13}N, high-spin assignments in the 1p-shell obtained with the J-dependent (p,α) reaction on ^{16}O 2—31544
^{13}N, obs. of lowest $T=_{3/2}$ state, 14 MeV resonance in ^{12}C(p,p)^{12}C 2—21428
^{13}N compound nucleus from 25 to 36 MeV excitation 2—38640
^{13}N saline solution production for research studies in pulmonary physiology 2—14031
^{14}N, deexcitation γ-rays after π- capture on ^{16}O 2—2691
^{14}N, dipole excitations calc. 2—21376
^{14}N, fragmentation at 2.1 GeV per nucleon 2—38651
^{14}N, fragmentation in collisions with ^{1}H and ^{12}C at 29 GeV, inclusive isotope spectra at 0° 2—35081
^{14}N, in rare earth nitrate soln., n.m.r. exchange effects 2—6254
^{14}N, n.m.r. in nucleic acid bases 2—7159
^{14}N, n.q.r. in hydrazides at 77K 2—24540
^{14}N, quadrupole coupling const. of methacrylonitrile 2—8799
^{14}N, spin and parity level obs., new level found 2—2690
^{14}N, stopped π^- capture, ^{8}B prod. 2—14996
^{14}N line width (T_2) meas. in solns. of symmetric Co (III) complexes 2—1119
^{14}N n.m.r. in paramag. complexes 2—8685
^{14}N n.m.r. relax. in pivalonitrile solns. 2—9154
^{14}N nuclear quadrupole resonance spectra in hydrazines 2—8784
^{14}N(^{14}N,^{4}He)^{24}Mg, 20.2 and 28.0 MeV, differential cross sections determ. search for transitions to high spin states 2—11873
^{14}N(^{3}He,p)^{16}O, structure of states of ^{16}O 2—8285
^{14}N(^{6}Li,^{7}Be)^{13}C, one-nucleon transfer reaction at 32 MeV, isospin and fractional parentage studies 2—11872
^{14}N(^{6}Li,^{7}Li)^{13}N, one-nucleon transfer reaction at 32 MeV, isospin and fractional parentage studies 2—11872
^{14}N(α,α), 26.6 MeV, diff. cross sections and angular distributions 2—38631
^{14}N(α,γ)^{18}F, 0.5 to 1.2 MeV, total cross section measurement 2—2807
^{14}N(α,n), excitation function 2—38641
^{14}N(d,α')^{12}C, investigation of α-particle unstable states in ^{12}C 2—18089
^{14}N(d,$\alpha'\alpha$)^{8}Be, investigation of α-particle unstable states in ^{12}C 2—18089
^{14}N(d,α)^{12}C, exptl. study at 1.7, 2.3, 2.9 MeV 2—31580

Nuclei with $6\leqslant A\leqslant 19$ continued
^{14}N(d,γ_0)^{16}O resonance in giant-dipole region of ^{16}O, 2.1-2.9 MeV, determ. of location 2—28076
^{14}N(e,e)^{14}N, form factor calc. 2—2768
^{14}N(n,p)^{14}C, 14 MeV, ang. distrib. and effective differential cross section meas. 2—5701
^{14}N(p,2p)^{13}C, DWA calc. of low energy reaction in 1p shell 2—21433
^{14}N(p,γ) ^{15}O , states in ^{15}O studied between 10.91 and 13.02 MeV excitation as resonances 2—27970
^{14}N(p,γ)^{15}O, determination of mass of ^{15}O 2—34913
^{14}N(p,p'γ), states in ^{15}O studied between 10.91 and 13.02 MeV excitation as resonances 2—27970
^{14}N(p,p)^{14}N, rel. to investigations of double level at 8.92 MeV in ^{15}O 2—8284
^{14}N(p,pd), 50 MeV, total cross sections, secondary p energy spectra, secondary nuclei momentum and angular distribs. 2—31535
^{15}N, deexcitation γ-rays after π- capture on ^{16}O 2—2691
^{15}N, dipole excitations calc. 2—21376
^{15}N, elastic and inelastic scattering of neutrons, cross sections and scattering amplitudes 2—31516
^{15}N, multilevel multichannel study of structure from 12-14 MeV excitation energy 2—11728
^{15}N, n.m.r. Fourier spectra 2—6262
^{15}N, nuclear structure investigations using ^{16}O and ^{19}F induced multinucleon transfer reactions in ^{12}C and ^{11}B 2—38654
^{15}N, observation of α-particle core excited threshold states 2—18091
^{15}N, polarized, calibration by polarized protons and deuterons 2—35021
^{15}N, spin-lattice relaxation in organic compounds, temp. depend. 2—13424
^{15}N(^{3}He,p)^{17}O double-stripping reaction at 18 MeV, study of 2p-1h structure of ^{17}O 2—24150
^{15}N(α,γ)^{19}F, study of resonance at 850 keV, spin parity, lifetime, M1 transition strength determ. 2—35069
^{15}N(d, ^{3}He)^{14}C, 52 MeV, high-lying T=1 states in mass-14 nuclei, $1p_{1/2}^{2}$ and $1p_{1/2}1p_{3/2}$ diagonal matrix elements 2—18233
^{15}N(d,p), proton spectra from stripping reaction leading to unbound states of ^{16}N 2—8361
^{15}N(γ,p)^{17}C, 19.6—38.3 MeV, proton spectra obs. at giant resonance energies cross-sections 2—5684
^{15}N(p,$\alpha\gamma$)^{12}C, shell model and rotational calcs. for ^{16}O 2—38481
^{15}N(p,n)^{15}O, threshold energy for reactions and mass of ^{15}O 2—31543
^{15}N(p,p')^{15}N*, excitation function meas. level structure of ^{16}O, from 20-23 MeV 2—14933
^{16}N, level scheme and spin and parity assignments using ^{14}C (^{3}He,p)^{16}N reaction 2—31449
^{16}N, resonance at 5.05 MeV interferes destructively with continuum, observed in ^{15}N(d,p) reaction 2—8361
^{16}N β decay, effect of ^{16}O 7.12 MeV level on α spectrum 2—2743
^{16}N giant reson. analogs and π^+ photoprod. from ^{16}O 2—35010
^{18}Ne, energies of lowest five T=1 states, Coulomb energy shifts 2—14935
^{19}Ne, excited state study and energy meas. using ^{20}Ne(^{3}He, ^{4}He)^{19}Ne 2—11862
^{19}Ne, observation of α-particle core excited threshold states 2—18091
^{19}Ne, study of levels using ^{16}O+^{3}He reactions 2—27967
N(n,γ), 15 MeV, meas. of γ-ray spectra and differential 80° cross sections for discrete γ-ray line production 2—31555
O, emulsion nucleus, identification of medium energy α-particle induced reactions 2—24237
O (A=16, 18), charge radius differences 2—14937
O (γ,n), cross sections, analysis of irregularities, Feynman diagram theory 2—28017
^{14}O, half life meas. 2—11792
^{15}O, determination of mass from ^{14}N(p,γ)^{15}O reaction 2—34913
^{15}O, double level at 8.92 MeV, investigation using ^{14}N(p,p)^{14}N scattering 2—8284
^{15}O, double level at 8.92 MeV, investigation using ^{14}N(p,p)^{14}N scattering 2—8284
^{15}O, levels populated in ^{13}C(^{3}He,n) reaction absolute differential cross sections 2—18090
^{15}O, observation of α-particle core excited threshold states 2—18091
^{15}O levels, spectroscopic factors deduced from ^{13}C(^{3}He,n) reaction at 6 MeV, test of coeffs. of fractional parentage 2—27966
^{15}O mass, and threshold energy for reaction ^{15}N(p,n)^{15}O 2—31543
^{15}O states studied as resonances in ^{14}N (p'γ) ^{15}O and ^{14}N(p,pγ) reactions between 10.91 and 13.02 MeV excitation 2—27970
^{16}O-^{16}O elastic scattering, energy dependence of real part of optical potential due to nuclear rotation 2—18240
^{16}O-^{16}O potential, dependence on ansatz prescribing density of compound system 2—11869
^{16}O, 7.12 MeV level, effect on α spectrum from ^{16}N β decay 2—2743
^{16}O, alpha-cluster ground state 2—31450
^{16}O, binding energy, third-order contribution 2—462
^{16}O, binding energy, variation calc. correction 2—5647
^{16}O, binding energy calculations and their dependence on the treatment of the Pauli operation in the G-matrix 2—31448
^{16}O, Brueckner Hartree Fock calcs., effect of variations in radial orbital wave functions and major shell mixing 2—11729
^{16}O, Coulomb excitation of ^{56}Fe rel. to static quadrupole moment determination from reorientation meas. 2—31472
^{16}O, disruption by capture of π^- in nuclear emulsion 2—38627
^{16}O, elastic scatt. of 30 MeV ^{6}Li ions 2—18239
^{16}O, elastic scattering from ^{12}C, phase shift analysis using optical potential 2—38657
^{16}O, fine structure in giant dipole resonance, interpretation questioned in light of expts. on ^{14}N(d,γ_0) reaction 2—28076
^{16}O, first excited state, triaxial shape study 2—11698
^{16}O, form factor in oscillator model including short range correlations, study by elastic electron scattering 2—38577
^{16}O, four particle four hole solution, instability against parity mixing 2—2692
^{16}O, ground state props. calc. using relativistic self consistent meson field theory 2—11704
^{16}O, K^--capture, study of binding energy of product $_{\Lambda}^{7}$Li 2—24146
^{16}O, K^- capture, study of deexcitation γ-rays, rates to proton or neutron single hole states in ^{15}O and ^{15}N 2—11850
^{16}O, level structure, 20-23 MeV, from meas. of excitation functions of ^{15}N(p,p')^{15}N* 2—14933
^{16}O, levels near excitation energies of 15, 20 MeV investigated by means of reactions, spin assignments 2—38481
^{16}O, low energy scatt. cross sections, Hartree-Fock approx. 2—11837

Nuclei with $6 \leqslant A \leqslant 19$ continued
^{16}O, many-particle excited states, calc. of energies, quadrupole moments and shapes 2—8283
^{16}O, muon capture, asymmetry of emitted neutrons 2—38582
^{16}O, negative-parity states populated in ^{12}C(^{6}Li,d) reaction 2—463
^{16}O, nuclear structure investigations using ^{16}O and ^{19}F induced multinucleon transfer reactions in ^{12}C and ^{11}B 2—38654
^{16}O, parity measuring α decay from 3^+ T=0 0.06 state calc. in Cabbibo model of weak interactions 2—24179
^{16}O, photoprod. of π^+, ^{16}N giant reson. 2—35010
^{16}O, photoprod. of π^+ 2—35011
^{16}O, pionic X-ray yields meas. using absolute efficiency technique, pion cascade calc. of 2p-level widths 2—28057
^{16}O, proton elastic scattering, optical model description improved by addition of surface- peaked term to real-central potential 2—24211
^{16}O, π- capture, nuclear deexcitation γ-rays from ^{14}N, ^{15}N and ^{14}C 2—2691
^{16}O, π^+ elastic and inelastic scattering, 385 MeV/c 2—24232
^{16}O, spectrum and asymmetry of neutrons emitted after polarized muon capture 2—35059
^{16}O, structure of states, study by ion reaction ^{14}N(^{3}He,p) at 18 MeV 2—8285
^{16}O, vector analysing power of (d,p) reactions at 12 MeV 2—35070
^{16}O + ^{16}O potential, shell model calc. 2—18241
^{16}O (γ,n), giant dipole resonance region, cross sections and scattering amplitudes 2—31516
^{16}O (p,2p), distorted momentum distrib. calc. with complex pot. consistent with nucleon density distrib. 2—488
^{16}O α-particle inelastic scattering, 40.5 MeV, excitation of 8.87 MeV 2- level, analysis including two-body spin-orbit force 2—35064
^{16}O elastic and inelastic scatt. of 30.4 MeV polarized protons 2—14983
^{16}O low energy neutron scattering, origin of damping of wave functions in nuclear interior 2—11700
^{16}O+^{12}C reaction, quasimolecular resonances 2—38656
^{16}O(^{3}He,^{3}He), 18 MeV, polarization of ^{3}He, cross sect. ang. distrib. 2—18219
^{16}O(^{3}He,^{3}He)^{16}O, study of levels of ^{19}Ne 2—27967
^{16}O(^{3}He,α)^{15}O, study of levels of ^{19}Ne 2—27967
^{16}O(^{3}He,p)^{18}F, 2.95 MeV, parity of 3134 keV J=1 state in ^{18}F 2—14936
^{16}O(^{6}Li,^{3}He)^{19}F, 24 MeV meas. of angular distrib. DWBA analysis comparison with ^{16}O(^{6}Li,t)^{19}Ne cross section 2—28083
^{16}O(^{6}Li,t)^{19}Ne, 24 MeV meas. of angular distrib. DWBA analysis comparison with ^{16}O(^{6}Li,^{3}He)^{19}F cross section 2—28083
^{16}O(α,α), 26.6 MeV, diff. cross sections and angular distributions 2—38631
^{16}O(α,α), 5-11 MeV, ^{20}Ne high-spin states study 2—21382
^{16}O(α,γ)^{20}Ne, 4.65 MeV, 5^- resonance located 2—503
^{16}O(d,d), backward scattering, cross sections and angular distributions 2—38629
^{16}O(d,n), excitation function 2—38641
^{16}O(n,n), low energy S-wave scattering, Hartree-Fock and Perey-Buck non-local potentials, comparison 2—18201
^{16}O(n,p)^{16}N, use for oxygen content determ. in Fe powder 2—16716
^{16}O(p,2p)^{15}N, angular correlations measured at 49.5 MeV, results compared with distorted wave impulse approx. 2—11830
^{16}O(p,2p)^{15}N, DWA, calc. of low energy reaction in 1p shell 2—21433
^{16}O(p,α)^{13}N, high-spin assignments in the 1p-shell of ^{13}N 2—31544
^{16}O(p,α)^{13}N astrophysical importance of rate and cross section of reaction for nucleo-synthesis 2—24217
^{16}O(p,d)^{15}O, 31.8-45.4 MeV, distorted wave calcs. in adiabatic deuteron model 2—24218
^{16}O(p,n)^{16}F, 23 MeV, excitation energies of levels in ^{16}F 2—18092
^{16}O(p,pd), 50 MeV, total cross sections, secondary p energy spectra, secondary nuclei momentum and angular distribs. 2—31535
^{17}O, 0.87-MeV state mean life, from γ-ray Doppler shifts 2—2693
^{17}O, 2p-1h structure studied via ^{15}N (^{3}He,p) reaction, data analysed in DWBA 2—24150
^{17}O, energy levels of low lying multiparticle, multihole states, analysis by weak coupling model 2—14934
^{17}O, hyperfine interaction of V_f centre in MgO, e.s.r. study 2—13528
^{17}O, in rare earth nitrate soln., n.m.r. exchange effects 2—6254
^{17}O, levels deduced from ^{14}C(^{3}He, ^{3}He), ^{14}C(^{3}He, α), ^{14}C(^{3}He, d) and ^{14}C(^{3}He, p) reactions at 2 to 7 MeV 2—38476
^{17}O, single-particle energies, third- order contributions 2—462
^{17}O, superhyperfine interaction, obs. in e.s.r. of $KZn(SO_4)_2.6H_2O:Cu^{2+}$ 2—26262
^{17}O, transitions from ^{16}O produced by (d,p) reaction at 12 MeV 2—35070
^{17}O n.m.r. in ruby 2—13548
^{17}O n.q.r., transition frequencies in powdered quinones and xanthene 2—37019
^{17}O(d,n)^{18}F, DWBA analysis, E_d=4 MeV, ^{18}F level obs. 2—504
^{18}O, energy levels, effect of higher order diagrams on effective interaction 2—38477
^{18}O, energy levels, shell model calculation, and effective interaction in s-d shell 2—464
^{18}O, experimental results on (p,p′) scattering, ground state deformation evidence 2—8286
^{18}O, hyperfine interactions of first excited 2^+ state in 7^+ and 6^+ ions 2—31451
^{18}O, identification of spin-parity combinations from ^{18}O(α,α) reaction 2—2694
^{18}O, in neat $H_2{}^{18}O$, anomalous proton chem. shift, mag. resonance obs. 2—6245
^{18}O, inelastic scattering cross sections for excitation of levels below 6.0 MeV measured 2—8326
^{18}O, low lying level calc. using harmonic oscillator and Woods Saxon wave functions 2—5646
^{18}O, low lying level calc. in harmonic oscillator shell model using one-boson exchange potentials 2—11731
^{18}O, neutron angular distribs., (p,n) reaction cross sections 2—14985
^{18}O+^{18}O, excitation functions for formation of ^{34}P, ^{30}Al and ^{27}Mg for ^{18}O energies of 13-41 MeV 2—28084
^{18}O(^{18}O, ^{16}O)^{20}O two-neutron transfer reaction, 13-41 MeV, determ. excitation functions, compared with other ^{18}O induced reactions 2—18243
^{18}O(^{18}O, 2pn), 23-40 MeV, production of new isotope ^{33}Si, meas. of lifetime and decay scheme 2—38535
^{18}O(^{3}He,d)^{19}F, distorted wave calculation of spectroscopic factors for T=$^{3}/_{2}$ states in ^{19}F 2—11720
^{18}O(α,α')^{18}O, energy spectra, 20-23.4 MeV, spin and parity combinations 2—2694

Nuclei with $6 \leqslant A \leqslant 19$ continued
^{18}O(d,p)^{19}O, distorted wave calculation of spectroscopic factors for T=$^{3}/_{2}$ states in ^{19}O 2—11720
^{19}O, T=$^{3}/_{2}$ states, calculation of spectroscopic factors from ^{18}O(d,p) reaction 2—11720
O(n,γ), 15 MeV, meas. of γ-ray spectra and differential 80° cross sections for discrete γ-ray line production 2—31555
Si, proton scattering, angular distributions for particles in 2 to 30 keV range 2—11824

Nuclei with $20 \leqslant A \leqslant 49$
2s-1d shell nuclei, quadrupole and hexadecapole deformation 2—21383
A=20, calculation of $T=2 \rightarrow T=1 \rightarrow T=0$ M1 decays 2—31456
A=23, 27, 38, 49 (n, n′γ) reaction, analysis of γ-ray spectra 2—35045
A=32, calculation of $T=2 \rightarrow T=1 \rightarrow T=0$ M1 decays 2—31456
A=40, 41, calc. of non normal parity states 2—8295
neutron capture cross sections in Mg, Al, Si, P and S from 20-80 keV 2—28047
nuclear component of primary cosmic radiation, observations from Cosmos 136 satellite 2—8215
shell model calculations, for nuclei with A=30-35 2—2702
16-18.2 MeV, search for nondirect effects in excitation functions 2—35026
^{40}(alt,d_0)^{41}Ca meas. of angular distribs, near Coulomb barrier, DWBA analysis gives spectroscopic factor 2—35074
^{a}Ca, A=39, 41, 43, 47, levels deduced from ^{40,42,44,48}Ca(p,d) reactions, spectroscopic factors derived from DWBA analysis, obs. of analogue states 2—35036
^{a}Ca(p,d)^{b}Ca A=40, 42, 44, 48, b=39, 41, 43, 47, 40 MeV, spectroscopic factors derived from DWBA analysis, obs. of analogue states 2—35036
A=20, prod. of K*- (890) at 10 and 12.7 GeV/c by K- 2—8158
^{24,24m}Al beta delayed alpha emission measured, deduced log fit values 2—18156
Al, ground state decay of levels, obs. of γ-rays from Al(n,xγ) 2—14989
Al, π photoproduction, 1160 MeV γ-quanta 2—14974
Al, ratio of photodisintegration to electrodisintegration for 5.0 GeV electron bombardment 2—11822
Al (A=31, 32, 33), production in bombardment of ^{232}Th with 290 MeV ^{40}Ar 2—5715
Al neutron total cross section between 23 and 45 MeV using time-of-flight technique with transmission method 2—38609
^{23}Al, β-delayed proton emission 2—24180
^{24}Al, β decay, half-life determ. 2—2744
^{24}Al, excitation energies of levels, study by ^{24}Mg(p,n)^{24}Al at 23 MeV 2—18092
^{26}Al, evidence for ground state rotational band of $K^{\pi}=5^+$ 2—2699
^{26}Al, level scheme, $4^+(d_{3/2})^{-2}$ state obs. 2—8290
^{26}Al, location of second $J^{\pi}=0^+$, T=1 state from ^{24}Mg(^{3}He,pγ), ^{25}Mg(^{3}He,dγ) and ^{27}Al(^{3}He,$\alpha\gamma$) reactions 2—38488
^{26}Al, mean lifetimes of levels and decay modes from ^{23}Na(α,n)^{26}Al reaction 2—14941
^{26}Al high spin states populated in ^{12}C(^{16}O,d)^{26}Al reaction 2—38655
^{26}Al nucleosynthesis in the early solar system and in cosmic rays 2—20470
^{26}Al$\rightarrow$^{26}Mg, positron emission and electron capture 2—11793
^{27}Al, excitation energies of excited states, γ-ray energy meas. 2—11724
^{27}Al, ground and excited states populated in β^+ decay of ^{27}Si branching ratios and log ft values obtained 2—18157
^{27}Al, Knight shift in Pd-Al dil. alloy, temp. depend. 2—40782
^{27}Al, lifetime of 1.013 MeV state 2—11736
^{27}Al, measurement of lifetime of the 1.01 MeV level 2—31457
^{27}Al, n.m.r., in GdAl and ErAl garnets 2—10542
^{27}Al, n.m.r. study of topaz, $Al_2SiO_4(F,OH)_2$ 2—10541
^{27}Al, oblate shape, agreement with calcs. in Coriolis band mixing model 2—31458
^{27}Al, quadrupole coupling constant for n.m.r. of $Gd_3Al_2(AlO_4)_3$ garnet 2—7139
^{27}Al dynamic polarization in ruby:Cr^{3+} 2—29856
^{27}Al high spin states populated in ^{12}C(^{16}O,p)^{27}Al reaction 2—38655
^{27}Al n.m.r. in ruby 2—13548
^{27}Al n.m.r. in type II superconductors 2—6777
^{27}Al proton reactions, resonance levels in ^{28}Si deduced 2—34915
^{27}Al spin-lattice relax. in $La_{1-x}Gd_xAl_2$ 2—33181
^{27}Al spin-lattice relax. in $LaAl_2Ce(Tm)$ 2—40580
^{27}Al(^{3}He,dγ)^{26}Al, location of second $J^{\pi}=0^+$, T=1 state in ^{26}Al 2—38488
^{27}Al(α,γ)^{31}P, investigation of ^{31}P energy levels 2—2703
^{27}Al(α,t), (α,α), 104 MeV, differential cross sections and normalization factors 2—21441
^{27}Al(α+pγ)^{30}Si, meas. of branching ratios and lifetimes of levels in ^{30}Si 2—34986
^{27}Al(d,p)^{28}Al, 23 MeV, low-lying states in ^{28}Al 2—34926
^{27}Al(γ,p), energy states from proton energy spectra 2—31523
^{27}Al(γ,π^+)^{27}Mg threshold to 1200 MeV, π production cross-section meas. 2—5682
^{27}Al(n,γ)^{28}Al, circular polarization meas., levels of ^{28}Al 2—18206
^{27}Al(n,p)^{27}Mg cross section meas. by β counting ^{27}Mg activity in Al foils, energies to 5.6 MeV 2—28049
^{27}Al(p,α,γ)^{24}Mg, 6.40 MeV, α-γ angular correlation 2—38594
^{27}Al(p,α)^{24}Mg, E_p=7.40 MeV, plastic detector study 2—14777
^{27}Al(p,α)^{24}Mg, low energy, rel. to investigation of states in ^{28}Si 2—31459
^{27}Al(p,α)^{24}Mg, meas. of reaction time at 633 and 1183 keV using blocking effect 2—24220
^{27}Al(p,γ)^{28}Si, excitation functions, resonances 2—28036
^{27}Al(p,γ)^{28}Si, investigation of ^{28}Si energy levels 2—34928
^{27}Al(p,γ)^{28}Si, yield curve obtained with implanted targets, determ. range of 50 keV Al^+ ions in C, Cu, Mo and Ta 2—19479
^{27}Al(p,n) reaction mechanism at intermediate energies ^{28}Si resonance 2—38595
^{27}Al(p,nγ)^{27}Si, 16 MeV, γ-spectrum 2—14986
^{28}Al, e.m. transition rates 2—34927
^{28}Al, low lying states, investigation using ^{27}Al(d,p)^{28}Al at 23 MeV 2—34926
^{28}Al, spin, parity assignments 2—18206
Al(n,γ), 15 MeV, meas. of γ-ray spectra and differential 80° cross sections for discrete γ-ray line production 2—31555
Al(n,xγ), 5.3-9.0 MeV, cross sect. meas. spectra, ground state decay of levels 2—14989
Al(p,x) reaction (X=p,d,t, ^{3}he, α), 19.8 GeV/c, energy distributions of light emission fragments 2—31545
^{36}Ar, energy levels and E2 transitions, Hartree-Fock and random phase approximations 2—38483
^{36}Ar magnetic transitions excited by 180° electron scatt. 2—11738
^{36}Ar(α,γ_0)^{40}Ca, giant resonance region 2—38642

Nuclei with 20≤A≤49 continued

^{36}Ar(d,p)^{37}Ar, E_d=18.00 MeV, proton ang. distrib. 2—2779
^{36}Ar(p,^{3}He)^{34}Cl deuteron transfer reaction enhanced by neutron-proton pairing correlations 2—11831
^{36}Ar(p,n)^{36}K, half life determ. for ^{36}K 2—2744
^{37}Ar, energy levels, from ^{36}Ar(d,p) study 2—2779
^{37}Ar, magnetic moments of 7/2^{-} mirror states 2—5652
^{37}Ar, transition strengths, investigation using ^{37}Cl(p,n)^{37}Ar reaction 2—5650
^{37}Ar perturbed ang. correl. in Ni 2—10292
^{38}Ar, mean lifetimes of 3.38 and 4.59 MeV levels prod. in ^{4}He(^{35}Cl,p)^{38}Ar reaction 2—21386
^{38}Ar lifetimes of levels at 3377, 4585, 4480 keV electron by Doppler shift attenuation and ^{38}Cl(α,pγ) reaction 2—27972
^{38}Ar(d,p)^{39}ar, 10.064 MeV, determ. of level structure of ^{39}Ar, orbital angular momentum transfer to target nucleus 2—34934
^{39}Ar, single neutron hole states populated in ^{40}Ar(^{3}He,α) reaction, spin and parity 2—27973
^{39}Ar from ^{39}Cl β-decay, energy levels investigation 2—11794
^{39}Ar level structure determ. from ^{38}Ar(d,p) reaction, orbital angular momentum transfer valves and spectroscopic factors 2—34934
^{40}Ar, experimental O_2^+(2.12 MeV)$\rightarrow 2_1^+$(1.46 MeV) B(E2) strength and pairing-vibration calculations 2—31463
^{40}Ar, level lifetimes from proton scatt., using Doppler shift attenuation method 2—38490
^{40}Ar+^{209}Bi transfer reactions, 190 to 270 MeV, determ. excitation function and recoil ranges of produced ^{211}At 2—11875
^{40}Ar(^{3}He,α)^{39}Ar, single neutron hole states population below 11.4 MeV excitation energy 2—27973
^{40}Ar(α,nγ)^{43}Ca, 13.5 MeV, study of excited state properties of ^{43}Ca, spin values 2—24155
^{40}Ar(n,γ)^{41}Ar circular polarization meas., levels of ^{41}Ar 2—18206
^{40}Ar(p,γ)^{41}K, investigation of excited states of ^{41}K 2—5653
^{40}Ar(p,p$'\gamma$)^{40}Ar, obs. of isobaric analogues of ^{41}Ar levels 2—34935
^{41}Ar, isobaric analogues, obs. through reaction ^{40}Ar(p,p$'\gamma$)^{40}Ar 2—34935
^{41}Ar spin, parity assignments 2—18206
Ca-Fe region even-target (^{3}He,p) reactions, search for 0^+ antianalog states 2—11858
Ca, isotope targets 29 MeV elastic scattering, determ. optical model parameters 2—18221
Ca, isotopes, phenomenological effective two body interaction 2—14943
Ca, proton elastic scattering, 5 to 6.4 MeV, excitation functions 2—38586
Ca isotopes, effective wave function calc. of J^π=0^+ states 2—14944
Ca isotopes, elastic scatt. of ^{16}O, ang. momentum effects 2—35082
Ca(^{3}He, ^{4}He), 13.0 MeV, on even isotopes, ang. distrib. of transitions 2—15012
Ca(^{16}O,^{16}O), A=40, 42, 44, 48, real part of optical potential combined microscopic and phenomenological approach 2—508
^{40}Ca, compressibility effect on shell model pot. 2—11711
^{40}Ca, elastic neutron scattering for energies up to 2 MeV 2—35054
^{40}Ca, elastic scatt. of 30 MeV ^{6}Li ions 2—18239
^{40}Ca, elastic scatt. of deuterons, coupled channel calc. 2—38632
^{40}Ca, ground state props. calc. using relativistic self consistent meson field theory 2—11704
^{40}Ca, low energy scatt. cross sections, Hartree-Fock approx. 2—11837
^{40}Ca, magnetic transition strength studied by 180° electron scattering 2—11737
^{40}Ca, muon capture, asymmetry of emitted neutrons 2—38582
^{40}Ca, nucleon triple scattering parameters, optical model analyses 2—18181
^{40}Ca, perturbative treatment of effective particle-hole interaction and transition moments 2—11739
^{40}Ca, polarization of emitted neutrons in muon capture 2—38584
^{40}Ca, quasi free scattering using Saclay linear accelerator, information on shell structure of nuclei obtained 2—5687
^{40}Ca, resonance wave functions and parameters from coupled channel method 2—14972
^{40}Ca, spectrum and asymmetry of neutrons emitted after polarized muon capture 2—35059
^{40}Ca, study of 6.75 MeV level populated in (p,p$'\gamma$) scattering 2—18101
^{40}Ca proton elastic scattering, optical model description improved by addition of surface- peaked term to real-central potential 2—24211
^{40}Ca(^{18}O, ^{14}C)^{44}Ti, pick up reaction at 48 MeV, ang. distrib. to final states, cross sections 2—28086
^{40}Ca(^{6}Li,2n)^{44}V, 18.5 MeV, production of highly neutron deficient vanadium isotope with half-life 90±25 ns 2—11795
^{40}Ca(α,^{3}He), (α,t), (α,α), 104 MeV, differential cross sections and normalization factors 2—21441
^{40}Ca(α,pγ)^{43}Sc, 7-12 MeV determ. lifetimes of levels populated in ^{43}Sc 2—18103
^{40}Ca(d,$\alpha\gamma$)^{48}K, 4.42, 5.08 MeV, levels of ^{48}K determ. from α-γ angular correlations 2—35075
^{40}Ca(d,n), neutron polarization meas., comparison with DWBA calc. 2—38614
^{40}Ca(d,p)^{41}Ca, effects of 2-step processes in reactions leading to $^{3}/_{2}{}^{+}$2.02 MeV state 2—28077
^{40}Ca(γ,np), threshold-200 MeV, direct excitation of two nucleons, neutron-proton correlations 2—38565
^{40}Ca(γ,np) 19-30 MeV, cross section determ. by counting residual γ-ray activity, comparison with calc. based on quasi-deuteron theory 2—485
^{40}Ca(γ,p) 15.2-24.6 MeV, determ. differential photoproton cross sections corresponding to different states of residual nucleus 2—14976
^{40}Ca(n,$\alpha\gamma$)^{37}Ar, 4.85≤E_n≤8.05 MeV, γ spectra 2—38615
^{40}Ca(n,γ)^{41}Ca circular polarization meas., levels of ^{41}Ca 2—18206
^{40}Ca(n,n$'\gamma$)^{40}Ca, 4.85≤E_n≤8.05 MeV, γ spectra 2—38615
^{40}Ca(n,pγ)^{40}K, 4.85≤E_n≤8.05 MeV, γ spectra, ^{40}K transitions 2—38615
^{40}Ca(p,p$'$), quasifree scattering at 1 GeV 2—31530
^{40}Ca(p,p$'\gamma$)^{40}Ca, doorway state structure in ^{41}Si 2—38598
^{40}Ca(t,d)^{41}Ca, effects of 2-step processes in reactions leading to $^{3}/_{2}{}^{+}$2.02 MeV 2—28077
^{41}Ca, energy levels of low lying multiparticle, multihole states, analysis by weak coupling model 2—14934
^{41}Ca, spin, parity assignments 2—18206
^{42}Ca, g factor of 6^+ state 2—24156
^{42}Ca, inelastic α scattering, relation between nuclear matter and nuclear potential 2—8355
^{42}Ca, inelastic scatt. of 50 MeV protons to deformed states 2—11835
^{42}Ca, static electric quadrupole moment of lowest rotational band 2—18102

Nuclei with 20≤A≤49 continued

^{42}Ca 6^+(3.19 MeV) state magnetic moment, comparison of theory and exptl. values 2—11740
^{43}Ca, e.m. decay of low-lying states populated in ^{43}Ca(p,p$'\gamma$) reaction 2—27974
^{43}Ca, excited state properties and spin values from ^{40}Ar(α,nγ) reaction at 13.5 MeV 2—24155
^{43}Ca, γ-decay schemes of resonant states and branching ratios and energies of bound states 2—14945
^{43}Ca, magneto moment determ. by optical pumping 2—18104
^{43}Ca(d,p)^{44}Ca, spectroscopic strengths and transition rates 2—31464
^{43}Ca(n,γ)^{44}Ca γ-ray spectra, assignment of transitions to levels in ^{44}Ca 2—24158
^{44}Ca, inelastic scattering by ^{3}He to positive parity states at 29 MeV, analysis within microscopic model 2—15013
^{44}Ca, level assignment, γ-ray spectra front transitions in reaction ^{43}Ca(n,γ) 2—24158
^{44}Ca, structure from Hamada-Johnston and Tabakin interactions 2—31464
^{45}Ca, transitions, ^{46}Ca(d,t) reaction study 2—2809
^{46}Ca(^{3}He,p)^{48}Sc, ^{48}Ca(^{3}He,p)^{50}Sc, obs. of strongly excited 1^+ states in Sc nuclei 2—34937
^{46}Ca(^{3}He,p)^{48}Sc, nuclear spectroscopy of ^{48}Sc 2—34938
^{46}Ca(α,d)^{48}Sc, study of levels of ^{48}Sc 2—31466
^{46}Ca(d,^{3}He)^{45}K, angular distrib. and spectroscopic strength 2—2809
^{46}Ca(d,t)^{45}Ca, angular distrib. and spectroscopic strength 2—2809
^{48}Ca, perturbative treatment of effective particle-hole interaction and transition moments 2—11739
^{48}Ca intermediate structure, S- and P-wave neutron spectroscopy 2—24160
^{48}Ca(^{3}He,t$'$)^{48}Sc, effect of two step process 2—21447
^{48}Ca(^{3}He,t)^{48}Sc, 23 MeV, study of levels of ^{48}Sc 2—31467
^{48}Ca(p,nγ)^{48}Sc, investigation of ^{48}Sc excited state properties 2—2705
^{49}Ca, gamma ray decay from the analogue state of the ground state 2—31469
^{49}Ca 2p-1h states, S- and P-wave neutron spectroscopy, neutron doorway escape widths determ. using theory of intermediate structure 2—24159
Ca(n,γ) A=40, 42, 44, gamma-ray spectra 2—2788
Ca(p,p), energetic dependence of elastic scattering cross sections on thick targets 2—28033
Ca(p,t), J^π=0^+ states, effective wave function calculation 2—14944
Ca(t,p), J^π=0^+ states, effective wave function calculation 2—14944
Cl (A=35, 37), magnetic moment determination from n.m.r. investigations in aqueous solutions 2—22007
Cl (A=41, 42), production in bombardment of ^{232}Th with 290 MeV ^{40}Ar 2—5715
^{32}Cl, β decay, half-life determ. 2—2744
^{33}Cl, single-particle strengths for quasibound levels determ. From ^{32}S(^{3}He,d) ^{33}Cl at 29.7 and 34.5 MeV 2—24153
^{33}Cl, studies by isospin forbidden resonances in ^{32}S(p,γ)^{33}Cl 2—34932
^{33}Cl analogue states of ^{33}P studied by isospin-forbidden resonances in ^{32}S(p,γ) reaction 2—34931
^{33}Cl energy levels, study by reaction ^{32}S(d,n) at 4.7 and 5.5 MeV 2—34930
^{34}Cl, levels, populated by γ ray decay of resonances in ^{33}S(p,γ)^{34}Cl reaction 2—11733
^{34}Cl, mean lives of 1230, 666, and 461 keV, levels, meas. by recoil-distance method 2—465
^{35}Cl, in powder sample, asymmetry parameter detn., n.q.r. obs. 2—7156
^{35}Cl, γ ray transitions 2—2704
^{35}Cl, lifetimes of first six excited states determ. from Doppler shift attenuation meas. on ^{35}Cl(p,p$'\gamma$) reaction 2—31462
^{35}Cl, n.m.r. in NaCl 2—7142
^{35}Cl, n.m.r. relaxation times meas. in PCl_3-PBr_3 liq. mixture and PCl_3 liq. 2—9178
^{35}Cl, n.q.r. in K_2SnCl_6 2—7158
^{35}Cl, n.q.r. spectra of chlorinated methylbenzenes 2—10590
^{35}Cl, transition strengths, investigation using ^{35}Cl(p,p$'$)^{35}Cl* reaction 2—5650
^{35}Cl (γ,p) and (γ,n) reactions at 30 MeV, meas. of de-excitation γ-rays in residual nuclei 2—38569
^{35}Cl and ^{37}Cl, kaon capture, obs. of γ-rays emitted from ^{32}P first excited state 2—28059
^{35}Cl n.m.r. in ClO_3F, spin-lattice relax. 2—8604
^{35}Cl n.m.r. in $CsNiCl_3$ 2—22703
^{35}Cl n.m.r. in TlCl, spin-lattice relax. 2—10262
^{35}Cl nuclear quadrupole resonance in P-Cl compounds and complexes 2—28317
^{35}Cl pion-capture obs. 2—5707
^{35}Cl quadrupole relax. in mol. cryst. 2—10276
^{35}Cl temp. depend. of nuclear quadrupole resonance and spin-lattice relaxation time in trichloroacetamide 2—10591
^{35}Cl(^{3}He,p)^{37}Ar, between 9 and 14 MeV, comparison with DWBA calc. 2—18235
^{35}Cl(α,pγ)^{38}Ar, 11.5 MeV, deduced lifetimes of levels in ^{38}Ar by Doppler shift method 2—27972
^{35}Cl(p,p$'$)^{35}Cl*, determination of ^{35}Cl transition strengths 2—5650
^{37}Cl, excitation energies of excited states, γ- ray energy meas. 2—11724
^{37}Cl, neutron angular distribs., (p,n) reaction cross sections 2—14985
^{37}Cl n.m.r. in TlCl, spin-lattice relax. 2—10262
^{37}Cl(d, pγ) ^{38}Cl, 3.1 MeV, study of levels below 2.75 MeV excitation energy in ^{38}Cl 2—24154
^{37}Cl(d,$\alpha\gamma$), ^{35}S, 4.25 MeV, study of states in ^{35}S 2—18100
^{37}Cl(γ,2p)^{35}P, half life and γ-ray energy meas. for new nuclide ^{35}P 2—5651
^{37}Cl(μ_e3-)^{37}Ar, cross section computation, detection of solar neutrinos 2—8329
^{37}Cl(p,n)^{37}Ar, determination of ^{37}Ar transition strengths 2—5650
^{38}Cl, study of levels below excitation energy 2.75 MeV with ^{37}Cl(d, pγ) reaction at 3.1 MeV 2—24154
^{39}Cl half-life determ. 2—11794
^{48}Cr, energy level study with ^{50}Cr(p,t)^{48}Cr reaction, spin and parity assignment 2—2706
^{48}Cr, energy levels populated in ^{50}Cr(p,t) reaction 2—467
^{49}Cr, beta decay to ^{49}V, lifetime of ^{49}V 90.65 keV state 2—2707
^{49}Cr, mean lifetimes of levels below 3 MeV excitation meas. using ^{49}To(α+nγ) reaction 2—18105
^{36}K, β decay, half-life determ. 2—2744
^{36}K, half life meas. with pneumatic shuttle system 2—31498
^{37}K, magnetic moments of 7/2^{-} mirror states 2—5652
^{38}K, γ decay of levels below 3-7 MeV excitation energy populated by ^{40}Ca(d,$\alpha\gamma$) reaction, multipole mixing ratios 2—35075

Nuclei with $20\leqslant A\leqslant 49$ continued
^{39}K, M2 and E3 radiation widths of 2.82 MeV level, comparison of experiment and theoretical predictions 2—8294
^{39}K, n.q.r. in $KBrO_3$ 2—40790
^{39}K, neutron elastic scatt., local optical nuclear model 2—5698
^{39}K double reson. and spin-lattice relax. in KH_2PO_4 2—10581
^{39}K(n,γ)^{40}K thermal neutron capture, meas. γ-ray spectra deduced Q-values, excitation energies of ^{40}K levels 2—18207
^{40}K, level lifetimes determ. from ^{40}Ar(p,p)^{40}K using Doppler shift attenuation method 2—38490
^{40}K, level transitions, from ^{40}Ca(n,pγ), $4.85\leqslant E_n\leqslant 8.05$ MeV 2—38615
^{40}K, short lived activities excited by 14.7 MeV fast neutrons 2—18093
^{40}K half-life for beta emission, undergraduate laboratory experiment 2—33843
^{41}K, excited states investigation from ^{40}Ar(p,γ)^{41}K reaction 2—5653
^{41}K, neutron angular distribs., (p,n) reaction cross sections 2—14985
^{41}K (n,γ)^{42}K thermal neutron capture, meas. γ-ray spectra deduced Q-values, excitation energies ^{42}K levels 2—18207
^{41}K(p,γ)^{43}Ca, 1400-1750 keV, investigation of excited states in ^{43}Ca 2—14945
^{45}K, transitions, ^{46}Ca(d,^{3}He) reaction study 2—2809
^{26}Kg(α,n)^{29}Si reaction, study of principal decay modes and lifetimes of levels below 7.2 MeV in ^{29}Si 2—27971
Mg (A=29, 30), production in bombardment of ^{232}Th with 290 MeV ^{40}Ar 2—5715
^{24}Mg, calculation of triaxial shapes 2—31424
^{24}Mg, deformations of ground-bands, rotational model analysis 2—31454
^{24}Mg, deuteron stripping, coupled channel Born approx. description 2—15011
^{24}Mg, energies, branching ratios, lifetimes, γ-ray transition, strengths of levels populated in ^{23}Na(p,γ) reaction 2—38591
^{24}Mg, energy gaps and momentum transfer 2—38486
^{24}Mg, energy levels, cluster model calcs. 2—38480
^{24}Mg, ground state, triaxial shape study 2—11698
^{24}Mg, high energy elastic electron scattering, analysed with phenomenological charge distribution and Woods-Saxon potential 2—8327
^{24}Mg, levels deduced from alpha particles emitted following β-decay of ^{24}Al 2—18156
^{24}Mg, lifetime meas. of 6.431 MeV (0^+) and 8.655 MeV (2^+) levels populated in ^{12}C(^{16}O,α)^{24}Mg reaction 2—38487
^{24}Mg, nuclear charge distributions from elastic electron scattering 2—34922
^{24}Mg, nuclear deformations from electron scatt. obs. 2—11783
^{24}Mg, role of spin transfer and multistep effects in transition to 5.22 MeV 3^+ state in ^{26}Mg(p,t) reaction 2—35035
^{24}Mg, vector analysing power of (d,p) reactions at 12 MeV 2—35070
^{24}Mg decay schemes from ^{23}Na(p,γ)^{24}Mg 2—38593
^{24}Mg Hartree-Fock model predictions of static and dynamic properties 2—11734
^{24}Mg high spin states populated in ^{12}C(^{16}O,α)^{24}Mg reaction 2—38655
^{24}Mg(^{16}O 2nγ)^{38}Ca, product study, including proton rich nuclei, 22-33 MeV 2—21450
^{24}Mg(^{3}He,pγ)^{26}Al, location of second $J^{\pi}=0^+$, T=1 state in ^{26}Al 2—38488
^{24}Mg(α,p), 28.8 MeV, study of J dependence for L=2 transfer 2—11863
^{24}Mg(d,n), neutron polarization meas., comparison with DWBA calc. 2—38614
^{24}Mg(e,e$'$), form factors using shell-model wave functions 2—35012
^{24}Mg(γ,xn), ^{26}Mg(γ,xn), structure in photoneutron cross section and giant resonance formation 2—38570
^{24}Mg(p,n)^{24}Al, 23 MeV, excitation energies of levels in ^{24}Al 2—18092
^{24}Mg(p,n)^{24}Al, half life determ. for ^{24}Al 2—2744
^{25}Mg, 975 keV $^{3}/_{2}{}^{+}$ state, half-life 2—18097
^{25}Mg, excited state mean life, from γ-ray Doppler shifts 2—2693
^{25}Mg, nuclear charge distributions from elastic electron scattering 2—34922
^{25}Mg, photoneutron cross section determ. 2—2762
^{25}Mg, spin of 4.075 MeV level determ. from gamma-ray polarization method 2—8289
^{25}Mg, transitions from ^{24}Mg produced by (d,p) reaction at 12 MeV 2—35070
^{25}Mg n.m.r. in aqueous phosphate solutions 2—28897
^{25}Mg(^{3}He,dγ)^{26}Al, location of second $J^{\pi}=0^+$, T=1 state in ^{26}Al 2—38488
^{26}Mg, calculation of triaxial shapes 2—31424
^{26}Mg, mean lifetimes of levels and decay modes from ^{23}Na(α,p)^{26}Mg reaction 2—14941
^{26}Mg, nuclear charge distributions from elastic electron scattering 2—34922
^{26}Mg ((p,n) charge exchange reaction to O^+ and 2^+ analogue states, channel coupling effects 2—28035
^{26}Mg from ^{26}Al ground state β-decay, excited states 2—11793
^{26}Mg(^{18}O, ^{16}O)^{28}Mg two-neutron transfer reaction, 20-45MeV determ. excitation functions, angular distributions and differential ranges 2—18243
^{26}Mg(^{3}He,t) charge exchange reaction to 0^+ and 2^+ analogue states, channel coupling effects 2—28035
^{26}Mg(^{6}Li,^{6}He)^{26}Al, charge exchange reaction, meas. and DWBA analysis of ang. distributions 2—28085
^{26}Mg(^{7}Li, ^{7}Be)^{26}Na, 36 MeV, used to meas. mass of ^{26}Na 2—34924
^{26}Mg(α,n)^{29}Si, level scheme for ^{29}Si 2—2701
^{26}Mg(d,$\alpha\gamma$)^{24}Na, investigation of low-lying levels of ^{24}Na 2—2698
^{26}Mg(d,p)^{27}Mg, 2.0 to 3.0 MeV, angular distributions and excitation functions 2—35072
^{26}Mg(d,pγ)^{27}Mg, mean life and mixing coeff. meas. for ^{27}Mg 2—18099
^{26}Mg(p,t)^{24}Mg, near 26 MeV, meas. of cross sections, angular distribs., excitation functions, DWBA calcs. 2—35035
^{27}Mg, mean life and mixing coeff. meas. using ^{26}Mg(d,pγ) reaction 2—18099
Mg(n,γ), 15 MeV, meas. of γ-ray spectra and differential 80° cross sections for discrete γ-ray line production 2—31555
^{20}Na, β decay, half life determ. 2—2744
^{20}Na, excitation energies of levels, study by ^{20}Ne(p,n)^{20}Na at 23 MeV 2—18092
^{20}Na, half life meas. with pneumatic shuttle system 2—31498
^{22}Na, cosmic ray produced, rel. to atmospheric exchanges 2—20324
^{22}Na, short lived activities excited by 14.7 MeV fast neutrons 2—18093
^{22}Na, slow neutron capture, charged particle emission 2—18205
^{22}Na, spin of 1984 keV level populated in ^{19}F(α,nγ)^{22}Na reaction 2—38485
^{23}Na, excitation energies and angular distributions of levels below 10.2 MeV determ. from ^{22}Ne(^{3}He,d) reaction 2—11735
^{23}Na, low-lying $K^{\pi}={}^{1}/_{2}{}^{-}$ band, E1 decay of members 2—24151

Nuclei with $20\leqslant A\leqslant 49$ continued
^{23}Na, mean lifetimes of levels and decay modes from ^{23}Na(p,p$'$)^{23}Na reaction 2—14941
^{23}Na, n.m.r. in NaCl 2—7142
^{23}Na, n.q.r. in $NaBrO_3$ 2—40790
^{23}Na, nuclear quadrupole spin-lattice relax. in $NaNO_3$, orientation depend. 2—26084
^{23}Na, photoneutron cross section determ. 2—2762
^{23}Na (γ,p) and (γ,n) reactions at 30 MeV, meas. of de-excitation γ-rays in residual nuclei 2—38569
^{23}Na bound states, assignment using ^{22}Ne(p,γ)^{23}Na reaction 2—24219
^{23}Na n.m.r. in hydrous and anhydrous Na_2MoO_4 and Na_2WO_4, meas. of quadrupole coupling consts., electric field gradient 2—37012
^{23}Na n.m.r. in perovskites 2—9816
^{23}Na nuclear quadrupole coupling constant in $NaNO_3$ low temperature behaviour 2—30034
^{23}Na quadrupole spin-lattice relax. in $NaNO_3$ 2—19933
^{23}Na spin-lattice relax. in NbN 2—13089
^{23}Na spin-lattice relax. in liq. alkali metal alloys 2—18855
^{23}Na(α,nγ)^{26}Al, γ-ray distrib. meas., spin assignment of positive parity levels, evidence for ground state rot. band 2—2699
^{23}Na(p,γ)^{24}Mg, accurate branching ratios 2—38593
^{23}Na(p,γ)^{24}Mg, resonance meas. 2—38592
^{23}Na(p,γ)^{24}Mg 0.3-1.9 MeV, meas. of proton energies and strengths of resonances, gamma decay, Q-value 2—38591
^{23}Na(p,p$'$)^{23}Na determ. of mean lifetimes and decay modes of levels populated in reaction 2—14941
^{24}Na, low-lying levels, investigation using ^{26}Mg(d,$\alpha\gamma$)^{24}Na reaction 2—2698
^{26}Na mass meas. using ^{26}Mg(^{7}Li, ^{7}Be)^{26}Na reaction 2—34924
Ne, K^- absorption 2—8354
Ne^{21} production in nuclear reactions, rel. yields and efficiencies 2—11816
^{20}Ne, ^{22}Ne, vapour pressure meas. from triple point to normal boiling point 2—30750
^{20}Ne, α-particle clustering, saturation mechanisms 2—38440
^{20}Ne, Brueckner Hartree Fock calc using density dependent effective interaction, binding energy estimate 2—11727
^{20}Ne, deformations of ground-bands, rotational model analysis 2—31454
^{20}Ne, determination of deformation parameters by inelastic scattering of polarized protons 2—35034
^{20}Ne, energy levels and E2 transitions, Hartree-Fock and random phase approximations 2—38483
^{20}Ne, excited levels, Tamm-Dancoff approx. 2—38484
^{20}Ne, excited state stability and band cut-off 2—38473
^{20}Ne, form factors of monopole transition, obs. using inelastic electron scattering 2—31455
^{20}Ne, Hartree-Fock model predictions of static and dynamic properties 2—11734
^{20}Ne, high-spin states studied in ^{16}O(α,α) scattering 2—21382
^{20}Ne, nuclear structure investigations using ^{16}O and ^{19}F induced multinucleon transfer reactions in ^{12}C and ^{11}B 2—38654
^{20}Ne, radiative width of 8^+ 11.948 MeV level, ^{4}He(^{16}O,γ) capture reaction study 2—18096
^{20}Ne, T=0 levels, generator coord. spectrum 2—34921
^{20}Ne(^{3}He, ^{4}He)^{19}Ne, 18 MeV, study of excited states in ^{19}Ne, energy meas. 2—11862
^{20}Ne(α,$\alpha_{1.63}$)^{20}Ne*, 20-24 MeV, anal. using strong absorption model, ang. distrib. 2—31565
^{20}Ne(d,α)^{18}F, $E_d<3.2$MeV, ang. distribs. and absolute cross section 2—5712
^{20}Ne(d,p)^{21}Ne, ang. distributions and excitation functions in incident energy range 0.9 to 2.4 MeV 2—31581
^{20}Ne(e,e$'$), form factors using shell-model wave functions 2—35012
^{20}Ne(p,n)^{20}Na, 23 MeV, excitation energies of levels in ^{20}Na 2—18092
^{20}Ne(p,n)^{20}Na, half life determ. for ^{20}Na 2—2744
^{22}Ne, determination of deformation parameters by inelastic scattering of polarized protons 2—35034
^{22}Ne(^{3}He,d)^{23}Na, 15 MeV, excitation energies and angular distributions of levels in ^{23}Na below 10.2 MeV 2—11735
^{22}Ne(d,α)^{20}F, $E_d<3.2$MeV, ang. distribs. and absolute cross section 2—5712
^{22}Ne(p,γ)^{23}Na, ang. distribution meas. of γ-rays 2—24219
Ni(p,p$'$), compound-nucleus contrib. 2—2771
P (A=35, 36, 37, 38), production in bombardment of ^{232}Th with 290 MeV ^{40}Ar 2—5715
^{28}P, β decay, half-life determ. 2—2744
^{28}P from ^{28}Si(p,nγ) at 23 MeV, γ-decay scheme and new levels detection 2—14986
^{29}P, radiative decay of 8.38 MeV level 2—34929
^{30}P, energy levels, from ^{29}Si(p,γ) reaction 2—31460
^{30}P, lifetime meas. for levels between 3.7 and 4.7 MeV excitation energy 2—21385
^{31}P, energy level investigation via alpha capture in ^{27}Al 2—2703
^{31}P, in aqueous H_3PO_4, effects of diamagnetic ions on relaxation 2—1121
^{31}P, in KH_2PO_4, chem. shift at 77K, rel. to H_3PO_4 2—13427
^{31}P, isobaric analog states, calc. in multishell configuration space 2—34912
^{31}P, n.m.r. obs. of antiferromagnetic transitions in $GdPO_4$, $TbPO_4$, $DyPO_4$ 2—6992
^{31}P, n.m.r. relaxation times meas. in PCl_3-PBr_3 and PCl_3-$PBrCl_2$-PBr_2Cl-PBr_3 liq. mixtures 2—9178
^{31}P, n.m.r. study of P=Se bond using ^{31}P-^{77}Se coupling 2—5903
^{31}P chemical shifts of cyclopentadienylnickel complexes 2—810
^{31}P n.m.r. in InP 2—33355
^{31}P(^{3}He,p)^{33}S, 6 to 14 MeV, angular distributions of four proton groups 2—8362
^{31}P(p,γ)^{32}S, 0.35-2.03 MeV, determ. proton energies and strengths of resonances, gamma decay, Q-value 2—38596
^{31}P(p,γ)^{32}S, resonance strengths 2—38597
^{32}P, β spectrum shape of mass separated source, precision measurement 2—2745
^{32}P, electromagnetic decays of lowest T = 2 state 2—8293
^{32}P, obs of γ-rays from 78.1 keV level following kaon capture in ^{32}S and ^{35,37}Cl 2—28059
^{32}P, spin of levels determ. by angular-correlation studies of ^{29}Si(α,p) reaction 2—8292
^{35}P, new nuclide prod. in ^{37}Cl(γ,2p) reaction half life and γ-ray energy meas. 2—5651
S, high energy elastic electron scattering, analysed with phenomenological charge distribution and Woods-Saxon potential 2—8327

Nuclei with $20\leqslant A\leqslant 49$ continued
- S (A=39, 40), production in bombardment of ^{232}Th with 290 MeV ^{40}Ar 2—5715
- ^{28}S, high energy elastic electron scattering, analysed with phenomenological charge distribution and Woods-Saxon potential 2—8327
- ^{31}S, 1p neutron strength, study of levels above E_x=4.5 MeV from ^{32}S(^{3}He, ^{4}He)^{31}S reaction 2—14942
- ^{32}S, calculation of triaxial shapes 2—31424
- ^{32}S, collective states obs. by inelastic scatt. of polarized protons 2—31461
- ^{32}S, energies, branching ratios, lifetimes, γ-ray transition strengths of levels populated in ^{31}P(p,γ) reaction 2—38596
- ^{32}S, energy gaps and momentum transfer 2—38486
- ^{32}S, ground state, triaxial shape study 2—11698
- ^{32}S, Hartree-Fock model predictions of static and dynamic properties 2—11734
- ^{32}S, inelastic electron scatt. through 180°, giant resonance structure 2—24205
- ^{32}S, kaon capture obs. of γ-rays emitted from levels in ^{32}P and ^{19}F 2—28059
- ^{32}S, magnetic transition strength studied by 180° electron scattering 2—11737
- ^{32}S, muon capture, asymmetry of emitted neutrons 2—38582
- ^{32}S, particle-hole excitation and surface excitation coupling 2—2668
- ^{32}S, polarization of emitted neutrons in muon capture 2—38584
- ^{32}S, static quadrupole moment of first excited state, width of $0^2\to 2^+$ transition obs. 2—2718
- ^{32}S energy levels, investigation using ^{28}Si(α,γ)^{32}S reaction 2—5649
- ^{32}S structure calc. using Strutinsky's theory of renormalization, comparison with HF results 2—24129
- ^{32}S(^{16}O,2nγ)^{46}G, product study, including proton rich nuclei, 22-33 MeV 2 -21450
- ^{32}S(^{3}He, ^{4}He)^{31}S, search for 1p neutron strength in ^{31}S, study of levels above E_x=4.5 MeV 2—14942
- ^{32}S(^{3}He,d) ^{33}Cl, 29.7 and 34.5 MeV, determ. single particle strengths for quasibound levels in ^{33}Cl 2—24153
- ^{32}S(α,p), 28.8 MeV, study of J dependence for L=2 transfer 2—11863
- ^{32}S(d,^{3}He)^{31}P, ^{32}S(d,t)^{31}S, charge-asymmetry meas., numerical estimate of isospin impurity in ^{32}S ground state 2—35073
- ^{32}S(d,n)^{33}Cl, 4.7 to 5.5 MeV, energy levels of ^{33}Cl 2—34930
- ^{32}S(d,p)^{33}S, E_d=18.00 MeV, proton ang. distrib. 2—2779
- ^{32}S(e,e′), form factors using shell-model wave functions 2—35012
- ^{32}S(γ-np) 19-30 MeV, cross section determ. by counting residual γ-ray activity, comparison with calc. based on quasi-deuteron theory 2—485
- ^{32}S(γ,n)^{31}S*, 16.3-27.3 MeV, cross sections 2—38571
- ^{32}S(γ,p)^{31}P*, 16.3-27.3 MeV, cross sections 2—38571
- ^{32}S(p,d)^{31}S, polarised protons at 24.5 MeV, asymmetry and differential cross sections 2—24221
- ^{32}S(p,γ)^{33}Cl, 3.36-5.41 MeV, studies on analogue states in ^{33}Cl by isospin forbidden resonances 2—34931
- ^{32}S(p,γ)^{33}Cl, isospin forbidden resonances rel. to analog states in ^{33}Cl 2—34932
- ^{32}S(p,n)^{32}Cl, half life determ. for ^{32}Cl 2—2744
- ^{33}S, detailed energy level schemes determ. from shell model calculations 2—28000
- ^{33}S, energy levels, from ^{32}S(d,p) study 2—2779
- ^{33}S, multipole mixing ratios of transitions between low-lying levels 2—18234
- ^{33}S(p,γ)^{34}Cl, 1058, 1098, 1121 keV, poperties of levels in ^{34}Cl studied 2—11733
- ^{34}S, collective states obs. by inelastic scatt. of polarized protons 2—31461
- ^{34}S, excitation energies of excited states, γ-ray energy meas. 2—11724
- ^{34}S(d,pγ)^{35}S, ang. correlations and decay of excited states 2—18100
- ^{34}S(d,pγ)^{35}S, lifetime of 1.99-MeV level of ^{35}S 2—2704
- ^{34}S(p,d)^{33}S, polarised protons at 24.5 MeV, asymmetry and differential cross sections 2—24221
- ^{34}S(p,γ)^{35}Cl, γ ray transitions of ^{35}Cl 2—2704
- ^{35}S, angular correlation meas. spin assignments and multipole mixing from ^{34}S(d,pγ)^{35}S, ^{37}Cl(d,$\alpha\gamma$)^{35}S 2—18100
- ^{35}S, lifetime of 1.99-MeV level from reaction ^{34}S(d,pγ)^{35}S 2—2704
- ^{36}S, γ transitions, mean lives and spin-parity assignments 2—34933
- ^{42}Sc, lifetimes of levels populated in ^{40}Ca(^{3}He,p) reaction at 8.4 and 8.6 MeV 2—8296
- ^{42}Sc(7$^+$)$\to$^{42}Ca(6$^+$) β decay ft values, discrepancy between theory and expt. not accounted for by two-hole admixtures 2—11740
- ^{43}Sc, determ. lifetimes and absolute transition strengths of $K^\pi=1/2^+$ rotational band 2—11741
- ^{43}Sc, g factor of $^{19}/_2{}^-$ isomeric state 2—24156
- ^{43}Sc 19/2$^-$ (3.12 MeV) state magnetic moment, comparison of theory and exptl. values 2—11740
- ^{43}Sc lifetimes measured by Doppler shift attenuation methods, determ. transition strengths 2—18103
- ^{44}Sc, 68 keV state, lifetime and magnetic moment meas. 2—34936
- ^{44}Sc, spherical states, shell model calculations 2—466
- ^{45}Sc, differential cross sections of excited states in ^{45}Sc(p,p′) reaction 2—18184
- ^{45}Sc, spins and parities of states investigated using ^{46}Ti(d,τ)^{45}Sc reaction 2—31465
- ^{45}Sc, total photoneutron cross section, threshold to 26 MeV, giant dipole states 2—38572
- ^{45}Sc spin-lattice relax. in Sc-rare earth dil. alloys 2—19934
- ^{45}Sc(γ,n)^{44m,g}Sc, isomeric cross section ratios 2—24202
- ^{45}Sc(n,2n)^{44m,g}Sc, isomeric cross section ratios 2—24202
- ^{45}Sc(p,p′), 49.75 MeV, differential cross sections of excited states 2—18184
- ^{48}Sc, excited states, investigation using ^{48}Ca(p,nγ)^{48}Sc reaction 2—2705
- ^{48}Sc, nuclear spectroscopy from ^{46}Ca(^{3}He,p) reaction 2—34938
- ^{48}Sc, strongly excited 1$^+$ states, obs. in ^{46}Ca(^{3}He,p)^{48}Sc and ^{48}Ca(^{3}He,p)^{50}Sc reactions 2—34937
- ^{48}Sc, study of levels using ^{48}Ca(^{3}He,t)^{48}Sc reaction at 23 MeV 2—31467
- ^{48}Sc, study of levels using ^{46}Ca(α,d)^{48}Sc reaction 2—31466
- ^{48}Sc$\to$^{48}Ti activity characts., transitions of ^{48}Ti 2—38536
- Si, low energy elastic scatt., tensor polarization and differential cross sections 2—18220
- Si (A=33, 34, 35, 36), production in bombardment of ^{232}Th with 290 MeV ^{40}Ar 2—5715
- ^{25}Si, excited state obs. using reaction ^{28}Si(^{3}He, ^{6}He)^{25}Si at 70.4 MeV 2—34923
- ^{27}Si, angular correlations and branching ratios of levels below 5 MeV excitation, spin assignments 2—24152
- ^{27}Si, β^+ decay to ground and excite states of ^{27}Al, position branching ratios and log ft values obtained 2—18157
- ^{27}Si, lifetimes of lower excited states using ^{28}Si(^{3}He,α)^{27}Si reaction 2—18098
- ^{27}Si from ^{27}Al(p,nγ) at 16 MeV, γ-spectrum 2—14986
- ^{28}Si, cross sections for inelastic interaction of neutrons, $E_n\lesssim 20$ MeV 2—28048
- ^{28}Si, deformations of ground-bands, rotational model analysis 2—31454
- ^{28}Si, elastic scatt. of 30 MeV ^{6}Li ions 2—18239
- ^{28}Si, energy gaps and momentum transfer 2—38486
- ^{28}Si, energy level investigation using ^{29}Si(p,d)^{28}Si and ^{30}Si(p,t)^{28}Si reaction 2—2700
- ^{28}Si, energy levels, study from reaction ^{29}Si(^{3}He,α)^{28}Si at 12 MeV 2—34925
- ^{28}Si, energy levels and E2 transitions, Hartree-Fock and random phase approximations 2—38483
- ^{28}Si, investigation using low energy ^{27}Al(p,α)^{24}Mg reaction 2—31459
- ^{28}Si, muon capture, asymmetry of emitted neutrons 2—38582
- ^{28}Si, nuclear deformations from electron scatt. obs. 2—11783
- ^{28}Si, polarization of emitted neutrons in muon capture 2—38584
- ^{28}Si, shell model calculations of excitation spectrum 2—21384
- ^{28}Si energy levels, investigation using ^{27}Al(p,γ)^{28}Si reaction 2—34928
- ^{28}Si Hartree-Fock model predictions of static and dynamic properties 2—11734
- ^{28}Si resonance and the ^{27}Al(p,n) reaction mechanism at intermediate energies 2—38595
- ^{28}Si resonance levels from ^{27}Al+p reactions, resonance strengths, partial proton width, spectroscopic factors deduced 2—34915
- ^{28}Si(^{16}O,2nγ)^{42}Ti, product study, including proton rich nuclei 22-33 MeV 2—21450
- ^{28}Si(^{3}He,^{6}He)^{25}Si, 70.4 MeV, obs. of ^{25}Si excited states 2—34923
- ^{28}Si(^{3}He,α)^{27}Si, lifetimes of lower excited states in ^{27}Si 2—18098
- ^{28}Si(^{3}He,$\alpha\gamma$)^{27}Si, angular correlations and branching ratios of levels in ^{27}Si below 5MeV excitation 2—24152
- ^{28}Si(α,γ)^{32}S, investigation of ^{32}S energy levels 2—5649
- ^{28}Si(d,n), neutron polarization meas., comparison with DWBA calc. 2—38614
- ^{28}Si(d,p)^{29}Si, E_d=18.00 MeV, proton ang. distrib. 2—2779
- ^{28}Si(d,pγ)^{29}Si, spectroscopic and reaction mechanism information from ang. correlations at 0° 2—2808
- ^{28}Si(e,e′), form factors using shell- model wave functions 2—35012
- ^{28}Si(n,p)^{28}Al and ^{28}Si(n,α)^{25}Mg cross-sections meas. to 5.6 MeV using Si semiconductor as target and detector 2—28049
- ^{28}Si(p,n)^{28}P, half life determ. for ^{28}P 2—2744
- ^{28}Si(p,nγ)^{28}P, 23 MeV, γ-spectrum 2—14986
- ^{29}Si, energy levels, from ^{28}Si(d,p) study 2—2779
- ^{29}Si, levels with excitation energy below 6.4 MeV 2—2701
- ^{29}Si, principal decay modes and lifetimes of levels below 7.2 MeV populated by ^{26}Mg(α,n)^{29}Si reaction 2—27971
- ^{29}Si, spin-lattice relax. in trichlorosilane 2—29845
- ^{29}Si(^{3}He,α)^{28}Si, 12 MeV, energy levels of ^{28}Si 2—34925
- ^{29}Si(α,p)^{32}P, spins of ^{32}P levels determ. by angular-correlation studies 2—8292
- ^{29}Si(n,α)^{26}Mg cross-sections meas. to 5.6 MeV using Si semiconductor as target and detector 2—28049
- ^{29}Si(p,d)^{28}Si, investigation of energy levels in ^{28}Si 2—2700
- ^{29}Si(p,γ)^{30}P, E_p=2-3MeV, ^{30}P levels 2—31460
- ^{30}Si, calculation of triaxial shapes 2—31424
- ^{30}Si γ decay studied by ^{27}Al(α,pγ) reaction, meas of branching ratios and lifetimes 2—34986
- ^{30}Si(^{3}He, pγ)^{32}p, γ-decays of lowest T=2 state of ^{32}p 2—8293
- ^{30}Si(α,nγ), γ-ray angular distribution, ^{33}S deduced levels 2—18234
- ^{30}Si(p,t)^{28}Si, investigation of energy levels in ^{28}Si 2—2700
- ^{31}Si, detailed energy level schemes determ. from shell model calculations 2—28000
- ^{32}Si, β decay, search for γ emission 20-200 kEV 2—38534
- ^{33}Si 6.3 sec, new isotope produced via ^{18}O(^{18}O,2pn) reaction, 23-40 MeV 2—38535
- ^{41}Si, doorway state structure from ^{40}Ca(p,p′γ)^{40}Ca reaction 2—38598
- Si(p,p), energetic dependence of elastic scattering cross sections on thick targets 2—28033
- ^{48}T,(p,γ)^{49}V, study of excited states of ^{49}V 2—27975
- Ti, isotope targets 29 MeV elastic scattering, determ. optical model parameters 2—18221
- ^{44}Ti, level structure study from ^{46}Ti(p,t) reaction at 51 MeV 2—24157
- ^{46}Ti, elastic scatt. of 37.7 MeV ^{3}He, global optical model analysis 2—38633
- ^{46}Ti, inelastic scattering by ^{3}He to positive parity states at 29 MeV, anaysis within microscopic model 2—15013
- ^{46}Ti(α+nγ)Cr, 6-10 MeV, Doppler-shift attenuation method used in nγ coincidence meas. deduced levels of ^{49}Cr 2—18105
- ^{46}Ti(d,τ)^{45}Sc, spins and parities of states in ^{45}Sc and evidence for single proton configurations in the ground state of ^{46}Ti 2—31465
- ^{46}Ti(p,t)^{44}Ti, 51 MeV, ang. distribs., level structure of ^{44}Ti 2—24157
- ^{47}Ti(t,p), 12 MeV, cross section meas., ^{49}Ti deduced levels 2—31468
- ^{48}Ti, inelastic scattering by ^{3}He to positive parity states at 29 MeV, analysis within microscopic model 2—15013
- ^{48}Ti transitions, ^{48}Sc decay obs. 2—38536
- ^{48}Ti(^{3}He,t′)^{48}V*, quasi-inelastic scatt., effect of 2 step processes coupling potentials 2—31532
- ^{48}Ti(d,p), 10 MeV, cross section meas., ^{49}Ti deduced levels 2—31468
- ^{48}Ti(n,γ)^{49}Ti, thermal, 2 keV and 25 keV neutrons, γ-spectra 2—14991
- ^{48}Ti(n,γ)^{49}Ti, transitiions in ^{49}Ti 2—31557
- ^{49}Ti, transitions studied by ^{48}Ti(n,γ)^{49}Ti reaction 2—31557
- ^{49}Ti level structure studied up to excitation energy of 6.3 MeV using ^{47}Ti(t,p), ^{48}Ti(d,p), ^{49}Ti(p,p′) reactions 2—31468
- ^{49}Ti(p,p′), 12 MeV, cross section meas., ^{49}Ti deduced levels 2—31468
- ^{44}V, highly neutron deficient isotope with half-life 90±25 ns produced in ^{40}Ca(^{6}Li,2n) reaction at 18.5 MeV 2—11795
- ^{46}V, excited states, study using (p,nγ) reaction 2—11742
- ^{48}V, L/K-capture ratio 2—34987
- ^{49}V, from ^{49}Cr beta decay, lifetime of 90.65 keV state 2—2707
- ^{49}V, L/K capture ratio 2—31499
- ^{49}V, study of excited states with ^{48}T,(p,γ)^{49}V reaction 2—27975

Nuclei with $50\leqslant A\leqslant 89$
- $59\leqslant Z\leqslant 69$, precise atomic mass differences 2—24306
- ^{55}Mn^{2+}, ENDOR IN K_2MgF_4, K_2ZnF_4, $ZnSiF_6$ crysts. with axial symmetry 2—30028
- ^{87}Rb maser, calc. on power output taking account of variations in optical pumping rate and density matrix elements 2—2377

Nuclei with $50\leqslant A\leqslant 89$ continued
— 2—21388
A~50, (^{3}He,n) reaction up to the continuum 2—31582
rare-earth nuclei, (d,t) reaction, angular distributions, two step model 2—38643
(n,2n) reactions in medium-, heavy-meass region, 14-15 MeV, determ. activation cross sections, isomeric cross section ratios, systematics 2—35047
(n,nγ) reaction cross sections, use of statistical models for A=46-88 mass range 2—31556
^{89}(α,^{3}He), 65.7 MeV, cross sections, shell model structure of ^{90}Y, l=5 transitions data 2—34950
As perturbed ang. correl. in Ni 2—36805
^{68}As, separated from ^{68}Se produced in ^{59}Ni(^{12}C,2n) reaction, meas. of half-life and γ ray spectra 2—38538
^{73}As, isobaric analogue states, study by reaction ^{72}Ge(p,p'e) at 3.3 to 4.7 MeV 2—34946
^{75}As, circular polarization of 401 keV γ ray determ. 2—11776
^{75}As, conversion electron spectrum, relative intensities of transitions 2—38542
^{75}As, decay, after effects, relaxation and recombination time constants 2—38541
^{75}As, half-lives of some excited states meas. using delayed coincidence technique 2—24165
^{75}As, half lives of short lived excited states 2—34948
^{75}As ENDOR in $NH_4H_2AsO_4$, KD_2AsO_4 and KH_2AsO_4 2—19376
^{75}As n.q.r. in $NH_4H_2AsO_4$ 2—10589
^{75}As perturbed ang. correl. in Ni and Co 2—36806
^{75}As quadrupole coupling const. in KD_2AsO_4 and CsD_2AsO_4 2—10554
^{75}As(n,n'γ), inelastic scattering at 0.8-2.2 MeV, energy levels and transitions determined 2—11750
^{75}As(p,nγ)^{75}Se, investigation of spins of low lying ^{75}Se levels 2—34947
^{76}As, $2\to2^+$ beta transition at 1200 keV 2—21414
^{76}As decay, γ-ray energies and relative intensities 2—38543
^{76}As decay scheme 2—18159
^{76}As$\to$^{76}Se, γ-γ coincidence obs., energy level scheme 2—31514
Au isotopes, theoretical decay rates analysed on shell model basis 2—11786
Br (A=79, 81), magnetic moment determination from n.m.r. investigations in aqueous solutions 2—22007
^{75}Br$\to$^{75}Se decay, obs. of γ-rays and conversion electrons rel. to ^{75}Se level scheme determination 2—24164
^{76}Br, decay scheme, incorporation of new positron emission and gamma transition data 2—11796
^{78}Br, γ-angular correlation of 120 μs state, time differential obs. of n.m.r. 2—5671
^{79}Br low-lying levels, intermediate coupling and core excitation models 2—38502
^{79}Br quadripolar linewidth in $KBrO_3$ and $NaBrO_3$ 2—7803
^{79}Br(p,n)^{79}Kr, conversion electron spectra, low lying states and transitions obs. 2—38501
^{81}Br, conversion coeffs. for 178, 260, 276 and 290 keV γ transitions 2—2746
^{81}Br n.q.r. in dibromo- and tribromoanisole, Zeeman effect 2—8745
^{81}Br quadripolar linewidth in $KBrO_3$ and $NaBrO_3$ 2—7803
^{81}Br(p,n)^{81}Kr, conversion electron spectra , low lying states and transitions obs. 2—38501
^{84}Br, decay to levels in ^{84}Kr, studied using gamma ray spectra 2—31502
^{85}Br, 3 minute decay, γ- rays assigned 2—5674
^{85}Br excited states, spins and parities assignment from ^{86}Kr(d, ^{3}He)^{85}Br 2—11865
^{87}Br, β decay, γ ray emission in competition with neutron emission 2—18160
^{87}Br and ^{88}Br as precursors for delayed neutrons, low energy spectrum 2—5728
^{79m}Br, half-life measurement 2—27980
Co, odd isotopes studied in unified vibrational model 2—8300
Co, total reaction cross section for 13.6 MeV deuterons 2—28068
^{54}Co, excited states, study using (p,nγ) reaction 2—11742
^{55}Co, e.m. transitions studied via ^{54}Fe(^{3}He,dγ)^{55}Co reaction 2—27976
^{55}Co, isobaric analogue states obs. in ^{54}Fe(p,γ) reaction at ~3 MeV 2—21387
^{55}Co energy levels, ^{54}Fe(p,γ) reaction study 2—38599
^{56}Co, energy levels, from ^{54}Fe(^{3}He,p)^{56}Co and ^{58}Ni(d,α)^{56}Co studies 2—2709
^{56}Co levels up to 2.6 MeV excitation studied by ^{56}Fe (p, nγ) coincidence expts. 2—24223
^{57}Co, energy level interpretation using particle-core coupling model 2—38491
^{57}Co, level half-life measurements 2—8297
^{57}Co, magnetic moment of oriented nucleus by n.m.r. 2—38506
^{57}Co, Mossbauer effect, second order Doppler shift elimination 2—36831
^{57}Co Mossbauer effect in Al and Si 2—19402
^{57}Co n.m.r. in Fe, radiative detection using Mossbauer effect 2—26301
^{58}Co, energy levels, high-resolution study by (d,α) and (^{3}He,d) reactions 2—34943
^{58}Co, magnetic moment of 10 μsec level 2—5654
^{59}Co, excited levels populated in proton and alpha induced reactions 2—24162
^{59}Co, half-life meas. of 1291.6 keV level 2—34944
^{59}Co, meas. of spin-spin effect in neutron total cross section from 0.3 to 8.0 MeV 2—18210
^{59}Co, n.m.r. in $CoCl_2.2H_2O$, approx. Ising system 2—33352
^{59}Co, n.m.r. in Gd_2Co_7, 77K 2—4555
^{59}Co, neutron angular distribs., (p,n) reaction cross sections 2—14985
^{59}Co, neutron elastic scatt., local optical nuclear model 2—5698
^{59}Co, T_1, self-diffusion and chemical shifts in solns. of symmetric Co (III) complexes 2—1119
^{59}Co broad-line n.m.r. in single crystal $CoMn(CO)_9$ 2—22842
^{59}Co cascades, γ-γ directional correl. obs. 2—34988
^{59}Co ENDOR in $KMnF_3$, hyperfine interactions 2—20144
^{59}Co n.m.r. in Co, impurity effects 2—13549
^{59}Co n.m.r. in V-Co alloys 2—10566
^{59}Co relax. times in dil. Ni alloys 2—40579
^{59}Co spin-lattice relax in dil. Fe-Co alloys 2—33180
^{59}Co transitions, internal conversion meas. 2—38537
^{59}Co(^{20}Ne,2n)^{77}Rb, production of new neutron deficient isotope ^{77}Rb, half-life and γ ray spectra meas. 2—34989
^{59}Co(^{3}He,α)^{58}Co, high-resolution study of ^{58}Co energy levels 2—34943

Nuclei with $50\leqslant A\leqslant 89$ continued
^{59}Co(α,α')^{59}Co, population of highly excited levels in ^{59}Co, energy spectra study 2—24162
^{59}Co(α,t)^{60}Ni, ang. distribution meas., DWBA analysis 2—2810
^{59}Co(n,γ)^{60}Co, polarized thermal neutrons, γ-ray circular polarization 2—18211
^{59}Co(p,p')^{59}Co, population of highly excited levels in ^{59}Co, energy spectra study 2—24162
^{59}Co(p,p)^{59}Co 5.8-6.5 MeV, p polarization and ang. distrib. obs. 2—8334
^{60}Co, investigation by the two-particle transfer reactions ^{62}Ni(d,α) and ^{58}Fe(^{3}He,p) 2—31474
^{60}Co, γ decay investigation using $\gamma\gamma$ ang. correlation meas. 2—2711
^{60}Co, spin assignments from ^{59}Co(n,γ) reaction 2—18211
^{60}Co disc isotropic sources, air-ground interface problem 2—28160
^{60}Co n.m.r. in Fe, single and multiple passage studies 2—1734
^{62}Co, investigation by two-particle transfer reaction ^{64}Ni(d, α) 2—31476
^{63}Co, decay scheme and period from γ-ray measurements 2—31501
^{60m}Co, K-conversion coefficients of gamma ray transitions 2—8223
Cr, isotope targets, 29 MeV elastic scattering, determ. optical model parameters 2—18221
Cr isotopes, elastic proton scattering, 2.8-6.3 MeV 2—489
Cr(A=50,52,54), elastic and inelastic scatt. at incident energies of 6 MeV 2—11823
^{50}Cr, (^{3}He,t) transitions isobaric analog ground states, energy dependence 2—31583
^{50}Cr, inelastic scattering by ^{3}He to positive parity states at 29 MeV, analysis within microscopic model 2—15013
^{50}Cr, study of excited states by means of decay of ^{50}Mn, ^{50}Cr(p,p'γ) and ^{52}Cr(p,t) reactions and Coulomb excitation with ^{35}Cl ions 2—34939
^{50}Cr(^{35}Cl, ^{35}Clγ), study of excited states of ^{50}Cr 2—34939
^{50}Cr(^{3}He,t), 21.4 to 37.5 MeV, energy dependence of transitions to isobaric analogue ground states 2—31583
^{50}Cr(^{3}He,t)^{50}Mn, ^{50}Mn levels obs. 2—11744
^{50}Cr(^{3}He,t)^{50}Mn, 21.4-37.5 MeV, differential cross sect., deduced level scheme ^{50}Mn, energy dependent effects 2—11743
^{50}Cr(α,nγ)^{53}Fe, 5.6 to 10.0 MeV, study of low lying states in ^{53}Fe 2—11748
^{50}Cr(α,pγ)^{53}Mn, mean lives of low lying levels of ^{53}Mn measured by Doppler shift attenuation with p-γ coincidences 2—18106
^{50}Cr(p,p'γ), study of excited states of ^{50}Cr 2—34939
^{50}Cr(p,p')^{50}Cr, using 12 MeV protons, ang. distrib. of absolute spin flip probability 2—18185
^{50}Cr(p,t)^{48}Cr, 51 MeV, energy level study of ^{48}Cr, spin and parity assignments 2—2706
^{50}Cr(p,t)^{48}Cr, study of populated energy levels 2—467
^{52}Cr, inelastic scattering by ^{3}He to positive parity states at 29 MeV, analysis within microscopic model 2—15013
^{52}Cr, lifetimes of levels to 4.5 MeV in excitation energy determ. by Doppler shift attenuation method 2—11746
^{52}Cr$^+$, ENDOR obs. in NaCl, superhyperfine struct. obs. 2—30029
^{52}Cr(^{3}He,p), 15 and 16.5 MeV, ^{54}Mn level scheme study 2—21448
^{52}Cr(p,p')^{52}G*, using 12 MeV protons, ang. distrib. of absolute flip probability 2—18185
^{52}Cr(p,p)^{52}Cr 5.8-6.5 MeV, p polarization and ang. distrib. obs. 2—8334
^{52}Cr(p,p) elastic scattering, 2.4-4.1 MeV, obs. of IAR to excited 2.321 MeV level in ^{53}Cr 2—18186
^{52}Cr(p,t), study of excited states of ^{50}Cr and spin and parity assignments 2—34939
^{53}Cr, 2.321 MeV excited level, obs. of IAR in ^{52}Cr(p,p) scattering 2—18186
^{53}Cr, e.m. properties studied with ^{50}Ti(α,nγ)^{53}Cr reaction 2—34940
^{53}Cr, n.m.r. in ferromag. CrO_2 2—13551
^{53}Cr, neutron angular distribs., (p,n) reaction cross sections 2—14985
^{53}Cr^{3+}, ENDOR, in YAG and LuAl garnet 2—10582
^{53}Cr(p,n)^{53}Mn, 2.6 to 5.9 MeV, differential cross sections meas. determ. levels and transition rates in ^{53}Mn 2—11747
^{53}Cr(p,nγ)^{53}Mn, 4.9 MeV, differential cross sections meas. determ. levels and transition rates in ^{53}Mn 2—11747
^{53}Cr(p,p)^{53}Cr 5.8-6.5 MeV, p polarization and ang. distrib. obs. 2—8334
^{54}Cr(^{3}He,p)^{56}Mn, 15 MeV, meas. of proton angular distributions, ^{56}Mn deduced levels 2—505
^{54}Cr(p,n) 1.8-2.9 MeV, isobaric analog states obs. in ^{55}Mn 2—2708
^{54}Cr(p,n)^{54}Mn, 2.6 to 3.1 MeV, energy levels of ^{54}Mn 2—38531
Cr(p,p)Cr A=50, 52, 54, 1.8-3.3 MeV, isobaric analogue states obs. in ^{51}Mn, ^{53}Mn, ^{55}Mn 2—2708
Cu, A=59, 61, 63, M1 transition from $g_{9/2}$ analogue to anti-analogue state 2—5655
Cu, A=63, 65, meas. of differential cross section for elastic scattering of 33 MeV ^{3}He particles, optical model analysis 2—28067
Cu, π photoproduction, 1160 MeV γ-quanta 2—14974
Cu isotopes from ^{238}U fission, spectra 2—11885
Cu neutron total cross section between 23 and 45 MeV using time-of-flight technique with transmission method 2—38609
^{58}Cu, excited states, study using (p,nγ) reaction 2—11742
^{58}Cu, γ-ray energies and relative intensities 2—18158
^{59}Cu, M1 transitions from $g_{9/2}$ analog-to-antianalog states 2—18109
^{61}Cu, Mi transitions from $g_{9/2}$ analog-to-antianalog states 2—18109
^{62}Cu, magnetic hyperfine interaction meas. on first excited state 2—5657
^{62}Cu levels deduced from ^{64}Zn(d,α) reaction with DWBA formalism 2—31475
^{63}Cu, electron scattering description using particle-core and particle-phonon coupling models 2—38578
^{63}Cu, M1 transitions from $g_{9/2}$ analog-to-antianalog states 2—18109
^{63}Cu n.m.r. in Cu-Fe dil. alloys 2—36657
^{63}Cu n.m.r. in dil. Cu-Ge alloys 2—10539
^{63}Cu n.m.r. in metallic Cu 2—1733
^{63}Cu spin-lattice relax. in dil. Cu-Mn alloys 2—16404
^{63}Cu(^{16}O,2n)^{77}Rb, production of new neutron deficient isotope ^{77}Rb, half-life and γ ray spectra meas. 2—34989
^{63}Cu(^{3}He,d)^{64}Zn, anal. of spectroscopic factors using intermediate coupling approach of unified model 2—2811
^{63}Cu(γ,n)^{62}Cu, threshold to 33 MeV, cross sections, obs. of induced activity 2—21424
^{63}Cu(p,p'), E_p=15.7 MeV, analysing power and spin dependence 2—28029
^{63}Cu(p,p') influence on isospin decay of composite ^{64}Zn system formed, Bohr independence hypothesis 2—24181
^{64}Cu, differential ranges of recoils meas. for ^{65}Cu(^{3}He,α) reaction at 32 MeV by electrostatic collection technique 2—35077
^{64}Cu, population and decay of levels up to 2300 keV, produced by thermal neutron capture in natural copper 2—14939

Nuclei with $50\leqslant A\leqslant 89$ continued
^{64}Cu, spins of low-lying states obs., $\gamma-\gamma$ directional correlation meas. 2—38496
^{65}Cu, n.m.r. in metallic Cu 2—1733
^{65}Cu, spallation, Monte Carlo simulation of nuclear cascade-evaporation 2—28037
^{65}Cu total reaction cross section for 13.6 MeV deuterons 2—28068
^{65}Cu(^{3}He,^{4}He), 32 MeV, differential ranges of ^{64}Cu recoils meas. by electrostatic collection technique 2—35077
^{65}Cu(^{3}He,d)^{66}Zn, anal. of spectroscopic factors using intermediate coupling approach of unified model 2—2811
^{65}Cu(α,αn), differential ranges of recoil product meas. over energy interval 24-42 MeV 2—35076
^{65}Cu(p,n)^{65}Zn, isobaric analogue resonance in ^{66}Zn 2—8339
^{65}Cu(p,nγ)^{65}Zn, isobaric analogue resonance in ^{66}Zn 2—8339
^{65}Cu(p,p′) influence of isospin on decay of composite ^{66}Zn system formed, Bohr independence hypothesis 2—24181
^{65}Cu(p.p′), E_p=15.7 MeV, analysing power and spin dependence 2—28029
^{66}Cu, spin and parity of 0.462 MeV level 2—8339
^{67}Cu, cumulative yield in natural U fission 2—35097
^{68}Cu isomer decay, meas. β- and γ-ray intensities γ-γ, β-γ coincidences, level structure of ^{68}Zn 2—38539
^{69}Cu^{2+}, distant ENDOR obs. in $ZnX_2(SO_4)_2.6H_2O$ where X=NH_4, K. Rb, Cs 2—30031
Dy, odd neutron number isotopes, mixing of components with $\Delta N=\pm 2$ 2—8301
Fe, 200 GeV proton interactions in accelerator cave, nucleon and charged pion albedo spectra 2—24222
Fe, keV resonance neutron capture 2—18194
Fe, natural, measurements of neutron cross-section minima 2—31558
Fe, neutron effective cross section in Doppler reson. region of large fast reactor 2—38726
Fe, proton interactions, 10 to 28 GeV, inelasticities and inelastic cross section 2—31541
Fe, proton scattering, angular distributions for particles in 2 to 30 keV range 2—11824
Fe, ratio of photodisintegration to electrodisintegration for 5.0 GeV electron bombardment 2—11822
Fe, total reaction cross section for 13.6 MeV deuterons 2—28068
Fe collective states excitation by 14 MeV neutrons 2—14990
^{53}Fe low lying states studied via ^{50}Cr(α,nγ) reaction 2—11748
^{54}Fe, (^{3}He,t) transitions isobaric analog ground states, energy dependence 2 -31583
^{54}Fe, mean lifetime and magnetic moment of 2.95 MeV (6^+) state 2—8298
^{54}Fe, substate excitation of 2^+ state by (p,p′γ) inelastic scatt. 2—34941
^{54}Fe elastic and inelastic scatt. of 30.4 MeV polarized protons 2—14983
^{54}Fe(^{18}O, ^{14}C)^{58}Ni, pick up reaction at 48 MeV, ang. distrib. to final states, cross sections 2—28086
^{54}Fe(^{3}He,n)^{56}Ni, 14 MeV, meas. angular distributions, deduced ^{56}Ni energy levels 2—27977
^{54}Fe(^{3}He,p)^{56}Co, levels of ^{56}Co 2—2709
^{54}Fe(^{3}He,t), 21.4 to 37.5 MeV, energy dependence of transitions to isobaric analogue ground states 2—31583
^{54}Fe(^{3}he, dγ)^{55}Co, e.m. transitions in ^{55}Co 2—27976
^{54}Fe(α,n)^{57}Ni, study of props. of levels at 2.443 and 3.003 MeV in ^{57}Ni 2—11749
^{54}Fe(p,γ), 1.7-3.0 MeV, ^{55}Co levels 2—38599
^{54}Fe(p,γ)^{55}Co, isobaric analogue states in ^{55}Co 2—21387
^{54}Fe(p,p′γ)^{54}Fe*, E_p=19.6 MeV, substate excitation of 2^+ state, transition from O^+ state 2—34941
^{55}Fe, excited state mean life, from γ-ray Doppler shifts 2—2693
^{56}Fe, cross sections for inelastic interaction of neutrons, $E_n\lesssim 20$ MeV 2—28048
^{56}Fe, determination of complete temp. dependence of hyperfine fields at five Fe sites in $SrFe_{12}O_{19}$ 2—22733
^{56}Fe, photonuclear reaction yields at 1.5 GeV 2—2763
^{56}Fe, reorientation effect and static quadrupole moment 2—2710
^{56}Fe, semi-microscopic model of two-proton hole cluster coupled to quadrupole vibrational field in ^{58}Ni 2—34942
^{56}Fe, static quadrupole moment, from reorientation meas. following Coulomb excitation by ^{4}He and ^{16}O 2—31472
^{56}Fe, total cross sections for (n,γ), (n,n′), (n,p) (n,2n) and (n,np), statistical model calcs. 2—494
^{56}Fe (^{3}He,t) charge exchange reaction to O^+ and 2^+ analogue states, channel coupling effects 2—28035
^{56}Fe (p,nγ) ^{56}Co, coincidence expts. in 7.7-10 MeV range, meas. γ-ray spectra, deduced levels in ^{56}Co 2—24223
^{56}Fe(^{3}He.p)^{58}Co, energy level scheme for ^{58}Co 2—21388
^{56}Fe(α,p)^{59}Co, population of highly excited levels in ^{59}Co, energy spectra study 2—24162
^{56}Fe(d,p)^{57}Fe*, polarization transfer to residual nucleus, Mossbauer measurements 2—18236
^{56}Fe(n,p), threshold detector for fast neutron spectrum investigations, meas. of activation integral 2—34822
^{56}Fe(p,n′)^{56}Co*, quasi inelastic scatt., effect of 2 step processes, coupling potentials 2—31532
^{56}Fe(p,n) charge exchange reaction to o^+ and 2^+ analogue states, channel coupling effects 2—28035
^{57}Fe, amplitude modulation of 14.4 keV gamma rays 2—24161
^{57}Fe, diffr. of reson. γ-rays due to to quadrupole interaction 2—16439
^{57}Fe, E_2:M1 multipole mixing ratio of excited state transitions 2—31473
^{57}Fe, energy level scheme, Mossbauer spectra in $FeOHSO_4$ 2—10325
^{57}Fe, meas. of perturbed angular correlation for 3/2+ excited state in compounds of Co 2—40595
^{57}Fe, Mossbauer effect, group II-IV-V compound, ABC_2 type 2—1669
^{57}Fe, Mossbauer effect, in $Dy_xR_{1-x}Fe_2$ and $Ho_xR_{1-x}Fe_2$, R=Tb, Er, Tm 2—26123
^{57}Fe, Mossbauer effect, in Fe (II) complex, bis(2,2′-bipyridyl) series, spin free spin paired solids 2—19984
^{57}Fe, Mossbauer effect, in FeSn, hyperfine field temp. depend. at Fe atoms 2—16434
^{57}Fe, Mossbauer effect, isomer shift, Pd-Fe, Pt-Fe, Ni-Fe solid solns. 2—4445
^{57}Fe, Mossbauer effect, proton irradiation damage in $K_4[Fe(CN_6)].3H_2O$ and $K_3[Fe(CN_6)]$ 2—16438
^{57}Fe, Mossbauer effect in Fe_3Pt 2—22737
^{57}Fe, Mossbauer effect in $Fe_{1-x}O$, non-stoichiometry effects 2—26129
^{57}Fe, Mossbauer effect in $Fe_{1-x}Co_x(Ni_x)Si$ 2—26127
^{57}Fe, Mossbauer effect in Fe, energy shift temp. and pressure depend. 2—36325

Nuclei with $50\leqslant A\leqslant 89$ continued
^{57}Fe, Mossbauer effect in polyacrylonitrile 2—22736
^{57}Fe, Mossbauer spectra, relax. due to s-d exchange interactions in Mo-Fe dil. system 2—40631
^{57}Fe, Mossbauer spectra 2—14938
^{57}Fe, Mossbauer spectra of iron (II)- phenanthroline complex 2—16432
^{57}Fe, n.m.r. hyperfine field spectra in magnetite, conduction model 2—7137
^{57}Fe, n.m.r. in $FeBO_3$ 2—36768
^{57}Fe, n.m.r. in $Li_{0.5}Fe_{2.5}O_4$, dipole and anisotropic hyperfine field effects 2—26304
^{57}Fe, n.m.r. in $YF3O_3$ ferromagnet, domain boundary oscills. 2—22681
^{57}Fe, n.m.r. obs. in $TmFeO_3$, 75- 114 K, spin reorientation 2—16663
^{57}Fe, nuclear quadrupole splitting in cummingtonites, Mossbauer spectra 2—10324
^{57}Fe, quadrupole shifts in $DyFe_2$ and $HoFe_2$, Mossbauer obs. 2—10318
^{57}Fe Mossbauer effect in amorphous Fe-Pd-P alloys 2—19877
^{57}Fe Mossbauer effect in au-Fe solid soln. 2—19828
^{57}Fe Mossbauer effect in $BaFe_{12-2x}Zn_xTi_xO_{19}$ 2—33216
^{57}Fe Mossbauer effect in β-Co fine particles 2—1626
^{57}Fe Mossbauer effect in $Cd_{0.98}Fe_{0.02}Cr_2S_4$ 2—26124
^{57}Fe Mossbauer effect in Co-Te system 2—16433
^{57}Fe Mossbauer effect in FeF_2, FeF_3, $FeCl_2$ and $KFeF_3$ 2—10323
^{57}Fe Mossbauer effect in $FeNi_3$ 2—40623
^{57}Fe Mossbauer effect in FeF_2 2—7057
^{57}Fe Mossbauer effect in γ-Mn, CoS_2, $MnFe_2O_4$ and $Fe_3(PO_4)_2.8H_2O$ 2—40617
^{57}Fe Mossbauer effect in $KMgF_3$ 2—29887
^{57}Fe Mossbauer effect in $LiAl_5O_8$ 2—40630
^{57}Fe Mossbauer effect in $PbTiO_3$ 2—36848
^{57}Fe Mossbauer effect in Si 2—1675
^{57}Fe Mossbauer source 2—38492
^{57}Fe Mossbauer spectroscopy, 3d wave functions 2—36835
^{57}Fe Mossbauer spectroscopy, quadrupole splitting due to single 3d electron 2—36834
^{57}Fe n.m.r. in α-Fe_2O_3 2—36770
^{57}Fe n.m.r. in Ferroxplana ferrites 2—10543
^{57}Fe n.m.r. in hexagonal ferrites 2—30024
^{57}Fe n.m.r. in Li-Al ferrites 2—10556
^{57}Fe n.m.r. in ordered $LiFe_5O_8$ 2—37010
^{57}Fe n.m.r. spin echo spectra in $Ga_xFe_{3-x}O_4$ and $GaNiFeO_4$ ferrimagnets 2—10547
^{57}Fe relax. times in Fe metal 2—40579
^{57}Fe spin echoes in YIG 2—10535
^{57}Fe(^{3}He,d)^{58}Co, high-resolution study of ^{58}Co energy levels 2—34943
^{57}Fe(d,^{4}He), new spin $^1/_2{}^-$ state observed in ^{55}Mn, shell model calculations 2—8287
^{57}Fe(γ,n), doorway state effects in M1 radiative excitation of p-wave resonances 2—18108
^{57}Fe(p,^{3}He), new spin $^1/_2{}^-$ state observed in ^{55}Mn, shell model calculations 2—8287
^{58}Fe, E_2:M1 multipole mixing ratio of excited state transitions 2—31473
^{58}Fe(^{3}He,p) two-particle transfer reaction, investigation of ^{60}Co 2—31474
^{58}Fe(n,γ)^{59}Fe, γ-ray spectra obs. following thermal neutron capture 2—5702
^{59}Fe, level transition scheme proposed, ^{58}Fe(n,γ)^{59}Fe ob. 2—5702
^{59}Fe$\rightarrow$^{59}Co decay, internal conversion meas. 2—38537
^{59}Fe$\rightarrow$^{59}Co decay, γ-γ directional correl. obs. of cascades 2—34988
^{60}Fe, astronomical gamma-ray flux det. by satellite 2—7504
Fe(μ,$W_0\nu$)Fe, 80-300 GeV, cross sections and differential distributions for W_0 prod. 2—27763
Fe(ν,$W_0\mu$)Fe, 80-300 GeV, cross sections and differential distributions for W_0 prod. 2—27763
Ga, A=65, 67, M1 transition from $g_{9/2}$ analogue to anti-analogue state 2—5655
^{65}Ga, decay scheme 2—24182
^{65}Ga, M1 transitions from $g_{9/2}$ analog-to-antianalog states 2—18109
^{67}Ga, low lying levels from ^{67}Zn(p,nγ)^{67}Ga 2—5658
^{67}Ga, M1 transitions from $g_{9/2}$ analog-to-antianalog states 2—18109
^{67}Ga$\rightarrow$^{67}Zn decay scheme, new γ-ray at 884 keV 2—38497
^{68}Ga, beta decay study 2—38540
^{69}Ga, fast neutron radiative capture cross section 2—8343
^{70}Ga 188 keV transition 2—38499
^{71}Ga, fast neutron radiative capture cross section 2—8343
^{71}Ga, in powder sample, asymmetry parameter detn., n.q.r. obs. 2—7156
^{76}Ga$\rightarrow$^{76}Ge, γ-ray decay scheme and nuclear energy levels in ^{76}Ge 2—11751
Ga(n,γ), γ-ray circular polarization, spin assignments 2—18209
Gd, odd neutron number isotopes, mixing of components with $\Delta N=\pm 2$ 2—8301
^{68}Ge from ^{70}Ge(p,t), excited levels study 2—18110
^{69}Ge from ^{70}Ge(p,d), excited levels study 2—18110
^{70}Ge, Coulomb excitation of excited 0^+ state with ^{35}Cl, ^{32}S ions 2—38498
^{70}Ge, thermal neutron capture, initial state excitation 2—11843
^{70}Ge,(p,d)^{69}Ge, 20 MeV, ^{69}Ge excited levels study 2—18110
^{70}Ge alpha particle elastic scattering, method of resolving real well depth ambiguities in optical model analysis 2—11856
^{70}Ge(p,t)^{68}Ge, 20 MeV, ^{68}Ge excited levels study 2—18110
^{71}Ge, level schemes from study of (n,γ)-reaction in natural Ge 2—27979
^{72}Ge, ^{84}Kr induced fusion reactions, effective threshold and minimum distance of approach meas. 2—24241
^{72}Ge(p,p’e), 3.3 to 4.7 MeV, isobaric analogue states in ^{73}As 2—34946
^{73}Ge, level schemes from study of (n,γ)-reaction in natural Ge 2—27979
^{74}Ge, level schemes from study of (n,γ)-reaction in natural Ge 2—27979
^{74}Ge polarized beams, relaxation time determ. 2—18116
^{75}Ge, level schemes from study of (n,γ)-reaction in natural Ge 2—27979
Hg isotopes, theoretical alpha decay rates analysed on shell model basis 2—11786
Kr, bombardment of compound nuclei for superheavy element synthesis 2—21451
^{72}Kr and neighbouring isotopes, oblate groundstate deformation predicted by Strutinsky-type calcs. of potential energy 2—24163
^{79}Kr, lifetimes of excited states, study from decay of ^{79}Rb 2—38500
^{79}Kr, low lying states and transitions, ^{79}Br(p,n) reaction obs. 2—38501
^{80}Kr, thermal-neutron capture cross section and resonance capture integral 2—8344
^{81}Kr low lying states and transitions, ^{81}Br(p,n) reaction obs. 2—38501
^{84}Kr, levels studied in decay of ^{84}Br using gamma ray spectra 2—31502
^{85}Kr, 10.7 year, thermal neutron capture cross section and resonance integral 2—31559
^{85}Kr, activity meas., in atmosphere 2—40972

Nuclei with $50\leqslant A\leqslant 89$ continued
^{86}Kr(d, ^{3}He(^{85}Br, ^{85}Br excited states, spins and parities assignment 2—11865
^{50}Mn, deduced levels, excited state study from ^{50}Cr(^{3}He,t)^{50}Mn reaction 2—11743
^{50}Mn, excited states, study using (p,nγ) reaction 2—11742
^{50}Mn, study of excited states of ^{50}Cr by means of 1.7 minute decay 2—34939
^{50}Mn levels obs. from ^{50}Cr(^{3}He,t)^{50}Mn 2—11744
^{52}Mn, level half-life measurements 2—8297
^{53}Mn, electromagnetic transitions, mean lives, multipole mixing ratios, probabilities 2—31470
^{53}Mn, levels and transition rates determ. from ^{53}Cr(p,n) reactions 2—11747
^{53}Mn, mean lives of low lying levels measured, electromagnetic transitions studied 2—18106
^{54}Mn, energy levels, study by reaction ^{54}Cr(p,n) at 2.6 to 3.1 MeV 2—38531
^{54}Mn, level scheme studied by ^{52}Cr(^{3}He,p) reaction 2—21448
^{54}Mn decay, K-X-ray γ directional correlations 2—18107
^{55}Mn, n.a.r. in MnTe 2—1426
^{55}Mn, n.m.r. spin echo in RbMnF$_3$, 4.2 K 2—16400
^{55}Mn, n.m.r. spin echo obs. in antiferromag. CsMnF$_3$ and MnCO$_3$ 2—16403
^{55}Mn, new spin $1/2^-$ state predicted from (p,^{3}He) and (d,^{4}He) reactions on ^{57}Fe, shell model calculations 2—8287
^{55}Mn, nuclear acoustic resonance in MnTe, mag. field depend. 2—20162
^{55}Mn^{2+}, e.p.r. and ENDOR in SrO, hyperfine struct. 2—26287
^{55}Mn broad-line n.m.r. in single crystal CoMn(CO)$_9$ 2—22842
^{55}Mn ENDOR in KMnF$_3$, hyperfine interactions 2—20144
^{55}Mn multiple spin echoes in Mn ferrites 2—4557
^{55}Mn n.m.r. in Mn$_4$N$_x$ 2—10557
^{55}Mn n.m.r. in MnCr$_2$O$_4$ 2—20163
^{55}Mn relax. times in dil. Ni alloys 2—40579
^{55}Mn(d,p)^{56}Mn, 10.1 MeV, energy levels of ^{56}Mn 2—31587
^{55}Mn(γ,3n)^{52m,g}Mn, isomeric cross section ratios 2—24202
^{56}Mn, energy levels deduced from ^{54}Cr(^{3}He,p) reaction at 15MeV 2—505
^{56}Mn, levels studied using ^{55}Mn(d,p) reaction 2—31587
^{56}Mn, lifetimes of 26 and 110 keV levels determ. using thermal neutron capture on natural Mn targets 2—8299
Mn(n,γ), γ ray circular polarization, spin assignments 2—18209
^{88}Nb$\to$^{88}Zr decay, γ-ray spectra tel. to ^{88}Zr level determination 2—21389
^{89}Nb, γ-decay process 2—477
Ni, 14 MeV neutron interactions, statistical emission of α-particles 2—35055
Ni, A=58, 60, 62, 64, meas. of differential cross section for elastic scattering of 33 MeV ^{3}He particles, optical model analysis 2—28067
Ni, elastic and inelastic deuteron scatt., differential cross sections, on neutron excessive and deficient nuclei 13.6 MeV 2—28065
Ni, neutron equilibrium pairing 2—38493
Ni, proton scattering, angular distributions for particles in 2 to 30 keV range 2—11824
Ni (A=58,60), excitation cross section of first 2$^+$ levels excited in (n, n$'\gamma$) reaction 2—11840
Ni isotopes, 0$^+$ states, broken-pair approximation and generator coordinate method 2—38494
Ni isotopes, calculation of quadrupole moments for $2_1{}^+$ state 2—31442
Ni total reaction cross section for 13.6 MeV deuterons 2—28068
^{56}Ni energy levels deduced from ^{54}Fe(^{3}He,n) reaction at 14 MeV 2—27977
^{57}Ni, 2.443 and 3.003 MeV level props. from ^{54}Fe(α,n)^{57}Ni reaction 2—11749
^{58}Ni, 11.8 MeV elastic scattering of deuterons, derivation of optical potential 2—2796
^{58}Ni, elastic scatt. of 30 MeV ^{6}Li ions 2—18239
^{58}Ni, substate excitation of 2$^+$ state by (p,p$'\gamma$) inelastic scatt. 2—34941
^{58}Ni levels populated in ^{58}Cu decay 2—18158
^{58}Ni(^{16}O, ^{16}O$'$)^{58}Ni* 34-58 MeV, excitation function obs. 2—35083
^{58}Ni(^{3}He,n)^{60}Zn, 15 MeV, meas. angular distributions, deduced ^{56}Ni energy levels 2—27977
^{58}Ni(^{3}He,p)^{60}Cu, shell model calculation 2—38644
^{58}Ni(d,α)^{56}Co, levels of ^{56}Co 2—2709
^{58}Ni(d,p)^{59}N, Coulomb stripping, energy levels of residual nucleus 2—31584
^{58}Ni(n,p), threshold detector for fast neutron spectrum investigations, meas. of activation integral 2—34822
^{58}Ni(p,γ), $g_{9/2}$ analog resonances, with strong M1 transitions to antianalog states 2—18109
^{58}Ni(p,p$'\gamma$)^{58}Ni*, E$_p$=20 MeV, substate excitation of 2$^+$ state, transition from O$^+$ state 2—34941
^{58}Ni(p,p)^{58}Ni 5.8-6.5 MeV, p polarization and ang. distrib. obs. 2—8334
^{59}Ni, energy levels from Coulomb stripping in ^{58}Ni(d,p)^{59}Ni reaction 2—31584
^{59}Ni(^{12}C,2n)^{68}Se, meas. of ^{68}Se half-life, separation of ^{68}As, assignment of γ ray transitions 2—38538
^{59}Ni(n,α) cross sections for thermal neutrons, calc. 2—5703
^{60}Ni, E2/M1 mixing ratio for $2_2{}^+\to 2_1{}^+$ transition 2—14946
^{60}Ni(^{3}He,t$'$)^{60}Cu*, quasi inelastic scatt., effect of 2 step processes, coupling potential 2—31532
^{60}Ni(α,α'), influence on isospin decay of composite ^{64}Zn system formed, Bohr independence hypothesis 2—24181
^{60}Ni(d,α)^{58}Co, energy level scheme for ^{58}Co 2—21388
^{60}Ni(d,α)^{58}Co, high-resolution study of ^{58}Co energy levels 2—34943
^{60}Ni(p,γ), $g_{9/2}$ analog resonances, with strong M1 transitions to antianalog states 2—18109
^{60}Ni(p,p)^{60}Ni 5.8-6.5 MeV, p polarization and ang. distrib. obs. 2—8334
^{61}Ni, electric quadrupole and mag. dipole moment of 67.4 keV level from Mossbauer study of NiCr$_2$O$_4$ 2—5656
^{62}Ni, (^{3}He,t) transitions isobaric analog ground states, energy dependence 2—31583
^{62}Ni, E2/M1 mixing ratio for $2_2{}^+\to 2_1{}^+$ transition 2—14946
^{62}Ni, elastic scatt. of 37.7 MeV ^{3}He, global optical model analysis 2—38633
^{62}Ni, proton scatt., E$_p$=2.43-2.63 MeV, rel. to isobaric analog states of ^{63}Ni 2—34945
^{62}Ni(^{3}He,t), 21.4 to 37.5 MeV, energy dependence of transitions to isobaric analogue ground states 2—31583
^{62}Ni(α,α'), influence on isospin on decay of composite ^{66}Zn system formed, Bohr independence hypothesis 2—24181
^{62}Ni(d,α) two-particle transfer reaction, investigation of ^{60}Co 2—31474
^{62}Ni(d,p)^{63}Ni, Coulomb stripping, energy levels of residual nucleus 2—31584

Nuclei with $50\leqslant A\leqslant 89$ continued
^{62}Ni(n,γ)^{63}Ni, thermal, 2 keV and 25 keV neutrons, γ-spectra 2—14991
^{62}Ni(p,α)^{59}Co, population of highly excited levels in ^{59}Co, energy spectra study 2—24162
^{62}Ni(p,γ), $g_{9/2}$ analog resonances, with strong M1 transitions to antianalog states 2—18109
^{63}Ni, energy levels from Coulomb stripping ^{62}Ni(d,p)^{63}Ni reaction 2—31584
^{63}Ni, isobaric analog states, spin assignment 2—34945
^{63}Ni, standardization, half-life and neutron capture cross-section 2—5679
^{64}Ni, 0$^+$ and 2$^+$ states, ^{68}Zn(d,^{6}Li) reaction study 2—2812
^{64}Ni, spin and parity assignments, gamma transitions 2—5693
^{64}Ni(d,α) two-particle transfer reaction investigation of ^{62}Co 2—31476
^{64}Ni(d,p)^{65}Ni, Coulomb stripping, energy levels of residual nucleus 2—31584
^{64}Ni(n, γ)^{65}Ni, thermal neutron capture, γ-ray spectra meas., ^{65}Ni energy levels deduced 2—28050
^{64}Ni(p,nγ)^{64}Cu $\leqslant$3.1 MeV, excitation function, gamma-ray ang. distrib. and nγ correlations determ. 2—5693
^{64}Ni(p,p)^{64}Ni, 3.150 to 4.050 ang. distribution and obs. of isobaric analog states in ^{65}Cu compound nucleus 2—35027
^{65}Ni, energy levels from Coulomb stripping in ^{64}Ni(d,p)^{65}Ni reaction 2—31584
^{66}Ni, cumulative yield in natural U fission 2—35097
Ni(n,γ), γ-ray circular polarization, spin assignments 2—18209
Ni(p,γ)Cu, M1 transition from $g_{9/2}$ analogue to anti-analogue state in Cu, A =59, 61, and 63 2—5655
Pb, size determ. from cross sections of K$^-$, π^- and $\bar{p}$ induced reactions at 20-60 GeV/c 2—11719
Pt isotopes, theoretical alpha decay rates analysed on shell model basis 2—11786
Rb, giant dipole states, photonuclear reaction study 2—2713
Rb, isotopic cross sections from 40- 60 MeV proton induced fission of ^{235}U, ^{238}U, ^{232}Th 2—11880
^{77}Rb, new neutron deficient isotope produced by ^{63}Cu(^{16}O,2n) and ^{59}Co(^{20}Ne, 2n) reaction, half-life and γ ray spectra meas. 2—34989
^{79}Rb, β transitions to excited states of ^{79}Kr 2—38500
^{84}Rb, form. cross section in proton interactions with U and Th 2—2826
^{84}Rb isomer ratios, residual effects during ^{85}Rb de- excitation 2—31585
^{85}Rb, alpha-particle induced reactions 2—11864
^{85}Rb, n.q.r. in RbBrO$_3$ 2—40790
^{85}Rb, short lived activities excited by 14.7 MeV fast neutrons 2—18093
^{85}Rb de-excitation, isomer ratios of ^{84}Rb, ^{85}Sr and ^{87,86,85}Y 2—31585
^{85}Rb spin-lattice relax. in liq. alkali metal alloys 2—18855
^{85}Rb(γ,n)^{84m,g}Rb, isomeric cross section ratios 2—24202
^{85}Rb(n,2n)^{84m,g}Rb, isomeric cross section ratios 2 -24202
^{86}Rb, form. cross section in proton interactions with U and Th 2—2826
^{87}Rb, n.q.r. in RbBrO$_3$ 2—40790
^{87}Rb levels deduced in ^{88}Sr(d,^{3}He) reaction at 35 MeV, determ. of transferred angular momenta, spectroscopic factors 2—38645
^{87}Rb spin-lattice relax. in liq. alkali metal alloys 2—18855
^{87}Rb(α,nγ)^{90}Y, γ-spectroscopic study of ^{90}Y levels 2—18112
^{88}Rb, 17.8 min. decay, meas. γ-γ angular correlations of four cascades, deduced ^{88}Sr levels 2—28006
^{88}Rb, β decay of 17.8 min state, population of levels in ^{88}Sr, γ-ray spectra 2—31477
^{50}Sc, strongly excited 1$^+$ states, obs. in ^{46}Ca(^{3}He,p)^{48}Sc and ^{48}Ca(^{3}He,p)^{50}Sc reactions 2—34937
Se, even isotopes, excitation cross sections of first 2$^+$ levels in (n,n$'\gamma$) reactions 2—28043
^{68}Se, produced by ^{59}Ni(^{12}C,2n) reaction, separation of ^{68}As, meas. of half-life and γ ray spectra 2—38538
^{75}Se, level scheme determination from obs. of γ-rays and conversion electrons following ^{75}Br decay 2—24164
^{75}Se, spins of low lying levels, investigation using ^{75}As(p,nγ)^{75}Se reaction 2—34947
^{75}Se decay, K-X-ray γ directional correlations 2—18107
^{76}Se, energy level scheme, ^{76}As decay obs. 2—31514
^{76}Se, level scheme deduced from ^{76}As decay 2—18159
^{76}Se(n,γ)^{77}Se, structure of ^{77}Se 2—18212
^{77}Se, structure study via (n,γ) reaction 2—18212
^{77}Se(n,γ)^{78}Se, structure of ^{78}Se 2—18212
^{78}Se, collective structure 2—14947
^{78}Se, structure study via (n,γ) reaction 2—18212
^{80}Se, thermal neutron capture, initial state excitation 2—11843
^{80}Se(n,γ)^{81}Se, captive mechanism, structure of ^{81}Se 2—18212
^{81}Se, conversion coeffs. for 103 keV γ transition 2—2746
^{81}Se, structure study via (n,γ) reaction 2—18212
^{82}Se, 14.8 MeV (n,2n), (n,p), (n,α) cross sections 2—18213
^{77m}Se, half-life measurement 2—27980
Se(n,n$'\gamma$), excitation cross sections of first 2$^+$ levels in even isotopes, energy dependence 2—28043
Sm, odd neutron number isotopes, mixing of components with ΔN=$\pm$2 2—8301
Sn, size determ. from cross sections of K$^-$, π^- and $\bar{p}$ induced reactions at 20-60 GeV/c 2—11719
Sr giant dipole states, photonuclear reaction study 2—2713
Sr isotopes, effective interaction among 1$g_{9/2}$ and 2$p_{1/2}$ neutrons, shell model calc. 2—11752
Sr isotopes from ^{238}U fission, spectra 2—11885
^{78}Sr prod. by ^{64}Zn(^{16}O,2n), half life determ. 2—28005
^{85}Sr, three particle level multiplets from decay 2—476
^{85}Sr bone scan in neoplastic disease 2—30675
^{85}Sr decay, K-X-ray γ directional correlations 2—18107
^{85}Sr isomer ratios, residual effects during ^{85}Rb de- excitation 2—31585
^{87}Sr, energy levels, study from reaction ^{89}Y(d,α) at 12 MeV 2—34949
^{87}Sr, fluorescence after thermal neutrons capture and levels 2—38503
^{87}Sr, level population in decay of ^{87}Y 2—5675
^{87}Sr, magnetic moment determ. by optical pumping 2—18104
^{88}Sr, nuclear structure investigations using inelastic electron scattering 2—18111
^{88}Sr, two hole and two particle four hole states populated in β decay of 17.8 min ^{88}Rb 2—31477
^{88}Sr levels deduced in ^{89}Y(d,^{3}He) reactions at 30, 35.5, 40 MeV, determ. of transferred angular momenta, spectroscopic factors 2—38645
^{88}Sr spins of levels and E2/M1 mixing ratio determ. from γ-γ angular correlations in decay of ^{88}Rb 2—28006
^{91}Sr 2p-1h states, S- and P-wave neutron spectroscopy, neutron doorway escape widths determ. using theory of intermediate structure 2—24159

Nuclei with $50 \leqslant A \leqslant 89$ continued
Sr(n,n), elastic and inelastic scatt., 14.8 MeV, differential cross sect., collective state excitation 2—21434
Ti collective states excitation by 14 MeV neutrons 2—14990
^{50}Ti, elastic scatt. of 37.7 MeV ^{3}He, global optical model analysis 2—38633
^{50}Ti, inelastic scattering by ^{3}He to positive parity states at 29 MeV, analysis within microscopic model 2—15013
^{50}Ti (n, γ)^{51}Ti, thermal neutron capture, γ-ray spectra meas., ^{51}Ti energy levels deduced 2—28050
^{50}Ti(α,nγ)^{53}Cr, e.m. props. of ^{53}Cr. 2—34940
V isotopes, elastic proton scattering, 2.8-6.3 MeV 2—489
^{51}V, cross sections for inelastic interaction of neutrons, $E_n \lesssim 20$ MeV 2—28048
^{51}V, elastic scatt. of 37.7 MeV ^{3}He, global optical model analysis 2—38633
^{51}V, electromagnetic transitions, mean lives, multipole mixing ratios, probabilities 2—31470
^{51}V, Knight shift in Pd-V dil. alloy, temp. depend. 2—40782
^{51}V, Knight shift in VO_2 2—33118
^{51}V, n.m.r. in $LiVO_2$ above and below transition temp. 2—7143
^{51}V, photonuclear reaction yields at 1.5 GeV 2—2763
^{51}V, theoretical internal conversion coefficients 2—11745
^{51}V in V_3Au, n.m.r. model proposed for normal and superconducting states 2—4564
^{51}V n.m.r. in Au-V dil. alloys 2—33114
^{51}V n.m.r. in dil. Au-V alloys 2—33350
^{51}V n.m.r. in V-Co alloys 2—10566
^{51}V n.m.r. in V-transition metal alloys and V-N(0) dil. solid solns. 2—26308
^{51}V n.m.r. in V_2O_3 2—10564
^{51}V n.m.r. in V_2O_5, $LiVO_3$ and $NaVO_3$ 2—10565
^{51}V spin-lattice relax. in V_3Pt 2—33183
^{51}V(^{3}He.d)^{52}Cr, 11.0 MeV, determ. of lifetimes of low- lying levels in ^{52}Cr 2—11746
^{51}V(p,p)^{51}V, 5.8-6.5 MeV, p polarization and ang. distrib. obs. 2—8334
Y collective states excitation by 14 MeV neutrons 2—14990
^{85}Y, decay, 5 hrs. and 2.68 hrs., three particle level multiplets in ^{85}Sr 2—476
^{85}Y isomer ratios, residual effects during ^{85}Rb de- excitation 2—31585
^{86}Y isomer ratios, residual effects during ^{85}Rb de- excitation 2—31585
^{87}Y, decay to levels in ^{87}Sr, log ft values 2—5675
^{87}Y isomer ratios, residual effects during ^{85}Rb de- excitation 2—31585
^{89}Y, excited levels, from decay of ^{89}Zr 2—2747
^{89}Y, inelastic nucleon scattering, features of core polarization knock-out exchange contributions 2—31527
^{89}Y giant dipole states, photonuclear reaction study 2—2713
^{89}Y levels deduced in ^{88}Sr(^{3}He,d) reaction at 33.4 MeV, determ. of transferred angular momenta, spectroscopic factors 2—38645
^{89}Y n.m.r. in Y and dil. Y-Ce alloys 2—13555
^{89}Y(^{3}He,t)^{89}Zr to $T_<$ states, shapes of angular distributions determ. 2—11866
^{89}Y(d,α)^{87}Sr, 12 MeV, study of ^{87}Sr levels 2—34949
^{89}Y(d,n)^{90}Zr stripping reaction, Coulomb effect 2—28078
^{89}Y(d,p), 33.3 MeV, cross sections, shell model structure of 90Y, l=5 transitions data 2—34950
^{89}Y(d,p)^{90}Y, 3 to 4.5 MeV and $\theta = 150°$, l_π-dependence of excitation functions 2—35078
^{89}Y(d,pγ)^{90}Y, γ-spectroscopic study of ^{90}Y levels 2—18112
^{89}Y(p,p'), excitation by 61.2 MeV protons of various states, differential cross sections 2—21429
^{86m}Y, investigation of β^+ and γ decay 2—38544
Zn, A=64, 66, 68, meas. of differential cross section for elastic scattering of 33 MeV ^{3}He particles, optical model analysis 2—28067
Zn, total reaction cross section for 13.6 MeV deuterons 2—28068
Zn (A=64, 66, 68), excitation cross section of first 2^+ levels excited in (n,n'γ) reaction 2—11840
Zn e scatt., stable even-even isotopes, cross-section ratios and rms radius 2—11819
Zn neutron total cross section between 23 and 45 MeV using time-of-flight technique with transmission method 2—38609
Zn(A=64, 66, 68), elastic scatt. and polarization of 30.5 MeV protons, optical model analysis 2—5690
^{60}Zn, half-life measurement using mass separated source 2—31500
^{60}Zn energy levels deduced from ^{58}Ni(^{3}He,n) reaction at 15 MeV 2—27977
^{61}Zn, half-life measurement using mass separated source 2—31500
^{64}Zn, composite system formed in ^{63}Cu+p and ^{60}Ni+α reactions, isospin effects in decay, Bohr independence hypothesis 2—24181
^{64}Zn foils, bombarded with ^{3}He 22.2-43.4 MeV, determ. γ-ray spectra, half lives of isotopes, cross sections, excitation functions, reaction mechanisms 2—24239
^{64}Zn(^{16}O,2n)^{78}Sr using 160 MeV oxygen ions 2—28005
^{64}Zn(d,α)^{62}Cu, 15 MeV, DWBA calcs., ^{62}Cu deduced levels 2—31475
^{64}Zn(n,p), threshold detector for fast neutron spectrum investigations, meas. of activation integral 2—34822
^{64}Zn(p,γ), $g_{9/2}$ analog resonances, with strong M1 transitions to antianalog states 2—18109
^{64}Zn(p,t)^{62}Zn, 27.5 MeV, angular distributions, ground state Q-value, levels of ^{62}Zn and spin-parity assignments 2—38495
^{65}Zn, low-lying levels obs. in ^{65}Cu(p,n) and (p,nγ) reactions 2—8339
^{65}Zn decay, K-X-ray γ directional correlations 2—18107
^{66}Zn, composite system formed in ^{65}Cu+p and ^{62}Ni+α reactions, isospin effects in decay. Bohr independence hypothesis 2—24181
^{66}Zn, isobaric analogue resonance obs. in ^{65}Cu(p,n) and (p,nγ) reactions 2—8339
^{66}Zn, lifetime of 1.037 MeV state 2—24147
^{66}Zn, lifetimes of levels excited by inelastic α particles 2—27978
^{66}Zn(p,γ), $g_{9/2}$ analog resonances, with strong M1 transitions to antianalog states 2—18109
^{67}Zn, half-life of $9/2^+$ state 2—8302
^{67}Zn, new level at 884 keV, ^{67}Ga decay obs. 2—38497
^{67}Zn(p,nγ)^{67}Ga, low lying levels of ^{67}Ga 2—5658
^{68}Zn, thermal neutron capture, initial state excitation 2—11843
^{68}Zn level structure deduced from decay of ^{68}Cu isomers 2—38539
^{68}Zn(d,^{6}Li)^{64}Ni, differential cross section, 27.2 MeV 2—2812
^{68}Zn(p,$p_1'\gamma$)^{68}Zn*, study of ^{69}Zn low lying states 2—2712
^{69}Zn, low lying states, from ^{68}Zn(p,$p_1'\gamma$)^{68}Zn* study 2—2712
Zn(p,γ)Ga, M1 transition from $g_{9/2}$ analogue to anti-analogue state in Ga, A=65, 67 2—5655
^{87}Zr, decay process, using Ge(Li) spectrometer 2—2747

Nuclei with $50 \leqslant A \leqslant 89$ continued
^{88}Zr, level scheme determination from obs. of γ-rays following ^{88g}Nb and ^{88m}Nb decay 2—21389
^{89}Zr, decay process, using Ge(Li) spectrometer 2—2747
^{89}Zr, one-neutron hole states, expt. study 2—38600
^{89}Zr, spin assignment, DWBA anal. of ^{91}Zr(p,t) reaction 2—38601
^{89}zr $T_<$ states from ^{89}Y(^{3}He,t) reaction angular distributions characteristic of nonallowed L transfers 2—11866
^{91}Zr, elastic scatt. of 37.7 MeV ^{3}He, global optical model analysis 2—38633

Nuclei with $90 \leqslant A \leqslant 149$
^{116}Sn(t,p), transitions to collective and non-collective states, DWBA analysis 2—28080
^{90}Zr giant dipole states, photonuclear reaction study 2—2713
^{92}Zr(α,n)^{95}Mo, 12-43 MeV, study of high spin levels in ^{95}Mo 2—21391
^{93}Y, decay, level scheme for ^{93}Zr 2—38505
^{94}Zr(α,n)^{97}Mo, 12-43 MeV, study of high spin levels in ^{97}Mo 2—21391
even-even nuclei, $80 < A < 160$, neutron capture cross sections at 25 keV 2—21439
heavy nuclei ($A \geqslant 130$), preformation of α particles by analysis of (n,α) reactions 2—21436
odd-mass nuclei, $51 \leqslant Z \leqslant 61$, level spectra and intermediate coupling model 2—27984
rare earth products of 28 GeV proton interaction with U, determ. charge and mass distribution 2—11834
rare-earth nuclei, (d,t) reaction, angular distributions, two step model 2—38643
spherical nuclei, equilibrium pairing energy gaps 2—38507
(n,2n) reactions in medium-, heavy-meass region, 14-15 MeV, determ. activation cross sections, isomeric cross section ratios, systematics 2—35047
^{a}Sb(^{3}He,d), A=121, 123, at 25 MeV determ. energy levels of ^{122,124}Te 2—18119
^{a}Sm A=144, 147, bombardment with 103 MeV ^{14}N ions, production of new α emitting isotopes ^{155,156}Tm 2—11801
^{a}Sn, A=116, 120, elastic scattering of ^{16,18}O at energies near the Coulomb barrier 2—11870
^{a}Te(p,t) A=124, 126 at 33 MeV determ. energy levels of ^{122,124}Te 2—18119
^{107,109,111}Ag, half-lives $^{9}/_{2}{}^{+}$ levels, M1 retardation and E2 enhancement factors of $^{9}/_{2}{}^{+} \to {}^{7}/_{2}{}^{+}$ transition, $^{7}/_{2}{}^{+}$ level structure 2—14949
Ag, proton induced fission, fragment energy spectra 2—2828
Ag binary fission cross- section induced by 29-GeV ^{14}N ions meas. 2—35093
^{107}Ag, single-particle density distributions in the extreme nuclear surface 2—14950
^{107}Ag alpha particle elastic scattering, method of resolving real well depth ambiguities in optical model analysis 2—11856
^{108}Ag→^{108}Pb, ^{108}Cd, β-decay, use of pneumatic irradiation apparatus with on-line measurement system 2—28001
^{112}Ag, β-decay, γ-ray assignment to level structure of ^{112}Cd 2—38547
^{112}Ag→^{112}Cd decay, γ-spectra meas., assignment of ^{112}Cd level scheme 2—21413
^{114}Ag, β-decay, γ-ray assignment to level structure 2—38547
^{114}Ag, decay scheme, formation by ^{114}Cd(n,p) reaction 2—31504
^{116}Ag, β-decay, γ-ray assignment to level structure 2—38547
^{110g}Ag 24 sec, β-decay of 1^+ ground state to low spin states in ^{110}Cd 2—31480
^{110m}Ag decay, γ-ray spectra meas., identification of weak transitions 2—28007
^{110m}Ag emitted gamma-rays, measurement of self-absorption in large cylindrical samples 2—24297
^{102m,g}Ag, 8 min and 13 min isotopically separated samples, meas. γ-ray spectra and $\gamma\gamma$ coincidences 2—14964
^{104m,g}Ag→^{104}Pd, 33 and 69 min isotopically separated samples, meas. γ-ray spectra and $\gamma\gamma$ coincidences 2—18168
Ba (A=134, 135, 136, 137), neutron resonances 2—11844
Ba isotopes from ^{238}U fission, spectra 2—11885
^{129}Ba decay, meas. γ-spectra with Ge(Li) and scintillation detectors deduced ^{129}Cs level scheme 2—18163
^{129}Ba decay, meas. γ spectra with Ge(Li) and scintillation detectors deduced ^{129}Cs level scheme 2—18163
^{130}Ba, isomeric transition $8 \to 6^+$, description using model 2—11762
^{132}Ba, E2/M1 mixing ratios of $2_2{}^+ \to 2_1{}^+$ gamma transition and corresponding E2% admixture determ. 2—2721
^{132}Ba levels obs. from ^{132}La decay 2—18120
^{133}Ba, P_k electron capture probabilities 2—14966
^{133}Ba decay, K-X-ray γ directional correlations 2—18107
^{133}Ba decay, L/K electron capture ratio 2—38532
^{134}Ba, excited levels, from decay of ^{134}La 2—8307
^{135}Ba, energy levels, lifetime meas. and spin and parity assignments 2—11763
^{135}Ba, magnetic moment determ. by optical pumping 2—18104
^{137}Ba, magnetic moment determ. by optical pumping 2—18104
^{138}Ba, level scheme construction, spin assignments from ^{138}Cs decay 2—24167
^{138}Ba(e,e'p) reaction, isobaric analogs 2—2770
^{140}Ca, energy levels formed in decay of ^{140}La determ. lifetime of 3^- octupolar level 2—18121
Cd isotopes, total neutron and scatt. cross-sections 2—24228
Cd^{113}, n.m.r. chemical shift in CdS, CdSe and CdTe 2—37005
^{110}Cd, low spin states populated by β-decay of 1^+ ground state of ^{110g}Ag, obs. of O^+ state of two phonon character 2—31480
^{111}Cd in Cd, quadrupole interaction of 247-keV state meas. 2—34956
^{112}Cd, level scheme from ^{112}Ag decay data 2—21413
^{112}Cd, level structure assignment from ^{112}Ag β-decay 2—38547
^{112}Cd, static quadrupole moment of 1° excited state, width of $0^2 \to 2^+$ transition 2—2718
^{112}Cd photoexcitation, study of energy levels 2—11758
^{113}Cd n.m.r. in CdTe 2—33351
^{114}Cd, level structure assignment from ^{114}Ag β-decay 2—38547
^{114}Cd, quadrupole moment of first excited state 2—5661
^{115}Cd, isomer ratio measured for charged particle induced fission of ^{238}U, ^{232}Th, ^{226}Ra, ^{209}Bi, deduced fragment angular momentum 2—11884
^{116}Cd, ^{84}Kr induced fusion reactions, effective threshold and minimum distance of approach meas. 2—24241
^{116}Cd, elastic and inelastic proton scattering at 12 MeV, determ. cross sections, deduced levels 2—18187
^{116}Cd, level structure assignment from ^{116}Ag β-decay 2—38547
^{116}Cd, study of ground state with (^{3}He,d) and (α,t) reactions 2—27983

Nuclei with 90$\leqslant$A$\leqslant$149 continued
^{116}Cd(^{3}He,d)^{117}In, study of In level scheme via proton transfer reactions 2—27983
^{116}Cd(α,t)^{117}In, study of In level scheme via proton transfer reactions 2—27983
Cd(p,p′), compound-nucleus contrib. 2—2771
^{139}Ce, P$_k$ electron capture probabilities 2—14966
^{140}Ce, gamma-gamma directional correlations 2—5665
^{140}Ce, neutron elastic scatt., local optical nuclear model 2—5698
^{140}Ce alpha particle elastic scattering, method of resolving real well depth ambiguities in optical model analysis 2—11856
^{140}Ce nuclear structure study by α scatt. 2—11764
^{140}Ce(e,e′p) reaction, isobaric analogs 2—2770
^{140}Ce(p,p′), isobaric analogue resonance properties of ^{141}Ce in a unified model calculation 2—31547
^{140}Ce(p,p), obs of resonances in ^{141}Pr corresponding to IAR's of low lying ^{141}Ce levels 2—18123
^{141}Ce, absolute disintegration rate det. by 4$\pi\beta$-γ coincidence meas. 2—11800
^{141}Ce, isobaric analogue resonance properties calculated in a unified model for ^{140}Ce(p,p′) 2—31547
^{141}Ce decay, $\beta\gamma$ correlatoon investigated using Compton backscattering to determ. circular polarization of γ-rays 2—14967
^{141}Ce half-life determ. 2—21412
^{144}Ce→^{144}Pr decay, γ-ray and conversion electron intensities 2—38515
Ce(n,γ), 14 MeV, spectra of photons 2—8345
Cs (A=131, 133), half lives of short lived excited states 2—34948
Cs isotopic cross sections from 40- 60 MeV proton induced fission of ^{235}U, ^{238}U, ^{232}Th 2—11880
^{129}Cs, level scheme deduced from ^{129}Ba decay 2—18163
^{131}Cs, half-lives of some excited states meas. using delayed coincidence technique 2—24165
^{132}Cs, form. cross section in proton interactions with U and Th 2—2826
^{133}Cs, half-lives of 81 keV and 161 keV excited levels 2—38514
^{133}Cs, half-lives of some excited states meas. using delayed coincidence technique 2—24165
^{133}Cs, n.m.r. in Cs_2O-B_2O_3 glasses and cryst. 2—30025
^{133}Cs, n.m.r. in Cs_2O-B_2O_3 glasses and cryst. 2—30026
^{133}Cs n.m.r., Bloch-Siegart shifts 2—38833
^{133}Cs n.m.r. in $CsNiCl_3$ 2—22703
^{133}Cs spin-lattice relax. in liq. alkali metal alloys 2—18855
^{133}Cs spin lattice relaxation rate in CsD_2AsO_4 2—29844
^{134}Cs, isomer ratio measured for charged particle induced fission of ^{238}U, ^{232}Th, ^{226}Ra, ^{209}Bi, deduced fragment angular momentum 2—11884
^{134}Cs isomers produced in α fission of ^{238}U, e.m. mass separator rel. to radiochemical 2—11881
^{136}Cs, form. cross section in proton interactions with U and Th 2—2826
^{138}Cs, energy level determ. 2—2770
^{138}Cs→^{138}Ba decay, level scheme construction, spin assignments 2—24167
^{147}Eu, level diagram from ^{147}Gd decay 2—24186
^{147}Eu, transition multipolarity and excited state characteristics 2—11766
Gd (A=145, 146), pattern of levels with large spin, spin and parity assignment 2—24169
^{144}Gd, quasirotational groundstate bands 2—18122
^{146}Gd, hindrance factor of E2 $6^+\to4^+$ transition, study using ^{144}Sm(α,2n)^{146}Gd 2—2723
^{147}Gd decay, conversion electron and γ-ray meas., ^{147}Eu level diagram 2—24186
^{1}H, total neutron cross sections in MeV region 2—28045
I, odd mass isotopes, positive parity level description using unified model 2—14953
^{121}I excited states obs. from ^{121}Xe decay 2—14965
^{123}I, level half-life measurements 2—8297
^{126}I decay, γ-ray obs. 2—38549
^{127}I, 360-58 keV cascade in Te crystal, ang. γ quanta correlation perturbation 2—29854
^{127}I, n.q.r. in $BaI_2.2H_2O$, struct. relns. between iodide, bromide and chloride dihydrates 2—30035
^{127}I, n.q.r. spectra of H_5IO_6 powder samples 2—10587
^{129}I Mossbauer effect in As_2Te_3 and $As_2Se_3.As_2Te_3$ 2—1670
^{129}I Mossbauer effect in GeTe, SnTe and PbTe 2—1673
^{129}I Mossbauer effect in tellurides 2—4446
^{130}I, ^{130*}I, β-decay, excitation of ^{130}Xe levels 2—24184
^{131}I, investigation of 636.3 and 722.9 keV transitions by gamma ray spectra and conversion electrons 2—479
^{132}I→^{132}Xe, γ-radiation, excited levels 2—5676
^{134}I level transitions obs. 4 new transitions found 2—2722
^{135}I shell-model predictions 2—8264
^{136}I, 45 sec and 83 isomers decay schemes 2—34990
^{137}I, β-delayed neutron energy spectrum meas. with high resolution neutron spectrometer 2—24185
In odd mass isotopes 109-117, application of unified model in intermediate coupling 2—27981
^{106}In, obs. of β decaying state in ^{92}Mo(^{16}O,pn)^{106}In reaction 2—18162
^{107}In→^{107}Cd, level scheme for ^{107}In and excited level spin and parity for ^{107}Cd 2—11798
^{113}In(n,n′)^{113m}In, reaction cross sections 2—31560
^{115}In, energy levels, photoactivation study 2—8303
^{115}In, excitation by positron annhilation cross sect. meas. 2—11759
^{115}In, muonic, $2s_{1/2}$ to $2p_{1/2}$ transition, magnetic hyperfine splitting 2—741
^{115}In, n.m.r. in $NiIn_xFe_{2-x}O_4$ 2—40778
^{115}In energy levels, inelastic neutron scattering study 2—27982
^{115}In Knight shifts in liq. dil. In-Pb alloys 2—22006
^{115}In n.m.r. in InAs and InSb, lineshifts 2—10551
^{115}In(n,n′), threshold detector for neutron spectrum investigations, meas. of activation integral 2—34822
^{116}In spin-lattice relax. in InAs, InP and InSb 2—7005
^{117}In, quadrupole moment of 660keV rotational level, meas. in $In_{0.99}Cd_{0.01}$ alloy at 4.2K 2—14951
^{117}In, study of level scheme via proton transfer reactions, (^{3}He,d) and (α,t) reactions 2—27983
^{115m}In, conversion electrons obs., evidence for positron annihilation without radiation emission 2—11759
^{132}La decay, ^{132}Ba levels obs. 2—18120
^{133}La excited states coexistence from correl. of quadrupolar moments 2—468
^{134}La decay, ^{134}Ba energy level study 2—8307
^{135}La, 119 keV level, lifetime meas. 2—31485
^{138}La, naturally recurring, decay 2—18164
^{139}La, Coulomb excitation by proton scattering at 12 MeV 2—5664

Nuclei with 90$\leqslant$A$\leqslant$149 continued
^{139}La, fast-neutron scattering, angular distributions 2—18202
^{139}La, fast neutron radiative capture cross section 2—8343
^{139}La nuclear structure study by α scatt. 2—11764
^{139}La spin-lattice relax. in $La_{1-x}Gd_xAl_2$ 2—33181
^{139}La spin-lattice relax. in La-Ce(Nd) dil. alloys 2—36786
^{139}La(n,γ), 14 MeV, spectra of photons 2—8345
^{140}La, β decay, determ. γ-ray transitions and internal conversion coefficients 2—18121
^{140}La, energy level determ. 2—2770
^{140}La, from thermal neutron induced fission of ^{249}Cf, fractional independent yield 2—35091
^{140}La decay, β spectrum analysed with Slatis Siegbahn β-ray spectrometer, study of outer β group with end point 2164 keV 2—28008
^{92}M., excitation functions and isomer ratios for (n,2n), (n,α) and (n,p) reactions 2—35056
Mo, A=95, 97, n.m.r. meas in hydrous and anhydrous Na_2MoO_4 2—37012
Mo(A=94, 98, 100), (p,d) reactions, evidence for neutron pick-up from interior core 2—35037
Mo(^{18}O, ^{16}O) two-neutron transfer reactions, E>Coulomb barrier 2—31589
^{92}Mo, 14.8 MeV (n,2n), (n,p), (n,α) cross sections 2—18213
^{92}Mo, deduced levels from ^{94}Mo(p,t) reaction at 40 MeV 2—18114
^{92}Mo, elastic electron scattering, 200 and 300 MeV 2—18177
^{92}Mo, magnetic moment of 2761 keV, 8^+ state 2—5659
^{92}Mo, short lived activities excited by 14.7 MeV fast neutrons 2—18093
^{92}Mo, spin and parity, assignment for levels populated in ^{94}Mo(p,t) reaction 2—2780
^{92}Mo collective states, assuming paired nucleons 2—18113
^{92}Mo(^{16}O,pn)^{106}In, obs. of β decaying state in ^{106}In 2—18162
^{92}Mo(^{3}He,d)^{93}Tc, levels up to a few MeV in ^{93}Tc 2—28079
^{92}Mo(^{3}He,dp)^{92}Mo, study of proton decay of six analogs of low-lying states in ^{93}Mo 2—28079
^{92}Mo(α,d)^{94}Tc, 50 MeV, high spin proton excited states population 2—31478
^{92}Mo(α,t)^{93}Tc, high spin proton states of ^{93}Tc 2—2696
^{92}Mo(d,n)^{93}Tc, DWBA calculations for reaction to unbound analog states, ang. distributions determ. 2—11867
^{92}Mo(d,n)^{93}Tc, E_d=12 MeV, neutron ang. distrib. 2—2717
^{92}Mo(d,pγ)^{93}Mo, coincidence meas. rel. to level structure and relative transition intensities in ^{93}Mo 2—34951
^{93}Mo, level structure and relative transition intensities from ^{92}Mo(d,pγ)^{93}Mo coincidence meas. 2—34951
^{94}Mo, isomeric $(g_{9/2})^2$ proton state observed in decay of ^{94}Tc 2—14960
^{94}Mo collective states, assuming paired nucleons 2—18113
^{94}Mo(d,n)^{95}Tc, E_d=12 MeV, neutron ang. distrib. 2—2717
^{94}Mo(p,p′γ)^{94}Mo, partial decay strengths, comparison with spectroscopic factors of ^{95}Mo(d,t)^{94}Mo reaction 2—18195
^{94}Mo(p,t)^{92}Mo, 40 MeV proton beam, spin and parity assessments 2—2780
^{94}Mo(p,t)^{92}Mo 40 MeV, deduced levels in ^{92}Mo 2—18114
^{95}Mo, quadrupole moment determ. using atomic beam magnetic resonance 2—21513
^{95}Mo(d,t)^{94}Mo, spectroscopic factors, comparison with partial decay strengths of ^{94}Mo(p,p′γ)^{94}Mo reaction 2—18195
^{95}Mo(n,γ)^{96}Mo, thermal, 2 keV and 25 keV neutrons, γ-spectra 2—14991
^{96}Mo(d,n)^{97}Tc, E_d=12 MeV, neutron ang. distrib. 2—2717
^{97}Mo, level structure investigation from Coulomb excitation meas. using α-particle and ^{16}O projectiles 2—34952
^{97}Mo, quadrupole moment determ. using atomic beam magnetic resonance 2—21513
^{97}Mo(n,γ)^{98}Mo, thermal, 2 keV and 25 KeV neutrons, γ- spectra 2—14991
^{102}Mo, levels studied using (t,p) reaction 2—31479
^{93m}Mo, magnetic moment of oriented nucleus by n.m.r. 2—38506
Mo(p,p), A=92,94,96,100, Ep=20,30,50 MeV, optical model analysis of cross sections and polarizations 2—28030
Mo(p,p′), compound-nucleus contrib. 2—2771
^{136}N, quasirotational groundstate bands 2—18122
Nb, A=92-96, high spin proton excited states population in Zr(α,d) and Zr(α,t) reactions 2—31478
^{90}Nb, γ-spectra and $\gamma\gamma$-coincidence spectra 2—478
^{90}Nb positron source, prep. 2—24177
^{91}Nb, excited states determ. from ^{91}Zr(p,nγ) reaction 2—2715
^{91}Nb, high spin proton states, from ^{90}Zr(α,t) reaction 2—2696
^{91}Nb, isobaric energy splitting between $T_>$- and $T_<$-single particle states 2—2716
^{92}Nb, isobaric analogue resonances observed in ^{91}Zr(p,n) reactions 2—5694
^{93}Nb, n.m.r. linewidth in nonstoichiometric lithium niobates 2—40777
^{93}Nb (^{3}He,^{7}Be), 41 MeV, α pickup, reaction cross section 2—11868
^{93}Nb giant dipole states, photonuclear reaction study 2—2713
^{93}Nb lower levels Coulomb excitation with ^{16}O ions from 25 to 42 MeV 2—14948
^{93}Nb(n,2n)^{92}Nb, cross section at 14.0 MeV meas. and apparent discrepancy with theory, relevance to fusion reactor technology 2—24227
^{96}Nb low-lying states study from ^{96}Zr(p,nγ)^{96}Nb 2—11754
^{90m}Nb, influence of chemical environment on decay constant of 2.38 keV isomeric transition 2—2714
^{94m}Nb, K-conversion coefficients of gamma ray transitions 2—8223
Nd, A=141, 143, coupled particle-pairing vibrational states excited via (p,t) reactions, level assignments made 2—11765
^{138}Nd→^{138}Pr, decay scheme, γ ray and conversion electron spectra 2—480
^{138}Nd→^{138}Pr, decay scheme, γ ray and conversion electron spectra 2—480
^{142}Nd, inelastic α scattering, relation between nuclear matter and nuclear potential 2—8355
^{142}Nd(e,e′p) reaction, isobaric analogs 2—2770
^{144}Nd, energy levels, neutron capture and gamma-ray spectra study 2—34960
^{147}Nd, study of nuclear matrix elements in 806 keV β transtiion 2—28009
^{147}Nd→^{147}Pm decay, γ-γ directional correl. obs. of ^{147}Pm cascades 2—34962
Nd(p,d), A=142-148, pairing vibrations 2—18196
Nd(p,t), A=142-150, energy gap 2—18196
^{208}Pb, self-absorption of gamma-rays produced by 7 MeV neutron interaction 2—24297
Pd isotopes, energies and intensities of conversion beta-ray spectra 2—38508
Pd isotopes from ^{238}U fission, spectra 2—11885
^{98}Pd→^{98}Rh, half-life meas. and level scheme for ^{98}Rh 2—38546

Nuclei with 90⩽A⩽149 continued

^{101}Pd→^{101}Rh positon decay spectrum investigated with double focussing spectrometer meas. of end point energies, log ft values and ^{101}Pd Q-value 2—31503
^{103}Pd, excited states, in-beam γ-ray meas. using ^{103}Rh(p,nγ)^{103}Pd reaction 2—11757
^{104}Pd, excited levels populated in decay of 33 min ^{104m}Ag and 69 min ^{104g}Ag 2—18168
^{104}Pd, excited state population in β^- decay of 4.3 sec and 4.41 min isomers of ^{104}Rh, spin values 2—34955
^{104}Pd, level structure determ. from ^{104}Rh decay 2—21392
^{112}Pd, levels studied using (t,p) reaction 2—31479
^{141}Pm, three quasiparticle multiplet population in electron capture decay of ^{141m}Sm 2—31505
^{143}Pm, effective coupling const. of M2 transition, $1h_{11/2}\rightarrow 1g_{7/2}$ state, half life meas. 2—18125
^{144}Pm, energy level determ. 2—2770
^{147}Pm cascades, γ-γ directional correl. obs., spin assignments 2—34962
^{148}Pm, structure of 1^- ground state 2—34963
^{138}Pr, decay scheme 2—38550
^{141}Pr, fast-neutron scattering, angular distributions 2—18202
^{141}Pr, fast neutron radiative capture cross section 2—8343
^{141}Pr, IAR's obs. in elastic and inelastic proton scattering from ^{140}Ce 2—18123
^{141}Pr, Mossbauer isomer shifts and hyperfine splitting of 145.4 keV γ-rays 2—18124
^{141}Pr(γ,n)^{140}Pr, threshold to 33 MeV, cross sections, obs. of induced activity 2—21424
^{142}Pr, $2\rightarrow 2^+$ beta transition at 587 keV 2—21414
^{142}Pr, energy level determ. 2—2770
^{143}Pr, level structure investigation using gamma rays produced in ^{143}Ce decay 2—21394
^{144}Pr, K-internal conversion coeff. of 53 keV transition, penetration study 2—24168
^{144}Pr, transitions, 80 keV, multipolarities 2—38515
^{144}Pr rot. of ang. correl. pattern of 53-80 keV cascade 2—34961
^{149}Pr(p,xn)$^{142-x}$Nd, 10.85 MeV, excitation function meas. 2—5695
^{103,105}Rh, half-lives $^9/_2{}^+$ levels, M1 retardation and E2 enhancement factors of $^9/_2{}^+\rightarrow{}^7/_2{}^+$ transition, $^7/_2{}^+$ level structure 2—14949
^{98}Rh, ^{99}Rh, excited states, from decay of Pd isotopes 2—38508
^{98}Rh, energy level properties from ^{98}Pd→^{98}Rh decay data 2—38546
^{98}Rh→^{98}Ru, half-life meas. and level scheme for ^{98}Ru 2—38546
^{99}Rh beta decay, energy level study of ^{99}Ru 2—34953
^{100}Rh time differential perturbed ang. correl. obs. in Ni 2—40487
^{103}Rh, negative parity states, model interpret. 2—38509
^{103}Rh half-life and magnetic moment determ. 2—5660
^{103}Rh in Fe, ion implanted, study of transient fields 2—7025
^{103}Rh negative parity levels, Coulomb excitation with ^{4}He and ^{16}O ions 2—18117
^{103}Rh polarized beams, relaxation time determ. 2—18116
^{103}Rh(n,n'), threshold detector for neutron spectrum investigations, meas. of activation integral 2—34822
^{103}Rh(n,n')^{103m}In, reaction cross sections 2—31560
^{103}Rh(p,nγ)^{103}Pd, in-beam γ-ray meas. of excited states in ^{103}Pd 2—11757
^{104}Rh, 43 sec and 4.41 min isomers, β^- decay to excited states of ^{104}Pd 2—34955
^{104}Rh decay, m and g isomers, ^{104}Pd levels and transitions 2—21392
^{104m}Rh→^{104}Pd β-decay, use of pneumatic irradiation apparatus with on-line measurement system 2—28001
^{93}Ru→^{93}Tc, γ ray decay, energy levels in ^{93}Tc studied 2—38545
^{94}Ru collective states, assuming paired nucleons 2—18113
^{96}Ru collective states, assuming paired nucleons 2—18113
^{96}Ru(p,α)^{93}Tc, α particle spectrum obs. at 120°, new levels in ^{93}Ti reported 2—38545
^{98}Ru, energy level properties from ^{98}Rh→^{98}Ru decay data 2—38546
^{99}Ru, study using ^{99}Rh beta decay 2—34953
^{102}Ru, collective structure 2—14947
^{102}Ru collective states, assuming paired nucleons 2—18113
^{103}Ru-^{103}Rh^m, low energy internal conversion electrons in $4\pi\beta$ counting, self and foil absorptions 2—14961
^{103}Ru half-life determ. 2—21412
^{106}Ru, levels studied using (t,p) reaction 2—31479
Sb, odd mass isotopes, positive parity level description using unified model 2—14953
Sb (A=126, 128, 130) beta decay scheme construction, quasi-particle levels of Te(A=126, 128, 130) with large spin 2—11799
Sb isotopes, neutron resons. 2—31561
^{117}Sb, g-factor meas. of isomeric state 2—5662
^{118}Sb, 0^+ analogue states, differential cross-sections for reaction ^{117}Sn(p,n)^{117}Sb 2—8340
^{120}Sb, 0^+ analogue states, differential cross-sections for reaction ^{119}Sn(p,n)^{119}Sb 2—8340
^{121}Sb, Mossbauer effect anisotropy in single crystals, 77 K 2—16440
^{121}Sb, spin lattice relaxation in $SbCl_3$ complexes, n.q.r. study 2—19937
^{121}Sb Mossbauer effect in Heusler alloys 2—40633
^{121}Sb Mossbauer effect in Pd_2MnSb alloy 2—33227
^{122}Sb low-lying states study from ^{122}Sn(p,n)^{122}Sb 2—11761
^{125}Sb, reduced transition rates from first excited state to ground state determ. from γ-γ angular correlations in decay of ^{125}mSn 2—28006
^{125}Sb β-decay to states in ^{125}Te, determ. of lifetimes of 35.5 and 465 keV states 2—34958
^{128}Sb 8.9h, β- decay, meas. of γ-ray and conversion electron spectra, ^{128}Te deduced levels 2—34959
^{133}Sb, shell-model predictions 2—8264
^{87}Se, ^{88}Se, ^{89}Se, half-lives determ. neutron emission probabilities and fission yields 2—5726
Sm (A=143, 144), pattern of levels with large spin, spin and parity assignment 2—24169
^{140}Sm, quasirotational groundstate bands 2—18122
^{142}Sm, quasirotational groundstate bands 2—18122
^{144}Sm, elastic and inelastic scattering of α particles and protons, structure of low lying levels studied 2—11857
^{144}Sm (p,p), (p,p'), 50.8 MeV, nuclear models' analysis 2—27985
^{144}Sm(^{3}He,α)^{143}Sm, 18 MeV, spectroscopic factors, momentum mismatch 2—506
^{144}Sm(α,2n)^{146}Gd, hindrance factor of E2 $6^+\rightarrow 4^+$ transition in ^{146}Gd 2—2723
^{144}Sm(e,e'p) reaction, isobaric analogs 2—2770
^{147}Sm, neutron resonances 2—31562
^{147}Sm^{3+} and ^{149}Sm^{3+} ENDOR in $LaCl_3$ 2—37016

Nuclei with 90⩽A⩽149 continued

^{148}Sm (p,p), (p,p'), 50.8 MeV, nuclear models' analysis 2—27985
^{148}Sm(p,p')^{148}Sm, 24.5 MeV, asymmetry measurements of low lying states, coupled channel analysis 2—469
^{149}Sm, neutron resonances 2—31562
^{149}Sm(n,α), cross sections for α transitions using thermal neutrons 2—14992
^{141m}Sm, electron capture decay, population of three quasiparticle multiplet in ^{141}Pm 2—31505
Sn, A=112, 120, 124, E_1 and E_2 transitions, 0 to 30 MeV interval, Fermi systems theory method 2—38511
Sn, even-mass-number-isotopes, effect of T=1 pairing correlations on nuclear deformation 2—31481
Sn, neutron equilibrium pairing 2—38493
Sn (A=116,118,124), charge density distribution parameters, electron scattering studies at 225.0 MeV 2—21393
Sn isotopes, calculation of quadrupole moments for $2_1{}^+$ state 2—31442
Sn isotopes, sub-barrier (p,n) reactions in single particle resonance region 2—11833
^{112}Sn(γ,p)^{111}In, cross section calc. from proton yield curve 2—8324
^{114}Sn, g-factor and half-life of isomeric state 2—38512
^{115}Sn, g-factor meas. of isomeric state 2—5662
^{115}Sn(n,γ)^{116}Sn, structure of low lying excited states of ^{116}SN 2—31484
^{116}Sn, 0^+ to 0^+ transition, strength parameter 2—31482
^{116}Sn, inelastic proton scattering, transitions to collective and non-collective states, DWBA analysis 2—28080
^{116}Sn, structure of low lying excited states populated in ^{115}Sn(n,γ), excitation energies and branching characteristics 2—31484
^{116}Sn excitation by heavy ion scatt. 2—31588
^{116}Sn(^{3}He,d)^{117}Sb*, strength of reaction to unbound final states 2—15005
^{117}Sn, 14.8 MeV (n,2n), (n,p), (n,α) cross sections 2—18213
^{117}Sn, half-life of 158 keV level 2—34957
^{117}Sn, γ-ray internal conversion coeff. 2—18118
^{117}Sn(p,n)^{117}Sb, 4.5 MeV, differential cross-sections near 0^+ analogue states 2—8340
^{118}Sn, g-factor of 7^- isomeric state 2—38512
^{118}Sn, inelastic proton scattering, transitions to collective and non-collective states, DWBA analysis 2—28080
^{118}Sn(t,p), transitions to collective and non-collective states, DWBA analysis 2—28080
^{119}Sn, Mossbauer effect and hyperfine parameters in FeSn 2—29884
^{119}Sn, Mossbauer effect in $BaTiO_3$, study of lower phase transitions 2—29463
^{119}Sn, Mossbauer effect in ferromag. alloys, Fe_3Si and Fe_3Al 2—7058
^{119}Sn, Mossbauer spectra, nuclear Zeeman effect in Gd-Sn alloy 2—13453
^{119}Sn, n.m.r. in $CeSn_3$, mag. ordering obs. 2—6941
^{119}Sn gamma recoilless reson. in rare earth iron garnets, h.f.s. 2—22741
^{119}Sn in YIG:Sn, temp. dependence of acticng hyperfine field 2—4354
^{119}Sn Mossbauer effect in $FeNi_3$ 2—40623
^{119}Sn Mossbauer effect in Ge-Sn solid soln. 2—29886
^{119}Sn Mossbauer effect in MnO 2—13450
^{119}Sn Mossbauer effect in rare gas solids, h.f.s., 4.2 K 2—19981
^{119}Sn n.m.r. in dil. Sn-In(Sb) alloys 2—37014
^{119}Sn(p,n)^{119}Sb, 4.5 MeV, differential cross-sections near 0^+ analogue states 2—8340
^{120}Sn, elastic scatt. of 30 MeV ^{6}Li ions 2—18239
^{120}Sn, inelastic proton scattering, transitions to collective and non-collective states, DWBA analysis 2—28080
^{120}Sn(p,p'γ), proton spin flip probability in excitation of first 2^+ states, 30 MeV 2—24212
^{122}Sn excitation by heavy ion scatt. 2—31588
^{122}Sn(p,n)^{122}Sb, ^{122}Sb low-lying states study 2—11761
^{124}Sn, excitation of particle-hole states by proton inelastic resonance scatt. 2—38513
^{124}Sn, isobaric analog resonances with direct reaction background, inelastic decay, investigation using ^{124}Sn(p,p') reaction 2—2720
^{124}Sn excitation by heavy ion scatt. 2—31588
^{124}Sn(d,p)^{125}Sn, sub Coulomb stripping 2—18237
^{124}Sn(γ,p)^{123}In, cross section calc. from proton yield curve 2—8324
^{124}Sn(p,p'), isobaric analog resonances of ^{124}Sn, inelastic decay with direct reaction background 2—2720
^{124}Sn(p,p'γ), proton spin flip probability in excitation of first 2^+ states, 30 MeV 2—24212
^{119m}Sn, Mossbauer spectroscopy using solid state detector 2—11760
^{125m}Sn, 9.7 min, decay, meas. γ-γ angular correlations of five cascades, deduced ^{125}Sb levels 2—28006
Sn(γ,n), A=114, 116, 117, 119 and 124, from threshold to 27 MeV, cross sections, neutron yield 2—28020
Sn(p,p'), compound-nucleus contrib. 2—2771
Sn(p,t), even isotopes, L=0 transitions analysis using pairing vibr. model, pairing and shell effects 2—31483
Sn(t,p), even isotopes, L=0 transitions analysis using pairing vibr. model, pairing and shell effects 2—31483
Sr isotopes, effective interaction among $1g_{9/2}$ and $2p_{1/2}$ neutrons, shell model calc. 2—11752
^{90}Sr, β decay, probability of production of internal bremsstrahlung 2—11797
^{92}Sr→^{92}Y, gamma-ray spectra, half-life obs. 2—2748
^{159}Tb, 14 MeV, spectra of photons 2—8345
^{93}Tc, energy levels, from ^{92}Mo(d,n) reaction 2—2717
^{93}Tc, high spin proton states, from ^{92}Mo(α,t) reaction 2—2696
^{93}Tc, study of levels up to a few MeV with ^{92}Mo(^{3}He,d)^{93}Tc reaction 2—28079
^{93}Tc levels populated in decay of ^{93}Ru and by the ^{96}Ru(p,α) reaction 2—38545
^{94}Tc, high spin proton excited states population in ^{92}Mo(α,d) reaction 2—31478
^{94}Tc decay, meas. of delayed γ-rays, comparison with data on ^{94}Mo levels indicate isomeric $(g_{9/2})^2$ proton state 2—14960
^{95}Tc, energy levels, from ^{94}Mo(d,n) reaction 2—2717
^{97}Tc, energy levels, from ^{96}Mo(d,n) reaction 2—2717
^{99}Tc, $\gamma\gamma$ ang. correlations and level lifetimes rel. to quantum characteristics of excited levels 2—11756
^{99}Tc Coulomb excitation with 52-64 keV ^{35}Cl ions, deduced level structure and lifetimes 2—18115
^{99}Tc γ cascades, directional correl. and multipole mixing 2—34954
^{99}Tc^m, low energy internal conversion electrons in $4\pi\beta$ counting, self and foil absorptions 2—14961
^{99m}Tc, E3 isomeric transition decay in ferroelec. $BaTiO_3$ 2—33056

Nuclei with 90⩽A⩽149 continued
Te, A=121, 123, 125, 127, 129, M4 transitions, ratios of internal conversion coefficients 2—38548
Te, separation into ground and metastable state isomers, γ-ray spectra 2—2719
Te (A=128, 130), 14.8 MeV (n,2n), (n,p), (n,α) cross sections 2—18213
^{121}Te, total particle parameter of 212keV transition 2—14952
^{122}Te, two-quasiparticle states, level systematics 2—8304
^{122}Te study of levels populated by (^{3}He,d) and (p,t) reactions 2—18119
^{124}Te, two-quasiparticle states, level systematics 2—8304
^{124}Te study of levels populated by (^{3}He,d) and (p,t) reactions 2—18119
^{125}Te, 35.5 keV level, gamma-gamma angular correlations 2—14954
^{125}Te, angular correlation study of 322-177 keV cascade 2—8305
^{125}Te, ion implantation perturbed angular correlation study of 443 and 463 keV levels 2—5663
^{125}Te Mossbauer effect in tellurides 2—4446
^{126}Te, two-quasiparticle states, level systematics 2—8304
^{127}Te, low energy internal conversion electrons in $4\pi\beta$ counting, self and foil absorptions 2—14961
^{128}Te, revised level scheme 2—8306
^{128}Te levels populated in 8.9h β- decay of ^{128}Sb, obs. of positive and negative-parity states 2—34959
^{129}Te Mossbauer effect in alkali halides 2—10319
^{134}Te shell-model predictions 2—8264
^{121}Xe→^{121}I decay scheme 2—14965
^{130}Xe, energy level excitation during β decay of ^{130}I, ^{13o*}I 2—24184
^{130}Xe, energy level excitation during γ decay of ^{130}I, ^{130*}I 2—24184
^{132}Xe, E2/M1 mixing ratios of $2_2{}^+\rightarrow 2_1{}^+$ gamma transition and corresponding E2% admixture determ. 2—2721
^{132}Xe, excited levels, ^{132}I decay obs. 2—5676
^{135}Xe, low energy neutron cross section analysed using S-matrix and R-matrix theory, different energy dependence of resonance widths related to unitarity 2—28044
^{143}Xe, fission prod. nuclide, identification, half life and γ-ray spectra 2—11886
^{90}Y, B decay, probability of production of internal bremsstrahlung 2—11797
^{90}Y, γ-decay of levels up to 3.2 MeV, study from ^{89}Y(d,pγ) and ^{87}Rb(α,nγ) 2—18112
^{90}Y, shell model structure, l=5 transition data from 89Y(d,p) and ^{89}Y(α, ^{3}He) 2—34950
^{92}Y level scheme obs. from ^{92}Sr decay 2—2748
^{94}Y decay, meas. energies and intensities of β- and γ-ray transitions, deduced levels ^{94}Zr 2—2749
^{94}Y→^{94}Zr decay scheme and new ^{94}Y transitions obs. 2—18161
^{95}Y→^{95}Zr decay scheme, γ-spectra study 2—18161
^{96}Y→^{96}Zr decay, new γ-transitions meas. 2—18161
^{90}Zn, 11.8 MeV elastic scattering of deuterons, derivation of optical potential 2—2796
Zr, A=90-92, 94, 96, elastic scattering of electrons, diff. cross sections at 300 MeV meas. 2—11820
Zr, A=91, 93, fluorescence after thermal neutrons capture and levels 2—38503
Zr, photonuclear giant dipole resonance, evidence for isobaric spin splitting 2—38561
Zr collective states excitation by 14 MeV neutrons 2—14990
^{90}Zr, (^{3}He,t) transitions isobaric analog ground states, energy dependence 2—31583
^{90}Zr, B(E2) for first 2^+ state 2—21390
^{90}Zr, elastic electron scattering, 200 and 300 MeV 2—18177
^{90}Zr, excitation functions and isomer ratios for (n,2n), (n,α) and (n,p) reactions 2—35056
^{90}Zr, fractionation of pair vibrational state 2—11753
^{90}Zr, ground state props. calc. using relativistic self consistent meson field theory 2—11704
^{90}Zr, neutron bombardment, isobaric analogue states in ^{91}Zr 2—38504
^{90}Zr, neutron inelastic scatt. cross section 2—2783
^{90}Zr, photoneutron cross section 2—38573
^{90}Zr, scattering, elastic and inelastic, of 185 MeV protons, differential cross sections and polarizations 2—8335
^{90}Zr alpha particle elastic scattering, method of resolving real well depth ambiguities in optical model analysis 2—11856
^{90}Zr magic number nucleus, high energy states, using ^{90}Nb decay 2—478
^{90}Zr(^{3}He,d)^{91}Nb, isobaric energy splitting between $T_>$- and $T_<$-single particle states 2—2716
^{90}Zr(^{3}He,t), 21.4 to 37.5 MeV, energy dependence of transitions to isobaric analogue ground states 2—31583
^{90}Zr(α,t)^{91}Nb, high spin proton states of ^{91}Nb 2—2696
^{90}Zr(γ,p)^{89}Y, search for isobaric analogue states 2—38574
^{90}Zr(p,α)^{87}Y, computation of pick-up form factors 2—2774
^{90}Zr(p,p′), excitation by 61.2 MeV protons of various states, differential cross sections 2—21429
^{91}Zr, isobaric analogue states excited by neutron bombardment of ^{90}Zr 2—38504
^{91}Zr 2p-1h states, S- and P-wave neutron spectroscopy, neutron doorway escape widths determ. using theory of intermediate structure 2—24159
^{91}Zr(p,n), isobaric analogue resonances in ^{92}Nb 2—5694
^{91}Zr(p,nγ)^{91}Nb, excited states determ. for ^{91}Nb 2—2715
^{91}Zr(p,t)^{89}Zr, E_p=51.7 MeV 2—38600
^{91}Zr(p,t)^{89}Zr, zero range DWBA anal. 2—38601
^{91}Zr(π^+,π^0)^{91}Nb, single charge exchange obs. by detecting decay proton from ^{91}Nb*, determ. cross section at 30 MeV 2—18215
^{92}Zr, α pickup, reaction cross section 2—11868
^{92}Zr(p,α)^{89}Y, computation of pick-up form factors 2—2774
^{93}Zr, level scheme, ^{93}Y decay study 2—38505
^{94}Zr, level scheme deduced from ^{94}Y decay 2—2749
^{94}Zr, modified level scheme from ^{94}Y decay 2—18161
^{94}Zr, neutron absorption cross sections, activation technique meas. 2—495
^{94}Zr(α,3n)^{95}Mo, 12-43 MeV, study of high spin levels in ^{95}Mo 2—21391
^{95}Zr, partial level scheme from ^{95}Y decay 2—18161
^{95}Zr half-life determ. 2—21412
^{96}Zr, neutron absorption cross sections, activation technique meas. 2—495
^{96}Zr(p,nγ)^{96}Nb, ^{96}Nb low-lying states study 2—11754
^{98}Zr, evidence for $J^\pi=o^+$ first excited state through meas. of internal conversion electrons from fission products 2—11755
Zr(α,d)Nb, 50 MeV, high spin proton excited states population 2—31478
Zr(α,t)Nb, 50 MeV, high spin proton excited states population 2—31478
Zr(p,p′), compound-nucleus contrib. 2—2771

Nuclei with 150⩽A
152<A<160, properties of β, γ vibrational bands 2—24170

Nuclei with 150⩽A continued
^{177}Hf transitions, penetration effects in internal conversion 2—38521
^{194}Au decay, exptl. investigation 2—11805
^{232}Th, independent yields of ^{133}I, ^{134}I and ^{135}I, reactor neutron induced 2—5727
^{232}Th neutron-induced fission, search for intermediate substructures in the fission cross section 2—31608
^{234m}Pa decay, gamma radiation obs. 2—24192
Z⩾114, possible existence of closed shells 2—5629
A=180-212, fission barriers calc. in two centre shell model using Strutinsky prescription 2—11876
A=200, neutron bound S-states, Woods-Saxon potential calc. 2—2673
A=200, neutron bound S-states, Woods-Saxon potential calc. 2—2673
A<226, influence of shells and pairing on the fission probabilities 2—31594
actinide nuclei, evidence for 2 shape isomers from fission studies in double humped barrier region 2—24149
actinide nuclei, sub Coulomb transfer reactions at low energy, cross section study 2—35066
actinides, 0^+ excited states 2—38479
actinides, 229⩽A⩽257, quasiparticle and vibrational excitations, evidence from radioactive decay meas. 2—21401
actinides, non collective description of low lying 0^+ states excited in (p,t) reactions 2—14940
actinides, odd-A with Z⩾100, nuclear spectroscopy and single particle states 2—21404
actinides, single nucleon transfer reactions rel. to nuclear structure studies 2—21420
average cross-section, neutrons of fission type reactor spectrum and γ-ray intensities of ^{231}Th 2—5705
deformed even-even rare-earth nuclear, spin-dependent force effect on moment of inertia 2—18127
doubly even actinide nuclei, α-decay, γ-ray spectra study, deduced levels of product nuclei 2—11780
doubly even actinide nuclei, prod. by α-decay deduced level energies of ground state rot. by bands 2—11780
effective quadrupole charges in the lead region 2—21371
element 104 isotopes possible prod. in heavy-ion bombardment of transuranic nuclei 2—14902
heavy nuclei, potential energy of deformation, fission barrier hts. 2—31595
heavy nuclei (A⩾130), preformation of α particles by analysis of (n,α) reactions 2—21436
rare earth isotopes, moments of inertia as function of neutron number 2—2726
rare earth nuclei in copper, time-dependent ang. correlations meas. 2—7021
rare earth products of 28 GeV proton interaction with U, determ. charge and mass distribution 2—11834
rare-earth isotopes, neutron capture cross-sections determ. by mass spectrometer 2—496
rare-earth nuclei, (d,t) reaction, angular distributions, two step model 2—38643
sample preparation for det. of ^{239}Pu, ^{241}Am and ^{242}Cm by liquid scintillation counting 2—14039
shell model states around ^{208}Pb, effective magnetic moment operator 2—27996
super-heavy, mass number >250, production of 2—11932
super-heavy nuclei, production using heavy ion accelerator 2—11696
superheavy, detection using mass recoil spectrograph 2—11929
superheavy element models, recent developments 2—34885
superheavy elements, possibility of occurrence in nature 2—24148
superheavy elements, recent theoretical developments 2—21403
superheavy elements, search in natural materials 2—34869
superheavy elements, synthesis using Kr bombardment of compound nuclei 2—21451
superheavy nuclei, formation by Kr bombardment of U, detection by mass measurement of fission products 2—21452
superheavy nuclei, potential energy of deformation, fission barrier hts. 2—31595
superheavy nuclei, prod. by bombardment of U or Pu with heavy ions 2—471
superheavy nuclei, stability against fission, alpha decay and electron capture 2—21454
superheavy nuclei, Z=112, 116, A=224-480 r.m.s. and binding energies 2—27998
trans bismuth nuclei, fission fross sections and spallation yields, >0.6 GeV 2—31593
transuranic, production from ^{238}Pu 2—27935
transuranium nuclides, formation, production and uses 2—11695
U, natural, cumulative fission yields of ^{66}Ni, ^{67}Cu, ^{172}Er, ^{175}Yb, ^{177}Lu 2—35097
W, A=182,184,186, Coulomb excitation of 2^+ states by ^{4}He, p and ^{16}O, B(E2) values 2—18142
(n,2n) reactions in medium-, heavy-meass region, 14-15 MeV, determ. activation cross sections, isomeric cross section ratios, systematics 2—35047
Dy, effect of nuclear deformation on K^- absorption 2—499
^{239} Pu fission, absolute meas. of α for neutron energies of 10 keV to 1 MeV 2—31603
$^{170, 172, 174, 176}$Yb(p,p′), 10-15 MeV, excitation functions leading to 0^+, 2^+, 4^+ and 6^+ states of ground state rot. bands, IAR study 2—18136
$^{180, 182}$W, relative quadrupole moments of first excited states, Mossbauer effect meas. after Coulomb excitation 2—11773
^{236*}U, fission, following thermal neutron irradiation of ^{235}U, search for long range fission products 2—24247
^{298}114, ground state props. calc. using relativistic self consistent meson field theory 2—11704
^{235}(d,p)^{236m}U, production of shape isomer via decay of class/states due to compound motion 2—11782
^{a}Hf, A=177, 179, 180, electric quadrupole and magnetic dipole moments of $^3F_2$ ground state determ. by atomic beam magnetic resonance meas. 2—18141
^{a}Pt(^{16}O,^{16}O′γ), A=194-196, 198, 35 MeV, meas. of hyperfine interactions of Pt nuclei recoiling into He, vacuum, g-factors determ. 2—38648
^{222}Ac, 66 sec isomer from bombardment of Pb with ^{18}O, decay with α emission 2—34994
^{225}Ac, α-spectrum, splitting of 5793 keV doublet 2—38554
^{227}Ac, det. of ^{227}Ac and ^{228}Th isotopes formed during irradiation in SM-2 reactor 2—40836
^{228}Ac→^{228}Th, excited level obs. from γ-γ coincidence meas. 2—483

Nuclei with 150$\leqslant$A continued
^{228}Ac$\rightarrow$^{228}Th, γ-spectra, level scheme of ^{228}Th 2—11808
^{228}Ac$\rightarrow$^{228}Th decay, internal conversion electrons 2—8317
Am, A=245, 246, spotnaneously fissioning isomers identification 2—31602
^{232}Am, neutron-deficient nucleus, explanation of retarded fission 2—31601
^{234}Am, neutron-deficient nucleus, explanation of retarded fission 2—31601
^{238}Am, electron capture decay 2—38530
^{241}Am, α-γ directional correl. in polycryst. source 2—34916
^{241}Am, neutron, absorption cross section meas. 2—498
^{241}Am(n,γ)^{242}Am fast neutron radiative capture cross-sections 2—11847
^{242}Am β-decay, det. of relative probability 2—38556
^{242}Am from ^{241}Am fast neutron radiative capture, spontaneous fission cross-section 2—11847
^{243}Am, isomer states, spontaneously fissioning, excitation in inelastic scatt. of γ quanta 2—15026
^{243}Am(n,γ)^{244}Am fast neutron radiative capture cross- sections 2—11847
^{244}Am from ^{243}Am fast neutron radiative capture, spontaneous fission cross-section 2—11847
^{205}At, three quasiparticle excitation in reaction ^{197}Au(^{12}C,4n)^{205}At 2—18147
^{207}At, decay to levels in ^{297}Po, level and transition study 2—18148
^{209}At decay scheme, γ-ray assignment and excited states 2—21415
^{209}At electron capture decay to levels of ^{209}Po, coupling of single-neutron-hole states obs. in ^{209}Po 2—31494
^{211}At, produced through ^{40}Ar+^{209}Bi transfer reactions, determ. excitation function and recoil ranges 2—11875
^{213}At, fission, fragment mass and charge distrib. 2—35085
Au, binary fission cross-section induced by 29-GeV ^{14}N ions meas. 2—35093
Au photofission, 250 to 1000 MeV, fragments angular distrib. meas. 2—15027
^{195}Au decay, precision determ. of high-Z K-shell fluorescence yields 2—15205
^{195}Au(n,2n) cross sections to 12^{-}, 5^{+} and 2^{-} states of ^{196}Au 2—2731
^{196}Au, 12^{-}, 5^{+}and 2^{-} states populated in (n,2n) reactions 2—2731
^{196}Au, mag. moment of 12- isomer, determ. by low temp. nuclear orientation 2—2732
^{197}Au, elastic scatt. of 30 MeV ^{6}Li ions 2—18239
^{197}Au, half-lives of some excited states meas. using delayed coincidence technique 2—24165
^{197}Au, half lives of short lived excited states 2—34948
^{197}Au, heavy-ion induced fission energetic balance 2—31610
^{197}Au n.m.r. in ordered Au$_4$Mn alloy 2—16656
^{197}Au(^{12}C, 4n)^{205}At, three quasiparticle excitation of ^{205}At 2—18147
^{197}Au(n,γ)^{198}Au cross-section at 22.8 keV, Monte Carlo calculation of neutron energy spectrum 2—5704
^{197}Au(p,p), using polarized protons, differential cross sect. and polarization meas., 11-14 MeV 2—14984
^{198}Au(n,γ)^{199}Au, level scheme ^{199}Au below 1 MeV, examination, determ. of level energies 2—5669
^{198}Au$\rightarrow$^{198}Hg decay, ang. correl. of 676-412 keV cascade 2—34976
^{198}Au$\rightarrow$^{198}Hg decay, angular correlation of γ-γ cascade 676-412 keV studied, mixing ratio of 676 keV transition determ. 2—31512
^{199}Au, core excitation model treatment of low lying levels, level sequence 2—27995
^{199}Au, level scheme below 1 MeV and level energies from ^{198}Au(n,γ) reaction 2—5669
^{202}Au, decay after production by ^{202}Hg (n,p), and ^{205}Tl (n,α) reactions 2—31513
^{202}Au, half life determ. and γ emission meas. based on beta counting 2—34992
^{204}Au, 40$\pm$3s activity assigned from ^{204}Hg(n,p) reaction 2—31513
^{197m}Au, half-life measurement 2—27980
Au(d,np)Au, 12 MeV, deuteron break up under Coulomb interaction of nucleus 2—35079
^{130}Ba(n,2p)^{131}Xe origin of excess ^{131}Xe in lunar rocks 2—7506
Bi, binary fission cross-section induced by 29-GeV ^{14}N ions meas. 2—35093
Bi, excitation rel. to hyperfine spectra of L and K X-ray emission from muonic atom 2—18370
Bi, proton scattering, angular distributions for particles in 2 to 30 keV range 2—11824
^{203}Bi decay, high resolution γ-ray studies, conversion coeffs. for transitions in ^{203}Pb 2—34993
^{204}Bi decay, high resolution γ-ray studies, conversion coeffs. for transitions in ^{204}Pb 2—34993
^{204}Bi mag. hyperfine interaction in Fe and Ni 2—29858
^{207}Bi, g-factors of $^{21}/_{2}{}^{+}$ isomer, stroboscopic meas. 2—38526
^{207}Bi, mag. moments 2—5670
^{207}Bi decay, K-X-ray γ directional correlations 2—18107
^{207}Bi decay, precision determ. of high-Z K-shell fluorescence yields 2—15205
^{208}Bi, force dependence of 0^{+} states 2—21399
^{209}Bi, 77.3 MeV-^{4}He induced fission, mass and energy distribs., test of liquid drop model 2—24249
^{209}Bi, analysis of muonic atom isomer shift 2—12063
^{209}Bi, charged particle induced, determ. ^{134}Cs and ^{115}Cd isomer ratios 2—11884
^{209}Bi, fast-neutron scattering, angular distributions 2—18202
^{209}Bi, heavy-ion induced fission energetic balance 2—31610
^{209}Bi, level structure from study of ^{210}Po IAR's in ^{209}Bi(p,p′) reaction 2—21400
^{209}Bi, Raman scattering of 10.38 MeV photons 2—24200
^{209}Bi, transfer reactions with ^{40}Ar, 190 to 270 MeV, determ. excitation function and recoil ranges of produced ^{211}At 2—11875
^{209}Bi α-decay, theoretical and exptl. investigation of half-life 2—38553
^{209}Bi comparison of energy levels excited by nonresonant 16.10 MeV proton scattering of 14.95 MeV scattering from isobaric analogue states 2—24175
^{209}Bi polarized target, production via low temp. polarization of Bi isotopes in ferromagnetic BiMn 2—36802
^{209}Bi(α,^{3}He)^{210}Bi, multiplet structure of ^{210}Bi 2—38529
^{209}Bi(d,p)^{210}Bi, 17.0 MeV, shell model structure of ^{210}Bi 2—24176
^{209}Bi(d,p)^{210}Bi, multiplet structure of ^{210}Bi 2—38529
^{209}Bi(p,2p)^{208}Pb, obs. of IAR's in ^{210}Po, as enhancements in excitation function 2—14959
^{209}Bi(p,α), level densities of near doubly magic nuclei 2—38527
^{209}Bi(p,p′), 14-21 MeV, ^{210}Bi and ^{209}Bi deduced level structure from ^{210}Po IAR's 2—21400

Nuclei with 150$\leqslant$A continued
^{209}Bi(p,p), using polarized protons, differential cross sect. and polarization meas., 11-14 MeV 2—14984
^{210}Bi, β decays, K-shell auto-ionization probability 2—18165
^{210}Bi, level structure from study of ^{210}Po IAR's in ^{209}Bi(p,p′) reaction 2—21400
^{210}Bi, multiplet structure from ^{209}Bi(d,p and ^{209}Bi(α,^{3}He) reactions 2—38529
^{210}Bi, shell model structure from ^{209}Bi(d,p) reaction at 17.0 MeV 2—24176
^{210}Bi, two-particle states, calc. with realistic forces 2—18149
^{211}Bi, level scheme from ^{211}Pb decay 2—27997
^{211}Bi, shell-model and β-decay calculations 2—2757
^{309}Bi, inelastic deuteron scattering, 13.1 MeV 2—18222
Bi(n,n) elastic and inelastic scatt., 14.8 MeV, differential cross sect., collective state excitation 2—21434
Bk, A=242, 244, spontaneously fissioning isomers identification 2—31602
^{249}Bk(^{16}O,4n)^{261}Ha, α-emitting isotope production 2—2740
^{249}Bk(^{18}O,5n)^{262}Ha, α-emitting isotope production 2—2740
^{249}Cf, fission cross section for thermal and fast neutrons 2—38662
^{249}Cf, neutron induced fission, mass distribution of fission products 2—5723
^{249}Cf, thermal-neutron fission cross sections and resonance integrals meas. 2—28088
^{249}Cf, thermal neutron induced fission, fractional independent yield of ^{140}La, nuclear charge distrib. 2—35091
^{249}Cf decay, L$_1$ subshell fluorescence and Coster-Kronig yields 2—21496
^{249}Cf decay, L$_2$ and L$_3$ subshell fluorescence and Coster-Kronig yields for Z=96 2—2933
^{249}Cf fission by neutrons at 0.16 to 1.6 MeV, cross section 2—15025
^{249}Cf fission by thermal neutrons, neutron yield and kinetic energy of fragments 2—15024
^{250}Cf(^{15}N,4n)^{261}Ha, α-emitting isotope production 2—2740
^{252}Cf, α-decay and associated L X-rays of Cm 2—18306
^{252}Cf, α-particle accompanied fission, ang. correlation 2—38659
^{252}Cf, fission, charge and mass distrib. determ. 2—2829
^{252}Cf, fission fragment γ-ray transitions, X-ray γ-ray coincidence study 2—2830
^{252}Cf, fission products, internal conversion cascades, X-ray coincidence study 2—2831
^{252}Cf, spontaneous fission, obs. of γ-rays from fission fragments 2—31611
^{252}Cf, spontaneous fission, K X-ray studies 2—38660
^{252}Cf, spontaneous fission, fragment K X-ray emission and nuclear charge distribution 2—11882
^{252}Cf asymmetrical fission, potential energy of heavy nuclei 2—8376
^{252}Cf fission fragments, energy loss measurements in elementary gases and solids as compared with theory 2—8377
^{252}Cf fission fragments, energy loss in composite systs., expt. 2—38666
^{252}Cf fission fragments energy straggling through air 2—8374
^{252}Cf fission product trace analysis by electron microscopy 2—21333
^{252}Cf fragments of specified atomic numbers, study of multiplicities of K X-rays 2—11883
^{252}Cf loaded fission ionization chamber, timing resolution 2—31373
^{252}Cf sources in tissue, calculated depth dose tables 2—41306
^{252}Cf spontaneous fission, neutron spectrum, fine structure 2—8370
^{252}Cf synthesis in underground thermonuclear explosion 2—35094
^{254}Cf asymmetrical fission, potential energy of heavy nuclei 2—8376
Cm, A=243, 245, spontaneously fissioning isomers identification 2—31602
^{242}Cm, asymmetric fission, two- centre shell model 2—15020
^{244}Cm, α-decay, self-radiation damage in CmO$_x$ and CmAlO$_3$ 2—12993
^{244}Cm, thermal-neutron fission cross sections and resonance integrals meas. 2—28088
^{244}Cm decay, L$_2$ and L$_3$ subshell fluorescence and Coster-Kronig yields for Z=94 2—2933
^{244}Cm spontaneous fission, prompt neutrons and kinetic energy of fragments 2—15021
^{245}Cm, thermal-neutron fission cross sections and resonance integrals meas. 2—28088
^{246}Cm, electron binding energy calc. from X-ray spectra and L-shell fluorescence yields 2—11784
^{246}Cm, thermal-neutron fission cross sections and resonance integrals meas. 2—28088
^{247}Cm, thermal-neutron fission cross sections and resonance integrals meas. 2—28088
^{248}Cm, population of 0^{+} states by (p,t) reaction 2—34920
^{248}Cm, thermal-neutron fission cross sections and resonance integrals meas. 2—28088
^{250}Cm synthesis in underground thermonuclear explosion 2—35094
^{155}Dy$\rightarrow$^{155}Tb decay, excited level obs. 2—24187
^{157}Dy levels deduced from ^{157}Ho decay using multidimensional coincidence device 2—34965
^{158}Dy, moment of inertia by excitation of ground-state band to spin 22 2—34966
^{158}Dy, nuclear moment of inertia at high rotational frequencies, levels populated with (α,xn) reaction 2—27988
^{160}Dy, formed in β-decay of ^{160}Tb study of hyperfine fields, in search for atomic after effects 2—18167
^{160}Dy, lifetimes of 2^{+}, 4^{+} states obs. 2—2726
^{160}Dy, mixing parameter for mixing of gamma vibrational and ground state bands 2—24171
^{160}Dy, nuclear moment of inertia at high rotational frequencies, levels populated with (α,xn) reaction 2—27988
^{160}Dy, transitions internal conversion coeffs. 2—38517
^{161}Dy, 26 keV Mossbauer transition, determ. of L-shell conversion coefficient 2—2728
^{161}Dy, interference of photoelectric and nuclear resonance absorption of 26 keV E1 γ rays studied by transmission and scattering Mossbauer expts. 2—2727
^{161}Dy, Mossbauer effect, in DyM, M=Cu, Ag, Zn, Rh 2—26125
^{161}Dy, neutron resonance, spin assignment 2—18131
^{161}Dy, rotation-particle coupling in ground state band studied using ^{160}Gd(α,3n)^{161}Dy reaction 2—31490
^{162}Dy, multiple Coulomb excitation of γ-vibrational bands using ^{16}O ions 2—14955
^{163}Dy, neutron resonance, spin assignment, hyperfine coupling constants 2—18131
^{165}Dy, β decay, level scheme of ^{165}Ho 2—21396
^{165m}Dy, β decay, level scheme of ^{165}Ho 2—21396
Er, A=164, 166, 167, 168, 170, neutron resonance spectroscopy, level spacings, Dyson's theory 2—34967

Nuclei with 150⩽A continued
Er, A=166, 168, 170, F test for missing levels, l=0 population 2—34969
Er, even A isotopes, distrib. of spacings between neutron capture levels 2—31453
Er, fast-neutron scattering, angular distributions 2—18202
Er (A=166, 168, 170) multiple Coulomb excitation of γ-vibrational bands using ^{16}O ions 2—14955
^{161}Er, decay to levels in ^{161}Ho 2—31508
^{162}Er, bombardment with 110 MeV ^{3}He particles, production of new α emitting isotopes ^{155,156}Tm 2—11801
^{162}Er, nuclear moment of inertia at high rotational frequencies, levels populated with (α,xn) reaction 2—27988
^{166}Er in Cu, time differential studies 2—7023
^{167}Er, n.m.r. in Er metal, 1.4K 2—33353
^{169}Er, β decays, K-shell auto-ionization probability 2—18165
^{171}Er β-decay to levels of ^{171}Tm, γ-ray transition properties 2—34970
^{172}Er, β-decay to levels of ^{172}Tm, proposed level scheme 2—18135
^{172}Er, cumulative yield in natural U fission 2—35097
^{167m}Er, half-life measurement 2—27980
^{254}Es, thermal-neutron fission cross section and fission resonance integral meas. by plastic fission track recorders 2—35087
Eu(A=153, 155) excited level lifetime and g-factor meas. at 103.2 and 105 keV 2—11768
^{151}Eu, Mossbauer effect in EuSe:Gd(La) 2—13444
^{151}Eu, muon capture, populations of individual final levels 2—18180
^{151}Eu^{2+}, ^{153}Fu^{2+}, ENDOR obs. in CdF$_2$, SrF$_2$, BaF$_2$, hyperfine interactions 2—30030
^{151}Eu isomer shift in EuF$_2$ and CaF$_2$:Eu^{2+} 2—19982
^{151}Eu Mossbauer effect in Eu$_2$TiO$_4$, h.f.s., quadrupole moment ratio 2—33218
^{151}Eu n.m.r. in EuFe garnet 2—36744
^{151}Eu n.m.r. in EuSe 2—10546
^{152}Eu decay, L/K electron capture ratio 2—38532
^{153}Eu, muon capture, populations of individual final levels 2—18180
^{153}Eu, muonic isomer shifts of γ-ray transitions, mean square radius of ground and excited states 2—18130
^{153}Eu n.m.r. in EuSe 2—10546
Fm isotopes, fission, mass division symmetry 2—21453
^{254}Fm, asymmetric fission, two- centre shell model 2—15020
^{254}Fm, fission, fragment mass and charge distrib. 2—35085
^{254}Fm, search for production by secondary nuclear reactions of 11.5 GeV protons on ^{238}U 2—28038
^{256}Fm, search for production by secondary nuclear reactions of 11.5 GeV protons on ^{238}U 2—28038
^{257}Fm, symmetry in mass distribution shown to be due to approach to ^{264}Fm nucleus 2—11877
^{257}Fm synthesis in underground thermonuclear explosion 2—35094
^{258}Fm, fission, fragment mass and charge distrib. 2—35085
Gd(A=20, 22), reactions with ^{22}Ne and ^{20}Ne, production of W isotopes 2—11769
^{150}Gd, excited state population in β decay of new 5.8 min ^{150}Tb isomer 2—31506
^{152}Gd, high spin state population via ^{152}Sm(α,4n) reaction 2—21395
^{152}Gd, level structure studies in 17.5h ^{152}Tb decay 2—11767
^{153}Gd, 363-keV γ-radiation, parity violating asymmetry 2—2750
^{153}Gd, high spin state population via ^{152}Sm(α,3n) reaction 2—21395
^{153}Gd, K capture decay, angular correlation, sum-peak coincidence spectra 2—481
^{153}Gd from ^{152}Sm(α,3nγ), high-spin states γ-spectroscopic study 2—18128
^{154}Gd, 123 keV K, L and M shell particle parameters 2—34964
^{154}Gd, multipolarity of 693 keV $2^{+\prime}\rightarrow2^{+}$ transition investigated 2—2725
^{154}Gd from ^{152}Sm(α,2nγ), high-spin states γ-spectroscopic study 2—18128
^{155}Gd, hyperfine struct. in GdIG, Mossbauer and n.m.r. obs. 2—7140
^{155}Gd, Mossbauer effect in double oxides, quadrupole splitting, isomer shift 2—10326
^{155}Gd, n.m.r. in Gd$_2$Co$_7$, 77K 2—4555
^{155}Gd(n,γ)^{156}Gd, gamma-ray transitions in ^{156}Gd 2—27987
^{156}Gd, gamma-ray transitions studied using ^{155}Gd(n,γ)^{156}Gd 2—27987
^{156}Gd, γ-γ directional correlation meas., M1 admixtures of transitions 2—31487
^{157}Gd, n.m.r. in Gd$_2$Co$_7$, 77K 2—4555
^{159}Gd, 363-keV γ-radiation, parity violating asymmetry 2—2750
^{160}Gd(α,3n)^{161}Dy, rotation-particle coupling in ground state band of ^{161}Dy 2—31490
^{157}Ge, perturbation effect on K- absorpt. 2—38628
^{261}Ha, new α-emitting isotope (Z=105), prod. by ^{250}Cf(^{15}N,4n) and ^{249}Bk(^{16}O,4n) 2—2740
^{262}Ha, new α-emitting isotope (Z=105), prod. by ^{249}Bk(^{18}O,5n) 2—2740
Hf recoiling into vacuum, perturbed γ-ray angular distributions 2—31491
^{172}Hf, half-life 2—11802
^{174}Hf, energy levels from ^{174}Ta decay 2—18137
^{176}Hf, half-life of 1247.7 keV level meas. in decay of ^{176}Ta, deduced E1M2E3 mixing of 1159.3 keV level 2—18140
^{177}Hf, internal conversion of 208keV E1 transition 2—14957
^{177}Hf, M1 and E2 transitions 2—38551
^{178}Hf, E0 and E2 transition probabilities 2—34972
^{178}Hf, level structure, study of decay of ^{178}Ta 2—11771
^{178}Hf(n,γ)^{179}Hf, investigation of low energy excited state structure of ^{179}Hf 2—38510
^{179}Hf, low energy excited state structure, investigation by ^{178}Hf(n,γ)^{179}Hf reaction 2—38510
^{180}Hf, magnetic moment of 1142 keV 8- state, two-quasiparticle state of Mossbauer experiments 2—8309
^{180}Hf, parity admixtures in nuclear forces γ transition study 2—31489
^{183}Hf, nonexistence of metastable state of 91 d half life 2—24190
^{179m}Hf, half-life measurement 2—27980
^{180m}Hf, 501-keV γ-radiation, parity violating asymmetry 2—2752
Hg (A=183,185), nuclear charge distribution obs. using optical pumping technique 2—27992
Hg isotopes, deformation energies for β_2, β_4 and γ distortions 2—27993
^{190}Hg, excited levels and 24.5 ns isomer, ^{181}Ta(^{14}N,5n) study 2—38523
^{197}Hg, 133 keV state, lifetime and g-factor by perturbated angle e$_{casc}$ γ correlation method 2—38524
^{198}Hg, low-energy level struct. 2—2733
^{198}Hg 676 keV transition, mixing ratio, ang. correl. obs. 2—34976
^{199}Hg, 13/2^{+} isomeric state decay modes determ. gamma-ray spectra obs. 2—5668
^{199}Hg, 208 keV state, IMPAC technique, measurement of precession angle 2—2697
^{199}Hg, half-life of 208.1 keV level and internal conversion coeffs. 2—38525

Nuclei with 150⩽A continued
^{199}Hg, slow neutron capture, meas. of conversion electron coeffs. and level scheme of ^{200}Hg 2—21397
^{200}Hg, level scheme and conversion electron coefficients from slow neutron capture in ^{199}Hg 2—21397
^{202}Hg (n,p), study of decay of ^{202}Au 2—31513
^{203}Hg, study of 279 keV transition to ^{203}Tl angular correlation meas. of asymmetry, deduced limit of parity mixing 2—2736
^{203}Hg$\rightarrow$^{203}Tl, β-γ directional correlation measurement for transition reveals parity violation in ^{203}Tl 2—11806
^{197m}Hg, decay, after effects, relaxation and recombination time constants 2—38541
^{199m}Hg, hyperfine structure and isomeric shift 2—34977
Ho, reactions with ^{22}Ne and ^{20}Ne, production of Ir isotopes 2—11772
^{157}Ho decay meas. γ-ray intensities, γ-γ coincidence with Ge(Li), Si(Li) detectors, ^{157}Dy levels deduced 2—34965
^{161}Ho levels, study from ^{161}Er decay 2—31508
^{163}Ho, rotational states differing by ΔK=2, 3, 4, evidence for configuration mixing 2—38519
^{164}Ho, spectra, static moments and transition probabilities 2—38518
^{165}Ho, level scheme from study of β decay of ^{165}Dy and ^{165m}Dy, Coriolis coupling between bands 2—21396
^{165}Ho, neutron cross section, parametric fit 2—497
^{165}Ho, nuclear quadrupole moment meas. by proton scattering from aligned target 2—34968
^{165}Ho n.m.r. in Ho alloys and intermetallics 2—10549
^{165}Ho n.m.r. in Ho metal 2—10550
Ir(A=179, 180, 181), production by irradiation of Ho with ^{22}He and ^{20}Ne 2—11772
Ir(^{14}N,xnγ) reaction study of isomeric states in neutron-deficient Po isotopes 2—21379
^{189}Ir, E2 and M1 transition probabilities between low energy states 2—18143
^{189}Ir, energy levels studied in decay of ^{189}Pt 2—31493
^{191}Ir, nuclear electric quadrupole interactions in dil. Fe and Ni alloys, n.m.r., 1.4 K 2—20160
^{191}Ir, proton states populated by ^{190,192}Os(^{3}He,d) and ^{190,192}Os(α,t) reactions 2—5666
^{191}Ir(^{14}N,xnγ) reaction study of isomeric states in neutron-deficient Po isotopes 2—21379
^{192}Ir, β decay, angular correlation between groups of γ-rays in ^{192}Pt, test of time reversal invariance 2—2753
^{192}Ir decay, γ transitions, relative intensities 2—38552
^{192}Ir$\rightarrow$^{192}Pt decay, triple γ ang. correl. obs. 2—34991
^{193}Ir, nuclear electric quadrupole interactions in dil. Fe and Ni alloys, n.m.r., 1.4 K 2—20160
^{193}Ir, proton states populated by ^{190,192}Os(^{3}He,d) and ^{190,192}Os(α,t) reactions 2—5666
^{193}Ir Mossbauer effect in Pt-Ir alloy 2—26306
^{191m}Ir, half-life measurement 2—27980
^{192m}Ir, L-conversion coefficients of gamma ray transitions 2—8223
^{175,176}Lu(α,xn), 24-48 MeV, study of decay of three-quasiparticle state in ^{177}Ta 2—11770
^{169}Lu, revised decay scheme 2—24188
^{171}Lu, $^{1}/_{2}^{-}$[541] and $^{3}/_{2}^{-}$[532] rotational bands, Coriolis pairs 2—18134
^{171}Lu, $^{1}/_{2}^{-}$[541] rotation band branching 2—18133
^{171}Lu, decay processes 2—2751
^{171}Lu, rotational states differing by ΔK=2, 3, 4, evidence for configuration mixing 2—38519
^{172}Lu, conversion electron spectra, transition conversion coeff. 2—24189
^{175}Lu, parity violation caused by vector meson exchange 2—38520
^{177}Lu, cumulative yield in natural U fission 2—35097
^{177}Lu transitions, penetration effects in internal conversion 2—38521
^{176m}Lu, K-conversion coefficients of gamma ray transitions 2—8223
^{177m}Lu decay, internal conversion meas., transitions 2—38551
^{204}Mg(n,p), study of new 40±3s activity of ^{204}Au 2—31513
^{150}Nd(p,d) 2—18196
^{150}Nd(p,t), pairing vibrations 2—18196
^{227}Np, neutron-deficient nucleus, explanation of retarded fission 2—31601
^{228}Np, neutron-deficient nucleus, explanation of retarded fission 2—31601
^{235}Np decay, precision determ. of high-Z K-sheel fluorescence yields 2—15205
^{237}Np, half life of $^{5}/_{2}^{-}$, 59.6 keV level, obs. using phoswich scintillators 2—38555
^{237}Np, in ThO$_2$, e.p.r. study 2—10486
^{237}Np, neutron induced fission of polarized nuclei, simultaneous determination of J and K quantum numbers 2—35089
^{237}Np aligned nucleus, neutron induced fission, determ. directional distrib. of fission fragments 2—35049
^{237}Np irradiation to form ^{234}Pu, minimum ^{236}Pu contamination 2—8394
^{237}Np neutron induced fission through double humped fission barrier, analysis of resonances in 20-60 eV range 2—2824
^{237}Np neutron irradiation, different energies, to produce ^{238}Np and ^{238}Pu 2—2789
^{237}Np(d,2n)^{237m}Pu 8.5-14.5 MeV, production of spontaneously fissioning isomers, meas. excitation function and cross sections 2—2821
^{239}Np$\rightarrow$^{239}Pu decay, γ spectrum, energies and intensities, ang. correl. obs. 2—34979
^{273}Np Mossbauer spectra of 59.54 keV γ rays obs. in neptunium (V) oxalate from 4.2 to 80K 2—19888
Os, A=186,188.190,192, Coulomb excitation of 2^{+}states by ^{4}He, p and ^{16}O, B(E2) values 2—18142
Os (A=184, 186, 188), $21^{+}\rightarrow0^{+}$ transition probabilities 2—14969
Os isotopes, deformation energies for β_2, β_4 and γ distortions 2—27993
^{182}Os, K-dependence of population of ^{182}Os levels from ^{185}Re(p,n)^{182}Os and ^{182}W(α,4n)^{182}Os reactions 2—27991
^{185}Os$\rightarrow$^{185}Re decay scheme 2—14969
^{186}Os, e.m. transitions 2—38522
^{186}Os, γ-γ ang. correl. obs. 2—34975
^{186}Os fission, fragment mass and charge distrib. 2—35085
^{188}Os, e.m. transitions 2—38522
^{189}Os, excited level lifetime and g-factor meas. at 69, 95 and 219 keV 2—11768
^{190}Os, ^{192}Os, ratio of moments of quadrupole moments of first excited states 2—5667
^{190}Os(^{3}He,d)^{191}Ir, proton state population in ^{191}Ir 2—5666
^{190}Os(α,t)^{191}Ir, proton state population in ^{191}Ir 2—5666
^{190}Os(n,p)^{190}Re, 14.8 MeV, excitation of 3 min activity in ^{190}Re 2—38616
^{192}Os(^{3}He,d)^{193}Ir, proton state population in ^{193}Ir 2—5666
^{192}Os(α,t)^{193}Ir, proton state population in ^{193}Ir 2—5666

Nuclei with 150$\leqslant$A continued
^{193}Os, isomerism investigation 2–18144
^{193}Os$\rightarrow$^{193}Ir decay scheme 2–14969
^{195}P Mossbauer effect in Fe-Pt alloy 2–10322
^{216}Pa production by bombardment of Os with P and Au with Mg 2–8365
^{231}Pa, proton reactions at 35 to 63 MeV, yields of α-radidactive products 2–35039
^{233}Pa, half life of $^{5}/_{2}{}^{+}$, 86.6 keV level, obs. using phoswich scintillators 2–38555
^{233}Pa, half life of $^{5}/_{2}{}^{+}$, 86.6 keV level using loaded scintillators 2–34995
^{234m}Pa and ^{234}Pa daughters with ^{238}U source, gamma-ray energies, precision meas. 2–11781
Pb, neutron equilibrium pairing 2–38493
Pb, photofission, 250 to 1000 MeV, fragments angular distrib. meas. 2–15027
Pb, proton interactions, 10 to 28 GeV, inelasticities and inelastic cross section 2–31541
Pb, π photoproduction, 1160 MeV γ-quanta 2–14974
Pb bombardment with ^{18}O ions, formation of 66 sec isomeric state of ^{222}Ac 2–34994
Pb isotopes, calculation of quadrupole moments for $2_1{}^{+}$ state 2–31442
Pb isotopes with A<208, extended shell-model calculations 2–8288
Pb target, A=206 to 208, inelastic scattering of neutrons at 13.7 MeV, angular distributions of neutrons 2–38617
^{197}Pb decay, partial energy level scheme of ^{197}Tl 2–31511
^{198}Pb, lower levels obs. from ^{203}Tl(p,6n)^{198}Pb 2–18146
^{200}Pb, lower levels obs. from ^{203}Tl(p,4n)^{200}Pb 2–18146
^{201}Pb$\rightarrow$^{201}Tl, γ-rays obs., conversion coeffs. calc. 2–2734
^{203}Pb, conversion coefficients, multipolarities of transitions following ^{203}Bi decay 2–34993
^{204}Pb, ^{206}Pb, ^{207}Pb and ^{208}Pb, inelastic deuteron scattering, 13.1 MeV 2–18222
^{204}Pb, conversion coefficients, multipolarities of transitions following ^{204}Bi decay 2–34993
^{204}Pb(n,γ), 2 keV capture, absolute cross sections determ. from prompt γ-ray spectrum 2–11845
^{205}Pb, $^{13}/_{2}{}^{+}$ level, magnetic moment and lifetime 2–8311
^{205}Pb, level scheme from absolute cross section meas. for 2 keV neutron capture in ^{204,209}Pb 2–11845
^{205}Pb isomers, mag. moments 2–5670
^{206}Pb/^{207}Pb ratio, radiohalos and unknown alpha radioactivity 2–2754
^{206}Pb, EO transition to ground state 2–11777
^{206}Pb, g-factors of 7^{-} isomer, stroboscopic meas. 2–38526
^{206}Pb, L-conversion coefficients of gamma ray transitions 2–8223
^{206}Pb isomers, mag. moments 2–5670
^{206}Pb(t,p)^{208}Pb, interpret. rel. to particle-core states in ^{208}Pb 2–35080
^{207}Pb, analysis of muonic atom isomer shift 2–12063
^{207}Pb intermediate structure, S- and P-wave neutron spectroscopy 2–24160
^{207}Pb(n,γ), 2 keV capture, absolute cross sections determ. from prompt γ-ray spectrum 2–11845
^{207}Pb(n,γ)^{208}Pb thermal neutron capture, γ-spectrum 2–11846
^{207}Pb(p,p), using polarized protons, differential cross sect. and polarization meas., 11-14 MeV 2–14984
^{208}Pb, and neighbouring nuclei, particle-oscillation coupling 2–14958
^{208}Pb, charge distribution, comparison of Hartree-Fock calc. with electronic scattering and muonic X-ray data 2–24174
^{208}Pb, coupling effects 2–38528
^{208}Pb, E_1 and E_2 transitions, 0 to 30 MeV interval, Fermi systems theory method 2–38511
^{208}Pb, effective interaction between $J^{\pi}=2^{+}$ two phonons states, existence of isovector quadrupole mode 2–8312
^{208}Pb, effective interaction between 2 phonon $J^{\pi}=O^{+}$ states, diagrammatic perturbation treatment 2–2739
^{208}Pb, elastic scatt. of 30 MeV ^{6}Li ions 2–18239
^{208}Pb, electron excitation of low-lying states 2–11778
^{208}Pb, excitation of first 2^{+}, 3^{-}, 4^{-} and 5^{-} levels in ^{208}Pb(^{3}He, ^{3}He′), ang. distrib. 2–24236
^{208}Pb, ground state props. calc. using relativistic self consistent meson field theory 2–11704
^{208}Pb, neutron radius determ. from sub Coulomb pick up reactions 2–2738
^{208}Pb, neutron radius from 166 MeV α-scattering 2–11779
^{208}Pb, nuclear structure investigations using inelastic electron scattering 2–18111
^{208}Pb, two-nucleon transfer cross sections for (p,t), (t,p), (^{3}He,n), (^{3}He,p) reactions, effect of ground state correlations 2–38602
^{208}Pb from ^{207}Pb(n,γ)^{208}Pb, excited states, γ-spectrum study 2–11846
^{208}Pb K^{-} capture, study of deexcitation γ-rays, rates to proton or neutron single hole states in ^{207}Pb and ^{207}Tl 2–11850
^{208}Pb particle-core states, rel. to ^{206}Pb(t,p)^{208}Pb reaction interpret. 2–35080
^{208}Pb(^{16}O,^{15}N)^{209}Bi, proton tunnelling, DWBA calc. of differential cross section 2–5714
^{208}Pb(^{16}O,^{17}O)^{207}Pb, neutron tunnelling, DWBA calc. of differential cross section 2–5714
^{208}Pb(^{3}He,^{3}He′), ang. distrib. of levels excited in ^{208}Pb, 43.7 MeV 2–24236
^{208}Pb($^{6}\alpha$d)^{208}Pb, ^{6}Li polarization effect on Coulomb breakup process 2–2816
^{208}Pb(α,2nγ), 43 MeV, study of high spin states in ^{210}Po 2–31495
^{208}Pb(α,α), E_{α}=166 MeV, neutron radius from optical potential anal. of data 2–11779
^{208}Pb(d,t), neutron pick up reaction at sub Coulomb energies, neutron radius 2–2738
^{208}Pb(e,e), 124, 167 MeV, elastic cross sections at moderate momentum transfers, model-independent description of nuclear charge distrib. 2–28023
^{208}Pb(p,α), level densities of near doubly magic nuclei 2–38527
^{208}Pb(p,d) neutron pick up reaction at sub Coulomb energies, neutron radius 2–2738
^{208}Pb(p,γ)^{209}Bi, 8.8 to 18.0 MeV, interfering giant dipole and isobaric analogue resonances 2–490
^{208}Pb(p,n), optical model potential, energy dependence of isospin dependent part 2–38603
^{208}Pb(p,p), using polarized protons, differential cross sect. and polarization meas., 11-14 MeV 2–14984
^{210}Pb, ground and low lying states obs. of isobaric analogs in T=23 states of ^{210}Po 2–14959
^{210}Pb, two-particle states, calc. with realistic forces 2–18149

Nuclei with 150$\leqslant$A continued
^{211}Pb, β-decay to first excited state of ^{211}Bi, directional correlation meas. β-matrix elements deduced 2–2756
^{211}Pb, shell-model and β-decay calculations 2–2757
^{211}Pb decay, level scheme of ^{211}Bi 2–27997
^{213}Pb, fission, fragment mass and charge distrib. 2–35085
Pb(e,e), A=206 to 208, 30 to 90 MeV, cross sections, charge distribution parameters 2–38579
Pb(n,n), A=206 to 208, 13.7 MeV, angular distributions of neutrons 2–38606
^{152}Pm, decay of isomers 2–31507
^{154}Pm, evidence for violation of Gallagher-Moskowski rules using Nilsson model 2–27986
^{154}Pm, isomerism in decay to levels of ^{154}Sm 2–18166
Po even-even isotopes, reduced widths of α-decay 2–24191
Po isotopes, neutron-deficient, A=200-203, isomeric states studied by (HI, xnγ) reactions 2–21379
^{202}Po, $(h_{9/2})^{2}$ two-quasiparticle isomeric state meas. half life and transition energies 2–2735
^{204}Po, J=8^{+} isomeric state, half-life meas. 2–2735
^{207}Po, levels and transitions study in decay of ^{207}At 2–18148
^{209}Po, coupling of single-neutron-hole states studied in electron capture decay of ^{209}At 2–31494
^{209}Po excited states, ^{209}At decay obs. 2–21415
^{210}Po, anomalous p orbital magnetic moment determ. 2–5638
^{210}Po, asymmetric fission, two-centre shell model 2–15020
^{210}Po, IAR obs. in ^{209}Bi(p,p′) reaction, level structure of ^{209,210}Bi 2–21400
^{210}Po, T=23 double analogue states of T=T_3=23 states in ^{210}Pb 2–14959
^{210}Po, two-particle states, calc. with realistic forces 2–18149
^{210}Po high-spin states studied in ^{208}Pb(α,2nγ) reaction 2–31495
^{211}Po, shell-model and β-decay calculations 2–2757
Pt, A=192,194,196,198, Coulomb excitation of 2^{+} states by ^{4}He, p and ^{16}O, B(E2) values 2–18142
Pt (A=192, 194, 196) monopole admixtures in $2'^{+}$-2^{+} transitions 2–11775
Pt isotopes, deformation energies for β_2, β_4 and γ distortions 2–27993
Pt(^{12}C,xnγ) reaction study of isomeric states in neutron-deficient Po isotopes 2–21379
^{189}Pt decay, study of levels in ^{189}Ir 2–31493
^{192}Pt triple γ cascade, multipolarity of 296 keV transition 2–34991
^{195}Pt, 130 keV state g-factor meas. by Mossbauer effect 2–18145
^{195}Pt, n.m.r. and Mossbauer effect in Pt-Ir alloy 2–26306
^{195}Pt, n.m.r. signals of Pt(II) complexes, anisotropy of displacement 2–26307
^{195}Pt, shift anisotropy in tetracyanoplatinates and 42O 2–10562
^{195}Pt relax. times in Ni 2–40579
^{196}Pt, population of 0^{+} states by (p,t) reaction 2–34920
^{195m}Pt, oriented in Fe, magnetic hyperfine splitting 2–27994
Pu, A = 239-241, absorption to fission rate 2–498
Pu, A=238, 239, neutron induced fission, ang. distrib. and kinetic energies of fragments 2–28094
Pu, prod. in fuel pin bundles of Canadian NPD reactor 2–5760
Pu (A=242, 244), population of 0^{+} states by (p,t) reaction 2–34920
96%^{239}Pu, 4%^{240}Pu, safe storage models11919 2–11919
^{234}Pu production, irradiation of ^{237}Np, minimum ^{236}Pu contamination 2–8394
^{237}Pu, properties of two spontaneously fissioning isomers studied, half-lives and energy dist. meas. 2–2821
^{238}Pu, alpha spectra, relative intensities and energies 2–8316
^{238}Pu, electric monopole transitions 2–38530
^{238}Pu, hard γ radiation associated with α decay, revised decay scheme 2–11810
^{238}Pu, production and applications 2–27935
^{238}Pu, spontaneous fission half-life 2–31598
^{238}Pu decay, L_2 and L_3 subshell fluorescence and Coster-Kronig yields for Z=92 2–2933
^{238}Pu nuclear characteristics and use as fuel in electric generators and heater units on spacecraft 2–8371
^{239}Pu, fission, det. of ^{238}U capture rate in mixed oxide fast reactor lattices 2–35103
^{239}Pu, fragment yield, neutron induced fission 5.5 and 15 MeV 2–5721
^{239}Pu, isomer states, spontaneously fissioning, excitation in inelastic scatt. of γ quanta 2–15026
^{239}Pu, level density and excitation energy relationship 2–27999
^{239}Pu, mixing ratios of transitions, half-lives, ^{239}Np decay obs. 2–34979
^{239}Pu, neutron induced fission, total delayed neutron yields as function of energy 2–31604
^{239}Pu, ratio of neutron cross sections of radiation capture and fission, $\lesssim$50 keV 2–8347
^{239}Pu, thermal neutron fission, fragment K X-ray emission and nuclear charge distribution 2–11882
^{239}Pu (n,γ), 0.5-5 MeV, relationship between level density and excitation energy in range 1-8 MeV 2–27999
^{239}Pu (n,n), 0.5-5 MeV, relationship between level density and excitation energy in range 1-8 MeV 2–27999
^{239}Pu and ^{235}U fission cross sections ratio meas. at 30 keV and from 0.5 to 5.4 MeV 2–28089
^{239}Pu fission, 0-1.6 MeV neutron induced, energy balance analysis of $\bar{\nu}$ values 2–38661
^{239}Pu fueled lattice, spectral neutron effects evaluation by foil activation 2–5732
^{239}Pu in PuO_2 fuel, Doppler effect measurements on small fuel samples, interpretation in fast reactor spectra 2–28137
^{239}Pu neutron number obs. in resonance neutron induced fission 2–5720
^{239}Pu(d,p) fission, two-centre model, cross-section calc., evidence for intermediate structure 2–38653
^{240}Pu, fast neutron total, elastic and inelastic scattering cross sections 2–8341
^{240}Pu, neutron coherent scatt. amplitude 2–5706
^{240}Pu, total spontaneous and isomer fission half-lives 2–31599
^{241}Pu, evaluation of neutron cross-sections in unresolved resonance region 2–38620
^{241}Pu, fission yield from freshly prepared specimen 2–28087
^{242}Pu, neutron coherent scatt. amplitude 2–5706
^{242}Pu, neutron induced fission, total delayed neutron yields as function of energy 2–31604
^{244}Pu(^{96}Zr,^{40}Ca)^{300}114, feasibility of producing superheavy nuclei of A$\approx$300 2–471
Ra even-even isotopes, reduced widths of α-decay 2–24191
^{224}Ra, alpha spectra, relative intensities and energies 2–8316

Nuclei with 150⩽A continued

- ^{226}Ra, charged particle induced, determ. ^{134}Cs and ^{115}Cd isomer ratios 2—11884
- ^{226}Ra, det. of ^{227}Ac and ^{228}Th isotopes formed during irradiation in SM-2 reactor 2—40836
- ^{226}Ra, neutron-induced fission, angular anisotropy of products 2—5722
- ^{226}Ra asymmetrical fission, potential energy of heavy nuclei 2—8376
- ^{236}Ra, conversion transitions accompanying ^{230}Th alpha decay 2—11809
- ^{177}Re rotational bands and quasiparticle levels studied via ^{169}Tm(^{12}C,4n) reaction 2—27989
- ^{179}Re rotational bands and quasiparticle levels studied via ^{172}Yb(^{11}B,4n) reaction 2—27989
- ^{182}Re, 64h isomer decay to excited states in ^{182}W, γ-ray spectra 2—14968
- ^{182}Re, internal conversion electrons, exptl. investigation of spectra 2—11804
- ^{185}Re(p,n)^{182}Os, K-dependence of population of ^{182}Os levels 2—27991
- ^{186}Re, K capture decay, angular correlation, sum-peak coincidence spectra 2—481
- ^{186}Re, nuclear structure and an isomer with half-life 2×10^5 years 2—34974
- ^{187}Re, gamma-gamma directional correlations of 552-134 keV cascade 2—8310
- ^{187}Re, half-lives of some excited states meas. using delayed coincidence technique 2—24165
- ^{187}Re, half lives of short lived excited states 2—34948
- ^{187}Re quadrupole interaction in Na_xWO_3 2—33187
- ^{190}Re, excitation of 3 min activity using 14.8 MeV ^{190}Os (n,p) reaction 2—38616
- ^{184m}Re decay, to levels of ^{184}W, γ-ray spectra, meas. 2—482
- Rn even-even isotopes, reduced widths of α-decay 2—24191
- Rn(A=206 to 212), alpha decay, exptl. investigation 2—11807
- ^{220}Rn decay products in air, coagulation rates 2—22018
- Sm isotopes, two-neutron transfer reactions rel. to coexistence of spherical and deformed states 2—14973
- ^{150}Sm, reduced transition probability B(E2) of first 2^+ level deduced from cross section for elastic and inelastic scattering of ^{4}He 2—2724
- ^{150}Sm (p,p), (p,p′), 50.8 MeV, nuclear models' analysis 2—27985
- ^{151}Sm, β decays, K-shell auto-ionization probability 2—18165
- ^{151}Sm, collective state population by (d,d′) and Coulomb excitation B(E2) values 2—18126
- ^{151}Sm(d,d′), 5, 12 MeV, B(E2) values of states populated 2—18126
- ^{152}Sm, determ. intrinsic quadrupole moments and shapes of ground and excited states 2—18082
- ^{152}Sm, g-factor of 2^+(122 keV) rotational state 2—8273
- ^{152}Sm (p,p), (p,p′), 50.8 MeV, nuclear models' analysis 2—27985
- ^{152}Sm recoiling into vacuum, obs. of spin precessions from static free hyperfine interaction 2—38516
- ^{152}Sm(α,xn)$^{152,\ 153}$Gd, 32-43 MeV, population of high spin states 2—21395
- ^{152}Sm(p,p′)^{152}Sm, 24.5 MeV, asymmetry measurements of low lying states, coupled channel analysis 2—469
- ^{153}Sm, calc. of positive and negative parity Nilsson orbitals including pairing, Coriolis and $\Delta N=2$ coupling 2—18129
- ^{154}Sm, lifetimes of ground-band states 2—31486
- ^{154}Sm (p,p), (p,p′), 50.8 MeV, nuclear models' analysis 2—27985
- Ta, ang. distrib. of products and fission time from shadow widths 2—28092
- Ta, photofission and photofragmentation 600-1700 MeV photon 2—31609
- Ta, π photoproduction, 1160 MeV γ-quanta 2—14974
- Ta, ratio of photodisintegration to electrodisintegration for 5.0 GeV electron bombardment 2—11822
- Ta neutron capture γ-ray yields 2—28051
- Ta photofission, 250 to 1000 MeV, fragments angular distrib. meas. 2—15027
- Ta target for 580 MeV and 19 GeV protons, excitation energy of residual lanthanide nuclei 2—35029
- ^{174}Ta decay, energy levels of ^{174}Hf and β-band mixing 2—18137
- ^{175}Ta→^{175}Hf, decay scheme investigation 2—11803
- ^{177}Ta, decay of three-quasiparticle state studied 2—11770
- ^{178}Ta, decay to levels in ^{178}Hf, structure study 2—11771
- ^{181}Ta, 77.3 MeV-^{4}He induced fission, mass and energy distribs., test of liquid drop model 2—24249
- ^{181}Ta, γ-ray quadrupole splitting at 6.2 keV in Re 2—36838
- ^{181}Ta, parity admixtures in nuclear forces γ transition study 2—31489
- ^{181}Ta, parity violation caused by vector meson exchange 2—38520
- ^{181}Ta, reactions induced with 40-110 MeV ^{11}B ions, excitation functions and recoil ranges determ. 2—11874
- ^{181}Ta in Ni lattice, temp. dependence of hyperfine field 2—36799
- ^{181}Ta(^{14}N,5n)^{190}Hg, excited levels and 24.5 ns isomer 2—38523
- ^{181}Ta(p,p), using polarized protons, differential cross sect. and polarization meas., 11-14 MeV 2—14984
- ^{181}Ta. Larmor precession of first rotational level determ. by perturbed angular correlation method 2—2729
- ^{182}Ta, oriented in Fe, β decay, structure and parity mixing in ^{182}W 2—31510
- ^{182}Ta decay, gamma- and beta-ray spectra obs. 2—31509
- ^{182}Ta→^{182}W, triple gamma cascade studies 2—2730
- ^{150}Tb, new 5.8 min isomer, β decay to ^{150}Gd excited states 2—31506
- ^{153}Tb, n.m.r., in ferromag. Tb 2—16662
- ^{155}Tb, excited levels, ^{155}Dy decay obs. 2—24187
- ^{155}Tb, rotational states and rotation- particle coupling 2—8308
- ^{157}Tb, rotational states and rotation-particle coupling 2—8308
- ^{159}Tb, 14 MeV, spectra of photons 2—8345
- ^{159}Tb, parity admixtures in nuclear forces γ transitions study 2—31489
- ^{160}Tb, in TbF_3 and $Eu_{1-x}Tb_xS$, β-decay search for atomic after effects 2—18167
- ^{161}Tb, 363-keV γ-radiation, parity violating asymmetry 2—2750
- Th, secondary effects produced by interaction with 28 GeV protons 2—35038
- Th (A=230, 232), population of 0^+ states by (p,t) reaction 2—34920
- Th even-even isotopes, reduced widths of α-decay 2—24191
- ^{228}Th, det. of ^{227}Ac and ^{228}Th isotopes formed during irradiation in SM-2 reactor 2—40836
- ^{228}Th, multipolarities of transitions 2—8317
- ^{228}Th excited levels, ^{228}Ac decay obs. 2—483
- ^{228}Th level scheme, ^{228}Ac decay obs. 2—11808
- ^{229}Th, $^{240-244}$Cm, ^{249}Bk and $^{249-252}$Cf, α-decay energy determ. of most intense α-groups 2—5677
- ^{230}Th, alpha decay, conversion transitions in ^{226}Ra 2—11809
- ^{230}Th, deformation parameters and E4 transition probabilities from Coulomb excitation expt. 2—8313

Nuclei with 150⩽A continued

- ^{232}Th, 3 MeV neutron induced fission yield, mass distribution determ. 2—5719
- ^{232}Th, bombardment with 290 MeV ^{40}Ar, production of new isotopes of Mg, Al, Si, P, Cl, S 2—5715
- ^{232}Th, charged particle induced, determ. ^{134}Cs and ^{115}Cd isomer ratios 2—11884
- ^{232}Th, F test for l=0 resonances, PT distrib. 2—34969
- ^{232}Th, level density and excitation energy relationship 2—27999
- ^{232}Th, photoneutron and photofission cross sections, intermediate structure 2—38575
- ^{232}Th, proton reactions at 35 to 63 MeV, yields of α-radioactive products 2—35039
- ^{232}Th, Raman scattering of 10.38 MeV photons 2—24200
- ^{232}Th 40-60 MeV proton induced fission, meas. of Rb and Cs isotopic cross sections 2—11880
- ^{232}Th (n,γ), 0.5-5 MeV, relationship between level density and excitation energy in range 1-8 MeV 2—27999
- ^{232}Th asymmetrical fission, potential energy of heavy nuclei 2—8376
- ^{232}Th fission, charge distrib. among products 2—11878
- ^{232}Th photofission using variable energy beam of γ-rays determ. cross sections from 5-8.3 MeV and transmission factors 2—21458
- ^{232}Th(n,n), 0.5-5 MeV, relationship between level density and excitation energy in range 1-8 MeV 2—27999
- Tl, secondary effects produced by interaction with 28 GeV protons 2—35038
- ^{198}Tl, decay, ^{198}Hg low-energy level structure 2—2733
- ^{201}Tl, fission, fragment mass and charge distrib. 2—35085
- ^{201}Tl, shell effects on saddle pt. deform. 2—34978
- ^{201}Tl, spin and parity assignments, level scheme proposed obs. of ^{201}Pb→^{201}Tl 2—2734
- ^{203}Tl, circular polarization of 279 keV γ ray determ. 2—11776
- ^{203}Tl, parity admixtures in nuclear forces γ transition study 2—31489
- ^{203}Tl, parity violation observed by meas. of β-γ directional correlation in ^{203}Hg→^{203}Tl decay 2—11806
- ^{203}Tl, study of 279 keV transition angular correlation meas.of asymmetry, deduced limit of parity mixing 2—2736
- ^{203}Tl and ^{205}Tl, inelastic deuteron scattering, 13.1 MeV 2—18222
- ^{203}Tl(p,4n)^{200}Pb, ^{200}Pb lower levels obs. 2—18146
- ^{203}Tl(p,6n)^{198}Pb, ^{198}Pb lower levels obs. 2—18146
- ^{204}Tl, internal bremsstrahlung spectrum, contribution of detour transitions 2—21398
- ^{204}Tl, nuclear energy level scheme, γ-spectroscopic analysis 2—2737
- ^{205}Tl, excitataion and resonance processes rel. to L and K X-ray emission from muonic ^{205}Tl 2—18371
- ^{205}Tl(n,α), study of decay of ^{202}Au 2—31513
- ^{206}Tl, decay to ^{206}Pb, strong EO transition in ^{206}Pb 2—11777
- ^{208}Tl, half-life precision measurement 2—2755
- ^{195m}Tl decay, partial energy level scheme of ^{197}Tl 2—31511
- ^{198m}Tl, decay, ^{198}Hg low-energy level structure 2—2733
- ^{155}Tm, new isotopes, α decay investigated, mass assignments made 2—11801
- ^{156}Tm, new isotopes, α decay investigated, mass assignments made 2—11801
- ^{167}Tm, level scheme investigated in 18 min. ^{167}Yb decay meas. of conversion electron and single γ-ray spectra, γ-γ coincidences 2—472
- ^{168}Tm, spectra static moments and transition probabilities 2—38518
- ^{169}Tm, gyromagnetic ratio of 316 keV $^7/_2{}^+$ state 2—18132
- ^{169}Tm, polarization by pumping circularly polarized light in Tm^{2+}:CaF_2 2—40596
- ^{169}Tm, structure determ. from energies and intensities of γ-rays following ^{169}Yb decay 2—470
- ^{169}Tm(^{12}C,4n), 62-76 MeV, study of ^{177}Re energy levels 2—27989
- ^{170}Tm, radiative constants, from magnetic and electric moments 2—24172
- ^{171}Tm, γ-ray transition properties following β-decay of 7.5h ^{171}Er 2—34970
- ^{172}Tm, proposed level scheme, β-decay of ^{172}Er 2—18135
- U, binary fission cross-section induced by 29 GeV ^{14}N ions meas. 2—35093
- U, bombardment with Kr, superheavy nucleus formation, detection by mass measurement of fission products 2—21452
- U, interaction with 28 GeV protons, charge and mass distribution of rare-earth products 2—11834
- U, secondary effects produced by interaction with 28 GeV protons 2—35038
- U (A=234, 236, 238), population of 0^+ states by (p,t) reaction 2—34920
- 93.4%^{235}U, safe storage models 11919 2—11919
- ^{232}U, alpha spectra, relative intensities and energies 2—8316
- ^{233}U, 77.3 MeV-^{4}He induced fission mass and energy distrib., test of liquid drop model 2—24249
- ^{233}U, neutron induced fission, total delayed neutron yields as function of energy 2—31604
- ^{233}U, thermal neutron fission, fragment K X-ray emission and nuclear charge distribution 2—11882
- ^{233}U aligned nucleus, neutron induced fission, determ. directional distrib. of fission fragments 2—35049
- ^{233}U and ^{235}U, fission, thermal neutron induced, nuclear charge distrib. 2—35086
- ^{233}U fission, 0-1.6 MeV neutron induced, energy balance analysis of $\bar{\nu}$ values 2—38661
- ^{233}U fission fragment yield, neutron induced fission 5.5 and 15 MeV 2—5721
- ^{234}U, thermal neutron ternary fission, yields and energy distribs. of ^{3}H, ^{4}He, ^{3}He 2—24248
- ^{234}U, total spontaneous and isomer fission half-lives 2—31599
- ^{235}U, 40-60 MeV proton induced fission, meas. of Rb and Cs isotopic cross sections 2—11880
- ^{235}U, fission, equilibrium deformation and quadrupole deformation parameter of even even fragments 2—28093
- ^{235}U, fission by thermal neutron, calc. of dipole excitation of fission fragments at scission point 2—18248
- ^{235}U, fission thermal neutron induced, search for long range fission products 2—24247
- ^{235}U, fragment ang. distrib. obs., saddle point transition states 2—38667
- ^{235}U, half-life and specific activity determ. 2—2758
- ^{235}U, neutron evaporation and energy distribution in individual fission fragments 2—35088
- ^{235}U, neutron induced fission, evaluation of direct meas. of no. of neutrons/fission ($\bar{\nu}$) 2—5724

Nuclei with 150$\leqslant$A continued

- ^{235}U, neutron induced fission total delayed neutron yields as function of energy 2—31604
- ^{235}U, neutron number obs. in resonance neutron induced fission 2—5720
- ^{235}U, new values of neutron nuclear data 2—28039
- ^{235}U, photofission using variable energy beams of γ-rays determ. cross section from 5-8.3 MeV 2—21458
- ^{235}U, thermal fission, energy and ang. distrib. of long range charged particles 2—35096
- ^{235}U, thermal neutron cross section 2—15023
- ^{235}U, thermal neutron fission, fragment K X-ray emission and nuclear charge distribution 2—11882
- ^{235}U, thermal neutron induced LRP fission, mass distrib. of products 2—21457
- ^{235}U, total neutron cross-section fluctuations in the keV range 2—28052
- ^{235}U aligned nucleus, neutron induced fission, determ. directional distrib. of fission fragments 2—35049
- ^{235}U and ^{239}Pu fission cross sections ratio meas. at 30 keV and from 0.5 to 5.4 MeV 2—28089
- ^{235}U fission, absolute meas. of α for neutron energies of 10 keV to 1 MeV 2—31603
- ^{235}U fission fragments, yields and kinetic energies depend. on energy of bombarding neutrons 2—8372
- ^{235}U neutron irradiation, different energies, to produce ^{238}Np and ^{238}Pu 2—2789
- ^{235}U thermal fission fragments, primary spins study from γ-emission 2—21459
- ^{235}U(n,f) investigation of conversion electrons from fragments and products, evidence for $J^{\pi}=o^{+}$ first excited state of ^{98}Zr 2—11755
- ^{236}U, asymmetric fission, two-centre shell model 2—15020
- ^{236}U, detection of γ-rays preceding isomeric fission induced by neutron capture in ^{235}U 2—24244
- ^{236}U, neutron-induced fission, high-resolution cross section meas. 2—31605
- ^{236}U, prompt neutrons from fission fragments 2—18246
- ^{236}U fragments, study of average emission times of K X-rays 2—11883
- ^{236}U neutron resonances, fission widths, 5.45-415 eV 2—21456
- ^{237}U, fission barrier parameters from fission widths of ^{236}U neutron resonances 2—21456
- ^{238}U/^{235}U cross sections ratio for radiative capture det. and reduction of systematic errors 2—38618
- ^{238}U, 40-60 MeV proton induced fission, meas. of Rb and Cs isotopic cross sections 2—11880
- ^{238}U, charged particle induced fission, determ. ^{134}Cs and ^{115}Cd isomer ratios 2—11884
- ^{238}U, deformation parameters and E4 transition probabilities from Coulomb excitation expt. 2—8313
- ^{238}U, det. of capture rate rel. to ^{239}Pu fission in mixed oxide fast reactor lattices 2—35103
- ^{238}U, F test for l=0 resonances, PT distrib. 2—34969
- ^{238}U, fast neutron induced LRP fission, mass distrib. of products 2—21457
- ^{238}U, fast neutron total and scattering cross sections 2—5699
- ^{238}U, fission by 16 and 42 MeV protons, α-particle emission 2—35095
- ^{238}U, fission induced by protons of 11.2 MeV and deuterons of 10.6 MeV, distribution of nuclear charge studied using Ge(Li) spectroscopy 2—35092
- ^{238}U, fragment energy distribution from neutron induced fission at 1.5 to 18.2 MeV 2—18247
- ^{238}U, half-life and specific activity determ. 2—2758
- ^{238}U, heavy-ion induced fission energetic balance 2—31610
- ^{238}U, neutron induced fission, total delayed neutron yields as function of energy 2—31604
- ^{238}U, photofission using variable energy beams of γ-rays determ. cross section from 5-8.3 MeV 2—21458
- ^{238}U, photoneutron and photofission cross sections, intermediate structure 2—38575
- ^{238}U, Raman scattering of 10.38 MeV photons 2—24200
- ^{238}U, relative neutron capture rate, meas. by foil activation 2—38619
- ^{238}U, yields of ^{131}Xe, ^{132}Xe, ^{134}Xe and ^{136}Xe obs. 2—5725
- ^{238}U α fission at medium energy, techniques for separation of ^{134}Cs isomers 2—11881
- ^{238}U fission by 2.2 GeV protons 2—11885
- ^{238}U in UO$_2$ fuel, Doppler effect measurements on small fuel samples, interpretation in fast reactor spectra 2—28137
- ^{238}U neutron resonance radiation widths 2—28053
- ^{238}U photofission fragment ang. distrib. obs. 2—2817
- ^{238}U(n,γ), γ-ray energy spectra, calculated and measured 2—8346
- ^{238}U(p,x)(x,y)^{254}Fm, search for ^{254}Fm production by secondary nuclear reaction of 11.5 GeV protons 2—28038
- ^{238}U(p,x)(x,y)^{256}Fm, search for ^{256}Fm production by secondary nuclear reactions of 11.5 GeV protons 2—28038
- ^{239}U, absorption to fission rate determ. 2—498
- ^{236m}U, shape isomer, production in ^{235}(d,p) reaction via decay of class I states 2—11782
- U(α,n), natural targets, effect of reactions on ratio of induced to spontaneous fission 2—35084
- W (A=182, 184, 186), population of 0$^+$ states by (p,t) reaction 2—34920
- W isotopes, deformation energies for β_2, β_4 and γ distortions 2—27993
- W neutron capture γ-ray yields 2—28051
- W(A=170, 171), production by irradiation of Gd with ^{22}Ne and ^{20}Ne 2—11769
- ^{182}W, excited levels study in decay of ^{182}Re, 64h isomer 2—14968
- ^{182}W, mag. moment of 1374 keV level 2—34973
- ^{182}W, magnetic moments of two excited states determ. by perturbed γ-γ angular correlation meas. in external mag. field 2—27990
- ^{182}W, parity admixtures in nuclear forces γ transition study 2—31489
- ^{182}W, produced in ^{182}Ta decay 2—2730
- ^{182}W, structure and parity mixing from ang. distrib. of γ rays in β decay of ^{182}Ta 2—31510
- ^{182}W Mossbauer spectra in W compounds 2—13452
- ^{182}W(α,4n)^{182}Os, K-dependence of population of ^{182}Os levels 2—27991
- ^{183}W, Mossbauer effect, recoilless fraction temp. variation and thermal shift 2—36327
- ^{183}W, Mossbauer linewidths and half-lives of 46.5 keV and 99.1 keV levels 2—11774
- ^{183}W(d,p), low lying levels of ^{184}W detn. 2—31492
- ^{184}W, level scheme from study of γ-ray spectra of decay of ^{184m,184}Re 2—482
- ^{184}W, low lying levels, (d,p) reaction obs. 2—31492
- ^{186}W, e.m. transitions 2—38522

Nuclei with 150$\leqslant$A continued

- ^{183m}W, half-life measurement 2—27980
- W(n,γ), γ-ray circular polarization, spin assignments 2—18209
- ^{131}Xe excess in lunar rocks due to ^{130}Ba(n,2p)^{131}Xe resonant capture 2—7506
- ^{167}Yb$\rightarrow$^{167}Tm, 18 min., electron capture decay, investigation of ^{167}Tm level scheme from conversion electron, single γ-ray spectra and γ-γ coincidences 2—472
- ^{168}Yb, nuclear moment of inertia at high rotational frequencies, levels populated with (α,xn) reaction 2—27988
- ^{169}Yb decay, energies and intensities of γ-rays, rel. to ^{169}Tm structure 2—470
- ^{170}Yb, half-lives of some excited states meas. using delayed coincidence technique 2—24165
- ^{170}Yb, half lives of short lived excited states 2—34948
- ^{170}Yb Mossbauer effect in Yb$_2$O$_2$S(Se) 2—26133
- ^{170}Yb Mossbauer effect in YbCl$_3$.6H$_2$O and Yb$_2$(SO$_4$)$_3$.8H$_2$O 2—10273
- ^{171}Yb, magnetic moment determ. by optical pumping 2—18104
- ^{171}Yb Mossbauer effect in YbCl$_3$.6H$_2$O and Yb$_2$(SO$_4$)$_3$.8H$_2$O 2—10273
- ^{172}Yb, Coriolis coupling of octupole states, empirical evidence from ^{173}Yb(^{3}He,α) and ^{173}Yb(d,t) reactions 2—24173
- ^{172}Yb(^{11}B,4n), 52-60 MeV, study of ^{179}Re energy levels 2—27989
- ^{173}Yb, magnetic moment determ. by optical pumping 2—18104
- ^{173}Yb(^{3}He,α)^{172}Yb, empirical evidence for Coriolis coupling of octupole states of ^{172}Yb 2—24173
- ^{173}Yb(d,t)^{172}Yb, empirical evidence for Coriolis coupling of octupole states of ^{172}Yb 2—24173
- ^{174}Yb, spin of 1518 keV level 2—14956
- ^{174}Yb (n, γ) ^{175}Yb, spectrum study, 26-1500 keV, level scheme of ^{175}Yb 2—18139
- ^{175}Yb, cumulative yield in natural U fission 2—35097
- ^{175}Yb, level scheme and energies, γ-branching ratios from ^{174}Yb (n, γ) reaction 2—18139
- ^{175}Yb, thermal neutron capture, ^{175}Yb energy level study 2—18138
- ^{175}Yb energy levels from primary transitions in thermal neutron capture by ^{174}Yb 2—18138
- ^{176}Yb, deuteron stripping, coupled channel Born approx. description 2—15011
- ^{176}Yb(n,γ)^{177}Yb, investigation of low energy excited state structure of ^{177}Yb 2—38510
- ^{177}Yb, low energy excited state structure, investigation by ^{176}Yb(n,γ)^{177}Yb reaction 2—38510
- ^{177}Yb decay, internal conversion meas., transitions 2—38551

Nucleic acids *see Macromolecules*

Nucleons and antinucleons

see also Cosmic rays/nucleons; Neutrons and antineutrons; Nuclear reactions and scattering due to/nucleons; Protons and antiprotons

- σ commutator, value derived from πN scatt. data, interpretation via chiral symmetry breaking Hamiltonian 2—428
- albedo spectra in accelerator cave from 200 GeV proton interaction in Fe 2—24222
- axial form factor, determ. from π electroproduction cross section 2—11633
- axial vector form factor from dispersion theory, A$_1$ dominance effects 2—31315
- coupling constants of isoscalar vector mesons to nucleon and dispersion-theoretic sum rules 2—31311
- Drell Yan relationship, effect of t-channel descript. of electroprod. 2—17832
- exchange, realistic model rel. to backward pd scatt. 2—8200
- form factor, examination using model describing elastic electron scattering 2—11602
- form factor derivation from pole dominance and Veneziano model 2—427
- form factors, axial vector, from threshold π electroprod. 2—27750
- form factors, validity of scaling relations 2—34707
- from protons evaluated in terms of p$_{11}$ pion-nucleon phase shift, asymptotic behaviour 2—38311
- isovector form factors, influence of higher order cut contributions and asymptotic behaviour of $\pi\pi$ scattering phase shift on decreasing properties 2—27769
- neutrino excitation, quark model 2—31332
- neutron stars, high-density nucleon localization 2—41103
- nucleon electromagnetic form factors, asymptotic form by Lorentz contraction and vector meson dominance 2—14687
- resonances, electroprod., helicity structure, symmetric quark model 2—31331
- subnucleonic particles, properties 2—5509

antinucleons

- No entries

interactions

- πN, 10.2 GeV/sec., coeff. of inelasticity 2—2614
- accelerator energies, multiplicity and ang. distrib. of prod. secondary particles 2—23881
- boson-nucleon collisions, single pion production, spectra and distributions in unitarized model of quasi-two-body contributions 2—23844
- electroproduction, scaling and form factors of nucleon in bremsstrahlung model 2—38313
- electroproduction from nucleons in relativistic quark model 2—14571
- hyperon-nucleon, separable two-channel potential model 2—38328
- hyperon-nucleon interactions, quark model rules for total cross-sections 2—11643
- meson-nucleon, produced pion spectra in diffractive model 2—31284
- multibaryon resonance, isobar- nucleon exchange interaction model 2—21308
- photoproduction, simple approach to Reggeization 2—8107
- photoproduction of vector neutral mesons on nucleons, Glauber model, quark model 2—14673
- subnucleonic particles, collisions at high relativistic energies 2—5509
- ultrahigh energy, inclusive N-body reactions 2—21299
- Δ resonance-nucleon total cross section estimated by analysing final state of weak or e.m. Δ-production on nuclei 2—34741
- eN, π^+ production, vector meson dominance model 2—17928
- eN, π production, threshold, low-energy theorems 2—14649
- eN, single π prod., multipole analysis by current algebra commutators 2—34680
- γn, forward π and η production, Regge models 2—17925
- γN, high energy pion production, s-channel dominance and charge ratios 2—8168

Nucleons and antinucleons continued
interactions continued
γN, pion photoproduction, construction of non minimal currents in chiral Lagrangians 2—14648
γn, pion production, sum rule determination from dispersion relations 2—17924
γN, π^0 photoprod., effect of ω and ρ complex Regge poles 2—27752
γN, π production, threshold, low-energy theorems 2—14649
γN, single pion prod. in first resonance region 2—31285
γN, single π prod., multipole analysis by current algebra commutators 2—34680
$\gamma N \to \Delta V^0 \pi$, method for experimental study of energy dependence of $V^0 \pi$ scattering amplitudes proposed 2—17935
$\gamma N \to N V^0$, charge exchange, Pomeranchuk theorem violation 2—8151
$\gamma N \to O^- B$ photoproduction, t-channel transformation matrices for helicity and invariant amplitudes 2—23781
$\gamma N \to (1/2)^+ + 2^+$, SU(6) symmetry study 2—5522
$\gamma N \to (3/2)^+ + 2^+$, SU(6) symmetry study 2—5522
$\gamma N \to \rho^0 N$, high energy role played by charged pion pairs mediating 2—31195
KN, medium energy, inclusive cross sections 2—34666
KN charge exchange reactions, rel. to tests of exchange degeneracy and duality 2—17908
KN partial cross sections deduced from K^+d interaction data from 865-1585 MeV/c 2—405
$KN \to K^0 N$ charge exchange, universality and complex Regge pole factorization 2—21264
$KN \to K^+ N$, near threshold, production and decay angular distributions interpreted in terms of t-channel phenomena 2—405
$\bar{K}N \to K\Xi$, exchange cross sections, Regge cut contributions 2—406
$K^- N$, in K mesic atoms 2—21555
$K^\pm N \to K^{*0} N$ charge exchange, difference between K^+ and K^- reactions obtained in absorption model using Reggeized π and ρ exchange 2—17956
ΛN, charge symmetry breaking interaction, rank-2 potentials 2—8208
$\Lambda \underline{N}$, charge symmetry breaking interaction, separable potentials 2—14708
$\underline{N}\bar{N}$ system, resonances 2—21300
$\bar{N}N \to \pi\pi$, finite energy sum rules on hyperbolas 2—17958
$N\gamma$, field-theoretic Reggeization in five- and six-point functions 2—347
νN, deep inelastic, study using conserved axial vector currents and current commutation relations 2—21241
νN interactions, quark model of resonance excitation 2—31332
pN, monopole production cross section 2—5485
pN is nuclear emulsions at 67 GeV/c, general characteristics, pp multiplicity 2—38320
π electroproduction on nucleon, phenomenological chiral Lagrangian model 2—31280
π photoproduction, presence of exotic currents in model 2—34678
π^- photoproduction, Glauber and symmetrization corrections to data from single arm spectrometer experiments 2—34677
πN, 60 GeV, energy characts. of secondary particles 2—2612
πN, 60 GeV, slow recoil proton 2—2613
πN, low energy phenomenology, review 2—38262
πN, multipion coherent interactions, very high energy 2—27702
πN bremsstrahlung, off- shell and structure effects discussed and calculated 2—14655
πN charge-exchange polarization, described by exchange of ρ-pole plus $\rho \otimes P$ Regge cut 2—413
πN secondary particle production at 60 GeV, comparison with particles prod. by cosmic rays 200-500 GeV 2—24027
$\pi^- N$, in nuclear emulsion, 45 and 60 GeV/c, prong number and ang. distrib. of secondary particles 2—23850
$\pi N \to K\Lambda$, dual amplitude and strange form factors, Veneziano model 2—17930
$\pi N \to XN$, diffractive production process, Pomeron exchange study 2—31294
$\pi N \to \omega N$, at high energy, 4.19 GeV 2—5538
$\pi N \to \pi\pi N$, diffractive $\pi\pi$ scattering at 13.1 GeV/c, factorized double exchange model 2—34681
$\pi N \to \rho\Delta(1236)$, Regge pole model, threshold constraints 2—38301
$\pi N \to \rho N$, photon exchange 2—5539
YN, recent developments 2—38329
$\gamma N \to \pi^+\pi^- N$, high energy role played by charged pion pairs mediating 2—31195
$\bar{N}N$ annihilation, cosmic rays, regularity of particle production 2—24032

interactions, nucleon-nucleon
10 GeV/c, secondary particles angular and energy distrib. 2—14688
application in many body problems 2—11707
diffraction-dissociation model, high energy interactions 2—34710
extended boson exchange model associated with hydrogen like Regge recurrence 2—31316
finity violating internucleon potential, pion exchange contributions 2—34877
high energy model, rel. to derivation of vertical sea-level muon spectrum and charge ratio 2—2602
low energy, below 1 GeV/c, recent developments 2—38314
multiple particle production at 250 GeV mean energy 2—2604
multiple production, fireball model 2—437
neutron stars, equation of state of matter at very high densities 2—10891
nuclear matter, approximation to reaction matrix 2—38446
OBEP potentials, vector meson contributions 2—8190
optimal relativity effects 2—27943
phase shift at high energies, rel. to nuclear matter binding energy 2—21356
recession velocity analysis of reactions at cosmic ray and machine energies 2—23882
$\bar{N}N$ annihilation at rest and hadronic production 2—34708
$\underline{N}N \to \Delta\underline{N}$ and its line-reversed reaction 2—34709
$\bar{N}N \to K\bar{K}$, low energy, effect of direct channel interference and meson towers 2—27770
$\underline{N}N \to NN^*$, $^1/_2{}^+$, 1400 MeV, exchange of pomeron as Regge cut 2—429
$\bar{N}\underline{N} \to 3\pi$ isospin analysis 2—34716
$N\bar{N} \to \pi\pi$ amplitude obtained by analytic continuation of the low energy πN scatt. amplitude 2—38315
$\bar{p}N \to \pi$-$\pi^+\pi^+$, Veneziano-type amplitudes, Dalitz plot analysis 2—5558
2π exchange contribution to NN potential calc. following Mandelstam representation method 2—38315
^{18}O, energy levels, effect of higher order diagrams on effective interaction 2—38477

interactions, pion-nucleon *see Pions/interactions, pion-nucleon*

Nucleons and antinucleons continued
scattering
μN, high energy inelastic scatt., secondary particle production and hypothesis of banking fragmentation 2—11579
Compton effect, ρ^0 photoproduction at high energies 2—8110
elastic, 300 to 3000 MeV, possibilities for study using polarized proton targets 2—34715
eN, deep inelastic, multiperipheral theory 2—11575
lepton nucleon deep inelastic scattering, Green's functions of Currents 2—27709
lepton-nucleon inelastic scattering, broken scale invariance 2—23790
lepton-nucleon scattering, relativistic quark parton model 2—14560
meson-nucleon, resonance generation, inverse problem study, partial waves 2—23831
meson-nucleon scattering, Feynman-diagram models of Fermion Regge-pole conspiracies 2—34655
eN, deep inelastic, electroproduction of resonances, structure functions in scaling limit 2—34713
eN, deep inelastic, scaling law as consequence of broken dilatation symmetry 2—8119
eN, deep inelastic, soft pion prod., current algebra 2—412
eN, deep inelastic scatt., inequalities for structure functions, algebraic structures, tests 2—27711
eN, deep inelastic scatt., polarization effects, quark parton model, parallel and antiparallel asymmetry 2—27712
eN, in elastic scattering, duality 2—23798
eN, inelastic, scaling and behaviour of nucleon resonances 2—14710
eN, inelastic rel. to e.m. p-n mass difference investigation 2—38312
eN, spin-dependent inelastic process 2—31205
eN deep inelastic scattering, parton dual-resonance model incorporating final-state interaction 2—14569
$\gamma N \to \gamma N$, Compton scattering, high energy role played by charged pion pairs mediating 2—31195
$\underline{K}N$, charge exchange, Veneziano model with cuts 2—38291
$\bar{K}N$, charge exchange, Veneziano model with cuts 2—38291
$\bar{K}N$, determ. of high energy scattering amplitudes from data on K-p elastic and charge exchange scattering 2—11600
$\underline{K}N$, differential cross section, Pomeranchuk theorem violation 2—8151
$\bar{K}N$, dual features of elastic scatt. amplitudes 2—34670
$\underline{K}N$, forward scattering, sum rules, zerology of amplitudes 2—2552
$\bar{K}N$, multichannel partial wave analyses in region 0 to 1400 MeV/c 2—17913
KN, regeneration $K_2^0 \to K_1^0$ in complex angular momentum theory 2—34671
KN, Reggeized multiple scattering quark model, total cross sections 2—17916
KN forward scattering, high energy phenomenology, Regge pole models tested 2—23859
$\bar{K}N$ scattering length calc. from X-ray transitions of K-mesic atoms 2—34672
$KN\Lambda$, coupling constants and zeros in ω-plane of T^+ and T^- KN amplitudes 2—2552
$N\bar{N}$, dual model construction 2—38317
$NN \to NN^*(I={}^1/_2)$, inelastic process, differential cross sections, Pomeron exchange study 2—31294
νN, deep inelastic scatt., inequalities for structure functions, algebraic structures, tests 2—27711
νN deep inelastic scattering, soft pion prod., current algebra 2—412
νN inelastic interactions, determ. of threshold relations following from scaling and duality 2—34613
νN Low Energy Theorems used to obtain sum Rules for critical cross sections at $Q^2=0$ 2—21240
pN, at 70 GeV IPHE proton synchrotron, magnetic monopole prod. 2—31181
Π N relativistic optical model, pion in 2-5 BeV/c range, determ. cross sections 2—23856
πN, 3-3 resonance, basic parameters 2—34690
πN, charge-exchange, polarization and sum rules in complex-Regge pole model 2—14662
πN, current algebra constraints on on-mass-shell amplitudes and Adler-Weisberger theorem 2—14661
πN, current algebra model, S-wave and P-wave scatt. lengths, low energy 2—23857
πN, dual relativistic quark model, low energy aspects 2—17945
πN, elastic, kinematical singularities in matrix decomposition 2—38185
πN, finite energy sum rules on hyperbolas 2—17936
πN, fixed pole effects, Regge parametrization based on very strong exchange degeneracy 2—31293
πN, helicity conservation from polarization data alone 2—11620
πN, low energy, direct expression for σ term 2—2563
πN, non-flip ρ exchange, cut correction generation 2—27758
πN, nucleon σ commutator derivation, interpretation via chiral symmetry breaking interaction 2—428
πN, peripherality from absorbed Reggeon exchange model 2—23862
πN, phase shift analyses, application of subtracted fixed-t dispersion relations 2—11619
πN, scattering amplitude, zero locations 2—8174
πN, short range potential, Reggeization using Veneziano amplitude 2—8175
πN, σ term, estimation from off mass shell Veneziano type amplitude 2—34687
πN, σ term calculation, model dependence 2—38306
πN, Veneziano representation, construction from isospin degeneracy patterns 2—23860
πN amplitudes and polarization parameters 2—23858
πN backward differential cross-section, t-channel contributions 2—14656
πN charge exchange data used for possible relation between absorptive and complex-Regge-pole models 2—17871
πN charge exchange scattering, considering Virasoro model 2—14660
πN coupling constant determ. by analytic extrapolation 2—415
πN forward scattering, high energy phenomenology, Regge pole models tested 2—23859
πN invariant amplitude at low energy, critical test of models 2—34688
πN isospin bounds for backward amplitude, saturation 2—23861
πN operator droplet model treatment, calc. diff. cross section, polarization and spin rotation parameters 2—14659
πN phase-shift analysis 2—34689
πN phase shift, p_{11}, rel. to evaluation of nucleon e.m. form factors 2—38311
πN scattering, nonanalytic behaviour of Σ term 2—14663

Nucleons and antinucleons continued
  scattering continued
    πN scattering amplitude high-energy behaviour of dual relativistic quark model 2—27731
    πN sigma term, determ. from pion nucleus scattering 2—14993
    $\pi N \rightarrow \omega N$, dual structure in scattering amplitude 2—2562
    $\pi N \rightarrow \pi N^*(I={}^1/_2)$, inelastic process, differential cross sections, Pomeron exchange study 2—31294
    $\pi N \rightarrow \pi' N'$, s-channel anal. in a scheme of higher baryon couplings 2—17937
    $\rho^0 N \rightarrow \rho^0 N$ elastic scattering, high energy role played by charged pion pairs mediating 2—31195
    ΣKN, coupling consts. and zeros in ω-plane of T^+ and T^- KN amplitudes 2—2552
    V^0N, slope parameter in differential elastic cross section 2—21421
    $\bar{K}$N, 800 to 1200 MeV/c, improved partial wave analysis 2—407
    $K^\pm$N, upper bounds on elastic cross section differences 2—2565
    Nd elastic scatt., cross-section, polarization formulas 2—38331
  scattering, nucleon-nucleon
    $^1S_0$ phase shift from Nambu Salpeter Bethe eqn. 2—8191
    amplitudes, bootstrap sum rules 2—11632
    dual model construction 2—38317
    elastic, experimental and theoretical results 2—14689
    elastic, relativistic one-boson-exchange model 2—34706
    high energy processes, W-boson prod. cross section 2—11624
    interaction potential including all exchanges involving single σ meson and pion-pair inserts 2—34712
    low-energy, rel. to relativistic eikonal approximation 2—31413
    low-energy, relativistic effects, soln of Bethe-Salpeter eqn. 2—2573
    mechanisms, phenomenological analysis at about 6 GeV 2—38316
    models, pseudoscalar and vector meson, for scattering outside phenomenological core 2—8192
    parity conservation test using 210 MeV proton beam, and C and polyethylene targets, use of impulse approx. 2—14690
    peripherality, semiquantitative test 2—8193
    phase parameters, damped one-and two pion exchange contributions 2—17957
    polarization expts. to test time-reversal invariance 2—34714
    soft pion emission study in asymptotic region 2—5531
    spin independence and s-channel helicity conservation, indistinguishibility 2—2572
    NN elastic scattering, OBE model improved by including inelastic effects, S-wave phase-shifts computed 2—34711
    $NN \rightarrow NN^*$ relationship between hadronic and electronic excitation of N* resonance 2—27777
  scattering, pion-nucleon *see Pions/scattering, pion-nucleon*
Nucleus
    see also Elements/origin; Hypernuclei; Radioactivity; Scattering, particles
    $Z \geqslant 114$, possible existence of closed shells 2—5629
    collapsed, observational consistency, properties and detection 2—8265
    constants, nuclear using level crossing in atomic spectra 2—2658
    deformed nuclei, exptl. values for nuclear constants, determination from rotational energy level characteristics 2—24125
    light nuclei with neutron excess, production 2—2686
    neutron-electron bound state, possibility for free existence 2—27938
    recoil nuclei from α decay, mass determ. and velocity meas. 2—11787
    rotation, various methods of analysis 2—14925
    surface energy and neutron-star matter 2—34887
    three-nucleon system, accurate numerical soln. to bound state problems 2—38470
    ^{4}He, form factor, elastic electron scattering with short range correlations 2—38577
    ^{16}O, form factor, elastic electron scattering with short range correlations 2—38577
  electric moment
    see also Molecules/nuclear coupling
    deformed nuclei, homogeneous charge distribution and rotational symmetry, calc. of multipole moments 2—31441
    effective quadrupole charges in the lead region 2—21371
    fission fragments, dipole excitations at scission point studied in a classical model 2—18248
    giant dipole resonance, isobaric analogue states, meson-induced 2—2790
    giant dipole resonance, isotopic structure and isospin impurity of low-lying nuclear states 2—18081
    intrinsic quadrupole moments of ground and excited states 2—18082
    intrinsic transition quadrupole moment, relationship with transition moments of inertia 2—34893
    multipole moments, shell model calc. for A=27, 28, 29 nuclei 2—38489
    multipole relaxation times determ. by meas. of statistically perturbed angular correlations 2—2684
    nonaxial quadrupole vibrational state, Nilsson model 2—8272
    quadrupole, comparison with molecular quadrupole moments 2—34275
    quadrupole Coulomb excitation, differential cross sections, computer program 2—34998
    quadrupole moments of excited states, determ. from perturbed angular correlation meas. 2—7026
    quadrupole moments of the 2_1^+ state of proton-closed-shell nuclei 2—31442
    quadrupole perturbations, theoretical aspects of time-integrated angular correlations 2—27957
    quadrupole radial matrix elements calc. for Coulomb excitation, computer program 2—21365
    static quadrupole moments, measurement 2—38455
    static quadrupole moments of sd-shell nuclei 2—2682
    summary of work presented to conference on hyperfine interaction detected by nuclear rotation 1970 2—5639
    by time differential studies following nuclear reaction implantation 2—34956
    $^{180,\ 182}$W, relative quadrupole moments of first excited states, Mossbauer effect meas. after Coulomb excitation 2—11773
    ^{a}Hf, A=177, 179, 180, quadrupole moments of $^3F_2$ ground state determ. by atomic beam magnetic resonance meas. 2—18141
    ^{12}B, nuclear quadrupole coupling in Be crystal 2—36998
    ^{42}Ca, static quadrupole moment of lowest rotational band 2—18102
    ^{111}Cd implanted in Cd, from quadrupole interaction meas. 2—34956
    ^{112}Cd static quadruple moment of first excited state meas. 2—2718
    ^{114}Cd, quadrupole moment of first excited state 2—5661

Nucleus continued
  electric moment continued
    ^{151}Eu Mossbauer effect in Eu_2TiO_4, h.f.s., quadrupole moment ratio 2—33218
    ^{56}Fe, static quadrupole moment, from reorientation meas. following Coulomb excitation by ^{4}He and ^{16}O 2—31472
    ^{56}Fe, static quadrupole moment, from reorientation effect 2—2710
    ^{164}Ho, static moments 2—38518
    ^{165}Ho, nuclear quadrupole moment meas. by proton scattering from aligned target 2—34968
    In odd-mass isotopes 109-117, unified model in intermediate coupling used to determ. quadrupole moments of ground states 2—27981
    ^{117}In, quadrupole moment of 660keV rotational level, meas. in $In_{0.99}Cd_{0.01}$ alloy at 4.2K 2—14951
    ^{24}Mg, excited-state quadrupole moment determ. using Hartree- Fock model predictions 2—11734
    ^{24}Mg, quadrupole and hexadecapole moments, electron scatt. obs. 2—11783
    ^{95}Mo, quadrupole moment determ. using atomic beam magnetic resonance 2—21513
    ^{97}Mo, quadrupole moment determ. using atomic beam magnetic resonance 2—21513
    ^{20}Ne, excited-state quadrupole moment determ. using Hartree-Fock model predictions 2—11734
    ^{61}Ni, quadrupole moment of 67.4 keV level from Mossbauer study of $NiCr_2O_4$ 2—5656
    ^{16}O, fine structure in giant dipole resonance, interpretation questioned in light of expts. on $^{14}N(d,\gamma_0)$ reaction 2—28076
    ^{16}O, many-particle excited states, calc. of energies, quadrupole moments and shapes 2—8283
    ^{190}Os, ^{192}Os, ratio of moments of quadrupole moments of first excited states 2—5667
    ^{32}S, excited-state quadrupole moment determ. using Hartree-Fock model predictions 2—11734
    ^{32}S, static quadrupole moment of first excited state meas. 2—2718
    ^{28}Si, excited-state quadrupole moment determ. using Hartree-Fock model predictions 2—11734
    ^{28}Si, quadrupole and hexadecapole moments, electron scatt. obs. 2—11783
    ^{168}Tm, static moments 2—38518
    ^{170}Tm, rel. to radiative constants 2—24172
  energy level transitions
    ^{203}Pb, conversion coefficients, multipolarities of transitions following ^{203}Bi decay 2—34993
    ^{22}Na, short-lived activities excited by 14.7 MeV neutrons 2—18093
    β, γ vibrational bands in nuclei with $152<A<160$ 2—24170
    γ-transitions and spectroscopic factor A=16-19 nuclei, weak coupling model 2—21377
    A=14 nuclei, e.m. transition strengths, weak coupling calc., E1 transition 2—21375
    A=20, calculation of $T=2 \rightarrow T=1 \rightarrow T=0$ M1 decays 2—31456
    A=32, calculation of $T=2 \rightarrow T=1 \rightarrow T=0$ M1 decays 2—31456
    actinides, odd-A with $Z \geqslant 100$, nuclear spectroscopy and single particle states 2—21404
    aligned nuclei, γ-ray direction correlation coefficients, graphical representation 2—11718
    amplitude mixing ratio, sign determ. using $\beta\gamma\gamma$ and $\gamma\gamma\gamma$ angular correlation 2—2681
    angular correlation of two gamma rays in asymmetric elec. field grad., effects of static and time depend quadrupole interactions 2—458
    computer program for calc. of gamma ray angular correlations for pure or mixed multipolarity transitions correcting states of high angular momenta 2—31431
    decay from doorway state, width relationship with ratio between nos. of correlating and open channels 2—14923
    deformed even nuclei, octupole moments and transitions, muclear rotational motion 2—31440
    deformed nuclei, importance of indirect transitions in (p,t) reactions 2—28031
    deformed nuclei, ratios of reduced probabilities of E2 transitions between rotational states 2—24135
    Doppler shift attenuation lifetime meas., method for determining recoil ion ranges 2—19479
    doubly even deformed nuclei strength functions for M1 transitions calc. in TDA and RPA approx. 2—27951
    doubly odd deformed nuclei, absolute electromag. γ-ray transition probabilities 2—18074
    E1 photoabsorption sum rule, relation to change in orbital g factors due to exchange currents 2—8268
    E2 radiative widths of highly excited levels 2—27950
    E2 transitions, calc. of reduced transition probabilities in sd-shell nuclei 2—2682
    E2 transitions, conversion coeff. ratios for M-, N-, and O-shell electrons 2—27956
    E4 transition probabilities, measurement 2—38455
    E1 transition strength distribs. estimated by direct reaction inelastic scattering 2—34892
    e.m. transitions internal conversion ratios meas. for several nuclei and compared with theor. values 2—18078
    excited nuclei, radiation widths, effect of shell structure spectrum 2—27955
    giant dipole and quadrupole resonances, excitation cross section calc. 2—2678
    ground state rotational band, phase transition from superfluid state to normal state 2—31438
    half-life measurement of short-lived isomers 2—27980
    heavy odd-A nuclei, nearly spherical, projected spectra 2—21380
    intra-band B(E2) transition rates of even nuclei in rare-earth region, centrifugal stretching model 2—8276
    j^n configuration states, calc. of excitation energies E2 transition rates and two particle transfer spectroscopic amplitudes 2—2674
    lifetime determinations of excited nuclear states 2—38464
    lifetime meas. of excited states, new version of microwave method 2—8274
    lifetime of excited states determ. by meas. Doppler broadening of emitted γ-rays 2—11240
    lifetime systematics 2—34982
    light nuclei, sum rule for M1 transitions, validity of SU(4) symmetry 2—38449
    M2/E1 mixing ratios in level decay at $\approx$ 7 MeV excitation 2—2680
    minor asymmetry in Gamow-Teller transitions of large ft value 2—18153
    M1 γ-transitions, single particle relativistic approach 2—31434

Nucleus continued
energy level transitions continued
Mossbauer absorption spectra of E2 and E2/M1 transitions, observation of interference effects 2—24136
multipole relaxation times determ. by meas. of statistically perturbed angular correlations 2—2684
odd A-nuclei, e.m. M1 reduced transition matrix elements between Nilsson states 2—38463
odd-odd nuclei, constancy of basis effect on transition probabilities 2—38454
p-wave neutron capture spectra 2—38611
pair conversion coeffs. for E1 and M1 multipolarities, up to 10 MeV 2—8277
parity non conserving electric multipole type transitions, exchange current contributions 2—31433
probabilities, modified quasiparticle model 2—21364
resonance wave functions and parameters from coupled channel method 2—14972
rigid asymmetric rotator model, E2-transition probabilities 2—38462
s-d shell, energy gaps and momentum transfer 2—38486
separated hyperfine transitions, angular correlation formalism 2—18079
spectra of simple nuclear systems, procedure for checking using c.m. potential energy 2—14908
spherical doubly even nuclei, reduced transition probabilities, many-body approximations using pairing-plus-quadrupole model 2—34871
spontaneous fission fragments of ^{252}Cf, γ transitions meas. 2—31611
T-invariance, Mossbauer tests 2—11717
time-reversal-invariance violation, limit imposed by neutron electric dipole moment 2—34901
transition moments of inertia, relationship with intrinsic transition quadrupole moments 2—34893
Z=40 isotope from ^{235}U(n,f) fission products, evidence that strong EO transition depopulates first excited state of ^{98}Zr 2—11755
^{107,109,111}Ag, half-lives $^9/_2{}^+$ levels, M1 retardation and E2 enhancement factors of $^9/_2{}^+ \to {}^7/_2{}^+$ transition. $^7/_2{}^+$ level structure 2—14949
Al, ground state decay of levels, obs. of γ-rays from Al(n,xγ) 2—14989
^{26}Al, mean lifetimes of levels and decay modes from ^{23}Na(α,n)^{26}Ap reaction 2—14941
^{27}Al, B(E2) transition rates, Coriolis bandmixing model calcs., agreement for oblate shape 2—31458
^{27}Al, lifetime of 1.013 MeV state 2—11736
^{27}Al, lifetime of 843 keV level determ. from ^{27}Al(^{35}Cl,^{35}Cl) reaction using recoil-distance method 2—8291
^{27}Al, measurement of lifetime of the 1.01 MeV level 2—31457
^{28}Al, e.m. transition rates 2—34927
^{28}Al, M1+E2 ground state transition from capturing state 2—18206
^{241}Am, α-γ directional correl. in polycryst. source 2—34916
^{36}Ar, E2 transitions, Hartree-Fock and random phase approximations 2—38483
$_{37}$Ar, transition strengths, investigation using ^{37}Cl(p,n)^{37}Ar reaction 2—5650
^{38}Ar, mean lifetimes of 3.38 and 4.59 MeV levels prod. in ^{4}He(^{35}Cl,p)^{38}Ar reaction 2—21386
^{38}Ar lifetimes of levels at 3377, 4585, 4480 keV electron by Doppler shift attenuation and ^{38}Cl(α,pγ) reaction 2—27972
^{40}Ar, experimental $O_2{}^+$(2.12 MeV)$\to 2_1{}^+$(1.46 MeV) B(E2) strength and pairing-vibration calculations 2—31463
^{40}Ar, level lifetimes from proton scatt., using Doppler shift attenuation method 2—38490
^{75}As, half-lives of some excited states meas. using delayed coincidence technique 2—24165
^{75}As, half lives of short lived excited states 2—34948
^{75}As, transitions determ. from inelastic neutron scattering expts. 2—11750
^{197}Au, half-lives of some excited states meas. using delayed coincidence technique 2—24165
^{197}Au, half lives of short lived excited states 2—34948
^{9}B, isospin forbidden particle decay of first T=3/2 state studied by ^{7}Li(^{3}He,pn) reaction 2—27964
^{130}Ba, isomeric transition 8-$\to$6$^+$, description using model 2—11762
^{132}Ba, E2/M1 mixing ratios of $2_2{}^+ \to 2_1{}^+$ gamma transition and corresponding E2% admixture determ. 2—2721
^{133}Ba, K-shell conversion coeffs. from γ-spectrum 2—14966
^{133}Ba decay, K-X-ray γ directional correlations 2—18107
^{135}Ba, lifetime of 481 keV level 2—11763
^{9}Be, decay properties of excited states studied in four-body break-up of ^{11}B(d,3α)n reaction 2—18230
^{9}Be, isospin forbidden particle decay of first T=3/2 state studied by ^{7}Li(^{3}He,pn) reaction 2—27964
^{207}Bi decay, K-X-ray γ directional correlations 2—18107
^{209}Bi, rel. to hyperfine structure of L and K X-rays in muonic atom 2—18370
^{211}Bi electromagnetic transition rate calc. comparison with expt. 2—2757
^{81}Br, conversion coeffs. for 178, 260, 276 and 290 keV γ transitions 2—2746
^{11}C, transitions to 4.31, 8.11 and unresolved doublet state in ^{12}C(p,d) reaction, evidence of nondirect reaction mechanism 2—31542
^{12}C, giant E1 resonances, study from ^{11}B(p, γ) reaction 2—31446
^{12}C 2$^+$ excited state, γ-ray decay, meas. of angular correlation with inelastically scattered α particles 2—38630
^{12}C decay studied via ^{11}B(p,2α)α reaction 2—18192
^{12}C γ-ray decay of 15.11 MeV t=1 state, determ. branching intensities 2—24144
^{14}C, deexcitation γ-rays after π- capture on ^{16}O 2—2691
^{40}Ca, γ-ray decay of 6.75 MeV level, lifetime, mixing ratio, electromag. transition strengths 2—18101
^{40}Ca, magnetic transition strength studied by 180° electron scattering 2—11737
^{40}Ca, resonance wave functions and parameters from coupled channel method 2—14972
^{40}Ca perturbative treatment of transition moments, transition probabilities calc. in Tamn-Dancoff approx. 2—11739
^{43}Ca, e.m. decay of low-lying states populated in ^{43}Ca(p,p$'\gamma$) reaction 2—27974
^{43}Ca, γ-decay schemes of resonance states produced in ^{41}K(p,γ) reaction 2—14945
^{45}Ca from ^{46}Ca(d,t)^{45}Ca study 2—2809
^{48}Ca, perturbative treatment of transition moments, transition probabilities calc. in Tamn-Dancoff approx. 2—11739
^{49}Ca, gamma ray decay from the analogue state of the ground state 2—31469

Nucleus continued
energy level transitions continued
^{112}Cd M2/E1 mixing ratio for transitions following nuclear photoexcitation 2—11758
^{112}Cd width of $0^+ \to 2^+$ meas. 2—2718
^{140}Ce, gamma-gamma directional correlations 2—5665
^{140}Ce, lifetime of 3$^-$ octupolar level 2—18121
^{252}Cf, fragment γ-ray transitions, X-ray γ-ray coincidence study 2—2830
^{33}Cl, γ-decay of isospin forbidden resonance states to first excited and ground states, M1 strength 2—34931
^{34}Cl, mean lives of 1230, 666, and 461 keV levels meas. by recoil-distance method 2—465
^{35}Cl, γ ray transitions 2—2704
^{35}Cl, lifetimes of first six excited states determ. from Doppler shift attenuation meas. on ^{35}Cl(p,p$'\gamma$) reaction 2—31462
^{35}Cl, transition strengths, investigation using ^{35}Cl(p,p$'$) ^{35}Cl* reaction 2—5650
^{38}Cl, multiple strengths of transitions linking levels below excitation energy 2.75 MeV to ground state 2—24154
^{246}Cm, X-ray spectra and L-shell fluorescence yields, rel. to electron binding energy calc. 2—11784
^{55}Co, e.m. transitions studied via ^{54}Fe(^{3}He,dγ)^{55}Co reaction 2—27976
^{57}Co, level half-life measurements 2—8297
^{59}Co, half-life meas. of 1291.6 keV level 2—34944
^{59}Co cascades, γ-γ directional correl. obs. 2—34988
^{59}Co internal conversion meas. 2—38537
^{60}Co, γ decay investigation using $\gamma\gamma$ ang. correlation meas. 2—2711
^{60m}Co, K-conversion coefficients of gamma ray transitions 2—8223
^{49}Cr, mean lifetimes of levels below 3 MeV excitation meas. using ^{49}Ti(α, nγ) reaction 2—18105
^{50}Cr, study of excited states by means of ^{50}Mn decay and ^{50}Cr(p,pγ) reaction 2—34939
^{52}Cr, lifetimes of levels to 4.5 MeV in excitation energy determ. by Doppler shift attenuation method 2—11746
^{53}Cr, e.m. properties studied with ^{50}Ti(α,nγ)^{53}Cr reaction 2—34940
Cs (A=131, 133), half lives of short lived excited states 2—34948
^{131}Cs, half-lives of some excited states meas. using delayed coincidence technique 2—24165
^{133}Cs, half-lives of 81 keV and 161 keV excited levels 2—38514
^{133}Cs, half-lives of some excited states meas. using delayed coincidence technique 2—24165
Cu, A=59, 61, 63, M1 transition from $g_{9/2}$ analogue to anti-analogue state 2—5655
^{59}Cu, M1 transitions from $g_{9/2}$ analog-to-antianalog states 2—18109
^{61}Cu, Mi transitions from $g_{9/2}$ analog-to-antianalog states 2—18109
^{63}Cu, M1 transitions from $g_{9/2}$ analog-to-antianalog states 2—18109
^{64}Cu, population and decay of levels up to 2300 keV, produced by thermal neutron capture in natural copper 2—14939
^{160}Dy, internal conversion coeffs. 2—38517
^{160}Dy, lifetimes of 2$^+$, 4$^+$ states obs. 2—2726
^{160}Dy, mixing parameter for mixing of gamma vibrational and ground state bands 2—24171
^{161}Dy, 26 keV Mossbauer transition, determ. of L-shell conversion coefficient 2—2728
^{161}Dy, interference of photoelectric and nuclear resonance absorption of 26 keV E1 γ rays studied by transmission and scattering Mossbauer expts. 2—2727
^{162}Dy, multiple Coulomb excitation of γ-vibrational bands using ^{16}O ions 2—14955
Er (A=166, 168, 170) multiple Coulomb excitation of γ-vibrational bands using ^{16}O ions 2—14955
Eu, transition multipolarity, investigation using angular $\gamma\gamma$ correlation method 2—11766
^{153}Eu, muonic isomer shifts of γ-ray transitions, mean square radius of ground and excited states 2—18130
^{18}F, short-lived activities excited by 14.7 MeV neutrons 2—18093
^{19}F, branching from levels observed using proton scatt. reaction 2—38482
^{19}F, obs. γ-rays from 110 and 197 keV levels following kaon capture in ^{32}S 2—28059
^{19}F, study of resonance at 850 keV is ^{15}N(α,γ) reaction, meas. of lifetime and M1 transition strength 2—35069
^{53}Fe mean life of low lying levels determ. by n-γ delayed coincidence meas. on ^{50}Cr(α,nγ) reaction 2—11748
^{54}Fe, mean lifetime of 2.95 MeV (6$^+$) state 2—8298
^{55}Fe, excited state mean life, from γ-ray Doppler shifts 2—2693
^{57}Fe, doorway state effects in M1 radiative excitation of p-wave resonances 2—18108
^{57}Fe, E_2:M1 multipole mixing ratio of excited state transitions 2—31473
^{58}Fe, E_2:M1 multipole mixing ratio of excited state transitions 2—31473
^{59}Fe, level transition scheme proposed, ^{58}Fe(n,γ)^{59}Fe ob. 2—5702
Ga, A=65, 67, M1 transition from $g_{9/2}$ analogue to anti-analogue state 2—5655
^{67}Ga, M1 transitions from $g_{9/2}$ analog-to-antianalog states 2—18109
^{70}Ga 188 keV transition 2—38499
^{146}Gd, hindrance factor of E2 $6^+ \to 4^+$ transition, study using ^{144}Sm(α,2n)^{146}Gd 2—2723
^{153}Gd, obs. of cascade of E2 transitions, following ^{152}Sm(α,3n) reaction 2—21395
^{153}Gd from ^{152}Sm(α,3nγ), high-spin states γ-spectroscopic study 2—18128
^{154}Gd, 123 keV K, L and M shell particle parameters 2—34964
^{154}Gd, multipolarity of 693 keV $2^{+\prime} \to 2^+$ transition investigated 2—2725
^{154}Gd from ^{152}Sm(α2nγ), high-spin states γ-spectroscopic study 2—18128
^{156}Gd, gamma-ray transitions studied using ^{155}Gd(n,γ)^{156}Gd 2—27987
^{156}Gd, γ-γ directional correlation meas., M1 admixtures of transitions 2—31487
^{70}Ge, Coulomb excitation, meas. of γ-ray yields, B(E2) transition to excited O$^+$ state 2—38498
^{76}Ge, γ-ray decay scheme investigation using ^{76}Ga$\to$^{76}Ge decay 2—11751
^{3}He, E2 transition in photodisintegration 2—21423
Hf recoiling into vacuum, perturbed γ-ray angular distributions 2—31491
^{176}Hf, half-life of 1247.7 keV level meas. in decay of ^{176}Ta, deduced E1M2E3 mixing of 1159.3 keV level 2—18140
^{177}Hf, internal conversion of 208keV E1 transition 2—14957
^{177}Hf, M1 and E2 transitions 2—38551
^{177}Hf, penetration effects in internal conversion 2—38521
^{178}Hf, E0 and E2 transition probabilities 2—34972
^{180}Hf, parity admixtures in nuclear forces γ transition study 2—31489
^{180m}Hf, E2/M2 and E3/M2 mixing ratios 2—2752
^{197}Hg, 133 keV state g-factor by perturbated angle e_{casc} γ correlation method 2—38524

Nucleus continued
energy level transitions continued
^{198}Hg 676 keV transition, mixing ratio, ang. correl. obs. 2—34976
^{199}Hg, $13/2^+$ isomeric state decay modes determ. gamma-ray spectra obs. 2—5668
^{199}Hg, half-life of 208.1 keV level and internal conversion coeffs. 2—38525
^{199m}Hg, hyperfine structure and isomeric shift 2—34977
^{164}Ho, transition probabilities 2—38518
^{123}I, level half-life measurements 2—8297
^{127}I, 360-58 keV cascade in Te crystal, ang. γ quanta correlation perturbation 2—29854
^{134}I obs. 4 new transitions found 2—2722
In odd-mass isotopes 109-117, unified model in intermediate coupling used to determ. M1 and E2 reduced transition probabilities 2—27981
^{115}In, muonic, $2s_{1/2}$ to $2p_{1/2}$ transition, magnetic hyperfine splitting 2—741
^{189}Ir, E2 and M1 transition probabilities between low energy states 2—18143
^{192m}Ir, L-conversion coefficients of gamma ray transitions 2—8223
^{38}K, γ decay of levels below 3-7 MeV excitation energy populated by ^{40}Ca(d,$\alpha\gamma$) reaction, multipole mixing ratios 2—35075
^{39}K, M2 and E3 radiation widths of 2.82 MeV level, comparison of experiment and theoretical predictions 2—8294
^{40}K, from ^{40}Ca(n,pγ), $4.85 \leqslant E_n \leqslant 8.05$ MeV 2—38615
^{40}K, level lifetimes determ. from ^{40}Ar(p,p)^{40}K using Doppler shift attenuation method 2—38490
^{40}K, short-lived activites excited by 14.7 MeV neutrons 2—18093
^{45}K from ^{46}Ca(d,^{3}He)^{45}K study 2—2809
^{79}Kr, conversion coeffs., ^{79}Br(p,n) reaction obs. 2—38501
^{79}Kr, lifetimes of excited states, study from decay of ^{79}Rb 2—38500
^{81}Kr, conversion coeffs., ^{81}Br(p,n) reaction obs. 2—38501
^{135}La, 119 keV level, lifetime meas. 2—31485
^{6}Li, isospin and decay modes from ^{7}Li(τ,α)^{6}Li and ^{7}Li(τ,α)^{6}Li*(d)^{4}He reactions at E_τ=1.5 MeV 2—27969
^{7}Li lifetime of 477 keV state determ. by meas. Doppler broadening of emitted γ rays 2—11240
^{8}Li, lifetime of first excited state, meas. using ^{9}Be(t,α) reactions 2—18088
^{171}Lu, $^1/_2{}^-$[541] rotation band branching 2—18133
^{171}Lu, 17 new transitions 2—2751
^{176}Lu, decay scheme investigation using ^{175}Lu(n,γ) reaction 2—34971
^{177}Lu, penetration effects in internal conversion 2—38521
^{176m}Lu, K-conversion coefficients of gamma ray transitions 2—8223
^{24}Mg, e.m. transition rates calculated using Hartree-Fock model predictions 2—11734
^{24}Mg, energies, branching ratios, lifetimes, γ-ray transition, strengths of levels populated in ^{23}Na(p,γ) reaction 2—38591
^{24}Mg, energy gaps and momentum transfer 2—38486
^{24}Mg, lifetime meas. of 6.431 MeV (0^+) and 8.655 MeV (2^+) levels populated in ^{12}C(^{16}O,α)^{24}Mg reaction 2—38487
^{24}Mg, role of spin transfer and multistep effects in transition to 5.22 MeV 3^+ state in ^{26}Mg(p,t) reaction 2—35035
^{24}Mg decay schemes from ^{23}Na(p.γ)^{24}Mg 2—38593
^{25}Mg, 975 keV $^3/_2{}^+$ state, half-life 2—18097
^{25}Mg, excited state mean life, from γ-ray Doppler shifts 2—2693
^{25}Mg, transitions from ^{24}Mg produced by (d,p) reaction at 12 MeV 2—35070
^{26}Mg, lifetime of 1809 keV level determ. from ^{12}C(^{19}F,$\alpha p\gamma$) reaction using recoil-distance method 2—8291
^{26}Mg, mean lifetimes of levels and decay modes from ^{23}Na(α,p)^{26}Mg reaction 2—14941
^{27}Mg, mean life and mixing coeff. meas. using ^{26}Mg(d,pγ) reaction 2—18099
Mn, A=51, 53, 55, fine structure meas. using p scatt. and ^{54}Cr(p,n) spins, parities and partial widths obtained 2—2708
^{52}Mn, level half-life measurements 2—8297
^{53}Mn, electromagnetic transitions, mean lives, multipole mixing ratios, probabilities 2—31470
^{53}Mn, mean lives of low lying levels measured, electromagnetic transitions studied 2—18106
^{53}Mn, transition rates determ. from study of ^{53}Cr(p,n) reactions 2—11747
^{54}Mn, $0^+ \to 0^+$ transitions, isobaric spin (^{3}He,p) intensity relations 2—21448
^{54}Mn, decay, K-X-ray γ directional correlations 2—18107
^{56}Mn, lifetimes of 26 and 110 keV levels determ. using thermal neutron capture on natural Mn targets 2—8299
^{92}Mo, short-lived activities excited by 14.7 MeV neutrons 2—18093
^{93}Mo, relative intensities from ^{92}Mo(d,pγ)^{93}Mo coincidence meas. 2—34951
^{13}N, obs. of lowest T=$_{3/2}$ state, 14 MeV resonance in ^{12}C(p,p)^{12}C 2—21428
^{14}N, deexcitation γ-rays after π- capture on ^{16}O 2—2691
^{15}N, deexcitation γ-rays after π- capture on ^{16}O 2—2691
^{23}Na, low-lying $K^\pi = {}^1/_2{}^-$ band, E1 decay of members 2—24151
^{23}Na, mean lifetimes of levels and decay modes from ^{23}Na(p,p$'$)^{23}Na reaction 2—14941
^{23}Na, resonance to bound states, multipole mixing ratios from ^{22}Ne(p,γ)^{23}Na meas. 2—24219
^{24}Na, low-lying levels, investigation using ^{26}Mg(d,$\alpha\gamma$)^{24}Na reaction 2—2698
^{89}Nb, γ-spectra 2—477
^{90m}Nb, influence of chemical environment on decay constant of 2.38 keV isomeric transition 2—2714
^{94m}Nb, K-conversion coefficients of gamma ray transitions 2—8223
^{144}Nd, gamma-ray spectra following resonance neutron capture in ^{143}Nd 2—34960
^{20}Ne, E2 transitions, Hartree-Fock and random phase approximations 2—38483
^{20}Ne, e.m. transition rates calculated using Hartree-Fock model predictions 2—11734
^{20}Ne, form factors of monopole transition, obs. using inelastic electron scattering 2—31455
^{20}Ne, radiative width of 8^+ 11.948 MeV level, ^{4}He(^{16}O,γ) capture reaction study 2—18096
^{57}Ni, mean lifetime of 3.003 MeV level 2—11749
^{60}Ni, E2/M1 mixing ratio for $2_2{}^+ \to 2_1{}^+$ transition 2—14946
^{62}Ni, E2/M1 mixing ratio for $2_2{}^+ \to 2_1{}^+$ transition 2—14946
^{64}Ni, spin and parity assignments, gamma transitions 2—5693
^{65}Ni level scheme deduced from meas. of thermal neutron capture in ^{50}Ti 2—28050
^{65}Ni level scheme deduced from meas. of thermal neutron capture in ^{64}Ni 2—28050
^{17}O, excited state mean life, from γ-ray Doppler shifts 2—2693
^{17}O, transitions from ^{16}O produced by (d,p) reaction at 12 MeV 2—35070

Nucleus continued
energy level transitions continued
^{18}O, hyperfine interactions of first excited 2^+ state in 7^+ and 6^+ ions 2—31451
^{18}O, probabilities for transitions to the ground state following excitation by inelastic electron scattering 2—8326
Os, A=186,188,190,192, Coulomb excitation of 2^+states by ^{4}He, p and ^{16}O, B(E2) values 2—18142
Os, isotopes, A=184, 186, 188, $21^+ \to 0^+$ transitions probabilities 2—14969
^{186}Os, e.m. transitions 2—38522
^{186}Os, γ-γ ang. correl. obs. 2—34975
^{188}Os, e.m. transitions 2—38522
^{189}Os, half lives at 69, 95 and 219 keV 2—11768
^{29}P, radiative decay of 8.38 MeV level 2—34929
^{30}P, lifetime meas. for levels between 3.7 and 4.7 MeV excitation energy 2—21385
^{31}P, investigation via alpha capture in ^{27}Al 2—2703
^{32}P, electromagnetic decays of lowest T = 2 state 2—8293
^{32}P, obs. of γ-rays from 78.1 keV level following kaon capture in ^{32}S and ^{35,37}Cl 2—28059
^{35}P, new nuclide prod. in ^{37}Cl(γ,2p) reaction half life and γ-ray energy meas. 2—5651
^{204}Pb, conversion coefficients, multipolarities of transitions following ^{204}Bi decay 2—34993
^{205}Pb, $^{13}/_2{}^+$ level, half-life and branching ratios 2—8311
^{206}Pb, EO transition to ground state 2—11777
^{208}Pb, E_1 and E_2 transitions, 0 to 30 MeV interval, Fermi systems theory method 2—38511
^{210}Pb, L-conversion coefficients of gamma ray transitions 2—8223
^{211}Pb, electromagnetic transition rate calc. comparison with expt. 2—2757
Pd (A=104, 106), rel. to assignment of levels excited in (α,xn) reactions 2—24166
^{103}Pd, excited states, in-beam γ-ray meas. using ^{103}Rh(p,nγ)^{103}Pd reaction 2—11757
^{104}Pd, multipolarities and mixing ratios 2—21392
^{143}Pm, effective coupling const. of M2 transition, $1h_{11/2} \to 1g_{7/2}$ state, half life meas. 2—18125
^{147}Pm cascades, γ-γ directional correl. obs., spin assignments 2—34962
^{202}Po, $(h_{9/2})^2$ two-quasiparticle isomeric state, meas. half life and transition energies 2—2735
^{204}Po, J=8^+ isomeric state, half-life meas. 2—2735
^{207}Po, establishment from decay of ^{207}At 2—18148
^{209}Po, M1 and E2 transition rates meas. in electron capture decay of ^{209}At 2—31494
^{211}Po, electromagnetic transition rate calc. comparison with expt. 2—2757
^{143}Pr, from ^{143}Ce decay, internal conversion coeff. and multipolarities rel. to level structure investigation 2—21394
^{144}Pr, 80 keV, multipolarities 2—38515
^{144}Pr, K-internal conversion coeff. of 53 keV transition, penetration study 2—24168
^{144}Pr rot. of ang. correl. pattern of 53-80 keV cascade 2—34961
Pt (A=192, 194, 196) monopole admixtures in $2'^+$-2^+ transitions 2—11775
^{192}Pt triple γ cascade, multipolarity of 296 keV transition 2—34991
^{195}Pt, 130 keV state g-factor meas. by Mossbauer effect 2—18145
^{195m}Pt, oriented in Fe, E2/M1 mixing ratio of 99 keV γ transition, n.m.r. study 2—27994
^{238}Pu, electric monopole transitions 2—38530
^{239}Pu, mixing ratios of transitions, half-lives, ^{239}Np decay obs. 2—34979
^{85}Rb, short-lived activities excited by 14.7 MeV neutrons 2—18093
^{186}Re, nuclear structure and an isomer with half-life 2×10^5 years 2—34974
^{187}Re, gamma-gamma directional correlations of 552-134 keV cascade 2—8310
^{187}Re, half- lives of some excited states meas. using delayed coincidence technique 2—24165
^{187}Re, half lives of short lived excited states 2—34948
^{103,105}Rh, half-lives $^9/_2{}^+$ levels. M1 retardation and E2 enhancement factors of $^9/_2{}^+ \to {}^7/_2{}^+$ transition, $^7/_2{}^+$ level structure 2—14949
^{103}Rh, half-life of 93 keV ($9/2^+$) level 2—5660
^{99}Ru, study using ^{99}Rh beta decay 2—34953
^{28}S, energy gaps and momentum transfer 2—38486
^{32}S, e.m. transition rates calc. using Hartree-Fock model predictions 2—11734
^{32}S, energies, branching ratios, lifetimes, γ-ray transition strengths of levels populated in ^{31}P(p,γ) reaction 2—38596
^{32}S, energy gaps and momentum transfer 2—38486
^{32}S, investigation using ^{28}Si(α,γ)^{32}S reaction 2—5649
^{32}S, magnetic transition strength studied by 180° electron scattering 2—11737
^{32}S width of $0^+ \to 2^+$ meas. 2—2718
^{33}S, multipole mixing ratios of transitions between low-lying levels 2—18234
^{35}S, angular correlation meas. spin assignments and multipole mixing from ^{34}S(d,pγ)^{35}S, ^{37}Cl(d,$\alpha\gamma$)^{35}S 2—18100
^{36}S, γ transitions, mean lives and spin-parity assignments 2—34933
^{125}Sb, determ. reduced transition rates from first excited state to ground state from γ-γ angular correlation meas. on decay of ^{125m}Sn 2—28006
^{42}Sc, lifetimes of levels populated in ^{40}Ca(^{3}He,p) reaction at 8.4 and 8.6 MeV 2—8296
^{43}Sc, determ. lifetimes and absolute transition strengths of $K^\pi = 1/2^+$ rotational band 2—11741
^{43}Sc lifetimes measured by Doppler shift attenuation methods, determ. transition strengths 2—18103
^{44}Sc, 68 keV state lifetime meas. 2—34936
^{48}Sc, excited states, investigation using ^{48}Ca(p,nγ)^{48}Sc reaction 2—2705
^{48}Sc, nuclear spectroscopy from ^{46}Ca(^{3}He,p) reaction 2—34938
^{75}Se decay, K-X-ray γ directional correlations 2—18107
^{81}Se, conversion coeffs. for 103 keV γ transition 2—2746
^{27}Si, angular correlations and branching ratios of levels below 5 MeV excitation, spin assignments 2—24152
^{27}Si, lifetimes of lower excited states using ^{28}Si(^{3}He,α)^{27}Si reaction 2—18098
^{28}Si, E2 transitions, Hartree-Fock and random phase approximations 2—38483
^{28}Si, e.m. transition rates calc. using Hartree-Fock model predictions 2—11734
^{28}Si, shell model calculations of excitation spectrum 2—21384
^{29}Si, lifetime of 3626 keV level determ. from ^{12}Cl^{19}F,n$p\gamma$) reaction using recoil-distance method 2—8291
^{29}Si, principal decay modes and lifetimes of levels below 7.2 MeV populated by ^{26}Mg(α,n)^{29}Si reaction 2—27971

Nucleus continued
energy level transitions continued
^{30}Si γ decay studied by ^{27}Al(α,pγ) reaction, meas of branching ratios and lifetimes 2—34986
^{144}Sm, transition strengths meas. for low lying states following elastic and inelastic scattering of α particles and protons 2—11857
^{150}Sm, reduced transition probability B(E2) of first 2$^+$ level deduced from cross section for elastic and inelastic scattering of ^{4}He 2—2724
^{151}Sm, collective state population by (d,d') and Coulomb excitation B(E2) values 2—18126
^{154}Sm, lifetimes of ground-band states 2—31486
Sn, A=112, 120, 124, E$_1$ and E$_2$ transitions, 0 to 30 MeV interval, Fermi systems theory method 2—38511
^{114}Sn, half-life of isomeric state 2—38512
^{116}Sn, 0$^+$ to 0$^+$ transition, strength parameter 2—31482
^{117}Sn, half-life of 158 keV level 2—34957
^{117}Sn, γ-ray internal conversion coeff. 2—18118
^{85}Sr decay, K-X-ray γ directional correlations 2—18107
^{87}Sr, fluorescence after thermal neutrons capture and levels 2—38503
^{87}Sr, half life of level at 388 keV, populated in decay of ^{87}Y 2—5675
^{177}Ta, decay of three-quasiparticle state, determ. E2/M1 mixing ratios, rotational-model parameters and half-life 2—11770
^{181}Ta, E2/M1 mixing ratio of 136 keV transition determ. by perturbed angular correlation methods 2—2729
^{181}Ta, parity admixtures in nuclear forces γ transition study 2—31489
^{182}Ta decay, gamma- and beta-ray spectra obs. 2—31509
^{159}Tb, parity admixtures in nuclear forces γ transitions study 2—31489
^{94}Tc decay, meas. of delayed γ-rays, comparison with data on ^{94}Mo levels indicate isomeric $(g_{9/2})^2$ proton state 2—14960
^{99}Tc, $\gamma\gamma$ ang. correlations and level lifetimes rel. to quantum characteristics of excited levels 2—11756
^{99}Tc Coulomb excitation with 52-64 keV ^{35}Cl ions, deduced level structure and lifetimes 2—18115
^{99}Tc γ cascades, directional correl. and multipole mixing 2—34954
^{99m}Tc, E3 isomeric transition decay in ferroelec. BaTiO$_3$ 2—33056
Te, A=121, 123, 125, 127, 129, M4 transitions, ratios of internal conversion coefficients 2—38548
Te, isomeric transition from ground to metastable state, isomer separation 2—2719
^{121}Te, total particle parameter of 212keV transition 2—14952
^{125}Te, 35.5 keV level, gamma-gamma angular correlations 2—14954
^{125}Te, angular correlation study of 322-177 keV cascade 2—8305
^{125}Te, lifetimes of 35.5 and 46.5 keV states populated in ^{125}Sb β-decay, M1 and E2 transition probabilities estimated 2—34958
^{228}Th, multipolarities 2—8317
^{230}Th, deformation parameters and E4 transition probabilities from Coulomb excitation expt. 2—8313
^{44}Ti, Q val. of ground state transition, L=2 and L=0 transitions 2—24157
^{48}Ti, crossover transition, ^{48}Sc decay obs. 2—38536
^{49}Ti, transitions studied by ^{48}Ti(n,γ)^{49}Ti reaction 2—31557
^{51}Ti level scheme deduced from meas. of thermal neutron capture in ^{50}Ti 2—28050
^{51}Ti level scheme deduced from meas. of thermal neutron capture in ^{50}Ti 2—28050
^{203}Tl, parity admixtures in nuclear forces γ transition study 2—31489
^{203}Tl, study of 279 keV transition angular correlation meas.of asymmetry, deduced limit of parity mixing 2—2736
^{204}Tl, internal bremsstrahlung spectrum, contribution of detour transitions 2—21398
^{168}Tm, transition probabilities 2—38518
^{170}Tm, radiative constants, from magnetic and electric moments 2—24172
^{171}Tm, γ-ray transition properties following β-decay of 7.5h ^{171}Er 2—34970
^{238}U, deformation parameters and E4 transition probabilities from Coulomb excitation expt. 2—8313
^{49}V, from ^{49}Cr beta decay, lifetime of 90.65 keV state 2—2707
^{51}V, electromagnetic transitions, mean lives, multipole mixing ratios, probabilities 2—31470
^{51}V, theoretical internal conversion coefficients 2—11745
^{182}W, parity admixtures in nuclear forces γ transition study 2—31489
^{183}W, Mossbauer linewidths and half-lives of 46.5 keV and 99.1 keV levels 2—11774
^{186}W, e.m. transitions 2—38522
^{132}Xe, E2/M1 mixing ratios of $2_2{}^+\rightarrow2_1{}^+$ gamma transition and corresponding E2% admixture determ. 2—2721
^{90}Y, shell model structure, l=5 transition data from 89Y(d,p) and ^{89}Y(α, ^{3}He) 2—34950
^{94}Y, four new transitions obs. from ^{94}Y→^{94}Zr decay 2—18161
^{96}Y, three new transitions obs. in ^{96}Y→^{96}Zr decay 2—18161
^{86m}Y, γ decay investigation 2—38544
^{170}Yb, half-lives of some excited states meas. using delayed coincidence technique 2—24165
^{170}Yb, half lives of short lived excited states 2—34948
^{65}Zn decay, K-X-ray γ directional correlations 2—18107
^{66}Zn, lifetime of 1.037 MeV state 2—24147
Zr, A=91, 93, fluorescence after thermal neutrons capture and levels 2—38503
^{89}Zr $T_<$ states from ^{89}Y(^{3}He,t) reaction angular distributions characteristic of nonallowed L transfers 2—11866
^{90}Zr, B(E2) for first 2$^+$ state 2—21390

energy levels
see also Nuclear structure; Radioactivity/decay schemes
0$^+$ states, excitation in two-particle transfer reactions 2—24134
2$^+$ level excitation in (n,n'γ) reactions, cross sections 2—18208
3 body problem, bound states and scattering processes, numerical study 2—38471
^{209}Bi, level structure from study of ^{210}Po IAR's in ^{209}Bi(p,p') reaction 2—21400
β, γ vibrational bands, properties in nuclei with 152<A<160 2—24170
(j-1) states anomalous coupling, excitation energies calc. 2—8275
A=11-40 population of levels following (n, n'γ) reactions by analysis of γ-ray spectra 2—35045
A=14 nuclei, weak coupling calc. 2—21375
A=18 nuclei, diagrams with 4p-2h intermediate states, contrib. to effective interaction 2—21378
A=18 to 40, kV neutron capture in 2s-1d shell 2—38610
A=6 to 9, Talmi-type calcs. 2—38469
A=8 system, excited states, investigation using ^{7}Li+n and ^{7}Li+p reactions 2—24141

Nucleus continued
energy levels continued
A<226, influence of shells and pairing on the fission probabilities 2—31594
actinides, 0$^+$ excited states 2—38479
actinides, 229⩽A⩽257, quasiparticle and vibrational character of excited levels, from radioactive decay meas. 2—21401
actinides, non collective description of low lying 0$^+$ states excited in (p,t) reactions 2—14940
actinides, odd-A with Z⩾100, nuclear spectroscopy and single particle states 2—21404
boson method, nuclear structure in ideal space 2—31423
bound states calc. in shell model using single particle spectra including the continuum 2—24130
collective levels, exchange exchange excitation problem 2—2676
conference on hyperfine interactions in crystals and nuclear props., Rehovot, Israel, 1970 2—5630
core-polarization correction in energy spectrum 2—38466
correlating and open channels, number ratio relationship with width for decay from doorway state 2—14923
Coulomb excitation, second-order quantum-mechanical theory 2—38450
deformed, collective 0$^+$ and 2$^+$ states 2—38452
deformed heavy nuclei, microscopic description of collective vibrational states, schematic approx. effects 2—38459
deformed nuclei, rotational level characteristics rel. to determination of exptl. values for nuclear constants 2—24125
deformed shell models of axial symmetry, spurious rotational states 2—21359
degenerate states, in j^n-config., and fractional parentage coeffs. 2—2670
densities, fermions, shell effects 2—27953
densities for random one- or two-body potentials 2—31430
dipole states, damping 2—38448
double even nuclei, asymmetric rotor with variable moment-of-inertia model for fitting ground state and γ-vibrational bands 2—14915
double-analog state formation in heavy nuclei, role of pairing 2—18188
doubly even actinide nuclei, prod. by α-decay deduced level energies of ground state rot. by bands 2—11780
doubly even deformed nuclei, properties of collective 1$^+$ states investigated in TDA and RPA approximations 2—27951
doubly open shell nuclei, quadrupole vibrational states, surface δ-interaction model 2—38458
Efimov states in a 3 body system 2—38457
electron scattering from one- and two-phonon vibrational states 2—31526
energies excited states prod. in (p,t) reaction on even even N=Z nuclei in 2s1d shell 2—24214
even-even, two particle multiplet configurations 2—24131
even-even Mo and Ru nuclei, paired nucleons, collective states 2—18113
even-even nuclei, phenomenological collective model for high angular momenta 2—31435
excited, investigation using γ-ray monochromator 2—2671
excited collective random phase approximation states, effect of various correlated ground states on energies 2—38460
excited level studies using Coulomb excitation 2—31588
Fermi gas theory, modifications caused by the existence of collective motions 2—38456
fermions in single particle level scheme, entropy, shell effects 2—27953
g-factor meas. of short-lived excited states with sum-technique 2—8273
giant dipole state, spreading width related to damping width of single particle states 2—14924
ground state correlations of vibrating closed shell nuclei due to residual interaction 2—8279
ground state energy, two and three nucleon, variation-iterational calc. 2—5635
ground state properties calc. using Λ_{00} and Λ_{10} theories 2—5633
ground state shell correction determ. method 2—34895
Hartree-Fock intrinsic states for sd shell 2—21351
heavy elements, single particle states and single particle models 2—21381
heavy nuclei, equilibrium deformations 2—27968
heavy nuclei, isotopic spin conservation for low lying collective states 2—21369
hyperfine structure, angular correlation, study, magnetic field r.f. modulation 2—8266
intrinsic states, variation after projection and projected Hartree methods, model comparison 2—38453
isobaric analog and configuration states, structure 2—5632
isospin splitting in giant dipole resonances, role of effective interactions 2—18076
level spacings calc. 2—34896
light nuclei, fractional parentage structure of ground state, influence on photodisintegration 2—21376
mass-14 nuclei, high-lying T=1 states, reaction ^{15}N(d, ^{3}He)^{14}C 2—18233
medium and heavy nuclei, low-lying many particle-many hole states, quartet model 2—14919
nuclei with closed shells of 50 or 82, det. by obs. of γ-decay of fission products and resonant scattering of neutron capture γ-rays 2—38441
odd-mass nuclei, 51⩽Z⩽61, level spectra and intermediate coupling model 2—27984
odd-odd nuclei, regularity in multiplet properties 2—11715
one particle fractional parentage coefficient, one-excited $U_{3(n-1)}$ states 2—18072
one-particle orbital fractional parentage coefficients, calc. method 2—14922
pairing vibrational state, study using two level model with pairing force 2—8278
pairing vibrational states in seniority-zero space, generator coordinate approach 2—21350
quadrupole vibr. bands, perturbation treatments 2—34899
quasirotational spectra, bootstrap theory 2—31437
rare earths, odd-mass alternating energy term for rot. levels 2—34917
rotational bands and SL(3,R) symmetry 2—34900
rotational spectra and shapes classification, phenomenological models 2—34886
rotational wavefunctions, I⩽13 and I⩽25/2 computer programme 2—38461
s-d shell, energy gaps and momentum transfer 2—38486
s-d shell nuclei, higher isospin states, Hartree-Fock-Bogoliubov model 2—14914
sd shell nuclei influence of pairing on rotational states, angular momentum projection method 2—27954
sd-shell nuclei, calculation of triaxial shapes 2—31424

Nucleus continued
energy levels continued
sd-shell nuclei, light, core excited states, α-cluster structure and weak coupling feature 2—38451
shell model calculations, A=27, 28, 29 nuclei 2—38489
shell model calculations, for nuclei with A=30-35 2—2702
single particle, in two-centre shell model 2—27946
single particle states of non-axially symmetric nuclei, numerical soln. to Schrodinger eqn. 2—2675
single-particle states 2—31429
spectra from nuclei in immediate vicinity of closed shells, analysis in terms of effective nucleon-nucleon interaction 2—8267
spherical nuclei, low spins, backward bending for quasirotational bands 2—31439
spherical nuclei, two-phonon quadrupole- octupole vibrations, microscopic theory 2—18077
spherical odd mass nuclei, structure of anomalous coupling state of spin I=(j-1) 2—31432
statistical description of a paired nucleus with the inclusion of angular momentum 2—34883
supermultiplet model for level densities 2—34897
Thomas-Fermi method formulation using realistic nucleon nucleon potential 2—31426
three body system, excited states calc. in local potential model 2—24132
two-particle orbital matrix of density for one-quanta oscillatory-excited SU_3-configs. 2—27936
unbound final states, strength of (^{3}He,d) reactions for their formation 2—15005
vibrational nuclei, low lying negative parity states 2—2677
yrast states, Coriolis effects at high angular momentum 2—27952
(γ,n), (γ,p), (γ,α), residual nuclei populated states 2—38563
^{298}114, ground state props. calc. using relativistic self consistent meson field theory 2—11704
^{a}Ca, A=39, 41, 43, 47, levels deduced from ^{40,42,44,48}Ca(p,d) reactions, spectroscopic factors derived from DWBA analysis, obs. of analogue states 2—35036
^{a}Pt, A=194-196, 198, levels deduced from recoil of Coulomb excited nuclei into He, vacuum, g-factors determ. 2—38648
^{107,109,111}Ag, structure of $^{7}/_{2}{}^{+}$ level 2—14949
^{24}Al, excitation energies of levels, study by ^{24}Mg(p,n)^{24}Al at 23 MeV 2—18092
^{26}Al, evidence for ground state rotational band of $K^{\pi}=5^{+}$ 2—2699
^{26}Al, level scheme, $4^{+}(d_{3/2})^{-2}$ state obs. 2—8290
^{26}Al, location of second $J^{\pi}=0^{+}$, T=1 state from ^{24}Mg(^{3}He,pγ), ^{25}Mg(^{3}He,dγ) and ^{27}Al(^{3}He,$\alpha\gamma$) reactions 2—38488
^{27}Al, (γ,p) reaction obs. 2—31523
^{27}Al, excitation energies of excited states, γ-ray energy meas. 2—11724
^{27}Al, ground and excited states populated in β^{+} decay of ^{27}Si, branching ratios and log ft values obtained 2—18157
^{28}Al, low lying states, investigation using ^{27}Al(d,p)^{28}Al at 23 MeV 2—34926
^{36}Ar, Hartree-Fock and random phase approximations 2—38483
^{37}Ar, from ^{36}Ar(d,p) study 2—2779
^{37}Ar, magnetic moments of $7/2^{-}$ mirror states 2—5652
^{39}Ar, single neutron hole states populated in ^{40}Ar(^{3}He,α) reaction, spin and parity 2—27973
^{39}Ar from ^{39}Cl β-decay 2—11794
^{39}Ar level structure determ. from ^{38}Ar(d,p) reaction, orbital angular momentum transfer valves and spectroscopic factors 2—34934
^{75}As, level scheme obtained from meas. of deexcitation γ rays from inelastic neutron scattering 2—11750
^{196}Au, 12^{-}, $5^{+}$and 2^{-} states populated in (n,2n) reactions 2—2731
^{199}Au, core excitation model treatment of low lying levels, level sequence 2—27995
^{199}Au, level scheme below 1 MeV and level energies from ^{198}Au(n,γ) reaction 2—5669
^{9}B, isospin mixing in $J^{\pi}={}^{3}/_{2}{}^{-}$ state, first $T={}^{3}/_{2}$ analogue states, Coulomb interaction contribution to width 2—14932
^{10}B, magnetic moment of 1^{+} first excited state 2—24142
^{10}B, spin-parity determinations by ^{11}B(^{3}He,α)^{10}B(α_0)^{6}Li correlations 2—5645
^{13}B, excitation energies of levels up to 8.7 MeV meas. by ^{7}Li(^{7}Li,p)^{13}B reaction 2—34911
^{132}Ba, obs. from ^{132}La decay 2—18120
^{134}Ba, excited levels, from decay of ^{134}La 2—8307
^{135}Ba, spin and parity assignment 2—11763
^{138}Ba, level scheme construction, spin assignments from ^{138}Cs decay 2—24167
^{7}Be, excitation energies of excited states, γ-ray energy meas. 2—11724
^{8}Be, spin and parity of 4.8 MeV level from Li(d,n) reaction 2—27963
^{9}Be, analysis of γ ray spectra from ^{7}Li(d,γ) at 361 keV, deduced branching ratios to levels 2—502
^{9}Be, isospin mixing in $J^{\pi}={}^{3}/_{2}{}^{-}$ state, first $T={}^{3}/_{2}$ analogue states, Coulomb interaction contribution to width 2—14932
^{9}Be, pionic X-ray yields meas. using absolute efficiency technique, pion cascade calc. of 2p-level widths 2—28057
Bi, collective state excitation cross sections 2—21434
^{208}Bi, force dependence of 0^{+} states 2—21399
^{209}Bi comparison of energy levels excited by nonresonant 16.10 MeV proton scattering of 14.95 MeV scattering from isobaric analogue states 2—24175
^{209}Bi(p,α), level densities of near doubly magic nuclei 2—38527
^{210}Bi, β decays, K-shell auto-ionization probability 2—18165
^{210}Bi, level structure from study of ^{210}Po IAR's in ^{209}Bi(p,p′) reaction 2—21400
^{210}Bi, multiplet structure from ^{209}Bi(d,p and ^{209}Bi(α,^{3}He) reactions 2—38529
^{210}Bi, shell model structure from ^{209}Bi(d,p) reaction at 17.0 MeV 2—24176
^{210}Bi, two-particle states, calc. with realistic forces 2—18149
^{211}Bi, level scheme from ^{211}Pb decay 2—27997
^{211}Bi, shell model wave function and energies obtained 2—2757
^{78}Br, γ-angular correlation of 120 μs state, time differential obs. of n.m.r. 2—5671
^{79}Br low-lying levels, intermediate coupling and core excitation models 2—38502
^{85}Br, ground and first four excited states, spins and parities assignment 2—11865
^{11}C levels studied in ^{12}C(p,d) reaction at 185 MeV, evidence of nondirect reaction mechanism 2—31542

Nucleus continued
energy levels continued
^{12}C, α-particle unstable states, investigation using nuclear reactions 2—18089
^{12}C, energy levels between 1.7 and 6.4 MeV using ^{9}Be(α,n)^{12}C reaction 2—31573
^{12}C, excited state stability and band cut-off 2—38473
^{12}C, low lying states structure study using cluster model with varying hinge angle 2—11725
^{12}C, lowest T=2 state, search for in isospin forbidden reactions 2—38474
^{12}C, many-particle excited states, calc. of energies, quadrupole moments and shapes 2—8283
^{12}C, particle vibration coupling, giant dipole resonance 2—18174
^{12}C, pionic X-ray yields meas. using absolute efficiency technique, pion cascade calc. of 2p-level widths 2—28057
^{12}C, variational calc. of quadrupole deformation energy and ground state energy 2—11726
Ca isotopes, effective wave function calc. of $J^{\pi}=0^{+}$ states 2—14944
^{40}Ca, ground state props. calc. using relativistic self consistent meson field theory 2—11704
^{40}Ca, perturbative treatment of collective particle-hole states, energy levels calc. in Tamn-Dancoff approx. 2—11739
^{40}Ca, study of 6.75 MeV level populated in (p,p′γ) scattering 2—18101
^{41}Ca, low lying multiparticle, multihole states, analysis by weak coupling model 2—14934
^{42}Ca, g factor of 6^{+} state 2—24156
^{42}Ca 6^{+}(3.19 MeV) state magnetic moment, comparison of theory and exptl. values 2—11740
^{43}Ca, energy values of branching ratios of bound states produced in ^{41}K(p,γ) reaction 2—14945
^{43}Ca, excited state properties and spin values from ^{40}Ar(α,nγ) reaction at 13.5 MeV 2—24155
^{44}Ca, level assignment, γ-ray spectra front transitions in reaction ^{43}Ca(n,γ) 2—24158
^{44}Ca, structure from Hamada-Johnston and Tabakin interactions 2—31464
^{48}Ca, perturbative treatment of collective particle-hole states, energy levels calc. in Tamn-Dancoff approx. 2—11739
^{48}Ca intermediate structure, S- and P-wave neutron spectroscopy 2—24160
^{49}Ca 2p-1h states, S- and P-wave neutron spectroscopy, neutron doorway escape widths determ. using theory of intermediate structure 2—24159
^{112}Cd, level scheme from ^{112}Ag decay data 2—21413
^{112}Cd, level structure assignment from ^{112}Ag β-decay 2—38547
^{112}Cd, study using photoexcitation, angular dist. of elastic and inelastic lines 2—11758
^{112}Cd static quadrupole moment of first excited state meas. 2—2718
^{114}Cd, level structure assignment from ^{114}Ag β-decay 2—38547
^{114}Cd, quadrupole moment of first excited state 2—5661
^{116}Cd, level structure assignment from ^{116}Ag β-decay 2—38547
^{116}Cd, study of ground state with (^{3}He,d) and (α,t) reactions 2—27983
^{116}Cd levels deduced from elastic and inelastic proton scattering measurements 2—18187
^{140}Ce levels formed in ^{140}La decay, new levels found at 2494 and 3474 keV 2—18121
^{33}Cl, single-particle strengths for quasibound levels determ. from ^{32}S(^{3}He, d) ^{33}Cl at 29.7 and 34.5 MeV 2—24153
^{33}Cl, study by reaction ^{32}S(d,n) at 4.7 and 5.5 MeV 2—34930
^{33}Cl analogue states of ^{33}P studied by isospin- forbidden resonances in ^{32}S(p,γ) reaction 2—34931
^{34}Cl, populated by γ ray decay of resonances in ^{33}S(p,γ)^{34}Cl reaction 2—11733
^{37}Cl, excitation energies of excited states, γ-ray energy meas. 2—11724
^{38}Cl, study of levels below excitation energy 2.75 MeV with ^{37}Cl(d, pγ) reaction at 3.1 MeV 2—24154
^{248}Cm, population of 0^{+} states by (p,t) reaction 2—34920
Co, odd isotopes, systematics explained by unified vibrational model 2—8300
^{54}Co, excited states, study using (p,nγ) reaction 2—11742
^{55}Co, ^{54}Fe(p,γ) reaction study 2—38599
^{56}Co, from ^{54}Fe(^{3}He,p)^{56}Co and ^{58}Ni(d,α)^{56}Co studies 2—2709
^{56}Co levels up to 2.6 MeV excitation studied by ^{56}Fe (p, nγ) coincidence expts. 2—24223
^{57}Co, interpretation using particle-core coupling model 2—38491
^{58}Co, energy level scheme from ^{56}Fe(^{3}He,p)^{58}Co and ^{60}Ni(d,α)^{58}Co reaction studies 2—21388
^{58}Co, high-resolution study by (d,α) and (^{3}He,d) reactions 2—34943
^{59}Co, excited levels populated in proton and alpha induced reactions 2—24162
^{60}Co, investigation by the two-particle transfer reactions ^{62}Ni(d,α) and ^{58}Fe(^{3}He,p) 2—31474
^{62}Co, investigation by two-particle transfer reaction ^{64}Ni(d,α) 2—31476
^{48}Cr, populated in ^{50}Cr(p,t) reaction 2—467
^{48}Cr, study with ^{50}Cr(p,t)^{48}Cr reaction, spin and parity assignment 2—2706
^{50}Cr, study of excited states by means of decay of ^{50}Mn, ^{50}Cr(p,p′γ) and ^{52}Cr(p,t) reactions and Coulomb excitation with ^{35}Cl ions 2—34939
^{53}Cr, 2.321 MeV excited level, obs. of IAR in ^{52}Cr(p,p) scattering 2—18186
^{129}Cs, level scheme deduced from ^{129}Ba decay 2—18163
^{138}Cs, 1- state determ. 2—2770
^{58}Cu, excited states, study using (p,nγ) reaction 2—11742
^{62}Cu, magnetic hyperfine interaction meas. on first excited state 2—5657
^{62}Cu levels deduced from ^{64}Zn(d,α) reaction with DWBA formalism 2—31475
^{64}Cu, spins of low-lying states obs., γ—γ directional correlation meas. 2—38496
^{157}Dy levels deduced from ^{157}Ho decay using multidimensional coincidence device 2—34965
^{161}Dy, rotation-particle coupling in ground state band studied using ^{160}Gd(α,3n)^{161}Dy reaction 2—31490
Er, A=164, 166, 167, 168, 170, neutron resonance spectroscopy, level spacings, Dyson's theory 2—34967
Er, A=166, 168, 170, F test for missing levels, l=0 population 2—34969
Er, even A isotopes, distrib. of spacings between neutron capture levels 2—31453
^{169}Er, β decays, K-shell auto-ionization probability 2—18165
^{147}Eu, excited state characteristics, investigation using angulat $\gamma\gamma$ correlation method 2—11766
^{147}Eu, level diagram from ^{147}Gd decay 2—24186

Nucleus continued
energy levels continued
^{151}Eu, muon capture, populations of individual final levels 2—18180
^{153}Eu, muon capture, populations of individual final levels 2—18180
^{16}F, excitation energies of levels, study by ^{16}O(p,n)^{16}F at 23 MeV 2—18092
^{18}F, energies of lowest five T=1 states, Coulomb energy shifts 2—14935
^{18}F, isospin mixed 5.61 and 5.67 MeV levels, spins determ. by angular correlation meas. 2—11730
^{18}F, low lying level calc. using harmonic oscillator and Woods Saxon wave functions 2—5646
^{18}F, shell model calculation and effective interaction in s-d shell 2—464
^{19}F, core excited states, α-cluster structure and weak coupling feature 2—38451
^{19}F, energy spectrum of non-normal-parity states produced using non-central particle- hole interaction 2—11732
^{19}F, new high spin states forming part of K=$^3/_2{}^+$ rotational bands 2—2695
^{19}F, resonances and resonance parameters deduced from ^{14}N(α,γ)^{18}F cross section measurement 2—2807
^{19}F, T=$^3/_2$ states, calculation of spectroscopic factors from ^{18}O(^{3}He,d) reaction 2—11720
Fe collective states excitation by 14 MeV neutrons 2—14990
^{53}Fe low lying states studied via ^{50}Cr(α,nγ) reaction 2—11748
^{57}Fe, Mossbauer spectra in $FeOHSO_4$, hyperfine field orientation, electric field gradient 2—10325
^{65}Ga, M1 transitions from $g_{9/2}$ analog-to-antianalog states 2—18109
^{67}Ga low lying levels from ^{67}Zn(p,nγ)^{67}Ga 2—5658
Gd (A=145, 146) pattern of levels with large spin, nuclear spin and parity assignment 2—24169
^{144}Gd, quasirotational groundstate bands 2—18122
^{150}Gd, excited state population in β decay of new 5.8 min ^{150}Tb isomer 2—31506
^{152}Gd, high spin state population via ^{152}Sm(α,4n) reaction 2—21395
^{152}Gd, level structure studies in 17.5h ^{152}Tb decay 2—11767
^{153}Gd, high spin state population via ^{152}Sm(α,3n) reaction 2—21395
^{68}Ge from ^{70}Ge(p,t), excited levels study 2—18110
^{69}Ge from ^{70}Ge(p,d), excited levels study 2—18110
^{70}Ge, Coulomb excitation of excited 0$^+$ state with ^{35}Cl, ^{32}S ions 2—38498
^{71}Ge level schemes from study of (n,γ)-reaction in natural Ge 2—27979
^{73}Ge level schemes from study of (n,γ)-reaction in natural Ge 2—27979
^{74}Ge, level schemes from study of (n,γ)-reaction in natural Ge 2—27979
^{75}Ge, level schemes from study of (n,γ)-reaction in natural Ge 2—27979
^{3}He, excitation energies up to 30 MeV examined in study of ^{6}Li(p,^{3}He) and ^{6}Li(p,α) reactions, search for broad resonances 2—18084
^{3}He, reaction ^{3}He(e,e'd)^{1}H study at 16 to 27 MeV 2—31443
^{4}He, new levels rel. to difference in ang. distribution for reactions ^{2}H(d,n)^{3}He and ^{2}H(d,p)^{3}H 2—27960
^{4}He, T=0 states study from ^{4}He(d,d't)^{1}H and ^{4}He(d,d'd)^{2}H at 52 MeV 2—14930
^{4}He ground state, long-range clustering correlation influence on photoreaction ^{4}He(γ,d)^{2}H 2—11818
^{5}He, excited states, study using ^{7}Li(d,α)^{5}He 2—24140
^{5}He, search for high lying levels using ^{7}Li(d,α)^{5}He reaction 2—31445
^{174}Hf, from ^{174}Ta decay 2—18137
^{178}Hf, level structure, study of decay of ^{178}Ta 2—11771
^{179}Hf, low energy excited state structure, investigation by ^{178}Hf(n,γ)^{179}Hf reaction 2—38510
^{190}Hg, ^{181}Ta(^{14}N, 5n) study 2—38523
^{198}Hg, low-energy level struct. 2—2733
^{199}Hg, excited levels, core particle model 2—38525
^{200}Hg, level scheme and conversion electron coefficients from slow neutron capture in ^{199}Hg 2—21397
^{161}Ho, study from ^{161}Er decay 2—31508
^{163}Ho, rotational states differing by ΔK=2, 3, 4, evidence for configuration mixing 2—38519
^{164}Ho, spectra calc. 2—38518
^{165}Ho, level scheme from study of β decay of ^{165}Dy and ^{165m}Dy, Coriolis coupling between bands 2—21396
I, odd mass isotopes, positive parity level description using unified model 2—14953
^{121}I, obs. from ^{121}Xe decay 2—14965
In odd-mass isotopes 109-117, unified model in intermediate coupling used to fit theoretical to exptl. energy spectra 2—27981
^{106}In, obs. of β decaying state in ^{92}Mo(^{16}O, pn)^{106}In reaction 2—18162
^{107}In, level scheme determination from ^{107}In→^{107}Cd decay studies 2—11798
^{115}In, inelastic neutron scattering study 2—27982
^{115}In, photoactivation study 2—8303
^{117}In, quadrupole moment of 660keV rotational level, meas. in $In_{0.99}Cd_{0.01}$ alloy at 4.2K 2—14951
^{117}In, study of level scheme via proton transfer reactions, (^{3}He,d) and (α,t) reactions 2—27983
^{189}Ir, energy levels studied in decay of ^{189}Pt 2—31493
^{191}Ir, proton states populated by ^{190,192}Os(^{3}He,d) and ^{190,192}Os(α,t) reactions 2—5666
^{193}Ir, proton states populated by ^{190,192}Os(^{3}He,d) and ^{190,192}Os(α,t) reactions 2—5666
^{37}K, magnetic moments of 7/2$^-$ mirror states 2—5652
^{40}K, excitation energies of levels deduced from ^{30}K(n,γ) reaction 2—18207
^{41}K, investigation using ^{40}Ar(p,γ)^{41}K reaction 2—5653
^{42}K, excitation energies of levels deduced from ^{42}K(n,γ) reaction 2—18207
^{79}Kr, low lying levels, ^{79}Br(p,n) reaction obs. 2—38501
^{81}Kr low lying levels, ^{81}Br(p,n) reaction obs. 2—38501
^{84}Kr, levels studied in decay of ^{84}Br using gamma ray spectra 2—31502
^{133}La excited states coexistence from correl. of quadrupolar moments 2—46[illegible]
^{140}La, 1- state determ. 2—2770
^{5}Li, deduced levels and transition intensities to ground and first excited state from ^{2}H(^{3}He,γ)^{5}Li reactions 2—11860
^{5}Li, energy dependence of phase shifts and spin and parity assignments from p-^{4}He elastic scattering data 2—35025
^{5}Li, search for high lying levels using ^{6}Li(^{3}He,α)^{5}Li reaction 2—31445
^{6}Li, pionic X-ray yields meas. using absolute efficiency technique, pion cascade calc. of 2p-level widths 2—28057
^{7}Li, ground and first excited state formation in ^{10}B(n,α)^{7}Li reaction at 0.48 MeV 2—11842
^{9}Li, from ^{7}Li(t,p)^{9}Li study 2—2689
^{171}Lu, $^1/_2{}^-$[541] and $^3/_2{}^-$[532] rotational bands, Coriolis pairs 2—18134
^{171}Lu, rotational states differing by ΔK=2, 3, 4, evidence for configuration mixing 2—38519
^{176}Lu, level structure investigation using ^{175}Lu(n,γ) reaction 2—34971

Nucleus continued
energy levels continued
^{24}Mg, cluster model calcs. 2—38480
^{24}Mg, energy gaps and momentum transfer 2—38486
^{24}Mg, levels deduced from alpha particles emitted following β-decay ^{24}Al 2—18156
^{24}Mg, spectra obtained using Hartree-Fock model predictions 2—11734
^{25}Mg, spin of 4.075 MeV level determ. from gamma-ray polarization method 2—8289
^{26}Mg from ^{26}Al ground state β-decay 2—11793
^{50}Mn, deduced levels, excited state study from ^{50}Cr(^{3}He,t)^{50}Mn reaction 2—11743
^{50}Mn, excited states, study using (p,nγ) reaction 2—11742
^{50}Mn, obs. from ^{50}Cr(^{3}He,t)^{50}Mn 2—11744
^{52}Mn levels and spectroscopic strengths deduced from ^{54}Fe(d,α) reaction at 15 MeV 2—31471
^{53}Mn, excitation energies and spin assignments determ. from study of ^{53}Cr(p,n) reactions 2—11747
^{54}Mn, level scheme studied by ^{52}Cr(^{3}He,p) reaction 2—21448
^{54}Mn, study by reaction ^{54}Cr(p,n) at 2.6 to 3.1 MeV 2—38531
^{55}Mn, new spin $^1/_2{}^-$ state predicted from (p,^{3}He) and (d,^{4}He) reactions on ^{57}Fe, shell model calculations 2—8287
^{56}Mn, levels studied using ^{55}Mn(d,p) reaction 2—31587
^{56}Mn deduced from ^{54}Cr(^{3}He,p) reaction at 15 MeV 2—505
^{56}Mn levels and spectroscopic strengths deduced from ^{58}Fe(d,α) reaction at 15 MeV 2—31471
^{92}Mo, deduced levels from ^{94}Mo(p,t) reaction at 40 MeV 2—18114
^{92}Mo, excitation functions and isomer ratios for (n,2n), (n,α) and (n,p) reactions 2—35056
^{93}Mo, level structure from ^{92}Mo(d,pγ)^{93}Mo reaction 2—34951
^{94}Mo, isomeric $(g_{9/2})^2$ proton state observed in decay of ^{94}Tc 2—14960
^{95}Mo, high spin levels from (α,xn) reactions 2—21391
^{97}Mo, high spin levels from (α,xn) reactions 2—21391
^{97}Mo, level structure investigation from Coulomb excitation meas. using α-particle and ^{16}O projectiles 2—34952
^{102}Mo, levels studied using (t,p) reaction 2—31479
^{14}N, new level found 2—2690
^{15}N, multilevel multichannel study of structure from 12-14 MeV excitation energy 2—11728
^{15}N, observation of α-particle core excited threshold states 2—18091
^{16}N, resonance at 5.05 MeV interferes destructively with continuum, observed in ^{15}N(d,p) reaction 2—8361
^{16}N, study using ^{14}C(^{3}He,p)^{16}N reaction 2—31449
^{136}N, quasirotational groundstate bands 2—18122
Na, collective state excitation cross sections 2—21434
^{20}Na, excitation energies of levels, study by ^{20}Ne(p,n)^{20}Na at 23 MeV 2—18092
^{23}Na, excitation energies and angular distributions of levels below 10.2 MeV determ. from ^{22}Ne(^{3}He,d) reaction 2—11735
^{24}Na, low-lying levels, investigation using ^{26}Mg(d,$\alpha\gamma$)^{24}Na reaction 2—2698
Nb, A=92-96, high spin proton excited states population in Zr(α,d) and Zr(α,t) reactions 2—31478
^{91}Nb, excited states determ. from ^{91}Zr(p,nγ) reaction 2—2715
^{91}Nb, high spin proton states, from ^{90}Zr(α,t) reaction 2—2696
^{91}Nb, isobaric energy splitting between $T_>$- and $T_<$-single particle states 2—2716
^{93}Nb lower levels Coulomb excitation with ^{16}O ions from 25 to 42 MeV 2—14948
^{96}Nb low-lying states study from ^{96}Zr(p,nγ)^{96}Nb 2—11754
Nd, A=141, 143, coupled particle-pairing vibrational states excited via (p,t) reactions, level assignments made 2—11765
^{144}Nd, neutron capture and gamma- ray spectra study 2—34960
^{18}Ne, energies of lowest five T=1 states, Coulomb energy shifts 2—14935
^{19}Ne, observation of α-particle core excited threshold states 2—18091
^{19}Ne, study of levels using ^{16}O+^{3}He reactions 2—27967
^{20}Ne, excited levels, Tamm-Dancoff approx. 2—38484
^{20}Ne, excited state stability and band cut-off 2—38473
^{20}Ne, generator coord. spectrum 2—34921
^{20}Ne, Hartree-Fock and random phase approximations 2—38483
^{20}Ne, high-spin states studied in ^{16}O(α,α) scattering 2—21382
^{20}Ne, spectra obtained using Hartree-Fock model predictions 2—11734
Ni isotopes, 0$^+$ states, broken-pair approximation and generator coordinate method 2—38494
^{56}Ni, deduced from ^{54}Fe(^{3}He,n) reactions at 14 MeV 2—27977
^{57}Ni, 2.443 and 3.003 MeV level props. from ^{54}Fe(α,n)^{57}Ni reaction 2—11749
^{58}Ni levels populated in ^{58}Cu decay 2—18158
^{59}Ni, energy levels from Coulomb stripping in ^{58}Ni(d,p)^{59}Ni reaction 2—31584
^{63}Ni, energy levels from Coulomb stripping in ^{62}Ni(d,p)^{63}Ni reaction 2—31584
^{64}Ni, 0$^+$ and 2$^+$ states, ^{68}Zn(d,^{6}Li) reaction study 2—2812
^{64}Ni, spin and parity assignments, gamma transitions 2—5693
^{65}Ni, energy levels from Coulomb stripping in ^{64}Ni(d,p)^{65}Ni reaction 2—31584
^{15}O, double level at 8.92 MeV, investigation using ^{14}N(p,p)^{14}N scattering 2—8284
^{15}O, observation of α-particle core excited threshold states 2—18091
^{15}O, populated in ^{13}C(^{3}He,n) reaction absolute differential cross sections 2—18090
^{15}O levels, spectroscopic factors deduced from ^{13}C(^{3}He,n) reaction at 6 MeV, test of coeffs. of fractional parentage 2—27966
^{15}O states studied as resonances in ^{14}N (p'γ) ^{15}O and ^{14}N(p,pγ) reactions between 10.91 and 13.02 MeV excitation 2—27970
^{16}O, 7.12 MeV level, effect on α spectrum from ^{16}N β decay 2—2743
^{16}O, alpha-cluster ground state 2—31450
^{16}O, four particle four hole solution, instability against parity mixing 2—2692
^{16}O, ground state props. calc. using relativistic self consistent meson field theory 2—11704
^{16}O, level structure, 20-23 MeV, from meas. of excitation functions of ^{15}N(p,p')^{15}N* 2—14933
^{16}O, many-particle excited states, calc. of energies, quadrupole moments and shapes 2—8283
^{16}O, negative-parity states populated in ^{12}C(^{6}Li,d) reaction 2—463
^{16}O, pionic X-ray yields meas. using absolute efficiency technique, pion cascade calc. of 2p-level widths 2—28057
^{16}O, structure of states, study by ion reaction ^{14}N(^{3}He,p) at 18 MeV 2—8285

Nucleus continued
energy levels continued
^{16}O near excitation energies of 15, 20 MeV investigated by means of reactions, spin assignments 2—38481
^{17}O, 2p-1h structure studied via ^{15}N (^{3}He,p) reaction, data analysed in DWBA 2—24150
^{17}O, levels deduced from ^{14}C(^{3}He, ^{3}He), ^{14}C(^{3}He, α), ^{14}C(^{3}He, d) and ^{14}C(^{3}He, p) reactions at 2 to 7 MeV 2—38476
^{17}O, low lying multiparticle, multihole states, analysis by weak coupling model 2—14934
^{17}O, single-particle energies, third- order contributions 2—462
^{18}O, effect of higher order diagrams on effective interaction 2—38477
^{18}O, excitation of levels below 6.0 MeV by inelastic electron scattering 2—8326
^{18}O, ground state deformation, low lying positive parity states analysed 2—8286
^{18}O, identification of spin-parity combinations from ^{18}O(α,α) reaction 2—2694
^{18}O, low lying level calc. in harmonic oscillator shell model using one-boson exchange potentials 2—11731
^{18}O, low lying level calc. using harmonic oscillator and Woods Saxon wave functions 2—5646
^{18}O, shell model calculation and effective interaction in s-d shell 2—464
^{19}O, T=$^{3}/_{2}$ states, calculation of spectroscopic factors from ^{18}O(d,p) reaction 2—11720
^{182}Os, K-dependence of population of ^{182}Os levels from ^{185}Re(p,n)^{182}Os and ^{182}W(α,4n)^{182}Os reactions 2—27991
^{31}P, investigation via alpha capture in ^{27}Al 2—2703
^{32}P, spectroscopic properties of levels determ. by angular correlation studies of ^{29}Si(α,p) reaction 2—8292
Pb, A=206 to 208, inelastic scattering of neutrons at 13.2 MeV, 2.6 MeV level observed 2—38617
^{198}Pb, obs. from ^{203}Tl(p,6n)^{198}Pb 2—18146
^{200}Pb, obs. from ^{203}Tl(p,4n)^{200}Pb 2—18146
^{205}Pb scheme from absolute cross section meas. for 2 keV neutron capture in ^{204,207}Pb 2—11845
^{207}Pb intermediate structure, S- and P-wave neutron spectroscopy 2—24160
^{208}Pb, coupling effects 2—38528
^{208}Pb, effective interaction between J$^{\pi}$=2^{+} two phonons states, existence of isovector quadrupole mode 2—8312
^{208}Pb, effective interaction between 2 phonon J$^{\pi}$=0^{+} states, diagrammatic perturbation treatment 2—2739
^{208}Pb, electron excitation of low-lying states 2—11778
^{208}Pb, excitation of first 2^{+}, 3^{-}, 4^{-} and 5^{-} levels in ^{208}Pb(^{3}He, ^{3}He'), ang. distrib. 2—24236
^{208}Pb, ground state props. calc. using relativistic self consistent meson field theory 2—11704
^{208}Pb from ^{207}Pb(n,γ)^{208}Pb, γ-spectrum study 2—11846
^{208}Pb particle-core states, rel. to ^{206}Pb(t,p)^{208}Pb reaction interpret. 2—35080
^{208}Pb(p,α), level densities of near doubly magic nuclei 2—38527
^{210}Pb, ground and low lying states obs. of isobaric analogs in T=23 states of ^{210}Po 2—14959
^{210}Pb, two-particle states, calc. with realistic forces 2—18149
^{211}Pb, shell model wave function and energies obtained 2—2757
Pd (A=104, 106), levels excited in (α,xn) reactions 2—24166
^{103}Pd, excited states, in-beam γ-ray meas. using ^{103}Rh(p,nγ)^{103}Pd reaction 2—11757
^{104}Pd, excited levels populated in decay of 33 min ^{104m}Ag and 69 min ^{104g}Ag 2—18168
^{104}Pd, excited state population in β^{-} decay of 4.3 sec and 4.41 min isomers of ^{104}Rh, spin values 2—34955
^{104}Pd, level structure determ. from ^{104}Rh decay 2—21392
^{112}Pd, levels studied using (t,p) reaction 2—31479
^{141}Pm, three quasiparticle multiplet population in electron capture decay of ^{141m}Sm 2—31505
^{144}Pm, 1- state determ. 2—2770
^{147}Pm level struct. 2—34962
^{148}Pm, structure of 1^{-} ground state 2—34963
^{154}Pm, evidence for violation of Gallagher-Moskowski rules using Nilsson model 2—27986
Po isotopes, neutron-deficient, A=200-203, isomeric states studied by (HI, xnγ) reactions 2—21379
^{202}Po, (h$_{9/2}$)^{2} two-quasiparticle isomeric state meas. half life and transition energies 2—2735
^{204}Po, J=8^{+} isomeric state, half life meas. 2—2735
^{207}Po, establishment from decay of ^{207}At 2—18148
^{209}Po excited states, ^{209}At decay obs. 2—21415
^{209}Po levels populated in electron capture decay of ^{209}At, coupling of single-neutron-hole states 2—31494
^{210}Po, two-particle states, calc. with realistic forces 2—18149
^{210}Po high-spin states studied in ^{208}Pb(α,2nγ) reaction 2—31495
^{211}Po, shell model wave functions and energies obtained 2—2757
^{142}Pr, 1- state determ. 2—2770
^{143}Pr, level structure investigation using gamma rays produced in ^{143}Ce decay 2—21394
^{196}Pt, population of 0^{+} states by (p,t) reaction 2—34920
Pu (A=242, 244), population of 0^{+} states by (p,t) reaction 2—34920
^{239}Pu, level density and excitation energy relationship 2—27999
^{87}Rb levels deduced in ^{88}Sr(d,^{3}He) reaction at 35 MeV, determ. of transferred angular momenta, spectroscopic factors 2—38645
^{177}Re, rotational bands and quasiparticle levels studied via ^{169}Tm(^{12}C,4n) reaction 2—27989
^{179}Re rotational bands and quasiparticle levels studied via ^{172}Yb(^{11}B,4n) reaction 2—27989
^{103,105}Rh, structure of $^{7}/_{2}{}^{+}$ level 2—14949
^{98}Rh, ^{99}Rh, excited states, from decay of Pd isotopes 2—38508
^{98}Rh, level scheme from ^{98}Pd decay data 2—38546
^{103}Rh, negative parity states, model interpret. 2—38509
^{103}Rh negative parity levels, Coulomb excitation with ^{4}He and ^{16}O ions 2—18117
^{219}Rn lifetime obs. of states excited by α-particle decay, microwave method 2—8222
^{98}Ru, level scheme from ^{98}Rh decay data 2—38546
^{99}Ru, study using ^{99}Rh beta decay 2—34953
^{102}Ru, collective structure 2—14947
^{106}Ru, levels studied using (t,p) reaction 2—31479
^{28}S, energy gaps and momentum transfer 2—38486

Nucleus continued
energy levels continued
^{31}S, 1p neutron strength, study of levels above E$_{x}$=4.5 MeV from ^{32}S(^{3}He, ^{4}He)^{31}S reaction 2—14942
^{32}S, collective states obs. by inelastic scatt. of polarized protons 2—31461
^{32}S, energy gaps and momentum transfer 2—38486
^{32}S, investigation using ^{28}Si(α,γ)^{32}S reaction 2—5649
^{32}S, spectra obtained using Hartree-Fock model predictions 2—11734
^{32}S, static quadrupole moment of first excited state meas. 2—2718
^{33}S, detailed energy level schemes determ. from shell model calculations 2—28000
^{33}S, from ^{32}S(d,p) study 2—2779
^{34}S, collective states obs. by inelastic scatt. of polarized protons 2—31461
^{34}S, excitation energies of excited states, γ-ray energy meas. 2—11724
Sb, odd mass isotopes, positive parity level description using unified model 2—14953
Sb isotopes, neutron resons. 2—31561
^{117}Sb, g-factor meas. of isomeric state 2—5662
^{122}Sb low-lying states study from ^{122}Sn(p,n)^{122}Sb 2—11761
Sc (A=48, 50), strongly excited 1^{+} states, obs. in ^{46}Ca(^{3}He,p)^{48}Sc and ^{48}Ca(^{3}He,p)^{50}Sc reactions 2—34937
^{43}Sc, g factor of $^{19}/_{2}{}^{-}$ isomeric state 2—24156
^{43}Sc 19/2^{-} (3.12 MeV) state magnetic moment, comparison of theory and exptl. values 2—11740
^{44}Sc, spherical states, shell model calculations 2—466
^{45}Sc, differential cross sections of excited states in ^{45}Sc(p,p') reaction 2—18184
^{48}Sc, excited states, investigation using ^{48}Ca(p,nγ)^{48}Sc reaction 2—2705
^{48}Sc, study of levels using ^{48}Ca(^{3}He,t)^{48}Sc reaction at 23 MeV 2—31467
^{48}Sc, study of levels using ^{46}Ca(α,d)^{48}Sc reaction 2—31466
Se, even isotopes, excitation cross sections of first 2^{+} levels in (n,n'γ) reactions 2—28043
^{75}Se, level scheme determination from obs. of γ-rays and conversion and electrons following ^{75}Br decay 2—24164
^{76}Se, level scheme, ^{76}As decay obs. 2—31514
^{76}Se, level scheme deduced from ^{76}As decay 2—18159
^{77}Se, structure study via (n,γ) reaction 2—18212
^{78}Se, collective structure 2—14947
^{78}Se, structure study via (n,γ) reaction 2—18212
^{81}Se, structure study via (n,γ) reaction 2—18212
^{25}Si, excited state obs. using reaction ^{28}Si(^{3}He, ^{6}He)^{25}Si at 70.4 MeV 2—34923
^{27}Si, angular correlations and branching ratios of levels below 5 MeV excitation, spin assignments 2—24152
^{28}Si, 1p hole and 2p particle configuration mixing, investigation via ^{29}Si(p,d)^{28}Si and ^{30}Si(p,t)^{28}Si reactions 2—2700
^{28}Si, Hartree-Fock and random phase approximations 2—38483
^{28}Si, investigation using ^{27}Al(p,γ)^{28}Si reaction 2—34928
^{28}Si, investigation using low energy ^{27}Al(p,α)^{24}Mg reaction 2—31459
^{28}Si, spectra obtained using Hartree-Fock model predictions 2—11734
^{28}Si, study from reaction ^{29}Si(^{3}He,α)^{28}Si at 12 MeV 2—34925
^{28}Si resonance levels from ^{27}Al+p reactions, resonance strengths, partial proton width, spectroscopic factors deduced 2—34915
^{29}Si, from ^{28}Si(d,p) study 2—2779
^{29}Si, levels with excitation energy below 6.4 MeV 2—2701
^{31}Si, detailed energy level schemes determ. from shell model calculation 2—28000
^{41}Si, doorway state structure from ^{40}Ca(p,p'γ)^{40}Ca reaction 2—38598
Sm (A=143,144), pattern of levels with large spin, nuclear spin and parity assignment 2—24169
Sm isotopes, two-neutron transfer reactions rel. to coexistence of spherical and deformed states 2—14973
^{140}Sm, quasirotational groundstate bands 2—18122
^{142}Sm, quasirotational groundstate bands 2—18122
^{148}Sm, low-lying states, coupled channel analysis of asymmetry meas. by inelastic proton scatt. 2—469
^{151}Sm, β decays, K-shell auto-ionization probability 2—18165
^{151}Sm, collective state population by (d,d') and Coulomb excitation B(E2) values 2—18126
^{152}Sm, g-factor of 2^{+}(122 keV) rotational state 2—8273
^{152}Sm, low-lying states, coupled channel analysis of asymmetry meas. by inelastic proton scatt. 2—469
^{152}Sm(α,xn)^{152}, ^{153}Gd, 32-43 MeV, population of high spin states 2—21395
^{153}Sm, calc. of positive and negative parity Nilsson orbitals including pairing, Coriolis and ΔN=2 coupling 2—18129
^{115}Sn, g-factor meas. of isomeric state 2—5662
^{116}Sn, structure of low lying excited states populated in ^{115}Sn(n,γ), excitation energies and branching characteristics 2—31484
^{124}Sn, excitation of particle-hole states by proton inelastic resonance scatt. 2—38513
Sr, collective state excitation cross sections 2—21434
Sr isotopes, effective interaction among 1g$_{9/2}$ and 2p$_{1/2}$ neutrons, shell model calc. 2—11752
^{85}Sr, three particle level multiplets 2—476
^{87}Sr, level population in decay of ^{87}Y 2—5675
^{87}Sr, study from reaction ^{89}Y(d,α) at 12 MeV 2—34949
^{88}Sr, two hole and two particle four hole states populated in β decay of 17.8 min ^{88}Rb 2—31477
^{88}Sr levels deduced in ^{89}Y(d,^{3}He) reactions at 30, 35.5, 40 MeV, determ. of transferred angular momenta, spectroscopic factors 2—38645
^{89}Sr 2p-1h states, S- and P-wave neutron spectroscopy, neutron doorway escape widths determ. using theory of intermediate structure 2—24159
^{181}Ta, Larmor precession of first rotational level determ. by perturbed angular correlation methods 2—2729
^{155}Tb, excited levels, ^{155}Dy decay obs. 2—24187
^{155}Tb, rotational states and rotation-particle coupling 2—8308
^{157}Tb, rotational states and rotation-particle coupling 2—8308
^{93}Tc, from ^{92}Mo(d,n) reaction 2—2717
^{93}Tc, high spin proton states, from ^{92}Mo(α,t) reaction 2—2696
^{93}Tc, study of levels up to a few MeV with ^{92}Mo(^{3}He,d)^{93}Tc reaction 2—28079
^{93}Tc levels populated in decay of ^{93}Ru and by the ^{96}Ru(p,α) reaction 2—38545
^{94}Tc, high spin proton excited states population in ^{92}Mo(α,d) reaction 2—31478
^{95}Tc, from ^{94}Mo(d,n) reaction 2—2717
^{97}Tc, from ^{96}Mo(d,n) reaction 2—2717
^{99}Tc Coulomb excitation with 52-64 keV ^{35}Cl ions, deduced level structure and lifetimes 2—18115
^{122}Te, two quasiparticle states, level systematics 2—8304

Nucleus continued
energy levels continued
^{122}Te study of levels populated by (^{3}He, d) and (p,t) reactions 2—18119
^{124}Te, study of levels of populated by (^{3}He, d) and (p,t) reactions 2—18119
^{124}Te, two-quasiparticle states, level systematics 2—8304
^{125}Te, ion implantation perturbed angular correlation study of 443 and 463 keV levels 2—5663
^{125}Te, phenomenological wave functions for ground, 35.5 keV, 463 keV states determ. from lifetime, transition probability data 2—34958
^{126}Te, two-quasiparticle states, level systematics 2—8304
^{128}Te, revised level scheme 2—8306
^{128}Te levels populated in 8.9h β- decay of ^{128}Sb, obs. of positive and negative-parity states 2—34959
Th (A=230, 232), population of 0^+ states by (p,t) reaction 2—34920
^{228}Th excited levels, ^{228}Ac decay obs. 2—483
^{228}Th level scheme, ^{228}Ac decay obs. 2—11808
^{232}Th, F test for l=0 resonances, PT distrib. 2—34969
^{232}Th, level density and excitation energy relationship 2—27999
Ti collective states excitation by 14 MeV neutrons 2—14990
^{44}Ti, structure study from ^{46}Ti(p,t) reaction at 51 MeV 2—24157
^{46}Ti, evidence for single proton configurations in the ground state from ^{46}Ti(d,τ)^{45}Sc reaction 2—31465
^{49}Ti level structure studied up to excitation energy of 6.3 MeV using ^{47}Ti(t,p), ^{48}Ti(d,p), ^{49}Ti(p,p′) reactions 2—31468
^{201}Tl, shell effects on saddle pt. deform. 2—34978
^{201}Tl, spin and parity assignments, level scheme proposed obs. of ^{201}Pb$\rightarrow$^{201}Tl 2—2734
^{204}Tl, γ-spectroscopic analysis 2—2737
^{207}Tl lifetime obs. of states excited by α-particle decay microwave method 2—8222
^{167}Tm level scheme investigated in 18 min. ^{167}Yb decay, meas. of conversion electron and single γ-ray spectra, γ-γ coincidences 2—472
^{168}Tm, spectra calc. 2—38518
^{169}Tm, from energies and intensities of γ-rays following ^{169}Yb decay 2—470
^{172}Tm, proposed level scheme, β-decay of ^{172}Er 2—18135
U (A=234, 236, 238), population of 0^+ states by (p,t) reaction 2—34920
^{238}U, F test for l=0 resonances, PT distrib. 2—34969
^{46}V, excited states, study using (p,nγ) reaction 2—11742
^{49}V, study of excited states with ^{48}T,(p,γ)^{49}V reaction 2—27975
W (A=182, 184, 186), population of 0^+ states by (p,t) reaction 2—34920
^{182}W, excited levels study in decay of ^{182}Re, 64h isomer 2—14968
^{182}W, mag. moment of 1374 keV level 2—34973
^{182}W, produced in ^{182}Ta decay 2—2730
^{182}W, structure and parity mixing from ang. distrib. of γ rays in β decay of ^{182}Ta 2—31510
^{184}W, level scheme from study of γ-ray spectra of decay of ^{184m,184}Re 2—482
^{184}W, low lying levels, (d,p) reaction obs. 2—31492
^{130}Xe, excitation during β decay of ^{130}I, ^{130*}I 2—24184
^{132}Xe, excited levels, ^{132}I decay obs. 2—5676
Y collective states excitation by 14 MeV neutrons 2—14990
^{89}Y, excited levels, from decay of ^{89}Zr 2—2747
^{89}Y levels deduced in ^{88}Sr(^{3}He,d) reaction at 33.4 MeV, determ. of transferred angular momenta, spectroscopic factors 2—38645
^{90}Y, levels up to 3.2 MeV study from ^{89}Y(d,pγ) and ^{87}Rb(α,nγ) 2—18112
^{90}Y, shell model structure, l=5 transition data from 89Y(d,p) and ^{89}Y(α, ^{3}He) 2—34950
^{92}Y level scheme obs. from ^{92}Sr decay 2—2748
^{172}Yb, Coriolis coupling of octupole states, empirical evidence from ^{173}Yb(^{3}He,α) and ^{173}Yb(d,t) reactions 2—24173
^{175}Yb, level scheme and energies, γ-branching ratios from ^{174}Yb (n, γ) reaction 2—18139
^{175}Yb, primary transitions in thermal neutron capture by ^{174}Yb 2—18138
^{177}Yb, low energy excited state structure, investigation by ^{176}Yb(n,γ)^{177}Yb reaction 2—38510
^{60}Zn, deduced from ^{58}Ni(^{3}He,n) reaction at 15 MeV 2—27977
^{62}Zn, study by reaction ^{64}Zn(p,t) at 27.5 MeV 2—38495
^{65}Zn, low-lying levels obs. in ^{65}Cu(p,n) and (p,nγ) reactions 2—8339
^{66}Zn, lifetimes of levels excited by inelastic α particles 2—27978
^{67}Zn, half-life of $9/2^+$ state 2—8302
^{67}Zn, new level at 884 keV, ^{67}Ga decay obs. 2—38497
^{68}Zn level structure deduced from decay of ^{68}Cu isomers 2—38539
Zr collective states excitation by 14 MeV neutrons 2—14990
^{88}Zr, level scheme determination from obs. of γ-rays following ^{88g}Nb and ^{88m}Nb decay 2—21389
^{89}Zr, one-neutron hole states, expt. study 2—38600
^{89}Zr, spin assignment, DWBA anal. of ^{91}Zr(p,t) reaction 2—38601
^{90}Zr, fractionation of pair vibrational state 2—11753
^{90}Zr, ground state props. calc. using relativistic self consistent meson field theory 2—11704
^{90}Zr magic number nucleus, high energy states, using ^{90}Nb decay 2—478
^{91}Zr 2p-1h states, S- and P-wave neutron spectroscopy, neutron doorway escape widths determ. using theory of intermediate structure 2—24159
^{93}Zr, ^{93}Y decay study 2—38505
^{94}Zr, level scheme deduced from ^{94}Y decay 2—2749
^{94}Zr, modified level scheme from ^{94}Y decay 2—18161
^{95}Zr, partial level scheme from ^{95}Y decay 2—18161
^{98}Zr, evidence for J^π=0^+ first excited state through meas. of internal conversion electrons from fission products 2—11755
excitation *see Nuclear excitation*
magnetic moment
see also Gyromagnetic ratio; Molecules/nuclear coupling; Nuclear magnetic resonance and relaxation
deformed even nuclei, octupole moments and transitions, muclear rotational motion 2—31440
deformed nuclei, magnetic dipole transitions, internal conversion, penetration factor calc. 2—8280
doubly even deformed nuclei, dipole sum rules calc. in TDA and RPA approx. 2—27951
light nuclei, effect of transition toroidal form factors 2—14906
multipole moments, shell model calc. for A=27, 28, 29 nuclei 2—38489
shell model interpretation 2—5640
shell model states around ^{208}Pb, effective magnetic moment operator 2—27996
single particle states, g_l factor deduction 2—2683
static, effect of exchange currents on orbital g factors 2—8268
static dipole moments of sd-shell nuclei 2—2682
summary of work presented to conference on hyperfine interaction detected by nuclear rotation 1970 2—5639

Nucleus continued
magnetic moment continued
p anomalous orbital magnetic moment confirmed from obs. on ^{210}Po 2—5638
^{a}Hf, A=177, 179, 180, dipole moments of $^3F_2$ ground state determ. by atomic beam magnetic resonance meas. 2—18141
^{37}Ar, magnetic moments of $7/2^-$ mirror states 2—5652
^{196}Au, of 12- isomer, determ. by low temp. nuclear orientation 2—2732
^{10}B, moment of 1^+ first excited state 2—24142
^{135}Ba, optical pumping determ. 2—18104
^{137}Ba, optical pumping determ. 2—18104
^{207}Bi, g-factors of $^{21}/_2{}^+$isomer, stroboscopic meas. 2—38526
^{207}Bi, operator represent. 2—5670
Br (A=79, 81), determination from n.m.r. investigations in aqueous solutions 2—22007
^{42}Ca, comparison of theoretical and exptl. values for $19/2^-$ (3.12 MeV) state 2—11740
^{43}Ca, optical pumping determ. 2—18104
Cl(A=35, 37), determinations from n.m.r. investigations in aqueous solutions 2—22007
^{57}Co, n.m.r. of oriented nucleus 2—38506
^{58}Co, of 10 μsec level, obs. 2—5654
^{54}Fe, 2.95 MeV (6^+) state 2—8298
^{157}Gd, Mossbauer effect theory 2—31488
^{3}H, operator for a three particle nucleus, calculated correction to moment 2—31444
^{3}He, operator for a three particle nucleus, calculated correction to moment 2—31444
^{180}Hf, 1142 keV 8- state, two-quasiparticle state by Mossbauer experiments 2—8309
^{199}Hg, 208 keV state, IMPAC technique, measurement of precession angle 2—2697
In odd-mass isotopes 109-117, unified model in intermediate coupling used to determ. dipole moments of ground and first excited states 2—27981
^{37}Ki magnetic moments of $7/2^-$ mirror states 2—5652
^{175}Lu, dipole from one-electron spectrum of Lu^{2+} 2—2943
^{56}Mn, ground state dipole moment determ. using thermal neutron capture on natural Mn targets 2—8299
^{92}Mo, of 2761 keV, 8^+ state, meas. 2—5659
^{93m}Mo, n.m.r. of oriented nucleus 2—38506
^{61}Ni, dipole moment of 67.4 keV level from Mossbauer study of NiCr$_2$O$_4$ 2—5656
^{205}Pb, $^{13}/_2{}^+$ level 2—8311
^{205}Pb isomers, operator represent. 2—5670
^{206}Pb, g- factors of 7^- isomer, stroboscopic meas. 2—38526
^{206}Pb isomers, operator represent. 2—5670
^{141}Pr, of 145.4 keV state, Mossbauer study 2—18124
^{195}Pt, 130 keV state, Mossbauer obs. 2—10322
^{195m}Pt, oriented in Fe, mag. moment of isomeric state, n.m.r. study 2—27994
^{103}Rh, of 93 keV($9/2^+$) level, determ. 2—5660
^{43}Sc, comparison of theoretical and exptl. values for $19/2^-$ (3.12 MeV) state 2—11740
^{44}Sc, 68 keV state 2—34936
^{87}Sr, optical pumping determ. 2—18104
^{169}Tm, 316 keV $^7/_2{}^+$ level 2—18132
^{170}Tm, rel. to radiative constants 2—24172
^{182}W, 1374 keV level 2—34973
^{182}W, of first 2^+ excited state and 1289 keV 2- state meas. by perturbed γ-γ angular correlation in external mag. field 2—27990
^{171}Yb, optical pumping determ. 2—18104
^{173}Yb, optical pumping determ. 2—18104
magnetic resonance *see Nuclear magnetic resonance and relaxation*
models
α cluster calc. on light 4N nuclei with density dependent forces 2—24139
(f,p) shell nuclei, single particle model rel. to structure information 2—34876
A=180-212, fission barriers calc. in two centre shell model using Strutinsky prescription 2—11876
A=6 to 9 systems, shell model calc. of normal parity states 2—11722
alpha-particle model for ^{12}C+^{12}C low energy reaction 2—24240
Amado model, use in calculation on D(p,2p)n reaction 2—8337
centrifugal stretching model for intra-band B(E2) transition rates of even nuclei in rare-earth region 2—8276
ckuster model, k-cluster configuration 2—38438
closed shell, particle-hole excitation and surface excitation coupling 2—2668
collective, semiclassical treatment of the dynamic ellipsoidal shapes 2—31420
collective model, even-even Mo and Ru nuclei 2—18113
collective model interpretation of α-scatt. data, ^{140}Ce and ^{139}La 2—11764
collective virtual core excitation model description of core polarization exchange contribs. to inelastic nucleon scattering 2—31527
Davydov-Chaban model analogue 2—38442
deformed shell of axial symmetry, spurious rotational states 2—21359
double even nuclei, asymmetric rotor with variable moment-of-inertia model for fitting ground state and γ-vibrational bands 2—14915
droplet model of Myers and Swiatecki, shape dependence, curvature and compressibility 2—8271
even-even nuclei, phenomenological collective model for high angular momenta 2—31435
exactly solvable model, RPA correlations in intrinsic state 2—38439
Fermi gas model for nuclear excited states, modifications caused by the existence of collective motions 2—38456
Fermi liquid drop, giant dipole resonance 2—14912
fission, asymmetric two centre shell model 2—31597
Goldhaber-Teller oscillating liquid-drop model and inelastic electron scattering in light nuclei 2—27945
Hartree-Fock-Bogoliubov model, higher isospin states in s-d shell nuclei 2—14914
heavy elements, single particle states and single particle models 2—21381
independent pair model, finite nuclei, nucleon correlation 2—2664
Kisslinger optical potential, calc. of pion-nucleus charge exchange scattering 2—8350
light nuclei, α-particle clustering, saturation mechanisms 2—38440
light nuclei, cluster structure, study from reaction C(p,α) at 660 MeV 2—38468
liquid-drop, application to fission of A=200 and actinide nuclei 2—11877
magnetic moment, shell model interpretation 2—5640

- **Nucleus** continued
  - **models** continued
    - matrix ensembles obtained from Brownian motion process and boundary conditions 2—2132
    - matter density models and antiproton-(emulsion) nuclei elastic scattering at 3GeV/c 2—24213
    - microscopic model interpretation of α-scatt. data, ^{140}Ce and ^{139}La 2—11764
    - model-space effective Hamiltonian, folded diagram expansion 2—2140
    - modified quasiparticle model, for determination of excitation energies and transition probabilities 2—21364
    - Nilsson, evidence for violation of Gallagher-Moskowski rules in ^{154}Pm 2—27986
    - Nilsson model, role of N-mixing 2—38437
    - Nilsson model calcs. of collective nuclear phenomena, effective force 2—8272
    - nucleon optical model pot., real part calc. 2—35017
    - odd-mass nuclei, electron scattering description using particle-core and particle-phonon coupling models 2—38578
    - optical, compound-nucleus and direct-reaction fast neutron total cross section of ^{240}Pu 2—8341
    - optical, proton and neutron scatt. analysis, A-depend. 2—35022
    - optical, rel. to p-wave neutron strength functions 2—35043
    - optical model analyses of elastic scattering, method of resolving real well depth ambiguities tested 2—11856
    - optical model analysis of elastic proton scattering at 16 MeV 2—31546
    - optical model appl. to quasielastic (p,n) reactions 2—11832
    - optical model for proton elastic scattering from ^{16}O, ^{40}Ca addition of surface peaked term to real-central potential 2—24211
    - optical model potential, energy dependence of isospin dependent part, study by ^{208}Pb(p,n) 2—38603
    - optical potential, neutron elastic scatt., shell effects 2—38605
    - optical potentials, nucleon-nucleus, $1/\gamma$ velocity dependence 2—24197
    - pairing-plus-quadrupole model, rel. to studies of many-body approximations 2—34871
    - particle-core coupling model, rel. to interpretation of ^{57}Co levels 2—38491
    - peripheral model for (d.p) stripping reaction to resonance state 2—21443
    - projected Hartree-Fock model, pairing effects 2—453
    - quartet Hartree-Fock model for sd shell 2—21351
    - quartet shell model, prediction of energies of intrashell quartet states 2—31422
    - rigid asymmetrical rotator, modified moments of inertia 2—14917
    - rotating nuclei with variable moment of inertia, model in which there is no upper limit on spin in rotational band 2—38465
    - sd-shell nuclei, light, α-cluster structure and weak coupling feature 2—38451
    - shell, Nilsson and excited core models of mass-27 systems, prediction for log ft values compared with experiment 2—18157
    - shell, quadrupling and pairing 2—21360
    - shell, two-centre, single-particle energy levels 2—27946
    - shell effects in excited nuclei, disappearance with excitation energy, statistical description 2—24133
    - shell model, A=27, 28, 29 nuclei, e.m. transition rates and multipole moments 2—38489
    - shell model, electrodisintegration cross sections, nuclear bond scheme 2—8328
    - shell model, rel. to theory of complex collisions 2—38649
    - shell model, shell structure influence on isobaric spin splitting 2—14913
    - shell model analysis of alpha decay rates of Pt, Au and Hg isotopes 2—11786
    - shell model calc. of mass 18 nuclei and effective interaction in s-d shell 2—464
    - shell model calcs. of level schemes of ^{31}Si and ^{33}S 2—28000
    - shell model calculations. for nuclei with A=30-35 2—2702
    - shell model calculations. Gartenhaus Schwartz transformation does not eliminate spurious effects 2—11712
    - shell model calculations. numerical approach 2—21362
    - shell model calculations of A<208 Pb isotopes 2—8288
    - shell model Hamiltonian, direct transcription from particle space to boson space 2—31423
    - shell model pot., compressibility effect 2—11711
    - shell-model bound state calcs. using single particle spectra including the continuum 2—24130
    - shells, diagonalization method compared to the strong channel coupling method 2—31518
    - spherical and deformed nuclei, shell correction approach to nuclear shell effects 2—34884
    - statistical description of a paired nucleus with the inclusion of angular momentum 2—34883
    - statistical model of compound nucleus, test using ^{195}Au(n,2n) cross sections 2—2731
    - superfluid model, pairing interactions, hydrodynamical limit 2—18069
    - superheavy elements, recent developments 2—34885
    - superheavy nuclei, shell-model calculations of fission decay widths and probabilities 2—18245
    - supermultiplet, for level densities 2—34897
    - surface δ-interaction model, quadrupole vibrations in doubly open shell nuclei 2—38458
    - unified model in intermediate coupling applied to odd mass isotopes 2—27981
    - unitary model for calculating nucleon polarization in elastic nucleon-deuteron scattering 2—24208
    - variable moment of inertia model, rot. spectra and shapes classification 2—34886
    - variable moment-of-inertia models for ground state collective modes of doubly even nuclei 2—21361
    - K- nucleus optical potential model role in K- mesonic atom spectra 2—35191
    - ^{8}Be structure in spherical shell, deformed shell and cluster models, appl. to fission problem 2—14931
    - ^{209}Bi, alternate models of particle-core coupling 2—24175
    - ^{12}C, three-alpha model 2—34910
    - ^{13}C, particle-rotator model of positive-parity states comparison of Feshbach and R-matrix theories for ^{12}C(n,n)^{12}C reaction 2—31549
    - ^{13}C, shell model for positive parity states, comparison of Feshbach and R-matrix reaction theories for ^{12}C(n,n)^{12}C reaction 2—31548
    - ^{40}Ca, compressibility effect on shell model pot. 2—11711
    - ^{56}Fe, semi-microscopic model of two-proton hole cluster coupled to quadrupole vibrational field in ^{58}Ni 2—34942
    - ^{93}Nb, shell model appl. to Coulomb excitation 2—14948
    - ^{58}Ni(^{3}He,p)^{60}Cu, shell model calculation 2—38644
    - ^{32}S, particle-hole excitation and surface excitation coupling 2—2668
    - ^{28}Si, shell model calculations of excitation spectrum 2—21384
    - Sm, 50.8 MeV proton scattering using simple optical model and reformulation DWBA and coupled channels 2—27985
  - **size**
    - 2s-1d shell nuclei, quadrupole and hexadecapole deformation 2—21383
    - β-decay, first-forbidden, finite-nuclear-size effect 2—21410
    - deformation producing character of T=1 interactions 2—38436
    - density, calculation by K-harmonic method 2—38427
    - density distribution, role of N-mixing in Nilsson model calc. 2—38437
    - ellipsoidal shapes, semiclassical treatment of dynamics of collective vibration and rotation 2—31420
    - finite effects on Fermi β-decay, radiative corrections 2—18151
    - giant resonance excitation, resolution into isospin components, rel. to neutron and proton r.m.s. radii 2—31407
    - light nuclei, relevance of shape charge distribution to ft values of superallowed Fermi transitions 2—21409
    - mass formula, inplications of fragment shell influences in nuclear fission 2—11877
    - mass sum rule, violation rel. to empirical determination of characteristics 2—34889
    - quadrupole perturbations, theoretical aspects of time-integrated angular correlations 2—27957
    - radii, hgh energy limit in elastic electron scattering 2—8325
    - recoil nuclei from α decay, mass determ. and velocity meas. 2—11787
    - r.m.s. radii, non static contribs. study by anal. of electron scattering 2—18176
    - rotational spectra and shapes classification, phenomenological models 2—34886
    - shape, relation to concept of intrinsic state, review of shape determ. 2—38447
    - shape, surface, in fission, three parameter description 2—24243
    - shape of ground and excited states determ. by new method 2—18082
    - shape of light even-even nuclei 2—5636
    - spherical and deformed nuclei, shell correction approach to nuclear shell effects 2—34884
    - superheavy nuclei, Z=112, 116, A=224-480 and r.m.s. radii r.m.s. radii 2—27998
    - Dy, effect of nuclear deformation on K^- absorption 2—499
    - Al, determ, from anal. of reaction cross sections due to π^-, K^- and $\bar{p}$ in range 20 to 60 GeV/c 2—11719
    - ^{27}Al, oblate shape, agreement with calcs. in Coriolis band mixing model 2—31458
    - C, determ. from anal. of reaction cross sections due to π^-, K^- and $\bar{p}$ in range 20-60 GeV/c 2—11719
    - ^{12}C, radius, variational calculation 2—11726
    - ^{252}Cf, spontaneous fission, fragment nuclear charge distribution 2—11882
    - ^{153}Eu, muonic isomer shifts of γ-ray transitions, mean square radius of ground and excited states 2—18130
    - ^{257}Fm, symmetry in mass distribution shown to be due to approach to ^{264}Fm nucleus 2—11877
    - Hg (A=183,185), nuclear charge distribution obs. using optical pumping technique 2—27992
    - Hg isotopes, deformation energies for β_2, β_4 and γ distortions 2—27993
    - ^{72}Kr and neighbouring isotopes, oblate groundstate deformation predicted by Strutinsky-type calcs. of potential energy 2—24163
    - ^{6}Li, electron elastic scattering at low momentum transfer. determ. charge form factors, model dependent and independent rms radii 2—24204
    - ^{6}Li shape, pion absorpt. study 2—38625
    - ^{24}Mg, calculation of triaxial shapes 2—31424
    - ^{24}Mg, deformations of ground-bands, rotational model analysis 2—31454
    - ^{24}Mg, ground state, triaxial shape study 2—11698
    - ^{24}Mg, nuclear charge distributions from elastic electron scattering 2—34922
    - ^{24}Mg, radius calc. using Hartree-Fock model 2—11734
    - ^{25}Mg, nuclear charge distributions from elastic electron scattering 2—34922
    - ^{26}Mg, calculation of triaxial shapes 2—31424
    - ^{26}Mg, nuclear charge distributions from elastic electron scattering 2—34922
    - N (A=14, 15), charge radius differences 2—14937
    - ^{26}Na mass meas. using ^{26}Mg(^{7}Li, ^{7}Be)^{26}Na reaction 2—34924
    - ^{20}Ne, deformations of ground-bands, rotational model analysis 2—31454
    - ^{20}Ne, radius calc. using Hartree-Fock model predictions 2—11734
    - O (A=16, 18), charge radius differences 2—14937
    - ^{16}O, first excited state, triaxial shape study 2—11698
    - Os isotopes, deformation energies for β_2, β_4 and γ distortions 2—27993
    - Pb, determ. from anal. of reaction cross sections due to π^-. K^- and $\bar{p}$ in range 20-60 GeV/c 2—11719
    - ^{208}Pb, charge distribution, comparison of Hartree-Fock calc. with electronic scattering and muonic X-ray data 2—24174
    - ^{208}Pb, model independent description of charge distrib. from elastic electron scattering data at moderate momentum transfers 2—28023
    - ^{208}Pb, neutron radius determ. from sub Coulomb pick up reactions 2—2738
    - ^{208}Pb, neutron radius from 166 MeV α-scattering 2—11779
    - ^{141}Pr, charge radius from Mossbauer isomer shifts. 145.4 keV γ-ray scattering 2—18124
    - Pt isotopes, deformation energies for β_2, β_4 and γ distortions 2—27993
    - ^{239}Pu, thermal neutron fission, fission fragment nuclear charge distribution 2—11882
    - ^{32}S, calculation of triaxial shapes 2—31424
    - ^{32}S, ground state, triaxial shape study 2—11698
    - ^{32}S, radius calc. using Hartree-Fock model predictions 2—11734
    - ^{28}Si, deformations of ground-bands, rotational model analysis 2—31454
    - ^{28}Si, radius calc. using Hartree-Fock model predictions 2—11734
    - ^{30}Si, calculation of triaxial shapes 2—31424
    - Sn, determ. from anal. of reaction cross sections due to π^-, K^- and $\bar{p}$ in range 20-60 GeV/c 2—11719
    - Sn, even-mass-number-isotopes, effect of T=1 pairing correlations on nuclear deformation 2—31481
    - Sn (A=116,118.124). charge density distribution parameters, electron scattering studies at 225.0 MeV 2—21393
    - ^{201}Tl, shell effects on saddle pt. deform. 2—34978
    - ^{233}U, thermal neutron fission, fission fragment nuclear charge distribution 2—11882

Nucleus continued
size continued
^{235}U, thermal neutron fission, fission fragment nuclear charge distribution 2—11882
W isotopes, deformation energies for β_2, β_4 and γ distortions 2—27993

spin and parity
see also Gyromagnetic ratio; Molecules/nuclear coupling
^{27}Al, levels below 5 MeV excitation 2—24152
A=14 nuclei, isospin mixture of negative parity states, weak coupling calc. 2—21375
A=40, 41, calc. of non normal parity states 2—8295
A=6 to 9 systems, normal parity states calculated in framework of shell model 2—11722
actinides, $229 \leqslant A \leqslant 257$, excited levels, from radioactive decay meas. 2—21401
deformed even-even nuclei, ground state moment of inertia 2—34902
excitation of unnatural parity states by inelastic scattering, extension of Satchler's microscopic formulation to spin orbit force 2—35064
giant dipole resonance, isotopic structure and isospin impurity of low-lying nuclear states 2—18081
ground state spins of doubly odd nuclei with valence electrons filling same subshell 2—457
heavy nuclei, isotopic spin conservation for low lying collective states 2—21369
isobaric spin splitting, influence of shell structure 2—14913
isospin, role in statistical processes, proton induced reactions 2—11815
isospin centroid energy calc. 2—34903
light nuclei prod. in (p,t) reaction on even even N=Z nuclei in 2s1d shell 2—24214
moments of inertia of light even-even nuclei 2—5636
parity mixing, exptl. investigation rel. to weak interaction theory 2—38216
parity non conserving electric multipole type transitions, exchange current contributions 2—31433
parity projection, spherical nuclei 2—18080
photonuclear reactions, consequences of isospin sum rules 2—31521
precession of spin under influence of crystalline elec. field gradient, meas. 2—7022
proton spin-flip in microscopic distorted wave approximation 2—18182
quasi-spin calculations, SO(5) Wigner coefficients for 14-dimensional representation 2—37574
rare earth isotopes, moments of inertia as function of neutron number 2—2726
rare earths, deformed, moment of inertia and vibr. energy under centrifugal stretching 2—34914
rare earths, deformed, rotations, moment of inertia, vorticity 2—34919
rare earths, odd-odd, ground state spin parity 2—34918
rotating nuclei with variable moment of inertia, model in which there is no upper limit on spin in rotational band 2—38465
spherical nuclei, low spins, backward bending for quasirotational bands 2—31439
spherical odd mass nuclei, structure of anomalous coupling state of spin I=(j-1) 2—31432
spin of energy levels, determ. from (γ,γ') reaction 2—2680
vibrational nuclei, low lying negative parity states 2—2677
p anomalous orbital magnetic moment confirmed from obs. on ^{210}Po 2—5638
^{26}Al high spin states populated in ^{12}C(^{16}O,d)^{26}Al reaction 2—38655
^{27}Al high spin states populated in ^{12}C(^{16}O,p)^{27}Al reaction 2—38655
^{28}Al, spin, parity assignments 2—18206
^{39}Ar, single neutron hole states populated in ^{40}Ar(^{3}He,α) reaction 2—27973
^{39}Ar, spin assignments of levels populated in ^{38}Ar(d,p) reaction made on basis of shell-model ordering of states 2—34934
^{41}Ar spin, parity assignments 2—18206
^{75}As, existence of parity non conserving nuclear potential confirmed in γ transition study 2—11776
^{9}B, high-spin assignments in the 1p-shell obtained with the J-dependent (p,α) reaction on ^{12}C 2—31544
^{10}B levels, determinations by ^{11}B(^{3}He,α)^{10}B(α_0)^{6}Li correlations 2—5645
^{11}B, isospin splitting of giant dipole reson. 2—34907
^{135}Ba, levels at 218, 481 and 852 keV 2—11763
^{138}Ba, level scheme construction, spin assignments from ^{138}Cs decay 2—24167
^{8}Be, 4.8 MeV level from Li(d,n) reaction 2—27963
^{79}Br low-lying levels, intermediate coupling and core excitation models 2—38502
^{85}Br, ground and first four excited states, assignment from ^{86}Kr(d,^{3}He)^{85}Br 2—11865
^{12}C, spin and spin-isospin dipole oscillations 2—24143
^{40}Ca, spin of 6.75 MeV level 2—18101
^{41}Ca, spin, parity assignments 2—18206
^{42}Ca deformed states, from inelastic scatt. of 50 MeV protons 2—11835
^{43}Ca, excited state properties and spin values from ^{40}Ar(α,nγ) reaction at 13.5 MeV 2—24155
^{107}Cd, excited levels, investigation using ^{107}In→^{107}Cd decay 2—11798
^{110}Cd, low spin states populated by β-decay of 1$^+$ ground state of ^{110g}Ag, obs. of O$^+$ state of two phonon character 2—31480
^{112}Cd, assignment from ^{112}Ag decay data 2—21413
^{112}Cd, assignments made for levels following nuclear photoexcitation 2—11758
^{38}Cl, assignments to levels below excitation energy 2.75 MeV 2—24154
^{56}Co, spin assignments to levels up to 2.6 MeV excitation 2—24223
^{59}Co, meas. of spin-spin effect in neutron total cross section from 0.3 to 8.0 MeV 2—18210
^{60}Co, spin assignments from ^{59}Co(n,γ) reaction 2—18211
^{60}Co, spin calc. from $\gamma\gamma$ ang. correlation meas. 2—2711
^{62}Co, investigation by two-particle transfer reaction ^{64}Ni(d,α) 2—31476
^{48}Cr, assignment for levels production in ^{50}Cr(p,t)^{48}Cr reaction 2—2706
^{49}Cr, spin assignments deduced from lifetimes of levels 2—18105
^{50}Cr study of excited states with ^{52}Cr(p,t) reaction 2—34939
^{53}Cr, e.m. properties studied with ^{50}Ti(α,nγ)^{53}Cr reaction 2—34940
^{64}Cu, spins of low-lying states obs., γ—γ directional correlation meas. 2—38496
^{66}Cu, 0.462 MeV level, study in ^{65}Cu(p,n) and (p,nγ) reactions 2—8339
^{158}Dy, moment of inertia by excitation of ground-state band to spin 22 2—34966
^{158}Dy, nuclear moment of inertia at high rotational frequencies, levels populated with (α,xn) reaction 2—27988
^{160}Dy, nuclear moment of inertia at high rotational frequencies, levels populated with (α,xn) reaction 2—27988
^{161}Dy, neutron resonance, spin assignment 2—18131

Nucleus continued
spin and parity continued
^{163}Dy, neutron resonance, spin assignment, hyperfine coupling constants 2—18131
^{162}Er, nuclear moment of inertia at high rotational frequencies, levels populated with (α,xn) reaction 2—27988
^{18}F, isospin mixed 5.61 and 5.67 MeV levels, spins determ. by angular correlation meas. 2—11730
^{18}F, parity of 3134 keV J=1 state using reaction ^{16}O(^{3}He,p) at 2.95 MeV 2—14936
^{18}F levels, ^{17}O(d,n)^{18}F reaction obs. 2—504
^{19}F, energy spectrum of non-normal-parity states produced using non-central particle- hole interaction 2—11732
^{19}F, new high spin states forming part of $K={}^3/_2{}^+$ rotational bands 2—2695
^{19}F, study of resonance at 850 keV in ^{15}N(α,γ) reaction, spin and parity assignment of 5/2$^-$ 2—35069
Ga(n,γ), γ-ray circular polarization, spin assignments 2—18209
Gd (A=145, 146), assignment from energy level pattern 2—24169
^{152}Gd, high spin state population via ^{153}Sm(α,4n) reaction 2—21395
^{153}Gd, high spin state population via ^{152}Sm (α,3n) reaction 2—21395
^{74}Ge polarized beams, relaxation time determ. 2—18116
^{76}Ge, investigation using ^{76}Ga→^{76}Ge decay 2—11751
^{4}He, isospin mixing in dipole states, ^{4}He(γ,n$_0$) reaction study 2—27959
^{4}He, spin and isospin in high energy proton elastic scattering and nuclear correlations 2—31529
^{180}Hf, parity admixtures in nuclear forces γ transition study 2—31489
^{198}Hg, from γ and conversion electron spectra and γ-γ ang. correlations 2—2733
^{38}K, assignments to second, third fourth excited states populated by ^{40}Ca(d,$\alpha\gamma$) reactions 2—35075
^{6}Li, isospin and decay modes from ^{7}Li(τ,α)^{6}Li and ^{7}Li(τ,α)^{6}Li*(d)^{4}He reactions at E_τ=1.5 MeV 2—27969
^{6}Li(d,pn), isospin selective reaction, obs. of spectral peaking characteristic of certain spin states 2—18227
^{175}Lu, parity violation caused by vector meson exchange 2—38520
^{24}Mg high spin states populated in ^{12}C(^{16}O,α)^{24}Mg reaction 2—38655
^{25}Mg, spin of 4.075 MeV level determ. from gamma-ray polarization method 2—8289
Mn, A=51, 53, 55, fine structure meas. using p scatt. and ^{54}Cr(p,n) spins, parities and partial widths obtained 2—2708
^{53}Mn levels, spin assignments made in study of ^{53}Cr(p,n) reactions 2—11747
^{54}Mn, assignments for levels populated in ^{52}Cr(^{3}He,p) reaction 2—21448
^{54}Mn, spins of low-lying levels studied by ^{54}Cr(p,n) reaction 2—38531
Mn(n,γ), γ-ray circular polarization, spin assignments 2—18209
^{92}Mo, assignment for levels populated in ^{94}Mo(p,t) reaction 2—2780
^{95}Mo, high spin levels from (α,xn) reactions 2—21391
^{97}Mo, high spin levels from (α,xn) reactions 2—21391
^{102}Mo, levels studied using (t,p) reaction 2—31479
^{13}N, high-spin assignments in the 1p-shell obtained with the J-dependent (p,α) reaction on ^{16}O 2—31544
^{14}N of 11.049 MeV state 2—2690
^{16}N, study using ^{14}C(^{3}He,p)^{16}N reaction 2—31449
^{22}Na, spin of 1984 keV level populated in ^{19}F(α,nγ)^{22}Na reaction 2—38485
^{23}Na, low lying negative states examined in terms of particle or hole character 2—11735
^{23}Na bound states, assignment using ^{22}Ne(p,γ)^{23}Na reaction 2—24219
^{20}Ne, assignments for levels studied by ^{16}O(α,α) scattering 2—21382
^{57}Ni, of 2.443 MeV level and possible assignment for 3.003 MeV level 2—11749
^{64}Ni, spin and parity assignments, gamma transitions 2—5693
Ni(n,γ), γ-ray circular polarization, spin assignments 2—18209
^{15}O, assignment for 10.47 MeV state 2—18090
^{16}O, four particle four hole solution, instability against parity mixing 2—2692
^{16}O, negative-parity states populated in ^{12}C(^{6}Li,d) reaction 2—463
^{16}O, spin assignments to levels near excitation energies of 15 and 20 MeV 2—38481
^{30}P, spin assignment for 3.834 and 3.927 MeV from lifetime meas. 2—21385
^{32}P, spins of levels determ. by angular-correlation studies of ^{29}Si(α,p) reaction 2—8292
^{203}Pb, assignments to levels populated in decay of ^{203}Bi 2—34993
^{204}Pb, assignments to levels populated in decay of ^{204}Bi 2—34993
^{103}Pd, assignments for excited states from ^{103}Rh(p,nγ)^{103}Pd reaction 2—11757
^{104}Pd, excited state population in β^- decay of 4.3 sec and 4.41 min isomers of ^{104}Rh, spin values 2—34955
^{104}Pd, spin of 1333.6 and 1792.7 keV levels 2—21392
^{112}Pd, levels studied using (t,p) reaction 2—31479
^{141}Pm, three quasi particle multiplet spin assignments 2—31505
^{147}Pm 91, 412 and 685 keV levels, spin assignments 2—34962
^{210}Po high-spin states studied in ^{208}Pb(α,2nγ) reaction 2—31495
^{138}Pr, assignment from log ft values of β transitions 2—38550
^{143}Pr, spin assignment of excited states using internal conversion coeff. 2—21394
^{195m}Pt, oriented in Fe, spin of isomeric state, n.m.r. study 2—27994
^{98}Rh, low excited levels, assignment from ^{98}Pd decay data 2—38546
^{103}Rh, negative parity states, model interpret. 2—38509
^{103}Rh negative parity levels, Coulomb excitation with ^{4}He and ^{16}O ions 2—18117
^{103}Rh polarized beams, relaxation time determ. 2—18116
^{98}Ru, low excited levels, assignment from ^{98}Rh decay data 2—38546
^{106}Ru, levels studied using (t,p) reaction 2—31479
^{32}S, isospin impurity in ^{32}S ground state numerical estimate from charge-asymmetry meas. in ^{32}S(d,^{3}He)^{31}P, ^{32}S(d,t)^{31}S reactions 2—35073
^{32}S, spins of levels populated in ^{31}P(p,γ) reaction determ. from angular distrib. meas. 2—38596
^{32}S levels, investigation using ^{28}Si(α,γ)^{32}S reaction 2—5649
^{35}S, angular correlation meas. spin assignments and multipole mixing from ^{34}S(d,pγ)^{35}S, ^{37}Cl(d,$\alpha\gamma$)^{35}S 2—18100
^{36}S, assignment using γ transition data 2—34933
Sb isotopes, neutron resons. 2—31561
^{117}Sb, g-factor meas. of isomeric state 2—5662
^{45}Sc, spins and parities of states investigated using ^{46}Ti(d,τ)^{45}Sc reaction 2—31465
^{48}Sc, excited states, investigation using ^{48}Ca(p,nγ)^{48}Sc reaction 2—2705
^{75}Se, assignment from ^{75}Br decay data 2—24164
^{75}Se, spins of low lying levels, investigation using ^{75}As(p,nγ)^{75}Se reaction 2—34947

Nucleus continued
spin and parity continued
^{28}Si, assignments for 9.76 and 9.93 MeV levels via ^{29}Si(p,d)^{28}Si and ^{30}Si(p,t)^{28}Si reactions 2–2700
Sm (A=143, 144), assignment from energy level pattern 2–24169
^{144}Sm, assignments made for low lying states following elastic and inelastic scattering of α particles and protons 2–11857
^{152}Sm recoiling into vacuum, obs. of spin precessions from static free hyperfine interaction 2–38516
^{152}Sm(α,xn)$^{152,\ 153}$Gd, 32-43 MeV, population of high spin states 2–21395
^{115}Sn, g-factor meas. of isomeric state 2–5662
^{88}Sr, determ. E2/M1 mixing ratio from γ-γ angular correlation meas. on decay of ^{88}Rb 2–28006
^{88}Sr, determ. spins of levels from γ-γ angular correlations meas. on decay of ^{88}Rb 2–28006
^{177}Ta, assignment to three- quasiparticle isomeric state at 1355 keV 2–11770
^{181}Ta, parity admixtures in nuclear forces γ transition study 2–31489
^{181}Ta, parity violation caused by vector meson exchange 2–38520
^{159}Tb, parity admixtures in nuclear forces γ transitions study 2–31489
^{99}Tc, 921 keV level, spin assignment 2–34954
^{99}Tc Coulomb excitation with 52-64 keV ^{35}Cl ions, spin and parity assignments mode for 726.3 and 761.8 keV levels 2–18115
^{44}Ti, levels up to 9.330 MeV excitation 2–24157
^{201}Tl, spin and parity assignments, level scheme proposed obs. of ^{201}Pb→^{201}Tl 2–2734
^{203}Tl, existence of parity non conserving nuclear potential confirmed in γ transition study 2–11776
^{203}Tl, parity admixtures in nuclear forces γ transition study 2–31489
^{203}Tl, parity violation observed by meas. of β-γ directional correlation in ^{203}Hg→^{203}Tl decay 2–11806
^{203}Tl, study of 279 keV transition angular correlation meas.of asymmetry, deduced limit of parity mixing 2–2736
^{182}W, parity admixtures in nuclear forces γ transition study 2–31489
^{182}W, structure and parity mixing from ang. distrib. of γ rays in β decay of ^{182}Ta 2–31510
W(n,γ), γ-ray circular polarization, spin assignments 2–18209
^{168}Yb, nuclear moment of inertia at high rotational frequencies, levels populated with (α,xn) reaction 2–27988
^{174}Yb, 1518 keV level 2–14956
^{62}Zn, study by reaction ^{64}Zn(p,t) at 27.5 MeV 2–38495
^{64}Zn, composite system formed in ^{63}Cu+p and ^{60}Ni+α reactions, isospin effects in decay, Bohr independence hypothesis 2–24181
^{66}Zn, composite system formed in ^{65}Cu+p and ^{62}Ni+α 2–24181
^{88}Zr, assignment from ^{88}Nb decay data 2–21389

theory
see also BCS theory; Nuclear forces; Nuclear structure
^{12}C, Brueckner Hartree Fock calc. using density dependent effective interaction, binding energy estimate 2–11727
Λ_{00} and Λ_{10} theories, application to calc. of ground state properties 2–5633
angular momentum projection from nonaxial intrinsic states 2–27944
boson method not violating Pauli principle, application to 3 quasiparticle system 2–18060
boundary condition model T matrix, in presence of tensor coupling 2–11705
coherent properties of systems with fixed particle number, field operator tensor properties 2–27102
correlated basis functions method, role of dispersion effect 2–34888
correlated wave functions of finite systems, cluster expansions 2–2663
correlation function between impurity particle and nucleon in nuclear matter 2–5634
Coulomb excitation, second-order quantum-mechanical theory 2–38450
damping of wave functions in nuclear interior, origin 2–11700
deformation of excited nuclei, and disappearance of shell effects with excitation energy, statistical description 2–24133
deformed, collective 0$^+$ and 2$^+$ states 2–38452
deformed even-even rare-earth nuclear, spin-dependent force effect on moment of inertia 2–18127
deformed nuclear density formalism of inelastic scattering, comparison with deformed optical potential formalism 2–8331
deformed nuclei, shell energies 2–14916
deformed nuclei with odd neutron number, mixing of components with ΔN=±2 2–8301
double even nuclei, asymmetric rotor with variable moment-of-inertia model for fitting ground state and γ-vibrational bands 2–14915
doubly even deformed nuclei, properties of collective 1$^+$ states investigated in TDA and RPA approximations 2–27951
ellipsoidal shapes, semiclassical treatment of dynamics of collective vibration and rotation 2–31420
energy and effective charge perturbation calculations, checking procedure using c.m. potential energy 2–14908
entropy, energy dependence at high excitation energy, Strutinski smoothing procedure 2–31409
even-even nuclei, p-f shell, Hartree- Fock-Bogoliubov calcs. 2–11703
exchange currents, effect on orbital g factors 2–8268
exchange currents and soft photon emission 2–2666
Faddeev equations for realistic three nucleon systems, solution 2–8269
fermion pair operators, boson expansion for nucleons with single j shell 2–2679
finite depth potential, two particle shell model wave function, separation of centre of mass motion 2–38430
finite nuclei, approx., Bethe Goldstone eqn., iterative solution 2–11701
gap equations, generalized, and coherence of α-α pair field 2–38429
Gartenhaus-Schwartz transformation, does not eliminate spurious effects in shell model calculations 2–11712
gas-liquid instability in many-fermion system, and breakdown of perturbation theory based on phase wave Hartree Fock hamiltonian 2–107
Gaussian overlap approx., conversion from integral to differential eigenvalue eqn. 2–18061
generator coordinate method and Bose expansions, connection 2–34891
generator coordinate method applied to pairing vibrations 2–31436
ground state shell correction determ. method 2–34895
group symmetries, classification and application 2–34875
group symmetry breaking, comparison of spectral and exact measures 2–24127
Hartree Fock constrained calcs., using Lagrange multipliers, modified procedure 2–2662
Hartree Fock contributions to the effective charge and interaction in the sd shell 2–2659

Nucleus continued
theory continued
Hartree-Fock calculations with Gaussian potentials, computer program 2–31403
Hartree-Fock theory of many-fermion system at high densities, exact results 2–108
heavy nuclei, antianalogous states 2–18150
hyperonic matter studied using lowest- order variational theory, equation of state determ. 2–18070
identical cluster systems, permutation symmetry 2–451
integral equations for four identical spinless particles obtained using Faddeev Yacubovsky approach 2–30788
interacting fermi gas, phase space analysis 2–23306
intranuclear-cascade calculations, Monte Carlo simulations, effect of nucleon-pair correlations 2–11708
Jastrow correlations, one-body and two-body 2–5151
Jastrow method, connection with Brueckner theory 2–27948
K-harmonic method, accuracy 2–14911
light nuclei wave function verification, in nuclear reactions with clusters 2–28012
many body problem, exact differential eigenvalue eqn. using generator coordinates 2–2660
many-body wave functions, with correlations, systematic theory 2–2141
matrix elements, approx. method based on identities 2–31406
matter, infinite, of interacting alpha-particles, excitation spectrum 2–38444
n-body problem, hyperspherical functions of tree type 2–14136
neutron and proton system, charge independent pairing interaction, generalized Bogolyubov-Valatin transformation 2–14904
neutron bound S-states, Woods-Saxon potential calc. 2–2673
nondegenerate system, collective rotational motion 2–24128
non-axially symmetric nuclei, fast numerical soln. to Schrodinger eqn. 2–2675
nuclear matter, approximation to reaction matrix 2–38446
nuclear matter, Green function treatment 2–2669
nuclear matter, N=Z, symmetry energy and single particle potential, rearrangement contribution 2–11713
nuclear matter, n-body clusters, cancellation effect 2–12596
nuclear matter, relation to nuclear potential in inelastic alpha-nucleus scattering 2–8355
nuclear matter, variational calc. of tensor force 2–18071
nucleon correlation, finite nuclei, Hartree-Fock approximation and independent-pair model 2–2664
nucleons behaviour inside nucleus 2–14903
one-particle jj-coupling coefficients of fractional parentage in T, J scheme 2–31405
one-particle quasistationary states, formula for width 2–8270
p-nuclei, unitary scheme, one-quanta oscill. excited states, two particle orbital density matrix 2–24126
pairing Hamiltonian, collective treatment, T=1 case 2–27941
pairing interactions, number-conserving algebraic method 2–34870
pairing plus monopole Hamiltonian on two shells, exact solution by boson representation of group Sp$_4$ 2–14097
pairing vibrational states in seniority-zero space, generator coordinate approach 2–21350
phase shift equivalent momentum dependent potentials, off-shell effects 2–18063
quadrupling and pairing in shell model 2–21360
quasi-particle RPA, test of consistency for rare-earth nuclei 2–34872
random phase approximation, consistency 2–38460
range of force, phase shift, binding energy, relation 2–31427
reaction matrix equation for nuclear matter, simple solution 2–18067
renormalized Brueckner-Hartree-Fock theory, analogue of Koopmans' theorem on separation energies 2–18062
residual two-body interactions, pairing and quadrupole-pairing type 2–11699
s-d shell nuclei, higher isospin states, Hartree-Fock-Bogoliubov model 2–14914
SCF theories, centre of mass corrections 2–2661
Schrodinger equation with Yukawa potential, bound state solutions by integral equations 2–14106
self-nuclear reactions, R-matrix 2–35003
single particle and collective degrees of freedom, interaction by perturbation treatment 2–14104
single particle wave functions, phenomenological models, variational calculations 2–38443
solvable Lipkin model, Brueckner theory applic. 2–21352
spherical nuclei, equilibrium pairing energy gaps 2–38507
spherical nuclei, Hartree Fock calcs. with Skyrme's interaction 2–27947
Strutinsky's theory of renormalization, validity examined by comparing predictions with those of HF calcs. for ^{32}S 2–24129
SU(3) fractional parentage in 1p-shell, computer program 2–21348
superconductivity and mass asymmetry in heavy nuclei, simultaneous coexistence 2–21363
superheavy elements, recent developments 2–21403
surface delta interaction and spherical Hartree-Fock Bogoliubov calcs. 2–11702
symmetry and group theory, basic principles 2–34874
Talmi coefficients, generalised, computer program 2–31404
tensor correlations in nuclear matter evaluation of three body contributions to factor cluster expansion of energy expectation value 2–27949
three-body problem, application of method of Pade approximants, determ. binding energy 2–2122
three-body problem, K-matrix theory 2–38428
two-body interactions, Hartree-Fock calculations 2–34873
two-particle orbital matrix of density for one-quanta oscillatory-excited SU_3-configs. 2–27936
vector bracket and transformed wave function of a few- body state 2–27937
Λ particle well depth, D$_\Lambda$ calc. by phase-shift approximation 2–450
Co, odd isotopes studied in unified vibrational model 2–8300
^{56}Fe, semi-microscopic model of two-proton hole cluster coupled to quadrupole vibrational field in ^{58}Ni 2–34942
^{2}H, optical model potential derivation using Glauber theory 2–18216
^{3}H, exchange magnetic form factor 2–5642
^{3}H, selection rule for K-harmonics 2–18086
^{3}He, exchange magnetic form factor 2–5642
^{3}He, vector-meson effects in electric form factor 2–14929
^{4}He, selection rule for K-harmonics 2–18086

Nucleus continued
theory continued
^{20}Ne, Brueckner Hartree Fock calc. using density dependent effective interaction, binding energy estimate 2—11727
Ni, neutron equilibrium pairing 2—38493
^{16}O, Brueckner Hartree Fock calcs., effect of variations in radial orbital wave functions and major shell mixing 2—11729
^{16}O, four particle four hole solution, instability against parity mixing 2—2692
Pb, neutron equilibrium pairing 2—38493
Pb isotopes with $A<208$, extended shell-model calculations 2—8288
^{208}Pb, isovector quadrupole mode, evidence for existence 2—8312
Sn, neutron equilibrium pairing 2—38493

Oceanography
see also Liquid waves; Seawater
acoustic attenuation due to fish in shallow water 2—1805
acoustic intensity calculations, multipath summability in ray-theory 2—14260
acoustic propag., layered model studies 2—30256
acoustic propagation and model of medium 2—37109
acoustic props. of sea beds 2—33443
acoustic wave fluctuations in a random medium, frequency correlation 2—2240
acoustic wave propagation in underwater sound channel, qualitative theory 2—2242
acoustic wave propagation in underwater sound channel, quantitative theory 2—2243
acoustic waves, extreme downward refraction, application of normal-mode and ray theory 2—14255
acoustics, coherent recombination of multipath signals 2—7755
air-sea interaction and the boundary layer, turbulent exchange processes 2—40930
Alaskan Stream, divergence studies 2—30245
altimeter experiment on Skylab S-193, objectives and capabilities 2—20225
M_2 amphidrome in Northeast Pacific 2—7238
Antarctic circumbipolar current, structure 2—16785
anticyclonic eddies formed from shoreward meanders of Gulf Stream, lifetime calc. 2—37103
Atlantic Ocean, characteristics of thermal inhomogeneities near Brazil current 2—33438
Atlantic Ocean, tropical zone water, thermohaline structure 2—13658
atmosphere interaction with ocean marine sediment formation 2—30288
atmospheric boundary layer and friction layer stratification effect on vertical profiles of turbulence, currents and wind 2—30277
atmospheric boundary layers, nonstationary interaction 2—20290
atmospherics infrasound, microbaroms caused by interfering ocean waves 2—37176
backscatter from sea surfaces at 2.25 cm 2—20282
backscatter model, of satellite altimeter 2—33569
bacteria distribution and activity 2—22945
barotropic waves and instabilities propagation along eastern continental shelf 2—7236
basic magmatism and continental drift in Guiana 2—7240
bathymetric chart from hydrographic survey, high resolution of morphological features 2—26428
Beaufort Sea, wind stress over ice and water 2—16827
Bering Sea, CO_2 conc. in surface waters, effect of upwelling mixing and high primary productivity 2—16784
bioluminescence in ship wake, in Atlantic, Mediterranean and Black Sea 2—13643
bitumen suspended particles, distribution, morphology and composition 2—13641
bottom current, temp. profiles and hydrographic data 2—10705
bottom reflectance, attenuation coefficients and water depth, multispectral scanner data 2—20297
bottom topography effect of oceanic circulation 2—20286
bottom-relief irregularity, quantitative evaluation 2—26479
boundary layer mixing and layer formation in a stratified fluid 2—30242
Bullard heat probe, extension of versatility 2—1808
Charlie-Gibbs Fracture Zone, flow of deep water 2—30237
circulation, effect of bottom topography for two layer model 2—26469
circulation, variations produced by bottom topography 2—1812
circulation linear theory, fundamental boundary value problem, unique solution 2—20293
circulation models, eddy and isentropic mixing 2—10714
coastal erosion study using satellite photographs 2—7202
coastal surface current rel. to wind velocity vector over the sea 2—13654
coastal upwelling, continental shelf water, along shore current 2—10711
coastal upwelling dynamics, simple theoretical model 2—4648
coherence of ocean currents over vertical distances, moored sensors 2—37106
contamination by artificial radioactivity, control and monitoring 2—40908
continental margin study by seismic wave refraction experiment 2—7206
contouring bottom features using side scanning sonar 2—37112
currents, equatorial, wind-driven, in homogeneous oceans 2—10709
currents theory, discussion 2—26480
data stations, unattended environmental oceanographic and meteorological monitoring equipment 2—40903
deep e.m. soundings, gradient methods 2—33436
deep sea, inertial oscillations 2—12528
deep sea basalt, U/He ages as indicators of excess Ar 2—33434
diffusion, vertical, in shallow waters 2—1813
diffusion processes, surface wind, quasi-periodic current structures 2—10713
dispersion studies, distorted hydraulic models, pollutant dispersal 2—28748
Doppler radar return from two-dimensional rough surfaces 2—20284
double Kelvin waves, experimental generation in laboratory 2—6182
eastern Pacific, vertical distribution of TcO_2, dissolved O, alkalinity and temp. 2—16781
electric and mag. fields motionally induced in sea, crust and mantle for large scale low frequency oceanic flows 2—1803
electrical conductivity of seawater, instrument for meas. from shipboard 2—26477
electronic equipment, conference, (Washington D.C., August 1971) 2—16723
e.m. flowmeter, two-component, for l.f. flows in shallow water 2—40906
energy spectra of sea, analysis and optical processing of photographs 2—22947

Oceanography continued
energy spectra of sea waves from photographic interpretation 2—20295
equations of dynamics, probability computing method for solutions 2—13661
expansion, oceanic, models for plate tectonics 2—30221
fluctuating hydrophysical elements, cyclic digital transformation, error determination 2—13660
fluctuation frequency of envelopes of sound signals reflected from ocean bottom 2—30250
geomagnetic prospecting methods, sediment thickness and rock base investigations 2—1785
gravity and magnetic anomalied over Bowers and Shirshov Ridges in Bering Sea 2—16780
gravity wave interaction with larger-scale motions, mass and momentum transfer 2—1806
gravity wave refraction in currents 2—20280
Gulf stream and Western Boundary Undercurrent observations at Cape Hatteras 2—22944
Gulf Stream cyclonic ring eddies in southern Sargasso Sea, available potential energy and decay rate 2—33432
heat circulation models, surface boundary conditions 2—30240
heat/NaCl system, stability of double-diffusive layers 2—20279
holographic weak-signal enhancement technique 2—14434
horizontal conversion coefficients, off-shore zones 2—30252
horizontal diffusion in stratified vertical shear flow 2—37119
hydrographic surveys, electronic positioning and minicomputer system 2—16791
hydrologic data collection, river and rainfall via geostationary satellite 2—20285
hydrologic data collection via geostationary satellite 2—16792
hydrological elements, reconstruction of fields from observational data 2—13657
hydrophysical fields, spectra in terms of wave numbers 2—12529
hydrophysical information output on a graph plotter 2—13662
hydrostatic stability conditions in atmospheric boundary layer above oceans 2—13635
ice drift determination using side looking airborne radar 2—16772
Icelandic region, upwelling, ocean waves, physics, chemistry, radiology 2—22949
inertial boundary layer, geostrophic approximation 2—13656
island arcs, anomalous structure, seismological evidence 2—16755
Lake Michigan, eddy diffusivity 2—10708
Lake Michigan, normalized and equilibrium spectra of wind waves 2—30241
Lake Ontario, equilibrium shape of a thermocline in a shore zone 2—30243
laser applications to depth sounding and underwater imaging 2—38000
long wave generation on sloping beach 2—20292
long waves sweeping through short waves, glitter photographs 2—13647
longshore current generation by obliquely incident internal gravity waves 2—7239
Lusitania deep current, rate and volume of geostrophic transport 2—26473
magnetic anomaly profiles correlated with model profiles for sea-floor spreading 2—1807
magnetic field vertical component in marine magnetic survey 2—13792
marginal seas, development mechanism 2—22935
marine environmental instrumentation testing laboratory 2—13652
marine frequency sounding, equivalency principle for multilayer media 2—30235
marine sediments, in-situ acoustic probe 2—40905
mean sea level of world ocean, nutational fluctuations 2—26472
Mediterranean Sea, bathymetric, magnetic field and gravity measurements 2—30236
monostatic scattering, from ocean bottom 2—37114
movements carrying and depositing waste, radioactive tracers for obs. 2—20294
noise, radiated ambient and self noise, identification generation and measurement 2—37110
nonlinear gravity waves on steady non uniform currents, application to deep water 2—37115
North Atlantic, evidence for ocean floor spreading from radioactive dating expt. 2—22950
North Atlantic Gilliss seamount, magnetization and gravity investigation using Poissons theorem 2—26401
North Atlantic thermocline, two-layer model 2—30244
North Pacific, geostrophic currents 2—26474
North Pacific, Heat storage and advection 2—1800
North Pacific and Bering Sea, CO_2 equilibrium conc. with respect to air in surface waters 2—1801
Northern Atlantic Ocean, tidal components in currents 2—13659
Norwegian-Greenland and Weddell seas, influence on bottom waters of the indian and Pacific Oceans 2—26466
ocean temperature response on atmospheric perturbations, statistical analysis 2—33440
Ocean Weather Station Juliett, upper 100 m temperature and salinity structure 2—37105
off-shore zone, peculiarities of horizontal turbulence 2—33439
oil on water, airborne optical detection 2—26464
optical, submersible spectroradiometer design 2—33431
optical methods of observing small-scale turbulence in seawater 2—13663
optical properties of clean naturally occurring water, prediction 2—13633
Pacific Ocean, northeastern, circulation, temporal variability 2—26475
particle dissolution during settling 2—22946
phytoplankton monitoring, airborne laser system 2—37121
planetary waves, solitary and cnoidal 2—7237
potential energy transfer to atmosphere by heating 2—26491
propagation and antennas, Conference, Los Angeles, (1971) 2—33486
pulse light fluorometer, for in situ and dredging use 2—30248
punched-card files of long-period average parameters, supplementary with current obs. 2—26478
radar backscatter meas. to classify sea state in Gulf of Mexico 2—16794
radar backscattering cross sections and wind velocity in ocean surface measurements, model 2—16788
radioactivity measurements of fission products in Atlantic and Pacific 2—16778
radionuclides, particulate and dissolved, concentration, sampler 2—4653
rare-earth elements distrib. in sediments of lagoon fed by hot springs 2—13642
resonant generation of internal waves through nonlinear interactions of surface waves 2—26468

Oceanography continued
resource problems, radar applications 2—33397
Rossby wake, cylindrical island in an eastward current in an unbounded ocean 2—10710
Rossby wake due to an island in an eastward current 2—30247
rough sea surface, Doppler return, two dimensional model 2—16790
Saanich Inlet, British Columbia, backscattering of underwater sound and scattering from fish school 2—37113
salt fingers convection, vertical thermohaline structure, double diffusivity mechanism 2—26470
Sargasso Sea, Gulf Stream rings 2—20479
satellite photographic studies 2—13650
sea currents, numerical method for solving theoretical equations of motion 2—13653
sea floor deformation, magnetic anomaly offsets, NE Pacific 2—10697
sea ice, thermodynamic model. surface-energy balances and diffusion equations 2—1794
sea level variations, non-regular spectra and rel. to atmospheric pressure and wind stress spectra 2—20289
sea photography, analysis and optical processing for wave energy spectra 2—16795
sea reverberation, autocorrelation function and spectrum 2—28765
sea roughness, variation of the normalized radar cross section with different windspeeds, North Atlantic Ocean 2—1802
sea surface roughness mapping using microwave radiometry 2—16783
sea surface slope and equilibrium wind wave spectra, wind induced growth of small waves 2—33441
sea surface slope and wind velocity, determination by sun glitter from a synchronous satellite 2—4650
sea temperature obs., effect of atmosphere when using multichannel i.r. remote sensing 2—13665
sea waves, interactions with geomagnetic field 2—33435
sea waves scatt. props. rel. to space time correlation coefficient 2—33445
seabed sediments, dynamic testing and engineering studies using seismic technique 2—13651
seamount, anticyclonic vortex 2—16782
seamount magnetism, average direction of magnetization by Backus' method 2—13800
seawaves angular spectrum by coherent h.f. backscatter 2—33444
sedimentary facies generation on spreading ocean ridge 2—26471
seismic surveys, signature of large air guns 2—30168
shallow water ambient noise, time variant characts. 2—30258
shallow water waves, propagation over random ocean bottom of constant average depth 2—40904
solar radiation transfer in atmosphere-ocean system, multiple scattering calculation 2—33467
sonic booms, underwater response, rapidly attenuated 2—37087
sound channel, focussing effects 2—30257
sound field amplitude fluctuations 2—30249
sound field analysis and transmission characts. 2—30254
sound impulse source, exploding wire 2—27297
sound refl. signal fluctuations 2—30255
sound transmission fluctuations in shallows at multiple frequencies 2—1804
soundings, nuclei condensation obs. in marine atmos. 2—37131
Southwestern IEEE Conference, Houston (1971) 2_4656
spectra of locally isotropic hydrophysical fields rel. to measuring instrument distortions 2—12516
statistical model, reverberation effected propagation 2—4657
STD, two-point, precise calculations 2—13634
stratified sea, surface and internal waves generated by a periodic travelling disturbance 2—13655
strong turbulent pycnoclines, approximate model 2—30238
structure of Scotia Sea and Falkland plateau from seismic refraction profiles 2—16779
subarctic surface water temperature computation in Pacific in winter 2—13639
submersibles, ocean platforms and continental shelf labs., place of man 2—13666
subsurface information by aerospace imaging of blue multispectral region 2—26408
subtropical mode water characteristics, insensitivity to meteorological fluctuations 2—37104
subtropical ocean interior, advective and diffusive heat balance 2—13649
surface current measurement by dynamics of temperature inhomogeneities 2—13644
surface generated ambient sea noise spectrum level logarithmic dependence on wind speed, effects of distant shipping 2—37111
surface layer of ocean, origin of thin temperature inversions 2—13636
surface temp., effects on cloud distribution over tropical oceans 2—1870
surface temperature mapping in west Atlantic 2—20298
surface temperatures, computer model for automated processing of satellite infrared information 2—20296
surface water movement, tracer dye imaging system, computer analysis 2—20299
surface wave dynamics with turbulent character of motion 2—20287
surface waves effects on thermal boundary layers 2—6181
surface wind fields det. by remote pasive microwave technique 2—16786
technology applied to the ocean, general paper 2—1809
temperature conductivity and salinity profiles under ice island T-3 2—10707
temperature discontinuity location using satellite television pictures 2—16789
temperature gradients from colour-enhanced satellite imageries 2—37118
temperature-salinity volumetric analysis, Nova Scotia shelf and Georges Bank area 2—13637
thermal emission, limiting factors of microwave measurement 2—16787
thermal probe for meas. vertical temp. profile 2—10717
thermal-sublayer thickness estimation 2—30246
thermohaline convection, turbulent transport processes 2—10712
thermohydrometers, tarring method for sensitivity determ. 2—9049
tidal components in currents in the Northern Atlantic Ocean 2—13659
tidal flow, one-dimensional, bottom friction 2—4647
tidal period of 1800 years, explanation 2—1814
tide theory, equilibrium tide height using barycentric coordinates 2—4646
tidel motions in Arctic seas, regime peculiarities and maps 2—33437
tides, co-oscillating semidiurnal in long, narrow bays 2—20278
tides, influence on evolution of Earth-Moon system 2—41190
tides calc. at Border Sea 2—20291
tides in shallow water, spectroscopy 2—13646

Oceanography continued
time of flight lidar measurements, as ocean probe, multiple scattering events 2—30234
transducer design and array configuration improvements for underwater generation and reception 2—34121
tropical east Pacific Ocean temperatures, influence on atmosphere 2—40907
tsunamis, secondary, detection using variable period band pass filter 2—4655
turbid medium, image of test-object, signal/noise ratio 2—4687
turbidity det., radiative transfer at atmosphere- ocean boundary 2—37157
turbulence in strongly stratified fluid, instability and density profile 2—37107
turbulence small scale, digital data recording and processing 2—20288
two layer frontal Kotschin model, baroclinic instability 2—26467
undersea noise level and wind speed dependence 2—10716
underwater acoustics past 20 years 2—37108
underwater laboratory, manned, Chernomor, some results 2—26476
underwater l.f. ambient noise theory 2—30253
underwater sound recording analysis 2—22951
upper layers, convective model for diurnal cycle 2—1799
US National Oceanic & Atmospheric Administration 1811 2—1811
velocity field in upper layer of ocean, rel. to surface waves 2—13631
Vema fracture zone and the tectonics of transverse shear zones in crustal ocean plates 2—4652
vertical distribution curves of hydrographic parameters, plotting method 2—13645
volcanism, rocks and structures of sea floor, review 2—1810
water mass exchange at mouth of Gulf of California 2—10706
wave field near smooth caustic, asymptotic evaluation 2—21940
wave follower for field study of air-sea interactions 2—20283
wave generation, wind duration and phase speed relation and drag coefficient relation to apparent roughness 2—26465
wave generation by wind, electro-hydraulic wave follower for wind field studies 2—16793
wave height measurement with a nanosecond radar 2—22952
wave spectra, in exposed and sheltered areas 2—13638
wave spectral analysis, low frequency waves and seiches 2—4654
wave transmission over shelf of arbitrary profile, new source potential 2—25021
waves, internal spectra in the presence of fine structure 2—4649
waves, nonlinear Kelvin and continental shelf. equations 2—30239
wind, velocity, temp. and humidity fluctuations, Kolmogoroff constants det. 2—7288
wind disturbed surface waves, curvature distrib. at different viewing angles 2—25020
wind disturbed water surfaces, diffusion sublayer thickness 2—4651
wind driven ocean, O_2, ^{14}C temp. velocity and salinity distributions, tracer model 2—13648
wind wave spectra in deep and shallow parts of bay 2—10715
CO_2 exchange between atmosphere and ocean in eastern South Atlantic 2—13640
H_2S concentration in the Black Sea, a photometric method of determination 2—13664

Octet theory *see SU(n) rules*

Omegatrons *see Leak detection; Mass spectrometers; Vacuum technique*

Onsager relations *see Statistical mechanics; Thermodynamics*

Optical activity *see Optical rotation*

Optical communication *see Laser beams/applications*

Optical constants
see also Absorption/light; Reflectivity
alkali halides, strain depend., calc. 2—40035
alkaline earth fluorides, photoelastic consts. 2—29870
alkaline earth metal film, reflectance and transmittance obs. 2—20017
anthracene, ε_2, determ. from refl. spectra 2—40651
anthracene, reflectivity, absorption band profile, exciton dynamics 2—9942
atmospheric aerosols, natural, in 2.5 to 40 μm range 2—37136
atmospheric gas solids, extreme u.v. reflection spectroscopy determ. 2—19995
benzene, solid, reflectivity determ. rel. to higher $\pi\rightarrow\pi^*$ transitions 2—20052
condensed matter, rel. to plasma wave damping rate 2—32903
contrast transfer coefficients of fibre optic bundles 2—38110
diamond, local effective fields calc., low frequency electronic dielec. const. umklapp effects 2—22745
dielectric coatings and films, determ. using parallel polarized radiation 2—13430
ellipsometric det. for absorbing substrates covered with transparent films 2—12651
ellipsometric determ. in extreme u.v. 2—16461
europium chalcogenides, optical transitions, magnetic order effect, energy level scheme 2—16488
exact equations, for detn. from reflection characs. 2—31086
film, calc. method 2—33195
film, from reflectance and transmittance meas. 2—33202
film, from reflectance and transmittance meas. 2—33203
film, light absorbing, refractive and absorption indices, ellipsometric meas. 2—6341
films, det. by ellipsometric method 2—11512
glass, Kerr constant and nonlinear indices 2—33201
glass fibres, clad. stress-optical coeffs., Tardy's method 2—33198
graphite, anisotropy, reflectance obs., 3-40 eV region 2—19997
group II-IV-V compounds, chalcopyrite semiconductors, absorption coefficients 2—26100
induced birefringence, two beam balanced method 2—38077
inerg gas solids, density of states and excitonic effects 2—20024
inert gas solids, extreme u.v. reflection spectroscopy determ. 2—19995
isotropic material, meas. by refl. 2—33196
lamellar crystals, u.v. obs. 2—10343
layer-type crystals, from reflectivity spectra obs., 2-10 eV rel. to ionicity 2—20005
liquid-vapour critical point, optical transmission and reflection coeff. 2—22038
metal, high temp. consts. 2—40605
metals, thin films, reflectance and transmittance from oblique incidence measurements 2—31088
molecular crystal, polarisability tensor calc. 2—33197
oxide layer, in situ method 2—25204

Optical constants continued
partially transmitting sample, transmittance method with polarized light 2—23708
polyethylene terephthalate film, band-averaged constants from i.r. data 2—40604
polyimide film, band-averaged constants from i.r. data 2—40604
polymethylpolyarsine, from reflectance spectrum 2—13431
polystyrene, vac. u.v. obs., free electron gas model 2—20009
rare earth sequisulphide, pyknometry, spectra, X-ray obs. 2—40671
refractory metal oxide, film, prep. by gaseous anodization 2—13301
semiconductor, amorphous, III-V, complex dielec. const. determ. 2—26104
semiconductor, amorphous, III-V and elemental, calc. 2—26105
semiconductor, anisotropic non-degenerate, rel. to band struct. and scatt. mechanisms 2—10298
semiconductor, carrier concentration, pseudo Brewster angle detn. 2—40282
semiconductor, heavily doped, i.r. reflectivity, free carriers 2—26140
solids, det. by reflectance-ratio obs. at non-normal incidence 2—36815
strongly absorbing solids, quantitative techniques in measuring and calculating i.r. props. 2—22721
styrene-MMA, vac. u.v. obs., free electron gas model 2—20009
surfaces, det. by ellipsometric method 2—11512
terrestrial analogs of lunar minerals, lunar origin det. 2—26813
toluene, Kerr constant and nonlinear indices 2—33201
transition metals, i.r. props., electron-phonon coupling 2—29646
vacuum u.v. reflectance meas. 2—14477
Ag-Au, determ. from energy loss functions by Kramers-Kronig analysis 2—19958
Ag, determ. from energy loss functions by Kramers-Kronig analysis 2—19958
Ag and Ag alloy films, 300 to 400 Å thick, determ. from 2.4 to 4.4 eV 2—22749
Ag films, from reflection and transmission coeff. meas. 2—26103
AgBr, u.v. determination 2—20018
AgBr(Cl), near and extreme u.v. obs. 2—1680
Ag_2O, thin Ag film oxidation 2—1656
Al, 10^{-2} to 10^5 eV range 2—19957
AlAs, absorpt., 4.2-293 K 2—19959
As_2Se_3, amorphous thin film, from i.r. refl. spectra 2—33200
Au, determ. from energy loss functions by Kramers-Kronig analysis 2—19958
Au and Au alloy films, 300 to 400 Å thick, determ. from 2.4 to 4.4 eV 2—22749
Au thin films, 0.3-1 μ, calc. of effective constants using approximate formulas relating meas. reflective transmission coeffs. 2—29871
C, amorphous, 1-4 eV, band struct. 2—26160
CdTe, piezo-optical constants at 10.6 μm, room temp. 2—36827
$Cd_xZn_{3-x}As_2$, from reflectivity obs., i.r.-vac. u.v. 2—20000
CsI, in excitonic region, reflection and luminesc. spectra obs. 2—20001
Ga, absorption spectra and interzone electron transitions 2—10297
GaAs, absorpt., 4.2-293 K 2—19959
GaP, nonlinear susceptibility, relative meas. and detn. of absolute value 2—40597
GaS(Se), temp. modulation, thermoreflectance obs. 2—10346
GaSb, Kramers-Kronig analysis 2—36857
GaSe(s) layer, thermoreflectance spectra, 77K, Kramers-Konig analysis 2—36858
Gd, polycryst., n and k consts., in i.r. range 2—19960
Ge, matrix elements in interband optical transitions 2—22746
GeO_2, i.r. reflectance obs. 2—20002
GeS, amorphous and crystalline, reflectivity obs., 0.5-21 eV 2—20015
KBr(Cl)(I), calc. from KKR energy bands 2—40703
KH_2PO_4 relative nonlinear coefficients, cw ruby laser as pump source 2—36814
KI, far-i.r. consts. and phonon freqs. 2—1681
KIO_3, ferroelectric, phase transition, electro-optical obs. 2—33211
KIO_3, ferroelectric, phase transition, electro-optical obs. 2—33211
K_3Sb purple film, Kramers-Kronig dispersion anal. 2—40601
La_2O_3-GeO_2 system, crystallization, X-ray and optical obs. 2—1209
La_2S_3, dielec. permittivity, i.r. spectra 2—40670
LiO_3 relative nonlinear coefficients, cw ruby laser as pump source 2—36814
MgF_2, extreme u.v. spectra obs. 2—33242
MgO, extreme u.v. spectra obs. 2—33242
NaCl, acqueous solution, relative spectral reflectance in i.r. 2—35766
$NaNO_3$, from vac. u.v. reflectivity spectra 2—16471
Nd_2S_3, dielec. permittivity, i.r. spectra 2—40670
Ni-P film surfaces, ellipsometric study 2—32370
Ni, magnetostriction effects rel. to magneto-optical anisotropy 2—16425
Ni, two-band conduction model 2—10299
$Ni_xZn_yFe_2O_4$, ellipsometric determ. 2—36816
O_2, adsorbed layer on Au, spectrophotometric method determ. 2—10300
$POCl_3$ Kerr constant and nonlinear indices 2—33201
p-$Pb_{1-x}Sn_xTe$, i.r. reflectivity spectra, free carrier parameters detn. 2—26148
Pr_2S_3, dielec. permittivity, i.r. spectra 2—40670
Rb, solid and liquid state, 0.3-2.4 μ wavelength region, temperature dependence 2—16417
Rb, spectral reflectance obs., 3.3-10.5 eV 2—26149
RbH_2AsO_4 relative nonlinear coefficients, cw ruby laser as pump source 2—36814
RbH_2PO_4 relative nonlinear coefficients, cw ruby laser as pump source 2—36814
S, orthorhombic, comparison with monoclinic Se 2—40128
Sb, film, meas. by ellipsometry, application of Maxwell Garnett theory 2—3541
Sb between 2 and 25 eV, by energy loss meas. with fast electrons 2—40603
Sb thin amorphous films, thickness dependence 2—32376
Se, amorphous thin film, from i.r. refl. spectra 2—33200
Se, anisotropy of dielec. const., 3-30 eV 2—22725
Se, monoclinic, comparison with orthorhombic S 2—40128
Si, at 5461 Å, etched and cleaved samples 2—36817
Si, matrix elements in interband optical transitions 2—22746
Si, pseudo-Brewster angle, carrier concentration detn. 2—13210
Si film on absorbing substrate, ellipsometric det. at 3655 Å 2—12651
αSiC and β-SiC, from energy loss expts. with 60 keV electrons 2—1445
SiO_2, at 5461 Å, etched and cleaved samples 2—36817
SiO_2 films formed on n-Si 2—40815
Sm_2S_3, dielec. permittivity, i.r. spectra 2—40670

Optical constants continued
Sn, grey, dielec. const., 1.18 to 4.95 eV 2—16475
$SrTiO_3$, permittivity from zero to optic freqs. 2—40359
Te, anisotropy of dielec. const., 3-30 eV 2—22725
TeO_2, dispersion characts. 2—1658

Optical dispersion *see Dispersion, optical*

Optical fibres *see Fibres/optical*

Optical films *see Films/liquid; Films, solid/optical properties*

Optical filters *see Filters, optical*

Optical images
see also Aberrations, optical; Holography; Resolving power, optics
'scattering-absorption' in image formation from phase objects, wave theoretical investigation 2—23684
aberrations effects on imaging with practically coherent illumination 2—23678
acoustic sources by diffraction of light by ultrasound 2—7959
aerospace imaging of blue multispectral region for ocean subsurface information 2—26408
analysis system, QMS, based on high speed roster scan principle 2—5407
analysis systems, automatic focus, cine and electron microscope facilities 2—5408
annular aperture resolution in partially coherent light 2—7977
coherent illumination of extended objects, apodisation functions for removing fringes 2—5418
coherent transfer function, for coherent imaging systems 2—14443
contrasting, projection and photography of microscopic objects 2—31116
conversion by nonlinear optical methods, longitudinal and transverse resolution 2—11504
dark field, of slits and opaque strips under coherent illumination, interference fringes 2—17686
data compression and enhancement below cut off frequency for sampled images 2—34454
deblurring, holographic principles and methods 2—23735
deblurring using holographic Fourier transform division method 2—34420
degradation by aliasing in planetary lander facsimile cameras 2—34458
depth and illumination, tutorial 2—17166
depth and illumination, tutorial 2—17167
depth with rear converter lens or afocal attachment 2—11510
diffraction, from telescope mirrors with random surface undulations, illuminance distribution 2—17677
diffraction, triangular wave targets in partially coherent light 2—27580
diffractional nature, demonstrated by expts. 2—17704
discernment between two dissimilar fields, Young's fringes of obs. of photographic negatives in coherent light 2—5419
discrete transfer functions 2—38046
enhancement of grey scale aerospace imagery for visual interpretation 2—31085
evaluation, history of Kodak Research Laboratory 2—11509
filtered, dimension obs. and defect detection 2—33862
formation, effect of aberrations, geometrical, physical and detector optics 2—5406
formation by lenses, classical theory 2—298
graded-index (GRIN) rods used as image relays, aberrations and design 2—5431
Herzberger's fundamental optical invariant and behaviour of lenses 2—11508
holographic, image quality of diffusely reflecting objects 2—38014
holographic, overlap prevention 2—27551
holographic formation, book 2—38004
holographic image deblurring for diffraction limited imaging attainment in electron microscopes 2—23540
holographic reconstruction of electron microscope image 2—17653
holographic sharpening 2—17658
illumination and depth, tutorial 2—17168
image treatment, computer simulation 2—27585
information processing, liq. cryst. applic. 2—11526
lenticular sheet three dimensional images, technical problems 2—38045
linear restoration of incoherently radiating objects by least squares estimate of radiance on photosensitive mosaic 2—27582
motion picture quality, information evaluation 2—5454
noise evaluation using two dimensional optical Fourier approach for space imagery 2—34456
oscilloscope traces, real-time holographic filtering 2—2413
phase determination from image and diffraction plane pictures 2—31097
photographic, line element broadening as function of emulsion exposure 2—38169
photographic data, superresolution, restoration with maximum entropy 2—34564
photographic transparencies, subjective image quality, relative effects of gaussian and Poisson noise 2—5455
photographically recorded imagery engancement 2—23732
point spreads approx. for deconvolution, applications to image improvement 2—7971
processing using geometric and spectral features 2—34457
quality, effect of optical contrast transfer functions 2—34440
real, formation, v.u.v. radiation, using Fresnel zone plate 2—38049
recording and reconstruction, 3D-holograms 2—23638
recording instrument with post recording bandpass selection 2—23712
recording processes, applic. 2—22636
restoration, 2-D, with signal dependent noise 2—34460
restoration, Bayesian based iterative method 2—7970
restoration in coherent processor using spatial filters 2—34459
restoration of degraded images using an information-theory model with maximum likelihood and entropy 2—31083
sector shaped apertures, far field diffraction pattern 2—34493
signal/noise ratio in image of test object observed through turbid medium 2—4687
sine wave patterns of constant luminance and varying chromacity 2—38050
spatially sampled, quality criteria 2—38047
spectrometric, signal to noise ratio in multiplex coding 2—31137
in spherical 27.5 metres mirror, photographic recording of optical effects 2—7965
in spherical 27.5m mirror, calc. of optical effects 2—7966
storage and decoding, white light three dimensional microscopy 2—34529
thermography, evaluation as composite material testing method 2—25554
three dimensional, of 2 dimensional object, prod., self reproduction phenomenon 2—11511

Optical images continued
three dimensional, projection type display, lenticular sheet picture 2—27567
three dimensional, storage methods, space-bandwidth requirements 2—2375
transmission by optical surface waves on glass 2—34471
turbulence, holographic compensation 2—23653
wave optical imaging performance of telescope system for different wavefront deviations 2—2422
waveguide, rectangular, transmission of visible coherent light images 2—27584
weak, detection with photon counting techniques 2—38048
weak phase-amplitude object, reconstruction 2—31084

Optical instrument testing
astronomical mirrors, surface quality determination by the slit and wire method 2—7580
baffle attenuation meas. in visible 2—5429
contact reflectometer and collimator photometer, inspection of large optical components 2—38082
flats and mirrors, interferometers for quality control 2—34518
i.r. spectrometers and spectrophotometers, wave number calibration of moderate and low resolution instruments 2—38156
lens test facility 2—31115
narrow band transmission interference filters, stabilization of optical characteristics 2—38131
optical flats, inspected by holographic interferometry 2—38098
plane parallel plates for mine interferometer, by interference pattern shift 2—38064
spherometry of concave surfaces, autoreflection method for centre of curvature location 2—2449
surface profile rectilinearity, measurement with photoelectric instruments 2—38099
surface roughness measurement, holographic interferometry 2—31089
telescopic instruments, quality evaluation, information theory criterion 2—38092
thermal i.r. imaging devices 2—27622
Yu 16 luxmeter, sensitivity and sources of error 2—21163

Optical instruments
Some instruments are listed separately, e.g. Refractometers
achromatic linear retarder, large angular aperture with thickened elements 2—27614
angular microdisplacement mechanism with a lamellar elastic element 2—23702
aspherical surfaces, uses 2—34520
aspherometer built from a GS-5 goniometer 2—27621
autocollimation focometer for measuring long focal lengths 2—5440
autocorrelator, application to MTF meas. 2—34512
automatic diopteremeter, improved accuracy 2—21164
automatic laser tracking and ranging system 2—23662
beam splitter, Jones's matrix representation 2—2444
beams couplers, unified theory of prism and grating types in pickup and launch modes 2—34475
two beams of different wavelength from single monochromator 2—2446
binoculars, information theory criteria for quality 2—38092
biplate compensator, optically active, alignment 2—2445
catadioptric imaging systems, meniscus aberration correctors, book 2—27626
for circular polarization of luminescence emitted by chiral molecules det. 2—31101
coatings, dye lacquered and constituents, reflectance in 210 to 2600 n.m. range 2—23707
coded gratings for narrow line width moire fringes 2—34487
colorimeter, tristimulus mask, double mirror grating dispersion system 2—5450
for control of radial intensity distribution of a light beam 2—23711
cooled photodetector with wheel type modulator, analysis at internal noise 2—37806
corneal topography measurement with autocollimating photokeratoscope 2—17128
correlator, multichannel, using two spatial dimensions 2—2443
design and aberrations, tutorial 2—38039
design and aberrations 2—21142
design with automatic computers 2—11519
dichrometer for near i.r. meas. 2—11538
differential interferometer, phase variations of transparent object using ground glass 2—31090
digital light deflector with prisms and polarization switch based on Pockels effect 2—11520
direct vision triple reflection prism, with ray path splitting 2—38096
distance measuring, two-laser, which corrects for atmospheric index of refraction 2—31105
durability under tropical conditions, microscope and photographic equipment 2—38093
durable nonabsorbing mirrors, produced by precipitation of oxides, for u.v. Fabry-Perot interferometers 2—38062
electro-optical light modulator, with birefringent beam splitter/ recombiner, patent 2—11521
electrooptic modulators, traveling wave, single and double pass, transient phase retardation 2—5397
embossed optical waveguides production 2—34524
endoscope, Hopkins, with air lenses and glass spacers, advantages 2—23153
fibre optic endoscope, flexible, diagnostic procedures and uses 2—26958
fibre optic information convertors 2—27630
flowmeter for local flow velocity, simulator for adjusting 2—28752
graded-index (GRIN) rods used as image relays, aberrations and design 2—5431
heterodyne spectroscopy, optical, local oscill. light mixing device 2—23729
holographic waveguide couplers for integrated optical circuits 2—34421
image recording with post recording bandpass selection 2—23712
imaging system, multispectral, using open Fresnel zone plate 2—318
i.r. absorption cells, optical behaviour 2—11534
laryngoscopic fibrescope, obs. of articulatory movements in speech 2—5072
laser telemeters, meas. accuracy with statistical properties of propagation, detection and meas. process 2—2442
lens sunshade, optical design, computation of residual light 2—38095
light beam oscillograph recordings, static error 2—21165
light source shutter, with magnetic control of transmission 2—38088
logarithmic detector for pulsed dye laser intensity variation obs. 2—23703

Optical instruments continued
micro densitometer, linear, demonstration of coherence effects 2—38179
microdensitometer, conditions for linearity 2—14458
microscopic systems, non-Airy pupil fns., influence of partially coherent illumination 2—27613
multispectral scanners, scan-angle effects 2—34526
near confocal optical scan amplifier based on split confocal resonator 2—34527
one dimensional phased array antenna, beam steering using electrooptical properties of $LiTaO_3$ 2—27365
optical distance measuring instruments, using electrooptical polarization modulators 2—30747
optimal design of lathes for making components by controlled shaping 2—34519
optoelectric sensor, diameter measurement of glass fibres during drawing 2—38097
OSCAR, optical surface contamination analysis reflectometer, vacuum u.v. 2—18929
particle size analyzer using gas laser, calc. from intensity variations in diffraction pattern 2—21158
phase shifts in balanced mixer system 2—17687
photo-optical instrumentation, symposium, Anaheim (1970) 2—21166
photodetectors, Schottky barrier diodes in hot-electron mode, model 2—5433
photoelectric localization of lines, optimal conditions determination 2—38087
polarization, vector methods 2—2435
polarization independent waveguide with coincident transverse electric and magnetic modes 2—34523
probe for powder mixture comp. meas. 2—19275
pulse light fluorometer, oceanographic measurements, for in situ and dredging use 2—30248
pulsed laser sensitometer using photographic plates and multiple imaging techniques 2—27615
rangefinder, phase detection and modulation error sources with microwave electro-optical modulator 2—31112
rangefinders, PMT's iwth external modulating electrodes 2—31111
rangefinders design, military 2—21159
recorder for simultaneous light pulses using fibre optic light guide 2—34532
reflectometer readings and absolute reflectances 2—8009
reflectometer/quart crystal microbalance combination for contamination meas. 2—41413
scales, grids and photomasks, development of manufacturing techniques 2—27623
scan and measure devices, systematic errors in optics 2—34516
scanning, fast retrace system using moving iron galvanometer 2—317
scanning spectrometers, use of rotating optical wedges 2—38157
scanning using pair of moving wedges 2—31113
screen, diffusing, with small angle light scatt. 2—320
sensor, contactless, for size distribution of drops in burning zone obs. 2—5434
shadowgraphs for spectral functional analysis by the methods of coherent optics 2—27645
signal processor with multiple orthogonal channels 2—27631
SIN interferometer bench, examination of holograms of stationary objects 2—38023
solarisation of glass transmitting u.v. light 2—11525
Soleil compensator, employing half shade plate, error in balancing 2—38091
spectroradiometer system, automatic recording, for spectral irradiance, transmittance, reflection or colour meas. 2—5430
spherometry of concave surfaces, autoreflection method for centre of curvature location 2—2449
sputtered glass waveguides, properties meas. 2—38115
teflon coated polishers for precision optical flats 2—31107
third order autocorrelator with diffused light source 2—31109
used in turbulent atmosphere, MTF determination 2—40966
TV laser microscope, magnification of 30 to 3000 on videocontroller 2—27616
Verdet constant of transparent materials 2—27617
vibrational amplitude measurement on diffuse surface, modulation of projected fringes 2—21160
visibility meter, portable version, disability glare factor 2—41334
waveguides, thin film, combining switching, coupling, modulation and guiding 2—38116
wedges with variable refracting angle 2—27577
window-heat sink sandwich for optical experiments using diamond (or sapphire)-semiconductor-In sandwich 2—20769
GaAs, proton implanted, waveguides 2—38100
HF i.r. absorption cell, construction, gas handling apparatus 2—37934
Si i.r. waveguides, doping, refractive index and losses relationship 2—38112

Optical materials
see also Filters, optical
absorbing spheroids, electrooptic properties 2—9186
antireflection coatings, laser induced damage 2—27632
apodizers, performance in partially coherent light 2—8025
coatings, dye lacquered and constituents, reflectance in 210 to 2600 n.m. range 2—23707
coloured glasses, heat resistant, low coefficient of expansion, light filters 2—38130
contamination, meas. using quartz crystal microbalance combined with reflectometer 2—41413
Corning crown glass, thermal expansion measurements from 30 to 250°C 2—36353
damage in laser materials, cont., Boulder, USA, May (1971) 2—23562
data need for newer optical materials 2—34509
dielectric coatings, effect of heat treatment 2—39485
diffusing, optical depth measurement 2—2434
discharge lamps, coolant liquid spectral characteristics 2—14469
F'-C' dispersions, mean reference index and wavelength 2—27588
glass, borosilicate, det. of acoustic wave velocity in, using vibration transducer 2—25672
glass, damage by Q-switched laser beam 2—33213
glass, electrostrictive laser beam focusing and small scale track formation 2—29862
glass, laser damage, thermoluminesc. obs. 2—1240
glass, low-loss, attenuation meas., using twin- beam spectrophotometer 2—8036

Optical materials continued
glass, optical, polishing mechanism, effect of surface layer hardness on rate 2—6305
glasses, commercial as selective transparent thermal insulation for solar devices 2—23705
holography, diffractive efficiency 2—2409
Kerr effect at 5 MHz in different optical glasses 2—23699
laser damage, probability and dynamics 2—29863
laser glass, BSC-2, direct nondestructive measurement of self focusing 2—26099
laser glass, Pt contamination due to melting in Pt crucibles 2—18895
laser glass, surface damage threshold studies using holography 2—27505
laser glass damage investigation, plasma formation and fracture 2—26098
laser materials, heat diffusion near absorbing centres 2—23608
laser materials, metallic and dielectric inclusions 2—23607
luminescence, electron-induced, meas. 2—33325
mechanical strength, variations due to external factors 2—39972
melinex, reflection and absorption coeff. at 338μ 2—19964
Mie scattering by spherical particles in low-loss glass for optical waveguides 2—7988
opt-electronic, single crystal, acousto-optic figure of merit estimation 2—4440
optical and coloured glasses, laser damage 2—27513
organosilicon films as light guides for integrated optics 2—38113
photochromic glass containing iodine, techniques for founding 2—5439
photoelastic polymers, method for making in cubic compression conditions 2—17705
photoresist films, Kodak KPR, as light guide for integrated optical circuits 2—38114
polymethyl methacrylate, Crofon optical fibre, bends to radius of curvature of five times own diameter 2—17712
quartz, microscopically damaged, laser beam catastrophic damage threshold 2—29859
quartz glass, high temp. and u.h.f. dielec. props. 2—19746
refractometer testing 2—5441
research history of Eastman Kodak Co. 2—14461
ruby, cryst. growth and characterization 2—25262
ruby, for use in lasers, growth by modified Verneuil process 2—18973
ruby, laser damage tracks, time evolution, scattering and luminesc. obs. 2—29861
ruby laser rod, optical homogeneity mosaic struct. effect 2—40600
sapphire, laser damage tracks, time evolution scattering and luminesc. obs. 2—29861
self focusing theory, rel. to laser beam damage in solids 2—29868
semiconductor, smooth uniform epitaxial layer growth method 2—32343
surface deterioration by formation of intermetallic compounds 2—14460
surface laser damage threshold, thermally stimulated electron emission image technique 2—19797
tellurite-based glasses, effect of added oxides on optical properties and crystallizability 2—27619
transition metal coatings, extreme u.v. reflectance spectra, characterization in 500-2000 Å region 2—17719
transparent dielectric, plasma formation on laser irrad. below damage threshold 2—29860
Ag_3AsS_3, laser damage using mode locked Nd:YAG laser 2—29864
AgCl antireflection coating for Si in 2.5-50μm region, transmittance obs. 2—8012
$Ba_2NaNb_5O_{15}$, catastrophic surface damage during intracavity freq. doubling for Nd:YAG laser 2—29869
$CaCO_3$3, calcite, cryst. growth at low temps. and low press. 2—35935
CaF_2, BaF_2 polycrystalline, i.r. transmitting, thermal expansion measurements from 10 to 300K 2—36356
$CdCr_2S_4$, hot pressed polycryst., for magneto-optic applic. 2—19970
CdS i.r. transmitting, thermal expansion measurements from 10 to 300K 2—36356
CdS polycrystalline, thermal expansion measurements from 30 to 250°C 2—36353
$CdS_xSe_{(1-x)}$ crystals diffusion processes, application to integrated optical circuit component fabrication 2—38102
CdTe i.r. transmitting, thermal expansion measurements from 10 to 300K 2—36356
CsI antireflection coating for Si in 2.5-50μm region, transmittance obs. 2—8012
GaAs, laser-type, refr. index peak at absorpt. edge freq. 2—36879
$Ge_{33}Se_{55}As_{12}$, chalcogenide glass 20, thermal expansion measurements from 30 to 250°C 2—36353
$Ge_{33}Se_{55}As_{12}$ glass, i.r. transmitting, thermal expansion measurements from 10 to 300K 2—36356
KCl:Pb laser window, 10.6μ absorpt., impurity effects 2—16416
KD_2PO_4, laser induced self focusing 2—22628
$KNbO_3$, crystal, growth by modified Kyropoulos technique 2—18978
$LiIO_3$, laser damage using mode locked Nd:YAG laser 2—29864
$LiNbO_3$, iron doped, holographic storage applic. 2—21131
$LiNbO_3$, laser damage using mode locked Nd:YAG laser 2—29864
$LiNbO_3$, luminesc., ruby laser beam induced rel. to optical index damage 2—26238
$LiNbO_3$, optical damage gree, light modulator, crystal growth and modulator construction 2—34428
$LiNbO_3$, use as nonlinear optical material 2—34367
$NH_4H_2PO_4$, laser induced self focusing 2—22628
$Pb_5(GeO_4)(VO_4)_2$, cryst. growth and acoustooptical effects 2—36828
SiO_2 film, prod. by reactive evap. rel. to opt. characterization 2—8021
SiO_xN_y film, prod. by reactive evap. rel. to opt. characterization 2—8021
TeO_2, acousto-optical device applic., melt-growth 2—15692
TiO_2 film, prod. by reactive evap. rel. to opt. characterization 2—8021
TlBr, TlCl antireflection coating for Si in 2.5-50μm region, transmittance obs. 2—8012
YAG:Lu, Nd, ion site distrib. and spectral line broadening 2—36853
YAG:Nd^{3+}, mechanism of Nd solubilization by Gd or Lu 2—29092
Optical mode, crystals *see Crystals/lattice mechanics*
Optical model *see Nucleus/models*
Optical properties of substances
see also Optical constants; Optical materials
absorptivity of metals and alloys, calorimetric method for scanning obs. 2—4431
adsorbed layers at interfaces, methods for obs. 2—9299
alkali halide, dielectric breakdown, laser induced 2—13428
alloys, absorptivity, calorimetric method for scanning obs. 2—4431
amylose triiodide complex, pulsed electric dichroism measurements 2—27600

Optical properties of substances continued
anisotropic scattering, many-molecular correlation induced, in simple fluids 2—6231
atmospheric aerosols, extinction coeff. 2—37135
birefringence, quartz, direct measurement by det. of thickness of half-wave plate 2—7048
carbonaceous mesophase, changes in pleochroism, extinction of contours, microstruct. 2—18826
coloured powders, light scattering, additive rule for mixtures 2—7042
det. from transmission meas. 2—4420
diamond, discrete variational method calc. 2—1525
diatomic molecules, inclusion of nuclear motion in calcs. of properties 2—24435
dichroic sheet, thermal lensing and optical damage 2—5396
disordered solids as filters for far infrared 2—31127
gas, study of reversal temp. as function of optical thickness 2—15541
glass, damage due to laser pulses 2—7912
glass MS19, light diffusing, spectrophotometric characteristics 2—33189
gradient-index, sine-wave optical paths 2—296
graphite d.c. arc burning in mag. field, spectrochemical aspects 2—35638
immersion liquids for holograms recorded on photographic film 2—5392
internal reflectance at boundary surface, diffuse and specular reflectance 2—17682
ionic crystal slab with NaCl structure, electric field calculation 2—4037
isomeric liquids, dipole interaction and flow birefringence 2—6013
liquids, light scattering, obs. of mechanism of structural rearrangement 2—18824
liquids, organic, shock compressed, opacity, absorpt. spectra 2—35770
liquids and solns., light scattering, structural investigations 2—32264
metal, nonlocal theory, specular and diffuse electron scatt. 2—16413
metal films, review 2—19956
metals, absorptivity, calorimetric method for scanning obs. 2—4431
modified Kramers-Kronig analysis of spectra 2—1678
molecular crystals, substitutionally disordered, electronic states 2—9937
natural waters 2—13632
nematic liquid, flow, orientation pattern, linearized continuum mechanics 2—9084
nitrobenzene, optical filament from., laser intensity inhomogeneities 2—6234
nonlinear crystals, unit for monitoring 2—17671
organic liquids, transparent dielectrics, mechanism of optical breakdown 2—39365
plasma, dense non-ideal, review 2—21768
polydimethylsiloxane rubber, swollen temp. dependence of anisotropy 2—1652
refraction coefficients determination for mixtures of solids, microscopic phase analysis 2—4428
resonant cavities, filled with excited gases 2—260
ruby, heavily doped, review 2—36868
ruby laser rod, optical homogeneity mosaic struct. effect 2—40600
secondary and trace ingredients in mixtures of solids, microscopic identification 2—3604
semiconductors, effect of ion bombardment 2—25803
strongly absorbing solids, quantitative techniques in measuring and calculating i.r. props. 2—22721
surfaces, iridescent and specular, difference 2—1158
tellurite-based glasses, effect of added oxides 2—27619
thermal blooming in gases, wind transverse to beam propagation 2—27581
transparent luminescent materials, det. of MTF and energy conversion efficiency 2—36924
window glass, change in stress- optical coeff. during stabilization 2—29879
Ag-Au alloys, determ. by energy loss spectra of electrons from 2 to 40 eV 2—19958
Ag, determ. by energy loss spectra of electrons from 2 to 40 eV 2—19958
$AgGaS_2$, linear and nonlinear 2—9364
Al_2O_3 film, electron beam evap., effect of substrate potential 2—40310
Al_2O_3 powder, from spectral normal emittance determ. using heated metal substrates 2—40088
AsSeI, vitreous, prep. and obs. of thermal and optical props. 2—3456
Au, determ. by energy loss spectra of electrons from 2 to 40 eV 2—19958
$BaTiO_3$:Nb crystal, dielec. props., prep. and substitution effect 2—16287
$Bi_4Ge_3O_{12}$:Nd, Er, Czochralski synthesis and properties 2—32405
$CaSO_4$ and Ca and Na double salts, double refraction and polarization and relations to structure 2—4434
$Cd_xHg_{1-x}Te$, rel. to 10μ band detectors 2—39577
CdS, photomechanical effect, converse piezoelectric effect 2—19972
CdTe, energy band pseudopotential model from optical props. 2—19666
$CuCl_2.2H_2O$, transmittance at elevated temps., passband characteristics 2—31145
$CuGa(In)S_2$, linear and nonlinear 2—9364
H_2O vapour, intensity-half-width products in 6.3 μm absorption band 2—32179
Hg vapour, measurement apparatus for transition metal to insulator density range 2—9036
KCl, cryst., optical defect characts., monochromatic photographic obs. 2—32500
$KMnO_3$, cluster model applic. 2—18961
$LiAlSiO_4$, β-eucryptite, crystal growth 2—9365
$LiIO_3$, beat generation, far i.r. 2—26102
$NH_4H_2PO_4$ 45° x-cut, four crystal monochromator 2—21132
Na, thin films, transmission of polarized light at oblique incidence 2—7045
NaCl, acqueous solution, optical constants in i.r. 2—35766
NaF, stress-optical dispersion, measurement by intensity method 2—26107
Na_2SO_4 and Ca and Na double salts, double refraction and polarization and relations to structure 2—4434
$(Pb,La)(Zr,Ti)O_3$ ceramics quality improvement 2—40616
$Pb_{1-x}Mn_xTe$ solid soln., optical permittivity, refl. spectra obs. 2—22539
$PbTiO_3$, single domain ferroelectric, nonlinear props. 2—19953
Sb_2S_3, anisotropy effects on (010) axis, obs. using polarization microscopy 2—19965
Si film, polycryst., i.r. optical props. 2—22076

Optical pumping
^{87}Rb maser, calc. on power output taking account of variations in optical pumping rate and density matrix elements 2—2377
alkali metal, atomic orientation, effect on mol. form. 2—18324
atom, coherent resons. induced by oscillating elec. field 2—38821
atom, in oscill. r.f. field, g-factor modification 2—31690
atomic $^1S_0$ ground states, method of orienting nuclei, using optical pumping and exchange collisions 2—15203

Optical pumping continued
atoms, as test of dressed atom theory of atomic interactions with r.f. photons 2—24305
atoms, effect of driving field on absorption and emission line shape functions 2—24353
atoms, r.f. experiments rel. to dressed atom theory, review 2—24312
atoms and ions, ground-state and metastable, survey of pumping mechanisms, light propagation, relaxation, spin exchange 2—35149
bromocresol green and purple dye amplifier, by one- and two-photon processes 2—21083
diaryl butadiene solutions, optical generation excited by ruby laser 2—6238
dye lasers, flashlamp efficiency improvement using light convertor 2—11474
dye lasers, Q-switched pulse stretching applications 2—14399
dye lasers, u.v. pulsed discharge Xe lamps 2—28670
electron beam, two-dimensional scanning laser production 2—7936
by electron beams, GaAs and CdS lasers 2—17640
flash, Nd:$CaWO_4$ laser with two step Q-switching technique, high power in single longitudinal mode 2—31046
flashlamp pumped rhodamine 6G, transient gain measurements on laser dyes 2—11477
flashlamp-pumped laser dye amplifiers properties, optimization for practical use 2—31044
formalism and proof 2—5340
gas, kinetic theory 2—28732
gas laser, allowed electron transitions 2—21063
gas laser, causing birefringence in active elements 2—17583
gas molecules, nonlinear level crossing in the standing wave field 2—31744
glass: Mn-R, R=Nd, Ho, Er, energy transfer between sensitizer-activator 2—4493
interference coatings, wide band, high reflectivity for laser pumping systems 2—27531
laser, molecular gas, electron beam controlled discharge method 2—34392
laser two step photodissociation of molecules as method of selective breaking of bonds 2—31759
masers, use of ruby crystals as active material 2—27452
methane and acetonitrile, generation of i.r. radiation by Raman scattering and difference frequency mixing with a Nd:YAG pump 2—23603
molecules, phosphorescent triplet states, optically detected adiabatic inversion 2—21581
monochromatic, of pulsed dye laser, spectral properties 2—37971
nuclear polarization in solids, ^{19}F and ^{169}Tm polarized in $Tm^{2+}:CaF_2$ by circularly polarized light 2—40596
organic molecules, triplet states, optically detectable double resonance 2—12198
photon counter, 10μ, noise due to laser pumping 2—37940
population inversion establishment by photoionization of inner shell electrons 2—27454
tunable dye laser pumped by ruby laser, frequency mixing in proustite crystal 2—27488
u.v. lasers, electron beam pumping 2—34381
YAG active crystal elements, temp. gradient and thermoelastic stresses 2—17621
Ar, Xe, Kr vortex discharge as pumping source for c.w. Nd:YAG laser, comparative study 2—27448
Ar laser, continuous action in fluorescein dyes, triplet quenching 2—276
CO_2, laser media, at high pressure, by electron beam controlled elec. discharge 2—17593
$CaWO_4:Nd^{3+}$, birefringence dispersion, population inversion 2—20030
CdS_xSe_{1-x} platelet laser, electron beam and laser beam pumping 2—37983
p-GaAs laser, electron beam pumped, wavelength tuning effects 2—14431
GaAs laser, microwave modulation using modulated electron beam 2—27522
He-He* collisions, metastability-exchange cross section, 15-115K, temp. dependence, optical pumping expt. 2—31732
He discharge, cumulative ionization, source of polarized electrons 2—12049
He discharge, population of 2^3S_1 spin states manipulated, dependence of electron production rate 2—12050
^{3}He, conservation of Hertzian coherence 2—721
^{4}He, depolarization of metastable 2^3S_1 level by collisions with Ne 2—31727
Hg (A=183,185), isotope shift obs. rel. to nuclear charge distribution 2—27992
^{199}Hg spin relaxation rate dependence on magnetic field 2—630
K, atomic orientation, effect on mol. form. 2—18324
Kr c.w. arc pumping, Nd:YAG laser, characteristics at 20 kW 2—21088
Mn, by Cs vapour, polarization of ground state due to spin exchange collisions 2—2932
N_2 laser, electron beam excited 2—23600
N_2 pumped dye laser, oscillator- amplifier system 2—11475
Nd:glass laser, effects of u.v. on performance characteristics, need to eliminate wavelengths corresponding to inactive absorption region 2—27501
Nd:YAG laser, solar pumping 2—21090
Nd^{3+}:YAG pulsed laser, influence of lamp filling 2—27500
Ne, of J=-J=1 transition by laser line, nonlinear effects 2—24358
^{21}Ne, excited levels orientation 2—18331
Rb_2, molecular vapour, dissociation mechanism 2—24485
^{85}Rb, D_2 optical pumping, nuclear decoupling in collisional relaxation 2—35172
^{87}Rb, D_2 optical pumping, nuclear decoupling in collisional relaxation 2—35172
Xe liquid, by electron beam, stimulated emission, vacuum u.v. region 2—28865

Optical quantum generators *see Lasers*

Optical rotation
see also Magneto-optical effects; Optical constants; Polarimeters; Polarization/light
arabinose, aqueous soln., γ-irrad., usefulness for dosimetry 2—5596
circular anisotropy, meas. using chromatic phase plates 2—23697
ferroelectric, influence on Mandelstam-Brillouin scatt. 2—26199
ferromagnet, magnetized, γ-quanta linear polarization, plane rot. 2—36819
fructose, aqueous soln., γ-irrad., usefulness for dosimetry 2—5596
glass, intensity-induced changes in ellipse rot. 2—16418
glucose, aqueous soln., γ-irrad., usefulness for dosimetry 2—5596
induced circular dichroism in cholesteric liquid crystals 2—28856
Kirkwood theory of natural optical activity 2—8508
liquid crystals, compensated cholesteric, optical rotatory dispersion meas. rel. to temp. and wavelength dependence of birefringence 2—28857

Optical rotation continued
magneto-optical rotation, computer program for dispersion curves distrib. 2—28253
material activity, phenomenological theory 2—7044
method for accurate small measurements 2—7995
molecules, optical activity, relation between static and dynamic perturbations 2—8518
nematic liquid crystal/chiralic compounds system, rotatory power. circular dichroism 2—18827
α-olefin isotactic copolymers, temp. coeff. of optical activity, rel. to conformational equilibria 2—35364
oriented molecule, ellipticity and rotatory strength of electronic transition 2—31761
alkyl orthozirconates, magneto-optical rotation determ. 2—6940
piezoelectric, influence on Mandelstam-Brillouin scatt. 2—26199
polymers, infinite single-stranded helical, theory 2—8841
α-quartz, impurities influence 2—10305
rotatory strength, upper and lower bounds for perturbed anisotropic harmonic oscillator one-electron model 2—31735
second and third order, rel. to biphotonic absorption and second harmonic generation 2—23698
second- and third-order, nonlinear response to laser light 2—21156
sucrose, aqueous soln., γ-irrad., usefulness for dosimetry 2—5596
symmetric molecule, optical activity in weak asymmetric field, adiabatic approx. 2—12064
uranyl butyrate optical activity studied 2—16421
Verdet constant of transparent materials, technique and instrument 2—27617
$ZnSeO_4.6H_2O:Cu^{2+}$, Co^{2+}, and $NiSeO_4.6H_2O$ 2—19966
$Bi_{12}GeO_{20}$, influence on light scatt. by phonons 2—16454
$NaBrO_3$, SHG 2—19952
$NaClO_3$, SHG 2—19952
$NaNO_2$, ferroelec., temp. depend. 2—19951
$5PbO3GeO_2$, switching of optical rotatory power 2—40615
TeO_2, rotatory power 2—1658
ZnO, Pockels effect 2—7051
$ZnSeO_4.6H_2O$: Cu^{2+}, Ni^{2+}, Co^{2+}, and $NiSeO_4.6H_2O$ 2—16420

Optical systems
see also Aberrations, optical; Lenses; Optical images; Optical instruments; Optical materials; Resolving power, optics
aberration correction, for spatial filtering 2—34451
acoustical-optical sonagraph, synthesis 2—38103
airborne photoreconnaissance image transmission system, end to end computer simulation 2—34521
aspheric surfaces, fabrication techniques 2—27586
aspherical elements testing, binary synthetic holograms by single sideband transmission 2—34442
aspherical surfaces, aberration theory and size/weight considerations 2—34517
asymmetric design using bicubic splines as interpolation formula 2—2423
attenuator, rotating step, wavelength independent, generating four radiance steps 2—27583
autocollimation focometer for measuring long focal lengths 2—5440
automatic dioptermeter, improved accuracy 2—21164
automatic lens design programs, convergence efficiencies of model functions 2—31081
catadioptric imaging systems, meniscus corrected for aberrations 2—27626
Cer-Vit mirror, lightweight, centre-mounted, for Lunar laser ranging pulses 2—21140
circle of confusion, graphical analysis of energy distribution 2—38043
circular aperture, far field diffraction pattern, partial coherent illumination, in presence of linear motion 2—38067
coherent data processing system for counting and identifying blood cells 2—37437
coherent processors, applic. to underwater acoustic signals 2—34530
coherent transfer function, for coherent imaging systems 2—14443
communication and detection receivers, error performance bounds 2—34511
concentric, aberration properties 2—27569
condensing, flat field 2—31114
contamination, meas. using quartz crystal microbalance combined with reflectometer 2—41413
contrasting, projection and photography of microscopic objects 2—31116
defocused, effects of amplitude filler on partially space coherent diffraction 2—11515
design, transfer function as an aid to design of optical systems, book 2—2452
design and aberrations 2—21142
design for space applications, rel. to meas. of refractive indices of fused SiO_2 at low temps. 2—26109
diffraction limited, imaging characteristics det. using Cooley-Tukey algorithm 2—17692
digital electrooptic light beam deflection technique for spectral wavelength modulation 2—31077
discrete transfer functions 2—38046
displays, nematic-liquid-crystal, two-frequency coincidence addressing scheme 2—8016
double beam interferometer, degradation eliminated using Moire method 2—21147
fibre, recent developments 2—38106
first order imagery, astigmatism and image rotation 2—23681
fly's eye lenses, with spherical lenslets, modulation transfer functions 2—38042
Fourier imaging systems, operating in white light, properties 2—300
guidance systems, u.v. optical designs, images of sky 2—10781
image position sensor for high resolution optical tracking 2—31106
image treatment, computer simulation 2—27585
imaginary-case optical-design modules 2—31079
imaging, for Martian Viking Mission 2—30567
imaging, for Viking Orbiter Expedition to Mars 2—33739
imaging, multispectral, using open Fresnel zone plate 2—318
imperfect, with annular aperture and amplitude filter, Fraunhofer diffraction under partially space coherent light 2—2430
integrated optics, light waves in thin films 2—2441
integrated optics, thin organosilicon films produced by r.f. discharge polymerization 2—27627
interferometric testing 2—34455
laser beam optics, filament form., self focusing, from beam focus on medium surface 2—11501

Optical systems continued
laser designated target tracker system with photoelectric detector 2—319
laser mirror mount, kinematic, allowing precise angular orientation 2—34410
light beam scanning, holographic techniques 2—5399
light guides, solution deposited thin films, doped with laser dyes for high optical gain 2—21167
light valve devices, photoactivated, photoconductive film/liquid crystal systems 2—21173
light valve display system, applic. of photoelectronic props. of CdS 2—22650
liquid crystals light valve arrays, matrix-addressed, turn-on time reduction and contrast enhancement 2—8015
liquid evaporation light deflector, electrically controlled varorization 2—27611
memories, acoustooptical arrays, deflection system for use with multi laser 2—1665
metal-dielectric multilayer application as optical element, book 2—2453
method of synthetic optical apertures 2—38059
modulation at high information rates of 1Gb/s 2—17664
modulation transfer functions of lenses, probable error in computation 2—38041
monitor for simultaneous obs. of angular and translational alignment 2—31108
multipass optical cell, 3rd order aberrations 2—31110
noncontacting sensor for ultrasonic surface waves 2—34528
obstructed apertures, near field diffraction pattern 2—38069
oceanographic research, methods of observing turbulence in seawater 2—13663
oscilloscope cathode ray tubes with fibre optic faceplate 2—34324
for particle size density distrib., f(x), determ., eqns. relating radii F(R) to f(x) 2—38086
planar scanning of band shape of interference field, systematic measurement errors 2—38058
polarization transfer function, ellipsometric measurement 2—23695
polarization transfer function as a bilinear transformation 2—14454
projection type measuring devices, sensitivity of lateral and longitudinal focusing adjustments 2—38090
pupil-scan aberration analyser and spot diagram measurement system 2—27574
quasioptimal filters, accuracy of signal timing in optical communication systems 2—34538
receiver, laser, electronically scanned, performance obs. 2—34525
response to polarization-modulated incident light 2—17678
ring-shaped aperture, averaging effect on amplitude fluctuations 2—31082
Ronchi grids, transmission of incoherent light between 2—34465
rotation-symmetrical centred, optical transfer function calc. using Diffieux integral 2—17709
scanning of a wave field by an optical system of arbitrary aperture as method for recording holograms 2—14436
scattering pattern recorder 2—21162
sensor, contactless, for size distribution of drops in burning zone obs. 2—5434
signal processing, Fresnel images of ultrasonic light modulators 2—34510
solar concentrator with stationary plane mirrors 2—23674
solar concentrator-receiver with equalized heat load 2—23673
spherically aberrated, far field diffraction 2—27597
super multifibre lightguides, structural and output image qulaity 2—38108
superachromatic glass triples and colour correction, tables 2—23682
synthetic apertures, assessment of alignment tolerances 2—38104
for thermographs, quantitative medical 2—2448
thick lens theory, use of matrices for simple treatment at sixth form level 2—38040
with time varying pupils, time averaged images 2—23710
transmittance of polarization attenuators, accuracies 2—27612
transmittance of systems with absorbing films, program for calc. 2—301
triple mirror reflection in a rectangular prims 2—7967
u.v. microscope, use of Vidicon-type TV camera tube for remote observation 2—38094
vacuum u.v. plane polarized monochromatic collimated beam production 2—17702
waveguides, self-focusing pulse channel resulting from striction nonlinearity 2—17715
X-horizon scanner for det. of attitude of spacecraft 2—37234
CaF_2 crystal components, grown from melt 2—39587

Optical waveguides *see Electromagnetic wave propagation/guided waves*

Optics
see also Aberrations, optical; Atmospheric optics; Lenses; Mirrors, etc.; Optical images; Quantum optics
annular aperture resolution in partially coherent light 2—7977
conference Optical Society of America (April 1971) 2—34426
design and aberration, tutorial 2—23212
divergent beam in turbulent medium, displacement 2—2424
fourier transformation of area-modulated spatial functions 2—2057
higher order moments or inverse or linear stochastic operator 2—11516
image depth and illumination, tutorial 2—17167
image illumination and depth, tutorial 2—17166
integrated, light waves in thin films 2—2441
integrated, organosilicon films as light guides for 2—38113
integrated, review 2—34540
integrated guided waves materials and devices, conference, Las Vegas (1972) 2—34368
Kodak research laboratories 2—11502
Kodak Research Laboratory history 2—14439
lateral localisation of periodic object by partially coherent light 2—17691
matrix formulation for propagation and reflection in stratified anisotropic media 2—34463
matrix multiplication by optical analogue methods 2—23663
processing of radar signals using Fresnel diffraction masks 2—7962
radiation patterns of Gaussian beams truncated by rectangular aperture 2—5410
rapid processes, new optical methods 2—23223
reversible semi symmetric systems, types I and II reversibility 2—31076
reversible semi symmetric systems, types I and II reversibility 2—31076
secondary standards, visible and γ-ray wavelength coupling 2—37553
surface wave guidance by periodic layers, effects of substrate curvature, and optical mode trapping 2—34473
surface waves, guidance, lateral wave phenomenon and image transmission 2—34471
ultrashort pulse propagation, local field effects in theory 2—34427

Optics continued
wave theoretical approach to 'scattering-absorption' in image formation from phase objects 2—23684

geometrical
anisotropic media, resonant modes 2—14440
aspheric surfaces, fabrication techniques 2—27586
cascade apertures, focusing capabilities 2—31096
circle of confusion, graphical analysis of energy distribution 2—38043
coma, optical design and aberrations 2—23676
complex potentials method for solution of problems 2—17276
contrasting, projection and photography of microscopic objects 2—31116
depth with rear converter lens or afocal attachment 2—11510
design and aberrations, field curvature and distortion, tutorial 2—27572
design modules, coupling problems 2—34443
electron emission microscope, axial chromatic aberration correction 2—17561
electron optical systems, correction of geometrical aberrations by octupoles 2—23533
first order imagery by a general optical system 2—23681
five-electrode e.s. immersion objective 2—27427
grating, spherical concave, stigmatic conditions, geometric optical theory 2—14444
Herzberger's fundamental optical invariant and image formation by lenses 2—11508
imaginary-case optical-design modules 2—31079
lens antennas, amplitude and phase transformation 2—20997
lens design program, Grey merit function 2—34444
lens testing and design, aberrations analysis, book 2—2421
matrix treatment of aberration theory 2—34446
Maxwell equations, based on Fermats principle and orthotomic system 2—34430
microscope objective, effect on images in quantitative microscopy 2—5406
modulation transfer functions of lenses, probable error in computation 2—38041
nonlinear, transition lines and singularities in the equations for nonlinear geometrical optics 2—31080
nonstationary surface roughness measurement by light scattering 2—17681
optical design and aberrations, astigmatism 2—27015
reflection of laser beam from arbitrary geometric surface, calc. of surface from response 2—21141
ring-shaped aperture, averaging effect on amplitude fluctuations 2—31082
thermal blooming in gases, wind transverse to beam propagation 2—27581
thermal blooming of laser beams in fluids 2—21108
thin film light guides and applications 2—5400
time dependent eqns. of motion of wave packets 2—23668
wave-optics computer model, comparison with nonlinear laser-propagation experiments 2—14432
weak phase-amplitude object, reconstruction 2—31084

nonlinear *see Nonlinear optics*

Orbital calculation methods
see also LCAO calculations
ab initio calcs. of nuclear spin spin coupling consts. in diatomic molecules 2—8502
ab initio CI theory, excited electronic states, application to ehtylene, formaldehyde, diimide and pyrazine 2—12086
ab initio method, application to electronic structure and geometry of oxygen containing molecules 2—28255
ab initio SCF MO calcs. of configuration and dissoc. energy of $(NO)_2$ 2—35268
ab initio SCF-MO calcs., test using core binding energy shift determ. 2—35341
ab initio SCF-MO calcs. of electronic structure of $Ni(CO)_4$ and $Cr(CO)_6$ 2—21634
all-valence-electron method for calc. X-ray emission energies and intensities of S and Cl inorganic anions 2—28267
atom, multiconfiguration approx. for ns^2 shells 2—18284
atomic configuration $1s^22s^22p^n3p$, non-orthogonal radial orbital appl. 2—28180
atoms, and ions, valence orbital ionization potential, general evaluation formulas for $K(2)L(8)3s^23p^63d^\alpha4s^\beta4p^\gamma$ or $1s^22s^m2p^n$ configurations 2—11964
barbituric acid and its 2-thio derivative, comparison between radicals formed by radiation 2—21662
4H-benzo[def]carbazole, absorption and emission spectra, comparison with MO calculations 2—24508
benzyl radical configuration calc. by π-SCF-MO and MINDO/1SCF-MO methods 2—38963
Bethe Goldstone equation, solution for transbutadiene molecule 2—35205
bond exciton model of alkenes and diene polymers 2—15348
butene, cis and trans, and their ions, ab initio MO calcs. 2—24520
CNDO, calc of K electron binding energy shifts in fluorinated methanes and benzenes 2—8771
CNDO, direct comparison with extended Huckel calculations of charge distributions for adenine 2—38957
CNDO and INDO appl. to electronic structure of formic acid in various conformations 2—24537
CNDO and INDO calcs. on isotopic ethyl fluorides 2—24535
CNDO calc. of potential energy for internal rotation of two rings in 5,5'-bisisoxazole 18493 2—18493
CNDO calc. of pseudorotational potential energy of five-membered rings 2—8546
CNDO method applic. to band struct. of solids 2—19494
CNDO method used to calc. force constants and equilibrium distances of diatomic molecules 2—771
CNDO potential model using intermediate-level MO wavefunctions for core-level binding energy shifts 2—35133
CNDO-CI studies of effects of multiple substitution on electronic spectrum of p-benzoquinone 2—12210
CNDO-CI wavefunctions for $n\pi^*$ states 2—8548
CNDO/2 approx. appl. to halogenated cyclophosphazenes 2—24481
CNDO/2 approx. molecular orbital method used in calc. of reaction pathway for photodissociation of acetone 2—31835
CNDO/2 calc. of quadrupole moments of molecules, including 2nd row elements 2—21576
CNDO/2 calc. on radical formed by electron irradiation of mesitylene 2—5980
CNDO/2 calcs. of intensity curves for SK_β spectra in SO_4^{2-} and SO_3^{2-} 2—35287

Orbital calculation methods continued
CNDO/2 calcs. used for assigning photoelectron spectra of halosilanes 2—24433
CNDO/2 calculation of graphitic BN chemisorption of H and O atoms 2—7177
CNDO/2 method, failure to predict barriers and conformations in some conjugated systems 2—3099
CNDO/2 method appl. to pyramidal inversion barriers calc. 2—24427
CNDO/2 SCF MO calcs. of charge distrib. in aromatic hydrocarbons and perfluoro analogues, comparison with exptl. ESCA results 2—31860
CNDO/2 study of 'Kekule' vibration assignment in benzene 2—21666
CNDO/S wavefunctions, use in perturbation treatment of spin-orbit coupling in formaldehyde and azulene 2—12091
configuration interaction calcs. on pi electron states of butadiene 2—8746
conjugated molecules, Wannier functions in π-electron problem in long polyenes 2—18477
core-level binding energy shifts calcs. 2—35195
coupled pair many electron theory extended 2—12105
cyclobuta[b]quinoxalines, Pariser Parr Pople calculation of electronic transition energy and oscillator strength values 2—12229
delta function model of one-electron diatoms, energy, branch-point singularities 2—15272
density localization of orbitals 2—35124
deoxycytidine-3'-monophosphate, semi-empirical MO calculations for isomeric structures 2—12235
distinguishable electron method appl. to three- and four-electron atoms 2—15199
eigenfunctions by projection operator technique 2—15184
electron correlation energy calc. method for closed shell atoms and molecules 2—35109
electron operator matrix elements, complex configuration, non-orthogonal radial orbitals 2—28179
energy-localized orbitals, local positive charge distribution definition 2—3086
ethane, ionization, ab initio MO studies of ground state support $^2A_{1g}$ assignment 2—21683
extended Huckel theory studies of ethylenediamine conformations 2—28375
formaldehyde protonation, electrostatic molecular potential study 2—18505
G1 effective potentials, ab initio, use for calc. of molec. excited states 2—28306
Gaussian basis sets for long range forces 2—35170
Gaussian orbitals in second- order correction calc. to interaction energy of two H atoms 2—21543
Gaussian type orbitals, field and field gradient integrals, computer programs 2—35206
general cluster expansion and general correlated functions method 2—15186
generalized valence bond wavefunctions for low lying states of methylene 2—21694
Goddard $O_{//}$ operator, alternative derivation 2—24300
group-theoretical det. of electronic states of polyatomic molecules and complexes in MO and HL schemes 2—15276
Hartree Fock atomic valence orbital effective principal quantum numbers from radial moments 2—15197
Hartree-Fock-Roothaan molecular orbital calc. of charge distribution of CS_2 2—21598
heavy ion-atom inelastic collisions, orbital energy- internuclear separation correlation diagrams determ. 2—28214
Heitler-London method for 2-electron problems, complete set of functions 2—15185
HFR operator, matrix elements, transformational properties 2—24423
Huckel approx., calc. of zero field splitting coeffs. of e.s.r. of lowest triplet state of polyacenes 2—12275
Huckel MO and SCF calcs. on 1,4- dimethylnaphthalenes, monomer and dimer cations 2—38976
Huckel molecular orbital calcs. of substit. benzenes, electronic structure, use as photographic developing agents 2—14494
hybrid Gaussian type orbital, test calc. with H atom 2—8486
hybrid orbitals used to describe molecular bonding 2—756
hydrogen-bonded molecular crystals, MO theory 2—22097
INDO, for 2-aminoacetophenone, calc. of free energy barrier to rotation of amino group around N-aryl bond 2—12206
INDO, hyperfine splittings for styrene radical anions 2—39008
INDO approx. SCF MO theory, nonplanarity of ketyls 2—8786
INDO calculation of inter-ring proton couplings 2—21583
INDO method, interproton spin-spin coupling in five-membered rings 2—28331
INDO SCF calcs. on e.s.r. spectra of carbomethoxycyanobenzyl radicals 2—31842
Karplus-Kolker approximate uncoupled Hartree-Fock perturbation theory 2—18269
LCAO MO SCF, approx. for Gaussian d-orbital exponents of second- row atoms 2—3020
LCAO wavefunctions of simple cubic lattice 2—19017
LCAO-MO-SCF ab initio calcs. of rotational barrier and electronic structure of monomethylphosphine 2—18515
LCAO-MO-SCF theory applied to closed- and open-ring structures of cyclopropanone 2—12228
LCGO MO SCF ab initio calc., C_3O_2 2—21591
LCOAO Ruedenberg expansion, ground and excited states 2—8545
localized orbitals construction, case of several partially filled bands, polyatomic systems 2—8540
many-electron systems, theory of separability 2—8417
matrix elements, spin free computation, simplificatons due to invariance group 2—8416
maximum overlap method, construction of hybrid orbitals, molecular polycentric systems 2—35201
MC SCF study of $X^1\Sigma^+$, $A^1\Sigma^+$, $^3\Sigma^+$ and $^{1,3}\Pi$ states of LiH 2—15314
MC-SCF theory, method of one-electron Hamiltonian 2—35106
methylenecyclopropane, INDO calculations on lowest energy singlet and triplet states, ring opening studied 2—8794
MIM (molecules in molecules) method applied to hydrocarbons 2—38987
MINDO/1 valence electron SCF MO method, ESCA chemical shifts of C and N 2—35209
MINDO/2 method study of radical configurations 2—827
minimal basis set radial orbitals improvement 2—28181
MO wavefunctions used to calculate diamagnetic susceptibilities of C_2H_2 and HCN molecules 2—35317

Orbital calculation methods continued
molecular, complexes and impurity molecules in crystals 2—3022
molecular conditionally convergent integrals, evaluation 2—28242
molecular orbitals, orthonormal basis set formulation, advantages 2—18388
molecular symmetry adapted linear combinations of atomic orbitals, computer generation 2—31756
molecules, efficacy of ab initio effective potentials as replacement for atomic core electrons 2—24421
multi-electron problem, permutation symmetry 2—11924
multiconfiguration SCF study of electron correlation effects in F_2 2—28289
multiconfiguration SCF wavefunctions, new computation techniques 2—15274
multiconfiguration self-consistent- field calcs. for several states of B atom 2—28186
multiconfiguration wavefunctions, application of generalized Brillouin theorem 2—8424
multiplet theory for single configuration for symmetric wave functions 2—3014
natural orbitals of Lowdin, approximation using Green's function method 2—38873
NEMO calculation of $Cr(CO)_6$ and $Cr(CO)_5$ NH_3 to interpret electronic spectra 2—12124
NEMO wavefunctions, applic. to indirect nucl. spin-spin coupling consts. calc. 2—8573
non empirical SCF calcs. on ethylene-Ag^+ complex 2—8766
nonorthogonal LMO's application to study of distorted atoms in HeNe and ions in LiF and NaCl 2—21610
one centre and poly centre mol. wavefunctions in HFR formulation, comparison for CH_4 and HF 2—35204
optimized valence configurations method, potential curve of F_2 ground state 2—28289
overlap integral of two atomic electron configurations, non-orthogonal radial orbitals 2—28178
pentalenoheptalene, nonbenzenoid hydrocarbons, 16 pi-electron systems 2—3067
polyatomic molecules, ab initio calcs. with small ellipsoidal gaussian basis sets 2—8543
polyatomic molecules, Gaussian expansion of Slater-type atomic orbitals 2—21575
polyatomic systems, localized HF orbitals for open shell case 2—8556
polyatomic systems, localized orbitals, open shell extended Huckel approximation 2—8557
population analysis, approximate MO method 2—8539
quadrupolar expansion for r_{12}^{-1} 2—35107
Rayleigh-Schrodinger perturbation theory, perturbation parameter, change of variable 2—14108
SCCC-DODS calcs. of spin density distribs. in aquo complexes of first transition metal ion series 2—12097
SCCC-MO calc. on ions TCO_4^-, Reo_4^- and ReS_4^- 2—18474
SCF, applic. to open-shell states of CO, N_2, O_2 2—8591
SCF calc. of low energy reaction paths for $HeH^+ + H_2 = He + He_3^+$ 2—18436
SCF calcs. on X-ray spectra of Dy ion 2—35135
SCF LCAO MO, ab initio calc. on cyclooctatetraene and related systems 2—3078
SCF LCGO MO calc. of coupling consts. of H_2, H_2O, C_2H_4 and C_2H_3F 2—8620
SCF MO calculations on small clusters of water molecules with an extra electron 2—12153
SCF MO P(LCGO) on H_2O molecule 2—3045
SCF semi-empirical pi-electron and Huckel methods, pentalenoheptalene 2—3067
SCF virtual orbitals, perturbational treatment 2—21480
SCF-CI ab initio minimal basis calculations for small molecules 2—38875
SCF-CI spin-restricted calculations of contact hyperfine splittings 2—18389
SCF-MO-LCAO calculation of vibrational spectra of excited states of conjugated molecules 2—12083
Schrodinger eqn., radial, for electron bound in central field potential, asymptotic solution 2—2130
self consistent random phase approx., analysis, application to ground state correlations 2—5771
self-consistent MO methods, organic molecules, Gaussian-type basis sets 2—21648
self-optimized self-consistent-field procedure generalized for atoms 2—24334
semiempirical CNDO approximated LCAO MO theory, elements of HFR operator matrix 2—24422
semiempirical MO calc., one-centre quantities for first and second transition metal series 2—3019
semiempirical MO methods, electron density distrib. in substituted phenols 2—24549
separated electron pair model 2—35262
separated electron pair model 2—35234
Slater orbitals, Gaussian approximations 2—38776
Slater type functions, for molecules containing second row atoms 2—8544
Slater type orbitals, expansion for four-centre integrals 2—35108
from soft-X-ray region photoionization cross sections, model 2—35219
STO-3G basis set and extended 4-31 G basis methods 2—24425
symmetric top molecules, matrix elements of powers of P and Q operators for isotropic two dimensional oscillator 2—37619
Theta-function overlap approximation applied to energy of cyclic polyenes 2—15392
three centre nuclear attraction integrals with Slater type atomic orbitals, analytic evaluation 2—8541
transcorrelated method for accurate correlation energies using gaussian-type functions 2—35105
two-electron integral evaluation using gaussian expansions of orbital products 2—8542
UHFMCZDO matrix element formalism, simplified calc. for inorganic systems 2—8577
uncoupled Hartree-Fock perturbation theory, improved, appl. to second order atomic props. 2—5772
valence bond/configuration interaction determ. of potential curve of metastable He_2 2—31802
valence electron pairs, Hylleraas-type correlated pair functions 2—18281
valence electron wavefunctions of adenine, electron density and dipole moment analysis 2—35302

Orbital calculation methods continued
vinyl cyanide, electronic structure and spectrum, valence shell calculations 2—18534
α-substituted vinyl radicals, electronic structure determ. from e.s.r. spectra and INDO calcs. 2—8712
$[NiCl_6]^{4-}$ semiempirical MO calc. 2—18459
F_2^+, 13 lowest electronic states, calculated potential energy curves 2—8613
F_3NO, electronic structure and conformation, CNDO and INDO approxs. 2—15299
H, radial matrix elements of radial-angular factorized atom 2—5849
H_2^+ molecular orbital used to calculate wavefunction of H_2 2—21606
HCP and HCN, comparison of molecular structure and properties by CNDO/2 method 2—18426
HD, Fermi contact nuclear spin-spin coupling, molecular orbital sum-over-states method 2—8636
$(He\text{-}Ar)^+$ system, 'ab initio' calculations using LCAO-STO-MO-SCF approximation 2—669
He_2^+, molecular screening, variational energy calc. 2—8653
Li atom, ground state, double perturbation theory calc. of total and hyperfine interaction energies 2—11957
N_2^- radical, calc. of contact hyperfine interaction, comparison with e.p.r. spectra 2—21629
N_4^- radical, calc. of contact hyperfine interaction, comparison with e.p.r. spectra 2—21629
$NH_3+HF \rightarrow NH_4F$ system, studies using extended nickel and CNDO/2 methods 2—20178

Orbitals *see LCAO calculations*

Order-disorder changes
AB substitutional solns., CuZnβ type, 'surrounded atom' model 2—15929
alloy, binary and ternary, model calcs. 2—15978
alloy, binary equiatomic, band model 2—19308
alloy, kinetics, model, role of long-range diffusion 2—9831
binary alloy, lattice vibration effects 2—19309
dynamic critical phenomena time depend fluctuations above order-disorder T_c 2—19818
dynamical mechanism, soft modes and critical fluctuations 2—15952
ferroelectric, phonon approx. 2—22392
ferroelectric phase transition, critical polarization fluctuations 2—36590
heavy ice, HF-doped, effect of defect sites and contaminants 2—29486
oxides, high temp., characterization using i.r. and Raman spectroscopy 2—9829
scaling theory 2—6631
steel, Fe-Ni type, rel. to resist. change during maraging process 2—15915
ternary alloy, f.c.c. lattice, interatomic interact. influence 2—39993
tetragonal (Li_0) superlattice formation 2—22355
triangular lattice gas, maximum temp. of transition between disordered and ordered phases 2—30803
Ag-Zn cold-worked alloy, electron irrad. enhanced diffusion 2—9614
Al-V alloy, X-ray and neutron diffr. obs. 2—39994
α- alloy, resist. vs quenching temp. and isothermal annealing time 2—1346
$AuCu_3$, influence on low temp. sp. ht. 2—1431
Au_3Cu, resist. and thermoelec. study 2—15979
Au_4V, short range order kinetics 2—39995
$BaSO_4$, during crystn. 2—36292
$BaTiO_3$, Raman scatt., temp. depend., linear disorder obs. 2—26188
CeD_x, nonstoichiometric, neutron diffr. obs. 2—25387
Co-Pd alloy, elec. diffr. obs. on evap. single crystal films 2—32781
Cu-Ni-Mn alloy, elec., mag. and thermal obs. 2—15981
Cu-Pt alloys, discrete two-phase region existence 2—15980
Cu_3Au:Fe alloy, atom ordering, electron struct. elec. resist., mag. susceptibility 2—9921
Cu_3Au alloy, ordering kinetics during quenching 2—29426
β-CuZn, kinetics and role of vacancies 2—13005
p-D_2, phase transition, order-disorder transition 2—22362
Fe-Al alloy, disloc. and antiphase boundaries, elec. microscope obs. 2—25406
Fe-Al alloy, quenching by laser pulse heating, limitations 2—19310
Fe-Co-V alloy, long range ordering kinetics 2—29487
Fe-Co, ordered state formation, X-ray spectral investigation of electronic energy spectrum 2—36920
Fe-Co alloy, effect on Co diffusion 2—39741
Fe-Co alloy, kinetics and role of vacancies 2—13005
Fe-Co alloy, long range ordering kinetics 2—29487
Fe-Si alloy, rel. to magnetic order 2—6636
Ge, ion irrad., sputtered atom ejection pattern studies 2—22370
o-H_2, phase transition, order- disorder transition 2—22362
O-H_2, solid, cluster expansion 2—22371
o-H_2, solid, mean-field theory 2—29473
Mg-In, alloy, calorimetric and dilatometric study 2—4010
$Mg_{0.993}Fe_{2.007}O_4$, kinetics of cation ordering 2—15985
$MgO.Al_2O_3.xSiO_2$, high quartz phase, growth from glass, X-ray obs. 2—9477
NH_4Cl, disorder-order transition, Raman scattering study 2—22372
NH_4Cl, effect on u.s. vel. 2—29528
NH_4Cl, meas. of variation of length of crystal at high pressure near order-disorder transition line 2—9830
$NaNO_2$, ferroelec. transitions 2—9866
$NaNO_2$, rel. to elec. field gradient temp. depend. in ferroelec. phase 2—25929
Nb_6C_5, transmission electron microscope obs. on slow cooling 2—9483
Ni-Fe-Nb alloys, magnetic properties, electrical resistivity and hardness 2—4372
Ni-Mn alloy, elec., mag. and thermal obs. 2—15981
Ni-Mo alloy, initial ordering mechanism 2—39996
Ni-Mo alloys, ordering kinetics, X-ray and electron microscope obs. 2—36293
Ni base alloys, Ni_8X, X=combinations of V, Nb, Ta, electron diffr., elec. resist. obs. 2—13007
Ni_2Cr alloy, critical shear stress, dislocation movement 2—9662
Ni_3Fe alloy, critical transformation temp., biphase domain 2—12780
Ni_3Mn, alloy, annealed, ordering during loading 2—15971
Ni_3Mn alloy, electron irrad. induced disorder 2—22373
Ni_4Mo, antiparallel twins, FIM study 2—22216
Ni_4Mo, kinetics, model, role of long-range diffusion 2—9831
Ni_4Mo alloy, ordering process during isothermal annealing, field-ion microscope obs. 2—36294
Ni_8Ti alloy single crystal, flow stress obs. 2—25504
Ni_4W, peritectoid growth 2—13006

Order-disorder changes continued
PtFe-PdFe(PtNi) alloy, magnetic transformation temp., lattice parameters, magnetization, coercive force 2—1633
Si, amorphization, ion bombardment induced 2—1242
Ti-Al-Ga, ordered phase formation, elec. microscope obs. 2—9774
Ti-Co, ordered state formation, X-ray spectral investigation of electronic energy spectrum 2—36920
Ti-Mo, ordered state formation, X-ray spectral investigation of electronic energy spectrum 2—36921
U-Si-Be system near saturation comp. 2—13016
$(U,Na)_{2-x}Nb_2O_{7-y}$, cryst. struct., X-ray obs. 2—32782
V-H system, H ordering in β-V_2H 2—32783
V-Ru alloy, high pressure resistivity obs.-rel. to anomaly in electronic props. 2—36290
VAu_4, magnetiz. and susceptibility study 2—19886
V_6C_5, residual resist. obs. 2—4219
VO, non-stoichiometric vacancy order 2—4011
WO_3, amorphization, ion bombardment induced 2—1242
Zr-Co, ordered state formation, X-ray spectral investigation of electronic energy spectrum 2—36920

Ordered structure *see Crystals/structure; Solids/structure*

Organic compounds
see also Free radicals; Macromolecules; Plastics; Polymers; Waxes
1,2-dichloroethane, liquid, p.m.r. obs., rel. to mol. motion 2—35794
1,3-thiazan, synthetic derivatives, absorption spectra, displacement according to solvent polarity 2—3122
1-amino, 4-hydroxyanthraquinone, sensitized emission spectra 2—31836
1-methylaminoanthraquinone, sensitized emission spectra 2—31836
bis-(bromomethyl)-mercury, vibrational assignment of i.r. and Raman spectra rel. to structure determination 2—21669
bis-(chloromethyl)-mercury, vibrational assignment of i.r. and Raman spectra rel. to structure determination 2—21669
1,8-bis(dimethylamino)naphthalene radical anion, hyperfine coupling consts., steric hindrance 2—21667
bis-(iodomethyl)-mercury, vibrational assignment of i,r. and Raman spectra rel. to structure determination 2—21669
$(TCNCl)_2$-3,3(DTC), exchange interaction anisotropy 2—4345
tert- butyl alcohol in cyclohexane, u.r. relaxation and kinetics of association 2—6229
1,2-dichloroethane, vibrational assignments made from study of far i.r. and Raman spectra 2—8759
o--xylene, phosphorescence spectra, frozen matrices, liq. nitrogen temps. 2—4502
m--xylene, phosphorescence spectra, frozen matrices, liq. nitrogen temps. 2—4502
acenaphthene: acenaphthylene, identification of two impurity sites 2—36891
acenaphthene, Hg heavy atom impurity effect on luminescence 2—3125
acenaphthene-d_{10}, i.r. and Raman spectra, fundamental assignment 2—28341
acenaphthenequinone vapour, singlet-triplet absorption spectrum, 5600 to 4300 Å 2—28336
acepleiadylene mol. cryst., electronic struct. and transitions 2—28340
acetaldehyde, force consts. from normal-coordinate analysis 2—8724
acetamide, monomeric, i.r. spectra, low temp. matrix isolation studies 2—8722
acetamide-^{15}N, n.m.r. spectra, solvent and temperature effects 2—15346
acetanalide, CNDO computations of electronic structure 2—829
acetanilides, disubstituted, ortho-effects in mass spectra, removal of excitation probability for low lying energy states of ion 2—38954
acetic acid, ^{13}C n.m.r. relaxation, temperature dependence 2—38951
acetic acid, ^{13}C spin-lattice relax. under proton decoupling conditions 2—10257
acetic acid, hydrogen bonded cyclic dimer, near i.r. spectra, vibrational analysis 2—21652
acetic acid, quantitative liquid-phase spectra, absorptivity in 2.5-13μm region 2—32270
acetic acid as impurity-sensitive etchant for NaF 2—25433
acetic acid dimers, matrix isolated, i.r. spectrum, interpretation of OH stretching absorption 2—8721
acetic acid in CCl_4, mol. assoc. effects on INDOR 2—25110
acetic acid single crystals, deuteron NMR spectra meas. determ. quadrupole coupling const. and asymmetry factors 2—20155
acetic acid-trichloroethylene system, liq.-vapour isobaric equilib., data consistency 2—1144
acetic anhydride, vibrational spectra, normal coordinate analysis and conformation 2—28338
acetic anhydride-CS_2 binary liq. system, critical phenomena in coexistence curve 2—3357
acetic anhydride-cyclohexane binary liquid system, crit. behaviour in phase boundary 2—35736
o-aceto benozoic acid, crystal structure, X-ray crystallographic data 2—6456
acetone, ^{13}C n.m.r. relaxation, temperature dependence 2—38951
acetone, calculation of band shapes and absorption coeffs. for electronic transitions 2—15259
acetone, dielectrophoretic force under action of nonuniform electric field 2—15600
acetone, Fourier transform obs. of Brillouin and Rayleigh line widths and shapes 2—1103
acetone, influence on photoelectric properties of Se 2—28992
acetone, interaction with compounds containing —OH, C=O valence oscillation line shift 2—8787
acetone, oriented p.m.r. spectra, rel. to MO studies of $^4J_{hh}$ 2—28339
acetone, partially deuterated, phosphorescence lifetime meas. 2—28337
acetone, permittivity, Deybe dispersion, l.f. meas. 2—9151
acetone, quantitative liquid-phase spectra, absorptivity in 2.5-13μm region 2—32270
acetone, reaction in gas discharge, polymer deposits 2—4580
acetone, reaction pathway for photodissociation calc. using CNDO/2 approx. molecular orbital method 2—31835
acetone, shock compressed, opacity, absorpt., spectra 2—35770
acetone, valence force field, Raman spectra obs. 2—18479
acetone-^{18}O, isotope effect on nonradiative relaxation 2—35301
acetonitrile, $2\nu_8$ state, effects of accidentally strong resonance in rot. spectrum, mol. consts. level separation 2—12203
acetonitrile, dielectric relaxation times as function of temperature 2—3410
acetonitrile, doubling excited degenerate vibr. state, rot. spectrum, anharmonicity const., transition study 2—12202

Organic compounds continued
acetonitrile, generation of i.r. radiation by Raman scattering and difference frequency mixing with a Nd:YAG pump 2–23603
acetonitrile, in benzene and carbon tetrachloride solutions, dielec. relaxation between 24 and 60°C 2–3401
acetonitrile, vibr. correl. functions determ. from i.r. spectra and r.f. data 2–31752
acetonitrile liquid, comparative study of quasielastic neutron scattering and nmr relaxation 2–1073
acetonitrile N-oxide, force field, mean square amplitudes of vibration, shrinkage effect, Coriolis coupling coeffs. 2–38958
acetonitrile-CCl_4, dipole moments calculation 2–39376
acetonitrile-CS_2 binary liquid system, coexistence curve 2–32243
acetonitrile-d_3 and water, H bonded complexes, obs. i.r. transitions involving vibrations 2–8754
acetonitrile-water complexes, OH group stretching vibrations, i.r. spectrum 2–25092
acetonitrile-water mixture, near critical point, u.s. absorp. 2–28854
acetophenone, interaction with compounds containing –OH, C=O valence oscillation line shift 2–8787
acetophenone, partially deuterated, phosphorescence lifetime meas. 2–28337
acetophenone, phosphorescence spectra, dynamic properties and zero field splittings of lowest excited triplet states 2–28335
acetophenone, single crystal e.p.r. studies of photoexcited states 2–26360
acetophenone anion radicals, restricted internal rotation influence on e.s.r. spectra 2–828
acetophenone in variety of matrices, phosphorescence, pseudo-Jahn-Teller distortion 2–29966
9-acetyl anthracene, in benzene, dielectric relaxation times from microwave obs. meas. of loss and constant 2–28342
acetyl chloride, force consts. from normal-coordinate analysis 2–8724
acetyl fluoride, force consts. from normal-coordinate analysis 2–8724
acetyl methionine, γ-irradiated, correlation between e.p.r. and positron annihilation 2–40752
N-acetyl-2-thiohydantoine, i.r. spectra 2–5957
N-acetyl-phenylhydroxylamine and its methyl ether, n.m.r. study of hindered internal rotation 2–38955
acetylacetone, structure of enol and keto tautomers determ. by electron diffraction 2–24498
acetylene, acetylene-d_2, acetylene-acetylene-d_2, mixed crystals. Raman spectra, assignments and relative intensities 2–16575
acetylene, adsorption on clean Ni surfaces, field-emission studies 2–1196
acetylene, assignment of bands at 2.1 to 2.2μ 2–21654
acetylene, bond orders and elec. quadrupole moments from point-charge model 2–28372
acetylene, fluorescence, by vacuum u.v. photolysis 2–830
acetylene, in compressed gaseous mixture, i.r. rotational correlation functions of bending vibr. 2–15315
acetylene, reaction in gas discharge, polymer deposits 2–4580
acetylene, spectra in 5 μm region, determination of anharmonic and rotation-vibration coupling constants 2–12200
acetylene and d_1 and d_2 deuterated species, rotational structure of vibrational bands 2–21653
acetylene crystal, n.m.r., second moment obs., molecular motion 2–7147
acetylene in soln., Fermi reson. 2–18478
acetylene molecule, magnetic anisotropy deduced from diamagnetic susceptibility, calc. by MO wavefunctions 2–35317
acetylenes, linear, ^{13}C chem. shift 2–8723
acetylenic organotin compounds, π-electron molecular interactions 2–15347
acids, thermal conductivity meas. with thermal comparator 2–25073
acridan in benzene, dielectric relaxation times from microwave obs. meas. of loss and constant 2–28342
acridine, e.s.r. spectra in metastable triplet state 2–4547
acridine dyes, crystallites, recombination delayed fluorescence 2–13506
acridine orange, e.s.r. triplet exciton spectrum 2–21651
acridine orange, triplet quantum yield study with tunable dye laser 2–26355
acridine red, mixed with rhodamine 6G, for wavelength tuning of Q-switched Nd:glass laser 2–5374
acridine yellow in polymethacrylate, fluoresc., preexcitation effect 2–4499
acridizinium ethylhexanesulphonate photodimer, providing distrib. feedback for dye laser 2–17612
acrolein, cis and trans isomers, mag. rotation spectrum, band assignment, energy level diagram 2–12204
acrolein, magnetic rotation and absorption spectra cis and trans isomer transitions 2–3069
acrolein and singly substituted methyl derivatives, bond order reversal and substituent interaction in $S_1(n,\pi^*)$ 2–35337
acrylonitrile, dielectric relaxation times as function of temperature 2–3410
acyl-pyrroles, electric dipole moments in solution 2–39380
acylfuranes, preferred conformation in benzene solution, determination from elec. moments 2–38956
adamantane, excited electrnic states, sharp vibronic structure 2–12205
adamantane, investigation of Rydberg states 2–31845
adamantane isotropic molecules, application of new formula for large mean-square amplitude matrices 2–24426
adamantanes, and 1-substituted derivatives, band assignments in i.r. spectra 2–8725
adenine, charge distributions, comparison of extended Huckel and CNDO calculations 2–38957
adenine, electron density and dipole moment analysis of valence electron wavefunctions 2–35302
adenosine triphosphate, hydrated disodium salt, cryst. and mol. structure 2–3744
L-alanine:Cu crystals, u.v.-induced conversion in Cu^{2+} complexes, e.p.r. study 2–10642
l-alanine, i.r. spectra, vibrational assignment allowing for dichroic behaviour 2–40682
L-alanine, sp. ht., 1.3 to 4.3K 2–29558
alcohol, in inert soln., intermol. nuclear relax. and mol. pair distrib. 2–6251
alcohol, solid, X-ray spectra, O_2 K-emission obs. 2–16598
alcohol solutions, association constants, i.r. spectra 2–18829
alcohol-alkyl halides mixtures, dielectric behaviour. meas. in 50 Hz to 5 MHz range 2–9152
alcohol-water mixtures, permittivity, temp. coeff., continuous analysis applic. 2–9153
alcohols, hydrogen bonding with alkylammonium salts 2–3068

Organic compounds continued
alcohols, liq. binary mixtures, surface tension, meas. at 25°C 2–32248
alcohols, normal aliphatic, dissolved in CCl_4, complex dielectric constant and domains of concentration 2–39381
alcohols, steric effects on hydrogen bond, i.r. spectra obs. 2–8726
alcohols, struct. absorpt. of u.s. waves 2–32259
alcohols in benzene solution, dielectric relaxation and microwave absorption 2–3400
alcohols on Al, low-energy surface, adsorption of alkanes 2–22081
aldehyde-BF_3 complexes, vibrational spectra 2–24501
aldehydes, fund. and harmonic vibrs., Fermi reson. 2–24499
aldehydes, saturated aliphatic, modulation of $n\rightarrow\pi^*$ absorption band 2–21689
aliphatic ketones in cyclohexane soln., dielectric relaxation 2–25099
alkali chloranilates, hydrated, crystal data, X-ray diffr. 2–19062
alkaline hydrazine sulphate soln., impurity centres in photographic emulsion, light sensitivity 2–27673
n-alkane, opt. absorpt., 6.5-35 eV 2–18492
n-alkane adsorption on Graphon, heat of immersion, calorimetry 2–35909
n-alkane/benzene (hexafluorobenzene) mixture, gas-liq. crit. temp. 2–25150
alkanecarbodithoic acids, i.r. spectra, n.m.r., dipolar moment 2–24500
alkanes, adsorption on alcohol-modified Al 2–22081
alkanes, collisions with I^+ and I_2^+, cross sections for positive ion prod. 2–24578
n-alkanes, configurational behaviour, computer simulation, Monte Carlo method 2–8727
n-alkanes, short chain, intrinsic viscosity 2–6222
alkanethiols, dielectric relaxation mechanism 2–39382
alkenes, adsorbed on synthetic zeolites, e.s.r. 2–21656
alkenes, bond exciton model 2–15348
alkoxynitroxide radicals, from photolysis of nitrobenzenes and heterocyclic nitro cpds., e.s.r. study 2–832
alkyl acetates, ultrasonic wave velocity, pressure and temp. dependences 2–25078
alkyl anthracene, fluorescence study of intramol. energy transfer 2–18481
alkyl fluorenole, fluorescence study of intramol. energy transfer 2–18481
alkyl platinum compounds, i.r. spectra 2–831
2- alkyl-iminobenzoxazolones, valence vibrations of azomethine group 2–835
alkylalkoxyamino radical, trapped in X-irradiated decanal oxime O-methyl ether-urea inclusion crystals, e.s.r. spectra 2–13592
alkylalkoxynitroxide radicals, e.s.r. study of decay processes and rotation 2–8728
alkylammonium salts, hydrogen bonding with alcohols 2–3068
alkylchlorosilanes, adsorption on quartz crystal surfaces 2–32394
peri-alkylnaphthalene anions 2–35303
allene, MO calc. of geometry, energy and polarity 2–28383
allene, vacuum u.v. spectra, preliminary ionization potential determination 2–21655
americium complex, $(C_5H_5)_3$ ^{241}Am(III), mag. susceptibility between 4.2 and 250K 2–22663
amide, in water, structure, n.m.r. obs. 2–6255
amides, n.m.r. ^{15}N and ^{13}C Fourier spectra, coupling constants, shifts 2–6262
amine, in soln., molecular dynamics, n.m.r. obs. 2–6256
amines, crystallites, recombination delayed fluorescence 2–13506
amino acid radicals in X-irrad. N-benzoylalanine single crysts., mol. struct., e.p.r. obs. 2–8735
amino acids, γ-irrad., polymorphic transform. 2–7187
amino acids, surface tension of aqueous solutions, applications of image potentials for multipoles embedded in a cavity 2–21002
amino anthracenes, nonsymmetrical, moment directions of electronic transitions 2–21657
amino phosphines and arsines, i.r. and Raman spectra, vibrational spectra 2–12207
amino-H-acid, aqueous solution, as radiator in Cherenkov counter 2–31366
2-aminoacetophenone, free energy barrier to rotation of amino group around N-aryl bond 2–12206
γ-aminobutyric acid, n.m.r. study, configuration 2–8730
ε-aminocaproic acid aqueous solns., Debye effect, conc. and temp. depend. 2–21996
α-aminoisobutyric acid, single crystal irradiated by γ rays at 77 K, identification of cation radical from e.s.r. spectra 2–22885
2-aminonaphthalene-6-sulphonate and derivatives, absorption and luminescence spectra 2–28343
2-aminonaphthalene-6-sulphonate and derivatives, solvent dependence, solvent effects on absorption and fluorescence spectra 2–28868
aminophenetoles, i.r. absorption spectra, vibrational analysis 2–3113
o-, m- and p-aminophenol, thermodynamic functions calc. from vibrational spectroscopy data 2–15350
p-aminophenol derivatives, hydrohalides, solid state ion exchange with matrix, i.r. spectra 2–10594
α aminophosphinic acids, i.r. spectra and structure 2–18523
3-aminopropyl dibutylboron with bases, vibrational spectra, hydrogen bonds and fermi resonance 2–31837
ammonium hydrogen di-chloroacetate, paraelect. phase, cryst. struct. 2–36002
ammonium oxalate monoperhydrate, cryst. struct. 2–36003
ammonium oxalate monoperhydrate, O-O bond shortening 2–39662
ammonium perfluoro octanoate+water systems, mesomorphic phases, n.m.r. obs. 2–9096
ammonium tartrate, cryst. struct. 2–22170
amphetamines and related compounds, p.m.r. and rotamer populations 2–8729
amylose films, anisotropic morphology obs. 2–3473
amylose tricarbanilate, chain length depend. of mean square radius of gyration 2–862
angelicin 2–30659
anhydrides, electronic absorption spectra, obs. bathochromic shift of $\pi\pi^*$-band of PA 2–28345
Δ-8,14-anhydrodigitoxigenine, cryst. struct. 2–25353
aniline, $^1B_2\leftarrow{}^1A_1$ transition, electric field induced perturbations 2–21658
aniline, hydrogen bonded complex with substituted phenols in benzene solution, far i.r. spectrum meas. 2–12277
aniline, partially deuterated derivatives, n.m.r., incremental aromatic solvent induced shifts 2–18488

Organic compounds continued
aniline, photoconductivity of matrix-isolated molecules at low temperature 2—25951
aniline and haloaniline complexes with 2, 4, 6-trihalophenols, crystalline, i.r. and n.q.r. spectra 2—10340
aniline in polar and apolar solvents, fluorescence quantum efficiencies 2—28876
aniline solutions, n.m.r. investigation of molec. association 2—22008
aniline-cyclohexane liquid mixtures, critical exponent determination by scattering studies 2—9133
aniline-nitrobenzene mixtures, sound propag., relax. processes 2—32260
aniline-nitrobenzene mixtures, structure of complex molecules formed by field ionization 2—15351
1-anilino-8-naphthalene sulphonate, solvent perturbation effects on spectra, nsec time resolved emission spectroscopy 2—8731
anisole drops suspended in water, coalescence of two colliding drops 2—9068
anisylidene para-aminophenylacetate, APAPA, liquid crystal, proton spin lattice relax. 2—6257
[10]annulenes, synthesis and geometry 2—3070
anthracene, 9-carbonyl derivs., temp. effect on fluorescence intensity due to intersystem crossing 2—24503
anthracene, absorption band profile, optical constants, exciton dynamics 2—9942
anthracene, absorption band profile of origin region of b polarized 4000 Å transition 2—10352
anthracene, avalanche breakdown and light emission 2—19754
anthracene, chemical shifts, ring current contribution 2—3072
anthracene, conduction processes, review 2—13246
anthracene, cryst., in soln., fluoresc. decay times, rel. to defects and reabsorpt., 2-350K 2—10442
anthracene, Debye temp., comparison of calc. methods 2—29511
anthracene, degradation luminescence for meas. of ionising emission in heterogeneous systems 2—38774
anthracene, diffusion length of singlet excitons 2—6737
anthracene, dislocations, electron microscopy, diffr. contrast method 2—25413
anthracene, effect of γ-ray induced impurities on semiconductive behaviour 2—19614
anthracene, electrogenerated chemiluminescence in solution 2—40821
anthracene, electron and hole generation 2—36521
anthracene, e.p.r. studies of deuteration effect on intersystem crossing 2—12208
anthracene, exciton induced photoemission 2—22659
anthracene, in n-paraffin monocrystals, dependence of luminescence spectrum on crystallization conds. and conc. 2—20098
anthracene, Kramers-Kronig relationships, refr. and extinction indices 2—15592
anthracene, librational modes, Raman spectra, pressure and temp. dependence 2—36896
anthracene, narrow band semiconduction, in review 2—9998
anthracene, optical anisotropy, 4.5-11.5eV 2—40651
anthracene, paramagnetic excitons, role in fluorescence and photoconductivity 2—25741
anthracene, photo-electret formation, effect of alternating field 2—4285
anthracene, photochemical reactions, role of dislocations and stacking faults, elec. microscope obs. 2—30088
anthracene, photocond., oxygen influence 2—33079
anthracene, p.m.r., exciton motion 2—7132
anthracene, proton relax. by excitons, low temp. 2—10277
anthracene, pure crystals, fluorescence rise and decay times 2—20107
anthracene, single cryst., field dependent electron and hole losses, drift current pulse obs. 2—13247
anthracene, single crystal, surface trapping, photoinjection obs. 2—13248
anthracene, thermal activation energies for hole injection 2—16318
anthracene, thin crystals, light absorption and fluoresc. spectra calcs. 2—10315
anthracene, transient photocurrents, exciton diffusion 2—4306
anthracene, triplet exciton dynamics, temp. depend. 2—33319
anthracene, triplet exciton generation at surfaces, effect on defect production 2—25740
anthracene, X-ray excited electron-hole pairs, geminate recombination 2—10040
anthracene alkyl-substituted analogues, films, elec. props. 2—13249
anthracene cryst., geometrical form 2—25247
anthracene cryst., triplet exciton quenching by internal β-irrad. 2—6736
anthracene crystal, spin-resonance absorpt., excition motion effects 2—22824
anthracene crystal metal interface, exciton dissoc. rate const. charge transfer 2—3490
anthracene crystal/electrolyte solution interface, quenching of excited states 2—26242
anthracene crystals, charge transfer exciton fission 2—36960
anthracene crystals, proton relaxation through triplet excitons 2—22845
anthracene derivates, polarization dependence on conc. of fluorescent derivatives 2—16622
anthracene derivatives, fluorescence spectra, polarization 2—4487
anthracene dissolved in organic liquid, two-photon laser photo-ionisation 2—30081
anthracene excimer, i.r. absorpt. study during pulse radiolysis of solns. in benzene 2—20203
anthracene film, γ-irrad., I-V characts. 2—29681
anthracene film, fluoresc. decay time 2—10443
anthracene film, space charge limited currents with uniform and non-uniform trap distrib. and size effects 2—40266
anthracene laser, triplet lifetimes meas. 2—17614
anthracene scintillation detector, response to electrons with energies from 2 to 10000 eV 2—34796
anthracene single cryst., opt. anisotropy from reflection spectra, 4.5-11.5 eV 2—20007
anthracene single crystals, recombination delayed fluorescence, origination from photoionization 2—22807
anthracene-d_{10}-fluorene mixed crystals, e.s.r., influence of deuteration and energy transfer 2—20154
anthracene/Al interface, exciton-induced photocurrents 2—25963
anthrapyridine, aminosubstituted, hydrogen bonds, i.r. and fluorescence spectra study 2—3071
anthraquinone in solutions, delayed thermal fluorescence 2—28874
anthraquinone molecules, adsorbed on W, energy distrib., of field emitted electrons 2—29075

Organic compounds continued
anti-tricyclo $[4.2.2.0^{2,5}]$-deca- 3,9-diene-7,8-endo-dicarboxylic anhydride, structure, X-ray diffraction investigation 2—833
antibiotics, charge transfer complex, conduction mechanism, conductivity and e.p.r. obs. 2—10526
antipyrine, 1-phenyl-2, 3-dimethyl-5-pyrazolone crystal structure obs. using physical techniques 2—9503
arabinose, aqueous soln., γ-irrad., optical rotation 2—5596
arcton 12, spark breakdown 2—9008
aromatic, photocond. activation energy, band struct. determ. 2—19791
aromatic azo compounds, reversible orientational photodichroism and photoisomerization, system model 2—33387
aromatic compounds, vitreous solutions, role of molec. association in temp. induced increase of delayed fluorescence 2—36947
aromatic crystals, triplet state exciton band structure from ^{13}C shallow trap states 2—19517
aromatic crysts., refr. indexes, optical anisotropies rel. to mag. anisotropy 2—33206
aromatic $d\pi^*$-$\pi\pi^*$ interactions, comparison with $n\pi^*$-$\pi\pi^*$ interactions in Ir(III) complexes 2—35300
aromatic hydrocarbon cryst., optical phonons and polaritons 2—19392
aromatic hydrocarbon cryst., phonon density of states 2—19400
aromatic hydrocarbon crystals, contact potential and work function 2—25849
aromatic hydrocarbon crystals, theory of electron-phonon interactions 2—25720
aromatic hydrocarbon dimers, absorpt. and emission spectra, radiative life times 2—10361
aromatic hydrocarbon dimers, Davydov splitting calc. 2—8717
aromatic hydrocarbon radicals, degenerate, g- factor deviations 2—18489
aromatic hydrocarbon radicals, e.p.r., proton hyperfine splitting and electron density relationships 2—18490
aromatic hydrocarbons, crystallites, recombination delayed fluorescence 2—13506
aromatic hydrocarbons, derivation and evaluation of electronic matrix elements governing intersystem crossing 2—31834
aromatic hydrocarbons, electrooptical polarisability in ground state and first excited singlet states 2—15381
aromatic hydrocarbons, intermediate level structure in highly excited electronic states 2—35214
aromatic hydrocarbons, magnetic field effect on photooxidation rate 2—33377
aromatic hydrocarbons, planewise summation of point dipole-dipole interactions rel. to exciton theory of strong transitions 2—13487
aromatic hydrocarbons and perfluoro analogues, charge distributions as determ. by ESCA 2—31860
aromatic hydrocarbons in poly(methylmethacrylate) temperature dependence of phosphorescence studied in 77-400K 2—20110
aromatic hydrocarbons in soln., triplet monomers and excimers, lifetimes 2—9143
aromatic molecular polycrystals, excitations and anharmonic effects, neutron scattering study 2—25667
aromatic molecule systems in rigid solution, donor phosphorescence quenching and decay in sensitized phosphorescence 2—13511
aromatic molecules, in nematic liq. cryst. relat. between orientation and principal polarizabilities 2—15352
aromatic molecules, magnetic anisotropies determ. using Cotton-Mouton effect 2—24495
aromatic molecules, optical nuclear polarization by selective population of nuclear sublevels 2—7027
aromatic nitriles, anion radicals, i.r. study of intramol. electron interaction 2—8732
aromatic single crystals, excitation of triplet excitons by guest-host energy transfer 2—4135
aromatic syst., energy trapping processes 2—36940
aryl cations, substituted, electronic structures, INDO calculations 2—28346
arylidene-1-3-indandiones, chromophoric conditioning 2—25962
7-azaindole dimer, potential energy curves of protons in H bonds in ground and excited states 2—5958
azide crystals, anisotropic thermal expansion by single crystal method 2—15734
2,6-bis(4-azidobenzylidene) cyclohexanone, stereoisomers, electronic structure and spectra, dipole moments, SCF MO LCAO methods 2—12233
azidotriphenyl derivatives of group IV elements, n.m.r. investigation 2—15395
azines, substituted by amine groups, amine-imine tautomerism 2—21659
1-aziridinyl carboxamide, i.r. and Raman spectra, vibrational analysis 2—12219
azo group, α,β-unsaturated, u.v electronic spectra, dipole moments, config. study 2—18483
azobenzene, p-monosubstituted derivs., polarization absorption spectra, electronic transitions 2—836
azobenzene, Raman spectra, meas. standard intensities, polarization ratio, determ. structure 2—24505
trans-azobenzene and isotopic derivatives, vibrational spectra 2—35304
azoethane, pyrolysis in reflected shock waves to produce ethyl radicals, reactions studied 2—20184
azolidones, mag. susceptibility, temp. and field depend. 2—19837
azomethane, ruby laser induced decomposition, cross section 2—26362
azonaphthalenes, basicity and electronic spectra, spectrophotometric study 2—28347
4,4′-azoxidianisole, electret thermal analysis 2—1078
azoxy compounds, nematic with dielectric anisotropies of different sign, electrohydrodynamic instabilities 2—39340
p-azoxyanisole, liquid crystal, phase transition, small angle X-ray obs. 2—3364
p-azoxyanisole, nematic, elasticity and orientational order 2—9089
p-azoxyanisole, nematic, self-diffusion tensor, temp. depend. 2—25045
p-azoxyanisole, nematic and isotropic, mobility, temp. depend. 2—39341
p-azoxyanisole, nematic liq. cryst., orientation, effect of flow 2—1077
p- azoxyanisole, nematic mesophase, proton spin lattice relaxation time 2—18856
p-azoxyanisole, nematic mesophase, spatial distrib. of light scatt. in applied elec. field 2—25087
p-azoxyanisole, PAA, order parameter, n.m.r. obs. 2—6261
p-azoxyanisole, phase transform., pressure effects, order parameter, n.m.r. spectra 2—6206
p-azoxyanisole, thermal, cond., interfacial and temp. gradient effects 2—6228

Organic compounds continued
p-azoxyanisole liq. cryst., self-diffusion anisotropy, coeffs., neutron diffr. obs. 2—6225
p-azoxyanisole liquid crystals, ultrasonic determ. of anisotropic shear and bulk viscosities 2—12552
azoxybenzenes, Raman scattering in solid, nematic and liquid phases 2—25088
p-azoxydianisole, equilibrium geometry, Raman spectrum and quantum chemical study 2—8733
p-azoxyphenetole, nematic, elasticity and orientational order 2—9089
p-azoxyphenetole lquid crystals, ultrasonic determ. of anisotropic shear and bulk viscosities 2—12552
azulene, deuterium isotope effect on fluorescence lifetime 2—21661
azulene, linewidths for $S_1 \leftarrow S_0$ and $S_2 \leftarrow S_0$ nonradiative processes 2—31838
azulene, perturbation treatment of spin-orbit coupling using CNDO/S wavefunctions 2—12091
azulene, $S_2 \rightarrow S_1$ emission 2—24504
azulene, spectral shifts in nonpolar solvents, mechanism 2—25093
azulene derivatives, room temp., effect of energy gap between states on fluorescence yields 2—24506
azulene solution. nonlinear absorption of ruby laser radiation 2—28859
azulenes, σ bonding polarization, comparison of results from i.r. intensity meas. and CNDO/2 calc. 2—21660
barbituric acid and its 2-thio derivative, comparison between radicals formed by radiation, e.s.r. study 2—21662
barium stearate, film, thickness dependence of dielectric breakdown 2—4278
benzaldehyde, ${}^1U(n\pi^*) \leftarrow S_0$ absorption spectra, vibronic intensification 2—12211
benzaldehyde, ${}^3U(n\pi^*) \rightarrow S_0$ phosphorescence, vibronic interactions 2—12212
benzaldehyde, conjugated system, pot. function for rotation about CC single bonds, CNDO/2 calc., inaccuracy of method 2—3099
benzaldehyde, phosphorescence spectra, dynamic properties and zero field splittings of lowest excited triplet states 2—28335
benzaldehyde, zero field splitting, phosphorescence rate consts. and vibronic activity in lowest triplet state by p.m.d.r. 2—28353
benzaldehyde anion radicals, restricted internal rotation influence on e.s.r. spectra 2—828
benzaldehyde in methyl cyclohexane. phosphorescence emission spectrum, mechanism 2—8739
benzaldehydes in benzene, substituted, dielectric relaxation and mutual viscosity 2—39383
1,2-benzanthracene, principal axis orientation of e.s.r. 2—15363
benzanthracene, zero field splitting coeffs. of e.s.r. of lowest triplet level, calc, using Huckel approx. 2—12275
1,2-benzanthracene solution, triplet decay mechanisms, kinetic and quantum yields of delayed fluorescence 2—21991
1,2-benzanthracene solution, triplet decay mechanisms, ratio of delayed monomer and excimer fluorescence of function of temp. 2—21993
benzene, ^{13}C n.m.r. chemical shift anisotropy 2—38964
benzene, 'Kekule' vibration assignment, CNDO/2 study 2—21666
benzene, absorpt. cross sections and photoionization efficiencies, 600-2200 Å 2—18491
benzene, adsorbed on C black, chem. pot., heat of adsorpt. rel. to surface coverage 2—35907
benzene, adsorbed on silica, mobility and diffusion, n.m.r. spin echo obs. 2—35929
benzene, adsorpt. on GeO_2, interactions with surface OH groups 2—35914
benzene, adsorption on glassy pyrogenic SiO_2 2—39565
benzene, adsorption on zeolites, ^{13}C n.m.r. investigation 2—39550
benzene, anal. of antiresonacnes in Rydberg spectrum in terms of theoretical line shape parameters 2—8802
benzene, benzene-d_6, radiational deuterium effect in triplet-single transition 2—21663
benzene, bond order in π-electron structure of molecules 2—18390
benzene, chemical shifts, ring current contribution 2—3072
benzene, computer calc. of true profiles of Raman lines 2—35311
benzene, electron impact, radiation emission for 0 to 500 eV incident energies 2—5961
benzene, excimer intrinsic fluorescence yield and lifetime, temp. dependence 2—28352
benzene, fluidized by water, coalescence rates 2—1126
benzene. fluorescence quantum yield and lifetime between —100 and 5°C 2—4500
benzene, Fourier transform obs. of Brillouin and Rayleigh line widyhs and shapes 2—1103
benzene, frozen, radiothermoluminescence studies of self absorption of emittted light 2—37058
benzene, in cycohexane, triplet yield as function of conc., intersystem crossing effects 2—28875
benzene, in non polar solvents, intensities of absorption bands, determ. from i.r. dispersion curves 2—18835
benzene, in solid HCl matrix. i.r. vibr. spectrum. phase effects, frequency changes 2—13486
benzene, influence of final-state spectrum in radiationless transitions studied by Laplace transform method 2—38962
benzene, i.r. exciton spectrum, density of states and absorption function calc. using ^{13}C shift data from a_{2u} mode 2—10397
benzene, jets, liquid-in-liquid, mass transfer, conc. driving force 2—3350
benzene, lattice frequencies calc. using pairwise potential function 2—25646
benzene, lifetimes of individual vibronic states 2—8734
benzene, liq., elec. current, high field strengths influence 2—25100
benzene, meas. of rotational diffusion tensor by Raman scattering 2—9135
benzene, methyl substituted derivatives, vibrational spectra 2—35309
benzene, monomer, and excimer, temp. dependence of specific rates describing fluorescence 2—8738
benzene, monosubstituted derivatives, dielectric relaxation in liquid phase at microwave frequencies 2—35779
benzene, non radiative relaxation of excited $A\,{}^1B_{2u}$ state 2—24511
benzene, opt. absorpt., 6.5-35 eV 2—18492
benzene, orbital determ., ESCA line intensities obs. 2—35219
benzene. r.f. irradiation effects on n.m.r. spectra 2—30032
benzene, S_1 state, fluorescence and intersystem crossing as function of rotational energy 2—24510
benzene, second harmonic light scatt. 2—35765
benzene, shock compressed, opacity, absorpt. spectra 2—35770
benzene, solid, higher $\pi \rightarrow \pi^*$ transitions, spectral obs. 2—20052
benzene, spin echo n.m.r. 2—35790
benzene, stimulated Raman scatt., temp. depend. 2—18831
benzene, stimulated scattering under picosecond laser excitation 2—1102
benzene, susceptibility anisotropy, from Cotton-Mouton effect meas. 2—18486
benzene, temperature dependence of flow birefringence 2—6232
benzene, temperature dependence of widths and integrated intensities of polarized Raman lines 2—28351
benzene, vapour, γ-irradiated, av. energy per ion pair 2—15498
benzene, velocity and absorption of shear waves near melting point 2—29536
benzene, Wannier functions in orbital theory 2—18477
benzene ${}^3B_{1u}$ state, obs. of Zeeman effect, evidence for dynamic pseudo Jahn Teller distortion 2—20109
benzene and -1-^{13}C deriv., isotropic and nematic soln., p.m.r. study of direct and indirect coupling 2—5962
benzene anion, g-factor deviations 2—18489
benzene anion radical. ion-pair formation, effect on meas. of spin-lattice relaxation 2—35308
benzene anion radical in liquid solution, investigation of c.w. saturation technique 2—35787
benzene cryst., far-i.r. absorpt. external vibr. lines broadening at melting pt. 2—20053
benzene crystals, pure exciton emission, 4 to 20K 2—13509
benzene derivatives, substituted, role of symmetry of a vibration in temperature dependence of i.r. band intensity 2—24509
benzene derivatives containing amino and carboxyl groups, absorption spectra 2—8741
benzene films, between differently polar fused silica surfaces, thermodynamic properties and molec. long range orientation 2—21947
benzene homologues, phosphorescence spectra, frozen matrices, liq. nitrogen temps. 2—4502
benzene host matrix to pyrimidine, zero-field microwave optical double resonance at 77 K 2—22818
benzene mol. ion, prod. by charge exchange, dissoc. lifetime 2—24513
benzene on NaY-zeolite, proton relax., —140 to 80°C 2—26086
benzene single crystals, self-diffusion, isotope mass effect 2—25464
5-benzene sulphonamido 3-phenyl 1-2-4 triazole, crystal structure 2—25354
benzene triplet absorption by monoolefins in gas phase, reaction rate determ. by kinetic absorption spectroscopy 2—13572
benzene vapour, adsorption on Saran charcoal, vol. change 2—3559
benzene vapour, optical absorption spectrum, photon energies 6-35 eV, electronic structure assignment 2—15358
benzene-acetic acid mixture, proton spin-lattice relax. 2—6252
benzene-borazine mixed crystals, electronic spectra, 4.2K 2—13485
benzene-chromium-tricarbonyl, Raman spectra, frequency assignment 2—28354
benzene/n-alkane mixture, gas-liq. crit. temp. 2—25150
benzenes, fluorinated, K electron binding energy shifts, CNDO potential model calc. 2—8771
benzenes, methyl substituted, radiative and nonradiative transitions from first excited singlet state, rate constant meas. 2—12209
benzenes, monosubstituted, electronic structure and spectra, variable electronegativity SCF-MO calc. 2—15353
benzenes, monosubstituted, in liquid state, coupling between rotational and translational motions, pressure dependence 2—39392
benzenes, substituted, electronic structures, use as photographic developing agents 2—14494
benzenes, trisubstituted, additivity relation for proton-proton coupling consts. 2—38961
benzenoid hydrocarbons, non-planar condensed, extension of Huckel London McWeeny theory of ring current effects on proton chemical shifts 2—24494
1:2 benznaphthacene, zero field splitting coeffs. of e.s.r. of lowest triplet level, calc. using Huckel approx. 2—12275
benznitrile, single crystal, e.p.r. studies of photoexcited states 2—26360
benzoates, proton spin-lattice relax. 2—29848
benzocyclobutene radical anion, ion pairing effects in K-THF and Cs-DME 2—18487
benzodioxane-1,4 and o-form, quasilinear fluoresc. spectra 2—28879
benzoic acid, dissolution of solids into turbulent liquid stream 2—28757
benzoic acid, effect of dimer formation on emission spectrum, position of (n,π^+) triplet state 2—35310
benzoic acid, single cryst., low freq. spectrum, GF method analysis 2—20079
benzoic acid cylinder rotating in water, mass transfer coeff. determ. from rate of dissolution 2—6218
benzol, adsorbed on Si, n.m.r. spin echo investigation 2—6374
benzonitrile, dielectric relaxation times as function of temperature 2—3410
benzonitrile, geometric distortion studied by high-resolution n.m.r. in the nematic phase 2—31840
benzonitrile, lowest-lying singlet $\pi^* \leftarrow \pi$ transition, rotational analyses, dipole moment changes 2—35343
benzonitrile and d_5 analogue, i.r. spectra, theoretical study of vibrational assignments 2—35312
benzonitrile in polycryst. matrices, vibr. anal. of luminescence in terms of excited state geometries 2—31839
benzonitrile mol. ion, prod. by charge exchange, dissoc. lifetime 2—24513
benzonitrile-heptane, dipole moments calculation 2—39376
benzophenone, 1.3K, principle phosphorescent trap, applic. of fast passage ODMR 2—22809
benzophenone, energy resolved decay, strong coupling between S_1 and T_1 vibronic levels 2—8737
benzophenone, partially deuterated, phosphorescence lifetime meas. 2—28337
benzophenone, radiative decay of lowest excited singlet state 2—3073
benzophenone, solns. and crystals, electronic and vibrational spectra, effect of u.v. illumination 2—26363
benzophenone and 1-methylcoronen mixed crystals, demonstration of delayed fluorescence 2—36939
benzophenone with diacetyl impurity, crystals, phosphorescence, transfer of excitation energy 2—1717
3,4-benzopyrene, fluorescence, effect of phase changes in cryst. cyclohexane matrix 2—33320
p-benzoquinone, effect of methyl and hydroxyl substituents on π-electron spectra 2—35307
p-benzoquinone adsorbed on TiO_2, bonding rel. to surface electronic state 2—29058
p- benzoquinone and derivatives phosphoresc. spectra 2—5959

Organic compounds continued
p-benzoquinone and methyl derivatives; CNDO-CI study of effects of substitutions on electronic spectrum 2—12210
p-benzosemiquinone in alcoholic soln., mol. motion e.p.r. obs. 2—35788
2,1,3-benzothiadiazole, in liq. cryst. phase, proton skeleton geometry, HCC angles, n.m.r. obs. 2—8566
benzotriazole, surface reaction film on Cu, i.r. and u.v.-visible refl. spectra 2—18959
benzoxazole, cryst., near u.v. absorption spectrum in polarized light 2—16502
benzoxazole, vibr. spectra 2—28348
2,6-[bis-2′-benzoxazolyl] pyridine, scintillation studies 2—3395
benzoyl fluoride, microwave spectrum from 26.5 to 40.0 GHz, rotational and vibrational assignments 2—15357
benzoyl fluoride microwave spectrum, rotational and vibrational assignments to ground and excited torsional states 2—15354
benzoyl peroxide on synthetic faujasite, decomp., chemiluminescence 2—13573
N-benzoylanine, X- irrad., radical prod., identification and mol. characterization, e.s.r. obs. 2—8735
2-benzoylpyridine, e.p.r., triplet state, g-tensor anisotropy 2—8762
benzo[cd]pyrenyl, assignment of proton hyperfine splitting constants 2—35305
4H-benzo[def]carbazole, absorption and emission spectra, comparison with MO calculations 2—24508
benzo[g,h,i,]perylene cryst. and mixed cryst. with perylene, spectral dependence of fluorescence lifetimes 2—22808
1,2- and 3,4- benzpyrene impurity molecules in isooctane crystals effect of polymorphic transformations on luminescence spectra 2—29959
benzyl, symmetry of first excited state determ. by rotational contour analysis of vibronic bands of emission spectra 2—15355
benzyl alcohol content in developing solution, effect on KP-4U film 2—5460
benzyl compounds, i.r. and Raman spectra, vibr. assignments, asymmetric structure 2—8742
benzyl derivatives, intramolecular charge-transfer mechanisms 2—38960
benzyl derivatives, para substit., i.r. and Raman spectra, vibr. assignment, asymmetric structure 2—8743
benzyl fluorides, inter and intramolecular movements studied by distortion in n.m.r. signals from ^{19}F 2—24512
benzyl radical, calculation of e.s.r. proton coupling constants 2—35306
benzyl radical, valence bond calculations of spin density distribution 2—38959
benzyl radical configuration calc. by π-SCF-MO and MINDO/1SCF-MO methods 2—38963
benzylamine tartrate, organic glass substrate for C film in elec. microscopy 2—9260
benzylidene-1,3-indandiones, chromophoric conditioning of photoelectric response 2—25962
benzylideneaminocinnamic acid derivs., effect of mol. struct. changes on mesomorphic transitions 2—9090
N-benzylidenemethylamines, para-substit. electronic absorption spectra, non-planar conformation 2—8740
benzylidine aniline, ASMO-CI calc. of electronic structure and molecular geometry 2—28350
benzyltin derivatives, far i.r. and Raman spectra, vibrational assignment 2—21665
1,1′-biaziridine, conformation from vibrational spectra data 2—38968
bicyanine dimer, electron- vibrational spectra, strong coupling case 2—12214
bicyclo [3.1.0] hexane substituted with O or CH_2, far i.r. spectra, ring-puckering vibration molecular confirmation studied 2—12215
bicyclo-[2,2,2]-octane, excited electronic states, sharp vibronic structure 2—12205
bicyclobutane, LCAO calculations 2—38965
bicyclobutane, molecular Zeeman effect and electronic charge distribution 2—35313
bicyclo[1.1.1]pentane, ab initio MO calculations 2—39011
bicyclo[2.1.0]pentane, microwave spectrum, structure and dipole moment 2—31841
bicyclo[2.1.1]hexan-2-one, microwave spectrum, dipole moment and rotational constants 2—8744
bicyclo[2.1.1]hexane, molecular structure 2—24514
bicyclo[2.2.2]octane, investigation of Rydberg states 2—31845
binary liquid solution, e.s.r. study of Heisenberg spin exchange near the critical point 2—32276
biological polymer, mobility, microwave Hall effect obs. 2—16216
biologically important aromatic acids, n.m.r. 2—35344
biomacromolecular system, microwave dielectric and Hall effect measurement 2—34286
biphenyl:naphthalene, obs. of localized rotational phonons 2—16014
biphenyl, conjugated system, pot. function for rotation about CC single bonds, CNDO/2 calc., inaccuracy of method 2—3099
biphenyl, in soln., ENDOR 2—15396
biphenyl, vibrational spectra and dihedral angles 2—38967
2,5-di(biphenyl)-1,4-oxazole), spectral intensity changes on excitation by N laser, quantum generation 2—3390
biphenyl based series, phenanthrene-carbazole-dibenzothiopene-dibenzofuran, polarization of electronic transitions 2—28355
biphenyl cryst., far-i.r. absorpt., external vibr. lines broadening at melting pt. 2—20053
biphenyl reaction with electrons produced by two-photon laser photolysis of molecules in liquids, rate constants meas. 2—30081
biphenyl type crystal, anomalous nuclear dipolar relaxation 2—7000
biphenyls, bridged, phosphorescence in fluid solution 2—39374
bis(acetic acid)-BF_3 complex, i.r. spectra, structure study 2—24546
4,4-bis(alkoxy)azobenzenes homologous series of nematic liquid crystals, n.m.r. relaxation 2—28898
bis(methanol)-BF_3 complex. i.r. spectra, structure study 2—24546
4,4′bis(n-hexyloxy)azoxybenzene- 4,4′bis (2-methylbutoxy)azoxybenzene mixtures, cholesteric liquid crystals, temp. dependence of order from reflectance spectra 2—28794
bis(pyridine)halogen(I) cations, CNDO/2 calculations 2—38966
bis(trifluoromethyl) diselenide molecular structure, electron diffraction determ. 2—24516
bis(trifluoromethyl) monoselenide, molecular structure, electron diffraction study 2—24515
bis-(4 n-alkoxybenzal)1-,4-phenylenediamines, liquid crystalline transitions, density obs. 2—18798

Organic compounds continued
bis-(maleonitriledithiolene)-metal chelate complex, semiconductor, e.p.r. spectra 2—16218
1,3-bisdiphenylene-2-phenylallyl-benzene complex, antiferromag. linear chains 2—26058
5,5’-bisisoxazole in liquid crystals, NMR spectra study, interpretation based on conformational equilibrium 18493 2—18493
2,2′-bis(6-methyl-3-pyridinol), crystal and molecular structure 2—29157
bitumen, suspended in seawater, distribution, morphology and composition 2—13641
boiling of liqs., u.s. wave effects 2—28959
borazole, Raman spectra 2—17731
boric phosphor of 2-phenylquinoline, photoluminescent properties 2—16614
2-bromo-1-butene vibrational assignment and rotational isomerism 2—24519
7-bromo-2,3-dihydro-1-methyl-5-phenyl-1,4-benzodiazepin- 2-one, 1:1 complex with chloral hydrate, molecular and crystal structure determ. by heavy atom method 2—9505
2-bromo-4-methyl acetanilide, ^{79}Br n.q.r., temp. variation, 77-302K 2—40793
bromobenzene, partially deuterated derivatives, n.m.r., incremental aromatic solvent induced shifts 2—18488
bromobenzene, quadrupole hyperfine structure in rotational spectrum analysed 2—12216
bromobenzene, stimulated scattering under picosecond laser excitation 2—1102
bromobenzene liquid core hollow fibres, optical transmission loss 2—21168
2-bromobutane, rotational isomerism from i.r. spectra in crystalline and glassy states 2—40685
p-bromochlorobenzene crystals, absorption spectra, 4K, exciton zone analysis 2—26208
bromocresol green and purple dye amplifier, optical pumping by one- and two-photon processes 2—21083
bromocyclobutane, ring-puckering vibration, far i.r. study 2—15366
bromoethane, gaseous, second density virial coeffs. 2—15535
bromoform, approx. force field 2—3076
bromoform, cryst. struct., 253K 2—32479
bromoform autocorrelation functions of dipole moment theoretical and experimental values compared 2—38985
bromoform-D_1, approx. force field 2—3076
bromoiodoacetylene, vibrational assignment rel. to force constant determination for dihaloacetylenes 2—38970
bromopropene, rotational isomerism 2—28381
2-bromothiazole, double-quantum effects in p.m.r. spectrum 2—38969
bromotricyanomethane, cryst. struct. 2—32478
bromoxylene, vibrational spectra 2—35309
s-trans-1,3- butadiene, ab initio investigations of $\sigma—\pi$ interactions in electronic states 2—24517
1,3-butadiene, ab initio SCF and CI calculations of barrier to internal rotation 2—38971
butadiene, bond order in π-electron structure of molecules 2—18390
butadiene, CI calcs. on pi-electron states 2—8746
1,3-butadiene, conjugated system, pot. function for rotation about CC single bonds, CNDO/2 calc., inaccuracy of method 2—3099
1,3-butadiene, electronic spectrum application of molecule within a molecule method to transitions 2—35298
1,3-butadiene, internal rotation, study via ab initio calcs. 2—28357
butadiene, new weak vibronic transitions predicted 2—12083
1,3-butadiene, solubility in liquid methane and liquid Ar 2—1080
trans butadiene, with four π-electrons, solution of molecular Bethe-Goldstone equation 2—35205
n-butane, produced in pyrolysis of azoethane in reflected shock waves, thermal decomposition meas. in 1160-1550K range 2—20184
n-butane free jets relaxation study from mass spectra temp. dependence 2—24518
butane-d_{10}, deuteron quadrupole coupling constant meas. via ^{2}H n.m.r. 2—10568
1,3-butanediol, pressure and temp. studies of n.m.r. translational relaxation 2—35795
butanes, adsorption on active C, pore struct. determ. 2—32751
1-butanol: porphyrexide, ^{13}C dynamic polarization rel. to polarized target production 2—36809
butanol, nuclear polarization, effect of absorbed power 2—34774
butanol-water-porphyrexide system, polarized proton target properties and performance 2—34779
1-butanol-water-porphyrexide system, proton polarization at 50kG and 1K, polarized target production 2—36808
1-butene, activation energy for addition of O(^{3}P) atoms 2—10614
butene, cis and trans, and their ions, ab initio MO calcs. 2—24520
butoxides of Na and K, vibrational spectra study of structure 2—5964
t-butyl alcohol, light scattering, additional maxima by addition of water and heavy water 2—9131
butyl alcohols, self association study using dielectric constant measurements 2—21956
n-butyl benzene, temperature dependence of flow birefringence 2—6232
t-butyl chloride, calorimetric, dielec. and i.r. obs. of phase transitions 2—36352
t-butyl chloride, comparison of electron diffraction and microwave spectroscopic structures 2—15359
t-butyl chloride, liquid, molecular rotation, dielec. relaxation 2—18843
t-butyl cyanide, i.r. and Raman spectra, vibrational assignment 2—5963
9-t-butyl-9,10-dihydroanthracene, struct., modified tangent procedure 2—3745
butyl-p-ethoxyphenyl terephthalate, electret thermal analysis 2—1078
n-butylacetate, fluidized by water, coalescence rates 2—1126
4- butyloxybenzal-4′-ethylaniline, liquid crystal smectic phase detn., X-ray obs. 2—32234
4-butyloxybenzylidene-4-acetoaniline, nematic A liquid crystal, e.s.r. obs. 2—18853
di-n-butylphthalate-water system, optical study of interfacial turbulence 2—6177
N-t-butylstyrenimine, solvent effects on proton-proton coupling consts. 2—35793
2-butyne, spin-lattice relaxation in various solutions 2—32279
butyric acid, u.s. absorption at 20 to 90°C 2—18819
γ-butyrolactone, i.r. spectral study of complexing and hydrogen bonding with o-cresol 2—28358

Organic compounds continued
- cadmium arachidate, organic monomolecular layers, in m.i.m. struct., neg. resistance obs. 2—36568
- caesium manganese oxalate tetrahydrate, cryst. struct., X-ray obs. 2—32482
- caesium manganese oxalate trihydrate, cryst. struct., X-ray obs. 2—32481
- calcium hydrazinecarboxylate, anhydrous, cryst. and mol. struct. 2—9504
- calcium tartrate, cryst. growth in gels, effect of Fe^{3+} contamination 2—15685
- caprolactam and N-methyl derivative, solution in toluene, ultrasonic relaxation processes analysed 2—12560
- caprone, temp. effects on i.r. absorption bands sensitive to H bonding 2—15362
- carbamyl fluoride, centrifugal distortion constants from microwave spectrum 2—35314
- carbazole, irradiated cryst., study of radical formation by e.s.r. 2—10489
- carbenes, spin dipole spin dipole contrib. to zero field splitting parameters 2—12220
- 2-carbethoxy-4-aminoindole, scintillation studies 2—3395
- carbomethoxycyanobenzyl radicals, e.s.r. spectra in 40°-200°C range, obs. of π- and σ- spin delocalization into the phenyl ring 2—31842
- carbon blacks, methods of investigating surface structure 2—6302
- carbon hexafluoride, γ-ray scintillation counter, comparison with NaI detector 2—31365
- carbon tebachloride- benzene system conc. gradient meas. as function of temp. grad. and flow rate 2—21977
- carbon tetrachloride, adsorption on active C, pore struct. determ. 2—32751
- carbon tetrachloride, collisions with NO in $^2\pi_{3/2}$, j=m$_j$=3/2 state, orientational anisotropy in total collision cross section 2—3150
- carbon tetrachloride, depolarization ratios of isotope lines 2—38941
- carbon tetrachloride, jets, liquid-in-liquid, mass transfer, conc. driving force 2—3350
- carbon tetrachloride, laser excited Raman bands, application of slit function corrections 2—9138
- carbon tetrachloride, matrix isolated in Ar, Raman spectra, intramolecular force field obs. 2—35315
- carbon tetrachloride, nonlinear refractive index due to nonlinear response of electronic currents 2—1096
- carbon tetrachloride, shock compressed, opacity, absorpt. spectra 2—35770
- carbon tetrachloride, solid, heat capacity, component vibrations detn. 2—6679
- carbon tetrachloride, vapour, γ-irradiated, av. energy per ion pair 2—15498
- carbon tetrachloride, vibratory spectra, intensities, electro-optical parameters 2—32267
- carbon tetrachloride effect on discharge behaviour of air in inhomogeneous electric field 2—24897
- carbon tetrachloride polarity in vibrational state obs., due to vibrationally induced dipole moment 2—12218
- carbon tetrachloride solution, proton spin-lattice relaxation of 1,2-dichloroethane 2—18857
- carbon tetrachloride-NO molecular beam collision, orientational anisotropy in total collision cross- section 2—8864
- carbon tetrafluoride, chemical shift of ^{19}F, press. and temp. depend. 2—5953
- carbon tetrafluoride, condensed phases, band moments and dipole autocorrelation functions 2—16503
- carbon tetrafluoride, gas phase Raman spectra, rotational profiles of vibrational bands 2—28250
- carbon tetrafluoride, Raman spectra 2—17731
- carbon tetrafluoride binary mixtures, phase equilibria and critical phenomena at low temp. and high pressure 2—9108
- carbon tetrafluoride polarity in vibrational state obs., due to vibrationally induced dipole moment 2—12218
- carbon tetrafluoride thermal conductivity and shear viscosity in static mag. field and field free space 2—35687
- carbon tetrafluoride-fluoroform system, heat capacity near consolute point 2—9123
- carbon tribromofluoride and trichlorobromide, crystal structure, i.r. absorption 2—40683
- carbonium ion, desorption from Pt and zeolite surfaces 2—6390
- carbonium ions, electronic structure, LCAO calculations 2—31843
- carbonyl compounds, conformation from obs. of n→π* transition sensitivity to solvent effects, importance of hindered carbonyl bisection 2—24521
- carbonyl fluoride, calc. of inertia defects, vibrational-rotational interaction constants and force constants 2—8749
- carbonyl group containing molecules, i.r. spectra, stretching and torsional modes obs. 2—8750
- carbonylbis(1-aziridine), vibrational analysis 2—15361
- carbonylbis (1-aziridine), i.r. and Raman spectra, vibrational analysis 2—12219
- carboxylic acid dimers, saturated, simulation of abnormal i.r. spectra due to H-band proton stretching vibrations 2—15360
- carboxylic acid hydracides, N-H vibration intensities calc. 2—8748
- carboxylic acid salts, H atom position in A-type H-bands 2—8747
- carboxymethylcellulose in water, free convection of heat from a vertical plate 2—37812
- catalase, electron microscopy, Fourier image processing 2—9417
- cellulose, paracryst. lattice disorder 2—25165
- cellulose acetate, surface cond., water vapour adsorption depend. 2—39547
- cellulose nitrate, use as detector film in alpha autoradiography 2—36191
- cellulose nitrate film used for detection of α-particles 2—11679
- cellulose nitrate for α-particle track visualisation, use in undergraduate laboratory 2—33840
- cellulose tricarbanilate, chain length depend. of mean square radius of gyration 2—862
- cetane-water interface, meas. of interfacial velocities 2—25053
- cetyl alcohol, adsorption on water drops 2—1061
- cetyl alcohol, proton injection measurements 2—25847
- n-cetyl alcohol and its solutions, solidification, dielec. anomalies 2—3443
- p-cetyloxybenzoic acid, p-methacrylyloxybenzoic axid and styrene liquid crystalline mixtures copolymerization 2—20185
- charge transfer complexes, sensitization of ZnO electrophotographic papers 2—40832
- 1-chlor-3-fluor-propyne, numerical stability of centrifugal distortion analysis 2—755
- p-chloranil, transient photocurrents, exciton diffusion 2—4306

Organic compounds continued
- chloranil amine charge transfer complex, e.p.r., elec. cond. 2—25832
- chloraniline+n-dinitrobenzene complex, geometry, molecular orbital calc. 2—35318
- chlorinated hydrocarbon residues, airborne fallout, anal. in freshwater ecosystem 2—37171
- chlorinated methylbenzenes, ^{35}Cl n.q.r. spectra, influence of vibr. and reorientations of CCl$_3$ groups 2—10590
- chloro maleic anhydride, vibrational spectra, assignment and force constant calc. 2—12223
- 2-chloro-1-butene vibrational assignment and rotational isomerism 2—24519
- 7-chloro-2,3-dihydro-1-methyl-5-phenyl-1,4-benzodiazepin-2-one, 1:1 complex with chloral hydrate, molecular and crystal structure determ. by heavy atom method 2—9505
- 1-chloro-2-bromoethane, i.r. band intensities, energy differences of rotational isomers 2—21677
- chloro-2-butyne, force constants determ. from normal cordinate calculations 2—21668
- 3-chloro-2-chloro-methyl-1-propene, rotational isomerism 2—28382
- chloro- and bromocyclopentane, vibrational spectra, conformational analysis 2—18495
- chloroacetaldehyde, microwave spectrum at 8 to 40 GHz, quadrupole coupling constant meas. 2—8752
- 4-chloroacetophenone, single crystal e.p.r. studies of photoexcited states 2—26360
- 2-chloroacrylonitrile, inter- and intramolecular dipole relaxation effects in double resonance spectra 2—21671
- p- chloroaniline, lowest singlet state in pure and mixed crystals 2—40684
- p-chloroaniline, pure cryst. absorption spectrum of lowest singlet state, vibronic intensity pattern 2—20054
- 2-chloroaniline-^{15}N, long-range coupling constants to amino protons from ring protons 2—21670
- chlorobenzene, Cotton-Mouton const. and absolute phase delay of light waves 2—15598
- chlorobenzene, far i.r. absorption interpreted by correlation function for rotational velocities 2—39368
- chlorobenzene, partially deuterated derivatives, n.m.r., incremental aromatic solvent induced shifts 2—18488
- chlorobenzene, quadrupole hyperfine structure in rotational spectrum analysed 2—12216
- chlorobenzene, temp. dependence of widths and integrated intnsities of polarized Raman lines 2—28351
- chlorobenzene-D$_5$, near u.v. absorption spectrum vibrational analysis 2—3075
- p-chlorobenzotrichloride, struct. and molecular motion, n.q.r. obs. 2—5966
- 1-chlorobenz[α]phenazine-7N-oxide, cryst. struct 2—12740
- 2-chlorobutane, rotational isomerism from i.r. spectra in crystalline and glassy states 2—40685
- chlorocyclobutane, ring-puckering vibration, far i.r. study 2—15366
- chloroethane, gaseous, second density virial coeffs. 2—15535
- chloroethylenes, π characteristics, SCF-LCAO theory 2—15364
- chlorofluorobenzene, transition moments, band contour anal., changes in rot. const. on excitation 2—12213
- chlorofluoroethylenes, far u.v. spectra, band assignment 2—12242
- chlorofluoromethanes, gaseous, second density virial coeffs. 2—15535
- chlorofluoromethanes, gaseous, second dielectric virial coeffs. 2—15536
- chlorofluoromethanes, gaseous total electric polarization 2—15543
- chloroform, ^{13}C n.m.r. relaxation, temperature dependence 2—38951
- chloroform, approx. force field 2—3076
- chloroform, Cotton-Mouton const. and absolute phase delay of light waves 2—15598
- chloroform, far i.r. absorption interpreted by correlation function for rotational velocities 2—39368
- chloroform, gaseous and solid, X-ray K-absorption spectra 2—3036
- chloroform, liq., proton spin lattice relaxation times, −54 to +90°C 2—9179
- chloroform, temp. dependence of proton spin-spin relaxation time over range −54 to +90°C 2—22009
- chloroform, temp. dependence of widths and integrated intensities of polarized Raman lines 2—28351
- chloroform and proton acceptor complexes, H bonded, obs. i.r. transitions involving vibrations 2—8754
- chloroform autocorrelation functions of dipole moment theoretical and experimental values compared 2—38985
- chloroform-carbon tetrachloride liquid system, tracer and mutual diffusivities 2—25065
- chloroform-D$_1$, approx. force field 2—3076
- chloromethyl radical, e.s.r. study in CH$_3$Cl single crystal 2—8792
- p- chlorophenol, α and β phases, crystal structure determ. by heavy atom method 2—6458
- chlorophyll-a films, conductivity and photovoltaic effects 2—26942
- chloropropene, rotational isomerism 2—28381
- 2-chloropropenes, deuterium substituted, microwave spectra, CH$_3$gp conformation 2—31844
- 3-chloropropyne, force constants determ. from normal coordinate calculations 2—21668
- p-chlorostyrene chains, dipole moments and random coil dimensions 2—8753
- chlorosubstituted, determ. of basicity from spectroscopic data 2—16670
- chlorotricyanomethane, cryst. struct. 2—32478
- chlorotrimethylsilane, mass transfer during film boiling, SiC deposition rel. to high modulus fibre preparation 2—1152
- chloroxylene, vibrational spectra 2—35309
- cholesteric esters, transparency characts., solid to isotropic liq. phase 2—9132
- cholesteric liq. cryst., ambient temp. rel. to liq. cryst. tape system 2—9124
- cholesteric liq. crystals, texture, pitch contraction, d.c. elec. field induced 2—6209
- cholesteric mixtures, flow behaviour 2—39338
- cholesterol acetate, stearate, laurate, and myristate, electret thermal analysis 2—1078
- cholesterol and thiocholesterol esters, high resolution NMR spectra, transition temps. 2—15574
- cholesterol esters, polymorphic and mesomorphic behaviour 2—25039
- cholesterol esters liquid crystals, Raman spectra 2—28869
- cholesteryl 2-(2-ethoxy ethoxy) ethyl carbonate liquid crystal, dynamical behaviour of ordering just above transition to cholesteric phase 2—32235

Organic compounds continued
cholesteryl acetate, liquid crystal, transformation kinetics and properties 2—6208
cholesteryl acetate, u.s. velocity near cholesteric-isotropic transition point 2—21983
cholesteryl benzoate, u.s. velocity near cholesteric-isotropic transition point 2—21983
cholesteryl bromide, liquid crystal, phase transition, small angle X-ray obs. 2—3364
cholesteryl formate, u.s. velocity near cholesteric-isotropic transition point 2—21983
cholesteryl laurate, dielec. const. temp. depend. on cycling, supercooling 2—35781
cholesteryl myristate, liquid crystal, transformation kinetics and pretransition effects 2—6207
cholesteryl myristate/p-methyoxybenzylidene- p′n-butyl aniline mixed system, helical liquid crystal phases 2—25050
cholesteryl nonanoate-iodide mixture, film, change of pitch on u.v. exposure 2—12541
chromium(III) trisacetylacetone film, semiconductivity 2—36522
chromium organometallic derivatives, correlation between ionization potentials of complexes and free ligands 2—18494
chromocene, photoelectron spectra, band intensities from theory for open shell molecules 2—31741
chromone, u.v. absorption spectra, band assignment, solvent and substituent effects 2—28360
chromones, 2-substituted, u.v. absorption spectra, band assignment, solvent and substituent effects 2—28360
chrysene, phosphorescent, in *p*-terphenyl host crystal, multiplet structure in low-field e.p.r. spectra 2—20139
chrysene, principal axis orientation of e.s.r. 2—15363
chrysene, single cryst., prep. and characterization 2—19009
chrysene, transient absorption spectra using laser photolysis apparatus 2—21672
cinnamaldehyde-imines, n.m.r. study 2—5967
N,N-cinnamamides, para- and meta-substituted, substituent effect on i.r. carbonyl stretching vibrations and hydroxyl frequency shifts 2—38977
clathrate-type double hydrates, n.m.r. study of molecular movement 2—847
clycocyamine hemihydrate, atomic struct., X-ray determ. 2—3748
clycol alcohol, mol. rot., influence of H-bond, cold neutron transmission obs. 2—15349
clyopentanone, photoelectron spectrum 2—838
cobalt (III) complexes, emission spectra of ^{57}Co following electron capture 2—19975
conjugated radicals, calculation of hyperfine splittings in e.s.r. spectra 2—38953
copper(II) acetates, low temperature infrared spectra 2—35320
copper (II) carboxylates, symmetry, e.p.r. obs. 2—28362
copper acetate power, e.s.r. spectrum at 12 katm. 2—27370
copper benzene sulphonate hexahydrate crystals, e.p.r. 2—13529
copper formate tetradeuterate, sublattice rotation and spin deviation, n.m.r. study 2—4410
copper formate tetrahydrate, dielec. response function 2—13322
copper formate tetrahydrate and deutero derivative, vibr. freqs. 2—10341
copper heteroorganic acetylenides, absorption and photoconduction spectra investigated by diffuse reflection spectroscopy 2—29922
copper hexadecachlorophthalocyanine, in epitaxial films 2—9292
copper phthalocyanine, band structure and deformation potentials 2—4128
copper phthalocyanine, thermo e.m.f. temp. depend. 2—36606
copper phthalocyanine films, photo-e.m.f. spectra, near i.r. 2—6907
copper stearate monolayers, struct., e.p.r. obs. 2—13546
coronene, Hg heavy atom impurity effect on luminescence 2—3125
coronene, in n-paraffin monocrystals, dependence of luminescence spectrum on crystallization conds. and conc. 2—20098
coronene, in paraffin solns. of naphthalene, dependence of fluorescence spectra sharpness on conc. 2—1714
coronene, internal conversion meas. of fluorescence yields and triplet state prod. 2—3121
coronene, reorientation of molecule in solid state, n.m.r. investigation 2—10567
coronene, spectral shifts in nonpolar solvents, mechanism 2—25093
coronene crystals, calculation of band structure and carrier mobilities 2—25727
coronene impurity molecules in isooctane crystals, effect of polymorphic transformations on luminescence spectra 2—29959
coumarin and related molecules, triplet-triplet absorption studies on 11000-27000 region 2—12225
coumarins, assignment of lowest excited singlet and triplet states on basis of luminescence measurements 2—12226
coumarins, u.v. spectra, description of $\pi-\pi^*$ transitions 2—8755
o-cresol, amorphous, deposited at low temperatures 2—28970
cresyl violet, flashlamp pumped dye lasers, mode locking and freq. tuning 2—17611
cresyl violet dye laser, continuous, mode locked, pumped in red. 2—17608
cresyl violet laser, flashlamp and laser pumped, characteristics 2—21082
crotonaldehyde, vibrational-electronic bands of $S_1(n,\pi^*)$ 2—35336
crude oil, p.m.r. freq. and temp. depend. 2—9165
crystal structure, approx. translation or rotation symmetry, X-ray method 2—32477
crystal violet dye, spectrophotometry, isomerism study 2—3077
crystals, low temp. study of radiation damage prod. by 100 keV electrons 2—25383
crystals, molecular interactions and molecular interaction energy 2—1199
cumene, phosphorescence spectra, frozen matrices, liq. nitrogen temps. 2—4502
cumulenes, rotating barrier end groups 2—837
cyanamide, electronic structure and nonplanarity, CNDO/2 calculations 2—28364
cyanamide group, electronic structure 2—28393
cyanide, CH_2N_2 isomer, N quadrupole coupling const. calc. 2—8751
cyanine dyes, triplet-state e.p.r. 2—38973
cyanine dyes for laser generation 7000-11000 Å 2—14423
cyanocyclobutane, ring-puckering vibration, far i.r. study 2—15366
cyanogen azide, infrared and Raman spectra measured 2—12232
2-cyanopyridine, microwave spectrum, assignment of transitions 2—840
cyanopyridine vapour, isomers, absorption spectra, $^1n\rightarrow{}^1\pi$ transition 2—31846

Organic compounds continued
cyanuric trifluoride, pure rotational Raman spectra and bond length det. 2—35357
cyclic alkanes, excited electronic states, sharp vibronic structure 2—12205
cyclic AMP, effect on lateral eye retinular cells in horseshoe crab 2—7627
cyclic molecules, contribution of trichloromethyl group to dipole moments 2—38952
cyclic phosphonium iodide, cryst. and mol. struct. 2—6465
1,3- cyclo-hexadiene, vibronic structure of first singlet calculated 2—12083
cyclobutane, i.r. and Raman spectra, vibrational assignments for D_{2d} symmetry 2—28365
cyclobutane, valence orbitals, symmetry properties 2—28363
cyclobutane carboxylate, structure investigation from vibrational, i.r. and Raman spectra 2—5969
cyclobutane-carboxylic acid vibrational spectra 2—24523
cyclobuta[b]quinoxalines, electronic spectra measured, calculated values of transition energies and oscillator strengths 2—12229
cyclohexane, delayed fluorescence, self-diffusion mechanism 2—4501
cyclohexane, excited electronic states, sharp vibronic structure 2—12205
cyclohexane, fluidized by water, coalescence rates 2—1126
cyclohexane, gaseous, conformation study by electron diffraction 2—5970
cyclohexane, investigation of Rydberg states 2—31845
cyclohexane, plastic phase, radical doped, molecular motion, e.p.r., ENDOR 2—26292
cyclohexane, self-diffusion in plastic crystals 2—32569
cyclohexane, solid, rot. transitions, obs. and theory 2—15977
cyclohexane, solid and liq., ionization cond., temp. and elec. field depend. 2—7188
cyclohexane, spin echo n.m.r. 2—35790
cyclohexane, translational self diffusion, press. depend. 2—29228
cyclohexane, vapour, γ-irradiated, av. energy per ion pair 2—15498
cyclohexane cryst., far-i.r. absorpt. external vibr. lines broadening at melting pot. 2—20053
cyclohexane diperoxide, chem. induced dynamic nucl. polarization, in biradical prods. 2—8756
cyclohexane on NaY-zeolite, proton relax., −140 to 80°C 2—26086
cyclohexane solution of octylamines, dielectric relaxation 2—35780
cyclohexane velocity and absorption of shear waves near melting point 2—29536
trans-cyclohexane-1,4-dicarboxylic acid, cryst. struct. 2—35999
trans-cyclohexane-1,4-dicarboxylic acid, K salt, struct., bond lengths 2—36000
cyclohexane-aniline binary liquid system near critical mixing temp., viscosity 2—1085
cyclohexane-aniline binary mixtures, study of critical behaviour by light diffusion 2—35764
cyclohexane-aniline mixture, scattered light intensity and turbidity meas. rel. to determination of criticial exponent 2—21987
cyclohexane-d_{12}, investigation of Rydberg states 2—31845
cyclohexane-d_{11}, liquid crystalline solvent, n.m.r. 2—6258
cyclohexanol, dendritic growth from stagnant or flowing liquid 2—3582
cyclohexanol, growth from the melt, anisotropy 2—1214
cyclohexanone, interaction with compounds containing –OH, C=O valence oscillation line shift 2—8787
cyclohexene on NaY-zeolite, proton relax., −140 to 80°C 2—26086
Δ^3cyclohexenecarboxylic acid, mol. association, proton mag. reson. chem. shift 2—28899
cyclohexyl benzene, Raman spectrum obs. 2—3079
cyclononane, conformation, from n.m.r. spectra 2—24522
cyclooctane, self-diffusion, vacancy mechanism, NMR linewidth meas. 2—15793
cyclooctanone, temperature and phase dependence of position lifetimes, -130-+56°C 2—29485
cyclooctatetraene and related systems, electronic structure, ab initio SCF LCAO MO calc. 2—3078
cyclopentadiene, vibrational analysis of photoelectron spectra 2—3097
cyclopentadienyl thallium, Coriolis consts. from microwave spectrum 2—15268
cyclopentane, barrier to planarity, Raman spectroscopic determination 2—15365
cyclopentane, CNDO calc. of pseudorotational potential energy 2—8546
cyclopentane, critical region scale law, verification 2—25151
cyclopentane, halogen derivatives, conformation and vibrational spectra 2—35323
cyclopentane, solubility in liquid methane and liquid Ar 2—1080
2- cyclopentane-1-one, molecular Zeeman effect 2—12231
cyclopentanone, far i.r. spectra and hindered pseudorotation 2—35322
cyclopentanone, gas phase and in solution, i.r. spectra study of Fermi resonance in $\nu_{c=o}$ region 2—24524
cyclopentanone in hexane soln., conc. depend. of absorpt. band 2—25096
cyclopentene, e.s.r. of cation radicals adsorbed on zeolites 2—21656
cyclopentene, Raman spectra, ring puckering vibrations, C-H stretching bands 2—35324
cyclopentenones, photoelectron spectra 2—838
cyclopropane, analysis of $\nu_5+\nu_{10}$ band, l-type resonance effects 2—8757
cyclopropane, generalized valence bond orbitals 2—8758
cyclopropane, i.r. absorpt. and Raman scatt., vibr. transitions 2—33278
cyclopropane, MO calc. of geometry, energy and polarity 2—28383
cyclopropane, solid, rot. transitions, obs. and theory 2—15977
cyclopropane, study of l-type resonance effects in $\nu_5+\nu_{10}$ band 2—21674
cyclopropane, valence bond calcs. of vicinal proton coupling consts. 2—38974
cyclopropane and derivatives, anisotropy of polarizability 2—839
cyclopropane intermediates, protonated, evidence for existence in crossed-beam ion reactions 2—37034
cyclopropane liquid, γ-irradiated, molec. structure effect on electron reaction kinetics 2—10649
cyclopropanone, closed- and open-ring structure investigated in LCAO-MO-SCF calculation 2—12228
cyclopropene, MO calc. of geometry, energy and polarity 2—28383
cyclopropyl carbinyl chloride, microwave spectrum and rotational isomerism 2—15367
cyclopropyl carbinyl fluoride, microwave spectrum and rotational isomerism 2—15367
cyclopropyl methyl ether, microwave spectrum, dipole moment component determination from quantitative Stark effect meas. 2—12230
cyclopropyl methyl ketone, microwave spectrum, barrier to internal rotation, dipole moment, conformation 2—21673
cyclopropylacetylene, microwave spectrum, structure, and dipole moment 2—35321

Organic compounds continued
- cyclorubber film with bis-azides, dependence of light sensitivity on solvent 2—27672
- cyclotrimethylene trinitramine, defect struct., X-ray determ. 2—9563
- cyclotrimethylene trinitramine, dislocations correl. with etch pits, X-ray obs. 2—3783
- L-cystine dihydrochloride, γ-irrad. cryst., photoinduced hole-electron recombination 2—22887
- decalin, nuclear spin-lattice relax. time calc. 2—32280
- decalin, supercooled, dielectric relaxation of rigid molecules in solution 2—35776
- decanal oxime O-methyl ether-urea inclusion crystals, X-irradiated, e.s.r. of trapped alkylalkoxyamino radical 2—13592
- n-decane, heat capacity at elevated press. 2—25072
- decane, liq., explanation for spectra in terms of 2-phonon absorption 2—1104
- decane-chlorex, liquid mixtures, critical exponent determination by scattering studies 2—9133
- n-decanol, self association study using dielectric constant measurements 2—21956
- 1-decanol-urea X-irradiated inclusion crystals, e.s.r. of trapped radicals 2—20153
- deoxycytidine-3′-monophosphate, energy calcs. for isomeric structure using extended Huckel theory 2—12234
- deoxycytidine-3’-monophosphate, semi-empirical MO calculations for isomeric structures 2—12235
- deuterated completely, ^{13}C-n.m.r. spectra, deuterium isotopic shift 2—8715
- deuteroethylene + F, crossed molecular beam study 2—37021
- dextrose, charred, e.p.r. meas., g-factor standard for wide temp. range 2—7126
- di(2-ethylhexyl) sebacate, viscosity, absolute measurement 2—39346
- di(2-ethylhexyl) sebacate, viscosity, absolute measurement 2—39347
- di(2-ethylhexyl)phthalate, viscoelasticity at pressures up to 1400 MN/m^2 2—39307
- di-t-butyl nitroxide, magnitude of multiplet splitting in X-ray photoelectron spectra, spin density implications 2—8672
- di-tert-butyl nitroxide, lipid spin labels in e.s.r. studies of biological membranes 2—20717
- 4,4′-dialkoxy-trans-stilbenes, phase transform, linkage group effects, permanent dipole 2—9099
- diamagnetic molecules, positronium quenching by carbonium ion 2—3065
- diaminodiphenylmethane isomers and their diisocyanates, i.r. and u.v. spectra 2—28371
- dianthracene anion radical, in γ-irradiated rigid ethereal solutions at 77K, absorption spectra 2—24502
- diaryl butadiene solutions, pumped by ruby laser, optical generation 2—6238
- diaryldialkoxysulphurane, X-ray crystal structure 2—25355
- diarylethanes, meas. by electron impact mass spectrometry, search for ring orbital interaction 2—35325
- diarylmethanes, meas. by electron impact mass spectrometry, search for ring orbital interaction 2—35325
- diarylthallium (III) derivatives, aromatic ring vibrations 2—21679
- 4,10-diazachryzene, in lowest triplet state, acid-base equilibria 2—18497
- 1,2- diazadiene-1,3 compounds, config. from electronic spectra 2—18483
- diazanaphthalenes, photoelectron spectra, ordering of π and nitrogen lone pair orbitals 2—15371
- diazanaphthalenes, triplet state population and depopulation, phosphorescence-microwave double-resonance meas. of zero field splittings and kinetic parameters 2—22810
- 9,10-diazaphenanthrene, rigid glass soln., intersystem crossing rate constants 2—10426
- diazaphenanthrenes, linear correlation between ^{1}H chem. shift and electron density 2—24551
- diazaphosphetidines, ^{19}F NMR spectra meas. and interpreted 2—28366
- 1,4-diazatriphenylene in frozen solns. at 77 K, phosphorescence kinetics 2—26244
- diazirine, CH_2N_2 isomer, N quadrupole coupling const. calc. 2—8751
- diazoaminobenzole, 2,5-dinitropyrole, spin-lattice relaxation of ^{15}N, temp. depend. 2—13424
- diazomethane, CH_2N_2 isomer, N quadrupole coupling const. calc. 2—8751
- diazomethane, comparative study of random phase approx. Hartree Fock of single excited configuration interaction methods of computing excitation energies 2—15277
- 1,2;5,6-dibenzanthracene, principal axis orientation of e.s.r. 2—15363
- 1,2,7,8 dibenzanthracene, transient absorption spectra using laser photolysis apparatus 2—21672
- dibenzene chromium TCQM complex, cryst. and molecular struct. 2—19066
- dibenzoylperoxide, chem. induced dynamic nucl. polarization, mag. field depend. 2—7182
- dibenzyl disulphide, space group ambiguity 2—22171
- dibenzyl ether, temperature dependence of flow birefringence 2—6232
- dibenzyl mercury, far i.r. and Raman spectra, vibrational assignment 2—21665
- dibromo maleic anhydride, vibrational spectra, assignment and force field derivation 2—12222
- α,ω-dibromoalkanes in benzene solutions, dielectric relaxation 2—1109
- 2,4-dibromoaniline, ^{79}Br n.q.r., temp. variation, 77-302K 2—40793
- 2,4-dibromoanisole, n.q.r. of ^{81}Br, Zeeman effect 2—8745
- 9, 10-dibromoanthracene, laser induced photocond. 2—16320
- p-dibromobenzene crystals, absorption spectra, 4K, exciton zone analysis 2—26208
- 1,4-dibromobutane solution, dielec. props., effect of solvent viscosity 2—18846
- 1,2-dibromoethane, i.r. band intensities, energy differences of rotational isomers 2—21677
- 1,6-dibromohexane solution, dielec. props., effect of solvent viscosity 2—18846
- 1,5-dibromopentane solution, dielec. props., effect of solvent viscosity 2—18846
- 1,2-dibromoperfluoropropane, ^{19}F n.m.r. spectra, conformational energy difference between gauche and trans isomers 2—28359
- 1,3-dibromopropane solution, dielec. props., effect of solvent viscosity 2—18846
- dibutyl phthalate aerosol, Brownian coagulation 2—32290
- dibutylphthalate aerosol, electric field effects on deposition in fibrous filters 2—28915
- dicalcium lead propionate, u.s. attenuation near phase transition 2—19415

Organic compounds continued
- dicarboxylic acid-NH_4ClO_4 mixtures, burning velocity dependence on pressure 2—7172
- dichloro maleic anhydride, vibrational spectra, assignment and force field derivation 2—12222
- dichloro-1,8 methyl-10 anthacene in solution, fluorescence spectra, observation of longer wavelength emission during freezing and reheating 2—9139
- 1,1-dichloro-1-nitroethane solution, dielec. props., effect of solvent viscosity 2—18846
- dichloro-difluoro-methane, visible luminescence, irradiation by 10.6μ CO_2 laser pulses 2—35273
- 9, 10-dichloroanthracene, laser induced photocond. 2—16320
- p- dichlorobenzene, α-ray irrad., impurity form., cryst. struct. effect, n.q.r. obs. 2—26317
- p-dichlorobenzene, γ-phase, polycrystalline, far i.r. spectra meas. 2—7077
- p-dichlorobenzene, first $^3\pi\pi^*$ state, optically detected mag. resonance 2—8763
- p-dichlorobenzene, phosphorescence microwave double resonance spectra 2—8568
- p-dichlorobenzene crystals, absorption spectra, 4K, exciton zone analysis 2—26208
- 2,5-dichlorobenzenesulphonic acid trihydrate, hydrogen bonding and cryst. struct. 2—29156
- dichlorodi fluoromethane, interference effect in nucl. mag. relax. 2—9180
- 4,4′- dichlorodiphenylamine, growth of pure single crystals from vapour 2—3577
- dichlorodurene, nuclear magnetic relaxation times meas. interpreted in terms of molecular reorientation 2—20167
- 1,2-dichloroethane, equil. const. and pot. barrier for rot. isomers 2—21676
- 1,2-dichloroethane, i.r. band intensities, energy differences of rotational isomers 2—21677
- 1,2-transdichloroethane, orientational disorder and i.r. and Raman spectra calc. using intermol. potentials 2—25357
- dichloroethane, shock compressed, opacity, absorpt. spectra 2—35770
- dichloroethane and d_3 analogue, primary steps in photolysis at 25°C 2—33384
- 1,1-dichloroethylene, crystal structure study by i.r. and Raman spectroscopy 2—6460
- 1,2-dichloroethylene, isomerization photosensitization by benzaldehyde 2—10637
- dichloroethylene, mol. orbital interpret. photoelectron and X-ray emission spectra 2—35328
- dichloroethylene, photoelimination reactions, tandem laser meas. of vibr. energy distrib. 2—33388
- dichlorofluoroacetamide, N,N-dichlorofluoroacetamide-d_2, X-irradiated, e.s.r. study of chlorofluoroacetamide radical 2—26267
- dichloromethane, vapour, γ-irradiated, av. energy per ion pair 2—15498
- 2,3dichloronaphthoquinone, i.r. and Raman spectra, vibr. assignment of obs. bands 2—31849
- 3,4-dichloronitrobenzene, n.q.r. Zeeman spectra of ^{35}Cl 2—13560
- 1,2-dichloroperfluoropropane, ^{19}F n.m.r. spectra, conformational energy difference between gauche and trans isomers 2—28359
- 3,5-dichlorophenol, temp. dependence of Cl.n.q.r. frequencies, torsional frequencies 2—28419
- dichlorophenols, and deuterated analogues, vibrational analysis of i.r. spectra 2—3080
- dichlorophenols, electronic absorption spectra in vapour phase, vibrational assignment 2—35319
- dichlorophenols, i.r. and Raman spectra, fundamental assignment 2—8764
- 4,11-dichloroquinacridone, vacuum sublimation and cryst. struct. 2—6466
- 2,3-dichloroquinoxaline, phosphorescent triplet $\pi\pi^*$ state, adiabatic inversion 2—21581
- dichlorosilicon, phthalocyanine, structure from i.r. spectrum 2—38972
- dichroic sheet, thermal lensing and optical damage 2—5396
- dicyclohexane, proton spin-lattice relax. and C-C bond pot. barrier 2—8760
- dicyclohexylhydroxymethylphosphine oxide, i.r. spectra rel. to H-bonding 2—15370
- N,N′-dicyclohexylurea, mol. packing determ. using pot. energy calcs. 2—6459
- dideutero methyl iodide, i.r. spectrum meas. analysis of fundamental bands, value for A_0 determ. 2—12221
- diethyl amine, vibrational spectra and rotational isomerism 2—3082
- diethyl ether, quantitative liquid-phase spectra, absorptivity in 2.5-13μm region 2—32270
- diethyl mercury, symmetry group for classification of vibrational modes 2—18503
- 1,1′-diethyl-2,2′-cyanine bromide, crystal structure determination by X-ray diffraction 2—3746
- 1,1′-diethyl-4,4′-cyanine bromide, crystal structure determination by X-ray diffraction 2—3746
- diethyl-α-hydroxyisopropylphosphonate, i.r. spectra rel. to H-bonding 2—15370
- N,N′-diethyl-pseudoisocyaninchloride, cryst. and mol. struct. 2—9506
- trans-15,16-diethyldihydropyrene, p.m.r. spectra, and π-electron loop separation 2—38979
- diethyleneglycoldiethylether-water mixture, near critical point, u.s. absorp. 2—28854
- 3,3′-diethylthiacarbocyanine iodide, photographic sensitizer, thermal activation energy of conducting process and electron trap depths 2—16319
- 3,3′-diethylthiacyanine iodide, photographic sensitizer, thermal activation energy of conducting process and electron trap depths 2—16319
- difluoro diazirine, centrifugal distortion constants 2—3081
- p-difluorobenzene in nonpolar solvents, power absorption coeff. and refractive index using submillimetre waves 2—39367
- difluorobenzenes, isomeric, electronic emission spectra, vibrational assignment 2—35330
- 2,2′-difluorobiphenyl, conjugated system, pot. function for rotation about CC single bonds, CNDO/2 calc., inaccuracy of method 2—3099
- 1,1-difluoroethylene, effect of pressure on gas permeability coefficients in polyethylene 2—35691
- 1,1-difluoroethylene, gaseous, second density virial coeffs. 2—15535
- 1,1-difluoroethylene, gaseous, second dielectric virial coeffs. 2—15536
- 1,1-difluoroethylene, gaseous, total electric polarization 2—15543
- difluoroethylene isomeric mols. in charge transfer reactions with rare gas ions 2—35384
- difluoroethylenes, solvent and temp. dependence of H—H, H—F and F—F coupling consts. 2—31851
- 2,2-difluoropropane, vibrational assignment of Raman and i.r. spectra 2—3083

Organic compounds continued
- diflurobenzene, transition moments, band contour anal., changes in rot. const. on excitation 2—12213
- digermane, bond flexibility force constants 2—31853
- diglycine monopicrate, atomic struct., X-ray determ. 2—3748
- diglycine sulphate, prep., struct., and dielec. props. 2—36594
- diglyme, solvent for investigation of Li isotope exchange reactions 2—22855
- dihaloacetylenes, force constant determination 2—38970
- 1,2-dihaloalkanes in various solvents, n.m.r., effect of solvent on vicinal proton coupling constants 2—12240
- dihalodiphenyl derivatives of group IV elements, n.m.r. investigation 2—15395
- 4,4′dihalogenobiphenyls, vibrational spectra and dihedral angles 2—38967
- 2,5-dihydrofuran, far i.r. spectrum, calc. using two-dimensional anharmonic oscillator 2—15368
- 2,3-dihydrofuran, microwave spectra for vibrational states of ring bending mode, Stark effect meas. 2—12237
- 2,5-dihydrofuran, Raman spectra, ring puckering vibrations, c-h stretching bands 2—35324
- 2,5-dihydropyrrole, microwave spectrum in ground and first vibrational excited states 2—18496
- 1,2-dihydroquinoline, photochromic, CNDO/CI study of electronic spectrum 2—28370
- 5,6-dihydrouracil-6-yl radical, conformation studies in mol. crysts. 2—15372
- diimide, ab initio CI treatment of ground and excited states 2—12086
- diiodomethyl radical, matrix i.r. spectrum, vibrational assignment 2—8800
- diisobutyl carbinol, fluidized by water, coalescence rates 2—1126
- diketene, molecular Zeeman effect, magnetic properties and electric moments 2—21675
- dimercaptodiethyl sulphide, i.r. spectra, configuration 2—8769
- dimethoxy di-benzo suberone, crystal structure, X-ray crystallographic data 2—6456
- 4,4′-dimethoxybenzophenone, e.p.r., triplet state, g-tensor anisotropy 2—8762
- dimethyl benzamide, hindered rotation, applic. of multi-site exchange theory 2—22853
- N,N-dimethyl carbamyl fluoride, hindered rotation, n.m.r. study 2—22852
- trans-15,16-dimethyl dihydropyrene, p.m.r. spectra, and π-electron loop separation 2—38979
- dimethyl ether, gaseous, second density virial coeffs. 2—15535
- dimethyl ether, gaseous, total electric polarization 2—15543
- dimethyl ether, gaseous second dielectric virial coeffs. 2—15536
- dimethyl ether+other polar gases, second dielectric virial coeffs. 2—15537
- dimethyl oxalate, valence field force constants obtained by normal coordinate analysis 2—8793
- dimethyl platinum, i.r. spectra 2—831
- dimethyl pyridine, vibratory spectra, interpretation and freq. calc. 2—38998
- dimethyl sulphide, vibrational spectra 2—38994
- dimethyl sulphone, vibrational spectra 2—38994
- dimethyl sulphoxide, oriented p.m.r. spectra, rel. to MO studies of $^4J_{hh}$ 2—28339
- dimethyl sulphoxide, permeability and diffusion coefficients in polyethylene membranes 2—35752
- dimethyl sulphoxide, vibrational spectra 2—38994
- dimethyl sulphoxide effects on conduction velocity of homarus axons 2—41279
- dimethyl trichalcogenocarbonate, Se-containing, mass spectra and n.m.r. spectra 2—21678
- dimethyl trifluoroacetamide, hindered rotation, applic. of multi-site exchange theory 2—22853
- 2,2-dimethyl-4-cyclopentene-3,5-dione, soln. and vapour, electronic spectra, absorption band assignment 2—8788
- N,N-dimethyl-thiourea S-trioxide, crystal- and molecular structure study by heavy atom method 2—5996
- N,N-dimethylacetamide, hindered internal rot., activation parameters, solvent effects, n.m.r. obs. 2—12255
- dimethylacetamide, hindered rotation, applic. of multi-site exchange theory 2—22853
- N,N-dimethylacetamide, valence force field and A′ symmetry vibrations 2—841
- dimethylalanine:Cu^{2+}, e.p.r. of cationic radicals formed by u.v. irradiation at 77K 2—30090
- dimethylallene, microwave spectrum, barrier to internal rot., rot. consts. dipole moment, r_0-type structural data 2—18499
- dimethylamine in solution 22-190°C, i.r. study of association and NH stretching vibration modes 2—28368
- p-dimethylaminobenzaldehyde hydrobromide, crystal and molec. structure, x-ray determination 2—39660
- dimethylaminodichloroarsine, vibrational spectrum and molecular structure 2—24528
- dimethylaminodichlorophosphine, vibrational spectra and structure 2—28369
- p-dimethylaminostyryl dyes, sensitization of nuclear track emulsions, creation of unstable traps for conductivity electrons 2—27916
- dimethylammonium trichlorocuprate (II), low-temp. mag. susceptibility 2—33177
- N,N-dimethylaniline systems, formation of ion radicals from the non-relaxed state of excited charge transfer systems 2—37039
- N,N-dimethylbenzamides, para- and meta-substituted, substituent effect on i.r. carbonyl stretching vibrations and hydroxyl frequency shifts 2—38977
- 2,3-dimethylbutane, solubility in liquid methane and liquid Ar 2—1080
- dimethylcadmium, structure study, normal coordinate analysis 2—21680
- 3,3′-dimethyldiazirine, electronic absorption spectra 2—24526
- dimethyldisulphide, molecular structure, electron diffraction study 2—24529
- 1,2- and 1,3-dimethylenecyclobutane, molecular symmetries determ. from vibrational spectra 2—12238
- 3,4-dimethylenecyclobutene, vapour and film, i.r. spectra 2—10398
- N,N-dimethylformamide, hindered internal rot., activation parameters, solvent effects, n.m.r. obs. 2—12255
- dimethylformamide, proton, deuteron and nitrogen resonance in nematic polypeptide liquid crystals 2—31847
- dimethylformamide as solvent for electrochemical study of H isotope exchange reactions 2—22854
- dimethylformamide in benzene, mol. assoc. effects on INDOR 2—25110

Organic compounds continued
- 1,3-dimethylindazole, electronically excited, temp. dependence of deactivation in solution 2—3119
- dimethylketene, rotational Zeeman effect in microwave spectrum, determ. of molecular g-tensor 2—38978
- dimethylmecury, structure study, normal coordinate analysis 2—21680
- dimethylmercury, valence force field determ. from vibrational freqs. of d_0 and d_6 species 2—5972
- 1,1′-dimethylmetallocenes, ^{13}C n.m.r. contact shift studies, spin delocalization 2—24531
- 1,6-dimethylnaphthalene, loaded liquid scintillator, measurement of decay times 2—11664
- 1,4-, 1,5-, 1,8-dimethylnaphthalenes, monomer and dimer cations, e.s.r. spectra, obs. of hyperfine splitting consts. 2—38976
- dimethylnitrosamine in benzene, mol. assoc. effects on INDOR 2—25110
- dimethylphenols, i.r. and Raman vibr. spectra, fundamental assignment 2—8764
- dimethylselenium difluoride and deuterium analogue, vibrational spectrum 2—12239
- unsym-dimethylselenourea and similar compounds, hindered rotation barrier 2—24527
- dimethylsulphoxide, long range ^{13}C-H coupling 2—28300
- dimethylsulphoxide, microwave complex permittivity measurement 2—21994
- dimethylsulphoxide, numerical stability of centrifugal distortion analysis 2—755
- N,N-dimethylthiopropionamide, normal coordinate analysis 2—5973
- dimethylzinc, structure study, normal coordinate analysis 2—21680
- dinaphtho[2,1-2′,3′]furan-8,13-dione, polymorphism, fluorescence with absorpt. spectra 2—25356
- dinaphtho[2,1-2′,3′]furan-8,13-dione and dinaphtho[1,2-2′,3′]furan-7,12 dione, electronic spectra 2—24538
- p-dinitrobenzene, geometric distortion studied by high-resolution n.m.r. in the nematic phase 2—31840
- 1-X-2,4-dinitrobenzenes, applic. of Shaefer's additivity rules for coupng constants 2—21681
- 1-X-2,4-dinitrobenzenes, applic. of Shaefer's additivity rules for coupng constants 2—21681
- 2,2′-dinitrobiphenyl electrogenerated radical anions, e.s.r. spectra, linewidths and spin densities 2—26368
- 1,8-dinitronaphthalene electrogenerated radical anions, e.s.r. spectra, linewidths and spin densities 2—26368
- 1,4- dioxadiene, conformation, ab initio study 2—18498
- dioxane cryst., far-i.r. absorpt., external vibr. lines broadening at melting pt. 2—20053
- 1,4-dioxane ring inversion barrier 2—28367
- dioxane-water mixture, proton spin-lattice relax. 2—6252
- 1,3-dioxolane, microwave spectra, pseudorotation 2—8761
- 2,4-dioxydithiobenzoic acid aqueous solution, i.r. and u.v. absorpt. spectra 2—39371
- dioxyphosphorane, bicyclic, crystal and molec. structure 2—25361
- dipeptides, γ-irrad., polymorphic transform. 2—7187
- α,α'-diphenyl, β-picrylhydrazyl, free radical, anomalous paramag. shift, proton mag. resonance obs. 2—7133
- diphenyl, Raman spectra, Davydov splitting magnitude, dependence on crystal elementary cell parameters 2—26183
- diphenyl ether, temperature dependence of flow birefringence 2—6232
- diphenyl ethers, highly substituted, energy barriers to rotation about Ar-O bond determ. from n.m.r. spectra 2—38975
- diphenyl monocrystal, low temps., far i.r. absorption spectra 2—16504
- diphenyl-α-hydroxyisopropylphosphine oxide, i.r. spectra rel. to H-bonding 2—15370
- N,N′- diphenyl-p-phenylenediamine, growth of pure single crystals from vapour, and meas. of photoconductivity data 2—3577
- diphenylacetylene in glasses at 77 K, photoexcited triplet state, e.p.r. detection 2—16690
- diphenylamine, calculation of electronic spectra 2—31848
- diphenylamine, photo-oxidation in presence of benzophenone, H-bonding effects 2—30064
- diphenylamine in CCl_4 solution, dipole-dipole interactions and solvent effects 2—15373
- 9,10-diphenylanthracene, electrogenerated chemiluminescence in solution 2—40821
- diphenyldiazomethane, irradiation in single crystal soln., e.p.r. and ENDOR study of rates and mechanisms 2—33363
- 1,1-diphenylethylene:diphenyldiazomethane, photolysis, spectral obs. rel. to cryst. struct. 2—37055
- diphenylhydroxymethylphosphine oxide, i.r. spectra rel. to H-bonding 2—15370
- diphenylmethane, phosphorescence enhancement mechanism 2—10449
- diphenylmethane, temperature dependence of flow birefringence 2—6232
- diphenylmethylene+1,1,diphenylethylene, in single crystal soln., e.p.r. and ENDOR study of rates and mechanisms 2—33363
- diphenylmethylene+diphenyldiazomethane, in single crystal soln., e.p.r. and ENDOR study of rates and mechanisms 2—33363
- diphenyloctatetracene mixed crystals, electronic spectroscopy and solubility 2—10362
- diphenylpolyene film, trap distrib., space charge limited current obs. 2—40267
- dipolar liquid, spin-lattice relax., elec. field effect 2—9160
- dipyrazolinylbenzene derivatives, solutions of 4 derivatives, quantum generation 2—27492
- 1,4-dipyrazolinylbenzenes, isomeric, lasing capacity 2—37975
- 1,4-diselenan, vibrational spectra, assignments and force constant calc. 2—12236
- disilane, bond flexibility force constants 2—31853
- disubstituted benzenes, influence of substituents and their position on diamagnetic susceptibility 2—28349
- 1,4-dithian, Raman spectra, force constant calc. and vibrational assignments 2—12285
- p-dithiin p.m.r. study of orientation in lyotropic liq. cryst. 2—18500
- DNA, computer controlled e.p.r. obs. of free radical formation after electron irradiation 2—22880
- DNA films, oriented, piezoelectric strain constants from —170 to 30°C 2—40364
- n-dodecane, heat capacity at elevated press. 2—25072
- dodecane-chlorex liquid mixtures, critical exponent determination by scattering studies 2—9133
- Dowtherem-A, neutron properties of moderators and coolants 2—28153
- DPPH, g-factor, low field meas., low temp. 2—10463

Organic compounds continued
DPPH and diphenylpicrylhydrazine, X-ray photoelectron spectra 2–7085
DPPH in polystyrene, dynamic nuclear polarization rel. to localization of energy in organic molecules 2–15369
DTDC in methanol dye laser, continuous, mode locked, pumped in red 2–17608
durene, e.p.r. of γ-irradiated crystals 2–36996
durene, iododurene and chlorodurene, crystalline potentials and l.f. phonon spectra 2–19393
dye, flash pumped, laser emission 2–32271
dye associates in solution, small angle X-ray scatt. 2–15567
dye laser, high gain, superrradiance 2–17616
dye lasers, efficiency and absorption of pumping radiation by excited molecules 2–37970
dye solns. reversible photobleaching under conds. of spontaneous and stimulated emission 2–20197
dye solution, fluorescence decay time rel. to viscosity 2–18837
dye solutions, e.s.r. of triplet states 2–5971
dye solutions, laser pumped, spectral shifts of laser emission 2–11476
dye-detergent micelle system, absorpt. and fluorescence spectra, comp. depend. 2–18839
dye-detergent solution, excited molecules local temp., fluorescence and absorpt. spectra 2–18838
dye-lasers, N_2 pumped, oscillator-amplifier system 2–11475
dyes, flashlamp-pumped lasers, survey 2–7926
dyes, laser application, comparison with ruby and Nd 2–275
dyes, laser generation, effect of photodecomposition on energy laser characteristics 2–27490
dyestuffs in viscous soln., conc. depolarization of fluoresc. 2–9142
ehtylene-CO_2-He system, immiscibility at 13 to 70°C and up to 5kb 2–12503
eicosane single cryst., internal friction loss peaks 2–3844
eosin, triplet quantum yield study with tunable dye laser 2–26355
eosine crystal, photographic sensitizer, thermal activation energy of conducting processes and electron trap depths 2–16319
epichlorohydrin, microwave spectrum and rotational isomerism 2–15367
epifluorohydrin, microwave spectrum and rotational isomerism 2–15367
esters, O-C (sp^3) single bond distance 2–8714
ethane, abstraction reactions in photolytic system with DBr and DI, threshold energy 2–13587
ethane, adsorpt. on zeolite Y, heat of adsorpt. 2–35927
ethane, adsorption on clean Ni surfaces, field-emission studies 2–1196
ethane, bond flexibility force constants 2–31853
ethane, bond orders and elec. quadrupole moments from point-charge model 2–28372
ethane, formation by insertion of photolysis produced methylene into methane C-H bond 2–22882
ethane, internal rotation barrier, determination by SCF-Xα scattered wave method 2–35326
ethane, internal rotation barrier, rel. to energy partitioning 2–3086
ethane, ion molecule reaction chemistry, low electron energy, study by ICR spectroscopy 2–33373
ethane, ion-molecule reactions, ion cyclotron double resonance 2–40807
ethane, ionization, ab initio MO studies of ground state support $^2A_{1g}$ assignment 2–21683
ethane, liquid, under saturated vapour pressure, sound velocity using law of corresponding states 2–35760
ethane, liquid density 2–15579
ethane, localized molecular orbitals and comparison with C-H bond in methane 2–35338
ethane, reaction in gas discharge, polymer deposits 2–4580
ethane, solid, rot. transitions, obs. and theory 2–15977
ethane, theory of internal rotation barriers 2–24532
ethane, use as calibration gas for CH_4 spectrophone meas. 2–12257
ethane, valence bond calcs. of vicinal proton coupling consts. 2–38974
ethane liquid, γ-irradiated, molec. structure effect on electron reaction kinetics 2–10649
ethane-d_3, i.r. spectrum, vibr. frequencies, force consts., Coriolis zetas 2–12243
ethane-d_6, deuteron quadrupole coupling constant meas. via ^2H n.m.r. 2–10568
ethanedithiol, i.r. spectra, configuration in solid and liquid 2–8769
ethanes, bromo-substituted, ^{13}C n.m.r. 2–21682
ethanes, disubstituted, Karplus equation failure to predict ang. depend. of J_{vic} 2–763
ethanethiol, energy disposal in photodissociation 2–33383
ethanol, adsorbed on C black, chem. pot., heat of adsorpt. rel. to surface coverage 2–35907
ethanol, chemisorption on CdS, electron emission temp. depend. 2–10153
ethanol, chemisorption on CdS surface, rel. to electron emission 2–10152
ethanol, dielectric relaxation studied by new methods of complex permittivity up to 13 GHz 2–9150
ethanol, influence on photoelectric properties of Se 2–28992
ethanol, quantitative liquid-phase spectra, absorptivity in 2.5-13μm region 2–32270
ethanol, solid, far i.r. spectra, torsional modes and barriers to internal rotation 2–28373
ethanol, structural absorption of u.s. waves, study based on structural relaxation theory 2–25075
ethanol, ultrasonic investigation of volume viscosity and structure 2–25056
ethanol, volume viscosities, acoustical study 2–12553
ethanol films, dry spot formation on heating from below 2–9122
ethanol molecules, physisorbed on LiF, establishment of ordered array 2–22080
ethanol-potassium ethylate, gamma-irrad., chem. shift 2–8765
ethene, adsorpt. on zeolite Y, heat of adsorpt. 2–35927
ether group, electronic structure 2–28393
ethers, divinyl, spectral evidence of vibrational coupling of double bonds 2–8770
ethionamide, crystal structure determ. 2–39659
3-N-(4′-ethoxybenzilideneamino)-6-n- butylpyridine. room temp. smectic morphology 2–15575
ethyl alcohol, mol. rot., influence of H-bond, cold neutron transmission obs. 2–15349
ethyl alcohol vapour, first Townsend coeff. meas. 2–15500
ethyl alcohol-dioxane mixture, proton spin-lattice relax. 2–6252
ethyl benzene in cyclohexane, intramolecular dielectric relaxation, numerical analysis 2–35774
ethyl chloride, gaseous, total electric polarization 2–15543

Organic compounds continued
ethyl compounds, ^{13}C-^{13}C coupling constants 2–842
ethyl ether of n-axisalaminocinnamic acid, nematic liquid crystal, interatomic distances cylindrical function 2–18797
ethyl fluoride, theory of internal rotation barriers 2–24532
ethyl fluorides, isotopically substituted, exptl. and theoretical N.M.R. studies of coupling constants and chemical shifts 2–24535
ethyl formate, formyl J_{ch}, solvent and temp. depend. 2–5976
trans ethyl methyl ether-type molecules, skeletal torsional frequencies 2–31852
ethyl nitrate, microwave spectrum, rotational constants of trans and gauche rotamers 2–12241
ethyl nitrate, photoionization mass spectra investigated 2–12224
ethyl radical, proton hyperfine splitting constants, interplay of direct and indirect coupling contributions 2–3085
ethyl radicals produced in the pyrolysis of azoethane in reflected shock waves, reactions studied in 1000-1540K range 2–20184
ethyl thiocyanate, microwave spectrum 2–35327
N-ethyl-phenothiazine-iodine complex, dielec. props. at 10 GHz 2–22544
ethylbenzene, phosphorescence spectra, frozen matrices, liq. nitrogen temps. 2–4502
ethylene, ab initio CI treatment of ground and excited states 2–12086
ethylene, activation energy for addition of $O(^3P)$atoms 2–10614
ethylene, atmospheric pollutant, tunable i.r. laser techniques for det. 2–40923
ethylene, bond orders and elec. quadrupole moments from point-charge model 2–28372
ethylene, chemisorbed on Pt LEED obs. 2–35918
ethylene, electronic transitions with large generalized oscillator strengths 2–8768
ethylene, ethylene-d_4, vibrational structure in photoelectron spectra rel. to vibrational spectrum of $K[PtCl_3(C_2H_4)].H_2O$ 2–3087
ethylene, Fermi contact contrib. to coupling consts., SCF LCGO MO calc. 2–8620
ethylene, force field and constants, determ. from SCF MO wavefunctions 2–8767
ethylene, gas, pressure effects under irradiation by CO_2 laser 2–1028
ethylene, gas phase thermal reaction with NO_2 at 25C, mechanism for formation of products, rate constants 2–22867
ethylene, ion-molecule reaction, product translational energy spectra 2–20175
ethylene, ion-molecule reactions, H scrambling 2–40808
ethylene, ionization potentials from photoelectron spectra 2–31854
ethylene, nonlinear i.r. absorp., excited state effects 2–18501
ethylene, photoionization cross sections calcs. using plane-wave method allowing orthogonality 2–31684
ethylene, reaction in gas discharge, polymer deposits 2–4580
ethylene, reaction with O^- adsorbed on MgO, e.s.r. study of resultant species 2–4578
ethylene, tissue equivalent gas, anomalous effect in cylindrical proportional counters 2–34788
ethylene + F, crossed molecular beam study 2–37021
ethylene + O_2, reaction rate constants in temp. range 232-500 K 2–40806
ethylene and ethylene-d_4, $N \rightarrow V$ transition calc. and vibrational structure of V band reproduced 2–12083
ethylene gas, solubility in water temp. dependence 2–25052
ethylene glycol, Cr complex doped, proton spin-lattice relax. 2–16669
ethylene glycol, pipe flow, low Reynolds no., turbulent vel. and temp. fields 2–9051
ethylene glycol, Raman spectra, chelate form. 2–18502
ethylene glycol, study of rotational isomers with i.r. absorption band spectra 2–38980
ethylene layers, prefrozen, adsorption of Ar, heats, entropies and hysteresis 2–22088
ethylene liquid, γ-irradiated, molec. structure effect on electron reaction kinetics 2–10649
ethylene molecule, ang. distribs. of photoelectrons 2–35329
ethylene oxide, adsorption on glassy pyrogenic SiO_2 2–39565
ethylene oxide, collisions study by broadening of microwave spectral lines 2–35385
ethylene photolysis at 147-193 nm, kinetic analysis of primary processes 2–40834
ethylene-Ag^+ complex, electronic structure calc. using nonempirical SCF theory 2–8766
ethylene-glycol-Cr(V) system, polarized proton target properties and performance 2–34779
ethylene/ammonia (methanol) mixtures, second virial coeff. 2–24976
ethylene/methane, ethylene/N_2 ethylene/CO_2, integral Joule-Thomson effect, exptl. check of predictive calculation methods 2–3325
ethylenediamine, conformations, extended Huckel theory study, minimal energy forms 2–28375
ethylenediamine salts, assignment of i.r. and far i.r. spectra 2–3089
ethyleneimine substitution structure from microwave gas spectra 2–24534
ethylenes, alkyl substituted, chem. shifts, coupling constants, n.m.r. obs. 2–12261
ethylenes, bromo-substituted, ^{13}C n.m.r. 2–21682
ethylgermanes, far i.r. spectra, torsional modes and barriers to internal rotation 2–28373
9-ethylguanine, polarization of electronic transitions 2–24533
ethylpentaborane, dissociation energy of B-ethyl bond in 1- and 2- isomers by electron impact and extended Huckel calcs. 2–12103
ethylsilanes, far i.r. spectra, torsional modes and barriers to internal rotation 2–28373
ethyltrichloroacetate, liquid, dielectric relax. processes rel. to mol. motions 2–35777
ethynylbenzene, lowest-lying singlet $\pi^* \leftarrow \pi$ transition, rotational analyses, dipole moment changes 2–35343
etioporphyrins, photoreduction products, n.m.r. spectra 2–28374
europium dibenzylmethane-piperidine chelates, luminesc. props. 2–36937
nfatty acid amides, i.r. spectra, vibrational analysis 2–15374
fatty acid salt monolayers between metal electrodes, tunnelling 2–1547
fatty acids, thickness meas. of monolayers by multiple beam interferometry 2–6357
ferric dithiocarbamate molecule, n.m.r. obs. 2–5965
ferrocene, bonding, mag. anisotropy study 2–36660
ferrocene, electron levels, collective motion model 2–28376
ferrocene, phase transitions at 164 K and 110 K, crystal shattering 2–4009
ferrous orthophenanthroline, Kramers-Kronig relationships, refr. and extinction indices 2–15592

Organic compounds continued
five-membered rings, CNDO calc. of pseudorotational potential energy 2—8546
five-membered rings, far i.r. spectra, effect of finite central barrier on pseudorotation 2—15343
fluoranthene, electrogenerated chemiluminescence in solution 2—40821
fluorene, irradiated cryst., study of radical formation by e.s.r. 2—10489
fluorene molecules in fluorene crystal, triplet states, e.p.r. and phosphorescence study 2—30089
9-fluorenone, emission and absorpt. spectra, low lying excited states 2—15375
9-fluorenone, obs. of low lying excited states in absorption spectrum 2—18504
fluorescein, exciton bands and aggregate emission studied in u.v. and visible region 2—35359
fluorescein, triplet quantum yield study with tunable dye laser 2—26355
fluorescein and halo-fluorescein dyes, dimerization thermodynamics 2—22876
fluorescein dye lasers, efficient phase- matched second harmonic generation 2—5368
fluorescein dyes, continuous laser action, triplet quenching 2—276
fluorinated heterocyclic compound, long range coupling consts. 2—5974
p-fluoro-α-methylstyrene radical anions, spin density distributions, unrestricted Hartree-Fock calculation 2—28388
fluorobenzene, far i.r. absorption interpreted by correlation function for rotational velocities 2—39368
fluorobenzene, partially deuterated derivatives, n.m.r., incremental aromatic solvent induced shifts 2—18488
fluorobenzenes, Rydberg states 2—21685
fluorobenzenes, valence-shell transitions in vacuum u.v. 2—38981
fluorocarbonium ions, $(FCH_2)^+$ and $(F_2CH)^+$, ab initio MO study of bonding 2—21684
fluorochloroacetones, ^{19}F n.m.r. and ^{13}C satellite spectra, conformational preferences, C-F coupling const. 2—28377
fluorocyclopentane, vibrational spectra and structure of ring 2—12245
fluorodichloromethane, ^{19}F rotating frame n.m.r. 2—9181
2-fluoroethanol, microwave spectrum obs. 2—8774
fluoroethylene, Fermi contact contrib. to coupling consts., SCF LCGO MO calc. 2—8620
fluoroform, approx. force field 2—3076
fluoroform, effect of pressure on gas permeability coefficients in polyethylene 2—35691
fluoroform, fluoroform-d, rotational hyperfine spectrum 2—12244
fluoroform, gaseous, second dielectric virial coeffs. 2—15536
fluoroform, gaseous, total electric polarization 2—15543
fluoroform, gaseous second density, virial coeffs. 2—15535
fluoroform, mol. beam meas. of hyperfine structure 2—8772
fluoroform, shear viscosity, room temp. mag. field effects 2—21925
fluoroform autocorrelation functions of dipole moment theoretical and experimental values compared 2—38985
fluoroform-D_1, approx. force field 2—3076
fluoroform-N_2 mixtures, heat conductivity change due to electric field parallel to temp. gradient 2—3326
fluoromethanes, HF chemical elimination lasers 2—31045
fluorophenols, o-, m- and p-, π-π^* emission spectra in near u.v. region 2—3090
2-fluoropropene, i.r. and Raman spectra, normal coordinate analysis 2—8773
2- fluoropyridine, rotational spectrum, Zeeman effect, g-vals. and susceptibility 2—843
fluorostyrenes, isomeric, emission spectra 2—3091
fluorotrichloromethane, ^{19}F rotating frame n.m.r. 2—9181
formaldehyde, 6 cm absorption, in Sgr A, Sgr B2 and galactic plane 2—17020
formaldehyde, ab initio CI treatment of ground and excited states 2—12086
formaldehyde, absorption, emission and n.m.r. studies of form as function of solvent and temp. 2—35771
formaldehyde, absorption in interstellar dark clouds 2—26758
formaldehyde, adsorption on Pt electrode, obs. using polarized light reflected intensity meas. 2—9309
formaldehyde, comparative study of random phase approx. Hartree Fock of single excited configuration interaction methods of computing excitation energies 2—15277
formaldehyde, in cometary spectra, detection 2—26863
formaldehyde, in Galaxy, correlation with continuum sources and OH clouds 2—10818
formaldehyde, interstellar, collisional pumping mechanism for anomalous 6 cm absorption 2—26750
formaldehyde, interstellar, detection of ^{18}O isotope at 4388 MHz 2—10916
formaldehyde, interstellar, photochemistry and lifetimes 2—4898
formaldehyde, mol. rot. transition by electron collision 2—18437
formaldehyde, perturbation treatment of spin-orbit coupling using CNDO/S wavefunctions 2—12091
formaldehyde, photodissociation, potential energy surfaces 2—20201
formaldehyde, photoionization, first ionization potential determination and ion yield curve interpretation 2—15378
formaldehyde, photoionization and absorption spectrum in vacuum u.v. 2—8775
formaldehyde, pressure dependence of i.r. microwave double resonance 2—38983
formaldehyde, radiationless transition probability, non-empirical study 2—8513
formaldehyde, Sgr A, absorption at +40 km/sec 2—37277
formaldehyde, singlet-triplet resonance interaction in A_2 states 2—31856
formaldehyde, spin-vibronic perturbations in $^1A_2$ state 2—15377
formaldehyde, valence and Rydberg transitions, dependence of generalized oscillator strength on momentum transfer 2—15376
formaldehyde, vertical ionization potential, calc. based on perturbation theory 2—3095
formaldehyde absorption at 4.83 GHz in dark galactic clouds 2—7396
formaldehyde absorption profile from HI region towards the K3-50 galactic nebula 2—33691
formaldehyde and ^{13}C and ^{18}O species, hyperfine components of 2_{11}-2_{12} transitions 2—35331
formaldehyde and ^{13}C species, mm wavelength spectrum, transition obs. 2—35332
formaldehyde and OH interstellar clouds, physical conditions and molecular formation and lifetimes 2—33694
formaldehyde in interstellar dust clouds 2—26757

Organic compounds continued
formaldehyde isotopes, molecular beam maser studies of transition 2—12247
formaldehyde line, lunar occultation studies of centre region of Galaxy 2—4788
formaldehyde mol. beam, multiphoton transition, 106 kHz 2—31855
formaldehyde oxime, Raman spectra obtained at room temp. and 120°C, results discussed with regard to molecular structure 2—8777
formaldehyde protonation, electrostatic molecular potential study 2—18505
formaldehyde-d_2, Coriolis perturbed absorpt. bands, rotational analysis 2—8776
formaldoxime, vibrational analysis of i.r. spectra, normal vibrations and torsional barrier 2—3094
formamide, high resolution rotational spectra 2—3093
formamide, interstellar, detection of 1_{11}-1_{10} transition at 1540 MHz in direction of Sgr A and B2 2—26761
formamide, molecular g values, molecular Zeeman effect 2—38982
^{15}N formamide, molecular Zeeman effect 2—12246
formic acetic anhydride, i.r. and Raman spectra, normal coord. anal. 2—8778
formic acetic anhydride, molecular structure, sector-microphotometer method of electron diffraction 2—18506
formic acid, ^{13}C spin-lattice relax. under proton decoupling conditions 2—10257
formic acid, adsorption on Pt electrode, obs. using polarized light reflected intensity meas. 2—9309
formic acid, comparative study of random phase approx. Hartree Fock of single excited configuration interaction methods of computing excitation energies 2—15277
formic acid, hydrogen bonded cyclic dimer, near i.r. spectra, vibrational analysis 2—21652
formic acid, quantitative liquid-phase spectra, absorptivity in 2.5-13μm region 2—32270
formic acid, rot. constants and structure using isotopic substitutions 2—18509
formic acid, rotational spectrum of vibrational ground state 8 to 300 GHz 2—18508
formic acid, various conformations, electronic structure, semiempirical CNDO and INDO calcs. 2—24537
formic acid dimer, nonempirical calc. of intramolecular rearrangement 2—3092
formic acid single crystals, deuteron NMR spectra meas. determ. quadrupole coupling const. and asymmetry factors 2—20155
formic acid vapour, h.f. discharge effect 2—1015
formyl formide, conformation and electronic structure, valence shell calc. 2—18507
4-formyl-2, 6-di-tert-butylphenoxy radical, e.s.r. and ENDOR spectra 2—5975
Freon 12, modelling of forced convection burnout in water 2—18264
Freon 12, saturated and superheated, heat transfer during film condensation 2—25000
Freon (R-113), supercooled, vapour injection effect on crit. ht. flux, high press. flow 2—24997
Freon-113, boiling, nucleate, saturated and subcooled, superheat layer thickness meas. 2—18885
Freon-11, critical heat flux data for scaling CHF in water 2—25003
Freon-water modelling of critical heat flux in uniformly heated annuli 2—24996
freons, thermal conductivity det., applic. of rule of continuity and law of corresponding states 2—28738
fructose, aqueous soln., γ-irrad., optical rotation 2—5596
fulminic acid, absorption spectrum from 200 to 450 cm^{-1} assignment 2—12248
fulminic acid, assignment of vibr. satellites obs. in rot. transition, vibr.-rot. interaction const. microwave and millimeter wave spectra 2—12268
fulminic acid, rotational spectrum 40-300 GHz, transitions of vibrationally excited states 2—21686
fulvenallene, vapour-phase i.r. spectrum and structure 2—28378
fulvene, microwave spectra, struct., dipole moment 2—8779
fulvene, vapour and mixed crystal spectra, lowest energy electronic transition 2—8780
fumarofine, molecular structure 2—3096
furan, orbital determ., ESCA line intensities obs. 2—35219
furan, valence charge distrib. calc. by charge iterative extended Huckel approach 2—5992
furan, vibrational analysis of photoelectron spectra 2—3097
furan, [2,5-D_2], rotational Zeeman effect in ground vibrational state 2—38984
furocoumarins, assignment of lowest excited singlet and triplet states on basis of luminescence measurements 2—12226
gas chemisorption on Si and Ge surfaces, ellipsometric and gas-volumetric obs. 2—10619
gases, chemisorption on Ge surfaces, structure of adsorption complexes 2—1749
gases for Stark modulating $00^{0}1$-$10^{0}0$ band in R branch of CO_2 laser 2—11467
germanium acetate, lattice parameters and space groups 2—19063
glass, nucl. mag. relax. by non-paramag. impurities, low temp. 2—10275
glucose, aqueous soln., γ-irrad., optical rotation 2—5596
glucose, time dependent heat capacity in glass transition region determ. by differential thermal analysis 2—6680
glycerin, Raman spectra, chelate form. 2—18502
glycerine/dye solution, fluorescence, depolarization, temp. and viscosity depend. 2—18840
glycerol, dynamic tensile failure 2—12525
glycerol, in soln., jets, liquid-in- liquid, mass transfer, conc. driving force 2—3350
glycerol, pressure and temp. studies of n.m.r. translational relaxation 2—35795
glycine:Cu^{2+}, e.p.r. of cationic radicals formed by u.v. irradiation at 77K 2—30090
glycine, polycrystalline, proton spin-lattice relaxation 2—1736
α-glycine, valence force field and conformation of $H_3NCH_2COO^-$ ion 2—28379
glycine isotopic species in Ar and N_2 matrices, i.r. spectra, band assignment 2—31857
glycol and water glass, trapped electron formation and decay during and after X-ray and U.V. irradiation 2—36951

Organic compounds continued

glycyl-L phenylamine chlorohydrate, monohydrate, crystal structure obs. 2—6461
glyoxal, $^{13}C_2$ substituted, visible electronic band, rotational analysis 2—8781
glyoxal, conjugated system, pot. function for rotation about CC single bonds, CNDO/2 calc., inaccuracy of method 2—3099
glyoxal, electronic structure and conformation 2—18510
glyoxal, glyoxal-d, vibrational assignment of i.r. spectra 2—3098
glyoxal vapour, fluorescence and phosphorescence from laser excited first singlet excited state 2—12249
glyoxylic acid, vibrational spectra and assignment, 4000 to 300 cm^{-1} 2—24539
gromo maleic anhydride, vibrational spectra, assignment and force constant calc. 2—12223
guanidinium aluminium sulphate hexahydrate, n.m.r., molecular motion 2—7131
guanine monohydrate, cryst. struct. 2—9507
haloalkenes, rotational isomerism 2—28382
haloalkenes, rotational isomerism 2—28381
halobenzenes, assignment to nu$_{19b}$ fundamental 2—35333
2-halocyclohexanols, OH-halogen intramolec, H-bond, potential function model 2—21687
2-haloethanols, OH-halogen intramolec. H-bond, potential function model 2—21687
haloethylamines, i.r. spectra, assignment of bands 2—3088
halogenated methanes, empirical correlation for gas thermal conductivity 2—24982
halogenated methyl radicals, substituent effects on geometry 2—31863
halogenoethylene and halogenogermane molecules, sum rules for vibration 2—8782
halogenomethanes, resonance Raman spectra excited by u.v. N_2 pulsed laser 2—28380
halomethanes, ^{13}C nuclear relaxation, field-dependent contributions 2—28333
halomethyl radicals, anharmonic potential functions for out-of-plane modes 2—21688
2-halomethyl-1,3-dioxans, double ultrasonic relaxation, ring inversion and internal rotation 2—24530
o-halophenols, OH-halogen intramolec. H-bond, potential function model 2—21687
hemin, calculation of spin-spin and spin-orbit contribution to zero-field splitting 2—31858
heneicosane velocity and absorption of shear waves near melting point 2—29536
heptane, solid, n.m.r. line shape 2—30033
n-heptane, thermal conductivity meas. from 20 to 300°C and 1 to 1000 bar 2—18768
n-heptane-polar cpd. solid solns., dielec. absorpt. phenomena 2—6876
heteroaromatic phosphine derivatives, ^{1}H- ^{31}P spin-spin long range coupling consts. 2—12250
heteroaromatics of type R_2X, calculation of electronic spectra 2—31848
N-heterocyclic compounds, ionization potentials, comparison of calculation with experiment 2—31869
heterocyclic nitro cpds., photolysis, e.s.r. study of alkoxynitroxide free radicals 2—832
heterocyclic quinones, spin density distrib., e.s.r. obs. 2—5995
heterocyclics, 5 membered, unsaturated, chem. shifts, H-H coupling consts., proton mag. reson. spectra 2—12256
β-1,2,3,4,5,6-hexachlorocyclohexane, ^{1}H and ^{13}C Fourier transform spectra 2—15356
hexachloroethane, lattice vibr., molecular rot. and C-Cl$_3$ group internal rot., n.q.r. obs. 2—16668
hexacosane-lauryl laurate mixture, dielec. loss, comp. depend. 2—40328
n-hexadecane, heat capacity at elevated press. 2—25072
hexadecane, liq., explanation for spectra in terms of 2-phonon absorption 2—1104
n-hexadecane, solidification rate determ. by acoustic method 2—39423
hexadecyl-trimethyl-ammonium bromide+Na p-chlorobenzoate+H_2O, light scatt. and transmission 2—9095
2,4-hexadiyne, spin-lattice relaxation in various solutions 2—32279
hexafluorobenzene, fluorescence decay times and radiative lifetimes, gas phase 2—24536
hexafluorobenzene, molecular reorientation between 77 to 270K, NMR study 2—26310
hexafluorobenzene, pure rotational Raman spectra and bond length det. 2—35357
hexafluorobenzene, Raman spectra 2—17731
hexafluorobenzene, solid, spin exchange, spin- lattice relax. 2—10278
hexafluorobenzene, spin echo n.m.r. 2—35790
hexafluorobenzene, susceptibility anisotropy, from Cotton-Mouton effect meas. 2—18486
hexafluorobenzene/n-alkane mixture, gas-liq. crit. temp. 2—25150
hexafluoropropene, C═C bond twisting, investigation using microwave spectrum 2—15380
hexahelicene, p.m.r. spectra, determ. chemical shifts, coupling constants at infinite dilution in CCl$_4$ 2—24507
hexahelicene anion radical, e.s.r. and ENDOR study 2—844
hexahydro-1,3,5-trichloro and trinitroso s-triazine, vibrational spectra 2—31859
hexahydro-1,3,5-trinitro s-triazine, monocrystal vibrational spectra, 10 to 200 cm^{-1} 2—15379
hexahydro-1,3,5-trinitro-s-triazine infrared and Raman spectra of single crystal and polycrystalline film 2—8783
1,2,3,6,7,8-hexahydropyrene, monovalent positive and negative ions, EPR spectra 2—18511
1,2,3,6,7,8-hexahydropyrene anion radical, liq. phase, ENDOR spectrum 2—5978
hexamethylbenzene, solid, nuclear spin states associated with protons of CH_3 group 2—40783
hexamethylcyclotrisiloxane, i.r. dichroism of oriented crystalline films 2—40686
hexamethyldisilane, solid, pulsed NMR studies of proton spin-lattice relaxation time in static and rotating frames 2—20168
hexamethyldisiloxane, antisymmetric valence vibrs. of Si-O-Si bridge 2—3101
hexamethyldisiloxine, polymerized thin film, prep., i.r. spectra, e.p.r. spectra, deposition rates 2—3550
hexamethylene tetramine, dislocation struct., X-ray topographic study 2—36037

Organic compounds continued

hexamethylenetetramine; HCl, proton magnetic resonance, orientational effects 2—33354
hexamethylenetetramine association phenomena rel. to alkali halides 2—9219
hexamethylethane, self-diffusion, vacancy mechanism, NMR linewidth meas. 2—15793
hexamethylethane, solid, pulsed NMR studies of proton spin-lattice relaxation time in static and rotating frames 2—20168
hexamethylethane cryst., mol. motions, n.m.r. obs. 2—13556
hexamethylphosphoramide, long range ^{13}C-H coupling 2—28300
hexamethyltrisiloxane, antisymmetric valence vibrs. of Si-O-Si bridge 2—3101
n-hexane, adsorption on quartz crystal piezogravimetric method of obs. 2—25223
n-hexane, electron mobility mechanism 2—35719
n-hexane, pulse radiolysis obs. of solvated electrons 2—22889
n-hexane, scattering cross section and mobility of excess electrons in liquid 2—35786
n-hexane, superheated tensile strength by ultrasonic cavitation 2—9066
n-hexane, vapour, γ-irradiated, av. energy per ion pair 2—15498
n-hexane droplets, evaporation in high temp. and pressure environment 2—39431
hexane-d$_{14}$, deuteron quadrupole coupling constant meas. via ^{2}H n.m.r. 2—10568
hexane-ethanol azeotropic mixtures, det. of critical temps. from ultrasonic data 2—39415
n- hexane-nitrobenzene mixture, near critical point, u.s. absorpt. 2—28854
n-hexane-o-toluidene, u.s. absorption around critical region 2—1094
hexatriene, new weak vibronic transitions predicted 2—12083
n-hexoic acid, ultrasonic relaxation 2—39362
L-histidine hydrochloride monohydrate:Cu(II), single crystal, lattice position of Cu from polarized absorption spectra and e.p.r. 2—36978
homocystine, polycrystalline, proton spin-lattice relaxation 2—1736
homologous series, regularities in diffusion coefficients 2—6166
hydantoine, Raman spectra 2—5979
hydrazides, ^{14}N n.q.r. at 77K 2—24540
hydrocarbon, chemisorption on W, field emission 2—25972
hydrocarbon, ion pumping, H_2 backstreaming 2—39545
hydrocarbon functional groups, in paraffins, near i.r. spectra 2—24541
hydrocarbon ions, CH_n^+, collision cross section meas. on gas targets 2—901
hydrocarbon ions, Ch_n^+, dissociation in collisions with N_2 at 40 to 140 keV 2—900
hydrocarbon molecules, charge distribution and diamagnetic susceptibility 2—35334
hydrocarbon vapours in air, mobile analysis instrument 2—22890
hydrocarbon-fluorocarbon mixtures, interaction virial coefficients 2—28734
hydrocarbon-sulphur systems, high temp. laser- induced reactions 2—30096
hydrocarbon-water mixtures, phase behaviour and critical phenomena 2—9109
hydrocarbons, C_3 molecules, MO calc. of geometries, energies and polarities 2—28383
hydrocarbons, C_3H_6, C_6H_{12}, C_6H_6, C_6H_{14} and C_8H_{10}, identification of localized bonds from Compton profiles 2—3103
hydrocarbons, closed shell alternant, PPP model, consequences of nonlinearity of Hartree-Fock approach 2—35203
hydrocarbons, conjugated, electric polarizabilities, perturbation theory calc. 2—38986
hydrocarbons, diffusion in air, regularity in coefficients of homologous series 2—32188
hydrocarbons, floating spherical Gaussian orbital model for ESCA chemical shifts for inner shells electrons 2—35335
hydrocarbons, generalized valence bond orbitals 2—8758
hydrocarbons, halogen substit., gas phase Raman intensities, vibrational study 2—12253
hydrocarbons, interstellar, absorption bands of type I supernovae spectra, laboratory simulation 2—7438
hydrocarbons, MIM calculations of electronic bands involving triplet states 2—38987
hydrocarbons, nonalternant, calc. of electronic absorption spectra 2—12252
hydrocarbons, proton polarization rel. to polarized target production 2—36810
hydrocarbons, residual, laser produced dissoc. and ioniz. 2—28386
hydrocarbons, saturated, 2nd virial coeffs., temp. dependence 300-500 K 2—28735
hydrocarbons, saturated, magnetic susceptibility, molecular orbital calc. 2—28384
hydrocarbons, solubility in liquid methane and liquid Ar 2—1080
hydrocarbons, vapour-liquid equilibrium distribution ratios computed by new equations 2—32308
hydrocarbons, viscosity press. depend. 2—35743
hydrocarbons in deuterated nitromethane, critical solution points 2—39343
β-hydrogen phthalocyanine, tight binding energy band calcs. 2—13261
4-hydroxy benzanthrone, absorption and fluorescence spectra 2—3102
2,2′-hydroxy-1,1′-naphthalazine phosphor abs. quantum efficiencies 2—4482
6-hydroxy-2-pyridone, strong hydrogen bonding, anomalous i.r. spectra 2—10360
2-hydroxycarboxylic acids, OH stretching vibrations 2—28385
hydroxyl group containing molecules, i.r. spectra, stretching and torsional modes obs. 2—8750
hydroxyphenazines, PPPMO calcs., charge density, bond order, oscillator strength and electronic transition energy 2—8785
hydroxyphenazines, PPPMO calcs., transition energies and oscillator strengths, electronic spectra 2—12251
8-hydroxyquinoline-N-oxide, cryst. and mol. struct. 2—9508
5- hydroxytryptophan metabolism in isolated perfused liver for X-irradiated rats 2—30667
hydrzines, ^{14}N nuclear quadrupole resonance spectra 2—8784
imidacarbocyanines containing residues of heterocyclic bases in benzene nuclei, photographic properties 2—27671
imidazole, H-bonded cryst. with protonic conductivity, γ-induced radicals, e.p.r. and ENDOR obs. 2—26293
imidazole cryst., hydrogen bonding 2—29159
2-iminothiazolidone-4, i.r. absorpt. spectra 2—1696

Organic compounds continued
2 iminothiazolidone-4, Raman spectra 2—5979
2-iminothiazolidone-4, Raman spectra 2—5979
iminoxy radical, formed from γ-radiation of 5-nitrouracil, e.s.r. structure study 2—10651
iminoxyl biradical solid solns., spin-lattice relax. 2—1731
1,3-indanione, spin-lattice relaxation in solution, microscopic molec. motions 2—28900
1-indanone, in divene host, optically detected e.s.r. study of lowest n-π^* triplet states 2—24542
indene, frozen hydrocarbon solns., phosphorescence spectra, liq. N temp. 2—16625
indenyl carbanion-alkali metal ion pairs, struct., n.m.r. obs. 2—18512
indole, frozen hydrocarbon solns., phosphorescence spectra, liq. N temp. 2—16625
indole, in naphthalene, conc. effect on local exciton spectra 2—13505
indole derivatives, aqueous, 77K, delayed fluorescence, role of photoejected electrons 2—10432
indole in water, fluorescence band-intensity distrib. 2—25095
indoles, temp. dependence of fluorescence in glass forming solvents in range 77-298 K 2—10435
intermolecular Overhauser effect 2—8719
interstellar, simulated chemistry 2—7463
iodo(methyl)germanes, infrared and Raman spectra 2—845
iodo-3 hydroxy-2 naphtho-quinone-1.4, crystal structure determ. 2—25358
iodobenzene, partially deuterated derivatives, n.m.r., incremental aromatic solvent induced shifts 2—18488
2-iodobutane, rotational isomerism from i.r. spectra in crystalline and glassy states 2—40685
iodoethane-d_2, quantum mechanical turinelling effects in methyl group n.m.r. line shape 2—10569
iodoform, l.f. Raman spectra, internal mode coupling 2—26198
iodoxylene, vibrational spectra 2—35309
ion chemistry, contrib. of electron spectroscopy 2—35297
ionone, α and β systems, nonplanarity in π radical 2—31861
iron chelates irradiated with electrons, Mossbauer absorption spectra meas. autoradiolysis mechanism present 2—19975
isobutane in gas mixture in multiwire proportional chambers, time degeneracy 2—27860
isobutene, activation energy for addition of O(^{3}P) atoms 2—10614
isobutene, ion-molecule reaction chains 2—10621
isobutene, vibronic structure of 1790 Å transition 2—12254
isobutene-d_0, -d_6, -d_8, Raman spectra of polycrystalline samples meas. assignments to fundamental modes made 2—13492
isocytosine, proton injection measurements 2—25847
isodiazomethane, CH_2N_2 isomer, structure, theoretical investigation 2—8751
isonicotinic acid, strong hydrogen bonding, anomalous i.r. spectra 2—10360
isooctane crystals, effect of polymorphic transformations on luminescence of impurity molecules coronene and benzpyrene 2—29959
isoprene, thermal polymerization with solid insoluble inhibitors, dynamics 2—21966
isopropyl alcohol, PVT behaviour for temperatures from 200-300°C and pressures from 1000 to 8000 lb./sq.in. 2—28949
isopropyl benzene in cyclohexane, intramolecular dielectric relaxation, numerical analysis 2—35774
isopropylalcohol, liquid state, i.r. study of molec. motion 2—15593
N-isopropylcarbazole, and radicals spectra, energy levels, splitting parameters 2—18513
isoquinoline, threshold electron excitation spectra, obs. of compound negative ion resonances and electronic transitions 2—35350
isorhodamine, i.r. absorp. spectra, rotatory oscillation and moments of inertia 2—39005
isothiazole series, meas. and calc. of ionization potential 2—846
isoxazole, electronic structure using improved LCAO method 2—18518
Kapton film, polyimide, Sn(II) sensitizer deposit, Mossbauer obs. 2—13588
kerosene drops in water, wakes of vertical and horizontal assemblages 2—25026
kerosene spray from atomizer, drop size determ. 2—6188
ketones, aliphatic, n$\rightarrow\pi^*$ transition shifts, contribs. from intermol. interactions and H bonds 2—3104
ketones, mechanism of energy transfer to rare earth ions, effect of electron density of CO group 2—31886
ketones, partially deuterated, solid and liquid, cross correlations and nonexponential spin-lattice relaxation 2—16406
ketones, saturated aliphatic, modulation of n$\rightarrow\pi^*$ absorption band 2—21689
ketones, saturated aliphatic, solvent effects in modulation of n$\rightarrow\pi^*$ absorption bands 2—21690
ketones, substituent constant derived from carbonyl stretching frequencies 2—15382
ketones, torsional vibrations, calc. using Green's function method 2—28387
ketyls, nonplanarity of carbonyl carbons from INDO approx. SCF MO theory 2—8786
lactones, O-C (sp^3) single bond distance 2—8714
lanthanum ethyl sulphate, spin-optical phonon relax. of Er^{3+} and Sm^{3+} 2—7011
lauryl laurate-hexacosane mixture, dielec. loss, comp. depend. 2—40328
lead acetate, lattice parameters and space groups 2—19063
lead dicalcium propionate, mol. motion, p.m.r. obs. 2—10574
DL-leucine, inhibition of positronium formation, after γ-irradiation 2—22888
leuco crystal violet, radiolytic oxidation, dosimeter for γ-rays 2—16689
lipids, bimolecular membranes, semiconductive and photoconductive properties 2—26941
liquid mixtures, dielectric constant 2—25098
liquid scintillation counting, sample preparation techniques 2—38363
liquid/saturated vapour equilib., crit. constants effects 2—28950
liquids, fluidized by water, coalescence rates 2—1126
liquids, isothermal compressibility determ. by ultracentrifugation, correlation with surface tension 2—24991
liquids, meas. of relative and absolute Raman scattering cross sections 2—28867
liquids, polar and nonpolar, far i.r. absorption spectra 2—1101
liquids, Rayleigh scatt., horizontal depolarization ratio 2—18841
liquids, spin lattice relaxation of ^{13}C nuclei 2—3408

Organic compounds continued
liquids, transparent dielectrics, mechanism of optical breakdown 2—39365
lithium formate monohydrate, cryst. struct. and ferroelec. props. 2—3747
lithium formate monohydrate, p-p vector length and orientation, proton mag. reson. 2—40785
lithium formate monohydrate, p.m.r. obs. 2—10570
lithium formate monohydrate single crystals, Raman and i.r. spectra at room and liquid nitrogen temps. 2—26180
lithium stearate, second moments and local mag. field vals. from adiabatic rapid passage n.m.r. 2—10544
lithium thallium tartrate, ferroelec. props. 2—29756
lithium thallium tartrate monohydrate, elec. control of elastic compliance 2—40360
long chain alcohols, permittivity and dipole moment in pure liquid states at varying temp. 2—39388
low-loss liquids, absorptivity measurement by measurement of change in refractive index caused by temp. change due to absorption 2—25083
lysine, polycrystalline, proton spin-lattice relaxation 2—1736
maleic anhydride, soln. and vapour, electronic spectra, absorption band assignment 2—8788
maleimide and isoelectronic molecules, electronic spectra, quantum chemical calc. 2—15383
malic acid free radical, conformational anal. using PCILO method, conformation by INDO calc. of coupling consts. 2—8789
manganese acetate tetrahydrate, e.p.r. absorpt. and dispersion obs., 16 GHz 2—16647
manganese organometallic derivatives, correlation between ionization potentials of complexes and free ligands 2—18494
manganic dithiocarbamate molecule, n.m.r. obs. 2—5965
Martian surface and atmosphere, proposed mass spectrometric anal. 2—30568
MBBA, electro-opt. effect in cells at room temp., characts. and mechanism 2—35763
MBBA, liquid cryst., electrohydrodynamic phenomena when subjected to unipolar injection 2—32228
MBBA, nematic, dielectric and resistivity obs. 2—25103
MBBA, nematic, elastic consts. of twist and bend 2—21964
melissic acid, thin film production, controlled evaporation in vacuum 2—1189
melting points, rel. to appl. as temp. standards 2—34224
mesitylene, ^{13}C containing, study of multiplet effect in dynamic polarization 2—24496
mesitylene, electron-irradiated, consequent radical, CNDO/2 calc. 2—5980
metal chelates, solid, electrical conductivity 2—26940
metal phthalocyanines, molecular electronic structure, molecular orbital treatment 2—15390
metalloporphyrins, probabilities of intercombination transitions 2—35347
methacrolein, vibrational-electronic bands of $S_1(n,\pi^*)$ 2—35336
methacrylonitrile, microwave spectrum, barrier to internal rot. of CH_3 and ^{14}N quad coupling const 2—8799
methane, absorption at 3.39 μ, temp. and press. depend., laser appl. 2—8797
methane, adsorption and displacement on W (111) surface 2—25235
methane, adsorption on stainless steel, isotherm meas. at 77 to 90 K and 10^{-9} to 10^{-4} torr 2—32390
methane, adsorption on W, flash desorption and work function study 2—12687
methane, analogue to ionized inert gas, mol. orbital determ. from vac. u.v. and photoelectron spectra 2—18409
methane, assignment of transitions in $\nu_3+\nu_4$ band 2—8790
methane, atmospheric release expts., thermospheric temp. obs. 2—16867
methane, bonds covalent, hybridization in context of separability of bond functions 2—28256
methane, collisions with Ar^+, Kr^+, Xe^+, charge transfer mechanism 2—659
methane, collisions with H and H^+ at 1 to 25 keV Lyman alpha emission cross sections 2—21544
methane, comparison of one centre and polycentre wavefunctions in HFR formulation 2—35204
methane, concentration in lower stratosphere over North America 2—37129
methane, deuterated, calculation of i.r. spectra of ν_3 and ν_4 modes in Kr and Xe matrices 2—40668
methane, deuterated, Gruneisen relation between expansion coeff. and heat capacity 2—16064
methane, effect on Ge(Li) diode preparation using Ti getter pumps 2—24088
methane, ejection of secondary electrons in collisions with 200-500 keV protons 2—12057
methane, excited in cavity, stimulated Raman scattering, threshold characteristics 2—850
methane, fluorinated, K electron binding energy shifts, CNDO potential model calc. 2—8771
methane, force constants and dipole moment derivatives, near Hartree-Fock calc. 2—21692
methane, formation of energetic protons by electron impact 2—3154
methane, generation of i.r. radiation by Raman scattering and difference frequency mixing with a Nd:YAG pump 2—23603
methane, ground state elec. dipole moment 2—849
methane, harmonic spectra of dense phases 2—36892
methane, high-resolution photoelectron spectra 2—35340
methane, influence of centrifugal distortion of molecule on spin lattice relaxation in gas 2—35316
methane, interpretation of mol. beam radiofrequency, ortho-para transitions 2—12266
methane, interstellar, photochemistry and lifetimes 2—4898
methane, ion-molecule reactions, H scrambling 2—40808
methane, i.r. absorption study of ν_4 band, 1225-1400 cm^{-1} 2—21696
methane, Jupiter, spectrophotometry of 1.5 μm window 2—26832
methane, kinetics of oxidation 2—33379
methane, leak rate through thin polycarbonate film 2—3816
methane, liq., eqn. of state, thermodynamic props. 2—12535
methane, liq., multiple neutron scatt. effects, atomic motions 2—9080
methane, liquid, solubilities of hydrocarbons and CO_2 2—1080
methane, liquid and gaseous, thermal cond. meas. 2—17427
methane, localized molecular orbitals and comparison with C-H bond in ethane 2—35338
methane, meas. and analysis of ν_3 band 2—38991
methane, nonlinear level crossing in the standing wave field 2—31744

Organic compounds continued
methane, obs. in spectrum of Uranus 2—30581
methane, photoelectron spectra 2—8795
methane, photolysis, methylene radical prod. followed by insertion into methane C-H bond 2—22882
methane, precision Stark- spectroscopy, nonlinear laser absorption 2—12217
methane, reaction in gas discharge, polymer deposits 2—4580
methane, reactions of positive ions in gas, pulsed ion cyclotron double resonance spectroscopy 2—24568
methane, rot. analysis of ν_3 band 2—12258
methane, rot. analysis of ν_4 band 2—31862
methane, shear viscosity, room temp. mag. field effects 2—21925
methane, solid, n.m.r. obs. of spin conversion 2—10571
methane, solid, proton spin-lattice relax., mol. reorientation 2—10279
methane, solid, sp. ht., low temp., impurities influence 2—9890
methane, solid, spin conversion and oxygen catalysis obs. 2—10572
methane, solid spin species conversion through level crossing with paramagnetic impurities, obs. using proton spin lattice relaxation time 2—33184
methane, thermal conductivity and shear viscosity in static mag. field and field free space 2—35687
methane, thermal conductivity meas. under the influence of a magnetic field 2—12510
deutero-methane, thermal conductivity meas. under the influence of a magnetic field 2—12510
methane, thermal dissociation on hot W emitter tips, field emission microscopy 2—30059
methane, tissue equivalent gas, anomalous effect in cylindrical proportional counters 2—34788
methane, vibrational relaxation times at increased pressure, effective specific heat ratio 2—14258
methane+H system, UHF LCAO MO GTO study of hydrogen exchange and abstraction 2—26336
methane absorption cell to produce contrast power resonances of He-Ne laser 2—27470
methane and ethane supersonic molecular beams, absolute intensities, vel. distrib. 2—21585
methane at high densities, positron annihilation 2—21922
methane at moderate and high densities, two potential models for equations of state 2—39273
methane Brillouin laser, single freq. 2—14405
methane gas, relative Raman cross section, rel. air pollution 2—35249
methane in Uranian spectrum, molecular absorptions 2—4978
methane molecule, photoionization total and differential cross sections, X- and u.v. excitation, calcs. 2—18458
methane radical cation, tetracoordinated three-centre bound config. 2—8791
methane-air combustion gases as aerodynamic test medium 2—39257
methane-argon liquid mixture, excess Gibbs energy 2—35753
methane-carbon dioxide system ion-molecule reactions studied at 0.1-0.4 torr in mass spectrometer, determ. rate constants 2—15421
methane-carbon tetrafluoride system, thermodynamic properties in neighbourhood of upper critical solution temp. 2—9111
methane-CO_2 mixtures, heat capacities up to 2250 psi 2—28736
methane-d_4, solid, orientational structures rel. to phase transitions 2—25359
methane-d, heat capacity in temp. region below 10K 2—16040
methane-H_2-N_2 mixtures, Joule Thomson effects 2—24980
methane-He-N_2, mixtures, Joule Thomson effects 2—24980
methane-perdeuteriopropane gas mixture, calc. of self and mutual diffusion coeffs. 2—32189
methane/CO_2, methane/ethylene, methane/N_2, integral Joule-Thomson effect exptal. check of predictive calculation methods 2—3325
methanes, mixed isotopic solid solutions, orientation effects on high resolution i.r. spectra 2—16505
methanol, adsorption of Pt electrode, obs. using polarized light reflected intensity meas. 2—9309
methanol, film boiling on vertical surfaces 2—32312
methanol, liquid proton motions studied by cold neutron scattering 2—25035
methanol, photoionization, first ionization potential determination and ion yield curve interpretation 2—15378
methanol, quantitative liquid-phase spectra, absorptivity in 2.5-13μm region 2—32270
methanol, reaction in gas discharge, polymer deposits 2—4580
methanol, triplet excitation by low energy electron impact spectroscopy, cross section determ. 2—15311
methanol, triplet excitation by low energy electron impact spectra 2—24453
methanol, volume viscosities, acoustical study 2—12553
methanol 2—25075
methanol at galactic centre, meas. of rest frequency of 36 cm radio line 2—33596
methanol solution, calc. of partial modal volumes of electrolytes at infinite dilution 2—15612
methanol vapour, adsorption on Saran charcoal, vol. change 2—3559
methanol-CS_2 system, specific heat and coexistance curve near critical point 2—35754
methanol/ethylene (n-pentane) mixtures, second virial coeff. 2—24976
methanols, isotopic, analysis of torsion-rotation spectrum, determ. molecular constants 2—8798
p-methoxy benzylidene p-n butylaniline, MBBA, order parameter, n.m.r. obs. 2—6261
m-methoxy phenol, near u.v. absorption spectrum 2—3106
4′-methoxy-benzylidene-4-acetoxyaniline, electret thermal analysis 2—1078
p-methoxy-benzylidine, p-n-butyl-aniline, nematic liquid crystal, dispersion and anisotropy obs. in u.s. velocity 2—32261
p-methoxybenzylidene p-n-butylanilene nematic liquid crystal, coherence length in isotropic phase 2—28795
p-methoxybenzylidene p-n-butylaniline, nematic proton spin-lattice relaxation 2—25113
p-methoxybenzylidene p-n-butylaniline, Raman spectra, solid, nematic and isotropic phases 2—13493
p′-methoxybenzylidene-p,n-butylaniline, liquid crystal, bending mode of curvature electricity 2—28889
p-methoxybenzylidine, p-n-butylaniline, liq. crystals, obs. of domains in longitudinal electric field 2—9100
p-methoxybenzyline-p-butylaniline, nematic liquid, refractive index and birefringence 2—18828

Organic compounds continued
methoxydifluorophosphine, microwave spectrum, rotational constants and molec. structure 2—15387
2-methoxyethanol, microwave spectrum, determination of rotational constants and dipole moment 2—12262
methyl(methylthio) mercury, vibrational assignment of i.r. and Raman spectra 2—21693
1-methyl 9-methyl 5,6,11,12-tri-hydro 5,11-dimethylphenhomazine, crystal structure, X-ray crystallographic data 2—6456
methyl acetate, ^{13}C n.m.r. relaxation, temperature dependence 2—38951
methyl acetate, valence field force constants obtained by normal coordinate analysis 2—8793
methyl alcohol, ^{13}C n.m.r. relaxation, temperature dependence 2—38951
methyl alcohol, laser excited Raman bands, application of slit function corrections 2—9138
methyl alcohol, mol. rot. influence of H-bond, cold neutron transmission obs. 2—15349
methyl alcohol and iodide, ^{13}C spin-lattice relax. 2—10257
methyl alcohol in Orion at $\lambda \sim 1$cm 2—7462
methyl alcohol vapour, first Townsend coeff. meas. 2—15500
methyl azidoformate, methyl azidoformate-d_3, microwave spectrum at 26.5 to 40.0 GHz, ground state rotational constants 2—15388
methyl bromide, ^{13}C n.m.r. relaxation, temperature dependence 2—38951
methyl bromide, gaseous total electric polarization 2—15543
methyl bromide, ground state geometry predicted from that of methyl iodide 2—12221
methyl bromide, molecules excited above first ionization potential, direct and pre-ionization, isotope effects on yields 2—759
methyl bromide -d_3, i.r. spectrum, analysis of ν_4, P and R structure 2—21695
methyl chloride, gaseous, second dielectric virial coeffs. 2—15536
methyl chloride, gaseous, total electric polarization 2—15543
methyl chloride, ground state geometry predicted from that of methyl iodide 2—12221
methyl chloride, Stark effect, applic. to Q-switching of CO_2 laser 2—3105
methyl chloride and fluoride, rot. collisional number and heat cond. 2—18767
methyl chloride ion molecule reactions, kinetics ion cyclotron resonance spectroscopy obs. 2—35114
methyl chloride single crystal, e.s.r. study of CH_2Cl radical 2—8792
methyl chloroformate, assignment of vibrational spectra 2—15384
methyl cyanide, in cometary spectra, detection 2—26863
methyl cyanide, vibrational analysis using empirical force field 2—21691
methyl cyanide and isocyanide, ab initio SCF calculations of electronic structure 2—38993
methyl cyanide mean vibration amplitudes calc. 2—24545
methyl cyanide-d_3, vibrational assignment of near i.r. spectra, derivation of Coriolis coupling const. and anharmonicity coeff. 2—38992
methyl cyanide-N_2 mixtures, heat conductivity change due to electric field parallel to temp. gradient 2—3326
methyl cyclopropanols, structure and isomerism of rotation about C-O determ. by solvent effect of pyridine on n.m.r. 2—5968
methyl derivatives of naphthalene, crystalline, proton spin relaxation investigation of methyl group motion 2—22844
methyl diboranes, proton magnetic resonance 2—35232
methyl fluoride, ^{13}C enriched, Stark effects 2—5357
methyl fluoride, investigation of $2\nu_4$ perpendicular band near 6000 cm^{-1} 2—38995
methyl fluoride+other polar gases, second dielectric virial coeffs. 2—15537
methyl fluoride-N_2 mixtures, heat conductivity change due to electric field parallel to temp. gradient 2—3326
methyl formate, valence field force constants obtained by normal coordinate analysis 2—8793
methyl group-containing solid, dynamic proton polarization due to temp. change 2—33361
methyl groups, ^{13}C spin-lattice relax. times and chem. polarization 2—8796
methyl halides, vibrational analysis using empiricial force field 2—21691
methyl iodide, ^{13}C n.m.r. relaxation, temperature dependence 2—38951
methyl iodide, collisional reaction with K atoms, energy dependence of differential and total reaction cross sections 2—678
methyl iodide, ground state geometry determ. from i.r. spectrum study of dideutero methyl iodide 2—12221
methyl iodide, as reactor gaseous fission product, ice absorption 2—543
methyl iodide, spin echo n.m.r. 2—35790
methyl iodide trapping, for removal of active iodine from reactor waste at high temp. and press. 2—5763
methyl isobutyl ketone, fluidized by water, coalescence rates 2—1126
methyl isocyanide, in cometary spectra, detection 2—26863
methyl isocyanide, isomerization, failure of RRKM theory 2—3109
methyl isocyanide, rot. spectrum for ν_8=1 and ν_8=2 excited vibr. states 2—24544
methyl malonic acid cryst., γ-irrad., methyl group tunnelling rot. freq. 2—22848
4-methyl N methyl pyridinium bromide, fused, n.m.r. spectra, specific conductance 2—4562
methyl naphthalene, cryst., rot., barriers of CH_3 groups 2—10573
methyl naphthalene, proton spin relaxation described by rotation of CH_3 groups 2—40786
1-methyl naphthalene in cyclohexane, intramolecular dielectric relaxation, numerical analysis 2—35774
methyl nitrate, microwave spectrum, structure and dipole moment 2—18514
methyl nitrate, photoionization spectra investigated 2—12224
methyl nitrate, solvent and temperature effects on ^{14}N nuclear spin relaxation 2—6259
3- methyl pentane-CS_2 glass system, γ-radiolysis 2—7185
methyl pyridine adsorption on Al_2O_3, i.r. spectroscopy study 2—6367
N-methyl pyridinium chloride (bromide), fused, n.m.r. spectra, specific conductance 2—4562
methyl radical, configuration interaction wavefunctions and computed inversion barriers 2—35277
methyl radical, hyperfine splittings, spin polarization contribution, first order perturbation treatment 2—15404
methyl radical reactions with HCl and H_2S, activation energies and kinetic isotope effects 2—26338
methyl silyl acetylene, mean amplitudes of vibration and Coriolis coupling constants 2—15385
methyl titanium halides, i.r. and n.m.r. spectra 2—38989
methyl torsional modes in molecular solids 2—12265

Organic compounds continued
methyl vinyl ketone, vibrational-electronic bands of $S_1(n,\pi^*)$ 2—35336
2-methyl-2, 4-pentanediol, pressure and temp. studies of n.m.r. translational relaxation 2—35795
3-methyl-pyrrole, analysis of NMR spectrum, assignments of chemical shifts and coupling constants 2—12260
methylacetylene, interstellar in Sgr B2, $^5O—^4O$ transition at 85457.29 MHz 2—7461
methylamine, vicinal H-H coupling, dihedral angle dependence, lone-pair orientation effect 2—5986
methylamine and deuterated derivatives, mass spectrometric study of negative ions formation by electron impact 2—38988
methylamine-d, inversion coordinate and barrier height for asymmetric amino group NHD determ. 2—12259
methylammonium, aluminium double sulphate dihydrate, far-i.r. absorpt., deuteration effects, vibrs. obs. 2—22756
methylammonium chloride, molecular reorientation, n.m.r. study 2—16407
methylated ethylenes, ionization potentials from photoelectron spectra 2—31854
methylated silanes, v.u.v. spectra 2—35299
methylbromide, collisions study by broadening of microwave spectral lines 2—35385
1- methylcoronen and benzophenone mixed crystals, demonstration of delayed fluorescence 2—36939
methylcyclohexane, gaseous, conformation study by electron diffraction 2—5970
methylcyclohexane, pulse radiolysis obs. of solvated electrons 2—22889
methylcyclohexane glass, biphenyl doped, isothermal deferred luminescence, electron tunnelling mechanism 2—4515
methylcyclohexane glass containing biphenyl, deferred luminescence at 4.2 K 2—7107
methyldifluorophosphine, microwave spectrum, rotational constants and dipole moment 2—15386
N-methyldiphenylamine, calculation of electronic spectra 2—31848
methylene, generalized valence bond wavefunctions for low lying states 2—21694
methylene, prod. in photolysis of methane, and insertion into C-H bond forming ethane 2—22882
methylene, singlet, vibrational deactivation by collision induced integration crossing 2—12311
methylene chloride, boiling, nucleation sites obs. by liq. crystals colour patterns 2—1151
methylene chloride, influence on photoelectric properties of Se 2—28992
methylene chloride, photoelectron-photoion coincidence spectra 2—28164
methylene difluoride, collisions study by broadening of microwave spectral lines 2—35385
methylene fluoride, high-resolution molecular Zeeman measurements of ^{19}F chemical shift anisotropy 2—35339
methylene groups, dihedral angle assignment by n.m.r. coupling constants 2—3066
methylene halides, rotation distortion constants 2—3108
methylenecyclopentane, liq. and vap. i.r. and Raman spectra, fundamental frequency assignment 2—12263
methylenecyclopropane, INDO calculations on lowest energy singlet and triplet states, ring opening studied 2—8794
methylhydrazine, N-N torsional potential function 2—38990
methylnaphthalenes in n-paraffins, obs. of fluorescence of free radicals, 77 and 55K 2—13510
methylpentaborane, dissociation energy of B-methyl bond in 1- and 2-isomers by electron impact and extended Huckel calcs. 2—12103
1-methylpentaborane(9), B-C coupling constants 2—24543
3-methylpentane, electron drift mobility in solid, photoinjection method temperature effects 2—22460
3- methylpentane + nitromethane binary mixture, decay rate of conc. fluctuations near critical mixing point 2—9110
3-methylpentane γ-irrad. at 77K, effects of optical bleaching on luminescence decay and trapped electron conc. 2—26229
methylpropenals, singly substituted, excited-state geometries 2—35336
methylpropenals, singly substituted, excited-state geometries 2—35337
5-methylrhodamine, far i.r. spectra, rotatory oscill. effects 2—39006
methylsilane, barrier to internal rotation and its derivatives w.r.t. vibrational coordinates 2—12264
α-methylstyrene radical anions, spin density distributions, unrestricted Hartree-Fock calculation 2—28388
o- and m-methylstyrenes, i.r. spectra, vibr. band assignment 2—3107
2-methyltetrahydrofuran, γ-irradiated at 4K, e.s.r. study of trapped electrons 2—36995
methyltetrahydrofuran glass energy levels structure of trapped electrons deduced from photoconducting and bleaching 2—36615
2- methyltetrahydrofuran irradiated glasses, study of trapped electron 2—26377
N-methylthioacetamide, i.r. spectra, normal coordinate anal., functional gp. frequencies 2—31864
4 methylumbelliferone solutions in $HClO_4$, high efficiency broad band tunable dye laser 2—37976
1-methylvinyl radical on silica gel surfaces, e.s.r. sppectra, temp. effects, h.f. linewidths 2—35358
Michler's ketone, glassy solns., environment effects on anomalous luminescence 2—36938
Michler's ketone, solid soln., phosphorescence from 2 levels populated by intersystem crossing 2—4504
mixed crystals, spin-phonon interaction for triplet state molecules 2—29847
molecular cryst., ^{35}Cl quadrupole relax., CCl_3-reorientation 2—10276
molecular cryst., charge-carrier injection, metal or electrolyte interface, theory 2—36520
molecular cryst., disordered, diffuse X-ray scatt. obs. 2—9375
molecular cryst., internal mobility, n.m.r. obs. 2—10538
molecular cryst., optical phonons and polaritons 2—19392
molecular cryst., Raman line shift and broadening due to mol. reorientation 2—10413
molecular cryst., tunnelling rot. of kindered methyl groups 2—26291
molecular crystal, exciton diffusion 2—36422
molecular crystals, sensitized luminesc. retardation effects 2—40712
molecular mobility of free radicals, e.p.r. obs. 2—26290
molecular solid, space charge limited current, effect of carrier dimerization 2—29689
molecules, laser induced i.r. fluorescence 2—826
molecules, self-consistent MO methods, Gaussian-type basis sets 2—21648

Organic compounds continued
molecules with one, two and three CH_3 tops, selection rules evaluated 2—8511
monochlorobenzene, cryst. struct. 2—9510
monocyclic molecules, diamag. susceptibility, small radius potential model, ring π-electron contrib. 2—38945
monodeuterobenzonitriles, in polycryst. matrices, vibr. anal. of luminescence in terms of excited state geometries 2—31839
monodeuteromethane, Coriolis resonance between ν_3, ν_6 and ν_5 bands 2—31753
monofluoroacetylene, rotational structure of ν, and 2ν, i.r. bands, centrifugal distortion const. 2—5983
monofluorobenzaldehydes and derivatives, n.m.r., conformations, spin coupling, and INDO-MO calculations 2—5982
monofluorobenzene, fluorescence decay times and radiative lifetimes, gas phase 2—24536
monofluorobenzene, lifetimes and quantum yields of fluorescence from vibronic states 2—21697
monoiodomethyl radical, matrix i.r. spectrum, vibrational assignment 2—8800
monomethylamine, vapour viscosity 2—32183
monomethyldiazirine, u.v. obs. spectrum, rotational fine structure of 0-0 band at 3424 Å 2—12267
monomethylphosphine, ab initio LCAO-MO-SCF calcs. of rotational barrier and electronic structure 2—18515
monosodium acetylide, neutron structure determ. at 293 and 5K 2—39661
N,N-dialkylhydrazones, i.r. spectra, absorption bands 2—3084
n-alkanes, Raman spectra and rotational isomerism 2—40696
N-halogen secondary amides, i.r. spectra, cis-trans isomerism 2—28344
naphthacene, exciton induction and echo 2—1705
naphthacene, spectral shifts in nonpolar solvents, mechanism 2—25093
1- and 2-naphthaldehydes, dielectric relaxation, microwave absorption meas. 2—15601
naphthalene, anal. of antiresonances in Rydberg spectrum in terms of theoretical line shape parameters 2—8802
naphthalene, and derivatives, crystalline state, emission spectra obs. 2—29964
naphthalene, chemical shifts, ring current contribution 2—3072
naphthalene, electrets, semiconducting, Schottky barrier formation 2—4191
naphthalene, emission and absorpt. spectra, charge transfer complexing effects 2—36893
naphthalene, equilibrium form, nonsingular surfaces 2—18925
naphthalene, fluorescence and nonradiative decay, excitation energy and deuteration dependence 2—28390
naphthalene, gas phase triplet absorption spectrum, obs. of 4 electronic transitions 2—8803
naphthalene, Herzberg-Teller theory and Duschinsky effect 2—12082
naphthalene, in biphenyl and durene, localized in-band rotational phonons, obs. in electronic spectra 2—29512
naphthalene, indole-doped, local exciton spectra, effect of impurity conc. 2—13505
naphthalene, isotopic mixed cryst., energy spectrum 2—33279
naphthalene, lattice frequencies calc. using pairwise potential functions 2—25646
naphthalene, librational modes, Raman spectra, pressure and temp. dependence 2—36896
naphthalene, mixed mol. cryst., Frenkel exciton states, density of states functions 2—19523
naphthalene, obs. of transient absorption bands in some regions in gas phase and soln. 2—3112
naphthalene, opt. absorpt., 6.5-35 eV 2—18492
naphthalene, optical detection of e.s.r. 2—10527
naphthalene, phosphorescence in vapour phase 2—35348
naphthalene, p.m.r., exciton motion 2—7132
naphthalene, proton relax. by excitons, low temp. 2—10277
naphthalene, Raman spectra, Davydov splitting magnitude, dependence on crystal elementary cell parameters 2—26183
$^1B_{2u}$ naphthalene, random lattice calculations on Frenkel exciton 2—1467
naphthalene, threshold electron excitation spectra, obs. of compound negative ion resonances 2—35350
naphthalene, triplet exciton lifetimes from delayed fluorescence and prompt phosphorescence 2—20108
naphthalene, vapour, fluorescence lifetimes of vibronic levels 2—3111
naphthalene absorbed on dispersed amumino- silicate absorbents, luminescence, 77K 2—4483
naphthalene crystals, proton relaxation through triplet excitons 2—22845
naphthalene in durene crystals, phosphorescence discussion in terms of phonons resonance pair interactions and intermol. energy transfer 2—20111
naphthalene radical ions, calculation of hyperfine splittings in e.s.r. spectra 2—38953
naphthalene type crystal, anomalous nuclear dipolar relaxation 2—7000
naphthalene-d_8, anisotropy of opt. polarizability from induced birefringence produced by photoselection 2—3110
naphthalene-d_8 in solid soln., X-ray excitation, triplet molecule formation 2—26364
naphthalene-d_8 interaction with singlet excitations of toluene 2—9140
naphthalene-pentacene mixed crystal, triplet energy transfer, delayed fluoresc. 2—40727
·naphthalene-tetracyanobenzene complex crystal effect of high density exciton on fluorescence decay curve 2—36948
2-naphthol, dissolution of solids into turbulent liquid stream 2—28757
2-naphthol cylinder rotating in water, mass transfer coeff. determ. from rate of dissolution 2—6218
2-naphthol in benzene, intramolecular dielectric relaxation, numerical analysis 2—35774
2-naphthyl radical, produced by ^3H decay synthesis in naphthalene-d_8, e.p.r. study 2—10650
1,8-naphthyridine, triplet state, e.s.r. studies using microwave and optical detection 2—10490
natural gas, CH_4, C_2H_6, C_3H_8, Joule- Thomson effect 2—24978
nematic liquid cryst., instabilities in pulsating elec. fields 2—12545
nematic liquid cryst., intermol. forces influence on positron annihilation 2—18796
nematic liquid cryst., stimulated Raman scatt. 2—12564
nematic phase, periodic struct. induced by rot. mag. field 2—18793
neodymium ethyl sulphate, spin-lattice relax., mag. field depend. 2—22719
neodymium ethylsulphate, paramagnetic relaxation, Pr^{3+} and Ce^{3+} cross-relaxation 2—26087

Organic compounds continued
- neopentane, electron mobility mechanism 2—35719
- neopentane, gaseous, Raman spectra 2—18520
- neopentane, scattering cross section and mobility of excess electrons in liquid 2—35786
- neopentane, self-diffusion in plastic crystals 2—32569
- neopentane, solubility in liquid methane and liquid Ar 2—1080
- neopentane and d_{12} analogue, normal coordinate anal. mean amplitudes of vibration 2—31865
- neopentane plastic phase transition 2—39976
- neopentane-1-bromo-2,2-dimethylpropane liq. mixture, excess free enthalpy calc. 2—28840
- neopentane-tetramethylsilane liq. mixture, excess free enthalpy calc. 2—28840
- neptunium (V) oxalate, properties studied from 2.4-37.5K, metamagnetic phase transition at 11.6K 2—19888
- Nile blue A dye laser, continuous, mode locked, pumped in red 2—17608
- nitramines, conjugated, electronic absorpt. spectra 2—8804
- nitriles, complexes formed with proton donors, structure from dipole moment measurements 2—28391
- nitroalkanes, in ethers, u.v. photolysis, prod. of alkylalkoxynitroxide radicals 2—8728
- m-nitroaniline, cryst. growth and electrooptic props. 2—16427
- m-nitroaniline, Pockels effect, half-wave voltage at 6328 Å 2—22732
- p-nitroaniline, single crystals, near i.r. spectrum, vibr. anal. 2—4461
- p-nitroaniline, thermal expansion, 290 to 380K 2—9898
- nitroanisoles, i.r. absorption spectra, vibrational analysis 2—3113
- nitroaromatics, study of luminescent emission characteristics 2—12269
- nitrobenzal anils, relaxation times and dipole moments, dil. solution method 2—31867
- nitrobenzene, optical filament from., laser intensity inhomogeneities 2—6234
- nitrobenzene, partially deuterated derivatives, n.m.r., incremental aromatic solvent induced shifts 2—18488
- nitrobenzene, stimulated scattering under picosecond laser excitation 2—1102
- nitrobenzene, structure relaxation during internal rotation of the nitro group 2—38997
- nitrobenzene-n-hexane binary mixtures near critical pt., sound velocity 2—28855
- nitrobenzene-n-hexane mixture, near critical point, u.s. absorp. 2—28854
- nitrobenzenes, photolysis, e.s.r. study of alkoxynitroxide free radicals 2—832
- p-nitrobenzonitrile, geometric distortion studied by high-resolution n.m.r. in the nematic phase 2—31840
- nitrobenzonitriles, electrogenerated radical anions, e.s.r. spectra 2—5985
- nitrocellulose and acetylcellulose, alpha particle track recording 2—18030
- nitroethane, symmetry group for classification of vibrational modes 2—18503
- 2-nitroethanol, rotational isomerism, i.r. spectra 2—28389
- nitroethyl, photoionization mass spectra investigated 2—12224
- nitrogen containing increased valence- formulae, generated from electronic structure studies of N_2O_4 2—12168
- nitroglycerine, explosion, laws of initiation during collapse of air cavities under impact 2—27293
- nitroglycerine, explosion in liquid layer under impact, bubble initiation mechanism 2—27292
- nitroglycerine powders, effective depth of light absorption required for ignition 2—27300
- nitromethane, shock compressed, opacity, absorpt., spectra 2—35770
- nitromethane, spin-lattice relaxation of ^{15}N, temp. depend. 2—13424
- nitromethane+alkene, binary system, liquid-liquid equilibria, miscibility gaps 2—1083
- nitromethane-CCl_4, dipole moments calculation 2—39376
- nitromethyl, photoionization mass spectra investigated 2—12224
- o- and p-nitrophenetoles, vibrational assignment of i.r. spectra 2—31866
- nitrorhodamine, far i.r. spectra, rotatory oscill. effects 2—39006
- p-nitrotoluene, polar liquid, induced dielectric alignment, n.m.r. obs. 2—9149
- 5-nitrouracil, e.s.r. study of iminoxy radical formed by γ-radiation 2—10651
- 5-nitrouracil, nonlinear optical susceptibility 2—19954
- nitroxide free radicals, e.p.r., coupling constants 2—5984
- nitroxide radicals, stable, mag. props. 2—25994
- nitroxide solid free radical, Overhauser effect 2—7152
- nitroxides, unsubstituted cyclic, photochem. production and e.s.r. studies 2—10643
- nomenclature, IUPAC rules, book 2—23211
- nonbenzenoid hydrocarbons, 16 pi-electron systems, molecular orbital calculations 2—3067
- norbornadiene, spin-lattice relaxation in solution, microscopic molec. motions 2—28900
- norbornanones and norbornenones, ionization potential, photoelectron spectroscopic determ. 2—3114
- norbornylene, translational self diffusion, press. depend. 2—29228
- normal alcohols, thermal conductivity meas. with thermal comparator 2—25073
- nucleic acid bases, thin films, energy loss functions for 25 keV electrons, inner shell excitation and inelastic scatt. cross sections 2—22446
- nucleic acid bases, thin films, energy loss functions for 25 keV electrons, outer shell excitation 2—22445
- nujol, liq., explanation for spectra in terms of 2-phonon absorption 2—1104
- $\alpha,\alpha,\alpha',\alpha'$,2,3,5,6-octachloro-p-xylene in benzene, dielectric relaxation times from microwave obs. meas. of loss and constant 2—28342
- n-octadecane, solification rate determ. by acoustic method 2—39423
- octamethylcyclotetrasiloxane, antisymmetric valence vibrs. of Si-O-Si bridge 2—3101
- octamethylcyclotetrasiloxane, equilib. props. near critical point, density, v.p. obs. 2—25154
- n-octane, heat capacity at elevated press. 2—25072
- octane, liq., explanation for spectra in terms of 2-phonon absorption 2—1104
- n-octane film, on quartz, interaction press.-thickness isotherms 2—39352
- 1,8-octanediol-glycol mixtures, dynamic proton polarization rel. to polarized target production 2—36811
- n- octanol in heptane solns., dielectric const. and dielectric loss meas. from microwave relaxation 2—6241
- octylamines, dielectric relaxation in cyclohexane solution 2—35780
- 4-octyloxybenzylidene-4′-ethylaniline 2—18853

Organic compounds continued
- oil, partially submerged drop, spreading on Plexiglas 2—1166
- oil, vacuum pump, torpidity phenomena 2—41409
- oils, pollution identification by flame photometric sulphur detector 2—7191
- α- olefin reaction products with tertiary butyl hydroperoxide, analysis by i.r. spectroscopy 2—16701
- olefin-O_3 chemiluminescent gas phase reactions, obs. of OH ground state vib.-rot. bands 2—22868
- olefins, plasma, prod. by laser heating, refl. rad. spectra 2—39156
- organic crystals, time resolved fluorescence spectrum, rel. to studies of two-photon excitation by dye laser 2—26361
- organo-montmorillonites, interstratified layer struct. 2—29081
- organoethoxysilanes, proton magnetic resonance 2—851
- organometallic β vinyl chloride (Hg, Sn, Tl, Sb), cis and trans. config., i.r. absorp. obs. 2—31872
- organometallic acetylides, i.r. and Raman spectra, vibrational assignment 2—15345
- organotin compounds, ^{119}Sn chemical shifts by double resonance 2—28332
- ovalene crystals, calculation of band structure and carrier mobilities 2—25727
- oxadiazole, electronic structure using improved LCAO method 2—18518
- oxalate, bond distance and coplanarity of $C_2O_4^-$ ion 2—32484
- oxalate dye, photocond., singlet exciton thermal ionization 2—19790
- oxalic acid, convective mass transfer coeffs. meas., Thoma method 2—4583
- oxalic acid as a chemical dosimeter, for mixed pile radiation in multimegarad range 2—5768
- oxazole, electronic structure using improved LCAO method 2—18518
- 3-oxetanone, microwave spectrum and ring-bending vibration 2—15389
- oximes, NH and CH spin couplings, effect of lone pair orientation 2—5986
- oxo-2 dioxaphosphorinane-1,3,2 derivatives, basicity of phosphoryl group 2—18517
- 5-oxybenzodioxane-1,4, in soln., infrared absorption bands, temp. dependence 2—18516
- oxyhaemoglobin, nitroxide radical spin labelled, effect of slow rotational motion on p.m.r. 2—25106
- oxyphosphorane, four-membered cyclic ring with pentavalent phosphorous, crystal and molec. structure 2—25360
- p-azoxyanisole, nematic, press. depend. of order parameter 2—15572
- palladium n-propyl mercaptide, bond lengths and angles 2—6464
- palladium porphyrin complexes, fast fluorescence, delayed fluorescence, quasiline structure studied 2—12276
- parabenzoquinone π-complexes, degree of delocalization of n-orbitals, calc. 2—18519
- 1,4-paradioxane in soln., mol. assoc. obs. 2—9172
- n-paraffin, doped, Shpol'skii spectra, 77K, polarization of multiplet components 2—20055
- paraffin, solidified in elec. and mag. fields, anisotropy, n.m.r. obs. 2—25939
- paraffin cryst., impure, phonon wings and zero-phonon lines in fluoresc. spectra 2—1715
- n-paraffins, high press. phase relations 2—15629
- paraffins, long-chain, u.v. absorpt., electronic excitations 2—40687
- n-paraffins, vibrational modes of Raman bands 2—28392
- paraxylene velocity and absorption of shear waves near melting point 2—29536
- penicillamine, polycrystalline, proton spin-lattice relaxation 2—1736
- pentabromotoluene, cryst. struct. 2—9511
- pentacene, exciton induction and echo 2—1705
- pentacene, triplet quantum yield study with tunable dye laser 2—26355
- pentacene-6 13-quinone, electronic spectra in solution 2—28394
- pentacene-naphthalene mixed crystal, triplet energy transfer, delayed fluoresc. 2—40727
- 2,4,α,α,α-pentachloro toluene, temp. dependence of Cl n.q.r. frequencies, torsional frequencies 2—28419
- pentaerythritol, elastic consts. determ. from u.s. velocity 2—25483
- pentaerythritol, hydrogen bonding, dispersion relations, from X-ray diffuse scatt. obs. 2—3749
- pentaerythritol, proton injection measurements 2—25847
- pentaerythritol-d_0 and -d_4, vibrational assignments vibrational crystal spectra 2—18521
- pentafluorobenzene, fluorescence decay times and radiative lifetimes, gas phase 2—24536
- pentafluoroiodomethane, photodissociation laser, Zeeman effects in hyperfine structure of atomic I emission 2—31038
- pentahalogenotoluenes, i.r. study of barriers to internal rotation form vibr. band width meas. 2—8806
- pentalenoheptalene, molecular orbital calculations 2—3067
- n-pentane, solubility in liquid methane and liquid Ar 2—1080
- n-pentane/methanol mixture, second virial coeff. 2—24976
- 1-pentanol-water-porphyrexide system, proton polarization at 50kG and 1K, polarized target production 2—36808
- pentaphenylcyclopentadienyl, methyl substituents effects on orbital degeneracy 2—24525
- 1-penten-3-yne, microwave spectrum, electric dipole moment, rotational constants 2—12270
- 2-(4-n-pentylphenyl)-5-(4-pentyloxyphenyl)- pyrimidine, smectic modifications detn. 2—25042
- 1-pentyne, rotational isomerism from microwave spectrum 2—8805
- peptide group, electronic structure 2—28393
- perdeuteriopropane-methane gas mixture, calc. of self and mutual diffusion coeffs. 2—32189
- perdeuterobenzene, lifetimes and quantum yields of fluoresence, from vibronic states 2—21697
- perdeuterobenzonitrile, in polycryst. matrices, vibr. anal. of luminescence in terms of excited state geometries 2—31839
- perdeuteromethane, thermal conductivity and shear viscosity in static mag. field and field free space 2—35687
- perfluoroalkanes, electron mobility, diffusion and attachment 2—39197
- perfluoroalkyl polyether fluids as a lubricant in vacuum pumps 2—23196
- perfluoroalkyliodide molecules in collision with iodine atoms, deactivation 2—8449
- perfluorocyclobutene and perfluorobutene, electron transport, attachment and ioniz. coeffs. 2—35588
- perfluoroethyl iodide, electron diffraction structure study r_g parameters 2—31868
- perfluoroheptane iso-octane critical mixture, correl. lengths 2—3430

Organic compounds continued
perfluoroisopropyl iodide, electron diffraction structure study r_g parameters 2—31868
perfluoromethyl iodide, electron diffraction structure study r_g parameters 2—31868
perfluoromethylcyclohexane, solid, phase transitions and molecular motions 2—1380
perfluoronaphthalene, chemical shift, inhomogeneous spin echoes, dipolar broadening 2—13422
perinaphthenyl radical, ENDOR spectra in liquid crystal 2—21647
perionaphthothioindigo and 2-perionaphthopentiophen-2′-(5′-methylthionaphthene)-indigo dyes, photochromic properties of coloured films 2—40833
peroxylamine disulphonate radical in liquid and frozen media, anisotropic rotational reorientation, e.s.r. study 2—16644
perylene, electrochromic spectra in polystyrene matrix, change in polarizability and dipole moment between ground and excited states 2—13488
perylene, film, pure and doped, bistable switching, metallic filament form. 2—16219
perylene, in paraffin solns. of naphthalene, dependence of fluorescence spectra sharpness on conc. 2—1714
perylene, photoionization in polar liquids, analysis of photochemical data 2—21701
perylene, possible reorientation of molecule in solid state, n.m.r. investigation 2—10567
perylene complex, semiconductor, e.p.r. spectra 2—16218
perylene thin films, bistable switching 2—25831
phenacyl chloride, temp. dependence of Cl n.q.r. frequencies, torsional frequencies 2—28419
phenantherene, Herzberg-Teller theory and Duschinsky effect 2—12082
phenanthrene, emission and absorpt. spectra, charge transfer complexing effects 2—36893
phenanthrene, emission spectra during irradiation with X-rays and U.V. light at 77°K 2—36951
phenanthrene, Kramers-Kronig relationships, refr. and extinction indices 2—15592
phenanthrene, rigid glass soln., intersystem crossing rate constants 2—10426
phenanthrene, single cryst., dielectric and dilation anomalies, capacitance meas., 23- 75C 2—10111
phenanthrene, zero field splitting coeffs. of e.s.r. of lowest triplet level, calc. using Huckel approx. 2—12275
phenanthrene in durene crystal system, absorption spectra, vibronic coupling 2—9322
phenanthrene/benzophenone in ethanol, 77K, two quanta sensitized photo-ionisation 2—1761
phenazine, i.r. and Raman spectra, vibrational assignments 2—8809
phenazine, Raman spectrum studied, purification of sample to reduce luminescence effects discussed 2—12273
phenazine-fluorene (anthracene) mixed crystals, e.s.r., influence of deuteration and energy transfer 2—20154
phenobarbital, N-H hydrogen bonding to electron donor, n.m.r. study 2—854
phenol crystallization of amorphous deposits 2—32314
phenol in polar and apolar solvents, fluorescence quantum efficiencies 2—28876
phenol intertiary and quaternary systems, i.r. spectra, proton accepting ability 2—28397
phenol vapour, intermolec. interactions, investigation using second virial coefficients and Stockmayer model 2—39027
phenol-methylpyridinoxide complex, H bond system, obs. of intra and inter-mol. vibrations 2—24548
phenolate ions, hydrated, isotopic, C-O stretching i.r. band frequency 2—28396
phenolic methacrylate anhydrides, i.r., n.m.r. and mass spectra, spectrometric data 2—28334
phenolic methacrylates, i.r., n.m.r. and mass spectra, spectrometric data 2—28334
phenols, chlorine substituted, complexes with acetonitrile, i.r. study of intermol. H bonds 2—856
phenols, halogenated, hydrogen bonding with N,N'-dimethyl formamide 2—3100
phenols, substituted, electron density distrib. calc. by semiempirical MO methods 2—24549
phenols, substituted, solns., electronic absorption spectra, waveband shifts obs. 2—12274
phenothiazine and N-substituted derivatives, configuration determination by n.m.r. 2—12271
phenothiazines, substituted dipole moments meas., bending of nucleus 2—38999
phenoxatiin, film, transport processes 2—16217
phenyl acetylene, glassy soln., thermolum. ascribed to fluoresc. of α-styryl radical 2—18528
phenyl alkyl ketones in glassy matrices, viscosity dependent dual phosphorescence 2—36950
phenyl compounds, monosubstituted, Gordy's rule applied to X bond 2—8810
phenyl isocyanide, lowest-lying singlet $\pi^*\leftarrow\pi$ transition, rotational analyses, dipole moment changes 2—35343
4-(N-phenyl piperizino)-6-methoxy quinaldine, atomic struct., X-ray determ. 2—3748
phenyl propanols, isomeric, dielec. const. and loss rel. to temp. 2—28886
5-phenyl-2-(4-dimethylaminophenyl)-oxadiazole- 1,3,4, electronic structure 2—3116
5-phenyl-2-(4-dimethylaminophenyl)-oxazole-1,3, electronic structure 2—3116
2-phenyl-naphthalene radical anion, ENDOR-in-solution spectra, hyperfine splitting, coherence effects 2—5988
phenylacetic acid and derivatives, n.m.r. 2—35344
phenylacetylene, i.r. spectra, theoretical study of vibrational assignments 2—35312
phenylacetylene, single crystal e.p.r. studies of photoexcited states 2—26360
phenylacetylene in glasses at 77K, photoexcited triplet state, e.p.r. detection 2—16690
phenylacetylenes, D-substituted, fluoresc., vibr. anal. 2—35345
phenylethylacetylene in glasses at 77K, photoexcited triplet state, e.p.r. detection 2—16690
phenyliodoacetylene, photolytic formation of free radical, e.s.r. obs. 2—4600

Organic compounds continued
phenylmethylacetylene in glasses at 77K, photoexcited triplet state, e.p.r detection 2—16690
pheophytin, spectral shifts in nonpolar solvents, mechanism 2—25093
phosphadiazetidinones, ^{19}F NMR spectra meas. and interpreted 2—28366
phosphadiazetidinones, ^{19}F NMR spectra meas. and interpreted 2—28366
phosphine oxides, spectroscopic study of intermolecular interactions 2—28434
phospholipids, mesomorphic phases rel. to cell membrane struct. and function 2—9097
phosphonic acid esters, e.s.r., angular dependence of β-P hyperfine couplings 2—15391
phosphorous compounds, n.m.r. spin-lattice relaxation in liquids 2—32277
photoconductor applic. to electrophotographic microimage recording 2—5464
phthalaldehyde, vibrational assignment of i.r. spectrum 2—35342
phthalazine, dipole moment changes for excitation to different levels, $n\rightarrow\pi^*$ transition 2—8811
phthalazine, intersystem crossing from higher excited singlet states 2—12272
phthalic anhydride derivatives, electronic absorption spectra 2—853
phthalimide gaseous derivatives, radiationless transitions, activation energy and excited state lifetimes 2—28395
phthalocyane, vapour, Q-switching of ruby laser radiation 2—17622
phthalocyanine, π-electron absorp., molecular orbital calc. 2—10399
phthalocyanine, band structure and deformation potentials 2—4128
phthalocyanine, metal-free, calc. of singlet exciton state transitions in visible region 2—39003
phthalocyanine metal complexes in solns. of Lewis acids, absorption spectra 2—1105
β-phthalocyanine single crystal, drift mobility, temp. depend. 2—32993
phthalocyanine single crystal, elec. and optical props. 2—33081
phthalocyanines, electronic structure 2—855
picoline, α-, β- and γ-, calc. vibr. spectra comparison with expt. 2—18842
picolines, spin-lattice relax. temp. depend., mol. rot. 2—9182
picolines, vibr. spectra, rel. to methyl substitution effects in pyridine 2—35346
pigments, surface free energy and polarity from contact angle obs. and surface tension eqn. 2—21968
pimelic acid single crystal, secondary processes caused by irradiation studied by e.s.r. technique 2—40835
pinacone-Cr(V) system, polarized proton target properties and performance 2—34779
piperidine hydrochloride, crystal and molecular structure determ. 2—25362
pirimidine derivatives, absorpt., fluoresc. spectra, scintillation props. 2—28877
pivalic acid, plastic crystalline phase, n.m.r. study of molecular motion 2—1737
pivalonitrile, dielec. and n.m.r. relax., mol. reorientation models 2—9154
pivalonitrile oxide, assignment of vibr. satellites obs. in rot. transition, vibr.-rot. interaction const. microwave and millimeter wave speectra 2—12268
pivalonitrile-N-oxide, microwave spectrum, bending mode estimate, symmetric top molecule 2—5989
plastic cryst., translational self diffusion, press. depend. 2—29228
platinum etioporphyrin complex, fast fluorescence, delayed fluorescence, quasiline structure studied 2—12276
platinum phthalocyanine, band structure and deformation potentials 2—4128
platinum square planar complex, conduction mechanisms 2—36523
plutonium complex, $(C_5H_5)_3\,{}^{239}$Pu(III), mag. susceptibility between 4.2 and 250K 2—22663
polar liquid, spin-lattice relax. temp. depend., mol. rot. 2—9182
poly(ethylene terephthalate), d.c. cond. at elevated temps. 2—22613
poly(methylmethacrylate) containing aromatic hydrocarbons, temperature dependence of phosphorescence in 77-400K range 2—20110
polyacenes, doped, anomalous exciton-quenching kinetics 2—6738
polyacenes, triplet-triplet absorption spectra 2—12201
polyacenes, zero field splitting coeffs. of e.s.r. of lowest triplet level, calc, uing Huckel approx. 2—12275
polycyclic aromatic hydrocarbons, magnetic circular dichroism of α bands 2—8801
polycyclic aromatic hydrocarbons, reversible photodimerization, applications to photochromism 2—33386
polyenes, Wannier functions in orbital theory, π-electron problem 2—18477
polyethylene, crystallization without chain folding, theory 2—22057
polyethylene, fibril structure, gold decoration 2—9226
polyethylene surface, flashover in vacuum, d.c., a.c., and surge voltages 2—22618
polymethine dye, flashlamp excited, green to i.r. 2—37974
polymethyl acrylate, molecular relax., Brillouin spectra obs. 2—26202
polythene, defect containing, vibrational props., numerical method 2—19394
polyurethane: rhodamine 6G, ring laser, unidirectional operation 2—17631
polyvinyl chloride, photocond., field and pressure depend. 2—33080
polyvinyl chloride, water vapour effects on thermoelectret behaviour 2—36602
polyvinylcarbazole, photoinduced current decay obs. 2—22648
polyvinylidene fluoride, film, second harmonic generation and pyroelectricity 2—19955
porphyrexide in n-butanol and water relax. rates and dynamic nuclear polarization 2—25114
porphyrin, π-electron absorp., molecular orbital calc. 2—10399
porphyrin, existence of tautomerism 2—28398
porphyrins, chlorines, electron excitation spectra, interpretation 2—39000
porphyrins, deuterated in photoreduction reactions 2—16688
potassium copper oxalate dihydrate, cryst. struct., X-ray study 2—32483
potassium homophthalate, X-ray diffraction study of crystal structure 2—3750
potassium hydrogen maleate, single cryst., dielec. relax. 2—10110
potassium hydrogen malonate, e.s.r. spectra of X-irradiated single crystals 2—20140
potassium hydrogen meso-tartrate, H-bonding 2—36001
potassium laurate-D_2O system, mesophases, mol. motion obs., n.m.r. meas. 2—6212
potassium mesaconate, crystal structure, X-ray crystallographic data 2—6456

Organic compounds continued
potassium sodium tartrate, far-i.r. absorpt., deuteration effects, vibrs. obs. 2—22756
potassium tartrate, electrooptical effects 2—26117
PPO styrene solutions during polymerization, decay times and radioluminescence yields 2—40809
predeuterated 1-butanol target, polarization of deuterons at 50 O 2 - 14742
prefabrication methods 2—18476
probenecid, crystal, structure, X-ray crystallographic data 2—6456
procaine hydrochloride, cryst. struct. 2—19064
proflavine, triplet quantum yield study with tunable dye laser 2—26355
proline in aqueous soln., Debye effect at microwave freqs. 2—3402
propane, gas and liq., permeation through polyethylene membranes 2—25066
propane, MO calc. of geometry, energy and polarity 2—28383
propane, reaction in gas discharge, polymer deposits 2—4580
propane, u.s. velocity, critical region phenomena 2—6283
propane gas, relative Raman cross section, rel. air pollution 2—35249
propane liquid, γ-irradiated, molec. structure effect on electron reaction kinetics 2—10649
propane premixed mixture with air, study of burning of vortex rings 2—6017
propane-air flame, Na seeded, fibre optics probe for line radiation intensity obs. 2—27311
propane-d$_6$, vibrational assignment of i.r. and Raman spectra, symmetric valence of vibrational frequencies of methylene and methyl groups 2—39002
propanes, methyl substituted, mol. structure effects on free ion yields and reaction kinetics 2—22886
propanol, aqueous solutions, determ. intensity of concentration scattering of light 2—15590
propargyl alcohol and deuterium analogues, vibrational assignment of i.r. and Raman spectra 2—5990
propene, MO calc. of geometry, energy and polarity 2—28383
propenes, chlorinated, rotational isomerism, steric effects, n.m.r. obs. 2—12227
prophyrins, probabilities of intercombination transitions 2—35347
1,3propidactone, ring puckering potential function 2—21698
β-propiolactone, molecular Zeeman effect, magnetic properties and electric moments 2—21675
propionic acid, vibrational spectra 2—28399
propionitrile, in benzene and carbon tetrachloride solutions, dielec. relaxation between 24 and 60°C 2—3401
propyl alcohol vapour, first Townsend coeff. meas. 2—15500
propyl cations, geometries and energies, ab initio MO calculations 2—39001
N-propyl derivatives, n.m.r. spectra, study of general features by subspectral methods 2—28400
propylene, activation energy for addition of O(^{3}P) atoms 2—10614
propylene, gas and liq., permeation through polyethylene membranes 2—25066
propylene, solvent for investigation of Li isotope exchange reactions 2—22855
propylene liquid, γ-irradiated, molec. structure effect on electron reaction kinetics 2—10649
propylene oxide, u.s. velocity in aqueous solutions 2—1095
propyne, as potential source for C_3 in comets 2—41206
propyne, H_2 formation in photolysis at 1236 Å 2—30091
propyne, MO calc. of geometry, energy and polarity 2—28383
propyne, vibrational analysis using empirical force field 2—21691
propynyl boron difluoride, i.r. spectrum, fundamental assignment, G_{12} symmetry group 2—8813
3-propynyl chloroformate, assignment of vibrational spectra 2—15384
pseudocumene, phosphorescence spectra, frozen matrices, liq. nitrogen temps. 2—4502
pseudoisocyanine, absorption spectra, highly- aggregated J-form 2—28401
psoralens, u.v. spectra, description of π-π^* transitions 2—8755
purine nucleic acid base, polycryst. powder, ^{14}N n.q.r., 77 K 2—7159
purine sodium salt, i.r. spectra, freq. variations due to proton loss 2—10342
purines temp. dependence of fluorescence in glass forming solvents in range 77-298 K 2—10435
PVK:TNF, electron transport, pulsed light transient photocond. obs. 2—13337
PVK, amorphous, field dependent drift mobility 2—16201
pyrazine, ab initio CI treatment of ground and excited states 2—12086
pyrazine, crystalline, phase transition at 29°C 2—29460
pyrazine, electronic structure, from photoelectron, u.v., mass and electron impact spectra 2—28403
pyrazine, frozen soln., obs. of additional bands in luminescence spectra due to emission from microcrystals 2—10445
pyrazine, photoelectron spectrum, correlation between ionization bands and electronic levels 2—28402
1-D- and 4-D-pyrazole, microwave spectra, hyperfine structure, quadrupole coupling 2—5993
pyrazole, microwave spectra, nuclear quadrupole coupling constants 2—8815
pyrazole, microwave spectrum, hyperfine structure, ^{14}N coupling consts., rotational constants 2—18526
pyrazolinone azomethine dyes, cryst. struct. 2—9512
$\text{pyrene}^+ + \text{pyrene} \rightleftharpoons (\text{pyrene})_2^+$, thermodynamic and rate constants 2—16674
pyrene, in n-paraffin monocrystals, dependence of luminescence spectrum on crystallization conds. and conc. 2—20098
pyrene, laser excited fluorescence S_2 emissions, intermediate strong coupling and vibr. redistrib. effects 2—15393
pyrene, location of triplet excimer level 2—4505
pyrene, phosphorescence in vapour phase 2—35348
pyrene, photionization in polar liquids, analysis of photochemical data 2—21701
pyrene, powdered, pressure effects on triplet excimer emission 2—4484
pyrene, temp. dependence of lifetime of triplet excimer emission 2—7099
pyrene, thermally activated exciton hopping process, fluorescence 2—25742
pyrene, vapour, effects of intramol. vibr. redistrib. in S_1 fluorescence 2—3117
pyrene and perylene excimer crystals, monomer emission, fluorescence spectra, 4.2K 2—16623

Organic compounds continued
pyrene complexes, stimulated emission when irradiated by Q-switched ruby laser 2—1706
pyrene dissolved in organic liquid, two photon laser photo- ionisation 2—30081
pyrene monomer and excimer, fluorescence and phosphorescence quenching rate parameter dependence on solvents 2—12571
pyrene soln. in toluene, excimer fluorescence, pressure dependence up to 10 kbar 2—15596
pyrene-d$_{10}$-fluorene mixed crystals, e.s.r., influence of deuteration and energy transfer 2—20154
pyreno-(1',2':1,2)-pyrene, cryst. struct., mol. struct. 2—32480
pyridazine, electronic structure, from photoelectron, u.v., mass and electron impact spectra 2—28405
pyridazine-d$_0$ and pyridazine-d$_4$, vibrational spectra 2—35349
2,2'- pyridil, $n \to \pi^*$ transition obs. 2—8814
pyridine, adsorption on $MgSiO_3$, hydrothermal treatment depend. 2—3562
pyridine, calc. vibr. spectra, comparison with expt. 2—18842
pyridine, electric dipole moment of lowest excited singlet state 2—12278
pyridine, freq. of non-polar vibr., influence of methyl substitution 2—35346
pyridine, gas obs. of singlet-triplet transition by ion and electron impact 2—21699
pyridine, hydrogen bonded complex with substituted phenols in benzene solution, far i.r. spectrum meas. 2—12277
2-amino-pyridine, in acetonitrile-water mixtures, phosphoresc., lifetime, intensity at 77K 2—7100
pyridine, n.m.r. ^{15}N and ^{13}C Fourier spectra, coupling constants, shifts 2—6262
pyridine, phys. sorbed on C, leaking curves 2—18958
pyridine, proton spin-lattice relax., solvent effects 2—6260
pyridine bromine charge transfer complexes in C_6H_6, far i.r. spectra, force consts., dipole moment 2—8816
pyridine-^{15}N, n.m.r. 2—24550
pyridine-halogen complexes, far i.r. intensity and normal coordinate studies, force consts., dipole moments 2—8817
pyridines, lactam and thione forms, electronic structure 2—28406
pyridinium.HBr, fused, specific conductance 2—4562
pyridinium.HCl, fused, n.m.r. spectra, specific conductance 2—4562
pyrimidine, electronic structure, from photoelectron, u.v., mass and electron impact spectra 2—28404
pyrimidine in benzene, zero-field microwave-optical double resonance at 77 K 2—22818
pyrimidine nucleic acid base, polycryst. powder, ^{14}N n.q.r., 77 K 2—7159
pyrimidines, lactam and thione forms, electronic structure 2—28406
pyrogallol, crystal structure at −150°C 2—39663
2-pyrone, molecular Zeeman effect 2—12231
4- pyrone, molecular Zeeman effect 2—12231
γ-pyrone series, aromatic derivs., obs. of $n\pi$-, $n\pi^*$- and $\pi\pi^*$- phosphorescence 2—857
pyrrole, effect of hydrogen bonding on NH stretching Raman band 2—21700
pyrrole, n.m.r. ^{15}N and ^{13}C Fourier spectra, coupling constants, shifts 2—6262
pyrrole, valence charge distrib. calc. by interative extended Huckel approach 2—5992
pyrrole, vibrational analysis of photoelectron spectra 2—3097
pyrylium cation and deuterated analogues, i.r. spectra, vibrational assignment 2—39004
quanidine aluminium double sulphate hexahydrate, far-i.r. absorpt., deuteration effects, vibrs. obs. 2—22756
quinacridone, vacuum sublimation and cryst. struct. 2—6466
quinoline, condensed states, intermolecular dynamics, vibr. spectra study 2—35377
quinoline, n.m.r. ^{15}N and ^{13}C Fourier spectra, coupling constants, shifts 2—6262
quinoline, threshold electron excitation spectra, obs. of compound negative ion resonances and electronic transitions 2—35350
quinoline and methyl derivatives, free radicals e.s.r. 2—8818
quinoline solutions, n.m.r. investigation of molec. association 2—22008
quinolines, hydrogenated, nature of electronic bands in luminescence spectra 2—4498
quinolinium, single cryst., elec. cond. temp. dependence 2—6754
quinolinium ion, n.m.r. ^{15}N and ^{13}C Fourier spectra, coupling constants, shifts 2—6262
quinone powders, meas. of naturally abundant ^{17}O n.q.r. transition frequencies 2—37019
quinones, PPPMO calcs., charge density, bond order, oscillator strength and electronic transition energy 2—8785
quinones, PPPMO calcs., transition energies and oscillator strengths, electronic spectra 2—12251
quinòsialine and d$_0$ deriv., electronic vapour absorption $(\pi^* \leftarrow n)$ spectra study 2—12279
quinoxaline, oriented in nematic phase, proton skeleton, spin spin coupling consts., n.m.r. obs. 2—9183
quinoxaline, vapour and mixed crystal spectra, $\pi^* \leftarrow n$ transition 2—10400
Raman spectra of small ring compounds in vapour state 2—12199
rare earth carboxylates, cryst. struct. 2—9513
retro-β-ionylidene acetic acid, conformational energy calc. by PCILO method 2—12293
rhodamine 6G: polyurethane film, ring laser, unidirectional operation 2—17631
rhodamine 6G, electrochromic spectra in polystyrene matrix, change in polarizability and dipole moment between ground and excited states 2—13488
rhodamine 6G, flashlamp pumped dye laser, mode locked, freq. tuning 584-645 nm 2—17611
rhodamine 6G, H-bonding effect on orientational relaxation in solutions, investigation using psec light pulses 2—3394
rhodamine 6G, laser, frequency tunable transform limited picosec. pulses 2—7927
rhodamine 6G, mixed with acridine red for wavelength tuning of Q-switched Nd:glass laser 2—5374
rhodamine 6G, multistage dye amplifier, absolute gain meas. 2—11473
rhodamine 6G, repetitively pulsed flashlamp pulsed dye laser 2—17613
rhodamine 6G, soln., intermol. energy transfer and conc. depolarization of luminescence 2—6237
rhodamine 6G dye laser, stabilized with Z cut KDP Lyot filter 2—17615
rhodamine 6G dye laser, wavelength selection using electrooptic ceramics 2—14425
rhodamine 6G dye lasers, with ultrafast transverse flow 2—7930

Organic compounds continued
Rhodamine 6G ethanol solutions, anti-Stokes luminesc. 2—35773
Rhodamine 6G in ethanol, stimulated emission excitation threshold lowering 2—21990
rhodamine 6G laser, flashlamp pumped, rate equation model 2—17614
rhodamine 6G solutions, fluorescence, concentration quenching by energy transfer 2—28878
rhodamine 6J, spectral intensity changes on excitation by N laser, quantum generation 2—3390
rhodamine 6J dye laser, construction 2—14424
rhodamine 6J laser, construction 2—27491
Rhodamine B, emission in vapour phase, possibility of lasing 2—39007
rhodamine B, flashlamp pumped dye laser, model locked, freq. tuning 584-645 nm 2—17611
rhodamine dye laser, photobleaching by flashlamp excitation 2—5370
rhodamine dye laser, plasma jet production 2—39159
rhodamine dye solns., superradiant laser emission using coaxial flashpump 2—15595
rhodamine dye solution, deformation of electronic absorption spectra rel. to associated molecule formation 2—39372
rhodamine S, i.r. absorption spectra, effect of inorganic peroxides and γ-irradiation 2—3118
rhodamine-thionine-detergent system, temp. effect on excitation energy migration 2—39375
rhodanine, vibr. spectra 2—8819
rhodopsin, linear birefringence in retinal rods, measurement of retardance of single unbleached rods 2—7613
rubrene, electrogenerated chemiluminescence in solution 2—40821
Rubrene, emission in vapour phase, possibility of lasing 2—39007
rubrene, hole mobility 2—25851
ruthenocene, mean amplitudes of vibration and perpendicular amplitude correction coeff. 2—28407
s-triazine, geometry in excited state determ. from rotational analysis of J-structure of band in 3100 Å system 2—12288
salicyclic acid, dissolution of solids into turbulent liquid stream 2—28757
salicylic acid cylinder rotating in water, mass transfer coeff. determ. from rate of dissolution 2—6218
salicylic acid esters, temp. variation of u.s. velocity 2—3388
salicylidene-m-hydroxyaniline, i.r. studies of H-bonding 2—28408
salol, cryst. growth from the melt, constant max. crystalliz. rate 2—19010
salol, crystal growth from the melt, constant max. crystalliz. rate 2—19011
salol velocity and absorption of shear waves near melting point 2—29536
Santowax-R, neutron properties of moderators and coolants 2—28153
saturated hydrocarbons, thermal conductivity meas. with thermal comparator 2—25073
Schiff's base, mesomorphism, chemical struct. depend. 2—25049
Schiff's base, mesomorphism, low thermal phase stability 2—25048
Schiff bases, aromatic, conformation in connection with liq. cryst. props. 2—6210
selenophene, oriented in lyotropic mesophase, n.m.r., direct couplings and interproton distance 2—28409
semicarbazide, e.s.r. spectra of X-irradiated single crystals 2—20141
semicarbazide hydrochloride, ferroelectric, dielec. meas. obs. 2—19770
semiconducting, electrical conductivities 2—4190
semiconductor molecular crysts., valence bandwidths, vac. u.v. photoemission obs. 2—19812
semiconductors, upper limit of effective electron mass 2—40228
semidiones, planarity of carbonyl carbons from INDO approx. SCF MO theory 2—8786
semiquinone solns., obs. using low power (25 watt) r.f. source 2—23470
semiquinones, planarity of carbonyl carbons from INDO approx. SCF MO theory 2—8786
silacyclobutane, mol. vibration, normal co-ordinate analysis, mean amplitudes detn. 2—18527
silico-organics, X-fluorescence, K-spectrum of Si 2—33312
silicon acetate, lattice parameters and space groups 2—19063
siloxanes, bond energy obs. from appearance potentials 2—15414
silyl methyl ether, microwave spectrum in 8 to 40 GHz region, dipole moment calc. from Stark splitting 2—15394
silyl radicals, trimethylsilyl substituted, substituent effects on geometry 2—31863
N-silylpyrrole, molecular structure investigation by electron diffraction 2—5994
sodium$_2$-pyrazine$^+$, computerized analysis of e.p.r. line-width variations 2—34266
sodium carboxymethyl cellulose, dielectric loss factor of aqueous solutions 2—39394
sodium palmitate-H$_2$O system, mol. order, relax. time and self-diffusion from n.m.r. obs. 2—35796
sodium salicylate in polar and apolar solvents, fluorescence efficiencies 2—28876
solid, electrical conduction 2—4221
solid solutions, lattice disorder effects on electronic spectra linewidths and multiplicities 2—36890
solid-state chemistry conf., Rehovot, Israel, (Sept. 1970) 2—37052
solvent, viscosity effect on dielec. props. of haloalkane solns. 2—18846
spin coupling ^{1}H—^{19}F, calc. by finite perturbation method 2—8571
spin-lattice relaxation of ^{13}C, temp. depend. 2—35296
spin-lattice relaxation of ^{13}C 2—15344
squalane, solutions with gas, viscosity-pressure dependence 2—9115
squalane, thermoluminescence and competitive electron trapping 2—7101
squalene, solutions with gas, viscosity-pressure dependence 2—9115
squalene with gases in solution, viscosity- pressure behaviour in saturated and unsaturated state 2—39349
Stark effect Q-switching of CO$_2$ gas lasers 2—7920
stearic acid, thin film production, controlled evaporation in vacuum 2—1189
cis-stilbene, calculation of band shapes and absorption coeffs. for electronic transitions 2—15259
stilbene, Raman spectra, Davydov splitting magnitude, dependence on crystal elementary cell parameters 2—26183
stilbene anion radical, electron transfer reaction with cis- and trans-stilbene, e.s.r. and u.v. study 2—37035
stilbene derivatives, thin films, bombardment in electron microscope, 3×10^{-7}-3×10^{-6} amps, structure determ. 2—19065
strontium dicalcium propionate, mol. motion, p.m.r. obs. 2—10574
strontium formate dihydrate, cryst. struct. 2—9514
structure analysis by mass spectra computer system 2—33391
styrene, absorpt. cross sections and photoionization efficiencies, 600-2200 Å 2—18491

Organic compounds continued
styrene, band contour anal., transition moments 2—12213
styrene monomer, fluorescence spectra dependence on rate of cooling 2—12569
styrene radical anions, INDO-MO calculations of hyperfine splittings 2—39008
styrenimine, solvent effects on proton- proton coupling consts. 2—35793
styryldiazines, linear correlation between ^{1}H chem. shift and electron density 2—24551
substituted benzenes, uncoupled Hartree-Fock calc. of ring currents 2—21664
6-substituted purines, n.m.r., assignment of individual proton signals 2—5991
succinonitrile, liquid and plastic phases, Raman spectra, vibrs. assignment 2—33288
succinonitrile, n.m.r. line narrowing study of translational mol. motion 2—1738
succinonitrile, plastic and liquid phases, mol. motion and lattice dynamics, light scattering obs. 2—16589
succinonitrile, plastic cryst. state, molecular motion, light scatt. obs. 2—26203
succinonitrile single crystal, Rayleigh scattering from entropy fluctuations 2—16443
sucrose, aqueous soln., γ-irrad., optical rotation 2—5596
sulfanilamides, charge transfer complex, conduction mechanism, conductivity and e.p.r. obs. 2—10526
sulfoxide complexes, quasi-octahedral, coordinate bond, vibrational model 2—12280
sulphinylbis (1-aziridine), i.r. and Raman spectra, vibrational analysis 2—12219
sulphuranes, X-ray crystal structure 2—25355
surface tension and polarity calc. from contact angle data 2—18808
surface-active organic cpds., spreading as monomolecular films on clean water surface 2—28775
sydnones, valence electron density and structure calculations 2—8820
(+)-tartaric acid, anomalous X-ray scatt. by oxygen 2—25363
taurine, e.s.r. of γ-irradiated crystal 2—33344
TBBA, disordered, diffuse X-ray scatt. obs. 2—9375
TCNQ, charge transfer complex, conduction mechanism, conductivity and e.p.r. obs. 2—10526
TCNQ anion radical salt, mag. susceptibility, Schottky type behaviour 2—25995
TCNQ charge-transfer complex, cond., Hall effect, Seebeck coeff. 2—40216
TCNQ complex, mobility, microwave Hall effect obs. 2—16216
TCNQ polymeric complex salts, factors affecting conductivity 2—25837
TCNQ salt, enhanced nuclear relaxation near Mott transition 2—33182
TCNQ salt, spin susceptibility and phase transitions 2—13094
TCNQ salts, compactions, Seebeck and Hall effects 2—25833
TCNQ-NMP, metal-insulator transition and antiferromag. obs. 2—19657
o-terphenyl, crystal, glass, liquid, heat capacity and thermodynamic properties 2—9891
p-terphenyl, doped and pure crystals, fluorescence rise and decay times 2—20107
o-, m- and p-terphenyl, in soln., ENDOR 2—15396
2-tert. butyl-4-methyl-indazole, electronically excited, temp. dependence of deactivation in solution 2—3119
tert-butyl alcohol, u.s. velocity in aqueous solutions 2—1095
tert-butyl-1,3-dioxanes, ^{13}C magnetic resonance spectra 2—3074
testosterone acetate, ODMR determination of zero field splitting parameters 2—35352
tetraalkylammonium iodide/glycerol solutions, viscosity 2—28813
tetraalkylammonium molten salts, configurational thermodynamic properties, internal Coulomb field contributions 2—28841
tetraalkylborate molten salts, configurational thermodynamic properties, internal Coulomb field contributions 2—28841
tetrabenzopentafulvalene derivatives, geometrical isomerism, n.m.r. obs. 2—12281
tetrabenzyl germanium, far i.r. and Raman spectra, vibrational assignment 2—21665
1,1,2,2-tetrabromoethane solution, dielec. props., effect of solvent viscosity 2—18846
tetracene, calculation of hyperfine splittings in e.s.r. spectra 2—38953
tetracene, charge carrier-exciton interaction, fluoresc. decay obs. 2—10446
tetracene, crystals, pentacene doped, heterofission of pentacene excited singlets 2—4136
tetracene, film, pure and doped, bistable switching, metallic filament form. 2—16219
tetracene, internal conversion meas. of fluorescence yields and triplet state prod. 2—3121
tetracene, paramagnetic excitons, role in fluorescence and photoconductivity 2—25741
tetracene, photooxidation kinetics, external mag. field effects 2—26365
tetracene, polarization data for triplet triplet absorption spectrum, band assignment 2—8823
tetracene films, photovoltages 2—1585
tetracene in p-terphenyl, 4.2 K, polarized fluorescence and absorption spectra 2—26175
tetracene thin films, bistable switching 2—25831
3,4,5,6-tetrachloro-2,7-dihydrothiepin, n.m.r. study of ring inversion 2—28413
tetrachloro-p-benzoquinone, cryst. struct. refinement at 110K 2—29158
2,3,4,5-tetrachloro-trans-hexatriene, obs. of conformational isomerism by rotation about single C-C bond 2—8825
s-tetrachlorobenzene, phosphorescence microwave double resonance spectra 2—8568
1,2,4,5-tetrachlorobenzene, temp. dependence of Cl n.q.r. frequencies, torsional frequencies 2—28419
tetrachlorohydroquinone cryst., mol. packing 2—22173
tetrachloroparaxylene, nuclear magnetic relaxation times meas. interpreted in terms of molecular reorientation 2—20167
tetrachlorosemiquinone in tetraethylene glycol, dynamic nuclear polarization 2—25111
tetracyano-p-quinodimethane, specular reflection spectra, anal. of metallic reflection influence of exciton phonon interaction 2—20008
tetracyanobenzene complexes, triplet-triplet absorption in visible and i.r. regions 2—35351
s-tetracyanobenzene-toluene complex, structure of fluorescent and phosphorescent states from absorption and emission spectra 2—15397
tetracyanoethylene oxide, aspherical electron charge density 2—28412

Organic compounds continued

- tetracyanoethylene oxide, crystal and molecular structure 2—28411
- tetracyanoethylene solution in mesitylene, π-π charge transfer complex, obs. of intermolecular vibrations in spectra 2—28426
- tetracyanoethylene tetrahydrofuran charge transfer complexes, ionic photodissociation and ionic photosensitized dissociation 2—30092
- tetracyanoethylene-trans-stilbene mol. complex, effect of external elec. field on abs. spectrum and electric dipole moment 2—31870
- tetracyanomethanes, molec. structure determination by electron diffraction 2—21702
- tetracyanoquinodimethane anthracene cryst. mol. complex, obs. of exciton interactions in polarized specular reflection spectra 2—13465
- tetracyanoquinodimethane complexes with different donors, e.p.r. spin echo study of excited triplet states 2—26269
- tetracyanoquinodimethane ion-radical salts, plasma oscillations of electrons 2—1682
- n-tetradecane, heat capacity at elevated press. 2—25072
- tetraenes, conformational energy and transition energy, u.v. spectra investigation 2—858
- tetraethylammonium bromide in methanol-dioxane mixture, elec. cond. 2—9159
- tetraethyllead, vapour state chem. thermodynamic props. 2—24553
- 1,2-disubstituted tetrafluoroethanes, n.m.r. spectra, rot. isomerism, coupling consts. 2—12283
- tetrafluoroethylene surface, flashover in vacuum, d.c., a.c., and surge voltages 2—22618
- tetrafluoromethane, orbital determ., ESCA line intensities obs. 2—35219
- tetrahydrobenzaldehyde, fluidized by water, coalescence rates 2—1126
- tetrahydrofuran, u.s. velocity in aqueous solutions 2—1095
- 4-tetrahydrothiapyranols, substituted, elec. dipole moments rel. to conformational studies 2—28410
- 4-tetrahydrothiapyranones, substituted, elec. dipole moments rel. to conformational studies 2—28410
- tetrakis (p-anisyl) pyrryl radical, spin density distrib. determ. from e.s.r. spectra 2—8807
- tetrakis (p-tolyl) pyrryl radical, spin density distrib. determ. from e.s.r. spectra 2—8807
- α-tetralone, in divene host, optically detected e.s.r. study of lowest n-π^* triplet states 2—24542
- tetramethyl ammonium nitrate, internal motion, proton mag. reson., 100-300K 2—40784
- tetramethyl ammonium perchlorate, internal motion, proton mag. reson., 100-300K 2—40784
- tetramethyl phosphorus nitride, i.r. and Raman spectra, vibrational assignment 2—8822
- 3,3,6,6,-tetramethyl-1-thiacycloheptine molecular structure 2—39010
- N,N,N′,N′-tetramethyl-p- phenylenediamine, recomb. luminesc. due to photoionization, 77 K 2—26230
- N, N, N′, N′ tetramethyl-para phenylenediamine, photoionization in polar liquids, analysis of photochemical data 2—21701
- tetramethylammonium trichloronickelate (II), low-temp. mag. susceptibility 2—33177
- tetramethylbenzene isomer, multiple proton relax. minima 2—8821
- tetramethylene cyclobutane-d_o and -d_8, vibrational spectra measured, symmetry determ. 2—12282
- tetramethylethylene, e.s.r. of cation radicals adsorbed on zeolites 2—21656
- tetramethylethylene, reaction with $O_2(^1\Delta_g)$, effect of pressure on rate 2—20180
- tetramethylsilane, n.m.r. chemical shift standard 2—31771
- tetramethylsilane, NMR study of ^{13}C chemical shifts, use of TMS as ^{13}C reference compound discussed 2—27376
- tetramethylsuccinonitrile, n.m.r. line narrowing study of translational mol. motion 2—1738
- tetranitro-1,3,5,7 octahydro tetrazocine-1,3,5,7, lattice vibrs. 2—9867
- tetraphenyl derivatives of group IV elements, n.m.r. investigation 2—15395
- tetraphenylditin (IV) carboxylates, Raman and i.r. spectra meas. for crystalline solids and in solution 2—24552
- tetraphenylpolyenes, electrooptical polarisability in ground state and first excited singlet states 2—15381
- tetraphenylporphine and Zn-tetraphenylporphine photoreduction, absorption spectra and e.p.r. of anion radicals 2—26366
- 1,3,6,8-tetraphenylpyrene, electrogenerated chemiluminescence in solution 2—40821
- tetraphenylpyrryl radical, spin density distrib. determ. from e.s.r. spectra 2—8807
- 4,4′,4″4‴-tetrasulphophthalocyanines, Cu and vanadyl derivatives, aggregates in solution, e.s.r. 2—9163
- s- tetrazine, resonance fluorescence and its quenching 2—39009
- s-tetrazine, vapour, rotational fine structure of 5500 Å band, electronic spectrum 2—8824
- tetrazole, polycryst., laser Raman and external optic phonon spectra 2—10414
- tetrile explosions, heat liberation in low and high velocity regimes 2—7174
- tetrolic acid, proton injection measurements 2—25847
- thallium(I) nitroparaffins, molec. structure determination from i.r. and n.m.r. studies 2—12287
- the dominant 6G dye laser, fluorescence analysis of Na subnanogram concentrations 2—7190
- 1,3,4-thiadiazole, microwave spectrum, nuclear quadrupole coupling and centrifugal distortion 2—18530
- thiathiophthenes, He584Å and X-ray photoelectron spectra 2—5997
- 1,3-thiazan, i.r. spectra, absorption band assignment 2—3124
- thiazolidindione-2,4, vibr. spectra 2—8819
- thiazolidine, 2-oxo- and 2-imino-, i.r. spectra absorption band assignment 2—3124
- thiazyl, bonding, increased valence theory 2—8679
- tri-2-thienylphosphine, tri-3-thienylphosphine assignments and signs of ^{13}C-^{31}P coupling constants from off-resonance proton decoupled ^{13}C spectra 2—31871
- thioformaldehyde, i.r. spectrum observed in C-H stretching region, rotational analyses of bands 2—12284
- thioformaldehyde, three bands of i.r. spectrum near 3μ measured and analysed, ground state constants obtained 2—12286
- thioketones, aliphatic, i.r. and Raman spectra, intensity and position of thiocarbonyl $\nu_{c=s}$ band 2—28414
- thionaphthene, frozen hydrocarbon solns., phosphorescence spectra, liq. N temp. 2—16625
- thionaphthene, Hg heavy atom impurity effect on luminescence 2—3125

Organic compounds continued

- thionine, protonation rate const. of triplet state by laser flash photolysis 2—37056
- thiophene, liq. and cryst. phases, i.r. spectra obs. 2—36004
- thiophene, orbital determ., ESCA line intensities obs. 2—35219
- thiophene, vibrational analysis of photoelectron spectra 2—3097
- thiophene and bromo-derivs., high-resolution photoelectron spectra 2—35340
- thiophene in thiophene-d_2, Davydov splitting in vibr. i.r. spectra 2—10401
- thiophene liquid proton spin relaxation and mol. motion, 300-550K 2—9184
- thiophene mol. ion, prod. by charge exchange, dissoc. lifetime 2—24513
- thiourea, aryl and antipyryl derivatives, i.r. spectra, absorption band assignment 2—3123
- Thiourea, ferroelec. phase, n.q.r. of ^{14}N, rel. to Stark effect 2—20171
- thiourea, ferroelec. phase, proton and deuteron mag. reson. 2—10575
- thiourea, ferroelec. transition, i.r. and Raman obs. 2—20080
- thiourea, inter- and intra-molecular force consts., i.r. and Raman active vibrations 2—29513
- thiourea, n.m.r., molecular motion 2—7131
- thiourea, satellite X-ray scatt., structural modulation 2—13320
- thiourea, temp. dependence of i.r. and Raman spectra, mol. and lattice vibrations phase transition 2—29923
- thiourea, vibr. modes, Raman spectra obs. 2—4040
- thiourea cryst., absorpt. spectrum, para- and ferroelec. phases 2—26176
- thiourea cryst., optical phonons and polaritons 2—19392
- thoacetamide-S-oxide, crystal and molecular structure by heavy atom method 2—18529
- 1,4-throxan, vibrational spectra, force constant calc. and vibrational assignments 2—12285
- thulium acetate tetrahydrate, absorption spectra over range 2500 - 9000 Å. Slater parameters, spin-orbit interaction 2—1697
- thulium ethyl sulphate, characterization of defect sites by e.p.r. investigations 2—33345
- thymine, computer controlled e.p.r. obs. of free radical formation after electron irradiation 2—22880
- tin (II) formate, difficulty in assigning unique unit cell to X-ray powder spectrum demonstrated 2—36005
- tin acetate, lattice parameters and space groups 2—19063
- TMMC, spin dynamics 2—22713
- TMMC, spin waves 2—22697
- TMPD chloranil single crystal, e.p.r. linewidth, ang. dependence 2—36981
- tobacco mosaic virus solution, mol. order, relax. time and self-diffusion from n.m.r. obs. 2—35796
- tolane, Raman spectra meas. standard intensities, polarization ratios, determ. structure 2—24505
- toluene, condensed states, intermolecular dynamics, vibr. spectra study 2—35377
- toluene, influence on photoelectric properties of Se 2—28992
- toluene, liquid, thermal cond. meas. 2—17427
- toluene, measurement of optical Kerr constant and nonlinear indices 2—33201
- toluene, phosphorescence enhancement mechanism 2—10449
- toluene, phosphorescence spectra, frozen matrices, liq. nitrogen temps. 2—4502
- toluene, polystyrene and poly(2,6-dimethyl-1,4-phenylene oxide, crystallization and melting of ternary mixtures 2—32319
- toluene, self-diffusion coeffs. and rotational correlation times 2—21973
- toluene, singlet excitations, interaction with triplet molecules of naphthalene-d_8 2—9140
- toluene, spin echo n.m.r. 2—35790
- toluene, spin-lattice relax. temp. depend., mol. rot. 2—9182
- toluene, spin-lattice relaxation of methyl and ring protons 2—32279
- toluene, stimulated scattering under picosecond laser excitation 2—1102
- toluene, temp. dependence of widths and integrated intensiteis of polarized Raman lines 2—28351
- toluene, thermal conductivity, hot wire method of obs., apparatus and results 2—9127
- toluene, thermal conductivity, hot wire method of obs., theory, review 2—9126
- toluene, toluene-d_5, rotational isomerism of methyl groups rel. to interpretation of i.r. spectra 2—15398
- toluene. Fourier transform obs. of Brillouin and Rayleigh line widths and shapes 2—1103
- toluene solutions, fluorescence, temp. dependence of singlet excitation transfer and quenching 2—3396
- toluene-bromine system, photochemical reaction velocity, rate constant of termination, quantum yield due to laser beam 2—20196
- toluic acid in polar and apolar solvents, fluorescence quantum efficiencies 2—28876
- p-toluidinium fluoride, cryst. struct. 2—12741
- 1,1-di-p-tolylethylene, conformational analysis 2—28415
- toulene, in microscopic capillaries, liq.-vapour equilib., concave surface effect on v.p. 2—35829
- transition metal carboxylates, cryst. struct. 2—9513
- transition metal layered dichalcogenide intercalation complex, elec. field gradient 2—19947
- transparent, dendrite morphology, holographic obs., rel. to metallurgical transforms. 2—15669
- tri (n-butyl) ammonium picrate and iodide, solutions in polar solvents, permittivity and loss 2—1110
- s-triazine, electronic structure, from photoelectron, u.v., mass and electron impact spectra 2—28416
- s- triazine, mixed mag. and electric dipole transition for absorption to lowest energy excited singlet state 2—8827
- triazole, H-bonded cryst. with protonic conductivity, γ-induced radicals, e.p.r. and ENDOR obs. 2—26293
- 2,4,6-tribromoanisole, n.q.r. of ^{81}Br, Zeeman effect 2—8745
- tribromomethane, ^{13}C n.m.r. relaxation, temperature dependence 2—38951
- tri-t-butylphenoxyl radical, ENDOR spectra in liquid crystal 2—21647
- 2,3,4-tricarbahexaborane(7), microwave spectrum at 8 to 38 GHz, rotational constants 2—15399
- 2,3,5-trichloro-p-benzoquinone, vibrational assignment of i.r. spectrum 2—35353
- trichloroacetamide, temp. depend. of ^{35}Cl nuclear quadrupole resonance and spin-lattice relaxation time 2—10591
- trichloroacetic acid dimer, neutron diffraction study of hydrogen bond 2—36006

Organic compounds continued
1,2,3-trichlorotrimethylbenzene, nuclear magnetic relaxation times meas. interpreted in terms of molecular reorientation 2—20167
triclooctadiene, interpretation of unusual electronic spectrum 2—28363
n- tricosane velocity and absorption of shear waves near melting point 2—29536
1,1,1-tricyanoethane, cryst. struct. 2—32478
tricyclo[1.1.1.0^{1,3}]pentane, ab initio MO calculations 2—39011
triethylamine, phys. sorbed on C, leaking curves 2—18958
trifloromethyl radical reactions with HCl and H_2S, activation energies and kinetic isotope effects 2—26338
trifluoroacetaldehyde, force consts. from normal-coordinate analysis 2—8724
trifluoroacetic acid, i.r. spectra, vibrational assignment 2—3126
trifluoroacetic anhydride, i.r. spectra, vibrational assignment 2—3126
trifluoroacetonitrile, force field, Coriolis consts., mean amplitudes, centrifugal distortion consts. 2—8828
trifluoroacetonitrile, microwave spectrum of excited vibr. states, obs. of $J \rightarrow J+1$ transitions 2—12292
trifluoroacetyl chloride, force consts. from normal-coordinate analysis 2—8724
trifluoroacetyl fluoride, force consts. from normal-coordinate analysis 2—8724
1,3,5- trifluorobenzene, susceptibility anisotropy, from Cotton-Mouton effect meas. 2—18486
trifluorobenzene pure rotational Raman spectra and bond length det. 2—35357
trifluorochloromethane, compressibility, abs. determination from light scattering meas. near critical point 2—9072
1htrifluorocyclopropene, i.r. spectra, vibrational assignment 2—12289
1,1,1-trifluoroethane, mass spectrum, appearance potentials and bond dissociation energies 2—15403
trifluoroethane, reactions with nuclear recoil ^{18}F atoms, approximate energetics and molec. dynamics 2—10616
trifluoroethane, reactions with nuclear recoil ^{18}F atoms, mechanism and systematics 2—10615
trifluoroethylamaine normal and deuterated, microwave spectrum rel. to intramolecular H-bonding 2—21703
2,2,2-trifluoroethylamine, microwave spectrum, intramolecular H-bonding investigation 2—12290
trifluoroiodoethane photodissociation laser, Zeeman effects in hyperfine structure of atomic I emission 2—31038
trifluoromethyl selenium cyanide, molecular structure electron diffraction determ. 2—24555
trifluoromethylquinoxalines, long-range H-F spin-spin coupling 2—24554
triglycine selenate, permittivity near phase transition pt. 2—29757
triglycine sulphate, γ-irradiated, displacive movement of the radical, e.s.r. obs. 2—26268
triglycine sulphate, acoustic emission on polariz. reversal and phase transition 2—13030
triglycine sulphate, applic. to pyroelec. thermal imaging devices 2—37797
triglycine sulphate, Cr^{3+} doped, internal elec. fields, e.p.r. obs. 2—10530
triglycine sulphate, critical phenomena 2—19771
triglycine sulphate, cryst. struct. 2—25364
triglycine sulphate, crystal growth from slightly supersaturated solns. 2—18993
triglycine sulphate, Curie temp., second harmonic scatt. 2—16294
triglycine sulphate, dielec. relax. 2—19758
triglycine sulphate, effect of X- and γ-radiation on permittivity and losses 2—1560
triglycine sulphate, elec. field gradients near domain walls 2—1565
triglycine sulphate, ferroelec., nonlinearity of dielec. const., second harmonic detection 2—33062
triglycine sulphate, ferroelec. switching, struct. inhibition, additives 2—33063
triglycine sulphate, ferroelectric, pyroelectric applications 2—6888
triglycine sulphate, noise and impedance meas., polarization fluctuations 2—33055
triglycine sulphate, peak voltage of pyroelec. response to short i.r. laser pulses 2—19774
triglycine sulphate, pyroelec. voltage response to rectangular i.r. signals 2—33064
triglycine sulphate, pyroelectric voltage response to step i.r. radiation signal 2—4283
triglycine sulphate, spontaneous polarization, laser irrad. effect 2—1574
triglycine sulphate, X-ray damaged, free radicals, e.p.r. study 2—5977
triglycine sulphate and fluoroberyllate, e.p.r. spectra of admixture ions 2—10528
triglycine sulphate targets for thermal imaging camera tubes 2—2366
triglycine sulphate-selenate mixed cryst., ferroelec. props., refr. index. 2—13321
triglycine sulphates, ENDOR on radicals of glycine II and III 2—10583
β-trihalogeno borazines of symmetry D_{3h}, electronic structure and strobilism 2—28356
trimeric clusters, Heisenberg-Dirac- van Fleck Hamiltonian, spin exchange, e.p.r. theory 2—30017
trimethyl acetonitrile, i.r. and Raman spectral, vibrational assignment 2—21704
1,2,4 trimethyl benzene based liquid scintillator 2—27866
trimethyl chlorosilane, chemisorption on SiO_2 2—39565
trimethyl germanium fluoride, i.r. and Raman spectra, normal coordinate anal. 2—24556
1,1,4-trimethyl-5-carboxy-cyclopentene-4, conformational energy calc. by PCILO method 2—12293
trimethylacetonitrile, p.m.r., second moment of absorption spectrum and spin-lattice relaxation time 2—16664
trimethylaluminium, use in epitaxial growth of AlN 2—12659
trimethylamine, gaseous, second density virial coeffs. 2—15535
trimethylamine, gaseous, total electric polarization 2—15543
trimethylamine, phys. sorbed on C, leaking curves 2—18958
trimethylamine, vapour viscosity 2—32183
trimethylamine borane, vacuum u.v. spectra, $\sigma \rightarrow \sigma^*$ electronic transitions 2—15401
trimethylamine borane, vacuum u.v. spectra, obs. of 2 electronic transitions 2—3127
trimethylamine borane-d_3, vacuum u.v. spectra, $\sigma \rightarrow \sigma^*$ electronic transitions 2—15401
trimethylamine complexes with I_2, Br_2, IBr and ICl, Raman and i.r. spectra band assignment to vibrations, force constants 2—12294

Organic compounds continued
trimethylarsenic dibromide and dichloride, i.r. and Raman spectra, vibr. assignments and force field calcs. 2—18536
2,4,5-trimethylbenzaldehyde, phosphorescence spectra, dynamic properties and zero field splittings of lowest excited triplet states 2—28335
2,4,5-trimethylbenzaldehyde in durene, assignment and location of 2nd triplet state 2—15402
trimethylene oxide, ring puckering vibr., vapour phase Raman spectrum 2—18531
trimethylene oxide in nematic liquid crystal, molecular structure determ. from NMR spectra 2—35354
trimethylene-2.1(α-phenyl α-hydroxypropyle-1 ferrocene, crystal structure determ. 2—6463
trimethylgallium, use in epitaxial growth of GaN 2—12659
2,4,6-trimethylphenol, asymmetry of absorpt. bands 2—8524
1,2,4-trioxacyclopentane, microwave spectrum, molec. structure determination 2—15400
1, 3, 5- trioxan, gaseous, molecular structure, electron diffraction investigation 2—18532
tripalavin-gelatin gel, phosphor, phosphoresc. decay kinetics, irrad. effects 2—36949
1,3,5-triphenylbenzene anion radical, orbital degeneracy obs., e.p.r., p.m.r. and d.m.r. 2—8808
triphenylbenzene triplet dianions, photo-oxidation in rigid solution, e.s.r. study 2—4601
triphenylene, possible reorientation of molecule in solid state, n.m.r. investigation 2—10567
triphenylene triplet dianions, photo- oxidation in rigid solution, e.s.r. study 2—4601
triphenylenes, 2-substituted, e.s.r. and luminesc. studies 2—35356
2,4,5-triphenylimidazyl radical, spin density distrib. determ. from e.s.r. spectra 2—8807
triphenylmethane, phosphorescence enhancement mechanism 2—10449
triphenylmethane, X-ray determ. of crystal structure 2—39664
triphenylmethane dye, saturable absorp. and Q-switching 2—21061
triphenylmethylhydroperoxides, H-bond study using n.m.r. and i.r. spectroscopy 2—28417
1,3,5- triphenylpyrazole, calculation of π-electron states by LACO MO method with Huckel approximation 2—3115
triphenyltin carboxylates, Mossbauer study of effect of helical chain 2—5954
triphenylverdasile, corresponding ions and the leucocompound, comparative study of i.r. spectra of radicals 2—39012
triplet excitons, prod. and annihilation near absorbing surfaces, delayed fluorescence 2—19522
triplet ketones, H abstraction, applicability of electronic-vibrational energy transfer model 2—30080
tripropargyl amine, i.r. and Raman spectra, vibr. assignments, rotational isomerism 2—18533
triptycene, cryst. struct. 2—12742
tris-(1,2-dimethylhydrazino)-diphosphine, cryst. and mol. struct. 2—6467
tris-sarcosine calcium chloride, Mn^{2+} doped, ferroelec., e.p.r. 2—10529
1,3,5-triselenan, vibrational spectra, assignments and force constant calc. 2—12236
1,3,5-trithian, force constant calc. and vibrational assignment 2—12236
trithienylphosphines, methyls substit., signs and magnitudes of long range $^1H-^{31}P$ spin coupling consts. 2—12291
trypsin, enthalpies for fixation of competitive inhibitors proflavin and benzamidine 2—40798
tryptophan in ethylene glycol-water glass, kinetics and cross section of 2-quantum ionization 2—1762
tryptophan in ethylene glycol-water glass, photoinduced trapped electrons, recombination luminescence study 2—4517
tryptophan in water, fluorescence band-intensity distrib. 2—25095
tryptophan molecule, in solid matrix, luminesc. and absorpt., 77K 2—35355
tungsten organometallic derivatives, correlation between ionization potentials of complexes and free ligands 2—18494
tyrosine, polycrystalline. proton spin-lattice relaxation 2—1736
6-undecanol-urea, X-irradiated inclusion crystals, e.s.r. of trapped radicals 2—20153
Uranium (3+) formate, low-temp. absorption spectrum, U^{3+} energy level scheme 2—10402
uranyl butyrate optical activity studied 2—16421
uranyl sulphate, luminescence in presence of nearly 100 electrolytes and organic substances 2—15597
urea, ^{15}N isotope effects on i.r. spectrum 2—28418
urea, fog seeding experiments, induced dissipation 2—16833
urea, lattice dynamics, molecular theory 2—22407
urea, urea-d_4, i.r. spectra, low temp. matrix isolation studies 2—8722
urea clathrate structure, ordering of 1,5-dichloropentane molecules 2—3751
u.s. diffraction of light, and elastic consts. determ. 2—1427
van der Waals complex molecules, structure investigation 2—21649
vapour pressures, melting pressures, meas. 2—25142
vegetable oils in liquid-solid transition, variation of dielectric properties 2—28881
vinyl bromide, i.r. vibration-rotation spectra, Coriolis interaction 2—8829
vinyl chloride, i.r. vibration-rotation spectra, Coriolis interaction 2—8829
vinyl cyanide, electronic structure and spectrum, valence shell calculations 2—18534
vinyl fluoride, vacuum u.v. photolysis, i.r. spectra of products, vibr. assignments 2—8830
vinyl germane, microwave spectrum at 12.4 to 40.0 GHz assignments and dipole moment calc. 2—15406
vinyl iodide, i.r. vibration-rotation spectra, Coriolis interaction 2—8829
vinyl radical, hyperfine splittings, spin polarization contribution, first order perturbation treatment 2—15404
vinyl radical on silica gel surfaces, e.s.r. spectra, temp. effects, h.f. linewidths 2—35358
α-substituted vinyl radicals, electronic structure determ. from e.s.r. spectra and INDO calcs. 2—8712
vinyl trifluorosilane, microwave spectrum, rotational constants 2—15405
l- vinyl-o-carborane, plastic crystalline behaviour, n.m.r. obs. 2—33358
vinylidene halides, normal and deuterated, generalised mean square vibration amplitudes 2—21705
vinyltrifluorosilane microwave spectrum, dipole moment from Stark shifts of rotational transitions 2—21706
vinyltrimethyl silane, polymerized thin film, prep., i.r. spectra, e.p.r. spectra, deposition rates 2—3550

Organic compounds continued
vinyltriphenyl derivatives of group IV elements, n.m.r. investigation 2—15395
violanthrene A, single cryst., intrinsic conduction 2—13250
violanthrene crystal, photo-e.m.f. 2—25849
warfare agents, phys. sorbed on C, leaking curves 2—18958
xanthate desorption from sulphide minerals, u.s. wave effects 2—29069
xanthene dyes, crystallites, recombination delayed fluorescence 2—13506
xanthene powders, meas. of naturally abundant ^{17}O n.q.r. transition frequencies 2—37019
xanthone, effects of medium on absorption and phosphorescence spectra 2—24557
o-xylene, exchange contribs. to internal rotation barrier 2—859
p-xylene, temperature dependence of flow birefringence 2—6232
xylene-water interface, meas. of interfacial velocities 2—25053
xylenes, liq., proton spin-lattice relax., mol. motion 2—9185
2,4-xylenol u.v. absorption spectrum, small spectrum 2—15407
xylols, ^{13}C containing, study of multiplet effect in dynamic polarization 2—24496
ytterbium ethyl sulphate, spin-orbital phonon relax. of Yb^{3+} 2—7011
ytterbium ethylsulphate, crystal field study 2—36794
yttrium ethyl sulphate, ^{3}Ho spin-lattice relax. 2—19936
yttrium ethyl sulphate, phonon bottleneck of spin-bath relax. of Yb^{3+} 2—19935
yttrium ethyl sulphate, ytterbium doped, proton polarization 2—19948
yttrium ethylsulphate:Dy^{3+}, paramag. relax., Orbach processes obs. 2—36982
zinc etioporphyrin, zero-field splitting of triplet state by optically detected magnetic resonance 2—35360
zinc phthalocyanine, photocond., light-intensity depend. 2—10143
zinc porphin, lowest triplet state, dynamics by microwave induced delayed phosphorescence 2—18535
zinc porphin, lowest triplet state, phosphorescence modulation by microwaves 2—21707
zinc tetrabenzporphin, fluorescence of second excited singlet and quasiline structure studied 2—12295
zinc uranyl acetate, electronic absorption spectrum and U—O bond distance 2—3128
AgI-KI acetone soln., emitted smoke ice forming ability 2—22972
anthracene, singlet exciton trapped carrier interaction 2—13508
bis(m-(m-phenoxy phenoxy)phenyl)ether, viscoelasticity at pressures up to 300 MN/m^2 2—39307
C_4, C_5 and C_6 hydrocarbons adsorption on CoO, gas chromatography determ. of heats of adsorption 2—25222
CH_2^+, ground and excited states, Hartree-Fock method using Slater basis set 2—8579
CH_3 radical, random motion and relax., e.p.r. obs. 2—26373
$CH_2CO_2^-$ radical, random motion and relax., e.p.r. obs. 2—26373
CHO^+, transient species obs. using photoelectron and chemielectron spectroscopy 2—35163
C—C bonds, single, double and triple, electron density distribs. 2—15679
cetylalcohol, effect on mass transfer, liquid-in- liquid jets 2—3350
^{35}Cl n.q.r. of 11 compounds, 77 K 2—24493
2,3-difluoroaniline, i.r. spectrum, vibr. assignment of fundamental frequencies 2—31850
HCO radical, e.p.r., microwave absorpt. spectra, rotational transition 2—8720
iso-amylol, jets, liquid- in-liquid mass transfer, conc. driving force 2—3350
methane, vibrational relaxation times meas. with spectrophone, use of NH_3 on C_2H_6 as calibration gas studied 2—12257
containing NO radicals, viscous medium, NO rotational correlation time calc. from e.s.r. calcs. 2—8686
Ni complex, $(n\text{-}C_4H_9)_4N.NiS_4C_4(CN_4)$, in n-butanol and $CHCl_3$, e.s.r. 2—9166
P compounds, partially deuterated, deuterium isotope effects on chemical shift and coupling consts. 2—8716
$PO_2(C_6H_5)_2(CF_3)_4C_3H_2$, crystal and molec. structure 2—25360
$PO_3(C_6H_5)_4(C_6H_4Br)C_5H_2$, crystal and molec. structure 2—25361
poly-L-lysine and salts in aqueous solution, dielectric studies 2—25101
propane-N_2 mixture, second virial coeffs., compressibility, 20-50°C 2—21915
S-Cl bonds in 59 compounds, ^{35}Cl n.q.r. 2—21650

Organometallic compounds *see Organic compounds*

Orthicons *see Electron tubes*

Oscillations
see also Electromagnetic oscillations; Liquid oscillations; Piezoelectric oscillations; Vibrations
beams, fundamental frequency by integral equation approach 2—17365
betatron, frequency measurement and damping, use of radial longitudinal accelerating field 2—18047
block on elastic surface, theory 2—27205
bubbles in water, natural frequencies 2—1065
circular membranes, transducer for monitoring 2—17358
computing method for periods of cyclic phenomena 2—11317
convective, l.f., in polytropic atmospheres in presence of mag. field 2—20706
coupled, transverse, in two circular beams, resonance 2—30993
curvilinear plate bending elements, new nonconforming family 2—27209
damped, approximate method of analysis, damping force determ. 2—17357
deflection of elastic plate on viscoelastic foundation under moving load 2—34056
displacement, moire analysis 2—14194
edge-tone in sub-sonic air flow by laser anemometer 2—15526
effects on temp. fluid through viscous dissipation in fluid flow 2—8886
electron beam, low velocity, obs. 2—17544
finite element eigenproblems, optimal gradient minimization 2—27194
flow in annular diffuser, induced vibration, expt. 2—39074
fluid, in a U tube, undergraduate expt. 2—15440
gas bubbles, free oscillation, thermal effects 2—1064
grid-stiffened simply supported plate, closed functional solution 2—14243
hoop, on elastic cylinder, theory 2—27205
hydromagnetic, fluid in a rotating cavity 2—8901
inertial oscillations in a deep sea, unsteady waves and currents, hydrodynamic considerations 2—12528
isochronous problem inside spherically uniform earth 2—14232
l.f. in low-conductivity GaAs 2—19642
light source fluctuation in Raman spectroscopy, compensation by quick analogue dividing 2—2471

Oscillations continued
liquid metal drops in non-conducting fluid, damping by transverse magnetic field 2—949
MHD dynamo action of fluid motions with two-dimensional periodicity 2—15441
nonlinear, restrictions on coeffs. of eqn. to ensure finite displacements at infinite time 2—5123
nonlinear systems, entropy and self-oscillations 2—30856
nonlinear transverse, at resonance in elastic layer and in layer of an ideally conducting fluid 2—37735
nonstationary random process, definition of spectrum 2—27214
optical parametric, focussing effect of wave interactions 2—23569
parametric phenomena, history and general characteristics 2—146
parametric pumping, method for studying magnetoelastic behaviour 2—25993
plate, in binary mixture of Newtonian fluids 2—6037
ponderomotive, in superconducting helical resonator 2—34865
pressure in shallow cavities in wind tunnel, Mach 0.8 to 3 2—1021
pressure pulse propagation through relaxing gas, distortion damping and dispersion 2—9015
resonant, of rotating pendulum, analytic investigation 2—37669
r.f. mode changes during calibration of low pressure Penning discharge vacuum gauge 2—23198
rheo nonlinear oscillator, stability of parameter excited pendulum 2—27119
rigid body motion, static displacement, holographic interferometry obs. 2—14233
rod, nonlinear theory 2—33968
rotating fluid, trapped modes in a thin spherical shell 2—24593
self of rotor shaft, lubricant effect 2—17292
slightly nonlinear systems, complex envelopes 2—34064
solar atmosphere, five-minute 2—20705
string, driven nonlinear, instabilities 2—34051
$^1/_2$-subharmonic, study by harmonic balance methods for single degree of freedom systems with nonlinear spring characteristics 2—34070
sun, higher and lower order modes 2—26875
surface and internal waves generated by a periodic travelling disturbance 2—13655
symmetrical autonomous systems with single degree of freedom, approximate min-max equivalent linearization 2—34047
Toroidal, Earth, attenuation 2—30173
torsion pendulum, damping, magnetoelastic effects 2—149
torsional loadings of perfectly conducting elastic half-space 2—27219
transverse, in intersecting storage rings, damping 2—14895
transverse, one-dimensional systems, finite difference methods 2—157
trapezodial plates, symmetric, simply supported, numerical analysis 2—17364
two-phase flow in hot channel influence of heat transfer characteristics on flow stability 2—39033
viscoelastic string, effect of stress relaxation 2—27208
CO_2 laser, hybrid injection locking 2—22576
Hg, surface waves, influence of spatially dependent electric fields on oscillation frequencies 2—9062

Oscillators
acoustoelectric, nonlinear theory applic. 2—25677
acoustoelectric, single-mode operated, nonlinear theory 2—19419
acoustoelectric, static field distrib. effect on mode behaviour 2—6672
acoustoelectric, with arbitrary static field distrib., linear theory 2—25676
a.f., measurement of magnetization 2—11432
charged particle oscillator, use as a u.h. vacuum gauge 2—41403
Colpitts, h.f., operation 2—7818
electrostatic, charged particle, ion source 2—21034
electrostatic oscillator experiment conducting sphere between two electrodes 2—17510
galvanomagnetic, utilizing magnetoresist. of a semicond. 2—21008
Gunn, ionizing radiation effects in microwave cavities 2—22596
Gunn diode, ionizing radiation effects 2—19716
Gunn effect, microwave, physical principles, material assessment, book 2—29731
Gunn oscillator, simple stabilized microwave source 2—20975
Josephson, intrinsic fluctuations 2—29648
laser, distributed feedback, using sinusoidal susceptibility modulation 2—37953
linear harmonic oscillator, derivation of generating function 2—17162
lumped element line low r.f. generator 2—17523
negative resist. charact. in cct. with Mylar film in series with resist. 2—11414
n.m.r. sideband-oscillator stability 2—7810
optical, unstable, performance on 30 kW dynamic laser obs. 2—262
optical parametric oscillation and second harmonic generation, simultaneous occurrence 2—10293
optical parametric oscillators, internal upconversion and frequency doubling 2—21051
parametric, optical, interferometric stabilization 2—21059
parametric, optical, using Ag3AsS$_3$ (proustite) 2—17578
parametric oscillator and coupled oscillator upconverter, plane-wave theory 2—21040
parametric oscillator tuning curve, parametric fluorescence 2—21048
pulse generator system for pulsed n.m.r. applications 2—2330
quartz, realizable precision in film thickness measurement 2—35879
simple harmonic oscillators, treatment using classical statistical Green functions 2—17160
superradiance in radiatively coupled tuning forks 2—14116
sweep generators for electrostatic analyzers for atomic collision expts. 2—2329
torsion, long period and relaxation time 2—17289
weak coupling effects on assembly of damped oscillators, application to ionic oscillations of unbounded plasma 2—28614
CO_2 laser, hybrid injection locking 2—22576
N_2, pumped dye-laser, oscillator-amplifier system 2—11475
ZnO, acousto-electric oscillator, effect of uniaxial stress on modes 2—4058

Oscillistor effect *see Semiconductors*

Oscillistors *see Semiconducting devices*

Oscillographs *see Electrical measurement*

Oseen method *see Flow; Hydrodynamics*

Osmium
atom, visualization, dark field electron microscopy, scattering cross sections 2—21521
atomic absorption spectrophotometry, N_2O-C_2H_2 flame 2—1771

Osmium continued
electrical and thermal conductivity, temp. depend. 2—29618
lattice parameters, −189 to 1709°C, solid equation of state 2—19304
Os-Pt-Hg abundance peak in Ap stars and very heavy cosmic rays 2—33624

Osmium compounds
Fe-Os dilute alloy, hyperfine field at Fe atoms, temp. depend. 2—16436
Os-Pt alloy, thermoelec. power, 4-300K 2—40373
Os-Th alloy, elec. and thermal cond., temp. depend. 2—29618
Os-V, alloy, dilate, mag. susceptibility, Knight shift 2—19836
Os complexes, hexahalometalate complexes, vibrational spectra, force constant calc. 2—16546
OsO_4 vapour, saturation of resonant absorption of CO_2-N_2-He laser 2—27494
V-Os alloy, VKβ_5 emission, electronic struct. 2—6728
W-Os alloy, work function of (111) and (100) faces, temp. depend. 2—19793

Osmosis
colloidal solutions, relation between osmotic equilib. and molecular buoyancy 2—35750
electrolyte solution, statistical theory 2—7181
electroosmosis in ion-exchange membranes, hydrodynamic model 2—28829
interpolymer membranes, investigation of water permeability and selection by 2—12557
non equilibrium osmometry, transport of molecules through non biological membranes 2—25067
polymer solution, osmotic press., solvent effects 2—18803
polymer solutions, osmotic pressure determ. by weighing 2—28831
reverse, concentration polarization at phase boundary of tubular membranes 2—12556
reverse, optimal performation spacing in support tubes 2—12555
vapour phase, application of minimizing program LETAGROP to colligative property type data 2—15561
^{3}He-^{4}He mixtures, osmotic pressure 2—9193
NaCl aqueous solution, coeff. calc. from vapour press. meas. 2—39433

Overhauser effect *see INDOR*

Oxidation
acetylene, d.c. discharge induced, CO molecule laser emission obs. 2—31787
ammonium compound explosives, oxidizer reactivity, rel. to combustion 2—33374
anodic oxide films, anodization 2—19745
aromatic hydrocarbons, magnetic field effect on photooxidation rate 2—33377
diphenylamine, photo-oxidation in presence of benzophenone, H-bonding effects 2—30064
electrochemical, u.s. wave applic. 2—30071
Fe-Al-Cr alloy, in Co_2, oxidation resist., effect of Ti and Mo 2—29430
graphite, for use in composites, improved oxidation resistance 2—39965
Hastelloy X, cyclic oxidation kinetics, 760-1200°C 2—40814
Incoloy 800, He environmental effects 2—12871
lanthanide and actinide oxides, reduction mechanism rel. to crystallographic shear relations between structure types 2—3738
leuca crystal violet, radiolytic oxidation, dosimeter for γ-rays 2—16689
metal, oxide film growth 2—3521
metal, parabolic oxidation, thin film parabolic growth low, elec. field effects 2—15660
metal, statical method of secondary ion mass spectroscopy 2—13594
metal, Y addition effects on resistance, void formation suppression mechanism 2—22877
methane, kinetics of reaction 2—33379
oxide and related phases prep. by chem. transport 2—10622
steel, stainless, He environmental effects 2—12871
steel casing, by neutron activated UPu oxide fuel 2—13577
sulphidized cermet, rel. to anitifriction props. 2—29342
tetracene, photooxidation kinetics, external mag. field effects 2—26365
thermodynamic potential variation during process, calc. method 2—40799
triphenylbenzene triplet dianions, photo-oxidation in rigid solution, e.s.r. study 2—4601
triphenylene triplet dianions, photo-oxidation in rigid solution, e.s.r. study 2—4601
wool fibre, surface discharge treated, S oxidation state obs. 2—37043
Zircaloy-2, radiation enhancement 2—13580
Ag-Cu alloys, evidence for preoxidation state and its characteristics 2—26347
Al:I, rate, effect of I traces 2—37044
Al, film, anodization, to inhibit hillock growth during semicond. device processing 2—3523
Al, oxide layer form., characteriz. by ellipsometry 2—22070
Al, rel. to creep near melting point 2—39798
Al, reversible transform., electron microscope obs. 2—40811
Al bicrystal, effects on grain boundary electromigration 2—39734
Al film, chemisorpt., incorporation-chemisorpt. transition 2—40810
Al films, freshly evaporated, glow- discharge-assisted oxide growth at 14°C 2—37042
α-Al_2O_3, doped, hydrogen incorporation by high temp. redox reactions 2—9584
$BaTiO_3$, reduced ceramic, O_2 plasma, F-centre formation, e.p.r. obs. 2—13576
Be, Auger electron spectra for various degrees of oxidation 2—6327
C, for use in composites, improved oxidation resistance 2—39965
C, pyrolytic, electrochemical oxidation, surface functional groups 2—4588
C fibre, composites, effect on flexure and shear strength 2—36266
C fibre, pyrolytic graphite coating effect on anti-oxidability 2—25610
CO, activation energy, from flame chemiluminesc. study 2—26344
CO, in shock waves with $Cr(CO)_6$ catalyst 2—20177
CO, reactant chemisorption on ZnO, a.c. cond. 2—25830
$CdSiP_2$, thermal analysis 2—1750
CeO_{2-x}, oxygen transport and effects on structure 2—10623
Co-Ni-Cr alloy, internal, rel. to precipitation 2—9796
Co-base alloy, Haynes No. 188, oxidation resist. 2—39920
Co, powder, aerosol, partial hysteresis cycles at various degrees 2—16376
CoO, to Co_3O_4, effect of porosity and crystallite size 2—22878
CoO_x, solidification temp. and nonstoichiometry in oxidizing atmos. 2—9333
Cr film, evaporation deposited, surface, rel. to oxidizing and nitriding treatments 2—39503
Cr surface, effect on soft X-ray appearance pot. spectra 2—35872

Oxidation continued
Cu-Cr-Si alloy, internal oxidation, precip. morphology 2—29427
Cu-Cr alloy, determ. of virtual product $N_0^{(s)}.D_0$ for scaling 2—26348
Cu-Mn alloy, MnO_2 growth on surface 2—19267
Cu, scale formulation, kinetics, diffusion mechanism 2—4589
Cu, surface struct., RHEED obs. 2—39457
Cu, thin layer formation or cathodic sputtering, plasma analysis rel. to thin film deposition 2—1011
Cu film, optical transmittance rel. to parallel layer oxidation model 2—40812
Cu films, in situ electron microscope obs. 2—18936
Cu_2S, chalcocite 2—9800
$D_2+{}^1/_2O_2 \rightarrow D_2O$, on Pt surface, reaction mechanism and rate 2—10629
$Dy^{3+} \rightarrow Dy^{2+}$, reduction in CaF_2 on X-ray irrad., colour centre formation 2—36063
Fe-Al-Cr alloys, H_2 permeability, 300-700°C, oxide film effect 2—29216
Fe, effect on high temp. tensile creep 2—12869
Fe, Mossbauer obs. 2—40813
Fe, single cryst. film, isolated oxide grains, elec. microscope obs. 2—9273
Fe compounds, pressure induced electronic changes, theoretical analysis 2—22098
Fe_2O_3-Fe_3O_4-liquid equilibrium conditions at oxygen pressures up to 53 bar 2—9808
α-Fe_2O_3, reduction to magnetite, kinetics, rel. to natural faces 2—16681
GaAs, in air, room temp. 2—33378
H_3AsO_4, u.s. field effect 2—30067
Mo, charact. electron energy loss spectra obs. 2—9250
Mo film, discontinuous, r.f. cond., oxidation and chemisorpt. of O_2 effects 2—40178
$(NH_4)_2U_2O_7 \rightarrow UO_2$ pellet, sintering/reduction 2—20187
Na, corrosion rate in drybox atmos. 2—20186
Nb-Cu alloy, reactions and resistance, effect of Cu content 2—30065
Nb, conc. variation with depth of absorbed oxygen 2—16682
Nb, reactions and resistance 2—30065
Nb, surface, effect on electron levels, X-ray photoelectron spectroscopic obs. 2—22505
Nb alloy, Cb-132, temp. range 550-1316°C 2—13578
Nb alloy, diffusion layers, struct. obs. 2—4590
Nb alloy, protection by Al coating containing additions of various elements 2—9267
Ni-Be alloy, internal oxidation, diffusivity determ. for O_2 in Ni 2—29221
Ni-Cr-Al alloy, 1000-1200°C 2—10624
Ni-Cr eutectic alloy, Cr_2O_3 layer formation and microstructure rel. to atmos. 2—4587
Ni-Fe alloy, kinetics and morphological development of oxide scale 2—16683
Ni-P film surfaces, ellipsometric study 2—32370
Ni, powder, aerosol, partial hysteresis cycles at various degrees 2—16376
Ni, Raney, mechanism obs. by sorption expts. 2—13575
Ni growth kinetics of absorbant layer and optical indices determ. 2—25204
Ni surface, effect on soft X-ray appearance pot. spectra 2—35872
Ni_3Ti, kinetic curves, 650-1000°C 2—20188
in plasma with r.f. discharge, study using KIO_3 2—4586
Pt-Rh-Zr alloys, internal oxidation and hardness 2—4591
S atom on surface of wool fibre, oxidation following corona discharge 2—37043
Si, anodic, impurity concentration profile analysis 2—3799
Si, anodic, SiO_2 layer growth 2—7179
n-Si, in 10-1400Å oxide thickness range 2—40815
Si, in air, room temp. 2—33378
Si, kinetics of SiO_2 thermal growth, ellipsometry obs. 2—39522
Si film, elec. stability, effect of HCl and Cl_2 2—39521
n-Si wafers, of varying thickness, photoconductivity, effect of thermal oxidation obs. 2—29769
SiO_x film growth using nitric acid, use in MNOS device 2—12666
Sm^{2+} to Sm^{3+} in KCl, spectroscopic evidence 2—10441
Sn film, oxide orientation rel. to substrate orientation 2—12667
Sn oxide film formation, chemical aspects of reactive sputtering 2—18944
Sr, studied by u.v. photoelectron spectroscopy 2—26349
Ta-Al alloy films, anodic oxide form. 2—3548
Ta film, sectioning by anodization and oxide stripping 2—9287
β-Ta film, sputtered, rel. to competitive diffusion of O_2 and N_2, at 828K 2—39531
Ta(110) surface, kinetic study using K_α X-ray emission 2—32385
Tho_2, reduction by C 2—30066
Ti-Mo-Zr, alloy, oxidation resist. rel. to Al content 2—29411
Ti films, in situ electron microscope obs. 2—18936
Ti surface, effect on soft X-ray appearance pot. spectra 2—35872
TiB_2, by dissolved oxygen in liq. steel 2—10625
$TiSi_2$, complex surface and diffusion limited mechanism 2—13579
U-Nb-Zr alloy, stress generation, flexure study 2—10627
UF_6, H_2 reduction mechanism 2—30063
W films, in situ electron microscope obs. 2—18936
$ZnIn_2S_4$, and $Zn_3In_2S_6$, thermal analysis 2—1750
$ZnSiP_2$, thermal analysis 2—1750
Zr alloy, radiation enhancement 2—13580
ZrB_2, by dissolved oxygen in liq. steel 2—10625

Oxide cathodes *see Cathodes/oxide*

Oxygen
$^1\Delta$ molecular oxygen, soln. in methanol, lifetime direct meas. by laser pulse technique 2—8688
absorption spectra, 20-100 Å 2—18463
abundance gradients across spiral galaxies, planetary nebulae rel. to interstellar medium enrichment 2—37269
acoustic dispersion at frequencies to 5.10^4 MHz/atm. 2—6160
adsorbed layer on Au, optical constants, spectrophotometric method determ. 2—10300
adsorbed layer on Pt, Au and Ni, specular reflection spectra, monolayer thickness range 2—9310
adsorbed on Mo, effect on emission electron microscope image 2—18960
adsorbed on W(100), influence on scattered electron intensity distribution rel. to surface meas. 2—25175
adsorption, on metal surface, oxidation 2—3521
adsorption and desorption on Ni by electron impact 2—6373
adsorption and displacement on W (111) surface 2—25235
adsorption by $CaCO_3$, influence on thermoluminesc. 2—10450
adsorption by porous Vycor glass, e.p.r. obs., 77K 2—35912
adsorption by Re, LEED structs., 293-1193 k 2—39563
adsorption on amorphous C, e.s.r. obs. 2—6378

Oxygen continued
adsorption on Fe, Co and Mn 2—12683
adsorption on graphite, physical 2—18957
adsorption on p-Ge field emitter, I-V characts., work function 2—25230
adsorption on Pt electrode, obs. using technique for polarized light reflected intensity meas. 2—9309
adsorption on SbSI and BiOI, thermostimulated currents, attachment levels 2—6805
adsorption on Si (111) surface, Auger electron spectroscopy 2—6386
adsorption on SiC, room temp. 2—29070
adsorption on Ta, RHEED obs. 2—12686
adsorption on W, LEED and Auger spectroscopy 2—35926
adsorption on W, sticking coeffs., electron desorpt. 2—35925
Andromeda galaxy, relative line strengths and abundances in emission regions in the nucleus and disk 2—13851
atmosphere, diurnal variation of density at 400 Km 2—20374
atmosphere, isotopic composition and soluble fractionation 2—37133
atmospheric, meridional model of mesosphere and lower thermosphere 2—7271
atmospheric, raman spectra, obs. using remote spectrometer 2—34553
atmospheric, Schumann-Runge bands, penetration of solar radiation 2—7299
atmospheric, thermal radiation meas. in 60 GHz band for temps. in stratosphere and lower mesosphere 2—16811
atmospheric, u.v. absorption cross section 2—7298
atmospheric bands, nightglow as alternative to auroral exploration 2—13751
atmospheric release expts., thermospheric temp. obs. 2—16867
atmospheric u.v. emission at 1304 Å, intensity variation with solar activity 2—26496
atom, effects of spatial symmetry restrictions on hyperfine splitting constants 2—8442
atom, K shell ionization cross sections due to proton impact 2—24381
atom $^1S_0$ metastable level, radiative life 2—28197
atomic, extreme u.v. absorption cross-sections in upper atmosphere 2—30318
atomic, photoioniz. of positive ions 2—18332
atomic, polarisability, unified treatment based on R-matrix theory 2—11931
atoms, collisions with CH, formation of CHO^+ by associative ionization, theoret. study 2—872
atoms, collisions with CO, calc. of CO_2 resonance formation probability 2—690
atoms, collisions with N_2, calc. of vibrational transition probabilities 2—15238
atoms, collisions with Na, K, Rb, Cs, charge exchange cross section, theoret. study 2—691
atoms, collisionwith H atoms, Oh formation through inverse dissociation 2—816
atoms, elastic scatt. of low energy electrons, cross section calc. 2—629
atoms, neutral and ionized, electronic structure and term energies 2—585
atoms, photoionization yields for high and low solar activity 2—4713
in blood, pressure flow meter, for obs. during artificial circulation 2—20730
in blood, pressure obs. during artificial circulation 2—20731
body, total content det. by fast neutron activation analysis 2—20718
c O_2+S, surface reaction kinetics on Cu (110), Auger spectroscopy 2—9248
charge transfer reactions with Ar^+, obs. using ion injection drift tube 2—24838
chemisorbed in Pt, LEED obs. 2—35918
chemisorbed on Ni, photoemission energy level meas. 2—4325
chemisorption, In PbI_2, ambient sensitive semiconduction 2—19650
chemisorption, on oxide surface, role in exo-emission 2—4314
chemisorption of Re, mol. beam obs. of adsorbed layer 2—35919
chemisorption on α-Cr_2O_3, i.r. study 2—6380
chemisorption on Bi-Te, thermoelectric semiconductor compounds, n-type, spectrophotometric obs. 2—16680
chemisorption on CdS, effect on elec. cond. 2—18956
chemisorption on CdS, effect on elec. cond. 2—32974
chemisorption on CdS, influence of surface struct. 2—29061
chemisorption on CdS, kinetics 2—29060
chemisorption on CdS surface, rel. to electron emission 2—10152
chemisorption on graphitic BN, CNDO/2 molecular orbital calc. 2—7177
chemisorption on Ir, kinetics 2—4584
chemisorption on Pt, model calcs. 2—35917
chemisorption on W or Ru, O_2 and CO_2 contiguous layer prep. 2—30062
chemisorption on ZnO, LEED study 2—18924
concentration variations in CO gas laser, effects on output power 2—31033
cosmic ray nuclei, interstellar propagation, differential kinetic energy/nucleon spectra 2—4764
V1057 Cygni, total absorption at λ7774 2—10876
desorption from Ag powder, microbalance obs. 2—35906
desorption from Nb, sticking probability and interaction kinetics 2—9308
diffusion, competitive in β-Ta film 2—39531
diffusion, in Nb alloy Cb-132, rel. to oxidation behaviour 2—13578
diffusion, in $TiSi_2$, oxidation mechanism 2—13579
diffusion, stress induced, in α-Zr 2—32568
diffusion, stress induced, in α-Zr 2—32567
diffusion in α-Zr, rel. to post-deform. ageing kinetics 2—9747
diffusion in Co_2SiO_4 2—32566
diffusion in Cu, coeff. determ. using solid electrolyte 2—25467
diffusion in liquid Ag, potentiostatic meas. method 2—12554
diffusion in Ni, determ. from internal oxidation kinetics of Ni-Be alloy 2—29221
diffusion in non-Newtonian saline solution 2—35749
diffusion in refractory oxide, mass spectrometer sectioning meas. technique 2—36250
diffusion in TiO_2, rutile, rel. to high temp. compressive creep 2—29273
diffusion in V, 60-1825°C 2—22252
diffusivity in H_2O, applicability of Stokes-Einstein equation 2—32251
dissociation in Ar, incubation time prediction 2—21587
dissolved in Nb, resist. hardness 2—3942
dissolved in wind driven ocean, distribution obs. tracer model 2—13648
in eastern Pacific, total dissolved, vertical distribution, multivariable regression analysis 2—16781
electron drift and diffusion, influence of H_2 traces 2—15501
electron impact dissoc., absolute prod. cross sect. of $O(^5S^0)$ 2—21520
electronic collisions, excitation, deactivation and attachment 2—5902

Oxygen continued
emission from Cytherean upper atmosphere 2—11011
enthalpies of reaction, dissolution in Cu-Ni, Cu-Co, Cu-Fe melts, e.m.f. obs. 2—3956
equilibrium charge state distributions of O and S ions in carbon stripper of tandem accelerator 2—27919
F-type supergiants, OI, Fe I and Fe II spectra, microturbulence 2—30458
flames, temperature det. using Raman scattering 2—37824
gas, solubility in water temp. dependence 2—25052
gaseous, broadening of fine structure Raman lines 2—815
glow discharge with Xe, clear emission of OIλ5577 2—15514
Herzberg Bands, excitation in nightglow 2—20382
Herzberg I bands, covariation with OI(5577) 2—13750
impurity in amorphous Ge, effect on absorption edge 2—40665
internal Penning source, for heavy ions 2—34861
interstitial, in Ti, mech. relax. and diffusion, internal friction obs. 2—36020
interstitial impurity in V, effect of annealing, 375-575K 2—25443
ion mobility in air, determ. using proportional counter 2—12457
ionospheric D-region, ionization process 2—7336
ionospheric ion density 2—41002
ions, channelling in Au, rel. to emerging charge-state distribs., 4-40 MeV 2—36383
ions, electron impact excitation cross sections 2—5822
ions, photoionization cross sections for excited states, emission models for gaseous nebulae 2—20506
isotopic analysis of O in solids using hollow cathode discharge 2—16697
jet, high-energy, gas flow obs. 2—8915
leak rate through thin polycarbonate film 2—3816
liquid, O_2 liquid, erosion intensity dependence on static pressure and ultrasonic frequency 2—39306
liquid, under saturated vapour pressure, sound velocity using law of corresponding states 2—35760
in liquid binary alloys, quasichem. eqns. activity coeff., bonding 2—25584
liquid/saturated vapour equilib., crit. constants effects 2—28950
Mars atmosphere, search using high dispersion spectroscopy 2—7526
martian atmosphere evolution 2—41194
Matrian atmosphere, u.v. spectrometry, Mariner 9 experiment 2—37361
migration on Mo-C-O alloy surface 2—9252
molecular core-level binding-energy shifts calcs. from Mo theories 2—35195
molecule, ^{17}O, quadrupole coupling const., electronic charge distrib. around O 2—5944
molecule, $^1\Sigma^+_g$ state, formation through sensitization by triplet state of aromatic molecules 2—13591
molecule, $^1\Sigma$ state, spectroscopic detection of photosensitized formation in gas phase 2—10641
molecule, absorpt. cross sections and ionization efficiencies 300-1000 Å region 2—21639
molecule, angular dependence of electron impact excitation cross sections 2—31817
molecule, collision induced vibrational and electronic spectra from 90 to 115 K 2—21635
molecule, collisions with K atom, K ionization cross section 2—31706
molecule, endothermic negative-ion charge transfer reactions, electron affinity meas. 2—8863
molecule, energies and properties of excited states, ab initio calcs. 2—8640
molecule, ionization potential, prod. of 1s hole states in O_2^+ ion 2—8689
molecule, pressure dependence of electron attachment relaxation and steady state microwave conductivity method 2—15326
molecule, Raman spectra, simulation of intensity contour allowing for spin splitting 2—21638
molecule, reactive scattering with Ba, study in crossed beam experiment 2—662
molecule, scattering of Ar, quantum state dependence 2—3152
molecule, singlet excited state, effects at ZnO surface to enhance conductivity 2—16317
molecule, slow electron attachment mechanism 2—12184
molecule, three-body electron attachment, investigation using electron beam techniques 2—15499
molecule, vibrational and electronic excitation due to low energy electron collisions 2—814
molecule, vibrational and rotational excitation in $He(2^3S_1)$ Penning ionization 2—21716
molecule, vibrational excitation by electrons at 10 to 100 eV 2—12171
molecule, vibrational structure from formation of $O_2^-X^2\Pi_g$ in electron scattering 2—24483
molecules, abs. absorption meas. in 2430 to 1920 Å continuum 2—5942
molecules, abs. absorption meas. on Herzberg I bands 2—5941
molecules, collisions with Cs atoms, analysis of ion production 2—899
molecules, collisions with Kr, charge transfer cross sections in thermal and suprathermal range 2—658
molecules, electron scattering, cross section meas. from 0 to 4eV rel. to negative molec. ion spectroscopy 2—819
molecules, electron scattering, resonance structure interpretation in 0 to 1.2 eV energy range 2—820
molecules, electronic structure of open shell states, SCF theory applic. 2—8591
molecules, ionization and dissociation by collision with Na^+ at 5 to 42 keV 2—883
molecules, neutron scatt. cross sections, cold and thermal, 173-373K 2—15327
molecules, reactive collisions with Ba, angular distribution meas. 2—4576
molecules, Schumann-Runge photodissociation continuum, theoretical calc. 2—818
multiply charged ion beam passing through celluloid film, determ. of electron loss and capture cross section 2—1447
multiply charged ion source, variable energy cyclotron 2—34859
negative ions, discharge, plasma anodization of Al 2—3199
nightglow F layer, 6300 A quantum efficiency of recombination mechanism 2—20417
Nova Delphini 1967 nebula, permitted line weakening in spectral range 5600 to 8800 Angstroms 2—13911
O_2, silent discharge, emission spectrum 2—12467
O_2 supersonic beams interacting with surface of Si crystal 2—6314
permeation through Ag membrane 2—25461
photochemistry in atmosphere, laboratory obs. 2—7273
photoelectron emission energy dependence of angular distribution 2—38826
photoionization yields for high and low solar activity using Monte Carlo simulation of model ionosphere 2—4713

Oxygen continued
plasma excitation and electron density meas. 2—15477
plasma jet, thermodynamic state calc. from dimensionless parameter 2—18590
polyatomic gas, shear viscosity, room temp. mag. field effects 2—21925
positive column, explan. of two different forms 2—24881
quenching of NO $A^2\Sigma^+$ by $O_2X^3\Sigma_g$- 2—28315
Raman spectrum, meas. of intensities of spin satellites of S(3) and S(5) lines 2—8695
self diffusion in titanate ceramics 2—12814
self-diffusion in BO_3 melt 2—15581
self-diffusion in $UO_{2\|x}$ 2—12815
singlet in $^1\Delta_g$ state, gas phase quenching by triplet state sensitizers 2—22856
solar corona abundance, det. from e.u.v. spectra 2—20692
solar energetic-particle events, composition, enrichment of very heavy nuclei 2—11082
solid, extreme u.v. reflection spectra 2—19995
sorption in mordenite 2—22082
sorption on PbSe epitaxial film 2—39561
in space, released from Apollo missions, interference with scientific observations 2—30600
stars in late stages of evolution and models of burnt-out cores 2—10868
surface impurity levels in Au, ang. distrib. of x-ray induced photoelectrons 2—19806
thermal cond., large mag. field effect, 77k 2—24981
thermal cond. coeff. dispersion in mag. field, reson. singularities, Scott effect 2—39283
thermophysical props. from melting line to 600 R for pressures to 5000 psia 2—12558
thermosphere, seasonal variation of concentration 2—20373
transient species, atomic and molecular, photoelectron and chemielectron spectroscopy 2—35163
vapour pressure equation 2—30749
vibrational relaxation times at increased pressure, effective specific heat ratio 2—14258
vibrationally excited, equilibrium densities for day and night, in upper atmosphere 2—22984
vibrationally excited $O_2(^3\Sigma\text{-}_g)$ formation in reactions of $O(^1D)$ atoms with O_2 and O_3 2—12183
in violanthrene A, single cryst., acceptor levels 2—13250
X-ray K-emission spectra, in ice, solid CO_2 and solid alcohols 2—16598
Ar-O_2, shock-heated, thermal ioniz. due to impurities 2—8992
C IV emission lines in HD45166 2—7430
CO-O flames, comparison of single- and double-probe meas. of electron temperature 2—37823
CS_2/O_2 chem. lasers, operative mechanisms 2—23587
CS_2-O_2, electric discharge, cw CO chemical laser 2—17592
Cs-O_2 vapour sources, applic. to thermionic energy converters 2—23496
Fe+N_2, O_2 reactions, ionization and spectral emission at simulated meteor conditions 2—33752
$Fe+O_2 \rightarrow FeO+O$, homogeneous gas phase reaction studied in N_2 bath at 1600 K using alumina fast-flow reactor in vacuum furnace 2—33367
GaP:O, liquid phase epitaxial growth, on oxygen incorporation, rel. to luminesc. props. 2—39593
GaP:Zn.O, annealing effects on luminesc. props. 2—26233
GaP:Zn.O growth from nonstoichiometric melt, red photoluminesc. 2—7098
Ge:O, ion implanted, absorpt. spectra before and after ion beam irrad. 2—22766
H-O_2 collisions at 10 to 35 keV, excitation of n=3 states in H 2—38849
H_2S-O_2 flame, vibr. temp. of SO radical 2—22874
$H^-+O \rightarrow H+O^-$, non resonant charge transfer, cross section calc. 2—692
$InAs_{1-x}P_x$(Cs-O), long-wavelength photoemission 2—6928
ion implantation, in Si, SiO_2 formation, i.r. absorp. obs. 2—26173
Mg-O complex, in GaP, yellow-orange bound excitonic transition 2—36941
N_2-O_2 mixtures, decay of luminescence, irradiated by alpha particles, emission spectra 2—35274
N_2 mixtures, d.c. and h.f. discharges, T-layers in positive column 2—28669
^{14}N, in rare earth nitrate soln., n.m.r. exchange effects 2—6254
inNb, interstitial solute pick-up, annealed sample, Hall-Petch plot 2—9544
O/H abundance ratio in dwarf blue galaxies 2—26625
O/He ratio enhancement during solar flares due to preferential acceleration 2—26897
O/N_2 conc. ratio in upper atmos. 2—22982
O/N_2 ratio in atmosphere above 400 km during magnetic storm 2—16871
O/O_2 and O/N_2 ratios in lower thermosphere, semiannual variations in the neutral composition of atmosphere 2—30309
O_2-H_2 detonations, effect of cool boundary layers on ionization probe obs. 2—35534
O_2-H_2 flames, premixed, spectroscopic applic. 2—22894
O_2-H_2 radicals low pressure discharges and surface reactions 2—35620
O- collisions with Na^+, mutual neutralization cross section, meas. with superimposed beams 2—688
O, absorption of electrons, rel. to atmospheric phenomena 2—8991
O, chemisorption of monolayer on Al film, sticking probability 2—3558
O and O^+, capture and loss of electrons in air, N_2 and O_2, corss sections 2—32115
O I and S II line intensity ratios in nuclei of galaxies and gaseous nebulae 2—37266
O I far u.v. emission spectrum from α Bootis (Arcturus) 2—41086
O I interstellear lines of Delta Scorpii and Zeta Ophiuchi 2—7429
O I λ7774 line in F-type supergiants, calibration and equivalent width 2—30457
O I λ7774 line in spectra of brightest stars in Magellanic Clouds 2—10875
O I total absorption measures, photoelectric photometry for 31 stars 2—33653
O II and O III multiplet levels with optical cascades, quantum beats in transitions 2—35143
O III, fine structure transitions, proton induced, cross sections 2—35160
O IV, electron impact ionization, cross section calc. for ground state config. 2—2953
O IV, s-p and p-d oscillator strength calc. using frozen core version of Hartree Fock approx. 2—8441
O resonance radiation in terrestrial airglow photoelectron excitation 2—13749
O VI, 2s→nf transitions, Coulomb-Born I cross sections 2—35151
O VII, dielectric recombination satellite line intensities, meas. and interpretation 2—28171

Oxygen continued
O VII line emission from coronal features and electron density 2—11146
O VII X-ray line emission, with rocket-borne spectrometer/chromator for solar corona mapping 2—11157
O^-, adsorbed on MgO, reactions with O_2, CO and ethylene, e.s.r. study of resultant species 2—4578
O^-, rate constant for conversion to $O_3^-(H_2O)_n$ in moist oxygen 2—30053
O^+, collisions with Ar and Ne at 50 to 200 keV, natural widths of kinetic energy loss distributions 2—15239
O^+, collisions with C foil, equilibrium charge distributions 2—5833
O^+, collisions with N_2 and Ne, at keV energies, KLL Auger electron emission 2—663
O^+, collisions with Ne, K-shell excitations, differential investigation of velocity dependence 2—2967
O^+, ionization by electrons in merging beams 2—38822
O^+, outer shell multi configuration approx., energy matrix elements 2—28196
O^+, reactive and charge transfer collisions with N_2, effects of metastable $O^+(^2D)$ 2—8482
O^+ ion beams, fast, obs. of Zeeman effect in optical spectra 2—34357
O^+ lateral diffusion in O_2 in electric field 2—24988
O_2-, adsorption on vacuum cleaved GaAs, LEED study 2—3561
O_2-, vibrational progression of resonances, association with Rydberg states 2—812
O_2- impurity centre in KI crystal, structure of phonon wing in spectra 2—26220
O_2, absorpt. spectra in solid O_2-N_2 mixture, 1.5K, mag. field effect 2—8694
O_2, charge exchange with alkali atoms, adiabatic electron affinities 2—388[illegible]8
O_2, collision with H and H^+ beams, Lyman-α emission cross sections 2—5868
O_2, dissociation rate constants in shock tube, u.v. absorpt. spectra 2—18461
O_2, dissociative ionization by 35 eV electron impact, energy spectrum of O^+ fragments meas. 2—3059
O_2, effect on Ge(Li) diode preparation using Ti getter pumps 2—24088
O_2, electron affinity from energy thresholds for negative-ion electron transfer reactions 2—5945
O_2, electron impact excitation selection rule for parity unfavoured transitions 2—12090
O_2, electron impact excitation, 4-45 eV, differential and integral cross sections determined 2—15328
O_2, i.r. fundamental vibration band obs., collision-induced 2—8697
O_2, ion-pair processes, by electron impact, mass spectrometric study 2—8623
O_2, photoelectron-photoion coincidence spectra 2—28164
O_2, photoelectron spectra of some autoionizing resonance states 2—8692
O_2, rate constant for conversion to $O_2^-(H_2O)_n$ in moist oxygen 2—30053
O_2, reaction with O^- adsorbed on MgO, e.s.r. study of resultant species 2—4578
α-O_2, solid, mag. form factor, neutron diffr. obs. 2—29839
O_2 adsorption structure on W obs. 2—6375
O_2 and mixtures with H_2, He_3, He_4, vibrational relaxation times determ. from sound absorption measurements 2—38932
O_2 and O_2-H_2O mixtures, u.s. attenuation temp. depend. 2—28740
O_2 Compton profile meas. using Ag and Mo X-rays 2—18451
O_2 Compton scattering of X-rays from gas, comparison of exptl. and theoretical profiles 2—15234
O_2 dissociation, by electron impact, translational spectroscopy of metastable and long-lived Rydberg fragments 2—3058
O_2 electron scatt., emission cross-sections for O I and O II multiplet radiation 2—2946
O_2 Herzberg I system, Franck-Condon factors, Klein- Dunham potentials calc. 2—38933
O_2 microwave spectrum, pressure broadening calc., strong-collision model 2—18460
O_2 molecular beam, mass spectrometric identification of paramagnetic component 2—18397
O_2 photoionization, effect of autoionization on angular distribution intensity of ejected photoelectrons 2—607
O_2 photoionization by soft X-rays at 0.28 and 1.49 keV, meas. of relative abundance of thermal energy ions 2—805
O_2 reaction with electrons produced by two-photon laser photolysis of molecules in liquids, rate constants meas. 2—30081
O_2 rotational excitation by slow positrons, cross section calc. in distorted wave approx. 2—24466
O_2 Senftleben effects, formal kinetic theory 2—15538
O_2^-, ground and excited states, potential energy calc. 2—15297
O_2^- centres in KCl, KBr, KI and NaI, elastic interaction 2—22186
O_2^- excitation spectra in alkali halide crystals, vibrational structure 2—813
O_2^+, electron-ion recombination, meas. in flowing afterglow 2—6108
O_2^+, ionospheric density, influence of neutral winds at night 2—23008
O_2^+, luminescence, Franck-Condon factors and collisional deactivation 2—15323
O_2^+, merging beam studies of ion-molecule reactions with Ba 2—12006
O_2^+, molecular ion, localized and delocalized 1s hole states 2—8689
O_2^+, O^-, O_2^- ions in lower ionosphere during solar eclipses, rocket measurements 2—33533
O_2^+, recombination coefficient meas. in flowing afterglow following electron-positive ion collisions 2—12000
O_2^+ collisions with He, Ne, Ar, meas. of differential scattering with single electron capture, 0.7-3.0 keV, interp. of curve crossing 2—672
$O_2 \rightarrow O(^3P)+O(^1S)$, vacuum u.v. photodissociation, time flight spectroscopy of metastable fragments 2—777
O_3-, on MgO, e.p.r. spectrum rel. to verification of formation 2—26263
O_3-, photodetachment study using tunable dye laser 2—817
O_3-, radical trapped at sites in $KClO_3$, due to X-irradiation e.p.r. study 2—10484
O_3 gas, relative Raman cross section, rel. air pollution 2—35249
O_4, cooperative optical transitions, dipole intensity computation, symmetry of dimeric and exciton states 2—24484
O^4 currents in exosphere 2—26522
O^{5+}, collisions at 30 MeV with Fe, multiple inner shell ionization, K_α spectrum 2—665
O^{5+} lithium like ions passing through C foil target, excitation of metastable autoionizing states, determ. of electron spectra 2—604
$O(^1D)$ atom reactions for chemical lasers 2—31045
$O_2(^1\Delta_g)$, reaction with tetramethylethylene, effect of pressure on rate 2—20180

Oxygen continued
- $O_2(^1\Delta_g)$, vacuum ultraviolet photoelectron spectrum 2—760
- $O_2(^1\Delta_g)$ concentration in D-region 2—33543
- $O_2(^1\Delta_g)$ luminescence, rate constants for quenching by 2,3-dimethyl-2-butene and triethylamine 2—21636
- $O_2(^1\Delta_g)+SO(^3\Sigma^-)\rightarrow SO(^1\Delta)+O_2(^3\Sigma_g^-)$, kinetic study by e.p.r., absolute rate constant 2—10612
- $O_2(^1\Delta_g\rightleftharpoons{}^3\Sigma^-_g)$ system, optical emission at 1.27 μm 2—7183
- $O_2^-(H_2O)_n$, formation from O_2^- in moist oxygen, rate const. 2—30053
- $O_3^-(H_2O)_n$, formation from O^- in moist oxygen, rate const. 2—30053
- OI, OII Nova Delphini 1967 nebula, forbidden transitions increased stability in spectral range 5600 to 8800 Angstroms 2—13911
- OI 5577 emission in SAR arc 2—20390
- OI 6300Å airglow, development during predawn enhancement 2—16879
- OI airglow emission, 6300 Å, intensity rel. to ionospheric scintillations 2—16882
- OI forbidden line intensities in the atmosphere during 1970, March 7 solar eclipse, properties of shadow bands 2—33473
- $O(^3P)$ atoms, activation energy of addition to olefins 2—10614
- $O(^3P)+CO$, reaction, kinetics and mechanism 2—22869
- $O(^1S)$ atoms, effective lifetime in pulsating aurora 2—20388
- $O(^5S^0)$, absolute prod. cross section due to electron impact dissoc. of O_2 2—21520
- OV emission spectra of WR stars 2—41102
- O_2—Ar^+ charge exchange collision, rate coeff. meas. 2—5832
- O_2—N^+ charge exchange collision, rate coeff. meas. 2—5832
- ^{16}O, abundance on surface of magnetic neutron stars 2—30477
- $^{16}O+{}^{16}O$ total reaction cross-section at astrophysical energies 2—37289
- $^{18}O/^{16}O$ in ice caps, for det. of past wind strengths 2—10727
- $^{18}O/^{16}O$ in stratospheric aerosol 2—10720
- $^{18}O/^{16}O$ isotopic analysis of Luna 16 soil 2—20667
- $^{18}O/^{16}O$ profiles through the Antarctic and Greenland ice sheets 2—22941
- ^{18}O and ^{14}C, isotope exchange between HCO_3 in saline solutions and solid $CaCO_3$ 2—16768
- $O_2^++Ba\rightarrow BaO^++O$ merging-beam study, determ. cross sections and kinetic energy of products 2—12005
- O_2+D_2 crossed beams elastic scattering, determ. of intermolecular potential 2—3145
- $O_2+Fe\rightarrow FeO+O$ reaction rate studied 2—35247
- O_2+H_2 crossed beams elastic scattering, determ. of intermolecular potential 2—3145
- $O_2+Li\rightarrow LiO_2$, cocondensation reactive collision, matrix laser Raman spectra of LiO_2 2—38921
- $O+Mo(CO)_6$ flames, chemiluminescence band system 2—22865
- O^++N_2 reaction, ab initio configuration interaction calculation of potential energy curves 2—12014
- $O+O^-$, adiabatic potential curves, ab initio calc. 2—12185
- $O+U\rightarrow UO^++e$, $O_2+U\rightarrow UO_2^++e$, collisional chemi-ionization processes, effective cross sections 2—33372
- O_2+ethylene, reaction rate constants, in temp. range 232-500K 2—40806
- SO_2/O_2 mixtures, meas. of sound absorption due to vibrational relaxation, existence of vib.-vib. coupling 2—15338
- $S(3^3P_3)+O\rightarrow SO+O$, absolute rate meas. using kinetic spectroscopy in vacuum u.v. 2—33371
- Si:O, annealed, neutron irrad., O conc., i.r. absorpt. spectra 2—22223
- Si:Sb,O, implantation disorder, ionization and thermal dependence 2—25376
- Ta:O film, sputtered, O_2 content rel. to struct. and elec. props. 2—39533
- Ti:O film, cermet, elec. resist., temp. and strain effects 2—40184
- W-O_2 system, gas phase constitution and chemical transport reactions, thermodynamic aspects 2—30057
- Zn:O liq., evaporation kinetics, equilib., v.p., rel. to surface active impurities, 563-623K 2—28951
- inZnS, melt grown or hydrothermally prep., optical spectra studies 2—36055
- ZnTe:In, O, luminesc., self-activated and isoelectronic O emission 2—20106

Oxygen compounds
- elementary reactions of neutral species 2—7165
- metal oxide, dielec. contact layer, stress/strain distrib. 2—25190
- OH $^2\Pi_{1/2}$ $J={}^1/_2$ line at 4660 MHz, obs. in Sagittarius B2 2—10934
- OH microwave emission in i.r. stars, effects of i.r. radiation and collisions on vibrational and rotational states 2—30528
- OH thermal emission from interstellar dust clouds of NGC 2264 yound open cluster 2—26735
- oxide:$Bi^{3+}(Eu^{3+})$, u.v. absorpt. band positions 2—20049
- oxide adsorption on Pt from perchloric acid, modulated specular reflection spectroscopy 2—9311
- oxide and related phases prep. by chem. transport 2—10622
- oxide ceramic, defects, porosity, elastic consts., u.s. and fluorescence obs. 2—12978
- oxide defect structures rel. to stoichiometry 2—9546
- oxide layer on Pt, Au and Ni, specular reflection spectra, monolayer thickness range 2—9310
- oxide single crystals, localized stresses due to thermal expansion 2—15821
- oxides, high temp., order-disorder, characterization using i.r. and Raman spectroscopy 2—9829
- oxides, K emission spectrum from O, chemical bonding obs. 2—13495
- oxides, positron lifetime spectra 2—40158
- oxides, tetrahedrally-coordinated, $LiPO_4$ type families 2—9335
- oxides of Al, Mg and Si, thermochemical props. of films at 2270 K 2—7161
- oxyfluorides and complex fluorides of group iv to vi elements, X-ray-electron investigation 2—33295
- perovskites, $A^{1+}B^{5+}O_3$-type, B=Ta,Nb,Sn, existence rel. to bonding, high press. synthesis, transforms. 2—9346
- semiconducting electroceramic oxides, control of properties by microstructure 2—32738
- Ag-O alloy, temp. and strain rate depend. of yield 2—32604
- Co-U-O system, $CoUO_4$ stability, $Co_3U_2O_8$ phase 2—15958
- Cu-Fe-S-O, phase equilibria, from 3-component phase diagrams 2—4012
- Fe-Mo(W)-O system, phase equilib. and thermodynamics 2—40008
- GaP:O, i.r. absorpt. spectra, localized phonon excitation, donor electron excitation 2—20037
- Mo-W-O system, ternary phase formation 2—22378
- Nb-O alloy, flow stress, soln. hardening 2—9661
- O_2, rotational Raman spectra 2—18464
- OCS, collisions study by broadening of microwave spectral lines 2—35385
- OCS, double resonance in microwave absorption spectrum 2—8693
- OCS, i.r. emission, rot.-vibr. struct. of transitions 2—28275

Oxygen compounds continued
- OCS, refractive index of liquid in temp. range 130-260 K 2—18825
- OCS in solution, determ. of band width and profile of ν_3 mode, separation of rotational and vibrational effects 2—38934
- OF, $^2\Pi$ state, ab initio calculations 2—31818
- OH, distribution in Galaxy, correlation with continuum sources and formaldehyde 2—10818
- OH, effective emitting populations for various collision frequencies 2—38870
- OH, electron scattering, quantum state dependence 2—3152
- OH, emission spectra associated with i.r. stars, position meas. 2—10968
- OH, emission spectrum in pulse discharge through H_2O vapour 2—28316
- OH, existence of free groups in liquid water 2—28786
- OH, formation through inverse predissociation 2—12186
- OH, formation through inverse dissociation 2—816
- OH, interstellar, search for emission in high galactic latitudes 2—13922
- OH, isotropic hyperfine coupling constants 2—31812
- OH, Λ-doublet transitions, detection in molecular beam maser 2—12187
- OH, predissociation by continuum of bound state without curve crossing 2—18462
- OH, production in $H+F_2O$ reactions 2—18545
- OH, reanalysis of $A^2\Sigma^+$-$X^2\Pi_i$ system 2—5943
- OH, rotational temp. in l.v. luminescent discharge and d.c. arc in Ar containing water vapour 2—24936
- OH, theoretical derivation of molecular parameters 2—12188
- OH (8-3) band airglow, nocturnal variations 2—7327
- OH and formaldehyde interstellar clouds, physical conditions and molecular formation and lifetimes 2—33694
- OH emission from i.r. stars 2—37296
- OH emission sources, interferometer positions 2—20594
- OH emission sources, search at 1665 MHz 2—7432
- OH excitation rates of vibrational levels, and nightglow intensities 2—40974
- OH ground state transition frequencies, beam maser measurements 2—21640
- OH ground state vib.-rot. bands, obs. in chemiluminescent O_3-olefin gas phase reactions 2—22868
- OH intensity variation in airglow spectrum between 3 and 4 microns meas. through morning and evening twilight 2—37194
- OH line, lunar occultation studies of centre region of Galaxy 2—4788
- OH molecules, Λ doubling in $^2\Pi$ states calc. from HF wavefunctions to test validity of Van Vleck's hypothesis 2—21637
- OH optical depth map of Carina Nebula 2—26643
- OH radical, high-field Stark effects on near u.v. spectrum 2—8698
- OH stellar sources of 1612 MHz, coincidence with M type Mira variables or M supergiants 2—23094
- OH‡, stimulated i.r. emission, produced by pulsed electric discharge 2—21077
- OH^- and OD^- impurities in alkali halides, absorpt. bands 2—4455
- OH^- in mesosphere, rocket measurement of 3064 Å $A^2\Sigma$-$X^2\Pi$ electronic transition 2—20349
- OH^+ molecule, fine structure of 3Π and $^3\Sigma^-$ states 2—21586
- $OH^-(H_2O)_n$, n=0-4, structures and energetics, ab initio MO calc. 2—24456
- OHX sources, interstellar, obs. of excited lines near 4700 MHz 2—10915
- $OSCl_2$, photodissociation in vacuum u.v., heat for formation of SO 2—33385
- Pu-C-O system, phase diagrams 2—12611
- Ti-O alloy, dil., comp. depend. of elastic const., u.s. velocity study 2—15802
- Ti-V-O and Ti-V-Al-O alloys, effect of O content on mech. props. 2—36144
- U-C-O system, phase diagrams 2—12611
- U-Pu-C-O system, phase diagrams 2—12611
- V-O solid solution, thermodynamic props., e.m.f. study 2—25602

Ozone
- absorption spectrum of $\nu_1+\nu_2+\nu_3$ band in 3.59 μm region, rigid rotator analysis 2—8696
- atmospheric, ground level density measurement 2—30276
- atmospheric, observations 2—13680
- atmospheric, spatial distribution, electronics for backscatter u.v. instrument, for obs. 2—16819
- atmospheric, u.v. absorption cross section 2—7298
- atmospheric, vertical distribution near equator 2—10721
- atmospheric meas. near sunrise 2—7265
- atmospheric number densities det. 30 to 75 km by lunar rocket photometry 2—30272
- atmospheric profile, Fourier spectroscopy from Nimbus meteorological satellite 2—22953
- chemiluminescent reaction with H_2S, CH_3SH, CH_3SH_3 and SO, visible and near u.v. spectra 2—20179
- Cologne, measurements of total 2—20316
- dissociation and reactions in atmosphere 2—7270
- electron attachment, low energy, using swarm techniques 2—32116
- flow metering system, design and operation 2—28702
- i.r. absorpt. bands, anharmonicity coeffs. 2—31816
- isotopic molecules, inert-gas matrix isolated, i.r. absorption spectra 2—8690
- mesosphere, from obs. of 1.27μ band 2—33452
- in middle stratosphere, horizontal distrib., macrosynoptic situations 2—30268
- molecule, energies and properties of excited states, ab initio calcs. 2—8640
- molecule, millimetre wave spectrum, rotational constants, Stark effect, dipole moment 2—8691
- photochemical dissociation with light of 3340 Å, kinetics and mechanism 2—37050
- photochemistry in atmosphere, laboratory obs. 2—7273
- photolysis obs. of primary products 2—7183
- reaction with $O(^1D)$ atoms, vibrationally excited $O_2(^3\Sigma^-_g)$ formation 2—12183
- spectral transmissivity of real gas, exponential model 2—21921
- troposphere and stratosphere, routine observations, comparison of Umkehr with i.r. method 2—30267
- tropospheric, gas phase destruction 2—22959
- O_3-olefin chemiluminescent gas phase reactions, vibration-rotation bands of ground state of OH 2—22868
- O_3+CS_2 reaction, CO laser emission 2—2392

Ozonosphere *see Atmosphere*

p-n junctions *see Semiconducting devices/junctions*

P-V-T relations *see Equations of state*
Pair creation *see Electron pairs; and under individual particles, e.g. Mesons*
Palaeomagnetism *see Rock magnetism*
Palladium
atom, visualization, dark field electron microscopy, scattering cross sections 2—21521
dielectric screening function 2—16111
diffusion of H and D, reversed isotope dependence, -60-200°C, dipole moment tensor 2—22236
electronic structure, conduction electron propag., electron-ion matrix element determ. 2—1460
e.p.r. of Dy^{3+}, weak h.f.s., ion ground state 2—33343
film, discontinuous, on dielec. substrate, electron cond., resist. coeff., 130-300K 2—40180
film, on Si single cryst., interdiffusion and compound formation 2—6352
film, single cryst. on NaCl, flash evap., struct. 2—9280
Hubbard's approx. band scheme, accuracy 2—13079
ion implanted, He release obs. 2—12751
lattice parameters, —189 to 1709°C, solid equation of state 2—19304
lattice vibration spectra, determination of specific heats and Debye temp. 2—22405
linear compressive strain, press. depend. to 20 kbar, phase transformations 2—9818
liquid, thermodynamic props. determ. by levitation calorimetry 2—21979
magnetic polarization of cond. electrons due to mag. moment 2—1632
magnetic susceptibility temp. depend. 2—29801
photoelectron spectra rel. to charge voltage on BaSO$_4$ substrate 2—13359
thermal conductivity, electrical resistivity absolute thermoelectric power meas. in 90-1300 K range, two-band model analysis 2—36367
valence band structure from u.v. photoelectron spectra 2—36650
X-ray spectra, relations between L_{III} absorp. limit and $L\beta_{2,15}$ lines 2—26206
CaS:Pd phosphor, electrolum., brightness rel. to voltage and freq. 2—36961
Pd/Ti thin film couples, diffusion and compound formation 2—39749
Pd^{2+}, in KI, e.s.r. obs. 2—4541
Palladium compounds
alloy, band struct., transport props., rel. to impurity scatt., model 2—40183
1,5-cyclooctadiene complexes, i.r. and Raman spectra, frequency dependence on metallic ion 2—15332
Ag-Pd dil. alloys, low field magnetoresistance 2—1474
Ag$_{.71}$Pd$_{.29}$ alloy, electronic structure studied by ESCA and X-ray spectroscopy, comparison with spectra of pure metals 2—32884
Al-Pd, X-ray emission spectrum study of band structure 2—36911
Au$_{.45}$Pd$_{.55}$ alloy, electronic structure studied by ESCA and X-ray spectroscopy, comparison with spectra of pure metals 2—32884
(Au$_{1-x}$Pd$_x$)Te$_2$ alloys, supercond. 2—19577
Ce$_x$La$_{1-x}$Pd$_3$ alloy, Kondo resistivity, crystalline elec. field effects 2—13112
Co-Pd-Si alloy, amorphous, ferromag, reson. 2—7110
Co-Pd alloy, ordered phases, elec. diffr. obs. on evap. single crystal films 2—32781
Cu-Ni-Pd system, struct., 400-700°C, X-ray obs. 2—3705
Cu-Pd bimetal film, diffusion kinetics, size effects 2—9618
β-CuPd, a/8[110](1$\bar{1}$0) faulting in prestrain induced transform. stage, X-ray obs. 2—32763
Cu$_3$Pd alloy long period ordered struct., phase transition, X-ray obs. 2—9799
Cu$_{.60}$Pd$_{.40}$ alloy, electronic structure studied by ESCA and X-ray spectroscopy, comparison with spectra of pure metals 2—32884
Fe-Pd-P alloys, amorphous, mag. props. 2—19877
Fe-Pd-Si, amorphous alloy, Mossbauer spectral study, magnetism model based on local ferromag. order 2—4375
Fe-Pd alloy powders, mag. reversal mechanism 2—40512
Fe-Pd dilute alloy, hyperfine field at Fe atoms, temp. depend. 2—16436
Fe-Pd dilute alloy, spin-lattice relax. time 2—19932
Fe-Pd epitaxial film, anisotropy 2—36724
Fe-Pd system, chemical diffusion and Kirkendall effect, 1100-1250°C 2—12804
Mn-Pd system, MnPd$_2$ phase, mag. and cryst. struct 2—16398
Mo-Pd system, diffusion, electron probe microanal. study 2—36078
Pd-20 at.%Si, amorphous phase, deform., time-depend mech. props. cryst. transform29264 2—29264
Pd-Ag-Au alloy system, Debye temp. and thermal expansion 2—4074
Pd-Ag-H system, elec. resist., 25°C, H$_2$ press. depend. 2—25769
Pd-Al dilute alloy, n.m.r. 2—40782
Pd-As(Sb) system, distorted CuZn struct. 2—29465
Pd-Co dil. alloys, elec. resist., giant moments, exchange coupling 2—26042
Pd-Cr alloys, electron transport props. and sp. ht., below Kondo temp. 2—29615
Pd-Cu, alloy, dilute, charge density oscill. around impurities n.q.r. obs. 2—16666
Pd-Er dilute alloy, e.p.r. 2—30014
Pd-Fe, ferromag., conc. depend. of av. mag. moment, Ising model calc. 2—16351
Pd-Fe, solid soln., positron annihilation and Mossbauer effect 2—4445
Pd-Fe alloys, elec. resist. temp. depend., mag. component 2—40181
Pd-Fe dil. alloy, low temp. resist. and large mag. scatt. 2—9959
Pd-H, positron annihilation, electronic structure detn. 2—19531
Pd-H system, ferroelasticity rel. to phase diagram determination 2—9694
Pd-H(B), Pd-M-H(B) (M=metal), dissociation thermodynamics, d-band effects 2—36247
Pd-H(D) solid solution, thermodynamic function, calc. 2—3961
Pd-Ir alloy, thermoelec. power, 4-300K 2—40373
Pd-Mn dil. alloys, acoustic-spin-wave stiffnesses and ordering temps. 2—10191
Pd-Mn dilute alloys, meas. of specific heat, critical behaviour and magnetic field dependence 2—13046
Pd-Ni-P alloy, amorphous, elec. resist., temp. coeff., rel. to P content, 4.2-300 K 2—40182
Pd-Ni, Pd-Cu, Pd-Ag, Pd-Au, X-ray spectra and band structure 2—36918
Pd-Ni alloy, electron transport props., 1.5-78 K 2—22494
Pd-Ni alloys, disordered, spin fluctuations 2—10173
Pd-Ni alloys, elec. resist., paramag.-ferromag. transition 2—1606
Pd-Pt-Fe, alloys, mag. hardening, mag. props., struct. 2—29813
Pd-Pt alloys, low temp. elec. resist. and thermopower 2—19551
(Pd$_{60-x}$-Pt$_x$-Ni$_{40}$)$_{75}$-P$_{25}$ alloy, elec. resist., 1.2-300 K 2—19550
Pd-Rh(Ru)dil. alloys, resist. minima 2—16147
Pd-Ru alloy, thermoelec. power, 4-300K 2—40373

Palladium compounds continued
Pd-Si:Fe, Cr, elec. resistivity, magnetiz., and magnetoresistance rel. to Kondo effect 2—25768
Pd-Si, Pd film on Si substrate, interdiffusion and compound form. 2—6352
Pd-Si alloy, phase diagram, metallography, X-ray and thermal analysis 2—3435
Pd-Si based metallic glasses, anomalous viscoelastic behaviour 2—32590
Pd-Ta system, diffusion investigation using electron probe 2—29205
Pd-Ti-Au film, struct. and mech. props., ageing effects 2—39534
Pd-V dilute alloy, n.m.r. 2—40782
α-Pd-W, alloy, homogeneous mag. behaviour 2—6939
Pd-W, system, X-ray diffraction study of phase diagram below 1100C 2—4022
Pd-Zn-Ga system, distorted CuZn struct. 2—29465
Pd complex, [Pd(NH$_3$)$_4$]Cl$_2$.H$_2$O, vibr. spectra 2—33270
Pd complex, bis-(π-allyl), orbital assignment from photoelectron spectra obs. 2—35280
Pd complex, C$_{14}$H$_{12}$N$_4$O$_4$Pd, cryst. struct. 2—12732
Pd complex, tetrabenzoporphine, quasilinear phosphorescence, fluorescence and absorption spectra 2—4486
Pd complexes, Pd phthalocyanine, relaxation mechanisms from excited singlet states, spin-orbit coupling effects 2—35279
PdAg:H, chem. pot and H conc. near critical point 2—19270
Pd$_3$Fe alloy, hydrogen absorpt., ordering depend. 2—9773
PdGe, dissociation energy, mass spectrometric Knudsen cell method 2—28321
PdH and PdD, mad. susceptibility temp. depend. 2—29801
PdH$_x$, electron-ion potential approx. model, muffin-tin potentials 2—1460
PdH(D), e.s.r. spectra of $^2\Sigma^+$ ground state, bonding nature, hyperfine coupling and g tensor components 2—12189
Pd$_2$MnSN alloy, Mossbauer effect study of hyperfine fields at Sn sites 2—36833
Pd$_2$MnSb Heusler alloy, giant hyperfine field at ^{121}Sb 2—33227
PdMnTe, cryst. struct. and mag. props. 2—33134
PdO, growth, semiconducting properties, bonding model, electrical meas. 2—3575
PdP$_y$S$_{2-y}$ phosphochalcogenides, synthesis and properties 2—3725
Pd$_3$(PS$_4$)$_2$ crystal structure, preparation 2—3725
Pd$_{81.8}$Si$_{18.2}$, amorphous, recrystallization, isothermal resistance obs. 2—15972
PdTiSi, PdZrGe, cryst. chemistry 2—9349
PdTiSi, PdZrGe struct. relns. with other transition metal silicides and germanides 2—18969
PtFe-PdFe alloy, order-disorder transformation, magnetization, coercive force, lattice parameters 2—1633
Rh$_{.60}$Pd$_{.40}$ alloy, electronic structure studied by ESCA and X-ray spectroscopy, comparison with spectra of pure metals 2—32884
ThPdSn, atomic struct., Debye-Scherrer determ. 2—3736
Ti-Pd system, phase diagram 2—40011
V-Pd alloy, X-ray spectral investigation 2—33301

Paper
cellulose paper for loudspeakers, sonic processing, electroacoustic characteristics 2—34125
conducting, strain gauge manufacture 2—20806
dielectric strength at cryogenic temps. for 50 HZ 2—40321
loudspeaker diaphragm papers, viscoelastic properties 2—30869
mica-paper-tape insulation, dielectric props., effects of manufacturing parameters 2—4261
onionskin, acoustic decoupling, performance degradation of deep-ocean transducers 2—14273

Paraelectric materials *see Dielectric properties of substances*

Paraelectric resonance
integrated absorpt. depend. on freq. and spin Hamiltonian parameters, non-Kramers doublet 2—26260
line profile and width, influence of elec. fields of charged defects 2—1566
KBr:OH$^-$, complex dielectric susceptibility, paraelectric relaxation, isotope effects 2—10116
KCl:Li, stress effects, coupling between lattice strain and multiplet tunnelling levels 2—22619
KCl:Li$^+$, dipole-lattice relaxation time detn. 2—36588
KCl, of Li$^+$, absorpt. spectra obs. 2—10115
RbCl:OH$^-$, complex dielectric susceptibility, paraelectric relaxation, isotope effects 2—10116
RbCl, of Ag$^+$, dipole moment obs. 2—33054

Paramagnetic resonance and relaxation
see also Acoustic paramagnetic resonance; ENDOR; Lasers; Masers; Spin-lattice relaxation; Spin-spin relaxation
(TCNQ)$_2$-3,3(DTC), exchange interaction anisotropy 2—4345
acetophenone, single crystal e.p.r. studies of photoexcited states 2—26360
acetophenone anion radicals, restricted internal rotation influence on e.s.r. spectra 2—828
acetyl methionine, γ-irradiated, correlation between e.p.r. and positron annihilation 2—40752
acridine, metastable triplet state, e.s.r. spectra 2—4547
acridine orange, e.s.r. triplet exciton spectrum 2—21651
adamite:Cu^{2+}, spin Hamiltonian parameters detn. 2—36994
adsorbed alkene molecules on synthetic zeolites 2—21656
L-alanine:Cu crystals, u.v.-induced conversion in Cu^{2+} complexes, e.p.r. study 2—10642
alkali borate glass, of VO^{2+} ion 2—40763
alkali borate glass, trapped electron centre, X-irradiation induced 2—20137
alkali halide, rel. to impurity precipitation, review 2—3794
alkali halide, rel. to weak mag. field enhancement of luminesc. from F-centres 2—26237
alkali halides, of F-centres optical detection 2—10491
alkaline earth fluorides, intrinsic pt. defects obs. 2—30006
alkaline earth fluorides, X-ray irrad., trigonal Gd^{3+} centres 2—13530
alkoxynitroxide radicals from photolysis of nitrobenzenes and heterocyclic nitro cpds. 2—832
alkyl radicals, conformations and hindered internal rotation calculation 2—18480
alkylalkoxyamino radical, trapped in X-irradiated decanal oxime O-methyl ether-urea inclusion crystals 2—13592
alkylalkoxynitroxide, study of decay processes and rotation 2—8728
peri-alkylnaphthalene anions, temperature effects 2—35303
α-aminoisobutyric acid, single crystal irradiated by γ rays at 77 K, identification of cation radical from e.s.r. spectra 2—22885
anisotropy of systems with monoclinic spin Hamiltonian 2—10472

Paramagnetic resonance and relaxation continued
- anthracene, e.p.r. studies of deuteration effect on intersystem crossing 2—12208
- anthracene-d_{10}- fluorene mixed crystals, influence of deuteration and energy transfer 2—20154
- antiferromagnet, scattering of low-freq. e.m. waves 2—7114
- apatite, of Mn^{2+}, impurity distrib. regularities 2—10498
- aromatic σ-type radicals 2—18482
- aromatic hydrocarbon radicals, proton hyperfine splitting and electron density relationships 2—18490
- arsenate single crystals, γ-irradiated ferroelectric and antiferroelectric, e.s.r. of free radicals 2—10122
- arseniates, ferroelec., γ-irrad., radicals obs. 2—10495
- atom, in oscill. r.f. field, g-factor modification 2—31690
- barbituric acid and its 2-thio derivative, comparison between radicals formed by radiation, e.s.r. study 2—21662
- benzaldehyde anion radicals, restricted internal rotation influence on e.s.r. spectra 2—828
- benzaldehyde anion radicals, restricted internal rotation influence on e.s.r. spectra 2—828
- 1,2-benzanthracene, principal axis orientation of e.s.r. 2—15363
- benznitrile, single crystal, e.p.r. studies of photoexcited states 2—26360
- benzocyclobutene radical anion, ion pairing effects in K-THF and Cs-DME 2—18487
- p-benzoquinone adsorbed on TiO_2, bonding rel. to surface electronic state 2—29058
- p-benzosemiquinone in alcoholic soln., mol. motion obs. 2—35788
- N-benzoylanine, X- irrad., radical prod., identification and mol. characterization, e.s.r. obs. 2—8735
- 2-benzoylpyridine, triplet state, g-tensor anisotropy 2—8762
- benzyl radical, calculation of e.s.r. proton coupling constants 2—35306
- biological membranes, use of lipid spin labels 2—20717
- bis-(maleonitriledithiolene)-metal chelate complex, organic semiconductor 2—16218
- butadiene, cis and trans, and their ions, e.s.r. coupling consts. from MO calcs. 2—24520
- carbazole, irradiated crystal, study of radical formation 2—10489
- carbomethoxycyanobenzyl radicals, e.s.r. spectra in 40°-200°C range, obs. of π- and σ- spin delocalization into the phenyl ring 2—31842
- charge transfer complexes, of thermally excited centres 2—10526
- chemisorption and catalysis, application of ESR methods 2—7176
- chloranil-amine charge transfer complex, elec. cond. 2—25832
- 4-chloroacetophenone, single crystal e.p.r. studies of photoexcited states 2—26360
- chloromethyl radical, e.s.r. study in CH_3Cl single crystal 2—8792
- chrysene, phosphorescent, in p-terphenyl host crystal, multiplet structure in low-field e.p.r. spectra 2—20139
- chrysene, principal axis orientation of e.s.r. 2—15363
- inclay minerals 2—10474
- complex, $[(C_2H_5)_4N]_2ZnCl_4$:Co, g-tensor orientation 2—33107
- computer anal. by least squares methods 2—11403
- conference, chemical applications 2—17499
- conjugated radicals, calculation of hyperfine splittings 2—38953
- copper (II) carboxylate, symmetry 2—28362
- copper benzene sulphonate hexahydrate crystals, e.p.r. 2—13529
- copper stearate monolayers, struct., obs. 2—13546
- Cu complex, diethyldithiophosphate, Cu-S hyperfine interaction study 2—36985
- cyanine dyes, triplet-state e.p.r. 2—38973
- cyclohexane, plastic phase, radical doped, molecular motion, ENDOR 2—26292
- cyclopentene adsorbed on zeolites 2—21656
- L-cystine dihydrochloride γ-irrad. cryst., observation of electron-hole recombination 2—22887
- 1-decanol-urea inclusion crystals, X-irradiated 2—20153
- dextrose, charred, g-factor standard for wide temp. range 2—7126
- di-tert-butyl nitroxide, lipid spin labels in biological membranes 2—20717
- diamagnetic crystal, magnetic impurity, e.p.r. line broadening rel. to phonon bottleneck in spin- lattice relax. 2—10532
- diamond, neutron-irradiated, e.s.r. spectra 2—40755
- diamond, rel. to opt. props., paramag. centres 2—26274
- diamond, synthetic, ^{61}Ni spectra 2—13535
- 4,10-diazachryzene, in lowest triplet state, rel. to acid-base equilibria 2—18497
- 1,2;5,6-dibenzanthracene, principal axis orientation of e.s.r. 2—15363
- dichlorofluoroacetamide, N,N-dichlorofluoroacetamide-d_2, X-irradiated, e.s.r. study of chlorofluoroacetamide radical 2—26267
- differential saturation method for overlapping spectra 2—7797
- diluted solutions with two paramag. species, exchange broadening of spectral lines 2—9162
- 4,4′-dimethoxybenzophenone, triplet state, g-tensor anisotropy 2—8762
- dimethylalanine:Cu^{2+}, e.p.r. of cationic radicals formed by u.v. irradiation at 77K 2—30090
- 1,4-, 1,5-, 1,8-dimethylnaphthalenes, monomer and dimer cations, e.s.r. spectra, obs. of hyperfine splitting consts. 2—38976
- 2,2′-dinitrobiphenyl electrogenerated radical anions, e.s.r. spectra, linewidths and spin densities 2—26368
- 1,8-dinitronaphthalene electrogenerated radical anions, e.s.r. spectra, linewidths and spin densities 2—26368
- diphenyldiazomethane, irradiation in single crystal soln., rates and mechanism 2—33363
- 1,1-diphenylethylene:diphenyldiazomethane, photolysis, spectral obs. rel. to cryst. struct. 2—37055
- diphenylmethylene+1,1,diphenylethylene, in single cryst. soln., rates and mechanics 2—33363
- diphenylmethylene+diphenyldiazomethane, in single cryst. soln., rates and mechanism 2—33363
- dipole-dipole system, temperature determ. 2—7028
- dispersion signal, rel. to abs. meas. of static susceptibility 2—16337
- DNA, after electron irradiation, computer controlled anal. of free radical formation 2—22880
- dyes, triplet states 2—5971
- electron electron double resonance in a two frequency spectrum, pulsed exchange model 2—8569
- electron spin induction cavities, decoupling perpendicular modes 2—17500
- electronic structure of point defects, Mossbauer and spin resonance obs., book 2—32876
- emerald, spin Hamiltonian Cr^{3+} ions in trigonal field 2—10494
- e.p.r. line observation as method of determ. nuclear polarization of low-energy polarized target 2—27833

Paramagnetic resonance and relaxation continued
- e.s.r. Lorentzian shaped lines, corrections to meas. of line width and resonance field 2—36975
- ethyl 4-azoxybenzoate, smectic mesophase, molecular organization 2—15576
- ferric dithiocarbamate, paramagnetic molecule 2—5965
- fluorene, irradiated crystal, study of radical formation 2—10489
- fluorene molecules in fluorene crystal, triplet states, e.p.r. and phosphorescence study 2—30089
- 4-formyl-2, 6-di-tert-butylphenoxy radical, temp. dependence 2—5975
- free radicals, hyperfine coupling, augmented basis functions 2—21579
- free radicals, transient, conformations and hindered internal rotation calculation 2—18480
- free-radical reaction products, electron spin polarizations 2—20183
- free-radicals, modulation effects in spin-echo signals 2—762
- frozen liquid crystals, orientation distribution function of aromatic molecules from triplet e.s.r. spectra 2—38950
- glass, computer simulation of spectra, struct. inference 2—39435
- glass, Fe_2O_3-rich, anomalous mag. behaviour 2—33132
- glass, org., γ-irradiated, scavenging kinetics of electrons, long range tunnelling 2—40831
- glass, soda, rare earth doped, sensitivity to crystalline environment or included impurity ions obs. 2—9223
- glass, Vycor, porous, obs. of O_2 adsorpt., 77K 2—35912
- glass fibre, Gd^{3+} activated, struct. obs. 2—10521
- glycine:Cu^{2+}, e.p.r. of cationic radicals formed by u.v. irradiation at 77K 2—30090
- graphite, natural and pyrolytic, low temp. behaviour 2—4548
- graphitizable substances, low temp. carbonization, mesophase formation 2—9784
- group III-V compound, review 2—33334
- H_3O and D_3O, refutation of reported discovery in e.s.r. studies of u.v. irradiated perchloric acid glasses 2—37054
- halogen atoms, forbidden transitions in gas phase spectra 2—2948
- Heisenberg ferromagnet, two-dimens. spin-1/2, exchange-energy consts. 2—40436
- heterocyclic quinones, spin density distrib. 2—5995
- hexahelicene anion radical, hyperfine coupling constants 2—844
- 1,2,3,6,7,8-hexahydropyrene, monovalent positive and negative ions, EPR spectra 2—18511
- h.f. voltages meas. by e.p.r. 2—27386
- high resolution, new developments review 2—7813
- L-histidine hydrochloride monohydrate:Cu(II), single crystal, lattice position of Cu from e.p.r. 2—36978
- homodyne spectrometer, improvement by filter in leakage branch 2—37861
- hyperfine intractions investigation by discrete r.f. saturation of inhomogeneously broadened lines 2—10473
- hyperfine multiplets, allowed and forbidden transitions, influence of nuclear Zeeman term 2—14343
- imidazole, H-bonded cryst. with protonic conductivity, γ-induced radicals, and ENDOR obs. 2—26293
- iminoxyl biradical solid solns., spin-lattice relax. 2—1731
- 1-indanone, in divene host, optically detected e.s.r. study of lowest n-π^* triplet states 2—24542
- inhomogeneously broadened line, dynamic nuclear polarization enhancement of solid effect 2—36977
- integrated absorpt. depend. on freq. and spin Hamiltonian parameters, non-Kramers doublet 2—26260
- intermolecular cation transfer reactions, e.p.r. studies of mechanism and detection of intermediate triple and quadruplet ions 2—26323
- interstellar dirty ice grains orientation and interstellar magnetic field strength 2—33689
- l.f. e.p.r. spectrometer 2—37859
- line shapes and saturation in slow motional region 2—18394
- line wing saturation, photon cascade 2—40749
- linewidths, Gaussian and Lorentzian broadening 2—22821
- liquid crystal, orientational order and motion 2—15594
- liquid crystals, e.s.r. line shapes of dissolved paramagnetic species 2—9161
- liquids, spin rotational relaxation in one dimension, calc. of angular momentum correlation functions 2—18852
- magnetic layer struct., line broadening due to uniaxial anisotropy 2—22672
- magnetic system of low dimensions, line broadening 2—20130
- malonic acid γ-irrad. cryst., modulation effects in spin-echo of $CH(COOH)_2$ radicals 2—4552
- manganese acetate tetrahydrate, absorpt. and dispersion obs., 16 GHz 2—16647
- manganic dithiocarbamate, paramagnetic molecule 2—5965
- metal, lineshape on localized spins 2—10477
- metal, spin-lattice relaxation, electron level width 2—22822
- metal plates, conduction e.s.r., theory 2—26270
- methyl radical, hyperfine splittings, spin polarization contribution, first order perturbation treatment 2—15404
- 2-methyltetrahydrofuran, γ-irradiated at 4K, e.s.r. study of trapped electrons 2—36995
- 1-methylvinyl radical on silica gel surfaces, temp. effects, h.f. linewidths 2—35358
- molecular cryst., h.f.s. of radicals with tunnelling methyl groups 2—26291
- molecules, pulsed excitation phosphorescence microwave double resonance rel. to intersystem crossing relative rate determination 2—8567
- Mossbauer spectra, hyperfine struct., effect of e.s.r. transitions 2—16429
- naphthalene, optical detection, phosphoresc. dynamics 2—10527
- 2-naphthyl radical, produced by ^3H decay synthesis in naphthalene-d_8 2—10650
- 1,8-naphthyridine, triplet state, microwave and optical detection 2—10490
- nematic mesophase, test of MHD effects in continuum theory 2—35445
- neodymium ethylsulphate, paramagnetic relaxation, Pr^{3+} and Ce^{3+} cross-relaxation 2—26087
- nitrobenzonitriles, electrogenerated radical anions, linewidth effects 2—5985
- 5-nitrouracil, study of iminoxy radical formed by γ-radiation 2—10651
- nitroxide free radicals, coupling constants 2—5984
- nitroxide radical complexes with transition metals, and n.m.r. obs. 2—26376
- nitroxides, photochemically produced, single-crystal e.s.r. studies 2—10643
- one-dimensional mag. systems, spin dynamics 2—40536
- organic binary liquid solution, e.s.r. study of Heisenberg spin exchange near the critical point 2—32276

Paramagnetic resonance and relaxation continued
organic crystal, molecular mobility of free radicals 2—26290
organic radicals in aq. solns., pulse radiolysis and e.p.r. 2—26372
oxyhaemoglobin, nitroxide radical spin labelled, effect of slow rotational motion 2—25106
perfluoromethylcyclohexane, solid, phase transitions 2—1380
perovskite fluorides, doped, first- and second-shell hyperfine interactions 2—20144
peroxylamine disulphonate radical in liquid and frozen media, anisotropic rotational reorientation, e.s.r. study 2—16644
perylene complex, organic semiconductor 2—16218
phenazine-fluorene (anthracene) mixed crystals, influence of deuteration and energy transfer 2—20154
phenyl radicals, matrix-trapped 2—18482
phenyl substituted imidazyl and pyrryl radicals, spin density distrib. determ. from e.s.r. spectra 2—8807
phenylacetylene, single crystal e.p.r. studies of photoexcited states 2—26360
conjugated phenylacetylenes in glasses at 77K, photoexcited triplet state, e.p.r. detection 2—16690
phenyliodoacetylene, e.s.r. obs. of photolytically formed free radical 2—4600
phonon spectroscopy through spin lattice coupling 2—9854
phosphonic acid esters, angular dependence of β-P hyperfine couplings 2—15391
pimelic acid single crystal, secondary processes caused by irradiation studied by e.s.r. technique 2—40835
polumethacrylate, acridine yellow activated, preexcitation effect 2—4499
polyethylene 2,6-naphthalene dicarboxylate, γ-irradiated, e.s.r. identification of trapped radicals 2—30097
polymer, semicrystalline, bond rupture, fracture mechanics 2—15886
polymer fibre, irradiated, straining, crystalline region, radicals 2—15846
polymeric fibres, reaction-rate model for fracture 2—3911
polymers, radicals formed as chains are broken by elongation 2—29292
polymers and liqs.; rot. diffusion and local conc. of radicals meas. 2—30018
polyphenoxy radicals, internal motion and conformation 2—35369
potassium hydrogen malonate, e.s.r. spectra of X-irradiated single crystals 2—20140
powder, line shape and spatial distrib. of line-width 2—36976
pyrene-d_{10}-fluorene mixed crystals, influence of deuteration and energy transfer 2—20154
2- pyridyl and 2-pyrimidinyl radicals, matrix-trapped 2—18482
pyrocarbons, low temp. spectral behaviour 2—10497
pyrrolidino and pyrrolino free radicals 2—18525
quadrupole interaction for cubic imperfections exhibiting dynamic Jahn-Teller effect 2—26259
α-quartz, X-irradiated, e.p.r. of Ti^{3+} centres 2—4543
α-quartz, X-irradiated, e.p.r. studies of Ti^{3+}-H^+ centres 2—22827
quartz dispersion in disintegrator, free radical formation 2—20151
quartz-Fe dispersion, mechano-chemical reactions 2—19988
quinoline and methyl derivatives, free radical obs. 2—8818
radical pairs radiation-produced in organic systems 2—20194
radicals, spin coupling consts. rel. to n.m.r. consts. 2—3026
Raman relaxation times, temp. depend., theory 2—40578
randomly oriented samples, simulation, approx. method 2—26258
rare earth cobalt intermetallics, mag. behaviour 2—10518
rare earth cobalt intermetallics, mag. behaviour 2—10519
rare earth impurities in metals, cond. electron coupling, review 2—4536
relaxation in magnetic resonance, book 2—1720
rubber, bond rupture, fracture mechanics, ozone effect 2—15886
ruby, exchange coupled ion clusters influence on line shape 2—13531
ruby, optically detected $E(^2E)\rightarrow{}^4A_2$ cross relax., detailed investig. 2—40714
ruby, spin Hamiltonian for Cr^{3+} ions in trigonal field 2—10494
ruby maser, e.s.r. transition spectra diagrams for X and K bands, determ. push-pull working point condition 2—11452
S-state ions in variable field config., theory 2—10479
sample orientation, three-axis goniometer 2—30967
sapphire, Fe, Ti doubly doped, study of biparticle formation and valency states after redox reactions 2—25241
saturation, phonon bottle neck in spin-lattice relax. 2—1646
scheelites, radiative paramag. defects obs. 2—13534
semicarbazide, X-irradiated single crystals 2—20141
semiconductor, combined resonance of band carriers, impurity effects 2—22823
signal, analysis of form 2—27372
silica gel γ-irradiated, with adsorbed gas molecules, luminescence and EPR spectra 2—6268
smectic A liquid crystal, molecular ordering, hyperfine splitting, mag. field orientation 2—18853
smoky quartz, impurity colour centres, e.p.r. and thermoluminescence studies, trapped electron dating 2—22226
sodaborate glasses with ZnO, X-irrad., comp. depend. of Zn^+ signal 2—26284
$sodium_2$-pyrazine$^+$, computerized analysis of line-width variations 2—34266
solutions of free radicals and transition metal complexes, spectral line exchange broadening 2—1117
spectrometer, superheterodyne, single klystron, application of serrodyne single sideband generator 2—2315
spectroscopy, conference, Clayton, Australia (1971) 2—8509
spherical harmonics, cartesian differentiation 2—6998
spin Hamiltonian parameter, determ., computational techniques 2—7802
spin system, phase shifted r.f. pulse irradiation, spin echoes and negative time evolution 2—33333
spin systems, quantum kinetic eqns. 2—10476
spin-lattice relaxation, quantum field theoretic analysis 2—29842
spin-phonon avalanche, spatial effects 2—40750
spin-phonon avalanche, spectral diffusion of mag. energy 2—40751
spin-phonon interaction, Fourier shapes of correlative functions 2—22715
spin-resonance absorption, effect of exciton motion, stochastic model 2—22824
spin-spin interactions, cross relaxation effect on dynamic nuclear polarization of protons in polystyrene 2—36997
stilbene anion radical, electron transfer reaction with cis- and trans-stilbene, u.v. study 2—37035
strain effects on coupling const. using dynamic nucl. polarization 2—10533
strontium borate compounds and glasses, e.s.r. of Mn^{2+} 2—16648

Paramagnetic resonance and relaxation continued
styrene radical anions, INDO-MO calculations of hyperfine splittings 2—39008
symmetry top molecules, oblate and prolate, in nematic solvents, spin relaxation 2—22004
taurine, γ- irradiated crystal 2—33344
TCNQ-NMP, metal-insulator transition and antiferromag. obs. 2—19657
temperature gradient effects on e.p.r. line shape and width, applications 2—33332
testosterone acetate, ODMR determination of zero field splitting parameters 2—35352
tetracyanoquinodimethane complexes with different donors, e.p.r. spin echo study of excited triplet states 2—26269
α-tetralone, in divene host, optically detected e.s.r. study of lowest n-π^* triplet states 2—24542
tetramethylethylene adsorbed on zeolites 2—21656
tetraphenylporphine and Zn-tetraphenylporphine, photoreduction, e.p.r. of anion radicals 2—26366
4,4′,4″4‴-tetrasulphophthalocyanines, Cu and vanadyl derivatives, aggregates in solution 2—9163
thulium ethyl sulphate, characterization of defect sites 2—33345
thymidine-5′-monophosphate, after electron irradiation, computer controlled anal. of free radical formation 2—22880
thymine, after electron irradiation, computer controlled anal. of free radical formation 2—22880
TMPD chloranil single crystal, e.p.r. linewidth, ang. dependence 2—36981
triazole, H-bonded cryst. with protonic conductivity, γ-induced radicals, and ENDOR obs 2—26293
triglycine sulphate, γ-irradiated, displacive movement of the radical in ferroelec. and paraelec. phases 2—26268
triglycine sulphate, Cr^{3+} doped, internal elec. field obs. 2—10530
triglycine sulphate and fluoroberyllate, admixture ion obs. 2—10528
trimeric clusters, Heisenberg-Dirac- van Fleck Hamiltonian, spin exchange, e.p.r. theory 2—30017
2,4,5-trimethylbenzyl radical in durene crystals 2—36996
1,3,5-triphenylbenzene anion radical, orbital degeneracy obs. 2—8808
triphenylbenzene triplet dianions, e.s.r. study of photo-oxidation in rigid solution 2—4601
triphenylene triplet dianions, e.s.r. study of photo-oxidation in rigid solution 2—4601
triphenylenes, 2-substituted, excited state reson. interactions 2—35356
triplet states in vitreous matrix, saturation of $\Delta m=1$ lines, anisotropy 2—13545
tris-sarcosine calcium chloride, Mn^{2+} doped, ferroelec. 2—10529
6-undecanol- urea inclusion crystals, X-irradiated 2—20153
unpaired spin number obs. 2—4535
vinyl radical, hyperfine splittings, spin polarization contribution, first order perturbation treatment 2—15404
vinyl radical on silica gel surfaces, temp. effects, h.f. linewidths 2—35358
α-substituted vinyl radicals, electronic structure determ. from e.s.r. spectra and INDO calcs. 2—8712
yttrium ethyl sulphate, ^{3}Ho spin-lattice relax. 2—19936
yttrium ethylsulphate:Dy^{3+}, Orbach processes obs. 2—36982
zeolites, linewidth temp. depend. 2—10478
zeolites, Y, copper exchanged, e.s.r. and i.r. studies of NO adsorption and disproportionation, effect of CO 2—25226
zero field direction lines 2—218
zinc tutton salts, spin-lattice relax. of Cu^{2+} 2—10274
$2MgO.2Al_2O_3.5SiO_2$,Ni, glass 2—30013
Ag atoms on porous glass and silica gel surfaces 2—1163
Ag atoms on porous glass and silica gel surfaces 2—1164
AgBr:Se, with different cationic impurities 2—4537
AgCl:S, paramag. centres, e.s.r. obs. 2—26271
AgCl, correl. with recomb. luminesc., hole self-trapping 2—16604
$Ag^{2+}(4d^9,{}^2D)$, in frozen acid solutions, study of core polarization 2—10481
Al, spin-flip scatt. of cond. electrons from transition metal impurities 2—40753
Al_2O_3-Cr_2O_3, containing 0.01-4.98% Cr, obs. 2—4549
Al_2O_3, γ-irradiated sample, study of holes trapped at Mg^{2+} Li^+ and cation vacancies 2—4538
Al_2O_3, of $3d^2$ ion, elec. field effect 2—13532
Al_2O_3, of Fe^{3+}, linewidth temp. depend., spin-phonon interaction 2—10493
Al_2O_3, pulverized, active centres, thermolum. 2—10522
Al_2O_3, spin-lattice relax. of Cr^{3+}, impurities influence 2—10264
Al_2O_3 corundum, Fe^{2+} effect on electron spin relax. for Fe^{3+} 2—13423
Ar, detection of $^3P_2$ metastable states, in gas phase, lifetime meas. 2—15211
Au:^{167}Er(^{171}Yb), hyperfine splitting parameter 2—26273
Au-Dy dil. alloys, Γ_8 (quartet) resonance obs. 2—26272
Au-Dy dil. alloys, quartet reson. of localized moment 2—40754
B, high temp. reson. line obs. 2—10170
B, low temp. variations of linewidth, relax. time and g-factor 2—30007
BN:C, F-centre, hyperfine splitting, g-factor 2—20131
B_2O_3-SiO film, e.s.r. obs. 2—40324
$BaBiO_3$, room temp. and liq. nitrogen temp. 2—4206
$BaBr_2$, electrolytically coloured, F-centre obs. 2—9600
$BaCl_2$, electrolytically coloured and X-ray irrad., F-centre obs. 2—9600
BaO-SiO_2 glass, γ-irrad., cation conc. and species effects 2—30015
BaO, of Mn^{2+} in trigonal sites 2—13533
BaO, point defects obs. 2—6478
BaO(S):Eu^{2+} dil. solid solns., linewidths and exchange interaction 2—7118
$BaSO_4$, pulverized, active centres, thermolum. 2—10522
$BaTiO_3$ ceramic, oxidation and reduction by O_2 plasma, F-centre formation 2—13576
BeD, ESR spectra meas. for ground state in solid Ar matrices, determ. hyperfine interaction and chemical bonding 2—15287
BeD, ESR spectra meas. for ground state in solid Ar matrices, determ. hyperfine interaction and chemical bonding 2—15287
BeF_2 glasses, of transition metal ions 2—10496
BeH, ESR spectra meas. for ground state in solid Ar matrices, determ. hyperfine interaction and chemical bonding 2—15287
C, pyrolytic, g anisotropy 2—22829
C amorphous, adsorption of paramagnetic O_2 and NO gases 2—6378
C fibre, structure and other electronic props. obs. 2—6289
CH_3 radical, random motion and relax. in crysts. 2—26373
$CH_2CO_2^-$ radical, random motion and relax. in crysts. 2—26373
Ca:Eu^{2+}, 5-30K, 35 GHz and 9 GHz 2—30003
CaF_2:Eu^{2+}, spin-lattice relaxation 2—22830
CaF_2:Fe^{3+}, cubic symmetry, spin parameters 2—1727
CaF_2:U^{3+}, discrete saturation spectrum, hyperfine interactions 2—30008

Paramagnetic resonance and relaxation continued

- CaF_2, containing ion pairs of Gd, Ce, Pr with H, D, T electron-phonon interactions 2—10499
- $CaO:Mn^{2+}$, isotropic exchange interaction, exchange striction 2—20146
- CaO, $[Na]^0$ and $[Li]^0$ centre obs. 2—33257
- CaO, of Ni^{2+}, linewidth ang. variation 2—7116
- $CaO(S):Eu^{2+}$ dil. solid solns., linewidths and exchange interaction 2—7118
- $CaS:Mn^{2+}$, cubic field splitting detn. 2—20132
- $CaWO_4$, neutron irradiated, point defects obs. 2—6478
- $CaWO_4$, neutron irradiated, $S=3/2$ defect obs. 2—20133
- $CaWO_4$, of $3d^2$ ion, elec. field effect 2—13532
- $Cd(BrO_2).H_2O$, γ-irradiated, free radicals, g-factors 2—10517
- $CdCl_2:Fe(II)$, determ. of strength of trigonal crystal field relative to spin-orbit coupling parameter, hence magnetic properties of $FeCl_2$ 2—1724
- $CdCl_2:Mn^{2+}$, zero field splitting temp. depend. 2—7117
- $CdF_2:Eu^{2+}$,77 to 300 K, 9 and 35 GHz, superhyperfine structure 2—1725
- $CdGa_2S_4$, of Mn^{2+}, spin Hamiltonian 2—10503
- $Cd_xHg_{1-x}Te$ mixed cryst., of Mn^{2+}, spectral parameters 2—13537
- $CdIn_2S_4$, zero-field splittings of Cr^{3+} 2—10501
- $Cd_{1-x}Mg_xTe:Mn^{2+}$, hyperfine interaction consts., g-factors, crystalline field consts. 2—26261
- $CdS:Mn^{2+}$, linear elec. field effect 2—22831
- $CdS:Ni^+$, g-factor and hyperfine struct. 2—30016
- $CdS:Ti^{2+}$, spin echo obs. 2—10500
- $CdS:Ti^{3+}$, 27 K 2—26275
- CdS-MnS coprecipitate 2—40762
- CdS, N_2 and lattice defect centres due to ion implantation 2—15774
- CdS, of $Fe^{3+}:Ag^{3+}$ associated centres 2—33338
- CdS, spin Hamiltonian for Cr^{2+} 2—13536
- n-CdS implantation of N ions, defect centres obs. 2—25422
- $CdS_{1-x}S_x$, mixed cryst., of Mn^{2+}, elec. effects 2—26276
- $CdS_{1-x}Te_x$, mixed cryst., of Mn^{2+}, elec. effects 2—26276
- $CdTe:Co^{2+}$, super-h.f.s., Koster-Statz effect 2—10502
- CdTe:Cu(Ga)(In), detector mat. evaluation 2—36539
- $Cd_{1-x}Zn_xS$, mixed cryst., of Mn^{2+}, elec. effects 2—26276
- CeO_2, spin-lattice interaction for Gd^{3+}, temp. depend. 2—26277
- $^{35}ClO(^2\pi_{3/2})$, $J=5/2$ and 3/2 rotational levels, hyperfine interactions in gas-phase EPR spectra 2—18413
- Cr(III) complexes with intramolecular exchange 2—8609
- Cs forbidden transitions in gas phase spectra 2—35169
- Cs_2HfCl_6, Nb^{4+} spectra, 4.2-77 K 2—4539
- $CsMnCl_32H_2O$, short range order effects 2—20148
- $CsMnCl_3.2H_2O$, linewidth anisotropy, spin correls. 2—40757
- CsN_3, photoinduced defect associated with an impurity, e.s.r. study 2—22825
- $CsPbCl_3$, of Gd^{3+}, phase transition obs. 2—12994
- Cs_2SO_4 single crystals, Mn^{2+} e.p.r. spectrum 2—4540
- $CsTi(SO_4)_212H_2O$ and deuterated system, g-values, Jahn-Teller effect 2—10288
- Cs_2ZrCl_6, W^{5+} and Mo^{5+} spectra, 4.2-77 K 2—4539
- Cu-Mn alloy, cond. electron loss effects 2—22832
- Cu (II) complex, binuclear chelate of ethylene glycol-bis (β aminoethylether) tetraacetic acid 2—9164
- Cu complex, copper (II) porphrins, dimeric, e.s.r. study of metal ion separation 2—18418
- Cu complex, powdered, e.s.r. lineshapes 2—40758
- Cu complexes, Cu(II)-amino acid complexes, e.p.r. spectra 2—10482
- Cu complexes, e.s.r. and optical absorption studies 2—7069
- Cu complexes, $M_2[M'Cu](NO_2)_6$ type, cooperative Jahn-Teller effect obs. 2—19943
- Cu complexes in soln., hyperfine coupling consts. and g-factor temp. depend. 2—25112
- Cu^{2+}, in complex halide, tetrahedral coordination 2—20134
- Cu^{2+} complexes with diethyldithiocarbamate and diethyldithiophosphate, ligand props. 2—24450
- Cu(II) complex, different symmetry axes for fine structure term and g-factor 2—10504
- Cu(II) complex, mixed ligand chelate, hyperfine splitting 2—36668
- Cu(II) complexes, ligand exchange influence 2—13538
- Cu(II) complexes with intramolecular exchange 2—8609
- Cu(II) morpholinebiguanide coord. cpds., bond covalence degree 2—26278
- $Cu(NH_3)_4(NO_3)_2$ in soln., e.p.r. study 2—21599
- Eu, Neel pt. phenomena, excitation of helical mag. struct. 2—40759
- FCl, radio frequency, spectrum obs., hyperfine parameters and dipole moment 2—8614
- Fe(III) complexes with intramolecular exchange 2—8609
- Fe(III) cpds. in ethylene glycol, liq. and frozen, τ_1 obs., structural determ. 2—12582
- $Fe(NH_4SO_4)_2.6H_2O:Cu^{2+}$, quadrupole hyperfine anisotropy obs. and mag. susceptibility 2—36843
- GaAs, doped, isotropic spectrum h.f.s., forbidden doublets 2—10505
- GaP, dynamical Jahn- Teller interaction effects on e.p.r. of shallow acceptors 2—7119
- Gd, microwave mag.-transmission reson. 2—36969
- $GdAl_2$, magnetization, Curie temp. 2—26040
- $GdNi_5$ mag. interactions obs. 2—16346
- $GdNi_x$, Gd_2Ni_7, $x=1$, 2, 3, 5, and susceptibility obs., temp. depend. 2—10506
- Ge:As, heavily doped, cond. electron spin relax. obs. 2—20135
- n-Ge:As, line profile distortion of donor electrons, 4.2 K 2—22833
- Ge:As, over wide impurity conc. range, line narrowing 2—26279
- Ge, from clean surfaces, surface energy states 2—30009
- GeO_2, of Mo^{5+}, A-tensor, charge compensation 2—33339
- GeO_2, pulverized, active centres, thermolum. 2—10522
- GeTe:Mn e.s.r. Lorentzian shaped lines, corrections to meas. of line width and resonance field 2—36975
- H radicals in flame 2—26342
- HCO radical, microwave absorpt. spectra, rotational transition 2—8720
- HgTe, HgSe, and mixed cpds., of Mn^{2+}, rel. to bonding 2—26280
- N-InSb, heavily doped, cond. electron spin relax. obs. 2—20135
- n-InSb line profile distortion of donor electrons, 4.2 K 2—22833
- InSe, press. and temp. induced phase 2—22156
- K complex, $K_2MCu(NO_2)_6$, (M=Ba, Pb), rel. to Jahn-Teller distortions 2—36988
- $KBr(I):M^{2+}$, M=Zn, Cd, reactions, coloration, spectra 2—19125
- $KCl:Eu^{2+}$, Z_l and Z_2 centres, optical absorpt. and e.p.r. obs. at 77K 2—36066
- KCl, $F_A(Li)$ centre spin lattice relaxation, 4.2K 2—10507
- KCl, F′- to F-conversion, thermal kinetics 2—1263

Paramagnetic resonance and relaxation continued

- KCl, off-centre behaviour of paramag. atom due to covalency 2—10509
- $KClO_3$, study of O_3- radical obtained by X-irradiation, trapping at 3 different sites 2—10484
- $KF.2(4)H_2O$, e.p.r. spectra, colour centres, 77K 2—1264
- KH_2AsO_4 and KD_2AsO_4, proton-lattice coupled mode obs. 2—19376
- $KH_2PO_4:Cr^{3+}$, effects of uniaxial stress and elec. fields 2—33340
- KI:Pd, hyperfine struct. 2—4541
- KIO_2F_2 γ-irrad. cryst., e.s.r. of IO_2F^- radical 2—20142
- $KMgF_3:V^{2+}$, covalent spin transfer obs. 2—20143
- $K_2Mg_2(SO_4)_3:Mn^{2+}$, ang. depend. of resonance lines 2—36987
- $KMnF_3$:Mg, linewidth decrease due to doping 2—10508
- $KMnF_3$, doped, first- and second-shell hyperfine interactions 2—20144
- $KN_3:KNO_2:KNO_3$, study of NO_2 and $NO_2{}^{2-}$ paramagnetic centers formed by irradiation of $NO_2{}^-$ and $NO_3{}^-$ 2—10483
- $K_2PbCu(No_2)_6$, cooperative distortion due to Jahn-Teller instability 2—15967
- $K_2SO_4:Cu^{2+}(Mn^{2+})$, hyperfine interactions, phase transition 2—9815
- K_2SO_4, irrad., SO_4 radical obs. 2—26375
- K_2SO_4, of Cd^+ in $^2S_{1/2}$ state 2—7120
- $K_2SeO_4:Cu^{2+}$, rel. to phase transitions 2—33341
- $KZnF_3$:Fe, Fe^{3+} (K^+ vacancy) centre obs. 2—36986
- $KZn(SO_4)_2.6H_2O:Cu^{2+}$, obs. of ^{17}O superhyperfine interaction, hyperfine tensor 2—26262
- $K_2Zn(SO_4)_2.6H_2O$, of Cu^{2+}, temp. and irrad. influence 2—13539
- $La_2Mg_3(NO_3)_{12}:Ce^{3+}$, conc. depend. Orbach relax. rates 2—10266
- $La_2Mg_3(NO_3)_{12}:Ce^{3+}$, phonon bottleneck and cross-relax. 2—10268
- $La_2Mg_3(NO_3)_{12}:Ni^{2+}$, spin-lattice relax. and phonon bottleneck 2—10267
- $La_2Mg_3(NO_3)_{12}$, of Pr^{3+}, spin lattice relax. 2—26080
- LaP, of Gd, cond. electron effects 2—40760
- Li dil. alloys, g-shift from conduction e.s.r. obs. 2—26281
- Li fine particles, relax. of cond. electron spins, size effect 2—20145
- $Li_2B_4O_7$ glass, thermoluminesc. processes, trapping centres, e.s.r. obs. 2—29976
- $LiF:Mn^{2+}$, 35 GHz, two kinds of centres 2—36989
- LiF, neutron irrad. defect obs., 77 K 2—13540
- $LiNbO_3:Cu^{2+}$, spectra at room temp., 77 K and 4.2 K 2—36990
- $LiNbO_3:Fe^{3+}$, e.p.r. investigation of crystal field parameters 2—30010
- $LiNbO_3:Gd^{3+}$, ferroelectric, e.p.r. of Gd^{3+} 2—10485
- $LiNbO_3$, of Fe^{3+} and Mn^{2+}, axial site obs. 2—30011
- $Li_2SO_4.H_2O$, irrad., SO_4 radical obs. 2—26375
- $LiVo_3$, of Mn^{2+}, n.m.r. comparison 2—10565
- Mg-Gd dil. alloy, effective exchange integral sign 2—16646
- Mg-Mn dil. alloys, interpret. rel. to relax. bottleneck theory 2—40761
- Mg, effects of surface oxide and nitride layers on cond. elec. spin resonance 2—33335
- $MgBrO_3.6H_2O$, γ-irradiated, free radicals, g-factors 2—10517
- MgF_2, F-centre obs. 2—19129
- MgF_2, F-centre obs. 2—19128
- $MgMn_2O_4$ spinel, line narrowing rel. to Mn_2O_3 2—30012
- $MgO:Mn^{2+}$, isotropic exchange interaction, exchange striction 2—20146
- $MgO:Mn^{2+}$ powder, defect effects 2—6479
- $MgO:Rh^{2+}(Pd^{3+})$, Jahn- Teller effect obs. 2—7121
- $MgO:V^{2+}$, Cr^{3+}, evidence for large amplitude localised vibrations from e.p.r. relaxation 2—30004
- MgO-Mn(Ni)O solid solns., lineshape evolution 2—1728
- MgO single crystal, e.s.r. study of ^{17}O hyperfine interaction of V_f center 2—13528
- MgO single crystals, e.s.r. 4d and 5d ions 2—4542
- MgTe, of Mn^{2+}, cryst. field parameters 2—13541
- Mn complex, $(CH_3)_4$ $NMnCl_3$, short range order effects 2—20148
- Mn II ions in solution, calc. of e.s.r. spectra 2—22005
- Mn^{2+}, impurity in newberyite, mag. complexes 2—26282
- Mn^{2+}, in polycryst. sample, spectra calc. 2—36979
- $MnCl_2.4H_2O$, absorpt. and dispersion obs., 16 GHz 2—16647
- $MnCl_2.4H_2O$ in DMF and DMA solutions 2—39391
- MnF_2, linewidth behaviour, diploar interaction and mag. lattice symmetry interplay 2—10510
- MnO_2, Hertzian Cotton-Mouton-VOigt effect 2—26283
- $MnSO_4.H_2O$, absorpt. and dispersion obs., 16 GHz 2—16647
- MoS_2:Nb, band structure investigation 2—32883
- N free radicals, coupling consts. determ. 2—26374
- $N_4{}^-$, molecular orbital calculation of contact hyperfine interaction, comparison with e.p.r. spectra 2—21629
- $NH_3{}^+$ radical, random motion and relax. in crysts. 2—26373
- N_2H_4 cation radicals 2—31810
- $NH_4Al(SO_4)_2$:Fe, e.s.r. spectrum obs. 2—7115
- NH_4Br:Pb(Sn,Cu,In), phosphor 2—1710
- NH_4Cl:Pb(Sn,Cu,In), phosphor 2—1710
- NH_4F, of Cu^{2+}, tetrahedral site obs. 2—20149
- $NH_4H_2AsO_4$, proton-lattice coupled mode obs. 2—19376
- $NH_4H_2PO_4$-(5wt%)KH_2PO_4 crystal, γ-irrad., $NH_3{}^+$ hyperfine coupling 2—10511
- $(NH_4)_2SO_4.Ga_2(SO_4)_3.24H_2O$, of Cr^{3+}, satellite line obs. 2—10512
- NO from u.v. irradiation of alkali azides 2—12182
- NO radicals, viscous medium, rotational correlation time calc. from e.s.r. calcs. 2—8686
- NO_2 impurity in KCl, hindered rotation at 2°K 2—15322
- $N(SO_3)_2{}^{2-}$, reorientational motion, e.s.r. study 2—22826
- $NaBr:Cr^+$, superhyperfine and quadrupole interactions 2—20170
- $NaBr(Cl):M^{2+}$, (M=Ba, Ca, Sr), irrad. type effects on symmetry of paramagnetic centres 2—26285
- $NaBrO_3$, γ-irradiated, free radicals, g-factors 2—10517
- $NaCl:Cr^+$, superhyperfine and quadrupole interactions 2—20170
- NaCl:Cu, new paramag. centre obs. 2—36980
- $NaCl:Cu^{2+}$, centres rel. to Cu^{2+} conc. 2—7123
- $NaCl:Fe^{3+}$, lines due to Fe_2O_3 agglomerates 2—10515
- $NaCl:Mn^{2+}$, neutral Mn centres 2—39716
- $NaCl:Mn^{2+}$, off-centre site obs. 2—10513
- NaCl, doped, trapped-hole centre parameters 2—10516
- NaCl, local defects study 2—16649
- NaCl, of Mn^{2+}, stress effects on ground state splitting 2—13542
- $NaF:Cr^+$, superhyperfine and quadrupole interactions 2—20170
- $NaH_3(SeO_3)_2$, external stress effects on unstable orientation 2—10514
- 2 $(Na_2Mg(SO_4)_2.4H_2O$, of Mn^{2+} impurities, hyperfine parameters, g 2—20136
- Na_2O-B_2O_3-Al_2O_3- SiO_2 and Na_2O-B_2O_3-Al_2O_3-Sb_2O_3-SiO_2 glasses, structure studies with e.p.r. 2—40679
- NaOH ice, resolution enhanced ESR spectra of trapped electrons, determ. hyperfine coupling const. and relax. characteristics 2—16645

Paramagnetic resonance and relaxation continued
Na_2SO_4, irrad., SO_4 radical obs. 2—26375
$NaVo_3$, of Mn^{2+}, n.m.r. comparison 2—10565
$Na_2Zn(SO_4)_2.4H_2O:Cu^{2+}$, elec. field symmetry, g-factors, hyperfine constants 2—7122
Ni complex, $(n\text{-}C_4H_9)_4N.NiS_4C_4(CN_4)$, in n-butanol and $CHCl_3$ 2—9166
Ni complex, α-bis(thiosemicarbazide) Ni(II) $SO_4.3H_2O$, Cu(II) doped, covalent bonding 2—26286
Ni complex $[TMPD^+]_2$ $[Ni(mnt)_2]^{2-}$, triplet exciton e.p.r. and structure 2—30005
Ni complexes, $M_2[M'NI](NO_2)_6$ type, cooperative Jahn-Teller effect obs. 2—19943
O^-, adsorbed on MgO, e.s.r. study of species formed in reactions with O_2, CO and ethylene 2—4578
O_3^-, on MgO, e.p.r. spectrum rel. to verification of formation 2—26263
$O_2(^1\Delta_g)+SO(^3\Sigma^-)\rightarrow SO(^1\Delta)+O_2(^3\Sigma_g^-)$, kinetic study, meas. of absolute rate constant 2—10612
$P_2O_5\text{-}Al_2O_3\text{-}Cs_2O:Cu(II)$ glass, struct., comp. depend. 2—18899
$P_2O_5\text{-}B_2O_3\text{-}Cs_2O$ glass, containing Cu^{2+}, struct. determ. 2—28976
$POCl_{3\odot}^-$, evidence for formation in γ-irradiated $POCl_3$ 2—821
$PbBr_2:Eu^{2+}$, spin Hamiltonian parameters detn. 2—33342
Pd-Er dilute alloy, g shift, rel. to host metal susceptibility 2—30014
Pd, of Dy^{3+}, weak h.f.s., ion ground state 2—33343
PdH(D), $^2\Sigma^+$ ground state, bonding nature, hyperfine coupling and g tensor components 2—12189
Pt-Er dilute alloy, g shift, rel. to host metal susceptibility 2—30014
Rb forbidden transitions in gas phase spectra 2—35169
$RbMnF_3$, linewidth behaviour, dipolar interaction and mag. lattice symmetry interplay 2—10510
RbN_3, X-irrad., trapped N atom obs. 2—22834
Rh, hyperfine splitting of Dy and Er localized moments 2—10520
$SO(^1\Delta)\rightarrow SO(^3\Sigma^-)$, study of decay mechanism at reactions vessel walls 2—10612
$SO(^3\Sigma^-)$, determ. of absolute conc. by gas phase e.p.r. using NO calibrant gas 2—10604
Se atoms in gas phase, e.s.r. spectrum, calc. of g-values including configuration interaction effects 2—24349
n-Si:P, absolute spin susceptibilities, impurity scatt. spin relax. 2—22835
Si:P, exchange coupling in donor atomic clusters 2—20150
Si:P, heavily doped, cond. electron spin relax. obs. 2—20135
Si:P ion implanted, divacancy radiation damage obs. 2—26265
p-Si:Zn, P, hyperfine splitting, hole-moment interaction 2—13543
$Si\text{-}SiO_2$, surface electron transport in m.o.s.f.e.t. and m.o.s. devices, paramag. centre effects 2—10095
Si, detection of optically induced divacancy 2—40764
Si, from clean surfaces, surface energy states 2—30009
Si, ion-implanted, ^{17}O h.f.s. of neutral vacancy-oxygen centre 2—40765
Si, ion implanted, paramag. defect inventory 2—26264
Si single crystal with ion implanted Sb, e.s.r. observation of defects produced 2—29191
SiC:N, discrete saturation of reson. lines 2—7124
SiC irrad., deffects obs. 2—1729
SiF_3 radical, hyperfine parameters 2—21642
$SiHF_2$ radical, hyperfine parameters 2—21642
SiH_2F radical, hyperfine parameters 2—21642
SiO_x, reactively evaporated film, spin density meas., electrical conduction props. 2—1726
$SmS:Eu^{2+}$, $Eu^{2+}\text{—}Sm^{2+}$ exchange interaction obs. 2—4544
SmS(Se)(Te), exchange interactions 2—36669
SmS(Se)(Te), of Eu^{2+} and Mn^{2+}, exchange interaction contribs. 2—36991
$SmSe:Eu^{2+}$, $Eu^{2+}\text{-}Sm^{2+}$ exchange interaction obs. 2—4544
$SmTe:Eu^{2+},Mn^{2+}$, $Eu^{2+}\text{—}Sm^{2+}$ and $Mn^{2+}\text{—}Sm^{2+}$ exchange interaction obs. 2—4544
$SnO_2:Fe^{3+}$, spin Hamiltonian parameter determ. 2—22847
SnO_2, pulverized, active centres, thermolum. 2—10522
$SrCl_2:Yb^{3+}$, cryst. field energies 2—36888
$SrCl_2$, alkali metal doped, colour centres obs. 2—3800
$SrCl_2$, F-centres obs. 2—33336
SrF_2, containing ion pairs of Gd, Ce, Pr with H, D, T electron-phonon interactions 2—10499
SrF_2, stress-induced g-shifts of Nd^{3+} and U^{3+}, freq. independ. 2—10524
$SrMoO_4:Gd^{3+}$, tetragonal active centre obs. 2—10523
$Sr_2Ni_xAl_{1-x}SbO_6$, solids solns., low-spin electron config. of Ni^{3+} 2—13378
$SrO:^{55}Mn^{2+}$, and ENDOR obs., hyperfine struct. 2—26287
$SrO\text{-}SiO_2$ glass, γ-irrad., cation conc. and species effects 2—30015
$SrO(S):Eu^{2+}$ dil. solid solns., linewidths and exchange interaction 2—7118
$SrTiO_3:Mn$, effect of annealing treatment 2—36992
$SrTiO_3$, Fe^{3+}- vacancy centre analysis 2—40766
$SrTiO_3$, fluctuations and correlations for $T \geqslant T_c$ 2—26266
$SrTiO_3$, phase transitions, critical dynamics for $T \geqslant T_c$ 2—25932
$SrTiO_3$ single crystals, Cr doped, e.s.r. of Cr^{5+} 2—20138
$TRO_2:^{237}Np^{4+}$, studies on strained and unstrained crystals, electronic state, of Np determ. 2—10486
Th, of rare earth ions, linewidth temp. depend., exchange coupling 2—20152
ThO_2, of $^{155}Gd^{3+}$, h.f.s. forbidden lines 2—13544
ThO_2, of $^{155}Gd^{3+}$, h.f.s. 2—26288
ThO_2, spin-lattice interaction for Gd^{3+}, temp. depend. 2—26277
TiO_2, e.s.r. and molecular adsorption, simultaneous investigation 2—10487
TiO_2, rutile, of Co^{2+}, impurity-vacancy assoc. 2—16650
TiO_2, rutile, of Co^{2+}, impurity-interstitial assoc. 2—16651
Ti_xO_{2x-1} system, mag. prop. obs. 2—36993
V complex vanadyl porphyrins, e.s.r. study of metal ion separation 2—18418
$V_2O_5:Cr^{3+}$, spin Hamiltonian parameters detn. 2—4545
$VO_2:Ti$, conduction band and impurity state electron lifetime, line broadening obs. 2—10037
$V_2O_5\text{-}P_2O_5$ glass, of V^{4+}, rel. to polar cond. and i.r. absorp. 2—10039
VO complexes in soln., hyperfine coupling consts. and g-factor temp. depend. 2—25112
VO_2^{2+} complexes with diethyldithiocarbamate and diethyldithiophosphate, ligand props. 2—24450
V_2O_5, doped, e.s.r. spectrum, motional narrowing 2—22828
Xe flash lamp for e.p.r. kinetic studies, pulse transmitted by silica light pipe 2—23716
Y:Gd, obs. of anisotropies in linewidth and resonance fields due to crystal field effects 2—4546
$YAG:Cr^{2+}$, rel. to recombination excitaton mechanism for X-ray and thermoluminesc. 2—40725
$YAlO_3:Cr^{3+}$, $EuAlO_3:Cr^{3+}$ comparison, exchange interactions 2—7125

Paramagnetic resonance and relaxation continued
$YAsO_4:Dy^{3+}$, Er^{3+}, ground doublet excited doublet transitions, relax. at liq. He temp. 2—10488
$YAsO_4:Dy^{3+}$, low lying ground level doublets obs. 2—33337
$YVO_4:Dy^{3+}$, Er^{3+}, ground doublet excited doublet transitions, relax. at liq. He temp. 2—10488
$Yb:Eu^{2+}$, 5-30K, 35 GHz and 9 GHz 2—30003
$Yb:Eu^{2+}$, dynamical effects, Ca impurity effect 2—22836
$YbCl_3.6H_2O$, relax. temp. depend., Mossbauer obs. 2—10273
$Yb_2(SO_4)_3.8H_2O$, relax. temp. depend., Mossbauer obs. 2—10273
$Zn(BrO_3).6H_2O$, γ-irradiated, free radicals, g-factors 2—10517
$ZnF_2:Fe^{2+}$, mag. dipole active lines 2—40555
$ZnGa_2O_4$, zero-field splittings of Cr^{3+} 2—10501
$ZnO:V^{2+}$, e.s.r. spectrum meas. at low temperature 2—25415
ZnO, surface Fermi level anchoring by chemisorbed species 2—4228
ZnO(Se), of Mn^{2+}, elec. field effect, piezoelec. and axial distortions influence 2—22837
$ZnS:Mn^{2+}$, axial impurity site obs. 2—26289
$ZnS:Ni^+$, g-factor and hyperfine struct. 2—30016
ZnS, additively coloured, F-centre stability obs. 2—19132
ZnS, of Cr^+, elec. field effect, piezoelec. and axial distortions influence 2—22837
$ZnSeO_4.6H_2O$, hydrated Ni^{2+}, Co^{2+} and Cu^{2+} ions, axial spin hamiltonian 2—10525
$ZnWO_4$, of Cr^{3+} and Mn^{2+}, linewidth temp. depend., spin-phonon interaction 2—10493
$ZnWO_4$ of Co^{2+} pairs 2—1730
measurement
aqueous sample cells for e.p.r., design considerations 2—37860
autodyne spectrometer with maser as oscillator 2—11404
cavity resonator for 8 mm. band with sample changing at liquid He temperatures 2—34265
computerized analysis of line-width variations 2—34266
c.w. saturation technique, electron spin-lattice relaxation of benzene anion radical in liquid solution 2—35787
e.p.r. magnetometers comparator for meas. of gyromagnetic ratio of free radicals 2—28261
EPR signals recording, applied methods, survey 2—217
g-factor, standard, for e.p.r., use of charred dextrose 2—7126
Hall probe magnetic field measurement, accuracy improvement 2—27369
hexamethyldisiloxine, polymerized thin film, e.p.r. spectra 2—3550
line narrowing due to automatic freq. control device 2—7800
optical detection of e.p.r. in solids at frequencies about 10 GHz 2—37858
polar solvents, special containing vessel made from high-pressure polyethylene 2—37523
signal dispersion meas. as method for meas. of static magnetic susceptibility 2—11431
spectrometer, automatic magnetic field calibrator 2—34264
spectrometer, high-sensitivity, design and assembly 2—34267
spectrometer, low/high power, resonance meas. to 0.5 W, saturation to 20 W 2—5303
spectrometer, modification for study of substances under hydrostatic pressure 2—27370
spectrometer, modifications for studies on solid samples at high hydrostatic pressures 2—27371
spectrometer, with Gunn-diode sitting in tunable re-entrant cavity 2—5300
spectrometer, with u.s. modulation, longit. strain modulations below 10^{-4} 2—5308
spectroscopy, signal detect., bimodal spin induction method 2—5301
spin conc. determ. by numerical double integration, error calcs. 2—30966
spin echo technique for broad line obs. 2—7798
strain modulation using sample in composite oscillator 2—7801
vinyltrimethylsilane, polymerized thin film, e.p.r. spectra 2—3550
Walsh-Rupp spectrometer modification for low-temp. ferromag. resonance meas. 2—27374
$Ca_5(PO_4)_3Cl:CrO^{3-}{}_4$, single crystals, at liquid helium temps. spectra, spin-Hamiltonian parameters 2—4550
Ge, amorphous, film, rel. to ageing process 2—4551

Paramagnetism
see also Magnetic properties of substances/paramagnetic
collective, deviation from ideal magnetization curve 2—6944
Curie temperature, classical-spin biquadratic exchange 2—19870
Heiseberg ferromagnet, decoupling scheme 2—36663
Heisenberg magnet, modified Callan decoupling in Green's function analysis 2—10184
Heisenberg magnet, one-dimensional, relaxation shape function 2—29799
Heisenberg magnet, spectral density moments, diagrammatic expansion 2—10169
Heisenberg model, transport coeff. calc. 2—36664
Heisenberg three dimensional ferromagnet Green's function decoupling approx. critical point exponents 2—26008
Hubbard's Hamiltonian using alloy analogy 2—6943
Hubbard model, localized moments form. 2—36399
Hubbard model, mag. order 2—40426
Hubbard model, tenfold d-electron degeneracy, para-ferromag. transition in transition metals 2—36676
isolated paramagnetic spin system, nonlinear response 2—20871
macromolecules with conjugated C=C bonds 2—35362
self-trapped paramagnetic spin polaron 2—22472
short range order paramagnet, neutron scatt., modified convolution approx. model 2—33112
solvents, susceptibilities determ. from proton shifts in n.m.r. 2—6247
spin-spin relaxation theory, relax. time, asymptotic value, and invariants of motion 2—26075
superconductor, Pauli spin effects on fluctuation-induced diamag. 2—25778
two magnon Raman scattering, at finite temps. 2—16516

Parametric amplifiers *see Amplifiers*

Parent *see Nucleus; Radioactivity*

Parity
see also individual particles, e.g. Mesons/spin and parity
baryons, duality formulation of parity-change rule 2—5550
spherical stellar systems, halo, random gravitational encounters 2—33639
strong interactions, parity violation, theory 2—17811

Particle accelerators
see also Ion beams
application in atomic spectroscopy 2—574
cavity, mechanical tolerances and h.f. loss distrib. rel. to e.m. field meas. 2—5608

Particle accelerators continued
characteristics and constraints within which they operate 2—27920
charged, with single or multimode operation, patent 2—18057
charged particle acceleration by nonstationary electric fields in magnetosphere 2—22989
circular, synchrotron radiation, coherent, model 2—372
closed electron drift plasma accelerator, with extended acceleration region 2—21813
collective, mag. field formation for electron-ion ring extraction 2—14800
collective effect accelerators 2—38416
collective heavy ion, transverse electron ring 2—14805
collective ion, research uses and applications to energy conversion 2—24259
collective ion, with transverse motion of electron ring 2—34863
computer controls, state of art and future development 2—14888
cylindrical cavity with H_{111} standing waves in axial magnetic field 2—21344
development of machines for yielding high resolution protons and deuterons at energies up to 40 MeV electrostatic and cyclotrons 2—38397
distortion of beams phase space volume configuration by nonlinear Coulomb forces 2—14795
dose and induced activity distrib., external proton beam targets 2—2878
dose distrib. of fast neutrons, in concrete labyrinth 2—2875
electron, problems in using polarized targets for electrons and muons 2—34767
electron, recycled, intensity limits and beam quality 2—14821
electron beams in circular cylindrical superconducting cavity 2—5615
electron bunch phase velocity, collective effects 2—5607
electron ring, Berkeley, stabilization of negative mass instability 2—14796
electron ring, betatron amplitude growth upon traversing resonances during the compression cycle 2—11689
electron ring, collective radial instabilities, enhancement of Landau-damping coefficients 2—14803
electron ring, cylindrical beam obs. 2—14841
electron ring, Erevan, meas. and monitoring of spatial characteristics of external beams 2—31401
electron ring, high current electron sources 2—14892
electron ring, ion loaded, mag. expansion self field effects 2—14804
electron ring, Karslruhe, status 2—14798
electron ring, static field, ion loading and acceleration 2—34862
electron ring accelerator, Gosching 2—14797
electron ring compressor design, implications of eddy currents for Landau-damping coefficients 2—14802
electron ring instabilities in waveguide 2—14801
electron rings for heavy ion acceleration 2—34848
electron-ion rings, resonant coupling of transversal oscillations due to polarization 2—14735
e.m. field distribution due to a beam-excited re-entrant cylindrical cavity mounted coaxially with a vacuum chamber 2—17471
e.m. impulse determ. of electron concentration using quadratic Stark effect 2—2653
environmental radiation and radioactivity from CERN high energy accelerators 2—2865
European 300 GeV Programme 2—14788
focusing action of microwave field on electron beam during capture in acceleration mode of cyclic accelerator 2—31392
heavy ion, applications in atomic physics 2—11932
heavy ion, design and research, review 2—34841
heavy ion, survey 2—5604
heavy ion, use in production of super-heavy nuclei 2—11696
heavy ion scattering to produce super heavy nuclei with $A>250$ 2—11697
heavy ions, acceleration by intense electron beams 2—34846
heavy ions from laser-produced metallic plasma subjected to high electric field 2—34843
high energy, conference, Geneva 1971 2—14787
intersecting, storage, 200 GeV, design using superconducting magnets 2—14836
ion implantation facility 2—39709
ion implantation machines, review 2—32546
ion implantation machines, review 2—32545
ions, acceleration by intense electron beams, collective ion acceleration model 2—34845
ions, by relativistic electron beams 2—34844
medical and industrial use 2—14786
multiple stage, heavy ion, charge exchange 2—5606
multiply charged heavy ions, conference (Gatlinburg, Tenn., USA, 1971) 2—34330
neutron leakage through penetrations in hadron shields 2—2874
neutron propagation in high energy proton accelerator access tunnels 2—2876
orbital, proton beams, neutralisation by slow electrons 2—2655
orbital, self-focussing of particles 2—14813
Pierce column, 750 keV exact, H^+ ion source, duoplasmatron feeding 2—8245
plasma, inductive-impulsive, current sheet structure 2—32011
plasma, quasi continuous inductive accelerator with standing r.f. waves 2—32015
plasma, simple unipolar pulsed 2—21793
proton-antiproton colliding beams, production and electron cooling 2—14790
protons, shielding, high energy muon transport 2—2870
pulsars, effect of near fields 2—41151
resonant instability of nonlinear oscillations, finite difference eqn. representation 2—14794
r.f. superconductivity applications 2—14789
Saturne, 750 keV preinjector beam, density distrib. obs. 2—8244
security systems, radiation accident prevention 2—2866
shielding, comparison of expt. data with Monte Carlo calcs. 2—2879
shielding and safety practices, dose rate monitoring 2—2884
shields, cascaded produced by high energy incident particles, mathematical model 2—2872
shields, mechanics of extra nuclear hadron cascades 2—5766
single cavity, radiation reaction force on electron ring passing through 2—14806
spherical aberrations due to dipole magnet 2—38423
stochasticity domain boundaries in Hamiltonian systems 2—14793
storage rings, intersecting CERN, preliminary health physics report 2—2897
superconducting helically loaded resonators, obs. at high field strength 2—27921

Particle accelerators continued
superconducting microtron type, theoretical study of losses by Joules effect and energy limitations 2—34840
superconducting ring 2—14855
Van de Graaff with optical detection system as pulse radiolysis apparatus 2—441
vertical Pelletron, in Canberra and Wisconsin, design features 2—38397
μ flux, in shields, calculation program 2—2873
for H granions, plasma formation 2—24788

accessories
see also Storage rings
autogenerator, h.f., stabilization modulation system 2—11653
automatic frequency control system for microtron 2—21342
beam current monitor and gated integrator 2—8260
beam monitor, coaxial transmission line, fine structure obs. 2—27926
Bevatron, pulsed ion source 2—34351
boat for arc discharge ion sources, liquid N_2 cooled 2—14856
CEA bypass, colliding electron and positron beams 2—14852
CEA low-β bypass performance 2—14868
CERN intersecting storage rings, proton-proton collisions at 15 GeV and other tests, parameters 2—449
compensated current magnetic channel, for 240 cm. isochronous cyclotron 2—24121
computer control of tandem accelerator, and meas. of yield functions 2—24124
current pulses, megampere, meas. by integrating Rogowski coil, nanosecond risetime 2—2321
cylindrical spark-chambers, used with ACO storage ring at Orsay 2—34839
electromagnet, computer calc. of mag. field 2—31395
electron ring compressors, conventional rel. to spring coil 2—14893
electron sources, high current, for electron ring accelerators 2—14892
electronic system for use with proportional counter for displaying beam profiles in secondary beam lines 2—14857
electrostatic septum for slow ejection of CPS 2—14849
energy spectrum display at output of linear ion accelerator using transparent induction pickup 2—31394
flash tube hodoscope chambers use in expts. 2—31359
HAIZY, isochronous cyclotron, beam transport system 2—31402
h.f. ion sources for protons for van de Graaff accelerator 2—38409
high power variable width slit system for Van de Graaff 2—34853
high power variable width slit system for Van de Graaff 2—24117
high voltage injector, for 6-10 MeV betatrons 2—38404
h.v. source, for 2MeV ion and electron accel., multiplication circuit 2—18054
injector of multiply charged ions for linac 2—18053
intersecting storage rings, coherent space charge instabilities 2—14885
intersecting storage rings, observation of beam behaviour 2—14884
intersecting storage rings, prevention of space charge neutralization of the beams 2—14886
ion source, Lamb shift, polarized for LAMP facility 2—8261
ion source, pulsed, producing pulses of nanosecond length 2—18031
ion sources, conference, New York (1971) 2—7873
ionization scanner signals, data acquisition and treatment 2—14799
isotope separator, on-line to heavy-ion accelerator 2—24123
LRL compressor 4, eddy currents effects on Landau-damping coefficients 2—14802
magnet coil power supply conductors, Cu, hollow, water-cooled 2—27931
magnetic screen for 240 cm. isochronous cyclotron 2—21345
matching of accelerating channels by cavity. and drift space and matching cavity methods 2—27923
modified flat pole for hard focusing channel 2—18038
multiple target extraction sharing scheme at CPS 2—14848
muon guide, made of units of magnetised Fe, identification of intermediate bosons 2—14883
negatively charged heavy ion beam production using less abundant isotopes 2—34353
neutron tube generators, high voltage multiplier as accel. voltage source 2—18051
oscillating quadrupole, h.f. for beam enlargement 2—18055
phase volume reduction of bunch by system for suppressing coherent phase oscillations 2—31398
pickups for beam position sensing of accelerated electrons 2—31400
polarized ion sources, atomic beam scattering 2—27930
preinjector, 500 kV medium gradient 2—38421
proportional chamber, large multiwire, characteristics 2—8230
pulsing system, nsec., for electrostatic accelerator 2—38400
radiation monitoring system 2—2898
radiation monitoring systems and instruments, NAL safety policy 2—2899
regenerative beam extractor, energy spread vs. radial oscillation amplitude 2—5627
r.f. beam separators, long duty cycle, room temp. and superconducting 2—14879
r.f. separators, particle deflection increased by feedback 2—14878
r.f. separators, phase slip and two-cavity separation 2—14880
ring electromagnet, equipment for mag. field obs. 2—21343
scattering chamber, charged particle, for obs. with polarized and unpolarized beams 2—14824
Serpujkhov 70 GeV proton synchrotron, fast ejection equipment 2—14850
slit collimator for external beam parameter improvement 2—18052
spectrometer with fixed setting for obs. of acceleration modes 2—21338
stigmatic grazing incidence monochromator for synchrotrons 2—34867
storage ring, radiation dangers of losses and bremmstrahlung 2—2864
storage rings, intersecting, radiation shielding and damage 2—2877
superconducting helical resonator for heavy ion accelerator, ponderomotive oscillations 2—34865
superconducting helically loaded resonators in proton accelerator 2—14853
superconducting magnet, performance in closed circuit cryogenic system 2—14870
superconducting magnet, pulsed, dipole, construction and testing for 1000 GeV synchrotron 2—14871
superconducting magnet design for synchrotron 2—14873
superconducting magnetic systems, air-core, winding configurations 2—14874
superconducting magnets, dipole, pulsed for synchrotron, testing 2—14872
superconducting magnets for synchrotrons of more than 1000 GeV, characteristics 2—14869
superconducting Mo test cavity, properties at 350 MHz 2—34866
superconducting pulsed magnets for 1000 GeV synchrotron 2—38420

Particle accelerators continued
accessories continued
superconducting r.f. separators, high field tests at 1.3 GHz 2—14876
superconducting synchrotron magnets, status 2—14846
synchrotron, proton, main ring magnet, 95 MVA motor-generator set employment 2—14859
synchrotron injector at Erevan, reducing energy spread 2—34852
target assembly, isopropanol-solid CO_2 cooled 2—2656
target coding system, calc. method for design 2—27932
three component separation of ultrahigh energy particles 2—14881
two gap ion buncher at input of linear accelerator 2—31399
u.h. vacuum system mating to ion accelerator 2—41412
vacuum system for superconducting linear accelerators 2—38398
valves, dual seal bakeable sector, CERN intersecting storage ring 2—23202
waveguide buncher electrical field characteristics, optimal design using hybrid computer 2—8262
C foils as heavy ion strippers, increase of lifetime at high temp. 2—14858
Nb cavities and structures, tests at S- and X-band frequencies 2—14875
Nb superconducting cavities, coated with Nb_2O_5, r.f. losses 2—14882
Nb superconducting cavities with high Q, r.f. beam separators 2—14815
Nb superconducting deflecting cavities, experimental investigation of Q values and peak fields 2—14877
betatrons
autoresonant, angular injection effects 2—34856
beam stacking in radial betatron phase space 2—14838
Bevatron, heavy ions, performance 2—34858
Bevatron, pulsed heavy ion source 2—34351
frequency measurement and damping of radial oscillations, use of radial longitudinal accelerating field 2—18047
head-tail instability, betatron and synchrotron oscillations 2—14840
high voltage injector, for 6-10 MeV betatrons 2—38404
iron-free strongly focussing, operating principles 2—18041
magnetic flux, rel. to energy increase from 5 to 10 MeV 2—38407
nonlinear resonances effects on beams dimensions in 70 GeV IFVE, accelerator 2—27928
on-line compouter control of Melbourne Univ. betatron 2—38408
oscillations, damping in weakly-focussing mag. field 2—34857
resonances, non-linear, at the IHEP 70 GeV accelerator 2—18046
synchrotron and betatron instabilities of stored electron and positron beams 2—14839
transportable, description and application 2—11692
cyclotrons
ALICE, heavy ion cyclotron, linear accelerator as injector 2—34854
AVF, isochronons field calc., instability problem 2—31397
AVF, isochronous field calc., instability problem 2—24120
beam dynamic stability 2—38402
beam energies obs. by time of flight method 2—8259
beam parameter improvement using slit collimator 2—18052
beam shadow measurements, computer controlled method 2—14823
circular, with isochronism of closed orbits, for high energy particles 2—14837
Cyclo-Graff, in Canberra, design features 2—38397
electron analogue of high energy proton cyclotron, orbit props. 2—38412
external beam matching to ion optical axis 2—8258
fringing field effects in quadrupole magnet 2—38424
HAIZY, isochronous cyclotron, beam transport system 2—31402
Harwell variable energy cyclotron, production of metal ions 2—34778
heavy ion, ALICE at Orsay 2—5614
internal Penning source, for heavy ions 2—34861
isochronous, 240 cm., compensated current magnetic channel 2—24121
isochronous, 240 cm., magnetic screen 2—21345
isochronous, resonance effects, particle trajectories and optimum slit width 2—38413
isochronous at Indiana University 2—5619
magnetic field meas. of 20 cm model magnet for 176 cm SF cyclotron, focusing and isochronism dependence on spiral shim, valley and hill gap 2—38396
medical, feasibility of production of ^{99m}Tc 2—3009
microsecond beam chopping by pulsing cyclotron deflector voltage, half-life measurements 2—24118
microtron, automatic frequency control system 2—21342
microtron for radiation physics of semiconductors 2—21341
multiply charged Ne, Ar, Kr, and Xe ions, by hot cathode source 2—34860
orbit props., mag. field error effects 2—38401
radial motion studies in central region 2—38403
radiation levels in experimental and associated areas 2—2881
review 2—27929
r.f. drive, computer compatible servo system 2—27933
r.f. system improvements to IPCR 160 cm machine 2—448
ring, l.f. injection mode 2—31396
ring, l.f. injection mode 2—24119
scattering chamber, charged particle, for obs. with polarized and unpolarized beams 2—14824
shield-leakage neutron spectra 2—2885
stripping to obtain high energy heavy ions 2—27927
superconducting magnet, performance in closed circuit cryogenic system 2—14870
synchrocyclotron, 600 MeV, CERN, magnet coil power conductors, Cu, water-cooled, hollow 2—27931
synchrocyclotron, h.f. autogenerator, stabilization modulation system 2—11653
trajectory positions for acceleration in three sector model with separate magnets 2—31393
variable energy, and source for multiply charged ions 2—34859
^{111}In, cyclotron production from ^{111}Cd, for nuclear medicine applications 2—28239
linear
805 MHz side-coupled, stopband hybrid computation 2—11690
acceleration mode obs using spectrometer with fixed setting 2—21338
beam, 40 MeV, duty-cycle smoothing using electron storage ring 2—14814
beam loading, operation with pulse modified high repetition frequency current 2—24115
Berkeley Hilac modification 2—5610
collective, at Dubna, status report 2—14816
c.w. heavy ion, combination of a helix and a tandem 2—5609
c.w. standing-wave, calc. of threshold current for transverse beam blowup including interaction of neighbouring modes 2—27924
electron, 30 MeV, positron acceleration and annihilation 2—24116

Particle accelerators continued
linear continued
electron, c.w. up to 4 MeV research and engineering at AECL 2—11691
electron, longitudinal dynamics in grouping sections 2—2654
electron, recirculation of beam, energy boost 2—14822
electron, S-band, accel. struct. temp. distrib., temp. eqns. 2—8248
electron multipactoring process in cavities 2—5618
electron rings, relativistic, single bunch, radiation, loss 2—14818
electron S-band, electron energy spectrum and instability design criteria 2—8247
electron U target, shielding requirements 2—2880
electrons, 30 MeV possible radiation hazards 2—2863
electrostatic, nsec. pulsing system 2—38400
energy storage processes, superconducting resonators use 2—38399
FN tandem Van de Graaff, equilibrium charge state distributions of O and S ions 2—27919
heavy ions, 100 keV, ion implantation studies 2—27925
induction longitudinal beam stability in ferromagnetic channel 2—21339
injection of relativistic particles into rapidly increasing mag. field 2—5624
injection system for heavy ions, ALICE at Orsay 2—5614
ion, beam energy spectrum display using transparent induction pickup 2—31394
ion beam axis calculation in inclined field tubes with equal maximum displacements of the tube 2—5611
ion linac output, synchronous beam, energy spectrum and instability 2—14817
matching of accelerating channels by cavity, and drift space and matching cavity methods 2—27923
modified flat pole for hard focusing channel 2—18038
as neutron source, isotropic 2—38417
proton, c.w., up to 3 MeV, research and engineering at AECL 2—11691
proton, longitudinal space-charge effects 2—18040
proton, operation and performance 2—14819
proton, review of work carried out in USSR 2—14820
proton, space charge effect obs. using electron model 2—5612
proton, supercond., at Karlsruhe, vacuum system 2—38398
proton, with space charge, computer obs. of beam dynamics 2—5613
proton beam control, Cu conductors for electromagnets 2—18039
superconducting heavy ion, advantages 2—34849
superconducting heavy ion, with independent accelerating gaps 2—34850
superconducting hilac, feasibility 2—34851
superHILAC, technology and facilities 2—21340
tandem, direct extraction negative ion source 2—8253
tandem, negative ion source 2—8254
tandem Van de Graaff, compact polarized ion source for high voltage terminal 2—8250
tandem Van de Graaff, ground state polarized ion source 2—8249
tandem Van de Graaff, HVEC diode ion source for injection of negative ions 2—8252
tandem Van de Graaff, Lamb shift polarized ion source 2—8246
teaching apparatus for simulation 2—33847
two gap ion buncher at input 2—31399
Van de Graaff, crossed field analyzer 2—11694
Van de Graaff, high power variable width slit system 2—34853
Van de Graaff, high power variable width slit system 2—24117
H- ion source 2—8251
U^{11+} UNILAC ion source and injection system 2—34842
synchrotrons
1000 GeV, superconducting pulsed magnet for use with 2—38420
adiabatic capture and accelerated intensity increase in CERN PS 2—14828
beam blow up due to magnet imperfections and corrective measures, CERN PS booster 2—14835
beam extraction techniques 2—14826
beam-bunch length matching at transition crossing 2—18049
Bevatron, transverse proton beam instabilities 2—18048
bevatron acceleration of beams of deuterons α-particles and nitrogen ions 2—38415
CEA bypass, colliding electron and positron beams 2—14852
CERN, 28 GeV, Cu hollow water-cooled conductors for magnet coil power supply 2—27931
CERN, testing of high dose-rate dosimeters 2—31632
CERN 300 GeV proton synchrotron, general information 2—8256
CERN proton synchrotron closed orbit at injection, on-line control 2—14854
CERN PS, passing transition 2—18043
CERN PS booster, multiturn injection, macroparticle computer simulation 2—14847
CERN PS damping of longitudinal instability 2—18042
coherent radial instability due to horizontal resistive walls, evaluation for Saturne 2—14834
CPS, electrostatic septum for slow ejection 2—14849
CPS, multiple target extraction sharing scheme 2—14848
dose monitoring, dismantling and disposal 2—2896
electron, 140 MeV, e.m. radiation strength 2—18045
electron, German type 2—18044
electron beam dimens., meas. using rot. disc, method 2—5617
electron synchrotron, 5 GeV, vacuum system problems 2—38405
equipment design criterion for CERN PS booster from stability considerations of coherent synchrotron motion 2—14833
heavy ion Princeton accelerator, N^{5+} and N^{6+} ions accelerated to 7.4 GeV 2—38414
high energy, analytic method for closed orbit correction 2—14825
induced radioactivity in ground water system near proposed 300 GeV accelerator 2—5622
injection and beam transfer scheme of Japanese 8 GeV proton synchrotron 2—14851
injection and ejection processes at Saturne 2—14827
injector at Erevan, reducing energy spread 2—34852
magnetic field flat top formation, time dependence 2—34864
National Accelerator Laboratory, proton description and problems 2—14842
NIMROD, attenuation of prod. radiation in access tunnels 2—5764
Nimrod operation and development report 2—5623
oscillations near transition energy, theory, equations in matrix form 2—27922
power supplies, using superconducting energy transfer principle 2—14832
Princetown, heavy ion acceleration 2—34855
proton, 28 GeV, main ring magnet, 95 MVA motor-generator set employment 2—14859

Particle accelerators continued
  synchrotrons continued
    proton, 70 GeV, IHEP, increasing intensity by increasing injection energy 2—14845
    proton, equipment for mag. field obs. in ring electromagnet 2—21343
    proton, high gradient column, ion source obs. 2—8257
    proton, NAL progress report 2—38411
    proton, orbit display, automatic 2—5620
    proton 76 GeV IHEP, status report 2—14843
    protons number optimisation by computer 2—38410
    quadrupole test, added multipole components 2—5621
    radiation problems in 300 GeV proton synchrotron 2—555
    radiation shielding, 300 GeV machine, dose rate below 5 rem/30y outside laboratories 2—2883
    radiation shielding requirements for a multi GeV electron ring 2—2869
    resonant vertical beam extraction, effect of nonlinear coupling 2—14829
    resonator matching to waveguide cct. 2—5616
    secondary beams at 70 GeV IHEP proton accelerator 2—14844
    Serpujkhov 70 GeV proton synchrotron, fast ejection equipment 2—14850
    slowing down electron bunch system conductivity determ. as function of synchronous energy at given bunch characteristics 2—24122
    stigmatic grazing incidence monochromator for use with 2—34867
    superconducting, 1000 GeV, design problems 2—14830
    superconducting, design w.r.t. magnet component error correction 2—14831
    superconducting magnet, pulsed, dipole, construction and testing for 1000 GeV machine 2—14871
    superconducting magnet design 2—14873
    superconducting magnets, dipole, pulsed for synchrotron, testing 2—14872
    superconducting magnets for machines of more than 1000 GeV, characteristics 2—14869
    synchrophasotron, accel. and extraction of D beam 2—18050
    syncrocyclotron, obs. of radiation levels in vicinity 2—2882
    zero gradient, electronic system for use with proportional counter for displaying beam profiles 2—14857
    zero gradient, ion source program, review 2—8255

Particle beams
  acceleration in proper fields of electron beam 2—14812
  alpha, acceleration in Bevatron 2—14809
  atomic, applic. to plasma diagnostics 2—32032
  bubble chamber beamline, computer control, software 2—14781
  bubble chamber beamline, computer control and acquisition system 2—14780
  bunches, high intensity, self focusing in periodic waveguide systems 2—14382
  centre of gravity obs. using proportional chamber 2—21024
  charged, acceleration mechanism in alternating mag. field 2—34313
  charged, intense, with nonstationary distrib. of transverse phase space density dynamics 2—5605
  charged, motion in axisymmetric magnetic fields 2—23518
  circular, resonance of coupled transverse oscillations 2—30993
  coherent radial instability due to horizontal resistive walls, evaluation for Saturne 2—14834
  colliding electron and positron beams in CEA bypass 2—14852
  Coulomb forces, nonlinear, effects on distortion of beam phase space volume configuration 2—14795
  coupling impedance, longitudinal, analogue method 2—18034
  cyclotron, energies obs. by time of flight method 2—8259
  cyclotron, external, matching to ion optical axis 2—8258
  cylindrical condenser, charged particle motion in normal section 2—34312
  density distribution, four dimensional, dependence on longitudinal coordinates 2—5327
  deuteron, Lamb shift polarized ion source 2—8246
  deuterons, acceleration in Bevatron 2—14809
  dynamics, in proton linear accelerator with space charge, computer obs. 2—5613
  electrical charge free, focussing 2—27418
  e.m. field distribution due to a beam-excited re-entrant cylindrical cavity mounted coaxially with a vacuum chamber 2—17471
  enlargement in accelerator, with h.f. oscillating quadrupole 2—18055
  formation with arbitrary conical surfaces as boundaries 2—21022
  injection into rapidly increasing mag. field, linear accelerator 2—5624
  insertion into bubble chamber calc. for choice of coordinates and angle of beam entry 2—31385
  intense, production with energies <10 keV, review 2—7881
  intense, with extraction energies >10 keV 2—7880
  ionization scanner signals, data acquisition and treatment 2—14799
  ISR, instrumentation and beam diagnostics 2—14785
  linac, 40 MeV, duty-cycle smoothing using electron storage ring 2—14814
  longitudinal beam stability in ferromagnetic channel, linear induction accelerator 2—21339
  momentum, direct meas. using time-of-flight and range techniques 2—7840
  monitor, coaxial transmission line, fine structure obs. 2—27926
  monitor, for symmetry and magnitude, using transmission ion chamber 2—34315
  monitor for pulsed accelerator 2—8260
  multiple aperture extractor design for producing intense neutral beams 2—34354
  multiple aperture extractor design for producing intense neutral beams 2—34354
  neutral atoms, injection in mirror systems, plasma production 2—24784
  neutron, calc. method for energy distrib. incident on circular disk 2—37894
  neutron, from cold source, production 2—27830
  neutron, interference, diffraction theory 2—17973
  neutron, monoenergetic eV-keV range, production using resonance scatterers in tangential beam tube of reactors 2—34752
  neutron, spectral characteristics obs. with direct charge detectors 2—27852
  neutron source, isotropic, use of linear accelerator 2—38417
  neutron spin-flip-chopper with high repetition rates 2—11656
  optics, Monte Carlo method studies 2—37893
  phase motion stability of bunch in storage ring, dependence on form of synchrotron frequency distribution function 2—14887
  phase space distribution in uniform longitudinal magnetic field 2—34314
  photonuclear expts. using combined energy and intensity sweeping 2—34751
  production, multiple aperture extractor design 2—7885
  proton, coasting, coherent instability due to electrons, at ISR 2—5628
  proton, duoplasmatron feeding of 750 keV exact Pierce column 2—8245

Particle beams continued
  proton, Lamb shift polarized ion source 2—8246
  proton, stability in storage-rings, effect of secondary charged particles 2—2652
  proton spreading by charge exchange, depend. on atmospheric structure 2—30291
  protons, aberrated cylindrically symmetrical, emittance obs. 2—7841
  protons, enhancement of ν-spread by the insertion of an electron beam 2—18032
  protons, pulsations of decreasing period as beam instability in plasma, model of geomagnetic variations 2—30367
  protons, transverse instabilities at the Bevatron 2—18048
  redistribution of beam on encountering object 2—7847
  resonant instability of nonlinear oscillations, finite difference eqn. representation, application to microtron 2—14794
  r.f.-knockout, determination of transverse coherent instability 2—18033
  scattered from thick target, spectrum shape in terms of energy losses 2—8321
  space charge dynamics, calculation by expansion method 2—18035
  spark spectrometer for investigations on 70 GeV beam, quark search 2—11688
  spatial characteristics meas. and monitoring of external beams of Erevan electron ring accelerator 2—31401
  stabilization of negative mass instability in Berkeley electron ring accelerator 2—14796
  stochasticity domain boundaries in Hamiltonian systems 2—14793
  in storage rings, coherent beams break up due to space charge 2—14901
  theory, technology and applications, conference, New York (1971) 2—7873
  three component separation of ultrahigh energy particles 2—14881
  trajectory positions for acceleration in three sector cyclotron model with separate magnets 2—31393
  transition acceleration, on passing vacuum-inverted dielectric boundary 2—23468
  transmission through porous material, path length distrib. 2—32284
  transverse stability of bunched beam in storage rings interacting with low Q-value systems 2—14791
  unbunched, relativistic, e.m. fields excited by longitudinal density fluctuations 2—27420
  universal diffractometer for neutrons, variable wavelength 2—24071
  H, neutral, energy dispersed 2—23523
  ^{2}H, accel. and extraction from synchrophasotron 2—18050

Particle detectors
  see also Bubble chambers; Cloud chambers; Counters; Ionization chambers; Nuclear track emulsions; Particle track visualization
  Anger scintillation camera, improved resolution using threshold preamplifiers 2—24098
  array position sensitive, for broad-range spectrograph 2—5578
  bubble chamber, 81 cm H_2, obs. of delta electrons 2—31381
  cellulose nitrate film used for detection of α-particles 2—11679
  using electrical impedance of electrolyte, patent 2—38389
  emulsion chamber expt. at Chacaltaya 2—8243
  energy loss correction for thick detectors 2—38352
  fission counters, Th coated, high energy neutron detection 2—23927
  flash tube hodoscope chambers use with particle accelerators 2—31359
  gamma-ray, background reduction using massive cosmic ray shielding 2—34795
  gaseous activities, short-lived, gas-sweeping system with semiconductor-counter telescope 2—8238
  geometric factor, circular or rectangular geometric types 2—21314
  high energy photoprotons, on-line counter hodoscope 2—34830
  msgnetic spectrograph for meas. of cosmic ray spectra at different altitudes in the atmosphere 2—27802
  multiwire proportional chambers, gas mixture for high gain 2—34786
  for neutral particles H, He, N atoms, by detection of secondary electron emission from Cu or AgMg surfaces 2—27885
  neutron, B lined chamber working under current collection and no multiplication conditions, for whole dynamic range of reactor 2—31375
  neutron, high intensity, with high neutron to gamma ray sensitivity ratio 2—18017
  neutron, nuclear reactor safety instruments, using multiplication 2—38763
  neutron, polycarbonate detector sandwiched between U fission foils, track obs. 2—38390
  neutron, using resonant scattering from ^{7}Li 2—38382
  neutron counter, high efficiency design for cosmic ray applic. 2—23930
  neutron detection using resonant scattering from ^{7}Li to identify levels following neutron producing reactions 2—27890
  neutron detector for location of beams in space, patent 2—21327
  neutron flux monitor, thin glass scintillation system, ^{6}Li(n, α)T 2—5588
  neutron sensor, self powered for flux obs. in high temp. nuclear reactor 2—11914
  neutrons, array of plastic scintillators, 1.0 to 450 MeV 2—34797
  neutrons, PENA flux measuring system with fast-response 2—5595
  neutrons, shelled activation detectors, measurement at kV energies 2—5580
  nomograms for calc. of error of energy of binary type nuclear reaction product and cross-section as function of emergence angle 2—27831
  optical with Van de Graaff accelerator as pulse radiolysis apparatus 2—441
  photon detectors, review article 2—38350
  phototube 8 channel amplifier modules for multidetector systems 2—31378
  pickups for beam position sensing of accelerated electrons 2—31400
  plastic foils, location of tracks aided by photodeposition of coordinate grids 2—27907
  polarity-correlation system for fast-reactor noise studies 2—11916
  pulse reactor radiation detection system using on-line computer 2—15173
  radioisotope distributions in human body true multiple scanning and obs. of absolute local activity 2—11206
  secondary particle identification from ionization losses in 81 cm H_2 bubble chamber 2—34832
  semiconductor detector with anticoincidence system for suppression of backscattered β-rays 2—14759
  solid state, det. of electron detection efficiencies 2—14770
  source strength intercomparisons, simple two-detector method 2—24094
  STEK, fast-thermal neutron measuring device, time of flight technique, 0.1 and 50 KeV 2—18005
  streamer chamber charging regulator system 2—34837
  time-of-flight system for heavy particle identification in nuclear reactions 2—442

Particle detectors continued
triple coincidence technique for inverse beta decay reactions 2—8237
ultrarelativistic, detection by transition radiation in X-ray frequency range 2—18020
n, threshold detectors of fast spectra, evaluation 2—38351
^{10}B, for γ-rays, det. of efficiency using Monte Carlo method 2—27892
CdTe:Cu (Ga)(In), detector-mat. evaluation by e.p.r. and channelling expts. 2—36539
CdTe, growth by travelling heater method 2—35944
CdTe, γ-ray detector material, conf., Strasbourg, France, June (1971) 2—34808
CdTe, nucl. rad. detector, ion implanted, performance 2—34815
Ci, used in heavy ion time-of-flight mass spectrometer 2—14745
n-GaAs, α-particle and γ-ray detection, liquid and vapour phase epitaxial layers 2—34816
GaAs, γ-detectors, conf. panel discussion 2—34817
Ge, with B implanted p^+ contacts, γ-detector 2—25883
Ge(Li), review 2—34818
Ge(Li) time characteristics calc., computer program 2—14763
^{3}H, liquid scintillation emulsions, using electrolytic enrichment 2—38366
^{3}He, polarization analyser, construction resolution and efficiency 2—8240
In foil neutron detector, Cd ratio for atmospheric neutrons 2—21331
Ne flash tubes, use at high repetition rates 2—38379
Si p-n junction, ion implantation fabrication 2—25896
Si surface barrier, correlation between etch pit density and performance 2—14761
SiC, α-particle detection at high temps. prod. and props. of diodes 2—34821
Si(Li), polarization sensitivity investigation using linearly polarized 121 keV γ-rays 2—438
W, as thermal neutron flux monitor at v. high temp. 2—8239

Particle focusing *see Particle optics*

Particle optics
see also Electron optics; Ion optics
μ in Fe with momentum 30 GeV/c, focusing properties and transport with energy decrease 2—21023
adiabatic orbits in magnetic null sheet 2—14380
beam formation with arbitrary conical surfaces as boundaries 2—21022
beam optics, Monte Carlo method studies 2—37893
beam redistribution on encountering object 2—7847
beam shadow measurements in cyclotron, computer controlled method 2—14823
bunches, high density, self focusing in periodic waveguide systems 2—14382
charged beam centered on privileged trajectory 2—34312
computer design and optimization of Fe cored focusing devices 2—30990
c.w. standing-wave linacs, calc. of threshold current for transverse beam blowup including interaction of neighbouring modes 2—27924
distribution function of charged particles in condensed dispersing medium with axially symmetric magnetic field 2—21023
electrical charge free, focussing 2—27418
focusing, two directional, with deflecting magnets, computer program 2—14381
focusing properties of crossed homogeneous mag. and hyperboloidal electric fields 2—2347
magnetic deflection system, fringing fields correction, design method 2—17535
neutron beams, interference, diffraction theory 2—17973
neutron collimator, forced reflection, n-n scattering experiment 2—14738
preinjector, 500 kV medium gradient 2—38421
quadrupole lenses, nonsymmetric, correction of geometric aberrations 2—23522
refraction at surfaces of discontinuities of e.m. potentials 2—30991
r.f. beam separators, long duty cycle, room temp. and superconducting 2—14879
r.f. separators, phase slip and two-cavity separation 2—14880
self focusing in cyclic accelerator 2—14813
systems of diaphragms with slit apertures, calculation of field 2—30992
waist to waist transfer for thick lens elements 2—23521

Particle range *see Energy loss of particles*

Particle size
see also Surface measurement
aerosols, calibration of apparatus for determining size distributions 2—6266
aerosols, det. in submicron range by thermophoresis 2—28917
aerosols, distribution det. from spectral attenuation meas. 2—4682
aerosols, glass substrates, particle conversion into droplet state 2—9191
aerosols, moving, holographic technique for obs. 2—6264
airborne, meas. by laser extinction and optical array spectrometers 2—16834
airborne Dow polystyrene spheres, electrical mobility and effective airborne radius 2—28914
alloy, f.c.c. cold worked, integral breadth, analysis X-ray line profile 2—22332
alloy crystal with dispersed precipitate, critical resolved shear stress 2—3861
atmospheric aerosol, variation of size distribution as function of relative humidity 2—13679
atmospheric spherical polydispersions, size distribution det. using light scattered data 2—7260
composite material containing spherical particles, theory of particle size meas. 2—3452
composite solids, effect on effective thermal conductivities 2—23396
density distribution, f(x), eqns. relating radii F(R) to f(x) 2—38086
disperse phases in alloy, coalescence kinetics 2—12961
disperse systems, low angle X-ray scatt. 2—3417
distorted polycrystal with generalized strain distrib., apparent particle size and strain 2—22199
droplets in clouds growing by condensation, effect of turbulence on distrib. 2—20345
drops in burning zone, contactless optical sensor for distribution obs. 2—5434
drops size distribution in immiscible binary liquid system, photoelectric probe 2—39316
granular solid, effect on angles of repose and bulk densities 2—25606
interstellar dirty ice grains with graphite cores, size distrib. around early type stars 2—33695
i.r. emission spectrum from single particles, variations with particle size 2—25118

Particle size continued
L1$_0$ superlattice, effect of twinning, calc. 2—3950
laser beam intensity variations in diffraction patterns for size analysis 2—21158
latex, distrib., determ. by flow ultramicroscopy 2—15617
latex, distribution det. by electron microscope 2—25117
light scattering determination, effect of refractive index 2—312
linear analysis, using automatic scanning microphotometer 2—5115
mean diameter of microparticles from size of projected images 2—37557
metal, fine particles produced by gas evaporation technique 2—25605
metal carbide particles, in metallic matrix, coarsening rate 2—29416
metallography, quantitative, principles and practical methods 2—25561
natural aerosol, dependence on relative air humidity 2—33463
optical microscopy 2—32681
polymer latex systems, size distribution analysis using extrema in unpolarized and horizontally polarized ang. light scatt. pattern 2—39397
polymer lattices, particle size distrib. assessment using 'quantimet'—electron microscope linkage 2—18858
polymer suspensions and dispersions, Quantimet image analysing computer linked to electron microscope for obs. 2—6265
polystyrene latex, light scattering during coagulation 2—15619
polyvinyl chloride latex, analytical centrifuge obs. 2—15894
powder, distrib. determ. by photomicrographic method 2—25608
powder, reaction kinetics, interfacial area 2—13565
quartz powder, grain size determ. by X-ray diffraction, extrapolation method 2—32744
raindrop analyzer for automatic counting and sizing 2—33464
rare earth oxide powder, crystallite growth, dynamic calcination effects 2—12980
sea water drops, size determination 2—32208
and shape, absolute meas., primary standard 2—5113
steel, mild, grain size effect on fracture initiation 2—29327
suspension in turbulent channel flow, rel. to entrainment 2—25124
suspension in turbulent jets, rel. to diffusion 2—25123
transition metals, grain size effect on supercond. T_c 2—19599
very small, crystalline, electron microscopy and diffr. 2—19256
water droplet generator for controlled pairs of equal and unequal size 2—18862
X-ray and light measurement applics. 2—37537
X-ray diffraction profile and moments, size broadening 2—3629
Zeiss-Endter analyzer, modification for data logging 2—19277
Zircalloy-2, cold-rolled, X-ray and electron microscope obs. 2—29185
Al-Cu alloy, coarsening of θ'' and θ' precipitates 2—9751
Al, cold worked and annealed, small angle X-ray scatt. obs. 2—25592
AlN, in low-C steel, at austenitic grain coarsening temp. 2—29433
Al_2O_3, coarsening in Ni-Al_2O_3-Mg alloy 2—32743
Al_2O_3, metallographic polishing powder, scanning electron microscope evaluation 2—36192
$CaTiO_3$ formation, solid state reaction kinetics, Carter's equation 2—13566
CdS-MnS powder, degree of dispersity, small angle X-ray scatt. 2—3970
Cu-Al, single cryst., internally oxidized, SEM obs. 2—15716
Cu-Al alloys, cold worked and annealed, small angle X-ray scatt. obs. 2—25592
2—3913
Cu-Ni alloy, effect on Debye temp. 2—19383
Cu, cold worked and annealed, small angle X-ray scatt. obs. 2—25592
Cu, effect on n.m.r. and mag. susceptibility 2—40772
CuAu effect of twinning, calc. 2—3950
Cu_2O inclusions in Cu, role in dislocation struct. 2—15761
Fe_2O_3 aerosols, labelled, variation of particle density with size 2—12590
Li fine particles, effect on e.p.r. line width 2—20145
MgIn effect of twinning, calc. 2—3950
Mn-Zn, alloy, age hardened, grain size, dependence of yield stress and flow stress 2—6546
$MnZnFe_2O_4$, of Fe_2O_3 and calcined spinel, rel. to mag. props. 2—33157
Mo wire, recrystallized, grain size and carbon content effects on ductility 2—29262
Ni-Fe films, grain size 2—36728
Ni-Th, and interparticle spacing, effects on mech. behaviour 2—3963
Ni, effect on Debye temp. 2—19383
Ni film, critical grain size for ferromag. 2—40510
Pb particles, size and surface effects on specific heat 2—32949
Pt/Al_2O_3 disperse catalyst, small angle X-ray scatt. obs. 2—3973
ThO_2, growth in dispersion strengthened Ni, electron microscopy 2—9734
TiC, stoichiometric, and morphology obs. 2—22347
WC-Co, hard alloy cermet, Co melt redistribution process 2—32736
WC_x powder, preparared by freeze-drying 2—29447
WO_3, non-stoichiometry, colour, micro-strain, Schottky defects, X-ray exam. 2—25246
ZrO_2, milled zirconia, monoclinic-tetragonal transformation, particle size effects 2—29484

Particle spectrometers
see also Alpha-particle spectrometers, etc.
area-of-interest unfolding of spectroscopic data 2—8221
automatic peak extraction technique using additive correlation procedure 2—34824
baseline restorer for higher resolving power 2—34782
broadband current preamplifier for high resolution energy and time information 2—27841
channel electron multipliers, charged particle detector units 2—17997
channel plate image intensifier for electrons 2—17565
charged, high resolution combining low dispersion magnet and Si(Li) drifted detectors 2—11659
coincidence, with NaI(Tl) scintillation crystals, counting efficiency and absorption factors for positron annihilation radiation 2—11662
computer program, LILY for automatic analysis of spectra, in FORTRAN IV 2—14736
continuous spectrum using position sensitive detector array 2—5578
cosmic ray muons, high energy spectrometer at SLAC, photographs of sea level muons zenith angles 45°-90° 2—27806
cosmic ray nuclei, superconducting magnet 2—21317
cosmic ray telescopes, contribution of scattered electrons to detected signal 2—27810
cylindrical mirror analyzer with surface entrance and exit slots, relativistic treatment 2—27426
design and calibration for satellites, using electron multipliers 2—31013
electron, amplifier for pulse counting applic. 2—34241
electron, attached to electron microscope for improved analysis 2—3661
electron, for use at u.h.v. conditions 2—2621

Particle spectrometers continued
electron, high-resolution high-efficiency double-focussing, design 2—23537
electron, low-energy, multi-plate analysers 2—18004
electron, obs. of photoionization of free atoms and molecules by radiation of resonant lines of inert gas 2—21323
electron energy analyzer, cylindrical mirror, design parameters 2—23536
electron energy distribution peak shift, high resolution measurement 2—6912
electron energy measurement with discrimination against hadronic background, lead glass 2—11661
electron field energy analyzer, retarding, high resolution 2—31352
electron trajectories reanalysis in 127° cylindrical 2—21318
electrostatic analysers, electrical insulation 2—17996
energy resolution, semiautomatic device, pulse amplitude distribution peak 2—24072
glass-scintillator ionization, hadron energy measurement 2—11657
heavy ion, time of flight measurement, Si detector 2—14745
h.f. amplifiers for semiconductor detectors at high loads 2—24066
linearity monitoring, pulse generator with equiprobable amplitude spectrum 2—24067
liquid scintillation, statistics of coincidence detection efficiency 2—5577
magnetic, 'ionographic' based, development 2—34781
magnetic, methods of analysing data from, for cosmic ray muons 2—8225
magnetic automated research spectrograph for meas. of cosmic ray muon spectrum 2—27799
magnetic deflection system, fringing fields correction, design method 2—17535
magnetic field, with periodic inhomogeneity with azimuth, geometric form 2—21319
magnetic for meas. of cosmic ray muon spectrum and charge ratio up to momentum of 3×10^{12} eV/c 2—27805
magnetic spark, investigations on 70 GeV beam, quark search 2—11688
magnetic spectrograph for primary cosmic ray studies 2—27797
multiple particle, measurement of p, α and β solar particle events 2—30619
narrow resonances, possible width determ. by missing mass interferometer 2—14744
neutron, application of threshold detectors using principle of neutron fission reaction 2—27853
neutrons, application of two- dimensional analyis mode for separation from gamma quanta 2—24082
particles experiment subsystem of Apollo 15 lunar subsatellite 2—30650
peak area det., effect of spectrum smoothing by digital filter 2—11658
photoelectron, He I, high resolution, performance obs. 2—8224
photoelectron, windowless for obs. of solids and surfaces 2—4102
proton, multichannel, modulated, for 0.03- 10keV energy range 2—27851
proton, performance of large plastic scintillation counters 2—8226
proton, with automatic follow-up of distribution maximum 2—21324
quadrupole lens pair and 60° spectrometer for broad range applic. 2—38356
semiconductor detector with anticoincidence system for suppression of backscattered β-rays 2—14759
semiconductor X-ray spectrometers, efficiency curves, and X/γ ratio for calibration sources 2—24068
Si surface barrier detectors for spectrometry of low energy ion beams 2—27840
SLAC 20 GeV, 400 wire proportional chamber system 2—27856
spectrograph with vertical double magnet for meas. of momentum spectrum and charge ratio of cosmic ray muons 2—27796
stigmatic focusing, with mass and energy dispersion 2—38778
time of flight, direct geometry, for pulsed reactor 2—8229
time of flight measurement of velocity spectrum of atoms from θ-pinch 2—34784
time-of-flight energy-mass-analyzer 2—21481
time-of-flight recording system, multichannel, design and performance 2—34783
total absorption, based on FEU-49 photomultiplier, time locking 2—21320
universal diffractometer for neutrons, variable wavelength 2—24071
wire chamber, h.v. pulsing system, read out and data acquisition systems 2—14750
X-ray photoelectron, use of electron flood gun to reduce surface charging 2—21030
μ, TeV energy, sea level spectra 2—31336
Si(Li), photon energies 5 to 125keV, absolute photopeak efficiency calibration 2—8223
TlCl(Be,I) scintillation, response to high energy electrons 2—2632
Particle symmetry *see Elementary particles/symmetry*
Particle track visualization
see also Bubble chambers; Cloud chambers; Luminescence chambers; Nuclear track emulsions; Spark chambers
cellulose nitrate, alpha particles, use in undergraduate laboratory 2—33840
cylindrical spark-chambers, used with ACO storage ring at Orsay 2—34839
dielectric detectors, track geometry 2—11683
electron microscopy replication study of fission product traces in plastic sheets 2—21333
emulsion chamber image intensifier system, for hadron studies in air showers 2—23931
etched holes in thin dielectric plastics, automatic fast counting system 2—38393
fission rate measurement, solid state track recorders 2—8411
formation of charged tracks in insulating materials 2—27908
gas track detectors, increase, modification of Sternheimer formula for energy loss of particles 2—21334
large wire spark chambers, with magnetostrictive read-out 2—31390
plastic detector, charged particle energy loss rel. to visualizable range 2—11682
plastic detector, for α-particle angular distrib. determ. 2—14777
plastic detectors, sensitivity determination rel. to cosmic ray applic. 2—23928
plastic sheets, thin, electrical method of location 2—27909
plastic track detector, particle identification characts. 2—38392
projection discharge chamber stacks with infinitely transparent electrodes 2—34833
in solids, use of interference-contrast microscopy 2—5597
spark chambers, wide-gap, compensation of drift of charged particles 2—18028
streamer chamber, memory time and dead time 2—24108
tracks storage using optical spark chamber pulsing 2—24111
Particle track visualization continued
H_2 bubble chamber photographs, scanning and meas. using computer 2—5601
U fission, location of minute grains by precise coordinate control 2—11685
Particle tracks
see also Energy loss of particles
bubble chamber photographs, track matching computer program 2—21335
bubble density obs. from p.p interactions using television measurement semi-automaton 2—31382
counting, automatic image analysis 2—24100
counting, automatic image analysis 2—5598
creation mechanisms 2—11684
density, bubble chamber, relativistic rise for fast charged particles 2—24103
density, bubble chamber, relativistic rise for fast charged particles 2—31384
in emulsion, simulation using δ-ray theory of track struct. 2—21337
fission products, density, automatic image analysis obs. 2—5599
fission rate measurement, solid state track recorders 2—8411
fission track annealing, radioactive dating, effect of water content 2—26463
formation in nitrocellulose plastic sheets, effect of etching interruptions 2—14776
fossil track studies of Luna 16 material 2—20660
geometry in dielectric nuclear detectors 2—11683
length obs. for heavy ions in mica 2—38391
location in thin plastic sheets using electrical method 2—27909
location on plastic detectors, photodeposition of coordinate grids 2—27907
meteorite Angra dos Reis fission origin of fossil 2—14006
microscope for, computer controlled 2—2450
multiwire proportional counters, array, process and coding system 2—27910
on-line counter hodoscope for high energy photoprotons 2—34830
Sea of Plenty soil 2—20658
solid state detectors, efficiency calibration 2—14775
Wilson cloud chamber, false curvature 2—24101
μ, and energy loss calcs. in various adsorbants, 2-600 GeV 2—5600
Particle velocity analysis
see also Alpha-particle spectrometers; Beta-ray spectrometers; Energy loss of particles; Ion velocity; Mass spectrometers
atomic beam velocity selection, using laser light resonances radiation pressure 2—34411
neutrons, cold, high resolution velocity selector using two rotor phased chopper system 2—27893
Particles *see Elementary particles; Energy loss of particles; Scattering, particles; and under individual particles, e.g. Protons and antiprotons*
Paschen-Back effect *see Spectra*
Patterson diagrams *see X-ray crystallography/calculation methods*
Peierls-Nabarro force *see Crystal imperfections/dislocations; Internal friction*
Peltier effect *see Thermoelectricity*
Pendellosung fringes *see X-ray crystallography*
Pendulums
critical points, as illustration in lattice dynamics teaching 2—17163
immersed in viscous fluid, reson. 2—30831
parameter excited, stability, rheo nonlinear oscillator 2—27119
reed, for internal friction meas. of ceramics 2—25604
rotating, analytic investigation of resonant oscillations 2—37669
simple, suspended from vibrator, Melde experiment to measure tension in cord 2—14148
torsion, oscillations, damping, magnetoelastic effects 2—149
torsional, calibration for measurement of liquid viscosities 2—39346
Periodic system
see also Elements
No entries
Permalloy *see Iron alloys; Nickel alloys*
Permeability, magnetic *see Magnetic properties of substances; Magnetization process*
Permeability, mechanical
see also Diffusion in solids
of anisotropic nonuniform porous media, second-order symmetric tensor regardless of preferred orientation of pores 2—1265
concrete, migration of moisture 2—15948
flow of gases through steel capillaries, temperature dependence 2—18731
interpolymer membranes, and selectivity 2—12557
polyethylene membranes, permeability and diffusion coefficients of dimethyl sulphoxide 2—35752
polyethylene membranes, permeation of gas and liq. propane and propylene 2—25066
polymeric membranes, press. effect on gas permeability coeffs. 2—35691
porous media, rel. to compaction press. 2—39966
quartz, fused, of gas 2—25471
rock from carboniferous strata, effect of triaxial stress 2—13603
zeolites, liquid metal filling of marrow channels 2—1384
O_2, through Ag membrane 2—25461
Permittivity
acetone, Deybe dispersion, l.f. meas. 2—9151
N-acetyl-2-thiohydantoine, i.r. spectra 2—5957
alcohol-alkyl halide mixtures, meas. in 50 Hz to 5 MHz range 2—9152
alcohol-water mixtures, temp. coeff., continuous analysis applic. 2—9153
alcohols, normal aliphatic, dissolved in CCl_4, complex dielectric constant and domains of concentration 2—39381
alkali halide, dielectric constant 2—32877
alkali halides, strain depend., calc. 2—40035
ε-aminocaproic acid aqueous solns., Debye effect, conc. and temp. depend. 2—21996
antiferromagnetic conductor, dielectric const., giant Zeeman effect 2—40540
benzene, monosubstituted derivatives, complex permittivities in liquid phase at microwave frequencies 2—35779
t-butyl chloride, liquid, molecular rotation, dielec. relaxation 2—18843
t-butyl chloride, rel. to solid state phase transitions 2—36352
butyl rubber, additive effects 2—22609
n-cetyl alcohol and its solutions, anomalies near f.p. 2—3443
cholesteryl laurate, temp. depend. on cycling, supercooling 2—35781
complex, derivation of phenomenological equation 2—220

Permittivity continued
complex, meas., quasioptical technique 2—23485
complex, measurement methods up to 13 GHz, application to water, ethanol and aqueous solutions 2—9150
copper formate tetrahydrate, from dielec. response function 2—13322
cubic crysts., dielec. const. static and h.f., strain dependence 2—36576
dielectric two phase media, ponderomotive force calc. 2—37870
diglycine sulphate, temp. depend. 2—36594
dimethylsulphoxide, microwave freq. region, dispersion obs. 2—21994
Earth half-space, from radiation impedance of a frame antenna 2—30220
effective dielectric tensor for e.m. waves in weakly inhomogeneous media 2—20979
egg yolk lecithin in hexane soln., high field meas. 2—28885
N-ethyl-phenothiazine-iodine complex, at 10 GHz 2—22544
ferrites with low losses in 2cm range of wavelengths unit for det. 2—34283
ferroelectric, displacive type, phenomenological theory 2—29751
ferroelectric ceramic, coarse grained, rel. to internal stresses 2—16280
ferroelectric solid solution, effect on transition temp., theory 2—19766
ferroelectric solid solution, thermodynamic theory 2—19767
ferroelectric-ferromagnetic ceramics, two- and three-phase 2—10117
ferroelectrics, temp. dependence of dispersion 2—16261
fused salts, Clausius-Mosotti relation, rel. to complex ion structure 2—39378
ground consts. determ. from mutual impedance of coplanar loops 2—30228
haloalkane solutions, effect of solvent viscosity 2—18846
hydrogen-bonded complex containing solvents, rel. to solvent effect on proton transfer 2—8555
ice:KCl, freq., conc. and temp. depend. 2—16264
ice, dielec. const. meas., 35.3 and 94.5 GHz 2—16265
kaolinite, dielectric constant and loss during dehydration 2—33045
Langmuir film, C-V relations 2—4273
liquid, low loss, dielec. const. and tan δ meas. in V-band 2—28880
long chain alcohols, meas. in pure liquid state at varying temp. 2—39388
lunar soil, and analogues, relative permittivity, determ. by Q-meter method 2—33727
measurement at X- and S-band frequencies 2—35779
measurement method at microwave frequencies using open resonator 2—2323
metahalloysite, dielectric constant and loss during dehydration 2—33045
metallic conductor, nearly-one-dimens., model 2—25761
m-nitroaniline, rel. to possible electrooptic appl. 2—16427
nylon-water suspension, using resonant cavity technique 2—9189
organic semiconductor, photodielec. effect 2—6898
perovskites, ferroelec. antiferroelec. and paraelec. comparative behaviour 2—1555
polar dielec. material, complex permittivity, theory 2—22604
polar liq., thermal variation of Cole-Cole distrib. parameter 2—9145
polar media, rel. to scattering of neutral particles, theory 2—22605
poly-L-lysine and salts in aqueous solution, relax. and dispersion 1 kHz-3 MHz 2—25101
polymer film, electron-beam-deposited, bombarding current depend. 2—32994
polytetrafluoroethylene film, r.f. sputtered 2—29049
polyvinyl chloride compound, degradation, dielec. spectra and a.c. cond. obs. 2—15645
polyvinyl chloride film, electric discharge effect, dielec. props., mechanical strength 2—16269
powder-like mixture for u.s. amplification 2—6670
powders, correlation with bulk permittivity 2—22602
proline in aqueous soln., Debye effect at microwave freqs. 2—3402
protein powders, temp. and hydration depend. 2—29057
quartz, capacitor meas. 2—33048
quartz glass, u.h.f. and high temp. 2—19746
refractory metal oxide, film, prep. by ionized gas anodization 2—13301
Rochelle salt, contrib. of domain wall motion 2—36575
semiconductor, Ge, amorphous film, effects of reactor irradiation 2—4232
semiconductor, microwave meas. 2—16233
semiconductor, zero-gap, in quantizing mag. field, l.f. case 2—22603
semiconductor prism, relation to reflection factor obs. using microwave technique 2—22555
semiconductors, det. at microwave frequencies 2—34239
1,2,4,5-tetrachlorobenzene, phase transition at ~233K, confirmation by dielec. const. meas. 2—28419
thermophysical properties of fluids 2—18813
transition metal nitrates, ethanol solutions, meas. at 28°C and 3.14 cm wavelength 2—35778
tri (n-butyl) ammonium picrate and diode, in polar solvents, permittivity and loss 2—1110
triglycine selenate, near phase transition pt. 2—29757
triglycine sulphate, effect of X- and γ- radiation 2—1560
triglycine sulphate, ferroelec., nonlinearity, second harmonic detection 2—33062
water, deionized, using resonant cavity technique 2—9189
water, microwave freq. region, dispersion obs. 2—21994
Ag halides, space charge layer contrib. to dielec. const. 2—33050
Ag halides, space charge layer contrib. to dielec. const. 2—40330
AgCl, rel. to exciton annihilation 2—4297
$AlCl_3$, hydrated and anhydrous, rel. to dielectric behaviour of water of hydration 2—36578
Al_2O_3, film, for gate insulation and passivation 2—1556
Al_2O_3, film, for gate insulation and passivation 2—1557
Al_2O_3, sintered with vitrifying additives 2—36199
Al_2O_3 film, formed by electron-beam evaporation 2—35884
B_2O_3, amorphous films, from in situ meas. of capacitance 2—4265
$Ba_2Na_{1-x}Li_xNb_5O_{15}$, ferroelectric, and cryst. growth obs. 2—29097
$BaTiO_3$:Nb, dielectric const., temp. and freq. dependencies, rel. to grain growth 2—1568
$BaTiO_3$, Al_2O_3 additive effects 2—16284
$BaTiO_3$, d.c. bias depend. 2—33049
$BaTiO_3$, dispersion characts. and freq. depend., 10^2-10^9 Hz range 2—6880
$BaTiO_3$, microwave freq. obs. 2—33046
$BaTiO_3$, temp. and heat treatment conditions depend. 2—16283
$BaTiO_3$, undoped, Sc_2O_3- and Ln_2O_3-doped 2—19761
$BaTiO_3$ powder, effect of adsorbed H_2O 2—16282
$Bi_4Ti_3O_{12}$, layer struct. ferroelec. 2—13316
$CaSO_4$, hydrated and anhydrous, rel. to dielectric behaviour of water of hydration 2—36578
Cd_2TiWO_7, growth, struct., dielec. loss 2—39638

Permittivity continued
$Cr_2(SO_4)_3$, hydrated and anhydrous, rel. to dielectric behaviour of water of hydration 2—36578
CuCl, temp. depend., rel. to Raman and electro-optic props. 2—22784
$Cu(NO_3)_2$, hydrated and anhydrous, rel. to dielectric behaviour of water of hydration 2—36578
n-GaAs, bulk, high-field microwave obs. 2—10015
GaSe, GaS, complex permittivity, evaluation from abs. reflectivity meas. 2—29741
Gd, polycryst., dielec. const freq. depend., optical consts., in i.r. range 2—19960
Ge, amorphous film, effects of reactor irradiation 2—4232
p-Ge, dielec. const., Drude-Zener formula, valence band interband transitions effects 2—25858
KAg_4I_5, cationically disordered compound 2—36585
$(K_{3/4}Bi_{1/4})(Zn_{1/6}Nb_{5/6})O_3$, temp. depend. 2—4266
KD_2PO_4, 300-500K, rel. to phase transition 2—22624
KH_2PO_4, 300-500K, rel. to phase transition 2—22624
KH_2PO_4, finely divided, Curie pt. phenomena 2—10121
KH_2PO_4, type ferroelectrics, temp. dependence of dispersion 2—16261
KH_2PO_4 and KD_2PO_4, high temp. anomalies 2—9814
KI, temp. dependence obs. 2—4267
K_2SO_4, microwave region using heterogeneous mixture method 2—36581
Li halides, rel. to Gruneisen parameter calc. 2—36319
$LiNbO_3$, temp. and freq. depend. 2—1571
Li_2O-BaO-Al_2O_3-SiO_2 system, equilibria, dielec. losses, specific vol. resist. 2—16266
Li_2SO_4, microwave region using heterogeneous mixture method 2—36581
$NH_4H_2PO_4$, far-i.r. absorpt. spectra in antiferroelec. and paraelec. phases 2—16494
$NH_4H_2PO_4$, finely divided, Curie pt. phenomena 2—10121
Na-NH_3 solution, 2.5-70 GHz, electron states determ. 2—12573
NaCl, epitaxial film, dielectric properties 2—10109
NaCl, solution in glycerol, rel. to ionic radii determination 2—15610
Na_2O-Al_2O_3-SiO_2 glass, temp. depend., X- and Q-band 2—29742
Na_2SO_4, microwave region using heterogeneous mixture method 2—36581
$Pb(Cd_{1/3}Nb_{2/3})O_3$ ferroelectric, cryst. growth, hysteresis, spontaneous polarization 2—19768
$Pb(Mg_{1/3}Nb_{2/3})O_3$-$PbTiO_3$-$PbZrO_3$ solid solution, piezoelec. characts. 2—13327
$PbNb_2O_6$-$BaNb_2O_6$, ceramic system, rel. to domain and grain struct. 2—29739
$5PbO.3GeO_2$, ferroelec. cryst., elastic, piezoelec. and dielec. constants 2—22617
$PbTiO_3$-$PbZrO_3$-$Pb(Zn_{1/3}Nb_{2/3})O_3$ system, dielec. props. near morphotropic phase boundary 2—33058
$Pb(zr_xTi_{1-x})O_3$, ceramic, maximum at morphotropic phase boundary 2—4280
RbH_2PO_4, 300-500K, rel. to phase transition 2—22624
RbH_2PO_4, high temp. anomalies 2—9814
SbSI, ferroelec. phase transition, long wavelength optical phonons, Raman spectra 2—16459
SbSI, ferroelectric, phase transition, soft mode coupling, Rayleigh scatt. 2—16012
SbSI, photon energy depend. of imaginary component 2—33059
SbSI, time depend. after polarization switching 2—10125
SbSI crystal, dielec. dispersion 2—29754
$Sb_2S_3(Se_3)$, 10 to 80 GHz 2—29743
Se-Te alloy, dielec. tensors 2—1558
Si:P complex permittivity obs. 2—22555
p-Si:Zn, P, photodielec. effect, polarizability of neutral atoms 2—13343
Si, freq. and wave vector depend. dielec. function 2—33018
Si, low temp. meas. 2—16241
α-SiC, determ. from refr. index 2—10395
$Sr_{0.75}Ba_{0.25}Nb_2O_6$ temperature dependence, freq. 10 kHz-10 MHz, use for light modulation 2—4268
$SrTiO_3$, d.c. bias depend. 2—33049
$SrTiO_3$, from zero to optic freqs. 2—40359
Ta_2O_5/Al_2O_3 mixture, anodic 2—3548
Ta_2O_5, film, effective dielec. const., current transport 2—6872
Ta_2O_5 film, amorphous, complex dielec. const., thickness effects 2—40326
TiO_2, rutile, dielectric loss mechanism 2—22608
TiO_2 film, amorphous, dielec. const. freq. depend., Cole-Cole diagrams 2—40327
TlBr, static dielec. const., isochoric temp. depend., anharmonic interactions 2—19403
$TlGaS_2(Se_2)$ single crystals 2—29677
$TlInS_2$ single crystals 2—29677
TlX, (X=halogen) and mixed systems, ferroelec. precursor 2—25933
V_2O_5-P_2O_5 glass, dielec. const., conductivity, 80-350 K 2—19749
VO_2, complex dielec. const., reflectivity obs. 2—33245
V_2O_5, single crystal, temp. dependence rel. to elec. props. 2—10038
Y_2O_3, sintered, relax. phenomena 2—16268
$Zn_xNi_{1-x}Fe_2O_4$, effect of Dy substitution 2—13413
ZnS, phosphor, photodielec. effect response. photocapacity measurement 2—10144

Perturbation theory
alloy, systematic treatment for Fermi energy and energy shift evaluation 2—40140
Brillouin -Wigner theory, derivation using Dirac formalism comparison with Rayleigh-Schrodinger theory 2—27062
Brown's lunar theory, analysis of approximations 2—1937
core polarization in alkali-like atoms, non-adiabatic approach 2—18279
coupled Hartree-Fock perturbation equations, exact solutions 2—31633
covalent semiconductors, vacancy formation and migration energies 2—18964
crystal electrons, in strong elec. field, Boltzmann equation 2—22450
delta function model of one-electron diatoms, energy, branch-point singularities 2—15272
diagrammatic representation arising from derivation of exchange interactions 2—11309
dislocation loop, electron micrographs, analytical expresson for black-white contrast figures 2—22204
dispersion theoretic perturbative methods 2—5142
distinguishable electron method appl. to three- and four-electron atoms 2—15199
e.m. cascades, perturbation theory formalism, study of transition effect 2—23949
e.m. radiation in magnetoplasma 2—35480

Perturbation theory continued
e.m. waves, scattering from perfectly conducting sinusoidal surface 2—30932
energy and effective charge calcs. in nuclear systems, procedure for checking 2—14908
expanding Universe spherical perturbations, rapid growth rel. to expanding anisotropic world models 2—26586
finite perturbation theory in INDO approximation for molecular calculations 2—28331
fluids, stationary homogeneous turbulence 2—15433
functional analysis calculations method compared 2—37617
generalized oscillator phase operators, continuity of spectra 2—5139
Green function derivation of stationary and time-dependent theory, distinction between real and virtual processes 2—11282
Hamiltonization of non-Hamiltonian systems, Lie transforms 2—17232
hard-sphere equation of state, calculation of high pressure vapour-liquid equilibria 2—22037
harmonic oscillator, large-ω asymptotic expansions, Pade approximants 2—17235
Hill determinant appl. to anharmonic oscillator 2—17233
inelastic electron scattering on finite nuclei, calc. of response function by solving Bethe-Goldstone like eqn. 2—2765
interacting bosons at absolute zero, perturbation theory based on currents 2—27100
intermolecular forces, appl. to H-bonds between first-row atoms 2—28257
Karplus-Kolker approximate uncoupled Hartree-Fock perturbation theory 2—18269
Kato perturbations, class of zero-dimensional models 2—2136
LEED, t-matrix formulation of perturbation approach, comparison of theory and expt. for Al, Ni 2—25169
ligand field theory calculations, effective perturbation method 2—38874
many electron atom, interaction with light and electronic interaction 2—28206
many-electron systems, many-particle correlations, all orders 2—27063
MHD flow, two-dimens., near mag. neutral line, perturbation theory 2—39078
molecular vibration-rotation energies, remarks on two-step procedure for calculation 2—8536
molecules, electric polarizabilities calc. 2—38986
nonlinear boundary value problems, perturbation operators 2—23276
nuclear anharmonic oscillations 2—34899
one- and two-electron diatomic molecules, ground state energy calc. by double perturbation theory with screening const. 2—8635
plasma, finite amplitude ion wave, nonlinear behaviour 2—15485
plasma, nonlinear wave with Landau damping 2—18651
probability density, classical limit for perturbed change in Hamiltonian 2—17227
prompt jump approximation, error estimation by singular perturbation theory 2—38692
quantum, microwave radiation on molecular dipoles, resonance interaction calculation 2—24419
quantum field theory, equal-time terms and convolutions of tempered distributions 2—8073
quantum field theory, nonpolynomial Lagrangian 2—8060
radial distribution function of a fluid with a soft core, expansion 2—21724
Rayleigh-Schrodinger, calc., of electron correlation energy of closed systems 2—35109
Rayleigh-Schrodinger, degenerate, soln. for energy and wave function 2—76
Rayleigh-Schrodinger, in calculations of hyperfine splittings 2—18389
Rayleigh-Schrodinger, perturbation parameter, change of variable 2—14108
Rayleigh-Schrodinger perturbation theory application to H atom 2—21539
Rayleigh-Schrodinger theory, derivation using Dirac formalism, comparison with Brillouin-Wigner theory 2—27062
reactor integral characteristics, relation with conventional perturbation theory 2—75
reduced Hamiltonian of near-symmetric rotor molecule deduced 2—21565
renormalizable massive vector meson theory, perturbation theory of the Higgs phenomenon 2—31303
renormalization perturbation theory and degenerate potential 2—74
rotating polytropes, series-expansion method employed 2—30451
scattering, high energy, cluster decomposition properties of φ^3 amplitudes 2—348
SCF LCAO MO constrained eqns. solution 2—31757
secular stability of stars, onset of complex roots 2—7415
self-consistent, solvent molecular motion effects on nuclear spin-spin coupling constants 2—18395
singular perturbation problems, degenerate forms having many solns. 2—33966
spin-orbit coupling in formaldehyde and azulene molecules studied using CNDO/S wavefunctions 2—12091
statistical semigroups, in quantum statistical mechanics 2—2162
stresses around elliptical hole in cylindrical shell 2—27131
thermal transport coeffs. calc. of self-diffusion coeff. using high temperature perturbation theory in Kubs-Green method shown to be invalid 2—30826
thermodynamic for fluid of molecules interacting via Stockmayer potential 2—39024
third order, for exponential Lagrangians 2—34570
three dimensional harmonic oscillator, high order theory for generalized central field perturbation 2—7680
three-body collisions, use of theory to overcome problems in separable expansion treatment 2—24195
three-electron atoms and ions, perturbation treatment of Hartree Fock equations for resonance states 2—8435
three-particle scattering, investigation of and relationship of two types of treatment 2—23278
uncoupled Hartree-Fock perturbation theory, improved, appl. to second order atomic props. 2—5772
Usachev-Gandini perturbation theory, formal functional treatment and variational principle 2—38684
variational, applic. to ground state energy calc. for ten-electron hydrides 2—15273
wave operator formalism, applic. of variational methods in variation-perturbation theory and energy bound theory 2—11283
ep scattering, deep inelastic 2—34619
ep scattering, derivation of asymptotic sum rule 2—383
Al_2O_3-Cr_2O_3, e.p.r. spectra, optical fluorescence spectra, obs., quantitative explanation 2—4549

Perturbation theory continued
Be atom, effect of unitary transformations among occupied orbitals, pair energies, relation to perturbation theory 2—35115
GaP, i.r. generation by coherent excitation of polaritons 2—16458
He atom, 1/Z expansion convergence 2—18307
Li atom, 1/Z expansion convergence 2—18307
MgO, iterative calc. by perturbation of configuration interaction for fundamental and first excited states 2—35263
N_2, SCF LCAO MO constrained eqns. soln. 2—31758

pH *see Electrochemistry*

Phase-contrast microscopy *see Microscopy*

Phase diagrams *see Phase equilibrium; Phase transformations*

Phase equilibrium
see also Solubility; Solutions
acetic acid-trichloroethylene system, isobaric equilib., consistency of data 2—1144
acetic anhydride-cyclohexane binary liquid system, crit. behaviour in phase boundary 2—35736
actinide-platinum metal-carbon system, C-stabilized ordered phase form. 2—29493
alkali metal tungsten bronzes, phase diag. determ. from electrochem. prep. process obs. 2—10633
alloy, binary, liquid-liquid equilibr., Gibbs energy of mixing 2—32241
alloy, binary liquid, elec. cond. obs. of critical behaviour 2—18790
alloy, binary system, T_0-p-c diagram 2—13009
binary alloy system, phase stability and bond types 2—39999
binary mixtures with component assoc., semi-integral criterion for consistency of liq.-vapour data 2—1143
boiling, binary and multicomponent systems 2—6286
boundary obs. using quantitative image analysis 2—6279
carbon tetrafluoride binary mixtures, critical phenomena at low temp. and high pressure 2—9108
critical point, microscopic foundation to scaling theory 2—15627
crystal growth, Czochralski method, crystn. front, effects of heat exchange 2—9362
cyclohexane-aniline binary mixtures, study of critical behaviour by light diffusion 2—35764
cyclopentane, critical region scale law, verification 2—25151
daltronides, berthollides and inorganic glasses, review 2—18896
diagram, digital computer calc. 2—13008
diagram, of the two ordering phases with $L1_0$, $L1_2$ superstructs., computer calcs. 2—32784
electron probe microanalysis appl. to determ. of equilibrium diagrams 2—4622
finite system, critical pts., and scaling laws 2—14133
fluid mixtures, calc. of phase behaviour under high pressure 2—9106
fluid mixtures, phase behaviour and critical phenomena under pressure 2—9105
gas, high temp., mass spectrometry appl. 2—18872
gas-gas, two-component lattice-gas model 2—9025
glass systems, phase separation 2—32316
group III-V systems, ternary, calcs. from thermodynamic props. 2—22354
high temp., electron microscope exam. techniques 2—9435
high temp. mats., conf., Gaithersburg, USA, Oct. (1971) 2—9326
hydrocarbon-water mixtures, phase behaviour and critical phenomena 2—9109
hydrocarbons, vapour-liquid equilibrium distribution ratios computed by new equations 2—32308
Laves phases, physical props. 2—9476
liquid crystal mixtures, mol. field treatment 2—9093
liquid-gas, semistatistical theory 2—9213
liquid-solid, coexistance, on melting of natural garnet and spinel lherzolites at high pressures 2—25155
liquid/saturated vapour, crit. constants effects 2—28950
macromolecular solutions, phase separations at high pressure 2—9076
metal interface, diffusional kinetics of intermetallic phase form., theory 2—36074
metal-B-N stystem, chemical bonding, crystal and electronic struct. 2—29489
metal-sulphur-oxygen systems, solid-gas equilib., chem. pot. diagram 2—22047
metallographic chart construction, statistical method 2—6642
mica solid solution, formation between $K_2Mg_6Al_2Si_6O_{20}F_4$ and Al-free mica 2—36302
multicomponent melts, liquidus temp. determ. 2—1140
multiphase molecular system, orbital electron photoexcitation effect, thermodynamics appl. 2—25136
Na_2O-B_2O_3 glass, effect of liquation on mech. and viscous props. 2—35848
Nb_3Al-Nb_3Ga-Nb_3Ge, alloy, pseudoternary system, investigation of certain sections 2—6617
noncondensed system, high pressure-high temperature, research techniques, book 2—41361
n-paraffins, high press. phase relations 2—15629
phase diagrams and their importance in non-destructive testing theory 2—6643
polystyrene-cyclohexane system near upper critical segregation temperature, thermodynamic functions determ. from light scattering meas. 2—35772
quartz-coesite equilibrium, anvil apparatus 2—15973
rare earth metal hectoboride phase, lattice parameters and Knoop hardness 2—9833
rare earth oxide (R_2O_3)-WO_3 system, cpd. formation, stoichiometry 2—9339
rare earth-platinum metal-carbon system, C-stabilized ordered phase form. 2—29493
refractory composition solid phase coexisting with periclase and liq. phase, microstruct. parameters 2—32776
solid soln., equil. estab. processes in non-equil. solns. with short-range order 2—9764
solid solution, as-cast struct., time-temp.-dissolution diagram 2—36297
spinel-type minerals, spin pairing of Fe(II), and corresponding phases 2—40584
steel, austenitic, interaction of C with Cr, Mo and W 2—32787
steel, austenitic stainless, 20%Cr-25%Ni, localized melting 2—36301
steel, basic metallurgy for non-destructive testing 2—29492
steel, high Al content, martensite and residual austenite struct. 2—12724
steel, low C, chemical analysis of Nb 2—1741

Phase equilibrium continued
steel, martensitic phase diagrams, mech. and thermal treatment effects 2—9834
toulene, in microscopic capillaries, liq.-vapour equilib., concave surface effect on v.p. 2—35829
transition metal oxides, mixed, phase diagram 2—36533
transition metal silicides and germanides, TT′Si(Ge) type, struct. relns. 2—18969
two phase system, dispersed particles, model, equilib. values, numerical solns. 2—29412
two phase systems, finely dispersed state, thermodynamic stability 2—25583
vapour-liquid, at high pressure, calculation with perturbed hard-sphere equation of state 2—22037
vapour-liquid equilibrium correlations, single-parameter equation describing binary and ternary behaviour 2—25147
water-inert gas mixtures, gas-liquid equilibria and critical curves 2—9107
Ag-Gd system, intermetallic cpd. formation 2—22375
AgI-Ag_2SO system, phase diagrams 2—39997
Al-Co system, intermetallic phases, peritectic transformations 2—4014
Al-Cu system, Al_2Cu phase dissolution 2—36297
Al-Ge system, metastable phases, obtained by rapid solidification 2—36296
Al-Mg system, with 0.5wt% Ag, solubility of α-phase 2—12955
Al-Mo system, high temp. phase struct. 2—4015
Al-Zn solid solution, activity meas., thermodynamic props. 2—4059
AmO_x, phase relns. and oxygen dissoc. press. obs. 2—9217
Ar, liquid-vapour isotope fractionation from triple point to critical point, mean Laplacian of intermolec. potential 2—39432
As-I system, interaction and vapour comp. 2—28934
As-S-Sn system, glass and cpd. formation, n.m.r. study 2—37003
As_2Se_3-Cu_2Se system, existence of ternary cpds. 2—29488
B-C-Si system, binary cpds. 2—32785
B_2Se_3-Tl_2Se system, DTA, X-ray, hardness and microstruct. study 2—36274
Ba-Cu, system, thermal and differential thermal analysis, phase diagram 2—3955
BaF_2-SrF_2 system, liquidus and solidus, DTA, X-ray diffr. 2—1407
BaO-B_2O_3 glass, effect of liquation on mech. and viscous props. 2—35848
BaO-Ln_2O_3 system, (Ln=rare earth), 1200-2450° C DTA and X-ray analysis 2—12991
BaO-Ni(Co)O-O-CO_2 systems, aragonite and 2H $BaNiO_3$ type phases structural relations 2—9454
BaO-TiO_2-Al_2O_3 system, ternary cpd. identification, X-ray anal. 2—29462
$Ba_xSr_{1-x}Nb_2O_6$ solid solution cryst. growth, stability regions 2—25271
Bi-Sn alloy, metastable phase BiSn formation under pressure, kinetics, Mossbauer obs. 2—9794
Bi, pressure-temp. phase diagram at low temp., elec. resistivity obs. 2—25619
Bi, triple pt., 41 kbar and 175°C, press.-temp. phase diagram 2—32304
Bi_2Te_3-BiI_3-Te, structure, phase composition and props. 2—3982
BkO_x, phase relns. and oxygen dissoc. press. obs. 2—9217
CO_2-HE-ethylene system, immiscibility at 13 to 70°C and up to 5kb 2—12503
CS_2-acetic anhydride binary liq. system, critical phenomena in coexistence curve 2—3357
Ca-Cu, system, thermal and differential thermal analysis, phase diagram 2—3955
CaO-Al_2O_3-CaF_2 system, diagram 2—15982
CaO-IrO_2-Ir system, phase relatives in air 2—25620
CaO-MnO-SiO_2 system, glass formation region 2—36579
CaO-Nb_2O_5-TiO_2-SiO_2, liquidus detn. in the 15% SiO_2 plane 2—9204
CaO-SiO_2-H_2O system, influence of surface-active materials on hydrosilicate comp. 2—36298
CaO-ZnO-B_2O_3 system, X-ray diffr. 2—22376
$CaO.Nb_2O_5$-$CaO.SiO_2$-TiO_2, plane in quaternary CaO-Nb_2O_5-TiO_2-SiO_2 system, liquidus temp. determ. 2—3431
$CaSo_4.{}^1/_2H_2O$, i.r. spectral characterization of γ and β phases 2—10367
Cd-Sn-Zn alloy system, liquidus temperature determ. 2—1140
Cd-Te, partial pressures and thermodynamic props. 2—12619
Cd-Te system, rel. to CdTe single cryst. growth 2—36500
CdF_2-$CaF_2(PbF_2)(ZnF_2)$ systems 2—15983
CdS-$CdCl_2$ system, differential thermal anal. 2—1408
CdSb-Ge system, diagram 2—29490
Cd_3Se_3-In_2Se_3, phase diagram 2—4017
CdTe, rel. to cryst. growth by modified Bridgman method 2—9363
Ce-Fe-B system, intermediate cpd. existence 2—29491
Ce-Ge system, diagram, existence of germanides 2—9832
CmO_x, phase relns. and oxygen dissoc. press. obs. 2—9217
Co-Se system, P-T diagram 2—12609
Co-Te system, phase relns. and thermodynamic props. 2—19311
Co, electrodeposited, phase comp. effect on mag. props. 2—1624
$Co_{3-x}Mn_xO_4$ solid soln., form. in O_2, Ar and air atm. at 1000°C 2—39921
Cr-Ge alloy, at high Cr content 2—32761
Cr-N system, thermodynamic relations 2—22377
Cr-Si-C, phase diagram, survey of Cr-rich area 2—40001
Cr-Tb system, diagram 2—40002
Cu-Al alloy, $(\alpha+\beta)$-two-phase region boundaries, metallography 2—22374
Cu-B, phase diagram, reassessment 2—3432
Cu-Fe-O, diagram, for construction of Cu-Fe-S-O diagram 2—4012
Cu-Fe-S-O, from phase diagrams for 3-component systems 2—4012
Cu-Fe-S, diagram, for construction of Cu-Fe-S-O diagram 2—4012
Cu-Ga, quenched hypereutectoid alloy, microstructure 2—9580
Cu-In-Te system, homogeneity region 2—1410
Cu-Mn, Cu-Ni alloys, diag. rel. to solidification 2—28936
Cu-Ni-Pd system, struct., 400-700°C, X-ray obs. 2—3705
Cu-Ni-Zn alloy, elec. resist. study 2—25641
Cu-S-O, diagram, for construction of Cu-Fe-S-O diagram 2—4012
Cu_3As-Cu_3P, constitution diagram 2—1409
Cu_2In, diagram, existence of NiAs struct. 2—32455
$Cu_{1-x}Ni_xCr_2O_4$, Jahn-Teller theory of crystal distortions 2—16411
EuO, phase diagram 2—32786
Fe-Cr-Zr system, α-γ-δ type polymorphism 2—4018
Fe-Cu-C system, diagram deduced from C activity study 2—40006
Fe-Mo-Co system, 1205, 1095 and 980C 2—40004
Fe-Mo-O system, 900°C section of phase diagram 2—40008
Fe-Ni-Cr-C system, austenite phase, equilib. C content determ. 2—40007
Fe-Ni-graphite, alloy, sintered, X-ray study 2—12938
Fe-Ni steel, austenitic phase stability, heat cycling effects 2—29436
Fe-Ni system, metastable equilib., T_0-p-c diagram 2—13009

Phase equilibrium continued
Fe-S-O, diagram, for construction of Cu-Fe-S-O diagram 2—4012
Fe-Si, high temp. phase stability, rel. to elastic consts. 2—9633
Fe-Sn compound, C influence, diffusion couple method 2—9835
Fe-W-O system, 900°C section of phase diagram 2—40008
Fe, cast, effects of O, S and trace elements on quality 2—12970
Fe rich alloy, δ-ferrite annealing, high temp. struct. 2—15964
Fe(N) sheets and foils, phase relations and epitaxy 2—39539
$Fe_{1-x}Ni_xCr_2O_4$, Jahn-Teller theory of crystal distortions 2—16411
Fe_2O_3-Fe_3O_4-liquid equilibrium conditions at oxygen pressures up to 53 bar 2—9808
FeO-SiO_2-TiO_2, phase relns. at high temp., high press. 2—9205
Ga-As-P system, rel. to $GaAs_{1-x}P_x$ prep. 2—12700
Ga-GaAs-GaP, phase diagram, liq.-solid curve, expts. and calcs. 2—22034
Ga-Hg system, shape of coexistence curve near T_c 2—15578
Ga-Sb-Se system, stratification region 2—35845
Gd_2O_3-SrO system, DTA study 2—29472
Gd_2O_2S-La_2O_2S, phosphor host material 2—13010
Ge-Cl_2-H_2 system, reactions 2—30037
Ge-S system, fusibility diagram 2—1138
Ge-Se-Te system, limits of glass-forming region 2—35846
$GeSe_2$-Te system, stratification regions and glass formation 2—35847
He-NH_3-N_2 system, immiscibility at 90 to 140°C and up to 3kb 2—12503
HfO_2-Y_2SiO_5 system, annealing, X-ray and optical studies 2—1411
HfO_yN_z, diagram 2—1397
HgS-HgI_2, system, existence of $Hg_3Si_2I_2$, rel. to electrooptic modulator prod. 2—35936
In-Ga-P system, rel. to epitaxial growth of $In_xGa_{1-x}P$ 2—9837
In-Ga-P ternary phase diagram 2—36295
In-Ga-Sb system, rel. to epitaxial growth of $In_xGa_{1-x}Sb$ 2—9836
In-Ga system, thermodynamics and phase diagram 2—15984
$In_xGa_{1-x}As$, phase diagram, crystal growth, and band struct. 2—19004
La_2O_3-GeO_2 system, crystallization, X-ray and optical obs. 2—1209
La_2O_3-Yb_2O_3 system, high temp. phase diagram 2—25642
Li-Se, miscibility gap and Li_2Se intermediate phase 2—13011
$LiAlSiO_4$-$LiGaSiO_4$-$LiAlGeO_4$-$LiGaGeO_4$ system, struct. 2—12728
Li_2O-Al_2O_3-SiO_2 glass, metastable phase separation and crystn. 2—25161
Li_2O-BaO-Al_2O_3-SiO_2 system, permittivity, dielec. losses, specific vol. resist. 2—16266
Li_2O-Na_2O-Fe_2O_3 system, intensification of ferrite formation 2—36303
$LiXO_4$, X=P, V, As, and $Li_2M^{2+}X_1{}^{4+}O_4$, M=Zn, Mg, X_1=Ge, Si 2—18966
Ln_2O_3-ZrO_2, phase transformations, phase diagrams, structure, thermal analysis, X-ray obs. 2—4008
$MgCO_3$-$NiCO_3$ system, crystal chemistry, stability relations 2—12999
MgO-Fe_2O_3-SiO_2 system, triangular phase diagram 2—29494
MnO-FeO-ZrO_2-SiO_2, liquidus temp. region, quenching technique 2—13012
MnO-P_2O_5-$MnCl_2$ system, rel. to Mn_2PO_4Cl cryst. growth 2—22111
Mo-Mn-C system, X-ray study 2—13013
Mo-Nb-Hf alloy, metallography, X-ray analysis, hardness 2—4019
Mo-W-O system, ternary phase formation 2—22378
NH_4HF_2, melting curve, high press. polymorphism 2—25141
$NaCl$-KCl-$CaCl_2$-UCl_3-UCl_4 solid systems, phase diagrams 2—39998
Nb-Al-Ce(La)(Y)(Pr) alloy, hardness rel. to comp. and annealing 2—4021
Nb-C-Re system, intermetallic cpd. structs. 2—36304
Nb-H system, ferroelasticity rel. to phase diagram determination 2—9694
Nb-Mo-N system, diagram 2—19314
Nb-Mo-N system, equilib. conc. and solubility of N_2 2—4020
Nb-Mo-N system, thermodynamics of α solid soln. 2—19313
Nb-Te system, phase study Nb_3Te_7 to Fe 2—9841
Nb-W system, phase diagram 2—39968
Nb_3Al-Ta_3Al system, annealing, solid solubility 2—9775
Nb_3Al-Ta_3Al system, solid solubility 2—9775
NbO_2-Nb_2O_5, Nb_2O_5-Nb_3O_7F systems, intergrowth phases, homogeneity 2—9336
Nd-Bi system, constitution diagram 2—1413
Nd_2O_3-ZrO_2 system, solid soln. and compound formation 2—29495
Ni binary alloys, solidified at fast cooling rates, metastable phases 2—36305
NiO-α-Fe_2O_3 fired mixtures, quantitative phase anal. 2—13014
NiO-MgO-Fe_2O_3 system, diagram 2—1414
NiS, press.-temp. phase diagram and cryst. struct. 2—26069
P-S(Se)-Sn system, glass and cpd. formation, n.m.r. study 2—37003
Pb-Bi system, contact melting 2—18879
Pb-Cd-Zn and Pb-Cd-Zn-Sn systems, digital computer calc. 2—13008
PbO-$PbSO_4$ system, diagram 2—36306
PbSe-SnSe, constitution diagram 2—1351
$PbZn_{1/3}Nb_{2/3}O_3$-$BaZn_{1/3}Nb_{2/3}$- $PbTiO_3$ system, struct. and dielec. study 2—25937
Pd-H, system, ferroelasticity rel. to phase diagram determination 2—9694
Pd-Si alloy, metallography, X-ray and thermal analysis 2—3435
Pd-W, system, X-ray diffraction study of phase diagram below 1100C 2—4022
Pu-C-O system, phase diagrams 2—12611
Re-O system, high press., $Re_{1\|x}O_3$ characterization 2—25346
$Sb_2Te_{2.9}$-Sb_2S_3, constitution diagram, in Sb-Te-S system 2—1415
Sb_2Te_3-Sb_2S_3, constitution diagram, in Sb-Te-S system 2—1415
ScO_x-actinide oxide systems, phase relationships 2—12610
Sn-Bi-As system Sn- and Bi-rich regions 2—22380
Sn-S-O-C, rel. to tin ore reduction 2—1150
Sn-S system, Mossbauer study 2—1674
Sn-Se system, Mossbauer study 2—1674
SnS-Sb_2S_3 system, compound formation 2—29496
SnS-Sb_2Se_3 system, diagram 2—29497
Sr-Cu, system, thermal and differential thermal analysis, phase diagram 2—3955
Ta-B system, diagram, determ. from thermal and X-ray anal. 2—13015
Ta-H system, ferroelasticity rel. to phase diagram determination 2—9694
Ta_2O_5-GeO_2 system, crystallization X-ray and optical obs. 2—1412
Ta_2VO_6-VO_2 system, evolution of crystallographic order 2—29153
Te-Ge-Se system, amorphous semiconductor, DTA obs. 2—29675
Th-N-O system, diagram 2—36307
Th binary alloys systems, phase diagrams 2—18262
Th hectoboride phase, lattice parameters and Knoop hardness 2—9833
Ti-Co system, intermediate phases 2—40010
Ti-Mo-Ni system, polythermal section, microstructure, resistivity, dilatometry, X-ray analysis 2—32788
Ti-Pd system, diagram 2—40011
Ti-Si-C system, rel. to complex carbide deposition 2—25213

Phase equilibrium continued
Ti-Zr-O alloys, phase characterisation 2—40009
Ti alloy, metastable phase decomp., volume changes 2—36308
Ti alloys, heat treatment microstructure 2—1350
(Tl, Na, Rb) NO_3, solid-liquid equilibria, polythermal projections 2—22035
(Tl,Na,Cs)NO_3 system, solid-liquid equilibria, polythermal projections 2—22035
(Tl,Na,Li)NO_3 system, solid. liquid equilibria, polythermal projections 2—22035
TlS-GaS system, diagram, intermediate compound form. 2—29498
U-C-O system, phase diagrams 2—12611
U-C-X, X=Ce, Nd, La, lattice parameter obs., solubility limits 2—9838
U-Pu-C-O system, phase diagrams 2—12611
U-Se-C ternary system, X-ray diffr., ceramography, electron microprobe analysis, 500-1400°C 2—29482
U-Si-Be system, phase relations 2—13016
U-Si system, diagram 2—40012
U-Te-C ternary system, X-ray diffr., ceramography, electron microprobe analysis, 500-1400°C 2—29482
UN-UC-Fe system, compatibility relationships 2—1416
U_2N_3, equilib. N_2 press., thermodynamic props. 2—7164
UO_2-$UO_{2.67}$-ThO_2 and $UO_{2\|x}$+NpO_2 systems, phase relations 2—1405
$UO_{2\pm x}$, composition changes, 1950 K 2—25637
V-D system, phase diagram 2—29247
V-H system, ferroelasticity rel. to phase diagram determination 2—9694
V_3Al-$Nb_3Al(Ta_3Al)$ system, annealing, solid solubility 2—9775
V_3Al-$Nb_3Al(Ta_3Al)$ system, solid solubility 2—9775
VN_xO_y, region of existence, cubic phase 2—1417
VO_2:Cr, struct. aspects of metal - insulator transition 2—25638
W-Mn-C system, X-ray study 2—13013
WC-Co, hard alloy cermet, Co melt redistribution process 2—32736
WV_2O_6-VO_2 system, evolution of crystallographic order 2—29153
Y-Ge system, thermal, microscopic, chemical and X-ray analysis 2—9839
Y_2O_3-Fe_2O_3-50PbO.40PbF_2.10B_2O_3 system, optimum comp. for ferrite and garnet crystn. 2—36291
Y_2O_2S-Gd_2O_2S, phosphor host material 2—13010
Y_2O_2S-La_2O_2S, phosphor host material 2—13010
Yb-Cd, system, phase diagram from differential thermal, microscopic and X-ray analysis 2—4024
Yb-Co system, cpd. formation, X-ray diffr. study 2—25349
Yb-Fe system, cpd. formation, X-ray diffr. study 2—25349
Yb-Ni system, cpd. formation, X-ray diffr. study 2—25349
Zn-Cu-Mg system, phase diagram, DTA, electron microprobe analysis 2—40013
Zn-Mg-Al system, constitution, metallography, magnetothermal and X-ray obs. 2—4025
Zn-Te, partial pressures and thermodynamic props. 2—12619
ZnO-B_2O_3 system, borate stability, temp. depend. 2—22368
ZnO-Nb_2O_5 system. cpd. formation 2—25644
ZrC-ZrO_2 system, oxycarbide stability 2—29499
ZrO_2-Gd_2O_3 system, d.t.a. and X-ray diffr. obs. 2—9840
Phase flow *see Flow/two-phase*
Phase meters *see Electrical measurement*
Phase transformations
Used for structural transitions only
alloy steels, critical points, influence of original structure 2—29469
amorphous deposits, transformation into supercooled liquids 2—32314
anharmonic Ising lattice first order phase transition, criteria 2—27084
p-azoxyanisole, pressure effects, order parameter, n.m.r. spectra 2—6206
binary mixtures, with two-particle interactions, theory 2—25148
Bose gas, Bogoliubov theory of condensation 2—7715
Calvet microcalorimetry appl. 2—23413
chemical potential in multiphase systems, nonhydrostatic thermodynamics 2—6278
cholesteryl acetate, liquid crystal, transformation kinetics and properties 2—6208
cholesteryl myristate, liquid crystal, transformation kinetics and pretransition effects 2—6207
condensed matter conference, Geneva, Switzerland, Sep. (1971) 2—12624
critical behaviour of model with coinciding transitions 2—14134
critical opalescence, height asymmetry 2—7989
critical opalescence of one component fluid, gravitational effects in small angle X-ray scattering expts. 2—22036
dense plasma, white dwarf star matter, equation of state, liquid-solid transitions, thermodynamics 2—30441
4,4′-dialkoxy-trans-stilbenes, phase transform., linkage group effects, permanent dipole 2—9099
dynamic critical phenomena, time depend fluctuations above order-disorder T_c 2—19818
dynamical mechanism, soft modes and critical fluctuations 2—15952
earth's core 2—26407
electrical resistivity determination at high temperatures and pressures 2—37528
eutectic and eutectoid, volume-diffusion controlled, Hillert theory, solute segregation 2—6280
Fermi systems, one-dimensional, introduction of correlation effects 2—11313
fluid system, multicomponent, correlation functions near crit. pt., thermodymamic struct. 2—15628
garnets and perovskites, high-pressure synthesis 2—17041
gas-liquid, nature of critical state, association theory 2—9214
gas-liquid, stochastic model applied to Monte-Carlo study 2—17268
gas-liquid instability in many-fermion system 2—107
glass-water system, phase transition, heat effects, dimens. changes in temp. cycles, 237-278K 2—35922
graph theory applic. 2—14131
group III-V, II-VI binary systems, phase diagram calc., liq. soln. models 2—3358
hard sphere Bose gas, computer simulation 2—15626
hard-core lattice gas, absence of Ehrenfest phase transition 2—11294
hard-ellipse system, classical, Monte Carlo calcs., relation to nematic liquid crystal 2—37639
ice, melting lines and triple points 2—25630
Ising lattice, spin pair correlation function calc. 2—5158
isopropyl alcohol, PVT behaviour for temperatures from 200-300°C and pressures from 1000 to 8000 lb./sq.in. 2—28949
Landau phase transition exactly solvable model 2—11296
lattice gas, existence of phase transitions with repulsive potential 2—17249
Lennard-Jones system, crit. phenomena, mol. dynamical calcs. 2—15999
Phase transformations continued
liquid, high press., photometer for obs., visible and i.r. spectral operation 2—38080
liquid, simple, liq.-vap. density transition 2—15631
liquid, solidification, acoustical technique applic. 2—28946
liquid and vapour density fluctuations at critical point, asymmetry 2—1146
liquid crystal cholesteryl bromide and p-azoxyanisole, small angle X-ray obs. 2—3364
liquid crystal system, H_2O-disodium chromoglycate 2—6211
liquid crystals, nematic to isotropic transition, study using two lattice model 2—21963
liquid crystals, n.m.r., n.q.r. and double resonance obs., review 2—6632
liquid-vapour critical point, optical transmission and reflection coeff. 2—22038
liquidus area exam. using new m.p. meas. technique for high temp. mats. 2—9793
mesomorphic, effect of mol. struct. changes 2—9090
mesomorphic, refractive index changes 2—9092
metal-sulphur-oxygen systems, solid-gas equilib., chem. pot. diagram 2—22047
metallurgical dendrite morphology, holographic obs. on transparent org. cpds., simulation expt. 2—15669
metals, microstructure deformations with temperature, emission electron microscope 2—3663
moving phase boundary, excess pressure 2—9201
multicomponent melts, thermal effect during crystallization of one constituent 2—1140
multicomponent system, scaling approach to tricritical phase transitions 2—23304
multiphase molecular system, orbital electron photoexcitation effect, thermodynamics appl. 2—25136
pressure induced, studied by monitoring Raman peak intensity 2—26181
quantum fluids, theoretical review 2—7714
random cluster model, relation to other models 2—20865
scaling laws, field-theoretic approach 2—3426
second-order, discussion of soft collective modes 2—23302
simple lattice gas with real phase changes 2—17256
softness of potential core 2—33954
solid to liquid, high pressure induced, review 2—15955
solid-liquid, thermodynamic resolution, simulated molecular dynamic calc. 2—25137
solution, multicomponent, quaternary mixtures, activity coeffs. 2—22032
superconducting colloids with multiple transition temperatures 2—19553
temperature and energy meas. using differential calorimeter 2—11384
thermophysical high temp. props., high speed meas. 2—19410
triple point, vapour pressure isotope effect 2—9202
two-dimensional system containing liquid, theory, applic. to surface tension calcs. 2—22033
two-phase systems, conf., Haifa, Israel, Aug-Sep (1971) 2—24624
vegetable oils in liquid-solid transition, variation of dielectric properties 2—28881
water adsorbed on silica 2—25233
white dwarf matter, applic. of Tisza theory 2—10853
Al, liquid-solid transition temp., γ-irrad. effect 2—6281
Ar, liq., liq.-vap. density transition 2—15631
Au-Sn alloy, liq., phase diagram modification from thermodynamic props. 380-1050°C 2—28837
B-C-Si, solid soln. formation, phase distribs., liquidus area determ. 2—9793
$BaTiO_3$, Al_2O_3 additive effects, liq. phase appearance and effect on densification 2—16284
C, from gas to condensed state in two dimensions of adsorbed layer on Ir(III) 2—9297
CO_2, compressibility, critical point, small angle X-ray scatt. obs. 2—3427
CaO-Al_2O_3-Fe-Fe_2O_3, applications to anhydrous high-alumina cements 2—1136
CaO-MgO-Al_2O_3-SiO_2 system, phase equilibria at akermanite-anorthite-forsterite join 2—39416
CaO-MgO-B_2O_3-SiO_2, refractory system, solid-liq. relationships at 1550°C, compatibility relationship diagrams 2—32305
CaO-Nb_2O_5-TiO_2-SiO_2, liquidus detn. in the 15% SiO_2 plane 2—9204
CdP_2-Ge, phase relns., congruent melting, eutectic formation 2—9795
Cu-Mn, liquidus and solidus curves, electron probe microanalysis, point counting obs. 2—3433
Cu-Ni, liquidus and solidus curves, electron probe microanalysis, point counting obs. 2—3433
FeO-SiO_2-TiO_2, high temp., high press., liquidus and solidus relns. 2—9205
$FeSO_4.7H_2O$, trimethylene glycol solution, molecular motion, diffusion, Mossbauer effect 2—22738
GdO, electron microscope obs. 2—9473
He II-He I transition temp. discrepancies 2—35811
He II, liquid-solid transition shown to result from instability of roton mode 2—25130
He superfluid, development of theory based on roton-roton interaction 2—9199
in Ising spin systems, characterisations 2—17247
KNO_3, first-order ferroelectric, study of phonon instability by Raman spectroscopy 2—25924
$LiNO_3$-$AgNO_3$, molten mixture, liquidus curve 2—25138
$LiNO_3$-KNO_3, molten mixture, liquidus curve 2—25138
$LiNO_3$-$NaNO_3$, molten mixture, liquidus curve 2—25138
Mn_7C_3, standard free energy of formation, e.m.f. measurements 2—3947
MnO-FeO-ZrO_2-SiO_2, phase relations, liquidus temp. region, quenching technique 2—13012
$Na_2[Fe(CN)_5NO].2H_2O$, trimethylene glycol solution, molecular motion, diffusion, Mossbauer effect 2—22738
Nb-Te system, thermodynamic parameters detn. 2—9841
SbSI, first-order ferroelectric, study of phonon instability by Raman spectroscopy 2—25924
Xe, adsorped on graphite, two dimensional phase change, LEED obs. 2—25224

solid-state
see also Ageing; Order-disorder changes
A-15 cpds., struct. instability model rel. to supercond. 2—40201
acetylene crystal, n.m.r., second moment obs., molecular motion 2—7147
alkali metal perchlorates and periodates, press. depend. 2—15956
alloy, ferromagnetic and antiferromagnetic, atomic ordering, spontaneous magnetization, stress effects 2—4369

- **Phase transformations** continued
  - **solid-state** continued
    - alloy, martensite transform. and shape memory 2—15953
    - alloy, quaternary, X-ray small angle scatt. 2—3654
    - amino acids, γ-irrad., polymorphic transform. 2—7187
    - ammonium Rochelle salt, ferroelectric phase superstructure 2—10119
    - anhydrite, exothermal effect rel. to hexagonal-orthorhombic transform 2—12992
    - austenite dispersion hardened system, martensite transition temp., excess phase particles depend. 2—6638
    - austenitic steels, giving ε and α martensite, proportion det. 2—19293
    - B2 structure, transform. twinning inhomogeneous shear model 2—13001
    - 3,4-benzopyrene, fluorescence, effect of phase changes in cryst. cyclohexane matrix 2—33320
    - boracites, atomic displacements due to polarity changes 2—32465
    - boracites, group-theoretical formulation of Landau theory 2—3695
    - brass, detect. by exoelectron emission method 2—36623
    - t-butyl chloride, calorimetric, dielectric and i.r. obs. 2—36352
    - Calvet microcalorimetry appl. 2—23413
    - carbonyl iron powder compact, struct. changes during sintering 2—39959
    - cermet steel, martensite transform. during cooling after sintering 2—12939
    - close-packed to b.c.c. transition, statistical mechanics of phase diagrams 2—22353
    - coke formation, obs. using microscopy and X-ray diffraction 2—1385
    - columbite transformation mechanism, cation displacements 2—3999
    - critical fluctuations, dynamical scaling 2—19482
    - crystallographic, electronically induced, solution of dynamic model including higher-order terms in distortion operator 2—25614
    - cyclooctanone, temperature and phase dependence of position lifetimes, -130-+56°C 2—29485
    - cyclopropane, cyclohexane, ethane, rot. transitions, obs. and theory 2—15977
    - diamagnetic metal, theory of nucleus formation in mag. field 2—25773
    - diamond synthesis, nuclei generation, liquid metal catalysis 2—19001
    - dicalcium lead propionate, u.s. attenuation obs. 2—19415
    - p- dichlorobenzene, α—γ transform. freq. temp. effect 2—26317
    - dielectric crystal, nomenclature and classification 2—12989
    - diglycine sulphate, rel. to temp. depend. of permittivity 2—36594
    - dipeptides, γ-irrad., polymorphic transform. 2—7187
    - displacive, soft mode phenomena 2—13017
    - displacive transitions, spurious first-order transitions in self-consistent phonon approximation 2—32758
    - double Bragg small-angle scatt. at phase transition 2—36279
    - dynamical mechanism, soft modes and critical fluctuations 2—15952
    - ferrocene, transitions at 164 K and 110 K, crystal shattering 2—4009
    - ferroelasticity, review 2—12988
    - ferroelectric, soft mode Raman spectroscopy, coupled modes 2—15995
    - ferroelectric, symmetry 2—19759
    - ferroelectric, symmetry of soft modes 2—22620
    - ferroelectric, thermodynamic theory, book 2—13314
    - ferroelectric crystal, double hysteresis loops and first order phase transitions 2—36589
    - ferroelectric phase transition, soft vibration modes, vibronic interaction 2—16281
    - ferroelectric phase transition of second kind, three-dimensional model 2—22621
    - ferroelectric solid solution, near transition temp., dielec. permeability 2—19767
    - ferroelectric solid solution, thermodynamic study 2—19766
    - ferroelectrics, microscopic theories 2—16279
    - ferroic crystal, nonmagnetic, state shift, elec., mech., and electromech. orders 2—40343
    - ferromagnet, metamagnetic transition, cluster model 2—16390
    - ferromagnet, MnBi film, and lattice parameters 2—4391
    - ferromagnetic bubble lattice, domain structures 2—16370
    - film, obs. by thin film thermocouple technique 2—39475
    - forsterite, natural, olivine-spinel transformation, 98-130 kb and 700-1100°C 2—9786
    - geological, explosive or detonative 2—7207
    - glass-crystal composite, internal stresses, transition temp., dilation obs. 2—6629
    - ground state rotational band, phase transition from superfluid state to normal state 2—31438
    - hexamethyldisilane, solid, discontinuity in proton spin- relaxation time plots at phase transition temp. 2—20168
    - hexamethylethane, solid, discontinuity in proton spin-relaxation time plots at phase transition temp. 2—20168
    - high pressure, model 2—39419
    - high pressure induced, review 2—15955
    - ice IV, isotopic substitution effects 2—25630
    - impurity ion probe study using transition metal and rare earth ions 2—20012
    - insulator-metal, and mag. phase transitions, thermodynamic model 2—29832
    - interference contrast method of obs. 2—25613
    - Invar, γ-phase stability, effect of alloying additions 2—36281
    - i.r. spectroscopy at high pressures using diamond- window cell 2—14474
    - isooctane crystals, effect of polymorphic transformations on luminescence of impurity molecules coronene and benzpyrene 2—29959
    - Jahn-Teller, derivation of model 2—32757
    - Landau theory, symmetry aspects 2—15954
    - Landau theory 2—19760
    - lead dicalcium propionate, phonons assoc. with 60°C phase transition, Raman spectra obs. 2—19405
    - linear, influence of molecular chain flexibility on glass transition temp. 2—28981
    - liquid crystals, cholesteric to nematic in strong magnetic field 2—28796
    - magnetic ordering, coexistence region, stress broadened 1st order transformation 2—10233
    - mantle dynamics 2—37091
    - martensite, χ-carbide formation and its transform. into cementite 2—39988
    - martensite concentration det. in 304 stainless steel by magnetometer, for failure prediction at low temp. 2—39977
    - martensitic, elec. resist. and magnetization study 2—39987
    - martensitic, f.c.c.$\rightleftharpoons$h.c.p., f.c.c.$\rightleftharpoons$d.h.c.p. type, strain relns. 2—25616
    - martensitic, low C Mn steel, rel. to damping effect 2—1395
    - metal, dislocation mobility prevention methods rel. to raising of yield pt. 2—12923
    - metal, martensite transform., shape memory effect 2—9789

- **Phase transformations** continued
  - **solid-state** continued
    - metal, rel. to friction and adhesion 2—3921
    - metallic, thermal pulser for obs. of kinetics 2—27303
    - methane-d$_4$, orientational structures 2—25359
    - molybdates, trivalent metal, struct. and phase relns. 2—9340
    - mullite decomp. under h.p. 2—33821
    - n-alkanes, Raman spectra and rotational isomerism 2—40696
    - neopentane plastic phase transition 2—39976
    - n.m.r., n.q.r. and double resonance obs., review 2—6632
    - olivine-spinel in silicates and germanates, crystal field effects and ionic radius ratio 2—1386
    - olivine-spinel phase boundary in descending lithosphere 2—22932
    - organic reactions, lattice and mol. considerations 2—35933
    - n-paraffins, high press. phase relations 2—15629
    - perfluoromethylcyclohexane 2—1380
    - perovskites, $A^{1+}B^{5+}O_3$-type, B=Ta,Nb,Sn, existence rel. to bonding, high press. synthesis, transforms. 2—9346
    - plastic crystals, rot. transitions, obs. and theory 2—15977
    - polyacrylonite, glass transitions region Mossbauer effect study of polymer dynamics 2—22736
    - polyethylene, crystalline, geometry of deformation twinning and phase transformations 2—9355
    - poly2-hydroxyethyl methacrylate, transition region from glassy to rubber-like state, relaxation behaviour 2—25514
    - polymeric and oligomeric systems, small angle X-ray scattering studies 2—18907
    - polymorphic transitions, molecular mechanism, model 2—32755
    - polyvinylcyclohexane, transition above glass transition temp., from elec. cond. 2—36582
    - pyrazine, crystalline, 29°C, i.r., differential scanning microscope and polarizing microscope evidence 2—29460
    - quartz, soft mode linewidth temp. depend., near α-β phase transition 2—20078
    - quartz-coesite transition, in anvil apparatus 2—15973
    - Raman spectroscopy, soft mode theory 2—29925
    - rare earth Co compounds, mag. transitions 2—25998
    - rare earth molybdates, $Ln_2(MoO_4)_3$, ferroelectric-paraelectric struct. transition, lattice parameters 2—9486
    - rare earth pnictides, quadrupole coupling interpret. 2—36792
    - rare earth pnictides lattice distortion model 2—1597
    - refractory oxide, high temp. DTA study 2—29472
    - review and theory 2—9785
    - Rochelle salt, local field model phase transitions, role Lorentz factors, rel. to ferroelec. phase 2—25931
    - sandstone, Coconino shock wave effects 2—4642
    - scaling theory for complex transitions 2—6631
    - second order, order parameter response in critical region 2—9787
    - second order, sp. ht., temperature coefficient, direct measurement 2—25683
    - second-order, discussion of soft collective modes 2—23302
    - semiconductor, amorphous to crystalline, effects on electronic processes 2—22515
    - solid-solid reaction, phase boundary reaction effects on diffusion 2—19134
    - steel, 18-8 stainless, tensile testing, −271°C-25°C 2—39785
    - steel, χ'-α_m, onset temp., effect of C content 2—1392
    - steel, χ'-martensite form., X-ray diffr. obs. 2—1393
    - steel, acceleration of pearlite spheroidization 2—32695
    - steel, as result of plasmic spraying 2—15900
    - steel, austenite, $\delta\to\gamma$ transformation on quenching, martensite and ferrite content 2—15951
    - steel, austenite, plastic deform. rel. to martensitic transform. 2—32764
    - steel, austenite- martensite due to deformation, effect of Ni 2—3979
    - steel, austenitic Cr-Ni with B additive, solid soln. decomp. 2—36240
    - steel, austenitization kinetics, form. from ferritic-pearlitic struct., at 1128K 2—32770
    - steel, austeno-martensitic, martensite reversion mechanism 2—29399
    - steel, bainite formation kinetics 2—40005
    - steel, carbide form. during tempering 2—39984
    - steel, casehardened, mech. props., B effect 2—12891
    - steel, Cr-Ni-Mn, ferritic phase changes rel. to strengthening 2—1318
    - steel, deformation martensite formation by cold rolling 2—3995
    - steel, effect of explosive deform. 2—39930
    - steel, eutectoid, lower bainite transform., effect of austenitising conditions 2—29470
    - steel, ferrite/austenite stabilising parameter of alloying elements 2—39985
    - steel, high C, containing Si, bainitic transform. 2—36300
    - steel, high-speed, austenite decomp. 2—36241
    - steel, isothermal bainitic transform., microstructure and mech. props. 2—9686
    - steel, low C, rel. to texture control in rapid annealing 2—39892
    - steel, low C Mn type, martensite, rel. to damping effect 2—1395
    - steel, maraging, austenite form. during ageing, X-ray obs. 2—32708
    - steel, maraging, hardening mechanism 2—36217
    - steel, martensitic phase diagrams, mech. and thermal treatment effects 2—9834
    - steel, martensitic stainless, 400-650°C, pulsed mag. field effects 2—36280
    - steel, martensitic transform., dislocation mechanism 2—6637
    - steel, martensitic transform., influence of thermomech. treatment and C conc. 2—15961
    - steel, martensitic transform., lattice parameter anisotropy 2—32766
    - steel, metallurgical phenomena accompanying structural hardening 2—3959
    - steel, metastable austenitic, martensite transform. and recrystn. texture 2—25596
    - steel, Mn, low C, rel. to temp. depend. of resist. 2—1394
    - steel, nitrification, struct. and hardness changes 2—15962
    - steel, quenched, martensite transformation, C interactions, resist., temp. depend. 2—3927
    - steel, reversible martensitic reaction, effect on recrystn. texture 2—3992
    - steel, rhenium, quenching, martensitic transformation, X-ray, dilatometric and resist. obs. 2—3994
    - steel, stainless, 17-4 PH, behaviour of weld heat affected zones 2—29410
    - steel, stainless, nitrided layer formation, plastic deformation 2—12927
    - steel, stainless stacking faults and $\gamma\to\varepsilon$ transform. 2—40003
    - steel, stainless TRIP, mech. props. rel. to austenite formation temp. 2—12857
    - steel, stainless TRIP, mech. props. rel. to austenite formation temp. 2—12857

Phase transformations continued
  solid-state continued
    steel, strainless, Cr-Ni type, $\alpha\rightarrow\gamma$ transform. and strengthening, alloying effects 2—39983
    steel, superplasticity, temp. cycling creep and transformation strain 2—12853
    steel, temp. distrib. during cooling, computer simulation 2—32689
    steel, transform. temp., meas. technique 2—19298
    steel, transition temp. increase due to form. of intercryst. cementite 2—29309
    steel, TRIP-type, rel. to fracture characts. 2—36172
    steel, weldable, heat treatment, hardenability rel. to comp. 2—12945
    steel components, carburized, phase transformation effects on bending stress distributions 2—36125
    strain-induced, contrib. to fatigue props. 2—32639
    substances with potash-tungsten-bronze structure, X-ray analysis, cell parameters 2—1399
    sulphospinels, AB_2S_4-type, synthesis, high pressure phenomena 2—9342
    superconductor, theory of nucleus formation in mag. field 2—25773
    surface creation during phase transformations 2—32754
    TCNQ salt, spin susceptibility and phase transitions 2—13094
    Teflon, shock-induced transition 2—9640
    ternary alloy, f.c.c. lattice, ordering phenomena, interatomic interact. influence 2—39993
    ternary systems, phase growth kinetics 2—39910
    1,2,4,5-tetrachlorobenzene, at ~233K, confirmation by dielectric const. meas. 2—28419
    tetragonal (Li_0) superlattice formation 2—22355
    tetramethylammonium halides, obs. using proton spin-lattice relaxation time meas. 2—29849
    thiourea, satellite X-ray scatt., structural modulation 2—13320
    thiourea, to ferroelectric modification, obs. in i.r. and Raman spectra 2—29923
    transition metal alloy, topologically close packed phases, band struct., elec. and mag. props. 2—35977
    transition metal solid solns., lattice instability 2—40214
    transition metal spinels, cryst. distortion, temp. depend. 2—3988
    triglycine sulphate, Curie temp., second harmonic scatt. 2—16294
    triglycine sulphate, ferroelec. single cryst., acoustic emission on phase transition 2—13030
    trirutile, transformation mechanism, cation displacements 2—3999
    tungstates, trivalent metal, struct. and phase relns. 2—9340
    uniaxial ferromagnet, field induced transitions 2—26056
    volume and thermal effects simultaneous meas. at high hydrostatic pressures 2—32756
    yttrium iron garnet, ferrimagnetic, field-induced, magnetic anisotropy effects 2—16387
    Ag-Cd alloy, stress-induced martensite transform. 2—36271
    Ag-Ge, thermodynamic analysis 2—22341
    Ag-Zn, electron microscopic investigation of ordered β' and ζ phases 2—32440
    β'-Ag-Zn alloy, martensite formation, electron microscopy 2—1387
    Ag-23 at.%Ge alloy, metastable h.c.p. phase decomp., precip. 39978 2—39978
    $AgCl(I)O_4$, press. depend. 2—15956
    AgF, B1-B2 change at high press. 2—36272
    Al-Au, solid soln., isothermal, rel. to supercond. props. 2—9790
    Al-Co system, intermetallic phases, peritectic transformations 2—4014
    Al-Cu alloy, struct. changes during long-term natural ageing 2—36213
    Al-$CuAl_2$, eutectic system, morphological obs. of eutectic-dendrite breakdown 2—3439
    Al-Mn, phase diagram, transform. equilib., homogeneity range 2—4013
    Al-Ni-Cu alloy, film, martensitic transform, growth of γ'-phase 2—29464
    Al-W alloy, rapidly quenched from the melt 2—25617
    Al-Zn, alloy, during ageing, X-ray diffr. obs. 2—19263
    Al-Zn, alloy, eutectoid, isothermal, growth rates, interlamellar spacings 2—12964
    Al-(15 at.%)Zn alloy, quenched, coherent phase separation kinetics, small angle X-ray scatt. 2—3980
    Al-Zn alloy, effect of Cu on phase transformation and ageing 2—29461
    Al-Zn alloy, in range of miscibility gap, effect of plastic deformation 2—29186
    $AlCu_3$, martensitic transform. 2—1657
    Al_2O_3, $\alpha-\gamma$ transition, impurity influence 2—1388
    Al_2O_3, film, gas-flame and plasma deposited 2—1389
    Al_2O_3, γ-α, rel. to exoelectron emission 2—4316
    $AlPO_4.2H_2O$, high temp., X-ray obs. 2—39979
    alloy, martensite transform., shape memory effect 2—9789
    As-Te-I glass, thermal, structural and elec. props., comp. depend. 2—22526
    $As_{1-y}Sb_yMn_3N$, metallic perovskite, orthorhombic deformation 2—25618
    Au-Cd alloy, martensitic transform., effect of solute substitution 2—12990
    Au-Ge, thermodynamic analysis 2—22341
    Au-Pb, diagrams, obs. in $AuPb_3$ region 2—4016
    Au-Si alloy, on Si substrate, as function of rate of cooling 2—39991
    AuCd, alloys, β-β'' martensitic transform. 2—6633
    AuZn, martensitic transform, rel. to elastic const. changes 2—3834
    BN polymorph form. under h.p. 2—33821
    $B_7O_{13}^{5-}$, cubic-orthorhombic phase transition, thermodynamic theory 2—9792
    $BaFe_2O_4$, polymorphic, transitions at 800 and 1000°C 2—39980
    $BaTiO_3$, ferroelec., Brillouin-Raman spectra, soft optic modes 2—16525
    $BaTiO_3$, ferroelec. single cryst., acoustic emission on phase transition 2—13030
    $BaTiO_3$, ferroelectric perovskite, spontaneous polarization, Curie temp., dielec. const., press. depend. 2—13319
    $BaTiO_3$, lower transitions, ^{119}Sn Mossbauer study 2—29463
    $BaTiO_3$, paraelec., linear disorder, Raman spectra obs. 2—20063
    $BaTiO_3$, Raman scatt., temp. depend., linear disorder obs. 2—26188
    Bi-Sn alloy, metastable phase BiSn formation under pressure, kinetics, Mossbauer obs. 2—9794
    Bi, comparison in liq. and solid h.p. systems 2—3983
    Bi, pressure-temp. phase diagram at low temp., elec. resistivity obs. 2—25619
    $(BiNa)_{1/2}TiO_3$, ferroelectric, rhombohedral to orthorhombic near 200°C . 2—29088
    β-brass, Ising model ferromagnet, neutron scatt. obs. 2—26029
    C-metal system, graphite- diamond transformation, X-ray obs. of ballas type synthetic diamond 2—32760

Phase transformations continued
  solid-state continued
    C fibre, graphitization, e.p.r. monitoring of struct. and electronic props. 2—6289
    C polymorph form. under h.p. 2—33821
    CO, exoelectron emission, temp. depend. 2—40386
    CO crystal, polymorphic transformations, chemical potential and transition temperature 2—39989
    $CaAl_2Si_2O_8$, metastable feldspar, displacive transformations, DTA obs. 2—22356
    $CaCrO_3$, O-orthorhombic to O′-orthorhombic, X-ray diffr. obs. 2—4407
    Ca_2GeO_4, stability relations, Bridgmann anvil obs., 500-1170°C 2—19300
    $3CaO.Al_2O_3.CaSo_4.xH_2O$, effects of temp. and humidity on stability 2—16677
    $CaZn_2(PO_4)_2.2H_2O$, scholzite, dehydration and transform. phases 2—19294
    Cd-Ge-As, ternary system, glass forming region, phase transition temps. 2—15636
    CdI_2, dislocation kinetics in polytype transform. 2—25622
    CdI_2, polytypic crystals, high temp., explanation in terms of movement of edge dislocations 2—1390
    CdI_2 polytypes, structural transformations, X-ray diffr. 2—25621
    CdI_2 polytypes, temp. depend. 2—25623
    CdS:Ga, spectra obs. of structure change dependent on impurity conc. 2—26162
    Ce, α-γ transform., f-bandwidth effects 2—19295
    $CeCo_5$-H, press. comp. isotherms, X-ray diffr. and mag. meas. 2—32774
    $Ce_{1-x}La_x$ alloys, $\alpha-\gamma$ electronic phase transitions 2—19507
    $CmAlO_3$, due to self-radiation from ^{244}Cm α-decay 2—12993
    CmO_x, due to self-radiation from ^{244}Cm and α-decay 2—12993
    Co-Fe-Ni-Nb alloys, semihard mag., partial f.c.c.-b.c.c. transform. 2—40463
    Co-Ni-Cr-Mo alloy, and precip. hardening 2—19296
    Co-Ni-Ti alloy, decomposition, modulated struct. 2—9467
    Co-Si system, eutectoid Co_3Si phase on unidirectional solidification 2—32723
    Co, recrystallization termination, interference of allotropic transform. at 440°C, internal damping obs. 2—39886
    Co complex, $[(C_2H_5)_4N]_2CoCl_4$, data from mag. susceptibility meas. 2—33105
    Co_2O_3, structural and low-spin high-spin transition 2—9468
    $Co_2SiF_6.6H_2O$, low temp. transition mechanism 2—25624
    Cr-Mn, itinerant electron model ferromagnet, neutron scatt. obs. 2—26029
    Cr-Ni, alloys containing B and Si, dilatometric investigation 2—9892
    $Cr_{0.8}Fe_{0.2}OOH$, thermal conversion to sesquioxide, paramag. to paramag. transform., Mossbauer obs., 400-900K 2—40628
    $CsBF_4$ high pressures, phase diagrams, differential thermal analysis, volumetric technique studies 2—3987
    CsCl, effect on inert gas diffusion and ionic conductivity 2—15788
    CsCl single crystals, vaporization rate in phase transition region meas., relation to bulk diffusion rate of Cs^+ discussed 2—12620
    $CsClO_4$ high pressures, phase diagrams, differential thermal analysis, volumetric technique studies 2—3987
    CsI, thin layers, low- temp. 2—9798
    $CsPbCl_3$, crysts., polarizing microscope obs. 2—12995
    $CsPbCl_3$, determined by e.p.r., DTA, and dielectric measurements 2—32762
    $CsPbCl_3$, dielec., DTA and e.p.r. obs. 2—12994
    Cu-Al-Ni alloy, martensitic transformation internal friction obs. 2—3842
    Cu-Al, β-phase transform. 2—36202
    β_1'—Cu-Al martensite, stress induced, rel. to shape memory effect 2—25626
    Cu-Al(Cr) alloy, second phase formation and solution kinetics, specific resist. obs. 2—29428
    Cu-15 at.%Sn, alloy, b.c.c. to orthorhombic martensite transform., shape strain obs. 6634 2—6634
    Cu-Fe, alloy, film, effect of precip. and matrix 2—6635
    Cu-Fe alloy, creep limit rel. to α-γ transform. 2—29269
    Cu-Fe alloys, transforms. of Fe precipitates 2—39981
    Cu-Ga, quenched hypereutectoid alloy, microstructure 2—9580
    Cu-Ge, thermodynamic analysis 2—22341
    Cu-Mn-Al, Heusler alloy, rel. to precipitation 2—9801
    Cu-Sb alloy, rel. to composition depend. of elastic moduli 2—39759
    Cu-Sn alloy, rel. to composition depend. of elastic moduli 2—39759
    Cu basic carbonates, study of amorphous-crystalline transformation involving nucleation and crystal proliferation kinetics 2—29103
    Cu complex, $Cu(C_2H_5NH_3)Cl_4$, diff. mag. susceptibility , phase diagram 2—16374
    Cu complexes, $M_2[M'Cu](NO_2)_6$ type, rel. to Jahn-Teller distortions, ligand field spectra interpret. 2—19943
    CuAu, first order change, two-dimens., Ising model 2—15960
    CuBr, 384 and 468°C 2—39581
    $Cu_{10}Ge_3$, distorted CuZn struct. 2—29465
    $Cu_3Ge_{0.5}Sb_{0.5}$, struct. phenomena, 2-electron correlation model 2—29466
    CuI, polymorphism at high pressure 2—3989
    $Cu(OH)_2$, reversible X-ray diffraction, infrared spectroscopy, 20-100°C 2—3991
    β-CuPd, a/8[110](1$\bar{1}$0) faulting in prestrain induced transform. stage, X-ray obs. 2—32763
    Cu_3Pd alloy, long period ordered struct., X-ray obs. 2—9799
    Cu_2S, temp. and oxygen effects 2—9800
    Cu_xS, (x = 1.85-2.0) elec. cond. study 2—13228
    $Cu_{10}Sn_3$, distorted CuZn struct. 2—29465
    $Cu_{10}Sn_3$, struct. phenomena, 2-electron correlation model 2—29466
    p-D_2, phase transition, order-disorder transition 2—22362
    $DyAsO_4$, at 11.17K, Raman scatt., degenerate phonon line splitting 2—16535
    $DyAsO_4$, Jahn-Teller induced, Raman scatt. obs. 2—16534
    $DyAsO_4$, low temp. X-ray diffr. obs. 2—25628
    $DyAsO_4$, mag. struct. 2—36765
    $DyAsO_4$, tetragonal- orthorhombic transform. 2—39982
    DySb, magnetic and structural phase transitions 2—33106
    $DyVO_4$, at 13.8K, Raman scatt., degenerate phonon line splitting 2—16535
    $DyVO_4$, elastic props. of mag. controllable Jahn-Teller distortion 2—9802
    $DyVO_4$, Jahn-Teller induced, Raman scatt. obs. 2—16534
    $DyVO_4$, Jahn-Teller system, electron-phonon coupled modes, Raman theory 2—20066
    $DyVO_4$, low temp. X-ray diffr. obs. 2—25628
    $DyVO_4$, mag. struct. 2—36765

Phase transformations continued
solid-state continued
$DyVO_4$, Raman and i.r. reflection spectra obs. 2—16533
$DyVO_4$, soft acoustic mode at cooperative Jahn Teller phase transition 2—25662
Eu, intermediate stage in mag. ordering 2—13371
EuO, Heisenberg ferromagnet, neutron scatt. obs. 2—26029
EuS, Heisenberg ferromagnet, neutron scatt. obs. 2—26029
Eu_2SiO_4, ferroelastic ferromag., optical absorpt. spectra, Faraday rotation, cryst. struct. 2—10195
Fe-7.8 wt % Cr alloy, potentiokinetic obs. 2—29431
Fe-C-Cr, alloy, transform. kinetics, austenite-proeutectoid ferrite, nucleation, growth rates 2—22359
Fe-C, alloy, martensitic and massive transform. temps. rel. to C content 2—22360
Fe-C alloy, second phase formation and solution kinetics, specific resist. obs. 2—29428
Fe-Co-V alloy, plastic deformation, $\gamma \rightarrow \alpha$, omnidirectional press. effect 2—9806
Fe-Co alloy, α-γ transition, effect on Co diffusion 2—39741
Fe-Co alloy, strength and struct. rel. to comp. 2—19268
Fe-Co alloy, thermal expansion, low temp. anomaly 2—13052
Fe-Cr-Mn, phase diagram calc., electron probe microanalysis, 750-950°C 2—6645
Fe-Cr-Ni-C-Si-Mn-P-Si-Nb, chill cast roll iron, isothermal austenite decomposition 2—3996
Fe-Cr-Ni, austenitic steel, antiferromag, transition to ferromag. martensitic on plastic temp. 2—26038
Fe-Mn-C alloys, martensite struct. rel. to metallurgical treatment 2—12997
Fe-Mn, alloy, cold rolled, annealed., α-γ transform. at 500°C, mag. props. 2—19876
Fe-Mn alloy, α' martensite nucleation, elec. microscope obs. 2—19301
Fe-Mn alloy, b.c.c.→(h.c.p., f.c.c.) transform., influence of shock and hydrostatic press. 2—32769
Fe-Mn alloy, microstruct. rel. to mech. props. 2—32767
Fe-Mo-Co, alloy, quenched from $\alpha+\gamma$ field, transform. microstructs. 2—12998
Fe-Ni-Co-Mo alloy, martensitic, ageing, formation of metastable ω phase 2—36299
Fe-Ni-Cr-Ti steel, austenitic, plastic deform. rel. to σ-phase form. 2—29471
Fe-Ni-Cr alloy, effect of austenitizing conditions on martensite formation 2—32768
Fe-Ni-Cr alloy, martensitic transform. kinetics 2—36277
Fe-Ni-Mn alloy, isothermal martensitic transform., kinetics 2—9804
Fe-Ni-Mn alloy, martensitic transformation, nucleation model 2—22357
Fe-Ni-Mo alloy, martensitic, rel. to cooling rate, plastic deform., hardening 2—29467
Fe-Ni alloy, f.c.c. lattice, para-process susceptibility rel. to comp. 2—29478
Fe-Ni alloy, impact loading, microstructure, hardness, α-γ transformation 2—3867
Fe-Ni alloy, martensitic transform. kinetics 2—36277
Fe-Ni martensite, transform. induced substructs., X-ray and elec. microscope obs. 2—22358
Fe-Zn system, reactive diffusion, pressure depend. 2—12996
Fe, cast, graphitizing tendency, effects of O, S and trace elements 2—12970
Fe, intermediate stage in mag. ordering 2—13371
Fe, temp. of $\gamma \rightarrow \alpha$ transform. rel. to cooling rate 2—19297
Fe, work function changes in α-γ transform. region 2—1587
Fe alloy, martensite transform, shape strains in deform. of lattices 2—29259
Fe polymorph form. under h.p. 2—33821
Fe rich alloy, δ-ferrite annealing, high temp. equilib. struct. 2—15964
Fe thin film, f.c.c.- b.c.c. transform., stress effects 2—9803
$Fe_3B_7O_{13}I$, phase transitions at low temp., X-ray obs. 2—36592
$FeCl_2$ amorphous frozen soln., glass transition 2—9220
$Fe_{1\|x}Cr_{2-x}O_4$, X-ray diffr. obs. 2—22361
$Fe_{3-x}Cr_xO_4$, ferrimagnetic, magnetization, phase transition effects 2—19903
Fe_2O_3-α-$Fe(OH)_3$, structural obs. over entire temp. range 2—29468
α-Fe_2O_3, reduction to magnetite, kinetics, rel. to natural faces 2—16681
Fe_3O_4, low temp. transition and multiple ordering 2—36278
Fe_3O_4, magnetite, low temp. Mossbauer effect rel. to structural vacancies 2—26130
Fe_3O_4, magnetite, magnetoresistance, 77-300K 2—25816
Fe_3O_4, magnetite, metal impurity effects on Verwey transition temp., magnetic obs. 2—25719
$Fe(OH)_2$, dehydration, haematite transformation, Mossbauer and i.r. spectra, mag. props. 2—22862
β-FeOOH, akaganeite→hematite conversion, charact. temp. 2—13038
FeOOH, β-δ in haematite, i.r. spectroscopic study of thermal conversion 2—40805
FeOOH, thermal conversion to sesquioxide, paramag. to antiferromag. transform., Mossbauer obs., 400-900K 2—40628
FeRh, ferro-antiferromag. transition, electron entropy contrib., positron annihilation obs. 2—16372
$FeS_{1\|x}$, Mossbauer obs. 2—15965
$Fe_2SiF_6.6H_2O$, low temp. transition mechanism 2—25624
Fe—Ni alloy, martensite transform, twinning 2—9807
Fe—Ni—Mo(V)—C alloy, martensite transform. twinning 2—9807
$Gd_2(MoO_4)_3$, elastic props. at ferroelastic transition 2—16009
$Gd_2(MoO_4)_3$, ferroelectric, elastic wave absorpt. 2—19299
$Gd_2(MoO_4)_3$, soft- zone boundary phonon driven 2—19763
Gd_2O_3-SrO system, DTA study, phase diagram determ. 2—29472
Ge, semiconductor, amorphous to crystn., assoc. with elec. transition, review 2—13238
$Ge_2(MoO_4)_3$, ferroelec. ferroelastic and paraelec.-paraelastic phases, X-ray obs. 2—19052
GeTe, thermal expansion near rhombohedral to f.c.c. transition 2—1396
GeTe film, semiconductor amorphous to polycrystalline phase transition kinetics rel. to switching 2—40256
H, transition from metallic to molecular form involving 'evaporation' of surface atoms 2—25631
O-H_2, cluster expansion 2—22371
o-H_2, phase transition, order-disorder transition 2—22362
HCl single crystal, X-ray and neutron diffr. obs. 2—32457
$H_5O_2{}^+AuCl_4{}^-.2H_2O$, obs. in ^1H, ^2H, n.m.r. and ^{35}Cl n.q.r. 2—10548

Phase transformations continued
solid-state continued
^3He, evidence for new phase 2—32303
$(Hf,Ta)V_2$ and $(Hf,Zr)V_2$ alloys, supercond. transition temp. correl with lattice instabilities 2—32937
Hf, α-β transformation effects on emissivity specific heat and temp. dependence of specific electrical resistance 2—29552
HfV_2, cubic- orthorhombic transform., low temp. 2—15966
HgI_2, Raman scatt. and i.r. absorp. obs. 2—16543
HgI_2, Raman spectra obs. at quadratic-orthorhombic transition pt. 2—29934
In-Al-P system, thermodynamic props. appl. to manufacture of $Al_xIn_{1-x}P$ 2—6788
In-Tl alloys, lattice stability near martensitic phase transformation, ultrasonic study 2—29474
Ir, with C adosrbed on (111) face, characteristics obs. using thermoelectron emission and surface ionization 2—22363
K and Na-K alloy films, rel. to photoelec. emission 2—33090
KD_2PO_4, high temp transitions 2—3997
KD_2PO_4, high temp. transition and metastability 2—22624
$K_4Fe(CN)_6.3H_2O$, ferroelec., Mossbauer investigation 2—29888
KH_2PO_4-type crystals, phonon spectra, Raman scatt. 2—16550
KH_2PO_4, ferroelec., soft modes, Raman spectra 2—16549
KH_2PO_4, high temp. transitions 2—3997
KH_2PO_4, high temp. transition and metastability 2—22624
KH_2PO_4, $KD_{2x}H_{2(1-x)}PO_4$, KH_2AsO_4, ferroelectric modes, Raman spectra 2—16551
KH_2PO_4, structural defects, phase transitions and dielectric props., radiation sensitive 2—1442
KH_2PO_4 and KD_2PO_4, high temp. transitions, atomic mechanism 2—9814
KIO_3, ferroelectric, electro-optical obs. 2—33211
$KMnF_3$, anomalous elastic behaviour obs. 2—19157
$KMnF_3$, of displacement type, X-ray investigation, thermodynamic description 2—1398
$KMnF_3$, para- to antiferromag. transition, Raman spectra obs. 2—16548
KNO_3-$Cd(NO_3)_2$ glass, positron lifetime, temp. depend. through phase transition 2—36374
KNO_3, thermal transform., elec. cond. obs. 2—32773
$KNbO_3$, cubic ferroelectric, phase transition, neutron diffuse scatt. obs. 2—13318
$KNbO_3$, ferro-antiferroelec., n.m.r. obs. 2—16661
K_2NiF_4, family, two dimensional antiferromag., n.m.r. obs. 2—16392
$K_2PbCu(No_2)_6$, cooperative distortion due to Jahn-Teller instability 2—15967
$K_2SO_4{:}Cu^{2+}(Mn^{2+})$, e.s.r., hyperfine interactions 2—9815
$K_2SeO_4{:}Cu^{2+}$, rel. to e.p.r. spectra 2—33341
K_2SnCl_6, ^{35}Cl n.q.r. obs., 77-320 K 2—7158
La-Ce alloy, high press. elec. resist. rel. to phase transform. 2—32775
$LaAlO_3$, transient n.m.r. obs. 2—9816
$LaCo_5$-H, press. comp. isotherms, X-ray diffr. and mag. meas. 2—32774
$LaCoO_3$, first order phase change, 648K 2—36283
$LaFeO_3$, ferroelastic effect 2—25633
Li, martensitic transform., nonlocal pseudopot. 2—15968
Li martensitic, effects on nuclear spin-lattice relax. time obs. 2—16660
$LiCr_{1-x}Fe_xO_2$, first order, Mossbauer obs. rel. to antiferromagnetic ordering and exchange 2—19924
Li_2MF_6, M=Ge, Ti, Sn, Zr, high pressure structural evolution 2—25632
$LiXO_4$, X=P, V, As, and $Li_2M^{2+}X_1{}^{4+}O_4$, M=Zn, Mg, X_1=Ge, Si 2—18966
Li_2ZrF_6, transformation mechanism, cation displacements 2—3999
Mg-Cu-Al alloy, enthalpies of form., Laves phases binding conditions 2—29475
Mg-Cu-Sn alloy, enthalpies of form., Laves phases binding conditions 2—29475
Mg-Cu-Zn alloy, enthalpies of form., Laves phases binding conditions 2—29475
$MgO.Al_2O_3.xSiO_2$ phase, growth from glass, X-ray obs. 2—9477
Mn-Fe-Ni alloy, isothermally treated, martensitic transform. characts. 2—32765
Mn-Fe, alloy, phase diagram rel. to hydrostatic extrusion 2—19312
$MnAl_2S_4$, pressure to 95 kb, temp. to 1000°C, decomposition to MnS 2—3998
$MnAs_{0.97}P_{0.03}$ para-ferromag. phase transition 2—4377
$MnAs_xSb_{1-x}$ solid solns., hexagonal-orthorhombic transition 2—19880
MnBi, film, ferromagnetic, and lattice parameters 2—4391
$MnGa_2S_4$, pressure to 95 kb, temp. to 1000°C, polymorphs. 2—3998
$MnSO_4(.H_2O)$, mag. transitions, sp. ht. meas. 2—22710
$Mn_2SiF_6.6H_2O$, low temp. transition mechanism 2—25624
$MnSiO_3$, high pressure transform., polymorphs, 1053-1673K 2—25634
N, α—γ phase transition, n.q.r. freq. shift at transition 2—26315
N_2 crystal, polymorphic transformations, chemical potential and transition temperature 2—39989
NH_4Br, proton spin-lattice relax. obs. 2—10272
$(NH_4)_2Cd_2(SO_4)_3$, ferroelec.-ferroelastic cryst., transformation mechanism 2—16291
$(NH_4)_2Cd_2(SO_4)_3$, mechanism of ferroelec. phase transformation 2—33057
NH_4ClO_4, low temperature 2—40675
$NH_4H_2PO_4$, Raman active ferroelectric modes 2—16551
$NH_4H_2PO_4$ structural defects, phase transitions and dielectric props., radiation sensitive 2—1442
NH_4NO_3, at 398K, cation diffusion study by proton spin relaxation 2—25465
NH_4NO_3IV, pseudosymmetry of twinning 2—9353
Na, martensitic, effects on nuclear spin-lattice relax. time obs. 2—16660
Na and Na-K alloy films, rel. to photoelec. emission 2—33090
$NaBD_4$, cubic to tetragonal transition observed in study of infrared Raman spectra 2—12181
$NaClO_3$, ferroelectric, relation to phonon structure 2—25930
$NaClO_3$, phase structure obs. 2—39990
$NaNbO_3$, cubic-tetragonal transition rel. to soft phonon modes 2—39648
$NaNbO_3$, ferro-antiferroelec., n.m.r. obs. 2—16661
NaOH, orthorhombic to monoclinic transition, obs. of diffuse X-ray scattering, change of lattice prameters 2—1400
Na_2SO_4, grinding effect differential thermal analysis study 2—29476
Na_2SiF_6, transformation mechanism, cation displacements 2—3999
Na_xWO_3, transient n.m.r. obs. 2—9816
Nb-Ge-Al alloy, low temp. cubic- tetragonal transform. 2—9817
Nb-H alloy, $\alpha \rightleftharpoons \alpha$ + hydride, rel. to plastic deform. effect on elec. cond. 2—39935
Nb_2O_5, high press. transforms. 2—29477

Phase transformations continued
solid-state continued
Nb_3Sb transition at 45 K, acoustic phonon instability and critical scattering 2—9864
Nb_3Sn, cubic-tetragonal transform. and supercond. 2—29637
Nb_3Sn, X-ray exam. 2—22364
Nd_2O_3, monoclinic to hexagonal, martensitic character, electron microscope and diffr. exam. 2—4000
Ni-Cr thick films, sputtered, deposition temp. effect on condensed phases 2—32371
Ni-Cu-Fe-graphite alloy, during sintering 2—1401
Ni-P films, resist. correl. and annealing effects 2—15969
Ni-Ta alloy, Ni_8Ta nucleation, structural processes 2—15970
Ni-Zn system, reactive diffusion, pressure depend. 2—12996
Ni-22.7-38 at.%Mn alloy, neutron diffr., X-ray scatt. obs., 673-908 K 2—25635
Ni, intermediate stage in mag. ordering 2—13371
Ni, linear compressive strain, press. depend. to 20 kbar 2—9818
Ni bronze, supersaturated soln. transformation, kinetics 2—9819
$NiCr_2O_4$, Jahn-Teller transition, X-ray crit. scatt. obs. 2—32777
Ni_3Mn, small angle neutron scatt. obs. 2—19303
NiTi, martensite transform., stacking faults role 2—15768
Ni_4W, peritectoid growth 2—13006
$(Pb,Ba)Nb_2O_6$, solid soln. reciprocal tetragonal and monoclinic phase transitions elec. field induced 2—1402
$PbMg_{1/3}Nb_{2/3}$, ferroelectric, temp. dependence of dielectric props., relaxation polarization, diffuse phase transition 2—16292
PbO, orthorhombic to tetragonal transform., induced by water 2—29480
PbO ceramic, effect on photocond. 2—36611
$PbSe-Ge_{1.5}As_{0.5}Se_3$, double glass transition, heat capacity obs. 2—18902
$PbTiO_3$, ferroelectric perovskite, spontaneous polarization, Curie temp., dielec. const., press. depend. 2—13319
$PbZrO_3$ and $PbTi_{0.2}Zr_{0.8}O_3$, Mossbauer obs. 2—4001
$Pb(Zr_xTi_{1-x})O_3$, ceramic, morphotropic phase boundary, electromech. activity 2—4280
Pd-As system, distorted CuZn struct. 2—29465
Pd-Sb system, distorted CuZn struct. 2—29465
Pd-Ta system, diffusion processes, investigation using electron probe 2—29205
Pd-Zn-Ga system, distorted CuZn struct. 2—29465
Pd, linear compressive strain, press. depend. to 20 kbar 2—9818
$Pd_{81.8}Si_{18.2}$, amorphous, recrystallization, isothermal resistance obs. 2—15972
$PrAlO_3$, Raman scatt. obs. 2—20077
$Pr_xNd_{1-x}AlO_3$, Raman scatt. obs. 2—20077
$PrO_{1.5}-PrO_{1.71}$ relationships, transitions, quenched samples and high temps., X-ray diffr. obs. 2—4002
$RbAg_4I_5$, press. effects, elec. resist., press. to 100 kbar, 293-453K 2—36285
RbCl, h.p. transition, thermal effects 2—1403
RbCl, press. induced polymorphic transition, hysteresis effect 2—9822
RbH_2PO_4, high temp. transitions, atomic mechanism 2—9814
RbH_2PO_4, high temp. transition and metastability 2—22624
$RbMnF_3$, Heisenberg ferromagnet, neutron scatt. obs. 2—26029
Rh_7B_3 and $RhB_{1.1}$, resist. and thermal e.m.f. extrema 2—1404
SF_6, at −180°C rel. to spin-lattice relax. 2—26085
SbSI, ferroelec. crysts., u.s. wave damping near phase transition, freq. depend., temp. depend. 2—29535
SbSI, ferroelec. phase transition, soft modes, Raman scatt. obs. 2—16564
SbSI, ferroelec. phase transitions, long wavelength optical phonons, Raman spectra 2—16459
SbSI, ferroelectric phase transition, soft mode coupling, critical Rayleigh scatt. 2—16012
Se-Sb, semiconductor, amorphous to crystn., assoc. with elec. transition, review 2—13238
Se, crystal-amorphous, shown to be cause of memory switching effect in bulk polycrystalline sample 2—4184
Se, hexagonal and amorphous, high-pressure transformations 2—25636
SiC, 2H type, low temp. transform. mechanism 2—32778
SiC, cubic-hexagonal transition 2—9823
SiC, single cryst. comparison with polycryst. 2—22365
SiC, single crystal, direct 2H-6H transformation on annealing at 2400C 2—4003
SiH_4, and SiD_4-SiH_4 mixtures, vibrational spectra, crystal and liquid 2—33272
SiO_2, quartz, diffuse X-ray scatt., near α-β transition 2—4038
SiO_2, tridymite, heats of transition, stacking disorder 2—9824
Sn-Ag alloy, rel. to composition depend. of elastic moduli 2—39759
Sn-Sb alloy, rel. to composition depend. of elastic moduli 2—39759
Sn, polymorphous beta-alpha transformation kinetics 2—4004
$SrAl_2Si_2O_8$, metastable feldspar, displacive transformations, DTA obs. 2—22356
$SrIrO_3$ high and low pressure forms, temperatures to 1200°C 2—3731
$SrTiO_3$, applic. of tetragonal phase e.p.r. spectrum 2—40766
$SrTiO_3$, critical behaviour near 105K 2—15974
$SrTiO_3$, critical dynamics for $T \geqslant T_c$ 2—25932
$SrTiO_3$, cubic-tetragonal phase transition, soft modes, Raman scatt. obs. 2—16569
$SrTiO_3$, displacive transition, u.s. vel., stress effects and interaction parameters 2—32780
$SrTiO_3$, displacive type transition, phonon freqs. 2—19305
$SrTiO_3$, u.s. attenuation and vel., temp. depend., 105 K transition, phonon modes 2—9879
$SrTiO_3$, u.s. props., anisotropy at phase transition 2—16022
$SrTiO_3$ of displacement type, X- ray investigation, thermodynamic description 2—1398
β-Ta film, sputtered, X-ray diffr. obs. 2—18945
TaC_x, lattice instability effects on supercond. 2—22509
$TbAsO_4$, second order, optical and mag. props. 2—10172
β-$Tb_2(MoO_4)_3$, ferroelec. ferroelastic crystal 2—3735
$Tb_2(MoO_4)_3$, ferroelectric transition, struct. and phase relns. 2—9340
$TbVO_4$, crystallographic distortion at 32 K, second order transition 2—19306
$TbVO_4$, Jahn-Teller induced, Raman scatt. obs. 2—16534
$TbVO_4$, Jahn-Teller system, electron-phonon coupled modes, Raman theory 2—20066
Te-As-Ge, semiconductor, amorphous to crystn., assoc. with elec. transition review 2—13238
$TeVO_4$, reversible polymorphic transformation at 650°C 2—9347
Ti-Al-Cr and Ti-Al-Cr-Mo alloy, effect on mech. props. 2—36142

Phase transformations continued
solid-state continued
β-Ti-Fe(Cr)(Mn)(Mo) alloys, isothermal transform. 2—12979
Ti-M alloy, M=Cr, Mn, V, Mo, continuous cooling transform., rel. to ω phase precipitation 2—29481
Ti-(25 at.%)Nb alloy, omega phase formation, mechanism and kinetics, X-ray obs., electron microscopy 2—4006
Ti-V and Ti-V-Al, rel. to props. and struct. 2—36141
Ti-Zr-O alloys, phase characterisation 2—40009
Ti alloy, β-stabilized, ω phase formation kinetics 2—36288
Ti alloy, martensite transform., shape strains in deform. of lattices 2—29259
Ti alloys, with metastable α-phase, under applied tensile stresses 2—13000
$TiCo_2$, Laves phase, electron microscope obs. 2—19105
$TiCr_2$, Laves phase, polytypism and stacking faults 2—19105
TiH_2, room temp. polymorphic transform 2—22366
TiNi, martensite struct., rel. to premartensitic instability 2—9825
TiNi, martensitic transformation, surface relief 2—6640
TiNi, martensitic transform. mechanism 2—13002
TiNi, resistivity peak on thermal cycling, shape memory effect 2—29479
TlI, 400-600K, elec. cond. study 2—9826
TmTe, pressure induced electronic and structural transform., X-ray and resistivity obs. 2—36289
U-Mo-Nb-Zr alloys, carbide inclusions effect 2—13004
U-Nb-Zr(Mo) system, kinetics of transform. of γ phase 2—36309
U-Se-C ternary system, solid state compatibility relationship at 600°C 2—29482
U-Te-C ternary system, solid state compatibilty relationship at 1200°C 2—29482
U-V-C system, C content effects 2—36310
U-V alloy, C content effect 2—13003
$UC-UC_2$, UC-UN alloys, lattice dimensions, X-ray diffr., 760-2250°C 2—19307
$UO_2-UO_3-LaO_{1.5}$, phase diagrams, single phase regions 2—4023
V-N alloy, banded microstructure 2—22367
VF_3, rel. to mag. ordering 2—36780
VO_2, monoclinic to tetragonal transition 2—4007
VO_2, semiconductor-metal, Raman scatt. obs. 2—16571
VO_x morphology and substruct. of b.c.c. to b.c.t. transform. induced by impurities 2—15976
V_2O_4, semiconductor-metal transition 2—29680
YZn, martensitic transform., rel. to elastic const. changes 2—3834
Yb, martensitic, X-ray diffraction obs. 2—6641
Yb film, h.c.p.$\rightleftarrows$f.c.c. martensitic transform., phase stability 2—39992
Zn-Nb alloy, $\beta \rightarrow \omega$ transform., u.s., elastic consts., and X-ray studies 2—40014
$ZnO-B_2O_3$ system, borate stability, temp. depend. 2—22368
$ZnO.Nb_2O_5$, $\alpha \rightleftarrows \beta$ polymorphic transition 2—25644
ZnS, effect of poyltypism, X-ray oscill. obs. 2—25351
ZnS, hexagonal, high press., investig. by Raman spectroscopy 2—22781
ZnS, polytypes, genesis and abundance 2—6454
ZnS, rel. to polytypism and Cu doping effects 2—25350
ZnSe, irrad., wurtzite-zincblende transform. 2—9529
α-$Zn_3(VO_4)_2$, low-temperature form 2—1230
Zr-(3 wt.%)Mo-(1 wt.%)Al alloy, thermal decomposition, Al effect 2—25640
Zr-Nb alloy, martensitic, comp. depend. of morphology 2—9827
Zr-Pu dilute alloy, $\beta \rightarrow \alpha$ transform., crystallographic study 2—29483
$ZrO_2-Gd_2O_3$ system, d.t.a. and X-ray diffr. obs. 2—9840
$ZrO_2-Ln_2O_3$, solidification diagrams, phase diagrams, near melting point, thermal analysis, X-ray obs. 2—4008
ZrO_2, milled zirconia, monoclinic-tetragonal, particle size effects 2—29484
Zr—Cu, Zr—Cu—M alloys, (M=Mo, Ni, Cr), on continuous cooling 2—1391
Zr—(3 wt.%)Mo-(1 wt.%)Al, tempering of strain induced martensitic phase, struct. and morphology 2—25639

Phase transitions *see Phase transformations*

Phonographs *see Sound reproduction*

Phonon bottleneck *see Crystals/lattice mechanics*

Phonon drag *see Crystal electron states/transport processes; Crystals/lattice mechanics*

Phonon-electron interactions *see Crystal electron states/transport processes; Crystals/lattice mechanics; Electron-phonon interactions*

Phonons
see also Crystals/lattice mechanics
A-15 compounds, theory 2—19333
acoustic, distrib. function for semiinfinite crystal or plate 2—6648
acoustic in metal surface, Brillouin scatt. 2—16453
acoustoelectric amplifier, reduced phonon noise 2—16028
alkali halide, dispersion, long-range three-centre potential effects 2—9852
alkali halide, role in internal friction process, theory 2—15806
alkali halide, single phonon X-ray scatt., eigenvector influence 2—9855
alkali halide, thermodynamic funcs., phonon freq. moments and Blackman rule of sums 2—40067
alkali halides, doped, thermal cond. 2—4077
alkali halides, exciton energy levels, exciton-phonon interaction influence 2—7067
alkali halides, two phonon Raman spectra 2—25658
alkali halides, two-phonon spectrum calc. using shell model theory of Raman scattering 2—26179
alkali metals, Drude absorption at a phonon, quantum mechanical calculation 2—36315
alkali metals, phonon dispersion 2—22386
alloy, lattice thermal resist. due to dislocations 2—32850
alloy, phonon spectrum, short range order effects, C.P.A. calc. 2—19334
alloys, binary disordered, frequencies using nonlocal pseudopotential methods 2—22385
amorphous materials, density of states and thermodynamic props., Raman scatt. 2—20061
anharmonic lattice, two-phonon response in first-order self-consistent phonon approx. 2—13019
antiferromagnet, critical phonon attenuation exponent 2—9872
ballistic heat pulse, phonon freq. distrib., mag. reson. obs. 2—13027
benzoic acid, single cryst., low freq. spectrum, GF method analysis 2—20079
biphenyl:naphthalene, obs. of localized rotational phonons 2—16014
bound phonon pairs, model 2—40021
boundary scatt., dislocation model, heat pulse detection process 2—9850
n-CdSe, conduction band edge, magnetophonon effect 2—19661

Phonons continued
- collision operators, Callaway model 2—9848
- conference, Rennes, France, July 1971 2—15987
- crystal spatially nonhomogeneous, acoustic phonon spectra 2—25647
- crystal surface, low energy electron inelastic scatt. by one phonon processes, theory 2—25170
- crystalline solid, spin-phonon interactions 2—22819
- crystals, multiphonon light scatt. from impurity centres 2—16452
- dielectric with high dislocation density, thermal phonon scatt. 2—6662
- diffusion, of localized defect, multi-phonon process 2—1266
- dislocation electrons and phonons, models of interactions 2—6492
- displacive phase transitions, soft mode phenomena 2—13017
- displacive transitions, spurious first-order transitions in self-consistent phonon approximation 2—32758
- duralumin, treated at 77K, phonon conductivity models, study 2—40086
- Einstein oscillators, interacting Helmholtz free energy 2—29500
- energy accommodation of gas at solid surface, contribs. from bulk, mixed and Rayleigh phonon modes 2—28994
- exciton-phonon complex, resonance interactions in strong mag. field 2—22457
- exciton-phonon interaction, coherent potential approx., applic. to optical spectra 2—26135
- exciton-phonon interaction theory, canonical transform. 2—25738
- f.c.c. lattice, thermodynamics of strongly anharmonic crystals 2—25653
- ferrodielectric, role in thermal cond. mechanism 2—6688
- ferroelectric, light scatt. by acoustic phonons 2—26199
- ferroelectric, order-disorder and displacive type, Raman spectra and phase changes 2—20062
- ferroelectric, tungsten bronze crystal structure, Raman scatt. temp. depend., polariton obs. 2—33281
- ferroelectric, wide-gap, vibr. mode freqs., dynamic perturbation 2—29749
- ferromagnet, critical phonon attenuation exponent 2—9872
- ferromagnetic insulator, coupled photon-magnon-phonon modes 2—10185
- ferromagnetic insulator, magnon-phonon interaction 2—36338
- Frenkel excitons strongly coupled with phonons, propagation in molecular crystals 2—32895
- frequencies in interatomic force constants derivation 2—4027
- frequency distribution function derivation, neutron inelastic coherent scatt. 2—25655
- graphite, surface phonon entropy calc. 2—32335
- graphite cryst., basal plane thermal cond. calcs., anharmonicity coeffs., phonon effects 2—19449
- group-theoretical analysis of vibrations, computer program 2—36311
- helium, liquid, dispersion described 2—9195
- Holstein process in superconductors, new sum rule 2—13120
- incoherent, with sharp energy distribs., exptl. detection processes 2—32796
- indirect two-photon interband transitions, analysis 2—22754
- inert gas solids, spectra studied using anharmonic potential parameters 2—4032
- insulator, role of three-phonon normal processes in phonon cond. 2—40016
- interference, in liquid He films 2—19319
- ionic cryst., impurity induced absorpt. and reduced thermal cond. vs. temp., correl. 2—19438
- ionic cryst., polariton modes classification 2—19328
- ionic Raman effect, i.r. active mode and second dipole moment effects 2—16521
- Jahn-Teller Hamiltonian for p-state equally coupled to E_{2g} and T_{2g} vibrs. 2—7012
- laser solid, detect migration due to laser excited photon-phonon conversion 2—29212
- lattice energy transport in linear atomic chain, Boltzmann transport equation rel. to thermal cond. derivation 2—36362
- lead dicalcium propionate, assoc. with 60°C phase transition, Raman spectra obs. 2—19405
- light scattering from polaritons in presence of lattice damping 2—29926
- liquid drag effects, momentum transfer through solid partition 2—39300
- liquid surface, mol. dynamics, stat. mech. calc. 2—6199
- liquid-filled resonant systems, excitation of fractional harmonic u.s. waves 2—28846
- Lyddane-Sachs-Teller relation at finite wave vector for NaCl type crystals 2—25648
- magnetic materials, zero and multiphonon Mossbauer line shape calc. 2—36323
- magnon-phonon interaction enhancement of electron effective mass 2—36423
- magnon-phonon interaction in a time-dependent magnetic field, quantum theory 2—40437
- metal, b.c.c., phonon dispersion, two parameter model potential method 2—19365
- metal, cubic, extended De Launay's model 2—19335
- metal, dirty normal, damping through electron phonon interaction, thermal Green function 2—13067
- metal, f.c.c., neutron scatt. by average phonons 2—9540
- metal, h.c.p., dispersion relation, Debye temp., modified axially symm. model 2—40049
- metal, h.f. phonons, detect. by photoemission 2—22393
- metal, nuclear spin phonon coupling, acoustic mag. reson. 2—40787
- metal, sound propagation, generalized transport eqns. taking account of phonon-phonon interactions 2—40059
- metal film, effects on electron energy loss spectra 2—6699
- metals, modified shell model treatment 2—19322
- methyl group-containing solid, coupling with combined spin and rotator system 2—33361
- molecular cryst., optical phonons and polaritons 2—19392
- molecular crystals, mechanical excitations and quantum theoretical formulation of linear electrodynamics 2—40015
- morphic effects, long wavelength optical phonons, external mag. field effects 2—19318
- naphthalene, in biphenyl and durene, localized in-band rotational phonons, obs. in electronic spectra 2—29512
- naphthalene in durene crystals, phosphorescence discussion in terms of phonons resonance pair interactions and intermol. energy transfer 2—20111
- noble metals, modified shell model treatment 2—19347
- non-crystalline solids, phonon-like excitations 2—32792
- nonlinear phonon-magnon inelastic scatt. processes 2—40066
- nonmagnetic crystal, first order photon-optical phonon interaction, mag. field effects 2—40688
- optical in Fe garnets 2—1700

Phonons continued
- Orbach relax. rate, interference and intermediate-level-width corrections 2—19930
- organic mixed crystals, spin-phonon interaction for triplet state molecules 2—29847
- organic solid solutions, lattice phonon structure rel. to electronic spectra 2—36890
- paraffin cryst., impure, phonon wings and zero-phonon lines in fluoresc. spectra 2—1715
- paramagnets, rotationally invariant theory of spin-phonon interactions 2—13376
- perovskite, ferroelec. transitions, theory 2—36591
- phonon sidebands, electronic transitions in molecular and mixed crystals 2—26134
- piezoelectric, light scatt. by acoustic phonons 2—26199
- piezoelectric crystal, polariton, Raman scatt. for general wave vectors 2—4026
- plane-parallel plate, spectrum of acoustic phonons, calc. 2—25652
- plasmas two-component systems with short-range interactions, phononlike surface modes 2—40153
- polar optical in piezoelectric and rhombic crystals, Raman studies on directional dispersion 2—25649
- polariton 2-photon absorption in noncentrosymmetric crystals 2—36865
- polariton wave propag. in cubic cryst. 2—4423
- polaritons, damped, light scatt., quantum theory 2—26138
- polaritons, Fermi resonance, manifestation of Raman spectra 2—29927
- poly-L-proline, forms I and II, dispersion curves, Higgs method 2—40050
- polymer, Raman scatt. from low freq. phonons 2—16577
- polymethylmethacrylate, hypersonic absorption by Brillouin scattering 2—40642
- polytetrafluoroethylene, dispersion curve, interchain force field and elastic constants 2—40039
- polythene, defect containing, vibrational props., numerical method 2—19394
- polyvinylchloride, hypersonic absorption by Brillouin scattering 2—40642
- pressure induced phonon frequency shift of LO and TO modes determ. from meas. of Raman spectra 2—26181
- quantum theory of light-matter interaction 2—16116
- quartz, fused, hypersonic, stimulated Brillouin scatt. obs. 2—16587
- quartz, hypersound attenuation by collinear phonon interactions 2—4048
- quartz, optical modes, stimulated Raman effect 2—16566
- Raman scatt. by LO phonons, electric-field-induced 2—33282
- Raman scatt. of phonons induced by polarons 2—16520
- Raman scattering, exciton mediated, resonance props., polariton theory 2—20058
- Raman scattering, phonon hybridization effects 2—20059
- Raman scattering by damped polaritons, quantum theory 2—16518
- Raman scattering from overtones and composite tones of optical vibrations 2—16519
- Raman scattering with polariton creation, theory 2—16451
- rare earth ion-cryst. host, multiphonon and Raman excitation 2—37940
- rare earth ions in crystals, rate of multiphonon relaxation 2—32799
- relaxation rate spectrum, infinite limit 2—15989
- resonance Raman scattering, intermediate state interactions 2—16510
- scattering effect in neutron scattering obs. of magnons 2—29808
- semiconductor, amorphous, one-phonon spectra 2—19332
- semiconductor, Boltzmann equation for acoustic phonon scatt. 2—16199
- semiconductor, degenerate nonpolar, hot carrier scatt. at optical phonons 2—19626
- semiconductor, diamond- and zinc-blende-type, stress-induced shifts of first- order Raman freqs. 2—20057
- semiconductor, hypersonic attenuation via exciton-phonon interaction 2—9876
- semiconductor, indirect-band-gap, participation in two-photon transitions 2—22753
- semiconductor, phonon-assisted indirect transitions, absorpt. spectra 2—7066
- semiconductor, photoelec. props., phonon heating effects 2—40375
- semiconductor, polar, d.c. mobility and disturbed phonon distrib. 2—40258
- semiconductor, polar, surface plasmon-phonon interaction 2—9947
- semiconductor, resonance Raman scatt. in electric fields 2—16512
- semiconductor, transport eqn., rel. to acoustic generation in mag. field 2—6671
- semiconductor, zero-gap, long wavelength acoustic phonons, effective dynamical matrix 2—9847
- semiconductor superlattice, phonon and polariton modes 2—19315
- semiconductors, n-type, light scattering by coupled Landau level LO phonon system 2—26185
- semiconductors, opaque, Raman spectra, mode Gruneisen consts. of optical phonons. 2—16539
- semimetal, spectra in mag. field 2—22395
- semimetal, transport eqn., rel. to acoustic generation in mag. field 2—6671
- silicate glasses, Raman spectra, phonon densities of states 2—19386
- spectra, transition metal carbides, correl. of physical and chemical props. 2—6655
- spectral line shifts, theory 2—16442
- spin-phonon avalanche, spatial effects 2—40750
- spin-phonon avalanche, spectral diffusion of mag. energy 2—40751
- spin-phonon interaction, effect on two-dimensional Ising system 2—4416
- spin-phonon interaction, Fourier shapes of correlative functions 2—22715
- spin-phonon interaction, theory 2—7014
- spin-phonon interaction in Heisenberg ferromag., magnon scatt. 2—26006
- spin-phonon interaction tensor components determ. 2—7113
- spin-phonon system, coupled, thermodynamic props. 2—6676
- superconducting films and small particles, phonon spectrum 2—13127
- superconducting transition-metal systems, relation of anomalies in phonon dispersion curves to acoustic plasmons 2—25771
- superconductor, A-15 cpds., transverse acoustic phonons role 2—29633
- superconductor, amorphous, phonon spectra 2—13157
- superconductor, generalized McMillan eqn. 2—16157
- superconductor, preferred direction tunnelling, phonon struct. 2—16155
- superconductor, type-II, mixed state, fluxoid-phonon interaction 2—13143
- superconductor, weak coupling, phonon spectrum 2—6771
- superconductor as phonon freq. convertor 2—40222
- superradiant effects in reson., medium 2—32836
- surface, inelastic slow electron scatt. by long wavelength phonons 2—39451
- surface polaritons and image charges at dielectric-vacuum interface 2—12640

Phonons continued
tetracene in p-terphenyl, 4.2 K, polarized fluorescence and absorption spectra rel. to electron-phonon coupling 2—26175
tetrazole, polycryst., laser Raman and external optic phonon spectra 2—10414
thermal conductivity, Callaway formula, generalization 2—9900
thermal conductivity, lattice formulation 2—4075
thin films, paraconductivity meas., effect of thermal phonon pair breaking on fluctuations 2—16150
thiourea, ferroelec. transition, i.r. and Raman obs. 2—20080
three phonon scatt. processes, variational treatment, Hamiltonian and Parrott model 2—40023
transition metal carbide, phonon spectra, pseudopot. approach 2—19321
transition metal compounds, phonon spectra anomalies, resonances electronic polarization 2—25657
transition metals, modified shell model treatment 2—19347
Urbach rule, unified theory, exponential absorpt. edges 2—20011
YAG, spectral linewidth studies of Pr^{3+} 2—10339
Ge, indirect phonon-assisted two-photon interband transitions 2—22754
Ag, dispersion and spectra, Debye temps., angular force effects 2—32807
Ag, dispersion curves, specific heat and vibr. spectra calc. from modified angular force model 2—32801
Ag alloys, phonon drag thermopower, 4-300K 2—40371
Ag_2MoO_4, normal spinel polarized Raman and phonon spectra 2—10408
Al, Wiedemann-Franz ratio, low temp. 2—40087
Al film, granular, supercond. enhancement mechanism 2—13154
Al film, supercond., reabsorpt. of phonons emitted during quasiparticle recomb. 2—13153
$Al_2O_3:Cr^{3+}$, resonant trapping, fluorescence obs. 2—19351
$Al_2O_3:Cr^{3+}$, ruby, γ-irradiated, thermal cond., Cr^{3+} spin-lattice relaxation, Cr^{2+} effect 2—40576
$Al_2O_3:Cr^{3+}$, spin-phonon interaction, ang. depend. 2—10286
$Al_2O_3:Fe^{3+}$, spin-phonon interaction 2—10493
Al_2O_3, lattice thermal conductivity 2—19447
Al_2O_3, phonon-phonon coupling, ang. depend. 2—16024
Ar, solid, dispersion curves and damping, calc. 2—32827
Ar, solid, phonon dispersion and damping 2—19407
Ar, spectra, lattice dynamics, central force rigid at. model 2—40040
Au, dispersion and spectra, Debye temps., angular force effects 2—32807
Au, dispersion curves, specific heat and vibr. spectra calc. from modified angular force model 2—32801
$BaCl_2.2H_2O$, i.r. spectra, optical phonons, water orientation, 80-473K 2—40041
BaF_2, critical point analysis of second-order Raman spectra 2—40691
$BaTiO_3$, ferroelec., Brillouin-Raman spectra, temp. depend., soft optic modes, phase transitions 2—16525
Be, lattice dynamics, freq. wave vector relations, phonon dispersion curves 2—40042
BeO, lattice thermal conductivity 2—19447
BeO, thermal cond. 2—4078
$BeSO_4.4H_2O$, Raman scatt. intensity of polaritons 2—16526
Bi, supercond., amorphous, phonon spectra 2—13157
$Bi_{12}GeO_{20}$, light scatt. by acoustic and optical phonons 2—16454
$Bi_{12}GeO_{20}$, phonon scatt. of laser radiation 2—10295
$Bi_{12}GeO_{20}$, scatt. of light 2—10335
CaF_2, critical point analysis of second-order Raman spectra 2—40691
$CaMoO_4$, direct optical coupling to surface phonons 2—33239
CaO, F^+ centre emission spectrum, one-phonon sidebands 2—29911
CaO, freq. wave vector rel., combined density of states calcs. 2—36329
CaO, second order Raman spectra 2—10407
CaO, vibronic props. of F^+ absorpt. band 2—7068
$CaWO_4$, hypersonic attenuation, phonon-phonon interactions 2—32833
$CdCl_2$ (Br_2) (I_2), Raman active modes 2—20064
$CdCr_2S_4$, $CdCr_2Se_4$, chalcogenide spinel, lattice dynamics and mag. ordering 2—32806
$Cd_xHg_{1-x}Te$, optical phonon scatt., rel. to electron mobility, under high hydrostatic pressure 2—10009
CdS, Brillouin scatt., acoustoelectric, anharmonic and resonance effects 2—26200
CdS, cathodolum., free exciton motion and exciton-phonon interaction studies 2—36958
CdS, electric field induced Raman scatt. by LO phonons 2—16528
CdS, evidence of bound exciton resonance in phonon Raman scattering 2—7079
CdS, inelastic polariton scatt. processes 2—16529
CdS, momentum in acousto-optical domain, light scatt. obs. 2—16455
CdS, optical modulation by acoustic phonon flux 2—22790
CdS, thermal Brillouin scatt., vel. and attenuation of sound 2—33289
CdS_xSe_{1-x}, solid soln., phonon. obs., reson. Raman effect 2—16583
CdSe, optical phonon drag effect 2—25813
$CdTe:Fe^{2+}$, phonon conductivity 2—40029
CdTe, Seebeck effect and Nernst-Ettingshausen effect, influence of optical phonons 2—25943
$Cd_{1-x}Zn_xS$, long wavelength phonon freq., conc. depend. Raman spectra 2—20065
$CrK(SO_4)_2.12H_2O$, soft-phonon mode near 193K, rel. to temp. variation in mean magnetic moment 2—6938
α-Cr_2O_3, paramag. phase, Raman scatt. 2—16532
$CsNO_3$, retaining site group in disordered crystal 2—36898
Cu-Au alloy, imperfect cubic lattice, dispersion relations 2—40045
Cu, densities of states, Brillouin zone integration by combined linear and quadratic interpolation 2—19501
Cu, dispersion and spectra, Debye temps., angular force effects 2—32807
Cu, phonon freq. distrib. functions determ. 2—13023
Cu, phonon freqs., static dielec. function, calc. from model band struct. 2—40043
CuCl, exciton spectra, line-width and phonon interaction 2—10378
CuCl, temp. depend., absolute Raman scatt., efficiencies 2—22784
CuI, dispersion curves and normal modes of vibrations 2—36328
Cu_2O powder, i.r. region transmittivity, optical phonons obs. 2—36878
Dy, magnetoelastic interaction, static and dynamic effects 2—25999
$DyAsO_4$, Jahn-Teller induced phase transition, Raman scatt. obs. 2—16534
$DyAsO_4$, phase transition 11.17K, Raman scatt., degenerate phonon line splitting 2—16535
$DyVO_4$, Jahn-Teller induced phase transition. Raman scatt. obs. 2—16534
$DyVO_4$, phase transition 13.8K, Raman scatt., degenerate phonon line splitting 2—16535
$DyVO_4$, Raman and i.r. reflection spectra, lattice vibrations and phase transition obs. 2—16533

Phonons continued
EuO, thermal cond., anomalous scatt. 2—19457
Fe, distrib. rel. to second order Doppler shift in Mossbauer effect 2—36325
$FeBO_3$, phonon Raman scatt. temp. depend., mag. contrib. to intensities 2—40692
$FeCl_2.2H_2O$, magnon-phonon interaction, microscopic description 2—40556
FeS_2, Raman scatt. from phonons 2—22785
Ga, supercond., amorphous, phonon spectra 2—13157
GaAs, amorphous, density of vibr. states, Raman spectra obs. 2—16541
n-GaAs, magnetophonon reson., many-phonon scatt. 2—19641
GaAs, non-thermal groups, X-ray and neutron scatt. obs. 2—4034
GaAs, observation of polaritons, new interpretation of pre-exciton reflectance and luminescence 2—13257
GaAs, phonon cond., Holland model applic. 2—4079
GaAs, refl. wavelength depend., optical phonon-plasmon coupling, Vargas theory 2—36859
GaAs, relaxation of photoexcited hot electrons through capture by ionized donors via emission of LO phonons 2—4527
n-GaAs, reson. Raman scatt. by electronic excitations, coupled plasmon-phonon modes 2—16538
GaAs, stress effect on reststrahlen spectrum 2—33284
GaP:Si,O, localized phonon excitation, i.r. absorpt. spectra 2—20037
GaP, dispersion of surface polaritons 2—33233
GaP, energy estimation from wavelength modulation of photoresponse 2—33074
GaP, i.r. generation by coherent excitation of polaritons 2—16458
GaP, indirect phonon-assisted two-photon interband transitions 2—22754
GaP, magneto-optical behaviour of no-phonon line 2—16606
GaP, polariton dispersion and damping, temp. depend., nonlinear spectra 2—4463
GaSb:Zn, low temp. phonon thermal cond., role of density of states effective mass 2—40092
p-GaSb, lattice thermal cond., 2 to 20 K 2—25694
$Gd_2(MoO_4)_3$, phase transition, soft-zone boundary phonon driven 2—19763
GdS, lattice contrib. to thermal conductivity 2—4080
Ge-Si alloy, Raman spectra, bond vibr. and interband resonance 2—20068
Ge, acoustical phonon generation rel. to electron drift vel. saturation 2—6846
Ge, amorphous, density of vibr. states, Raman spectra obs. 2—16541
Ge, amorphous film, energy loss spectra of 25 keV electrons, two phonon excitation 2—19481
Ge, bounds of three phonon U-resistances 2—32808
Ge, dispersion curve, perturbation theory calc. 2—12692
Ge, energy estimation, from wavelength modulation of photoresponse 2—33074
Ge, hypersonic attenuation via exciton-phonon interaction 2—9876
n-Ge, low temp. lattice cond. 2—4081
n-Ge, phonon scatt. by neutral donors, low temp. 2—6691
Ge, Raman scatt., temp. depend., cryst. vibrs. anharmonic props. 2—16540
Ge, Raman scattering, carrier conc. effects 2—26192
Ge, Raman spectra, resonant peak nature 2—33285
Ge, scattering of dislocations rel. to u.s. attenuation 2—40062
GeO_2, optical phonon freq., i.r. reflectance obs. 2—20002
H_2, D_2, HD, hexagonal phase, Raman active optical phonons 2—22397
H_2, solid, phonon-libron coupling calc. 2—19370
H_2, solid and in solid soln., near i.r. absorp., phonon spectra 2—19371
He, liquid, phonon roton interaction Hamiltonian construction 2—28927
He II, phonon lifetimes 2—6273
He II, scattering from impurities in an imperfect Bose gas 2—30821
He solid, phonon spectral functions and ground state energy in bcc phase 2—35814
^3He, b.c.c., lattice dynamics, dispersion curves calculated using T-matrix method 2—9200
^3He, heat pulse propag., umklapp processes, second sound 2—18871
^4He, b.c.c. solid and superfluid, interaction processes from inelastic neutron scattering 2—35815
^4He, density matrix of liquid at low temp. 2—32297
^4He, onset of ballistic flow of phonons temp. pulse technique, 1st sound velocities 2—15624
^4He, solid, lifetime, stimulated Brillouin scatt. obs. 2—16585
^4He b.c.c. single crystal, evidence of strong phonon relaxation from inelastic neutron scattering expts. 2—25135
HfC, dispersion calc. 2—19373
p-HgTe, lattice thermal cond. 2—32855
InAs, low temp. phonon cond. 2—25695
$InBO_3:Tb^{3+}$, Ce^{3+}, calcite type cryst., luminesc., 4f-5d transitions, phonon sidebands 2—29962
$InBO_3$, phonon Raman scatt. temp. depend., mag. contrib. to intensities 2—40692
n-InP, magnetophonon oscillations of longit. magnetoresist. 2—10018
InSb-NiSb eutectic alloy, rel. to anisotropy of thermal cond. 2—19460
InSb, coupled cyclotron-plasmon-phonon modes for sample configs. ranging from Faraday to Voigt 2—22769
n-InSb, d.c. mobility and disturbed phonon distrib. 2—40258
InSb, hole-optical phonon coupling magneto-optical study 2—36822
n-InSb, magnetophonon resonance of hot electrons at 77K 2—36527
InSb, phonon cond., Holland model applic. 2—4079
K, phonon dispersion calc. using pseudopotential approach 2—36318
K complex, $K_2MCu(NO_2)_6$, (M=Ba, Pb), Jahn-Teller distortion and optical phonons 2—36988
KBr, two phonon Raman spectra 2—25658
KCl, laser-stimulated atomic migration 2—25463
KI: O_2-(S_2-), luminescence spectra, structure of phonon wing 2—26220
KI, dispersion relations, anharmonicity 2—1681
KI, i.r. absorpt., two-phonon processes 2—40677
KI, multiphonon absorpt. bands, i.r. transmission spectra 2—36883
$KMnF_3$, anomalous elastic behaviour near struct. phase transition 2—19157
$KMnF_3$, para- to antiferromag. transition, Raman spectra obs. 2—16548
KNO_3 instability in ferroelectric phase transition studied by Raman spectroscopy 2—25924
$K_{1-x}Na_xTaO_3$ mixed cryst., ferroelec. transitions, soft modes 2—25928
$KTa_{0.64}Nb_{0.36}O_3$, Raman spectrum, paraelec. and ferroelec. phases, phonon modes 2—36905
$Kta_{0.63}Nb_{0.37}O_3$, cubic ferroelectric, soft modes, neutron scatt. obs. 2—13029

Phonons continued
LaF_3, nonresonant energy transfer from Er^{3+} to Yb^{3+}, phonon emission and absorpt. 2—40718
$La_2Mg_3(NO_3)_{12}$:Ce^{3+}, conc. depend. Orbach relax. rates 2—10266
$La_2Mg_3(NO_3)_{12}$:Ce^{3+}, phonon bottleneck and cross-relax. 2—10268
$La_2Mg_3(NO_3)_{12}$:Ni^{2+}, spin-lattice relax. and phonon bottleneck 2—10267
Li, dispersion relation, screening effects 2—40046
$LiAl_5O_8$:Fe^{3+}, fluoresc. and excitation spectra, ordered and disordered phases 2—36945
LiF, deformed, thermal phonon scatt. by mobile dislocations 2—13026
LiF, dynamics of F_2^+-centres, one phonon sideband and Raman scatt. 2—22772
LiF, thermal cond. and Ziman limit 2—25696
LiF, thermal phonon-dislocation interaction 2—32856
$LiIO_3$, polaritons and oblique phonons, Raman scatt. and i.r. refl. 2—4447
$LiNbO_3$, directional dispersion of phonon frequencies and polariton scatt. 2—16553
$LiNbO_3$, eigenfrequency, eigenvector and Raman scatt. cross section of polaritons 2—16554
$LiNbO_3$, polariton dispersion, temp. depend., soft modes 2—16552
$LiNbO_3$, polariton eigenfrequencies and eigenvectors, calc. in long optical phonon limit 2—22475
Lif, scatt. at dislocations, thermal cond. obs. 2—16069
$LuBO_3$:Tb^{3+}, Ce^{3+}, calcite type cryst., luminesc., 4f-5d transitions, phonon sidebands 2—29962
$MgCl_2$, crystalline and molten, Raman spectra phonon frequencies, residual lattice bands 2—20073
MgO:Cr^{3+}, Raman relax. rates of Cr^{3+}, Debye model of phonons 2—40044
MgO:Fe^{2+}, ballistic heat pulse scatt. by resonant spins, phonon freq. distrib. 2—13027
MgO:Fe^{2+}, sp. ht., spin-phonon interaction contrib. 2—6676
MgO:Ni, mag. circular dichroism, vibr. induced d→d transitions 2—22773
MgO:Ni, paramag. cryst., phonon avalanche, Brillouin scatt. 2—16018
MgO:Ni^{2+}, Raman relax. rates of Ni^{2+}, Debye model of phonons 2—40044
MgO, lattice thermal conductivity 2—19447
Mg_2X, X=Si, Ge, Sn, Pb, resonant scatt. by F_{1u} type phonons 2—20075
Mg_2X, X=Si, Ge, Sn, Pb, resonant scatt. by F_{2g}-type phonons 2—20074
$MgZn_2$, phonon spectra, group theoretical calc. 2—22402
$MnPt_3$, ferromag., neutron scatt. obs. 2—22676
NH_3, solid, freq. distrib. func., neutron scatt. obs. 2—36321
NH_3, solid, molecular and lattice vibrations, Raman obs. 2—19382
Na, anharmonic lattice dynamics 2—19380
Na, phonon aided optical absorp. theory 2—20045
$NaBrO_3$, fund. band edge absorpt., temp. shift, band transitions, phonon emission absort. 2—36884
NaCl, thermal cond., temp. range 1-80 K, phonon contrib calc. 2—40094
$NaClO_3$, ferroelectric phase transition, relation to phonon structure 2—25930
$NaClO_3$, vibr. spectrum and dielec. behaviour, Raman obs. 2—33286
NaF, thermal cond. and Ziman limit 2—25696
NaI, i.r. absorpt., two-phonon processes 2—40677
NaI, multiphonon absorpt. bands, i.r. transmission spectra 2—36883
$NaNbO_3$, cubic-tetragonal transition rel. to soft phonon modes 2—39648
$Na_2ZnCl_4.3H_2O$, $Na_2ZnCl_4.3D_2O$, long wavelength phonon spectra, assignment using Raman data 2—40036
Nb, dislocation damping by phonon viscosity 2—29183
Nb_3Sb, acoustic-phonon instability and critical scattering near phase transition at 45 K 2—9864
Ne solid, dispersion curves, calc. using modified Morse pot. 2—40047
Ni, phonon freq. distrib. functions determ. 2—13023
NiO Raman, scattering by phonons, magnons and phonon- magnon interactions from 10-650K 2—26195
NiS, acoustic and optical modes, rel. to struct. phase transition 2—16349
p-GaP, luminescence spectrum, phonon lines and bands 2—20096
Pb-Bi amorphous alloys, supercond., phonon spectra 2—13172
Pb, supercond., amorphous, phonon spectra 2—13157
Pb, supercond., splitting of phonon struct. in tunnelling characts. 2—19595
PbF_2, critical point analysis of second-order Raman spectra 2—40691
n-PbTe, i.r. magnetoabsorpt., phonon-cyclotron and carrier-transfer reson. 2—40678
Pd-Mn dil. alloys, acoustic-spin-wave stiffnesses and ordering temps. 2—10191
$PrAlO_3$, low temp. phase transition, Raman obs. 2—20077
$Pr_xNd_{1-x}AlO_3$, low temp. phase transition, Raman obs. 2—20077
$RbClO_3$, phonon Raman spectrum and optical phonon damping 2—16563
$RbClO_3$ anisotropic crystals, polarized Raman obs. by immersion technique 2—26196
RbCs, alloy binary disordered, frequencies using nonlocal pseudopotential methods 2—22385
RbH_2PO_4, Brillouin scatt., soft mode behaviour 2—7083
SbSI, instability in ferroelectric phase transition studied by Raman spectroscopy 2—25924
SbSI, long wavelength, ferroelec. phase transitions, Raman spectra 2—16459
SbSI, soft phonon couplings in press.-induced phase transition 2—19385
$ScBO_3$:Tb^{3+}, Ce^{3+}, calcite type cryst., luminescence, 4f-5d transitions, phonon sidebands 2—29962
Se, dispersion curves, neutron inelastic scattering obs., non-bonded force model 2—4042
Se, long wave optical phonon freq., comparison with Te 2—22406
Si:P, effect on impurity photocond. spectra 2—33075
Si, amorphous, density of vibr. states, Raman spectra obs. 2—16541
Si, amorphous film, energy loss spectra of 25 keV electrons, two phonon excitation 2—19481
Si, dispersion curve, perturbation theory calc. 2—12692
Si, energy estimation, from wavelength modulation of photoresponse 2—33074
Si, ion implanted, SiC, Si_3N_4, SiO_2 formation, i.r. phonon absorp. bands obs. 2—26173
Si, l.f. phonon scattering mechanization by acceptor holes rel. to u.s. attenuation 2—13037
n- Si, m.o.s. structure, tunnelling characteristics, phonon structure 2—16255
n-Si, phonon drag influence on piezothermopower 2—4239
p-Si, phonon transmission, impurity effects 2—32832
Si. Raman scattering, carrier conc. effects 2—26192
α-SiC, optical phonon energy range, determ. from i.r. absorpt. 2—10395
SiO_2, quartz, diffuse X ray scatt., near α-β transition 2—4038

Phonons continued
SrF_2, critical point analysis of second-order Raman spectra 2—40691
SrO powder, far-i.r. surface-activated band-mode absorpt. 2—7074
$SrTiO_{3-x}$ and $Ca_ySr_{1-y}TiO_{3-x}$, soft mode supercond. 2—19598
$SrTiO_3$, differential second order Raman spectroscopy 2—16568
$SrTiO_3$, displacive transition, u.s. vel., stress effects and interaction parameters 2—32780
$SrTiO_3$, optic modes and permittivity 2—40359
TaC, dispersion calc. 2—19373
Tb, magnetoelastic interaction static and dynamic effects 2—25999
$TbVO_4$, Jahn-Teller induced phase transition, Raman scatt. obs. 2—16534
Te:Sb, coupled plasmon-LO phonon modes, reflectivity obs. 2—32906
Te, long wave optical phonon freq., comparison with Se 2—22406
TlBr, exciton-optical phonon interaction, reson. Raman scatt., hot luminesc. 2—16588
V, phonon freq. distrib. functions determ. 2—13023
VBO_3, phonon Raman scatt. temp. depend., mag. contrib. to intensities 2—40692
VO_2, phonon softening effect rel. to metal-insulator transition 2—29679
VO_2, semiconductor- metal transition, Raman scatt. obs. 2—16571
YAG:Cr^{3+}, vibronic spectrum and fluoresc. lifetime, temp. depend. 2—13507
$YbCl_3.6H_2O$, Orbach processes 2—10273
Zn, dispersion relations and lattice specific heat calc. 2—19391
$ZnAl_2O_4$, normal spinel polarized Raman and phonon spectra 2—10408
ZnO:Li, lattice cond. 2—19471
ZnO, Raman spectra, hydrostatic pressure effect, Gruneisen parameters 2—16574
ZnS, hexag. single cryst., Raman dispersion of selected phonons 2—16572
ZnS, Raman dispersion cross section, TO and LO modes 2—16573
ZnS, Raman spectra, hydrostatic pressure effect, Gruneisen parameters 2—16574
ZnSe, Raman dispersion cross section, TO and LO modes 2—16573
$ZnWO_4$:$C4^{3+}(Mn^{2+})$, spin-phonon interaction 2—10493
ZrB_{12}, supercond. isotope effect due to optical phonon modes 2—6782

Phosphorescence
acenaphthene, Hg heavy atom impurity effect on luminescence 2—3125
acetone, partially deuterated, lifetime meas. 2—28337
acetone-^{18}O, isotope effect on nonradiative relaxation 2—35301
acetophenone, dynamic properties and zero field splittings of lowest excited triplet states 2—28335
acetophenone in variety of matrices, pseudo-Jahn-Teller distortion 2—29966
acetophenone partially deuterated, lifetime meas. 2—28337
aromatic compounds, donor phosphorescence quenching and decay in sensitized phosphorescence 2—13511
aromatic hydrocarbons in poly(methylmethacrylate) temperature dependence studied in 77-400K 2—20110
benzaldehyde, $^3U(n\pi^*) \rightarrow S_0$ phosphorescence, vibronic interactions 2—12212
benzaldehyde, dynamic properties and zero field splittings of lowest excited triplet states 2—28335
benzaldehyde, zero field splitting, phosphorescence rate consts. and vibronic activity in lowest triplet state by p.m.d.r. 2—28353
benzaldehyde in methyl cyclohexane, emission spectrum, mechanism 2—8739
benzene, benzene-d_6, radiational deuterium effect in triplet-single transition 2—21663
benzene, photoexcitation spectrum, Zeeman effect, dynamic pseudo Jahn-Teller distortion 2—20109
benzene homologues, spectra, frozen matrices, liq. nitrogen temps. 2—4502
benzonitrile in polycryst. matrices, vibr. anal. in terms of excited state geometries 2—31839
benzophenone, 1.3K, principle phosphorescent trap, applic. of fast passage ODMR 2—22809
benzophenone, partially deuterated, lifetime meas. 2—28337
benzophenone, solns. and crystals, effect of u.v. illumination 2—26363
benzophenone with diacetyl impurity, crystals, transfer of excitation energy 2—1717
p benzoquinone and derivatives, vapour spectra 2—5959
benzyl derivatives, intramolecular charge-transfer mechanisms 2—38960
biphenyls, bridged, in fluid solution 2—39374
boric phosphor of 2-phenylquinoline, spectra, intensity and decrease with time at different temperatures 2—16614
coronene, Hg heavy atom impurity effect on luminescence 2—3125
diamond, semicond., and thermoluminesc. 2—26245
4,10-diazachryzene, in lowest triplet state, rel. to acid-base equilibria 2—18497
diazanaphthalenes, triplet state population and depopulation, phosphorescence-microwave double-resonance meas. of zero field splittings and kinetic parameters 2—22810
1,4-diazatriphenylene in frozen solns., at 77 K 2—26244
diphenylmethane, enhancement mechanism 2—10449
fluorene molecules in fluorene crystal, triplet states, e.p.r. and phosphorescence study 2—30089
glyoxal vapour, fluorescence and phosphorescence from laser excited first singlet excited state 2—12249
halophosphate synthesis, elec. microscope obs. 2—4571
indene, frozen hydrocarbon solns., liq. N temp. 2—16625
indole, frozen hydrocarbon solns., liq. N temp. 2—16625
isooctane cryst. with impurity mols., polymorphic transform. effects 2—29959
Michler's ketone, solid soln., from 2 levels populated by intersystem crossing 2—4504
molecules, phosphorescent triplet states, optically detected adiabatic inversion 2—21581
molecules, pulsed excitation phosphorescence microwave double resonance rel. to intersystem crossing relative rate determination 2—8567
monodeuterobenzonitriles in polcryst. matrices, vibr. anal. in terms of excited state geometries 2—31839
naphthalene, charge transfer complexing effects 2—36893
naphthalene, optical detection of e.s.r. 2—10527
naphthalene, phosphorescence in vapour phase 2—35348
naphthalene, triplet exciton lifetimes from delayed fluorescence and prompt phosphorescence 2—20108
naphthalene in durene crystals, discussion in terms of phonons, resonance pair interactions and internal energy transfer 2—20111
naphthalene-d_8 in solid soln., X-ray phosphorescence triplet molecule formation 2—26364

Phosphorescence continued
perdeuterobenzonitrile in polycryst. matrices, vibr. anal. in terms of excited state geometries 2—31839
phenanthrene, charge transfer, complexing effects 2—36893
phenyl alkyl ketones in glassy matrices, viscosity dependent dual phosphorescence 2—36950
phosphor, Eu^{3+} activated, colour shift mechanism 2—1716
phosphorescence microwave double resonance spectroscopy, quadrature phase relationships 2—8568
pyrazine, frozen soln., obs. of additional bands from microcrystals due to emission 2—10445
pyrene, location of triplet excimer level 2—4505
pyrene, phosphorescence in vapour phase 2—35348
pyrene, temp. dependence of lifetime of triplet excimer emission 2—7099
pyrene monomer and excimer, quenching rate parameter dependence on solvents 2—12571
2-amino-pyridine, in acetonitrile-water mixtures, lifetime, intensity, at 77K 2—7100
pyrimidine in benzene, zero-field microwave-optical double resonance at 77 K 2—22818
γ-pyrone series, aromatic derivs., obs. of $n\pi$-, $n\pi^*$- and $\pi\pi^*$- phosphorescence 2—857
rare earth trifluoride, up-conversion phosphor, prep. method 2—33321
s-tetracyanobenzene-toluene complex, structure of fluorescent and phosphorescent states from absorption and emission spectra 2—15397
thionaphthene, frozen hydrocarbon solns., liq. N temp. 2—16625
thionaphthene, Hg heavy atom impurity effect on luminescence 2—3125
toluene, enhancement mechanism 2—10449
transients induced magnetic resonance fast passage 2—22809
2,4,5-trimethylbenzaldehyde, dynamic properties and zero field splittings of lowest excited triplet states 2—28335
2,4,5-trimethylbenzaldehyde in durene, assignment and location of 2nd triplet state 2—15402
tripalavin-gelatin gel, phosphor, phosphoresc. decay kinetics, irrad. effects 2—36949
triphenylmethane, enhancement mechanism 2—10449
tryptophan molecule, in solid matrix, 77K 2—35355
X-ray and U.V. induced, obs. during and after irradiation 2—36951
xanthone, effects of medium on polarized phosphorescence spectra 2—24557
zinc borates, thermal activation energies of electron traps 2—10448
zinc porphin, delayed phosphorescence of lowest triplet state by microwaves 2—18535
zinc porphin, lowest triplet state, phosphorescence modulation by microwaves 2—21707
CO_2 photodissociation obs. of phosphorescence from $CO(a^3\Pi\text{-}X^1\Sigma)$ Cameron bounds 2—28276
CaS-SrS-Ce, Sm phosphors, energetic structure of capture centres 2—16624
Cas phosphor, decay time reduced with Co addition 2—26248
Cd complex, tetrabenzoporphine, quasilinear spectra, vibration structure 2—4486
Cr complexes solid-state and rigid glass 2—10376
Fe^{3+} ions in oxide host lattices 2—10447
$Hg(6^3P_2)\rightarrow Hg(6^3P_1)$ transition, relative intramultiplet quenching cross sections 2—28192
KCl, γ-irrad., F-centre obs. 2—16630
Mg complex, tetrabenzoporphine, quasilinear spectra, vibration structure 2—4486
Pd complex, tetrabenzoporphine, quasilinear spectra, vibration structure 2—4486
SO_2 neat crystals, optical detection of zero field splittings in phosphorescent triplet state 2—13512
SnO_2, stimulated photoluminesc. emission 2—26243
Zn complex, tetrabenzoporphine, quasilinear spectra, vibration structure 2—4486
ZnS:Cu, freq. domain meas., green emission mechanism 2—33322
ZnS rel to photodielec. effect response 2—10144

Phosphors *see Luminescence; Luminescent devices*

Phosphorus
atom, 2p binding energies, correlation with at. charge and group shifts 2—35167
black, vapour phase growth of crysts. at h.p. 2—25252
diffusion, intergranular, in α—Fe 2—12807
diffusion in Fe, grain boundary, effects of C 2—22249
diffusion in Si 2—12785
gas, ^{31}P n.m.r. chemical shifts 2—32181
ion implantation in diamond, p-n junction form. 2—36045
ion implanted GaAs, i.r. localized vibr. mode absorpt. 2—13474
ion implanted Si, additional ion bombardment effects 2—25434
meteorite content, chemical analysis 2—11020
molecule, dissoc. energies and potential curves 2—31819
Ge:B,P, amorphous, ion implanted, path length distrib., 25-150 keV 2—25710
Ge:Ga, P, single cryst. growth, compensated, programmed growth rate 2—3572
Ge:P, As, single cryst. growth, uniform impurity distrib., growth rate program 2—1211
Ge:P, γ-irrad., impurity-vacancy complexes 2—15741
Ge:P, γ-irradiated, vacancy-donor complexes 2—29704
Ge:P, γ-ray irrad., role of impurity in defect form 2—15777
Ge:P ion implanted, elec. props. and doping profile 2—25859
P I to PV, excited level lifetimes, evaluation from beam foil spectra 2—5792
P IV, extreme u.v., Hartree-Fock theoretical wavelengths, accuracy 2—24336
P^+, collisions with Ar, Auger electron energy distribution for fixed impact parameters 2—693
Si:B,P, lattice contraction coefficients detn. 2—22225
n-Si:P, D irrad., effect on Hall mobility, carrier density 2—22566
n-Si:P, e.s.r. parameters, spin susceptibilities, impurity scatt. spin relax. 2—22835
Si:P, elec. active damage in hot implantations 2—25869
Si:P, exchange coupling in donor atom clusters, e.s.r. study 2—20150
Si:P, first order Stark effect in impurity photocond. 2—10140
Si:P, heavily doped, cond. electron spin relax., e.s.r. obs. 2—20135
Si:P, impurity photocond., influence of phonons 2—33075
Si:P,As, simultaneous diffusion, backscatt. He ion and radioactive analysis obs. 2—32551
n-Si:P,Fe, vacancy-interstitial interaction 2—6485

Phosphorus continued
Si:P ion implanted, amorphization 2—25381
Si:P ion implanted, channelling profiles 2—19111
Si:P ion implanted, crystal damage and elec. props. 2—25380
Si:P ion implanted, divacancy radiation damage, e.p.r. obs. 2—26265
Si:P ion implanted, non-Gaussian profile, mechanisms discussed 2—25437
Si:P ion implanted, profiles and elec. activity 2—25866
p-Si:Zn, P, photodielec. effect, polarizability of neutral atoms 2—13343
inSi, homogeneity breakdown, during joint diffusion of Ni and P 2—36058
Si crystal, P ion implanted, profiles, calc. 2—25426
inSi epitaxial layer, temp. depend. of doping conc. 2—25209
TlCl:P, luminesc., effect of i.r. irrad. 2—10430

Phosphorus compounds
halophosphate phosphors-glass interaction, Mn effect on binder burning-out 2—29965
cis-1,3-$P_3N_3F_4(C_6H_5)_2$, P-P coupling constants 2—15329
1,1-$P_3N_3F_4(C_6H_5)_2$, P-P coupling constants 2—15329
1,1,3,3-$P_3N_3F_4(C_6H_5)_2$, P-P coupling constants 2—15329
partially deuterated, deuterium isotope effects on chemical shift and coupling consts. 2—8716
phosphate containing molecules, effects on ^{25}Mg n.m.r. in MgCl 2—28897
phosphides, arsenophosphides, struct. evolution 2—18968
phosphine oxides, spectroscopic study of intermolecular interactions 2—28434
ultraphosphates, definition and cryst. chemistry 2—6395
$Al_xIn_{1-x}P$, thermodynamic props. of In-Al-P system appl. to manufacture 2—6788
Co-P, noncryst. films, structure, electron diffraction obs. 2—6429
Co-P film, chemical deposition, magnetization 2—13404
Fe-Ni-P film, mag. field induced anisotropy 2—36725
Fe-P-B, amorphous ferromagnetic, splat cooling prep. 2—10211
Fe-P-C alloy, intergranular brittleness, rel. to P and C content 2—36235
Fe-Pd-P alloys, amorphous, mag. props. 2—19877
H_3PO_4, effects of diamagnetic ions on relaxation of ^{31}P in aqueous solutions 2—1121
In-Ga-P, phase diagram, rel. to epitaxial growth of $In_xGa_{1-x}P$ 2—9837
In-Ga-P ternary phase diagram 2—36295
$Li_2O.P_2O_5.SiO_2$ glass, lithium disilicate crystn., electron microscope obs. 2—39440
Mn-P-C alloy, amorphous, atomic and radial distrib. functions 2—15933
$NH_4H_2PO_4$ crystals, double refraction, temp. dependence, spectrographic meas. over 20 to 65°C and λ=400 to 650 nm 2—7046
$Nd^{3+}:POCl_3:ZrCl_4$ liq. laser, Q-switched, output characts. 2—7928
$Nd:SnCl_4POCl_3$ circulation type, spatial and energy characteristics 2—273
Ni-P film surfaces, ellipsometric study 2—32370
Ni-P films, struct. and elec. resist., annealing effects 2—15969
Ni-P layers, imperfectly crystallized quasi-amorphous, struct. 2—22074
Ni-Pt-P-Cr alloys, amorphous, elec. resist. and mag. susceptibility 2—6761
P-Cl compounds and complexes, ^{35}Cl nuclear quadrupole resonance 2—28317
P-Ni-Pd alloy, amorphous, elec. resist., temp. coeff., rel. to P content, 4.2-300 K 2—40182
P-S(Se)-Sn system, glass and cpd. formation, n.m.r. study 2—37003
PCl_3-PBr_3, liq. mixture, ^{31}P and ^{35}Cl n.m.r. relaxation times meas. 2—9178
PCl_3-$PBrCl_2$-PBr_2Cl-PBr_3, liq. mixture, ^{31}P n.m.r. relaxation times meas. 2—9178
PCl_3, condensed states, intermolecular dynamics, vibr. spectra study 2—35377
PCl_3, i.r. spectra, symmetric top force constants 2—38935
PCl_3, liq. ^{35}Cl n.m.r. relaxation times meas. 2—9178
PF_3, liquid, significant structure theory, degrees of freedom, thermodynamic properties 2—28785
PF_2CN gas, molecular structure, electron diffraction det., sector-microphotometer method 2—18466
PF_2NH_2, microwave spectrum, structure, dipole moment and quadrupole coupling consts. 2—31820
PH_2, electron affinity determ. from cross section for photodetachment of electrons from PH_2- 2—15331
PH_3, adsorption on SiC, room temp. 2—29070
PH_3, effects of Coriolis resonance in ν_2 and ν_4 bands, spectral determ. 2—8700
PH_3, partially deuterated and tritiated, harmonic wavenumbers and normal coords. calc. 2—18444
PN, rotation spectrum, new constants 2—38936
$(PNCl_2)_3$, ^{15}N-labelled, vibrational assignment of i.r. spectra 2—28319
PNF_{11}, N=As, Sb, Ta, Nb, chem. shift, spin coupling, mag. resonance obs. 2—5927
$(PNF_2)_3$, gas phase, electron diffraction study of molecular structure 2—5946
P_2O_5-B_2O_3-Cs_2O glass, containing Cu^{2+}, struct., e.p.r. study 2—28976
PO, emission spectrum attributed to $^2\Sigma$-$^2\Sigma$ transitions, rotational structure of bands 2—18465
PO, Rydberg states converging to ground state of PO^+, LCAO-MO SCF calculations 2—35278
PO_4 glasses:Nd, lasing and spectral line characteristics 2—17627
PO_4^{3-}, bonding investigations using X-ray spectroscopy and ab initio SCF-MO calc. 2—31821
PO_4^{3-}, crystal structure, bond length data 2—6447
P_2O_5 orthorhombic form, i.r. absorption spectra and X-ray powder diffraction 2—15729
P_4O_{10}, normal coordinate analysis, force consts., mean amplitudes of vibration from spectral study 2—18467
P_4O_{10} molecule, normal coordinates and force field 2—28318
P_4O_6, normal coordinate analysis, force consts., mean amplitudes of vibration from spectral study 2—18467
$POCL_3$—$ZrCl_4$:Nd^{3+}, liquid laser system 2—27497
$POCl_2$:Nd liquid laser, lasing and spectral line characteristics 2—17627
$POCl_3$:Nd laser solns., Brillouin and Rayleigh scatt. 2—32269
$POCl_3$:Nd liquid laser, spectral output props. 2—34399
$POCl_3$:Nd^{3+} laser amplifier, performance 2—23605
$POCl_3$:Nd^{3+} liquid laser systems properties 2—17610
$POCl_3$ measurement of optical Kerr constant and nonlinear indices 2—33201
$POCl_3$ solid, analysis of i.r. and Raman spectra, determ. of structure 2—13491
$POCl_{3\odot}^{-}$, radical anion, e.s.r. spectrum and structure 2—821
$P_2O_5.SiO_2$, In m.i.s. struct., charge distribution 2—10102
P_4S_{10} powder, ^{31}P n.m.r. chemical shielding anisotropy at 99.4 MHz 2—10561

Phosphorus compounds continued
  P_4S_3 single crystal, ^{31}P n.m.r. chemical shielding anisotropy at 99.4 MHz 2—10561
  ^{31}P compounds, spin rotation interaction constants derived from chemical shift data, and from NMR relaxation and viscosity data 2—15281
  ^{31}P n.m.r. spin-lattice relaxation in liquid compounds 2—32277
  $(Pd_{60-x}—Pt_x—Ni_{40})_{75}—P_{25}$ alloy, elect. resist., 1.2-300 K 2—19550
  V_2O_5-P_2O_5 glass, in m-i-m struct., high resistance, negative resistance and high conductivity obs. 2—40314
  V_2O_5-P_2O_5 glass, polar conductivity and i.r. absorp. 2—10039

Photochemistry
  see also Photochromism; Photographic process
  acetophenone, single crystal e.p.r. studies of photoexcited states 2—26360
  acetylene, fluorescence, by vacuum u.v. photolysis 2—830
  acridine orange, triplet quantum yield study with tunable dye laser 2—26355
  L-alanine:Cu crystals, u.v.-induced conversion in Cu^{2+} complexes, e.p.r. study 2—10642
  alkali halides, u.v. and pulse irradiated, heavy atom effects on electronic processes 2—26370
  anthracene, role of dislocations and stacking faults, elec. microscope obs. 2—30088
  anthracene dissolved in organic liquid, two photon laser photo-ionisation 2—30081
  anthraquinone in solutions, delayed thermal fluorescence 2—28874
  aromatic azo compounds, reversible orientational photodichroism and photoisomerization, system model 2—33387
  aromatic $d\pi^*$-$\pi\pi^*$ interactions, comparison with $n\pi^*$-$\pi\pi^*$ interactions in Ir(III) complexes 2—35300
  azomethane, ruby laser induced decomposition, cross section 2—26362
  benzaldehyde, zero field splitting, phosphorescence rate consts. and vibronic activity in lowest triplet state by p.m.d.r. 2—28353
  benzene, in cyclohexane, triplet yield as function of conc., intersystem crossing effects 2—28875
  benznitrile, single crystal, e.p.r. studies of photoexcited states 2—26360
  benzophenone, solns. and crystals, electronic and vibrational spectra, effect of u.v. illumination 2—26363
  bleached phase hologram fade resistance stability improvement method 2—27548
  4-chloroacetophenone, single crystal e.p.r. studies of photoexcited states 2—26360
  chrysene, transient absorption spectra using laser photolysis apparatus 2—21672
  coumarin and related molecules, triplet-triplet absorption studies on 11000-27000 region 2—12225
  L-cystine dihydrochloride, γ-irrad. cryst., photoinduced hole-electron recombination 2—22887
  decanal oxime O-methyl ether-urea inclusion crystals, X-irradiated, e.s.r. of trapped alkylalkoxyamino radical 2—13592
  1,2,7,8 dibenzanthracene, transient absorption spectra using laser photolysis apparatus 2—21672
  dibenzoylperoxide, chem. induced dynamic nucl. polarization, mag. field depend. 2—7182
  dichloroethane and d_3 analogue, primary steps in photolysis at 25°C 2—33384
  1,2-dichloroethylene, isomerization photosensitization by benzaldehyde 2—10637
  dichloroethylene, photoelimination reactions, tandem laser meas. of vibr. energy distrib. 2—33388
  dimethylalanine:Cu^{2+}, e.p.r. of cationic radicals formed by u.v. irradiation at 77K 2—30090
  N,N- dimethylaniline systems, formation of ion radicals from the non-relaxed state of excited charge transfer systems by laser photolysis 2—37039
  1,3-dimethylindazole, electronically excited, temp. dependence of deactivation in solution 2—3119
  diphenylamine, photo-oxidation in presence of benzophenone, H-bonding effects 2—30064
  1,1-diphenylethylene:diphenyldiazomethane, photolysis, spectral obs. rel. to cryst. struct. 2—37055
  dye solns. reversible photobleaching under conds. of spontaneous and stimulated emission 2—20197
  electron primary emission during γ transmission of two component medium 2—30079
  eosin, triplet quantum yield study with tunable dye laser 2—26355
  ethanethiol, energy disposal in photodissociation 2—33383
  ethylene photolysis at 147-193 nm, kinetic analysis of primary processes 2—40834
  excimer-monomer transfer in electrochemiluminesc. 2—13525
  flash photolysis apparatus for 90-300 K 2—22881
  fluorene molecules in fluorene crystal, triplet states, e.p.r. and phosphorescence study 2—30089
  fluorescein, triplet quantum yield study with tunable dye laser 2—26355
  formaldehyde, interstellar, primary decomposition to give H and H_2 and photoionization 2—4898
  formaldehyde, photodissociation, potential energy surfaces 2—20201
  glass, organic, γ-irradiated scavenging kinetics of electrons, long range tunnelling 2—40831
  glycine:Cu^{2+}, e.p.r. of cationic radicals formed by u.v. irradiation at 77K 2—30090
  halide, layer structure, optical props. and chemical decomposition, review 2—16686
  heterocyclic nitro cpds., photolysis, e.s.r. study of alkoxynitroxide free radicals 2—832
  hydrocarbon-sulphur systems, high temp. laser- induced reactions 2—30096
  in ionosphere, study with air release instrument and r.f. mass spectrometer 2—13764
  Kapton film, Mossbauer obs. of Sn(II) sensitizer deposits 2—13588
  latent photographic image formation mechanism 2—30082
  methane, interstellar, primary decomposition to give H and H_2 and photoionization 2—4898
  methane, photolysis, methylene radical prod. followed by insertion into methane C-H bond 2—22882
  methylated silanes, v.u.v. spectra 2—35299
  3-methylpentane γ-irrad. at 77K, effects of optical bleaching on luminescence decay and trapped electron conc. 2—26229
  methyltetrahydrofuran glass energy levels structure of trapped electrons deduced from photoconducting and bleaching 2—36615
  monolayer assemblies, chromophore interactions 2—35374

Photochemistry continued
  naphthalene-d_8 in solid soln., X-ray excitation, triplet molecule formation 2—26364
  nitroalkanes, in ethers, u.v. photolysis, prod. of alkylalkoxynitroxide radicals 2—8728
  nitrobenzoenes, phtolysis, e.s.r. study of alkoxynitroxide free radicals 2—832
  nitroxide production from nitramines, e.s.r. studies 2—10643
  organic crystals, two-photon excitation by dye laser 2—26361
  organic solid-state chemistry, conf. Rehovot, Israel, (Sept. 1970) 2—37052
  ozone, photochemical dissociation with light of 3340 A, kinetics and mechanism 2—37050
  pentacene, triplet quantum yield study with tunable dye laser 2—26355
  perylene , photoionization in polar liquids, analysis of photochemical data 2—21701
  phenanthrene/benzophenone in ethanol, 77K, two quanta sensitized photo-ionisation 2—1761
  phenylacetylene, single crystal e.p.r. studies of photoexcited states 2—26360
  phenyliodoacetylene, photolytic formation of free radical, e.s.r. obs. 2—4600
  photolysis, laser induced two photon process, role of self-focusing 2 21110
  photopolymerization, applic. in optical memories and optical logic circuits 2—37051
  poly-P2VB, solid-state photopolymerization, X-ray diffr. obs. 2—3477
  polyethylene, vibrational excitation rel. to photochemical decomp. 2—33389
  polymers, photolysis, continuous light scatt. technique 2—37057
  porphyrins, deuterated in photoreduction reactions 2—16688
  proflavine, triplet quantum yield study with tunable dye laser 2—26355
  propyne, H_2 formation in photolysis at 1236 Å 2—30091
  pyrene, photoionization in polar liquids, analysis of photochemical data 2—21701
  pyrene dissolved in organic liquid, two photon laser photo-ionisation 2—30081
  radical pairs produced in organic systems, e.s.r. and ENDOR 2—20194
  reaction kinetics, applic. of spectrophotometer 2—17736
  reactions, effects on laser beams transmission through absorbing medium 2—20196
  relaxation in excited molecules 2—35200
  rhodamine dye laser, photobleaching by flashlamp excitation 2—5370
  ruby, colour stability when annealed or exposed to UV irradiation 2—22883
  solvated electron, quantum yield from $Fe(CN)_6^{4-}$ in water-alcohol mixtures 2—26369
  stilbene anion radical, electron transfer reaction with cis- and trans-stilbene, u.v. study 2—37035
  2-tert. butyl-4-methyl-indazole, electronically excited, temp. dependence of deactivation in solution 2—3119
  tetracene, photooxidation kinetics, external mag. field effects 2—26365
  tetracyanoethylene tetrahydrofuran charge transfer complexes, ionic photodissociation and ionic photosensitized dissociation 2—30092
  N, N, N′, N′ tetramethyl-para phenylenediamine, photoionization in polar liquids, analysis of photochemical data 2—21701
  tetraphenylporphine and Zn-tetraphenylporphine photoreduction, absorption spectra and e.p.r. of anion radicals 2—26366
  thionine, protonation rate const. of triplet state by laser flash photolysis 2—37056
  toluene-bromine system, reaction velocity, rate constant of termination, quantum yield due to laser beam 2—20196
  trifluoromethylbenzene, fluorescence and intersystem quantum crossing yields 2—10644
  triphenylbenzene triplet dianions, photo-oxidation in rigid solution, e.s.r study 2—4601
  triphenylene triplet dianions, photo-oxidation in rigid solution, e.s.r. study 2—4601
  triplet ketones, H abstraction, applicability of electronic-vibrational energy transfer model 2—30080
  tryptophan in ethylene glycol-water glass, photoinduced trapped electrons, recombination luminescence study 2—4517
  tryptophan molecule, in solid matrix, triplet-triplet annihilation rel. to fluoresc. 2—35355
  two-quanta photoprocesses, aromatic molecules 2—20198
  vinyl fluoride, vacuum u.v. photolysis, i.r. spectra of products, vibr. assignments 2—8830
  water vapour photolysis between 1500 and 1700 angstroms, micrometer-sizer particle formation 2—26359
  AgBr, chemical model of latent image 2—4599
  AgBr, field injected electrons, photographic action 2—31150
  AgBr microcrystalline emulsion, deep latent image formation mechanism 2—26358
  AgBr(Cl)(I) emulsion films pulse photolysis obs. 2—20195
  AgCl, chemical model of latent image 2—4599
  As-S glass, hologram formation mechanism 2—23634
  AsH_3, flash photolysis giving vacuum u.v. absorption spectrom of As_2 molecule 2—18402
  $As_2S_3(Se_3)$, amorphous, photodecomp. and optical densification 2—13589
  CO, vibrational excitation in the spin-orbit relaxation $Hg(6^3P_{1\to0})$ 2—15292
  CO_2, photolysis at 1633 Å, material balance of product CO, O_2 and O_3, reaction mechanism 2—10639
  CO_2, photolysis at 1849 and 2139Å 2—10638
  C_3O_2, photolysis generation of electronically excited $C(2^1D_2)$ atoms 2—15232
  C_3O_2, vacuum u.v. photolysis in presence of CH_4 and Ar, 25°C, reaction products study, and mechanism 2—30083
  $CS_2 \to CS(A^1\Pi)+S(^3P_2)$, photodissociation in vacuum u.v., determ. of $D_0^0(SC\text{-}S)$ 2—37053
  CS_2+NO_2 flash photolysis, CO laser emission 2—2393
  $CS_2+O(^3P)$ flash-initiated reaction, vibrational relaxation of CS 2—5917
  CdS, photosensitivity, rel. to photochem. reactions, heat treatment 2—22639
  ClF, reactions with H_2 and methane, basis for chain branching chemical laser 2—7918
  ClF_3, reactions with H_2 and methane, basis for chain branching chemical laser 2—7918
  Co, interstellar, primary decomposition to give H and H_2 and photoionization 2—4898
  $F+H_2(HCl)(CH_4)$, photolysis, chemical laser signal pulse shape 2—20199

Photochemistry continued
$Fe(CN)_6^{4-}$, photoexcited in 10N NaOH glasses, electron formation quantum yields at 77K 2—26357
$GeBr_4$ flash photolysis, u.v. absorption spectrum of GeBr 2—5928
GeH_4, in Ar matrix, vacuum u.v. photolysis products 2—16687
GeH_4, vacuum u.v. photolysis, i.r. spectra of prod. GeH_2 and GeH_3 2—8616
GeH_3Br, vacuum u.v. photolysis, i.r. spectra of prod. matrix isolated GeH_2Br 2—12127
GeH_3Cl, vacuum u.v. photolysis, i.r. spectra of prod. matrix isolated GeH_2Cl 2—12127
H_2, atmospheric, ecape efficiency 2—7272
H_2 photodissociation by u.v. radiation, preventing existence of enough H_2 to stabilize clusters of galaxies and close Universe 2—10816
HBO molecule produced in photolysis of $H_2B_2O_3$ in Ar matrix 2—28293
HO_2-, from photolytic reactions, kinetic analysis of absorption spectrum 2—24460
H_2O, interstellar, primary decomposition to give H and H_2 and photoionization 2—4898
H_3O, and D_3O, refutation of reported discovery in e.s.r. studies of u.v. irradiated perchloric acid glasses 2—37054
I atom recombination in presence of I_2 and He, Ar, Xe, N_2 and CO, studied by flash photolysis 300-1173K 2—26356
I_2, quantum yield for unimolecular dissociation in visible absorption 2—31803
Ir(III) complexes, comparison of $n\pi^*$-$\pi\pi^*$ interactions with $d\pi^*$-$\pi\pi^*$ interactions in aromatics 2—35300
KBr(Cl):OH, optical bleaching of F-centres, low temp. 2—29200
N_2F_4-$NO(N_2)$(CF) systems, laser irradiation effect 2—20200
N_2F_4, laser induced dissoc., rate 2—31808
N_2F_4+RH systems, flash photolysis chemical HF lasers 2—270
NH_3, Hg-photosensitized UV luminescence, evidence for cluster attachment 2—30084
NH_3, interstellar, primary decomposition to give H and H_2 and photoionization 2—4898
NO_2 photodissociation, angular distribution of recoil O atoms 2—30086
NO_2 photodissociation, energy partitioning 2—30085
NOCl photodissociation, energy partition and recoil photofragment angular distributions 2—30087
NO+H_2 mixtures, flash photolysis, far u.v. spectrum of HNO 2—18430
Ni complex, $[TMPD^+]_2[Ni(mnt)_2]^{2-}$, triplet exciton e.p.r. and structure 2—30005
O_3-O_2-O system in atmosphere 2—7273
O_2, $^1\Sigma$ state, spectroscopic detection of photosensitized formation in gas phase 2—10641
O_3 photolysis, obs. of primary products 2—7183
$OSCl_2$, photodissociation in vacuum u.v., heat of formation of SO 2—33385
$O_2(^1\Sigma^+_g)$, formation through sensitization by triplet state of aromatic molecules 2—13591
SF_6-NO system, laser irradiation effect 2—20200
SO_2, fluorescence and predissociation 2—35286
SbH_3, flash photolysis giving vacuum u.v. absorption spectrum of Sb_2 molecule 2—18402
SiH_3I flash, photolysis, obs, of new absorption spectrum 4600-5600Å, assigned by rotational analysis to HSiI radical 2—35260
$SnBr_4$ flash photolysis, u.v. absorption spectrum of SnBr 2—5928
SrS(Cu) phosphors, spectral distrib. of luminescent emission, excitation spectra, decay and thermoluminescence 2—33310
ZnO, sensitization by organic charge transfer complexes 2—40832

Photochromism
e.m. field mapping applic. 2—11387
glass, activated, use as 3-D holographic media 2—11492
perionaphthothioindigo and 2 perionaphthopentiophen-2′-(5′-methylthionaphthene)-indigo dyes, photochromism of coloured films 2—40833
photosensitive emulsion sensitization applic. 2—23733
reversible photodimerization applications using polycyclic aromatic hydrocarbons 2—33386
sodalite, cathodochromic props. 2—13590
CaF_2, rare earth coloured crystal behaviour 2—10640

Photoconducting devices
diode, spacing of photocurrent and external emission spectra maxima 2—20117
electrophotographic microimage recording by organic photoconductor 2—5464
ferroelectric-photoconductor memory, electrode requirements 2—40339
ferroelectric-photoconductor memory, equiv. cct. analysis 2—40337
ferroelectric-photoconductor optical storage medium 2—40349
ferroelectric-photoconductor storage device, thin film, design and performance 2—40336
films, deformation due to electrostatic forces 2—22636
h.v. photoelec. convertors, array-type, microcells with p-n junctions 2—13348
laser-photocell combination, vibrations of structures meas., in-plane 2—2227
light valve devices, photoactivated, photoconductive film/liquid crystal systems 2—21173
light valve display system, applic. of photoelectronic props. of CdS 2—22650
light-sensitive frequency convertor, relaxation generator with controllable base bias 2—36619
p-n, impurities with deep energy levels, compensation of spectral characteristics 2—29772
photocell densitometer construction 2—5458
thermoplastic sandwich, applications to data storage and interferometry 2—6910
transistor, photocurrent due to photon drag of carriers 2—6909
Au-GaAs diode, surface-barrier, photosensitivity spectra 2—6908
$CdCr_2Se_4$:In, bolometer material assessment 2—1512
CdS-CdSe cell, degradation mechanism and reliability estimation 2—29773
CdS, diodes, implanted, negative photovoltage, spectral response 2—15774
CdS single-crystal/amorphous-semiconductor heterojunction pickup tube 2—10147
CdTe junction, surface-barrier, photoelectret effect on γ-irrad. 2—13349
GaAs p^+-n solar cell, electron irrad., capacity and defect levels 2—29775
GaAs photodiode, electron bombard., I-V and spectral characts. 2—36620
Se film, integrating cell having anomalous photoconductivity 2—37799
Si-CdS p-n heterojunctions, photo- e.m.f. characts. 2—6859

Photoconducting devices continued
Si p-n diode, fabricated by B ion implantation 2—25968
Si photoconvertor, study of behaviour in i.r. region 2—14365
Si photodetector, for satellite appl., radiation damage 2—25967
Si photodiode, nonuniformly illuminated, frequency characteristics 2—29725
Si photodiode, thin-base, photocurrent kinetics 2—29724
ZnO-Si, heterojunction, elec. and optical props. 2—10088

Photoconductivity
see also Photoconducting devices
anilines in solid Xe 2—25951
anthracene, diffusion length of singlet excitons 2—6737
anthracene, role of paramagnetic excitons 2—25741
anthracene, sensitivity to oxygen impurities 2—33079
anthracene, transient photocurrent, exciton diffusion 2—4306
anthracene alkyl-substituted analogues, films, temp. depend. 2—13249
anthracene crystal/electrolyte solution interface, quenching of excited states 2—26242
anthracene/Al interface, exciton-induced photocurrents 2—25963
aromatic crystals, band struct. determ. 2—19791
arylidene-1-3-indandiones, chromophoric conditioning 2—25962
benzylidene-1,3-indandiones, chromophoric conditioning 2—25962
chalcogenides, amorphous, model analysis 2—36609
p-chloranil, transient photocurrent, exciton diffusion 2—4306
condensed media, multiquantum photocurrent 2—25977
condensed media, review 2—19800
copper heteroorganic acetylenides, absorption and photoconduction spectra investigated by diffuse reflection spectroscopy 2—29922
copper phthalocyanine films, photo-e.m.f. spectra, near i.r. 2—6907
cryostat, metal, and sample holder, for photo Hall effect studies on high ohmic crystals from 10-300 K 2—30721
cyanine dyes, photographic sensitizing, activation energy 2—16319
decay time constant, temp. depend., by least squares method 2—4295
9, 10-dibromoanthracene, ruby laser induced, carrier generation by triplet exciton process 2—16320
9, 10-dichloroanthracene, ruby laser induced, carrier generation by triplet exciton process 2—16320
dielectric, instrumentation and data reduction technique for obs. 2—19780
N,N′- diphenyl-p-phenylenediamine, data from pure single crystal 2—3577
electrophotographic plate, photodischarge process 2—22635
ferroelectric semiconductor, surface layer effects 2—4296
finite layer, photocurrent and carrier distribs. due to steady absorbed light 2—16307
group II-VI cpds., impurity spectra 2—6901
inhomogeneous material, numbers and barrier mechanisms 2—16209
inhomogeneous material, numbers and barrier mechanisms 2—16208
initial photocurrent due to pulsed light absorbed in finite thickness 2—25952
insulator, with discrete traps, high field and thermally stimulated currents, optically excited 2—22521
insulator with field-depend. mobility, transient photocurrent 2—16308
lipids, bimolecular membranes 2—26941
methyltetrahydrofuran glass energy levels structure of trapped electrons deduced from photoconducting and bleaching 2—36615
m.i.m. struct., interface barrier energies from photoresponse, electron scatt. effect 2—33039
molecular crystal, spectral distrib. of quantum yield 2—19801
molecular crystals, exciton-induced photocurrents 2—25963
molecules, matrix-isolated at low temperature 2—25951
M.O.S. struct., direct meas. of built-in voltage, method 2—13295
m.o.s. structure, deep electronic traps obs. 2—36574
noise, band to band Auger processes 2—19781
organic crystals, chromophoric conditioning in polar molecules 2—25962
organic crystals of anthracene type, advances since 1967 2—25961
organic semiconductor, photodielec. effect 2—6898
oxalate dye, singlet exciton thermal ionization 2—19790
p-type crysts., negative photocond. rel. to elec. instability, single recomb. model 2—33067
photo-Hall mobility meas. on high impedance materials using double modulation method 2—27387
photoconductor/liquid crystal sandwich, coloured image formation 2—31133
photoconductors, acoustoelec. aftereffect 2—36345
photodischarge process, quasi-steady- state analysis rel. to electrophotography 2—2480
photoelectret regime, photopolarization, thermally stimulated currents 2—33065
β-phthalocyanine single crystal, drift mobility, temp. depend., photocond. obs. 2—32993
phthalocyanine single crystal, spectra snd laser induced obs. 2—33081
polyethylene, γ-ray irrad. effects 2—25964
polymer film, electron-beam-deposited, bombarding current depend. 2—32994
polystyrene, vacuum u.v. range, memory effects 2—10142
polyvinyl chloride, field and pressure depend. 2—33080
polyvinylcarbazole, photoinduced current decay obs. 2—22648
PVK:TNF, transient, pulsed light illumination, electron transport 2—13337
response times det. method 2—19783
scattering mode ferroelectric-photoconductor image storage and display devices 2—21172
semiconductor, amorphous thin film, review 2—10005
semiconductor, deep-trapping kinematics 2—36481
semiconductor, effect of multiple trapping centres in presence of radiative interband recombination 2—36608
semiconductor, elemental, photomodulated r.f. cond., diffusion coeff. determ. 2—1509
semiconductor, frequency-contrast characts. for image converter applic. 2—6895
semiconductor, in quantizing mag. fields 2—1583
semiconductor, inhomogeneous, local photocond. signal rel. to carrier lifetime 2—22634
semiconductor, phonon heating effects 2—40375
semiconductor, quadratic processes 2—10436
semiconductor, quasi-monopolar, intrinsic photocond. in depletion layer 2—40377
semiconductor, recomb. domains, analytic theory 2—13204
semiconductor-insulator powder system, transient effects 2—19782
semiconductors, det. at microwave frequencies 2—34239

Photoconductivity continued
    tetracene, photocurrent obs. of photooxidation kinetics, external mag. field effects 2—26365
    tetracene, role of paramagnetic excitons 2—25741
    transparent dielectric subjected to laser light, surface photocurrent 2—19784
    transport process, two dimensional, fluctuation theory 2—25953
    u.v. microprobe technique for minority-carrier diffusion length meas. 2—6815
    zinc phthalocyanine, light-intensity depend. 2—10143
    AgBr:S, annealed crystals, dark conductivity meas., obs. of complex formation and photoreduction processes 2—6900
    AgCl, exciton mechanism 2—4297
    β-B, rhombohedral, transient rel. to trapping level detn. 2—19665
    $Bi_{12}GeO_{20}$, light- and elec.-field-depend. oscillation of space-charge-limited current 2—25955
    $CdCr_2S_4$, impurity level obs., Ag and In doped crysts. 2—40659
    $CdCr_2Se_4$, rel. to bolometer application 2—1512
    $CdGa_2Se_4$, band struct. 2—16309
    $Cd_xHg_{1-x}Te$, quantum efficiency, 78 K 2—22638
    $CdIn_2S_4$, rel. to band struct. 2—22760
    $CdIn_2S_4$, resist., Hall mobility, stoichiometry effect 2—10008
    p-CdP_2, forbidden band width, acceptor level depth, and compensation detn. 2—40248
    CdS:Cu, photo-Hall effect, i.r. quenching 2—33068
    CdS/liquid cryst. system, photoactivated light valve devices 2—21173
    CdS-Cu_2S heterojunction, photosensitivity 2—36492
    CdS, change in properties during passage of double-injection currents 2—40245
    CdS, crystals grown by sublimation under excess pressure of Cd and S 2—13339
    CdS, disintegration, effect on photoelectric properties of heterophase electrophotographic layers 2—2479
    CdS, electrophotographic properties, effect of macromolecular binding agents 2—337
    CdS, excitation spectra rel. to luminescence excitation spectra, intensity of illumination dependence 2—1719
    CdS, low temp. spectra, exciton diffusion length detn. 2—10047
    CdS, photoconductor preparation and characteristics 2—4471
    CdS, photoelectronic props. rel. to light valve display applics. 2—22650
    CdS, photosensitive u.s. attenuation obs. 2—16025
    CdS, photosensitivity, rel. to photochem. reactions, heat treatment 2—22639
    CdS, photovoltage inversion effect rel. to semiconductor surface states 2—6896
    CdS, sintered layer, rel. to microstructure obs. 2—19046
    CdS, temp. depend. 0.9 eV quenching band peak position 2—4298
    CdS film, vacuum evaporated, photosensitivity 2—36492
    CdS layers, photothermoelec. analysis, carrier density and mobility 2—16310
    CdS photoelectrets, lifetime under different polarization conditions 2—22640
    CdS platelets, thermally stimulated currents in range of unity gain factor, frozen-in current 2—19777
    $CdS_{1-x}Se_x$, Ar laser irrad., free carrier generation by exciton-donor interact. and exciton impact ioniz. 2—19635
    CdSe:Cu, Cl layer, sintered, operation in longitudinal mode 2—29764
    CdSe, carrier mobility rel. to excitation intensity, in negative photocond. conditions 2—32976
    CdSe, elec. domain motion obs. 2—29771
    CdSe, low temp. spectra, exciton diffusion length detn. 2—10047
    CdSe, photocurrent kinetics and instability 2—16313
    CdSe, photoelectronic props. of electronically active defects 2—13338
    CdSe, single cryst., effects of HNO_3 etching 2—16312
    CdSe, single cryst., nonactivated, stationary characts., electronic processes 2—29770
    CdSe, single cryst., transient, small signal case 2—16311
    CdSe, transient photocond., monovalent donors 2—4299
    CdSe film, photoelec. props. during activation 2—22641
    CdTe:Fe, impurity level obs. 2—36538
    CdTe, double acceptor obs. 2—36528
    n-CdTe, electron irrad. defects, annealing and recovery 2—15739
    n-CdTe, impurity photocond., recomb. centres 2—6902
    CdTe, impurity spectra 2—6901
    n-CdTe, obs. of defect levels before and after electron-irrad. 2—36537
    Cu phthalocyanine, surface trap distribution 2—29765
    $(CuInTe_2)_x(2CdTe)_{1-x}$ alloys, 0.7-1.6eV 2—6899
    $CuPbAsS_3$ single crystals, 90 to 300 K 2—22762
    Eu_3As_2 film, spectral depend., rel. to mag. order determ. 2—36722
    Eu_3P_2 film, spectral depend., rel. to mag. order determ. 2—36722
    EuS, ferromag. semiconductor, transient, photocond., magnetoresist. 2—10136
    FeS_2, low temp. 2—4300
    GaAs:Cr, in high electric fields 2—4301
    GaAs:Cr, photoinjected carrier recomb. and trapping processes 2—33069
    GaAs-SiO_2 interface, photocond. spectrum of GaAs 2—22642
    GaAs, electron and neutron irrad., band edge density of states detn. 2—29916
    n-GaAs, evaporated films, transient response meas. in electronic transport props. determ. 2—40244
    n-GaAs, hydrogenic donor levels in mag. field 2—10058
    n-GaAs, intrinsic photocond. in depletion layer 2—40377
    GaAs, low resistivity, carrier lifetime, electron bombardment and annealing effects 2—36508
    GaAs, proton irrad., role of recomb. centres 2—36610
    GaAs, rel. to free excitons, function of free electron density 2—25954
    GaAs, two photon excitation processes 2—19785
    GaAs, u.s. rel. and attenuation in photocond. cryst., illumination depend. 2—19413
    GaAs, Zeeman splitting of donor states 2—16229
    n-GaAs film, epitaxial, influence of state of surface 2—22643
    GaAs obs. of nonhydrogenic exciton and energy gap 2—22549
    GaAs with deep acceptors, spectral depend. 2—40250
    n-$GaInS_3$, slow recomb. level obs. 2—6903
    GaP, epitaxial, minority carrier diffusion length, impurity conc. depend., Schottky diode photocurrent obs. 2—29670
    GaP, wavelength modulation near indirect absorpt. edge 2—33074
    GaSe:Sn(Ge)(Cu)(I), i.r. photolum., recombination centres 2—7093
    GaSe, layer semicond., elec. and optical props. 2—10016
    Ge:Hg, grown by gas transport, spectral photosensitivity 2—29095

Photoconductivity continued
    Ge:Sb, neutron irrad., carrier lifetime detn. 2—40285
    n-Ge, carrier recombination, dislocation quenching 2—25956
    Ge, dielectric-metal transitions, excitons 2—16235
    Ge, effect of surface barrier on spectral distrib., photoeffect 2—4303
    Ge, electron irrad., steady-state photocond. lifetime, influence of temp. 2—19685
    Ge, extrinsic, gain saturation, low temp. 2—13340
    p-Ge, minority carrier lifetime, photocond. and photo-magnetoelec. obs. 2—22563
    Ge, photo-effect on sheet cond. along grain boundary 2—4302
    p-Ge, photon drag tensor 2—13341
    n-Ge, recomb. at dislocations, effect on high field photocond. 2—29766
    n-Ge, screw dislocations contrib. 2—10064
    Ge, wavelength modulation near indirect absorpt. edge 2—33074
    GeO_2, amorphous, fluctuation levels 2—10137
    GeO_2, vitreous, wavelength, field, and temp. depend. 2—22644
    HgCdTe, minority carrier sweepout, high field obs. 2—22645
    HgI_2, photopolarization current and photoelectret state 2—19786
    HgO, spectral response of surface photoconductivity 2—4304
    I_2 in solid CO_2 2—25951
    n-InAs, low temp., carrier mobility obs. 2—6904
    InAs, microwave biased, free carrier screening effects 2—19787
    InP, two photon excitation processes 2—19785
    n-InSb, carrier numbers and mobility, effects of intense i.r., photocond. and photo Hall effect obs. 2—32908
    n-InSb, negative photocond. in transverse mag. field 2—33070
    n-InSb, photoelec. Hall effect in quantizing mag. fields 2—4305
    InSb, spectra, impact ionization thresholds, quantum efficiency, 295K, 90K 2—22646
    n-InSb, transverse mag. field effects 2—29767
    In_2Te_3-Hg_3Te_3 alloy, spectral distrib. 2—33071
    KCl, Hall mobility of electrons meas. by double modulation method 2—27387
    KCl, multiphoton absorption processes obs. 2—22637
    KI, F-centre, laser induced, 40 and 100 K 2—1584
    KI, multiphoton absorption processes obs. 2—22637
    LiH, temp. depend. 2—6905
    $LiNbO_3$, nonstoichiometric, defect study 2—19083
    $MoSe_2$, exciton-exciton interaction during laser irrad. 2—19788
    NaCl, multiphoton absorption processes obs. 2—22637
    NaI, impurity photocond. due to excitonic-energy transfer 2—16314
    NiO, epitaxial, hole drift mobility, photoexcitation obs. 2—10027
    NiO, single cryst., visible and near u.v. region, impurity controlled p-type processes 2—10138
    PbI_2 films, anomalous photovoltages 2—13342
    PbO ceramics, spectral depend. 2—36611
    PbS film, mechanisms of photosensitivity 2—36613
    PbS films, effects of baking 2—22647
    PbS films, effects of gas treatment on temp. coeffs. 2—36612
    PbS films, spectral response 2—16315
    PbS films, struct. defects depend. 2—3773
    $Pb_{1-x}Sn_xTe$ epitaxial film 2—32375
    $Pb_{1-x}Sn_xTe$ epitaxial layers, bulklike photocond. 2—10139
    S, orthorhombic crystal, carrier generation by pulsed X-rays 2—29768
    Sb_2S_3, rel. to local levels in the forbidden band 2—40262
    Se/poly(N-vinyl carbazole), transient photoinjection of holes and xerographic layer sensitization 2—33072
    Se/poly(N-vinyl carbazole), transient accumulation of interfacial charge, xerographic layer sensitization 2—33073
    Se, amorphous film 2—32989
    Se, films, amorphous, exponential hole trap distrib. in forbidden band, photoresponse obs. 2—25957
    Se, ionization coeff. for holes 2—4217
    Si:B, carrier recomb., electron and hole lifetimes, 1.7-4.2 K 2—16244
    Si:B, high resistivity, gain saturation 2—19789
    Si:B ion implanted, defect effects obs. 2—25960
    Si:Li, radiation-induced extrinsic photocond. and radiation damage 2—25958
    Si:Ni diode, impurity photocond., negative photocond. 2—22586
    Si:P, first order Stark effect in impurity photocond. 2—10140
    Si:P, impurity spectra, influence of phonons 2—33075
    Si, meas. at two modulation frequencies, for simultaneous det. of specific resistance and excess carrier lifetime homogeneities 2—29707
    Si, radiation induced defects obs. 2—25959
    Si, wavelength modulation near indirect absorpt. edge 2—33074
    n-Si wafers, of varying thickness, theraml oxidation effect obs. 2—29769
    SiO_2, amorphous, band edge obs. 2—16316
    $TiO_2:Fe^{3+}$, Fe level determ. 2—10141
    TlBr, photo-excited, Hall effect and magnetoresist., temp. depend. 2—40264
    $TlGaS_2(Se_2)$, temp. depend. 2—29677
    TlI-TlBr, KRS-5 ionic crystal, negative photocond., electrolysis effects 2—13303
    $TlInS_2$, temp. depend. 2—29677
    Tl_2S binder layers, IV characts., photocurrent spectral distrib. 2—33076
    $ZnIn_2S_4$, quenching due to hot electron capture, electric field variation 2—36614
    ZnO, enhancement by energy transfer mechanism, evidence from electrochem. obs. 2—16317
    ZnO, sensitization by organic charge transfer complexes 2—40832
    ZnS:Ga, description by donor-acceptor pair model 2—29957
    ZnS;Cu, Cl film, switching phenomena at 77K 2—40380
    ZnTe:Al, defect levels assignment 2—13244
    ZnTe:Ga, negative photocond., room temp. 2—33078
    ZnTe-CdTe solid solution, negative photocond., room temp. 2—33077
    ZnTe-GaSb, p-p heterojunc., elec. and optical props. 2—10087

Photodisintegration *see Deuterons/photodisintegration; Nuclear reactions and scattering due to/photons*

Photodissociation *see Photochemistry*

Photoeffect, nuclear *see Gamma-rays/effects; Nuclear reactions and scattering due to/ photons*

Photoelasticity
    see also Double refraction/mechanical; Piezo-optical effects
    alkaline earth fluorides, consts. meas. 2—29870
    anisotropic media, rotational contribution to higher order photoelastic interactions 2—16423
    cellulose derivatives, stressed films with various substitution degrees 2—7047

Photoelasticity continued
crack propagation, edge crack panels, elastic fields 2–2214
epoxy-diane resin, γ-irrad. effects 2–39803
ethylene propylene terpolymer stress optical coeffs. of rubbery state, dependence, chain length 2–25507
glass, different compositions, thermal expansion determ., fusion method 2–25687
holographic application 2–27541
holographic interferometry applications 2–14212
holography applications, conference (Los Angeles August 1971) 2–14147
incompressible media, rel. between absolute photoelastic coefficients 2–135
isochromatic elimination in double exposure photoholoelasticity 2–143
mechanically anisotropic bodies, calibration tests 2–23327
organic crystal, u.s. freq. 2–1427
photoelasto plasticity method for orthogonal cutting 2–126
polybutadiene, stress optical coeffs. of rubbery state, temp. dependence, chain length 2–25507
polyisoprene, stress optical coeffs. of rubbery state, temp. dependence, chain length 2–25507
pressure vessel models, stress effects 2–29238
principal stress characterization, two- and three-dimensional analysis 2–37681
α-quartz, dispersion of stress- birefringence meas. using Soleil Babinet compensator 2–36820
relaxation of stress concentration using supplementary curvature, photoelastic investigation 2–2218
residual stresses in metals, measurement by photoelastic gauges 2–17316
solid surface, diffraction of light wave by Rayleigh wave, refl. obs. 2–7053
stress-induced optical activity effects 2–36825
structural analysis, applications of holographic technique 2–11338
styrene-butadiene copolymer stress optical coeffs. of rubbery state, temp. dependence, chain length 2–25507
turbine blade fastenings, stress analysis 2–5180
two dimensional orthotropic bodies, photoelastic determ. of state of stress and strain 2–5186
CdTe layers, concentration due to monochromatic illumination 2–29877
Cu^+ halides, piezooptical coefficients, phase matching of nonlinear optical processes 2–26119
α-HgS, cinnabar rel. to acousto-optical props. 2–19973
NaF, stress-optical dispersion, measurement by intensity method 2–26107
TeO_2, dispersion characts. 2–1658
TiO_2, rutile, Brillouin scatt., antisymmetric susceptibility obs. 2–16423
α-ZnS, consts. meas. by u.s. pulse method 2–25482

Photoelectrets *see Electrets; Photography*

Photoelectric cells *see Photoconducting devices; Photoconductivity; Photoelectricity; Photovoltaic effects*

Photoelectric effect, atomic *see Atoms*

Photoelectric emission *see Electron emission/photoelectric*

Photoelectricity
see also Electron emission/photoelectric; Photoconductivity; Photovoltaic effects
amplifier for photoelectric effect 2–2325
diodes obtained by bombarding Si surface with positive ions 2–36618
metal whisker diodes, thermal field emission as i.r. light rectification mechanism 2–16323
m.i.m. system, contact-limited transient photoinjection currents 2–13288
optophotoelectric sensor, diameter measurement of glass fibres during drawing 2–38097
planar scanning of band shape of interference field, systematic measurement errors 2–38058
semiconductor, photoelectret state, non-isothermal relaxation, trapping levels, thermally stimulated currents 2–25950
semiconductor, photon pressure effect 2–13344
semiconductors, det. at microwave frequencies 2–34239
solar cells, direct conversion to electricity, review of research 2–34296
surface profile rectilinearity, measurement with photoelectric instruments 2–38099
timing accuracy of readout pulses in photoelectric systems 2–27388
xerographic discharge characts. of photoreceptors 2–23744
xerographic discharge characts. of photoreceptors 2–23743
AsS, photopolarization and photoelectret state of crystalline and vitreous samples 2–40369
Bi_2S_3-Sb_2Se_3 film, photoelec. props., sensitivity, sp, resist. 2–36607
CdS-S solid solution, photoelectret state formation and high photosensitivity and resistivity obs. 2–36603
CdS, disintegration, effect on photoelectric properties of heterophase electrophotographic layers 2–2479
CdS, film, photoelectret phenomena and dark polarization current 2–10130
CdS, photovoltage inversion effect rel. to semiconductor surface states 2–6896
CdS, surface photovoltage 2–13264
CdS, wavelength depend. of surface photovoltage 2–13345
CdS p-n junction, formed by N ion implantation on n-type layer 2–25422
CdS solar cells, manufacturing processes 2–34298
CdTe film, photodielectric effect, model based on conductivity hypothesis 2–40376
Cu phthalocyanine, negative photoeffect 2–29765
GaAs, effect of adsorbed H_2O on surface photovoltage 2–13346
GaAs film, heteroepitaxial, grown on sapphire, in m.i.s. config., photoelec. studies 2–40379
Ge, photogradient e.m.f. of hot carriers 2–16322
KN_3, internal photoemission of electrons and holes 2–40260
SbI_3 crystal, photoelectret state relaxation, space charge relocalization effect 2–6906
SbSI, photoelectric state and photopolarization 2–33060
SbSeI, photoelectric state and photopolarization 2–33060
Se/poly(N-vinyl carbazole) layered struct., space-charge-perturbed xerographic discharge 2–40378
Se, influence of organic solvents and thermoplastic polymers 2–28992
Se photocell, thermally stimulated current, energy spectrum of localized centers 2–29687
p-Si:Zn, P, photodielec. effect, polarizability of neutral atoms 2–13343
Si, photogradient e.m.f. of hot carriers 2–16322
Si film, heteroepitaxial, grown on sapphire, in m.i.s. config., photoelec studies 2–40379

Photoelectricity continued
ZnO, diffusion of photoelectrically excited electrons, d.c. effect coefficients 2–4294
ZnS:Cu, photoelectret properties, surface charge and depolarization current studies 2–36604
ZnS, phosphor, photodielec. effect response 2–10144

Photoelectromagnetic effects
charge carrier mobility measurement in inhomogeneous semiconductors 2–4099
metal-semiconductor contact, Dember effect interpretation 2–13282
semiconductor, intrinsic, Dember effect 2–4193
semiconductor, phonon heating effects 2–40375
semiconductor, transient characts., theory 2–25966
vibrators, effects of resonance on distortion and sensitivity threshold 2–23480
$FeBO_3$, photomag. effect, domain struct. 2–33174
GaAs:Cr, photoinjected carrier recomb. and trapping processes 2–33069
n-InAs, low temp., carrier mobility obs. 2–6904
p-iNAs, low temp. photomag. effect 2–13347
p-InSb, h.f. response 2–4309
PbI_2 films, anomalous Dember photo-e.m.f.'s 2–13342
Si:Au Dember cell, visible and near i.r. photodetection 2–10149
Si:Au photomagnetoelectric light detector characteristics over −20°C to +60°C range 2–34506

Photofission
low energy, of heavy elements, barrier heights 2–28091
near barrier, even targets, induced by dipole and quadrupole photons 2–28090
threshold, using bremsstrahlung beams from low energy electron accelerators 2–38664
Au, 250 to 1000 MeV, fragments angular distrib. meas. 2–15027
Pb, 250 to 1000 MeV, fragments angular distrib. meas. 2–15027
Ta, 250 to 1000 MeV, fragments angular distrib. meas. 2–15027
Ta, 600-1700 MeV photons 2–31609
Ta, photofission, ang. distrib. of products and fission time from shadow widths 2–28092
^{232}Th near threshold using variable energy beam of γ rays determ. cross sections from 5-8.3 MeV and transmission factors 2–21458
^{235}U, near threshold usinv variable energy beam of γ-rays determ. cross sections from 5-8.3 MeV 2–21458
^{238}U, near threshold usinv variable energy beam of γ rays determ. cross sections from 5-8.3 MeV and transmission factors 2–21458
^{238}U, yields of ^{131}Xe, ^{132}Xe, ^{134}Xe and ^{136}Xe obs. 2–5725
^{238}U photofission fragment ang. distrib. obs. 2–2817

Photographic light sources *see Light sources; Photography*

Photographic materials
see also Nuclear track emulsions
bleached density-log exposure curve and MTF curve from optical path variation 2–14493
cellulose nitrate, use as detector film in α-autoradiography 2–36191
cellulose nitrate film used for detection of α-particles 2–11679
coherent light characteristics, rel. to holography, optical data processing 2–5457
colour film, visual eval. of density differences 2–34562
colour film materials, quantitative analysis by thin layer chromatography 2–2474
colour positive film type 650, graininess, definition, colour separation, saturation and fidelity 2–2478
developing agents, electronic structures of substituted benzenes 2–14494
emulsion, hologram recording on, compensation for aberrations 2–11497
emulsion, processing and cameras, review 2–38173
emulsions, crowded, granularity theory for multilayers 2–38167
emulsions, crowded, granularity theory for multilayers 2–38172
emulsions, relative detective quantum efficiency obs., used with new developer 2–5456
emulsions with high efficiency in blue-green, rel. to phase holograms 2–31071
frequency conversion of weak light fluxes by photographic materials 2–11449
high image resolving power materials 2–38168
holographic recording of Fourier transform of slit, effect of nonlinearity 2–23637
immersion liquids for holograms recorded on photographic film 2–5392
light scattering and Wiener spectrum meas. for fine grained materials for holography 2–14492
for microphotography, contributions of Kodak Research Laboratories 2–14491
non Ag-halides, photosensitive props. 2–21182
nucleation imaging media, applications 2–23731
parasitic interference, effects on investigation of spatial frequency response 2–21183
photochromic materials, phase holographic response function 2–34412
photoemulsions, bleached, high resolution, diffraction effectiveness for holography 2–23639
photoplastic films for holographic recording 2–17661
photoresist, adhesion 2–3518
photoresist films, Kodak KPR, as light guide for integrated optical circuits 2–38114
plate, deform. during exposure, detect. by holographic interferometry 2–27669
properties from the point of view of use in electron microscopy tested with 60 keV electron exam. 2–23734
retina image transformation comparison with films 2–23182
semiconductor-insulator powder system, transient photocond. effects 2–19782
silver halide emulsion films, photochemistry 2–20195
transparencies, subjective image quality, relative effects of gaussian and Poisson noise 2–5455
Ag halide for X-ray films, grain size distribution using electron microscope 2–38171
Ag halides, effects of electron and positive hole traps 2–14495
Ag halides, space charge layer contrib. to dielec. const. 2–33050
Ag halides, space charge layer contrib. to dielec. const. 2–40330
Ag sol filter, reduction of $AgNO_3$ with $NaBH_4$ in presence of gelatin 2–27675
AgBr, field injected electrons, photographic action 2–31150
AgBr dispersion in polyvinyl alcohol, influence of mechanical agitation on growth and crystal habit 2–27666

- **Photographic materials** continued
  - AgBr emulsions, latent image formation, contribution of interstitial Ag^+ ions 2—2475
  - CdS, disintegration, effect on photoelectric properties of heterophase electrophotographic layers 2—2479
  - CdS, electrophotographic properties, effect of macromolecular binding agents 2—337
  - Na halide emulsions, line element image broadening as a function of exposure 2—38169
  - Se/poly(N-vinyl carbazole) layered struct., space-charge-perturbed xerographic discharge 2—40378
  - Zn, photopolymers, based on polyamides, wear resistance 2—3917
  - **sensitivity**
    - colour, photographic papers, resolution and definition 2—27677
    - copolymer of acryl amide and methylene-bis-acryl amide, and resolving power, application to holography 2—34416
    - cyanine dyes, thermal activation energy of conducting process and electron trap depths 2—16319
    - cyclorubber film with bis-azides, dependence of light sensitivity on solvent 2—27672
    - dyes, sensitizing and desensitizing, desensitization, effects of electron and positive hole traps 2—14495
    - electroradiographic Se, amorphous, charged with X-rays 2—338
    - impurity centres, formed by alkaline hydrazine sulphate soln. 2—27673
    - latent photographic image formation mechanism 2—30082
    - nuclear emulsions, noise in photographic trace due to grain size 2—27917
    - optical density curves in relation to exposure to ^{192}Ir and development times for two films 2—8050
    - photochromic reaction use for selective sensitization of photosensitive emulsion 2—23733
    - response to c.r.t., redefinition based on radiometric exposure units 2—11548
    - silver halide, for holography 2—34563
    - spectral sensitization and special materials for scientific use 2—11546
    - AgBrI emulsions, with imidacarbocyanines containing residues of heterocyclic bases in benzene nuclei 2—27671
    - AgCl, photocond. mechanism 2—4297
    - Se/poly(N-vinyl carbazole), transient photoinjection of holes and xerographic layer sensitization 2—33072
    - Se/poly(N-vinyl carbazole), transient accumulation of interfacial charge, xerographic layer sensitization 2—33073
    - Se, amorphous, electroradiographic, charged with X-rays 2—338
    - ZnO electrophotographic papers, sensitization by organic charge transfer complexes 2—40832
- **Photographic process**
  - *see also Photochemistry*
  - electron microscope imaging of neurons laboratory processing and handling 2—17759
  - emulsion, processing and cameras, review 2—38173
  - film copying, sharpness estimation using modulation transfer function 2—332
  - film copying operations, rationalization using $(NH_4)_2S_2O_3$ solution and precision doping pumps 2—331
  - film reporting, i.r., fluoroscopic image photography 2—2476
  - film transfer mechanisms, influence on prints quality 2—31151
  - grain, definitions 2—11547
  - image shaping, focal series, Golden Section ratio 2—27664
  - latent photographic image formation mechanism 2—30082
  - masked and unmasked negatives, influence on colour reproduction and definition 2—27684
  - microfilm recording by computer, precision high-resolution c.r.t. 2—27670
  - printout effect suppression in photographic phase holograms 2—5388
  - prints, gradation changes, characteristics 2—31152
  - release printing for widescreen anamorphic films 2—5459
  - stereoscopic pictures, moon, (1840-1864) 2—30534
  - X-ray films rel. to grain size distribution 2—41418
  - $As_2S_3(Se_3)$, amorphous, photodecomp. and optical densification 2—13589
  - **development**
    - benzyl alcohol content in developing solution, effect on KP-4U film 2—5460
    - colour films, positive, technique 2—23739
    - colour negative printing, colorverter and translator 2—27667
    - image sharpening, holography 2—333
    - intensification of low density images by autoradiography 2—27668
    - nuclear track emulsions, acoustic treatment at 50 Hz of mounted layers, accelerated diffusion of developer 2—27918
    - optical density curves in relation to exposure to ^{192}Ir for two films 2—8050
    - tanning action and coloured image formation for several developers 2—27674
    - Ag thread-like crystals, formation in physical development 2—27676
- **Photography**
  - *see also Cameras; Cinematography; Lenses/photographic; Radiography*
  - astronomical, automatic drive for photographic plates 2—2006
  - background diffusion, controlled 2—17749
  - blockadjustment methods in photographic astrometry 2—37424
  - blurred photographs made in partially coherent light, program for calc. of error in resolution enhancement 2—34565
  - bubble chamber, photographs, automatic analysis 2—27912
  - cameras, high definition, resolving power, calc. 2—23736
  - contrasting, projection and photography of microscopic objects 2—31116
  - contrography, electrostatic imaging by charge transfer 2—14500
  - dosimetry, applic. of radioisotope X-ray fluorescence spectrometry 2—330
  - Earth from satellite, uses for forest fire detection, cloud cover, automatic cartography, coastal erosion 2—7202
  - electro, charged pigment, imaging systems 2—21184
  - electrophotographic discharge process, quasi- steady-state analysis 2—2480
  - electrophotographic microimage recording by organic photoconductor 2—5464
  - electrophotographic plate, photodischarge process 2—22635
  - electrophotography, review 2—31158
  - enhancement of grey scale aerospace imagery for visual interpretation 2—31085
  - exposure meters with indicating light diodes for amateur cameras 2—38166
  - exposure transfer function for system using focal plane slit shutter, diffraction effects and interaction with uniform linear image motion 2—31148
  - film printing, frequency contrast response of image, obs. 2—38170

Photography continued
  - flashguns with optical feedback 2—14497
  - gamma camera dynamic flow studies on single film by colour coding of time 2—26961
  - high-speed, Q-switched pulse stretching applications 2—14399
  - holograms, pre- and post-exposure, effects on recording and reconstruction 2—5389
  - holographic image sharpening 2—17658
  - image deblurring, holographic principles and methods 2—23735
  - image depth and illumination, tutorial 2—17167
  - image illumination and depth, tutorial 2—17168
  - image illumination and depth, tutorial 2—17166
  - image processing using geometric and spectral features 2—34457
  - image shaping, focal series, Golden Section ratio 2—27664
  - imagery enhancement 2—23732
  - kinoforms, optically generated 2—17751
  - lenses, thin, with variable spherical power 2—34452
  - meteorological, transmitted by satellite, recuperation 2—37127
  - microcircuit printing, optoelectronic system 2—37906
  - microphotography, contributions of Kodak Research Laboratories to sensitised materials 2—14491
  - modulation transfer function det. by generation of sinusoidal test image by incoherent spatial filtering 2—31149
  - object motion simulator with photographic recording of image velocity and velocity compensation in cameras 2—5462
  - objective prism Schmidt camera, prismatic correction plate 2—20715
  - photoresist AZ111, modulation transfer function 2—5463
  - pinhole, fly's eye and holographic stereograms, comparison 2—8056
  - pseudocolour image enhancement by two separation photographic process 2—31156
  - remote control system for cinecameras, soundtrack synchronization 2—27682
  - remote photogeology applied to ground current paths in h.v. d.c. systems 2—16763
  - resolution, dependence on objective aperture 2—27665
  - sea, analysis and optical processing for wave energy spectra 2—16795
  - simulated space, information content as a function of image resolution 2—16937
  - stereophotogrammetric, short-range 2—31157
  - superresolution of data, restoration with maximum entropy 2—34564
  - supplementary lenses and reversal, effect on field depth 2—8052
  - tanning action and coloured image formation for several developers 2—27674
  - thermal i.r. imaging devices, studying quasistationary thermal fields 2—37805
  - xerographic discharge characts. of photoreceptors 2—23743
  - xerographic discharge characts. of photoreceptors 2—23744
  - xerography, electrostatics application 2—34280
  - xerography, optical techniques 2—17752
  - xeroradiography, automated system and industrial application 2—23745
  - on Fe-Ni magnetic films, vacuum deposited on glass, using i.r. laser pulses 2—27683
  - **applications**
    - axial impact on mild steel rod, theoretical and experimental treatment 2—9716
    - back reflection Kossel camera, modification to electron proton analyser 2—38178
    - baroclinic waves, study using three-level streak photography 2—39076
    - bubble chamber film analysis, techniques and applic. 2—14779
    - bubble chamber photographs, track matching computer program 2—21335
    - cellulose nitrate film used for detection of α-particles 2—11679
    - cine films, use as a higher education aid 2—12
    - communication channel, information storage capacity calc. 2—14499
    - copying holograms on photoresist with thermal source 2—23636
    - corneal topography measurement with autocollimating photokeratoscope 2—17128
    - dryout obs., combined photographic film thickness and temp. technique 2—24275
    - electron microscope imaging of neurons laboratory processing and handling 2—17759
    - electronic imaging devices in astronomy 2—17099
    - energy spectra of sea waves from photographic interpretation 2—20295
    - fluorescence colour photography of the eye 2—17757
    - frequency conversion of weak light fluxes by photographic materials 2—11449
    - gated picture ranging in picosecond range, applications 2—5453
    - high speed transient deformation, three dimensional Moire fringe technique 2—27187
    - image storage, three dimensional, space-bandwidth product 2—2375
    - interfacial tension between two liquids 2—9118
    - Kerr-cell photographs of arc formation in h.v. vacuum discharge 2—24918
    - liquid drops, recording 2—23742
    - Mercury passage, along disk of Sun, position angles and contact instants 2—7534
    - meteor trail speed obs. using optical wedge shutter 2—7538
    - nondestructive exam. of irrad. fuel pins 2—38753
    - optical correlation for real time strain obs. 2—14193
    - particle size density distrib., f(x), determ., eqns. relating radii F(R) to f(x) 2—38086
    - plasma diagnostics, nanosecond transmission photography using pulse clipped Q-switched laser 2—35543
    - pulses in mode-locked Nd:glass laser radiation 2—5453
    - pyrometer, IF-87, radiance temp. measurement 2—27332
    - raindrop growth, coalescence with cloud droplets 2—1863
    - relativistic object: dumbell-like formed by two packets of light 2—5453
    - relief reproduction, review of photographic methods 2—27686
    - roentgenography with high-energy X-rays, luminescence yield 2—27687
    - screenless precession photography for refl. intensity meas. in crystallography 2—9386
    - sea energy spectra, analysis and optical processing 2—22947
    - shock induced elastic ripples on electronic circuitry components 2—8055
    - solar spectra recording 2—11057
    - space research 2—1917
    - spectral anal. using a camera, in introductory physics lab. 2—16698
    - stress wave propagation and fracture in thin curved bars 2—5214
    - Technocart, stereoplotter for terrestrial photogrammetry 2—27685
    - tornado-producing thunderstorms, prediction by aerial photography 2—13703
    - vibration analysis by moire contour-sum contour-difference 2—8054

Photography continued
- **applications** continued
  - vibration analysis of tuning fork of electronic watch, by holographic and photographic methods 2—14234
  - vibrational amplitude measurement on diffuse surface, modulation of projected fringes 2—21160
  - weld metal strain measurement in brittle temperature range 2—12956
  - X-ray intensifying screen using Gd_2O_2S:Tb phosphor 2—30672
  - X-ray photographs, intensitometer applications 2—17758
  - KCl, crystal, grown from melt, optical defects, monochromatic photographic obs. 2—32500
- **colour**
  - under available light conditions Super 8 film and cameras 2—2473
  - with black-and-white film, review 2—336
  - diffuse reflection density of multilayer colour prints 2—17756
  - distortion due to substandard film, effectiveness of RGB and FBAS colour correctors 2—23737
  - film recording from TV, mechanized procedure 2—23738
  - fluorescence, obs. of eye 2—17757
  - image retrieval from monochromatic transparencies, influence of film 2—34567
  - masked and unmasked negatives, influence on colour reproduction and definition 2—27684
  - photo-colourprint paper, resolution and definition 2—27677
  - positive film type 650, graininess, definition, colour separation, saturation and fidelity 2—2478
  - positive films, processing technique 2—23739
  - printing of colour negatives, colorverter and translator 2—27667
  - TV and film lighting requirements and lamp characteristics 2—5444
- **high-speed**
  - under available light conditions Super 8 film and cameras 2—2473
  - frame rate of a million per second 2—17750
  - graphite fibre-epoxy resin composite, tensile fracture, photographic obs. 2—36167
  - in-flight, stop—motion flash photography 2—38177
  - picosecond streak camera, laser triggered avalanche transistor voltage generator 2—17753
  - relativistic object: dumbell-like formed by two packets of light 2—5453
  - obs. of shock induced elastic ripples in electronic circuitry components 2—8055
  - spark light source for framewise photography of fast processes 2—38174
  - ultrahigh speed, mode-licked Nd:glass laser pulses 2—5453
  - Ar arc discharge, anode spot behaviour during retrograde motion obs. 2—24935

Photoionization
- $2p^q$ configurations, multichannel photodetachment cross section, calc. using polarized orbital close-coupling approx. 2—5851
- anilines in solid Xe 2—25951
- anthracene single crystals, rel. to recombination delayed fluorescence 2—22807
- atom, multi-electron, photoionization section of 1s and 2s states, computer calcs. 2—31642
- atoms, cross sections, R-matrix theory 2—599
- atoms, effect of light polarization on multiphoton ionization, cross section variation 2—28203
- atoms, many-electron correlations, calc. using random phase approx. with exchange 2—598
- benzene, efficiencies and absorpt. cross sections, 600-2200 Å 2—18491
- cross section depend. on photoelectron energy 2—31683
- cross sections, atomic, unified treatment based on R-matrix theory 2—11931
- cross sections calcs. using plane-wave method allowing orthogonality 2—31684
- double photoionization, L=1 final states, energy dependence, threshold law 2—11965
- ethyl nitrate, mass spectra investigated, determ. electron affinities of NO_2, NO_3 and heat formation of NO_3 2—12224
- ethylene molecule, ang. distribs. of photoelectrons 2—35329
- formaldehyde, insterstellar, photochemistry 2—4898
- formaldehyde, investigation in vacuum u.v. 2—8775
- halogen and interhalogen, hot band effects on ionization threshold 2—18420
- indole derivatives, aqueous, 77K, delayed fluorescence 2—10432
- inert gas atoms, calc. cross sections and angular distributions using HF wave functions 2—11981
- many electron atom, including electron correlation effect 2—28206
- mass spectrometry electron energy deposition spectra estimated from photoelectron and photoionization cross sections 2—8418
- methane, total and differential cross sections, calcs. 2—18458
- methanol, first ionization potential determination and ion yield curve interpretation 2—15378
- methyl nitrate, mass spectra investigated, determ. electron affinities of NO_2, NO_3 and heat of formation of NO_3 2—12224
- Millikan apparatus for meas. on solids and liquids 2—31007
- moleculaes, photosensitized ionization, by Ar 2—8551
- molecular crystal, photon energy larger than band gap 2—19801
- molecular ion, fluorescence as interpreting aid in photoelectron spectroscopy 2—35220
- molecular ions, photodetachment spectrometry, crossed beam technique 2—761
- molecular photoelectron spectroscopy, autoionization obs. at different wavelengths 2—31770
- molecules, matrix-isolated at low temperature 2—25951
- nitro-methyl, mass spectra investigated determ. electron affinities of NO_2, NO_3 and heat of formation of NO_3 2—12224
- nitroethyl, mass spectra investigated, determ. electron affinities of NO_2, NO_3 and heat of formation of NO_3 2—12224
- photoelectron spectra and partial photoionization cross sections 2—12167
- photoelectron spectroscopy of transient species, vacuum ultraviolet 2—760
- pyrazine, photoelectron spectra 2—28403
- pyrene in polar liquids, analysis of photochemical data 2—21701
- pyridazine, photoelectron spectra 2—28405
- pyrimidine, photoelectron spectra 2—28404
- pyrylene, in polar liquids, analysis of photochemical data 2—21701
- quasistellar objects, emission line intensities 2—10922
- styrene, efficiencies and absorpt. cross sections, 600-2200 Å 2—18491
- N,N,N′,N′-tetramethyl-p- phenylenediamine, recomb. luminesc. due to photoionization, 77 K 2—26230
- N, N, N′, N′ tetramethyl-para phenylenediamine, in polar liquids, analysis of photochemical data 2—21701

Photoionization continued
- s-triazine, photoelectron spectra 2—28416
- tryptophan in ethylene glycol-water glass, kinetics and cross section of 2-quantum ionization 2—1762
- Al cross-sections for all levels belonging to $1s^22s^22p^63s^23p^q$ configurations 2—24337
- Ar, cross section calcs., effect of core polarizability 2—11973
- Ar atoms, variation of angular distribution of ejected photoelectrons 2—607
- Ar cross-sections for all levels belonging to $1s^22s^22p_63s^23p^q$ configurations 2—24337
- Au, extreme u.v., calcs. using final state correls. 2—31675
- Au atoms, inclusion of intrachannel interactions in calc. 2—601
- Ba atoms, metastable 2—18327
- Be, effect of two electron autoionizing levels on cross sections 2—8461
- Bi, cross section meas. between 250 eV and 4o eV in X-ray-u.v. wavelength region, use of two grating spectrograph 2—608
- Bi, extreme u.v., calcs. using final state correls. 2—31675
- Bi atoms, inclusion of intrachannel interactions in calc. 2—601
- Br, photoelectron spectra, total and partial photoionization cross sections 2—15312
- CO, by soft X-rays at 0.28 and 1.49 keV, meas. of relative abundance of thermal energy ions 2—805
- CO fluorescence band intensities, $CO^+ (A^2\Pi_i \rightarrow X^2\Sigma^+)$ transition 2—21593
- CO molecule, efficiencies and absorpt. cross sections in 300-1000 Å region 2—21639
- CO photoelectron spectra and partial photoionization cross sections 2—12167
- CO^+, enhancement of vibrational level population by photoelectron spectrometry 2—35265
- CO_2, by soft X-rays at 0.28 and 1.49 keV, meas of relative abundance of thermal energy ions 2—805
- CO_2 photoelectron spectra and partial photoionization cross sections 2—12167
- Ca, effect of two electron autoionizing levels on cross sections 2—8461
- Cl_2, cross sections of valence mol. orbitals, valence electron approx. 2—8621
- Cs, cross sections and spin orientation of ejected electrons 2—31677
- Cs, excited atoms, cross section determ. 2—602
- Cs, principal series oscillator strengths and ground state photoionization cross sections 2—31679
- Cs atoms, using laser at 6943Å, 3 photon process, ratio of transition rates for circularly and linearly polarized light meas. 2—603
- F_2, cross sections of valence mol. orbitals, valence electron approx. 2—8621
- Fe neutral atom, cross section calc. for photon energies from threshold to 10 keV 2—11976
- Fr atoms, inclusion of intrachannel interactions in calc. 2—601
- GaAs:Cu,GaAs:Ag, deep acceptors, i.r. investigations of optical absorption cross sections 2—6831
- H-, photodetachment cross section, calculation 2—696
- H, multichannel photodetachment cross section, calc. using polarized orbital close-coupling approx. 2—5851
- H^-, static and dynamic polarizabilities, via asymptotic approx., photodetachment cross sect. 2—18347
- H_2, ang. distrib. of phoeoelectrons, rot. ionization range 2—35255
- H_2, simultaneous excitation and photoionization, obs. from photoelectron spectra at 247 Å 2—35256
- HCl, cross sections of valence mol. orbitals, valence electron approx. 2—8621
- HF, cross sections of valence mol. orbitals, valence electron approx. 2—8621
- H_2O, interstellar, photochemistry 2—4898
- H_2O, total and differential cross sections, calcs. 2—18458
- H S, total and differential cross sections, calcs. 2—18458
- He, photon energies from threshold-160.6 eV, determ. of partial cross sections and ang. distrib. of ejected n=2 photoelectrons 2—31673
- Hg atoms, inclusion of intrachannel interactions in calc. 2—601
- Hg cross sections for ion production meas. by photoelectron spectroscopy 2—2947
- I_2, photoelectron spectra, total and partial photoionization cross sections 2—15312
- I_2 in solid CO_2 2—25951
- K, cross sections and spin orientation of ejected electrons 2—31677
- K, multiphoton ioniz. probability, 1.06 and 0.53 μ 2—35157
- K, polarized atomic beam, production of polarized electrons 2—11978
- K, principal series oscillator strengths and ground state photoionization cross sections 2—31679
- K atoms, cross sections, model potential calc. 2—605
- Kr, cross section profiles of resonances in continuum 2—597
- Kr, resonances in continuum 2—596
- Kr atoms, variation of angular distribution of ejected photoelectrons 2—607
- Li, polarized atomic beam, production of polarized electrons 2—11978
- Mg, effect of two electron autoionizing levels on cross sections 2—8461
- N_2, by soft X-rays at 0.28 and 1.49 keV, meas. of relative abundance of thermal energy ions 2—805
- N_2, effect of autoionization on angular distribution intensity of ejected photoelectrons 2—607
- N_2, vibrationally excited, spectrum meas. in 79.58-84.20 nm region 2—18446
- N_2, vibrationally excited, spectrum in 79.5-84.0 nm region, appearance of new bands 2—3053
- N_2 mol., multiphoton ioniz. and dissoc. at $\lambda=0.53\ \mu$ 2—35272
- N_2 molecule, efficiencies and absorpt. cross sections in 300-1000 Å region 2—21639
- N_2 vibrationally excited, study of spectrum in flowing N_2 afterglows, application to kinetic processes 2—806
- N_2 yields for high and low solar activity, using Monte Carlo simulation of model ionosphere 2—4713
- N_2^+, enhancement of vibrational level population by photoelectron spectrometry 2—35265
- NH_3, interstellar, photochemistry 2—4898
- NO, by soft X-rays at 0.28 and 1.49 keV meas. of relative abundance of thermal energy ions 2—805
- NO, photoelectron spectra and partial photoionization cross sections 2—12167
- NO, to $X^1\Sigma^+$ state of NO^+, vibrational transition probabilities 2—21625
- N_2O photoelectron spectra and partial photoionization cross sections 2—12167

Photoionization continued
N_2O^+, selection rules for $^2\Pi$ states 2—12163
Na, principal series oscillator strengths and ground state photoionization cross sections 2—31679
Na atoms, cross sections, model potential calc. 2—605
Ne, total and differential cross sections, calcs. 2—18458
Ne atom, cross section partition, exptl. obs. in soft-X-ray region 2—35166
O, positive ions, cross section calc. 2—18332
O yields for high and low solar activity, using Monte Carlo simulation of model ionosphere 2—4713
O_2, by soft X-rays at 0.28 and 1.49 keV, meas. of relative abundance of thermal energy ions 2—805
O_2, effect of autoionization on angular distribution intensity of ejected photoelectrons 2—607
O_2, molecule, efficiencies and absorpt. cross sections in 300-1000 Å region 2—21639
O_2, photoelectron spectroscopy of O_2 ($^1\Delta_g$), vacuum ultraviolet 2—760
O_2 yields for high and low solar activity, using Monte Carlo simulation of model ionosphere 2—4713
O_3-, photodetachment study using tunable dye laser 2—817
Ra atoms, inclusion of intrachannel interactions in calc. 2—601
Rb, principal series oscillator strengths and ground state photoionization cross sections 2—31679
Rb vapour, selective two step using laser radiation 2—21524
Rn atoms, inclusion of intrachannel interactions in calc. 2—601
SF_6, molecule, efficiencies and absorpt. cross sections in 300-1000 Å region 2—21639
SF_6, of atoms in soft X-ray spectrum 2—35285
Si cross-sections for all levels belonging to $1s^22s^22p^63s^23p^q$ configurations 2—24337
SiF_4, of atoms in soft X-ray spectrum 2—35285
Tb, cross sections and spin orientation of ejected electrons 2—31677
Xe, cross section profiles of resonances in continuum 2—597
Xe, resonances in continuum 2—596
Xe atoms, variation of angular distribution of ejected photoelectrons 2—607

[illegible]
astronomical clouds, non-thermal radiation spectra, emission line intensities of quasars 2—10842
atmospheric gases, partial cross sections, photoelectron spectroscopy obs. 2—8990
cross sections for excited states of O, S, and Ar ions, emission model for gaseous nebulae 2—20506
formaldehyde, first ionization potential determination and ion yield curve interpretation 2—15378
light source using sliding spark over solid Xe insulator, for plasma production 2—35508
metal vapour, cross-section meas. 2—18297
methylene chloride, photoelectron-photoion coincidence spectra 2—28164
molecules, X-ray photoionization, relative abundances and recoil energies of fragment ions 2—28310
photoelectron-photoion coincidence spectrometer, design and performance 2—28164
photoelectron-photoion coincidence spectroscopy, principles and theory 2—28260
population inversion establishment by photoionization of inner shell electrons 2—27454
precursor, for elimination of atom-atom collision region 2—39193
quantum yields of selected compounds at 58.4 and 73.6-74.4 nm 2—28269
Ag I, autoionization lines in vac. u.v. spectra determ. by photoionization and emission 2—18309
Ar, ion source, charge transfer efficiency Ar^+-Ar detn. 2—18342
AsH_2^-, photodetachment of electrons, electron affinity 2—35587
Au I, autoionization lines in vac. u.v. spectra determ. by photoionization and emission 2—18309
Cu I, autoionization lines in vac. u.v. spectra determ. by photoionization and emission 2—18309
GeH_2X_2 (X=F, Cl, Br, or I), photoelectron spectra 2—21643
GeH_3X (X=F, Cl, Br, or I), photoelectron spectra 2_21643
H, intergalactic, heating mechanism of QSO radiation 2—26611
H_2, 21.22 eV photoelectron spectrum, rotation structure 2—18431
H_2, by double electron excitation, photoelectron spectroscopy obs. 2—18423
Kr, ion source, charge transfer efficiency Kr^+-Kr detn. 2—18342
Li vapour, autoionizing spectra, vac. u.v. obs. 2—18308
NH_2^-, photodetachment of electrons, electron affinity 2—35587
Na vapour, autoionizing spectra, vac. u.v. obs. 2—18308
O_2, photoelectron-photoion coincidence spectra 2—28164
Rb vapour, two-photon ionization by ruby laser beam 2—6106
SiH_2X (X=F, Cl, Br, or I), photoelectron spectra 2—21643
SiH_3X (X=F, Cl, Br, or I), photoelectron spectra 2—21643
Xe, ion source, charge transfer efficiency Xe^+-Xe detn. 2—18342

Photolysis *see Photochemistry*

Photomagnetic effects *see Photoelectromagnetic effects*

Photomagnetoelectric effects *see Photoelectromagnetic effects*

Photometers
see also Spectrophotometers
absolute u.v. calibration to update Orbiting Astronomical Observatory calibration 2—11189
Auto-Spot 1°, construction, function and applications 2—2440
calibration of photometer intended for study of polar aurorae 2—27606
calibration using synchrotron radiation from electron storage ring as absolute standard 2—7640
contact reflectometer and collimator photometer, inspection of large optical components 2—38082
dual probe, for luminance comparison 2—34507
error analysis 2—314
exposure meters with indicating light diodes for amateur cameras 2—38166
goniophotometer, automatic, use of time shared computers in connection with 2—23701
IFO-453, automatic absorption photometer 2—38084
integrating two-dimensional Si diode array vidicon astronomical photometer 2—27605
light distribution, state of development in Japan, review 2—7999
light scattering, evaluation of methods for determining refraction correction 2—31104
for liquid phase conversion obs. under high press., visible and i.r. spectral operation, construction 2—38080

Photometers continued
masks for altering the spectral distribution 2—5442
MF-4 microphotometer, recording section 2—27607
microphotometer, transmission, area-scanning, photon noise limited for films or plates 2—7583
photocells, evaluation of the spectral response using luminescense-measuring photoelectric technique 2—6897
photoelectric, maximum sensitivity det. for pulsed and continuous radiation sources 2—34505
scanning photometer, rotating interference filter, auroral sounding rockets 2—23052
single particle, for latex particle size distrib. determ. 2—15617
small surface area, used with He-Ne laser for studying diffraction 2—34503
spherical scatterers dependence of extinction efficiency on instrument geometry 2—14456
for stellar radial velocity meas. 2—7582
total light absorption in high-transmission glass 2—5427
CdS cells, photoconductivity and limitations detected in calibration 2—17698
Si:Au photomagnetoelectric light detector characteristics over −20°C to +60°C range 2—34506
Si-target vidicon photometer, two-dimensional photometric images of planets and stars 2—41268

Photometry
see also Brightness; Densitometry; Illumination; Spectrophotometry
close binary stars 2—41123
ϵ Coronae Austrinae, light and colour curves in RI 33648 2—33648
3CR catalogue radiosources 2—13966
critical fusion frequency, brightness measurement 2—26982
V1057 Cygni, UBVRI photometry10876 2—10876
daylight, photometric flux derivation from filtered meas. of global radiant energy 2—7296
definition problems of luminance and brightness 2—8004
double beam compensation type, dynamics of servosystems 2—38083
electronic imaging devices in astronomy 2—17099
faint clusters in Large Magellanic Cloud, colour-magnitude diagrams 2—37314
fluorescent lamp, assessment of effect of screen in integrating sphere 2—8001
four-colour photographic analysis of stellar distributions in high galactic latitudes 2—10820
IES practical guide to photometry 2—38081
illumination measurement for buildings, open spaces, and highways 2—2438
integrating sphere, view into through observation window 2—8002
isophote map of chromospheric bright and dark mottles on the solar disk 2—23132
isophotic contours and monochromatic photographs of planetary nebulae NGC 2392, 6210, 6826, 6720 and 6853 2—16963
light distribution, state of development in Japan, review 2—7999
luminaires, det. of average luminance 2—38140
luminosity and CFF thresholds in deuteranopes and protanopes 2—11224
multichannel area photometry for stars of low apparent brightness 2—41269
N-galaxies 3C390.3 and PKS 0521-36 2—10828
narrow band and broadband i.r. of IRC stars 2—4865
near i.r. obs. of θ CrB binary system 2—23080
origin and history, review 2—5426
photoelectric receivers, relative spectral sensitivity distributions, apparatus for automatic obs. 2—8000
photoelectric scanning echelle spectrograph, nebula photometry 2—26937
photon scalar irradiance as optimum measure of radiant energy available for photosynthesis, measurement and calibration of underwater photon scalar irradiance collector 2—33775
plasma diagnostics, electron number density profiles det. using optical switch 2—28599
relative spectral power distribution, standards, verification by filter radiometry 2—8003
six colour system, revised indices for G and K dwarf stars 2—13902
speckle noise elimination by stirring of sample in laser light scattering photometery 2—31056
standards, candela, lumen, review 2—7998
star clusters, Ca K-line photometry of A stars 2—7445
supergiant stars, colour excesses 2—33647
tasks, problems and organizations, review 2—5425
UBV, centred on NGC 6522, red giants in nuclear bulge of the Galaxy 2—13838
UBV, early-type stars at high galactic latitudes 2—13836
UBV and Hβ, faint OB star groups in Monoceros 2—13837
ubvyβ system, calibration in terms of intrinsic colour indices and absolute magnitude for B-type stars 2—4864
units and terminology, new British standard, review 2—34504
Uranus, multicolour photoelectric wavelengths 0.315 to 1.06 μ 2—4978
u.v., from OAO, interstellar extinction obs. 2—10912
uvbyβ and gnkmf systems, obs. of consistency of calibrations 2—5021
white dwarfs, uvby, magnitudes and colours 2—33663
H_2S concentration in the Black Sea, a photometric method of determination 2—13664

light sources
of galaxies with integrating television 2—7383
light measurement, monochrome and colour TV studios 2—14457
applications of digital computers, methods 2—23700
pulsation coefficient meas., relative spectral sensitivity 2—17133
testing programme, developments 2—2439
u.v., secondary standard, calibration by synchrotron and plasma-blackbody radiation 2—8023
vacuum u.v., CI multiplet transition proximity meas., 170-250 nm, using plasma rad. and synchrotron sec. standards 2—17747
vacuum u.v., stabilized H_2 arc 2—17748
vacuum u.v. standard radiators, comparison between synchrotron and plasma blackbody radiation 2—17746

Photomultipliers
calibration using synchrotron radiation from electron storage ring as absolute standard 2—7640
channel, efficiency for 10-1000 eV electrons 2—8236
channel, efficiency for protons of 0.2-10 keV 2—2638
channel, gain variations throughout operating history 2—24095
channel, operation in analog continuous current mode 2—2637

Photomultipliers continued
channel plate electron multipliers, operational gain characteristics 2—14394
channel-electron, construction, properties, applic. as vacuum u.v. detector 2—14393
Channeltron gain in magnetic fields 2—37931
compensated leading edge timing 2—34828
cooling effect on dark pulses 2—37929
dark current, method of reduction at room temperature 2—34328
diffuse reflection and fluorescence measurement, powered solids 2—20103
EAS recording, background radiation interf. minimization 2—2625
fast, in single-photoelectron limit, late output pulses 2 27432
FEU-49, time locking circuit for operation in Cerenkov total absorption spectrometer 2—21320
head-on cathode, effects of external mirror coatings 2—31012
housing, compact, with controlled cooling 2—41364
image dissector, statistical analysis of signal and noise pulses 2—27434
image intensifier, single photoelectron excitation of phosphors, output intensity distribution 2—38089
ionizing radiation effects on output current, sensitivity and resolution, review 2—21330
as light source, evaluation 2—17721
lightning observations and recording using photoelectron multiplier system 2—37164
multianode photomultiplier, matrix anode design 2—37930
nanosecond signal sampling circuit 2—7871
noise characteristics, selection and counting of irregular pulses 2—24093
noise statistics 2—34327
one electron, effects of prolonged operation on spectral sensitivity, gain, noise level and plateau length 2—37928
optical communication and detection receivers, error performance bounds 2—34511
optical enhancement at u.v. wavelengths 2—2371
optical rangefinders, PMT's with external modulating electrodes 2—31111
parallel-plate, characts., applic. to low-energy electron spectroscopy 2—31006
photocathode average integral sensitivity characteristics 2—21033
photon counting, discusses detection techniques 2—14766
photon counting, effect of afterpulses 2—38380
photon counting, emission spectroscopy 2—14767
pulse counting using amplifier 2—34241
RCA 6217, 5819, variations of spectral sensitivity at low temp. 2—7870
RCA C31000E, quantum enhancement 2—2372
recording capacity for reception of weak signals in large backgrounds, choice of photoreceivers 2—37927
sensitivity threshold for scintillation measurements of soft beta radiation 2—23549
signal-to-noise ratio depend. on operating voltage 2—2370
subnanosecond response time with chevron microchannel plate for electron multiplication 2—27433
threshold characteristics of photoelectron multipliers at wavelength 530 nm 2—37926
transient response det. using light emitting GaP diodes 2—17723
tube, for thermolum. dosimetry, a.c. heater current rel. to readings 2—27897
in ultravacuum micromanometer, for discharge light flux detection 2—30734
Cu-Be, procedure for restoring signal- to-noise ratio 2—2373
GaP dynode, dynamical gain measurement 2—6935

Photons
see also Cosmic rays/photons; Gamma-rays; Nuclear reactions and scattering due to/photons; X-rays
bremsstrahlung emission, coherent, from electrons, ~1000 GeV 2—27702
concepts, short review article 2—38222
correlation measurements, effect of incomplete spatial coherence 2—7910
counter, 10μ, noise due to laser pumping and internal upconversion 2—37940
counting cumulants, coherent and chaotic mixtures, lognormal fading 2—23559
counting distrib. of Brillouin scattered light from amplified vibr. noise in ZnO 2—13494
counting experiment, rel. to determination of coherence surface 2—37937
counting statistics, spectral distrib. probabilities 2—7909
detectors, review article 2—38350
echo resonance, in ruby 2—33232
evanescent photons, absorption and emission in fluorescence of excited molecules 2—31736
fluctuating dielectric permeability medium, photon flux 2—5339
gaussian light of arbitrary spectral profile, generating function of photocounts 2—37941
as Goldstone particle, theoretical investigation 2—17793
Goos-Hanchen and Imbert effects 2—34231
isovector, rel. to algebra of couplings in chiral symmetry 2—38212
mass, experimental results on longitudinal displacements of laser beams near total reflection 2—34370
monorefringent medium, spatial distribution of refr. index 2—23664
multiphoton theory, experimental test 2—27447
optical, detected in coincidence with β rays from $Sr^{90} \to Y^{90}$ source, detection and identification of internal bremsstrahlung 2—11789
particle aspect formulation 2—23782
photocount statistics, spectral truncation effects 2—23560
production, application of Chew Pignotti duality 2—11590
production by various atomic processes described as source term in Boltzmann equation 2—23286
propagator corrections due to hadron vacuum polarization 2—5483
radiation press. in refractive media 2—21136
Raman amplifier, quantum statistics 2—31020
rest mass, rel. to velocity of light in gravitational field 2—37589
rest mass, rel. to Weber's experiment for gravitational wave observation 2—26583
size, clarification based on physical picture 2—17816
spectra from $\nu\mu$ inelastic scatt., effect of lepton polarization properties 2—27710
in spectral line, escape probability, isothermal atmosphere 2—11451
statistical effects and optical birefringence 2—31021
statistics of a composite photon formed of two fermions 2—38223
statistics of phase locked coupled light beams 2—34371
two photon (different modes) amplifier, quantum statistics 2—21039
two-photon amplifier, quantum statistics 2—21038

Photons continued
two-photon process studied in colliding beam experiments, $e+e \to e+e+\Gamma$ 2—14553
in unified spinor field theory of relativity 2—17215
universe, effective transparency to very high energy photons 2—16950
virtual, investigation in $e+p \to e+\rho+p$ reaction using quantum electrodynamics and multiperipheral and constituent models 2—34617
virtual, magnetic monopole pair prod. in pp collisions 2—31180

interactions
$\gamma p \to \rho^0 p$ s-channel helicity conserving amplitude, dual extension to $\gamma p \to \pi^+ \pi^- p$ 2—373
backward photoprod., phenomenological anal. in terms of kinetic cut model 2—8108
bootstrap self consistency conditions for amplitudes in photon meson meson and photon baryon baryon reactions 2—17820
colliding photon beams, hadron production, difficulties in theory 2—14578
deep inelastic photoproduction, specific multi-Regge model 2—23796
gamma ray absorption in and critical energies for supernovae and Crab Nebula 2—10925
gas with H-He plasma, dynamics described by Boltzmann equation 2—23286
hydride molecules, photoejection of proton 2—24472
pair production by γ rays method for determ. effects of screening 2—21248
photon-photon interactions, Sun, Freundlich red shift 2—17049
photoproduction, inelastic of W^+ bosons in quark parton model 2—17949
photoproduction from nucleons, simple approach to Reggeisation 2—8107
photoproduction of ρ, existence of fixed pole 2—424
photoproduction of ρ, Regge pole analysis, deep inelastic region 2—14681
photoproduction of φ at 5.2 GeV by obs. of $\varphi \to K^+K^-$ decays 2—14678
photoproduction of ions, mesons and vector mesons, conference 2—31258
photoproduction of pseudoscalar mesons, consequences of SU_3 invariance, absence of exotic resonances and duality 2—23832
photoproduction of single pions, in first resonance region dispersion relations and isotensor e.m. current 2—8166
photoproduction of vector neutral mesons on nucleons, Glauber model, quark model 2—14673
photoproduction reactions on polarized protons, construction of butanol target and effects of radiation damage 2—34766
r.f. photons, with atoms, optical pumping experiments as test of dressed atom theory 2—24305
SU(3) for photoproduction, tests taking account of mass differences 2—34635
virtual photon photon annihilation, pion mass differences 2—17822
$_\gamma{}^3He \to K^+{}_\Lambda{}^3H$, current algebra study 2—18094
$e_+e \to e+e+$hadrons, representation as photon-photon interaction, scaling 2—14567
e^+e^- photoproduction, effect of magnetic field 2—5506
$ep \to e'p'\pi^0$, recoil proton polarization, first nucleon resonance energy region 2—27751
η, photoproduction on hydrogen, 4 and 8 GeV, differential cross section measured 2—8153
η photoproduction, apparent anomaly and stray baryonic states 2—21281
$2\gamma \to 3\pi$, total cross section 2—21231
$2\gamma \to (2n+1)\pi$, gauge invariance rel. to chiral symmetry 2—38224
$2\gamma \to (2n+1)\pi$, gauge invariance and chiral symmetry 2—38225
$\gamma + \to \pi^- + p + p$, pp final state interactions, separable potential model 2—8199
γd, multipion photoproduction at energies up to 5 GeV, partial cross sections meas. 2—27749
γd photoproduction, isostructure of e.m. currents 2—34588
$\gamma d \to \rho^0 d$, 6 to 18 GeV, ρ^0 meson-nucleon cross section 2—14683
$\gamma e \to e^+e^-$, cross section calc., possible use to meas. photon beam polarization 2—5507
$\gamma e \to eW^- + W^-$, cross sections 2—14674
$\gamma\gamma$, virtual interaction, investigations in e^-e^- and e^+e^- collisions 2—11573
$\gamma\gamma$ collisions in electron-positron storage rings, introduction of realistic experimental conditions 2—14554
$\gamma\gamma \to e^+e^-$ in magnetic field, polarization effects 2—8122
$\gamma\gamma \to e^+e^-$ in magnetic field, role of Compton effect 2—8111
$\gamma\gamma \to$ hadrons, parton model 2—34601
$\gamma\gamma \to \nu\bar{\nu}$, effective cross section calc. by using IVB theory 2—21239
$\gamma\gamma \to \pi\pi$, calculation of cross sections 2—34600
$\gamma\gamma \to \pi\pi$, low energy, simple phenomenological description 2—21230
$\gamma\gamma \to \pi\pi$, virtual photon interaction, analysis 2—34599
$\gamma\gamma \to \pi\pi\pi$, low energy theorems from PCAC hypothesis 2—14556
γn, formation of $P_{11}(1470)$ resonance 2—8182
γn, forward π and η production, Regge models 2—17925
γN, high energy pion production, s-channel dominance and charge ratios 2—8168
γN, pion photoproduction, construction of non minimal currents in chiral Lagrangians 2—14648
γn, pion production, sum rule determination from dispersion relations 2—17924
γN, π^0 photoprod., effect of ω and ρ complex Regge poles 2—27752
γN, π production, threshold, low-energy theorems 2—14649
γN, single pion prod. in first resonance region 2—31285
γN, single π prod., multipole analysis by current algebra commutators 2—34680
$\gamma N \to \Delta V^0 \pi$, method for experimental study of energy dependence of $V^0\pi$ scattering amplitudes proposed 2—17935
$\gamma N \to NV^0$, charge exchange, Pomeranchuk theorem violation 2—8151
$\gamma N \to O^-B$ photoproduction, t-channel transformation matrices for helicity and invariant amplitudes 2—23781
$\gamma N \to (1/2)^+ + 2^+$, SU(6) symmetry study 2—5522
$\gamma N \to (3/2)^+ + 2^+$, SU(6) symmetry study 2—5522
$\gamma n \to \pi^- p$, polarization parameters, target asymmetry 2—34675
$\gamma n \to \pi^+ p$, 0.5 to 2.5 GeV, differential cross section polarization and asymmetry ratio 2—34653
$\gamma N \to \rho^0 N$, high energy role played by charged pion pairs mediating 2—31195
γp, muon pair production at high energies, field theoretical parton model 2—11577
γp, photoprod. of resonances with annihilation radiation, 3 prong events 2—17821
$\gamma p \to K^0 \Sigma^+$, differential cross sections and asymmetry coefficients, Regge pole model with cuts 2—34660
$\gamma p \to K^+ \Lambda$, differential cross sections and asymmetry coefficients, Regge pole model with cuts 2—34660

Photons continued
- **interactions** continued
  - $\gamma p \to K^+\Delta^0$, differential cross section meas. at constant momentum transfer between 1.05 and 2.2 GeV 2—34661
  - $\gamma p \to K^+\Lambda$, 0.5 to 2.5 GeV, differential cross sections, polarization and asymmetry ratios 2—34653
  - $\gamma p \to K^+\Lambda^0$, differential cross section meas. at constant momentum transfer between 1.05 and 2.2 GeV 2—34661
  - $\gamma p \to K^+\Sigma^0$, 0.5 to 2.5 GeV, differential cross sections, polarization and asymmetry ratios 2—34653
  - $\gamma p \to K^+\Sigma^0$, differential cross sections and asymmetry coefficients, Regge pole model with cuts 2—34660
  - $\gamma p \to K^+ + \Lambda(\Sigma^0)$, low energy description and duality relations 2—34662
  - $\gamma p \to \eta p$, 0.5 to 2.5 GeV, differential cross sections, polarization and asymmetry ratios 2—34653
  - $\gamma p \to \eta p$, photoproduction, dip mechanism 2—14557
  - $\gamma p \to \omega p$, comparison of experimental data with VDM predictions 2—34703
  - $\gamma p \to p'\pi^0$, recoil proton polarization, first nucleon resonance energy region 2—27751
  - $\gamma p \to p\pi^+\pi^-$, cross sections, ρ^0 and Δ^{++} production in bubble chamber with 2.8 and 4.7 GeV polarized photons 2—27707
  - $\gamma p \to \varphi p$, comparison of experimental data with VDM predictions 2—34703
  - $\gamma p \to \pi^-$+anything, inclusive reaction in proton fragmentation region, differential cross sect. 2—374
  - $\gamma p \to \pi^-\pi^+p$, 1GeV, energy spectra and excitation yields 2—23845
  - $\gamma p \to \pi^0 p$, 0.5 to 2.5 GeV, differential cross sections, polarization and asymmetry ratios 2—34653
  - $\gamma p \to \pi^0 p$, unpolarized and linearly polarized photons, 4 to 18 GeV 2—11606
  - $\gamma p \to \pi^+ n$, 0.5 to 2.5 GeV, differential cross sections, polarization and asymmetry ratios 2—34653
  - $\gamma p \to \pi^+ n$, polarization parameters, target asymmetry 2—34675
  - $\gamma p \to \pi^+\pi$-p, s-channel resonance region, cross sections 2—34679
  - $\gamma p \to \pi^+\pi^- p$, diffraction-dissociation model for high energy ρ production, comparison with empirical data 2—23875
  - $\gamma p \to \pi^+\pi^- p$ dual extension of photoproduction reaction $\gamma p \to \rho^0 + p$ 2—373
  - $\gamma p \to \pi^+\pi^0 n$, 1Gev, energy spectra and excitation yields 2—23845
  - $\gamma p \to \pi$+anything, pion distrib., extension of nova model 2—17819
  - $\gamma p \to \rho^0 p$, 5.5 to 18 GeV, determ. cross section for p meson production 2—14552
  - $\gamma p \to \rho^0 p$, comparison of experimental data with VDM predictions 2—34703
  - $\gamma\pi \to \pi\pi$, amplitude, anomalous divergence of neutral axial vector current 2—31288
  - $\gamma\pi \to \pi\pi$, Veneziano amplitude 2—14555
  - $\gamma Z \to Ze^+e^-\ e^+e^-$, test of cross section of $\gamma\gamma \to e^+e^-e^+e^-$ at high energy 2—11572
  - K photoproduction, apparent anomaly and stray baryonic states 2—21281
  - $N\gamma$, field-theoretic Reggeization in five- and six-point functions 2—347
  - ω photoproduction, effect of natural parity exchange 2—34700
  - $p\gamma \to pX^0$, electromag. X^0 prod., spin parity determ. 2—31309
  - π- photoproduction, parametrization, complex Regge poles 2—11608
  - π photoproduction, presence of exotic currents in model 2—34678
  - π photoproduction, Regge pole model including kinematic cuts study 2—23846
  - π photoproduction in $\Delta(1230)$ resonance region, multipole amplitudes 2—31286
  - π photoproduction near first resonance, isotensor terms and T violation 2—11607
  - π production, at high energies 2—5534
  - π production, inelastic backward scattering and $O_{3,1}$ symmetry 2—31275
  - π^- photoproduction, Glauber and symmetrization corrections to data from single arm spectrometer experiments 2—34677
  - π^+ photoproduction, parametrization, complex Regge poles 2—11608
  - π^o photoproduction from H at 4 GeV, polarized target asymmetry 2—23847
  - ρ^0 photoproduction, closure approx. in deuterium and non-diffractive amplitudes 2—425
  - ρ^0 photoproduction, Regge pole model analysis 2—27766
  - ρ^0 photoproduction from H, D and complex nuclei, 4-9 GeV, determ. detailed dipion mass-spectrum fits 2—14684
  - ρ° photoproduction, effect of natural parity exchange 2—34700
  - W boson, spin-1, protoproduction at high-energies 2—17948
  - $\gamma N \to \pi^+\pi^- N$, high energy role played by charged pion pairs mediating 2—31195
  - γp photoproduction, isostructure of e.m. currents 2—34588
- **polarization**
  - in gravitational field of rotating objects, quantum field theory 2—34598
  - $\gamma e \to e^+e^-$, cross section calc., possible use to meas. photon beam polarization 2—5507
  - $^{27}Al(n,\gamma)^{28}Al$, circular polarization meas., levels of ^{28}Al 2—18206
  - $^{40}Ar(n,\gamma)^{41}Ar$ circular polarization meas., levels of ^{41}Ar 2—18206
  - Ca atomic cascade, linear correlation rel. to exptl. test of local hidden variable theories 2—31659
  - $^{40}Ca(n,\gamma)^{41}Ca$ circular polarization meas., levels of ^{41}Ca 2—18206
  - $^{59}Co(n,\gamma)^{60}Co$, polarized thermal neutrons, γ-ray circular polarization 2—18211
  - Si(Li) detector, sensitivity investigation using linearly polarized 121 keV γ-rays 2—438
- **scattering**
  - Compton, induced by relativistic particles 2—11571
  - Compton, on fast electrons, rel. to vacuum light vel. meas. 2—23667
  - hypothetical scalar particles, current conservation and double-spectral representation 2—17818
  - ionization, multiphoton, local laser-beam intensity fluctuations 2—35148
  - light scattering by light using e^-e^+ colliding beams 2—23783
  - photoproduction data against ω_w analysis of scaling and local duality of two structure functions 2—34618
  - $e\gamma \to e\nu\bar{\nu}$, effective cross section calc. by using IVB theory 2—21239
  - $\gamma\gamma \to \gamma\nu\bar{\nu}$, effective cross section calc. by using IVB theory 2—21239
  - γp, Compton scattering, 3.2-3.7 GeV, cross section asymmetry 2—2515
  - γp below pion production threshold, polarization of recoil proton calc. using second order Compton amplitude 2—31323
  - $\gamma p \to \pi^0 p$, calc. of phase of forward amplitude using modulus dispersion relations 2—34723
  - $\gamma\pi$, off-shell $\rho\pi$ summ rules, applic. to π and K e.m. mass differences 2—2512
  - $\gamma\rho$, inelastic photoabsorption asymptotics 2—8121

Photons continued
- **scattering** continued
  - $p\gamma \to p\pi^+\pi^-$, total and differential cross sections evaluated using relativistic covariant and gauge invariant amplitude 2—34676
  - $\pi\gamma$ elastic, kinematical singularities in matrix decomposition 2—38185
  - He, atom, excited in plasma, resonance scatt. using dye laser 2—15247
  - $\gamma\gamma$, kinematics, invariant amplitudes 2—2513

Photonuclear reactions *see Nuclear reactions and scattering due to/photons*

Photophoresis
- No entries

Photoproduction *see Gamma-rays/effects; Nuclear reactions and scattering due to/ photons; Photons/interactions*

Photoresistors *see Photoconducting devices; Semiconducting devices*

Photosphere
- acoustic natural modes in a model solar atmosphere rel. to 5 minute periodicity in gas vel. 2—14018
- active region, distribution of electrical conductivity and gradients 2—26904
- bright points, intensity distribution, CN spectroheliogram 2—26906
- bright points, intensity distribution, CN spectroheliogram 2—26906
- chemical composition from spectral observations 2—23129
- chromosphere transition region, spectral line variations 2—41225
- continuous spectrum intensities rel. to convergency of photospheric models 2—37398
- dynamics of a toroidal magnetic ring rel. to sunspots and spicules 2—17075
- faculae rel. to photospheric network and magnetic fields 2—30624
- fine structure elements as origin of magnetic field 2—11038
- fluctuations, power, coherence and, phase spectra calc. by fast Fourier transform techniques 2—37401
- mag. field strength correlation with coronal brightness 2—41260
- mag. fields meas. at time of solar eclipse of 7 March 1970 2—41248
- magnetic and velocity fields and brightness 2—17076
- magnetic field, 5-minute oscillations 2—11036
- magnetic field, model of fine structure 2—11097
- magnetic field, purely toroidal, time development and interaction with poloidal mag. field 2—30623
- magnetic field, rel. to X-ray corona 2—11067
- magnetic field patterns, association with $H\alpha$ flares 2—11129
- magnetic field spectroheliograms 2—11034
- magnetic fields, arch filaments, new magnetic flux at solar surface 2—5009
- magnetic fields, Joule dissipation, effect of anisotropy of electric conductivity 2—17077
- magnetic fields, weak, detection using 40-channel magnetograph 2—14019
- magnetic fields at different levels 2—11112
- magnetic fields rotation, differential, rel. to coronal induction currents 2—37423
- microturbulent vel., analysis of Goldberg-Unno method 2—17074
- microturbulent velocities in an atmosphere with convection 2—37397
- motions, association with magnetic field structure and flare occurrence in active region 2—11101
- neutron as source of corona energy 2—7570
- oscillations, five-minute, in an isothermal atmosphere 2—20705
- plage region, vertical velocities and magnetic fields 2—11100
- solar cosmic rays model, low rigidity flare particles released from trapping field, plasma heated by flare process 2—17069
- streamline analysis test on terrestrial wind data 2—11094
- supergranulation at the centre of the disc 2—11098
- supergranule velocity and magnetic field 2—11099
- temp. and density fluctuations, contribution of granulation and oscillations 2—30622
- temperature profile, gas motions into upper chromosphere 2—5012
- transition zone with chromosphere, inhomogeneities study from the CaII i.r. lines 2—11052
- turbulent velocity in undisturbed and active photosphere 2—41240
- upper, variations of temperature with latitude 2—11092
- velocity fields, long periods, 5 min oscillations and supergranulation at lower layers 2—37400
- CN λ3883 spectroheliograms to map weak magnetic fields 2—11093
- CN network, intensity variations with time 2—17050
- Ca flocculi, Kodaikanal Observatory, second half of 1967 obs. 2—41242

Photovoltaic effects
- benzylidene-1,3-indandiones, chromophoric conditioning 2—25962
- charge carrier mobility measurement in inhomogeneous semiconductors 2—4099
- chlorophyll-a films 2—26942
- detectivity calc. for n-p heterojunction detectors 2—17410
- electro-optical device, radiant to electrical energy, vice versa, solid with excited electron states, Fresnel optical system, patent 2—34299
- electroluminescence in ZnSe-In junction, reverse biased 2—29996
- ionization chamber, liq. filled, X-ray and γ-ray induced 2—38360
- photocell, efficiency optimization 2—2334
- Schottky barriers, epitaxial PbTe, i.r. detection 2—7769
- semiconductor, anisotropic effect 2—36488
- semiconductor, optical energy gaps determ. from surface photovoltage meas. 2—40381
- semiconductor, photon pressure effect 2—13344
- semiconductor heterojunction, cond. band discontinuity determ. from photovoltage meas. 2—19701
- semiconductor material and devices, process control 2—29694
- semiconductor materials, high resolution measurement, photo- and electroluminescence, photo-e.m.f. 2—36959
- tetracene films, photovoltages 2—1585
- violanthrene crystal, e.m.f. 2—25849
- $Cd_xHg_{1-x}Te$, epitaxial layers, i.r. detector 2—6911
- CdS-PbS heterojunction, visible and near i.r., elec. props. 2—10148
- CdS-SnS heterojunctions 2—33082
- CdS, surface state parameters, determ. from surface photovoltage transients 2—29603
- CdS, surface states, photovoltage spectroscopy study 2—32892
- CdS, wavelength depend. of surface photovoltage 2—13345
- CdS cell prep. in soln. with Bi ions 2—10145
- CdTe-HgTe heterostruct. with built-in homojunctions 2—13350
- $Cu_{2-x}S$-CdS photocell, scanning light microprobe obs. 2—4307
- Cu_2S-CdS, heterojunc., heat treated, optical degradation effects 2—10146
- $Cu_{2-x}Se$-CdSe cells, heat treatment effects 2—29774
- p-GaAs-n-ZnSe diode, I-V characts., junction capacitance, optical collection efficiency 2—25894

Photovoltaic effects continued
GaAs, surface photovoltage, rel. to temp. and illum. depend. of work function 2–33006
GaP, wavelength modulation near indirect absorpt. edge 2–33074
Ge, in contact with electrolyte, photo-e.m.f. obs., surface barriers 2–22649
Ge, photogradient e.m.f. of hot carriers 2–40382
Ge, photogradient e.m.f. of hot carriers 2–16322
Ge, wavelength modulation near indirect absorpt. edge 2–33074
Ge film, obliquely deposited, photovoltage and resistance obs. 2–36616
Ge films, photovoltages larger than band gap 2–16321
InSb, optical energy gaps determ. from surface photovoltage meas. 2–40381
In_2Te_3-Hg_3Te_3 alloy, 2-12 μm 2–33071
PbS-Ge heterojunction, cond. band discontinuity determ. from photovoltage 2–19701
$Pb_{1-x}Sn_xTe$ diode, produced by proton bombardment 2–29776
PbTe:Sb p-n junction photovoltaic detector, prep. by ion implantation 2–40383
Si, photogradient e.m.f. of hot carriers 2–40382
Si, photogradient e.m.f. of hot carriers 2–16322
Si, wavelength modulation near indirect absorpt. edge 2–33074
Si cell spectral response, expt. 2–13351
Si radiation detectors, temperature depend. of photocurrents produced by X- and γ-rays 2–38383
Si(Li)-containing solar cells, damage and recovery characteristics after electron irradiation 2–21013
Te, Dember effect, i.r. detector 2–4308
ZnO-Si, heterojunction, elec. and optical props. 2–10088
ZnS, anomalous effect, origin 2–25965
ZnS, comparative study of thermally, stimulated voltaic effects and luminescence, role of traps and luminescence centres 2–16301

Physical chemistry
chemical fluid mechanics 2–28441
colligative properties, application of minimizing program LETAGROP to data 2–15561
dissipative systems, localized spatial structures and nonlinear chemical waves 2–22849

Physical effects of radiations
see also Under individual radiations. e.g. Neutrons and antineutrons/ effects
acoustic, loudness function, psychophysical correlates 2–27286
acoustic waves, frequency dependence of complex elastic constants of building materials 2–17399
antireflection coatings, laser induced damage 2–27632
atomic collisions in solids IV-physics of channelling and related phenomena, conference Gausday, Norway, Sept. (1971) 2–36379
basalt, saturation remanence 2–1912
binary solid solution, radiation- induced strengthening, model 2–36224
carbazole, crystal, study of paramag. radiation defects 2–10489
chromel-alumel thermocouple, reactor rad. influence on thermo-e.m.f. 2–16305
cladding strength analysis under combined effect of creep and plasticity, in fast-reactor environment 2–21465
CMNOS structures, electronic recovery 2–19735
creep in liquid metal fast breeder reactors, application of finite element methods 2–15082
L-cystine dihydrochloride, γ-irrad. cryst., photoinduced hole-electron recombination 2–22887
damage, nuclear polarization and target uniformity 2–34772
damage in laser materials 2–33191
damage to nuclear reactors, safety and economics, review of problems 2–2844
deformation centre formation, changes in structure of layer of material 2–3752
desorption, photon induced, primary excitation process 2–39567
dielectric, charged, rel. to short circuit currents and motion of zero field planes 2–22610
dielectric, solid, conductivity 2–40159
dielectrics, thermal breakdown voltage changes expression for 2–16274
diffusion controlled reaction kinetics, rel. to damage in solids 2–19070
dislocation loop nucleation model for irradiated solids 2–25396
dose and induced activity distrib., external proton beam targets 2–2878
epoxy resin/glass composites, stability 2–1382
ethylene, gas, pressure effects under irradiation by CO_2 laser 2–1028
fast fracture behaviour of metals and critical crack size 2–15877
fatigue crack propagation in reactor components due to acoustically induced stress, fracture mechanics approach 2–15171
films, metallic, surface polygonization, influence of light 2–15662
fission fragment energy degradation in elementary gases and solids, semi-empirical approach 2–8373
fluorene, crystal, study of paramag. radiation defects 2–10489
fracture toughness, prediction of radiation induced changes 2–15148
fuels, γ-ray spectra obs. 2–8410
graphite components, THTR temperature and radiation induced stresses 2–15132
graphite fuel elements, helium-cooled HTR, shrinking and induced stresses 2–15131
graphite reactor components, stress analysis 2–15128
on Gunn diode oscillators 2–19716
Gunn microwave oscillators, ionizing effect 2–22596
inert gas bubbles intersected by dislocations on atomic steps 2–9553
junction field effect transistors, transient response 2–19713
laser beams effects on matter, book 2–6696
laser induced damage, avalanche breakdown and probabilistic nature 2–21114
lattice-directed trajectories, wave theory 2–19476
linear electron accelerator, 30 MeV possible radiation hazards 2–2863
LMFBR core design analysis, radiation induced swelling and creep 2–15045
Mare Fecunditatis, extreme radiation damage in soil 2–20659
metal, radiation damage, computer simulation 2–15737
metals, secondary defects, nucleation, growth, annihilation 2–3766
microcircuits, modelling for normal and radiation effects behaviour 2–17518
m.i.s. structs., interface elec. props., irrad. effects 2–40315
m.i.s. structures, radiation induced perturbations in electrical properties 2–6874
m.o.s., and bipolar circuits, testing at dose rates from 10^9 to 10^{12} Rad (Si)/s 2–22599

Physical effects of radiations continued
m.o.s. memory, non-volatile, preprogrammed by use of ionizing radiations 2–19736
m.o.s. structures, stability and sensitivity 2–19731
on m.o.s./LSI devices, transient ionizing radiation 2–19737
m.o.s.t., hardening processes against ionizing radiation 2–19738
multiphase molecular system, phase transitions and equilibr., electronic photoexcitation effect 2–25136
nematic solution, partially deuterated molecules, H-D dipolar coupling removal, n.m.r. obs. 2–9170
neutron, effect on tangential and axial elastic limits of Zircaloy-2-fuel casings 2–11900
nuclear fuel, coated particle, rel. to stress and strain calcs. 2–15119
nuclear reactors, effect on fuels, fuel materials and assemblies 2–24282
nuclear reactors internal and structural materials, radiation damage 2–28145
optical, explosive evaporation of water drops, dynamics 2–28957
optically initiated electrical breakdown in gas, mechanism of development 2–24891
organic crystals, low temp. study of radiation damage prod. by 100 keV electrons 2–25383
organic materials, dose per unit electron current, high energy electrons on a thin target 2–2895
p-m.o.s. devices radiation hardening by optimization of thermal SiO_2 gate insulator 2–19734
photochromic liquids, optical tagging for liquid velocity distrib. obs. 2–28754
photomultiplier output current, sensitivity and resolution, review 2–21330
plastics, ABS, colour stability expt. 2–7032
polyethylene, effect of γ- irradiation on plastic deformation 2–36124
polyethylene, polystyrene, polymethacrylate, polycarbonate and PTFE, radiation- induced electrical conductivity 2–6752
polyethylene crystal, electron microscopy, contrast effects 2–22185
polymer, effect on creep and deform. relax. 2–39793
polymer fibre, straining, crystalline regions, radicals, e.p.r. obs. 2–15846
polymeric materials, testing apparatus, extension, creep, relax., in ionizing rad. 2–39880
polyvinyl chloride solutions, gamma irradiation induced branching, viscosity obs. 2–18804
polyvinylcyclohexane, change in dielectric properties 2–36582
radiothermoluminescence and analysis of structure of polymers 2–37061
on reactor pressure vessel, current trends in control, surveillance of 2–28126
ruby, u.v. irradiated, colour stability, rel. to dopants and annealing 2–25450
scientific instruments in space missions 2–10782
semiconductor, Ge, amorphous film, reactor irrad. effect on elec. props. 2–4232
semiconductor detectors, radiation damage, general patterns 2–27874
semiconductor devices, system for meas. of characteristics after radiation pulses 2–29727
on shock wave flow variables 2–12496
shrinking of graphite components, strength and durability rel. to construction problems of a THTR 2–18265
solar, plastics ageing, in natural and laboratory conditions 2–1156
solar cell radiation damage, results from ATS-1 satellite experiment 2–27400
solar cells, Li-containing, damage and recovery characteristics 2–21013
solid, defect formation and diffusion on heavy particle bombardment 2–39666
solids, nuclear recoil, knock out effects, emission probability 2–25702
sonic boom responses and damage to buidling structures 2–34153
sonic booms, building responses, flight trials of Concorde 2–34154
sonic booms, conference, Acoustical Soc. America, (Houston Texas 1970) 2–34102
sonic booms, effects of exposure on buildings 2–37466
space and nuclear radiation effects, conference, Durham USA 1971 2–19697
steel, stainless, radiation-induced swelling 2–24283
storage ring, radiation dangers of losses and bremmstrahlung 2–2864
storage rings, colliding beam experiments, radiation damage 2–2877
storage rings, intersecting CERN, preliminary health physics report 2–2897
stress distributions in fuelled graphite bricks, HTGR, finite element analysis 2–15127
stresses in fuel elements, HTGR, finite element analysis 2–15125
stresses in graphite fuel elements, HTGR, radiation induced creep 2–15126
structural design of nuclear reactors, criteria from high temp. material properties 2–15110
superconducting magnets, synchrotron 2–14372
superconducting weak link, microwave radiation influence on IV charact. 2–36477
syncrocyclotron, obs. of radiation levels in vicinity 2–2882
thermal radiation during ultrasonic cavitation, obs. 2–18781
thermo-luminescent characteristics of environmental substances, accident dosimetry 2–5767
track formation by charged particles in insulating materials 2–27908
transistor, characts. 2–40305
transistors, bipolar, gain degradation mechanism, neutron irradiation 2–22591
tripalavin-gelatin gel, phosphor, phosphoresc. decay kinetics, irrad. effects 2–36949
vacuum system for in-pile irradiation studies 2–41411
Zircaloy, fuel claddings and pressure tubes in water cooled reactors 2–18257
AgI-KI acetone soln., emitted smoke ice forming ability, effect of u.v. irrad. 2–22972
Al, shear modulus, effect of neutron irradiation at 4K, variation with Frenkel defects concentration 2–22278
Al grain boundaries, relaxation on neutron irradiation 2–22218
Al_2O_3-CdSe thin-film transistor, effects of ionzing radiation 2–22595
Al_2O_3 m.o.s. devices, radiation-induced trapped charge, relaxation phenomena 2–19739
As-Ge-Se, amorphous semiconductor, film, memory state optically induced reversible change 2–13256
Au-15 at.%Ag alloy, rad. damage interpretation, ordering props., elec. resist. obs. 2–36009
$BaCO_3$, Tn nuclear recoil, knock out effects, emission probability 2–25702

Physical effects of radiations continued
C, glassy, induced length changes 2—39439
CaF$_2$ crystal, F$_3^-$ centre, zero-phonon lines 2—19124
CaF$_2$ crystal diffusion of ^{133}Xe, 750-1000°C, defect trapping 2—22245
CdS:Cu, i.r. quenching of photo-Hall effect 2—33068
CdS, high field domain velocity, anode-cathode direction, i.r. irradiation 2—25815
CdS, photodesorption mechanism 2—12681
CdS thin film, ion bombardment, conductivity obs. 2—23204
^{252}Cf fission fragments, energy loss measurements in elementary gases and solids as compared with theory 2—8377
Cs$_3$Sb layers, i.r. radiation causing filling or emptying of surface traps causing reversible bending of energy bands at solid surface as explanation of photoemission current anomalies 2—36634
Cu-Be alloy changes in tensile properties during irradiation and post-irradiation ageing 2—29284
Cu, shear modulus, effect of neutron irradiation at 4K, variation with Frenkel defects concentration 2—22278
Cu$_2$O, elec. cond., illum. effects, electron trapping, photomemory effect 2—40276
Fe$_3$Al, radiation damage, computer simulation 2—39671
p-GaAs:Si, electron radiative recomb. during epitaxial growth 2—20095
onGaAs, ion implantation damage, flux dependence, investigation using ^{85}Kr channelling, Rutherford backscattering methods 2—25369
GaAs p-n junction, illumination influence, Cu diffusion 2—10085
Ge, amorphous film, reactor irrad. effect on elec. props. 2—4232
Ge, illumination effect on dislocation mobility 2—32521
Ge, light-sensitive defect form. by electron and neutron irrad. 2—12749
Ge(Li) diodes in γ-ray detector fast neutron damage 2—24092
GeTe film, semiconductor, amorphous to polycrystalline phase transition, light pulse heating 2—40256
n-InP:Cu, illuminated, l.f. current oscill. 2—22538
p-InSb, irrad. defects, cond. changes 2—6819
KBr (I), u.v. excitation, thermally stimulated cond. obs. 2—19074
KCl:Ag$^-$, C-band light irrad., absorpt. bands attributed to paired Ag$^-$ ions 2—15784
KCl:Ag$^-$. C-band light irrad., absorpt. attributed to paired Ag$^-$ cons., theory 2—19126
KCl, defect annealing, absorp. band obs. 2—36011
KH$_2$PO$_4$, structural defects, phase transitions and dielectric props. 2—1442
K$_2$ReCl$_6$, irradiated, mag. susceptibility and structure modifications 2—4344
LiF, deep electron trap props., thermoluminesc. obs. 2—29981
LiF, hardening, thermal deformation, role of entropy 2—3869
LiF, thermoluminescence efficiency 2—27894
LiF dosimetry phosphor, radiation-induced increase of thermoluminesc. sensitivity 2—13516
MgF$_2$, phys., elec., opt. props., damage obs. 2—1237
MgO, MgF$_2$ damage processes, review 2—19076
Mg$_2$SiO$_4$:Tb, OH, radio-thermoluminesc., illum. effects 2—29978
Mo, void lattice and regular arrays 2—1231
NH$_4$H$_2$PO$_4$ structural defects, phase transitions and dielectric props. 2—1442
NaBr(Cl):M^{2+}, (M=Ba, Ca, Sr), irrad. type effects on symmetry of paramagnetic centres 2—26285
NaReO$_4$, irradiated, mag. susceptibility and structure modifications 2—4344
Pt, shear modulus, effect of neutron irradiation at 4K, variation with Frenkel defects concentration 2—22278
β-Pu, length change due to self- irradiation damage, 4K 2—19080
S, electrification in darkness and under illimination 2—25914
Si:Ni diode, parameters, illumination effects 2—22586
Si, double injection and space charge currents, illumin. effects 2—22569
Si, e.p.r. detection of optically induced divacancy 2—40764
Si, surface characterization by ellipsometry 2—25187
on Si diodes, near and in avalanche breakdown 2—19710
Si npn transistors, effects of intense ionizing radiation 2—13287
p-SiC, alloyed with Pt-B-Sn, space charge limited currents, illum. effects 2—22565
Si$_3$N$_4$ film, deposition control by 2537Å rad., thickness limiting 2—39520
SiO$_2$ densification, bond polarizability, hole trapping and defect structure 2—19733
SiO$_2$ glass, sputtering yields and damage depths caused by 5.6 keV inert gas ions, energy losses 2—25713
SiO$_2$ polymorphs, irrad.-induced changes in density and molar fraction 2—18904
SiO$_2$ v.u.v. radiation charging in m.o.s. structure 2—19741
SrF$_2$ crystal, F$_3^-$ centre, zero-phonon lines 2—19124
Ta, electron irradiation, 4.5 K, study of spontaneous recombination and Frenkel defects prod. 2—22195
ThO$_2$-15% UO$_2$ pellets, possible fuel for homogeneous aqueous suspension reactor, neutron irradiation studies 2—5754
TlCl:p, luminesc., effect of i.r. irrad. 2—10430
U, Pu nuclear fuel compositions, properties before and after fast neutron irradiation 2—15112
UO$_2$, fission induced creep, instrumented capsule for meas. 2—11917
W-Re, thermocouple, reactor rad. influence on thermo-e.m.f. 2—16305
W, photon induced residual gas desorption by synchrotron radiation 2—6387
(Zn,Cd,Hg)S:Cu,In electroluminor, electrolum., radiation enhancement 2—36968
Zr-25%Nb fuel claddings and pressure tubes in water cooled reactors 2—18257

Physics
see also Biographies; History; Nuclear physics; Teaching
astronomically determined dates and geometrical alignments, tutorial article 2—11236
computer, instructional uses, and quantum scattering theory 2—2051
computer applications undergraduate course 2—37545
concept formulation and exchange of knowledge in education 2—17147
conference, Israel Physical Society, Haifa (1971 2—2048
continuum physics, mathematical background, multi author book 2—26
coronas without space charge and at static voltages 2—21891
critical phenomena, basic theoretical concepts and problems 2—7691
critical phenomena, conference, Bochum, Germany (1971) 2—7689
critical phenomena, theoretical survey 2—7690
education, engineering syllabuses at GCE A level which have attempted to unite physics and technical studies 2—37544
education in underdeveloped countries 2—2

Physics continued
history, relevance to education of physics teachers 2—37541
human mind, effective theory based on merger of physics and psychology 2—23209
inquiry aspects, emphasis rel. to teaching 2—17146
interspeciality relationships in a physics journal 2—37538
macromolecular solutions, viscoelasticity meas. 2—25015
measurement of time varying phenomena, book 2—5112
for musicians 2—4
Nuffield advanced physics course, kit of modules for electronics option 2—37547
open-ended cumulative expts. in advanced laboratory 2—14058
parametric phenomena, history and general characteristics 2—146
physicists, survey of occupation in Czechoslovakia 2—37539
solid state, materials, book 2—5110
teachers, pedagogical formation, discussion of learning process in schools 2—37542
teaching, elementary schools, aid from univ. dept. 2—27003
teaching, nonscience students, noncalculus derivation of Coulomb potential 2—27007
teaching, role for history of physics 2—37540
teaching, theory, scientific value 2—26998
teaching science to nonscience majors 2—5
teaching strategy to develop physicist's skills early 2—14057
team teaching, freshman courses 2—14061

Physics fundamentals
see also Cosmology; Elementary particles; Field theory, classical; Field theory, quantum; Indeterminacy; Mechanics; Parity; Probability; Quantum theory; Relativity; Thermodynamics; Units
causality, one-dimensional tachyon theory 2—17199
causality, test in ρ meson system using e.m. corrections to $\pi^-p\to\pi^+\pi^-n$ reaction 2—34704
constants, universal, ratios rel. to expansion 2—20465
elementary matter, electromagnetic and inertial manifestations of new theory 2—17144
elementary matter, philosophical approach and general implications of new theory 2—20794
fundamental constants, constancy with time 2—17169
hadron theory rel. to classical space-time 2—21268
optical image depth and illumination tutorial 2—17168
photon concept, short educational article 2—38222
Planck's constant determ. from Wien's displacement law 2—27005
Planck's constant expt., amplifier 2—2325
Planck radiation law, dimensional considerations in its development 2—14123
pleochroic halos, reexamination of constancy of nature 2—23210
principle of equivalence and electromagnetism 2—37833
Soviet standard of units based on SI system 2—5108
symmetry, physical laws of phenomenological type 2—26997

Physiology
see also Biological technique and instruments; Blood; Hearing; Vision
acoustical stimulus response, rel. to architectural acoustics 2—34156
animal, effect of continuous low level e.m. fields 2—5041
cardiac output, averaging computer analysis of displacement ballistocardiograms 2—23142
cell membrane resistance and polarization meas. using chopped-current clamp with single electrodes of changing resistance 2—2014
cochlea, 'place' theory of hearing 2—20748
cricothyroid activity correl. with pitch raising 2—33794
e.m. flowmeter sensitivity 2—32196
foetus, u.s. effects 2—5245
industrial noise effects on adolescents and standardization 2—26972
infrasound emission effects 2—37443
laryngeal adjustments in devoicing of vowels 2—30683
mammalian central nervous system, intense u.s. interaction 2—30668
microscope equipment for cyto- and histophotometric and spectrophotometric analyses 2—5054
microstructure of thick biological specimens and organs by contact fluorescence microscopy 2—33783
muscle response to drug, applic. of results of heat diffusion from disjoint plane domains 2—2151
musculus temporalis in basic movements of jaw, electromyographic analysis 2—41287
nervous system information processing rel. to psychophysical and electrophysiological analysis 2—7592
neural network model for residue pitch perception 2—33802
peripheral fasciculations, neurophysiological method 2—41288
psychophysiological factors due to environmental noise 2—30686
pulmonary, ^{13}N-saline solutions for research studies 2—14031
Purkinje system, dog, collision of excitation waves 2—37432
rats and rabbits, variations in arterial blood flow during electrical stimulation near the heart 2—30655
squid axons, fluorescence signals in ANS-stained axons during voltage clamp 2—30661
time perception mechanisms 2—17

Piezo-optical effects
alkali haldies, piezobirefringence in vac. u.v. 2—16470
alkaline earth fluorides, piezobirefringence in vac. u.v. 2—16470
mechanically anisotropic bodies, photoelasticity, calibration tests 2—23327
piezoreflective-magnetostrictive film transducer, patent 2—13332
BaF$_2$, piezobirefr. coeff., energy band deform. pot. 2—26167
CaF$_2$, piezobirefr. coeff., energy band deform. pot. 2—26167
CdTe, constants at 10.6 μm, room temp. 2—36827
Cu$^+$ halides, photoelastic properties, phase matching of nonlinear optical processes 2—26119
GaAs, stress effect on reststrahlen spectrum 2—33284
Ge:Zn, symmetries and deform. pot. consts. of singly ionized Zn 2—29890
Ge, illumination induced stresses, surface pot. depend. 2—10314
KCl, piezobirefr. coeff., energy band deform. pot. 2—26167
KCl, stress induced linear dichroism of Ag$^-$ and Cu$^-$ 2—33208
LiF, piezobirefr. coeff., energy band deform. pot. 2—26167
NaCl, piezobirefr. coeff., energy band deform. pot. 2—26167
NaCl, stress induced linear dichroism of Ag$^-$ and Cu$^-$ 2—33208
Ni, piezo soft X-ray effect, band struct. 2—22792
Si:Mg, excitation spectra and piezospectroscopic effects of donors 2—10338
Si, radiation-induced absorpt. bands, piezospectroscopic obs. of group V—defect complex 2—16499

Piezo-optical effects continued
SrF_2, piezobirefr. coeff., energy band deform. pot. 2—26167

Piezoelectric oscillations
annular ceramic disc with concentric electrodes, radial displacement 2—22626
ceramic rectangular plate, thickness vibrations 2—11352
flexurally oscillating rectangular plate, analogue network 2—23373
neutron diffraction, mosaic blocks 2—25317
piezo-semiconductor resonator, damping suppression by drifting electron field 2—4287
prestrained composite transducer, mechanical response 2—10126
quartz, piezogravimetric method of studying adsorption 2—32394
quartz, X-cut plates, coupled vibrs., reson. freq. temp. depend. 2—29758
quartz microbalance, temperature range expansion 2—27028
quartz vibrators, effect of neutron and X-radiation of resonance frequency and elastic properties 2—25934
quartz X-cut surface wave transducer, impulse response in Rayleigh wave system 2—5239
radially polarized ceramic rings, axisymmetric modes and electrical impedance 2—27231
semiconductor platelet, nonlinear theory 2—19419
slab, bounded on one side by viscoelastic medium 2—17377
transducers, review of definitions relating to conversion losses 2—5238
u.s. instrument, electroacoustic channel, mathematical modelling 2—25935
LiF, mech. vibrs., elec. field pulse influence 2—10128
$LiNbO_3$, Y-cut, Z-propagating surface wave, parameters determined by numerical analysis 2—5216
α-N, cryst. struct., piezoelec. reson. obs. 2—32466
ZnO, acousto-electric oscillator, effect of uniaxial stress on modes 2—4058

Piezoelectricity
see also Electrostriction; Piezoresistance
acoustic generator loaded through intermediate layer in pulse mode, natural frequency 2—27265
acoustic surface wave convolution, nonlinear material evaluation 2—19414
acoustoelectric oscillations, computer simulation 2—29540
acoustoelectric oscillator, static field distrib. effect on mode behaviour 2—6672
acoustoelectric oscillators with arbitrary static field distrib., linear theory 2—25676
acoustoelectric phenomena, nonlinear theory, amplitude saturation, oscillator applic. 2—25677
acoustoelectric transverse, surface domains, structure by linear approx. for generation threshold conditions 2—25669
actin film, oriented muscle protein 2—1577
amorphous semiconductor, resistance, in review of elec. props. 2—13215
anisotropic cryst., acoustic surface wave beam diffr. 2—9868
ceramic, surface wave scatter loss, optical measurement 2—36337
ceramic resonators, review of developments in Europe 2—40340
ceramic transducers, fund. modes 2—29519
ceramics, appl. in telecommunications 2—6887
ceramics for electronics, conf., Hradec Kralove, Czechoslovakia, (1971) 2—12977
coupling, effect on second order elastic constants of compound crystals and ceramics 2—17376
crystal volume acoustic modes interaction with conducting pseudoperiodic grating described by acoustoelectric periodic structure 2—25679
crystals, Raman studies on polar phonons 2—25649
derivation, from bulk properties 2—22627
dicalcium lead propionate, u.s. attenuation near phase transition 2—19415
diffusion layer, transducers, losses due to inactive layer on working surface 2—7753
DNA films, oriented, piezoelectric strain constants from −170 to 30°C 2—40364
dynamometer, for notched bar impact tests 2—121
elastic waveguide, coupling to volume waves 2—6658
electromechanical coupling due to charged dislocations 2—40363
electrostriction coefficients of dielectrics, measurement using method of induced induction e.m.f. 2—34277
ferroelectric memory array, response 2—40362
gas suspension flow, solid particle conc. determ. 2—28912
geodesy, applications in recorders and as standards 2—40869
interdigital acoustic surface wave grid response 2—32819
liquid crystal, nematic, piezoelec. domain formation, theory 2—6240
liquid crystals, Meyers coeffs. calc. 2—18845
long interdigital transducer, distortion of central resonance, back-piezoelec. effects 2—40361
Mandelstam-Brillouin scattering, effect of piezoelc. props. 2—26199
materials, ceramics, book 2—36597
p′-methoxybenzylidene-p,n-butylaniline, liquid crystal, bending mode of curvature electricity 2—28889
myosin film, oriented muscle protein 2—1577
nonlinear acoustical props. and elastic wave equations 2—29516
nonlinear elastic medium, surface wave vel. and second harmonic generation 2—25671
nonlinear interaction between Bleustein-Gulyaev waves in plate and adjacent semiconductor 2—32824
piezo-e.m. interaction between u.s. and nucl. spin systems 2—32825
piezoelectric polaron, energy spectrum calc. 2—13098
poly(γ-benzyl-L-glutamate), oriented films, real and imaginary components of complex strain constant in temp. range −180 to +180°C 2—22630
poly(vinyl fluoride), electret film, piezoelec. props., piezoelec., dielect., elastic consts. 2—10131
potential distrib. and tertiary pyroelec. effect 2—6886
in PVC and PVF films, induced by rolling during processing19773 2—19773
quartz, fused, surface wave vel. and second harmonic generation 2—25671
α- quartz, hysteresis phenomena in deform. 2—16296
quartz, nonlinear polarization coeffs. determ. 2—36601
quartz, surface elastic waves, surface motion obs. 2—40056
quartz, x-cut, piezoelec. current due to short duration shock wave loading 2—22629
quartz crystals, use in measuring the thickness of films during deposition 2—35881
quartz gauge, shock wave induced polarization 2—14356
Raman scattering, of polaritons for general wave vectors 2—4026
Schottky barrier diode as press. transducer 2—29719
semiconductor, acoustic amplification, associated microwave radiation power 2—36342

Piezoelectricity continued
semiconductor, acoustic two-wave interaction in alternating elec. field 2—29514
semiconductor, acoustoelec. high field domains, Fourier analysis 2—29544
semiconductor, acoustoelec. surface domains 2—29543
semiconductor, acoustoelectric parametric interactions 2—4054
semiconductor, carrier interaction with Lamb wave 2—1424
semiconductor, III-V and II-VI, effective charge and piezoelec. effect 2—36596
semiconductor, intrinsic and impurity absorpt., calc. 2—40653
semiconductor, non-normalizability of hot electron distrib. function 2—29653
semiconductor, nonlinear excitation of acoustoelec. fluctuations 2—19418
semiconductor, piezoelec. scatt. at high elec. fields, electron energy distrib. function validity 2—9988
semiconductor, plasmon-enhanced sound amplification 2—36346
semiconductor, Rayleigh wave amplification, in transverse elec. field 2—6668
semiconductor, reduced phonon noise in acoustoelec. amplifier 2—16028
semiconductor, u.s. amplification in oscillator platelets 2—19419
single crystal piezoelectric materials for surface acoustic waves 2—20933
sound propagation, relations between electromechanical coupling and elastic consts. 2—32826
strain, small homogeneous, X-ray detn. for piezoelectric consts. 2—4282
surface acoustic wave coupling in semiconductors 2—22413
surface acoustic wave nonlinearity enhancement due to charge carrier coupling 2—40051
surface acoustic waves, optical probing of internal behaviour 2—29517
surface acoustic waves 2—32821
surface elastic waves, electromech. coupling 2—29542
Teflon cable, effective piezoelec. consts., strain transducer applic. 2—25938
tourmaline, assessment as acoustic surface wave delay medium 2—40055
transducer, complex impedance meas. in operational conditions 2—23376
transducer, freq. and transient response rel. to intermediate layers and matching ccts. 2—29520
transducer, mech. loaded, vibr. patterns 2—29521
transducer, thin film, efficiency and optimum thickness 2—29525
transducer, thin film, precip. under electron bombardment 2—4046
transducer, u.s. focussing, with Gaussian vel. distrib. 2—27270
transverse surface waves, spontaneous oscillations generator 2—25680
u.s. Rayleigh waves on boundary with semicond. 2—29524
wurtzite type cryst., theory 2—36595
zincblende type cryst., theory 2—36595
$B_7O_{13}^{5-}$, temp. dependence near cubic orthorhombic phase transition temp. 2—9792
$BaTiO_3$, bias field influence on internal friction near Curie pt. 2—29244
$Ba(Ti_{0.95}Zr_{0.05})O_3$ ceramic plates, surface wave propag. characts. 2—19408
$Bi_{12}GeO_{20}$, consts. determ. by light scatt. 2—10335
$Bi_{12}GeO_{20}$, Rayleigh wave propagation 2—19412
$Bi_{12}GeO_{20}$, rel. to light scatt. by phonons 2—16454
$Bi_{12}GeO_{20}$ surface wave velocities, electromechanical coupling 2—29539
$Bi_{12}GeO_{20}$ thin plates, const. meas. 2—10127
C, amorphous film, rel. cond. mechanisms 2—13221
CdS, Bragg diffr. on surface acoustoelec. domains 2—29547
CdS, Brillouin scatt., acoustoelectric, anharmonic and resonance effects 2—26200
CdS, carrier interaction with Lamb wave 2—1424
CdS, flexural wave amplification 2—6674
CdS, off-axis acoustoelec. domains, Brillouin scatt. 2—4056
CdS, photomechanical effect, converse piezoelectric effect 2—19972
CdS, surface-wave interactions, nonlinear, acoustic convolution 2—4055
CdS, surface effect 2—36598
CdS, u.s. amplification, temp. depend. 2—29545
CdS, u.s. amplification in continuous drift field 2—29546
CdS transducer, thin film, precip. under electron bombardment 2—4046
CdS transducer, wedge-shaped, for u.s. surface waves 2—6660
CdS type crystal, effect on elastic waves 2—16295
$Co_3B_7O_{13}I$, ferroelec., coeff. meas. 2—22622
GaAs, depletion layer transduction of surface waves 2—13324
GaAs, phonon-electron interactions rel. to u.s. generation, amplification 2—4049
GaAs, u.s. rel. and attenuation in photocond. cryst., illumination depend. 2—19413
n-Ge, piezo-Hall e.m.f. 2—19684
KIO_3, phase transition, electro-optical obs. 2—33211
$LiIO_3$, dielec. behaviour, barrier layer effects 2—25936
$LiNbO_3$, acoustic correl. and convolution using nonlinear surface wave interactions 2—29548
$LiNbO_3$, ferroelec., piezoelec. leaky surface wave propagation and amplification 2—22412
$LiNbO_3$, leaky surface wave 2—29526
$LiNbO_3$, mixing of noncollinear elastic surface waves 2—9869
$LiNbO_3$, surface wave amplification 2—29527
Mn-$ZnSiO_4$, response values rel. to hydrothermal synthesis from Na_2N-ZnO-SiO_2 system 2—29087
$Pb(Mg_{1/3}Nb_{2/3})O_3$-$PbTiO_3$-$PbZrO_3$ solid solution, permittivity, mechanical Q-factor 2—13327
$PbNb_2O_6$-$BaNb_2O_6$ ceramic system, props. rel. to domain and grain struct. 2—29739
$5PbO.3GeO_2$, ferroelec. cryst., elastic, piezoelec. and dielec. constants 2—22617
$Pb_{0.95}Sr_{0.05}(Ti_{0.48}Zr_{0.52})_3$, 0.8 wt.% Cr_2O_3, paraelectric to ferroelectric phase transition effect on dielectric and piezoelectric props. 2—1576
$PbTiO_3$-$PbZrO_3$-$Pb(Zn_{1/3}Nb_{2/3})O_3$ system, ferro- and piezoelec. props. near morphotropic phase boundary 2—33058
$PbTiO_3$ ceramic, effect of additives on piezoelec. and related props. 2—36599
$PbZn_{1/3}Nb_{2/3}O_3$-$BaZn_{1/3}Nb_{2/3}O_3$-$PbTiO_3$ ternary system 2—25937
$Pb(Zr,Ti)O_3$ ceramic plate, surface elastic wave propagation characts. 2—29531
$Pb(Zr,Ti)O_3$ ceramic transducer, electromechanical coupling coeffs. 2—13326
$Pb(Zr_xTi_{1-x})O_3$, ceramic, electromech. activity, morphotropic phase boundary 2—4280
$Pb(Zr.Ti)O_3$, ceramic, mech. quality factor, impurity effects 2—13325
$Pb(Zr.Ti)O_3$ ceramic/Ge wafer layers, surface acousto-electric amplification 2—19677
SbSI, rel. to eleotrostrictive effect 2—19772

Piezoelectricity continued
Se-Te single crystal alloy, piezoelec. and elastic props. 2—36600
Se_xTe_{1-x}, single cryst., piezoresistivity 2—4216
n-Si, piezothermopower, in region of phonon drag 2—4239
$Sr(ClO_3)_2$, r.f. absorpt. during n.q.r. due to piezoelec. props., 77-200K 2—40792
ZnO, off-axis acoustoelec. domains, Brillouin scatt. 2—4056
ZnO, photon counting distrib. of Brillouin scattered light from amplified vibr. noise 2—13494
ZnO film u.s transducers for longit. and shear modes, fabrication 2—29549
ZnO films, sputtered, c-axis polarity obs. 2—6356
ZnO(S)(Se), influence on elec. field effect in e.p.r. 2—22837

Piezomagneto-optical effects *see Magneto-optical effects*

Piezoreflectance
No entries

Piezoresistance
see also Piezoelectricity
film, metal, resist. strain coeff. 2—40163
Ag films, plasma oscillation obs. 2—29893
Al films, longit. gauge factor 2—16139
CuCl, uniaxial stress effects on excitons 2—13461
Ge, Γ transitions in E_0' region 2—10348
Ge, n-type inversion layers, quantum limit piezoresist. 2—25853
n-Si, electron irrad., influence of O_2 vacancy complex (A-centre) 2—25861
Si, film, polycryst., resist. temp. coeff., gauge factor 2—10072
Si, intervalley scatt. mechanism 2—22568
Si, n-type inversion layers, quantum limit piezoresist. 2—25853
n-Si, plasma reflectivity minimum, freq. shift due to uniaxial stress 2—33244
Si, stress depend. of E'_0 refl. peak 2—16474
Si ion implanted resistor, gauge factor and temp. coeff. 2—25880
Si m.o.s. inversion layer, transport phenomena, effective mass approach 2—19744
ZnS, deformed, exciton spectra and exchange interaction 2—29902

Piles, nuclear fission *see Nuclear reactors, fission*

Pinch effect *see Discharges, electric; Plasma/confinement; Semiconducting materials*

Pions
cancer radiotherapy applications 2—41290
charge radius, possible lower and upper bounds 2—31279
charge radius calculated from sum rule for slope of pion charge form factor 2—21290
chiral symmetric pion Lagrangian, perturbation series check of Ward identity 2—23758
distribution in pp$\to\pi$ + anything reaction, incoherent droplet model 2—17920
dual, quark model 2—410
dual models with no tachyon 2—17922
dual pion-quark model, equivalence of fermions in individual models 2—17844
electromagnetic form factor, modification of ρ meson propagator by insertions of vacuum polarization tensor 2—27764
electromagnetic mass difference, chiral dynamical calc. 2—14645
e.m. form factor, information inside analyticity region provided by bounds on modulus on cut $(t \geqslant 4m^2)$ 2—34673
e.m. form factor meas. in lepton pair production cross-sections $\geqslant 40$ GeV 2—14628
e.m. form factors, calc. from finite energy sum rules 2—11609
e.m. form factors, possibility of meas. from $(\pi,\pi l^+l^-)$ reactions 2—14644
e.m. mass differences, applic of off-shell $\rho\pi$ sum rules 2—2512
energy spectrum in $K^+\to\pi^+\pi^+\pi$- decay at rest, analysis 2—11591
finity violating internucleon potential, pion exchange contributions 2—34877
form factor, electromag., investigation using dispersion relations 2—2553
form factor, examination using model describing elastic electron scattering 2—11602
form factor analyticity and e.m. radius calc. 2—27744
hard pion current algebra models, restrictions of unitarity and analyticity for pion form factor 2—34586
mass differences, rel. to virtual photon photon annihilation 2—17822
massive, constrained to be a free field if exact field-current identity is consistent with broken chiral symmetry 2—21295
mechanical form factor, behaviour rel. to dimensions of scale invariance breaking 2—21289
multiple pion exchange, statistical approach to unitarity damping 2—17921
pion model identical to Bardakci's sector of dual quark model 2—21252
pion-fermion system, embryonic dual model 2—411
radii, m.s.r., determ. based on analytical properties of form factors 2—31277
radiology, human kidney T-1 cells, RBE and OER of π^- mesons 2—37440
spatial distribution for stopping in tissue, techniques for mapping 2—11200
stopped negative pion interaction with C, obs. of emitted charged secondaries 2—35058
three-pion intermediate state, determ upper bound for contribution to imaginary part of amplitude for $K^0_L\to\mu^+\mu^-$ 2—17896
three-pion states, contribution to $K_L\to\mu^+\mu^-$ puzzle 2—31269
tumor therapy applic. stopping region visualization expts. 2—20728
two-pion system, S-matrix model applied to P-wave, ρ-meson radius determination 2—34596
$A\sigma\pi$ vertices, hard meson calc. 2—31308
π^+-π^0 mass difference, computation using gravity-modified hadron electrodynamics 2—5532
2π exchange contribution in NN potential calc. following Mandelstam representation method 2—38315
$\pi\rho\omega$ decoupling, vector dominance model and partial conservation of axial vector current 2—14643
$\sigma\pi\pi$ vertices, hard meson calc. 2—31308
CsI energy loss and range-energy relation 2—4091

decay
diffractive dissociation, natural parity exchange and Gribov-Morrison parity rule 2—404
γ-ray production, rel. to cosmic radiation 2—4782
π^0, rel. to gamma radiation from the Galaxy 2—10819
$\pi^0\to e^+e$-, upper bound to decay rate used to determ contrib. of 3π intermediate state to $K^0_L\to\mu^+\mu^-$ puzzle 2—17896
$\pi^0\to\gamma\gamma$, decay of parallel beams, kinematics 2—23843

Pions continued
decay continued
$\pi^0\to\gamma\gamma$ decay of parallel beams, kinematics 2—34674
$\pi^+\to\mu^++\nu_\mu$, determ. of ν_μ mass upper limit 2—379
$\pi^+\pi$-, coherent decays from 3-10 GeV/c K_L^0 beam in liq. H_2, proper time distrib. 2—2545

interactions
coherent prod. of 3π and 5π, 17-200 GeV, energy dependence of cross section 2—27702
dual-pion model satisfying current-algebra constraints 2—31281
multiparticle sum rules, soft-pion theorems applied to dispersion relations 2—31278
in photographic emulsion, function of energy for 20, 60 and 200 GeV 2—23934
$\gamma\pi\to\pi\pi$, amplitude, anomalous divergence of neutral axial vector current 2—31288
$\gamma\pi\to\pi\pi$, Veneziano amplitude 2—14555
$K\pi$, low energy phenomenology, review 2—38262
π-nucleus interaction, 200 GeV and 60 GeV, reaction analysis 2—23938
π-, 60 GeV/c interactions with light and heavy nuclei, investigation using standard and enriched emulsions 2—34685
π^- on emulsion nuclei, 45 and 60 GeV/c, coherent production of particles 2—23849
π-d$\to$nnγ, soft-photon cross sections 2—38298
π^+d, 5.1 and 9 GeV/c, f^0 production and decay 2—31312
π^+d, structure in f^0-mass region 2—23872
$\pi^+d\to dA_3^+\to d\pi^+\pi^+\pi$-, 13 GeV/c, nonconservation of s-channel helicity 2—2554
$\pi^+d\to\gamma pp$, radiative absorption, 290 MeV/c, determ. total cross section and differential cross section 2—414
$\pi^+d\to p_sp\pi^+\pi^-$, structure in f^0 mass region 2—21297
$\pi^+d\to pp$, non radiative absorption, 290 MeV/c, determ. total cross section and differential cross section 2—414
$\pi^+n\to K^+\Lambda$, differential cross section and polarization, model with exchange degeneracy and duality failure of Regge cut models 2—17911
$\pi^+n\to\omega p$, density matrix element meas. rel. to dip mechanism tests 2—8134
$\pi^+n\to p\pi^+\pi^-$, 7 GeV/c, $\pi\pi$ scattering studied, obs. of S-wave resonance in the f^0 mass region 2—17950
$\pi^+n\to p\pi^+\pi^-$, f^0 mass region, evidence for structure 2—31307
$\pi^-p\to\eta n$, direct channel description at high energy 2—11616
$\pi^-p\to\pi^0n$, direct channel description at high energy 2—11616
$\pi^-P\to\pi^0n$, two-pion exchange contribution 2—17929
$\pi+p\to p+A_2$, self-absorption of single peak rel. to A_2 double peaking 2—8186

interactions, pion-nucleon
10.2 GeV/sec, coeff. of inelasticity 2—2614
60 GeV, energy characts. of secondary particles 2—2612
bremsstrahlung, off-shell and structure effects discussed and calculated 2—14655
charge-exchange polarization, described by exchange of ρ-pole puls $\rho\otimes P$ Regge cut 2—413
low energy phenomenology, review 2—38262
multipion coherent interactions, very high energy 2—27702
secondary particle production at 60 GeV, comparison with particles prod. by cosmic rays 200-500 GeV 2—24027
π^- interaction with nuclear emulsion, 7.5, 17 and 60 GeV 2—11612
πN, 60 GeV, slow recoil proton 2—2613
π^-N, in nuclear emulsion, 45 and 60 GeV/c, prong number and ang. distrib. of secondary particles 2—23850
$\pi^+n\to p\pi^+\to\omega\Delta^{++}$, rel. to decisive tests for dip mechanisms 2—2508
$\pi N\to K\Lambda$, dual amplitude and strange form factors, Veneziano model 2—17930
$\pi N\to XN$, diffractive production process, Pomeron exchange study 2—31294
$\pi N\to\omega N$, at high energy, 4.19 GeV 2—5538
$\pi N\to\pi\pi N$, diffractive $\pi\pi$ scattering at 13.1 GeV/c, factorized double exchange model 2—34681
$\pi N\to\rho\Delta(1236)$, Regge pole model, threshold constraints 2—38301
$\pi N\to\rho N$, photon exchange 2—5539

interactions, pion-pion
Kang-Lee model, analysis 2—31292
low energy phenomenology, review 2—38262
S-matrix, internal symmetry propagation 2—368
$\pi\pi\to N\bar{N}$, constraints and bounds on partial waves 2—2560
$\pi^+\pi^-\to\pi^0\pi^0$ Van Hove model, explicit realization 2—2559

interactions, pion-proton
double Regge pole exchange model, applic. to 8 and 16 GeV/c reactions 2—34682
leading-particle distribution determ. universality relation shown to exist between πp and pp processes 2—11635
Pi$^+p\to\pi^+\pi^+\pi^-p$, 11.7 GeV/c, spin and parity analysis of charged 3π system in mass region of 1400-1900 MeV 2—14682
$P^\pm\pi\to\pi^0$+anything study of triple-Reggeon couplings 2—2556
$\pi^-\to\omega^0n$, determ. of ω spin density matrix elements 2—14676
$\pi^+\to X+$ anything ($X=\pi^+$, π-, K_s^0), inclusive reaction at 6 and 22 GeV/c, charged multiplicity distribs. single particle spectra 2—27755
π-p, 60 GeV/c, investigation using standard and enriched emulsions 2—34685
π-p$\to$ two charged final particles, 11.2 GeV/c, strange particle production 2—38304
π-p$\to K^+\Sigma$-, 2.75 to 10 GeV/c, differential cross sections for peripheral K^+ production 2—17905
π-p$\to K^+Y^*$- (1385) 2.75 to 10 GeV/c, differential cross sections for peripheral K^+ production 2—17905
π-p$\to$Xn, differential cross section, Pomeranchuk theorem violation 2—8151
π-p$\to\eta$n, differential cross section, Pomeranchuk theorem violation 2—8151
π-p$\to$neutral particles, total cross-section meas. for incident momenta from 250 to 1800 MeV/c 2—2555
π-p$\to\pi$-D_{13}^+, $\pi D_{13}D_{13}$ coupling constant and PCAC consistency condition 2—38302
π-p$\to\pi$-N^{+*}, s-channel helicity conservation 2—8172
π-p$\to\rho$-p, 3 to 8 GeV/c, expt. data analysis by complex angular momentum method 2—14658
π-p$\to\rho^0$n, 3 to 8 GeV/c, expt. data analysis by complex angular momentum method 2—14658

Pions continued
  interactions, pion-proton continued
    π^-p, 4 GeV/c, thermodynamical description secondary pion distribution 2—14654
    π^-p, 4 GeV/c, with strange particle production, phenomenological model 2—5541
    π^-p, $K_1^0K_1^0$ effective mass spectra, 4.0 and 5.0 GeV/c 2—11613
    $\pi^-p \to A_2^- + p, A_2^- \to \pi^-$+neutrals, near threshold, A_2 mass spectrum evidence for structure in resonance 2—5548
    $\pi^-p \to K^+\Sigma^-$, exchange cross sections, Regge cut contributions 2—406
    $\pi^-p \to K^+ + \Sigma^-$, two body process, prediction of energy dependence 2—2576
    $\pi^-p \to K^+ + Y^{*-}(1385)$ two body process, prediction of energy dependence 2—2576
    $\pi^-p \to K^{*0}\Lambda(\Sigma^0)$, 3.9 GeV/c, interpretation by simple exchange processes 2—34683
    $\pi^-p \to M^0n$, obs. of narrow neutral mesons near 950 MeV 2—23870
    $\pi^-p \to (p\pi^+\pi^-)\pi^-$, 16 GeV/c, observation of $(p\pi^+\pi^-)$ mass enhancement 2—430
    $\pi^-p \to \eta^0n$, separated function proton rich frozen target, polarized, prototype 2—5575
    $\pi^-p \to \eta n$, total cross sections constancy 2—17931
    $\pi^-p \to$missing mass+n meson mass spectrum near $X^0(958)$ studied near threshold of reaction 2—38308
    $\pi^-p \to n6\gamma$, 2.94 GeV/c, cross sections, study of $3\pi^0$ and $\pi^0\pi^0\eta$, $\eta \to 2\gamma$ systems 2—27757
    $\pi^-p \to ne^+e^-$, cross section sensitive to universality relation of coupling constraints of vector mesons 2—8100
    $\pi^-p \to nm\gamma$, $m \geqslant 3$, 2.94 GeV/c, study of π^0 and γ-quanta systems, cross sections 2—23854
    $\pi^-p \to n\varphi$, obs. of $\varphi \to \eta\gamma$ decay, branching ratio 2—17953
    $\pi^-p \to n\pi^+\pi^-$, 7 GeV/c, $\pi\pi$ scattering studied, obs. of S-wave resonance in the f^0 mass region 2—17950
    $\pi^-p \to p+(\pi^-\gamma)+m\pi^0$, possible existence of π-γ resonance at 270 MeV 2—11627
    $\pi^-p \to pd$, 5 GeV/c, differential cross section 2—23852
    $\pi^-p \to p\pi^+\pi^-\pi^-$, 13 and 20 GeV/c, A3 region of three-pion mass spectrum 2—31314
    $\pi^-p \to p\pi^+\pi^+\pi^-\pi^-\pi^-$, 7 GeV/c, single particle distributions 2—23851
    $\pi^-p \to p\pi^+\pi^+\pi^-\pi^-\pi^-\pi^0$, 7 GeV/c, single particle distributions 2—23851
    $\pi^-p \to \pi^-p\pi^+\pi^-$(16 GeV/c), factorization of diffraction dissociation amplitude 2—391
    $\pi^-p \to \pi^-\pi^-\pi^+p$, 16 GeV/c, Van Hove analysis 2—11617
    $\pi^-p \to \pi^-\pi^+n$, 4.45 GeV/c, cross sections, ρ^0 and f^0 resonance prod. 2—23855
    $\pi^-p \to \pi^-\pi^+n$, single pion prod. processes, one pion and pomeron exchange model, non dual property 2—2557
    $\pi^-p \to \pi^-\pi^+n$, single pion prod. processes, one pion and pomeron exchange model, non dual property 2—2557
    $\pi^-p \to \pi^0(\eta)n$ charge exchange, universality and complex Regge pole factorization 2—21264
    $\pi^-p \to \pi^0n$, high energy, described by exchange of ρ-pole plus $\rho \otimes P$ Regge 2—413
    $\pi^-p \to \pi^0n$, origin of zeros in ρ-Regge residues 2—8173
    $\pi^-p \to \pi^0n$, separated function proton rich frozen target, polarized, prototype 2—5575
    $\pi^-p \to \pi^+\pi^-X^0$, 15 GeV/c, $\pi^+\pi^-$ scatt. study via Chew Low extrapolation 2—31291
    $\pi^-p \to \pi^+\pi^-n$, 15 GeV/c, ρ-ω interference effects and $\omega \to 2\pi$ branching ratio 2—27756
    $\pi^-p \to \pi^+\pi^-n$, e.m. corrections rel. to causality test in ρ meson system 2—34704
    $\pi^-p \to \pi\pi N$, reactions in c.m. energy range 1400-2000 MeV, meas. cross sections and angular distribution 2—14657
    $\pi^-p \to \rho^-p$, Reggeon-particle spin couplings in Feynman-diagram models of Reggeization 2—14589
    π^+p, 3.5 GeV/c, study of four prong events and quasi two body reactions 2—31289
    π^+p, 5.45 GeV/c, $\Delta^{++}\eta$ and $\Delta^{++}x^0$ production, and η-x^0 mixing 2—31290
    π^+p, at 5.45 GeV/c, A_2^+ production 2—17955
    π^+p, strange particle production in c.m. energy range 1820 to 2090 MeV 2—11615
    π^+p 15-60 GeV/c., total cross sections meas. 2—5556
    π^+p bremsstrahlung, calc. of photon angular distributions and cross sections using soft photon theorem 2—14655
    π^+p inclusive reactions at 8 and 16 GeV/c, with exotic and non-exotic particle combinations, limiting properties 2—11614
    π^+p six prong interactions, at 8 GeV/c, determ. single particle distributions, cross section for production of mesons and meson resonances 2—17934
    $\pi^+p \to \Delta^{++}K^+K^-$, 7 GeV/c, analysis of observed anomaly in $\pi\pi$ s-wave scattering near $K\bar{K}$ threshold 2—23865
    $\pi^+p \to \Delta^{++}\omega^0$, 5.45 GeV/c, study of final states prod. 2—5542
    $\pi^+p \to \Delta^{++}\pi^+\pi^-$, 7 GeV/c, analysis of observed anomaly in $\pi\pi$ s-wave scattering near $K\bar{K}$ threshold 2—23865
    $\pi^+p \to \Delta^{++}\pi^+\pi^-$, study of ρ—ω interference and exchange degeneracy at 5.45 GeV/c 2—5540
    $\pi^+p \to \Delta^{++}\pi^+\pi^-\pi^0$, study of ρ—ω interference and exchange degeneracy at 5.45 GeV/c 2—5540
    $\pi^+p \to \Delta^{++}\rho^0$, 5.45 GeV/c, study of final states prod. 2—5542
    $\pi^+p \to K^+\Sigma^+$, between 3.5 and 14 GeV/c, meas. differential cross section and polarization 2—17933
    $\pi^+p \to K^+\Sigma^+$, polarization of resisting sigma meas. at 1.11 GeV/c 2—38305
    $\pi^+p \to K^+Y^{*+}(1385)$, between 3.5 and 14 GeV/c meas. differential cross section and polarization 2—17933
    $\pi^+p \to \Sigma^+K^+$, 1.28 and 1.41 GeV/c, additional data, charge independence test 2—2558
    $\pi^+p \to (p\pi^+\pi^-)\pi^+$, 8 and 16 GeV/c, observation of $(p\pi^+\pi^-)$ mass enhancement 2—430
    $\pi^+p \to \omega\Delta^{++}$, density matrix element meas. rel. to dip mechanism tests 2—8134
    $\pi^+p \to pA_3^+ \to p\pi^+\pi^+\pi$-, 13 GeV/c, non-conservation of s-channel helicity 2—2554
    $\pi^+p \to p\pi^+\pi^0$, multibody final states, analysis using prism plot 2—2507
    $\pi^+p \to p\rho^+$ backward reaction, as test of Regge dip mechanism 2—17885
    $\pi^+p \to \pi^+p\pi^+\pi$-, at 11.7 GeV/c, longitudinal phase space analysis, comparison with $\pi^\pm p \to \pi^\pm\pi^+\pi$-p at same energy 2—21292
    $\pi^+p \to \pi^+\pi^0p$, 13.1 GeV/c, study of Δ^{++} production and decay angular distributions 2—14713
    $\pi^+p \to \pi^+\pi^+\pi$-p, 16 GeV/c, Van Hove analysis 2—11617
    $\pi^+p \to \rho^0\Delta^{++}$, applic. of electric Born model 2—17927

Pions continued
  interactions, pion-proton continued
    $\pi^+p \to \rho^+p$, Reggeon-particle spin couplings in Feynman-diagram models of Reggeization 2—14589
    $\pi^\pm p$, scaling of high energy total cross sections, angular momentum cuts 2—8197
    $\pi^\pm p \to \pi$-π-+anything, two particle inclusive reactions, 18.5 GeV/c dependence of correlation functions on rapidities of final state particles 2—23853
    $\pi^\pm p \to \pi(N\pi)$, dominance of isospin zero exchange at 16 GeV/c and production of a low mass $(N\pi)$ enhancement 2—34684
    $\pi p \to n\pi N$ absorption model 2—38303
    $\pi p \to \pi^0n$, differential cross section, Pomeranchuk theorem violation 2—8151
    $\pi p \to \pi N^*$, diffractive production of isobars, quark model with quark spin flip 2—23813
    $\pi p \to \rho N$, 6 GeV/c, study of ω exchange isolated in the reactions 2—14677
    $\pi p \to$soft π^0+anything, soft pion theorems consequences 2—14588
    $\pi^\pm\rho$, 5 GeV/c, comparison of A_1-A_2 interference 2—17932
  production
    $\pi^+p \to \pi^+\pi^+\pi^-p$, 16 GeV/c, Van Hove analysis 2—11617
    boson-nucleon collisions, spectra and distributions in unitarized model of quasi-two-body contributions 2—23844
    coherent, 3 pions, by action of π^- mesons on C nuclei 2—11610
    coherent diffraction generation by protons on photoemulsion nuclei 2—23848
    coherent prod. of 3π and 5π from pions, 17-200 GeV, energy dependence of cross section 2—27702
    coherent reactions of 67 GeV/c protons in nuclear emulsion, cross section for production of particles 2—38321
    cosmic ray muon photo nuclear interaction at $3 \div 50$ GeV 2—23935
    cosmological mechanism for production near Friedmann type singularity 2—26598
    deep inelastic scattering, electrons and neutrinos on nucleons, current algebra 2—412
    distribution in $\gamma p \to \pi$+anything, nova model 2—17819
    double pion photoproduction off protons below 1 GeV 2—23845
    double-pion photoproduction, effective Lagrangian model 2—34676
    electron production, threshold cross section, axial form factor 2—11633
    electroproduction, polarized electrons on polarized protons, reaction cross-section 2—14651
    electroproduction, refined vector meson dominance analysis 2—11629
    electroproduction amplitude, determ. by current algebra 2—5535
    electroproduction cross sections, e^+e^- annihilation, 1.4-2.4 GeV 2—31206
    electroproduction in deep inelastic region, means of meas. dimension of chiral symmetry breaking 2—14647
    electroproduction in low energy resonance region, form factors and ang. distribs. 2—31287
    electroproduction in nucleon, phenomenological chiral Lagrangian model 2—31280
    electroproduction near threshold, axial nucleon form factor 2—5537
    electroproduction on protons, determ. values of axial-vector nucleon form factor 2—11611
    elementary particle collisions, kinematical region, scaling law 2—2506
    forward photoproduction off nucleons, Regge models 2—17925
    in hadron collisions, investigation of pion distribution 2—27761
    high energy reactions, inclusive and exclusive, producing large nos. of particles 2—27723
    high multiplicity interactions, p_t and p_l distributions 2—34625
    inclusive particle producing reaction, strong exchange process thermodynamic model 2—27724
    inclusive spectra and baryon exchange in single pion production processes 2—38297
    inclusive spectra reproduced in model calc. which emphasizes diffractive excitation of target or projectile 2—11605
    isospin analysis with emphasis on separation of Pomeron exchange 2—14652
    large angle pair prod., high energy collision of electron and positron beams 2—14573
    meson-nucleon collisions, pion spectra in diffractive model 2—31284
    multipion prod in $\bar{p}p$ non annihilation reactions of 6.94 GeV/c cross sections 2—5552
    multiplicities of pion production, distributions found 2—2536
    one pion prod. processes, turnover points, statistical treatment 2—14646
    photo and electroprod. on nucleons, multipole analysis by current algebra commutators 2—34680
    photoproduction, at high energies 2—5534
    photoproduction, high-energy, s-channel dominance and charge ratios 2—8168
    photoproduction, in first resonance region, dispersion relations and isotensor e.m. current 2—8166
    photoproduction, inelastic backward scattering and $O_{3,1}$ symmetry 2—31275
    photoproduction, low energy, chiral transformation property of e.m. current 2—8169
    photoproduction, polarization parameters, target asymmetry 2—34675
    photoproduction, presence of exotic currents in model 2—34678
    photoproduction, Regge pole model including kinematic cuts study 2—23846
    photoproduction, rel. to ρ meson production, vector meson dominance model 2—8188
    photoproduction, rel. to vector meson production, vector meson dominance model 2—8184
    photoproduction, unpolarized and linearly polarized photons, 4 to 18 GeV 2—11606
    photoproduction and electroproduction, conference 2—31258
    photoproduction from nuclei at high energy, effect of two body correlations 2—31520
    photoproduction in $\Delta(1230)$ resonance region, multipole amplitudes 2—31286
    photoproduction near first resonance, isotensor terms and T violation 2—11607
    photoproduction off nucleons, sum rule determination from dispersion relations 2—17924
    photoproduction on nuclei with nucleon emission 2—8323
    photoproduction on nucleons in first resonance region 2—31285
    photoproduction on protons of multiple particles, s channel resonance region, cross sections 2—34679
    pionization, multiperipheral and polyperipheral approaches 2—11604

Pions continued
  production continued
    proton interactions in Fe in accelerator cave, charged pion albedo spectra 2—24222
    single particle distribs. from $\bar{p}p$ annihilation at 2.32 GeV/c 2—27743
    soft pion emission, forbidden at asymptotic energy, operator droplet model study 2—5531
    soft-pion theorems rel. to direct nuclear reactions 2—24199
    threshold π electroproduction at transferred 4 momenta squared up to 10.4 F^{-2}, form factors 2—27750
    $ee\to ee+3\pi$, total cross section calc. using model incorporating gauge invariance and PCAC 2—21246
    eN interactions, threshold, low-energy theorems 2—14649
    γd, multipion photoproduction at energies up to 5 GeV, partial cross sections meas. 2—27749
    $\gamma\gamma\to\pi\pi$, virtual photon interaction, analysis 2—34599
    γN, photoproduction, construction of non minimal currents in chiral Lagrangians 2—14648
    γN interactions, threshold, low-energy theorems 2—14649
    $\gamma N\to\Delta V^0\pi$, method for experimental study of energy dependence of $V^0\pi$ scattering amplitudes proposed 2—17935
    $\gamma p\to\pi^0 p$, calc. of phase of forward amplitude using modulus dispersion relations 2—34723
    K/π ratio, angular behaviour at high energy in multi-Regge model 2—17904
    $K\to 2\pi$, contribution of isospin-violating nonelectromagnetic term 2—11597
    $K\to 3\pi$, contribution of isospin-violating nonelectromagnetic term 2—11597
    $N\bar{N}\to\pi\pi$ amplitude obtained by analytic continuation of the low energy πN scatt. amplitude 2—38315
    p-Be collisions, 12.4 GeV/c, π^+ and π- production 2—11825
    $Pi^+p\to\pi^+\pi^+\pi^-p$, 11.7 GeV/c, spin and parity analysis of charged 3π system in mass region of 1400-1900 MeV 2—14682
    pn collisions at 7.0 GeV/c, isospin analysis of single pion production 2—27748
    $\bar{p}n$ interactions in flight, odd-even ratio for pionic annihilation 2—5559
    $pn\to\pi^+\pi$-π-, comparison of analyses by rising-shift model and Veneziano model 2—34730
    pp, structure of inclusive pion spectrum near x=0 at energies of CERN intersecting storage rings 2—5545
    $\bar{p}p$ annihilation at 7 GeV/c, investigation of pion multiplicity distribution 2—27745
    pp collisions, 28.5 to 10^3 GeV/c, inclusive pion spectrum properties 2—17963
    pp collisions at 7.0 GeV/c, isospin analysis of single pion production 2—27748
    pp inelastic collisions up to 700 GeV, prong distribs. 2—34725
    pp interactions, 12, 24 GeV/c, meas. of $\pi^+\pi^-$ distrib., evidence for pionization 2—38296
    pp interactions, π and K spectra, empirical formula 2—21303
    $pp\to\pi^\pm$+anything, pion distributions near kinematical boundary, Deck effect description 2—2575
    $pp\to\pi$+(anything), very high energies, small K/π ratio shown to be due to difference in longitudinal mass 2—23837
    π- photoproduction, parametrization, complex Regge poles 2—11608
    π electroprod. on protons, ang. dependence of cross section 2—31202
    π^-, in interactions of relativistic deuterons with nuclei 2—21288
    π^- electroprod. on neutron in threshold region 2—5536
    π^- from 11.8 GeV/c K^+p, isotropic reaction obeying Bose Einstein distribution, temperature of hadronic matter 2—5544
    π^- photoproduction, Glauber and symmetrization corrections to data from single arm spectrometer experiments 2—34677
    π^0, cross section for $^1H(p,p\pi^0)^1H$ at 600 MeV 2—17923
    π^0, electroproduction, in first resonance region at momentum transfer of 0.3, 0.45, 0.60 and 0.76 $(GeV/c)^2$ 2—5533
    π^0, photoproduction on nucleons, effect of ω and ρ complex Regge poles 2—27752
    π^0 electroproduction, backward, coincidence meas. 2—8167
    π^0 electroproduction on protons, recoil proton polarization 2—27751
    π^0 multiplicities for scattering processes, bounds from isospin invariance 2—27746
    π^0 photoproduction at 4 GeV, meas. of polarized target asymmetry in 0.25-1.05 $(GeV/c)^2$ range 2—34768
    π^0 photoproduction on protons, recoil proton polarization 2—27751
    π^+, electroprod, deep inelastic region, general survey 2—8117
    π^+, electroprod near w=2 GeV, form factor determ. 2—17926
    π^+, π- produced in inclusive π^+p reactions, distributions in Feynman variable compared at 8 and 16 GeV/c 2—11614
    π^+ electroproduction, vector meson dominance model 2—17928
    π^+ electroproduction, vector meson dominance predictions 2—27747
    π^+ from 11.8 GeV/C K^+p isotropic reaction obeying Bose Einstein distribution, temperature of hadronic matter 2—5544
    π^+ photoproduction, parametrization, complex Regge poles 2—11608
    π^+ photoproduction from ^{16}O 2—35011
    π^+ production in $^2H(p,\pi^+)^3H$, $^3He(p,\pi^+)^4He$, and $^4He(p,\pi^+)^5He$ reactions 2—35030
    π^+ yield from 70 GeV p interaction obs. 2—5555
    $\pi^\pm$, inclusive single particle spectra in pp collisions, triple Regge limit, 14-70 GeV/c 2—27773
    $\pi^\pm$, photoprod. from complex nuclei, 2 and 3 GeV 2—31283
    $\pi\to 3\pi,\pi\to 5\pi$ coherent processes on nuclei, rise of total cross-section 2—14653
    π^o photoproduction from H at 4 GeV, polarized target asymmetry 2—23847
    π^o electroproduction in second resonance region, determ. of virtual photoproduction differential cross sections 2—31282
    π^-A, A=nuclei from Be to Pb, determ. of unstable boson nucleon total cross sections 2—420
    $\pi^\pm\Delta$ electroproduction in electric Born model 2—17927
    $\pi\Delta(1236)$ electroprod, prediction within framework of vector meson dominance model 2—11603
    π-$p\to\pi$-π-π^+p, 16 GeV/c, Van Hove analysis 2—11617
    $\pi^+\pi$-, from proton-antiproton annihilation from 700 to 1100 MeV/c, determ. diffr. cross sections 2—14700
    $\pi^+\pi^-$, by e^+e^- annihilation in ρ energy range with Orsay storage ring 2—38241
    $\pi^+\pi^-$ from π^+p reaction, 7 GeV/c, analysis of observed anomaly in $\pi\pi$ s-wave scattering near $K\bar{K}$ threshold 2—23865

Pions continued
  production continued
    $\pi^+\pi^-$ photoproduction, diffraction- dissociation model for high energy ρ production, comparison with empirical data 2—23875
    $\Sigma(1385)\pi$ production near $\Lambda(1520)$ resonance from K^-p reaction, analysis by partial waves and moments 2—17981
    $^{27}Al(\gamma,\pi^+)^{27}Mg$ threshold to 1200 MeV, π production cross-section meas. 2—5682
    $^{11}B(\gamma.\pi^-)^{11}C$ threshold to 1200 MeV, π production cross-section meas. 2—5682
    π^+ photoproduction from ^{16}O 2—35010
  scattering
    amplitudes construction from experimental data and analyticity 2—2509
    Compton scattering, model formulation on basis of Regge poles and scale invariance 2—11609
    dual-resonance model for any target, set of constraints 2—21291
    generalized Veneziano model, for pion scattering off isovector currents and scaling limit 2—31276
    normalization factor for one pion distrib. function 2—8165
    $(K\pi)$ S-scattering, effective range approx. in sum rules for K_{l3} form factors 2—38286
    $\gamma\pi$, off-shell $\rho\pi$ summ rules, applic. to π and K e.m. mass differences 2—2512
    $K\pi$, K_{l3} divergence form factor and Pade approximations 2—23833
    $K\pi$, T=3/2 elastic scatt. cross section using Durr-Pilkuhn form factor 2—14640
    $\Lambda\pi$, pomeron coupling 2—17980
    $p\pi^+\pi^-$, low mass system prod. in 16 GeV/c pp interactions, helicity conservation study 2—5551
    πd, importance of off-energy-shell scatt. and Fermi motion 2—8170
    πd, low energy Faddeev equations 2—38300
    πd high-energy elastic, deuteron spin alignment as test for double scattering contributions in Glauber theory 2—14714
    $\pi^+d\to\pi^0pp$, charge exchange, 290 MeV/c, determ. total cross section and differential cross section 2—414
    $\pi^+d\to\pi^+d$, elastic, 290 MeV/c, determ. total cross section and differential cross section 2—414
    $\pi^+d\to\pi^+pn$, inelastic, 290 MeV/c, determ. total cross section and differential cross section 2—414
    $\pi\Delta$ charge exchange, dual approach to Regge dips 2—399
    $\pi\gamma$ elastic, kinematical singularities in matrix decomposition 2—38185
    πK, backward, possible difficulties with u-channel exchange degeneracy 2—34686
    πK, dual resonance model with exotic resonances 2—31295
    πK, low energy, K-matrix model 2—27754
    πK, unitarity sum rule, one term Veneziano model 2—2561
    πK scatt., low energy, consequences of broken $SU(3)\otimes SU(3)$ 2—14650
    $\pi\Lambda$, $\pi\Sigma$, implications of finite energy sum rules 2—8171
    πN, dual relativistic quark model, low energy aspects 2—17945
    πN, low energy, direct expression for σ term 2—2563
    πN sigma term, determ. from pion nucleus scattering 2—14993
    $\pi^-n\to n\pi^-$, elastic backward scatt., 23 and 40 GeV/c, differential cross sections 2—27753
    $\pi\pi$, dual relativistic quark model, low energy aspects 2—17945
    $\pi\Xi$ backward, possible difficulties with u-channel exchange degeneracy 2—34686
    $V^0\pi$ elastic-scattering amplitudes, method for experimental study of energy dependence in vector-dominance model 2—17935
    π^-d, backward elastic scattering, obs. of energy-dependent structure between 496 and 1050 MeV/c 2—11618
  scattering, pion-nucleon
    3-3 resonance, basic parameters 2—34690
    σ term, estimation from off mass shell Veneziano type amplitude 2—34687
    σ term calculation, model dependence 2—38306
    absorptive and complex-Regge-pole models, possible relation 2—17871
    amplitudes and polarization parameters 2—23858
    backward differential cross-section, t-channel contributions 2—14656
    charge exchange scattering, considering Virasoro model 2—14660
    charge-exchange, polarization and sum rules in complex-Regge pole model 2—14662
    coupling constant determ. by analytic extrapolation 2—415
    cross section, Pomeranchuk theorem violation 2—8151
    current algebra model, S-wave and P-wave scatt. lengths, low energy 2—23857
    current-algebra constraints on on-mass-shell amplitudes and Adler-Weisberger theorem 2—14661
    dual relativistic quark model, high-energy aspects 2—27731
    elastic, kinematical singularities in matrix decomposition 2—38185
    finite energy sum rules on hyperbolas 2—17936
    fixed pole effects, Regge parametrization based on very strong exchange degeneracy 2—31293
    forward scattering, high energy phenomenology, Regge pole models tested 2—23859
    helicity conservation from polarization data alone 2—11620
    invariant amplitude at low energy, critical test of models 2—34688
    isospin bounds for backward amplitude, saturation 2—23861
    non-flip ρ exchange, cut correction generation 2—27758
    nonanalytic behaviour of Σ term 2—14663
    nucleon σ commutator derivation, interpretation via chiral symmetry breaking interaction 2—428
    operator droplet model treatment, calc. diff. cross section, polarization and spin rotation parameters 2—14659
    peripherality, from absorbed Reggeon exchange model 2—23862
    phase shift, p_{11}, rel. to evaluation of nucleon e.m. form factors 2—38311
    phase shift analyses, application of subtracted fixed-t dispersion relations 2—11619
    phase-shift analysis 2—34689
    polarization in backward elastic scattering at high-energy, meas. at low cross sections 2—34691
    relativistic optical model, pions in 2-5 BeV/c range, determ. cross sections 2—23856
    scattering amplitude, zero locations 2—8174
    short range potential, Reggeization using Veneziano amplitude 2—8175
    Veneziano representation, construction from isospin degeneracy patterns 2—23860
    $\pi N\to\omega N$, dual structure in scattering amplitude 2—2562
    $\pi N\to\pi N^*(I=^1/_2)$, inelastic process, differential cross sections, Pomeron exchange study 2—31294
    $\pi N\to\pi' N'$, s-channel anal. in a scheme of higher baryon couplings 2—17937

Pions continued
- **scattering, pion-pion**
  - amplitude construction, inelastic unitarity constraints and crossing symmetry, total cross sections 2—34695
  - amplitude unitarization, current algebra beyond tree approx. 2—419
  - continuous-moment sum rule analysis, possible violation of exchange degeneracy 2—11621
  - diffractive, in $\pi N \to \pi\pi N$ interaction at 13.1 GeV/c, factorized double exchange model 2—34681
  - dual N-spin amplitude 2—34696
  - dual relativistic quark model, high-energy aspects 2—27731
  - dual resonance model, chirality, generalization of Lovelace Shapiro formula 2—8178
  - dual resonance model with exotic resonances 2—31295
  - electromagnetic form factor by dispersion relations 2—8180
  - length anal., based on sigma commutator 2—17944
  - lengths, crossing symmetry restrictions on dispersion relations rel. to sum rules 2—416
  - low energy, application of axiomatic field theory, construction of S, P, and D-wave models 2—11622
  - low energy models to satisfy exact results of axiomatic field theory 2—5543
  - low energy scattering and Veneziano model with subtraction constant, simple model proposed 2—31296
  - off-mass-shell continuation in ABFST multiperipheral model, $\pi\pi$ scattering considered 2—17870
  - P wave, exchange forces determ., N/D solutions 2—31299
  - partial waves, Veneziano and physical, asymptotic behaviour and complex zeros 2—417
  - phase shift, influence of asymptotic behaviour on decreasing properties of isovector nucleon form factors 2—27769
  - phase shift and length, energy dependence from K_{e4} decay study 2—31264
  - phase shifts calc. by means of Roskies' crossing constraints 2—2567
  - S and P waves, improvement of some rigorous inequalities 2—17946
  - S-wave scattering, phase shifts in effective-potential model 2—14669
  - S-wave scattering, simple solvable neutral model 2—2568
  - s-wave scattering amplitude near 980 MeV determ. from $\pi^+p \to \Delta^{++}\pi^+\pi^-$ and $\Delta^{++}K^+K^-$ at 7 GeV 2—23865
  - Shirkov eqns., modification to remove divergences 2—27760
  - triple-pomeron vertex at t=0, indirect calc. 2—14609
  - unitarized Veneziano model, search for complex poles 2—14668
  - unitarized Veneziano partial wave amplitudes, unique solution of dispersion relations found 2—14666
  - Veneziano amplitudes, applic. of inverse amplitude (K-matrix) method for unitarization 2—398
  - Veneziano amplitudes, K-matrix unitarization, positivity and crossing symmetry constraints 2—14670
  - Veneziano model, normalization using a multiperipheral model with π, K and ω exchange 2—38299
  - Veneziano partial waves, with essential singularities, dispersive approximations 2—418
  - f^0 mass region, observation of S-wave resonance 2—17950
  - $\pi^-\pi^+$, elastic, cross sections, 0.28-1.5 GeV/c from $\pi^-p \to \pi^-\pi^+n$ reaction 2—23855
  - $\pi^0\pi^0$, general crossing symmetric amplitude, analysis of 'best' positivity and analyticity inequalities 2—14667
  - $\pi^+\pi$- ang. distrib. at 980 MeV, anomalous behaviour of $\langle Y_1{}^0 \rangle$ moment 2—31297
  - $\pi^+\pi^-$, in $\pi^-p \to \pi^+\pi^-X^0$ at 15 GeV/c, Chew Low extrapolation 2—31291
  - $\pi^0\pi^0$, constraints on *s*-wave amplitude 2—8179
- **scattering, pion-proton**
  - cross section difference between π^+p and π-p charge exchange scattering, Regge pole-cut model 2—34693
  - polarization meas. in backward elastic scattering at 6 GeV/c, effect of signal-to-background ratio 2—34691
  - $\pi^\mp p$ forward elastic scattering, 6-17.5 GeV/c, trends in polarization data 2—34726
  - π-p elastic data exclusion in calculating multiplicities, role of diffractive contributions 2—2535
  - π^-p, charge exchange, s-channel anal. in a scheme of higher baryon couplings 2—17937
  - π^-p, comparison of on- and off-mass-shell elastic and inelastic scatt., one-pion-exchange dominance 2—34692
  - π^-p charge-exchange scattering, polarization and differential cross section at large angles 2—14665
  - π^-p elastic and charge exchange data at 5GeV/c fitted by geometric s-channel model 2—17940
  - π^-p elastic scattering, 865 to 2732 MeV/c, polarization distributions and differential cross section 2—23864
  - $\pi^-p \to \pi^-p$, coupled channel process, Coulomb corrections calc. using S-matrix theory 2—2564
  - $\pi^-p \to \pi^0n$, 20-50 GeV/c, charge exchange scattering, cross section data 2—17939
  - $\pi^-p \to \pi^0n$, coupled channel process, Coulomb corrections calc. using S-matrix theory 2—2564
  - $\pi^-p \to \pi^0n$ charge-exchange above 5 GeV, structure of absorptive Regge cuts 2—17943
  - $\pi^-p \to \pi^0n$ differential cross section in wide-angle region, ρ trajectory 2—17942
  - π^+p, elastic, differential cross section calc. from impact parameters 2—8177
  - π^+p elastic and charge exchange data at 5 GeV/c fitted by geometric s-channel model 2—17940
  - π^+p elastic scatt., differential cross sections between 0.6 and 0.8 GeV/c 2—17938
  - π^+p elastic scattering from 2.74-4.0 GeV/c at all angles, analysis in terms of s-channel helicity amplitudes 2—14664
  - $\pi^+p \to \Sigma^+K^+$, intermediate energies, meas. of the polarization parameter in backward scattering on polarized target 2—34694
  - $\pi^+p \to p\pi^+$, intermediate energies, meas. of the polarization parameter in backward scattering on polarized target 2—34694
  - $\pi^\pm p$, determ. of dip structure of differential cross section from phase behaviour of scattering amplitude 2—2566
  - $\pi^\pm p$, dispersion relation calc. of scattering amplitudes 2—17941
  - $\pi^\pm p$, elastic, dual absorption model comparison with pp, $\bar{p}p$ and $K^\pm p$ elastic scattering near 8 and 16 GeV/c 2—34724
  - $\pi^\pm p$, elastic scatt. amplitudes 2—8176
  - $\pi^\pm p$, high energy total and differential cross sections using shielded fixed Pomeranchon model 2—23863
  - $\pi^\pm p$, large angle, 5 GeV/c, differential cross section 2—31298

Pions continued
- **scattering, pion-proton** continued
  - $\pi^\pm p$ elastic scatt., 180°, 0.60-1.60 GeV/c, differential cross section 2—27759
  - $\pi^\pm p \to \pi^\pm p$, s-channel anal. in a scheme of higher baryon couplings 2—17937
  - $\pi p \to \pi\Delta$, study of dip at $t \simeq o$ for high s, upper limit of quark mass. 2—17866
  - $\pi^\pm p$, upper bounds on elastic cross section differences 2—2565

Pitch detection *see Acoustical measurement; Hearing*

Plages *see Sun*

Planetary atmospheres
- barotropic boundary layer, exchange coeffs., vertical profiles 2—4989
- circulation, similarity theory relations from hydrothermodynamic equations 2—1986
- composition, miniature Mattauch-Herzog mass for rockets 2—566
- composition and structure, review 2—26829
- Cytherean, circulation problems 2—4990
- Cytherean, interpretation of CO_2 band and H_2O line 2—33747
- cytherean, O I and H I emission from upper atmosphere 2—11011
- Cytherean, occurrence of $FeCl_2.2H_2O$ particles in clouds 2—26859
- Cytherean, presence of $FeCl_2$ in clouds 2—26860
- Cytherean, upper, retrograde motion 2—26856
- Cytherean topside ionosphere, existence of thermal protons 2—17143
- Cytherian, numerical modelling of radiative convective heat transfer 2—26857
- Cytherian, radiative heat transfer below clouds 2—26858
- Cytherlan cloud tops, chemical composition, aqueous HCl 2—11012
- Earth, nonstationary problem in boundary layer 2—26827
- exospheric temperature variations rel. to solar cycle 2—7520
- inhomogeneous, technique for calc. line profiles 2—20677
- Io, occultation of β Sco, photoelectric obs. 2—26835
- Jovian, absorption coeff and brightness temp. calc. in 6-14 micron range 2—26837
- Jovian, circulation problems 2—4990
- Jovian, H/He ratio, calc. from obs. of occultation of β Sco 2—7523
- Jovian, optical properties and structure 2—7522
- Jovian, scale height from occultation of β scorpii 2—26834
- Jovian, vertical shear at visible cloud level 2—30555
- Jovian and other gaseous systems, dynamic aspects 2—26833
- Jovian ionosphere model 2—30545
- Jupiter, decametric L burst, long baseline analysis 2—37355
- Jupiter, implications of GeH_4 i.r. absorption spectra 2—12128
- Jupiter, inhomogeneous models 2—26831
- Jupiter, isodensity maps of planet in 1968 and Great Red Spot (1968-70) 2—13998
- Jupiter, occultation curves of β Scorpii 2—4963
- Jupiter, solar-composition, from observations of β Sco occultations 2—4966
- Jupiter, u.v. photometric observation of occultation of β Scorpii 2—4964
- Jupiter's satellite, Io, atmos. density upper limit from light curve during occultation of β Scorpii C 2—4968
- Jupiter's satellite, Io, atmos. density upper limit from light curve during occultation of β Scorpii C 2—4971
- Jupiter's satellite, Io, upper limit for surface pressure of various possible atmospheric compositions 2—4970
- laboratory investigation of CO_2 infrared spectral absorption line broadening at 207 and 298 K 2—18406
- light scattering, effect of absorption 2—1987
- Mars, atmospheric features, two-dimensional digital vidicon photometry 2—30560
- Mars, atomic carbon by photodissociation of CO and CO_2 2—11004
- Mars, chemical composition, pressure and thickness, cosmic and terrestrial obs. 2—26842
- Mars, CO in CO_2 atmosphere, strength of rotational lines in R branch, det. at 298, 202 and 132 K, and of self and CO_2 broadening 2—31788
- Mars, F_2 region, electron collision freq. 2—17037
- Mars, history and development of its atmosphere, organic synthesis 2—7532
- Mars, Mariner 9 i.r. spectroscopy experiment, water vapour and dust 2—37359
- Mars, Mariner 9 science experiments, resume 2—37365
- Mars, O_2 search using high dispersion spectroscopy 2—7526
- Mars, occultation experiment, Mariner 9 S-band 2—37362
- Mars, wind regimes, topographic maps 2—7531
- Mars and Venus, rate constants for $CO_2{}^+$+H and CO_2+H^+, measurements in flowing afterglow system 2—17038
- Mars exosphere, H Lyman-α u.v. spectra, photodissociation of water vapour 2—13997
- Mars i.r. radiometry, Mariner 9 of experiment 2—37360
- Mars study of evolution 2—41194
- Mars u.v. spectrometry, Mariner 9 experiment 2—37361
- Martian, circulation problems 2—4990
- Martian, data obtained by Mariner 4, 6 and 7, review 2—30566
- Martian, effects of large scale temp. advection, model 2—26843
- Martian, proposed detection and mapping of water vapour during Viking Mission 2—30564
- Martian, proposed expt. for mass spectrometric anal. of organic constituents and water content, Viking Mission 2—30568
- Martian, Viking Mission, proposed anal. of data from radar and radio systems 2—33740
- Martian, Viking Mission, proposed meteorological expts. 2—30573
- Martian clouds, mapping from 1969 photographs 2—4976
- Martian dust storm, CO_2 absorption spectra 2—37364
- Martian polar cap surface, photometric function and roughness 2—26844
- Martian south polar cap, identiciation of carbon dioxide frost 2—14001
- Neptune, thermal opacity due to methane- H_2 collisions 2—26823
- from occultation light curves with spatial and spectral resolution 2—4959
- radiation content determ. 2—7249
- radiative transfer problems in isotropic scattering homogeneous spherical media by combined operational method 2—20676
- Saturn, faint atmospheric belts, photographic obs. 2—26850
- Saturn, microwave brightness temperatures, He:He mixing ratios 2—26848
- Saturn, NH_3 abundance in sub-cloud atmosphere, radio astronomical obs. 2—30580
- seasonal variations in planetary circulations, comparison of Earth, Jupiter and Saturn 2—41193
- spectroscopy 2—1990

Planetary atmospheres continued
structure and composition using Planetary Atmosphere Experiments Test 2—4962
terrestrial, temp. turbulent fluctuations, radiative damping rate 2—4960
Uranus, spectrum obs. 2—30581
Uranus, thermal opacity due to methane-H_2 collisions 2—26823
u.v. region studies, upper atmosphere examination by near fly by 2—11009
Venus, American Astronomical Society, Amherst, USA 1971, conference 2—26623
Venus, atomic carbon by photodissociation of CO and CO_2 2—11004
Venus, cloudy, theory of formation of spectral lines 2—23117
Venus, comet-like interaction with solar wind, characteristics of atmosphere, Venus probes data 2—37376
Venus, double cloud model and CO_2 absorption lines in spectrum 2—26851
Venus, i.r. and microwave transmission 2—41200
Venus, microwave brightness temp. and interpretations of radio and radar spectra 2—30582
Venus, numerical experiments on general circulation 2—26855
Venus, spectroscopic evidence for structure of visible clouds 2—23114
Venus, upper clouds, composition from occultation, transit and spectral data 2—41199
Venus review of data obtained by space probes and earth based investigations 2—26854
Venusian, spectral composition emissivity and absorptivity of 91% CO_2 9% N_2 mixtures at 8500-11500 K 2—30584
CO_2, photolysis at 1849 and 2139Å 2—10638
H_2-He collision induced absorption in major planets 2—26825
H_2 nil, gravitational instabilities prevented by solar tidal force 2—26824

Planetary nebulae
see also Galaxies; H I regions; H II regions
chemical composition, analysis of emission spectra and photometry 2—23065
continuum and line radiation from i.r. 2—16962
in Cygnus-Perseus region, Schmidt camera survey 2—26642
DR 21, radio recombination line obs. of H85α line 2—23061
Dumbell, NGC 6853, obs. at [NII] 6584Å 2—20502
ejection at stellar envelope from long period variables 2—26719
ejection of matter, model 2—23062
evolution of close binary system, mass loss evidence 2—37290
evolution theories 2—7419
filamentary structure, origin 2—7386
filamentary structure caused by radiation pressure gradients 2—20504
IC 418, H paschen and HeI emission 2—4803
IC 418, i.r. spectrum, Paschen lines, reddening constants 2—1950
IC 418, radio recombination line obs. of H85α line 2—23061
internal motions and kinematics, review 2—23063
interstellar medium enrichment by planetary nebulae, N/O abundance gradients across spiral galaxies 2—37269
ionization structure, optically thick condensations and associated luminous shadows 2—26641
inLarge Magellanic Cloud, radial distribution 2—20503
maser sources, review 2—30401
model nuclei, evolutionary computations of single stars 2—26687
NGC 1514, spectral obs. of control star 2—26684
NGC 2392, 6210, 6826, 6720 and 6853, monochromatic photographs and isophotic contours 2—16963
NGC 40, line intensities, photoelectric and photographic obs. 2—16961
NGC 6720 ring, plate form, model obs. 2—23062
NGC 7027, Balmer line intensities near series limit 2—4804
NGC 7027, NGC 6210, NGC 6888, radio recombination line obs. of H85α line 2—23061
NGC 7027, recombination spectrum 2—20501
NGC 7293, filamentary structure, model of orbiting comet-like structures 2—23064
NGC 7293, filamentary structure, origin 2—7386
NGC 7293, helix, west-south-west extension 2—41067
NGC 7662, Bowen fluorescence mechanism 2—5109
O and Of-type central stars, effective temperature calculations 2—10886
Orion, radio recombination line obs. of H85α line 2—23061
physical state parameters from total spectral line intensities 2—35679
radio observations at 2700 MHz, extinction coeff. determ. 2—33613
Rosette, radio recombination line obs. of H85α line 2—23061
He I triplet spectrum, theory, interpretation 2—10838
He triplet state population obs. 2—5057

Planets
see also Asteroids; Jupiter; Mars; Mercury, planet; Neptune; Planetary atmospheres; Saturn; Solar system; Uranus; Venus
capture of comets, restricted three body problems 2—7713
disturbing function, expansion by binomial and Laplace series 2—20678
earth, albedo from turbidity obs. 2—37077
elastic properties of interior 2—41219
extrasolar, photometric indices 2—7405
extrasolar, technique for photometric detection 2—37354
fluid motions, large-scale 2—20688
formation, gasdynamics 2—41166
Grand Tour missions to Jupiter, Neptune, Pluto, Saturn, and Uranus, calculation of expected radiation doses 2—23113
interplanetary scintillations, simultaneous observations of radio sources 2—26899
Jupiter, capture of outer satellites, three-body elliptical problem, capture at perihelion or aphelion 2—23115
liquid planets, third order approx. equilibrium figure, homogeneous model 2—26393
magnetic field free, solar wind induced mass loss 2—4961
major, H_2-He collision induces rotational translational absorption 2—26825
major and minor, meridian obs. for 1963-67, positions 2—1989
mass, determination, review 2—11001
mass effects on orbits of first four asteroids and determination of the mass of Ceres 2—11013
masses, analysis of independent determinations 2—11003
masses, from optical and radar data 2—30579
minor, orbital elements, radar obs. 2—2007
minor, photographic obs. (1970) catalogue 2—20683
motion, Kepler's laws derivation 2—37353
motion parameters normalized to obtain dimensionless eqns. 2—7373
motions from N-body problem solution with recurrent power series 2—1942
oblate, gravitational field, quasiperiodic motion of particle 2—45

Planets continued
orbits, computerized series solution of relativistic equations of motion 2—11008
origin, astronomical evidence in other stars 2—41165
origin, plasma to planets, conference (Saltsjobaden, Sweden, Sept 1971) 2—41164
outer planets, limitations on mass determinations from mutual perturbations 2—30546
perturbation of orbits of long-period comets with large perihelion distances 2—26862
pulsar planetary systems, possible method of detection from perturbation on time of arrival of pulses 2—17021
radiation, visible scanning photoelectric polarimeter for Stokes parameter 2—11175
satellite capture in the three-body elliptical problem 2—33590
secular disturbing function, influence of great inequality 2—20680
surface organic chemistry exploration, mass spectrometers for spacecraft 2—41191
two-dimensional photometric images of planets and stars using a Si-target vidicon photometer 2—41268
X and gamma radiation in planetary system 2—41192

Plasma
see also Discharges, electric; Electrons; Ions; Space charge; Thermonuclear reactions
Abel integration equation inversion 2—35456
air, nonisothermal, radiative heat transfer mechanism 2—18589
alkali, complete local thermodynamic equilibrium 2—31938
alkali metal, spectroscopic meas. of electron density and temp. 2—15472
anisotropic, rotational discontinuities, rel. to solar wind 2—11086
anodization, thin film growth, review 2—3520
anodization of Al, Langmuir probe cleaning, O discharge 2—3199
anomalous d.c. resistivity, computer simulation 2—8923
anomalous resistivity, effect of external circuit 2—18665
arc, capillary, d.c., for excitation of aerosol for spectrochemical anal. of metals 2—20215
arc, low pressure, state in nonhomogeneous medium 2—24693
arc, meas. of voltage and current by digital method, computation of turbulent resistivity 2—21775
arc, modes of current existence in heterogeneous medium 2—24694
arc, periodically repeating pulses of current, investigation 2—985
Astron type E layer generation using high current electron beams 2—3221
in astrophysics, phenomena in Sun, stars, interplanetary space and upper atmos. 2—23083
astrophysics and origin of solar system in terms of plasma physics 2—7359
atomic spectra, forbidden line profiles, ion dynamic correction 2—24318
auroral zone and polar caps, distribution 2—13753
beam-plasma discharges, inertial effects in current risetime 2—35474
Boltzmann integrals for inelastic collision and radiative processes in monatomic plasma 2—6068
bounded, thermonuclear, quasistationary states, heated by laser 2—28502
canonical theory, Hamiltonian and statistical electrohydrodynamics 2—35455
cathodic sputtering, Ar-O_2 mixture, discharge obs. rel. to Ni, Fe and $NiFe_2O_4$ deposition 2—1012
cathodic sputtering, discharge analysis rel. to thin film prod. processes 2—1011
characteristic surfaces for supersonic flow of guiding centre plasma 2—28497
characteristics, rel. to ion probe current in nonstationary conditions 2—8958
cold, transition layer with confined mag. field, structure, model 2—995
collisional, theory of electron energy distribution obs. 2—35457
collisionless heating, using oscillating external currents 2—31942
collisionless interactions between counterstreaming ions in laser produced plasma 2—15452
collisionless plasma 2—989
collisionless relaxation, interpenetrating ionic streams 2—6065
collisionless relaxation of ultrarelativistic electron beam 2—24696
colloidal, duration of afterglow 2—35472
column, warm, interaction with plane e.m. wave 2—991
computer simulation 2—8908
condensation, chemical effects, solar system origin 2—41167
conference on plasma physics and controlled thermonuclear fusion, Madison, USA (1971) 2—21760
contamination by anode channel erosion 2—9013
controlled nuclear fusion research and plasma physics— conference (Vienna, 1971) 2—24644
Coulomb gas, classical, nodal expansion of free energy 2—3195
crossed field, average potential 2—31962
cylindrical gravitational waves in hot plasma with constant axial magnetic field 2—28495
degenerate, at relativistic temperature, dielectric function 2—8927
degenerate electron gas, neutrino bremsstrahlung, in high dense stars 2—8113
degenerate electron type, in mag. field, dielectric function at relativistic temps. 2—24687
deionisation of plasma dispersing in vacuum, distribution of charged particles 2—21759
dense, nonideal, cluster formation 2—28528
deuterium, X-ray continuum radiation from high temp. plasma 2—35499
dielectric, maximization of e.m. energy transmission 2—30916
diffusion type, transition to positive column discharge 2—31947
discharge, electrochemistry 2—21778
discharge, electron distribution calc. from spectral line intensities by Tikhonov's regularization method 2—35607
discharge, hot cathode, noise in plasma ion frequency band 2—35488
discharge, impulsive, physical processes in dielectric chambers 2—31965
discharge, nonselfsustaining, mass-charge composition of ions in mag. field 2—24691
discharge, velocity of gas flow, stabilization 2—15442
dispersion function, general recurrence relation, evaluation of integrand moments 2—24647
distribution function, spherical harmonics and Cartesian tensor product expansions 2—39092
distribution of charged and neutral particles across positive column in power discharge 2—21882
dynamics, rel. between space charge and spatial potentials, conditions for instability 2—8912

Plasma continued
- electric field and impedance of planar capacitor containing warm inhomogeneous magnetized plasma 2—39119
- electric fields, Langmuir-Bohm criteria and boundary conditions 2—31964
- electric microfield distribution in stationary turbulent plasma 2—35451
- electrodeless discharge, closed-form solns. 2—12462
- electron, with self-consistent field interaction, varational and statistical methods 2—33958
- electron and population densities for nonequilibrium plasma 2—35469
- electron beam injection, relativistic, induced and transitional fields and currents 2—21776
- electron beam interaction using Marx generator technology 2—39091
- electron beams, relativistic, intense, expansion in preionized gas 2—11440
- electron density, influence on products of reactive cathodic sputtering of Cu in O_2 2—3527
- electron distribution function, deformation under influence of large amplitude wave 2—28529
- electron emission over dielectric in vacuo 2—35605
- electron energy distrib. function, effect of near-wall h.f. oscills. 2—1002
- electron energy distribution function at low pressures in pulsed high-frequency discharge 2—12365
- electrostatic field excitation by incident plane transverse e.m. waves 2—18583
- energy conversion research recommendations 2—5319
- equilibrium magnetoplasma with linear inhomogeneities, propagation of magnetoacoustic waves 2—28496
- equilibrium turbulent boundary layers, mean and fluctuating electron density 2—28526
- even velocity moments of nonlinear distribution function 52] 2—39094
- excited level occupation numbers, escape factor, model calcs. 2—35450
- experimental data smoothing for performance of inverse Abel transformation, numerical procedure 2—33859
- fluctuation spectrum, with few electrons in Debye volume, obs. by collective light scattering 2—18618
- fundamentals of plasma state in class environment, book 2—6058
- gap to positive electrode, electrical breakdown 2—12375
- hard X-ray spectrum, produced by thermal Bremsstrahlung 2—24650
- heating, by h.f. field of ion cyclotron frequency, calc. 2—15445
- heating, electron beam injection into magnetic trap 2—6087
- heating, influence of laser pulse dynamics 2—35461
- heating and contraction, effects of trapped particle pinch effect in Tokamak plasmas 2—28575
- heating by dissipation of current driven turbulence 2—24657
- heating by focused pulsed laser radiation, dynamics 2—28506
- heating by laser, heat conduction mechanism considering recovery of fusion energy 2—28602
- heating by neutral injection in toroidal mag. field 2—32021
- heating of spherically and elliptically confined plasma influence of form of laser pulse 2—35458
- heating with very short pulses, neutron yield and e.m. radiation 2—24651
- h.f. discharge, capacitative bright and dark, identity 2—983
- h.f. radiation spectrum, possibility of narrowing at development of beam-plasma instability 2—35578
- high beta plasma 2—989
- high ion density, D ions, electrons, controlled nuclear fusion 2—38665
- hydrodynamic induced scattering in isotropic and magnetoactive plasma 2—31953
- hydrodynamics, statistical 2—979
- induction, for heating powders, work coil performance 2—3222
- induction, press. and flow obs. 2—12374
- induction coupled spectroscopic source, applic. in trace element det. 2—14489
- interaction of colliding laser beams, radiation amplification 2—12388
- interaction with high intensity laser pulse, fundamental equations 2—8909
- interplanetary, radio scintillations due to irregularities with power law spectra 2—11025
- interplanetary, satellite observations, average field strength of solar wind 2—14008
- ion heating by fast magnetoacoustic waves 2—21766
- ion heating by modulated electron beam 2—18587
- ion heating in Tokamak with transit time magnetic pumping 2—31940
- ion sound waves, growth rates in constant electric field 2—39111
- ion temp. with hot electrons 2—35459
- ionosphere, intensities of plasma lines obs. 2—23010
- jet, thermodynamic state, dimensionless parameter, calcs. for Ar, H, N, O, He plasmas 2—18590
- kinetic theory and evolution of relativistic plasma in uniform ambient magnetic field 2—8911
- kinetics of coeff. of reflection and energy distribution and electron current at plasma boundary calc. 2—21763
- Kubo conductivity of strongly magnetized, two-dimensinal, plasma 2—984
- Langevin eqn. of motion for electrons in inhomogeneous plasma 2—18585
- laser heating, fusion effects for spherical thermal wave 2—32007
- laser heating, fusion effects for spherical thermal wave 2—32006
- laser heating and fusion energy region of D-T plasma by mechanical magnetic cumulation 2—31983
- laser irradiation causing anomalous heating 2—28505
- laser light scattering, comparison of calc. and obs. spectra in mag. field 2—32010
- laser production and heating Moscow 1970 conference 2—28604
- layer in optical resonator, det. of radiation temp. 2—35495
- l.f. electric microfield distrib. in plasma containing multiply charged ions 2—24688
- light scattering frequency spectrum effect of magnetic field 2—32009
- Liouville equation, approximate solutions and truncation scheme for distribution functions 2—14142
- magnetised plasma, plane layer, average force on electrons and ions 2—3202
- magnetized, nonstationary collisionless shock waves prod; ion gyroperiod time scale 2—15457
- magnetized, study of optical mixing 2—8938
- magnetized arc, anomalous scattering of laser light 2—35497
- magnetoplasma, nonisothermal, excitation of ion waves by nonlinear wave mixing 2—8974
- magnetosphere, motion produced in electric field produced by geomagnetic disturbance 2—13735
- magnetospheric, conference (New Delhi, Feb. 1971) 2—20401
- magnetospheric, sources, wave-particle interactions and acceleration mechanisms 2—20365

Plasma continued
- magnetotail sheet thinning during auroral substorms 2—16885
- microwave, control of electrical parameters and spectral radiation by variation of gas conc., field frequency and power level 2—8929
- models, partial local thermodynamic equilibrium 2—21764
- models of topside ionosphere and electrostatic wave propagation 2—10756
- modulating electron beam, nonlinear bunching 2—251
- moving, heating by fast large amplitude magnetosonic wave 2—6063
- neutral beam injection heating of toroidal plasmas 2—31939
- neutral sheet, magnetospheric, at lunar distance, preceding substorm onset 2—4955
- noble gas, metastable densities 2—8922
- non-ideal, dense, thermodynamical, transport and optical props., review 2—21768
- nonideal, kinetic equations, Boltzmann and Landau 2—28499
- nonideal, relationship of thermopower to conductivity 2—28518
- nonlinear pondermotive forces in interaction with laser radiation 2—8918
- nonlinear response of weakly ionized system to pulsed elec. field 2—8928
- nonlinear response theory, h.f. conductivity and sum rules 2—35452
- numerical simulation with periodic smoothing in phase space 2—28512
- optical transmission of nonequilibrium inhomogeneous plasma 2—28565
- pair correlation function, asymptotic solution of Frieman-Book equation 2—6062
- periodic electron, one-dimensional, quasilinear theory and numerical simulation 2—24646
- phase space density granulation 2—12366
- θ-pinch, heating by CO_2 laser radiation 2—39151
- plasmatron discharge as source for spectrochemical analysis 2—4618
- plasmoids, formation in electric breakdown of air in superimposed d.c. and h.f. electric fields 2—8998
- polymerization process, thin film formalism 2—3550
- positive column diffusion controlled, self-contraction mechanism in medium pressure range 2—12470
- positive column theory 2—21762
- potential distribution and ionic charge near equipotential sphere moving in low density plasma 2—24686
- proton, energy for inflation of geomagnetic field during magnetic storm 2—30370
- quantum electrodynamics of nonthermal relativistic kinetic theory 2—31936
- quiescent, 3rd international conference at Elsinore (September 1971) 2—12353
- radiation power as function of discharge parameters in Tokamak 3 device 2—31945
- radiative recombination of hydrogenic ions 2—16964
- rare gas, afterglow, decay in magnetic field 2—28570
- relativistic, resonance states of total charge density 2—24643
- relativistic particles interaction with turbulent plasma 2—31996
- relaxation processes enhancement by collective effects 2—41076
- resistivity, anomalous h.f., driven by large electric field oscillating near electron plasma frequency 2—18601
- resonant line broadening by electrons in nonequilib. partly ionized plasma 2—18289
- reverse behaviour in boundary value problem of rotationally symmetric infintely conducting static incompressible plasma 2—24645
- short theta pinch, refractivity obs. using laser interferometry 2—23686
- simulation, computer 2—39095
- simulation, initial particle distributions 2—978
- solar, rotation phenomena 2—41230
- solar flare plasma, heating by high energy electrons 2—37409
- solar flares, cooling, energy input for flash phase, heating to produce optical and soft X-ray emission 2—30631
- solar system, conference (Saltsjobaden, Sweden, Sept 1971) 2—41164
- solar wind, flow through Earth's bow shock, ratio of specific heats 2—16874
- solar wind, higher moment equations and distribution function 2—20701
- solid surface interaction with low energy noble gas ions, energetic neutrals scatt. 2—6332
- spark, influence on sample surface in laser microspectral analysis 2—37066
- spatial time evolution of plasma with Tokamak type discharge 2—28500
- spectroscopy, high temp. plasma 2—994
- spraying using Ta-Hf mixture as sputtering source 2—5106
- static shielding, quantum theory, intermediate magnetic field strength 2—8926
- statistical thermodynamics, thermodynamic potentials and plasma stability and equilibrium 2—39093
- stepwise ionization in discharge plasmas, electron ionization cross section of excited H 2—35597
- stopping power for relativistic heavy ion 2—28498
- stream, reflection by combined barrier on upper hybrid resonance 2—31991
- strongly correlated, scatt. of light 2—28564
- supersonic flow, possibility in collapsing post-sunset ionosphere 2—20418
- surface grafting of textiles 2—3504
- technological process for strong adhesive bond productions 2—39973
- temperature, radial distribution, from lateral radiance ratio 2—28507
- temperature and electrical conductivity in Fe welding arc, radial distribution by optical investigation 2—1017
- temperature and pressure calc. for optically dense plasma obtained by discharge with evaporating wall 2—28527
- temporal evolution of distribution function in external electric field perpendicular and parallel to mag. field 2—24649
- thermal, l.f. induction 2—35462
- thermal contraction, quasi-one-dimensional model 2—12358
- thermal induction, between coaxial cylinders, equil. temp. profiles 2—8913
- thermodynamics of relaxation of temperature anisotropy 2—28504
- thermonuclear fusion, plasma heating by relativistic electrons 2—24654
- time dependent linear Vlasov eqn. soln. for Case-Van Kampen modes by multiple time scale method 2—8910
- topside thermal protons, plasmapause variations, corotating plasma tail 2—13786
- turbulence, shift and broadening of resonance 2—31937
- turbulent, energy density spectrum of elec. field 2—31963
- turbulent heating 2—12357
- turbulent heating and magnetic confinement 2—24655
- two component, inhomogeneous, first order relativistic kinetic equation 2—3192
- unmagnetised, theory, book 2—18586

Plasma continued

- Vlasov, linearized variational analysis of single- species, one-dimensional 2—12355
- Vlasov, self consistent electric field det. 2—28514
- Vlasov equation, time development solution 2—24648
- wake behind body in motion parallel to magnetic field, effects of periodically varying cross section of body 2—21773
- warm, impedences near lower hybrid resonance, electron pressure effects 2—18602
- wave kinetic equation, produced entropy as Liapunov stability function 2—35454
- weakly coupled, weakly inhomogeneous, in mag. field, kinetic and macroscopic equations deriv. 2—35453
- A arc, Boltzmann equilibrium between spectral energy levels 2—6061
- Ar, emission line profile broadening, correction curve 2—8440
- Ar, heating by fast magnetic compression 2—28546
- Ar, high pressure, as high radiance standard 2—24659
- Ar, induction, temp. profiles 2—3196
- Ar, light scattering and density inhomogeneity broadening of plasma satellites 2—3213
- Ar, positive column, pressure dependence of neutral flow effusing from 2—24873
- Ar, relaxation process and population inversion 2—976
- Ar, seeded with K vapour, d.c. conductivity meas. 2—31703
- Ar, shock produced, ioniz. 2—18606
- Ar, stable, electron-ion recombination coeff. det. by probe method 2—24840
- Ar arc, effect of Cs seeding on cathode temp. 2—12373
- Ar arc, electrical conductivity and optical reduction of ionization potential, correlation of peculiarities 2—39120
- Ar constricted arc plasma, thermochemical nonequilibrium 2—28501
- Ar jet, as excitation source, interference obs. 2—16704
- Ar jet from h.f. induction discharge gas and electron temps. dependence on input power and flow rate 2—28503
- Ar supersonic flows in arc plasmatron, optical meas. of electronic parameters 2—39113
- CO afterglow, obs. of emission of C_2 Swan bands 2—24697
- CO_2 laser, vibrational temp. obs. in i.r. using line reversal method 2—24447
- Cs-Ar discharge, electron distrib. function, kinetic coeffs. 2—15443
- Cs-Ar positive column, electron temp. and radial density distrib. of Cs atoms 2—12464
- Cs, conc. gradient determ. from hook distortion 2—39112
- Cs, Cs-He, electrical conductivity obs. 2—24690
- Cs, dense, Coulomb interaction contribution to specific electrical resistance 2—39121
- Cs, ionic species determ. using d.c. and r.f. excitation 2—3204
- Cs, l.v. arcs, electron temp. and charged particle distrib. in gap 2—12376
- Cs, spectroscopic meas. of electron density and temp. 2—15472
- Cs afterglow, excited states relaxation in presence of reabsorption 2—24355
- Cs discharge, influence of resonant illumination on props. and parameters 2—31956
- Cs discharge plasma, spectral emission, level population and plasma decay and development processes 2—35610
- Cs pulsed discharge, spontaneous emission 2—2935
- Cu, exploding wires, radiation in infrared, visible, u.v. and vacuum u.v. spectral ranges 2—3214
- Cu I, line broadening consts., theoretical estimation 2—2919
- D-T, thermal balance equation 2—509
- H, absorption spectra of laser flashes 2—21541
- H, Balmer spectrum meas. for temps. 12000-20000 K 2—35177
- H, decaying, population inversion and atomic relaxation 2—35496
- H, laser-produced, photon absorpt. coeff. calc. 2—12387
- H, local thermodynamic equilibrium, continuous emission calc. 2—24715
- H, turbulent heating of plasma column in linear arc discharge 2—24658
- H afterglow, one dimensional numerical model 2—24698
- H plasma absorption coeffs. at laser frequencies 2—12390
- H_2, continuous emission at bound-to-free transition regions 2—35500
- H_2, discharge, inductive, electron energy distrib. function 2—988
- H_2, radiative attachment and photodetachment of free electrons in arc, cross sections 2—35586
- H_2 discharge, h.f., luminous radiation, radial distrib. 2—986
- H_2 discharge, inductive, electron temp. and density obs. 2—987
- ^2H-^3H, cumulation-laser heating, average value model description for cylindrical wave 2—24652
- ^2H-^3H, nuclear, microfusion during laser heating process, methods for raising the energy recovery 2—24653
- ^2H, heating by fast magnetic compression 2—28546
- He-Cs, decay, luminescence flare up and population of Cs levels 2—977
- He-N, time dependence of number densities of N^+, N_2^+, N_3^+, N_4^+ during decay period 2—24703
- He-like ion line emission in solar plasmas 2—37381
- He, afterglow, effect of elevated, time varying neutral gas temp. 2—24702
- He, containing C impurities, pressure broadened profiles of C III and C IV lines 2—28188
- He, cryogenic, afterglow obs. 2—24701
- He, decaying, electron conc. meas. 2—980
- He, different absorption and emission line shapes for Stark broadened resonance lines 2—8495
- He, excited atom population densities, determination by electron impact spectroscopy 2—28530
- He, hollow cathode discharge, nonthermal plasma, excited level population, electron temp. 2—6060
- He, large time constant emission in decaying plasma in Kovarglass built discharge tube 2—6059
- He, recombining, spectroscopic study of early afterglow 2—24700
- He, spectral line shapes, photoelectric recording 2—3191
- He and He-Ne, metastable densities 2—8922
- He arc plasma jet, profiles of isolated He I lines 2—35184
- He I 4471 Å line and forbidden components, Stark profiles in laser produced plasma 2—39136
- He laser produced, Stark profiles of forbidden and allowed transitions 2—6078
- He recombining plasma, formation of He_2^+ by associative ionization 2—24672
- HeI, influence of distant electron collisions on plasma broadened 4471.48 Å line 2—35183
- Hg arc, electrical conductivity and optical reduction of ionization potential, correlation of peculiarities 2—39120
- Hg arc, l.p., efflux of atoms from cathode spots 2—12479
- interaction with a photon gas, Boltzmann equation 2—23286
- K afterglow, excited states relaxation in presence of reabsorption 2—24355
- Kr, shock heated, electron densities and ionization relaxation times 2—35470
- Li ionization and recombination rates calcs. 2—6105
- N_2, arc, effect of curvature on thermal and dynamic props. 2—24692
- N_2, electron distribution function and mean energy 2—21769
- N_2, radial temp. distrib., emission spectra obs. 2—28510
- Ne-He, low pressure discharge, dependence of electron distrib. function on discharge current 2—15444
- Ne-He afterglow, electron density decay after cataphoresis 2—24677
- Ne, low pressure discharge, dependence of electron distrib. function on discharge current 2—15444
- Ne and He-Ne, metastable densities 2—8922
- Ne arcs, l.v., ionisation mechanism 2—12372
- O, r.f. discharge, oxidation study using KIO_3 2—4586
- SF_6, thermal conductivity 10^3 to 20×10^3 K and pressures 1 to 10 atm., calc. 2—12511
- U, electron density and temp. rel. to continuum source applic. 2—14487
- Xe, continuum absorption coefficient det. 2—35475
- Xe, saturable absorpion effects, YAG:Nd^{3+} radiation 2—18619
- Xe discharge, initial stages at high pressure, current growth and broadening of current carrying channel 2—31966
- **collision processes**
  - beam discharge, heating of electrons by electron beam 2—3198
  - Boltzmann integrals for inelastic collision and radiative processes in monatomic plasma 2—6068
  - Brownian motion, Kubo's modified theory 2—31951
  - cathodic sputtering, reactive processes, rel. to thin film prod. processes 2—1011
  - cold ion collection by means of Langmuir probes, effect of collision in transitional regime 2—28572
  - collisional distributions in mirror plasma 2—31950
  - collisional trapped-particle instability, radial dependence 2—21850
  - Coulomb, effects on maintenance of Landau damping of electron oscillations 2—6093
  - Coulombic interactions, many body, influence on thermodynamical and kinetic props. 2—28525
  - decay of weakly ionized plasma, in electrically conducting plasma, in longitudinal magnetic field 2—31952
  - diffusion near rational surface, enhancement factor 2—15448
  - drift instability driven by axial current observed in double-ended Q-machine cesium plasma 2—3245
  - electron distribution function in an electric field, influence of inelastic scattering 2—8919
  - electron impact ionizing collisions, perturbing effect of weak r.f. signals 2—28523
  - electron loss, distortion of radio pulse 2—20402
  - electron-ion, using BGK model 2—39131
  - electron-ion interaction in weakly ionized system 2—18597
  - electron-neutral collisions, effects on propagation of electron plasma waves 2—32062
  - energy deposition from nuclear elastic scattering 2—6067
  - gas-plasma interaction, hetegonic relevance, critical velocity, solar system formation 2—41171
  - H cascade excitation on passing through dense plasma and gaseous targets 2—15246
  - interstreaming ions interaction in laser produced plasma 2—18598
  - inverse electron-ion bremsstrahlung and stimulated Compton scattering in heating of confined plasma, influence of laser pulse form 2—35458
  - ion cloud, effect of ion-electron collisions on motion 2—18599
  - ion heating in h.v.θ plasma 2—28509
  - ion ion collisions prod. transport across mag. field, analogy to turbulent transport in velocity space 2—15449
  - ion-molecular reactions in plasma containment devices due to impurities in device 2—12364
  - ion-neutral gas mols., effects on ion acoustic waves 2—32059
  - Kr, afterglow, highly ionized, recombination 2—24676
  - Langmuir probe response in transitional regime, effect of collisions on ion-saturation current 2—28586
  - Lorentz plasma, Boltzmann collision integral, role of high momentum transfer collisions 2—31949
  - parameters, Langmuir probe determination 2—28589
  - positive column, pulsed, electron drift speed and multiplication obs. 2—8996
  - Ramsauer effect system, effect on stability 2—32090
  - Ramsauer gases, exact theoretical treatment of cyclotron echoes 2—18596
  - relaxation of cathode beam, factors leading to accel. and decel. 2—8920
  - relaxation processes enhancement by collective effects, applications to stellar dynamics 2—10851
  - single component plasma, Boltzmann collision integral, role of high momentum transfer collisions 2—31949
  - solar magnetoplasma partially ionized, electrical conductivity 2—30636
  - spatial ion wave echoes in Q-machine plasma 2—39110
  - thermal, ionization and recombination at various plasma temps. 2—28524
  - Thomson scatt. of laser light in collision dominated system 2—12389
  - transverse instabilities of colliding plasma, roles of ion motion and return currents 2—8986
  - Ar, afterglow, highly ionized, recombination 2—24676
  - Ar II, ionic levels, study of inversion of population state at collision of shock waves 2—28547
  - Cs-Ar discharge, effect of electron atom and electron electron collisions 2—15443
  - H, injection into transverse mag. field, X-rays and microwave radiation 2—39109
  - H_2, interaction with He gas, excitation transfer 2—35189
  - He^+-N_2 reactions in plasma containment device due to N_2 impurity in device 2—12364
  - He, afterglow, highly ionized, recombination 2—24676
  - He, afterglow, validity of quasisteady state and collisional radiative recombination 2—3197
  - He, inelastic collision cross section, from electron energy distrib. function 2—8921
  - Ne, afterglow, highly ionized, recombination 2—24676
- **confinement**
  - *see also Stellarators*
  - ^2H, hot, high density in magnetic mirror trap, turbulent heating 2—24747

- **Plasma** continued
  - **confinement** continued
    - θ-pinch with azimuthal magnetic field, betatron acceleration mechanism 2—21795
    - adiabatic compression 2—39138
    - Alcator, nonlinear feedback control 2—6084
    - alkali-plasma column structure in weak mag. field 2—12396
    - Astron, equilibrium magnetic field, E-layer and plasma equilibria calc. 2—12399
    - Astron, injection, equilibrium and stability of E-layer and confined plasma 2—21765
    - Astron. Trapping experiments 2—21808
    - Astron-type, application of intense relativistic electron beams 2—21809
    - beam moving along curved mag. field lines, reverse deflection and contraction 2—18625
    - Burnout V d.c. magnetic mirror machine, lifetime of hot-ion plasma 2—24741
    - canted mirror, hot electron equilibrium, distrib. fn. 2—39145
    - circular quadrupole magnetic well, DECA IIB 2—24734
    - CLIMAX toroidal quadrupole device, convective motion 2—21806
    - closed line device, injection system, numerical control 2—21789
    - closed line systems, equilibrium, theory 2—28571
    - coaxial injector, mechanism of focus formation 2—24724
    - collective modes, collisionless kinetic modes involving trapped particles MHD stability 2—24731
    - combined pinch, heating and stability 2—21796
    - configurational properties of fusioning plasma, confinement by fuel injection 2—32014
    - cool electron θ-pinches, turbulent heating and resistivity 2—39139
    - curved θ pinch, dynamic equilib. achieved by effect of oscillating axial current on toroidal drift of column 2—12430
    - cylindrical cavity, variable length, high density resonantly sustained plasma 2—21826
    - d.c. octopole, decay 2—21802
    - dense plasma focus, ion energy 2—24720
    - dense plasma focus, restrike or subsidiary break-down 2—24722
    - diffusive Tokamak equilibrium, time dependent solutions 2—32018
    - drift cone instability, finite beta stabilization 2—39187
    - drift motion and instability in curved mag. field 2—18677
    - drift wave stability, growth rate and boundary, under linear theta pinch conditions 2—18679
    - Duoplasmatron ion source, high containment device for medium charge states 2—34332
    - between electrodes, stability analysis 2—3216
    - electron cyclotron radiation measurements in magnetic mirror plasma system 2—28566
    - electrostic-inertial confinement 2—32012
    - e.m. trap, accumulation by ionization of residual gas 2—39141
    - equilibrium configurations for sphere, generalization, application to confinement and ball lightning 2—32013
    - feedback stabilization of kink modes in current carrying plasma 2—6082
    - finite pressure minimum-B config., magnetostatic equilibria 2—35505
    - focus, dense pinch phase, MHD model 2—24735
    - focus, non-adiabatic ion distribution function from self-consistent calc. 2—24725
    - focus, Thomson scattering and neutron anisotropy during neutron emission 2—24721
    - focus system, radiation losses in thermonuclear reactions 2—24729
    - focus type, high current gas discharge 2—24723
    - hard core pinch, Cartesian model, parallel viscous modification of resistive tearing instability 2—18621
    - heating by skin current 2—39097
    - heavy sheath, laser impulse, initial stage of expansion 2—3217
    - Heliotron-D machine, gun plasma confinement times 2—28585
    - h.f. heating in closed mag. trap 2—21810
    - high beta (l=1) stellarator experiments, shock wave heating 2—24738
    - homopolar device, stability 2—39142
    - hot electron, by electron cyclotron resonance wrapping in cusped magnetic field 2—18628
    - injector-divertor device, trapped plasma density, microwave meas. 2—6088
    - instabilities, mirror and fire hose, rel. to Larmore radius 2—15488
    - internal ring device F IV, heating 2—21804
    - ion-molecular reactions in plasma containment devices due to impurities in device 2—12364
    - JAERI hexapole with high toroidal field 2—21805
    - J.I.P.P. stellarator, dependence of plasma confinement on magnetic configuration and plasma properties 2—24762
    - laser cavity, TEA, intracavity lens arrangement 2—9004
    - levitated toroidal multipole, design and optimization 2—24740
    - linear screw pinch, dynamic stabilization of helical m=1 instability 2—32102
    - mag. multipole confinement of mag. field- free plasma 2—12402
    - magnetic, effects of turbulence at high electric fields 2—24807
    - magnetic bottle, non-resonant large diameter plasma 2—24742
    - in magnetic field, decay rate variations 2—28570
    - magnetic field, structure of transition layer, model 2—995
    - magnetic fields with spherical separatrix 2—8946
    - magnetic guarding of hoop supports in Wisconsin toroidal octupole 2—39144
    - magnetic mirror, cyclotron-resonance heating, rel. to theory of stochastic acceleration of particles 2—30814
    - magnetic mirror field, asymmetrically burning pulsed Penning discharge, cathode heating 2—32023
    - magnetic mirror trap, conditions for suppressing h.f. cone instability 2—24752
    - magnetic mirror trap, ion-cyclotron instability obs. 2—24825
    - magnetic mirror trap, reversal of axial mag. field by injection of high current electron beams 2—3221
    - magnetic mirror with low-freq. short-wavelength fluctuations 2—18630
    - magnetic of turbulently heated plasma 2—24655
    - magnetic trap, axially symmetric, effects of electric field on transfer processes 2—28520
    - magnetic well build up by neutral atoms injection with different injection energies and angles 2—28580
    - magnetoelectric fields 2—24719
    - MHD equilibrium of elliptic cylinder, current distributions and magnetic surfaces 2—12368
    - MHD pinch, nonlinear surface waves 2—3234

- **Plasma** continued
  - **confinement** continued
    - mirror, flutelike microinstabilities in plasma with broad perpendicular velocity distributions 2—3243
    - mirror confinement, microinstability in r.f. elec. field 2—24808
    - mirror containment problem, direct re-injection solution 2—8953
    - mirror trap, limitations on equilibrium and stability of high beta plasma ring 2—24749
    - moving cylindrical incompressible plasma, magnetic field diffusion 2—21794
    - multiple-mirror, examination using fixed scattering centre model 2—12401
    - multipole configuration of counter-rotating high-frequency fields, behaviour of interacting plasma 2—8950
    - multipole structures, plasma injection, heating and losses 2—21801
    - neutral injection mirro machine, build up and microinstability obs. 2—24753
    - nonadiabatic energy limit for ions and mirror ratio in magnetic well geometry 2—39146
    - nuclear fission, controlled international efforts 2—2842
    - nuclear fusion, current outputs, control techniques 2—18647
    - octopolar magnetic well, heating expt. 2—24748
    - off-resonance heating of mirror confined plasmas 2—28555
    - PHOENIX II mirror machine, effects of feedback system on losses and flute instability 2—32019
    - θ pinch, bending into torus, Scyllac theory 2—24739
    - θ-pinch, CO_2 laser heating by inverse bremsstrahlung and induced Compton processes 2—21790
    - θ pinch, conditions and mechanism of heating 2—24785
    - θ pinch, expt. to determine shift in Thomson scattered spectrum due to electron drift 2—35498
    - θ pinch, helical equilibrium fields in 5 meter toroidal sector and 3 meter linear device 2—28578
    - theta pinch, high β, anisotropic equilibrium 2—18622
    - θ pinch, h.v., ion heating obs. 2—28509
    - θ pinch, rotation during implosion 2—18623
    - θpinch, shock heating and shock structures in 2—28546
    - θ pinch accelerator, multiturn, efficiency obs. 2—35513
    - Z-pinch experiments with shock heating 2—21797
    - in poloidal heliotron magnetic field, stagnation region effect 2—18626
    - Polytron configuration, simulation 2—24736
    - PR-6 adiabatic temp., decay obs. 2—24751
    - probkotron, loss of particles with radial electric field 2—3218
    - Proto-Cleo stellarator, confinement times and unidirectional current 2—24761
    - Q-machine, single-ended, perturbed ion velocity distribution meas. at wave exciting grid 2—12403
    - Q-machine at Innsbruck 2—35510
    - quadrupole device, high-energy gun-injected toroidal 2—21807
    - radiation power as function of discharge parameters in Tokamak 3 device 2—31945
    - reverse field diffuse pinch, hydromagnetic and resistive instabilities 2—39184
    - r.f. supplemented magnetic mirror 2—32025
    - rotating plasma, rarefied, in trap with magnetic mirrors 2—21800
    - rotations in hollow cathode low pressure magnetically confined Ar arc discharge 2—24937
    - runaway electrons, observed lack, explanation based on model relying on particle trapping in plasma waves 2—15449
    - SATURN-three turn stellarator-torsatron, confinement and magnetic surfaces 2—24763
    - screw pinch, dynamic stabilization of m=1 mode 2—28649
    - sheath convection effects with flush-mounted electrostatic probes 2—3220
    - sheath with secondary electron emission, model 2—32016
    - spatially periodic magnetic field, h.f. interaction with plasma bursts 2—35565
    - spherator, fluctuation level and confinement times dependence on magnetic field configuration 2—12400
    - spherator with levitated superconducting ring 2—21803
    - spherical and elliptical confinement, influence of form of laser pulse on heating 2—35458
    - ST Tokamak, particle and energy balance 2—24744
    - stabilized magnetic mirror traps, hot electron target plasma for accumulation of energetic ions 2—24750
    - stellarator, JIPP, results using $J\times B$ gun and ECRH plasma 2—3219
    - stellarator, Uragan, hot-electron collisionless plasma containment 2—15467
    - stellarator field, l=3, convective motion of trapped particles 2—3194
    - superconducting Levitron ring, negative feedback position control system 2—28567
    - synchrotron radiation to ionize wall originated impurities in thermonuclear reactors 2—18253
    - tetrahedral spire with improved magnetic well using superimposed d.c. baseball field 2—18629
    - thermonuclear device, effect of fusion reactions 2—24754
    - thermonuclear reactions, prospects for control 2—24260
    - theta pinch with superposed fields 2—39140
    - theta-pinch, toroidal equilibrium for a high-β 2—12397
    - Tokamak, $\beta \gg 1$ and arbitrary current distribution 2—24733
    - Tokamak, det. of mag. field direction using laser light scattering 2—32022
    - Tokamak, dynamics at high temp. 2—24746
    - Tokamak, feasibility of steady state operation for controlled fusion 2—39147
    - Tokamak, imperfect axisymmetry and computer program for avoidance of particle losses 2—32020
    - Tokamak, neutral beam injection heating of toroidal plasmas 2—31939
    - Tokamak, non-round loop cross section 2—39143
    - Tokamak, nonlinear saturation of collisional trapped particle instability 2—32097
    - Tokamak, radial dependence of collisional trapped-particle instability 2—21850
    - tokamak, sharp-boundary model of a high- pressure system 2—12392
    - ST Tokamak, stability experiments, dependence on plasma profile 2—24730
    - Tokamak, TO-1, equilibrium using feedback system 2—28653
    - Tokamak and hybrid systems, toroidal equilibria 2—24681
    - Tokamak devices, macroscopic instabilities of plasma column 2—24728
    - Tokamak discharges, effect of non-axisymmetric confining fields 2—24745
    - Tokamak machine, thermonuclear plasma, ion cyclotron oscills., transverse current excitation 2—28609
    - Tokamak models, stationary, comparison 2—8952

Plasma continued
  confinement continued
    Tokamak system, possibility of stationary thermonuclear reactor 2—24732
    Tokamak system, radiation losses in thermonuclear reactions 2—24729
    Tokamak T-4 device, energy balance and electron and ion heating 2—24743
    Tokamak TM-3, electron-cyclotron heating 2—39098
    Tokamak type toroidal plasma column, equilibrium 2—8951
    Tokamak-6, experiments under macroscopically stable discharge conditions 2—24737
    Tokamaks, energy loss due to electrons trapped in drift waves 2—18627
    Tokamaks, equilibrium, transport coeffs., stability design diagnostics and heating methods 2—35503
    Tokamaks, nonlinear kink and tearing mode effects 2—24824
    Tokamaks, open confinement and turbulence, Vienna 1971 conference 2—24726
    tokamaks, spatial det. of poloidal mag. field 2—18610
    TOR-1 stellarator, confinement rel. to collision frequency, rotational transform angle and magnetic field intensity 2—28583
    TOR-2 two-turn stellarator, rotational transform angle resonance values 2—28584
    Tornado trap, experimental investigation of the structure and stability of the magnetic field 2—8948
    Tornado-2 trap, stability of the topology of magnetic field 2—8947
    toroidal, axially symmetric systems, equilib. config., flux functions method 2—21791
    toroidal, by hard core theta pinch with poloidal field coils 2—6081
    toroidal axisymmetric systems, conditions for stability regions of dissipative trapped ion instability 2—18678
    toroidal configuration of relativistic electron beams 2—15465
    toroidal devices, pseudo classical diffusion across magnetic field 2—24727
    toroidal discharge, high voltage, early departure from free acceleration and turbulent heating of electrons 2—39209
    toroidal geometry, transit time magnetic pumping for heating of low beta plasma 2—24683
    toroidal high-β experiments in compact axisymmetric configurations 2—28577
    toroidal mag. fields, ion acceleration, charge exchange ionization and fast ion trajectories, reviewed 2—32021
    toroidal MHD-equilibria, stability criteria 2—8899
    toroidal pinch, high β, experimental and theoretical studies 2—21799
    toroidal plasma, low-β, rotational transform effects 2—35506
    toroidal screw pinch, containment with various field programming 2—28573
    toroidal screw pinch with non-circular cross- section, equilibrium and stability 2—28574
    toroidal screw pinches, longitudinal current decay 2—21798
    toroidal system, high β with long wavelength helical fields 2—28654
    toroidal theta-pinch, confinement in periodic caulked-cusp field 2—28576
    transport in toroidal systems 2—12360
    Tuman 2 toroidal device and plasma heating 2—24755
    vintotron, magnetic configuration 2—6080
    vintotron, motion of trapped particles 2—15468
    Wendelstein II-a stellarator, confinement minima 2—24760
    Z pinch, combination of intense relativistic electron beams 2—15466
    D-T, laser channelled gas embedded z pinch, theoretical estimate of structure 2—18646
    H, discharge, spherical diode, charged particle, confinement, concentric grids 2—21877
    H, fields and pressure gradient during collapse of θ-pinch, ion azimuthal velocity calc. 2—18623
    H, injection into transverse mag. field, X-rays and microwave radiation 2—39109
    H, turbulent heating in magnetic mirror 2—24656
    H plasma motion, on injection into cusp field 2—21792
    H with ionic impurities, radiation losses in plasma focus type Z-pinch 2—8943
    H_2^+ long diffused column, dissoc. recomb. as cause of axial density decay 2—28569
    ^2H-^3H and ^2H-^3He mirror reactors, multi-species Fokker-Planck calculations 2—28579
    ^2H, open-ended magnetic well system, density and ion energy obs. 2—24756
    He, ion cyclotron resonance plugging and heating of cusped plasma 2—39137
    N, fields and pressure gradient during collapse of θ-pinch, ion azimuthal velocity calc. 2—18623
  devices
    see also Plasma diodes; Stellarators
    for acceleration, collisionless, in l.p. discharge 2—35515
    acceleration, model similar to 'snow-plough' one examined 2—21811
    accelerator, impulsive erosion, electron concentration distribution and electric and mag. fields 2—3226
    accelerator, quasi continuous inductive, with standing r.f. waves 2—32015
    accelerator, simple unipolar pulsed 2—21793
    arc constrictor, heat transfer distribution on variable cross sectional area 2—35502
    arc generators, construction, mode of operation, characts. 2—35554
    arc source, d.c., capillary, for use in spectrochemical analysis 2—10657
    Astron, injection, equilibrium and stability of E-layer and confined plasma 2—21765
    Astron. Trapping experiments 2—21808
    automatic control and stabilization of temp. of plasma jet 2—6102
    beam torch efficiency rel. to anode and cathode fall 2—6089
    for coating production, self lubricating anti friction type 2—6335
    long coaxial, outflow of plasma into vacuum 2—3232
    coaxial accelerator, strong turbulence and shock 2—35514
    current amplifier 2—6079
    dense plasma, focus, structure, neutron meas. and phenomenological description 2—24778
    dense plasma focus, ion energy 2—24720
    dense plasma focus, restrike or subsidiary break-down 2—24722
    dense plasma focus structure, numerical calc. X-ray and optical meas. 2—24777
    direct conversion of energy to electricity, fuel cycle obs. and calcs. 2—27398
    Duoplasmatron ion source, high containment device for medium charge states 2—34332
    echo holophone, content addressable recorded information 2—35507

Plasma continued
  devices continued
    electrical gas gun, discharge chamber parameters 2—35516
    electrode emissivity, limitation of layers in gas-electrode boundary 2—35511
    ELMAN II, beam-plasma interaction in relatively short beam-plasma system 2—28644
    focus, laser-heated, soft X-ray generation 2—14055
    focus, velocity distribution of ions producing neutrons 2—12393
    gun, conical Z-pinch, design and operation 2—12394
    Harmonica 2 and Tokamak, nonlinear expressions for displacement 2—31958
    Heliotron-D machine, gun plasma confinement times 2—28585
    hollow cathode arcs applications 2—28680
    impulsive erosion accelerator, coefficient of monochromaticity on occurrence of distributed discharge 2—32028
    induction conical source, acceleration of plasma clusters 2—32027
    induction plasma torches, review 2—39149
    inductive-impulsive accelerator, current sheet structure 2—32011
    injectors with capacitive and inductive energy storage, plasma clusters acceleration 2—3231
    internal ring device F IV, confinement and heating 2—21804
    ion engine, microanomalous diffusion and critical magnetic flux density 2—21812
    ion production, heavy highly charged 2—5625
    jet, mag. field and gas flow effects on anode root motion 2—32140
    jet, turbulent, structure and behavior obs. 2—35523
    jet in high current capillary discharge, meas. of front of streaming velocities 2—32121
    jets, protruding from capillary in high current discharge, investigation 2—32120
    jets, radial arc burning between concentric cylinders with axial mass inflow, numerical description 2—35518
    jets, source with non-cylindrical electrode geometry 2—24764
    laser heating enhancement by addition of heavy impurities to target, thermonuclear reactions 2—18591
    low-velocity, flowing gas mass fraction determ. 2—18593
    mirror fusion reactor, fast neutral injection for plasma heating and reactor start-up 2—28142
    mirror machine, r.f. heating of decaying H plasma 2—35509
    mirror machine, turbulent plasma heating ion component parameters 2—6083
    mirror machine reactors with direct conversion, engineering and economics 2—28130
    mirror machines, critical length criteria 2—32026
    mirror reactor, efficient recirculation on power model 2—28133
    mirror type experiments, 2X II and Baseball II, diagnostics 2—28591
    MPD accelerator, axisymmetric, influence of mass velocities on current distribution 2—35512
    multiple aperture extractor design for producing intense ion and neutral beams 2—34354
    multipole structures, plasma injection, heating and losses 2—21801
    neutron energy spectra and flux distributions for D-D reactions in plasma focus type z-pinch discharges 2—24718
    ORMAK expt., theoretic and experimental results 2—28581
    θ pinch accelerator, multiturn, efficiency obs. 2—35513
    plasma spraying, effect of powder feed rate upon quality of coating 2—3215
    plasmatron, high pressure, pulsed 2—6086
    plasmatron, high-frequency, Ar flow parameters 2—12363
    plasmatron, thoriated W cathodes, erosion in N_2 2—24757
    plasmatron jet, velocity meas. of weakly ionized gas stream using MHD pickup 2—15470
    plasmatron output parameters, spectroscopic study 2—8993
    Pleiade, developments, ion accumulation 2—24759
    PR-6 adiabatic trap, decay obs. 2—24751
    Q-machine, grid-excited waves, perturbed density and ion velocity distribution function 2—12437
    Q-machine, ion-acoustic collisionless shocks caused by microwave heating of electrons 2—21781
    Q-machine, single-ended, perturbed ion velocity distribution meas. at wave exciting grid 2—12403
    Q-machine, two ion beam instability with inhomogeneous B-field 2—18692
    Q-machine, wake behind obstacle in plasma flow as diagnostic for ion distribution function 2—21823
    Q-machine at Innsbruck 2—35510
    Q-machine source with rotationally symmetric temp. profile due to rotating cathode 2—39148
    Q-machine with end plates, parallel current and sheath effects on collisional drift waves 2—12428
    r.f. supplemented magnetic mirror 2—32025
    source with arc stabilized by supersonic airstream parameters 2—6085
    space vehicle neutralization, generator 2—20438
    ST Machine, computer assistance using interfacing and control hardware 2—28568
    Tokamak, dynamics at high temp. 2—24746
    Tokamak, heat flux and energy losses calc., due to electrons trapped in drift waves 2—18627
    Tokamak, imperfect axisymmetry and computer program for avoidance of particle losses 2—32020
    Tokamak, ORMAK expt., theoretic and experimental results 2—28581
    Tokamak, poloidal magnetic field measurement, polarization of e.m. wave propagating in plasma with magnetic shear 2—28554
    Tokamak, TO-1, equilibrium using feedback system 2—28653
    Tokamak 3, radiation power as function of discharge parameters 2—31945
    Tokamak discharges, radial transport 2—28519
    Tokamak fusion reactors, model design studies and economic feasibility 2—28141
    Tokamak plasma heating, axisymmetric magnetic pumping 2—28535
    Tokamak T-4 device, energy balance and electron and ion heating 2—24743
    Tokamak-6, experiments under macroscopically stable discharge conditions 2—24737
    Tokamaks, equilibrium, transport coeffs., stability design diagnostics and heating methods 2—35503
    torch, a.c., thermal characteristics modelling 2—18632
    torch, d.c., energy characteristics 2—35521
    torch, energy transfer distrib., secondary gas flow effect 2—8949
    torch, generation of high enthalpy gas streams 2—35517

Plasma continued
devices continued
torch, ion flow velocity and efficiency 2—35522
torch jet, effect of flow rate of stabilizing gas on electron concentration 2—35520
torches, influence of geometry on h.f. voltage component in d.c. arc 2—35519
toroidal turbulent heating machine, cross field ion acoustic instability 2—18686
torus devices for thermonuclear fusion equipment 2—11915
transformer with single plasma turn as secondary 2—24717
Tuman 2 toroidal device, and plasma heating 2—24755
vintotron, magnetic configuration 2—6080
Z pinch as a spectroscopic source, influence of shock-piston separation 2—11545
Z-pinch focus, X-ray spectra measurement by time resolved Ross filter system 2—18624
H plasma r.f. heating in mirror machine near ion cyclotron frequency 2—35509
diagnostics
see also Langmuir probes
accelerators, magnetic field intensity and density measurements, by neutral and charged particle beams 2—35550
air, electrical and thermal conductivity obs. using stabilized electric arc 2—6071
alkali metal, spectroscopic methods for electron density and temp. meas. 2—15472
alleviant effectiveness, electrostatic probe technique 2—28588
ambipolar diffusion coeff., meas. by Langmuir probes from cross spectrum of thermal density fluctuations 2—12410
analogue system, calibrated oscilloscope display 2—28598
anomalous heating by resonant excitation of magnetoacoustic waves 2—35501
boundary layers, electron-density and electron-temp. meas. 2—24767
bremsstrahlung continuum, absolute intensity calc., i.r. technique 2—8957
conductivity probe for turbulent systems 2—12407
d.c. octopole, observation of neoclassical, intermediate and Pfirsch-Schulter diffusion 2—35464
delayed microwave scanning technique for meas. of periodically varying parameters 2—31977
dense plasma focus, location and dimensions, X-ray method 2—24777
density, self-consistent stationary distributions in weakly inhomogeneous constant mag. field 2—8939
density meas., applic. of K-H$^+$ charge exchange cross section meas. in 150-8000 eV range 2—18343
density ratio determ., spectroanalysis, analytical line pairs 2—4609
dielectric props., system penetrated by helicon waves and effect on microinstabilities 2—35473
diffusion type plasma, transition to positive column discharge 2—31947
discharge under external h.f. field, microwave probing 2—28600
divided Langmuir probe method for meas. of ion temp. 2—35533
Doppler and Stark shifts in spectra of arc heated flow from plasma jet, interferometric meas. 2—24765
double Langmuir probes in dense flowing transient plasmas, perturbations caused by presence 2—35532
drift waves in strongly sheared magnetic field 2—18668
duoplasmon arc discharge, inhomogeneous axial magnetic field 2—24772
electron conc. det. by Faraday splitting of laser modes 2—35542
electron conc. in stabilized plasmas, laser interferometer method 2—32049
electron concentration distribution and electric and mag. fields in impulsive erosion plasma accelerator 2—3226
electron concentration laser interferometer study in resonator 2—3227
electron cyclotron radiation measurements in magnetic mirror plasma system 2—28566
electron cyclotron reson. obs. from light scatt. cross section 2—12404
electron density, CO_2 laser absorpt. and interferometry method 2—15473
electron density, continuous obs. using cavity resonators 2—32047
electron density, laser interferometer obs. 2—28594
electron density, velocity and gas dynamic pressure obs. 2—35528
electron density and temp., direct- display meter 2—8956
electron density meas., comparison of Langmuir probe with microwave interferometer and cavity methods 2—35527
electron density meas. by Langmuir probes from cross spectrum of thermal density fluctuations 2—12410
electron density meas. in cylindrical microwave cavity resonators, influence of discharge tube configuration 2—32038
electron density meas. with i.r. Schlieren interferometer 2—21822
electron density profiles determ. from Tonks-Dattner reson. 2—8955
electron energy distribution det., collisionless probe theory 2—35457
electron energy distribution functions, meas. by sample and hold method 2—24770
electron number density profile, photometric technique using optical switch 2—28599
electron plasma interaction with large amplitude wave, trapping effects 2—18672
electron plasma wave echo amplitude 2—18670
electron temp., cumulative ionization effect, floating double probe method 2—21819
electron temp. and concentration det. by laser radiation scattering 2—32039
electron temp. and density of Ar ion laser discharge by Tonks-Dattner resonances 2—39132
electron temp. det., effect of time averaging spectral line intensities in presence of fluctuations 2—32044
electron temp. det. from rate of ionization 2—32036
electron temp. meas. by radiofrequency probe method, low density plasma 2—15478
electron temperature, effect of beam like electrons on double probe 2—15474
electron temperature, electrostatic probe and radar backscatter obs., reasons for two distinct physical quantities 2—15475
electron trapping, test wave amplification and instability 2—18674
electronic temp. determ., effect of impurities on X-ray continuum radiation 2—35499
electrostatic energy analyser for ion velocity measurement 2—18639
electrostatic fluctuations under conditions of turbulent heating, spectral obs. using probe 2—32035
electrostatic probe, induced current 2—12408
electrostatic probes, spectroscopic, laser, microwave and r.f. techniques, conference (Oxford, September 1971) 2—24828

Plasma continued
diagnostics continued
electrostatic probes, spectroscopic, laser, microwave and r.f. techniques, conference (Oxford, September 1971) 2—21860
electrostatic refr. probe 2—12406
electrostatic wave ionograms, ray tracing and ionograms 2—35547
e.m. absorption, meas. using laser with reformed emission frequencies between 460 and 700 nm 2—39135
e.m. interactions, nonlinear, for remote control, heating and meas. of electron distributions and trapped particles 2—24774
energy distrib. of ions and electrons in injector-diverter apparatus of stellarator 2—32040
energy exchange between large amplitude waves and the electron energy distribution 2—18673
floating double-probe method, mag. field effect 2—12409
flow velocity obs. in T-tube 2—24769
fluctuation data, FFT spectral analysis techniques for acquisition and processing 2—18638
fluctuations, digital spectral analysis 2—32048
gas diode microphone, plasma acoustics 2—35548
glow discharges, pressure considerations associated with ion sampling 2—32125
Hall potential difference obs. 2—24868
helical, three-frame pulsed holographic interferometry 2—24776
h.f. electrical probe 2—28595
high-energy supersonic streams, expts. with two flow-swallowing enthalpy probes 2—28587
holographic camera, ultra-fast 2—7953
immersion-type electrical conductivity probe for anisotropic plasmas 2—32029
inert gases, use of bremmstrahlung continuous spectrum, electron density obs. 2—35531
interferometry 2—35526
ion acoustic instability, cross-field current-driven 2—18693
ion and electron temp. det. using laser light scattering in e.m. shock tube 2—35540
ion attracting cylindrical probe, Sonin-Laframboise-Chen paradox 2—32042
ion distribution function for single ended Q-machine by wake behind obstacle in plasma flow 2—21823
ion temperature, obs. using transient current in cylindrical Langmuir probe 2—18634
ion velocity in accelerated beam, optical method of obs. 2—32045
ion-acoustic waves, trapped-ion instability 2—18694
ionic composition meas. by Langmuir probes from cross spectrum of thermal density fluctuations 2—12410
ionization degree on anode side of electrical double sheath in low press. Hg discharge 2—8924
ionization wave electron energy distrib. function det. by sample and hold technique 2—32072
ionospheric laboratory 2—33529
ionospheric probes for Japan Antarctic Research Expedition rockets 2—10761
Langmuir probe measurements, area influences and floating potentials 2—21818
Langmuir probes in plasma with anisotropic velocity distribution 2—35524
Langmuir sheath thickness meas. using ion acoustic waves and hot probe 2—32031
laser beam refr. method for electron density determ. 2—3223
laser light scattering homodyne technique for obs. of drift waves 2—35541
laser light scattering technique 2—39151
laser probing of weakly ionised turbulent gas flow, comparison of neutral and plasma fluctuations 2—3291
laser produced plasma, in keV temp. range 2—24775
line emission profile obs. in X-ray region, mechanism of formation and heating det. 2—35537
linear antenna probe, near zone fields 2—35544
local properties, technique for use in turbulent system 2—35536
magnetic field direction meas. in Tokamak plasma by laser scattering 2—35525
magnetic field measurement by laser dispersion 2—32034
magnetic field strength obs. using charge particle beams 2—8959
mass: charge ratio, techniques for obs. 2—3224
in MHD generator, effects of ambipolar diffusion 7821 2—7821
microwave, active single wire Fabry-Perot interferometer 2—35546
microwave electron density measuring systems used in controlled fusion research 2—28592
microwave holography application 2—17650
microwave holography application 2—18640
microwave interferometry in high temp. partially ionized dense gases 2—39150
microwave scattering, by surface charge waves 2—35481
microwave set-up for electron density meas. 2—24768
microwave signal attenuation in plasma-beam discharge, effect of low frequency oscillations 2—24798
microwave spectra in toroidal apparatus with turbulent heating 2—3211
in mirror type experiments, 2X II and Baseball II 2—28591
applic. of models, partial local thermodynamic equilibrium 2—21764
moving arc column, use of probes to determine cross sectional size 2—35634
multichannel energy anal. of ions and fast charge exchange atoms 2—18633
multimode cavity for simultaneous excitation and electron density meas. 2—15477
multiply charged heavy ion content, energy and spatial distrib. obs. 2—35529
nanosecond transmission photography using pulse clipped Q-switched laser 2—35543
neutral atom spectrometer, calibrated, for ion temp. meas. for 0.165-10keV energy region 2—15479
non-resonant large diameter plasma confined in magnetic bottle 2—24742
nonequilibrium plasma, H line ratios as electron temp. indicator 2—21820
applic. of nonlinear wave-wave coupling, scattering and radiation 2—21824
optical magnetic probe, magneto-optical effect 2—35551
optically thin sources, applixation of Abel integral eqn. for calc. radial distribution of emitters 2—15469
plasmatron jet, weakly ionized gas stream velocity meas. using MHD pickup 2—15470

Plasma continued
diagnostics continued
positron interaction method 2—12405
potential distribution in space charge sheath by nondisturbing probe method 2—32043
potential meas. in streaming plasma by production of cold ions in plasma and electrostatic energy analyser 2—18635
potential measurement using probe with small openings 2—3225
potential surrounding moving test-particle in a quiescent plasma 2—18595
probe, plane, sheath, positive ion, thickness, probe pot., parabolic approx. 2—12395
probe behaviour in high-speed collision free flow 2—6090
probes, large, theory of h.f. props. in isotropic plasma 2—35535
pulsed atom system applic. 2—12033
pulsed discharge, electron concentration determination 2—32119
pulsed discharge plasma, density by optical interferometer 2—28601
Q-switched pulse stretching applications 2—14399
radiation temp. of layer in optical resonator 2—35495
rarefied, penetration of ions to collector of multielectrode probe 2—32030
r.f. probes, resonance effect and admittance in ion rich plasma sheath 2—35545
rotation asymmetry meas. in self-magnetic field of plasma discharge by coil systems 2—18636
Rozhdestvenskii-Hook method, for plasma in MHD generator 2—31959
scattering and interferometric studies using CO_2 laser light 2—35539
scattering method, for low-temp. plasmas 2—32037
seven channel Fabry-Perot spectrum analyzer for laser scattering meas. in θ-pinch 2—24766
shock produced plasma, laser detectors obs. interferometer, X-ray bremsstrahlung spectra, probe and neutron 2—28508
space potential det. from max. amplitude of l.f. noise 2—24771
space potential obs., review 2—15476
spectroscopic study of homogeneous plasma column using h.f. generator 2—39153
static spherical probe theory verification in moving h.p. plasma 2—8954
stellarator, plasma trapped in injector-divertor device, microwave study 2—6088
streaming measurements in arc, drag force on probe 2—35637
subnanosecond interferometry of plasma filaments in laser produced spark 2—39157
temperature electron and ion measurements of laser created plasma 2—24773
temperature meas. in laser pulse induced gas breakdown by soft X-ray continuum emission technique 2—32033
temperature measurement, field absorption method 2—35553
temperature measurement, hot W-wire method 2—35549
temperature measurements, theory of diffraction interferences 2—35552
temperature obs., effect of electron diffusion 2—35530
temperature waves meas. connection with drift type instability 2—21856
time of flight measurement of velocity spectrum of atoms from θ-pinch 2—34784
in Tokamak devices 35503 2—35503
transient, pulsed submillimeter interferometer 2—28593
transient technique using simultaneous CO_2 laser interferometry and absorpt. 2—15471
turbulent, study of probe geometry effects 2—21816
turbulent plasma studied by external ion beam 2—32041
vapour density pulses meas. from arc discharge using ionization gauge with current stabilisation circuit 2—18719
velocity diffusion in an electron beam-plasma interaction 2—18637
wave growth in a large unmagnetized electron beam-plasma system 2—18671
X-ray and neutron emission from laser produced plasmas 2—21814
Ar, shock produced, electron density profiles, ioniz. relax. 2—24768
Ar, viscosity meas. 2—3228
Ar beam, optical spectroscopy obs. of ionic axial energy 2—35538
Ba, ion temp. obs. using Zeeman scanning technique 2—32046
CO-O flames, comparison of single- and double-probe meas. of electron temperature 2—37823
CO_2, electrical and thermal conductivity obs. using stabilized electric arc 2—6071
Cs, dependencies on pressure of various ion species, mass spectral obs. 2—24779
Cs, low pressure discharge, electron energy distrib. function meas. 2—21821
Cs resonance charge exchange cross section at 2eV 2—18603
CsI determ. of electron density of an ionized plasma 2—12367
H, ion density and electron temp. using atomic beams 2—32032
^{2}H, confined in open-ended magnetic well system, density and ion energy obs. 2—24756
He, absorption methods for measuring absolute concentration of metastable atoms 2—31954
He, discharge, frequency and strength of applied microwave electric field 2—18359
Hg, concentration measurement behind a shock front using continuous recording of interference fringe shift 2—28596
K, selective excitation spectroscopy using laser source 2—18642
K h.f. fluctuations in the density gradient 2—18643
LiI, determ. of electron density of an ionized plasma 2—12367
N_2, viscosity meas. 2—3228
Ne positive column, time resolved meas. of electron distribution function in low-pressure arc 2—39096
O_2-H_2 detonations, effect of cool boundary layers on ionization probe obs. 2—35534
Xe, laser produced, schlieren cinematographic and holographic obs. 2—21825
Xe, radiating plasma flow produced by shock waves, conductivity probe obs. 2—32050
Xe plasma produced in cascaded arc 2—21761
electromagnetic waves
absorption, by linear layer in resonance region 2—215
absorption, from v.h.f. discharge 2—8961
absorption, meas. using laser with reformed emission frequencies between 460 and 700 nm 2—39135
absorption by inhomogeneous plasma 2—32001
absorption for mirror and diffuse boundaries, limited magnetoactive plasma 2—31990
absorption of incident wave on warm homogeneous plasma half-space 2—31979

Plasma continued
electromagnetic waves continued
aerial-plasma interaction, effect of mesh size on admittance of plane grid capacitor 2—35491
anisotropic electron plasma, Cherenkov type radiation 2—8935
anisotropic plasmas, strong field e.m. wave interaction 2—39126
anomalous heating by resonant excitation of magnetoacoustic waves 2—35501
anomalous skin effect in semibounded plasma studied using results on specular reflection of electrons 2—990
antenna, cylindrical, in weakly ionized plasma, radiation resistance 2—14337
antenna immersed in warm plasma 2—35490
antenna in magnetically active plasma, quasi-electrostatic field, quasi-one-dimensional structures 2—28560
attenuation due to scatter 2—35493
back scattering in magnetoactive plasma containing random inhomogeneities in electron density, correlation theory 2—31973
backscattered cross section computation, turbulent media, expansion scheme 2—12386
bremsstrahlung emissivity of turbulent plasma particles 2—31996
in cavity, rad. spectrum 2—12422
circularly polarized field, high-frequency, stability of plasma boundary in transverse constant mag. field 2—8982
circularly polarized field, high-frequency self-consistent stationary distributions in weakly inhomogeneous constant mag. field 2—8939
collisionless, dense, penetration, self-action 2—12384
continuum radiative transfer, application to Scorpius X-1 2—37337
cosmic media, current-optical effects 2—33696
cosmological model, photon rest mass effect on e.m. dispersion 2—20463
coupled longitudinal and transverse waves propagation normal to magnetic field, three fluid theory 2—31993
coupled mode propagation, in presence of shear 2—18610
crossover frequencies in plasmas with two species in presence of Coriolis force 2—18613
cyclotron modulation of scattered waves, optimal experimental conditions 2—35492
cyclotron resonance interaction, algebraic solutions 2—15462
cyclotronic harmonic waves, dispersion characts. 2—12383
dense electron plasma, intensity- dependent propagation characteristics of circularly polarised high power laser radiation 2—28559
diffraction, at impedance wedge in an anisotropic plasma 2—39127
diffraction, by moving semi-infinite screen 2—15464
dipole, short, in hot uniaxial plasma 2—30963
dipole antenna, in space-time periodic media, radiation patterns 2—34262
drifting uniaxial magnetoplasma, phase group velocity of e.m. waves 2—31974
dynamo-optical effects, cold inhomogeneous moving electron plasma, no collisions, no external magnetic field 2—35482
electron cyclotron radiation measurements in magnetic mirror plasma system 2—28566
electron cyclotron reson. obs. from light scatt. cross section 2—12404
electron density meas. in cylindrical microwave cavity resonator, influence of discharge tube configuration 2—32038
electron-cyclotron wave reson. in inductively coupled h.f. discharges 2—12382
electrostatic plasma waves conversion, dispersion relation for all wavelenghts 2—31986
e.l.f./v.l.f. radiation resist. of finite dipole in multicomponent system 2—31978
e.m. instabilities in anisotropic plasma, nonlinear development 2—8987
extraordinary wave collision-induced instability of extraordinary wave 2—39183
far i.r. laser radiation, cooperative enhanced scattering from nonthermal theta-pinch plasmas 2—39134
field detection in microwave plasma interaction and wave transformation 2—32005
fluctuations in layer 2—6075
f.m. wave propag., nonlinear phenomena 2—28550
generation by microwaves in crossed and parallel fields 2—24781
growth rate and stability in counterstreaming plasmas 2—31981
gyrosynchrotron radiation fields and its transfer in magnetoactive system 2—31972
half-space, e.m. field fluctuations, external currents, elec. field correl. spectral density 2—39130
heating at lower hybrid resonance 2—31997
heating by wave transformation at frequency close to lower hybrid frequency 2—24713
heating in toroidal trap by h.f. waves 2—24716
heating in Tuman 2 toroidal device 2—24755
helical slow wave system 2—35485
h.f. field distribution in absorption region 2—32002
h.f. heating 2—24714
hybrid freq. range propag. and heating 2—24792
hybrid-frequency cutoffs in gyrotropic waveguides, axially magnetized 2—17486
induced Compton scattering and nonlinear propagation, laser-created plasmas 2—28558
induction discharge plasma, density fluctuations, e.m. scatt. study 2—31989
interactions, nonlinear, for remote control, heating and meas. of electron distributions and trapped particles 2—24774
interface between vacuum and anisotropic Vlasov plasma 2—18616
ion cyclotron resonance plugging and heating of cusped He plasma 2—39137
ion-acoustic two-stream instability in unstable radiofrequency generated plasma 2—28645
ionosphere, dispersion and absorption, oblique sounding experiments 2—33514
large amplitude whistler, computer simulation of collisionless damping 2—31980
laser light absorption, resonant mechanism 2—32008
light phenomena in interaction of oppositely directed shock waves and gas-discharge plasma 2—12378
linear lossy inhomogeneous cold magnetoplasma, radiation from arbitrary source, integral eqns. 2—993
linear wave conversion in inhomogeneous warm plasma 2—35486
lower hybrid wave plasma interaction and heating by collisionless absorption 2—31998
magnetic field, investigation of characteristics of waves 2—8940

Plasma continued
electromagnetic waves continued
magnetic line source, with moving sheath 2—31985
magneto-ionic medium, e.m. pulse propagation 2—21782
magnetoactive, excitation with opposite polarization to helicon 2—16117
magnetoactive plasma, plane layer, high-amplitude TM waves 2—21785
magnetoplasma, electron drift vel. meas. by microwave dragging 2—8917
magnetoplasma, perturbation theory 2—35480
magnetoplasma, propagation discussed for frequencies near electron-cyclotron resonance frequency 2—15459
magnetoplasmas, electromagnetic instability, relativistic streaming effects 2—32100
magnetosphere, helicon, whistler propagation, non-linear effects 2—13746
microwave, nonlinear scattering from a plasma column 2—18614
microwave, scattering by surface charge waves 2—35481
microwave attenuation due to coating of aperture antenna 2—14332
microwave combination scattering from plasma waves in electron beam-plasma 2—28615
microwave emission resonance for bounded magnetoplasma 2—15484
microwave heating of electrons in Q-machine causing ion-acoustic collisionless shocks 2—21781
microwave phase shift, interferometer zebra stripe method 2—23436
microwave propagation in circular waveguide partially filled with cold plasma dielectric 2—28561
microwave radiation interaction with solid state plasma 2—992
microwave scattering from underdense and overdense turbulent plasmas 2—31982
microwave signal attenuation in plasma-beam discharge, effect of low frequency oscillations 2—24798
microwave spectra in toroidal apparatus with turbulent heating 2—3211
microwaves, off-resonance heating of mirror confined plasmas 2—28555
microwaves, Tonks-Dattner resonances in Ar ion laser discharge, det. of plasma electron density and temp. 2—39132
microwaves propagating through r.f. plasma, amplitude modulation 2—28553
mode conversion in inhomogeneous plasma 2—12385
modulation, percentage calculation, meas. of associated varying parameters 2—31977
monochromatic wave excitation during injection of electron beam into plasma 2—15461
multipole h.f. fields for dynamic stabilization of MHD instabilities 2—18680
near electron cyclotron resonance, asymptotic theory of electron motion 2—28563
nonhomogeneous magneto-active plasma, hybrid resonances 2—21784
nonlinear cond. induced by freq. modulated e.m. wave propag. 2—28548
nonlinear harmonic generation in thermal magnetized plasma of incident microwave beam 2—31995
nonlinear interaction between charged particle and two h.f. waves beating near cyclotron frequency 2—32000
nonlinear interaction in magnetized electron beam 2—12381
nonlinear penetration of plane plasma layer by e.m. waves 2—3208
nonlinear scattering from inhomogeneous column 2—31992
obliquely incident, scattering by inhomogeneous column 2—14321
opacity considerations and nonlinearity 2—35483
overdense plasma, propagation of strong waves 2—3209
penetration, at frequencies close to lower hybrid resonance, into magnetised plasma 2—21788
penetration into semi-infinite collisional plasma 2—39131
plane antenna, ‘entry’ admittance 2—28549
plane pulse propagation asymptotic representation 2—14304
plane wave interaction with inhomogeneous warm plasma column 2—991
polarization of e.m. wave, effect on wave energy absorption caused by linear transformation of waves 2—18608
polarization of wave propagating in plasma with magnetic shear, poloidal magnetic field in Tokamak 2—28554
propagation along static magnetic field, effect of static electric field 2—18615
propagation and absorption of ion hybrid waves in weakly inhomogeneous plasma layer 2—28557
propagation and absorption of ion hybrid waves in weakly inhomogeneous plasma layer 2—28556
propagation in infinite circular cylinder in absence of collisions 2—39125
propagation of strong field modulated waves in anisotropic plasma 2—18607
propagation perpendicular to static magnetic field in nonuniform magnetized plasma, conversion of fast waves to slow 2—31988
radar scattering cross sections of space vehicles in electron plasma medium 2—33568
radiation propagation, correlation function 2—15453
reflection, plasma and e.m. waves at moving dielec. medium and compressible plasma interface 2—21783
reflection and transmission by moving plasma slab, coeff. calc. 2—31976
retarded, influence of acceleration on radiation from inhomogeneous plasma beams 2—3210
review, whistler modes and helicon waves correlation 2—24710
r.f., lower hybrid heating in Alcator 2—6076
r.f. helix excitation of densities high above critical in cylindrical plasma sources, effects of magnetic field 2—24711
r.f. transmission between two whip antennae in warm plasma 2—15463
r.f. wave negative absorpt. near electron cyclotron harmonics 2—8936
scattering, from turbulent plasma slab 2—35484
scattering, generation of enhanced electrostatic oscillations in magnetized plasma 2—8938
scattering by electron density space time fluctuations 2—3207
scattering by underdense plasma layer, perturbation technique for Gaussian, sech, parabolic density distribution 2—31975
scattering cross section with wave vector perpendicular to confining magnetic field 2—15460
second harmonic generation in laser created plasma 2—31994
semi-infinite, moving, anisotropic, reflection and transmission 2—21787
s.h.f. oscillations interaction with low temp. gas discharge plasma 2—39204
simulation methods, generation of radiation field noise 2—39128
simultaneous absorption of quasitransverse and quasilongitudinal waves in plasma 2—32003
singly scattered radiation, depolarization in turbulent plasma 2—39129
slab, isotropic, impulse reflection 2—31987
solid-state and gaseous discharge, non linear theory of propagation 2—4142

Plasma continued
electromagnetic waves continued
stability in relativistic plasma 2—6074
stimulated scattering and self-focusing in laser produced plasma 2—3212
stochastic heating by random microwave noise 2—32004
stratified plasma with dielectric window, input admittances of pair of identical rectangular slot antennas studied 2—8934
superluminous and subluminous waves, stability in streaming relativistic magnetoplasma 2—24814
supraluminous, instability, in weakly turbulent plasma, growth, damping, and bifurcation 2—18612
surface wave modes, excitation and detection 2—15458
surface waves interaction with electron beam, cylindrical geometry 2—21786
synchrotron emitting plasmoid in coronal magnetic field, moving Type IV radio burst 2—17087
Thompson scattering of laser light, six channel interference filter spectrum analyser 2—39133
three wave resonant interaction in magnetized plasma 2—28552
total dipole radiation intensity 2—35489
transformation and absorption of h.f. waves into rapidly damped longitudinal plasma waves 2—24712
transverse, energy and momentum exchange 2—18609
transverse mode, nonlinear focusing 2—31984
travelling ionization disturbances, undamped nonlinear oscillations 2—21832
travelling-wave antenna excitation of cyclotron waves 2—12424
upper hybrid frequency, nonlinear resonant mode conversion 2—28638
upper hybrid frequency zone, linear mode conversion 2—28562
upper hybrid resonance, reflection of stream by combined barrier of Pleiade type 2—31991
v.h.f., absorption in plasma inhomogeneous along mag. field 2—8942
v.h.f. absorption, non- linear effects 2—8941
warm, lossy two-layer, admittance of half-wavelength slot antenna radiating into, electron temperature effects 2—30958
waveguide, flanged, covered with dielectric or plasma slab, radiation 2—18617
waveguide, unpaired dipolar mode, quasistatic approx. 2—23460
weak r.f. signals, perturbing effect on electron impact ionizing collisions 2—28523
weakly ionized plasma, wave propag. equations 2—28551
whistler, stability of steady, large amplitude 2—18611
whistler instability in electron plasma with anisotropic and non-Maxwellian velocity distributions 2—8937
whistler-mode in magneto-active plasma penetrated by particle beam 2—30346
X-band microwaves, thermal self focusing 2—35487
Ar, r.f. induction, departure from equilibrium, spectroscopic obs. 2—39107
Cs, currentless photoresonance 2—35494
D targets, enhanced absorption of incident laser energy 2—12417
H, generation by microwaves in axial magnetic fields below electron cyclotron resonance 2—31999
H with ionic impurities, radiation losses in plasma focus type Z-pinch 2—8943
He, afterglow slab, propagation of strong circularly polarized wave near electron cyclotron frequency 2—8944

magnetohydrodynamics
see also Magnetohydrodynamic waves
adiabatic flow along magnetic lines of force, exact solution of equations of motion 2—28532
Alfven waves, amplification in time varying magnetic field 2—28621
alfven waves, in anisotropic plasma under hose instability conditions 2—6069
Alfven waves, parametric amplification 2—39173
arc dynamics in transverse magnetic field, energy dissipation and momentum transport 2—24930
axisymmetric flows in external magnetic fields with Hall effect 2—31960
axisymmetric MHD equilibria, stability to localized modes 2—21852
beam moving along curved mag. field lines, reverse deflection and contraction 2—18625
closed electron drift accelerator with extended acceleration region 2—21813
collective modes, collisionless kinetic modes involving trapped particles 2—24731
collisionless hydromagnetic shock waves propagating along magnetic field, existence conditions 2—8932
collisionless shock waves, radiation from, wave generation and transformation processes 2—31957
combustion products from turbulent plasma under channel flow, electric conductivity dependence on turbulence 2—28533
cumulation of plasma and magnetic field as a result of implosion of a strongly conducting liner 2—39114
current-carrying, helical equilibrium configurations obtained by means of MHD approx. 2—12449
cyclotron waves, dispersion, perpendicular to magnetic field 2—32064
cylindrical capacitor with crossed fields, resonant properties 2—21771
d.c. arc, rotational properties in unhomogeneous magnetic field 2—24931
decay of weakly ionized plasma, in electrically conducting plasma, in longitudinal magnetic field 2—31952
density and radial density variation, ambipolar diffusion theory 2—31955
dielectric operator, exact and linear, for stratified streams with velocity gradients 2—15456
drift motion and instability in curved mag. field 2—18677
duct flow, magneto-viscous interaction effects 2—3200
duct flow at moderate Hartmann number 2—3201
elliptical cylinder, current distributions and magnetic surfaces 2—12368
e.m. propagation, along static magnetic field, effect of static electric field 2—18615
equilibrium and stability by dynamic techniques 2—15455
equilibrium configurations for sphere, generalization, application to confinement and ball lightning 2—32013
fast compression, low-β stellarators, plasma shift with finite electrical conductivity 2—24682
filamentary mag. structure on current sheath of coaxial accelerator, solar flare type processes 2—11135
finite β cylindrical, equilibrium with bumpy field 2—12354
finite pressure minimum-B config., magnetostatic equilibria 2—35505
flux conservation theorem 2—24678
free atom and ion concentration, Rozhdestvenskii-Hook method 2—31959
h.f. discharge, nonequilibrium plasma subsonic jet 2—28531

Plasma continued
- **magnetohydrodynamics** continued
  - high beta (l=1) stellarator experiments, shock wave heating 2—24738
  - inhomogeneous high pressure plasma, driving of Alphven type waves 2—21838
  - instability dynamic stabilization by multipole h.f. fields 2—18680
  - instability theory for interpretation of magnetic perturbations in Tokamak 2—24824
  - integrability of MHD eqns. for rotational symmetric configuration of plasma with infinite conductivity 2—12370
  - ionosonic oscillations, stability, in variable magnetic field 2—32065
  - linear equilibrium in helicoidal image, displacement in Harmonica 2 and Tokamak 2—31958
  - Lorentz plasma in strong magnetic field, electron distribution function calc. 2—12369
  - magnetic and gravitational energy release by resistive instability, application to solar flares 2—982
  - magnetic nozzle flow, fully ionized, quasi-one-dimensional anaysis 2—35471
  - magnetic pumping for plasma heating 2—24684
  - magnetic pumping in toroidal geometry for heating of low beta plasma 2—24683
  - magnetic structure of ionizing skew shock waves, MHD downstream interaction 2—28540
  - magnetization and determination of hydromagnetic equilibrium 2—28534
  - magnetoacoustic waves, mutual transformation at plasma inhomogeneities 2—39115
  - magnetopause, Kelvin-Helmholtz instability 2—16877
  - magnetoplasma, thermal spread and wave propagations near resonances 2—15459
  - magnetoplasma with skin current, instability due to electron temperature gradient in ion and electron acoustic branches 2—12356
  - model for dense pinch phase of focus 2—24735
  - motion in field of two-dimensional magnetic dipole 2—6064
  - MPD accelerator, axisymmetric, influence of mass velocities on current distribution 2—35512
  - non-linear waves in cold collisionless plasma 2—8968
  - nonequilibrium MHD plasmas at high magnetic field strengths, current and potential distributions 2—21770
  - parametric instability of magnetoactive plasma, excitation by nonpotential vibrations 2—32103
  - particle acceleration, cylindrical cavity with H_{111} standing waves in axial magnetic field 2—21344
  - pinch, diffuse reverse field, instabilities 2—39184
  - plane plasma capacitor in crossed fields, perturbation of parameters 2—21772
  - plasmoid motion in axially symmetrical mag. field 2—981
  - potential created by sinusoidally varying imobile point charge 2—15454
  - Rayleigh Taylor instability of viscous Hall plasma with magnetic field 2—28641
  - relaxation, quasi-linear, of fast ions moving transverse to magnetic field 2—8925
  - solar magnetic field, oscillatory hydromagnetic dynamo 2—14017
  - solar wind, effect of interplanetary magnetic field 2—14014
  - solar wind, hydromagnetic waves and discontinuities 2—26903
  - spatial diffusion in magnetic field, anomalous contribution of l.f. fluctuations 2—24668
  - stability, hydromagnetic analysis by finite element method 2—32094
  - stability, non-localized higher-m instabilities 2—24822
  - stability in field of finite amplitude Alfven wave 2—32093
  - stability in magnetogasdynamics, generalized theory 2—8933
  - stability in Tokamak and hybrid systems, toroidal equilibria 2—24681
  - stability of stratified atmosphere flowing over liquid 2—26657
  - straight high current discharge, anomalous energy losses, plasma heating 2—24685
  - streaming relativistic magnetoplasma, stability of superluminous and subluminous waves 2—24814
  - surface waves, nonlinear, on axisymmetric MHD pinch 2—3234
  - Tokamak, $\beta \gg 1$ and arbitrary current distribution 2—24733
  - Tokamak plasma heating, axisymmetric magnetic pumping 2—28535
  - Tokamak system, toroidal plasma column, maintenance of longitudinal current 2—24732
  - toroidal, low press. discharge, radial field 2—18600
  - two dimensional model, Earth's magnetic tail, plasma trapped on current sheet in dipole field 2—22992
  - two fluid model in crossed E and B fields for hydrodynamic instability obs. 2—6097
  - two-stream instability turbulent heating in computer simulations 2—12371
  - undamped transverse plane waves in fluid of finite diffusivities 2—18579
  - velocity meas. of weakly ionized gas stream from plasmatron by MHD pickup 2—15470
  - wall stabilized arc in transverse magnetic field, coupled distrib. of viscous flow and temp. 2—24680
  - waves, coupled resonances 2—15446
  - waves, in a field of particular structure, coupling 2—15458
  - weakly ionized radiating plasma, MHD waves, unified linear theory 2—21848
    - Ar cross-flow arc, transverse magnetic field effects 2—28678
    - Cu vacuum arc, effect of axial magnetic fields $\leqslant 1$ kG 2—24679
    - He, in cond. wall tube, ion density radial distribs., field fluctuations 2—21774
    - W vacuum interrupting arc, transverse magnetic field 2—24947
- **measurement technique** *see Plasma/diagnostics*
- **oscillations**
  - *see also Magnetohydrodynamic waves;*
  - acoustic, linear theory obs. of stability 2—6096
  - acoustic in low temp. plasma, effects of magnetic field on stability 2—39164
  - acoustic instability of two temp. plasma in crossed electric and magnetic fields 2—28639
  - acoustic wave, ion, dispersion in magnetized plasma 2—3233
  - acoustic wave amplification in presence of electric field 2—28629
  - acoustic wave amplification in sheath 2—28628
  - acoustic wave propagation, production and amplification 2—18620
  - Alfven wave finite amplitude, and hydrodynamoc plasma stability in field 2—32093
  - Alfven waves, amplification in time varying magnetic field 2—28621
  - Alfven waves, nonlinear Landau damping 2—1000
  - Alfven waves, parametric amplification 2—39173

Plasma continued
- **oscillations** continued
  - Alphven type waves, inhomogeneous high pressure plasma, instabilities 2—21838
  - aurora, radio, ion-acoustic waves 2—40988
  - beam-plasma instabilities, high-order wave mixing 2—24796
  - beam-plasma interaction, phase focusing 2—6094
  - beam-plasma system, higher harmonics of electron oscillation 2—32058
  - beam-plasma system, Langmuir noise levels, H spectra, Stark broadening 2—18667
  - Bernstein-Greene-Kruskal wave with trapped electrons 2—28643
  - at bow shock crossings, distant 2—20370
  - bursts, h.f. interactions with spatially periodic magnetic field 2—35565
  - Cherenkov emission in presence of finite amplitude wave 2—8966
  - cold collisionless plasma, non-linear hydromagnetic waves 2—8968
  - cold electron, stability with electron beam in presence of h.f. electric field 2—28633
  - collective, of relativistic radiating electron plasma 2—3236
  - collective, resulting in drift beam instability for ion beam-plasma interaction 2—35574
  - collisional drift waves, effects of heat transport 2—21844
  - collisional drift waves, end plate damping in Q-machines 2—18669
  - collisional drift waves in presence of coherent ion acoustic or Langmuir waves, dispersion properties 2—8969
  - collisional drift waves in presence of coherent ion acoustic or Langmuir waves 2—32109
  - collisional drift waves in Q-machine with end plate, parallel current and sheath effects 2—12428
  - convection of weakly ionized plasma in a nonuniform magnetic field, computer study 2—12427
  - current driven turbulence, dissipation and plasma heating 2—24657
  - current free, weakly ionized, in mag. field, l.f. oscill. buildup 2—32063
  - cyclotron absorpt. region, relativistic effects 2—8976
  - cyclotron harmonic waves in inhomogeneous plasma 2—39174
  - cyclotron harmonic waves in inhomogeneous plasma theory 2—39180
  - cyclotron harmonic waves in reflex discharge, dispersion relation 2—39176
  - cyclotron waves, anomalous reflection and transmission 2—24793
  - cyclotron waves, dispersion, perpendicular to magnetic field 2—32064
  - cyclotron waves, theory and computer expt. on self-trapping instability 2—35568
  - cylindrical waves in anisotropic plasma 2—35557
  - decay instability, weakly inhomogeneous system 2—28648
  - density fluctuation instability in mag. field 2—32108
  - density perturbations and waves in Q-machines, collective interaction and freely streaming ions 2—12440
  - digital spectral analysis, diagnostics 2—32048
  - dispersion in beam systems with external magnetic field 2—999
  - dispersion in beam systems with pressure anisotropy 2—998
  - dispersion relation for bounded systems 2—18669
  - dispersion relations for bounded systems, application to plasma 2—28612
  - dissipative drift modes in Tokamak type configurations 2—24823
  - distribution function, fine structure due to interaction with electron beam 2—28632
  - Doppler spectrum of source moving through warm electron plasma, effect of spatial dispersion 2—32067
  - drift oscillations in stellarator, large electron free-path lengths 2—28582
  - drift wave propag., effect of ion mixtures 2—18658
  - drift wave stabilization by magnetic shear feedback and dynamic methods 2—28651
  - drift waves, dynamic stabilization 2—32106
  - drift waves, h.f., dispersion relation 2—28623
  - drift waves, mechanism of energy loss in Tokamaks due to electron trapping 2—18627
  - drift waves in strongly sheared magnetic field 2—18668
  - drift waves laser light scattering homodyne technique for obs. 2—35541
  - electrical, wall influence in d.c. glow discharge 2—32128
  - electron, effects of Coulomb collisions on maintenance of Landau damping 2—6093
  - electron, obs. of nonlinear decay by induced scattering on ion-waves 2—32086
  - electron and ion wave echoes, effect of relaxation, review 2—21846
  - electron and ion waves, incomplete dispersiion function 2—24803
  - electron beam, highly energetic, interaction with dense plasma 2—18594
  - electron beam interaction, electron distrib. function oscills. 2—35556
  - electron beam space-charge wave propagation 2—27422
  - electron beams, relativistic and nonrelativistic, interactions with waves in plasma beam discharge, non-linear effects 2—24805
  - electron Bernstein mode propagation expts. 2—32085
  - electron cyclotron damping 2—12426
  - electron cyclotron heating in nonuniform magnetic field, computer calc. 2—3193
  - electron cyclotron waves, excitation 2—8979
  - electron plasma interaction with large amplitude wave, trapping effects 2—18672
  - electron plasma ion acoustic waves, modulational instabilities due to trapped electrons 2—18685
  - electron plasma wave coupling to ion acoustic waves 2—997
  - electron plasma wave echo, second order, structure 2—3237
  - electron plasma wave echo amplitude 2—18670
  - electron streams, multi-velocity, effect of inhomogeneity on electrostatic oscillations 2—15483
  - electron trapping, test wave amplification and instability 2—18674
  - electron trapping by electron plasma wave, nature of instability 2—35570
  - electron wave, nonlinear frequency shift, obs. by numerical simulation and perturbation expansion 2—32060
  - electron wave propag. in inhomogeneous system, ballistic waves detection 2—18656
  - electron waves, electron-neutral collision effects on propagation 2—32062
  - electron waves in magnetoplasma, obs. of line structure in light scattering spectrum 2—35566
  - electron-cyclotron wave reson. in inductively coupled h.f. discharges 2—12382
  - electronic shock waves in collisionless plasma, expt. obs. 2—21779
  - electrostatic ion wave propagation perpendicular to mag. field, amplitude depend. 2—21834
  - electrostatic oscillators, enhanced, generation in magnetized plasma by e.m. waves 2—8938
  - electrostatic wave propag. and instabilities 2—32091

Plasma continued
oscillations continued
electrostatic wave propagation near electron cyclotron harmonics, dispersion relation 2—8972
electrostatic waves, enhanced damping due to combination scatt. from density oscillation 2—39169
electrostatic waves, h.f., models for propagation 2—32070
electrostatic waves, large amplitude, trapping of beam electrons from beam plasma interaction 2—18584
electrostatic waves, perturbed distribution functions, exact calc. 2—12435
electrostatic waves convers. to e.m. dispersion relation for all wavelengths 2—31986
electrostatic waves in Vlasov plasma undergoing E×B drift 2—8971
electrostatically driven oscillations near lower-hybrid resonance frequency, direct observation 2—21835
caused by e.m. wave penetration at frequencies close to lower hybrid resonance, into magnetised plasma 2—21788
e.m. wave transformation at frequency close to lower hybrid frequency for plasma heating 2—24713
e.n. perturbations, negative absorption of microwaves 2—35561
energy exchange between large amplitude waves and the electron energy distribution 2—18673
excitation by electron beam-plasma interaction 2—39191
excitement by relativistic and nonrelativistic electron beams, instabilities and wave transformation, nonlinear theory 2—24806
explosive three wave interaction, wave coupling 2—28637
extraordinary modes, nonlinear resonant interactions mode conversion at upper hybrid frequency 2—28638
extraordinary wave collision-induced instability of extraordinary wave 2—39183
fluctuation data, FFT spectral analysis techniques for acquisition and processing 2—18638
flute, stabilisation in rarefied magnetised plasma by feedback with finite number of stabilising elements 2—3239
Fokker-Planck treatment of non-linearly interacting waves 2—8967
frequency shift due to trapped particles and time asymptotic distribution functions 2—24794
frequency shifts and broadening, nonlinear theory 2—18661
gas discharge in neon, magnetized, obs. 2—32055
generation and transformation, radiation from collisionless MHD shock waves 2—31957
glow discharge, correlations between self-excited moving striations and plasma parameters at points along discharge tube 2—21881
gun plasma, optical meas. of degree of turbulence from He I and II spectral lines 2—39170
gyro-resonance absorption in the corona and the fine structure of solar radio bursts 2—11075
heat conductivity mechanism for laser heating in case of spherical and cylindrical waves 2—39162
helicon wave, effect on microinstabilities 2—35473
h.f. discharge, resonances under transverse mag. field 2—3203
h.f. oscillation spectrum, phase velocities 2—24797
h.f. resonance excitation of moving striations 2—12481
high speed nonlinear plasma waves 2—39177
hot collisionless plasma, nonlinear evolution of wave packet, effect of trapped particles 2—18663
impulse arc, spark expansion, cylindrical non-equilibrium thermal wave model for 2—15521
inert gas heavy current column at low press., ionization waves 2—28607
initial value problems for nonrelativistic linearised Vlasov-Maxwell equations in uniform magnetic field 2—15482
ion acoustic, parametric resonance in alternating electric field 2—28635
ion acoustic resonances, refined fluid theory for bounded nonuniform plasmas 2—28626
ion acoustic shocks, post frontal turbulence 2—39172
ion acoustic solitary waves in collisionless warm plasma, formation and interaction 2—8978
ion acoustic turbulence, turbulent heating theory 2—28616
ion acoustic wave excitation by parametric heating and strong high-frequency fields 2—12439
ion acoustic wave growth in presence of two beam plasma with high temp. ratio 2—18692
ion acoustic wave propagation in non Maxwellian plasma of single ended Q-device 2—12436
ion acoustic wave propagation in plasma with double-humped ion velocity distribution function 2—12442
ion acoustic waves, causing ion heating 2—3240
ion acoustic waves, influence of collisions 2—32059
ion acoustic waves, ion ballistic contribution 2—15486
ion acoustic waves, parametric excitation by high-frequency electric fields 2—15493
ion acoustic waves, propagation from and to spherical or cylindrical conductor 2—28608
ion acoustic waves causing ion heating in ion streaming plasma 2—12431
ion acoustic waves in ion streaming plasma causing ion heating 2—21839
ion acoustic waves use for Langmuir sheath thickness meas. 2—32031
ion and electron waves propagation and damping in thermally ionized collisionless plasma 2—21841
ion beam thermalization 2—28642
ion cyclotron heating by modulated electron beam 2—18655
ion cyclotron wave, resonant excitation, h.f. heating 2—21810
ion cyclotron waves, excitation using travelling-wave antenna 2—12424
ion cyclotron waves, parametric instabilities 2—35569
ion density perturbations propagation in Q-machine with double-humped velocity distribution functions 2—12441
ion free streaming wave propagation 2—18653
ion heating by fast magnetoacoustic waves 2—21766
ion plasma, parametric excitation 2—32056
ion sound decay instability induced by large amplitude Bernstein mode 2—18675
ion sound oscills. of plasma cylinder, surface acoustic waves 2—15487
ion sound wave propag. in presence of large neutral background 2—24791
ion velocity distributions meas. at wave exciting grid of single ended Q-machine 2—12403
ion virtual wave props. 2—39168
ion wave, finite amplitude, nonlinear partial differential equation 2—15485
ion wave, propagation in presence of ion- neutral collisions, Boltzmann collision operator approx. 2—28624
ion wave excitation by tenuous modulated beam or high energy electrons 2—21840

Plasma continued
oscillations continued
ion waves, asymmetric sidebands in current carrying plasma 2—32057
ion waves, interference pattern 2—18659
ion waves, resonant excitation by v.l.f. and whistler waves 2—8974
ion waves instability when $T_e \gtrsim T_i$, destabilizing effect of current 2—21853
ion-acoustic resonances in cylindrical plasma, comparison with refined fluid theory 2—21843
ion-acoustic wave dispersion in cylindrical column 2—21836
ion-acoustic waves, trapped-ion instability 2—18694
ion-acoustic waves and ionization waves review comparisons of phenomenological props. and physical mechanisms, review 2—21847
ion-cyclotron, in magnetic mirror trap 2—24825
ion-sound turbulence, anomalous resistivity calc., inconsistency 2—18654
ionic of bounded plasma, derivation from treatment of effects of weak coupling in assembly of oscillators 2—28614
ionic waves, first order ion distribution function in Q-machine 2—12434
ionization waves, backward and forward, time and space interference 2—32079
ionization waves, moving and standing striations, electron energy distribution functions, obs. by sample and hold techn. 2—32072
ionization waves, nonlinear interaction with sound waves 2—32083
ionization waves, self-excited, in positive column 2—32076
ionization waves, standing striations as solutions of Pekarek equation 2—32071
ionization waves, theory of wave-mode coupling 2—32080
ionization waves, unstable, discontinuity formation 2—32077
ionization waves, unstable, mode coupling 2—32081
ionization waves, wake of acoustic pulse moving to cathode 2—32075
ionization waves in positive column, influence of longitudinal mag. field 2—32074
ionization-recombination oscillations, in magnetic traps 2—12433
ionizing electron waves, laser induced plasmas 2—24799
ionosonic, parametric amplification mechanism in weakly ionised plasma in variable electric field 2—3238
ionosonic, stability in variable magnetic field 2—32065
ionosonic microturbulence, anisotropy of the electric fields in a powerful h.p. discharge 2—8988
Landau damping, nonlinear and longitudinal wave growth in magnetic field 2—8977
Landau damping, second order, secularity, free theory 2—24802
Langmuir and acoustic wave fluctuations, nonlinear level, excited by parametric decay instability 2—32096
Langmuir and acoustic waves, nonlinear saturation 2—21849
Langmuir waves, parametric coupling in inhomogeneous plasma 2—39165
large amplitude electron wave, nonlinear frequency shift formulated by subtraction procedure 2—18664
large amplitude wave, deformation of electron distribution function 2—28529
large amplitude waves, diffusion effects on damping 2—28631
large-amplitude electron plasma oscillation, effect of external circuit on anomalous resistivity 2—18665
l.f., drift-dissipative instabilities, in limited gas discharge plasma 2—32104
l.f. and instability in plasma with anisotropic electron temp. 2—35558
l.f. eigenmodes, parametric excitation, comparison 2—32061
l.f. oscillations, microwave signal attenuation 2—24798
linear mode conversion in upper hybrid frequency zone 2—28562
linear wave conversion in inhomogeneous warm plasma 2—35486
linear waves in mixed imcompressible barotropic beam plasmas 2—24804
longidutinal, in mag. field, fast electron excitation 2—1001
longitudinal, contributions to transport processes in stellar media 2—7411
longitudinal, Landau treatment of collisionless damping 2—24800
longitudinal, nonlinear instability 2—32095
longitudinal waves, instabilities and induced scattering due to nonlinear Landau damping in magnetic field 2—8985
longitudinal waves, non linear interaction in two fluid plasma, excitation of solar type II burst emission 2—6095
low r.f., excitation by lumped element line generator 2—17523
low-frequency, drift-diffusion instability of weakly ionised inhomogeneous plasma 2—3247
magnetic drift waves near proton cyclotron frequency 2—12391
in magnetic field, weakly ionized currentless plasma of r.f. discharge 2—32066
magnetic perturbations in Tokamak 2—24824
magnetoacoustic resonance in nonuniform current carrying plasma column 2—8973
magnetoactive plasma, effect of strong homogeneous h.f. electric field 2—35559
magnetoplasma, l.f. waves, spectral broadening, nonlinear theory 2—18657
magnetosonic solitary waves, laminar motion obs. 2—35563
magnetosonic waves in reacting thermonuclear plasma 2—39171
magnetosonic waves in relativistic anisotropic plasmas, dispersion relation 2—8970
magnetosphere, excitation of ion acoustic waves 2—30315
magnetosphere, helicon, whistler propagation, non-linear effects 2—13746
metallic colloids, absorption spectra, influence of plasma waves 2—36864
microwave combination scattering from plasma waves in electron beam-plasma 2—28615
modulated RF discharge, neutral acoustic 2—18703
multimode cavity for simultaneous excitation and electron density meas. 2—15477
near-wall h.f., rel. to electron energy distrib. function 2—1002
nonhomogeneous magneto-active plasma, hybrid resonances 2—21784
nonlinear electrostatic waves construction 2—28611
nonlinear ionization waves in unstable positive column, response to weak pulse disturbance 2—24790
nonlinear wave, maximum amplitude 2—39178
nonlinear wave, with Landau damping, perturbation theory 2—18651
nonlinear wave interactions 2—28636
nonlinear wave-wave coupling, applic. to diagnostics 2—21824
nonlinear waves in nonuniform plasma 2—28613
parametric coupling between electron and ion waves in self resonant plasma 2—39175
parametric decay instability, saturation and threshold, obs. of new oscillatory saturation states 2—18687
phase velocity and stabilization, non linear variation 2—12425
positive column, Fourier analysis of nanosecond pulses 2—28619
potential surface waves in non-homogeneous plasma at plasma resonance in transition layer 2—39167

Plasma continued
oscillations continued
precursor and wake effects 2—3206
propagation, parallel, of nonlinear l.f. waves to mag. field in high β plasma 2—3235
propagation and absorption of ion hybrid waves in weakly inhomogeneous plasma layer 2—28557
propagation and absorption of ion hybrid waves in weakly inhomogeneous plasma layer 2—28556
pseudowaves and ion acoustic waves, simulation 2—12438
pulsations of decreasing period as proton beam instability in plasma, model of geomagnetic variations 2—30367
pump waves, self-induced resonant decay processes 2—28634
Q-machine, grid-excited waves, perturbed density and ion velocity distribution function 2—12437
quasi static waves of inhomogeneous bounded plasma, approx. dispersion relation 2—28610
quasielectrostatic cyclotron harmonic wave propagation in topside ionosphere, energy reflection in warm magnetosphere 2—28630
quasimonochromatic, steady state, excitation by relativistic electron beam, nonlinear theory 2—39161
radial distribution in development of instability in mag. field 2—12450
radiation temperatures, upper limits, near fundamental and harmonics of electron plasma frequency 2—8963
reflection at moving dielec. medium and compressible plasma interface 2—21783
reflex-arc, turbulence, spectral characts. 2—12423
resonant, nonlinear interaction 2—39166
resonant beam-plasma interaction mechanism for glow discharge breakdown 2—15513
resonant behaviour of column in axial mag. field, effect of temp. inhomogeneities 2—8964
review 2—24710
saturation of current driven ion wave turbulence 2—32088
short beam-plasma devices, h.f. beam instability excitation 2—18649
short-wave, electron Larmor radius finiteness rel. to mirror instabilities and h.f. fire hose 2—15488
slow surface wave propagation, in ionic sheaths 2—28618
space charge waves in bounded anisotropic systems, dispersion relations 2—8965
spatial and temporal response of electrons in h.f. plasma to small amplitude fast voltage pulse 2—21842
spatial evolution of low-freq. perturbations produced by a grid 2—18662
spatial ion wave echoes, collisional effects 2—39110
spatial structure, arising from drift dissipative instability in mag. field 2—32084
stability of anisotropic plasma to almost perpendicular magnetosonic waves 2—8980
stationary solitary wave, with finite temperature, conditions for propagation 2—24801
stimulated ion acoustic wave generator in laser created plasma, red shift explanation 2—32087
Sun, energy transport by longitudinal plasma waves, solar neutrinos 2—33757
superhighfrequency noise signal modulation, plasma-electron beam system 2—39106
surface waves, nonlinear, on axisymmetric MHD pinch 2—3234
surface waves at plasma vacuum interface, dispersion relation, disappearance of plasmon effect 2—18650
surface waves on border of half spaced plasma with metal grating 2—32068
temperature waves meas. connection with drift type instability 2—21856
thermal density fluctuation cross spectrum use in meas. of plasma properties 2—12410
thermal wave, fusion energy considerations during laser heating of plasma 2—39163
thermal waves, self similar in two temperature system 2—28622
thermonuclear plasma, ion cyclotron oscills., transverse current excitation 2—28609
thermonuclear reaction waves, in solid density D-T plasma 2—18660
Tonks-Dattner reson., electron density profiles determ. 2—8955
Tonks-Dattner reson., parametric excitation 2—28664
toroidal plasma, effect of an electrostatic turbulence on trapped particles 2—12429
toroidal turbulent heating machine, cross field ion acoustic instability 2—18686
transformation and absorption of h.f. waves into rapidly damped longitudinal plasma waves 2—24712
transition from amplitude oscillation to linear Landau damping, numerical investigation 2—39179
turbulence, heating in θpinch devices 2—28546
turbulence, theory, based on a Weiner type process of diffusion in phase space 2—24795
turbulence in magnetically confined plasmas at high electric fields 2—24807
turbulent heating of dense isothermal system, transverse current 2—21837
two-stream, electrostatic, under conditions of turbulent heating, spectral obs. using probe 2—32035
u.h.f. drift waves from electron stream drifting through density gradient in plasma, dispersion relation 2—18666
u.h.f. signal, parametric amplification in beam-plasma system in finite magnetic field 2—35564
undamped, nonlinear, effects of strong e.m. field on electron ionization, temperature 2—21832
unstable mode, large amplitude, parametric suppression by pumping 2—18688
unsteady weak nonlinear modulated waves, propagating along mag. field in multicomponent quasineutral plasma 2—32069
Vlasov-Maxwell equations in collisionless plasma, deviation from uniform state 2—989
warm plasma, two-component, propagation of waves perpendicular to magnetic field 2—21833
wave functions, quantum analogy, restatement of transformation 2—28617
wave growth in a large unmagnetized electron beam-plasma system 2—18671
wave induced losses from double ended Q-machine at onset of current driven collisional drift instability 2—21854
wave process generated by local source or disturbance in plasma subjected to magnetic field 2—39160

Plasma continued
oscillations continued
wave propag. in hybrid freq. range and heating 2—24792
wave propagation in presence of Coriolis force, multispecies plasma 2—28620
wave propagation props. in streaming molecular electronic system 2—35562
wave spectrum found from non-linear saturation theory for decay-type parametric instability 2—15494
waves, transverse and longitudinal, parametric excitation by intense laser light near plasma frequency 2—12432
weak nonlinear waves, collisional theory, based on moment equations of Boltzmann equations 2—35477
Ar, cylindrical inductively-coupled h.f. discharge at low pressure, electron-cyclotron resonance 2—39181
Ar, ion waves, suppression by r.f. electric field 2—32089
Ar, magnetoplasma, resonances in microwave emission 2—15484
Ar column, ionization waves, suppression using Takayama grids 2—32078
Ar positive column, interference of l.f. waves 2—8997
CO and CO mixtures, turbulent ionization waves 2—32082
H drift waves, collisionless, resonant characteristics, comparison of exprt. with linear theory 2—21845
He, field free magneto-plasma, rel. to perpendicular diffusion 2—8975
He, ion acoustic waves, externally excited, existance range 2—28625
He, magnetoplasma, resonances in microwave emission 2—15484
He, weakly ionized, acoustic wave generation in low pressure afterglow 2—12443
Hg positive column, feedback control of self-excited electrostatic waves 2—18652
Hg vapour, parametric excitation 2—32056
K, fluctuations in the density gradient 2—18643
Ne, ionization waves, time resolved obs. of electron energy distribution function 2—32073
Ne, kinetic theory of externally excited ionization waves in the weak current column, electron velocity distribution function 2—6092
Ne, magnetoplasma, resonances in microwave emission 2—15484
Xe pulsed gas discharge, dependence of frequency on conditions 2—28627
production
on absorbing materials, by rhodamine laser radiation 2—39159
arc generators, construction, mode of operation, characts. 2—35554
arc source, d.c., capillary, for use in spectrochemical analysis 2—10657
long coaxial, outflow of plasma into vacuum 2—3232
collisional type in magnetic mirror trap 2—24752
duoplasmatron ion source, intense beam with extraction energies >10 keV 2—7880
duoplasmatron ion source, model of arc 2—7877
duoplasmatron ion source, use with spike cathode 2—7876
expansion cup design, analysis 2—8962
film cooling on anode, use of refractory material for anode 2—18631
generator cooling water temperature meas. with resistor-thermometers 2—34226
HELIOS facility for quiescent, steady- state plasma studies 2—12420
high-energy ion prod. in laser-produced plasma 2—39154
homogeneous column by means of h.f. generator 2—39153
injection and dissociation of accelerated H_2 granions 2—24788
injectors with capacitive and inductive energy storage, plasma clusters acceleration 2—3231
ion beam, collisionless, to simulate ionospheric plasma 2—18644
ion source, large area, high current, for controlled fusion experiments 2—7882
ion source, multi-aperture, for 1 kV injection into controlled fusion expt. 2—7884
ion source for high current operation 2—7891
ionization of residual gas in e.m. trap 2—39141
jets, source with non-cylindrical electrode geometry 2—24764
laser, expanding, precursor ionization fronts 2—12379
laser, heating mechanism, electron temp. and refl. study 2—24780
laser, heating mechanisms for nuclear fusion 2—8960
laser, interferometry 2—35526
laser, obs. of highly charged heavy ion content 2—35529
laser created, thin target, electron temp. scaling laws 2—21827
laser generated, characterization 2—15481
laser glass, rel. to damage investigation 2—26098
laser glass surface damage, holographic obs. 2—27505
laser irradiation of solid targets, effects of magnetic field on plasma 2—39158
laser on metal surface, breakdown products 2—996
laser produced dense plasma application to controlled fusion 2—24783
laser produced spark, subnanosecond interferometry of plasma filaments in spark 2—39157
laser radiation in keV temp. range on solid H and D 2—24775
with laser system, multibeam 2—3230
laser-solid interaction, ioniz. model, Raman-antistokes light 2—12415
laser-solid interaction, one-dimens. 2—12414
laser-solid interaction, pondermotive forces 2—8918
in magnetic trap, by injecting electron beam, heating condition 2—6087
by microwaves, in crossed and parallel fields 2—24781
neutral beam injection in mirror systems 2—24784
olefins, by laser heating, refl. rad. spectra 2—39156
θ pinch, conditions and mechanism of heating 2—24785
plasmatron jet, velocity meas. of weakly ionized gas stream using MHD pickup 2—15470
plasmoids, propagation in nonlinear Alfven wave 2—12416
quiescent large volume collisionless plasma sustained by high frequency voltage 2—12418
quiescent plasmas in magnetic field by beam- plasma discharge 2—28605
relativistic by adiabatic compression 2—39138
sliding spark light source with solid Xe insulator for photoionization of gases 2—35508
spark discharges, supply processes, hydrodynamic characteristics of discharge channel 2—21889
superconducting Levitron, and heating 2—21829
thermal electrodeless plasmas generation below r.f. range 2—24717
thermonuclear, laser-solid interaction 2—32052
on transparent dielectric, by laser irrad. below damage threshold 2—29860
Al, by laser heating, refl. rad. spectra 2—39156
Al emission spectra from a ruby laser- produced plasma, 35 to 50 Angstroms 2—18283
Al foil, laser irrad. 2—21828
Ar, by v.h.f. discharge, obs. of absorption lines 2—8961

Plasma continued
production continued
Ar, Co_2 laser produced, magnetic field dependent breakdown 2—32053
Ar, discharges, ion production probabilities 2—21876
Ar, non-equilibrium, in mag. field 2—24786
Ba, photoionized, from metastable atoms 2—18327
CO_2 TEA laser. from solid H_2 targets 2—24782
Cs nonideal plasma, electric-discharge shock tube 2—28603
D-T, laser channelled gas embedded z pinch, theoretical estimate of structure 2—18646
D, by laser beam, spectral investigation of reflected light 2—18645
D targets, neutron production by incident laser energy 2—12417
D_2, dense high vel., from coaxial accelerator 2—39155
D_2O ice, by laser heating, refl. rad. spectra 2—39156
H, by CO_2 TEA laser-solid H_2 interaction 2—24787
H, rotating system form. in homopolar config. 2—32051
H_2, 0.1 to 10 mtorr, microwave generation by end-on and side-on irradiation 2—32054
^2H, by collisional shock waves 2—28508
^2H, electrodeless generation in axisymmetric toroidal vessel 2—24699
^2H, nanosecond laser focussed on solid target 2—35555
^2H blob, laser generation from ice pellet freely falling within superconducting mag. bottle 2—15480
He, by CO_2 laser, structure of fireball 2—6091
He, CO_2 laser produced, magnetic field dependant breakdown 2—32053
He, quiescent column, in skipping B-fields 2—24789
Hg, dense quiescent, using long capillary positive column 2—24876
Hg lamp with sodium thallium and indium iodides 2—3229
Li, arc source, principal characteristics 2—12419
LiD, by laser heating, refl. rad. spectra 2—39156
Mg, laser beam production on solid surface 2—21830
N, quasistationary, using rectangular current pulse 2—28606
U in Q-device BARBARA, single-ended opteration, applications 2—12421

shock waves
attenuation obs. for flow velocity det. in T-tube 2—24769
collective dissipation obs. in θ pinch expts. 2—28545
collisional, produced in e.m. shock tube, numerical obs. 2—31968
collisional theory, based on moment equations of Boltzmann equations 2—35477
collisionless, electronic shock waves, expt. obs. 2—21779
collisionless, laser scatt. meas. of turbulence 2—39122
collisionless, propagation, turbulent heating and non linear processes 2—28544
collisionless perpendicular, jumps in electron temp., pot. and mag. field 2—28543
collisionless plasma, near-steady oblique shock waves 2—39123
collisionless plasma, quasi-shock waves in longit. mag. field 2—31967
collisionless resistive turbulent low-Mach-number shocks, self-consistent theory 2—24707
conservation relations, laminar, magnetosonic, oblique, electrostatic and turbulent, book 2—3206
electron density and diffusion velocity of ionised air in front of shock wave 2—28539
electron heating in perpendicular collisionless shock 2—8931
electrostatic, space charge condition and Mach number 2—3205
electrostatic, stable high-Mach-no. in collisionless system 2—24704
electrostatic ion-acoustic shocks produced by density steps 2—24706
explosive interaction of negative energy Bernstein and ion acoustic waves 2—18683
heating and structures in θpinch devices 2—28546
heating in collisionless plasma, high Mach numbers 2—24708
heating to fusion temps. 2—28508
high-Mach number, oblique and collisionless, ion heating, numerical simulation study 2—18605
hydromagnetic, propagating in collisionless plasma along mag. field, existence conditions 2—8932
hydromagnetic shock waves in collisionless plasma 2—989
ion-acoustic, slug and piston problems, particle-in-cell computer simulation 2—35476
ion-acoustic, weak, propagating in uniform state, long time behavior of precursor 2—31969
ion-acoustic collisionless, by microwave heating of electrons in Q-machine 2—21781
light phenomena in interaction of oppositely directed shock waves and gas-discharge plasma 2—12378
magnetic structure of ionizing skew shock waves, MHD downstream interaction 2—28540
magnetic structure of normal ionizing shock waves 2—28542
magnetic structure of oblique ionizing shock waves 2—28541
magnetosonic shock formation, ion and electron pressure effects 2—39124
MHD, radiation from, wave generation and transformation processes 2—31957
nonequilibrium viscous shock layer of blunt body, structure 2—24705
nonstationary, collisionless, formation in wind tunnel device, ion gyroperiod time scale 2—15457
oscillation profile, effect of intrinsic viscosity in electron and ion components 2—6072
precursor ionization fronts ahead of expanding laser plasma 2—12379
rel. to pressure anisotropy 2—989
propagating perpendicular to mag. field, profile, charge separation effects 2—18604
propagation initiated by local energy release, two temperature hydrodynamic equations 2—28622
pulsed cylindrical converging shock waves, decreasing density medium 2—31971
radioisotope emission alpha particles alteration 2—35676
shock thickness, upstream and downstream magnetic field, particle density and temperature meas. 2—21780
solar corona, interaction between type III bursts and a collisionless shock wave 2—17055
solar wind 2—17059
stability in magnetogasdynamics, generalized theory 2—8933
supersonic flow around plate and cylinder bodies 2—12377
thermonuclear reactions behind shock waves due to absorption of laser radiation 2—6077
toroidally confined plasma, equilibrium potential distribution 2—24709
Ar, filamentary structure of shock driving current sheath, turbulence 2—35514
Ar, shock-heated, influence of wall boundary layer on plasma flow 2—6073

Plasma continued
shock waves continued
Ar, supersonic flow in transverse mag. field, discharge characteristics in induced electric field 2—12380
Ar II, ionic levels, study of inversion of population state at collision of shock waves 2—28547
Cs, sound emission by front of shock wave due to ionization and electron excitation 2—31970
H_2, $^2H_2$, filamentary structure of shock driving current sheath, turbulence 2—35514
^2H, highly ionized with low internal mag. field, collision-dominated shock structure 2—35478
He, electric field, densities, temperatures and shock velocities 2—35479
He, filamentary structure of shock driving current sheath, turbulence 2—35514
Kr plasma, shock heated, electron densities and ionization relaxation times 2—35470
Xe, radiating plasma flow production, conductivity probe obs. 2—32050

stability
absolute and convective instabilities, saddlepoint treatment 2—32099
acoustic instability, linear theory obs. 2—6096
acoustic instability of two temp. plasma in crossed electric and magnetic fields 2—28639
adiabatic compression 2—39138
afterglow, weakly ionized, enhanced diffusion assoc. with instabilities 2—15447
alfven waves, in anisotropic plasma under hose instability conditions 2—6069
anisotropic, magnetosonic wave near ion cyclotron frequency, almost-perpendicular to mag. field 2—8980
axisymmetric MHD equilibria, stability to localized modes 2—21852
beam cyclotron instability, theory and computer simulation 2—24813
beam instability, in equatorial electrojet, excitation of longitudinal waves 2—22998
beam plasma instability obs. 2—3242
beam-plasma instabilities, high-order wave mixing 2—24796
beam-plasma instability, effects of inhomogeneities in density 2—12447
beam-plasma instability, possibility of narrowing h.f. radiation spectrum at development 2—35578
Bernstein-Greene-Kruskal wave with trapped electrons 2—28643
BGK equilibrium, accessibility of exact nonlinear stationary states in water bag model computer expts. 2—28646
boundary in transverse constant mag. field and high-frequency circularly polarized field 2—8982
cold electron oscillations, with electron beam in presence of h.f. electric field 2—28633
collective modes, collisionless kinetic modes involving trapped particles 2—24731
collision-induced instability of extraordinary wave 2—39183
collisional cyclotron instability in Ramsauer effect ionized gases 2—32090
collisional drift instability driven by axial current observed in double-ended P-machine cesium plasma 2—3245
collisional drift waves in presence of coherent ion acoustic or Langmuir waves 2—32109
collisional trapped particle instability, nonlinear saturation in Tokamak geometry 2—32097
collisional trapped-particle instability, radial dependence 2—21850
collisionless plasma, Vlasov equation and stellar gas 2—41083
constricted arc, influence of plasma nonequilibrium and radiation transfer 2—24925
constricted plasma , between 2 electrodes, stability analysis 2—3216
contrastreaming instability in a one- dimensional finite-length system 2—12446
convective instability of cyclotron resonance interaction 2—15462
counter beam, energy distrib. function 2—39185
crossed field instabilities driven by electron beam produced radial d.c. electric field and ion reaction 2—24820
cumulation of plasma and magnetic field as a result of implosion of a strongly conducting liner 2—39114
current driven collisional drift instability in Q-machine, wave induced losses and anomalous resistivity 2—21854
current driven turbulence, dissipation and plasma heating 2—24657
current-carrying, helical equilibrium configurations obtained by means of MHD approx. 2—12449
curved magnetic field destabilization, electronic electrical cond. finiteness 2—18691
cyclotron instability in finite pressure plasma 2—32092
decay instability, weakly inhomogeneous system 2—28648
density fluctuation instability in mag. field 2—32108
diffuse linear pinch, growth rates of instabilities 2—39186
discharge, velocity of gas flow, stabilization 2—15442
dispersion relation for bounded systems 2—18669
dissipative drift modes in Tokamak type configurations 2—24823
dissipative trapped ion instability, conditions for stability in axisymmetric toroidal confinement systems 2—18678
Dory-Guest-Harris instability, nonlinear evolution 2—12448
drift, and meas. of temp. waves 2—21856
drift beam instability, plasma-ion beam system in longitudinal magnetic field 2—35574
drift cone instability, finite beta stabilization 2—39187
drift cyclotron instability, effect of finite β plasma 2—24812
drift diffusion, instability in mag. field 2—32107
drift dissipative instability, dynamic stabilization 2—32106
drift dissipative instability, spatial structure of oscillations arising 2—32084
drift dissipative instability in cont. r.f. plasma, frequencies and growth rate 2—21859
drift instability in Q-machine column, passive feedback control by tunable series resonance circuit 2—21858
drift motion and instability in curved mag. field 2—18677
drift wave, growth rate and boundary under linear theta pinch conditions 2—18679
drift wave stabilization by magnetic shear feedback and dynamic methods 2—28651
drift waves, h.f., dispersion relation 2—28623
drift waves laser light scattering homodyne technique for obs. 2—35541
drift-diffusion instability of weakly ionised inhomogeneous plasma 2—3247
drift-dissipative, l.f. oscillations in limited gas discharge plasma 2—32104

Plasma continued
stability continued
dynamic equilib. of curved θ pinch achieved by effect of oscillating axial current on toroidal drift of column 2—12430
dynamic stabilization of m=1 mode on screw pinch 2—28649
dynamic stabilization of transverse Kelvin Helmholtz instability by a.c. electric field 2—21857
Earth's radiation belt, mag. scattering of charged particles on cyclotron instability waves 2—10750
electromagnetic instability in magnetoplasmas, relativistic streaming effects 2—32100
electromagnetic waves in relativistic plasma 2—6074
electron beam stability, problem of critical currents 2—3246
electron beams, counter streaming, gyrating linear theory of 2-beam instability 2—15489
electron beams, relativistic and nonrelativistic effects on instabilities and wave transformation, nonlinear theory 2—24806
electron cyclotron and ion acoustic instabilities and turbulent heating in Tokamak devices 2—24821
electron cyclotron drift, and anomalous diffusion, resistivity, and turbulent heating 2—24667
electron cyclotron drift instability and turbulence, obs. of cross field anomalous resistivity 2—3244
electron stream drifting through density gradient in plasma, dispersion relation for u.h.f. drift waves produced 2—18666
electron trapping, test wave amplification and instability 2—18674
electron trapping by electron plasma wave, nature of instability 2—35570
electron-beam filamentation in strong magnetic fields 2—39188
electron-plasma ion-acoustic decay instability, saturation for comparable electron and ion temperatures 2—18690
electrostatic instabilities at electron cyclotron freq. harmonics 2—32091
electrostatic instabilities in equational electrojet 2—7329
electrostatic instabilities in two component anisotropic system 2—35573
electrostatic plasma wave with trapped electrons modulational instabilities 2—18685
electrostatic theory, Tokamak plasma, development from two component fluid equations 2—24811
electrostatic two ion beam instability mechanism for ion heating in oblique collisionless shock waves 2—18605
e.m. instabilities in anisotropic plasma, nonlinear development 2—8987
e.m. instability, counterstreaming with anisotropic temps., theory, review 2—35572
e.m. wave propagation, energy and momentum exchange 2—18609
e.m. waves in symmetric counterstreaming plasmas 2—31981
e.n. perturbations, negative absorption of microwaves 2—35561
equatorial electrojet, two stream instability stabilization 2—33510
equilibrium in TO-1 Tokamak using feedback system 2—28653
explosive interaction of negative energy Bernstein and ion acoustic waves 2—18683
feedback and dynamic stabilization of drift and transverse Kelvin-Helmholtz instabilities 2—28652
feedback control, by linked internal and external feedback 2—15492
feedback stabilization of flute instability in PHOENIX II mirror machine 2—32019
feedback stabilization of kink modes in current carrying plasma 2—6082
fluctuation data, FFT spectral analysis techniques for acquisition and processing 2—18638
fluctuations in unstable relativistic plasma 2—39192
flute oscillations, stabilisation in rarefied magnetised plasma by feedback with finite number of stabilising elements 2—3239
flute stabilization via electrostatically confined cold electrons 2—6098
flutelike microinstabilities in mirror confined plasma with broad perpendicular velocity distributions 2—3243
force free fields effects 2—15495
helical m=1 instability in linear screw pinch, dynamic stabilization 2—32102
h.f. beam plasma instabilities, nonlinear phenomena 2—24818
h.f. beam-instability in relatively short beam-plasma system 2—28644
h.f. beam-plasma instabilities, degree of coherence det. 2—35577
h.f. cone instability, conditions for suppressing in open traps 2—24752
h.f. field stabilization of nonuniform magnetized plasma 2—6101
h.f. instability in decay in adiabatic trap 2—24751
h.f. instability of finite press. plasma in presence of loss cone, effects of Landau damping 2—21851
h.f. stabilization of current carrying toroidal plasma column in longitudinal magnetic field 2—24815
high beta ring, confined in mirror trap 2—24749
high beta toroidal system with long wavelength helical fields 2—28654
hole equil. in quasi-cold system 2—15491
homopolar device 2—39142
hose-pipe in stellar systems 2—41072
hydrodynamic in field of finite amplitude Alfven wave 2—32093
hydrodynamic instabilities, in transverse magnetic field 2—6097
hydromagnetic analysis by finite element method 2—32094
hydromagnetic stability of stratified atmosphere flowing over liquid 2—26657
induction discharge plasma, density fluctuations, e.m. scatt. study 2—31989
induction heated plasma, effective voltage- current characteristic calc. from solution of plasma energy balance 2—39182
inhomogeneous high pressure plasma, driving of Alphven type waves 2—21838
of inhomogeneous Vlasov equilibria, by statistical thermodynamics 2—39189
instabilities due to nonlinear Landau damping of longitudinal waves in magnetic field 2—8985
instabilities leading to microturbulence, collective dissipation in shock waves 2—28545
instabilities of force free high β plasma 2—6099
instability excitation by almost monoenergetic electron beam 2—21831
instability of currents in gas at pressures of 1-50 torr. 2—21874
instability of inhomogeneous streams with non- uniform velocity profile with and without longitudinal mag. field 2—18648
interchange instability, in gravitational field, stabilization by combined effects of viscosity and resistivity 2—32098
interplanetary, microinstabilities in solar exosphere, model 2—33767
ion acoustic and beam, due to turbulent heating by intense pulsed discharges in OGRA-2T device 2—24816
ion acoustic instability, cross-field current-driven 2—18689
ion acoustic instability, cross-field current-driven 2—18693

Plasma continued
stability continued
ion acoustic instability due to ion streaming across magnetic field, spatial growth 2—35571
ion acoustic instabilty and collisionless thermalization 2—28642
ion acoustic microinstability, turbulent field characteristics of strong current Z discharge 2—24817
ion acoustic wave propagation in plasma with double-humped ion velocity distribution function 2—12442
ion sound decay instability induced by large amplitude Bernstein mode 2—18675
ion sound instability, current driven, and anomalous resistance, computer simulation 2—24695
ion sound instability effects for subharmonic and harmonic forcing oscillations 2—8981
ion wave current instability and anomalous resistivity 2—3241
ion-acoustic instability in two-temp. collisional system 2—24810
ion-acoustic instability of two temp. collisional fully ionized plasma, destabilizing effect of current 2—21853
ion-acoustic two-stream instability in unstable radiofrequency generated plasma 2—28645
ion-acoustic waves, trapped-ion instability 2—18694
ion-cyclotron instability in magnetic mirror trap 2—24825
ion-ion two stream instability, and collisional dissipation, between counter-streaming ions 2—15452
ionosonic oscillations, in variable magnetic field 2—32065
jet, device for automatic control and stabilization of temp. 2—6102
laser produced plasma, parametric instability rel. to heating mechanism 2—24780
l.f., anisotropic electron temp. 2—35558
l.f., nonuniform radial elec. field effects 2—8984
l.f. instability in system produced by local electron cyclotron reson. 2—15490
longitudinal instabilities, ion-acoustic and ionization waves, review 2—21847
loss cone modes in inhomogeneous mirror machines 2—24826
low current d.c. discharge, anomalous behaviour of electron gas 2—32105
magnetic fields effects on stability of acoustic oscillations in low temp. plasma 2—39164
magnetized toroidal plasma with h.f. current flow 2—28650
magnetohydrodynamic, Tokamak and hybrid systems, toroidal equilibria 2—24681
magnetoplasma with skin current, instability due to electron temperature gradient in ion and electron acoustic branches 2—12356
magnetosphere, ion e.m. cyclotron instabilities 2—20372
magnetospheric, Kelvin-Helnholtz instability 2—33500
magnetospheric instability theories, review 2—1887
MHD, by dynamic techniques 2—15455
MHD, non-localized higher-m instabilities 2—24822
MHD instabilities, dynamic stabilization by multipole h.f. fields 2—18680
MHD instabilities in weakly ionized, radiating plasma 2—21848
MHD instability theory for interpretation of magnetic perturbations in Tokamak 2—24824
microinstabilities, excitation and stabilization by r.f. electric field 2—24809
microinstabilities, in neutral injection mirror machine, threshold density 2—24753
microinstabilities or high pressure plasma and ion viscosity dependence of longitudinal thermal flux 2—39190
microinstability, influence of helicon 2—35473
mirror confined plasma, anisotropic vel. distrib., electrostatic instabilities 2—18676
mirror confined plasma, microinstability in r.f. elec. field 2—24808
modulated wave instability in multicomponent quasineutral plasma, influence of weak dissipation 2—32069
non-isothermic, electron Larmor radius finiteness rel. to mirror instabilities and h.f. fire hose 2—15488
nonlinear instability of longitudinal oscillations 2—32095
nonlinear interaction with electron beam, phase focusing of beam 2—32101
oscillating two stream instability, coupled mode analysis 2—35575
parametric decay instability, saturation and threshold, obs. of new oscillatory saturation states 2—18687
parametric instabilities, nonlinear saturation 2—21849
parametric instabilities of ion cyclotron waves 2—35569
parametric instability, nonlinear saturation, theory and applic. to ionosphere 2—32096
parametric instability of electron-ion system driven by h.f. wave 2—12445
parametric instability of magnetoactive plasma, excitation by nonpotential vibrations 2—32103
parametric instability of waves in a magnetic field due to high-frequency electric fields 2—15493
parametric suppression of large amplitude unstable mode, due to pumping 2—18688
parametrically unstable system, Cherenkov wave interaction and particle velocity 2—12444
polytropes, rotating supermassive magnetic, instabilities 2—13815
positive columns, effect of helical instability on radial density distribution, calculational method 2—24673
pulsations of decreasing period as proton beam instability in plasma, model of geomagnetic variations 2—30367
quasi-linear approx. for turbulent plasma, validity tests by application to bump-in-tail and two stream instabilities 2—18681
quasistationary longitudinal ion streams in the L-1 stellarator 2—24827
radial distribution of perturbations in mag. field 2—12450
Rayleigh Taylor instability of viscous Hall plasma with magnetic field 2—28641
Rayleigh-Taylor instability, in presence of vertical mag. field, finite Larmor radius effects 2—8983
resistive instability and magnetic and gravitational energy release, application to solar flares 2—982
resistive tearing instability, parallel viscous modification in Cartesian model of hard core pinch 2—18621
reverse field diffuse pinch, hydromagnetic and resistive instabilities 2—39184
r.f. system, nonlinear effects, l.f. instability 2—18682
saturated parametric instability, spectrum and anomalous resistivity 2—15494
saturation of instabilities excited by electron beam 2—35576
self-trapping instability of cyclotron waves, theory and computer expt. 2—35568

Plasma continued
stability continued
short beam-plasma devices, role of initial suppression of beam-plasma interaction 2—18649
slipping mode in weakly ionized system, kinetic theory 2—28647
spiraling electron beam-plasma interaction, electrostatic instability 2—39191
stabilization by h.f. rotational field 2—35567
stationary rotating plasma, hollow anode arc 2—24758
stellar gas, encounterless, self-gravitational 2—10866
streaming instability driven by d.c. electric fields in cold collisionless plasma, model of end state 2—24819
streaming plasma, nonlinear instabilities 2—6100
streaming relativistic magnetoplasma, stability of superluminous and subluminous waves 2—24814
surface waves, nonlinear, on axisymmetric MHD pinch 2—3234
thermal, with velocity shear, due to tangential discontinuity 2—12359
thermal instability, feedback stabilisation, for fusion reactors 2—24268
thermodynamic potentials for soln. 2—39093
with thermonuclear reaction products, linear theory 2—24754
Tokamak, non-round loop cross section 2—39143
ST Tokamak, stability experiments, dependence on plasma profile 2—24730
in Tokamak devices 35503 2—35503
toroidal, axially symmetric systems, equilib. config., flux functions method 2—21791
toroidal equilibrium for a high-β theta- pinch 2—12397
toroidal plasma with non-circular cross section, MHD stability 2—24670
toroidal screw pinch with non-circular cross-section 2—28574
toroidal turbulent heating machine, cross field ion acoustic instability 2—18686
transverse instability of colliding plasma, roles of ion motion and return currents 2—8986
triggering of instabilities in magnetic mirror field 2—35560
two ion beam instability in Q-machine with inhomogeneous B-field 2—18692
two-stream instability and anomalous resistivity, numerical investigation 2—8930
two-stream instability turbulent heating in computer simulations 2—12371
velocity space instabilities, driven by anisotropy 2—18684
water-bag model computer experiments, exact nonlinear stationary states 2—28513
weak D-type ionisation waves behind optically thick layer of ionised gas 2—28640
whistler instability in electron plasma with anisotropic and non-Maxwellian velocity distributions 2—8937
whistler wave, steady, large amplitude 2—18611
H plasma motion, on injection into cusp field 2—21792
K, collisional drift instability, effects of parallel wavelength 2—21855

transport processes
afterglow, diffusion cooling of electrons 2—31943
afterglow, longitudinal thermal conductivity of electron gas 2—24689
afterglow, weakly ionized unstable, ambipolar diffusion 2—15447
afterglow diffusion, space charge controlled 2—32126
anomalous resistivity in r.f. confined plasma 2—28537
background plasma creation by relativistic electron beam injection 2—15496
betatron acceleration mechanism for θ pinch with azimuthal magnetic field 2—21795
bounded system, mean diffusive motion time of charges 2—15450
charged particle motion, in axially symmetric magnetic field 2—14378
chemical transport in nonisothermal plasma, using glow discharge 2—35467
coefficients by generalized Langevin equation 2—39105
collective motions, method of redundant variables 2—27096
collisional a.c. electrical conductivity of anisothermal magnetoplasma from convergent classical kinetic equation 2—39117
collisional a.c. electrical conductivity tensor of multispecies magnetoplasma from quantum mechanical convergent kinetic equation 2—39118
collisional transport across mag field, analogy to turbulent transport in velocity space 2—15449
collisionless relaxation of ion streams 2—24666
conductivity, relationship to thermopower in nonideal plasma 2—28518
conductivity of high temperature plasma under current heating in high-shear Uragan stellarator 2—24674
constricted arc, influence of plasma nonequilibrium and radiation transfer 2—24925
convective motion due to trapped particles of plasma in l=3 stellarator field 2—3194
current layer development in mag. field with neutral line 2—39100
cut off criteria of electronic partition function and transport properties of thermal plasmas 2—28511
d.c. arc, mass transport, oscilloscopic registration method of obs. 2—24663
d.c. octopole, observation of neoclassical, intermediate and Pfirsch-Schulter diffusion 2—35464
dense non-ideal plasma, review 2—21768
dielectric function, self consistent electric field det. 2—28514
diffusion, anomalous, and turbulent heating in pinch plasmas 2—24667
diffusion, collisional, in axisymmetric torus, finite-β Tokamak plasma 2—28516
diffusion, effect on damping of large amplitude waves 2—28631
diffusion, thermodiffusion, mobility and ambipolar diffusion of electrons 2—12362
diffusion, three dimensional, in v. strong magnetic field 2—31946
diffusion and recombination in a dense Ar plasma 2—35465
diffusion in axisymmetric torus in banana regime 2—24664
diffusion near rational surface, enhancement factor 2—15448
diffusive Tokamak equilibrium, time dependent solutions 2—32018
discharge, velocity of gas flow, stabilization 2—15442
disperse flow, low temp. spectra 2—39101
drift waves in strongly sheared magnetic field 2—18668
electric field effects in axially symmetric magnetic traps 2—28520
electrical conductivity, det. from electric arc obs. 2—28515
electrical conductivity and current heating in a strong magnetic field 2—28538
electrical conductivity of two- dimensional guiding centre plasma 2—28536
electron and ion counterflow between parallel surfaces 2—24662
electron beam dynamics in longitudinal magnetic field 2—23528

Plasma continued
transport processes continued
electron diffusion, effect on gas temp. obs. 2—35530
electron pitch angle diffusion driven by oblique whistler mode turbulence 2—8916
electron plasma, nonlinear correction to conductivity tensor 2—27108
electron swarms, mobility and amplification, radial diffusion coeff. 2—35463
electron thermal conductivity, noble gases, arbitrary degree of ionization 2—28521
electron velocity distribution relaxation, calc. 2—31944
fusion, discussion of transport properties using first order relativistic kinetic equation 2—3192
fusion plasma, discussion using first order relativistic kinetic equation 2—3192
gas discharge plasma, detector characteristics, interaction with h.f. fields 2—21777
heating and cooling mechanisms, tangential discontinuity, causing thermal instability 2—12359
ion beam thermalization 2—28642
ion enhanced diffusion in quasistable drift waves 2—39104
laser focussing in conduction heating, spherical electron thermal wave 2—18592
Lorentz plasma, Boltzmann collision integral, role of high momentum transfer collisions 2—31949
low-current relativistic beam equilibria, current profile, energy distribution 2—24661
magnetoplasma, electron drift vel. meas. by microwave dragging 2—8917
magnetron, smooth-bore, turbulent diffusion study by Brownian motion 2—37925
nonlinear cond. induced by freq. modulated e.m. wave propag. 2—28548
particle acceleration, relativistic, by hydromagnetic turbulence 2—8914
potential surrounding moving test-particle in a quiescent plasma 2—18595
quasilinear diffusion of axisymmetric toroidal plasma 2—39103
radial in Tokamak discharges 2—28519
radical conditions obtained on SiO 2—35466
resonant diffusion, electron cyclotron heating by microwave fields 2—24660
self-focussing beam of ions and electrons, stationary states 2—21767
single component plasma, Boltzmann collision integral, role of high momentum transfer collisions 2—31949
solar wind, electron energy flux, parallel to interplanetary mag. field 2—17068
spatial diffusion in magnetic field, anomalous contribution of l.f. fluctuations 2—24668
temperature relaxation processes, in magnetic field 2—31941
thermal conductivity of stationary toroidal plasma 2—18588
thermalization rate and non- Maxwellian ion vel. distrib. 2—35460
thermoelectric, corrections calc. from electron distribution function for Lorentz plasma in strong magnetic field 2—12369
in Tokamak devices 35503 2—35503
toroidal and poloidal flows in axisymmetric collisional plasmas 2—24669
toroidal confinement systems 2—12360
toroidal devices, pseudo classical diffusion across magnetic field 2—24727
toroidal plasma with non-circular cross section, MHD stability 2—24670
transient response to pulsed elec. field 2—31961
turbulent diffusion in phase space 2—24795
velocity diffusion in an electron beam-plasma interaction 2—18637
water-bag model computer experiments, exact nonlinear stationary states 2—28513
waves, longitudinal, in stars 2—7411
weakly ionized, current constriction 2—24867
weakly ionized nonequilibrium flow, electron energy transfer processes 2—39099
weakly ionized plasma, conductivity rel. to microscopic density functions 2—39102
Wiedmann-Franz law for a high-frequency fully ionized plasma 2—12361
Z pinch, combination of intense relativistic electron beams 2—15466
Ar-Cs discharge, electron distrib. function, kinetic coeffs. 2—15443
Ar, electrical conductivity, in cascaded arcs, effect of deviations from LTE 2—28522
Ar, flow parameters in channel of high-frequency plasmatron 2—12363
Ar, flux, by mag. field, to 100 kOe, broadening 2—31948
Ar hydrodynamic drag on a small sphere moving relative to the plasma in local thermodynamic equilib. theoretical and exptl. study 2—35468
CO_2 jet, high-energy, vel. attenuation 2—8915
Cs, electrical conductivity, dense nonideal plasma, high temp. obs. 2—28517
Cs, electron velocity distribution functions 2—6066
Cs, turbulent diffusion, heating and resistivity 2—24665
^2H inhomogeneous plasma, hydrodynamic behaviour under heating by CO_2 laser 2—24675
He, electrical conductivity, in cascaded arcs, effect of deviations from LTE 2—28522
He, electron energy distrib. function at cyclotron reson. 2—39108
He, field free magneto-plasma, perpendicular diffusion rel. to oscillation 2—8975
He, flux, by mag. field, to 100 kOe, broadening 2—31948
He, in cond. wall tube, ion density radial distribs., field fluctuations 2—21774
Hg, electrical conductivity, dense nonideal plasma, high temp. obs. 2—28517
Hg plasma diffusion velocity 2—1009
Kr, electrical conductivity, in cascaded arcs, effect of deviations from LTE 2—28522
La free particles in dc arc plasmas burning in air 2—15451
Ne, electrical conductivity, in cascaded arcs, effect of deviations from LTE 2—28522
Ne, partially ionized, low temp., conductivity tensor 2—24671
Ne jet, high-energy, vel. attenuation 2—8915
O_2 jet, high-energy, vel. attenuation 2—8915
Sm free particles in dc arc plasmas burning in air 2—15451

Plasma diodes
high-current quasi-steady MPD accelerators, anode phenomena 2—27397
Cs, Knudsen, mechanism of current oscillations 2—21011
Cs thermionic, electric space potential 2—14362

Plasma guns *see Plasma/devices*

Plasma in solids *see Crystal electron states/plasma; Electron gas; Semiconductors; Solids*

Plasma jets *see Plasma/devices*
Plasma sheath *see Plasma confinement*
Plasma thermocouples *see Electricity/direct conversion; Plasma/devices*
Plasma torches *see Plasma/devices*
Plasma waves *see Plasma/oscillations*
Plasmoids *see Plasma*
Plasmons *see Crystal electron states/plasma*
Plastic deformation
see also Slip
acoustic emission study, review 2—22314
Al alloys, effects on fracture toughness 2—15837
alkali halide, rigidity, dislocation rosettes 2—6562
alkali halides, deformed by ultrasound, elec. field effect on internal stresses 2—6537
alloy, creep deform., electron microscope obs. 2—35978
alloy, f.c.c., Portevin-Le Chatelier bands 2—12849
alloy, martensite transform. and shape memory 2—15953
alloy crystal with dispersed precipitate, critical resolved shear stress 2—3861
alloys, light, hot torsion testing 2—9648
aluminosilicate rod, quenched, strength rel. to thermal shock 2—3887
anisotropic media, displacement and plastic distortion fields produced by dislocations 2—34038
anisotropic rigid-plastic material exhibiting plastic dilatation, plane deformation 2—2219
anisotropic yield of some common metals 2—29255
artificial earthquakes, response spectrum analysis with two ground predominant modes 2—16743
artificial graphite, rel. to elastic-plastic theory 2—15831
Au-Cu alloy, Portevin-Le Chatelier bands 2—12849
beams, segmentwise cross section, Foulkes mechanism in optimal plastic design for alternative loads 2—27144
bending, slow and dynamic, crack critical openeing, double notched sample 2—9706
β-brass, annealing, discontinuous yielding, superdislocation climb, temp. depend. 2—39781
brass, effects on fracture toughness 2—15837
α-brass, grain growth rates 2—39924
β- brass, single crystals, dynamic compressive behaviour, yield stresses 2—3853
β-brass, yield stress, anomalous temp. depend. 2—29258
buckling, of nearly cylindrical shells under lateral pressure 2—33982
buckling of cylindrical shells under compression, design criteria 2—17302
buckling of roof shell models with free edges under pressure 2—127
buckling tests on thin leaf springs 2—25476
ceramic crystal, press forging, recrystallization, fracture, strength 2—36249
circular hole, thermal stress conc., for elastic plastic strains 2—7738
composite plates and shells, buckling analysis 2—17338
compressed rigid-plastic body, breaking stresses and deformation speeds along rupture 2—5201
concrete, under repeated compressive loads, effect of understressing 2—22345
conglomerate plastics, effect of temperature and saturated humidity 2—29268
creep buckling of a curved column under a time- varying axial load 2—37680
cryostat, for study of thermally activated processes during deform. 2—25559
crystal, considered in colloidal chem. framework 2—32514
crystals, elastic twin formation, dislocation theory 2—25398
cylindrical shell, finite length, creep buckling under uniform external pressure 2—7746
cylindrical shell with circular cut-out, effect of slot on buckling load 2—33981
dynamic elastic-plastic deformation of rings produced by pulsed electron beam, numerical predictions 2—34046
Earth's upper mantle elastico-plastic 2—26453
elastic-plastic, at finite strain, non-isothermal theory 2—5196
elastic-plastic, yield condition and flow rule under finite elastic volume change 2—33980
elastic-plastic media, superposed motions 2—27184
energy considerations, rel. crack growth energy balance criterion 2—29314
fatigue test, energy dissipation meas. 2—25538
f.c.c. crystal, stage III work hardening, hydrostatic press. effects 2—19179
ferroelasticity, review 2—12988
ferromagnetic film, deformed, magnetoelastic energy calc. 2—36720
frames, segmentwise cross section, Foulkes mechanism in optimal plastic design for alternative loads 2—27144
frictional behaviour of S-137 material and surface layer struct. 2—29341
grain boundary, by glide dislocations 2—25390
graphite, high press., stress-strain curves 2—32607
graphite, pyrolytic, compression annealed, preferred orientation and degree of graphitization 2—22327
high temp., constant stress continuous load compression creep machine for small single crystals 2—36193
hot workability, torsion testing study 2—39861
hydrostatic extrusion, rods, residual stress distribution obs. 2—3883
imperfect circular ring, radially constrained, buckling 2—11340
impulsive loading of clamped beams, plastic deflection 2—37708
impulsive loading problems, lower bound on deformations 2—2192
Inconel 600, explosive shock deformation, thermal recovery 2—9656
inhomogeneous, emission electron microscopy, microhardness 2—19174
laminated plastics materials, spontaneous 2—22270
Laves phases, physical props. 2—9476
low cycle deformation and failure resistance, transverse deformation measurements 2—29345
machined surface layer by grinding, struct., thermal residual stress, temp. distrib. 2—1284
martensite, strain ageing mechanism 2—32700
martensitic transforms., f.c.c.⇌h.c.p., f.c.c.⇌d.h.c.p. type, strain relns. 2—25616
meas. by means of ultrasonic surface waves 2—29378
metal, allotropic transition, adhesion and friction rel. to struct. 2—3921
metal, cold working, reduction of latent energy in heat cond. equation 2—39883
metal, computer estimation of deformation parameter 2—32601
metal, conical turning, lubrication and rate of rotation 2—12844

Plastic deformation continued
metal, cubic, anisotropy in sheet forming operations 2—25582
metal, cyclic stressing by u.s. waves for testing and quality control 2—19233
metal, deform. texture, theory 2—39916
metal, dislocation vel. and density determ. from deform. waves of continuous yielding 2—36108
metal, dispersion hardening rel. to Bauschinger effect 2—25574
metal, fatigue failure prediction, complicated stress-strain history 2—39817
metal, f.c.c., struct. changes, stacking fault energy depend. 2—39681
metal, f.c.c. and b.c.c., conical flow in metal forming 2—36211
metal, high temp., rel. to self diffusion 2—12875
metal, high voltage electron microscopy 2—3863
metal, martensite transform., shape memory effect 2—9789
metal, phenomenological theory, static recovery effects 2—39794
metal, review 2—12845
metal, strain hardening, strengthening coeff. 2—12951
metal, stressed state diagram, anal. 2—1377
metal, thermoactivation parameters determ. 2—36126
metal, treatment to raise yield point 2—12923
metal, under dynamic loading, dissipation and damage, theory 2—15828
metal, weakening and superconductivity transition 2—22499
metal, yield pt. under tension, plotting unit 2—41354
metal crystals, energy relations, method of temp. meas. 2—19178
metal fibre, porous, pressing and sintering, dimensional changes, residual stress relaxation 2—29257
metals, dislocations, review 2—39778
metals and alloys, superplasticity, origin of quasiliquid states 2—32614
necking instabilities in elastic-plastic plates 2—17336
Ni-Cr alloy, influence of diffusion creep on precipitate-free zone form 2—29270
nonlinear, direct meas. method 2—25536
notch in round beam under cyclic impact bending, kinetics 2—25498
nuclear fuel and cladding, parametric analysis 2—15826
nuclear fuel element cladding, ratchetting growth 2—15825
nuclear reactor, heat exchanger tubesheets, plastic strain analysis 2—15141
nuclear reactor cores critical buckling, calc. by variational methods to optimize core geometry 2—24269
nuclear reactors, structural components, branch-pipe tee connection, limit analysis and plastic collapse 2—15142
plastic, optical yield and birefr. 2—19969
plasticity, finite deformation theory for elastic response, yield and plastic flow, application to geologic materials 2—14214
plates in uniaxial compression, various support boundary conditions 2—11341
polyamides, doubly-oriented, small angle X-ray diffr. obs. 2—18909
polycarbonate, uniaxial compression and tensile yield stress, temp. depend. 2—22272
polycrystal, microdeform., stat. theory 2—6541
polycrystal, microdeform., stat. theory 2—6542
polyethylene, cold-drawn, retraction effect, role of cryst. morphology 2—32593
polyethylene, high density cold-rolled, tensile props. 2—39792
polyethylene, press. depend. 2—3874
polyethylene irradiated crystals 2—36124
polyethylene terephthalate, self- oscillation mechanism of necking 2—19186
polyformaldehyde, mullite filled, tensile rupture, fracture microstructure 2—29293
polymer, crystalline, morphology, X-ray obs. and electron microscopy 2—3462
polymer, crystalline, morphology 2—15824
polymer, effect on internal friction 2—6525
polymer, elastic-plastic behaviour in the softening range 2—29266
polymer, fracture initiation rel. to network orientation and microstructure 2—15869
polymer, glassy amorphous, yielding behaviour 2—3872
polymer, isotropic, plastic stress-strain behaviour 2—19185
polymer, molecular motion, microstructure, rotational isomerism 2—15640
polymer, relax., irrad. effects 2—39793
polymer, strained crystalline, fracture, chain scission 2—15845
polymer, volume changes, yield stress press. depend. 2—3873
polymer molecular order and motion, seminar, Seattle, USA, Oct. (1970) 2—15639
polymer network, micromechanics 2—15844
polymeric fibres, reaction-rate model 2—3911
polymeric materials, testing apparatus, extension, creep, relax., in ionizing rad. 2—39880
polymers, crystalline, change to oriented fibre structure during elongation 2—29292
polymers, oriented, yield behaviour 2—6540
polystyrene, thin sections, crazing, fibrillar struct., electron microscope obs. 2—3912
polyvinyl chloride, compression yield stress rel. to loss tangent, β-transition range 2—15854
polyvinyl chloride, oriented sheet, yielding and internal stress effects 2—15847
porous solid under press., quasistatic deform. 2—39773
Prandtl-Reuss materials, generalized, equation for finite deformation 2—17339
pressure-induced ductility, microstruct. influence 2—39780
pressurized shell, plastic growth through interaction of steady press. with thermal stresses 2—37723
quartzites, creep, from various regional metamorphic environments 2—9668
quasi-linear M/V model of solid, rheological props. 2—2193
ratchetting, in nuclear reactions, design criteria from high temp. material properties 2—15110
rheological material, internal struct. changes, gradient theory, thermodynamic theory 2—20901
rheological materials with internal changes, gradient theory 2—5178
ribbon cathode in device for meas. internal stress in electrolytic coatings 2—39859
of rigid/plastic media, principal- and slip-line methods of numerical analysis 2—12842
rolling of cylinder on rigid/perfectly plastic half-space 2—37671
rough surfaces, energy balance approach 2—32602

Plastic deformation continued
sandstone, effect of size and stress concentration on dilatancy and fracture 2—29320
screw dislocation generation, from grain boundary ledges 2—15758
semi-infinite rods, determ. applied load which maximizes the permanent displacement of the end of the rod 2—20905
semiconductor, Ge, effect on thermoelectric power 2—4233
serrated yielding, vacancy annihilation 2—32503
serrated yielding due to solute locking, effect of vacancy sinks and sources 2—25500
shock wave propagation in elasto-plastic media, conditions for existence of continuous plastic deformations 2—37786
simple structures, finite-element analysis of large elastic-plastic transient deformations 2—27152
single crystal, pure, load-elongation and creep curves computed 2—25499
small elastic-plastic deformations of thin shells, allowance for material compressibility 2—37696
solid solns., diffusional homogenisation during deform., energy stability, free energy 2—29413
stainless steel, shock loading, recovery and recrystallization 2—9657
stainless steel, type 304, residual microstructure, explosive shock 2—9655
stall, micro-alloyed, hot rolling, recrystallization 2—9735
stee, superplasticity, temp. cycling, creep and transformation strain 2—12853
steel, 18-8 stainless, tensile testing, —271°C-25°C 2—39785
steel, 1X12VNMO, effect of thermomechanical working on cavitation resistance 2—6597
steel, 9Ni-4Co-0.20C weldment, post-irrad., notch ductility 2—15834
steel, γ' phase precip., effect of degree of deform. 2—36215
steel, acceleration of pearlite spheroidization 2—32695
steel, alternating deform., plastic strain mech., substruct. 2—32610
steel, austenite, carbide precipitation kinetics 2—32772
steel, austenite, hot rolled, recrystallization 2—12943
steel, austenite, rel. to martensitic transform. 2—32764
steel, austenitic, deform. resist., C content effects in types 304 and 316 2—1304
steel, austenitic, deform. texture, influence of form of stress state 2—36233
steel, austenitic, effect of thermomechanical treatment on cyclic strength 2—9688
steel, austenitic, hot working struct, and strength 2—9729
steel, austenitic stainless, mathematical model 2—12858
steel, blue brittleness, tensile testing study 2—36115
steel, bulk and micro-flow fracture behaviour, neutron irrad. effects 2—25525
steel, cementite particle fracture 2—39839
steel, cold-rolled, spontaneous formation of stacking faults 2—36040
steel, cyclic stressing, fatigue fracture 2—9707
steel, deformation martensite formation by cold rolling 2—3995
steel, dynamic softening, differential equations 2—36116
steel, effects on carbide precipitation 2—32771
steel, effects on fracture toughness 2—15837
steel, embrittlement by H_2, obs. 2—29318
steel, fatigue crack growth, stress cycle asymmetry effects 2—39840
steel, fatigue strength under axial load, effect of surface hardening 2—36150
steel, Fe-Cr-Ni, dilatometric obs. rel. to hardening process during ageing 2—32697
steel, hardness and struct., effect of explosive deform. 2—39930
steel, high C, cold drawn, ageing and recovery 2—9757
steel, high-speed, quench deform. due to complex carbide precip. 2—29392
steel, high-speed, resist. to microplastic deform. 2—36114
steel, low C, grain size depend. of yield 2—12855
steel, low C, stress strain curve after cyclic deform. 2—1285
steel, low C Mn type, damping, rel. to martensitic transform. 2—1395
steel, low-C, dislocation struct. form. under static and cyclic loads 2—39783
steel, Luders bands, impurity-dislocation reactions, deform. kinetics rel. to serrated yielding 2—22208
steel, maraging, yield strength, rel. to hardening mechanism 2—36217
steel, martensite, impact deformation strengthening 2—39901
steel, microcrack formation, density meas. obs. 2—32584
steel, neutron irrad., rel. to defect struct. obs. 2—1232
steel, notched, fatigue loading, crack development, stress distrib. 2—29325
steel, notched, stressed, yield stress, tensile strength, area reduction, elongation at rupture 2—12890
steel, phase transformation austenite- martensite effect of nickel 2—3979
steel, plastic zone form. and fatigue crack extension during bending 2—19215
steel, plastic zones in double cantilever beam specimens 2—19216
steel, pre-strained, stresssed, ductility, yield and tensile strength, permanent strain 2—12854
steel, rel. to effect of nonmetallic inclusions on strength 2—36139
steel, rel. to strength drop at cryogenic temps. 2—36138
steel, rolled, recrystallization, u.s. attenuation obs. 2—25572
steel, soft polycrystalline, stress/strain, temp. and grain dia. depend. 2—12856
steel, stainless, ductibility at rupture 2—3880
steel, stainless, neutron irradiation, void formation, thermo-mechanical treatment effect 2—6469
steel, stainless, nitrided layer formation, austenitic → ferrite transformation 2—12927
steel, stainless, stacking faults and $\gamma \to \epsilon$ transform. 2—40003
steel, stainless, type 304, elastic-plastic constitutive equations 2—15823
steel, stainless austenitic, effect of carbides on high strain fatigue 2—9651
steel, stainless TRIP, mech. props. rel. to austenite formation temp. 2—12857
steel, static and dynamic loading, reproducible procedures 2—1303
steel, strengthening using hydroextrusion 2—9745
steel, transformer, deform. texture, effect of initial state 2—12936
steel, weldable structural, isothermal recrystallization kinetics 2—12942
steel, with and without u.s. vibr., second order residual stress 2—36117
steel bimetal structure, cohesion dependence of layers 2—1363
steel welds, repeated static loads, effect of heat treatments 2—3895
steels subjected to thermomechanical treatment, modelling 2—22275
strain, high rate, twinning and slip, single crystal niobium 2—3884
strain, low rate, segment of sessile dislocations, nonhomogeneous slip 2—3884
strain rate sensitivity, temp. depend. 2—19177
stress sensitivity, stress and temp. depend. 2—9647

Plastic deformation continued
structural metals, mathematical model for elevated temperature deformation 2—15827
superconductor, electron-dislocation interaction 2—13164
surface metal layers, analysis for tools and dies 2—34000
system buildings, spatial stability against buckling 2—20888
tensile testing, 'machine hardness' concept 2—29379
testing, fatigue testing, biaxial stress, stress conc. and pure bending conditions 2—19229
rel. to thermal strain measurement, contact method 2—1435
thin infinite plate, geometrically similar expansion of hole 2—7744
transition metal, cubic, shear strain effects, interaction with nucl. spins 2—25997
ultimate tensile stress, structure sensitivity 2—25492
void growth under applied stress, strain energy effects 2—22187
wear tracks, plastic flow, asperities, electron microscopy 2—9720
work hardening, stage I, temp. depend. due to jog dragging 2—9743
yielding of structural members, effect of shear 2—14163
Zircaloy tubing, influence of reduction values on texture formation 2—25569
Zn, electrically induced deform., before brittle fracture 2—36121
A crystal, slip band formation round indentation figures, Schmid factors 2—1297
Ag-Cd alloy, stress-induced martensite transform. 2—36271
Ag-Cd alloy, tensile deform., X-ray diffr. study 2—15829
Ag-O alloy, temp. and strain rate depend. of yield 2—32604
Ag, effect of evaporated metal coatings 2—1286
Ag, thick film, single cryst., Luders deform., dislocation struct. 2—6543
Ag, thin cryst., slip morphology size depend. 2—22206
Ag_3Mg, long period ordered, dislocation splitting, stacking faults 2—25501
Al-0.05%Fe alloy, grain boundary sliding in presence of second phase particles 2—32605
Al-Mg-Zn alloy, cyclic stressing, fatigue fracture 2—9707
Al-Mg, recovery and stacking fault energy, 77-500K 2—36112
Al-Mg alloy, effect on elastic limit, discontinuities 2—36104
Al-Mg alloy, fracture in tension, influence of alloying additions 2—12846
Al-Zn alloys, effect on phase transformations in range of miscibility gap 2—29186
Al, 99.5% pure, solute redistrib. during grain boundary migration 2—36229
Al, anelastic behaviour, dislocation-point defect interaction, internal friction meas. 80-500K 2—12830
Al, anodically oxidised, effects on electron emission 2—10157
Al, creep, stress and temp. depend. 2—9671
Al, deformed at 77K, ageing 2—19245
Al, electron microscope study of ductile rupture surface 2—39812
Al, exoelectron energy and intensity meas. rel. to low temp. working 2—29779
Al, fine subgrain struct. adjacent to fatigue cracks 2—32543
Al, loading path effect on yield surface at temp. from 70 to 305°F 2—25502
Al, low temp. intermittent deform., specimen size effect 2—36111
Al, monocrystal, polygonization under elongation stress and crystal orientation 2—39570
Al, oriented tricrystals, bending joints, intergranular energy 2—12848
Al, recovery and stacking fault energy, 77-500K 2—36112
Al, rolling, recrystallization, grain growth 2—12926
Al, single cryst., extruded rod, deform. band form. along flow directions in plastic zone 2—19110
Al, yield point, temp. depend., after high press. treatment 2—19182
Al, yield stress, effect of grain boundaries 2—12847
Al alloy, age hardened extruded rod, mechanical anisotropy rel. to texture 2—3856
Al alloy, complicated stress-strain history, fatigue failure 2—39817
Al wire, u.s. bonding mechanism 2—15830
Al_2O_3, corundum whiskers, flow stress 2—6545
Al_2O_3, sapphire, prismatic slip, 1150°-1750°C 2—36130
Al_2O_3 anodic coating on Al 2—1286
alloy, martensite transform., shape memory effect 2—9789
Au-(14 at.%)Cu alloy, Portevin-Le Chatelier effect22265 2—22265
B/epoxy shear panels, diagonal tension behaviour 2—22350
Be-1%Fe, Mossbauer obs. 2—32722
Be, hot pressed, tensile props., temp. strain rate depend. 2—29283
Bi, motion of non-coherent twin boundaries under repeated loadings 2—19107
C, graphite, shock compacted, hardness and microstruct. 2—9714
C fibre, hot stretching effects on struct. and electronic props. 2—6289
Cd-Mg alloys, crit. resolved shear stresses 2—32608
Cd crystal, tensile testing, 77-295K 2—29261
Cd single crystal, torsionally stressed, shear stress distrib. in various slip systems 2—29275
CdS, dislocations influence on optical props. 2—10369
Cr-V steels, effect of Mo content and yield point on creep rupture strength 2—29286
Cr-Zr-Nb-C alloy, rel. to stress rupture and ductility control by microstruct. modification 2—9692
Cr, containing Cr_2O_3 particles, pressurization induced dislocation density 2—12850
CsI, laser irrad. induced crowdion deform. mechanism 2—6495
Cu-Al-Fe alloy, superplasticity, rel. to microstructure 2—32606
Cu-Al-Fe alloy, superplastic, high temp. tensile testing 2—15832
Cu-Al, aluminium bronze, superplastic, tensile props. 2—15833
Cu-Al, liquid metal embrittlement, role of plastic deformation 2—3898
Cu-Al alloy, effect of deform. temp. on struct. and props. 2—12888
Cu-Al alloy, microstruct. following explosive shock deformation, 1 megabar pressure 2—9650
Cu-Al alloy, thermomechanically treated 2—36202
β_1'-Cu-Al martensite, shape memory effect rel. to stress induced phase transformations 2—25626
Cu-(1.9 wt.%)Be alloy, microscopic yield stress precip. substruct. depend., rel. to fatigue strength 22283 2—22283
Cu-Ni-Zn alloy, effect on elec. resist. 2—25641
Cu-Ni alloys, resistivity changes arising from cyclic deformation 2—15905
Cu, cold rolling, orientation stability, strain rate depend., electron diffr. 2—39899
Cu, creep, stress and temp. depend. 2—9671
Cu, dislocation cell size and density, elec. microscope obs. 2—36031
Cu, dislocation motion before and after yielding 2—1289
Cu, dynamic recrystallization during hot torsion 2—29450
Cu, electrolytic, extrusion, recrystallization, texture, mech. props. 2—3926

Plastic deformation continued
Cu, electron microscope study of ductile rupture surface 2—39812
Cu, exposed to u.s. vibr., time depend. of yield stress 2—36195
Cu, fatigue by unidirectional repeated tensile loading 2—12893
Cu, flow stress, effect of pressurizing 2—12851
Cu, high purity, recovery, elec. resistivity obs., deviations from Matthiessen's rule 2—25579
Cu, microstruct. following explosive shock deformation, 1 megabar pressure 2—9650
Cu, polycryst., low temp. plastic flow, stacking fault energy, flow stress 2—12868
Cu, radiation-induced hardening after deform. by rolling 2—39898
Cu, shear strained, stored energy, yield stress and recrystn. 2—19181
Cu, sintered, stress-strain curve rel. to degree of deform. 2—19172
Cu, stored energy, calorimetric determ. 2—9649
Cu, stored energy, room temp. deformed 2—3864
Cu, strain, substruct. misorientation and hardness characts. 2—29334
Cu, with oxide inclusions, dislocation struct. formed by pressurizing 2—15761
Cu, yield point, temp. depend., after high press. treatment 2—19182
Cu alloys, role of Cr and Zr on rolling and annealing texture 2—3946
Cu crystal, conical indentation, dislocation reactions 2—1288
$CuAl_2$, compressive and tensile deform. 2—19180
Eu_2SiO_4, ferroelastic ferromag., optical absorpt. spectra, Faraday rotation, cryst. struct. 2—10195
F-(3 wt.%)Si, alloy single crystals, yielding between 113 and 473 K 22271 2—22271
Fe-Al alloy, ordered, vacancy elimination due to linear defect form. 2—39695
Fe-Al_2O_3, dispersion hardened, at elevated temp. 2—9658
Fe-C alloy, brittle fracture initiation, carbide particle size effects 2—39823
Fe-C system, microstructure stability during cyclic deformation 2—32724
Fe-Co-V, hot drawing, dislocation movement, electron microscopy 2—9780
Fe-Co-V alloy, $\gamma \rightarrow \alpha$ transformation, omnidirectional press. effect 2—9806
Fe-Cr-Ni, steel, antiferromag. austenitic-ferromag. martemsitic transition at liq. He temp. 2—26038
Fe-Cr alloy, yield strength, 77-400K 2—39786
Fe-Mn alloy, shock deformed, recovery, role of point defects 2—9653
Fe-Mn alloy, shock loaded, twins, electron microscopy 2—9744
Fe-1.1at%Nb, substitutional dynamic strain ageing effects 2—3866
Fe-(1.1 at%)Nb alloy, substitutional strain ageing, serrated flow6536 2—6536
Fe-Ni-C alloy, martensite, morphology, rel. to formation temp. 2—12775
Fe-Ni-Cr-Ti steel, austenitic, rel. to σ-phase form. 2—29471
Fe-Ni-Mo, alloy, lattice distortion due to deformation 2—15721
Fe-Ni-Mo alloy, effect on martensitic transform. 2—29467
Fe-Ni alloy, effect on Hall coeff. and resist. 2—22492
Fe-Ni alloy, impact loading, microstructure, hardness, α-γ transformation 2—3867
Fe-Ni system, explosively loaded, hardening, recrystallization, grain boundaries 2—9575
Fe-Si, rel. to effect of nonmetallic inclusions on strength 2—36139
Fe-Si, texture variations during recovery stage 2—12935
Fe-Si alloy, edge and screw dislocation mobility, h.v. elec. microscope obs. 2—25407
Fe-Si single crystals, crack propag., effect of prestrain and ageing 2—12909
Fe-V alloy, yield strength, 77-400K, comp. depend. 2—39786
Fe, Armco, cyclic bending, microstructure, absorptional fatigue 2—29300
Fe, Armco, effect on Hall coeff. and resist. 2—22492
Fe, carbonyl, H permeability, 100-650°C 2—29218
Fe, cast, deformation heat treatment for dimens. stabilization of parts 2—36205
Fe, cast, electron microscope study of ductile rupture surface 2—39812
Fe, changes in thermo e.m.f., resistivity and X-ray spectra, due to increase in defect conc. 2—3865
Fe, dislocation structs., HVEM analysis 2—39696
α-Fe, grain growth rates 2—39924
Fe, grains, quenching after heat treatment 2—19242
Fe, mag. fields effects 2—32603
Fe, rupture and fatigue testing, Al particles effect 2—9693
Fe, sintered, stress-strain curve rel. to degree of deform. 2—19172
Fe, strain distrib. within and around deform. twin bands 2—29188
Fe, work hardened by strain rate cyclic changes, high temp. deform., slip 2—19244
Fe, yield point, temp. depend., after high press. treatment 2—19182
Fe alloy, martensite transform., shape strains in deform. of lattices 2—29259
Fe crystal, tension deformation, elastic limit, yield stress 2—15835
Fe crystal annealed, laminated, twisted, primary recrystallization texture 2—15901
αFe single crystal, creep, under stress lower than yield stress 2—12870
Fe single crystal, reactivation of mechanical aftereffect by discontinuous change of external mag. field 2—25473
Ge, dislocation half-loop formation by microhardness indentor 2—36032
Ge, effect on thermoelectric power 2—4233
Ge, internal friction in deformed single cyst. 2—19165
GeTe powder, during pressing 2—1379
In, superconductor, compression effects on T_c, role of pt. defects 2—25787
InAs, deformed in torsion, coherent twin boundaries 2—19106
K, annealing and recovery spectrum 2—19089
K, annealing and recovery spectrum 2—19090
KCl-KBr, solid soln., polygon wall motion, load compression curve 2—9659
KCl, dislocation shift, stress induced, local obstructions 2—19100
KCl, effect of strain on γ-ray induced F-centre colouring at room temp. 2—3803
KCl, γ-irradiated, stress relaxation 2—9660
$LaFeO_3$, ferroelastic effect 2—25633
LiF, acoustic emission, correl. with dislocation kinetics 2—4044
LiF, deformation defects, annealing effects, u.s. acoustic wave attenuation obs., 78-350K 2—12859
LiF, radiation hardened, thermal, role of entropy 2—3869
Mg-Ag alloy, serrated yielding 2—29260
Mg-Cd alloy, role of slip and twinning, 77 K and room temp. 2—9679
Mg, neutron irrad., yield stress obs. 2—36119
Mg, role of slip and twinning, 77 K and room temp. 2—9679
Mg crystal, tensile testing, 77-295K 2—29261
MgO, annealing, dislocation loops 2—32524

Plastic deformation continued
Mn-Fe, alloy, hydrostatic extrusion rel. to phase diagram, constitution and props. 2—19312
Mo-Ti-C alloy, deformed, subgrain growth during annealing 2—12946
Mo, cryst, effect on paramag. susceptibility 2—16347
Mo, deformed, subgrain growth during annealing 2—12946
Mo, fine struct. changes during rolling 2—32508
Mo, high temp. recovery 2—15743
Mo, precip., rel. to grain size depend. of elastic limit 2—12860
Mo, yield, strain-rate and temp. depend. 2—39790
Mo crystal, dislocational internal friction, u.s. attenuation 2—6497
MoS_2, natural molybdenite, cold working. microstructure, X-ray line broadening 2—25409
NaCl, acoustic emission, correl. with dislocation kinetics 2—4044
NaCl, deformed surface struct., electron microscope obs. 2—9251
NaCl, dislocation struct. rel. to n.m.r. line broadening anisotropy 2—10560
NaCl, γ-irradiated, stress relaxation 2—9660
NaCl, mechanism, temp. and strain rate sensitivity 2—39789
NaCl, substruct. components, Kossel line obs. 2—9547
NaF, point defect formation 2—1245
NaI, dislocation struct. rel. to n.m.r. line broadening anisotropy 2—10560
Nb-H alloy, effect on elec. resistivity 2—39935
Nb-H system, ferroelasticity rel. to phase diagram determination 2—9694
Nb, temp. effects on stage III recovery 2—25575
Nb, yield, strain-rate and temp. depend. 2—39790
Nb single crystal, strain deformation, high and low rate strain 2—3884
Nb single crystal, twinning, pre-strain effects 2—32538
NbC, diamond grinding. surface work hardening, microstructure 2—3871
NbC_x, shock wave effects 2—29328
Ni/ZrO_2 composite, low temp. 2—12874
Ni-Al-W-Mo-Co alloy, effect on struct. and props. 2—9733
Ni-Co alloy single crystal, magneto-plastic effects 2—33144
Ni-Cr alloy, low temp. recovery, elec. cond. study 2—36120
Ni-Cu, Ni-Cu-C alloys, at temperatures between 78 and 523 K 2—1278
Ni-Fe alloy, deformability, initial permeability, de-oxidation elements addition effect 2—4367
Ni-M solid soln. alloys, (M=Al, Cr, Si, Sb, Ti), effect of solute on yield stress temp. depend. 2—25505
Ni, deformed at high press., dislocation struct., flow stress 2—22210
Ni, effect on ferromag. reson. 2—36972
Ni, effect on Hall coeff. and resist. 2—22492
Ni, effect on magnetomech. damping 2—19890
Ni, high strain rate deformation, recovery and recrystallization, polygonisation 2—9748
Ni, low temp. recovery, elec. cond study 2—36120
Ni, mag. props. anisotropy 2—40450
Ni, microhardness increase under action of u.s. waves 2—9663
Ni, tensional deformation, secondary recrystallisation structure 2—12947
Ni, twinning struct. growth, X-ray obs. 2—12862
Ni alloy, dispersion hardened 2—1293
Ni alloy, Mar-M200, Hf doped, ductility enhancement 2—15865
Ni and alloys, dispersion hardened, role of microstruct. in strengthening 2—39936
Ni single crystal, magneto-plastic effects 2—33144
Ni solid solns., non-equil., short-range order estab. 2—9772
Ni super-alloy, microstructure 2—12863
Ni_3Al, yield point and flow stress, temp. and strain depend. 2—12861
Ni_3Al alloy, flow stress, anomalous temp. depend. 2—6548
Ni_3Al alloy, slip and dislocation motion, hardening mechanism 2—6547
Ni_2Cr alloy, critical shear stress, ordering effects 2—9662
Ni_3Ga, yield stress, anomalous temp. depend. 2—3870
Ni_3Ti alloy single crystal, partially ordered, flow stress obs. 2—25504
Pb-Sn eutectic alloy, superplasticity 2—29263
Pb, creep, stress and temp. depend. 2—9671
Pb, etch pit dislocation density, critical resolved solar stress 2—6549
PbSn eutectic alloy, extrusion in superplastic region 2—12864
PbTe powder, during pressing 2—1379
Pd-H system, ferroelasticity rel. to phase diagram determination 2—9694
Pu-Ga alloy, strength rel. to working temp. and homogeneity 2—15839
α-Pu, extruded, elongation rel. to grain size 2—6550
Re, low temp. recovery spectrum 2—15744
Si epitaxial slices, central region obs. 2—12865
Sn-Pb eutectic alloy, superplastically deformed, texture 2—12975
Sn, superconductor, compression effects on T_c, role of pt. defects 2—25787
SnTe powder, during pressing 2—1379
Ta-H system, ferroelasticity rel. to phase diagram determination 2—9694
Ta, $\langle 100 \rangle$ and $\langle 110 \rangle$ single crysts., prestrain effects on micro- and macro-yielding 2—25496
Ti-Al-V, alloy, effect on creep, tensile and torsional loading effects 2—19188
Ti-Mo alloys, effect on supercond. T_c 2—6781
Ti, resistance due to dispersed phase, 150-300°C 2—9664
Ti, yield stress reduction by dynamic strain ageing, 77-1026K 2—25581
Ti alloy, fine subgrain struct. adjacent to fatigue cracks 2—32543
Ti alloy, martensite transform., shape strains in deform. of lattices 2—29259
TiC, diamond grinding, surface work hardening, microstructure 2—3871
TiC_x, shock wave effects 2—29328
TiH_x, yield stress, temp. and vacancy content depend. 2—19183
α-U, stress relaxation, apparent activation enthalpy 2—25494
V-H system, ferroelasticity rel. to phase diagram determination 2—9694
V-Ti alloy, solid soln. strengthening and weakening 2—29441
W-Re alloy, electronic struct., positron annihilation 2—22483
W-Re alloys, comp. and annealing temp. depend. elongation 2—1290
W, effect of degree of deform. on hardening coeff. 2—9746
W, single crystals, (110)[001] and (001)[110] orientations, rolling workability 2—3451
WC-Co alloy, slip lines, deform. mech., electron microscope obs. 2—32531
WC-Co cemented carbide compressive deform., microstruct. and mech. props. obs. 2—39791
Zn-Mg dilute alloy, age hardening, effect of cold rolling 2—29405
Zn, acoustic emission, correl. with dislocation kinetics 2—4044
Zn, electron irrad., rel. to deform. resist. 2—25506
Zn, electroplastically deform. effects, shift in cold brittleness limit 2—32611
Zn, hydrostatic extrusion, struct. and strength 2—19184

Plastic deformation continued
Zn, motion of non-coherent twin boundaries under repeated loadings 2—19107
Zn, surface deform. during sliding, surface films effect 2—22304
Zn single crystal, by sliding friction, surface film effects 2—15890
Zn single crystal, Peierls mechanism significance at low temps. 2—36122
Zr-Sn solid soln., substruct. strengthening 2—12953
Zr, low temp. recovery and recrystallization, resist. obs. 2—15911
Zr, rel. to texture and anisotropy 2—15892
Zr, resistometric recovery above room temp. 2—36219
Zr, role of dislocations with (c+a) type Burgers vector 2—36123
Zr alloy, high temp. 2—12875
α-Zr substruct. strengthening 2—12953
ZrB$_2$ single crystal, slip plane, Burgers vector and shear stress 2—15841
ZrC, diamond grinding, surface work hardening, microstructure 2—3871
ZrC$_x$, shock wave effects 2—29328

Plastic flow
see also Rheology
alloy, substitutional, serrated flow, Portevin-Le Chatelier effect 2—22263
amorphous polymer, tensile strength, internal friction, ductile-brittle transition 2—36145
α-brass, fatigue ductility 2—12905
brass, fatigue rupture, fracture surface morphology 2—12907
Charpy impact test, computer-assisted 2—36186
colloidal suspension, coagulated, as repeptization phenomenon, viscous energy 2—15618
composite, fibre-reinforced, theory 2—15848
concrete, strain and ultimate strength under triaxial compressive stress 2—15859
diamond-type cryst., dislocation dissoc. and mobility 2—39702
dislocation motion through array of discrete obstacles, viscous drag effects 2—12764
ductile crack growth role in failure of structures 2—25527
finite deformation theory analysis, application to geologic material 2—14214
fluid-like viscoplastic substances, yield stress meas. 2—28746
graphite, ductility, temp. and stress effects 2—32615
Gyarmati's principle, construction of dissipation potentials for nonlinear problems 2—37649
high temp., empirical power law, activation parameters 2—32620
hot forming without lubrication 2—9678
incompressible continuous medium, spatial plastic flows with instantaneously inextensible planes 2—20899
incompressible power law pseudoplastic fluid, converging channel 2—12326
metal, ductile, critical plane-strain stress intensity factor 2—19208
metal, f.c.c. and b.c.c., conical flow in metal forming 2—36211
metal, negative friction stress during high temp. creep, theory 2—12866
metal, phenomenological theory, static recovery effects 2—39794
metal, strain amplitude dislocation damping 2—3775
non-elliptic first order systems, Riemann invariants method, flow theory 2—20900
around notch, applicability of slip-line field theory 2—12881
orthotropic materials in tension and in compression 2—15852
plate, orthotropic, perfect plastic flow eqns., yield criterion 2—20902
polyethylene, press. depend. 2—3874
polymer, flow processes in the softening range 2—29266
polymer, isotropic, plastic stress-strain behaviour 2—19185
rate-dependent cracks, unsteady motion preceded by thin plastic zones 2—9700
rotating cylinder, velocity field determination 2—30844
serrated yielding due to solute locking, effect of vacancy sinks and sources 2—25500
sintering, material transport mech. in early stages 2—36255
slip-line field in strain hardening material, plane strain extrusion 2—12880
stee, superplasticity, temp. cycling, creep and transformation strain 2—12853
steel, 18-8 stainless, tensile testing, —271°C-25°C 2—39785
steel, alternating deform., plastic strain mech., substruct. 2—32610
steel, austenitic, level of uniform ductility 2—36233
steel, austenitic stainless, hot ductility, effect of N$_2$ and Ni 2—9672
steel, austenitic stainless, mathematical model 2—12858
steel, cast high-speed, effect of Ti and V 2—36176
steel, Cr-Mo-V, ductility, effect of enhanced purity 2—32617
steel, Cr-Ni-Mn type, effect of nitrogen 2—9654
steel, discontinuous twinning during essentially elastic compression, 4.2 K 2—39787
steel, ductility in hot working, O content effects 2—39893
steel, effect of ageing conditions 2—36118
steel, effect of comp. on Pb embrittlement 2—9652
steel, effect of Ge content 2—36203
steel, ferritic, ductile-brittle transition, additive effects 2—25518
steel, high strength construction, ductile-brittle transition, rare earth additions effect 2—15797
steel, low temp. 2—36113
steel, maraging, heat treatment effects 2—36204
steel, maraging, high-strength 2—36218
steel, maraging stainless, ductility 2—36243
steel, martensitic stainless, effect of thermomagnetic treatment 2—36280
steel, neutron irrad., rel. to defect struct. obs. 2—1232
steel, of machined surface layer 2—29001
steel, pre-strained, stressed, ductility, yield and tensile strength, permanent strain, cracks 2—12854
steel, stacking faults influence on flow velocity 2—3868
steel, stainless, AISI type 446, ductility, high temp. effects 2—29335
steel, stainless, ductibility at rupture 2—3880
steel, stainless, fatigue ductility 2—12905
steel, wear-resistant, effect of C and V content 2—36237
steel, XC 38, ductility, inclusions effects 2—15853
strain hardening, bifurcation and instability modes in thick walled cylinders under pressure 2—12879
superalloy, superplastic props. 2—29387
superconductor, dislocation motion, supercond. and normal states, theory 2—12766
superconductor, electron-dislocation interaction 2—13164
surface metal layers, analysis for tools and dies 2—34000
tensile tests, determ. of stress- strain flow curve 2—36189
visioplasticity method appl. to soln. of problems 2—5194
wear tracks, asperities, electron microscopy 2—9720
zircaloy, effect on hydrogen embrittlement 2—29311

Plastic flow continued
Zircaloy tubing, rupture ductility, hydride platelets orientation effect 2—15842
Al-Mg alloy, in uniaxial tension, ductility, influence of alloying additions 2—12846
Al, fatigue ductility 2—12905
Al, influence of specimen dimensions, macroscopic simulation 2—3905
Be, microscale, by slip and twinning 2—12906
CaF$_2$, sintering mechanism 2—32741
Cr-V steels, effect of Mo content and yield point on creep rupture strength 2—29286
Cu-Al-Fe alloy, superplasticity, rel. to microstructure 2—32606
Cu-Al, effect of thermomechanical treatment 2—36202
Cu-Al alloy, internally oxidized, ductility 2—39887
Cu-(1.9 wt.%)Be alloy, microscopic yield stress precip. substruct. depend., rel. to fatigue strength 22283 2—22283
Cu-(1.9wt.%)Co, Cu-(2wt.%)Co-(6wt.%)Zn alloys, agehardening mechanism, precip. effects 2—3913
Cu-(1wt.%)Si, microdynamics, slip initiation 3885 2—3885
Cu-2at.%(10at.%Al, work hardened, stage II, flow stress, forest stress, electron microscope obs. 2—3788
Cu, ductile fracture, unidirectional repeated tensile loading 2—12893
Cu, ductility, temp. depend., effect of annealing in vacuum or air 2—12882
Cu, flow stress, effect of pressurizing 2—12851
Cu, microdynamics, slip initiation 2—3885
Cu, polycryst., low temp., deform., stacking fault energy, flow stress 2—12868
Cu, torsional fatique, 78 K, shear modulus, internal friction 2—22260
CuAl$_2$, ductility, in compressive and tensile testing 2—19180
Fe-C alloy, ductility, carbide particle size effects 2—39823
Fe-Cr-Co system, ductile permanent magnet 2—40474
Fe-(1.1 at%)Nb alloy, substitutional strain ageing, serrated flow6536 2—6536
Fe, cast, ductile-brittle transition temp, heat treatment depend. 2—39832
Fe, ductile-brittle transition, N$_2$ effect, annealing depend. 2—15836
in Fe, ductile brittle transition, effect of added nitrogen 2—25503
Fe, hardness-flow stress-grain-size relationship 2—22289
Fe, plastic zone around fatigue cracks 2—39782
Fe, rel. to conc. of impurities 2—40859
Fe, work hardened by strain rate cyclic changes, flow stress 2—19244
α-Fe, yield, flow stresses, grain size dependence dislocation model 2—3854
Fe alloys, low temp. ductile fracture, meeting report 2—32646
Fe crystal, tension deformation, elastic limit, yield stress 2—15835
Fe polycrystal, pure, hydrostatic pressure effects on flow stress 2—39801
Ge, ductility and brittleness rel. to molten metal contact 2—29310
HfC, hardness meas., indentation and cracking 2—1294
LiF:Mg^{2+}, impurity influence on flow stress 2—9561
Mg-Ag alloy, serrated yielding 2—29260
Mg-Zn alloys, yield strength rel. to age-hardening 2—6599
Mg alloy, cavity growth caused by flow, density and metallographic obs. 2—39788
Mn-Zn, alloy, age hardened, grain size, dependence of yield stress and flow stress 2—6546
Mo, strain-rate and temp. depend. 2—39790
Mo polycrystal, pure, hydrostatic pressure effects on flow stress 2—39801
Mo wire, ductility, effect of grain size and C content 2—12884
Mo wire, recrystallized, grain size and carbon content effects on ductility 2—29262
NaCl, flow stress temp. and strain rate sensitivity 2—39789
Nb-N alloy, flow stress, solution hardening 2—9661
Nb-O alloy, flow stress, solution hardening 2—9661
Nb, strain- rate and temp. depend. 2—39790
Nb alloy, deformed, annealing, struct. and ductility 2—9646
Ni/ZrO$_2$ composite, dispersion-strengthening 2—12874
Ni-Al alloy, precipitation-hardened 2—29404
Ni-Cr-Fe alloys, neutron irradiation, extension rate, grain size, ductility 2—25513
Ni-Cr alloys, influence of grain size and precip. parameters 2—12872
Ni-M solid soln. alloys, (M=Al, Cr, Si, Sb, Ti), effect of solute on yield stress temp. depend. 2—25505
Ni, deformed at high press., dislocation struct., flow stress 2—22210
Ni, flow stress rel. to dynamic recrystallisation 2—32699
Ni, neutron irradiation, extension rate, grain size, ductility 2—25513
Ni$_3$Al, yield point and flow stress, temp. and strain depend. 2—12861
Ni$_8$Ti alloy single crystal, partially ordered, flow stress obs. 2—25504
Pb-Sn:Cu uniaxial metal matrix composite, subjected to axial and normal lateral loads 2—15851
α-Pu, extruded, elongation rel. to grain size 2—6550
Si, glide band form. 2—36036
SiC:Ti uniaxial metal matrix composite, subjected to axial and and normal lateral loads 2—15851
TaC, hardness meas., indentation and cracking 2—1294
Ti-Al-Cr and Ti-Al-Cr-Mo alloy, after annealing 2—36142
Ti-Al-Sn-Zr-Mo alloy, rel. to microstruct. 2—39942
Ti-V-O and Ti-V-Al-O alloys, ductility, effect of O content 2—36144
Ti-V and Ti-V-Al alloys, after quenching, comp. depend. 2—36141
α-Ti, dislocation dynamics, activation enthalpy 2—22211
α-Ti and alloys, effect of B-stabilizer 2—36143
W, microdynamics, slip initiation 2—3885
Zn-Al eutectoid alloy, superplasticity, effect of processing history 2—29265
Zn polycrystal, hydrostatic pressure effects on flow stress 2—39802
Zr, effect on hydrogen embrittlement 2—29311
Zr polycrystal, hydrostatic pressure effects on flow stress 2—39802

Plasticity
see also Viscoelasticity
anisotropic shells, analysis of viscoelasto- plastic structural behaviour by finite element method 2—14220
anisotropy of some common metals 2—29255
artificial graphite, rate-independent continuum theory, experimental verification 2—39779
beam, elastic plastic and infinite, impact by semi-infinite elastic rod 2—5172
beams, thin-walled, local buckling and post local buckling behaviour 2—3860
beams, wide, dynamic behavior 2—6539
book on theory of plasticity, book 2—27189
composite, unidirectional, elastic-plastic analysis for longit. loading 2—36109

Plasticity continued
constitutive equations, determination procedure for materials with both time-dependent and time-independent plasticity 2—23335
continuous media, rigid, perfectly plastic, limit analysis 2—33989
cracked plate, elastic-plastic analysis 2—14213
dislocation movement slip planes 2—19176
elastic-plastic materials, work hardened, model of, based on elastic model of materials with microstructure 2—29248
elastic-plastic media, superposed motions 2—27184
elastic-plastic solid, anisotropic, plane-wave propag. 2—39767
elastic-plastic wave cancellation in energy absorbing materials 2—27217
elastic/viscoplastic hollow sphere, wave propagation 2—27223
elasto-plastic system, one degree of freedom, effect of heavy vibrations 2—27199
elasto-plasticity, matrix differential equation and numerical solution 2—17301
finite deformation theory for elastic response, yield and plastic flow, application to geologic materials 2—14214
fluid-like viscoplastic substances, yield stress meas. 2—28746
fracture mechanics, finite element method 2—23336
group II-VI compound, photoplasticity 2—19175
half-space punching in Tresca material 2—37706
incompressible continuous medium, spatial plastic flows with instantaneously inextensible planes 2—20899
limit analysis and design of plates, shells and discs, book 2—39881
mechanical props. of solids and fluids, book 2—39752
metal, f.c.c. and b.c.c., empirical stress-strain relationships in conical flows in metal forming 2—36211
metal, weakening and superconductivity transition 2—22499
metal systems, superplasticity, heat resist. 2—36110
metals, constitutive relations, internal variable thermodynamic theory 2—12843
metals, statistical interpretation 2—3875
model for cyclic strain accumulation 2—34039
neopentane plastic phase transition 2—39976
non-elliptic first order systems, Riemann invariants method, flow theory 2—20900
nuclear equipment design, use of inelastic analysis 2—14215
nuclear reactor fuel cladding, under combined effect of creep and plasticity, strength analysis 2—21465
one-dimensional non-viscous dynamic theory, applicability 2—37707
plane delatational plasticity 2—2219
plate, orthotropic, perfect plastic flow eqns., yield criterion 2—20902
plate of finite thickness with penny-shaped crack, plastic energy dissipation 2—34019
plates, rectangular, flat, dynamic behavior 2—6539
polymer, yield behaviour 2—15843
Prandtl-Reuss materials, generalized, characteristic surfaces and acceleration wave propagation 2—17340
Prandtl-Reuss materials, generalized, equation for finite deformation 2—17339
Prandtl-Reuss materials, generalized growth and decay of acceleration waves, propagating boundary surfaces 2—17341
Riemann invariants method applic. 2—37705
rigid shell, moderately large deflections theory 2—17342
shells, rotationally symmetric, numerical solution of elastic plastic problems 2—138
shells of revolution, large deflection elastic plastic analysis 2—14208
shock wave propagation in elasto-plastic media, conditions for existence of continuous plastic deformations 2—37786
slip and resistance to shear, elastic limits 2—17356
slip spread in notched half-plane, screw dislocation distrib. 2—11333
steady plastic cycles in structures 2—14216
steel, austenitic, rel. to martensitic transform. 2—32764
steel, effect of Ni and S content 2—6538
steel, highchrome, hot-rolling effects 2—1362
strain, allowable amount as basis for design 2—17344
stress analysis, notched bar in plane strain bending 2—12838
stress analysis of two dimensional problems under simultaneous creep and plasticity 2—14186
stress and displacement velocity in plastic rotationally symmetric flow zones, application to reactor structure 2—14175
stress invariants, teaching paper 2—27186
structural optimization with piece-wise concave cost functionals 2—30851
superplastic metallic alloys, steady extrusion 2—32709
superplasticity, in metals and alloys, origin of quasiliquid state 2—32614
thermal behaviour of solids of revolution, analysis by finite element method, application to nuclear reactor technology 2—17355
thin sheet materials, method based on torsion testing 2—39878
Tresca material, effective plastic strain 2—34040
two-layer viscoplastic media, circular motion between two coaxial surfaces 2—5202
viscoplastic props. of metal crystals 2—6492
viscoplasticity, non-associated constitutive law 2—27183
wave propagation, effect of Young's modulus variation with plastic strain of temp. 2—14254
weightless cohesive frictional material, equations of plasticity, method of integration 2—37709
Cu-Al, aluminium bronze, superplastic, tensile props. 2—15833
Fe-Ti alloy, ductile-brittle transition, cold working effects 2—29307

Plastics
see also Polymers
ABS, colour stability 2—7032
adhesive bond production by surface treatment via plasma processing 2—39973
ageing, under solar radiations, in natural and laboratory conditions 2—1156
bearings, operational behaviour, structure effects 2—32653
conglomerate plastics, effect of temperature and saturated humidity on deformation 2—29268
creep of thermoplastics in tension, measurement at high pressure in petroleum-vapour atmospheres 2—39970
cryogenic props., used in low temp. normal and superconducting magnets 2—14371
development, review 2—18908
durability, freq. depend. of fatigue limit, relax. phenomena effects 2—32630
fibre reinforced, dynamic properties 2—3832
fibre reinforced, NDT using u.s. reson. method 2—32658
foam, compressive strength, meas. apparatus 2—25542
foamed, heat transfer, thickness and temp. effects 2—28924
for low temp. normal and superconducting magnets 2—14371
glassy, mechanism of molec. wt. dependence of brittle strength 2—39830
high-pressure polyethylene containing vessel for e.p.r. studies of polar solvents 2—37523
HIPS, creep mechanisms, crazing, rubber-toughening obs. 2—22274
laminated, spontaneous deformations 2—22270
loading process behind fronts in reflected and refracted waves in plastic layered media 2—30879
methacrylate, lesion development by focused ultrasound 2—37441
Mylar, ionic thermocurrent 2—4270
mylar films, electroluminescence, non destructive electric breakdown 2—20118
mylar liquid H_2 target with thin mylar sidewalls and vacuum housing 2—31344
NE 110 scintillator, cylindrical, smoothing of light collection 2—27870
nitrocellulose sheets, particle track formation in, effect of etching interruptions 2—14776
non-dispersive X-ray fluorescence in analysis 2—39971
nuclear track detector, efficiency calibration 2—14775
nylon, stress ageing, water content influence 2—3937
nylon, thermal cond., 4 to 350 K 2—19473
nylon 6, fatigued fibres temp. dependence of dynamic viscoelasticities 2—3846
Nylon 6, ortho-positronium annihilation obs. of glass transition 2—15646
nylon fibres, reaction-rate model for fracture 2—3911
optical yield and birefringent phenomena 2—19969
perspex, elastic consts. 2—3839
Perspex, elec. strength, voltage rise time depend. 2—29747
photoconductive-thermoplastic sandwich's applications to data storage and interferometry 2—6910
Plexiglas, as Cherenkov counter radiator, threshold properties 2—31366
Plexiglas, electret state form. under electron beam bombardment 2—29760
plexiglass, Cu film, diffusion processes occurring during blast compression time 2—29203
PMMA, eqn. of state, u.s. vel. obs. 2—25479
polycarbonates, automatic counting of holes etched by fission fragments 2—38393
polyethylene, electron induced cond., carrier mobility detn. 2—22543
polyethylene, thermal cond., 3 to 300 K 2—22434
polyethylene terephthalate, amorphous and cryst., fracture behaviour 2—39845
polyethylene terephthalate, electron induced cond., carrier mobility detn. 2—22543
polyethylene terephthalate, i.r. radiation of thin films 2—40604
polyimide, i.r. radiation of thin films 2—40604
polypropylene film, metallic filler, strength rel. to mag. field 2—29406
polystyrene, electron induced cond., bulk excitation 2—25808
polystyrene, electron induced cond., carrier mobility, detn. 2—22543
polystyrene, eqn. of state, u.s. vel. obs. 2—25479
polystyrene, photocond., vacuum u.v. range, memory effects 2—10142
polyvinylidene fluoride, pyroelec. props., i.r. detectivity 2—13329
PVC foams, aged, heat transmission factor meas., cryogenic temp. 2—17433
rocket motors, low-cost moulded 2—20436
shock wave propagation in polytropic plastic body with elastic unloading props., closed form soln. 2—30878
stacks, heavy primary measurement in the region of supersonic aircraft 2—2893
strength, thickness depend. 2—15885
surface composition anal. using ion scattering spectrometry 2—20216
Teflon, ^{19}F n.m.r. line narrowing by rotary spin echoes 2—20156
Teflon, shock compression and induced phase transition 2—9640
Teflon, surface cond., water vapour adsorption depend. 2—39547
Teflon cable, effective piezoelec. consts., strain transducer applic. 2—25938
teflon-FEP, vacuum deposition and struct. 2—12676
tensile testing at a constant rate of stress change 2—29355
thermoplastics, carbon fibre reinforced, tribological characteristics 2—1336
thermoplastics, shear creep test apparatus 2—29370
water containing, heat shielding props. 2—36262
Young's modulus and creep in flexure meas., apparatus and technique 2—29371

Platinum
adsorption obs. using technique for polarized light reflected intensity meas. 2—9309
adsorption of Ag, H, O oxides, specular reflection spectra, monolayer thickness range 2—9310
atom, visualization, dark field electron microscopy, scattering cross sections 2—21521
black on stainless steel, secondary electron emission coeff., reflection characteristics for Pt blacked screened collector 2—22660
carbide overlayer on (111) surface, Auger effect, LEED 2—6385
chemisorption of O_2, model calcs. 2—35917
desorption of carbonium ions, field ionization 2—6390
deuteron irradiated, defect production and recovery 2—22194
diffraction grating, Al coating reflection deterioration because of diffusion 2—1661
electron irrad., dislocation, defect interactions, pinning, depinning, anelastic effects 2—1239
epitaxial particles, contamination of $Sr_{1-x}Ba_xNb_2O_6$ grown in Pt crucible 2—39579
fast neutron irradiation, resist. recombination volume 2—25763
film, discontinuous, on dielec. substrate, electron cond., resist. coeff., 130-300K 2—40180
film, on Si, low temp. migration of Si 2—15791
film, on Si single cryst., interdiffusion and compound formation 2—6352
film, vapour deposition on emission tip substrates, field ion microscopy 2—12663
film grown in elec. field, elec. resist. 2—9953
in glass, contamination due to melting in Pt crucibles 2—18895
hardening under press., vacancy volume of formation 2—15898
i.r. absorptivities at room and liquid He temperatures, derived from reflectivity measurements 2—26106
lattice parameters, −189 to 1709°C, solid equation of state 2—19304
linear thermal expansion, determ. by X-ray diffraction 2—16059
neutron activation analysis of ^{199}Pt, in biological tissue by analysis of daughter ^{199}Au 2—10678

Platinum continued
optical coating, characterization in 500-2000 Å region, extreme u.v. reflectance spectrum 2—17719
photoemission, band struct. 2—19810
plate in Wilhelmy method for interfacial tension determ., improvement by covering with Pt black 2—1087
polarograph, sensing element with rotating platinum anode 2—30101
quenching, dilatometry 2—39895
reflectivity changes in perchloric acid rel. to cathodic H adsorpt. and oxide formation 2—9311
resistance thermometer, accuracy improvements 2—20964
resistance thermometers, resistance meas., a.c. bridge 2—2281
shear modulus, effect of neutron irradiation at 4K on polycryst. sample 2—22278
specific heat, high temp., thermal vacancies influence 2—13047
stacking fault energy, twin boundary energy temp. coeff. 2—32533
stepped surface, chemisorbed gases, LEED obs. 2—35918
surface struct. of high Miller index surfaces, LEED obs. 2—35873
thermal expansion, 293 to 1900 K, Fizeau interferometer and twin-microscope method 2—16058
thermal expansion, cooperative measurement using pushrod dilatometers 2—16045
thermal expansion, low temp. 2—32848
wall reaction preparation of ^{217}At atomic beam 2—38846
wire, vacancy thermal equilibration kinetics, millisecond heat pulse obs. 2—39680
X-ray spectra, band struct. 2—7087
Os-Pt-Hg abundance peak in Ap stars and very heavy cosmic rays 2—33624
Pt/Al_2O_3 composite, grain boundary grooving 2—19287
Pt/Al_2O_3 composite, grain boundary grooving 2—19288
Pt/Al_2O_3 disperse catalyst, metal particle size distrib., small angle scatt. 2—3973
Pt/Au thin films couples on Si substrate, adhesion and diffusion obs. 2—39745
Pt/H system, electron impact desorption, active site obs. 2—39562
Pt/Ti thin film couples, diffusion and compound formation 2—39749
Pt-10%Rh/Pt and Pt-13%Rh/Pt thermocouples, reference tables 2—37830
Si:Pt diode, charge state and thermal generation in space charge region 2—10091

Platinum compounds
coordination, photoelectron spectroscopy 2—35281
1,5-cyclooctadiene complexes, i.r. and Raman spectra, frequency dependence on metallic ion 2—15332
X-ray photoelectron spectroscopy 2—31824
$[Pt(NH_3)_4]Cl_2.2H_2O$, anisotropy of chem. shift of ^{195}Pt nmr signal, position of Pt in unit cell 2—26307
Au-Pt alloy, discussion of spinodal hypotheses and precipitation 2—29425
Cu-Pt alloys, ordering 2—15980
Fe-Ir-Pt alloys, appearance of ferromagnetism 2—40473
Fe-Pt-Mn martensitic alloys, age-hardening 2—3941
Fe-Pt alloy, ^{195}Pt Mossbauer effect 2—10322
Fe-Pt alloy film, spin wave resonance 2—10468
Fe-Pt dilute alloy, hyperfine field at Fe atoms, temp. depend. 2—16436
$Fe_{65}(Pt_xIr_{1-x})_{35}$, f.c.c. alloy, mag. props., temp. and comp. effects 2—29817
Mn_3Pt alloys, local antiferromag. ordering 2—36774
Ni-Pt-P-Cr alloys, amorphous, elec. resist. and mag. susceptibility 2—6761
Ni-Pt alloys, ferromag.-paramag. transition 2—40489
Pd-Pt alloys, low temp. elec. resist. and thermopower 2—19551
$(Pd_{60-x}\text{-}Pt_x\text{—}Ni_{40})_{75}\text{—}P_{25}$ alloy, elec. resist., 1.2-300 K 2—19550
Pd complex, $[Pd(NH_3)_4]Cl_2.H_2O$, vibr. spectra 2—33270
Pt-Au alloy films, elec. conducting, on ceramics, prep. technique 2—1182
Pt-Co dil. alloy, magnetiz. and magnetoresist. 2—16344
Pt-Cr alloys, electron transport props. and sp. ht., below Kondo temp. 2—29615
Pt-Cu, alloy, dilute, charge density oscill. around impurities n.q.r. obs. 2—16666
Pt-Er dilute alloy, e.p.r. 2—30014
Pt-Fe, solid soln., positron annihilation and Mossbauer effect 2—4445
Pt-Fe dil. alloys, spin fluctuation effects in resist. 2—36445
Pt-Ir alloy, Mossbauer effect and n.m.r., ^{195}Pt and ^{193}Ir 2—26306
Pt-Ir solid solution alloys, shape of field ion image points, halo effect 2—12963
Pt-Ni alloys, mag. props. in ordered and disordered states 2—40419
Pt-Os alloy, thermoelec. power, 4-300K 2—40373
Pt-Pd-Fe, alloys, mag. hardening, mag. props., struct. 2—29813
Pt-Rh-Zr alloys, internal oxidation and hardness 2—4591
Pt-Si, Pt film on Si substrate, interdiffusion and compound form. 2—6352
Pt, complex, tetracyanoplatinates, n.m.r. study, anisotropy of ^{195}Pt shift 2—10562
Pt (IV) ammine complexes, substituted, i.r. and Raman spectra, factor group, space group symm. 2—10412
Pt complex, bis(triphenylphosphine) platinum dioxide chloroform adduct, crystal and molecular structure 2—29149
Pt complex, dichloro(ethylenediamine)platinum(II), polarized crystal spectra and ionic exciton states 2—29920
Pt complex, $K[PtCl_3(C_2H_4)].H_2O$, vibrational spectrum, relationship with vibrational structure in photoelectron spectra of ethylene and ethylene-d_4 2—3087
Pt complexes, Pt(II)-olefin, Br n.q.r. 2—5947
Pt complexes of types K_2PtX_4, K_2PtX_6 and $(PPh_3)_2PtX_2$ X-ray investigation 2—33300
$PtCl_{2(4)}$, isomer shift meas. of ^{195}Pt 99 keV transition 2—10322
PtCo alloy, domain wall pinning as source of mag. hardening 2—19858
PtFe-PdFe(PtNi) alloy, order-disorder transformation, lattice parameters, magnetization, coercive force 2—1633
PtI_2, isomer shift meas. of ^{195}Pt 99 keV transition 2—10322
Pt(II) complex, PtX_2L_2, X=Cl, Br and I, L=dialkyl sulphide, i.r. and Raman spectra, fundamental assignment 2—28322
$PtI_4.2H_2O$, prep. and structure 2—9356
PtO_2, isomer shift meas. of ^{195}Pt 99 keV transition 2—10322
PtOH, two species detected on Pt surface by i.r. spectroscopy 2—8699
PtP_yS_{2-y} phosphochalcogenides, synthesis and properties 2—3725
$PtSb_2$, valence band struct. 2—25842
PtSi, sputtered film, microstruct., electron microscope obs. 2—3540
ThPtGe, atomic struct., Debye-Scherrer determ. 2—3736

Pleochroism
l-alanine, i.r. spectra, vibrational assignment allowing for dichroic behaviour 2—40682

Pleochroism continued
alkali halides, mag. circular dichroism of centres produced by electrolytic reduction 2—10359
transazobenzene and isotopic derivatives, i.r. dichroism of oriented crystal 2—35304
carbonaceous mesophase, extinction of contours, microstruct. 2—18826
circular dichroism induced in symmetric cations by dissymmetric anions 2—19967
Cotton-Mouton effect, applics. 2—13470
dichroic reflector lamps for colour projection, rapid selection 2—23717
dichroism, linear birefringence in retinal rods, measurement of retardance of single unbleached rods 2—7613
dichroism, retinal rods of frogs, examination by polarizing microscope 2—11219
dichroism, u.v., visible or i.r., apparatus for instantaneous meas. in thin polymer during high-speed stretching 2—29874
hexamethylcyclotrisiloxane, i.r. dichroism of oriented crystalline films 2—40686
induced circular dichroism in cholesteric liquid crystals 2—28856
ionic cryst., mag. circular dichroism, freq. dispersion theory 2—10358
magnetic circular dichroism, computer program for dispersion curves distrib. 2—28253
magnetic circular dichroism, new applications to atomic and molecular systems 2—4432
magnetic circular dichroism, oscillatory behaviour in Jahn Teller coupled system 2—26154
molecules, magnetic circular dichroism 2—18381
molecules, vibrational-electronic circular dichroism spectra, low resolution spectra 2—8528
nematic system, chiralic molecules addition, optical rotatory power, circular dichroism 2—18827
nonmagnetic crystal, circular dichroism of optical phonons 2—40688
polycyclic aromatic hydrocarbons, magnetic circular dichroism of α bands 2—8801
polystyrene-polybutadiene-polystyrene macroscopic ‘single crystal’, i.r. dichroism 2—15417
polyvinyl alcohol films, study of chain orientation by visible and i.r. dichroism 2—6004
pulsed electric dichroism measurements of macromolecular solutions 2—27600
rare earth garnets, dichroism due to site selectivity of ions 2—40639
tetrapyrrole pigments, triplet-triplet absorption, dichroism 2—3120
transient electric dichroism of macromolecules using simple spectrophotometer 2—5999
$Ba(ClO_4)_2.3H_2O:MnO_4^-$, mag. circular dichroism spectrum of MnO_4^- at 4.2K 2—36870
$Bi_{3-2x}Ca_{2x}V_xFe_{5-x}O_{12}$, mag. circular dichroism 2—40611
CaO, stress-induced dichroism in F^+ centre emission spectrum 2—29911
$Co(H_2O)_6^{2+}$ in chiral lattice, circular dichroism spectra, Cotton effects obs. 2—26163
Co(III) complexes, trigonal MS_6 type, MCD spectra 2—12161
Cr(III) complexes, trigonal MS_6 type, MCD spectra 2—12161
$Cs_2ZrBr_6:Ir^{4+}$, high resolution magnetic circular dichroism spectra, assignment 2—26164
CuCl-CuBr solid solns., mag. circular dichroism spectra 2—16486
$Cu(H_2O)_6^{2+}$ in chiral lattice, circular dichroism spectra, Cotton effects obs. 2—26163
n-Ge, uniaxially stressed, i.r. dichroism due to free carriers 2—19968
Ir(III) complexes, trigonal MS_6 type, MCD spectra 2—12161
KCl, stress induced linear dichroism of Ag^- and Cu^- 2—33208
$KNiF_3$, antiferromagnet, mag. circular dichroism rel. to magnon sideband identification in optical absorption spectra 2—36882
LiF, moment anal. of mag. circular dichroism assoc. with allowed electronic transitions of impurity F-centres 2—10306
MgO:Ni, mag. circular dichroism, vibr. induced d→d transitions 2—22773
Mn complex, Mn(III) porphyrins, magnetic circular dichroism far red spectra 2—8667
NaCl, stress induced linear dichroism of Ag^- and Cu^- 2—33208
Rh(III) complexes, trigonal MS_6 type, MCD spectra 2—12161
Si, neutron irrad., stress induced dichroism of divacancy associated i.v. absorp. bands 2—22777
n-Si, uniaxially stressed, i.r. dichroism due to free carriers 2—19968
$Y_{3-2x}Ca_{2x}V_xFe_{5-x}O_{12}$, mag. circular dichroism 2—40611
YIG:Si, polarization-depend. photoinduced effects 2—26116
YIG:Si, spontaneous and photoinduced linear dichroism 2—22730
$ZnSeO_4.6H_2O:Cu^{2+}$, Co^{2+}, and $NiSeO_4.6H_2O$, dichroism, optical activity 2—19966
$ZnSeO_4.6H_2O:Cu^{2+}$, Ni^{2+}, Co^{2+}, and $NiSeO_4.6H_2O$, dichroism, optical activity 2—16420

Plexiglas *see Plastics*

Pluto
light curve analysis in terms of geometrical model 2—37368
mass, from optical and radar data 2—30579
mass determination from obs. of 5 outer planets and 7 minor planets 2—11002

Plutonium
atom, relative X-ray transition probs. to K-shell 2—21510
potentiometric determination in mixed oxides 2—30104
spin fluctuations and anomalous resist. 2—40409
superconductivity, review 2—13147
α-Pu, extruded, elongation rel. to grain size 2—6550
β-Pu, length change due to self- irradiation damage, 4K 2—19080
α-Pu, mag. susceptibility, localized moments 2—19835
^{238}Pu, production and applications 2—27935
^{238}Pu growth, neutron irradiation of ^{235}U and ^{237}Np 2—2789
^{239}Pu-Be(α,n) sources of different sizes, neutron energy spectra 2—28010
^{244}Pu, detection in nature 2—5678
^{244}Pu extinct, in meteorites and history of solar system 2—1996

Plutonium compounds
intermetallics, cubic, mag. props. 2—40562
nuclear fuel compositions, properties and irradiation behaviour 2—15112
Pu-C-O system, phase diagrams 2—12611
Pu-Cu, Pu-Ga-Cu, Pu-Ga-Ni systems, unit cell parameters, X-ray diffr. 2—15730
Pu-Ga alloy, plastic deformation, strength rel. to working temp. and homogeneity 2—15839
PuH_2, nonstoichiometric, variation of lattice parameter with H content 2—29150

Plutonium compounds continued
- $Pu(NO_3)_4$ neutron spectrum measurements, scattering kernels of ^{239}Pu and H compared with theoretical calculations in three different solutions 2—520
- PuO_2/UO_2 fast nuclear reactor fuel, fluoridation method for reprocessing 2—15111
- PuO_2-UO_2 fuel mixtures, neutron radiography testing with TiO_2, Eu_2O_3, RhO_2 mixtures as analogues 2—550
- PuO_2-UO_2 microlattice, expts. in LWR for design of fuel elements 2—24270
- PuO_2-UO_2 nuclear reactor fuels, det. of ^{238}U capture rates rel. to ^{239}Pu fission 2—35103
- PuO_2, nuclear fuel, operational and design experience for fast reactors in USSR 2—15099
- PuO_2, thermal cond., high temp. 2—19465
- PuSb, mag. props. 2—33140
- $^{238}PuO_2$, lattice parameters meas. by X-rays, temp. and long exposure effects 2—39651
- $^{239}PuO_2$ single cryst., high temp. soln. growth 2—25266
- U-Pu-C-O system, phase diagrams 2—12611
- $(U, Pu)O_2$ fuel, creep, irrad. effect 2—11902
- $(U, Pu)O_2$ fuel, in-pile thermal cond. meas. 2—18266
- $(U, Pu)O_2$ mixed oxides, thermal cond., high temp. 2—19465
- UO_2-PuO_2 fuel, O_2:metal ratio effects 2—2862
- UO_2-PuO_2 fuels melting heat rating 2—2860
- $(U_{0.8}Pu_{0.2})O_{1.97}$, enthalpy, 2350 to 3000K 2—13040
- Zr-Pu dilute alloy, $\beta \rightarrow \alpha$ transform., crystallographic study 2—29483

Pockels effect *see Electro-optical effects*

Point defects *see Crystal imperfections*

Point groups *see Crystal structure, atomic*

Poiseuille flow *see Flow; Hydrodynamics*

Poisson ratio *see Elastic constants*

Polar cap absorption *see Electromagnetic wave propagation/ionosphere*

Polar cap flow *see Airglow*

Polarimeters
- *see also Ellipsometry*
- for circular polarization of luminescence emitted by chiral molecules det. 2—31101
- Compton, multiple scattering, Monte Carlo calc. 2—11660
- digital light deflector with prisms and polarization switch based on Pockels effect 2—11520
- electronic, with Faraday compensation 2—14453
- Jones matrices for Fourier spectropolarimeters 2—8033
- optical saccharimeters, measurement accuracy in sugar production 2—38076
- photoelectric, for remote sensing of atmosphere 2—16799
- polarimeter, scanning photoelectric, obs. of all four Stokes parameters of visible radiation of Sun, Moon, corona and planets 2—11175
- radio frequency polariscope, for defectoscopy 2—9384
- solar activity at 7 GHz homologous events from different active centres 2—7552
- spectropolarimeter, JASCO model J20, review 2—7994
- stress analysis, using optically sensitive coatings 2—34501
- stress distribution measurement in transparent cubic crystals, attachment 2—23696
- u.s. polarimetry, vibrs. generation 2—29523
- X-ray, astronomical, incoherent Thomson scatter in Li metal 2—10981
- X-ray, examination of astronomical sources 2—10982
- NaI(Tl) single crystal polarimeters, polarization sensitivities 2—27889

Polarisability
- aromatic hydrocarbons, electrooptical polarisability in ground state and first excited singlet states 2—15381
- aromatic molecules, in nematic liq. cryst. relat. between orientation and principal polarizabilities 2—15352
- atomic, unified treatment based on R-matrix theory 2—11931
- atoms, cross sections, R-matrix theory 2—599
- atoms, neutral, ground states, static dipole polarisabilities 2—8421
- atoms alignment of excited states due to isotropic irradiation 2—8432
- complex atom, calc. of perturbed orbital wavefunction giving full polarizability of ground and excited states 2—21489
- conjugated molecules, π-electron polarizability, multiconfiguration approx. 2—12089
- cyclobutane carboxylate ion, aqueous, degree of polarization determ. 2—5969
- cyclopropane and derivatives, anisotropy 2—839
- diatomics in soln., spectroscopic method for determ. dipole moment and polarizability function 2—18377
- dispersion interaction const. for polyelectronic systems, limits, from dynamic polarizability 2—31697
- electron gas, degenerate, temp. depend. of h.f. polarizability 2—37658
- 9-ethylguanine, polarization of electronic transitions 2—24533
- hydrocarbons, conjugated, perturbation theory calculation 2—38986
- hyperpolarisabilities, coupled Hartree- Fock calculation 2—35182
- metallic particles in quasistatic elec. field 2—36434
- molecular, as basis for energy partitioning estimates in radiolysis 2—22884
- molecular crystal, polarisability tensor, refractive index calc. 2—33197
- molecules, calc. using expressions for derivatives of eigenvalues of hamiltonian 2—37616
- naphthalene-d_8, anisotropy of opt. polarizability from induced birefringence produced by photoselection 2—3110
- open shell ions, self consistent calc. of dynamic multipole polarizabilities 2—35123
- chain optical anisotropy, matrix anisotropy, multiplication analysis 2—12296
- organic molecules, σ- and π-electrons 2—18475
- perturbation theory for excited states, electric polarizabilities 2—38986
- perylene, electrochromic spectra in polystyrene matrix, change in polarizability and dipole moment between ground and excited states 2—13488
- point dipole near metal surface, Thomas-Fermi response, effective polarizability 2—15652
- polar gases, total electric polarizations 2—15543
- rhodamine 6G, electrochromic spectra in polystyrene matrix, change in polarizability and dipole moment between ground and excited states 2—13488
- tetraphenylpolyenes, electrooptical polarisability in ground state and first excited singlet states 2—15381
- three- and four-electron atoms, distinguishable electron method 2—15199
- two electron atoms, lower-bound procedure 2—31726

Polarisability continued
- Ar, core polarizability effects on photoionization cross section calc. 2—11973
- Ar atom, hyperpolarizability, Hartree-Fock calc. 2—11955
- Au particles in quasistatic elec. field 2—36434
- BaS, dynamic ion charge determ., i.r. spectra and static dielectric props. obs. 2—22396
- Be atom, Hartree-Fock calc. of hyperpolarizability 2—11955
- C, dipole polarisability in ^3P ground state 2—18341
- CaS, dynamic ion charge determ., i.r. spectra and static dielectric props. obs. 2—22396
- H, ground-state hyperfine splitting, polarizability correction, rel. to structure functions of inelastic ep scatt. 2—38236
- H, static relativistic polarisability, closed analytic expression 2—28227
- H^-, static and dynamic polarizabilities, via asymptotic approx., photodetachment cross sect. 2—18347
- H_2, ground-state, computation of frequency dependent polarizability 2—792
- H_2, variational calculation of static polarisability 2—21717
- HCL, spectroscopic method for determ. dipole moment and polarizability function 2—18377
- He atom, dynamic polarizability and dipole shielding factor at imaginary frequencies calc. by coupled HF approx. 2—28232
- He atom, Hartree-Fock calc. of hyperpolarizability 2—11955
- He sequence, hyperpolarisability, coupled Hartree-Fock calculation 2—35182
- He_2, long-range expansion, coeff. calc. 2—8654
- $^{39}K^{19}F$, rel. to Stark effect, molec. beam resonance meas. 2—21646
- Li ion sequence, self consistent calc. of dynamic multipole polarizabilities 2—35123
- Mn complex, $Mn_2Fe(CO)_{14}$, atomic, bond and molecular polarizabilities 2—18442
- NCl_3, isotopic species, atomic, bond, and mol. polarizabilities, root mean square amplitudes statistical thermodynamics 2—5937
- Ne, correlation corrections, error due to use of commuting potential 2—21516
- Ne atom, dynamic, polarizability and dipole shielding factor at imaginary frequencies calc. by coupled HF approx. 2—28232
- Ne atom, hyperpolarizability, Hartree-Fock calc. 2—11955
- O, unified treatment based on R-matrix theory 2—11931
- SrS, dynamic ion charge determ., i.r. spectra and static dielectric props. obs. 2—22396
- $^{205}Tl^{19}F$, rel. to Stark effect, molec. beam resonance meas. 2—21646
- Xe-H^+ collisions, 15 eV, possibility of producing spin polarized H atoms 2—5867

Polarization
- 3C58, supernovae remnant, brightness and polarization structure, obs. at 2.8 cms 2—26791
- alkali halide, anomalous d.c. polariz. current due to surface effects 2—10107
- alkali halides in crystal, polarization effects in electron binding energy 2—31685
- alkali-inert gas collisions, alkali depolarization, time reversal in classical path approx. 2—5843
- alkali-like atoms, core polarization, non-adiabatic approach 2—18279
- atmospheric signals from severe thunderstorms 2—13706
- azulenes, σ bonding polarization, comparison of results from i.r. intensity meas. and CNDO/2 calc. 2—21660
- 3C 273, circular 2—26692
- 3 C 279, polarization at 8GHz during 1966-70 outburst4910 2—4910
- VY Canis Majoris, circular 2—26692
- Cassiopeia A, distribution of linear polarization at 9.8 and 11.1 cm wavelengths 2—33708
- circular, radio source obs. 2—30522
- circular, reduction of parasitical signal on antenna of variable profile using grating 2—11179
- circular of synchrotron radiation in presence of hydromagnetic waves due to pitch angle anisotropies in relativistic electron gas 2—30909
- collision spectra optical broadening and depolarization of lines 2—31698
- Compton polarimeter for resonantly scattered neutron-capture gamma rays 2—11651
- cross-polarization distortion in microwave radio transmission due to rain 2—22980
- depolarization ratios meas. in Raman spectroscopy, factors influencing precision 2—27647
- drifting subpulses of pulsar 0809+74 2—10943
- elastic dielectrics, polarization gradient contribution in continuum theory 2—19150
- elastic waves in crystals 2—1282
- electron spin, photoelectrons from alkali metals illuminated with circularly polarized light 2—33089
- electrostrictive ceramics, method 2—30874
- e.m. wave, in anisotropic medium, corrections 2—11389
- excitonic states, rel. to resonance Raman scatt. in electric fields 2—16512
- extended extragalactic radiosources, obs. at 6 cm wavelength 2—20613
- extended galactic radio sources, obs. of supernova remnants at 6 cm wavelength 2—20614
- ferroelectric, displacive, ionic displacement, Curie temp., spontaneous polarization 2—13310
- ferroelectric, KH_2PO_4 and KD_2PO_4, polarization relax., u.s. obs. 2—4279
- ferroelectric, macroscopic stimulated polarization echo 2—1569
- ferroelectric phase transition, critical polarization fluctuations 2—36590
- fluorescence, conc. quenching by excitation transfer, anisotropy and 2nd nearest neighbour consideration 2—8552
- fused salts, rel. to complex ion structure 2—39378
- GaAs injection laser, anisotropy of active field and radiation polarisation 2—27525
- HD 226868, circular 2—26692
- horizontal meas. rel. to Peake's model 2—2282
- IC443, supernova remnent brightness and polarization structure, obs. at 2.8 cms 2—26791
- ice:KCl, dielec. props. 2—16264
- insulator, electron states, electronic polarization effect, review 2—40136
- isotropic rigid solution, fluorescence depolarization by excitation transfer 2—20099
- laser beam, energy of linear components of polarization at 1.060 μ 2—2407
- leptons, effect on electron and photon spectra from $\nu\mu$ inelastic scatt. 2—27710

Polarization continued
- light nuclei, disintegration during inelastic scatt. of electrons, nucleon polarization 2—31525
- lunar crater Posidonius 2—30535
- magnetic monopole moving in constant elec. field, polarization of radiation 2—7835
- metal particles in glass matrices, elec. polarizability 2—22606
- microwaves, vertically, diffraction by two long parallel inclined strips 2—11392
- mixed conductor, method for partial electronic/ionic cond. determ. 2—16271
- molecular fluid, depolarized light scatt. 2—18832
- naphthalene electrets, Schottky barrier formation 2—4191
- NGC 1068, circular 2—26692
- NGC 4151, circular 2—26692
- non-polar liquid mixtures, collisional polarization 2—1107
- NP 0532, upper limit to circular polarization 2—10935
- optical nuclear spin, in molecular crystals 2—16665
- partially polarized waves, emission and detection by two channel antennas 2—23442
- plasma surface waves, on border of half spaced plasma with metal grating 2—32068
- polar vacancies, dielec. loss angle, freq. and temp. dependence 2—40323
- polyvinylidene fluoride, polarization reversal 2—13329
- proton target, Davis, computerized n.m.r. system 2—24064
- pulsar, PSR 0833-45, measurements at 400 MHz 2—37332
- pulsar 0809+74, drifting subpulses 2—4931
- quartz, nonlinear polarization coeffs. determ. 2—36601
- quartz gauge, shock wave induced polarization 2—14356
- quasar 3C 273, circular 2—4944
- quasars at 49 cm 2—13939
- quasi stellar radiosources, depolarization at long wavelength, correlation with redshift 2—41146
- radio waves reflected from ionosphere, Stokes parameters for anal. 2—22999
- radiofrequency, millimeter wavelengths, Sun active regions 2—5005
- radiofrequency, Sun, mapping at 7.8 GHz 2—5004
- radiosources, extragalactic, in 3C catalogue 2—20624
- radiosources, quasars and radiogalaxies, high resolution obs. 2—30521
- reversal in ferroelectrics, hysteresis loop, coercive field, domain shape effect 2—13311
- rhodamine 6G, soln., intermol. energy transfer and conc. depolarization of luminescence 2—6237
- scattering processes, electromagnetic and weak, secondary particle polarization 2—27705
- Sco X-1 X-ray source, 3C 273 quasar and NGC 1068 Seyfert galaxy 2—37334
- seismic waves, total volume 2—30186
- Seyfert galaxies NGC 4151, NGC 1068, circular 2—4944
- shellac wax, magnetoelectret effect 2—1578
- soda lime glass, ionic cond., electrode polariz. effects 2—22611
- solar emission at 7.8 GHz, two-dimensional maps 2—7554
- solar microwave bursts observed at 17 GHz 2—11078
- solar radio emission in active centre 2—11120
- stellar atmospheres, extended, radiation transfer 2—4820
- Sun S-component radiation at 81 and 250GHz 2—23125
- supernovae remnants emission, and magnetic field structure 2—26718
- suspension, rel. to pulsed electrical breakdown 2—39396
- tetracene, data for triplet triplet absorption spectrum, band assignment 2—8823
- transition metal compounds, phonon spectra anomalies, resonances electronic polarization 2—25657
- triglycine sulphate, Cr^{3+} doped, spontaneous polarization, rel. to e.p.r. 2—10530
- triglycine sulphate, critical phenomena 2—19771
- triglycine sulphate, ferroelec. single cryst., acoustic emission on polariz. reversal 2—13030
- triglycine sulphate, spontaneous polarization, laser irrad. effect 2—1574
- triglycine sulphate-selenate mixed cryst., spontaneous polarization 2—13321
- tris-sarcosine calcium chloride, Mn^{2+} doped, spontaneous polarization rel. to e.p.r. spectra 2—10529
- two dimensional solns., conc. quenching of fluorescence polarization 2—8553
- W28, supernova remnant brightness and polarization structure, obs. at 2.8 cms 2—26791
- W44, supernova remnant brightness and polarization structure, obs. at 2.8 cms 2—26791
- waves propagating in uniaxially stressed elastic media 2—34080
- X-radiation, from atoms excited by electron impact theoret. study 2—617
- X-ray emission from Crab Nebula, det. 2—41155
- X-ray source Sco X-1, circular 2—4944
- X-rays, solar, anisotropy during flares 2—17054
- $Ag^{2+}(4d^9,{}^2D)$, in frozen acid solutions, e.p.r. study of core polarization 2—10481
- β-Al_2O_3, ionic cond., electrode polariz. effects 2—22611
- Al_2O_3, time dependent polarization 2—36584
- $Ba_2Na_{1-x}Li_xNb_5O_{15}$, ferroelectric, and cryst. growth obs. 2—29097
- $BaTiO_3$, ferroelec. single cryst., acoustic emission on polariz. reversal 2—13030
- $BaTiO_3$, spontaneous, phase transition, dielec. const., press. and temp. depend. 2—13319
- $BaTiO_3$, spontaneous, temp. depend., ferroelectric phase transition, soft vibration modes 2—16281
- $BaTiO_3$, switching processes in low temp. phases 2—29752
- $Bi_4Ti_3O_{12}$ films, domain struct. and polarization reversal 2—40350
- CdS, excitonic states, rel. to electric field induced Raman scatt. 2—16528
- CdS photoelectrets, effects on lifetime 2—22640
- $CuCl_2.2H_2O$, e.m. wave absorption 2—7043
- Fe_3S_4 film, electrostatic polarization, electron diffr. 2—19751
- $Gd_2(MoO_4)_3$, ferroelec., elec. field depend. 2—19971
- $Gd_2(MoO_4)$, pyroelec. effect, ferroelectric phase transition 2—13328
- H(1s), Glauber calcs. polarization fraction of Lyman-α radiation emitted in collisions with e- 2—21540
- Hg resonance radiation, collisional quenching and depolarization 2—5841
- K atomic beam, properties 2—24390
- KBr single crystal, surface polarization capacitance 2—16270
- KH_2PO_4:D, KD_2PO_4:H, ferroelec., impurity effects, zero-temp. Green function method 2—19765
- KH_2PO_4, KD_2PO_4, polarization relax., u.s. obs. 2—4279

Polarization continued
- KH_2PO_4, macroscopic stimulated polarization echo 2—1569
- Mn, ground state due to spin-exchange collisions with optically pumped vapour 2—2932
- $NH_4Fe(SO_4)_2$, Mossbauer spectral dip rel. to spontaneous polarization 2—6885
- NO, γ, ε and δ system, fluorescence spectrum polarization of rotational lines, vibr. band intensities 2—8675
- Na, atoms, excited, polarization transfer in sensitizing collisions with inert gas atoms in strong mag. field, polarization transfer 2—2978
- NaCl, ionic cond., electrode polariz. effects 2—22611
- NaCl, polarization impedance of pure and doped crysts. 2—16273
- $NaNO_2$, polarization reversal mechanism, X-ray obs. 2—40353
- $NaNO_2$, spontaneous polarization temp. depend. 2—19951
- $(Pb,La)(Zr,Ti)O_3$ ceramics, ferroelec. domain switching 2—40355
- $Pb(Cd_{1/3}Nb_{2/3})O_3$ ferroelectric, cryst. growth, dielec. hysteresis 2—19768
- $PbMg_{1/3}Nb_{2/3}$, ferroelectric, temp. dependence of dielectric props., relaxation polarization, diffuse phase transition 2—16292
- $PbTiO_3$, phase transition, spontaneous polarization, dielec. const., press. and temp. depend. 2—13319
- $Pb(Zr_{0.65}Ti_{0.35})O_3$ with Nb_2O_5, oxygen depleted surface layers, ferroelec. field effect 2—40357
- Rb atoms, electron beam scatt., electrons polarization 2—28209
- S, electrification in darkness and under illimination 2—25914
- SbSI, ferroelectric, phase transition, soft mode coupling, Rayleigh scatt. 2—16012
- SbSI, injection currents and polarization charge accumulation 2—6822
- SbSI, instability of ferroelec. polarization 2—29753
- SbSI, photopolarization 2—33060
- SbSI, polarization switching in two-phase coexistence region 2—10125
- SbSI, spontaneous polarization, rel. to piezoelectricity 2—19772
- SbSeI, photopolarization 2—33060
- Si_3N_4 layers, effect of irradiation with low energy electrons 2—1561
- SiO_2 layer in m.o.s. system, relaxation polarization, surface potential stability 2—4269
- Sr^+, optically pumped, spin depolarization in collisions with inert gas atoms 2—5846

light
- *see also Double refraction; Optical rotation; Photoelasticity; Polarimeters*
- anthracene derivates, polarization dependence on conc. of fluorescent derivatives 2—16622
- anthracene derivatives, fluorescence spectra 2—4487
- atmospheric depolarization, effect of electrostrictively induced stimulated Brillouin scattering 2—10730
- atoms, effect of light polarization on multiphoton ionization, cross section variation 2—28203
- bicyanine dimer, electron- vibrational spectra, strong coupling case 2—12214
- characteristic and losses of anisotropic laser resonators 2—21057
- circular, luminescence emitted by chiral molecules, sensitive instrument for obs. 2—31101
- circular components, Jones vectors, matrices for transformation from linear to circular basis 2—17695
- circularly polarized beam, calculation and experimental proof of the transverse shift on total internal reflection 2—31100
- coherence measurement of one dimensional wavefront 2—7907
- coherence properties in weak magnetic fields 2—7908
- corona, green line, det. of magnetic field orientation 2—11151
- V 1057 Cygni, variable star 2—41113
- daytime sky during solar eclipses, in visible region 2—33471
- dense gases, scattered light depolarization in critical region, molecular theory 2—9035
- depolarization and angular dependences of n-harmonic scattered light in statistically inhomogeneous media 2—38074
- depolarization when scattered by anisotropic molecules 2—9033
- eigenstates of anisotropic resonators, Jones matrx calc. 2—27463
- ellipsometry, equi-azimuth and equi-ellipticity contour charts 2—31102
- ferroelectric polarization-reel, type modulator 2—38028
- ferromagnet, magnetized, γ-quanta linear polarization, plane rot. 2—36819
- film, single-wavelength 2—313
- effects in fourier spectroscopy, coherency matrix representation 2—23723
- gas laser beam, intensity obs. for det. of birefringence in active elements 2—17583
- glycerine/dye solution, fluorescence, depolarization, temp. and viscosity depend. 2—18840
- gratings, formation of moire fringes 2—34486
- handedness of polarization after total reflection of linearly polarized light 2—14442
- holography, photoelasticity study 2—27541
- holography, recording and reconstruction processes 2—7950
- interference fringe shifter 2—27592
- interference of elliptically polarized beams 2—34478
- interference-polarizing filter for magnetic field studies, electrically controlled 2—27634
- interferometry, complex amplitude addition and detection of pattern differences 2—5415
- interstellar, general law 2—7428
- interstellar absorption band at 4430 Å wavelength dependence of polarization 2—20595
- i.r. diffraction-grating spectrophotometer, degree of polarization 2—31142
- laser array, uniform polarization 2—37994
- laser beam, total refl. and separation into two rectilinearly polarized beams 2—2405
- laser beam depolarization in a turbulent medium, gaussian and Kolmogorov spectra 2—31058
- laser beams, induced by scattering, teaching demonstration 2—8
- magnetic circular dichroism, new applications to atomic and molecular systems 2—4432
- microscopy, obs. of anisotropy effects on (010) axis of stibnite 2—19965
- mode filters for integrated optics 2—38129
- modulated, response of optical system 2—17678
- modulated interference-polarization filter, transmission band and secondary max. obs. 2—31129
- moisture content of soil applic. 2—20275
- multiple backward-scattered radiation, luminance and polarization properties in fogs and smokes 2—4690
- multiple forward scatt. in artificial fogs and smokes 2—5421
- NGC 2264, polarization of pre-main sequence stars 2—26700

Polarization continued
light continued
normal oscillation modes in anisotropic travelling wave resonator 2—37950
optical devices, vector methods 2—2435
optical distance measuring instruments, using electrooptical polarization modulators 2—30747
n-paraffin, doped, Shpol'skii spectra, 77K, multiplet components 2—20055
photoelectric measurements of sunspot magnetic fields 2—11108
propagation through rectangular light pipe or flat lightguide plates 2—34500
rare earth iron garnet, at mag. compensation point 2—16457
reflection transmission and phase shift by imbedded optical films 2—7974
scattered in atmosphere, det. of atmospheric turbidity 2—37159
scattering, Rayleigh and isotropic, exact closed form solution for discrete eigenvalue 2—23694
scattering in a plane-parallel atmosphere 2—13720
Sco X-1, wavelength and time dependence 2—20629
scrambler plates used to depolarize visible radiation, using Raman effect 2—7991
semi-plane diffracted wave, conducting screen effect 2—7993
sky radiation at twilight, effect of atmospheric aerosol layers 2—20335
skylight near sun, effects on polarimetric K corona obs. 2—37418
solar active regions, mangetic field determination by circular polarimetry 2—11114
solar corona, white-light photographs 2—41256
solar corona meas. 2—41257
solar coronal emission lines 3400 to 9000 Å, linear polarization in inner corona 2—41258
sunspots, circular polarization components, crossover and magneto-optical effects in spectra 2—37406
surface scattered, rel. to birefringence meas. method 2—4433
transfer function of an optical system as a bilinear transformation 2—14454
transmittance of polarization attenuators, accuracies 2—27612
u.v. polarizers and reflectors 2—7976
vacuum u.v. plane polarized monochromatic collimated beam production 2—17702
vacuum u.v. polarizers at CNRS Bellevue, review 2—14477
X-ray star Sco X-1, variable circular polarization in visible region, periods and amplitudes 2—33718
Ag_3SbS_3, polarisation shift of absorption edge, simplified band model 2—29906
Al_2O_3 film, porous anodic, effects on light scatt. 2—19949
$CsNO_3$, Raman spectra in solid and molten phases 2—36898
GaAs junction laser, conservation of polarization 2—23616
GaAs laser array fabrication 2—17633
Ge, i.r. absorption of dislocations 2—10381
HIO_3, nonlinear 2—26101
I_2, collisional depolarization of laser excited fluorescence 2—38919
$NaNO_3$, polarization dependence of reflectivity spectral lines in vac. u.v. 2—16471
Ne-He, internal-mirror lasers, polarization props. at 6328 Å 2—23595
Rb solid and liquid, optical constants in 0.3-2.4 μ region determ. from polarization of reflected radiation 2—16417
Polarography *see Chemical analysis/electrochemical*
Polarons *see Crystal electron states/polarons*
Polishing *see Surface structure*
Polonium
in troposphere, origin from ^{210}Pb in atmosphere 2—37134
Polonium compounds
No entries
Polyelectrolytes *see Electrochemistry; Polymers; Solutions*
Polymerization
p-cetyloxybenzoic acid, p-methacrylyloxybenzoic axid and styrene liquid crystalline mixtures copolymerization 2—20185
fluorescein and halo-fluorescein dyes, dimerization thermodynamics 2—22876
glass, GeO_2-$Tl_2O(Ag_2O)$ and Tl_2O-Al_2O_3-GeO_2, i.r. study 2—15638
isobutene, ion-molecule reaction chains 2—10621
isoprene with solid insoluble inhibitors, dynamics with modified Ubbelohde viscometer 2—21966
photodimerization by polycyclic aromatic hydrocarbons, applications to photochromism 2—33386
plasma process, thin film formalism 2—3550
poly-P2VB, solid-state photopolymerization, X-ray diffr. obs. 2—3477
poly-p-xylylene, morphology obs. 2—3480
polyethylene, high-crystallinity, prep. at low press. 2—3475
polymer film, growth from gaseous phase 2—3551
polyoxymethylene, in aqueous soln., epitaxial crystallization 2—35954
PPO styrene solutions during polymerization, decay times and radioluminescence yields 2—40809
4,4',4''4'''-tetrasulphophthalocyanines, Cu and vanadyl derivatives, aggregates in solution, e.s.r. 2—9163
NO adsorbed on Li halides, dimerization 2—15677
Pb, matrix isolated, absorption spectra study 2—15223
S, liquid, chain dissociation, ring scission, elec. resist. obs. 2—35785
Se, liquid chain dissociation, ring scission, elec. resist. obs. 2—35785
SeO_2 to dimer and higher aggregates 2—28326
Polymers
see also Plastics
A-B block copolymer, isolated molecule, block segregation study 2—24560
acrylic fibres, heat treated, meridional peaks in X-ray small angle scatter pattern 2—9221
adsorption, applic. of ellipsometry 2—9303
adsorption, at solid-solvent interface, adsorption isothermal, layer thickness 2—15671
aliphatic chain crystallization, example of even fold surface with adjacent fold reentry and transition to chain extension 2—35850
aliphatic chains, crystallization, general chain-folding behaviour 2—32317
aliphatic polyesters, epitaxial growth on uniaxially oriented polyethylene, polypropylene, polycaprolactam and polyoxymethylene 2—29106
aliphatic polyesters, epitaxial growth on uniaxially oriented polyethylene 2—29105
n-alkanes, short chain, intrinsic viscosity 2—6222
n-alkanes in 1-chloronaphthalene solvent, effect of molecular weight on refractive increment 2—6235
amorphous, PVT props. and transitions 2—3478

Polymers continued
amorphous, rot. and progressive diffusion, local conc. of radicals, e.p.r. obs. 2—30018
amorphous, tensile strength, internal friction 2—36145
amorphous PVC, PS, PMMA, PPO, time dependent heat capacity in glass transition region determ. by differential thermal analysis 2—6680
biopolymers, mol. config. and conform. changes, u.s. absorpt. obs. 2—28422
biopolymers, ultrasonic absorption spectroscopic study of conformational modifications 2—30653
block copolymers, depolarized light scattering in terms of birefringent domains 2—16422
butadiene-styrene block copolymers, branched, steady flow and dynamic viscosity studied 2—6179
carbonized polymer fibers, low angle electron scattering, surface structure 2—22058
carboxymethylcellulose, u.s. absorption of salts in aqueous solutions 2—25079
carboxypolymethylene in water, free convection of heat from a vertical plate 2—37812
β-cellotetraose, cell dimensions of the cellulose II model compound 2—32486
Celluloid, mechanics of upper and lower yield points 2—3474
chain, cluster expansion, random walks 2—39019
chain, configuration-dependent properties, mathematical methods 2—15409
chain molecule, asymptotic behaviour of distribution functions 2—8844
chain rupture in strained crystalline polymers, molecular mechanism 2—29292
chemical equilibrium, stress effects 2—4570
chlorinated polyethylenes, volume and thermal relaxation, at glass-rubber transition 2—16065
chlorinated polyvinyl chloride, capillary flow, melt fracture 2—15548
coating, application and drying, mech. relax. 2—15668
coating for metals by electrophoretic deposition 2—1760
composite, SBS copolymer, mech. props. 2—29235
composite and interpenetrating networks, non-Gaussian elasticity 2—32318
conference on polymer chemistry, New Orleans, USA (1970) 2—30036
contact lenses, manufacture from LSO-M plastic 2—27620
copolymer of acryl amide and methylene-bis-acryl amide, sensitivity and resolving power, application to holography 2—34416
crystalline, deformation mechanisms and morphology 2—15824
crystalline, elastic moduli using composite theory 2—39763
crystalline, plastic deformation, morphology, small angle X-ray scatt. obs., electron microscopy 2—3462
crystalline, thermodynamic and morphological properties 2—28969
crystallization, chain folding, spherulite growth 2—35851
crystallization, effect of a secondary process, branching mechanism 2—39444
crystallization, without chain folding, theory 2—22057
cyclic polyenes, energy, Theta-function overlap approximation 2—15392
deformation, linear, automatic recording of thermal stability 2—29351
dielectric breakdown, review 2—10114
dielectric properties, measurement in field of 10^4MHz γ-rays from ^{60}Co 2—29740
dielectric properties, thermodynamical treatment 2—6875
diene, bond exciton model 2—15348
diffusion in turbulent boundary layer, drag reduction 2—25013
dilute solutions, calc. of torque induced on free and enclosed rotating discs 2—35703
dilute solutions, normal stress effects, Fixman's viscosity theory 2—25057
disordered spherulites, scattering of light, effect of disorder in magnitude of anisotropy 2—7041
DNA type, intercalation interaction of small molecules 2—8842
Dow Corning 200 fluids, anomalous acoustic behaviour 2—32830
drag reducing, dil. solution, turbulent pipe flow, laser dopplermeter velocity obs. 2—25007
drag reduction in liquids, nonuniform concentration as mechanism 2—32218
elastic, fatigue strength and ageing under artificial climatic conditions, simulation device 2—25557
elastic-plastic behaviour, and flow processes, in the softening range 2—29266
elastomer, friction and area of contact with solid surface 2—3922
elastomers, triaxial tension, fracture 2—15885
electric discharge, film surface 2—6116
electrical conduction mechanism, mass spectrometry determ. 2—4277
electron and optical microscopy, state-of-the-art 2—35857
entangled, statistical mechanics 2—39018
epoxy cast resin, mechanics of upper and lower yield points 2—3474
epoxy resin, high pressure compressibility, dynamic obs. 2—22269
epoxy resin, linear viscoelastic range from uniaxial tension tests 2—1279
epoxy resin, plastic flow 2—19185
epoxy resin, struct., effects of plasticizers and modifiers 2—35855
epoxy resin composite, glass bead filled, fracture toughness 2—36105
epoxy resin/glass composite, post irrad. mech. props. 2—1382
epoxy resins, ionic dissoc. energy in elect. cond. behaviour 2—25912
epoxy resins, velocity meas. of polarized ultrasonic wafes in temp. range 4-100 K, calc. of specific heat and elastic moduli 2—40058
epoxy-diane resin, γ-irrad. effects on mech. and optical props. 2—39803
epoxypolyamide varnish film, ionic conduction rel. to Fe_2O_3 pigmentation 2—1564
ethyl carbamate, copolymers with diethylene glycol etc., crystal study, i.r. spectra 2—4462
ethylene acrylic acid copolymer, X-ray scatt. invariant, density, crystallinity 2—25163
ethylene propylene terpolymer stress optical coeffs. of rubbery state, dependence, chain length 2—25507
ethylene vinyl acetate copolymer, X-ray scatt. invariant, density, crystallinity 2—25163
ethylene-chlorotrifluoroethylene copolymers, structure investigation by i.r., n.m.r. and X-ray diffraction examination 2—39446
ethylene-vinyl acetate copolymers, microstructure study by n.m.r. 2—4563
failue surface in principle stress space 2—15815
fibre, irradiated, straining, crystalline regions, radicals e.p.r. obs. 2—15846
fibre, semicrystalline, strength rel. to mol. wt. and struct. 2—15643
fibrous, paracrystalline structure, X-ray study 2—28979
filled, thermophys. props., 10 to 400 K 2—19429
film, bistable electrical switching 2—6873

Polymers continued
  film, electron-beam-deposited, bombarding current depend. of elec. props. 2—32994
  film, polymerization from gaseous phase 2—3551
  films, apparatus for instantaneous meas. of u.v., visible or i.r. dichroism during high-speed stretching 2—29874
  films, measurement of tensile strain curves 2—29367
  flow, quasisteady, dilute, centreline-Bernoulli eqn. 2—9055
  fluorocarbon, film struct., x-ray and i.r. obs. 2—9228
  foil, prod. of high quasipermanent charge densities by breakdown fields 2—25923
  fracture initiation rel. to network orientation and microstructure 2—15869
  fracture mechanics, bond rupture, e.s.r. obs. 2—15886
  friction coeff., press. depend. 2—3923
  friction process with metals, in s.h. vacuum, 300-10K 2—36179
  gels and solutions, anomalous freezing 2—1142
  glass transition, hole theory applic. 2—3460
  glassy, oriented, elastic consts. 2—3839
  glassy amorphous, yielding behaviour 2—3872
  guar gum, expansion-contraction behaviour of dilute solution, capillary jets 2—32202
  high polymer solns., dilute, viscosity rel. to conc. 2—3377
  high-polymer physics, conf., Cleveland, USA, Mar.-Apr. 1971 2—3459
  hydrocarbon-type chain, matrix formalism 2—15416
  hydrogels, use in contact lens applications, bibliography 2—11222
  insulating, electron induced cond., bulk excitation 2—25808
  intercrystalline links eval. 2—3461
  at interfaces, symposium, Chicago, USA, (Sep 1970) 2—15654
  interfacial properties between two immiscible polymers theory 2—28802
  i.r. spectroscopy at high pressures using diamond- window cell 2—14474
  lactone, glass transition temp. of monomeric lactones and polymers 2—32321
  latex systems, size distribution analysis using extrema in unpolarized and horizontally polarized ang. light scatt. pattern 2—39397
  linear, Fourier representation methods for electronic structure 2—35367
  linear, influence of molecular chain flexibility on glass transition temp. 2—28981
  linear, origin of internal viscosity 2—39013
  linear, rheological properties at temp. above glass transition region and melting point 2—15855
  linear polyethylene, fractionation during bulk crystallization under high pressure 2—19012
  liquid, polymer system, interfacial tension, surface tension, polarity 2—18808
  macromolecules, adsorpt. from soln., conditions for form. of multilayers 2—35930
  Makrofol E, particle track visualisation in dosimetry of high energy radiation 2—2890
  mechanical props., dynamic, rel. to mol. packing 2—3840
  mechanical props. torsion balance with air bearings for obs. 2—22310
  mechanical rupture processes 2—1746
  melinex, reflection and absorption coeff. at 338μ 2—19964
  melts, flow in entrance region of circular tube, wall normal stresses 2—25006
  melts, surface tension, wetting, pendent drop-sessile drop method 2—35746
  metal/polymer composite, elec. resist. 2—40160
  methacrylate and polybutyl acrylate with low crosslinking, comparison of viscoelastic properties with poly(2-hydroxymethyl methacrylate) crosslinked solutions in dithylene glycol 2—35711
  methacrylate copolymer, —196-20°C, side chain relaxation, comp. depend. 2—36101
  methene dye laser, u.v. emission by second harmonic in $NH_4H_2PO_4$ or $LiIO_3$ crystals 2—27498
  Methocell in water, velocity profiles on downstream side of contraction 2—35702
  methyl cellulose solution, effect of ageing on flow birefringence 2—35740
  N- methylmethacrylamide - styrene copolymers, molecular interaction, spectroscopic study 2—863
  molecular motion, microstructure, rotational isomerism, relaxation processes 2—15640
  molecular motion in solid amorphous polymers 2—6877
  molecular motions struct. and temp. depend., 4-300 K 2—15807
  molecular order and motion, seminar, Seattle, USA, Oct. (1970) 2—15639
  molecular orientation meas., fluoresc. technique 2—9227
  molecular rheology 2—18538
  molten, liquid, surface tension and interfacial tension meas., Vonneguts rot. drop procedure 2—18809
  monomer-trimer problem, series expansion, general formulation and applic. to square lattice 2—20861
  morphology, transmission electron microscope obs. 2—35853
  network, molecular deformation field 2—15844
  networks, statistical thermodynamics at large deformations 2—28980
  nylon, stress ageing, water content influence 2—3937
  nylon, velocity meas. of polarized ultrasonic waves in temp. range 4-100 K, calc of specific and elastic moduli 2—40058
  nylon 12, polymorphism, X-ray diffraction study 2—25167
  nylon 66, doubly oriented, n.m.r. absorption spectrum studied, second moments found at 180°C 2—7148
  nylon 66, n.m.r. investigations of chain mobilization and water mobility 2—22846
  nylon 6, fatigued fibres temp. dependence of dynamic viscoelasticities 2—3846
  nylon 6, glass fibre reinforced, plane bending fatigue crack propagation 2—29305
  nylon 6, glass fibre reinforced effect of glass fibre content on temp. dependence of dynamic viscoelasticity 2—25486
  nylon 6, uniaxially aligned fibre reinforced composites 2—6627
  nylon fibres, reaction-rate model for fracture 2—3911
  nylon-6,6 and nylon-6,10 copolymers with nylon-6T, melting and crystallization 2—9210
  nylon-6, effect of mol. wt. on isothermal crystallization kinetics 2—3471
  nylon-6, kinetics of primary isothermal crystallization, 201-213C 2—3470
  α-olefin isotactic copolymers, conformational equilibria 2—35364
  optical rotation of infinite single-stranded polymers, theory 2—8841
  organosilicon thin films, produced by r.f. discharge polymerization for integrated optics 2—27627
  paraffin chains, CNDO calc. of side chain main chain ang. dependence 2—24562

Polymers continued
  particle size distrib. assessment using 'quantimet'—electron microscope linkage 2—18858
  pentaerythritol alkyd varnish film, ionic conduction rel. to Fe_2O_3 pigmentation 2—1564
  perspex magneto-electrets, dielectric behaviour 2—4286
  phase transitions, small angle X-ray scattering studies 2—18907
  phenol-formaldehyde polymer, study of fracture surface regularity 2—3485
  phenolformaldehyde tung oil varnish film, ionic conduction rel. to Fe_2O_3 pigmentation 2—1564
  phenyl containing, cryogenic relaxation, internal friction 2—36098
  photoelastic, optically sensitive method for making in cubic compression conditions 2—17705
  photoemission under irradiation by 15 to 25 keV photons, intensities 2—19813
  photolysis, continuous light scatt. technique 2—37057
  photopolymer holography, fixing techniques and signal-to-noise studies 2—23647
  plastic deform., volume changes, yield stress press. depend. 2—3873
  Plexiglas, with water film, spreading of partially submerged oil drop 2—1166
  PMMA, fatigue fracture and striations 2—25535
  p.m.r. line narrowing due to rot. 2—13557
  poly(2,6-dimethyl-1,4-phenylene oxide) in ternary mixtures with toluene and polystyrene, crystallization and melting 2—32319
  poly(2-hydroxethyl methacrylate), water swollen gel, tensile strength, crosslinking effect 2—35807
  poly(2-hydroxymethyl methacrylate) crosslinked solutions in diethylene glycol, comparison of viscoelastic properties with methacrylate and polybutyl acrylate with low crosslinking 2—35711
  poly(β-benzyl L-aspartate), crystallinity and conformational changes 2—22059
  poly(γ-benzyl L-glutamate) in dichloromethane, liquid cryst. solutions 2—28796
  poly(γ-benzyl-L-glutamate), oriented films, real and imaginary components of complex strain constant in temp. range —180 to +180°C 2—22630
  poly(amide-imide) friction and wear in dry air at 260°C, obs. 2—12918
  poly(ethylene o-phthalate) adsorption, applic. of ellipsometry 2—9303
  poly(ethylene oxide) of low molecular weight, study of melting behaviour 2—39422
  poly(L-alanine), α-proton chem. shift 2—38982
  poly(N-vinyl carbazole)/Se, transient accumulation of interfacial charge, xerographic layer sensitization 2—33073
  poly(N-vinyl carbazole)/Se, transient photoinjection of holes and xerographic layer sensitization 2—33072
  poly(N-vinyl carbazole)/Se layered struct., space-charge- perturbed xerographic discharge 2—40378
  poly(orthomethylstyrene) PVT props. and transitions 2—3478
  poly(tetramethylene oxide), crystallization, small angle X-ray scatt. obs. 2—3469
  poly(vinyl fluoride), electret film, piezoelec. props., piezoelec., dielect., elastic consts. 2—10131
  poly 2-vinyl naphthalene, in fluid and glassy solvents, obs. of temp. dependent excimer emission in fluorescence spectra 2—8849
  poly 4-methyl pentene-1, high field cond. 2—22615
  poly N-vinyl carbazole films, thermal activation energy of elec. conductivity and trap structure 2—36524
  poly-α-methylstyrene, optical anisotropy, light scatt. and thermal transition meas. 2—15415
  poly-α-methylstyrene chain fractions in solution, particle scattering factor and segment-segment distance distribution 2—12563
  poly-α-methylstyrene chain fractions in solution, particle scattering factor and segment-segment distance distribution 2—12562
  poly-β-benzyl-L-aspartate, helix coil transition region of dielectric relaxation due to dipolar orientation 2—8846
  poly-γ-benzyl-L-glutamate, electrically oriented X-ray diffr. patterns 2—15577
  poly-γ-benzyl-L-glutamate, two phase solution 2—25038
  poly-DL-alanine, poly-L-alanine, chain conformation from neutron scattering study 2—35368
  poly-L-alanine, helix to coil transition, chemical shift change prediction from Zeeman effect of formamide 2—12246
  poly-L-alanine, sp. ht., 1.3 to 4.3K 2—29558
  poly-L-proline, forms I and II, dispersion curves, Higgs method 2—40050
  poly-n-lauryl methacrylate, dielec. relaxation as function of frequency, temp. and pressure 2—6877
  poly-n-vinylcarbazole, thin film, radiation induced conductivity, charge carrier yields obs. 2—19535
  poly-nonyl methacrylate, dielec. relaxation as function of frequency, temp. and pressure 2—6877
  poly-P2VB, solid-state photopolymerization, X-ray diffr. obs. 2—3477
  poly-p-xylylene, morphology obs. 2—3480
  α-poly-p-xylylene, oriented, crystal struct. 2—3481
  polyacid aqueous solns., effect of degree of neutralization on u.s. absorpt. 2—32262
  polyacrylamide solution, non-Newtonian pipe flows, laser anemometer obs. of turbulence structure 2—28758
  polyacrylates, ionic, glass transition temp. 2—28982
  polyacrylic acid, u.s. absorption of salts in aqueous solutions 2—25079
  polyacrylonite, glass transitions region Mossbauer effect study of polymer dynamics 2—22736
  polyacrylonitrile, dielec. dispersion, pyrolysis effect 2—30041
  polyacrylonitrile, evaporated film, electrical and optical properties 2—29650
  polyacrylonitrile, mechanical relaxation properties 2—35859
  polyacrylonitrile, mechanical relaxation props. of drawn samples 2—35858
  polyacrylonitrile, Raman spectra rel. to i.r., structural model 2—8845
  polyacrylonitrile based C fibre, structure and other properties obs., using e.p.r. 2—6289
  polyacrylonitrile thin film formation by vacuum deposition 2—29048
  polyalkylmethacrylates, transient state diffusion of water 2—15794
  polyamide, lamellar crystals, X-ray diffraction analysis 2—3464
  polyamides, chain folding, X-ray exam. 2—3465
  polyamides, doubly-oriented, small-angle X-ray diffr. diagrams 2—18909
  polybenzoxazole, props. 2—35978
  poly-p-bromostyrene, dynamic mechanical properties studied from 4 to 250K 2—6518

Polymers continued
polybutadiene, stress optical coeffs. of rubbery state, temp. dependence, chain length 2—25507
cis-polybutadiene, tack mechanism 2—39975
polybutene-1, isotactic and polyethylene glass transition temp., small angle X-ray diffr. 2—3463
polycaproamide, static and fatigue strength, liquid immersion effect 2—29289
polycaprolactam, deform. effect on internal friction 2—6525
poly-ε-caprolactam, electric properties, static field effects 2—19750
polycaprolactam, epitaxial growth on uniaxially oriented polyethylene, polypropylene, polycaprolactam and polyoxymethylene 2—29106
polycarbonate, effects of cold rolling on tensile strength 2—1308
polycarbonate, elastic consts. 2—3839
polycarbonate, glass fibre reinforced, plane bending fatigue and crack propagation 2—29304
polycarbonate, glassy, optical and mechanical limits of linear relaxation behaviour 2—25495
polycarbonate, injection moulded, molec. orientation and weight effects on Izod impact strength 2—22280
polycarbonate, radiation-induced electric conductivity, dose rate dependence 2—6752
polycarbonate, uniaxial compression and tensile yield stress, temp. depend. 2—22272
polycarbonate styroflex, creep, deform. relax., irrad. effects 2—39793
polycarbonates, irrad., proton spin-lattice, relax., obs. 2—10280
polychloroprene, recrystallization after partial melting 2—6403
poly-p-chlorostyrene, dynamic mechanical properties studied from 4 to 250K 2—6518
polyconjugated systems, intermolecular interaction, supramolecular structure and paramagnetism 2—6001
polydecamethylene 1,16-hexadecanedicarboxylate, morphological habit rel. to chemical structure 2—22109
polydimethylsiloxane, spreading kinetics on solid surface 2—25177
polydimethylsiloxane fluids, broad dielectric loss peaks, a.f., −120 to −100°C 2—13302
polydimethylsiloxane melts, molec. weight dependence of viscosity under high pressure 2—25059
polydimethylsiloxane rubber, swollen, temp. dependence of optical anisotropy 2—1652
polydimethylsiloxane shown to be main constituent of pseudo-'polywater' by mass spectrometric study 2—28801
polydiphenylacetylene films, hole mobility 2—1530
polydisperse systems of low molecular weight, refractive index increments and light scattering 2—39402
polyelectrolyte solutions, conc. dependence of reduced viscosity 2—25058
polyene, electronic spectra, SCFMO calc. with configuration interaction 2—8847
polyester systems, glass-reinforced, compression moulded, mech. props., analysis 2—29290
polyester-diisocyanate, reaction kinetics, spectroscopic method 2—4575
polyester-styrene copolymers, viscoelasticity, effect of 3-dimensional network density 2—25485
polyether urethanes, relaxation and crystallization props, temp. behaviour 2—3482
polyethylene, α-relax., temp. peak 2—12837
polyethylene, γ-irrad., elec. cond., pre-exponential factor 2—25834
polyethylene, amorphous surface layers, thickness, with rel. to supercooling, loops, cilia 2—18949
polyethylene, analogies between chain- folded and extended-chain crystallization 2—9369
polyethylene, branched, structural evaluation by combined gel-permeation chromatography and gradient electron fractionation 2—28424
polyethylene, cold-drawn, retraction effect, role of cryst. morphology 2—32593
polyethylene, cold-drawn, struct. during annealing 2—39897
polyethylene, configurational statistics on chain placed on rigid lattice 2—21710
polyethylene, confined growth crystallization, crystallite orientation 2—39445
polyethylene, crystalline, geometry of deformation twinning and phase transformations 2—9355
polyethylene, crystalline, thermodynamic and morphological properties 2—28969
polyethylene, deform. effect on internal friction 2—6525
polyethylene, drawn, morphology and molecular motion, n.m.r. obs. 2—15641
polyethylene, echelon gratings and combination filters long wave i.r, spectral regions 2—34539
polyethylene, effect of pressure on gas permeability coefficients of 1,1-difluoroethylene and fluoroform, free volume theory application 2—35691
polyethylene, electrical breakdown, in non-uniform fields polarity and neg. space charge effects 2—22616
polyethylene, electrical stability under action of powerful high voltage impulses 2—21995
polyethylene, fibril structure, gold decoration 2—9226
polyethylene, friction meas. 2—12919
polyethylene, high and low density, comparison of twinning produced by rolling and annealing 2—32320
polyethylene, high density, plastic flow 2—19185
polyethylene, high density cold-rolled, tensile props. 2—39792
polyethylene, high mol. wt., flow behaviour 2—1043
polyethylene, high-crystallinity, prep. at low press. 2—3475
polyethylene, hot stretched, recrystallization, x-ray small angle scatt. 2—15893
polyethylene, irrad., small-angle scatt. obs., ordered and disordered regions 2—25384
polyethylene, irradiated at 4°K, i.r. spectra 2—29924
polyethylene, linear, affine deformation of colloidal superstructure 2—29249
polyethylene, linear, internal friction, relax. phenomena, low temp. 2—3845
polyethylene, low density, cold rolled, superstruct., XYZ photographic light scatt. obs. 2—12632
polyethylene, low density, low temp. brittleness 2—22284
polyethylene, low density, uniaxially orientated, hot- and cold-drawn, tensile creep behaviour 2—12877
polyethylene, low press., mech. props. rel. to molecular struct. 2—28978

Polymers continued
polyethylene, low-density, molecular weight distribution and long-chain branching 2—8848
polyethylene, low-pressure, i.r. spectroscopic study of branching 2—31875
polyethylene, mol., vibrational excitation rel. to photochemical decomp. 2—33389
polyethylene, photocond., γ-ray irrad. effects 2—25964
polyethylene, photoemission in vac. u.v. 2—29787
polyethylene, plastic deform., h.p. 2—3874
polyethylene, radiation-induced electric conductivity, dose rate dependence 2—6752
polyethylene, relax. times and elastic moduli, temp. depend. 2—32583
polyethylene, rheology at high pressures 2—15857
polyethylene, shock compression effect on elec. resist. 2—40161
polyethylene, single crystal, mosaic struct. 2—15647
polyethylene, solid and molten, diffusion mechanism and solubility of small molecules 2—22237
polyethylene, strength characts., rel. to surface active media, stress, electron irrad. 2—39811
polyethylene, supermolecular struct., opt. microscope obs. 2—35854
polyethylene, supermolecular structure, light- microscopic investigation 2—3132
polyethylene, superstructure, optical microscopy 2—32684
polyethylene, u.v. absorpt. spectra, electronic excitations 2—40687
polyethylene 2,6-naphthalene dicarboxylate, γ-irradiated, e.s.r. identification of trapped radicals 2—30097
polyethylene crystal, electron microscopy, contrast effects 2—22185
polyethylene crystals, lateral surface energy from interatomic potentials 2—28993
polyethylene crystals, review of morphology, crystallization and dissolution modes, structural study 2—25164
polyethylene gratings, shortwave depression in interference for spectral regions 15-50 μm 2—31130
polyethylene in 1-chloronaphthalene solvent, effect of molecular weight on refractive increment 2—6235
polyethylene irradiated crystals, plastic deformation 2—36124
polyethylene melt, flow behaviour, influence of dissolved gases 2—18778
polyethylene melt, shear rate dependent relax. spectrum 2—15552
polyethylene melts, high density, molec. weight distribution effect on capillary flow 2—21944
polyethylene melts, high density, molec. weight distribution effects on rheological properties 2—21929
polyethylene melts, viscoelastic fluid, flow through rectangular duct 2—25008
polyethylene membranes, permeability and diffusion coefficients of dimethyl sulphoxide 2—35752
polyethylene membranes, permeation of gas and liq. propane and propylene 2—25066
polyethylene oriented films, change in supramolecular organization during reorientation 2—28983
polyethylene oxide, expansion-contraction behaviour of dilute solutions, capillary jets 2—32202
polyethylene oxide solution, non-Newtonian pipe flows, laser anemometer obs. of structure of turbulence 2—28758
polyethylene sebacate, morphological habit rel. to chemical structure 2—22109
polyethylene steel composites, dynamic modulus changes under repeated plane bending 2—29236
polyethylene terephthalate, laser-Raman study of crystallinity changes 2—35861
polyethylene terephthalate, plastic flow 2—19185
polyethylene terephthalate, self- oscillation mechanism of necking 2—19186
polyethylene terephthalate fibre, texture rel. to tension and annealing temp. 2—15642
polyethylene terephthalate film, effect of sorbed I on small angle X-ray diffraction 2—35860
polyethylene terephthalate films, anomalous induced transient cond. 2—32995
polyethylene valence band, exptl. and theoretical study 2—16115
polyethylene wax blends, effects of long and short branches on steady state flow, application of concentration superposition 2—35441
polyethylene with simple orientation texture, small-angle X-ray diffr. diagrams 2—18910
polyethylenephthalate and solutions in anisole and nitrobenzene, viscosity 2—9116
polyethylenes, chlorinated, n.m.r., assignation of lines and analysis of Cl content 2—3130
polyethyleneterephthalate, crystallinity determ. from combination of heat capacity and enthalpy measurements 2—6293
polyethyleneterephthalate, small angle X-ray scatt., absolute intensity, correlation function 2—3467
polyethyleneterephthalate dielectric strength meas. at cryogenic temps. for 50 HZ 2—40321
polyferrocene, phthalocyanines, polyvinyl pyridine and TCNQ complex, d.c. dark cond., Seebeck meas. 2—36475
polyformaldehyde, mullite filler, deformation, rupture, microstructure 2—29293
polyformaldehyde, rigid partially deuterated, quantitative interpretation of B-n.m.r. spectra 2—6002
polyhexadecyl acrylate, molecular mobility 2—3131
polyhexadecyl methacrylate, molecular mobility 2—3131
polyhexamethylene sebacate, morphological habit rel. to chemical structure 2—22109
polyhexane-1, sp. ht., abnormal behaviour in region of γ and δ relax. peaks 2—25686
poly2-hydroxyethyl methacrylate, effect of low mol. wt compounds on relaxation behaviour 2—25514
polyhydroxyethyl methacrylate preswollen network, mech. props. 2—3827
polyimide friction and wear in dry air at 260°C, obs. 2—12918
polyisobutene soln., viscometric functions in steady shear flows 2—3341
polyisobutylene, dil. soln., excluded volume effects on viscosity, mol. dimensions and 2nd virial coeffs. 2—25033
polyisobutylene, interconversion of viscoelastic functions by linear programming 2—14217
polyisobutylene, verification of empirical equations for viscoelastic functions 2—14218
polyisobutylene in ethyl heptanoate, meas. of sedimentation coeffs., second virial coeffs., intrinsic viscosities near θ-point 2—39395

Polymers continued
polyisobutylene solution, falling sphere viscometry for det. of zero shear viscosity 2—35745
polyisoprene, stress optical coeffs. of rubbery state, temp. dependence , chain length 2—25507
polylysine in solution, diffusion coeff. as function of concentration determ. from spectrum of scattered light 2—39403
polymeric materials, testing apparatus, extension, creep, relax., in ionizing rad. 2—39880
polymers, substituted, electronically excited state, properties 2—864
polymers, vibronic interaction theory 2—6000
polymethacrylate, acridine yellow activated, fluoresc., preexcitation effect 2—4499
polymethine dye thin films, bleachable Q-switch for GOS-1000 laser 2—17575
polymethonium-AgI cpds., solid electrolytes, ionic cond. 2—22614
polymethyl acrylate, infrared spectrum in region 4000 to 150 cm^{-1} 2—18539
polymethyl acrylate, molecular relax., Brillouin spectra obs. 2—26202
polymethyl methacrylate, concentrated solns. in toluene and methyl ethyl ketone absorption of ultrasound 2—27253
polymethyl methacrylate, Crofon optical fibre, bends to radius of curvature of five times own diameter 2—17712
polymethyl methacrylate, plastic flow 2—19185
polymethyl methacrylate, radiation- induced electric conductivity, dose rate dependence 2—6752
polymethyl methacrylate, shear creep, energy spectra 2—12878
polymethyl methacrylate, short cylinders, longitudinal mode resonances 2—17361
polymethyl methacrylate, thermodynamic props., press. depend. 2—13048
polymethyl methacrylate (perspex), linear viscoelastic range from uniaxial tension tests 2—1279
polymethyl methacrylate preswollen network, mech. props. 2—3827
poly-N-methyl-l-alanine, Monte Carlo calculations of average dimensions using hard-sphere models 2—24564
polymethylammonium ions, n.m.r. spectra, narrowing by rot. motions 2—13552
polymethylene, short model chains, configurational statistics 2—24561
polymethylmethacryalate, electrical breakdown, in non-uniform fields, polarity and neg. space charge effects 2—22616
polymethylmethacrylate, crack growth 2—9712
polymethylmethacrylate, crack propagation and arrest 2—15887
polymethylmethacrylate, creep, deform. relax., irrad. effects 2—39793
polymethylmethacrylate, drawn, meas. of molecular orientation by broad line n.m.r. 2—10576
polymethylmethacrylate, effects of creep on elastic modulus and critical load of shallow circular arch 2—1296
polymethylmethacrylate, hypersonic absorption by Brillouin scattering 2—40642
polymethylmethacrylate, in benzene-carbon tetrachloride and chloroform-carbon tetrachloride solutions, proton spin-lattice relaxation times for solvent mols. rel. to selective adsorption 2—39393
polymethylmethacrylate, moderately conc. soln., viscosity, solvent effects 2—18803
polymethylmethacrylate, optical density, light exposure effect 2—38386
polymethylmethacrylate, stressed in liquid media, crack growth 2—29332
polymethylmethacrylate, temp. rise in craze region during fast crack propagation 2—9713
polymethylmethacrylate electret form., press. depend. 2—16297
polymethylmethacrylate in diethylphthalate, time dependent rheology under constant stress and shear 2—34017
polymethylpolyanine, refl. spectrum, optical consts. determ. 2—13431
polynucleotides, Fermi resonance of i.r. vibrations in NH_2 groups 2—28423
polyoxymethylene, epitaxial crystallization during polymerization in aqueous soln. 2—35954
polyoxymethylene, in interstellar clouds, thermodynamic stability 2—20604
polyoxymethylene, internal friction, relaxation processes, 4.2-300 K 2—6592
polyoxymethylene, orthorhombic, determ. lattice modes and intermolecular potential 2—16576
polyoxymethylene cryst., morphological changes on annealing and melting 2—3476
polyphenoxy radicals, e.s.r. determ. of internal motion and conformation 2—35369
polyphenyleneaminochloranils, electrical and magnetic properties 2—25835
polyphenylmethacrylyl ester of hexyloxybenzoic acid, soln. in benzene, liquid-crystalline behaviour 2—25051
polyphosphonitrilic chloride crystal, Young's modulus calc. from spectroscopic force consts. 2—15798
polypropylene, β-form crystals in types III and IV isotactic spherulites, characterization of structure and organization 2—39447
polypropylene, anomalously low friction with MoS_2 and graphite under He atom irrad. 2—32657
polypropylene, atactic and isotactic, molecular motion, spin-spin and spin-lattice relaxation 2—33178
polypropylene, glass reinforced, cyclic creep testing 2—39871
polypropylene, isotactic, row nucleation on graphite fibres 2—9231
polypropylene, isotactic, small- and wide-angle X-ray diffr., solid-solid transition 2—3468
polypropylene, structure of spherulites from birefringence measurements 2—35862
polypropylene dielectric strength at cryogenic temps. for 50 HZ 2—40321
polypropylene dielectric strength meas. at cryogenic temps. for 50 HZ 2—40321
polypropylene film, metallic filler, strength rel. to mag. field 2—29406
polypropylene film, two step biaxial stretching, orientation behaviour 2—25475
polypyrimidine, elec. cond., temp. depend. 2—25836
polyquinoline carboxylic acid, metal-polymer-metal sandwich, electrical conductivity study 2—19721
polysaccharide solution, stiff chain parameters, light and X-ray small angle scatt. 2—3369
polysarcosine, randomly coiling, Monte Carlo calculations of average dimensions using hard-sphere models 2—24564
polyselenomethylene, hexagonal, assignment of vibrational spectra 2—15418
polystyrene, and derivs., spin lattice proton relaxation 2—4414

Polymers continued
polystyrene, concentrated solns. in toluene and methyl ethyl ketone, absorption of ultrasound 2—27253
polystyrene, crack growth 2—9712
polystyrene, crazing, fibrillar struct., electron microscope obs. 2—3912
polystyrene, dynamic nuclear relaxation of protons, cross relaxation due to electronic spin-spin interactions 2—36997
polystyrene, effect of halogen ring substitution and crazing on low temp. dynamic mechanical damping peak 2—6518
polystyrene, elastic consts. 2—3839
polystyrene, equation of state parameters 2—1072
polystyrene, hot-stretched, activation energy for retraction 2—12878
polystyrene, in benzene-cyclohexane solution, proton spin-lattice relaxation times for solvent mols. rel. to selective adsorption 2—39393
polystyrene, inherent flow size and fracture energy 2—1330
polystyrene, isotactic, strain-induced crystn. 2—3479
polystyrene, isotactic stretched, crystal nucleation 2—22060
polystyrene, moderately conc. soln., viscosity, solvent effects 2—18803
polystyrene, opt. props., vac. u.v. obs., free electron gas models 2—20009
polystyrene, plastic flow 2—19185
polystyrene, poly(2,6-dimethyl-1,4-phenylene oxide) and toluene, crystallisation and melting of ternary mixtures 2—32319
polystyrene, PVT props. and transitions 2—3478
polystyrene, radiation-induced electric conductivity, dose rate dependence 2—6752
polystyrene, short cylinders, longitudinal mode resonances 2—17361
polystyrene, strength, crazes and cracking 2—15888
polystyrene, vitreous solidification thermodynamics 2—12625
polystyrene adsorbed layer on Au film, calorimetric i.r. spectroscopy 2—18955
polystyrene adsorption, applic. of ellipsometry 2—9303
polystyrene and polymethyl methacrylate, specific heat, thermal cond. 2—22427
polystyrene bead aerosols, monodisperse, generation 2—12591
polystyrene composites, dynamic mech. props. 2—36096
polystyrene in cyclohexane, meas. of sedimentation coeffs. second virial coeffs., intrinsic viscosities near θ-point 2—39395
polystyrene in organic solvent, ultrasonic relaxation spectrum associated with three state conformational change 2—35761
polystyrene in water sols, effect of dispersing agents on angular dependence of light scattering 2—6267
polystyrene latex, light scattering during coagulation 2—15619
polystyrene latex, particle size distrib. determ. by flow ultramicroscopy 2—15617
polystyrene solution, X-ray obs. 2—3370
polystyrene solutions, moderately concentrated, storage and loss shear moduli 2—21930
polystyrene solutions in tetrachloroethylene. effect of molecular weight on ^{13}C spin lattice relaxation times 2—28901
polystyrene sphere-water sols, effects of dispersing agents on angular dependence of scattered light 2—28921
polystyrene spheres, Dow, airborne, electrical mobility and effective airborne radius 2—28914
polystyrene-cyclohexane system near upper critical segregation temperature, thermodynamic functions determ. from light scattering meas. 2—35772
polystyrene-polybutadiene-polystyrene macroscopic 'single crystal', i.r. spectroscopy, dichroism and molecular orientation 2—15417
polytetrafluoroethylene, core and valence energy levels by electron spectroscopy 2—6003
polytetrafluoroethylene, gamma radiation effects on fine structure 2—39448
polytetrafluoroethylene, interchain force field and elastic constants from phonon dispersion curve 2—40039
polytetrafluoroethylene, radiation-induced electric conductivity, dose rate dependence 2—6752
polytetrafluoroethylene, shock compression effect on elec. resist. 2—40161
polytetrafluoroethylene dielectric strength meas. at cryogenic temps. for 50 HZ 2—40321
polytetrafluoroethylene film, r.f. sputtered, elec. and chem. props. 2—29049
polythene, carrier transport 2—13251
polythene, defect containing, vibrational props., numerical method 2—19394
polythiomethylene, hexagonal, assignment of vibrational spectra 2—15418
polyurethane, thermoplastic elastomers, crystallization behaviour 2—3472
polyurethane thermoplastic elastomers based on polybutylene adipinate, thermomechanical props. and phase state 2—6522
polyurethanes, segmented, anisotropic superstructure meas. by photographic light scattering 2—15648
polyvinyl acetate, dried samples, dielec. γ relax. 2—25916
polyvinyl acetate solution, moderately concentrated, storage and loss shear moduli 2—21930
polyvinyl alcohol, solns. in CCl_4 and dimethylsulphoxide, i.r. absorption spectra study 2—3133
polyvinyl alcohol fibres, stretching, effects on tensile strength and solubility 2—15649
polyvinyl alcohol films, optical study of chain orientation 2—6004
polyvinyl alcohol solution, effect of ageing on flow birefringence 2—35740
polyvinyl chloride, annealing, 80-260°C, crystallization 2—18906
polyvinyl chloride, cleavage fracture, birefringence obs. 2—15889
polyvinyl chloride, compression yield stress rel. to loss tangent, β-transition range 2—15854
polyvinyl chloride, filled plasticized, viscoelastic properties 2—6524
polyvinyl chloride, hysteresis effect in variation of electrical conductivity with field and temp. 2—4264
polyvinyl chloride, IUPAC symposium on macromolecules, Prague, Czechoslovakia, September (1970) 2—15644
polyvinyl chloride, oriented sheet, yielding and internal stress effects 2—15847
polyvinyl chloride, photocond., field and pressure depend. 2—33080
polyvinyl chloride, plane bending fatigue of specimens prepared by different mould methods 2—25517
polyvinyl chloride, plastic flow 2—19185
polyvinyl chloride, plasticized, creep obs., 20-100°C 2—19189
polyvinyl chloride, unplasticized, creep susceptibility, stress level depend. 2—25511
polyvinyl chloride compound, degradation, dielec. spectra and a.c. cond. obs. 2—15645

Polymers continued
polyvinyl chloride film, electric discharge effect, dielec. props., mechanical strength 2—16269
polyvinyl chloride latex, particle size, meas. using analytical centrifuge 2—15894
polyvinyl chloride molten, viscosity meas. 2—25060
polyvinyl chloride solutions, gamma irradiation induced branching, viscosity obs. 2—18804
polyvinyl chloride-dioctyl phthalate-dioctyl sebacate system, elastic modulus depend. on composition 2—6523
polyvinyl fluoride, thermal molec. motion meas. by viscoelastic method 2—22061
polyvinyl stearate molecular mobility 2—3131
polyvinylacetate, at water/air interface, monolayer collapse 2—1090
polyvinylacetate, at water/air interface, monolayer collapse 2—1089
polyvinylchloride, hypersonic absorption by Brillouin scattering 2—40642
polyvinylcyclohexane, relaxation processes study by dielectric method, phase transition 2—36582
polyvinylfluoride, pyroelectric effect when irradiated with i.r. 2—6889
polyvinylfluoride film, pyroelectric, application to i.r. detector, high D* 2—7770
polyvinylidene chloride-co-methacrylonitrile, monomer sequence distributions by p.m.r. spectroscopy 2—28425
polyvinylidene fluoride films, poled, pyroelec. and nonlinear optical props. 2—40367
polywater, interpretation of i.r. spectra of clay adsorbed water 2—3393
propylene-butadiene alternating copolymers, 220 MHz n.m.r. evidence of alternating sequences 2—35370
propylene-vinlcyclohexane copolymers, structure study from i.r. spectra 2—24563
PVC, $Cl^- L_{2,3}$ absorpt. spectra regularities 2—20032
PVC, $L_{2,3}$ absorpt. edge of Cl^- 2—33293
PVC and PVF films, piezoelectric effect induced by rolling during processing 2—19773
pyrrone friction and wear in dry air at 260°C, obs. 2—12918
quenched linear chains, solutions of master equations and related random walks 2—37629
radiation damage of crysts. in electron microscope 2—19081
Raman scattering, from low freq. phonons 2—16577
random, atomic vibrational properties, numerical studies 2—36313
random coile chains, Monte Carlo studies of relaxation of vector end-to-end length 2—24559
resins under axial compression, relaxation characteristics 2—29382
rheology, molecular theories 2—15856
rheology integral constitutive eqn. and rate dependent relaxation spectrum 2—34014
semicrystalline, crystal orientation rel. to spherulite deformation 2—18905
semiflexible helices, chain length depend. of mean square radius of gyration 2—862
semiflexible helices, mean square raius of gyration and end-to-end distance rel. to degree of polymerization 2—861
silico-organic film, metal-dielectric-metal structure in glow discharge, threshold breakdown potentials 2—4258
skeletal vibration bands, effect of anharmonicity on half widths 2—31874
small angle X-ray scattering studies, state-of-the- art 2—35852
in solution, methods for calc. refractive index increment from properties of polymer and solvent 2—39401
solution, partial specific volume determination from relation between refractive index and density increments 2—39342
solution, polyisobutylene in petroleum, stress effects, deform., relax. phenomena 2—28806
solution, weak aqueous, flow, continuum mech. approach 2—35697
solutions, degradation by ultrasound 2—39020
solutions, dilute, diffusion of fluids 2—1091
solutions, dilute, limiting stretch rate 2—3346
solutions, osmotic pressure determ. by weighing 2—28831
solutions, thermodynamic props. 2—15583
spherulites, growth, branching mechanism 2—39443
spreading kinetics on solid surface 2—25177
strained crystalline, plastic deformation, fracture, chain scission 2—15845
structure analysis and radiothermoluminescence 2—37061
styrene methacrylic acid copolymer ionomers, stress relaxation investigation 2—25491
styrene-α-methylstyrene block copolymers, conformations in dilute solution 2—35371
styrene-butadiene copolymer stress optical coeffs. of rubbery state, temp. dependence, chain length 2—25507
styrene-isoprene-styrene copolymers, solvent cast films domain structure and bulk properties 2—25162
styrene-MMA, opt. props., vac. u.v. obs., free electron gas models 2—20009
surface molecule contact interaction with adsorbed solid particles 2—25232
TCNQ charge-transfer complex, cond., Hall effect, Seebeck coeff. 2—40216
TCNQ polymeric complex salts, factors affecting conductivity 2—25837
Teflon, photoemission in vac. u.v. 2—29787
teflon, proton and fluorine spin lattice relax. time meas., CW-methods 2—7151
teflon, velocity meas. of polarized ultrasonic waves in temp. range 4-100 K, calc. of specific heat and elastic moduli 2—40058
terephthalamide-nylon, isolation of single crystals from dilute solutions of hexafluoro-2,2-propandiol 2—18994
textiles, polyacrylic acid grafting, by plasma generated free radical sites 2—3504
thermal conductivity, review 2—29568
thermal decomp., activation energies 2—1746
thermoplastic, brittle fracture and chemical constitution 2—6570
thermoplastic, effect of fusible alloys on wear characteristics 2—6589
thermoplastics, mineral fibres for reinforcing 2—39964
torque reduction in finite amplitude secondary flows of dilute solution 2—3372
transitions at low temperatures in amorphous substances, detection by Rayleigh scattering 2—9229
Treloar's distribution for length of freely connected chain, derivation and numerical implications 2—8843
turbulent boundary layer, suppressed diffusion of drag-reducing 2—25014
two-phase systems, mech. props., time-temp. superposition 2—15809
vacuum deposition for encapsulation of electronic circuitry 2—14054
vibrational spectra, defect induced 2—16506

Polymers continued
vinyl chloride chains, random coil dimensions and dipole moments, effect of isotacticity 2—8840
viscoelastic behaviour during crosslinking reactions, prediction 2—15810
viscoelastic properties, high freq., shear mode strip delay line study 2—15811
viscoelastic relaxation, conf., Los Angeles, USA, March (1971) 2—15808
viscosity of dilute solutions, Mark-Houwink equation and Flory constant 2—15580
wire insulation PVC, dry blending improvement 2—10106
worm like chains, end-to-end distance calc., X-ray obs. 2—3371
X-ray diffraction characterization studies, state-of-the-art 2—35856
yield behaviour, plasticity and nonlinear viscoelasticity 2—15843
yield behaviour of oriented materials 2—6540
Young's modulus of crystalline and amorphous polymers rel. to structure 2—15796

Polymorphism
see also Crystal structure
alkali halide, transition pressure, fourth order anharmonic theory 2—19317
amino acids, γ-irrad., polymorphic transform. 2—7187
cholesterol esters 2—25039
dinaphtho[2,1-2′,3′]furan-8,13-dione, X-ray obs., spectra 2—25356
dipeptides, γ-irrad., polymorphic transform. 2—7187
glasses with small amounts of K_2CO_3 thermal treatment leading to polymorphism 2—28973
halide, layer structure, rel. to optical props. and chemical decomposition, reveiw 2—16686
ice, amorphous deposits formed at low temperatures 2—28970
isooctane cryst. with impurity mols., polymorphic transform. effects on luminesc. 2—29959
liquid crystals, and birefringence 2—9092
metal, Debye temp. effects analysed 2—25323
nylon 12, X-ray diffraction study 2—25167
organic solid-state reactions 2—35933
perovskites, $A^{1+}B^{5+}O_3$-type, polytypes and transforms. 2—9346
phase transitions, review and theory 2—9785
platelet-shaped polytypic crysts., streaking of X-ray diffraction spots 2—3608
polytypes, cyclicity hexagonality, Zhdanov symbol 2—35955
polytypism in crysts., n.m.r. obs. 2—26298
rutile structures, pressure induced polymorphism 2—15732
smectic, effect of mol. struct. changes 2—9090
smectic, rel. to mol. geom. 2—9091
smectic liquid crystal, (modifications A, B and C), X-ray diffr. obs. 2—18794
sulphospinels, AB_2S_4-type, synthesis, high pressure phenomena 2—9342
transitions, molecular mechanism, model 2—32755
BN polymorph form. under h.p. 2—33821
$BaFe_2O_4$, transitions at 800 and 1000°C 2—39980
$BaMnO_3$ modifications, prep. by hydrothermal and high-pressure prep. 2—19918
C polymorph form. under h.p. 2—33821
CO crystal, transformations, chemical potential and transition temperature 2—39989
$CaCO_3$, characterization of vaterite and calcite crysts. grown in gels 2—15684
CdI_2, dislocation kinetics in polytype transform. 2—25622
CdI_2, polytypic crystals, high temp. phase transformation 2—1390
CdI_2, rhombohedral polytype form. 2—12772
CdI_2 polytypes, struct. phase transform. with temp. 2—25623
CdI_2 polytypes, structural transformations, X-ray diffr. 2—25621
CdI_2 polytypes, Zhdanov numbers in Zigzag sequence 2—25329
$CsBF_4$, high pressure, with $RbBF_4$ 2—3987
$CsClO_4$, high pressure, with $CsClO_4$ 2—3987
$CsHF_2$ rel. to melting at high pressures 2—36282
$Cu(OH)_2$ phase transition, X-ray diffraction, infrared spectroscopy, 20-100°C 2—3991
CuSe alloy, prod. and struct. determ. by electron microscopy 2—29139
Fe-Cr-Zr system, α-γ-δ type 2—4018
Fe polymorph form. under h.p. 2—33821
$K_3Co(CN)_6$, cryst. struct. 2—29144
KHF_2, rel. to melting at high pressures 2—36282
$LiXO_4$, X=P, V, As, and $Li_2M^{2+}X_1{}^{4+}O_4$, M=Zn, Mg, X_1=Ge, Si 2—18966
MnAs, rel. to crystal growth, horiz. zone melting method 2—19005
Mn_2GeO_4, polymorphs, high-pressure, cryst. structs., X-ray obs. 2—25337
$MnSiO_3$, transform, high-pressure, polymorphs, 1053-1673K 2—25634
N_2 crystals, transformations, chemical potential and transition temperature 2—39989
NH_4HF_2, melting curve, high press. 2—25141
$NaClO_3$, phase structure obs. 2—39990
Nb_2O_5, high pressure phase transitions 2—29477
Ni, high strain rate deformation, recovery and recrystallization, polygonisation 2—9748
RbCl, press. induced polymorphic transition, hysteresis effect 2—9822
$RbHF_2$ rel. to melting at high pressures 2—36282
S, purple form, Raman spectrum 2—29936
SiC, single crystal, direct 2H-6H transformation on annealing at 2400C 2—4003
SiC film, reactive sputtering of 2H polytype 2—32377
SiO_2, vapour transport and deposition conditions for polymorphs 2—39583
Sn, beta-alpha transformation kinetics 2—4004
β-Ta, film, sputtered, X-ray diffr. obs. 2—18945
$TeVO_4$, reversible transformation at 650°C 2—9347
$TiCo_2$, Laves phase, electron microscope obs. 2—19105
$TiCr_2$, Laves phase, electron microscope obs. 2—19105
TiH_2, room temp. polymorphic transform 2—22366
$ZnO.Nb_2O_5$, $\alpha \rightleftharpoons \beta$ polymorphic transition 2—25644
ZnS, polytypes, with number 1 in their Zhdanov symbols 2—22166
ZnS, polytypism and phase transformations, Cu doping effects 2—25350
ZnS, polytypism effects on electroluminesc. 2—26253
ZnS, rel. to phase transformation, X-ray oscill. obs. 2—25351
ZnS polytypes, disordered, probability of layer superposition 2—9498
ZnS polytypes relative abundance 2—9497
$ZrO_2.12Nb_2O_5$, polymorph characterization, structure and intergrowth obs. 2—9500

Polynomials *see Algebra; Functions*
Polytypism *see Polymorphism*

Pomeranchuk poles and trajectories
ABFST model, Regge slopes and schizophrenic pomeron 2–34647
Amati-Bertocchi-Fubini-Stanghellini-Tonin multiperipheral model, Regge trajectories and pomeron slope 2–8145
coupling theorems for tri-Regge vertex including pomeron 2–402
diffractive Pomeranchukon bootstrap, application to inclusive expts. 2–17884
dual Pomeron amplitude, asymptotic behaviour 2–23827
fixed pole Pomeranchukon bootstrap in asymptotic high energy hadron hadron scattering 2–14605
Freund model for Pomeranchuk term, in near forward direction 2–2539
hadron interactions, Pomeranchuk theorem violation 2–8151
inclusive reactions near boundary of phase space, Pomeranchuk theorems 2–31239
inelastic processes, disturbance of relation 2–2540
inelastic reactions, validity of Pomeranchuk hypothesis 2–38269
Pomeranchon coupling ratios, self consistency in multiperipheral model 2–14611
Pomeranchuk singularity, unitary models 2–8150
Pomeranchukon, connection with f and f' Regge trajectories from multiperipheral model 2–14613
Pomeranchukon, dynamically based coupling scheme 2–14612
Pomeranchukon, role of strangeness in generation 2–14614
Pomeranchukon singularities, self-consistent 2–401
pomeron, model diffraction term. 2–27732
Pomeron, phenomenological explanation of experimental results indicates fixed cut of changing character 2–8146
Pomeron cut, dipole and Cheng-Wu forms for leading Pomeranchuk term in total cross sections of hadron interactions 2–34626
Pomeron dominance and inclusive multiparticle cross sections 2–11568
Pomeron exchange, separation in pion production processes 2–14652
pomeron exchange as Regge cut in $NN \to NN^*$ 2–429
Pomeron exchange in diffractive production and inelastic processes 2–31294
pomeron fine structure and diffraction peak slope parameter 2–14608
pomeron model, comparison of predictions with experiment 2–17878
pomeron properties illustrated model having these properties suggested 2–23826
Pomeron proton scattering, phenomenological duality 2–17967
quasistability of pomeron, bootstrap model proposed 2–31253
singularities, functional self-consistency equation 2–34651
three Pomeron vertex, zero demonstration by multiparticle unitarity 2–17882
triple Pomeron vertex, lower bound 2–21277
triple Pomeron vertex, vanishing, nonsense wrong signature zero 2–17881
triple-Pomeron coupling in longitudinal and transverse momentum correlation of proton spectrum 2–38325
triple-pomeron vertex at $t=0$, indirect calc. 2–14609
two body scattering amplitudes, helicity structure of P and P' contributions 2–14606
two-Pomeranchukon cuts and vanishing of triple-Pomeranchukon coupling 2–34650
Veneziano amplitude, vacuum singularity on nondual part 2–27730
vertices, single, double and triple-Pomeron, relations between 2–2537
violation of theorem by high-energy scattering models, phenomenological comparison of models 2–34639
f^0 proportionality in inclusive reactions 2–423
KN and $\bar{K}N$ scatt., Veneziano model, exotic trajectories 2–11601
K^+p elastic scattering, residue of Pomeranchukon trajectory 2–17917
$K^{\pm}p$ elastic scattering, residue functions obtained from description combining Regge and absorption models 2–409
$\Lambda\pi$ scattering, pomeron coupling 2–17980
pp scatt., differential cross sects., slope determ. using Regge pole model, average Pomeranchuk slope 2–14698

Pomeranchuk rule *see Elementary particles/scattering*

Population inversion *see Lasers; Masers; Optical pumping*

Porosity *see Porous materials*

Porous materials
see also Permeability, mechanical; Surface measurement
adsorbents, adsorbate solidification rel. to meniscus curvature 2–35928
adsorption in micropores, thermodynamics, generalized thermal eqn. 2–35901
alumina, hydrous film, porosity 2–9264
beds effective thermal conductivitv determ. from transient heat conduction studies 2–29564
calcium silicates, hydrated, pore struct. analysis by water vapour adsorpt. 2–35910
cement, portland, hydrated, pore struct. analysis by water vapour adsorpt. 2–35910
cement, portland, hydrated paste, pore struct. analysis by water vapour adsorpt. 2–36269
cement paste, hydrated, pore size generalized log-normal distrib. 2–36268
ceramic, porosity reduction, by impregnation with salt soln. 2–29442
ceramic composites, internal stresses deform., finite element analysis 2–32597
ceramics, field distortion and dielec. strength rel. to porosity 2–13299
coalescence of oil-in-water dispersion induced by flow through porous media 2–32281
compaction, shock-wave struct. 2–12836
composite, porosity source 2–22349
conccrete, microporosity obs. using colour film 2–39967
concrete, water migration, action of temperature gradient and pore pressures 2–15948
consolidation, displacement functions 2–17351
creep, during sintering 2–1344
drying, nonlinear heat and mass transfer, extended variational formulation 2–183
ductile, static and dynamic pore-collapse relations 2–32750
evaporation kinetics 2–6287
ferromagnet, anisotropy due to nonsphericity of pores and inclusions 2–40451
ferromagnet, approach to saturation, internal strain effect 2–1623
fibrous absorbents, sound propag. 2–34172
fluid flow in porous medium, equations of motion and continuity 2–28446
fluid linear flow, math. model 2–3342
fluoroescent tracer penetration, ultraviolet absorber dye usage 2–25094
gas diffusion, limitation of rates of reaction 2–3307
gas flow, compressible adiabatic, one-dimensional theory 2–1018
gas flow, Klinkenberg effect, meas. of coeff. b 2–15528
gas flow meas. in region of molecular, transition and slip flow 2–24956

Porous materials continued
glass, e.s.r. of Ag atoms on surface 2–1164
glass, e.s.r. of Ag atoms on surface 2–1163
glass, Vycor, adsorpt. of O_2, surface area, heat of adsorpt., e.p.r. obs., 77K 2–35912
glass adsorbed water layer, Ar adsorpt., thermodynamic props. 2–35913
glass diaphragm, sintered, plugging by distilled water 2–25611
glass fibrous mats, coalescence of oil-in-aqueous suspensions induced by flow through mats 2–32282
glass-water system, phase transition, heat effects, dimens. changes in temp. cycles, 237-278K 2–35922
graphite, damage during pore struct. determ. by Hg under press. 2–3975
graphite, neutron irrad., porosity 2–3756
graphite, neutron irrad., submicroporosity, temp. and dose depend. 2–29165
heat sources, transpiration cooling 2–2270
heat transfer, fluid with phase change 2–11375
heat transfer and fluid flow in a porous media, two-dimensional analysis 2–21757
heat transfer during filtration flow of a liq. 2–35422
heat transfer during kinetic burning in turbulent boundary layer on porous surface 2–27317
ion exchange resins and pelletized particles, sorption and bidisperse model of transient diffusion 2–1192
light scatt. cross sections, photon diffusion model, pore size meas. 2–32285
liquid filled in elastic skeleton, consolidation, constitutive relations derivation 2–21933
magnetization saturation, Neel theory 2–10203
melting, liquid phase capillarity 2–3434
melting characts. determ. by n.m.r. 2–9208
metal, eqn. of state under strong shock compression 2–3847
metal, porosity effect on shock melting and vaporization 2–39420
metal fibre, pressing and sintering, deformation, residual stress relaxation 2–29257
MHD flow between two-porous discs 2–39079
microporous solid, texture, DTA study 2–9783
non-destructive techniques for flaw size determination, reviews 2–32571
open porosity det. by hydrostatic weighing 2–19289
oxide ceramic, porosity, defects, elastic consts., u.s. obs. 2–12978
P-α model modification 2–15947
particle beam transmission, path length distrib. 2–32284
permeability rel. to compaction press. 2–39966
permeability tensor for anisotropic nonuniform media, regardless of preferred orientation of pores 2–1265
phosphors-glass interaction, halophosphate, Mn effect on binder burning-out 2–29965
pore size, porosity, meas. methods 2–36267
pore size distribution, determ. by photomicrographic method 2–25608
pore size distribution, meas. method and apparatus 2–32749
pore visualization, by filling with liquid and dissolving material after hardening 2–29455
quasistatic deform. with press. 2–39773
reactor fuel element, fission gas diffusion conditions 2–31628
Saran charcoal, adsorption of H_2O, methanol, or benzene vapour, vol. change 2–3559
scalar transport, dispersion vector, functional depend. 2–9057
silica gels, specific surface areas, pore struct., adsorpt. and i.r. spectra obs. 2–35920
silicas, porous and nonporous, adsorpt. of N_2, surface area calcs. by BET and α_s methods 2–35923
specific surface, N_2 thermal desorption obs. 2–15938
squeeze film, between porous rectangular plates, velocity slip effects 2–39850
steel, Cr-Mn, effect of alloying elements on porosity 2–1359
substrates for Pt-Au films, porosity rel. to prep. technique 2–1182
thermal diffusivity, steady-state approx. 2–19440
thermoelastic consolidation of material subjected to mechanical and thermal disturbance 2–22352
transient 3-dimensional natural convection 2–11379
X-ray scatt. intensity, absolute scale 2–15701
zeolites, liquid metal filling of marrow channels 2–1384
Al, coating, porosity, microscopy 2–25612
Al_2O_3, porosity reduction, by impregnation with salt soln. 2–29442
Au, electroless deposit, porosity, effect of growth conditions 2–3524
C, active, effect of heat treatment on pore struct., adsorption study 2–32751
CoO, oxidation to Co_3O_4, effect of porosity 2–22878
CrCx, production by vibration compaction 2–19290
Cu pure, porous-homogeneous couple, vacancy migration, pore redistrib. 2–12986
Fe, hydraulic resist. determ. 2–29456
Fe powder, pore struct. and compressibility 2–39958
KCl films, energy distrib. of transmitted secondary electrons 2–25985
LiF, reactor irrad., macropore formation 2–19075
Ni/Cu, pure, porous-homogeneous couple, vacancy migration, pore redistrib. 2–12986
Ni, porosity effect on elec. and thermal cond. 2–19464
SiO_2 microporous film, characterization by repeated interference of total internal reflection 2–39529
ThO_2 water vapour treated, adsorpt. of Ar and N_2, pore struct. 2–35924
Ti powder rolled metal, sintering 2–15926
TiC-NbC, high porosity complex carbide prep. 2–39969
TiC-ZrC, high porosity complex carbide prep. 2–39969
UP powder, sintering, 1500-2000°C 2–3935

Porterin-LeChatelier effect *see Stress/strain relations*

Positive column *see Discharges, electric*

Positive ray sources *see Ion sources*

Positive rays *see Chemical analysis/by mass spectrometry; Ion beams*

Positons *see Positrons*

Positronium
annihilation in gases, method of improving statistical accuracy in lifetime obs. 2–34620
atom, exchange scattering by H atom, cross section calc. 2–5873
atom, on H atom, exchange scattering cross section calc. 2–2991
chemical interaction with O_2 in liq. N_2 2–33366
formation and quenching in condensed media 2–28778
formation inhibition in DL-leucine after γ-irradiation 2–22888

Positronium continued
- polar media, positronium scatt. rel. to permittivity dispersion 2—22605
- quenching by carbonium ion in diamag. organic molecules 2—3065
- silicone fluids, three quantum annihilations 2—38237
- on solid surface, weakly bound states 2—9296
- in SiO_2 powders, ang. correl. obs. of formation 2—40110

Positrons
- *see also Electron pairs; and Electrons, which include both negative and positive electrons when the differences between them are of no special significance*
- acceleration, using 30 MeV electron linear accelerator 2—24116
- annihilation angular correlation obs., using spark chamber 2—2647
- annihilation in gases, method of improving statistical accuracy in lifetime obs. 2—34620
- annihilation in liquids 2—28778
- annihilation radiation, counting efficiency of coincidence spectrometer, Monte Carlo calc. 2—11662
- colliding beams, high energy, large angle muon and pion pairs prod. 2—14573
- core annihilation in metals 2—22482
- g factor, new precision measurement 2—11576
- interaction with Ar atom, semiphenomenological model 2—38832
- metal, negative work function 2—25969
- passage through solids and liqs., study by Monte Carlo method, in comparison with positrons 2—5502
- silicone fluids, three quantum annihilations 2—38237
- spectra, obtained from linear accel. of electrons at 8-30 MeV, energy distrib. 2—23801
- $3^+e\text{-}\rightleftarrows pp$, tests of T invariance 2—2503
- e^+e^- scattering, high energy, radiative corrections to coincidence experiments 2—21245
- Au, emission, negative work function 2—25970
- ^{90}Nb positron source, prep. 2—24177
- Si thin crystal, channelling 2—29580

Potassium
- activation analysis in solid rocket propellants 2—1772
- adsorption on Cu, low and high conc. states 2—29063
- afterglow discharge plasma, excited states relaxation in presence of reabsorption 2—24355
- Apollo 15 samples, primordial radioelements and cosmogenic radionuclides 2—41188
- atom, $4^2S_{1/2}\to 4^2P_{1/2,3/2}$ excitation by electrons, differential cross sections with spin analysis 2—18335
- atom, cold surface ionization on Ta and W ribbons 2—13364
- atom, collisions with diatomic molecules, thresholds and energy dependence of excitation cross sections, meas. from 1 to 10 eV 2—2977
- atom, collisions with H_2, N_2, O_2, CO, ionization cross sections 2—31706
- atom, electron impact excitation cross sections calc. using regional trial function in variational principle for R matrix 2—24364
- atom, ionization by 20-100 keV protons, electron prod. and ion formation cross sections 2—11979
- atom, low energy electron scattering, absolute elastic and inelastic differential cross sections 2—35168
- atom, multiphoton ioniz. probability 1.06 and 0.53μ 2—35157
- atom, optically oriented, collision rates 2—8479
- atom, photoionization cross section and spin orientation of ejected electrons 2—31677
- atom, principal series oscillator strengths and ground state photoionization cross sections 2—31679
- atom, spin-orbit perturbation in P-state continuum 2—24362
- atomic beam, applic. to plasma diagnostics 2—32032
- atomic beam, properties and polarization 2—24390
- atomic beam scatt. from [100] surface of Cu 2—6312
- atomic orientation by optical pumping, effect on mol. form. 2—18324
- atomic spectra, highly excited levels, absorption line broadening and shift in K vapour 2—11956
- atoms, collision with CO_2, long lived collision complex formation, comparison of experiment with statistical model 2—676
- atoms, collision with I_2, cross section meas., comparison with harpooning model predictions 2—686
- atoms, collisional reaction with methyl iodide, energy dependence of differential and total reaction cross sections 2—678
- atoms, collisions with Be_2, chemi-ionization differential cross section 2—680
- atoms, collisions with Br_2, negative ion formation, mass analysis 2—681
- atoms, collisions with Hg, differential scattering cross sections and intermolecular potential energy curves 2—888
- atoms, collisions with O atoms, charge exchange cross section, theoret. study 2—691
- atoms, electron scatt., differential direct scatt. cross section meas. at 4 eV 2—624
- atoms, electron scatt., differential spin-flip cross sections 2—623
- atoms, ionization by 20 to 100 keV protons 2—2949
- atoms, photoionization cross sections, model potential calc. 2—605
- atoms, superthermal, collisions with Hg and I_2, ang. scattering cross sections 2—682
- atoms scatt. by inert gases, total cross sections meas. theory 2—12009
- binding energy and lattice constants, pseudopotential calc. 2—40139
- circumstellar absorption components of U Mon 2—26709
- de Haas-van Alphen effect and spin-splitting g-factor 2—36428
- Debye-Waller factor 2—1422
- deformed, annealing and recovery spectrum 2—19089
- deformed, model for stage-B recovery 2—19090
- desorption from Nb, activation energies, mean adsorption lifetimes 2—6384
- dimers, reactive scattering with halogen molecules, cross sections and mechanisms 2—890
- electrical resistivity, low temp., Bloch T^5 law failure 2—16145
- electrical resistivity below 4.2 K 2—4157
- electron collision cross sections for momentum transfer 2—31703
- electrucal, resist. low temp. pure and impure cryst. 2—4158
- film, collective electron oscillations obs. by photoemission 2—16329
- film, photoelec. emission, 2.3-4.6 eV 2—33090
- film, thermal cond., calc. from elec. cond. 2—29567
- flame, K-seeded, acoustic wave excitation 2—39284
- Hall effect meas. in solid and liquid state 2—16137
- interstellar absorption line, bright O- and B-type stars in Orion region 2—4870
- ion velocity in He, Ne, Ar, H, N, gases pressure dependence obs. 2—3253
- lattice dynamics using pseudopotential approach 2—36318

Potassium continued
- liquid, interionic potential calc. 2—21955
- liquid, meas. of electrical properties in liquid-gas critical region 2—9157
- liquid, meas. of vapour pressure curve up to critical point, determ. vaporization entropy as function of temp. 2—28963
- liquid, oscillation spectra, variational calc. 2—9077
- liquid, sp. ht., spline correl. function 2—18812
- longitudinal plasmons, optically excited 2—10385
- magnetoresistance, model for analysis 2—1590
- multiphoton ionization, role of multiphoton resonance, two-step four-photon process 2—35158
- multiphoton ionization at 1.06 microns 2—35153
- plasma, collisional drift instability, effects of parallel wavelength 2—21855
- plasma, h.f. fluctuations in the density gradient 2—18643
- plasma, laser diagnostics using selective excitation spectroscopy 2—18642
- plasma column structure in weak mag. field 2—12396
- polarized atomic beam, photoionization, production of polarized electrons 2—11978
- polycrystalline, magnetoresistance, impurity, strain, temp., and size depend. 2—40176
- in rare gas matrices, absorpt. and luminesc. 2—24387
- recharging target for recharging protons to give H^- beams 2—7900
- in soils, remote sensing by low altitude gamma spectrometric surveys 2—37096
- solar absorption line at 7699 Å, red shift, atomic beam resonance-scatt. meas. 2—33762
- solid, cohesive energies and radii of metal cells calc. by ab initio method 2—1198
- spin wave transmission, 120 GHz 2—40745
- superconducting transiion temperature, pressure depend., pseudopot. approach 2—36454
- thermal desorption from α-Fe 2—32393
- twilight airglow observations, vertical abundance characteristics 2—30321
- work function and surface structure, calc. 2—39455
- atoms, collisions with I atoms, chemi-ionization cross section 2—684
- BeO:K, phosphor, thermolum. props. 2—29970
- CsCl:K, i.r. lattice absorpt., breathing shell model 2—36875
- $CsI:K^+$, impurity-induced i.r. absorpt., lattice dynamical calc. 2—40661
- K/A radiometric age determination, Freetown Igneous Complex, Sierra Leone, combined with palaeomagnetic evidence 2—16931
- K/Ca dates from pegmatitic micas 2—16767
- K-Ar technique, Apollo sample 15555 dating 2—41180
- K^+-Ar, atomic collisions, rel. to transparency 2—11992
- K-Cs crossed beams, thermal energy, velocity dependence of total elastic scattering cross section, determ. of long range potential 2—2975
- K-H^+ charge exchange cross section meas. in energy, range 150-8000 eV, applic. to plasma diagnostics 2—18343
- K-H_2 mixtures with pulsed infection of metal vapour into gas discharge plasma, obs. laser section 2—23601
- K-Hg, high resolution meas. of differential scattering cross section, intermolecular potential determ. by inversion of data 2—28427
- K-Kr binary collision broadening of K absorption line, contribution of dipole-quadrupole dispersion 2—31667
- in K, enhancement of self-diffusion 2—32564
- K I emission cross-section, radiative efficiency for atoms and ions emitted by high speed meteor 2—26865
- K II and K III spectra, radiative lifetimes 2—31678
- K multiphoton ionization probability, experiments rel. to theory 2—35159
- K X, extreme u.v., Hartree-Fock theoretical wavelengths, accuracy 2—24336
- K XVII spectrum in e.u.v. identification and classification of spectral lines 2—31666
- K^+, collisions with Ar, ion-atom potentials, derivation from intermediate and strong elec. field mobility data 2—2966
- K^+, collisions with He, Ne, Ar, Kr, determination of repulsive potentials from total scattering cross sections 2—12010
- K^+, excitation by collisions with Ar atoms, cross section meas. 2—18329
- K^+, head-on collisions with He, H_2, D_2, energy loss meas. 2—679
- K^+, refl. from Ag and Au targets 2—22065
- K^+, repulsive interaction potentials, calc. from total scattering cross sections 2—12011
- K^+ and inert gas atom collisions, determination of repulsive potentials 2—38840
- K^+ beam, excitation by scatt. on solid target 2—31678
- K^+ collisions with inert gas atoms, study of excitation mechanism, inelastic transitions 2—674
- K^+ impact on solid surface, emission of optical radiation 2—36956
- K^+ in $BaCl_2$, e.p.r. spectra 2—9600
- K^+ ion, on collision with He, Ne, Ar atoms, excitation section structure, applicability of three term model 2—38841
- KVIII Mg I-like spectra, analysis, isoelectronic comparison with spectra of CaIX, ScX, TiXI 2—28198
- ^{39}K, h.f.s. splitting consts. of first excited state 2—8451
- ^{41}K, h.f.s. splitting consts. of first excited state 2—8451
- ^{42}K production in nuclear reactor, biomedical applications 2—41291
- $K^+ + Ar \to K^{+*} + Ar$, collisions, threshold behaviour of excited cross section of KII resonance line 2—2951
- $K + Br_2 \to K^+ + Br_2^-$, mechanism near threshold 2—7167
- $K + Br_2 \to K^+ + Br + Br^-$. differential cross section for chemi- ionization in inelastic collisions 2—28223
- $K_2 + Br_2$, comparison of ang. distrib. of K atom reactive scattering and KBr ang. distrib. 2—26339
- $K_2 + Br_2$, ICl, IBr, BrCN, reactive scatt., ang. distribution meas. and total reaction cross sections 2—31885
- K_2+BrCN, comparison of ang. distrib. of K atom reactive scattering and KCN distribs. 2—26339
- K+HBR→KBr+H, trajectory calc. in eV region, computer program 2—33370
- K+HBr→KBr+H, total reaction cross section, computer trajectory calc. in eV region 2—677
- $K + I_2 \to K^+ + I + I^-$, differential cross section for chemi- ionization in inelastic collisions 2—28223
- NaCl:K, field gradient tensor calcs. for nuclei round substitutional ion 2—26093

Potassium compounds
- aqueous salt solutions, effect on metal transfer during CO_2 welding 2—19250
- borate glass, trapped electron centre, X-irradiation induced, e.s.r. and optical obs. 2—20137
- chloranilates, hydrated, crystal data, X-ray diffr. 2—19062

Potassium compounds continued
- graphite intercalation compounds, physical sorption of molecular H_2 at low temp. 2—6370
- graphite intercalation cpds., photoelectron spectra, electronic props. 2—10158
- halide, ionic transport parameters 2—33051
- halides, core exciton decay, photoemission obs. 2—19802
- halides, elastic consts., temp. depend. 2—29231
- halides, extreme u.v. spectral obs. 2—20042
- halides, far-i.r. anharmonic self-energy of long wave phonons 2—19348
- halides, Pb-doped, crysts. and aq. solns., optical absorpt. 2—20039
- hexacyanoferrate (II), photoelectron spectra meas. using Millikan apparatus 2—31007
- hydrogen maleate, single cryst., dielec. relax. 2—10110
- $K_2SeO_4:Cu^{2+}$, e.p.r., rel. to phase transitions 2—33341
- Luna 16 soil conc. 2—20664
- mica solid solution, formation between $k_2Mg_6Al_2Si_6O_{20}F_4$ and Al-free mica 2—36302
- muscovites, i.r. spectroscopic study of isomorphic changes 2—29919
- potassium copper oxalate dihydrate, cryst. struct., X-ray study 2—32483
- salt of trans-cyclohexane-1,4-dicarboxylic acid, struct., bond lengths 2—36000
- substances with potash-tungsten-bronze structure, attempt at synthesis 2—1399
- meso-tartrate, H-bonding, cryst. struct., X-ray analysis 2—36001
- c $KH_2PO_4:Cr^{3+}$, e.p.r., effects of uniaxial stress and elec. fields 2—33340
- K-Cs alloys, liq., nucl. spin-lattice relax. 2—18855
- K^+-indenyl ion pairs, struct., n.m.r. obs. 2—18512
- K complex, $K_2MCu(NO_2)_6$, (M=Ba, Pb), Jahn-Teller distortion and optical phonons 2—36988
- K complex, $K_2MFe(NO_2)_6$, (M=Ca, Sr, Ba, Pb), Mossbauer spectra 2—36846
- K complex, $K_2Pt(CN)_4X_{0.3}.2.6H_2O$, (X=Cl, Br), transport props., optical refl. study 2—19546
- KAg_4I_5, cationically disordered compound, elec. conductivity and dielec. const. 2—36585
- KAg_4I_5, cationically disordered compound, thermoelec. props. 2—40332
- KAg_4I_5, single crystal growth and crystal struct. 2—12698
- KAg_4I_5 solid electrolyte, thermopower 2—25947
- $KAl(NH_2)_4$, crystal structure determ. 2—39643
- $KAlO_2$-TiO_2; $KAlO_2$-SiO_2, crystal structure 2—3719
- KBH_4 and KBD_4, i.r. and Raman low temp. vibrational spectra 2—10384
- $(K_{3/4}Bi_{1/4})(Zn_{1/6}Nb_{5/6})O_3$, prep. and dielec. props. 2—4266
- $KBrO_3$, n.q.r. of ^{39}K 2—40790
- $KBrO_3$, nucl. quadripolar linewidth of ^{79}Br and ^{81}Br 2—7803
- $KBrO_3$ film, polycrystalline, preparation, thickness obs. and uniformity evaluation 2—9278
- KCL+CsCl, collision complex formation cross sections, ang. distrib. from mol. beams 2—28429
- KCN, single crystal neutron diffraction study rel. to disorder of CN^- ions in cubic phase 2—32461
- KCN IV, cryst. struct. at 50 kbar 2—12726
- $K_2CO_3.CaCO_3.SiO_2$ glasses, structural changes, analysis by I.R. and X-rays 2—1154
- $KCl:Sr^{2+}$ cluster formation of ion-defect pairs 2—15776
- KCl solid, meas. of thermal shift of electron binding energy traceable to Madelung energy 2—35931
- $KClO_3$, e.p.r. study of O_3- radical obtained by X-irradiation, trapping at 3 different sites 2—10484
- $KClO_3$, temp. dependence of n.q.r. frequencies from 77 to 350K 2—37018
- $KClO_3$ film, polycrystalline, preparation, thickness obs. and uniformity evaluation 2—9278
- $K(Co, Mn)F_3$, disordered antiferromagnet, study of mag. excitations by inelastic neutron scattering 2—4405
- $K_3Co(CN)_6$, cryst. struct. 2—29144
- $KCoF_3$, one and two exciton Raman scatt., magnon scatt. 2—36902
- $KCoF_3$, Raman spectrum, double magnons 2—20071
- K_2CoF_4, two-dimensional antiferromagnet, ^{19}F n.m.r. anomaly near critical temp. 2—30027
- $K_3Cr(CN)_6$, exptl. investigation of $^4A_2 \rightarrow {}^2E$, $^2T_1$ transitions 2—29918
- $K_4Cr(CN)_5NO$, i.r. spectra, vibr. modes, cryst. struct. 2—22770
- K_2CrO_4, ionizing radiation effects on thermal annealing in crossover region 2—10645
- K_2CrO_4 $K\alpha$ doublet intensity distribution 2—20056
- $K_2Cr_2O_7$, Kramers-Kronig relationships, refr. and extinction indices 2—15592
- $K_2Cr_2O_7$ liquid filters for visible and i.r. regions 2—8013
- K_2CsSb photocathode as high-gain secondary emitter 2—40392
- $K_2CuCl_4.2H_2O$, morphology deduction from cryst. struct. 2—39644
- K_2CuF_4, n.m.r. of ^{19}F, hyperfine interaction, unpaired spin densities 2—10552
- KD_2AsO_4, ^{75}As quadrupole coupling const. 2—10554
- KD_2AsO_4, γ-irradiated single crystal, e.s.r. of free radicals 2—10122
- $K(D_{2x}H_{2-2x})PO_4$, absorption coefficients, obs. 2—36824
- $KD_{2x}H_{2(1-x)}PO_4$, phonon modes and phase changes, Raman spectra 2—20062
- KD_2PO_4, double-loop dielec. hysteresis 2—6883
- KD_2PO_4, efficient second harmonic generation of Nd^{3+}:glass picosec. laser pulses 2—37984
- KD_2PO_4, electro-optic Q-switch, simulation by programmable desk calculator 2—4437
- KD_2PO_4, high temp. phase transition and metastability 2—22624
- KD_2PO_4, high temp. phase transitions 2—3997
- KD_2PO_4, Landau-Khalatnikov damping of transverse elastic waves 2—29533
- KD_2PO_4, statistical perturbation theory, order-disorder ferroelec. 2—10124
- KD_2PO_4, u.s. waves, diffraction of polarized light 2—19974
- $KDy(MoO_4)_2$, paramag. absorpt. in parallel fields 2—6947
- KF, electron density distribution, Lowdin approx. 2—32865
- KF, ultrasonic velocity and adiabatic compressibility in aqueous solution 2—21982
- KF aqueous solutions, nuclear Overhauser effect, relaxation times meas. 2—28896
- $KF.2(4)H_2O$, γ-irrad., colour centre formation, optical, e.p.r. spectra 2—1264
- $K_3Fe(CN)_6$, Kramers-Kronig relationships, refr. and extinction indices 2—15592
- $K_3Fe(CN)_6$, quadrupole interaction and paramagnetic anisotropy temp. depend. 2—36845

Potassium compounds continued
- $K_4Fe(CN)_6.3H_2O$, ferroelec., Mossbauer investigation of phase transition 2—29888
- $K_4Fe(CN)_6.3H_2O$, para and ferroelectric, n.m.r. obs. of ^1H 2—4556
- $KFeF_3$, Mossbauer effect, temp.-depend. cryst. field and electronic charge density 2—10323
- $KFeF_3$, weak covalency effects on cryst. field and nucl. quadrupole splittings 2—36788
- $KFeF_4$, 2-dimens. antiferromagnet, mag. struct. and props. 2—26067
- $KFeF_4$, mag. struct., Mossbauer spectra 2—40564
- $KFeO_2$-TiO_2, crystal structure 2—3719
- KH, potential energy curves, applicability of Morse potential, rot. consts., r-centroids, Franck Condon factors 2—18457
- KH_2AsO_4, ferroelectric. long range correlation, n.m.r. and dielectric relax. obs. 2—10553
- KH_2AsO_4, ferroelectric, proton-lattice interactions, dynamic susceptibility, Raman spectra 2—19377
- KH_2AsO_4, γ-irradiated single crystal, e.s.r. of free radicals 2—10122
- KH_2AsO_4, paraelectric phase, proton-phonon coupling, Raman spectra 2—19364
- KH_2AsO_4, phonon modes and phase changes, Raman spectra 2—20062
- KH_2AsO_4, polarized i.r. transmission spectrum in paraelectric phase 2—40709
- KH_2AsO_4 and KD_2AsO_4, proton-lattice coupled motion 2—19376
- KHF_2, crystal and molec. dynamics, i.r., Raman and neutron studies 2—26169
- KHF_2, lattice energy calc. using multipole moments from LCAO-MO calcs. 2—22093
- $KH_2PO_4:D$, $KD_2PO_4:H$, ferroelec., impurity effects, zero-temp. Green function method 2—19765
- KH_2PO_4/semiconductor contact surface, edge electro-optical effect 2—13439
- KH_2PO_4, chem. shift, of ^1H at 300K rel. to C_6H_{12}, ^{31}P at 77K rel. to H_3PO_4 2—13427
- KH_2PO_4, cryst. growth rate, rel. to degree of supercooling 2—35946
- KH_2PO_4, dipolar spin-lattice relax. study of l.f. motion 2—10259
- KH_2PO_4, double reson. of ^{39}K, spin- lattice relax., ferroelec. transition phenomena 2—10581
- KH_2PO_4, dynamical model, elec. susceptibility, sp. ht., isotope effect, crit. behaviour 2—19764
- KH_2PO_4, ferroelec., existence of dislocations at domain tips 2—22623
- KH_2PO_4, ferroelec., phase transitions, Landau theory 2—19760
- KH_2PO_4, ferroelec., soft modes, Raman spectra 2—16549
- KH_2PO_4, ferroelec. phase transform., lattice modes 2—19398
- KH_2PO_4, ferroelectric, temp. dependence of dielectric permittivity dispersion 2—16261
- KH_2PO_4, finely divided, permittivity 2—10121
- KH_2PO_4, first-order ferroelec. transition 2—10123
- KH_2PO_4, high temp phase transitions 2—3997
- KH_2PO_4, high temp. phase transition and metastability 2—22624
- KH_2PO_4, $KD_{2x}H_{2(1-x)}PO_4$, KH_2AsO_4, ferroelectric modes, Raman spectra 2—16551
- KH_2PO_4, KD_2PO_4, KH_2AsO_4, ferroelectric phase transitions, phonon spectra, Raman scatt. 2—16550
- KH_2PO_4, KD_2PO_4, soft optic and acoustic modes, light scatt. obs. 2—20072
- KH_2PO_4, KD_2PO_4, u.s. vel. and attenuation, dielec. susceptibility, polarization relax. 2—4279
- KH_2PO_4, macroscopic stimulated polarization echo 2—1569
- KH_2PO_4, ordinary+extraordinary→extraordinary type interaction, vector synchronism conditions 2—10296
- KH_2PO_4, parametric light sources, frequency stability 2—38141
- KH_2PO_4, phonon modes and phase changes, Raman spectra 2—20062
- KH_2PO_4, pressure effects on lattice parameters and structure 2—32459
- KH_2PO_4, proton-phonon interactions 2—32811
- KH_2PO_4, self-focussing of ultrashort pulses and filamentary damage 2—13429
- KH_2PO_4, spin-spin cross relax., double r.f. field irrad. influence 2—10254
- KH_2PO_4, tunable four photon parametric fluorescence 2—29866
- KH_2PO_4, vanishing of ferroelec. at high press. 2—22625
- KH_2PO_4, vibr. spectra 2—13490
- KH_2PO_4, X-ray irrad., light pulse emission accompanied current pulses 2—13515
- KH_2PO_4 and KD_2PO_4, quantum acoustics of ns. hypersound pulses 2—32822
- KH_2PO_4 and KD_2PO_4, high temp. dielec. anomalies, phase transitions 2—9814
- KH_2PO_4 circle theorem for zeroes distribution of partition function, breakdown 2—1570
- KH_2PO_4 crystals, det. of refractive index in i.r. region using parametric scattering of light 2—40607
- KH_2PO_4 electro-optical modulator, with low modulator voltage 2—17669
- KH_2PO_4 electronic beam-light modulator 2—7964
- KH_2PO_4 Lyot filter, stabilization of rhodamine 6G dye laser 2—17615
- KH_2PO_4 radiation effects on structure, phase transitions and dielectric props. 2—1442
- KH_2PO_4 relative nonlinear coefficients, cw ruby laser as pump source 2—36814
- KH_2Po_4 electro-optic light deflectors, max deflection and resolving power 2—38078
- $KH_3(SeO_3)_2$, dipolar spin-lattice relax. study of l.f. motion 2—10259
- KI: O_2-(S_2-), luminescence spectra, structure of phonon wing 2—26220
- KI:Au, optical absorpt. and Raman scatt. 2—40676
- $KI:In^+$, $KI:Sn^{2+}$ magnetic field dependence of radiative lifetime of A-band emission 2—36930
- KI:KOH, microwave absorption, 8 to 40 GHz, 1.3K 2—13479
- KI:KOH, thermal cond., continuum of tunnelling levels 2—19446
- $KI:M^{2+}$, M=Zn, Cd, reactions, coloration, spectra 2—19125
- KI:Pd, e.s.r. obs. 2—4541
- KI:Tl phosphor, luminescence kinetics, electron-hole centre interaction 2—40711
- KI:Tl type phosphors, Jahn-Teller effect in emission spectra, $^3T_{1u}$ adiabatic potential-energy surfaces 2—33314
- $KI:Tl^+$, u.v. absorp. bands, uniaxial stress effects 2—10386
- KI-AgI acetone soln., emitted smoke ice forming ability 2—22972
- KI-KBr mixed cryst., Raman scatt. from phonons 2—40694
- KI, dielectric constant, temp. dependence obs. 2—4267
- KI, diffusion coefficient of hydrogen and activation energy 2—19139
- KI, diffusion of rare gases 2—3809
- KI, elastic interaction of O_2^- centres 2—22186

Potassium compounds continued

- KI, elec. field gradient around point defects, continuum elasticity calc. 2—25385
- KI, energy bands and optical consts. 2—40703
- KI, exciton structure, vacuum u.v. reflectivity obs. 2—16469
- KI, excitonic structure, obs. using reflectivity meas. in vacuum u.v. 2—4137
- KI, excitons perturbed by self-trapped excitons 2—26156
- KI, F-centre luminesc., weak mag. field enhancement 2—26237
- KI, far-ir. optical consts. and phonon freqs. 2—1681
- KI, Faraday rot. of excitons 2—22731
- KI, i.r. active two-phonon processes 2—40677
- KI, i.r. transmission spectra, multiphonon absorpt. bands 2—36883
- KI, laser induced photoconductivity of F-centre, 40 and 100 K 2—1584
- KI, multiphoton transitions, photocond. obs. 2—22637
- KI, proton irrad., beam intensity depend. of F-centre yield 2—12788
- KI, proton irrad., defect formation, channelling effects 2—19130
- KI, U-centre induced Raman scatt. 2—36904
- KI, u.v. excitation, thermally stimulated cond. obs. 2—19074
- KI, X-irradiated, role of Auger effect in thermostimulated phenomena 2—33323
- KIO_3, appl. to oxidation mechanism study in O plasma with r.f. discharge 2—4586
- KIO_3, phase transition, electro-optical obs. 2—33211
- KIO_2F_2 γ-irrad. cryst., e.s.r. of IO_2F^- radical 2—20142
- KI+CsCl, collision complex formation cross sections, ang. distrib. from mol. beams vel. distrib. 2—28429
- $K_2MFe(NO_2)_6$, (M=Ca, Sr, Ba, Pb), Mossbauer obs. 2—36836
- $K_2Mg(CrO_4)_2.2H_2O$ crystal structure determ. 2—6443
- $K_2MgF_4:Mn^{2+}$, $K_2ZnF_4:Mn^{2+}$, spin-Hamiltonian higher order parameters, from ENDOR, at 4.2K 2—30028
- $KMgF_3:V^{2+}$, coalent spin transfer, e.p.r. and ENDOR obs. 2—20143
- $KMgF_3$, luminesc. from colour centres 2—32556
- $KMgF_3$, Mossbauer effect of ^{57}Fe, h.f.s., Fe^{2+} electronic props. 2—29887
- $KMg_3FeSi_3O_{10}(OH)_2$, synthetic ferriphlogopite, tetrahedral Fe^{3+} Mossbauer parameters 2—10327
- $KMg_{1-x}Mn_xF_3$, lattice consts. 2—29145
- $K_2Mg(MoO_4)_2.2H_2O$ crystal structure determ. 2—6443
- $K_2Mg_2(SO_4)_3:Mn^{2+}$, e.s.r. spectra 2—36987
- $K_2Mg(WO_4)_2.2H_2O$ crystal structure determ. 2—6443
- $KMnF_3:Mg$, Neel temp. shift and e.p.r. linewidth 2—10508
- $KMnF_3:Ni^{2+}$, ion absorpt. transition temp. depend rel. to mag. ordering effects 2—33267
- $KMnF_3:Ni(Co)$, spectra, exciton-magnon absorpt. structure, impurity effects 2—6993
- $KMnF_2$, sound velocity and elastic consts., Mandelstam-Brillouin scatt. obs. 2—16580
- $KMnF_3$, anomalous elastic behaviour near struct. phase transition 2—19157
- $KMnF_3$, disordered, cryst. struct., diffuse X-ray scatt. 2—9375
- $KMnF_3$, dispersion and damping of soft zone-boundary phonons 2—22409
- $KMnF_3$, doped, first- and second-shell hyperfine interactions 2—20144
- $KMnF_3$, n.m.r. linewidth, critical behaviour 2—10555
- $KMnF_3$, para- to antiferromag. transition, Raman spectra obs. 2—16548
- $KMnF_3$, phase transformations of displacement type, X-ray investigation thermodynamic description 2—1398
- K_2MnF_4, antiferromag., ENDOR, hyperfine splitting of Mn^{2+} 2—7154
- K_2MnF_4, n.m.r. linewidth, critical behaviour 2—10555
- $KMnO_3$, paramag., optical props., cluster model applic. 2—18961
- $KMnO_4$ dilute solutions, Resonance Raman effect studied 2—12565
- $KMnO_4$ Raman spectra using rotating sample technique 2—10410
- $KMn_{1-x}X_xF_3$, (X=Zn,Ni,Fe), local susceptibility 2—40417
- K_2MoO_4-Li_2MoO_4 molten system, surface tension, comp. depend. 2—28818
- $K_{0.85}Mo_6O_{17}$, single cryst. struct. determ. 2—9480
- $KN_3:NO_3$-, u.v. irradiation, e.s.r. in NO molecule 2—12182
- KN_3, internal photoemission of electrons and holes 2—40260
- KN_3, lattice dynamics 2—4035
- KNO_3-$Cd(NO_3)_2$ glass, positron lifetime, temp. depend. through phase transition 2—36374
- KNO_3-$LiNO_3$, molten mixture, liquidus curve, thermodynamic props. 2—25138
- KNO_3, elec. cond., thermal transform. 2—32773
- KNO_3, material coeffs. and micropolar theory 2—25650
- KNO_3 first-order ferroelectric phase transition, Raman spectroscopy of phonon instability 2—25924
- KNO_3+AgNO_3, system, molten salts, equivalent conductivity 2—1112
- KN_3;KNO_2;KNO_3, e.p.r. study of NO_2 and NO_2^{2-} paramagnetic centers formed by irradiation of NO_2^- and NO_3^- 2—10483
- KNa, molecular beam resonance study 2—38920
- $K_{1-x}Na_xTaO_3$ mixed cryst., ferroelec. transitions, soft modes 2—25928
- $KNbO_3$, crystal, growth by modified Kyropoulos technique 2—18978
- $KNbO_3$, cubic ferroelectric, phase transition, neutron diffuse scatt. obs. 2—13318
- $KNbO_3$, disordered, cryst. struct., diffuse X-ray scatt. 2—9375
- $KNbO_3$, ferro-antiferroelec. phase transition, n.m.r. obs. 2—16661
- $KNbO_3$, orthorhombic, elastic consts., X-ray diffuse scatt. obs. 2—32578
- $KNb(Ta)O_3$-$W(Te)O_3$ system, crystal chemistry 2—15682
- $KNiF_3$, covalency and ligand field effects, Hartree-Fock calcs. 2—40590
- $KNiF_3$, magnon sideband in optical absorption spectra, positive identification using mag. circular dichroism 2—36882
- $KNiF_3$, n.m.r. of ^{19}F 2—13554
- $KNiF_3$ Raman scatt. by four magnons 2—36903
- K_2NiF_4, anisotropy, antiferromag. reson. study 2—36974
- K_2NiF_4, family, two dimensional antiferromag., phase transition and crit. phenomena 2—16392
- $K_4Ni(NO_2)_6H_2O$, multiple internal reflection i.r. spectroscopy, effect of different prism angles 2—27646
- KNi_1-xMg_xF_3, Ni^{2+} ion absorpt. transition temp. depend rel. to mag. ordering effects 2—33267
- K_2O-SiO_2, glass, electrical conductivity, activation energies, models 2—3458
- K_2O-SrO-Nb_2O_5 system, ferroelec. characterization 2—40352
- KO dissociation energy and ground state calc. from ion model 2—28266
- K_2O, prod. in matrix reaction, i.r. spectrum, force constants 2—12158
- KOH, stabilized in Ar matrix at 4.2 K, i.r. absorption spectra, force field calc. 2—28304
- $(KOH)_2$, stabilized in Ar matrix at 4.2 K, i.r. absorption spectra, frequencies of OH vibrations and configurations determ. 2—28304

Potassium compounds continued

- $K_2O.3SiO_2$ glass, diffusion coeff., effect of specific activity 2—15792
- $K_2O.3SiO_2$ glasses, Frenkel pairs form. 2—1249
- $(KPO_3)_n$, small angle X-ray scatt., desmearing obs. by computer program 2—3628
- KPb_2Cl_5, $KPbCl_3$, fused salts, polarizability rel. to complex ion structure 2—39378
- $K_2PbCu(NO_2)_6$, phase transitions, heat capacity and e.s.r. obs. 2—15967
- $K_2Pt(CN)_4Br_{0.3}.(H_2O)_n$, one-dimens. metallic behaviour confirmation by far-i.r. refl. 2—33241
- K_2PtCl_6 type structures, effect of radius ratio on distortion 2—32460
- $K_2Pt(Pd)Cl_4$, cryst. struct. and factors affecting accuracy 2—29143
- K_2PtS_2, prep. and cryst. struct. 2—32462
- K_2ReCl_6, irradiated, mag. susceptibility and structure modifications 2—4344
- $K_2SO_4:CrO_4^{2-}$, optical absorption spectra, fine structure 2—22771
- $K_2SO_4:Cu^{2+}(Mn^{2+})$, e.s.r., hyperfine interactions, phase transition 2—9815
- K_2SO_4, dielec. const., microwave region using heterogeneous mixture method 2—36581
- K_2SO_4, e.p.r. of Cd^+ in $^2S_{1/2}$ state 2—7120
- K_2SO_4, irrad., SO_4 radical obs. using e.p.r. 2—26375
- K_3Sb, purple film, optical constants det. using Kramers Kronig dispersion anal. 2—40601
- $KSbF_x$, (x=4,5,6) and KSb_2F_4, ^{121}Sb Mossbauer data rel. to structural parameters 2—1668
- K_2SnCl_6, ^{35}Cl n.q.r. obs., 77-320 K 2—7158
- $KTaGe_3O_9$, $K(Ta_{1-x}Nb_x)Ge_3O_9$, $KTa(Ge_{3-y}Si_y)O_9$, atomic positions 2—25334
- $KTa_{0.63}Nb_{0.37}O_3$, cubic ferroelectric, soft phonon dispersion modes, neutron scatt. obs. 2—13029
- $KTa_{0.64}Nb_{0.36}O_3$, Raman spectrum, paraelec. and ferroelec. phases, phonon modes 2—36905
- $KTa_xNb_{1-x}O_3$ solid solns., cryst. growth 2—25264
- $KTaO_3$, linear-displacement correls. neutron scatt. analysis 2—22408
- K_2TeI_6, cryst. structure. X-ray study effect of radius ratio 2—32460
- α-KTh_6F_{25}, cryst. struct. 2—15722
- $K_7Th_6F_{31}$, cryst. struct. 2—6436
- $KTiOPO_4$, space group, X-ray exam. 2—15723
- K_3TlF_6, $K_2Tl_7F_{23}$ crystal structure, characterized MF-TlF_3 system, M=Li, Na, K 2—3737
- $K_3UO_2F_5$, i.r. absorption spectrum, normal coordinate analysis 2—40667
- $KX:Tl^+$, X=Halogen, Tl^+ induced electron-phonon interactions rel. to Raman spectra 2—16086
- $KY(MoO_4)_2:Er^{3+}$, empirical energy level diagram for Er^{3+} from absorption and luminescence spectra 2—26166
- $KY(WO_4)_2:Nd^{3+}$, laser, transition cross sections, fluorescent line width and branching ratios 2—31051
- $KY(WO_4)_2:Nd^{3+}$ stimulated emission and laser props. 2—27508
- $KZnF_3:Fe$, ENDOR and e.s.r., Fe^{3+} (K^+ vacancy) centre obs. 2—36986
- $KZnF_3:Mn^{2+}$, Cu^{2+}, optical absorpt. spectra 2—10388
- $KZn(SO_4)_2.6H_2O:Cu^{2+}$, e.s.r., obs. of ^{17}O superhyperfine interaction, hyperfine tensor 2—26262
- $K_2Zn(SO_4)_2.6H_2O$, e.s.r. of Cu^{2+}, temp. and irrad. influence 2—13539
- $^{39}K^{19}F$, Stark effect, molec. beam resonance meas. 2—21646
- $K_3[Fe(CN)_6]$, proton irradiation damage, Mossbauer obs. 2—16438
- $K_4[Fe(CN_6)].3H_2O$, proton irradiation damage, Mossbauer obs. 2—16438
- $K_2[Pt(CN)_4]Br_{0.3}$-$2,3H_2O$, n.m.r. study, anisotropy of ^{195}Pt shift, line broadening 2—10562
- $K_2[Pt(C_2O_4)_2].2H_2O$, anisotropy of chem. shift of ^{195}Pt nmr signal, position of Pt units in unit cell 2—26307
- Kh_2PO_4 loaded waveguide, application to coherent light-phase modulator 2—11500
- Na-K alloy, liquid, partial structure factors 2—6200
- Na-K alloy film, photoelec. emission and phase transitions 2—33090
- Na-K eutectic alloy, critical heat flow during boiling in conditions of free convection 2—28954
- Na-K liquid alloy, electrotransport theory 2—21999
- Na-K liquid alloys, volume thermal expansion coefficients 2—25068
- Na-K solutions electrical transfer, resistivity and density of electron states meas. 2—39386
- Na-K system, liq., electronic struct. 2—9078
- NaOH-KOH-ZnO mixture, flux for tinning Al wire 2—41357
- Pt, complex, tetracyanoplatinates, anisotroy of ^{195}Pt shift 2—10562

potassium bromide

- colour centres, bleaching and annealing attributed to D_3-centres 2—36065
- colour centres, colloidal Pb centres 2—29196
- coloured crystals, i.r. absorption of molecular centres 2—26153
- diffusion coefficient of hydrogen and activation energy 2—19139
- doping by dynamic compression of layer on surface 2—9587
- elastic constants, and Debye temp. in single crysts. and KCl-KBr solid soln. 2—19375
- electrical breakdown, in non-uniform fields, polarity and neg. space charge effects 2—22616
- electron emission under atom and ion bombardment, gamma ratio and energy distribution 2—36648
- energy bands and optical consts. 2—40703
- exciton structure, vac. u.v. reflectivity obs. 2—16469
- excitonic structure, obs. using reflectivity meas. in vacuum u.v. 2—4137
- F-centre, asymptotics of weakly bound electron wave function and photodisintegration cross section 2—32552
- F-centres, luminesc., weak mag. field enhancement 2—26237
- Faraday rot. of excitons 2—22731
- impurity-induced far-i.r. absorpt., phonon spectra 2—26168
- K′-centres, high press. ENDOR study 2—39715
- photoelectric emission from complex F-centres 2—6929
- point defects, elec. field gradient, continuum elasticity calc. 2—25385
- positron trapping, by F- and F′-centres, theory 2—25448
- Raman spectra, two phonon scatt. 2—25658
- reflectivity spectra, far-u.v., electronic struct. 2—13457
- rigidity, dislocation rosettes 2—6562
- sputtering, by Ar^+ and Xe^+, mass spectrometry obs. 2—22447
- surface, Cl- substitution, cooperative interactions including surface transition 2—29059
- surface polarization capacitance, single cryst. 2—16270
- thermally stimulated conductivity of u.v. excited crystals 2—19074
- thermodynamic functions, phonon freq. moments, and Blackman rule of sums 2—40067
- twist grain boundaries 2—9579
- U-centre induced Raman scatt. 2—36904
- X-ray irrad., optical absorpt. and thermoluminesc. 2—40728

Potassium compounds continued
potassium bromide continued
X-ray irrad. defects, annealing, low temp. 2—3760
X-ray scattering on single phonon, eigenvector influence 2—9855
$KBR_{1-x}I_x$ mixed cryst., Raman scatt. from phonons 2—40694
KBr:Au, optical absorpt. and Raman scatt. 2—40676
KBr:Cl, field gradient tensor calcs. for nuclei round substitutional ion 2—26093
KBr:I, luminesc. from bound excitons, polarized light obs. 2—26236
KBr:KI, colour centre prod. rates 2—32555
KBr:Li^+, lattice reson. in far i.r. h.p. obs. 2—6650
KBr:M^{2+}, M=Zn, Cd, reactions, coloration, spectra 2—19125
KBr:OH, optical bleaching of F-centres, low temp. 2—29200
KBr:OH^-, complex dielectric susceptibility, paraelectric relaxation, isotope effects 2—10116
KBr:$SeO^{2-}{}_3$, $SeO^{2-}{}_4$, i.r. absorp. spectra 2—10387
KBr:Tl, vac. u.v.- X-u.v. excited, photo- and electrophotoluminescence processes 2—16603
KBr/$CdBr_2$(Cl_2) and KBr/LiBr(Cl) molten mixtures, u.s. velocity and compressibility 2—25076
KCl:KBr, luminesc., transitions to exciton and cond. band states 2—36932
KCl-KBr, solid soln., polygon wall motion, load compression curve 2—9659
KCl-KBr powder mixtures, mixed cryst. form. 2—32742
$KCl_{1-x}Br_x$, mixed system, Debye-Waller factors, calc. by virtual cryst. model 2—36334
O_2^- centres, elastic interaction 2—22186

potassium chloride
absorption spectra, 12-25 eV 2—20034
$Cl^-{}_{II,III}$ absorption spectra, pure and KCl-NaCl, KCl-RbCl solid solns. 2—20041
aqueous solns., Brillouin scattering of laser light 2—3392
band structure, calc. using pseudopotential approach 2—29598
brine-ice interface, kinetics determ. from temp.-gradient zone migration of droplets 2—9240
channelling, MeV protons and He^+ ions 2—3754
channelling of low-energy alkali ions 2—36391
colour centre formation in pure and I^- doped cryst., irrad. intensity effects 2—22230
colour centres, colloidal Pb centres 2—29196
crystals, containing complex impurity ions, Raman scatt. spectra 2—16547
crystals, grown from melt, optical defects, monochromatic photographic obs. 2—32500
crystals, grwon from melt, cleavage, computer simulation 2—29083
Debye-Waller B-values, interionic interaction model 2—22404
diffusion coefficient of hydrogen and activation energy 2—19139
diffusion of Tl, electron probe analysis 2—9607
dislocation shift, stress induced, local obstructions 2—19100
droplet migration in thermal gradient 2—9523
effusion from cylindrical orifice, ang. distrib. study by mass spectra 2—9017
elastic constants, and Debye temp. in single crysts. and KCl-KBr solid soln. 2—19375
electromechanical coupling due to charged dislocations 2—40363
electron irradiation damage, low temp., dislocation loops 2—12750
energy bands, ab initio calcs. 2—4123
energy bands and optical consts. 2—40703
e.p.r., off-centre behaviour of paramag. atom due to covalency 2—10509
F′- to F-conversion, thermal kinetics 2—1263
F-aggregate centre form. 2—15783
F-aggregate centres, radiation annihilation 2—32554
F-centre, asymptotics of weakly bound electron wave function and photodisintegration cross section 2—32552
F-centre, step diffusion activation energy 2—15782
F-centre accumulation kinetics, X-irrad., pure and Pb-doped crysts. 2—36069
F-centre accumulation kinetics, X-irrad. pure and Pb-doped crysts. 2—36070
F-centre colouring, γ-ray induced at room temp., effect of colouring 2—3803
F-centre diffusion, temp. and conc. depend. 2—32553
F-centre luminescence during X-ray irradiation at low temperatures 2—29953
F-centre prod. efficiency, in electron irrad. cryst. 2—6507
F-centres, elastic scatt. of polarons 2—9598
F-centres, luminesc., weak mag. field enhancement 2—26237
F-centres and F_2-centres, conversion and equilib. during warming 2—22228
F-centres in γ-irrad. cryst., thermoluminesc. and annealing 2—16630
F-centres in X-ray coloured cryst., thermoluminesc. 2—4512
Faraday rot. of excitons 2—22731
film, porous, energy distrib. of transmitted secondary electrons 2—25985
films, energy losses of slow electrons, resonance potentials 2—25711
Hall mobility of electrons meas. by double modulation method 2—27387
heat capacity inversion by quadratic programming 2—6678
in ice, dielec. props. 2—16264
impurity-induced far-i.r. absorpt., phonon spectra 2—26168
ionic cond., defect interactions 2—1247
irradiated, defect annealing, absorp. band obs. 2—36011
laser-stimulated atomic migration 2—25463
M-centre optical bleaching, quantum yield 2—9602
M-centre triplet form. 2—9601
M-centres, relaxed excited triplet state decay 2—22229
Mossbauer spectra of ^{129}Te, local environment of impurity 2—10319
multiphoton transitions, photocond. obs. 2—22637
paraelectric reson. of Li^+ 2—10115
photoelectric emission from complex F-centres 2—6929
piezobirefringence coeff., energy band deform. pot. 2—26167
piezobirefringence in vac. u.v. 2—16470
positron annihilation rel. to positive ion vacancies and F-centres 2—19530
positron trapping, by F- and F′-centres, theory 2—25448
projection grown on W substrate, field emission microscopy 2—6358
proton bombardment, H-defects, U centre, i.r. and u.v. absorpt. spectra 2—22227
proton irrad., U-centre obs. 2—25453
proton irradiated, defect formation, channelling effects 2—19130
reflectivity spectra, far-u.v., electronic struct. 2—13457
rigidity, dislocation rosettes 2—6562
self diffusion, ionic conductivity, vacancy defect study 2—19140

Potassium compounds continued
potassium chloride continued
single crystals, vaporization of H_2O liq. inclusion 2—3762
solid-liquid phase transformation, thermodynamic resolution, simulated molecular dynamic calc. 2—25137
spin lattice relaxation of F_A(Li) relaxation, 4.2K 2—10507
stress induced linear dichroism of Ag^- and Cu^- 2—33208
stress relaxation, dislocation movement in γ-irradiated crystal 2—9660
substrate, Brownian motion of Al crystallites, rel. to epitaxy 2—32359
thermal expansion and free energy from the deformation dipole model 2—16054
thermodynamic fnctions, phonon freq. moments and Blackman rule of sums 2—40067
thermoluminescence of X-ray coloured cryst., relax. process parameters 2—4512
thermomigration of biphase vapour-liq. droplets 2—25375
X-ray irrad., F-, F_2-centres, dynamic equilibrium, temp. depend. 2—25452
X-ray irrad., hole centre obs. 2—1262
X-ray scattering on single phonon, eigenvector influence 2—9855
yield point, effect of colour centre conc. by γ-irradiation 2—15838
Fa(Li) colour centre, impurity displacement, absorp. band posn., isotropic hyperfine interaction 2—9599
K-KCl, melts, electron mobility calc. 2—6243
KCl:Ag^-, C-band light irrad., absorpt. bands attributed to paired Ag^- ions 2—15784
KCl:Ag^-. C-band light irrad., absorpt. attributed to paired Ag^- cons., theory 2—19126
KCl:CN^-, doped, thermal cond., phonon scatt. 2—4077
KCl:Ca, formation of paramagnetic V-centres 2—29202
KCl:Ca, Sr, Ba, thermal electric alignment and Stark effect of Z_1-centres 2—20040
KCl:Ca, vaporization rate meas., 430-550°C 2—9218
KCl:Co(Ba)(Cd), X-irrad., optical belaching and F- to M-centre conversion 2—22231
KCl:Cu, thermolum., glow curves, trap parameters 2—36953
KCl:Eu^{2+}, Z_l and Z_2 centres, optical absorpt. and e.p.r. obs. at 77K 2—36066
KCl:I, Ag, impurity induced Raman spectra 2—26194
KCl:In, luminesc. due to hole trapping by In^+ and $In^+v_{c^-}$ centres 2—36943
KCl:In, polarized luminesc. of In^{2+} and $In^{2+}v_{c^-}$ centres 2—33315
KCl:In^+, u.v. absorp. bands, uniaxial stress effects 2—10386
KCl:KBr, luminesc., transitions to exciton and cond. band states 2—36932
KCl:KNO_3, electrolytically coloured, X-ray generation of stable centres 2—36067
KCl:KOH, thermal cond., continuum of tunnelling levels 2—19446
KCl:Li, nonlinear susceptibility of tunnelling ions 2—29738
KCl:Li, paraelec. reson., stress effects 2—22619
KCl:Li^+, dipole-lattice relaxation time, paraelec. resonance obs. 2—36588
KCl:Li^+, n.m.r., quadrupole line splitting in elec. field 2—37009
KCl:Li^+ linear thermal expansion coefficients below 30 K 2—16055
KCl:Mn, central hyperfine splitting temp. depend., l.f. local mode obs. 2—10291
KCl:NH_4Cl, local torsional and translational modes 2—19399
KCl:NO_2-, absorpt. and emission spectra, effect of impurities 2—16492
KCl:OH, optical bleaching of F-centres, low temp. 2—29200
KCl:O^{2-}($SO_4{}^{2-}$), electron excess colour centres 2—25451
KCl:Pb, crysts. and aq. solns., optical absorpt. 2—20039
KCl:Pb, spectroscopic determination of conc. limits of isomorphic substitution 2—39711
KCl:Pb laser window, 10.6μ absorpt., impurity effects 2—16416
KCl:Pb^{2+}, polarized luminesc. of impurity-vacancy complexes 2—16609
KCl:$SeO^{2-}{}_3$, $SeO^{2-}{}_4$, i.r. absorp spectra 2—10387
KCl:Sm^{2+} fluoresc. sites, canonical distrib. law and C_{2v} paradox 2—40723
KCl:Sm^{2+} single crystal, theory of Zeeman anisotropy fluorescence spectroscopy, numerical fit of low-J transitions 2—22804
KCl:Sr^{2+} resolution of Z_1-band by numerical methods 2—3805
KCl:Tl, luminescence, thermal broadening 2—4528
KCl:Tl, photoluminescence on band region excitation 2—36933
KCl:Tl phosphorus, origin of 4750 Å emission 2—36931
KCl:U, γ-irradiated, colouring and hardening due to secondary interstitial processes 2—36060
KCl/$CdCl_2$(Br_2) and KCl/LiBr molten mixtures, u.s. velocity and compressibility 2—25076
KCl/XCl fused mixture (X=Rb,Cs,Li), u.s. velocity and compressibility 2—25077
KCl-KBr, solid soln., polygon wall motion, load compression curve 2—9659
KCl-KBr powder mixtures, mixed cryst. form. 2—32742
KCl-LiCl, eutectic melt, viscosity, 400-500°C 2—28811
KCl-NaCl-$CaCl_2$-UCl_3-UCl_4 solid systems, phase diagrams 2—39998
KCl-NaCl solid solns., Cl^--$L_{II,III}$ absorpt., band struct. 2—7072
K_2Cl_2, mass spectrometric ang. distrib. study of effusion from cylindrical orifices 2—9017
$KCl_{1-x}Br_x$, mixed system, Debye-Waller factors, calc. by virtual cryst. model 2—36334
KCl;Au, optical absorpt. and Raman scatt. 2—40676
(NaCl-KCl):Sn, mixed crysts., thermolum., 300-500K 2—36954
O_2^- centres, elastic interaction 2—22186

Potential energy, gaseous molecules *see Molecules/intermolecular mechanics*

Potential energy, single molecules *see Molecules/internal mechanics; Molecules/vibration*

Potentiometers *see Electrical measurement*

Powder diffraction cameras *see X-ray crystallography/apparatus*

Powder metallurgy *see Metallurgy; Sintering*

Powders
see also Granular structure; Particle size; Sintering; Surface measurement
annular shear cell, failure plane rotation 2—19278
binary mixture, reflection coefficient, comp. depend. 2—33207
burning, interaction with acoustic fields 2—37036
carbonyl iron, structural changes during sintering 2—39959
characterization by adsorption, automated gravimetric system 2—22079
compaction and flow under constant pressure 2—39957
crystalline particle identification, very small size by electron microscopy and diffraction 2—19256
crystalline particles, adhesion forces distrib. during compression 2—32752
densification kinetics, sintering eqns. at const. rates of heating 2—32740
dusty gases, shock waves, theoretical-kinetic approach 2—35675
e.p.r., line shape and spatial distrib. of line-width 2—36976

Powders continued
- e.s.r. spectra obs. under hydrostatic pressure, spectrometer modification 2—27370
- frost suceptibility and crystal structure 2—3971
- handling system, vacuum 2—5107
- heating in induction plasmas, work coil performances 2—3222
- highly dispersive, X-ray chamber for obs. in temp. range from −175 to +400°C 2—19023
- magnetoplumbite powders, mag. spectra before and after annealing, 30-52 GHz meas. range 2—16643
- metal, energy absorption during compaction 2—39955
- metal, sintering, shrinkage equation 2—6620
- metal, stressed state diagram, anal. 2—1377
- metal oxide, specific surface meas. by air permeability 2—1376
- metallurgy, applic. to nuclear industry 2—8408
- metallurgy, Conf., London, England, Nov. (1971) 2—9726
- metallurgy, material and process improvements 2—3969
- mixture composition meas. using optic probe 2—19275
- particle density determ. by air pycnometer 2—3858
- particle size distribution, determ. by photomicrographic method 2—25608
- particulate mixture, sampling, statistical analysis 2—19276
- particulate mixture, statistical anal. using social survey techniques 2—25607
- permittivity, correlation with bulk permittivity 2—22602
- phosphor, halophosphate, synthesis, elec. microscope obs. 2—4571
- production by plasma techniques 2—35978
- protein, complex permittivity, rel. to sorption props. 2—29057
- quartz, grain size determ. by X-ray diffraction, extrapolation method 2—32744
- rare earth oxide, crystallite growth, dynamic calcination effects 2—12980
- reaction kinetics, particle size and interfacial area 2—13565
- refractory compound, supersonic grinding kinetics 2—15939
- semiconductor-insulator system, transient photocond. effects 2—19782
- sintering equations analysis, densification kinetics, under constant heating conditions 2—9778
- sintering mech., viscous sphere fusion rel. to surface tension forces 2—36256
- sorption process measurement, spectroscopy in diffuse i.r. transmission 2—6362
- specific mass, determ. by hydrostatic press. meas. 2—15937
- specific surface, N_2 thermal desorption obs. 2—15938
- steel, X-ray line broadening study 2—3706
- transition metal oxides, hot pressing, densification, mech. props. 2—39954
- visualization of vortices in liquids using Al powder 2—28759
- X-ray diffr., integrated intensity changes, effective temp. factor, rel. to powder cryst. state 2—12714
- Zeiss-Endter particle size analyzer, modification for data logging 2—19277
- Ag, structure, comparison of methods 2—15940
- Al-Al_2O_3 alloy, ball milled, mach. props. rel. to particle size 2—6622
- Al, friction and slip resist. 2—12920
- Al_2O_3, metallographic polishing powder, scanning electron microscope evaluation 2—36192
- Al_2O_3, pulverized, active centres, e.p.r., thermolum. 2—10522
- BN-TiB_2-Al system, evaporating element prep. 2—39956
- $BaSO_4$, pulverized, active centres, e.p.r., thermolum. 2—10522
- $BaTiO_3$, dielec. props., effect of adsorbed H_2O 2—16282
- BeSe, Bes, synthesis and properties 2—20027
- $BiRhO_{3\|x}$ system, pyrochlore and perovskite prep. 2—25242
- $CaTiO_3$ formation, solid state reaction kinetics, Carter's equation, particle size distrib. 2—13566
- Cd-Pb-Sn mixture, sintering above the ternary eutectic temp. 2—29451
- CdS:Cu phosphor, prep. and electrolum. 2—40733
- CdS-MnS, degree of dispersity, particle size distrib., small angle X-ray scatt. 2—3970
- CdSe:Cl, pressed, nonlinear current-voltage curve, interparticle contact depend. 2—4211
- Co_3O_4, formation and elementary grain substructure obs. 2—25330
- CsF, submicron particle prod., evap. and meas. in shock tube 2—12981
- Cu-Fe-Al_2O_3,sintering, shrinkage equation 2—6620
- Cu, pressing, effect of press. and temp. 2—3972
- Cu_9Al_4—X, X=Mn, Fe, Ni, ternary mixed powder compacts, Kirkendall diffusion, sintering behavior 2—19279
- Er_2O_3, high temp. enthalpy and specific heat obs. using method of mixtures 2—29556
- Fe-Pd alloy, mag. reversal mechanism 2—40512
- Fe, cast, laboratory scale melting and solidification method 2—35818
- Fe, friction and slip resist. 2—12920
- Fe, hot pressing, supersonic oscillation effect 2—15923
- Fe, pore struct. and compressibility 2—39958
- Fe, pressing, effect of press. and temp. 2—3972
- Fe, vacuum hot pressing, effect of u.s. waves 2—1347
- Fe, X-ray line broadening study 2—3706
- α-Fe_2O_3:Co micropowders, mag. props., lattice parameters 2—16386
- GeO_2, pulverized, active centres, e.p.r., thermolum. 2—10522
- GeTe, pressed powders 2—1379
- Hg-In alloy, grain model 2—12983
- KCl-KBr mixtures, mixed cryst. form. 2—32742
- MgO:Mn^{2+}, e.p.r., defect effects 2—6479
- MgO, containing LiF, cold-pressed, temp. depend. of elec. cond. 2—36210
- NO_3^- containing, diffuse reflectance spectra 2—29899
- Ni-Cr-Mo alloy, heat treatment effects on props. 2—19280
- Ni-Mo alloy, heat treatment effects on props. 2—19280
- Ni, effect of H_2 on crystalline struct. imperfection 2—15941
- Ni, mag. props., particle size depend. 2—40513
- Ni, pressing, effect of press. and temp. 2—3972
- Ni, vacuum hot pressing, effect of u.s. waves 2—1347
- Ni compacts, verification of existence of oriented microstresses by X-ray examination 2—39960
- NiO, degassing temp. rel. to sp. surface area and heat of wetting 2—6623
- P_2O_5 orthorhombic form, X-ray diffraction, and i.r. absorption spectra 2—15729
- PbTe, pressed, texture 2—1379
- $PbZrO_3$-$PbTiO_3$ ceramic, sintering, calcining temp. effects 2—39953
- Se-As glass, sintering 2—19281
- SiO_2, positronium form., ang. correl. obs. 2—40110
- SnO_2, pulverized, active centres, e.p.r., thermolum. 2—10522
- SnTe, pressed powders 2—1379
- Ti, rolled metal sintering 2—15926
- TiC, stoichiometric, crystallinity and particle morphology 2—22347
- Tl_2S binder layers, photocond. 2—33076

Powders continued
- UO_2, cold pressing, energetic study 2—6624
- UP, sintering and porosity, 1500-2000°C 2—3935
- V_2O_5, diffuse reflectance spectra 2—29901
- WC_x, prep. by freeze-drying 2—29447
- Y_2O_3-Fe_2O_3 mixture, ferrite form. at 1100°C 2—30058
- ZnO catalyst., chemisorption of CO oxidation reactants, a.c. cond. 2—25830
- ZrB_2-W, mixtures, sintering, solid solution formation, phases 2—6626
- ZrB_2-W alloy, sintering, effect on struct. and props. 2—12950

Praseodymium
- fcc, dispersion of singlet triplet magnetic excitons as function of temperature 2—6963
- magnetic props. 2—40418
- X-ray excited optical fluorescence, in Gd_2O_3, La_2O_3, and Y_2O_3 2—22805
- Pr^{2+}, Pr^{3+}, configuration interactions, Trees parameters 2—5793
- Pr^{3+}, in $PrCl_3$, anisotropic spin-orbit coupling in cryst. fields 2—29851
- Pr^{3+} e.p.r. in $La_2Mg_3(NO_3)_2$ 2—26080
- Pr^{3+} emission in La_2O_2S, thermal quenching 2—1709
- Pr^{3+} in lanthanide fluorides, far-i.r. Stark and Zeeman splitting 2—40669
- Pr^{3+} in YAG, spectral linewidth studies of Pr^{3+} 2—10339
- Pr(IV), formation by pulse radiolysis of aqueous Pr(III) solution, spectrum and chemical properties 2—30095

Praseodymium compounds
- oxide-oxygen system, phase relationships and transitions, X-ray diffr. obs. 2—4002
- La-2.01 at.% Pr alloy, cryst. elec. field, lattice contrib., cond. electron contrib., shielding 2—40591
- Nb-Al-Pr alloy, hardness rel. to comp. and annealing 2—4021
- Pr-Dy-Co ternary, magnetic characteristics 2—10213
- $PrAlO_3$, phase transition, Raman scatt. obs. 2—20077
- PrC_2, vaporization and surface ionization 2—35840
- $PrCO_3$, mag. structure, neutron diffraction obs. 2—36703
- $PrCl_3$:Pr^{3+}, anisotropic spin- orbit coupling, in cryst. fields 2—29851
- $PrCl_3$, magnetostriction model, second order phase transition 2—6985
- $PrCo_2$, heat capacity obs., 8-300K, rel. to mag. transitions 2—19869
- $PrCo_3$, e.p.r., mag. behaviour 2—10518
- $Pr_2Co_{1.7}$, atomic struct., X-ray determ. 2—3726
- $PrCrSe_3$, elec. props., semicond. behaviour 2—10029
- $Pr_{0.333}Cu_{0.1}Al_{0.566}$, magnetic and neutron diffraction studies 2—10216
- PrF_3, X-ray spectra, energy shift of K-lines 2—16599
- $PrFe_2$, Laves phase compound, synthesis method 2—22343
- $PrFeO_3$, mag. struct. 2—40565
- PrH_2-PrH_3 system, dissoc. press., thermodynamic props., and soln. parameters 2—22379
- $Pr_xLa_{1-x}OCl$, phosphor, concentration quenching of luminescence by dipole quadrupole mechanism 2—36927
- $Pr_2Mn_{3-x}Zn_3(NO_3)_{12}.24H_2O$, Zeeman effect, satellite structures 2—4458
- $Pr_2(MoO_4)_3$, precision lattice parameters, ferroelectric-paraelectric structural transition 2—9486
- $Pr_xNd_{1-x}AlO_3$, phase transition, Raman scatt. obs. 2—20077
- $PrNi_5$, sp. ht. obs., 1.6-4K 2—16037
- PrO_2 and Pr_2O_3, X-ray spectra, energy shifts of K-lines 2—16599
- Pr_nO_{2n}, cryst. growth and reduction to Pr_nO_{2n-2}, struct. obs. 2—9366
- $PrP_3O_9.3H_2O$, prep. and X-ray exam. 2—15724
- $PrPb_3$, magnetic props., temp. range 2.8-300K 2—4346
- $PrPd_3$, mag. props. 2—19829
- Pr_2S_3, lattice oscillations, dielec. permittivity, molar heat capacity, i.r. spectra 2—40670
- Pr_2S_3, struct., density, reflection spectra 2—40671
- $Pr_2Si_2O_7$, cryst. struct. 2—9485
- $PrTl_3$, Curie temp. calc. 2—13377
- Pr_3Tl dispersion of singlet triplet magnetic excitons as function of temperature 2—6963
- $Sm_{1-x}Pr_xCo_5$ series, magnetic properties, variation between cast and annealed compounds, aligning methods 2—13386

Precipitation
- *see also Atmosphere/precipitation*
- alkali halide, of impurities, review 2—3794
- alloy, autoradiographic study of amount of B segrated to precipitates 2—16713
- alloy, coalescence kinetics of disperse phases 2—12961
- alloy, coherency-loss problem 2—19258
- alloy, dispersed precipitate, critical resolved shear stress 2—3861
- alloy, nimonic-type, aged, elastically strained by precipitates, X-ray diffr. intensity distrib. 2—15928
- alloys, solid solns., volume fraction rel. to particle coarsening, modified Liftshitz-Slyozov-Wagner theory 2—6606
- Alnico alloys, ferromagnetic phases, indirect evaluation of individual props. using electrochem. means 2—26031
- Alnico-V alloy, 0.5%Ti, metallurgical and mag. props. 2—4368
- backscattering cross section in submillimeter range 2—16832
- cladding materials, carburization obs. using single-stage extraction replicas 2—36228
- coherent cryst. interfaces as two-dimens. superlattices 2—25324
- dendritic precipitate growth kinetics 2—19262
- diamond, inhomogeneous, impurity platelet distrib. and size 2—9588
- grain boundary precipitates, diffusion controlled coarsening behaviour 2—32539
- grain boundary segregation, equilib., thermodynamic bounds 2—25615
- hardening, analogy with magnetic and superconductor hardening 2—39912
- hardening system, electron microscope preshadowed extraction replica technique, analytical method 2—12703
- helices and loop formation mechanism at precip. particles 2—25397
- ice melting electrification depend. on earlier freezing rate 2—7292
- Inconel 700 alloy, γ' precip. growth on ageing 2—39986
- Inconel 706, rel. to optimum combination of props. and fabricability 2—29395
- martensite, of χ-carbide and its transform. into cementite 2—39988
- metal, alloy, at phase transform. rel. to double Bragg scatt. 2—36279
- metal, intergranular force from free electron energy variation 2—29014
- metal carbide particles, in metallic matrix, coarsening rate 2—29416
- metal system, dislocation mobility prevention methods rel. to raising of yield pt. 2—12923
- metallic system, hardening by ordered coherent precipitates 2—19259
- permanent magnet materials characterization 2—40514
- phototropic Ag-halide containing glass, elec. microscope obs. 2—12627
- Pyromet 860, precip. strengthening, effect of Ti and Al content 2—29394
- solid soln., supersaturated, form of coherent precipitates 2—39911

Precipitation continued
- solid solns., diffusional homogenisation during deform., energy stability, free energy 2—29413
- solid solution, supersaturated, grain orientation and boundary struct. 2—9788
- stainless steel, containing Ti oxides, influence on creep at rupture 2—9674
- steel, γ' phase precip. mechanism, solid soln. hardening effects 2—36215
- steel, acceleration of pearlite spheroidization 2—32695
- steel, austenite, of carbides, kinetics 2—32772
- steel, austenitic, of carbides, hardening in types 304 and 316 2—1304
- steel, austenitic, of NbN, effect of Mn, Si, Cr or Ni 2—12968
- steel, austenitic, precipitation-hardening, fatigue limit and durability 2—36152
- steel, austenitic Cr-Ni with B additive, solid soln. decomp. 2—36240
- steel, austenitic stainless, interdendric regions 2—9212
- steel, austeno-martensitic, precip. at martensite-austenite reversion interfaces 2—29399
- steel, cast V, hardening 2—9749
- steel, chromium, martensite decomp. rel. to carbide formation during tempering 2—32727
- steel, Cr-Mo, electron microscope and X-ray study 2—9770
- steel, effect of ageing conditions on mech. props. 2—36118
- steel, high C martensite, carbide structure and morphology 2—32725
- steel, high strength Ti-structural type, recrystn. study 2—29391
- steel, high-speed, austenite decomp. and carbide precip. 2—36241
- steel, high-speed, quench deform. due to complex carbide precip. 2—29392
- steel, high-speed W-Cr-V-Co, effect of C content on phase comp. 2—32726
- steel, influence of precip. hardening on recrystn. texture 2—3992
- steel, low C Nb-structural type, electron diffr. obs. 2—32707
- steel, maraging, hardening mechanism 2—36217
- steel, martensite, impact deformation strengthening 2—39901
- steel, Mn-Si low C, influence of Nb addition on structure 2—9812
- steel, Nb-stabilized austenitic stainless, rel. to fatigue failure 2—32629
- steel, of carbide phase during tempering, effect of rate of heating 2—36216
- steel, of carbides, cold and hot plastic deformation effects 2—32771
- steel, stainless, 17-4 PH, behaviour of weld heat affected zones 2—29410
- steel, stainless, irrad. enhanced precip. 2—39931
- steel, stainless, secondary defects formed on quench-ageing 2—1244
- steel, stainless, type 304, creep rupture specimens 2—39800
- steel, stainless, types 304 and 316, fast reactor irrad. damage 2—1236
- steel, with Nb additive, effect on mech. props. 2—9738
- steel austenitic, form. of NbC inclusions, effect of hardening conditions 2—36234
- steel maraging, rel. to optimum heat treatment 2—36204
- steels, austenitic, carbide precipitation effect on grain boundary internal friction peak 2—29246
- superalloy, control of microstruct. and props. using precip. phases 2—29387
- Zircaloy, tetragonal hydride, elec. diffr. obs. 2—9828
- Zircaloy tubing, hydride platelets orientation and effect on mech. props. 2—15842
- Ag-23 at.%Ge alloy, metastable h.c.p. phase decomp. 2—39978
- Al-Ag-Zn alloy, X-ray diffr. and electron microscope obs. 2—3938
- Al-Ag alloys, dil., vacancy form. energy rel. to solute-solute interaction 2—9537
- Al-Cu-Cd(In) alloy, rel. to elec. resist. change on ageing 2—9755
- Al-Cu alloy, coarsening of θ'' and θ' precipitates 2—9751
- Al-Cu alloy, internal friction obs. 2—9791
- Al-Cu alloy, loss of coherency of θ' precipitates 2—12966
- Al-Cu alloy, rel. to recovery 2—9756
- Al-Cu alloys, resist. peaks 2—9955
- Al-Cu film conductors, effects on electromigration life 2—39735
- Al-3wt.%Cu, aged, fatigue life 2—3952
- Al-4%Cu film, resistance changes due to precipitation during power annealing 32759 2—32759
- Al-(4 wt.%)Cu alloy, fibrous struct. of precipitates produced at scratch 2—39917
- Al-Cu(Zn, Mg,Mg_2Si) alloys, pre-precipitate formation and reversion 2—25590
- Al-Fe-Si, cast, segregation of Fe and Si 2—15957
- Al-Ge system, rel. to metastable phase decomp. 2—36296
- Al-Mg-Li system, age hardening 2—12954
- Al-Mg-Si alloy, electron microscope obs. 2—25576
- Al-Mg-Si alloy, rel. to inverse Portevin-Le Chatelier effect 2—32595
- Al-Mg alloy, effect of 0.5wt% Ag 2—12955
- Al-Mg alloy, of Mg at dislocations, elastic limit obs. 2—36104
- Al-(1.3wt.%)Mg_2Si alloy, age hardening, Guinier Preston zone formation, Sn addition effect 2—12987
- Al-Si, alloy, vacancies, Si atoms, vacancy enhanced nucleation 2—3953
- Al-Zn-Mg, effect of Ag, correl. with stress corrosion behaviour 2—3951
- Al-Zn-Mg alloy, quenched, aged, metastable miscibility gap, small angle X-ray obs. 2—3981
- Al-Zn-Mg alloy, transition phase, X-ray obs. 2—9753
- Al-Zn, alloy, during ageing, X-ray diffr. obs. 2—19263
- Al-Zn alloys, of stable β-phase, Mg additive effects 2—39919
- Al-Zr alloy, of cubic Al_3Zr phase, elec. microscope obs. 2—36273
- Al-Zr solid soln., supersatured, fan-shaped precip. form. during decomposition 2—32719
- Al-2.8 at%Zn-1.4 at%Mg, alloy, rel. to neutron irrad. 2—29418
- Al-5.0 at%Ag-5.0 at%Zn, alloy, rel. to neutron irrad. 2—29418
- Al, 99.5% pure, precip. dissolution during grain boundary migration 2—36229
- Al alloy, duraluminium, rel. to hydrostatic pressure effects on ageing 2—15913
- Al metallization, on integrated circuits, of Si 2—25876
- AlCu, AlMgSi alloy, temper vacancy elimination, resist. obs. 2—15897
- Au-Fe solid soln., solute clustering and mag. order 2—19828
- Au-N, alloys, discussion of spinodal hypotheses 2—29425
- Au-Pt alloys, discussion of spinodal hypotheses 2—29425
- C, glasslike, of graphite, isothermal dissolution 2—3985
- CdS-MnS coprecipitate, e.p.r. study 2—40762
- Co-Al, alloy, coercivity 2—22686
- β-Co-γ-Co_2Ta, eutectic system, strengthening, Ta lateral diffusion 2—12720
- Co-8.8 wt.%Cu alloy, complex form., X-ray and electron microscope obs. 2—25593
- Co-Ni-Cr-Mo alloy, hardening and phase transformations 2—19296
- Co-Ni-Cr alloy, formation by internal oxidation 2—9796
- Co-Ti-X alloy, X=Cr, Fe, Ni, of γ'-Co_3Ti 2—9797

Precipitation continued
- Co-W, supersaturated solid solution, decomposition, thermomagnetic obs. 2—3986
- Co alloy, WC grain growth kinetics 2—12933
- Cr-Ni-Ti, austenitic steel, precip. processes rel. to creep resist. 2—9675
- Cr-W alloy, grain boundary diffusion, interface reaction, Kirkendall effect 2—22246
- Cu-(14.3 wt.%)Al, interphase boundary diffusion 2—22248
- Cu-(14.3 wt.%)Al alloy, equilib. surface segregation, Auger electron spectroscopy meas. 2—25625
- Cu-Ag alloy, associated dislocation climb 2—1367
- Cu-Al alloy, equilib. surface segregation, Auger electron spectroscopy meas. 2—25627
- Cu-Be alloys, during ageing under neutron irradiation, 100-160°C 2—39905
- Cu-(1.9 wt.%)Be alloy, precip. substructure depend. of fatigue props. 2—22283

2—3913
- Cu-Co, coherent, single crystals, plastic behaviour, dislocation arrangement 2—3936
- Cu-Co alloy, single crystal, precip. hardening, dislocation arrangement 2—19243
- Cu-Cr-Si alloy, internal oxidation, precip. morphology 2—29427
- Cu-Fe, alloy, film, effect on phase transform. 2—6635
- Cu-Fe alloys, mag. and struct. transforms. of Fe precipitates 2—39981
- Cu-Mn-Al, Heusler alloy, and phase transformation identification 2—9801
- Cu-Mn, solid solution, annealing, coherent ordered phase 2—3990
- 59wt.%Cu-12wt.%Ni-29wt.%Zn alloy, and recrystn., rel. to cold working 2—32688
- Cu-Ni-1 wt.%Si alloy, ageing behaviour 2—25578
- Cu-Ni-Si-Mg(Cr) alloy, cold working rel. to age hardening behaviour 2—32706
- Cu-Zn alloy, dendritic precipitate growth kinetics 2—19262
- Cu-1%Co, single-multi domain transition of ferromag. precipitates, neutron scatt. obs. 2—4361
- Cu-1%Co, single ferromag. domain precipitates, neutron scatt. obs. 2—4360
- Cu_3Au-Co alloy, precip.-hardening 2—29383
- Cu_3Se, formed by solid state reaction, microstruct., elec. microscope obs. 2—36043
- Fe-B-N alloy, rel. to formability and texture 2—32728
- Fe-Base superalloys, review 2—29437
- Fe-C, Fe-C-Cr and Fe-C-Si alloys primary graphite obs. by thermal differential analysis 2—6615
- Fe-C alloy, cluster formation kinetics 2—15963
- Fe-C alloy, nonisothermal conditions 2—9811
- Fe-Cr-C steel, martensitic, tempering, internal friction peaks due to precip. 2—29393
- Fe-Cr-Ni-P, steel, stainless, austenitic, of Cr_3P, quenching defects, microstruct. 2—6483
- Fe-Cr-Ni, alloy, transitional ferrite phase form. 2—29435
- Fe-Cr-Ni alloy, transitional ferrite phase form. 2—29434
- Fe-7.8 wt % Cr, alloy, carbide precip., potentiokinetic obs. 29431 2—29431
- Fe-Cu-C steel, sintered, precip. process during ageing 2—25580
- Fe-In alloy, Fe-rich, slowly cooled 2—39932
- Fe-Mo alloy, nitrided, FIM study 2—12969
- Fe-N, martensite, of Fe_4N, interstitial ordering, Mossbauer obs., 293-353K 2—9543
- Fe-N solid solution, mag. field orienting of Fe_8N platelets 2—3993
- Fe-Nb-C, steel, segregation mech., phase struct., annealing tests, electron refr. obs. 2—32729
- Fe-Ni-Co-Mo, steel, pre-precipitation and reversion, resistivity and elec. microscope obs. 2—9809
- Fe-Ni-Co-Mo alloy, martensitic, ageing, formation of metastable ω phase 2—36299
- Fe-Ni-Cr austenitic matrix, carbide nucleation, B effect 2—9810
- Fe-Ni-CrTi alloy, γ' hardened, strengthening mech., γ_{apb} calcs. 2—32733
- Fe-P-C alloy, intergranular brittleness, rel. to P and C at boundaries 2—36235
- Fe-S alloys, of Fe sulfides during tempering 2—39891
- Fe-Ti-C alloy, rel to formability and texture 2—32728
- Fe-Ti, steel, work hardened, annealed, recrystn., recovery, segregation, electron and optical microscope obs. 2—32698
- Fe-V-Nb-C alloy, of VC_x, electron microscope obs. 2—9769
- Fe-W-Mo steel, tempered, precip., of carbide 2—29384
- Fe-W steel, tempered, precip. of carbide 2—29384
- α-Fe, age hardening rel. to quenching rate 2—22328
- Fe, of C, effects on grain boundary diffusion of P 2—22249
- Fe, of H, in cavities during diffusion 2—6514
- Fe alloys, graphite precipitate, formation and spatial configuration 2—15908
- Fe austenite, of NbC, impurity addition effects 2—12962
- Fe f.c.c. thin film, of b.c.c. phase, stress effects 2—9803
- Fe—(1.4at.%)Cu alloy, clustering, atom probe field ion microscopy 2—3960
- GaAs:Zn, of Zn in Zn diffused region 2—22224
- Ge:Te, precipitate form. on growth dislocations 2—12770
- Ge-Cu solid soln., kinetics 2—6639
- Ge-Li, gamma-ray spectrometer production 2—11674
- Ge-Li system, of Li, at 60°C 2—3815
- Ge, of Li, anomalous X-ray transmission obs. 2—15778
- Ge, of Li, kinetics, correl. with dislocation character 2—3798
- Ge, of Li, X-ray diffr. obs. 2—9813
- Ge crystals investigation of Li precipitates 2—19093
- LiF, LiF:Mg, precip. hardening, crit. resolved shear stress 2—32705
- Mg-Zn alloy, hardening mechanism 2—6599
- Mg-Zn alloy, yield stress grain size depend. and strengthening 2—6546
- MgO-Fe-Ni, rel. to fracture props. 2—39842
- MgO-$MgFe_2O_4$, rel. to fracture props. 2—39842
- MgO, precip. strengthening by $MgFe_2O_4$ 2—29402
- Mo-N, solid soln., supersaturated, effect of isochronic ageing, electron microscope obs., 200-500°C 2—25599
- Mo, rel. to grain size depend. of elastic limit 2—12860
- Nb-Ti alloy, Young's modulus temp. depend., precip. effect 2—36095
- Ni-Al-Nb alloy, Ni rich 2—19302
- Ni-Al alloy, of γ' phase, FIM obs. 2—39907
- Ni-Al alloy, of Ni_3Al, morphology and effect on mech. props. 2—29404
- Ni-22.7-38 at.%Mn alloy, during phase transform., 673-908 K 2—25635
- Ni-Co-Cr-Mo alloy, heat resistant, σ-phase precip. mechanics 2—9821

Precipitation continued
Ni-Cr-Nb-Co, alloy quenched and reheated, study of cell precipitation 2—25563
Ni-Cr base alloys, influence on creep props. 2—12872
Ni-(33 at.%) Cu alloy, clustering kinetics 2—15934
Ni-(11.1, 13.8 at.%)Al, alloy, at 425°C and 450°C, Curie temp. change, magnetization vs temp. 2—29403
Ni alloy, Inco 718, hardening, effect of Ti, Al, Nb and Mo content changes 2—9820
Ni superalloy, of intermetallic cpds. and carbides, electron microscope obs. 2—32731
Ni(20 wt.%)Cr alloy, effects of Al+Ti complex additions rel. to recrystallization 2—25573
Ni_8Ta phase, in Ni-Ta alloy 2—15970
Ni—V—C alloy, of VC_x, electron microscope obs. 2—9769
Pt-Ir, Rh-Ir alloys solid solutions shape of field ion image points, halo effect 2—12963
Si-Fe solid soln. 2—1533
Si, habit and morphology of Cu precipitates 2—39939
Si, homogeneity breakdown, during joint diffusion of Ni and P 2—36058
Si, of Li, and driftability 2—27880
Si, of Li, X-ray topography obs. 2—19115
Si, precipitate colonies of Cu 2—36286
Si, precipitate colonies of Cu 2—32779
Si(Li), Li precipation and Li-B ion pair formation 2—1255
Sn-Cd alloy, Cd segregation during melting, neutron radiography obs. 2—15633
Sn-Sb-Cu alloy, η phase segregation prevention 2—3965
Ti-Al, alloy, microsegregation of Al, rel. to cooling rate, comp., electron-probe analysis 2—29440
β-Ti-Fe(Cr)(Mn)(Mo) alloys, of α-phase 2—12979
Ti-M alloy, M=Cr, Mn, V, Mo, of ω phase, continuous cooling transform. obs. 2—29481
Ti-Mo, alloy, microsegregation, rel. to cooling rate, comp., electron-probe analysis 2—29439
Ti-$TiC_{0.52}$ two-phase platelets, optical metallography, electron microfractography 2—6582
Ti-V, alloy, microsegregation, rel. to cooling rate, comp., electron-probe analysis 2—29439
Ti-55 at.%Ni alloy, hardening, rel. to Ti_2Ni_3 precip.39903 2—39903
Ti alloy, β-stabilized, ω phase formation kinetics 2—36288
Ti alloys, nitriding by ionic bombardment, skin microstructure and corrosion resistance 2—12928
V, of $V_{16}N$ superlattice, elec. microscope and X-ray diffr. obs. 2—15975
Zn-Mg dilute alloy, ageing characts. 2—29405
Zr-(3 wt.%)Mo-(1 wt.%)Al alloy, thermal decomposition, Al effect 2—25640
Zr and zircaloy-2, zirconium hydride, struct. and distrib. rel. to heat treatment 2—22369
ZrB_2 single crystal, during plastic deform. 2—15841
Zr—(3 wt.%)Mo-(1 wt.%)Al, tempering of strain induced martensitic phase, struct. and morphology 2—25639

Pressure
see also Atmospheric pressure and density; High pressure phenomena and effects; Radiation pressure; Vapour pressure
delta wings leeward surfaces, bow shock waves at high supersonic speeds 2—6147
electrolyte pressure and flow distrib. in fuel cell batteries 2—5315
hydrostatic, effect on velocity of sound in rocks 2—26391
liquid, magnetic, effects of magnetic field 2—1062
non-spherical globule, pressure distribution on the surface 2—37667
oscillations in shallow cavities in wind tunnel, Mach 0.8 to 3 2—1021
of plane wedge punch on infinite elastic plane, calc. by asymptotic method 2—37700
quartz, thermolum., press. effect 2—29986
squalene with gases in solution, viscosity- pressure behaviour in saturated and unsaturated state 2—39349
thermodynamic in quantum statistical mechanics, review 2—5163
$Ge_{15}Te_{81}S_2As_2$, amorphous semiconductor, effect of hydrostatic pressure on VA characteristics 2—9984
^3He-^4He mixtures, pressure-temp-density relations near liq.-vapour critical point 2—22025
^3He-^4He mixtures, pressure and density meas. along boiling and dew curves 2—22026
SF_6 along critical isochore determ. from spectrum and intensity of scattered light 2—12512

Pressure measurement
see also Manometers; Vacuum gauges; Vapour pressure measurement
articulatory behavior during alteration of vocal effort 2—37452
atmospheric surface pressure measurements from a satellite 2—40911
blood, using piezoelectric transducer 2—14042
capillary discharge, high current, piezoelectric meas. 2—32121
composite piston systems for measuring high pressures 2—27033
delta wing in low-speed wind tunnel, oscillatory deformation 2—6145
diaphragm pressure transducer, strain gauge type, nonlinearity 2—20809
differences in gas flow, transducer for obs. 2—3294
differential-transformer type pressure transducers, calculation of temperature errors 2—23228
fast response gauge for shock reflection obs. ionized gases 2—30751
floating vacuum gauges, optical readout 2—26996
in flow, low velocity, water 2—20807
inertia and sensitivity relationship for high press. meas. systems 2—23229
instrument for meas. small press. differences 2—33915
piezoceramic pickup flashlamps obs. 2—27278
pulsed arc, pressure meas. from specimen displacement 2—37567
transducer discrimination, fluctuations beneath turbulent boundary layer in air 2—15527
u.h., 10^{-1} to 10^{-13} torr, using hot cathode ionization gauges 2—23199

Primary cells *see Electric cells*

Prisms, optical
direct vision triple reflection, with ray path splitting 2—38096
electrostatic, use in photo-electron spectrometer 2—7852
at high flux densities, prevention of premature damage at high flux densities 2—17707
isosceles passing a conical beam 2—5404
liquid biprisms, determination of refr. index of liquids, teaching experiment 2—33850
refraction, relation for refractive index 2—17672
thin film light guides, geometrical optics 2—5400

Prisms, optical continued
total reflection, for ellipsometer aligning 2—38038
Wallaston, analyzer for single beam Schlieren interferometer 2—34479

Probability
see also Random processes; Statistical analysis
computing method for solving equations of dynamics of the ocean 2—13661
Jaynes's information-theoretic entropy and probability theory 2—2165
low angle scattering curve, proportion of particles with specific radius of gyration 2—27094
quantum optics, phase variables, statistical characts. 2—17569

Probes
see also Plasma/diagnostics
acoustic, in-situ obs. of sea bed sediments 2—40905
Bullard heat, extension of versatility, oceanographic use 2—1808
calorimetric, supersonic gaseous flow, thermal meas. 2—28721
capacitive for Fourier analysis of hydrodynamic surface waves 2—28761
coil, near stratified conductor, eddy current analysis 2—5310
conductivity, r.f., for turbulent plasmas 2—12407
cooled spherically electrostatic, in quiescent continuum slightly ionized chemically frozen gas, theory 2—21815
in dense flowing transient plasmas, perturbations caused by presence 2—35532
double probe method, reliability of anode as probe potential reference point in d.c. gas discharge 2—21817
double probe technique for obs. of pulsed discharge 2—3257
eddy current, for obs. of fluctuations in electrical conductivity of liquid metals at high temps. 2—34285
electric and mag. probe investigations of parameters of impulsive erosion plasma accelerator 2—3226
electrometer, solid state, miniature, construction details 2—21007
electron beam microprobe use for wide angle reflection method in crystallography 2—39605
electron microprobe, operation 2—7196
electron temp., cumulative ionization effect, floating double probe method 2—21819
electron temperature meas. in a.c. discharge excited between insulating electrodes 2—39205
electrostatic, flush-mounted, effect of negative ions 2—8945
electrostatic, flush-mounted, sheath convection effects for fast flowing plasma 2—3220
electrostatic, in nonstationary plasma 2—8958
electrostatic, induced current, for plasma diagnostics 2—12408
electrostatic, plasma diagnostics, conference (Oxford, September 1971) 2—21860
electrostatic, plasma diagnostics, conference (Oxford, September 1971) 2—24828
electrostatic, technique for determining effectiveness of plasma alleviants 2—28588
electrostatic refr., for plasma diagnostics 2—12406
e.m., Earth crust characteristics obs. 2—33420
ferroprobes with longitudinal excitation over wide intensity range 2—23514
fibre optics, water cooled, for spectrally resolved radiation obs. 2—27311
flame, temperature meas. 2—27306
floating double-probe method, mag. field effect 2—12409
four-point, resistivity meas. on GaAs epitaxial layers 2—29696
gas-liquid high velocity flows, local velocity and void fraction meas. technique 2—24633
gases, binary mixtures, continuous unsteady concentration meas., hot wire technique 2—18771
geometry effects on turbulent plasma diagnostics when used to measure local statistical properties 2—21816
Hall, incremental field meas. of multipole admixtures in quadrupole fields 2—11433
hot film, obs. of velocity distrib. and transition turbulences in arteries 2—26945
hot-wire aerodynamic disturbances caused by different parts of probe in circular jet 2—35673
immersion-type electrical conductivity probe for anisotropic plasmas 2—32029
impedance of symmetric spherical probe in presence of spacecraft body 2—21001
ion, mass analyzer, applic. to surface and bulk solids 2—20217
ion, ultramicro analysis 2—7195
ion attracting cylindrical, Sonin-Laframboise-Chen paradox 2—32042
ion microprobes for investigation of solid substances, state of development 2—30107
ionospheric plasma, for Japan Antarctic Research Expedition rockets 2—10761
Langmuir, area influences and floating potentials, rel. to plasma diagnostics 2—21818
Langmuir, effect of collision on cold ion collection in transitional regime 2—28572
Langmuir, electron density meas., comparison with microwave interferometer and cavity methods 2—35527
Langmuir cylindrical, exptl. study of response in transition regime 2—28586
Langmuir probe response, end effect, rel. to ionospheric satellite conditions 2—39152
laser microprobe use in identification of inclusions in Lydian gold coins 2—22901
linear antenna, near zone fields in plasma 2—35544
moveable, for semicond. diode studies, potential distrib. at surface of n-region 2—19709
multi-electrode, in rarefied problem, penetration of ions to collector 2—32030
negative glows, electrical probe characteristics 2—35614
for neutron activation analysis in boreholes, using ^{252}Cf and Ge(Li) detector 2—34803
for n.m.r., damper design 2—2331
n.m.r. high press. studies of liquids 2—18854
optic, for powder mixture comp. meas. 2—19275
optical, for liquid insulants mobility meas. 2—32272
optical interferometer, density of pulsed discharge plasma 2—28601
optical magnetic, magneto-optical effect 2—35551
parachuted, obs. of ion densities in lower D-region 2—7341
photoelectric method of drop size distribution meas. in immiscible binary liquid system 2—39316
plasma, behaviour in high-speed collision free flow 2—6090

Probes continued
plasma, double probe, effect of beam like electrons 2—15474
plasma, h.f. electrical 2—28595
plasma, spherical, r.f. sheath model, admittance characteristics 2—32017
plasma potential measurement 2—3225
plasma streaming measurements in arc 2—35637
quadripolar probe for hot collisionless isotropic plasma 2—28597
radiometric, aerated water flow applics. 2—39296
r.f., dipolar, admittance and performance obs. in simulated atmosphere 2—26534
r.f., for meas. of electron temp. in low density plasma 2—15478
r.f., resonance effect and admittance in ion rich plasma sheath 2—35545
scintillation, for thyroid surgery, radioactive I tracers 2—2029
semiconductor junction detection 2—19699
semiconductor potential sampling, low temp., electrical point contact 2—40284
sheath, positive ion, thickness, probe pot., parabolic approx. 2—12395
space charge problems in measurements 2—12411
split film anemometer, det. of azimuthal convective heat transfer coeff. 2—21756
static spherical probe theory verification in moving h.p. plasma 2—8954
tandem isothermal calorimetric for atomic flow rate det. 2—28703
theory of h.f. props. in isotropic plasma 2—35535
thermal, for temp. meas. by ref. to heat flow, for use in flame type furnaces 2—20961
thermal cond. meas. method 2—17436
thermoconductimeter applic. for low vel. meas. in liqs. 2—25009
thickness meas. of dielectric layers 2—32351
two flow-swallowing enthalpy, expts. in high-energy supersonjc streams 2—28587
for two-phase flow velocity and void fraction determ. at high press. 2—24630
u.s., for steel roll hardening depth meas. 2—1332
u.v. microprobe technique for minority-carrier diffusion length meas. 2—6815
variable temp. for obs. of magnetic transitions in 4.2-300 K range 2—27406
void fraction measurement in reactors 2—553
CO-O flames, comparison of single- and double-probe meas. of electron temperature 2—37823
CdTe, medical, γ-ray detection, compared to Si(Li) probe 2—33785
CdTe, medical, γ-ray detection, compared to Si(Li) probe 2—26947
TiO$_2$ chemisorption probe for detection of H atoms 2—30106
Procopiu effect *see Films, solid; Magnetoelectric effects; Magnetomechanical effects*
Programming *see Calculating apparatus/digital computer programmes*
Projectiles *see Ballistics*
Projectors, optical
dichroic reflector lamps for colour projection, rapid selection 2—23717
Fresnel lenses for condenser systems 2—5405
measuring devices, sensitivity of lateral and longitudinal focusing adjustments 2—38090
scan and measure devices, systematic errors in optics 2—34516
for stereo slides, system development and design 2—316
Promethium
No entries
Promethium compounds
Pr complex, promethium tris-2,2,6,6-tetramethyl-3,5-heptanedione 2—18441
Prominences, solar *see Sun/prominences*
Propagation *see Acoutsic wave propagation; Electromagnetic wave propagation*
Propagators *see Field theory, quantum; Quantum electrodynamics*
Proportional counters *see Counters/proportional*
Prospecting *see Geophysical prospecting*
Protactinium
superconductivity, review 2—13147
Protactinium compounds
PaO$_2$-ThO$_2$-UO$_2$ solid soln. formation, exchance of Pa^{4+} in molten LiF-BeF$_2$-ThF$_4$ with U^{4+} and Th^{4+} 2—10593
Proteins
actin, orientated film, piezoelectric effect 2—1577
carbonic anhydrase at 77 K in water-ethylene glycol glasses, obs. of delayed fluorescence from tryptophan residues 2—28420
crystal structure, direct determ. of heavy atom positions in isomorphic substitution 2—32485
crystallography, least-squares refinement 2—25287
crystallography, semi-isomorphism test using higher moments of intensities 2—9501
crystallography techniques, contemporary developments 2—15735
cylindrical rod molecule, model, electron micrograph contrast calc. 2—9412
dextran and globular, ultrasonic absorption 2—30658
egg yolk lecithin in hexane soln., high field permittivity meas. 2—28885
ferrodoxin, X-ray photoelectron spectroscopy 2—31873
food materials, liq., apparent thermal diffusivity meas. procedure 2—17441
glycera haemoglobin, phase determination using tangent formula, and isomorphous replacement 2—3743
haemoglobin and derivatives electronic state of Fe determ. from X-ray fluorescence spectra 2—24558
heavy-atom derivatives, crystallographic analysis 2—9502
insulin, cryst. struct. 2—9509
molecular config. and conform. changes, u.s. absorpt. obs. 2—28422
molecules, X-ray diffraction examination 2—15412
Mossbauer spectroscopy, structure and mag. properties 2—17122
myoglobin, Patterson function, vector space search methods applic. 2—22172
myoglobin, vibration and defect contribs. to temp. factors, Mossbauer and X-ray obs. 2—4041
myoglobin and derivatives electronic state of Fe determ. from X-ray fluorescence spectra 2—24558
myosin orientated film, piezoelectric effect 2—1577
nucleoprotein, energy transfer between protein and DNA 2—26943
pepsin at 77 K in water-ethylene glycol glasses, obs. of delayed fluorescence from tryptophan residues 2—28420
peptide chains, CNDO calc. of side chain main chain ang. dependence 2—24562
powders, complex permittivity, rel. to sorption props. 2—29057
Proteins continued
protein crystals, electron microfractography 2—25278
serum albumin, resolved Raman spectra and fluoresc. 2—39014
in solution, detection, absorption spectra obs. 2—10665
solutions, dilute, diffusion of fluids 2—1091
tertiary structure, freedom of dihedral angles and energy calc. 2—39017
tertiary structure, representation and computation of conformations 2—39016
thermodynamics of growth, elementary biochemical explanation of instability, role of ATP 2—15411
tryptophan-containing absorption and luminescence spectra 2—8832
X-ray crystallography, phase determ., anomalous dispersion method 2—32419
X-ray effect on glycoproteins and related carbohydrates 2—7600
Proton magnetic resonance
acetone, oriented spectra, rel. to MO studies of $4J_{hh}$ 2—28339
2-aminoacetophenone, free energy of activation for hindered rotation around N-aryl bond 2—12206
ammonium salts, spin symmetry sites 2—40776
amphetamines and related compounds, rotamer populations 2—8729
anthracene, exciton motion 2—7132
anthracene crystals, proton relaxation through triplet excitons 2—22845
aqueous electrolyte solns., concentrated, pressure effect on proton spin-lattice relaxation 2—1118
AX$_2$ system, proton cross relaxation effect 2—765
benzene and 1-^{13}C deriv., isotropic and nematic soln., study of direct and indirect coupling 2—5962
benzene on NaY-zeolite, proton relax., -140 to 80°C 2—26086
benzenes, trisubstituted, additivity relation for proton-proton coupling consts. 2—38961
biological macromolecules, water eliminated Fourier transform n.m.r. technique 2—23474
N-t-butylstyrenimine, solvent effects on proton-proton coupling consts. 2—35793
camera design and applics. 2—23476
carbon tetrachloride solution, proton spin-lattice relaxation of 1,2-dichloroethane 2—18857
2-chloroaniline-^{15}N, long-range coupling constants to amino protons from ring protons 2—21670
chloroform, liq., proton spin lattice relaxation times, -54 to $+90$°C 2—9179
chloroform, temp. dependence of proton spin-spin relaxation time over range -54 to $+90$°C 2—22009
copper formate tetradeuterate, sublattice rotation and spin deviation study 2—4410
cyclohexane, cyclohexene on NaY-zeolite, proton relax., -140 to 80°C 2—26086
Δ^3cyclohexenecarboxylic acid, mol. association, chem. shift 2—28899
trans-15,16-diethyldihydropyrene, chemical shift calc. π-electron ring current hypothesis 2—38979
trans-15,16-dimethyl dihydropyrene, chemical shift calc. using π-electron ring current hypothesis 2—38979
dimethyl sulphoxide, oriented spectra, rel. to MO studies of $^4J_{hh}$ 2—28339
dimethylformamide in nematic polypeptide liquid crystals 2—31847
1-X-2,4-dinitrobenzenes, applic. of Shaefer's additivity rules for coupng constants 2—21681
1,4-dioxane ring inversion barrier 2—28367
α,α'-diphenyl, β-picrylhydrazyl, free radical, anomalous paramag. shift 2—7133
p-dithiin study of orientation in lyotropic liq. cryst. 2—18500
free precession decay of pairs in rigid lattice 2—7130
fumarofine, molecular structure 2—3096
glycine, polycrystalline, proton spin-lattice relaxation 2—1736
heterocyclic, 5 membered, unsaturated, chem. shifts, H-H coupling consts., spectra, $223\leqslant T\leqslant 383$K 2—12256
hexamethylethane cryst., mol. motion obs. 2—13556
homocystine, polycrystalline, proton spin-lattice relaxation 2—1736
hydroxyl groups on solids, line shape problem 2—10536
1,3-indanione, spin-lattice relaxation in solution, microscopic molec. motions 2—28900
lead dicalcium propionate, mol. motion 2—10574
liquid crystal, orientational order and motion 2—15594
lithium formate monohydrate, p-p vector length and orientation 2—40785
lithium formate monohydrate, splitting caused by H_2O molecules 2—10570
lysine, polycrystalline, proton spin-lattice relaxation 2—1736
measurement under magic angle rot., apparatus 2—7804
methane, solid spin species conversion through level crossing with paramagnetic impurities, obs. using proton spin lattice relaxation time 2—33184
P-methoxy benzylidene p-n-butylaniline, nematic, spin-lattice relaxation 2—25113
methyl derivatives of naphthalene, crystalline, proton spin relaxation investigation of methyl group motion 2—22844
methyl nitrate, solvent and temperature effects on ^{14}N nuclear spin relaxation 2—6259
methylammonium chloride, temp. depend. of spin lattice relax. time 2—16407
molecular paramagnetic moment, collision time correlation 2—5905
monofluorobenzaldehydes and derivatives 2—5982
multispin p.m.r., digitization and computer processing of data 2—2316
naphthalene, exciton motion 2—7132
naphthalene crystals, proton relaxation through triplet excitons 2—22845
norbornadiene, spin-lattice relaxation in solution, microscopic molec. motions 2—28900
olfactory nerve of garfish, water metabolism 2—7587
organoethoxysilanes 2—851
penicillamine, polycrystalline, proton spin-lattice relaxation 2—1736
polar liquid, spin-lattice relax. temp. depend., mol. rot. 2—9182
polar solutes, proton shifts in various solvents 2—28895
polymer, line narrowing due to rot. 2—13557
polymethylmethacrylate, drawn, meas. of molecular orientation by broad line n.m.r. 2—10576
polymethylmethacrylate, in benzene-carbon tetrachloride and chloroform-carbon tetrachloride solutions, spin-lattice relaxation times for solvent mols. rel. to selective adsorption 2—39393
polystyrene, in benzene-cyclohexane solution, spin-lattice relaxation times for solvent mols. rel. to selective adsorption 2—39393
polyvinylidene chloride-co-methacrylonitrile, monomer sequence distributions by p.m.r. spectroscopy 2—28425
rubber, line narrowing due to rot. 2—13557

Proton magnetic resonance continued
  spectrometer adaptation for ^{19}F 2—7806
  spectroscopy, conference (Toronto, October 1971) 2—13597
  spectroscopy, high resolution, at 60, 100 and 220 MHz 2—11407
  strontium dicalcium propionate, mol. motion 2—10574
  styrenimine, solvent effects on proton-proton coupling consts. 2—35793
  tetramethyl ammonium nitrate, internal motions, 100-300K 2—40784
  tetramethyl ammonium perchlorate, internal motions, 100-300K 2—40784
  tetramethylammonium halides, spin-lattice relaxation times rel. to molec. motion and phase transition investigations 2—29849
  thiophene liquid proton spin relaxation and mol. motion, 300-550K 2—9184
  thiourea, ferroelectric phase 2—10575
  trimethylacetonitrile, second moment of absorption spectrum and spin-lattice relaxation time 2—16664
  trithienylphosphines, methyls substit., signs and magnitudes of long range ^{1}H$-^{31}$P spin coupling consts. 2—12291
  tyrosine, polycrystalline, proton spin-lattice relaxation 2—1736
  water, adsorbed molecules, hydrogen bond and intermol. interactions 2—10618
  B_2H_6, and methyl and chloro derivatives 2—35232
  Co complex, acetylacetonate alkylamine complex resonance shifts study 2—28283
  $CoCl_22H_2O$, antiferromag., high mag. field, metamagnetic transitions, 4.2 K 2—20157
  Co(III) complex, NN′-dialkyldithiocarbamates, anomalous spectra, hindered rotation about C-N bond 2—21595
  $CsMnCl_3.2H_2O$, motion of crystalline H_2O 2—7135
  D_2 liquid, longitudinal relaxation times, molecular rotation 2—6249
  Fe complex, FeEDTA- in water, hydrolysis products 2—3409
  Fe complexes, derivatives of $[SCH_3Fe(CO)_3]_2$ 2—785
  H_2- inert gas mixtures, spin lattice relaxation time meas. from 165 to 265 K, collisional contrib. 2—24986
  HCl molecules in hexamethylenetetramine crystals, orientational effects 2—33354
  HD, solid, spin lattice relaxation and nuclear polarization at $T<1K$ 2—37008
  H_2S, line shape and second moment at 58K, H-H distances 2—26302
  H_2Se, line shape and second moment at 58K, H-H distances 2—26302
  $HSiBr_{3-n}I_n$, identification from spectral parameters 2—24487
  $HSiCl_{3-n}I_n$, identification from spectral parameters 2—24487
  Hg complexes, bis(perfluorovinyl)mercury and methyl(perfluorovinyl)mercury, magnetic nonequivalence 2—15310
  LaH_xD_y, x, y $\leqslant 2$, $2\leqslant x+y\leqslant 3$, proton mag. reson., isotope effects 2—26303
  $La_2Mg_3(NO_3)_{12}.24H_2O$, Nd- doped, spin-lattice relax. 2—10269
  Lu-H system, linewidth temp. depend., second moment calc. 2—7144
  $Mg_2Al_4Si_5O_{18}.nH_2O$, low temperature form, rel. to investigations of H_2O molecule positions 2—30019
  $MgSiF_6.6H_2O$, nuclear spin lattice relaxation study and internal rotations 2—10577
  Mn, complex, $Mn(CO)_3C_5H_5$, in nematic solvent, geometry of C_5H_5 ring 2—8666
  NH_4BF_4, polycryst., NH_4^+ reorientation 2—10559
  NH_4Cl, proton spin-lattice relax. times 2—7007
  NH_4ClO_4, polycryst., NH_4^+ reorientation 2—10559
  NH_4NO_3, cation diffusion study by proton spin relaxation 2—25465
  $(NH_4)_2SiF_6$, ionic motion study 2—37011
  $(NH_4)_2SnBr_6(Cl_6)$, ionic motion study 2—37011
  Ni complex, acetylacetonate alkylamine complex resonance shifts study 2—28283
  Pb complex, bis acetylacetonato dimethyllead, ^{13}C-H and ^{207}Pb-C-H coupling consts. 2—28320
  Rh(III) complex, NN′-dialkyldithiocarbamates, anomalous spectra, hindered rotation about C-N bond 2—21595
  Ta-H system, 77-300 K 2—20165

Proton spectra
  antiproton steady-state spectrum in cosmic rays calc. by statistical model of two fire-balls 2—37246
  ^{2}H(n,p)2n, analysis using diagram summing method 2—31553
  ^{2}H(n,p)2n, E_n=14.1 MeV, energy spectra of breakup protons 2—18203
  ^{2}H(n,p)nn, effect of quasifree scattering on shape of kinematically incomplete spectra at forward angles 2—38612

Protonium *see Protons and antiprotons*

Protonosphere *see Atmosphere/upper*

Protons and antiprotons
  see also Cosmic rays/protons; Nuclear reactions and scattering due to/protons; Nucleons and antinucleons
  beam stability in storage-rings, effect of secondary charged particles 2—2652
  blood, adsorption, applic. of ellipsometry 2—9303
  channelling, axial, temp. depend. of critical angle 2—29571
  charge, interpretation as quantized magnetic flux and relation to scaling 2—14691
  colliding beams, production and electron cooling 2—14790
  dose and induced activity distrib., external proton beam targets 2—2878
  electron-proton charge difference, upper limit det. by acoustic method 2—5499
  e.m. form factors, calc. from finite energy sum rules 2—11609
  energy loss and straggling of 0.6 to 2.0 MeV protons in Fe, Co and Sb, meas. by gamma resonance shift method 2—4088
  energy loss of channelled protons in single crystals, new indirect method applied to CaF_2 and BaF_2 crystals 2—19480
  film, stopping powers 2—32862
  form factors, deviations from scaling law when momentum transfer is not restricted to small values 2—38318
  form factors 2—21301
  geomagnetically trapped, distribution intensity changes due to magnetic storm of 17 Apr 1965 2—4709
  gyromagnetic ratio, basis of n.m.r. standardization method for ampere 2—5312
  ice, channelling and backscatt., surface struct. determ. 2—35871
  in intersecting storage rings, incoherent space charge phenomena and beam lifetime 2—14792
  mass and radius of protons by general relativity 2—31176
  mass difference between proton and neutron 2—17971
  properties and uses, educational article 2—8194
  proton structure, SLAC 20 GeV electron scattering experiments using liquid H and D targets 2—2574

Protons and antiprotons continued
  proton-neutron mass difference, finite difference in structure functions, scale invariance 2—17959
  α-quartz, axial and planar channelling 2—29579
  radii, m.s.r., determ. based on analytical properties of form factors 2—31277
  structure function, sum rule for difference from neutron structure function 2—27774
  structure functions, inelastic, scaling, from ep scatt. 2—31203
  structure functions, ratio with neutron functions, effect of t-channel descript. of electroprod. 2—17832
  N*(1470)-p, M1 transition form factor calc., using Chou Yang model 2—17983
  np, mass difference, calc. taking into account i.r divergent contributions to mass shift 2—5142
  p-n e.m. mass difference and inelastic electron scattering 2—38312
  p-n mass difference, computation in Sudarshan theory of universal primary interactions 2—17960
  Al, energy straggling, as a function of foil thickness 2—36382
  Au thin crystals, channelling effects on Rutherford scatt. yield 2—40104
  BaF_2, channelling in $\langle 111\rangle$ direction, comparison with CaF_2 2—29574
  $BaTiO_3$, cubic and tetragonal phases, proton channelling 2—29573
  CaF_2, channelling in $\langle 111\rangle$ direction, comparison with BaF_2 2—29574
  CaF_2 channelling in single crystals, energy 0.67 to 4.00 MeV 2—9905
  CdTe:Cu(Ga)(In), channelling obs. rel. to detector mat. evaluation 2—36539
  Cr film, deceleration phenomena 2—6702
  CsI energy loss and range-energy relation 2_4091
  Cu, dechannelling, backscatt. and X-ray yield study 2—40106
  Cu, film, deceleration phenomena 2—6702
  Nb, dechannelling, min. yield 2—40109
  Si, backscattering, angular width of blocking, cryst. struct. study 2—25705
  Si, dechannelling, backscatt. obs. 2—36388
  Si, dechannelling, channelled fraction rel. to penetration depth calcs. 2—36389
  Si, penetration depth depend. of angular dips, for H^+ and D^+, backscatt. study 2—40111
  Si, proton channelling, ion implantation damage study 2—22182
  W, dechannelling, 77-873K 2—36392
  W, dechannelling, channelled fraction rel. to penetration depth calcs. 2—36389
 absorption
  range with depth in Ne-H liquid mixtures 2—2644
  p, 1-3.3 GeV/c, cross section on C and Cu 2—17918
  Ni foils, energy loss distribution 2—6703
 angular distribution
  $K^{\pm}p$ elastic scattering, description combining Regge and absorption models 2—409
  ^{36}Ar(d,p)^{37}Ar, E_d=18.00 MeV 2—2779
  ^{12}C(d,n)^{13}N*(p)^{12}C, measurement of neutron-proton correlations 2—31578
  ^{3}He(^{3}He,2p)^{4}He, meas. at seven energies below Coulomb barrier 2—2800
  ^{3}He(d,p)^{4}He, 2-6 MeV, angular distributions of proton polarization 2—38639
  ^{3}He(d,p)^{4}He, <1 MeV, ang. distrib. of outgoing protons 2—38638
  ^{4}He, spin and isospin in high energy proton elastic scattering and nuclear correlations 2—31529
  ^{6}Li(γ,p), ang. distribution of high energy photoprotons 2—28019
  ^{24}Mg(^{3}He,pγ)^{26}Al, rel. to location of second $J^{\pi}=0^+$, T=1 state in ^{26}Al 2—38488
  ^{26}Mg(d,p)^{27}Mg, 2.0 to 3.0 MeV, angular distributions and excitation functions 2—35072
  ^{64}Ni(p,p)^{64}Ni, obs. at 3.150 to 4.050 MeV and lab. angles of 89°, 125°, 140°, 165° 2—35027
  ^{32}S(d,p)^{33}S, E_d=18.00 MeV 2—2779
  ^{28}Si(d,p)^{29}Si, E_d=18.00 MeV 2—2779
 antiprotons
  No entries
 detection, measurement
  antiproton abundances and zenithal assymetries in the primary cosmic radiation 2—10778
  channel electron multiplier, efficiency for protons of 0.2-10 keV 2—2638
  polarization during elastic scattering, energy dependence meas. 2—440
  solar wind, average proton properties from Pioneers 6 and 7 2—20698
  spectrometer, multichannel, modulated, for 0.03-10keV energy range 2—27851
 effects
  alkali halide, channelling, radiation damage 2—3754
  chromosome rupture 2—2021
  diamond, chemical reactions 2—20202
  excitation of He-like ions in solar corona 2—20708
  glass, multicomponent silicate optical, radioluminescence 2—4519
  lasers, stripe geometry, heterostructure, proton bombardment method 2—21096
  solar cells, nonpenetrating proton damage 2—23501
  solar flare effects on lunar Xenon 2—10994
  target behaviour in external photon beam used in photoproduction reactions 2—34766
  Ag film, radiation defect annealing, 93-263K 2—22174
  Al, microhardness 2—39847
  BaF_2, depth and temperature dependence of channelling effect studied by interactions of fast proton with sublattice 2—32863
  Ca, microhardness 2—39847
  CaF_2:Ho^{3+},Nd^{3+}, irrad., elec. resist. 2—10007
  CaF_2, depth and temperature dependence of channelling effect studied by interactions of fast proton with sublattice 2—32863
  Cu film, radiation defect annealing, 93-263K 2—22174
  GaAs, irrad., photocond. 2—36610
  Ge, irradiation damage, rel. to exo-electron emission 2—4318
  Ge, thin cryst., channelling, continuum picture 2—36386
  KCl, H-defects, U centre, i.r. and u.v. absorpt. spectra 2—22227
  KCl, irrad., defect formation, channelling effects 2—19130
  KCl, irrad., U-centre form. 2—25453
  KI, irrad., beam intensity depend. of F-centre yield 2—12788
  KI, irrad., defect formation, channelling effects 2—19130
  $K_3[Fe(CN_6)]$, radiation damage, Mossbauer obs. 2—16438
  $K_4[Fe(CN)_6].3H_2O$, radiation damage, Mossbauer obs. 2—16438
  LiF, irrad., defect formation, channelling effects 2—19130
  MgO, channelling, radiation damage 2—3754
  NaCl, irrad., beam intensity depend. of F-centre yield 2—12788

Protons and antiprotons continued
effects continued
NaCl, irrad., defect formation, channelling effects 2—19130
NaF, irrad., defect formation, channelling effects 2—19130
Ni, microhardness 2—39847
Ni, void formation by flash heating 2—22177
$Pb_{0.76}Sn_{0.24}Te$, p-type to n-type conversion 2—36514
$Pb_{1-x}Sn_xTe$, p-n junction formation, photovoltaic and laser diodes 2-29776
Si:B ion implanted, conc. distrib. and atom location by induced x-ray emission 2—25436
Si, irradiation damage, rel. to exo-electron emission 2—4318
Si, thin cryst., channelling, continuum picture 2—36386
Si epitaxial layer, enhanced diffusion of substrate impurities 2—25902
SrF_2, channelling, radiation damage 2—3754

interactions
see also Nuclear reactions and scattering due to/protons
70 GeV, yields of various particle obs. 2—5555
annihilation reactions, exptl. investigations 2—38326
beam spreading by charge exchange depend. on atmospheric structure 2—30291
bremsstrahlung cross section at 20 MeV 2—2775
coherent reactions of 67 GeV/c protons in nuclear emulsion, cross section for production of particles 2—38321
electron beam insertion, enhancement of ν-spread 2—18032
emulsion nuclei interaction with 76 GeV proton 2—31534
inclusive reactions negative particle prod. at CERN ISR 2—23885
matter density models and antiproton-(emulsion) nuclei elastic scattering at 3GeV/c 2—24213
photoproduction of π^0 at 4 GeV, meas. of polarized target asymmetry in 0.25-1.05 $(GeV/c)^2$ range 2—34768
$dp\rightarrow N+$meson, spin effects 2—14627
$e\rightarrow e\text{-}p\pi^0$, coincidence measurement of backward π^0 electroproduction 2—8167
e p, electroproduction of pions determ. values of axial-vector nucleon form factor 2—11611
$e\text{-}p\rightarrow e\text{-}K^+\Lambda(\Sigma^0)$ obs., e-K coincidence meas. 2—34616
ep, electroprod. cross section, upper limit of isotensor contrib. in $\Delta(1236)$ region 2—23797
ep collisions, deeply inelastic, hadron momentum distrib. 2—8130
$e^-p\rightarrow e^-p\pi^0$, in first resonance region at momentum transfers of 0.3, 0.45, 0.60 and 0.76 $(GeV/c)^2$ 2—5533
$ep\rightarrow e'n\pi^+(p'\pi^0)$, pion electroprod., polarized electrons on polarized protons, reaction cross-section 2—14651
$ep\rightarrow e'p'\pi^0$, recoil proton polarization, first nucleon resonance energy region 2—27751
$ep\rightarrow en\pi^+$, effect of form factors F_π and G_{en} 2—14572
$ep\rightarrow en\pi^+$, near w=2 GeV, pion form factor 2—17926
$ep\rightarrow e\pi^+\Delta^\circ$, predictions for $\pi\Delta(1236)$ prod. within framework of vector meson dominance model 2—11603
$ep\rightarrow e\rho p$, size of virtual photon, investigation using quantum electrodynamics and multiperipheral and constituent models 2—34617
$\gamma\gamma\rightarrow\pi^0\pi^0\pi^0$, low energy limit of one loop contribution, linear σ model calculation 2—8109
$\gamma\gamma\rightarrow\pi^+\pi\text{-}\pi^0$, low energy limit of one loop contribution, linear σ model calculation 2—8109
γp, muon pair production at high energies, field theoretical parton model 2—11577
γp, photoprod. of resonances with annihilation radiation, 3 prong events 2—17821
$\gamma p\rightarrow K^0\Sigma^+$, differential cross sections and asymmetry coefficients, Regge pole model with cuts 2—34660
$\gamma p\rightarrow K^+\ \Lambda$, differential cross sections and asymmetry coefficients, Regge pole model with cuts 2—34660
$\gamma p\rightarrow K^+\Delta^0$, differential cross section meas. at constant momentum transfer between 1.05 and 2.2 GeV 2—34661
$\gamma p\rightarrow K^+\Lambda$, 0.5 to 2.5 GeV, differential cross sections, polarization and asymmetry ratios 2—34653
$\gamma p\rightarrow K^+\Lambda^0$, differential cross section meas. at constant momentum transfer between 1.05 and 2.2 GeV 2—34661
$\gamma p\rightarrow K^+\Sigma^0$, 0.5 to 2.5 GeV, differential cross sections, polarization and asymmetry ratios 2—34653
$\gamma p\rightarrow K^+\Sigma^0$, differential cross sections and asymmetry coefficients, Regge pole model with cuts 2—34660
$\gamma p\rightarrow K^++\Lambda(\Sigma^0)$, low energy description and duality relations 2—34662
$\gamma p\rightarrow\eta p$, 0.5 to 2.5 GeV, differential cross sections, polarization and asymmetry ratios 2—34653
$\gamma p\rightarrow\eta p$, photoproduction, dip mechanism 2—14557
$\gamma p\rightarrow\omega p$, comparison of experimental data with VDM predictions 2—34703
$\gamma p\rightarrow p'\pi^0$, recoil proton polarization, first nucleon resonance energy region 2—27751
$\gamma p\rightarrow p\pi^+\pi^-$, cross sections, ρ^0 and Δ^{++} production in bubble chamber with 2.8 and 4.7 GeV polarized photons 2—27707
$\gamma p\rightarrow\varphi p$, comparison of experimental data with VDM predictions 2—34703
$\gamma p\rightarrow\pi^-+$anything, inclusive reaction in proton fragmentation region, differential cross sect. 2—374
$\gamma p\rightarrow\pi^-\pi^+p$, 1GeV, energy spectra and excitation yields 2—23845
$\gamma p\rightarrow\pi^0p$, 0.5 to 2.5 GeV, differential cross sections, polarization and asymmetry ratios 2—34653
$\gamma p\rightarrow\pi^0p$, unpolarized and linearly polarized photons, 4 to 18 GeV 2—11606
$\gamma p\rightarrow\pi^+n$, 0.5 to 2.5 GeV, differential cross sections, polarization and asymmetry ratios 2—34653
$\gamma p\rightarrow\pi^+n$, polarization parameters, target asymmetry 2—34675
$\gamma p\rightarrow\pi^+\pi\text{-}p$, s-channel resonance region, cross sections 2—34679
$\gamma p\rightarrow\pi^+\pi^-p$, diffraction-dissociation model for high energy ρ production, comparison with empirical data 2—23875
$\gamma p\rightarrow\pi^+\pi^-p$ dual extension of photoproduction reaction $\gamma p\rightarrow\rho^0+p$ 2—373
$\gamma p\rightarrow\pi^+\pi^0n$, 1Gev, energy spectra and excitation yields 2—23845
$\gamma p\rightarrow\pi+$anything, pion distrib., extension of nova model 2—17819
$\gamma p\rightarrow\rho^0p$, 5.5 to 18 GeV, determ. cross section for p meson production 2—14552
$\gamma p\rightarrow\rho^0p$, comparison of experimental data with VDM predictions 2—34703
$\gamma p\rightarrow\rho^0p$ s-channel helicity conserving amplitude, dual extension to $\gamma p\pi^+\pi^-p$ 2—373
$K^-+p\rightarrow\Lambda+$anything, inclusive reactions, scaling properties 2—34665
$K^0(\bar{K}^0)p\rightarrow Q^0(\bar{Q}^0)p$, cross over obs. in production differential cross sections 2—31302

Protons and antiprotons continued
interactions continued
K-p, 10 GeV/c quasi two-body reactions, study of $K^*(890)$ and $K^*(1420)$ production 2—14685
K-p, 3.9 and 4.6 GeV/c, production and decay properties of $K^*(890)$ and $K^*(1420)$ 2—14686
K-p, channel cross sections from 1.26 to 1.84 GeV/c 2—21285
K-p at 10 GeV/c, study of Σ production 2—34735
$K\text{-}p\rightarrow\bar{K}N\pi$, study at 4.2 GeV/c 2—34669
$K\text{-}p\rightarrow Y^0+$vector meson, 3.15 and 3.3 GeV/c, comparison of data with quark model predictions 2—27740
$K\text{-}p\rightarrow\omega\Lambda$, 1915-2168 MeV, differential cross sections, density matrices, partial wave anal. 2—14641
K^-p, 10 GeV/c, diffraction dissoc. and charge, strangeness exotic exchange processes in 4-body final states 2—5529
K^-p, 3.95 GeV/c, search for Ξ^* resonances 2—23895
K^-p to $O^{-1}/_2{}^+$ final states, 3.95 GeV/c, determ. cross sections, angular distr. and polarizations 2—14636
$K^-p\rightarrow K^-p\pi^0$, study of $\Sigma(1760)$ formation 2—38330
$K^-p\rightarrow K^-\pi^+n$, 1.33.to 11.2 GeV/c, applic of dual resonance model for $K^-K^+pn\pi^-$ system 2—17906
$K^-p\rightarrow K^0\pi^-p$, inclusion of spin in Veneziano model 2—17912
$K^-p\rightarrow K^{*-}p$, inclusion of spin in Veneziano model 2—17912
$K^-p\rightarrow K^{*0or-}(1420)N$, 14.3 GeV/c, three body final states, cross sections and density matrix elements 2—23840
$K^-p\rightarrow K^{*0or-}(890)N$, 14.3 GeV/c, three body final states, cross sections and density matrix elements 2—23840
$K^-p\rightarrow\bar{K}^{*0}\pi^-p$, dual five-point amplitude study 2—31270
$K^-p\rightarrow K^*(890)\pi^-p$, Reggeon-particle spin couplings in Feynman-diagram models of Reggeization 2—14589
$K^-p\rightarrow\Lambda(1327)\pi^0\rightarrow\Lambda\gamma\pi^0$ 740 MeV/c, search for $\Lambda(1327)$ 2—17979
$K^-p\rightarrow Q^-p$, 8.25 GeV/c, helicity conservation 2—8160
$K^-p\rightarrow\Sigma(1385)\pi$, production mechanism with total energy in vicinity of $\Lambda(1520)$ resonance 2—17981
$K^-p\rightarrow\Xi^-\pi^+K^0$, obs. of $\Xi\pi$ resonance with mass 1606 MeV/c^2 2—21307
$K^-p\rightarrow(p\pi^+\pi^-)K^-$, 10 GeV/c, observation of $(p\pi^+\pi^-)$ mass enhancement 2—430
$k^-p\rightarrow k^-\pi^+n$, study at 3 GeV/c 2—2550
$K^-p\rightarrow\omega\Lambda$, bubble chamber investigation at 1915 to 2168 MeV, energy dependent partial wave analysis 2—34664
$K^-p\rightarrow\pi^-\Sigma^+$, duality diagrams for forward reaction amplitude, predictions tested 2—14637
$K^-p\rightarrow\pi^+\Sigma^-$, exchange cross sections, Regge cut contributions 2—406
K^+p, 2.1- to 2.7 GeV/c, cross sections 2—8161
k^+p, rapidity correlations between negative pions produced 2—31271
K^+p 15-60 GeV/c., total cross sections meas. 2—5556
$K^+p\rightarrow K^0\Delta^{++}$, 2.25 GeV/c incident momentum, meas. of differential cross-section, spin density matrix elements 2—38289
$K^+p\rightarrow K^0\Delta^{++}$, higher spin production processes, Veneziano model with absorptive corrections applied 2—38288
$K^+p\rightarrow K^0+$anything, inclusive reaction, Reggeon total cross sections 2—31231
$K^+p\rightarrow K^0+n(charged)+X^0$ semi-inclusive reaction at 5, 8.2, 16 GeV/c, scaling properties 2—38290
$K^+p\rightarrow KN\pi$, resonance production in intermediate energy range 2—17907
$K^+p\rightarrow K^{*0}\pi^+p$, dual five-point amplitude study 2—31270
$K^+p\rightarrow K^*$ (890 or 1420) + X^+, inclusive reactions at 8.2 GeV/c 2—17909
$K^+p\rightarrow K^*(890)\pi^+p$, Reggeon-particle spin couplings in Feynman-diagram models of Reggeization 2—14589
$K^+p\rightarrow\pi^-+$anything, analysis using peripheral representation, two body exotic exchange amplitude 2—2576
$K^+p\rightarrow\pi^+{}_k{}^0$, 12 GeV/c, detailed fits to data using generalized Veneziano model 2—17910
$K^\pm p$, scaling of high energy total cross sections, angular momentum cuts 2—8197
$K^\pm p\rightarrow K^{*\pm}(1420)N$, energy dependence of cross sections 2—23841
$K^\pm p\rightarrow K^{*\pm}(890)p$, energy dependence of cross sections 2—23841
$K^+p\Sigma K^{*+}p$, higher spin production processes, Veneziano model with absorptive corrections applied 2—38288
$\mu^-p\rightarrow n\nu_\mu$, radiative corrections 2—34621
$np\rightarrow d\gamma$, study of meson exchange effects 2—23890
$np\rightarrow pp\pi^-$, 2-30 GeV, theoretical analysis in framework of Reggeized OPE model 2—27772
νp interactions, at CERN synchrotron, cross sections, status report 2—23793
p-C inelastic cross section meas., 20-600 GeV 2—24029
p absorption, 1-3.3 GeV/c, cross section on C and Cu 2—17918
pd collisions, $\Lambda(\Sigma)$ production below $pp\rightarrow\bar{\Lambda}\Lambda$ threshold, possible study of $\bar{Y}N$ annihilation 2—432
$pd\rightarrow{}^3He+$ missing mass, evidence for neutral boson of mass 953 MeV and narrow width from neutral meson spectrum 2—2542
$pd\rightarrow\Lambda^0+$ anything at 1.09-2.90 GeV/c, double scattering effect and missing mass spectrum 2—34736
$pd\rightarrow d(p\pi^+\pi\text{-})$, study at 28 GeV/c 2—34717
$pd\rightarrow pd\pi^+\pi^-$, 7 GeV/c, coherent production of final state 2—23883
$Pi^+p\rightarrow\pi^+\pi^+\pi^-p$, 11.7 GeV/c, spin and parity analysis of charged 3π system in mass region of 1400-1900 MeV 2—14682
$p\gamma\rightarrow pX^0$, electromag. X^0 prod., spin parity determ. 2—31309
pn, isospin analysis of single pion production at 7.0 GeV/c 2—27748
pN, monopole production cross section 2—5485
pn interactions in flight, odd-even ratio for pionic annihilation 2—5559
pN is nuclear emulsions at 67 GeV/c, general characteristics, pp multiplicity 2—38320
$pn\rightarrow3\pi$, at rest, resonance structure of Veneziano model 2—17970
$pn\rightarrow pp\pi\text{-}$, isobar production and diffraction dissociation at 7.0 GeV/c 2—34731
$pN\rightarrow\pi\text{-}\pi^+\pi^+$, Veneziano-type amplitudes, Dalitz plot analysis 2—5558
$pn\rightarrow\pi^+\pi\text{-}\pi\text{-}$, comparison of analyses by rising-shift model and Veneziano model 2—34730
$pn\rightarrow\pi^+\pi^-\pi^-$, exptl. investigations 2—38326
$pn\rightarrow\pi^+\pi^-\pi^-$ at rest, duality and final-state interaction 2—23888
$pp\rightarrow\pi\text{-}\pi^+$, asymmetries of differential cross sections using polarized protons 2—34719
$pp\rightarrow\pi^+\pi\text{-}$, comparison with $e^+e\rightarrow\pi^+\pi\text{-}$ using generalized vector meson dominance 2—17968
$pp\rightarrow\pi^\pm+$(anything), covariant function of longitudinal mass used to describe inclusive transverse momentum distribution 2—23884
$P^\pm\pi\rightarrow\pi^0+$anything study of triple-Reggeon couplings 2—2556
$\pi^+\rightarrow\rho^+p$, Reggeon-particle spin couplings in Feynman-diagram models of Reggeization 2—14589

Protons and antiprotons continued
interactions continued
$\pi^- \to \omega^0 n$, determ. of ω spin density matrix elements 2—14676
$\pi^+ \to X +$ anything ($X = \pi^+$, π^-, K_s^0), inclusive reaction at 6 and 22 GeV/c, charged multiplicity distribs. single particle spectra 2—27755
π-p, 60 GeV/c, investigation using standard and enriched emulsions 2—34685
π-p→ two charged final particles, 11.2 GeV/c, strange particle production 2—38304
π-p→$K^+\Sigma^-$, 2.75 to 10 GeV/c, differential cross sections for peripheral K^+ production 2—17905
π-p→$K^+\Sigma^-$, exchange cross sections, Regge cut contributions 2—406
π-p→Xn, differential cross section, Pomeranchuk theorem violation 2—8151
π-p→ηn, differential cross section, Pomeranchuk theorem violation 2—8151
π-p→neutral particles, total cross-section meas. for incident momenta from 250 to 1800 MeV/c 2—2555
π-p→π-D_{13}^+, $\pi D_{13} D_{13}$ coupling constant and PCAC consistency condition 2—38302
π-p→π-N^{+*}, s-channel helicity conservation 2—8172
π-p→π-π-π^+p, 16 GeV/c, Van Hove analysis 2—11617
π-p→ρ-p, 3 to 8 GeV/c, expt. data analysis by complex angular momentum method 2—14658
π-p→ρ^0n, 3 to 8 GeV/c, expt. data analysis by complex angular momentum method 2—14658
πp leading-particle distribution determ. universality relation shown to exist between πp and pp processes 2—11635
π^-p, 4 GeV/c, thermodynamical description secondary pion distribution 2—14654
π^-p, 4 GeV/c, with strange particle production, phenomenological model 2—5541
π^-p, $K_1^0 K_1^0$ effective mass spectra, 4.0 and 5.0 GeV/c 2—11613
π^-p→$K^+ Y^{*-}$(1385), 2.75 to 10 GeV/c, differential cross sections for peripheral K^+ production 2—17905
π^-p→$K^+ + \Sigma^-$, two body process, prediction of energy dependence 2—2576
π^-p→$K^+ + Y^{*-}$(1385), two body process, prediction of energy dependence 2—2576
π^-p→$K^{*0}\Lambda(\Sigma^0)$, 3.9 GeV/c, interpretation by simple exchange processes 2—34683
π^-p→M^0n, obs. of narrow neutral mesons near 950 MeV 2—23870
π^-p→$(p\pi^+\pi^-)\pi^-$, 16 GeV/c, observation of $(p\pi^+\pi^-)$ mass enhancement 2—430
π^-p→η^0n, separated function proton rich frozen target, polarized, prototype 2—5575
π^-p→ηn, direct channel description at high energy 2—11616
π^-p→ηn, total cross sections constancy 2—17931
π^-p→missing mass+n meson mass spectrum near X^0(958) studied near threshold of reaction 2—38308
π^-p→n6γ, 2.94 GeV/c, cross sections, study of $3\pi^0$ and $\pi^0\pi^0\eta$, $\eta \to 2\gamma$ systems 2—27757
π^-p→ne^+e^-, cross section sensitive to universality relation of coupling constraints of vector mesons 2—8100
π^-p→nmγ, $m \geqslant 3$, 2.94 GeV/c, study of π^0 and γ-quanta systems, cross sections 2—23854
π^-p→nφ, obs. of $\varphi \to \eta\gamma$ decay, branching ratio 2—17953
π^-p→n$\pi^+\pi^-$, 7 GeV/c, $\pi\pi$ scattering studied, obs. of S-wave resonance in the f^0 mass region 2—17950
π^-p→p+$(\pi^-\gamma)$+mπ^0, possible existence of π-γ resonance at 270 MeV 2—11627
π^-p→pd, 5 GeV/c, differential cross section 2—23852
π^-p→$p\pi^+p^+\pi^-\pi^-\pi^-\pi^0$. 7 GeV/c, single particle distributions 2—23851
π^-p→$p\pi^+\pi^-\pi^-$, 13 and 20 GeV/c, A3 region of three-pion mass spectrum 2—31314
π^-p→$p\pi^+\pi^+\pi^-\pi^-\pi^-$, 7 GeV/c, single particle distributions 2—23851
π^-p→$\pi^- p\pi^+\pi^-$(16 GeV/c), factorization of diffraction dissociation amplitude 2—391
π^-p→$\pi^-\pi^+$n, 4.45 GeV/c, cross sections, ρ^0 and f^0 resonance prod. 2—23855
π^-p→$\pi^-\pi^+$n, single pion prod. processes, one pion and pomeron exchange model, non dual property 2—2557
π^-p→$\pi^-\pi^+$n, single pion prod. processes, one pion and pomeron exchange model, non dual property 2—2557
π^-p→$\pi^0(\eta)$n charge exchange, universality and complex Regge pole factorization 2—21264
π^-p→π^0n, direct channel description at high energy 2—11616
π^-p→π^0n, high energy, described by exchange of ρ-pole plus $\rho \otimes P$ Regge 2—413
π^-p→π^0n, origin of zeros in ρ-Regge residues 2—8173
π^-p→π^0n, separated function proton rich frozen target, polarized, prototype 2—5575
π^-p→$\pi^+\pi^- X^0$, 15 GeV/c, $\pi^+\pi^-$ scatt. study via Chew Low extrapolation 2—31291
π^-p→$\pi^+\pi^-$n, 15 GeV/c, ρ-ω interference effects and $\omega \to 2\pi$ branching ratio 2—27756
π^-p→$\pi^+\pi^-$n, e.m. corrections rel. to causality test in ρ meson system 2—34704
π^-p→$\pi\pi$N, reactions in c.m. energy range 1400-2000 MeV, meas. cross sections and angular distribution 2—14657
π^-p→ρ^-p, Reggeon-particle spin couplings in Feynman-diagram models of Reggeization 2—14589
π^+p, 3.5 GeV/c, study of four prong events and quasi two body reactions 2—31289
π^+p, 5.45 GeV/c, $\Delta^{++}\eta$ and $\Delta^{++}x^o$ production, and η-x^o mixing 2—31290
π^+p, at 5.45 GeV/c, A_2^+ production 2—17955
π^+p, strange particle production in c.m. energy range 1820 to 2090 MeV 2—11615
π^+p 15-60 GeV/c., total cross sections meas. 2—5556
π^+p bremsstrahlung, calc. of photon angular distributions and cross sections using soft photon theorem 2—14655
π^+p inclusive reactions at 8 and 16 GeV/c, with exotic and non-exotic particle combinations, limiting properties 2—11614
π^+p six prong interactions, at 8 GeV/c, determ. single particle distributions, cross section for production of mesons and meson resonances 2—17934
π^+p→$\Delta^{++}K^+K^-$, 7 GeV/c, analysis of observed anomaly in $\pi\pi$ s-wave scattering near $K\bar{K}$ threshold 2—23865
π^+p→$\Delta^{++}\omega^0$, 5.45 GeV/c, study of final states prod. 2—5542
π^+p→$\Delta^{++}\pi^+\pi^-$, 7 GeV/c analysis of observed anomaly in $\pi\pi$ s-wave scattering near $K\bar{K}$ threshold 2—23865

Protons and antiprotons continued
interactions continued
π^+p→$\Delta^{++}\pi^+\pi^-$, study of π—ω interference and exchange degeneracy at 5.45 GeV/c 2—5540
π^+p→$\Delta^{++}\pi^+\pi^-\pi^0$, study of ρ—ω interference and exchange degeneracy at 5.45 GeV/c 2—5540
π^+p→$\Delta^{++}\rho^0$, 5.45 GeV/c, study of final states prod. 2—5542
π^+p→$K^+\Sigma^+$, between 3.5 and 14 GeV/c, meas. differential cross section and polarization 2—17933
π^+p→$K^+\Sigma^+$, polarization of resisting sigma meas. at 1.11 GeV/c 2—38305
π^+p→K^+Y^{*+}(1385), between 3.5 and 14 GeV/c meas. differential cross section and polarization 2—17933
π^+p→Σ^+K^+, 1.28 and 1.41 GeV/c, additional data, charge independence test 2—2558
π^+p→$\omega\Delta^{++}$, density matrix element meas. rel. to dip mechanism tests 2—8134
π^+p→pA_3^+→$p\pi^+\pi^+\pi^-$, 13 GeV/c, non-conservation of s-channel helicity 2—2554
π^+p→$p\pi^+\pi^0$, multibody final states, analysis using prism plot 2—2507
π^+p→$p\rho^+$ backward reaction, as test of Regge dip mechanism 2—17885
π^+p→$\pi^+ p\pi^+\pi^-$, at 11.7 GeV/c, longitudinal phase space analysis, comparison with $\pi^\pm$p→$\pi^\pm\pi^+\pi^-$p at same energy 2—21292
π^+p→$\pi^+\pi^0$p, 13.1 GeV/c, study of Δ^{++} production and decay angular distributions 2—14713
π^+p→$\pi^+\pi^+\pi^-$p, 16 GeV/c, Van Hove analysis 2—11617
π^+p→$\rho^0\Delta^{++}$, applic. of electric Born model 2—17927
$\pi^\pm$p, 8 and 16 GeV/c, double Regge pole exchange model 2—34682
$\pi^\pm$p, scaling of high energy total cross sections, angular momentum cuts 2—8197
$\pi^\pm$p→π-π-+anything, two particle inclusive reactions, 18.5 GeV/c dependence of correlation functions on rapidities of final state particles 2—23853
$\pi^\pm$p→$\pi(N\pi)$, dominance of isospin zero exchange at 16 GeV/c and production of a low mass $(N\pi)$ enhancement 2—34684
πp→nπN absorption model 2—38303
πp→π^0n, differential cross section, Pomeranchuk theorem violation 2—8151
πp→πN^*, diffractive production of isobars, quark model with quark spin flip 2—23813
πp→ρN, 6 GeV/c, study of ω exchange isolated in the reactions 2—14677
$\pi^\pm\rho$, 5 GeV/c, comparison of A_1-A_2 interference 2—17932
Ξ^0p, cascade reactions, cross section calc. in elastic and inelastic channels 2—17982
Fe in accelerator cave, nucleon and charged pion albedo spectra 2—24222
$K^+p \to K^*$ $K^+p \to K^{*0}N^{*++}$, quark model predictions, expt. verification 2—5527
pp→p+(anything), covariant function of longitudinal mass used to describe inclusive transverse momentum distribution 2—23884
π+p→p+A_2, self-absorption of single peak rel. to A_2 double peaking 2—8186
π^+p→$(p\pi^+\pi^-)\pi^+$, 8 and 16 GeV/c, observation of $(p\pi^+\pi^-)$ mass enhancement 2—430

interactions, proton-proton
15-60 GeV/c., total cross sections meas. 2—5556
γ production in interstellar gas 2—26756
angular distribution of charged particles emitted around 90° in centre of mass produced at very high energies 2—38322
Bremsstrahlung, coplanar symmetric geometry, 51.8 MeV 2—31317
calorimeter events above 100 GeV, multiplicities, angular distributions and total inelastic cross sections 2—24028
final state interactions, in $\gamma + d \to \pi^- + p + p$, separable potential model 2—8199
four-prong events, exptl. study at 13.1 GeV/c 2—8195
fragmentation into protons and pions, peripheral dynamics studied 2—11636
high energy, analysis by solvable model 2—17961
inclusive particle producing reaction, strong exchange process thermodynamic model 2—27724
inclusive pion spectrum, 28.5 to 10^3 GeV/c 2—17963
inclusive reaction, effects of unitarity symmetry constraints 2—31318
inclusive single particle spectra in triple Regge limit of produced $\pi^\pm$, $K^\pm$, p and $\bar{p}$ 2—27773
inelastic cross section meas., 20-600 GeV 2—24029
pionization at 12, 24 GeV/c, scaling and factorization properites 2—38296
prong distribution, applic. of cluster expansion 2—17964
rapidly rising p-p total cross section, evidence from cosmic-ray data 2—34718
scaling of high energy total cross sections, angular momentum cuts 2—8197
single γ-ray spectra, at c.m. energies 30 to 50 GeV 2—17962
transverse momentum distribution of photons produced at intersecting storage rings 2—11637
Δ(1236) production, parameter-free Reggeized absorption model 2—34742
N^* production and elastic scatt., 6 to 30 GeV/c 2—34720
$p + p \to D + e^+ + \nu$ solar primary nuclear processes, dependence on deuteron structure 2—17047
$p + p \to p + \pi^- + \Delta^{++}$, double Regge pole analyses, comparison with data at 22 GeV/c 2—8198
$\bar{p}$p, annihilation, 2.3 GeV/c, ρ/ω interference, cross sections, absence of discrete s-channel resonances 2—8202
$\bar{p}$p, non annihilation reactions of 6.94 GeV/c, 4 and π prod., cross sections 2—5552
$\bar{p}$p, scaling of high energy total cross sections, angular momentum cuts 2—8197
$\bar{p}$p annihilation, duality violating model 2—17969
$\bar{p}$p annihilation at 7 GeV/c, investigation of pion multiplicity distribution 2—27745
$\bar{p}$p annihilation cross sections at low energy, effect of annihilations of stopping antiprotons 2—34729
$\bar{p}$p annihilation into $\pi^+\pi^-$ and K^+K^- from 700 to 1100 MeV/c, determ. cross sections 2—14700
$\bar{p}$p annihilations, 2.2 GeV/c, $K^+K^-\pi^+\pi^-$ and $K^+K^-\pi^+\pi^-\pi^0$ final states, K^*, ρ and ω production 2—34727
$\bar{p}$p annihilations at rest, two-meson production in gauge-invariant chiral Lagrangian model 2—31326
pp→$\Delta\Delta$, dominance of electromag. interactions due to s and t dependence 2—27771
pp→K_1^0+ anything, 13-28 GeV/c, test of limiting behaviour for K_1^0 2—17978

Protons and antiprotons continued
interactions, proton-proton continued
$pp\to K^0$+(anything), very high energies, small K/π ratio shown to be due to difference in longitudinal mass 2—23837
$pp\to\bar{K}K\pi\pi\pi$, final-state investigations at 1.6 to 2.2 GeV/c 2—11638
$pp\to\Lambda$ + anything, 13-28 GeV/c, test of limiting behaviour 2—17978
$pp\to\eta^0\pi^+\pi^-$, 3-body annihilation at rest, anal. using final state interaction model 2—11634
$pp\to nX$, pion exchange and inclusive spectra 2—31320
$pp\to p\Delta$, dominance of electromag. interactions due to s and t dependence 2—27771
$pp\to pn\pi^+$, applic. of Reggeized one pion exchange model 2—21302
$pp\to ppX$, differential meson multiplicity in bremsstrahlung model, contrast with multiperipheral model 2—14694
$pp\to pp\pi^+\pi^-$, 16 GeV/c, enhancements in $p\pi^+\pi^-$ mass spectrum at 1450 and 1700 MeV 2—14693
$pp\to pp\pi^+\pi^-$, 16 GeV/c, study of helicity conservation in low mass $p\pi^+\pi^-$ systems 2—5551
$pp\to pp\pi^+\pi^-$(19 GeV/c), factorization of diffraction dissociation amplitude 2—391
$pp\to pp\pi^+\pi^+\pi^-\pi^-$, 23 GeV/c, long range correlations and dynamics of multiparticle production 2—11566
$pp\to p\pi^+$, nucleon exchange mechanism in the inclusive reaction 2—31319
$pp\to\pi^-$+anything, experimental scaling tests for reaction at 19 GeV/c 2—5553
$pp\to\pi^0\pi^0$ at rest, s-state annihilation, evidence 2—8196
$pp\to\pi$ + anything, anal of π distrib. using incoherent droplet model 2—17920
$pp\to\pi^+np$, 650 MeV, cross-section meas. and compared with one π exchange model 2—5554
$pp\to\pi^+\pi^-\pi^0$ stopping process interpreted by introduction of a resonance ρ' 2—31325
$pp\to\pi^+\pi^+\pi^-\pi^-\pi^0$, 3.25 GeV/c, phenomenology of multi pion production 2—14701
$pp\to\pi^\pm$+anything, pion distributions near kinematical boundary, Deck effect description 2—2575
$pp\to\pi$+(anything), very high energies, small K/π ratio shown to be due to difference in longitudinal mass 2—23837
$pp_{\to\pi^+}$anything at 2.32 GeV/c, analysis of double differential cross section 2—14692
$pp\rightleftharpoons e^+e^-$, tests of T invariance 2—2503
π and K spectra, empirical formula 2—21303
π production, single, in collisions at 7.0 GeV/c, isospin analysis 2—27748
πp leading-particle distribution determ. universality relation shown to exist between πp and pp processes 2—11635
^3H and ^3He, ^1S scattering length rel. to binding energy difference 2—2687
$pp\to pX$, duality predictions on exptl. data near phase space boundary 2—23886
$pp\to p(p\pi^+\pi^-)$, study at 28 GeV/c 2—34717
magnetic moment
anomalous orbital magnetic moment confirmed from obs. on ^{210}Po 2—5638
polarization
beams, use in high energy physics expts. on elastic and inelastic processes 2—34728
bounds to contrib. to H atom hyperfine structure from ep scattering 2—2984
butanol target for study of photoproduction reactions, construction and effects of radiation damage 2—34766
Davis target, computerized n.m.r. system 2—24064
inelastic scatt. from Zn nuclei at 30.5 MeV, optical model analysis 2—5690
elastic scattering, energy dependence meas. 2—440
recoil p in π^0 electro- and photoproduction 2—27751
recoil proton, for γp Compton scatt., below π prod. threshold 2—31323
sudden approx. calc. for $^{12}C(d,p_o)^{13}C$ reaction 2—31579
target for polarization meas. of high energy charge exchange reactions, discussion of background due to bound protons 2—34765
transverse, in elastic ep scattering, derivation of rigorous bounds 2—8118
(d,p) Coulomb stripping reaction, cross-section and proton polarization 2—5708
$K\mp p$ forward elastic scattering, 6-17.5 GeV/c, trends in polarization data 2—34726
μp high energy scattering, weak neutral currents and polarization effects 2—34622
pd elastic scattering, meas. at 1.0 GeV/c 2—8204
pp elastic scattering, 0.9 to 2.5 GeV/c, polarization and differential cross section by diffraction model 2—23889
pp forward elastic scattering, 6-17.5 GeV/c, trends in polarization data 2—34726
pp forward elastic scattering, 6-17.5 GeV/c, trends in polarization data 2—34726
$\pi\mp p$ forward elastic scattering, 6-17.5 GeV/c, trends in polarization data 2—34726
$\pi^-p\to\gamma n$ polarized target, test of time reversal invariance 2—34769
$\pi^+p\to p\pi^+$, intermediate energies, meas. of the polarization parameter in backward scattering on polarized target 2—34694
$^{12}C(d,p)^{13}C$, 3.9 to 5.8 MeV, polarization meas. 2—31577
$^{12}C(p,p)$, at energies around 4.81 MeV resonance, excitation function and polarization meas. 2—31531
$^{12}C(t,p)^{14}C$, polarization of ground state proton 2—28075
$^{52}CR(p,p)^{52}Cr$ 5.8-6.5 MeV, p polarization and ang. distrib. obs. 2—8334
$^{59}Co(p,p)^{59}Co$ 5.8-6.5 MeV, p polarization and ang. distrib. obs. 2—8334
$^{53}Cr(p,p)^{53}Cr$ 5.8-6.5 MeV, p polarization and ang. distrib. obs. 2—8334
$^2H(d,p)^3H$, polarization transfer 2—38637
$^3He(d,p)^4He$, 2-6 MeV, angular distributions of proton polarization 2—38639
$^4He(p,p)$ elastic scattering, 20-45 MeV, angular distrib. of polarization and cross sections meas. across 23.4 MeV resonance 2—35024
$^{58}Ni(p,p)^{58}Ni$ 5.8-6.5 MeV, p polarization and ang. distrib. obs. 2—8334
$^{60}Ni(p,p)^{60}Ni$ 5.8-6.5 MeV, p polarization and ang. distrib. obs. 2—8334
^{62}Ni, scattered protons, rel. to isobaric analog states of ^{63}Ni 2—34945
$^{51}V(p,p)^{51}V$, 5.8-6.5 MeV, p polarization and ang. distrib. obs. 2—8334
production
high energy reactions, inclusive and exclusive, producing large nos. of particles 2—27723
inclusive particle producing reaction, strong exchange process thermodynamic model 2—27724
inclusive single particle spectra in pp collisions, triple Regge limit, 14-70 GeV/c 2—27773

Protons and antiprotons continued
production continued
$\bar{p}$, inclusive single particle spectra in pp collisions, triple Regge limit, 14-70 GeV/c 2—27773
scattering
amplitudes construction from experimental data and analyticity 2—2509
Compton scattering, 2.2-7 GeV, forward cross sections calc. 2—2514
dp, both polarized, spin correlation coefficients at 29 MeV 2—34743
ep, inelastic, leading contribs. to structure function for massive QED 2—14513
inclusive spectrum, longitudinal and transverse momentum correlation in terms of Regge formula 2—38325
polarized beams, use in high energy physics expts. on elastic and inelastic processes 2—34728
ep, asymptotic sum rule, derivation in perturbation theory 2—383
ep, bounds to part of p polarizability contrib. to H atom hyperfine structure 2—2984
ep, deep-inelastic, spin- dependent effects 2—23800
ep, deep inelastic, cross sections, in vector and pseudo-scalar meson theories 2—2521
ep, deep inelastic, in proton fragmentation region 2—38233
ep, deep inelastic, parton model, contrib. of resonances to scaling behaviour of structure function 2—14574
ep, deep inelastic, perturbation theory 2—34619
ep, deep inelastic, scaling behaviour of e.m. structure functions in chiral dynamics 2—38235
ep, elastic, transverse polarization of protons, derivation of rigorous bounds 2—8118
ep, electroproduction of pions in deep inelastic region, means of meas. dimension of chiral symmetry breaking 2—14647
ep, finite energy sum rules and scaling 2—23799
ep, inelastic, backward production of ρ^0 and ω mesons 2—34702
ep, inelastic, Regge pole model 2—38234
ep, inelastic, structure, functions rel. to polarization contribution to H hyperfine structure 2—38236
ep, inelastic at large momentum transfers, cross sections, scaling of inelastic proton structure functions 2—31203
ep, inelastic coincidence expt. in region of $\Delta(1236)$ at $q^2=-0.35$ and -1.0 $(GeV/c)^2$ 2—31202
ep, inelastic in region of Δ_{1236} 2—5501
ep, inelastic strength function, fragmentation approach 2—17833
ep, N^* electroproduction, relativistic quark model 2—8209
ep, pion production near threshold, axial form factor 2—5537
ep, polarized target, electron asymmetry induced by final e.m. interaction 2—27713
ep, radiative corrections, renormalization group approach 2—2519
ep, thermodynamical model, interpretation of scaling behaviour of structure functions 2—14695
ep consistency relation of sum rule, applicable to elastic and inelastic cross sect. data 2—14697
ep deep inelastic scattering in massive QED 2—382
ep deep inelastic scattering, phenomenological formula, cross sections 2—27714
ep deep inelastic scattering, structure functions 2—31200
ep inelastic, Regge pole analysis 2—38319
ep inelastic scattering, phenomenological scaling by vector-meson dominance 2—14575
$e^\pm p$, validity of weak interaction renormalizable theory of Tanikawa-Watanabe 2—27704
$ep\to e$+hadron+anything, inelastic process, nucleon fragmentation 2—31204
$ep\to ep'\rho^0$ differential cross section determ. 2—27765
$ep\to ep\gamma$, investigation below pion threshold 2—17834
$ep\to epx^0$, missing mass in ρ meson region 2—23876
$e\rho$, inelastic electroproduction of resonances, asymptotics 2—8121
γp, Compton scattering, 3.2-3.7 GeV, cross section asymmetry 2—2515
γp below pion production threshold, polarization of recoil proton calc. using second order Compton amplitude 2—31323
$\gamma p\to\pi^0p$, calc. of phase of forward amplitude using modulus dispersion relations 2—34723
$\gamma\rho$, inelastic photoabsorption asymptotics 2—8121
$K\mp p$ forward elastic scattering, 6-17.5 GeV/c, trends in polarization data 2—34726
$K_lp\to K_sp$, 15-35 GeV, K^0 regeneration amplitude 2—31273
K-p elastic and charge exchange date, determ. high energy $\bar{K}N$ scattering amplitudes 2—11600
Kp, 2.11-2.72 GeV/c, analysis of elastic channel, differential cross-sections 2—5530
K^-p, elastic, connection with $K^-p\to(K^-\pi^+\pi^-)p$ dissociation, dual diffractive model 2—408
K^-p, elastic scatt. round 1950 MeV 2—2549
K^-p, low energy, Coulomb and mass difference corrections to charge independent parameters 2—17914
K^-p forward scatt. amplitudes, real parts 2—8162
$K^-p\to(\kappa^-\pi^+\pi^-)p$ dissociation, connection with elastic K^-p scatt., dual diffractive model 2—408
K^+p, elastic, finite-energy sum rules and fixed poles 2—17917
K^+p, phase-shift analyses of zeros of scattering amplitudes obtained by shortest path method, study of discontinuities 2—38293
K^+p elastic, between 432 and 939 MeV/c, determ. cross sections 2—14642
K^+p elastic scattering, 0.5 to 2.5 GeV/c, phase shift analyses 2—23842
K^+p forward scatt. amplitudes, real parts 2—8162
K^+p low-energy scott data below 1 GeV/c re-analysis 2—2551
$K^+p\to K^0\Delta^{++}(1236)\to K^0p\pi^+$, 0.9-1.5 GeV/c, partial wave analysis 2—27741
$K^\pm p$, elastic, angular dist. above 3 Gev/c, description combining Regge and absorption models 2—409
$K^\pm p$, forward scatt., dispersion relations 2—8163
$K^\pm p$, high energy total and differential cross sections using shielded fixed-Pomeranchon model 2—23863
$K^\pm p$ elastic scatt., 5 GeV/c, obs. of K-p backward peak, cross sections 2—31274
$K^\pm p$ forward scattering amplitudes, theoretical model independent determ. of zeros 2—27742
μp, high energy, weak neutral currents and polarization effects 2—34622
μp, question of anomalous interaction discussed 2—11578
np, calcs. using finite difference soln. of partial wave Schrodinger eqn. 2—7672
np charge exchange scatt., comparison of Michigan and mixed model 2—8207

Protons and antiprotons continued
scattering continued
np elastic, 4.8 GeV/c, small angle differential cross section over four momentum transfer range 2—11641
np inelastic cross sections, 100 and 130 GeV/c for cosmic ray neutrons 2—23940
np scatt., n polarization meas., n energy=16.2 MeV 2—38327
pd, backward scatt., with relativistic model of N and N* exchanges 2—8200
Pd, elastic, differential cross section and polarization meas. at 1.0 GeV/c 2—8204
pd, high-energy elastic, deuteron spin alignment as test for double scattering contributions in Glauber theory 2—14714
pd elastic at high energies, results from virtual pion exchange model compared with experiment 2—8203
$p\gamma \to p\pi^+\pi^-$, total and differential cross sections evaluated using relativistic covariant and gauge invariant amplitude 2—34676
pN, at 70 GeV IPHE proton synchrotron, magnetic monopole prod. 2—31181
pn, elastic, near 1.8 GeV/c, differential cross sections 2—31324
pn, elastic scatt., cross section estimates from pd scattering data at 24.0 GeV/c 2—34721
pp, low energy elastic, antishrinkage 2—34729
pp charge exchange scatt., comparison of Michigan and mixed model 2—8207
$p\pi^+\pi^-$, low mass system prod. in 16 GeV/c pp interactions, helicity conservation study 2—5551
$\pi^{\mp}p$ forward elastic scattering, 6-17.5 GeV/c, trends in polarization data 2—34726
π-p elastic data exclusion in calculating multiplicities, role of diffractive contributions 2—2535
πp, cross section difference between π^+p and π-p charge exchange scattering, Regge pole-cut model 2—34693
πp polarization meas. in backward elastic scattering at 6 GeV/c, effect of signal-to-background ratio 2—34691
π^-p, charge exchange, s-channel anal. in a scheme of higher baryon couplings 2—17937
π^-p, comparison of on- and off-mass-shell elastic and inelastic scatt., one-pion-exchange dominance 2—34692
π^-p charge-exchange scattering, polarization and differential cross section at large angles 2—14665
π^-p elastic and charge exchange data at 5 GeV/c fitted by geometric s-channel model 2—17940
π^-p elastic scattering, 865 to 2732 MeV/c, polarization distributions and differential cross section 2—23864
$\pi^-p \to \pi^-p$, coupled channel process, Coulomb corrections calc. using S-matrix theory 2—2564
$\pi^-p \to \pi^0n$, 20-50 GeV/c, charge exchange scattering, cross section data 2—17939
$\pi^-p \to \pi^0n$, coupled channel process, Coulomb corrections calc. using S-matrix theory 2—2564
$\pi^-p \to \pi^0n$ charge-exchange above 5 GeV, structure of absorptive Regge cuts 2—17943
$\pi^-p \to \pi^0n$ differential cross section in wide-angle region, ρ trajectory 2—17942
π^+p, elastic, differential cross section calc. from impact parameters 2—8177
π^+p elastic and charge exchange data at 5 GeV/c fitted by geometric s-channel model 2—17940
π^+p elastic scatt., differential cross sections between 0.6 and 0.8 GeV/c 2—17938
π^+p elastic scattering from 2.74-4.0 GeV/c at all angles, analysis in terms of s-channel helicity amplitudes 2—14664
$\pi^+p \to \Sigma^+K^+$, intermediate energies, meas. of the polarization parameter in backward scattering on polarized target 2—34694
$\pi^+p \to p\pi^+$, intermediate energies, meas. of the polarization parameter in backward scattering on polarized target 2—34694
$\pi^{\pm}p$, determ. of dip structure of differential cross section from phase behaviour of scattering amplitude 2—2566
$\pi^{\pm}p$, dispersion relation calc. of scattering amplitudes 2—17941
$\pi^{\pm}p$, elastic scatt. amplitudes 2—8176
$\pi^{\pm}p$, high energy total and differential cross sections using shielded fixed-pole Pomeranchon model 2—23863
$\pi^{\pm}p$, large angle, 5 GeV/c, differential cross section 2—31298
$\pi^{\pm}p$ elastic scatt., 180°, 0.60-1.60 GeV/c, differential cross section 2—27759
$\pi^{\pm}p \to \pi^{\pm}p$, s-channel anal. in a scheme of higher baryon couplings 2—17937
$\pi p \to \pi\Delta$, study of dip at $t \simeq o$ for high s, upper limit of quark mass. 2—17866
$\Sigma^{\pm}p$, total and differential cross sections, 130-180 MeV/c, allowed regions for singlet and triplet scattering lengths 2—5561
ep deep inelastic region, ρ prod., Regge pole analysis 2—14681
H_2, fast proton impact, Lyman-α radiation prod. cross-section 2—18427
Kp, high-energy forward scattering amplitudes and asymptoticity, dispersion relation investigation 2—38292
K^+p, with strong p-waves at low energies, phase shifts 2—38294
$\pi^{\pm}p$, upper bounds on elastic cross section differences 2—2565
scattering, proton-proton
bremsstrahlung cross-sections at 156 MeV obs. 2—34603
consistency relation or sum rule, applicable to elastic and inelastic cross sect. data 2—14697
differential cross sect., dip bump structure determ. from phase behaviour of scattering amplitude 2—2566
differential cross section calc., high energy elastic scattering using non local model 2—2578
differential cross sects., slope determ. using Regge pole model, average Pomeranchuk slope 2—14698
elastic, differential cross section meas. at intermediate momenta and large angles 2—11640
elastic, dual absorption model comparison with $\bar{p}p$, $K^{\pm}p$ and $\pi^{\pm}p$ elastic scattering near 8 and 16 GeV/c 2—34724
elastic, experimental and theoretical results 2—14689
elastic, in 1.3-3.0 GeV/c energy range and 50°-90° angular range, meas. of differential cross sections of angular distribs. 2—27775
elastic, investigation of new set of kinematic variables 2—2579
elastic diffraction slopes and total cross section determ. by use of covariant function in phenomenological description 2—23884
exchange degeneracy scheme, cross-over and slope parameter 2—17966

Protons and antiprotons continued
scattering, proton-proton continued
forward peak shrinkage in elastic scatt., consistency of 2-channel diffraction model 2—11639
four momentum transfer of recoil proton, differential cross sect. 2—17965
head on collision at 15 GeV, CERN intersecting storage rings 2—449
high energy total and differential cross sections using shielded fixed pole Pomeranchon model 2—23863
high-energy calc. of total and differential cross section using droplet model with current current interaction 2—21305
inelastic at 500-1500 GeV, inclusive cross section meas. 2—21304
inelastic collisions up to 700 GeV, prong distribs. 2—34725
infinite one boson exchange type model for high energy elastic scatt. 2—31321
leading particle energy loss, relationship with multiplicity growth 2—14696
magnetic monopole pair prod. cross section from internal virtual photons 2—31180
multiparticle prod., single particle spectra, 28.5 GeV, comparison with cosmic ray data above 10^4 GeV 2—8201
proton beams in intersecting storage rings, effect on beams lifetime 2—14792
quasifree, in reaction $^2H(p,2p)n$, 21.5-56.4 MeV 2—2776
Regge absorption model for small angle elastic scattering 2—23887
semiclassical model of high energy scattering 2—38323
total cross sections, asymptotic behaviour, and additional odd-signature meson trajectories 2—21306
$K^{\pm}p$, elastic, dual absorption model comparison with pp, $\bar{p}p$ and $\pi^{\pm}p$ elastic scattering near 8 and 16 GeV/c 2—34724
p-p elastic scatt., 5GeV/c, evidence for backward peak, differential cross section 2—31322
pp, asymmetries of differential cross sections using polarized protons 2—34719
pp, elastic, dual absorption model comparison with pp, $K^{\pm}p$ and $\pi^{\pm}p$ elastic scattering near 8 and 16 GeV/c 2—34724
pp elastic, investigation of new set of Kinematic variables 2—2579
pp elastic scattering, 0.9 to 2.5 GeV/c, polarization and differential cross section by diffraction model 2—23889
pp forward elastic scattering, 6-17.5 GeV/c, trends in polarization data 2—34726
pp forward elastic scattering, 6-17.5 GeV/c, trends in polarization data 2—34726
pp total cross sections, asymptotic behaviour, and additional odd-signature meson trajectories 2—21306
$pp \to \bar{\Lambda}\Lambda$ studying using Regge pole model with exchange degeneracy and absorption 2—5557
$pp \to \bar{\Lambda}\Sigma^0$, study using Regge pole model with exchange degeneracy and absorption 2—5557
$pp \to \bar{\Sigma}^0\Sigma^0$, study using Regge pole model with exchange degeneracy and absorption 2—5557
$pp \to pN^*$, 5-30 GeV/c, Pomeron scattering obs. of phenomenological duality 2—17967
$pp \to pX$ duality predictions in high energy missing mass spectra 2—23814
$pp \to pp\omega$, simple Regge pole model 2—2577
$pp \to x\pi$, x=4, 5, 6, 7, 2.32 GeV/c, single particle distribs. of π 2—27743
π-p elastic data exclusion in calculating multiplicities, role of diffractive contributions 2—2535
$\pi^{\pm}p$, elastic, dual absorption model comparison with pp, $\bar{p}p$ and $K^{\pm}p$ elastic scattering near 8 and 16 GeV/c 2—34724
scattering proton-deuteron
amplitude, real part at 3 GeV 2—38324
elastic, 3.6 GeV/c, spin alignment of deuterons 2—11646
elastic, both polarized, 10 MeV, analysing powers A_{1111} 2—38332
momentum loss spectra, 24.0 GeV/c, Glauber theory interpretation 2—34722
momentum loss spectra, 24.0 GeV/c rel. to estimates of elastic pn scattering cross sections 2—34721
nonelastic shadow corrections, 15 to 30 GeV 2—14699
Pseudopotential methods
alkali metal, electron-ion pseudopot. form factor 2—1455
alkali metals, band struct., phase-shift analysis 2—36403
alkali metals, mag. susceptibility change due to pseudopot. mag. field depend. 2—1604
alkali metals, variable phase approach to scatt. theory 2—29592
alkaline earth metals, liq., resist. calcs. using model pseudopots. 2—18849
alloy, binary ordering, cubic lattice, electron energy 2—9920
alloy, dil. binary, residual resist. determ. 2—36441
chalcopyrite lattice, band struct. calc. 2—13260
covalent semiconductors, vacancy formation and migration energies 2—18964
disordered system, band struct. and transport props. 2—16102
divacancy migration in metals 2—15748
electron-neutral atom scattering 2—38829
Fong-Cohen d-pseudopot, for energy bands 2—40138
KKRZ-pseudopotential, construction from relativistic theory of LEED 2—22062
lattice dynamics, unified microscopic approach 2—19325
liquid metals, absolute thermoelectric forces 2—21998
liquid metals, electronic structure from nonlocal energy dependent model potential 2—39328
magnetic energy bandstructure and magnetic breakdown in metals 2—32913
metal, band struct., phase-shift pseudopot. 2—36402
metal, binding energy and lattice consts. calc. 2—40139
metal, d-band, electronic struct. 2—25723
metal, quasiparticle damping, electron-phonon effects 2—16084
metal simple, binding energies, struct. and lattice consts. calcs. 2—9317
metallic self-diffusion applic. 2—12791
periodic lattice pot., matrix elements 2—6718
semiconductor, cubic, electronic struct. determ. 2—16225
solid spectra interpret., combined OPW, inner shell photoabsorpt. features 2—16480
zincblende alloy, charge distribution 2—6716
zincblende alloy, energy gap, comparison pseudopotential and dielectric methods 2—6717
Al, liquid, specific resist. correlation with short range order 2—1116
Al energy band determ. via model-pseudopotential approach 2—29616
Hg, cryst., Fermi surface 2—1464
Li, b.c.c. and h.c.p., binding energy and compressibility 2—6391
Mg, elastic consts. derivation from local pseudopot. 2—3837
Pb, liquid, specific resist. correlation with short range order 2—1116

Pseudopotential methods continued
  Sn, white, pseudopot. form factors 2—13091
  Zn liquid specific resist. correlation with short range order 2—1116
  ZnGeP$_2$, band struct. calc. 2—13260

Pulsars
  γ sources search at 10^{11}-10^{12}eV, null result 2—33722
  γ-quanta fluxes, upper limits point source search 2—17025
  absorption of gamma rays by photons 2—26771
  analysis of experimental observations 2—7475
  AP 2016+28, polarization properties at 430 MHz 2—30515
  astrophysical and cosmological problems 2—16949
  braking index and period pulse width distribution 2—20610
  Centaurus X-3, reconsiders the white dwarf model 2—7501
  charged particle motion near, models and synchrotron radiation 2—4940
  cosmic ray injection, possible periodic flux 2—10955
  cosmic ray production, origin of light elements 2—16955
  cosmic ray production 2—4929
  CP0329, CP0950, CP1133, CP1919, obs. of pulse height fluctuations 2—10942
  CP0950 interplanetary scintillation and interstellar scattering at 318MHz, upper circuit on angular size 2—26776
  CP 0328, NP 0531, twinkling from passage of Alfven waves through thermal plasma in interstellar space 2—30506
  CP 0328, wide-band radiofrequency spectra, peroidicity 2—10948
  CP 1919, polarization properties at 430 MHz 2—30515
  Crab, braking index and period pulse width distribution 2—20610
  Crab, oblique rotator model for radiation mechanism 2—10953
  Crab, optical pulsations, absence of amplitude or pulsar-shape variations 2—20616
  Crab, polarization at low radio frequencies 2—41150
  Crab, pulsed γ-ray det. of 10^{12} eV 2—41163
  Crab, radio emission, rotation measure and intrinsic angle 2—7478
  Crab, rotation axis and magnetic field axis 2—7479
  Crab, timing, dispersion, morphology and 430 MHz polarimetry 2—26787
  Crab Nebula, delay of polarization minima after pulse peaks 2—7487
  Crab Nebula, interstellar scattering two-region model 2—4934
  Crab Nebula, mechanism of glitches 2—4938
  Crab Nebula, search for pulsed γ-ray emission above 50 MeV 2—26812
  Crab Nebula 0532, gamma ray telescope for obs., using multiplate spark chamber 2—10989
  Cyg X-1, hard X-ray pulsations, upper limits 2—7484
  Cyg X-1, search for pulsed radio emission at 327 MHz 2—10954
  Cyg X-1, X-ray pulsations, mechanism 2—13973
  declination, average pulse energy, and pulse shape of 12 weak pulsars at 327 MHz 2—10963
  Doppler period variations of high velocity pulsars 2—10946
  drifting subpulse phenomena, use as general classification scheme 2—4930
  dynamics and electrodynamics 2—26793
  electron gas behaviour in superstrong magnetic fields 2—33959
  e.m. wave emission, quantum treatment of electron emission in 2—5479
  energy release and nonthermal radiation, explanation using field modific. of classical gravitational theory 2—16948
  fluctuation spectra analysis, polarization of subpulse structure 2—26786
  flux meas., 1420 MHz 2—10951
  formed by type II supernova explosion, mass ejection 2—10892
  frictional heating model of neutron stars 2—7435
  gamma ray absorption by photons 2—10925
  hard X-ray pulsations from Vela supernova remnant 2—26800
  intensity, long-term variations at 149 MHz, (0329+54, 1919+21, 2016+28 and 2217+47) 2—4932
  interferometric observations between 2.7 and 8.1 GHz 2—10959
  limiting mass of neutron stars 2—7436
  magnetic field effects on outermost crust 2—10956
  magnetosphere, model 2—30517
  magnetosphere structure, evaporation and accumulation of gas 2—26779
  maser emission mechanism 2—30518
  microquakes and macroquakes, frequency jumps in radiation 2—30479
  models, e.m. features and predictions 2—4939
  multiple model for QSOs and Seyfert galaxies 2—20617
  ND 0532 in Crab nebula, review of theories 2—23084
  neutron matter, magnetic properties 2—30482
  neutron matter, magnetic susceptibility 2—33660
  NP0527 interplanetary scintillation and interstellar scattering at 318MHz det. of angular diameter 2—26776
  NP0532, radiation and dispersion relation for light 2—23102
  NP0532, search for pulsed γ-ray emission above 50 MeV 2—7485
  NP0532, very long baseline interferometry at 121.6 MHz 2—26788
  NP 0532, delay of polarization minima after pulse peaks 2—7487
  NP 0532, gamma ray spectra 25-975 keV 2—17026
  NP 0532, hard X-ray spectrum 2—7503
  NP 0532, long baseline interferometry at decametric wavelength 2—26780
  NP 0532, position of local sources of radiation calc. and polarization characteristics 2—13958
  NP 0532, precursor pulse, explanation as result of scattering 2—10941
  NP 0532, pulsed gamma radiation from the Crab Nebula, balloon observations at 50 MeV 2—10952
  NP 0532, pulsed gamma rays at about 10^{12} eV 2—10987
  NP 0532, pulsed X-ray emission in 20 to 200 keV range 2—7481
  NP 0532, strong interpulses detection 2—10947
  NP 0532, upper limit to circular polarization 2—10935
  NP 0532, X-ray observations, 30-100 keV 2—7482
  oblique rotator model and a dense magnetosphere 2—7486
  OP 1914 period, position, pulse shape and timing obs. 2—26699
  origin, number density of Ap stars 2—33643
  origin, theory of evolution of growing stellar cores up to C ignition 2—16989
  parameters, table 2—23087
  particle acceleration, effect of near fields 2—41151
  period-luminosity function, reliability reviewed 2—10962
  periods, period derivatives and positions from timing observations 2—26773
  planetary systems, possible method of detection from perturbation on time of arrival of pulses 2—17021
  polarization of 0809+74, drifting subpulses 2—4931
  polarization properties at 430 MHz 2—30515
  PP 0943, bursts in radioemission 2—10944
  PSR 0532+22, rotation axis and magnetic field axis 2—7479
  PSR 0809+74, polarization of drifting subpulses 2—10943
  PSR 0833-45, period characteristics and timing obs. 2—30516
  PSR 0833-45, polarization measurements at 400 MHz 2—37332

Pulsars continued
  PSR 0835-45 γ spectra 25-975 keV 2—17026
  PSR 1929+10, polarization properties at 430 MHz 2—30515
  radiation and baryon matter in neutron stars, American Astronomical Society, Amherst, USA 1971, conference 2—26623
  radiation diagrams formation and relativistic motion of radiation source 2—13958
  radiation from fragmentation of supermassive disks 2—7366
  radiation mechanism rel. to relativistic electrons in spiral orbits, polyscrew streams 2—33705
  radio spectra, average, 53-606 MHz 2—26789
  radiosources, redshifts and fluxes 2—1968
  relative space positions with supernova remnants, and period-luminosity relation 2—23088
  resonant pulsations in polytropic models, coupling between fundamental and overtone 2—26766
  rotation and dispersion measures from polarization and pulse time of arrival obs., galactic mag. field 2—13952
  rotation measures for linearly polarized pulsars north of −19° declination 2—4794
  rotational theories 2—30525
  scattering of pulsar radiation in interstellar medium 2—4937
  Sco X-1 and Cyg X-1, search for pulsar like emissions at 400 MHz 2—23090
  slowdown rate relaxation, from calc. of electron velocity relaxation in rotating neutron superfluid 2—7491
  speedups related to metastability of superfluid neutron star core 2—37324
  synchrotron instability, linear theory 2—30514
  synchrotron radiation, coherent, model 2—372
  synchrotron radiation from ultra-anisotropic particle distributions 2—26790
  theoretical concepts including nature, structure and radiation 2—4908
  universal X-ray background 2—20625
  Vela, second decrease in period 2—10957
  X-ray, near NP 0527, search for emission over 100 keV 2—41160
  X-ray, NP 0532, near Crab nebula 2—30529
  X-ray observations of a new pulsed source near the Crab Nebula 2—20635

Pulse generators *see Circuits*

Pulse-height analysers *see Counting circuits*

Pumps
  see also Vacuum pumps
  helico-centrifugal, anticavitation by using reverse currents 2—30714
  magnetohydrodynamic pump, operating characteristics in braking regime for liquid ferrous metals 2—8898
  for nuclear reactor circulation, stress analysis 2—15036
  oil, air driven with valve and connector for 20 kbars 2—41373
  submerged A.C. conduction, for pumping liquid Mg 2—960

Purkinje effect *see Vision*

Pyroelectricity
  uses for acoustical meas. 2—5246
  ferroelectrics applics., review of developments in Europe 2—40340
  lithium formate monohydrate, cryst. struct. and ferroelec. props. 2—3747
  measurement technique and applic. to response time detector 2—40365
  piezoelectric, potential distrib. and tertiary pyroelec. effect 2—6886
  polar crystal, pyroelectric coeff. measurement 2—10129
  polar crystals, rel. to optical rectification by impurities 2—33210
  polyvinylfluoride film, application to i.r. detector, High D* 2—7770
  polyvinylfluoride when irradiated with i.r. 2—6889
  polyvinylidene fluoride, film 2—19955
  polyvinylidene fluoride, rel. to i.r. detectivity 2—13329
  polyvinylidene fluoride films, poled 2—40367
  radiation detector, responsivity enhanced by PbZrTiO$_3$ pyroultrasonic parametric amplifier 2—20952
  radiation receivers, co-ordinate sensitive 2—17411
  thermal imaging devices 2—37797
  triglycine sulphate, i.r. detector 2—6888
  triglycine sulphate, peak voltage of response to short i.r. laser pulses 2—19774
  triglycine sulphate, pyroelectric voltage response to step i.r. radiation signal 2—4283
  triglycine sulphate, voltage response to rectangular i.r. signals 2—33064
  triglycine sulphate targets for thermal imaging camera tubes 2—2366
  Ba$_x$Sr$_{1-x}$Nb$_2$O$_6$, voltage response to rectangular i.r. signals 2—33064
  (BiNa)$_{1/2}$TiO$_3$, current obs. up to 400°C rel. to ferro-/antiferroelec. nature 2—29088
  CdS:Li, exhibiting tap effect, differences in surface charges during cooling and heating 2—19775
  CsPbCl$_3$, phase transition obs. 2—12994
  Gd$_2$(MoO$_4$)$_3$, ferroelec. phase transition, spontaneous polarization 2—13328
  NaBa$_2$Nb$_5$O$_{15}$ pyroelectric voltage response to step i.r. radiation signal 2—4283
  (Pb,La) (Zr,Ti)O$_3$ ceramics, rel. to i.r. detector applic. 2—40366
  PbNb$_2$O$_6$-BaNb$_2$O$_6$, ceramic system, props. rel. to domain and grain struct. 2—29739
  PbTiO$_3$, i.r. detector noise performance and neutron irradiation resistance 2—17414
  Pb(Zr, Ti)O$_3$ detector, high D*, fast 2—34196
  SrO.BaO.Nb$_2$O$_5$ peak voltage of response to short i.r. laser pulses 2—19774

Pyrolysis *see Chemical reactions*

Pyrometers
  disappearing filament, optics and residual aberrations 2—34197
  with electron optical converters, calc. relating min. meas. temp. to converter and optics parameters 2—20965
  i.r. radiation detector, performance parameters 2—11370
  low temp. obs. of objects located at considerable distance away 2—23407
  optical, three colour, with microsecond resolution time 2—2285
  photographic, IF-87, radiance temp. measurement 2—27332
  radiation, attachment for obs. of high temps. of small surfaces 2—23395

Q-switching
  electro-optical, KD$_2$PO$_4$ crystals, simulation by programmable desk calculator 2—4437
  high power laser, passive method for compression of light pulses 2—27559
  laser, flash pumped, high gain type, obs. 2—21086
  laser, patent 2—7913
  laser amplifier, superregenerative 2—23572
  laser damage of i.r. nonlinear materials 2—21047

Q-switching continued
- laser Q switch design, deuterated KDP, absorption data 2—36824
- lasers, production of ultra-short pulses 2—23659
- model selection, in continuously pumped Q-switched, lasers 2—17579
- polymethine dye thin films, bleachable Q-switch for GOS-1000 laser 2—17575
- pulse stretching, applications 2—14399
- pulsed, of c.w. laser cavity, output pulse intensity meas. 2—23571
- randomly polarized laser sources, electrooptical technique 2—17573
- ruby laser, high repetition rate, obs. 2—21087
- ruby laser, radiation by phthalocyanine vapour 2—17622
- ruby lasers, high-coherence, mode selection 2—17623
- triphenylmethane dye, and saturable absorption, ruby laser pumped 2—21061
- two-step technique for producing high power in single longitudinal mode, use with Nd:$CaWO_4$ laser 2—31046
- ultra short pulse lasers, review 2—5351
- CO_2-N_2-He laser using saturable filter containing OsO_3 vapour 2—27494
- CO_2 gas lasers, by molecular gases exhibiting Stark effect 2—7920
- CO_2 laser, by use of the Stark effect in methyl chloride 2—848
- CO_2 laser, intracavity lens arrangement, air breakdown characteristics 2—9004
- CO_2 laser, passive Q-switching using ^{13}C enriched methyl fluoride 2—5357
- CO_2 laser, passively Q switched, frequency stabilization 2—21069
- CO_2 laser, pulsed discharge, numerical modelling, output pulse characts. 2—34390
- CO_2 laser, single rotational line selection 2—7954
- CO_2 laser, Stark effect driven Q-switching 2—21068
- He-Xe laser, amplitude characteristics 2—23599
- $LiNbO_3$, in Nd:YAG laser, damage obs. 2—29864
- Nd:glass laser, for discrete train of light pulses, applications to high speed cinematography 2—27499
- Nd:glass laser, wavelength tuned by mixing acridine red and rhodamine 6 G in dye cell 2—5374
- Nd:YAG laser, using acousto-optic beam deflector 2—17629
- Nd laser, radiation statistics 2—21084

Quadrupole crystal field interactions *see Crystals/hyperfine field interactions*

Quadrupole moments, molecular *see Molecules/moments*

Quadrupole moments, nuclear *see Nucleus/electric moment*

Quanticule theory (of chemical binding) *see Bonds*

Quantization *see Field theory, quantum/quantization; Quantum theory/quantization*

Quantum chemistry
- p-azoxydianisole, rel. to equilibrium geometry study 2—8733
- bimolecular reactions, quantum transition probabilities in multidimensional systems with potential barriers 2—33365
- electron spectroscopy, review 2—31003
- exclusion principle violating diagrams, generalization of many body-theory 2—28163
- Gaussian type orbitals, field and field gradient integrals, computer programs 2—35206
- harmonic oscillator two-centre integrals, application 2—27068
- hydrides, groups IV to VII, quantum mechanical calc. of molecular radii 2—35227
- maleimide and isoelectronic molecules, electronic spectra, quantum chemical calc. 2—15383
- non-crossing rule in molecular quantum mechanics 2—35202
- non-partial wave treatment of reactive and non-reactive scattering, coupled integral equations formalism 2—37026
- orbital exponents choice, semiempirical method, evaluation by variational energy calculations for He_2^+ 2—8653
- reactions, quantum-mechanical Hamiltonian, practical considerations 2—33362
- reactive scattering, Volterra equation formalism for coupled channel amplitude densities 2—37025
- H+DCl, comparison of isotope exchange and abstraction mechanisms 2—16671
- $H+H_2$, collinear reactive scattering, quantum mechanical soln., numerical methods comparison 2—26322
- $H+H_2$ collinear reaction, quantum mechanical computational study, close-coupling method 2—20172
- $H+H_2$ collinear reaction, quantum mechanical reaction probabilities and rate constants 2—22859
- $H+H_2$ reaction, quantum calculations of planar reactivity. development of mathematical techniques 2—33368
- $H+H_2$ reaction, quantum calculations of planar reactivity, application of mathematical techniques 2—33369

Quantum counters *see Photons; Radiation detectors*

Quantum electrodynamics
- *see also Electrodynamics; Electromagnetism*
- analytic vertex expansion 2—34582
- canonical dimensions for the electromagnetic field and current 2—357
- canonical transformation by computer 2—14146
- charged particle, coherent states in time- dependent uniform e.m. field of plane current 2—34583
- connection with dual resonance model, consequences of gauge invariance studied 2—14594
- constants ratio to cosmological constants, rel. to universe expansion 2—20465
- Coulomb Green function in the x-representation, Lagerr polynomial expansion 2—28227
- cyclotronic resonance in vacuum polarization 2—23769
- electromagnetic field interaction with matter, angular momentum basis 2—23768
- electron and photon Green's function, Dyson eqns. soln., $\alpha(\alpha,L)^n$ approx. 2—14517
- electron emission in strong e.m. wave 2—5479
- electron propagator, μ-mesic hydrogen and (g—2) of muon as possible tests 2—38200
- equal time canonical current commutators calc., absence of noncanonical behaviour 2—14515
- external field problems 2—8085
- Fermi-Dirac vacuum plus one electron, quantum kinematics 2—5481
- fourth-order Lamb shift, crossed-graph contribution 2—21203
- free electron between conducting plates, magnetic moment 2—8087
- gauge invariance, manifest covariance and observer dependence relations and Bergmann quantization 2—2497
- gauge-independent spin-1 field, vacuum polarization 2—31175

Quantum electrodynamics continued
- generalized Lorentz gauge description 2—27698
- Goto-Imamura-Pradhan-Schwinger term, killing mechanism 2—21201
- hadron electrodynamics, gravity-modified, rel. to π^+-π^0 mass difference computation 2—5532
- Hamiltonian of quantum electronics 2—34366
- indefinite metric applications 2—38202
- in intense crossed field, radiative corrections and their analytical properties 2—23767
- kinetic theory of nonthermal relativistic plasma 2—31936
- Lamb shift, as consequence of finite size of electron 2—24325
- Lamb shift, contribution of α^2 slope of Dirac form factor of free electron 2—23771
- Lamb shift, multipole expansions 2—21495
- Landau gauge, generalization to massive vector meson field 2—38197
- Landau-gauge zero-fermion-mass, vanishing of second-order correction to triangle anomaly 2—8089
- limit of validity determ. by $e^+e \rightarrow \mu^+\mu$- reaction 2—11556
- loosely bound composite system, radioactive transition probabilities, relativistic corrections 2—35116
- massive, canonical approach, to high energy scattering 2—5482
- massive, in infinite momentum frame 2—8088
- massive, inelastic e-p scattering 2—382
- massive, leading controls to structure function in inelastic region of ep scatt. 2—14513
- molecular, critical analysis of hamiltonian theory 2—21574
- multiple quantum transition probabilities 2—24301
- neutral atoms, spin-dependent effects between conducting plates 2—8086
- optical activity theory 2—5480
- photon as Goldstone particle, theoretical investigation 2—17793
- photon propagator, corrections due to hadron vacuum polarization 2—5483
- photon self energy parts omission, application of Callan Symanzik scaling eqns. 2—14516
- regularization induced by nonpolynomial Lagrangian 2—2496
- regularization through non-polynomial Lagrangians 2—23766
- relativistic particle, high spin in e.m. field, Hamiltonian and wave eqns. 2—23772
- spin-zero particles, bound-state problem, relativistic corrections to Coulomb binding energies 2—38201
- spinor, covariant axial vector current and its divergence equation 2—21202
- spinor electrodynamics, axial vector vertex, examination using analytic regularization method 2—14512
- stress tensors and conformal invariance, quantum corrections 2—17796
- sum rule for charge renormalization constant 2—38199
- test, using $e^+e^- \rightarrow \mu^\pm\mu^\mp$ reaction 2—17794
- test, using e^+e^- interactions at high q^2 values 2—17795
- transitions in e.m. fields of abitrary intensity, nonperturbative method 2—17465
- two dimensions, Schwinger model, operator solns. in several gauges 2—2495
- two-body system, applic. to H atom theory 2—14519
- vacuum polarisation, rel. to modification of Coulomb law in uniform static magnetic field 2—38203
- vacuum polarization, intense e.m. field, photon splitting 2—21205
- vacuum polarization, stability in limiting field 2—21204
- vacuum polarization corrections to photon propagator and pi magnetic moment 2—5483
- vacuum polarization in mag. field, dispersive props. of free space 2—11557
- vacuum polarization insertions in ρ-dominance electromagnetic pion form factor 2—27764
- validity study using storage rings 2—14783
- vertex function on mass shell, eikonal approx. 2—350
- violation at small distances in annihilation of polarized nonpoint leptonic pairs 2—23788
- wave equations, infinite components, props. after inclusion of external electromag. fields 2—14514
- e^-e^+ colliding beam experiments, test of theory 2—23802
- $ep \rightarrow e\rho p$, size of virtual photon 2—34617
- μ magnetic moment corrections due to hadron vacuum polarization 2—5483
- H atom, scalar, spinor, mass levels, derivation on basis of micro-noncausal theory 2—38848

Quantum electronics *see Lasers; Masers; Photons; Quantum optics*

Quantum field theory *see Field theory, quantum*

Quantum fluids
- δ-function gases, cluster coefficient computation through U functions 2—2173
- critical phenomena, theoretical review 2—7714
- dense gas, physical particle description of equilibrium props. 2—2176
- hard sphere mixtures, osmotic pressure 2—9193
- liquid, superfluid, vortices, quantum mech. form. 2—35808
- liquids, phonon-like excitations, study of disordered systems 2—32792
- off-diagonal long range order systems, canonical ensemble perturbation eval. 2—17265
- phase transitions, theoretical review 2—7714
- vapour-superfluid interface, temp. fluctuations associated with gravity waves 2—30819
- ^3He, quantum crystal, interior of neutron stars 2—30478
- ^4He, density matrix of liquid at low temp. 2—32297

boson systems
- Bose condensation, phenomenological theory of superfluidity, hydrodynamics 2—28929
- Bose gas. Bogoliubov theory of condensation 2—7715
- Bose-Einstein system, finite, density fluctuations and onset of superfluidity 2—7716
- charged boson gas, corrections to variational ground state 2—14140
- charged gas, calc. of generalized dielectric constant in random phase approximation 2—30824
- charged gas, investigation at intermediate densities 2—27098
- coherent properties of systems with fixed particle number, field operator tensor properties 2—27102
- dumped, Green function theory 2—11308
- dynamic structure factor 2—14139
- dynamics, in action angle variables 2—103
- free systems, approach to equilibrium 2—7710
- Glauber representation (coherent states) approach 2—11307
- homogeneous, with condensate, bound states of excitations 2—37653

Quantum fluids continued
boson systems continued
interacting bosons at absolute zero, perturbation theory based on currents 2—27100
interacting gas, quantum condensation, rel. to thermodynamic limit and dimensionality 2—27103
liquid, critical indices calc. 2—17266
liquid, gauge symmetry breakdown, hydrodynamical limit properties 2—104
many particle Bose system, variational calc. of ground state 2—37655
nonideal Bose gas, Green functions and thermodynamics 2—37654
nonuniform states of an imperfect Bose gas 2—30820
phase changes, computer simulation 2—15626
with repulsive core and attractive tail, Green-function methods 2—20874
structure function and self energy from generalized Hartree approx. 2—30823
superconductivity applic. 2—19567
superfluid system, Gross Pitaevskii eqn. for order parameter 2—20875
thermodynamic properties, variational model 2—14138
thin films, Bose Einstein condensation 2—27099
tunnel model for hard-sphere bosons in their ground state 2—105
zero temperature, validity of hydrodynamic model for a Bose liquid 2—30822
He II, general theory, Bogoliubov model and excitation 2—12599
He II, quasi-particle scattering from impurities in an imperfect Bose gas 2—30821
^{3}He-^{4}He, solution, second sound excitation 2—15623

fermion systems
antiferromagnetic linear chains, Fermi liquid theory, residual interaction and collective mode 2—40541
Bose condensation in interacting systems 2—5165
Bose Einstein gas, hard core, relationship of properties to physical ^{4}He system 2—17267
coherent properties of systems with fixed particle number, field operator tensor properties 2—27102
collision processes, effect of strong repulsion at short distances 2—23298
compressibility and current parameters of Fermi-liquid 2—9944
dynamic structure factor 2—14139
electron fermi liquid, in mag. field, applicability of kinetic eqns. of Landau Silin theory 2—2179
exchange interactions in Fermi systems, derivation 2—11309
Fermi gas model for nuclear excited states, modifications caused by the existence of collective motions 2—38456
Fermi liquid, charged and neutral, kinetic Landau equations 2—11311
four-fermion model with indefinite metric, fine structure constant 2—37657
free systems, approach to equilibrium 2—7710
gas-liquid instability in many- fermion system, and breakdown of perturbation theory based on plane wave Hartree Fock hamiltonian 2—107
ground-state ideal gas, effective pair potential 2—7717
Hartree-Fock theory of many-fermion system at high densities, exact results 2—108
infinite system, limiting procedure for obtaining physical states 2—2178
interacting gas, one dimensional model, solution in thermodynamic limit 2—37656
interacting gas, phase space analysis 2—23306
internal coordinates 2—33955
liquid, in constant mag. field, kinetic equation 2—11310
liquid ^{3}He and nuclear matter, n-body clusters, cancellation effect 2—12596
nonequilibrium systems, time-dependent Liouville theory, Hartree-Fock resummation techniques 2—20876
nuclear binding energy shell correction calculations 2—5637
pairing interaction, approximate fulfilment of the Pauli principle in the Green function technique 2—33956
phase transition in one- dimensional Fermi systems, introduction of correlation effects 2—11313
quasirelativistic N-fermion problem, reduction to the Pauli formalism 2—2177
Schrodinger eqn. of finite systems, approx. soln. appl. to nucleon correlation in finite nuclei 2—2664
spin susceptibility in nearly- ferromagnetic, temp. depend. 2—36682
structure function and self energy from generalized Hartree approx. 2—30823
superfluid nuclear model, pairing interactions, hydrodynamical limit 2—18069
surface wave, weakly damped 2—20877
two-dimensional Fermi gas instabilities studied in Hartree Fock approximation 2—11312
^{3}He-^{4}He, solution, second sound excitation 2—15623
^{3}He liquid interface with solid, Fermi-gas model of Kapitza resistance 2—35810

Quantum generators *see Lasers; Masers*
Quantum mechanics *see Quantum theory*
Quantum optics
amplified spontaneous emission, spectral distribution, dependence on length and inversion density of active medium 2—37936
anisotropy induced by resonant absorption or amplification of radiation 2—2374
and astrophysics, overlap of fields of interest, review 2—30401
atomic and molecular coherence, review 2—27445
density matrix of matter interacting with nonmonochromatic radiation 2—17571
division of wavefront sideband Fresnel holography, using field emission electrons 2—31068
electronic materials, chemical analysis 2—4604
fluctuating dielectric permeability medium, photon flux 2—5339
fluctuation theory, detuned single mode laser 2—2381
four photon parametric frequency selection in wide stimulated emission lines of dye laser 2—27487
frequency conversion of weak light fluxes by photographic materials 2—11449
Hamiltonian, multiatom, multimode, eigenvalues and eigenvectors 2—7904
Hamiltonian of quantum electronics 2—34366
incoherent emission, description of interaction with substances, using Fokker-Planck-Kolmogorov equation 2—34369
informational properties of linear optical systems, effect of energy sensitive detector 2—14437
ladder approx., Wigner-Weisskopf theory 2—17570

Quantum optics continued
laser, maser operation principles, derivation from Einstein's basic radiation laws 2—37942
laser, quantum theory 2—5348
light beam propagation in atmosphere, obs. by laser-radar techniques 2—16841
light beams, phase-locked, coupled, photon statistics 2—34371
Lorentz spectral line, width meas. using digital photoelectron correlation device 2—7905
microwave nonlinear interaction in acentric crystals 2—23556
multiphoton theory, experimental test 2—27447
multiquantum process, integral characts. rel. to radiation intensity 2—21042
nonlinear effects, second harmonic generation 2—27442
nonlinear optical signals, tunable four photon parametric fluorescence 2—29866
one-photon amplifiers 2—2376
optical and magneto-optical activity rel. to biphotonic absorption and second harmonic generation 2—23698
optical parametric oscillators, internal upconversion and frequency doubling 2—21051
optoelectronics, development (1970-72) 2—34472
paramagnetic 3-resonator amplifier with 30 cm output 2—34373
parametric amplifier in optical information systems 2—7906
parametric oscillator and coupled oscillator upconverter, plane-wave theory 2—21040
parametric oscillator tuning curve, parametric fluorescence 2—21048
phase variables, statistical characts. 2—17569
photocount distrib. in L space points for partially coherent Gaussian light 2—17568
photoelectron statistics, due to mixing of different types of fields 2—27444
photon and electron, interference and correlations in Young-type expts., prod. of beats in photocurrents, optical modulation of electron beams 2—31019
photon counting, improvement using pulse height analyser 2—2640
quantum mechanical systems, in monochromatic and nearly monochromatic fields 2—14105
Raman photon amplifier, quantum statistics 2—31020
spatial correlations and photon counting 2—7910
spontaneous emission from driven Doppler line 2—11934
Superconducting Quantum Interferometer Device and its applications 2—4180
two photon (different modes) amplifier, quantum statistics 2—21039
two-photon amplification, quantum correlations 2—34374
two-photon amplifier, quantum statistics 2—21038
ultra-short pulses, stability and excitations 2—14396
CdF$_2$:Er^{3+}, i.r. quantum counter, by generation of C$_{3v}$ local site symmetry 2—37939
H frequency shift of hyperfine transitions by coherent perturbations 2—31710
Nd^{3+}, amplification cross-section in POCl$_3$-SnCl$_4$-(H$_2$O) system 2—21081
Quantum statistics *see Statistical mechanics/quantum*
Quantum theory
see also Electron theory; Elementary particles; Field theory, quantum
adiabatic invariance for slow disturbance 2—11279
Aharanov-Bohm effect and many body problem, reply to Janossy's treatment 2—70
algebraic, automorphism groups of C*-algebras, fell bundles and W*-bigebras, internal symmetry description 2—7664
analyticity of regularized integrals containing eigenfunctions with complex momentum, use in resonant states 2—7673
angular momentum and spin, relation between classical and quantal theorem 2—14110
angular momentum operators in theory of atomic levels in fields, asymmetric top moments 2—17219
angular momentum theory, graphical methods 2—14099
atom electron shell, energy operators matrix elements, recurrent relations 2 28177
Bell's inequality, stronger form 2—33916
Boltzman eqn. resolution for spin lattice relaxation of electronic spin systems 2—10255
book, conceptual foundations of quantum mechanics 2—37605
book, lectures in mathematical physics 2—37569
book, practical quantum mechanics 2—37606
book, practical quantum mechanics 2—37607
book, waves in physical systems 2—33887
bounded observables, minimal uncertainty states 2—2118
Brownian motion including inter-particle interactions 2—11295
canonical transformations, necessary and sufficient conditions 2—27034
charge, quantized, in terms of pure geometry 2—7678
charged particle in alternating mag. field, Schrodinger eqn. soln. 2—27066
charged scalar particle, mass shift in intense standing e.m. wave 2—37891
classical limit, solution to Schrodinger equation in limit when h→0 2—14094
classical parastochastics and quantum mechanics 2—27087
complex atom, calc. of perturbed orbital wavefunction giving full polarizability of ground and excited states 2—21489
complex semi-simple Lie algebras concerning dynamical symmetries, structure discussed 2—23268
conformal dilatation pictures with scale invariant operators 2—14098
continuous spectrum, perturbation by near-lying level 2—5146
cosmological phenomena and microphysics, unified approach to theory of matter 2—4768
Coulomb functions in entire (η,ρ) plane, computer program 2—34997
Coulomb Green function, equivalence of expressions 2—2905
Coulomb potential, diffusion and drift 2—17231
Coulomb potential, screened, properties 2—5774
Coulomb problems, canonical transformations 2—33925
Coulomb T-matrix, on-shell 2—2906
cyclotron resonance spectrometer, quantum mechanical description, noise analysis 2—14375
decay, new theories for interpretation of measurements 2—5492
decay expts. interpret. 2—31187
decomposition of quantum systems into sub-systems 2—7670
density matrices, positivity constraints 2—5148
diagonal hypervirial theorems, derivation for bound state trial wavefunction 2—11272
dibaric particle in constant magnetic field 2—7674
Dirac current, Gordon decomp. method 2—27064

Quantum theory continued
- Dirac Feynman Gell-Mann equation, classical counterpart rel. to classical spin variables 2—20843
- Dirac matrix for spherically symmetric potentials 2—27058
- Dirac particle, stigma in even environment 2—37613
- Dirac particle, stigma in even environment 2—37612
- Dirac particle in scalar Coulomb field 2—37621
- dispersion at resonance, formulae 2—20844
- eigenfunctions of spin and orbital angular momentum by projection operator technique 2—15184
- eigenvalue problem, square well in phase plane, film demonstration 2—27051
- eigenvalues of Hermitian operators, limits to the accuracy of Cohen Feldmann bounds 2—7679
- eigenvalve of hamiltonian, derivatives determ. from general matrix formalism, calc. of molecular properties 2—37616
- elastic collision trajectories, uniformization, semiclassical transition probability theory 2—27065
- electron plasma, static shielding, intermediate magnetic field strength 2—8926
- electrons, behaviour, free electron physics, book 2—17831
- elementary excitation observables, conditions for simple bounds given a single measured observable 2—30784
- elementary systems, invariance requirements for determ. of localized states 2—5140
- equation of motion with higher derivatives, derivation 2—14092
- fine structure constant, investigation of Wyler's expression 2—2133
- fractional parentage coeffs. rel. to matrix elements of irreducible tensorial operators 2—24324
- free particle Hamiltonian, complex energy eigenstates, function spaces 2—17220
- free particle positron uncertainty, time variation, matrix derivation 2—14093
- gaussian functions, rapid calc. of integrals 2—15271
- generalized oscillator phase operators, continuity of spectra 2—5139
- generalized wave operators, existence and completeness for spherically symmetric asymptotically Coulomb potentials 2—11278
- gravitation, redundancy of constraints 2—20830
- Green's functions, determ. by orthogonal operator expansion method 2—33924
- Hamiltonian eigenvalue parameter derivatives 2—37618
- Hamiltonian for molecular rotation and vibration examined, analysis of effect of a change in molecular-fixed axes 2—8535
- Hamiltonian ground state determ., application to pairing interactions 2—11709
- hamiltonian matrices, lower bound on eigenvalues, application to n-electron systems 2—23270
- Hamitonian, for system with nonlinear Lagrangian 2—37604
- harmonic oscillator, forced, correspondence principle methods 2—5773
- harmonic oscillator, large-ω asymptotic expansions, Pade approximants 2—17235
- harmonic oscillator field, Brownian motion of particle 2—37635
- harmonic oscillator functions, computer program for generalised transformation brackets 2—30793
- harmonic oscillator two-centre integrals, Gauss potentials 2—27068
- harmonic oscillators, orthogonality relations of many time generating functionals 2—27067
- Hartree approx. generalization, space time correlation function 2—30823
- heat transport, in isotopically substituted one dimensional harmonic crystal 2—25689
- Heisenberg uncertainty relation, geometrical approach 2—2135
- Hilbert space sequences, applications to quantum mechanics 2—2116
- Hilbert space structure, axiomatic foundation, improved formulation 2—30782
- hyperdifferential operators appl. to quantum mech. 2—5125
- integral equations for four identical spinless particles obtained using Feddeev Yacubovsky approach 2—30788
- interacting spin systems, calc. of time dependent correlation functions 2—2137
- interstellar formaldehyde, collisional pumping mechanism for anomalous 6 cm absorption 2—26750
- intravectorial formalism 2—7675
- ionic. cryst., Hartree-Fock eqns., Lowdin's approx. 2—25240
- isotropic two-dimensional oscillator, matrix elements of powers of P and Q operators 2—37619
- Jost function of central momentum-dependent S-state interaction 2—2144
- Kapur-Peierls eigenstates for S- and P-wave scattering by square well potential 2—27070
- Kato perturbations, class of zero-dimensional models 2—2136
- Lagrangian and Hamiltonian formalism consistency for const. curvature space 2—33917
- Laplacian operator, alternative derivation in spherical coordinate system 2—27050
- Lie algebras and quantum mechanics, textbook 2—32
- linear chain with free end boundary conditions, quantum field theory operators derived 2—11290
- Lippman Schwinger kernel, determ. of eigenvalues 2—7672
- local hidden variable theories, exptl. test using linear polarization correlation of photons in Ca atomic cascade 2—31659
- local hidden variable theories, proposed experimental test 2—2117
- local hidden variables theories, proposed exptl. test 2—69
- Lorentz invariant particles, classical system 2—2087
- m-dimensional anisotropic harmonic oscillator, translational degrees of freedom, exact solutions in magnetic field 2—20850
- many electron systems of interacting particles, calc. of second order physical props by Green's functions 2—8415
- many-body problem in one dimension, exact results 2—27097
- many-body systems, continuity equations 2—14112
- master equations with canonical invariance 2—11274
- matrix equations, failure to satisfy algebraic relations of operators 2—30791
- measured quantal object, entropy changes 2—7665
- measurement, space-time structure 2—17234
- measurement theory, entropic processes 2—67
- minimum uncertainty and density matrices 2—30783
- minimum uncertainty packets, equivalence classes 2—5149
- molecular Bethe Goldstone equation, solution for transbutadiene molecule 2—35205
- molecular crystals, mechanical excitations and quantum theoretical formulation of linear electrodynamics 2—40015

Quantum theory continued
- molecular solids, treatment of lattice dynamics 2—32789
- momentum space probability distribution for 1 d wave packet impinging on square well potential, illustrative film 2—14102
- monatomic gases, second virial coeff. and Ursell Mayer function, quantum mechanical perturbation expansion 2—32173
- multichannel problems, WKB solns. and semiclassical scattering matrix elements 2—23282
- multilevel quantum system, interact with polychromatic e.m. field, semiclassical and quantum treatment 2—5138
- multiparticle partial-wave amplitudes, inelastic unitarity, Racah coeffs. for Poincare group 2—17813
- N-completeness problem, relationship with N- representability, geminal expansions 2—23269
- n-dimensional anisotropic oscillator in uniform mag. field, exact solutions 2—20849
- N-particle noninteracting Green function 2—33921
- N-particle system, permutation symmetry, energy lower bound method 2—37650
- nonlinear wave mechanics 2—17224
- nonseparable systems, classical quantization using classical limit Green's function 2—7666
- observables, exact and simultaneous measurements 2—23267
- one dimensional mechnaicl continuum, relativistic quantum mechanics, subsid. cond. of dual resonance model 2—7669
- one electron systems, pointwise bounds for eigenfunctions 2—15240
- one-dimensional potential, bound states 2—20847
- one-electron atomic wave functions, analysis in modern physics course 2—17221
- operator algebra, use of coherent states 2—27053
- operator construction methods 2—7677
- oscillator, nonlinear conservative, periodic to stochastic transition, Zwanzig theory 2—11286
- oscillator phase operators, states minimizing uncertainty product 2—23280
- pairing plus monopole Hamiltonian on two shells, exact solution by boson representation of group Sp_4 2—14097
- particle scattering by exponential potential, distortion operator method 2—20853
- particles, probability interpretation along classical trajectories 2—17225
- particles with spin zero and one half in external fields 2—23279
- Pauli and Dirac matrices, trace of product 2—11280
- phase space description of quantum system 2—14096
- position-momentum uncertainty relation 2—33927
- potential scatt, validity of modified Glauber eikonal approx. 2—11288
- potential scattering, inverse problem from Dirac eqn. 2—27071
- potentials, with suppressed S-wave phase shift at low energies 2—23285
- prediction, consequences of dropping reduction postulate 2—5141
- probability density, classical limit for perturbed change in Hamiltonian 2—17227
- product representation of exponential Hamiltonian operator, convergence of density matrix 2—14126
- propagator, canonical functional integral representation 2—27061
- proposition systems, closure of gap in covering law 2—23266
- pseudopotential theory, similarity transformation of Schrodinger eqn. 2—20817
- pure operations, theory 2—17218
- quantum measurement problem, existence 2—33918
- quantum measurement problem, existence 2—30785
- quantum mechanical expectation values, upper and lower bounds 2—2904
- quantum mechanical systems, in monochromatic and nearly monochromatic fields 2—14105
- quantum mechanics, decision procedures 2—33920
- quantum mechanics, formulation in auxiliary algebras 2—20841
- quantum mechanics, inverse decay problem 2—2138
- quantum mechanics, operator valued measures, finite and infinite processes 2—11277
- quantum mechanics, reduction to classical mechanics 2—17223
- quantum mechanics, spectrum generating Lie algebras and symmetries 2—33923
- quantum mechanics, spectrum generating Lie algebras and symmetries 2—33922
- quaternionic wavefunctions for triply degenerate states 2—23272
- radial oscillator, canonical transformations 2—33925
- radiative electron transitions, microscopic model 2—7687
- recurrence relations, approx. solution technique, applic. to 3-J and 6-J symbols 2—2127
- reduced density matrices, necessary conditions for N-representability 2—11281
- reformulation, deterministic ensemble theory 2—68
- relativisitic, deviation of infinitesimal particle propagator by consideration of nature of mass 2—17237
- relativistic, spin independent energy shifts for free electron 2—8087
- relativistic exchange operator, partial wave expansion, Coulomb integral calc. 2—14107
- relativistic particle with spin, position operator 2—5152
- relativistic quantum dynamics of string model of hadrons, wave eqn. and dual amplitude 2—8126
- relativistic quantum mechanics, projective representations and relation of internal to space-time symmetries 2—20846
- relativistic quantum mechanics and S-matrix theory 2—14511
- relativistic two-body problem, quantum mechanics solution 2—33890
- resonance quasi-projection operators, Feshbach formation, examination of idempotency requirement 2—11988
- scattering, Fredholm and Pade approx. for coupled channels 2—20852
- scattering, instructional uses of computers 2—2051
- scattering, spin-$^1/_2$ particles, polarization vector description of spin effects 2—27069
- scattering 2—33928
- scattering amplitudes, in non-physical region 2—37625
- scattering by spherical well, Pade approximants used to calculate bound states and phase shifts 2—30796
- Schwarz-Hora effect, treatment as one-electron quantum mechanical phenomenon 2—6707
- single particle and collective degrees of freedom, interaction by perturbation treatment 2—14104
- singular potentials, duality rel. to potential scatt. with indefinitely high spin 2—7685
- space-time and general relativity 2—2103
- space-time code, position operators 2—27052

Quantum theory continued

spherical-top molecules, collision-induced far i.r. rotation-translation spectrum 2—5896
spin-1 particle motion, in homogeneous magnetic field, multispinor formalism 2—17238
statistical system satisfying axioms of quantum logic 2—2119
stochastic quantum mechanics, derivation of electron anomalous magnetic moment 2—30795
structure concept from magnetic moments 2—37603
superoperator transformation thories of Prigogine and Kummer, equivalance 2—30794
symmetry group, relativistic quantum mechanical 2—17216
systems of atoms, nuclei and electrons, second quantization representation 2—2121
teaching of introductory quantum mechanics using a computer 2—11271
three body bound state, high energy phase shift behaviour 2—17236
three body rearrangement scattering, comment on quantum mechanical collinear model 2—20851
three dimensional harmonic oscillator, high order perturbation theory for generalized central field perturbation 2—7680
three particle problem, numerical calcs. in continuous spectrum 2—27093
three-body problem, exterior-interior separation 2—37620
three-body problems, quantum mechanical approach 2—77
time of arrival operator, Hermitian operators 2—17217
two dimensional harmonic oscillator, recursion relations for matrix elements 2—11285
two particle harmonic oscillator wavefunctions, product expansion using 2nd quantization 2—14111
unstable quantum systems, decay theory 2—17229
vibration rotation Hamiltonian, 4th order of bent XYX type molecule 2—15275
wave mechanics, hydrodynamical model, limitation of one body treatment 2—2125
wave mechanics, hydrodynamical model, treatment of Stern Gerlach effect of H atoms 2—2124
wave mechanics, statistical foundations and nonsymmetric binomial distribution, application of computer 2—27012
wave packets, three-dimensional, time dependence of resonance dispersion 2—37608
wave transmission through potential barriers, approximation theory 2—23277
Wigner 9j coefficients, structure in Bargmann approach 2—2139
Wigner quantum distribution function, kinetic equation integration 2—37602
WKB approximation, polarised medium, nonadiabatic transition probability 2—865
WKB method, generalized, second approx. 2—24203
$H+H_2$ collinear reaction, quantum mechanical computational study, close-coupling method 2—20172

application methods
atom-diatom collisions, reactive, exact quantum cross sections for three-dimensional angle dependent model 2—4568
atomic systems, many-body methods 2—562
Casimir-Polder interactions, long-range, quantum- mechanical sum rules 2—21529
chemical reactions, quantum-mechanical Hamiltonian 2—33362
complementary variational principles in Thomas-Fermi theory for neutral atoms 2—38805
crystalline defect motion 2—19071
damped linear-vibration systems, local modifications, procedure for determ. eigenvalues and eigenvectors 2—17362
deformed nuclear shell models of axial symmetry, spurious rotational states 2—21359
dislocation motion 2—15759
electron removal, wave function determ. 2—18323
electron-atom collisions, cross sections calc., Vainshtein and Born approx. 2—5857
electrostatic interaction matrix element calc., relativistic correction 2—27059
expansion technique for electron-atom inelastic scatt. 2—35178
gas-surface interaction theory, rate of attractive potential 2—9234
Green's functions of Schrodinger equation for simplest systems 2—14109
harmonic oscillator evolution of quantum states in a uniform time varying electric field 2—11284
harmonic oscillator potential interaction, two-particle case 2—27056
harmonic oscillator quark model for decay widths of meson resonances 2—21293
Hartree- Fock-Roothaan equation, relations for supermatrices 2—2903
Hill determinant appl. to anharmonic oscillator 2—17233
interaction between two quantum-mechanical systems, effect on measurements 2—5137
interpolation theory for quantum mechanics 2—30792
Jastrow correlations, one-body and two-body 2—5151
Landau-Teller interaction, exact quantum-mechanical transition probabilities 2—21713
liquid crystals, calc. of spectrum of elementary excitation 2—15568
many-electron systems, theory of separability 2—8417
matrix elements, spin-free computation, simplificatons due to invariance group 2—8416
matrix elements in orthogonal scheme 2—27060
metal, adsorption, book 2—15672
metal, adsorption, review 2—15676
model-space effective Hamiltonian, folded diagram expansion 2—2140
molecular systems, many-body methods 2—562
nonlinear optical effects, variation-perturbation method 2—15540
nuclear binding energy, K-harmonic method, accuracy 2—14911
nuclear fission, approach to asymmetry of process 2—31596
nuclear model, matrix ensemble obtained from Brownian motion process and boundary conditions 2—2132
open systems, time evolution, harmonic oscillator model 2—20869
parametrically interacting e.m. oscillations 2—30917
quantum mechanical impulse approx., applic. to vibrational inelastic scattering 2—3134
Raman scattering by damped polaritons 2—16518
Rayleigh-Schrodinger perturbation theory application to H atom 2—21539
renormalization perturbation theory and degenerate potential 2—74
scattering, reactive and nonreactive, nonpartial wave treatment, coupled integral equation formalism 2—2902

Quantum theory continued
application methods continued
Schrodinger eqn., radial, for electron bound in central field potential, asymptotic solution 2—2130
Takabayashi angle calc. for hydrogen atom 2—8483
transcorrelated method for accurate correlation energies using gaussian-type functions 2—35105
tunnelling, classical trajectory contribution, semiclassical limit of Feynman path integrals 2—7668
van der Waals potentials, long-range, sum-rule moment bounds 2—21528
variational methods for electron plasma with self-consistent field interaction 2—33958
Wiener-Khintchine theorem for e.m. fields, new formulation of quantum-mechanical analogue 2—33926
$H+H_2$ reaction, quantum calculations of planar reactivity, application of mathematical techniques 2—33369
$H+H_2$ reaction, quantum calculations of planar reactivity, development of mathematical techniques 2—33368
He, unbound states and asymptotically correct bound states, least squares calc. 2—18355
$LiNbO_3$, eigenfrequency, eigenvector and Raman scatt. cross section of polaritons 2—16554

many-particle systems *see Helium/liquid; Quantum fluids; Statistical mechanics/quantum; Superconductivity; Superfluidity*

quantization
see also Field theory,quantum/quantization
Bergmann technique, application to electrodynamics and relationship between gauge invariance manifest covariance and observer dependence 2—2497
dynamic systems, application of analyticity 2—14095
dynamical quantization procedure 2—23238
dynamical systems, classification theory 2—11275
eigenprobabilities 2—2120
Einstein equations, local quantum theory formulation, locality 2—17202
general Lagrangian systems, Hamiltonian formalism for exceptional case 2—20840
gravitational waves, cylindrical, canonical quantization 2—57
kinetic energy with variable inertia, operator determ. by fundamental properties 2—17239
magnon-phonon interaction in time- dependent magnetic field, theory based on quantization of magnetoelastic field 2—40437
spinning particle, quantization of relativistic classical mechanics equation of motion 2—27117
stress waves, rel. to fracture theory 2—37673

wave equations
see also Dirac equation
alkali halide, M′-centre, weakly bound electron wave function 2—25449
alkali metal atom, nonrelativistic wave functions and eigenvalues 2—18317
alkali metal atom, optical electron transitions, wave function calc. 2—18313
atoms, $2\leqslant Z\leqslant 126$, relativistic Hartree-Fock-Slater eigenvalues, radial expectation values and potentials 2—572
construction when mass levels known 2—37611
coupled eqn. system in hyperspherical formalism, reduction 2—20842
detailed wave eqn. theory, for extended model underlying dual amplitude 2—31212
eigenfrequency density oscillations, wave equation in finite domain 2—14103
Gaussian wave functions, many body problem 2—33952
Gel'fand-Yaglom, finite dimensional, construction for arbitrary integral spin particles 2—37610
helium-like atomic systems, correlated wavefunctions 2—31724
hypergeometric difference equation for Stark-ladder effect in crystals 2—25726
interacting spin particles, separation of angular and radial variables 2—2123
kinetic energy expectation values with discontinuous approximate wave functions 2—23275
Klein-Gordon, persistence of S-matrix singularities 2—2131
Klein-Gordon field eqns, with self-interactions, particular solns. 2—2483
linear relativistic wave equations of particles with spin $^1/_2$ 2—30790
many-body wave functions, with correlations, systematic theory 2—2141
massless, conformal group 2—37615
Mathieu equation, complex eigenvalue determ. 2—17228
neutrino, relativistic wave equation 2—23792
nonlinear Klein-Gordon eqn., theory and appl. 2—2064
p-nuclei, unitary scheme wave function, decomp. coeffs. 2—24126
partial wave Schrodinger eqn. finite difference soln. 2—7672
partial-wave Lippmann-Schwinger equation, simple numerical solution 2—20845
periodic lattice, rel. to dynamical theories of X-ray and electron diffr. 2—3617
permutation symmetries of wave functions, applications to density matrix theory 2—72
plane wave factors, Euler Lagrange optimization, atomic collisions 2—73
quasi relativistic equations for charged fermions in external e.m. field, deduced from electrodynamics 2—71
quasi-hole states, singly-occupied orbit model 2—35122
relativistic, massive particles with arbitrary spin 2—17230
relativistic function, effective potential method 2—37609
relativistic Hamilton-Jacobi equation, rel. to construction of Dirac equation 2—2128
relativistic spin-zero equations, solutions 2—23273
Schrodinger, error analysis in numerical algebraic method 2—27055
Schrodinger, independent particle eqn. for non-axially symmetric nuclei, numerical soln. 2—2675
Schrodinger's eqn. and radial elec. fields 2—23274
Schrodinger's equation, derivation 2—10804
Schrodinger eqn., one-variable, generated by hypergeometric eqn., potential construction 2—2134
Schrodinger eqn., periodic potential, N dimensions 2—5147
Schrodinger eqn., radial, for electron bound in central field potential, asymptotic solution 2—2130
Schrodinger eqn. derivation from Newtonian mechanics 2—30789
Schrodinger eqn. radial part, appl. to particle scatt., soln. using minicomputer 2—5153
Schrodinger eqn. separation in thin films 2—13066
Schrodinger eqn. soln. in terms of wavefunctions least distorted from prods. of atomic wavefunctions 2—2126

Quantum theory continued
wave equations continued
Schrodinger eqn. soln. in two media joined on surface, Green function technique 2—16091
Schrodinger eqn. with δ-function potentials, exact soln. 2—16095
Schrodinger equation, computer solutions, undergraduate teaching 2—33844
Schrodinger equation, heuristic approach for elementary students 2—14100
Schrodinger equation, identities involving coefficients in asymptotic expansion of outgoing scattering solution 2—33929
Schrodinger equation, least squares solution by Monte Carlo method 2—30786
Schrodinger equation, path integral solution in curved spaces 2—2129
Schrodinger equation, wave-packet solution in WKB approximation, classical limit 2—17222
Schrodinger equation for alpha decay of Pt, Au and Hg isotopes 2—11786
Schrodinger equation for molecular vibration rotation energies, remarks on two-step procedure for calculation 2—8536
Schrodinger equation with central potential, exact solution 2—7671
Schrodinger equation with Yukawa potential, bound state solutions by integral equations 2—14106
Schrodinger equations, application of generalization of concept of invariance of differential equations 2—33870
Schrodinger operators, one-particle, application of criterion for rigged Hilbert spaces 2—37614
Schrodinger time dependent eqn., approx. soln., application to atomic and mol. scatt. 2—27054
Schrodinger wave eqn. for 3 nucleon system 2—38470
Schroedinger, tight-binding, time dependent Green's function 2—27076
Schroedinger, time dependent, solution for harmonic oscillator in electric field 2—11284
semicylinder, Schrodinger eqn., reduction of elliptic integral boundary problems to mixed problems 2—30754
spherically symmetric potentials, Dirac and t matrices 2—11276
spin maximum 1 particle 2—27057
spinor space approach to hadron mass formula 2—31209
statistical distrib. general dynamical model, analogy with Schrodinger eqn. 2—33945
statistical moments of a wave packet, time evolution 2—14101
variational wavefunctions, adiabatic theorem 2—30787
wavefunction, SCF, used to calculate X-ray scattering factor and diamagnetic susceptibility of H_2S gas 2—786
wavefunctions of bound states in potential well, normalisation of higher-order phase-integral approximations 2—20848
CO, electron scatt. at near thermal energies, effect of molecular wavefunction 2—18405
H_2^+, variational wavefunctions, exact radial elliptic coordinate dependence 2—31796
Na atom, nonrelativistic wave functions and eigenvalues 2—18317
Rb atom, nonrelativistic wave functions and eigenvalues 2—18317

Quarks
additive quark model, statistical tensors, bounds for linear combinations 2—8125
axial quark number in framework of chiral Lagrangians, investigation of η meson 2—14625
bootstrap origin 2—23807
bound state, self-consistent model 2—31218
collapsed nuclei, quark model 2—8265
cosmic ray experiments compared with limits attainable using CERN intersecting storage rings 2—23901
cosmic rays at sea level and mountain altitude, search for quarks 2—23905
current-current quark model, hadronic hyperon decays 2—11642
delayed penetrating particles near air shower cores 2—23903
dual model possessing gauge identities 2—386
dual pion-quark model, equivalence of fermions in individual models 2—17844
dual pions, quark model 2—410
dual quark-gluon model of hadrons, derivation of quark emission vertex 2—8128
dual realistic quark model 2—31215
dual relativistic model for $\pi\pi$ and πN scattering amplitudes, high energy aspects 2—27731
dual relativistic quark model, low energy aspects for $\pi\pi$ and πN scattering amplitudes 2—17945
dual resonance model, quark spin 2—31240
gluon model, scalar and pseudoscalar, implications of bound states problem in relativistic field theory 2—38198
gluon-quark model, light-cone structure of current commutators 2—2522
hadronic interactions, small distances 2—390
hadrons, quark-parton model for e.m. mass differences 2—11581
harmonic oscillator quark model for decay widths of meson resonances 2—21293
hyperon-nucleon interactions, quark model rules for total cross-sections 2—11643
hyperons, nonleptonic decay, current current quark model 2—17977
lepton scatt., inelastic, quark models 2—17826
leptons and quarks, U(4) symmetry scheme 2—38228
light cone structure of model, proposed scaling law for hadron electroprod. 2—14583
lightlike model, current densities 2—17845
magnetic and electric quarks in hadrons, Diracs magnetic monopoles 2—34623
mass, upper limit, from study of dip in $\pi p \to \pi \Delta$ reaction 2—17866
meson model based on principle of temperate interaction 2—403
model, for $K^+p \to K^{*0}N^{*++}$, expt. verification 2—5527
model fo diffractive production with quark spin flip 2—23813
nonlinear interactions, e.m. and weak interactions 2—8101
nuclear resonances, quark model of neutrino excitation 2—31332
O(3,1) quark group model, with mesons having an inner structure 2—38247
partons, calculation of mass 2—31214
photoproduction of vector neutral mesons on nucleons, Glauber model, quark model 2—14673
pion model identical to Bardakci's sector of dual quark model 2—21252
quark model double scattering relations, accuracy 2—31250
quark parton model, application to calc. of constraint relations for structure functions of inelastic Compton scattering 2—17817
quark parton model, structure analysis, configuration mixing 2—23806
relativistic model, hadron interaction study 2—34631

Quarks continued
relativistic quark models, evaluation 2—14590
relativistic scalar model with strong binding, dynamics discussed with Bethe-Salpeter equation 2—17842
search, in air showers of energies between 10^{13} and 10^{15} eV 2—17843
search for beyond the atmosphere using proton-3 satellite 2—23904
eN, deep inelastic scatt., polarization effects, quark parton model, parallel and antiparallel asymmetry 2—27712
N* electroproduction in quark model 2—23897

Quartz
α, photoelastic dispersion of stress-birefringence meas. using Soleil Babinet compensator 2—36820
β, single crystal, polarized Raman spectra meas. determ. characteristics of fundamental optical modes 2—16507
β-quartz models used to determ. optically active vibrational modes of vitreous SiO_2 and BeF_2 2—22382
acoustic diffr. beam spreading for propagating modes 2—32820
acoustic resonator, disc shaped u.s. resonance method study 0.8-26 MHz 2—5218
acoustic vibration, laser beam intensity modulation obs. 2—16019
adsorption of akylchlorosilanes on crystal surfaces 2—32394
adsorption of Ar, n-hexane, and water vapour, piezogravimetric method of obs. 2—25223
artificial, growth, passive faces and imperfection surfaces 2—18970
birefringence, direct measurement by det. of thickness of half-wave plate 2—7048
Brillouin and Raman scattering, absolute cross-sections 2—16522
channelling, of H^+, D^+ and He_4^+ 2—29579
colour centre, interstitial Fe^{3+} in synthetic brown quartz 2—3806
coupled vibrs. of X-cut plates, reson. freq. temp. depend. 2—29758
creep deformation, from various regional metamorphic environments 2—9668
crystal, deposition monitor 2—3510
crystal microbalance, use for outgassing and opt. contamination meas. 2—41413
dielectric consts. meas. 2—33048
diffuse X-ray scattering, near α-β transition 2—4038
diffusion of implanted He, gas release monitoring 2—9627
dispersion in disintegrator, S-O band rupture, free radical formation, e.p.r. obs. 2—20151
elastic surface waves, collinar nonlinear interaction 2—40057
electrical conductivity, OH diffusion 2—6751
electrolytic sweeping of alkali ions 2—4598
electroptic coeff., dispersion and temp. dependence, light modulation 2—13440
fibre manometer, bakeable to 520°C, for 10^{-1} to 10^{-6} torr 2—20785
filter crystals, v.h.f. waves, mode control 2—5235
fired, thermoluminesc. sensitivity, radiation-induced increase 2—13517
fused, gas permeability 2—25471
fused, hypersonic phonons at low temp., stimulated Brillouin scatt. obs. 2—16587
fused, surface wave vel. and second harmonic generation 2—25671
fused sheets drilled using CO_2 laser, meas. of hole depth vs. absorbed laser intensity 2—36220
gauge, shock wave induced polarization 2—14356
glass, high temp. and u.h.f. dielec. props. 2—19746
hypersound attenuation by collinear phonon interactions 2—4048
imperfections, positron annihilation applic. as probe 2—32488
interstellar grains, irradiated, to account for interstellar extinction 2—10920
laser induced damage, dependence on mode structure 2—12743
laser radiation self-focussing and filamentary damage 2—13429
light diffraction efficiency of acoustic surface waves on quartz 2—5423
mechanical activation during grinding. ^{57}Fe Mossbauer obs. 2—32712
mechanical strength, temperature dependence of ultimate strength 2—39879
microscopically damaged, laser beam catastrophic damage threshold 2—29859
molten, struct. 2—9222
nonlinear polarization coeffs. determ. 2—36601
optical absorpt. and rotatory power, impurities influence 2—10305
optical interband transitions, X-ray spectra obs. 2—20085
optical modes, stimulated Raman effect 2—16566
optical vessel for gases and liquids at elevated pressures and temperatures 2—37532
oscillator, realizable precision in film thickness measurement 2—35879
phenolic, laser-induced stress waves 2—15814
piezoelectric crystals, use in measuring the thickness of films during deposition 2—35881
piezoelectric current, x-cut sample subjected to short duration shock wave loading 2—22629
piezoelectric deform. of X-cut discs, hysteresis 2—16296
piezoelectric vibrators, effect of neutrons and X-radiation on resonance frequency and elastic properties 2—25934
position annihilation in single crystals, expts. confirming peaks on momentum distrib. of annihilation photon 2—29582
powder grain size determ. by X-ray diffraction, extrapolation method 2—32744
α-quartz, Ag electromigration paths and cryst. perfection 2—29223
α- quartz, synthetic, dynamics of impurities 2—19387
α-quartz, X-irradiated, e.p.r. of Ti^{3+} centres 2—4543
quartz-Fe dispersion, mechano-chemical reactions, e.p.r. and Mossbauer obs. 2—19988
radiative emission meas. of sinters by cooling or specimen 2—27309
refractive index modification, by ion implantation 2—25417
resonator for simultaneous stress and mass change meas. in films 2—35878
resonators, Na_2CO_3 process cultured, Q capability from i.r. absorption meas. 2—14301
resonators as thermally sensitive elements of frequency transducers 2—37826
shock propag. produced by planar impact 2—9637
smoky, inpurity colour centres, e.p.r. and thermoluminescence studies, trapped electron dating 2—22226
soft mode linewidth, temp. depend., near α-β phase transition 2—20078
solid state isotherms 2—4642
solubility in NH_4F aqueous solution, temp. and conc. depend. 2—35739
spectral emission capacity in 2-25 μm region 2—40724
spectral reflectance in near i.r. 2—26112
stress corrosion cracking, static fatigue 2—1327

Quartz continued
substrate. meas. of helium film profile at 2.10 K 2—3419
surface acoustic waves, optical probing of internal behaviour 2—29517
surface cond., water vapour adsorption depend. 2—39547
surface elastic waves, surface motion obs. 2—40056
thermal conductivity det. by steady state method, fused and crystalline forms 2—16732
thermoluminescence, press. and thermal effects, pot. as rad. dosimeter 2—29986
ultrasonic delay lines with zero temperature coeff. of delay 2—5231
vectors, determ. of sign by X-ray topography 2—32534
vibrating cryst., neutron time spectrum 2—9430
X-cut, surface wave transducer, impulse response in Rayleigh wave system 2—5239
X-irradiated α-quartz, e.p.r. studies of Ti^{3+}-H$^+$ centres 2—22827
X-ray spectral characteristics from dynamical diffr. theory 2—33292
yellow colour centres, Fe^{3+} and Co^{3+} doping 2—19131

Quartz resonators *see Piezoelectric oscillations; Resonators; Transducers*

Quasars
see also Cosmic radiations, radiofrequency; Cosmology; Galaxies; Stars
3C173, electronographic obs. 2—10926
3C273B, radio and optical positions 2—7472
3C455, optical object 2—10949
3C 273, observation of periodicies of light variations 2—23086
3C-279, two components moving apart at super-light velocities 2—30513
3 273, circular polarization obs. 2—37334
γ sources search at 10$_{11}$-10^{12} eV, null result 2—33722
absorption line redshifts 2—13932
absorption spectra 2—13931
analysis on basis of radio and optical observations 2—20609
astrophysical and cosmological problems 2—16949
b2 1215+30, brightness meas. 2—37327
BL LAC, relation between the optical and centrimetric polarized emission 2—13935
BL LAC and five other variables, polarization and colour variation 2—33702
bright galaxy association, study of 222 QSRS's and 166 QSO's 2—37326
3C273, association with NGC 4151, optical and i.r. curves 2—20491
3C273, gravitational deflection of radio waves 2—30510
3C279, gravitational deflection of radio waves 2—30510
3C279 and 273, fine structure variations at 7840 MHz 2—4911
3C 173, identification and UBV photometry with an electronic camera 2—30508
3C 273, γ-ray obs. 2—4948
3C 273, circular polarization 2—4944
3C 273, obs. at 8.2 mm 2—13963
3C 273, randomness of optical fluctuations 2—13937
3C 273, UBV observations during 1970-71 period 2—20608
3C 273, X-ray spectrum, determ. heavy element abundance in intergalactic medium 2—26612
3 C 279, polarization at 8GHz during 1966-70 outburst4910 2—4910
3C 279, Q.S.S., detection of double source structure in nucleus 2—4936
3C 345, obs. at 8.2 mm 2—13963
3C 84, obs. at 8.2 mm 2—13963
3C-273, critique of periodicity 2—33701
catalogue of optical data 2—4918
chronology of condensed matter from collective evolution 2—17015
classification, optical form. 2—13858
compact objects, energy conversion by rotation of massive objects with magnetic fields 2—13941
compact objects, magnetoid instability in twisted magnetic fields and repeated explosions 2—13944
compact objects, optical classification 2—13860
conference, Dordrecht (1970) 2—13847
cosmic rays, ultra high energy, quasars as possible sources 2—1931
cosmological evidence 2—13951
cosmological evolution 2—20462
density and luminosity evolution 2—33703
depolarization at long wavelength, correlation with redshift 2—41146
differentially expanding atmospheres, line profiles 2—30509
distribution in space 2—13931
distributions of size and brightness, 8 GHz obs. 2—30520
emission line intensities from predictions of photoionization of gas clouds 2—10842
energy release and nonthermal radiation, explanation using field modific. of classical gravitational theory 2—16948
energy source, construction and theories of behaviour 2—30511
evolution of massive cores in post quasar phase 2—13945
evolution of radio and optical luminosity 2—10927
faint spectra using Lick Observatory image-dissector scanner 2—41270
fragmentation of supermassive disks 2—7366
galaxies with u.v. continuum, list of 99 objects including Seyfert galaxies and quasars 2—33599
high brightness, circular polarization obs. 2—30522
identification of 18 southern QSOs 2—33700
i.r. observations 2—13934
local and cosmological, two classes proposal to explain redshifts 2—26772
luminosity function and bivariate ratio obs. 2—20611
luminosity functions and density evolution, method allowing for observational selection for 3CR quasars 2—4915
magnetoid expulsion and momentum conservation in metagalactic astronomy 2—13940
mass-distance relations 2—13931
masses, upper limits 2—7470
matter-antimatter model 2—13947
models for cosmic evolution 2—17017
and N galaxies, properties, comparison 4916 2—4916
OJ 287, energy distribution between 0.36 and 3.4 μm 2—10930
optical large scale variations and history 2—13942
optical variability 2—13936
optically variable, PKS 0906+01, PKS 2345-16, NRAO 512 and OX 074, characteristic behaviour 2—4914
origin, blueshift obs. 2—30512
PHL 5200, CIII and CIV lines in nebula, indirect evidence for presence of dust 2—33704
PHL 5200, RS 23, physical properties of absorption envelopes 2—13933
PHL 957, absorption line profiles 2—37325
PHL 957, QSO, photometry, absorption lines 2—20618
PHL 957, radio quiet, spectrum 2—10923

Quasars continued
photoelectric obs. of stars nearby 2—20554
photoionization of intergalactic hydrogen, heating mechanism 2—26611
PKS 0237-23, C/Si and Al/Si abundance ratios 2—4909
PKS 2134+004, speed of light received greater than 440,000 km/sec 2—23085
PKS 2251+11, spectra of two associated galaxies 2—13845
polarization, linear, obs. at 49 cm 2—13939
QSO, absorption lines and low mass protogalaxies 2—20612
QSO, angular distribution of those associated with 4C radiosources 2—10928
QSO, Balmer lines, effect of flue of relativistic electrons on relative intensity 2—30434
QSO, compact, radio emission 2—13959
QSO, energy source and structure, from collision of two gas clouds 2—26768
QSO, gamma ray absorption by photons 2—10925
QSO, redshift periodicities 2—26770
QSO, southern, redshift obs. 2—26769
QSO, spectra and time variations 2—13965
QSO, time dependence of emission line strengths 2—10840
QSO's, optical and radio luminosity functions 2—1966
QSO's and Seyfert galaxies, radiation from, size limitations on thermal and nonthermal models 2—17018
QSO's multiple pulsar model 2—20617
QSOs absorption of gamma rays by photons 2—26771
QSS, extragalactic, intensity variations, rel. to spectra 2—13962
quasi stellar objects, optical monitoring 2—4913
quasistellar object, PHL 957, spectrum 2—10923
quasistellar objects, luminosity function at 400 and 2700 MHz 2—4923
quasistellar objects, photoionization and emission line spectra 2—10922
quasistellar sources, compact, polarimetric obs. 2—10929
quasistellar sources, redshifts and luminosities rel. to optical quasistellar objects 2—10931
radiation pressure driven mass loss 2—33699
radio structure, diameter-redshift relationship 2—13938
radiosources, redshifts and fluxes 2—1968
radiostructure mapping 2—4912
redshift distribution, influence of observational selection 2—26767
redshift distribution and radiosource counts 2—13949
redshifts, selection effect in meas. 2—7471
redshifts and photon abs. of γ radiation, American Astronomical Society, Amherst, USA 1971, conference 2—26623
relativistic ejection of particle by radiation pressure 2—13930
screening probability as restriction on cosmological models 2—13824
single electron synchrotron radiation model 2—13943
small diameter, linear polarization obs. 2—30521
Southern Hemisphere, spectroscopic and photographic identifications 2—4917
spectra, origin of absorption lines 2—10924
spectroscopic observations of 22 QSO's, redshift measurements 2—41145
statistical properties 2—13948
structure and evolution 2—17016
supermassive disc as ultimate energy source for compact objects 2—13946
synchrotron radiation circular polarization in presence of hydromagnetic waves due to pitch angle anisotropies in relativistic electron gas 2—30909
theory, redshift, geometry, physical props. and explosion mechanism 2—1965
He primordial abundance correlation with absolute luminosity prediction 2—13950

Quasi-particles
see also Crystal electron states/excitons; Crystal electron states/plasma; Crystal electron states/polarons; Helicons; Spin waves
neutron matter first and zero sound propagation 2—30481
scattering from impurities in an imperfect Bose gas 2—30821
Al film, supercond., quasiparticle recomb. time, thickness depend. 2—13153

Quenching, optical *see Luminescence*

Quenching, thermal *see Heat treatment*

Racah coefficients *see Quantum theory*

Radiation
see also Acoustic radiations; Bremsstrahlung; Cherenkov radiation; Electromagnetic waves; Electrons/radiation; Emissivity Radiative transfer; Stars/radiation; Sun/radiation; Sunlight
absorption, bulk materials from which low-loss glass fibres are drawn 2—34531
anisotropic media in presence of boundary, Vavilov-Cerenkov radiation of moving charged particle 2—34243
attenuation in snowfalls, submillimetre range, computations 2—16836
black body, and attractive force between two metal plates 2—34194
black body, and matter in a uniform model universe 2—10795
black body, in cavity, photon thermalization process 2—33962
black body spectrum, statistical mechanical derivation 2—7702
charged particle, gyrotropic medium, intensity 2—244
dipole antenna, in space-time periodic media, radiation patterns 2—34262
dipole oscillators, homogeneous uniformly moving medium, frequency spectrum 2—11399
Earth, between 5 and 20 microns obtained by NIMBUS III satellite 2—26830
e.m., from flanged waveguides, mathematical theory 2—23462
e.m., from source above perfectly conducting extending sphere 2—30957
e.m. waves, cylindrical antenna in weakly ionized plasma, radiation resistance 2—14337
e.m. waves, theory of antenna arranged in parallel to cylindrical dielectric rod 2—23467
fluctuation spectrum transformation, resonant medium interaction 2—21139
gas dynamics, plane phase method analysis 2—39256
glass, semi-transparent filament, radiative transfer through axially symmetric boundary layer 2—6685
high energy, interaction with matter 2—38766
intensity, emergent, fast method of obs. in radiative transfer theory 2—5261
ionizing, effect on breakdown of air 2—18712
i.r., atmospheric flux, dependence of spectral distrib. on CO$_2$ concentration 2—26498
i.r., interferometry 2—7979
i.r., reflection by plane layer, applic. to finding height of cloud tops 2—26497

Radiation continued
  i.r. attenuation in rain and snow, computations 2—16837
  i.r. lunar, directional characteristics 2—1978
  Kirchhoff theory, scalar, vector, dyadic formulation 2—30925
  linear electron accelerator, 30 MeV possible radiation hazards 2—2863
  losses in electroluminescent grain 2—16635
  microwave, reflection from water surface, underwater sound sources detection 2—14274
  nonstationary processes, fast meas. of integral characteristics of spectrum using two-beam interferometer 2—23690
  plasma, fluctuating radiation propagation 2—15453
  shielding and monitoring, accelerators, CERN conference 2—2868
  shielding requirements for multi-GeV electron synchrotron ring 2—2869
  solar, global study of heat flow, investigation of changes caused by industry 2—4663
  solidification of semi-transparent materials, effect of radiative heat transfer 2—6282
  spectral distribution, arising from Thomson scattering of e.m. wave by ultrarelativistic electrons 2—5291
  spectral power density within symmetric closed cavities in good conductors, effect of wall roughness 2—30883
  temperature of plasma layer in optical resonator 2—35495
  terrestrial emission, mapping using an image radiometer 2—20233
  transition, in resonator with anisotropic medium 2—34240
  v.u.v., real image formation with Fresnel zone plate 2—38049
  Ar arc, high pressure, radiation transport mechanism 2—3275
  FeO vibration-rotation radiative band intensity meas. 2—35247
  87%H_2-13%He, 10000-25000 K, radiative intensity calc. 38911 2—38911
  H_2, 10000-25000 K, radiative intensity calc. 2—38911
 heat
  atmosphere, thermal i.r. radiation meas. by radioprobes 2—7309
  atmosphere, thermal i.r. radiation spectrum, synthetic represent. 2—7307
  atmospheric, energy balance methods for det. comparison 2—30266
  atmospheric i.r. emission, influence of aerosols, clouds and molecular absorption 2—1817
  blackbodies, freezing point, quality 2—5257
  blackbody, emissivity of ceramic cylindrical cavity with circular baffles 2—37796
  blackbody, plane beam, coherence props. 2—30828
  cooling bodies, heat-conduction capacity and optimization of radiating elements on surface 2—11376
  critical point during in-blow of ablating body products into a boundary layer 2—5265
  cylindrical particle cloud, importance of anisotropic scattering and searchlight effect on angular dist. of thermal radiation determ. 2—17415
  degree of blackness meas. method for small specimens, quartz and cordierite sinters 2—27309
  dust suspensions, radiation characteristics, calc. 2—27313
  geological interpretation of i.r. images using a mathematical model 2—22921
  global, dependence on turbidity and cloud cover, calc. 2—37076
  heat transfer in non-grey medium, interaction of radiation with conduction 2—5268
  i.r. technique, applic. 2—17408
  medical thermography, diagnostic value and design of thermographs 2—26957
  effect on natural convection boundary layer 2—27321
  nonisothermal nongray atomic gases, continuum radiative flux 2—21916
  radiometer, for black body temps. at rate of 15000 per second 2—2284
  radiometer, high-sensitivity absolute pulse, calibration by calculation 2—11369
  real bodies, review 2—17409
  refractories, dielectrics, spectral emission, normal total, temp. range 1000-1500°C 2—4454
  solar cavity receivers, analysis of thermal regimes 2—23393
  solar concentrators, application of theory at similarity 2—34433
  stellate radiator with mirror-polished surfaces, performance 2—11368
  thermal boundary layer of thin plate heated on reverse side by radiation 2—27305
  transient conduction in slab with radiation, perturbation type analysis 2—5274
  unsteady radiant heating of conical foil receptors, effects of heat sinks at base and vertex on time response and sensitivity 2—27310
  Nb, high-speed (subsecond) measurements, 1500-2700K 2—40076
  W, black body radiators, calculated with new valves of Planck's radiation constants 2—14283
Radiation belts *see Atmosphere/radiation belts*
Radiation chemistry *see Chemical effects of radiations/ionizing radiations; Radiochemistry*
Radiation damage *see Physical effects of radiation*
Radiation detectors
  see also Bolometers; Photometry; Radioactivity measurement
  Anger scintillation camera, improved resolution using threshold preamplifiers 2—24098
  anisotropic inhomogeneous crystal, thermoelec. eddy currents in unsteady temp. field 2—40370
  anisotropic thermopile made from low-symmetry single crystals 2—5262
  anticoincidence method, $4\pi\beta$-γ, for radioactive conc. obs. of solutions 2—14768
  cavity-type receivers, black lacquer coated, absorptance obs. 2—2269
  CO_2 pressure modulated radiometer for atmospheric temp. sounding in 40-80 km region 2—26483
  conical foil receptors, effects of heat sinks at base and vertex on time response and sensitivity during unsteady radiant heating 2—27310
  crescograph, magnetic, theory of operation 2—2053
  ferroelectrics applics., review of developments in Europe 2—40340
  fibre optics probe, water cooled, spectrally resolved obs. 2—27311
  Fritschen and Funk net radiometers, for atmospheric obs., comparison of Funk and Idso techniques 2—37151
  gas filled, application of ultra high vacuum technology to purification 2—30738
  glancing incidence optics for astronomical instruments 2—11161
  Golay cell, thermal and mechanical properties, equivalent electrical circuit and performance optimization 2—5259
  gravitational, directivity pattern, theory of ang. dependence 2—14078
  infrared imaging, thermal features of Lake Ontario 2—16733
  i.r., Dember effect in Te single cryst. 2—4308
  i.r., high D*, using pyroelectric polyvinylfluoride detectors 2—7770
  i.r., industrial applics. 2—34547

Radiation detectors continued
  i.r., influence of predetector conversion of carrier frequency on sensitivity 2—37800
  i.r., Schottky barrier diodes, applic. 2—22585
  i.r. detectors and their applications 2—7771
  i.r. liquid crystal for inspecting semiconductors 2—33008
  i.r. method of temperature measurement 2—7772
  i.r. microscope for temperature measurement of small areas 2—7764
  i.r. radiation rel. to earthquake activity associated with the volcanic eruption of Akita-komaga-take 2—10689
  i.r. radiometer, error in measuring temperature of nonblack bodies 2—37803
  i.r. radiometer, low noise, with metallic bolometer 2—37798
  i.r. radiometer, theory and design 2—5263
  i.r. sensing systems 2—2267
  i.r. spin scan radiometer, for spin-stabilized geostationary satellite 2—16735
  i.r. thermometer, room temperature thermometer 2—7773
  long wavelength i.r., cooled photodetector with wheel type modulator, analysis at internal noise 2—37806
  low temperature bolometer detector, for differential molecular beam scattering apparatus 2—18398
  millimetric, n-InSb low-inertia detector 2—17496
  Montes Apenninus LAC 14, comparison with radar obs. 2—33732
  moving or stationary scanners, intrinsic plane sensitivity det. 2—38378
  multichannel radiometer for i.r. thermal mapping of Mars, proposed for Viking Mission 2—30565
  nuclear power plant, radiation detection monitors 2—38773
  nuclear reactor system, using on-line computer 2—31630
  nuclear reactor system, using on-line computer 2—24289
  nulled system for photon-momentum radiometry 2—34198
  particle, e.m. wave, characteristics 2—38348
  photoelectric convertors, h.v. array-type microcells with p-n junctions 2—13348
  using photon drag effect, CO_2 laser output obs. 2—21067
  photovoltaic n-p heterojunction, detectivity calc. 2—17410
  pile-up correction in meas. of lifetimes 2—17990
  pneumatic, boundary effects and thermodynamic equilibrium 2—27308
  polyvinylidene fluoride, i.r. detectivity 2—13329
  portable detector for automatic gain stabilization of radiometers 2—23394
  pulse height analysers for improved photon counting 2—2640
  pyroelectric, co-ordinate sensitive, advantages 2—17411
  pyroelectric, responsivity enhanced by $PbZrTiO_3$ pyroultrasonic parametric amplifier 2—20952
  pyroelectric, variable response time 2—40365
  pyroelectric thermal imaging devices 2—37797
  pyrometers performance 2—11370
  radiometer, high-sensitivity absolute pulse, calibration by calculation 2—11369
  radiometer calibration, low energy i.r. targets 2—7768
  radiometer sonde, for obs. of stratospheric emission due to water vapour in its rotational band 2—20308
  radiometric integrals in closed form 2—2266
  rocket borne radiometer, low pass i.r. filter 2—34195
  Schottky barriers, epitaxial PbTe 2—7769
  scintillation crystals, recording flash X-ray burst times 2—2630
  self-powered, precision monitoring of intense bremsstrahlung pulses 2—27891
  self-scanned ferroelec. image sensor 2—38145
  semiconductor, charge collection efficiency analysis 2—31368
  semiconductor, photon pressure effects 2—13344
  semiconductor, preparation and applications, book 2—27886
  semiconductor, process control, thermal and elec. meas. 2—29694
  spectroradiometry standards, review 2—7998
  submersible spectroradiometer, for optical oceanography 2—33431
  superconducting point contact junction arrays, broad band detection 2—13194
  thermal i.r. imaging devices, studying quasistationary thermal fields 2—37805
  thermal i.r. imaging in aerial surveys of natural resources 2—30131
  thermoelements connected to compensating circuit 2—17422
  thermomicrography 2—37802
  thermopile, for c.w. and laser pulse obs. 2—2268
  triglycine sulphate, pyroelectric i.r. detector 2—6888
  wideband i.r., bandwidth measurement 2—30884
  X-rays with bandpass response characteristics 2—18021
  BaF_2 thermoluminescence in det. of radiation quality 2—38385
  CdF_2:Er^{3+}, i.r. quantum counter, by generation of C_{3v} local site symmetry 2—37939
  $Cd_xHg_{1-x}Te$, 10μ band, crystal growth, optical, and elec. props. 2—39577
  $Cd_xHg_{1-x}Te$, epitaxial, i.r. photovoltaic detector 2—6911
  CdS:Ag, Al, i.r. detection, by high field domain reconfiguration 2—29714
  CdS, detector for h.f. electric signals using acoustoelectric surface wave field in piezo- photo-conducting crystal 2—23429
  CdTe, nuclear radiation detector, transport processes 2—34811
  CdTe detector for nucleonic propellant gauging in zero-G environment 2—34814
  GdTe detector device characterization, temp. range 60-80°C 2—34813
  Ge, high purity, planar and coaxial, fabrication 2—18016
  Ge, high purity neutron damage and annealing 2—24091
  HgCdTe i.r. detectors at 4 to 6 μm and room temperature 2—7774
  $Hg_{1-x}Cd_xTe$ for 1-14 μ region, preparation and spectral response 2—17412
  InSb tunable detector, for far i.r. spectroscopy 2—27659
  InSb tunable detector for far i.r. spectroscopy 2—8047
  $PbNb_2O_6$-$BaNb_2O_6$ ceramic system, applic. to i.r. detectors 2—29739
  $PbTiO_3$ pyroelectric i.r. detector, noise performance and neutron irradiation resistance 2—17414
  Pb(Zr, Ti)O_3 pyroelectric, high D*, fast 2—34196
  Se film, integrating cell having anomalous photoconductivity 2—37799
  Si, temperature dependence of photocurrents produced by X- and γ-rays 2—38383
  Si mesa photodiodes for improved demodulation of light 2—38036
  Si photocells for solar radiation meas. 2—23499
Radiation effects *see Biological effects of radiations; Chemical effects of radiations; Physical effects of radiations*
Radiation monitoring
  see also Dosimetry
  accelerators, and radiation shielding, CERN conference 2—2868
  accelerators and storage rings, high energy, induced radiation 2—2898

Radiation monitoring continued
environmental radiation and radioactivity from CERN high energy accelerators 2—2865
environmental radioactive purity near the IRT-2000 reactor 2—8413
in-core self-powered neutron detectors, high- temp. performance 2—15172
instrumented capsule for meas. of fission induced creep of UO_2 reactor fuel 2—11917
laser-beam skin damage and exposure level monitoring 2—7597
medical dose rates, instrument for measuring small differences 2—2039
m.o.s.f.e.t.s. in nuclear instrumentation amplifiers 2—31377
nuclear power plant, radiation detection monitors 2—38773
nuclear power plants, radiation releases and radiation in closed loops 2—28162
in nuclear power stations review 2—38765
proton synchrotron problems 2—555
reactor pressure vessels current trends in control, surveillance of neutron irradiation effects 2—28126
reactors, development of safety systems in USSR 2—15182
safety regulations, instruments 2—38348
SOLRAD 10(C) satellite for solar radiation and activity 2—23131
systems and instruments, NAL safety policy 2—2899
thermoelectromotive force obs. 2—8389
γ-rays, perimeters and surrounding of nuclear power stations 2—5769
B neutron detector system for monitoring whole dynamic range of reactor 2—31375
^{60}Co disc isotropic sources, air-ground interface problem 2—28160
Radiation pressure
see also Acoustic streaming
acoustic, nuclear reactor design factor, Windscale High Intensity Noise Rig 2—38707
acoustic, pulsed cylindrical and spherical shells, radiated pressure in unbounded acoustic medium 2—34101
rel. to acoustoelectric effect 2—25678
Earth's shadowing effect on satellite orbital elements, solar radiation pressure 2—30392
laser light, applic. to isotope separation and atomic beam velocity selection 2—34411
laser light pressure, applications 2—27566
photons propagating in refractive media 2—21136
planetary nebulae, filamentary structure caused by radiation pressure gradients 2—20504
relativistic ejection of particle due to point source field, application to quasi stellar objects 2—13930
semiconductor, photon pressure effects 2—13344
on test particle in general relativity 2—37593
thermal waves in liquids made to flow by temperature gradient, direct measurement 2—35692
He-burning shell in red supergiant stars of 15 solar masses, thermal stability 2—10867
Radiation protection
see also Radiation monitoring
accelerator, CERN 300 GeV, dose-rate below 5 rem/30y outside laboratories 2—2883
accelerator prod. radiation, attenuation in access tunnels 2—5764
accelerator shielding and safety practice at NAL 2—2884
accelerators, CERN conference 2—2868
accelerators, high energy protons, muon transport 2—2870
active nondestructive assay techniques for nuclear materials 2—28159
aircraft, SST, general survey of problem 2—2894
concrete biological shield, energy absorption under shock loading 2—15183
cosmic ray enders in human tissue, evaluation at level of SST flight from solar minimum to maximum 2—5050
cosmic ray shielding, background reduction obtained with γ-ray detectors 2—34795
cosmic rays protection, spacemen helmet shielding 2—16935
cyclotron, radiation levels in experimental and associated areas 2—2881
cylindrical duct with helical iron plug, spatial distributions of neutrons and photons 2—5765
induced disease problems of response relation to dose, dose-rate and quality 2—5047
dose, effect after repeated exposure, assessment of radiation hazard in space flights 2—5061
dose distrib. of fast neutrons, in concrete labyrinth 2—2875
dose rate rel. to shielding thickness requirement, charts 2—28161
electron beam welders and evaporators 2—557
electron bem TREE expts., electron shielding r.f. shielding 2—8414
electron synchrotron ring, shielding requirements for a multi-GeV machine 2—2869
e.m., potential hazards and safety standards 2—33786
fusion reactors, radiological impact 2—24298
gamma ray shielding, dose rate calculations using Monte Carlo technique 2—558
gamma-ray albedo calculation using moments method 2—8412
gamma-ray sources, computer program for shielding calculations, PEL—SHIE 2—38770
Grand Tour missions to Jupiter, Neptune, Pluto, Saturn, and Uranus calculation of expected doses 2—23113
heat dissipation from radioactive materials during transport 2—18267
heterogeneous passive and active shields, external proton beam target 2—2871
laser beam properties and hazards, review 2—2408
laser beams, biological effects, safe levels of radiation 2—17648
mathematical model for dependence of injury cross section on LET 2—5049
microwave safety standards 2—5039
monitoring systems and instruments, NAL safety policy 2—2899
neutron leakage through penetrations in hadron shields 2—2874
neutron propagation in high energy proton accelerator access tunnels 2—2876
neutrons and secondary γ-rays in atmosphere, effects of ground on steady state and time dependent transport 2—7318
nuclear fission reactors, irradiation damage, review of problems of safety and economics 2—2844
nuclear power plant, radiation detection monitors 2—38773
nuclear reactors, Geneva 1971, conference 2—24257
nuclear reactors, safety analysis, accident occurrence probability 2—38725
particle accelerator shields, mechanics of extra nuclear hadron cascades 2—5766
Radiation protection continued
portable TV X-ray introscope, with autonomic biological safeguard 2—30744
proton synchrotron problems 2—555
quality factor and dose equivalent 2—41299
radiation loop parameter optimization for gamma sources 2—38767
radioactive waste disposal, review of management and handling 2—2858
reactor safety requirements, development of systems in USSR 2—15182
reactor shielding, computer graphic-aided design 2—38772
reactor shields, strength when subject to dynamic load, steel ferrules with fillers 2—15042
reactors two-dimensional shielding calculations using combination of diffusion theory and line-of-sight method 2—38771
research projects, UKAEA reports 2—5035
security systems in vicinity of accelerators, accident prevention 2—2866
shield-leakage neutron spectra from synchrocyclotron 2—2885
shielding, comparison of expt. data with Monte Carlo calcs. 2—2879
shielding, electrostatic, against radiation in space 2—2867
shielding, external Be target in intense intermediate energy proton beam 2—34756
shielding materials, attenuation of fast neutrons 2—38769
shielding of intersecting proton storage rings, radiation damage within the rings 2—2877
shielding required for use of U target with a linear electron accelerator 2—2880
shields, cascaded produced by high energy incident particles, mathematical model 2—2872
shields, multilayer, physical interpretation and structure of build-up factor asymptotic and transient components 2—11920
Solar cosmic rays, protection of astronauts 2—4759
space and supersonic transport, conf. 2—5048
space flights, assessment of radiation hazard 2—5062
storage of fissile metals, models 2—11919
storage ring, radiation dangers of losses and bremmstrahlung 2—2864
synchrocyclotron, personnel dose monitoring, dismantling and disposal 2—2896
syncrocyclotron, obs. of radiation levels in vicinity 2—2882
waste disposal in subsurface cavity, temp. increase 2—22916
X-ray machines, exposure characteristics 2—17109
x-ray safety systems for use with Philips PW 1016 and PW 1316 tube shields 2—19024
μ flux, program for calculation in actual configurations 2—2873
Pb shield manufacture 2—556
^{90}Y rods, shielded assembly for handling 2—15181
Radiative recombination *see Luminescence*
Radiative transfer
absorbing emitting medium involving specular directional surfaces, pseudo hemispherical properties 2—23309
atoms, multilevel, infinite fine structure coupling 2—5781
blackbody radiation, coherence props. 2—30828
boundary value problems, Green's methods for stellar atmospheres 2—4821
clouds, transfer of i.r. radiation 2—26494
combined operational methods for transfer problems in isotropic scattering homogeneous spherical media 2—20676
continuum, in hot plasma, application to Scorpius X-1 2—37337
cooling effects behind reflected shock wave in absorbing gas 2—7762
cooling of shock heated air in explosively driven shock tube 2—12509
Cytherian atmosphere, heat transfer below clouds 2—26858
Cytherian atmosphere, numerical modelling 2—26857
Earth's atmosphere-ocean system 2—37157
gases, application of mean absorption coeff. non nonisothermal i.r. radiative transfer 2—21909
heat, near critical point during in-blow of ablating body products into boundary layer 2—5265
laser-heated foil, Laplace transform method for predicting losses 2—17419
linearization of radiation heat transfer, methods compared 2—27314
Monte Carlo method for estimation of solns. 2—23311
multiregional analysis of temp. fields in finite rod bundles cooled by liquid metals 2—15166
photon scattering in atmosphere of atoms, statistical functions 2—14144
planar medium nongray, heat transfer interaction by cond. and radiation 2—17418
plasma, air, nonisothermal, radiative heat transfer mechanism 2—18589
power reactor fuel element dynamic heat transfer analysis 2—15165
effects on reflected shock waves in gas flow 2—3293
regional averaging method for real stellar atmospheres 2—1958
relativistic, moment method 2—2265
semiinfinite space, temperature waves 2—27316
singular integral eqn. rel. to polynomial scatt. indicatrices 2—17273
solar chromosphere coupling 2—23133
spheres, concentric, approx. soln. to radiative equilibrium with gray gas layer 2—39279
spherical harmonics method applic. 2—7728
spherically symmetric, appl. of S_n method 2—30827
spherically symmetric, half-range differential approx. 2—27312
stellar atmospheres, real regional averaging 2—1958
superradiant pulses, quantum statistics 2—27110
theory, application of τ_{ef} method 2—5260
theory, method for obs. of emergent intensities 2—5261
time dependent, damping of temp. fluctuation, near L.T.E. grey approx. 2—27111
time dependent, damping of temp. fluctuation, two level atom case, applic. to interstellar medium 2—23312
time-freq. dependent calculation by Monte Carlo method 2—14143
two-dimensional transfer, synthesis methods 2—11316
variable Eddington method, for Christy's model of W Virginis 2—20517
Ar arcs, high pressure, gradient- current characteristics, radiated power and spectral intensities of lines 2—24934
N_2 arcs, exptal. det. 2—24943
N_2 cascade arc, energy balance 2—24913
OH, H_2O maser emission in envelope of infrared star 2—30447
Radiators *see Electromagnetic waves/radiators; Transducers*
Radicals *see Free radicals*
Radioactive dating
basaltic glass from North Atlantic bed, evidence for ocean floor spreading 2—22950
constancy of nature, reanalysis of measurements of pleochroic halos 2—23210

Radioactive dating continued
- fission track technique, fossil radiation damage, in Indian muscovites 2—7227
- Fra Mauro formation, Rb-Sr age 2—1974
- Franciscan metamorphic rocks, K-Ar dating 2—33425
- geological specimens 2—16717
- Indian biotites, fission track ages 2—4645
- in Jurassic intrusions, and magnetic remanence measurements13804 2—13804
- lunar rock, breccia and soil samples, ^{40}Ar-^{39}Ar ages and cosmic ray exposure ages 2—4951
- lunar rocks, crystalline, Rb/Sr, ^{40}Ar/^{39}Ar or cosmic ray methods 2—4950
- lunar rocks, igneous, Rb-Sr ages 2—1972
- meteorites, stony, terrestrial age 2—26869
- minerals, nondestructive preliminary determ. of U and Th content 2—4608
- rocks and minerals, from retention of radiogenic gases 2—7229
- rocks from extinct volcano, obs. of anomalously weak geomag. field during Matuyama reversed epoch 2—16934
- volcanic glass, effect of water content of fission track annealing 2—26463
- $_{38}$Ar-^{37}Ar cosmic ray exposure age of lunar basalts from Mare Fecunditatis 2—20654
- ^{38}Ar-Ca, Apollo 15 rock 15555, cosmic-ray exposure ages 2—41182
- ^{40}Ar/^{39}Ar age spectrum technique for rocks and minerals 2—16766
- ^{40}Ar/^{39}Ar technique of K-Ar dating. comparison with conventional technique 2—7228
- ^{40}Ar-^{39}Ar, Apollo 15 rock 15555, gas retention age 2—41182
- ^{40}Ar-^{39}Ar, Apollo sample 15555 2—41179
- ^{40}Ar-^{39}Ar gas retention age of lunar basalts from Mare Fecunditatis 2—20654
- ^{14}C and ^{18}O, isotope exchange between HCO$_3$ in saline solution and solid CaCO$_3$ application to groundwater age 2—16768
- K/A evidence for Freetown Igneous Complex, Sierra Leone combined with palaeomagnetic evidence 2—16931
- K/Ca dates from pegmatitic micas 2—16767
- K-Ar, γ-irradiated minerals, mica samples 2—26462
- K-Ar, Jurassic Chon Aike formation 2—26564
- K-Ar age of Raco, meteorite 2—11018
- K-Ar dating of miopliocene volcanic rocks 2—16765
- K-Ar technique. Apollo sample 15555 dating 2—41180
- Rb-Sr ages of lunar basalts and model age of soils 2—20653
- Rb-Sr technique. Apollo sample 15555 dating 2—41180

Radioactive tracers
- biological trace elements using gamma ray spectroscopy, nuclear activation analysis, radioactive tracers 2—17123
- chloroform-carbon tetrachloride liquid system, tracer and mutual diffusivities 2—25065
- diffusion coefficients in glass, specific activity effects 2—15792
- flow meas. in hydroelectric turbines by constant rate injection method 2—6176
- ions, reflection from solid surfaces, radiotracer technique meas. 2—7901
- ocean nuclides, particulate and dissolved, concentration sampler 2—4653
- pipeline interface detector, gas chromatograph 2—4606
- in waste, tracking of path and deposition site in sea 2—20294
- ^{14}C, dissolved in wind driven ocean, distribution obs. model 2—13648
- Hg, for liquid-vapour interface transport obs. 2—25004
- ^{22}Na, atmospheric exchange study 2—20324
- ^{212}Pb, scattered on monotonic gases, cross section measured from distribution of α particle tracks 2—12015
- ^{233}U, diffusion penetration plot in Ta crystal, α-energy spectra 2—6516
- ^{133}Xe intracarotid injection, cerebral blood flow det. 2—23148

Radioactivity
- *see also Alpha-particles; Beta-rays; Gamma-rays; Atmosphere/radioactivity; Beta-decay theory; Chemical analysis, radioactive; Chemical effects of radiations/ionizing radiations; Fallout; Geophysical prospecting; Nuclear decay theory; Nuclear bombardment targets; Nuclear excitation; Nuclear reactions and scattering; Radiochemistry*
- ^{234m}Pa decay, gamma radiation obs. 2—24192
- β decay, sudden change of nuclear charge, excitation mechanism of optical transitions 2—18296
- β-decay, unique first forbidden, matrix elements, spin isospin core polarization, $A\approx 90$ 2—11788
- A=15 and 17, first-forbidden non-unique β transitions and mirror comparisons 2—18154
- actinides, $229\leqslant A\leqslant 257$, decay meas. rel. to quasiparticle and vibrational excitations 2—21401
- aeroradioactivity survey, applic. to geological mapping 2—16764
- alpha decay, calc. of overlap integral 2—11785
- alpha decay, velocity meas. of recoil nuclei and determ. of their mass 2—11787
- cosmic ray induced, in detectors effect on diffuse γ-ray obs. 2—4779
- doubly even actinide nuclei, α-decay, γ-ray spectra study, deduced levels of product nuclei 2—11780
- Earth's internal heat as a source for a volcanic-orogenic cycle 2—7205
- fermi type β-transition from odd odd nucleus to even even nucleus 2—21369
- heavy nuclei, antianalogous states, β- and γ-transitions 2—18150
- highly excited nuclei, correlations of identical particles emitted 2—21408
- hydrology applics. of tritium as a radioactive indicator 2—33428
- maria, formation in a convective cell theory 2—7205
- moon rock and terrestrial basalt, Th-content rel. Moon origin 2—30547
- ocean, pollution measurements 2—16778
- odd A nuclei, surface distributions of α-particles 2—34983
- pre-equilibrium decay, nuclear density distribution 2—31496
- radiation emitted by sources, large course phenomena 2—24193
- radioisotopes, peaceful uses 2—24251
- remote sensing of Th, U and K in soils and rocks, low altitude gamma spectrometric surveys 2—37096
- sources, Ra, intercomparison using γ ray intensity measurements 2—5672
- sources of ^{59}Fe, ^{114}In^{m}, ^{115}Cd^{m}, ^{113}Sn, ^{125}Sb, ^{207}Bi, ^{204}Tl, by electrodeposition on thin metallized plastic films 2—5673
- statically oriented nuclei, symmetry properties of decay processes 2—36801
- successive decay and related equilibria, computer simulation 2—30745
- superheavy nuclei, stability against alpha decay, potential energy surface calc. 2—21454
- surface heat flow in Earth's crust, heat transfer mechanisms 2—22920
- ^{222}Ac, 66 sec isomer, α particle emission, electron capture and isomer transition mechanism 2—34994
- ^{225}Ac, α-spectrum, splitting of 5793 keV doublet 2—38554

Radioactivity continued
- ^{228}Ac→^{228}Th, excited level obs. from γ-γ coincidence meas. 2—483
- ^{228}Ac→^{228}Th decay, internal conversion electrons 2—8317
- ^{112}Ag, β-decay, γ-ray assignment to level structure of ^{112}Cd 2—38547
- ^{112}Ag→^{112}Cd decay, γ-spectra meas., assignment of ^{112}Cd level scheme 2—21413
- ^{114}Ag, β-decay, γ-ray assignment to level structure 2—38547
- ^{116}Ag, β-decay, γ-ray assignment to level structure 2—38547
- ^{23}Al, β-delayed proton emission 2—24180
- ^{238}Am, electron capture decay 2—38530
- ^{242}Am β-decay, det. of relative probability 2—38556
- ^{75}As, after effects, relaxation and recombination time constants 2—38541
- ^{75}As, conversion electron spectrum, relative intensities of transitions 2—38542
- ^{76}As, 2→2^{+} beta transition at 1200 keV 2—21414
- ^{76}As decay, γ-ray energies and relative intensities 2—38543
- ^{76}As→^{76}Se, γ-γ coincidence obs., energy level scheme 2—31514
- ^{207}At, decay to levels in ^{297}Po, level and transition study 2—18148
- ^{198}Au→^{198}Hg decay, ang. correl. of 676-412 keV cascade 2—34976
- ^{12}B, β decay, Coulomb and nuclear structure effects 2—11791
- ^{210}Bi, β decays, K-shell auto-ionization probability 2—18165
- ^{75}Br→^{75}Se decay, obs. of γ-rays and conversion electrons rel. to ^{75}Se level scheme determination 2—24164
- ^{86}Br, ^{87}Br γ-rays differentiated 2—5674
- ^{87}Br, β decay, γ ray emission in competition with neutron emission 2—18160
- ^{10}C, superallowed Fermi decay, branching ratio, significance for weak vector interaction 2—21411
- ^{143}Ce→^{143}Pr, level structure of ^{143}Pr, investigation using decay associated gamma rays 2—21394
- ^{144}Ce→^{144}Pr decay, γ-ray and conversion electron intensities 2—38515
- ^{249}Cf, L$_2$ and L$_3$ subshell fluorescence and Coster-Kronig yields for Z=96 2—2933
- ^{249}Cf decay, L$_1$ subshell fluorescence and Coster-Kronig yields 2—21496
- ^{252}Cf, α-decay and associated L X-rays of Cm 2—18306
- ^{244}Cm, L$_2$ and L$_3$ subshell fluorescence and Coster-Kronig yields for Z=94 2—2933
- ^{49}Cr, beta decay to ^{49}V, lifetime of ^{49}V 90.65 keV state 2—2707
- ^{138}Cs→^{138}Ba, level scheme construction, spin assignments 2—24167
- ^{58}Cu, γ-ray energies and relative intensities 2—18158
- ^{155}Dy→^{155}Tb decay, excited level obs. 2—24187
- ^{165}Dy, β decay, level scheme of ^{165}Ho 2—21396
- ^{165m}Dy, β decay, level scheme of ^{165}Ho 2—21396
- ^{169}Er, β decays, K-shell auto-ionization probability 2—18165
- ^{172}Er, β-decay to levels of ^{172}Tm, proposed level scheme 2—18135
- ^{59}Fe→^{59}Co decay, internal conversion meas. 2—38537
- ^{59}Fe→^{59}Co decay, γ-γ directional correl. obs. of cascades 2—34988
- ^{68}Ga, beta decay study 2—38540
- ^{147}Gd decay, conversion electron and γ-ray meas., ^{147}Eu level diagram 2—24186
- ^{153}Gd, 363-keV γ-radiation, parity violating asymmetry 2—2750
- ^{159}Gd, 363-keV γ-radiation, parity violating asymmetry 2—2750
- ^{3}H, atomic effects in β-spectrum 2—14963
- ^{3}H→^{3}He+e-+v-$_{e}$, calc. of meson exchange corrections using realistic nuclear wave functions 2—18155
- ^{4}H meson-less decay model 2—24145
- ^{261}Ha, new isotope of element 105, α-particle spectra 2—2740
- ^{262}Ha, new isotope of element 105, α-particle spectra 2—2740
- ^{4}He, meson-less decay model 2—24145
- ^{183}Hf, nonexistence of metastable state of 91 d half life 2—24190
- ^{180m}Hf, 501-keV γ-radiation, parity violating asymmetry 2—2752
- ^{197m}Hg, after effects, relaxation and recomination time constants 2—38541
- ^{130}I, ^{130*}I, β-decay, excitation of ^{130}Xe levels 2—24184
- ^{132}I→^{132}Xe, γ-radiation, excited levels 2—5676
- ^{106}In, obs. of β decaying state in ^{92}Mo(^{16}O, pn)^{106}In reaction 2—18162
- ^{107}In→^{107}Cd, level scheme for ^{107}In and excited level spin and parity for ^{107}Cd 2—11798
- ^{192}Ir, β decay, angular correlation between groups of γ-rays in ^{192}Pt, test of time reversal invariance 2—2753
- ^{192}Ir decay, γ transitions, relative intensities 2—38552
- ^{192}Ir→^{192}Pt decay, triple γ ang. correl. obs. 2—34991
- ^{134}La decay, ^{134}Ba energy level study 2—8307
- ^{138}La, γ-ray intensity and energy meas. 2—18164
- ^{177m}Lu decay, internal conversion meas., transitions 2—38551
- $_{\Lambda}^{7}$Li→^{4}He ^{3}He π^{-}, energy and angular distributions of decay products 2—38478
- $_{\Lambda}^{7}$Li→pd$\alpha\pi^{-}$, energy and angular distributions of decay products 2—38478
- ^{12}N, β decay, Coulomb and nuclear structure effects 2—11791
- ^{16}N β decay, effect of ^{16}O 7.12 MeV level on α spectrum 2—2743
- ^{88}Nb→^{88}Zr decay, γ-ray spectra rel. to ^{88}Zr level scheme determination 2—21389
- ^{89}Nb, γ-decay process 2—477
- ^{90}Nb, γ-spectra and $\gamma\gamma$-coincidence spectra 2—478
- ^{90}Nb positron source, prep. 2—24177
- ^{147}Nd→^{147}Pm decay, γ-γ directional correl. obs. of ^{147}Pm cascades 2—34962
- ^{20}Ne, α-decay widths 2—21382
- ^{237}Np, half life of $^{5}/_{2}^{-}$, 59.6 keV level, obs. using phoswich scintillators 2—38555
- ^{239}Np→^{239}Pu decay, γ spectrum, energies and intensities, ang. correl. obs. 2—34979
- ^{16}O, parity measuring α decay from 3^{+} T=0 0.06 state calc. in Cabbibo model of weak interactions 2—24179
- ^{32}P, β spectrum shape of mass separated source, precision measurement 2—2745
- ^{233}Pa, half life of $^{5}/_{2}^{+}$, 86.6 keV level, obs. using phoswich scintillators 2—38555
- ^{206}Pb/^{207}Pb ratio, radiohalos and unknown alpha radioactivity 2—2754
- Pd isotopes, energies and intensities of conversion beta-ray spectra 2—38508
- ^{98}Pd→^{98}Rh, level schemes for ^{98}Rh 2—38546
- ^{154}Pm, decay to levels of ^{154}Sm, isomerism 2—18166
- Po even-even isotopes, reduced widths of α-decay 2—24191
- ^{142}Pr, 2→2^{+} beta transition at 587 keV 2—21414
- ^{189}Pt decay, study of levels in ^{189}Ir 2—31493
- ^{238}Pu, alpha spectra, relative intensities and energies 2—8316
- ^{238}Pu, L$_2$ and L$_3$ subshell fluorescence and Coster-Kronig yields for Z=92 2—2933
- ^{244}Pu, detection in nature 2—5678
- Ra even-even isotopes, reduced widths of α-decay 2—24191

Radioactivity continued
^{224}Ra, alpha spectra, relative intensities and energies 2—8316
^{77}Rb, new neutron deficient isotope produced by ^{63}Cu(^{16}O,2n) and ^{59}Co(^{20}Ne,2n) reactions, half-life and γ ray spectra meas. 2—34989
^{79}Rb, β transitions to excited states of ^{79}Kr 2—38500
^{88}Rb, β decay of 17.8 min state, population of levels in ^{88}Sr, γ-ray spectra 2—31477
^{182}Re, 64h isomer decay to excited states in ^{182}W, γ-ray spectra 2—14968
^{190}Re, excitation of 3 min activity using 14.8 MeV ^{190}Os (n,p) reaction 2—38616
^{184m}Re decay, to levels of ^{184}W, γ-ray spectra, meas. 2—482
^{98}Rh→^{98}Ru, level schemes for ^{98}Ru 2—38546
^{104}Rh, 43 sec and 4.41 min isomers, β^- decay to excited states of ^{104}Pd 2—34955
^{104}Rh, m and g isomers, ^{104}Pd levels and transitions 2—21392
Rn even-even isotopes, reduced widths of α-decay 2—24191
Rn(A=206 to 212), alpha decay, exptl. investigation 2—11807
^{68}Se, produced by ^{59}Ni(^{12}C,2n) reaction, separation of ^{68}As, meas. of half-life and γ ray spectra 2—38538
^{81}Se, conversion coefficients for low-energy gamma radiation 2—2746
^{32}Si, β decay, search for γ emission 20-200 kEV 2—38534
^{151}Sm, β decays, K-shell auto-ionization probability 2—18165
^{85}Sr, three particle level multiplets 2—476
^{174}Ta, energy levels of ^{174}Hf and β-band mixing 2—18137
^{178}Ta, decay to levels in ^{178}Hf, structure study 2—11771
^{182}Ta, oriented in Fe, β decay, structure and parity mixing in ^{182}W 2—31510
^{150}Tb, new 5.8 min isomer, β decay to ^{150}Gd excited states 2—31506
^{160}Tb, in TbF$_3$ and Eu$_{1-x}$Tb$_x$S, β-decay search for atomic after effects 2—18167
^{161}Tb, 363-keV γ-radiation, parity violating asymmetry 2—2750
Th even-even isotopes, reduced widths of α-decay 2—24191
^{230}Th, alpha decay, conversion transitions in ^{226}Ra 2—11809
^{198}Tl, decay, energy levels of ^{198}Hg 2—2733
^{206}Tl, decay to ^{206}Pb, strong EO transition in ^{206}Pb 2—11777
^{198m}Tl, decay, energy levels of ^{198}Hg 2—2733
^{232}U, alpha spectra, relative intensities and energies 2—8316
^{85}Y, 5 hrs and 2.68 hrs, three particle level multiplets in ^{85}Sr 2—476
^{87}Y, decay to levels in ^{87}Sr, log ft values 2—5675
^{96}Y→^{96}Zr, new γ-transitions meas. 2—18161
^{86m}Y, investigation of β^+ and γ decay 2—38544
^{169}Yb, energies and intensities of γ-rays, rel. to ^{169}Tm structure 2—470
^{177}Yb decay, internal conversion meas., transitions 2—38551
^{64}Zn, composite system formed in ^{63}Cu+p and ^{60}Ni+α reactions, isospin effects in decay, Bohr independence hypothesis 2—24181
^{65}Zn, branching ratio investigation 2—24183
^{66}Zn, composite system formed in ^{65}Cu+p and ^{62}Ni+α 2—24181
^{87}Zr, using Ge(Li) spectrometer 2—2747
^{89}Zr, using Ge(Li) spectrometer 2—2747

dating *see Radioactive dating*

decay periods
beta-decay, crystal field effects on half-life 2—475
Doppler shift attenuation factor, Monte Carlo method 2—34981
half-lives of isotopes produced by ^{3}He bombardment of ^{64}Zn foils 2—24239
high pressure effect on decay constant 2—14962
highly excited nuclei, lifetime meas. in 10^{-18} to 10^{-22} sec region 2—21408
lifetime systematics 2—34982
superheavy nuclei, electron capture and alpha-decay half life calc. 2—21454
time meas. with 2 photomultipliers in single photoelectron condition 2—8314
^{114}Ag, half-life determ. 2—31504
^{23}Al, β-delayed proton emission, half-life determination 2—24180
^{24}Al, β decay, half-life determ. 2—2744
^{26}Al→^{26}Mg half-life determ. 2—11793
Au isotopes, theoretical decay rates analysed on shell model basis 2—11786
^{202}Au, half life determ. and γ emission meas. based on beta counting 2—34992
^{209}Bi α-decay, theoretical and exptl. investigation of half-life 2—38553
^{141}Ce half-life determ. 2—21412
^{249}Cf, ^{243}Am, ^{239}Np and ^{243}Cm, as standards for efficiency calibration of Ge(Li) detectors 2—27884
^{32}Cl, β decay, half-life determ. 2—2744
^{39}Cl half-life determ. 2—11794
^{63}Co, decay scheme and period from γ-ray measurements 2—31501
^{172}Hf, half-life 2—11802
Hg isotopes, theoretical alpha decay rates analysed on shell model basis 2—11786
^{36}K, β decay, half-life determ. 2—2744
^{36}K, half life meas. with pneumatic shuttle system 2—31498
^{40}K half-life for beta emission, undergraduate laboratory experiment 2—33843
^{85}Kr, leak detection applic., soak procedure and counting equipment 2—30731
^{94}Kr, fission prod. nuclide, identification, half life and γ-ray spectra 2—11886
^{94}Kr, fission prod. nuclide, identification, half life and γ-ray spectra 2—11886
^{138}La, partial half-lives of EC and β branches 2—18164
^{20}Na, β decay, half-life determ. 2—2744
^{20}Na, half life meas. with pneumatic shuttle system 2—31498
^{88}Nb→^{88}Zr, half-lives for decay of ground state and excited state isomers 2—21389
^{22}Ne, lifetime, Doppler shift attenuation method, measurements in slowing materials 2—34985
^{63}Ni, half-life measurement from activity and isotopic abundance 2—5679
^{14}O, half life meas. 2—11792
^{28}P, β decay, half-life determ. 2—2744
^{233}Pa, half life of $^{5}/_{2}{}^{+}$, 86.6 keV level using loaded scintillators 2—34995
^{98}Pd→^{98}Rh, half-life meas. 2—38546
^{152}Pm isomers 2—31507
Pt isotopes, theoretical alpha decay rates analysed on shell model basis 2—11786
^{240}Pu, total spontaneous and isomer fission half-lives 2—31599
^{186}Re, nuclear structure and an isomer with half-life 2×10^5 years 2—34974
^{98}Rh→^{98}Ru, half-life meas. 2—38546
^{103}Ru half-life determ. 2—21412
^{87}Se, ^{88}Se, ^{89}Se, half-lives determ. 2—5726

Radioactivity continued
decay periods continued
^{33}Si 6.3 sec, new isotope produced via ^{18}O(^{18}O,2pn) reaction, 23-40 MeV 2—38535
^{78}Sr half-life determ. 2—28005
^{92}Sr half life obs. as 2.71 hours 2—2748
^{177}Ta half-life measurement using microsecond beam chopping by pulsing cyclotron deflector voltage 2—24118
^{208}Tl, half-life precision measurement 2—2755
^{234}U, total spontaneous and isomer fission half-lives 2—31599
^{235}U, half-life and specific activity determ. 2—2758
^{238}U, half-life and specific activity determ. 2—2758
^{44}V, highly neutron deficient isotope with half-life 90±25 ns produced in ^{40}Ca(^{6}Li,2n) reaction at 18.5 MeV 2—11795
^{143}Xe, fission prod. nuclide, identification, half life and γ-ray spectra 2—11886
^{60}Zn, half-life measurement using mass separated source 2—31500
^{61}Zn, half-life measurement using mass separated source 2—31500
^{65}Zn, half-life meas. 2—24183
^{95}Zr half-life determ. 2—21412

decay schemes
^{211}Pb, level scheme of ^{211}Bi 2—27997
transuranium nuclides, formation, production and uses 2—11695
^{185}Os→^{185}R3, nuclear decay investigation 2—14969
^{193}Os→^{193}Ir, nuclear decay investigation 2—14969
^{138*}Pr→^{138}Ce, γ ray and conversion electron spectra 2—480
^{228}Ac→^{228}Th, γ-spectra, level scheme of ^{228}Th 2—11808
^{108}Ag→^{108}Pb, ^{108}Cd, β-decay, use of pneumatic irradiation apparatus with on-line measurement system 2—28001
^{112}Ag→^{112}Cd, half life determination 2—21413
^{114}Ag, production by ^{114}Cd(n,p) reaction 2—31504
^{110g}Ag 24 sec, β-decay of 1$^+$ ground state to low spin states in ^{110}Cd 2—31480
^{110m}Ag, γ-ray spectra meas., identificatikn of weak transitions 2—28007
^{102m,g}Ag, 8 min and 13 min isotopically separated samples, meas. γ-ray spectra and $\gamma\gamma$ coincidences 2—14964
^{104m,g}Ag→^{104}Pd, 33 and 69 min isotopically separated samples, meas. γ-ray spectra and $\gamma\gamma$ coincidences 2—18168
^{24,24m}Al beta delayed alpha emission measured, deduced log ft values 2—18156
^{26}Al→^{26}Mg, positron emission and electron capture 2—11793
^{68}As, separated from ^{68}Se produced in ^{59}Ni(^{12}C, 2n) reaction, meas. of half-life and γ ray spectra 2—38538
^{76}As, γ-ray intensities and energies 2—18159
^{209}At, γ-ray assignment and excited states 2—21415
^{194}Au, beta and gamma spectra 2—11805
^{195}Au, precision determ. of high-Z K-shell fluorescence yields 2—15205
^{198}Au→^{198}Hg, angular correlation of γ-γ cascade 676-412 keV studied, mixing ratio of 676 keV transition determ. 2—31512
^{202}Au, studied after production by ^{202}Hg(n,p) and ^{205}Tl(n,α) reactions 2—31513
^{204}Au, studied after production by ^{204}Hg(n,p) reaction 2—31513
^{129}Ba→^{129}Cs, β- and γ-activity, meas. γ-ray spectra, deduced levels of ^{129}Cs 2—18163
^{203}Bi, high resolution γ-ray studies, conversion coeffs. for transitions in ^{203}Pb 2—34993
^{204}Bi, high resolution γ-ray studies, conversion coeffs. for transitions in ^{204}Pb 2—34993
^{207}Bi, precision determ. of high-Z K-shell fluorescence yields 2—15205
^{211}Bi, transition rates and log ft values calculated, comparison with expt. 2—2757
^{76}Br, incorporation of new positron emission and gamma transition data 2—11796
^{84}Br, decay to levels in ^{84}Kr, studied using gamma ray spectra 2—31502
^{85}Br, 3 minute decay, γ- rays assigned 2—5674
^{141}Ce $\beta\gamma$ correlation investigated using Compton backscattering to determ. circular polarization of γ-rays 2—14967
^{63}Co, decay scheme and period from γ-ray measurements 2—31501
^{68}Cu isomers, meas. β- and γ-ray intensities γ-γ β- γ coincidences, level structure of ^{68}Zn 2—38539
^{161}Er to levels in ^{161}Ho 2—31508
^{171}Er β-decay to levels of ^{171}Tm, γ-ray transition properties 2—34970
^{65}Ga, gamma-ray meas. 2—24182
^{67}Ga→^{67}Zn, new γ-ray at 884 keV 2—38497
^{76}Ga→^{76}Ge, γ-ray decay scheme and nuclear energy levels in ^{76}Ge 2—11751
^{203}Hg, study of 279 keV transition to ^{203}Tl angular correlation meas. of asymmetry, deduced limit of parity mixing 2—2736
^{203}Hg→^{203}Tl, β-γ directional correlation measurement for transition reveals parity violation in ^{203}Tl 2_11806
^{157}Ho, meas. γ-ray intensities, γ-γ coincidence with Ge(Li), Si(Li) detectors, ^{157}Dy levels deduced 2—34965
^{126}I, γ-ray obs. 2—38549
^{131}I, investigation of 636.3 and 722.9 keV transitions by gamma ray spectra and conversion electrons 2—479
^{136}I, 45 sec and 83 sec isomers 2—34990
^{137}I, β-delayed neutron energy spectrum meas. with high resolution neutron spectrometer 2—24185
^{132}La→^{132}Ba 2—18120
^{140}La, β decay, determ. γ-ray transitions and internal conversion coefficients 2—18121
^{140}La, β spectrum analysed with Slatis Siegbahn β-ray spectrometer, study of outer β group with end point 2164 keV 2—28008
^{6}Li excited states decay 2—8315
^{169}Lu, revised scheme 2—24188
^{138}Nd→^{138}Pr, γ ray and conversion electron spectra 2—480
^{147}Nd, study of nuclear matrix elements in 806 keV β transtiion 2—28009
^{235}Np, precision determ. of high-Z K-shell fluorescence yields 2—15205
^{28}P γ-decay scheme study from ^{28}Si(p,nγ) at 23 MeV 2—14986
^{201}Pb→^{201}Tl, γ-rays obs., conversion coeffs. calc. 2—2734
^{211}Pb, β-decay to first excited state of ^{211}Bi, directional correlation meas. β-matrix elements deduced 2—2756
^{211}Pb, β-decay transition rates and log ft values calculated, comparison with expt. 2—2757
^{195m}Pb, partial energy level scheme of ^{195}Tl 2—31511
^{197m}Pb, partial energy level scheme of ^{197}Tl 2—31511
^{101}Pd→^{101}Rh positon decay spectrum investigated with double focussing spectrometer meas. of end point energies, log ft values and ^{101}Pd Q-value 2—31503
^{152}Pm isomers 2—31507

Radioactivity continued
decay schemes continued
^{211}Po transition rates and log ft values calculated, comparison with expt. 2—2757
^{138}Pr, single and coincidence γ-ray spectra 2—38550
^{238}Pu, α decay, revised scheme based on investigation of hard γ radiation 2—11810
^{88}Rb→^{88}Sr, 17.8 min, meas. γ-γ angular correlations of four cascades, level structure of ^{88}Sr 2—28006
^{99}Rh beta decay, energy level study of ^{99}Ru 2—34953
^{104m}Rh→^{104}Pd β-decay, use of pneumatic irradiation apparatus with on-line measurement system 2—28001
^{93}Ru→^{93}Tc, γ ray decay, energy levels in ^{93}Tc studied 2—38545
Sb (A=126, 128, 130), beta decay, quasi-particle levels of Te(A=126, 128, 130) with large spin 2—11799
^{125}Sb β-decay to states in ^{125}Te, determ. of lifetimes of 35.5 and 465 keV states 2—34958
^{128}Sb 8.9h, β- decay, meas. of γ-ray and conversion electron spectra, ^{128}Te deduced levels 2—34959
^{42}Sc(7$^+$)→^{42}Ca(6$^+$) β decay ft values, discrepancy between theory and expt. not accounted for by two-hole admixtures 2—11740
^{48}Sc→^{48}Ti activity characts., transitions of ^{48}Ti 2—38536
^{27}Si,B$^+$ decay to ground and excited states of ^{27}Al, position branching ratios and log ft values obtained 2—18157
^{33}Si 6.3 sec, new isotope produced via ^{18}O(^{18}O,2pn), reaction 23-40 MeV, γ-ray intensities and decay 2—38535
^{125}Sn→^{125}Sb, 9.7 min, meas. γ-γ angular correlations of five cascades, level structure of ^{125}Sb 2—28006
^{90}Sr, β decay, probability of production of internal bremsstrahlung 2—11797
^{92}Sr→^{92}Y, gamma-ray spectra, half-life obs. 2—2748
^{175}Ta→^{175}Hf, excited states in ^{175}Hf 2—11803
^{176}Ta→^{176}Hf, meas. half life of 1247.7 keV level is ^{176}Hf deduced E1M2E3 mixing of 1159.3 keV level 2—18140
^{182}Ta→^{182}W, triple gamma cascade studies 2—2730
^{152}Tb→^{152}Gd, rel. to level structure studies in ^{152}Gd 2—11767
^{155}Tm, new isotopes, α decay investigated, mass assignments made 2—11801
^{156}Tm, new isotopes, α decay investigated, mass assignments made 2—11801
^{44}V, β-delayed α-particle decay observed in highly neutron deficient isotope produced in ^{40}Ca(^{6}Li,2n) reaction 2—11795
^{121}Xe→^{121}I 2—14965
^{90}Y, β decay, probability of production of internal bremsstrahlung 2—11797
^{94}Y, energies and intensities of β- and γ-ray transitions to levels of ^{94}Zr 2—2749
^{94}Y→^{94}Zr, γ-spectra study 2—18161
^{95}Y→^{95}Zr, γ-spectra study 2—18161
^{86m}Y, β^+ and γ decay 2—38544
^{167}Yb→^{167}Tm, 18 min, electron capture decay, investigation of ^{167}Tm level scheme from conversion electron, single γ-ray spectra and γ-γ coincidences 2—472
^{60}Zn, γ-ray spectra using mass separated sources 2—31500
^{61}Zn, γ-ray spectra using mass separated sources 2—31500

electron capture
bremsstrahlung, theoretical results from Morrison-Schiff, Glauber-Martin and Zon-Rapoport theorems 2—34980
superheavy nuclei, stability against electron capture, potential energy surface calc. 2—21454
^{209}At decay scheme, γ-ray assignment and excited states 2—21415
^{209}At decay to levels of ^{209}Po, coupling of single-neutron-hole states obs. in ^{209}Po 2—31494
^{133}Ba, P_k electron capture probabilities 2—14966
^{134}Ba decay, L/K ratio 2—38532
^{139}Ce, P_k electron capture probabilities 2—14966
^{152}Eu decay, L/K ratio 2—38532
^{153}Gd, angular correlation, sum-peak coincidence spectra 2—481
L/K ratio meas. from γ-ray X-ray sum peak in Ge(Li) spectra 2—38532
^{138}La→^{138}Ba, partial half-life 2—18164
^{186}Re, angular correlation, sum-peak coincidence spectra 2—481
^{141m}Sm population of three quasiparticle multiplet in ^{141}Pm 2—31505
^{48}V, L/K-capture ratio 2—34987
^{49}V, L/K capture ratio 2—31499

protection *see Radiation protection*

Radioactivity measurement
see also Dosimetry; Radiation monitoring; and the specific radiation, e.g. Gamma rays
in atmosphere, equilibrium between Rn and daughters 2—13726
decay time meas. with 2 photomultipliers in single photoelectron condition 2—8314
electron capture, L/K ratio, from γ-ray X-ray sum peak in Ge(Li) spectra 2—38532
intercomparison of Ra sources by measurements of γ-ray intensity 2—5672
ocean contamination monitoring 2—40908
recoil nuclei from α-decay, velocity measurement and mass determination 2—28003
solutions, $4_{\pi}\beta$-γ anticoincidence method 2—14768
thick sources, effect of $\beta\gamma_{cp}$ correlation experiments 2—28002
^{141}Ce, absolute disintegration rate det. by $4\pi\beta$-γ coincidence meas. 2—11800
$4\pi\beta$-X coincidence method and $4\pi e$ counting for self and foil absorptions of low energy internal conversion electrons 2—14961
^{131}I, concn. in air, automatic instrument for continuous obs. 2—4698
^{233}Pa, half life of $^{5}/_{2}{}^{+}$, 86.6 keV level using loaded scintillators 2—34995

apparatus
see also Particle detectors
aerosols, instruments and methods for characterizing 2—28911
anticoincidence method, $4\pi\beta$-γ, for solutions 2—14768
beta ray spectrometer, Siegbahn-Slatis type, modification 2—38358
flash tubes, computer simulation at diffusion and drift of electrons 2—34789
laboratory γ spectroscopy and solid-state detectors 2—7197
nonlinear pulse height compensator for use with time to amplitude convertor for walk corrections 2—34827
pneumatic irradiation apparatus with on-line measurement system for the study of short lived isotopes 2—28001

Radioactivity measurement continued
apparatus continued
portable gamma-ray scintillometer for radioactive ore prospecting 2—33423
X- and gamma ray differentiation in radioactive material 2—34829

Radioastronomy
see also Cosmic radiations, radiofrequency; Sun/radiation, radiofrequency
almucantar telescope, capabilities 2—26934
Arecibo radio-radar telescope, improvements 2—30645
cosmological models testing methods 2—41033
and cosmology 2—4772
Culgoora radioheliograph for generation of diffraction patterns 2—5020
fan-beam survey near declinations +28° and +41°, catalogues of 320 detected sources 2—26795
fully steerable decametric array at Clark Lake 2—20711
geodesic precision measurements using very long baseline radio interferometry 2—30132
information processing using computer 2—7572
interferometer, Ku-band, for mapping discrete radio sources 2—5026
interferometer visibility scintillation due to interstellar and interplanetary refractive index variations 2—33707
interferometry, joint Soviet-American project 2—7573
interferometry, very-long-baseline, whole-Earth array 2—33773
interplanetary scintillations, simultaneous observations of radio sources 2—26899
interstellar communications technology 2—17096
Jupiter, 1964 apparition, observations at decameter wavelengths 2—11007
Jupiter, decametric L burst, long baseline analysis 2—37355
Jupiter, decametric radio noise, Faraday rotation in Earth ionosphere 2—1992
long baseline interferometry 2—26935
long baseline interferometry of 3C sources at decametric wavelength 2—26780
Mercury, topography and scattering characteristics at 3.8 cm radar wavelength 2—33746
microwave radiometer for daily measurement of solar flux at 2800 MHz 2—30615
microwave receivers for molecular line radio astronomy 2—11168
propagation and antennas, Conference, Los Angeles, (1971) 2—33486
radio recombination lines, historical development 2—23067
radio reflectors, deformation monitoring, experimental laser system 2—2009
radiotelescopes, interferometers, sensitivity and future developments 2—7574
RAE-1 satellite, design, calibration, performance, magnetosphere long wave radio phenomena studies 2—30389
23 cm. receiver for Cracow radiotelescope 2—11169
23 cm. receiver for Cracow radiotelescope 2—11169
satellite, l.f. observatory, design, calibration and performance 2—33570
satellite instruments and techniques for frequencies down to 30 kHz 2—11167
solar radioelectric activity at 600 MHz in 1967 2—7551
space, obs. of solar bursts at all frequencies, the STEREo project 2—11081
spectra found in 8000 MHz survey 2—4935
telescope, effects on amplitude scintillation spectrum 2—37167
telescope, paraboloidal, radiation pattern obs. using interferometer 2—17097
telescope spectrograph, computer-run 2—23137
telescopes, review 2—2008
very-long-baseline interferometry of exploding quasar 3C-279 2—30513
white dwarfs, magnetic, obs. at 10.63 GHz 2—4872

Radiocarbon dating *see Radioactive dating*

Radiochemistry
see also Chemical analysis/radioactive; Chemical effects of radiations/ionizing radiations; Radioactive tracers
lunar rocks, radioactive heat sources rel. to interior temperature profile 2—20671
2-naphthyl radical, ^{3}H decay synthesis in naphthalene-d$_8$, e.p.r. study 2—10650
perturbed angular correlations of gamma radiation, effect of slow rotational diffusion 2—20204
polycarbonates, irrad., proton spin-lattice, relax., obs. 2—10280
pulse radiolysis system, using kinetic spectrophotometry, design considerations 2—37059
radionuclides, particulate and dissolved, concentration, from natural waters with sampler 2—4653
recovery, precipitation of UN from liquid U-Sn alloy 2—8405
^{234}Pu production, irradiation of ^{237}Np, minimum ^{236}Pu contamination 2—8394
UC spheres preparation by carbothermic reduction of sol-gel UO$_2$-C spheres 2—7189

Radiography
see also Luminescent devices; X-ray tubes
alpha autoradiography, use of cellulose nitrate detector films 2—36191
autohistoradiograms, determ. of grain counting efficiency 2—11687
autoradiography, quantitative method for B content determ. 2—16713
body doses, film-thermoluminescent dosimetry method 2—41311
bone turnover assessment by micro- and auto-radiography 2—30674
computer controlled, for articulatory movement tracking 2—30685
computer controlled, state-of-the-art 2—34568
conccrete, microporosity obs. using colour film 2—39967
diffusion in aqueous gels, monitoring of concentration charges 2—12592
electron beam depth dose curves, surface ionization ratio for 3 to 11 MeV 2—37451
electron beam depth dose curves, theoretical and experimental curves for 3 to 11 MeV 2—33790
flash X-ray of electron beam weld cavities 2—25551
flying spot X-ray imaging system 2—32675
image enhancement, math. concepts. 2—32672
image enhancement problems 2—32673
image quality in radiographic inspection, rel. to welds 2—14056
marrow scanning with radiocolloids 2—30678
medical stereoscopic X-ray TV system 2—7635
minification for low information density scanning, advantages 2—33788
neutron, applic. of low power nuclear reactor 2—38736
neutron, development using research reactors 2—39872
neutron, imaging process in direct conversion method, model 2—5576

Radiography continued
neutron, position sensitive proportional counter 2—27862
neutron, testing for PuO_2-UO_2 fuels using TiO_2, Eu_2O_3, RhO_2 mixtures as analogues 2—550
neutron, use as practical clinical tool 2—5059
neutron, visual image quality indicator 2—39863
neutron imaging, multiwire proportional chambers adaption with delay-line readouts 2—27863
neutron of nuclear fuel elements and valve packings 2—18258
non-destructive techniques for flaw size determination, review 2—32571
pelvimetry, simplified determination of correction factors 2—33784
radiometric density error analysis for thin material sections 2—32661
reactor fuel, fission product release performance, post-irrad. exam. techniques 2—38761
reactor fuel, post-irrad. exam. techniques at Studsvik 2—38750
reactor fuel post-irrad. exam. facilities 2—38751
reconstruction of three dimensional object from its transmission shadowgraph using convolutions instead of Fourier transforms 2—112
roentgenography with high-energy X-rays, luminescence yield 2—27687
scanners, working region 2—41307
skeletal imaging agents 2—30677
spatial freq. filtering 2—32674
three dimensional reconstruction of substance from shadow 2—2833
three-dimensional reconstruction from radiographs and electron micrographs by convolution method 2—29108
tomography, detection of small intrarenal calcifications 2—33787
X-ray, contact radiography using cold cathode discharge 2—25552
X-ray, single shot contact, applications 2—6409
X-ray and neutron, facilities at Univ. of Missouri 2—38768
X-ray intensifying screen using Gd_2O_2S:Tb phosphor 2—30672
X-ray pulses from a tube with a rotating target and 2.5 MV accelerating voltage 2—11234
X-ray tube design for aerospace component inspection 2—32665
zonography of the petrous temporal bone 2—7601
Ca, whole body content det. by in vivo neutron activation analysis 2—26956
$^{144}Ce^{3+}$ radioactive ions, diffusion in ion-exchange resins 2—7162
$^{137}Cs^{+}$ radioactive ions, diffusion in ion-exchange resins 2—7162
^{18}F for bone scanning, review of 10 years experience 2—30676
$^{212}Pb^{2+}$ radioactive ions, diffusion in ion-exchange resins 2—7162
Sn-Cd alloy, Cd segregation during melting, neutron radiography obs. 2—15633
^{85}Sr bone scan in neoplastic disease 2—30675
α-Zr, thermally oxidised, autodiffusion of O, meas. by obs. nuclear reaction $^{18}O(p,\alpha)^{15}N$ 2—12818

Radiolysis *see Chemical effects of radiations/ionizing radiations*

Radiometer gauges *see Vacuum gauges*

Radiosondes *see Meteorological instruments*

Radiosources
3C58, brightness and polarization structure of supernova remnant, obs. at 2.8 cms 2—26791
3C 391 supernova remnant, effects of interstellar gas on continuum spectrum and cut off of low frequencies 2—37329
3C 455, optical object 2—10949
4C catalogue, 2700 MHz obs. in declination zone +4° to —4° 2—20615
408 MHz, a sample of 4C sources, study 2—4921
1410 MHz, low latitude survey of milky way from 355° to 5° longitude 2—4922
absorption measurements at 21-cm on low-latitude sources south of declination —46° 2—10966
RAgl, OH emission, interferometer positions 2—20594
Antares B, interferometric obs. 2—4919
apparent size, interstellar scattering, Galactic structure 2—41057
B3V companion to Antares B 2—7474
BL Lac, 21 cm H absorption, line produced by local intervening cloud 2—13967
3C120, 3C273, 3C279, expanding source model of radio outbursts 2—4941
3C196, long baseline interferometric obs. 2—5022
5C1 and 5C2, spectral properties and comparison of spectral index distributions between 1400 and 408MHz 2—26775
3C273-3C279 position difference using long-baseline interferometry fringe phase obs. 2—30519
3C274, galaxy, high resolution obs. at 8 GHz 2—30520
3C279, rapid differential proper motion in radio fine structure 2—33606
3C459, long baseline interferometric obs. 2—5022
4C51.12, radio nebula, centimetre wavelength observations 2—41148
3C84, galaxy, high resolution obs. at 8 GHz 2—30520
4C 05.34, HI clouds in 2—20612
3 C 120, Seyfert galaxy, rapid change in visibility function 2—37265
3C 173, identification and UBV photometry with an electronic camera 2—30508
3C 279, gravitational deflection of signal near sun 2—4991
3C 279, quasistellar, detection of double source structure in nucleus 2—4936
3C 279, variable, direct obs. of diameter changes, models 2—13964
3C 391, H absorption profile and microwave continuum emission 2—13954
3C 48, long baseline interferometric obs. 2—5022
3C 61.1, optical identification 2—1966
Cas A, flux density obs. at cm. wavelengths 2—4920
Cassiopeia A, absolute meas. of flux at 16 GHz 2—37330
Cassiopeia A, absolute spectra 2—37333
Cassiopeia A, decrease of flux density at 1.4 and 3 GHz 2—37333
Cassiopeia A, distribution of linear polarization at 9.8 and 11.1 cm wavelengths 2—33708
Cen A, X-ray emission spectrum 2—26803
cluster galaxies, magnitude-redshift diagram interpretation and deceleration parameter 2—13870
compact, angular structures 2—13960
compact, high resolution obs. at 13 cm 2—17019
compact, in nuclei of elliptical galaxies 2—13961
compact objects, stars assoc. with galaxies and QSO's 2—13959
conference (San Juan, December 1971) 2—26582
core-halo, brightness distribution 2—26781
cosmological import of counts 2—13970
counts at 430 MHz 2—26783
counts in cosmological models, evolution rates 2—1967
3CR catalogue, optical identification and photometry 2—13966

Radiosources continued
Cyg. A, flux density obs. at Cm. wavelengths 2—4920
Cyg X-1, hard X ray pulsations, upper limits 2—7484
Cyg X-1, recent appearance 2—7477
Cyg X-1, search for pulsed radio emission at 327 MHz 2—10954
Cygnus A, absolute spectra 2—37333
Cygnus A, power spectra of intensity fluctuations, for obs. of small scale structure in ionosphere 2—4715
Cygnus A radio clouds, structure and spectrum 2—33709
Cygnus X region, continuum emission at 74, 111, and 196 MHz 2—30524
Cygnus X-1, identification with HDE 226868 2—23098
Cyrus X-1, position and identification 2—23092
density and luminosity evolution of source populations, errors in theory 2—7468
depolarization at long wavelength, correlation with redshift for quasars 2—41146
discrete, mapping with Ku-band radio interferometer 2—5026
double, fluid dynamic stability, evolution 2—26796
double, morphological difference between those in and out of clusters, as evidence for intergalactic medium 2—26609
double, relative orientation of major axes 2—20623
DR21, planetary nebula, H85α recombination lines 2—33614
DR 21-OH, microwave emission from nonmetastable levels of NH_3 2—10933
DW 0224+67, DW 0727-11, variations at microwave frequencies 2—7488
emission model based on radiation from relativistic particles 2—33714
extended, discrete, as ghost images in universe of strong positive curvature and inhomogeneous mass distribution 2—13825
extended, in Coma Cluster, origin of mag. field 2—37335
extended galactic, polarization of supernova remnants at 6 cm wavelength 2—20614
extra-galactic, structure and evolution 2—17016
extragalactic, in 3C catalogue polarization props. 2—20624
extragalactic, intensity variations 2—13962
extragalactic, interpretation of variable components by synchro-Compton theory 2—23089
extragalactic, linearly polarized brightness distribution at 2695 MHz 2—20622
extragalactic, Parkes survey of 21-cm absorption spectra 2—10964
extragalactic, spectral index distributions 2—26785
extragalactic, spectral indices at 1.4 GHz 2—26794
extragalactic distributions of size and brightness, 8 GHz obs. 2—30520
extragalactic extended, polarization at 6 cm wavelength 2—20613
extragalactic objects, observational paradoxes about red shifts, ages and origins 2—26608
fan-beam survey near declinations +28° and +41°, catalogues of 320 detected sources 2—26795
fine structure at 81.5 MHz, technique of interplanetary scintillation for angular diameter obs. 2—26777
G55.7+3.4, mapping at 11 and 21 cm wavelengths, possible association with CP1919 2—10961
G55.7+3.4, non-thermal shell source close to the directon of CP 1919 2—10960
galactic, 21-cm absorption measurements, north of declination -48° 2—10965
galactic, and galactic disk obs. at meter wavelengths 2—33706
in galactic centre, interferometric obs. at 5 GHz 2—10940
galactic nebulae 2—33618
galactic plane 100μ survey 2—20627
galactic radio objects toward galactic centre, 21-cm line interferometry 2—33713
galaxies, continuum, origin of emission in spirals 2—4925
galaxies, luminosity function at 400 and 2700 MHz 2—4923
galaxies, optical and radio luminosity functions 2—1966
galaxies, positions, and flux densities in continuum 2—4924
galaxies, redshift meas. 2—37252
galaxies, redshifts and fluxes 2—1968
galaxies, redshifts from spectroscopic observations 2—20488
galaxies, Seyfert and normal, obs. at 1415 Mhz 2—4926
galaxies, spectra between 10 and 10000 MHz 2—13956
galaxies, tidally interacting, obs. at 4.2 and 2.2 cm 2—7378
galaxies γ sources search at 10^{11}-10^{12} eV, null result 2—33722
galaxies and quasars, models fo cosmic evolution 2—17017
galaxies at 2695 and 8085 MHz, mapping the distribution of polarized radiation 2—26782
giant loops, new interpretation as supernovae remnants 2—13913
glitches in the Crab Nebula pulsar 2—4938
high brightness, circular polarization obs. 2—30522
IC443, brightness and polarization structure of supernova remnant, obs. at 2.8 cms 2—26791
IC 410, meter wavelength obs. 2—33706
IC 418, planetary nebula, H85α recombination lines 2—33614
IC 443 nebula, supernova remnant, obs. at 408 MHz 2—16967
interferometer visibility scintillations due to interstellar and interplanetary refractive index variations 2—33707
interferometry, very-long-baseline, whole-Earth array 2—33773
interplanetary scintillation at metre wavelengths 2—17022
Jupiter, emission at 80 MHz 2—33734
Jupiter decametric radiation enhancement caused by photoelectron emission from Io 2—33735
BL Lacertae, variable, photoelectric obs.30488 2—30488
lower limit to angular size, baseline length for interferometric observations 2—20621
lunar occultation obs. 2—37331
β Lyrae, eclipsing binary 23091 2—23091
M17, Stark broadening in radio recombination lines 2—4927
M31, metre wavelength radio observations 2—26637
M33 spiral galaxy, obs. at 318 and 606 MHz, brightness temp. distribution and spectrum 2—37328
M51 nucleus, high resolution radio continuum survey at 1415 MHz 2—37263
Maffei 1, radio luminosities 2—10894
methanol, rest frequency of 36 cm radio line from galactic centre 2—33596
microwave and i.r. continuum flux, time variations monitoring 2—4933
microwave receivers for molecular line radio astronomy 2—11168
N132D supernova remnant in Large Magellanic Cloud, obs. at 408 MHz 2—7490
N49 supernova remnant in Large Marellanic Cloud, obs. at 408 MHz 2—7490

Radiosources continued
- N63A supernova remnant in Large Magellanic Cloud, obs. at 408 MHz 2—7490
- N(S) relationship at 1400 MHz 2—13968
- N-galaxies 3C 120, 371, detection of redshifted H I line 2—13929
- NGC 1068, neutral H obs. at 21 cms., integrated profiles, H and total masses meas. 2—13868
- NGC 1499, NGC 2175, NGC 2244, meter wavelength obs. 2—33706
- NGC 3227, neutral H obs. at 21 cms., integrated profiles, H and total masses meas. 2—13868
- NGC 4051, neutral H obs. at 21 cms., integrated profiles, H and total masses meas. 2—13868
- NGC 4151, neutral H obs. at 21 cms., integrated profiles, H and total masses meas. 2—13868
- NGC 5128, radio emission from nucleus, nonthermal source within infrared object, 11.1 and 3.7 cm wavelength 2_1948
- NGC 5195 nucleus, high resolution radio continuum survey at 1415 MHz 2—37263
- NGC 7027, planetary nebula, H85α recombination lines 2—33614
- nonlinear spectra interpretation, general empirical expression 2—10945
- nonthermal, galactic, soft X-ray emission, implications in Galactic background and interstellar medium 2—7473
- Nova Delphini 1967, radio variations 2—33666
- Nova Serpentis 1970, radio variations 2—33666
- NP0532, long baseline interferometric obs. 2—5022
- NP0532, very long baseline interferometry at 121.6 MHz 2—26788
- NRAO 588/589, radio nebula, centimetre wavelength observations 2—41148
- NRAO 589A and 4C51.12, radio nebulae, distance estimates 2—41149
- number counts and spectral distribution at centimetric wavelengths 2—13969
- observation of, principles employed in 2—7476
- Ohio, spectra and position det. 2—10932
- Ohio optical variation in 11 sources with unusual spectra 2—10936
- OJ 287, energy distribution in optical and infrared regions 2—10930
- OJ 287, obs. at optical and mm wavelengths 2—10938
- OJ 287, UBV photometry obs., 3900-4900 Å 2—26792
- OJ 287, variability of optical intensity and plane polarization 2—41152
- OJ 287, variable, obs. at cm. wavelengths 2—10939
- optical position obs. 2—7489
- optical positions of 9 compact radio sources relative to AGK 3 2—33711
- Orion A, OH emission, interferometer positions 2—20594
- Orion A, Stark broadening in radio recombination lines 2—4927
- P 1934-63, structure, interferometer obs. 2—13955
- Parkes 2700 MHz survey, catalogue for 03^h, 11^h, 19^h, 23^h zone, declinations −33° to −75° 2—13953
- β Persei, eclipsing binary23091 2—23091
- PHL 957, HI clouds in 2—20612
- photoelectric obs. of stars nearby 2—20554
- PKS 1514-24, lunar occultation measurements linking it with AP Lib 2—10958
- planetary nebulae at 2700 MHz, extinction coeff. determ. 2—33613
- precise positional measurement of 28 sources 2—7483
- pulsar radiation mechanism rel. to relativistic electrons in spiral orbits, polyscrew streams 2—33705
- pulsars, average radio spectra 53-606 MHz 2—26789
- pulsars, fluctuation spectra analysis, polarization of subpulse structure 2—26786
- pulsars, redshifts and fluxes 2—1968
- QSO, absorption lines and low mass protogalaxies 2—20612
- QSO, spectra and time variations 2—13965
- QSO's and Seyfert galaxies, radiation from, size limitations on thermal and nonthermal models 2—17018
- QSO's multiple pulsar model 2—20617
- QSOs and galaxy in southern hemisphere, redshift obs. 2—26769
- QSS, 3C 273, 1510-08, detection of redshifted H I line 2—13929
- QSS, expanding source model of radio outbursts 2—4941
- quasars, associated with bright galaxies, study of 222 QSRS's and 166 QSO's 2—37326
- quasars, redshifts and fluxes 2—1968
- quasi-stellar objects, luminosity function at 400 and 2700 MHz 2—4923
- quasistellar, compact, polarimetric obs. 2—10929
- quasistellar, luminosity function and bivariate ratio obs. 2—20611
- quasistellar, redshifts and luminosities rel. to optical quasi-stellar objects 2—10931
- radio recombination line emission in four sources formerly considered supernova remnants 2—26778
- radiogalaxy, γ-quanta fluxes, upper limits point source search 2—17025
- Ryle Neville survey (1962) optical identification 2—1966
- Sagittarius B2, obs. of $^2\Pi_{1/2}$ J=½ line of OH at 4660 MHz 2—10934
- sample complete to 3 p.u. at 430 MHz 2—26784
- scintillation, interplanetary, electron density variations in solar wind 2—11024
- scintillations due to plasma interplanetary medium irregularities with power law spectra in interplanetary medium 2—11025
- Sco X-1, observations at 80 MHz to show existence of radio flares 2—4945
- Sco X-1, search for pulsed emission 2—7493
- Sco X-1 and Cyg X-1, search for pulsar like emissions at 400 MHz 2—23090
- Seyfert 3C 120, correlated optical and radio variability 2—23060
- Seyfert galaxies, high brightness, circular polarization obs. 2—30522
- Seyfert galaxies, multiple pulsar model 2—20617
- Seyfert galaxies, NGC 1068, 1275, detection of redshifted H I line 2—13929
- Seyfert galaxies nuclei, expanding source model of radio outbursts 2—4941
- VXSgr, OH emission, interferometer positions 2—20594
- Sgr A, compact components, interferometric obs. at 5 GHz 2—10940
- Sgr A, Sgr B2, 6 cm formaldehyde absorption 2—17020
- Sgr A at 22.2 GHz with a beamwidth of 1.5 arcminutes 2—4928
- small diameter, linear polarization obs. 2—30521
- small galactic nebulae, radio emission at 606 MHz, identification with optical objects 2—33616
- Solar type III burst events, fine structure 2—5002
- southern, optical obs., spectroscopic features 2—10937
- spectra found in 8000 MHz survey 2—4935
- stars, discussion of available information, radio astronomy 2—7492
- sun, local sources, two groups 2—2002
- supernova 1970g, first epoch radio obs. identification with pointlike source 2—37303
- supernova of 1006 A.D. radio obs. search 2—4874
- supernova remnant Puppis A, radio map at 408 MHz 2—4875
- supernova remnants, redshifts and fluxes 2—1968
- supernova remnants, soft X-ray emission, implications in galactic background and interstellar medium 2—7473
- supernovae remnants in distant normal spiral galaxies 2—13854
- surface brightness, observation for differing counts 2—26765
- survey at 5GHz, faint sources, positions and flux densities 2—13957
- synchrotron radiation from relativistically expanding source 2—33715
- Tau A, flux density obs. at cm. wavelengths 2—4920
- Tau A, Vir A, Cyg A, Cas A, absolute flux density measurements at 26.3 MHz 2—20619
- Taurus A, absolute meas. of flux at 16 GHz 2—37330
- Taurus A absolute spectra 2—37333
- thermal, model distribution, est. of r.m.s. confusion levels in galactic plane 2—16970
- variable, in association with X-ray source GX9+1 2—23093
- variable, models, testing by obs. of diameter changes 2—13964
- variable, obs. at 8.2 mm 2—13963
- variable extragalactic sources at 3.8 cm., deductions from sky survey 2—41147
- variable structures, model as outbursts of clouds of relativistic electrons into stationary magnetic field tubes 2—33710
- variables, associated with centimeter excess spectral type 2—41153
- variables at 8000 MHz, obs. 2—26774
- Virgo A, l.f. high resolution obs. of angular structure of central region at 151 and 408 MHz 2—33716
- VRO 42.22.21 (BL Lac), new phase of activity 2—20620
- W28, brightness and polarization structure of supernova remnant, obs. at 2.8 cms 2—26791
- W3-OH, microwave emission from nonmetastable levels of NH_3 2—10933
- W43, microwave emission from nonmetastable levels of NH_3 2—10933
- W44, brightness and polarization structure of supernova remnant, obs. at 2.8 cms 2—26791
- W49, galactic H_2O sources, very low baseline interferometry, high resolution 2—30523
- W49, W51, W56, meter wavelength obs. 2—33706
- W49 and Orion A, H_2O line emission, very long baseline interferometry 2—33712
- W51, microwave emission from nonmetastable levels of NH_3 2—10933
- weak, in Parkes catalogue for declinations +20° and −20°, identifications 2—20607
- H I absorption spectra at 21 cm, statistics of concentration in the galactic disk 2—10967
- H_2O emission at 22.23508 GHz associated with OH emission in southern Milky Way 2—33597
- H_2O line emission regions in Orion A study by very long baseline interferometry 2—41154
- H_2O microwave sources associated with H II regions, laser pumping 2—30526
- OH emission sources, interferometer positions 2—20594

Radiostars *see Radiosources*

Radiotelescopes *see Radioastronomy*

Radiowave propagation *see Electromagnetic wave propagation*

Radiowave spectra *see Nuclear magnetic resonance and relaxation; Paramagnetic resonance and relaxation; Spectra*

Radium
- atom, L_{II} subshell fluorescence, Auger and Costner Kronig yields 2—18321
- atoms, photoionization calc., inclusion of intrachannel interactions 2—601
- intercomparison of sources, Ge(Li) detector, γ-ray intensity measurements 2—5672

Radium compounds
- No entries

Radium emanation *see Radon*

Radon
- atoms, photoionization calc., inclusion of intrachannel interactions 2—601
- radioactive equilibrium with daughters in atmosphere 2—13726
- turbulent transfers inside vegetative canopy, use of Rn for meas. of diffusivity profiles 2—22963
- ^{219}Rn, lifetime obs. of states excited by α-particle decay, microwave method 2—8222
- ^{222}Rn, distribution on surface of Moon 2—7514

Rain
- *see also Condensation; Snow*
- anomalies in e.m. attenuation at 37 GHz 2—37165
- anomalous attenuation of millimetre, microwaves 2—30301
- atmospheric attenuation, at 15 and 35 GHz 2—16850
- attenuation, weather radar meas. at 10 GHz 2—33492
- attenuation at 15.3 and 35 GHz over 15.5 km path 2—37168
- attenuation meas., of radiowaves, in submillimetre range, experimental study 2—16828
- attenuation meas. at 18.5 to 30.9 GHz on 2.6 kilometre propagation path 2—20353
- attenuation of e.m. waves, statistical study 2—16851
- attenuation on earth-space communication 2—37162
- contaminant concentrations during convective rains, correlations with intensity of downpour 2—1866
- contamination precipitation and diffusion from clouds to great distances 2—20398
- density quantitative determ. using digital meas. values input and processing 2—7246
- Department of Katowice, specific β-radioactivity in rain 2—30303
- design storm for hilly catchment with inadequate raingauge network 2—20340
- digital measuring unit 2—7248
- distribution in warm sector depression 2—40955
- drop spectra, interference phenomena calc. 2—7306
- droplet growth, coalescence process, photographic and visual observation 2—1863
- effect on radar orthognal detection at Ku band 2—13725
- e.m. millimetre wave attenuation 2—37166
- e.m. wave propagation, 6.25 mm wavelength, rainfall attenuation obs. 2—16835
- e.m. waves propagation, millimetre, in tropical and equatorial regions 2—16865

- **Rain** continued
  - evaporated, optical constants in 2.5 to 40 μm range 2—37136
  - extraterrestrial particles, magnetic spheroids, global deposition, association with rainfall 2—22969
  - fall, daily mean, accuracy of estimates 2—1871
  - fall, spatial variation, effect of wind direction and speed 2—1854
  - forecasting heavy rainfall along Gujarat coast in association with Bay depressions 2—20338
  - forecasting over small catchment areas by synoptic typing 2—20339
  - freezing by passage through strong electric fields 2—1864
  - gauges, ground-level 2—1823
  - hydrometeors in troposphere, e.m. wave scatt., interference study 2—33490
  - intensity determination, drop size spectra 2—30289
  - i.r. radiation, attenuation, computations 2—16837
  - microwave attenuation, rainfall effect 2—26506
  - microwave attenuation, rainfall effect 2—26507
  - microwave radio transmission, cross-polarization distortion 2—22980
  - monsoon, break type, and dynamic instability of zonal current 2—1869
  - monsoon, vertical coupling between upper and lower tropospheres 2—7278
  - monsoons in the Amazon Basin 2—1868
  - Narmada Basin, hydrometeorological aspects 2—20337
  - pluviometric possibility indicating line for durations shorter than 24 hours, evaluation of parameter values 2—20336
  - radar characteristics, in submillimeter range 2—16832
  - radar measurement as specific identification task 2—22970
  - radioactive fallout in atmospheric dust and rain during 1971, effect of Chinese and French nuclear tests 2—40973
  - radiowave attenuation above 10 GHz, equivalent precipitation model 2—10736
  - radiowave attenuation for frequencies above 10 GHz, calc. 2—10735
  - radiowave interference, bistatic scatter expt., high resolution L-band radar meas. 2—33487
  - radiowaves, submillimetre, attenuation, computations 2—16852
  - radiowaves attenuation, 11 and 18 GHz, meas. at higher angles of elevation 2—16866
  - rain intensity, droplet spectra and radar reflectivity, comparative study 2—7247
  - raindrop analyzer for automatic counting and sizing 2—33464
  - scatter, coordination area for mainlobe to mainlobe coupling 2—33491
  - scatter computer model, predictions for ATS-F/G radio interference expt. at 6 GHz 2—33489
  - scatter interference statistics between terrestrial microwave and satellite communication systems at 4 to 8 GHz 2—33488
  - scattering effects, radiometric measurements 2—33493
  - S, Cl- content, meteorological interpretation 2—1821
- **Raman spectra** *see Scattering/light, Raman spectra*
- **Ramsauer effect** *see Electron beams; Electrons/absorption; Energy loss of particles*
- **Random functions** *see Random processes*
- **Random processes**
  - *see also Brownian motion; Fluctuations; Statistical analysis*
  - Fokker-Planck and random walk models, interrelation, with application to Coulomb interactions 2—37659
  - Fourier holography at type-written text, effect of weighting the random distrib. 2—5390
  - heavy particle motion in an infinite one dimensional gas of hard spheres 2—7721
  - hypersurface generation by computer 2—14119
  - kinetic turbulence in random function theory, growing modes eliminated by physical causality 2—37235
  - measurement processes, dynamics, application of information theory 2—20795
  - multiple scattering of particles, random walk theory 2—2155
  - noise, 1/f, random walk model 2—25805
  - noise, 1/f, random walk model 2—25806
  - one-dimensional walks with boundary, expansion of master equation 2—33934
  - percolation model, large range connectivity criteria 2—27079
  - product reliability, random fatigue analysis 2—7734
  - random lattices, double site approx., applic. to calculation of frequency spectra of disordered systems 2—37634
  - random walk, on two-dimensional substrate lattices, detailed calc. of number distinct sites visited 2—30801
  - random walk, rel. to corrections to expressions for saturation density of stable clusters in solid films 2—32345
  - random walks, in polytype structures 2—20864
  - self-excluding walk of N-jumps, mean square extension 2—23289
  - selfavoiding rings on lattice, number 2—37633
  - selfavoiding walk problem, numerical investigation of closure approximations 2—20863
  - selfavoiding walks and returns, two and three dimensional lattices, asymptotic behaviour 2—37632
  - stochastic approach to nonlinear damper of vibrs. 2—37726
  - stochastic master equations, perturbative approach 2—20856
  - walk, linear response theory 2—7696
  - wave propagation in one-dimensional random media 2—5167
  - H_2 glow discharge, Monte Carlo simulation 2—35617
  - He, random walk theory of elastic and inelastic time dependent collisional processes in electric field 2—18711
- **Range of particles** *see Energy loss of particles*
- **Rapid recovery** *see Recovery*
- **Rare earth compounds**
  - *see also the compounds of the individual metals; Ferrites*
  - 4f bonding study, new model of electronic configuration 2—4106
  - alloys, Ln-Rh system, atomic struct. 2—22161
  - borides, B-rich, synthesis and characterization 2—9337
  - carboxylates, cryst. struct. 2—9513
  - chalcogenides, ternary, cryst. chemistry and mag. props. 2—9341
  - chromoselenides, elec. props., semicond. behaviour 2—10029
  - cobalt alloy permanent magnet characterization 2—40515
  - cobalt alloys, permanent magnet characts. 2—40516
  - cobalt intermetallics, coercive force, nucleating fields, ang. depend. 2—40491
  - cobalt intermetallics, mag. behaviour, e.p.r. obs. 2—10518
  - cobalt intermetallics, mag. behaviour, e.p.r. obs. 2—10519
  - cobalt intermetallics, mag. ordering temp., proess. depend. 2—33142
  - cobalt magnet processing 2—39896
- **Rare earth compounds** continued
  - cobaltates, high spin-low spin equilib., mag. susceptibility, elec. cond. and Mossbauer study 2—36656
  - cobaltides, RCo_5 permanent magnet, prep. by pressing and sintering 2—19883
  - complexes, β-diketonates, i.r. absorption spectra in region 750 to 250 cm^{-1} 2—21620
  - dielectric film formation by vaporization of the oxides with electron beam 2—29017
  - ferrite garnet, mag. struct., phase transition 2—4396
  - fluorides, far-i.r. Stark and Zeeman splitting of rare earth ions 2—40669
  - gallium garnets, Czochralski growth 2—19003
  - gallium garnets, for appl. as substrates, Czochralski growth 2—29099
  - garnet, dichroism due to site selectivity of ions 2—40639
  - garnet, growth-induced anisotropy, theory 2—13372
  - garnet films, bubble parameters, temp. depend. 2—36749
  - garnets, growth-induced anisotropy, sign and magnitude 2—4363
  - hectoboride phase, lattice parameters and Knoop hardness 2—9833
  - hexaborides, single crystal, vapour liquid solid growth mechanism 2—1204
  - hydroxyfluorides, synthesis and cryst. struct. 2—3728
  - insulators, ionic, Gd^{3+}-Gd^{3+} exchange coupling 2—1610
  - intermetallic, Cu_3LnTe (Ln=Sm, Gd, Dy, Yb, Y), prep. and props. 2—36230
  - intermetallic, Laves phase, spin-lattice relax. time temp. depend. 2—40581
  - intermetallic, $Ln_2X_{\sim 9}$(X=Zn or Cd), cryst. struct. 2—39656
  - intermetallic, spin-lattice relax., dynamic effects of paramag. ions 2—26078
  - intermetallic compounds, $Eu_xLa_{1-x}Al_2$ ternaries, reversal of coupling, RKKY analysis 2—4412
  - intermetallic compounds, role of mag. exchange and crystal field interactions in determining physical properties 2—10206
  - iridates, electronic characterization, cryst. chem. considerations, elec. and mag. meas. 2—10076
  - iron garnet, hyperfine field on ^{119}Sn, rare earth contrib. 2—22741
  - iron garnets, control of bubble domain props. by Co^{3+} addition 2—22692
  - iron garnets, film/substrate matching requirements for bubble form. 2—36750
  - iron garnets, noncubic mag. anisotropy mechanism and vacancy ordering 2—10202
  - iron garnets, optical birefringence and magnetocryst. anisotropy 2—40530
  - Laves phase compounds with Co and Ni, thermal expansion behaviour 2—4073
  - Luna 16 fines, conc. 2—20662
  - magnetic properties 2—25987
  - magnetic props., itinerant electronic system, theory 2—16342
  - Mischmetal-Mg alloys, metallographic prep. 2—12974
  - molybdates, $Ln_2(MoO_4)_3$, ferroelectric-paraelectric struct. transition, lattice parameters 2—9486
  - molybdates, struct. and phase relns. 2—9340
  - monochalcogenides, electronic collapse at high pressure 2—29589
  - monochalcogenides, synthesis and melt-growth 2—9367
  - nickel oxides, cryst. and mag. struct. 2—3727
  - niobates, $RENbO_4$ type, cryst. struct. 2—6448
  - nitrate, exchange effects, ^{1}H, ^{17}O and ^{14}N resonances 2—6254
  - nuclear spin-lattice relax. in paramagnetic state, model 2—7009
  - optical spectra, magnetic ordering effects 2—33259
  - orthoaluminate cryst. chemistry, struct. obs. on orthorhombic $SmAlO_3$ and trigonal $NdAlO_3$ 2—19058
  - orthochromites, supertransferred hyperfine fields 2—7029
  - orthochromites, thermomagneto-optical memory in regions with modified mag. struct. 2—1620
  - orthoferrite, crystal growth by floating zone method 2—32403
  - orthoferrite, growth by floating zone method and mag. props. 2—22113
  - orthoferrites, anisotropy in domain wall mobility 2—10252
  - orthoferrites, annealing induced domain wall mobility changes 2—10199
  - orthoferrites, domain wall energies 2—13419
  - orthoferrites, $Ln_{1-x}Ca_xFe_{1-x}Sn_xO_3$, hyperfine interactions of Sn, Mossbauer obs. 2—7059
  - orthoferrites, magnetoelastic properties near spin reorientation temperature 2—4395
  - orthoferrites, props. and use as logic elements 2—16366
  - orthoferrites, Sm-doped, low birefringence 2—40613
  - orthoferrites, supertransferred hyperfine fields 2—7029
  - orthoferrites, temp. sensitivity of bubble domains 2—26022
  - orthoferrites, thermomagneto-optical memory in regions with modified mag. struct. 2—1620
  - oxide, in $BaTiO_3$, effect on microstructure and dielec. props. 2—19761
  - oxide, powder crystallite growth, dynamic calcination effects 2—12980
  - oxide (R_2O_3)-WO_3 system, cpd. formation, stoichiometry 2—9339
  - oxides, crystallographic shear relations between α-UO_3, CaF_2, La_2O_3 and NaCl structure types 2—3738
  - oxides, $Ln_2O_3.2ZrO_2$, synthesis and cryst. struct. 2—36284
  - oxides, X-ray $L_{\gamma 2,3}$ spectrum 2—33298
  - oxides and oxysalts, union centred coordination polyhedra and related props. 2—9338
  - palladium intermetallics, R Pd_3 type, 1.5 to 300K 2—19829
  - paramagnetic complexes, use as chem. shift reagents in n.m.r. 2—5304
  - permanent magnet materials characterization 2—40514
  - perovskites, Dzialoshinsky-Moriya type ferromagnet, spin flop weak ferromag. transition 2—19874
  - phosphates, antiferromagnetic transitions, ^{31}P n.m.r. obs. 2—6992
  - phosphor, Yb^{3+}-sensitized, i.r.-visible conversion processes 2—33308
  - platinum metal-rare earth-carbon system, C-stabilized ordered phase form. 2—29493
  - pnictides, energy level scheme, absorpt. spectra, magneto-optical effect, elec. transport 2—4203
  - pnictides, quadrupole coupling interpret. of phase transitions 2—36792
  - pnictides, structural and magnetic phase transitions, lattice distortion model 2—1597
  - refractory tungstates, mats. charact. 2—29449
  - RPb_3, R=Ce, Pr, Nd, Eu, Gd, Sm, magnetic props., temp. range 2.8-300K 2—4346
  - ruthenates, electronic characterization, cryst. chem. considerations, elec. and mag. meas. 2—10076
  - silicates, of type $RE_2[SiO_4]O$, cryst. struct., X-ray diffr. 2—6450
  - transition metal intermetallics, model calcs. for s- and d-bands 2—40142
  - transition metal intermetallics, strong field magnetiz. 2—33159
  - trichlorides, Kramers-Kronig relationships, refr. and extinction indices 2—15592

Rare earth compounds continued
- trifluorides, X-ray photoelectron spectroscopy, multiplet splitting and 2-electron excitation 2—35282
- tungstates, struct. and phase relns. 2—9340
- ultraphosphates, definition and crystal chemistry 2—6395
- Ag-R dil. alloys, R=rare earth metal, resist., magnetoresist., thermopower, review 2—13110
- BaO-Ln$_2$O$_3$ system, (Ln=rare earth), phase relations, DTA and X-ray analysis 2—12991
- Be intermetallic, ^{9}Be spin-lattice relax. 2—26078
- Co-rare earth metals alloys, permanent magnet, magnetization changes, under heating up to 650°C 2—26035
- Co intermetallic, magnetiz. and specific heat rel. to mag. transitions 2—25998
- Fe garnet, critical light scatt. at mag. compensation point 2—16457
- Fe garnet, mag. anisotropy control by ion implantation 2—25417
- LnTiNbO$_6$,Ln=Ce, Pr, Nd, Sm, Eu, luminescence and diffuse reflection spectra obs. 2—4448
- Sc-rare earth dil. alloys, localized moments influence on spin-lattice relax. 2—19934

Rare earth metals
- *see also the individual metals*
- 4f bonding study, new model of electronic configuration 2—4106
- abyssal and plateau basalts, element abundances 2—10698
- in Ap star β CrB4829 2—4829
- atoms, $4f^{n-1}6s^26p$ configurations, lowest six-level structures 2—2937
- cobaltides, Ln-Ln′-Co ternaries; Ln, Ln′=Gd, Nd, Dy, Pr, Ho, magnetic characteristics 2—10213
- critical u.s. vel. and spin diffusion coeff. 2—29530
- crystal field potential, conduction electron enhancement, resonance amplitudes 2—10282
- crystalline electric field parameters, OPW calc. 2—26092
- crystalline electric field potentials, conduction electron enhancement 2—10283
- dopants in soda glass sensitivity to crystalline environment or impurity ions, meas. techniques 2—9223
- energies of electronic configurations of singly, doubly, and triply ionized 2—2942
- energy differences between two systems in singly and doubly ionized and neutral 2—590
- energy spectra and electronic configurations 2—28182
- e.p.r. obs., rare earth impurities in metals, cond. electron coupling, review 2—4536
- exchange interaction, symmetry of wave functions 2—33108
- Fermi contact hyperfine constants moment perturbed calc. 2—579
- Gruneisen const. calc. 2—22431
- h.c.p., deform. struct. obs. from X-ray line broadening 2—3772
- heavy, electric field gradient estimated from exptl. hyperfine interaction obs. 2—26091
- ion activated cryst., i.r.-visible conversion 2—26222
- ion in cryst. fields, anisotropic spin-orbit coupling 2—29851
- ion systems in solids, stepwise energy transfer and i.r. to visible conversion 2—10427
- ions, $4f^n6s$ configuration, accurate numerical HF SCF wave functions 2—573
- ions, cryst. fields, config. interaction influence 2—13425
- ions, energy transfer mechanism from ketones, effect of electron density of CO group 2—31886
- ions, expectation values of $\langle r^n \rangle_{4f}$ calc. using self-consistent-field wave functions 2—28184
- ions, form factor calcs. 2—3595
- ions, mag. reson., matrix elements, relativistic calcs. 2—10480
- ions, multiplet splitting of 4s and 5s electrons 2—19945
- ions, substituion in MgFe$_2$O$_4$, effect on props. 2—13412
- ions, use as probes in study of interactions in solids 2—20012
- ions in CaF$_2$, trigonol symmetry complexes with hydride ions 2—19113
- ions in cryst. host, multiphonon, Raman and two- photon excitation 2—37940
- ions in crystals, ionic model calc. d cryst. field parameters without charge compensation 2—1650
- ions in crystals, rate of multiphonon relaxation 2—32799
- lanthanide ions, Zeeman splitting of cubic cryst. field levels, covalent and vibronic contributions 2—19944
- luminescence, in fluoroberyllate laser glass 2—29961
- luminescence, in solid matrices, review 2—36923
- Luna 16 soil conc. 2—20664
- Luna 16 soil levels A and D, conc. 2—20665
- in lunar minerals by ion microprobe mass analysis 2—37344
- magnetic interactions, review 2—16341
- magnetic properties 2—25987
- magnetocrystalline anisotropy, zero-point energy effect 2—40452
- magnetostriction, in terms of exchange coeffs. and cryst. potential parameters 2—40415
- melting, volume contraction 2—35825
- neutral atoms, energy difference between f^qps^2 and $f^{q+1}s^2$ electron configurations 2—592
- neutron diffraction, theory 2—36698
- as nuclear control materials 2—18260
- partition functions, polynomial approx. for det. of stellar abundances and line profile 2—20518
- photoabsorption, potential barrier effects 2—20047
- photoabsorption, potential barrier effects 2—22775
- photoabsorption, potential barrier effects 2—22776
- sedimentary material, distrib. and composition in lagoon fed by hot springs 2—13642
- spectrographic determination in minerals 2—1768
- stars, Ap, opacities, effect of rare earths 2—26704
- Sun, lower chromosphere, meas. of non-thermal velocities from rare-earth emission lines 2—17088
- superconductivity, press. depend. 2—29639
- thin films, direct absorption transitions at optical frequencies 2—26151
- transition probabilities for f-electron J-multiplets in cubic cryst. fields 2—19939
- trivalent ions, electronically excited in electrode processes electroluminescence 2—21992
- u.s. investigation of spin-phonon interaction 2—40189
- valence levels from X-ray photoelectron spectra 2—36628
- X-ray tubes, alloying elements in Cr-Cu mirrors 2—30743
- in yttrium orthovanadate phosphors, dependence of luminescence intensity on ion concentration 2—16608

Rare earth metals continued
- Zeeman effect for ions in crystal field with C_{3h} symmetry 2—36863
- in CaF$_2$, photochromic behaviour 2—10640

Rare gases *see Inert gases*

Rayleigh scattering
- acetone, Fourier transform obs. of line widths and shapes 2—1103
- air pollution detection comparison with laser radar method 2—26481
- amorphous polymers, detection of low temperature transitions 2—9229
- aprotic laser solns. with Nd, scatt. coeffs. determ. 2—32269
- benzene, Fourier transform obs. of line widths and shapes 2—1103
- cholesteryl 2-(2-ethoxy ethoxy) ethyl carbonate liquid crystal, dynamical behaviour of ordering just above transition to cholesteric phase 2—32235
- conductor irradiated by electromagnetic wave, dipole moments 2—37848
- depolarization when scattered by anisotropic molecules 2 9033
- depolarized light scatt., theory of sharp and broad Rayleigh lines 2—18821
- electromagnetic waves, by obliquely oriented uniform needles 2—5292
- fluids, role of electrostriction, absorption and electrocaloric effect 2—32178
- isotropic gyrotropic continuous medium, with rot. degrees of freedom 2—6019
- laser-radar, resonance-scattering, suppression of spurious signals 2—7304
- liquid, continuous spectrum intensity distrib. 2—9134
- liquids, collision induced effects 2—12561
- liquids, collison-induced scattering, isolated binary collision model 2—25082
- mechanism of rearrangement from light scattering and molecular motion obs. 2—18824
- molecules in magnetic fields, polarization dependence of intensity 2—31745
- organic liquids, horizontal depolarization ratio 2—18841
- polymers, photolysis, continuous light scatt. technique 2—37057
- spectroscopy, exptl. methods, cont. contrib. 2—16446
- succinonitrile, plastic and liquid phases, molecular motion and lattic dynamics obs. 2—16589
- succinonitrile single crystal, scattering from entropy fluctuations 2—16443
- toluene, Fourier transform obs. of line widths and shapes 2—1103
- X-rays from heterogeneous materials 2—7060
- CS$_2$, Fourier transform obs. of line widths and shapes 2—1103
- H$_2$ isotopes, collision cross sections, interrelationships with other transport and relaxation phenomena 2—39026
- H$_2^+$ molecules, inclusion of nuclear motion in calc. of optical properties 2—24435
- LiCl aqueous soln., suggesting low temp. immiscibility 2—15589
- NH$_4$Cl, as function of pressure and temperature in region of order-disorder transition 2—13456
- RbH$_2$PO$_4$, line intensities at ferroelec. transition 2—40697
- SF$_6$, gaseous, depolarization of scattered Rayleigh radiation 2—35283
- SF$_6$, Rayleigh linewidth measured near critical point 2—9038
- SbSI, ferroelec., critical scatt. 2—19769
- SbSI, ferroelectric phase transition, soft mode coupling 2—16012

Rayleigh waves *see Elastic waves; Seismic waves*

Re(h)binder effect *see Mechanical strength; Surface phenomena*

Reaction kinetics
- *see also Catalysis; Chemical reactions; Exchanges, chemical; Explosions*
- anthracene crystal metal interface, exciton dissoc. rate const. charge transfer 2—3490
- beam-foil-gas spectroscopy, technique for studying steady-state non-equilibrium processes 2—26319
- benzene triplet absorption by monoolefins in gas phase, reaction rate determ. by kinetic absorption spectroscopy 2—13572
- bimolecular reaction, diffusion- controlled 2—22860
- bimolecular reactions, obs. rate constants and cross sections 2—10599
- biphenyl reaction with electrons produced by two-photon laser photolysis of molecules in liquids, rate constants meas. 2—30081
- bound state formation and dissociation in 2d gases, rate constant 2—15533
- brucite, dehydroxylation, solid state 2—36253
- 1-butene, activation energy for addition of O(^{3}P) atoms 2—10614
- dichloroethylene, photoelimination reactions, rate const. ratios for vibr. transistions 2—33388
- diphenyldiazomethane, irradiation in single crystal soln., e.p.r. and ENDOR study of rates and mechanisms 2—33363
- diphenylmethylene+1,1,diphenylethylene, in single crystal soln., e.p.r. and ENDOR study of rates and mechanisms 2—33363
- diphenylmethylene+diphenyldiazomethane, in single crystal soln., e.p.r. and ENDOR study of rates and mechanisms 2—33363
- electrogenerated chemiluminescence 2—30075
- ethylene, activation energy for addition of O(^{3}P) atoms 2—10614
- ethylene, gas phase thermal reaction with NO$_2$ at 25C, mechanism for formation of products, rate constants 2—22867
- ethylene, ion-molecule reaction, product translational energy spectra 2—20175
- ethylene photolysis at 147-193 nm, kinetic analysis of primary processes 2—40834
- ferrite formation in MgO-Fe$_2$O$_3$ powders 2—1378
- fluid-solid, continuously weighed rotating disk reactor 2—30043
- gas mixture, relaxation 2—13563
- grapitization of pitch coke and acetylene black, activation energy determ. 2—29388
- halogen atom conc. meas. in discharge flow systems using atomic resonance absorption 2—15229
- Hastelloy X, cyclic oxidation kinetics, 760-1200°C 2—40814
- highly reactive mixture, relativistic kinetic theory 2—26331
- hot-atom reactions limits of validity of the kinetic theory 2—30040
- hydrated electron, diffusion-controlled reactions, pulse radiolysis measurement of rate at high pressures 2—37060
- ion cyclotron resonance mass spectrometry, determ. of rate consts. of ion-molecule reactions 2—28165
- ionization rate constant, testing by principle of detailed balancing 2—24839
- ionosphere, ion-molecule, ion-electron reaction rate constant from in situ obs. 2—7331
- ionospheric D-region, rate constant for NO$_2$-+H=OH-+NO reaction 2—30353
- isobutene, activation energy for addition of O(^{3}P) atoms 2—10614
- kaolinite, dehydroxylation, solid state 2—36253
- low density gases dimerizing 2—40800

Reaction kinetics continued
  M/M^{3+} electrode reaction kinetics, steady-state intermediate ion concs. 2—10631
  master equation for dissociation of dilute diatomic gas 2—30038
  in metallurgy, adaptation of theory of thermodynamic potentials 2—40799
  methane, kinetics of oxidation 2—33379
  methyl chloride ion-molecule reactions, ion-cyclotron resonances spectroscopy obs. 2—35114
  methyl radical reactions with HCl and H_2S, activation energies and kinetic isotope effects 2—26338
  molecular beam collisions, potential energy surfaces and reactive scattering 2—12298
  Nb carburization, in methane atmosphere 2—26341
  $2NO_2 \rightarrow 2NO+O_2$, thermal conductivity meas. made from 548-792K, deduced chemical kinetic constants 2—26321
  normally reactive mixtures, relativistic kinetic theory 2—26330
  organic radicals in aq. solns., pulse radiolysis and e.p.r. 2—26372
  oscillating reaction, stochastic analysis 2—40795
  oxides of Al, Mg and Si, decomposition at 2270 K 2—7161
  ozone, photochemical dissociation with light of 3340 A, kinetics and mechanism 2—37050
  partial charge-transfer reactions at thermal energies, rate constants 2—26325
  photochemical, applic. of spectrophotometer 2—17736
  polyester-diisocyanate, spectroscopic method 2—4575
  propanes, methyl substituted, mol. structure effects in radiolysis, ion and electron mobilities 2—22886
  propylene, activation energy for addition of $O(^3P)$ atoms 2—10614
  proton transfer reactions, determination of relative proton affinities 2—10597
  proton transfer reactions of type $XH^+ + Y \rightleftharpoons YH^+ + X$, kinetics and energetics studied by flowing afterglow method 2—12303
  $pyrene^+ + pyrene \rightleftharpoons (pyrene)_2^+$, thermodynamic and rate constants 2—16674
  radical reactions, nuclear and electron spin polarizations 2—20183
  rate measurements in shock tubes, effects of laminar and turbulent boundary layer buildup 2—1748
  recombination of isolated pairs in condensed media, application of diffusion model 2—33364
  reduced time usuage in data plotting 2—37022
  relaxation amplitudes for systems of two coupled equilibria 2—40798
  rotating disk apparatus for studies of fluid-solid surface reactions in corrosive liquid environments 2—30042
  solid phase reactants, activation energy 2—10611
  solid state, particle size and interfacial area 2—13565
  sorption, linear isotherm range, external diffusion kinetics 2—22078
  steel decarburization, in H_2 and H_2-steam mixture 2—36242
  stilbene anion radical, electron transfer reaction with cis- and trans-stilbene, e.s.r. and u.v. study 2—37035
  stochastic description, birth and death model replaced by phase-space description 2—87
  surface diffusion processes, influence on kinetics of heterogeneous nucleation 2—1170
  temperature jump apparatus, nanosecond, for chemical kinetics obs. 2—4572
  tetracene, photooxidation kinetics, external mag. field effects 2—26365
  thermal decomposition, simultaneous calorimeter and const. decomp. rate thermal anal. study 2—37024
  thionine, protonation rate const. of triplet state by laser flash photolysis 2 -37056
  transition state theory, collision complexes, product translational energy distrib. 2—20174
  trifloromethyl radical reactions with HCl and H_2S, activation energies and kinetic isotope effects 2—26338
  trifluoroethane, with nuclear recoil ^{18}F atoms, approximate energetics and molec. dynamics 2—10616
  trifluoroethane, with nuclear recoil ^{18}F atoms, mechanism and systematics 2—10615
  Ar, liquid, mol. structure effects in radiolysis, ion and electron mobilities 2—22886
  $BaCO_3$, decomposition, solid state 2—36253
  Br_2 recombination from atoms in inert gas, rate constants determ. 2—37028
  CO^+ charge exchange with O and NO, thermal energy reaction rate consts. 2—26329
  CO_2, photolysis at 1633 Å, reaction mechanism 2—10639
  $CO_2(xyo)+CO_2 \rightarrow CO_2(001)+CO_2$ shock tube meas. of vibrational relaxation, reaction rate obtained 2—35235
  $CaTiO_3$, formation, Carter's equation, appl., particle size distrib., X-ray obs. 2—13566
  CeO_{2-x}, oxygen transport and effects on structure 2—10623
  $CuFe_5O_8$, eutectoid decomp. 2—15959
  D_2, oxid. on Pt surface 2—10629
  DBr+ethane photolytic system abstraction reaction, threshold energy 2—13587
  DI+ethane photolytic system, abstraction reaction, threshold energy 2—13587
  $F+H_2(HCl)(CH_4)$, HF chemical laser signal pulse shape 2—20199
  $Fe+O_2 \rightarrow FeO+O$, homogeneous gas phase reaction studied in N_2 bath at 1600 K using alumina fast-flow reactor in vacuum furnace 2—33367
  H^+ charge exchange with O and NO, thermal energy reaction rate consts. 2—26329
  HCl adsorbed on rutile, i.r. spectra 2—15678
  HO_2-, from photolytic reactions, kinetic analysis of absorption spectrum 2—24460
  HO_2 radical in gas phase 2—37038
  H_2O proton affinity studied using elevated pressures in ion source of quadrupole mass filter 2—22863
  H_2+Br_2, obs. of laser action on several vibration-rotational transitions in bands of HBr 2—27467
  H_2+Cl_2, obs. of laser action on several vibration-rotational transitions in bands of HCl 2—27467
  $H+H_2$, collinear exchange reactions, with vibr. excitation reaction probabilities and thermal rate consts. 2—10608
  $H+H_2$ collinear reaction, quantum mechanical reaction probabilities and rate constants 2—22859
  $H_2^+ + H_2$ and isotopic variations, from ion cyclotron resonance 2—30048
  $H+H+H \rightarrow H_2+H$, collisional reaction, rate constant estimation using Monte Carlo simulation 2—715
  $K+Br_2 \rightarrow K^+ + Br_2^-$, mechanism near threshold 2—7167

Reaction kinetics continued
  K_2+Br_2, comparison of ang. distrib. of K atom reactive scattering and KBr ang. distrib. 2—26339
  K_2+BrCN, comparison of ang. distrib. of K atom reactive scattering and KCN distribs. 2—26339
  $K+HBR \rightarrow KBr+H$, trajectory calc. in eV region, computer program 2—33370
  Mg, nitrogenation with simultaneous metal sublimation 2—30051
  Mg nitrogenation, effect of N_2 purity 2—30050
  NO_2 gas phase thermal reaction with ethylene at 25°C, mechanism for formation of products, rate constants 2—22867
  $NO^- + X \rightarrow NO+X+e$, rate constants for collisional detachment, 193-506K, 2—21718
  $N_2^+(X^2\Sigma_g^+, v''=0)$ rate constants of various reactions, study by kinetic absorption spectroscopy 2—22866
  $^{14}N(\alpha,\gamma)^{18}F$ rate obs., w.r.t. stellar evolution 2—20530
  NaOH, vitrified aqueous solution, irradiated, 77 K, electron tunnelling 2—30093
  Nb carburization, in acetylene atmosphere 2—26340
  Nd_2O_3-ZrO_2 system, high temp. compound formation 2—29495
  Ni_3Ti, oxidation, 650-1000°C 2—20188
  O^-, rate constant for conversion to $O_3^-(H_2O)_n$ in moist oxygen 2—30053
  O_2, bimol. rate constants for quenching in $^1\Delta_g$ state 2—22856
  O_2, rate constant for conversion to $O_2^-(H_2O)_n$ in moist oxygen 2—30053
  O_2 reaction with electrons produced by two-photon laser photolysis of molecules in liquids, rate constants meas. 2—30081
  O_3 decomposition during photolysis by 2537Å radiation 2—7183
  $O_2(^1\Delta_g)$ with tetramethylethylene, effect of pressure on rate of reaction 2—20180
  $O_2(^1\Delta_g)+SO(^3\Sigma^-) \rightarrow SO(^1\Delta)+O_2(^3\Sigma_g^-)$, kinetic study by e.p.r., absolute rate constant 2—10612
  $O(^3P)$ atoms, activation energy of addition to olefins 2—10614
  $O(^3P)$+CO, rate constant, pressure dependence 2—22869
  O_2+ ethylene, absolute rate constants in temp. range 232-500K 2—40806
  O_2+S, adsorbed on Cu(110) surface, Auger spectroscopy 2—9248
  $PbO+ZrO_2+TiO_2$, high temp. obs. 2—13571
  PuO_2/UO_2 reactor fuel, fluoridation method of reprocessing 2—15111
  $ReO_3^- + Cl_2$, rate const. meas. in drift tube/mass spectrometer apparatus 2—10613
  $ReO_3^- + NO_2$, rate const. meas. in drift tube/mass spectrometer apparatus 2—10613
  $SO(^1\Delta) \rightarrow SO(^3\Sigma^-)$, mechanism of decay at reaction vessel walls, e.p.r. study 2—10612
  $SO(^3\Sigma^-)$, determ. of absolute conc. by gas phase e.p.r. using NO calibrant gas 2—10604
  $S(3\,^3P_3)+O_2 \rightarrow SO+O$, absolute rate meas. using kinetic spectroscopy in vacuum u.v. 2—33371
  β-SiC formation, pyrolysis of CH_3SiCl in H_2 2—18985
  SiO_2 film, dissolution rates in acidic fluoride solns. 2—10628
  $Sm_2O_3+Cr_2O_3$, activation energy and rate controlling step 2—30054
  Ta oxidation, X-ray emission study 2—32385
  $TiO_2(g)+Ti(g)=2TiO(g)$ studied in 2150-2500 K range using Knudsen effusion-mass spectrometric technique, dissociation energy determ. 2—28329
  $TiO_2(g)=TiO(g)+O(g)$ studied in 2000-2250 K range using Knudsen effusion-mass spectrometric technique, dissociation energy determ. 2—28329
  $(WO_3)^-_{n=1,2,3}+Cl_2$, rate const. meas. in drift tube/mass spectrometer apparatus 2—10613
  $(WO_3)^-_{n=1,2,3}+NO_2$, rate const. meas. in drift tube/mass spectrometer apparatus 2—10613
  ZnO, hydrothermal growth 2—29093
  Zr-Cr alloy, corrosion in steam, 325-700°C, rate law 2—20191
  Zr, corrosion in steam, 325-700°C, rate law 2—20191

Reactors *see Nuclear reactors, fission; Nuclear reactors, fusion*

Recombination *see Ions, recombination; Semiconductors*

Recombination radiation *see Luminescence*

Recording
  advanced sonar recording techniques, fibre optic cathode ray tubes 2—27629
  audio-visual, super-8 film plus optical sound 2—8049
  automatic, of linear deformation and thermal stability of elastic polymers 2—29351
  automatic, relaxation curves of dielectrics 2—34282
  automatic balance with moving coil weight compensator, recording of rapid mass variations 2—23221
  buffer store with 256 channels for cosmic ray expts. 2—31335
  colour, for electron microscopes and probes 2—7866
  colour holographic technique 2—17660
  computer-synthesized sounds 2—23383
  discrete, i.r. absorption spectra, attachment for UR-20 i.r. spectrometer 2—27658
  electrical signals, using ink jets, intensity modulation, electric control 2—32201
  electron density fluxes following mag. disturbance in upper atmos. 2—22983
  electron microscope, trajectory displacement, calc. 2—14392
  electron microscope image recording system, dynamical obs. 2—7862
  electrophotographic microimage recording by organic photoconductor 2—5464
  holographic, electrooptic materials and fixing techniques 2—21121
  holographic, in photochromic CaF:La, application to holographic interferometry 2—17657
  holographic, physics and technology 2—38017
  holographic system, stabilization with intermittent exposure control 2—38021
  impulse noise, temporary threshold shift studies 2—11361
  laser beam system, patent 2—37520
  light beam oscillograph, static error 2—21165
  light pulses, simultaneous, applic. of fibre optic light guide 2—34532
  liquid drops, photographic techniques 2—23742
  magnetic, Mn-Zn ferrite head, grain size effects on noise 2—10224
  magnetic, relationship of vector and scalar magnetization 2—6972
  magnetic on thin films, domain studies by longitudinal Kerr magnetooptic effect 2—19861
  magnetic recording heads, efficiency analysis 2—7832
  magnetic thin film system for fast transients in nuclear diagnostics 2—30715
  materials in holography 2—17659
  mechanical test data, automatic device 2—20766
  memory cathode ray tubes, use in standard oscilloscopes 2—17562

Recording continued
n.m.r. signals, using mag. field intensity meter with improved signal-to-noise ratio 2—17503
optical images, recording processes 2—22636
optical images, weak, using photon counting techniques 2—38048
optical images with post recording bandpass selection 2—23712
seismic system, lightweight low power portable 2—30158
spectrometer and spectrophotometer systems, working region effects on contour distortion of spectral lines 2—38160
system for MF-4 microphotometer 2—27607
systems for spectrometers dynamic errors during tracing individual spectral line 2—31146
ultrasonic amplitude and phase in liquid by double interaction with light 2—37762
video, electron source using directly heated LaB$_6$ emitter 2—2352
video recorder, technique for recording rapidly changing mass spectra 2—38791
X-ray diffraction patterns, flash X-ray tube and image intensifier 2—12707
yield pt. of metals under tension, plotting unit 2—41354
^{19}F n.m.r. spectra, double frequency conversion circuit for adapting proton radiospectrometer 2—27377
MnBi homogeneous films, thermomagnetic writing 2—1636

Recovery
alloy with 10% carbides, sintering process, coercivity and resist. obs. 2—19240
creep, recovery-work hardening model 2—9669
dislocation creep, work hardening/recovery model, mech. eqns. of state 2—39691
metal, b.c.c. and f.c.c., point defects produced after irrad. 2—15745
metal, rel. to friction stress during high temp. creep, theory 2—12866
metal, rel. to phenomenological theory of plastic flow 2—39794
neutron irradiated materials, depletion zone recovery 2—6471
steel, high C, cold drawn wire 2—9757
Al-Cu alloy, after tempering, cold working and reversion 2—9756
Al-Mg, plastically deformed, 77-500K 2—36112
Al-Zr alloy, cold worked at liq. N$_2$ temp. 2—15912
Al, electron irrad., stage III 2—6473
Al, plastically deformed, 77-500K 2—36112
Au-(15 wt.%)Ag alloy, static crowdion behaviour, resist. obs.15754 2—15754
Au film on cold substrate 2—32360
C, pyrolytic, neutron irrad., annealing, phys. props. 2—3757
Cd, cold working, defect production, 77K, elec. resist. obs. 2—25411
Cd, low temp. electron irrad., stage III, elec. resist. study 2—39669
Cd, plastically deformed, resist. and supercond. transition temp. 2—19559
n-CdTe, electron irrad. defects 2—15739
Cu, electron irrad., rel. to lattice parameter/resistivity change ratio 2—15740
Cu, high purity, plastic deformation, elec. resistivity obs., deviations from Matthiessen's rule 2—25579
Cu, neutron irradiation, elastoresistivity, 20K 2—25371
Fe-Mn alloy, shock deformed, role of point defects 2—9653
Fe-Si, heavily deformed, texture variations 2—12935
Fe alloy, martensite, Mossbauer obs. of carbide particles 2—10320
In, plastically deformed, resist. and supercond. transition temp. 2—19559
K, deformed, model for stage-B recovery 2—19090
K, deformed, residual resist. obs. 2—19089
Mg, cold working, defect production, 77K, elec. resist. obs. 2—25411
Mg, electron irrad. damage 2—36012
Mo, neutron irrad. and cold worked high temp. recovery 2—15743
Nb, stage III, deformation temp. effects 2—25575
Ni-Cu alloy, radiation damage in 500 kV electron microscope, dislocation loops 2—1238
Ni, high strain rate deformation, recrystallization, polygonisation 2—9748
Ni, laser irrad., of elec. resist. 2—9533
Pn, plastically deformed, resist. and supercond. transition temp. 2—19559
Pt, deuteron irrad., defect production and recovery 2—22194
Re, fast particle irrad. and cold worked, low temp. recovery spectrum 2—15744
Sn, plastically deformed, resist. and supercond. transition temp. 2—19559
TiO$_2$, rutile, high temp. creep-resistant substruct. 2—29272
Zr, cold rolled, polygonization, recrystallization, electron microscopy 2—6502
Zr, low temp. deformation and recrystallization, resist. obs. 2—15911

Recrystallization (metals) *see Heat treatment*

Rectifiers
see also Electron tubes; Semiconducting devices
metal whisker diodes, thermal field emission as i.r. light rectification mechanism 2—16323
CuSe-Mg contact, rectifying properties studied under low frequency A.C. conditions 2—16249
Si controlled, use in microsecond pulse generator 2—37873

Red giants *see Stars*

Red shift
astronomical spectra, cosmological origin 2—33594
cluster galaxies, magnitude-redshift diagram interpretation and deceleration parameter 2—13870
Coma Cluster, correlation with magnitude 2—7381
cosmological, expanding Universe postulate rel. tired light effect for explanation 2—33572
3CR catalogue radiosources 2—13966
diameter relation for galaxies 2—13875
elliptical galaxies in clusters, angular diameter and aperture correction 2—33601
elliptical giant galaxies, stellar evolution models, colour-redshift relation 2—10832
evolution rate of nearby giant ellipticals rel. to magnitude-redshift relation and q$_0$, deceleration parameter 2—37240
extragalactic, mechanism based on ageing of e.m. wave group 2—42
galaxies, clusters, rel. to apparent magnitudes 2—26593
galaxies, in terms of types, magitudes, diameters, colours and inclinations 2—13846
galaxies, Markarian's second list, low-dispersion spectra, redshifts, absolute magnitudes and space density 2—26624
galaxies in distant clusters, evolutionary effects 2—30429
galaxies near Hercules cluster, image tube spectra 2—30428
galaxies near PKS 2251+11, spectra 2—13845
galaxy cluster, selection effects on model of universe 2—10790
gamma rays in expanding Universe 2—7375

Red shift continued
gravitational, deduction from finite rest masses of wave quanta in material media 2—17201
gravitational, three-body effect 2—17200
Maffei No. 2, intrinsic colour index 2—4800
magnitude relation including possible effects of evolution of cluster galaxies 2—13876
non-velocity, in galaxies 2—30433
Palacios' gravitational theory explanation by wavelength considerations 2—27040
periodicites and QSO's 2—26770
photons, for optical depth to be unity 2—7375
plasma, stimulated decay of transverse wave impinging on plasma as explanation 2—32087
QSO's, gravitational component 2—33699
QSO's, spectroscopic observations of 22 objects with redshift measurements 2—41145
QSOs and radio galaxy in southern hemisphere 2—26769
QSS's rel. to QSO's 2—10931
quasars, absorption line spectra 2—13932
quasars, distribution, influence of observational selection 2—26767
quasars, distribution and radiosource counts 2—13949
quasars, selection effect in meas. 2—7471
quasars, two classes, local and cosmological to explain anomalies 2—26772
quasi stellar radiosources, correlation with depolarization at long wavelengths 2—41146
radio galaxies, southern 2—10937
radio galaxies, spectroscopic observations 2—20488
radiogalaxies, meas. 2—37252
radiosources, extragalactic, rel. to intensity variations 2—13962
radiosources, galaxies and quasars 2—1968
random shuffling, insensitivity of $\langle V/V_m \rangle$ in luminosity-volume test 2—41032
solar K absorption line at 7699 Å, atomic-beam resonance-scatt. meas. 2—33762
$10^3 M_\odot$ star and relativistic evolution 2—16980
van Maanen 2, cool white dwarf 2—26685
H$_2$, frequency shifts of rotational lines, collision induced 2—8651

Reflectance *see Electroreflectance; Magnetoreflectance; Piezoreflectance; Reflectivity; Thermoreflectance*

Reflection
see also Neutrons/reflection; X-ray reflection
coefficients, power, random medium 2—38
dilute non-electrolyte solutions, coefficient 2—28830
gamma quanta reflection factor in graphite cylinders 2—38738
i.r., metal crysostat for obs. 2—41372
i.r. in rhodochrosite, effects on complex refractive index 2—7040
i.r. radiation, by plane layer, applic. to finding height of cloud tops 2—26497
laser light, technique for obs. of dynamic changes in surface morphology 2—35865
matter waves, the Goos-Haenchen effect for grazing incidence 2—78
plasma wave, at moving dielectric medium and compressible plasma interface 2—21783
seismic P-waves, from 20° discontinuity 2—33403
seismic waves, coeff. for solid wedge embedded in solid medium 2—7213
seismic waves, effective velocity obs., effect of correlated errors in hodographs on accuracy 2—7210
seismic waves, effective velocity obs. from hodographs, effect of dip in intermediate interface on accuracy 2—7211
seismic waves, main types obs. of great distance from source 2—33411
SH-waves, propagation in linear viscoelastic solids 2—26429
shock waves, in ionized gases, pressure gauge for obs. 2—30751
shock waves, prediction of wave pattern 2—180
shock waves in absorbing gas, radiative cooling effect behind waves 2—7762
shock waves loading process behind fronts in plastic layered media 2—30879
stress wave at plane boundary between anisotropic media 2—14250
thermal radiation props. of solids 2—19474
waves in rotating fluid nearly parallel to boundary viscous effects 2—3180

acoustic waves
see also Echo; Reverberation
fluctuation frequency of envelopes of sound signals reflected from ocean bottom 2—30250
grating, dense doubly peridoic, in presence of rigid baffle 2—5232
layer with space dependent velocity 2—14259
multiple reflections, perceptible limit of echo 2—34112
ocean bottom, signal fluctuations 2—30255
ocean bottom refl. coeff ang. depend. 2—30254
plane, interference obs. 2—30867
Rayleigh waves, reflection and transmission in wedge 2—11350
shock wave, analysis method 2—27258
shock wave, at boundary, wave form 2—27257
by small conducting solid cylinder in viscous conducting fluid 2—14264
transient echo pulse from rigid sphere in fluid 2—34113
viscous isothermal atmosphere, downward reflection of acoustic-gravity waves 2—903

acoustic waves, ultrasonic
delay lines, zero temperature coeff., synthetic quartz crystals 2—5231
half-value depth, flaw testing 2—11356
inspection technique, surface crack and flow detection 2—1321
materials testing using reflection from targets of simple geometry 2—30873
optical sensor, noncontacting 2—34528
optical sensor, noncontacting 2—34528
schlieren visualisation of radiated field in water above and below Al plates illuminated by short ultrasonic pulses 2—34099
seawater surface, diffuse refl. mechanism 2—30259
surface, and multipath propagation, application to underwater telemetry 2—164
visualization in solids and liquids, Schlieren apparatus 2—37765

electromagnetic waves
52-GH$_z$ beams, focusing by cylindrical mirrors 2—23438
dielectric media, effect of moving boundary 2—20982
Doppler radar return from two-dimensional rough surfaces 2—20284
E-region, m.f. radiowaves, amplitude and phase obs. 2—41007
f.m., ice thickness measurement method, patent 2—37098
Goos-Hanchen and Imbert effects 2—34231

Reflection continued
- **electromagnetic waves** continued
  - guided, in longitudinal moving stratified medium 2—2310
  - hybrid, TE and TM, cylindrically guided, reflection and transmission properties 2—23461
  - inhomogeneous medium, convex metallic cylinder 2—23439
  - interface between vacuum and anisotropic Vlasov plasma 2—18616
  - internal, total, particle motion near surface 2—14379
  - ionosphere, horizontally stratified, radiowaves propagated at oblique incidence 2—40992
  - ionosphere, region of signal formation 2—33515
  - by ionosphere, Stokes parameters for anal. of polarization 2—22999
  - ionosphere E_s region, numerical calc. of coeff. 2—4723
  - ionosphere model, linear, perturbed 2—30965
  - ionosphere model, linearly varying, with vertical magnetic field 2—23006
  - ionospheric layer, frequency shift of radiowaves 2—40998
  - l.f. radio waves, distance attenuation at vertical incidence to ionosphere 2—10758
  - from lunar surface 2—30536
  - melinex, coeff. at 338μ 2—19964
  - microwave, from water surface underwater sound sources detection 2—14274
  - moving dielectric medium and compressible plasma interface 2—21783
  - optics in stratified anisotropic media, 4 by 4 matrix formulation for propagation and reflection 2—34463
  - partial reflection method, ionospheric D region, electron density profiles, collision number 2—30921
  - planar surface waveguide junction, modal-matching method 2—17484
  - plane, by moving dielectric taper, boundary value problem 2—30923
  - plane, from sea ice, equivalent frequency charact. modelling 2—203
  - plane e.m. wave incident on conductive moving mirror 2—30920
  - from plasma, lossy, inhomogeneous, distortion of radio pulse 2—20402
  - plasma, semi-infinite, moving, anisotropic 2—21787
  - plasma slab, isotropic, transient response 2—31987
  - plasma slab, moving, power reflection coeff., calc. 2—31976
  - propagation in ionosphere as atmosphere, inhomogeneous 2—14338
  - radio waves, in dissipative media, calc. 2—20981
  - radio-echo sounding, focussing effects in wavy strata 2—13613
  - radiowaves, vertically polarized, propagation parameter calc. 2—1892
  - real-time measurement of microwave parameters and e.m. fields 2—20986
  - r.f. Brewster angles and Fresnel coefficients by computer programs 2—17474
  - r.f. from meteor trails, effects of multicomponent composition of meteorites 2—33753
  - rough sea surfaces, two dimensional, Doppler return 2—16790
  - rough surfaces, effect of curvature variation 2—2305
  - spatially dispersive medium, exact soln. by Maxwell's theory 2—29891
  - spatially dispersive medium, mode coupling and exciton polarization 2—29892
  - spherical shell, radially inhomogeneous, field calc. 2—30922
  - by stratified moving media, field intensities calculated 2—7788
  - total reflection, as filter of polarization states 2—34246
  - two layer ground in quasi-static regime, magnetic dipole transient response 2—33398
  - wave obliquely incident on nonuniform magnetized plasma 2—31988
  - p-Ge, free carrier magneto- microwave Kerr effect 2—40612
  - n-InSb, microwave, mag. field dependence during helicon wave propagation 2—16601
- **light**
  - *see also Films, solid/optical properties; Mirrors*
  - adsorbed layers, theory 2—9300
  - adsorbed layers at interfaces, conf., London England, Dec (1970) 2—9298
  - adsorbed layers at interfaces, internal reflection spectroscopy 2—9302
  - albedo from turbidity obs. 2—37077
  - alkaline earth metal film, optical consts. detn. 2—20017
  - alkaline earth titanates and zirconates, diffuse refl. spectra, band struct. 2—1526
  - angular scintillations in laser return from retroreflector, effects of atmospheric turbulence 2—22973
  - anharmonicity of crysts. heated by intense i.r. radiation 2—19345
  - anthracene, 4.5-11.5 eV, anisotropy 2—40651
  - anthracene single cryst., opt. anisotropy from reflection spectra, 4.5-11.5 eV 2—20007
  - antiferromagnet, magnon-photon coupling 2—22747
  - from arbitrary geometric surface, calc. of surface from response of laser beam 2—21141
  - atmospheric gas solids, extreme u.v. reflection spectroscopy 2—19995
  - benzene, solid, higher $\pi\rightarrow\pi^*$ transitions, spectral obs. 2—20052
  - beryl, i.r. spectra, anharmonicity 2—26143
  - beryl, spectra in the i.r. measured with polarized light 2—10365
  - bounded media propagation, spatial coherence enforcement 2—5379
  - catadioptric imaging systems, meniscus aberration correctors, book 2—27626
  - circularly polarized beam, calculation and experimental proof of the transverse shift on total internal reflection 2—31100
  - coatings, dye lacquered and constituents, reflectance in 210 to 2600 n.m. range 2—23707
  - colour prints, multilayer, diffuse density 2—17756
  - critical angle for total reflection, relativistic change for moving media 2—33899
  - datolite, spectra in the i.r. measured with polarized light 2—10365
  - diffuse, powdered solids, photomultiplier measuring apparatus 2—20103
  - electrode/electrolyte interface, specular reflection obs. of adsorbed layers 2—9301
  - electrostatically scanned film reflectors for interferometer and laser applications 2—23671
  - ellipsometric determ. in extreme u.v. of opt. constants 2—16461
  - exchange splitting in excitons, interatomic distance depend. 2—29903
  - film-substrate with randomly rough boundaries 2—3509
  - from fundus of eye, effect on retinoscopy 2—41321
  - handedness of polarization after total reflection of linearly polarized light 2—14442
  - by imperfect cube corners, dot patterns 2—34469
  - inert gas solids, extreme u.v. reflection spectroscopy 2—19995
  - inhomogeneous media, effects of sample imperfections 2—22743
  - integrating sphere, view into through observation window 2—8002
  - internal reflectance at boundary surface, diffuse and specular reflectance 2—17682
  - i.r., coeffs. for multigrid interference filters 2—17718
  - i.r., cryostat with pneumatic device, semiconductor specimens 2—20778

Reflection continued
- **light** continued
  - for i.r. spectral reflectance of ADP, KDP, NaCl, KBr, CsBr, CsI, TlBr, TlCl and KRS6 2—4430
  - l 2—13461
  - laser beams, results on longitudinal displacement and photon mass 2—34370
  - lidar reflectance of fair weather cumulus at 0.903 μ 2—30283
  - liquid evaporation light deflector, electrically controlled varorization 2—27611
  - liquid-vapour critical point 2—22038
  - by machine finished surface, roughness obs. using speckle patterns formed in broad band illumination 2—35869
  - magnetised medium with weak spatial dispersion, field boundary conditions 2—19962
  - magneto-Kerr effect, Voigt configuration, reflected wave polariz. rotation 2—10307
  - metal surface, spectra 2—16460
  - metals, thin films, reflectance and transmittance from oblique incidence measurements 2—31088
  - mica, vacuum u.v. props. 2—40648
  - multiple, illumination of coaxial cylinders 2—27568
  - multiple beam reflection interferometer with matched front mirror, exptl. study 2—14448
  - mylar reflective plastic film, ageing and effects of bonding to substrate metallized side down 2—23704
  - optical constants, exact eqns. from reflection characs. 2—31086
  - oriented molecular layers, specular reflectance and ellipsometric spectroscopy 2—26110
  - oxide layer on Pt, Au and Ni, specular reflection spectra, monolayer thickness range 2—9310
  - oxygen on Pt, Au and Ni, specular reflection spectra, monolayer thickness range 2—9310
  - parabolic solar concentrators, estimation of accuracy of reflecting surfaces 2—34432
  - polarized, by imbedded optical films 2—7974
  - polycrystalline materials, specular reflectance i.r. spectroscopy, LO mode frequency meas. 2—15992
  - powder, binary mixture, comp. depend. 2—33207
  - prisms, use in ellipsometer aligning 2—38038
  - Raman spectra by reflection 2—40693
  - rectangular prism for use as a triple mirror 2—7967
  - reflectometer, opt. surface contamination analysis, OSCAR system, vacuum u.v. 2—18929
  - reflectometer readings and absolute reflectances 2—8009
  - reflectometer/quart· crystal microbalance combination for contamination meas. 2—41413
  - rough surfaces, effect of depth on apparent plane of reflection for surfaces having centres of symmetry 2—23689
  - scattering of laser beam at polished glass surfaces, sensitive dark-field examination of polished sample 2—14447
  - semiconductor, carrier concentration, pseudo Brewster angle detn. 2—40282
  - semiconductor, heavily doped, optical const. free carriers 2—26140
  - semiconductor, layered inhomogeneous structures, transmission and reflection spectra, layer thickness detn. 2—40643
  - silicate glaze, i.r. spectra rel. to comp. 2—36854
  - silicate glaze, i.r. spectra rel. to struct. 2—28972
  - soil, spectral reflectance and daylight spectral energy distribution using characteristic vector analysis 2—16773
  - solar concentrators, application of theory at similarity 2—34433
  - solar concentrators, construction and power characteristics of paraboloidal concentrators composed of doubly curved facets 2—23675
  - solar energy concentration, review 2—34437
  - solar reflectors, energy transport and distribution characteristics in reflection field as whole 2—23672
  - spatially dispersive model medium 2—38054
  - specular from echelette grating, use as far i.r. filter 2—23692
  - specular optics, surface properties, theory and applications, measurement of reflectance, book 2—2420
  - stacked glass plates, calibration of spectrophotometer for specular light 2—17734
  - sunlight from oil water, airborne optical detection 2—26464
  - surface structure, fatigue failure, optical correlation function 2—9725
  - from surface waves, intensity distrib. and phase modulation 2—14446
  - tetracyano-p-quinodimethane, specular reflection spectra, anal. of metallic reflection influence of exciton phonon interaction 2—20008
  - tetracyanoquinodimethane anthracene cryst. mol. complex, obs. of exciton interactions in polarized specular reflection spectra 2—13465
  - topaz, spectra in the i.r. measured with polarized light 2—10365
  - transition metal complexes, crystallizing in columnar structure, one-dimensional metallic properties from reflectance spectra 2—15681
  - at uniaxial crystal and isotropic medium boundary 2—1660
  - u.v. reflectors and polarizers 2—7976
  - u.v. wide-band reflectors, chemical deposition from Th and Si oxides 2—34515
  - zoisite, spectra in the i.r. measured with polarized light 2—10365
  - Ag and Ag alloy films, 2.4 to 4.4 eV, optical consts. detn. 2—22749
  - Ag films, optical constants from reflection and transmission coeff. meas. 2—26103
  - Ag films on Pt, specular reflection spectra, monolayer thickness range 2—9310
  - β-AgI, hexag. single cryst., exciton spectra, large angle reflection obs. 2—16462
  - Ag_3SbS_3, 2-5 eV, energy levels determ. 2—29894
  - Al_2O_3, corundum, i.r. spectra, phonon distrib. 2—26142
  - As, amorphous, reflector power 2—29896
  - As_2S_3, amorphous, i.r. spectra, reststrahlen band 2—16465
  - As_2S_3, glass and cryst., interband spectra, Kramers-Kronig analysis of interband refl. 2—22748
  - As_2Se_3, amorphous, i.r. spectra, reststrahlen band 2—16465
  - As_2Se_3, amorphous thin film, optical consts. determ. from i.r. spectra 2—33200
  - As_2Se_3, glass and cryst., interband spectra, Kramers-Kronig analysis of interband refl. 2—22748
  - Au, direct optical coupling to surface plasmons 2—33239
  - Au and Au alloy films, 2.4 to 4.4 eV, optical consts. detn. 2—22749
  - Au film, laser modification of reflectance 2—36813
  - Au thin films, 0.3-1 μ, optical constants determ. from reflection and transmission meas. 2—29871

Reflection continued
  light continued
    B, β-rhombohedral, 0.4 to 16μ, anisotropy 2—40644
    $Ba(NO_3)_2$, i.r. spectra, anharmonicity 2—19354
    Bi_2Te_3, reflectivity spectra, intensive interband transitions identified 2—19996
    CO_2, solid, reflection spectra from 4 to 22 eV 2—16466
    $CaCO_3$, fundamental vibrational modes, far i.r. spectra 2—19998
    $CaMoO_4$, direct optical coupling to surface phonons 2—33239
    $CdAs_2$, for i.r. spectra, classical non-interacting oscillator model applied 2—19999
    CdF_2, bandedge, spectral obs. 2—26144
    $CdGeAs_2(P_2)$, band struct. obs. 2—13458
    $CdIn_2Se_4$, spectra, band gap determ. 2—20031
    $CdIn_2Se_4(S_4)$, band struct. calc. 2—29898
    $CdSiP_2$, band struct. obs. 2—13459
    $CdSnAs_2$, spectra, energy band struct. correlation 2—10345
    CdTe, exchange splitting in excitons, interatomic distance depend. 2—29903
    Co^{2+} complex, 'oxinate', u.v. and visible spectra 2—22751
    Cs halide, between 12.5 and 26 eV, Cs-5p core level excitation 2—36856
    CsI, rel. to optical constants in excitonic region 2—20001
    Cu, treated with benzotriazole, surface film, i.r. and u.v.-visible refl. spectra 2—18959
    CuBr, exciton spectrum, band struct. 2—33236
    CuCl, single crystal, exciton spectra, Kramers Kronig analysis, phonon interaction 2—10378
    D plasma, laser beam produced, spectral investigation of reflected light 2—18645
    $DyVO_4$, i.r. spectra, lattice vibrations and phase transition obs. 2—16533
    GaAs, spectra, energy band struct. correlation 2—10345
    GaAs, wavelength depend., optical phonon-plasmon coupling, Vargas theory 2—36859
    GaP, ATR obs. of dispersion of surface polaritons 2—33233
    GaP, and log. derivative between 2.5 and 6.0 eV 2—22765
    GaP, cryst. orientation determ from light refl. pole figures 2—39571
    GaP, Raman reflection spectra 2—40693
    $Ga_2S_3(Se_3)(Te_3)$, band struct. calc. 2—29898
    β-GaSe, layer compound, i.r., interlayer bonding and lattice vibrations 2—25663
    Ge, doped, direct optical coupling to surface plasmons 2—33239
    p-Ge, i.r. spectra, hole relax. and effective masses 2—6847
    Ge, ion irrad., refl. coeff. near fund. absorpt. edge 2—22727
    GeO_2, i.r. spectra, phonon freq. and dielectric const. detn. 2—20002
    He-Ne laser beam, on surface of off-axis parabolic mirror 2—34435
    $HgCr_2Se_4$, semicond. spinel, i.r. spectra, lattice vibrations 2—19374
    InAs, spectra, energy band struct. correlation 2—10345
    $In_2S_3(Se_3)(Te_3)$, band struct. calc. 2—29898
    KD_2PO_4, i.r., high temp. phase transition study 2_22624
    KH_2PO_4, i.r., high temp. phase transition study 2—22624
    KH_2Po_4 electro-optic light deflectors, max deflection and resolving power 2—38078
    KI, far-i.r. consts. and phonon freqs. 2—1681
    LiF, i.r. spectra, reliability of classical dispersion analysis 2—20003
    LiH, exciton form. 2—7094
    $LiIO_3$, polaritons and oblique phonons 2—4447
    MgO-Al_2O_3-SiO_2 system, cordierite glass crystallization i.r. spectra, D.T.A. 2—1155
    MgO, i.r. spectra, phonon distrib. 2—26142
    MgO, i.r. spectra, reliability of classical dispersion analysis 2—20003
    MnF_2, magnon-photon coupling 2—22747
    NO_3^- in powder state, diffuse reflectance spectra 2—29899
    Na, optical cond., Drude tail anomaly 2—10349
    $Na_4Al_3Si_3O_{12}Cl$, sodalite, doped, refl. spectra 2—22806
    NaF, temp. depend. of long-wavelength phonons 2—40649
    Nd^{3+} complex, energy levels, spectroscopic parameter, diffuse refl. spectra 2—26147
    Ni^{2+} complex, 'oxinate', u.v. and visible spectra 2—22751
    NiO-α-Fe_2O_3 fired mixtures, i.r. refl., phase anal. 2—13014
    $Ni_xZn_yFe_2O_4$, ellipsometric determ. of optical consts. 2—36816
    $Pb_{0.95}Cd_{0.05}Te$ solid soln., i.r. refl. spectrum, transport props. determ. 2—22540
    $Pb_{1-x}Mn_xTe$ solids soln., refl. spectra, cond. effective mass 2—22539
    $Pb(NO_3)_2$, i.r. spectra, anharmonicity 2—19354
    $Pb_{0.75}Sn_{0.25}Te$ solid soln., i.r. refl. spectrum, transport props. determ. 2—22540
    p-$Pb_{1-x}Sn_xTe$, i.r. spectra, free carrier parameters detn. 2—26148
    $PbTe_{0.8}Se_{0.1}S_{0.1}$ solid soln., i.r. refl. spectrum, transport props. deeterm. 2—22540
    $PbTi(Zr)O_3$, diffuse refl. spectra, band struct. calc. 2—1526
    Pt electrode/adsorbed layers, polarized light intensity meas. technique for adsorpt. obs. 2—9309
    Pt in perchloric acid, modulated specular reflection spectroscopy, cathodic H adsorpt., oxide formation 2—9311
    Rb thin films, meas. as a function of thickness for polarised monochromatic radiation in 3000-6000Å range 2—16472
    RbH_2PO_4, i.r., high temp. phase transition study 2—22624
    Sb, optical Shubnikov-de Haas effect obs. 2—22480
    SbSI, density of electron states 2—33059
    Se, amorphous thin film, optical consts. determ. from i.r. spectra 2—33200
    Si, ion implanted, effects of Al film, recrystallization and interfacial migration 2—19120
    Si, ion irrad., refl. coeff. near fund. absorpt. edge 2—22727
    Si, pseudo-Brewster angle, carrier concentration detn. 2—13210
    $Sr(NO_3)_2$, i.r. spectra, anharmonicity 2—19354
    Ta_2O_5-GeO_2 system, crystallization, i.r. spectrum 2—1412
    Te:Sb, coupled plasmon-LO phonon modes, reflectivity obs. 2—32906
    V_2O_5 powder, diffuse reflectance spectra 2—29901
    Xe, liquid and solid, Wannier exciton peaks obs. 2—10351
    Y_2O_3:Eu^{3+}, random substitution of Eu^{3+} for Y^{3+} 2—13464
    YbS, YbSe, YbTe, powder, energy band struct. and bond ionicity 2—16476
    $ZnGeAs_2$, spectra, energy band struct. correlation 2—10345
    $ZnIn_2S_4$ and $Zn_3In_2S_6$, band struct. calc. 2—29898
    ZnS, deformed, exciton spectra and exchange interaction 2—29902
    ZnS, with stacking faults, exciton refl. spectra 2—22752
    $ZnSnAs_2$, electrorefl. spectra, electron transitions 2—20006
    ZnTe, exchange splitting in excitons, interatomic distance depend. 2—29903
    ZnTe, exciton reflection spectra, stress induced splitting 2—16477
    ZuTe film, stoichiometry depend. 2—25829

Reflectivity
    see also Diffusion/light; Electroreflectance; Films, solid/optical properties; Magnetoreflectance; Modulation spectroscopy; Optical constants; Piezoreflectance; Thermoreflectance
  absolute reflectances from reflectometer readings 2—8009
  adsorbed layers at interfaces, conf., London England, Dec (1970) 2—9298
  alkali halides, vacuum u.v. region, excitonic struct. 2—16469
  anthracene, absorption band profile of origin region of b polarized 4000 Å transition 2—10352
  anthracene, optical constants, absorption band profile, exciton dynamics 2—9942
  atmosphere, isothermal scattering and absorptive, proof of relation between reflectivity and emissivity 2—40965
  benzene, solid, opt. constants determ. rel. to higher $\pi \rightarrow \pi^*$ 2—20052
  cavity radiators, emissivity calc. 2—7767
  cholesteric liquid crystals, reflectance spectra rel. to temp. dependence of order 2—28794
  coatings, dye lacquered and constituents, reflectance in 210 to 2600 n.m. range 2—23707
  diffraction grating near shortwave limit, effect of ruling distortion 2—5420
  diffraction gratings in vacuum u.v., decreased by mineral oils using during ruling 2—34494
  Earth, moonlit, birectional obs., compared to atmospheric models 2—7297
  film, double layer formulae, rel. to optical consts. determ. 2—33202
  film, normal incidence, optical consts. determ. 2—33203
  glass, spectral reflectance in near i.r. 2—26112
  graphite, anisotropy obs., 3-40 eV region 2—19997
  of integrating sphere, diffused illumination, general theory for measurement 2—27589
  ionic cryst., far-u.v. spectra, electronic struct. 2—13457
  i.r. internal reflection spectroscopy, review and future prospects 2—11531
  i.r. reflection spectroscopy, applic. to adsorption metal surfaces 2—12679
  lamellar crystals, u.v. obs. 2—10343
  laser reflectors 2—34384
  layer-type crystals, obs. in 2-10 eV range, plasmon and excitonic processes rel. to ionicity 2—20005
  metal, high temp. consts. 2—40605
  metal/electrolyte interfaces, double-layer structure models 2—9235
  of mirror surfaces, normal incidence method 2—34466
  normal incidence modulated reflection spectrometer, cryst. reflectivity meas. 2—8039
  plasma, laser produced, heating mechanism determ. 2—24780
  plastic film on Al substrate, spectral normal reflectance 2—40604
  polymethylpolyarsine, 0.17-13 μ 2—13431
  quartz, spectral reflectance in near i.r. 2—26112
  rare earth sequisulphide, spectra, density, struct., band structure 2—40671
  reflectance, scalar diffuse and specular, vector representation 2—34467
  reflectance spectroscopy, diffuse theory and applic. 2—11532
  reflectance spectroscopy, principles, applic. and advantages of the various methods 2—11530
  reflectance-ratio obs. at non-normal incidence for det. of optical constants of solids 2—36815
  Saturnian satellite, Iapetus, polarization observations rel. to albedo differences 2—41197
  semiconductor, amorphous, III-V, complex dielec. const. from refl. meas. 2—26104
  semiconductor, heavily doped, optical const. free carriers 2—26140
  semiconductor, interband transitions and excitonic effects 2—10044
  tetracyanoquinodimethane ion-radical salts, plasma oscillations of electrons 2—1682
  transition metal coatings, extreme u.v. reflectance spectra, characterization in 500-2000 Å region 2—17719
  u.v.-near i.r. reflectance spectros. analytical applic. and instruments 2—11541
  vacuum u.v. meas., opt. const. determ., methods at CNRS Bellevue, review 2—14477
  water, clean, naturally occurring, irradiance reflectance prediction as function of wavelength 2—13633
  Ag, interband transitions 2—10344
  Ag, wavelength modulation spectra, effective mass 2—26141
  AgBr, u.v. determination 2_20018
  $AgGaS_2(Se_2)$, energy band gap obs. 2—4223
  Al-Cu(Mn) dil. alloys, impurity effects on band struct. 2—16463
  Al, effects of roughness of dielectrics, obs. in surface plasmon excitation spectral range 2—16464
  Al, surface plasmons excitation, effects of different roughnesses 2—13102
  Al films, reflectance drops and surface oscillations, roughness spectra 2—4130
  As, plasma reson. refl. 2—7063
  Au/electrolyte interface, electromodulation mechanism 2—9246
  Au, electroless deposit, effect of deposition conditions 2—3524
  Au, interband transitions 2—10344
  Au, wavelength modulation spectra, effective mass 2—26141
  Au black, theory at i.r. optical properties 2—26111
  $CdIn_2S_4$, rel. to band struct. 2—22760
  CdTe, band struct. obs. 2—33303
  $Cd_xZn_{3-x}As_2$, i.r.-vac. u.v. obs., opt. const. determ. 2—20000
  Cr, antiferromag. energy gap obs. 2—36763
  Cr, i.r. absorptivities at room and liquid He temperatures, derived from reflectivity measurements 2—26106
  Cu, interband transitions 2—10344
  $CuCr_2Se_{4-x}Br_x$, specular refl. obs. 2—40645
  Fe, i.r. absorptivities at room and liquid He temperatures, derived from reflectivity measurements 2—26106
  GaAs epitaxial layers at low temp., polariton and spatial dispersion effects seen for n=1 free exciton 2—13257
  GaS, GaSe, abs. reflectivity rel. to complex permittivity of GaS and GaSe 2—29741
  GaSb, 7.7 to 25 eV, and photoelectric emission, band struct. obs. 2—19808
  GaSb, Kramers-Kronig analysis 2—36857
  n-Ge, laser-excited, carrier relaxation times and recombination, optical obs. 2—16231
  GeS, amorphous and crystalline, opt. constants determ., 0.5-21 eV 2—20015
  $Hg_{(1-x)}Cd_{(x)}Te$, 20-400 cm^{-1}, using far i.r. reflection interferometer 2—34480

Reflectivity continued
HgTe, band struct. obs. 2—33303
K complex, $K_2Pt(CN)_4X_{0.3}.2.6H_2O$, transport props. determ., (X=Cl, Br) 2—19546
KBr, in vacuum u.v., rel. to excitonic structure studies 2—4137
KI, in vacuum u.v., rel. to excitonic structure studies 2—4137
$K_2Pt(CN)_4Br_{0.3}.(H_2O)_n$, one-dimens. metallic behaviour confirmation by far-i.r. refl. 2—33241
K_3Sb purple film. Kramers-Kronig dispersion anal. 2—40601
LiF coated Al mirror, effect of deposition rate, substrate temp. and aging 2—34434
MgF_2, extreme u.v. spectra, extinction coeffs. 2—33242
MgF_2 coated Al mirror, effect of deposition rate, substrate temp. and aging 2—34434
MgO, extreme u.v. spectra, extinction coeffs. 2—33242
Mg_2X, (X=Si, Ge, Sn, Pb), band struct., refl. spectra study 2—26146
MoS, u.v. spectra, interband transitions, plasma reson. 2—13463
NaCl, aqueous solution, optical constants in i.r. 2—35766
NaI, in vacuum u.v., rel. to excitonic structure studies 2—4137
$NaNO_3$, vac. u.v. spectra 2—16471
$NbSe_2$, anisotropy band struct. 2—10350
$NbSe_2$, u.v. spectra, interband transitions, plasma reson. 2—13463
Ni, i.r. absorptivities at room and liquid He temperatures, derived from reflectivity measurements 2—26106
$Pb_{1-x}Sn_xTe$, wavelength modulation derivative reflection spectra, assignment of obs. structures with band calcs. 2—4449
Pt, i.r. absorptivities at room and liquid He temperatures, derived from reflectivity measurements 2—26106
Pt in perchloric acid, changes, rel. to cathodic H adsorpt. and oxide formation 2—9311
Rb, optical and dielec. consts., band struct. 2—26149
Rb, solid and liquid, values obtained for perpendicular incidence 0.3-2.4 μ wavelength radiation 2—16417
S, orthorhombic, comparison with monoclinic Se 2—40128
Sb_2S_3, reflectance as function of wavelength on (010) axis 2—19965
Sb_2Te_3:I, i.r. refl., rel. to impurity effect on elec. cond. 2—19651
Se, dielec. const. anisotropy determ., 3-30 eV 2—22725
Se, monoclinic, comparison with orthorhombic S 2—40128
Si, amorphous, electronic struct. obs. 2—33017
Sn, grey, optical consts., band struct. 2—16475
α-Sn, RPA dielec. function in far-i.r. 2—10051
Te, dielec. const. anisotropy determ., 3-30 eV 2—22725
p-Te, laser-excited, carrier relaxation times and recombination, optical obs. 2—16231
Te films, obliquely deposited, determ. for 2-25 μ radiation 2—19963
VO_2 films, optical consts., band assignments 2—33245
$ZrZn_2$, electronic struct. 2—40650
Refraction
particles, at surfaces of discontinuities of e.m. potentials 2—30991
seismic waves, computations for ray segments in media with continuous velocity distrib. 2—30160
seismic waves, obs. of deep sedimentary basin in continental shelf west of Shetlands 2—30192
seismic waves, statistics of time term method of analysis 2—26420
shock waves loading process behind fronts in plastic layered media 2—30879
stress wave at plane boundary between anisotropic media 2—14250
acoustic waves
see also Dispersion/acoustic
by jet flow, numerical ray tracing study 2—20929
jet flow, numerical study by wave acoustics 2—20930
lenses, closed homogeneous cylindrical, gain calc. 2—37758
lenses, homogeneous spherical, sound field in focal region 2—5219
through model cylindrical vortex, with viscous core, angular deflection and ray paths 2—17381
ocean, application of normal-mode and ray theory 2—14255
by wind, power profiles 2—13731
acoustic waves, ultrasonic
No entries
electromagnetic waves
see also Electromagnetic wave propagation
air, refractive index obs. as function of height radiosondes 2—1834
atmosphere, refractometer calibration instabilities related to electrical characteristics of sensor 2—1882
focussing, cascaded annular lens system 2—5403
lens antennas, amplitude and phase transformation 2—20997
lunar surface, reception of post-occultation transmissions 2—4953
microwave, on short tropospheric paths, high resolution meas. 2—20357
plane e.m. wave incident on conductive moving mirror 2—30920
radio refractivity, vertical structure, super-refraction over India obs. 2—33484
radio refractivity gradients obs., in Mekong Delta 2—33483
radiowaves in Venus atmosphere, height dependence of refractive index using results of direct measurements 2—41198
spatially dispersive medium, exact soln. by Maxwell's theory 2—29891
spatially dispersive medium, mode coupling and exciton polarization 2—29892
three centimeter waves, illustrative experiments on birefringence using artificial dielectrics 2—2302
v.l.f. radio waves, in Earth-ionosphere waveguide 2—16894
N_2, liquid, submillimeter wave region 2—32266
Si, electron wave refraction LEED obs. 2—15658
refraction
light
see also Double refraction
apical refraction of spectacle lenses, measurement in dioptres 2—27573
atmosphere, from mean data and iteration method 2—10731
catadioptric imaging systems, meniscus aberration correctors, book 2—27626
coma, optical design and aberrations 2—23676
focusing by concave magnetic domain wall yttrium orthoferrites 2—7969
internal conical refraction, analytical approach to theory 2—23677
lasers, pulse modulation, using acoustooptic refraction 2—21134
lenses and prisms, prevention of premature damage at high flux densities 2—17707
prism, relation for refractive index 2—17672
solar energy concentration, review 2—34437
spatially dispersive model medium 2—38054
spherical wavefronts in stratified isotropic media 2—33474
refraction continued
light continued
wedges with variable refracting angle 2—27577
$CaSO_4$ and Ca and Na double salts, relation between optical properties and structure 2—4434
CuBr characterization 2—39581
Na_2SO_4 and Ca and Na double salts, relation between optical properties and structure 2—4434
Refractive index
air, portable modification to Jamin interferometer 2—34483
air, radio waves, obs. as function of height radiosondes 2—1834
atmosphere, correlation with microwave fading, statistics 2—40971
atmospheric, mean monthly values, computation errors 2—13670
dielectric liquids, correlation with surface tension 2—28815
p-difluorobenzene in nonpolar solvents, using submillimetre waves 2—39367
e.m. wave propagation effect, refractive index structure function constant over 28 im at 35 GHz 2—37169
gas discharge medium in CO_2 laser 2—27495
gases, laser interferometer based on fringe counting technique 2—21146
long chain alcohols, meas. in pure liquid state at varying temp. 2—39388
nonlinear, cubic lattice, correction for higher induced multipoles 2—17674
plasma, optically thin sources, application of Abel integral eqn. for calc. refractive index distribution 2—15469
radio, mean monthly values, computation errors 2—13670
rhodochrosite, complex index in range 0.33 to 2.5 μm 2—7040
solid dielectrics and magnetic materials, sub mm wavelengths 2—34237
$BaTiO_3$ film, r.f. sputtered, rel. to deposition temp. 2—40347
$LiNbO_3$, nonlinear crystal, influence of transverse inhomogeneity on second harmonic generation 2—27562
light
see also Disperions, optical; Double refraction; Optical constants
n-alkanes in 1-chloronaphthalene solvent, effect of molecular weight on refractive increment 2—6235
anisotropic crystals, influence of interband transitions 2—16478
anthracene, Kramers-Kronig relationships 2—15592
arc discharges, distrib. det. by quantitative laser Schlieren technique 2—35636
atmosphere, fluctuation profile, laser remote sensing 2—40963
atmospheric, optical distance correction for fluctuation, Lidar technique using depolarization factor 2—1875
atmospheric, structure parameter behaviour near ground 2—1874
benzene, solid, reflectivity determ. rel. to higher $\pi \to \pi^*$ transitions 2—20052
carbon tetrachloride, nonlinear, due to nonlinear response of electronic currents 2—1096
cutoff interference filter, conditions for selecting refractive indices of layers and substrates 2—14464
dielectric film, optical props. rel. to interference coatings and waveguides 2—40599
dielectric layers, modified interference method for meas. dispersion 2—13432
diffusion meas., conc. gradient by immersion method 2—19135
ellipsometric determ. in extreme u.v. 2—16461
ferrous orthophenanthroline, Kramers-Kronig relationships 2—15592
fields, three dimensional, reconstruction using holographic interferometry 2—11498
films, thin, det. from interference maxima and minima of transmitted light 2—27591
Fourier transform interferometry, general equations for determination of complex indices 2—38061
gas, transparent in vacuum u.v., Perot-Fabry interferometric obs. 2—15208
glass, effects of temp. on index and optical path length 2—7038
gradient media, sine-wave optical paths 2—296
group II-IV-V compounds, chalcopyrite semiconductors 2—26100
intensity dependent, rel. to third harmonic generation 2—17670
internal reflectance at boundary surface, diffuse and specular reflectance 2—17682
i.r., dry and natural atmospheric aerosols and sea salt 2—37128
liquid, thermal changes induced by laser beam 2—25081
liquid biprism, teaching experiment 2—33850
liquid crystals, changes at transition temp. 2—9092
liquid crystals, compensated cholesteric, principal values 2—28857
metal, high temp. consts. 2—40605
p-methoxybenzyline-p-butylaniline, nematic liquid, temp. depend. 2—18828
mica solid solution, formed between $K_2Mg_6Al_2Si_6O_{20}F_4$ and Al-free mica 2—36302
microscopic phase analysis of mixtures of solids 2—4428
Mie scattering, modification of van de Hulst relation 2—24983
molecular crystal polarisability tensor calc. 2—33197
moment equations for waves propagated in random media 2—7997
monorefringent medium, spatial distrib. possibilities 2—23664
m-nitroaniline, rel. to possible electrooptic appl. 2—16427
nonuniform refractive index fibre, mode propagation 2—31121
organic aromatic crysts., optical anisotropies rel. to mag. anisotropy 2—33206
phenanthrene, Kramers-Kronig relationships 2—15592
polydisperse systems of low molecular weight, refractive index increments and light scattering 2—39402
polyethylene in 1-chloronaphthalene solvent, effect of molecular weight on refractive increment 2—6235
polymer solutions, relation between refractive index and density increments rel. to polymer partial specific volume determination 2—39342
polymers in solution, methods for calc. refractive index increment from properties of polymer and solvent 2—39401
polypropylene, β-form crystals in types III and IV isotactic spherulites 2—39447
polystyrene, vac. u.v. obs., free electron gas model 2—20009
prism 2—17672
quartz, control by ion implantation 2—25417
rare earth trichlorides, Kramers-Kronig relationships 2—15592
semiconductor, group II-VI cpds., dispersion props. 2—13435
separation of scattering and absorption components in nonhomogeneous media 2—34468
sputtered glass waveguides 2—38115
styrene-MMA, vac. u.v. obs., free electron gas model 2—20009
triglycine sulphate-selenate mixed cryst., 2—13321
u.s. wave density and press. distrib. plotting method 2—27250

Refractive index continued
light continued
H, dilute gases, one term Sellmeier formula for optical dispersion 2—39287
Ag film, aggregated, ellipsometric det., effect of anisotropy 2—40606
AgBr(Cl), dispersion relation 2—1680
AgF, high frequency determ. by ellipsometry 2—32802
$AgGaS_2$, meas. 2—1654
Al, 10^{-2} to 10^5 eV range 2—19957
Al films, variation on annealing 2—1659
Al_2O_3, defects in synthetic corundum crystals grown by the Czochralski method 2—29872
As_2Se_3 film, glassy, electric fields effects 2—19961
BN film, optical props. 2—26159
$Ba_2NaNb_5O_{15}$, temperature dependence obs. 2—10302
CO_2 films, condensed on cryogenic surfaces, refractive indices and densities 2—7039
$Ca_{10}(PO_4)_6F_2$-$Ca_4Y_6(SiO_4)_6F_2$ solid solution, comp. depend. 2—36275
$Ca_{10}(PO_4)_6(OH)_2$, melt grown single crysts. 2—15690
Cl_2 liquid in temp. range 130-260 K 2—18825
Cs_2O-M_2O-SiO_2 glass, (M=Li,Na), rel. to struct. 2—28975
$CuGaS_2$, meas. over range of transparency of crystal 2—1654
CuI, nonlinear index, dispersion 2—1655
$CuInS_2$, refractive index meas. 2—1654
GaAs, laser-type, peak at absorpt. edge freq. 2—36879
GaN film, r.f. sputtered 2—18937
GaP, i.r., evaluation from emitted i.r. intensity and polariton field 2—16458
GaP film, forbidden band width, absorpt. spectra 2—1691
Ge, Brillouin scattering, at 6328 and 4880 Å, linewidths analyzed to give real and imaginary part of refractive indices 2—20082
Ge, coeff. of temp. 2—7954
Ge, in 77 to 300K range obs. using modification of minimum deviation technique 2—36818
Ge semiconductor, i.r., doped and compensated 2—16482
$Ge_{55}As_{33}Se_{12}$ TI-20 glass, index homogeneity 2—34541
H glow discharge, degree of dissociation determ. from refractive index, manometric of energy dissipation data 2—15512
HBr liquid in temp. range 130-260 K 2—18825
HCl liquid, in temperature range 130-260 K 2—18825
H_2O films condensed on cryogenic surfaces, refractive indices and densities 2—7039
H_2S liquid, in temperature range 130-260 K 2—18825
HfO_2-Y_2SiO_5 solid solutions 2—1411
InN film, r.f. sputtered 2—18937
$K_2Cr_2O_7$, Kramers-Kronig relationships 2—15592
$K_3Fe(CN)_6$, Kramers-Kronig relationships 2—15592
KH_2PO_4 crystals, i.r. region using parametric scattering of light 2—40607
K_3Sb purple film, Kramers-Kronig dispersion anal. 2—40601
MgO-Fe_2O_3-SiO_2 system, rel. to phase diagram 2—29494
MgO film, in 0.22-8 μm wavelength range 2—34476
Mn_2PO_4Cl, grown from $MnCl_2$ flux 2—22111
NH_2 liquid, in temperature range 130-260 K 2—18825
NH H_2PO_4 crystals, i.r. region using parametric scattering of light 2—^{4}40607
N_2O liquid, in temperature range 130-260 K 2—18825
Ni film, polarimetric obs. 2—33199
$Ni_xZn_yFe_2O_4$, rel. to atomic struct. and energy levels 2—36816
OCS liquid, in temperature range 130-260 K 2—18825
$PbCl_2$, Kramers-Kronig relationships 2—15592
$PbMg_{1/3}Nb_{2/3}O_3$, elec. field effect 2—10312
PbTe film, deposition parameter effects rel. to i.v. multilayer filters 2—40602
$PbTiO_3$, single domain ferroelectric, rel. to nonlinear optical properties 2—19953
Rb, spectral reflectance obs., 3.3-10.5 eV 2—26149
SO_2 liquid, in temperature range 130-260 K 2—18825
Si, at 5461 Å, etched and cleaved samples 2—36817
Si, Brillouin scattering at 6328 and 4880 Å, linewidths analyzed to give real and imaginary part of refractive indices 2—20082
Si, in 77 to 300K range obs. using modification of minimum deviation technique 2—36818
Si, near i.r., press. depend. 2—10303
Si i.r. waveguides, doping, refractive index and losses relationship 2—38112
Si semiconductor, i.r., doped and compensated 2—16482
α-SiC, 6H polytype, dielec. const. determ. 2—10395
2HSiC, minimum deviation method, calculation of birefringence 2—26108
SiO_2, at 5461 Å, etched and cleaved samples 2—36817
SiO_2, fused, 404.7 to 667.8 nm, −200 to +20°C 2—26109
SiO_2, SiO_xN_y evaporated films 2—8021
SiO_2 films formed on n-Si 2—40815
SiO_x evaporated film, rel. to deposition conditions 2—10394
Ta_2O_5/Al_2O_3 mixture, anodic 2—3548
Ta_2O_5-GeO_2 solid solutions 2—1412
TeO_2, dispersion characts. 2—1658
TiO_2 evaporated film 2—8021
VO_2, complex const., reflectivity obs. 2—33245
ZnS dielectric layers, modified interference method for meas. dispersion 2—13432
Refractive index measurement
dielectrics, at mm wavelengths 2—34238
low-loss liquids, absorptivity, measurement of change in refractive index caused by temp. change due to absorption 2—25083
low-temperature liquids 2—18825
method for nematic liquids 2—18828
plasma electrostatically driven oscillations near lower hybrid resonance frequency 2—21835
Refractometers
atmosphere humidity meas. over water, comparison of spectra with Ly-α humidiometer 2—22955
laser interferometric differential refractometer for chromatographic effluent detection 2—17706
microwave, single cavity frequency and bandwidth stabilized, patent 2—216
optical material testing 2—5441
Refractories
borides, high temp. enthalpy 2—19274
carbide layer build up on steel open arc 2—32739
carbides, packing and vacancy ordering 2—9329
ceramic fibres, prod., applications 2—39950
Refractories continued
chemical vapour deposition techniques 2—32349
compression testing, high temp., const. press. 2—25548
crystal growth, cold metal crucible system 2—25267
crystal growth, review 2—39576
dielectric film production, gaseous phase reaction 2—3507
fibres, bonded to ceramics to improve thermal properties of latter 2—3967
furnace design for studying refractory oxides 2—30719
i.r. spectra, temp. range 1000-1500°C, wavelength range 1-15μ 2—4454
magnesia, modulus of rupture, effect of silicate phases 2—1310
metal, dispersion hardening, review 2—32747
oxide, droplet solidification, spheroidization times, supercooling 2—12613
oxides, fusion, obs. by use of rotary furnace 2—37524
oxides, growth by floating zone method and mech. props. 2—29098
oxides, phase transitions, DTA study 2—29472
oxides, reactions with carbon, temps. to 2400°C, X-ray obs. 2—3636
pore size distribution, meas. method and apparatus 2—32749
rare earth oxides and oxysalts, textured films 2—9338
rare earth tungstates, mats. charact. 2—29449
sintered, polycryst. props. rel. to monocryst. props. 2—22254
sintering, high-temp., densification, rel. to dislocations 2—36260
sulphides, metal-rich, cryst. chemistry, significance of Kasper polyhedra 2—9351
thermal conductivity at high temperatures 2—19445
transition metal borides, carbides and silicides, shock compression 2—12841
transition metal carbides, stability, model 2—9330
transition metal cpds. with high coord., valence bonding 2—9328
vaporization rate, determined in solar and arc furnaces 2—35831
zirconia, stabilized, applic. to thermal probe construction 2—27331
$Ca_3Cr_2(SiO_4)_3$, synthesis from $CaCO_3$, Cr_2O_3 and SiO_2 using 03 flux 2—1375
CaO-MgO-B_2O_3-SiO_2, solid-liq. relationships at 1550°C, compatibility relationship diagrams 2—32305
from Eu_2O_3+W reaction at 1900-2000°C in high vacuum 2—28967
β-Ga_2O_3, growth by floating zone method and mech. props. 2—29098
Gd_2O_3-SrO system, phase diagram, DTA study 2—29472
$MgCr_2O_4$, solid phase coexisting with periclase and liq. phase, microstruct. parameters 2—32776
NbC_x, shocked, microcrack form. and plastic deform. 2—29328
NbC_x, thermodynamic props., determ. from sp. ht. 2—13044
Ni alloy, super-refractory, dynamic recrystallization 2—12948
SiC, 2H type, low temp. phase transform. mechanism 2—32778
TaC_x, 0-3000°K, sp. ht. and thermodynamic props. 2—1436
TaC_x, lattice instability effects on supercond. 2—22509
ThO_2-SrO, ThO_2-BaO systems, charact. using specially designed furnace 2—30719
TiC_x, shocked, microcrack form. and plastic deform. 2—29328
V_8C_7, cryst. struct. 2—29154
ZrC_x, shocked, microcrack form. and plastic deform. 2—29328
Zr_9S_2, and other metal-rich refractory sulphides, significance of Kasper polyhedra 2—9351
Refractory materials *see Refractories*
Refrigerators *see Low-temperature production*
Regge poles and trajectories
ABFST model, Regge slopes and schizophrenic pomeron 2—34647
absorption model for small angle elastic pp scattering 2—23887
Amati-Bertocchi-Fubini- Stanghellini-Tonin equation, forward direction, validity of trace approx. and spectrum of output poles 2—8149
Amati-Bertocchi-Fubini-Stanghellini-Tonin multiperipheral model, Regge trajectories and pomeron slope 2—8145
amplitudes with Schwartz type Regge trajectories 2—14610
asymptotic behaviour of trajectories and widths 2—23825
chiral and gauge field theories, Regge pole content 2—17790
complex angular momentum theory including pole and cut contributions for regeneration $K_2^0 \rightarrow K_1^0$ on nucleons 2—34671
complex angular momentum theory including poles and cuts for high energy scattering and charge exchange processes 2—34641
complex conjugate pairs of trajectories, calc. using scalar Bethe Salpeter eqn. 2—31251
complex poles, theory and practice 2—8144
complex-Regge-pole and absorptive models, possible relation, πN scattering considered 2—17871
coupling theorems for tri-Regge vertex including pomeron 2—402
cut, pomeron exchange in NN→NN* 2—429
cut contrib., formulated on basis of complex Regge poles and duality 2—34646
cut model, phenomenological model based on reggeon diagram technique 2—5518
cut theories, review 2—38259
cuts, t-channel functions proposed which reproduce successes of dual absorptive model 2—14607
cuts and related topics, review 2—38258
deep Regge limit, connection with deep light cone limit for electroprod. and massive lepton pair prod. 2—17865
diffraction scattering, complex trajectories 2—11588
dual absorptive models, properties of trajectories following from analyticity 2—38272
dual amplitude with arbitrary trajectories 2—34642
dual crossing symmetric models with Regge cuts 2—34649
dual crossing symmetric representations with finite width resonances 2—21274
dual N-Reggeon vertex, field operator formalism 2—2538
duality constraints in inclusive reactions, vanishing of pomeron-pomeron-reggeon coupling 2—8133
elementary discontinuity formulas, Mueller's Regge hypothesis 2—21278
e.m. scattering, self-consistent dispersion theoretic amplitudes 2—17814
exchange diagrams used to suggest sufficient condition for energy independence of inclusive reactions 2—27722
exotic boson exchange cross sections, Regge cut contributions 2—406
extended boson exchange model associated with hydrogen like Regge recurrence 2—31316
f′ and φ trajectories, implication of introducing strangeness into multiperipheral model 2—14614
f and f′ trajectories connection with Pomeranchukon from multiperipheral model 2—14613
factorizable models, construction of N-reggeon vertex 2—11586
geometric and Regge models, equivalence 2—17886
hadron inclusive reactions, cross section calc. in triple Regge limit using dual models 2—17849

Regge poles and trajectories continued
high energy models and geometrical duality, new model proposed 2—31254
high energy scatt., explanation of fixed pole at J=1 2—14604
hypercharge exchange reactions, complex Regge poles 2—17852
inclusive processes, reggeon reggeon total cross sections 2—14593
inclusive reactions, application of Regge phenomenology 2—21254
inclusive reactions, phenomenological extension of triple Regge behaviour 2—21259
inclusive reactions, triple Regge domain, exchange degeneracy and total cross sections 2—31231
inclusive reactions in the Regge pole model and duality 2—31224
inclusive spectra, shapes, function of longitudinal momentum, Regge phenomenology 2—27719
infinitely rising, existence of the Mandelstam representation 2—34648
interacting Reggeons, role in field-theoretic investigations of high-energy scattering 2—17780
meson-nucleon scattering, Feynman-diagram models of Fermion Regge-pole conspiracies 2—34655
multi-Regge amplitudes, factorization 2—34652
multi-Regge amplitudes, factorization in dual resonance model 2—8148
multi-Regge model for deep inelastic electro and photoproduction 2—23796
multi-Reggeon vertex, expressions obtained by multiple factorization and mathematical induction techniques 2—21276
multiperipheral model, extended, low energy zeros and Regge poles 2—392
multiperipheral model, final state spectra 2—31252
N-Reggeon vertex from n-particle Veneziano amplitude 2—27728
Nakanishi representation, Regge behaviour 2—17787
nonpomeron Regge cuts, dual representation 2—21275
one pion exchange model, and applic. to $pp \to pn\pi^+$ reaction 2—21302
P′ and ω poles, use in discussion on nature of Pomeron 2—8146
parameters, improved coupled integral equations 2—17879
partial waves, finite energy sum rules and formulation for N/D equations 2—34597
photoproduction, Regge model for forward π and η production off nucleons 2—17925
photoproduction from nucleons, simple approach to Reggeization 2—8107
pole dominance amplitude, high energy, space time correlation function properties 2—31255
pole residues, closed form expressions, Virasoro model 2—14600
pole-cut model, application to difference in cross section between π^+p and π-p charge exchange scattering 2—34693
potential scattering, numerical determination of Regge poles 2—38275
proton spectrum, longitudinal and transverse momentum correlation in terms of Regge formula 2—38325
Regge behaviour and duality, approach based on infinite sum of one-particle-exchange amplitudes 2—23829
Reggeon graph scheme, 10 to 100 GeV 2—14551
relativistic trajectories, from configuration space δ-shell interaction 2—8147
residues, above threshold, predictions using dual absorptive model applied to t-channel 2—17864
residues, rel. to partial widths in dual resonance models 2—8139
resonant amplitude, new interpretation of duality and structure 2—23828
rising trajectories, Bethe Salpeter model construction 2—23761
rising trajectories, dual absorptive model study 2—23823
scattering, elementary particles, theoretical difficulties of Regge-eikonal model 2—38276
scattering amplitudes role of fixed angular momentum plane branch points with regard to t=0 singularity structure 2—17880
strong interactions, very high energy, nonlocal theory 2—8098
symmetric N-Reggeon vertex with nonequal Regge trajectories, dual resonance model 2—14616
three-to-three scattering amplitudes triple-Regge coupling and diffractive spin dependence 2—17877
threshold behaviour in simple field theoretic model 2—17781
trajectories, standing-wave modified, applic. to ion-atom scattering 2—642
triple Regge vertex, anomalies in inclusive reactions 2—23824
triple-Regge region, resonance contribution from high energy missing mass spectra 2—23814
triple-Regge vertex, helicity pole and related asymptotic behaviours of six-line amplitude studied using DRM 2—17883
u-channel exchange degeneracy in $\pi\bar{K}$ and $\pi\Xi$ backward scattering 2—34686
Δ trajectory, calc. using N/D formalism 2—17954
Δ_δ, trajectory behaviour and nondegenerate parity partners 2—8210
e, A_2 trajectory exchange degeneracy, evidence from KN charge exchange reactions 2—17908
ep inelastic scattering, Regge pole model 2—38234
ep inelastic scattering data, Regge pole analysis 2—38319
K/π ratio, angular behaviour at high energy in multi-Regge model 2—17904
K photoproduction, Regge pole model with cuts 2—34660
$\bar{K}N$, determ. of high energy scattering amplitudes from data on K-p elastic and charge exchange scattering 2—11600
$KN \to K^0N$ charge exchange, universality and complex Regge pole factorization 2—21264
$K^\pm N \to K^{*0}N$ charge exchange, difference between K^+ and K^- reactions obtained in absorption model using Reggeized π and ρ exchange 2—17956
$K^-n \to \pi^-\Lambda$, differential cross section and polarization, model with exchange degeneracy and duality, failure of Regge cut models 2—17911
$K^\pm p$ elastic scattering, description combining Regge and absorption models 2—409
$N\bar{N}$ system, Regge trajectories, resonance widths 2—21300
$N\gamma$ interactions, field theoretic Reggeization in five- and six-point functions 2—347
ω complex Regge poles, in π^0 photoproduction on nucleons 2—27752
$p+p \to p+\pi^-+\Delta^{++}$, double Regge pole analyses, comparison with data at 22 GeV/c 2—8198
pp reactions, $\Delta(1236)$ production, parameter-free Reggeized absorption model 2—34742
pp scatt., differential cross sects., slope determ. using Regge pole model, average Pomeranchuk slope 2—14698
$pp \to pp\omega$, simple Regge pole model 2—2577
$P^\pm\pi \to \pi^0$+anything study of triple-Reggeon couplings 2—2556
π Compton scattering, model formulation on basis of Regge poles and scale invariance 2—11609
π photoprod., Regge pole model including kinematic cuts study 2—23846
π^- photoproduction, parametrization, complex Regge poles 2—11608
π^+ photoproduction, parametrization, complex Regge poles 2—11608
$\pi\Delta$ charge exchange, dual approach to Regge dips 2—399
πN charge-exchange polarization, described by exchange of ρ-pole plus $\rho \otimes P$ Regge cut 2—413
πN charge-exchange scattering, polarization and sum rules in complex-Regge-pole model 2—14662
πN scattering, fixed pole effects, Regge parametrization based on very strong exchange degeneracy 2—31293
πN scattering, peripherality from absorbed Reggeon exchange model 2—23862
$\pi^+n \to K^+\Lambda$, differential cross section and polarization, model with exchange degeneracy and duality, failure of Regge cut models 2—17911
$\pi N \to \rho\Delta(1236)$, Regge pole model, threshold constraints 2—38301
$\pi^-p \to \pi^0(\eta)n$ charge exchange, universality and complex Regge pole factorization 2—21264
$\pi^-p \to \pi^0n$, origin of zeros in ρ-Regge residues 2—8173
$\pi^-p \to \pi^0n$ charge-exchange above 5 GeV, structure of absorptive Regge cuts 2—17943
$\pi^+p \to p\rho^+$ backward reaction, as test of Regge dip mechanism 2—17885
$\pi^\pm p$ reactions, 8 and 16 GeV/c, double Regge pole exchange model 2—34682
ρ, trajectory, calc. using N/D formalism 2—17954
ρ complex Regge poles, in π^0 photoproduction on nucleons 2—27752
$pp \to pX$, duality predictions on exptl. data near phase space boundary 2—23886
ρ, photo- and electroprod. in deep inelastic region, Regge pole analysis 2—14681

Relativity
bivectorial and spinorial fields, energy- momentum tensor 2—27042
charge, quantized, in terms of pure geometry 2—7678
conference, Technion City, Israel (1969) 2—2077
cosmological models with pressure, analytic solns. for all values of space curvature constant 2—10791
dynamical, with noncanonical positions 2—11259
dynamics of a particle of variable mass 2—33895
electrons, behaviour, free electron physics, book 2—17831
gravitational theories, characterization by cumulative effects in free particles motion and in behaviour of clocks 2—14074
isometric relativistic motions with respect to particle 2—14157
lightlike particle states, wave packet realization parton model of hadrons 2—30763
long range interactions due to geometrical props. of spaces with curvature 2—58
Lorentz invariant one-body problems, Lagrangians for approximately relativistic interactions 2—11257
momentum and angular momentum in relativistic classical particle mechanics 2—30769
multiply connected universe and excluded possibilities of geometrodynamical analogue to electric charge 2—47
nonlinear electromagnetic Lagrangian, linear field equations 2—17540
planetary motion, computerized series soln. of relativistic equations 2—11008
quasi relativistic equations for charged fermions in external e.m. field, deduced from electrodynamics 2—71
relativistic classical particle mechanics, example construction 2—33894
relativistic two-body problem, quantum mechanics solution 2—33890
relativistic two-body problems, classical mechanics solutions 2—33889
scalars, Lorentz and metric invariant 2—20821
singularities, new technique for analysis 2—2060
super light velocities in exploding quasar 2—30513
teaching, didactic approach 2—17165
thermodynamic irreversibility of signal sending and expanding universe 2—2264

general
see also Cosmology, Gravitation; Red shift; Space-time configurations
black holes, detection using gravitational lens effect 2—7367
black holes, limits on amount of energy which may be extended 2—23256
boundary conditions, stability of cosmological models 2—37596
Brans-Dicke cosmologies, exact solutions in flat Friedmann universes 2—1927
Brans-Dicke theory, generalized field equations 2—7657
Brans-Dicke theory, vacuum field solutions 2—20828
centrally symmetric field, De Donder model for liquid sphere 2—17197
Chaplygins gas movement, hydrodynamical analogy for astrophysical effects 2—14090
charged bodies, equations of motion determ. from Einstein-Maxwell field equations 2—37599
clock paradox, Schwarzschild's line element application 2—50
complex recurrent space-times 2—33908
cosmological models with non-zero pressure 2—4769
cosmological phenomena and microphysics, unified approach to theory of matter 2—4768
curved spaces, e.m. radiation from charged particles 2—2089
distribution theory and thin shells 2—2101
Ehrenfest paradox, statements and procedures 2—30778
Einstein's eqns., Robinson-Trautman soln. 2—11266
Einstein's equations, approx. solns. 2—2106
Einstein's field eqns. closed cosmological solutions 2—41031
Einstein's field equation, derivations 2—14081
Einstein's field equations with perfect fluid, soln. 2—2110
Einstein's relativistic field theory, particle motion, coordinate conditions 2—17213
Einstein equation, method for generating new solutions 2—23259
Einstein equations, local quantum theory formulation, locality 2—17202
Einstein equations, spherically symmetric time dependent solutions 2—14088
Einstein equations, Vaidya soln. 2—11263
Einstein equations, with cosmological term, homogeneous anisotropic solns. 2—17204
Einstein equations of evolution, geometric approach 2—23262
Einstein field equations, axial symmetry case, gravitational radiation 2—17203
Einstein relativistic field theory, particle motion, consideration of diffused and localized electric charge 2—20831
Einstein-Maxwell equations, approximate radiative soln. 2—2291
Einstein-Maxwell field equations, class of plane solutions 2—23254
Einstein-Rosen bridge, rotating, and neutron stars 2—2100
electromagnetic Thirring problem 2—17212

Relativity continued
general continued
e.m. energy confined to finite volume, inertia and passive gravitational props. rel. to principle of equivalence 2—37833
e.m. fields, static 2—2114
embedded space-times, remark on energy and momentum 2—33909
energy complex in tetrad formulation 2—5134
energy tensor for gravitational field 2—33892
energy-momentum complex of gravitational field, construction of new formalism for solution 2—52
energy-momentum tensor of system of charged particles 2—2346
equations of motion 2—2104
equilibrium figure for axisymmetrical celestial bodies equations, soln. by Lichtenstein method 2—27047
exact cosmological solutions in Brans and Dicke's scalar tensor theory 2—33575
field equations derived from SL_{2c} symmetry representation of gravitational-field dynamical variables 2—17187
field theories, general, energy of stationary system 2—37591
fluid, perfect, bounded source, news function 2—7661
fluid dynamics with dissipation, formulation of eqns. application to expanding universe 2—14087
fluid spheres, differential equations for non-charged spheres of perfect fluid 2—53
fluid spheres, physically meaningful, differential conditions 2—23265
fluid spheres, static, spherically symmetrical, stability 2—14084
four-dimensionality of space, Einstein tensor 2—33905
fusion of gravitational and e.m. theories for geometry of world manifold 2—59
gaseous sphere without energy flow, gravitational collapse, hydrodynamical equations 2—30779
global properties 2—64
gravitatational waves, toroidal and cylindrical, correspondence 2—27049
gravitating spherical shell, surface density of matter 2—37590
gravitational collapse and event horizons 2—1929
gravitational collapse of uniformly rotating current carrying thin disk 2—4773
gravitational deflection, measurement on 3C273 and 3C279 quasars 2—30510
gravitational deflection of microwave radiation near sun 2—4991
gravitational field angular momentum transfer 2—27048
gravitational field eqns. for metric field of rotating rod, loss of mass 2—14083
gravitational field equations, noncharged static spheres of perfect fluid in isotropic coordinates 2—37581
gravitational fields with groups of motions on two-dimensional transitivity hypersurfaces, model with matter and magnetic field 2—30775
gravitational quadrupole radiation 2—33896
gravitational radiation from particle falling radially into Schwarzschild black hole 2—2097
gravitational theory, construction of consistent boundary conditions in presence of strong discontinuities 2—37583
gyroscope expt., summary of important perturbations 2—17196
irrotational dust solutions of Einstein equations, velocity-dominated singularities 2—2091
Jordan-Brans-Dicke theory, field theoretical construction 2—20836
junction conditions at discontinuous surfaces 2—30774
Kerr metric of rotating body, test particle motion 2—2085
Kerr type space-times, sources 2—37592
and kinetic theory of gases 2—3322
Landau-Lifshitz pseudotensor analogues 2—2108
Lense-Thirring type gravitational forces between spinning cylinders and disks 2—5136
level surfaces inside relativistic rotating stars, Poincare's limit 2—26648
light deflection by gravitational field of Sun 2—23250
light tracks near dense charged body 2—26653
Lorentz cobordism and gravitational collapse 2—30776
Lorentz covariant theory of gravitation, deduction 2—14076
Lorentz invariant particles, classical system 2—2087
Lorentz transformations in uniform gravitational field, application to clock paradox 2—51
magnetized deformable media, theory 2—17308
mass and radius of elementary particles, structure study by general relativity 2—31176
massive sphere with 2 density distrib., exact internal solutions 2—14089
metrics, Reissner-Nordstrom, Newman-Unti-Tamborino, Kerr, study of singularities 2—11261
motion in two space-like dimensions, set of coordinate transformations 2—23258
motion of a point body with variable rest mass, covariant equations 2—33975
neutrino-gravitational fields, combined 2—2090
Newman-Penrose equations in Minkowski space 2—33903
null e.m. field propagation 2—11265
NUT metric, generating potential 2—33907
observables, via Hamilton Jacobi functionals 2—55
particle motion in monopole-prolate quadrupole gravitational field 2—2098
particle production and vacuum polarization, anisotropic gravitational field 2—20837
plane inverse potential problem, nonuniquness of the soln. 2—30768
principle, proposed redefinition 2—2081
projective field theory, axialsymmetric stationary solns. 2—7653
quantization, Sommerfeld-Wilson, of metric field 2—62
quantum cosmology, quaternion formulation 2—26587
and quantum space time 2—2103
radially symmetric radiation field, associated spinorial solution 2—30773
radiation pressure on test particle 2—37593
radiative transfer, moment method 2—2265
Ricci scalar curvature invariant, appl. of new invariance property of field theories 2—7645
Riemann spaces, 4-dimens., filled with ideal fluids, Riemann curvature 2—33904
Robinson-Trautmann solutions on compact manifolds 2—30777
scalar-tensor universe, motion of a structureless free particle 2—2095
Schwarzschild field, Maxwell equations 2—11268
Schwarzschild exterior space-time, gravitational field outside a sphere of matter 2—2092
Schwarzschild gravitational field, light beam deviation calc. 2—2086
Schwarzschild metric, spinor solutions 2—7658

Relativity continued
general continued
singularities and possible prevention due to vacuole rotation 2—4770
space homogeneity criteria 2—23255
space-time code, algebriac quantization 2—20834
space-time curvature tensor, classification 2—2109
spherically symmetric centripetal e.m. wave 2—17207
spherically symmetric spacetimes, invariant formulation of Einstein's eqns. 2—23264
spin 1/2 particles, bound states 2—27045
spinor fields, generalized field equations and application to the Dirac field 2—2094
spinor fields, Noether's theorem and the conservation laws in Riemann-Cartan space 2—2093
spinor vacuum, polarization by slowly varying gravit. field 2—43
static field eqns., division into types, supermassive star models 2—26659
static multiparticle systems, exact solutions to field equations 2—14085
static perfect fluids, Einstein field equation solutions 2—20823
stellar evolution, relativity parameter at high degeneracy 2—20529
SU(2) technique applications for gravitational radiation problems 2—2099
tachyons, instability of Green function for Klein-Gordon waves 2—2501
Taub-NUT metric, Kruskal-like extension, geodesic incompleteness 2—17211
test, using spinning body acceleration in gravitational field 2—17209
test using spinning body acceleration in gravitational field 2—17210
testing, progress, problems and prospects 2—27046
thermodynamics, nonstationary, kinetic derivation from Chernikov thirteen moment approx. 2—33947
thin sandwich theorem, solution 2—56
third principle and generalization of geometric object 2—2107
topological formulation, space-time, reference frames and relativity group structure 2—30772
topological methods and magnetic charge, holonomy and characteristic classes 2—63
topological questions in canonical formulation of gravitation 2—46
trapped surfaces in strongly curved space-times 2—2080
twin paradox, free fall consideration, asymmetrical aging 2—33901
twistors, symplectic structure and Lagrange's identity 2—2102
uniqueness and existence theorems, and global hyperbolicity in Cauchy problem 2—61
universe model, anisotropic, Einstein eqn., soln. with cosmological term 2—44
vacuum fields, characteristic initial data 2—54
waves in Schwarzschild field 2—37586
weak gravitational fields, covariant Green functions of photon and electron 2—2070
white dwarfs, rotating, integral parameter calc., rel. to Newtonian theory values 2—10844
$e\mu$ mass doublet, derivation 2—20827
special
see also Tachyons
angular momentum in special relativity 2—37587
canonical dynamics of charged particles 2—7651
clock paradox resolved 2—27043
critical angle for total reflection, effect of moving media 2—33899
Ehrenfest paradox pertaining uniformly rotating cylinder 2—17198
equilibrium 2—2072
experimental tests 2—2078
generalized Lorentz transformations, implications for observability of tachyons 2—33900
Lorentz transform., rel. to charge motion in constant homogeneous e.m. field 2—7652
Lorentz transformation, Bargmann-Hall-Wightman- Jost theorem, version using hyperfunctions 2—2076
Lorentz transformation, derivation based on Newtonian mechanics 2—27123
Lorentz transformation, general, matrix identities 2—48
magnetic field as mechanism to preserve relativistic momentum 2—33893
magnetic field origin 2—27044
mass increase, undergraduate laboratory demonstration 2—14080
observer in uniformly accelerated translating motion, behaviour w.r.t. inertial observer 2—37588
paradoxes based on consideration of forces resolved by introducing concept of hidden momentum 2—33898
rotating relativistic ring, disk problem 2—11260
simple introduction 2—5132
textbook on relativistic mechanics 2—49
thermodynamic inequalities 2—30770
time, nature and its measurement, cosmological interpretation of theory 2—23252
time for terrestrial circumnavigation relative to clock on earth, dependence on direction 2—11258
twin paradox effect, relation to theory 2—33897
vector fields, dynamical characts., transform. props. 2—7660
velocity addition theorem, invariance of 4D-scalar product 2—30771
unified field theories
Bonnor's unified field theory, external field of nonstatic isolated system 2—14091
charge-to-mass ratio, conservation 2—17214
charged bodies, equations of motion determ. from Einstein-Maxwell field equations 2—37599
Einstein, empirical test based on nonconventional e.m. interaction 2—33914
Einstein's equations, static cylindrically symmetric solutions derived 2—66
Einstein's equations, static uniform line charge solution derived 2—65
Einstein-Maxwell equations, null e.m. radiation, exact solutions 2—37600
Einstein-Maxwell equations, soln. using null bundle transform. 2_7662
Einstein-Maxwell equations, soln. using null bundle transform. 2—11269
Einstein-Maxwell equations, solutions representing fields of spinning sources 2—11267
Einstein-Maxwell equations with many black holes, solutions 2—33912
Einstein-Maxwell field, models of static cylindrically symmetric solutions 2—20839
Einstein-Maxwell field equations, class of plane solutions 2—23254
e.m. fields in curved space-time invariant 2—7663
e.m. vacuum fields, stationary class 2—33913
isolated charged monopoles, nonexistence 2—20838
neutrinos in Rainich geometry 2—2115
Riemannian spaces admitting certain types of Killing's motion, geodesics 2—11270

Relativity continued
unified field theories continued
spinor theory, properties of photons, neutrinos, electrons and baryons 2–17215
time-symmetric electrodynamics, general relativity as source of difficulties 2–37601
Relaxation
see also Acoustic wave propagation. Dielectric phenomena; Elastic relaxation; Ferroelectric phenomena; Ferromagnetic relaxation; Molecules/relaxation; Nuclear magnetic resonance and relaxation; Paramagnetic resonance and relaxation; Spin-lattice relaxation
alkali halides, aqueous solutions ultrasonic absorption, kinetic model of structural relaxation processes 2–39361
anisotropic, in gaseous binary mixtures, of temp. differences, stresses and heat fluxes 2–39280
atomic multipole relaxation cross section calc. by matching method 2–5826
atoms, following optical pumping of ground and metastable states 2–35149
caprolactam and N-methyl derivative, solution in toluene, ultrasonic relaxation processes 2–12560
cathode beam in low temp. plasma, factors leading to accel. and decel. 2–8920
chemical, rel. to evaluation of micelle formation kinetics using two-state model 2–26324
chemically reacting fluids, internal relaxation 2–22857
clay soil, effects of water content on mechanical properties 2–37102
collisionless of ultrarelativistic electron beams in plasma 2–24696
dipole, weak and strong elec. fields 2–23420
effect on plasma wave echoes, electron and ion 2–21846
electron gas in afterglow plasma in mag. field 2–24689
ethanol, structural absorption of u.s. waves, study based on structural relaxation theory 2–25075
flexible macromolecule solutions, stress relaxation after shearing flow 2–24995
galactic disk systems, no Vlasov limit, application to structure 2–16958
gas, pressure pulse propagation, distortion, damping and dispersion 2–9015
gases, dilute diatomic, derivation of master eqn. for vibrational relaxation 2–9024
heredity theory, analytical relations between creep and relaxation functions 2–30842
n-hexoic acid, ultrasonic 2–39362
ionisation, and light absorption, on strong shock waves in H_2 2–21867
Knudsen's gas, temp. relaxation 2–18752
light scatt. in medium characterized by single relaxation process, temp. and internal parameter fluctuation effects 2–5422
metal fibre, porous, pressing and sintering, deformation, residual stress relaxation 2–29257
methanol 2–25075
photochromic glass, model, kinetic equations 2–3454
plasma, collisionless, of ion streams 2–24666
plasma, collisionless, thermodynamics of relaxation of temp. anisotropy 2–28504
plasma, of fast ions moving transverse to magnetic field 2–8925
plastic around strong inclusions rel. to primatic punching 2–22329
polycarbonate, glassy, optical and mechanical limits of linear relaxation behaviour 2–25495
polyether urethanes, and crystallization props, temp. behaviour 2–3482
polyhexadecyl acrylate, molecular mobility 2–3131
polyhexadecyl methacrylate, molecular mobility 2–3131
poly2-hydroxyethyl methacrylate, effect of low mol. wt compounds on relaxation behaviour 2–25514
polymer coating, role in application and drying 2–15668
polyoxymethylene, relaxation processes, internal friction, 4.2-300 K 2–6592
polystyrene, hot-stretched, activation energy for retraction 2–12878
polyvinyl stearate, molecular mobility 2–3131
pulsar slowdown rate, from calc. of electron velocity relaxation in rotating neutron superfluid 2–7491
reacting gas, rate constant as function of time 2–13563
resins under axial compression direct measurement method 2–29382
restrictions on isothermal relaxation functions in linear viscoelasticity 2–14219
solution, polyisobutylene in petroleum, stressed, deformed 2–28806
spin-1/2 probe system, rel. to time correlations of infintely large systems 2–5159
stars, collective, of two phase space density collisionless one dimensional self gravitating systems 2–10850
steel, structural, welded, heat treatment and residual stress 2–12944
stellar dynamics, collisional processes, gravitational polarization 2–16971
stellar dynamics, deflection of velocity vector of test star in stellar field 2–10847
stochastic Ising model, critical relaxation 2–14120
stress, and strain hardening effects on fatigue crack propagation 2–15876
stresses, temperature type in anisotropic cylinder 2–145
styrene methacrylic acid copolymer ionomers, stress relaxation investigation 2–25491
systems of two coupled equilibria 2–40798
thermal, in solids propagating thermoelastic waves 2–27215
velocity of micron sized particles in shock waves, det. by laser radiation 2–22010
water, structural absorption of u.s. waves, study based on structural relaxation theory 2–25075
Al grain boundaries, on neutron irradiation 2–22218
Ar, ionization behind leading edge of reflected shock wave 2–39198
CO_2-N_2-He, Michelson laser interferometer, phase modulated Q-factor, relaxation processes 2–17688
CO_2 TEA laser 2–37966
$COFe_2O_4$, spinel, relaxation of electrical conductivity 2–19533
Cs afterglow discharge plasma, excited states relaxation in presence of reabsorption 2–24355
H, and population inversion in decaying plasma 2–35496
He gas, n=3 states, collision relaxation by associative ionization 2–15251
He gas, n=3 states, collisional relaxation processes 2–18364
^{3}He polarized gas, relaxation on solid surfaces rel. to polarized nucl. bombardment target applic. 2–34762
^{199}Hg magnetic field dependence of spin relaxation rate 2–630
K, afterglow discharge plasma, excited states relaxation in presence of reabsorption 2–24355
Relaxation continued
KCl, γ-irradiated, stress obs., dislocation movement 2–9660
$MgFe_2O_4$, spinel, relaxation of electrical conductivity 2–19533
$MnFe_2O_4$, spinel, relaxation of electrical conductivity 2–19533
N_2O in laser, upper energy level relaxation 2–272
NaCl, γ-irradiated, stress obs., dislocation movement 2–9660
Rb atoms, polarized, in inert gases, exptl. evidence for Rb inert gas molecules 2–28224
Ti, of O interstitials, internal friction obs. 2–36020
TiO_2, e.s.r. and molecular adsorption, simultaneous investigation 2–10487
Xe laser oscillations, time behaviour and spectra 2–14421
$ZnFe_2O_4$, spinel, relaxation of electrical conductivity 2–19533
Remanence *see Magnetization state*
Renner effect *see Molecules*
Replica techniques *see Electron microscopy*
Reproduction *see Sound reproduction*
Resistance, electrical *see Conductivity, electrical*
Resistance thermometers *see Thermometers/resistance*
Resistivity *see Conductivity, electrical*
Resolving power, optics
see also Optical instrument testing
autocorrelation of wavefront in focus of homogeneous sphere 2–14435
cameras, high definition, calc. 2–23736
deflectors, resolution 2–14455
electron microscope, scanning, testing with specimens of precise dimensions 2–7859
electron-optic image tube, rel. to mag. flux density 2–2359
information content of simulated space photographs, function of image resolution 2–16937
photography, dependence of resolution on objective aperture 2–27665
X-ray image intensifier using channel plate, time and space resolution 2–20792
X-ray spectrometer with cooled Si(Li) detector, tested on 6.4 KeV line of ^{57}Co 2–20791
KH_2Po_4 electro-optic light deflectors 2–38078
Resonance, elementary particles *see Baryons/resonances; Hyperons/resonances; Mesons/resonances*
Resonance, magnetic *see Magnetic resonance and relaxation*
Resonance spectra *see Spectra*
Resonators
anisotropic laser cavity, magnetooptic mode splitting 2–31026
anisotropic optical, Jones matrix method for calc. of polarization eigenstates, review 2–27463
anisotropic optical travelling wave, polarization of normal oscillation modes 2–37950
astigmatically compensated cavities, CW dye lasers 2–21079
bar, designed to have specified end reactance in a certain frequency range 2–2230
cavities, filled with excited gases, optical props. 2–260
cavity, ferrite-filled, approximation technique calculation 2–30908
cavity for pulsed lasers 2–27461
circular, excitation of travelling wave regime 2–23430
confocal-laser, unstable, design criteria 2–34378
convex-concave, for TEM_{00} operation of solid-state ion lasers 2–37980
curved-junction injection laser, patent 2–11491
c.w. chemical laser, employing supersonic jet, cavity studies 2–23574
c.w. dye laser cavity, stable, efficient and damage resistant, review of designs 2–34376
c.w. laser cavity, pulsed Q-switching, output pulse intensity meas. 2–23571
diffraction grating as passive optical valve in laser 2–34375
diffractive laser, mode structure det. using iterative computer program 2–34379
energy guides, polyhedral, Nd glass, design and performance 2–27464
e.p.r. cavity resonator for 8 mm. band with sample changing at liquid He temperatures 2–34265
Fabry-Perot, infinite-strip, quasi-stationary wave patterns 2–2382
Fabry-Perot with smooth parallel mirrors, mode equation determination 2–17580
Fabry-Perot with smooth parallel mirrors, mode equation solution 2–17581
Fokker-Planck equation in detailed balance, solutions 2–27109
fundamental mode radiation, thermal lensing 2–17619
gas laser, coupled linear cavities, patent 2–11479
gas laser, stabilized by thermal compensation system 2–17585
Gunn oscillator cavity, ionizing radiation effects 2–22596
internally scanned lasers, cavity mode mixing effects 2–11459
Josephson weak-link junctions, cylindrical cavity modes 2–1499
laser, confocal spherical 2–27465
laser, emission focusing in spherical resonator 2–5352
laser, Nd-Glass, pulse duration by varying cavity length and dye transmission 2–34401
laser cavity, stabilization device, patent 2–34380
laser cavity characteristics, effect of inserted optical delay line 2–27502
laser ring resonators, diffraction grating coupled, high power type 2–21058
lasers, mode selection techniques 2–31028
l.f., design, from obs. of stepped bar vibrating transversely 2–17366
matching, influence on output power of YAG laser 2–17644
microwave refractometer having single cavity frequency and bandwidth stabilized, patent 2–216
mirror, open, with saturable gain medium, modal field distributions det. 2–5350
mode selection by linear polarizer with anisotropic metal film 2–21053
non-instantaneous inclusion, generation of monoimpulsive radiation 2–31048
nonlinear, second harmonic generation, pulse shortening, calc. 2–14402
open, compound mirror, obs. of losses and field patterns 2–34377
optical, det. of radiation temp. of plasma layer 2–35495
optical, picosecond stimulated Raman spectra pulse generation 2–34498
optical cavity, light modulation, obs. 2–38032
optical cavity, oscillations, interferometric stabilization 2–21059
optical parametric oscillator, focussing effect 2–23569
optical strength, dependence of breakdown threshold on purity of element 2–39365
optical with paraxial modes 2–23568
parametric pumping, method for studying magnetoelastic behaviour 2–25993

Resonators continued
piezo-semiconductor, damping suppression by drifting electron field 2—4287
polarization characteristics and losses of anisotropic laser resonators 2—21057
prism dispersion, of Nd laser, frequency tuning and extraction of second harmonic radiation 2—37988
quartz, thermally sensitive elements of frequency transducers 2—37826
quartz crystal, Na_2CO_3 process cultured, Q capability from i.r. absorption meas. 2—14301
saturable optical resonator, nonlinear characts. 2—31027
spherical for free laser generation in ruby, electro- optical smoothing of spatial inhomogeneities 2—21095
spherical mirror, self-collimation method of adjustment 2—21055
split confocal, applic. to near confocal optical scan amplifier 2—34527
stable and unstable cavities, pulsed N_2/CO_2 laser single mode operation 2—11470
superconducting, helically loaded, in proton accelerator 2—14853
superconducting cavity, TE_{011} mode, with high critical mag. and Q-value 2—25798
superconducting Mo test cavity, properties at 350 MHz 2—34866
system of 3-resonators in paramagnetic maser 2—34373
tilted mirror type, losses and amplitude distribution for oscillation 2—200
transition radiation in resonator with anisotropic medium 2—34240
unstable, influence of edge effects 2—27462
unstable, with large Fresnel no's., generation of single transverse mode in homogeneous active medium 2—27507
CO_2 laser, effect of output-coupling apertures on spatial coherence 2—11458
HCN, pulsed 337 μm laser, mode sweeping obs. 2—23590
InSb microwave resonators, plasma coupling 2—27347
Nb cavity, Q-value, X-band 2—4181
Nb superconducting cavity, resistance ratio meas. for material evaluation 2—25800
acoustic *see Acoustic resonators*
electromagnetic *see Electromagnetic oscillations*
Reverberation
see also Architectural acoustics; Echo
acoustic laboratories, at the Building Research Station 2—11359
acoustic waves, in statistical ocean 2—4657
analogue reverberation processor design 2—30875
in caves, meas. of reverberation times 2—27254
chamber, 100-4000 Hz, homogeneous sound field study 2—27238
chamber, stereophonic sound enhancement system, patent 2—20948
concert auditoria, subjective acoustic experience, results of questionnaire 2—17401
in concert halls, space-acoustic measurements 2—17403
decays, and sound pressure levels measurement using a rotating microphone system 2—2246
dimension ratios of rectangular rooms with good distribution of eigentones 2—17400
electroacoustic reproduction of perceived reverberation for quality judgements in architectural acoustics 2—20947
large rooms, Sabine reverberation time 2—34161
model room, diffusion and absorpt. of sound 2—34178
multipurpose hall, acoustical planning 2—34176
power emitted by small noise sources in reverberant rooms 2—37779
rooms in acoustical laboratories in Southampton England 2—172
scale-model room, comparison with actual room 2—34177
scattering and echo structure 2—34111
suppression using electroacoustic devices 2—5243
talks studios, permissible bass rise obs. 2—27232
time control by direct feedback 2—17392
Reviews
γ-ray astronomy 2—11160
acceleration of intense electron beams, collective ion acceleration model 2—34845
acoustic propagation in, and model of ocean 2—37109
acoustic signal processing 2—34127
acoustic wave diffraction theory 2—20931
active island arc characteristics 2—22935
active nondestructive assay techniques for nuclear materials 2—28159
adhesives, use for assembly of instruments or associated parts 2—19291
aeronautical acoustics, noise, units for nuisance measurement 2—17396
aerosol chemistry, development from colloid and surface chemistry, review 2—12588
alkali halide, ionic transport parameters 2—29745
alkali halide, ionic transport parameters 2—33051
analytic function theory review 2—29
anechoic and reverberant rooms at the Building Research Station 2—11359
antimatter, symmetric existence in universe 2—16951
Ap stars, magnetic 2—26668
Ap stars abundance anomalies 2—13891
archeomagnetic methods, history of geomagnetic field 2—13807
aspherical surfaces in optical instruments 2—34520
asteroid and meteor streams 2—41213
asteroids, physical parameters, interrelations with comets 2—41202
astronomical magnetic fields 2—26584
atmospheric humidity measuring techniques 2—1844
atmospheric metal ion chemistry, problems and laboratory data 2—4699
atomic spectroscopy in the last 20 years 2—2929
Auger electron spectroscopy 2—13598
Auger neutralization of singly-charged ions and de-excitation of excited atoms 2—22651
basalts, Apollo 11, petrogenesis and implications of lunar origin 2—23106
breeder reactors and advanced converters, international development 2—2843
bubble chambers, supersonic 2—31386
calibration of goniometric scales and instruments, certification of reference standards 2—23216
camera lens design at Kodak, history 2—14496
Canada's nuclear power program 2—5741
canonical quantization of gravitational field, status 2—2494
carbon fibre composites 2—1381
catadioptric imaging systems, meniscus aberration correctors, book 2—27626
ceramic, work of fracture determ. 2—39951
cerebral rhythms in waking EEG 2—2017
Reviews continued
chemical lasers, dynamics and operating characteristics 2—17584
chemical lasers 2—23578
chromatography, gas 2—4605
clay soil, rheological behaviour under dynamic loading 2—1298
colour photography with black-and-white film 2—336
colour vision mechanism 2—30707
cometary meteoroids 2—41212
cometary origins 2—1995
concrete containment structures in India, design and structural analysis 2—15097
contact discharges, spectroscopic study 2—3261
controlled thermonuclear fusion 2—28124
cosmic rays, primary, historical background, interactions, detection, spectra, origin and cosmological significance 2—8217
cosmic rays, solar modulation, long and short term variations 2—30411
cosmological theories 2—13826
CP violation 2—38214
crystals, vibrational modes and spectra, factor group analysis for known struct. 2—25645
c.w. dye laser cavity, stable, efficient and damage resistant, designs 2—34376
cyclotron 2—27929
data need for newer optical materials 2—34509
defects on magnetic insulators 2—40543
desorption, electron impact induced 2—39543
detector photocathode developments 2—40384
diffusion in thin films 2—39724
disordered systems, numerical studies of vibrational properties 2—36313
earthquakes and explosions discrimination, surface wave measurement 2—22924
elastic glass fibres, strength and treatments for enhancement 2—36263
electrodynamics of ionosphere and magnetosphere 2—20405
electron microscope design, applications and accessories 2—39609
electronic imaging devices in astronomy 2—17099
electrophotography 2—31158
elementary particle properties 2—34584
e.m. wave scintillation studies in ionosphere, atmosphere, interplanetary space, and communication problems 2—20358
e.m. waves in plasma 2—24710
energy and material, global exchange 2—4663
ESCA 2—40856
evoked retinal responses 2—5080
fault detection based on meas. of mechanical noise of deformation 2—29160
field theory, one dimensional space time 2—27692
films, magnetic, flux reversal 2—40503
flow meas. techniques, present state and latest developments 2—918
flux quantization theories 2—1488
focused ultrasound, for local treatment of biological tissue 2—30666
Forbush decreases in cosmic rays 2—26558
foveal colour vision responses, variations due to macular pigmentation 2—20757
free electron physics, optics, detection, spin, magnetic moment and relativistic behaviour, book 2—17831
frequency and time standards, atomic and molecular 2—30748
galactic cosmic ray intensity, effects of active solar regions 2—17081
gas-cooled fast breeding, nuclear reactors 2—38698
gas-cooled nuclear reactors 2—2852
geodetic techniques, using satellites 2—7204
geophysical prospecting, newly developing fields 2—4631
globular cluster stars, evolution and pulsation, comparison of theory and obs. 2—20583
gravitational collapse and event horizons 2—1929
gravitational wave formation 2—16946
great earthquakes, aftershock zones and seismicity gaps, earthquake prediction 2—22923
group III-V compound, e.p.r. 2—33334
Gum nebula 2—23066
hadron dynamics, medium energy, two-body and quasi-two-body reactions 2—38257
hadron e.m. interactions with colliding rings, investigation of parton and light cone contributions 2—38245
hadron inelastic interactions, limiting behaviour, diffraction and fragmentation 2—38256
hadron interactions, duality and symmetry rel. to low energy phenomenology 2—38263
hadron interactions, low energy phenomenology 2—38262
hadron multiparticle production exprts. on sealing, limiting fragmentation and factorization 2—21265
hadron spectroscopy, low energy 2—38261
hadron strong interactions, exptl. results at energies >10GeV 2—38265
hadron symmetries, broken chiral and scale invariance 2—38249
hadronic multiparticle, reactions of very high energies 2—34633
hadronic weak interactions, CP violation, review 2—38266
harmonic analysis, functions useful to geomagnetism 2—4749
heart disease, diagnosis, treatment, electronic tools 2—2032
heart rate measurement 2—23151
heat transfer, 1970 literature 2—5266
heat transfer, problems in the Seventies, area of application and type of mechanism 2—5267
heavy ion accelerators of the future 2—5604
heavy ion particle accelerators, design and research 2—34841
high polymers, thermal conductivity 2—29568
holographic applications 2—38024
holographic image deblurring methods and principles 2—23735
holographic interferometry 2—23656
holography, applications, areas for future development 2—38019
holography, conception, development and uses 2—290
holography, new techniques 2—23641
holography, physical basis 2—27544
holography, science and engineering uses 2—5391
holography and applications 2—21125
hot wire method of fluid thermal conductivity obs. theory 2—9126
hydrogel polymers, use in contact lens applications 2—11222
hydrologic data collection via geostationary satellite 2—16792
hydrophilic lenses 2—21144
image formation in quantitative microscopy, factors affecting 2—5406
IMFBR wire wrapped fuel assemblies, interchannel mixing 2—8406
induction plasma torches 2—39149

Reviews continued
industrial ultrasonics applications, current and future status 2—20937
initial F_2-layer frequencies variation with stratospheric circulation 2—33548
instruments for thermophysical investigations 2—37831
insulator, electron states, electronic polarization effect 2—40136
integrated optics 2—34540
interaction between atmosphere and ocean, fog, cloud and marine sediment formation 2—30288
interferometric testing of optical systems and components 2—34455
intergalactic matter and radiation and origin and evolution of universe 2—13834
intergalactic medium, X-ray observations, interpretations 2—26610
interstellar cloud chemical constituents 2—10918
interstellar molecules 2—26764
ion and neutral beam production, with energies <10 keV 2—7881
ion bombardment induced radiation damage in solids 2—15736
ion containment sources 2—34344
ion implanters 2—32545
ion injection techniques, for semicond. technology 2—32547
ion injector, for semicond. technology 2—32546
ion sources, design and assembly technology 2—7887
ion sources, high vacuum 2—5336
ion sources, new techniques for production of heavy highly charged 2—5625
ion sources, polarized Lamb shift 2—7894
ion sources and beams, state of development 2—27439
ion sources polarized, ground state atomic beam 2—7893
ion molecule reactions 2—24567
ionizing radiation effects on photomultipliers 2—21330
ionosphere, sky-wave backscatter 2—40999
ionosphere, sporadic E-region, formation mechanisms and hydromagnetics 2—4744
ionosphere D-region ion chemistry 2—16909
ionospheric changes which accompany geomag. storms 2—20409
ionospheric electron and ion temp. det., processes and mechanisms involved 2—20404
ionospheric movements, obs. by incoherent scatter 2—16902
ionospheric radiopropagation 2—26527
i.r. astronomy, emission from galactic and extra galactic sources 2—7469
i.r. lasers, tunable, applic. 2—17636
i.r. obs. of blue stars 2—20557
i.r. radiation from compact objects 2—13934
kaon decays, experimental data 2—21287
laboratory instruments, safety considerations in design and operation 2—30713
Lagrangians and finite field theories, major coupling constant specification in elementary particle interactions 2—27691
laser anemometers, operation and applications 2—3283
laser application, geodetic and industrial metrology 2—40873
laser dyes, flashlamp pumped 2—7926
laser gyro, construction and operation 2—41029
lasers, stimulated emission, historical development 2—23563
lasers and light scattering 2—310
LEED, crystal surface obs. 2—15650
lepton g factors 2—34604
leptonic and semi-leptonic weak interactions 2—23779
light water reactors 2—2851
linear proton accelerators, work carried out in USSR 2—14820
liquid crystals 2—15573
liquid metals and alloys density meas. 2—39344
liquid semiconductors electrophysical properties and chemical bond characteristics, fine arrangement, zone structure and Fermi surface det. 2—35784
loudness function, psychophysical correlates 2—27286
luminescence of rare earth activated solids 2—36923
luminescence petrography 2—1795
lunar seismology and other experiments left by Apollo missions 2—33729
magnetic fields in sunspots and active regions 2—11106
magnetopause, internal structure 2—16878
magnetosphere, e.l.f. and v.l.f. fluctuations, satellite observations 2—33507
magnetosphere plasma instability, theories 2—1887
magnetospheric plasma, sources, wave-particle interactions and acceleration mechanisms 2—20365
many-particle reactions, longitudinal phase space technique and inclusive reactions 2—38260
Martian and Venus research projects 2—7529
Martian atmosphere, data obtained by Mariner 4, 6 and 7 2—30566
mass flow meas. 2—12520
mass spectrometry, field-ionization type, surface applics. 2—38785
mass spectrometry 2—570
matter, unified theory, cosmological phenomena and microphysics 2—4768
measurement of time varying phenomena, book 2—5112
medical and industrial use of particle accelerators 2—14786
mesomorphic materials for electro-optical applications 2—32263
meson-meson scattering 2—14624
metal, refractory, dispersion hardening, review 2—32747
metal ion laser 2—34387
meteoritic complex in solar system 2—41214
meteors, NASA Faint Meteor Spectra Patrol 2—14004
MHD fluids, equilibrium and stability by dynamic techniques 2—15455
MHD power generation 2—232
microsound, assessment for signal processing 2—20939
microwave diagnostic techniques for semiconductor obs. 2—22555
microwave electron density measuring systems used in controlled fusion research 2—28592
microwave exposure, biological effects 2—30665
microwave propagation, tropospheric 2—20356
microwave radiation dangers for the human body 2—30664
mise-a-la-masse measurements, feasibility study 2—16759
molecular and atomic collision processes 2—35380
moon, Apollo 11, 12 and 14 data 2—1981
Mossbauer spectroscopy applications to chemical engineering 2—1666
multibeam holography characteristics, optimal recording parameters 2—2414
multicharged ion sources, production by electron-atom collisions 2—34331
musical acoustics, electro-acoustics 2—34096
N-body problem, numerical methods of integration and exprts. 2—14149

Reviews continued
negative ions, properties and reactions 2—21872
networks for particle identification according to shape of scintillation signals 2—31363
neutron activation analysis of semiconductors 2—16715
neutron diffraction examination of inorganic materials 2—29133
nitride and carbide nuclear fuels, for fast breeder reactors 2—28148
n.m.r. techniques 2—14350
non-destructive techniques for flaw size determination 2—32571
nuclear fast breeder reactors, development and experiences 2—2846
nuclear fission reactors, fuel utility and supply problems 2—2859
nuclear fission reactors, irradiation damage, problems of safety and economics 2—2844
nuclear fuel fabrication processes and costs 2—24277
nuclear fuel manufacture and development 2—2856
nuclear fuel materials, development 2—24279
nuclear fusion research in USSR, Tokamak systems 2—15018
nuclear physics, pure and applied research with 3 MeV Van de Graaff accelerator at Australian Inst. Nucl. Sci. 2—38426
nuclear physics studies using fast neutrons 2—491
nuclear power plant instrumentation, w.r.t. operation and design 2—21475
nuclear reactor noise analysis data extraction methods 2—31620
nuclear reactor noise analysis data extraction methods 2—24265
nuclear reactor pressurized water coolant system support structures, design 2—15053
nuclear reactors, fast breeder type 2—28125
nuclear shape determ., relation to concept of intrinsic state 2—38447
nuclear structure, study from weak and related processes 2—31410
nucleation kinetics 2—39592
oceanic volcanism 2—1810
optical design and aberrations, astigmatism 2—27015
optical fibre waveguides 2—38120
optical fibres, flexible light guides 2—2458
optical methods of studying upper atmosphere and space 2—7301
optical pumping 2—35149
optical surface waves, guidance, lateral wave phenomenon and image transmission 2—34471
optical systems for u.v. space researches 2—10781
optical tracking of satellites 2—7352
optoelectronics, development (1970-72) 2—34472
paleomagnetism of deep-sea cores from central Pacific 2—41018
particle accelerators, development of machines for yielding high resolution protons and deuterons at energies up to 40 MeV 2—38397
particle accelerators computer control 2—14888
phase holograms reconstructions, depth removal effect on exposure 2—7948
photoconductivity in organic crystals, advances since 1967 2—25961
photoelectric instruments for measurement of surface profile rectilinearity 2—38099
photoemissive effect and photocurrent in condensed media 2—19800
photographic emulsion, processing and cameras, review 2—38173
photometric measurement of illumination for buildings, open spaces, and highways 2—2438
photometric units and terminology, new British standard 2—34504
photometry, light distribution, state of development in Japan 2—7999
photometry, origin and history 2—5426
photometry, tasks, problems and organizations 2—5425
photon concept, short educational article 2—38222
photon detectors 2—38350
piezoelectric transducers, definitions relating to conversion losses 2—5238
planetary atmospheres, composition and structure, review 2—26829
planetary atmospheres, u.v. region studies, upper atmosphere examination by near fly by 2—11009
planetary mass determination 2—11001
planetary nebulae, internal motions and kinematics 2—23063
plasma, non-ideal, dense, thermodynamical, transport and optical props. 2—21768
plasma confinement in toroidal mag. fields, ion acceleration, charge exchange, ionization and fast ion trajectories 2—32021
plasma diagnostics, space potential obs. 2—15476
plasma e.m. instability theory 2—35572
plasma ion-acoustic and ionization waves comparisons of phenomenological props. and physical mechanisms 2—21847
plasma wave echoes, electron and ion, effect of relaxation 2—21846
plastic deformation in metals 2—39778
plastic lens cameras, development 2—17755
plastics development 2—18908
p.m. and coding techniques in telecommunications, large area photometry 2—14438
polar magnetic substorms 2—41012
pore size, porosity, meas. methods 2—36267
precession determination 2—10808
pressure meas. techniques, ionization gauges 2—41392
prestressed concrete containment structures, design procedures and test results 2—15164
problems in high energy physics 2—21207
proportional counters, multiwire chamber 2—34787
proton synchrotron, NAL, description and problems 2—14842
pulsars, rotational theories 2—30525
pulsars 2—23084
quantum frequency standards, status and development prospects 2—37561
quasar structure and evolution 2—17016
radiation damage processes in MgO and MgF_2 2—19076
radiation monitoring in nuclear power stations 2—38765
radio telescopes 2—2008
radio-astronomy, space instruments and techniques for frequencies down to 30 kHz 2—11167
radioactive waste disposal, management and handling 2—2858
radiological protection in SST aircraft 2—2894
radiosource counts and cosmology 2—13970
radiothermoluminescence and analysis of structure of polymers 2—37061
reflection and refraction, stress wave at plane boundary between anisotropic media 2—14250
refractometer calibration instabilities related to electrical characteristics of sensor 2—1882
refractory compounds, crystal growth 2—39576
Regge cut theories 2—38259
Regge cuts and related topics 2—38258
relief reproduction, photographic methods 2—27686

Reviews continued
remote sensing for use in mineral exploration 2—4625
resonance parameters of fissionable nuclei 2—8366
resonators, anisotropic optical, Jones matrix method for calc. of polarization eigenstates 2—27463
reverberation scattering and echo structure 2—34111
ruby, heavily doped, optical props. 2—36868
satellite instrumentation, high sensitivity survey for X- and γ-ray sources 2—10985
satellite oceanography 2—13650
satellites in heliocentric orbit, listing of all known to have entered solar orbit 2—13813
seismic data processing and analysis, computer developments 2—30163
semiconductivity in organic crystals, advances since 1967 2—25961
semiconductor, III-V and II-VI effective charge and piezoelec. effect 2—36596
semiconductor electron emitters with negative electron affinity 2—22652
semiconductors, charge state effects in displacement damage 2—19660
semiconductors, compound, for radiation detectors 2—27875
SI units, developments in changeover and modification to metric system 2—2052
cohesionless soil, rheological behaviour under dynamic loading 2—3886
solar cycle models and numerical studies 2—11124
solar energy concentration 2—34437
solar large scale magnetic field theories and magnetic activity cycle 2—11047
solar magnetic field measuring methods 2—11028
solar magnetic fields, large scale activity 2—4993
solar magnetic fields, small scale, theories 2—11037
solar magnetic fields, small scale structure 2—4992
solar magnetic fields in association with flares 2—11129
solar magnetic fields large scale and their consequences 2_11039
solar space research, techniques and discoveries 2—23123
solar system space research using cosmic rays as probes 2—4949
solar u.v., observational methods and results 2—11058
solid, theoretical strength 2—22277
solid solns., thermodynamic props. 2—29414
sonic boom generation theory and prediction methods 2—35667
sonic boom simulation, devices and techniques 2—34188
sonic booms, animal responses 2—37500
sonic booms, seismic and underwater responses 2—37087
space environment monitoring data, solar terrestrial relationships 2—16939
space station development 2—7355
space telemetry by satellite borne laser stations 2—26576
spectral distribution meas. of radiant energy, comparative study of methods 2—8028
spectroscopy, internal reflection i.r. 2—11531
spherical and deformed nuclei, shell correction approach to nuclear shell effects 2—34884
sporadic-E theory, recent developments in wind-shear theory, midlatitude E_s theory 2—37210
standards in photometry and spectroradiometry 2—7998
stars, parallaxes and proper motions 2—13888
stellar evolution theories 2—7419
stochastic processes, elements, review 2—86
storage rings, electron and positron, present state and future prospects 2—14860
strain gauges, resistance and piezoresistance 2—30663
submarine basalts, characteristic thermomagnetic curve 2—23042
sun, gamma-ray and neutron emissions 2—11090
superconducting ring accelerators 2—14855
superconducting synchrotron magnets 2—14846
superconductor, spin excitation effects 2—29623
superheavy elements, recent theoretical developments 2—21403
supernova remnants and their significance to astrophysics 2—7440
surface plasmon effects, expt. obs. 2—16119
surface wave electron interactions in solids 2—22416
surface waves, propagation, transduction and scattering, Rayleigh waves 2—20921
synchrotron, zero gradient, ion source program 2—8255
ternary fission, ^{235}U, thermal neutron induced 2—2822
thermodynamic pressure in quantum statistical mechanics 2—5163
thermonuclear fusion obtained by laser irradiation 2—2818
thermospheric solar tides 2—10742
thermospheric winds in F-region, equations of motion 2—10770
thunderbolts 2—20351
Titan III L, space booster 2—20433
Tokamaks, equilibrium, transport coeffs., stability design diagnostics and heating methods 2—35503
tornadoes, prediction from h.f. radio noise from thunderstorms 2—13705
transducer design and array configuration improvements for underwater generation and reception 2—34121
transition metal superconductors, exptl. survey 2—29641
transition metals, lattice dynamics 2—32814
transition metals and cpds., energy bands, review 2—29599
transplutonium elements, reserach status report 2—21347
two wavelength interferometric techniques 2—34490
ultrasonic applications in electrochemical processes 2—40818
ultrasonic B-scanning methods, for head and eye 2—20735
ultrasonic crystal filters, application to communications monolithic IC's 2—20938
ultrasonic nondestructive testing, development trends 2—2251
ultrasonic time position and B-scanning of heart 2—17117
ultrasonic transducers 2—23359
underwater acoustic noise, radiated ambient and self noise, identification generation and measurement 2—37110
underwater acoustics past 20 years 2—37108
underwater sound propagation 2—34103
u.v. intensity calibration in spectral range 10-4000 Å 2—8024
vacuum technology, use of graphite in high and ultrahigh vacuum 2—5102
variable rotation of Earth, work of R.T.A. Innes 2—7519
Venus, atmosphere 2—26854
viscous dissipation and effects on viscosity obs. by capillary rheometers 2—21754
water flow at base of glacier or ice sheet, general theory 2—40901
wave drag, reduction by antisymmetric arrangement of wings and bodies 2—35657
weak interaction theory, Cabibbo, nonleptonic, leptonic and semileptonic interactions 2—21220

Reviews continued
weak interactions, experimental problems and prospects 2—21221
weak interactions, progress and problems in exptl. investigations 2—38216
welding, temporary strength of metals during solidification 2—15916
X-ray analysis, electron microscopy and electron probe anal., computer applications 2—25282
X-ray astronomy instruments, satellites and focusing X-ray telescopes 2—10979
X-ray powder diffractometry, automatic 2—15707
X-ray sources, discrete and diffuse, identification with known astronomical objects 2—10978
X-ray structural analysis equipment 2—19022
Zircaloy, fuel claddings and pressure tubes in water cooled reactors 2—18257
e^+e^- colliding beams, theoretical aspects 2—38242
NN interactions, energies below 1GeV/c, recent developments 2—38314
YN interactions, recent developments 2—38329
^{13}C n.m.r. spectroscopy, chemical applic. and instrumentation 2—27375
Cs III atomic time scales, construction techniques and improvement suggestion 2—5118
Fe-base superalloys, microstruct. and mech. props. 2—29437
GaAs, etching 2—32338
GaAs, etching fluids 2—32339
GaS, GaP semiconductor characterization by photoluminescence and optical absorption 2—16641
He, liquid, fundamental properties 2—1127
Hg chalcogenides fundamental features of energy band structure 2—4121
$Hg_{1-x}Cd_xTe$ epitaxial growth, for i.r. detectors 2—17412
$Na+H_2O$ reaction, research rel. to nuclear reactor applic. 2—40801
^{210}Po in troposphere, origin from ^{210}Pb in atmosphere 2—37134
Se, general properties and applications 2—19615
Si surface transport properties 2—36547
U isotope enrichment for nuclear fission reactors, present trends and techniques 2—3010
Zr-25%Nb fuel claddings and pressure tubes in water cooled reactors 2—18257

Reynolds number *see Flow; Hydrodynamics*

Rhenium
adsorption of CO and O_2, LEED structures, 293-1193 k 2—39563
chemisorption of O_2, mol. beam obs. of adsorbed layer 2—35919
electrical and thermal conductivity, temp. depend. 2—29618
h.c.p., point defect prod. on irrad., recovery 2—15745
LEED pattern, (0001) surface, C effects 2—29004
optical coating, characterization in 500-2000 Å region, extreme u.v. reflectance spectrum 2—17719
quadrupole splitting of 6.2 keV γ rays of ^{181}Ta in Re metal 2—36838
recovery after fast particle irrad. and cold work 2—15744
solubility of N_2, 2000-2700°C, 200-600 torr 2—32734
surface microstruct., scanning electron microscope obs. 2—39464
Ni:Re, hyperfine field at ^{187}Re nuclei, time differential perturbed angular correl. obs. 2—36798
W-Re thermocouple, for oxidizing media at v. high temps. 2—27336

Rhenium compounds
VR-20 alloys, electrical resistivity 1200 to 2800°K 2—13114
Cu-Re dilute alloy, magnetoelastic props. 2—13416
Fe-Re dilute alloy, hyperfine field at Fe atoms, temp. depend. 2—16436
K_2ReCl_6, irradiated, mag. susceptibility and structure modifications 2—4344
Mo-Re alloys, supercond., u.s. attenuation, energy gap anisotropy 2—16180
Mo-Re dil. alloys, elastic consts. 2—29234
Mo-(35 at. %)Re alloy, slip patterns and deform. twins correl. 2—15765
$NaReO_4$, irradiated, mag. susceptibility and structure modifications 2—4344
Nb-C-Re system, intermetallic cpd. structs. 2—36304
Re-Mo-C alloy, C distrib. and diffusional mobility 2—36052
$Re-Mo_2C$ solid solution, comp. depend. of supercond. crit. temp. 2—22498
Re-Th alloy, elec. and thermal cond., temp. depend. 2—29618
Re-V, alloy, dilate, mag. susceptibility, Knight shift 2—19836
Re-W, alloy, thermocouple, reactor rad. influence on thermo-e.m.f. 2—16305
ReC_x, high press. synthesis, struct., superconductivity 2—19057
ReF_6, $^2E_{5/2g} \leftarrow {}^2E_{3/2g}$ transition, Jahn-Teller effects 2—3060
ReF_6, i.r. spectra, Jahn Teller vibrations, zeta const. 2—31825
ReF_6, multiple intramolec. scattering effects on electron diffraction patterns 2—38937
ReO_3, de Haas-van Alphen effect, Fermi surface obs. 2—4149
ReO_3, Fermi surface, press. derivatives 2—13090
ReO_3, positron lifetime correlations 2—4150
ReO_3, valence band structure, X-ray photoemission spectroscopy 2—36639
ReO_3^-, ReO_4^- ion source, using thermionic emission and hot cathode arc discharges 2—23551
ReO_4^-, SCCC-MO calc. 2—18474
ReO_4^-, vibr. spectra, r.m.s. amplitude 2—3064
$Re_{1||x}O_3$, nonstoichiometric phase in high press. Re-O system, characterization 2—25346
$ReO_3^-+Cl_2$, rate const. meas. in drift tube/mass spectrometer apparatus 2—10613
$ReO_3^-+NO_2$, rate const. meas. in drift tube/mass spectrometer apparatus 2—10613
ReS_4^-, SCCC-MO calc. 2—18474
W-Re alloy, annealed, plastic deformation, electronic struct., positron annihilation 2—22483
W-Re alloy, diffusion of ^{14}C, carbide layer source, temp. range 1500-1800°C 2—9629
W-Re alloy, elec. resist. and Hall effect, conc. depend. 2—36447
W-Re alloys, phys. props., thermocouple 2—1290
W-Re alloys, self-diffusion, 1935-2500°C 2—36086
W-Re solid solution, Hall coeff. and resist., rel. to struct. 2—39944

Rheology
see also Plasticity; Viscoelasticity
biorheology, apparatus for producing mechanical step pulses 2—33779
blood, conference (Heidelberg 1969) 2—14032
buckling of roof shell models with free edges under pressure 2—127
chlorinated polyvinyl chloride, capillary flow, melt fracture 2—15548
clay soil, effects of water content on mechanical behaviour, creep and relaxation tests 2—37102
clay soil behaviour under dynamic loading 2—1298

Rheology continued
- Cosserat medium, principle of virtual work 2—34015
- cumulative fatigue damage under stress controlled conditions 2—36154
- curvilinear laminated composites, continuum model 2—23323
- Earth, tectonically significant layers obs. using seismic wave data 2—30212
- fluid saturated porous solid, wave propagation effects 2—22261
- hereditary media, linear theory 2—33987
- heredity theory, analytical relations between creep and relaxation functions 2—30842
- mechanical hysteresis-determ. using Boltzmann superposition principle 2—37689
- memory effects and internal changes of a material 2—27141
- polyethylene, high pressures 2—15857
- polymers, integral constitutive eqn. and rate dependent relaxation spectrum 2—34014
- polymers, linear, at temp. above glass transition region and melting point 2—15855
- polymers, molecular theories 2—15856
- polymethylmethacrylate in diethylphthalate under constant stress and shear, transient and steady state data 2—34017
- Prandtl-Reuss materials, generalized, equation for finite deformation 2—17339
- quasi-linear M/V model of solid, rheological props. 2—2193
- rheological material, internal struct. changes, gradient theory, thermodynamic theory 2—20901
- rheological materials with internal changes, gradient theory 2—5178
- rheometer, concentric cylindrical design for high pressure applic. 2—24990
- rheometer comparison, for evaluation of fluids exhibiting drag reducing properties 2—28478
- rheometer designs for elastico-viscous liquid 2—3344
- snow behaviour under stress conditions 2—33426
- cohesionless soil behaviour under dynamic loading 2—3886
- spherical shell, loss of stability, external press effects 2—30843
- stress overshoot, elasticity breakdown, stress relaxation and elastic recoil 2—14162
- suspension, shear stress, rel. to velocity gradient, Casson equation 2—15614
- torsional moment impedance of infinite plate 2—27148

Rhodium
- atoms, imaging with high resolution electron microscope 2—9404
- electrical resist. anomaly due to dil. mag. impurities 2—25770
- e.s.r., hyperfine splitting of Dy and Er localized moments 2—10520
- film, discontinuous, on dielec. substrate, electron cond., resist. coeff., 130-300K 2—40180
- lattice parameters, −189 to 1709°C, solid equation of state 2—19304
- optical coating, characterization in 500-2000 Å region, extreme u.v. reflectance spectrum 2—17719
- photoemission, band struct. 2—25736
- positron annihilation radiation, angular correl., calc. 2—36433
- thermal cond., high temp., Lain-Krishnan method 2—13059
- thermal conductivity at liquid helium temperatures and in magnetic fields 2—4082
- thermoelectric power meas., 4-300K 2—4290
- X-ray spectra, relations between L_{III} absorp. limit and $L\beta_{2,15}$ lines 2—26206
- Pt-10%Rh/Pt and Pt-13%Rh/Pt thermocouples, reference tables 2—37830
- Rh/Fe-Ni, plated alloy, lattice parameters during heat treatment 2—9471

Rhodium compounds
- carbides, ordered phase form. in Ln-Rh-C and actinide-Rh-C systems 2—29493
- 1,5-cyclooctadiene complexes, i.r. and Raman spectra, frequency dependence on metallic ion 2—15332
- rare earth alloys, Ln_3Rh, Ln_7Rh_3 and $LnRh_3$ phases, cryst. struct. 2—22161
- Cu-Rh dilute alloy, magnetoelastic props. 2—13416
- Fe-Rh alloys, model of antiferromag.-ferromag. transition 2—29836
- Fe-Rh dilute alloy, hyperfine field at Fe atoms, temp. depend. 2—16436
- Fe-Rh dilute alloy, spin-lattice relax. time 2—19932
- FeRh, ferro-antiferromag. transition, electron entropy contrib., positron annihilation obs. 2—16372
- FeRh alloy, ordered, diffuse scatt. of neutrons, mag. moment obs. 2—10247
- FeRhIr alloy, magnetic transitions, pressure dependence 2—4374
- Mo-Rh alloys, spin fluctuation effects on supercond. 2—19600
- Ni-Rh alloy, low temp. heat capacity anomaly, superparamag. behaviour 2—13045
- Ni-Rh alloys, elec. resist., giant mag. polarization clouds 2—22493
- Ni-Rh alloys, giant moments 2—40486
- Pd-Rh dil. alloys, resist. minima 2—16147
- Pt-Rh-Zr alloys, internal oxidation and hardness 2—4591
- PtP, upper limit of dissoc. energy 2—5948
- Rh-Fe(Mn) dil. alloys, J_{sd} values determ. from n.m.r. linewidth obs. 2—10563
- Rh-Ir solid solution alloys, shape of field ion image points, halo effect 2—12963
- Rh-Mn-Sb alloy, cryst. struct., mag. props. 2—22160
- Rh-Mn dil. alloys, mag. susceptibility and low temp. sp. ht. 2—19827
- Rh-V, alloy, dilate, mag. susceptibility, Knight shift 2—19836
- Rh-0.5 wt.%Fe alloy, resist., localized spin fluctuations 2—6763
- Rh complexes, Rh phthalocyanine, relaxation mechanisms from excited singlet states, spin-orbit coupling effects 2—35279
- Rh_7B_3 and $RhB_{1.1}$, resist. and thermal e.m.f. extrema 2—1404
- $Rh_4(CO)_{12}$, i.r. spectra, derivation of stretching frequencies, interatomic forces and bonds 2—38900
- Rh(III) complex, NN′-dialkyldithiocarbamates, anomalous p.m.r. spectra, hindered rotation about C-N bond 2—21595
- Rh(III) complexes, luminesc., emission lifetimes, quantum yields 2—26223
- Rh(III) complexes, trigonal MS_6 type, MCD spectra 2—12161
- Rh_7Mg_{44}, crystal structure determ. by X-ray diffraction 2—29151
- Rh_2MnAl alloy, cryst. struct., mag. props. 2—22160
- RhP, identification and dissoc. energy 2—5948
- $Rh_{.60}Pd_{.40}$ alloy, electronic structure studied by ESCA and X-ray spectroscopy, comparison with spectra of pure metals 2—32884
- RhT, T=Tb, Dy, Ho, Er, mag. props. compared with crystal field calc. 2—19884
- RhTi(Mn)Si, RhZr(Nb)Ge, cryst. chemistry 2—9349
- RhTiSi, RhMnSi, RhZrGe, RhNbGe, struct. relns. 2—18969
- Ru-Rh alloys, spin fluctuations effects on supercond. 2—19600
- ThRhIn(Sn,Sb), atomic struct., Debye-Scherrer determ. 2—3736

Riemann-Cristoffel tensors *see Relativity; Tensors*

Righi-Leduc effect *see Magnetothermal effects*

Ring currents *see Atmosphere; Ionosphere*

Riometers *see Ionosphere measuring apparatus*

Rochelle salt
- ammonium salt, ferroelectric phase superstructure 2—10119
- dielectric const. and relax. time 2—16293
- permittivity, contrib. of domain wall motion 2—36575
- phase transitions, local field model, role of Lorentz factors rel. to ferroelec. phase 2—25931

Rock magnetism
- Aegean deep sea core 2—26565
- anisotropy, numerical evaluation of uncertainties in experimental measurements 2—37228
- Antarctica, secular variation of declination from 1774 to 1965 2—33556
- archeomagnetic methods, history of geomagnetic field 2—13807
- Atlantic Ocean, mid-oceanic ridge samples, magnetic susceptibility and natural remanent magnetization 2—26566
- Aubepin clays, NRM analysis 2—16930
- Baffin Island, n.r.m. of lower teriary lavas 2—26559
- basalt, effect of neutron irradiation on saturation remanence 2—1912
- basalts, evidence for normal geomagnetic field polarity event at 263 m.y. BP 2—7346
- basalts, oxidized, remanent magnetization, geophysical interpretation 2—1907
- basalts, petrology rel. to mag. props. 2—1906
- basement rocks, magnetometer spectral determination of depth 2—13625
- Bergell granite, remanent 2—1914
- chronostratigraphy, miopliocene volcanic rocks 2—16765
- rel. to continental drift and other geophysical phenomena 2—33414
- Coronation Sills, thermal and magnetic cleaning, pole positions calc. 2—26561
- dolerites, Permo-Triassic and Precambrian, in Suriname 2—4755
- extinct volcano, anomalous weak field during Matuyama reversed epoch 2—16934
- ferrimagnetic minerals, obs. using resonance of spin precession of electrons causing ferromagnetism 2—1908
- flux magnetometers applications 2—23510
- fossils, origin of solar system 2—41019
- Gauss-Matuyama paleomagnetic transition and volcanic formation of Escandorgue Range 2—33559
- Georgian SSR, inclination and declination over past 2500 years 2—26547
- Grenville Front origin det. 2—37227
- igneous, natural remanent magnetization 2—1915
- impact breccias, origin of magnetization 2—1913
- Iran, archeomagnetic dating of baked earths 2—33563
- isothermal residual magnetization and coercive force, effect of high pressure and temp. on changes 2—33561
- Jurassic Chon Aike formation, NRM and reversed remanence 2—26564
- Labrador coast, igneous rock units, pole position calc. 2—26562
- Laschamp polarity event, evidence against occurrence 13300-30400 years ago 2—13803
- lavas, intensity of geomag. field in geological time, pleistocene and pliocene data 2—16933
- lunar samples, remanence 2—13979
- maghemitization, magnetic processes in oceanic ridge 2—13802
- magnetic remanence and radiometric dating in Jurassic intrusions 2—13804
- magnetometers, astatic, using negative feedback 2—26560
- mapping by high sensitivity airborne magnetometers, tectonics of sediments 2—33560
- oceanic crust, record of geomag. polarity events, binary model for anomalies 2—1905
- ophiolites, thermomag. props., Curie temp. 2—1916
- Pacific, West-central, deep-sea sediments 2—23041
- palaeomagnetism of Indian rock, rel. to continental drift 2—33558
- paleomagnetic properties of Middle-Upper Devonian Volcanics of Orkney Islands 2—37226
- paleomagnetism of deep-sea cores from central Pacific, review 2—41018
- Phanerozoic geomagnetic reversals, maximum entropy power spectrum method 2—20420
- polar movement, Great Logan Loop, Canadian shield rocks during Neohelikian era 2—7350
- polarity of miopliocene volcanic rocks 2—16765
- polarity reversals in volcanic samples 2—26563
- red beds, device for chemical demagnetization 2—1911
- remanent, viscous, A.F. demagnetization 2—1909
- remanent magnetisation in lake sediments, variation in direction of horizontal component 2—7351
- remanent magnetisation measurements, slow spinner magnetometer with digital computer 2—13805
- Rochechouart impact structure, paleomagnetic age determination 2—37229
- seamount magnetism, average direction of magnetization by Backus' method 2—13800
- Sierra Leone, Freetown Igneous Complex, age estimation combined with K/A radiometric evidence 2—16931
- Southern Africa and North America, Precambrian drift from pole paths 2—33562
- spherical analysis, from measured declination nondipole component 2—13806
- stable magnetic remanence of recent sediments, anal. for det. of geomag. secular variations 2—26544
- stratigraphy and nomenclature for geological time 2—20429
- strongly oxidised rocks, palaeomagnetism 2—1910
- submarine basalts, characteristic thermomagnetic curve 2—23042
- testing unit vectors for correlation 2—23043
- thermal demagnetization, progessive method, electrically heated furnace 2—4756
- thermoremanent magnetization, effect of thermal fluctuations during a.c. field treatment 2—30380
- titanomaghemite, saturation magnetization reversal on heating 2—16932
- titanomagnetites, exchange anisotropy 2—41017
- Fe_2O_3-α-$Fe(OH)_3$ temperature phase transition, structural obs. over entire temp. range, formation of chemical remanent magnetization 2—29468
- $Mg_2Fe_2TiO_4$, self reversal due to interaction with Fe_3O_4 2—30381

Rockets
- Aerobee, solar spectrum 2100 to 3200 Å 2—33758
- burning of solid fuel in hybrid engine 2—7168

Rockets continued
- elastic launch vehicles, separated flow, dynamic effects 2—26568
- flight, meas. of ram effect and ion density calc. in ionosphere 2—4760
- frequency shift in air coupled surface waves originated by rocket launches 2—16738
- generation and propagation of shock waves from Apollo rockets at orbital altitudes 2—37178
- guidance system figure-of-merit, saving in mid-course correction velocity 2—20437
- infrasonic signal propagation, launch and re-entry of Saturn V 2—37177
- ionosphere, E-region, measurements of horizontal winds at night 2—4736
- ionosphere, sporadic and night-time E-region, observations of upper layers 2—4735
- ionosphere, sporadic E layers, observations of structure and size 2—4734
- ionosphere, sporadic E-region, altitude profile of the vertical wind, measurement by rocket trails 2—4737
- ionosphere, sporadic E-region, measurement of horizontal wind profiles, energy dissiptation 2—4738
- ionosphere, sporadic E-region, measurement of wind shear and electron density 2—4727
- ionosphere, sporadic E-region, vapour trail rocket experiments to determine wind profiles 2—4733
- ionosphere, sporadic E-region, vector magnetometer measurements of ionospheric currents 2—4739
- Japan Antarctic Research Expedition ionospheric plasma probes 2—10761
- launching system programme for European satellite 2—4757
- low thrust, minimum-fuel orbital transfers 2—13810
- motors, low-cost moulded plastic sounding 2—20436
- multistage booster, powered flight performance computer program 2—13812
- orbital dynamics, motion in gravitational field of mass point, separable KS-variables 2—20434
- retrorocket exhaust effect on subsonic drag of 120° conc. 2—16940
- Saturn, singular optimal guidance problem, switching conditions and synthesis technique 2—20435
- solid motor thrust vector control, omnidirectional flexible seals 2—13811
- sondes, history of French rockets 2—41023
- spinning missile, gravity induced angular motion 2—26569
- obs. of sporadic E layers in midlatitudes, probe, propagation experiments 2—37219
- thermosphere measurements with mass spectrometer 2—40976
- thrust, math. derivation of optimum exit pressure condition 2—30382
- Titan III L, space booster 2—20433
- transfer trajectories, minimum impulse, specified transfer time 2—30395
- X-ray flux meas., Norma X-2, Cetus X-2 at 2 to 10 keV 2—10977
- N_2^+ u.v. auroral emissions, spectrographic recordings from rocket 2—30327

Rolling *see Forming processes*

Rotating bodies
- *see also Angular velocity measurement; Centrifuges; Earth/rotation; Gyroscopes*
- artificial satellites, periodic solutions of slowly spinning gravity gradient system, motion in circular and elliptic orbits 2—41028
- asymmetric, motion in rotating liquid 2—6168
- automobile wheels, static vs spin balancing 2—17279
- autorotation of flat plate about spanwise axis, unsteady lift, drag, angular acceleration meas. 2—9020
- bearing geometry effects on low-speed torque ripple 2—5176
- compact objects, energy conversion by rotation of massive objects with magnetic fields 2—13941
- cylinders and spheres, scattering of sound waves 2—14266
- disc, causing turbulent gas flow 2—3292
- discrete, continuous, boundary value problems solns. 2—20884
- discs, free and enclosed, resistance to station at high Reynolds number, calc. of fluid-induced torque 2—35703
- discs, stress analysis of compounded discs 2—7743
- discs in liquid metal in magnetic field 2—943
- disk, asymptotic solution 2—34031
- fluid annulus, hydromagnetic stability 2—31927
- freely spinning gyrostat satellites with energy dissipation, equations of motion 2—30383
- Lense-Thirring type gravitational forces between spinning cylinders and disks 2—5136
- liquid planets, third order approx. equilibrium figure, homogeneous model 2—26393
- magnetized, equatorial satellite in geomagnetic field, permanent rotations 2—37233
- main sequence stars, angular momentum variations 2—20520
- motion of rigid body, Weierstrass p-function, half-periods evaluation 2—117
- motion of rigid body, Weierstrass p-function 2—116
- neutron stars, stability and radial pulsations 2—33656
- neutron stars and white dwarfs, quasiradial pulsations in Newton's theory of gravity, central density 2—33657
- planetary ellipsoids, MHD of liquids, exact solutions of equations 2—13889
- polytropes, supermassive, magnetic, structure and evolution 2—13815
- relativistic ring, disk problem 2—11260
- shaft, symmetrical, vibration frequencies using 'Timoshenko beam' theory 2—151
- shaft self oscillations, lubricant effect 2—17292
- spin up, hydromagnetic, of fluid confined by two flat electrically conducting boundaries 2—8902
- spin-up of stratified fluid, theory and experiment 2—8885
- stationary rotating relativistic star, magnetic field generation 2—37282
- steady and oscillating blunt bodies, theory of supersonic flow 2—28687
- stellar collapse of a rotating star, instability and separation of small mass envelope, relativistic effects 2—33580
- tuning forks as inertial sensors 2—5175

Rotation, molecular *see Molecules/rotation*

Rotatory power, dispersion *see Optical rotation*

RS coupling *see Atoms; Spectra/atoms*

Rubber
- adhesion, with cord, fatigue characteristics 2—29459
- butyl rubber, additive effects on dielectric properties 2—22609
- for car tyres, thermic aging resistance obs. 2—1430
- chemical structure changes during ionization ageing 2—37041

Rubber continued
- chloroprene caoutchouk, thin films, formation of structures in presence of constant magnetic field 2—25166
- creep and tensile properties, effects of cross linking by dicumyl peroxide 2—25508
- crosslinked by S, viscoelastic meas. of width and time position of retardation spectrum 2—9635
- elasticity, statistical mechanics, applic. of modified description for systems with internal constraints 2—7699
- elastomeric materials, internal strain meas. using radioactive implants 2—19226
- elastomers, stress relaxation rel. to molecular struct. 2—25487
- fracture mechanics, bond rupture, e.s.r. obs., ozone effect 2—15886
- mechanical props., dynamic, rel. to mol. packing 2—3840
- perbunan, dielectric props., temp. dependence in microwave region 2—25915
- p.m.r. line narrowing due to rot. 2—13557
- RTV-60 silicone in two- and three-phase heterogeneous mixtures with Al, Pb, Ni, Bi, meas. of thermal conductivity 2—22432
- stretched, fibrillar to lamellar morphology transformation 2—9230
- styrene-butadiene, unfilled vlucanizate, simple tension, fracture 2—15885
- Viton A-HV vulcanizates, effect of crosslink density on time-temp. dependence of tensile properties 2—25512
- Young's modulus determ. from indentation of sheets by spherically tipped indentors 2—22256

Rubidium
- adsorption on Mo, Auger electron spectroscopy 2—12684
- atom, collisions with alkali metal ions, charge transfer cross sections 2—2981
- atom, in Ar buffer gas, cross-section for spin depolarization, indirect optical pumping 2—664
- atom, nonrelativistic wave functions and eigenvalues 2—18317
- atom, Penning ionization in slow collisions with Ar 2—11982
- atom, photoionization cross section and spin orientation of ejected electrons 2—31677
- atom, principal series oscillator strengths and ground state photoionization cross sections 2—31679
- atom, spin-orbit perturbation in P-state continuum 2—24362
- atom, two-photon excitation, transitions, scattering mechanisms 2—15224
- atoms, collision with I_2, cross section meas., comparison with harpooning model predictions 2—686
- atoms, collisions with O atoms, charge exchange cross section, theoret. study 2—691
- atoms, electron beam scatt., polarization 2—28209
- atoms, polarized, relaxation in inert gases, exptl. evidence for Rb inert gas molcules 2—28224
- atoms, relativistic HFS calcs. of electronic levels and equation of state for arbitrary temp. and matter density 2—28185
- atoms, self-induced transparency 2—31671
- diffusion in CsI, temp. depend. 2—22247
- excited atoms colliding with inert gas atoms, theory of fine structure transitions 2—21535
- film, thermal cond., calc. from elec. cond. 2—29567
- gas phase, fornidden p.m.r. transitions 2—35169
- Hall effect meas. in solid and liquid state 2—16137
- liquid, interionic potential calc. 2—21955
- liquid, temperature dependence of resistivity evaluated using a model potential in the Ziman formula 2—3405
- nuclear spin-lattice relax. times, many-electron enhancement effects 2—16660
- optical props., band struct. 2—26149
- photoemission from core states 2—4118
- saturated vapour pressure, 707 to 1541°K 2—12622
- solid and liquid, optical constants meas. in 0.3-2.4 μ wavelength region, temperature dependence 2—16417
- vapour, 4-photon parametric processes following excitation by 2 lasers 2—606
- vapour, phase-matched, third harmonic generation 2—9037
- vapour, selective two step photoionization using laser radiation 2—21524
- vapour, two-photon ionization by ruby laser beam 2—6106
- work function and surface structure, calc. 2—39455
- CsCl:Rb, i.r. lattice absorpt., breathing shell model 2—36875
- $CsI:Rb^+$, impurity-induced i.r. absorpt., lattice dynamical calc. 2—40661
- Rb-He, cross section for spin relaxation in ground state calc. 2—8457
- Rb-Rb collisions, thermal energies, spin dependence of total cross section 2—12016
- Rb-Sr ages on density and size fractions of Apollo 11 fine soil sample 2—13988
- Rb-Sr technique, Apollo sample 15555 dating 2—41180
- Rb-Xe vapour, third harmonic generation 1.06 μ radiation 2—6161
- Rb II resonance-line spectrum in the vacuum u.v. 2—18312
- Rb thin films, excitation by light, properties of volume and surface plasma oscillations 2—16472
- Rb^+, in $KCl:NO_2$, effect on low temp. spectra 2—16492
- Rb_2, molecular vapour, opt. pumping and mol. dissociation under laser pulse irrad. 2—24485
- $RbTaGe_3O_9$, $RbNbGe_3O_9$, $Rb(Ta_{1-x}Nb_x)Ge_3O_9$, $RbTa(Ge_{3-y}Si_y)O_9$, atomic points 2—25334
- ^{85}Rb, D_2 optical pumping, nuclear decoupling in collisional relaxation 2—35172
- ^{85}Rb maser, frequency standard, pumping light and buffer gas frequency shifts 2—27449
- ^{87}Rb, D_2 optical pumping, nuclear decoupling in collisional relaxation 2—35172
- ^{87}Rb, hyperfine shift, clock transition 2—18319
- ^{87}Rb, modulated fine and hyperfine components of absorbed light beams 2—8458
- ^{87}Rb, r.f. field induced mag. relax. 2—18318
- $Rb^+ + Ar \rightarrow K^{+*} + Ar$, collisions, threshold behaviour o excited cross section of RbII resonance line 2—2951

Rubidium compounds
- chloranilates, hydrated, crystal data, X-ray diffr. 2—19062
- halides, core exciton decay, photoemission obs. 2—19802
- halides, elastic consts., temp. depend. 2—29231
- halides, extreme u.v. spectral obs. 2—20042
- halides, lattice dynamics 2—25666
- halides, off-centre potential of Cu^+ and Ag^+ defects, uniaxial stress effects 2—20020
- halides, with O^{2-} at vacancies, dielectric loss measurements 2—6484
- Na-Rb alloys, liquid, electrotransport obs. 2—25104

Rubidium compounds continued
Rb-Cs alloys, liq., nucl. spin-lattice relax. 2—18855
$RbAg_4I_5$, press. effects, elec. resist., press. to 100 kbar, 293-453K 2—36285
$RbAg_4I_5$, single crystal growth and crystal struct. 2—12698
$RbBr:Pb^{2+}$, C-band peak position determ. using extended Mollwo-Ivey reln. 2—29197
RbBr/XBr fused mixture, (X=Li,Na), u.s. velocity and compressibility 2—25077
RbBr, low temp. sp. ht. 2—25685
$RbBrO_3$, n.q.r. of ^{85}Rb and ^{87}Rb 2—40790
$RbCl:OH^-$, complex dielectric susceptibility, paraelectric relaxation, isotope effects 2—10116
RbCl:RbOH, thermal cond., continuum of tunnelling levels 2—19446
RbCl/XCl fused mixture, (X=K,Li,Cs), u.s. velocity and compressibility 2—25077
RbCl, containing F-centres, raman scatt., 80K 2—22789
RbCl, far-u.v. reflectivity spectra, electronic struct. 2—13457
RbCl, h.p. phase transition, thermal effects 2—1403
RbCl, low temp. sp. ht. 2—25685
RbCl, paraelec. reson. of Ag^+ 2—33054
RbCl, press. induced polymorphic transition, hysteresis effect 2—9822
RbCl, second order Raman frequencies in terms of phonon frequencies 2—29935
RbCl and KCl-RbCl solid solns., $Cl^-_{II,III}$ absorpt. spectra 2—20041
$RbClO_3$, phonon Raman spectrum and optical phonon damping 2—16563
$RbClO_3$ anisotropic crystals, polarized Raman obs. by immersion technique 2—26196
$Rb_2CoCl_4.2H_2O$, paramag.-antiferromag. transition, sp. ht. obs. 2—6996
$RbCoF_3:Ni^{2+}$, absorpt. transition temp. depend. rel. to mag. ordering effects 2—33267
$RbCoF_3$, u.s. vel., Neel pt. phenomena, elastic consts. 2—32828
Rb_2CoF_4, two-dimensional antiferromagnet, ^{19}F n.m.r. anomaly near critical temp. 2—30027
RbCs, alloy, binary disordered, phonon frequencies using nonlocal pseudopotential methods 2—22385
$RbCsMn_2Cl_6$, atomic struct. 2—22159
RbD_2PO_4, crystn. from RbDP in heavy water soln. 2—1210
RbF, elastic consts., 300 to 4.2K 2—32579
$RbFaF_3:Ni^{2+}$, absorpt. transition temp. depend. rel. to mag. ordering effects 2—33267
$RbFeCl_3$, one-dimens. mag. ordering obs. 2—40563
$RbFeF_3$, n.m.r. of ^{19}F 2—13554
α-$RbFeF_4$, mag. struct., Mossbauer spectra 2—40564
RbH, potential energy curves, applicability of Morse potential, rot. consts., r-centroids, Franck Condon factors 2—18457
RbH_2AsO_4, proton and fluorine spin lattice relax. time meas., CW-methods 2—7151
RbH_2AsO_4 relative nonlinear coefficients, cw ruby laser as pump source 2—36814
$RbHF_2$, lattice energy calc. using multipole moments from LCAO-MO calcs. 2—22093
RbH_2PO_4, Brillouin and Rayleigh line intensities at ferroelec. transition 2—40697
RbH_2PO_4, Brillouin scatt., soft mode behaviour 2—7083
RbH_2PO_4, dipolar spin-lattice relax. study of l.f. motion 2—10259
RbH_2PO_4, ferroelectric phase transition, phonon spectra, Raman scatt. 2—16550
RbH_2PO_4, high temp. dielec. anomalies, phase transitions 2—9814
RbH_2PO_4, high temp. phase transition and metastability 2—22624
RbH_2PO_4, u.s. absorpt., near ferroelec. phase transition temp., critical effects 2—36341
RbH_2PO_4 relative nonlinear coefficients, cw ruby laser as pump source 2—36814
RbI/NaI fused mixture, u.s. velocity and compressibility 2—25077
RbI, diffusion of rare gases 2—3809
RbI, Faraday rot. of excitons 2—22731
RbI, low temp. sp. ht. 2—25685
RbI, V_k-polaron diffusion obs. from opt. anisotropy decay 2—22233
RbI excitons perturbed by self-trapped excitons 2—26156
$Rb_2MnBr_4.2H_2O$ magnetic transitions, exchange and anisotropy fields from spin flop and saturation fields 2—29834
$Rb_2MnCl_4.2H_2O$ magnetic transitions, exchange and anisotropy fields from spin flop and saturation fields 2—29834
$RbMnF_3:Ni$, antiferromag., impurity mode energy calc. 2—16562
$RbMnF_3:Ni^{2+}$, absorpt. transition temp. depend. rel. to mag. ordering effects 2—33267
$RbMnF_2$, sound velocity and elastic consts., Mandelstam-Brillouin scatt. obs. 2—16580
$RbMnF_3$, antiferromag., ^{55}Mn n.m.r. spin echo, 4.2 K 2—16400
$RbMnF_3$, antiferromag., nuclear acoustic reson., u.s. wave propag. 2—40789
$RbMnF_3$, antiferromagnetic, equilib. spin configuration calc. 2—26070
$RbMnF_3$, e.p.r. linewidth behaviour, dipolar interaction and mag. lattice symmetry interplay 2—10510
$RbMnF_3$, Heisenberg ferromagnet, phase changes, neutron scatt. obs. 2—26029
$RbMnF_3$, mag. susceptibility, 55 to 300 K 2—36778
$RbMnF_3$, magnetoelastic effects in thermal cond. 2—40096
$RbMnF_3$, two-magnon Raman scatt. 2—16509
$RbMnF_3$, u.s. coupling to ^{19}F spins 2—37013
$RbMnF_3$ antiferromag., magnon sideband temp. depend. calc. 2—33163
$RbMnF_3$ antiferromagnet, dynamic magnetoelastic coupling 2—26045
Rb_2MnF_4, antiferromag., ENDOR, hyperfine splitting of Mn^{2+} 2—7154
$RbN_3:NO_3$-, u.v irradiation, e.s.r. in NO molecule 2—12182
RbN_3, X-irrad., e.s.r. study of trapped N atom 2—22834
$RbNO_3$, molten, diffusion coeff. of I^- and CO_3^{2-} 2—21976
$RbNb(Ta)O_3$-$W(Te)O_3$ system, crystal chemistry 2—15682
RbO dissociation energy and ground state calc. from ion model 2—28266
Rb_2O, prod. in matrix reaction, i.r. spectrum, force constants 2—12158
RbOK, prod. in matrix reaction, i.r. spectrum, force constants 2—12158
Rb_2PtS_2, prep. and cryst. struct. 2—32462
$RbTiOPO_4$; space group, X-ray exam. 2—15723
^{87}RbF, h.f.s., Stark and Zeeman effect, molec. beam resonance meas. 2—21641
$(Tl,Na,Rb)NO_3$ system, solid-liquid equilibria, polythermal projections 2—22035

Ruby
absorption spectra, conc. broadening of lines 2—1686

Ruby continued
acoustical dynamic nucl. polarization of ^{27}Al in Cr^{3+} doped crysts. 2—29856
active material for optically pumped masers 2—27452
bearings, operational behaviour, structure effects 2—32653
colour stability when annealed or exposed to UV irradiation 2—22883
cooled ruby laser, frequency shifted by adding He gas to vapour phase of liquid N_2 bath 2—34400
cross relaxation between $\bar{E}(^2E)$ and $^4A_2$ states of Cr^{3+}, optically detected, detailed investig. 2—40714
crystal growth, modified Verneuil process, for laser material 2—18973
crystal growth and characterization 2—25262
ENDOR, spin echo, hyperfine and quadrupole interaction parameters 2—26311
e.p.r., exchange coupled ion clusters influence on line shape 2—13531
e.p.r., spin Hamiltonian for Cr^{3+} ions in trigonal field 2—10494
fluorescence, resonant phonon trapping detected 2—19351
generation spectrum, three level centres, laser parameters 2—4485
heavily doped, optical props., review 2—36868
laser, complex resonator with optical delay line, operating mode 2—31047
laser, effect of selective loss on generation spectra at 80K 2—27504
laser, emission focusing in spherical resonator 2—5352
laser, emission obs. under self-Q-switching conditions 2—277
laser, fluctuations in output energy, with passive Q-switch optomechanical switch 2—27506
laser, for generating microsecond light pulses having narrow spectrum 2—37979
laser, frequency mixed with tunable dye laser in proustite crystal 2—27488
laser, generation in intense mag. field, 77k 2—278
laser, generation of monoimpulsive radiation on non-instantaneous inclusion of resonator 2—31048
laser, operation in the purely transverse electric mode TE_{01} 2—31049
laser, Q switched, high repetition rate, obs. 2—21087
laser, Q-switching of radiation by phthalocyanine vapour 2—17622
laser, single mode, wake visualization of hypersonic projectiles 2—3284
laser, single transverse-mode, mode-locked 2—23610
laser, stimulated radiation irradiated by ^{60}Co gamma rays 2—31050
laser, with KDP electro-optical modulator with low modulator voltage 2—17669
laser crystals, trace elements determ. by neutron activation analysis 2—30126
laser damage tracks, time evolution, scattering and luminesc. obs. 2—29861
laser for hologram recording 2—21129
laser generation, free, with spherical resonator, electro- optical smoothing of spatial inhomogeneities 2—21095
laser induced breakdown of He at high pressure 2—24896
laser Q-switched, single mode, use in high speed holography 2—38016
laser rod, optical homogeneity mosaic struct. effect 2—40600
laser with controlled lasing time, coherent characteristics 2—14426
laser with delay line 2—27502
lasers, mode selection with slow Q-switching 2—17623
lasers, pulsed, for holography, recent improvements 2—23646
lasers, self-induced transparency and pulse delay, exptl. investigation 2—11481
losses in superconducting helical resonator from 130 to 450 MHz at low temp. 2—36577
maser, theoretical and experimental conditions for achieving push-pull working point condition 2—11452
maser, t.w., nonreciprocal element for low-field version 2—27451
multiple three level laser, emission spectra, transition dipole moment orientation depend. 2—4470
n.m.r. of ^{27}Al and ^{17}O with dynamic polarization 2—13548
photon echo behaviour near 2.06 kG 2—26158
photon echo decay, Cr conc. depend. 2—40636
photon echo resonance 2—33232
photon echoes, area theorem applic. 2—7031
pink, radiation imprisonment and mag. field effects on luminesc. 2—1708
press. forging, deformation, recrystallization, strength, fracture 2—36249
spin-lattice relax., temp. depend., 0.15 to 40K 2—33179
spin-lattice relaxation, γ-irradiation Cr^{2+} production effect, thermal cond. 2—40576
u.v. irradiated, colour stability rel. to dopants and annealing 2—25450
Cr^{3+} spin-lattice relaxation field depend. 2—22717

Rupture *see Mechanical strength*

Russell-Saunders coupling
electron g^3 configurations 2—18282
Se atoms, calc. of g-value based on R-S coupling scheme and taking configuration interaction into effect 2—24349

Ruthenium
chemisorption, O_2 and CO_2 contiguous layer prep. 2—30062
diffusion in Cu single crystals, dislocations effect, 725-1062°C 2—12803
electromechanical polishing, etching, prep. for optical metallography 2—12650
lattice parameters, -189 to 1709°C, solid equation of state 2—19304

Ruthenium compounds
carbides, ordered plase form. in Ln-Ru-C and actinide-Ru-C systems 2—29493
niobate, single cryst. struct. determ. 2—9480
ruthenates, pyrochlores, electronic characterization, cryst. chem. considerations, elec. and mag. meas. 2—10076
$[Ru^{II}(CN)_5NO]^{2-}$, electronic absorption spectrum calc. and obs. 2—5949
$CeRu_{2-x}Co_x$ dil. alloys, supercond. T_c depression and mag. susceptibility 2—1495
Cr-Ru dilute alloy, magnetoelastic props. 2—13416
Fe-Ru dilute alloy, hyperfine field at Fe atoms, temp. depend. 2—16436
Fe-Ru dilute alloy, spin-lattice relax. time 2—19932
Mn-Ru dil. alloys, complex mag. interactions, resist. obs. 2—40561
Pd-Ru dil. alloys, resist minima 2—16147
Ru-Ir(Pt)(Rh)(Co)(Ni) alloys, spin fluctuation effects on supercond. 2—19600
Ru-Pd alloy, thermoelec. power, 4-300K 2—40373
Ru complex, $[Ru(NH_3)_5.DMSO]^{2+}$ $2PF_6^-$, crystal structure 2—22162
RuO_4, i.r. and Raman spectra, coriolis consts., quadratic force constants 2—12190
$RuZn_6$, crystal structure of primitive cubic, non-centrosymmetric phase by X-ray phase determ. 2—29152
RuZrSi, RuTiSi, struct. relns. 2—18969
$[Ru^{II}Cl_5NO]^{2-}$ electron absorption spectrum 2—38938

Ruthenium compounds continued
V-Ru alloy, high pressure resistivity obs. rel. to anomaly in electronic props. 2—36290
V-Ru alloy, VKβ_5 emission, electronic struct. 2—6728
Rutile *see Titanium compounds*
S-matrix theory
see also Dispersion relations
analytic properties, and perturbation of continuous spectrum by near-lying level 2—5146
collisions, inelastic reactive, uniformization using exact trajectories of S matrix 2—7667
conserved currents and symmetry transformations, investigations in Wightman field theory 2—8065
functional matrix, for nonrelativistic spin 1/2 fermions 2—353
lepton weak interactions, high energy behaviour 2—21235
nonlocal, Regge poles, very high energy strong interactions 2—8098
normalizable wave functions for bound states and resonances 2—34596
nuclear resonances, dynamical approach 2—18073
nucleus with A=200, S-state energy level calc. 2—2673
particles with spin zero and one half in external electric fields 2—23279
potential scattering of S-waves, correspondence between resonances and Kapur Peierls eigenstates 2—27070
relativistic dressed particle scattering, functional matrix 2—354
and relativistic quantum mechanics 2—14511
S-wave phase-shifts in N$\bar{N}$ elastic scattering with inelastic effects 2—34711
scalar fields, nonlocal theory, S-matrix satisfying unitary and macrocausality conditions 2—8082
scattering of 'soft nucleons' from a target calc. from closed linear algebra of currents and interpolating fields 2—17791
scattering S-matrix existence 2—38181
semiclassical transition probability theory, uniformization with elastic collision trajectories 2—27065
singularities in nonrelativistic potential theory associated with non-L^2 wave functions 2—2131
strong interactions, bootstrapping rel. to classical space-time, unique S-matrix requirement 2—21268
strong interactions, internal symmetry propagation 2—368
unitary covariant S-matrices, defined by convergent perturbation series, construction 2—8071
^{135}Xe, low energy neutron cross section analysed using S-matrix and R-matrix theory, different energy dependence of resonance widths related to unitarity 2—28044
Safety precautions *see Radiation protection*
Sakata model *see Elementary particles*
Samarium
atom, Ab initio HF calculations of core relaxation and screening effects on s-electron density at nucleus 2—21522
free particles in dc arc plasmas, transport mechanism 2—15451
lunar rocks, neutron capture on ^{149}Sm 2—13980
magnetic props. 2—40495
magnetic struct. 2—40494
neutron capture on Gd and Sm in Luna 16, G-2 soil 2—20655
optical spectra, plasma and relax. freqs. of cond. electrons 2—40640
X-ray excited optical fluorescence, in Gd_2O_3, La_2O_3, and Y_2O_3 2—22805
Sm^{2+} in KCl, fluoresc. sites 2—40723
Sm^{2+} in KCl, theory of Zeeman anisotropy fluorescence spectroscopy, numerical fit of low-J transition 2—22804
Sm^{2+} to Sm^{3+} oxidation in KCl, spectroscopic evidence 2—10441
Sm^{3+}, absorption spectra in $POCl_3$:$SnCl_4$ solution 2—9141
Sm^{3+}, in metallic solid, paramag. susceptibility calc. 2—26002
Sm^{3+} in $CaWO_4$, spin-lattice relax. 2—1649
Sm^{3+} spin-phonon relax. in lanthanum ethyl sulphate 2—7011
Sm(II), formation spectrum and chem. props. from pulse radiolysis of tervalent ion 2—30094
Sm(III), aqueous soln., pulse radiolysis, formation spectrum and chem. props. of divalent ion formed 2—30094
$^{147}Sm^{3+}$ and $^{149}Sm^{3+}$ ENDOR in $LaCl_3$ 2—37016
Samarium compounds
chalcogenides, prep. and resistivity rel. to vacancy conc. 2—9367
Sm complexes, ethyl 1-methyl acetoacetates and ethylbenzoylacetates, force constant determination from i.r. absorption spectra 2—28328
$SmAlO_3$, orthorhombic, cryst. struct. refinement from single cryst. X-ray data 2—19058
$SmAu_6$, cryst. struct. 2—35997
$SmCO_5$ magnet for focusing in millimeter wave tubes 2—21032
$SmCl_2$ molecule, in Ar, Kr or N_2 matrix, i.r. absorpt. studies 2—28327
$SmCo_5$, as magnet material in astatic magnetometer 2—30983
$SmCo_5$ alloy, domain wall pinning as source of mag. hardening 2—19858
$SmCo_5$ magnet, props. as function of Sm_3Co sintering aid 2—33143
$SmCo_5$ magnets, domain wall energy and coercive force 2—10200
SmF_2 molecule, in Ar, Kr or N_2 matrix, i.r. absorpt. studies 2—28327
SmF_3, anomalous n.m.r. shift of ^{19}F 2—7145
$SmFeO_3$ and $Sm_xTb_{1-x}(Er_{1-x})FeO_3$, growth and mag. props. 2—22113
$Sm_3Ga_5O_{12}$ and $Sm_3Ga_5O_{12}$-$Ln_3Ga_5O_{12}$ solid soln., Czochralski growth 2—19003
SmH_2-SmH_3 system, dissoc. press., thermodynamic props., and soln. parameters 2—22379
$Sm_xLa_{1-x}OCl$, phosphor, concentration quenching of luminescence by dipole quadrupole mechanism 2—36927
Sm_6Mn_{23}, ferrimag. probe, meas. of mag. field at site of Sm nuclei 2—1651
$Sm_2(MoO_4)_3$, precision lattice parameters, ferroelectric-paraelectric structural transition 2—9486
$xSm_3NbO_7+(1-x)La_3NbO_7$, dielectric constant and loss tangent, $0 \leqslant x \leqslant 1$ 2—1559
SmO, antiphase boundaries 2—25333
SmO, cryst. struct., electron diffr. obs. 2—12733
Sm_2O_3, solid phase interaction with Cr_2O_3 2—30054
$SmPb_3$, magnetic props., temp. range 2.8-300K 2—4346
$SmPd_3$, mag. props. 2—19829
$Sm_{1-x}Pr_xCo_5$ series, magnetic properties, variation between cast and annealed compounds, aligning methods 2—13386
SmS:Eu^{2+}, Eu^{2+}-Sm^{2+} exchange interaction, e.p.r. obs. 2—4544
Sm_2S_3, lattice oscillations, dielec. permittivity, molar heat capacity, i.r. spectra 2—40670
Sm_2S_3, struct., density, reflection spectra 2—40671
SmS(Se)(Te), e.p.t. of Eu^{2+} and Mn^{2+}, exchange interaction contribs. 2—36991
SmS(Se)(Te), exchange interactions 2—36669
Samarium compounds continued
SmS(Se)(Te), i.r. absorpt. peaks, semicond.-metal transition 2—33274
SmSe:Eu^{2+}, Eu^{2+}-Sm^{2+} exchange interaction, e.p.r. obs. 2—4544
$Sm_{0.55}Tb_{0.45}FeO_3$, annealing induced domain wall mobility changes 2—10199
$Sm_{0.55}Tb_{0.45}FeO_3$, domain wall mobility enhancement through X-irrad. compared with annealing 2—26071
$Sm_{0.55}Tb_{0.45}FeO_3$ platelets, bubble domain propag. 2—6967
$Sm_xTb_{1-x}FeO_3$, growth from PbO-PbF_2-B_2O_3 melts 2—22114
SmTe:Eu^{2+},Mn^{2+},Eu^{2+}—Sm^{2+} and Mn^{2+}—Sm^{2+} exchange interactions, e.p.r. obs. 2—4544
Sampling *see Statistical analysis*
Sand
heat and moisture transfer in wet sand during freezing 2—20956
Satellites, artificial
air traffic control system, channel characterisation 2—16862
altimetry, ocean backscatter model 2—33569
amplitude scintillations, axial asymmetry in F-region irregularities 2—26542
with arbitrary inclination and eccentricities within Laplace's limit, coordinates computation 2—26575
attitude stabilization system, movable mass. for artificial g space stations 2—26577
AZUR, misalignment of magnetic orientation due to geomagnetic field 2—20451
Brouwer's theory, use of Hills variables 2—30384
communication under unfavourable geographic and atmospheric conditions 2—7314
communications, with narrow-beam antennas, attitude stabilization 2—26578
communications rel. to atmospheric inhomogeneities 2—7317
COS-B, spectral analysis of gamma rays technique 2—11182
COS-B instrumentation for galactic γ meas. 2—30398
dose measurement of integrated radiation 2—5066
dual spin, in circular orbit, stability by method of averaging formulation 2—20449
Earth, motion under influence of tesseral harmonics 2—37232
Earth's shadowing effects on orbital elements, solar radiation pressure 2—30392
electron multiplier detection efficiency for low-energy electrons 2—31013
Eole project, operations 2—16942
evolution of French satellites 2—41025
Explorer 28, ephemeris of highly eccentric orbit 2—41027
F-region, fast Faraday fading of long range satellite signals 2—10762
fibres, gravity-gradient stabilization systems 2—20452
Galilean satellite exploration 2—20447
geostationary, equatorial, momentum wheel stabilization 2—13814
geostationary, Faraday rotation of signals, ionospheric electron content, from Faraday rotation of geostationary satellite signals 2—30350
geostationary, total electron content of ionosphere, measurement 2—13770
ground testing attitude control system, special purpose machine 2—1919
information processing for meteorology and Earth resources 2—7253
INTELSAT network, present and future trends of telecommunication satellites 2—7357
inversion of spin-stabilized spacecraft by mass translation 2—20448
ISIS-I, spin rate behaviour, despin torque mechanisms 2—20441
Jupiter nonsphericity, perturbation to orbit 2—1924
Langmuir probe response, end effect, rel. to ionospheric satellite conditions 2—39152
Large Space Telescope instrumentation, observing programme 2—41265
laser range observation, earth's pole of rotation 2—1777
launching system programme for European satellite 2—4757
Liapunov stability of spinning satellites with long flexible appendages 2—20439
low atmosphere studies of temperature and pressure, microwave propagation 2—10719
luni-solar effects on motion 2—20442
magnetized, equitorial in geomagnetic field, permanent rotations 2—37233
magnetopause attitudes, determined from satellite crossings 2—13740
magnetopause structure during magnetic storm, satellite observations 2—13739
meteorological, information on winds, temperatures, pressures from instrumented balloons 2—1920
meteorological data collection, satellite and earth stations system 2—30262
microaccelerometer, with drag compensation, geodesy obs. 2—16728
motion around oblate planet, method of averaging appl. 2—20450
motion of Earth satellites using correlations between solar activity indices 2—33565
motion of freely spinning gyrostat satellites with energy dissipation 2—30383
motion parameters normalized to obtain dimensionless eqns. 2—7373
NASA GEOS-11, for worldwide time synchronization 2—33865
Nimbus satellite, Fourier spectroscopy 2—22953
oceanography, photographic analysis 2—13650
OGO-V corssings of plasmapause, comparison with ground-based observations of Pi micropulsation events 2—30313
optical tracking, Moonwatch program, laser and radar obs. 2—7352
optimal transfer to gravitationally stable position 2—30386
orbit, libration points in limited generalized problem of three bodies 2—37248
orbit, variations, meas. of variations in upper atmosphere during geomag. storm 2—16868
orbit evolution rel. to solar radiation pressure 2—30397
orbital elements, perturbation due to solar radiation pressure and Earth oblateness 2—1925
orbital equation of motion in an axially symmetric gravitation field, integrability cases 2—1936
orbital inclination changes caused by rotating atmosphere with day-to-night density variation 2—33567
orbital inclination of an Earth satellite, recurrence relation for inclination function 2—1940
orbital motion of near-Earth satellites, determ. of orientation of Earth's rotation axis 2—30544
orbital solns. with geopotential coefficients, GEOS, optical observations 2—20443
Orbiting Astronomical Observatory calibration updating by absolute u.v. calibration of rocket photometers 2—11189
orbits with small eccentricities, second order theory problems 2—1922

Satellites, artificial continued
- OSO, real time control of observing program 2—11165
- periodic solutions of slowly spinning gravity gradient system, motion in circular and elliptic orbits 2—41028
- photography for geographical use 2—7202
- planetary, in near circular orbits, relation for estimation of lifetime 2—30387
- polar cusp observations during magnetic storm, satellite penetration into magnetosheath plasma 2—13741
- probes and electrodes, application of plasma studies 2—6090
- process control and EDP 2—7356
- proton flux and energy spectra measurement from sun 2—5008
- proton flux and energy spectra measurement using nuclear emulsions on a space station 2—4784
- radio astronomy, l.f. observatory, design, calibration and performance 2—33570
- radioastronomical instruments and techniques for frequencies down to 30 kHz 2—11167
- RAE-1, for radioastronomical studies, design, calibration and performance 2—30389
- SAS-D u.v. astronomical satellite, stellar spectra studies 2—41024
- shadow effects, influence on motion 2—41026
- simulation of polar satellites flight through ionosphere by wake behind obstacle in plasma flow from Q-machine 2—21823
- solar orbit, listing of all known to have entered solar orbit 2—13813
- SOLRAD 10(C) solar radiation and activity expt. 2—23131
- space station orbit calculations round an oblate Earth, first order soln. 2—20445
- space stations, dynamically unbalanced dual-spin rigid or low-coupling interconnections 2—20440
- space stations, general summary of principles 2—7355
- space telemetry by satellite borne laser stations 2—26576
- spin stabilised in solar orbit, attitude deviations 2—20444
- spin-stabilized lunar satellites, attitude determination using Kalman filter 2—20453
- stability of circular orbits, estimation of deviations 2—30391
- stability of method for regulating motion 2—30385
- stationary Earth-satellite orbit injection by use of Moon's gravitational field 2—30393
- stellar spectra study, design 2—7354
- superconducting magnetic systems, removable current lead for power supply 2—34309
- surface materials, photoelectron flux and solar irrad. 2—33566
- tracking, using satellites 2—16941
- transfer orbits, Lawden's spiral, non-optimality of intermediate-thrust arcs 2—30390
- TRANSIT system for worldwide synchronization 2—33864
- triple calibration sphere expt. test of Cook's (1965) theory 2—1923
- X-ray observations of sun from Vela 2—11066

Saturn
- atmosphere, microwave brightness temperatures, He:He mixing ratios 2—26848
- atmospheric entry simulation, use of higher performance electric-arc-driven shock tube 2—20949
- disk, monochromatic coefficient of brightness 2—30554
- faint atmospheric belts and bright spot photographic obs. 2—26850
- gravitational moments, for rotating planet, computed from available models 2—37356
- great inequality, influence on secular disturbing function 2—20680
- Iapetus, polarization observations rel. to albedo differences 2—41197
- magnetospheric, estimation of characteristics 2—30548
- mass determination from obs. of 5 outer planets and 7 minor planets 2—11002
- perturbation of orbits of long-period comets with large perihelion distances 2—26862
- position, meridian obs. for 1963-67 2—1989
- radio emission obs. at 49.5 cm 2—26849
- ring system, phase curves, model for non-atmospheric bodies 2—20637
- rings, polytropic and isothermal plane symmetric configurations 2—10784
- satellites, physical and chemical nature 2—7535
- seasonal variations in planetary circulations, comparison with Earth and Jupiter 2—41193
- Titan, obs. of temp. at 20 microns 2—37369
- u.v. photometry from the Orbiting Astronomical Observatory 2—20675
- H_2 rich atmosphere gravitational instabilities prevented by solar tidal force 2—26824
- NH_3 abundance in sub-cloud atmosphere, radio astronomical obs. 2—30580

SC (sudden commencement) *see Magnetic storms*

Scalers *see Counting circuits*

Scandium
- atomic spectra and energy level det. 2—35145
- Auger spectrum, LLM and LMM transitions 2—13361
- Compton profile, band struct. 2—1704
- film, in multilayer structure, in backscattering analysis 2—15659
- ions, in Li isoelectronic sequence, spectra 2—2995
- magnetic anisotropy, temp. depend. 2—40420
- Sc I to Sc III lifetimes of excited levels, spectra from 600 to 6000 Å 2—15225
- Sc XIX spectrum in e.u.v. identification and classification of spectral lines 2—31666
- Sc XVI, carbon-like spectra in the range 16 to 22 Angstroms 2—15220
- ScX MgI-like spectra, analysis isoelectronic comparison with spectra of KVIII, CaIX, TiXI 2—28198

Scandium compounds
- alloy, dil., mag. anisotropy, temp. depend. 2—40420
- alloy, dil., with rare earths, localized moments influence on spin-lattice relax. 2—19934
- carbides, struct. chemistry 2—9327
- ferrites, $Fe_{3-x}Sc_xO_4$, $Li_{0.5}Fe_{2.5-x}Sc_xO_4$ and $Mg_wMn_xFe_ySc_zO_4$, magnetostructural props. 2—36751
- Luna 16 soil conc. 2—20664
- oxide, nonstoichiometric, plasma-synthesized, prep. and physico-chem. props. 2—9344
- ScAs epitaxial layers, vapour growth, elec. and optical props. 2—9282
- ScB_2, ultra soft X-ray spectra 2—29943
- $ScBO_3:Tb^{3+}$, Ce^{3+}, calcite type cryst., 4f-5d transitions studied, luminescence obs. 2—29962
- ScH_x, proton motion, n.m.r. obs. 2—20164

Scandium compounds continued
- Sc_3In, ferromag. transition, mag. entropy, heat capacity obs. 2—40493
- Sc_3In, resist., sp. ht., mag. props. 2—40492
- $Sc_2(MoO_4)_3$, struct. and phase relns. 2—9340
- ScO_x-actinide oxide systems, phase relationships 2—12610
- ScO, low-lying electronic states, interpretation 2—5950
- Sc_2O_3, in $BaTiO_3$, effect on microstructure and dielec. props. 2—19761
- Sc_2O_3 doping, use in stabilisation high temperature form Ta_2O_5 2—3734
- Sc_2O_3 film, stopping power for low energy protons 2—32862
- ScP epitaxial layers, vapour growth, elec. and optical props. 2—9282
- $ScVO_4:Er^{3+}$, mag. props. and sp. ht., calc. from cryst. field parameters 2—40421
- SiO, orange system, $^2\Pi$ to $^2\Sigma$ transition, rotational analysis of band (0,0) 2—31827
- $SrSc_xFe_{12-x}O_{19}$, elec. cond., temp. and comp. depend. 2—29674

Scattering
- amplitudes, in non-physical region 2—37625
- amplitudes construction in non renormalizable quantum field theories 2—31159
- analytic continuation procedure, Fredholm determinant (Jost function) applic. 2—83
- backscattering and internal rarefied gas flows 2—32155
- book, scattering theory 2—37626
- Born approximations, unitarized 2—21477
- classical, exact soln. from repulsive inverse power potential 2—39
- classical deflection function, approx. expression, linear in potential 2—40
- collisions, inelastic reactive, uniformization using exact trajectories of S matrix 2—7667
- Coulomb scattering, two body, off-shell and on-shell unitary relations 2—80
- cross sections, Jost function interpolation 2—14114
- by dipolar charges, fixed, model 2—754
- dynamic, from potential periodically varying with time 2—5155
- energy dependent amplitudes, computation via analytic continuation of Fredholm determinant 2—7682
- error-affected data, rigorous lower bound on amplitude maximum 2—33931
- flat slab, particle transmission through, Monte Carlo calc. 2—23310
- Fredholm theory, classical limit, for general multichannel scatt. system 2—7684
- gas scattering function, ellipsoidal molecule model 2—1031
- gases at surfaces, molecular beam system for obs. 2—32324
- gravitational waves, smooth toroidal 2—20820
- inelastic calc. of energies and widths of resonances by stabilization method 2—27073
- inelastic two-channel problems, uniform asymptotic solutions and semiclassical S-matrix elements 2—7683
- integral equations for four identical spinless particles obtained using Feddeev Yacubovsky approach 2—30788
- inverse problem, reaction matrix approach 2—33928
- isotropic case of noncoherent scattering in plane-parallel finite layer 2—30760
- Jost function of central momentum-dependent S-state interaction 2—2144
- Lamb wave obliquely incident on one dimensional irregularities 2—5215
- Lyman α radiation in geocorona, intensity rel. to solar activity 2—30314
- molecular nozzle beams, gas density determination 2—38882
- multichannel problems, WKB solns. and semiclassical scattering matrix elements 2—23282
- non-relativistic, test of least squares variational method 2—2146
- nonreactive, nonpartial wave treatment, coupled integral equation formalism 2—2902
- nonrelativistic, existence and completeness of wave operators 2—27072
- on-shell Coulomb T-matrix 2—24299
- operator multiple-scattering series, breakdown of simple cancellation 2—30761
- P- and S-wave by square well potential, correspondence between resonances of Kapur Peierls eigenstates 2—27070
- partial scattering amplitudes, analytical props., power series expansion 2—23281
- phase shift, as continuous functional 2—2142
- phase shift, as continuous functional 2—2143
- phase shifts, Fredholm integral equation method 2—23284
- plasma, induced by nonlinear Landau damping of longitudinal plasma waves in magnetic field 2—8985
- potential, from regular lattices, evanescent waves 2—37580
- potential, impact parameter representation of amplitude for all scatt. angles 2—17240
- potential, off energy shell phase shifts 2—17241
- potential, proof of Schwinger's action principle 2—34574
- potential, relation between three-dimensional Fredholm determinant and Jost functions 2—33930
- potential, study of resonances, energy derivative of phase shift rederived in computationally useful form 2—12001
- potential, validity of modified Glauber eikonal approx. 2—11288
- potential, variational principles for phase function method 2—23283
- potential, with indefinitely high spin, duality of singular potentials 2—7685
- potential scattering, Born series for T matrix with potentials tr^2) 2—17243
- potentials, with suppressed S-wave phase shift at low energies 2—23285
- quantum theory, instructional uses of computers 2—2051
- on smooth quasipotential, exchange forces studied 2—5154
- Rayleigh waves, review 2—20921
- reactive, nonpartial wave treatment, coupled integral equation formalism 2—2902
- resonances, interpretation method using Fredholm determinant (Jost function) 2—83
- Schrodinger, equation error analysis in numerical algebraic method 2—27055
- Schrodinger equation, identities involving coefficients in asymptotic expansion of outgoing scattering solution 2—33929
- seismic P-waves, crustal effect 2—16737
- shallow water waves, propagation over random ocean bottom of constant average depth 2—40904
- short wavelength regime, formulation in near classical limit 2—5150
- simple fluids, equilibrium fluctuations, nonhydrodynamic aspects, projection operator formalism 2—8869
- on singular potentials, power series for phase shift 2—14115
- spherical well, Pade approximants used to calculate bound states and phase shifts 2—30796

Scattering continued
three body rearrangement, comment on quantum mechanical collinear model 2—20851
three-body breakup processes, Kohn-type variational principle 2—37623
three-body breakup processes, variational principles 2—37624
three-body problem, eikonal formulation 2—81
two-body, on-shell Coulomb T-matrix derivation 2—82
unitarity relation for scattering by arbitrary noncentral force used to determ. phase of scattering amplitude from diff. cross section 2—37622
by van der Waals forces in Born approximation 2—79
water waves, acoustic model for experimental study 2—9060
waves, from thin comb with hard boundaries 2—20819
acoustic waves
air bubbles in water, coherence of sound 2—17384
backscattering from rough surface, in water, surface spectrum dependence 2—14263
by Eaton lenses, spherical and cylindrical fluid 2—17385
elastic cylinder, circumferential and transmitted waves 2—27263
elastic cylindrical shell, integral represent. 2—27262
by fixed rigid prolate spheroids, short wave asymptotic behaviour 2—27260
monostatic from ocean bottom 2—37114
plane waves, by circular cylinder 2—165
pressure release spherical surface, Kirchoff integral formulation 2—27259
reverberation and echo structure 2—34111
Saanich Inlet, British Columbia, backscattering of underwater sound and scattering from fish school 2—37113
by small conducting solid cylinder in viscous conducting fluid 2—14264
by uniformly rotating systems, wave equations for cylinders and spheres 2—14266
by vegetation and ground, transmission of random noise 2—14265
acoustic waves, ultrasonic
cavity in solid medium, longit. wave scatt. 2—9874
heterogeneous systems, direct wave attenuation 2—28907
piezoelectric ceramic, surface wave scatter loss, optical measurement 2—36337
seawater surface, spectral analysis 2—30260
shrimp egg suspensions 2—28922
electromagnetic waves
active corrugated struct., plane wave scatt. 2—14315
anisotropic composite obstacles, reciprocity 2—11396
antiferromagnet, fluctuations near crit. mag. field 2—6988
axially moving concentric dielectric system, oblique incidence 2—14316
backscattering, of plane wave pulses, by low-density dielectrics 2—14317
backscattering from rough surface, simulation using acoustic waves 2—14263
bidirectional scatt. from rough surfaces 2—11395
conducting cylinder, dielectric half space, multipole methods 2—11402
by conducting sphere near the ground, quasi-static soln. in bispherical coords., calc. of response to ground wave 2—34250
from curve rough surfaces, waves transmitted through turbulent media 2—30929
cylindrical, by spherical object 2—14320
dielectric, local defects detection using radiodefectoscope in reflection regime 2—29373
discontinuities in waveguides, ray-optical calculation 2—17481
distributed radar targets props. 2—30943
doppler return from two dimensional random rough sea surfaces 2—30944
Earth's atmosphere, backscattering by turbulent irregularities 2—20355
fog, attenuation at millimeter wavelength 2—33494
frequency cross correlation of wideband signals 2—23448
with Gaussian amplitude distribution, from dielectric cylinders14314 2—14314
Gaussian beam, as bundle of complex rays 2—2299
ground backscatter observed with high resolution oblique sounders, h.f. waves 2—30933
group of point reflectors, inverse problem 2—27356
h.f. backscattering from conducting sphere coated with radially inhomogeneous dielectric 2—20988
h.f. radiowaves, by spherical electron cloud, numerical, analytical solutions 2—30934
homogeneous bodies of arbitrary shape, scattering characteristics 2—2304
in homogeneous isotropic turbulent medium with ellipsoidal inhomogeneities, statistics 2—20985
Huygens' principle, electrodynamic formulation for smooth inhomogeneous medium, rotation of plane of polarization. 2—23444
hydrometeors in troposphere, interference study 2—33490
by ice cylinders, arbitrarily oriented, cloud microstructure 2—30282
by inhomogeneities, limits of applicability of approximate solutions 2—37849
integral equations, noniterative solution 2—34252
ionosphere, near field correction for backscatter gain, theory and exp. 2—33516
ionosphere, sky-wave backscatter, review 2—40999
ionosphere, sporadic E-region, a new model 2—4732
ionosphere D-region, amplitude distributions of partial reflections 2—16907
ionosphere E-region, meas. of ion conc. and composition 2—33547
ionosphere F-region, analysis of incoherent data 2—4746
ionospheric propagation, power spectrum of waves 2—14325
i.r. in rhodochrosite, effects on complex refractive index 2—7040
from irregularities in magneto-ionic medium, theory using Green's dyadic 2—30935
Kirchhoff method, for layer with plane interface at front and rough interface at back 2—27354
by lunar surface 2—30536
in magnetoactive plasma, correlation theory of back scattering field 2—31973
metal rod, elliptic 2—207
microwave, by surface charge waves, excited on plasma column 2—35481
microwave combination scattering from plasma waves in electron beam-plasma 2—28615
microwave scattering pattern from dielectric target, inversion 2—17479
Mie, scattering by sphere, calculation by computer program 2—11397
moving objects, energy balance and radiation forces 2—20989
multiple, propagation through random media 2—14324
nonlinear from inhomogeneous plasma column 2—31992
obliquely incident, by inhomogeneous cylinders 2—14321
ocean backscatter model, of satellite altimeter 2—33569
ocean surface, foam emissivity at microwaves 2—34253

Scattering continued
electromagnetic waves continued
ocean surface, wind dependences of radar return 2—30939
ocean surface winds rel. to radar scatt. coefficient, expts. (1969-1971) 2—34255
ocean-like one-dimensional random surfaces 2—30937
orthogonally polarized components, cross correlation, extended object scattering 2—23447
perfect conductor, inverse identity for monostatic far field cross section 2—34257
perfectly conducting bodies, transient fields rel. to free oscillations 2—34251
phase of scattered amplitude from systems of unknown charge distribution determ. from exptl. data 2—20987
plane wave pulse, backscattering from dielectric sphere 2—14313
plasma, rel. to e.m. wave attenuation 2—35493
plasma, with e.m. wave vector perpendicular to confining magnetic field 2—15460
plasmas, turbulent, modified Born backscattering 2—12386
polygonal cylinders, point-matching technique 2—30941
pulsar radiation in interstellar medium 2—4937
pulse, from grounded dielectric slab, at polarizing incidence 2—14323
pulse scattering with grounded dielectric slab 2—17477
radar cross sections of space vehicles in electron plasma medium 2—33568
radar scattering properties of Mercury backscattering properties, rotation period 2—14000
by radially inhomogeneous cylinders constructed of artificial dielectric, experimental study 2—7790
radio, backscattering cross section, in rain 2—16832
radiowaves, from sporadic-E region, measurement of ordinary, extraordinary critical, blanket frequencies using ionosonde 2—37217
rain, radiometric measurements 2—33493
rain-scatter interference between terrestrial microwave and satellite comunication systems at 4 to 8 GHz 2—33488
Rayleigh, by obliquely oriented uniform needles 2—5292
Rayleigh hypothesis, modified, mode-matching method 2—17468
retrieval of electrical radius ka from scattered field, in circular, cylindrical and spherical coordinates 2—14319
r.f., forward and backscatter, by spherical overdense clouds 2—33485
rough sea surfaces, two dimensional, Doppler return 2—16790
rough surfaces, effect of curvature variation 2—2305
sea, lowest order interaction between radio and ocean wave fields 2—30940
sea, second order Doppler sidebands in h.f. echo 2—30919
sea waves, correlation methods 2—33445
seawaves angular spectrum by coherent h.f. backscatter 2—33444
secondary diffraction of close edges, conducting bodies 2—23443
sinusoidal surface, perfectly conducting, perturbation soln. 2—30932
by small body, primary field determination 2—27357
solar radiation, by corona, transfer characteristics 2—30614
sphere, radially inhomogeneous 2—210
by spherically symmetric objects, vector potential solutions 2—37847
statistically rough surface, calculation 2—27355
surface back scattering patterns, effective beamwidth, distribution of reflected signals, meter, decimetre waves 2—30928
surface current density on perfectly conducting polygonal cylinders when incident field is polarized in axial direction 2—23446
target with higher order diffraction components, coherent short-pulse meas. data processing method 2—34256
by thin conducting wires, least-squares solution using numerical basis transformation technique with point matching methods 2—30930
transient, by arbitrary wire structure 2—14318
transient plane wave, by periodic grating 2—20990
tropospheric scatter propagation, communication channels 2—17478
turbulent plasmas, overdense and underdense, scattering of microwaves 2—31982
two dimensional body, of arbitrary cross section, calc. 2—30931
two dimensional slightly rough random surface 2—30938
two inclined half planes, theory 2—14322
by ultrarelativistic electrons, spectral distrib. of resultant radiation 2—5291
by underdense plasma layer, Gaussian, sech, parabolic density distribution, perturbation technique 2—31975
in velocity dependent systems, arbitrary objects moving in free space 2—30936
waveguide, rectangular, with perfectly conducting cylindrical obstacle, calc. 2—14327
by wind waves at 9.4, 24, 70 GHz, windspeed dependences 2—34254
wires associating three dimensional conducting surfaces 2—30942

light
see also Diffusion, light; Rayleigh scattering
'scattering-absorption' in image formation from phase objects, wave theoretical investigation 2—23684
absorbing spheres, Mie scattering 2—21153
alignment fluctuations of mag. tapes, continuous monitoring 2_239
amylose films, anisotropic morphology obs. 2—3473
aniline-cyclohexane liquid mixtures, critical exponent determination by scattering studies 2—9133
anisotropic, manymolecular correlation induced, in simple fluids 2—6231
anti-Stokes secondary radiation from impurity centres, interference effects from vib. sublevels 2—10403
atmosphere, angular volume-scattering function, nephelometer obs. above 26 km 2—37158
atmosphere, climatic changes 2—13719
atmosphere, optical inhomogeneous region near the critical point 2—40967
atmosphere, turbidity det. from obs. of polarization 2—37159
atmosphere turbidity characterization from solar radiation intensity profiles meas. 2—7310
atmospheric spherical polydispersions, size distribution det. using light scattered data 2—7260
atmospheric turbidity, wavelength depend. of aerosol or haze scattering 2—22976
atomic vapour, coherence properties, level crossing expt. 2—11937
p-azoxyanisole, nematic mesophase, spatial distrib. of light scatt. in applied elec. field 2—25087
benzene, second harmonic, induced by quadrupolar mol. fluctuational elec. fields 2—35765
block copolymers, depolarized light scattering in terms of birefringent domains 2—16422
bubble-size distribution determination 2—21945

Scattering continued
light continued
t-butyl alcohol, additional maxima by addition of water and heavy water 2—9131
carbon tetrachloride, scatt. and i.r. absorpt. spectra 2—32267
chemically reacting fluids, intensity of scatt. light rel. to concentration fluctuations 2—22857
clouds, visible light scattering, angular transmittance 2—22967
clouds of elongated particles 2—10729
from coated spheres, biological cells model 2—30654
coherent system of two-level particles 2—26136
coloured powders, optical properties of mixtures 2—7042
contribution to refractive index in nonhomogeneous media, separation from absorption component 2—34468
critical binary mixture, signal correl. obs. 2—25064
critical opalescence, height asymmetry 2—7989
critical opalescence, review 2—9130
crystal, surface vibration modes, light scatt. 2—29505
crystals, multiphonon scatt. from impurity centres 2—16452
cyclohexane-aniline mixture, intensity and turbidity meas. rel. to determination of critical exponent 2—21987
cyclopentane, critical region scale law, verification 2—25151
daytime sky, degree of linear polarization rel. to multiple scattering during solar eclipses, visible region 2—33471
decane-chlorex, liquid mixtures, critical exponent determination by scattering studies 2—9133
dense gases, depolarization in critical region, molecular theory 2—9035
depolarization and angular dependences of n-harmonic scattered light in statistically inhomogeneous media 2—38074
depolarization when scattered by anisotropic molecules 2—9033
dielectric film, optical props. rel. to interference coatings and waveguides 2—40599
by disordered spherulites, effect of disorder in the magnitude of anisotropy 2—7041
disperse systems, agglomeration measurement using laser light scatt. 2—1122
disperse systems, smallangle theory for optically anisotropic spheres and discs, exptl. verification 2—28903
dispersion and asymmetry, empirical relationship at critical point 2—1145
dodecane-chlorex, liquid mixtures, critical exponent determination by scattering studies 2—9133
electric field stimulated interserial combination scattering, from excitons 2—16449
electron fluid, in mag. field, theory 2—36849
exciton-phonon interaction, coherent potential approx. 2—26135
ferrimagnetic system, magnon-photon interactions 2—36850
ferromagnet, near antiferromag. transition point 2—1615
ferromagnets, magnetized, Faraday effect, 0.1-0.5 MeV γ quanta 2—16419
by fluid binary mixtures, analysis using stochastic hydrodynamic equations 2—7990
fluids, eqns. in terms of invariant expansion of 2-body statistical correlation function 2—7700
fluids, Onsager symmetry relations rel. to spectral distribution 2—32177
fog, determination of particle size distribution from scattering function 2—33462
fogs and smokes, multiple forward scatt., intensity and polarization 2—5421
by free electron oscillating charge, phase of scatterd amplitude determ. from exptl. data 2—20987
in glass fibre waveguide, angular distribution 2—38124
glasses, low loss, for optical fibres 2—38111
Heisenberg antiferromagnet, magnon-magnon interaction effects 2—16391
higher order moments or inverse or linear stochastic operator 2—11516
homodyne detection of signal scattered by moving surface of normally distributed roughness 2—21116
by ice cylinders, large infinite, at normal incidence 2—34497
impurity crystal, antiresonance theory 2—16447
inhomogeneous media, nonlinear scatt. theory 2—16450
instrument for recording scattering patterns 2—21162
interference in atomic absorption anal. of biological materials 2—22893
intrinsic semiconductor thermal balance in presence of laser beam with photon energy<band gap 2—22742
inverse problem, sampled data solution 2—311
isotropic approximate forms for the H-function 2—7986
Jahn-Teller centre, elementary excitations 2—19991
laser beam at polished glass surfaces 2—14447
laser beams, induced polarization, teaching demonstration 2—8
laser beams in θ-pinch plasma, meas. by seven channel Fabry-Perot spectrum analyzer 2—24766
laser hypersonic emission, generation in Mandelstam-Brillouin stimulated scattering process, in isotropic dielectric 2—257
laser light scattering homodyne technique for obs. of plasma drift waves 2—35541
liquid, stimulated temp. scatt. 2—1097
liquid crystal, nematic, heterodyne meas. in applied d.c. field 2—18834
liquid crystal, nematic, orientational order and elasticity 2—9089
liquid crystal, nematic, two-dimensional, possible exptl. obs. 2—9087
liquid crystal, nematic dynamic scatt. in homeotropic and homogeneous textures 2—32233
liquid crystal matrix display, additional solid layers for parasite current suppression 2—25084
liquids, at small angles, molecular weight determination 2—3391
liquids, collison-induced scattering, isolated binary collision model 2—25082
liquids, obs. of mechanism of structural rearrangement 2—18824
liquids, VH-depolarized spectra, at high $k^2\eta/\rho\Gamma$ 2—21988
liquids and solns., structural investigations 2—32264
Lorenz-Mie, comparison using three model size distributions at laser wavelengths 2—34496
low absorption medium, application of Rozenberg's theory to determ. coeffs. of deep attenuation and absorption 2—27599
low temperature plasma diagnostics 2—32037
macromolecular solns., quasielastic scatt., internal modes of motion 2—15591
macromolecular solutions, rel. to investigation of virial coeff. changes and phase separations at high pressure 2—9076
macromolecular suspensions and solns., transient scatt. processes induced by pulsed fields 2—15621
macromolecules in solution, structural evaluation 2—18537

Scattering continued
light continued
magnetic material, anomalies near critical pt. 2—10331
MBBA, coherence length in isotropic phase of room- temp. nematic crystal 2—35734
medium characterized by single relaxation process, temp. and internal parameter fluctuation effects 2—5422
metal surface, rough, photon interactions 2—4427
metallic particles, submicron size, plasma resonance description of white light scattering characteristics 2—13471
p-methoxybenzylidene p-n-butylanilene nematic liquid crystal, coherence length in isotropic phase 2—28795
microporous materials, photon diffusion model, pore size meas. 2—32285
Mie, modification of van de Hulst relation 2—24983
Mie calculations, synthetic distributions using a dual-computer technique 2—7987
Mie scattering by spherical particles in low-loss glass for optical waveguides 2—7988
milky glass, depth attenuation and absorption coeff., calc. from two-parameter approx. theory and Rozenberg theory 2—26113
molecular fluid, spectra 2—18832
molecular liquids, depolarized light scatt., existence of central diffuse line and broad background 2—21985
multiple backward-scattered radiation, luminance and polarization properties in fogs and smokes 2—4690
nonstationary surface roughness measurement 2—17681
parametric and polariton in KH_2PO_4 and $NH_4H_2PO_4$ crystals, obs. using Ar laser 2—40607
particle-size determination, effect of refractive index 2—312
in photographic fine grained materials for holography, Wiener spectrum meas. 2—14492
photon exit from spectral line formed in a scattering atmosphere, probability distribution 2—11451
plane-parallel atmospheres, partially polarized light 2—13720
by planetary atmospheres, effect of absorption 2—1987
by plasma, CO_2 laser light, diagnostic technique 2—35539
plasma, collisional dominated, Thomson scatt. of laser light 2—12389
plasma, collisionless shock wave, turbulence meas. 2—39122
plasma, frequency spectrum effect of magnetic field 2—32009
plasma, laser light, comparison of calc. and obs. spectra in mag. field 2—32010
plasma, laser light, det. of ion and electron temp. in e.m. shock tube 2—35540
plasma, mag. field meas., laser dispersion 2—32034
plasma, magnetized arc, anomalies using laser light 2—35497
plasma, six channel interference filter spectrum analyser 2—39133
plasma, solid state, hot, collision controlled light scatt., response rel. to fluctuations 2—16121
plasma, strongly correlated, charged particle ordering influence 2—28564
plasma electron waves, obs. of line structure 2—35566
by plasma with few electrons in Debye volume, fluctuation spectrum obs. 2—18618
polaritons, damped, quantum theory 2—26138
polarized, half-range orthogonality theorem 2—34495
polarized beam, rel. to birefringence meas. method 2—4433
poly-α-methylstyrene, optical anisotropy meas. 2—15415
poly-α-methylstyrene chain fractions in solution, particle scattering factor and segment-segment distance distribution 2—12563
poly-α-methylstyrene chain fractions in solution, particle scattering factor and segment-segment distance distribution 2—12562
polydisperse systems of low molecular weight, refractive index increments and light scattering 2—39402
polydispersed indicatrices of small angle scattering, asymptotic formulas for calc. angular structures 2—25115
polylysine in solution, diffusion coeff. as function of concentration determ. from spectrum of scattered light 2—39403
polymer latex systems, size distribution analysis using extrema in unpolarized and horizontally polarized ang. light scatt. pattern 2—39397
polymers, photolysis, continuous light scatt. technique 2—37057
polysaccharide solution, stiff chain parameters, small angle X-ray scatt. 2—3369
polystyrene, coagulating latex 2—15619
polystyrene in water sols, effect of dispersing agents on angular dependence 2—6267
polystyrene sphere-water sols, effect of dispersing agents on angular dependence 2—28921
polystyrene-cyclohexane system near upper critical segregation temperature, determ. turbidity curve, thermodynamic functions 2—35772
polyurethanes, segmented, anisotropic superstructure meas. by photographic light scattering 2—15648
polyvinyl chloride solutions, gamma irradiation induced branching, viscosity obs. 2—18804
propanol, aqueous solutions, determ. intensity of concentration scattering 2—15590
quartz, microscopically damaged, laser beam catastrophic damage threshold obs. 2—29859
quasielastic, from non Gaussian concentration fluctuations 2—21986
quasielastic, under optical microscope, dynamic properties of macromolecules 2—34514
radiance distribution inside sphere for nonuniform nonlambertian diffusely scattering surfaces and surface scattering transfer characteristics calc. spherical harmonic moments meas. 2—31099
rare earth iron garnet, at mag. compensation point 2—16457
Rayleigh and isotropic, exact closed form solution for discrete eigenvalue 2—23694
review, use of lasers as light source 2—310
by rough surfaces, determ. by direct solution of Maxwell's equations 2—17693
ruby, from laser damage tracks, time evolution studies 2—29861
sapphire, from laser damage tracks, time evolution studies 2—29861
screen, diffusing, with small angle light scatt. 2—320
in seawater, Monte Carlo simulation 2—37120
seawater, total coefficient, nephelometric obs. 2—13630
seawater particles, scattering of light from underwater laser, determination of size distribution 2—1798
semiconductor, differential scatt. cross section for strong electric field 2—19993
semiconductor, magnetoplasma quasi- elastic light scatt. 2—16448
semiconductor, parametric excitation of density waves, direct conversion of photons, into plasmons 2—13200

Scattering continued
light continued
semicondutror, many-valley, scatt. cross section 2—16515
simple fluids, density and temperature dependence of spectrum of depolarized light 2—3160
sky brightness, approximate equation from atmospheric transmittance and albedo 2—1888
small-angle, by anisotropic cylinder 2—17694
solids, conf., Paris, France, Jul. 1971 2—16445
speckle patterns in unfiltered sunlight 2—14452
spectrophotometric examination of light scattering media 2—2466
spherical dielectric particles, scatt. efficiency factor for radiative transport 2—21154
spherical scatterers, dependence of extinction efficiency on photometer geometry 2—14456
starlight, by interstellar dust grains, to produce diffuse galactic light, absolute intensity obs. 2—7459
stimulated, and self-focusing in laser produced plasma 2—3212
stimulated, of Rayleigh line wing, amplification coeff. 2—5447
stimulated, on free liquid surface at full Fresnel reflection 2—31055
stimulated, stationary regime establishment time 2—38073
stimulated thermal scattering, review 2—1099
sunlight, resonance scattering by spherically symmetric optically thick Sr gas cloud 2—30319
by surface, flaw detection using oblique angle illumination 2—35868
surfactant+additive+water systems 2—9095
Thomson scattering of laser light, by plasma, shift due to electron drift in θ-pinch 2—35498
transient, in pulsed nematic liquid crystal cells 2—3389
trifluorochloromethane, near critical point, rel. to abs. determination of compressibility 2—9072
triglycine sulphate, Curie temp., second harmonic scatt. 2—16294
in turbid media, polarization phenomenon illustrated by three centimeter e.m. wave expt. 2—2302
turbid medium, characteristics of thin beam from exact solution of transport equation 2—2433
vertex functions, scattering amplitudes, high-energy asymptotic form 2—38072
water, clean, naturally occurring prediction as function of wavelength 2—13633
Al coated flat glass samples small angle obs. 2—38075
Al films, surface-roughness spectra 2—4130
Al_2O_3, refractive index of defects in synthetic corundum crystals grown by the Czochralski method 2—29872
Al_2O_3, sapphire, high power laser beam scatt., nonlinear effects 2—16450
Al_2O_3 film, porous anodic, polariz. effects 2—19949
Al_2O_3 porous anodic film, coloration 2—13454
Ar plasma, and density inhomogeneity broadening of plasma satellites 2—3213
$Bi_{12}GeO_{20}$, by acoustic and optical phonons 2—10335
$Bi_{12}GeO_{20}$, scatt. by acoustic and optical phonons 2—16454
CS_2, second harmonic, induced by quadrupolar mol. fluctuational elec. fields 2—35765
CdS, by acousto-optical domains and inhomogeneities induced by domain propagation 2—16455
CoF_2, antiferro- and paramag. phases, exciton relaxation 2—16456
CoF_2, two-magnon scatt. 2—40545
Cu_2O, combination scatt., exciton level determination, cross-section calc. 2—16449
FeF_2, antiferromag., one magnon spectrum, temp. dependence 2—16537
GaAs, differential scatt. cross section for strong elec. field 2—19993
$GeCl_4$, scatt. and i.r. absorpt. spectra 2—32267
H_2O turbidity, correlation of optical models and aircraft data 2—1815
He I liq. and ^{4}He gas, h.f. depolarized scatt. 2—12597
^{4}He, superfluid, from density variations generated in sound modes by thermal transducer 2—18869
He+^{114}Cd mixture, laser for exciting spectra 2—23594
Hg vapour, resonance radiation, forward scattering 2—8448
n-InSb, differential scatt. cross section for strong elec. field 2—19993
MnF_2, antiferromag., magnon pairs at spin flop transition 2—16537
MnF_2, antiferromagnet, two-spin fluctuation scattering, analysis based on frequency moments 2—33280
N_2, resonance scattering of first positive system in dayglow 2—40985
NO^{2-}, in alkali halide cryst., reson. secondary radiation spectra, hot and scatt. luminesc. 2—16639
Na, particles, submicron size, plasma resonance description of white light scattering characteristics 2—13471
NiF_2, antiferromag., magnetic field effects 2—16537
$PbCl_4$, scatt. and i.r. absorpt. spectra 2—32267
Rb atom, two-photon excitation, transitions 2—15224
SF_6-He, stimulated concentration scattering 2—28860
SF_6, spectrum and intensity meas. at critical density in range $0.048\ K<(T-T_c)<2.4\ K$ 2—12512
$SiCl_4$, scatt. and i.r. absorpt. spectra 2—32267
SiO_2, bulk fused silica, materials testing, fibre optic communications 2—33190
$SnCl_4$, scatt. and i.r. absorpt. spectra 2—32267
$TiCl_4$, scatt. and i.r. absorpt. spectra 2—32267
Xe-He, stimulated concentration scattering 2—28860
Xe, intensity magnitude and angular dependence, meas. near critical point 2—9034

light, Brillouin spectra
acetone, Fourier transform obs. of line widths and shapes 2—1103
anisotropic media, rotational contrib. antisymmetric susceptibility obs. 2—16423
aprotic laser solns. with Nd, scatt. coeffs. determ. 2—32269
benzene, Fourier transform obs. of line widths and shapes 2—1103
crystal vibration modes 2—29505
dielectric cryst., scatt. by thermal fluctuations 2—16578
electrolyte solutions, hypersonic vel. meas. 2—28862
experimental methods, conf. contrib. 2—16446
ferroelectric, Mandelstam-Brillouin scatt., review 2—26199
fluids, role of electrostriction, absorption and electrocaloric effect 2—32178
gas mixtures, Brillouin-Mandelstam lines broadening 2—35685
laser, ultrashort pulses 2—37949
liquid, stimulated Mandelstam-Brillouin scatt. 2—1097
metal surface, acoustic phonons 2—16453
methane, single freq. laser 2—14405
piezoelectric, Mandelstam-Brillouin scatt., review 2—26199

Scattering continued
light, Brillouin spectra continued
polymethyl acrylate, molecular relax. 2—26202
polymethylmethacrylate, hypersonic absorption, meas. of linewidths as function of temperature 2—40642
polyvinylchloride, hypersonic absorption, meas. of linewidths as function of temperature 2—40642
quartz, absolute scatt. cross-section 2—16522
quartz, fused, stimulated scatt., hypersonic phonons at low temp. 2—16587
stimulated, electrostrictively induced, effect on atmospheric depolarization 2—10730
stimulated lines in crysts., small shift differences, optical heterodyne meas. 2—20081
succinonitrile, plastic and liquid phases, molecular motion and lattic dynamics obs. 2—16589
succinonitrile, plastic cryst. state, molecular motion obs. 2—26203
toluene, Fourier transform obs. of line widths and shapes 2—1103
$Ba_2NaNb_5O_{15}$, stimulated scatt. rel. to catastrophic surface damage during intracavity freq. doubling for Nd:YAG laser 2—29869
$BaTiO_3$, ferroelec., temp. depend., soft optic modes 2—16525
CS_2 Fourier transform obs. of line widths and shapes 2—1103
CdS, acousto-elec. domain, acoustic strain detn. 2—26114
CdS, acousto-electric oscill., scatt. from coherent ultrasound 2—16584
CdS, acoustoelectric, anharmonic and resonance effects 2—26200
CdS, elastic anisotropy effects on acoustoelectric domain propagation 2—36348
CdS, off-axis acoustoelectric domains 2—4056
CdS, optical modulation by acoustic phonon flux 2—22790
CdS, reson. scatt and fund. absorpt. edge 2—33290
CdS, thermal scatt., vel. and attenuation of sound 2—33289
CoF_2, Mandelstam-Brillouin scatt., sound velocity and elastic consts. detn. 2—16580
Ge, at 6328 and 4880 Å, linewidths analysed to give real and imaginary part of refractive indices 2—20082
He II, components of first and second sound, intensity ratio 2—35813
^{4}He, solid, sound velocity and phonon lifetime detn. 2—16585
KCl aqueous solns., Brillouin scattering of laser light 2—3392
KH_2PO_4, KD_2PO_4, soft optic and acoustic modes 2—20072
$KMnF_3$, Mandelstam-Brillouin scatt., sound velocity and elastic consts. detn. 2—16580
LiCl aqueous soln., suggesting low temp. immiscibility 2—15589
LiCl aqueous solns., Brillouin scattering of laser light 2—3392
MgO:Ni, paramag. cryst., scatt. by phonon, avalanche 2—16018
MnF_2, Mandelstam-Brillouin scatt., sound velocity and elastic consts. detn. 2—16580
NH_4Br, disordered cubic phase, hypersound attenuation and dispersion 2—26201
NaCl aqueous solutions, Brillouin scattering of laser light 2—3392
Ne, single cryst., elastic const. detn. 2—16586
RbH_2PO_4, line intensities at ferroelec. transition 2—40697
RbH_2PO_4, soft mode behaviour 2—7083
$RbMnF_3$, Mandelstam-Brillouin scatt., sound velocity and elastic consts. detn. 2—16580
Si, at 6328 and 4880 Å, linewidth analyzed to give real and imaginary part of refractive indices 2—20082
TiO_2, rutile, antisymmetric susceptibility obs. 2—16423
Xe, single cryst., elastic const. detn. 2—16586
Xe cryst., elastic consts. determ. 2—3838
ZnO, off-axis acoustoelectric domains 2—4056
Zno, photon counting distrib. of scattered light from amplified vibr. noise 2—13494

light, Raman spectra
β-quartz, single crystal, determ. polarization characteristics of fundamental optical modes 2—16507
air pollution detection comparison with laser radar method 2—26481
antiferromagnet, scattering of low-freq. e.m. waves 2—7114
atmosphere, N_2/water vapour ratio, laser backscatter 2—16816
atmospheric pollutant remote detection, methods compared 2—1876
atmospheric pollution detection systems, remote 2—37137
atmospheric temp. obs., vertical profiles from backscatter from N_2 2—10718
condensed media, relation between Einstein coeffs for spontaneous and stimulated scattering 2—18376
crystal, from overtones and composite tones of optical vibrations 2—16519
crystal vibration modes 2—29505
crystalline materials, effect of laser fundamental radiation on excitation of stimulated Raman scattering by its second harmonic 2—28861
crystals, shell model description, application to two-phonon spectrum of alkali halides 2—26179
crystals, theory, role of intermediate state interactions and use of group theory analysis 2—26178
degenerate Fermi system, intermediate state interactions 2—16510
depolarization ratios meas., factors influencing precision 2—27647
dielectric crystals, response functions in scattering by vibrational and polariton modes 2—16508
dimers, determ. first three spectroscopic moments of collision induced spectra 2—21561
electronic spectra, collision induced, symmetry selection rules 2_15255
electronic transitions, laser excitation 2—10333
energy band structure, determ. by interband Raman scatt. 2—25716
exciton mediated, resonance props., polariton theory 2—20058
experimental methods, conf. contrib. 2—16446
Fermi resonance of polaritons, manifestation in spectra 2—29927
ferroelectrics, soft mode spectroscopy, coupled modes 2—15995
ferromagnetic cryst., magnons effects 2—40609
gas mixing, unsteady, conc. meas. 2—21902
gas phase Raman spectroscopy, new accessory 2—11544
gases, high resolution technique 2—17731
gases, high-resolution rotation-vibrational spectroscopy with laser excitation 2—24417
gases, l.p., high resolution Raman spectra using single mode Ar laser 2—31135
gases, obs. using plane parallel Fabry-Perot interferometer 2—17732
hexahydro-1,3,5-trinitro-s-triazine, 3200-200 cm^{-1} single crystal and polycrystalline film 2—8783
high source fluctuation compensation by quick analogue dividing 2—2471
holographic interferograms of phase irregularities in stimulated Raman emission light 2—17656

Scattering continued
light, Raman spectra continued
hydrogen bonded molec. fluids, exponential spectral shape rel. to collision induced scatt. 2—3016
impurity centre, asymmetric vibration, resonant scatt. 2—16513
inelastic scattering, by paramagnetic spin waves 2—26184
insulator, transparent, intermediate state interactions 2—16510
intensities, correlation between liquids and gases 2—1098
inverse, in threshold region of stimulated Raman scattering explanation as interference effect 2—18830
iodoform, i.f. spectra, internal mode coupling 2—26198
i.r. generation in acetonitrile and methane by Nd:YAG laser 2—23603
isolation of weak stimulated Raman scattering lines by selective absorption of strongest Stokes component 2—39364
laser, ultrashort pulses 2—37949
light beam propagation in atmosphere, obs. by laser-radar techniques 2—16841
liquid, effect of laser fundamental radiation on excitation of stimulated Raman scattering by its second harmonic 2—28861
liquid, stimulated scatt., temp. depend. 2—18831
liquid two component mixtures, inverse Raman scattering 2—18822
liquids, analysis of orientational broadening of line shapes 2—8514
liquids, and solutions, local field effect obs. 2—35767
liquids, baffle technique for l.f. obs., Starunov's theory 2—18833
liquids, determ. of rotational correlation times from bandshapes 2—25089
liquids, orientational broadening of lineshapes 2—12566
liquids, single crystals and crystalline powders, applic. of Ar laser 2—17744
liquids, study of reorientational motions about different axes 2—9135
matrix isolation spectroscopy, experimental technique 2—11527
matrix Raman spectroscopy, depolarization methods and isotope splitting 2—8529
matrix spectroscopy, isolation laser, developments and applic. 2—11533
meteorological state variable determinations by laser backscatter 2—16808
molecular vibration, book on the foundations of the subject 2—5899
molecule, resonance effect due to excitation in absorpt. continuum 2—745
molecules, first order j-dependent line shifts, classical path impact theory 2—28244
molecules, first order j-dependent line shifts, classical path impact theory 2—28245
molecules, laser spectra, minimisation of emission background 2—31743
molecules in magnetic fields, polarization dependence of intensity 2—31745
nonmagnetic crystal, first order Raman activity, mag. field effects 2—40688
nontransparent samples, relative intensities and depolarization ratios 2—29929
nuclear Raman scattering, 10.38 MeV photons by ^{238}U, ^{232}Th, ^{209}Bi 2—24200
optical filter-cum-condenser lens system 2—38161
phonon hybridization effects 2—20059
phonon scatt. induced by polarons 2—16520
piezoelectric and rhombic crystals, theory of directional dispersion of polar-optical phonons 2—25649
piezoelectric crystal, polariton, Raman scatt. for general wave vectors 2—4026
Placzek-Teller coefficients $b_{j',k}{}^{j,k}$ for negative ΔJ derived 2—12071
withpolariton creation, theory 2—16451
polariton in presence of lattice damping 2—29926
from polariton modes, effect of lattice damping, quantum theory 2—16518
preresonance scatt. tensor study by resolvant method 2—26177
quantum kinetic equation for system with discrete energy levels 2—29928
Raman photon amplifier, quantum statistics 2—31020
reflection spectra 2—40693
rotating sample technique for coloured crystals 2—10410
selection rules, resonance Raman scatt. 2—16511
selection rules in crystals, breakdown of group theory 2—36895
self-action of light arising from stimulated Raman scattering 2—23666
semiconductor, large band, localised energy levels, impurity levels 2—16579
semiconductor, resonance Raman scatt. in electric fields 2—16512
semiconductors, applic., development of tunable sources of i.r. radiation 2—16523
semiconductors, n-type, scattering by coupled Landau level LO phonon system 2—26185
solids, first and second order spectral obs. under hydrostatic pressure, pressure and temp. dependence 2—36896
solids, review of exptl. and theoretical aspects., impact of laser developments on field 2—26182
solids under hydrostatic pressure, meas. of first and second order spectra 2—26181
spectrometer remote, field tests, O_2, N_2, H_2O and CO_2 obs. at 1.6 km range in atmosphere 2—34553
spectroscopy, with tunable dye laser and narrow band filter 2—27644
spherical top molecules, gas phase spectra, rotational profiles of vibrational bands 2—28250
spin flip laser, tunable direct meas. of linewidth 2—23613
stimulated, as technique for generation of coherent light 2—34498
stimulated, excitation coherence in cryst. 2—10404
structural phase transitions, Raman spectroscopy, soft mode theory 2—29925
transient scattering, study of spectral line shape and cross section 2—24416
transient stimulated, exptl. investigation in linearly dispersionless medium 2—11454
transition metal ion and rare earth ion doped crystals 2—20012
two magnon, at finite temperatures 2—16516
variable angle reflection cell, for obs. of matrix trapped molecules and radicals 2—34557
vibrational spectra, effect of phase and pressure changes, review of work 1963-1970 2—8516
visualisation of objects in ultrasonic fields by ultrasonic Raman light diffraction 2—27275
^{209}Bi, nuclear Raman scattering of 10.38 MeV photons 2—24200
CdS, inelastic polariton scatt. 2—16529
α-Cr_2O_3, antiferro- and paramag. phase, phonon mode and magnon scatt. 2—16532
CsH_2AsO_4, paraelectric phase, proton-phonon coupling 2—19364

Scattering continued
light, Raman spectra continued
D metastable atoms, singly stimulated two-photon emission, laser induced quenching 2—24393
EuGa garnet, symmetry labeling of low lying electronic levels 2—20067
GaP thin films, as technique for structure and composition analysis of films 2—29933
H_2, rotational Raman lines, anisotropy in Dicke narrowing rel. to measure of nonsphericity of intermolecular forces 2—38903
I vapour resonant Raman effect, time ordered diagrams for creation of higher vibrational levels 2—12073
I_2, det. of line intensity and importance of virtual transitions 2—18439
InSb, stimulated around 5 μm, investigation of input power and focussing, magnetic field and sample temp. effects 2—20070
KCl, laser-stimulated atomic migration 2—25463
KH_2AsO_4, paraelectric phase, proton-phonon coupling 2—19364
Mg_2X, X=Si, Ge, Sn, Pb, resonant scatt. by F_{2g}-type phonons 2—20074
Mg_2X, X=Si, Ge, Sn, Pb, resonant scatt. by F_{1u} type phonons 2—20075
NaCl:Cu^+ Raman active resonance modes, overtones and anharmonicity 2—20076
$POCl_3$, shifts of crystals meas. with laser Raman spectrometer, structure determination 2—13491
$PbBr_2$ single crystal, obs. 2—7081
$PbCl_2$, single crystal, obs. 2—7081
SbSI, ferroelec. phase transition, long wavelength optical phonons 2—16459
UCl_6, assignment 2—29937
$_{232}$U, nuclear Raman scattering of 10.38 MeV photons 2—24200
^{238}U, nuclear Raman scattering of 10.38 MeV photons 2—24200
XeF_6, vapour and in isolation matrix 2—38944

light, Raman spectra, inorganic
alkali halides, two phonon spectra 2—25658
alkali metal atoms, multi-photon and parametric coupling processes 2—2920
amorphous materials, density of states and thermodynamic props. 2—20061
antiferromagnet, two-magnon scatt., amplitude renormalization factor 2—40689
antiferromagnet, two-magnon scatt. 2—16509
antiferromagnetic transition metal fluorides, study of mixed crystals 2—40543
2,3dichloronaphthoquinone, and i.r. spectra, vibr. assignment of obs. bands 2—31849
dilute solutions of highly coloured compounds, resonance Ramon effect studied 2—12565
dysprosium aluminium garnet, electronic Raman scatt. theory 2—29938
dysprosium gallium garnet, electronic Raman scatt. theory 2—29938
electric-field-induced scatt. by LO phonons in external mag. field 2—33282
ferrimagnetic crystal, by high amp. spin waves 2—20060
ferroelectric, lattice vibr. modes, powder Raman spectra 2—13021
ferroelectric, order-disorder and displacive type, phonon modes and phase changes 2—20062
ferroelectric, tungsten bronze crystal structure, polariton results 2—33281
ferromagnet, scatt. from impurity pairs 2—22669
formates, and i.r. spectra., props. rel. to spectra 2—16542
glass optical waveguide, stimulated scattering 2—17618
group IVa dihalides isolated in solid Ar, N_2 matrices, vibrational spectra and depolarization meas. 2—38884
hexafluorides, spectral analysis, thermodynamic props. 2—823
hexahaloiridates, alkali salts, lattice vibration obs. and force constant calc. 2—40673
hydroxyapatites, hydrothermally prepared, vibr. spectra 2—16527
ice, Ih, polarized domains mixed coulomb valence dynamical models 2—20069
ionic contribution, i.r. active mode and second dipole moment effects 2—16521
lithium formate monohydrate single crystal and aqueous solution, polarization and orientation studies of intense lines 2_26180
metal, line broadening, rel. to electron-phonon interaction 2—16514
metal oxides, with C-type rare earth oxide structure, comparison with theoretical predictions 2—22755
oxides, high temp., characterization of order-disorder 2—9829
quartz, absolute scatt. cross-section 2—16522
quartz, optical modes study 2—16566
quartz, soft mode linewidth temp. depend., near α-β phase transition 2—20078
α- quartz, synthetic, dynamics of impurities 2—19387
rare gas cryst., mol. impurity motion 2—26187
semiconductor, amorphous state produced by ion bombardment 2—26186
semiconductor, diamond- and zinc-blende-type, stress-induced shifts of first-order freqs. 2—20057
semiconductor, magneto-Raman scatt. and lack of inversion symmetry 2—10405
semiconductor, stimulated plasma wave scattering 2—16517
semiconductor superlattice, phonon and polariton modes 2—19315
semiconductors, opaque, hydrostatic pressure effects, Gruneisen const. 2—16539
silicate glasses, phonon densities of states 2—19386
transition metal tetrathio and tetraselenometallates, normal coordinate analysis 2—15340
two-magnon scatt., review 2_36894
ytterbium aluminium garnet, electronic Raman scatt. theory 2—29938
ytterbium gallium garnet, electronic Raman scatt. theory 2—29938
Ag olefin complexes, rel. to νC=C stretching frequencies 2—15282
AgCl from modified shell model, comparison with expt. 2—40024
Ag_2MoO_4, normal spine polarized spectra 2—10408
Al complexes, vibrational assignment 2—15283
$AlCl_3$-$ZnCl_2$, molten system study 2—28863
Ar:$N_2(O_2)$, impurity motion 2—26187
As_4 vapour at elevated temp. in-cavity laser spectroscopy 2—24438
As_4O_6 vapour at elevated temp. in-cavity laser spectroscopy 2—24438
As_2S_3, amorphous 2—22782
$AuAl_2(Ga_2)(In_2)$, scatt. tensor freq. and linewidth, phonon modes 2—16524
B complexes, vibrational assignment 2—15283
B_2Br_4, crystalline and liq., to 40 and 30 cm^{-1} respectively 2—15284
BF_3, BCl_3, BBr_3 and BI_3, crystalline, 77 K, factor group analyses 2—22783
B2O_3 glass, assignments made for observed lines, existence of B=O double bond 2—26189

Scattering continued
light, Raman spectra, inorganic continued
BaF_2, second-order Raman spectra, critical point analysis 2—40691
$BaTiO_3$, ferroelec., temp. depend., soft optic modes 2—16525
$BaTiO_3$, paraelec., linear disorder obs. 2—20063
$BaTiO_3$, temp. depend., linear disorder obs. 2—26188
$Ba_3(XO_4)_2$, X=P, As, V, Cr, Mn, i.r. and Raman vibr. spectra, interpretation based on crystal structure 2—8586
$BeSO_4.4H_2O$, polariton scatt. efficiency 2—16526
$Bi_{12}GeO_{20}$, lattice vibrs. 2—40690
$Bi_{12}SiO_{20}$, lattice vibrs. 2—40690
Br_2, reson. effect in absorpt. continuum, degree of depolarization of vibr. bands 2—24440
C_2N_4, infrared 2—38895
C_3N_2O, crystalline and non-crystalline forms, 77 K 2—29931
$(CO)Fe(PF_3)_4$, C_{3v} and C_{2v} isomers, vibrational assignments and enthalpy difference 2—24446
CS_2 picosecond laser excitation new lines 2—1102
CSClBr, vibrational analysis 2—38896
$CaCO_3III$, high pressure phase, prep. from calcite by method giving Raman spectrum free of $CaCO_3II$ features 2—10406
CaF_2, linewidth temp. depend. and anharmonicity 2—7078
CaF_2, phonon spectra, second order scatt. calc. 2—16004
CaF_2, second- order Raman spectra, critical point analysis 2—40691
$Ca_2NaZn_2V_3O_{12}$, $Ca_2NaMg_2V_3O_{12}$ garnets, stretching modes 2—4464
CaO, second order spectra, polarizability tensor, phonon modes 2—10407
$Ca(OH)_2$ and Ca(OD) , band assignments 2—26190
Cd complex, tetramethylammonium cadmium chloride, l.f.lattice modes compared with $(CH_3)_4NMnCl_3$ 2—1699
$CdCl_2$ (Br_2) (I_2), phonon freq. 2—20064
$CdCr_2S_4$, $CdCr_2Se_4$, chalcogenide spinel, lattice dynamics and mag. ordering 2—32806
CdS, bound exciton reson. Raman effect, temp. depend. line shape obs. 2—16581
CdS, electric field induced by LO phonons 2—16528
CdS, evidence of bound exciton resonance in phonon Raman scattering 2—7079
CdS, reson. and near reson., role of bound exciton states 2—16582
CdS, reson. cancellation of scatt. from lattice vibrs. 2—36897
CdS_xse_{1-x}, solid soln., reson. Raman effect 2—16583
$Cd_{1-x}Zn_xS$, long wavelength phonon freq. conc. depend 2—20065
Ce complex, cerium tris-2,2,6,6-tetramethyl-3,5-heptanedione 2—18441
Cl_2, computer simulation of rotational structure 2—21594
Cl_2O_7 obs. and attributions 2—779
$CoCl_2$, electronic scatt. by Co^{2+} ion 2—16531
CoF_2, antiferro- and paramag. by excitons 2—16530
Co_2GeO_4, normal spinel polarized spectra, electronic scattering of Co^{2+} 2—10408
$Cr(CO)_6$, liquid, automatic assignment of observed frequencies and combinations 2—39369
CsBr, second order Raman frequencies in terms of phonon frequencies 2—29935
CsCl, impurity induced scatt., phonons 2—22410
$Cs_3In_2Cl_9$ 2—31773
$CsNO_3$, polarized Raman spectra in solid and molten phases 2—36898
Cs_2SO_4 single crystal, Ar^+ laser excitation, polarization of Raman lines under different crystal orientations 2—36899
Cs_2ZnCl_4, molten system study 2—28863
CuBr(Cl)(I), second order lines, assignment 2—33283
CuCl, temp. depend., absolute scatt. efficiencies 2—22784
o-D_2, single cryst., rot. spectra, polarization studies 2—26193
DyAl garnet, reson. cancellation of scatt. from electronic levels 2—36897
DyAl garnet, reson. electronic effect 2—26191
$DyAsO_4$, Jahn-Teller induced phase transitions obs. 2—16534
$DyAsO_4$, phase transition 11.17K, degenerate phonon line splitting 2—16535
$DyVO_4$, Jahn-Teller system, electron-phonon modes, theory 2—20066
$DyVO_4$, lattice vibrations and phase transition obs. 2—16533
$DyVO_4$, phase transition 13.8K, degenerate phonon line splitting 2—16535
$DyVO_4$ Jahn-Teller induced phase transitions obs. 2—16534
EuO, 1.8-300K 2—36900
EuO, two magnon spectra and bound state 2—16536
EuS, 1.8-300K 2—36900
EuSe, 1.8-300K 2—36900
EuTe, 1.8-300K 2—36900
F_2O, crystalline 2—29932
$FeBO_3$, phonon Raman scatt. temp. depend., mag. contrib. to intensities 2—40692
FeF_2, electronic scatt., rel. to mag. ordering 2—36901
FeS_2, Raman scatt. from phonons 2—22785
GaAs, amorphous, density of vibr. states. detn. 2—16541
p-GaAs, interband electronic Raman scatt. 2—16567
n-GaAs, scatt. by electronic excitations, coupled plasmon-phonon modes 2—16538
$GaAs_xP_{1-x}$, resonant scatt. 2—22786
$GaCl_3$-CsCl molten mixture, study of melt structure 2—28864
GaP, polariton dispersion and damping, temp. depend. 2—4463
GaP, reflection spectra 2—40693
β-GaSe, layer compound, interlayer bonding and lattice vibrations 2 -25663
Gd complex, gadolinium tris-2,2,6,6-tetramethyl-3,5-heptanedione 2—18441
$Gd_2(MoO_4)_3$, ferroelec.-ferroelastic domain wall struct. 2—16290
Ge-Si alloy, bond vibr. and interband resonance 2—20068
Ge, amorphous, density of vibr. states detn. 2—16541
Ge, carrier conc. effects 2—26192
p-Ge, interband electronic Raman scatt. 2—16567
Ge, resonant peak nature 2—33285
Ge, temp depend., cryst. vibrs. anharmonic props., phonons 2—16540
H_2, D_2, HD, hexagonal phase, phonon scatt. 2—22397
p-H_2, single cryst., rot. spectra, polarization studies 2—26193
H_2 gas, relative Raman cross section, rel. air pollution 2—35249
H_2^+ molecules inclusion of nuclear motion in calc. of optical properties 2—24435
HCl, HBr, orthorhombic crystals, crystal size effects 2—29930
HCl, pressure broadening of rotational Raman lines 2—38913
HCl, rotational Raman lines, meas. of pressure broadening 2—3039
HD, single cryst., rot. spectra, polarization studies 2—26193
H_2O, D_2O, H_2O-D_2O mixtures, stimulated and spontaneous 2—21989
H_2O, in OH stretching region, contours of Raman bands 2—18433

Scattering continued
light, Raman spectra, inorganic continued
HOD in OH stretching region, contours of Raman bands 2—18433
$HSiBr_{3-n}I_n$, ground vibrations determ. 2—24487
$HSiCl_{3-n}I_n$, ground vibrations determ. 2—24487
$HSiI_3$, ground oscillations determ. 2—24487
HTO in H_2O, laser Raman spectra, contributions of OT and OH stretching vibrations 2—32268
He, liquid, Raman diffusion investigation of excited state above phonon-roton spectrum 2—15620
^3He, liquid and solid, meas. of inelastic scattering intensities and spectral forms 2—9194
^4He, liquid and solid, meas. of inelastic scattering, intensities and spectral forms 2—9194
Hg atom, anti- Stokes Raman transition 2—24342
HgI_2, l.f. line, solid-solid phase change, external vibr. mode 2—29934
HgI_2, phase transition 2—16543
HgO cinnabar, lattice vibrations studied with Raman laser and far i.r. techniques 2—32810
I_2, 213 cm-$_1$ line, exciting freq. depend., relative scattering cross section, by resonant Raman effect 2—5933
I_2, reson. effect in absorpt. continuum, degree of depolarization of vibr. bands 2—24440
I_2, reson. fluoresc. continuous passage to reson. Raman effect 2—8660
I_2 dilute solutions, Resonance Raman effect studied 2—12565
InAs, and $InAs_{1-x}Sb_x(P_x)$, resonant scatt. 2—22786
$InBO_3$, phonon Raman scatt. temp. depend., mag. contrib. to intensities 2—40692
$InCl_2$ 2—31773
InSb, resonance enhancement of spontaneous spin-flip Raman scattering and polarization selection rules 2—13489
InSb, spin-flip laser, high intensity 2—16544
InSb, stimulated tunable spin-flip scatt., polarization, cavity and saturation effects 2—16545
InSb, tunable stimulated spin-flip, at various wavelengths 2—10409
InSb spin-flip Raman laser, fund. loss mechanisms 2—34406
Ir complexes, hexahalometalate complexes, force constant calc. 2—16546
KBr:Au, coloured and uncoloured crysts. 2—40676
KBr, two phonon spectra 2—25658
KBr, U-centre localized modes 2—36904
$KBr_{1-x}I_x$ mixed cryst., scatt. from phonons 2—40694
KCl:Au, coloured and uncoloured cysts. 2—40676
KCl:I, Ag, impurity induced 2—26194
$KCoF_3$, mag. excitations 2—20071
$KCoF_3$, one and two exciton Raman scatt., magnon scatt. 2—36902
KH_2AsO_4, ferroelectric, proton-lattice interactions, dynamic susceptibility 2—19377
KHF_2, rel. to crystal and molec. dynamics 2—26169
KH_2PO_4-type crystals, phase transitions, phonon spectra 2—16550
KH_2PO_4, ferroelec. modes 2—13490
KH_2PO_4, ferroelec. phase transition, soft modes 2—16549
KH_2PO_4, $KD_{2x}H_{2(1-x)}PO_4$, KH_2AsO_4, temp. depend., lattice modes, internal vibrations, ferroelectric phase transition 2—16551
KH_2PO_4, KD_2PO_4, soft optic and acoustic modes 2—20072
KH_2PO_4, proton-phonon interactions 2—32811
KI:AU, coloured and uncoloured crysts. 2—40676
KI, U-centres localized modes 2—36904
KM_nO_4 dilute solutions, Resonance Raman effect studied 2—12565
$KMnF_3$, para- to antiferromag. transition 2—16548
$KMnO_4$, rotating sample technique 2—10410
KNO_3 investigation of phonon instability in first-order ferroelectric phase transition 2—25924
$K_{1-x}Na_xTaO_3$ mixed cryst., ferroelec. transitions, soft modes 2—25928
$KNiF_3$, four magnon scatt. 2—36903
$KTa_{0.64}Nb_{0.36}O_3$, paraelec. and ferroelec. phases, phonon modes 2—36905
KX:Tl^+, X=Halogen, Tl^+ induced electron-phonon interactions rel. to Raman spectra 2—16086
KcL, crystals, containing complex impurity ions 2—16547
La complex, lanthanum tris-2,2,6,6-tetramethyl-3,5-heptanedione 2—18441
LiF:Mn, localized vibr. modes 2—25668
LiF, dynamics of F_2^+-centres 2—22772
$LiIO_3$, polaritons and oblique phonons 2—4447
$LiNbO_3$, cross section determ. from polariton eigenfrequency and eigenvector 2—16554
$LiNbO_3$, directional dispersion of phonon frequencies and polariton scatt. 2—16553
$LiNbO_3$, polariton dispersion, temp. depend., soft modes 2—16552
$LiNbO_3$, tunable stimulated scattering, power and linewidth obs. 2—17626
LiO_2, from $Li+O_2$ cocondensation reaction, matrix laser Raman spectra 2 38921
LiO_2 molecule in oxygen matrices obs. of O isotopic shifts for assignment to symmetric O-O vibrational mode 2—28308
$LiTaO_3$ polariton dispersion, temperature tunability 2—1698
$MgCl_2$, crystalline and molten, phonon frequencies, residual lattice bands 2—20073
MgO:Co^{2+} first order, impurity induced lattice vibrs. 2—16555
Mg_2SiO_2, forsterite, vibr. modes 2—22411
MnF_2:Co^{2+}, antiferro- and paramag. phases, by localized modes 2—16530
MnF_2:Ni,Fe, antiferromag., impurity mode energy calc. 2_16562
MnF_2:Zn^{2+}, two-magnon region obs. 2—7080
MnF_2, two-magnon scatt. 2—36906
Mo(CO) , liquid, automatic assignment of observed frequencies and combinations 2—39369
N_2, electrically discharged, relaxation rate and energy transfer 2—38930
N_2 flames, temperature det. 2—37824
NCl_3, isotopic species evaluation of pot. energy constants 2—5937
ND_4ReO_4, far i.r. and laser-excited Raman spectra, librational mode obs. 2—10411
ND_4XO_4 (X=I,Re), ND_4 fundamentals and lattice modes rel. to anomalous temp. dependence of n.q.r. 2—16556
NH_3, solid, molecular and lattice vibrations 2—19382
NH_4BF_4, 77 to 300K 2—24482
NH_4Cl, rel. to study of disorder-order phase transition 2—22372
NH_4ClO_4, low temperatures 2—40675
$NH_4H_2PO_4$, temp. depend., lattice modes, internal vibrations, ferroelectric phase transition 2—16551
NH_4ReO_4, far i.r. and laser-excited Raman spectra, librational mode obs. 2—10411

Scattering continued
light, Raman spectra, inorganic continued
$(NH_4)_2SO_4$, $(ND_4)_2SO_4$, and i.r. spectral variations at ferroelectric T_c 2—22787
$(NH_4)_2SO_4$ solutions, viscosity independence of half-width of $\nu_1(A_1)$ line of SO_4 ion 2—1100
NH_4XO_4 (X=I,Re), NH_4 fundamentals and lattice modes rel. to anomalous temp. dependence of n.q.r. 2—16556
NO, backscatt. cross sections 2—15542
NO gas, relative Raman cross section, rel. air pollution 2—35249
NO_2, wavelength and pressure dependence obs. 2—38929
N_2O gas, relative Raman cross section, rel. air pollution 2—35249
N_2O_4, scatt. cross section detn., Q-switched ruby laser excitation 2—5940
$NaBD_4$, high and low temperature modification, assignment of bands due to isotopic splitting 2—12181
$NaBO_2$, ^{18}O-labelled aqueous solns. 2—21589
NaCl:Au, coloured and uncoloured crysts. 2—40676
NaCl:Br, I, Li, impurity induced 2—26194
$NaCl:Cu^+$ lattice reson., even parity, anharmonic coupling, Raman scatt. obs. 2—16558
NaCl:H first order, field induced, scatt. by localised impurity modes 2—16560
NaCl first and second order, defect induced, F-centre defect 2—16559
$NaClO_3$, vibr. spectrum and dielec. behaviour 2—33286
NaF, second order spectrum, analysis 2—16557
$NaHF_2$, rel. to crystal and molec. dynamics 2—26169
$NaNO_2$, temp.-depend. phonon struct. 2—9866
$NaNO_2$, two-phonon scatt., Curie pt. behaviour 2—6657
$NaNO_3$, disordered phase, correl. field splitting of vibr. modes 2—19378
$NaPF_6$, $NaSbF_6$, $NaClO_4$, aqueous solutions, stimulated and spontaneous 2—21989
$Na_2ZnCl_4.3H_2O$, $Na_2ZnCl_4.3D_2O$, long wavelength phonon spectra, assignment using Raman data 2—40036
Nd complex, neodymium tris-2,2,6,6-tetramethyl-3,5-heptanedione 2—18441
NiO, four magnon scatt. 2—36903
NiO, scattering by phonons, magnons and phonon-magnon interactions from 10-650K 2—26195
NiO, two-magnon scatt. 2—16509
O_2, gaseous, broadening of fine structure Raman lines 2—815
O_2, rotational spectrum, meas. of intensities of spin satellites of S(3) and S(5) lines 2—8695
O_2, simulation of intensity contour allowing for spin splitting 2—21638
O_2 flames temperature det. 2—37824
O_3 gas, relative Raman cross section, rel. air pollution 2—35249
Os complexes, hexahalometalate complexes, force constant calc. 2—16546
$PbCl_4$, neat liquid at 20°C and n-pentane solutions at −40°C, fundamental values determ. force constant and thermodynamic properties recalculated 2—12568
PbF_2, second-order Raman spectra, critical point analysis 2—40691
p- PbS, semiconductor, surface electric-field induced scatt. 2—16561
p- PbSe, semiconductor, surface electric-field induced scatt. 2—16561
p- PbTe, semiconductor, surface electric-field induced scatt. 2—16561
$PbTiO_3$, apparent soft mode line width divergence near transition temp. 2—22788
Pd complexes, frequency dependence on metallic ion 2—15332
Pr complex, promethium tris-2,2,6,6-tetramethyl-3,5-heptanedione 2—18441
$PrAlO_3$, low temp. phase transitions obs. 2—20077
$Pr_xNd_{1-x}AlO_3$, low temp. phase transitions obs. 2—20077
Pt (IV) ammine complexes, substituted, factor group, space group symm. 2—10412
Pt complexes, frequency dependence on metallic ion 2—15332
Pt olefin complexes, rel. to $\nu C=C$ stretching frequencies 2—15282
Pt(II) complex, PtX_2L_2, X=Cl, Br and I, L=dialkyl sulphide, fundamental assignment 2—28322
RbCl, containing F-centres, 80K 2—22789
RbCl, second order Raman frequencies in terms of phonon frequencies 2—29935
$RbClO_3$, phonon Raman spectrum 2—16563
$RbClO_3$ anisotropic crystals, polarized Raman obs. by immersion technique 2—26196
$RbMnF_3$:Ni, antiferromag., impurity mode energy calc. 2—16562
$RbMnF_3$, two-magnon scatt. 2—16509
Rh complexes, frequency dependence on metallic ion 2—15332
RuO_4, i.r. and Raman spectra, coriolis consts., quadratic force constants 2—12190
S, purple form 2—29936
SO_2, backscatt. cross sections 2—15542
SO_4 ions in sulphate solutions, viscosity independence of half width of $\nu_1(A_1)$ line 2—1100
SbSI, investigation of phonon instability in first-order ferroelectric phase transition 2—25924
SbSI, soft phonon couplings in press.-induced phase transition 2—19385
SbSI ferroelectric semiconductor, Curie temp., soft modes 2—16564
SeO_2 and $(SeO_2)_2$, matrix spectra 2—28326
Si, amorphous, density of vibr. states. detn. 2—16541
Si, carrier conc. effects 2—26192
Si, stimulated, using Nd:glass laser 2—33287
$SiBr_{4-n}I_n$, ground vibrations determ. 2—24487
n-SiC:N, Raman scatt., interf. between donor electrons and pure crystal phonons 2—16565
SiC, Kohn-Luttinger interference effect and cond. band minima 2—26197
$Si(CH_3)_4$, gaseous E and F_2 band contours 2—18520
$SiCl_2Br_3$, r_6 value in agreement with calcs. 2—18470
Si_2F_6 vibr. spectra, normal coordinate anal., stretching force constants 2—8709
SiH_4 and SiD_4-SiH_4 mixtures, crystal and liquid 2—33272
Sn, gray, spectrum shape, polarization selection rules, rel. to mag. field 2—16567
$SnCl_2$, matrix Raman spectra, 4.2K, Ar and N_2 matrices 2—12196
p- SnTe, semiconductor, surface electric-field induced scatt. 2—16561
SrF_2, second-order Raman spectra, critical point analysis 2—40691
$Sr_3Ge_3O_9$ and $Sr_3Si_{3-x}Ge_xO_9$, vibr. spectra 2—36907
$Sr_3Si_3O_9$ and $Sr_3Si_{3-x}Ge_xO_9$, vibr. spectra 2—36907
$SrTiO_3$, cubic-tetragonal phase transition, soft modes 2—16569
$SrTiO_3$, differential second order spectroscopy 2—16568
$Sr_3(XO_4)_2$, V=P. As, V, Cr, Mn, i.r. and Raman vibr. spectra, interpretation based on crystal structure 2—8586
$TbVO_4$, Jahn-Teller induced phase transitions obs. 2—16534

Scattering continued
light, Raman spectra, inorganic continued
$TbVO_4$, Jahn-Teller system, electron-phonon modes, theory 2—20066
Te, mode linewidths, polarization selection rules, wavevector shifts, second order struct. 2—16570
Te, thin surface layer on CdTe, Raman detect. 2—7082
TeO_2, phonon modes 2—40695
$TiCl_nBr_{4-n}$, and i.r. spectra, force consts. 2—18471
Tl vapour, electronic stimulated scatt., Stokes shift 2—35146
TlBr, reson., hot luminesc., exciton-optical phonon interaction 2—16588
TlBr, second order Raman frequencies in terms of phonon frequencies 2—29935
$Tl_3In_2Cl_9$ 2—31773
VBO_3, phonon Raman scatt. temp. depend., mag. contrib. to intensities 2—40692
VO_2, semiconductor-metal transition obs. 2—16571
$W(CO)_6$, liquid, automatic assignment of observed frequencies and combinations 2—39369
$Y_3Fe_5O_{12}$ garnet, stretching modes 2—4464
$ZnAl_2O_4$, normal spinel polarized spectra 2—10408
ZnO, hydrostatic pressure effects, Gruneisen parameters 2—16574
ZnS, hexag. single cryst., Raman dispersion of selected phonons 2—16572
ZnS, hexagonal, high press. obs., phase transform. investig. 2—22781
ZnS, hydrostatic pressure effects, Gruneisen parameters 2—16574
ZnS, resonant cancellation 2—16573
ZnSe, resonant cancellation 2—16573

light, Raman spectra, organic
bis-(bromomethyl)-mercury, vibrational assignment rel. to structure determination 2—21669
bis-(chloromethyl)-mercury, vibrational assignment rel. to structure determination 2—21669
1,2-dichloroethane, low and high temperature modifications, assignments made for lattice vibrations 2—8759
acenaphthene-d_{10}, fundamental assignment 2—28341
acetic anhydride, interpretation of vibrational spectra 2—28338
acetone, valence force field obs. 2—18479
acetylene, acetylene-d_2, acetylene-acetylene-d_2 mixed crystals, assignments and relative intensities 2—16575
acetylene and d_1 and d_2 deuterated species, rotational structure of vibrational bands 2—21653
amino phosphines and arsines, i.r. and Raman spectra, vibrational spectra 2—12207
aziridines, vibrational analysis 2—12219
azobenzene, meas. standard intensities, polarization ratio, determ. structure 2—24505
trans- azobenzene and isotopic derivatives 2—35304
azoxybenzenes, in solid, nematic and liquid phases 2—25088
p-azoxydianisole, rel. to equilibrium geometry study 2—8733
benzene, computer calc. of true profiles of Raman lines 2—35311
benzene, meas. of rotational diffusion tensor 2—9135
benzene, methyl substituted derivatives 2—35309
benzene, picosecond laser excitation new lines 2—1102
benzene, stimulated scatt., temp. depend. 2—18831
benzene, temperature dependence of widths and integrated intensities of polarized Raman lines 2—28351
benzene-chromium- tricarbonyl, frequency assignment 2—28354
benzoic acid, single cryst., low freq. spectrum, GF method analysis 2—20079
benzoxazole, vibr. spectra 2—28348
benzyl compounds, vibr. assignments, asymmetric structure 2—8742
benzyl derivatives, para substit., vibr. assignment, asymmetric structures 2—8743
benzyltin derivatives, vibrational assignment 2—21665
1,1′-biaziridine, vibrational assignment and conformation determination 2—38968
biphenyl 2—38967
borazole, rotation spectra 2—17731
bromo maleic anhydride, vibrational assignment and force constant calc. 2—12223
3- bromo-2-bromomethyl-propene, rotational isomers 2—18524
bromobenzene, picosecond laser excitation new lines 2—1102
bromoiodoacetylene, vibrational assignment rel. to force constant determination for dihaloacetylenes 2—38970
bromoxylene 2—35309
t-butyl cyanide, vibrational assignment 2—5963
carbon tetrachloride, laser excited bands, application of slit function corrections 2—9138
carbon tetrachloride matrix isolated in Ar, intramolecular force field obs. 2—35315
carbon tetrafluoride, gas phase spectra, rotational profiles of vibrational bands 2—28250
carbon tetrafluoride, rotation spectra 2—17731
carbonylbis(1-aziridine), vibrational analysis 2—15361
3- chloro-2-chloromethyl-propene, rotational isomers 2—18524
chloro- and bromocyclopentane, conformational analysis 2—18495
chlorobenzene, temperature dependence of widths and integrated intensities of polarized Raman lines 2—28351
chloroform, temperature dependence of widths and integrated intensities of polarized Raman lines 2—28351
chloromaleic anhydride, vibrational assignment and force constant calc. 2—12223
chloroxylene 2—35309
cholesterol esters liquid crystals in crystal, cholesteric and isotropic phases 2—28869
cyanogen azide, spectra with polarizations obtained 2—12232
cyanuric trifluoride, rotational spectra, and bond length det. 2—35357
cyclobutane, vibrational assignments for D_{2d} symmetry 2—28365
cyclobutane-carboxylic acid vibrational spectra 2—24523
cyclohexyl benzene, Raman spectrum obs. 2—3079
cyclopentane, halogen derivatives, at very low temperature 2—35323
cyclopentane, rel. to determination of barrier to planarity 2—15365
cyclopentene, ring puckering vibrations, C-H stretching bands 2—35324
cyclopropane, vibr. transitions 2—33278
dibenzyl mercury, vibrational assignment 2—21665
dibromo maleic anhydride, vibrational assignment and force field derivation 2—12222
dichloro maleic anhydride, vibrational assignment and force field derivation 2—12222
1,2-dichloroethane, equil. const. and pot. barrier for rot. isomers 2—21676

Scattering continued
  light, Raman spectra, organic continued
    1,2-transdichloroethane, orientational disorder and spectra calc. using intermol. potentials 2—25357
    dichlorophenols, i.r. and Raman spectra, fundamental assignment 2—8764
    diethyl amine, vibrational assignment rel. to rotational isomerism 2—3082
    2,2-difluoropropane, vibrational assignment 2—3083
    4,4′dihalogenobiphenyls 2—38967
    2,5-dihydrofuran, ring puckering vibrations, C-H stretching bands 2—35324
    dimethyl sulphide 2—38994
    dimethyl sulphone 2—38994
    dimethyl sulphoxide 2—38994
    dimethylaminodichloroarsine, structure study and vibrational assignment 2—24528
    dimethylaminodichlorophosphine 2—28369
    1,2- and 1,3-dimethylenecyclobutane, spectra obtained for solids at low temps. and liquids 2—12238
    dimethylphenols, i.r. and Raman spectra, fundamental assignment 2—8764
    diphenyl, Davydov splitting magnitude, dependence on crystal elementary cell parameters 2—26183
    1,4-diselenan, vibrational assignments and force constant calc. 2—12236
    1,4-dithian, force constant calc. and vibrational assignments 2—12285
    ethers, divinyl, spectral evidence of vibrational coupling of double bonds 2—8770
    ethylene glycol, OH band obs., chelate form. 2—18502
    ethylgermanes, solid, torsional modes 2—28373
    ethylsilanes, solid, torsional modes 2—28373
    ferroelectric, thiourea, lattice modes 2—4040
    fluorocyclopentane, vibrational spectra and structure of ring 2—12245
    2-fluoropropene, normal coordinate analysis 2—8773
    formaldehyde oxime, spectra obtained at room temperature and 120°C 2—8777
    formic acetic anhydride, normal coord. anal. 2—8778
    glycerin, OH band obs., chelate form. 2—18502
    glyoxylic acid, 4000 to 300 cm^{-1}, vibrational assignment 2—24539
    halogenomethanes, resonance Raman spectra excited by u.v. N_2 pulsed laser 2—28380
    hexafluorobenzene, rotation spectra 2—17731
    hexafluorobenzene, rotational spectra, and bond length det. 2—35357
    hexahydro-1,3,5,trinitro s-triazine, monocrystal vibrational spectra, 10 to 200 cm^{-1} 2—15379
    hexahydro-1,3,5-trichloro and trinitroso s-triazine 2—31859
    hydantoine, vibrs. freqs. 2—5979
    hydrocarbons, halogen substit., gas phase Raman intensities, vibrational study 2—12253
    2-iminothiazolidone-4, vibr. freqs. 2—5979
    iodo(methyl)germanes 2—845
    iodoxylene 2—35309
    isobutene-d$_0$, -d$_6$, -d$_8$, polycrystalline, spectra recorded from 100 to 4000 cm^{-1} 2—13492
    lead dicalcium propionate, phonons assoc. with 60°C phase transition, Raman spectra obs. 2—19405
    l.f., at large angular dispersions of three-prism spectrograph, Starunov's theory 2—28866
    liquids, meas. of relative and absolute scattering cross sections 2—28867
    macromolecules, in physiologically realistic conditions 2—15413
    methane, excited in cavity, stimulated Raman scattering, threshold characteristics 2—850
    methane gas, relative Raman cross section, rel. air pollution 2—35249
    p-methoxybenzylidene p-n-butylaniline, solid, nematic and isotropic phases 2—13493
    methyl(methylthio) mercury, vibrational assignment 2—21693
    methyl alcohol, laser excited bands, application of slit function corrections 2—9138
    methyl chloroformate, vibrational assignments 2—15384
    methylenecyclopentane, liq., fundamental frequency assignment 2—12263
    molecular, cryst., line shift and broadening due to mol. reorientation 2—10413
    n-alkanes, Raman spectra and rotational isomerism 2—40696
    naphthalene, Davydov splitting magnitude, dependence on crystal elementary cell parameters 2—26183
    nematic liquid cryst., stimulated scatt. 2—12564
    neopentane, gaseous, E and F_2 band contours 2—18520
    nitrobenzene, picosecond laser excitation new lines 2—1102
    organometallic acetylides, vibrational assignment 2—15345
    n-paraffins, vibrational modes of Raman bands 2—28392
    pentaerythritol-d$_0$ and -d$_4$, vibrational assignments 2—18521
    phenazine, purification of sample to reduce luminescence effects in spectrum discussed 2—12273
    phenazine, vibrational assignments 2—8809
    picoline, α-, β- and γ-, calc. frequencies, comparison with expt. 2—18842
    polyacrylonitrile, polarized rel. to i.r., structural models 2—8845
    polyethylene terephthalate, laser-Raman study of crystallinity changes 2—35861
    polymer, scatt. from low freq. phonons 2—16577
    polymers, defect induced, vibrational properties 2—16506
    polyoxymethylene, orthorhombic obs. of lattice modes, evaluation of intermolecular potential 2—16576
    polyselenomethylene, hexagonal, vibrational assignment 2—15418
    polythiomethylene, hexagonal, vibrational assignment 2—15418
    propane gas, relative Raman cross section, rel. air pollution 2—35249
    propane-d$_6$, vibrational assignment, symmetric valence of vibrational frequencies of methylene and methyl groups 2—39002
    propargyl alcohol and deuterium analogues, vibrational assignment 2—5990
    propionic acid 2—28399
    3-propynyl chloroformate, vibrational assignments 2—15384
    pyridazine-d$_0$ and pyridazine-d$_4$ 2—35349
    pyridine, calc. frequencies, comparison with expt. 2—18842
    pyrrole, effect of hydrogen bonding on NH stretching Raman band 2—21700
    Raman spectroscopy of organic gases, high resolution, photographic, experimental technique 2—11528
    rhodanine, vibr. freqs. 2—8819
    serum albumin, resolved spectra and fluoresc. 2—39014
    small ring compounds in vapour state 2—12199
    stilbene, Davydov splitting magnitude, dependence on crystal elementary cell parameters 2—26183

Scattering continued
  light, Raman spectra, organic continued
    succinonitrile, liquid and plastic phases, vibrs. assignment 2—33288
    tetrabenzyl germanium, vibrational assignment 2—21665
    tetramethyl phosphorus nitride, vibrational assignment 2—8822
    tetramethylene cyclobutane-d$_0$ and -d$_8$, vibrational spectra measured, symmetry determ. 2—12282
    tetranitro-1,3,5,7 octahydro tetrazocine-1,3,5,7, lattice vibrs. 2—9867
    tetraphenyldítin (IV) carboxylates, spectra from 50-4000 cm^{-1} meas. for crystalline solids in solution 2—24552
    tetrazole, polycryst., laser Raman and external optic phonon spectra 2—10414
    thiazolidindione-2,4, vibr. freqs. 2—8819
    thioketones, aliphatic, intensity and position of thiocarbonyl $\nu_{c=s}$ band 2—28414
    thiourea, ferroelec. transition, obs. 2—20080
    thiourea, inter- and intra-molecular force consts., i.r. and Raman active vibrations 2—29513
    thiourea, lattice modes 2—4040
    thiourea, temp. dependence, mol. and lattice vibrations entropy 2—29923
    1,4-thioxan, force constant calc. and vibrational assignments 2—12285
    tolane, meas. standard intensities, polarization ratios, determ. structure 2—24505
    toluene, temperature dependence of widths and integrated intensities of polarized Raman lines 2—28351
    toulene, picosecond laser excitation new lines 2—1102
    trifluorobenzene, rotational spectra, and bond length det. 2—35357
    trimethyl acetonitrile, vibrational assignment 2—21704
    trimethyl germanium fluoride, normal coordinate anal. 2—24556
    trimethylamine complexes with I_2, Br_2, IBr and ICl, band assignment to vibrations, force constants 2—12294
    trimethylarsenic dibromide and dichloride, vibr. assignments and force field calcs. 2—18536
    trimethylene oxide, vapour phase spectra, rel. to ring puckering transitions 2—18531
    tripropargyl amine, vibr. assignments, rotational isomerism 2—18533
    1,3,5-triselenan, vibrational assignments and force constant calc. 2—12236
  X-rays *see X-ray scattering*
Scattering, elementary particles *see Elementary particles/scattering*
Scattering, nuclear *see Nuclear reactions and scattering*
Scattering, particles
    see also Collision processes; Energy loss of particles; Field theory, quantum/interactions; Elementary particles/scattering; Nuclear forces; Nuclear reactions and scattering; Particle tracks; S-matrix theory; and under individual particles, e.g. Alpha-particles
    book, scattering theory 2—37626
    bubble chamber tracks, least squares fit taking into account multiple scattering 2—14739
    distortion operator method, application to elastic scattering 2—20853
    elastic scattering phase shifts, computation via analytic continuation of Fredholm determinants constructed using L^2 basis 2—17242
    electrons, spectrum shape at high energies, application to proton and deuteron targets 2—2520
    fast particle with arbitrary spin in slowly varying external e.m. field, eikonal approximation, exponentiation and sum rules 2—14113
    Fredholm and Pade approx. for coupled channels 2—20852
    heavy ions, multiple scattering in stripper foils 2—34362
    ions, 90° forward scattering through thin targets for det. of lighter impurities on Si 2—16714
    at lattice site, model for blocking effect 2—9904
    many-particle scattering equations, distortion potentials and reduction method 2—30797
    molecules, differential scattering, low temperature bolometer detector 2—18398
    multiple, random walk theory 2—2155
    plural scatt., small-angle, Monte Carlo calcs. 2—2145
    potential scattering, inverse problem from Dirac eqn. 2—27071
    quasi-particle, from impurities in an imperfect Bose gas 2—30821
    relativistic dressed particle functional S-matrix 2—354
    spin-$^1/_2$ particles, polarization vector description of spin effects 2—27069
    thin absorbers, energy spread for a range of incident particles and targets 2—4089
    Thomson scattering, analogy with double Compton scattering 2—21229
    three-body, K-matrix formalism 2—20854
    three-body, operator connection between Faddeev and Lovelace approaches 2—7681
    three-particle, investigation of two distinct types of perturbation theories 2—23278
    transport processes, order-of-scattering theory 2—37663
    two-particle, relativistic kinematics, hyperbolic surface representation 2—8104
    variable-phase method, perturbation method 2—11287
Schizons *see Elementary particles; Field theory, quantum/interactions, weak*
Schlieren systems
    boundary layer separation measurement, relative merit of monochrome and colour 2—2258
    cinematographic, Xe plasma diagnostics applic. 2—21825
    laser, dark field, for study of gas mixing in unsteady flows 2—21901
    laser technique for det. of refractive index distrib. in arc discharges 2—35636
    single beam interferometer, using Wallaston prism analyzer 2—34479
    ultrasonic pulse propagation and reflection in solids and liquids, visualization 2—37765
    visualisation of radiated field in water above and below Al plates illuminated by short ultrasonic pulses 2—34099
Schottky barriers *see Semiconductor-metal boundaries*
Schottky defects *see Crystal imperfections/vacancies*
Schottky effect (noise) *see Electron tubes; Noise/electrical; Semiconducting devices*
Schrodinger equation *see Quantum theory/wave equations*
Schwarzschild space *see Cosmology; Gravitation; Relativity/general*
Scintillation *see Luminescence*
Scintillation chambers *see Luminescence chambers*
Scintillation counters *see Counters/scintillation*
Seals
    electrical feedthroughs for high pressure low temp. applications 2—20765

Seals continued
- four lip for use in ultra-high vacuum, description and performance 2—17139
- high pressure liquid, for pressure cell 2—26994
- interface contact vacuum sealing processes, phenomena affecting leak rate 2—41408
- materials, stress-strain diagram, testing device 2—22313
- O-rings, metallic 2—5105
- omnidirectional flexible, for thrust vector control of solid rocket motors 2—13811
- rapidly demountable connection using rubber sealing ring for liquid N_2 line 2—41406
- for testing tubes by internal pressure 2—23191
- tests using halide leakage detector 2—30730
- vacuum, demountable, thermoelastic 2—33824
- vacuum and pressure release valve combined for low temp. use 2—23201
- valve, constant volume, pneumatically operated for pressures to 1400 bars 2—23193
- valves, UHV, in vacuum chamber 2—5101
- AgCl for two glass components, using r.f. heating of sealing surfaces 2—20787
- F compatible for sealing electric leads into high press. low temp. cell 2—23192
- In, in low temp. devices 2—41366
- In, ultrahigh-vacuum valve 2—20786

Seawater
- acoustic attenuation due to fish in shallows 2—1805
- Atlantic Canada, continental margin, conductivity structure by geomagnetic induction 2—33419
- atmosphere interaction with ocean marine sediment formation 2—30288
- bioluminescence in ship wake, in Atlantic, Mediterranean and Black Sea 2—13643
- bitumen suspended particles, distribution, morphology and composition 2—13641
- brightness temp. det. from attenuation of i.r. thermal radiation by atmospheric particulates 2—16844
- brine, atomic absorption obs. of trace elements 2—10661
- bubble column, CO_2 desorption 2—1194
- Charlie-Gibbs Fracture Zone, flow of deep water 2—30237
- coherence of ocean currents over vertical distances, moored sensors 2—37106
- diffusion, vertical, in shallow waters 2—1813
- dispersion studies, distorted hydraulic models, pollutant dispersal 2—28748
- drops, size determination 2—32208
- electrical conductivity meas. from shipboard, instrument 2—26477
- fluctuation frequency of envelopes of sound signals reflected from ocean bottom 2—30250
- geochemical 'salt' cycle to explain ocean salinity 2—7205
- heat/NaCl system, stability of double-diffusive layers 2—20279
- horizontal diffusion in stratified vertical shear flow 2—37119
- ice identification with side-looking air-borne radar 2—1793
- isothermal compressibility near 1 atm. 2—33433
- light propagation in, multiple scattering calcs. 2—37120
- light scattering total coefficient, nephelometric obs. 2—13630
- Ocean Weather Station Juliett, upper 100 m temperature and salinity structure 2—37105
- particle dissolution during settling 2—22946
- particle size distribution, scattering of light from underwater laser source, c.r.o. recording 2—1798
- photoluminescence, spectral variations with differences in salinity and concentration of yellow matter 2—1797
- radionuclides, particulate and dissolved, concentration, sampler 2—4653
- rare-earth elements distrib. in sediments of lagoon fed by hot springs 2—13642
- salinity, geochemical 'salt' cycle 2—7205
- sea currents, numerical method for solving theoretical equations of motion 2—13653
- small-scale turbulence, optical methods of observations 2—13663
- sound transmission fluctuations in shallows at multiple frequencies 2—1804
- spray relation to wind-stress discontinuity 2—20281
- STD, two-point, precise calculations 2—13634
- subarctic surface water temperature computation in Pacific in winter 2—13639
- subtropical mode water characteristics, insensitivity to meteorological fluctuations 2—37104
- surface current measurements by dynamics of temperature inhomogeneities 2—13644
- surface diffuse refl. of u.s. wave 2—30259
- surface layer of ocean, origin of thin temperature inversions 2—13636
- surface scatt. of u.s. waves 2—30260
- temperature and salinity profiles under ice island T-3 2—10707
- temperature inhomogeneities, determ. of shape and size 2—30251
- temperature obs., effect of atmosphere when using multichannel i.r. remote sensing 2—13665
- temperature-salinity volumetric analysis, Nova Scotia shelf and Georges Bank area 2—13637
- thermal emissivity, cm wavelength, variations with temperature and salinity 2—1783
- thermohaline convection, turbulent transport processes 2—10712
- thermohaline structure of the Atlantic Ocean tropical zone water 2—13658
- transparency, meas. of locally isotropic hydrophysical fields and measuring instrument distortions 2—12516
- wave refraction in ocean currents 2—20280
- waves, erosion patterns on beach sand due to hyperbolic outer flow 2—3349
- waves, interactions with geomagnetic field 2—33435
- waves, spectral analysis, low frequency waves and seiches 2—4654
- CO_2 concentration at surface, effect of upwelling, mixing and high primary productivity 2—16784
- CO_2 exchange between atmosphere and ocean in eastern South Atlantic 2—13640
- Co uptake by Aeolian dust 2—22948
- H_2S concentration in the Black Sea, a photometric method of determination 2—13664
- N_2O concentration in North Atlantic, rel. to surface air 2—10722

Second sound
- *see also Helium/liquid, sound propagation*
- evaporation of neutral atoms, stimulation 2—6276

Second sound continued
- ionic lattice, velocity calc. 2—32851
- He II, Brillouin components, intensity ratio calc. 2—35813
- He II, uniformly rotating, coupling from second to first sound 2—35812
- He liquid, vel. decrease rel. to mutual friction force 2—18867
- HeII, increase in attenuation in an annulus due to rotation 2—9198
- ^{3}He-^{4}He solution, excitation 2—15623
- ^{3}He, solid, rel. to heat pulse propag. 2—18871
- ^{4}He, superfluid, light scattering from thermal transducer generated density variations 2—18869
- Li^{7}F, drifting sound vel. 2—13033
- NaF, drifting sound vel. 2—13033

Secondary cells *see Electric cells*

Secondary electron emission *see Electron emission/secondary*

Sedimentation
- dilute dispersion of spheres falling in Newtonian fluid, velocity obs. 2—28904
- drops submerged in velocity field in presence of surfactants 2—39314
- marine sediments, in-situ acoustic probe 2—40905
- polyisobutylene in ethylheptanoate, meas. of sedimentation coeffs. near θ-point 2—39395
- polystyrene in cyclohexane, meas. of sedimentation coeffs. near θ-point 2—39395
- velocity, pressure dependent diffusion 2—32283

Seebeck effect *see Thermoelectricity*

Seidel theory *see Aberrations, optical*

Seignette salt *see Rochelle salt*

Seignettoelectric materials *see Ferroelectric materials*

Seismic waves
- *see also Seismology*
- air coupled surface waves, frequency shift, originated by rocket launches 2—16738
- attenuation, lateral variations in upper mantle above inclined earthquake zone 2—22925
- attenuation in a inhomogeneous medium performed on short baselines 2—26437
- body wave magnitudes, basis for seismic discriminant 2—30156
- body- and surface-wave data, determination of focal mechanism and source depth of shallow earthquakes 2—20245
- co-phase analysis technique for detection and parameter est. 2—37140
- coda, det. of crustal layer thickness 2—40893
- crustal transfer ratios of short- and long-period body waves 2—20257
- deep level mines, tabular excavations, seismic events from rockbursts 2—20252
- distant, caused by reflection of spherical shock wave from Earth's surface 2—37085
- earth, attenuation meas. rel. to geophysical prospecting, patent 2—20300
- earthquake focal mechanism, combination of P and S data 2—26416
- earthquakes, effect on nuclear power plants, mathematical model derived from experimental data 2—15098
- elastic wave solns. in stratified media, Thomson-Haskell methods 2—26424
- elastic-wave propagation in two evenly-welded quarter-spaces, numerical solutions 2—17372
- energy release from the aftershock activity of the high yield nuclear explosion BENHAM 2—20240
- explosions, generation in prestressed media 2—26414
- explosions in aeolian soil, effect of rate of detonation of explosives and construction of charges 2—30162
- focal mechanism of Miake-sima volcano earthquakes 2—26443
- focus size estimations of weak earthquakes in the Caucasus 2—26442
- general linear inverse problem, surface waves and free oscillations in determination of earth structure 2—40884
- grouting in dam construction elastic wave velocity meas. before and after 2—4637
- hodochrone inversion for nonplanar waves 2—10688
- Japan, upper mantle P-wave velocity structure from travel time studies of deep earthquakes 2—26411
- long period obs., criteria for identification of nature of first wave 2—40878
- longitudinal, velocity, Black Sea region 2—33407
- longitudinal spectra, Earth's crust structure beneath seismic station 2—40894
- longitudinal waves generated in remote earthquakes, frequency spectrum 2—26444
- Love, finite, propagation in heterogeneous elastic half space 2—34082
- Love and Rayleigh, comparison of multipath propagation at LASA 2—20242
- Love waves and toroidal oscillations of Earth, attenuation data 2—30173
- Montana earthquake, obs. of radiated 2—37082
- multiply reflected, obs. of great distance from source 2—33411
- noise obs. in Greece 2—13611
- NORSAR theoretical model of seismic noise field 2—30172
- nuclear reactor equipment, mechanical supports, dynamic analysis 2—15140
- nuclear reactors, pressure tubes, stress analysis 2—15051
- numerical simulation of seismic sources 2—26425
- outer core, travel times and velocities from PmKP 2—33405
- P, vertical component, energy spectra, crustal effects 2—16737
- P signals, absorption and complexity, from underground ex. 2—7209
- P-wave magnitudes, method of correcting for effect of earthquake focal mechanism 2—30155
- P-wave notion, amplitude spectra of G_2 and G_3 waves, det. of earthquake source mechanism and rupture propagation 2—37088
- P-wave residuals and amplitudes at Iberian stations 2—26447
- P-wave signal from underground explosions, generation by Rayleigh-wave scattering 2—22915
- P-wave travel time gradients, obs. of double discontinuity in upper mantle 2—10690
- P-wave velocities in Upper Mantle from earthquake data 2—4630
- P-waves, reflected from 20° discontinuity 2—33403
- P-waves, reflection from boundaries in lower lithosphere, obs. of nonuniformities 2—33415
- P-waves and Rayleigh waves propagation in Melanesia, structural implications 2—16740
- phase velocities, errors from frequency wavenumber spectral sections 2—37083
- propagation, relationship, between two- and three-dimensional 2—26413
- propagation of Love waves across nonhorizontally layered structures 2—20238

Seismic waves continued
- prospecting, quantitative evaluation of dynamic meas. 2—26434
- ray paths determ. by velocity logging with sets of detectors 2—4635
- Rayleigh waves, reflection and transmission in wedge 2—11350
- reflected, effective velocity obs., effect of correlated errors in hodographs on accuracy 2—7210
- reflected, effective velocity obs. from hodographs, effect of dip in intermediate interface on accuracy 2—7211
- reflection coeff. for solid wedge embedded in solid medium 2—7213
- reflection of shear waves from the reclaimed island in the Kobe Harbour 2—4636
- refraction, obs. of deep sedimentary basin in continental shelf west of Shetlands 2—30192
- refraction, statistics of time term method of analysis 2—26420
- refraction computations for ray segments in media with continuous velocity distrib. 2—30160
- refraction waves for concave bed time-distance curves researched 2—4638
- regional variations on earthquake source spectra from short- to long-period amplitudes ratio 2—20234
- S and P arrival time obs. for estimation of firing depth of underground explosions 2—40879
- S-wave arrival time, overestimation of epicentral distances for earthquakes 2—20247
- SH wave equation, in transversely isotropic inhomogeneous elastic media 2—34081
- SH waves, incident plane, surface motion of semi-cylindrical alluvial valley 2—30151
- SH-waves, propagation in linear viscoelastic solids 2—26429
- shear wave velocities in the Earth's mantle 2—20258
- Skidaway Island, air coupled seismic waves from Apollo launching 2—37081
- surface, damped, saddle point approximation 2—4628
- surface, excitation, earthquakes and underground explosions, periods of 15 to 70 seconds 2—22922
- surface wave propagation in anisotropic media, particle motion in upper mantle 2—30176
- surface waves, Haskell's matrix method, considerations of singularities 2—26430
- synthetic seismograms generation using linear systems theory 2—13605
- teleseismic P waves, apparent velocity variation across large-aperture seismic array 2—22927
- teleseismic P-waves from a 10 ton underwater explosion in North Sea 2—33413
- time-dependent waveforms, extrapolation along path of propagation 2—37084
- transmission and damping in tectonosphere, for rheology det. 2—30212
- transmission and reflection of elastic- viscoelastic interface 2—30174
- travel times and amplitudes, numerical interpolation of velocity profiles 2—17373
- underground hollows determ. by the use of artificial seismic waves 2—4639
- velocigraph, ultralong period, with galvanometric registration 2—40877
- velocities in 3km borehole core in precambrian crystalline rocks 2—16753
- velocity anisotropy in upper mantle in Pacific Ocean 2—22930
- velocity anomalies in upper mantle beneath Tonga-Kermadec island arc 2—16739
- velocity of propagation in sedimentary rocks, effect of depth 2—30195
- vertical profiling data, estimation of intensity of multiply reflected waves 2—30194
- viscoelastic separation from elastic waves in the soft ground 2—4634
- volume, polarization properties in determined and stochastic variants 2—30186
- yield defendence of magnitudes from underground nuclear explosions 2—30175

Seismographs *see Seismology*

Seismology
- *see also Geophysical prospecting; Seismic waves*
- accelerometer, effect of large accelerations on accuracy 2—16746
- Aegean Island arc, geophysical and tectonic features 2—22926
- Alaskan earthquake, 28 March 1964, source mechanism 2—20256
- Alpide Belt-Sunda Arc and adjoining areas, quantitative seismicity maps 2—20239
- Altay mountain region, tectonics and seismicity 2—26449
- anomalous microtilt preceding local earthquake 2—30154
- Antarctica, reflections from discontinuities beneath Novaya Zemlya 2—20251
- artificial earthquakes, response spectrum analysis with two ground predominant modes 2—16743
- Atlantic, absence of anisotropy of the uppermost mantle beneath the East flank of the Reykjanes Ridge 2—20244
- Australian continent, various zones 2—10691
- Baffin Bay, reflection profiling obs. 2—40892
- Black Sea region, velocity field of longit. seismic waves 2—33407
- California, northern and central, seismicity (for 1965-1969) 2—30157
- catastrophic earthquakes, energy estimates of preceding processes 2—26435
- Caucasian weak earthquakes, focus size estimations 2—26442
- Caucasus macroseismic data, earthquake recurrence graphs and seismic activity map, 1961-66 period 2—26441
- Chandler wobble, excitation by earthquakes, realistic Earth model 2_30179
- characterization of region around Dushanbe 2—20255
- Chilean earthquake of 1960, force system 2—30182
- colour sonagrams, data interpretation 2—30164
- continental margin study by refraction experiments 2—7206
- continental shelf west of Shetlands, refraction obs. of deep sedimentary basin 2—30192
- converted earthquake wave method, comparison with deep seismic sounding 2—30196
- crack propagation, Kostrov theory, computational procedure 2—3902
- Crater Lake collapse structure obs., S.E. Saskatchewan 2—26422
- crustal movements in the seismically active areas of Middle Asia 2—7219
- crustal transfer ratios of short- and long-period body waves 2—20257
- data processing and analysis, computer developments 2—30163
- data storage, for offshore recordings 2—1786
- deconvolution of seismogram by reiterative convolution 2—30184
- deep level mines, tabular excavations, seismic events from rockbursts 2—20252
- deformation of a multilayered half-space by stress dislocations and conc. forces 2—23322

Seismology continued
- digital data analysis facility 2—16745
- discriminant based on focal mechanism 2—30156
- displacement fields of inclined faults, analytical expressions 2—20250
- dynamic shear cracks with friction, model for shallow focus earthquakes 2—30180
- Earth, inner core solidity from normal mode observations 2—13618
- Earth's core, fine structure using velocity variation of waves 2—10693
- Earth motion caused by local atmospheric pressure changes 2—37080
- earthquake analysis, structural dynamics in areas of low and average seismic activity 2—16742
- earthquake epicentral distances, overestimation from incorrect S-wave arrival times 2—20247
- earthquake focal mechanism, method of correcting effects on P-wave magnitude det. 2—30155
- earthquake prediction, local movements above active faults, Middle Asia 2—7219
- earthquake prediction, meas. of forerunner indications 2—4632
- earthquake response analysis, nuclear reactor structures evaluated for damping efficiencies 2—15080
- earthquake sequence; absence of accompanying geodetic strain 2—30153
- earthquake sequence near Danville, California (1970) 2—30152
- earthquakes, det. of max. magnitude and max. scale intensity 2—30189
- earthquakes, in SW Germany 2—40880
- earthquakes, influence on Earth's rot. 2—22905
- Earthquakes, mid-Atlantic ridge, statistical study, evidence of clustering 2—4629
- earthquakes, strong, est. of probability 2—30191
- earthquakes and explosions discrimination, surface wave measurement 2—22924
- earthquakes at island arcs and lithosphere 2—26448
- elastic multipole theory and seismic moment 2—20241
- elastic waves parameters det. from pattern obtained by acoustic logging 2—160
- elasto-plastic system, one degree of freedom, effect of heavy vibrations, aid to design of seismic resistant structures 2—27199
- electronic seismometer using a water well as sensing element 2—37086
- exploration, interpretation of data 2—30197
- fault detection from data 2—7212
- Fennoscandian continental array, P-wave velocity anomalies 2—30171
- free oscillations of the Earth from power spectra recorded during periods of low earthquake activity 2—10702
- frictional fault model, relation between apparent stress and stress drop 2—20246
- geoacoustic data, digital acquisition and processing system 2—37078
- great earthquakes, aftershock zones and seismicity gaps, earthquake predictions 2—22923
- Grenville Front, obs. of crust and Moho 2—26423
- ground motion, method for realistic synthesis 2—26419
- ground response of soil deposit on base-rock, surface accelerations 2—20237
- Gulf of Finland, spectral composition of underwater seismic noise 2—26436
- Hamilton County Indiana, analysis using potential field continuation for basement anomaly shape 2—26400
- higher activity during night, rel. to position of Sun 2—1784
- hodochrone inversion for nonplanar waves 2—10688
- holographic weak-signal enhancement technique 2—14434
- hypocentres, calculation for ten earthquakes in Western Sicily 2—10686
- island arcs, anomalous structure, seismological evidence 2—16755
- isochrons in three-dimensional systems 2_30165
- isolines, automatic construction, using computer and plotter 2—30183
- Italian Region, epicentre and maximum observed intensity maps 2—26421
- Kii peninsula in Japan, spatial distrib. of earthquakes 2—30207
- Lesser Antilles, fault plane solutions of earthquakes 2—16736
- l.f. electrochemical filters, application to seismological investigations 2—30147
- long period seismograph, 330 second galvanometer 2—26433
- long-period seismic noise, local fluctuations in atmospheric pressure field 2—37079
- magnitude-energy relation for large and small earthquakes 2—4633
- magnitude-frequency relation and deep-focus earthquakes 2—20243
- marine surveys, signature of large air guns 2—30168
- microseisms, comparison at Berggiesshubel, Moxa and Cuba 2—26431
- microtremors, predominating period of subsoil, from exponential freq. distrib. 2—37090
- MILROW underground nuclear explosion, seismic motion in the distance range 7 to 377 km 2—20253
- Missouri and Tennessee, microearthquake survey 2—26418
- monitoring equipment, electronic, conference, (Washington D.C., August 1971) 2—16723
- Moon, internal friction, dislocation mechanism, lunar rock quality factor from mechanical vibrations and moonquakes 2—13993
- Moon, LM and S-IVB impacts interpreted as modulation mirage 2—13977
- moonquakes, recording by stations installed by Apollo 12 and 14 2—37349
- MRW seismogram transformation, algorithm 2—33408
- Mudurnu Valley Turkey earthquake, source mechanism and rupture propagation 2—37088
- multichannel correlation apparatus, directional properties 2—7214
- Nevada, Rainbow Mountain-Dixie Valley- Fairview Peak area, earthquake distribution and mechanism of faulting 2—13607
- Nevada Seismic Zone, microseismicity and tectonic activity 2—20249
- NORSAR array, technical description and preliminary results of data analysis 2—30178
- nuclear explosion, underground, accompanying strain and its relation to geology 2—26412
- nuclear explosions, atmospheric, ground motions 2—7208
- nuclear reactor building, aseismic design, stress analysis by finite element method 2—15081
- olivine-spinel phase boundary in descending lithosphere 2—22932
- optimal frequency range det. for exploration at various depths 2—30185
- optimization of seismic obs. system, methodical principles 2—40876
- Pacific Ocean, earthquake swarm on the Queen Charlotte Islands fracture zone 2—26410
- permafrost regions, low-noise dynamite experiment 2—30167
- phase transitions, explosive or detonative 2—7207
- PKIKP times and S station anomalies 2—13608
- potentialscope use in discrete-analog system for rapid processing of information 2—30199

Seismology continued
recorders, applic. of piezoelectric devices 2—40869
recording channel response to single pulse 2—30193
recording system, lightweight low power portable 2—30158
records, statistical method for evaluating the correlational properties 2—30198
reflected-wave method, modes of occurrence of reflecting areas on sea bottom 2—13610
San Fernando, California, accelogram of 9 Feb. 1971 earthquake 2—20248
seabed sediments, technique for dynamic testing and engineering studies 2—13651
seismic array data processing, digital techniques 2—26409
sensor array processing with channel recursive Bayes technique 2—26426
sensors, nonlinear equations of motion with two degrees of freedom 2—26432
shear wave velocities in the Earth's mantle 2—20258
shock wave, plane, nonstationary, propagation in soil 2—26446
sonic booms, seismic response below damage threshold 2—37087
source layering function of underground explosions and earthquakes, application of common path method 2—20254
source-generated noise 2—30166
South Sandwich Islands earthquake, focal process, source parameters 2—40881
southern California, regional variations of earthquake source spectra 2—20234
stiffness in faulting and friction laboratory experiments 2—22928
strong-motion accelerograms, zero baseline correction 2—20236
structure of Scotia Sea and Falkland plateau from seismic refraction profiles 2—16779
synthetic seismogram computation from acoustic log 2—40875
synthetic seismograms for deep seismic sounding studies using asymptotic ray theory 2—20235
synthetic seismograms generation using linear systems theory 2—13605
teleseismic P-waves, bandpass spectra, recorded at Hagfors Observatory 2—30177
terrestrial line spectra, realistic Earth models, earthquake source-mechanism 2—30181
theoretical seismograms in heterogeneous media, calc. taking into account absorption and phase velocity dispersion 2—33410
tiltmeter, Hg, development, reduction of sensitivity to temp. and pressure changes 2—16747
time term method of analysing refraction data, statistics 2—26420
timing module for strong motion seismographs 2—30159
Tokachi-Oki earthquake, focal mechanism and contortion of the lithosphere at a junction of two trenches 2—7218
transducers, response to nonharmonic input, analogue simulation 2—30187
travel-time errors in laterally inhomogeneous Earth 2—26415
tsunamis, secondary, detection using variable period band pass filter 2—4655
Turkey, 1970 Gediz earthquake in western Anatolia 2—26390
underground explosions, estimation of firing depth 2—40879
underground nuclear explosions, analysis of signals in four geological environments 2—13606
underground nuclear explosions, effects of water in rocks 2—22929
underground nuclear explosions, elastic energy and magnitude determinations 2—26417
underground nuclear explosions, seismic spectrum scaling 2—30150
underground nuclear explosions and earthquakes, identification 2—40883
underthrusting in southwest Japan, model for convergent plate interactions 2—13609
underwater automatic-buoy seismic station 2—26445
upper mantle structure variation in Australia, from obs. of P-wave anomalies of Cannikin explosion 2—26457
USSR, Western Tuva, energy classification and focal dimensions of micro-earthquakes 2—30188
Venusian experiment at end of decade 2—26826
volcanic activity, correlation between i.r. radiation and earthquake activity of Akita-komaga-take 2—10689
volcanic earthquakes, focal mechanism of Miake-sima volcano 2—26443
volcanism, oceanic, rocks and structures of sea floor, review 2—1810
western Brazil large deep-focus earthquake, 9 November 1963, source process and its tectonic implications 2—20259
western Greece, microearthquakes, interpretation of recordings 2—37089
world-wide detection and identification of underground nuclear explosions 2—16741
World-Wide Network of Seismograph Stations, history and operation 2—30206

Selenium
absorption and electroabsorption near fund. edge 2—33271
aerosol electric field effects on deposition in fibrous filters 2—28915
amorphous, atomic distribution curves 2—22049
amorphous, attenuation length of excited electrons 2—32987
amorphous, crystallization behaviour 2—39434
amorphous, electrical conduction, in review 2—10000
amorphous, electrical props., in review 2—13215
amorphous, field dependent drift mobility 2—16201
amorphous, high field transport and impurity effects 2—10032
amorphous, time dependent heat capacity in glass transition region determ. by differential thermal analysis 2—6680
amorphous film, elec. cond., temp. depend. and mechanism 2—25826
amorphous film, photocond. and optical props. 2—32989
amorphous layers, effective lifetime of charge carriers 2—29673
amorphous thin film, optical consts. determ. from i.r. refl. spectra 2—33200
atoms in gas phase, e.s.r. spectrum, calc. of g-values including configuration interaction effects 2—24349
bulk polycrystalline sample, memory switching effect, crystallization 2—4184
coherent emission from ionic transitions 2—594
compressibility of hexagonal crysts. 2—32600
crystallization from amorphous phase, dislocation form. and motion 2—32525
dielectric constant anisotropy, 3-30 eV 2—22725
diffusion, in ZnSe 2—3825
diffusion in CdS(Te), possible ternary cpd. prep. 2—3820
electrical conductivity anisotropies in molten state and chain structure 2—28893
electroabsorption, temp. depend., indirect edge obs. 2—13480

Selenium continued
electronic bands, Fourier expansion 2—22466
electrophotographic coatings, fatigue phenomenon 2—1316
electroradiographic amorphous Se, charged with X-rays 2—338
extended chain crystals, formation mechanism and occurrence of lamellar and fibrillar spherulites 2—35952
film, amorphous, exponential hole trap distrib. in forbidden band, photoresponse obs. 2—25957
film, amorphous, space charge I-V characts. 2—13259
film, deposition on glass substrate, crystallite orientation 2—1183
film, integrating cell having anomalous photoconductivity 2—37799
film, polarized memory effect 2—32988
film, recrystallization, electron microscopy 2—18934
general properties and applications, review 2—19615
heavy ions, collsions on O_2, Ar, Kr, Xe, C and Au, determ. of charge state fractions 2—668
impurity in Cu, spiral elongation test for annealability 2—3932
ionization coefficient, for holes, photocurrent obs. 2—4217
liquid, current instability 2—12580
liquid, nonlinear IV charact., Poole-Frenkel effect 2—1115
liquid, polymerization, chain dissociation, ring scission, elec. resist. 2—35785
liquid, switching, I-V characts. mag. field effect 2—25105
liquid, switching and memory effects 2—22002
long wave optical phonons, comparison with Te 2—22406
magnetic props. in the solid-state and in soln. 2—13375
memory switching, in bulk crystalline material, amorphous layer formation 2—16212
mobility, microwave Hall effect obs. 2—16216
molecular vapour condensation on epitaxial substrate 2—6337
molten, switching effect 2—12579
monoclinic, band struct., transport and optical props., comparison with orthorhombic S 2—40128
neutron, irrad. effects on resist. and thermopower 2—6823
p-type, trigonal single crystal, barrier limited conduction mechanism 2—10030
phase transformations in amorphous and hexagonal Se at high pressure 2—25636
phonon dispersion curves, neutron inelastic scattering obs., non-bonded force model 2—4042
photocell, thermally stimulated current, energy spectrum of localized centers 2—29687
photodischarge process, quasi-steady- state analysis rel. to electrophotography 2—2480
photoelectric properties, influence of organic solvents and thermoplastic polymers 2—28992
rectifier, hot hole mobility, avalanche Hall effect obs. 2—36559
single crystal film, Cd, Te electrodes, space charge limited current 2—10031
solid target, collisional X-ray excitation by I^- bombardment 2_15226
thermal expansion, negative, role of elastic consts. 2—25688
vitreous, sp. ht., 1.0-0.1 K 2—22425
vitreous, surface tension determination from obs. of thermal healing of scratches 2—39465
AgBr:Se, e.s.r. spectra with different cationic impurities 2—4537
Au-Se system, transient internal photoemission of carriers 2—13209
in Fe-Si alloy, effect on grain growth rate in primary recrystn. 2—39890
in GaAs epitaxial layers, effect of $AsCl_3$ conc. on incorporation 2—9276
GaAs$_{-x}$P$_x$:Se, epitaxial, cathodoluminesc. assessment for light emitting diodes 2—10459
He-Se laser, construction and performance rel. to He-Ne He-Cd and He-Zn lasers 2—27475
InSb:Se, heavily doped, mobility, pressure depend. 2—10020
Se:I, In, molten, impurity influence on props. 2—3406
Se:Tl, trigonal crystal grown by travelling solvent method, d.c. conductivity 2—40263
Se/poly(N-vinyl carbazole), transient accumulation of interfacial charge, xerographic layer sensitization 2—33073
Se/poly(N-vinyl carbazole), transient photoinjection of holes and xerographic layer sensitization 2—33072
Se-CdSe heterojunction strain sensor, properties 2—2056
Se, hexagonal, determ. of anisotropic compressibility and thermal expansion 2—15731

Selenium compounds
monohalides, mol. force field 2—8701
Se-Cu-As, glass, switching phenomena, elec. behaviour, rel. to Cu content 2—13227
As-Se amorphous layers, effective lifetime of charge carriers 2—29673
As-Te alloy, amorphous, photogeneration and high field effects on mobility 2—10032
Co-Se system, P-T phase diagram 2—12609
CuSe alloy, prod. and struct. determ. by electron microscopy 2—29139
Ga-Sb-Se system, stratification region 2—35845
Ge-Se-In system, cryst. samples, switching phenomena 2—25822
Ge-Se-In system, cryst. samples, elec. props. 2—25821
Ge-Se-Te glass, density, softening temp., hardness and elec. props. 2—35846
Ge_2SeTe_7, amorphous semicond., transient characteristics, filamentary plasma model 2—16248
Li-Se, phase equilibrium, miscibility gap and Li_2Se intermediate phase 2—13011
P-Se-Sn system, glass and cpd. formation, n.m.r. study 2—37003
PbSe-$Ge_{1.5}As_{0.5}Se_3$, double glass transition, heat capacity obs. 2—18902
$(Sb\text{-}Bi)_2$ $(Te\text{-}Se)_3$ quaternary solid solutions, thermoelectric properties 2—13335
Se-As-Ge, amorphous semiconductor, film, memory state optically induced reversible change 2—13256
Se-As, chalcogenide, glass transition 2—9225
Se-As glass, powder, sintering 2—19281
Se-Au alloy, cryst. struct. 2—32442
Se-Ge-Sb(As), elec. cond., effect of low temp. annealing 2—36516
Se-Sb, amorphous to crystalline transition assoc. with elec. transition, review 2—13238
Se-Te-As, chalcogenide, glass transition 2—9225
Se-Te alloy, amorphous, microhardness, density, X-ray scatt. and heat capacity relax. effects 2—39772
Se-Te alloy, dielec. tensors 2—1558
Se-Te alloy, elastic stiffness consts., comp. depend. 2—25481
Se-Te alloy, liquid, electrical switching 2—3407
Se-Te single crystal alloy, piezoelec. and elastic props. 2—36600

Selenium compounds continued
Se-U-C ternary system, phase equilibrium, solid state compatibility relationship 2—29482
$Se(GeH_3)_2$ gas, molecular structure sector-microphotometer method of electron diffraction 2—18468
SeN, electronic spectra, vibrational and rotational analysis 2—35288
SeO Cl_2, ^{35}Cl n.q.r., 77 K 2—24493
SeO_2, matrix isolated i.r. spectrum and thermodynamic functions 2—8705
SeO_2, microwave spectrum, 3rd order potential constants and dipole moment 2—31828
SeO_2 and $(SeO_2)_2$, matrix Raman spectra molec. structure, and vibrational analysis 2—28326
$SeO^{2-}{}_3$, in KCl and KBr, i.r. absorp. spectra 2—10387
$SeO^{2-}{}_4$, in KCl and KBr, i.r. absorp. spectra 2—10387
$SeOCl_2$:Nd laser solns., Brillouin and Rayleigh scatt. 2—32269
$SeOCl_2$:Nd liquid laser, lasing and spectral line characteristics 2—17627
Se_xTe_{1-x}, single cryst., piezoresistivity 2—4216
Sn-Se films, vacuum deposition 2—3547
Sn-Se system, Mossbauer study 2—1674
Te-Ge-Se system, amorphous semiconductor, structure and elec. props. 2—29675
Te-Se, liquid alloy, Hall coeff. detn. 2—12581
ZnSe, light emission at n-i junction when forward biased 2—29997

Self-diffusion *see Diffusion in gases, in liquids, in solids*

Semi-insulating materials (high-resistivity semiconductors) *see Semiconducting materials*

Semiconducting devices
see also Counters/semiconductor; Lasers/semiconductor; Masers
5th international vacuum conference, Boston, Mass., USA, Oct. (1971) 2—41374
amplifier-discriminator system for operation with proportional slow-neutron counters 2—17521
avalanche multiplication device, fabrication by ion implantation 2—25882
basic principles, book 2—6856
bimolecular lipid membranes, rectifier behaviour 2—26941
bulk, scanning electron microscope cond.-mode signals 2—4241
chalcogenide switches and memory 2—29716
characteristics meas. after radiation pulses, apparatus 2—29727
charge coupled device, with ion implanted barrier and two nonoverlapping electrodes per bit 2—19695
conference, developments in film and device fabrication, New York (1971) 2—1537
continuously ON, prediction of transistor annealing factors from electrical obs. 2—17519
d.c. thermistor thermometer, numerical method of linearizing 2—20963
design and production, book 2—19612
dictionary in seven languages 2—11243
discrete charge models 2—10080
electric field distrib. meas. using edge electro-optic effect in KDP 2—13439
electron emitters with negative electron affinity 2—22652
electronic engineering materials and devices, book 2—4187
EPIC technology, two step impurity diffusion into finite crystals 2—36552
geometry, conditions for space charge free currents 2—4202
group IV-VI compound semicond. films, device applications 2—40297
Gunn effect, structural features of alloyed contacts to GaAs 2—33037
Gunn oscillator, simple stabilized microwave source 2—20975
h.f. generation and amplification, conference, Ithaca (1971) 2—23573
IC resistors, ion implanted, improvements 2—25879
ICs, defect filtering with orientation dependence 2—6853
integrated circuit, Si precipitation from Al metallization 2—25876
integrated optics guided waves materials and devices, conference, Las Vegas (1972) 2—34368
i.r. detector, Dember effect in Te single cryst. 2—4308
light-sensitive frequency convertor, relaxation generator with controllable base bias 2—36619
material process control, elec. and thermal meas. 2—29694
measurement methods 2—36540
measurement methods 2—19682
microwave field configuration display 2—27348
m.o.s. technology, advances in ion implantation 2—25878
p-n, electrical breakdown, review 2—9982
photocells, $Cu_{2-x}S$-CdS, scanning light microprober obs. 2—4307
photoconductors, effect of multiple trapping centres in presence of radiative interband recombination 2—36608
piezo-semiconductor resonator, damping suppression by drifting electron field 2—4287
power dissipation, diamond/metal contact behaviour 2—15950
processing, use of silane SiO_2 films in control of oxide step contours 2—19693
research application 2—34325
reverse currents apparatus using multivibrator for meas. 2—22574
scanning electron microscopy, informational signal processing 2—3668
sensor applications, state-of-the-art 2—33022
shift register, charge-transfer, surface transport obs. 2—40317
silicon device fabrication by ion implantation doping 2—3793
solar air conditioning, thermoelectric method 2—34297
space and nuclear radiation effects, conference, Durham USA 1971 2—19697
structural elements, laser apparatus for obs. of amplitude and resonance frequency of vibrations 2—27211
surface, Auger spectroscopy 2—1503
surface potential gradients, scanning electron microscopy 2—10077
surface states rel. to surface struct. 2—33005
switch, thin film, negative resist. and filamentary cond. 2—10079
switching and memory devices, amorphous semiconductors, review 2—10001
testing and fabrication, using scanning electron microscope 2—3664
thermistors, design of thermal compensation circuit 2—23489
thermoelectric solar heat transformer 2—34294
thermoelectric transducers, heat resistant 2—11429
thin film, chalcogenide glass threshold switches, frequency dependence of negative capacitance effects obs. 2—6854
three-layer structs., n′-n-n′, n-p-n types, switching fields 2—22573
u.h.f. and mat. technology 2—36553
vidicon, Si, spectral response, effect of SiO_2 chem. vapour deposited film 2—13277
Al film ion impression onto GaAs wafers 2—32358
Al interconnection, anodization, to inhibit hillock growth during high temp. processing 2—3523

Semiconducting devices continued
Bi_2Te_3-Bi_2Se_3 and Bi_2Te_3-Sb_2Te_3 thermoelements, for i.r. radiation power det. 2—17422
$Cd_xHg_{1-x}Te$, epitaxial, i.r. photovoltaic detector 2—6911
CdS-CdSe photoconductive cell, degradation mechanism and reliability estimation 2—29773
GaAs, transferred electron, scanning electron microscope cond.-mode signals 2—4241
GaAs bulk devices, computer simulation on lateral spreading of space charge 2—19698
GaAs Gunn device, high field diagnostics, magnetoresistance technique 2—36564
GaAs(Cs-O), photocathode, photoyield decay characteristics 2—25981
GaInAs (Cs,O), photocathode, interfacial barrier effects, thermally assisted emission 2—19807
GdS:Ag, Al, i.r. detector, high field domain reconfiguration 2—29714
Ge-Si, thermoelectric element, prep. by hot pressing 2—6857
Ge, with B implanted p^+ contacts, γ-detector 2—25883
Ge nuclear counter, low temp. behaviour 2—8234
Ge(Li), γ-ray detector, peak efficiency calibration 2—5592
InAsP (Cs,O), photocathode, interfacial barrier effects, thermally assisted emission 2—19807
InSb tunable detector, for far i.r. spectroscopy 2—27659
Si, masking and passivating layers, parasitic p-n junction form 2—40298
Si, neutron displacement energy effects, requirements for standardization of damage curves 2—19692
Si ion implanted resistor, piezoresistive props., gauge factor and temp. coeff. 2—25880
Si ion implanted thermoresistive sensor, for cryogenic temperatures 2—25884
Si photodetector, for satellite appl. radiation damage 2—25967
SiC, figures of merit and technological problems 2—19696
Te, Dember effect, i.r. detector 2—4308
$Te_{40}As_{37}Ge_7Si_{18}$/Ge electrode, ovonic threshold switching 2—10082
$Te_{40}As_{35}Ge_7Si_{18}$ threshold switch, nature of ON-state 2—22577
VO_2 coplanar, switching initiation and thermal breakdown 2—4243

diodes
amorphous, a.c. voltage amplification 2—10089
avalanche, small signal analysis of p-n junction in breakdown 2—4250
avalanche, triggering behaviour, breakdown voltage detn. 2—10083
BARITT, small-signal negative conductance 2—40301
BARITT, transit-time oscillations 2—36556
electroluminescent, carrier recomb., recomb. rad. intensity, transient characts. 2—19705
electroluminescent, operating characteristics and radiation effects 2—20116
electroluminescent, spacing of photocurrent and external emission spectra maxima 2—20117
glass, transient characteristics, filamentary plasma model 2—16248
Gunn, impact ionization effect on domain potential 2—29722
Gunn, math. model for arbitrary diffusion conditions 2—6867
Gunn, oscillators, ionizing radiation effects 2—19716
Gunn, over critically doped, switching behaviour 2—19704
Gunn, resistively loaded, transverse mag. field effect 2—33036
Gunn, temperature distribution and constant resistance 2—6868
Gunn-effect diode e.p.r. spectrometer 2—5300
integrating two-dimensional Si diode array vidicon astronomical photometer 2—27605
laser, large optical cavity, high power 2—21103
laser, radiation trapping 2—21104
loss resistance meas. 0.2 to 30 ohms using pulse method 2—25874
luminescent, form. by liq. phase epitaxy 2—32343
metal-chalcohalide glass- metal struct., freq. characts. 2—6862
metal-Se, I-V characteristics, Schottky rectification 2—4251
metal-semiconductor-metal, velocity fluctuation noise 2—36565
neutron damage effects, step- recovery frequency multipliers 2—22582
p^+-n, junction noise at high injection 2—36558
p-i-n, large signal theory and performance, use of model 2—6861
p-i-n, volt-ampere characteristics, effect of concentration dependence of excess-carrier lifetime 2—29721
p-i-n microwave switches, neutron damage 2—22583
phase shifters for i.r. radiation 2—40303
photodiodes, obtained by bombarding Si surface with positive ions 2—36618
power diodes, contact joints quality monitoring, high-speed instrument 2—25893
Schottky, recomb. current 2—25891
Schottky barrier, in hot-electron mode as photodetectors, model 2—5433
Schottky barrier, press. sensitivity for press. transducer applic. 2—29719
Schottky barriers, epitaxial PbTe, application to i.r. detection 2—7769
Scottky barrier, with high breakdown voltages, fabrication 2—22584
surface-barrier, electron-hole pair no. depend. on proton energy 2—6702
TRAPATT operation, threshold conditions 2—36557
tunnel, group III-V alloy, tunnel mechanisms and junction characteriz. 2—25897
zener, investigation of microplasma noise with scanning electron microscope 2—6863
Al-GaAs double-heterostructure, electroluminescent diode source for optical fibre transmission lines 2—29991
(AlGa)As-GaAs lasers, heterojunction, narrow active regions, symmetrical 2—11486
$Al_xGa_{1-x}As$, light emitting, partial dissolution during LPE 2—1541
Au-GaAs, surface-barrier, photosensitivity spectra 2—6908
Au-GaAs contact, barrier height depend. on surface layer thickness 2—33030
Au-GaP Schottky barriers, green injection luminesc. 2—13523
CdS, formed by N ion implantation on n-type material 2—25422
CdS, implanted, photoelec. props. 2—15774
CdSe-Cu point contact, polarized memory mechanism 2—16250
CdTe-Au, IV characts, Schottky theory and tunnelling 2—29733
CuSe-Mg contact, rectifying properties studied under low frequency A.C. conditions 2—16249
GaAlAs laser diodes, characteristics 2—21102
$Ga_{1-x}Al_xAs$, tunnel, Au-Ge doped, photosensitive impurity-assisted tunnelling 2—40304
$Ga_{1-x}Al_xAs$ electroluminescent diodes, formation by Al^+ implantation, emission spectra 2—9585
$Ga_xAl_{1-x}As$, electroluminescent, fabrication improved technique 2—16636
GaAs:Ge, luminesc., low-energy emission band obs. 2—26251
GaAs:Zn, high-efficiency electroluminescent, fabrication effects 2—26250

Semiconducting devices continued
- **diodes** continued
  - $GaAs$-$Ga_{1-x}Al_xAs(Zn)$, heterostruct., electroluminesc. diode 2—10454
  - p- GaAs-n-ZnSe, photovoltaic props., I-V characts. junction capacitance, optical collection efficiency 2—25894
  - GaAs, applic. in infrared detection 2—22585
  - GaAs, electroluminescent, degradation with prolonged operation, role of Cu 2—40734
  - GaAs, emitter current limited injection 2—33021
  - n-GaAs, free-running Gunn diode, fluctuations in drift velocity of high- field domains 2—36562
  - GaAs, IV characts., transition processes switching 2—6864
  - n- GaAs, ion implantation, fabrication 2—6838
  - GaAs, surface-barrier structures by chemical deposition of Au, Ni, Ag, In, Sn and Zn 2—25892
  - GaAs, two-stage epitaxial growth on spinel 2—10090
  - GaAs electroluminescent, optical matching methods 2—11523
  - GaAs emission, with transistor structures, characts. meas. 2—1542
  - GaAs Gunn diode, microwave perform. degrad. due to thermocompression bonding effects 2—36563
  - GaAs photodiode, electron bombard., I-V and spectral characts. 2—36620
  - GaAs Schottky barrier, generation rate conversion factor det. using ionizing radiation pulse 2—19706
  - n-GaAs Schottky barrier, tunnelling resist. 2—10092
  - $GaAs_{1-x}P_x$ light emitting diodes, operating parameters, laboratory investigation 2—29723
  - $GaAs_{1-x}P_x$:Se, light emitting, material assessment by cathodoluminesc. 2—10459
  - GaAsP, light emitting, photolum. props., optimum device fabrication procedure 2—40716
  - $GaAs_{0.5}P_{0.5}$, Schottky barrier, generation rate conversion factor det. using ionizing radiation pulse 2—19706
  - $GaAs_{0.6}P_{0.4}$, pn-Schottky hybrid cold cathode diode 2—13353
  - $GaAs_{1-x}P_x$, electro luminescent, defect centres generation during forward-bias degradation 2—7104
  - GaN, blue electroluminescence 2—36962
  - GaP:Mg-O, light emitting, yellow 2—36941
  - GaP:N, p-n junct., efficient yellow electroluminesc. 2—7092
  - GaP, electroluminescent, substrate-epitaxial interface quality effects 2—25199
  - GaP, light-emitting, degradation reduction by chemical passivation 2—7105
  - GaP, light emitting, connected in back direction, time characteristics det. 2—17723
  - GaP, light emitting, neutron damage 2—20094
  - GaP, red emitting, injection and quantum efficiencies 2—33328
  - GaP, technology and electroluminesc. props. 2—29994
  - Ge:Au, n^+pp^+, prebreakdown behaviour 2—13283
  - Ge, reverse biased, i.r. radiation response, impurity and defect levels detn. 2—19707
  - Ge p-n junction, current-voltage characteristic, excess current carriers drift effects 2—25898
  - Ge(Li), γ-ray detector, resolution deterioration caused by fast neutron damage 2—24092
  - p-PbS point contact diodes, hysteresis effect in breakdown region 2—33031
  - $Pb_{1-x}Sn_xSe$, laser emission and band crossing under press. 2—37998
  - $Pb_{1-x}Sn_xTe$ photovoltaic diode, produced by proton bombardment 2—29776
  - PbTe:Sb p-n junction photovoltaic detector, prep. by ion implantation 2—40383
  - Se rectifier, hot hole mobility, avalanche Hall effect obs. 2—36559
  - Si:Ni, current-voltage characts., turnover voltage, photocond., diode parameters 2—22586
  - Si:Pt, charge state and thermal generation in space charge region 2—10091
  - Si, avalanche injection, n′-n-n′ struct., transient characts., switching time 2—22587
  - Si, carrier lifetimes rel. to temp., light spot method, 293-523K 2—33033
  - Si, electronic thermometer 2—2283
  - Si, potential distrib. at surface or n-region 2—19709
  - Si, transient radiation effects near and in avalanche breakdown 2—19710
  - Si diode array camera tube with fibre optic faceplate 2—31155
  - Si image intensifier target for electron microscopy 2—17563
  - Si mesa photodiodes for improved demodulation of light 2—38036
  - Si p-n junction nuclear particle detector, ion implantation fabrication 2—25896
  - Si p-n junction thermometer, forward voltage-temp. characts. 2—40302
  - Si p-n photodiode, fabricated by B ion implantation 2—25968
  - Si photodiode, nonuniformly illuminated, frequency characteristics 2—29725
  - Si photodiode, thin-base, photocurrent kinetics 2—29724
  - Si radiation detectors, temperature depend. of photocurrents produced by X- and γ-rays 2—38383
  - Si Schottky barrier, current limiting processes, fabricating, characts. 2—25895
  - Si Schottky barrier, generation rate conversion factor det. using ionizing radiation pulse 2—19706
  - Si Zener, planar, correlation between lattice defects and elec. props. 2—33032
  - Si Zener diode as transducer for high press. meas. in gaseous H_2 at 15000 atm. 2—20782
  - SiC, diffused, cathodoluminesc., radiative recomb. quantum efficiency 2—16633
  - SiC, epitaxial, prep. and props. 2—22588
  - SiC, light emitting, neutron damage 2—19708
  - SiC, prod. and props. rel. to α-particle detection at high temps. 2—34821
  - α-SiC epitaxial, p-n junc., light emitting 2—9370
  - ZnO-Si, heterojunc., light detector, elec. and optical props. 2—10088
- **junctions**
  - avalanching p-n, submicrosecond transient thermal response, double pulse meas. 2—29718
  - cathode, multi-emitter p-n junction, activation 2—4312
  - conduction band discontinuity, determ. from photovoltage meas. 2—19701
  - detection using optical probe 2—19699
  - diamond, p-n junction form. by ion implantation of B and P 2—36045
  - electroluminescent efficiency, theory 2—4524
  - ion implanted junction device technology, recent advances 2—25875
  - j.f.e.t., transfer power characteristic at liquid air temp. 2—29728
  - laser, curved-junction injection type, patent 2—11491

Semiconducting devices continued
- **junctions** continued
  - lasers, stripe geometry, heterostructure, proton bombardment method 2—21096
  - neutron irradiated, capacitance-voltage characteristics of n^+pp^+ and p^+nn^+ 2—22579
  - p-n, abrupt analytical expressions for elec. field and capacitance 2—6858
  - p-n, avalanche breakdown criterion from doping profile integral 2—33025
  - p-n, breakdown voltage detn., triggering behaviour avalanche diode 2—10083
  - p-n, carrier conc. profiling technique 2—36554
  - p-n, c.w. injection laser thermal problems 2—11485
  - p-n, depth meas. using scanning electron microscope 2—4245
  - p-n, diffusion coeff., impurity conc. depend. 2—10084
  - p-n, electron beam scanning of angle- lapped surface, induced current meas. 2—32958
  - p-n, formation by in-pile irradiation doping of Si^{30} 2—13280
  - p-n, impurities with deep energy levels, compensation of spectral characteristics 2—29772
  - p-n, lasers, principles 2—23614
  - p-n, reactance inversion, band gap depend. 2—33026
  - p-n, small signal response, capacitance calc. for deep traps 2—16245
  - p-n, some problems of the theory of forward biasing 2—1539
  - p-n, space charge region, carrier generation-recombination 2—16246
  - p-n-p-n structs., pot. distrib. during switching transients 2—22578
  - photocathode, field-assisted infrared, feasibility and design 2—25976
  - photocathode, heterojunction, interfacial barrier 2—6922
  - photoelectric convertors, h.v. array-type 2—13348
  - planar avalanching p-n, hole currents in thermally grown SiO_2 2—40306
  - Schottky barriers, epitaxial PbTe 2—7769
  - sensor applications, state-of-the-art 2—33022
  - surface electric field distribution, electron mirror microscope 2—4227
  - tunnel, interactions between mag. scatterers 2—13284
  - CdS-Cu_2S heterojunction, elec. props., photosensitivity 2—36492
  - CdS-$Cu_{2-x}S$ n-p heterojunction, energy band diagram 2—4247
  - CdS-PbS heterojunction, photovoltaic effect visible and near i.r. 2—10148
  - CdS-SnS heterojunctions, photovoltaic effect 2—33082
  - CdS single-crystal/amorphous-semiconductor heterojunction pickup tube 2—10147
  - CdTe-HgTe, heterostruct. with built-in homojunction, photovoltaic effect 2—13350
  - CdTe, p-n formation and conductivity inversion obs. on ion implantation 2—36047
  - CdTe, p-n junction, volume charge region recombination centre parameters 2—34809
  - CdTe, surface-barrier, photoelectret effect on γ-irrad. 2—13349
  - $CuInS_2$, p-n formation and stimulated emission obs. on scanning visible spectrum 2—10416
  - Cu_2S-CdS, heterojunc., photovoltaic cell, optical degradation effects 2—10146
  - n-GaAs-p-AlGaAs heterojunctions, Auger effect and radiative recombination 2—10086
  - GaAs, p-n, illumination influence, Cu diffusion 2—10085
  - GaAs, p-n, recomb. emission, varying local delay time and doping depend. 2—19700
  - GaAs, p-n, Si-doped, impedance, freq. characts. 2—13279
  - GaAs p^+-n solar cell, electron irrad., capacity and defect levels 2—29775
  - n-GaAs Schottky barrier, bistable switching and memory 2—33024
  - $GaAs_{0.6}P_{0.4}$:Te, diffusion of Zn, from G-P-Zn source, p-n junction form., junction profile 2—9586
  - $GaAs_{0.6}P_{0.4}$, ion implanted p-n, annealing effect on characts. 2—25887
  - $GaAs_{0.6}P$, pn-Schottky hybrid cold cathode diode 2—13353
  - $GaAs_{0.6}P^{0.4}_{0.4}$, pn-Schottky hybrid cold cathode diode 2—13353
  - GaP, epitaxial p-n junc., X-ray topography obs. of misfit dislocations 2—4248
  - GaP, light emitting diode material, cathodoluminesc., scanning elec. microscope obs. 2—22813
  - GaP, Zn-diffused, emission spectra 2—36507
  - GaP p-n junction material, minority-carrier diffusion length 2—6815
  - GaP p-n junctions, excess current- and luminescence-noise 2—22581
  - GaSb, p-n junc., carrier conc. and thermal e.m.f. in p-region 2—1540
  - Ge/ZnSe/GaAs(Cs), heterojunc. photocathode 2—6926
  - Ge-GaAs p-n heterojunction, prep. and I-V characts. 2—29720
  - Ge, p-i-n struct., formed by electron irrad., s.c.l. current 2—25889
  - Ge, p-i-n struct. production by electron irrad. 2—25888
  - Ge, self energy effects in tunnelling 2—40290
  - InSb-CdTe heterojunctions, liquid phase epitaxy 2—1178
  - InSb, tunnel, electron-phonon interactions 2—33027
  - PbS-Ge heterojunction, cond. band discontinuity determ. from photovoltage 2—19701
  - Se-CdSe heterojunction strain sensor, properties 2—2056
  - Se photocell, thermally stimulated current, energy spectrum of localized centers 2—29687
  - Si:Au, reverse-biased p^+-n, freq. response of Au centres in depletion layer 2—33028
  - p-Si:B Schottky-barrier tunnel junction, effects of uniaxial compression on zero-bias anomaly 2—19703
  - Si:Cu n^+-p junction, characts., dopant conc. profile 2—25890
  - Si:Fe p-n, switching behaviour, lifetime and photoeffect obs. 2—33029
  - Si-CdS, p-n, elec. and photoelec. characts. 2—6859
  - p^+-n Si-Ge, heterojunction, alloyed, transport mechanism 2—19702
  - Si, masking and passivating layers, parasitic p-n junction form 2—40298
  - Si, N^+-p-n planar struct., prep. by anomalous diffusion of Ga 2—9595
  - Si, p-n, avalanche breakdown, oxygen conc. depend. 2—13281
  - Si, p-n, diffusion, impurity distribution, potential distribution 2—4246
  - Si, p-n, electron beam induced current, model 2—40295
  - Si, p-n, Zener effect, impact ionization 2—13278
  - Si, p-n heterogeneity, surface microscopy charge visualization, electron 2—4244
  - Si, p-n junc., trap parameters, thermally stimulated capacitance obs. 2—25886
  - Si, pnp, with asymmetrical impurity density, method of obs. 2—16247
  - Si detector, rad. enhanced diffusion, defect prod. ratio 2—33023
  - Si p-n, junction, mesoplasma, isothermal dynamic I-V characts. 2—40300
  - n-Si Schottky barrier, bistable switching and memory 2—33024
  - α-SiC, p-n, shallow ion- implanted, electron emission 2—40299
  - SiC, p-n prod. and props. rel. to α-particle detection at high temps. 2—34821
  - α-SiC epitaxial, p-n junc., light emitting 2—9370
  - SiC p-n, cold cathode, multi-emitter activation 2—4312

Semiconducting devices continued
junctions continued
SiC p-n junction cold cathode, elec. characts. analysed 2—22654
ZnO-Si, heterojunc., light detector, elec. and optical props. 2—10088
ZnS-GaP n-p heterojunction, prep. and I-V characts. 2—29720
ZnSe-GaP n-p heterojunction, prep. and I-V characts. 2—29720
ZnSe-Ge heterojunctions, switching and memory characts. 2—6860
ZnSe-ZnTe heterojunction, epitaxial growth, green electroluminesc. 2—40735
ZnTe-GaSb, p-p heterojunc., elec. and optical props. 2—10087
transistors
17th International Electron Devices Meeting, Washington (1971) 2—22575
annealing, short term, by neutrons in biased off mode 2—19711
avalanche, volt-ampere characteristics and method for obtaining 2—23543
bipolar, ^{60}Co γ-irrad. effects on noise parameters 2—22594
bipolar, high performance and stability due to surface passivation of semiconductors 2—4186
bipolar, integral charge-control model, hot carriers effect 2—36560
bipolar, ultrahard, design criteria, neutron tolerance 2—19714
circuit behaviour, computer simulation with systematic selection of transistor models 2—17516
with circular emitter, thermal resist. 2—36561
delay time bridge, displacement damage effects in bipolar transistors 2—21009
fabrication, enhanced diffusion 2—9590
f.e.t., small source-drain voltage case, nonlinear resist. 2—13285
field effect, in spectrometric amplifiers for semiconductor detectors 2—19715
gain degradation mechanism, neutron irradiation 2—22591
gamma-ray and neutron effects on current gain response 2—22590
gated, emitter avalanche currents 2—6866
j.f.e.t., ceramic encapsulation, manufact. process and statistical analysis of noise and elec. parameters 2—29726
j.f.e.t., fabrication by ion implantation 2—25899
j.f.e.t., transfer power characteristic at liquid air temp. 2—29728
j.g.f.e.t., thermal noise behaviour at 77 to 300K 2—1543
junction field effect, transient radiation response 2—19713
metal-nitride-oxide-semiconductor, charge storage at electric fields near gate insulator breakdown 2—6865
microwave, fabrication by ion implantation 2—25900
m.i.s. memory transistor, charge transport time depend., direct tunnelling model 2—22598
m.o.s., radiation hardening 2—19738
m.o.s., Si inversion layer, electron conductivity-mass anisotropy calc. 2—36569
m.o.s., silicon-on-sapphire, characteristics for radiation hardened aerospace systems 2—19742
m.o.s. self aligned gate, speed improvement by ion implantation 2—25901
m.o.s.f.e.t., X-irrad. effects 2—13296
m.o.s.t., surface capture centres 2—22580
m.o.s.t. inversion layer, hole mobility, low temp. Hall effect obs. 2—16254
neutron-hardened, role of emitter area 2—22592
nuclear irradiation effects 2—40305
p-n-p, alloy junc., minority carrier diffusion, intense mag. field effects 2—22589
photocurrent due to photon drag of carriers 2—6909
shock induced elastic ripples on surface, obs. by nsec. photography 2—8055
surface-charge, quasistatic and transient response 2—4252
synchronous detector, transistor-switch, based on integrated microcircuits 2—23487
temperature measurement of surface by means of fluorescence of coating of phosphor 2—5281
Al_2O_3-CdSe thin-film transistor, effects of ionzing radiation 2—22595
GaAs emission diode with transistor structures, characts. meas. 2—1542
GaAs semi-i.g.f.e.t., compensation by proton bombardment applic. 2—25820
Mo/Au-Ge/Ge/n-GaAs/Ge/Pb-Ge layer composition and microhardness 2—4249
Si, bipolar, dislocation and stacking fault generation at surface heterogeneities 2—33035
Si, j.f.e.t. neutron and γ-ray responses 2—22593
Si, junction, effect of electron bombardment on shot noise 2—13286
n-p-n-Si, performance rel. to slip plane dislocations 2—1544
Si f.e.t., noise temp. at 2 and 4 GHz, obs. 2—4253
Si junction f.e.t., neutron produced trapping centres 2—19712
Si junction f.e.t. neutron radiation effects, defect formation in space-charge region rel. to characts. degradation 2—10093
Si m.o.s.f.e.t., differential negative resistance of n-type inversion layer 2—19740
Si m.o.s.t., inversion layer, hole drift vel. 2—19743
Si n-p-n, fabrication by ion implantation 2—29729
Si n-p-n microwave, applic. of enhanced diffusion by proton irrad. 2—25902
Si n-p-n planar, gamma and electron irrad. effects 2—10094
Si npn, effects of intense ionizing radiation 2—13287
tunnel and interface devices
see also Metal-insulator-metal structures and devices; Metal-insulator-semiconductor structures and devices; Tunnelling
17th International Electron Devices Meeting, Washington (1971) 2—22575
junction, interactions between mag. scatterers 2—13284
metal-semiconductor-metal diode velocity fluctuation noise 2—36565
reliability physics, 9th annual proceedings, New York (1971) 2—6869
thin film triode, amplification of injected current from tunnel cathode in p-type amorphous layer 2—33034
tunnel diode transistor binary counter 2—31372
tunnel diodes, group III-V alloy, tunnel mechanisms and junction characteriz. 2—25897
tunnel junctions, preparation by glow-discharge oxidation of freshly evaporated Al films 2—37042
$Ga_{1-x}Al_xAs$ tunnel diodes, Au-Ge doped, photosensitive impurity- assisted tunnelling 2—40304
n-GaAs-metal tunnel contact, ion bombardment effects on tunnelling characts. 2—16251
n-GaAs Schottky barrier, tunnelling resist. 2—10092
Ge, heteroepitaxial film on GaAs, stress, orientation thickness effects 2—3534
InSb tunnel junction, electron-phonon interactions 2—33027

Semiconducting devices continued
tunnel and interface devices continued
p-Si:B Schottky-barrier tunnel junction, effects of uniaxial compression on zero-bias anomaly 2—19703
Si-Si_3N_4- SiO_2-Si, s.n.o.s. diode, instability, diffusion effects 2—10097
Si-SiO_2 interface device, performance, stability 2—40307
Te-TeO_2-Pb, tunnelling junction, phonon assisted tunnelling effect 2—29688
Semiconducting materials
see also Ion implantation; Magnetoelectric effects; Photoconductivity; Photovoltaic effects; Semimetals
alkaline earth titanates and zirconates, band gap determ. 2—1526
alloy, disorder effects on band gaps 2—32997
alloy, substitutional, origin of energy gap bowings 2—40270
amorphous, anomalous relative sign of Hall and Seebeck coeff. 2—22519
amorphous, charge carrier mobility at mobility edge 2—40237
amorphous, electrical props., review 2—13215
amorphous, in thin film switch, negative resist. and filamentary cond. 2—10079
amorphous, switching, differentiation between electronic and thermal 2—13216
amorphous, switching, thermal effects 2—6794
amorphous, switching and memory effects, review 2—10001
amorphous, tetrahedrally bonded, elastic deform. effect on elec. cond. 2—36489
amorphous, thin film, review 2—10005
amorphous alloys, electronic basis of switching 2—36485
amorphous films, condition for memorization by laser light pulse 2—4188
anthracene, avalanche breakdown and light emission 2—19754
anthracene, conduction processes, review 2—13246
anthracene, diffusion length of singlet excitons 2—6737
anthracene, effect of γ-ray induced impurities on semiconductive behaviour 2—19614
anthracene, electron and hole generation 2—36521
anthracene, exciton induced photoemission 2—22659
anthracene, narrow band semiconduction, in review 2—9998
anthracene, photo-electret formation, effect of alternating field 2—4285
anthracene, photocond., oxygen influence 2—33079
anthracene, single cryst., field dependent electron and hole losses, drift current pulse obs. 2—13247
anthracene, single crystal, surface trapping, photoinjection obs. 2—13248
anthracene, thermal activation energies for hole injection 2—16318
anthracene, X-ray excited electron-hole pairs, geminate recombination 2—10040
anthracene alkyl-substituted analogues, films, cond., photocond., optical absorpt. 2—13249
anthracene film, γ-irrad., I-V characts. 2—29681
anthracene film, space charge limited currents with uniform and non-uniform trap distrib. and size effects 2—40266
aromatic hydrocarbon crystals, contact potential and work function 2—25849
arylidene-1,3-indandiones, effects of polar molecules chromophoric conditioning 2—25962
benzylidene-1,3-indandiones, effects of polar molecules chromophoric conditioning 2—25962
biological materials, microwave dielectric and Hall effect measurements 2—26939
biological polymer, microwave Hall effect, mobility detn. 2—16216
bis-(maleonitriledithiolene)-metal chelate complex, conductivity and e.p.r. obs. 2—16218
CdS, photoconductive and luminescent properties obs. 2—13339
n-CdSe, conduction band edge, magnetophonon effect 2—19661
cetyl alcohol, proton injection measurements 2—25847
chalcogenide bonding bands, lone-pair bands and impurity states 2—19662
chalcogenide glass, between metal electrodes, switching processes 2—19634
chalcogenide glass, model for elec. cond. mechanism 2—19628
chalcogenide glass, thin films threshold switches, frequency dependence of negative capacitance effects obs. 2—6854
chalcogenide glasses, metal- semiconductor transition 2—40439
chalcogenide glasses, small polaron hopping motion, investigation via measurements of charge transport processes 2—32986
chalcogenides, amorphous, a.c. cond. 2—16205
chalcogenides, amorphous, photocond. analysis 2—36609
charge transfer complexes, conduction mechanism, conductivity and e.p.r. obs. 2—10526
chloranil-amine charge transfer complex, elec. cond., e.p.r. 2—25832
chlorophyll-a films, conductivity and photovoltaic effects 2—26942
chromium(III) trisacetylacetone film, IV characts. 2—36522
chrysene, single cryst., prep. and characterization 2—19009
conductivity and Hall effect, measurement by computer controlled automatic system 2—19680
conductivity measurements, transmission of TE_{11} microwaves in circular waveguide 2—19679
copper heteroorganic acetylenides, absorption and photoconduction spectra investigated by diffuse reflection spectroscopy 2—29922
copper phthalocyanine, thermo e.m.f. temp. depend. 2—36606
copper phthalocyanine films, photo-e.m.f. spectra, near i.r. 2—6907
coronene, calculation of band structure and carrier mobilities 2—25727
diamond, electronic struct. and optical props. calc. using discrete variational method 2—1525
diamond, resist., heavy neutron irrad. effect 2—36496
diamond, thermoluminesc., phosphoresc. 2—26245
diamond, thermoluminesc. theory, kinetic eqns., recomb., trapping 2—26246
diamond, X-ray photoelectron spectrum, valence band width, density of states 2—25978
diamond-type, dielec. function 2—6826
diamond-type, stress-induced shifts of Raman freqs. 2—20057
dictionary in seven languages 2—11243
diphenylpolyene, film, trap distrib., space charge limited current obs. 2—40267
electrical breakdown, review 2—9982
electrical resistivity determination at high temperatures and pressures, phase transformations 2—37528
electroceramic oxides, control of properties by microstructure 2—32738
electronic specific heat, heavily doped, in weak mag. field, Geeen's function method 2—9886
electronic transitions at high press., reveiw 2—15955

Semiconducting materials continued
- elemental, ambipolar diffusion coeff. determ. 2—1509
- elemental, amorphous, band struct. and transport props. 2—19646
- epitaxial layer growth, from soln. in liq. metal theory 2—18930
- N-ethyl-phenothiazine-iodine complex, dielec. props. at 10 GHz 2—22544
- europium chalcogenides, halide doped resistivity increase 2—4353
- europium monochalcogenides, prep. and resistivity rel. to vacancy conc. 2—9367
- ferroelectric, effect of charge carrier on behaviour 2—16276
- ferroelectric, photocond. due to surface layers 2—4296
- ferromagnet, $CdCr_2Se_4$, elec. props. and photocond. 2—1512
- field electron emission, saturation region in Fowler-Nordheim characts. 2—6917
- film, diamond and zincblende struct., twinning probability calc. 2—39525
- film, surface plasma losses, dispersion 2—29691
- film characterization during deposition from field-effect meas. 2—40231
- GaP, cond., surface and contact effects 2—19675
- glass, chalcogenide, pressure and frequency dependences of threshold voltage, delay time, thermal switching 2—16220
- glass, electron conductivity, bistable behaviour in covalent thin films, uses 2—16202
- glass, endothermic phenomena in switch-on process 2—32960
- glass, $Ge_xSe_{1-x}(Te_{1-x})$, thin film struct. and neutron damage 2—1516
- glass, Ovshinsky switching, double injection 2—32990
- glass, protonic, elec. cond. 2—40232
- glass, transient characteristics, filamentary plasma model 2—16248
- glass filter 2—22757
- glassy chalcogenide, standard state choice for physicochemical studies 2—32966
- graphite, colloidal sheet of paper with random holes, percolation theory and bulk conductivity 2—9983
- graphite, Hall effect and thermoelec. power minority carrier study 2—36497
- graphite, irrad., elec. resist. rel. to thermal cond. 2—13220
- graphite, pyrolytic, electrical resistivities from charge carrier transport parameters 2—29661
- graphite, transport props., temp. depend. doping influence 2—1510
- group cpds., III-V cpds. photocathode, major detector development 2—40389
- group I-III-VI$_2$ cpds., resist., annealing effects 2—40242
- group II-IV-V compound, ABC_2 type, Mossbauer obs. 2—1669
- group II-IV-V compounds, chalcopyrite semiconductors, linear and non-linear optical properties 2—26100
- group II-VI, effective charge and piezoelec. effect 2—36596
- group II-VI and III-V cpds., displaced atomic species 2—6487
- group II-VI compound, F^+ centre, electronic struct. 2—1261
- group II-VI compounds, single cryst. growth from gel 2—18989
- group II-VI cpds., high symmetry pts. in Brillouin zone 2—19361
- group II-VI cpds., impurity photocond. spectra 2—6901
- group II-VI cpds., interband Faraday effect 2—13435
- group II-VI cpds., interband Faraday effect 2—13437
- group II-VI cpds., interband Faraday effect 2—13436
- group II-VI cpds., rare earth photoluminesc., sensitization 2—20092
- group II-VI cpds., sensitization of rare earth photoluminesc. 2—22801
- group IIB-VIA, upper d-levels from X-ray and u.v. photoelectron spectra 2—36633
- group III-V, effective charge and piezoelec. effect 2—36596
- group III-V, II-VI binary systems, phase diagram calc., liq. soln. models 2—3358
- group III-V, II-VI cpds., semiconductor- metal transition at high press. 2—15955
- group III-V, optical effective mass of electrons, temp. dependence 2—36525
- group III-V compound, e.p.r., review 2—33334
- group iii-v compounds, crystalline and amorphous, density of states calc. 2—10049
- group III-V compounds, hot electron galvanothermomagnetic props., low temp. 2—19779
- group III-V compounds, review of vapour-phase-growth method 2—3573
- group III-V cpds., n.m.r. lineshifts 2—10551
- group IV-VI compound semicond. films, device applications 2—40297
- β-hydrogen phthalocyanine, tight binding energy band calcs. 2—13261
- impurity analysis, group concentration methods 2—20205
- impurity distribution in thermoelectric material, from radioactive analysis 2—30125
- impurity states, redistrib. due to impurity-phonon interaction 2—40028
- indirect-band-gap, two-photon transition 2—22753
- inhomogeneous, high apparent mobility 2—4204
- ion implantation, anomalous penetration 2—25419
- ion implantation, techniques, processes, equipment, applications 2—25418
- isocytosine, proton injection measurements 2—25847
- isoelectronic impurities, screened potential 2—13201
- layered inhomogeneous structures, transmission and reflection spectra, layer thickness detn. 2—40643
- lipids, bimolecular membranes, conductivity and photoconductivity 2—26941
- liquid, charge carrier mobility at mobility edge 2—40237
- measurement methods, microwave 2—16233
- measurement methods 2—19682
- metal-insulator transition, coherent- potential approximation solution of Falicov-Kimball model 2—19663
- molecular cryst., charge-carrier injection, metal or electrolyte interface, theory 2—36520
- n-type, analysis of two band Hall effect and magnetoresistance 2—9987
- n-type, light scattering by coupled Landau level LO phonon system 2—26185
- naphthalene electrets, polarization, Schottky barrier formation 2—4191
- organic, electrical conductivities 2—4190
- organic, H-bonded crystals, proton injection measurements 2—25847
- organic, single cryst., Hall effect d.c. measurement technique 2—16215
- organic, upper limit of effective electron mass 2—40228
- organic molecular crysts., valence bandwidths, vac. u.v. photoemission obs. 2—19812
- organic semi-insulators, electrical conduction 2—4221
- organic thin films, bistable switching 2—25831
- ovalene, calculation of band structure and carrier mobilities 2—25727
- oxide, with metal or higher valence state oxide inclusions, elec. cond. calc. 2—40241
- p- PbTe Raman scatt., surface electric-field induced 16561 2—16561
- pentaerythritol, proton injection measurements 2—25847

Semiconducting materials continued
- perylene complex, conductivity and e.p.r. obs. 2—16218
- phenoxatiin, film, transport processes 2—16217
- photo- and electroluminescence, photo-e.m.f., high-resolution measurements 2—36959
- photocathode, field-assisted infrared, feasibility and design 2—25976
- photoelectric properties, phonon heating effects 2—40375
- β-phthalocyanine single crystal, drift mobility, temp. depend. 2—32993
- piezoelectric, non-normalizability of hot electron distrib. function 2—29653
- piezoelectric, Rayleigh wave amplification, in transverse elec. field 2—6668
- piezoelectric, u.s. amplification in oscillator platelets 2—19419
- piezosemiconducting plate, transverse surface waves, spontaneous oscillations generator 2—25680
- piezosemiconductor, transverse acoustoelectric surface domain structure 2—25669
- piezothermopower, phonon drag effect in n-type material 2—4239
- plasma, solid state, collision dominated, interaction of randomly phased vibrational waves 2—1428
- polyacrylonitrile thin film formation by vacuum deposition 2—29048
- polydiphenylacetylene films, hole mobility 2—1530
- polypenyleneaminochloranils, electrical and magnetic properties 2—25835
- polypyrimidine, elec. cond., temp. depend. 2—25836
- Poole-Frenkel constant evaluation 2—1524
- powder-like mixture for u.s. amplification, elec. and mech. props. 2—6670
- PVK, amorphous, field dependent drift mobilities 2—16201
- rare earth monochalcogenides, electronic collapse at high pressures 2—29589
- rare earth ruthenates and iridates, electronic characterization, cryst. chem. considerations, elec. and mag. meas. 2—10076
- resistivity measurement, microwave technique 2—19681
- rubrene, hole mobility 2—25851
- samarium monochalcogenides, prep. and resistivity rel. to vacancy conc. 2—9367
- semi-insulators, trap-controlled space-charge-limited current rel. to Poole-Frenkel barrier 2—40230
- sisal wax, elec. conductivity rel. to suitability for electret preparation 2—29759
- small gap semiconductor, effect of transverse elec. field on Landau diamag. and Pauli paramag. quantization of conduction band 2—9981
- solid solution, supersaturated, precip. kinetics 2—6607
- space-charge-limited currents, in presence of traps with Coulombic potential 2—29656
- surface conductivity, measurement by field effect obs. 2—19676
- TCNQ complex, microwave Hall effect, mobility detn. 2—16216
- TCNQ polymeric complex salts, factors affecting conductivity 2—25837
- TCNQ salt, enhanced nuclear relaxation near Mott transition 2—33182
- TCNQ salt, spin susceptibility and phase transitions 2—13094
- TCNQ salts, compactions, Seebeck and Hall effects 2—25833
- TCNQ-NMP, metal-insulator transition 2—19657
- ternary, external luminescent efficiency, theory 2—4524
- tetrolic acid, proton injection measurements 2—25847
- transition metal compounds, nonstoichiometric, semiconductor-metal transition, magnetic and electrical properties 2—4218
- transition metal cpds., metal-insulator transition 2—13241
- transition metal oxide, free and bound charge carriers 2—10028
- transition metal oxides, mixed, phase diagram 2—36533
- tubular semiconductor specimens, measurement of Hall coefficient 2—29692
- violanthrene A, single cryst., intrinsic conduction 2—13250
- vitreous, chemical bonding, theory 2—19613
- wurtzite cpds., excition energy levels 2—4222
- wurtzite-type, energy spectrum of direct excitons 2—36526
- zero gap semiconductor, HgTe type, electron and heavy hole Landau level crossing 2—9981
- zinc-blende-type, stress-induced shifts of Raman freqs. 2—20057
- Zincblende alloy, charge distribution, pseudopotential approach 2—6716
- zincblende alloy, energy gap, comparison pseudopotential and dielectric methods 2—6717
- zincblende alloys, atomic displacement effect on energy gap bowing 2—25839
- zincblende-type, dielec. function 2—6826
- zirconia, solid electrolyte, n-type cond. 2—22542
- p-,CdP_2, band gap, acceptor level depth and compensation, dark and photoconductivity obs. 2—40248
- Ag_3AsS_3, for electrooptic modulator, cryst. growth 2—35936
- $AgGaS_2$, n-type conduction obs. 2—9364
- $AgGaS_2(Se_2)$, optical props., band struct. 2—4223
- $AgGaS_2(Se_2)$, resist., annealing effects 2—40242
- $AgGa(Se)_2$, stimulated emission obs. on scanning visible spectrum 2—10416
- $AgInS_2(Se_2)$, resist., annealing effects 2—40242
- $Ag_2S(Se)(Te)$, single cryst. growth and struct. 2—1203
- Ag_3SbS_3, refl. spectrum and energy levels 2—29894
- $A^{II}B^{V}$ compound, film, prep. by crystalliz. of melt compressed between two backings, elec. props. 2—32975
- Al base electrodes, tunneling into both sides of weakly coupled Pb-Cu proximity sandwiches 2—19558
- AlAs-GaAs mixed crystals, solution growth technique 2—18939
- AlAs, anisotropic electron effective mass, Faraday rotation study 2—22547
- AlAs, enhanced indirect optical absorpt., direct band gap 2—33252
- AlAs, optical absorption constant, 4.2-293 K 2—19959
- $Al_{1-x}Ga_xAs$, photoluminesc., liquid N_2 temp. 2—4489
- $Al_xGa_{1-x}As$ lasers, double- heterostructure, highly uniform characteristics at room temperature 2—7938
- $Al_xGa_{1-x}As$, light emitting diode, partial dissolution during LPE 2—1541
- $Al_xGe_{1-x}As$, solubility of Zn, anomalies obs. using different diffusion sources 2—9592
- $Al_xIn_{1-x}P$, thermodynamic props. of In-Al-P system appl. to manufacture 2—6788
- AlN film, prep. from trimethylaluminium 2—12659
- AlSb, band struct., interband transitions and excitonic effects 2—10044
- AlSb, Raman spectra, hydrostatic pressure effects, Gruneisen consts. 2—16539
- As-Ge-Se, amorphous, film, memory state optically induced reversible change 2—13256
- As-Ge-Se glass, elec. cond., effect of low temp. annealing 2—36516
- As-Se amorphous layers, effective lifetime of charge carriers 2—29673

Semiconducting materials continued
As_{20}-Te_{70}-Ge_{10}, amorphous films, condition for memorization by laser light pulse 2—4188
As-Te-I glass, thermal, structural and elec. props., comp. depend. 2—22526
As-Te alloy, amorphous, photogeneration and high field effects on mobility 2—10032
As-Te glass, switching processes 2—29658
As_2S_3-Sb_2S_3, cond., hopping mechanism 2—36493
As_2S_3, amorphous, field dependent drift mobilities 2—16201
As_2S_3 films, amorphous, a.c. and d.c. cond. 2—10006
$As_2S_3Ag_x$, glass, $x<0.977$, elec. props. transport mechanism 2—13217
As_2Se_3-Cu_2Se system, phase diagram, ternary cpd. existence 2—29488
$As_2(Se,Te)_3$, vitreous, Hall coeff., cond., annealing effects 2—40243
As_2Se_3, amorphous, band struct. and transport props. 2—19646
As_2Se_3, amorphous, thermopower, 120 to 200 C 2—16303
As_2Se_3, vitreous, charge carrier mobility, cond., band struct., bistable switching action 2—4205
As_2Se_3, vitreous, elec. cond. and Hall coeff., 180-225°C 2—22527
As_2Se_3 amorphous thin film, optical consts. determ. from i.r. refl. spectra 2—33200
As_2Se_3 glass, crystallization rate, control by impurity addition 2—28974
AsSeI, vitreous, prep. and obs. of thermal and optical props. 2—3456
As_2Te_3, chalcogenide, vaporization and sublimation 2—25156
Au-GaP Schottky barriers, green injection luminesc. 2—13523
Au-Si interface, possible cpd. form., resist. and electron microscopy 2—3493
Au-SiO films, elec. cond. 2—12656
B, β-rhombohedral, energy gap, optical determ. 2—40644
β-B, rhombohedral, trapping levels and parameters detn. 2—19665
BAs, cryst. growth, elec. props. 2—15686
BN, pseudo current glow curves 2—40275
BP, refractory, single crystal growth from B-Ni-P soln. 2—9358
$BaBiO_3$, prep., elec. and mag. props. 2—4206
Ba_2MReO_6, ordered perovskite, M=Mn, Co, Ni, Mg and Y, elec. and mag. props. 2—22691
BaO, elec. cond., thermal e.m.f. and thermionic emission 2—29659
$BaTiO_3$, doped, positive temp.-coeff. of resist., Nb_2O_5 and MnO_2 effect 2—36494
$BaTiO_3$, polycryst. nonstoich., high temp. cond. measurement 2—13218
$BaTiO_3$, Ti-rich, elec. cond., rel. to defect struct. 2—15751
$BaTiO_3$ ceramic, barrier layer formation, Mn^{2+} diffusion 2—13219
BeTe, BeSe, Bes, synthesis, and bandgap by optical absorp. obs. 2—20027
Bi-Sb alloy, transport properties 2—29660
Bi-Sb alloys, elec. props., press. influence 2—32968
Bi-Sb films, low temp. elec. props. 2—36495
Bi_2-Te_3-Bi_2Se_3 alloy, n-type, thermoelec. props. 2—36605
Bi-Te, n-type, spectrophotometric obs. of O_2 chemisorption 2—16680
BiOI crystal, adsorption of O_2, attachment levels, thermo-stimulated current 2—6805
$Bi_{95}Sb_5$:Te, Shubnikov-de Haas and band structure investigations 2—29683
$Bi_{1-x}Sb_x$ alloys, metal-semicond. transitions under press. 2—6810
$Bi_{1-x}Sb_x$ solid solns., Ettingshausen effect 2—13336
Bi_2Te_3-Sb_2Te_3-Sb_2Se_3 alloy, p-type, thermoelec. props. 2—36605
Bi_2Te_3, diamagnetic susceptibility, 90-650 K, energy gap calc. 2—25996
Bi_2Te_3, reflectivity spectra, intensive interband transitions identified 2—19996
C, amorphous, hopping cond., trap density distrib. elec. props. 2—4207
C, amorphous film, electrical transport 2—13221
C, amorphous film, tunnelling between localized states 2—13222
C, pyrolytic graphite, c-axis conductivity, detailed interpretation 2—36486
C fibre, polyacrylonitrile-based, electronic props. 2—13266
$CdAs_2$, far i.r. reflctivity, classical non-interacting oscillator model applied 2—19999
Cd_3As_2, cryst. platelets, growth from vapour, elec. props. 2—40274
Cd_3As_2, single cryst., quantum oscills. of thermoelec. power thermal cond. coeffs., effective mass calcs. 2—16226
$Cd_3(As_xP_{1-x})_2$ alloys, optical transmission edge, temp. depend. 2—10336
$CdCr_2S_4(Se_4)$, optical props. of impurity levels, Ag and In doped crysts. 2—40659
$CdCr_2Se_4$:Ga, current noise measurements 2—40278
$CdCr_2Se_4$-metal junction, magnetocapacitance effect 2—36555
$CdCr_2Se_4$, elec. props. and photocond. 2—1512
p-$CdCr_2Se_4$, ferromagnetic semiconductor, elec. field dependent magnetoresistance 2—32972
CdF_2, bandedge, spectral obs. 2—26144
$CdGa_2S_4$, heat capacity, 14-300K, Debye temp., thermodynamic props. 2—25684
$CdGa_2Se_4$, band struct., photocond. 2—16309
$CdGa_2Se_4$, optical absorpt., indirect transitions 2—16485
$CdGeAs_2$, amorphous, Faraday rotation nr. absorp. edge 2—1663
$CdGe_xAs_2$ glass, i.r. absorpt., rel. to struct. 2—10374
$CdGeAs_2(P_2)$, band struct. and optical props. 2—13458
$CdGeP_2$, glassy, elec. cond., 450-860K 2—36498
$CdGe_xP_2$ glass, i.r. absorpt., rel. to struct. 2—10374
$Cd_{0.1}Hg_{0.9}$ Te, film, Hall coeff. and mobility thickness depend. 2—10012
$Cd_xHg_{-x}Se$, mixed cryst., energy gap, composition depend. 2—10046
$Cd_xHg_{1-x}Se(Te)$, interband Faraday rot. 2—13435
$Cd_xHg_{1-x}Se(Te)$, interband Faraday effect 2—13436
$Cd_xHg_{1-x}Te$, energy gap, pressure and temp. depend., Hall coeff. obs. 2—19667
$Cd_xHg_{1-x}Te$, Shubnikov-de Haas oscillation, Landau level splitting 2—32998
$Cd_xHg_{1-x}Te$ alloys, relativistic effects on energies of optical transitions 2—29684
$Cd_xHg_{1-x}Te$, crystal growth, optical and elec. props. rel. to 10μ band detectors 2—39577
$Cd_xHg_{1-x}Te$, electron mobility, under high hydrostatic pressure 2—10009
$Cd_xHg_{1-x}Te$, epitaxial, i.r. photovoltaic detector 2—6911
$Cd_xHg_{1-x}Te$ alloys, Hall mobilities, press. and temp. depend. 2—4209
$CdIn_2S_4$(:Sb), Hall coeff., elec. cond., carrier mobility, temp. depends., 200-500K 2—22529
$CdIn_2S_4$, contact, I-V characts., switching and memory effects 2—19719
$CdIn_2S_4$, Hall mobility, resist., photocond. stoichiometry effect 2—10008
$CdIn_2S_4$, heat capacity, 14-300K, Debye temp., thermodynamic props. 2—25684
$CdIn_2S_4$, optical and photoelec. props., rel. band struct. 2—22760
$CdIn_2S_4(Se_4)$, refl. spectra, band struct. determ. 2—29898
$CdIn_2Se_4$-$CdInTe_4$ solid solution, electron effective mass determ. 2—19638

Semiconducting materials continued
$CdIn_2Se_4$, refl. and transmission spectra, band gap determ. 2—20031
CdO-Bi_2O_3, elec. cond., temp. depend. 2—1511
CdO, donor diffusion, activation energy 2—15781
CdP_2, band struct. and exciton behaviour 2—26215
CdS:Ag:Cl, residual cond., model 2—4208
CdS:Ag, Al, i.r. detection, by high field domain reconfiguration 2—29714
CdS:Ag,Er^{3+} photoluminesc., sensitization 2—20092
CdS:Cu, i.r. luminesc. 2—13503
CdS:Cu, photo-Hall effect, i.r. quenching 2—33068
CdS:Cu, trap parameters, thermolum. study 2—19668
CdS:Cu crystal, Hall mobility rel. to doping 2—29664
CdS:Cu powder phosphor, prep. and electolum. 2—40733
CdS:Mn, high symmetry pts. in Brillouin zone 2—19361
CdS:Ni^+, e.p.r., g-factor and hyperfine struct. 2—30016
CdS:Te, conc. depend. of emission intensity 2—4490
CdS:Ti^{3+}, e.p.r. study, 27 K 2—26275
CdS/In boundary, contact barrier development, current instability 2—4254
CdS-CdSe photoconductive cell, degradation mechanism and reliability estimation 2—29773
CdS-$Cu_{2-x}S$ n-p heterojunction, energy band diagram 2—4247
CdS-Ni, absorption spectra, charge transfer band region, bound state formation 2—36889
CdS-PbS heterojunction, photovoltaic effect visible and near i.r. 2—10148
CdS-electrolyte interface, electron transfer, surface states contrib. 2—13225
CdS, n-CdTe, exciton carrier binding time, cathodoluminescence obs. 2—7102
CdS, acousto-elec. domain, acoustic strain detn., Brillouin spectra and birefringence obs. 2—26114
CdS, acousto-elec. oscill., Brillouin scatt. by coherent ultrasound 2—16584
CdS, acoustoelec. current instabilities unified model 2—36347
CdS, acoustoelec. domain form., low temp effects 2—16029
CdS, acoustoelectric surface domains investigation by method of acoustoelectric detection and properties of detector 2—25681
CdS, band gap reduction due to high photoinjected carrier injection 2—29949
CdS, birefringence spectral depend. 2—7061
CdS, Bragg diffr. on surface acoustoelec. domains 2—29547
CdS, Brillouin scatt., acoustoelectric, anharmonic and resonance effects 2—26200
CdS, cathodolum., free exciton motion and exciton-phonon interaction studies 2—36958
CdS, change in properties during passage of double-injection currents 2—40245
CdS, chemisorption of oxygen, effect on elec. cond. 2—32974
CdS, cubic, carrier effective masses, f- sum rule 2—4224
CdS, difffusion of Se and Te, possible ternary cpd. prep. 2—3820
CdS, dispersion of nonlinear optical susceptibilities 2—4426
CdS, domain formation, threshold elec. field 2—13224
CdS, elastic anisotropy effects on acoustoelectric domain propagation, Brillouin scatt. obs. 2—36348
CdS, elec. cond., effect of chemisorbed oxygen 2—18956
CdS, elec. props. rel. to growth conditions 2—19636
CdS, electron conc. and mobility, resist. and Hall meas. 2—10010
CdS, electron damping and amplification of Lamb waves 2—22414
CdS, electronic attenuation and intensification of Lamb waves 2—1424
CdS, film, photoelectret phenomena and dark polarization current 2—10130
CdS, flexural wave amplification 2—6674
CdS, high field domain velocity, anode-cathode direction 2—25815
CdS, in $Cu_{2-x}S$-CdS photocell 2—4307
CdS, in m.i.s.m. thin film device, electron emission 2—10098
CdS, inelastic polariton scatt. processes 2—16529
CdS, ion-implanted Bi depth distrib. 2—39710
CdS, ion implantation of N_2, diode form., photoelec. props., e.p.r. of implanted centres 2—15774
CdS, light emission associated with high field domains 2—13502
CdS, light scattering from acousto-optical domains 2—16455
CdS, low temp. photocond. spectra, exciton diffusion length detn. 2—10047
CdS, off-axis acoustoelec. domains, Brillouin scatt. 2—4056
CdS, off-axis domain formation and current anomaly 2—40246
CdS, optical-transmission modulation by acoustoelec. domains 2—7062
CdS, oxygen chemisorption, influence of surface struct. 2—29061
n-CdS, p-type layer formation by N ion implantation 2—25422
CdS, photocond., 0.9 eV quenching band temp. depend. 2—4298
CdS, photodesorption mechanism 2—12681
CdS, photoluminescence, i.r. and thermally stimulated luminesc., comparison 2—10420
CdS, photomechanical effect, converse piezoelectric effect 2—19972
CdS, photosensitive u.s. attenuation as tool for photocond. and optical absorpt. obs. 2—16025
CdS, photosensitivity, rel. to photochem. reactions, heat treatment 2—22639
CdS, photovoltage inversion effect rel. to surface states 2—6896
CdS, reson. cancellation of Raman scatt. from lattice vibrs. 2—36897
CdS, single cryst., layer like electroluminesc. 2—4525
CdS, single crystal, symmetrical surfaces, field emission 2—6918
CdS, surface-wave interactions, nonlinear, acoustic convolution 2—4055
CdS, surface photovoltage, wavelength depend. 2—13345
CdS, surface state parameters, determ. from surface photovoltage transients 2—29603
CdS, surface states, photovoltage spectroscopy study 2—32892
CdS, thermostimulated capacitor discharge, pseudo current glow curves 2—40275
CdS, transient photoemission of carriers from Cu 2—13209
CdS, u.s. amplification, temp. depend. 2—29545
CdS, u.s. amplification in continuous drift field 2—29546
CdS, X-ray spectra, band structure 2—16595
CdS acoustoelec. amplifier, reduced phonon noise 2—16028
CdS electron-beam-pumped, temp.-induced wavelength shift 2—2403
CdS epitaxial film, effect of substrate orientation on struct. 2—29031
CdS film, epitaxial, grown from vapour, struct., resist., cathodolum. 2—39535
CdS film, He ion bombarded, elec. cond., trapped electron release 2—40247
CdS film, in Al-(Al_2O_e)-CdS-Al switching element, post-breakdown conduction 2—19720

Semiconducting materials continued
CdS film, solution spray prep., Hall mobility, rel. to cryst. orientation 2–32971
CdS film, vacuum evaporated, elec. and physical props. 2–36492
CdS lasers, electron beam pumped, increased power output 2–17640
CdS lasers, stimulated emission of polaritons 2–34404
CdS layer on W, photo-field emission 2–4319
CdS layers, photothermoelec. analysis, carrier density and mobility 2–16310
CdS surface, contact potential difference meas. 2–13264
CdS transducer, wedge-shaped, for u.s. surface waves 2–6660
$CdS_{1-x}Se_x$, Ar laser irrad., free carrier generation by exciton-donor interact. and exciton impact ioniz. 2–19635
CdS_xSe_{1-x}, directional strain effect on birefringence 2–29912
CdS_xSe_{1-x} platelet laser, optically pumped by electron beam or laser beam, spectral characs. obs. 2–37983
CdS_xSe_{1-x}, graded band gap material, fluorescence 2–26231
CdS(Se)(Te), u.v. photoemission obs. of upper d levels 2–25979
CdS(Se)(Te) film, twinning probability calc. 2–39525
CdS. recomb. luminesc., rel. to adsorption, elec. field 2–22795
CdSb:Ag(Ge)(Te) layers, doping and elec. props. 2–36046
CdSb:Te, Hg(In), influence of double doping on elec. props. and band struct. 2–36499
CdSb, band struct., elec. cond. and thermal e.m.f. study 2–29662
CdSb, impurity state redistrib. due to impurity-phonon interaction 2–40028
CdSe:Cl, pressed powder, nonlinear current-voltage curve, interparticle contact depend. 2–4211
CdSe:Cr,Fe, photoionization absorp. spectra 2–10373
CdSe:Cu, Cl layer, sintered, operation in longitudinal photoconductivity mode 2–29764
CdSe-$BaTiO_3$, two- layer system, u.s. amplification and absorpt. 2–13032
CdSe-Cu point contact, polarized memory mechanism 2–16250
CdSe-SiO_x, in m.i.s. struct. vol. and interface states detn. 2–4259
CdSe-electrolyte interface, electron transfer, surface states contrib. 2–13225
CdSe, carrier mobility rel. to excitation intensity, in negative photocond. conditions 2–32976
CdSe, cubic, carrier effective masses, f-sum rule 2–4224
CdSe, dielec. coated, laser emission 2–11487
CdSe, diffusion of S and Te, possible ternary cpd. prep. 2–3820
CdSe, dispersion of nonlinear optical susceptibilities 2–4426
CdSe, elec. cond., high temp., in Se atmosphere 2–32973
CdSe, in m.i.s. struct., flat band shift, controlled charge injection 2–4260
CdSe, in metal-CdSe-SiO_x- metal struct., conduction mechanisms 2–13291
CdSe, low temp. photocond. spectra, exciton diffusion length detn. 2–10047
CdSe, optical phonon drag effect 2–25813
CdSe, photocurrent kinetics and instability 2–16313
CdSe, photoelectronic props. of electronically active defects 2–13338
CdSe, single cryst., photocond., effects of HNO_3 etching 2–16312
CdSe, single cryst., transient photocond., small signal case 2–16311
CdSe, solubility of Cu_2Se, 600-850°C 2–36248
CdSe, surface morphology, rel. to sublimation mechanism 2–12645
CdSe, temp.-elec. skin effect rel. to continuous sound generation 2–13223
CdSe, transient photocond., monovalent donors 2–4299
CdSe, two-electron transitions of donor 2–10337
CdSe electron-beam-pumped, temp.-induced wavelength shift 2–2403
CdSe film, cond. mechanism, effect of annealing 2–10011
CdSe film, evaporation in high vacuum, energy relns. 2–29030
CdSe film, heat treatment in air, Cd crystallite growth 2–18935
CdSe film, on CaF_2, refl. electron diffr. obs. 2–39500
CdSe film, photoelec. props. during activation 2–22641
CdSe film on $Ba_xSr_{1-x}TiO_3$ substrate, I-V characts., supersonic carrier drift vel. 2–19416
CdSe films, photoemission obs. of energy struct. 2–6925
CdSe(Te), interband Faraday rot. 2–13435
CdSe(Te) and mixed crysts., interband Faraday effect 2–13436
$CdSiP_2$, band struct., refl. and absorpt. spectra obs. 2–13459
$CdSiP_2$, thermal oxidation 2–1750
$CdSnAs_2$, band struct., electrefl. spectra 2–13460
$CdSnAs_2$, reflectivity spectra, energy band struct. correlation 2–10345
$CdSnP_2$, with different impurities, cathodoluminesc. and photoluminesc. 2–10452
CdTe:Cd film, annealed in Cd vapour, elec. cond. rel. to annealing temp. 2–29663
CdTe:Cu (Ga)(In), detector-mat. evaluation by e.p.r. and channelling expts. 2–36539
CdTe:Fe, impurity levels, elec. props. photoconductivity, absorpt. and electro-absorpt. spectra 2–36538
CdTe:In, photoluminesc., donor-acceptor pair spectrum 2–40722
p-CdTe:S, i.r. absorpt. spectra, 90-470K 2–22761
CdTe:Ti(V)(Cr), absorpt. spectra and crystal field parameters 2–22759
CdTe-Au diode, IV characts, Schottky theory and tunnelling 2–29733
CdTe-HgTe, heterostruct. with built-in homojunction, photovoltaic effect 2–13350
CdTe, band struct. determ. 2–40279
CdTe, Bi ion implantation, inversion layer formation, damage and unnealing obs. 2–36049
CdTe, conductivity inversion obs. on ion implantation 2–36047
CdTe, crystal growth, modified Bridgman technique 2–9363
CdTe, crystal growth, vapour transport method 2–18980
CdTe, crystal growth using modified Bridgman method 2–35949
n-CdTe, defect levels before and after electron-irrad., photoconductivity spectra obs. 2–36537
CdTe, diffusion of S and Se, possible ternary cpd. prep. 2–3820
CdTe, donor-Cd vacancy complexes, annealing effects 2–36535
CdTe, double acceptor obs. 2–36528
CdTe, electroabsorpt., Franz-Keldysh effect, internal microfields 2–36873
CdTe, electron beam landing energy, optical modulation 2–22554
n-CdTe, electron irrad. defects, annealing, photocond. obs. 2–15739
CdTe, exchange splitting in excitons, interatomic distance depend. 2–29903
CdTe, for i.r. modulator, cryst. growth 2–29089
CdTe, growth and doping by travelling heater method 2–35944
n-CdTe, impurity photocond., recomb. centres 2–6902
CdTe, impurity photocond. spectra 2–6901
CdTe, γ-ray detection, 60-80°C, device characterization 2–34813

Semiconducting materials continued
CdTe, γ-ray detector for nucleonic propellant gauging in zero-G environment 2–34814
CdTe, γ-ray detector material, conf., Strasbourg, France, June (1971) 2–34808
CdTe, γ-ray spectrometer mat. characterization by nuclear methods and trapping analyses 2–34810
CdTe, γ-ray spectrometer material, crystal growth recombination centre parameters 2–34809
CdTe, γ-ray spectrometer mat., trapping analysis, transient charge technique 2–34801
CdTe, lattice disorder on Bi and Tl ion implantation, annealing obs. 2–36048
CdTe, localized levels, elec. and opt. obs. 2–36667
CdTe, metallurgical and electronic props. rel. to single cryst. growth 2–36500
CdTe, Monte Carlo calc., high field transport props. 2–32970
CdTe, n.m.r. of ^{113}Cd, cond. electron g-factor 2–33351
n-CdTe, non-Γ donor levels and electron transfer kinetics 2–33003
CdTe, nucl. rad. detector, ion implanted, performance 2–34815
CdTe, optical, photoemissive props., energy band pseudopotential model 2–19666
CdTe, purification by vertical zone melting, compensation and conductivity type determ. 2–35950
CdTe, quality as γ-ray spectrometer 2–38367
CdTe, reflectivity and band struct. 2–33303
CdTe, Seebeck effect and Nernst-Ettingshausen effect, influence of optical phonons 2–25943
CdTe, stoichiometry rel. to conc. and type of electrically active defect 2–36536
CdTe, thermo-e.m.f. of hot electrons, field depend. 2–19778
CdTe, transport processes, nucl. rad. detector characterization 2–34811
CdTe, X-ray and X-ray spectrometers, device and mat. evaluation, trapping obs. 2–34812
CdTe characterization for γ detector 2–2634
CdTe film, photodielectric effect, model based on conductivity hypothesis 2–40376
CdTe junction, surface-barrier, photoelectret effect on γ-irrad. 2–13349
$CdTl_{0.8}As_2$, glassy, elec. cond and band gap 2–19637
CdX, x=chalcogen, core electron levels, x-ray induced electron emission obs. 2–19811
$Cd_{1-x}Zn_xSb$, temp. dependence thermoelectric power and resistivity 2–4210
Cds, ion implanted, shallow hole levels 2–6836
Co II complexes, $A_2A'Co^{II}(NO_2)_6$ type 2–9980
$CoAl_2O_4$, transport phenomena, small polaron model 2–25814
$CoIn_2S_4$, prep., elect. resist., mag. props. 2–29800
CoO:Li, current noise measurements 2–40278
CoO, high temp. defect struct. and transport props. 2–36501
CoO, hole drift mobility at high temp. 2–13226
CoO, undoped and Cr or Ti-doped, Hall mobility and defect struct., high temp. 2–36502
Cr_2S_3, elec. and mag. props., rel. to deviation from stoichiometry 2–40522
Cr_xSn_1- Te alloys, prep. and mag. props. 2–33131
CsI, luminesc., kinetics of self trapped exciton recomb. 2–4472
Cu-As-Se, glass, switching phenomena, elec. behaviour, rel. to Cu content 2–13227
$CuAlS_2(Se_2)$, resist., annealing effects 2–40242
$Cu_xCd_{1-x}Cr_2Se_4$, ferromag., cryst. growth and props. 2–39585
$CuCr_2Se_{4-x}Br_x$, optical props., Curie temp., band obs. 2–40645
$CuGaS_2$, $CuInS_2$, p-type prep. and stimulated emission obs. on scanning visible spectrum 2–10416
$CuGaS_2$, p-type conduction obs. 2–9364
$CuGaS_2(Se_2)$, resist., annealing effects 2–40242
CuI, photoelectric emission in spectral region 500 to 1700 A 2–40391
$CuInS_2$, p- and n-type conduction obs. 2–9364
$CuInS_2(Se_2)$, resist., annealing effects 2–40242
$Cu_2In_4Te_7$, preparation and properties 2–25807
$CuInTe_2)_x(2CdTe)_{1-x}$ alloys, photoconductivity, 0.7-1.6eV 2_6899
Cu_2O-Hg contact, barrier capacitance anomaly of Hg melting pt. 2–25885
CuO_2, exciton luminesc., elec. cond., adsorpt. effects 2–22796
Cu_2O, elec. cond., effect of surrounding atm. and impurities 2–4212
Cu_2O, elec. cond., illum. effects, electron trapping, photomemory effect 2–40276
Cu_2O, exciton electrorefl. spectra, ang. depend. 2–29897
Cu_2O, u.v. electroreflectance, band assignments 2–33237
Cu_2S-CdS, heterojunc., photovoltaic cell, optical degradation effects 2–10146
$Cu_{2-x}S$-CdS p-n heterojunction, energy band diagram 2–4247
CuS film, thermal expansion oscillations, 60-300K 2–40084
$Cu_{2-x}S$, in photocell, photovoltaic effect, scanning light microprober obs. 2–4307
Cu_xS, ($x = 1.85$-2.0), elec. cond., temp. depend. 2–13228
$Cu_{2-x}Se$, cubic, room temp. stable, elec. cond. and thermopower, composition depend. 2–36503
Eu_3As_2 film, mag. ordering, photocond. and optical absorpt. study 2–36722
EuB , indirect exchange interactions 2_10171
$EuCr_2S_4$, lattice defects, electron microscope obs. 2–32507
EuO:Gd, free carrier conc., scatt. time and mobility, effective mass 2–40662
EuO, cond. mechanisms 2–19639
EuO, i.r. absorpt., elec. cond. and stoichiometry correl., phase diagram 2–32786
EuO, insulator-metal transition rel. to long range mag. order 2–36529
EuO films, resist. temp. depend., spin flip scatt. 2–36504
Eu_3P_2 film, mag. ordering, photocond. and optical absorpt. study 2–36722
EuS, ferromag., transient photocond., magnetoresist. 2–10136
EuS, magnetiz., tunnelling obs. 2–36709
EuSe, luminesc. decay time 2–4474
EuTe, mag. props., charge carrier effects 2–29835
EuTe, resist., Hall effect, mag. transition 2–29665
$FeCr_2S_4$, ferrimag., elec. transport props. 2–32977
$FeIn_2S_4$, $FeIn_2S_{4-x}Se_x$ 2–29800
Fe_3O_4, magnetite, cond. above Verwey transition 2–36505
Fe_3O_4, magnetite, n.m.r., ^{57}Fe hyperfine spectra, conduction model 2–7137

Semiconducting materials continued
FeP_2 single crystals, prepared by chemical transport reaction magnetic susceptibility, electrical resistivity, Hall effect meas. 2—29798
FeS_2 low temp. photoconduction phenomenon 2—4300
$FeTiO_3$, elec. cond., temp. variation 2—40249
(GaAl)As, injection laser, double- heterostructure, pulsation due to lateral optical coupling 2—7939
$Ga_{1-x}Al_xAs$, ion implantation of GaAs, electroluminescent emission spectrum obs. 2—9585
$GaAs/Al_xGa_{1-x}As$, periodic band gap structures, molecular beam epitaxy 2—6404
GaAs-AlAs heterojunction injection laser, internal parameters at 300K 2—37992
GaAs-AlAs injection laser, stimulated emission threshold dependence on duration of pumping current 2—37997
GaAs-GaAlAs heterostructure layers, for laser at room temperature 2—27521
p-GaAs-n-ZnSe diode, I-V characts., junction capacitance, optical collection efficiency 2—25894
GaAs, for Gunn effect microwave oscillators, book 2—29731
GaAs, stress-modulated magnetoreflectivity, band parameters 2—33234
GaAs injection laser, energy depend. of internal losses 2—11490
GaAsP:N, indirect semiconductor, stimulated emission and laser operation `(cw, 77K) associated with deep isoelectronic traps 2—17635
$GaAs_{1-x}P_x$:Se, epitaxial, cathodoluminesc. assessment for light emitting diodes 2—10459
$GaAs_{0.6}P_{0.4}$:Te, diffusion of Zn, from G-P-Zn source, p-n junction form., junction profile 2—9586
$GaAs_{0.5}P_{0.5}$, Schottky barrier diodes, generation rate det. using ionizing radiation pulse 2—19706
$GaAs_{0.6}P_{0.4}$, pn-Schottky hybrid cold cathode diode 2—13353
$GaAs_{1-x}P_x$, indirect gap, no phonon and phonon assisted exciton absorp. 2—36880
$GaAs_{1-x}P_x$, photoluminesc. spectra 2—10440
$Ga_{0.12}As_2Se_{3-x}Te_x$, glassy, I-V characts., chem. comp. influence, switching 2—13229
GaInAs (Cs,O), photocathode, interfacial barrier effects, thermally assisted emission 2—19807
$Ga_xIn_{1-x}P$ alloys, energy band struct., electrorefl. obs. 2—33238
$Ga_xIn_{1-x}P$, heteroepitaxial growth, PCl_3 reaction 2—19015
$Ga_xIn_{1-x}P$, photoluminesc., band struct. determ. 2—10422
$Ga_xIn_{1-x}P$ alloys, band struct. 2—22550
n-$GaInS_3$, photocond. and photoluminesc., slow recomb. level obs. 2—6903
$Ga_xIn_{1-x}Sb$, growth and properties 2—19002
GaN, epitaxial growth rel. to luminescent elements 2—39595
GaN blue light-emitting diode 2—36962
GaN epitaxial layers, photolum., carrier conc. depend. 2—36928
GaN film, elec. and optical props. 2—18937
GaN film, prep. from trimethylgallium 2—12659
GaP:B, optical absorpt. by lattice and local vibrs. 2—1690
GaP:B, radiation damage centre, local mode absorpt. 2—29167
GaP:Be,(Mg)(Zn),O, luminescence 2—10421
GaP:C, acceptor concs., ioniz. energy 2—25845
n-GaP:Fe, electron traps, e.p.r. and Hall coeff. obs. 2—40251
GaP:MgO complex, yellow-orange bound excitonic transition 2—36941
GaP:N, epitaxial, efficient yellow luminesc. 2—7092
GaP:N, undulation spectra, rotational levels of shallow acceptor states 2—33304
GaP:O, liquid phase epitaxial growth, on oxygen incorporation, rel. to luminesc. props. 2—39593
GaP:Si, bound excitons, and donor ground state, optical study 2—36530
GaP:Te, Zn, epitaxial single cryst., Hall mobility and resistivity obs. 2—40255
GaP:Zn, impurity-to-band activation energies, conc. and temp. depend. 2—10057
GaP:Zn, O, luminesc., minority carrier lifetimes and Zn-O centre conc. 2—4478
GaP:Zn,O, annealing effects on luminesc. props. 2—26233
GaP:Zn,O, recomb. centres characteriz. from photoluminesc. temp. depend. 2—29951
GaP:Zn,O, red photoluminesc. efficiency, minority carrier lifetime 2—7098
GaP-GaAs, electrolum. and elec. props., donor conc. effects 2—29993
GaP-GaAs mixed crystal, reson. Raman scatt. 2—22786
GaP-ZnS(Se) p-n heterojunction, prep. and I-V characts. 2—29720
GaP, amorphous, complex dielec. const. calc. 2—26105
GaP, annealing behaviour after Ne^+ irrad. 2—25374
GaP, band struct., interband transitions and excitonic effects 2—10044
GaP, band struct. 2—29593
n-GaP, chem. polishing by etching soln. 2—32340
GaP, diffusion of Be, profiles and coeffs. determ 2—25444
GaP, discrete pair line emission from Ge donor and acceptor 2—36929
GaP, donor-electron transitions assoc. with cond. band minima 2—6832
GaP, dynamical Jahn- Teller interaction effects on e.p.r. of shallow acceptors 2—7119
GaP, electrolum. diode material, struct. defects 2—29992
GaP, electronic structure, empirical pseudopotential method 2—16225
GaP, enhanced indirect optical absorpt., direct band gap 2—33252
GaP, epitaxial, minority carrier diffusion length, impurity conc. depend., Schottky diode photocurrent obs. 2—29670
GaP, epitaxial p-n junc., X-ray obs. misfit dislocations 2—4248
GaP, extrinsic minority carrier lifetime meas., electroluminesc. 2—26249
GaP, high purity, cryst. growth 2—12694
GaP, i.r. generation by coherent excitation of polaritons 2—16458
GaP, indirect band gap semiconductor-containing isoelectronic traps, observation of super radient laser emission 2—11489
GaP, indirect phonon-assisted two-photon interband transitions 2—22754
GaP, ion implantation induced disorder, annealing, study using Rutherford backscattering, channelling techniques with 1 MeV He ions 2—25421
GaP, ion implantation of Bi, hot-implant behaviour 2—25432
GaP, light-emitting diodes, degradation reduction by chemical passivation 2—7105
GaP, light emitting diode material, cathodoluminesc., scanning elec. microscope obs. 2—22813
GaP, low energy exciton state parameters, 77-300K 2—9918
GaP, nonlinear susceptibility, relative meas. and detn. of absolute value 2—40597
GaP, orange luminesc. spectrum with V_{ga}-O_p centre 2—16606
GaP, orientation of low-indexed faces, optical determ. 2—39571

Semiconducting materials continued
GaP, photocond. and photovoltage, wavelength modulation 2—33074
GaP, radiation damage due to implantation 2—25373
GaP, reflectivity and log. derivative between 2.5 and 6.0 eV 2—22765
GaP, vapour phase epitaxy and defects 2—29032
GaP diode, technology and electroluminesc. props. 2—29994
GaP epitaxial layer, doping gradient, C-V characts. 2—22222
GaP epitaxial layer perfection, substrate prep. influence 2—25199
GaP film, forbidden band width, absorption. spectra, refractive index 2—1691
GaP heteroepitaxial films on sapphire, crystalline nature characterization 2—32368
GaP layers on Ge substrates, autodoping effect 2—36507
GaP light emitting diode, neutron damage 2—20094
GaP light emitting diodes, connected in back direction, time characteristics det. 2—17723
GaP p-n junction material, minority-carrier diffusion length 2—6815
GaP p-n junctions, excess current- and luminescence-noise 2—22581
GaP red emitting diodes, injection and quantum efficiencies 2—33328
GaP whiskers, growth and morphology 2—9294
GaP(Zn,O), liquid encapsulation Czochralski grown, luminesc. and doping characts. 2—22798
GaS, GaP, characterization by photoluminescence and optical absorption 2—16641
n-GaS, hopping cond. 2—13231
GaS, n- and p-type, band scheme from dark cond. obs. 2—29669
GaS, optical consts., temp. modulation 2—10346
GaS crystal, dark cond., temp. depend. 2—25818
$Ga_2S_3(Se_3)(Te_3)$, refl. spectra, band struct. determ. 2—29898
p-GaSb:Si, photoluminesc., shallow acceptor obs. 2—7090
GaSb:Te, conduction band, Hall and conductivity obs. 2—4225
GaSb:Te, Hall coeff., mobility, and resistivity, from thermal cond. data 2—22532
GaSb:Te, phonon scatt. at low temp. 2—22533
GaSb:Zn, low temp. phonon thermal cond., role of density of states effective mass 2—40092
GaSb, acceptor states, effective mass approx. 2—19670
GaSb, amorphous, complex dielec. const. calc. 2—26105
GaSb, band struct., interband transitions and excitonic effects 2—10044
p-GaSb, cryst. growth, carrier conc. reduction 2—25273
p-GaSb, doped, thermopower temp. depend. 2—16306
GaSb, energy relax. time, microwave harmonic mixing and transport phenomena obs. 2—19644
GaSb, high field transport props., Faraday rotation obs. 2—32978
p-GaSb, lattice thermal cond., 2 to 20 K 2—25694
GaSb, p-n junc., carrier conc. and thermal e.m.f. in p-region 2—1540
GaSb, photoelectric emission and reflectivity, 7.7 to 25 eV, band struct. obs. 2—19808
p-GaSb, photoluminesc. under uniaxial compression, impurity levels 2—4477
n-GaSb, piezo-Hall effect, cond. band obs. 2—10013
GaSb, Raman spectra, hydrostatic pressure effects, Gruneisen consts. 2—16539
GaSb, stress-modulated magnetoreflectivity, band parameters 2—33234
GaSb, stress-modulated magnetoreflectivity, band parameters 2—33234
p-GaSb, ultrasonic attenuation, pulse echo method, microwave freq. 2—16026
GaSb, wavelength modulation spectra, rel. to band struct. 2—1692
GaSb amorphous film, tunnelling, effect of temp. and doping 2—19647
GaSb optical props., interband transitions 2—36857
GaSe:Sn(Ge)(Cu)(I), photocond., photolum., recombination centres 2—7093
GaSe, absorpt., 1.8-4.2 eV, excitonic effect 2—29939
GaSe, electron beam induced luminesc., exciton-exciton interaction 2—20115
GaSe, electroreflectance in higher interband transition region 2—40647
GaSe, energy band struct. 2—6830
GaSe, GaS, complex permittivity, evaluation from abs. reflectivity meas. 2—29741
GaSe, layer compound, elec. and optical props. 2—10016
GaSe, layer type, exciton binding energy from absorp. spectra 2—10380
GaSe, layered, resist. changes due to decomp., switching effects 2—32991
GaSe, optical consts., temp. modulation 2—10346
GaTe, electroabsorption spectra, band gap and exciton role detn. 2—20038
GaTe, layer type, exciton binding energy from absorp. spectra 2—10380
Ga_2Te_3, elec. cond., impurity conc. and temp. depend. 2—10014
Gd_3S_4, transport props., localization, vacancies and mag. interaction 2—32981
Ge/ZnSe/GaAs(Cs), heterojunc. photocathode 2—6926
Ge-Se-In system, cryst. samples, elec. props. 2—25821
Ge-Se-In system, cryst. samples, switching phenomena 2—25822
Ge-Se-Te glass, density, softening temp., hardness and elec. props. 2—35846
Ge-Si alloy, thermoelectric element, prep. by hot pressing 2—6857
Ge-Si alloys, heavily doped, resistivity, electron scatt. by phonon, acoustic and ionized impurity modes 2—32982
Ge-Te alloy, amorphous, band struct. and transport props. 2—19646
Ge(Li) diodes in γ-ray detector fast neutron damage 2—24092
Ge(Li) gamma-ray spectra, minimum detectable photopeak areas 2—21322
GeO_2, amorphous, fluctuation levels, photocond. obs., −180 to 100°C 2—10137
GeO_2, vitreous, photocond., rel. to band struct. model 2—22644
GeSe, liq., Hall effect 2—9156
Ge_xSe_{1-x} glass, thin film struct. and neutron damage 2—1516
$GeSi_{1.2}As_3Te_{4.8}$ film, glass switching noise 2—22530
GeTe-$AgSbTe_2$, band gap width dependence on composition from thermoelectric power and elec. conductivity meas. 2—32999
GeTe-SnTe, alloy, film, plasma energy, electron energy loss spectra, electron micorscope obs. 2—4143
GeTe film, amorphous, recording of optical information 2—40225
GeTe film, amorphous to polycrystalline phase transition light pulse heating 2—40256
Ge_xTe_{1-x} glass, thin film struct. and neutron damage 2—1516
$Ge_{15}Te_{81}S_2As_2$, amorphous, effect of hydrostatic pressure on VA characteristics 2—9984
HfO_2, hole mobility, elec. cond., Seebeck coeff. and thermogravimetric obs. 2—10017
Hg, in chrysotile asbestos., supercond. and semicond. transition 2—29634

Semiconducting materials continued
HgCdTe, photocond., minority carrier sweepout, high field obs. 2—22645
p-$Hg_{1-x}Cd_xTe$, carrier conc. press. depend., 4.2 and 77K 2—32983
$Hg_{1-x}Cd_xTe$, epitaxial vapour growth 2—29036
$Hg_{1-x}Cd_xTe$, cryst. growth, homogeneous, Bridgman method, comp. distrib. rel. to growth interface 2—25275
$Hg_{1-x}Cd_xTe$, electron mobility 2—25823
$Hg_{1-x}Cd_xTe$, galvanothermomagnetic obs. det. of nonuniform thermal gradients using liquid crystals 2—34225
$Hg_xCd_{1-x}Te$, dislocations, etching study 2—9558
$HgCr_2Se_4$, spinel, lattice vibrations, i.r. reflection and transmission spectra 2—19374
HgI_2, spectral distrib. of photopolarization current 2—19786
HgS, for electrooptic modulator, cryst. growth 2—35936
HgS, thermomodulation of edge absorpt. 2—40666
HgS_xSe_{1-x}, transport props., temp. depend. 2—13233
HgSe, annealing in Se, effect on resist. and stoichiometry 2—25442
HgSe(Te), u.v. photoemission obs. of upper d levels 2—25979
HgTe, band struct. determ. 2—40279
p-HgTe, lattice thermal cond., thermopower 2—32855
HgTe, reflectivity and band struct. 2—33303
HgX, x_chalcogen, core electron levels, x-ray induced electron emission obs. 2—19811
In-In_2S_3 liquid partial system, resist. and thermoelec. 2—1114
p-InAs-metal barrier, CV characts., inversion layer effect 2—10081
InAs, amorphous, complex dielec. const. calc. 2—26105
InAs, amorphous, complex dielec. const. from refl. meas. 2—26104
InAs, band struct., interband transitions and excitonic effects 2—10044
InAs, deformed in torsion, coherent twin boundaries 2—19106
n-InAs, free electron conc., quantized mag. field effect 2—6829
InAs, ion-electron emission, relaxation process and defects 2—19815
n-InAs, low temp. non-Ohmic galvanomag. effects 2—16211
InAs, low temp. phonon cond. 2—25695
p-iNAs, low temp. photomag. effect 2—13347
n-InAs, low temp. photomagnetoelec. and photocond. effects 2—6904
InAs, microwave biased photocond., free carrier screening effects 2—19787
n-InAs, rad. recomb. mech., photoluminesc. spectra, 30-77 K 2—22799
InAs, reflectivity spectra, energy band struct. correlation 2—10345
InAs, wavelength modulation spectra, rel. to band struct. 2—1692
InAs and $InAs_{1-x}Sb_x(P_x)$, reson. Ramon scatt. 2—22786
InAs film, sputtering and elec. props. 2—10023
n-InAs fund. absorpt. edge, optical transitions, 300 and 100 K 2—13477
InAs quantized surface accumulation layer, electron tunnelling 2—13265
p-InAs surface, clean cleaved, anomalous magnetoresist., resist., <4.2K 2—10019
InAsP (Cs,O), photocathode, interfacial barrier effects, thermally assisted emission 2—19807
n-$InAs_{1-x}P_x$, electroreflectance spectra, Γ_{15}—Γ_1 transitions, composition depend. 2—16468
$InAs_{1-x}P_x$(Cs-O), long-wavelength photoemission 2—6928
$InAs_xSb_{1-x}$, film, absolute zero energy gap, optical, photoelec. and galvanomag. obs. 2—40277
$In_xGa_{1-x}As$, optically pumped at room temp., laser action 2—17643
$In_xGa_{1-x}As$, epitaxial growth and properties 2—1216
$In_xGa_{1-x}As$, phase diagram, crystal growth, and band struct. 2—19004
$In_xGa_{1-x}As$ solid solns., fund. absorpt. edge obs. 2—13478
$In_{1-x}Ga_xP$:N, indirect and direct crystals, cw laser operation on A-line transition 2—17642
$In_{1-x}Ga_xP$, radiative recomb. processes, band transitions 2—7091
$In_{1-x}Ga_xP$, mixed crystals, homogeneous, solution-growth reproducible preparation 2—9359
$In_{1-x}Ga_xP$, photoluminesc. assoc. with multivalley resonant states of N isoelectronic trap 2—26219
$In_{1-x}Ga_xP$ platelet laser, optically pumped, 8900-5800 Å 2—23617
$In_xGa_{1-x}P$, phase diagram for In-Ga-P system, rel. to epitaxial growth 2—9837
$In_{1-x}Ga_xP(x \leqslant 0.60)$ platelet laser, optically pumped volume excited cw room temp. operation 2—23612
$In_xGa_{1-x}Sb$, phase diagram for In-Ga-Sb system, rel. to cryst. growth 2—9836
InN film, elec. and optical props. 2—18937
n-InP:Cu, l.f. current oscill., bulk negative resist., electron transfer, trapping 2—22538
InP, amorphous, complex dielec. const. from refl. meas. 2—26104
InP, amorphous, complex dielec. const. calc. 2—26105
InP, band struct., interband transitions and excitonic effects 2—10044
InP, bound exciton lifetime, emission decay and osc. strength 2—10423
InP, cond., surface and contact effects 2—19675
n-InP, electron drift vel., microwave meas. 2—25824
n-InP, magentophonon oscillations of transverse magnetoresist. 2—6820
n-InP, magnetophonon oscillations of longit. magnetoresist. 2—10018
n-InP, microwave velocity/field characteristics obs., comparison with n-GaAs 2—6811
InP, solution grown, unstable domains, obs. 2—40257
n-InP, velocity-field charact. for electrons 2—19648
n-InP, velocity-field characteristic, microwave measurement 2—32984
$In_2S_3(Se_3)(Te_3)$, refl. spectra, band struct. determ. 2—29898
InSe, press. and temp. induced phase, synthesis and props. 2—22156
In_2Te_3-Hg_3Te_3 alloy, photocond. and photovolt. effect, 2-12 μm 2—33071
In_2Te_3, elec. cond., impurity conc. and temp. depend. 2—10014
$In[M^{2+}In]S_4$ spinel, (where M=Fe, Co and Ni), electron correlations and antiferromag. interactions 2—26000
KN_3, internal photoemission of electrons and holes 2—40260
LiH, elec. and photo-cond. 2—6905
Mg_2Ge, Raman spectra, hydrostatic pressure effects, Gruneisen consts. 2—16539
Mg_2Ge, thermal cond., two mode anal. 2—40093
Mg_2Pb, heat capacity, lattice heat capacity, thermodynamic functions, Debye temp., temp. range 5-300K 2—4066
Mg_2Si, Raman spectra, hydrostatic pressure effects, Gruneisen consts. 2—16539
Mg_2Si, thermal cond., two mode anal. 2—40093
Mg_2Sn, Raman spectra, hydrostatic pressure effects, Gruneisen consts. 2—16539
Mg_2Sn, thermal cond., two mode anal. 2—40093
$Mn_{-x}Cr_x(Fe_x)Si_{1.7}$ solid solns., thermopower cond., electron and hole densities 2—10024
$MnIn_2S_4$, $Mn_2S_{4-x}Se_x$, prep., elec. resist., mag. props. 2—29800

Semiconducting materials continued
MnO, Hall mobility of electrons, high temp. ionized impurity influence 2—10025
MnO, hole drift mobility at high temp. 2—13226
MnO, single cryst., nonstoich. disorder 2—1519
$MnSi_{2-x}$, x=0.25-0.28, cond. mechanism, thermoelec. power calc. 2—40261
MoO_3:Ni, defect struct. and elec. cond. 2—10026
MoS_2, u.v. spectra, interband transitions, plasma reson. 2—13463
MoS_2 molybdenite, mag., elec., thermoelec. props. and Hall effect 2—36513
$MoSe_2$, exciton-exciton interaction during laser irrad. 2—19788
Nb_3(Al, Ge) films, vacuum deposited, T_c and current capacity 2—40208
NbC, band structure, tight binding method 2—4124
$NbSe_2$, reflectivity anisotropy band struct. 2—10350
Nd-Bi alloy, phase diagram and elec. props. 2—1413
$NiIn_2S_4$, $NiIn_2S_{4-x}Se_x$, prep., elec. resist., mag. props. 2—29800
NiO:Li, current noise measurements 2—40278
NiO, epitaxial, hole drift mobility, photoexcitation obs. 2—10027
NiO, hole drift mobility at high temp. 2—13226
NiO, single cryst., photocond. in visible and near u.v. region 2—10138
$Pb_{1-x}Ge_xTe$, effect of alloying on energy gap, calc. 2—22552
PbI_2, ambient sensitive semiconduction 2—19650
PbI_2 films, anomalous photovoltages 2—13342
$Pb_{1-x}Mn_xTe$ solid soln., density of states effective mass, and effective mass determ. 2—22539
PbS-Ge heterojunction, cond. band discontinuity determ. from photovoltage 2—19701
n-PbS, Nernst effects, scatt. mechanisms, 1-80K 2—25949
PbS, photocond., effect of gas treatment on temp. coeffs. 2—36612
p-PbS, Raman scatt., surface electric field induced 2—16561
PbS, X-ray spectra, band struct. determ. 2—29945
PbS film, epitaxial growth, multilayer approach using NaCl as a parting layer 2—39518
PbS film, mechanisms of photosensitivity 2—36613
p- PbSe, Raman scatt., surface electric field induced 2—16561
PbSe films, vacuum deposited, electrical properties 2—6821
$Pb_{0.918}Sn_{0.082}Se$ epitaxial growth on BaF_2 and CaF_2 substrates 2—25205
$Pb_{1-x}Sn_xSe$, elec. props., rel. to band struct. model 2—25825
$Pb_{1-x}Sn_xSe$, Shubnikov-de Haas effect, Fermi surface 2—25841
$Pb_{1-x}Sn_xSe$ diodes, laser emission and band crossing under press. 2—37998
$Pb_{0.76}Sn_{0.24}Te$, effects of proton bombardment, p-type to n-type conversion 2—36514
$Pb_{1-x}Sn_xTe$, epitaxial growth, heat treatment and elec. props. 2—32375
$Pb_{1-x}Sn_xTe$, effect of alloying on energy gap, calc. 2—22552
p-$Pb_{1-x}Sn_xTe$, free carrier parameters detn., i.r. reflectivity spectra obs. 2—26148
$Pb_{1-x}Sn_xTe$, photovoltaic and laser diodes produced by proton bombardment 2—29776
$Pb_{1-x}Sn_xTe$ epitaxial layers, bulklike photocond. 2—10139
$Pb_{1-x}Sn_xTe$ film, epitaxy 2—39517
PbTe:Gd, mag. characts., localized moments 2—33141
PbTe:Sb p-n junction photovoltaic detector, prep. by ion implantation 2—40383
p-PbTe-metal barrier, CV characts., inversion layer effect 2—10081
PbTe, e.m. wave propag., effect of quantized mag. field 2—16228
PbTe, effect of impurities on homogeneity and dislocation struct. 2—36035
p-PbTe, elastic consts., electronic contrib. 2—32582
n-PbTe, i.r. magnetoabsorpt., phonon-cyclotron and carrier-transfer reson. 2—40678
PbTe, thermal cond., hydrostatic press. influence 2—19436
PbTe and $Pb_{1-x}Sn_xTe$ epitaxial layers, Hall mobilities 2—4214
PbTe epitaxial films, microstruct. and elec. props. 2—9279
PbTe films, electron-electron scatt. effects in photoelec. emission 2—10160
$PbTi(Zr)O_3$, band gap determ. 2—1526
$PbZrO_3$, thermoelec. effect 2—25948
$Pb(Zr_{0.65}Ti_{0.35})O_3$ with Nb_2O_5, oxygen depleted surface layers, ferroelec. field effect 2—40357
PdO, growth, electrical meas., bonding model 2—3575
Pt square planar complex, conduction mechanisms 2—36523
$PtSb_2$, valence band struct. 2—25842
α-S, electron irrad. carrier generation, temp. and field depend. 2—36515
S, orthorhombic, band struct., transport and optical props., comparison with monoclinic Se 2—40128
Sb-Ge-Se glass, elec. cond., effect of low temp. annealing 2—36516
Sb_2O_3, Sb_2O_5 nonstoichiometric and controlled valence n-type semicond. 2—40226
Sb_2S_3-SbI_3-In, glass forming region detn., optical and elec. props. obs. 2—39441
Sb_2S_3, local levels in the forbidden band, photocond. obs. 2—40262
Sb_2S_3, molten, switching effect 2—12579
SbSI, acoustic second harmonic generation 2—6666
SbSI, ferroelec. phase transition, soft modes, Raman scatt. obs. 2—16564
SbSI, first-order ferroelectric phase transition, Raman spectroscopy of phonon instability 2—25924
SbSI, injection currents and polarization charge accumulation 2—6822
$Sb_2S_3(Se_3)$, permittivity, 10 to 80 GHz 2—29743
Sb_2Se_3, liq., Hall effect 2—1108
SbSeI, photopolarization and related capture centres 2—33060
SbSi, photopolarization and related capture centres 2—33060
SbSi crystal, adsorption of O_2, attachment levels, thermo-stimulated current 2—6805
Sb_2Te_3:I, elec. cond., effect of impurity content 2—19651
Sb_2Te_3, cryst. growth, chemical transport method 2—29096
Sb_2Te_3, de Haas-van Alphen effect 2—32877
Sb_2Te_3, dislocation loops, electron microscope obs. 2—12771
Sb_2Te_3, thermal cond., hydrostatic press. influence 2—19436
ScAs(P) epitaxial layers, vapour growth, elec. and optical props. 2—9282
Se:Tl, trigonal crystal grown by travelling solvent method, d.c. conductivity 2—40263
Se-Sb, amorphous to crystalline transition assoc. with elec. transition, review 2—13238
Se-Te alloy, liquid, electrical switching 2—3407
Se, absorpt. and electroabsorpt. near fund. edge 2—33271
Se, amorphous, attenuation length of excited electrons 2—32987
Se, amorphous, field dependent drift mobilities 2—16201
Se, amorphous, high field transport and impurity effects 2—10032
Se, amorphous film, photocond. and optical props. 2—32989
Se, anisotropy of dielec. const., 3-30 eV 2—22725

Semiconducting materials continued
Se, bulk crystallized, memory switching, amorphous layer formation 2—16212
Se, bulk polycrystalline sample, memory switching effect, crystallization 2—4184
Se, films, amorphous, exponential hole trap distrib. in forbidden band, photoresponse obs. 2—25957
Se, general properties and applications, review 2—19615
Se, hole ionization coeff., from photocurrent obs. 2—4217
Se, liq., current instability 2—12580
Se, liq., nonlinear IV charact., Poole-Frenkel effect 2—1115
Se, liq., switching and memory effects 2—22002
Se, liquid, switching, I-V characts. mag. field effect 2—25105
Se, metal-Se diode, rectification 2—4251
Se, microwave Hall effect, mobility detn. 2—16216
Se, molten, anisotropy of electrical conductivity in laminar flow and chain structure 2—28893
Se, molten, switching effect 2—12579
Se, monoclinic, band struct., transport and optical props., comparison with orthorhombic S 2—40128
Se, neutron irrad. effects on resist. and thermopower 2—6823
Se, single cryst. film, Cd, Te electrodes, space charge limited current 2—10031
Se, transient photoemission of carriers from Au 2—13209
Se, trigonal, electronic bands, Fourier expansion 2—22466
Se, trigonal, temp. depend. electroabsorpt. on indirect edge 2—13480
p-Se, trigonal single cryst., barrier limited conduction mechanism 2—10030
Se amorphous film, elec. cond., temp. depend. 2—25826
Se amorphous layers, effective lifetime of charge carriers 2—29673
Se amorphous thin film, optical consts. determ. from i.r. refl. spectra 2—33200
Se film, amorphous, space charge I-V characts. 2—13259
Se film, polarized memory effect 2—32988
Se photocell, thermally stimulated current, energy spectrum of localized centers. 2—29687
Se rectifier, hot hole mobility, avalanche Hall effect obs. 2—36559
Se_xTe_{1-x}, single cryst., piezoresistivity 2—4216
Si:B, doping by BF_2 molecule implantation 2—25429
Si-As-Te and Si-Ge-As-Te glasses, glass-forming region and DTA study 2—15637
Si film, on sapphire, elec. props. depth variation, m.o.s. Hall technique 2—19688
Si surface barrier detectors effects of neutron irradiation on meas. of fission fragment properties 2—27873
SiAs, melt grown, elec. props. 2—10033
SiC:Al(N), diffusion of boron, heavy doping influence 2—29222
SiC:In, implanted, backscatt. analysis, disorder and p-type cond. 2—25827
SiC:N, i.r.absorpt. and thermally stimulated luminesc. due to impurity level nonequiv. population 2—13481
n-SiC:N, Raman scatt., interf. between donor electrons and pure crystal phonons 2—16565
SiC-Co_3O_4, electrical properties obs. 2—6792
α-SiC, 6H polytype, optical phonon energy range and dielec. const. 2—10395
SiC, diode prod. and props. rel to α-particle detection at high temps. 2—34821
α-SiC, epitaxial, from vapour phase, struct. and p-n junc. 2—9370
SiC, epitaxial growth of p-n junctions 2—22588
α-SiC, etching in molten NaOH or KOH, melt temp. effects 2—35874
n-SiC, exciton-exciton interaction in photoluminescence spectrum 2—1712
SiC, figures of merit and technological problems 2—19696
β-SiC, formation kinetics, pyrolysis of CH_3SiCl_3 2—18985
SiC, ion-implanted, photoluminesc. of radiation defects 2—33309
SiC, Kohn-Luttinger interference effect and cond. band minima 2—26197
SiC, oxidation resistant layer formation by reaction of Si and CH_4 2—29040
SiC, polar surface identification, in alkaline soln. 2—18923
α-SiC, single cryst. growth, vapour transport method 2—18986
SiC, triboluminesc., sand blasting technique 2—4526
SiC diffused diode, cathodoluminesc., radiative recomb. quantum efficiency 2—16633
SiC film, twinning probability calc. 2—39525
SiC p-n junction cold cathode, multi-emitter, activation 2—4312
SiC p-n junction cold cathode, elec. characts. analysed 2—22654
n- SiC polytype, i.r. impurity absorp. bands 2—16498
α-SiC:N, impurity adsorpt., electron transitions 2—7073
Si(Li) and Ge(Li) X-ray detectors, efficiency curves, and X/γ ratio for calibration sources 2—24068
SiO_2 thermally grown, conduction mechanisms 2—10034
SiO_x films, doped and undoped, Poole-Frenkel effect 2—1527
Si_2Te_3, amorphous, band struct. and elec. props. 2—19671
SmS(Se)(Te), i.r. absorpt. peaks, semicond.-metal transition 2—33274
Sn, grey, optical consts., band struct. 2—16475
n-Sn, grey, stress-induced band gap 2—36531
α-Sn, RPA dielec. function in far-i.r. 2—10051
SnO_2:Sb, resist., anomalous press. depend. 2—16213
SnO, SnO_2, nonstoichiometric and controlled valence n-type semicond. 2—40226
SnO_2, density of states effective mass 2—4226
SnO_2, electrotransmission spectra near fundamental threshold 2—40641
SnO_2, polycryst., prep. by precip. from soln. and props. 2—40227
SnS_2, layered, resist. changes due to decomp., switching effects 2—32991
$SnS_2(Se_2)$, electron energy band struct. 2—33001
p- SnTe, Raman scatt., surface electric field induced 2—16561
SnTe, supercond., low temp. heat capacity 2—19427
p-SnTe, valence band struct., weak field magnetoresist. 2—25843
$SrCr_2S_4$, lattice defects, electron microscope obs. 2—32507
SrO, elec. cond., thermal e.m.f. and thermionic emission 2—29659
$SrSc_xFe_{12-x}O_{19}$, elec. cond., temp. and comp. depend. 2—29674
$SrTiO_3$-In barrier, tunnelling, rel. to polaron transitions 2—4139
$SrTiO_3$, supercond., low temp. heat capacity 2—19427
TaS_2, 1s-form, diamag., spin-orbit coupling 2—16412
Te:Ag(Sb) layers, doping and elec. props. 2—36046
Te:Sb, coupled plasmon-LO phonon modes, reflectivity obs. 2—32906
Te-As-Ge, amorphous to crystalline transition assoc. with elec. transition, review 2—13238
Te-Ge-Se system amorphous, structure and elec. props. 2—29675
Te-Se, liquid alloy, Hall coeff. detn. 2—12581

Semiconducting materials continued
Te, acceptor states, Hall effect obs. 2—10053
Te, acoustoelectric amplification, studied using epitaxial Se transducers 2—10035
Te, anisotropy of dielec. const., 3-30 eV 2—22725
Te, cyclotron reson. absorpt. struct. in valence band 2—33002
Te, Dember effect, i.r. detector 2—4308
Te, electron-phonon interaction, rel. to temp. depend. of microwave absorpt. 2—25844
Te, Hall coeff. and elec. cond., 1.4-77K 2—29676
Te, intervalence band traisition, modulation by acoustoelec. domains 2—7075
p-Te, laser-excited, carrier relaxation times and recombination, optical obs. 2—16231
Te, liquid, Hall coeff. detn. 2—12581
Te, mobility and microhardness, Sn impurity conc. depend. 2—13239
Te, press. coeff. of resist., rel. to pressure sensor appl. 2—20780
Te, supercurrent tunnelling junction 2—13183
Te, surface defects influence on carrier density and elec. cond. 2—10062
Te, surface quantum states in accumulation layer 2—16232
Te, trigonal, electronic bands, Fourier expansion 2—22466
Te, valence band transformation under pressure, Shubnikov-de Haas effect obs. 2—10052
Te film, on TGS substrate, ferroelec. field effect temp. dependence 2—36517
Te film characterization during deposition from field-effect meas. 2—40231
$Te_{40}As_{37}Ge_7Si_{18}$ films, ovonic threshold switching 2—10082
$Te_{48}As_{30}Ge_{10}Si_{12}$, glass, switching and memory behaviour 2—16214
$Te_{81}Ge_{15}As_4$, glass, switching and memory behaviour 2—16214
$Te_{81}Ge_{15}Sb_2S_2$, amorphous film, light induced memory 2—19653
ThO_2, hole mobility, elec. cond., Seebeck coeff. and thermogravimetric obs. 2—10017
TiN, pulsed compression, electron energy spectra 2—36532
TiO_2:Al, current noise measurements 2—40278
TiO_2:Fe^{3+}, photocond. spectra, Fe level 2—10141
TiO_2-Nb_2O_5 ceramic, electrical properties, influence of Nb_2O_5 percentage 2—6793
TiO_2, electrical ageing mechanism 2—36518
TiO_2, reduced, electric charge transport, nonstoichiometry, defect ordering 2—29171
TiO_2, reduced, O vacancy diffusion 2—39748
TiO_2, surface electronic state, rel. to adsorbed p-benzoquinone molecules bonding 2—29058
TlBr, photo-excited, Hall effect and magnetoresist., temp. depend. 2—40264
$TlGaS_2$, synthesis, cryst. struct., and band gap 2—29498
$TlGaS_2(Se_2)$, elec. and photoelec. props. 2—29677
$TlInS_2$, elec. and photoelec. props. 2—29677
$Tl_2Ru_2O_7$, electronic characterization, cryst. chem. considerations, elec. and mag. meas. 2—10076
Tl_xTe_{1-x}, liq., Hall mobility, temp. and comp. depend. 2—39387
U_3O_8, sintered, elec. cond. and thermopower 2—22541
β-US_2, mag. moment, cryst. struct. refinement 2—25828
$(U_yTh_{1-y})O_{2\|x}$ solid solution, elec. cond., O_2 press. depend. 2—40265
VC, band structure, tight binding method 2—4124
V_6C_5, electron scatt. by vacancies, residual resist. 2—4219
VO_2:Cr, struct. aspects of metal - insulator transition 2—25638
VO_2:Ti, conduction band and impurity state electron lifetime, e.s.r. obs. 2—10037
V_2O_5-P_2O_5 glass, dielec. props., a.c. cond., 80-350 K 2—19749
V_2O_5-P_2O_5 glass, in m-i-m struct., high resistance, negative resistance and high conductivity obs. 2—40314
V_2O_5-TeO_2 glass, between metal electrodes, I-V characts., —100-200°C 2—36519
VO_2, band struct., LCOAO approach 2—6834
VO_2, energy gap, charge carrier mobility, semiconductor to metal transition 2—4007
VO_2, film, fast metal-insulator transition, laser beam induced 2—10054
VO_2, in thin film switch negative resist. and filamentary cond. 2—10079
VO_2, metal-insulator transition 2—29679
VO_2, microhardness and cond. in semicond.-metal transition region 2—29678
VO_2, optical props., band struct. 2—33245
VO_2, semiconductor- metal transition, Raman scatt. obs. 2—16571
VO_2, susceptibility, correl. with Knight shift, rel. to band struct. 2—33118
VO_2 film, thermoelec. power, Hall mobility, struct. dependence 2—19654
VO_x, highly correlated electron gas props. 2—19633
VO_x, polaron morphology, band struct. transitions 2—10055
$V_2O_{3\|\delta}$, metal-semicond. transition 2—10167
V_2O_4, semiconductor-metal transition 2—29680
V_2O_5, Hall and drift mobilities 2—10036
V_2O_5, single crystal, elec. cond. and dielectric props. 2—10038
V_2O_5 electron hopping, two-level, high and low temperatures, dislocation model 2—4220
$VO_{2-x}F_x$ $0<x<0.2$, metallic to semiconductor transition, single crystal resistivity data 2—3739
$V_2O_{5-x}F_x$, $0<x<0.025$, single crystal resistivity data 2—3739
VO_2; Ti, impurity conduction, microwave freq. cond. obs. 2—19655
α-WC, low temp. resist. and Hall effect 2—1521
WSe_2, energy gap, effect of dislocation struct. 2—36534
YbTe, 4f-5d electron collapse, pressure induced 2—10056
$Zn_xCd_{1-x}S$:Ag,Ni, photoluminescence mechanism, energy band model 2—4480
$Zn_xFe_{3-x}O_{4-x}F_x$, prep., mag. props. and elec. cond. 2—22695
$ZnGeAs_2$, reflectivity spectra, energy band struct. correlation 2—10345
$ZnGeP_2$, band struct., empirical pseudopotential calc. 2—13260
$ZnGeP_2$, crysts., p-type, Hall effect, thermoelec. power, hole conc., hole effective mass 2—13245
$ZnIn_2S_4$, photocond. quenching due to hot electron capture, electric field variation 2—36614
$ZnIn_2S$ and $Zn_3In_2S_6$, thermal oxidation 2—1750
$ZnIn_2S_4^4$ and $Zn_3In_2S_6$, refl. spectra, band struct. determ. 2—29898
ZnO:Li, thermal cond. 2—19471
ZnO-Si, heterojunc., lifht detector, elec. and optical props. 2—10088
ZnO, electron-beam-pumped, lasing action 2—16611
ZnO, far-i.r. free carrier absorpt. 2—16500
ZnO, luminesc., band-band recomb. and cond. electron conc. 2—16613
ZnO, off-axis acoustoelec. domains, Brillouin scatt. 2—4056

Semiconducting materials continued
ZnO, one-equivalent adsorbates, intergranular contact resist, surface energy states 2—6840
ZnO, photoluminesc., mixed-mode excitons, reabsorpt. and exciton diffusion 2—16612
ZnO, photon counting distrib. of Brillouin scattered light from amplified vibr. noise 2—13494
ZnO, polar surfaces, LEED study 2—18924
ZnO, stimulated emission and excited states of donor electron 2—4481
ZnO, surface Fermi level anchoring by chemisorbed species e.p.r. study 2—4228
ZnO electron-beam-pumped, temp.-induced wavelength shift 2—2403
ZnO surface, electronic, LEED and Auger diagnostics 2—29012
ZnO(Se)(Te), u.v. photoemission obs. of upper d levels 2—25979
Zn_3P_2-Cd_3As_2 solid solution, Hall coeff., resist., 300-800K, X-ray analysis, dilatometry 2—19656
ZnP_2, cathodoluminesc., interband transitions and exciton behaviour 2—26227
ZnS:Cu, Cl film, optical and electrical switching of dark cond., and photocond. at 77K 2—40380
ZnS:Cu, temp. effect on electrolum. decay 2—20120
ZnS:Ga, luminescence and photoconductivity, description by donor-acceptor pair model 2—29957
ZnS:I, low voltage electrolum., due to acoustoelectric instability 2—36966
ZnS:Mn, elec. cond., temp. depend. and impurity effects 2—13243
ZnS:Mn, high symmetry pts. in Brillouin zone 2—19361
ZnS:Mn, population inversion, electrolum. excitation, impurity impact excitation 2—13524
ZnS:Ni, ion-hole complexes formed in charge exchange between impurities 2—29956
ZnS:Ni^+, e.p.r., g-factor and hyperfine struct. 2—30016
ZnS:Tb^{3+} films, hot- electron impact excitation of electroluminesc. 2—16637
ZnS-GaP n-p heterojunction, prep. and I-V characts. 2—29720
ZnS-Ni, absorption spectra, charge transfer band region, bound state formation 2—36889
ZnS, comparative study of thermally stimulated voltaic effects and luminescence, role of traps and luminescence centres 2—16301
ZnS, electronic structure, empirical pseudopotential method 2—16225
ZnS, epitaxial growth on GaAs substrate 2—9289
ZnS, growth impurities, optical spectra studies 2—36055
ZnS, in m.i.s.i.m. struct., electrolum. quantum yield 2—20121
ZnS, photoluminescence, elec. field quenching mechanism 2—36935
ZnS, powder layer, rare-earth activated, d.c. electroluminesc. 2—10455
ZnS, with stacking faults, exciton refl. spectra 2—22752
ZnS epitaxial film, prep. by r.f. sputtering 2—29047
ZnS epitaxial layer, electrooptical quality, growth and props. 2—9290
ZnS film, epitaxial, grown from vapour, struct., resist., cathodolum. 2—39535
ZnS film, on Si, triode r.f. sputtering system 2—32384
ZnS phosphor, low temp. stimulation by elec. field 2—26252
ZnS thin film, rare earth doped, prep. by ion implantation, and luminesc. 2—19119
ZnS(Se)(Te) film, twinning probability calc. 2—39525
ZnSb, p- and n- type, electrical transport values 2—1522
ZnSe:Er^{3+}, site sensitive excitation mechanisms, photoluminesc. 2—22801
ZnSe:Ni, two-stage excitation of anti-Stokes luminesc. 2—33311
ZnSe:Tm, Li, luminesc., absorpt., and Zeeman effect 2—40721
ZnSe-GaP n-p heterojunction, prep. and I-V characts. 2—29720
ZnSe-Ge heterojunctions, switching and memory characts. 2—6860
ZnSe-Ni, absorption spectra, charge transfer band region, bound state formation 2—36889
ZnSe-ZnTe heterojunction, epitaxial growth, green electroluminesc. 2—40735
ZnSe, band struct. determ. 2—40279
ZnSe, elec. cond., high temp., in Se atmosphere 2—32973
ZnSe, electronic structure, empirical pseudopotential method 2—16225
ZnSe, solubility of Cu_2Se, 700-1000°C 2—36248
ZnSe epitaxial layer, electrooptical quality, growth and props. 2—9290
ZnSe film, epitaxial, grown from vapour, struct., resist., cathodolum. 2—39535
ZnSe film, epitaxial deposition on Ge substrate 2—18948
ZnSe m.i.s. electroluminescent device, exhibiting switching and memory 2—33327
ZnSe(Te), exciton carrier binding time, cathodoluminescence obs. 2—7102
$ZnSiP_2$, thermal oxidation 2—1750
$ZnSnAs_2$, electrorefl. spectra, electron transitions 2—20006
ZnTe:Al, defect levels assignment, elec. transport and photoelectronic props. 2—13244
ZnTe:Ga, negative photocond., room temp. 2—33078
ZnTe:In, O, luminesc., self-activated and isoelectronic O emission 2—20106
ZnTe-CdTe solid solution, negative photocond., room temp. 2—33077
ZnTe-GaSb, p-p heterojunc., elec. and optical props. 2—10087
ZnTe, band struct. determ. 2—40279
ZnTe, electron trapping-detrapping effect in cond. band, hydrogenlike donor obs. 2—13263
ZnTe, electronic structure, empirical pseudopotential method 2—16225
ZnTe, exchange splitting in excitons, interatomic distance depend. 2—29903
ZnTe, interband Faraday effect 2—13436
ZnTe, interband Faraday rot., low mag. field 2_7049
ZnTe, interband Faraday rot. 2—13435
ZnTe film, gas phase deposition 2—35898
ZnTe film, recrystallization rel. to struct., elec. and optical props. 2—29046
ZnX, x=chalcogen, core electron levels, x-ray induced electron emission obs. 2—19811
ZrC, band structure, tight binding method 2—4124
ZrH, magnetoresistance, Hall effect, field and H content depend. 2—6824
ZrO-Nb_2O_5, ceramic, electrical properties, influence of Nb_2O_5 percentage 2—6793
ZrO_2, hole mobility, elec. cond., Seebeck coeff. and thermogravimetric obs. 2—10017

gallium arsenide
γ-detectors, conf. panel discussion 2—34817
acceptor effects, transport and photoelec. props. 2—40250
acceptor states, effective mass approx. 2—19670
acoustic sum-frequency generation, discontinuities in nonlinear increase 2—13214

Semiconducting materials continued
gallium arsenide continued
acoustic surface wave propagation, meas. in 100 MHz region 2—14256
acoustoelectric amplifier, reduced phonon noise 2—16028
acoustoelectric current, linear and nonlinear growth 2—16030
adsorption of H_2O, effect on surface photovoltage 2—13346
amorphous, complex dielec. const. calc. 2—26105
amorphous, complex dielec. const. from refl. meas. 2—26104
amorphous state, produced by ion bombardment, Raman spectra obs. 2—26186
Auger recomb. quadruplets and impact ioniz. 2—33096
band edge density of states, electron and neutron irradiated sample, optical props. obs. 2—29916
band struct., interband transitions and excitonic effects 2—10044
barrier-metal contact six-parameter model values using iterative error-minimizing multiparameter computer technique 2—19694
bulk devices computer simulation 2—19698
carrier concentration profiles, compensation for effects of stray capacities 2—22535
cathodoluminescence investigation, clean vacuum electron beam drive, temperature dependence of bandgap 2—17549
crystal growth, gas etching method 2—12695
density of states, crystalline and amorphous, pseudopot. and CBS calc. 2—10049
dielectric constant microwave perturbation meas. of temp. dependence method for minimizing airgap contact impedances 2—25850
diffusion of Zn, isoconcentration technique 2—15789
diode, IV characts., transition processes, switching 2—6864
dominant scatt. mechanisms, Hall and Seebeck coeffs., 300 to 700K obs. 2—6816
donor states, effective mass theory 2—16229
doping, thermodynamic study for care of epitaxial growth 2—3530
doping and process impurities, characterization using mass spectrometry 2—16696
doping anomalies, analysis by Si-O complex model 2—33004
electrical characterization using Hall, magnetoresistance measurements 2—33009
electroabsorption, nonlinear effects 2—7071
electroluminescent diode, degradation with prolonged operation, role of Cu 2—40734
electroluminescent diode, spacing of photocurrent and external emission spectra maxima 2—20117
electroluminescent small area diodes, shot-noise in output 2—22817
electronic structure, empirical pseudopotential method 2—16225
electroreflectance meas. by electrolyte method, galvanoluminesc. role 2—40646
emission diode with transistor structures, characts. meas. 2—1542
energy gap, temp. depend., from thermodynamic data 2—13258
epitaxial, γ-irrad. damage, energy levels 2—16227
epitaxial, characterization using Schottky barriers 2—33010
epitaxial, two-stage growth on spinel, diode form. 2—10090
epitaxial film, prep. by r.f. sputtering 2—29047
epitaxial films, Hall effect, cond., impurity levels, carrier mobility 2—6812
epitaxial growth, effects of $AsCl_3$ conc. on impurity incorporation 2—9276
epitaxial growth, liquid phase 2—32366
epitaxial growth, transitional layer formation 2—9275
epitaxial growth, vapour, liquid phase methods, growth conditions, mechanisms 2—32401
epitaxial high purity growth 2—35891
epitaxial layer growth, from soln. in liq. metal theory 2—18930
epitaxial layers, Cu-contaminated, acceptor levels 2—19669
epitaxial layers, doping profile, Schottky contact study 2—25431
epitaxial layers, effect of substrate temp. on doping level and impurity distrib. 2—18938
epitaxial multilayer vapour growth 2—35892
epitaxial vapour growth 2—32365
etching, dissolution kinetics in HNO_3, NaClO and HF/CrO_3 2—39460
etching, rate-controlling process, review 2—32338
etching fluids, review 2—32339
excitation and modulation of 10.6 μm guided waves in epitaxial thin films, Ge prisms and phase grating couplers 2—38117
film, cond., field depend., low temp. 2—6814
film, epitaxial, photocond., influence of state of surface 2—22643
film, evaporated, fundamental electronic props. 2—40244
film, heteroepitaxial, grown on sapphire, in m.i.s. config., photoelec. studies 2—40379
film, heteroepitaxial growth on insulating substrates 2—39510
film, magnetoresist. anisotropy, thickness, field and temp. depend. 2—19678
film growth, nucleation on W (111) face 2—29033
films, n and n^+ type, homoepitaxial, impurity obs. using ion microanalyzer 2—16694
Franz-Keldysh effect, studied by 3 methods 2—7052
Franz-Keldysh effect anisotropy 2—10379
growth, on GaAs substrate at const. temp. 2—39588
Gunn device, high field diagnostics, magnetoresistance technique 2—36564
Gunn devices, transverse spreading velocity, high field domain 2—29730
Gunn diode, microwave perform. degrad. due to thermocompression bonding effects 2—36563
Gunn domains, quenching due to surface effects 2—4213
Gunn effect generation parameters, temperature dependence, meas. 2—16252
Hall consts., cond., forbidden band width, carrier mobility, high press. effects 2—36506
heterostructure injection lasers 2—11484
high voltage microwave e.m.f. 2—29668
impurity centres, Fe-group, ground states and photoioniz. 2—19672
impurity distribution, n-type of n^+-type films 2—1259
inhomogeneous, high apparent mobility 2—4204
injection laser, gradual degradation rates 2—21099
injection laser, mesa stripe geometry, fabrication 2—21105
injection laser, spontaneous emission intensity to full operating power 2—5377
injection laser with power about 200 W 2—27524
ion implantation, retention and build up of heavy implanted Bi ions 2—25424
ion implantation by Al^+, electroluminescent diode formation 2—9585
ion implantation of Zn, 1 MeV 2—25423
ion implanted, elec. activity 2—25372

Semiconducting materials continued
- **gallium arsenide** continued
  - i.r. photoionization of deep acceptors of Cu and Ag doped GaAs 2—6831
  - irradiation, correlation of heavy ion data 2—39469
  - junction, p-n, illumination influence, Cu diffusion 2—10085
  - junction, p-n, Si-doped, impedance, freq. characts. 2—13279
  - laser, double-diode, dynamics of emission, saturable-absorber effect 2—17632
  - laser, effects of 250-800 keV electron beam bombardment on threshold and power characteristics 2—27516
  - laser, electron beam pumped, wavelength tuning effects 2—14431
  - laser, electron-beam pumped, wavelength tuning rel. to lasing threshold 2—11488
  - laser, frequency modulation by injection current 2—27518
  - laser, influence of inhomogeneous distribution of minority carriers on doping dependence of threshold current 2—17634
  - laser, injection, ageing and injected carrier lifetime 2—7940
  - laser, injection, influence of spiking on spectral characteristics 2—27520
  - laser, junction, conservation of polarization 2—23616
  - laser, lightly doped, long-wavelength shift in operation 2—37990
  - laser, microwave modulation by pumping with electron beam modulated by microwave signal 2—27522
  - laser, multielement, electron bombardment pumping, emitting mirror type 2—37996
  - laser, oscillation delay times distrib. over emitting surface 2—5378
  - laser array, uniform polarization 2—37994
  - laser diodes, under inhomogeneous excitation conditions 2—17639
  - lasers, electron beam pumped, increased power output 2—17640
  - lasers, self pulsing, transitions between mode configurations due to mode locking 2—11456
  - light scattering under strong elec. field ·2—19993
  - liq. phase epitaxy in Ga soln., computer simulations 2—3531
  - liquid phase epitaxial growth, doping, and properties 2—29104
  - low conductivity, l.f. current pulses 2—19642
  - low resistivity, carrier lifetime, electron bombardment and annealing effects 2—36508
  - metallurgical structure of alloyed contacts to 2—33037
  - microsconic analogue to laser oscillating acoustoelec. domains 2_36349
  - m.i.s. formation, deposition of Si_3N_4 and flat-band parameters 2—15665
  - n type, carrier wave under crossed d.c. electric and magnetic fields 2—40254
  - n-type, arsenic implantation effects on elec. props. 2—25846
  - n-type, bulk, high- field microwave permittivity 2—10015
  - n-type, bulk effect devices, deep level determination from C-V measurements 2—13268
  - n-type, cathodoluminesc., donor conc. depend. 2—13519
  - n-type, compensated, low field mobility at low temperatures 2—36491
  - n-type, compensation by proton bombardment 2—25820
  - n-type, current carrier concentrations by Faraday effect 2—29695
  - n-type, epitaxial layers, carrier conc. rel. to impurity conc. 2—29685
  - n-type, far i.r. cyclotron resonance, effective mass ratio, and impurities scatt. time detn. 2—19528
  - n-type, gain and frequency conversion efficiency, under microwave heating, effect of charge carrier mobility 2—25819
  - n-type, Hall mobility and factor calc. using linearized Boltzmann eqn. 2—16080
  - n-type, heavily doped, resist. temp. depend. 2—13230
  - n-type, high field cond., displaced Maxwellian distrib. func., diffusion approx. calc. 2—19645
  - n-type, hole lifetime doping depend. obs. 2—1514
  - n-type, hydrogenic donor levels in mag. field 2—10058
  - n-type, intrinsic photocond. in depletion layer 2—40377
  - n-type, ion implanted layers, carrier conc., diode prep. 2—6838
  - n-type, ionization inhomogeneities in S-type characteristics 2—25817
  - n-type, ionized impurity density and mobility 2—13232
  - n-type, magnetophonon reson., many-phonon scatt. 2—19641
  - n-type, microwave velocity/field characteristics obs., comparison with n—InP 2—6811
  - n-type, negative resist. in strong microwave field 2—6813
  - n-type, nuclear radiation detector, low temperature performance 2—38372
  - n-type, photoluminesc., vacancy correl. with dislocations 2—16607
  - n-type, reson. Raman scatt., electronic excitations, coupled plasmon-phonon modes 2—16538
  - n-type, Schottky barrier, bistable switching and memory 2—33024
  - n-type, slow domains and negative resist. via transferred electron effects 2—19643
  - n-type, space -charge scatt. and electron transport 2—13267
  - n-type, specific resistance for Sn, Sn-Ag, and Au-Ge-Ni ohmic contacts 2—29715
  - n-type, spontaneous emission, doping depend. 2—29950
  - n-type, thermoelec. force measurement 2—25944
  - n-type, velocity-field characts., temp. depend. 2—32979
  - n-type, velocity-field characts. at low temps. 2—29672
  - n-type high purity epitaxial surface-barrier diode, room temperature operation as detector of photons and charged particles 2—38374
  - n-type layer, field profile above transferred electron threshold 2—29671
  - negative differential mobility, nonuniform d.c. field effects on carrier waves 2—19619
  - negative mobility, emitter current limited injection 2—33021
  - neutron induced metallic spike zones, effects on electrical properties 2—19621
  - neutron irradiation effects on diffused laser diodes 2—21098
  - nonhydrogenic exciton and energy gap, photoluminescence and photoconductivity 2—22549
  - nonrectifying contacts dependence of resistance on frequency and density of current 2—19718
  - nonsaturating velocity/field characteristics 2—36480
  - nuclear radiation detection, liquid and vapour phase n-type layers 2_34816
  - optical, crystallographic characterization 2—32364
  - optical absorption constant, 4.2-293 K 2—19959
  - optical interband threshold, 4.5 eV, symmetry determination from polarisation dependence of transverse electroreflectance spectrum 2—26145
  - optical props. of laser-type crysts. 2—36879
  - optical waveguide, phase matched parametric interactions 2—38119
  - oxidation in air, room temp. 2—33378
  - p^+-n solar cell, electron irrad., capacity and defect levels 2—29775
  - p-n junction, recomb. emission, varying local delay time and doping depend. 2—19700
  - p-type, band splitting, electron spin optical orientation obs. 2—13475

Semiconducting materials continued
- **gallium arsenide** continued
  - p-type, electron beam excited, spontaneous emission internal quantum efficiency 2—29947
  - p-type, galvanomag. effects in impurity zone cond. region, 300 and 77 K 2—32980
  - p-type, heat treatment effect on 0.93 eV luminesc. band 2—36942
  - p-type, hole vel., temp. depend. 2—40253
  - p-type, hole vel., temp. depend. 2—40252
  - p-type, interband electronic Raman scatt. 2—16567
  - p-type layer, by ion implantation of Be and Mg 2—22220
  - p-type pulse excited cathodoluminescence, relaxation kinetics, non-radiative recombination 2—7102
  - passivation with Si_3N_4 2—35893
  - periodic structures, p/n, molecular beam epitaxy 2—6404
  - photocathode, caesiated, photoyield decay characteristics 2—25981
  - photocathode, Cs_2-O activated, electron energy loss in band bending region 2—6927
  - photoconductivity, in high electric fields 2—4301
  - photoconductivity, rel. to free excitons 2—25954
  - photodiode, electron bombard., I-V and spectral characts. 2—36620
  - photoemission ang. distrib. rel. to energy distrib. struct. 2—36638
  - photoluminescence, 1.5141 eV line, of lifetime of weakly bound excitons 2—29952
  - photoluminescence, radiative recomb. obs. using impact ioniz. of donors 2—16602
  - photoluminescence excitation spectra, capture of hot electrons by ionized donors 2—4527
  - piezoelectric, ion implantation, monolithic acoustic surface wave amplifier formation 2—29190
  - plasmon-enhanced sound amplification 2—36346
  - polaritons observation, new interpretation of free-exciton reflectance and luminescence 2—13257
  - proton irradiated, photocond., role of recomb. centres 2—36610
  - Raman spectra, hydrostatic pressure effects, Gruneisen consts. 2—16539
  - reflectivity spectra, energy band struct. correlation 2—10345
  - reflectivity wavelength depend., optical phonon-plasmon coupling, Vargas theory 2—36859
  - resistivity measurement by four probe method 2—29696
  - Schottky barrier, tunnelling resist. 2—10092
  - Schottky barrier diode, generation rate det. using ionizing radiation pulse 2—19706
  - Schottky barrier junction, elec. and crystallographic props. 2—33038
  - solar cell, photoluminesc. spectra, current-voltage characts., impurity influence 2—21012
  - spontaneous emission, electron beam excited, intensity depend. on excitation level 2—4521
  - surface, electron characteristic loss spectrum, fine struct. 2—6330
  - surface barrier detector for α-particles, β- and γ-rays 2—11677
  - surface contamination, organic solvents 2—32367
  - surface states, intrinsic, localized, estimation at cleavage plane 2—25848
  - surface-barrier diode, photosensitivity spectra 2—6908
  - surface-barrier structures by chemical deposition of Au, Ni, Ag, In, Sn and Zn 2—25892
  - transferred electron devices, scanning electron microscope cond.-mode signals 2—4241
  - trap levels, thermostimulated current study 2—10048
  - tunnel contact, ion bombardment effects on tunnelling characts. 2—16251
  - tunnelling in n-GaAs-Pb contact, press. depend. 2—40221
  - two photon absorption, photocond. obs. 2—19785
  - u.s. generation and amplification in single crysts. 2—4049
  - u.s. velocity and attenuation, in photocond. cryst., illumination depend. 2—19413
  - vapour phase epitaxy, Si contamination, electron probe microanalysis obs. 2—39594
  - wafer, ion impression of Al films 2—32358
  - Wannier levels, optical absorp. in an elec. field 2—22764
  - wavelength modulation spectra, rel. to band struct. 2—1692
  - work function, temp. and illumination depend., contact potential study 2—33006
  - Al-GaAs double-heterostructure, electroluminescent diode source for optical fibre transmission lines 2—29991
  - AlGa:As-GaAs, heterojunction laser diode 2—21103
  - (AlGa)As-GaAs heterojunction lasing transitions investigated 2—23615
  - (AlGa)As-GaAs lasers, heterojunction, narrow active regions, symmetrical 2—11486
  - (AlGa)As-GaAs single heterojunction laser diode, Fabry-Perot cavity parameter effects on threshold current and efficiency 2—21100
  - Al_xGa_{1-x}As-GaAs heterojunction laser diode, large-optical-cavity, threshold and efficiency 2—17637
  - Al_xGa_{1-x}As, light emitting diode, partial dissolution during LPE 2—1541
  - AlGaAsGaAs, laser diodes, radiation trapping 2—21104
  - Au-GaAs contact, barrier height depend. on surface layer thickness 2—33030
  - Au, evaporated layer, interdigital transdducer form., Schottky barrier, surface elastic wave obs. 2—13324
  - Cd^+, Te^+ implanted, single crystal, electrical activity, effect of implanting into substrate heated to 180°C 2—25804
  - Ga_{1-x} Al_xAs tunnel diodes, Au-Ge doped, photosensitive impurity- assisted tunnelling 2—40304
  - Ga_xAl_{1-x}As-GaAs-Ga_xAl_{1-x}As double heterostruct. lasers with very narrow active regions, operation 2—34405
  - GaAlAs laser diodes, characteristics 2—21102
  - GaAs:Cd, implantation damage, annealing 2—9521
  - GaAs:Cr, photocond. in high electric fields 2—4301
  - GaAs:Cr, photoinjected carrier recomb. and trapping processes 2—33069
  - p-GaAs:Cr cathode, photosensitive and thermostimulated emission, spectral distrib. 2—6920
  - GaAs:Cu, i.r. absorpt., complex nature of Cu acceptor 2—16490
  - p-GaAs:Cu, radiative recomb. under carrier heating conditions 2—4476
  - GaAs:Ge diodes, luminesc., low-energy emission band obs. 2—26251
  - p-GaAs:Si, electron radiative recomb. during epitaxial growth 2—20095
  - GaAs:Si, implanted, localized vibr. mode absorpt. 2—40664
  - GaAs:Si, laser, amphoterically doped, one step liquid phase epitaxy 2—5376
  - GaAs:Si layers, n- to p-type conversion, substrate orientation depend. 2—1515
  - GaAs:Sn, Ge, Mg molecular-beam epitaxy, surface structure observation, electrical and optical evaluation of layers grown 2—3553
  - GaAs:Sn, Zeeman spectra of principal bound exciton 2—33306

Semiconducting materials continued
gallium arsenide continued
n-GaAs:Te, Dingle temp., cyclotron mass, Hall mobility, Dingle mobility, Shubnikov-de Haas effect, 1.9-4.2 K 2—22548
GaAs:Zn, carrier and Zn concs. in Zn diffused region 2—22224
GaAs:Zn, Cd film, heteroepitaxial, formation and elec. props. 2—22531
GaAs:Zn, impurity conc. determ. from Hall effect and hole mobility 2—6837
n-GaAs:Zn, ion bombarded, enhanced diffusion, luminesc. 2—25446
GaAs:Zn, Te, radiative recomb. time characts. 2—33305
GaAs:Zn,Fe, impurity interactions at m.p., calc. 2—29667
GaAs:Zn electroluminescent diodes, high-efficiency, fabrication effects 2—26250
GaAs/Al$_x$Ga$_{1-x}$As, periodic band gap structures, molecular beam epitaxy 2—6404
GaAs- GaAlAs diode, lasers, minimum threshold current 2—5375
GaAs-AlAs solid solution, valence band spin-orbit splitting, optical spin orientation of non-equilib. electrons 2—26218
GaAs-Al$_x$Ga$_{1-x}$As double- heterostructure, light modulator 2—17710
GaAs-Au surface-barriers, capacitance relax. determ. 2—4242
GaAs-Ga-GaP, phase diagram, liq.-solid curve, expts. and calcs. 2—22034
GaAs-Ga$_{1-x}$Al$_x$As(Zn), heterostruct., electroluminesc. diode 2—10454
GaAs-Ge n-p heterojunction, prep. and I-V characts. 2—29720
GaAs-InAs, solid solns., fund. absorpt. edge obs. 2—13478
GaAs-SiO$_2$ interface, photocond. spectrum of GaAs 2—22642
p-GaAs-n-ZnSe diode, I-V characts., junction capacitance, optical collection efficiency 2—25894
n-GaAs, Cu diffused, photoluminesc., donor-Cu complex 2—10439
n-GaAs, free-running Gunn diode, fluctuations in drift velocity of high- field domains 2—36562
n-GaAs, i.r. absorpt., carrier conc. and temp. depend. 2—29915
on GaAs, ion implantation damage, flux dependence, investigation using ^{85}Kr channelling, Rutherford backscattering methods 2—25369
GaAs, semiempirical calculation of electronic zones 2—29686
GaAs, stress-modulated magnetoreflectivity, band parameters 2—33234
GaAs, valence band spin-orbit splitting, optical spin orientation of non-equilib. electrons 2—26218
GaAs laser frequency separation between adjacent longitudinal modes meas. and second order dispersion 2—14429
GaAs$_{1-x}$P$_x$:N, stimulated emission and laser action on isoelectronic trap transitions 2—37995
GaAs$_{1-x}$P$_x$:Se, epitaxial, cathodoluminesc. assessment for light emitting diodes 2—10459
GaAsP wafer, photolum., laser induced, rel. to use as light emitting diode 2—40716
GaAs$_{0.6}$P$_{0.4}$, pn-Schottky hybrid cold cathode diode 2—13353
GaAs$_{0.6}$P$_{0.4}$ ion implanted p-n junctions, annealing effect on characts. 2—25887
GaAs$_{1-x}$P$_x$, indirect gap, no phonon and phonon assisted exciton absorp. 2—36880
GaAs$_{1-x}$P$_x$ electroluminescent diodes, defect centres generation during forward-bias degradation 2—7104
GaAs$_{1-x}$P$_x$, electrolum. and elec. props., donor conc. effects 2—29993
GaAs$_{1-x}$P$_x$, photoluminesc. spectra 2—10440
GaAs$_x$P$_{-x}$, reson. Raman scatt. 2—22786
GaAs;Te influence of dislocation densities on output characteristics of injection lasers 2—17641
Ge/ZnSe/GaAs(Cs), heterojunc. photocathode 2—6926
In$_x$Ga$_{1:x}$As, optically pumped at room temp., laser action 2—17643
In$_x$Ga$_{1-x}$As, epitaxial growth and properties 2—1216
In$_x$Ga$_{1-x}$As, phase diagram, crystal growth, and band struct. 2—19004
InP, two photon absorption, photocond. obs. 2—19785
Mo/Au-Ge/Ge/n-GaAs/ Ge/Pb-Ge, complex diode, layer composition and microhardness 2—4249
n-type, Hall effect, conc. and mag. field intensity depend. 2—22534

germanium
(110) and (100) surface band structures, computation 2—16230
acceptors due to lattice defects 2—29698
acoustic amplification, 9.3 GHz, deformation potential constants 2—19417
acoustoelectric effects, transport theory 2—9880
amorphous, complex dielec. const. calc. 2—26105
amorphous, electronic density of states 2—10073
amorphous, hopping cond., trap density distrib. elec. props. 2—4207
amorphous, optical absorption, temp. depend. at band edge 2—4457
amorphous, Poole-Frenkel cond., comparison of theory and expt. 2—22452
amorphous, seach for anisotropy in low field and high-field resistivity 2—25856
amorphous, short range order and pseudogaps 2—22545
amorphous, switching, rel. to crystn. 2—33014
amorphous film, elec. props., electrode effects 2—10066
amorphous film, e.p.r., resistivity, rel. to ageing process 2—4551
amorphous films, photoemission, electronic struct. 2—4324
amorphous in m.i.s. structure/tunnelling 2—13298
amorphous state, produced by ion bombardment, Raman spectra obs. 2—26186
amorphous to crystalline transition assoc. with elec. transition, review 2—13238
band struct., interband transitions and excitonic effects 2—10044
band struct., photoemission obs. 2—33015
band-band impact recomb. 2—33011
Boltzmann eqn., method of soln. using spherical harmonic approx. 2—16199
conductivity along grain boundary, photo-effect 2—4302
crystal growth, role of dynamic props. of dislocations 2—6400
cyclotron absorption, crossed fields 2—1472
decoration, microtopography and physical properties of (111) face 2—12639
depletion-barrier modulation, thire-derivative spectra 2—33240
detector, γ-rays from ^{60}Co, using impulse 2—24090
detector fabrication and performance 2—27876
detector variation in molten salt Li electroplating method of fabrication 2—21329
detector variation in molten salt Li electroplating method of fabrication 2—31370
detectors, comparative study of timing techniques 2—14762
diamagnetic excitons, energy spectrum, band degeneracy influence 2—13271
diamagnetic excitons in degenerate bands 2—26152

Semiconducting materials continued
germanium continued
dielectric-metal transitions excitons, photocond. 2—16235
diffusion of an electron-hole plasma in crystal, effect of a magnetic field 2—13074
diode, reverse biased, i.r. radiation response, impurity and defect levels detn. 2—19707
domains, static, magnetic fields effect obs. 2—29705
doped and compensated, i.r. refractive index and absorption spectra rel. to conduction processes 2—16482
doped crystal, conductivity at low temperatures, 1.3-4.2K 2—40287
double acceptor, ground state splitting 2_6848
effective mass tensor and donor ground state, strain effects 2—16237
electroabsorption, excitonic effects 2—7066
electron and hole ioniz. rates 2—6849
electron drift vel., saturation, acoustical phonon generation 2—6846
electron irrad., elec. and photoelec. props., influence of temp. 2—19685
electron-hole liquid model, metallic state calcs. 2—36416
electron-hole pair prod. and radiation detector energy resolution 2—10063
electron-hole recombination, band-to-band Auger process 2—7089
electronic states of dislocations, absorpt. study 2—40289
electronic structure, empirical pseudopotential method 2—16225
electronic transitions at high press., review 2—15955
energy loss spectra of 25 keV electrons and 2 phonon excitation in amorphous films 2—19481
epitaxial layer growth, from soln. in liq. metal theory 2—18930
even Hall effect, at orientation of current along low symmetry axis 2—4234
Fermi level of heavily doped crysts., density of states approx. 2—36059
field emission IV charact., Au adsorption effect 2—29782
film, amorphous, annealed, elec. and optical props. 2—40291
film, amorphous, extrinsic and hopping cond., thermoelec. obs. 2—10069
film, amorphous, interelation of transport, optical and structural props. 2—13273
film, amorphous, reactor irrad. effect on elec. props. 2—4232
film, amorphous, struct., elec. resist., band gap, crystn. 2—40286
film, charge carrier mobility thickness depend. 2—1532
film, epitaxial, elec. cond. and Hall effect 2—10067
film, on Ge and sapphire substrates, conduction rel. to crystalline struct. 2—36542
film, p-type, deform. splitting of impurity absorpt. band 2—13476
film, photovoltages larger than band gap 2—16321
film, twinning probability calc. 2—39525
galvanomagnetic recomb. effect in inhomogeneous elec. field, carrier density distribs. 2—25854
galvanomagnetic-recombination effect, non-stationary 2—29700
Hall effect and cond., irrad. induced defect obs. 2—12749
heavily doped levels, estimation of amount of compensation 2—19686
high purity, coaxial detector, timing properties rel. to Ge(Li) detectors 2—21328
high purity radiation detector, neutron damage and annealing 2—24091
high-field conductivity in n-type, non-equiv. intervalley scatt. effects 2—13272
hot carrier energy relax. time, meas. method 2—29652
hot carriers, photogradient e.m.f. 2—16322
hypersonic attenuation due to optically excited carriers 2—9875
hypersonic attenuation via exciton-phonon interaction 2—9876
impurity scatt., energy depend., model for heavily doped n-type 2—10065
indirect phonon-assisted two- photon interband transitions 2—22754
injecting and blocking contacts, Al and Sb/Ge/Sb evap. layers 2—40296
interband transitions, e_1 and E_1, thermoabsorpt. study 2—40288
intervalley scattering selection rules 2—22561
intrinsic, self- magnetoconc. effect 2—33012
intrinsic absorpt., radiation induced increase 2—26165
ion irradiated, defect production and removal, secondary electron emission monitoring 2—29169
ion scattering, directional effects 2—25986
ion-electron emission, relaxation process and defects 2—19815
i.r. dichroism due to free carriers in n-type uniaxially stressed Ge 2—19968
luminiescence, free exciton condensation into electron- hole drops 2—33307
magneto microwave Kerr effect, amplitude ratio meas. and Hall mobility estimation 2—36821
magnetoresistance, quantum transfer, on uniaxial elastic deformation 2—4235
measurement methods, for resist., lifetime and inhomogeneities 2—36540
minority carrier heating under strong electron-hole interaction conditions 2—6844
n,p-doped, structure of electroreflectance spectra 2—16467
n-type; bulk negative differential conductivity 2—10068
n-type, compensated, electron-phonon scattering 2—36544
n-type, current carriers, dislocations effect, 77-300K 2—22564
n-type, current instability and intervalley redistrib. of electrons 2—6845
n-type, current oscillations, low temp. 2—25852
n-type, degenerate, hot carrier scatt. at optical phonons 2—19626
n-type, elec. effects on screw dislocations 2—10064
n-type, electric current density v. electric field, computation 2—4229
n-type, electron irrad., E_c- 0.2 eV level, isochronal annealing effects 2—22560
n-type, e.m. wave propag., effect of quantized mag. field 2—16228
n-type, fast CO$_2$ laser modulation by hot carriers 2—40598
n-type, Hall coeff., mobility anisotropy coeff., from helicon reson. freq. meas. 2—25855
n-type, injected carrier instability in high electric field 2—33013
n-type, intrinsic photocond. quenching, edge dislocation effect 2—25956
n-type, laser-excited, carrier relaxation times and recombination, optical obs. 2—16231
n-type, magnetoresistivity rel. to elec. field strength 2—29701
n-type, negative long. magnetoresistance of hot electrons 2—29703
n-type, phonon scatt. by neutral donors, low temp. 2—6691
n-type, piezo-Hall e.m.f. 2—19684
n-type, recomb. at dislocations, effect on high field photocond. 2—29766
n-type, saturation stressed degenerately doped, longitudinal resistivity and Hall effect 2—22562
n-type, self energy effects in tunnelling 2—40290
n-type, strong-field magnetoresist. and impurity hopping cond. 2—6850
n-type, transverse galvanomag. coeffs. in strong elec. fields 2—6851
n-type ste-junction nuclear radiation detector, low temperature performance 2—38372

Semiconducting materials continued
  germanium continued
    network of cracklike voids, evidence from study of u.v. dielectric constants 2—9711
    nonlinear I-V characts., optical charge exchange between impurity centres 2—13269
    nonlinear S-type IV characts., double injection influence 2—6843
    nuclear counter, low temp. behaviour 2—8234
    optical absorpt. by holes, indirect transitions role 2—1693
    p-i-n structure formation, by electron irrad. 2—25888
    p-type, dielectric const., plasma freq, Drude-Zener formula, valence band interband transitions effects 2—25858
    p-type, epitaxial film, surface electron states 2—16238
    p-type, field electron emission, transient processes 2—13355
    p-type, free carrier magneto-microwave Kerr effect 2—40612
    p-type, impurity ionization by hot electrons, electron temp. calc. 2—4120
    p-type, interband electronic Raman scatt. 2—16567
    p-type, i.r. refl. spectra, hole relax. and effective masses 2—6847
    p-type, magnetothermal conductivity, evidence for Jahn-Teller effect 2—33185
    p-type, minority carrier and ion drift mobilities, oxygen conc. correl. 2—1531
    p-type, minority carrier lifetime, photocond. and photo-magnetoelec. obs. 2—22563
    p-type, non-equilib. plasma osc., anisotropic band struct. 2—10003
    p-type, photon drag tensor 2—13341
    p-type field emitter, O_2 adsorption, I-V characts., work function 2—25230
    phonon transmission, impurity effects 2—32832
    photoconductive responsive, gain saturation low temp. 2—13340
    photoconductivity and photovoltage, wavelength modulation 2—33074
    photoelectromagnetic effect, confirmation of theory of transient characts. 2—25966
    photoemission, two-electron transitions 2—16331
    photogradient e.m.f. of hot carriers 2—40382
    photovoltaic effect, surface barriers 2—22649
    piezoreflectance, Γ transitions in E_0' region 2—10348
    piezothermoelectric power anisotropy 2—4292
    positron annihilation, surface effects 2—32911
    radiation counter, applic. to nuclear radiation spectrometry 2—34819
    radiation detector, hot carrier phenomena 2—8233
    radiation detectors, planar and coaxial fabrication 2—18016
    radiation effects, 10.6 μm, interaction with current carriers 2—16236
    radiative recomb. of biexcitons 2—4479
    Raman scattering, carrier conc. effects 2—26192
    Raman spectra, hydrostatic pressure effects, Gruneisen consts. 2—16539
    recombination waves, by electron mirror microscope 2—4236
    refractive index in 77 to 300K range obs. using modification of minimum deviation technique 2—36818
    selective epitaxial deposition, growth mech. near Ge-SiO_2 boundary 2—25203
    solid phase growth, from evap. Al layer 2—39512
    submillimetre wave modulation, by free carrier absorption 2—21137
    surface, laser damage 2—12647
    surface barrier effect on spectral distrib. of photoconductivity and photoeffect 2—4303
    surface charging by adsorption 2—12648
    surface states, localized, in (111) planes 2—36543
    surfaces, sulphurization technique for stabilization 2—3488
    thermoelectric power, effects of plastic deformation 2—4233
    transport properties, dislocation effects 2—29697
    trapezoidal filtering of signals from detectors at high rates 2—31367
    u.s. attenuation, effect of dislocations 2—40062
    u.s. attenuation and thermal cond., low temp. 2—29532
    V-I characteristics by broad pressure contacts 2—4230
    vacancy formation energy, specimen thickness effects 2—36018
    wavelength modulation spectra, rel. to band struct. 2—1692
    dislocation electronic states, Hall effect obs. 2—25857
    n-Ge:As, e.p.r. line profile distortion of donor electrons, 4.2 K 2—22833
    Ge:As, e.s.r. line narrowing over wide impurity conc. range 2—26279
    Ge:As, heavily doped, cond. electron spin relax., e.s.r. obs. 2—20135
    Ge:Au diodes, n^+pp^+ prebreakdown behaviour 2—13283
    Ge:B, Ga, P, As ion implanted, elec. props. and doping profiles 2—25859
    Ge:B,P, amorphous, ion implanted, path length distrib., 25-150 keV 2—25710
    Ge:Co, Fe, Ni, Ag, Au, excited by laser rad., electron-hole recomb. at deep impurity centres 2—22558
    p-Ge:Cu, impurity compensation effect on elec. props. under press. 2—19687
    Ge:Ga, P, single cryst. growth, compensated, programmed growth rate 2—3572
    Ge:Hg, growth by gas transport, and specific resist. meas. 2—29095
    Ge:Nd,Eu, magnetoresist., paramag. susceptibility 2—13270
    n-Ge:Ni, hot electron lifetime temp. depend., photocurrent decay obs. 2—29702
    Ge:P, As, single cryst. growth, uniform impurity distrib., growth rate program 2—1211
    Ge:P, electron-phonon scatt. and phonon cond. 2—32854
    Ge:P, γ-irrad., n-p conversion due to impurity-vacancy complex form. 2—15741
    Ge:P, γ-irradiated, vacancy-donor complexes 2—29704
    Ge:Sb, hypersonic attenuation, temp. dependence, donor electronic relaxation 2—9877
    Ge:Sb, irradiated with 14 MeV neutrons, resistance and carrier lifetimes 2—40285
    Ge:Sn, radiative recomb. at isoelectronic point defects 2—10429
    Ge:Zn, symmetries and deform. pot. consts. of singly ionized Zn 2—29890
    Ge/ZnSe/GaAs(Cs), heterojunc. photocathode 2—6926
    Ge-GaAs p-n heterojunction, prep. and I-V characts. 2—29720
    Ge-PbS heterojunction, cond. band discontinuity determ. from photovoltage 2—19701
    Ge-Si alloy, thermoelectric element, prep. by hot pressing 2—6857
    Ge-Si solid soln., forbidden band width determ., 900-1200K 2—22559
    Ge-electrolyte interface, surface recomb. states 2—22557
    p-Ge, Ag doped, temp. depend. of lifetime, PCD method 2—27881
    Ge, Ge:Sb, electronic effects on u.s. wave propagation 2—40054
    Ge, n-type inversion layers, quantum limit piezoresist. 2—25853
    Ge, p-i-n struct., formed by electron irrad., s.c.l. current 2—25889
    p-Ge, PCD lifetime meas. as function of temp. in detector grade and impurity doped 2—29699
    Ge, with B implanted p^+ contacts, γ-detector 2—25883

Semiconducting materials continued
  germanium continued
    Ge film, obliquely deposited, photovoltage and resistance obs. 2—36616
    Ge(Li), γ-ray detector, peak efficiency calibration 2—5592
    Ge(Li) counters for analysis of X-ray K-spectra of elements 2—24089
    Ge(Li) detector, for registering soft γ-rays 2—34806
    Ge(Li) detector, numerical calculation of prompt coincidence curve 2—11671
    Ge(Li) detector characteristics, correlation with recent developments in Ge 2—27879
    Ge(Li) detector performance, Fano factor 2—38369
    (Ge(Li) detectors, review 2—34818
    Ge(Li) gamma-ray detectors, relative efficiency from 0.5 to 12 MeV 2—14764
    Ge(Li) γ-ray detector, calibration and photoefficiency 2—18015
    Ge(Li) γ-ray detector, hollow core coaxial, fabrication 2—14765
    Ge(Li) planar detector, shape distrib. by differential pulse shape selection method 2—34804
    Ge(Li) planar detector, subnanosecond timing of charge pulses 2—34805
    interband optical transitions, matrix elements 2—22746
    Li precipitation and driftability, gamma-ray spectrometer production 2—11674
    p-n junction diode, current-voltage characteristic, excess current carriers drift effects 2—25898
    Pb(Zr.Ti)O_3 ceramic/Ge wafer layers, surface acousto-electric amplification 2—19677
    p^+-n Si-Ge, heterojunction, alloyed, transport mechanism 2—19702
    ZnSe-Ge heterojunctions, switching and memory characts. 2—6860
  indium antimonide
    acceptor states, effective mass approx. 2—19670
    acoustic amplification, crossed elec. and mag. fields 2—32835
    acoustic wave interaction with hot electrons 2—32841
    acoustic waves, thermal amplification, current decay time dependence 2—4051
    acoustoelectric current, magnetic field dependence 2—4057
    amorphous, complex dielec. const. calc. 2—26105
    amorphous, complex dielec. const. from refl. meas. 2—26104
    amorphous film, tunnelling, effect of temp. and doping 2—19647
    amorphous state, produced by ion bombardment, Raman spectra obs. 2—26186
    band struct., interband transitions and excitonic effects 2—10044
    coupled cyclotron-plasmon-phonon modes for sample configs. ranging from Faraday to Voigt 2—22769
    density of states, crystalline and amorphous, pseudopot. and CBS calc. 2—10049
    diamagnetic excitons, wave function 2—6735
    diamagnetic excitons in degenerate bands 2—26152
    electron mobility in high elec. fields, electron-phonon interaction 2—22537
    electron scatt. mechanisms 2—36509
    electron velocity, in strong electric and magnetic fields 2—16210
    electron-phonon interaction, direct exptl. obs. 2—16082
    electronic plasma fluctuations rel. to external elec. and mag. fields 2—16224
    epitaxy, liquid phase, on CdTe 2—1178
    film, amorphous, recording of optical information 2—40225
    Hall effect transducer, for mag. bubble domain detection 2—40445
    hole-optical phonon coupling, magneto-optical study 2—36822
    hot electron galvanothermomagnetic props., low temp. 2—19779
    intrinsic, plasma compression caused by θ pinch at 300K 2—4189
    intrinsic carrier conc. temp. depend. helicon interferometry obs. 2—36512
    intrinsic Hall voltage, spatial distribution for semicond. slab 2—10022
    magnetic susceptibility, low temp. in strong mag. field 2—33110
    magnetoresistance, 77K, anisotropy 2—6807
    magnetoresistance, bulk and surface props. 2—19728
    magnetotransmission expt. effect of electron plasmon coupling 2—16424
    microwave detector with low inertia, volume effects 2—17496
    n-type, cond. band nonparabolicity influence on electron heating 2—13252
    n-type, cond. in Wigner lattice in mag. field 2—13236
    n-type, Corbino disc in galvanomag. oscill. 2—21008
    n-type, d.c. field-induced anisotropy of microwave cond. 2—13234
    n-type, d.c. mobility and disturbed phonon distrib. 2—40258
    n-type, electric field dependent motion of acoustic domains 2—36350
    n-type, electrical properties at 77 K, effect of tempering between 0 and 150°C 2—22516
    n-type, electron temp. determ. from Shubnikov-de Haas oscills. 2—36510
    n-type, energy relax. mechanisms, low temp. 2—32985
    n-type, free electron conc., quantized mag. field effect 2—6829
    n-type, frequency conversion of e.m. radiation 2—10050
    n-type, heavily doped, cond. electron spin relax., e.s.r. obs. 2—20135
    n-type, heavily doped with Se, Te and S, mobility, pressure dependence 2—10020
    n-type, high field electron transport, effects of electron-hole pair prod. 2—36511
    n-type, high field transport, drifted Maxwellian approach 2—22536
    n-type, i.r. Faraday rotation, low temp. electron impurity scatt. detn. 2—22729
    n-type, laser cyclotron resonance. pulsed elec. field modulated 2—9948
    n-type, light scattering under strong elec. field 2—19993
    n-type, magnetophonon resonance of hot electrons at 77K 2—36527
    n-type, microwave reflectance, mag. field dependence during helicon wave propagation 2—16601
    n-type, mode I acoustoelec. excitations in transverse mag. fields 2—19420
    n-type, negative photocond. in transverse mag. field 2—33070
    n-type, nonequil. carrier phenomena 2—19627
    n-type, nonlinear oscillations 2—6817
    n-type, photocond., transverse mag. field effects 2—29767
    n-type, photoelec. Hall effect in quantizing mag. fields 2—4305
    n-type, plasma pinch effect, Hall and inductance obs. 2—25751
    n-type, rel. to stimulated plasma wave Raman scattering 2—16517
    n-type, saturation of impurity cyclotron resonance and effect of 337 μm radiation on carrier numbers and mobility 2—32908
    n-type, scattering on short-range potential centres 2—10021
    n-type, surface helicon waves 2—6841
    n-type, surface plasmon-phonon coupling 2—9947
    n-type, third harmonic generation at millimetre wavelengths at 77°K 2—33000
    n-type, u.s. amplification in electron-hole plasma 2—36343
    n-type, u.s. attenuation in magnetothermally pinched plasma 2—36340
    n-type, warped Fermi surface conc. depend., from period anisotropies in SdH and dHvA obs. 2—19509

- **Semiconducting materials** continued
  - **indium antimonide** continued
    - optical energy gaps determ. from surface photovoltage meas. 2—40381
    - p-type, absorpt. spectrum, fund., absorpt. mech. 2—22768
    - p-type, absorpt. spectrum, fund., temp. effect., forbidden band width temp. coeff., 83-300K 2—22767
    - p-type, decay of injected electron-hole plasmas 2—13235
    - p-type, Hall coeff. field depend., constant energy surface, 77 K 2—22551
    - p-type, h.f. photoelectromag. effect 2—4309
    - p-type, hyperfreq. surface waves, crossed mag. and elec. fields 2—6842
    - p-type, irrad. defects, cond. changes 2—6819
    - p-type, optical absorpt. coeff. changes due to plasma and hole current effects 2—16491
    - photoconductivity spectra, quantum efficiency, impact ionization threshholds, 295K, 90K 2—22646
    - plasma, parametric excitation of density waves, direct conversion of photons into plasmons 2—13200
    - plasma, sausage instability, stabilization by axial mag. field 2—6818
    - plasma, temperature gradient- induced instability 2—29606
    - plasma pinch channel, effective cross-section, microwave measurement 2—25750
    - Raman lasers and parametric amplifiers, review 2—5345
    - Raman spin flip laser, high intensity 2—16544
    - second harmonic generation, coherence lengths and susceptibilities near band edge 2—7036
    - spin-flip Raman laser, fund. loss mechanisms 2—34406
    - spin-flip Raman laser, tunable, in 400 G mag. field 2—5372
    - stimulated spin-flip Raman scattering, at various wavelengths 2—10409
    - surface, magnetoconductance oscillations of n-type inversion layers 2—33007
    - transport coefficients, use for bulk material characterization 2—40240
    - tunnel junction, electron- phonon interactions 2—33027
    - u.s. attenuation, electron-phonon interaction 2—32838
    - u.s. generation and amplification, crossed electric and magnetic fields 2—4050
    - wavelength modulation spectra, rel. to band struct. 2—1692
    - Au-InSb, oxide-InSb struct., charge exchange between traps 2—13297
    - $\mathrm{InAs}_x\mathrm{Sb}_{1-x}$, film, absolute zero energy gap, optical, photoelec. and galvanomag. obs. 2—40277
    - InSb-GaSb, phase diagram for In-Ga-Sb system, rel. to cryst. growth 2—9836
    - n-InSb, e.p.r. line profile distortion of donor electrons, 4.2 K 2—22833
    - p-InSb, Shubnikov-de Haas oscills., Hall effect obs. 2—40259
    - $\mathrm{InSb}_{1-x}\mathrm{Bi}_x$, cryst. growth by Czochralski method 2—25263
  - **silicon**
    - (110) and (100) surface band structures, computation 2—16230
    - (110) surface n-channel m.o.s.f.e.t., conductivity anisotropy obs. 2—16239
    - acoustic amplification, deformation potential constants 2—19417
    - acoustoelectric effects, transport theory 2—9880
    - amorphous, complex dielec. const. calc. 2—26105
    - amorphous, elec. cond., band tail model 2—13275
    - amorphous, electronic density of states 2—10073
    - amorphous, photoemission and optical obs. of electronic struct. 2—33017
    - amorphous, short range order and pseudogaps 2—22545
    - amorphous, switching, rel. to crystn. 2—33014
    - amorphous in m.i.s. structure/tunnelling 2—13298
    - amorphous state, produced by ion bombardment, Raman spectra obs. 2—26186
    - anomalous diffusion, of Ga, rel. to n^+-p-n struct. prep. 2—9595
    - avalanche breakdown, statistical theory 2—29712
    - band struct., interband transitions and excitonic effects 2—10044
    - band-band impact recomb. 2—33011
    - bolometer, compensated impurity cond. role in performance 2—11371
    - Boltzmann eqn., method of soln. using spherical harmonic approx. 2—16199
    - carrier conc. profiles in amorphous layer 2—25425
    - carrier concentration, pseudo Brewster angle detn. 2—40282
    - carrier concentration, pseudo-Brewster angle obs. 2—13210
    - carrier props. determ. from electron beam generation model 2—40295
    - cesiated, secondary i.r. radiation effect on photoelectron energy distrib. curve 2—40393
    - charge carrier relax. times and far-i.r. spectra 2—33273
    - charged vacancy equil. conc., complex form. influence 2—1528
    - contamination, by Na, from water and alcohol 2—3501
    - crystal growth, role of dynamic props. of dislocations 2—6400
    - cyclotron absorption, crossed fields 2—1472
    - cyclotron resonance, Landau levels and hole resonance 2—4146
    - defect recomb. centre parameters determ. from carrier functions 2—32959
    - detectors, surface stability to neutron bombardment 2—38376
    - dielectric constant microwave perturbation meas. of temp. dependence method for minimizing airgap contact impedances 2—25850
    - dielectric function, freq. and wave vector depend. 2—33018
    - dielectric props., low temp. 2—16241
    - diffusion, of Ni and P, homogeneity breakdown 2—36058
    - diffusion of B, P, and As impurities 2—39712
    - diode, carrier lifetimes rel. to temp., light spot method, 293-523K 2—33033
    - diode, potential distrib. of surface of n-region 2—19709
    - diode, transient radiation effects near and in avalanche breakdown 2—19710
    - diode array camera tube with fibre optic faceplate 2—31155
    - dopant distribution, laser irrad. effect 2—3797
    - doped and compensated, i.r. refractive index and absorption spectra rel. to conduction processes 2—16482
    - doping and process impurities, characterization using mass spectrometry 2—16696
    - double injection and space charge currents, illumin. effects 2—22569
    - effective mass tensor and donor ground state, strain effects 2—16237
    - electrical crystal disturbances depiction, with electron beam probe 2—29706
    - electroabsorption, excitonic effects 2—7066
    - electron beam landing energy, optical modulation 2—22554
    - electron drift velocity and mobility at 4.2K, elec. field dependence 2—22572
    - electron irradiated, low temp. a.c. hopping cond. 2—29170
    - electron-hole pair prod. and radiation detector energy resolution 2—10063
    - electron-hole recombination, band-to-band Auger process 2—7089
    - electronic structure, empirical pseudopotential method 2—16225
    - electronic transitions at high press., review 2—15955
    - energy bands and soft X-ray absorpt. 2—40144
- **Semiconducting materials** continued
  - **silicon** continued
    - energy loss spectra of 25 keV electrons and 2 phonon excitation in amorphous films 2—19481
    - epitaxial film on Si substrate, thickness and orientation determ. 2—39526
    - epitaxial films, four-probe resist. meas. 2—16234
    - epitaxial layer, enhanced diffusion of substrate impurities by proton irrad. 2—25902
    - epitaxial layer, far i.r. interference thickness measurement 2—25207
    - epitaxial layer noise temp. at 2 and 4 GHz, obs. 2—4253
    - epitaxial layer resistance profile meas. method 2—19683
    - epitaxial layers, surface morphology, model derivation 2—3544
    - epitaxial wafer, resistivity measurement using voltage relax. technique 2—29708
    - extreme u.v. transmission, crystalline and amorphous specimens, conduction band structure obs. 2—26172
    - film, chem. vapour deposition and elec. props. 2—1536
    - film, epitaxial on sapphire, carrier transport mechanisms, m.i.s. deep depletion Hall effect struct. obs. 2—40293
    - film, heteroepitaxial, grown on sapphire, in m.i.s. config., photoelec. studies 2—40379
    - film, on sapphire, elec. props. depth variation, m.o.s. Hall technique 2—19688
    - film, oxidation, elec. stability, effect of HCl and Cl_2 2—39521
    - film, piezoresist. props., resist. temp. coeff., gauge factor 2—10072
    - film, polycryst., chemically deposited, resistivity 2—22570
    - film, twinning probability calc. 2—39525
    - film, vapour deposited, struct. rel. to growth conditions 2—39524
    - gamma-ray detector, response 2—38373
    - Hall effect of hot electrons, elec. and mag. field depend. 2—36546
    - heteroepitaxial film on spinel, carrier recomb. and trapping, transient response to elec. irrad. 2—25860
    - hole capture by neutral B atoms, hole conc. and lifetimes 2—16243
    - hot carrier energy relax. time, meas. method 2—29652
    - hot carriers, photogradient e.m.f. 2—16322
    - impact ionization of In, Ni, Au deep impurities 2—36545
    - impurity complexes, Be and Be-Li, acceptor level obs. 2—33019
    - impurity profile estimation near N-N^+ epitaxial layer interface 2—15779
    - inhomogeneous, high apparent mobility 2—4204
    - intervalley scattering mechanism 2—22568
    - intervalley scattering selection rules 2—22561
    - intrinsic absorpt., radiation induced increase 2—26165
    - ion implantation, electrical properties 2—22221
    - ion implanted, B^+, P^+, and Ne^+ ions, crystal damage and elec. props. 2—25380
    - ion implanted, defect energy levels detn., thermally stimulated current obs. 2—25865
    - ion implanted, defects, electron microscope obs. and elec. meas. 2—22181
    - ion implanted dopants, rapid electrical profile meas. using ion beam etching 2—19116
    - ion implnated thermoresistive sensor, for cryogenic temperatures 2—25884
    - ion scattering, directional effects 2—25986
    - i.r. dichroism due to free carriers in n-type uniaxially stressed Si 2—19968
    - i.r. waveguides, doping, refractive index and losses relationship 2—38112
    - irradiation, correlation of heavy ion data 2—39469
    - isolated interstitials and band gap obs. 2—40143
    - j.f.e.t., neutron and γ-ray responses 2—22593
    - junction, p-n, avalanche breakdown, oxygen conc. depend. 2—13281
    - junction, reverse-biased p^+-n, freq. response of Au centres in depletion layer 2—33028
    - junction f.e.t., neutron produced trapping centres 2—19712
    - junction f.e.t. neutron radiation effects, defect formation in space-charge region rel. to characts. degradation 2—10093
    - junction transistors, junction, effect of electron bombardment on shot noise 2—13286
    - masking and passivating layers, fault localization 2—40298
    - measurement methods, for resist., lifetime and inhomogeneities 2—36540
    - mesa photodiodes for improved demodulation of light 2—38036
    - metal-Si contacts, density of states and barrier height 2—10071
    - m.i.s. negative resistance diode 2—40316
    - m.i.s. struct., flat band shift, controlled charge injection 2—4260
    - m.i.s. structure, anomalous recombination 2—25908
    - in m.i.s.i.m. structure, nonlinearity of capacitance 2—19729
    - m.o.s. inversion layer, transport phenomena, effective mass approach 2—19744
    - m.o.s. structure, 20-40 Å oxide film on nondegenerate Si, interface states 2—22601
    - m.o.s. structure, I-V characts., effect of dislocations in Si 2—36573
    - m.o.s.t., interface-state density and mobility ratio obs. 2—16240
    - m.o.s.t., inversion layer, hole drift vel. 2—19743
    - m.o.s.t. inversion layer, electron conductivity-mass anisotropy calc. 2—36569
    - n-p-n planar transistor, gamma and electron irrad. effects 2—10094
    - n-p-n planar transistor performance rel. to slip plane dislocations 2—1544
    - n-type, anodic dissolution, etch channel form. 2—40830
    - n-type, bulk negative differential cond. 2—25863
    - n-type, current oscillations 2—4240
    - n-type, electron irrad., influence of O_2 vacancy complex (A-centre) on piezoresistance 2—25861
    - n-type, e.m. wave propag., effect of quantized mag. field 2—16228
    - n-type, Hall scattering coeff. 2—1535
    - n-type, hetero-diffusion of Zn and Au, reactor irrad. enhanced 2—29193
    - n-type, hole cond., warm carrier energy relax. time, rel. to uniaxial stress at 90K 2—16242
    - n-type, lightly doped, negative differential cond. and current oscillations 2—22571
    - n-type, mobilities due to impurities and lattice, meas. by microwave transmission 2—4238
    - n-type, m.o.s. structure, tunnelling characteristics, phonon structure 2—16255
    - n-type, phonon drag, thermopower, Nernst-Ettingshausen effect 2—6894
    - n-type, photogradient e.m.f. of hot carriers 2—40382
    - n-type, plasma reflectivity minimum, freq. shift due to uniaxial stress 2—33244
    - n-type, polar Hall effect and magnetoresistance 2—29711
    - n-type, Schottky barrier, bistable switching and memory 2—33024
    - n-type, transverse magnetoresist. in heating elec. fields 2—4237
    - n-type, wafers of varying thickness, photoconductivity, effect of thermal oxidation obs. 2—29769

Semiconducting materials continued
  silicon continued
    n-type, warm electron cond., anisotropy, high temp. 2—29709
    n-type, warm-carrier d.c. transport 2—36550
    n-type, warm-carrier microwave transport 2—36551
    n-type guarded contact surface barrier device, detector in X-ray spectrometer 2—38371
    n-type inversion layer, in m.o.s.f.e.t., differential negative resistance 2—19740
    n-type inversion layer, surface quantization 2—40292
    n-type ste-junction nuclear radiation detector, low temperature performance 2—38372
    neutron activation anal. technique 2—16715
    neutron displacement energy effects, requirements for standardization of damage curves 2—19692
    neutron irrad., defect annealing obs. by space-charge-limited current 2—33020
    neutron irradiated, divacancy associated i.v. absorp. bands 2—22777
    npn transistor effects of intense ionizing radiation 2—13287
    oxidation in air, room temp. 2—33378
    p-n diffusion junction, impurity distribution, potential distribution 2—4246
    p-n heterojunction, elec. and photoelec. characts. 2—6859
    p-n junction, mesoplasma, isothermal dynamic I-V characts. 2—40300
    p-n junction, trap parameters, thermally stimulated capacitance obs. 2—25886
    p-n junction, Zener effect, impact ionization 2—13278
    p-n junction diode thermometer, forward voltage-temp. characts. 2—40302
    p-n junction formation by in-pile irradiation doping of Si^{30} 2—13280
    p-type, ion-implanted, secondary electron emission coeff. 2—33098
    p-type, space-charge-limited currents and negative differential resist. 2—19691
    p-type, u.s. attenuation quenching by mag. field 2—40063
    p-type diffusion using boric acid in methanol as impurity source 2—36057
    passivation of silicon surfaces with thermally grown silicon oxide films 2—4186
    phonon transmission, impurity effects 2—32832
    photocell, effects of electric field on collection efficiency 2—23498
    photoconductivity, radiation induced defects obs. 2—25959
    photoconductivity and photovoltage, wavelength modulation 2—33074
    photodetector, for satellite appl., radiation damage 2—25967
    photodiode, nonuniformly illuminated, frequency characteristics 2—29725
    photodiode, thin-base, photocurrent kinetics 2—29724
    photodiodes, obtained by bombarding Si surface with positive ions 2—36618
    piezoreflectivity, stress depend of E'_0 refl. peak 2—16474
    plasmon excitations, energy depend., low energy electron backscattering 2—6747
    pnp junctions with asymmetrical impurity density, method of obs. 2—16247
    process control, device appl., elec. and thermal meas. 2—29694
    process control, device appl., elec. and thermal meas. 2—29694
    Raman scattering, carrier conc. effects 2—26192
    Raman spectra, hydrostatic pressure effects, Gruneisen consts. 2—16539
    refractive index in 77 to 300K range obs. using modification of minimum deviation technique 2—36818
    reversed annealing calc. for neutron damaged p-type 2—19690
    Schottky barrier diode, generation rate det. using ionizing radiation pulse 2—19706
    Schottky diode, current limiting processes, fabrication, characts. 2—25895
    s.n.o.s. diode, instability, diffusion effects 2—10097
    space-charge-limited current flow in metal-p$^+$-p-p$^+$-metal dielec. devices 2—13292
    specific resistance and excess carrier lifetime homogeneity, det. by photoconductivity meas. at two modulation frequencies 2—29707
    substrate, effect of crystallographic orientation on effective surface state charge density of m.o.s. structures 2—25909
    (110) surface, electron mobility anisotropy at low temp. 2—36548
    surface barrier detectors, effect of electron bombardment on operating characteristics 2—38375
    surface barrier detectors for spectrometry of low energy ion beams 2—27840
    surface charge visualization, transition metal solution treatment, electron microscopy 2—4244
    surface state calculation for (100), (110) and (111) faces 2—25864
    surface states, localized, in (111) planes 2—36543
    surface transport properties, state-of-the-art 2—36547
    thermionic electron emission, Maxwellian energy distrib. 2—33084
    thermoelectromotive force in p-type under compression 2—4293
    transient cond., trap behaviour 2—13274
    transistor, bipolar, dislocation and stacking fault generation at surface heterogeneities 2—33035
    transport properties, dislocation effects 2—29697
    u.s. attenuation and thermal cond., low temp. 2—29532
    u.s. attenuation by acceptor holes 2—13037
    V-I characteristics by broad pressure contacts and method of determining n- or p-type nature 2—4230
    wavelength modulation spectra, rel. to band struct. 2—1692
    Zener diode, planar, correlation between lattice defects and elec. props. 2—33032
    Zener diode as transducer for high press. meas. in gaseous H_2 at 15000 atm. 2—20782
    Al-Al$_2$O$_3$-Si system, internal photoemission, energy band diagram 2—13358
    Au doped photomagnetoelec. and Dember cells, visible and near i.r. photodetection 2—10149
    B ion-implanted layers, sheet resistivity meas. 2—10075
    p-GaAs:Si, electron radiative recomb. during epitaxial growth 2—20095
    Ge-Si alloy, thermoelectric element, prep. by hot pressing 2—6857
    Ge, n-type inversion layers, quantum limit piezoresist. 2—25853
    interband optical transitions, matrix elements 2—22746
    P ion implanted, profiles, calc. 2—25426
    PtSi-Si-PtSi, m.s.m. struct., current transport 2—10096
    S$^+$ donor, electronic structure by semiempirical LCBO method 2—29710
    SI:B, doping profile, from BN film diffusion source 2—3796
    Si:Al, core correction to ground state energy 2—40294
    Si:Al, solid solubility, electron microprobe analysis 2—3795
    Si:Au, impedance and g-r noise under space-charge conditions 2—22567
    Si:Au acceptor state, resolution of an anomaly 2—19689

Semiconducting materials continued
  silicon continued
    Si:Au photomagnetoelectric light detector characteristics over −20°C to +60°C range 2—34506
    Si:B, electron irrad. damage and cond. 2—22178
    Si:B, high resistivity photoconductor, gain saturation 2—19789
    n-Si:B, implanted, acceptor conc. obs. 2—25868
    p-Si:B, subthreshold electron irrad. effects 2—12752
    Si:B,Au, electron irrad., annealing, elec. cond., Hall effect 2—10070
    Si:B carrier recombination, electron lifetime; hole lifetime, 1.7-4.2K 2—16244
    Si:B implanted, acceptor profiles, damage depth distrib. 2—6504
    Si:B implanted, annealing behaviour and elec. props. 2—33016
    Si:B implanted, deep level centre obs. 2—4231
    Si:B ion implanted, elec. profile and annealing behaviour 2—25867
    Si:B ion implanted, enhanced annealing effects, by postimplantation of Si ions 2—19112
    Si:B ion implanted, photocond. obs. of defects 2—25960
    p-Si:B Schottky-barrier tunnel junction, effects of uniaxial compression on zero-bias anomaly 2—19703
    Si:C, impurity conc. effects on thermal donor formation 2—19117
    Si:Cu n$^+$-p junction, characts., dopant conc. profile 2—25890
    Si:Fe, impurity levels 2—1533
    Si:In, implanted, elec. cond and Hall effect 2—6852
    Si:In, Sb ion implanted, conc. profiles, Hall effect 2—25439
    Si:In ion implanted, ionization energy detn. 2—25872
    Si:In ion implanted, mobility, resistivity, and carrier conc. 2—25871
    Si:Li, radiation-induced extrinsic photocond. and radiation damage 2—25958
    Si:Li,B, ion pairing and ground state degeneracy, resistivity and Hall effect obs. 2—36053
    Si:Li neutron irradiated and heat treated, carrier removal effects 2—19652
    Si:Li solar cell, neutron irradiation damage, thermal annealing 2—22179
    Si:Mg, excitation spectra and piezospectroscopic effects of donors 2—10338
    p-Si:N ion implanted at cryogenic temps., elec. props. 2—25430
    Si:N ion implanted buried layer, electrical properties 2—25440
    Si:Ni diode, current-voltage characts., turnover voltage, photocond., diode parameters 2—22586
    Si:P, As, additional ion bombardment effects 2—25434
    Si:P, complex permittivity obs. using microwave technique 2—22555
    n-Si:P, D irrad., effect on Hall mobility, carrier density 2—22566
    n-Si:P, e.s.r. parameters, spin susceptibilities, impurity scatt. spin relax. 2—22835
    Si:P, elec. active damage in hot implantations 2—25869
    Si:P, exchange coupling in donor atom clusters, e.s.r. study 2—20150
    Si:P, first order Stark effect in impurity photocond. 2—10140
    Si:P, heavily doped, cond. electron spin relax., e.s.r. obs. 2—20135
    Si:P, impurity photocond., influence of phonons 2—33075
    n-Si:P,Fe, acceptor levels and vacancy-interstitial interaction 2—6485
    Si:P ion implanted, channelling profiles 2—19111
    Si:P ion implanted, deep localized energy levels obs. 2—25870
    Si:P ion implanted, profiles and elec. activity 2—25866
    Si:Pt diode, charge state and thermal generation in space charge region 2—10091
    Si:S$^+$, LCAO MO treatment 2—10074
    Si:Y, γ-irrad., and thermally processed, A-centre form. 2—1534
    n-Si:Zn, p-n junctions, impurities with deep energy levels, compensation of spectral characteristics 2—29772
    p-Si:Zn, P, photodielec. effect, polarizability of neutral atoms 2—13343
    Si:Zn, slow recombination wave motion obs. 2—25862
    p-Si:Zn,P, e.p.r. of Zn, hole-moment interaction 2—13543
    Si/SiO$_2$ system, surface charge density analysis with oxygen and nitrogen annealing 2—1529
    Si-Al$_2$O$_3$, effects of heat treatment on Si surface potential 2—29736
    Si-Au interface, possible cpd., form., resist. and electron microscopy 2—3493
    n-Si-Fe, recombination at Fe atoms and thermally generated lattice defects 2—36549
    p$^+$-n Si-Ge, heterojunction, alloyed, transport mechanism 2—19702
    Si-LiNbO$_3$, layered struct., transverse acoustoelec. effect 2—13036
    Si-SiO$_2$-Al$_2$O$_3$, effects of heat treatment on Si surface potential 2—29736
    Si-SiO$_2$, interface density and pot., v.l.f. m.o.s. capacitance meas. 2—6833
    Si-SiO$_2$ interface, nonuniform lateral ionic impurity distribs. 2—40313
    Si-SiO$_2$ interface, positive surface charge control by Cs implantation 2—10078
    Si-SiO$_2$ interface, surface state annealing parallel to B$_2$ centre annealing in irrad. SiO$_2$ 2—40312
    Si-SiO$_2$ interface device, performance, stability 2—40307
    Si-SiO$_2$ interface state parameters, m.o.s. capacitor obs. 2—40320
    Si-SiO$_2$ interface states, generation and distrib. obs. using bias temp. treatment 2—29737
    Si-SiO$_2$ system, elec. and recombination props. 2—6855
    Si-SiO$_2$ systems, transmission lines, characteristics 2—20991
    Si, screened exchange and Slater approx. comparison 2—22467
    Si p-n junction nuclear particle detector, ion implantation fabrication 2—25896
    Si p-n photodiode, fabricated by B ion implantation 2—25968
    Si$_{1-x}$Al$_x$ ion implanted, elec. props. 2—25873
    SiAs source material, capsule diffusion process 2—22240
    p-SiC, alloyed with Pt-B-Sn, space charge limited currents, current-voltage characts. 2—22565
    SiGe solid soln., forbidden band width determ., 900-1200K 2—22559
    Si(Li) driftability and precipitation 2—27880
    SiO$_2$-Si, m.o.s. struct., surface state characterization, quasi-static technique 2—16253
    SiO$_2$-Si interface, surface states induced by ion implantation of N$^+$, K$^+$ and Si$^+$ ions 2—25881
    ZnO-Si, heterojunc., lifht detector, elec. and optical props. 2—10088

Semiconductor lasers *see Lasers/semiconductor*

Semiconductor-metal boundaries
    backscattering and channelling analysis 2—25877
    Cu-CdS system transient internal photoemission of carriers 2—13209
    dielectric-metal, electron injection, arbitrary band structure 2—4256
    rectification, Se diodes, Schottky theory 2—4251
    Schottky, determination of deep level density and energy of impurities by C-V measurement 2—13268
    Schottky barriers, characterization of epitaxial GaAs 2—33010
    Schottky barriers, epitaxial PbTe 2—7769

Semiconductor-metal boundaries continued
- Schottky junction, avalanche breakdown criterion from doping profile integral 2—33025
- Al thin film interconnections, crossing Si-SiO$_2$ steps temperature cycling effects 2—1538
- Au-GaAs contact, barrier height depend. on surface layer thickness 2—33030
- Au-Se system, transient internal photoemission of carriers 2—13209
- CdCr$_2$Se$_4$-metal junction, magnetocapacitance effect 2—36555
- CdIn$_2$S$_4$ metal contact, I-V characts., switching and memory effects 2—19719
- CdS/In boundary, contact barrier development, current instability 2—4254
- CdTe-Au, IV characts, Schottky theory and tunnelling 2—29733
- Cu$_2$O-Hg contact, barrier capacitance anomaly of Hg melting pt. 2—25885
- GaAs-Au surface-barriers, capacitance relax. determ. 2—4242
- GaAs-metal, contact technology for Gunn devices metallurgical structure of interface after alloying 2—33037
- n-GaAs-metal tunnel contact, ion bombardment effects on tunnelling characts. 2—16251
- GaAs, Schottky barrier, form. by Au deposition, surface elastic waves, depletion layer transduction 2—13324
- n-GaAs, specific resistance for Sn, Sn-Ag, and Au-Ge-Ni ohmic contacts 2—29715
- GaAs alloy Schottky barrier junction, elec. and crystallographic props. 2—33038
- GaAs barrier contact, six-parameter model values using iterative error-minimizing multiparameter computer technique 2—19694
- GaAs epitaxial layers, doping profile, Schottky contact study 2—25431
- n-GaAs Schottky barrier, bistable switching and memory 2—33024
- Ge, linearized third-derivative spectra with depletion-barrier modulation 2 -33240
- p-InAs-metal barrier, CV characts., inversion layer effect 2—10081
- p-PbTe-metal barrier, CV characts., inversion layer effect 2—10081
- PtSi-Si-PtSi, m.s.m. struct., current transport 2—10096
- Se, rectification, Schottky theory 2—4251
- Si-metal, contacts, density of states and barrier height 2—10071
- n-Si Schottky barrier, bistable switching and memory 2—33024
- Si Schottky diode, current limiting processes, fabrication, characts. 2—25895
- SrTiO$_3$-In, tunnelling, rel. to polaron transitions 2—4139

Semiconductors
- *see also Crystal electron states; Ion implantation; Magnetoelectric effects; Photoconductivity; Photovoltaic effects*
- absorption coefficient for two-photon transitions in a magnetic field 2—4450
- acceptor impurities, substitutional, deep level obs. 2—6835
- acoustic surface wave amplification due to discontinuous periodic coupling 2—4053
- acoustic wave generation in mag. field 2—6671
- acoustic waves coupling 2—22413
- acoustoelectric effects, transport theory 2—9880
- acoustoelectric oscillations, computer simulation 2—29540
- acoustoelectric oscillators with arbitrary static field distrib., linear theory 2—25676
- acoustoelectric phenomena, nonlinear theory, amplitude saturation, oscillator applic. 2—25677
- acoustomagnetoelectric and acoustoelec. effects 2—9881
- admittance det. at microwave frequencies 2—34239
- alloy semiconductors, dielectric measurements in microwave frequency region 2—4262
- amorphous, band struct., cycle-free approx. 2—25840
- amorphous, covalent network model, electronic struct. 2—19658
- amorphous, elec. props., band models, review 2—13203
- amorphous, elec. props. rel. to struct. 2—32967
- amorphous, electronic processes, phase transition effects 2—22515
- amorphous, electronic states and elec. transport, review of current theories 2—40233
- amorphous, elemental covalent, short range order and pseudogaps 2—22545
- amorphous, forbidden optical and elec. bands, Fritzsche model 2—16223
- amorphous, Hall conductivity, random phase model 2—16200
- amorphous, localized states in band gaps, perturbed atomic orbitals 2—16222
- amorphous, negative resistance arising from thermal effects 2—19620
- amorphous, one-phonon spectra 2—19332
- amorphous, percolation on continuum and localization-delocalization transition 2—6791
- amorphous, phys. props., review 2—40224
- amorphous, trial wavefunctions for valence band 2—13253
- amorphous, weak absorpt. tails and localized states 2—33248
- amorphous and cryst., energy gaps and ordering 2—13254
- amorphous and doped, conduction via percolation processes 2—13072
- amorphous films, electro-thermal switching, model 2—9994
- amorphous state, produced by ion bombardment, Raman spectra obs. 2—26186
- anisotropic, excess-carrier transport and photovoltaic effect 2—36488
- anisotropic, mod. potential probe for location of principal axes of cond. tensor 2—29693
- anisotropic band structure, non-equilib. plasma osc. 2—10003
- anisotropic non-degenerate, optical props. rel. to band struct. and scatt. mechanisms 2—10298
- antiferromagnetic, electromagnetic fluctuations in a mag. field 2—6989
- Auger recomb. quadruplets and impact ioniz. 2—33096
- band struct., interband transitions and excitonic effects 2—10044
- band struct., muffin tin model, general potentials 2—16221
- band structure, surface curvature detn. 2—10060
- biexciton binding energy, rel. to electron-hole effective mass ratio 2—9940
- binary, cubic, Debye temps. from Lindemanns melting law 2—40048
- binding energy of excitonic mols. 2—32896
- Boltzmann eqn., exact soln. 2—16080
- Boltzmann eqn., method of soln. using spherical harmonic approx. 2—16199
- carrier concentration, pseudo Brewster angle detn. 2—40282
- carrier concentration, pseudo-Brewster angle obs. 2—13210
- carrier distribution, convergence of Gummel's numerical algorithm 2—9992
- carrier effective mass., far i.r. cyclotron reson. meas. technique 2—25757
- carrier local drift mobility, pulse method 2—13206

Semiconductors continued
- carrier waves, non-isothermal analysis 2—1508
- channelling effect meas., ion implantation 2—36044
- characterization, kinetics of one energy level recomb. and surface states 2—22523
- charge carrier capture by deep traps 2—10045
- charge carrier mobility measurement for inhomogeneous 2—4099
- charge carriers transport, short life-time in homogeneous 2—4100
- charge state effects in displacement damage 2—19660
- charge-carrier equilibrium according to mass-action law 2—13202
- charged impurity influence on dislocation mobility in systems with high Peierls barriers 2—29177
- charged vacancy equil. conc., complex form. influence 2—1528
- chemical vapour deposition techniques 2—32349
- chemisorption, effect on elec. cond., book 2—15672
- chemisorption, effect on elec. cond., review 2—18956
- chemisorption, electronic phase transitions and instability phenomena 2—6839
- combined resonance of band carriers, impurity effects 2—22823
- compensated, current instability rel. to carrier lifetimes 2—6797
- compensated, Gunn effect 2—1504
- compensated, low field mobility at low temperatures 2—36491
- compensated, S-type IV charact., low temp. 2—6795
- conduction in narrow energy bands, theory 2—40236
- conductivity oscillations in surface layers under quantizing mag. fields 2—6800
- contact, metal-semicond., filling of local levels, applied voltage effects 2—19659
- cryostat with pneumatic device, optical measurements in the far i.r. 2—20778
- crystal growth, cold metal crucible system 2—25267
- crystal growth, role of dynamic props. of dislocations 2—6400
- current fluctuations in presence of external field 2—29649
- cyclotron echo 2—22477
- cylindrical, four point probe resistivity 2—9986
- deep-trapping kinematics 2—36481
- defect electronics, book 2—5111
- defect recomb. centre parameters determ. from carrier functions 2—32959
- degenerate, longit. magnetoacoustic phenomena 2—36344
- degenerate nonpolar, hot carrier scatt. at optical phonons 2—19626
- degenerately doped, complementary variational bounds for low temp. resistivity 2—6789
- diamagnetic excitons in degenerate bands 2—26152
- diamond (or sapphire)-semiconductor-In sandwich as window-heat sink sandwich for optical expts. 2—20769
- diamond-type, electronic props. of point defects, extended Huckel method applic. 2—13085
- diamond-type, electronic props. of point defects, extended Huckel method applic. 2—13084
- diamond-type acceptor level ground state energy 2—13262
- dictionary in seven languages 2—11243
- dielectric props., low temp. 2—16241
- dielectric relaxation effect on travelling carriers 2—36482
- diffused structure, carrier equiv. lifetime, impurity deionization and temp. effects 2—25809
- diffusion constant for electrons in nonequilibrium system 2—22520
- disordered, optical absorpt. coeffs., calc. 2—40653
- disordered solids, dielectric theory many electron effects 2—1502
- disordered system, band struct. and transport props. 2—16102
- disordered system, density of states, gap existence 2—4110
- disordered systems, thermoelec. behaviour 2—10132
- dispersed in insulator, transient photocond. effects 2—19782
- doped, dielec. function and effective band edge concept 2—29596
- doped, electron shielding 2—4200
- doped, highly correlated electron gas props. 2—19633
- double injection current, a new approach 2—22522
- dynamic negative differential conductivity 2—6803
- Einstein relation, in the presence of a magnetic field 2—36490
- electric field distrib. meas. using edge electro-optic effect in KDP 2—13439
- electric field intensity meas. by β-conductive method 2—40234
- electrical conductivity, in strong electric fields 2—4198
- electroabsorption, excitonic effects 2—7066
- electron concentration, quantized mag. field effect 2—6829
- electron energy quantization in mag. field 2—25838
- electron gas, degenerate, temp. depend. of h.f. polarizability 2—37658
- electron gas, Landau level broadening and transverse magnetocond. 2—16197
- electron gas, thermodynamics in crossed fields 2—6745
- electron gas, two-dimens., transverse magneto-cond. 2—40229
- electron gas with random impurity scatt., Hall effect 2—16207
- electron heating, cond. band nonparabolicity influence 2—13252
- electron transfer to electrolyte calc. of impedance and noise thro surface states 2—13585
- electron transport coefficients and scattering of acoustic phonons 2—12362
- electron-electron interactions, Monte Carlo calcs. 2—16206
- electron-hole pair prod. 2—10063
- electron-hole pair prod. by impact ioniz., threshold energies 2—29655
- electron-hole pair production, threshold energy calc. 2—32996
- electron-hole recombination at dislocations and possible negative differential cond. 2—9990
- electron-phonon interaction, direct exptl. obs. 2—16082
- electronic basis of switching in amorphous alloys 2—36485
- electronic engineering materials and devices, book 2—4187
- excitonic absorption coefficient 2—10355
- extrinsic, n- and p-type, concepts of donors and acceptors, charge carrier production 2—32957
- Faraday effect, influence of uniform electric field 2—33209
- ferroelectric, photocond. due to surface layers 2—4296
- ferromagnetic, electron-spin interaction influence on carrier transport 2—6740
- ferromagnetic, energy spectrum and mobility of small polaron, s-d interaction influence 2—6739
- ferromagnetic, galvanomag. and thermomag. effects 2—13333
- ferromagnetic, heavily doped, metal- insulator transition 2—32961
- ferromagnetic, high field transport 2—4199
- field electron emission, saturation region in Fowler-Nordheim characts. 2—6917
- film, conductivity and Hall mobility, van der Pauw method 2—9991
- film, current calc. by method of damped electron waves 2—16196

Semiconductors continued
film, current calc. by method of damped resist. meas. 2—16234
film, optical absorpt. under size quantization conditions 2—7064
film, size-quantized, cond. temp. depend. 2—4194
fluorescence, quadratic processes 2—10436
four point probe Hall effect and resistivity measurements 2—40223
four point probe resistivity, correction devisors for parallelepiped, Green's func. method 2—40283
Franz-Keldysh effect, internal fields 2—4438
frequency-contrast characts. for image converter applic. 2—6895
galvanomagnetic effect, pulsed magnetic field measurement 2—19776
Green's function method for calc. of impurity energy levels in the band gap 2—18543
group III-V cohesive energy and compressibility, perturbation theory calc. 2—12691
group IV, cohesive energy and compressibility, perturbation theory calc. 2—12691
group IV-VI compound semicond. films, device applications 2—40297
growth, automatically controlled, with aid of digital computer, patent 2—18995
Gunn domain avalanching, theory 2—4196
Gunn domain phenomena, direct microscopic simulation 2—19618
Gunn domains, instability growth factor under d.c. conditions 2—6798
Gunn effect materials with field-dependent diffusion, Shockley's positive conductance theorem 2—4195
Hall effect for polarized electrons, Kane model calc. 2—22525
Hall effect in heavily doped materials near metal- insulator transition 2—19623
Hall effect in impurity conduction 2—13212
Hall effect meas., continuous recording equipment 2—22556
Hall voltage in inhomogeneous systems, photocond. mechanism 2—16208
Hall voltage in inhomogeneous systems, photocond. mechanism 2—16209
heavily doped, diffusion, density of states approx. 2—36059
heavily doped, low temp. thermoelec. effects, Green's function method 2—25942
heavily doped, mag. suscept. in weak mag. fields 2—4192
heavily doped, thermoelec. effect, weak mag. field depend., calc. 2—40268
heavily doped, thermomagnetic and adiabatic effects, low temp. 2—40269
heavily doped, transport props., at low temp. in weak mag. fields 2—19625
heavy ion bombardment, amorphous film production 2—25367
helicon modes, reflectivity, localized carrier distrib. influence 2—10059
heterogeneous layers, concl. meas., four-probe method 2—6801
high field domain theory in presence of trapping 2—32963
high field transport, drifted Maxwellian approach 2—16204
high-field transport, resonant type current anomalies 2—32965
high-resist, space-charge-limited current, current-voltage characts. 2—22514
homogeneous, with exponential band tail, laser generation threshold, theory 2—20090
homogeneous, with exponential band tail, laser generation threshold, theory 2—20090
homopolar, charge carrier capture by deep traps, hot electrons 2—29657
hopping conduction, in strong mag. field, theory 2—6808
hot carrier energy relax. time, meas. method 2—29652
hot electron transverse conductivity in quantizing magnetic fields 2—9995
hot electrons, inelastic impurity scattering 2—1507
impurity analysis by spark source mass spectrometry 2—16691
impurity band hopping cond., theory 2—16198
impurity centres, Fe-group, ground states and photoioniz. 2—19672
impurity concentration estimation, spectral analysis after chemical laminar etching 2—29194
impurity det. by emission spectros. 2—16708
impurity distrib., direct meas. method 2—15775
impurity level density and energy from C-V meas. 2—13268
impurity levels, periodic lattice Green functions applic. 2—6718
impurity segregation coeff., compensation effect from resist. meas. 2—32548
impurity-to-band activation energies, conc. and temp. depend. 2—10057
indirect gap, band-to-band Auger model 2—7089
indirect transitions, resonant magnetooptical absorpt. 2—40610
indirect-band-gap, two-photon transition 2—22753
inhomogeneous, anomalously high mobility model 2—16195
inhomogeneous, Hall effect anomaly calc. 2—22518
inhomogeneous, local photocond. signal rel. to carrier lifetime 2—22634
inhomogeneous, simple model for high apparent mobility 2—25810
inhomogeneous, thermally stimulated cond., rel. to trapping levels 2—6796
inspection with liquid crystal detector 2—33008
insulator-metal, and mag. phase transitions, thermodynamic model 2—29832
interstitial migration mechanism 2—19091
intrinsic, Hall and Dember effects 2—4193
intrinsic, many-photon photoelectric emission 2—6921
intrinsic, self- magnetoconc. effect 2—33012
intrinsic, trap-free, double injection, space charge limited current 2—40329
intrinsic carrier conc. temp. depend., helicon interferometry obs. 2—36512
ion bombardment effects on physical properties 2—25803
ion implantation, conf., Garmisch-Partenkirchen, Germany, May 1971 2—25416
ion implantation, retention, saturation effects, effect of sputtering 2—25420
ion implantation, spatial distrib. of energy deposited by energetic heavy ions 2—15773
ion implantation 2—9583
ion implantation application 2—1256
ion implantation damage, Rutherford scatt. and channelling obs. 2—19068
ion injection techniques, state-of-the-art 2—32547
ion injector, review 2—32546
i.r. reflectivity of heavily doped material, optical const., free carriers 2—26140
isoelectronic impurities, screened potential 2—13201
Kane model, small-gap, energy levels and wavefunctions in mag. fields 2—6827
Knight shift oscillations and nucl. relax. times in crossed elec. and mag. fields 2—40768
Landau-Coulomb levels in degenerate band 2—10041
large band, resonant Raman effect localised energy levels, impurity levels 2—16579
light scatt., magnetoplasma quasi-elastic 2—16448
light scattering under strong elec. field 2—19993

Semiconductors continued
liquid, electrophysical properties, chemical bond characteristics, fine arrament, zone structure and Fermi surface det. 2—35784
low compensated, impurity conductivity 2—25811
low mobility, switching, thermal mechanism 2—10002
low mobility materials, conf., Eliat, Israel, Apr. 1971 2—9996
luminescence, recomb. radiation decay calc. 2—7088
luminiescence, free exciton condensation into electron- hole drops 2—33307
magnetic, emission and absorption spectra 2—26150
magnetic, energy levels, elec. transport, magneto- optical effects 2—4203
magnetic, properties 2—40439
magnetic susceptibility, low temp. in strong mag. field 2—33110
magneto-optical obs. in far i.r. regions 2—36541
magneto-Raman scatt. and lack of inversion symmetry 2—10405
magnetoplasma, sound amplification, nonlinear theory 2—32839
magnetoresistance, hopping, gauge invariance 2—9993
many valley, galvomag. effects in strong mag. field and heating elec. field 2—16203
many valley, shallow donor impurity states. ground state levels 2—40280
many-valley, density of states and electron mobility 2—6825
many-valley, light scatt. cross section 2—16515
materials, process control and devices, meas. methods 2—6790
materials and devices, book 2—19612
measurement methods 2—36540
metal-insulator transitions, coherent pot. approx. 2—40271
Meyer-Neldel rule, thermally assisted tunnelling and pseudointrinsic cond. 2—13211
microwave conductivity, non-parabolic energy dispersion 2—10004
microwave diagnostic techniques, review 2—22555
microwave emission and kink in IV charact. 2—1505
minority carrier diffusion path length in rectangular specimen, probe obs. 2—1506
minority carrier diffusion profiles, electron-beam excited 2—32958
mixed valence, hopping transport 2—9997
m.o.s. inversion layer mobility, theory 2—22553
Mott exciton dissoc. in random field 2—6733
Mott transition, impurity effects 2—40273
multiphoton intraband transitions, uniform mag. field, e.m. wave interaction 2—6828
multivalley, domain struct., Sasaki effect 2—1501
multivalley, multivalued equilib. distrib. of current carriers 2—22546
multivalley, size effect, heating electronic field 2—6804
negative differential mobility, nonuniform d.c. field effects on carrier waves 2—19619
negative magnetoresistance in semiconductors with overlapping impurity and conduction bands 2—29682
negative mobility, emitter current limited injection 2—33021
negative-mobility amplifiers in emitter current limited injection mode, space charge effects 2—6809
neutron activation analysis, review 2—16715
noise, 1/f, random walk model 2—25806
noise, 1/f, random walk model 2—25805
non-crystalline, non-ohmic behaviour and switching 2—19632
noncentrosymmetric, spin relax. of cond. electrons 2—29841
noncrystalline, elec. cond., review 2—10000
nondegenerate, acoustoelec. gain in magnetic fields 2—22415
nondegenerate, galvanomag. and thermomag. effects, theory 2—29651
nondegenerate, pseudoresonances in magnetophonon structure 2—19624
nonlinear effects, electron recomb. influence 2—6799
nonlinear optical effects in crysts. with variable effective mass 2—7033
nonlinear optical phenomena, rel. to free carriers 2—36484
nonparabolic, d.c. field-induced anisotropy of microwave cond. 2—13234
ohmic and nonohmic transport, nonparabolicity and overlap effects 2—19622
optical absorpt. by impurity centre with deep level in static elec. field 2—10353
optical energy gaps determ. from surface photovoltage meas. 2—40381
organic, electrical conductivities 2—4190
organic, photodielec. effect 2—6898
organic crystals of anthracene type, advances since 1967 2—25961
oxide structures, inhomogeneous distribution of free charge carriers in space charge region 2—25801
p-type, relax.-case, sign of Hall coeff. 2—13208
p-type crysts., negative photocond. rel. to elec. instability, single recomb. model 2—33067
phonon transmission, impurity effects 2—32832
photoconduction, noise, band to band Auger processes 2—19781
photoconductivity, decay time const., temp. depend., by least squares 2—4295
photoconductivity, quadratic processes 2—10436
photoconductivity in quantizing mag. fields 2—1583
photoelectret state, non-isothermal relaxation, trapping levels, thermally stimulated currents 2—25950
photoelectric emission, deviation from the Schottky line, theory 2—4323
photoelectromagnetic effect, transient characts., theory 2—25966
photoemission and photocurrent, review 2—19800
photoemission characts., surface elec. field effects 2—36640
photoluminescence, radiative recomb. obs. using impact ioniz. of donors 2—16602
photon drag of holes for degenerate hole distrib. case 2—6711
photon pressure effect 2—13344
piezoelectric, acoustic amplification, associated microwave radiation power 2—36342
piezoelectric, acoustic two-wave interaction in alternating elec. field 2—29514
piezoelectric, acoustoelec. high field domains, Fourier analysis 2—29544
piezoelectric, acoustoelec. surface domains 2—29543
piezoelectric, acoustoelectric domains on transverse surface wave 2—29690
piezoelectric, acoustoelectric parametric interactions 2—4054
piezoelectric, electronic attenuation and intensification of Lamb waves 2—1424
piezoelectric, nonlinear excitation of acoustoelec. fluctuations 2—19418
piezoelectric, piezoelec. scatt. at high elec. fields, electron energy distrib. function validity 2—9988
piezoelectric, plasmon-enhanced sound amplification 2—36346
piezoelectric, reduced phonon noise in acoustoelec. amplifier 2—16028
plasma, electron-hole, non-stationary pinch 2—4141
plasma, e.m.-waves, dispersion relation 2—32888

Semiconductors continued

- polar, d.c. mobility and disturbed phonon distrib. 2—40258
- polar, high freq. conductivity 2—9989
- polar, longit. magnetoresist., displaced- Maxwellian analysis 2—36487
- polar, surface plasmon-phonon interaction 2—9947
- polar degenerate, current fluctuations, carrier scatt. by optical phonons 2—6806
- polar mobility of electrons and holes 2—32964
- polaron-polaron interaction, theory 2—25743
- polycrystal, free carrier absorption 2—13469
- positron annihilation, surface effects 2—32911
- potential sampling probe, low temp., electrical point contact 2—40284
- process control, device appl., elec. and thermal meas. 2—29694
- quasi-monopolar, intrinsic photocond. in depletion layer 2—40377
- quasineutral wave instability for field depend. electron density case 2—13205
- radiative electron capture by impurities 2—40713
- Raman scattering, development of tunable sources of i.r. radiation 2—16523
- Raman scattering, exciton mediated, resonance props., polariton theory 2—20058
- recombination centres characteriz. from photoluminesc. temp. depend. 2—29951
- recombination domains, analytic theory 2—13204
- recombination domains, illumination effect 2—22524
- relaxation, carrier transport 2—29654
- residual cond., model 2—4208
- residual impurity det. using photoelectric spectroscopy 2—40841
- resonance Raman scattering, in electric fields 2—16512
- resonant interaction with ultrashort coherent light pulse 2—38051
- resonator method of parameter meas. 2—4185
- Seebeck effect of paramag. polaron 2—10133
- small polaron transport and narrow band semiconduction, review 2—9998
- sorption on IV-VI single crystal films, chemical sensing 2—19674
- space charge, equil. distrib. 2—4197
- space charge current-voltage characts. for uniform trap distribution 2—13255
- space charge free currents, conditions for 2—4202
- space group D^{12}_{2d}, band structure 2—10042
- spatially inhomogeneous system, hot electron theory, local approx. 2—25812
- sputtering, photon emission during ion bombardment 2—10357
- sputtering resulting from 20-500 keV Ar bombardment, measurement of step height, scanning electron microscopy study 2—25704
- stimulated Raman scattering, from plasma waves 2—16517
- strongly doped, dielectric constant, giant Zeeman effect 2—40540
- structure and physical properties, book 2—27886
- superconducting, low temp. heat capacity 2—19427
- superlattice, phonon and polariton modes 2—19315
- surface, Auger spectroscopy 2—1503
- surface, carrier wave motion, transverse diffusion effects 2—19673
- surface, ionic thermally stimulated cond. of water vapour 2—29744
- surface, nonlinear interaction between Bleustein- Gulyaev waves in piezoelec. plate 2—32824
- surface, self-consistent potential, elec. and mag. fields effects 2—10061
- surface electric field distribution, electron mirror microscope 2—4227
- surface inversion layer, quantization of carriers 2—40235
- surface props. obs with u.h. vacuum cryostat 2—26990
- surface states rel. to surface struct. 2—33005
- thermal cond., hydrostatic press. influence 2—19436
- thermal instability in laser beam with phonon energy<band gap 2—22742
- thermal resist. due to electron-phonon scatt., trial function 2—9901
- thermally stimulated cond. and thermoluminesc., simultaneous meas. 2—13513
- thermionic emission, deviation from the Schottky line, theory 2—4323
- thermodynamics, statistical, of electron transport, undergraduate book 2—13068
- thermoelectric power meas. by Seebeck effect of sintered semiconductors 2—17509
- three-photon absorpt. rel. to energy band models 2—10356
- trace analysis, emphasis on impurity distribution 2—30098
- transport coefficients, use for bulk material characterization 2—40240
- transport eqn., heterogeneous semicond. 2—19617
- transport eqn., heterogeneous semicond. thread 2—19616
- transport phenomena in strong elec. field 2—9985
- transport processes, equivalent circuit models 2—4201
- transverse negative differential cond. possibility 2—32962
- two-electron transition process, elec. field depend. 2—13237
- two-valley, negative differential cond., carrier redistrib. inertia 2—36483
- U.S. Rayleigh waves on boundary with piezoelec. 2—29524
- valence electrons, energy operator, approx. diagonalization 2—19486
- warm-electron distrib., maximum anisotropy approx. applic. 2—13207
- X-ray topography, scanning oscillator method for bent slices 2—39601
- zero-gap, long wavelength acoustic phonons, effective dynamical matrix 2—9847
- zero-gap, permittivity in quantizing mag. field, l.f. case 2—22603
- zincblende type, dielectric function, Penn model 2—10043
- zincblende-type, charge density 2—12690
- zincblende-type, semimetal-semicond. transitions 2—19664
- ZnSe, electroluminescence in ZnSe-In junction, reverse biased 2—29996

Semimetals

- acoustic wave generation in mag. field 2—6671
- antiferromagnet, dielectric constant, giant Zeeman effect 2—40540
- electron gas, degenerate, temp. depend. of h.f. polarizability 2—37658
- e.m. excitation of sound, deformation mechanism 2—6673
- excitonic phase, effect of paramagnetic impurities 2—32914
- graphite based synthetic metals, electrical anisotropy 2—40171
- magnetoacoustic phenomena, longit. 2—36344
- microwave emission and kink in IV charact. 2—1505
- nuclear quadrupole interaction, sp. ht. obs. on As 2—4419
- phonon spectra in mag. field 2—22395
- theory, applic. of consistent theory of fluctuations in superconductors 2—16151
- u.s. wave amplification in elec. field 2—40064
- As, i.r. reflectivity, plasma reson. freqs. 2—7063
- Bi:Te, hyperfine heat capacity and nucl. quadrupole interaction 2—16657
- Bi, Alfven wave second harmonic generation 2—40156
- Bi, damped wave size effect, carrier mobilities 2—32905
- Bi, Fermi surface, r.f. size effect obs. 2—9956
- Bi, interband transitions, i.r. magnetoreflectivity 2—16473

Semimetals continued

- Bi, low field thermomag. power tensor 2—25945
- Bi, magnetosonic-elec. effect 2—16125
- Bi, pure and doped, magnetoacoustic attenuation, Landau level broadening 2—29537
- Bi, thermomag. power tensor and Umkehr effect 2—22633
- Bi film, galvanomag. effects, quantum size effect 2—25765
- NiS, metal-nonmetal transition 2—19515
- Sb-Bi alloys, interband transitions, i.r. magnetoreflectivity 2—16473
- Sb, resistivity and Hall coeff. temp. variation above 4.2K 2—36446

Series

- planetary motion, computerized soln., relativistic orbital motion 2—11008
- planetary motion, disturbing function, expansion by binomial and Laplace series 2—20678
- summation of series of the form Σnx^n occuring in specific heat theory 2—14068
- truncation, new method, applied to supersonic flow past steady of oscillating blunt bodies of resolution 2—28687

Sferics *see Atmospherics*

Shadow universe *see Cosmology; Elementary particles*

Shear strength *see Mechanical strength/shear*

Shell model *see Nucleus/models*

Shielding *see Radiation protection*

Shock tubes

- acoustic absorption measurement coeff., sound reductions in jet engine nacelles 2—4045
- arc driven, theoretical performance 2—2259
- attenuation-free, design 2—11362
- cylindrical, geometry effects on normal ionizing shock waves 2—17405
- diaphragmless electrothermal, using preheated Ar 2—20950
- discharge tubes with diaphragms, characteristics study 2—32145
- effects of laminar and tubulent boundary layer buildup on chemical rate measurements 2—1748
- electric-arc-driven, high performance for simulation of Jupiter and Saturn atmosphere entry 2—20949
- electromagnetic, inversion of population state 2—28547
- high performance, with air driver, design for undergraduate lab. 2—27290
- high-performance, using e.m. forces, test meas. 2—14281
- linear explosive-driven, trajectories of gas shocks 2—37782
- magnetic, digital computer solution 2—7760
- real gas tailoring, analytical method, Mach number 2—28715
- reflected shock, duration of const. temp. in overtailored condition 2—28682
- shock wave deceleration effects on ionization levels 2—34185
- sonic boom simulation, devices and techniques 2—34188
- Cs nonideal plasma, electric-discharge shock tube 2—28603

Shock waves

- *see also Detonation; Explosions; Plasma/shock waves; Supersonic flow*
- acceleration in gas with density gradient 2—21905
- acoustic, reflected, analysis method 2—27258
- acoustic wave refl. and transmission at boundary, wave form. 2—27257
- acoustic-gravity wave generation at 120 km by sea level detonation 2—37190
- around afterbody in wake of 120° cone, wind tunnel investigation at Mach 3.0 2—12498
- air-water two-phase system, propagation 2—39285
- anisotropic elastic media, shock propag. produced by planar impact 2—9637
- atmosphere, generation and detection 2—13689
- atmospheric, produced by focusing of shocks generated by supersonic aircraft, detection 2—4672
- axisymmetric, quasi-stationary velocity approx. for time development, applic. to stellar explosions 2—23391
- axisymmetric cone in steady supersonic flow, approx. analytic soln. 2—24969
- B-G-K model, density slope shock thickness, approx. solutions for structure 2—5251
- blast wave propagation in inhomogeneous atm. 2—10739
- blast waves, contour image improvement by use of striped background in photogrammetry 2—27291
- blast waves, general formulation of conservation equations governing nonsteady flow field 2—37788
- bubble-liquid mixtures, propag. 2—32214
- chromosphere, discrepancies in weak shock theory 2—26926
- closed form soln. for propagation in polytropic plastic body with elastic unloading props. 2—30878
- collision, initial phase 2—6142
- collisionless perpendicular shock, leading edge, distribution function 2—34190
- collisionless shocks, temp. gradient instability 2—34191
- composite, anisotropic plates, wave surfaces due to impact 2—36099
- composite, Elkonites, response to shock loading 2—36100
- composite, fibre reinforced, steady wave propag., Hugoniot 2—25489
- composite, reinforced, finite-amplitude wave propag. 2—12835
- coordinate measurement in spark chambers, using shock wave generated by sparks 2—34835
- curved characteristics, elementary function expression 2—17406
- damping conditions, treatment using continuum model of two-dimensional flow 2—5250
- damping in liquid containing gas bubbles 2—39319
- delta wings leeward surfaces, high supersonic speeds 2—6147
- diffracting and reflecting wave pattern prediction 2—180
- diffraction on wedge moving with supersonic velocity 2—27294
- dusty gases, theoretical-kinetic approach 2—35675
- elastic-plastic solid, anisotropic, plane-wave propag. 2—39767
- elastoplastic material, rate-sensitive, nonlinear waves 2—34078
- electrodynamic explosions 2—5254
- energy release from the aftershock activity of the high yield nuclear explosion BENHAM 2—20240
- exothermic gaseous mixtures, development of instabilities in flow field 2—39233
- explosion of cylindrical charge, finite length, flow analysis 2—30881
- exponential atmosphere propagation 2—7320
- finite difference approach, supersonic flow over aerodynamic wing-body configurations 2—32160
- formation and propagation from a concave boundary in simple and complex wave fields 2—11364
- galactic, link between interstellar gas and spiral structure in a galaxy 2—20486

Shock waves continued
galactic interstellar medium in spiral mag. field 2—20597
galaxies, spiral, barred structure and motions 2—4799
gas, generation and propag., applic. to nonlinear props. 2—39261
in gas statistical models evaluation using shock structure problem 2—6143
generation and propagation, from Apollo rockets at orbital altitudes 2—37178
high velocity impacts in metals, investigation of temperature increases 2—9645
high-Mach number, oblique and collisionless, in magnetized plasma, ion heating, numerical simulation study 2—18605
hydromagnetic, propagation in a self-gravitating gas 2—12493
hypersonic air flow around spherical segment 2—39250
hypersonic flow past wedges and cones, perturbation analysis 2—3303
in immiscible displacement in fissured porous medium 2—179
impact stress waves in composite structures 2—14231
incidence on blunt body in supersonic flow 2—32165
infinite circular cylinder, phase structure of near field pressure and speed of vibrations 2—27296
internal structure 2—37785
interplanetary, directional and temporal properties of solar protons 2—14015
interplanetary space, formation and propagation of shocks after chromospheric flares 2—37375
interstellar, supernovae cooling effects 2—26717
isolator, optimum 2—177
jets, axisymmetric, supersonic, impingement on perpendicular flat plate 2—3306
laminar boundary -layer/shock wave interactions on flared axisymmetric bodies under adiabatic conditions 2—18723
large angle cones, surface pressure distrib. and sonic point location 2—6148
laser glass, rel. to laser beam damage, holographic obs. 2—27505
liquid, generation and propag., applic. to nonlinear props. 2—39261
liquid, nonlinear acoustic problem obs. using X-ray flashes 2—32192
liquid containing gas bubbles, weak shock waves, Crespo two phase flow model 2—25016
loading process behind fronts in reflected and refracted waves in plastic layered media 2—30879
Mach wave, tailoring, analytical method 2—28715
magnetogasdynamics, cylindrical blast wave propagation 2—18575
magnetosphere, var. of the bow shock wave during geomag. storms 2—10773
material relax. props. determ. from decaying elastic shock fronts 2—15813
materials exposed to explosive waves, test method 2—39868
mechanical shock and single impulse frequency analysis 2—2257
metals, bulk modulus, press depend., calc. from shock wave data 2—32573
N-waves, dynamic magnification factor for sonic booms on complicated structures 2—7761
nonlinear dissipative, in inhomogeneous media 2—14071
normal flowfield, radiative cooling and nonequilibrium chemistry cooling 2—34186
normal ionizing, effects of cylindrical geometry 2—17405
one-dimensional, in elastic non-conductors, external influences on growth and decay 2—2260
one-dimensional, propagation in inhomogeneous elastic materials 2—23390
passage through curved interface of two media 2—37783
plane, ionizing, stability in magnetic field 2—37784
plane, nonstationary propagation in inelastic medium such as soil 2—26446
plane ionizing, supersonic, stability in mag. field 2—18747
profile equation, variational approach 2—12491
propagating boundary surfaces between elastic and plastic state, growth and decay of acceleration waves 2—17341
propagation in air due to Tunguska meteorite, rel. to atmos. inhomogeneity 2—30269
propagation in elasto-plastic media, conditions for existence of continuous plastic deformations 2—37786
propagation in free space 2—6125
propagation in gaseous media, diagnostic techniques, kinetics 2—24970
propagation in uniform or non-uniform media, uniformly valid analytic solution 2—27295
radiation gas dynamics, plane phase method analysis 2—39256
radiation resisted, in gas particle flows 2—24967
radiative cooling effects in absorbing gas behind reflected shock wave 2—7762
rare gas solid, mol. dynamic simulations 2—32592
rarefied plasma, supersonic flow around plate and cylinder bodies 2—12377
reflected, effects of radiative transfer 2—3293
reflected shock, duration of const. temp. in overtailored condition 2—28682
reflection in ionized gases, pressure gauge for obs. 2—30751
relativistic flow, propagation into region of decreasing density 2—3171
reproduction of shock spectra for testing with electrodynamic shakers 2—37787
rocks, attenuation, Q values, in granite and limestone 2—3841
RR Lyrae, calculation for atmosphere 2—7439
self similar blast waves, parametric study 2—34189
in solar wind, reverse and forward slow 2—20703
solar wind plasma 2—17059
solid, generation and propag., applic. to nonlinear props. 2—39261
solid media, physical processes 2—11363
sonic bang, characteristic overpressure as typifying parameter 2—15531
sonic boom generation theory and prediction methods 2—35667
sonic boom in turbulence, statistics of random overpressure peaks 2—9023
sonic boom minimization, modification of aircraft configuration 2—35668
sonic boom propagation, effects of atmospheric irregularities 2—37186
sonic boom propagation through stratified atmosphere 2—35669
sonic boom simulation, devices and techniques 2—34188
sonic booms, behavioural awakening study 2—7591
sonic booms, loudness heard outdoors as function of overpressure and rise time 2—3315
spherical wave propagation in Maxwell and Voigt type media 2—17346
spiral nature of the Galaxy, speed determination of density waves near inner Lindblad resonance 2—4791
stability of shock accelerated interface between two gases 2—32144
in stellar envelope, propagation, associated with collapsing Fe cores, matter ejection 2—26663

Shock waves continued
stellar interiors, spherically symmetric stellar models, propagation 2—30448
strong, normal, influence of radiation and equilibrium reactions on flow variables in front of and behind 2—12496
strong in monatomic gas, structure determ. using Fokker-Planck model 2—28726
structure in binary gas mixtures 2—3314
structure in diatomic gas, using loaded sphere molecular model for computer simulation 2—18743
supernovae, relativistic shock propagation and search for e.m. pulses 2—37306
supersonic aircraft, high speed wind tunnels for studying transonic phenomena 2—18745
in supersonic flow, axisymmetric, non-equilibrium, decay 2—6131
supersonic flow from slender bodies, theory of characteristics, PLK method 2—18737
supersonic flow through, formulae for stagnation conditions 2—35651
in supersonic flows, determ. structure of viscous flowfield downstream from a centre line Mach reflection 2—21735
thermal, pulsed nuclear reactor fuel elements, viscous damping 2—15105
thin disc, uniformly charged, moving in dielectric Cerenkov field 2—2345
Timoshenko beams, continuous, natural frequencies 2—11348
trajectories in linear explosive-driven shock tubes, blast wave theory 2—37782
transonic flow past two-dimensional symmetrric profile 2—917
troposphere, oblique propagation 2—26509
turbulent boundary-layer shock interaction with and without injection 2—28710
visco-elastic waves, weak shock structure study by wavefront theory 2—159
viscous compressible fluid, viscosity influence on blast wave solns. 2—35666
viscous inviscid and inviscid flow problem, by numerical method 2—28459
in water due to explosion, effects of bottom coverings 2—6180
weak, propagation in inhomog. medium, Reed-Ottermann theory, second order correction 2—34187
weak nonlinear waves, propagation through turbulence 2—30877
X-type pseudo shock comparison with λ type pseudo shock 2—178
Al alloy, plane shock structures, comparison of steady and unsteady profiles 2—3848
in Al and duraluminium, effects of elastic limit 2—6569
Ar-He mixtures, velocity distribution functions, electron beam fluorescence obs. 2—24962
Ar, ionized, corner expansion flow induced over range of Mach numbers 13-18 and pressures 1-10 torr at 300 K 2—3302
CO_2-N_2-He mixtures, vibrational population inversions behind normal shock waves 2—24442
CO_2 flow parameters, boundary layers, Mirels principle 2—28693
H_2, ionization relaxation and light absorption on strong shock waves 2—21867
H_2, magnetic shock structure, shock thickness, magnetic field jump and ion temp. meas. 2—12502
N_2 flow parameters, boundary layers, Mirels principle 2—28693

effects
aerospace materials and structures, sensitivity, fracture 2—9703
air heating in shock tube, radiative cooling and enthalpy profiles 2—12509
alpha particle radioisotope emission alteration 2—35676
arc column in forced axial convection 2—9011
boundary-layer interaction problems, shock- induced solution by integral mthod 2—35674
composite, Hugoniot analysis 2—19167
composite, Hugoniot synthesis using theory of mixtures 2—19169
detonation initiation in low density explosives 2—5252
elastic ripples on surface of electronic circuitry components 2—8055
ferromagnet, shock-induced anisotropy, demagnetiz., domain theory analysis 2—36706
ferromagnet, shock-induced anisotropy, demagnetiz., mag. grain interaction 2—33130
flow of initially cold gas influenced by short shock, perturbation methods 2—5249
glycerol, dynamic tensile failure 2—12525
heating in collisionless plasma, high Mach numbers 2—24708
Inconel 600, explosive shock deformation, thermal recovery 2—9656
initiation problem, collisionless solution, transport phenomena 2—1029
ion acoustic shocks in plasma, post frontal turbulence 2—39172
liquid droplet breakdown dynamics in gas flow 2—1063
liquids, laser induced breakdown, short duration photography 2—9144
metal, eqn. of state under strong shock compression 2—3847
metal, shock compression, effects of electronic struct. 2—39769
metal, shock melting and vaporization 2—39420
metallic system, idealized dynamic stress/strain curve of uniaxial compression 2—32594
metals, shock vaporization, rel. to equation of state determ. above 200 kbar 2—22044
noise generation from supersonic shear layers, generalized convective wave theory 2—14276
nuclear reactor shield, energy absorption obs. 2—15183
plasma heating, Z-pinch experiments 2—21797
plasma heating and production 2—28508
polymer, compression effect on elec. resist. 2—40161
porous solid, dynamic compaction 2—12836
quartz, x-cut, piezoelectric currents 2—22629
quartz gauge, induced polarization 2—14356
response of viscoelastic sphere to a pulse from a point source at the centre 2—17345
sandstone, Coconino, solid phase effects 2—4642
solid, broken by shock loading, dispersion 2—32625
sonic boom, response of box structure 2—153
sonic boom responses and damage to buidling structures 2—34153
sonic booms, animal responses 2—37500
sonic booms, building responses, flight trials of Concorde 2—34154
sonic booms, conference, Acoustical Soc. America, (Houston Texas 1970) 2—34102
sonic booms, effect of exposure of humans and buildings 2—37466
sonic booms, human response, in laboratory and community 2—37465
sonic booms, seismic and underwater responses 2—37087
stainless steel, shock loading, recovery and recrystallization 2—9657
stainless steel, type 304, residual microstructure, explosive shock 2—9655
steel, hardness and struct., effect of explosive deform. 2—39930

Shock waves continued
- **effects** continued
  - steel, precompression effect on dynamic fracture strength 2—12889
  - Teflon, shock compression and induced phase transition 2—9640
  - toroidally confined plasma, equilibrium potential distribution 2—24709
  - transition metal borides, carbides and silicides, shock compression 2—12841
  - turbulent boundary layer parameters 2—32167
  - u.v. emission from K2 III p Arcturus 2—26695
  - velocity relaxation of micron sized particles det. by laser radiation 2—22010
  - wedge-shaped cavity, processes 2—29250
  - Al, precompression effect on dynamic fracture strength 2—12889
  - Ar, ionization, obs. by microwave radiation measurement 2—3308
  - Ar, ionization relaxation behind leading edge of reflected shock wave 2—39198
  - Br_2, dissociation, rate meas. at 1500 to 2700K 2—24459
  - C, graphite, shock compacted, hardness and microstruct. 2—9714
  - Cs nonideal plasma, electric-discharge shock tube 2—28603
  - Cu-Al alloy, microstruct. following explosive deform., 1 megabar pressure 2—9650
  - Cu, microstruct. following explosive deform., 1 megabar pressure 2—9650
  - Cu film on LiF or plexiglass, diffusion processes occurring during blast compression time 2—29203
  - Fe-Ni alloy, impact loading, microstructure, hardness, α-γ transformation 2—3867
  - Fe-Ni system, explosively loaded, hardening, recrystallization, grain boundaries 2—9575
  - HBr, dissociation, rate meas. at 1500 to 2700K 2—24459
  - LiF, elastic precursor decay, point defect effects 2—39770
  - LiF, electric precursor decay, impurity clustering effects 2—39771
  - LiF, X-ray diffr. obs. 2—3715
  - N_2 dissociation, obs. of induction time 2—24479
  - N_2 rotational states, electron beam fluorescence investigations 2—39265
  - NbC_x, microcrack form. and plastic deform. 2—29328
  - TiC_x, microcrack form. and plastic deform. 2—29328
  - Xe plasma, radiating plasma flow production, conductivity probe obs. 2—32050
  - YIG, shock-induced anisotropy, demagnetiz., mag. grain interaction 2—33130
  - YIG, shock-induced anisotropy, demagnetiz., domain theory analysis 2—36706
  - ZrC_x, microcrack form. and plastic deform. 2—29328

Shot noise *see Noise/electrical*

Showers *see Cosmic rays/showers and bursts*

Shubnikov-de Haas effect *see Magnetoresistance*

Silicon
- *see also Semiconducting devices; Semiconducting materials/silicon*
- adsorption of O_2, Auger electron spectroscopy 2—6386
- amorphization, by 30 keV P ion implantation 2—25381
- amorphous, Raman spectra, density of vibr. states detn. 2—16541
- amorphous layer form. by ion bombardment 2—25425
- angular dips, depth depend. for H^+ and D^+, backscatt. study 2—40111
- anharmonicity and temp. depend. of forbidden (222) refl. 2—13028
- annealing temp. of A and E centres, interference effect 2—9539
- anodic oxidation, SiO_2 layer growth 2—7179
- antireflection coatings for 2.5-50μm region, transmittance obs. 2—8012
- atom, collisional charge exchange formation of excited Si- 2—5835
- atom, electron impact L-shell ionization calc., occurrence of delayed maxima 2—8467
- atom, Kα-X-ray spectra produced by 30 MeV oxygen bombardment 2—24350
- atomic collision with Ar ions, radiative transitions between quasimolecular levels 2—28215
- atomic mismatch on closure of controlled partial splits, shear displacement 2—19095
- atomic spectral line intensities, dependence on temp. of CaF_2-Al_2O_3 fused systems 2—40849
- Auger spectra, electron-induced, backscatt. effects 2—33095
- backscattering spectra of mol. hydrogen ions 2—9908
- barrier detector, operating in d.c. mode, detection of H^+, H_2^+, H_3^+ 2—18013
- benzol, adsorbed, n.m.r. spin echo investigation 2—6374
- bremsstrahlung photon emission, 1 BeV electron and positron interaction 2—13498
- Brillouin scattering, at 6328 and 4880 Å, linewidth analyzed to give real and imaginary part of refractive indices 2—20082
- channelling, effects of thermal vibrs. and impurity atoms 2—40108
- channelling of He^+ ions in crysts. overlaid with amorphous films 2—4092
- channelling of ion beams, minimum yield temp. depend. 2—13063
- channelling of light ions, energy loss determ. 2—40118
- chemisorption of organic gases, ellipsometric and gas-volumetric obs. 2—10619
- contamination, in GaAs during vapour phase epitaxial growth 2—39594
- crystal, etching structure 2—39572
- crystal, interaction of impinging O_2 supersonic beam 2—6314
- crystal, single, crystallographic defects detection 2—1241
- crystal growth, vacancy cluster prevention 2—9357
- crystal struct. factors meas. using Pendellosung and interferometry fringes 2—9487
- crystalline-amorphous transition, ion bombardment effects 2—25159
- Czochralski growth, crystn. front and impurity zone study 2—9368
- dechannelling of protons, channelled fraction rel. to penetration depth calcs. 2—36389
- dechannelling of protons and He ions, backscatt. obs. 2—36388
- defect struct., high-resolution phase-contrast electron microscopy obs. 2—6491
- detector, rad. enhanced diffusion, defect prod. ratio 2—33023
- diamondlike lattice, dynamics and vibrational spectra, valence force pot. calcs 2—19357
- diffusion, in W, in field emission microscope 2—12816
- diffusion, of Al metallization, enhanced effects due to ion implantation 2—25472
- diffusion in α-Fe, 800-1300°C, conc. depend. 2—12805
- diffusion in Zn_2SiO_4 2—32566
- diffusion of As, profile estimation 2—25447
- diffusion of elec. active impurities 2—12785
- diffusion of Fe, coeff. determ. 2—1533
- diffusion of impurity C, Ge traps 2—15780

Silicon continued
- diffusion of ion implanted Sb 2—29191
- diffusivity and solubility, in Al film, rel. to integrated circuit metallization 2—19142
- dislocation, i.r. transmission microscope obs. 2—15763
- dislocation dissoc. and mobility 2—39702
- dislocation dissociation and stacking fault energy calc. 2—3781
- disturbed layer structure 2—36010
- effect of Si on joints in austenitic steel 2—3957
- elastic consts., anisotropy, 293-873K 2—6520
- electric wave refraction, LEEd obs. 2—15658
- electron diffraction scattering on (111) surface, comparison of Bethe theory calc. of specular intensity with exptl. values 2—29117
- electron irrad., isothermal annealing of luminesc. 2—10428
- electron microscope sample prep. for transmission mode expts. 2—19032
- electron microscopy, transmission electron channelling patterns 2—9490
- epitaxial, dislocations at film-substrate interface 2—1184
- epitaxial film, on sapphire, structural defects 2—6354
- epitaxial growth, effects of grown in and process induced defects 2—25248
- epitaxial growth, on Si through Si_3N_4 window 2—9285
- epitaxial layer, crystal imperfections, ion channelling studies 2—19084
- epitaxial layer, stacking fault elimination by heat treatment 2—39705
- epitaxial layer, temp. depend. of doping conc. of As and P 2—25209
- epitaxial slices, plastic deform. in central regions 2—12865
- epitaxy, introd. of slip 2—25208
- e.p.r. detection of optically induced divacancy 2—40764
- e.p.r. from clean surfaces, surface energy states 2—30009
- exo-electron emission, after proton irradiation 2—4318
- exo-emission, thermally excited, effects of pretreatment of crystals 2—16326
- fast io dechannelling, theory and expt. 2—40099
- film, condensed, effect of deposition conditions on profile and props. 2—32353
- film, electron diffr. rel. to channelling 2—35969
- film, epitaxial growth mechanism 2—3542
- film, epitaxy, by silane pyrolysis, HEED and Auger spectroscopy obs. 2—39523
- film, homoepitaxial, grown by SiH_4 pyrolysis, quality, HEED and Auger spectroscopy obs. 2—39528
- film, Kikuchi pattern, electron channeling 2—9399
- film, polycryst., deposition in-process thickness monitor, i.r. interferometry method 2—22077
- film, polycryst., thickness determ. by i.r. interferometry 2—22076
- film, single cryst., dimpling, ion produced lattice damage 2—25368
- film, vapour deposited, struct. rel. to growth conditions 2—39524
- film growth, open method, thermodynamics of gas transport 2—3543
- foil, electron diffr. contrast profiles of vacancy clusters 2—6486
- growth twins, high order, orientation calc. 2—3570
- Harwell-Lintott industrial ion implantation machine, evaluation by making Si planar resistors 2—37935
- implantation disorder, ionization and thermal dependence 2—25376
- impurities in GaSb, microanalysis by direct obs. of resonant nuclear reactions 2—10681
- impurity concentration profiles, anodic oxidation technique 2—3799
- ion channelling, of H^+ and D^+, quantum effects, backscatt. obs. 2—36387
- ion implanated, effects of Al films, recrystalliz. and interfacial migration 2—19120
- ion implantation damage, stress measurements 2—25379
- ion implanted, disorder, effects of flux, temp., and ionization 2—22182
- ion implanted, elastic and anelastic behaviour 2—19166
- ion implanted, localized surface defects 2—9527
- ion implanted, paramag. defect inventory, e.p.r. obs. 2—26264
- ion implanted, SiC, Si_3N_4, SiO_2 formation, i.r. absorp. obs. 2—26173
- ion implanted, struct. differences in light and heavy ion disorder, channelling obs. 2—25378
- ion implanted crystal, precision lattice parameter, X-ray obs. 2—3763
- ion implanted dopants, rapid electrical profile meas. using ion beam etching 2—19116
- ion irradiation damage, in transmission elec. microscope 2—6477
- ion-bombarded, amorphous layers depth meas. 2—39675
- ion-bombarded, lattice strain 2—36021
- ion-implanted, ^{17}O h.f.s. of neutral vacancy-oxygen centre 2—40765
- i.r. thickness meas. of epitaxial layers, interpretation of phase shift at substrate layer interface 2—29039
- L-emission spectra 2—20086
- lattice mechanics, variable bond charge model 2—36335
- lighter impurities on, det. by 90° forward ion scattering through thin targets 2—16714
- mean square displacement, bulk and surface atoms 2—22389
- microdefects, disloc. free float-zone cryst., annealing and etching obs. 2—3569
- migration, at low temp. into Au and Pt films 2—15791
- migration, low temp., through Au and Ag films 2—3812
- Mossbauer effect of ^{57}Fe, interstitial and cobalt-vacancy complex obs. 2—1675
- neutron Pendellosung fringes obs. in wedged shaped cryst. 2—9429
- neutron total effective cross section for 130 eV neutrons 2—19478
- nuclear backscattering, by ^4He ions, random spectrum defined 2—25715
- nucleosynthesis in silicon burning in stellar explosions with various initial compositions 2—26673
- optical constants at 5461 Å, etched and cleaved samples 2—36817
- oxidation in 10-1400Å oxide thickness range 2—40815
- oxidized, floating-zoned, dislocation free, spotty defects, X-ray diffr. obs. 2—19104
- perfect crystal, multiple beam Borrmann effect 2—39602
- phonon dispersion curve, perturbation theory calc. 2—12692
- photocells for solar radiation meas. 2—23499
- photoconvertor, study of behaviour in i.r. region 2—14365
- photoionization cross-sections for all levels belonging to $1s^22s^22p^63s^23p^q$ configurations 2—24337
- photovoltaic cell spectra response, expt. 2—13351
- plasma, free carrier, laser generated, optical and elec. props. 2—29876
- plasmon excitations, energy depend., low energy electron backscattering 2—6747
- plastic flow, glide band form. 2—36036
- plate, use in high resolution focussing X-ray monochromator 2—25285
- positron channelling, in thin crysts. 2—29580
- powder compact, nitriding, N_2 diffusion process 2—39961
- precipitate colonies of Cu 2—36286
- precipitate colonies of Cu 2—32779

Silicon continued
  precipitates of Cu, habit and morphology 2—39939
  precipitation, in integrated circuit Al metallization 2—25876
  proton backscattering, angular width of blocking, interatomic dist. determ. 2—25705
  protons backscattering, fast 2—22441
  radiation detectors, temperature depend. of photocurrents produced by X- and γ-rays 2—38383
  radiation-induced absorpt. bands, piezospectroscopic obs. of group V—defect complex 2—16499
  recombination rad. spectrum, temp. shift and width of 0.970 eV no-phonon line, 6-110K 2—22800
  reflection coeff., ion irrad. effects 2—22727
  refractive index, near i.r., press. depend. 2—10303
  scattering or Ar ions, directional effects 2—36647
  six coordinated in SiO_6 polyhedron, by study of crystal structure of various Si containing complexes 2—6393
  solar abundance, Doppler shifted spectra of forbidden Si I lines 2—4998
  solar abundance from forbidden lines of Si I 2—4995
  solar cells, nonpenetrating proton damage 2—23501
  solar corona abundance, det. from e.u.v. spectra 2—20692
  solar energetic-particle events, composition, enrichment of very heavy nuclei 2—11082
  solid-state control-detector, high energy solar X-rays 2—11071
  sputtered, surface damage, depth of damage 2—39467
  sputtering ratios under heavy ion bombardment, energy and ang. depend. 2—25706
  sputtering yield and sticking probability by ellipsometry 2—32378
  stacking faults conc., rel. to epitaxial growth rate 2—6499
  in steel, austenitic, effect on NbN solubility and precip. 2—12968
  steel impurity, effect on H crack corrosion resistance 2—6579
  stimulated Raman scattering, using Nd:glass laser 2—33287
  stopping power of energetic He ions, channelling and random directions 2—40117
  structure factor, and absorption potentials, elec. diffraction obs. 2—3729
  substrate for Ag film, deposited by Si reaction with AgF vapour 2—39487
  surface, secondary electron emission yield, fine struct. detection 2—32322
  surface, thermal desorption of H, CO and CO_2 2—9312
  surface, thermally oxidized, cryst. orientation effect on fault form. 2—9570
  surface barrier detector, correlation between etch pit density and performance 2—14761
  surface barrier detector, correlation between etch pit density and performance 2—14761
  surface barrier detectors, pulse height characteristics for heavy ions 2—31371
  surface characterization by ellipsometry, treatment effects 2—25187
  surface phonons, inelastic slow electron scatt. 2—39451
  surface structure, (111), glancing incidence HEED obs. 2—9236
  surface structure, (111), glancing incidence HEED obs. 2—9238
  surface structure, (111) face, LEED-AES obs. 2—39470
  surface structure, LEED, Auger spectroscopy 2—3502
  thermal diffuse scatt. at Bragg refls., Mossbauer obs. 2—19402
  thermal expansion, low temp. behaviour 2—19434
  thermomigration of Au-rich droplets 2—39746
  thin cryst., particle channelling, angular distrib., continuum picture 2—36386
  thin crystal, channelling of supercollimated beam of H^- ions 2—22436
  thin crystal, ion irrad. damage and annealing 2—22180
  thin section prep. by fracture-extraction technique 2—6414
  u.s. attenuation and thermal cond., low temp. 2—29532
  vacancy formation and migration energies, pseudopotential calc. 2—18964
  vacuum u.v. spectra, expts. using storage ring light source 2—16479
  wafer, stacking fault and dislocation loop generation 2—25181
  wafer, thermal conditions for dislocation generation 2—32526
  X-ray diffr. meas., F_{222} obs., bonding electron density meas. 2—3702
  X-ray examination of thin crystals, equal inclination interference fringe obs. 2—6449
  X-ray spectra, high-energy satellites of $L_{2,3}$ emission bands 2—33299
  Al/Si abundance ratio in quasar PKS 0237-23 det. from absorption spectrum 2—4909
  in Al film, electromigration induced failure 2—6510
  in As_2Se_3 glass, effect on crystn. rate 2—28974
  BeO:Si, phosphor, thermolum. props. 2—29970
  C/Si abundance ratio in quasar PKS 0237-23 det. from absorption spectrum 2—4909
  in Fe, cast, effect on carbonitride case after low temp. cyaniding 2—36245
  GaAs:Si, laser, amphoterically doped, one step liquid phase epitaxy 2—5376
  in GaAs epitaxial layers, effect of $AsCl_3$ conc. on incorporation 2—9276
  GaP:Si, bound excitons, and donor ground state, optical study 2—36530
  lattice defects, surface layers, lapping 2—36270
  Si:As, lattice location, beam effects in He ion channelling 2—32550
  Si:B, epitaxial grwth, effect of water vapour on doping 2—12665
  Si:B, ion implanted, lattice parameters 2—9488
  Si:B,P, lattice contraction coefficients detn. 2—22225
  Si:B diffused, surface layer conc. of boron 2—9589
  Si:B ion implanted, conc. distrib. and atom location, ion produced x-ray obs. 2—25436
  Si:B ion implanted, post implantation of Si ions, enhanced annealing effects 2—25428
  Si:B ion implanted, random and channelled distrib. 2—25427
  Si:C ion implanted, substitutional, localized mode obs. 2—25377
  Si:Ga, In ion implanted, atom location, enhanced diffusion case, He ion backscatt. obs. 2—25438
  Si:H, Si-H bond parameters rel. to atomic muon dimens. 2—28225
  Si:In, Sb ion implanted, conc. profiles and enhanced diffusion 2—25439
  Si:In, Sb ion implanted, enhanced migration in presence of Al film 2—19121
  Si:O, annealed, neutron irrad., O conc., i.r. absorpt. spectra 2—22223
  Si:P,As, simultaneous diffusion, backscatt. He ion and radioactive analysis obs. 2—32551
  n-Si:P,Fe, vacancy-interstitial interaction 2—6485
  Si:P ion implanted, divacancy radiation damage, e.p.r. obs. 2—26265
  Si:P ion implanted, non-Gaussian profile, mechanisms discussed 2—25437
  Si:Yb, ion backscatt., channelling, flux peaking, energy and depth depend. 2—36054
  Si:Yb ion implanted, atom location, flux peaking 2—25435
  p-Si:Zn,P, e.p.r. of Zn, hole-moment interaction 2—13543
  Si/He ratio enhancement during solar flares due to preferential acceleration 2—26897

Silicon continued
  Si-Fe p-n junction, switching behaviour, lifetime and photoeffect obs. 2—33029
  Si-metal film, low-temp. Si migration, ion backscatt. obs. 2—39468
  Si, amorphization, bombardment induced, by Ar, As, B, Ne, P, Sb, Si 2—1242
  Si, precipitation of Li, X-ray topography obs. 2—19115
  Si I, van der Waals broadening of shock excited emission lines, about 5000K 2—15227
  Si I lines in the extreme u.v. solar spectrum 2—26882
  Si II absorption lines in HD45166 2—7430
  Si II from spectroscopic observations of quasars, redshift measurements 2—41145
  Si II interstellar lines of Delta Scorpii and Zeta Ophiuchi 2—7429
  Si III, cryst. struct. stability, force constant study 2—22096
  Si III, Si IV photospheric lines of Delta Scorpii and Zeta Ophiuchi 2—7429
  Si III and Si IV, u.v. spectrometry experiment on Mariner 9 for early type stars 2—37300
  Si III in B-type stars, failure in explanation by rapid rotation effects 2—37280
  Si IX, fine structure transitions, proton induced, cross sections 2—35160
  Si V, extreme u.v., Hartree-Fock theoretical wavelengths, accuracy 2—24336
  Si_2, absorption spectrum between 4800 and 3000 Å, yielding new data on first excited state 2—8706
  Si^{2+}, normal config., non-orthogonal radial orbitals applic. 2—28175
  Si^{4+} in $Gd_3Fe_5O_{12}$, uniaxial mag. anisotropy 2—10229
  Si^{7+}, outer shell multi configuration approx., energy matrix elements 2—28196
  Si(Li), Li-B ion pair formation and Li precipitation 2—1255
  Si(Li) and Ge(Li) X-ray detectors, efficiency curves, and X/γ ratio for calibration sources 2—24068
  Si(Li) detector in a single cryostat, X-ray spectrometer 2—20791
  $_{28}Si$, abundance on surface of magnetic neutron stars 2—30477
  YIG;Si, a.c. hopping cond. 2—13242

Silicon compounds
  see also Quartz
  acetate, lattice parameters and space groups 2—19063
  alkali silicate glasses, electrical conductivity, activation energy, models 2—3458
  binary borosilicate glass films, vapour deposited, i.r. absorption spectra 2—16484
  disordered solids, vitreous silica and ice I 2—31127
  fused silica, thermal expansion standard ref. mat. 739, 80-1000 K 2—14289
  glass, sputter topographies, evolution, secondary processes 2—39466
  hydroxylic silica surfaces, H_2O adsorption, anomalous water formation 2—9074
  leonhardite, crystal structure determ. by X-ray diffractometry 2—6426
  lunar silicate materials, angular azimuthal distributions of high energy cosmic rays 2—10801
  magnetic silicate liquids, SiO_2 concentrations rel. to viscosity, model for calculation 2—40889
  organic polymer film, metal-dielectric-metal structure in glow discharge, threshold breakdown potentials 2—4258
  oxide films, thermochemical props. at 2270 K 2—7161
  oxides, chemical deposition of u.v. wide- band reflectors 2—34515
  oxynitride, film, prep. and props. 2—3545
  quartz-coesite transition, in anvil apparatus 2—15973
  silane SiO_2 film, control of oxide step contours, in semiconductor processing 2—19693
  silica, adsorpt. of benzene, mobility and diffusion, n.m.r. spin echo obs. 2—35929
  silica, fused, solubility of gases 2—35849
  silica, phase transitions in adsorbed water 2—25233
  silica (l'Aerosil), i.r. study of physical adsorption of CO and N_2O 2—9304
  silica film, preparation by chemical vapour deposition 2—1185
  silica gel, e.s.r. of Ag atoms on surface 2—1163
  silica gel γ-irradiated, with adsorbed gas molecules, luminescence and EPR spectra 2—6268
  silica gels, specific surface areas, pore struct., adsorpt. and i.r. spectra obs. 2—35920
  silicas, fused, electron induced luminesc. meas. 2—33325
  silicas, highly dispersive, methods of investigating, surface structure 2—6302
  silicas, porous and nonporous, adsorpt. of N_2, surface area calcs. by BET and α_s methods 2—35923
  silicate glasses, fatigue, dynamic and static, fatigue curves 2—32591
  silicate glasses, Raman spectra, phonon densities of states 2—19386
  silicate layers, diffusion controlled growth, multiphase reaction product 2—25258
  silicate phases in MgO, effect on hot strength 2—1310
  silicate systematics, tetrahedral and octahedral coordination 2—9345
  silicates, olivine-spinel transformation, crystal field effect and ionic radius ratio 2—1386
  silicates, quantitative differential thermal analysis without standard for heat effects obs. 2—19430
  silicates, surface struct., Si peaks in Auger spectra 2—25180
  silicia gel, sorption-desorption hysteresis, cavity theory, elec. discharge effect on entrapped water 2—35921
  silicides, Si L-emission spectra 2—20086
  silicides, struct. chemistry 2—9327
  silicides, transition metal, crystal chemistry 2—9349
  silicides, TT′Si type, T and T′=d-type transition metals, struct. relns. 2—18969
  silicone fluids, positronium, three quantum annihilations 2—38237
  SiO_2, amorphous, photocond. and photoinjection obs. of band edge 2—16316
  v.u.v. radiation charging in m.o.s. structure 2—19741
  X-ray fluorescence K-spectrum of Si 2—33312
  zeolites, adsorption of benzene, ^{13}C n.m.r. investigation 2—39550
  zeolites, Y, copper exchanged, e.s.r. and i.r. studies of NO adsorption and disproportionation, effect of CO 2—25226
  zeolote, desorption of carbonium ions, thermal ionization 2—6390
  Al-Fe-Si, cast, segregation of Fe and Si 2—15957
  Al-Mg-Si, alloy, split aged, internal friction obs. 2—29243
  Al-Mg-Si alloy, inverse Portevin-Le Chatelier effect 2—32595
  Al-Mg-Si alloy, precip., electron microscope obs. 2—25576

Silicon compounds continued
Al-Si alloy, flake/fibre morphology transition rel. to directional freezing rate 2—22337
Al-Si alloy, Na effects on Si growth vel. and morphology 2—32720
Al-Si eutectic, melt refinement 2—18875
Al-Si eutectic alloy, directional solidification, convection influence 2—25146
Al-Si eutectic alloy, directional solidification, convection influence 2—25145
Al-Si eutectic alloy, unidirectional solidification, convection effects 2—12614
Al-SiO$_x$-Ag cold cathode, electron emission, attenuation length 2—25971
Al-Zn-Si alloy, clustering and solute-vacancy interactions, elec. resistivity obs. 2—32693
AlMgSi alloy, temper vacancy elimination, correl. with precipitation stages 2—15897
AlSi dil. alloy, hardening, vacancy-solute atom interaction 2—15749
Au-Ge-Si alloy, viscosity and glass formation 2—32721
Au-Si alloy, on Si substrate, phase transformations 2—39991
Au-Si interface, possible cpd. form., resist. and electron microscopy 2—3493
Au-SiO films, elec. cond. and substruct. 2—12656
B-C-Si system, phase equilib. 2—32785
BC$_x$, impact strength determ., drop weight test method 2—29443
C-Si, fuel coating, neutron irrad. induced dimens. change 2—22176
CaO-MgO-Al$_2$O$_3$-SiO$_2$ system, phase equilibria at akermanite-anorthite-forsterite join 2—39416
CaO-Nb$_2$O$_5$-TiO$_2$-SiO$_2$, liquidus detn. in the 15% SiO$_2$ plane 2—9204
CdSe-SiO$_x$, in m.i.m. struct., conduction mech., interface phenomena 2—13291
Co-Pd-Si alloy, amorphous, ferromag, reson. 2—7110
Co$_3$Si eutectoid phase, unidirectional solidification of Co-Si 2—32723
Cr-Si-C, phase diagram, survey of Cr-rich area 2—40001
CrNi-Si film, struct. and elec. props. 2—39505
Cu-Cr-Si alloy, internal oxidation, precip. morphology 2—29427
Cu-(1wt.%)Si, flow, microdynamics, slip initiation 2—3885
Fe:Si, film, thickness rel. to domain struct. and mag. props. 2—16368
Fe-Al-Si alloy, fine structure, X-ray obs. 2—9470
Fe-C-Si alloy, non-eutectic solidification 2—28948
Fe-5-13 at.%Si, alloy, ordering, struct. singularities, X-ray obs. 2—29429
Fe-Ni-Cr:Si, steel, Si content rel. to B solubility, intermetallic form. 2—22339
Fe-Pd-Si, amorphous alloy, Mossbauer spectral study, magnetism model based on local ferromag. order 2—4375
Fe-(3.2 wt.%) Si alloy single crystals, twinning, influence of normal stress on critical resolved shear stress 2—22215
Fe-(11.6 wt.%SI, deformation in compression, two modes of slip 2—3784
Fe-(3 wt.%)Si, alloy, domain struct. and mag. losses in hard direction 2—40448
Fe-Si, annealing, 800°C, grain growth, texture, magnetostriction effects 2—9805
Fe-Si, dislocation-ferromag. domain interaction, x-ray obs. 2—10198
Fe-Si, heavily deformed, texture variation during recovery stage 2—12935
Fe-Si, high temp. creep, dislocation dynamics 2—39799
Fe-Si, high temp. elastic consts., rel. to phase stability 2—9633
Fe-Si, in alterniating mag. field, domain boundary displacement 2—36701
Fe-Si, internal friction in alternating mag. field 2—12834
Fe-Si, primary recrystn., impurity-drag effect on grain growth rate 2—39890
Fe-Si, strength, effect of nonmetallic inclusions 2—36139
Fe-Si, temp. depend. of domain struct. 2—36689
Fe-Si alloy, edge and screw dislocation mobility, h.v. elec. microscope obs. 2—25407
Fe-Si alloy, magnetostrictive deform., X-ray diffr. obs. 2—19889
Fe-Si alloy, magnetostriction, surface Ni film thickness depend. 2—1635
Fe-Si alloy, order-disorder transition, rel. to mag. order 2—6636
Fe-Si alloy, ordered solid soln. struct., Mossbauer obs. 2—19987
Fe-Si alloy, recrystn. texture, effect of S 2—12937
Fe-Si alloys, ordered, cond. electron spin density oscillations 2—1611
Fe-Si alloys, spin density distrib. 2—29809
Fe-Si alloys, struct., X-ray exam. 2—6202
Fe-Si ordered alloys, n.m.r., enhancement factors and relax. times 2—1648
Fe-Si single crystal, mag. domain struct., X-ray topographical obs. 2—29814
Fe-Si single crystals, crack propag., effect of prestrain and ageing 2—12909
Fe-Si thin tape, texture and mag. props., effect of heat treatment 2—36717
Fe-(3.2 wt.%)Si alloy, deformed, Barkhausen jumps 2—40475
Fe-(3 wt.%)Si alloy, freq. depend. domain struct. rel. to losses 2—40449
Fe-(3 wt.%)Si alloy single crystals, plastic yielding between 113 and 473 K 22271 2—22271
Fe-7 wt.% Si, evidence for {112} slip planes 2—39704
Fe$_3$Si, mag. hyperfine fields for impurity Sn atoms, Mossbauer obs. 2—7058
GaP:Si, i.r. absorpt. spectra, localized phonon excitation, donor electron excitation 2—20037
Ge-Si alloy, Raman spectra, bond vibr. bond vibr. and interband resonance 2—20068
Ge-Si alloys, heavily doped, resistivity, electron scatt. by phonon, acoustic and ionized impurity modes 2—32982
Li-Na-Si glass, partially recrystallized, spontaneous deformation phenomena 2—12629
Li$_2$O-BaO-Al$_2$O$_3$-SiO$_2$ system, phase equilib., permittivity, dielec. losses, specific vol. resist. 2—16266
Mn-Co-Si system, cryst. struct. of Mn$_{45}$Co$_{40}$Si$_{15}$ phase 2—39646
MnO-FeO-ZrO$_2$-SiO$_2$ phase equilibria, liquidus temp. region, quenching technique 2—13012
MnSi$_{1.73}$, heat capacity, temp. range 50-500K 2—40074
Ni-Cu-Si alloy, reciprocal mag. susceptibility, antiparallel coupling 2—4347
Ni-Cu-Si alloys, mag. and struct. props. 2—33116
Ni-Si alloy, energy changes in magnetiz. 2—33139
P$_2$O$_5$.SiO$_2$, In m.i.s. struct., charge distribution 2—10102
Pd-20 at.%Si, amorphous phase, deform., time-depend mech. props. cryst. transform29264 2—29264
Pd-Si:Fe, Cr, elec. resistivity, magnetiz., and magnetoresistance rel. to Kondo effect 2—25768
Pd-Si, Pd film on Si substrate, interdiffusion and compound form. 2—6352
Pd-Si alloy, phase diagram, metallography, X-ray and thermal analysis 2—3435

Silicon compounds continued
Pd-Si based metallic glasses, anomalous viscoelastic behaviour 2—32590
Pd$_{81.8}$Si$_{18.2}$, amorphous, recrystallization, isothermal resistance obs. 2—15972
Pt-Si, Pt film on Si substrate, interdiffusion and compound form. 2—6352
PtSi, sputtered film, microstruct., electron microscope obs. 2—3540
ScO, electronic states, energy of $^2\Delta$ state, high resolution analysis 2—12192
Si-Al, alloy, vacancy enhanced nucleation of Si atoms, precipitation 2—3953
Si-As-Te and Si-Ge-As-Te glasses, glass-forming region and DTA study 2—15637
Si-C-B system, solid soln. formation, phase distribs., liquidus area determ. 2—9793
Si-Cu-Ni-Mg(Cr) alloy, age hardening behaviour rel. to cold working 2—32706
1 wt.%Si-Cu-Ni alloy, ageing behaviour, precip., GP zone form., struct. 2—25578
Si-Fe laminates, analytical correlation between rotational and alternating hysteresis losses 2—10204
Si-Fe solid soln., precip. 2—1533
Si-Ge alloys, helical surface, etch pit obs. of impurity segregation 2—6331
Si-Ge alloys, i.r. absorpt. of lattice and local modes 2—13483
Si-Ge alloys, localized vibr. modes of B-Li pairs 2—13482
Si-SiO$_2$ interface, positive surface charge control by Cs implantation 2—10078
Si-SiO$_2$ interface state parameters, m.o.s. capacitor obs. 2—40320
SiAs, melt grown, elec. props. 2—10033
SiBr molecule, matrix element of dipole moment of transition, depend. on r-centroid intensities 2—18469
SiBr$_4$, force constant relationships, derivative 2—18470
SiBr$_4$, i.r. spectra, frequency assignment 2—35248
SiBr$_{4-n}$I$_n$, ground vibrations determ. from Raman spectra 2—24487
SiC:Al(N), diffusion of boron, heavy doping influence 2—29222
SiC:In, implanted, backscatt. analysis, disorder and p-type cond. 2—25827
SiC:N, 6H polytype, Zeeman effect of the absorp. lines R_0 and S_0 2—36885
SiC:N, e.p.r. lines, discrete saturation 2—7124
SiC:N, i.r.absorpt. and thermally stimulated luminesc. due to impurity level nonequiv. population 2—13481
SiC-C alloy, struct., fracture stress, Youngs modulus 2—32447
SiC-Co$_3$O$_4$, electrical properties obs. 2—6792
SiC, 2H type, low temp. phase transform. mechanism 2—32778
α-SiC, 6H polytype, optical phonon energy range and dielec. const. 2—10395
SiC, abrasive, action on Ti alloy, Si saturation of ground surface 2—6604
SiC, α-particle detection at high temps. prod. and props. of diodes 2—34821
2HSiC, birefringence, calculated from refractive indices, found by minimum deviation method 2—26108
β-SiC, chemically vapour deposited, stacking faults, electron diffr. obs. 2—12774
SiC, coated fuel particles for gas cooled fast reactor 2—28149
α-SiC, cryst. growth using induction-heated furnace 2—29091
SiC, cubic-hexagonal transition 2—9823
SiC, dense polycryst., temp. depend. of elastic modulus 2—22257
SiC, deposition during film boiling of chlorotrimethylsilane, rel. to high modulus fibre preparation 2—1152
SiC, elec. microscope obs. of fracture chips 2—9691
α and βSiC, energy loss function and optical constant determination from electron beam experiment 2—1445
α-SiC, epitaxial, from vapour phase, struct. and p-n junc. 2—9370
SiC, epitaxial growth of p-n junctions 2—22588
SiC, equation for enthalpy and specific heat in temp. range 273.15-2900K 2—40077
α-SiC, etch hillocks on carbon faces 2—29005
α-SiC, etching in molten NaOH or KOH, melt temp. effects 2—35874
n-SiC, exciton-exciton interaction in photoluminescence spectrum 2—1712
SiC, figures of merit and technological problems, for semiconductor devices 2—19696
β-SiC, film, growth kinetics on Si substrate methyltrichlorosilane decomposition 2—39527
β-SiC, formation kinetics, pyrolysis of CH$_3$SiCl$_3$ 2—18985
SiC, fracture energy determ. 2—29317
SiC, fracture surface, scanning and transmission electron microscopy 2—9697
SiC, ion-implanted, photoluminesc. of radiation defects 2—33309
SiC, irrad., e.p.r., defects obs. 2—1729
SiC, Kohn-Luttinger interference effect and cond. band minima 2—26197
SiC, light emitting diode, neutron damage 2—19708
SiC, microregion in C ion implanted Si, i.r. absorp. obs. 2—26173
SiC, oxidation resistant layer formation by reaction of Si and CH$_4$ 2—29040
α-SiC, p-n shallow ion-implanted junction, electron emission 2—40299
SiC, phase transform., single cryst. comparison with polycryst. 2—22365
SiC, polar surface identification, in alkaline soln. 2—18923
SiC, room temp. adsorption of O$_2$, HBr, H$_2$S(Se), NH$_3$, and PH$_3$ 2—29070
SiC, self-bonded, factors affecting fracture strength 2—29329
SiC, Si L-emission spectra 2—20086
α-SiC, single cryst. growth, vapour transport method 2—18986
SiC, single crystal, direct 2H-6H transformation on annealing at 2400C 2—4003
α-SiC, sintered, polycryst. props. rel. to monocryst. props. 2—22254
SiC, twinning probability calc. 2—39525
SiC, whiskers, ribbon-like, tensile strength, etching, surface defects 2—12673
SiC and SiC/graphite composite, thermal cond. 2—19466
SiC diffused diode, cathodoluminesc., radiative recomb. quantum efficiency 2—16633
SiC film, reactive sputtering of 2H polytype 2—32377
SiC grains, cause of violet opacity in S and C-S stars 2—4823
SiC light emitting diodes, operating characteristics and radiation effects, review 2—20116
SiC p-n junction cold cathode, multi-emitter, activation 2—4312
SiC p-n junction cold cathode, elec. characts. analysed 2—22654
n- SiC polytype, i.r. impurity absorp. bands 2—16498
SiC powder, supersonic grinding kinetics 2—15939
β-SiC whiskers, form. and morphology 2—29050
α-SiC whiskers, La-stimulated high temp. growth 2—25217

Silicon compounds continued
SiC whiskers, neutron irrad. damage 2—39674
SiC whiskers, nucleation, growth and morphology, from SiO_2-C-H system 2—18952
SiC_2 free radical, absorption bands obs., 4300 to 5000 Å 2—12195
$Si(CH_3)_4$, gaseous, Raman spectra, E and F_2 band contours 2—18520
α-SiCiN, impurity adsorpt., electron transitions 2—7073
SiCl molecule, matrix element of dipole moment of transition, depend. on r-centroid intensities 2—18469
$SiCl_4$, depolarization ratios of isotope lines 2—38941
$SiCl_4$, i.r. spectra, frequency assignment, symmetry forbidden bands from ν_2(e) mode 2—35248
$SiCl_4$, influence on TiO_2 whisker growth in vapour phase reaction 2—29051
$SiCl_4$, vibratory spectra, intensities, electro-optical parameters 2—32267
$SiCl_4$ polarity in vibrational state obs. due to vibrationally induced dipole moment 2—12218
$SiCl_nBr_{4-n}$, force constants and ground oscillations 2—18470
SiD, 3250Å bands, rotational analysis 2—5952
SiD_3NCO, mean amplitudes and shrinkages from spectroscopic data 2—3062
SiD_3NCS, mean amplitudes and shrinkages from spectroscopic data 2—3062
SiF molecule, matrix element of dipole moment of transition, depend. on r-centroid intensities 2—18469
SiF_2, vacuum u.v. spectra, assignment 2—12194
SiF_3, radical, e.s.r. spectra, hyperfine parameters 2—21642
SiF_4, chemical shift of $_{19}F$, press. and temp. depend. 2—5953
SiF_4, soft X-ray spectrum, effect of symmetry, photoionization of atoms 2—35285
SiF_4, ultrasoft X-ray absorption spectra of Si and F 2—31830
SiF_4 visible luminescence, irradiation by 10.6μ CO_2 laser pulses 2—35273
Si_2F_6, i.r. and Raman vibr. spectra, normal coordinate anal., stretching force constants 2—8709
SiH, 3250Å bands, rotational analysis 2—5952
SiH, Franck-Condon factor and true potential energy curves 2—5951
SiH^+, Franck-Condon factor and true potential energy curves 2—5951
SiH^+, Franck Condon factors and r-centroids for $A'\pi-X'\Sigma^+$ band system 2—31829
SiH_4, analogue to ionized inert gas, mol. orbital determ. from vac. u.v. and photoelectron spectra 2—18409
SiH_4, and deuterated species, matrix isolated, i.r. spectra 2—8707
SiH_4, and SiD_4-SiH_4 mixtures, vibrational spectra, crystal and liquid 2—33272
SiH_4, photoelectron spectra 2—8795
SiH_4, vacuum u.v. spectra, expts. using storage ring light source 2—16479
SiH_4 molecule, force constants and dipole moment derivatives calc. for symmetric and antisymmetric stretching and bending vibr. modes 2—12193
$SiHCl_3$, Overhauser effect, ^{29}Si spin-lattice relax. 2—29845
SiH_3D, high resolution i.r. spectrum of Si-H stretching region 2—8710
$SiHF_2$, radical e.s.r. spectra, hyperfine parameters 2—21642
SiH_2F radical, e.s.r. spectra, hyperfine parameters 2—21642
SiH_3I flash, photolysis, obs, of new absorption spectrum 4600-5600Å, assigned by rotational analysis to HSiI radical 2—35260
SiH_3NCO, mean amplitudes and shrinkages from spectroscopic data 2—3062
SiH_3NCS, mean amplitudes and shrinkages from spectroscopic data 2—3062
SiH_2X (X=F, Cl, Br, or I), photoelectron spectra 2—21643
SiH_3X (X=F, Cl, Br, or I), photoelectron spectra 2—21643
SiH_xX_{4-x}, X=halogen, photoelectron spectra studied to obtain information on bonding 2—24433
SiI_4, force constant relationships, derivative 2—18470
SiN, violet electronic emission 2—38940
Si_2N_4, in m.n.o.s. diode, two carrier charge transport and storage model 2—36570
β-Si_3N_4, dislocation generation 2—19102
Si_3N_4, elec. corona streamers, fossilization 2—39220
Si_3N_4, film, SiH_4-NH_3 catalysis, electron microscope obs. 2—9257
Si N_4, in m.n.o.s. memory device, influence of charge storage mechanisms 2—36572
Si_3N_4, in s.n.o.s. diode, instability, diffusion effects 2—10097
Si_3N_4, microregion in N ion implanted Si, i.r. absorp. obs. 2—26173
Si_3N_4, Si L-emission spectra 2—20086
α-Si_3N_4 filamentous crystals, elastic consts., determ. from supersonic velocity 2—39761
Si_3N_4 film, deposited on Si by silane press. lowering 2—1186
Si_3N_4 film, deposition control by 2537Å rad., thickness limiting 2—39520
Si_3N_4 films, sputtered from hot pressed targets, contamination levels 2—32383
Si_3N_4 insulating film deposition on GaAs by r.f. glow discharge 2—15665
Si_3N_4 layers, effect of irradiation with low energy electrons 2—1561
Si_3N_4 layers, electron traps, thermally stimulated electron emission spectra obs. 2—13354
SiO-B_2O_3 film, a.c. and d.c. cond., and e.s.r. obs. 2—40324
SiO_2-CaO-MgO-B_2O_3, refractory system, solid-liq. relationships at 1550°C, compatibility relationship diagrams 2—32305
SiO_x-CdSe, m.i.s. struct., vol. and interface traps, from C-V characteristics 2—4259
SiO_2-MO glass, (M=Ba, Sr), γ-irrad., e.p.r. and absorpt. spectra 2—30015
SiO_2-MgO-Fe_2O_3 system, triangular phase diagram 2—29494
SiO-Ni, composite film, tensile strength, microhardness 2—15666
SiO_2-Si, m.o.s. struct., surface state characterization, quasi-static technique 2—16253
SiO_2-Si interface, nonuniform lateral ionic impurity distribs. 2—40313
SiO_2-Si interface, surface state annealing parallel to B_2 centre annealing in irrad. SiO_2 2—40312
SiO_2-Si interface, surface states induced by ion implantation of N^+, K^+ and Si^+ ions 2—25881
SiO-SiN dielectric films, optical guided propagation 2—38101
SiO, amorphous, Poole-Frenkel cond., comparison of theory and expt. 2—22452
SiO, electronic transitions in region 3700 to 3950 Å 2—35289
SiO, potential curves for valence-excited states 2—8702
SiO, radiative lifetimes and absolute oscillator strengths for $A^1\Pi-X^1\Sigma^+$ transition 2—35290
SiO molecule, $E^1\Sigma^+$-$X^1\Sigma^+$ system in vacuum u.v. region 2—8708
SiO molecule, first ionization potential, obs using electron impact mass spectrometry 2—12102

Silicon compounds continued
SiO_2, amorphous, photoemission measurements of valence levels 2—10162
SiO_2, amorphous, structure, pair distrib. function detn. 2—22050
SiO_2, amorphous, total small angle slow neutron scatt. cross-section 2—22051
SiO_2, bulk fused silica, total optical absorp., materials testing for fibre optics 2—33190
SiO_2, evap. quarterwave coating, ruby laser damage threshold 2—27636
SiO_2, film, on Si, dielec. breakdown 2—10103
SiO_2, film, on Si, Na redistrib. 2—3546
SiO_2, film, sputtered, field dependence of relaxation phenomena 2—19747
SiO_2, fused, optical absorpt., irrad. effects 2—15785
SiO_2, fused, refractive indices, 404.7 to 667.8 nm, −200 to +20°C 2—26109
SiO_2, glassy pyrogenic, surface, adsorption study 2—39565
SiO_2, in m.a.o.s. diode, two carrier charge transport and storage model 2—36571
SiO_2, in m.a.o.s. struct., charge injection 2—1548
SiO_2, in m.a.o.s. struct., charge storage 2—13293
SiO_2, in m.i.s. struct., flat band shift, controlled charge injection 2—4260
SiO_2, in m.n.o.s. diode, two carrier charge transport and storage model 2—36570
SiO_2, in m.n.o.s. memory device, influence of charge storage mechanisms 2—36572
SiO_2, in m.o.s. structure, deep electronic traps, photocond. and CV characts. obs. 2—36574
SiO_2, in s.n.o.s. diode, instability, diffusion effects 2—10097
SiO_2, in Si-SiO_2-Al_2O_3 struct., effect of heat treatment 2—29736
SiO_2, measurement of thickness and indices of films using ellipsometry 2—6353
SiO_2, microregion in O ion implanted Si, i.r. absorp. obs. 2—26173
SiO_2, noncrystalline, X-ray diffraction patterns and structure determ. at 25°C 2—22054
SiO_2, on Si, Na contamination from water and alcohol 2—3501
SiO_2, optical constants at 5461 Å, etched and cleaved samples 2—36817
SiO_2, photoemission props., rel. to use as satellite surface material 2—33566
SiO_2, quartz, diffuse X-ray scatt., near α-β transition 2—4038
SiO_2, quartz, optical interband transitions, X-ray spectra obs. 2—20085
SiO_2, radical conditions obtained by applic. of h.f. plasma 2—35466
SiO_2, rutile-type, cryst. struct. 2—6435
SiO_2, SiO, Si L-emission spectra 2—20086
SiO_2, thermally grown, hole currents 2—40306
SiO_2, thin dielectric film, study using method of multiple frustrated total internal reflection 2—20004
SiO_2, trapping efficiency of low energy Au ions 2—12783
SiO_2, tridymite, phase transition shift, heat of transformation 2—9824
SiO_2, vapour transport and deposition conditions for polymorphs 2—39583
SiO_2, vitreous, press. induced conformational changes, bond polarizability 2—18903
SiO_2 colloidal, adhesion of monolayer on glass 2—32395
SiO_2 electron injection, scatt. in image pot. well 2—40319
SiO_2 electron irradiated, short term charge annealing 2—19732
SiO_2 evaporated film, refractive index, absorptance, i.r. transmittance, stress, stability and structure 2—8021
SiO_2 film, chem. vapour deposited on Si vidicon, effect on spectral response 2—13277
SiO_2 film, dissolution rates in acidic fluoride solns. 2—10628
SiO_2 film, impurity depth profile, secondary ion emission study 2—16333
SiO_2 film, on Si, kinetics of thermal growth, ellipsometry obs. 2—39522
SiO_2 film, on Si, thickness meas. using IOTA, computer controlled scanning spectrophotometer 2—29713
SiO_2 film local stress meas. method 2—12664
SiO_2 film thermally grown on Si, buckling rel. to thickness/window width ratio 2—9283
SiO_2 films, electrochem. charging by injected electron currents 2—13304
SiO_2 films, prep. by oxidation of n-Si 2—40815
SiO_2 films, production by reactive evaporation in ionized gases 2—3505
SiO_2 films, sputtered, thermoluminesc., colour centres 2—40729
SiO_2 films, thermal-grown, characteristics 2—18942
SiO_2 gate insulators, thermally grown, optimization for radiation hardening of p-m.o.s. devices 2—19734
SiO_2 glass, H_2 dissolution, i.r. absorp. spectra obs. 2—12630
SiO_2 glass, sputtering yields and damage depths caused by 5.6 keV inert gas ions, energy losses 2—25713
SiO_2 glass, strengthening by high pressure Ar impregnation 2—12892
SiO_2 ion implanted film, chemical and elec. props. rel. to semicond. device technology 2—25210
SiO_2 layer, defects, activation energy of charge carrier diffusion 2—25911
SiO_2 layer, growth by anodic oxidation of Si 2—7179
SiO_2 layer in m.o.s. system, relaxation polarization, surface potential stability 2—4269
SiO_2 microporous films, characteristics by repeated interference of total internal reflection 2—39529
SiO_2 noncrystalline, defect structure and irradiation behaviour 2—19733
SiO_2 on Si substrate, ellipsometry for Hg and He-Ne laser spectral lines, book of tables 2—6355
SiO_2 phases in deep sea cherts of the North Atlantic 2—10699
SiO_2 plate, wetting by molten Fe 2—3496
SiO_2 polymorphs, irrad.-induced changes in density and molar fraction 2—18904
SiO_2 polymorphs, π bonding and delocalization effects 2—9319
SiO_2 powders, positronium form., ang. correl. obs. 2—40110
SiO_2 single crystals, suitability as filters for high intensity neutron beams 2—15029
SiO_2 surface layers, Auger spectrum, chem. shift obs. 2—29006
SiO_2 surface reactions, O_2-H_2 radicals, low pressure discharges 2—35620
SiO_2 thermally grown, conduction mechanisms 2—10034
SiO_2 vitreous, migration and solubility of He 2—36083
SiO_2 vitreous, optically active vibrational modes calc. using β-quartz models determ. from X-ray diffraction 2—22382
SiO_x, anodic oxide film, electrolytic breakdown products, morphology 2—9284
SiO_x, film, r.f.-sputtered, i.r. spectra near 9μm, rel. to sputtering voltage, thickness, heat treatment conditions 2—13484
SiO_x, in m.i.m. thin film cathode 2—19723
SiO_x, reactively evaporated film, e.s.r. study, spin density meas., electrical conduction props. 2—1726
SiO_x evaporated film, optical props., rel. to deposition conditions 2—10394

Silicon compounds continued

SiO_x film, depth composition profile by ion scatt. spectroscopy 2—39454
SiO_x film, oxidation by nitric acid, use in MNOS device 2—12666
SiO_x films, doped and undoped, Poole-Frenkel effect 2—1527
SiO_xN_y evaporated film, refractive index, absorptance, i.r. transmittance, stress, stability and structure 2—8021
SiO N_y films, production by reactive evaporation in ionized gases 2—3505
SiO_2.CaO-Nb_2O_5.CaO-TiO_2, plane in quaternary CaO-Nb_2O_5-TiO_2-SiO_2 system, liquidus temp. determ. 2—3431
SiP_2O_7, monoclinic AIV modification, band lengths and angles 2—9489
Si_2Te_3, amorphous, band struct. and elec. props. 2—19671
Te-As-Ge-Si glass switching system, nature of ON-state 2—22577
$Te_{48}As_{30}Ge_{10}Si_{12}$, glass, switching and memory effects 2—16214
Ti-Si-C system, phase equilib., rel. to complex carbide deposition 2—25213
TiO_2-SiO_2 glass, binary system, thermal expansion significance of bridging oxygens 2—16062
U-Si-Be system, phase relations 2—13016
U-Si system, phase diagram 2—40012
V-Ti-Si, V-Ti-Nb-Si, Si alloying effects on creep and creep strength 2—1295
V_3Si, single cryst., supercond. critical current peak effect 2—16169

Silver

(111) surface, scatt. of Ar beams up to 20 eV 2—15657
acoustic cyclotron reson., phase shift 2—32907
activator, NaCl, vac. u.v.-X-u.v. excited, photo- and electrophotoluminescence processes 2—16603
activator of thermolum. $Li_2B_4O_7$ 2—27900
anode, ablation in short duration spark discharges 2—24905
atom, autoionization lines in vac. u.v. spectra determ. by photoionization and emission 2—18309
atom, electron bombardment, inner shell ionization 2—18326
atom, K and L X-ray yields, study by 2 to 30 MeV proton bombardment 2—38808
atom, multiple ioniz. and Auger transitions by electron impact 2—11972
atoms, inner shell excitation by protons, impact parameter dependence 2—600
atoms on porous glass and silica gel surfaces, e.s.r. 2—1163
atoms on porous glass and silica gel surfaces, e.s.r. 2—1164
Auger spectra, electron-induced, backscatt. effects 2—33095
Bordoni peak height, meas. freq. depend. 2—15803
bremsstrahlung absolute cross sections determ. 2—22437
cold worked, internal friction, lattice defects, low temp. 2—12828
contamination by S adsorption from SO_2, Auger spectra and work function obs. on polycryst. samples 2—39552
crystal struct., symmetry of electron diffr. diagrams 2—9442
crystals, electrolytic growth, effect of twin defects 2—25261
Debye-Waller factor, temp. dependence, theory 2—6649
dendritic cryst., growth, electrolysis of $AgNO_3$ soln., rel. to current fluctuation 2—9295
diffusion, in Ce f.c.c. γ-phase and b.c.c. δ-phase 2—29215
diffusion, of Pb and Au along grain boundaries in Au/Ag/Pb film struct. 2—22243
diffusion in CdS, coeff. determ., electric and opto- photoelectric meas. methods 423-773K 2—9617
diffusion in Mg single cryst., diffusion constant, anisotropy, valence effect, activation energy 2—6515
diffusion in Ni, lattice coeff. 2—12811
diffusion of ^{110}Ag in Sn and Pb 2—22250
diffusion of In impurities in thermal gradient 2—29214
diffusion of interstitial H, lattice relaxation 2—9613
diffusion simultaneous of ^{105}Ag and ^{110}Ag, isotope effects, 1046-1227K 2—25466
disclination, involving five twins, de Wit characts. obs. 2—32517
dislocation etchant characts. 2—9556
doping of p-Ge and Ge(Li) detectors, lifetime killer and hole trap 2—27881
electrical resistivity, temp. depend. oxygen-bearing Ag 2—40168
electrocrystallization from $AgNO_3$ melt, morphology of growth of (100) and (111) faces 2—1202
electromigration paths in α-quartz 2—29223
electroreflectance spectra in range 3 to 4 eV 2—29895
e.m. wave propagation, non-local regime 2—16120
epitaxy on molybdenite, substrate temp. effect 2—25192
etch pits on (100) and (111) surfaces, orientation 2—3567
evaporation heats, spectroscopic determ. 2—28960
fast neutron irradiation. resist. recombination volume 2—25763
Fermi surface interpolation schemes, muffin tin zero 2—16099
film, 300 to 400 Å thick, optical consts. determ. from 2.4 to 4.4 eV 2—22749
film, aggregated, effect of optical anisotropy on ellipsometric det. of n, k and d 2—40606
film, annealing, hole growth, island formation 2—25194
film, atomically smooth (111), vacuum deposited on NaCl 2—39488
film, deposition on Si by reaction with AgF vapour, 80-600°C 2—39487
film, deposition on SiO, effect of ion beam bombardment 2—29041
film, electromigration direction 2—36075
film, epitaxial deposition on molybdenite 2—29024
film, growth and struct., thickness depend. 2—3522
film, laser beam irrad., rupture threshold 2—9263
film, nucleation and growth on SiO_2 in ultra-high vac. 2—32355
film, nucleation and growth on SiO_2 in ultra-high vac. 2—32356
film, on Si substrate, low temp. migration of Si 2—3812
film, on Si substrate, low-temp. Si migration, ion backscatt. obs. 2—39468
film, paratransmission of electrons 2—22440
film, photoemission 2—13357
film, piezorefl., plasma oscillation obs. 2—29893
film, polycryst., geometrical size effect 2—19542
film, preferential deposition induced by Au ion implantation of substrate 2—12784
film, proton bombardment, radiation defect annealing, 93-263K 2—22174
film, resist. and Hall coeff., geom. size effect 2—1481
film, reson. effect in photoemission 2—16328
film, smooth detachable, deposition method 2—1173
film, struct. modification due to mech. vibration, adhesion measurement 2—18931
film, surface diffusion, hillock formation 2—25193
film, technique for stripping from mica substrates 2—39489
film, thermopower, electronic struct. 2—16302
film, thin, optical properties, modification under action of oxygen 2—1656
film, transition radiation ang. distrib., reson. behaviour near plasma freq. 2—33229

Silver continued

film, vacuum deposited, internal friction, 4.2-77 K 2—29245
film deposition on SiO_2, nucleation rates 2—12652
film grown in elec. field, elec. resist. 2—9953
film growth on graphite, size distrib. of nuclei 2—29023
film on Al substrate, at. intermixing with Au, x-ray photoemission obs. 2—19805
film on Pd, partial misfit dislocations 2—9262
film on Pt, specular reflection spectra, monolayer thickness range 2—9310
films, deposition and detection below 0.01 monolayer 2—32354
films, optical constants from reflection and transmission coeff. meas. 2—26103
fretting, spherical particle form. 2—39852
getter-ion pump, with cold cathode characteristics 2—33827
impurity levels in Au, ang. distrib. of x-ray induced photoelectrons 2—19806
interfacial layers, informational props. 2—39456
lattice dynamics 2—32803
lattice parameters and thermal expansion coeff. determ., 30-180K, X-ray method 2—3694
liquid, diffusion of oxygen, potentiostatic meas. method 2—12554
magnetic pseudopotential, spin and spin-orbit interaction dependent 2—36659
melting, incipient, in presence of S and O_2 2—1260
microwave transmission spectroscopy, cyclotron phase resonances 2—19527
Nernst-Ettinghausen effect, phonon drag contrib. 2—1581
optical film, thickness uniformity det. when produced by evaporation in standard and ultrahigh vacuum 2—35883
permeation membrane, O_2 passage through 2—25461
phonon dispersion and spectra, Debye temps., angular force effects 2—32807
phonon dispersion curves, specific heat, vibr. spectra from modified angular force model 2—32801
phonon dispersion relations 2—4030
plastic deformation, effect of evaporated metal films 2—1286
polycrystalline, Na, K, Kr ion refl. coeffs., electronic stopping. surface effects 2—7902
polycrystalline layer, on NaCl, transmission of struct. information 2—6333
powder, O_2 desorpt., microbalance obs. 2—35906
powder, structure, comparison of methods 2—15940
recrystallization, role of impurities, internal friction meas. 2—9736
reflection coefficients, for keV Na^+ and K^+ beams 2—22065
reflectivity spectra, interband transitions 2—10344
resistivities, electrical and thermal, temp. dependence 2—22490
single crystal, strain free prep. of thinned specimens 2—22126
sintering, material transport kinetics 2—6621
solar abundance from near u.v. studies, spectrum synthesis method, agreement with type I carbonaceous chondrites 2—26880
solid, optical properties determ. by energy loss spectroscopy of electrons from 2-40 eV 2—19958
solubility in molten halides 2—9103
sputtering yield for single crystal bombarded by 6 keV Ne and Kr ions at temps. from 200-600°C 2—32859
stacking fault, twin and point defect energies, pair pot. calcs. 2—15747
stacking fault energy, electron microscope obs., weak beam method 2—3787
stacking fault energy twin boundary energy temp. coeff. 2—32533
stopping powers for fission fragment transmission 2—1446
strain coefficients, for electron mean free path and free electron density, thin film obs. 2—9954
surface, intensities of Auger lines excited by electron and X-ray irrad. 2—12638
thermal diffusion in Pb, heats of transport 2—22242
thermal expansion, anharmonic contrib., high temp. 2—32845
thermal expansion, at high temps., anharmonic contribs. 2—40081
thermal expansivity data, rel. to thermal vacancies 2—16042
thermal props. and i.r. absorbing power of thin layers 2—19448
thick film, single cryst., dislocation struct., Luders deformation 2—6543
thin cryst., slip morphology size depend. 2—22206
thin slabs, microwave transmission, discrete waves 2—19532
thread-like crystals, formation in physical development 2—27676
valence band struct. from u.v. photoelectron spectra 2—36650
vapour pressure obs. at 800-1600°K, low pressure 2—3450
wavelength modulation spectra, effective mass 2—26141
whiskers, electrocrystallization, dislocation mechanism 2—25215
X-ray spectra, relations between L_{III} absorp. limit and $L\beta_{2,15}$ lines 2—26206
Ag^{3+}:Fe^{3+} centres in CdS, e.p.r. 2—33338
Ag:PO glass dosimeter, delta-ray theory of track structure, energetic heavy ion detection 2—34823
Ag/GaAs, surface-barrier structures by chemical deposition 2—25892
Ag/Pd, psuedomorphic layer/substrate system, Rutherford scatt. study 2—40103
Ag-MgO, cold cathode, self-sustained emission stability 2—25975
Ag-MgO cold cathode, self sustained emission 2—25974
Ag-O-Cs photocathode, emission mechanism, cpd. form. on sensitizing oxidized layers 2—33086
Ag^- in KCl and NaCl, stress induced linear dichroism 2—33208
Ag^+, adsorption from soln, by activated C 2—39556
Ag^+ in alkali halides, uniaxial stress effects on off-centre pot. 2—20020
Ag^+ in RbCl, paraelec. reson. 2—33054
$Ag^{2+}(4d^9,{}^2D)$, in frozen acid solutions, e.p.r. study of core polarization 2—10481
in Al-Mg alloy, effect on ageing 2—12955
Al-SiO_x-Ag thin film cathode, elec. props. 2—19723
CdS:Ag, Al, i.r. detection, by high field domain reconfiguration 2—29714
CdS:Ag film, evaporated, recrystalliz., electron micrograph obs. 2—35888
CdSb:Ag layers, doping and elec. props. 2—36046
Ge:Ag, excited by laser rad., electron-hole recomb. at deep impurity centres 2—22558
KCl:Ag, impurity induced Raman spectra 2—26194
KCl:Ag^-, C-band light irrad., absorpt. bands attributed to paired Ag^- ions 2—15784
KCl:Ag^-. C-band light irrad., absorpt. attributed to paired Ag^- cons., theory 2—19126
Te:Ag layers, doping and elec. props. 2—36046
Zn-Al-Mg, effect on precipitation, correl. with stress corrosion behaviour 2—3951

Silver continued
$Zn_xCd_{1-x}S$:Ag,Ni, photoluminescence mechanism, energy band model 2—4480
ZnS:Ag,Cl phosphor, luminesc., long decay, trap depth 2_36936
Silver compounds
Al-5.0 at%Ag-5.0 at%Zn, alloy, neutron irrad. rel. to precip. and G.P.zones 2—29418
alloy film, optical consts. detn. 2.4-4.4eV 2—22749
alloys, phonon drag thermopower, 4-300K 2—40371
c.p. alloys, stacking order stability 2—12713
electron density distribution, Lowdin approx. 2—32865
germanate glass, polymerization, i.r. study 2—15638
halide, heat of transport, linear chain model 2—25690
halide, in phototropic glass, phase separation 2—12627
halide, ionic transport parameters 2—33051
halide, vacuum u.v. spectra, expts. using storage ring light source 2—16479
halide for X-ray films, grain size distribution using electron microscope 2—38171
halide in photographic emulsion grain size distribution rel. to X-ray film processing 2—41418
halide photographic emulsions, line element image broadening as a function of exposure 2—38169
halides, molten, solubility of Ag 2—9103
halides, photographic emulsion, processing and cameras 2—38173
halides, space charge layer contrib. to dielec. const. 2—33050
halides, space charge layer contrib. to dielec. const. 2—40330
silica gel, e.s.r. of Ag atoms on surface 2—1164
silver halide light sensitive photographic material for holography 2—34563
Ag-Al alloy, quenched, GP zones, Perod's law, X-ray Laue scatt. 2—32441
Ag-Al alloys, liq., config. transition of Ho impurities 2—39390
Ag-Au, at. intermixing, x-ray photoemission obs. Al substrates 2—19805
Ag-Au alloys, optical properties determ. by energy loss spectroscopy of electrons from 2-40 eV 2—19958
Ag-Au system, liq., electronic struct. 2—9078
Ag-Au(Pd) dil. alloys, low field magnetoresistance 2—1474
Ag-Cd alloy, stress-induced martensite transform. 2—36271
Ag-Cd alloy, tensile deform., X-ray diffr. obs. 2—15829
Ag-Co(Ni) two-phase targets, reduced, sputtering yields 2—32864
Ag-Cu, liq. binary, excess Gibbs energies, heats of mixing, mass spectrometric intensity ratio method, 1000-1250°C 2—18814
Ag-Cu alloys, evidence for preoxidation state and its characteristics 2—26347
Ag-23 at.%Ge alloy, metastable h.c.p. phase decomp., precip. 39978 2—39978
Ag-Ga system, 3/2 electron cpds., thermodynamic props. 2—39934
Ag-Ga(Ge)(Ni)(Zn) alloys, electronic sp. ht.. 2—25732
Ag-Gd system, phase equilibra 2—22375
Ag-Ge, thermodynamic analysis 2—22341
Ag-H(D) solid solution, thermodynamic function, calc. 2—3961
Ag-In-Cd plate type shim rods, MTR fuel elements, flux density and reactivity measurements 2—15040
Ag-(5 at.%) Ir alloy, evaporation, beta irradiation effect 2—28965
Ag-Mn alloy, nondilute, Kondo effect, elec. resist. study 2—19917
Ag-Mn dil. alloys, optical props., electronic struct. 2—20019
Ag-O alloy, temp. and strain rate depend. of yield 2—32604
Ag-R dil. alloys, R=rare earth metal, resist., magnetoresist., thermopower, review 2—13110
Ag-Sn alloy, solid and liq. phases, thermodynamic props. 2—40000
Ag-Zn, electron microscopic investigation of ordered β' and ζ phases 2—32440
β'-Ag-Zn alloy, martensite formation, electron microscopy 2_1387
Ag-Zn alloy, radiation enhanced diffusion 2—3817
Ag-Zn cold-worked alloy, electron irrad. enhanced diffusion 2—9614
Ag alloy, welding techniques in controlled atmospheres, MIG and TIG welding 2—3943
Ag halides photographic effects of electron and positive hole traps 2—14495
Ag olefin complexes, νC=C stretching frequencies rel. to i.r. and Raman spectra 2—15282
Ag sol light filter, reduction of $AgNO_3$ with $NaBH_4$ in presence of gelatin 2—27675
$AgAl_{11}O_{17}$, sodium β-alumina isomorph., stoichiometry and defect struct. rel. to cation mobility 2—18965
Ag_3AsS_3, for electrooptic modulator, cryst. growth 2—35936
Ag_3AsS_3, proustite, i.r. parametric oscillator 2—17578
Ag_3AsS_3, proustite, parametric image upconversion of 10.6 μm illuminated objects 2—21060
$AgAuZn_2$, solid soln, first and second neighbour ordering, stability criterion 2—19257
AgBi mol., rot. and vibr. consts. determ. 2—24434
AgBi mol., rot. consts. determ. from spectra with unresolved rot. struct. 2—18399
AgBr:Cr^{2+}, near i.r. absorpt., temp. depend., Jahn-Teller effect 2—40656
AgBr:$Cr^{2+}(Fe^{3+})(Ti^{3+})$, near i.r. absorpt., temp. depend., Jahn-Teller effect 2—40657
AgBr:S, annealed crystals, dark conductivity meas., obs. of complex formation and photoreduction processes 2—6900
AgBr:Se, e.s.r. spectra with different cationic impurities 2—4537
AgBr-NaCl solid solutions, thermodynamic properties from miscibility gap meas. 2—22417
AgBr, Ag 4d levels from temp.-dependent photoelectron spectroscopy 2—36626
AgBr, chemical model of latent image 2—4599
AgBr, field injected electrons, photographic action 2—31150
AgBr, intrinsic contrib. to thermotransport of Sr^{2+}, Cd^{2+} and Mn^{2+} 2—19141
AgBr, optical constants, reflectivity and absorption spectra in the u.v. region 2—20018
AgBr, optical response in near and extreme u.v. 2—1680
AgBr, polaron cyclotron reson., temp. depend., energy depend. of cyclotron mass, 1.7-25K 2—22473
AgBr, polaron self-energy, temp. depend. 2—22474
AgBr, surface, self-diffusion of Ag^+, tracer technique 2—3491
AgBr dispersion in polyvinyl alcohol, influence of mechanical agitation on growth and crystal habit 2—27666
AgBr microcrystalline emulsion, deep latent image formation mechanism 2—26358
Silver compounds continued
AgBr photographic emulsion, latent image formation, contribution of interstitial Ag^+ ions 2—2475
AgBr(Cl)(I) emulsion films pulse photolysis obs. 2—20195
AgBrI, photographic properties of emulsions with imidacarbocyanines containing residues of heterocyclic bases in benzene nuclei 2—27671
AgCl:Cr^{2+}, near i.r. absorpt., temp. depend., Jahn-Teller effect 2—40656
AgCl:$Cr^{2+}(Fe^{2+})(Ti^{3+})$, near i.r. absorpt., temp. depend., Jahn-Teller effect 2—40657
AgCl:Cu, ionic cond., temp. and Cu conc. effects 2—36583
AgCl:Mn^{2+} monocrystals, luminescent properties, effect of Mn^{++} concentration 2—4488
AgCl:S, paramag. centres, e.s.r. obs. 2—26271
AgCl-NaCl solid solutions, thermodynamic properties from miscibility gap meas. 2—22417
AgCl, AgBr, AgI, microwave rotation spectrum 2—28270
AgCl, chemical model of latent image 2—4599
AgCl, Debye-Waller B-values, interionic interaction model 2—22404
AgCl, diffusion and electrolytic migration of Mn^{2+} ions, temp. depend. 2—29213
AgCl, dynamical behaviour, modified shell model 2—40024
AgCl, hole self-trapping and recomb. luminesc., low temp. 2—16604
AgCl, intrinsic contrib. to thermotransport of Sr^{2+}, Cd^{2+} and Mn^{2+} 2—19141
AgCl, optical response in near and extreme u.v. 2—1680
AgCl, photographic sensitivity and exciton absorpt. 2—4297
AgCl, pure and Cd-doped, Cd diffusion, temp. depend. 2—39733
AgCl antireflection coating foSi, in 2.5-50 μm region, transmittance obs. 2—8012
AgCl crystals, slip at room temp. 2—19103
AgCl seal for two glass components, using r.f. heating of sealing surfaces 2—20787
$AgClO_4$, phase transitions, press. depend. 2—15956
Ag_2CrO_4, dissolution in aqueous solutions, analysis of mass transport 2—30072
AgF, B1-B2 phase change at high press. 2—36272
AgF, far i.r. transmission spectrum, lattice vibrations, cryst. structure, dielec. props. and elastic consts. 2—32802
AgF, valence band struct. 2—25728
AgGaS , prep. and props. 2—9364
$AgGaS_2^2$, refractive indices and second harmonic generation coeffs. meas., possibility of laser application 2—1654
$AgGaS_2$, visible cathodoluminesc., free exciton annihilation 2—33324
$AgGaS_2(Se_2)$, elec. props., room temp. 2—40242
$AgGaS_2(Se_2)$, optical props., band struct. 2—4223
$AgGa(Se)_2$, stimulated emission obs. on scanning visible spectrum 2—10416
$Ag_2H_3IO_6$ single crystals, gel growth technique 2—22101
AgHal crystal, photoelectron capture in surface trap 2—29585
AgHal lattice, energy depths of potential holes 2—29584
Ag_2HgI_4, thermochromic, ^{127}I n.q.r. frequencies and critical broadening 2—10584
$Ag_2Hg_3IO_6$, cryst. growth by hybrid gel technique 2—25269
AgI-AgBr solid solution, lattice parameters, rel. to ice crystal nucleation 2—3693
AgI-Ag_2SO_4, ionic conductivity, obs. 2—39997
AgI-KI acetone soln., emitted smoke ice forming ability 2—22972
AgI-PbI_2 solid mixture, emitted smoke ice forming ability 2—22971
AgI-polymethonium cpds., solid electrolytes, ionic cond. 2—22614
β-AgI, hexag. single cryst., exciton spectra, large angle reflection obs. 2—16462
AgI, reduction of effect on water drops due to multiple freezing 2—39425
AgI aerosol, nucleation of water drops by Brownian contact 2—18859
AgI molten, self-diffusion between 580° and 620°C, porous-frit technique 2—28824
$AgIO_4$, phase transitions, press. depend. 2—15956
$AgInS_2(Se_2)$, elec. props., room temp. 2—40242
Ag_3Mg, long period ordered, plastic deformation, stacking faults, dislocation splitting 2—25501
Ag_5MnAl alloy, remanent magnetiz., coercivity 2—10207
Ag_2MoO_4, normal spinel polarized Raman and phonon spectra 2—10408
$AgNO_3$-$LiNO_3$, molten mixture, liquidus curve, thermodynamic props. 2—25138
$AgNO_3$-$NaNO_3$ ($LiNO_3$) molten salt mixtures, ion migration 2—28892
$AgNO_3$, internal electromigration mobilities of ^{22}Na and ^{24}Na, relative difference 2—28827
$AgNO_3$ melts, thermodynamic properties from e.m.f. meas. 2—21980
$AgNO_3$+KNO_3, system, molten salts, equivalent conductivity 2—1112
Ag_2O-P_2O_5, glass, i.r. and visible spectra, struct. 2—40655
Ag_2O, contaminated, nucleation of water drops by Brownian contact 2—18859
Ag_2O, lattice expansion by annealing 2—29560
Ag_2O, optical constant determination 2—1656
$(AgPO_3)_n$, dehydration product from $(AgPO_3)_3.H_2O$, surface tension 2—30045
$(AgPO_3)_3.H_2O$, dehydration, thermograms and diffractograms 2—30045
$Ag_{.71}Pd_{.29}$ alloy, electronic structure studied by ESCA and X-ray spectroscopy, comparison with spectra of pure metals 2—32884
α-Ag_2S, ionic cond., and derivation of self diffusion coeffs. 2—16272
Ag_2S, single cryst. growth and struct. 2—1203
Ag_3SbS_3, polarisation shift of absorption edge, simplified band model 2—29906
Ag_3SbS_3, refl. spectrum and energy levels 2—29894
Ag_2Se, single cryst. growth and struct. 2—1203
Ag_2Te, single cryst. growth 2—1203
Al-Ag-Zn alloy, precipitation phenomena 2—3938
Al-Ag, quenched from liq. state, ageing, X-ray diffraction obs. 2—25577
Al-Ag alloy, thermopower, Nielsen- Taylor effect 2—22632
Al-Ag alloy, X-ray scatt., Laue intensity 2—9444
Al-Ag alloys, dil., vacancy form. energy rel. to solute-solute interaction 2—9537
Al-Ag alloys, vacancy-solute interaction energies, clustering kinetics obs. 2—22190
Al-Ag metastable solid solution, supercond. transition temp. 2—16171
Au-15 at.%Ag alloy, rad. damage interpretation, ordering props., elec. resist. obs. 2—36009
Au-(15 wt.%)Ag alloy, static crowdion behaviour, resist. obs. 2—15754
Au-Ag alloy, short-range order formation, vacancy influence, elec. resistivity obs. 2—32596
Au-Ag alloys, electron irrad. effects on diffusion 2—39737

Silver compounds continued
  Cu-Ag-Au alloys, sp. ht. low temp. meas. 2—4065
  Cu-Ag alloy, discontinuous precip. and dislocation climb 2—1367
  Cu-Ag bimetal film, diffusion kinetics, size effects 2—9618
  Cu-Ag eutectic alloy system, elastic moduli, u.s. wedge method obs. 2—39760
  Cu-Ag films, sputtered, investigation of factors affecting composition 2—32363
  Ga-Ag, thermodynamic props. for solid and liquid solns. 2—32730
  GeTe-AgSbTe$_2$, band gap width dependence on composition from thermoelectric power and elec. conductivity meas. 2—32999
  Mg-Ag alloy, serrated yielding 2—29260
  NaCl-AgCl solid solution, decomp., X-irrad. effects 2—36246
  Ni-Ag alloy, spring characteristics of thin leaf springs 2—25476
  Pd-Ag-Au alloy system, Debye temp. and thermal expansion 2—4074
  Pd-Ag-H system, elec. resist., 25°C, H$_2$ press. depend. 2—25769
  Pd-Ag, X-ray spectra and band structure 2—36918
  PdAg:H, chem. pot and H conc. near critical point 2—19270
  Pt olefin complexes, νC=C stretching frequencies rel. to i.r. and Raman spectra 2—15282
  Sn-Ag, ohmic contact on n-GaAs, specific resistance 2—29715
  Sn-Ag alloy, elastic moduli, phase and composition depend. 2—39759
  Sn-Ag liquid alloy, Knight shift comp. depend. rel. to conduction electron density 2—9177
  ZnS: AgAlS$_2$ liminescence, thermal and i.r. stimulation 2—29958
Sinanoglu's theory *see Atoms/structure*
Sintering
  carbonyl iron powder compact, structural changes obs. 2—39959
  cermet steel, effect on vol. 2—12939
  densification kinetics, analysis, under constant heating conditions 2—9778
  electroceramics, control of properties by microstructure 2—32738
  feldspar, isothermal sintering, shrinkage obs. 2—29445
  ferrographite, effect of sintering conditions on props. 2—12940
  material transport mech. in early stages 2—36255
  metal, enhancement by impurity addition, prediction and control 2—22326
  metal fibre, porous, pressing, deformation, residual stress relaxation 2—29257
  metal powder, shrinkage equation 2—6620
  molten carbonate fuel cell anodes, inhibition 2—11420
  oxide-metal, carbide-metal, liq.-solid systems, rel. to wetting 2—6316
  porous body, steady-state and transient creep 2—1344
  powder, viscous sphere fusion rel. to surface tension forces 2—36256
  powders, densification kinetics, sintering eqns. at const. rates of heating 2—32740
  press-, for sprayed coating, properties 2—1339
  rare earth cobaltide RCo$_5$ permanent magnet prep. 2—19883
  rare earth-cobalt alloy permanent magnet characterization 2—40515
  rare earth-cobalt magnet processing 2—39896
  refractories, effect of dislocations 2—36260
  refractories, polycryst. props. rel. to monocryst. props. 2—22254
  spinel ferrite, cation distrib. rel. to elec. cond. relaxation 2—10112
  steel, super-high-density sintered, fatigue and fracture props. 2—6561
  Ag, material transport kinetics 2—6621
  Al$_2$O$_3$:MgO, alumina, densification and grain size control 2—29444
  Al$_2$O$_3$:MgO, initial sintering, effect of green density 2—36257
  Al$_2$O$_3$-MoMn bond strengths, sintering conditions effect 2—32753
  Al$_2$O$_3$, effect of TiO$_2$ addition 2—36194
  Al$_2$O$_3$, Mo-dispersed, hot pressing and mech. props. 2—15862
  Al$_2$O$_3$, Mo-dispersed, hot pressing and mech props. 2—15863
  Al$_2$O$_3$, sintering temp. reduction by vitrifying additives 2—36199
  Al$_2$O$_3$, synergetic press. method, densification 2—39875
  BaTiO$_3$: Nb, Nb diffusivity rel. to grain growth 2—1269
  BaTiO$_3$, effect of conditions on dielec. props. 2—16283
  BaTiO$_3$, liquid phase, exaggerated grain growth 2—1374
  BeO-Cu$_2$O$_2$ ceramics, electrical resistivity effect of temperature and sintering pressure 2—6753
  BeO-Fe$_3$O$_4$ ceramics, electrical resistivity effect of temperature and sintering pressure 2—6753
  CaF$_2$, densification, sintering mechanism, effect of additives 2—32741
  Cd-Pb-Sn powder mixture, sintering above the ternary eutectic temp. 2—29451
  Co alloys with 10% carbides, recovery and recrystallization, coercivity and resist. obs. 2—19240
  Cu-Fe-Al$_2$O$_3$ powder, shrinkage equation 2—6620
  Cu, powder, kinetics, mass transport mechanism 2—22346
  Cu, powder pressing, effect of press. and temp. 2—3972
  Cu based compacts, dimensional changes 2—1358
  Cu$_9$Al$_4$—X, X=Mn, Fe, Ni, ternary mixed powder compacts, expansion, Kirkendall diffusion 2—19279
  Fe-Cr, powders, coarse and fine, isothermal sintering, exponential law, logarithmic time law 2—12982
  Fe-Mo, powders, coarse and fine, isothermal sintering, exponential law, logarithmic time law 2—12982
  Fe-Ni-graphite, 1050-1200°C 2—12938
  Fe, powder pressing, effect of press. and temp. 2—3972
  Fe, vacuum hot pressing, effect of u.s. waves 2—1347
  LiF, phosphor, prep. method, thermolum. prop. changes during prep. 2—27901
  Mg$_x$Mn$_y$Fe$_{3-x-y}$O$_{4\|y}$, swelling effect 2—36258
  MnZnFe$_2$O$_3$, rel. to microstructure and mag. props. 2—33157
  (NH$_4$)$_2$U$_2$O$_7$→UO$_2$ pellet, reduction 2—20187
  NaF, kinetics, non-isothermal conditions, isothermal annealing time effects, dilatometric method exam. 2—12984
  Ni-Cu-Fe-graphite alloy, phase and struct. changes 2—1401
  Ni, active powder, mass transport mech. 2—36259
  Ni, powder pressing, effect of press. and temp. 2—3972
  Ni, vacuum hot pressing, effect of u.s. waves 2—1347
  Ni$_{1-x}$Co$_x$Fe$_2$O$_4$, effect of sintering temp. on mag. props. 2—29829
  PbZrO$_3$-PbTiO$_3$ ceramic, calcining temp. effects 2—39953
  Se-As glass powder 2—19281
  SmCo$_5$ magnet, props. as function of Sm$_3$Co sintering aid 2—33143
  Ti powder rolled metal, hold time detn. 2—15926
  TiC-Ni alloy, for optimal wear resist. 2—9777
  TiC-ZrC(NbC), high porosity complex carbides, compaction 2—39969
  Tl$_2$O$_3$-Ta$_2$O$_5$ mixture, tantalate prep. 2—29396
  UO$_2$, powders, cold pressing, energetic study 2—6624
  UP powder, porosity, 1500-2000°C 2—3935
  W, Ni activated, kinetics 2—6625
  WC, powder, rel. to milling, dislocation density effects 2—22348
  ZrB$_2$-W, powder mixtures, solid solution formation, phases 2—6626
Sintering continued
  ZrB$_2$-W alloy powders, effect on struct. and props. 2—12950
Skin effect
  anomalies in semibounded plasma study using results on specular reflection of electrons 2—990
  classical skin depth found by meas. of change in mutual inductance between coaxial coils, undergraduate expt. 2—37551
  conducting slabs, parallel, transient proximity effect 2—37867
  ferrite, Mn-Fe, effect on ferromag. resonance 2—4533
  ferromagnet, in alternating mag. field equations 2—36435
  gas discharge, high frequency, theory 2—6112
  normal and anomalous in the nonlinear theory of e.m. wave propagation in solid state plasmas and gas discharges 2—4142
  plasma, magnetized toroidal, with h.f. current flow as function of density temp. and ion mass 2—28650
  semimetal, e.m. excitation of sound, deformation mechanism 2—6673
  CdSe, temp.-elec. skin effect rel. to continuous sound generation 2—13223
  Mn$_x$Fe$_{3-x}$O$_4$, effect on ferromag. resonance 2—4533
  Na optical conductivity, exponential dependence of Drude tail anomaly 2—10349
Sky brightness
  see also Airglow; Twilight
  approximate equation from atmospheric transmittance and albedo 2—1888
  atmospheric model, luminosity distrib., cloud cover effect 2—26499
  aureole, application to atmospheric aerosol measurement 2—16818
  night, influence of Quadrantids shower 2—4986
  nightglow rel. to precipitating energetic electrons in midlatitude nighttime D-region 2—37206
  optical methods obs., review 2—7301
Sliderules *see Calculating apparatus*
Slip
  air-water mixture, slip distrib. and ave. void fraction meas. techniques 2—24628
  Al crystal, band formation round indentation figures, Schmid factors 2—1297
  anisotropic cryst., displacement fields of straight dislocations 2—32511
  b.c.c. metals, slip geometry 2—6498
  brass, fatigue rupture, fracture surface morphology 2—12907
  ceramic crystal, press forging, recrystallization, strength, fracture 2—36249
  critical two-phase flows, one- and two-component, variable slip model 2—35437
  diamond-type cryst., dislocation dissoc. and mobility 2—39702
  double ended dislocation array, slip line model 2—19099
  field theory, applicability of elastic-plastic flow around notch 2—12881
  flow fields, strain hardening material, plane strain extrusion 2—12880
  frictional behaviour and surface struct. of S-137 material 2—29341
  graphite, role in high press. deform. 2—32607
  homogeneous, high strain rate deformation, single crystal niobium 2—3884
  ice, systems rel. to hardness anisotropy 2—9717
  initiation and microdynamics of flow in tungsten and other metals 2—3885
  metal, dispersion hardening rel. to initial fine slip 2—25574
  metal, f.c.c., twinning-gliding dislocation interaction in various slip systems 2—15766
  metal, rel. to friction stress during high temp. creep, theory 2—12866
  nonhomogeneous, low strain rate deformation, single crystal niobium 2—3884
  parallel edge dislocations, slip stability, analysis 2—36038
  plane, dislocation movement, plasticity theory 2—19176
  plastic, spread in notched half-plane 2—11333
  plasticity theory 2—17356
  screw dislocation generation, from grain boundary ledges 2—15758
  single crystal, pure, load-elongation and creep curves computed 2—25499
  slip-line field technique appl. to rolling of cylinder on plastic half-space 2—37671
  steel, stainless, rel. to stacking faults and $\gamma\to\varepsilon$ transform. 2—40003
  steel, stainless bicrystals, high temp. intergranular creep 2—12876
  steel, substruct., plastic strain mech., alternating deform. 2—32610
  two-phase flow, high-velocity, transverse slip of gas and energy migration 2—35439
  velocity and temp., coeffs. for gas-surface scattering kernels 2—39230
  rel. to X-ray crystallography, Fresnel formulae 2—35963
  Ag, thin cryst., slip morphology size depend. 2—22206
  AgCl crystals, room temp. 2—19103
  Al-Mg, recovery and stacking fault energy, 77-500K 2—36112
  Al, impact loaded, deform. bands, secondary slip system 2—32621
  Al, low temp. intermittent deform., specimen size effect 2—36111
  Al, recovery and stacking fault energy, 77-500K 2—36112
  Al, rel. to grain boundary behaviour 2—12847
  Al$_2$O$_3$, sapphire, 1150°-1750°C 2—36130
  Be, temp. depend. of cct. resolved shear stresses for basal and prismatic slip 2—32622
  Bi, slip planes, compression tests, shear stresses 2—32530
  Cd-Mg alloys, crit. resolved shear stresses 2—32608
  Cd single crysal, torsionally stressed, shear stress distrib. 2—29275
  CoO crystal, creep, temp. and O$_2$ press. effects 2—6553
  Cr, polycryst., high-temp. creep, surface slip lines 2—32616
  Cu-(1wt.%)Si, initiation and microstrain behaviour rel. to dislocation struct., single cryst. 2—3885
  Cu, initiation and microstrain behaviour rel. to dislocation struct., single cryst. 2—3885
  Cu, rel. to internal friction under neutron irrad. and fatigue 2—15805
  Cu crystal, conical indentation, dislocation reactions 2—1288
  Cu crystal, fatigue cracks 2—3908
  CuAl$_2$, compressive and tensile deform. 2—19180
  Cu$_3$Au, single cryst., fine struct. of slip lines, elec microscope obs. 2—15717
  Fe-7 wt.% Si, evidence for {112} slip planes 2—39704
  Fe-(11.6 wt.%SI, deformation in compression, two modes of slip 2—3784
  Fe, Armco, cyclic bending deformation, absorptional fatigue 2—29300
  α-Fe, cleavage fracture initiation and propagation, twin intersection 2—12883
  Fe, work hardened by strain rate cyclic changes, high temp. deform., slip 2—19244
  Fe crystal, annealed, laminated, twisted, primary recrystallization texture 2—15901
  Fe crystal, tension deformation, elastic limit, yield stress 2—15835

Slip continued
Ge-Cu solid soln., slip twinning interaction 2—29182
LiF:Mg^{2+}, dislocation struct. parameters, impurities influence 2—9561
Mg-Cd alloy, plastic deform. mechanism, 77 K and room temp. 2 9679
Mg-Zn alloys, age-hardened, Ashby second slip theory applic. 2—6599
Mg, MgO-dispersion strengthened, rel. to high temp. creep 2—25598
Mg, plastic deform. mechanism, 77 K and room temp. 2—9679
MgO, high temp. fatigue fracture initiation mechanism 2—29302
Mo-(35 at. %)Re alloy, slip patterns and deform. twins correl. 2—15765
Mo, single cryst., slip bands obs. by X-ray diffr. 2—15726
MoS$_2$, natural molybdenite, cold working, microstructure, X-ray line broadening 2—25409
NaCl, birefringence slip bands 2—39789
NaCl, dislocation mechanism, 1.4 to 573 K 2—32623
Nb, dislocation damping by phonon viscosity 2—29183
Nb single crystal, high and low strain rate deformation 2—3884
NbC, slip system determination by hardness anisotropy 2—9564
Ni$_3$Al alloy, hardening mechanism 2—6547
Ni$_3$Al alloy, superdislocation braking, defect capture 2—6548
Sb cleavage foil, rel. to dislocation geometry 2—19101
Si, glide band form. 2—36036
Si epitaxial slices, central region obs. 2—12865
Si epitaxy, thermal stress 2—25208
SiC, 2H type, low temp. phase transform. mechanism 2—32778
β-Si$_3$N$_4$, dislocation generation 2—19102
SrSO$_4$, active slip planes computation 2—3782
Te, temp. dependence of elastic limit 2—3855
Ti, high localized strains at solitary slip bands 2—9696
TiC, slip system determination by hardness anisotropy 2—9564
TiH$_x$, plastically deformed, slip plane 2—19183
UO$_2$, deform. in compression, slip planes, shear stresses, dislocation structs. 2—32527
VC, slip system determination by hardness anisotropy 2—9564
W, initiation and flow microdynamics 2—3885
WC-Co alloy, slip lines, deform. mech., electron microscope obs. 2—32531
Zn, surface deform. during sliding, surface films effect 2—22304
Zr-Nb alloy, martensite phase 2—9827
Zr, slip planes, and dislocations with (c+a) type Burgers vectors 2—36123
ZrB$_2$ single crystal, plastic deform., active slip planes 2—15841
ZrC, slip system determination by hardness anisotropy 2—9564

Smectic phase *see Liquid crystals*

Smokes *see Aerosols*

Snoek effect *see Crystal imperfections/interstitials; Elastic relaxation*

Snow
anomalous attenuation of radiowaves, models for 2—30299
anomalous attenuation of radiowaves in millimetre, microwave range 2—30300
density gauge by gamma ray attenuation, telemetered profiling 2—30284
evaporated, optical constants in 2.5 to 40 μm range 2—37136
falling, effects on millimetre wave propagation 2—30298
falling, laser beam propagation 2—30294
falling rate measuring gauges, heat-plate, water-drop types, construction, characteristics 2—30286
falling velocity measurement, optical, supersonic methods 2—30285
i.r. radiation, attenuation, computations 2—16837
microwave emission, brightness temp. 2—16770
radiation attenuation, in submillimetre range, computations 2—16836
rheological behaviour under stress conditions 2—33426
snowstorms of 1970, March 4 in central and south-east England 2—40916
spatial distribution, sizes of snowflakes during snowfall tabulated against radiowave attenuation coefficients due to snowfall 2—30287
thunderstorms, proximity soundings 2—13710
transparency rel. to density and air permeability in natural snow cover 2—16831

Sodium
activation analysis in solid rocket propellants 2—1772
anharmonic lattice dynamics 2—19380
atmospheric abundance rel. to radio meteor rate 2—17040
atmospheric layer, laser excitation 2—20314
atom, 3^{2}P$_{3/2}$ state, crossings of Zeeman sublevels calc. using dipolar magnetic and quadripolar electric interaction constants as parameters 2—18316
atom, charge transfer cross-section measured for various ions, 1-500 eV 2—35162
atom, collision with H$^+$ and He$^+$, two electron loss 2—5870
atom, collisions with diatomic molecules, thresholds and energy dependence of excitation cross sections, meas. from 1 to 10 eV 2—2977
atom, D-line radiation excitation in collisions with internally excited H$_2$, D$_2$, N$_2$ 2—35161
atom, electron excitation cross section and polarization of unresolved doublet resonance radiation 2—5803
atom, electron impact excitation cross sections calc. using regional trial function in variational principle for R matrix 2—24364
atom, electron impact ionization, abs. cross section meas. in 100eV to 2keV energy range 2—5798
atom, electron scattering, cusp observation due to opening of inelastic 3^{2}P channel 2—11986
atom, electronic excitation in collisions with Li$^+$, Na$^+$, K$^+$, cross sections 2—2980
atom, extreme u.v. photoabsorpt. spectra 2—18310
atom, nonrelativistic wave functions and eigenvalues 2—18317
atom, principal series oscillator strengths and ground state photoionization cross sections 2—31679
atom, stopping power in Ni film, transmission method of obs. 2—16077
atomic flame spectra, D line reversal, chemiluminescence effects 2—8452
atomic spectra, pressure broadening of 5889 Å and 5895 Å lines by thermal and high temperature He 2—31669
atoms, charge rearrangement reactions with CO$^+$ 2—12012
atoms, collision with I$_2$, cross section meas., comparison with harpooning model predictions 2—686
atoms, collisions, with SO$_2$ and NO$_2$, 1 to 30 eV, electronic excitations 2—687
atoms, collisions with O atoms, charge exchange cross section, theoret. study 2—691
atoms, low energy elastic electron scatt. 2—2956
atoms, photoionization cross sections, model potential calc. 2—605
binding energy and lattice constants, pseudopotential calc. 2—40139
boiling phenomena, direct heating in forced convection loop 2—31629

Sodium continued
Compton profile and momentum distrib. of interacting cond. electrons 2—19513
core annihilation rates, calc. 2—36431
D-line, solar spectrum, broadening by H 2—7548
Debye parameter and vibration amplitude from Bragg intensity data 2—9862
Debye-Waller factor, temp. dependence, theory 2—6649
desorption from Nb, activation energies, mean adsorption lifetimes 2—6384
determination in pyrographite by neutron activation using alternating irradiation regimes method 2—40861
diffusion, in Li, electro- and thermotransport 2—15787
electrical cond., 40 to 360K 2—19463
electrical resistivity, low temp., Bloch T^5 law failure 2—16145
electron beam analysis, glass and raw materials 2—22899
electron-phonon interaction, local field effects 2—1456
excited atom, sensitizing collisions with inert gas atoms in strong mag. field, polarization transfer 2—2978
film, photoelec. emission, 2.3-4.6 eV 2—33090
film, vapour quenched and annealed, photoelectric electron emission 2—6930
fluorescence analysis in subnanogram concentations, stimulated by narrow-band dye laser 2—7190
Hall effect meas. in solid and liquid state 2—16137
impurity in plasma arc, effect on spectral intensities of Ti and Mn 2—15524
in interstellar clouds, ionization equilibria as a function of position 2—33687
interstellar lines, formation in H I cloud or interstellar region 2—4897
ionization constants for NO-acetylene flames 2—22897
lattice mechanics, f.c.c. and b.c.c. structure, de Launay and CGW models 2—19379
liquid, corrosion of Ni, rel. to temp. and Na vel. 2—37046
liquid, corrosion of transition metals 2—37045
liquid, interionic potential calc. 2—21955
liquid, oscillation spectra, variational calc. 2—9077
liquid, solubilities of Ar and He as functions of temperature and pressure 2—6213
liquid, sp. ht., spline correl. function 2—18812
liquid, speed of sound, 1000 to 1500C 2—15588
liquid, static struct. factor 2—35728
liquid, statistical error due to finite time averaging in computer expts. on number density and kinetic energy-density autocorrelation 2—32220
liquid, velocity autocorrel. function and self-diffusion coeff. 2—32226
liver, transport-rate constants, kinetic basis of computer simulation 2—41281
melting curves calc. 2—9207
melting pt. behaviour of vol. expansion, thermal cond. and elec. resist. 2—16070
metal, lattice relaxation, effect on soft X-ray spectra near Fermi edge 2—20083
on metal films, methods of determ. conc. 2—6366
nuclear spin-lattice relax. times, many-electron enhancement effects 2—16660
optical conductivity, exponential dependence of Drude tail anomaly 2—10349
oxidation by gases, corrosion rate in drybox atmos. 2—20186
particles, submicron size, plasma resonance description of white light scattering characteristics 2—13471
phonon meas., resolution effects 2—4036
plasma, propagation and damping of small amplitude electron and ion waves in thermally ionized collisionless plasma 2—21841
in rare gas matrices, absorpt. and luminesc. 2—24387
recharging target for recharging protons to give H$^-$ beams 2—7900
self-diffusion enhancement by K additions 2—32564
self-diffusion mechanisms 2—39744
solar corona abundance, det. from e.u.v. spectra 2—20692
solid, cohesive energies and radii of metal cells calc. by ab initio method 2—1198
spin wave transmission, 120 GHz 2—40745
stellar compositions, measurements in the Hyades and field giants with narrow-band photometry 2—16993
superconducting transiion temperature, pressure depend., pseudopot. approach 2—36454
surface states, abnormal absorpt. maxima 2—16495
thermal cond., 40 to 360K 2—19463
thermal desorption from α-Fe 2—32393
thin films, transmission of polarized light at oblique incidence 2—7045
twilight airglow observations, vertical abundance characteristics 2—30321
vapour, test of pair potential theory 2—9029
vapour arc, high pressure, radial temp. distrib. det. 2—24945
vapour obs. of amplitude modulated train pulse 2—23665
vapour pressure, over Na$_2$O, torsion effusion determ. 2—22048
work function and surface structure, calc. 2—39455
X-ray spectra, absorpt. in X-u.v. range 2—1702
x-ray spectra, electron gas correls. and core hole effects 2—1701
X-ray spectra, high-energy satellites of L$_{2,3}$ emission bands 2—33299
Ar arc, introduction of Na, effect on spectral intensity 2—15523
atoms, collisions with I atoms, chemi-ionization cross section 2—684
BeO:Na, phosphor, thermolum. props. 2—29970
Ca^0, Ca$^+$ interstellar, basis of model of interstellar medium 2—30505
Ge:Na, constant vapour source diffusion, solubility detn. 2—36056
K multiphoton ionization probability, experiments rel. to theory 2—35159
Li$^+$, collisional rotational excitation of N$_2$ 2—894
LiF:Na, radiothermolum., trap elimination by Na incorporation 2—27903
Na-Ar, two phase flow invertical channel, void fraction and heat transfer coefficients 2—21932
Na-H$_2$ mixtures with pulsed infection of metal vapour into gas discharge plasma, obs. laser section 2—23601
Na-He cross-section for spin relaxation in ground state calc. 2—8457
Na-Li liquid system, critical opalescence, small angle X-ray scatt. obs. 2—3428
Na$^+$-Na charge transfer cross section calc. obs. of oscillations 2—24378
Na$^+$-Na resonance charge transfer, cross section calc. from Na$_2^+$ potential curves 2—3055
Na I interstellar, relative line strengths in e.u.v., use in abundance estimations 2—10913
Na$^-$ multiconfiguration method calc. of low-lying autoionization states 2—11959

Sodium continued
- Na^+, collision with O-, mutual neutralization cross section, meas. with superimposed beams 2—688
- Na^+, collisional rotational excitation of N_2 2—894
- Na^+, collisions with H_2, H_2 dissociation 2—882
- Na^+, collisions with H_2, N_2, O_2 at 5 to 42 keV, ionization and dissociation 2—883
- Na^+, collisions with Ne, K-shell excitations, differential investigation of velocity dependence 2—2967
- Na^+, diffusion in NaCl, temp. depend. of isotope effect 2—39742
- Na^+, enhancement of colour centre formation in CaF_2 2—36063
- Na^+, refl. from Ag and Au targets 2—22065
- Na^+ collisions with inert gas atoms, study of excitation mechanism, inelastic transitions 2—674
- Na_2, collision-induced rotational transitions, asymmetries, Born approximation treatment 2—18380
- Na_2, ionization potential 2—6104
- Na_2^+, potential curve calc., Na^++Na resonance charge transfer cross sections 2—3055
- Na_2^+ dissociation energy 2—6104
- ^{22}Na, cosmic ray produced, rel. to atmospheric exchanges 2—20324
- ^{22}Na, diffusion in Li, under temp. gradients and elec. fields 2—19145
- ^{23}Na, hyperfine constants of $3^2P_{3/2}$ state, level crossing method 2—11960
- ^{24}Na production in nuclear reactor, biomedical applications 2—41291
- Na+H_2O reaction, research review rel. to nuclear reactor applic. 2—40801
- Na^++Li _Na+Li^+, cross sections for nonresonant charge capture in energy range 100 eV to 12 keV 2—24388
- Na^++Ne, low energy collisions, phase interference effects obs. in total cross section 2—2979
- $Na^*(3p^2P)$ D lines obs. on photodissociation of NaI 2—12180
- $Na_2(b^1\pi_u)$ state, collision induced energy transfer 2—3151
- Ni/Na overlayer system, surface struct. 2—28985
- Si, SiO_2, contamination, from water and alcohol 2—3501
- SiO_2:Na, redistrib. on immersion in hot electrolyte 2—3546

Sodium compounds
- borate glass, trapped electron centre, X-irradiation induced, e.s.r. and optical obs. 2—20137
- channelling, MeV protons and He^+ ions 2—3754
- chloranilates, hydrated, crystal data, X-ray diffr. 2—19062
- cryolite-alumina mixtures, alumina diffusion, temp. and comp. depend. 2—28825
- cryolite-alumina mixtures, viscosity obs., 980, 1000, 1020, 1050°C 2—28812
- goetzenite, cryst. struct. 2—9463
- halides, elastic consts., temp. depend. 2—29231
- NaI:Tl, light sum storage process rel. to anionic impurities 2—10425
- $NaNO_2$, polarization reversal mechanism, X-ray obs. 2—40353
- soda-baria-silica glass system, crystallization, nucleation 2—3457
- sodaborate glasses with ZnO, X-irrad., e.p.r., comp. depend. of Zn^+ signal 2—26284
- sodalite, cathodochromic props. 2—13590
- surfactants, stratification of stabilized free liquid films 2—6192
- tourmaline, assessment as acoustic surface wave delay medium 2—40055
- zeolite lattices with Hg filled channels, struct. behaviour 2—6444
- zeolites, liquid metal filling of marrow channels 2—1384
- AlNa silicate glasses, Nd-doped, Al coordination effect on spectroscopic properties of activator 2—26211
- $Ba_2NaNb_5O_{15}$, refractive indices meas., temperature dependence obs. 2—10302
- $Ba_2NaNb_5O_{15}$, second harmonic generation, dielec. consts., electro-optic coeffs. 2—13315
- $Ba_2NaNb_5O_{15}$ as intracavity nonlinear element for Nd:YAl garnet laser 2—281
- $Cd(NO_3)_2$ and NaCl solutions as detector for recording of neutrons 2—38365
- CdS_xse_{1-x}, solid soln., reson. Raman effect 2—16583
- $K_{1-x}Na_xTaO_3$ mixed cryst., ferroelec. transitions, soft modes 2—25928
- Li-Na-Si glass, partially recrystallized, spontaneous deformation phenomena 2—12629
- Li_2O-Na_2O-Fe_2O_3 system, intensification of ferrite formation 2—36303
- Na-Cs alloys, liq., nucl. spin-lattice relax. 2—18855
- Na-K alloy, liquid, partial structure factors 2—6200
- Na-K alloy film, photoelec. emission and phase transitions 2—33090
- Na-K eutectic alloy, critical heat flow during boiling in conditions of free convection 2—28954
- Na-K liquid alloy, electrotransport theory 2—21999
- Na-K liquid alloys, volume thermal expansion coefficients 2—25068
- Na-K solutions, electrical transfer, resistivity and density of electron states meas. 2—39386
- Na-K system, liq., electronic struct. 2—9078
- Na-Li alloys, electrical resistivity meas. 100 to 1050°C 2—12578
- Na-NH_3 solution, electron states, near metal-nonmetal transition 2—12573
- Na-Rb alloys, liquid, electrotransport obs. 2—25104
- Na^+-indenyl ion pairs, struct., n.m.r. obs. 2—18512
- NaA, hydrated synthetic zeolite, pseudosymmetric struct. refinement 2—9479
- $NaAlF_4$, i.r. spectra of matrix isolated vapours 2—797
- Na_3AlF_6, cryolite film, struct., rel. to sorption behaviour 2—9291
- $Na_4Al_3Si_3O_{12}Cl$, sodalite, doped, fluoresc. and refl. spectra 2—22806
- $NaBD_4$, infrared and Raman spectra of high and low temperature modifications, cubic to tetragonal symmetry transition studied 2—12181
- $NaBH_4$ and $NaBD_4$, i.r. and Raman low temp. vibrational spectra 2—10384
- $NaBO_2$, ^{18}O-labelled, vibrational spectra 2—21589
- $Na_2B_4O_7$, mechanism of crystallisation from melt 2—1213
- $NaBa_2Nb_5O_{15}$ pyroelectric voltage response to step i.r. radiation signal 2—4283
- $NaBa_3[Si_2O_7](OH)$, linear diortho group Si_2O_7, structure detn. 2—35995
- NaBr:Cr^+, superhyperfine and quadrupole interactions, e.p.r. and ENDOR obs. 2—20170
- NaBr:F-, impurity tunnelling, thermal and dielec. props. 2—33052
- NaBr:M^{2+}, (M=Ba, Ca, Sr), irrad. type effects on symmetry of paramagnetic centres 2—26285
- NaBr/RbBr fused mixture, u.s. velocity and compressibility 2—25077
- NaBr, single phonon X-ray scatt., eigenvector influence 2—9855
- NaBr surface, Cl- substitution, cooperative interactions including surface transition 2—29059
- $NaBrO_3$, fund. band edge absorpt., temp. shift, band transitions, phonon emission absort. 2—36884
- $NaBrO_3$, γ-irradiated, free radicals, e.p.r., g-factors 2—10517

Sodium compounds continued
- $NaBrO_3$, n.q.r. of ^{23}Na 2—40790
- $NaBrO_3$, nucl. quadripolar linewidth of ^{79}Br and ^{81}Br 2—7803
- $NaBrO_3$, SHG, optical rotatory power 2—19952
- $NaBrO_3$ film, polycrystalline, preparation, thickness obs. and uniformity evaluation 2—9278
- Na_2CO_3 anhydrous pile, meas. of neutron spectrum with time-of-flight method by an electron linac 2—28101
- Na_2CO_3 dilute solution, determ. heat transfer rate from electrically heated thin Pt wire under influence of electrolytic currents 2—21981
- $NaClO_3$, double n.m.r., by acoustic excitation 2—33356
- $NaClO_3$, ferroelectric phase transition, relation to phonon structure 2—25930
- $NaClO_3$, γ-irradiated, real structure detn., X- ray obs. 2—36013
- $NaClO_3$, multiple internal reflection i.r. spectroscopy, effect of different prism angles 2—27646
- $NaClO_3$, n.q.r. of ^{35}Cl, press. and vol. depend., press. to 20 kbar 2—40791
- $NaClO_3$, nucleation by collision process at supersaturation, followed by dilution 2—18991
- $NaClO_3$, phase structure obs. 2—39990
- $NaClO_3$, SHG, optical rotatory power 2—19952
- $NaClO_3$, single crystals, electrical conductivity, 100-250C, effect of cation impurity 2—1478
- $NaClO_3$, temp. dependence of n.q.r. frequencies from 77 to 350K 2—37018
- $NaClO_3$, vibr. spectrum and dielec. behaviour, Raman obs. 2—33286
- $NaClO_3$ film, polycrystalline, preparation, thickness obs. and uniformity evaluation 2—9278
- $NaClO_4$, aqueous solution, stimulated and spontaneous Raman scattering 2—21989
- NaF:Cr^+, superhyperfine and quadrupole interactions, e.p.r. and ENDOR obs. 2—20170
- NaF:Cr^+, superhyperfine struct. obs. using ENDOR 2—30029
- NaF, channelling, MeV protons and He^+ ions 2—3754
- NaF, electron density distribution, Lowdin approx. 2—32865
- NaF, impurity-sensitive etchant 2—25433
- NaF, lattice dynamics, rigid ion model limitations 2—40017
- NaF, long-wavelength optic phonons, temp. depend. 2—40649
- NaF, point defects, formation and annealing 2—1245
- NaF, proton irrad., defect formation, channelling effects 2—19130
- NaF, second order Raman spectrum analysis 2—16557
- NaF, second sound vel. 2—13033
- NaF, single phonon X-ray scatt., eigenvector influence 2—9855
- NaF,. sintering kinetics, non-isothermal conditions, isothermal annealing time effects, dilatometric method exam. 2—12984
- NaF, stress-optical dispersion, measurement by intensity method 2—26107
- NaF, thermal cond. and Ziman limit 2—25696
- NaF, ultrasonic velocity and adiabatic compressibility in aqueous solution 2—21982
- NaF, X-ray scatt. factor, calc. 2—32435
- NaF absorption spectra, between 25 and 72 eV 2—26170
- $Na_2Fe(CN)_5NO.2H_2O$, nucl. diffr. of reson. γ-rays due to quadrupole interaction 2—16439
- $Na_3Fe(CN)_6.nH_2O$, Mossbauer study of hydration phenomena 2—33215
- $NaFeO_2$-TiO_2, crystal structure 2—3719
- Na_2GeS_3, crystal structure determ. 2—39628
- NaH, potential energy curves, applicability of Morse potential, rot. consts., r-centroids, Franck Condon factors 2—18457
- $NaHF_2$, crystal and molec. dynamics, i.r., Raman and neutron studies 2—26169
- Na_2HPO_4, fog seeding experiments, induced dissipation 2—16833
- $Na_4HP_3O_{10}.H_2O$, thermogravimetric dehydration curves 2—30052
- $NaH_3(SeO_3)_2$, dipolar spin-lattice relax. study of l.f. motion 2—10259
- $NaH_3(SeO_3)_2$, e.p.r., external stress effects on unstable orientation 2—10514
- $NaH_3(SeO_3)_2$, effect of γ-radiation on dielectric properties 2—1553
- NaI:Pb^{2+}, C-band peak position determ. using extended Mollwo-Ivey reln. 2—29197
- NaI/RbI fused mixture, u.s. velocity and compressibility 2—25077
- NaI, dislocation struct. rel. to n.m.r. line broadening anisotropy 2—10560
- NaI, elastic interaction of O_2^- centres 2—22186
- NaI, excitonic structure, obs. using reflectivity meas. in vacuum u.v. 2—4137
- NaI, i.r. active two-phonon processes 2—40677
- NaI, i.r. transmission spectra, multiphonon absorpt. bands 2—36883
- NaI, impurity photocond. due to excitonic-energy transfer 2—16314
- NaI, radiation detector, escape peak to photopeak photons ratio calculation 2—5593
- NaI, self-diffusion, n.m.r. relax. obs. 2—9626
- NaI, self-diffusion, vacancy mechanism 2—9625
- NaI, single phonon X-ray scatt., eigenvector influence 2—9855
- NaI, thermodynamic funcs., phonon freq. moments, and Blackman rule of sums 2—40067
- NaI, V_K-polaron diffusion obs. from opt. anisotropy decay 2—22233
- NaI exciton structure, vac. u.v. reflectivity obs. 2—16469
- NaI photodissociation fluorescence of $Na^*(3p^2P)$ D lines obs. 2—12180
- NaI plasma production in high pressure mercury lamps 2—3229
- $NaIO_4$, thermal expansion, rel. to cryst. chemistry 2—22430
- NaI(Tl)-Ge(Li) coincidence-anticoincidence gamma ray spectrometer 2—24070
- NaI(Tl), anticompton $4\pi\gamma$ detector system at NBS 2—27867
- NaI(Tl) crystal counters, efficiency of recording gamma radiation from point isotropic sources 2—24085
- NaI(Tl) detector system, pulse height shift or single escape peak 2—446
- NaI(Tl) Harshaw 7F8 well crystal, total and photopeak efficiencies for cylindrical γ sources 2—24081
- NaI(Tl) γ-ray spectrometer, solar monitoring in OSO-7 spacecraft 2—30610
- NaI(Tl) monocrystal scintillator for use with gamma automat. 2—2629
- NaI(Tl) well-type detectors, γ-ray efficiency values 2—38364
- $NaI.2H_2O$ and $NaI.2D_2O$, far-i.r. absorpt., deuteration effects, vibrs. obs. 2—22756
- $NaK_2Ca_2TiSi_7O_{19}(OH)$, tinaxite, cryst. struct. 2—1229
- $Na_{0.88}Li_{0.12}NbO_3$-Li_2O ceramic, cryst. symm., lattice parameters, 293-783K, X-ray and thermal expansion obs. 2—32470
- $NaMgAl(C_2O_4)_3.9H_2O$:Cr^{3+}, luminesc. emission spectra rel. to Cr^{3+} conc. 2—26221
- $Na_2Mg(MoO_4)_2.2H_2O$, crystal structure determ. 2—6443

Sodium compounds continued
$2(Na_2Mg(SO_4)_2.4H_2O$, e.s.r. of Mn^{2+} impurities, hyperfine parameters, g 2—20136
$Na_2Mg(SeO_4)_2.2H_2O$ crystal structure determ. 2—6443
$Na_2Mg(WO_4)_2.2H_2O$ crystal structure determ. 2—6443
Na_2MoO_4-Li_2MoO_4 molten system, surface tension, comp. depend. 2—28818
$Na_{0.9}Mo_6O_{17}$, single cryst. struct. determ. 2—9480
Na_2MoO_4, hydrous and anhydrous, ^{23}Na n.m.r., meas. of quadrupole coupling constants, electric field gradient 2—37012
NaN_3, cryst. struct., refinement 2—3721
$NaNH_4CrO_4.2H_2O$, cryst. struct. 2—35993
$Na_4(NH_4)P_5O_{15}.4H_2O$, cryst. struct. 2—35994
$NaNO_3$-$AgNO_3$ melts, thermodynamic properties from e.m.f. meas. 2—21980
$NaNO_3$-$AgNO_3$ molten salt mixtures, ion migration 2—28892
$NaNO_3$-$LiNO_3$, molten mixture, liquidus curve, thermodynamic props. 2—25138
$NaNO_2$, anharmonicity 2—25665
$NaNO_2$, ferroelectric phase, electric field gradient and long range order parameter 2—25929
$NaNO_2$, force consts. of NO_2^-, temp. depend. 2—6652
$NaNO_2$, nonlinear optical coeffs., temp. depend. 2—19951
$NaNO_2$, Raman spectra, two-phonon scatt., Curie pt. behaviour 2—6657
$NaNO_2$, spt. ht. near antiferroelec. transition pt. critical exponents 2—9889
$NaNO_2$, temp.-depend. phonon struct. in Raman spectra 2—9866
$NaNO_2$ liquid filters for visible and i.r. regions 2—8013
$NaNO_2$ liquid optical filters for lasers, corrosion of circulation system materials 2—30068
$NaNO_3$, ^{23}Na nuclear quadrupole spin-lattice relax., orientation depend. 2—26084
$NaNO_3$, anharmonicity 2—25665
$NaNO_3$, disordered phase, correl. field splitting of vibr. modes 2—19378
$NaNO_3$, enthalpy calculations, Frenkel defects, Schottky defects, formation 2—3767
$NaNO_3$, lattice dynamics 2—19381
$NaNO_3$, low temperature behaviour, 42-308K, of nuclear quadrupole coupling constant of ^{23}Na 2—30034
$NaNO_3$, molten, diffusion coeff. of F^-, Br^-, I^-, CO_3^{2-}, SO_4^{2-} 2—21976
$NaNO_3$, nucl. quadrupole spin-lattice relax., orientation depend. 2—19933
$NaNO_3$, single crystal, nuclear quadrupole coupling constant of ^{23}Na, pressure and temp. dependence 2—16659
$NaNO_3$, vac. u.v. reflectivity spectra 2—16471
$NaNbO_3$, disordered, cryst. struct., diffuse X-ray scatt. 2—9375
$NaNbO_3$, ferro- and antiferroelec., diffuse X-ray scatt., static model of one dimensional disorder 2—32469
$NaNbO_3$, ferro-antiferroelec. phase transition, n.m.r. obs. 2—16661
T_2-$NaNbO_3$, struct. at 600°C, cubic-tetragonal transition rel. to soft-phonon modes 2—39648
Na_2O-Al_2O_3-SiO_2 glass, dielec. props., microwave 2—29742
Na_2O-B_2O_3-SiO_2 glass fibre, quick loading tensile strength, comp. depend. 2—19194
Na_2O-B_2O_3 glass, effect of liquation on mech. and viscous props. 2—35848
Na_2O-Cs_2O-SiO_2 glass, refr. index, density and thermal expansion 2—28975
Na_2O-Fe_2O_3-TiO_2-SiO_2 glass, mag. susceptibility, temp. depend. 2—1598
Na_2O-SiO_2, glass, electrical conductivity, activation energies, models 2—3458
NaO, NaO^+, NaO^-, Hartree-Fock molec. orbital studies, deduction of Na-O species properties 2—37032
NaO dissociation energy and ground state calc. from ion model 2—28266
Na_2O, evaporation process, Na vapour pressure, torsion effusion determ. 2—22048
Na_2O, standard enthalpy of formation calculated from enthalpy of reaction of hydrolysis 2—37031
NaOH-KOH-ZnO mixture, flux for tinning Al wire 2—41357
NaOH, orthorhombic to monoclinic transition, obs. of diffuse X-ray scattering, change of lattice prameters 2—1400
NaOH, vitrified aqueous solution, irradiated, reaction kinetics, 77 K, electron tunnelling 2—30093
NaOH dilute solution, determ. heat transfer rate from electrically heated thin Pt wire under influence of electrolytic currents 2—21981
NaOH ice, resolution enhanced ESR spectra of trapped electrons, determ. hyperfine coupling const. and relax. characteristics 2—16645
$Na_2O.SiO_2$ glass, low temp. thermal props., rel. to low lying vibrs. 2—40075
$Na_2O.SiO_2$ glass, relax. characts., effect of struct. heterogeneity 2—1283
$Na_2O.SiO_2.6H_2O$, location of hydrogen atoms 2—6442
$Na_2O.3SiO_2$ glass, diffusion coeff., effect of specific activity 2—15792
$Na_2O.3SiO_2$ glasses, Frenkel pairs form. 2—1249
$NaPF_6$, aqueous solution, stimulated and spontaneous Raman scattering 2—21989
$NaReO_4$, irradiated, mag. susceptibility and structure modifications 2—4344
Na_2SO_4, dielec. const., microwave region using heterogeneous mixture method 2—36581
Na_2SO_4, grinding effect on phase transformation, differential thermal analysis study 2—29476
Na_2SO_4, irrad., SO_4 radical obs. using e.p.r. 2—26375
Na_2SO_4, vaporization thermodynamics, study by transpiration method 2—28961
Na_2SO_4 and Ca and Na double salts, relation between optical properties and structure 2—4434
$NaSbF_4$, ^{121}Sb Mossbauer data rel. to structural parameters 2—1668
$NaSbF_6$, aqueous solution, stimulated and spontaneous Raman scattering 2—21989
Na_2SiF_6, phase transformation mechanism, cation displacements 2—3999
$Na_4Si_4S_{10}$, crystal structure determ. 2—39658
Na_6Tl, cryst. struct. 2—32468
Na_6Tl, space group and lattice parameters 2—3720
Na_3TlF_6, $Na_5Tl_9F_6$ crystal structure, characterised MF-TlF_3 system, M=Li, Na, K 2—3737
α-Na_2UO_4, U-O lattice vibrations from i.r. absorption spectra 2—40680
β $Na_xV_{2-x}Mo_xO_5$ bronzes, cryst. struct. 2—3714
$NaVO_3$, ^{51}V n.m.r., Mn^{2+} e.p.r., comparison 2—10565
Na_2WO_4, ^{182}W Mossbauer spectra 2—13452
Na_xWO_3, cryst. growth, electrolytic adaptation of Kyropoulos technique 2—18979

Sodium compounds continued
Na_xWO_3, optical transition to Fermi level 2—33243
Na_xWO_3, sodium ordering, ^{187}Re nucl. quadrupole interaction obs. 2—33187
$Na_2ZnCl_4.3H_2O$, $Na_2ZnCl_4.3D_2O$, long wavelength phonon spectra, assignment using Raman data 2—40036
$Na_2Zn(SO_4)_2.4H_2O$:Cu^{2+}, elec. field symmetry, g-factors, hyperfine constants, e.s.r. obs. 2—7122
$Na_2[Fe(CN)_5NO].2H_2O$, trimethylene glycol solution Mossbauer effect, molecular motion, diffusion 2—22738
$Na[Fe(CN)_5x].nH_2O$, elec. field gradient sign determ. 2—36790
$(Tl,Na,Li)NO_3$, $(Tl,Na,Rb)NO_3$, $(TlNa,Cs)NO_3$ systems, solid-liquid equilibria, polythermal projections 2—22035
$(U,Na)_{2-x}Nb_2O_{7-y}$, cryst. struct., order-disorder transform. X-ray obs. 2—32782

sodium chloride
$Cl^-_{II,III}$ absorption spectra, pure and KCl-NaCl solid solns. 2—20041
acoustic diffr. beam spreading for propagating modes 2—32820
acoustic emission, correl. with dislocation motion 2—4044
additively coloured, self- diffusion 2—39743
aqueous salt solutions, effect on metal transfer during CO_2 welding 2—19250
aqueous solns., Brillouin scattering of laser light 2—3392
aqueous solution, optical constants in i.r. 2—35766
aqueous solution, vapour press. meas. and osmotic coeff. calc. 2—39433
band structure, calc. using pseudopotential approach 2—29598
brine inclusions in salt mines, r.f. absorption measurement 2—7222
brine-ice interface, kinetics determ. from temp.-gradient zone migration of droplets 2—9240
channelling, MeV protons and He^+ ions 2—3754
cleaved, sublimation rate, activation energy estimation 2—32313
coloration, first stage, of pure and Ca-doped crysts. 2—12789
colour centres, colloidal Pb centres 2—29196
crystal, impurity Mn diffusion from vol. to surface growth of MnO films 2—3536
Debye-Waller B-values, interionic interaction model 2—22404
diffusion of impurity Ca^{2+} ions, investigation of eqns. 2—9591
diffusion of Pb^{2+} and Cd^{2+}, simultaneous, effects of common ion interaction and effusion during quenching 2—12810
dislocation damping coeffs. variation during γ-irrad. 2—3780
dislocation motion at low temps. 2—39700
distortion of ions, study by nonorthogonal least distorted localized molecular orbitals in restricted H-F approx. 2—21610
doping by dynamic compression of layer on surface 2—9587
electric relief, meas. by interfacial layers 2—39456
electrolytic conductance, meas. in sulfolane water mixtures at 25 and 35°C 2—22000
electron density distribution, Lowdin approx. 2—32865
electron emission under atom and ion bombardment, gamma ratio and energy distribution 2—36648
energy band structure, resolution of apparent APW-OPW differences 2—16109
epitaxial film, dielectric properties 2—10109
e.p.r. of Mn^{2+}, stress effects on ground state splitting 2—13542
e.s.r. trapped-hole centre parameters, doped crysts. 2—10516
etching, inhibition kinetics at dislocation sites 2—3568
F- and X-centres, radiation prod., thermal destruction 2—6506
F-centre, asymptotics of weakly bound electron wave function and photodisintegration cross section 2—32552
F-centre accumulation, proton beam intensity depend. 2—12788
F-centre optical bleaching in X-irradiated crystals 2—9597
film with adsorbed CO_2, vibration frequency shifts and splittings 2—5914
films, energy losses of slow electrons, resonance potentials 2—25711
fog seeding experiments, induced dissipation 2—16833
fracture toughness of Al improvement by environmental exposure to salt solution 2—1302
habit growth, phenol effect 2—39578
impurity-enhanced dissolution studies 2—32398
impurity-vacancy complex reorientation for crysts. doped with Ca^{2+}, Cd^{2+}, Mn^{2+}, Mg^{2+} 2—12757
internal stresses in crysts. deformed by ultrasound, elec. field effect 2—6537
ion implantation of P, Kr, Xe, range distribs., diffusion processes, sectioning technique 2—9594
ionic conduction, electrode polariz. effects 2—22611
ionic transport parameters 2—29745
lattice dynamics, rigid ion model limitations 2—40017
luminescence, shock wave induced 2—10417
Lyddane-Sachs-Teller relation at finite wave vector for NaCl type crystals 2—25648
Mossbauer spectra of ^{129}Te, local environment of impurity 2—10319
multiphoton transitions, photocond. obs. 2—22637
n.m.r., ^{23}Na and ^{35}Cl spin-spin reservoir 2—7142
n.m.r. line broadening anisotropy due to plastic deform. 2—10560
parting layer in epitaxial growth of PbS using multilayer approach 2—39518
piezobirefringence coeff., energy band deform. pot. 2—26167
piezobirefringence in vac. u.v. 2—16470
plastic deform., strain hardening mechanisms, internal stresses, flow stress 2—39789
plastically deformed, substruct. components, Kossel line obs. 2—9547
polarization impedance of pure and doped crysts. 2—16273
positron annihilation, laser beam irrad. effects 2—29578
positron trapping, by F- and F′-centres, theory 2—25448
potential distribution, graphite electrodes 2—4272
proton irradiated, defect formation, channelling effects 2—19130
pure and doped, linear thermal expansion coefficients below 30 K 2—16055
Raman spectra, first and second order, defect induced, F-centre defect 2—16559
rigidity, dislocation rosettes 2—6562
sea salt, i.r. refractive index 2—37128
self diffusion, ionic conductivity, vacancy defect study 2—19140
self diffusion activation volume 2—29204
self-diffusion of Na^+, temp. depend. of isotope effect 2—39742
self-diffusion of Na, X-irradiation effects 2—32559
single crystals, vaporization of H_2O liq. inclusion 2—3762
slip mechanism, 1.4 to 573 K 2—32623
solution in glycerol, viscosity, dielectric constant and conductivity rel. to ionic radii determination 2—15610

Sodium compounds continued
sodium chloride continued
spectral emission capacity in 24-25 μm region 2—40724
stability, fourth order anharmonic theory 2—19317
stress induced linear dichroism of Ag^- and Cu^- 2—33208
stress relaxation, dislocation movement in γ-irradiated crystal 2—9660
substance for Au film nucleation and growth, high-resolution shadow casting obs. 2—39495
surface reactions, with alkali halides, ang. distribution of reaction and vaporization products 2—10609
surface relief of plastically deformed crystals 2—9251
thermal conductivity, temp. range 1-80 K, phonon contrib. calc. 2—40094
thermal expansion, shell model 2—16056
thermodynamic fnctions, phonon freq. moments and Blackman rule of sums 2—40067
transmission of struct. information with Bi, Ni, Ag, Au, Zn, Pb, Sn, Al polycryst. interfacial layers 2—6333
transmission spectra, elec. field influence 2—1695
triboluminescence, low temp. obs. 2—10456
twist grain boundaries 2—9579
u.s. attenuation, dislocations influence 2—29534
vacancy pair form. entropy calcs. 2—36019
X-ray intensities, thermal diffuse scatt. influence 2—12704
X-ray irrad., F-centres isothermal decay, opt. absorpt. obs. 2—36068
X-ray line profiles, intensity corrections 2—9385
X-ray scattering on single phonon, eigenvector influence 2—9855
yield point, effect of colour centre conc. by γ-irradiation 2—15838
AgCl-NaCl, AgBr-NaCl solid solutions, thermodynamic properties from miscibility gap meas. 2—22417
Na-NaCl, melts, electron mobility calc. 2—6243
NaCl:Ag, vac. u.v.-X-u.v. excited, photo- and electrophotoluminescence processes 2—16603
NaCl:Au, optical absorpt. and Raman scatt. 2—40676
NaCl:Br, $(Br^-)_2$-centre, luminesc. and absorp. 2—33316
NaCl:Br, field gradient tensor calcs. for nuclei round substitutional ion 2—26093
NaCl:Br, I, Li, impurity induced Raman spectra 2—26194
NaCl:Br^-, luminesc. of localized excitons at 4.0 eV and 5.15 eV 2—16610
NaCl:$CaCl_2$, dielectric loss study, effect of impurity vacancy complexes 2—16267
NaCl:Cr^+, superhyperfine and quadrupole interactions 2—20170
NaCl:Cr^+, superhyperfine struct. obs. using ENDOR 2—30029
NaCl:Cu, new paramag. centre, e.s.r. obs. 2—36980
NaCl:Cu, thermolum., glow curves, trap parameters 2—36953
NaCl:Cu^+ lattice reson., even parity, anharmonic coupling, Raman scatt. obs. 2—16558
NaCl:Cu^+ Raman active resonance modes, overtones and anharmonicity 2—20076
NaCl:Cu^{2+}, paramag. centres rel. to Cu^{2+} conc., e.s.r. obs. 2—7123
NaCl:F, impurity pair resonant modes, i.r. absorp 2—22774
NaCl:Fe^{3+}, e.s.r. lines due to Fe_2O_3 agglomerates 2—10515
NaCl:H Raman scatt., first order, by localised impurity modes, field induced 2—16560
NaCl:K, field gradient tensor calcs. for nuclei round substitutional ion 2—26093
NaCl:M^{2+}, (M=Ba, Ca, Sr), irrad. type effects on symmetry of paramagnetic centres 2—26285
NaCl:Mn^{2+}, e.p.r., off-centre site obs. 2—10513
NaCl:Mn^{2+}, neutral Mn centres, e.p.r. and optical absorpt. studies 2—39716
NaCl:NaOH, thermal cond., continuum of tunnelling levels 2—19446
NaCl:Pb, spectroscopic, determination of conc. limits for isomorphic substitution 2—39711
NaCl:Pb^{2+}, polarized luminesc. of impurity-vacancy complexes 2—16609
NaCl:Tl, x-irrad., thermoluminesc. glow peaks 2—29988
NaCl-AgCl solid solution, decomp., X-irrad. effects 2—36246
(NaCl-KCl):Sn, mixed crysts., thermolum., 300-500K 2—36954
NaCl-KCl-$CaCl_2$-UCl_3-UCl_4 solid systems, phase diagrams 2—39998
NaCl-KCl solid solns., Cl^-—$L_{II,III}$ absorpt., band struct. 2—7072
NaCl-water-ice, interfacial free energy detn. 2—18971
NaCl, local defects, e.s.r. study 2—16649
NaF absorption spectra, between 25 and 72 eV 2—26170
$ThCl_4$-NaCl melt, complex ion formation, e.m.f. obs. 2—32256
Sofar *see Sound ranging*
Sogicons *see Semiconducting devices*
Soil
Apollo 11 fine sample 10084, Rb-Sr ages on density and size fractions 2—13988
Apollo 15 lunar samples, description of finds 2—41176
Apollo 15 sample 15531, geochemistry 2—41183
Apollo 15 samples, geologic setting 2—41177
clay, rheological behaviour under dynamic loading 2—1298
cohesionless, rheological behaviour under dynamic loading 2—3886
earthquake ground motions of a soil deposit on base-rock 2—20237
hydrorheology of clay, effects of water content on mechanical behaviour, creep and relaxation tests 2—37102
identification from spectral reflectance and daylight spectral energy distribution using characteristic vector analysis 2—16773
Iran, archeomagnetic dating of baked earths 2—33563
layer display using impulsive sound wave method 2—30223
lunar, bearing strength and mechanical props. 2—26819
lunar, friction and abrasion props. 2—33726
lunar, Mare Fecundatitis, relative proportions and petrology significance of particles 2—20646
lunar, Mare Fecunditatis, shock metamorphic effects 2—20649
lunar, model age and Rb-Sr age of basalt fragments 2—20653
lunar, noble gas analysis of KREEP fragments 2—7507
lunar, relative permittivity, dielec. loss tangents, elec. resist. 2—33727
lunar, Sea of Fertility, petrology of basaltic and monomineralic fragments 2—20647
lunar, silicate melt inclusions and glasses 2—20645
lunar, thermal props, rel. to terrestrial analogs 2—33725
lunar, TOR-1 vacuum apparatus for obs. 2—33825
lunar mare soil, cracking and formation of clods 2—13990
lysimeter, weighing, mechanical balance—electrical readout 2—22942
mapping of soil types from multispectral scanner data, computerized 2—16776
microwave radiometry, temperature, rel. to subsurface structure 2—20267
moisture content measurement by polarization of reflected sunlight 2—20275
Soil continued
moisture detection, imaging radars and aerial photography 2—30208
permafrost, electric props., and radio wave absorption 2—30231
permeability of beds, determ. by meas. of streaming potentials in a well 2—7233
remote sensing of composition applic. to limitations in agriculture 2—20274
remote sensing of Th, U and K in soils and rocks, low altitude gamma spectrometric surveys 2—37096
resistivity meas. method 2—30229
shock wave propagation 2—26446
surface characteristics determined remotely from microwave radiation 2—16774
B, Li, N_2, Th, U determination using nuclear track technique 2—7200
$FePO_4.2H_2O$, solubility equilibrium constant and saturation curve for synthetic strengite in dilute phosphoric acid solutions 2—40890
Solar activity
11 year cycle and unipolar magnetic regions rel. to geomagnetic disturbances 2—30365
1969, methods and instruments 2—7560
association with geomagnetic storm of 8 March 1970 2—7561
association with geomagnetic storm of 8 March 1970 2—7347
asymmetrical activity in the 1959-1969 period 2—17079
effects on atmospheric u.v. emission by OI at 1304 Å, intensity variations 2—26496
auroral phenomena for 30 substorms during IQSY (1964-5) and IASY (1969), geographical distribution 2—20389
chromospheric flares as sources of directed corpuscular streams 2—30630
classification Oct-Dec 1967, comparison with Jul-Sep 2—4711
coronal condensations after long-enduring microwave events 2—41234
coronal magnetic field map, calculated from photospheric magnetic data 2—17095
coronal magnetic fields above active regions 2—11150
coronal streamers, correlation from OSO-7 white light coronograph studies 2—26930
cosmic ray bursts, energy changes in interplanetary space 2—17057
cosmic ray intensity, 27-day recurrence and long term modulation 2—11089
cosmic ray intensity time variation 2—14715
cosmic ray intensity variations study 2—17043
cosmic rays, sporadic and annual variations 2—14717
cycle, intensity variations in cosmic radiation, simulation 2—37395
cycle, models and numerical studies 2—11124
cycle No. 19, number of spotgroups formed and average liftetime 2—30627
distribution large scale, planetary tidal forces influences 2—5013
dynamo theory of solar cycle and application of mean- field MHD 2—11048
dynamo theory of solar cycle and observational models 2—37404
electron density indicator using ratio of line intensities in He like ions 2—20710
galactic cosmic ray distrib. effect, Oct. and Nov. 1968 2—16957
galactic cosmic ray intensity, effects of active solar regions 2—17081
geomagnetic activity, annual variation according to character figures and sunspot cycle 2—30374
geomagnetic results 2—20425
global distribution asymmetry and time variations of solar differential rotation law 2—37405
homologous events from different active centres, microwave burst analysis 2—7552
ionosphere, effect on yearly variations of the sporadic E-region 2—4729
effects on ionospheric characteristics 2—13767
jet structure evolution during late phase of complex outburst 2—7557
large-scale motions 2—30628
l.f. bursts, coronal density above active regions 2—26908
lower thermosphere, seasonal effects on distributions of minor neutral constituents 2—33451
magnetic cycle and large scale field theories 2—11047
magnetograph obs. of the 5-min. oscillations, interference effects 2—17073
maximum, 1968-70, Wolf numbers 2—7559
mesosphere, seasonal effects on distributions of minor neutral constituents 2—33451
phenomena occurring in magnetos., ionos. and atmos., geomag. field variations 2—20419
phenomena rel. to broad band micropulsation activity 2—16923
quiet-Sun centre-limb observations at 6 and 11 cm. during cycle maximum 2—37399
radio burst activity index and burst incidence computed for 1968-69 period 2—41235
radiofrequency, 1969 activity at 600 and 151.5 MHz 2—26892
regions, effect on interplanetary mag. field 2—2000
relationship with N_2 conc. in upper atmos. 2—22982
relationship with phenomena in lower atmosphere of Earth 2—23130
rel. to sector structure of photospheric magnetic field 2—11045
short radio waves reflection from ionosphere, measurement during solar eclipse 2—13761
solar cycle, effect on temperature of exospheres in planetary atmospheres 2—7520
SOLRAD 10(C) satellite experiment 2—23131
space environment monitor, satellite burst, solar activity and geometric disturbances 2—16938
sunspot cycle, 1958/70, effect on ionospheric absorption and stratospheric temperature 2—4720
Sunspot cycle 20, prediction (1972) 2—37403
sunspot cycle 21, probable behaviour 2—26911
theories, refinement from artificial satellite study of corona 2—17092
v.h.f. radio signals, 30 to 100 MHz, propagation in atmosphere 2—16849
videomagnetograms, during subflare, prior to major flare 2—5010
X-ray emitting regions, temporal behaviour, results from OSO-IV 2—37385
Zurich sunspot number rel. to radio emission at 10.7 cm at Ottawa 2—26895
Solar batteries *see Electricity, direct conversion*
Solar cells *see Electricity, direct conversion/solar cells*
Solar constant *see Sunlight*
Solar corona *see Sun/corona*
Solar corpuscular streams *see Sun/radiation corpuscular*
Solar eclipses *see Sun/eclipses*
Solar flares *see Sun/flares*

Solar furnaces *see Heating; High-temperature phenomena and effects*

Solar noise *see Sun/radiation, radiofrequency*

Solar prominences *see Sun/prominences*

Solar system
see also Planets, etc.
conference (San Juan, December 1971) 2—26582
cosmic rays, obs. of mag. field structures 2—4949
Crater 9 meteorite, possible masses, entry trajectory and orbital calculations 2—23118
early, conditions inferred from meteorites 2—41168
evolution, nucleo synthesis theories 2—20461
evolution obs. using automatic vehicles on Moon 2—41169
evolutionary processes 2—20638
exploration, contribution of U.S. space program 2—41170
formation, critical velocity of gas-plasma interaction, hetegonic relevance 2—41171
formation, gasdynamics 2—41166
galactic protons, radial gradient, Mariner 4 measurement 2—16954
geosciences, evolution and movement of matter, principles 2—30130
history from extinct ^{129}I, ^{244}Pu and superheavy elements in meteorites 2—1996
Jacobian integral as classificational and evolutionary paratmeter of interplanetary bodies 2—30533
mass distrib., compatible with ring shaped rotating clouds of particles in plant of single nebula 2—10990
meteoritic complex, reviews 2—41214
origin, astronomical evidence in other stars 2—41165
origin, chemical effects in plasma condensation 2—41167
origin, obs. from fossil magnetic fields 2—41019
origin, plasma to planets, conference (Saltsjobaden, Sweden, Sept 1971) 2—41164
origin in terms of plasma physics 2—7359
planetary system, characteristic X and gamma radiation 2—41192
trans Saturnian belt of particulate matter 2—41205
^{26}Al nucleosynthesis, heat source in the early solar system 2—20470

Solar wind *see Sun/radiation, corpuscular*

Solid solutions
see also Alloys; and under compounds of the individual elements. Solid solutions such as Au-Cu, Au-Cu-Zn are indexed under compounds of the named elements, i.e. 'Gold compounds', 'Copper alloys', 'Zinc compounds' in these examples
AB substitutional solns., CuZnβ type, 'surrounded atom' model 2—15929
acetonitrile-water, at 77K, effect of matrix on phosphoresc. props. of 2-amino-pyridine 2—7100
aromatic compounds, vitreous solutions, role of molec. association in temp. induced increase of delayed fluorescence 2—36947
as-cast structure, time-temp.-dissolution diagram 2—36297
binary, radiation-induced strengthening, model 2—36224
binary, static displacement of atoms, determ. using anomalous scattering 2—3691
binary system, utility of first order Wagner interaction coeffs. in evaluation of thermodynamic data 2—29415
clustering and ordering, stability criterion 2—19257
defective, AB_x, clastic model 2—36007
defective, nonequivalent nodes, cluster model 2—9763
di-substitutional, concentrated, form. conditions 2—19261
diffusional homogenisation during deform., energy stability, free energy 2—29413
equilibrium estab. processes in non-equil. solns. with short-range order 2—9764
ferroelectric, dielec. permeability, thermodynamic theory 2—19767
ferroelectric, thermodynamic study 2—19766
fluorescence, averaging procedure in reson. energy transfer theory 2—10433
interstitial, precipitation of cubic centred lattice 2—15963
interstitial, statistical mech. calc. of thermodynamic props., entropy, enthalpy 2—6605
interstitial, thermodynamic props. of C in Ni, Co and Fe 2—32717
ionic crystals, with tellurates and tellurites impurity induced i.r. absorptions 2—16481
isotropic rigid solution, fluorescence depolarization by excitation transfer 2—20099
liquid crystal phase, H_2O-disodium chromoglycate 2—6211
luminescence, theory of the influence of concentration 2—4469
metallic, binary f.c.c., free energy relations 2—25322
methane isotopes, high resolution i.r. spectra, orientation effects 2—16505
molecular bodies, symmetry relationships 2—9377
multicomponent, quaternary mixtures, activity coeffs. 2—22032
neutron irradiation, computer simulation 2—3753
ordered, lattice parameter near antiphase boundary 2—9433
organic, lattice disorder effects on electronic spectra linewidths and multiplicities 2—36890
precipitation, volume fraction rel. to particle coarsening, modified Liftshitz-Slyozov-Wagner theory 2—6606
quasi-chemical theory 2—89
self diffusion rel. to periodic law of electronic layers and solid solubility 2—12792
semiconductor, supersaturated, precip. kinetics 2—6607
spinodal decomposition of supersaturated system, thermodynamics 2—3949
supersaturated, decomp., form of coherent precipitates 2—39911
supersaturated, intergranular precipitation, orientation, grain boundary structure 2—9788
ternary carbides, nonstoichiometric, thermodynamic model allowing for comp. depend. of parameters 2—25603
thermodynamic props. review 2—29414
two phase system, dispersed particles, model, equilib. values, numerical solns. 2—29412
two phase systems, finely dispersed state, thermodynamic stability 2—25583
AgBr-NaBr, thermodynamic properties from miscibility gap meas. 2—22417
AgCl-NaCl, thermodynamic properties from miscibility gap meas. 2—22417
AgI-Ag_2SO_4, ionic conductivity, obs. 2—39997
Al-Au, isothermal phase transformations, rel. to supercond. props. 2—9790
Al-Zn, Guinier Preston zone formation, X-ray scatt. obs. 2—9448
Al-transition metal, supersaturated, residual resistivity 2—25764

Solid solutions continued
Al_2O_3-Cr_2O_3, containing 0.01-4.98% Cr, e.p.r. spectra, optical fluorescence spectra, obs. 2—4549
Ar-Xe, absorpt. spectra, 8-11 eV, exciton effects 2—20025
$AuCu_3$, antiphase boundary influence on lattice parameters 2—39631
B-C-Si system, formation and phase distrib. 2—9793
p-$Bi_{0.5}Sb_{1.5}Te_{3-x}Se_x$, x=0 to 0.6, influence of internal conductivity on properties 2—29762
$CaCl_2.2CH_3OH$ solid solution, X-ray determ. of crystal structure 2—6425
CdF_2-MF_2, F=Ca,Sr,Pb, crystalline miscibility, X-ray obs. 2—22338
Cd_3Se_3-In_2Se_3, phase diagram 2—4017
CdTe-In_2Te_3, formation rel. to In doping of CdTe by travelling heater method 2—35944
$Cd_{1-x}Zn_xS$, long wavelength phonon freq., conc. depend. Raman spectra 2—20065
$Co_{3-x}Mn_xO_4$, form. in O_2, Ar and air atm. at 1000°C 2—39921
Cu-Al, liquid metal embrittlement, role of plastic deformation 2—3898
Cu-Cd, bare alloy, increase in critical resolved shear stress in temp. independent region 2—9766
Cu-In, bare alloy, increase in critical resolved shear stress in temp. independent region 2—9766
Cu_3As-Cu_3P, constitution diagram 2—1409
Cu_3Au, single cryst., fine struct. of slip lines, elec microscope obs. 2—15717
Fe-Ti oxides, rhombohedral, magnetic domain study 2—4341
Fe_3O_4-FeV_2O_4, spinels, magnetic properties, preparation 2—10212
Ga-M, M=Au, Ag, Cu, thermodynamic props, calorimetry obs. 2—32730
Gd_2O_2S-La_2O_2S, subsolidus phase relations, phosphor host material 2—13010
Ge-Li system, free energy of mixing 2—1370
KCl-KBr, polygen wall motion, load compression curve 2—9659
KCl-NaCl, KCl-RbCl, $Cl^-_{II,III}$ absorpt. spectra obs. 2—20041
$La_xSr_{1-x}RuO_3$, effects of Sr substitution by La on elec. and mag. behaviour 2—22708
LiBr-NaBr, absorpt., 6-9.5 eV. comp. depend. 2—16493
LiF, LiF:Mg, solid soln. hardening, crit. resolved shear stress 2—32705
$Mn_{5-x}Fe_xGe_3$, (x=0.5, 1.0 and 1.5), effects of Fe substitution in $Mn_5Ge_3D8_8$ struct. 2—19867
NaCl-NaBr, luminesc. of localized excitons at 4.0 eV and 5.15 eV 2—16610
Nb-Te system, rel. to phase study 2—9841
Nb_3Al-Ta_3Al system, annealing 2—9775
Ni-Fe, positron annihilation and Mossbauer effect 2—4445
Ni-M alloys, hardening effect of solute atoms (M=Al, Cr, Si, Sb, Ti) 2—25505
Ni bronze, supersaturated soln. transformation, kinetics 2—9819
NiO-MgO, thermodynamic properties 2—4061
NiO-ZnO, limits of solubility, NiO in ZnO, X-ray studies, magnetic investigation 2—3962
Pb, impurity solid-solubility correl., atom size, heat of solution 2—3964
PbSe-SnSe, constitution diagram 2—1351
$Pb_{0.95}Sr_{0.05}(Ti_{0.48}Zr_{0.52})_3$, 0.8 wt.% Cr_2O_3, paraelectric to ferroelectric phase transition effect on dielectric and piezoelectric props. 2—1576
Pd-Fe, positron annihilation and Mossbauer effect 2—4445
Pd-H(B), Pd-M-H(B) (M=metal), dissociation thermodynamics, d-band effects 2—36247
PdAg:H, chem. pot. and H conc. near critical point 2—19270
Pt-Fe, positron annihilation and Mossbauer effect 2—4445
Pt-Ir, Rh-Ir alloys, shape of field ion image points, halo effect 2—12963
$(Sb\text{-}Bi)_2(Te\text{-}Se)_3$, thermoelectric properties 2—13335
ThO_2-PaO_2-UO_2, formation, exchange of Pa^{4+} in molten LiF-BeF_2-ThF_4 with U^{4+} and Th^{4+} 2—10593
TlBr—TlI lattice constant dependence on composition, powder method 2—1372
TlCl-TlBr lattice constant dependence on composition, powder method 2—1372
V_3Al-$Nb_3Al(Ta_3Al)$ systems, annealing 2—9775
W-ZrB_2, powder mixture, formation, sintering, phases 2—6626
Y_2O_2S-Gd_2O_2S, subsolidus phase relations, phosphor host material 2—13010
Y_2O_2S-La_2O_2S, subsolidus phase relations, phosphor host material 2—13010
Zr-Nb carbide, thermodynamic model allowing for comp. depend. of parameters 2—25603
ZrO_2-Gd_2O_3, phase transformations, d.t.a. and X-ray diffr. obs. 2—9840

Solidification *see Freezing*

Solids
see also Crystals; Films, solid; Metals; Plastics; Powders; Semiconductors; Vitreous state
alkali fluorides electron affinities determ. from photoemission spectra 2—19803
book 2—18891
book 2—18892
condensed matter conference, Geneva, Switzerland, Sep. (1971) 2—12624
conference, nuclear and solid state physics, Bombay (1972) 2—34868
dictionary of solid state physics and electronics, German and English 2—28968
e.m. and critical phenomena 2—19482
heavy ion strippers, average equilibrium charge states 2—34359
ion beam interactions, conference contrib. 2—25703
specific surface area meas. by adsorption method 2—27021
ultrasonic pulse propagation and reflection, schlieren apparatus 2—37765

structure
see also Crystal structure; Crystals; Electron diffraction examination of materials; Electron microscope examination of materials; Films, solid; Granular structure; Hartree-Fock method; Lattice energy; Metals; Neutron diffraction examination of materials; Plastics; Powders; X-ray examination of materials
close-packed to b.c.c. transition, statistical mechanics of phase diagrams 2—22353
conference, Ames, USA, Aug. (1971) 2—3591
ethylene-chlorotrifluoroethylene copolymers, i.r., n.m.r. and X-ray diffraction examination 2—39446
fibrous polymers, paracrystalline structure, X-ray study 2—28979
glass, structural relaxation, multiparameter model 2—12626
layer of material, structural change due to deformation centre form by radiation damage 2—3752
metals, logarithmic central potential between atom pairs 2—15680
perfluoromethylcyclohexane, molecular reorientation 2—1380

Solids continued
  structure continued
    polyethyleneterephthalate, crystallinity determ. from combination of heat capacity and enthalpy measurements 2—6293
    polymethylmethacrylate, drawn, meas. of molecular orientation by broad line n.m.r. 2—10576
    polystyrene-polybutadiene- polystyrene macroscopic 'single crystal', from i.r. spectra 2—15417
    polytetrafluoroethylene, gamma radiation effects on fine structure 2—39448
    polyurethanes, segmented, anisotropic superstructure meas. by photographic light scattering 2—15648
    refractory transition metal cpds. with high coord., Madelung const. calcs. 2—9328
    steel, two-layered corrosion resistant, technol. processing effects 2—1365
    As–S, glassy, chemical structure transformations 2—4340
    BeF_2, noncrystalline, X-ray diffraction patterns and structure determ. at 25°C 2—22054
    C vitreous, electron microscope study of structure 2—6290
    $K_2CO_3.CaCO_3.SiO_2$ glasses, analysis by i.r. and X-rays 2—1154
    SiO_2, noncrystalline, X-ray diffraction patterns and structure determ. at 25°C 2—22054
  theory
    book, introduction to solid state physics 2—5110
    brittle solids, erosion, multiple drop impact, statistical model 2—29306
    conference, Ames, USA, Aug. (1971) 2—3591
    cracking in solids containing inclusions 2—32636
    crystal, dislocated, shear wave propag. 2—20919
    crystals, anharmonic, free energy, sp. ht. at high temps. 2—40069
    cubic lattice, cooperative phenomena, extended Watson integral 2—19484
    defect electronics in semiconductors, book 2—5111
    electrical cond., impurity scatt. in presence of e.m. field, impurity conc. effects 2—16081
    hexamethylenetetramine association phenomena rel. to alkali halides 2—9219
    ice, cavity model for localized electrons and microscopic relaxation time 2—29078
    materials with simple microstructure, equations of motion 2—36087
    mechanical props. of solids and fluids, book 2—39752
    nonlinear Klein-Gordon eqn., theory and appl. 2—2064
    space-charge-limited currents in presence of traps 2—22517
    two phase system, dispersed particles, model, equilib. values, numerical solns. 2—29412
    two phase systems, finely dispersed state, thermodynamic stability 2—25583
    two-dimensional crystal, melting, molecular dynamics study 2—28942
    Van der Waals forces calc. for dissipative media 2—12623
    X-ray scatt., inelastic, by electrons in solids 2—16591
    Ne, modified Morse pot., pot. energy curves, phonon dispersion curves 2—40047
Solions *see Transducers*
Sols
    see also Colloids; Sedimentation
    polystyrene in water, effect of dispersing agents on angular dependence of light scattering 2—6267
    polystyrene sphere-water, light scattering, effect of dispersing agents on angular dependence 2—28921
    H_2SiO_3, possible identity with anomalous water 2—9074
Solubility
    see also Phase equilibrium
    acetonitrile-CS_2 binary liquid system, coexistence curve 2—32243
    alloy, ordering intrusion, volume effects 2—6610
    austenite, of graphite and cementite, calc. 2—25597
    binary ordering alloy, of interstitial impurities, vol. effect 2—22334
    binary ordering alloy, of interstitials, press. depend. 2—22333
    cupronickel melts, of graphite, 1300, 1400 and 1500 rotating disc method 2—6216
    diphenyloctatetracene mixed crystals, solid solubility in durene, diphenyl and bibenzyl 2—10362
    gases, temp. coeff. for regular solns., semiempirical method for determ. 2—28797
    gases in liquids, calc. of Gibbs free energy of cavity formation, use in study of solvophobic interaction 2—9102
    gases in water, temp. dependence 2—25052
    Henry's law constant for simple mixtures, temp. depend. 2—3368
    hydrocarbons in deuterated nitromethane, critical solution points 2—39343
    hydrocarbons in liquid methane and liquid Ar 2—1080
    ice, of helium, activation energies 2—9620
    metal, f.c.c., of H/D, isotope effect, calc. 2—19260
    metal, solid phase dissolution in liq. phase 2—32242
    nitromethane+alkene, binary system, liquid-liquid equilibria, miscibility gaps 2—1083
    organic cylinders rotating in water, mass transfer coeff. determ. from rates of dissolution 2—6218
    Pierotti's theory for solubility of gases in liquids 2—35735
    polyethylene, solid and molten, of small molecules 2—22237
    polyvinyl alcohol fibres, effects of stretching 2—15649
    silica, fused, of gases 2—35849
    solute in flowing solvent, cumulants of the distribution of concentration 2—12517
    steel, austenitic, of NbN, effect of Mn, Si, Cr or Ni 2—12968
    steel, austenitic stainless, of nitrogen 2—9212
    steel, liquid, of nitrogen, calc. 2—9771
    transition metals, IVA to VIIA, of elements in groups IIIA to IB 2—22335
    Ag, of Gd, phase diagram 2—22375
    Ag, of H and D, calc. 2—3961
    Ag molten halides, of Ag 2—9103
    AgBr-NaBr solid solutions, miscibility gap meas. rel. to determination of thermodynamic properties 2—22417
    AgCl-NaCl solid solutions, miscibility gap meas. rel. to determination of thermodynamic properties 2—22417
    Al-Mg alloy, containing 0.5 wt% Ag, of α-phase 2—12955
    Al, of H and D, calc. 2—3961
    $Al_xGa_{1-x}As$, of Zn, anomalies using different diffusion sources 2—9592
    Ar in liquid Na, as function of temperature and pressure 2—6213
    Au- In solid solution, lattice parameters, solubility limit, thermal expansion, density 2—19265
    CO_2 in liquid methane and liquid Ar 2—1080
Solubility continued
    CS_2- methanol system, coexistence curve near critical point 2—35754
    CdSb, of Ge, thermal analysis study 2—29490
    CdSe, of Cu_2Se, 600-850°C 2—36248
    Co, of H and D, calc. 2—3961
    Co alloys, molten, of nitrogen 2—9767
    Co liquid, of N and C, scaled particle theory 2—21965
    Cu-Al(Cr) alloy, second phase formation and solution kinetics, specific resist. obs. 2—29428
    Cu-Cr system, solubility limits determ. 2—39923
    Cu, of H and D, calc. 2—3961
    Fe-C alloy, second phase formation and solution kinetics, specific resist. obs. 2—29428
    Fe-Ni-Cr, steel, of B, solubility curve, solubility boundary 2—22340
    Fe-Ni-Cr, steel, of B 2—22339
    Fe, of H and D, calc. 2—3961
    Fe, study of activity and solubility of C 2—25585
    Fe alloys, molten, of nitrogen 2—9767
    Fe austenite, of NbC, impurity addition effects 2—12962
    Fe liquid, of N and C, scaled particle theory 2—21965
    GaAs, of Zn, rel. to Zn vapour press. and As press. 2—15789
    GeO_2 vitreous and partially devitrified, diffusion and solubility coeffs. of He, Ne, Ar 2—39730
    H and D in metals 2—29229
    He in liquid Na, as function of temperature and pressure 2—6213
    LaF_3, of Nd^{3+} and Er^{3+}, conc. quenching obs. 2—10424
    NH_4F aqueous solution, of quartz, temp. and conc. depend. 2—35739
    Nb-C solid soln., of C, 1500-2150°C 2—32718
    Nb-Mo-N system, of N_2, press., temp. and comp. depend. 2—4020
    Ni, of H and D, calc. 2—3961
    Ni alloys, molten, of nitrogen 2—9767
    Ni liquid, of N and C, scaled particle theory 2—21965
    Pb, of impurities, solid-solubility correl., atom size, heat of solution 2—3964
    $PbO-PbF_2-B_2O_3$, of YIG 2—29101
    Pd, of H and D, calc. 2—3961
    Pd_3Fe alloy, hydrogen absorpt., ordering depend. 2—9773
    Re, of N_2, 2000-2700°C, 200-600 torr 2—32734
    SiO_2, vitreous, of He 2—36083
    SiO_2 film, dissolution rates in acidic fluoride solns. 2—10628
    Sn alloys, impurity solubility limits, residual resist. obs. 2—39940
    Ti-Al-Sn alloy, of H_2, rel. to stress corrosion cracking 2—19147
    U-C, Ce,Nd,La, sol. limits rel. to phase diagrams 2—9838
    V-O solid solution, e.m.f. study 2—25602
    YAG:Nd^{3+}, mechanism of solubilization of Nd by Gd or Lu 2—29092
    ZnSe, of Cu_2Se, 700-1000°C 2—36248
Solution energy *see Heat of solution*
Solutions
    see also Heat of solution; Liquids; Solid solutions
    1-1 electrolyte solns., calcs. on restricted primitive model 2—10630
    tert- butyl alcohol in cyclohexane, u.r. relaxation and kinetics of association 2—6229
    acetic anhydride-cyclohexane binary liquid system, crit. behaviour in phase boundary 2—35736
    acyl-pyrroles, electric dipole moments in solution, solvent-solute interactions 2—39380
    additive, expt. on turbulent diffusion 2—32249
    alcohol-water mixtures, permittivity, temp. coeff., continuous analysis applic. 2—9153
    alkali halides, aqueous, ultrasonic absorption, kinetic model of structural relaxation processes 2—39361
    alkali metal, struct. transition of Sn impurities 2—18799
    aniline-nitrobenzene mixtures, sound propag., relax. processes 2—32260
    aqueous, dielectric relaxation studied by new methods of complex permittivity up to 13 GHz 2—9150
    aqueous, drops, explosive evaporation in field of optical radiation, dynamics 2—28957
    aqueous, structure 2—35730
    binary, dilute, interfacial hydrodynamics of pools heated from below obs. using linear stability anal. 2—15545
    binary, normal freezing eqns. 2—1139
    binary, surrounded atom model 2—28816
    binary liq. critical mixtures, conc. fluctuations decay rate, vertex correction contribution 2—12534
    binary liquid alloys, calculation from surrounded atom model 2—28816
    binary liquid mixtures, viscosity prediction from thermodynamic properties 2—6221
    binary mixtures, compressibility, theory and u.s. meas. 2—28803
    binary mixtures, hydrodynamic correl. functions 2—3367
    binary mixtures near critical soln. pt., anomalies, sound propag. anomalies 2—28845
    2,5-di(biphenyl)-1,4-oxazole), spectral intensity changes on excitation by N laser, quantum generation 2—3390
    carbon tetrafluoride binary mixtures, phase equilibria and critical phenomena at low temp. and high pressure 2—9108
    chloroform-carbon tetrachloride mixtures, tracer and mutual diffusivities 2—25065
    clathrate-like shells in nonelectrolyte-water mixtures 2—1095
    complex formation, solvation effects, enthalpy-entropy compensation 2—6214
    concentrated electrolytes, generalized Debye Huckel theory 2—28781
    concentration consts., least squares estimation pilot study 2—12549
    condensation phenomenon near limit of inifinite dilution based on Poisson-Boltzmann eqn. 2—9101
    critical binary mixture, mass diffusion and correl. length 2—25064
    cyclohexane-aniline binary liquid system near critical mixing temp., viscosity 2—1085
    cyclohexane-aniline binary mixtures, study of critical behaviour by light diffusion 2—35764
    diamagnetic and paramagnetic susceptibilities determ. from proton shifts in n.m.r. 2—6247
    diphenylamine in CCl_4 solution, dipole-dipole interactions and solvent effects 2—15373
    dissolution of crystals in its own melt 2—35822
    dissolution of solids into turbulent liquid stream 2—28757
    electrolyte, aqueous, sound vel. 2—28853
    electrolyte, primitive model calc. of thermodynamic properties compared with Debye model 2—28835
    electrolyte solutions, theory of Onsager transport coeffs. l_{ij} and R_{ij} 2—6219

- **Solutions** continued
  - electrolytes, hypersonic vel. meas. by Brillouin scattering spectra 2—28862
  - e.s.r. spectra obs. under hydrostatic pressure, spectrometer modification 2—27370
  - fluid mixtures, calc. of phase behaviour under high pressure 2—9106
  - fluid mixtures, phase behaviour and critical phenomena under pressure 2—9105
  - group III-V, II-VI binary systems, liq. soln. models 2—3358
  - hard sphere mixtures, conformal solution theory 2—904
  - hexane-ethanol azeotropic mixtures, det. of critical temps. from ultrasonic data 2—39415
  - hydrated electron, semicontinuum model 2—1079
  - hydrocarbon-water mixtures, phase behaviour and critical phenomena 2—9109
  - hydrocarbons in deuterated nitromethane, critical solution points 2—39343
  - hydrogen-bonded complexes, proton transfer, environment effects, dielectric obs. 2—8555
  - interaction of particles immersed in solvent 2—1082
  - intramolecular dielectric relaxation, numerical analysis 2—35774
  - ionic, infinite dilution, electrical and electromag. conductivity application of classical statistics 2—15604
  - ionic, primitive model, accuracy of theories 2—28799
  - Kirkwood-Buff theory 2—6215
  - light scattering structural investigations 2—32264
  - macromolecular, intramol. pot. barrier determ., from u.s. absorpt. 2—28800
  - macromolecular, quasielastic light scatt., internal modes of motion 2—15591
  - macromolecular, virial coeff. changes and phase separations at high pressure 2—9076
  - macromolecules, computerized meas. of viscoelasticity 2—25015
  - methane-carbon tetrafluoride, thermodynamic properties in neighbourhood of upper critical solution temp. 2—9111
  - methane-carbon tetrafluoride system, thermodynamic properties in neighbourhood of upper critical solution temp. 2—9111
  - methyl cellulose, ageing effect on flow birefringence 2—35740
  - methyl nitrate, solvent and temperature effects on ^{14}N nuclear spin relaxation 2—6259
  - molecules, Stepanov's relation between absorption and luminescence, realizability condition 2—8517
  - multicomponent, quaternary mixtures, activity coeffs. 2—22032
  - nonelectrolyte-water, u.s. velocity 2—1095
  - polar solutes in various solvents, n.m.r. proton shifts 2—28895
  - polydisperse systems of low molecular weight, refractive index increments and light scattering 2—39402
  - polyelectrolyte solutions, conc. dependence of reduced viscosity 2—25058
  - polyelectrolytes, u.s. absorption 2—25079
  - polyheavy water identification as complex ionic salts soln. 2—35737
  - polyisobutylene, dil. soln., excluded volume effects on viscosity, mol. dimensions and 2nd virial coeffs. 2—25033
  - polyisobutylene in ethyl heptanoate, meas. of sedimentation coeffs., second virial coeffs., intrinsic viscosities near θ-point 2—39395
  - polyisobutylene in petroleum, stress effects, deform., relax. phenomena 2—28806
  - polymer, anomalous freezing 2—1142
  - polymer, drag reducing, turbulent pipe flow, laser dopplermeter velocity obs. 2—25007
  - polymer, moderately conc., viscosity, solvent effect 2—18803
  - polymer, partial specific volume determination from relation between refractive index and density increments 2—39342
  - polymer, weak aqueous, flow, continuum mech. approach 2—35697
  - polymers, immiscible, theory of the interface 2—28802
  - polymers, scaling of heat transfer 2—3384
  - of polymers methods for calc. refractive index increment from properties of polymer and solvent 2—39401
  - polystyrene in cyclohexane, meas. of sedimentation coeffs., second virial coeffs., intrinsic viscosities near θ-point 2—39395
  - polystyrene-cyclohexane system near upper critical segregation temperature, thermodynamic functions determ. from light scattering meas. 2—35772
  - polyvinyl alcohol, ageing effect on flow birefringence 2—35740
  - polywater identification as complex ionic salt soln. from distillation and ESCA obs. 2—35738
  - Raman scattering spectra, local field effect 2—35767
  - reflection coefficient for dilute non-electrolyte solutions 2—28830
  - rhodamine 6J, spectral intensity changes on excitation by N laser, quantum generation 2—3390
  - rodlike marcomolecules, time-dependent shearing flow of dilute solutions 2—28798
  - saturated, freezing inside or outside spheres, analytical solutions 2—9211
  - solute properties, behaviour near critical point in almost pure solvent 2—9104
  - squalane-gas, viscosity-pressure dependence 2—9115
  - squalene-gas, viscosity-pressure dependence 2—9115
  - statistical distributions and structure 2—1081
  - thermodynamics of nonuniform solutions, baric interface theory, higher derivatives 2—32254
  - tobacco mosaic virus solution, mol. order, relax. time and self-diffusion from n.m.r. obs. 2—35796
  - two component system in 2D, hydrophobic interaction simulation 2—3366
  - uranyl sulphate, luminescence in presence of nearly 100 electrolytes and organic substances 2—15597
  - u.s. absorption measurement by differential zero method 2—20927
  - viscosity meas. in presence of solid components with modified Ubbelohde viscometer 2—21966
  - viscous, dynamic nuclear polarization, Overhauser effect 2—25107
  - viscous, effect of particle charge on radiationless energy transfer 2—28871
  - viscous, paramag. impurities, Overhauser effect, nuclear polarization 2—25108
  - water, hydrogen bonded solvent, effect of solute on hydrogen bond formation 2—32240
  - water-inert gas mixtures, gas-liquid equilibria and critical curves 2—9107
  - Ar-methane, liq. mixt., excess Gibbs energy 2—35753
  - Ar+Kr liquid mixtures, density and excess properties 2—15579
  - Cu complexes, solvent effects on hyperfine coupling consts. and g-factor 2—25112
  - $FeCl_2$ frozen soln., Mossbauer meas. from −180°C to melting point 2—10316
- **Solutions** continued
  - HCl, aqueous, radial distribution functions, X-ray diffraction study 2—21958
  - HCl in formamide, relative partial molal heat capacity and enthalpy of HCl from e.m.f. meas. 2—28834
  - Kr+Xe liquid mixtures, density and excess properties 2—15579
  - LiCl aqueous soln., Rayleigh and Brillouin scatt. suggesting low temp. immiscibility 2—15589
  - ^{13}N, saline, production for research studies in pulmonary physiology 2—14031
  - VO complexes, solvent effects on hyperfine coupling consts. and g-factor 2—25112
- **Sonar** *see Sound ranging*
- **Sonic boom** *see Aerodynamics; Shock waves/effects*
- **Sonoluminescence** *see Luminescence/liquids and solutions*
- **Soret effect** *see Diffusion in liquids, thermal*
- **Sorption**
  - *see also Adsorption; Chemisorption; Desorption*
  - convective mass transfer coeffs. meas.. Thoma method 2—4583
  - dynamics, linear isotherm range, external diffusion kinetics 2—22078
  - group IV-VI single crystal films, chemical sensing 2—19674
  - hydroxyapatite, powder, compacted membrane, of Ar, N_2, CO_2, 77-303K 2—39554
  - maximum rate obtainable in vacuum metallurgical treatments 2—41415
  - mordenite, of N_2, O_2, and Ar 2—22082
  - polyalkylmethacrylates, sorption-rate curves for water 2—15794
  - polyethylene terephthalate film, effect of I on small angle X-ray diffraction 2—35860
  - porous solids, bidisperse model of transient diffusion for ion exchange resins and pelletized particles 2—1192
  - protein powders, rel. to complex permittivity meas. 2—29057
  - silica gel, sorption-desorption hysteresis, cavity theory 2—35921
  - stainless steel, of CO and S, effect of Au coating 2—39558
  - steel, medium carbon, aluminized, effect of barrier layer on resorption of Al layer 2—3876
  - structure effectiveness in vacuum systems with quasi point gas sources 2—32392
  - vacuum trap using $Fe_2O_3.Fe_3O_4$ for N-5S pump 2—20783
  - water vapour on activated C, hysteresis, mathematical model 2—25229
  - X-ray camera for obs., vapour thermostatted 2—3619
  - zeolite, simple theoretical absorption isotherms for sorption of gases 2—6368
  - Zircaloy tubing, hydrogen pick-up, environmental effects 2—11907
  - Al_2O_3, of water, dielec. loss factor 2—16263
  - C, activated, of Ag^+ ions from soln. 2—39556
  - C, of trimethylamine, triethylamine, and pyridine, leaking curves 2—18958
  - CO_2, solid, characteristics, electron bombardment effects 2—3556
  - $CaCO_3$, calcite, of water vapour and N_2, effect of ball-milling 2—35911
  - K-graphite intercalation compounds, of molecular H_2 at 90 K and below 2—6370
  - Ni, Raney, for study of oxid. and reduction mechanism 2—13575
  - PbSe epitaxial film, of H and O_2 2—39561
- **Sound** *see Acoustics*
- **Sound field** *see Acoustic radiators; Acoustics; Intensity measurement/acoustics*
- **Sound ranging**
  - calibration of underwater sonar, ping-pong balls as standard small targets 2—27279
  - echo sounding system using impulsive source 2—30865
  - marine frequency sounding, equivalency principle for multilayer media 2—30235
  - monopulse processor, bearing estimation performance for passive linear arrays 2—7756
  - oceanography, contouring bottom features using side scanning sonar 2—37112
  - passive sonar processing of noise with unknown covariance structure 2—11360
  - scattering by fixed rigid prolate spheroids, short wave asymptotic behaviour 2—27260
  - sonar, medical diagnosis of blighted ovum 2—17114
  - sonar, scanning, performance and resolution of Canadian and Japanese instruments 2—171
  - sonar applications in medic diagnosis conference (Glasgow, December 1971) 2—17113
  - underwater transducers, calibration at high u.s. frequencies 2—34124
- **Sound recording** *see Recording*
- **Sound reproduction**
  - *see also Acoustic radiators; Recording; Transducers*
  - cellulose paper for loudspeakers, sonic processing, electroacoustic characteristics 2—34125
  - with cine film, super-8 film plus optical sound 2—8049
  - electrodynamic loudspeakers, spectral characteristics of nonlinear sound components 2—34126
  - electrodynamic loudspeakers, with short circuited windings, input impedance 2—34093
  - impulse noise, temporary threshold shift studies 2—11361
  - impulse noise meas. and temporary threshold shifts, tape recording limitations 2—37484
  - loudspeaker diaphragm papers, viscoelastic properties 2—30869
  - loudspeakers, on-load life test facility 2—34092
  - pillow type loudspeakers, sensitivity measurement device 2—34142
- **Space charge**
  - acetone, permittivity variation obs. 2—9151
  - afterglow, space-charge-controlled diffusion 2—32126
  - bounded electron beam, space-charge wave propagation 2—27422
  - coherent-beams break-up in storage rings 2—14901
  - concentric spheres and cylinders, space-charge-limited thermionic emission 2—14383
  - density distribution during corona discharge calculation method based on conformal mapping 2—15517
  - density in atmosphere 2—40969
  - dynamics, calculation by expansion method 2—18035
  - effect in low energy electron guns 2—21036
  - effect in proton linacs, obs. using electron model 2—5612
  - electron, compensation by ion counter-flow, bipolar current produced between spherical electrodes 2—24849
  - electron beam blow-up and loss 2—18036

Space charge continued
electron-positron colliding beams, non-linear space charge effects 2—18037
electrostatics, plane 2—14354
in intersecting storage ring, incoherent space charge phenomena and beam lifetime 2—14792
klystron type bunchers, radiation intensity calc. 2—34326
liquid dielectrics, d.c. conduction regimes 2—32275
m.a.o.s. diode, rel. to two carrier charge transport and storage model 2—36571
negative-mobility amplifiers in emitter current limited injection mode 2—6809
plasma, bounded anisotropic, dispersion relations of space charge waves 2—8965
plasma, potential det. from max. amplitude of l.f. noise 2—24771
problems in probe obs. 2—12411
proton beam, enhancement of ν-spread by insertion of an electron beam 2—18032
proton lines; longitudinal effects 2—18040
semi-insulators, trap-controlled space-charge-limited current rel. to Poole-Frenkel barrier 2—40230
temporal growth injected into long air gaps under long front impulse voltages 2—24901
p-SiC, alloyed with Pt-B-Sn, space charge limited currents, current-voltage characts. 2—22565

gas
atmosphere, potential gradient measurements using field mills 2—4692
diode, gas filled, planar, potential distrib. 2—39203
diode, space-charge-limited current 2—7869
electron distribution function, validity of two term approximation 2—18749
glow corona, rod-plane gaps in air, breakdown times obs. and calculations 2—18709
Townsend Huxley diffusion, inelastic collisions 2—18750
Cs thermionic diode electric space potential 2—14362

solid
amorphous film, dielec. polarization current, space charge contrib. 2—4271
anthracene film, space charge limited currents with uniform and non-uniform trap distrib. and size effects 2—40266
borosilicate glass film in m.i.m. structure, effect on electric strength depend. on insulator thickness 2—29734
current-voltage characteristics for uniform trap distrib. 2—13255
dielectric, charged, rel. to short circuit currents and motion of zero field planes 2—22610
dielectric with shorted electrodes, decay of excess charge 2—4270
diphenylpolyene, film, trap distrib., space charge limited current obs. 2—40267
film, space charge limited conduction, image force effects 2—19630
film insulators, d.c. conduction mechanism, book 2—29732
glass, doped with transition metal ions, space charge limited hopping cond. 2—40239
insulators with Gaussian distrib. of traps 2—19752
limited currents in insulators, in presence of traps with Coulombic potential 2—29656
metal-insulator system, space-charge- limited current 2—13209
m.i.m. system, space-charge-limited currents 2—13288
m.o.s. structure, electron traps, trapped space charge model 2—36574
m.o.s. structure, polarization effects 2—22600
organic molecular solid, space charge limited current, effect of carrier dimerization 2—29689
Plexiglas, negative charge under electron beam bombardment 2—29760
poly(N-vinyl carbazole)/Se, perturbed currents and transient photoinjection of holes 2—33072
poly(N-vinyl carbazole)/Se, rel. to transient accumulation of interfacial charge 2—33073
poly 4-methyl pentene-1, high field cond. 2—22615
poly N-vinyl carbazole films, thermal activation energy of elec. conductivity and trap structure 2—36524
polyethylene, rel. to elec. breakdown in non-uniform fields 2—22616
polyethylene terephthalate films, anomalous induced transient cond. 2—32995
polymethylmethacryalate, rel. to elec. breakdown in non-uniform fields 2—22616
Poole-Frenkel effect, under space charge limited current conditions 2—19629
semiconductor, double injection, a new approach 2—22522
semiconductor, equil. distrib. 2—4197
semiconductor, film, conductivity and Hall mobility, van der Pauw method 2—9991
semiconductor, high-resist, space-charge-limited current, current-voltage characts. 2—22514
semiconductor, intrinsic, trap-free, double injection, space charge limited current 2—40329
semiconductor, negative mobility, emitter current limited injection 2—33021
semiconductor, relax., recombinative space-charge injection 2—29654
semiconductor junction, p-n, diffusion profile from C-V curves 2—10084
semiconductor-oxide structure, inhomogeneous distribution of free charge carriers due to insulating layer 2—25801
semiconductors, charge state effects in displacement damage 2—19660
space charge limited current, in samples containing fully ionized donors 2—19631
space charge limited current, large drift velocity 2—6709
space-charge-limited currents in presence of traps 2—22517
Zincblende alloy, charge distribution, pseudopotential approach 2—6716
Ag halides, space charge layer contrib. to dielec. const. 2—40330
Ag halides, space charge layer contrib. to dielec. const. 2—33050
Al_2O_3 film in m.i.m. structure, effect on electric strength depend. on insulator thickness 2—29734
As_2S_3 films, amorphous, recombinative space charge injection 2—10006
Au-Se system, space-charge-limited current 2—13209
β-B, rhombohedral, s.c.l.c. obs. of trapping levels 2—19665
$Bi_{12}GeO_{20}$, light- and elec.-field-depend. oscillation of space-charge-limited current 2—25955
CdS, change in properties during passage of double-injection currents 2—40245
Cu-CdS system, space-charge-limited current 2—13209
n-GaAs, evaporated film, SCL current meas. in electronic transport props. determ. 2—40244

Space charge continued
solid continued
n-GaAs, space-charge scatt. and electron transport 2—13267
GaAs bulk devices, lateral spreading analysis using computer simulation 2—19698
Ge, p-i-n struct. formed by electron irrad. 2—25889
Ge film, amorphous, elec. props., space charge limited cond. interpretation 2—40291
GeO_2, vitreous, photocond. study 2—22644
KBr, rel. to elec. breakdown in non-uniform fields 2—22616
$Pb(Zr.Ti)O_3$, ceramic, mech. quality factor rel. to space charge 2—13325
SbI_3 crystal, photoelectret state relaxation, space charge relocalization effect 2—6906
SbSI, ferroelec., space charge limited current, influence on switching behaviour 2—29755
Se/poly(N-vinyl carbazole) layered struct., space-charge-perturbed xerographic discharge 2—40378
Se, single cryst. film, Cd, Te electrodes, space charge limited current 2—10031
Se film, amorphous, I-V characts. 2—13259
Si:Au, impedance and g-r noise under space-charge conditions 2—22567
Si:Pt diode, charge state and thermal generation in space charge region 2—10091
Si, defect annealing obs. by space-charge-limited current 2—33020
p-Si, space-charge-limited currents 2—19691
Si, space charge currents, illumin. effects 2—22569
Si metal-p^+-p-p^+- metal dielec. devices, space-charge-limited current flow 2—13292
SiO_2 electron irradiated, short term charge annealing 2—19732
SiO_2 v.u.v. radiation charging in m.o.s. structure 2—19741
ZnTe-GaSb, p-p heterojunc., elec. and optical props. 2—10087

Space groups
benzoxazole crystals 2—16502
2,2′-bis(6-methyl-3-pyridinol) 2—29157
cosine seminvariant formulas 2—3599
not derivable by parallelohedra and subdivision into stereohedra, work by Federov 2—9378
derivation by means of parallelhedra and steriohedral subsets, impossibility 2—25281
derivative lattices, determ., transform. matrices 2—32408
dibenzyl disulphide, space group ambiguity 2—22171
generalised Herring's criterion 2—35958
grid points, rotational, optimal spacing 2—3601
magnetic, irreducible representations, rel. to phase transitions 2—6936
magnetic, n.m.r. techniques for investigating possible generation by crystallographic space groups 2—29792
orthorhombic space groups, mag. struct. classification 2—33101
p-coloured groups, 3-dimens., derivation using 4-dimens. space symmetry groups 2—3594
Patterson vectors of lattice complexes 2—9381
primitive, struct. semi invariant, symmetry applic. 2—22118
selection rules, methods and application to Fd3m 2—3597
spin space groups, Bravais lattices 2—36655
spin space groups, point groups 2—36654
tetragonal lattice, dispersion laws 2—9374
tetragonal symmetry, homogeneous sphere packing 2—9379
BN, hexagonal cryst., representations for symmetric points 2—3696
$Ca_3Fe_2(GeO_4)_3$, mag. groups 2—33169
$CaGeN_2$; $Ca_{1-x}eN_2$, cryst. struct., cell parameters 2—15714
Cu (II) complex, bis biguanidium copper (II) nitrate dihydrate 2—22154
Cu (II) complex, bis(N-n-hexyl-o-hydroxyacetophenominato) copper (II) 2—25331
$DyAsO_4$, mag. struct. 2—13417
$LiCu_2P_2$ and $Li_{1.75}Cu_{1.25}P_2$, cryst. struct. 2—19054
$MgCr_2O_4$, structural distortion due to siting of Cr^{3+} ion 2—6438
Mg_3N_2, cryst. struct., cell parameters 2—15725
$PbO_{1.57}$, cryst. struct., X-ray obs. 2—15728
$Pb_3O_2Cl_2$, synthetic, cryst. struct. 2—15727
Pt complex, bis(triphenylphosphine) platinum dioxide chloroform adduct 2—29149
SiH_4, cryst., factor groups of low-temp. phase 2—33272
Ti_2ZrO alloy, $\omega'(0)$ phase 2—39653

Space research
see also Atmosphere
ablating bodies, surface patterns of 2—1918
acronyms and abbreviations in use at Kennedy Space Center 2—11237
advanced X-ray observations, instrumentation 2—41262
American and Soviet studies of Moon Mars and Venus, review 2—17028
antennas, circularly symmetric retrodirective 2—16944
balloon techniques 2—41021
cabin atmosphere, effects of hyperoxia on lung ultrastructure 2—11197
cosmic rays protection, spacemen helmet shielding 2—16935
electronics and aerospace systems conference, Washington, D.C. (1971) 2—13809
energetically optimal trajectories for Earth-planet-Earth flights 2—30394
environment monitor of solar activity and geometric disturbances 2—16938
environment monitoring data, solar terrestrial relationships 2—16939
experiment planning 2—41022
ground station, Telespace 2—16936
information content of simulated space photographs, function of image resolution 2—16937
ISIS-II for ionosphere and magnetosphere studies 2—20411
laser beams tracking and pointing as prerequisite to communications, application to large space telescope 2—37231
laser location of reflector on board Lunokhod-1 2—41020
laser radar, scanning system 2—23044
lunar surface electrical props., Apollo 17 experiment 2—33733
Moon, summary of scientific results from Soviet robots 2—7518
Moon, unmanned Rover exploration, objectives and requirements 2—1980
Newtonian lift and drag of blunt-cone cylinder bodies representing rockets or reentry vehicles 2—35658
nuclear and space radiation effects, conference, Durham USA 1971 2—19697
nuclear radiation interference and damage effects in charged particle expts. for deep space missions 2—20430
optical system design for space applications, rel. to meas. of refractive indices of fused SiO_2 at low temps. 2—26109
optical system design for space applications, rel. to meas. of refractive indices of fused SiO_2 at low temps. 2—26109

Space research continued
optical tracking of satellites, Moonwatch program, laser and radar obs. 2—7352
optimal control of motion of material point in thin spherical layer of central gravitational field 2—26574
periodic swing-by orbits connecting Earth and Mars 2—20446
progress of exploration and research 2—4758
projects scheduled for the 1970's are summarized 2—7353
radar scattering cross sections of space vehicles in electron plasma medium 2—33568
radiation effects on scientific instruments 2—10782
role of photography 2—1917
simulation of polar satellites flight through ionosphere by wake behind obstacle in plasma flow from Q-machine 2—21823
Solar flares, protection of astronauts from Solar cosmic rays 2—4759
space simulation, use of Ti evaporation pump 2—41376
telemetry by satellite borne laser stations 2—26576
thermophysics, NASA programmes 2—20432
Titan III L, space booster 2—20433
TV systems, design and applic. 2—26580

Space-time configurations
asymptotically flat spaces, coordinate conditions 2—2088
asymptotically Friedmann, radiation and energy 2—7654
complex recurrent space-times 2—33908
correlation function properties for high energy Regge behaved pole dominance amplitude 2—31255
cosmology, topological properties of universe 2—1928
curved space time, restrictions from geometry on quantization 2—17193
electric charge of collapsed objects and black hole formation 2—20467
electric Weyl spacetimes and stationary soln. 2—37594
e.m. fields in curved space-time, invariant 2—7663
embedded space-times, remark on energy and momentum 2—33909
flatness conditions, asymptotic form of Weyl tensor 2—5135
gravitational geons, angular momentum and mass 2—23261
ideal points representing points at infinity and singular points, construction 2—37595
indefinite metric spaces, geometry 2—33869
Kerr type space-times, sources 2—37592
Lorentz cobordism and topology of spacelike hypersurfaces 2—30776
measurement theory, space-time structure 2—17234
neo-geodesics in a Riemannian space 2—14075
NUT metric, generating potential 2—33907
particle scattering, generalized O(2,1) expansions for asymptotically growing amplitudes 2—31192
proper vibration of space 2—17179
quantal correlation function, Hartree approx. 2—30823
quantum, and general relativity 2—2103
quantum manifold, position operators 2—27052
relativistic quantum mechanics, projective representations and relation of internal to space-time symmetries 2—20846
Schwarzschild, gravitational synchrotron radiation, particle source in highly relativistic circular geodesic 2—33910
Schwarzschild's, propagation of spherical waves 2—60
Schwarzschild exterior space-time, gravitational field outside a sphere of matter 2—2092
space-time code, algebriac quantization 2—20834
spherically symmetric spacetimes, invariant formulation of Einstein's eqns. 2—23264
spinorality applied to space-time in relativity 2—2066
static, event horizons, proof of vacuum Israel theorem 2—2082
stationary and static space-times, new physical characterization 2—23251
tensor bundles, b-boundary construction 2—2083
tetrads, anholonomic co-ordinates and space-time geometry 2—2079
topological formulation 2—30772
trapped surfaces in strongly curved space-times 2—2080
uniqueness theorem, global, geometric for solns. of Einstein equations 2—61

Space vehicles
see also Rockets; Satellites, artificial
aerodynamic torque effects and design criteria 2—10780
Airborne Astrographic Camera System at Air Force Eastern Test Range 2—37230
Apollo 14 for lunar surface obs. applying dual frequency bistatic-radar 2—33731
Apollo 15, analysis of anorthosite from Moon 2—7511
Apollo command module, Monte Carlo simulation of land landing 2—20431
comet rendezvous missions, trajectory requirements 2 26864
dual spin, flexibly coupled, nutation damping and vibration isolation 2—26570
Earth planet Earth flights, energetically optimal trajectories 2—30394
experiment to determine G from an orbiting space laboratory 2—37582
flight trajectory parameters evaluation, unknown matrix of second moments of navigation meas. errors 2—26571
guidance system figure-of-merit, saving in mid-course correction velocity 2—20437
heat shield material, graphite ablation characteristics 2—4060
Jovian atmosphere, component survivability during entry 2—17036
landing impact protection through hybrid attenuation system 2—26579
Liapunov stability of spinning satellites with long flexible appendages 2—20439
location, using atomic clocks 2—7358
Mariner, orbiting 2—1994
Mariner 1969 orbit det. using overlapping TV pictures 2—26845
Mariner spacecraft, features and purposes of Mariner 9 project 2—30388
modularized space station, design 2—23050
multiple elliptic orbit re-entry parameters, isotopic heaters 2—30396
navigation, attitude control in near earth orbits, use of noctilucent-layer effect 2—33564
navigation meas. optimization 2—26573
orbit around Mars, determination by optical sighting of Martian moons 2—16943
orbital space stations, McDonnell Douglas proposal, design 2—23051
orbiting space station, N. American Rockwell proposal, design 2—23047
plasma generator for neutralization during electron ejection 2—20438
process control and EDP 2—7356
re-entry, aerodynamics, flow 2—35670
re-entry bodies, heat-sink type, separated flow, dynamic effects 2—26568
Salyut space station, design and objectives 2—23049
shuttle, designs 2—1921

Space vehicles continued
Skylab, specifications and instruments 2—23048
Skylab S-193, altimeter expt., objectives and capabilities 2—20225
space station orbit calculations round an oblate Earth, first order soln. 2—20445
stars, visual detection through windows on illuminated side 2—26567
trajectory det. errors, geometrical interpretation of maximum likelihood method of estimation 2—26572
transfer orbits, Lawden's spiral, non-optimality of intermediate-thrust arcs 2—30390
^{238}Pu fuel characteristics for electric generators and heater units on spacecraft 2—8371
instrumentation
see also Langmuir probes
attitude determ., spin-stabilized lunar satellite, using Kalman filter 2—20453
attitude stabilization system, movable mass. for artificial g space stations 2—26577
camera, facsimile for planetary landers, aliasing image degradation 2—34458
computer, repairable via command and telemetry links by reprogramming around failed unit 2—23046
COS-B satellite for galactic γ meas. 2—30398
electron multiplier detection efficiency for low-energy electrons 2—31013
electronics for backscatter u.v. instrument for atmos. O_3 obs. 2—16819
fuel gauging system in zero-G environment with CdTe γ-ray detector 2—34814
gravimeter, semiautomatic, self-levelling for lunar surface 2—17034
guidance systems, u.v. optimal designs, images of sky 2—10781
high-current quasi-steady MPD accelerators, anode phenomena 2—27397
infrared and solar sensors, analysis of, for satellite attitude determination 2—1926
laser gyro, construction and operation 2—41029
lunar orbital mass spectrometer 2—41174
Mariner Mars 1969 infrared spectrometer 2—31139
Martian orbiter, for obs. of orbits of moons 2—16943
mass spectrometer for planetary surface exploration (Mars 1976) 2—41191
micromotors run on liquid N_2, specific impulse calc. 2—30399
miniature Mattauch-Herzog mass spectrometer for investigation of planetary atmospheres 2—566
multispectral scanners, scan-angle effects 2—34526
photoelectric equipment, housing in rocket expts. 2—10783
rockets for O_2 and methane release expts. 2—16867
satellites for altimetry obs. 2—16727
scanning photometer, rotating interference filter, auroral sounding rockets 2—23052
simulator for opt. equipment testing 2—14471
Skylab space station 2—23048
X-horizon scanner for attitude det. 2—37234

Spallation *see Nuclear spallation*

Spark chambers
coordinate measurement, using shock waves generated by sparks 2—34835
current limited, cosmic ray applic. 2—23932
cylindrical, used with ACO storage ring at Orsay 2—34839
device for automatic filling after evacuation 2—31388
edge profiles, field distortion at gas dielectric interface 2—34836
fission, spatial velocity distrib. meas. in critical assembly channel 2—5602
gamma ray telescope, digitized, satellite borne 2—26811
gamma ray telescope, digitized, satellite dome 2—33721
low pressure, parallel plate, operational characteristics, efficiency 2—24110
low pressure, parallel plate, operational characteristics, efficiency 2—31389
low voltage, detection efficiency 2—24106
magnetostriction, characteristics under conditions of large background levels 2—24109
with magnetostrictive read-out, construction and performance 2—31390
with magnetostrictive readout, increasing magnetostrictive signals 2—2648
magnetostrictive wire readouts, multiwire Ni arrangement and dual pickup on single Remendur wire 2—38394
magnets, superconducting, design and manufacture 2—24105
magnets, superconducting, design features 2—27914
memory time of wire devices 2—24107
modular, pressure <1 atm, Ar and Ne filling 2—2646
multiplate in gamma ray telescope for obs. of Crab Nebula pulsar 0532 2—10989
multiple used as targets in high energy particle and cosmic ray physics expts., design theory 2—27801
multitrack sealed, efficiency meas. as function of delay between passage of cosmic ray particle and application of h.v. pulse 2—27787
piezoelectric detection of torsional waves 2—27915
positron ang. correl. meas. apparatus 2—29569
for positron annihilation angular correlation obs. 2—2647
projection discharge chamber stacks with infinitely transparent electrodes 2—34833
resolution, for γ-ray astronomy 2—8242
spark calorimeter, calibration using pions 2—2586
streamer, compact high speed low impedance Blumlein line for h.v. pulse shaping 2—38395
track localization, effect of magnetic field 2—18029
tracks storage using optical spark chamber pulsing 2—24111
two dimensional, with low delay trigger system, combined digital and analogue readout techniques 2—34834
wide gap, spatial accuracy, particle track drift compensation 2—11686
wide gap, with Al foil electrodes, testing 2—31387
wide-gap, compensation of drift of charged particles 2—18028
wire, for clinical imaging of gamma rays 2—2650
wire, read-out system with core memory 2—34838
wire, shift register readout 2—2649
X-rays, characteristics measurement of narrow-gap instrument 2—24112
gamma ray, use as high energy astronomical detector 2—11181
γ rays spectral analysis in COS-B satellite for astronomical meas. 2—11182
Ne/He streamer chamber, Lichtenberg figure ringing 2—21336

Spark counters *see Counters/spark*

Sparks, electric
see also Breakdown, electric; Lightning
air, thermal reignition of high current spark channel 2—24899
astigmatic optical image transfer, for spectrographic system 2—14473
breakdown, statistical variation, expt. 2—35630
breakdown in SF_6 and arcton 12 2—9008
channel resist., temporal variation 2—32136
charge transfer excitation in atmospheric pressure discharges 2—15520
current growth during breakdown of short vacuum gap 2—1013
discharge electrode ablation studied using spectrophotometric technique 2—9005
exploding wire as underwater sound impulse source 2—27297
exploding wires, temporal behaviour of input power and conductivity 2—24900
gaps, under high pressure, voltage breakdown 2—15519
gas discharge gap, ignition potential stabilisation for large pressures 2—3271
growth in long gaps in air, effect of space charge 2—24901
high current, high pressure, explosive erosion of anode 2—12476
high pressure, mechanism 2—24890
h.v. gap triggering, laser beam suitability 2—3270
laser, solid state, ignition, pulse generator 2—17620
laser-triggered gap, ps. triggering 2—9007
light source for framewise photography of fast processes 2—38174
long spark mechanism, effect of floating particles 2—24902
Lyman discharge, use as light source for v.u.v. spectroscopy 2—38164
medium voltage, use as spectrochemical light source 2—20213
plasma, influence on sample surface in laser microspectral analysis 2—37066
power systems, flashover analysis, spark gaps 2—18713
produced by output of TEA CO_2 laser, two wavelength interferometry 2—35632
r.f. discharge, high speed gas flow, sparking potential 2—35629
short duration, anode ablation, in air 2—24905
spectral analysis of blast formed disperse particles in spark discharge 2—4616
spectroscopy source, spectrochemical analysis of wear- metals in oils 2—14488
supply processes, hydrodynamic characteristics of discharge channel 2—21889
surface, cathode directed, formation 2—24903
vacuum gap breakdown probability, dependence on surface condition of electrodes 2—35627
v.h.v., in u.h. vacuum, formation mechanisms from breakdown delay time meas. 2—39219
Al, source parameters and excitation process 2—28673
Ar v.u.v. emission from high density spark discharge, spectral radiant intensity saturation and self reversal and effects of voltage increases 2—32135
CO_2, small gap width, current steps 2—24908
H_2, spark channel spectroscopic investigation, voltage collapse 2—15518
He v.u.v. emission from high density spark discharge, spectral radiant intensity saturation and self reversal and effects of voltage increases 2—32135
I_2, low pressure, negative ion to electron density ratio and ionization obs. in non-uniform field conditions 2—24909

Specific heat
see also Debye temperature; Gruneisen relation; Thermodynamic properties
calorimeter for heat capacity meas. on small samples in temp. range 1-35 K using Si chip bolometer as sample holder, temp. sensor and heater 2—30726
carbon tetrafluoride-fluoroform system, heat capacity near consolute point 2—9123
critical scaling in linear model for fluids 2—3425
fluids, isochoric heat capacity, gravity influence on behaviour near critical point 2—8874
fluids, singularity at critical point 2—8873
ideal Bose gas, confined in thin film geometry 2—27099
magnetic transition temperature, determ. using differential scanning calorimeter 2—13414
molecules adsorbed on homogeneous surface, heat capacity 2—35902
solar wind plasma flow, ratio of values in upstream and downstream regions of earths bow shock 2—16874
theory, summation of series of the form Σnx^n 2—14068
thermophysical properties of fluids 2—18813
^{3}He, ^{4}He submonolayer films, meas. at 0.04 to 4.2 K 2—32292
$Ni(NO_3)_2.6H_2O$, low temp., antiferromag. interactions 2—1434
gases
Cp/Cv meas. for gases with steady oscillations new apparatus described for method of Ruchardt 2—32176
methane, deuterated, Gruneisen relation between expansion coeff. and heat capacity 2—16064
monatomic ionized, numerical method for 2—18758
multiatomic, degrees of freedom, textbook error 2—27014
CO_2-methane mixtures up to 2250 psi, determ. by heat exchanger method 2—28736
CO_2, isobaric, at subcritical pressures, experimental data 2—1036
liquids
alkali metals, sp. ht. prediction 2—28788
aqueous solutions of organic compounds, rapid determ. by hydrocarbon mixing 2—25070
benzene, adsorbed on C block, heat capacity rel. to surface coverage 2—35907
Calvet microcalorimetry appl. 2—23413
constant volume, of almost pure solvent, behaviour near solution critical point 2—9104
n-decane, elevated press., from p,V,T meas. 2—25072
ethanol, adsorbed on C black, heat capacity rel. to surface coverage 2—35907
n-hexadecane, elevated press., from p,V,T meas. 2—25072
metal, Pb, adiabatic calorimetry, 300-850K 2—4068
n-octane, elevated press., from p,V,T meas. 2—25072
o-terphenyl, heat capacity and thermodynamic properties 2—9891
n-tetradecane, elevated press., from p,V,T meas. 2—25072
water adsorbed on silica, heat capacities rel. to phase transitions 2—25233
CS_2- methanol system, meas. near critical point 2—35754
Co, determ. by levitation calorimetry 2—21979
D_2O, 0.1-21 MN/m² absolute press., 20-640K, tables 2—35755
n-dodecane, elevated press., from p,V,T meas. 2—25072

Specific heat continued
liquids continued
HCl solutions in formamide, relative partial molal heat capacity of HCl from e.m.f. meas. 2—28834
He submonolayer, heat capacity 2—28926
^{3}He-^{4}He mixtures, near tricritical pt., lambda anomaly 2—15622
^{3}He-^{4}He mixtures, specific heat near junction of λ and phase separation curves 2—1129
^{3}He, metastable, obs. of lifetimes following cooling at constant density 2—3421
^{4}He, heat capacity anomaly near λ transition, density depend. 2—25127
^{4}He films, thick, superfluid phase transition phenomena 2—9196
Hg, spline correl. function 2—18812
I, system of equations 2—6226
K, spline correl. function 2—18812
Na, spline correl. function 2—18812
Pb, adiabatic calorimetry, 300-850K 2—4068
Pd, determ. by levitation calorimetry 2—21979
solids
L-alanine and poly-L-alanine, 1.3 to 4.3K 2—29558
alkali metals, const. volume values calc. 2—29503
alloy, dil., linear low temp. sp. ht. due to superparamag. clusters 2—29554
K-alumina, heat capacity obs. 2—16033
amorphous, Raman scatt. obs. 2—20061
anthracene, rel. to Debye temp. calc. methods 2—29511
binary alloy, rel. to order- disorder transformation, lattice vibration effects 2—19309
1,3-bisdiphenylene-2-phenyallyl-benzene complex, heat capacity anomaly rel. to paramag.-antiferromag. transition 2—26058
Calvet microcalorimetry appl. 2—23413
carbon tetrachloride, component vibrations detn. 2—6679
crystals, anharmonic, free energy, sp. ht. at high temps. 2—40069
cubic crystal, characteristic temp. rel. to Lindemann melting criterion 2—35820
dilute magnetic alloy, electronic props. below Kondo temp., model Hamiltonian approach 2—36439
electron gas at metallic densities 2—19423
electronic specific ht and free energy due to electron ion pseudopotential interaction 2—16092
epoxy resins calc. from ultrasonic velocity, 4-100 K, existence of localized modes and extrapolation below 4 K 2—40058
ferroelectric, dynamical model applic. 2—19764
ferroelectric solid solution, effect on transition temp., theory 2—19766
four point Hubbard model, specific heat maxima, rel. to Mott transition 2—33167
$GdCl_3.6H_2O$, heat capacity from 5 to 300K rel. to entropies and crystal field splittings 2—16035
glass, temp. depend., rel. to lattice mechanics 2—22419
glass systems, low temp. anomalies 2—9885
glasses and their crystals, low temp. heat capacity differences 2—9882
glucose, time dependent heat capacity in glass transition region determ. by differential thermal analysis 2—6680
graphite, rel. to thermal expansion calc. 2—32846
grease Apiezon N and T, correlation with thermal conductance and glass transition temp. 2—30728
Heisenberg lattice films 2—40424
Hubbard model, one-dimens. half-filled 2—40537
Hubbard model, one-dimens. half-filled-band 2—22670
Hubbard model, rel. to change in local mag. moment. 2—22701
Hubbard model, rel. to change in local mag. moment. 2—22700
ice, pure and doped, 80 to 230 K 2—19426
inert gas solids, heat capacity studied using anharmonic potential parameters 2—4032
Ising ferromagnet, three dimens., behaviour above Curie temp. 2—40429
itinerant electron system, high temp. 2—10183
lattice vibrations, Debye temps., const. vol. specific ht. 2—29503
lunar soil, rel. to terrestrial analogs 2—33725
magnetic impurity model, solvable, thermodynamics 2—40402
metal, electronic sp. ht. rel. to electronic struct. 2—40121
metal, Pb, adiabatic calorimetry, 300-850K 2—4068
metals, apparatus for temp. dependence of thermal diffusion and true specific heat 2—29553
metals in normal and superconducting states, method of determ. 2—16032
methane, low temp., impurities influence 2—9890
methane-d, heat capacity in temp. region below 10K 2—16040
molar heat content, dependence of electrical resistance, obs. by impulsive method 2—22487
noble metals, matrix element studies 2—32803
nylon, calc. from ultrasonic velocity, 4-100 K, existence of localized modes and extrapolation below 4 K 2—40058
perfect non-Bravais cryst. with internal strains 2—9883
polyethyleneterephthalate, crystallinity determ. from combination of heat capacity and enthalpy measurements 2—6293
polyhexane-I, abnormal behaviour in region of γ and δ relax. peaks 2—25686
polymer, filled, 10 to 400 K 2—19429
polymers, PVC, PS, PMMA, PPO, time dependent heat capacity in glass transition region determ. by differential thermal analysis 2—6680
polymethyl acrylate, from Brillouin spectra obs. of molecular relax. 2—26202
polymethyl methacrylate, press. depend. 2—13048
polystyrene and polymethyl methacrylate, thermal cond. 2—22427
rare earth Co compounds, mag. transitions 2—25998
semiconductor, heavily doped, in weak mag. field, Green's function method 2—9886
steel, Cr-type, apparent sp. ht. variation during ageing 2—39900
superconducting degenerate semiconductors 2—19427
superconducting film, effect of order parameter fluctuations 2—32935
superconductor, dimensionality change in fluctuation specific heat 2—36448
superconductor, very small size, from Landau-Ginzberg eqn. 2—16152
synthetic sapphire alumina, heat capacity obs. 2—16033
TCNQ-NMP, metal-insulator transition and antiferromag. obs. 2—19657
teflon calc. from ultrasonic velocity, 4-100 K, existence of localized modes and extrapolation below 4 K 2—40058
temperature coefficient, direct measurement 2—25683
o-terphenyl, crystal and glass, heat capacity and thermodynamic properties 2—9891
thermophysical high temp. props., high speed meas. 2—19410
tohdite, heat capacity and heat of dehydration obs. 2—16033

Specific heat continued
solids continued
transition metal alloys, dil., low temp. anomalies 2—19827
transition metal alloys, f.c.c., electronic component, interstitial carbon influence 2—16114
transition metal borides, heat capacities in temp. range 1.5 to 15 K 2—22418
ytterbium ethylsulphate, calc. from cryst. field parameters 2—36794
zeolite, synthetic, sp. ht. vs. temp., heat of fusion of absorbed water 2—19424
Ag-Ga(Ge)(Ni)(Zn) alloys, electronic band struct. obs. 2—25732
Ag, and phonon dispersion curves and vibr. spectra from modified angular force model 2—32801
Al-Zn alloy, study of solvus curve of Guinier-Preston zones 2—29422
Al, model potential calcs. 2—32804
α-Al_2O_3, NBS standard reference material 2—29555
Ar, central force rigid at. model, lattice dynamics, heat capacity 2—40040
Ar, low-temp. limit 2—32842
As, semimetal, meas., 0.017-0.3K, determ. of nuclear quad. coupling const. 2—4419
Au-V, dilute, low temp. sp. ht. rel. to simple powers of T in Kondo effect 2—29613
Au-V dil. alloys, electronic contrib., impurity effects 2—16034
Au-Zn alloys, electronic sp. ht. below 3K 2—4064
Au, and phonon dispersion curves and vibr. spectra from modified angular force model 2—32801
$AuCu_3$, electronic coeffs., ordering influence 2—1431
$AuSb_2$, low temperature measurements 2—4065
AuSn, low temperature measurements 2—4065
Au_4Ti, ordered states, mag. entropy 2—40070
Au_4V, ordered and disordered states, mag. entropy 2—40070
$Ba(NO_3)_2$, anharmonicity obs. 2—19354
Bi:Te, hyperfine heat capacity and nucl. quadrupole interaction 2—16657
$Bi_{0.4}Sb_{0.6}$, superconducting thin film, fluctuation heat capacity near T_c 2—9887
$CdGa_2S_4$, heat capacity, 14-300K, Debye temp., thermodynamic props. 2—25684
$CdIn_2S_4$, heat capacity, 14-300K, Debye temp., thermodynamic props. 2—25684
Ce-La alloys, supercond., Fermi surface obs. 2—19578
$CeIn_3$, 1.5-4.2K 2—16036
$Ce_{1-x}La_xAl_3$, low temp. meas., crystal field splitting data 2—1432
$Ce_xLa_{1-x}Pd_3$, rel. to electronic struct. and Kondo effect 2—19832
$CeNi_5$, 1.6-4K 2—16037
$CePt_2$, low temp. heat capacity and mag. susceptibility 2—22424
$Co_3B_7O_{13}I$, anomaly at Ferroelectric phase transition 2—25926
$CoCl_2.6H_2O$, critical phenomena 2—6677
$CoF_2SHF.6H_2O$, anomalies in 240-275 K region 2—22421
CoS_2, at low temps., density of states of $d\gamma$ band 2—22420
$CoSiF_6.6H_2O$, anomalies in 240-275 K region 2—22421
Cr, calorimetric obs. of first order transition at 311K 2—36762
Cr, determination from lattice vibration spectra 2—22405
Cr complex, $[Cr_4(OH)_6(en)_6](SO_4)_3.10H_2O$, magnetic contribution 2—19920
CrAs, mag. transition, neutron and X-ray diffr., latent heat at transformation 2—10242
CrB_2, mag. props. 2—33171
CrB_2, substituted, antiferromag. transition region obs. 2—16395
Cu-Ag-Au alloys, low temperature measurements, agreement with Stern's theory 2—4065
Cu-Ga(Ge)(Ni)(Zn) alloys, electronic band struct. obs. 2—25732
Cu-Ni alloy, low temp., dil. Fe effect 2—40071
Cu, heat capacity inversion by quadratic programming 2—6678
Cu, molar heat content, dependence of electrical resistance, obs. by impulse method 2—22487
Cu complex, $(C_nH_{2n\|1}NH_3)_2CuX_4$ (n=1-10, X=Cl, Br) specific heat meas. deviations from ideal Heisenberg ferromagnet 2—13041
DyAl garnet, rel. to two-sublattice Ising model characteriz. 2—40552
$DyPO_4$, antiferromagnet 2—26063
$ErCrO_3$ single crystal, deduced from optical data of Er^{3+} ground state 2—16487
Er_2O_3, obs. using method of mixtures 2—29556
EuSe, polycryst., temp. range 0.5-16K 2—22423
Fe-Cr alloy, low temp. anomaly, ferromagnetic transition effects 2—13398
FeF_2, Ising behaviour 2—40072
$Fe_{65}(Ni_{1-x}Mn_x)_{35}$, low temp., rel. to mag. props. 2—33133
Fe_3O_4, low temp. phase transition and multiple ordering 2—36278
Fe_3Pt, low temp., study of electronic contrib. 2—26039
Gd, ferromag. ordering, carrier contrib. 2—40372
Gd, spin wave contrib. 2—13042
β-$Gd_2(MoO_4)_3$, antiferromag., ferroelectric, heat capacity 0.4-4.2K 2—10239
$GdNi_5$, 1.6-4K 2—16037
^4He monolayers, Debye temperatures and 'melting' anomalies 2—32302
Hf high temps. including β phase and thermal effects of $\alpha \rightarrow \beta$ transformation 2—29552
$HoCl_3.6H_2O$, heat capacity from 5 to 300K rel. to entropies and crystal field splittings 2—16035
I, system of equations 2—6226
InPb superconducting alloys, deduction of electronic sp. ht. from magnetostriction and magnetization curves 2—19823
InSb(II), ht. capacity, 80-100K, comparison with isoelectronic Sn 2—13043
KCl, heat capacity inversion by quadratic programming 2—6678
KH_2PO_4, dynamical model applic. 2—19764
$K_2PbCu(NO_2)_6$, heat capacity anomalies, 273 and 280 K 2—15967
Kr, low-temp. limit 2—32842
$LaAl_2$, Laves phase compound, at low temp., and supercond. transition 2—19425
$LaIn_3$, 1.5-4.2K 2—16036
$LaIn_3$, supercond., mag. interactions 2—16179
$LaNi_2$, 1.6-4K, electronic and vib. contribs. 2—16038
$LaNi_5$, 1.6-4K 2—16037
$LaPt_2$, low temp. heat capacity 2—22424
La_2S_3, molar thermal capacity, dielec. permittivity, i.r. spectra 2—40670
$La_2S_3(Se_3)(Te_3)$, electronic component 2—1433
Li^7F, heat capacity per unit. vol. 2—13033
$LiYF_4:Er^{3+}$, temp. depend., determ. from cryst. field parameters 2—40421
$LuAl_2$, Laves phase compound, at low temp. 2—19425

Specific heat continued
solids continued
$LuCl_3.6H_2O$, heat capacity from 5 to 300K rel. to entropies and crystal field splittings 2—16035
$Lu_{0.9035}Er_{0.0965}$, heat capacity from 6 to 300K rel. to cryst. field energy levels 2—26088
$MgO:Fe^{2+}$, spin phonon interaction contrib. 2—6676
Mg_2Pb, semiconductor, temp. range 5-300 K 2—4066
MnBi, preparation by solid diffusion, total excess sp. ht. for mag. transition at 640K 2—6962
MnF_2, magnon sp. ht. 2—40073
$MnSO_4(.H_2O)$, mag. transitions, sp. ht. meas. 2—22710
$MnSi_{1.73}$, temp. range 50-500K, carrier and lattice components discussed 2—40074
β-N_2, rotational heat capacity from heat capacity of N_2-Ar mixture, barrier to rotation 2—4067
NH_3, from freq. distrib. func., neutron scatt. obs. 2—36321
NaBr:F-, rel. to impurity tunnelling 2—33052
NaF, heat capacity per unit vol. 2—13033
$NaNO_2$ near antiferroelec. transition pt., critical exponents 2—9889
$Na_2O.SiO_2$ glass, low temp., rel to low lying modes 2—40075
Nb-Mo alloy, supercond. T_c anomaly 2—13167
Nb-Ti system, supercond., rel. to electronic structure 2—40195
Nb, determination from lattice vibration spectra 2—22405
Nb, high-speed (subsecond) measurement of heat capacity, 1500-2700 K 2—40076
Nb and Nb-Ta alloys, rel. to supercond. props. 2—19588
NbC_x, thermodynamic props., determ. from sp. ht. 2—13044
$NdCo_2$, heat capacity obs. 8-300 K, rel. to mag. transitions 2—19869
$NdNi_2$, 1.6-4K, mag. contribs. 2—16038
$NdNi_5$, 1.6-4K 2—16037
Nd_2S_3, molar thermal capacity, dielec. permittivity, i.r. spectra 2—40670
Nd_2S_3(Se)(Te_3), electronic component 2—1433
Ni-Co alloys, f.c.c., electronic component, interstitial carbon influence 2—16114
Ni-Rh alloy, low temp. heat capacity anomaly, superparamag. behaviour 2—13045
Ni-transition metal dil. alloys, electronic component 2—16039
Ni, magnetic internal energy, temp. depend. 2—40457
Ni_3Al, rel. to mag. props. 2—40442
$NiCl_2.2H_2O$, low temp. anomalous mag. sp. ht. 2—22712
Ni_3Ga alloys, nearly-ferromag., low temp. meas. rel. to clustering and spin fluctuations 2—19856
Pb-In alloys, jump obs. at supercond. T_c 2—19593
Pb, adiabatic calorimetry, 300-850K 2 4068
Pb and Pb-30% Bi disordered superconducting films, rel. to determination of electronic props., comparison with tunnelling data 2—9979
Pb particles, size and surface effects 2—32949
$Pb(NO_3)_2$, anharmonicity obs. 2—19354
PbSe-$Ge_{1.5}As_{0.5}Se_3$, rel. to double glass transition 2—18902
Pd-Cr alloys, electron transport props and sp. ht., below Kondo temp. 2—29615
Pd-Mn dilute alloys, meas. of specific heat, critical behaviour and magnetic field dependence 2—13046
Pd, determination from lattice vibration spectra 2—22405
$PrCo_2$, heat capacity obs., 8-300 K, rel. to mag. transitions 2—19869
$PrIn_3$, 1.5-4.2K 2—16036
$PrNi_5$, 1.6-4K 2—16037
Pr_2S_3, molar thermal capacity, dielec. permittivity, i.r. spectra 2—40670
Pt-Cr alloys, electron transport props. and sp. ht., below Kondo temp. 2—29615
Pt, high temp., thermal vacancies influence 2—13047
RbBr(Cl)(I), low temp. 2—25685
$Rb_2CoCl_4.2H_2O$, mag. transition phenomena 2—6996
Sc_3In, ferromag. transition, mag. entropy, heat capacity obs. 2—40493
Sc_3In, mag. transition obs. 2—40492
$ScVO_4:Er^{3+}$, temp. depend., determ. from cryst. field parameters 2—40421
Se-Te alloy, amorphous, heat capacity relax. effects 2—39772
Se, time dependent heat capacity in glass transition region determ. by differential thermal analysis 2—6680
Se, vitreous, 1.0-0.1 K 2—22425
SiC, equation for enthalpy and specific heat in temp. range 273.15-2900K 2—40077
Sm_2S_3, molar thermal capacity, dielec. permittivity, i.r. spectra 2—40670
β-Sn, Mossbauer recoilless fraction temp. variation 2—36326
SnTe, lattice and electronic contribs. 2—19427
$SrMoO_4:Er^{3+}$, temp. depend., determ. from cryst. field parameters 2—40421
$Sr(NO_3)_2$, anharmonicity obs. 2—19354
$SrTiO_3$, lattice and electronic contribs. 2—19427
Ta, calculated on the basis of lattice dynamical model of Sharma and Joshi 2—4039
Ta, determination from lattice vibration spectra 2—22405
TaC_x, 0.3000°K, thermodynamic props. determ. 2—1436
$TbCl_3.6H_2O$, heat capacity from 5 to 300K rel. to entropies and crystal field splittings 2—16035
Th-U dilute alloy, low temp., rel. to mag. props. 2—29557
Ti, heat capacity in temp. range 1000 to 1700 K 2—29551
$Ti_2O_3:V$, low temp. anomaly, electronic origin 2—40078
$Ti_2O_3:V_2O_3$, low temp., contribution by one dimensional electron gas 2—4069
$Tm_2(SO_4)_3.8H_2O$ rel. to mag. ordering 2—16399
$TmVO_4$, Lande g-factor value determ. by sp. ht. meas. 2—22665
UN, 298-1700K 2—40796
UN, heat capacity, 386.8-701.3K 2—19428
V, 1200-1800 K 2—19469
VAu_4, rel. to order-disorder transformation 2—19886
$V_{1-x}Cr_xB_2$, antiferromagnetic, spin fluctuation effects 2_19927
VF_3, mag. ordering obs. 2—36780
V_3Si, low temp., mag. contrib. in mixed supercond. state 2—16190
W, heat capacity, 2000-3600K, high-speed meas. 2—25682
W, temp. modulation method 2—4070
WSi_2, W_5Si_3, enthalpy, heat capacity, 1200-2200K 2—29559
Xe, low-temp. limit 2—32842
$YAG:Er^{3+}$, calc. from cryst. field parameters 2—36794
YAl_2, Laves phase compound, at low temp. 2—19425
$YPO_4:Er^{3+}$, temp. depend., determ. from cryst. field parameters 2—40421
$Y_{1-x}Th_xAl_3$, low temp. meas., influence of Brillouin zones on electronic density of states 2—1432
$YVO_4:Er^{3+}$, temp. depend., determ. from cryst. field parameters 2—40421

Specific heat continued
solids continued
YbFe garnet, mag. phase transition obs. 2—33160
Yb_2O_2S, and mag. props. rel. to Yb^{3+} crystalline field 2—19928
Zn, lattice contrib. from phonon dispersion relations 2—19391
Zr, heat capacity 2—32816
$ZrZn_2$, low temp. heat capacity anomaly 2—40079

Spectra
see also Absorption/light; Astronomical spectra; Atmospheric spectra; Chemical shift; Colour; Isotope shift; Mass spectra; Scattering/light, Raman spectra; Spectrochemical analysis; Spectroscopy; Stark effect; X-ray spectra; Zeeman effect
absorption, E→F optical transition in centre of cubic symmetry, method of moments 2—13467
absorption, of isolated spectral line, used in determining instrument function of i.r. spectrometer 2—27655
absorption i.r., determ. by multiple, attenuated total refl. method 2—34543
adsorbed layers, reflection spectra, theory 2—9300
adsorbed layers at interfaces, conf., London England, Dec (1970) 2—9298
adsorbed layers at interfaces, internal reflection spectroscopy 2—9302
adsorbed layers at interfaces, methods for obs. 2—9299
alkali metal plasma, electron density meas. from Stark profiles 2—15472
analysis, iterative least squares procedure using digital computer 2—7731
analysis based on analog technique, bandpass filtering 2—325
bleaches, luminescent, spectral and colour characteristics 2—16444
charged particles and gamma-rays, in FORTRAN IV 2—14736
composite, evaluation rel. to wavelength dependent lightpaths 2—34544
compressed liqs., i.r. absorption, cell for study up to 1600 bar 2—2468
condensed medium, optical transition energy calc. 2—36407
contact discharges, spectroscopic study 2—3261
crossed transitions, localised and delocalised states in crystals 2—29904
crystal vibration modes, i.r. absorpt. 2—29505
crystals, inverse hydrogen-like series 2—29905
crystals, orientationally disordered, i.r. spectra discussion, effect of short range correlation of orientations 2—10354
defect activated transitions, selection rules for point group compatibility tables 2—19989
direct electronic transition, near Van Hove singularities 2—4451
disordered solid, i.r. vibr. spectrum, theory 2—22388
disperse flow, radiation spectra 2—39101
electronic transitions, in molecular and mixed crystals, phonon sidebands 2—26134
emission spectra of crystals for which the effective mass approx. is valid, annihilation of excitons and exciton phonon interaction 2—4133
fluctuation of radiation passing through resonant medium 2—21139
Fourier transform spectrometer generated, elimination and reduction of background 2—8026
gas, modification of resonant r.f. absorption under influence of nonresonant h.f. field 2—38866
gas, study of reversal temp. as function of optical thickness 2—15541
hadrons, basis set of spinless mass quanta and fermion spinor defined, used to describe meson and baryon resonances 2—31210
hyperfine multiplets, allowed and forbidden transitions, influence of nuclear Zeeman term 2—14343
impurity crystal, absorpt. and light scatt., antiresonance theory 2—16447
impurity spectral lines in solids, new mathematical technique for deriving Stokes' shift 2—36860
impurity spectral lines in solids, relation between new method for deriving Stokes' shift and adiabatic approx. approach 2—36861
inductive resonance energy transfer, theory 2—1677
injection laser under spiking conditions instantaneous and averaged emission spectra 2—37991
inner shell photoabsorpt., correl. of atomic, mol. and crystn. spectra 2—15207
i.r. absorption spectra, recorded in holographic memory device, substance identification 2—11493
i.r. emission of hot jets, determ. of turbulence strength and characteristic parameters 2—39263
line shape absorption, influence of coupled coherent and incoherent motion of excitons 2—19520
liquids, VH-depolarized light scattering spectra, at high $k^2\eta/\rho\Gamma$ 2—21988
Lorentz absorption lines, new analysis procedures 2—8030
metallic colloids, absorption spectra, influence of plasma waves 2—36864
metallo-organic layered media, exciton mechanism of high temp. supercond. 2—1683
microwave and far i.r., pressure broadening and line shift, impact theory 2—17730
molecular fluid, depolarized light scatt. 2—18832
Newton's spectrum, absence of indigo in spectral projections 2—27608
olefins, plasma, prod. by laser heating, refl. rad. spectra 2—39156
optical, effects of sample imperfections 2—22743
optical, modified Kramers-Kronig analysis 2—1678
photocount statistics, truncation effects 2—23560
photon exit from spectral line in isothermal atmosphere 2—11451
planetary atmospheres 2—1990
plasma, high temperature 2—994
polariton 2-photon absorption in noncentrosymmetric crystals 2—36865
quantum kinetic equation for system with discrete energy levels 2—29928
Renner-type systems, optical band shape for A→E transition 2—33228
resonance radiation self-imprisonment 2—1707
ruby laser, effect of selective loss on generation spectra at 80K 2—27504
semiconductor, heavily doped, i.r. reflectivity, free carriers 2—26140
semiconductors in a magnetic field, absorption coeff. for two photon transitions 2—4450
solid, double-exciton excitation effects in absorpt. spectra 2—20014
solid, exciton interference with continuum absorpt., origin, lineshape calcs. 2—20013
solid, inner shell photoabsorpt., giant, subgiant and fine structure interpret. 2—16480
solid, photoelectron, multiplet splittings 2—35226
solid, spectra, calc. high resolution method, life-time effects 2—22744
solid, vacuum u.v., expts. using storage ring light source 2—16479
solid X-ray photoelectron spectral shifts, thermochemical estimates 2—35223
spatially dispersive medium, mode coupling and exciton polarization 2—29892
spatially dispersive medium, reflection and refraction, exact soln. by Maxwell's theory 2—29891
spectroscopy, conference, Clayton, Australia (1971) 2—8509
speech, information compression, maximum likelihood estimation 2—5076

Spectra continued
sputtered particles, during ion bombardment 2—10357
superradiance on exciton levels 2—26137
superradiant damping, multimode Maxwell-Bloch eqns. 2—11947
superradiant damping and absorpt. 2—8434
surface plasmon effects, expt. obs., review 2—16119
surface waves, seawater, low frequency waves and seiches 2—4654
transparent materials, mag. spin reson. influence on laser radiation spectrum 2—10332
vacuum u.v., conf., Tokyo, Japan, Aug.-Sep. (1971) 2—14470
Al, plasma, prod. by laser heating, refl. rad. spectra 2—39156
Ar laser in strong magnetic field, study of emission intensities 2—14411
Ar plasma, r.f. induction, departure from equilibrium, spectroscopic obs. 2—39107
D_2O, plasma, prod. by laser heating, refl. rad. spectra 2—39156
H plasma absorption coeffs. at laser frequencies 2—12390
He, superfluid, excitation spectrum, criticism of single particle Green function approach 2—12602
LiD, plasma, prod. by laser heating, refl. rad. spectra 2—39156
N_2 plasma jet, radial temp. distrib., emission spectra obs. 2—28510
Nd laser with narrow spectral lines, method of generation and increasing emission 2—27512

atomic
see also Atoms/excitation; Atoms/structure; Auger effect; Russell-Saunders coupling
absorption, flame furnace studies, optimization of conditions 2—30115
absorption, hyperfine struct. 2—8437
absorption, noise and detection limits 2—8042
absorption, non-dispersive optical systems 2—8041
absorption and emission line-shape functions, effect of a driving or pump field 2—24353
absorption coeff. in l.f. spectral line, influence of strong e.m. radiation 2—10845
absorption data processing, computer program 2—21497
absorption series, suppression of levels of high principal quantum number when using intense flash background sources 2—24322
absorption spectrophotometry, internal standards evaluation 2—10667
absorption spectroscopy, significanfe of thermally assisted processes 2—2462
absorption spectroscopy techniques, non-flame carbon rod atomizers 2—8045
absorption spectrum of nonmonochromatic radiation, broadening mechanism effect 2—31650
actinides, interpretation problems 2—21501
actinides, rel. to metallurgical properties 2—21502
actinides and lanthanides energies of electronic configurations of singly, doubly, and triply ionized 2—2942
alkali, metals, probability of stimulated microwave emission from Zeeman levels 2—31665
alkali metal, line broadening due to collisions with H 2—15209
alkali metal, nonrelativistic wave functions and eigenvalues 2—18317
alkali metal, optical transitions, wave function and oscillator strength calc. 2—18313
alkali metal halide ions, core electron binding energies from X-ray photoelectron spectra 2—31685
alkali metals, multi-photon and parametric coupling processes 2—2920
alkali-He collisions, elastic approx. for fine structure transition cross sections 2—5842
alkaline earth metals, singly ionized, Stark shifts of isolated spectral lines 2—15206
alloy, sputtered vapour, atomic fluorescence analysis 2—10666
arc discharge, upper electrode effect on excitation spectra 2—39227
atomic spectroscopy applications 2—38798
atoms in plasma, forbidden line profiles, ion dynamic correction 2—24318
Auger and Coster-Kronig transition probabilities to 2s state for $33\leqslant Z\leqslant 85$ atoms 2—2930
Auger lines in X-ray photoelectron spectroscopy 2—35164
Auger transition rate in mixed coupling scheme 2—24361
beam foil spectroscopy, technique and appls. 2—574
beam-foil excitation mechanism using $^4He^+$, $^6Li^+$ and ^7Li ions 2—8481
binary collision broadening, impact theory predictions for shift and width of isolated electronic spectral lines 2—18339
broadening of spectral lines by perturber gas, unified theory including impact and statistical theories 2—38804
broadening shift of atomic lines produced by fast electron collisions 2—28167
collision spectra optical broadening and depolarization of lines 2—31698
collisions in gases, study of Doppler shift of light emitted by excited atoms at 10-100keV energies 2—2964
Cotton-Mouton effect, time-dependent double perturbation investigation 2—15201
dielectric recombination satellite line intensities, meas. and interpretation 2—28171
double-ionization effects on radiative rates, Auger rates and fluorescence yields calc. by Gryzinski methods 2—31682
dressed atom, semiclassical theory of radiofrequency transitions 2—11938
electron correlations in unified line shapes and Stark broadening by electrons 2—35129
electron impact meas. of polarization free vacuum uv excitation functions 2—5796
elements $18\leqslant Z\leqslant 39$, $K\beta/D\alpha$ X-ray transition probability ratios 2—31657
elements between $Z=58$ and 94, L fluorescent X-ray relative intensities 2—31660
experimental studies, historical developments, review 2—21486
Fermi contact hyperfine constants for rare earth atoms and ions, moment perturbed calc. 2—579
fourth-order Lamb shift, crossed-graph contribution 2—21203
gases, atmospheric, monochromatic absorpt. coeff., high speed laser spectroscopy 2—33620
halogen, transient species obs., photoelectron and chemielectron spectroscopy 2—35163
Hanle effect, quantum approach, at system reson. interaction with laser, reson. interaction r.f. field 2—15204
He-Ar gas mixture, translational absorption spectra computed 2—5791
hyperfine structure correction for configuration interaction 2—8425
impact and Doppler broadening of lines 2—31638
impact broadened multiplets, collapse, theoretical study 2—11940
inert gas, electron impact excitation cross sections determ. from spectral line intensities, simultaneous calibration of apparatus 2—5797

Spectra continued
atoms continued
inert gas, transition probabilities and near configuration interactions 2—8433
interaction of atoms with polarized light 2—35128
isoelectronic series, F(I)...Cu(XXI) wavelengths and oscillator strengths of $2p^5$-$2p^43s$ transition 2_587
kaonic atoms, light, strong interaction shifts and widths of X-ray transitions 2—21556
Kerr effect, time dependent double perturbation-variation formulation 2—15200
kinematics of inelastic collisions, influence on optical spectra and spectra of ejected electrons 2—5828
Lamb shift, as consequence of finite size of electron 2—24325
Lamb shift, external field effects 2—21488
Lamb shift, multipole expansions 2—21495
lanthanides, energy differences between two systems in singly and doubly ionized and neutral 2—590
laser spectra; collection of 800 lines of 38 elements 2—582
lasing spectra, Stark effect constants calc. 2—577
level crossing used to determine nuclear constants 2—2658
line breadth, collisional braodening, cross sections for resonance lines 2—2961
line broadening, determination using correspondence principle 2—11939
line broadening, unified theories 2—5778
line formation in inhomogeneous magnetic fields 2—11056
line profile narrowing, by alignment in case of radiation trapping 2—31649
line shapes, kinetic theory 2—576
line shapes, pressure effects of inert gas mixtures 2—24331
loosely bound composite system, radioactive transition probabilities, relativistic corrections 2—35116
M-shell Auger and Coster-Kronig electron specctra 2—24332
magnetic circular dichroism, new applications to atomic and molecular systems 2—4432
many-body calculations of energies and transition probabilities 2—21499
metals, absorption and emission data and formation in flames 2—5279
metals, spectral study of collisions of second kind 2—2960
modified adiabatic approximation in theory 2—28183
monatomic gases, role of off diagonal resolvent matrix elements in resonance absorption line shape derivation 2—31653
multiphoton ionization processes in gases, role of atomic spectra 2—35583
multiple quantum resonances caused by large r.f. field, calc. of positions and shapes using continued fraction solution 2—31645
multiple quantum transition probabilities 2—24301
muonic ^{209}Bi, hyperfine spectra of L and K X-rays, analysis in terms of nuclear excitation 2—18370
muonium, hyperfine interval, precision meas. using Ramsey resonance in zero field 2—3011
muonium, in Ar and Kr, quadratic h.f.s. pressure shifts 2—3012
N two-level atoms, intensity fluctuations in spontaneous emission 2—24335
nf series, general relations, of Al-I, Ga-I, In-I, Tl-I 2—8438
nonlinear interference effect in a field modulated by random Markoff process 2—24326
nonspherical hadronic atoms, second-order vacuum polarization energies of X-ray transitions 2—18368
normal absorption processes, Taylor expansion of expression for transition probability 2—31634
one-electron atoms, line broadening calc. 2—15242
optical line spectrum, radiative and collisional interactions, astrophysics 2—21500
Pb autoionized emission lines 2—35140
photoabsorption cross section, universal nature 2—18292
photoelectron, angular distribs. obs. 2—31769
photoelectron, photoionization cross section depend. on photoelectron energy 2—31683
planetary nebulae, chemical composition, analysis of emission spectra and photometry 2—23065
pollutants, nonflame atomic absorption techniques 2—22892
pressure broadening, unified classical path theories 2—2926
quasistatic wings of broadened lines, rel. to determination of interatomic potentials 2—21485
radio recombination lines, pressure broadening, rel. to emission from HII regions 2—2924
rare earth elements, electronic configurations, energy spectra 2—28182
rare earth metals, multiplet splitting in X-ray photoelectron spectra of trifluorides 2—35282
rare earth metals, potential barrier effects in photoabsorpt. 2—20047
rare earth metals, potential barrier effects in photoabsorpt. 2—22775
rare earth metals, potential barrier effects in photoabsorpt. 2—22776
resonance fluorescence, excited state struct. and lifetimes 2—8436
resonance lines from hollow cathode lamps, selective modulation, gating technique 2—34556
resonance radiation imprisonment, relax. of atom velocity and polarization distrib. 2—5782
resonance transition probabilities, asymptotic expansions in 1/Z in perturbation theory 2—31648
resonant level population in cylindrical config. discharge 2—18288
review of atomic spectroscopy in the last 20 years 2—2929
r.f. dressed atom theory, review of experimental and theoretical investigations 2—24312
r.f. resonance measurement on doublet excited state, saturation effects computed by continued fraction solution 2—31644
single-electron atom in black-body radiation, Lamb shift temp.-dependent correction 2—12020
solar mag. regions, collision effect on line formation 2—11055
solar physics and gaseous nebulae, conference (Cambridge, USA, April 1971) 2—23122
spontaneous emission from driven Doppler line 2—11934
spreading of Compton lines, comparison of intensity distributions computed using three different models 2—15194
stimulated emission and absorption near resonance 2—34372
submicrosecond laser pulse sampling and atomic vapour production, physical chemical processes 2—15230
superradiance, phenomenological theory 2—24327
superradiance master equation, approx. soln. 2—581
third-row atoms and ions, resonance transition probabilities including correlation effects 2—35156
transfer equation, line formation with general redistribution 2—35118
transition amplitudes, transitions between highly excited states 2—24321

Spectra continued
atoms continued
transition metals, spin exchange splitting in Auger spectra 2—11983
transition probability measurements by incorporation of cascade decay curves 2—591
two-electron atoms, radiative transition rates from 2p3p ^3P and 2p3d $^{1,3}D$ states 2—18361
two-level, line source fn., in inhomogeneous finite atmosphere 2—4851
two-level problems, spin 1/2 formalism 2—21557
two-level system driven near resonance, linewidth corrections 2—31654
two-level systems, superradiant effects 2—24309
wave numbers, computers program for calculation from least squares level values 2—31640
X-ray photoelectron spectral shifts, thermochemical estimates 2—35223
X-ray rates, for 2p shell 2—584
X-ray satellite emission by single electron jump 2—28172
X-rays, cosmic, characteristic line spectra, mode of excitation 2—7370
XUV, Hartree-Fock theoretical wavelengths for AlIV-CaXI, accuracy 2—24336
Ag, 2 to 30 MeV proton bombardment, K and L X-ray yields 2—38808
Ag I, autoionization lines in vac. u.v. spectra determ. by photoionization and emission 2—18309
Al, is cathode torch discharge 2—3265
Al emission line obs., vac. u.v., stimulated emission 2—18305
Al IX, Al XI emission lines from a ruby laser-produced plasma, 35 to 50 Angstroms 2—18283
Al ix, x, xi, obs. 2—8439
Al^{3+} ion spectrum of laser-produced plasma, autoionizing series 2—18298
Am core electron binding energies determ. from photoelectron spectra 2—35165
Ar, emission line profile broadening, correction curve 2—8440
Ar, ion laser transitions, spontaneous emission profiles, line profile anal. 2—24329
Ar, isoelectronic wavelength calc. 2—24338
Ar, light emission from pulsed corona discharge in cylindrical electrode geometry 2—32137
Ar, mean lives of levels of first two ionized states determ. by Hanle-effect meas. on aligned fast ions 2—11945
Ar, time-dependent study of VUV emission following excitation by 250 keV pulsed electron beam 2—28204
Ar hydrogen and helium-like ions, study of forbidden decay modes, determ. lifetimes of states 2—28226
Ar II, transition probabilities rel. to configuration temps. in hollow cathode Ar arc 2—39229
Ar II, transition probabilities and excitation temps. from study of spectral lines 2—21492
Ar II ion spectrum, excitation mechanisms 2—18300
Ar IX, XI and XII, overlap with satellites to Lyman alpha lines of C and B 2—15210
Ar ii, Larmor precession of excited states 2—11944
Ar impulse discharges, emission spectra studied by photography in 1000-2000Å region 2—28667
Ar line, brightness meas., plasma parameters at plasmatron output 2—8993
Ar long induction discharge, spectral and calorimetric meas. of radial temp. distribution and energy deposited respec. 2—28661
Ar monochromatic absorption coeff. at high temps. and pressures 2—39288
Ar VIII transitions between levels of principal quantum numbers 3, 4 and 5, identification and transition probabilities 2—31656
Ar v.u.v. emission from high density spark discharge, spectral radiant intensity saturation and self reversal and effects of voltage increases 2—32135
Ar^+, transition probabilities for f-d transitions 2—24347
Ar^+ ion beams, fast, obs. of Zeeman effect ion optical spectra 2—34357
$^{16}Ar^+$, lifetimes of 2^3S_1 and 2^3P_1 levels 2—18299
As II, Zeeman effect in electrodeless discharge tubes, 24025 Gauss 2—15217
As K-shell fluorescence yield meas. 2—38809
Au hollow-cathode lines, effects of hyperfine structure on measured widths 2—15218
Au I, autoionization lines in vac. u.v. spectra determ. by photoionization and emission 2—18309
Au I, hyperfine structure sign determination by Starke effect investigation of 6p $^2P_{3/2}$ state 2—21503
B, effects of spatial symmetry restrictions on hyperfine splitting constants 2—8442
B, lifetimes and oscillator strengths from decay curves, beam-foil technique 2—18484
B discharge lamp emission, line width 2—8048
B I, v.u.v., solar abundance studies 2—15213
Ba, electron impact excited resonance transitions, minima in generalized oscillator strengths 2—5816
Ba, lifetime of 5d6p $^1P_1$ level determ. from meas. of Hanle resonance, calc. of absolute oscillator strengths 2—2940
Ba, resonance line excitation by electron impact 2—11948
Ba II, electron impact broadening of lines in electric shock tube plasma 2—5783
Be, lifetimes and oscillator strengths from decay curves, beam-foil technique 2—18484
Be I isoelectronic sequence, transition probabilities and excitation cross sections 2—28187
Be II, electron impact broadening of lines in electric shock tube plasma 2—5783
Bi i multipole line at 4615 Angstroms, total intensity 2—38810
Bk I, Bk II, emission spectra, electron configuration determination 2—21508
Bk III, Bk IV, absorption and luminescence spectra, energy level assignments 2—21504
Br, wavelengths in 1.8-4.0 μm region 2—28190
C, effects of spatial symmetry restrictions on hyperfine splitting constants 2—8442
C, ground state, $^3P_1$ and $^3P_2$ levels, Zeeman effect, Lande factors calc. 2—8450
C, hydrogenic, determ. of Lamb shift via $2S_{1/2}$ metastable quenching 2—18301
C, lifetimes and oscillator strengths from decay curves, beam-foil technique 2—18484
C I isoelectronic sequence, Sc-V, in the range 16 to 22 Angstroms 2—15220

- **Spectra** continued
  - **atoms** continued
    - C II to C V ions, beam foil spectra in 300Å- 1300Å region, meas. of mean lives of excited levels 2—31658
    - C III and C IV pressure broadened profiles in the plasma 2—28188
    - C IV ion, radiative transition probabilities and recombination coefficients 2—21491
    - CIII, emission from WR stars 2—41102
    - CS, highly excited levels, absorption line broadening and shift in Cs vapour 2—11956
    - CV, C VI, line broadening calc. 2—15242
    - C$^+$(2p)-H(2s) collisions, fine structure excitation cross sections at low energies 2—5834
    - Ca, Comet Bennett (1969 i), emission from nucleus 2—4981
    - Ca, highly ionized in the Li isoelectronic sequence, transition energy values 2—2995
    - Ca, resonance line excitation by electron impact 2—11948
    - Ca collisional cross-sections for emission and luminous efficiencies in spectra of meteors 2—4983
    - Ca I interstellar line at λ4226 for four stars with strong Ca II K-lines 2—4900
    - Ca II, crossed beams of electrons and Ca$^+$ used to meas. cross sections for excitation of H and K lines of polarization fraction 2—5799
    - Ca to Th, M-shell Coster-Kronig, Auger and radiative rates, and fluorescence yields 2—24311
    - Ca XVIII in e.u.v., Li like spectra, identification and classification of spectral lines 2—31666
    - CaIX MgI-like spectra, analysis, isoelectronic comparison with spectra of KVIII, ScX, TiXi 2—28198
    - Cd, effective cross sections of excited ion formation in electronic collisions, calc. by meas. line intensities 2—5800
    - Cd, energy loss spectra, rel. to electron impact excitation studies 2—619
    - Cd, Lande factors of 5s6s $^3S_1$ levels 2—24341
    - Cd I, energy dependence of resonance line excited in Cd-Zn collisions 2—2968
    - Cd II, isotope shifts in resonance lines, size of specific mass shifts in alkali-like resonance lines 2—5784
    - Cd oscillator strengths semiempirical calc. 2—24344
    - ^{110}Cd, spectral analysis by isotopic dilution method 2—37067
    - Ce V and Ce VI, resonance lines 2—28189
    - Cf I, Cf II, emission spectra, electron configuration determination 2—21508
    - Cl, wavelengths in 1.8-4.0 μm region 2—28190
    - Cl I and Cl II lines, Stark shifts 2—11952
    - Cl II, stark broadening 2—35138
    - Cl II, Stark broadening meas. 2—2941
    - Cl$_{II}$-Cl$_{VII}$ energy levels and mean lives 2—589
    - Cm, L X-rays, energies and intensities, associated with $_{252}$Cf α-decay of ^{252}Cf 2—18306
    - Cm I, Cm II, emission spectra, electron configuration determination 2—21508
    - Co, Lα line shapes near threshold of excitation 2—21506
    - Co, soft X-ray spectra, classification 2—5786
    - Co X-XVII, classification of emission lines from $3s^23p^n$—$3s3p^{n+1}$ and $3p^n$—$3p^{n-1}3d$ transitions 2—21519
    - Co XVII, relativistic corrections to ionization energies and dipole oscillator strengths 2—8445
    - Cr, soft X-ray spectra, classification 2—5786
    - Cr X to XII, classification of emission lines from $3s^2\ 3p^n$-$3s\ 3p^{n+1}$ and $3p^n$-$3p^{n-1}3d$ transitions 2—2936
    - Cr XXII in e.u.v., Li like spectra, identification and classification of spectral lines 2—31666
    - Cs, absorption, line shapes, pressure effects of inert gas mixtures 2—24331
    - Cs, collisional excitation transfer cross sections 2—2971
    - Cs, comparison of experimental and theoretical pressure broadened line shapes 2—21507
    - Cs, relative oscillator strengths for transitions in diffuse series 2—8444
    - Cs I, satellites of principle lines 2—18303
    - Cs I, van der Waals broadening of shock excited emission lines, about 5000K 2—15227
    - Cs I (6G-5D) forbidden component, ionic profiles calc. 2—24345
    - Cs II, on excitation in collisions with He, Ne, Ar in energy range from threshold to 28 keV 2—2969
    - Cs multiphoton ionization at 1.06 and 0.53 microns 2—35153
    - Cs pulsed discharge, spontaneous emission 2—2935
    - ^{133}Cs, hyperfine structure of 6p $^2P_{3/2}$ level redetermined by zero field optical double resonance method, deduced g_J factor 2—24339
    - Cu, Lα line shapes near threshold of excitation 2—21506
    - Cu, soft X-ray spectra, classification 2—5786
    - Cu atomic cascade, linear polarization correlation of photons rel. to exptl. test of local hidden variable theories 2—31659
    - Cu I, autoionization lines in vac. u.v. spectra determ. by photoionization and emission 2—18309
    - Cu I, line broadening consts., theoretical estimation 2—2919
    - D, metastable, laser induced quenching, single stimulated two-photon emission and anti-Stokes Raman scattering 2—24393
    - Dy i, atomic isotope shifts in visible region of spectra 2—31661
    - Dy I, classif. 2—11953
    - Er i, atomic isotope shifts in visible region of spectra 2—31661
    - Es I, Es II, emission spectra, electron configuration determination 2—21508
    - Es III, luminescence spectra, energy level assignments 2—21504
    - Eu^{3+}, absorption spectra in $POCl_3$:$SnCl_4$ solution 2—9141
    - Eu(II), formation spectrum and chem. props. from pulse radiolysis of tervalent ion 2—30094
    - F, effects of spatial symmetry restrictions on hyperfine splitting constants 2—8442
    - F^{6+} lithium like ions passing through C foil target, excitation of metastable autoionizing states, determ. of electron spectra 2—604
    - Fe, soft X-ray spectra, classification 2—5786
    - Fe collisional cross-sections for emission and luninous efficiencies in spectra of meteors 2—4983
    - Fe I, Fe II, oscillator strength, obs. using shock tube emission spectroscopy 2—18280
    - Fe I line, magneto-optical effect on circular polarization in sunspots 2—17080
    - Fe I oscillator strengths det. from anomalous dispersion of shock heated gases 2—18304
    - Fe XI to XV, classification of emission lines from $3s^2\ 3p^n$-$3s\ 3p^{n+1}$ and $3p^n$-$3p^{n-1}3d$ transitions 2—2936
    - Fe XVI, relativistic corrections to ionization energies and dipole oscillator strengths 2—8445
    - FeI oscillator strengths and f-values, arc meas. 2—35139
    - Fe+N_2, O_2 reactions, ionization and spectral emission at simulated meteor conditions 2—33752
    - Gd I, arc spectrum, line splittings, assignments 2—15214
    - Gd II, spark spectrum, line splittings, assignments 2—11954
    - H-H spin-exchange collisions, radiation frequency shifts 2—31719
    - H^1-He collisions, determ. of excitation cross section ratios $\sigma_3 1_p/\sigma_4 1_s$ and $\sigma_3 1_p/\sigma_4 1_d$ and the polarization of 3^1P-2^1S transition 2—5883
    - H-like, quantum induced $2S_{1/2}$-$1S_{1/2}$ photon-plasma transitions, probability 2—31709
    - H, $2^2S_{1/2}$-$2^2P_{3/2}$ interval meas. by decay in magnetic field 2—2985
    - H, absorption spectra of laser flashes 2—21541
    - H, anticrossings on n=3 levels, Lamb shift 2—5848
    - H, atomic relaxation contributing to population inversion in H plasma 2—35496
    - H, Balmer spectrum meas. for plasma at temps. 12000-20000 K 2—35177
    - H, collisional and radiative transition rates for bound-bound and bound-free transitions, approximate formulae 2—31715
    - H, dipole oscillator strengths, square of radial integral 2—31712
    - H, fine and hyperfine structure 2—15243
    - H, isotope effect in d.c. arc plasma 2—695
    - H, Lamb shift, contribution of α^2 slope of Dirac form factor of free electron 2—23771
    - H, line broadening calc. 2—15242
    - H, lines at optical wavelengths in recombination spectra of gaseous nebulae 2—13879
    - H, Lyman-α emission following quenching process on electron impact excitation of 2s metastable state 2—8489
    - H, Lyman-α radiation from 2p and 2s states formed by collisions of H$^+$ and H with H_2 2—15245
    - H, metastable, polarization of quench-induced Lyman-α radiation 2—12035
    - H, obs. of H_β satellites in presence of turbulent electric fields 2—8487
    - H, ratio of intensities of Balmer lines as indicator of electron temp. in nonequilib. plasma 2—21820
    - H, role in multiphoton ionization 2—35583
    - H, Stark broadening obs. of beam-plasma system, Langmuir oscills. 2—18667
    - H, Stark effect produced in Lyman-α line by weak electric fields 2_18349
    - H, transient species obs., photoelectron and chemielectron spectroscopy 2—35163
    - H, transitions between highly excited states, cross section calc. 2—8488
    - H,H$^+$, Lyman alpha emission cross sections for collisions with CO, CO_2, methane and NH_3 at 1 to 25 keV 2—21544
    - H frequency shift of hyperfine transitions by coherent perturbations 2—31710
    - H hyperfine separation, Stark shift measured in maser 2—12021
    - H Lyman-β line, classical calcs. for broadening 2—38847
    - H Stark components in Coulomb field, perturbation theory calc. 2—15215
    - H$^-$, collisions with neutral atomic or molecular targets, energy spectrum of emitted electrons studied 2—12023
    - H_α line, brightness meas., plasma, parameters at plasmatron output 2—8993
    - H_β lines, Stark broadening 2—15241
    - H_γ and H_β Stark broadened Balmer lines, asymmetries 2—35176
    - H$^+$+He, ejected electron spectrum, profiles of $2s^2(^1S)$ autoionizating state in He 2—12025
    - H(2p) from fast proton impact on H_2, Lyman-α radiation prod. cross-section 2—18427
    - He-Ne mixture, laser transition $3s_2$-$3p_1$ 2—38814
    - He-like ions, magnetic quadrupole decay of low-lying n^3P_2 states 2—21547
    - He, 1s ns ^1S states, improved lower bounds to energy levels calc. with analytical orbital wave function 2—21550
    - He, absolute cross sections for n^1P excitation by electrons calc. from spectral line intensities in uv region 2—5880
    - He, asymptotic values of quantum defect, variational calc. 2—18356
    - He, doubly excited states, line identification from beam foil meas. 2—31725
    - He, electron bombardment, $2s2p(^1p)$ and $2p^2(^1D)$ states in electron emission spectrum studied 2—12047
    - He, energy spectra of ejected electrons from autoionizing states excited by electron bombardment 2—15248
    - He, energy spectrum of electrons emitted in collisions with 10-130 keV H_1^+, H_2^+, H_3^+, excitation functions determ. 2—12046
    - He, excitation by 20-100 keV h$^+$, H, He$^+$, He beams, cross section determ. from spectroscopic analysis of emitted radiation 2—3000
    - He, expectation values for ^1S state, Delves principle applied using numerical excited Hartree orbitals 2—35185
    - He, ionized in plasma, Stark broadened resonance lines, difference in absorption and emission line shapes 2—8495
    - He, lines at optical wavelengths in recombination spectra of gaseous nebulae 2—13879
    - He, near threshold electron impact excitation of n=2 states, study of trapped electron spectra 2—12041
    - He, ortho., collisional excitation, obs. in plasma by emission spectroscopy 2—12037
    - He, radiative transition rates from 2p3p ^3P and 2p3d $^{1,3}D$ states 2—18361
    - He, spectral line profile, λ=5876Å, afterglow emission obs. 2—18354
    - He, zero-field level crossing used to measure upper-state lifetimes 2—28233
    - He I, combined Zeeman and h.f. Stark effects, calcs. of various spectral lines 2—18359
    - He I, mean life meas. by Hanle effect on high vel. atoms excited in gaseous target 2—2997
    - He I, profiles of isolated lines, in He arc plasma jet 2—35184
    - He I 4471 Å line and forbidden components, Stark profiles in laser produced plasma 2—39136
    - He I lines, absorption profiles, broadening 2—7427
    - He II, n=4-5 and n=4-6 line complexes, obs. of relative positions intensities and widths in low temp. hollow cathode 2—31723
    - He isoelectronic sequence, radiative transitions 2—21548
    - He lines, Stark broadening 2—15241
    - He to Kr oscillator strength sums and average dispersion coefficients calculated from analytical HF wavefunctions 2—11943
    - He transitions, calc. of electric quadrupole multiplet strengths, study length and velocity matrix elements 2—21549

Spectra continued
atoms continued
He v.u.v. emission from high density spark discharge, spectral radiant intensity saturation and self reversal and effects of voltage increases 2—32135
He$^+$, 3P-state lifetime determ. from half-widths of r.f. signals 2—5878
He$^+$, light emission from ion beams excited by crysts., channelling 2—15252
He$^+$, line broadening calc. 2—15242
He$^+$, n=3 state, $P_{3/2}$-$D_{3/2}$ splitting and crossing signals detection 2—5877
He$^+$, n=4, fine structure splittings S-D, Lamb shift $P_{3/2}$-$D_{3/2}$ 2—12036
He$^+$, n=5, electric field induced anticrossing, fine structure splitting 2—18357
He$^+$, time-resolved spectroscopy of 4686 line to study simultaneous ionization and excitation of He by electrons 2—28235
He$^+$ triplet line intensity, 2 ^{3}S metastable level 2—31721
HeI, influence of distant electron collisions on plasma broadened 4471.48 Å line 2—35183
HeI lines, electron collision excitation functions, cross section variations 2—8497
^{3}He structure of 2^3P-2^3S_1 optical transition studied by emission of absorption spectroscopy 2—24402
^{4}He, meas. of electrostatic fine structure intervals 7^1D-7F, microwave optical determ. 2—18358
Hg-Cd, mixture, sensitized fluorescence, width of 3261 Å spectral line 2—8447
Hg, 6^3P_1 state, coherent diffusion of radiation in modulation resonance expt. 2—31646
Hg, effective cross sections of excited ion formation in electronic collisons, calc. by meas. line intensities 2—5800
Hg, electron impact excited resonance transitions, minima in generalized oscillator strengths 2—5816
Hg, finite continuous emission spectrum, press. depend. 2—35137
Hg, in Mg-Ar discharge, influence of N_2 and CO impurities 2—2939
Hg, Lande factors of 6s7s $^3S_1$ levels 2—24341
Hg, radiative level shifts and Raman effect under laser irrad. 2—24342
Hg, resonance radiation, collisional quenching and depolarization 2—5841
Hg, Stark shift in $6s6p^3P_1$ state 2—38811
Hg a.c. arc discharge lamps, modulated spectra 2—38163
Hg spectrum, electron impact meas. of absolute oscillator strengths of 3 transitions 2—8446
Hg vapour, resonance radiation, forward scattering 2—8448
^{199}Hg, hyperfine struct., Fourier spectroscopy obs. 2—588
$Hg(6^3P_2) \rightarrow Hg(6^3P_1)$ transition, relative intramultiplet quenching cross sections 2—28192
Hγ line strengths in early-type stars, photoelectric measurements 2—4844
I, wavelengths in 1.8-4.0 μm region 2—28190
I in CF_3 and C_2F_5I photodissociation lasers, Zeeman effect in hyperfine structure of emission 2—31038
K, highly excited levels, absorption line broadening and shift in K vapour 2—11956
K, ionized, radiative lifetimes 2—31678
K binary collision broadening of absorption line induced by Kr, contribution of dipole-quadrupole dispersion 2—31667
K multiphoton ionization at 1.06 microns 2—35153
K XVII in e.u.v., Li like spectra, identification and classification of spectral lines 2—31666
KVIII Mg I-like spectra, analysis, isoelectronic comparison with spectra of CaIX, ScX, TiXI 2—28198
^{39}K, h.f.s. splitting consts. of first excited state 2—8451
^{41}K, h.f.s. splitting consts. of first excited state 2—8451
Kr I sequence, Rydberg series and ionization potential 2—15219
Kr II, transition probabilities of ionic lines 2—5788
KrI isoelectronic sequence Rb-Mo, resonance-line spectra, vacuum u.v. 2—18312
La, potential barrier effects in photoabsorpt. 2—22776
Li, perturbed by He. violet satellite bands 2—38813
Li I, doubly excited levels, induced by Li$^+$-He collisions in 10-75keV region 2—5801
Li I^a, I^b, II^a, new spectral lines obs. between 200 and 600 nm, possible classification 2—28195
Li vapour, autoionizing spectra, vac. u.v. obs. 2—18308
Li$^-$ free-free transitions, calc. of absorption coefficient from elastic electron scattering data 2—28170
Li$^+$ transitions, calc. of electric quadrupole multiplet strengths, study length and velocity matrix elements 2—21549
Lu I, hyperfine structure and lifetime determ. by level cross technique 2—593
Lu IV lines from sliding spark, wavelengths 400 to 3200 Angstroms, energy levels 2—31668
Lu^{2+}, one-electron 2—2943
Mg, Comet Bennett (1969 i), emission from nucleus 2—4981
Mg collisional cross-sections for emission and luminous efficiencies in spectra of meteors 2—4983
Mg III, extended analysis 2—5789
Mn, soft X-ray spectra, classification 2—5786
Mn IX to XIV, classification of emission lines from $3s^2\ 3p^n$-$3s\ 3p^{n+1}$ and $3p^n$-$3p^{n-1}3d$ transitions 2—2936
Mn spectral intensity increases due to presence of Na impurities in C arc 2—15524
Mn violet triplet, pressure broadening and shift due to foreign gases 2—31664
Mn XXIII, e.u.v., identification and classification of spectral lines 2—31666
Mo, ESCA study of $2p^43d^{10}$ to $2p^33d^9$ transition, L-series 2—31641
Mo, transition probabilities, absolute, 450-510 nm 2—2944
N, beam foil excited, lifetimes of NII-NV energy levels 2—35142
N, excitation in He afterglow with traces of N_2 2—28194
N, meas. in long wavelength and vacuum u.v. region 2—5790
N, transient species obs., photoelectron and chemielectron spectroscopy 2—35163
N VI, dielectric recombination satellite line intensities, meas. and interpretation 2—28171
N$^-$, in plasma, photodecay cross sect. meas. 2—18315
N$^+$, collisional excitation spectrum at 50 keV from He target 2—18344
NIV, emission from WR stars 2—41102
Na, $3^2P_{3/2}$ state, crossings of Zeeman sublevels calc. using dipolar magnetic and quadripolar electric interaction constants as parameters 2—18316
Na, D-line radiation excitation in collisions with internally excited H_2, D_2, N_2 2—35161
Spectra continued
atoms continued
Na, electron excitation cross section and polarization of unresolved doublet resonance radiation 2—5803
Na, extreme u.v. photoabsorpt. spectra 2—18310
Na, nonrelativistic wave functions and eigenvalues 2—18317
Na collisional cross-sections for emission and luminous efficiencies in spectra of meteors 2—4983
Na D line reversal, premixed flames, chemiluminescence effects 2—8452
Na pressure broadening of 5889 Å and 5895 Å lines by thermal and high temperature He 2—31669
Na vapour, autoionizing spectra, vac. u.v. obs. 2—18308
^{23}Na, hyperfine constants of $3^2P_{3/2}$ state, level crossing method 2—11960
Na*($3p^2P$) D lines obs. on photodissociation of NaI 2—12180
Ne-Ar gas mixture, translational absorption spectra computed 2—5791
Ne, $^3P_1$ resonance level, lifetime estimate using interference phenomena 2—31670
Ne, 350 to 920Å, spectra and mean lives, beam-foil studies 2—15222
Ne, electron collisions, vacuum u.v. spectra 2—18454
Ne, energy spectra of ejected electrons from autoionization states excited by electron bombardment 2—15248
Ne, isotope shifts, gain method of measurement 2—21514
Ne, metastable levels and isotopic effects 2—8453
Ne, photoionization cross sections partition, exptl. obs. in soft-X-ray region 2—35166
Ne, shape of absorbed spectral line at λ=743 Å, Doppler and Lorentz broadening 2—15221
Ne I 743 Å line, accurate measurement to fifth order, calculation of other lines in vacuum u.v. 2—8427
Ne II, cross section for 3p states meas. for excitation by electron collision 2—5804
Ne ions, continuous free-free absorption 2—15202
Ne VIII transitions between levels of principle quantum numbers 3, 4 and 5, identification and transition probabilities 2—31656
Ne$^+$, transition probabilities for f-d transitions 2—24347
^{20}Ne, $3S_2$-$3p_4$ transition 2—8454
^{20}Ne, $3s_2$-$3p_4$ laser transition, pressure dependence of radiation width, broadening and frequency 2—8455
^{21}Ne, hyperfine structure of excited states and quadrupole moment, using laser-induced line-narrowing technique 2—24346
^{22}Ne, pressure broadening and shift of 1.15 μm line, constants in Lennard Jones interatomic potential determ. 2—21517
Ni, Lα line shapes near threshold of excitation 2—21506
Ni, soft X-ray spectra, Classification 2—5786
Ni, XVIII, relativistic corrections to ionization energies and dipole oscillator strengths 2—8445
Ni I, lifetime obs. of optical levels using phase shift method 2—31680
Ni XI-XVII, classification of emission lines from $3s^23p^n$—$3s3p^{n+1}$ and $3p^n$—$3p^{n-1}3d$ transitions 2—21519
O, $^1S_0$ metastable level, radiative life 2—28197
O, effects of spatial symmetry restrictions on hyperfine splitting constants 2—8442
O, energy dependence of angular distribution of photoelectrons 2—38826
O, transient species obs., photoelectron and chemielectron spectroscopy 2—35163
O I and O II multiplet radiation following e scatt. from O_2 2—2946
O VII, dielectric recombination satellite line intensities, meas. and interpretation 2—28171
O$^+$ ion beams, fast, obs. of Zeeman effect in optical spectra 2—34357
OV, emission from WR stars 2—41102
P I to PV, excited level lifetimes, evaluation from beam foil spectra 2—5792
Pb, matrix isolated, absorption spectra 2—15223
Pb arc spectra, autoionized lines 2—38815
Pb I reson. line, press. effect, absorpt. spectrum in presence of Kr 2—24348
Pb X-ray L_2-L_3 Coster-Kronig transition probability meas. 2—11961
Rb, nonrelativistic wave functions and eigenvalues 2—18317
Rb, self-induced transparency 2—31671
Rb, two-photon excitation, transitions, scattering mechanisms 2—15224
Rb excited atoms colliding with inert gas atoms, theory of fine structure transitions 2—21535
^{87}Rb, hyperfine shift, clock transition 2—18319
^{87}Rb, modulated fine and hyperfine components of absorbed light beams 2—8458
S IX, S X, S XI, S XII, calc. of energies of $1s^22s^22p^k$ to $1s^22s2p^{k+1}$ to $1s^22p^{k+2}$ transitions 2—35144
SI, absorption in vac. u.v. 2—20691
Sc, highly ionized in Li isoelectronic sequence, transition energy values 2—2995
Sc I to Sc III, 600 to 6000 Å, lifetimes of excited levels 2—15225
Sc III, anal. giving new energy levels 2—35145
Sc XIX in e.u.v., Li like spectra, identification and classification of spectral lines 2—31666
ScX Mg I-like spectra, analysis isoelectronic comparison with spectra of KVIII, CaIX, TiXI 2—28198
Se, coherent emission from ionic transitions 2—594
Si I, van der Waals broadening of shock excited emission lines, about 5000K 2—15227
Sm ions, 2+ and 3+, evidence for oxidation in KCl 2—10441
Sm^{3+}, absorption spectra in $POCl_3$:$SnCl_4$ solution 2—9141
Sm(II), formation spectrum and chem. props. from pulse radiolysis of tervalent ion 2—30094
Sn IV, isotope shifts in resonance lines, size of specific mass shifts in alkali-like resonance lines 2—5784
Sr, Comet Bennett (1969 i), emission from nucleus 2—4981
Sr, electron impact excited resonance transitions, minima in generalized oscillator strengths 2—5816
Ta trapped in Ar matrices at 4.2K, absorption spectrum 2—36869
Tb I, analysis of structure of sextet system of $4f^8(^7F)5$ of $6s^2$ 2—21523
Th, excited in interrupted vacuum arc, mag. enhancement 2—38799
Ti, highly ionized in Li isoelectronic sequence, transition energy values 2—2995
Ti I, atomic g_J-values and lifetimes of z^3F- states 2—28200
Ti spectral intensity increases due to presence of Na impurities in C arc 2—15524
Ti VI and VIII, meas. $3s^23p^k$-$3s3p^{k+1}$ transitions, determ. ground configuration intervals 2—28199
Ti XX in e.u.v., Li like spectra, identification and classification of spectral lines 2—31666

- **Spectra** continued
  - **atoms** continued
    - TiXI Mg I-like spectra, analysis and comparison with iso-electronic spectra of KVIII, CaIX, ScX 2—28198
    - Tl I absorption spectrum in v.u.v. 2—18320
    - ^{203}Tl, spectral analysis by isotopic dilution method 2—37067
    - ^{205}Tl, muonic, resonance processes and nuclear excitation rel. to L and K X-rays 2—18371
    - Tm I, lifetimes of 14 levels meas. using technique of zero field level crossing 2—24351
    - V, photoionization cross sections calcs. using plane-wave method allowing orthogonality 2—31684
    - V IX,X, classification of emisssion lines from $3s^2\ 3p^n$-$3s\ 3p^{n+1}$ and $3p^n$-$3p^{n-1}3d$ transitions 2—2936
    - Va XXI in e.u.v., Li like spectra, identification and classification of spectral lines 2—31666
    - Xe, collective reson. in $4d^{10}$ shell 2—11963
    - Xe, photoabsorption spectra, collective effects, study of $5p^6$ shell, excitations into $5p$-nd^1P channel 2—11962
    - Xe, photoabsorption spectrum of $5p^6$ shell, collective effects and screening 2—595
    - Xe, singly and multiply ionized, excited by electron collision, vacuum u.v. spectra observed 2—8465
    - Xe discharge lamp, long linear, with metallic halide additives, continuous emission spectra 2—3254
    - Xe I i.r. laser lines, h.f.s. 2—31672
    - Xe II, transition probabilities of ionic lines 2—5788
    - Xe impulse discharges, emission spectra studied by photography in 1000-2000 Å region 2—28667
    - Xe lamps, emission 2—27641
    - Xe laser relaxation oscillations 2—14421
    - Xe laser relaxation oscillations 2—14421
    - ^{129}Xe arc spectrum hyperfine structure 2—31651
    - Y, V, anal. to give energy level structure and configuration 2—38817
    - YIV, transitions to the ground level 2—38816
    - Yb(II), formation spectrum and chem. props. from pulse radiolysis of tervalent ion 2—30094
    - Zn, electron impact spectrum at 50 to 150 eV and 0 to 11° range 2—28210
    - Zn, Perot-Fabry interferometric obs. in vac. u.v. 2—15208
    - Zn I, excitation functions, in Zn^+-Zn and Cd^+-Zn collisions 2—2982
    - Zn level lifetimes meas. by delayed coincidence method 2—8459
    - Zn vapour, atom conc. determ. by absorpt. method 2—20212
    - ^{68}Zn, spectral analysis by isotopic dilution method 2—37067
  - **inorganic liquids and solutions**
    - alkali metal nitrates, vibrational spectra as functions of phase 2—35768
    - alkali molybdates and tungstates, molten 2—35844
    - aprotic laser solns. with Nd, scatt. coeffs. determ. 2—32269
    - hydrated electron, absorption spectra, –4 to 390°C, pulse radiolysis study 2—7184
    - pirimidine derivatives, absorpt., fluoresc. spectra, scintillation props. 2—28877
    - polywater, interpretation of i.r. spectra of clay adsorbed water 2—3393
    - potassium halides, Pb-doped, aq. soln., optical absorpt. 2—20039
    - rare earth trichlorides, Kramers-Kronig relationships, refr. and extinction indices 2—15592
    - water, existence of free OH groups 2—28786
    - water, i.r. absorpt., after passage through mag. field 2—3397
    - water adsorbed on dispersed silica, absorpt. spectra 2—29064
    - CS_2, Fourier transform obs. of Brillouin and Rayleigh line widths and shapes 2—1103
    - CS_2, solvent dependence of absorption band at 316 nm 2—9137
    - $Ca(NO_3)_2$-KNO_3 melt, glass transition, u.v. absorpt. spectra 2—18901
    - $Cr(CO)_6$, Raman spectra, automatic assignment of observed frequencies and combinations 2—39369
    - $CsNO_3$, polarized Raman spectra 2—36898
    - GeCl, vibratory spectra, intensities, electro-optical parameters 2—32267
    - HNCS, liquid, temp. dependence of vibr. band intensities in i.r. spectra 2—12567
    - H_2O, in organic solvents, possible motional effects on vibrational spectrum in fundamental stretching region 2—39370
    - He-Ar, dilute solutions, far i.r. absorption spectrum arising from collision induced dipole moments 2—9136
    - He, excitation spectrum from small angle scattering of nuclear γ-rays 2—22021
    - He, superfluid, u.v. emission spectrum on electron bombardment 2—12604
    - I_2, lattice absorp. near melting point 2—33266
    - KCl:Pb, aq. soln., optical absorpt. 2—20039
    - $K_2Cr_2O_7$, Kramers-Kronig relationships, refr. and extinction indices 2—15592
    - $K_3Fe(CN)_6$, Kramers-Kronig relationships, refr. and extinction indices 2—15592
    - $MnCl_2.4H_2O$ in DMF and DMA solutions, absorption 2—39391
    - $Mo(CO)_6$, liquid, Raman spectra, automatic assignment of observed frequencies and combinations 2—39369
    - N_2, vibrational lifetimes 2—19360
    - $NaBO_2$, ^{18}O-labelled aqueous solns., i.r. absorption and Raman spectra 2—21589
    - $Nd(O_2PCl_2)_3/POCl_3/ZrCl_4$, liq. laser soln. i.r. spectrum, relative intensities and frequency assignment 2—35769
    - Ne-Ar, dilute solutions, far. i.r. absorption spectrum arising from collision induced dipole moments 2—9136
    - $PbCl_4$, vibratory spectra, intensities, electro-optical parameters 2—32267
    - $PbCl_4$ in n-pentane solution at 20°C, electronic spectrum measured 2—12568
    - Pr(IV), formed by pulse radiolysis of aqueous Pr(III) solution 2—30095
    - $SiCl_4$, vibratory spectra, intensities, electro-optical parameters 2—32267
    - SiH_4 and SiD_4-SiH_4 mixtures, i.r. vibrational spectra 2—33272
    - $SnCl_4$, vibratory spectra, intensities, electro-optical parameters 2—32267
    - SnI_4, bond- bending oscillation 2—15563
    - $TiCl_4$, vibratory spectra, intensities, electro-optical parameters 2—32267
    - $W(CO)_6$, Raman spectra, automatic assignment of observed frequencies and combinations 2—39369
    - Xe, reflection spectra, Wannier exciton peaks obs. 2—10351
  - **inorganic molecules**
    - *see also Molecules*
    - dense fluid, i.r. high pressure study, intermol. forces and mol. motion 2—18789
    - ethane, ion molecule reaction chemistry, low electron energy, study by ICR spectroscopy 2—33373

- **Spectra** continued
  - **inorganic molecules** continued
    - group V and VI hydrides, photoelectron spectra and valence shell orbital structures 2—8576
    - pseudoisocyanine, absorption spectra, highly- aggregated J-form 2—28401
    - silicone grease, i.r. emission 2—27642
    - He-Ar mixture, vac. u.v. emission band spectrum 2—18401
    - Hg compounds in water pollution, Raman spectra 2—12150
  - **inorganic molecules, diatomic**
    - electronic-vibrational band, intensity distribution of rotational lines, Honl London factors, normalization 2—8512
    - Group VI elements, compared with formulas for rotational line strengths in $^3\Sigma^\pm$—$^3\Sigma^\pm$ transitions with intermediate coupling 2—3015
    - halogen and interhalogen, hot band effects on ionization threshold 2—18420
    - heavy, rot. consts. determ. 2—18399
    - metal halides, ionic, single ion transitions 2—31805
    - rotation and vibr. consts. determ. from spectrum with unresolved rot. struct. 2—24434
    - vibration-rotation line broadening in rare gas perturbed systems 2—8575
    - AgBi, rot. and vibr. consts. determ. from spectrum with unresolved rot. struct. 2—24434
    - AgBi, rot. consts. determ. 2—18399
    - AgCl, AgBr, AgI, microwave rotation spectrum 2—28270
    - AlCl, AlBr, AlI, millimetre wave rotational spectra, determination of rotation-vibration interaction 2—21588
    - AlO emitted from H flame at atmospheric pressure, 2300-2700 K, intensity of first Al resonance doublet meas. 2—10617
    - Ar_2, absorption spectrum, 780-1080 Å, intermolecular pair potential 2—18544
    - Ar_2, determ. of pair potential and second virial coeffs. 2—3027
    - As_2, vacuum u.v. absorption spectrum 2—18402
    - AsF, emission spectrum, 7320-7400 Å, obs. of new $^1\Pi$ state, rotational constants 2—18403
    - AsF absoprtion spectrum analysed, 2 new singlet systems 2—773
    - AsO, flame emission spectrum, chemical excitation 2—38886
    - BF, microwave spectrum, molecular constant determination for vibrational ground state 2—15285
    - BH, Franck- Condon factors and r-centroids of A-X band systems 2—3028
    - BaO, $A^1\Sigma$—$X^1\Sigma$ system, Franck-Condon factors, r-centroids and oscillator strength 2—15286
    - BaO, band 4700-15500Å synthetic and from atmospheric release at 170km 2—10744
    - BaO, microwave optical double resonance spectroscopy 2—35231
    - BeCl, rotational analysis of $A^2\Pi$-$X^2\Sigma^+$ band system, determ. of principle molecular constants 2—28271
    - BeD, ESR spectra meas. for ground state in solid Ar matrices, determ. hyperfine interaction and chemical bonding 2—15287
    - BeH, ESR spectra meas. for ground state is solid Ar matrices, determ. hyperfine interaction and chemical bonding 2—15287
    - Bi_2, new band system in emission spectrum 2—28272
    - BiCl, A-X system, transition moment as function of internuclear separation 2—3029
    - Br, photoelectron spectra, total and partial photoionization cross sections 2—15312
    - Br_2, extreme red absorption spectrum $A^3\pi(1_u)\leftarrow X^1\Sigma_g^+$, vibrational and rotational assignment 2—38889
    - Br_2, vibrational structures of $E\rightleftarrows B$ emission systems 2—21618
    - $^{79}Br^{81}Br$, $A^3\pi(1)$—$X^1\Sigma^+$ system, Franck-Condon factors and r-centroids 2—38890
    - $^{79}Br^{81}Br$, Franck-Condon factors and r-centroids for $B^3\Pi(0_u^+)$—$X^1\Sigma_g^+$ system 2—38891
    - C_2^-, matrix isolated, laser excited fluorescence study 2—35236
    - C_2^-, two photon photodetachment of electrons, confirmation of $^2\Sigma_g^+$ ground state 2—24444
    - C_2^+ new spectrum associated with diatomic carbon obs. in absorption in flash discharge, probably due to C_2^+ ion 2—24443
    - CN, Comet Bennett (1969 i), emission from nucleus 2—4981
    - CN radical, mag. resonance and level anti-crossing 2—5922
    - CN vibration-rotation interaction effects on Franck-Condon factors for $B^2\Sigma^+$-$X^2\Sigma^+$ transition by asymptotic expansion method 2—28282
    - CO, 2.7 μm band, narrow band model parameters 2—35237
    - CO, A $^1\Pi$ state, measured lifetimes of first seven vibrational levels 2—3030
    - CO, $a^3\Pi$-$^1\Sigma$ Cameron system, oscillator strength and lifetimes calc. 2—12119
    - CO, absorpt. cross sections and photoionization efficiencies in 300-1000 Å region 2—21639
    - CO, absorption spectrum in Hopfield helium continuum region, obs. of Rydberg series 2—31785
    - CO, adsorbed on Cs halide films, i.r. and shifts 2—5918
    - CO, adsorbed on Cu surface, obs. using multiple specular reflection 2—12679
    - CO, band strength of 0,0 band of $a^3\Pi$-$X'\Sigma$ transition, radiative lifetime of $a^3\Pi$ state 2—18407
    - CO, electron impact excited emission cross sections, meas. from 1260 to 5000Å 2—5919
    - CO, electron impact spectrum, abs. generalized oscillator strengths for $B^1\Sigma^+\leftarrow X^1\Sigma^+$ and $C^1\Sigma^+\leftarrow X^1\Sigma^+$ transitions 2—12115
    - CO, energy loss spectrum rel. to determination of cross section for electron impact excitation of electronic states 2—15293
    - CO, from photodissociation of CO_2, meas. of fourth positive system 2—778
    - CO, half-width computation for air- broadened lines 2—12114
    - CO, i.r. chemiluminescence, effective energy transfer to admixed COS 2—28428
    - CO, i.r. emission, vibr. transitions 2—28275
    - CO, inner shell electrons, ionization by 10 keV electron as function of energy loss 2—39195
    - CO, K-absorpt. structs. of O and C, 20-100 Å 2—18463
    - CO, lifetimes of two vibronic levels of $B^1\Sigma^+$ state and transition moment of $B^1\Sigma^+$—$X^1\Sigma^+$ transition 2—35244
    - CO, line shape of i.r. emission from flames 2—28278
    - CO, linewidth self-broadening and broadening by Ar and N additions 2—38885
    - CO, new absorption bands and studies of known isotopic bands 2—28277
    - CO, obs. of spectral emission due to excited states prod. in $He(2^3S)+CO_2$ reaction 2—24445

- **Spectra** continued
  - **inorganic molecules, diatomic** continued
    - CO, oscillator strengths, deduction from vibrational level lifetime meas. 2—5921
    - CO, photoelectron spectra, study of autoionization, vibrational structure 2—8674
    - CO, profiles of i.r. absorption bands in liquids, rotational motion 2—775
    - CO, pulsed laser emission 2—2395
    - CO, r.f. spectroscopy of perturbed excited states 2—8599
    - CO, vacuum u.v., cascade arc, absorpt. and photoionization fluoresc. 2—21593
    - CO,absolute oscillator strengths of transitions of vibration-rotation spectra 2—12113
    - CO ($a^3\pi$), lifetime and quenching in flowing in He afterglow 2—12117
    - CO adsorpt. or Ni at low temps., i.r. obs. 2—22086
    - CO in CO_2 atmosphere, strength of rotational lines in R branch, det. at 298, 202 and 132 K, and of self and CO_2 broadening 2—31788
    - CO physically adsorbed on siica, i.r. study 2—9304
    - CO^+, enhancement of vibrational level population by photoelectron spectrometry 2—35265
    - CO^+ comet-tail band system, calc. of Einstein A coefficients, band oscillator strengths and absolute band strengths 2—18417
    - CS, photoelectron spectrum of short lived species in product of CS_2 discharge assigned to this molecule, determ. ionization potential 2—31789
    - CS, vacuum u.v. photoelectron spectrum values for first two ionization potentials obtained 2—28285
    - $C^{34}S$, rotational, structure in $^1\Pi-^1\Sigma^+$ transition 2—8590
    - $^{13}C\,^{18}O$, band origins in Angstrom system 2—31779
    - Ca_2 vapour, $^1\Sigma$-$^1\Sigma$ transition, rotational and vibrational structure 2—8601
    - CaO, investigation of ground state, matrix spectra of Ca and CaO 2—35241
    - Cl_2 vibrational structures of $E\rightleftharpoons B$ emission systems 2—21618
    - ClF, photoelectron spectrum meas. adiabatic ionization potentials obtained 2—12121
    - Co, valence electrons, ionization by 10 keV electrons as function of energy loss 2—39194
    - CoO, observed in low-pressure arc with Co electrode 2—14485
    - CsBr, quadrupole hyperfine structure 2—38901
    - CsSb, visible spectrum 2—8607
    - CuAs, emission spectrum, intensity distrib. 2—24449
    - $^{63}Cu_2$, rot. analysis of A-X system bands 2—783
    - D_2, absorption spectrum below 840 Å 2—12125
    - D_2, emission continuum, oscillator strength 2—12143
    - D_2, metastable, lifetime of $c^3\Pi_u$ state 2—24471
    - D_2, photoelectron, use of cylindrical-mirror analyzer 2—35293
    - D_2, vacuum u.v. emission spectrum, vibr. and rot. consts. of ground and excited states 2—18419
    - DBr, hyperfine structure and Stark effect of $J=O\rightarrow$rotational transition 2—8648
    - DCl, electronic absorption spectra, states assoc. with $(\sigma^2\pi^3)c\pi$ and $(\sigma^2\pi^3)c\sigma$ configuration 2—18424
    - DCl, far i.r. rotational spectra, line shape parameters, interferometric meas. 2—15302
    - DCl in Ar and other matrices, i.r. spectra at 20 K 2—24452
    - DF, photoelectron use of cylindrical-mirror analyzer 2—35293
    - DI, extinction coeffs. in 32000-52000 cm^{-1} region, repulsive potential curve determ. 2—3043
    - DI, repulsvie potentials from electronic absorption spectra 2—12144
    - $EuF_2(Cl_2)$, in Ar, Kr or N_2 matrix, i.r. absorpt. 2—28327
    - F_2, electronic states, absorption and emission spectra 2—38907
    - F_2, vacuum u.v. obs. below 1200 Å 2—18378
    - FCl, radio frequency, spectrum obs., hyperfine parameters and dipole moment 2—8614
    - FeO, observed in low-pressure arc with Fe electrode 2—14485
    - FeO vibration-rotation radiative band intensity meas. 2—35247
    - GaD, structure of $A^1\Pi$-$X^1\Sigma^+$ transition measured and analysed 2—12126
    - GaH, Franck-Condon factors and r-centroids of A-X band systems 2—3028
    - GaH, structure of $A^1\Pi$-$X^1\Sigma^+$ transition discussed 2—12126
    - GeBr, u.v. absorption 2—5928
    - ^{72}GeO, ^{74}GeO, electronic transition and isotopic effect 2—31793
    - 87%H_2-13%He, 10000-25000 K, radiative intensity calc. 38911 2—38911
    - H_2-He, H_2-Ne pairs, collision-induced absorption band 2—8652
    - H halides, gas phase absolute intensities of i.r. vibrational bands, influence of bond and lone pair moments on total dipole moment 2—28298
    - H halides, in CCl_4 soln., absolute intensity of i.r. bands, signs of M_l quantities in dipole moment 2—28299
    - H_2, 10000-25000 K, radiative intensity calc. 2—38911
    - H_2, ang. distrib. of phoeoelectrons, rot. ionization range 2—35255
    - H_2, dissociative photoionization, photoelectron spectroscopy obs. 2—18423
    - H_2, emission continuum, oscillator strength 2—12143
    - H_2, excited, microwave optical magnetic resonance induced by electrons, g value 2—12147
    - H_2, fine structure of $N=1(1s3p)^3\Pi_u$ state, determination by magnetic resonance 2—18429
    - H_2, fluorescent spectra in Werner system 2—38912
    - H_2, frequency shifts of quadrupolar components of collision induced fundamental i.r. band 2—31799
    - H_2, frequency shifts of rotational lines, collision induced 2—8651
    - H_2, Lyman and Werner bands, electron impact excitation 2—5931
    - H_2, Lyman bands, relative line intensities 2—28301
    - H_2, metastable, lifetime of $c^3\Pi_u$ state 2—24471
    - H_2, parity forbidden transitions, excitation by energetic electronics 2—12141
    - H_2, photoelectron use of cylindrical-mirror analyzer 2—35293
    - H_2, Rydberg series and ionization potential 2—38908
    - H_2, simultaneous excitation and photoionization, obs. from photoelectron spectra at 247 Å 2—35256
    - H_2, u.v. obs., predissociation 2—18432
    - H_2, vacuum u.v. obs. below 1200 Å 2—18378
    - H_2, zero field level crossing in excited rotational levels, radiative lifetime meas. 2—35250
    - $H_2\,(d^3\pi_u)$ meas. of fine structure by microwave optical magnetic resonance induced by electrons 2—24462
    - H_2 and HD, i.r. emissivities and interstellar D abundances 2—41141
    - H_2 continuum, lifetime and quenching rates 2—12134
    - H_2 following electron impact excitation 2—35253
    - H_2 Lyman-α radiation, transmission props. of LiF-O_2 filter 2—23728
    - H_2 rotational line narrowing in inert gas mixtures due to pressure 2—8649

- **Spectra** continued
  - **inorganic molecules, diatomic** continued
    - H_2 spontaneous radiative dissociation calc., fluorescent spectra 2—38912
    - H_2 Werner band, obs. of gain by stimulated emission of vacuum u.v. radiation 2—24469
    - H_2 Werner bands, 1161-1240 Å, obs. of vacuum u.v. laser action 2—24470
    - H_2^+, Rydberg states, calculations 2—8644
    - HBr, absolute i.r. intensity meas., value of terms Mi of dipole moment function 2—28297
    - HCl, absolute i.r. intensity meas., values of terms Mi of dipole moment function 2—28297
    - HCl, electronic absorption spectra, states assoc. with $(\sigma^2\pi^3)c\pi$ and $(\sigma^2\pi^3)c\sigma$ configuration 2—18424
    - HCl, far i.r. rotational spectra, line shape parameters, interferometric meas. 2—15302
    - HCl, far i.r. spectra in liquid Ar and Kr 2—35252
    - HCl, perturbed by Ar, vibr.-rot. spectrum, line widths and shifts 2—8618
    - HCl, profiles of i.r. absorption bands in liquids, rotational motion 2—775
    - HCl adsorbed on rutile, i.r. spectra 2—15678
    - HCl molecular beam electric resonance spectroscopy, Stark-Zeeman spectra obs. 2—12145
    - HD, fluorescent spectrum in Lyman system 2—38912
    - HD, Lyman bands, relative line intensities 2—28301
    - HD, metastable, lifetime of $c^3\Pi_u$ state 2—24471
    - HD molecule, Rydberg series obs., 700-1000 Å 2—18435
    - HF, electronic states, absorption and emission spectra 2—38907
    - HF, line strengths and collision broadened half-widths obs. 2—8650
    - HF, meas. of pressure broadening of rotational line at 40 cm^{-1} using far i.r. spectrometer 2—8634
    - HF, photoelectron, use of cylindrical-mirror analyzer 2—35293
    - HF, strengths and widths of first overtone band 2—38910
    - HF, vacuum u.v. obs. below 1200 Å 2—18378
    - HF, vibration rotation bands, evaluation of r-centroids and higher terms of elec. dipole moment 2—21609
    - HF dimer, rotational structure 2—8639
    - HF molecular beam electric resonance spectroscopy, Stark-Zeeman spectra obs. 2—12145
    - HI, absolute i.r. intensity meas., values of terms Mi of dipole moment function 2—28297
    - HI, extinction coeffs. in 32000-52000 cm^{-1} region, repulsive potential curve determ. 2—3043
    - HI, repulsive potentials from electronic absorption spectra 2—12144
    - HO_2-, absorption spectrum, kinetic analysis 2—24460
    - Hd, photoelectron, use of cylindrical-mirror analyzer 2—35293
    - He_2, description of $3p\pi$, $^{1,3}\Pi_g\rightarrow 2s^{1,3}\Sigma_u^+$ band system, characterization of 2s, $a^3\Sigma_u^+$, $A^1\Sigma_u^+$ $3p\pi$, $e^3\Pi_g$ and $E^1\Pi_g$ states 2—12149
    - He_2 $X^1\Sigma_g^+$-$A^1\Sigma_u^+$, potential curves from continuous electronic spectra 2—38917
    - HeH, translational absorption, line shape calc. from dipole moment and potential curve 2—796
    - HeH^+, Franck Condon factors for bound state-continuum transitions 2—8656
    - HfO, band spectrum 2300 to 11500 Å 2—8658
    - I_2, photoelectron spectra, total and partial photoionization cross sections 2—15312
    - I_2, reson. fluoresc. continuous passage to reson. Raman effect 2—8660
    - I_2 bands, spectrum and excitation functions 2—31804
    - I_2 vibrational structures of $E\rightarrow B$ and $F\rightarrow X$ emission systems 2—21618
    - ICl, microwave absorption and dispersion 2—38918
    - $^{127}I_2$, nuclear hyperfine structure in electronic spectrum obs. by saturated absorption spectroscopy 2—12156
    - InBr, emission band spectrum, vibrational analysis 2—21619
    - InH, Franck-Condon factors and r-centroids of A-X band systems 2—3028
    - LaO, $B\rightarrow X$ system, relative band strengths and intensities 2—28305
    - LaO, band spectrum, rotational constants 2—12159
    - LaO, rotational analysis of O-O band of $C^2\Pi\rightarrow X^2\Sigma^+$ transition 2—3049
    - LiH, rotation vibrational spectra, calculation using MC SCF formalism 2—15314
    - $^7Li^{16}O$, $X^2\Pi$ state, fine structure parameters 2—15313
    - LuO, rot. and vibr. analsysis 2—799
    - Mg_2, Franck-Condon effect, calculations 2—8601
    - Mg_2, in solid rare gas matrices, absorption spectrum, correlation of bands to $A^1\Sigma\leftarrow X^1\Sigma$ transition 2—8665
    - N_2-O_2 mixtures, decay of luminescence, irradiated by alpha particles, emission spectra 2—35274
    - N_2, absorpt. cross sections and photoionization efficiencies in 300-1000 Å region 2—21639
    - N_2, C $^3\Pi_u$ state, electron impact excitation of $v'=3$ and 4 levels, electron emission band obs. 2—5938
    - N_2, collision induced i.r. absorption, study in temp. range 77 to 297K 2—8668
    - N_2, ESCA line intensities, orbital determ. 2—35219
    - N_2, electronic transition moment variation in first and second positive band systems 2—38927
    - N_2, high resolution absorpt., 730-980 Å 2—18453
    - N_2, high resolution absorption study from 73 to 980 Å 2—35269
    - N_2, i.r. absorpt., elec. field induced 2—31807
    - N_2, inner shell electrons, ionization by 10 keV electron as function of energy loss 2—39195
    - N_2, intensity of first positive bands, study of region in which 2 and 3 body processes compete 2—18345
    - N_2, laser transitions, excitation mechanisms 2—5367
    - N_2, N_2^+, decay of electron impact excited states, time resolved studies 2—5939
    - N_2, photoelectron spectra, study of autoionization, vibrational structure 2—8674
    - N_2, pulsed laser action 2—5365
    - N_2, rotational Raman 2—18464
    - N_2, second positive bands in afterglow of N_2 and O_2 mixture 2—3052
    - N_2, vacuum u.v. absorption spectrum, o-X system, rot. consts. of vibr. levels 2—15325
    - N_2, vacuum u.v. emission features, dissociative excitation by electron impact 2—8669
    - N_2, vacuum u.v. emission from Lewis Rayleigh afterglow, rel. to recombination of N atoms via $N_2(a'\pi_g)$ and $N_2(a'1\Sigma_u^-)$ states 2—804
    - N_2, valence electrons, ionization by 10 keV electrons as function of energy loss 2—39194

spectra continued
  inorganic molecules, diatomic continued
    N_2, vibrationally excited, transient species obs. using pehotoelectron and chemielectron spectroscopy 2—35163
    N_2, vibrationally excited photoionization spectrum meas. in 79.58-84.20 nm region 2—18446
    N_2 impulse discharges, emission spectra studied by photography in 1000-2000Å region 2—28667
    N_2^+, enhancement of vibrational level population by photoelectron spectrometry 2—35265
    N_2^+ u.v. auroral emissions, spectrographic recordings from rocket 2—30327
    NO-, vibrational progressions of resonances, association with Rydberg states 2—812
    NO, $^2\pi_{3/2}$-$^2\pi_{1/2}$ transition 2—8687
    NO, $A^2\Sigma^+$ state, lifetimes of v'=0,1,2, levels 2—12164
    NO, absolute oscillator strength measurements of γ-system 2—38925
    NO, electron impact dissociative excitation in vacuum u.v. 2—3054
    NO, hyperfine structure states mixing in magnetic field 2—12174
    NO, laser magnetic resonance obs., magnetic and electrical dipole transitions obs., g factor and hyperfine structure separation calc. 2—38928
    NO, magnetic dipole transitions in far infra-red spectrum 2—38931
    NO, magnitude of multiplet splitting in X-ray photoelectron spectra, spin density implications 2—8672
    NO, monochromatic excitation of rotational levels in vibrational levels of $A^2\Sigma^+$ state 2—12175
    NO, obs. absorption meas. of $\beta(B^2\Pi-X^2\Pi)$ band system 2—5935
    NO, photoelectron spectra, study of autoionization, vibrational structure 2—8674
    NO, rotational Raman 2—18464
    NO $A^2\Sigma^+$, electronic quenching by $O_2X^3\Sigma_g$ 2—28315
    NO $A^2\Sigma^+$ state, radiative lifetime determ. from Hanle effect measurement 2—28314
    NO abs. oscillator strength estimates for some bands of β system 2—35271
    NO adsorbed on Li halides, i.r. spectra 2—15677
    NO vacuum-u.v. excitation cross sections, electron impact determ. 2—21627
    NO^+, photoelectron, obtained with He 584 and Ar 1048-1067 lines 2—15316
    $NO^+ \to O^+ + N$ unimolecules dissociation, translational spectroscopy 2—21624
    NSe, electronic spectrum, 2800-3200Å, vibr. and rot. analysis of 12 red degraded bands 2—18456
    $N_2^+(X^2\Sigma_g^+, v''=0)$, reactions with N_2 and other substances, study by kinetic absorption spectroscopy 2—22866
    $^{14}N^{16}O$, hyperfine Λ-doubling transitions obs. by molecular beam electric resonance method 2—8681
    $N_2(a\ ^1\Pi_g)$, radiative lifetime and formation of metastable $N_2(a'\ ^1\Sigma_u$-) by intrasystem cascading 2—35270
    NaO, NaO^+, NaO^-, spectroscopic constants from Hartree-Fock molec. orbital studies, deduction of Na-O species properties 2—37032
    $Na_2(b^1\pi_u)$ state, collision induced energy transfer 2—3151
    NiO, observed in low-pressure arc with Ni electrode 2—14485
    O_2-, vibrational progressions of resonances, association with Rydberg states 2—812
    O_2, abs. absorption meas. in 2430 to 1920 Å continuum 2—5942
    O_2, abs. absorption meas. on Herzberg I bands 2—5941
    O_2, absorpt. cross sections and photoionization efficiencies in 300-1000 Å region 2—21639
    O_2, absorption in solid O_2-N_2 mixture, 1.5K mag. field effect 2—8694
    O_2, collision induced vibrational and electronic spectra from 90 to 115 K 2—21635
    O_2, dissociation rate constants in shock tube, u.v. absorpt. obs. 2—18461
    O_2, i.r. fundamental vibration band obs., collision-induced 2—8697
    O_2, K-absorpt. structures, 20-100 Å 2—18463
    O_2, photoelectron spectra of some autoionizing resonance states 2—8692
    O_2, resonance electron spectrometric obs. of electronic collisions 2—5902
    O_2, rotational Raman 2—18464
    O_2, Schumann-Runge photodissociation continuum, theoretical calc. 2—818
    O_2, vibrationally excited, absorption in Schumann Runge continuum 2—3057
    O_2 Herzberg I system, Franck-Condon factors, Klein- Dunham potentials calc. 2—38933
    O_2 microwave spectrum, pressure broadening calc., strong-collision model 2—18460
    O_2^- excitation in alkali halide crystals, vibrational structure 2—813
    $O_2(^1\Delta_g)$, vacuum ultraviolet photoelectron spectrum 2—760
    $O_2(^1\Delta g)$, transient species obs. using pheoelectron and chemielectron spectrosocopy 2—35163
    OF, $^2\Pi$ state, ab initio calc. of spectroscopic constants 2—31818
    OH, effective emitting populations for various collision frequencies 2—38870
    OH, emission in pulsed discharge through H_2O vapour 2—28316
    OH, excitation rates of vibrational levels, and nightglow intensities 2—40974
    OH, Λ-doublet transitions, detection in molecular beam maser 2—12187
    OH, predissociation by continuum of bound state without curse crossing 2—18462
    OH, reanalysis of $A^2\Sigma^+$-$X^2\Pi_i$ system 2—5943
    OH, rotational temp. in night airglow, temporal variations 2—30322
    OH Comet Bennett (1969 i), emission from nucleus 2—4981
    OH ground state vibr.-rot. bands, obs. in chemiluminescent O_3-olefin gas phase reactions 2—22868
    OH radical, high-field Stark effects on near u.v. spectrum 2—8698
    OH‡, stimulated i.r. emission, produced by pulsed electric discharge 2—21077
    $O_2(^1\Sigma^+_g)$, emission at 7620 Å rel. to detection of sensitized formation 2—13591
    PN, rotation spectrum 2—38936
    PO, emission spectrum attributed to $^2\Sigma$-$^2\Sigma$ transitions, rotational structure of bands 2—18465
    PO, Rydberg states converging to ground state of PO^+, LCAO-MO SCF calculations 2—35278
    Pb_2, matrix isolated, absorption spectra 2—15223
    PbO, i.r. spectra and structure, matrix isolation study 2—15330
    Rb_2, laser pulse radiation absorpt., mol. dissociation mechanism 2—24485
    ^{87}RbF, h.f.s., Stark and Zeeman effect, molec. beam resonance meas. 2—21641

Spectra continued
  inorganic molecules, diatomic continued
    S_2^- excitation in alkali halide crystals, vibrational structure 2—813
    $SO(^3\Sigma_g)$, transient species obs. using photoelectron and chemielectron spectroscopy 2—35163
    Sb_2, vacuum u.v. absorption spectrum 2—18402
    SbBr, electronic spectra, band system classification 2—28325
    SbF, effective vibrational temperature in A_2 system 2—3061
    SbF, rotational analysis of C_2 system 2—824
    SeN, electronic spectra, 3500-5500Å 2—35288
    Si halide, matrix element of dipole moment of transition, depend. on r-centroid intensities 2—18469
    Si_2, absorption between 4800 and 3000 Å, new data on first excited electronic state 2—8706
    SiD, 3250 Å bands, rotational analysis 2—5952
    SiH, 3250Å bands, rotational analysis 2—5952
    SiH, Franck- Condon factor and true potential energy curves 2—5951
    SiH^+, Franck-Condon factor and true potential energy curves 2—5951
    SiH^+, Franck Condon factors and r-centroids for $A'\pi-X'\Sigma^+$ band system 2—31829
    SiN, violet electronic emission 2—38940
    SiO, electronic transitions in region 3700 to 3950 Å 2—35289
    SiO, orange system, $^2\Pi$ to $^2\Sigma$ transition, rotational analysis of band (0,0) 2—31827
    SiO, radiative lifetimes and absolute oscillator strengths for $A^1\Pi-X^1\Sigma^+$ transition 2—35290
    SiO molecule, $E^1\Sigma^+$-$X^1\Sigma^+$ system in vacuum u.v. region 2—8708
    $SmF_2(Cl_2)$, in Ar, Kr or N_2 matrix, i.r. absorpt. 2—28327
    SnBr, u.v. absorption 2—5928
    SnCl, rotational analysis of visible band systems 2—31831
    Te_2 gas, $A0_u^+$, $B0_u^+-X0_g^+$ systems, rotational analysis 2—35292
    TiO, $^1\Delta$ to $a^1\Delta$ transition, rotational analysis 2—31832
    TiO, in inert matrices at 4°K 2—24489
    TlBi, gaseous, determ. dissociation energy from thermodynamic treatment of Knudsen cell-mass spectrometric data 2—21644
    TlCl, TlBr, TlI photoelectron spectra, analysis 2—24490
    TlCl isotopes, h.f.s. and Zeeman and Stark effects, molec. beam resonance meas. in different vibrational states 2—21645
    $^{205}Tl^{19}F$, Stark effect, molec. beam resonance meas. 2—21646
    UO, matrix isolated, i.r. spectrum 2—825
    Xe_2, absorption coeff. in u.v. near 147-nm resonance line 2—8713
    Xe_2, absorption spectrum, vacuum u.v. region, evidence for molecule formation 2—24492
    $YbF_2(Cl_2)$, in Ar, Kr or N_2 matrix, i.r. absorpt. 2—28327

  inorganic molecules, polyatomic
    alkali metal nitrates, vibrational spectra of monomer and dimer, cation association effects 2—8610
    borine carbonyl, high resolution spectrum of ν_5 perpendicular band 2—8582
    dihalocompounds, molecular orbital assignment from photoelectron spectra 2—35242
    hexafluorides, analysis of i.r. absorption spectra, thermodynamic props. 2—823
    hydrides, analogues to ionized inert gases, mol. orbitals from vac. u.v. and photoelectron spectra 2—18409
    metal tetrachlorides, electronic spectra, assignment of electronic transitions 2—12100
    rare earth β-diketonates, i.r. absorption spectra in region 750 to 250 cm^{-1} 2—21620
    rare earth metal fluorides, multiplet splitting in X-ray photoelectron spectra 2—35282
    thulium acetate tetrahydrate, ansorption over range 2500 - 9000 Å, Slater parameters, spin-orbit interaction 2—1697
    transition metal salts, bonding from multiplet splitting in X-ray photoelectron spectra 2—35291
    transition metal tetrathio and tetraselenometallates, i.r. spectra, normal coordinate analysis 2—15340
    triatomic C_{2v} type, mech. anharmonicity contrib. to i.r. band intensities 2—35228
    water, triplet excitation by low energy electron impact spectra 2—24453
    water, using far i.r. spectrometer 2—8634
    $[Ru^{II}(CN)_5NO]^{2-}$, electronic absorption spectrum calc. and obs. 2—5949
    Ag olefin complexes, i.r. spectra rel. to $\nu C=C$ stretching frequencies 2—15282
    Al complexes, vibrational assignment of i.r. spectra 2—15283
    $AlCl_3$, Al_2Cl_6, matrix isolated, i.r. spectrum rel. to structure investigations 2—31775
    $AlCl_3$, matrix isolated spectrum 2—12101
    B complexes, vibrational assignment of i.r. spectra 2—15283
    BBr_3, i.r. intensity of A_2 bands 2—38888
    B_2Br_4, crystalline and fluid, vibrational spectra and molecular symmetry 2—15284
    BD_4^- ions, solid solutions imbedded in f.c.c. alkalai halide lattices, infrared spectra 2—12181
    BF_2OH, structure and dipole moment from microwave spectrum 2—35230
    BO_2-, i.r. spectra, isotope effects 2—24439
    $BaCl_22(ONH_3)$ i.r. absorption spectra, vibrational analysis 2—15294
    Bi, complex, $Bi(S_2C_2H_4)X$, i.r. spectra, ligand configuration, vibr. assignment 2—8769
    BrCN, i.r. matrix- isolated spectra, 20K 2—8588
    BrCN, matrix isolation, i.r. spectra, Fermi resonance and dimer structure 2—12122
    C_4, C_5 and C_6, pure and mixed-isotope, Σ_u^+ freqs. and stretching force consts. 2—3031
    CCO, transient absorption spectrum observed in flash photolysis of C_2O_2 studied in 5000-9000 Å region 2—8603
    CN_2, infrared band in low temperature matrix 2—31782
    C_2N_2, rotational and vibrational structure of 2500 Å system 2—12109
    C_2N_2, rotational structure in $^1\Sigma_u \leftarrow {}^1\Sigma_g^+$ transition at 2200A, vibrational anal. 2—21592
    C_2N_4, infrared 2—38895
    CNBr, photoelectron spectra, geometries of various states of positive ions 2—774
    CNBr, vibr.-rot. spectrum, Fermi reson. 2—15288
    CNCl, photoelectron spectra, study of geometry of positive ions 2—774
    CNI, photoelectron spectra, geometries of various states of positive ions 2—774
    CO_2:O_2 mixtures, reflection spectra from 4 to 22 eV 2—16466
    CO_2-N_2-He plasma, electrically excited spectrum from 4.2 to 5.5 μm 2—12118

Spectra continued
  inorganic molecules, polyatomic continued
    CO_2-N_2* flowing mixtures, i.r. emission at 2.7 μm 2—21590
    CO_2, 10.4 μm band, N_2 broadened collisional width, variation with rot. quantum no. 2—38899
    CO_2, absorption in 1750 to 1200 Å region, temp. dependence calc. 2—12116
    CO_2, adsorbed on NaCl film, new bands obs. 2—5914
    CO_2, collision broadened line widths, effects of Coriolis interaction on line strengths of 3339 cm^{-1} band 2—18410
    CO_2, effect of Fermi resonance on temp. dependence of intensity of i.r. absorption bands 2—776
    CO_2, electron impact excited emission cross sections, meas. from 1260 to 5000Å 2—5919
    CO_2, Fermi Polyads at 5μm 2—8596
    CO_2, i.r. vibrational relaxation times, using spectrophone 2—18415
    CO_2, induced fluoresc. and temp. jump by resonant absorpt. of laser radiation 2—38893
    CO_2, near i.r. absorption spectra, vibr. energy levels and rot. const. determ. 2—12111
    CO_2, pure and N_2 perturbed, linewidths of ν_3-ν_1 transition 2—31781
    CO_2, threshold electron impact excitation spectra studied by SF_6 scavenger technique 2—28313
    CO_2 91% and N_2 9% mixture as Venusian atmosphere, spectral composition, emissivity and absorptivity 2—30584
    CO_2 dimers in 'locked' configuration, i.r. spectrum studied 2—8605
    CO_2 extinction coefficient meas. in 1700-3000 Å region 2—15296
    CO_2 infrared absorption line broadening at 207 and 298 K 2—18406
    CO_2 photodissociation obs. of phosphorescence from $CO(a^3\Pi$-$X^1\Sigma)$ Cameron bounds 2—28276
    CO_2 vibrational states lifetimes, spectrophone measurements interpretation 2—24436
    CO_2^+, obs. of spectral emission due to excited states prod. in $He(2^3S)+CO_2$ reaction 2—24445
    CO_2^{2-}, in anisotropic $CaCO_3$ crystal, Einstein coefficient spectra, light wave fields differences 2—801
    C_3O, infrared band in low temperature matrix 2—31782
    C_3O_2, ESCA line intensities, orbital determ. 2—35219
    C_3O_2, high-resolution photoelectron spectra, vib. analysis 2—35240
    $CO(CN)_2$, vacuum u.v. absorption spectrum, vibrational assignments 2—3032
    $CO(CN)_2$, X=F, Cl, Br, photoelectron spectra, 6-21 eV 2—28279
    COF_2, Fermi resonant 1943 cm^{-1} band, temp. dependence of spectral intensity 2—8592
    $(CO)Fe(PF_3)_4$, C_{3v} and C_{2v} isomers, i.r. spectra, vibrational assignments and enthalpy difference 2—24446
    COS, temperature dependence of u.v. continuous absorption spectrum, 210-260 nm 2—15291
    COS, threshold electron impact excitation spectra studied by SF_6 scavenger technique 2—28313
    COX_2, X=F, Cl, Br, photoelectron spectra, 6-21 eV 2—28279
    CS_2, afterglow emission studied following excitation in microwave or Ar discharges, 360-640 nm 2—24448
    CS_2, threshold electron impact excitation spectra studied by SF_6 scavenger technique 2—28313
    CSClBr, i.r. and Raman spectra, vibrational analysis 2—38896
    CSClF, u.v. band spectra, identification of electronic transitions, vibronic assignments 2—12120
    $CaCl_22(ONH_3)$ i.r. absorption spectra, vibrational analysis 2—15294
    $CaSO_4$-1/2H_2O, infrared observations of supposed α and β forms 2—5923
    $CdCl_22(ONH_3)$ i.r. absorption spectra, vibrational analysis 2—15294
    Ce complex, cerium tris-2,2,6,6-tetramethyl-3,5-heptanedione, vibrational, i.r. and Raman obs. 2—18441
    ClCN, i.r. matrix-isolated spectra, 20K 2—8588
    ClCN, matrix isolation, i.r. spectra, Fermi resonance and dimer structure 2—12122
    ClO_3- anion, Kβ X-ray emission spectrum calc. with all valence electron molecular orbital method 2—28267
    ClO_4- anion, Kβ X-ray emission spectrum calc. with all valence electron molecular orbital method 2—28267
    Cl_2O_7 obs. and attributions 2—779
    $Co_4(CO)_{12}$, i.r. spectra, derivation of stretching frequencies, interatomic forces and bonds 2—38900
    Co(III) complexes, trigonal MS_6 type, MCD spectra 2—12161
    $Cr(CO)_6$, complex, electronic spectra interpreted using non-empirical molecular orbital calcs. 2—12124
    $Cr(CO)_5NH_3$ complex, electronic spectra interpreted using non-empirical molecular orbital calcs. 2—12124
    CrF_4, mol. rotation spectrum, rel. to bond nature 2—8606
    Cr(III) complexes, trigonal MS_6 type, MCD spectra 2—12161
    CrIII complexes, tris chromium sulphur chelates, absorption and emission spectra, vibr. structure, energy forbidden transitions 2—21596
    $Cs_3In_2Cl_9$, i.r. 2—31773
    Cs_2SO_4 in inert gas matrices, 4.2 K, i.r. absorption spectra, vibr. assignment 2—31790
    $Cu(NO_3)_2$, vibrational spectra of monomer and dimer, cation association effects 2—8610
    D_2O, high resolution photoelectron spectrum meas. rotational structure partialy resolved 2—12151
    D_2S, nuclear hyperfine structure and mol. constants from mol. beam expt. 2—8611
    FD_2^+, i.r. spectrum, determ. of structure and force constants 2—8612
    FHD^+, i.r. spectrum, determ. of structure and force constants 2—8612
    Fe complexes, derivatives of $[SCH_3Fe(CO)_3]_2$ 2—785
    $FeCl_2$, matrix- isolated, nuclear gamma resonance studies at 4.2°K 2—35246
    Fh_2^+, i.r. spectrum, determ. of structure and force constants 2—8612
    Gd complex, gadolinium tris-2,2,6,6-tetramethyl-3,5-heptanedione, vibrational, i.r. and Raman obs. 2—18441
    $GeBr_4$, i.r. spectra, frequency assignment 2—35248
    $GeCl_4$, i.r. spectra, frequency assignment, symmetry forbidden bands from ν_2(e) mode 2—35248
    GeF_2, vacuum u.v. spectra, assignment 2—12194
    GeH_2, prod. in vacuum u.v. photolyisis of GeH_4, i.r. spectrum, frequency assignment 2—8616
    GeH_3, prod. in vacuum u.v. photolysis of GeH_4, i.r. spectrum, frequency assignment 2—8616
    GeH_4, absorption spectra, 2-17 μ region, vibrational band analysis 2—21601
    GeH_4, i.r. absorption spectra, 250 to 5000 cm^{-1} 2—12128

Spectra continued
  inorganic molecules, polyatomic continued
    GeH_4, photoelectron spectra 2—8795
    GeH_2Br, prod. in vacuum u.v. photolysis of GeH_3Br, i.r. spectrum, normal coordinate anal. 2—12127
    GeH_2Cl, prod. in vacuum u.v. photolysis of GeH_3Cl, i.r. spectrum, normal coordinate anal. 2—12127
    GeH_2X_2 (X=F, Cl, Br, or I), photoelectron spectra 2—21643
    GeH_3X (X=F, Cl, Br, or I), photoelectron spectra 2—21643
    H_2, high resolution photoelectron spectrum meas. rotational structure partially resolved 2—12151
    HBO isolated in Ar matrix, i.r. spectrum 2—28293
    HCN isotopes in Ar matrices, i.r. spectra 2—8643
    HCNO, i.r. spectrum, hot band analysis, l-type doubling const. 2—8632
    HCl complexes, effect of intermolecular Van der Waals interactions on i.r. spectra 2—24575
    $HD^{80}Se$, hyperfine structure of $4_2 \rightarrow 4_1$ rotational transition by beam maser spectroscopy 2—24455
    HF_2, i.r. spectrum, null gap region, rotational structure 2—12133
    HN_3, rotation-vibration spectrum in near i.r. and visible 2—15303
    HNCO, microwave obs. of rotational transitions 2—38902
    HNO, far u.v. system, oscillator strength meas. 2—18430
    HNSO, ultraviolet, diffuse bands between 2690 and 2387Å 2—35251
    HO_2 radical in gas phase, absorption spectra 2—37038
    H_2O, CO_2 and O_3 spectral transmissivity of real gas, exponential model 2—21921
    H_2O, emission spectrum of oxy-hydrogen flame observed, rotational analysis 2—12152
    H_2O, i.r. absorpt., after passage through mag. field 2—3397
    H_2O, optical and electron scatt. spectra, theoretical interpretation 2—12138
    H_2O, triplet excitation by low energy electron impact spectroscopy, cross section determ. 2—15311
    H_2O, vacuum u.v. obs. below 1200 Å 2—18378
    H_2O i.r. spectra of deformation vibration in micas 2—15304
    H_2O vapour, intensity-half-width products in 6.3 μm absorption band 2—32179
    H_2O vapour, measurement and interpretation of near i.r. bands 2—8659
    $H_2{}^{18}O$, i.r. spectra of vapour, rotational structure of ν_2 band, vals. of energy levels of 1st excited state 2—12132
    HOCl, i.r. spectrum, gas phase, ν_2 band study 2—18425
    HOF, in dil. N_2 matrix, i.r. spectrum, obs. of fundamental frequencies 2—8638
    H_2PPF_2, microwave spectrum, conformation determination from Stark effect analysis 2—15305
    H_2S, structure of ^2A, band in photoelectron spectrum correlated with transitions to vibrational-rotational levels 2—24474
    H_2S photoelectron spectrum, calc. of vibrational envelope and bond angle in first excited state of H_2S^+ 2—28303
    H_2S^+ radical ion, comparison of photoelectron and optical spectroscopy 2—21616
    H_2S_n (n=2,3...8), predicted and observed spectral properties 2—15336
    HSiI absorption spectrum 4600-5600Å, obs. in flash photolysis of SiH_3I, geometry of upper and lower states 2—35260
    I complexes, electronic, spectra, effect of intermolecular interactions 2—8578
    $InCl_2$, i.r. 2—31773
    Ir(III) complexes, comparison of $n\pi^*$-$_{\pi\pi}{}^*$ interactions with $d\pi^*$-$\pi\pi^*$ interactions in aromatics 2—35300
    Ir(III) complexes, trigonal MS_6 type, MCD spectra 2—12161
    $K_3Cr(CN)_6$, exptl. investigation of $^4A_2 \rightarrow {}^2E$, $^2T_1$ transitions 2—29918
    $K_4Cr(CN)_5NO$, vibr. modes 2—22770
    K_2O, prod. in matrix reaction, i.r. spectrum, force constants 2—12158
    KOH, stabilized in Ar matrix at 4.2 K, i.r. absorption spectra, force field calc. 2—28304
    $(KOH)_2$, stabilized in Ar matrix at 4.2 K, i.r. absorption spectra, frequencies of OH vibrations and configuration determ. 2—28304
    La complex, lanthanum tris-2,2,6,6-tetramethyl-3,5-heptanedione, vibrational, i.r. and Raman obs. 2—18441
    $LiAlF_4$, i.r. spectra of matrix isolated vapours 2—797
    $LiCrO_2$, electronic struct., absorpt. spectrum obs. 2—19512
    LiO_2 in oxygen matrices, assignment of vibrational modes in i.r. and Raman spectra 2—28308
    ^7LiCN and ^6LiCN, matrix isolated, i.r. spectra, vibrational modes band assignment 2—12160
    Mn (II) complex, $MnX_4(C_5H_5NH)_2$ vibr. spectra 2—25338
    Mn complex, Mn(III) porphyrins, far red MCD spectra 2—8667
    $MnCl_22(ONH_3)$ i.r. absorption spectra, vibrational analysis 2—15294
    MoO_4^{2-}, vibrational spectra and force constants 2—35264
    MoS_4^{2-}, vibrational spectra and force constants 2—35264
    N_2, in solid Ar matrix, induced fundamental i.r. band 2—18472
    N_2 9% and CO_2 91% mixture as Venusian atmosphere, spectral composition, emissivity and absorptivity 2—30584
    N_3^-, NO_2^-, NO_3^-, valence shell electronic structure photoelectronic spectroscopy obs. 2—35276
    N_3^-, valence electronic struct. from X-ray photoelectron spectroscopy 2—35225
    NCl_3, isotopic species, i.r. evaluatiln of pot. energy constants 2—5937
    NF_3, high resolution study of l-type resonance in ν_4 band 2—8673
    NH_3-H_2 collisions, observation of $\Delta k=\pm3$ transitions 2—24579
    NH_3, electron collisions, vacuum u.v. spectra 2—18454
    NH_3, far i.r., cross relaxation in rotational inversion doublets 2—38923
    NH_3, ground state to $^2A_1''$ ionic state transition, Franck Condon factors 2—8671
    NH_3, rotational spectra, analysis, determ. of structural parameters 2—802
    NH_3, Stark effect on vibr.-rot. transition, h.f.s. 2—24476
    NH_3, using far i.r. spectrometer 2—8634
    NH_3, vibr.-rot. transition, absortion saturation 2—5934
    NH_3, vibration-rotation spectrum, rotational analysis of 6450 A band 2—28312
    NH_3 gas, vibration- rotation spectrum, vibr. assignments 2—21631
    NH_3 infrared spectra in the atmosphere 2—37138
    NH_3 Stark effect on vibr.-rot. transition, h.f.s. 2—24476
    NH_4BF_4, i.r. spectra, 17 to 300K 2—24482
    NO_2, electronically excited, short radiative lifetimes 2—8680
    NO_2, resnance fluorescence spectrum, interpretation 2—12172
    NO_3-, in anisotropic $NaNO_3$ crystal, Einstein coefficient spectra, light wave fields differences 2—801
    N_2O, electron collisions, vacuum u.v. spectra 2—18454
    N_2O, harmonic oscillator Franck Condon factors for ionization 2—15317

Spectra continued

inorganic molecules, polyatomic continued

N_2O, i.r. absorption of fundamental bands, spectral mean parameters 2—15321

N_2O, in solid N_2 matrix, i.r. spectra, anharmonic force constants 2—12169

N_2O, intensity and half-width meas. of (00°2-00°0) band 2—38926

N_2O, line strengths of bands in 2.9 micron region, dipole moment matrix element 2—18448

N_2O, relative rotational line intensities of various transitions, 250 and 300 K 2—24480

N_2O, threshold electron impact excitation spectra studied by SF_6 scavenger technique 2—28313

N_2O absorption lines, foreign-gas broadening coefficients 2—28309

N_2O high resolution determ. of line intensities 2—12176

N_2O physically adsorbed on silica, i.r. study 2—9304

N_2O_3, gaseous, i.r. spectrum, −120°C, assignment of vibration rotation bands 2—12178

NSF, triplet state at 5360 Å, Zeeman study and preliminary rotational analysis 2—3051

$^{15}NH_3$, i.r. microwave two-photon transitions 2—8683

$NaAlF_4$, i.r. spectra of matrix isolated vapours 2—797

$NaBD_4$, infrared spectra of high and low temperature modification, assignment of bands due to isotopic splitting 2—12181

$NaBO_2$, ^{18}O-labelled, vibrational spectra 2—21589

Nd complex, neodymium tris-2,2,6,6-tetramethyl-3,5-heptanedione, vibrational, i.r. and Raman obs. 2_18441

Ni, complex, of dimercaptodiethyl sulphide, i.r. spectrum, configuration 2—8769

Ni complex, bis-(π-allyl), orbital assignment from photoelectron spectra obs. 2—35280

No, integrated intensity of fundamental band 2—21632

O_3, high resolution meas. of $\nu_1 + \nu_2 + \nu_3$ absorption band in 3.59 μm region, rigid rotator analysis 2—8696

O_3, i.r. absorpt. bands, anharmonicity coeffs. 2—31816

O_3 isotopic molecules, inert-gas matrix isolated, i.r. absorption spectra 2—8690

O_3 with H_2S, CH_3SH, CH_3SCH_3 and SO, chemiluminescent reaction, visible and near u.v. spectra 2—20179

O_4, cooperative optical transitions, dipole intensity computation, symmetry of dimeric and exciton states 2—24484

OCS, i.r. emission, rot.-vibr. struct. of transitions 2—28275

OCS in solution, determ. of band width and profile of ν_3 mode, separation of rotational and vibrational effects 2—38934

PCl_3, i.r. spectra, symmetric top force constants 2—38935

$(PNCl_2)_3$, ^{15}N-labelled, vibrational assignment of i.r. spectra 2—28319

P_4O_{10}, normal coordinate analysis, force consts., mean amplitudes of vibration from spectral study 2—18467

P_4O_6, normal coordinate analysis, force consts., mean amplitudes of vibration from spectral study 2—18467

$POCl_3$, isolated in Ar, CO_2 and CH_4 at liquid He temperature, i.r. spectra 2—13491

Pb_2O_2, i.r. spectra and structure, matrix isolation study 2—15330

Pb_4O_4, i.r. spectra and structure, matrix isolation study 2—15330

PbX_2, (X=Br, Cl,I), photoelectron, use of cylindrical-mirror analyzer 2—35293

Pd complex, bis-(π-allyl), orbital assignment from photoelectron spectra obs. 2—35280

Pd complexes, 1,5-cyclooctadiene complexes, i.r. spectra, frequency dependence on metallic ion 2—15332

Pr complex, promethium tris-2,2,6,6-tetramethyl-3,5-heptanedione, vibrational, i.r. and Raman obs. 2—18441

Pt complex, $K[PtCl_3(C_2H_4)].H_2O$, vibrational spectrum, relationship with vibrational structure in photoelectron spectra of ethylene and ethylene-d_4 2—3087

Pt complexes, 1,5-cyclooctadiene complexes, i.r. spectra, frequency dependence on metallic ion 2—15332

Pt coord. cpds., photoelectron spectroscopy 2—35281

Pt olefin complexes, i.r. spectra rel. to $\nu C{=}C$ stretching frequencies 2—15282

Pt(II) complex, PtX_2L_2, X=Cl, Br and I, L=dialkyl sulphide, i.r. and Raman spectra, fundamental assignment 2—28322

PtOH on surface of Pt, i.r. spectra of OH groups 2—8699

Rb_2O, prod. in matrix reaction, i.r. spectrum, force constants 2—12158

RbOK, prod. in matrix reaction, i.r. spectrum, force constants 2—12158

ReF_6, $^2E_{5/2g} \leftarrow {}^2E_{3/2g}$ transition, Jahn-Teller effects 2—3060

ReF_6, i.r. spectra, Jahn Teller vibrations, zeta const. 2—31825

Rh complexes, 1,5-cyclooctadiene complexes, i.r. spectra, frequency dependence on metallic ion 2—15332

$Rh_4(CO)_{12}$, i.r. spectra, derivation of stretching frequencies, interatomic forces and bonds 2—38900

Rh(III) complexes, trigonal MS_6 type, MCD spectra 2—12161

RuO_4, i.r. and Raman spectra, coriolis consts., quadratic force constants 2—12190

$[Ru^{II}Cl_5NO]^{2-}$ electron absorption spectrum 2—38938

S_3, S_4, identification in unsaturated S spectrum at 300 to 650°C 2—15334

SCN- anion, Kβ X-ray emission spectrum calc. with all valence electron molecular orbital method 2—28267

SF_6, absorpt. cross sections and photoionization efficiencies in 300-1000 Å region 2—21639

SF_6, ESCA line intensities, orbital determ. 2—35219

SF_6, K-absorpt. structures of S, 20-100 Å 2—18463

SO_2, $^3B_1$ state, radiative lifetimes 2—8704

SO_2, rotational analysis of $^3\beta_1 \leftarrow {}^1A_1$ bands 2—12191

SO_2, single vibronic level lifetimes of first excited singlet state 2—8703

SO_2, vibrational structure of 2348 Å system 2—15335

SO_2 detection in air, by dual beam Fourier transform spectroscopy 2—10671

$SO_3{}^{2-}$ anion, KB X-ray emission spectrum calc. with all valence electron molecular orbital method 2—28267

$SO_4{}^{2-}$ anion, Kβ X-ray emission spectrum calc. with all valence electron molecules orbital method 2—28267

$SO_2{}^{35}Cl^{35}Cl$, ^6R type transitions identification 2—24486

SeO_2, matrix isolated, i.r. spectrum and thermodynamic functions 2—8705

$SiBr_4$, i.r. spectra, frequency assignment 2—35248

SiC_2 free radical, absorption bands obs., 4300 to 5000 Å 2—12195

$SiCl_4$, i.r. spectra, frequency assignment, symmetry forbidden bands from ν_2(e) mode 2—35248

SiF_2, vacuum u.v. spectra, assignment 2—12194

SiF_4, ultrasoft X-ray absorption spectra of Si and F 2—31830

Spectra continued

inorganic molecules, polyatomic continued

Si_2F_6, i.r. and Raman vibr. spectra, normal coordinate anal., stretching force constants 2—8709

SiH_4, and deuterated species, matrix isolated, i.r. spectra 2—8707

SiH_4, photoelectron spectra 2—8795

SiH_4, SiF_4, vacuum u.v. expts. using storage ring light source 2—16479

SiH_3D, high resolution i.r. spectrum of Si-H stretching region 2—8710

SiH_2X_2 (X=F, Cl, Br, or I), photoelectron spectra 2—21643

SiH_3X (X=F, Cl, Br, or I), photoelectron spectra 2—21643

SiH_xX_{4-x}, X=halogen, photoelectron spectra studied to obtain information on bonding 2—24433

Sm complexes, ethyl 1-methyl acetoacetates and ethylbenzoylacetates, force constant determination from i.r. absorption spectra 2—28328

Sn, chain and ring conformation, predicted and observed spectral properties 2—15336

SnH_4, photoelectron spectra 2—8795

SrF_2, hydrogenated, deuterated, containing Pr, i,r. local mode spectra vibronic splittings 2—10368

$TiCl_nBr_{4-n}$, i.r. and Raman spectra, force constants 2—18471

TiO_2, in inert matrices at 4°K 2—24489

$Tl_3In_2Cl_9$, i.r. 2—31773

$TlNO_3$, vibrational spectra of monomer and dimer, cation association effects 2—8610

TlX, (X=Br, Cl,I), photoelectron, use of cylindrical-mirror analyzer 2—35293

$tMVO_4$, ground state doublet splitting, g-factor, mol. field effects below T_d 2—22665

U complexes, mono and tri-fluoro-oxalate, luminescence and i.r. absorption spectra 2—28330

UO_2 ion, vibronic spectra, correlation with coordination geometry 2—15341

$UO_2{}^{2+}$, new absorption bands, assignment rel. to vibr. levels of ground state 2—35294

$VOCl_25NH_3$ absorption spectra corresponding to deformation oscillations of coordinated molecule 2—15342

XeF_6, Raman spectra and i.r., visible, u.v. absorption spectra in vapour and matrix isolation 2—38944

inorganic molecules, polyatomic, radiofrequency

see also Nuclear magnetic resonance and relaxation; Paramagnetic resonance and relaxation

molecule, and isotopic species, submillimeter wave spectra, rotational transition assignment 2—12146

vapour, resolution of anomalies in resonance dispersion of pressure broadened line at 22 GHz 2—8633

BrF_5, microwave spectrum 2—5912

COS gas, microwave spectrum, line shape study, low pressures 2—12165

CsF, molecular beam, r.f. spectra, electric dipole moment and quadrupole coupling const. up to v=8 2—5926

$(DF)_2$, microwave and r.f. spectra 2—8645

$(DF)_2$, study of r.f. and microwave spectra by molecular beam electric resonance method 2—21614

DOF microwave spectra, rotational constants and structural parameters 2—8626

D_2S, millimeter and submillimeter wave rotational spectrum, rotational constants and centrifugal distortion effects 2—21600

DSSD, rotational spectrum anomalous K doubling by centrifugal distortion 2—24461

DSSD millimetre wave rotational spectrum, Q branches 2—24451

F_3SiSiH_3, microwave spectrum at 8 to 38 GHz, rotational constant determination 2—15300

GeH_3Br, six isotopic species, microwave pure rotational spectra 2—18421

GeH_3I, four isotopic species, microwave pure rotational spectra 2—18421

HDS, microwave rotational spectrum, centrifugal distortion analysis and rotational constants 2—8631

$(HF)_2$, microwave and r.f. spectra 2—8645

$(HF)_2$, study of r.f. and microwave spectra by molecular beam electric resonance method 2—21614

HFDF, study of r.f. and microwave spectra by molecular beam electric resonance method 2—21614

HNCO and DNCO, molecular-beam microwave spectra 2—31795

HNO_2, cis and trans, microwave spectra for eight isotopic species 2—788

H_2O, HDO, D_2O, isotopic species, microwave spectrum 2—12148

$H_2{}^{16}O$, submillimeter microwave spectrum, rotational transition meas. 2—18400

HOF, microwave spectra, rotational constants and structural parameters 2—8626

H_2S, and isotopic species, submillimeter wave spectra, rotational transition assignment 2—12146

H_2S, microwave spectrum and centrifugal distortion effects 2—38904

HSSD, millimetre wave rotational spectrum, $^rQ_0$ branch 2—38909

HSSH millimetre wave rotational spectrum, P,Q and R branches 2—28294

HfI, obs. of new band spectrum in emission from radiofrequency discharge 2—8657

LiOH(D), molecular beam electric resonance spectra 2—8663

NF_2 free radical, microwave rotational spectrum 2—12179

NF_2 radical, microwave Zeeman spectra, electron spin-rotation interaction 2—8678

NH_3, collision induced rotational transition, microwave double resonance study 2—12177

NH_3 dimers, presence deduced from spectra near 10 cm^{-1} 2—38924

NH_3 gas, microwave spectrum, line shape study, low pressures 2—12165

$^{14}NH_3$, quadrupole tensor evaluated first and second order Zeeman effects obs. 2—8682

O_3, millimetre wave spectrum, rotational constants, Stark effect, dipole moment 2—8691

OCS, collisions study by broadening of microwave spectral lines 2—35385

OCS, double resonance in absorption spectrum 2—8693

PF_2NH_2 2—31820

SF_5Cl, quadrupole hyperfine effects in microwave spectrum 2—38939

SeO_2, microwave spectrum, 3rd order potential constants and dipole moment 2—31828

SnH_3Br, microwave spectrum, molec. structure and constant determination 2—15337

SnH_3I, microwave spectrum, molec. structure and constant determination 2—15337

inorganic solids

α-Al_2O_3, concentration profiles of coloured transition metal ions, meas. 2—17741

Spectra continued
inorganic solids continued
alkali borate glass, absorpt. of VO^{2+} ion 2—40763
alkali borate glass, trapped electron centre, X-irradiation induced, absorp. obs. 2—20137
alkali fluorides, photoemission spectra, 10-40 eV photon energy range, electron affinities determ. 2—19803
alkali halide, optical absorp., Bi^{3+}, Hg^0, Cd^0 centres 2—3801
alkali halide, rel. to impurity precipitation, review 2—3794
alkali halides, band density approach, expts. using storage ring light source 2—16479
alkali halides, exciton energy levels, exciton-phonon interaction influence 2—7067
alkali halides, mag. circular dichroism of centres produced by electrolytic reduction 2—10359
alkali halides, matrix shifts of h.f.s. consts. of Mn and Mn^+ centres 2—7024
alkali halides, uniaxial stress effects on off-centre pot. of Cu^+ and Ag^+ 2—20020
alkali halides, u.v. absorpt. of heavy ions, fine struct. 2—33250
alkali halides, vac. u.v. reflectivity, excitonic struct. 2—16469
alkali halides with s^2 ions, charge transfer effects on optical transitions 2—33230
alkali iodides, excitons perturbed by self-trapped excitons 2—26156
alkali metal nitrates, vibrational spectra as functions of phase 2—35768
alkali metal sulphate, Co^{2+}-doped, crystal field parameter determ. at low temps. 2—36866
alkaline earth metal film, reflectance and transmittance, optical consts. detn. 2—20017
alkaline earth titanates and zirconates, diffuse refl. spectra, band struct. 2—1526
amorphous and cryst. material, exponential tail behaviour of fund. absorpt. edge 2—40652
anharmonicity of crysts. heated by intense i.r. radiation 2—19345
antiferromagnet, magnon sideband temp. depend. calc. 2—33163
antiferromagnet, magnon-photon coupling 2—22747
antiferromagnetic transition metal fluorides, study of mixed crystals 2—40543
apatite, i.r. spectral investigation of structural changes during hydrothermal treatment 2—39635
atmospheric gas, extreme u.v. reflection spectra 2—19995
band structure studies 2—36406
beryl, i.r. refl., anharmonicity 2—26143
beryl, transmission and reflection in the i.r., measured with polarized light 2—10365
binary borosilicate glass films, vapour deposited, i.r. absorption spectra 2—16484
boron suboxide, i.r. and soft X-ray emission rel. to cryst. chemistry 2—9331
borosilicate glass, film, i.r. absorp., nondestruct. detn. of comp. and thickness 2—1174
borosilicate glass, film, on Si, B diffusion source, i.r. absorp. 2—16483
caesium halides, core exciton decay obs., photoemission spectra 2—19802
calcium hydroxyapatite, i.r. spectra of OH groups, H bonding, fluoridation effects 2—36872
CdX, x=chalcogen, d-levels location from u.v. photoemission obs., comparison with other spectra 2—22658
chlorides, Cl^- $L_{2,3}$ absorpt. spectra regularities 2—20032
coatings, dye lacquered and constituents, reflectance in 210 to 2600 n.m. range 2—23707
corundum, i.r. reflection spectra effect of impurity ions 2—33235
crystallographic axes determ. in single crysts. at high pressures 2—15683
datolite, transmission and reflection in the i.r., measured with polarized light 2—10365
diamond, absorpt. rel. to e.p.r. spectra, paramagnetic centres 2—26274
diamond, impurity induced one phonon absorpt. 2—20028
diamond, i.r. spectra, absorption lines, bond vibrations 2—10366
diamond, local effective fields calc., low frequency electronic dielec. const. umklapp effects 2—22745
diamond, two-phonon i.r. spectrum, elec. field effect 2—20029
disordered solids as filters for far infrared, absorptivities 2—31127
divalent complexes of cis chelating bidentate ligands, effect of d-orbital splitting on i.r. spectra 2—10363
electrode/electrolyte interface, specular reflection obs. of adsorbed layers 2—9301
europium chalcogenides, optical transitions, magnetic order effect, energy level scheme 2—16488
exchange splitting in excitons, interatomic distance depend. 2—29903
exciton-phonon interaction, coherent potential approx. 2—26135
exploding wire binary alloy, width of absorption lines 2—38812
α-Fe_2O_3, with chemisorbed CO, detection 2—7178
α-Fe, absorpt. spectra, self-absorpt., theoretical forms of emission L_{III} bands 2—16489
fluoroberyllate laser glass, rare earth doped, absorption 2—29961
formates, i.r. and Raman spectra, props. rel. to spectra 2—16542
germanate glass:Nd^{3+}, absorp. and laser props. 2—20102
germanates, normal II-IV spinels, i.r. spectra, vibrational assignment 2—10382
graphite, reflectivity, 3-40 eV region, opt. anisotropy obs. 2—19997
group IIB-VIA semiconductors, upper d-levels from X-ray and u.v. photoelectron spectra 2—36633
halide, layer structure, optical props., review 2—16686
heavy rare earths, direct absorption transitions at optical frequencies 2—26151
hexahaloiridates, alkali salts, Raman and i.r. spectra, lattice vibration obs. and force constant calc. 2—40673
hydrates, far-i.r. absorpt., deuteration effects, vibrs. obs. 2—22756
hydrates of various salts, i.r. spectra, stretching frequencies of H_2O molecules 2—20016
hydroxyapatites, hydrothermally prepared, vibr. spectra 2—16527
inert gas, density of states and excitonic effects 2—20024
inert gas, extreme u.v. reflection spectra 2—19995
insulator, double-exciton excitation effects in absorpt. spectra 2—20014
ionic cryst., far-i.r. anharmonic self-energy of long wave phonons 2—19348
ionic cryst., far-u.v. reflectivity, electronic struct. 2—13457
ionic cryst., i.r. absorpt. due to surface modes 2—19340
ionic cryst., multiphonon impurity absorpt. bands, magneto-optical effects 2—10358
ionic cryst., phonon press. depend. 2—19336

Spectra continued
inorganic solids continued
ionic cryst. two- and three-phonon processes in far-i.r. absorpt. 2—16000
ionic crystal, impurity ion octahedral complex, overlapping and covalency effects 2—19990
ionic crystal, i.r. absorp., temp. depend. of nonlinear lattice resonance damping 2—22390
ionic crystals, tellurate and tellurite doped, impurity induced absorption 2—16481
i.r., transition metal ion and rare earth ion doped crystals 2—20012
i.r. emission from single particles, variations with particle size 2—25118
KCl, absorpt., 12-25 eV 2—20034
lamellar cryst., u.v. reflectivity and optical consts. 2—10343
lanthanide fluorides, far-i.r. Stark and Zeeman splitting of rare earth ions 2—40669
layer-type crystals, reflectivity, 2-10 eV, plasmon and excitonic processes rel. to ionicity 2—20005
layer-type crystals, u.v. and soft X-ray absorpt. spectra 2—20033
Lyddane-Sachs-Teller relation, finite wave vector effects 2—19327
magnetic, emission and absorption spectra 2—26150
magnetic insulator, exciton line broadening and Hubbard model 2—19519
metal, dielec. function and effective band edge concept 2—29596
metal oxides, with c-type rare earth oxide structure, vibrational spectra, comparison with theoretical predictions 2—22755
metal particle, in transparent medium, rel. to surface plasmon energy 2—40152
metal-oxide boundary, contact interaction, i.r. spectroscopy obs. 2—15656
mica, Siberian deposits, i.r. spectra, 0.75 - 15 μm 2—1685
mica, vacuum u.v. props. 2—40648
mica solid solution, formed between $K_2Mg_6Al_2Si_6O_{20}F_4$ and Al-free mica 2—36302
mixed valence semiconductor, absorp. rel. to hopping conduction 2—9997
molybdates, normal I-VI spinels, i.r. spectrum, vibrational assignment 2—10382
muscovites, i.r. spectroscopic study of isomorphic changes 2—29919
optical absorption, Urbach's rule, with dispersion of frequencies 2—4452
orientationally disordered cryst., line profiles of exciton absorpt. 2—7065
oxide:Bi^{3+}(Eu^{3+}), u.v. absorpt. band positions 2—20049
oxide layer on Pt, Au and Ni, specular reflection spectra, monolayer thickness range 2—9310
oxides, high temp., i.r. and Raman, characterization of order-disorder 2—9829
oxygen layer on Pt, Au and Ni, specular reflection spectra, monolayer thickness range 2—9310
phosphate glasses containing Eu^{3+}, transition probabilities 2—29914
polycrystal, free carrier absorption 2—13469
polycrystalline materials, specular reflectance i.r. spectroscopy, LO mode frequency meas. 2—15992
potassium halides, core exciton decay obs., photoemission spectra 2—19802
potassium halides, extreme u.v. absorpt. spectra 2—20042
potassium halides, Pb-doped, optical absorpt. 2—20039
α- quartz, synthetic, dynamics of impurities 2—19387
rare earth, sequisulphide, reflectivity, band struct., density 2—40671
rare earth compounds, magnetic ordering effects 2—33259
rare earth garnets, dichroism due to site selectivity of ions 2—40639
rare earth ion-cryst. host, multiphonon, Raman and two-photon excitation 2—37940
rare earth metals, potential barrier effects in photoabsorpt. 2—20047
rare earth metals, potential barrier effects in photoabsorpt. 2—22775
rare earth metals, potential barrier effects in photoabsorpt. 2—22776
rare earth oxides and oxysalts, nephelauxetic effect rel. to anion centred coordination polyhedra 2—9338
rare gas, induced far-i.r. phonon spectra 2—19353
reflection spectroscopy, metals and alloys 2—16460
refractories, dielectrics, i.r. characteristics over temp. range 1000-1500°C 2—4454
resonance phenomena for local oscillations at multiple and combined frequencies 2—40654
rubidium halides, core exciton decay obs., photoemission spectra 2—19802
rubidium halides, extreme u.v. absorpt. spectra 2—20042
ruby:Cr, conc. depend. photon echo decay 2—40636
ruby, colour stability when annealed or exposed to UV irradiation 2—22883
ruby, conc. broadening of lines 2—1686
ruby, generation spectrum, three level centres, laser parameters 2—4485
ruby, heavily doped, optical props., review 2—36868
ruby, photon echo behaviour near 2.06 kG 2—26158
ruby, photon echo resonance 2—33232
sapphire, absorption, origin of colours, rel. to impurity ion interactions 2—10364
sapphire, Fe, Ti doubly doped, redox reaction, e.s.r. and optical spectra, biparticle formation, valency states 2—25241
semiconductor, absorpt. by impurity centre with deep level in static elec. field 2—10353
semiconductor, amorphous, weak absorpt. tails and localized states 2—33248
semiconductor, diamag. excitons in degenerate bands 2—26152
semiconductor, disordered, intrinsic and impurity absorpt., calc. 2—40653
semiconductor, doped, dielec. function and effective band edge concept 2—29596
semiconductor, electroabsorpt., excitonic effects 2—7066
semiconductor, excitonic absorption coefficient 2—10355
semiconductor, GaAs(Sb), InAs(Sb), Ge, Si, wavelength modulation, rel. to band struct. 2—1692
semiconductor, Ge, absorpt. by holes, indirect transitions role 2—1693
semiconductor, interband transitions and excitonic effects 2—10044
semiconductor, layered inhomogeneous structures, transmission and reflection spectra, layer thickness detn. 2—40643
semiconductor, magnetic, energy levels 2—4203
semiconductor glass filter, absorpt., transmission, luminescence 2—22757
silica gels, specific surface areas, pore struct., adsorpt. and i.r. spectra obs. 2—35920
silicate glass, u.v. absorpt. of Pb 2—16497
silicate glaze, i.r. reflection rel. to comp. 2—36854
silicate glaze, i.r. reflection rel. to struct. 2—28972
silver germanate glass, polymerization, i.r. study 2—15638
silver halides, valence band struct., expts. using storage ring light source 2—16479

Spectra continued
 inorganic solids continued
  soda, glass, pure earth doped, sensitivity to crystalline environment or included impurity ions obs. 2—9223
  sulphides and sulphates, visible and near i.r. of minerals and rocks 2—20010
  thallium aluminogermanate glass, polymerization, i.r. study 2—15638
  thallium germanate glass, polymerization, i.r. study 2—15638
  thin conducting slabs, absorption spectra, influence of plasma waves 2—36864
  thin crystal, electro-reflectance and absorption spectra, multiple reflection effects 2—19994
  topaz, transmission and reflection in the i.r., measured with polarized light 2—10365
  transition metal, vacuum u.v. photoelectron spectra, density of states in conduction band 2—9929
  transition metal coatings, extreme u.v. reflectance spectra, characterization in 500-2000 Å region 2—17719
  transition metal complexes, crystallizing in columnar structure, one-dimensional metallic properties from reflectance spectra 2—15681
  transition metal dichalcogenides, group IVA, selection rules for optical transitions 2—36417
  transition metal dichalcogenides, group VIA, fine struct. interpret. 2—32886
  transition metal niobates, i.r. absorpt. cryst. chem. 2—10396
  transition metal oxide, i.r. optical props. rel. to charge transport, review 2—9999
  tungstates, normal I-VI spinels, i.r. spectrum, vibrational assignment 2—10382
  Urbach rule, review 2—4453
  valence band structure from u.v. photoelectron spectra 2—36650
  vanadates, normal I-III-V spinels, i.r. spectrum, vibrational assignment 2—10382
  water adsorbed on alkali halide films, H-bond vibration, i.r. spectra 2—9305
  wurtzite type crystal, piezospectroscopy of defects 2—33247
  X-ray photoelectron, valence level obs. 2—36628
  YAG, Pr^{3+} linewidth obs. 2—10339
  zeolites, Y, copper exchanged, e.s.r. and i.r. studies of NO adsorption and disproportionation, effect of CO 2—25226
  ZnX, x=chalcogen, d-levels location from u.v. photoemission obs., comparison with other spectra 2—22658
  zoisite, transmission and reflection in the i.r., measured with polarized light 2—10365
  α-Al_2O_3:Fe^{3+}, optical absorption spectrum, assignment based on d^5 crystal field calc. 2—26157
  α-$2CaO.GeO_2.H_2O$, i.r., 3600-400 cm^{-1} 2—36871
  $3Al_2O_3$. $2SiO_2$, i.r. freq. calc. 2—36867
  AlN, polycrystalline, Kramers-Kronig analysis 2—40658
  Ag-Au, energy loss spectra of fast electrons, determ. optical properties 2—19958
  Ag-Mn dil. alloys, intraband absorpt., interband transitions 2—20019
  Ag, electron irrad., radiation emission 2—4085
  Ag, electroreflectance spectra in range 3 to 4 eV 2—29895
  Ag, energy loss spectra of fast electrons, determ. optical properties 2—19958
  Ag, interband transitions 2—10344
  Ag, vibrational spectra, phonon dispersion curves and specific heat calc. from modified angular force model 2—32801
  Ag, wavelength modulation spectra, effective mass 2—26141
  Ag and Ag alloy films, 2.4 to 4.4 eV, reflection and transmission, optical consts. detn. 2—22749
  Ag film, abnormal absorpt. band drift under action of O_2 2—1656
  Ag film on Pt, specular reflection spectra, monolayer thickness range 2—9310
  Ag films, transition radiation ang. distrib., reson. behaviour near plasma freq. 2—33229
  AgBr:Cr^{2+}, near i.r. absorpt., temp. depend., Jahn-Teller effect 2—40656
  AgBr:Cr^{2+}(Fe^{2+})(Ti^{3+}), near i.r. absorpt., temp. depend., Jahn-Teller effect 2—40657
  AgBr, Ag 4d levels from temp.-dependent photoelectron spectroscopy 2—36626
  AgBr, u.v. determination of absorption peaks 2—20018
  AgBr, wavelength modulation spectrum, determ. of polaron self-energy temp. depend. 2—22474
  AgBr(Cl), near and extreme u.v. obs. 2—1680
  AgCl:Cr^{2+}, near i.r. absorpt., temp. depend., Jahn-Teller effect 2—40656
  AgCl:Cr^{2+}(Fe^{2+})(Ti^{3+}), near i.r. absorpt., temp. depend., Jahn-Teller effect 2—40657
  AgCl, i.r. absorpt., from modified shell model, comparison with expt. 2—40024
  AgF, far i.r. transmission spectrum in lattice vibr. region, structure, dielec. props., elastic constants 2—32802
  $AgGaS_2(Se_2)$, energy band gap obs. 2—4223
  β-AgI, hexag. single cryst., exciton spectra, large angle reflection obs. 2—16462
  Ag_2O-P_2O_5, glass, i.r. and visible spectra, struct. 2—40655
  Ag_3SbS_3, polarisation shift of absorption edge, simplified band model 2—29906
  Ag_3SbS_3, refl. spectrum, energy levels determ. 2—29894
  Al-Au, Al-Ti alloys, comparison with sandwich struct. vac. u.v. spectra 2—20021
  Al-Cu(Mn) dil. alloys, impurity effects on band struct. 2—16463
  Al, absorpt., band struct. 2—29907
  Al, absorpt. and reflectance, 10^{-2} to 10^5 eV range, opt. constants determ. 2—19957
  Al, radiative decay of surface plasmons, photon emission 2—33251
  Al, reflectance in surface plasmon excitation region, surface roughness effects 2—16464
  Al, thermomodulation, interband region interpret. 2—36855
  AlAs, enhanced indirect absorpt., direct band gap 2—33252
  AlAs, optical absorpt., 4.2-293 K 2—19959
  Al_2O_3: Cr absorption spectra 2—33253
  Al_2O_3: Mn: Mg absorption spectra 2—33253
  Al_2O_3, corundum, colour centre activation energies 2—29198
  Al_2O_3, corundum, i.r. refl. phonon distrib. 2—26142
  Al_2O_3, corundum, production by Czochraslki and Verneuil method, absorption spectra 2—29908
  Al_2O_3, quartz, interstitial Fe^{3+}, absorp. 2—3806
  Al_2O_3, ruby, Cr^{3+} pairs, level scheme and energy transfer 2—33249

Spectra continued
 inorganic solids continued
  α-Al_2O_3, sapphire, transition metal doped, H incorporation by H_2, high temp., i.r. study 2—9584
  Al_2O_3 ceramic, thermolum. emission spectra, continuous determ. 2—29982
  Ar:Cs, absorpt., dynamical Jahn-Teller effect 2—10392
  Ar-Xe solid solns., exciton effects, 8-11 eV range 2—20025
  Ar, absorpt. of Li, K, Na and Cs atoms 2—24387
  Ar, doped, induced far i.f. phonon spectra 2—19353
  Ar, i.r. absorption of interstitial H and D atoms 2—33264
  Ar matrix shifts obs. in absorption spectra of trapped Ta atoms 2—36869
  As, amorphous, reflector power and fund. absorpt. edge 2—29896
  As, plasma reson. refl. 2—7063
  As_2S_3, amorphous, i.r. absorp. and reflectivity 2—16465
  As_2S_3, glass and cryst., interband spectra, Kramers-Kronig analysis of interband refl. 2—22748
  As_2S_3, glassy, thermoabsorpt. spectra, forbidden band widths, at 300 K and 130 K 2—22758
  $\alpha(\beta)$-As_4S_3, far i.r., n.q.r., cryst. struct., point charge calcs. 2—10586
  As_2Se_3, absorpt. and thermoabsorpt. near fund. edge 2—20026
  As_2Se_3, amorphous, i.r. absorp. and reflectivity 2—16465
  As_2Se_3, amorphous thin film, optical consts. determ. from i.r. refl. 2—33200
  As_2Se_3, glass and cryst., interband spectra, Kramers-Kronig analysis of interband refl. 2—22748
  As_2Se_3, glassy, thermoabsorpt. spectra, forbidden band widths, at 300 K and 130 K 2—22758
  Au-Mn dil. alloys, intraband absorpt., interband transitions 2—20019
  Au, direct optical coupling to surface plasmons 2—33239
  Au, energy loss spectra of fast electrons, determ. optical properties 2—19958
  Au, interband transitions 2—10344
  Au, photoelectron, density of states in conduction band 2—9929
  Au, photoemission spectra, temperature modulated, agreement with one-electron band theory and reflectance data 2—36627
  Au, spin-orbit coupling effects in u.v. and X-ray photoelectron spectra 2—36629
  Au, thermomodulation, interband region interpret. 2—36855
  Au, valence bands determ. from X-ray photoelectron spectra, comparison with relativistic calcs. 2—36630
  Au, vibrational spectra, phonon dispersion curves and specific heat calc. from modified force model 2—32801
  Au, wavelength modulation spectra, effective mass 2—26141
  Au and Au alloy films, 2.4-4.4 eV, reflection and transmission, optical consts. detn. 2—22749
  B, β-rhombohedral, refl., 0.4 to 16μ, anisotropy 2—40644
  BN film, absorption edge detn. 2—26159
  $B(OH)_3$ and its thermal decomposition products, i.r. vibrational spectra 2—29909
  $BaAl_{12}O_{19}$, doped with Fe group ions, absorption spectra, valency and coord. nos. of impurity ions 2—1687
  $Ba(ClO_4)_2.3H_2O$:MnO_4^-, mag. circular dichroism spectrum of MnO_4^- at 4.2K 2—36870
  $BaCl_2.2H_2O$, i.r. spectra, optical phonons, water orientation, 80-473K 2—40041
  BaF_2:Sr, X-irrad., absorp. spectra, F_{ae} centres 2—33256
  $Ba_{0.25}Mg_{2.75}Y_2Ge_3O_{12}$:$Nd^{3+}$, absorpt., laser action 2—16616
  $Ba(NO_3)_2$, i.r. refl., anharmonicity 2—19354
  BaO-SiO_2 glass, γ-irrad., optical absorpt. 2—30015
  BaS, dynamic ionic charge determ. from i.r. spectra and static dielec. props. 2—22396
  $BaSb_2O_6$, i.r. absorpt., cryst. chem. 2—26161
  $BaSiO_3$-Nd_2SiO_5, amorphous system, apatite phase, comp. depend., i.r. obs. 2—18894
  $Ba_3(XO_4)_2$, X=P, As, V, Cr, Mn, i.r. and Raman vibr. spectra, interpretation based on crystal structure 2—8586
  Be, calc. of soft X-ray photoelectron spectra using band theory of metals 2—36631
  BeTe, BeSe, BeS, optical absorp., bandgap detn. 2—20027
  $Bi_{12}GeO_{20}$, scatt. by phonons 2—10335
  Bi_2Te_3, reflectivity, intensive interband transitions identified 2—19996
  CO, adsorbed on Cu and CuO, .r. spectrum, reflection-absorption spectroscopy 2—7070
  CO_2, solid, reflection spectra from 4 to 22 eV 2—16466
  $Ca_2BaSi_3O_9$, vibr. spectrum interpretation 2—36908
  $CaCO_3$, fundamental vibrational modes, far i.r. reflection 2—19998
  $CaCO_3$, optical phonon lifetimes 2—19360
  $CaCO_3$, vaterite and calcite crysts. grown in gels, i.r. spectra 2—15684
  $CaCO_3$, absorpt. spectrum, effect of electrolysis and cryst. conditions 2—33255
  CaF_2:Dy^{3+}, noncubic components of emission spectra 2—26213
  CaF_2:Eu, zero phonon line, concentration dependence 2—4456
  CaF_2:Mn, thermolum. emission spectra, continuous determ. 2—29982
  CaF_2:Sr, Ba, X-irrad., absorp. spectra, F_{ae} centres 2—33256
  CaF_2, colour centres, electron-phonon interaction 2—13472
  CaF_2, F_3 centre, absorpt. band, zero-phonon line, fluorescence 2—19122
  CaF_2, hydrogenated, deuterated, containing Pr, i.r. local mode spectra, vibronic splittings 2—10368
  CaF_2, containing ion pairs of Gd, Ce, Pr with H, D, T, optical and i.r., electron-phonon interactions 2—10499
  CaF_2, lanthanide ion doped, far i.r., low freq. lattice resonant modes 2—9858
  CaF_2, low temp irrad., F_3^- centre, zero-phonon line 2—19124
  CaF_2, Mn- and Ce:Mn doped, cathode ray irrad., absorpt. rel. to colour centres 2—12787
  CaF_2, oscillator strengths of α- and β-bands 2—29199
  CaF_2, thermolum. emission spectra, 300-823 K 2—29973
  CaF_2, zero-phonon line, F_3 centre, quadratic Stark effect 2—19123
  $CaMoO_4$, direct optical coupling to surface phonons 2—33239
  $Ca_4Nd_6(SiO_4)_6F_2$, britholite, synthetic, i.r. absorption spectra, effect of replacing Ca by Mg, Sr, or Ba 2—33258
  CaO, $[Na]^0$ and $[Li]^0$ centre obs. 2—33257
  CaO, F^+ centre emission spectrum, one-phonon sidebands 2—29911
  CaO, vibronic props. of F^+ absorpt. band 2—7068
  $Ca(OH)_2$ microcryst., vibr. freqs. 2—16005
  $Ca_{10}(PO_4)_6F_2$-$Ca_4Y_6(SiO_4)_6F_2$, i.r. 2—36275
  CaS:Zr, Mn phosphor, luminesc. emission spectra, luminesc. mech. 2—36925

Spectra continued
  inorganic solids continued
    CaS, dynamic ionic charge determ. from i.r. spectra and static dielec. props. 2—22396
    $CaSb_2O_6$, i.r. absorpt., cryst. chem. 2—26161
    $CaSiO_3$-Nd_2SiO_5, amorphous system, apatite phase, comp. depend., i.r. obs. 2—18894
    $CaSo_4.{}^1/_2H_2O$, i.r. spectral characterization of γ and β phases 2—10367
    $CaWO_4$:Er, visible absorption spectrum of Er identification of upper electronic levels 2—29910
    $CaWO_4$:Nd^{3+}, optical pumping, birefringence dispersion, population inversion 2—20030
    Cd, optical absorption peaks explained in terms of direct transitions by APW calculations of band structure 2—4116
    Cd complex, tetrabenzoporphine, quasilinear spectra, vibration structure 2—4486
    $CdAs_2$, for i.r. reflectivity, classical non-interacting oscillator model applied 2—19999
    $Cd_3(As_xP_{1-x})_2$ alloys, optical transmission edge, temp. depend. 2—10336
    $CdCr_2S_4$, $CdCr_2Se_4$, chalcogenide spinel, lattice dynamics and mag. ordering, i.r. obs. 2—32806
    $CdCr_2S_4(Se_4)$, impurity level obs., Ag and In doped crysts. 2—40659
    CdF_2, absorpt. and refl., bandedge obs. 2—26144
    $CdGa_2Se_4$, abosprt., indirect transitions 2—16485
    $CdGe_xAs_2$ glass, i.r. absorpt., rel. to struct. 2—10374
    $CdGeAs_2(P_2)$, band struct. obs. 2—13458
    $CdGe_xP_2$ glass, i.r. absorpt., rel. to struct. 2—10374
    $Cd_xHg_{1-x}Se$, mixed crystal, absorp., energy gap, composition depend. 2—10046
    $Cd_xHg_{1-x}Te$, spectra, energy band gap, comp. depend. 2—10370
    $Cd_xHg_{1-x}Te$ alloys, relativistic effects on energies of optical transitions 2—29684
    $CdIn_2S_4$, absorpt. and refl., rel. to band struct. 2—22760
    $CdIn_2S_4(Se_4)$, refl. spectra, band struct. calc. 2—29898
    $CdIn_2Se_4$, refl. and transmission spectra, band gap determ. 2—20031
    CdS:Ga, absorp. and emission, rel. to structure change dependent on impurity conc. 2—26162
    CdS:Ti^{2+}, absorpt. Jahn-Teller struct. 2—10371
    CdS-Ni, absorption spectra, charge transfer band region, bound state formation 2—36889
    CdS, B, n=1 exciton line, electric field effect 2—10372
    CdS, birefringence spectral depend. 2—7061
    CdS, dislocations influence 2—10369
    CdS, optical-transmission modulation by acoustoelec. domains 2—7062
    CdS, optical phonons bound to neutral acceptors 2—19992
    $CdSb_2O_6$, i.r. absorpt., cryst. chem. 2—26161
    CdSe:Cr,Fe, photoionization absorp. 2—10373
    CdSe, B, n=1 exciton line, electric field effect 2—10372
    CdSe, two-electron transitions of donor 2—10337
    $CdSiP_2$, band struct. obs. 2—13459
    $CdSnAs_2$, electrorefl., band struct. obs. 2—13460
    $CdSnAs_2$, reflectivity, energy band struct. correlation 2—10345
    $CdSnP_2$, single cryst., thermoreflectance spectra 2—29900
    CdTe:Fe, impurity levels, photoconductivity, absorpt. and electro-absorpt. spectra obs. 2—36538
    p-CdTe:S, i.r. absorpt., 90-470K 2—22761
    CdTe:Ti(V)(Cr), absorpt., crystal field parameter determ. 2—22759
    CdTe, analysis in terms of energy band pseudopotential model 2—19666
    CdTe, electroabsorpt., Franz-Keldysh effect, internal microfields 2—36873
    CdTe, exchange splitting in excitons, interatomic distance depend. 2—29903
    CdTe, photoluminesc. spectra, spontaneous, edge emission band fine struct. 2—40715
    CdTe, reflectivity and band struct. 2—33303
    CdTe, u.v., rel. to band struct. determ. 2—40279
    CdX, x=chalcogen, core electron level obs., x-ray induced electron emission obs. 2—19811
    $Cd_xZn_{3-x}As_2$, reflectivity, i.r.-vac. u.v. obs., opt. const. determ. 2—20000
    Ce, soft x-ray absorpt. and photoemission obs. of electronic energy states 2—22791
    $CeO_2.TeO_3.4.5H_2O$, i.r. thermal stability study 2—29079
    ClO_3^-, in alkali halide matrices, i.r. spectra, site symm., Cl isotope effects 2—36874
    Co^{2+} complex, 'oxinate', u.v. and visible reflectance 2—22751
    Co^{2+} octahedral complex, overlapping and covalency effects 2—19990
    $CoCl_2$, exchange splitting of excited Kramers doublet in i.r. spectra 2—40660
    $Co_3IB_7O_{13}$, ceramic, visible and i.r. 2—15936
    $Co(NH_3)_6I_2$, internal rot. of NH_3 groups, i.r. spectra obs. 2—10375
    CoO, valence band structure, X-ray photoemission spectroscopy 2—36639
    Cr-Mn alloys, comparison with sandwich struct. vac. u.v. spectra 2—20021
    Cr, antiferromag. energy gap obs. 2—36763
    Cr (III) binuclear complex, $[(NH_3)_5Cr(OH)Cr(NH_3)_4(H_2O)]Cl_5.H_2O$, electronic spectra, 4.2-300 K 2—10377
    Cr complexes, solid-state and rigid glass, refl. and emission 2—10376
    Cr^{3+} octahedral complex, overlapping and covalency effects 2—19990
    α-Cr_2O_3, adsorption of CO_2, i.r. study 2—6381
    α-Cr_2O_3, adsorption of H_2O, D_2O and CO, i.r. study 2—6379
    α-Cr_2O_3, O_2 chemisorption, i.r. study 2—6380
    Cr_2O_3, optical-exciton absorption sepctrum changes observed for stress-induced spin flop 2—4403
    Cs halide, reflection between 12.5 and 26 eV, Cs-5p core level excitation 2—36856
    Cs halides, far-i.r. anharmonic self-energy of long wave phonons 2—19348
    CsBr:Pb^{2+}, A-band peak position determ. using extended Mollwo-Ivey reln. 2—29197
    CsBr(I), far-i.r. absorpt. due to impurities, phonon density 2—19366
    CsCl:K(Rb), i.r. lattice absorpt., breathing shell model 2—36875
    CsF, CsI, extreme absorpt., spectra, multiplet exciton band obs. 2—22793
    CsI, CsBr, CsCl, absorpt., 12-25 eV region, 300, 77 and 20K 2—20034
    CsI, impurity induced i.r. absorpt., lattice dynamical calc. 2—40661
    CsI, reflection, rel. to optical constants in excitonic region 2—20001
    $CsNO_3$, polarized Raman spectra 2—36898
    Cs_2ZrBr_6:Ir^{4+}, high resolution absorption spectra, assignment 2—26164
    Cu-Ni alloys, comparison with sandwich struct. vac. u.v. spectra 2—20021
    Cu, interband absorption, one- electron analysis 2—29913
    Cu, interband transitions 2—10344
    Cu, thermomodulation, interband region interpret. 2—36855

Spectra continued
  inorganic solids continued
    Cu complexes, e.s.r. and optical absorption studies 2—7069
    CuB_2O_4 and $Cu_3B_2O_6$ pellets characterization 2—13568
    CuBr, exciton spectrum, band struct. 2—33236
    CuBr(Cl)(I), deform. potentials for excitons 2—33231
    CuCl-CuBr solid solns., Zeeman effect of exciton bands 2—16486
    CuCl, exciton spectra, line-width and phonon interactions 2—10378
    CuCl, u.v. and soft X-ray absorpt. spectra 2—20033
    CuCl, uniaxial stress effects on excitons 2—13461
    CuCl(Br), shakeup photoelectron spectra 2—36636
    $CuGaS_2$, absorpt. and electroreflectance 2—9364
    $CuInS_2$, electroreflectance 2—9364
    CuN_6, infrared spectrum, rel. to explosive props. 2—1688
    CuO, Cu_2O, valence band structure, X-ray photoemission spectroscopy 2—36639
    Cu_2O, exciton electrorefl. spectra, ang. depend. 2—29897
    Cu_2O, green series n=1 exciton line, diffr. electroabsorp. obs. 2—36876
    Cu_2O, i.r. absorp. after annealing in O_2 and α-particle bombardment 2—36877
    Cu_2O, shakeup photoelectron spectra 2—36636
    Cu_2O, u.v. electroreflectance, band assignments 2—33237
    Cu_2O powder, transmittivity, i.r. region, optical phonons 2—36878
    $Cu(OH)_2$ infrared, temperature range 20-100°C 2—3991
    $CuPbAsS_3$ single crystals, absorption curves, 90-300K 2—22762
    D_2, adsorbed on NaCl and CsI, i.r. absorpt. spectra, 20K 2—36881
    $DyAlO_3$, absorpt., magnetic ordering effects 2—33259
    $DyAsO_4$, phase transition 11.17K, far i.r. spectra 2—16535
    $DyVO_4$, i.r. reflection, lattice vibrations and phase transition obs. 2—16533
    $DyVO_4$, phase transition 13.8K, for i.r. spectra 2—16535
    Er^{3+}, electric-dipole intensities calc., ligand field interactions 2—20035
    Er^{3+}, in fluorides, luminesc., emission spectra, excitation mechanism 2—26217
    $ErCrO_3$ single crystal, optical ${}^4I_{15/2}\rightarrow{}^4S_{3/2}$ transition of Er^{3+} studied with polarized light as function of temp. and applied mag. field 2—16487
    ErFe garnet, exchange interactions, far-i.r. Zeeman obs. 2—40637
    Eu complex, dibenzoylmethane, absorption and luminescence symmetry surrounding central ion 2—40663
    Eu^{3+} in phosphate glasses, transition probabilities 2—29914
    Eu_3As_2 film, absorpt., rel. to mag. order determ. 2—36722
    EuO:Gd, magneto-optical props. 2—40662
    Eu_3P_2 film, absorpt., rel. to mag. order determ. 2—36722
    Eu_2SiO_4, ferroelastic ferromag., optical absorpt., Faraday rotation, cryst. struct. 2—10195
    F_2O, crystalline, i.r. spectrum 2—29932
    Fe-Mn alloys, comparison with sandwich struct. vac. u.v. spectra 2—20021
    Fe^{3+}-doped oxides, phosphorescence and excitation spectra 2—10447
    Fe complexes, $Fe(py)_2\ Cl_2$ and $Fe(py)_4Cl_2$, electronic and Mossbauer spectra and mag. moment 2—16431
    $FeCO_3$, far-i.r. transmission, Neel pt. phenomena 2—40638
    $FeNbO_4$ and $FeNb_2O_6$, cryst. chem. 2—13473
    $Fe(OH)_2$, dehydration, haematite transformation, magnetic props., Mossbauer and i.r. spectra 2—22862
    FeOOH, β-δ in haematite, i.r. spectroscopic study of thermal conversion 2—40805
    Ga, optical constants, interzone electron transitions 2—10297
    GaAs:Al(P), implanted, i.r. localized vibr. mode absorpt. 2—13474
    GaAs:Co, absorp., optical transitions from valence band to acceptor states 2—33260
    GaAs:Cu, i.r. absorpt., calc. 2—36316
    GaAs:Cu, i.r. absorpt., complex nature of Cu acceptor 2—16490
    GaAs:Si, implanted, localized vibr. mode absorpt. 2—40664
    GaAs, absorp. in an elec. field, Wannier levels obs. 2—22764
    GaAs, electroabsorpt. and polarization anisotropy 2—7071
    GaAs, electron and neutron irrad., i.r. absorp., band edge density of states detn. 2—29916
    GaAs, electroreflectance meas. by electrolyte method, galvanoluminesc. role 2—40646
    GaAs, Franz-Keldysh effect anisotropy 2—10379
    n-GaAs, i.r. absorpt., carrier conc. and temp. depend. 2—29915
    GaAs, i.r. absorpt. bands due to localized vibrs. of B and C 2—33263
    p-GaAs, interband absorpt., band splitting, electron spin optical orientation obs. 2—13475
    GaAs, laser-type, refr. index peak at absorpt. edge freq. 2—36879
    GaAs, optical absorpt., 4.2-293 K 2—19959
    GaAs, reflectivity, energy band struct. correlation 2—10345
    GaAs, stress-modulated magnetoreflectivity, band parameters 2—33234
    GaAs, stress effect on reststrahlen spectrum 2—33284
    GaAs, transverse electroreflectance rel. to 4.5 eV interband threshold symmetry 2—26145
    GaAs, wavelength modulation, rel. to band struct. 2—1692
    GaAs refl. wavelength depend., optical phonon-plasmon coupling, Vargas theory 2—36859
    GaAs solar cell, photoluminesc. spectra, current-voltage characts., impurity influence 2—21012
    $GaAs_{1-x}P_x$, indirect gap, no phonon and phonon assisted exciton absorp. 2—36880
    $Ga_xIn_{1-x}P$ alloys, energy band struct. 2—33238
    GaP:B, optical absorpt. by lattice and local vibrs. 2—1690
    GaP:B, radiation damage centre, local mode absorpt. 2—29167
    GaP:Si, absorpt., rel. to bound excitons and donor ground state 2—36530
    GaP:Si,O, i.r. absorpt. spectra, localized phonon excitations, donor electron excitations 2—20037
    GaP, ATR obs. of dispersion of surface polaritons 2—33233
    GaP, donor-electron transitions assoc. with cond. band minima 2—6832
    GaP, enhanced indirect absorpt., direct band gap 2—33252
    GaP, i.r. generation by coherent excitation of polaritons 2—16458
    GaP, localized vibr. modes of light impurities 2—13025
    GaP, low energy exciton state parameters, 77-300K 2—9918
    GaP, photocond. and photovoltage, wavelength modulation near absorpt. edge 2—33074
    GaP, reflectivity and log. derivative between 2.5 and 6.0 eV 2—22765
    GaP film, forbidden band width, absorpt., refractive index 2—1691
    GaP(Zn, O), impurity absorpt. 2—22797
    GaS, GaP, absorption, characterization and impurity det. 2—16641
    GaS(Se), thermoreflectance, temp. modulation of optical consts. 2—10346
    $Ga_2S_3(Se_3)(Te_3)$, refl. spectra, band struct. calc. 2—29898
    GaSb, optical consts., interband transitions 2—36857

Spectra continued
  inorganic solids continued
    GaSb, photoelectric emission and reflectivity, 7.7-25 eV, band struct. obs. 2—19808
    GaSb, stress-modulated magnetoreflectivity, band parameters 2—33234
    GaSb, wavelength modulation, rel. to band struct. 2—1692
    GaSe, absorpt., 1.8-4.2 eV, excitonic effect 2—29939
    GaSe, absorpt. spectra, absorpt. near fund. edge due to two dimens. excitons, 4.2 K 2—20036
    GaSe, electroabsorp. in the hyperbolic exciton region 2—33262
    GaSe, electroreflectance in higher interband transition region 2—40647
    β-GaSe, layer compound, i.r. reflectivity, interlayer bonding and lattice vibrations 2—25663
    GaSe, layer semicond., absorption, elec. and optical props. 2—10016
    GaSe, layer type semicond., absorp., exciton binding energy 2—10380
    Ga_2Se, indirect optical transitions, electroabsorp. obs. 2—33261
    GaSe(s), layer, thermoreflectance, 77K, Kramers-Kronig analysis 2—36858
    GaTe, electroabsorption, band gap and exciton role detn. 2—20038
    GaTe, layer type semicond., absorp., exciton binding energy 2—10380
    Gd^{3+} in hexagonal crystals nephelauxetic effects, departures from electrostatic crystal field models 2—40582
    $GdAlO_3$:Er^{3+}, absorp., rel. to energy level diagram 2—33313
    $GdAlO_3$:Nd^{3+}, optical absorpt. 2—20097
    $Gd_3Al_5O_{12}$, melt grown, optical absorpt. 2—22110
    Ge:O, ion implanted, absorpt. spectra before and after ion beam irrad. 2—22766
    Ge:Zn, symmetries and deform. pot. consts. of singly ionized Zn 2—29890
    Ge, absorpt. by holes, indirect transitions role 2—1693
    Ge, amorphous, temp. depend. absorp. edge 2—4457
    Ge, amorphous, variation in absorption edge due to impurity O 2—40665
    Ge, amorphous film, i.r. absorpt. rel. to transport and structural props. 2—13273
    Ge, doped, direct optical coupling to surface plasmons 2—33239
    Ge, e_1 and E_1 interband transitions, thermoabsorpt. study 2—40288
    Ge, electronic states of dislocations, absorpt. obs. 2—40289
    Ge, electroreflectance spectra, direct verification of third derivative nature 2—13462
    p-Ge, i.r. refl., hole relax. and effective masses 2—6847
    Ge, linearized third-derivative spectra with depletion-barrier modulation 2—33240
    Ge, magneto-electroreflection spectrum at low temp., apparatus and heterojunction for obs. 2—22750
    Ge, photocond. and photovoltage, wavelength modulation near absorpt. edge 2—33074
    Ge, piezoreflectance, Γ transitions in E_0' region 2—10348
    Ge, polarization and i.r. absorp. of dislocations 2—10381
    Ge, semiconductor, i.r. absorption, doped and compensated state 2—16482
    Ge, thermoreflectance in E_0 region 2—10347
    Ge, wavelength modulation, rel. to band struct. 2—1692
    Ge film, amorphous, annealed optical absorpt. 2—40291
    p-Ge films, deform. splitting of impurity absorpt. band 2—13476
    GeO_2, adsorpt. of benzene, interactions with surface OH groups, i.r. spectra obs. 2—35914
    GeO_2, i.r. reflectance, phonon freq. and dielectric const. detn. 2—20002
    GeS, amorphous and crystalline, reflectivity obs., 0.5-21 eV 2—20015
    H atom layer on Pt, inverse electroreflectance 2—9310
    H_2, adsorbed on NaCl and CsI, i.r. absorpt. spectra, 20K 2—36881
    H_2, and in solid soln., near i.r. absorp., phonon spectra 2—19371
    HCN, crystalline, absorption intensity of librational mode 2—10383
    HD, adsorbed on NaCl and CsI, i.r. absorpt. spectra, 20K 2—36881
    HfO_2:Nd^{3+}, absorpt. spectra and emission of Nd^{3+} 2—33269
    $HgCr_2Se_4$, semiconducting spinel, lattice vibrations, reflection and transmission obs. 2—19374
    HgI_2, 2-6 eV region, 4.2K and 79K 2—33265
    HgI_2, i.r. absorp., phase transition 2—16543
    HgS, thermomodulation of edge absorpt. 2—40666
    HgSe(Te), d-levels location from u.v. photoemission obs., comparison with other spectra 2—22658
    HgTe, reflectivity and band struct. 2—33303
    HgTe, u.v., rel. to band struct. determ. 2—40279
    HgX, x=chalcogen, core electron ~~level~~ obs., x-ray induced electron emission obs. 2—19811
    I_2 single crystal, lattice absorp. 2—33266
    InAs, reflectivity, energy band struct. correlation 2—10345
    InAs, single cryst., thermoreflectance spectra 2—29900
    InAs, wavelength modulation, rel. to band struct. 2—1692
    n-InAs fund. absorpt. edge, optical transitions, 300 and 100 K 2—13477
    n-$InAs_{1-x}P_x$, electroreflectance, Γ_{15}—Γ_1 transitions, composition depend. 2—16468
    $In_xGa_{1-x}As$ solid solns., fund. absorpt. edge obs. 2—13478
    InP, single cryst., thermoreflectance spectra 2—29900
    InP, zero-phonon and phonon assisted optical transitions from Γ_{1c} to subsidiary X_{1c} conduction bands 2—36851
    β-In_2S_3, with spinel defect structure, normal coordinate analysis of far i.r. spectra rel. to lattice vibration spectra 2—29917
    $In_2S_3(Se_3)(Te_3)$, refl. spectra, band struct. calc. 2—29898
    p-InSb, absorpt. coeff. changes due to plasma and hole current effects 2—16491
    p-InSb, absorpt. spectrum, fund., temp. effect., 83-300K 2—22767
    p-InSb, absorpt. spectrum, fund., absorpt. mech. 2—22768
    InSb, coupled cyclotron-plasmon-phonon modes for sample configs. ranging from Faraday to Voigt 2—22769
    n-InSb, microwave reflectance, mag. field dependence during helicon wave propagation 2—16601
    InSb, photocond. spectra, 295K, 90K 2—22646
    InSb, semiconductor effect of electron plasmon coupling on magnetotransmission expts. 2—16424
    InSb, wavelength modulation, rel. to band struct. 2—1692
    InSb type cryst., diamag. excitons 2—6735
    Inert gas, extreme u.v., review 2—20023
    Ir complexes, hexahalometalate complexes, i.r. spectra, force constant calc. 2—16546
    K halides, far-i.r. anharmonic self-energy of long wave phonons 2—19348
    K thin films, absorption, oscillatory structure 2—10385
    KBH_4 and KBD_4, i.r. and Raman low temp. vibrational spectra 2—10384
    KBr:Li^+, lattice reson. in far i.r. h.p. obs. 2—6650
    KBr:$SeO^{2-}{}_3$, $SeO^{2-}{}_4$, i.r. absorp. 2—10387
    KBr, X-irrad., F- and V_2-centre obs. 2—40728

Spectra continued
  inorganic solids continued
    KBr coloured crystals, i.r. absorption of molecular centres 2—26153
    KBr(Cl), impurity-induced far-i.r. absorpt., phonon spectra 2—26168
    KBr(Cl)(I), KKR energy bands and optical consts. 2—40703
    KBr(I):M^{2+}, M=Zn, Cd, reactions, coloration, spectra 2—19125
    K_2CO_3-SiO_2 glass system, i.r. and X-ray spectra study 2—28973
    $K_2CO_3.CaCO_3.SiO_2$ glasses, i.r. spectral study of structural changes 2—1154
    KCl:Ag^-, C-band light irrad., absorpt. bands attributed to paired Ag^- ions 2—15784
    KCl:Ag^-, C-band light irrad., absorpt. attributed to paired Ag^- cons., theory 2—19126
    KCl:In^+, u.v. absorp., uniaxial stress effects, molecular treatment 2—10386
    KCl:KBr, luminesc. emission spectra, transitions to exciton and cond. band states 2—36932
    KCl:NO_2-, absorpt. and emission, effect of impurities 2—16492
    KCl:Pb, determination of conc. limits for isomorphic substitution 2—39711
    KCl:Pb, optical absorpt. 2—20039
    KCl:$SeO^{2-}{}_3$, $SeO^{2-}{}_4$, i.r. absorp. 2—10387
    KCl-NaCl solid solns., Cl^--$L_{II,III}$ absorpt., band struct. 2—7072
    KCl, absorp. band position, F_A(Li) colour centre 2—9599
    KCl, irradiated, defect annealing, absorp. band obs. 2—36011
    KCl, KCl-RbCl, KCl-NaCl solid solns., $Cl^-{}_{II,III}$ absorpt. spectra 2—20041
    KCl, proton bombardment, U centre, H defects, i.r. and u.v. absorpt. 2—22227
    KCl, proton irrad., U-centre obs. 2—25453
    KCl, Raman scattering and i.r. absorption, laser-stimulated atomic migration 2—25463
    $KClO_3$, $KBrO_3$ polycrystalline film, i.r. transmission 2—9278
    $K_3Cr(CN)_6$, exptl. investigation of ${}^4A_2 \rightarrow {}^2E$, ${}^2T_1$ transitions 2—29918
    $K_4Cr(CN)_5NO$, cryst. struct., vibr. modes 2—22770
    KF.2(4)H_2O, optical, colour centres, 77K 2—1264
    KH_2AsO_4, polarized i.r. transmission spectrum in paraelectric phase 2—40709
    KHF_2, i.r. spectra rel. to crystal and molecular dynamics studies 2—26169
    KH_2PO_4, ferroelec. modes 2—13490
    KI:Pd, absorp., rel. to impurity state and e.s.r. obs. 2—4541
    KI:Tl^+, u.v. absorp., uniaxial stress effects, molecular treatment 2—10386
    KI, far-i.r. consts. and phonon freqs. 2—1681
    KI, i.r. absorpt., two-phonon processes 2—40677
    KI, i.r. transmission spectra, multiphonon absorpt. bands 2—36883
    KI, X-irradiated, absorption spectra rel. to role of Auger effect in thermostimulated phenomena 2—33323
    KMF_3:Ni^{2+}, (M=Mg,Mn), absorpt. transition temp. depend. rel. to mag. ordering effects 2—33267
    $KMnF_3$:Ni(Co), exciton-magnon absorpt. struct., impurity effects 2—6993
    $KNiF_3$, antiferromagnet, magnon sideband in optical absorption spectra, positive identification using mag. circular dichroism 2—36882
    $K_4Ni(NO_2)_6.H_2O$, multiple internal reflection i.r. spectroscopy, effect of different prism angles 2—27646
    $K_2Pt(CN)_4Br_{0.3}.(H_2O)_n$, one-dimens. metallic behaviour confirmation by far-i.r. refl. 2—33241
    K_2SO_4:$CrO_4{}^{2-}$, optical absorption spectra, fine structure 2—22771
    $K_3UO_2F_5$, i.r. absorption spectrum, normal coordinate analysis 2—40667
    $KY(MoO_4)_2$:Er^{3+}, absorption and luminescence spectra rel. to empirical energy level diagram for Er^{3+} 2—26166
    $KZnF_3$:Mn^{2+}, Cu^{2+}, optical absorpt., temp. depend. 2—10388
    Kr:Fe, absorpt. linewidth temp. depend., Debye temp. obs. 2—1694
    Kr, absorpt. of Li, K, Na and Cs atoms 2—24387
    Kr, doped, induced far-i.r. phonon spectra 2—19353
    Kr, i.r. absorption of interstitial H and D atoms 2—33264
    La, potential barrier effects in photoabsorpt. 2—22776
    La, soft X-ray absorpt. and photoemission obs. of electronic energy states 2—22791
    $LaBr_3$:Tb^{3+}, absorpt. and fluorescence. spectra, Tb^{3+} excited states determ., 77K 2—36946
    LaF_3, extreme u.v. spectra interpret. 2—36852
    La_2O_3-GeO_2 system, crystallization, X-ray and optical obs. 2—1209
    La_2S_3, lattice oscill., dielec. permittivity, carrier conc., i.r. obs. 2—40670
    Li, absorpt., band struct. 2—40672
    $LiBH_4$ and $LiBD_4$, polycrystalline, i.r. and Raman vibrational spectra, 80K 2—10389
    LiBr-NaBr solid solns., absorpt., 6-9.5 eV, comp. depend. 2—16493
    LiF:OH, i.r. absorption obs., thermoluminesc. 2—29977
    LiF, absorp., $F_2{}^+$ centre evolution by α-particle and deuteron irrad. 2—29201
    LiF, coloration, α- and deuteron irradiation, F-centres 2—25454
    LiF, dynamics of $F_2{}^+$-centres, one phonon sideband 2—22772
    LiF, i.r. reflectance, reliability of classical dispersion analysis 2—20003
    LiF, thermoluminescence emission spectra, continuous determ. 2—29982
    LiH, refl., exciton form. 2—7094
    $LiIO_3$, polaritons and oblique phonons 2—4447
    $LiNbO_3$, Fe group doped, Coulomb interaction, internal field 2—26094
    $LiNbO_3$, nonstoichiometric, absorpt. 2—19083
    $LiNbO_3$ absorption spectra 2—33253
    $LiTmF_4$:Nd^{3+}, absorption, possible use as laser material 2—36944
    $LiYF_4$:Nd^{3+}, absorp., ground term energy states 2—20043
    $LnTiNbO_6$,Ln=Ce, Pr, Nd, Sm, Eu, luminescence and diffuse reflection spectra obs. 2—4448
    Mg complex, tetrabenzoporphine, quasilinear spectra, vibration structure 2—4486
    $MgBr_2$, optical absorp. in the vicinity of Mg L-shell transitions 2—33268
    $MgCl_2$, optical absorp. in the vicinity of Mg L-shell transitions 2—33268
    MgF_2, extreme u.v. spectra, extinction coeffs., interband transitions 2—33242
    MgF_2, F-centre obs. 2—19129
    MgF_2, irrad., absorpt. band obs., M centre stability 2—1237
    MgF_2, optical absorp. in the vicinity of Mg L-shell transitions 2—33268
    $MgNb_2O_6$, i.r. absorpt. cryst. chem. 2—10396
    MgO:Ni, mag. circular dichroism, vibr. induced d→d transitions 2—22773
    MgO-Al_2O_3-SiO_2 system, cordierite glass crystallization, i.r. reflection, D.T.A. 2—1155
    MgO, extreme u.v. spectra, extinction coeffs., interband transitions 2—33242
    MgO, i.r. refl., phonon distrib. 2—26142
    MgO, i.r. reflectance, reliability of classical dispersion analysis 2—20003

- **Spectra** continued
  - **inorganic solids** continued
    - MgO, small cryst., i.r. absorpt., anharmonicity and particle density effects 2—40033
    - MgO, small cryst., i.r. absorpt., lattice dynamical calc. 2—40034
    - $MgUO_4$, U-O lattice vibrations 2—40680
    - Mg_2X, (X=Si, Ge, Sn, Pb), band struct., refl. spectra study 2—26146
    - $M^{II}U_2{}^{V}F_{12}.4H_2O$ (M=Co,Ni, or Cu), absorption 1500-33000 cm^{-1} 2—33275
    - Mn complexes, tetrahalomanganate (II), low-temperature single crystal absorption and emission, obs. of fine structure 2—40674
    - $MnCl_2$, $2MgCl_2$, $12H_2O$, absorption spectrum in near u.v., Zeeman splitting of 12 sharp lines 2—20044
    - MnF_2:Ni,Fe, Raman, i.r., and neutron, impurity mode energy calc. 2—16562
    - $MnF_2:Ni^{2+}$ absorpt. transition temp. depend. rel. to mag. ordering effects 2—33267
    - $MnF_2:Zn^{2+}$, two-magnon region obs. 2—7080
    - MnF_2, magnon-photon coupling 2—22747
    - MnO, valence band structure, X-ray photoemission spectroscopy 2—36639
    - Mn_2PO_4Cl, absorpt., 200-20000nm. 2—22111
    - MnS, antiferromag., spin wave dispersion, effect of magnon-magnon interact., and magnon sidebands 2—33176
    - Mo-O system, optical absorpt. 2—26174
    - MoS_2, u.v. reflectivity, interband transitions, plasma reson. 2—13463
    - ND_4ReO_4, far i.r. and laser-excited Raman spectra, librational mode obs. 2—10411
    - ND_4XO_4 (X=I,Re), ND_4 fundamentals and lattice modes rel. to anomalous temp. dependence of n.q.r. 2—16556
    - NH_3-Ar(N_2) systems, NH_3 molecule rotation 2—10391
    - NH_4ClO_4, low temperature i.r. spectra 2—40675
    - $NH_4H_2PO_4$, far-i.r. absorpt. in antiferroelec. and paraelec. phases 2—16494
    - NH_4HSP_4 and ND_4DSO_4, i.r. spectra, temp. range 285 to 17°K 2—20046
    - NH_4ReO_4, far i.r. and laser-excited Raman spectra, librational mode obs. 2—10411
    - $(NH_4)_2SO_4$, $(ND_4)_2SO_4$, Raman and i.r. spectral variations at ferroelectric T_c 2—22787
    - NH_4X, X-halide, effects of H bonding on i.r. spectra from vibr. study 2—10390
    - NH_4XO_4 (X=I,Re), NH_4 fundamentals and lattice modes rel. to anomalous temp. dependence of n.q.r. 2—16556
    - NO, adsorbed on evaporated alkali halide films, i.r. spectra 2—1195
    - NO^{2-}, in alkali halide cryst., reson. secondary radiation spectra, hot and scatt. luminesc. 2—16639
    - NO_3^- in powder state, diffuse reflectance spectra 2—29899
    - Na, absorpt., abnormal maxima 2—16495
    - Na, phonon aided optical absop. theory 2—20045
    - Na, reflectance, optical cond., Drude tail anomaly 2—10349
    - $Na_4Al_3Si_3O_{12}Cl$, sodalite, doped, fluoresc. and refl. spectra 2—22806
    - $NaBH_4$ and $NaBD_4$, i.r. and Raman low temp. vibrational spectra 2—10384
    - $NaBrO_3$, fund. band edge absorpt., temp. shift, band transitions, phonon emission absort. 2—36884
    - NaCl:Br, absorp. band of $(Br^-)_2$- centre 2—33316
    - NaCl:F, i.r. absorp., impurity pair resonant modes 2—22774
    - $NaCl:Mn^{2+}$, neutral Mn centres, absorpt. study 2—39716
    - NaCl:Pb, determination of conc. limits for isomorphic substitution 2—39711
    - NaCl, elec. field influence 2—1695
    - NaCl, NaCl-KCl solid soln., $Cl^-{}_{II,III}$ absorpt. spectra 2—20041
    - $NaClO_3$, multiple internal reflection i.r. spectroscopy, effect of different prism angles 2—27646
    - $NaClO_3$, $NaBrO_3$ polycrystalline film, i.r. transmission 2—9278
    - NaF, temp. depend. of long-wavelength phonons 2—40649
    - $NaHF_2$, i.r. spectra rel. to crystal and molecular dynamics studies 2—26169
    - $NaI:Pb^{2+}$, C-band peak position determ. using extended Mollwo-Ivey reln. 2—29197
    - NaI, i.r. absorpt., two-phonon processes 2—40677
    - NaI, i.r. transmission spectra, multiphonon absorpt. bands 2—36883
    - $NaMgAl(C_2O_4)_3.9H_2O:Cr^{3+}$, luminesc. emission spectra rel. to Cr^{3+} conc. 2—26221
    - $NaNO_3$, disordered phase, i.r. study 2—19378
    - $NaNO_3$, vac. u.v. reflectivity 2—16471
    - Na_2O-B_2O_3-Al_2O_3-SiO_2 and Na_2O-B_2O_3-Al_2O_3-Sb_2O_3-SiO_2, glasses, structure studies with i.r., e.p.r. and electronic absorption spectroscopy 2—40679
    - Na_2O-Fe_2O_3-TiO_2-SiO_2 glass, optical absorpt. 2—1598
    - α- Na_2UO_4, U-O lattice vibrations from i.r. absorption spectra 2—40680
    - Na_xWO_3, optical transition to Fermi level 2—33243
    - $Na_2ZnCl_4.3H_2O$, $Na_2ZnCl_4.3D_2O$, long wavelength phonon spectra, assignment using Raman data 2—40036
    - $NbSe_2$, reflectivity anisotropy band struct. 2—10350
    - $NbSe_2$, superconducting layer structure, far i.r. transmission spectrum, energy gap meas. 2—4165
    - $NbSe_2$, u.v. reflectivity, interband transitions, plasma reson. 2—13463
    - Nd:glass laser, effect of Nd absorption bands on generation energy 2—280
    - Nd^{3+} complex, energy levels, spectroscopic parameter, diffuse refl. spectra 2—26147
    - Nd_2S_3, lattice oscill., dielec. permittivity, carrier conc., i.r. obs. 2—40670
    - Ne:Cs, absorpt., dynamical Jahn-Teller effect 2—10392
    - Ni, d-band photoelectron energy distrib. near Curie temp., exchange splitting 2—33091
    - Ni, energy gap obs. 2—25735
    - Ni, i.r. and visible absorpt., 4K, band struct. 2—16496
    - Ni, optical constants, band struct. 2—10299
    - Ni,Ni base alloys, light cond., interband transitions 2—26171
    - Ni or CO adsorpt. at low temps., i.r. obs. 2—22086
    - Ni^{2+} complex, 'oxinate', u.v. and visible reflectance 2—22751
    - Ni^{2+} octahedral complex, overlapping and covalency effects 2—19990
    - $Ni_3IB_7O_{13}$, ceramic, visible and i.r. 2—15936
    - $Ni(NH_3)_6I_2$, internal rot. of NH_3 groups, i.r. spectra obs. 2—10375
    - NiO, shakeup photoelectron spectra 2—36636
    - NiO, valence band structure, X-ray photoemission spectroscopy 2—36639
    - $Ni_xZn_yFe_2O_4$, rel. to atomic struct. and energy levels 2—36816
    - Os complexes, hexahalometalate complexes, i.r. spectra, force constant calc. 2—16546

- **Spectra** continued
  - **inorganic solids** continued
    - P_2O_5 orthorhombic form, i.r. absorption spectra and X-ray powder diffraction 2—15729
    - $POCl_3$, vibrational i.r. spectrum, analysis of band splitting and polarization for structure determ. 2—13491
    - $PbBr_2$, film, exciton absorp., thickness effects 2—10393
    - $Pb_{0.95}Cd_{0.05}Te$ solid soln., i.r. refl. spectrum, transport props. determ. 2—22540
    - $PbCl_2$, Kramers-Kronig relationships, refr. and extinction indices 2—15592
    - $Pb_{1-x}Mn_xTe$ solids soln., refl. spectra, cond. effective mass 2—22539
    - $Pb(NO_3)_2$, i.r. refl., anharmonicity 2—19354
    - PbO-$PbSO_4$ system, i.r. spectra of xPbO.$PbSO_4$, and phase diagram 2—36306
    - PbS, film, thermoreflectance spectra 2—29900
    - $PbSb_2O_6$, i.r. absorpt., cryst. chem. 2—26161
    - $Pb_{0.75}Sn_{0.25}Te$ solid soln., i.r. refl. spectrum, transport props. determ. 2—22540
    - p-$Pb_{1-x}Sn_xTe$, i.r. reflectivity, free carrier parameters detn. 2—26148
    - $Pb_{1-x}Sn_xTe$, wavelength modulation derivative reflection spectra, assignment of obs. structures with band calcs. 2—4449
    - n-PbTe, i.r. magnetoabsorpt., phonon-cyclotron and carrier-transfer reson. 2—40678
    - $PbTe_{0.8}Se_{0.1}S_{0.1}$ solid soln., i.r. refl. spectrum, transport props. deeterm. 2—22540
    - $PbTi(Zr)O_3$, diffuse refl. spectra, band struct. calc. 2—1526
    - Pd complex, $[Pd(NH_3)_4]Cl_2.H_2O$, vibr. spectra 2—33270
    - Pd complex, tetrabenzoporphine, quasilinear spectra, vibration structure 2—4486
    - $Pr_2Mn_{3-x}Zn_x(NO_3)_{12}.24H_2O$. Zeeman effect, satellite structures 2—4458
    - Pr_2S_3, lattice oscill., dielec. permittivity, carrier conc., i.r. obs. 2—40670
    - Pt, in perchloric acid, modulated specular reflection, cathodic H adsorpt., oxide formation 2—9311
    - Pt (IV) ammine complexes, substituted, i.r. and Raman, factor group, space group symm. 2—10412
    - Pt complex, dichloro(ethylenediamine)platinum(II), polarized crystal absorption spectra 2—29920
    - Rb, optical and dielec. consts., band struct. 2—26149
    - $RbBr:Pb^{2+}$, C-band peak position determ. using extended Mollwo-Ivey reln. 2—29197
    - RbCl, RbCl-KCl solid soln., $Cl^-{}_{II,III}$ absorpt. spectra 2—20041
    - $RbMF_3:Ni^{2+}$, (N=Fa,Co,Mn), absorpt. transition temp. depend. rel. to mag. ordering effects 2—33267
    - $RbMnF_3$:Ni, Raman, i.r., and neutron, impurity mode energy calc. 2—16562
    - ReO_3, valence band structure, X-ray photoemission spectroscopy 2—36639
    - SO_2 neat crystals, optical detection of zero field splittings in phosphorescent triplet state 2—13512
    - Sb, magnetorefl., band struct. obs. 2—32909
    - Sb and Sb-Bi alloys, interband transitions, i.r. magnetoreflectivity 2—16473
    - SbSI, density of electron states 2—33059
    - Se, absorpt. and electroabsorpt. near fund. edge 2—33271
    - Se, amorphous thin film, optical consts. determ. from i.r. refl. 2—33200
    - Se, trigonal, temp. depend. electroabsorpt. on indirect edge 2—13480
    - Si:C, absorp., rel. to impurity conc. effect on thermal donor formation 2—19117
    - Si:Mg, excitation spectra and piezospectroscopic effects of donors 2—10338
    - Si:O, i.r. absorpt. spectra before and after annealing and neutron irrad. 2—22223
    - Si-Ge alloys, i.r. absorpt. of lattice and local modes 2—13483
    - Si-Ge alloys, localized vibr. modes of B-Li pairs 2—13482
    - Si-SiO_2-Al gamma radiation damage studies by internal photoemission 2—19730
    - Si-SiO_2-Cr gamma radiation damage studies by internal photoemission 2—19730
    - Si, amorphous, electronic struct. obs. 2—33017
    - Si, core excitation, expts. using storage ring light source 2—16479
    - Si, crystalline and amorphous, extreme u.v. transmission rel. to conduction band structure 2—26172
    - Si, far-i.r. obs., rel. to charge carrier relax. times determ. 2—33273
    - Si, neutron irradiated, divacancy associated absorption bands 2—22777
    - Si, photocond. and photovoltage wavelength modulation near absorpt. edge 2—33074
    - n-Si, plasma reflectivity minimum, freq. shift due to uniaxial stress 2—33244
    - Si, radiation-induced absorpt. bands, piezospectroscopic obs. of group V—defect complex 2—16499
    - Si, recomb. rad. spectrum, temp. shift and width of 0.970 eV no-phonon line, 6-110K 2—22800
    - Si, semiconductor, i.r. absorption, doped and compensated state 2—16482
    - Si, stress depend. of E'_0 refl. peak 2—16474
    - Si, wavelength modulation, rel. to band struct. 2—1692
    - Si ion implanted, SiC, Si_3N_4, SiO_2 formation, i.r. transmission obs. 2—26173
    - SiC:N, 6H polytype, Zeeman effect of the absorp. lines R_o and S_o 2—36885
    - SiC:N, i.r. absorpt. due to impurity level nonequiv. population 2—13481
    - α-SiC, 6H polytype, i.r. absorpt., optical phonon energy range determ. 2—10395
    - n- SiC polytype, i.r. impurity absorption 2—16498
    - α-SiCiN, impurity adsorpt., electron transitions 2—7073
    - SiH_4 and SiD_4-SiH_4 mixtures, i.r. vibrational spectra 2—33272
    - SiO_2, glassy pyrogenic, adsorption, i.r. studies 2—39565
    - SiO_2, thin dielectric film, study using method of multiple frustrated total internal reflection 2—20004
    - SiO_2 glass, H_2 impregnated, i.r. absorp. 2—12630
    - SiO_x evaporated film, absorpt., rel. to deposition conditions 2—10394
    - SiO_x film, r.f.-sputtered, i.r. spectra near 9μm, rel. to sputtering voltage, thickness, heat treatment conditions 2—13484
    - Sm, i.r. obs., plasma and relax. freqs. of cond. electrons 2—40640
    - $Sm_2O_3+Cr_2O_3$ reaction, i.r. spectra of products 2—30054
    - Sm_2S_3, lattice oscill., dielec. permittivity, carrier conc., i.r. obs. 2—40670
    - SmS(Se)(Te), i.r. absorpt. peaks, semicond.-metal transition 2—33274
    - Sn, grey, optical consts., band struct. 2—16475
    - α-Sn, RPA dielec. function in far-i.r. 2—10051
    - SnO_2, electrotransmission spectra near fundamental threshold 2—40641

Spectra continued
inorganic solids continued
SnO_2 layers, absorption spectra meas. in 3.1-5.2 eV region, obs. characteristic absorption 2—29921
$SrCl_2$:Yb^{3+}, cryst. field energies 2—36888
$SrCl_2$, absorp., F-centres obs. 2—33336
$SrCl_2$, alkali metal doped, colour centres obs. 2—3800
SrF_2:Ca, Ba, X-irrad., absorp. spectra, F_{ae} centres 2—33256
SrF_2, F_3 centre, absorpt. band, zero-phonon line, fluorescence 2—19122
SrF_2, containing ion pairs of Gd, Ce, Pr with H, D, T, optical and i.r., electron-phonon interactions 2—10499
SrF_2, low temp. irrad., F_3^- centre, zero-phonon line 2—19124
SrF_2, zero-phonon line, F_3 centre, quadratic Stark effect 2—19123
$Sr_3Ge_3O_9$, vibr. spectrum interpretation 2—36908
$Sr_3Ge_3O_9$ and $Sr_3Si_{3-x}Ge_xO_9$, i.r., vibr. spectra 2—36907
$Sr(NO_3)_2$, i.r. refl., anharmonicity 2—19354
SrO-SiO_2 glass, γ-irrad., optical absorpt. 2—30015
SrO powder, far-i.r. surface-activated band-mode absorpt. 2—7074
$Sr(OH)_2$, $Sr(OD)_2$, i.r. absorption spectra, normal coordinate analysis rel. to lattice vibration spectra 2—40037
SrS, dynamic ionic charge determ. from i.r. spectra and static dielec. props. 2—22396
$SrSb_2O_6$, i.r. absorpt., cryst. chem. 2—26161
$SrSiO_3$-Nd_2SiO_5, amorphous system, apatite phase, comp. depend., i.r. obs. 2—18894
$Sr_3Si_3O_9$ and $Sr_3Si_{3-x}Ge_xO_9$, i.r., vibr. spectra 2—36907
$SrTiO_3$:Nb, free carrier optical absorpt. 2—36887
$SrTiO_3$, band structure determ. from X-ray photoelectron spectra 2—33092
$SrTiO_3$, wavelength-modulated absorption, reinterpretation not involving coexisting phases 2—20048
$Sr_3(XO_4)_2$, X=P, As, V, Cr, Mn, i.r. and Raman vibr. spectra, interpretation based on crystal structure 2—8586
Ta_2O_5-GeO_2 system, crystallization, i.r. refl. 2—1412
TbF_3 trapped in N_2, i.r. obs., vibr. spectrum 2—13455
$TbPO_4$, mag. ordering and Jahn-Teller distortion 2—36779
Te, absorpt., 36-246 eV, conduction band obs. 2—20050
Te, intervalence band traisition, modulation by acoustoelec. domains 2—7075
Ti-O system, optical absorpt. 2—26174
Ti to Co series, photoabsorption cross sections calcs. 2—22779
TiO_2:Fe^{3+}, photocond., Fe level 2—10141
TiO_2, surface properties, i.r. study of H_2O and surface OH species 2—1197
V-O system, absorpt. 2—26174
V complex, $[V(urea)_6]^{3+}$, ligand field analysis 2—13374
V film, interband transitions 2—7076
V^{3+}, octahedral complex, overlapping and covalency effects 2—19990
V_2O_5-P_2O_5 glass, i.r. absorp. rel. to polar conduction 2—10039
VO_2 films, reflectivity, electroabsorpt., band assignments 2—33245
V_2O_5 powder, diffuse reflectance spectra 2—29901
W-O system, absorpt. 2—26174
WOI_2, absorpt. bands 2—25254
Xe:Cs, absorpt., dynamical Jahn-Teller effect 2—10392
Xe:Li solid, luminescence and absorpt., 4-80 K 2—29963
Xe, absorpt. of Li, K, Na and Cs atoms 2—24387
Xe, reflection spectra, Wannier exciton peaks obs. 2—10351
Y, soft x-ray absorpt. and photoemission obs. of electronic energy states 2—22791
YAG:Cr^{3+}, excitation and fluorescence 2—26241
YAG:Cr^{3+}, vibronic spectrum and fluoresc. lifetime, temp. depend. 2—13507
YAG:Lu, Nd, ion site distrib. and spectral line broadening 2—36853
$YAlO_3$:Nd^{3+}, intensity parameters 2—4496
$YAsO_4$:Dy^{3+}, absorp., low lying ground level doublets obs. 2—33337
YIG, excitons, spin wave sidebands and exchange interactions 2—40681
Y_2O_3:Eu^{3+}, reflection, random substitution of Eu^{3+} for Y^{3+} 2—13464
Yb^{3+}, in fluorides, luminesc., emission spectra, excitation mechanism 2—26217
YbS, YbSe, YbTe, reflection and absorp., energy band struct. and bond ionicity 2—16476
Zn, band struct. obs. 2—33276
Zn complex, tetrabenzoporphine, quasilinear spectra, vibration structure 2—4486
$ZnGeAs_2$, reflectivity, energy band struct. correlation 2—10345
$ZnIn_2S_4$ and $Zn_3In_2S_6$, refl. spectra, band struct. calc. 2—29898
ZnO_2:Nd^{3+}, absorpt. spectra and emission of Nd^{3+} 2—33269
ZnO, far-i.r. free carrier absorpt. 2—16500
ZnO, Zn 3d states location from u.v. photoelectron spectra 2—36641
$Zn_5(OH)_8(NO_3)_2.2H(D)_2O$ i.r. spectrum, compared with results of crystal structure determ. 2—4460
ZnS:Ni, ion-hole complexes formed in charge exchange between impurities 2—29956
ZnS:TbF_3 films, i.r. obs., vibr. spectrum 2—13455
ZnS-Ni, absorption spectra, charge transfer band region, bound state formation 2—36889
ZnS-SnO_2 systems, absorption spectra meas. in 3.1-5.2 eV region 2—29921
ZnS, deformed, exciton spectra and exchange interaction 2—29902
ZnS, with stacking faults, exciton refl. spectra 2—22752
ZnS layers, absorption spectra meas. in 3.1-5.2 eV region, obs. characteristic absorption 2—29921
β-$Zn(SCN)_2$, pure and Pb-activated, absorption spectra 2—16501
ZnSe:Tm, Li, absorpt. 2—40721
ZnSe-Ni, absorption spectra, charge transfer band region, bound state formation 2—36889
ZnSe, u.v., rel. to band struct. determ. 2—40279
$ZnSnAs_2$, electrorefl., electron transitions 2—20006
ZnTe, exchange splitting in excitons, interatomic distance depend. 2—29903
ZnTe, stress induced splitting of exciton reflection spectra 2—16477
ZnTe, u.v., rel. to band struct. determ. 2—40279
ZnX, x=chalcogen, core electron level obs., x-ray induced electron emission obs. 2—19811
$Zr(As,P)_2O_7$ solid solns., As and P distrib. obs. 2—9499
ZrO_2:Er^{3+},Y_2O_3 stabilized, absorp., oxygen ion co-ordination obs. 2—33277
$ZrZn_2$, electronic struct. 2—40650
ZuTe film, stoichiometry depend. 2—25829

Spectra continued
inorganic solids, radiofrequency
see also Nuclear magnetic resonance and relaxation; Paramagnetic resonance and relaxation
Al_2O_3, ruby, Cr^{3+} pairs, level scheme and energy transfer 2—33249
Fe garnets, optical phonons 2—1700
KI:KOH, microwave absorption, 8 to 40 GHz, 1.3K 2—13479
Te, temp. depend. of microwave absorpt., interpretation 2—25844

molecules
absorption, elec. field effects, theoretical study considering field fluctuation 2—15260
absorption and fluorescence in Herzberg-Teller theory inolusion of Duschinsky effect discussed 2—12082
absorption and fluorescence use to determ. dipole moment of electronically excited molecules 2—8554
band shapes and absorption coefficients for electronic transitions 2—15259
in binary solvent, rel. to universal van der Waal's interactions 2—24574
calculation from mol. dynamics data using fast fourier transform 2—20855
collisional relaxation and rotational intensity distributions 2—38870
complex, far i.r., band shape anharmonicity 2—8533
complex, use of mathematical logic to determ. structure from i.r. vibration spectra 2—28246
computers and calculating machines, use in spectroscopy 2—31138
conference, Columbus, Ohio, USA (1971) 2—8521
conjugated, vibrational spectra of excited electronic states calc., evaluation of vibronic transition intensities 2—12083
continuous absorption spectra, Franck-Condon factor 2—15263
rel. to cool giant stars, calc. using model atmospheres 2—16996
core electron ESCA spectra, shake-up satellite line intensities 2—35219
Cotton-Mouton effect, time-dependent double perturbation investigation 2—15201
diatomic, photoelectron spectra and molec. constants of autoionizing states 2—8565
diatomic, r-centroid approx. in intensity theory 2—15258
diatomic molecules, internuclear distance from estimated spectroscopic intensities 2—8531
diatomic molecules, vibrational transition probabilities theoretical determ. 2—24418
dimers, determ. spectroscopic moments of collision induced for i.r. and Raman spectra 2—21561
elastic quadrupole radiation processes, effects of molecular interactions on line shape 2—12299
electronic absorption spectra, collision induced, symmetry selection rules 2—15255
electronic spectra, determ. of vibr. and rot. consts. 2—18386
electronic transitions, vibronically-induced symmetry-forbidden, theoretical formalism 2—12084
energy loss spectra for electron transmission, excitation of vibr. levels 2—12099
Franck-Condon factor for a Morse oscillator when z is small, contribution to theory of radiationless transitions 2—28259
Franck-Condon factors for radiationless transitions, polyatomic 2—8506
Franck-Condon factors rel. to method of steepest descent 2—8507
ground state vibrational temp. determ. by reversal of spectral lines in i.r. region of CO_2 laser 2—15256
harmonic oscillator two-centre integrals, application 2—27068
high resolution, in 8 to 20 μm region, vibration rotation band meas. 2—12079
infrared spectra, first order j-dependent line shifts, classical path impact theory 2—28244
interstellar, use as probes of dense clouds 2—41144
i.r. absorption, impurity matrix studies, validity of use of cell model 2—13466
i.r. bands in gases, possibilities and limitations of a schematic model 2—38869
i.r. emission by nonisothermic gaseous layers 2—3329
i.r. intensity sum rule and effective charges 2—35208
i.r. spectra, effect of phase and pressure changes, review of work 1963-1970 2—8516
i.r. spectra, first order j- dependent line shifts, classical path impact theory 2—28245
i.r. spectra, influence of lone pair of nitrogen of molecules with few rotamer forms 2—21563
Kerr effect, time dependent double perturbation-variation formulation 2—15200
laser pyrolysis plumes in ambient gases, spectral emission 2—20176
line broadening, unified theories 2—5778
linear mol., dipolar absorpt. theory 2—31740
liquid state, translation motion 2—15563
Lorentz gas, induced infra-red spectra, intercollisional interference effects, kinetic theory 2—31876
magnetic circular dichroism, new applications to atomic and molecular systems 2—4432
microwave, press. induced line shift 2—8519
microwave absorption spectra, collisional relaxation rel. to rotational energy transfer investigation 2—12297
microwave and far infrared regions, pressure broadening and shift 2—28243
microwave astronomy, galactochemistry 2—10921
modified adiabatic approximation in theory 2—28183
molecular dimers, absorption bandshape 2—31746
multiplet theory for single configuration for symmetric wave functions 2—3014
$n \leftarrow \pi^*$ transitions, CNDO-CI predictions of energies and intensities 2—8548
nonpolar, purely rot. spectra from vib. ground states 2—21570
nonresonant Autler and Townes effect on a line broadened by saturation 2—35194
normal absorption processes, Taylor expansion of expression for transition probability 2—31634
open shell molecules, theory for band intensities of photoelectron spectra 2—31741
optical activity, relation between static and dynamic perturbations 2—8518
optical oscillator strengths by electron impact spectroscopy 2—8515
pair of linear molecules, interpretation of i.r. spectra 2—39023
Penning ionization electron spectroscopy 2—35222
photoelectron, angular distribs., review 2—31768

Spectra continued
molecules continued
photoelectron, angular distribs. obs. 2—31769
photoelectron, autoionization obs. at different wavelengths 2—31770
photoelectron, molecular ion fluorescence interpreting aid 2—35220
photoelectron, multiplet splittings 2—35226
photoelectron, orbital assignments, use of perfluoro and He(II) intensity effects 2—35221
photoelectron, photoionization cross section depend. on photoelectron energy 2—31683
photoelectron, vacuum ultraviolet, study of transient species 2—760
photoelectron spectra, X-ray and u.v. sources, rel. to orbital structure determination 2—8564
photoelectron spectroscopy, review of work at Oxford Univ. 2—35218
polyatomic, approx. charact. normal vibrations, least squares criterion 2—8532
polyatomics, forbidden rotational spectra, intensity acquirement by centrifugal distortion mech. 2—18383
polyatomics, relative nonradiative decay rates of initially selected vibronic levels 2—21558
pressure broadening of spectral lines, classical path approx. 2—748
pressure broadening phenomena discussed using analogy between theory of foreign-gas broadening and self broadening 2—31747
radiationless transition probability, multi- phonon transition, Franck-Condon factor 2—24415
radiationless transitions, influence of final-state spectrum studied by method based on Laplace transform 2—38868
resonance broadening of spectral lines in gases, many-body aspects 2—753
rotational spectra, systematic interpretation based on Stark effect 2—38871
rotational transition determ. from microwave optical double resonance 2—35231
Rydberg spectra, term value trends discussed for wide range of compounds 2—8522
self broadening of spectral lines 2—747
spectroscopy, conference, Clayton, Australia (1971) 2—8509
spherical-top molecules, collision-induced far i.r. rotation-translation spectrum, quantum theory 2—5896
Stepanov's relation between absorption and luminescence, realizability condition 2—8517
symbolic logic appl. to analysis of spectra and planning of spectral investigations 2—5894
symmetric top molecules, determ. of axial rotation const. from vibr. rot. spectra 2—8534
system with quasi-two-level centres and emission, spectral eqns. 2—31749
tetrahedral molecules, pure rotational transitions from ground vibronic states 2—12081
two-level problems, spin 1/2 formalism 2—21557
vacuum u.v., high resolution, research at Nat. Res. Council, Canada 2—18378
vibrating i.r. and Raman spectra, book on the foundations of the subject 2—5899
vibration-rotation absorption, using wavelength tunable lasers 2—749
vibrational, undergraduate paperback 2—5898
vibrational correl. functions determ. from i.r. spectra and r.f. data 2—31752
vibrational rotational spectra, line intensity eqns. taking into account accidental Coriolis resonance 2—746
vibrational spectra rel. to dipole-dipole interaction, influence of solvents 2—25090
vibrational-electronic circular dichroism spectra, low resolution analysis 2—8528
X-ray, vertically oriented double-crystal attachment for spectrograph 2—21580
X-ray absorption spectra, evidence of effective potential barrier 2—35193
X-ray emission and electron spectroscopy, review 2—31003
X-ray photoelectron spectral shifts, thermochemical estimates 2—35223

organic molecules and substances
see also Molecules
1,3-thiazan, synthetic derivatives, absorption spectra, displacement according to solvent polarity 2—3122
acenaphthene: acenaphthylene, identification of two impurity sites 2—36891
acenaphthenequinone vapour, singlet-triplet absorption spectrum, 5600 to 4300 Å 2—28336
acetanilides, disubstituted, ortho-effects in mass spectra, removal of excitation probability for low lying energy states of ion 2—38954
acetone, calculation of band shapes and absorption coeffs. for electronic transitions 2—15259
acetone, Fourier obs. of Brillouin and Rayleigh line widths and shapes 2—1103
acetone-^{18}O, isotope effect on nonradiative relaxation 2—35301
acetonitrile, $2\nu_8$ state, effects of accidentally strong resonance in rot. spectrum, mol. consts. level separation 2—12203
acetonitrile, doubling excited degenerate vibr. state, rot. spectrum, anharmonicity const., transition study 2—12202
acetophenone, phosphorescence spectra, dynamic properties and zero field splittings of lowest excited triplet states 2—28335
acetylene in soln., Fermi reson. 2—18478
acetylenic organotin compounds, UV spectroscopy 2—15347
acrolein, cis and trans isomers, mag. rotation spectrum, band assignment, energy level diagram 2—12204
acrolein, magnetic rotation and absorption spectra cis and trans isomer transitions 2—3069
adamantane, excited electronic states, sharp vibronic structure 2—12205
adamantane, investigation of Rydberg states 2—31845
alcohol glasses, electron trapping spectra 2—13593
alcohol solutions, association constants 2—18829
aldehydes, saturated aliphatic, modulation of $n\rightarrow\pi^*$ absorption band 2—21689
n-alkane, opt. absorpt., 6.5-35 eV 2—18492
allene, vacuum u.v. spectra, preliminary ionization potential determination 2—21655
2-aminonaphthalene-6-sulphonate and derivatives, electronic spectra 2—28343
2 aminonaphthalene-6-sulphonate and derivatives, solvent dependence 2—28868
p aminophenol derivatives, hydrohalides, solid state ion exchange with matrix, i.r. spectra 2—10594

Spectra continued
organic molecules and substances continued
anhydrides, electronic absorption spectra, obs. bathochromic shift of $\pi\pi^*$-band of PA 2—28345
1-anilino-8-naphthalene sulphonate, solvent perturbation effects, nsec time resolved emission spectroscopy 2—8731
anthracene, absorption band profile of origin region of b polarized 4000 Å transition 2—10352
anthracene, Kramers-Kronig relationships, refr. and extinction indices 2—15592
anthracene, refl., 4.5-11.5 eV, anisotropy 2—40651
anthracene alkyl-substituted analogues, films, temp. depend. 2—13249
anthracene single cryst., opt. anisotropy from reflection spectra, 4.5-11.5 eV 2—20007
aromatic $d\pi^*$-$\pi\pi^*$ interactions, comparison with $n\pi^*$-$\pi\pi^*$ interactions in Ir(III) complexes 2—35300
aromatic hydrocarbon dimers, absorpt. and emission spectra, radiative lifetimes 2—10361
aromatic hydrocarbon dimers, Davydov splitting calc. 2—8717
aromatic hydrocarbons, electrooptical polarisability in ground state and first excited singlet states 2—15381
aromatic molecule systems in rigid solution, donor phosphorescence quenching and decay in sensitized phosphorescence 2—13511
aromatic nitro-substituted anion-radicals, electronic spectra 2—834
2,6-bis(4-azidobenzylidene) cyclohexanone, stereoisomers, electronic structure and spectra, dipole moments, SCF MO LCAO methods 2—12233
azines, substituted by amine groups, amine-imine tautomerism 2—21659
azo group, α,β-unsaturated, u.v electronic spectra, dipole moments, config. study 2—18483
azobenzene, p-monosubstituted derivs., polarization absorption spectra, electronic transitions 2—836
azonaphthalenes, basicity and electronic spectra, spectrophotometric study 2—28347
azulene, linewidths for $S_1\leftarrow S_0$ and $S_2\leftarrow S_0$ nonradiative processes 2—31838
azulene, $S_2\rightarrow S_1$ emission 2—24504
azulene, spectral shifts in nonpolar solvents, mechanism 2—25093
azulene vapour, single vibronic level lifetimes 2—8736
benzaldehyde, $^1U(n\pi^*)\leftarrow S_0$ absorption spectra, vibronic intensification 2—12211
benzaldehyde, $^3U(n\pi^*)\rightarrow S_0$ phosphorescence, vibronic interactions 2—12212
benzaldehyde, phosphorescence spectra dynamic properties and zero field splittings of lowest excited triplet states 2—28335
benzene, absorpt. cross sections and photoionization efficiencies, 600-2200 Å 2—18491
benzene, anal. of antiresonances in Rydberg spectrum in terms of theoretical line shape parameters 2—8802
benzene, benzene-d_6, radiational deuterium effect in triplet-single transition 2—21663
benzene, electron impact, radiation emission for 0 to 500 eV incident energies 2—5961
benzene, ESCA line intensities, orbital determ. 2—35219
benzene, ESCA spectra, core binding energies and chemical shifts 2—5960
benzene, Fourier obs. of Brillouin and Rayleigh line widths and shapes 2—1103
benzene, influence of final-state spectrum in radiationless transitions studied by Laplace transform method 2—38962
benzene, opt. absorpt., 6.5-35 eV 2—18492
benzene, solid, higher $\pi\rightarrow\pi^*$ transitions, spectral obs. 2—20052
benzene, u.s. excited shift in u.v. absorption band spectra 2—18485
benzene, vapour, single vibronic level lifetimes 2—8736
benzene anion radical, metal hyperfine splitting by line-shape analysis, effect of exchange processes 2—35308
benzene derivatives containing amino and carboxyl groups, absorption spectra 2—8741
benzene triplet absorption by monoolefins in gas phase, reaction rate determ. by kinetic absorption spectroscopy 2—13572
benzene vapour, optical absorption spectrum, photon energies 6-35 eV, electronic structure assignment 2—15358
benzene-borazine mixed crystals, electronic spectra, 4.2K 2—13485
benzenes, methyl substituted, radiative transitions from first excited singlet state, rate constant meas. 2—12209
benzenes, monosubstituted, variable electronegativity SCF-MO calc. 2—15353
benzonitrile, lowest-lying singlet $\pi^*\leftarrow\pi$ transition, rotational analyses, dipole moment changes 2—35343
p- benzoquinone, effect of methyl and hydroxyl substituents 2—35307
p-benzoquinone and methyl derivatives CNDO-CI study of effects of substitutions on electronic spectrum 2—12210
benzotriazole, surface reaction film on Cu, i.r. and u.v.-visible refl. spectra 2—18959
benzoxazole, cryst., near u.v. absorption spectrum in polarized light 2—16502
benzo|cd|pyrenyl, assignment of proton hyperfine splitting constants 2—35305
benzyl, symmetry of first excited state determ. by rotational contour analysis of vibronic bands of emission spectra 2—15355
N-benzylidenemethylamines, para-substit. electronic absorption spectra, non-planar conformation 2—8740
bicyanine dimer, electron- vibrational spectra, strong coupling case 2—12214
bicyclo-|2,2,2|-octane, excited electronic states, sharp vibronic structure 2—12205
bicyclo|2.2.2|octane, investigation of Rydberg states 2—31845
2,5-di(biphenyl)-1,4-oxazole), spectral intensity changes on excitation by N laser, quantum generation 2—3390
biphenyl based series, phenanthrene-carbazole-dibenzothiopene-dibenzofuran, polarization of electronic transitions 2—28355
p-bromochlorobenzene crystals, absorption spectra, 4K, exciton zone analysis 2—26208
1,3-butadiene, electronic spectrum application of molecule within a molecule method to transitions 2—35298
carbon tetrachloride, depolarization ratios of isotope lines 2—38941
carbon tetrachloride, vibratory spectra, intensities, electro-optical parameters 2—32267
carbonyl compounds, conformation from obs. of $n\rightarrow\pi^*$ transition sensitivity to solvent effects, importance of hindered carbonyl bisection 2—24521
p- chloroaniline, lowest singlet state in pure and mixed crystals 2—40684
p-chloroaniline, pure cryst. absorption spectrum of lowest singlet state, vibronic intensity pattern 2—20054

Spectra continued
organic molecules and substances continued
chlorobenzene, quadrupole hyperfine structure in rotational spectrum analysed 2—12216
chlorobenzene-D_5, near u.v. absorption spectrum vibrational analysis 2—3075
chlorofluoroethylenes, far u.v. spectra, band assignment 2—12242
cholesteric esters, transparency characts., solid to isotropic liq. phase 2—9132
cholesteric liquid crystals, reflectance spectra rel. to temp. dependence of order 2—28794
chromocene, photoelectron spectra, band intensities from theory for open shell molecules 2—31741
chromone, u.v. absorption spectra, band assignment, solvent and substituent effects 2—28360
chromones, 2-substituted, u.v. absorption spectra, band assignment, solvent and substituent effects 2—28360
chrysene, transient absorption spectra using laser photolysis apparatus 2—21672
copper formate tetrahydrate and deutero derivative, vibr. freqs. 2—10341
copper heteroorganic acetylenides, absorption and photoconduction spectra investigated by diffuse reflection spectroscopy 2—29922
coronene, spectral shifts in nonpolar solvents, mechanism 2—25093
coumarin and related molecules, triplet-triplet absorption studies on 11000-27000 region 2—12225
coumarins, u.v. spectra, description of π—π^* transitions 2—8755
cyanine dyes, triplet-state e.p.r. 2—38973
cyanopyridine vapour, isomers, absorption spectra, $^1n \rightarrow {}^1\pi$ transition 2—31846
cyclic alkanes, excited electronic states, sharp vibronic structure 2—12205
cyclobuta[b]quinoxalines, electronic spectra measured, calculated values of transition energies and oscillator strength 2—12229
cyclohexane, excited electronic states, sharp vibronic structure 2—12205
cyclohexane, investigation of Rydberg states 2—31845
cyclohexane-d_{12}, investigation of Rydberg states 2—31845
cyclopentadiene, photoelectron spectra, vibrational analysis 2—3097
cyclopentanone in hexane soln., conc. depend. of absorpt. band 2—25096
cyclopentenones, photoelectron spectra 2—838
cyclopropane, study of l-type resonance effects in $\nu_5 + \nu_{10}$ band 2—21674
cylopentanone, photoelectron spectrum 2—838
L-cystine dihydrochloride γ-irrad. cryst., observation of electron-hole recombination 2—22887
decane, liq., explanation for spectra in terms of 2-phonon absorption 2—1104
di-t-butyl nitroxide, magnitude of multiplet splitting in X-ray photoelectron spectra, spin density implications 2—8672
diaminodiphenylmethane isomers and their diisocyanates, i.r. and u.v. spectra 2—28371
diazanaphthalenes, photoelectron spectra, ordering of π and nitrogen lone pair orbitals 2—15371
1,2,7,8 dibenzanthracene, transient absorption spectra using laser photolysis apparatus 2—21672
p-dibromobenzene crystals, absorption spectra, 4K, exciton zone analysis 2—26208
p-dichlorobenzene crystals, absorption spectra, 4K, exciton zone analysis 2—26208
dichloroethylene, mol. orbital interpret. photoelectron and X-ray emission spectra 2—35328
dichlorophenols, electronic absorption spectra in vapour phase, vibrational assignment 2—35319
difluorobenzenes, isomeric, electronic emission spectra, vibrational assignment 2—35330
1,2-dihydroquinoline, photochromic, CNDO/CI study of electronic spectrum 2—28370
dimethyl pyridine, vibratory spectra, interpretation and freq. calc. 2—38998
2,2-dimethyl-4-cyclopentene-3,5-dione, soln. and vapour, electronic spectra, absorption band assignment 2—8788
3,3′-dimethyldiazirine, electronic absorption spectra 2—24526
1,3-dimethylindazole, electronically excited, temp. dependence of deactivation in solution 2—3119
dinaphtho[2,1-2′,3′]furan-8,13-dione, fluorescence and optical absorpt. 2—25356
dinaphtho[2,1-2′,3′]furan-8,13-dione and dinaphtho[1,2-2′,3′]furan-7,12-dione, electronic 2—24538
2,4-dioxydithiobenzoic acid aqueous solution, absorption spectra 2—39371
diphenylamine, calculation of electronic spectra 2—31848
1,1-diphenylethylene: diphenyldiazomethane, photolysis and struct. obs. 2—37055
diphenyloctatetracene mixed crystals, electronic spectroscopy and solubility 2—10362
discharge lamps, coolant liquid spectral characteristics 2—14469
dye solutions, laser pumped, spectral shifts of laser emission 2—11476
dye-detergent micelle system, absorpt. and fluorescence spectra, comp. depend. 2—18839
dye-detergent solution, excited molecules local temp., fluorescence and absorpt. spectra 2—18838
emission, nucleoprotein, energy transfer between protein and DNA 2—26943
eosin, exciton bands and aggregate emission studied in u.v. and visible region 2—35359
erythrosin, exciton bands and aggregate emission studied in u.v. and visible region 2—35359
ethyl radical, proton hyperfine splitting constants, interplay of direct and indirect coupling contributions 2—3085
ethylene, ethylene-d_4, vibrational structure in photoelectron spectra rel. to vibrational spectrum of $K[PtCl_3(C_2H_4)].H_2O$ 2—3087
ethylene, ionization potentials from photoelectron spectra 2—31854
ethylene, photoionization cross sections calcs. using plane-wave method allowing orthogonality 2—31684
ethylene molecule, ang. distribs. of photoelectrons 2—35329
9-ethylguanine, polarized specular reflectance 2—24533
ethynylbenzene, lowest-lying singlet $\pi^* \leftarrow \pi$ transition, rotational analyses, dipole moment changes 2—35343
ferrous orthophenanthroline, Kramers-Kronig relationships, refr. and extinction indices 2—15592
9-fluorenone, emission and absorpt., low lying excited states 2—15375
9-fluorenone, obs. of low lying excited states in absorption spectrum 2—18504

Spectra continued
organic molecules and substances continued
fluorescein, exciton bands and aggregate emission, studied in u.v. and visible region 2—35359
fluorobenzenes, Rydberg states 2—21685
fluorobenzenes, Valence-shell transitions in vacuum u.v. 2—38981
fluoroform, mol. beam meas. of hyperfine structure 2—8772
fluorophenols, o-, m-, and p-, π-π^* emission spectra in near u.v. region 2—3090
2- fluoropyridine, rotational spectrum, Zeeman effect, g-vals. and susceptibility 2—843
fluorostyrenes, isomeric, emission spectra 2—3091
formaldehyde, absorption, emission and n.m.r. studies of form as function of solvent and temp. 2—35771
formaldehyde, absorption spectrum in vacuum u.v. 2—8775
formaldehyde, spin-vibronic perturbations in $^1A_2$ state 2—15377
formaldehyde, valence and Rydberg transitions, dependence of generalized oscillator strength on momentum transfer 2—15376
formaldehyde and ^{13}C and ^{18}O species, hyperfine components of 2_{11}-2_{12} transitions 2—35331
formaldehyde and ^{13}C species, at mm wavelengths, transition obs. 2—35332
formaldehyde isotopes, molecular beam maser studies of transition 2—12247
formaldehyde-d_2, Coriolis perturbed absorpt. bands, rotational analysis 2—8776
formamide, high resolution rotational spectra 2—3093
formic acid, rotational spectrum, isotopic substitutions 2—18509
fulvene, vapour and mixed crystal spectra, lowest energy electronic transition 2—8780
fumarofine, molecular structure 2—3096
furan, ESCA line intensities, orbital determ. 2—35219
furan, ESCA spectra, core binding energies and chemical shifts 2—5960
furan, photoelectron spectra, vibrational analysis 2—3097
glasses, γ-irradiated, scavenging kinetics of electrons, long range tunnelling 2—40831
glyoxal, $^{13}C_2$ substituted, visible electronic band, rotational analysis 2—8781
heteroaromatics of type R_2X, calculation of electronic spectra 2—31848
hexadecane, liq., explanation for spectra in terms of 2-phonon absorption 2—1104
1,2,3,6,7,8-hexahydropyrene, monovalent positive and negative ions, conformational interconversion 2—18511
L-histidine hydrochloride monohydrate:Cu(II), single crystal, lattice position of Cu from polarized absorption spectra 2—36978
hydrocarbons, MIM calculations of electronic bands involving triplet states 2—38987
hydrocarbons, nonalternant, calc. of electronic absorption spectra 2—12252
4-hydroxy benzanthrone absorption and fluorescence spectra 2—3102
1-amino, 4-hydroxyanthraquinone, sensitized emission spectra 2—31836
2-hydroxycarboxylic acids, OH stretching vibrations 2—28385
hydroxyphenazines, PPPMO calcs., transition energies and oscillator strengths, electronic spectra 2—12251
ion-radicals, electronic spectra and molecular orbital interpretation 2—834
N-isopropylcarbazole, and radicals; energy levels, splitting parameters 2—18513
isoquinoline, threshold electron excitation spectra, obs. of compound negative ion resonance and electronic transition 2—35350
ketones, saturated aliphatic, modulation of $n \rightarrow \pi^*$ absorption band 2—21689
ketones, saturated aliphatic, solvent effects in modulation of $n \rightarrow \pi^*$ absorption bands 2—21690
liquid crystal, orientational order and motion 2—15594
liquids, shock compressed, opacity absorpt. spectra 2—35770
maleic anhydride, soln. and vapour, electronic spectra, absorption band assignment 2—8788
maleimide and isoelectronic molecules, electronic spectra, quantum chemical calc. 2—15383
mercury compounds in water pollution, Raman spectra 2—12150
metalloporphyrins, probabilities of intercombination transitions 2—35347
methane, assignment of transitions in $\nu_3+\nu_4$ band 2—8790
methane, meas. and analysis of ν_3 band 2—38991
methane, obs. in spectrum of Uranus 2—30581
methane, photoelectron spectra 2—8795
methane, reactions of positive ions in gas, pulsed ion cyclotron double resonance spectroscopy 2—24568
methane, rot. analysis of ν_3 band 2—12258
methanol, triplet excitation by low energy electron impact spectroscopy, cross section determ. 2—15311
methanol, triplet excitation by low energy electron impact spectra 2—24453
methanols, isotopic, analysis of torsion-rotation spectrum, determ. molecular constants 2—8798
m-methoxy phenol, near u.v. absorption spectrum 2—3106
methyl chloride, Stark effect, applic. to Q-switching of CO_2 laser 2—3105
methyl fluoride, ^{13}C enriched, Stark effects 2—5357
methyl isocyanide, rot. spectrum for ν_8=1 and ν_8=2 excited vibr. states 2—24544
3-methyl-pyrrole, analysis of NMR spectrum, assignments of chemical shifts and coupling constants 2—12260
1-methylaminoanthraquinone, sensitized emission spectra 2—31836
methylated ethylenes, ionization potentials from photoelectron spectra 2—31854
methylated silanes, v.u.v. spectra 2—35299
N-methyldiphenylamine, calculation of electronic spectra 2—31848
molecular cryst., optical phonons and polaritons 2—19392
molecular crystal, radiative corrections and transitions 2—10334
monomethyldiazirine, u.v. obs. spectrum, rotational fine structure of 0-0 band at 3424 Å 2—12267
naphthacene, spectral shifts in nonpolar solvents, mechanism 2—25093
naphthalene, anal. of antiresonances in Rydberg spectrum in terms of theoretical line shape parameters 2—8802
naphthalene, charge transfer complexing effects 2—36893
naphthalene, gas phase triplet absorption spectrum, obs. of 4 electronic transitions 2—8803
naphthalene, in biphenyl and durene, localized in-band rotational phonons, obs. in electronic spectra 2—29512
naphthalene, indole-doped, local exciton spectra, effect of impurity conc. 2—13505

Spectra continued
organic molecules and substances continued
naphthalene, isotopic mixed cryst., energy spectrum 2—33279
naphthalene, obs. of transient absorption bands in some regions in gas phase and soln. 2—3112
naphthalene, opt. absorpt., 6.5-35 eV 2—18492
naphthalene, phosphorescence in vapour phase 2—35348
naphthalene, threshold electron excitation spectra, obs. of compound negative ion resonances 2—35350
naphthalene vapour, single vibronic level lifetimes 2—8736
nematic liq. cryst., cholesteric additives effect 2—12540
nitramines, conjugated, electronic absorpt. 2—8804
norbornanones and norbornenones, photoelectron spectra, rel. to ionization potential 2—3114
nujol, liq., explanation for spectra in terms of 2-phonon absorption 2—1104
octane, liq., explanation for spectra in terms of 2-phonon absorption 2—1104
oxysubstituted aromatic compounds, electronic, calculation using molecular orbital theory - LACO approach 2—852
palladium porphyrin complexes, fast fluorescence, delayed fluorescence, quasiline structure studied 2—12276
n-paraffin, doped, Shpol'skii spectra, 77K, polarization of multiplet components 2—20055
paraffins, long-chain, u.v. absorpt., electronic excitations 2—40687
pentacene-6 13-quinone, electronic spectra in solution 2—28394
perionaphthothioindigo and 2-perionaphthopentiophen-2′-(5′-methylthionaphthene)-indigo dyes, photochromism of coloured films 2—40833
perylene, electrochromic spectra in polystyrene matrix, change in polarizability and dipole moment between ground and excited states 2—13488
phenanthrene, charge transfer, complexing effects 2—36893
phenanthrene, Kramers-Kronig relationships, refr. and extinction indices 2—15592
phenanthrene in durene crystal system, absorption spectra, vibronic coupling 2—9322
phenols, substituted, solns., electronic absorption spectra, waveband shifts obs. 2—12274
phenyl isocyanide, lowest-lying singlet $\pi^*\leftarrow\pi$ transition, rotational analyses, dipole moment changes 2—35343
phenyl substituted imidazyl and pyrryl radicals, spin density distrib. determ. from e.s.r. spectra 2—8807
pheophytin, spectral shifts in nonpolar solvents, mechanism 2—25093
phthalazine, intersystem crossing from higher excited singlet states 2—12272
phthalic anhydride derivatives, electronic absorption spectra 2—853
phthalocyanine, π-electron absorp., molecular orbital calc. 2—10399
phthalocyanine. metal-free, calc. of singlet exciton state transitions in visible region 2—39003
phthalocyanine metal complexes in solns. of Lewis acids, absorption spectra 2—1105
platinum etioporphyrin complex, fast fluorescence, delayed fluorescence, quasiline structure studied 2—12276
polyacenes, triplet- triplet absorption spectra 2—12201
polycyclic aromatic hydrocarbons, α bands, magnetic circular dichroism 2—8801
polyene, electronic spectra, SCFMO calc. with configuration interaction 2—8847
polyethylene, u.v. absorpt., electronic excitations 2—40687
polymers, i.r. absorption, defect induced, vibrational properties 2—16506
polymethacrylate, acridine yellow activated, preexcitation effect 2—4499
polystyrene, vac. u.v. obs., opt. constants, free electron gas model 2—20009
porphyrin, π-electron absorp., molecular orbital calc. 2—10399
porphyrins, probabilities of intercombination transitions 2—35347
protein, non-heme iron, X-ray photoelectron spectroscopy 2—31873
proteins, tryptophan-containing absorption and luminescence spectra 2—8832
psoralens, u.v. spectra, description of $\pi-\pi^*$ transitions 2—8755
pyrazine, photoelectron spectrum, correlation between ionization bands and electronic levels 2—28402
pyrazine, u.v. and electron impact spectra 2—28403
pyridazine, u.v. and electron impact spectra 2—28405
2,2′- pyridil, $n\to\pi^*$ transition obs. 2—8814
pyridine, gas obs. of singlet-triplet transition by ion and electron impact 2—21699
pyrimidine, u.v. and electron impact spectra 2—28404
pyrrole, ESCA spectra, core binding energies and chemical shifts 2—5960
pyrrole, photoelectron spectra, vibrational analysis 2—3097
quinoline, threshold electron excitation spectra, obs. of compound negative ion resonances and electronic transitions 2—35350
quinones, PPPMO calcs., transition energies and oscillator strengths, electronic spectra 2—12251
quinosialine and d_0 deriv., electronic vapour absorption ($\pi^*\leftarrow n$) spectra study 2—12279
quinoxaline, vapour and mixed crystal spectra, $\pi^*\leftarrow n$ transition 2—10400
radiationless transitions, chem. reactions, relaxation phenomena in excited mols. 2—35200
radiationless transitions, electronic relax. processes 2—35196
Raman spectroscopy of organic gases, high resolution, photographic, experimental technique 2—11528
retinal and rhodopsin solutions, rel. to capacitance before and after visible light absorp. 2—37508
rhodamine 6G, electrochromic spectra in polystyrene matrix, change in polarizability and dipole moment between ground and excited states 2—13488
rhodamine 6G, H-bonding effect on orientational relaxation in solutions, investigation using psec light pulses 2—3394
Rhodamine 6G ethanol solution, optical absorpt. 2—35773
rhodamine 6J, spectral intensity changes on excitation by N laser, quantum generation 2—3390
rhodamine dye solns., superradiant laser emission using coaxial flashpump 2—15595
rhodamine dye solution, deformation of electronic absorption spectra rel. to associated molecule formation 2—39372
riboflavin, electronic spectra, binary solvents influence 2—28870
s-triazine, n, π^* absorption spectra meas. study of 3100 Å system 2—12288
solid solutions, lattice disorder effects on electronic spectra linewidths and multiplicities 2—36890
solid-state chemistry conf., Rehovot, Israel, (Sept. 1970) 2—37052

Spectra continued
organic molecules and substances continued
cis-stilbene, calculation of band shapes and absorption coeffs. for electronic transitions 2—15259
styrene, absorpt. cross sections and photoionization efficiencies, 600-2200 Å 2—18491
styrene-MMA, vac. u.v. obs., opt. constants, free electron gas model 2—20009
succinonitrile single crystal, Rayleigh scattering from entropy fluctuations 2—16443
2-tert. butyl-4-methyl-indazole, electronically excited, temp. dependence of deactivation in solution 2—3119
tetracene, polarization data for triplet triplet absorption spectrum, band assignment 2—8823
tetracene in p-terphenyl, 4.2 K, polarized fluorescence and absorption spectra 2—26175
tetracyano-p-quinodimethane, specular reflection spectra, anal. of metallic reflection influence of exciton phonon interaction 2—20008
tetracyanoethylene-trans-stilbene mol. complex, effect of external elec. field on abs. spectrum and electric dipole moment 2—31870
tetracyanoquinodimethane anthracene cryst. mol. complex, obs. of exciton interactions in polarized specular reflection spectra 2—13465
tetracyanoquinodimethane ion-radical salts, plasma oscillations of electrons 2—1682
tetraenes, conformational energy and transition energy, u.v. spectra investigation 2—858
tetrafluoromethane, ESCA line intensities, orbital determ. 2—35219
tetraphenylpolyenes, electrooptical polarisability in ground state and first excited singlet states 2—15381
tetraphenylporphine and Zn-tetraphenylporphine photoreduction, absorption spectra and e.p.r. of anion radicals 2—26366
tetrapyrrole pigments, triplet-triplet absorption, dichroism 2—3120
s-tetrazine, vapour, rotational fine structure of 5500 Å band, electronic spectrum 2—8824
thiathiophthenes, He584Å and X-ray photoelectron spectra 2—5997
thiophene, ESCA line intensities, orbital determ. 2—35219
thiophene, ESCA spectra, core binding energies and chemical shifts 2—5960
thiophene, photoelectron spectra, vibrational analysis 2 3097
toluene, Fourier obs. of Brillouin and Rayleigh line widths and shapes 2—1103
s-triazine, u.v. and electron impact spectra 2—28416
triclooctadiene, interpretation of unusual electronic spectrum 2—28363
trimethylamine borane, vacuum u.v. spectra, $\sigma\to\sigma^*$ electronic transitions 2—15401
trimethylamine borane, vacuum u.v. spectra, obs. of 2 electronic transitions 2—3127
trimethylamine borane-d_3, vacuum u.v. spectra, $\sigma\to\sigma^*$ electronic transitions 2—15401
2,4,5-trimethylbenzaldehyde, phosphorescence spectra, dynamic properties and zero field splittings of lowest excited triplet states 2—28335
triphenylenes, 2-substituted, excited state reson. interactions 2—35356
tryptophan molecule, in solid matrix, absorpt., 77K 2—35355
Uranium (3+) formate, low-temp. absorption spectrum, U^{3+} energy level scheme 2—10402
valence electronic struct. from X-ray photoelectron spectroscopy 2—35225
vinyl cyanide, valence shell calculations 2—18534
X-ray photoelectron spectra of DPPH and diphenylpicrylhydrazine 2—7085
xanthone, effects of medium on absorption spectra 2—24557
2,4-xylenol u.v. absorption spectrum, small spectrum 2—15407
zinc etioporphyrin, zero-field splitting of triplet state by optically detected magnetic resonance 2—35360
zinc tetrabenzporphin, fluorescence of second excited singlet and quasiline structure studied 2—12295
zinc uranyl acetate, electronic absorption spectrum and U—O bond distance 2—3128
CHO^+, transient species obs. using photoelectron and chemielectron spectroscopy 2—35163
$GeCl_4$, depolarization ratios of isotope lines 2—38941
H complexes, H_2 phthalocyanines, relaxation mechanisms from excited singlet states, spin-orbit coupling effects 2—35279
Mg complexes, Mg phthalocyanines, relaxation mechanisms from excited singlet states, spin-orbit coupling effects 2—35279
Pd complexes, Pd phthalocyanines, relaxation mechanisms from excited singlet states, spin-orbit coupling effects 2—35279
Rh complexes, Rh phthalocyanines, relaxation mechanisms from excited singlet states, spin-orbit coupling effects 2—35279
$SiCl_4$, depolarization ratios of isotope lines 2—38941
$SnCl_4$, depolarization ratios of isotope lines 2—38941

organic molecules and substances, infrared
bis-(bromomethyl)-mercury, vibrational assignment rel. to structure determination 2—21669
bis-(chloromethyl)-mercury, vibrational assignment rel. to structure determination 2—21669
bis-(iodomethyl)-mercury, vibrational assignment rel. to structure determination 2—21669
1,2-dichloroethane, low temperature modification, assignments made for lattice vibrations 2—8759
acenaphthene-d_{10}, fundamental assignment 2—28341
acetamide, monomeric, low temp. matrix isolation studies 2—8722
acetic acid, hydrogen bonded cyclic dimer, near i.r. spectra, vibrational analysis 2—21652
acetic acid, quantitative liquid-phase spectra, absorptivity in 2.5-13μm region 2—32270
acetic acid dimers, matrix isolated, interpretation of OH stretching absorption 2—8721
acetic anhydride, interpretation of vibrational spectra 2—28338
acetone, quantitative liquid-phase spectra, absorptivity in 2.5-13μm region 2—32270
acetonitrile, vibr. correl. functions determ. 2—31752
acetonitrile-d_3 and water, H bonded complexes, obs. i.r. transitions involving vibrations 2—8754
acetonitrile-water complexes, OH group stretching vibrations 2—25092
N-acetyl-2-thiohydantoine, temp. depend. 2—5957
acetylene, in 5 μm region, determination of anharmonic and rotation- vibration coupling constants 2—12200
adamantanes, and 1-substituted derivatives, band assignments 2—8725
l-alanine, vibrational assignment allowing for dichroic behaviour 2—40682

Spectra continued
organic molecules and substances, infrared continued
alcohols, steric effects on hydrogen bond 2—8726
aldehyde-BF$_3$ complexes, vibrational spectra 2—24501
alkanecarbodithoic acids, partial assoc. in form of dimers by hydrogen bridges 2—24500
alkyl platinum compounds 2—831
2- alkyl-iminobenzoxazolones, valence vibrations of azomethine group 2—835
amino phosphines and arsines, i.r. and Raman spectra, vibrational spectra 2—12207
aminophenetoles, absorption spectra, vibrational analysis 2—3113
α- aminophosphinic acids, zwitterionic structure 2—18523
3-aminopropyl dibutylboron with bases, vibrational spectra, hydrogen bonds and fermi resonance 2—31837
aniline, hydrogen bonded complex with substituted phenols in benzene solution, far i.r. spectrum meas. 2—12277
aniline and haloaniline complexes with 2, 4, 6-trihalophenols, crystalline, i.r. and n.q.r. spectra 2—10340
anthracene dimer anion, in γ-irradiated rigid ethereal solutions at 77K, absorption spectra 2—24502
anthracene dimer anion, in γ-irradiated rigid ethereal solutions at 77°K, absorption spectra 2—24502
anthracene excimer, absorpt. study during pulse radiolysis of solns. in benzene 2—20203
anthrapyridine, aminosubstituted, hydrogen bond study 2—3071
aromatic nitriles, anion radicals, study of intramol. electron interaction 2—8732
aziridines, vibrational analysis 2—12219
trans- azobenzene and isotopic derivatives 2—35304
azulenes, σ bonding polarisation from i.r. intensity meas., comparison with CNDO/2 calc. 2—21660
benzene, adsorbed layers on glassy pyrogenic SiO$_2$ 2—39565
benzene, in non polar solvents, intensities of absorption bands, determ. from i.r. dispersion curves 2—18835
benzene, in solid HCl matrix, vibr. spectrum, phase effects, frequency changes 2—13486
benzene, i.r. exciton spectrum, density of states and absorption function calc. using ^{13}C shift data from a$_{2u}$ mode 2—10397
benzene, methyl substituted derivatives 2—35309
benzene cryst., far-i.r. absorpt., external vibr. lines broadening at melting pt. 2—20053
benzene derivatives, substituted, role of symmetry of a vibration in temperature dependence of i.r. band intensity 2—24509
benzonitrile and d$_5$ analogue, theoretical study of vibrational assignments 2—35312
benzophenone, solns. and crystals, effect of u.v. illumination 2—26363
p-benzoquinone adsorbed on TiO$_2$, bonding rel. to surface electronic state 2—29058
benzoxazole, vibr. spectra 2—28348
4H-benzo[def]carbazole, absorption and emission spectra, comparison with MO calculations 2—24508
benzyl compounds, vibr. assignments, asymmetric structure 2—8742
benzyl derivatives, para substit., vibr. assignment, asymmetric structures 2—8743
benzyltin derivatives, vibrational assignment 2—21665
1,1′-biaziridine, vibrational assignment and conformation determination 2—38968
bicyclo [3.1.0] hexane substituted with O or CH$_2$, far i.r. spectra investigated 2—12215
biphenyl, vibrational spectra and dihedral angles 2—38967
biphenyl cryst., far-i.r. absorpt., external vibr. lines broaden at melting pt. 2—20053
bis(acetic acid)-BF$_3$ complex, molecular structure study 2—24546
bis(methanol)-BF$_3$ complex, molecular structure study 2—24546
bromo maleic anhydride, vibrational assignment and force constant calc. 2—12223
2-bromo-1-butene vibrational assignment and rotational isomerism 2—24519
2-bromobutane, crystalline and glassy states, rotational isomerism 2—40685
bromocyclobutane, ring-puckering vibration, far i.r. study 2—15366
bromoiodoacetylene, vibrational assignment rel. to force constant determination for dihaloacetylenes 2—38970
bromopropene, rotational isomerism 2—28381
bromoxylene 2—35309
t-butyl chloride, rel. to solid state phase transitions 2—36352
t-butyl cyanide, vibrational assignment 2—5963
γ- butyrolactone, i.r. spectral study of complexing with o-cresol 2—28358
caprone, temp. effects on i.r. absorption bands sensitive to H bonding 2—15362
carbon tetrafluoride, condensed phases, band moments and dipole autocorrelation functions 2—16503
carbon tribromofluoride and trichlorobromide, crystal structure 2—40683
carbonyl group containing molecules, i.r. spectra, stretching and torsional modes obs. 2—8750
carbonylbis(1-aziridine), vibrational analysis 2—15361
carboxylic acid dimers, saturated, simulation of abnormal spectra due to H-bond proton stretching vibrations 2—15360
chloro maleic anhydride, vibrational assignment and force constant calc. 2—12223
2-chloro-1-butene vibrational assignment and rotational isomerism 2—24519
1-chloro-2-bromoethane, band intensity calc., energy differences between rotational isomers 2—21677
3-chloro-2-chloro-methyl-1-propene, rotational isomerism 2—28382
chloro- and bromocyclopentane, conformational analysis 2—18495
chlorobenzene, far i.r. absorption interpreted by correlation function for rotational velocities 2—39368
2-chlorobutane, crystalline and glassy states, rotational isomerism 2—40685
chlorocyclobutane, ring-puckering vibration, far i.r. study 2—15366
chloroform, far i.r. absorption interpreted by correlation function for rotational velocities 2—39368
chloroform and proton acceptor complexes, H bonded, obs. i.r. transitions involving vibrations 2—8754
chloropropene, rotational isomerism 2—28381
chlorosubstituted compounds, determ. of basicity from spectroscopic data 2—16670
chloroxylene 2—35309

Spectra continued
organic molecules and substances, infrared continued
N,N-cinnamamides, para- and meta-substituted, substituent effect on i.r. carbonyl stretching vibrations and hydroxyl frequency shifts 2—38977
copper(II) acetates, low temperatures 2—35320
crotonaldehyde, vibrational- electronic bands of S$_1$(nπ^*) 2—35336
crystal hydrates, far-i.r. absorpt. deuteration effects, vibrs. obs. 2—22756
cyanocyclobutane, ring-puckering vibration, far i.r. study 2—15366
cyanogen azide in several solvents, spectra measured from 33 to 4000 cm^{-1} 2—12232
cyclobutane, vibrational assignments for D$_{2d}$ symmetry 2—28365
cyclobutane carboxylate ion, aqueous and crystalline, study from 4000 to 250 cm^{-1} 2—5969
cyclobutane-carboxylic acid vibrational spectra 2—24523
cyclohexane cryst., far-i.r. absorpt. external vibr. lines broadening at melting pt. 2—20053
cyclopentane, halogen derivatives, matrix trapped 2—35323
cyclopentanone, far i.r. spectra and hindered pseudorotation 2—35322
cyclopentanone, gas phase and in solution, study of Fermi resonance in $\nu_{c=o}$ region 2—24524
cyclopropane, vibr. transitions 2—33278
diaminodiphenylmethane isomers and their diisocyanates 2—28371
dianthracene anion radical, in γ-irradiated rigid ethereal solutions at 77K, absorption spectra 2—24502
diarylthallium (III) derivatives, aromatic ring vibrations 2—21679
dibenzyl mercury, vibrational assignment 2—21665
dibromo maleic anhydride, vibrational assignment and force field derivation 2—12222
1,2-dibromoethane, band intensity calc., energy differences between rotational isomers 2—21677
dichloro maleic anhydride, vibrational assignment and force field derivation 2—12222
p- dichlorobenzene, γ-phase, polycrystalline 2—7077
1,2-dichloroethane, band intensity calc., energy differences between rotational isomers 2—21677
1,2-transdichloroethane, orientational disorder and spectra calc. using intermol. potentials 2—25357
1,1-dichloroethylene, crystal structure investigation 2—6460
2,3dichloronaphthoquinone, and Raman spectra, vibr. assignment of obs. bands 2—31849
dichlorophenols, and deuterated analogues, vibrational analysis 2—3080
dichlorophenols, i.r. and Raman spectra, fundamental assignment 2—8764
dichlorosilicon phthalocyanine, structure studies 2—38972
dicyclohexylhydroxymethylphosphine oxide, H-bonding investigation 2—15370
dideutero methyl iodide, analysis of fundamental bands, value for A$_0$ determ. 2—12221
diethyl amine, vibrational assignment rel. to rotational isomerism 2—3082
diethyl ether, quantitative liquid-phase spectra, absorptivity in 2.5-13μm region 2—32270
diethyl-α-hydroxyisopropylphosphonate, H-bonding investigation 2—15370
2,2-difluoropropane, vibrational assignment 2—3083
4,4′dihalogenobiphenyls, vibrational spectra and dihedral angles 2—38967
2,5-dihydrofuran, far i.r. spectrum, calc. using two-dimensional anharmonic oscillator 2—15368
diiodomethyl radical, matrix spectrum, vibrational assignment 2—8800
dimercaptodiethyl sulphide, configuration 2—8769
dimethyl platinum, assignment of CH stretching modes of methyl group 2—831
dimethyl sulphide 2—38994
dimethyl sulphone 2—38994
dimethyl sulphoxide 2—38994
dimethylamine in solution, 22-190°C, meas. of association of NH stretching vibration modes 2—28368
dimethylaminodichloroarsine vibrational assignment 2—24528
dimethylaminodichlorophosphine 2—28369
N,N-dimethylbenzamides, para- and meta-substituted, substituent effect on i.r. carbonyl stretching vibrations and hydroxyl frequency shifts 2—38977
1,2- and 1,3-dimethylenecyclobutane, spectra obtained from 33 to 4000 cm^{-1} in solid and gas states 2—12238
3,4- dimethylenecyclobutene, vapour and film 2—10398
dimethylphenols, i.r. and Raman spectra, fundamental assignment 2—8764
dioxane cryst., far-i.r. absorpt., external vibr. lines broadening at melting pt. 2—20053
2,4-dioxydithiobenzoic acid aqueous solution, absorption spectra 2—39371
diphenyl monocrystal, low temps., far i.r. absorption spectra 2—16504
diphenyl-α-hydroxyisopropylphosphine oxide, H-bonding investigation 2—15370
diphenylamine in CCl$_4$ solution, of X-H absorption band 2—15373
diphenylhydroxymethylphosphine oxide, H-bonding investigation 2—15370
1,4-diselenan, vibrational assignments and force constant calc. 2—12236
DNA, correlation between theoretical and obs. frequencies 2—21709
DNA, Fermi resonance of i.r. vibrations in NH$_2$ groups 2—28423
epoxy resin, struct., additive effects, obs. 2—35855
ethane-d$_3$, vibr. frequencies, force consts., Coriolis zetas 2—12243
ethanediol, configuration in solid and liquid 2—8769
ethanol, quantitative liquid-phase spectra, absorptivity in 2.5-13μm region 2—32270
ethanol, solid, far i.r. torsional modes 2—28373
ethers, divinyl, spectral evidence of vibrational coupling of double bonds 2—8770
ethyl carbamate, copolymers with diethylene glycol etc., crystal study 2—4462
ethylene glycol, study of rotational isomers with absorption band spectra 2—38980
ethylene oxide, adsorbed layers on glassy pyrogenic SiO$_2$ 2—39565
ethylenediamine salts, assignment of i.r. and far i.r. spectra 2—3089
ethylgermanes, solid, far i.r. torsional modes 2—28373
ethylsilanes, solid, far i.r. torsional modes 2—28373
nfatty acid amides, vibrational analysis 2—15374
five-membered rings, far i.r. spectra, effect of finite central barrier on pseudorotation 2—15343
fluorobenzene, far i.r. absorption interpreted by correlation function for rotational velocities 2—39368
fluorocarbon film, struct. determ. 2—9228

Spectra continued
organic molecules and substances, infrared continued
fluorocyclopentane, vibrational spectra and structure of ring 2—12245
2-fluoropropene, normal coordinate analysis 2—8773
formaldehyde, pressure dependence of i.r. microwave double resonance 2—38983
formaldehyde-d$_2$, Coriolis perturbed absorpt. bands, rotational analysis 2—8776
formaldoxime, vibrational analysis, normal vibrations and torsional barrier 2—3094
formic acetic anhydride, normal coord. anal. 2—8778
formic acid, hydrogen bonded cyclic dimer, near i.r. spectra, vibrational analysis 2—21652
formic acid, quantitative liquid-phase spectra, absorptivity in 2.5-13μm region 2—32270
fulminic acid, absorption spectrum from 200 to 450 cm^{-1} assignment 2—12248
fulvenallene, vapour phase 2—28378
glycine isotopic species in Ar and N$_2$ matrices, band assignment 2—31857
glyoxal, glyoxal-d, glyoxal-d$_2$, vibrational assignment 2—3098
glyoxylic acid, 4000 to 300 cm^{-1}, vibrational assignment 2—24539
halobenzenes, assignment to nu$_{19b}$ fundamental 2—35333
haloethylamines, assignment of bands 2—3088
3-1 halogano-2-halogenomethyl-propene, vibrational spectra, rotational isomers 2—18524
hexahydro-1,3,5-trichloro and trinitroso s-triazine 2—31859
hexahydro-1,3,5-trinitro s-triazine, monocrystal vibrational spectra, 10 to 200 cm^{-1} 2—15379
hexahydro-1,3,5-trinitro-s-triazine, 3200-200 cm^{-1} single crystal and polycrystalline film 2—8783
hexamethylcyclotrisiloxane, i.r. dichroism of oriented crystalline films 2—40686
hexamethyldisiloxine, polymerized thin film 2—3550
hexamethylenetetramine association phenomena rel. to alkali halides 2—9219
hydrocarbon functional groups, in paraffins, near i.r. spectra 2—24541
6-hydroxy-2-pyridone, strong hydrogen bonding 2—10360
hydroxyl group containing molecules, i.r. spectra, stretching and torsional modes obs. 2—8750
2-iminothiazolidone-4 absorpt. 2—1696
iodo(methyl)germanes 2—845
2-iodobutane, crystalline and glassy states, rotational isomerism 2—40685
iodoxylene 2—35309
isonicotinic acid, strong hydrogen bonding 2—10360
isopropylalcohol, liquid state, rotational autocorrelation functions rel. to molec. motion 2—15593
isorhodamine, absorp., rotatory oscillation and moments of inertia 2—39005
ketones, interaction with compounds containing —OH, C=O valence oscillation line shift 2—8787
liquid crystal, orientational order and motion 2—15594
liquids, polar and nonpolar, far i.r. absorption spectra 2—1101
lithium formate monohydrate and partially deuterated compound, i.r. spectra of single crystals 2—26180
methacrolein, vibrational-electronic bands of $S_1(n,\pi^*)$ 2—35336
methane, absorption at 3.39 μ, temp. and press. depend., laser appl. 2—8797
methane, absorption study of ν_4 band, 1225-1400 cm^{-1} 2—21696
methane, deuterated, calculation of i.r. spectra of ν_3 and ν_4 modes in Kr and Xe matrices 2—40668
methane, harmonic spectra of dense phases 2—36892
methane, precision Stark- spectroscopy, nonlinear laser absorption 2—12217
methane, rot. analysis of ν_4 band 2—31862
methanes, mixed isotopic solid solutions, orientation effects on high resolution spectra 2—16505
methanol, quantitative liquid-phase spectra, absorptivity in 2.5-13μm region 2—32270
methyl(methylthio) mercury, vibrational assignment 2—21693
methyl bromide -d$_3$, analysis of ν_4, P and R structure 2—21695
methyl chloroformate, vibrational assignments 2—15384
methyl cyanide-d$_3$, vibrational assignment of near i.r. spectra, derivation of Coriolis coupling const. and anharmonicity coeff. 2—38992
methyl fluoride, investigation of 2ν_4 perpendicular band near 6000 cm^{-1} 2—38995
methyl pyridine adsorption on Al$_2$O$_3$, i.r. spectroscopy study 2—6367
methyl titanium halides 2—38989
methyl vinyl ketone, vibrational-electronic bands of $S_1(n,\pi^*)$ 2—35336
methylamine-d, inversion splittings interpreted by simple theory of asymmetric inverter 2—12259
methylenecyclopentane, liq. and vap., fundamental frequency assignment 2—12263
methylhydrazine, cis and trans barrier heights, far i.r., N-N torsional potential function 2—38990
in methylmethacrylamide-styrene copolymers, in region of ν NH bond 2—863
5-methylrhodamine, molecule rotatory oscill. effects 2—39006
methylsilane, barrier to internal rotation and its derivatives w.r.t. vibrational coordinates 2—12264
o- and m-methylstyrenes, vibr. bands assignment 2—3107
N-methylthioacetamide, normal coordinate anal., functional gp. frequencies 2—31864
monofluoroacetylene, rotational structure of ν, and 2ν, i.r. bands, centrifugal distortion const. 2—5983
monoiodomethyl radical, matrix spectrum, vibrational assignment 2—8800
N,N-dialkylhydrazones, absorption bands 2—3084
N-halogen secondary amides, cis-trans isomerism 2—28344
p-nitroaniline, near i.r., vibr. anal. 2—4461
nitroanisoles, absorption spectra, vibrational analysis 2—3113
2-nitroethanol, rotational isomerism 2—28389
nitromethane, nitromethane-d$_3$, matrix-isolated, i.r. spectra and intermolec. potentials 2—24547
o- and p-nitrophenetoles, vibrational assignment 2—31866
nitrorhodamine, molecule rotatory oscill. effects 2—39006
α- olefin reaction products with tertiary butyl hydroperoxide, analysis by i.r. spectroscopy 2—16701
organometallic β vinyl chloride (Hg, Sn, Tl, Sb), cis and trans config. detn. 2—31872
organometallic acetylides, vibrational assignment 2—15345

Spectra continued
organic molecules and substances, infrared continued
5-oxybenzodioxane-1.4, in soln., absorption bands temp. dependence 2—18516
pentaerythritol-d$_0$ and -d$_4$, vibrational crystal spectra 2—18521
pentahalogenotoluenes, study of barriers to internal rotation from vibr. band width meas. 2—8806
phenazine, vibrational assignments 2—8809
phenol intertiary and quaternary systems, i.r. spectra, proton accepting ability 2—28397
phenolate ions, hydrated, isotopic, C-O stretching i.r. band frequency 2 -28396
phenolic methacrylate anhydrides, and n.m.r. and mass spectra, spectrometric data 2—28334
phenolic methacrylates and n.m.r. and mass spectra, spectrometric data 2—28334
phenols, chlorine substituted, complexes with acetonitrile, study of intermol. H bonds 2—856
phenylacetylene, theoretical study of vibrational assignments 2—35312
phosphine oxides, spectroscopic study of intermolecular interactions 2—28434
phthalaldehyde, vibrational assignment 2—35342
polyethylene, low-pressure, i.r. spectroscopic study of branching 2—31875
polyethylene irradiated at 4°K 2—29924
polyethylene terephthalate, thin plastic films 2—40604
polyethylene terephthalate fibre, annealing, folded chains, absorption spectra 2—15642
polyimide, thin plastic films 2—40604
polymethyl acrylate, in region 4000 to 150 cm^{-1} 2—18539
polymethylpolyarsine, refl., optical consts. determ. 2—13431
polynucleotides, Fermi resonance of i.r. vibrations in NH$_2$ groups 2—28423
polyselenomethylene, hexagonal, vibrational assignment 2—15418
polystyrene-polybutadiene-polystyrene macroscopic 'single crystal' 2—15417
polythiomethylene, hexagonal, vibrational assignment 2—15418
polyvinyl alcohol, solns. in CCl$_4$ and dimethylsulphoxide 2—3133
porphyrins, chlorines, electron transitions, absorption spectra 2—39000
propane-d$_6$, vibrational assignment, symmetric valence of vibrational frequencies of methylene and methyl groups 2—39002
propargyl alcohol and deuterium analogues, vibrational assignment 2—5990
propionic acid 2—28399
propylene- vinylcyclohexane copolymers, structure study 2—24563
propynyl boron difluoride, fundamental assignment, G$_{12}$ symmetry group 2—8813
3-propynyl chloroformate, vibrational assignments 2—15384
purine sodium salt, freq. variations due to proton loss 2—10342
pyridazine-d$_0$ and pyridazine-d$_4$ 2—35349
pyridine, hydrogen bonded complex with substituted phenols in benzene solution, far i.r. spectrum meas. 2—12277
pyridine bromine charge transfer complexes in C$_6$H$_6$, force consts., dipole moment 2—8816
pyridine-halogen complexes, far i.r. intensity and normal coordinate studies, force consts., dipole moments 2—8817
pyrrole, liquid and crystalline samples and a solution in carbon tetrachloride 2—21700
pyrylium cation and deuterated analogues, vibrational assignment 2—39004
rhodamine S, effect of inorganic peroxides and γ-irradiation 2—3118
rhodanine, vibr. freqs. 2—8819
rubber, chemical struct. changes during ionization ageing, obs. 2—37041
salicylidene-m-hydroxyaniline. H-bonding studies 2—28408
tetrabenzyl germanium, vibrational assignment 2—21665
tetracyanobenzene complexes, triplet-triplet absorption in visible and i.r. regions 2—35351
tetracyanoethylene solution in mesitylene, π-π charge transfer complex, obs. of intermolecular vibrations in spectra 2—28426
tetramethyl phosphorus nitride, vibrational assignment 2—8822
tetramethylene cyclobutane-d$_0$ and -d$_8$, vibrational spectra measured, symmetry determ. 2—12282
tetranitro-1,3,5,7 octahydro tetrazocine-1,3,5,7, lattice vibrs. 2—9867
tetraphenylditin (IV) carboxylates, spectra from 30-4000 cm^{-1} meas. for crystalline solids and in solution 2—24552
thallium(I) nitroparaffins, i.r. spectra rel. to molec. structure determination 2—12287
1,3-thiazan, absorption band assignment 2—3124
thiazolidindione-2,4, vibr. freqs. 2—8819
thiazolidine, 2-oxo- and 2-imino-, absorption band assignment 2—3124
thioformaldehyde, spectrum observed in C-H stretching region, rotational analyses of bands 2—12284
thioformaldehyde, three bands near 3μ measured and analysed, ground state constants obtained 2—12286
thioketones, aliphatic, intensity and position of thiocarbonyl $\nu_{c=s}$ band 2—28414
thiophene, liq. and cryst. phases, absorpt. obs. 2—36004
thiophene in thiophene-d$_2$, Davydov splitting in vibr. spectra 2—10401
thiourea, aryl and antipyryl derivatives, absorption band assignment 2—3123
thiourea, ferroelec. transition, obs. 2—20080
thiourea, inter- and intra-molecular force consts., i.r. and Raman active vibrations 2—29513
thiourea, temp. dependence, mol. and lattice vibrations entropy 2—29923
thiourea cryst., absorpt. spectrum, para- and ferroelec. phases 2—26176
1,4-thioxan, force constant calc. and vibrational assignments 2—12285
toluene, toluene-d$_5$, interpretation in terms of rotational isomerism of methyl groups 2—15398
2,3,5-trichloro-p-benzoquinone, vibrational assignment 2—35353
trifluoroacetic acid, vibrational assignment 2—3126
trifluoroacetic anhydride, vibrational assignment 2—3126
1h-trifluorocyclopropene, vibrational assignment 2—12289
trimethyl acetonitrile, vibrational assignment 2—21704
trimethyl chlorosilane, adsorbed layers on glassy pyrogenic SiO$_2$ 2—39565
trimethyl germanium fluoride, normal coordinate anal. 2—24556
trimethylamine complexes with I$_2$, Br$_2$, IBr and ICl, band assignment to vibrations, force constants 2—12294
trimethylarsenic dibromide and dichloride, vibr. assignments and force field calcs. 2—18536
2,4,6-trimethylphenol, asymmetry of absorpt. bands 2—8524

Spectra continued
organic molecules and substances, infrared continued
triphenylmethylhydroperoxides, H-bond study using n.m.r. and i.r. spectroscopy 2—28417
triphenylverdasile, corresponding ions and the leucocompound, comparative study of i.r. spectra of radicals 2—39012
tripropargyl amine, vibr. assignments, rotational isomerism 2—18533
1,3,5-triselenan, vibrational assignments and force constant calc. 2—12236
urea, ^{15}N isotope effects 2—28418
urea, urea-d$_4$, low temp. matrix isolation studies 2—8722
vinyl bromide, vibration rotation spectra, Coriolis interaction 2—8829
vinyl chloride, vibration rotation spectra, Coriolis interaction 2—8829
vinyl fluoride, vacuum u.v. photolysis prods., vibr. assignment and force field, bonding 2—8830
vinyl iodide, vibration rotation spectra, Coriolis interaction 2—8829
vinyltrimethyl silane, polymerized thin film 2—3550
2,3-difluoroaniline, vibr. assignment of fundamental frequencies 2—31850

organic molecules and substances, radiofrequency
see also Nuclear magnetic resonance and relaxation; Paramagnetic resonance and relaxation
acetonitrile, vibr. correl. functions determ. 2—31752
9-acetyl anthracene, in benzene, dielectric relaxation times from microwave obs. meas. of loss and constant 2—28342
acridan in benzene, dielectric relaxation times from microwave obs. meas. of loss and constant 2—28342
benzoyl fluoride, microwave spectrum from 26.5 to 40.0 GHz, rotational and vibrational assignments 2—15357
benzoyl fluoride microwave spectrum, rotational and vibrational assignments to ground and excited torsional states 2—15354
bicyclo[2.1.0] pentane, microwave spectrum 2—31841
bicyclo[2.1.1]hexan-2-one, microwave spectrum, dipole moment and rotational constants 2—8744
t- butyl chloride, microwave spectroscopic structures compared with electron diffraction studies 2—15359
carbamyl fluoride, centrifugal distortion constants from microwave spectrum 2—35314
chloroacetaldehyde, microwave spectrum at 8 to 40 GHz, quadrupole coupling constant meas. 2—8752
2-chloropropenes, deuterium substituted, microwave spectra, CH_3gp conformation 2—31844
2-cyanopyridine, microwave spectrum, assignment of transitions 2—840
cyclopentadienyl thallium, Coriolis consts. from microwave spectrum 2—15268
cycloprolydrin, microwave spectrum and rotational isomerism 2—15367
cyclopropyl carbinyl chloride, microwave spectrum and rotational isomerism 2—15367
cyclopropyl carbinyl fluoride, microwave spectrum and rotational isomerism 2—15367
cyclopropyl methyl ether, microwave spectrum, dipole moment component determination from quantitative Stark effect meas. 2—12230
cyclopropyl methyl ketone, microwave spectrum, barrier to internal rotation, dipole moment, conformation 2—21673
cyclopropylacetylene, microwave spectrum 2—35321
p-dichlorobenzene, phosphorescence microwave double resonance spectra 2—8568
2,3-dihydrofuran, microwave spectra for vibrational states of ring bending mode, Stark effect meas. 2—12237
2,5-dihydropyrrole, microwave spectrum in ground and first vibrational excited states 2—18496
dimethylallene, microwave spectrum, barrier to internal rot., rot. consts. dipole moment, r_0-type structural data 2—18499
dimethylketene, rotational Zeeman effect in microwave spectrum, determ. of molecular g-tensor 2—38978
1,3-dioxolane, microwave spectra, pseudorotation 2—8761
epichlorohydrin, microwave spectrum and rotational isomerism 2—15367
epifluorohydrin, microwave spectrum and rotational isomerism 2—15367
ethyl nitrate, microwave spectrum, rotational constants of trans and gauche rotamers 2—12241
ethyl thiocyanate 2—35327
ethylene oxide, collisions study by broadening of microwave spectral lines 2—35385
ethyleneimine microwave gas spectra, substitution structure study 2—24534
2-fluoroethanol, microwave spectrum obs. 2—8774
fluoroform, fluoroform-d, rotational hyperfine spectrum 2—12244
formaldehyde, pressure dependence of i.r. microwave double resonance 2—38983
formaldehyde absorption at 4.83 GHz in dark galactic clouds 2—7396
formic acid, rotational spectrum of vibrational ground state 8 to 300 GHz 2—18508
fulminic acid, assignment of vibr. satellites obs. in rot. transition, vibr.-rot. interaction const. microwave and millimeter wave spectra 2—12268
fulminic acid, rotational spectrum 40-300 GHz, transitions of vibrationally excited states 2—21686
fulvene, microwave spectra, struct., dipole moment 2—8779
hexafluoropropene, C=C bond twisting, investigation using microwave spectrum 2—15380
methacrylonitrile, microwave spectrum, barrier to internal rot. of CH_3 and ^{14}N quad coupling const 2—8799
methane, interpretation of mol. beam radiofrequency, ortho-para transitions 2—12266
methanol at galactic centre, meas. of rest frequency of 36 cm radio line 2—33596
methoxydifluorophosphine, microwave spectrum, rotational constants and molec. structure 2—15387
2-methoxyethanol, microwave spectrum, determination of rotational constants and dipole moment 2—12262
methyl azidoformate, methyl azidoformate-d$_3$, microwave spectrum at 26.5 to 40.0 GHz, ground state rotational constants 2—15388
methyl nitrate 2—18514
methylamine-d, inversion splitting obs. in microwave spectrum interpreted by theory of asymmetric inverter 2—12259
methylbromide, collisions study by broadening of microwave spectral lines 2—35385
methyldifluorophosphine, microwave spectrum, rotational constants and dipole moment 2—15386
methylene difluoride, collisions study by broadening of microwave spectral lines 2—35385
methylhydrazine, cis and trans barrier heights, N-N torsional potential function 2—38990

Spectra continued
organic molecules and substances, radiofrequency continued
methylsilane, barrier to internal rotation and its derivatives w.r.t. vibrational coordinates 2—12264
monofluoroacetic acid, structure determination 2—38996
$\alpha,\alpha,\alpha',\alpha'$,2,3,5,6-octachloro-p-xylene in benzene, dielectric relaxation times from microwave obs. meas. of loss and constant 2—28342
3-oxetanone, microwave spectrum and ring-bending vibration 2—15389
1-penten-3-yne, microwave spectrum, electric dipole moment, rotational constants 2—12270
1-pentyne, rotational isomerism from microwave spectrum 2—8805
phosphorescence microwave double resonance spectroscopy, quadrature phase relationships 2—8568
pivalonitrile oxide, assignment of vibr. satellites obs. in rot. transition, vibr.-rot. interaction const. microwave and millimeter wave speectra 2—12268
pivalonitrile-N-oxide, microwave spectrum, bending mode estimate, symmetric top molecule 2—5989
1-D- and 4-D-pyrazole, microwave spectra, hyperfine structure, quadrupole coupling 2—5993
pyrazole, microwave spectra, nuclear quadrupole coupling constants 2 -8815
pyrazole, microwave spectrum, hyperfine structure, ^{14}N coupling consts., rotational constants 2—18526
2- pyrone, microwave spectra assignment and rotational consts. determ. 2—12231
silyl methyl ether, microwave spectrum in 8 to 40 GHz region, dipole moment calc. from Stark splitting 2—15394
s-tetrachlorobenzene, phosphorescence microwave double resonance spectra 2—8568
1,3,4-thiadiazole, microwave spectrum, nuclear quadrupole coupling and centrifugal distortion 2—18530
2,3,4-tricarbahexaborne(7), microwave spectrum at 8 to 38 GHz, rotational constants 2—15399
trifluoroacetonitrile, microwave spectrum of excited vibr. states, obs. of $J \to J+1$ transitions 2—12292
2,2,2-trifluoroethylamine, microwave spectrum, intramolecular H-bonding investigation 2—12290
trifluoroethylamine, normal and deuterated, microwave spectrum rel. to intramolecule H-bonding 2—21703
trifluoromethylhypofluorite, microwave spectrum at 8 to 40 GHz, rotational constants for ground state 2—8826
1,2,4-trioxacyclopentane, microwave spectrum, molec. structure determination 2—15400
vinyl germane, microwave spectrum at 12.4 to 40.0 GHz, assignments and dipole moment calc. 2—15406
vinyl trifluorosilane, microwave spectrum, rotational constants 2—15405
vinyltrifluorosilane microwave spectrum, dipole moment from Stark shifts of rotational transitions 2—21706
HCO radical, e.p.r., microwave absorpt. spectra, rotational transition 2—8720

Spectral line breadth
see also Doppler effect; Stark effect; Zeeman effect
absorption lines produced by exploding wire binary alloy 2—38812
peri-alkylnaphthalene anions, linewidth attenuation effects in e.p.r. 2—35303
asymmetric top molecules, collision broadening of absorption lines 2—15257
atom, absorption spectrum of nonmonochromatic radiation, broadening mechanism effect 2—31650
atom, impact and Doppler broadening 2—31638
atomic, broadening of lines by perturber gas, unified theory including impact and statistical theories 2—38804
atomic, collisional broadening, cross sections for resonance lines 2—2961
atomic lines, broadening and shift produced by fast electron collisions 2—28167
atoms, collapse of impact broadened multiplets, theoretical study 2—11940
atoms, line broadening, unified theories 2—5778
atoms, line broadening determination using correspondence principle 2—11939
atoms, profile narrowing by alignment in case of radiation trapping 2—31649
atoms, two-level system driven near resonance, linewidth corrections 2—31654
atoms in plasma, forbidden line profiles, ion dynamic correction 2—24318
azulene, linewidths for $S_1 \leftarrow S_0$ and $S_2 \leftarrow S_0$ nonradiative processes 2—31838
band shapes and absorption coefficients for electronic transitions 2—15259
Be stars, emission line profiles 2—16987
beam foil spectroscopy, reduction of Doppler broadened line widths by accepting only parallel rays of light 2—31136
benzene, anal. of antiresonances in Rydberg spectrum in terms of theoretical line shape parameters 2—8802
benzene, computer calc. of true profiles of Raman lines 2—35311
binary collision broadening, contribution of dipole- quadrupole dispersion 2—31667
binary collision broadening, impact theory predictions for shift and width of isolated electronic spectral lines 2—18339
Brillouin spectra, benzene, toluene, acetone and CS_2 2—1103
broadening in ^{19}F n.m.r. spectra due to N-F coupling, elimination by lowering temp. 2—5306
collision spectra optical broadening and depolarization of lines 2—31698
computer evaluation of integrals, asymptotic estimation 2—37664
crystal, impure, interference narrowing of hot luminescence lines 2—1450
Doppler and dispersion linewidth of Voigt profile, optimization of parameters of Fabry-Perot interferometer 2—8037
Doppler broadened resonance radiation, Monte Carlo investigation 2—8426
Doppler broadening from isotropic case of noncoherent scattering in plane-parallel finite layer 2—30760
Doppler profile rel. to reabsorbed radiation profile and Ladenburg-Levi function 2—38162
dye laser for spectroscopic investigations, efficient spectral narrowing and accurately reproducible tuning 2—37972
elastic quadrupole radiation processes, effects of molecular interactions on line shape 2—12299
e.p.r., computerized analysis 2—34266
e.p.r. line shape and width, temp. gradient effects in single crystal. applications 2—33332

Spectral line breadth continued
e.s.r. exchange broadening in solutions of free radicals and transition metal complexes 2—1117
e.s.r. line shapes in slow motional region 2—18394
e.s.r. Lorentzian shaped lines, corrections to meas. of line width and resonance field 2—36975
ethylene oxide, collisions study by broadening of microwave spectral lines 2—35385
gases, pressure line shape and Dicke effect 2—38806
glass:Nd, laser induced fluorescence line narrowing 2—33317
heptane, solid, n.m.r. line shape 2—30033
i.r. gas lasers, overlapping and high-pressure broadening in CO_2 and HF lasers 2—5361
l 2—27483
laser doppler velocimeter, signal broadening effects 2—23224
laser induced line narrowing effects in coupled Doppler broadened transition, standing wave features 2—21494
laser radiation spectrum broadening due to increase in transmission of nonlinear filter 2—27530
line shapes, pressure effects of inert gas mixtures 2—24331
liquids, orientational broadening of Raman lineshapes 2—12566
liquids, rotational correlation times determ. from Raman bandshapes 2—25089
Lorentz spectral line, width meas. using digital photoelectron correlation device 2—7905
Lorentzian dispersion lines, unsaturated, effect of modulation broadening on shape 2—14346
Lyman alpha line of hydrogen 2—2986
method of measurement 2—38149
methylbromide, collisions study by broadening of microwave spectral lines 2—35385
methylene difluoride, collisions study by broadening of microwave spectral lines 2—35385
1-methylvinyl radical on silica gel surfaces, e.s.r. sppectra, temp. effects, h.f. linewidths 2—35358
microwave and far infrared regions, pressure broadening and shift 2—28243
microwave and far i.r., pressure broadening and line shift, impact theory 2—17730
molecular pressure broadening phenomena discussed using analogy between theory of foreign-gas broadening and self broadening 2—31747
molecules, line broadening, unified theories 2—5778
multiple quantum resonances caused by large r.f. field, calc. of positions and shapes using continued fraction solution 2—31645
naphthalene, anal. of antiresonances in Rydberg spectrum in terms of theoretical line shape parameters 2—8802
n.m.r., line shapes in pulsed single resonance, analogue computer calculation 2—34271
n.m.r., motional narrowing, macroscopic and microscopic motions, rot. and concomitant motions 2—13552
n.m.r. line broadening, effect of macroscopic rot. of solid 2—26297
non resonant feedback laser, spectral profile meas. of cw amplified spontaneous emission by heterodyne method 2—21062
nonresonant Autler and Townes effect on a line broadened by saturation 2—35194
O stars line broadening as evidence for macroturbulence in atmospheres 2—33649
one-electron atoms, general program for calculation 2—15242
organic solid solutions, lattice disorder effects 2—36890
phonon-induced line shifts, theory 2—16442
polymers, skeletal vibration bands, effect of anharmonicity on half widths 2—31874
polyphenoxy radicals, linewidth effect in e.s.r. 2—35369
powder, e.p.r. line shape, spatial distrib. of line-width 2—36976
pressure broadening, molecular gases, classical path approx. 2—748
pressure broadening, unified classical path theories 2—2926
radiation from monokinetic atomic beam, broadening and narrowing by amplification 2—38845
radio recombination lines, pressure broadening, rel. to emission from HII regions 2—2924
Raman scattering, transient, study of spectral line shape and cross section 2—24416
Raman specta, liquids, analysis of orientational broadening of line shapes 2—8514
Rayleigh spectra, benzene, toluene, acetone and CS_2 2—1103
resonance broadening in gases, many-body aspects 2—753
resonant line broadening by electrons in nonequilib. partly ionized plasma 2—18289
self broadening, gas molecules 2—747
spin flip Raman laser, tunable direct meas. of linewidth 2—23613
Stark broadening, unified classical path theory 2—24319
Stark broadening by electrons and electron correlations in unified line shapes 2—35129
Stark broadening theory, exact line profile with model microfield 2—8430
Stark broadening theory of atomic lines, soluble scalar model as test 2—8429
succinonitrile, n.m.r. line narrowing study of translational mol. motion 2—1738
tetramethylsuccinonitrile, n.m.r. line narrowing study of translational mol. motion 2—1738
TMPD chloranil single crystal, e.p.r. linewidth, ang. dependence 2—36981
unified theory of spectral line broadening 2—2986
vapour, resolution of anomalies in resonance dispersion of pressure broadened line at 22 GHz 2—8633
vinyl radical on silica gel surfaces, e.s.r. spectra, temp. effects, h.f. linewidths 2—35358
WUMa systems, rotationally broadened line profiles 2—20546
X-ray Kα linewidths for Z=12—55 and 60, 65, 70, 75, 80, 85 with 2p shell vacancy 2—578
X-ray line shape and position, effect of emitting atom symmetry 2—35192
YAG, Pr^{3+} linewidth obs. 2—10339
Ar, ion laser transitions, spontaneous emission profiles, line profile anal. 2—24329
Ar ion laser transitions interference obs. 2—15195
Ar plasma beam ion line, Doppler broadening, obs. for det. of ionic axial energy 2—35538
Au hollow-cathode lines, effects of hyperfine structure on measured widths 2—15218
B discharge lamp emission 2—8048
Bi arc spectra, autoionized lines 2—38815

Spectral line breadth continued
C III and C IV pressure broadened profiles in the plasma 2—28188
C V, C VI, line profile calc. 2—15242
CO, half-width computation for air- broadened lines 2—12114
CO, i.r. emission lines 2—28278
CO, profiles of i.r. absorption bands in liquids, rotational motion 2—775
CO, self-broadening and broadening by Ar and N additions 2—38885
CO rotational lines in R branch, self and CO_2 broadening at 298, 202 and 132 K 2—31788
CO_2, 10.4 μm band, N_2 broadened collisional width, variation with rot. quantum no. 2—38899
CO_2, collision broadened line widths, effects of Coriolis interaction on line strengths of 3339 cm^{-1} band 2—18410
CO_2 infrared absorption line broadening at 207 and 298 K 2—18406
COS gas, microwave spectrum, line shape study, low pressures 2—12165
Cl II, stark broadening 2—35138
Cl II, Stark broadening meas. 2—2941
Co, Lα line shapes near threshold of excitation 2—21506
Cs, absorption, line shapes, pressure effects of inert gas mixtures 2—24331
Cs, comparison of experimental and theoretical pressure broadened line shapes 2—21507
Cs, highly excited levels, absorption line broadening in Cs vapour 2—11956
Cs I, van der Waals broadening of shock excited emission lines, about 5000K 2—15227
Cu, Lα line shapes near threshold of excitation 2—21506
Cu I, line broadening consts., theoretical estimation 2—2919
DCl, far i.r. rotational spectra, line shape parameters, interferometric meas. 2—15302
Eu^{3+} in phosphate glasses and aqueous solutions 2—29914
H, line profile calc. 2—15242
H, Stark broadened Balmer lines H_γ, and H_β, asymmetries 2—35176
H, Stark broadening theory, each line profile with model microfield 2—8430
H Lyman-β line, classical calcs. for broadening 2—38847
H radio recombination line broadening by electron collisions 2—37273
H_2, rotational Raman lines, anisotropy in Dicke narrowing rel. to measure of nonsphericity of intermolecular forces 2—38903
H_2 rotational line narrowing in inert gas mixtures due to pressure 2—8649
H_β lines, Stark broadening 2—15241
HCl, far i.r. rotational spectra, line shape parameters, interferometric meas. 2—15302
HCl, pressure broadening of rotational Raman lines 2—38913
HCl, profiles of i.r. absorption bands in liquids, rotational motion 2—775
HCl, rotational Raman lines, meas. of pressure broadening 2—3039
HF, line strengths and collision broadened half-widths obs. 2—8650
HF, meas. of pressure broadening of rotational line at 40 cm^{-1} using far i.r. spectrometer 2—8634
HF, strengths and widths of first overtone band 2—38910
HN_3, rotation-vibration spectrum in near i.r. and visible 2—15303
H_2O vapour, intensity-half-width products in 6.3 μm absorption band 2—32179
He-Ar, dilute solutions, far. i.r. absorption spectrum arising from collision induced dipole moments 2—9136
He-Ne laser, steady state amplitude fluctuations, natural spectral line width 2—31036
He, Stark broadening theory, exact line profile with model microfield 2—8430
He I, with forbidden components, absorption profiles, broadening 2—7427
He II, n=4-5 and n=4-6 line complexes, obs. in low temp. hollow cathode 2—31723
He lines, Stark broadening 2—15241
He plasma, Stark broadened resonance lines, difference in absorption and emission line shapes 2—8495
He^+, line profile calc. 2—15242
HeI, influence of distant electron collisions on plasma broadened 4471.48 Å line 2—35183
K, binary collision broadening of absorption line induced by Kr, contribution of dipole- quadrupole dispersion 2—31667
K, highly excited levels, absorption line broadening in K vapour 2—11956
$K_2[Pt(CN)_4]Br_{0.3}$.2,3H_2O, broadening of ^{195}Pt resonances in n.m.r. study 2—10562
Mn violet triplet, pressure broadening and shift due to foreign gases 2—31664
$Mn_xFe_{3-x}O_4$ ferrites, ferromagnetic resonance linewidth broadening, independent cluster model 2—20127
NH_3 gas, microwave spectrum, line shape study, low pressures 2—12165
N_2O, half-width meas. of (00°2-00°0) band 2—38926
N_2O, self and N_2 broadened lines direct meas. 2—18449
N_2O, self broadened and N_2 broadened half widths, 297K, quadrupole moments 2—15324
N_2O absorption lines, foreign-gas broadening coefficients 2—28309
Na, interstellar, as discriminant between models for galactic HI regions 2—4897
Na D-line, solar, broadening by H 2—7548
Na pressure broadening of 5889Å and 5895Å lines by thermal and high temperature He 2—31669
Ne-Ar, dilute solutions, far. i.r. absorption spectrum arising from collision induced dipole moments 2—9136
Ne, shape of absorbed spectral line at λ=743 Å, Doppler and Lorentz broadening 2—15221
^{20}Ne, 3S$_2$-3p$_4$ transition 2—8454
^{20}Ne, 3s$_2$-3p$_4$ laser transition, pressure dependence of radiation width, broadening and frequency 2—8455
^{22}Ne, pressure broadening and shift of 1.15 μm line, constants in Lennard Jones interatomic potential determ. 2—21517
Ni, Lα line shapes near threshold of excitation 2—21506
O_2, gaseous, broadening of fine structure Raman lines 2—815
O_2 microwave spectrum, pressure broadening calc., strong-collision model 2—18460
OCS, collisions study by broadening of microwave spectral lines 2—35385
Pb arc spectra, autoionized lines 2—38815
SF_6/D_2O clathrate hydrate, powder, ^{19}F n.m.r. lineshapes, chemical shift and anisotropy, correlation times 2—28323
SO_4 ions in sulphate solutions, viscosity independence of half width of $\nu_1(A_1)$ Raman line 2—1100
Si I, van der Waals broadening of shock excited emission lines, about 5000K 2—15227
SiC:N, e.p.r. lines, discrete saturation 2—7124

Spectral line breadth continued
Xe, spectral profile meas. of cw amplified spontaneous emission by heterodyne method 2—21062
Xe laser spectral narrowing dependence on line broadening mechanism, saturation and distributed loss effects 2—14398
Y:Gd, obs. of anisotropies in e.p.r. linewidth and resonance fields due to crystal field effects 2—4546
YH_3 diffusion of H, n.m.r. study, spin lattice relaxation time, resonance line shapes 2—29207

Spectrochemical analysis
see also Chemical analysis/by mass spectrometry; Spectroscopy
air pollution diagnostics, comparison of correlation spectroscopy and tunable diode laser-absorption 2—10663
alloy, sputtered vapour, atomic fluorescence analysis 2—10666
in arc source, calibration curve rules 2_4617
aromatic hydrocarbons and perfluoro analogues, charge distributions as determ. by ESCA 2—31860
astigmatic optical image transfer, for spectrographic system 2—14473
atmospheric, pollutant molecules, global survey by high speed interferometer 2—13683
atmospheric, pollutants, concentrations meas. by molecular spectroscopy 2—13682
atmospheric, pollution, high resolution correlation spectroscopic study 2—11529
atmospheric pollutants, atomic absorption 2—13685
atomic absorption, flame furnace studies, optimization of conditions 2—30115
atomic absorption, light scattering and molecular absorption interferences 2—22893
atomic absorption, noise and detection limits 2—8042
atomic absorption, non-dispersive optical systems 2—8041
atomic absorption, p.m.r., i.r., Raman and X-ray, conference (Toronto, October 1971) 2—13597
atomic absorption, use of Massmann furnace 2—8046
atomic absorption analysis, detection limit improvement using graphite vessels 2—40843
atomic absorption analysis, use of a.c. arc 2—40845
atomic absorption meas. using graphite vessels, optimal conditions for recording analytical signals 2—30112
atomic absorption rel. to atomic emission, choice considerations and advantages 2—16709
atomic absorption spectrophotometry, internal standards evaluation 2—10667
atomic absorption techniques, non-flame carbon rod atomizers 2—8045
atomic fluorescence analysis, sensitivity test 2—16699
atomic spectros. atomization efficiency of sample introduction vaporization systems 2—20218
Auger electron spectroscopy, chem. effects 2—35863
Auger electron spectroscopy, metal surface obs. 2—9242
Auger electron spectroscopy, review 2—13598
Auger electron spectroscopy, surface chemical analysis, review 2—10670
automatic chemical analysis by infrared absorption spectra 2—4614
benzene homologues, phosphorescence spectra, frozen matrices, liq. nitrogen temps. 2—4502
biological trace elements using gamma ray spectroscopy, nuclear activation analysis, radioactive tracers 2—17123
borosilicate glass films, vapour-deposited, i.r. method 2—13596
brine, atomic absorption obs. of trace elements 2—10661
CAMSPEK, microwave analysis for industrial laboratories 2—26383
ceramic glazes, Ti determ. by spectrophotometric method 2—40850
contact discharges, spectroscopic study 2—3261
correlation spectrometry and interferometry 2—38150
disperse particles in spark discharge, blast formed 2—4616
electrically conductive materials, device using d.c. arc to produce aerosol for analysis 2—10657
electron spectroscopy, conf., Pacific Grove, U.S.A., Sept. (1971) 2—31002
electron spectroscopy 2—40856
electron spectroscopy for polymer chemistry, core and valence energy level det. of PTFE 2—6003
electron spectrosocpy, review 2—31003
electronic microanalysis appl. to hot metallurgical samples 2—12925
elementary, in introductory physics lab., using grating in front of camera 2—16698
emission analysis by multichannel photoelectric quantometer 2—40847
emission analyzer, 2000 channel, direct reading, rapid 2—16706
emission spectra, automatic determinations 2—40846
ESCA, new photoelectron spectrometer and applics. 2—19805
ESCA, principles and recent developments 2—30111
excitation source, Ar plasma jet, interference obs. 2—16704
film surface contamination analysis using vacuum u.v. reflectometer 2—18929
flame atomic emission spectroscopy, scanning technique for multielement analysis 2—40842
flame emission spectros. using NO-acetylene flame and atomic absorption spectros., comparison of detectioc limits for 68 elements 2—10660
flame spectros., APCE-MIBK extraction system 2—20207
geological materials, using pulsed laser source coupled to double focusing mass spectrograph 2—18276
glass, lead borate, water content determ., i.r. absorpt. method 2—28977
glow discharge, applications 2—15511
graphite d.c. arc burning in mag. field, analytical application 2—35638
Grimm glow discharge lamp for spectrochemical analysis, electrical properties and discharge characteristics 2—4613
instrumentation for i.r. and atomic absorption analysis 2—10669
ionization spectroscopy, principle and applications 2—36646
i.r. absorption, Hadarard-transform spectrometry 2—40839
i.r. gas analysers, operation and applications 2—13595
i.r. gas analysis 2—10664
i.r. internal reflection spectroscopy, review and future prospects 2—11531
i.r. non-dispersive gas analysers 2—40840
iron ore, X-ray fluorescence 2—10675
lanthanide elements, UV bands, comparison with chromatographic analysis 2—1768
laser microspectral analysis, influence of spark plasma on sample surface 2—37066
laser sampling, Q-switched, and resulting plumes, atmospheric effects 2—10659
laser-Raman radar techniques for sensing molecular constituents in atmosphere 2—13681

Spectrochemical analysis continued
light source, Q-switched Ne laser with high pulse repetition rate 2 16705
linear light source 2—40838
luminescence spectra, excitation and emission, corrected to relative quanta, instrument technique 2—14483
lunar and geochemical samples, using large low background gamma ray spectrometer 2—18000
matrix Raman spectroscopy, isotope splitting and depolarization methods 2—8529
metal disk samples, flat, rotating disc sample holder for sparking 2—10662
metal samples, direct nebulization 2—10658
metallic film thickness measurement by means of absorption of coloured complexes 2—35880
metallic samples, using laser light sources 2—37065
metallurgy, atomic absorption spectrophotometry, emission spectrography 2—27649
metals, aerosol generation direct from surface 2—20215
Michelson interferometer for continuous gas analysis in far i.r., application to UF_6 2—37064
in nitrogen industry, for quality control, product analysis 2—16702
non metallic impurities extracted from steel 2—1770
nonflame atomic absorption technique 2—22896
α-olefin reaction products with tertiary butyl hydroperoxide, analysis by i.r. spectroscopy 2—16701
optically thin gases, total line intensities and physical state parameters 2—35679
oxide layers on metals, use of 'shake- up' satellites in photoelectron spectra 2—7192
Pb-Bi eutectic mixtures, obs. of Zr content 2—16703
plasmas, density ratio determ., analytical line pairs 2—4609
plasmatron discharge as source 2—4618
plastic, non-dispersive X-ray fluorescence in analysis 2—39971
pollutants, nonflame atomic absorption techniques 2—22892
polycrystalline metals, study of scattered electrons in X-ray spectral microanalysis 2—26385
polyethylene, low-pressure, i.r. spectroscopic study of branching 2—31875
polyheavywater, composition determ. 2—35737
polywater, ESCA spectra and distillation at 360 and 800°C 2—35738
potassium halides, Pb dopant conc. determ. for optical absorpt. studies 2—20039
proteins, in soln., detection, absorption spectra obs. 2—10665
reflectance spectroscopy, diffuse theory and applic. 2—11532
reflectance spectroscopy, principles, applic. and advantages of the various methods 2—11530
rocket propellants, solid, trace impurities, γ-ray spectroscopy 2—1772
semiconductor epitaxial structures, impurity concentration estimation, spectral analysis after chemical laminar etching 2—29194
semiconductors, det. of residual impurities using photoelectric spectroscopy 2—40841
semiconductors, impurity det. by emisssion spectros. 2—16708
sensitivity, spectrometer parameter effects 2—40844
sensitivity using adjustable-waveform, high voltage spark source 2—14482
spark, medium voltage, use as spectrochemical light source 2—20213
spark source, controlled waveform, analytical characterization 2—14484
sparksource, wear-metals in oils 2—14488
substance identification from i.r. spectra using holographic memory device 2—11493
surface, electron scatt., ionization spectroscopy 2—6309
surface Auger electron spectroscopy and appearance potential spectroscopy comparison 2—9233
surface composition, using ion scattering spectrometry 2—20216
time resolved direct reading analysis using laser source with medium pulse repetition rate 2—20214
titano-magnetite ores, in spark discharge of blast-formed disperse particles 2—4616
wool fibre, surface discharge treated, S oxidation state obs. 2—37043
X-ray, detection limits improvement using double-crystal spectrometer 2—4612
X-ray, detection limits rel. to spectrometer parameters 2—4610
X-ray, optimum spectrometer parameters rel. to detection limits 2—4611
Al, angular distribution of backscattered inelastic electrons in X-ray spectral microanalysis, 3-30 keV 2—26384
Al, using atomic fluorescence flame spectrometry 2—22898
Ar plasma, emission line profile broadening, correction curve 2—8440
Ca, using atomic fluorescence flame spectrometry 2—22898
CaF_2-Al_2O_3, dependence of atomic spectral line intensites of Fe, Cr and Si mixtures on the temp. 2—40849
Cd in solution, effect of magnetic field on excitation spectra 2—40848
CdTe, compensation determ. rel. to purification by vertical zone melting 2—35950
^{110}Cd, spectral analysis by isotopic dilution method 2—37067
Cm_2O_3, Am content, emission spectroscopy 2—30109
Co in Fe and steel, interferences 2—10668
Cr, using atomic fluorescence flame spectrometry 2—22898
Cu-Zn alloys, in elec. discharge, role of controlled atmos. in suppressing 'third' element effect 2—4615
Cu, angular distribution of backscattered inelastic electrons in X-ray spectral microanalysis, 3-30 keV 2—26384
CuO layer on Cu alloy, use of 'shake-up' satellites in photoelectron spectra 2—7192
F in geochemical samples, by projection of all arc flames onto the aperture of a spectrograph 2—30113
Fe, using atomic fluorescence flame spectrometry 2—22898
Ga, using atomic fluorescence flame spectrometry 2—22898
GaP thin films, Raman spectra as technique for structure and composition analysis of films 2—29933
H in Cr-Ni steels and Ni alloys 2—16700
H_2, small amounts, isotopic analysis based on compression of sample into discharge tube 2—30108
H_2O-D_2O mixtures, isotopic analysis with spectrophotometer 2—16692
H_2O, quantitative determ. in mica using i.r. spectroscopy 2—30114
H_2O vapour, small amounts, isotopic analysis based on compression of sample into discharge tube 2—30108
Hg traces in host material detected by new atomic absorption spectrometer from hyperfine structure lines in mag. field 2—8038
In, using atomic fluorescence flame spectrometry 2—22898
Ir, atomic absorption spectrophotometry 2—1771
Mn, using atomic fluorescence flame spectrometry 2 22898
NO_2 concentration in $N_2O_4 \rightleftharpoons 2NO_2 \rightleftharpoons 2NO+O_2$ system, use of Beer Lambert law 2—1769

Spectrochemical analysis continued
  Na D line reversal, premixed flames, chemiluminescence effects 2—8452
  NiO layer on Ni alloy, use of ‘shake-up’ satellites in photoelectron spectra 2—7192
  O_2-H_2 premixed flames, applic. 2—22894
  Os, atomic absorption spectrophotometry 2—1771
  S_2F_2, ion cyclotron resonance spectrometry investigation of ion molecule reactions 2—22871
  SO_2 detection in air, by dual beam Fourier transform spectroscopy 2—10671
  Sn quantitative analysis in NBS SRM Cu-base alloys and ore concentrates by Mossbauer spectroscopy 2—16710
  Sr, using atomic fluorescence flame spectrometry 2—22898
  Ta oxide film on Ta substrate, quantitative X-ray emission analysis 2—12670
  Ti, using atomic fluorescence flame spectrometry 2—22898
  ^{203}Tl, spectral analysis by isotopic dilution method 2—37067
  W, angular distribution of backscattered inelastic electron in X-ray spectral microanalysis, 3-30 keV 2—26384
  Zn vapour, atom. conc. determ. by atomic absorpt. method 2—20212
  ZnS, melt grown or hydrothermally prep., oxygen impurity study 2—36055
  ^{68}Zn, spectral analysis by isotopic dilution method 2—37067
  ZrO_2 rare earth neutron poisons, X-ray excited optical fluorescence 2—4506

Spectrometers
  see also Mass spectrometers; Monochromators; Particle spectrometers; Spectrophotometers; X-ray spectrometers
  astigmatic optical image transfer, general method 2—14473
  atomic absorption, detection of trace Hg in host material, based on hyperfine Zeeman effect 2—8038
  atomic absorption, Fabry-Perot interferometer 2—17738
  atomic absorption flame, with Xe arc continuum sources 2—17737
  calibration from calc. intensities of vibr. bands in fluorescence of NO 2—8675
  calibration to meas. absolute intensity and centre-to-limb variation of sun in v.u.v. region 2—11063
  Cassegrain, high resolution balloon-borne spectrograph, near solar u.v. 2—11061
  computer analysis of instrument function of slit-type instruments 2—27656
  computer control, digital data communication network 2—21175
  diffuse reflection and fluorescence measurement, powered solids 2—20103
  dispersive, multiplexing with nineteen entrance and exit slots 2—8034
  double beam, single detector, wavelength modulation 2—31140
  double beam vacuum u.v. spectrometer and logarithmic ratiometer 2—27652
  Ebert Fastie, quantitative eval. of unwanted doubly diffracted radiation 2—326
  efficiency, comparison criteria for instruments measuring radiation of remote objects 2—23724
  electron, cylindrical electrostatic analyzer, resolution 2—31005
  electron, low-energy, multidetector system 2—31006
  electron, spherical-grid-retarding potential analyzer, resolution and sensitivity 2—31004
  electron, time-of-flight spectrometer for total-cross-section-meas. at low energies 2—31009
  emission, production problems with inflexible specification 2—14478
  Fabry-Perot, stabilized multipassed interferometer, high contrast ratio 2—17739
  Fabry-Perot and complex S.I.S.A.M., theoretical instrument function 2—31143
  Fabry-Perot interferometer, u.v. spectroscopic studies, orbiting astronomical telescopes 2—11171
  Fabry-Perot interferometer with birefringent elements, tuning elements for dye lasers 2—27654
  far i.r. for studies of gases, performances studies from spectra of water and NH_3 2—8634
  far i.r. Fourier, Double beam interferometer 2—38159
  field-compensated Michelson spectrometers 2—27651
  fixed setting for obs. of acceleration modes in linear ion accelerator 2—21338
  Fourier-transform, based on Michelson interferometer, undergraduate expt. 2—14475
  Hadamard transform spectrometer, 0.1 cm^{-1} resolution 2—11539
  Hadamard-transform, multiplexing techniques 2—34546
  high resolution Hadamard transform spectrometer, modes of operation 2—27650
  i.r., demountable with gallery cut in rear salt window, for use with semisolids 2—34551
  i.r., grating, high resolution, design and construction 2—8032
  i.r., possibilities of determining instrument function from absorption spectra 2—27655
  i.r., wave number calibration of moderate and low resolution instruments 2—38156
  i.r., with monochromators, efficiency factor 2—38158
  i.r. absorption, Hadarard-transform spectrometry 2—40839
  i.r. and atomic absorption analyses, instrumentation 2—10669
  i.r. for measuring sorption processes on powder substances 2—6362
  i.r. using Ge:Hg detector for 9-14 μ, application to ν_1-band of gaseous COS 2—34548
  Jones matrices for Fourier interferometers 2—8033
  kinospectrograph, recording of emission spectra (3000 - 9000 Å on 16 mm cine film 2—328
  laser, to study absorption spectra of atmospheric gases 2—2464
  laser extinction and optical array, for airborne particle size meas. 2—16834
  mag. resonance, pulsed gas laser, dual-beam, for magnetooptic studies of solids 2—5449
  magnetic, for electron spectroscopy, design 2—34321
  Mariner Mars 1969 infrared spectrometer 2—31139
  for Martian atmosphere water vapour detection and mapping during Viking Mission 2—30564
  Michelson interferometer with tunnel effect beam splitter, use as Fourier spectrometer in far infrared 2—14476
  microwave, study of line shapes in gases at low pressures 2—12165
  multichannel, for flame emission and atomic absorption obs. 2—17733
  n.m.r., frequency modulated, with Robinson-type oscillator for internal mag. field meas. 2—2319
  normal incidence modulated reflection spectrometer, cryst. reflectivity meas. 2—8039

Spectrometers continued
  oblique incidence concave grating objective spectroscope 2—5448
  optical sound spectrograph synthesis 2—20940
  photoelectron, soft X-ray source, design 2—11235
  photoelectron, spectroelectrostatic prism 2—7852
  photoelectron, x-ray induced, construction and use in ESCA 2—19805
  photoelectron 584 Å commercial spectrometer, design and applications 2—8043
  plane grating, elimination of aberrations 2—27570
  radial velocity spectrometer, rapid scanning, construction and testing 2—37428
  Raman, FORTRAN ray tracing program for use in design 2—34554
  Raman, remote, field tests, O_2, N_2, H_2O and CO_2 obs. at 1.6 km range in atmosphere 2—34553
  saturation RPE spectrograph, power and frequency stabilized 2—34549
  scanning, use of rotating optical wedges 2—38157
  scanning, using rotating optical wedges for 1-6 μm region 2—34552
  seven channel Fabry-Perot spectrum analyzer for laser scattering meas. in θ-pinch 2—24766
  signal to noise ratio in multiplex coding of optical images 2—31137
  six channel interference filter spectrum analyser, examination of Thompson scattering by pulsed plasma 2—39133
  solar, multichannel, electronic systems 2—41221
  solar spectroscopic equipment for use in rockets 2—41224
  spectrofluorimeter system, on-line, for rapid collection of absolute luminescence spectra 2—11535
  spectrograph, plane grating 2—2465
  spectrograph for cometary u.v. obs. 2—10911
  spectroscopy, conference, Clayton, Australia (1971) 2—8509
  spherical-grid retarding potential analyzer, resolution and sensitivity 2—37907
  stroboscopic, ultra-high speed, using image converter camera as signal sampling system 2—27653
  submersible spectroradiometer, for optical oceanography 2—33431
  for thermoluminescence emission spectra, continuous determ. 2—29982
  time-of-flight, for short laser pulse spectral density determ. 2—27557
  triple system for Raman and luminescence spectroscopy 2—34555
  ultrasonic, continuous wave, for simultaneous obs. of sound velocity and attenuation variations 2—23378
  u.v., calibration 2—8035
  visual using graphite block for obs. of pulsed CO_2 laser line 2—17735
  Wisconsin echelle spectrograph, automatic data handling by computer 2—38155
  X-ray photoelectron, small-size, performance tests 2—31010

 accessories
  atomic absorption, Massmann furnace 2—8046
  atomic absorption techniques, non-flame carbon rod atomizers 2—8045
  cavity type absorption cell for double resonance microwave spectroscopy 2—37857
  cell housing, variable temp. −160 to 150°C for pulse radiolysis flow systems 2—14480
  compressed liqs., i.r. absorption, cell for study up to 1600 bar 2—2468
  computer-coupled Ge(Li) spectroscopy, neutron activation analysis 2—26388
  counting interval normalization circuit 2—27660
  cryostats for vacuum u.v. spectroscopy, temp. 77 to 300 K and 4.2 K 2—17135
  crystal current leveller for microwave spectrometer 2—17497
  digital computer measurement and detection of spectral lines 2—23727
  for discrete recording of i.r. absorption spectra 2—27658
  double beam, compensating wedge, errors and elimination 2—327
  double beam spectrophotometer, automatic level controller, electronic accessory 2—17742
  double monochromator, Heath EU-700 in tandem, low cost device 2—21178
  e.p.r., aqueous sample cells, design considerations 2—37860
  e.p.r., automatic magnetic field calibrator 2—34264
  e.s.r., modifications for studies on solid samples at high hydrostatic pressures 2—27371
  four channel timeshare oriented data acquisition interface unit for atomic absorption spectrophotometers 2—17743
  gas phase Raman spectroscopy, new accessory 2—11544
  gated image converter for meas. of fluorescence rise and decay time 2—20107
  gating technique for selective modulation of resonance lines from hollow cathode lamps 2—34556
  goniometer, three axis, for e.p.r. sample orientation 2—30967
  graphite block in spectrometer for visual obs. of pulsed CO_2 laser line 2—17735
  heterodyne spectroscopy, optical, local oscill. light mixing device 2—23729
  hydropneumatic drive for scanning system of Fabry-Perot 2—17740
  image-tube scanner for Wisconsin echelle spectrograph 2—38148
  i.r. cell, demountable gallery, for soft semisolids 2—34551
  luminescence excitation and emission spectra free of disturbing instrument characteristics 2—14483
  Mossbauer, doppler drive design 2—14743
  optical filter-cum-condenser lens system for Raman spectroscopy 2—38161
  proton radiospectrometer, attachment for recording ^{19}F n.m.r. spectra 2—27377
  R12B n.m.r. spectrometer, new variable temp. accessory 2—5305
  Raman, precision frequency calibrator 2—23720
  recording system, dynamic errors during tracing individual spectral line 2—31146
  recording systems, working region effects on contour distortion of spectral lines 2—38160
  rotating disc sample holder for sparking of flat-metal-disc samples 2—10662
  spark source, controlled waveform, analytical applications 2—14484
  spark source, high voltage, adjustable waveform, spectrochemical sensitivity 2—14482
  spherical specularly reflecting nonresonant cavities as long path absorption cell for far i.r. 2—31144
  transmission filters, far i.r. applic. of disordered solids 2—14481
  u.v. visible spectra meas. of single crystals with local reproducibility 2—17741
  vacuum u.v. detector, construction and props. of channel-electron multiplier 2—14393
  variable angle reflection cell for laser Raman obs. of matrix trapped molecules and radicals 2—34557

Spectrometers continued
- **accessories** continued
  - $CuCl_2,2H_2O$ filter, transmittance at elevated temps., passband characteristics 2—31145
  - InSb tunable detector, for far i.r. spectroscopy 2—27659
  - InSb tunable detector for far i.r. spectroscopy 2—8047
  - LiF-O_2 filter for Lyman-α radiation from electron impact on H_2, transmission properties 2—23728

Spectrometers, radiofrequency
- *see also Nuclear magnetic resonance and relaxation/measurement; Paramagnetic resonance and relaxation/measurement*
- autodyne, using resonance BWT 2—2314
- CAMSPEK, microwave chemical compounds analysis 2—26383
- construction and application at La Plata University 2—14342
- ENDOR, working at X-band for the microwave pumping 2—5303
- e.p.r., automatic magnetic field calibrator 2—34264
- e.p.r., homodyne, improvement by filter in leakage branch 2—37861
- e.p.r., low/high power, resonance meas. to 0.5 W, saturation to 20 W 2—5303
- EPR, problems of sensitivity and stability 2—217
- e.p.r., superheterodyne, single klystron, application of serrodyne single sideband generator 2—2315
- e.p.r., with Gunn-diode sitting in tunable re-entrant cavity 2—5300
- e.p.r., with u.s. modulation, longit. strain modulations below 10^{-4} 2—5308
- e.p.r. autodyne spectrometer with maser as oscillator 2—11404
- e.s.r., high-sensitivity, design and assembly 2—34267
- e.s.r., modification for study of substances under hydrostatic pressure 2—27370
- ferrites, susceptibility down to 10^{-5}, ultrasensitive technique 2—23469
- f.m. n.m.r., for meas. of internal magnetic fields 2—17495
- l.f. e.p.r. spectrometer 2—37859
- microwave, Camspek 2—2312
- microwave, crystal current leveller 2—17497
- microwave, double resonance, cavity type absorption cell 2—37857
- microwave, n.m.r., e.s.r., data acquisition system, computer instrument interfaces 2—7796
- microwave receivers for molecular line radio astronomy 2—11168
- microwave solar burst spectrographic radiometer 2—26893
- microwave-microwave double resonance spectrograph with crossed fields 2—27368
- n.m.r., pulsed, coherent, stabilization of resonance conditions 2—34270
- n.m.r., pulsed, with phase detection 2—34269
- n.m.r., tunable, for v.h.f.-u.h.f. range 2—37865
- n.m.r., variable frequency, double resonance probe 2—5303
- n.m.r., Varian 4200 spectrometer, mode of operation 2—7151
- n.m.r., Varian-XL-100 modification for Fourier transform operation 2—34272
- n.q.r., super-regenerative centre-shift elimination and lineshape response control 2—7807
- nuclear quadrupole resonance, wide range, superregenerative, with varactor diode frequency modulation 2—17505
- p.m.r., adaptation for ^{19}F n.m.r. 2—7806
- polariscope, for defectoscopy 2—9384
- variable frequency audio modulator for, patent 2—11408
- n-InSb, low inertia detector of millimetric radiation 2—17496

Spectrophotometers
- absolute u.v. calibration to update Orbiting Astronomical Observatory calibration 2—11189
- atomic absorption, double beam, with push button calibration and automatic zero, spectral anal. 2—21177
- atomic absorption, four channel timeshare oriented data acquisition interface unit 2—17743
- atomic absorption system with automatic base line, for process control 2—22895
- automatic chemical analysis by infrared absorption spectra 2—4614
- calibration for specular light by means of stacked glass plates 2—17734
- cell for in situ catalyst identification, high-pressure, high-temperature 2—16707
- computer analysis of instrument function 2—27656
- double beam, automatic level controller, electronic accessory 2—17742
- double beam u.v.-VIS, beam balance, optical geometries, accuracy, ccts. 2—8040
- double mirror grating dispersion system 2—5450
- errors due to inaccurate emission flow 2—2467
- Eskalab alpha, use in non-Eskalab procedures 2—21174
- Fabry-Perot, for observation of airglow 2—11537
- far i.r., quantitative spectral purity meas. 2—23726
- IOTA, computer controlled, for thin film thickness meas. 2—29713
- i.r., optical behaviour of absorption cells 2—11534
- i.r., wave number calibration of moderate and low resolution instruments 2—38156
- i.r. diffraction-grating spectrophotometer, degree of polarization 2—31142
- i.r. reflectance attachment for examination of surface chemistry of powder adsorbents 2—38154
- limiting factors, u.v.-near i.r. reflectance spectroscopy 2—11541
- Raman, modification for use with laser exciting source 2—34550
- rapid readout from dual wavelength 2—23725
- recording, applic. to photochemical reaction kinetics 2—17736
- recording systems, working region effects on contour distortion of spectral lines 2—38160
- twin-beam attenuation meas., in low-loss optical glass 2—8036
- u.v., stellar, high resolution, satellite borne 2—10887
- vacuum u.v., 10m concave grating spectrograph 2—18378
- vacuum u.v., at CNRS Bellevue, review 2—14477
- vacuum u.v., photoionization apparatus, opt. layout, for metal vapour obs. 2—18309
- $FeSO_4$ dosimeter, measurement precision below 1000 rads 2—5058

Spectrophotometry
- *see also Colorimetry*
- afocal instruments, complete optical integration 2—17729
- atomic absorption, instrumentation and application 2—27649
- auroral measurements 2—33508
- automatic control of nuclear fuel recycling processes applic. 2—28144
- ceramic glazes, Ti determ. by spectrophotometric method 2—40850
- crystal violet dye, isomerism study 2—3077
- derivative absorption and emission, numerical methods for generation 2—11536
- differential technique for determining the optical constants of very thin film 2—10300

Spectrophotometry continued
- Earth, colorimetry, aurora, optical struct., brightness, obs. from space 2—7241
- electrode ablation in a spark discharge studied 2—9005
- glass MS19, light diffusing, spectrophotometric characteristics 2—33189
- kinetic, design considerations for nanosecond pulse radiolysis 2—37059
- microscope equipment for tissue analysis 2—5054
- multispectral scanner data, used in water depth and characteristic determination 2—20297
- optical density errors due to inaccurate emission flow, estimation 2—2467
- vacuum u.v., double-beam methods at CNRS Bellevue, review 2—14477
- weakly absorbing and light scattering media examination 2—2466
- weakly absorbing media, new method of study 2—27657
- X-rays, soft, solar spectrum, grating with parallel grazing incidence 2—11069
- H_2O-D_2O mixtures, isotopic analysis with spectrophotometer 2—16692
- Ir determination, air-C_2H_2 flame 2—1771
- Os determination, N_2O-C_2H_2 flame 2—1771

Spectroscopy
- *see also Modulation spectroscopy; Spectra; Spectrometers; Spectrophotometry*
- absorption spectra, i.r., determ. by multiple attenuated total refl. method 2—34543
- applied, conference, New York, (October 1971) 2—14472
- atmospheric, gases and aerosols, absorption, emission and scattering remote sensing 2—16840
- atom, review of last 20 years 2—2929
- atomic, atomization efficiency of sample introduction vaporization systems 2—20218
- atomic absorption, anal. of several elements in one sample 2—21177
- atomic absorption, noise and detection limits 2—8042
- atomic absorption, obs. of pollutants in atmosphere 2—13685
- atomic absorption, p.m.r., i.r., Raman and X-ray, conference (Toronto, October 1971) 2—13597
- atomic absorption spectroscopy, significance of thermally assisted processes 2—2462
- atomic resonance absorption applied to chemically reacting systems 2—15229
- Auger electron, principles and applications, review 2—35866
- Auger electron spectroscopy, review 2—10670
- Auger spectroscopy, principles, techniques, and appl. to surface analysis 2—6303
- beam foil, reduction of Doppler broadened line widths by accepting only parallel rays of light 2—31136
- beam-foil-gas technique for studying steady-state non-equilibrium processes 2—26319
- Brillouin, absolute scatt. cross-section for quartz standard 2—16522
- colour film three band technique 2—34545
- computer assisted measurements 2—21175
- concave grating theory 2—14450
- conference, Clayton, Australia (1971) 2—8509
- correlation, applic. to remote sensing of air pollution gases 2—16822
- correlation interferometry, 0.1 cm^{-1} resolution 2—8031
- correlation spectrometry and interferometry, spectrochem. analysis 2—38150
- crystallographic axes determ. in single crysts. at high pressures 2—15683
- data indexing for fast accurate retrieval 2—21180
- diffuse reflectance, theory and applic. 2—11532
- digital spectrum analysis, effect of aliasing, averaging and smoothing 2—324
- electrode processes, optical methods for studying 2—40823
- electron, conf., Pacific Grove, U.S.A., Sept. (1971) 2—31002
- electron, material and structural analysis, applic. to glass research 2—22141
- electron, review 2—31003
- electron, review 2—31750
- electrooptic spectral scanning, high speed 2—5451
- emission, instrumentation and application 2—27649
- emission, photon counting and photographic detection 2—14767
- emission spectra, study of intense sharp bands on Cary 14 spectrophotometer, Wood's diffraction grating anomalies 2—21179
- erythrocyte ghosts, light-beating spectrum, technique for macromolecular studies in solution and suspension 2—37433
- excitation source, Ar plasma jet, interference obs. 2—16704
- far i.r., using InSb tunable detector 2—27659
- far i.r. gas laser applic. 2—17728
- flame atomic emission, scanning technique for multielement analysis 2—40842
- fluorescence flame, laser excited, applic. to steel analysis 2—22898
- Fourier, from Nimbus meteorological satellite 2—22953
- Fourier, high resolution, i.r. interferometer 2—34492
- fourier, polarization effects, coherency matrix representation 2—23723
- Fourier transform, elimination and reduction of background 2—8026
- Fourier transform, spectral errors resulting from random sampling position errors 2—27643
- Fourier transforms, S/N ratio 2—38152
- gases, atmospheric, photoelectron photoionization partial cross section determ. 2—8990
- gases, l.p., high resolution Raman spectra using single mode Ar laser 2—31135
- heat-pipe oven, operation for metallic vapours 2—8044
- high resolution correlation spectroscopy and air pollution 2—11529
- holographic, use of hologram as dispersive and focussing element of spectroscope 2—289
- internal reflection, applic. to adsorbed layer obs. at interfaces 2—9302
- internal reflection i.r., review and future prospects 2—11531
- inverse Fourier, spectra reconstruction, harmonics generated by Michelson interferometer 2—5446
- ion cyclotron resonance, trapped ion cell 2—35114
- ion scattering, surface composition analysis 2—20216
- ionization, principle and applications 2—36646
- i.r., adsorbed layers on metal surfaces, sensitivity improvements 2—15673
- i.r., applications to bacterial biology 2—11194
- i.r., det. of compos. of water vapour using spherical specularly reflecting nonresonant cavities as long path absorption cell 2—31144
- i.r., device using microwave techniques 2—17498
- i.r., emission, basic principles 2—27642
- i.r., industrial applics. 2—34547
- i.r., inert gas matrix technique 2—2463
- i.r., recording techniques at low signal levels 2—323

Spectroscopy continued
i.r. at high pressures using diamond-window cell 2—14474
laser, absorption spectra determ. 2—11543
laser, monochromatic absorpt. coeff. determ. 2—11542
laser 2—8029
laser Raman spectroscopy, minimizing emission background 2—31743
laser-Raman radar techniques for sensing molecular constituents in atmosphere 2—13681
light scattering, exptl. methods, cont. contrib. 2—16446
line shapes in plasma, photoelectric recording 2—3191
low-temperature, book 2—38151
luminescence excitation and emission spectra free of disturbing instrument characteristics 2—14483
matrix Raman, isolation laser, developments and applic. 2—11533
microsecond. use of high current capillary discharge as radiation standard 2—32120
molecular, computer applic. using interferometer 2—21176
molecular, normalization of Honl-London factors 2—8512
molecular, symbolic logic appl. to analysis of spectra and planning of spectral investigations 2—5894
molecular, use of computers and calculating machines 2—31138
Mossbauer, applications to chemical engineering 2—1666
Mossbauer, real shape of spectral lines, effect of exptal. geometry on shape 2—34904
Mossbauer, resolution improvement, Fourier transform. method 2—29889
multiple internal reflection i.r. spectroscopy, methods and advantages 2—27646
multiplexing techniques, applic. of various interferometers 2—34546
n.m.r., nuclear spin relaxation, Fourier transform analysis 2—7149
nuclear, on-line, retention of inert gases ion implanted in transport tapes 2—12060
optical, instrument for study of mag. ions in crysts. 2—33249
microwave optical double resonance, new technique 2—35231
optimal conditions for selecting spectra 2—4575
oriented molecular layers, specular reflectance and ellipsometric spectroscopy 2—26110
Perot-Fabry, vacuum u.v., construction and operation 2—15208
photoelectron, meas. using Millikan apparatus 2—31007
photoelectron, review 2—23721
physical metallurgy, tools and techniques, book 2—29372
plasma column, Doppler broadening 2—39153
Raman, absolute scatt. cross-section for quartz standard 2—16522
Raman, gases, high resolution, developments 2—17731
Raman, laser technology, development and applic. 2—16523
Raman, macromolecules in physiologically realistic conditions 2—15413
Raman, with tunable dye laser and narrow band filter 2—27644
Raman matrix isolation spectroscopy, experimental technique 2—11527
Raman spectroscopy of organic gases, high resolution, photographic, experimental technique 2—11528
reflectance principles, applic. and advantages of the various methods 2—11530
reflection, i.r., applic. to adsorption metal surfaces 2—12679
relative spectral power distribution, standards, verification by filter radiometry 2—8003
second derivative, applic. to air pollution trace gases anal. 2—16821
shadowgraphs for spectral functional analysis by the methods of coherent optics 2—27645
solar u.v. techniques 2—11059
solid, effective sampling depths in X-ray photoelectron spectroscopy 2—36632
spark, electrode erosion obs. 2—12476
spectra, composite, evaluation rel. to wavelength dependent lightpaths 2—34544
spectral distribution meas. of radiant energy, comparative study of methods 2—8028
spectral path, measurement errors, light absorbing media 2—327
spectroradiometry, extended wavelength 2—14479
spectroradiometry standards, review 2—7998
stimulated light scattering of Rayleigh line wing, amplification coeff. 2—5447
surface chemical analysis, Auger electron spectroscopy and appearance potential spectroscopy comparison 2—9233
time-of-flight, optimization problem 2—14746
transient plasma obs. in vac. u.v., techniques at CNRS Bellevue, review 2—14477
ultra-weak, study of detection methods 2—23722
ultrasonic absorption for conformational modifications of biopolymers 2—30653
u.s., of liquids, piezotransducer applics. 2—29520
u.v., stellar using Cassegrain-echelle optics with image intensification, rocket payload 2—11163
u.v.-near i.r., analytical applic. and instruments 2—11541
vacuum UV, beam splitting technique 2—20021
vacuum u.v., conf., Tokyo, Japan, Aug.-Sep. (1971) 2—14470
vacuum u.v., description of undergraduate laboratory and experiments 2—11242
vacuum u.v., instrumentation and techniques, CNRS Bellevue 2—14477
vacuum u.v. absolute intensity meas. by thermocouple recording of H arc spectrum 2—14490
vacuum u.v. spectrum obtained by holographic method 2—2461
vacuum u.v. with cascade arcs, use of He, Ar and Ar in He 2—21593
Walsh functions for det. of spatial frequency content of scene brightness distribution 2—34462
Ar plasma beam ionic axial energy det. 2—35538
W vortex plate, cracking, gas combustion, defects 2—32641

light sources
a.c. arc lamps, modulated spectra 2—38163
arc between parallel electrodes, stability of emission 2—34561
atomic absorption analysis, comparison of hollow cathode and h.f. electrodeless lamps 2—40843
atomic absorption method for determ. atomic and ionic fields 2—27663
BRV continuum, soft X-ray- u.v., visible, opt. and elec. characts. 2—14487
compensation of fluctuations in Raman spectroscopy by quick analogue dividing 2—2471
continuous, for vacuum u.v. spectroscopy 2—38164
dye laser, repetitive (up to 20 Hz) 2—17607
dye laser for spectroscopic investigations, efficient spectral narrowing and accurately reproducible tuning 2—37972
exploding wires, influence of atmospheric props. on self-absorption 2—34558

Spectroscopy continued
light sources continued
flames as source of metal atoms, formation processes and spectral data 2—5279
gas discharge lamp, spectral composition meas. 2—38143
Grimm glow discharge lamp for spectrochemical analysis, electrical properties and discharge characteristics 2—4613
high current capillary discharges 2—39210
impulse, determination from temps. in the region 600-1000 n.m. 2—31147
impulse lamp, absorption of energy emission in Nd glasses 2—27662
i.r. source, 0.6-5.6 μm spectral region 2—23730
lamps, h.f. modulation 2—329
laser light sources in spectrochemical analysis 2—37065
laser with high pulse repetition rate for time rsolved direct reading spectrochemical analysis 2—16705
lasers, for atomic fluorescence, characteristics 2—21181
linear, for spectral analysis 2—40838
longwave i.r., gas discharge lamp with metallic body 2—34560
low-pressure arc as source for molecular spectra 2—14485
microwave plasma burner, operation and props. 2—5452
multiple tape, for β-ray spectrometers for internal conversion electrons 2—18003
plasma, induction coupled, applic. in trace element det. 2—14489
reabsorbed radiation profile, influence of source geometry 2—38162
repetitively pulsed tunable dye laser 2—31043
semiconductor lasers as emission sources for spectral measurements 2—2472
spark, medium voltage, use as spectrochemical light source 2—20213
sparks, spectrochemical analysis of wear- metals in oils 2—14488
spectral lamp, multielement, twin- discharge for 6-8 elements 2—27648
Stark effect in methyl chloride, application to Q-switching of the CO_2 laser 2—848
storage ring, applic. to solid- state vacuum u.v. spectra 2—16479
storage ring developments at Univ. Wisconsin 2—17745
u.v., secondary standard, calibration by synchrotron and plasma-blackbody radiation 2—8023
u.v. standard radiators, vacuum photometric comparison between synchrotron and plasma blackbody radiation 2—17746
vacuum u.v., at CNRS Bellevue, review 2—14477
vacuum u.v., CI multiplet transition proximity meas., 170-250 nm, using plasma rad. and synchrotron sec. standards 2—17747
for vacuum u.v., modifications in systems rel. to lamp type 2—18378
vacuum u.v. lasers, high power 2—14415
vacuum u.v. photometric standard, stabilized H_2 arc applic. 2—17748
visible and near u.v. spectra of low- pressure rare gas microwave discharges 2—2469
v.u.v. atomic line source, 35 GHz microwave excitation of gas discharge in tapered waveguide 2—27661
Z pinch, influence of shock-piston separation 2—11545
Ar laser for Raman spectros. 2—17744
Ar with small amount Xe, vac. u.v. spectral region 2—14486
B discharge lamp, spectral line width 2—8048
He discharge lamps, windowed, for photoelectron spectroscopy 2—31008
He(II) intensity effects in photoelectron spectral transition identification 2—35221
Hg arc modulated 2—2470
Nd, Q-switched laser, medium pulse repetition rate, spectrochemical source 2—20214
Xe, current stabilization 2—38165
Xe pulsed discharge lamp, optical and electrical characteristics 2—34559

Spectroscopy, radiofrequency
see also Nuclear magnetic resonance and relaxation; Paramagnetic resonance and relaxation; Spectrometers, radiofrequency
applications, work of La Plata University 2—14342
double resonance experiment for splitting molecular stark-effect levels 2—38879
e.p.r., signal detect., bimodal spin induction method 2—5301
Fourier difference, with analogue Fourier analyzer 2—14349
Fourier transformation spectroscopy, double resonance methods 2—14344
i.r., device using microwave techniques 2—17498
i.r., using proustite crystal, applic. 2—23570
Jupiter, spectral properties in the decameter wavelength region, 1964 apparition 2—11007
microwave, backward diodes as detectors 2—27367
microwave, instrument for study of mag. ions in crysts. 2—33249
microwave, press. induced line shift 2—8519
microwave, Stark modulator, simple and versatile 2—2313
microwave double-resonance experiment, prevention of higher-frequency pump radiation from reaching detector 2—27373
p.m.r., high resolution, at 60, 100 and 220 MHz 2—11407
pulsed NMR spectroscopy, digital pulse programmer 2—37862
^{13}C n.m.r., chemical applic. and instrumentation, review 2—27375

Speech
see also Hearing
accent patterns, EMG obs. 2—33794
adaptive voice recognition system 2—37459
analysis and synthesis by linear prediction of the speech wave 2—14043
articulatory movement tracking using computer controlled radiography 2—30685
articulatory movements, observed by laryngoscipic fibrescope, inserted via nose 2—5072
articulatory movements by time optimal control 2—30691
artificial mouth design, diffraction coeff. of various shaped objects for human mouth and spherical sound source 2—26966
auditory frequency analysis, filter characteristics from psychoacoustics and neurophysiology 2—26967
automatic recognition system, dictionary and phonological rule 2—5077
bass singers, voice source props. 2—37456
bilabial closure duration for /p/, influence of utterance length 2—23155
cepstrograms and spectrograms, computer generated 2—7606
dynamic patalography using computer and oscilloscope 2—30684
evaluation, rank ordering procedure for auditory stimuli 2—37480
formant freq., auditory meas. 2—30689
formant-coded voiced, effects of smoothing and quantizing parameters 2—11207
harmonic synthesizer, vowel perception 2—20932
hearing role, alterations in S/N ratio, timing and sidetone spectrum 2—30680
identification, formant freq. shapes 2—37460

Speech continued
- identification of place of consonant articulation from vowel formant transitions 2—23175
- information compression, maximum likelihood spectral estimation 2—5076
- intelligibility, environmental noise effect 2—30686
- intercostal muscles, electromyography in connected speech 2—41314
- interference test for transmission quality meas. 2—37457
- Japanese word accent, model for generation of fundamental frequency contours 2—5074
- lossy vocal tract shape determ. 2—30687
- loudness increase on applic. of ear protector, interpret. as cybernetical process 2—37454
- mean energy spectrum, six languages spoken in chorus 2—20745
- musculature, studies of single motor units 2—37453
- perception, discrimination of synthetic speech sounds 2—5075
- physiology of production and features specifying vowels 2—7605
- preceding vowel duration as cue to perception of voicing characteristics of word final consonants in American English 2—41317
- recognition, continuously spoken words, time-normalization by dynamic programming 2—5078
- recognition of synthetic vowels, durations as cue 2—23174
- segment duration, threshold tracking method of obs. of incremental and decremental just noticeable differences 2—37474
- spectral waveforms of speech sounds, computer simulation 2—20746
- subglottal air pressures associated with /p/ and /b/ 2—23154
- subjective intelligibility tests objectification 2—37458
- synthesis, model of articulatory organs with physiological parameters 2—5073
- talks studios, permissible bass rise obs. 2—27232
- temporal phenomena, perception 2—37475
- timbre eval. and subjective perception 2—37461
- vocal effect alteration, pressure obs. of articulatory behavior 2—37452
- vocal fry, slope discontinuities in glottal pulse shapes 2—11208
- vocal signal visual pattern 2—30690
- vocal tract resonances with losses 2—33795
- vocal tract resonances with losses det. of frequencies and bandwidths 2—30681
- vocal tract sound transmission, parametric represent. 2—30688
- vowel devoicing, physiological laryngeal adjustments 2—30683
- vowels, component loudnesses in recognition, individual spectral components 2—30682
- word stress prod. in Russian 2—37455

Spherical aberration *see Aberrations, optical*

Spicules *see Sun/prominences*

Spin *see Elementary particles; Hyperons/spin and parity; Mesons/spin and parity; Nucleus/spin and parity; Rotating bodies*

Spin echo *see Nuclear magnetic resonance and relaxation*

Spin-lattice relaxation
- 1,2-dichloroethane, liquid, p.m.r. obs., rel. to mol. motion 2—35794
- acetic acid, temperature dependence of ^{13}C relaxation 2—38951
- actinide cpds., nuclear relax. times in paramag. state, model 2—7009
- alkali halide, rel. to weak mag. field enhancement of luminesc. from F-centres 2—26237
- alkali metal alloys, liq., Korringa relation, correl. effects 2—18855
- anthracene crystals, proton relaxation through triplet excitons 2—22845
- aqueous electrolyte solns., concentrated, pressure effect on proton spin-lattice relaxation 2—1118
- p- azoxyanisole, nematic mesophase, proton spin lattice relaxation time 2—18856
- benzene anion radical, ion-pair formation, effect on meas. of spin-lattice relaxation 2—35308
- benzene anion radical in liquid solution, investigation of c.w. saturation technique 2—35787
- benzoates, proton relaxation 2—29848
- p-benzosemiquinone in alcoholic soln., mol. motion e.p.r. obs. 2—35788
- binary liquid mixture, molecular interaction free 2—6252
- binary liquid mixtures, ^{1}H relaxation, determ. of mixed translational contribs. 2—9169
- 4,4-bis(alkoxy)azobenzenes homologous series of nematic liquid crystals 2—28898
- 1,3-butanediol, pressure and temp. studies of n.m.r. translational relaxation 2—35795
- 2-butyne, temperature dependence in various solutions 2—32279
- carbon tetrachloride solution, proton spin-lattice relaxation of 1,2-dichloroethane 2—18857
- chlorinated methylbenzenes, temp. dependence 2—10590
- chloroform, liq., proton spin lattice relaxation times, −54 to +90°C 2—9179
- chloroform, temperature dependence of ^{13}C relaxation 2—38951
- conduction electrons, at high mag. fields, theory 2—26077
- coronene, relaxation time n.m.r. measurements, study of reorientation of molecule in solid state 2—10567
- crystals temperature dependence calc. using defect mechanisms of self diffusion 2—7001
- cyclohexane, translational self diffusion obs. 2—29228
- decalin, relax. time calc. 2—32280
- diamagnetic crystal, magnetic impurity, e.p.r. line broadening rel. to phonon bottleneck in spin- lattice relax. 2—10532
- diazoaminobenzole, 2,5-dinitropyrole, of ^{15}N, temp. depend. 2—13424
- dichlorodi fluoromethane, interference effect in ^{19}F relax. 2—9180
- dicyclohexane, proton relax. and C-C bond pot. barrier 2—8760
- diffusion mechanism in solids applic. 2—25458
- diffusion mechanism influence on time meas. in rot. frame 2—10262
- dilute paramagnetic systems, from n.m.r. of nuclei near impurity, technique 2—37015
- dipolar liquid, elec. field effect 2—9160
- dipolar relax. in spin systems 2—10260
- dispersion singularities, saturation, appl. to molecular triplet states 2—7002
- electronic spin system, resolution of Boltzman quantum equations 2—10255
- ethylene glycol, Cr complex doped, proton relax. 2—16669
- ferroelectric, hydrogen- bonded, dipolar relax. study of l.f. motion 2—10259
- ferroelectric transition, critical dynamics 2—10258
- Fourier transform n.m.r., relaxation times 2—27380
- glycerol, pressure and temp. studies of n.m.r. translational relaxation 2—35795

Spin-lattice relaxation continued
- glycine, polycrystalline, proton spin-lattice relaxation 2—1736
- guanidinium aluminium sulphate hexahydrate, n.m.r., molecular motion 2—7131
- halomethanes, ^{13}C relaxation, field-dependent contributions 2—28333
- 2,4-hexadiyne, temperature dependence in various solutions 2—32279
- hexafluorobenzene, solid, and spin exchange 2—10278
- hexafluorobenzene, solid, molecular reorientation study 2—26310
- hexamethyldisilane, solid, pulsed NMR studies of proton spin-lattice relaxation time in static and rotating frames 2—20168
- hexamethylethane, translational self diffusion obs. 2—29228
- hexamethylethane cryst., mol. motions, n.m.r. obs. 2—13556
- homocystine, polycrystalline, proton spin-lattice relaxation 2—1736
- hydrogen bonded liquids, pressure and temp. studies of n.m.r. translational relaxation 2—35795
- iminoxyl biradical solid solns. 2—1731
- 1,3-indanione, relaxation in solution, microscopic molec. motions 2—28900
- ketones, partially deuterated, nonexponential behaviour in solid and liquid 2—16406
- lanthanide cpds., nuclear relax. times in paramag. state, model 2—7009
- lanthanum ethyl sulphate, spin-optical phonon relax. of Er^{3+} and Sm^{3+} 2—7011
- liquid, mol. motion determ. from relax. time freq. depend. 2—9173
- liquid, nucl. relax. by multipole interactions 2—32278
- liquid, nucl. relax. times freq. depend., correl. time distrib. influence 2—35791
- liquid crystal, molecular orientational motion, magnetic resonance spectra 2—15594
- liquids, n.m.r. apparatus for obs. at high pressures 2—37864
- liquids, using triplet pulse sequences 2—34273
- lyotropic liquid crystal, relax. time obs. 2—35796
- lysine, polycrystalline, proton spin-lattice relaxation 2—1736
- mechanisms, Fourier shapes of phonon operator correlative functions 2—22715
- metal, electron transition, non-mag. impurity effect 2—22716
- metal, e.p.r. width, temp. depend. 2—22822
- metal, nucl. relax. times, crossed elec. and mag. fields 2—40768
- metal, relax. time due to nuclear quadrupole interaction, calc. 2—19931
- metal, temp.-independ. relax. time, n.m.r. 2—29843
- methane, influence of centrifugal distortion of molecule on nuclear spin relaxation in gas 2—35316
- methane, solid, mol. reorientation obs. 2—10279
- methane, solid, spin conversion and oxygen catalysis obs. 2—10572
- methane, solid, spin species conversion through level crossing with paramagnetic impurities, obs. using proton spin lattice relaxation time 2—33184
- p-methoxybenzylidene p-n-butylaniline, nematic, p.m.r., anisotropic fluctuations 2—25113
- methyl alcohol, temperature dependence of ^{13}C relaxation 2—38951
- methyl bromide, temperature dependence of ^{13}C relaxation 2—38951
- methyl derivatives of naphthalene, crystalline, proton spin relaxation investigation of methyl group motion 2—22844
- methyl groups, of ^{13}C 2—8796
- methyl groups in molecular liquids 2—32279
- methyl iodide, temperature dependence of ^{13}C relaxation 2—38951
- 2-methyl-2, 4-pentanediol, pressure and temp. studies of n.m.r. translational relaxation 2—35795
- methylammonium chloride, temp. depend. n.m.r. study 2—16407
- molecular cryst., ^{35}Cl quadrupole relax., CCl$_3$-reorientation 2—10276
- molecular cryst., proton relax. due to tunnelling methyl groups 2—26291
- molecular paramagnetic moment, collision time correlation 2—5905
- monosubstituted benzenes, in liquid state, pressure dependence of relaxation times 2—39392
- naphthalene crystals, proton relaxation through triplet excitons 2—22845
- nematic liquid crystal, APAPA, temp. range 290-425 K 2—6257
- nematic liquid crystal, T$_1$ angular dependence 2—6246
- nematic liquid crystals, homologous series 2—28898
- neodymium ethyl sulphate, mag. field depend. 2—22719
- neodymium ethylsulphate, paramagnetic relaxation, Pr^{3+} and Ce^{3+} cross-relaxation 2—26087
- nitromethane, of ^{15}N, temp. depend. 2—13424
- nitroxide radical complexes with transition metals, effect on e.p.r. obs. 2—26376
- n.m.r. spectra, high resolution, selective relax. time meas., spin-echo signal 2—7150
- n.m.r. spectroscopy, Fourier transform analysis 2—7149
- norbornadiene, relaxation in solution, microscopic molec. motions 2—28900
- norbornylene, translational self diffusion obs. 2—29228
- nuclear, for case of anisotropic diffusion, longitudinal and transversal relaxation time determ. 2—26076
- Orbach relax. rate, interference and intermediate-level-width corrections 2—19930
- organic compounds, of ^{13}C, temp. depend. 2—35296
- organic compounds, of ^{13}C 2—15344
- organic free radicals, electron times 2—5955
- organic mixed crystals, spin-phonon interaction for triplet state molecules 2—29847
- 1,4-paradioxane in soln., mol. assoc. obs. 2—9172
- paramagnetic, quantum field theoretic analysis 2—29842
- penicillamine, polycrystalline, proton spin-lattice relaxation 2—1736
- perylene, relaxation time n.m.r. measurements, study of possible reorientation of molecule in solid state 2—10567
- phonon avalanche, spatial effects 2—40750
- phonon avalanche, spectral diffusion of mag. energy 2—40751
- phonon bottle neck, on e.p.r. saturation 2—1646
- phonon spectroscopy through spin lattice coupling 2—9854
- plastic cryst., translational self diffusion obs. 2—29228
- polar liquid, proton relax. temp. depend., mol. rot. 2—9182
- polycarbonates, irrad., proton relax. obs. 2—10280
- polymethylmethacrylate, in benzene-carbon tetrachloride and chloroform-carbon tetrachloride solutions, proton spin-lattice relaxation times for solvent mols. rel. to selective adsorption 2—39393
- polypropylene, atactic and isotactic, molecular motion study 2—33178
- polystyrene, and derivs., spin lattice proton relaxation 2—4414
- polystyrene, in benzene-cyclohexane solution, proton spin-lattice relaxation times for solvent mols. rel. to selective adsorption 2—39393
- polystyrene solutions in tetrachloroethylene. effect of molecular weight on ^{13}C spin lattice relaxation times 2—28901
- population inversion of spin levels in paramag. cryst. 2—6714

Spin-lattice relaxation continued

- pyridine, solvent effects 2—6260
- quadrupole relax., two-freq. methods 2—10263
- quadrupole spin echo obs. by two-freq. methods 2—7805
- quantum kinetic equation for system with discrete energy levels 2—29928
- quasi-nematic system, two-dimens., nucl. relax. time 2—32236
- quasilocalized lattice modes influence on quadrupolar relax. rate 2—10261
- Raman relaxation times, temp. depend., theory 2—40578
- rare earth Be compound, of ^{9}Be 2—26078
- rare earth intermetallic compounds, dynamic effects of paramag. ions 2—26078
- rare earth intermetallic cpds. in Laves phase, relax. time temp. depend. 2—40581
- ruby, heavily doped, optical props., review 2—36868
- ruby, temp. depend., 0.15 to 40K 2—33179
- semiconductor, nucl. relax. times, crossed elec. and mag. fields 2—40768
- solids, calc. of ^{1}H relaxation by quantum mechanical treatment of methyl group rotation 2—1647
- spin-phonon interaction, effect on two-dimensional Ising system 2—4416
- spin-temperature hypothesis, violation, Loschmidt paradox 2—7704
- TCNQ salt, enhanced nuclear relaxation near Mott transition 2—33182
- teflon, proton and fluorine, time, CW-method meas. 2—7151
- tetramethylammonium halides, proton spin-lattice relaxation times rel. to molec. motion and phase transition investigations 2—29849
- tetramethylbenzene isomer, multiple proton relax. minima 2—8821
- thiophene liquid proton spin relaxation and mol. motion, 300-500K 2—9184
- thiourea, n.m.r., molecular motion 2—7131
- time meas. by pulse and harmonic saturation methods 2—19929
- toluene, intra- and inter-molecular contributions 2—32279
- transition metal phosphides, Ti_3P structure type, measurements 2—4559
- tribromomethane, temperature dependence of ^{13}C relaxation 2—38951
- triphenylene, relaxation time n.m.r. measurements, study of possible reorientation of molecule in solid state 2—10567
- triplet states in vitreous matrix, saturation of $\Delta m=1$ lines, anisotropy 2—13545
- two proton system, tunnelling 2—10256
- tyrosine, polycrystalline, proton spin-lattice relaxation 2—1736
- xylenes, liq., of protons, mol. motion 2—9185
- ytterbium ethyl sulphate, spin-orbital phonon relax. of Yb^{3+} 2—7011
- yttrium ethyl sulphate:Yb^{3+} and Nd^{3+}, effect of paramagnetic impurity on n.m.r. studies 2—37015
- yttrium ethyl sulphate, of ^{3}Ho, Orbach and Raman processes 2—19936
- yttrium ethyl sulphate, phonon bottleneck of spin-bath relax. of Yb^{3+} 2—19935
- yttrium ethylsulphate:Dy(Yb), rel. to proton polarization by rot. cooling at $T<1K$ 2—29846
- zinc tutton salts, of Cu^{2+} 2—10274
- Al, solid and liquid phases, pulsed n.m.r. meas. 2—4112
- Al, temp. depend., melting effects, rel. to electronic struct. 2—7136
- Al superconducting, calc. of temp. variation in nuclear spin-lattice relaxation rate including anisotropy in energy gap 2—36450
- Al_2O_3:Cr^{3+}, ruby, field depend. 2—22717
- Al_2O_3:Cr^{3+}, ruby, γ-irradiated, phonon scatt., Cr^{2+} effect, thermal cond. obs. 2—40576
- Al_2O_3, corundum, of Fe^{3+} ions, temp. and conc. depend. 2—26079
- Al_2O_3, of Cr^{3+}, impurities influence 2—10264
- Al_2O_3 corundum, Fe^{2+} effect on electron spin relax. for Fe^{3+} 2—13423
- $AsCl_3$ complex, relax. time, n.q.r. obs. 2—26314
- AsH_3, AsD_3, liquids As-p, As-d spin-spin coupling constants meas., spin-lattice relaxation times 2—35792
- $AuAl_2$-$AuGa_2$-$AuIn_2$ pseudobinary alloys, satellite resons. 2—37004
- CS_2, ^{13}C relaxation, field-dependent contributions 2—28333
- CS_2, temperature dependence of ^{13}C relaxation 2—38951
- ^{13}C, field-dependent contributions 2—28333
- ^{13}C, n.m.r. satellite lines 2—5906
- ^{13}C, n.m.r. spectroscopy, Fourier transform techniques 2—5907
- ^{13}C, relax. times and chem. polarization 2—8796
- ^{13}C, under proton decoupling conditons 2—10257
- ^{13}C nuclei, meas. in organic liquids 2—3408
- ^{13}C relaxation, small molecules, temperature dependence 2—38951
- CaF_2:Eu^{2+}, e.p.r. obs. 2—22830
- CaF_2:Eu^{2+}, effect of paramagnetic impurity on n.m.r. studies 2—37015
- $CaWO_4$, of Sm^{3+} and Ho_{3}^{+}, temp. depend. 2—1649
- CdTe, n.m.r. of ^{113}Cd, cond. electron g-factor 2—33351
- $CeSn_3$, nuclear relax. times rel. to mag. ordering obs. 2—6941
- ClO_3F, n.m.r. of ^{35}Cl and ^{19}F 2—8604
- ^{35}Cl temp. depend. of nuclear quadrupole resonance and spin-lattice relaxation time in trichloroacetamide 2—10591
- CrO_2, ferromag., n.m.r. obs. 2—13551
- CsD_2AsO_4, ^{133}Cs relaxation rate 2—29844
- CsD_2AsO_4, ferroelectric phase transition, ^{133}Cs spin-lattice relax. temp. depend. obs. 2—6881
- Cu-Cr(Fe) dil. alloys, impurity induced relax. of host nuclei 2—36785
- Cu-Cr(Mn) dilute alloys, nuclear relax. times, obs. and analysis 2—7003
- Cu-Fe of ^{63}Cu, dil. alloys, rel. to Kondo effect 2—36657
- Cu-Mn dil. alloys, of ^{63}Cu, electron spin relax. obs. 2—16404
- Cu, nuclear relax. time, 1-10 mK 2—13553
- Cu, solid and liq., temp. depend. 2—10545
- Cu, temp. depend., melting effects, rel. to electronic struct. 2—7136
- Cu fine particles, size effect 2—40772
- Cu^{2+}, in complex halide, tetrahedral coordination, e.s.r. obs. 2—20134
- D_2, solid, h.c.p. 2—10253
- D_2, solid and liq., relax. of (J=0) mols. 2—22718
- Er, conically ordered ferromagnet, ^{167}Er n.m.r. study 2—33353
- Fe-Co dil. alloy, of ^{59}Co 2—33180
- Fe-transition metal dilute alloy, pulsed n.m.r. study 2—19932
- Fe(III) cpds. in ethylene glycol, liq. and frozen, τ_1 obs., structural determ. 2—12582
- Ga halides in aqueous solutions 2—1120
- GeH_4 and GeD_4, solid, mol. motion obs. 2—10265
- H_2-He, mixtures, test of linearity of time as function of percentage of adulterant gas 2—8628
- H_2-inert gas mixtures, proton spin lattice relaxation time meas. from 165 to 265K, collisional contrib. 2—24986
- HBr in DBr solution, molecular motion 2—6253
- HCl in DCl solution, molecular motion 2—6253
- HD, solid, p.m.r. obs. at $T<1K$ 2—37008
- ^{3}He, solid, mag. field orientation depend., autocorrel. function 2—15625
- Hf-H system, electronic contrib., spin echo method 2—16405

Spin-lattice relaxation continued

- InAs(P)(Sb), of ^{116}In, temp. depend. 2—7005
- K-Cs alloys, liq., Korringa relation, correl. effects 2—18855
- KCl, F_a(Li) centre, saturation recovery ESR obs., 4.2K 2—10507
- $K_4Fe(CN)_6.3H_2O$, para and ferroelectric, of ^{1}H 2—4556
- KH_2PO_4, of ^{39}K, rel. to ferroelec. transition 2—10581
- $KNbO_3$, ferro-antiferroelec. phase transition, n.m.r. obs. 2—16661
- K_2SnCl_6, of ^{35}Cl, 77-320 K, phase transitions obs. 2—7158
- La-Ce(Nd) dil. alloys, of ^{139}La 2—36786
- $LaAl_2Ce(Tm)$, impurity-induced relax. of ^{27}Al 2—40580
- $LaAlO_3$, of ^{23}Na, phase transitions obs. 2—9816
- $La_{1-x}Gd_xAl_2$, of ^{139}La and ^{27}Al, impurity contrib. 2—33181
- $La_{3-x}Gd_xAl$, of ^{27}Al, rel. to gapless supercond. 2—6777
- $La_2Mg_3(NO_3)_{12}$:Ce^{3+}, conc. depend. Orbach relax. rates 2—10266
- $La_2Mg_3(NO_3)_{12}$:Ce^{3+}, phonon bottleneck and cross-relax. 2—10268
- $La_2Mg_3(NO_3)_{12}$:Ni^{2+}, phonon bottleneck obs. 2—10267
- $La_2Mg_3(NO_3)_{12}$, of Pr^{3+}, Raman process 2—26080
- $La_2Mg_3(NO_3)_{12}24H_2O$ crystal with Nd, proton spin-lattice relaxation, 1.5 to 40 K and 0.7 to 20 kG 2—7010
- $La_2Mg_3(NO_3)_{12}.24H_2O$, Nd-doped, proton relax. 2—10269
- $La_2Mg_3(NO_3)_{12}.24H_2O$, of nucl. Zeeman and spin-spin energy 2—10270
- LaP, e.s.r. of Gd, cond. electron effects 2—40760
- Li, nuclear relax. times, many-electron enhancement effects 2—16660
- Li, of conduction electrons, mechanism 2—26081
- Li metal, effect on soft X-ray spectra near Fermi edge 2—20083
- LiF, proton and fluorine, time, CW-method meas. 2—7151
- $LiN_2H_5SO_4$, n.m.r., dipolar relaxation of ^{7}Li, hindered rotation 2—7006
- $MgSiF_6.6H_2O$, ^{1}H and ^{19}F nuclear spin lattice relaxation study and internal rotations 2—10577
- $MnSiF_6.BH_2O$, direct process for Mn^{2+} in strong magnetic fields 2—10271
- NH_4Br, of protons, phase transition phenomena 2—10272
- NH_4Cl:$Cu^{2+}(2H_2O)$, effect of paramagnetic impurity on n.m.r. studies 2—37015
- NH_4Cl, proton relaxation times 2—7007
- NH_4NO_3, cation diffusion study by proton spin relaxation 2—25465
- NH_4PF_6, and spin exchange 2—10278
- $(NH_4)_2SO_4$, ferroelectric, anomalies at 4 K, n.m.r. obs. 2—26082
- $(NH_4)_2SiF_6$, ionic motion, p.m.r. study 2—37011
- $(NH_4)_2SnBr_6(Cl_6)$, ionic motion, p.m.r. study 2—37011
- $(NH_4)_2SnCl_6$, tunnelling- assisted proton relax. of NH_4^+, 20-125 K 2—26083
- Na-Cs alloys, liq., Korringa relation, correl. effects 2—18855
- Na, nuclear relax. times., many-electron enhancement effects 2—16660
- Na metal, effect on soft X-ray spectra near Fermi edge 2—20083
- Na_2MoO_4, hydrous and anhydrous powder, meas. of ^{23}Na relaxation time using tone burst technique 2—37012
- $NaNO_3$, ^{23}Na nuclear quadrupole relax., orientation depend. 2—26084
- $NaNO_3$, nucl. quadrupole relax. of ^{23}Na, orientation depend. 2—19933
- $NaNbO_3$, ferro-antiferroelec. phase transition, n.m.r. obs. 2—16661
- Na_xWO_3, of ^{23}Na, phase transitions obs. 2—9816
- Na_2Wo_4, hydrous and anhydrous powder, meas. of ^{23}Na relaxation time by tone-burst technique 2—37012
- Nb:^{2}H, and quadrupole coupling 2—7129
- Nb-H system, proton relax. times, conc. depend. 2—7008
- NbN, of ^{23}Na, s-band state density at Fermi energy 2—13089
- ^{31}P in liquid organic and inorganic compounds 2—32277
- $PbMoO_4$, of Ho^{3+}, temp. depend. 2—1649
- Pd-Al dilute alloy, conc. depend. 2—40782
- Pd-V dilute alloy, conc. depend. 2—40782
- Rb-Cs alloys, liq., Korringa relation, correl. effects 2—18855
- Rb, nuclear relax. times, many-electron enhancement effects 2—16660
- RbH_2AsO_4, proton and fluorine, time, CW-method meas. 2—7151
- SF_6, in liq.-vapour critical region 2—39426
- SF_6, solid, dipolar and Zeeman relax., 300-4.2 K 2—26085
- $SbCl_3$ complexes, temp. dependence of relaxation of ^{121}Sb nuclei, n.q.r. study 2—19937
- Sc-rare earth dil. alloys, localized moments influence 2—19934
- $SiHCl_3$, of ^{29}Si, Overhauser effect obs. 2—29845
- Ta_3Sn, type II supercond., hyperfine interactions 2—4173
- Tb, ferromag., n.m.r. of ^{153}Tb 2—16662
- Ti-H system, electronic contrib., spin echo method 2—16405
- Ti-H system, spin echo study 2—16401
- TlCl, diffusion mechanism influence on time meas. in rot. frame 2—10262
- UF_6, ^{19}F rotating frame spin-lattice relaxation, obs. via anisotropic chemical shift 2—4561
- V_3Pt, of ^{51}V, near supercond. transition 2—33183
- Y-H, system, electronic contrib., spin echo method 2—16405
- YH_3, n.m.r. meas. of time as function of temp. 2—29207
- $YbCl_3.6H_2O$, temp. depend., Mossbauer obs. 2—10273
- $Yb_2(SO_4)_3.8H_2O$, temp. depend., Mossbauer obs. 2—10273
- Zr-H system, electronic contrib., spin echo method 2—16405
- ZrH_n, n=1.0-1.9, relax. time temp. depend., spin-echo obs. 2—16402

Spin-spin relaxation

- alkali metal alloys, liq., Korringa relation, correl. effects 2—18855
- 1,3-butanediol, pressure and temp. studies of n.m.r. translational relaxation 2—35795
- chloroform, temp. dependence of proton spin-spin relaxation time over range −54 to +90°C 2—22009
- electronic, cross relaxation effect on dynamic nuclear polarization of protons in polystyrene 2—36997
- ferromagnet, planar, in zero field exchange narrowing limit 2—40575
- gas, n.m.r. obs., quadrupole moments 2—12095
- glycerol, pressure and temp. studies of n.m.r. translational relaxation 2—35795
- hydrogen bonded liquids, pressure and temp. studies of n.m.r. translational relaxation 2—35795
- liquid, mol. motion determ. from relax. time freq. depend. 2—9173
- liquid, nucl. relax. times freq. depend., correl. time distrib. influence 2—35791
- lyotropic liquid crystals, relax. time obs. 2—35796
- 2-methyl-2, 4-pentanediol, pressure and temp. studies of n.m.r. translational relaxation 2—35795
- n.m.r. spectra, high resolution, selective relax. time meas., spin-echo signal 2—7150
- n.m.r. spectroscopy, Fourier transform analysis 2—7149
- nuclear coupling consts., relativistic corrections, higher-order combinations 2—13547
- nuclear double resonance, cross-relaxation 2—36999
- paramagnetic system, relax. time, asymptotic value, and invariants at motion 2—26075

Spin-spin relaxation continued
polypropylene, atactic and isotactic, molecular motion study 2—33178
Al_2O_3:Cr^{3+}, ruby, γ-irradiated, phonon scatt., Cr^{2+} effect, thermal cond. obs. 2—40576
$AsCl_3$ complex, relax. time, n.q.r. obs. 2—26314
AsH_3, AsD_3, liquids As-p, As-d spin-spin coupling constants meas., spin-lattice relaxation times 2—35792
$Co_xZn_{1-x}Fe_2O_4$ ferrite, mixed, Mossbauer obs. 2—40577
$CsMnF_3$, antiferromag., ^{55}Mn n.m.r. spin echo obs. 2—16403
D_2, solid, h.c.p. 2—10253
Er, conically ordered ferromagnet, ^{167}Er n.m.r. study 2—33353
Ga halides in aqueous solutions 2—1120
GeH_4 and GeD_4, solid, mol. motion obs. 2—10265
K-Cs alloys, liq., Korringa relation, correl. effects 2—18855
KH_2PO_4, cross relax., double r.f. field irrad. influence 2—10254
$MnCO_3$, antiferromag., ^{55}Mn n.m.r. spin echo obs. 2—16403
Na-Cs alloys, liq., Korringa relation, correl. effects 2—18855
$Ni_xZn_{1-x}Fe_2O_4$ ferrite, mixed, Mossbauer obs. 2—40577
Rb-Cs alloys, liq., Korringa relation, correl. effects 2—18855
Tb, ferromag., n.m.r. of ^{159}Tb 2—16662
Ti-H system, spin echo study 2—16401
$YbCl_3.6H_2O$, paramag. relax. temp. depend. 2—10273
ZrH_n, n=1.0-1.9, relax. time temp. depend., spin-echo obs. 2—16402

Spin waves
see also Ferromagnetism/spin wave theory
algebraic realization, perturbation calculation 2—13380
antiferrimagnet, uniaxial two-sublattice Neel-type, energy spectra 2—33154
antiferrimagnet, unixial two-sublattice Neel-type, energy spectra 2—36730
antiferrodielectric, spin excitation, exciton model 2—4281
antiferromagnet, anisotropic, critical damping of uniform mode 2—26068
antiferromagnet, coupled magnetohydrodynamical-spin wave reson. 2—26257
antiferromagnet, critical fluctuations 2—26055
antiferromagnet, Heisenberg model, temp. depend. of impurity modes, Green function theory 2—19911
antiferromagnet, interacting magnons 2—22696
antiferromagnet, interaction with acoustic waves 2—32831
antiferromagnet, isotropic, surface spin wave energy spectrum 2—40544
antiferromagnet, itinerant electron model, wave vel. calc. 2—6987
antiferromagnet., localized impurity influence 2—16388
antiferromagnet, magnon sideband temp. depend. 2—33163
antiferromagnet, magnon-photon coupling 2—22747
antiferromagnet, semiconductor and metal, electromagnetic fluctuations in a mag. field 2—6989
antiferromagnet, two-magnon Raman scatt., amplitude renormalization factor 2—40689
antiferromagnet, two-magnon Raman scatt. 2—16509
antiferromagnet with two different impurities, localized spin wave spectrum, theory 2—40538
antiferromagnetic model, excited states, indication of magnons 2—36757
antiferromagnetic spin-1/2 Heisenberg chains 2—22697
ferrimagnet, pulse propag. of exchange-dominated waves 2—19900
ferrimagnetic crystal, inelastic scatt. and magneto-optical props. 2—20060
ferrimagnetic system, light scattering, magnon-photon interactions 2—36850
ferrite, density of states singularities 2—10177
ferrite, parametric excitation with second magnetization harmonic frequency 2—16385
ferrite discs, magnetoacoustic resonance, two-stage parametric excitation 2—30001
ferro- and ferrimagnets, non-metallic, thermal conductivity 2—19844
ferrodielectric, thermal cond., role of magnons 2—6688
ferromagnet, near antiferromag. transition point 2—1615
ferromagnetic magnons, inelastic ultracold neutron scattering 2—19039
Heisenberg antiferromagnet, dil., Green function calc. 2—19912
Heisenberg antiferromagnet, dynamical susceptibility, magnon-magnon interaction effects 2—16391
Heisenberg antiferromagnet, non-collinear sublattices, linear defect 2—22698
Heisenberg antiferromagnet, one-dimensional, spin-wave theory and static correlations 2—10232
Heisenberg systems, dynamical scaling and kinetic equations just below critical temperature 2—26003
interacting magnon system, applic. of Green function theory of damped boson system 2—11308
magnetic insulator, e.m. modes coupling to magnetostatic modes 2—26009
magnetically ordered cryst., coupled e.m.-spin waves 2—10175
magnon Raman effects in ferromag. crysts. 2—40609
magnon relaxation, dislocation density depend. 2—3774
magnon-phonon interaction enhancement of electron effective mass 2—36423
magnon-phonon interaction in a time-dependent magnetic field, quantum theory 2—40437
metal, spin wave theory, weakly attenuating, in electron liq. 2—26007
neutron scattering in magnon studies, effect of phonon scattering 2—29808
nonlinear phonon-magnon inelastic scatt. processes 2—40066
paramagnetic, inelastic scattering of light 2—26184
paramagnons, applic. of consistent theory of fluctuations in superconductors 2—16151
periodic arrays, soft mode instabilities 2—19852
rare earth compounds, optical spectra, magnetic ordering effects 2—33259
semiconductor, ferromag., electron-magnon coupling 2—6740
semiconductor, ferromag., mobility of polarons interacting with magnons 2—6739
semiconductor, ferromag., spectrum of subthermal magnons 2—13333
spin-phonon interaction in Heisenberg ferromag., magnon scatt. 2—26006
three magnon bound states, numerical soln. 2—36683
TMMC, neutron scatt. obs. 2—22697
TMMC, spin dynamics 2—22713
transition metals, quadratic dispersion 2—6948
two magnon Raman scattering, at finite temps. 2—16516
two-magnon Raman scatt., review 2—36894
u.s. wave interaction with nuclear spin waves 2—40189
p-$CdCr_2Se_4$, ferromagnetic semiconductor, spin wave carrier interaction rel. to elec. field dependent magnetoresistance 2—32972
$CoCl_2.2H_2O$, interacting magnons 2—22696
CoF_2, two-magnon light and neutron scatt. 2—40545
Cr-Co(Fe) dil. alloys, localized impurity influence 2—16388

Spin waves continued
Cr-Fe dilute alloy, rel. to hyperfine fields 2—40622
Cr, rel. to anisotropic resistivity, crit. exponent in vicinity of Neel temp. 2—25767
$CuCl_2.2H_2O$, parallel pumping of spin waves 2—40551
Dy, magnetoelastic interaction, static and dynamic effects 2—25999
Dy, magnon energy spectrum 2—40441
Er, at 4.6 K in magnetic cone phase, study of neutron scattering 2—10189
Er, electron-magnon scatt. 2—6759
EuO, dispersion curves, neutron scatt. obs. 2—40472
EuO, magnon side-bands in luminesc. spectrum 2—36926
EuS, dispersion curves, neutron scatt. obs. 2—40472
Fe-Si ordered alloys, virtual magnon levels 2—1648
$FeBO_3$, ferromag., spin wave energy gaps, acoustic reson. 2—22675
$FeBO_3$, phonon-magnon interaction effect on Raman scatt. intensity 2—40692
$FeCl_2$, magnon dispersion relations 2—26066
$FeCl_2.2H_2O$, magnon-phonon interaction, microscopic description 2—40556
α-Fe_2O_3, ferromag., spin wave energy gaps, acoustic reson. 2—22675
Fe_3O_4, magnon dispersion relations, neutron diffr. obs. 2—36748
Gd, contrib. to sp. ht. 2—13042
Gd, polycryst., generation by optically excited electrons 2—19960
$GdAlO_3$, u.s.-spin wave interaction 2—32837
$GdVO_4$, magnetothermal resist., spin wave dispersion curves 2—22706
$InBO_3$, phonon-magnon interaction effect on Raman scatt. intensity 2—40692
$KCoF_3$, one and two exciton Raman scatt., magnon scatt. 2—36902
$KCoF_3$, Raman spectrum, double magnons 2—20071
$KMnF_3$:Ni(Co), absorption spectra, exciton-magnon struct., impurity effects 2—6993
$KNiF_3$, antiferromagnet, magnon sideband in optical absorption spectra, positive identification using mag. circular dichroism 2—36882
$KNiF_3$ Raman scatt. by four magnons 2—36903
K_2NiF_4 family, two dimensional antiferromag., phase transition, spin wave theory 2—16392
Li ferrite, Co^{2+} effect on spin wave decay 2—36971
$MnCO_3$, excitations, dispersion waves, neutron inelastic scattering study 2—36760
$Mn_{1.88}Cr_{0.12}Sb$, obs. of acoustical branch of magnon dispersion relation 2—22699
MnF_2:Zn^{2+}, far i.r. and Raman spectra in two-magnon region 2—7080
MnF_2, antiferromag., spin wave relaxation theory 2—36772
MnF_2, antiferromagnet, two-spin fluctuation light scattering, analysis based on frequency moments 2—33280
MnF_2, mag. Raman scatt. 2—36906
MnF_2, magnon-photon coupling 2—22747
MnF_2, magnon sp. ht. 2—40073
$MnFe_2O_4$, magnon dispersion relations, neutron diffr. obs. 2—36748
MnO, neutron diffr. obs., 4.2K 2—36775
$MnPt_3$, ferromag., dispersion, neutron scatt. obs. 2—22676
MnS, antiferromag., spin wave dispersion, effect of magnon-magnon interact., and magnon sidebands 2—33176
Ni, spin-wave reciprocal effective mass 2—9935
Ni film, microwave helicon- magnon interaction 2—16382
NiO, antiferromag, magnon excitation by electron tunnelling through Ni-NiO-Pb junctions 2—10240
NiO, Raman scatt. by four magnons 2—36903
NiO, two-magnon Raman scatt. 2—16509
NiO Raman, scattering by phonons, magnons and phonon- magnon interactions from 10-650K 2—26195
NiS, magnon dispersion 2—16349
Pd-Mn dil. alloys, acoustic-spin-wave stiffnesses and ordering temps. 2—10191
$RbMnF_3$, magnetoelastic effects in thermal cond. 2—40096
$RbMnF_3$ two-magnon Raman scatt. 2—16509
Tb, magneto-elastic coupling, acoustic wave vel., magnon-phonon interactions 2—13393
Tb, magnetoelastic interaction, static and dynamic effects 2—25999
VBO_3, phonon-magnon interaction effect on Raman scatt. intensity 2—40692
V_2O_3, Suhl-Nakamura interaction 2—10564
Y-(10 wt.%) Tb alloy, spin wave dispersion relation 2—40569
YIG, absorpt. spectra obs. 2—40681
YIG, axially magnetized single cryst., magnetostatic reson. absorpt. modes 2—19909
YIG, e.m. modes coupling to magnetostatic modes 2—26009
YIG, fine struct. of spin wave instabilities 2—40748
YIG, standing wave modulation, mag. anisotropy effects 2—13387
YbFe garnet, spin waves near mag. reorientation transition 2—40570

Spinors *see Quantum theory/wave equations*

Spions (pions with spin) *see Pions*

Spirality *see Elementary particles; Field theory, quantum*

Sporadic-E *see Ionosphere/E-region*

Sprays
see also Aerosols; Drops; Jets
combustion products of N_2H_4 and N_2O_4 liquid streams, photographic study 2—7170
evaporation, computer model 2—12615
heat transfer amplification in liquid-gas spray flows 2—32215
liquid, drop size determ. 2—6188
plasma spraying, effect of powder feed rate upon quality of coating 2—3215

Spurions *see Elementary particles*

Sputtering
a.c., d.c. biased, compositional control of Ta-Al alloy films 2—39478
alloy vapour, atomic fluorescence analysis 2—10666
amorphous solids, sputtered, topography, computer simulation 2—39449
atmosphere actuated linear motion device, preparation of samples free from surface contamination 2—41410
cathode, heated metal surfaces 2—35604
cathode, vacuum system for deposition of optical coatings 2—32352
cathode in glow discharge, heat transfer effects 2—35611
cathodic, reactive, of CuO thin films, plasma generator analysis 2—1011
computer simulation of sputtering of polycrystalline materials 2—4084
cosputtered film, compositional analysis and deposition profile calc. 2—39477
double electrode r.f. sputtering system, discharge characteristics 2—30741

Sputtering continued
double electrode r.f. sputtering system, effect of secondary circuit resonant frequency 2—30742
film deposition, focusing effects 2—3515
film deposition profiles calc. and comp. analysis 2—32344
film preparation using double-cathode discharge 2—29043
films deposition, increased adhesion 2—9255
glass, sputter topographies, evolution, secondary processes 2—39466
glow discharge, film growth, material transport, review 2—3519
high vacuum water cooled cathode assembly and feed through 2—41414
ion, vacuum pumps 2—23195
ion source for etching 2—37933
ion sources, machining of small structures 2—7890
Josephson tunnelling barriers fabrication by r.f. sputter etching 2—6783
metal atoms, mean energy meas. 2—36370
metal film, nucleation, growth, electron microscope obs. 2—6343
metal surface emission properties, effect of bombarding ions energy 2—36371
metals, on plastic film substrate, two-station r.f. sputtering system 2—39504
photon emission, by sputtered particles, during ion bombardment 2—10357
photon emission during alkali ion bombardment of solids, mechanism 2—36955
plasma spraying as source using Ta-Hf mixtures 2—5106
polytetrafluoroethylene film, r.f. sputtered, elec. and chem. props. 2—29049
reactive, metal film deposition, influence of surface adsorp. characts. 2—22068
r.f., on the nature of the discharge 2—39206
r.f., techniques for control of thin film properties 2—3512
r.f. diode system, operation and performance 2—41375
r.f. glow discharge, application to elemental analysis of thin surface layers 2—9232
semiconductor, effect on ion retention, saturation effects during implantation 2—25418
semiconductor, effect on ion retention, saturation effects during implantation 2—25420
semiconductor, from 20 to 500 keV Ar bombardment, step height measurement, scanning electron microscopy 2—25704
sputter ion mass spectrometers, sensitivity 2—565
superconducting A-15 film prep. by co-sputtering 2—29013
surface chem. profiles, inert gas sputtering obs. 2—39452
Ag-Co(Ni) two-phase targets, reduced, sputtering yields 2—32864
Ag single crystal, yield, bombarded by 6 keV Ne and Kr ions at temps. from 200-600°C 2—32859
Au, energy distrib. of sputtered atoms 2—40105
Au, laser-produced, film condensation inhibition 2—9270
Au, scatt. of Ar ions 2—36384
Au, sputtered ejection patterns, contribution from atomic collision sequences 2—40113
Au, structure in <110> spots on sputtered ejection patterns 2—6697
Au film, residual gas pressure effect on cross-section structure 2—25196
Au films, gas incorporation 2—35882
$BaTiO_3$ film, prep. by reactive cathode sputtering 2—29028
$BaTiO_3$ film, r.f., on Si, struct. and refr. index rel. to deposition temp. 2—40347
$BaTiO_3$ film, r.f., props. rel. to deposition temp. 2—40347
Bi-Sn sintered cathode, composition and deposition rate of r.f. sputtered films 2—39497
Cu-Ag films, investigation of factors affecting composition 2—32363
Cu, atomic number depend. of heavy ion sputtering yield 2—40114
Cu, ion products from 10 keV Ar^+ collisions, energy spectra 2—36651
Cu in O_2, influence of plasma electron density 2—3527
Cu target, sputtered-particle velocity spectra 2—16076
EuO-(6at.%)Fe, by r.f. discharge, Penning ionization obs. 2—4087
EuO film deposition 2—12658
Fe cathode, in Ar-O_2 mixtures, molecular sputtering mode obs. 2—1012
Fe foil, by fast neutrons 2 40107
GaAs, r.f. deposition, NaCl substrate 2—29047
GaAs single crystals, with inert gas ions, sputtered elements spatial distrib. 2—1441
GaSb single crystals, with inert gas ions, sputtered elements spatial distrib. 2—1441
Ge, energy and ang. depend. of sputtering ratios under heavy ion bombardment 2—25706
Ge, ion bombardment induced disorder, sputtered atom ejection pattern studies 2—22370
$Hf_yTa_{1-y}N_x$ film preparation 2—9277
InAs film, d.c. method 2—10023
InSb single crystals, with inert gas ions, sputtered elements spatial distrib. 2—1441
KBr, by low energy Ar^+ and Xe^+, mass spectrometry obs. 2—22447
Mo film, sputter deposition and removal from metal surfaces, Auger analysis 2—39514
Mo surface, low energy noble gas ion bombardment, energetic neutrals scatt. 2—6332
Nb, by Nb, H, D and He ions, 10 to 80 keV 2—4086
Nb film fabracation 2—25788
Ni-Cr thick films, deposition temp. effect on condensed phases 2—32371
Ni-Cu, differential sputtering yield 2—19477
Ni cathode, in Ar-O_2 mixtures, molecular sputtering mode obs. 2 1012
$NiFe_2O_4$ cathode, in Ar-O_2 mixtures, molecular sputtering mode obs. 2—1012
PbO_x film, prep. by reactive cathodic sputtering 2—22075
Si, energy and ang. depend. of sputtering ratios under heavy ion bombardment 2—25706
Si, rel. to surface damage, depth of damage 2—39467
Si, sputtering yield and sticking probability by ellipsometry 2—32378
Si_3N_4 films, from hot-pressed targets, contamination levels 2—32383
SiO_2 glass, yields and damage depths caused by 5.6 keV inert gas ions, energy losses 2—25713
SiO_x, film, r.f.-sputtered, i.r. spectra near 9μm, rel. to sputtering voltage, thickness, heat treatment conditions 2—13484
Sn oxide film formation, chemical aspects of reactive sputtering 2—18944
Ta-Ti, alloy, film, d.c. glow discharge diode co-sputtering, struct. rel. to sputtering conditions 2—12671
Ta film, cathodic sputtered, form. features. 2—29042
Ta film, in Ar-H_2O mixture, resist. rel. to O_2 content 2—39532
Ta film, self-induced sputtering during electron- beam evap. 2—12669

Sputtering continued
β-Ta film, sputtered, O_2 and N_2 competitive diffusion at 828K 2—39531
Ta film, sputtered in Ar-O_2, struct. and props., oxygen content depend. 2—29044
Ta film, struct. and elec. props. rel. to O_2 content 2—39533
β-Ta film, very pure, formation conditions 2—1187
β-Ta film sputtered, elec. cond., struct., transform., X-ray diffr. obs. 2—18945
W, 150 keV ion bombardment, cluster yield 2—40112
W films, from hot-pressed targets, contamination levels 2—32383
Zn, anomalous behaviour under metal ion bombardment 2—13062
ZnO acoustic transducer, r.f. diode production process 2—14269
ZnO film, d.c. and r.f. sputtered, struct., elec. and optical props. 2—39536
ZnO film deposition, transducer prep. 2—29549
ZnS, on Si, triode r.f. sputtering system 2—32384
ZnS, r.f. deposition, NaCl substrate 2—29047

Stacking faults
alloy, f.c.c., decorated faults, electron microscope image 2—36039
alloy, f.c.c., energy determ. 2—9565
anthracene, elec. microscope obs., role in photochemical reactions 2—30088
dechannelling cross section, calc. 2—40100
electron diffraction, many beam dynamical theory 2—32532
energy, dislocation multiribbon interaction with twin domain boundaries 2—25394
eutectic, coarsening by fault migration 2—9577
graphite, eutectic flake, electron microscope obs. 2—9568
graphite, in electron diffr. patterns 2—9438
metal, f.c.c., deformed, energy depend. of struct. changes and mech. props. 2—39681
metal, f.c.c. and h.c.p., energy rel. to impurity conc. 2—22212
metal, f.c.c. and h.c.p., pair pot. calc. for fault energies 2—15747
metal, f.c.c. twin boundary energy, temp. coeff., stacking fault energy 2—32533
MoS_2, natural molybdenite, cold working. microstructure, X-ray line broadening 2—25409
polytypic structures, energy, rel. to atomic struct. 2—3785
quartz, determ. sign of fault vectors by X-ray topography 2—32534
rare earth metals, h.c.p., deform. struct. obs. from X-ray line broadening 2—3772
scanning electron microscopy, defect images calc. 2—19036
scanning electron microscopy obs. 2—19037
steel, cold-rolled, spontaneous fault formation 2—36040
steel, decorated faults influence on flow velocity 2—3868
steel, Nb-stabilized austenitic stainless, rel. to fatigue failure 2—32629
steel, stainless, rel. to $\gamma \rightarrow \varepsilon$ transform. 2—40003
vectors, determ. of sign by X-ray topography 2—32534
Ag-Cd alloy, plastically deformed, X-ray diffr. obs. 2—15829
Ag, energy, electron microscope obs., weak beam method 2—3787
Ag film on Pd, extrinsic faults assoc. with partial misfit dislocations 2—9262
Ag_3Mg, long period ordered, plastic deformation, dislocation splitting 2—25501
Al-Mg, platically deformed, stacking fault energy and recovery 2—36112
Al-Zn, alloy, energy, rel. to dislocation interactions 2—9566
Al-Zn alloys, energy variation, influence of Zn, effect on decomposition mechanism 2—29186
Al, plastically deformed, stacking fault energy and recovery 2—36112
β-AlNi, anisotropic broadening and separation of strain and fault effects 2—32535
Au-0.65at%Zn, nucleation, electron microscope obs., 251-393 K 2—3589
Au, nucleation, electron microscope obs., 251-393 K 2—3589
Au, quenched, vacancy sink efficiency of stacking-fault tetrahedra 2—9567
CdI_2, kinetics, role in formation of polytypes 2—1390
CdI_2 polytypes, Zhdanov numbers in Zigzag sequence 2—25329
CdI_2 rhombohedral structures, energy calcs. 2—12772
Co, crystal thickness depend. of stacking fault contrast 2—9569
Cu-Al-Ni alloy, γ'-phase, electron microscope obs. 2—36042
Cu-Al-Zn alloy, stacking fault energy, electron microscope obs. 2—12773
Cu-(10 at.%)Al alloy, computer simulated dislocation image comparison 2—22207
Cu-Al solid solution, effect on steady state creep rate 2—15850
Cu-Ga(Ge)(Al) solid solutions, anelasticity 2—9636
Cu-Ni alloy, effect on Debye temp. 2—19383
Cu-Zn solid solution, effect on steady state creep rate 2—15850
Cu, defect clusters produced by ion irrad. 2—39670
Cu, energy, electron microscope obs., weak beam method 2—3787
Cu, energy, electron microscope obs. weak beam method 2—3786
Cu, polycryst., low temp. plastic flow, stacking fault energy, flow stress 2—12868
β-CuPd, a/8[110](1$\bar{1}$0) faulting in prestrain induced transform. stage, X-ray obs. 2—32763
$EuCr_2S_4$, electron microscope obs. 2—32507
Fe-Ni-Cr alloy, rel. to martensitic transform. kinetics 2—36277
Fe-Ni alloy, rel. to martensitic transform. kinetics 2—36277
Fe_2O_3, magnetite, X-ray diffr. obs. 2—15767
Fe_7S_8, pyrrhotite, defect struct., electron microscope obs. 2—22201
GaP, electrolum. diode material, electron microscope obs. 2—29992
Ni, effect on Debye temp. 2—19383
NiTi martensite, diffr. patterns analysis 2—15768
Si, conc., rel. to epitaxial growth rate 2—6499
Si, energy calc. from dislocation dissociation 2 3781
Si, grown in and process induced defects, effect on epitaxial growth 2—25248
Si, oxidized, floating-zoned, dislocation free, spotty defects, extrinsic stacking faults 2—19104
Si, thermally oxidized, cryst. orientation effect on fault form. 2—9570
Si epitaxial film on Si substrate, rel. to thickness and orientation determ. 2—39526
Si epitaxial layer, elimination by heat treatment 2—39705
Si transistor, bipolar, generation at surface heterogeneities 2—33035
Si wafers, thermal oxidation effects 2—25181
β-SiC, chemically vapour deposited, electron diffr. obs. 2—12774
SiC, fracture surface, scanning and transmission electron microscopy 2—9697
SiO_2, tridymite, phase transition shift, heat of transformation 2—9824
$SrCr_2S_4$, electron microscope obs. 2—32507
$TiCo_2$, Laves phase, electron microscope obs. 2—19105
$TiCr_2$, Laves phase, electron microscope obs. 2—19105

Stacking faults continued
Yb, rel. to martensitic transformation, X-ray diffraction obs. 2—6641
Zn, electron microscope obs. 2—15764
ZnS, deformed, effect on exciton spectra 2—29902
ZnS, effect on exciton refl. spectra 2—22752
Standards
see also Constants; Units
absolute vacuum wavelength standard, gas laser theory 2—31029
of ampere, n.m.r. method 2—5312
ASTM, magnetic properties, metallic materials for thermostats, electrical resistance, heating, contacts, electronics, book 2—37552
atomic absorption spectrophotometry, internal standards evaluation 2—10667
block gauges measurement, pneumatic compensator for a double-beam interferometer 2—27594
Brillouin and Raman scattering, absolute cross-sections for quartz 2—16522
Coordinated Universal Time scale, 1972 change 2—5117
density meas. by precision comparison using buoyant force gradient method for small samples 2—17173
dielectric constant and loss angle tangent meas. methods standardization 2—21005
electron microscopy, high resolution, prep. of metal films 2—9259
force, loading machines employment 2—22
frequency, ^{85}Rb maser, pumping light and buffer gas frequency shifts 2—27449
frequency, and time signals, broadcast by radio stations, details of services 2—18
frequency, based on stabilized lasers 2—23624
frequency, hydrogen maser wall shift variation with storage bulb diameter 2—5342
frequency, of Physikalisch-Technische Bundesanstalt 2—5119
frequency, of Physikalisch-Technische Bundesanstalt 2—5119
frequency and time, atomic and molecular, review 2—30748
frequency stabilization, He-Ne gas laser, compared with r.f. standard 2—17604
g-factor for e.p.r., use of charred dextrose 2—7126
gamma ray sources, allowance for effect of radioactive impurities 2—21405
gamma sources, class I spectrometric certification 2—473
glassy carbon, for normalization of small-angle X-ray scatt. intensities 2—25295
heat capacity and enthalpy, NBS standard α-Al_2O_3 reference material, thermodynamic functions 2—29555
high-radiance, high pressure Ar plasma 2—24659
laser reson., narrow, optical freq. standards, microwave standards, interferometry applications 2—34383
long lived, for efficiency calibration of Ge(Li) detectors 2—27884
magnification test specimen for scanning electron microscope 2—5331
mass and weight standard meas. 2—23219
materials properties and composition 2—19234
microwave radiation safety 2—5039
neutron flux density, correction factor for perturbations caused by activation probe 2—5731
n.m.r., TMS chemical shift standard 2—31771
noise, for environmental pollution 2—30876
noise levels at industrial plants 2—23386
noise levels in industry 2—26972
particle size and shape, absolute meas., primary standard 2—5113
photometric units, review 2—34504
photometry, candela, lumen review 2—7998
piezoelectric, applic. in goedesy 2—40869
policy of Acoustical Society of America 2—27285
quantum frequency standards, status and development prospects 2—37561
safety, from e.m. radiation 2—33786
scanning electron microscopy, resolution standard, comparison and evaluation of specimens 2—39621
secondary, visible and γ-ray wavelength coupling 2—37553
spectral radiance calibration standard, rel. to calc. continuous emission of LTE hydrogen plasma 2—24715
spectroradiometry, W strip lamp, Xe arc and anode of C arc 2—7998
synchrtron radiation, 1100 to 3000 Å, from electron storage ring 2—7640
temperature, international practical scale 2—37825
temperature, organic reference substances, calorimetric evaluation 2—34224
temperature lamp, stabilized d.c. source 2—23715
thermal conductivity meas. 2—17413
thermal expansion, 80-1000 K, fused silica ref. mat. 739 2—14289
thermal insulator conductivity meas. standards, guard-ring method 2—23190
time signals and frequency standards, broadcast by radio stations, details of services 2—18
u.v. light source, calibration by synchrotron and plasma- blackbody radiation 2—8023
for vacuum gauge calibration, piston manometer 2—41400
for vacuum meas. accuracy 2—41399
vacuum u.v., CI multiplet transition proximity meas., 170-250 nm, using plasma rad. and synchrotron sec. standards 2—17747
vacuum u.v. photometric standard, stabilized H_2 arc applic. 2—17748
vacuum u.v. radiators, photometric comparison between synchrotron and plasma blackbody radiation 2—17746
voltage, superconducting tunnel junction 2—6784
water, volume mass, absolute value 2—23220
water density at atmospheric pressure, 0° to 100°C, revision of USSR standard tables 2—3375
Cs beam frequency standards, cavity phase dependent frequency shifts 2—30746
H arc for vacuum u.v. 2—7639
He-Ne laser, cw at 88 THz, absolute frequency measurements 2—17174
Ne I 743 Å line, accurate measurement to fifth order, calculation of other lines in vacuum u.v. 2—8427
Pt-10%Rh/Pt and Pt-13%Rh/Pt thermocouples, reference tables 2—37830
Stark effect
accelerators, e.m. impulse, determ. of electron concentration using quadratic Stark effect 2—2653
alkali metal plasma, electron density meas. from Stark profiles 2—15472
alkali metals, ground state hyperfine structure 2—24333
alkaline earth metals, singly ionized, Stark shifts of isolated spectral lines 2—15206
Stark effect continued
aniline, $^1B_2 \leftarrow {}^1A_1$ transition, electric field induced perturbations 2—21658
asymmetric rotors, dipole moment determ., new approach 2—8547
atomic lasing spectra, constant calc. 2—577
atoms, with hyperfine structure, matrix elements of quadratic effect 2—15192
broadening, theory of atomic lines, soluble scalar model as test 2—8429
broadening by electrons and electron correlations in unified line shapes 2—35129
broadening theory, exact line profile with model microfield 2—8430
crystals, Stark-ladder picture of tilted energy band, hypergeometric solution 2—25726
cyclopropyl methyl ether, microwave spectrum, dipole moment component determination from quantitative Stark effect meas. 2—12230
2,3-dihydrofuran, meas. in microwave spectra for vibrational states of ring bending mode 2—12237
double resonance experiment for splitting molecular stark-effect levels 2—38879
enlightenment of absorptive medium induced by Stark shift of multiphoton resonance 2—35117
gas, modification of resonant r.f. absorption under influence of nonresonant h.f. field 2—38866
H line broadening, h.f. discharge 2—8988
interferometric method of meas. in spectra by arc heated flow from plasma jet 2—24765
lanthanide fluorides, far-i.r. splitting of rare earth ions 2—40669
Lyman alpha line of hydrogen 2—2986
Lyman alpha line of hydrogen 2—2986
M17, broadening in radio recombination lines 2—4927
methane, precision Stark- spectroscopy, nonlinear laser absorption 2—12217
2-methoxyethanol, Stark effect meas. in microwave spectrum, total dipole moment determination 2—12262
methyl chloride, applic. to q-switching of CO_2 laser 2—3105
methyl chloride, spectroscopic study, application to Q-switching of the CO_2 laser 2—848
methyl fluoride, ^{13}C enriched, modulated absorpt. of CO_2 laser radiation 2—5357
methyldifluorophosphine, meas. in microwave spectrum, dipole moment calc. 2—15386
microwave spectroscopic modulator 2—2313
molecular beam. Zeeman-Stark effect due to translational motion 2—28264
organic gases for CO_2 laser modulation in 00°1-10°0 band in R branch 2—11467
Orion A, broadening in radio recombination lines 2—4927
Q-switching in CO_2 lasers by molecular gases 2—7920
rotational spectra, systematic interpretation based on Stark effect 2—38871
silyl methyl ether, Stark splitting in microwave spectrum in 8 to 40 GHz region, dipole moment calc. 2—15394
spectral line breadth 2—2986
Thiourea, ferroelec. phase, n.q.r. of ^{14}N, rel. to Stark effect 2—20171
time ordering 2—2986
unified classical path theory of Stark broadening 2—24319
unified theory of spectral line broadening 2—2986
vinyl germane, meas. in microwave spectrum at 12.4 to 40.0 GHz, dipole moment calc. 2—15406
vinyltrifluorosilane microwave spectrum, dipole moment from Stark shifts of rotational transitions 2—21706
Al atomic constant meas. for several lines 2—2653
Au I, 6p $^2P_{3/2}$ state, investigation rel. to hyperfine structure sign determination 2—21503
Ba II lines in electric shock tube plasma 2—5783
Be II lines in electric shock tube plasma 2—5783
BeO, shift of spin levels of ^{9}Be 2—22840
C atomic constant meas. for several lines 2—2653
CO_2 gas laser, modulation of 10.4 μ band 2—27558
CO_2 laser, Stark effect driven Q-switching 2—21068
CaF_2, zero-phonon line, F_3 centre, uniaxial stress effect 2—19123
CdS, B, n=1 exciton line, electric field effect 2—10372
CdSe, B, n=1 exciton line, electric field effect 2—10372
Cl I and Cl II lines, Stark shifts 2—11952
Cl II, stark broadening 2—35138
Cl II spectra, meas. 2—2941
Cs I (6G-5D) forbidden component, ionic profiles calc. 2—24345
Cu I, line broadening consts., theoretical estimation 2—2919
DBr, hyperfine structure and Stark effect of J=O→rotational transition 2—8648
F atomic constant meas. for several lines 2—2653
$Gd_2(MoO_4)_3$: Nd^{3+}, level positions of Nd^{3+} ions 2—1679
H, broadening theory, exact line profile with model microfield 2—8430
H, Lyman-α line, effect produced by weak electric field 2—18349
H, shift of atomic hyperfine separation measured in maser 2—12021
H, Stark broadened Balmer lines H_γ and H_β, asymmetries 2—35176
H atom in Coulomb field, perturbation theory calc. 2—15215
H Lyman-β line, classical path calcs. for broadening 2—38847
H spectra, beam-plasma system, Langmuir oscills. 2—18667
H_β lines, broadening 2—15241
HCl molecular beam electric resonance spectroscopy, Stark-Zeeman spectra obs. 2—12145
HF molecular beam electric resonance spectroscopy, Stark-Zeeman spectra obs. 2—12145
H_2PPF_2, analysis in microwave spectrum rel. to conformation determination 2—15305
He, broadening theory, exact line profile with model microfield 2—8430
He I, combined Zeeman and h.f. Stark effects, calcs. of various spectral lines 2—18359
He I 4471 Å line and forbidden components, Stark profiles in laser produced plasma 2—39136
He lines, broadening 2—15241
He plasma, laser produced, profiles of forbidden and allowed transitions 2—6078
He plasma, Stark broadened resonance lines, difference in absorption and emission line shapes 2—8495
Hg, 6s6p$^3P_1$ state, differential Stark shift 2—38811
KCl:Ca, Sr, Ba, electro-optic study of Z_1-centre and thermal electric alignment 2—20040
^{39}K ^{19}F, molec. beam resonance meas. 2—21646

Stark effect continued
LiOH(D), molecular beam electric resonance spectra, vibrational states 2—8663
NH_3, vibr.-rot. transition, h.f.s. 2—24476
NH_2D, modulation of CO_2 laser 2—17589
O_3, from millimetre wave spectrum, value of dipole moment 2—8691
OH radical, high-field Stark effects on near u.v. spectrum 2—8698
^{87}RbF, molec. beam resonance meas. 2—21641
Si:P, first order Stark effect in impurity photocond. 2—10140
SrF_2, zero-phonon line, F_3 centre, uniaxial stress effect 2—19123
TlBr, derivation of electric dipole moments from Stark effect meas. on pure rotational transitions 2—8711
TlCl isotopes, molec. beam resonance meas. in different vibrational states 2—21645
TlI, derivation of electric dipole moments from Stark effect meas. on pure rotational transitions 2—8711
$^{205}Tl^{19}F$, molec. beam resonance meas. 2—21646

Stars
see also Multiple stars, Nebulae; Novae; Planetary nebulae; Stellar atmospheres; Sun; Variable stars
1061 OB stars and Cepheids, radial velocities 2—33635
A_0, radial velocities in South Galactic Cap 2—13885
A-type, peculiar nuclear processes producing anomalous abundances of elements 2—4837
activity cycles, rel. between magnetic field angular velocity and period 2—33636
Am phenomenon, origin 2—20527
American and Soviet space research studies, review 2—17028
angular momentum, changes due to neutrino emission 2—37286
anharmonic pulsations of massive star in He burning phase 2—33672
Ap type, surface peculiarities, effect of rotational circulation, convection, accretion and mass loss 2—7409
asymptotic branch stars, luminosity functions 2—33626
B3V companion to Antares B, radio emission 2—7474
B8-A3 stars distribution near galactic plane, contour maps and space densities 2—13840
BD+40°4124 and surrounding young stellar group, i.r. and optical observations 2—33682
blue horizontal branch in ω Cen colours, temp. and gravities 2—10873
blue horizontal branch in globular clusters, gravities 2—10906
blue stragglers, in old galactic cluster M67, masses 2—4891
blue stragglers in old disk population, presence of ultrashort period cepheids 2—20570
VY Canis Majoris, polarization and structure of surrounding nebulosity 2—16966
carbon-oxygen strs of $5M_{\odot}$, $10M_{\odot}$ and $30M_{\odot}$, evolution towards pre-supernova stage 2—16985
η Carinae, interstellar Co feature in region 20605 2—20605
η Cassiopeiae, parallax and mass ratio13883 2—13883
Cen X-3, X-ray pulsations due to occulting binary system 2—26799
WX Centauri region, positions and proper motions 26669 2—26669
β Cephei, low luminosity boundary of instability strip13898 2—13898
Cepheids, proper motions, corrections of lunisolar precession and notion of the ecliptic 2—13831
cepheids, Wesselink radii, suggested reduction in p factor 2—7404
charged and dense, investigation of circular photon orbits 2—26653
cluster, vinal theorem estimates of mass 2—10898
cluster 47 Tucanae two-dimensional photometric images using a Si-target vidicon photometer 2—41268
cluster models for binary evolution 2—10865
clustering and evolution, American Astronomical Society conference, Amherst, USA (1971) 2—26623
clustering near NGC68-72 group of galaxies, fluctuation in foreground star denstiy 2—20587
clusters, binary evolution 2—41130
clusters, Cepheid loops, envelope opacities at 5 $M_{\odot}$ 2—33676
clusters, disruption through passing interstellar clouds, numerical experiments 2—41128
clusters, early type, total mass content 2—26728
clusters, non-isolated, escape rates, numerical experiments 2—41129
clusters, nonisolated, rate of escape from, formation of multiple stars 2—13914
clusters, Perseus and Coma, extended X-ray sources, comparison with optical and radio emission 2—30499
clusters, spherical, Monte Carlo models of dynamical evolution 2—10902
clusters of low mass objects isolated in the interstellar medium, basic data 2—4886
clusters of neutron stars as mechanism for injection of cosmic rays 2—7480
collapse of a rotating star, instability and separation of small mass envelope, relativistic effects 2—33580
collapsing clusters, reproducibility of run-away stars formed 2—10905
collapsing clusters, run-away stars, trajectories stability 2—41132
collisional relaxation in stellar systems 2—41069
collisionless one dimensional systems, Vlasov equation, phase-space boundary integration 2—41074
collisionless self-gravitational gas, stability properties 2—41083
collisionless systems, dynamics, numerical integration methods 2—41077
collisions, head-on, numerical hydrodynamic study of coalescence 2—30413
Coma cluster, abundances in F dwarfs 2—4893
Coma Cluster, origin of mag. field in extended radio and X-ray source 2—37335
conference (San Juan, December 1971) 2—26582
γ Corvi, Hg-Mn type, rotation 2—4828
P Cygni, movement of matter in envelope 2—10854
Cygnus X-1 radiosource, position and identification 2—23092
DB white dwarfs, accretion and convective envelopes 2—7418
degenerate, effect of nuclear reactions on stability toward adiabatic radial perturbations 2—26678
degenerate, X-ray emission 2—4946
dense, neutrino bremsstrahlung in degenerate electron gas 2—8113
density wave interactions at Lindblad resonances in disc like collisionless system, energy and angular momentum exchanges 2—4832
diameters, diffraction limited meas. by 200 inch telescope and speckle interferometry 2—26662
distributions in high galactic latitudes, four-colour photographic photometery 2—10820
double, image prod. using electron camera 2—10882

Stars continued
dwarfs, nearby K3 and M2, space motions correl. with solar motion and apex 2—4812
dynamical friction and polarization clouds 2—41070
dynamical system with three degrees of freedom, number of isolating integrals 2—41073
dynamics, and discontinuous Markov process 2—16972
dynamics, collective processes in plasma physics 2—41076
dynamics, collisional relaxation, gravitational polarization 2—16971
dynamics, collisionless, applications of plasma physics methods 2—10848
dynamics, collisionless 2—41136
dynamics, discontinuous Markov process 2—41071
dynamics, gravitational N-body problem, IAU colloquium, Cambridge (1970) 2—41042
dynamics, relaxation times, numerical experiments 2—41134
dynamics evolution and instabilities of plane stellar systems 2—16974
early-type, photoelectric measurements of $H\gamma$ line strengths 2—4844
effective temp. of normal late type stars, broad band index 2—30439
explosion, time development of axisymmetric shock, quasi-stationary velocity approximation 2—23391
faint blue, in anticentre region, finding charts 2—13839
faint clusters in Large Magellanic Cloud, colour-magnitude diagrams 2—37314
flare, in Pleiades cluster 2—10843
fluid motions, large-scale 2—20688
formation, cluster mass and radius and galactic shape 2—33625
G-giant stars, new classs at the Galactic Pole 2—20514
late G-giants, Fe I and Ti I excitation temps. by curves of growth 26660 2—26660
galactic, cluster, H 20, UBV photometry 2—4887
galactic cluster, lifetimes, tidal fields of passing interstellar clouds 2—10903
galactic cluster, old, M67, masses of blue straggler and horizontal branch stars 2—4891
galactic clusters, Population I, K-line strengths in A stars 2—20548
galactic clusters, radio emission at 1.4 GHz and 2.7 GHz 2—17006
galactic clusters, rich, dynamic evolution, King type equil. models 2—13921
galactic clusters, rich, dynamic evolution, mass function 2—13920
galactic clusters, young shock waves as link with interstellar gas 2—20486
giants, late-type, space velocities and CN anomalies 2—1956
globular cluster, evolution and pulsation, comparison of theory and obs. 2—20583
globular cluster, NGC 6171, periods and period changes in variable stars 2—20568
globular cluster in M31, scanner abundance obs. 2—10897
globular cluster NGC 6171, studies of RR Lyrae stars 2—17009
globular cluster subsystem of the Andromeda galaxy 2—13849
globular clusters, dependence of Q parameter on mass distribution function 2—16979
globular clusters, M5, M13, M92, evolutionary interpretation of luminosity function 2—30502
globular clusters, M5 and M13, luminosity function 2—33686
globular clusters, NGC 6304, NGC 6401, photometric obs. 2—26734
globular clusters, RR Lyr. stars, blue edges and He abundance 2—26738
globular clusters, surface gravities of blue horizontal branch stars 2—26701
globular clusters, UV-bright stars 2—26737
globular clusters NGC6362 and 6752 BV photographic calibration 2—23081
gravitational n-body problem, collisionless systems, numerical experiments 2—41048
gravitational N-body problem, treatment of close approaches in numerical integration 2—17287
grazing occultations over Canada in (1972) 2—37346
H II region model with first generation on newborn second generation stars and OH emission sources coincidence with point sources 2—37274
HD 143448, probable member of NGC 6025 open cluster 2—20584
HD 149 382, OB sub-dwarf 2—10890
HD 45677, variability obs. 2—30484
HD 77581, as optical candidate for X-ray 2—37340
Herstmonceux astrolabe observations, analysis and discussion 2—1951
horizontal branch, in old galactic cluster M67, masses 2—4891
hose pipe instability in stellar systems 2—16973
HR, Southern, photoelectric radial velocities 2—26670
Hyades open cluster, Li abundance obs. 2—10900
IC 4665, open cluster, spectroscopic binaries, orbital elements and radial velocities 2—10895
IC 4665, open cluster membership probabilities from relative proper motions 2—37311
interiors, thermohaline convection 2—10857
IRC 20385 galaxy or rich globular cluster, distance 2—26739
K-giants Fe I and Ti I excitation temps. by curves of growth 2—26660
late F dwarfs, ages and kinematics rel. to chemical compos. 2—26654
lunar occultations, photoelectric observations 2—13975
M15 globular cluster giant branch, gaps due to fast rotating cores 2—26716
M67, old galactic cluster masses of blue straggler and horizontal branch stars 2—4891
M67 galactic cluster blue stars, horizontal branch and blue stragglers hypotheses 2—20539
M supergiants, coincidence with OH 1612 MHz sources from i.r. obs. 2—23094
main sequence, C-burning, equilibrium pulsational and secular stability properties 2—10855
main sequence model of 2.25 $M_{\odot}$, opacity corrections 2—37279
massive, gravitational collapse, obs. of neutrinos, data on neutrino oscillations 2—26752
massive cluster stars, evolution of velocity distribution function 2—33675
mean places for supplementary stars in the Tokyo PZT star list 2—30440
metallic line, explanation for appearance position in H-R diagram and absence among rapidly rotating stars 2—20527
models, computed, semiconvection 2—7412
N-body problem, direct integration methods, and close encounters and binary orbits 2—17286
near sun, characteristics 2—4810
neutron, accretion of matter, equations of motion for flow in and out 2—7434
neutron, accretion of matter 2—30407
neutron, and rotating Einstein-Rosen bridge 2—2100

Stars continued
neutron, calculations of central densities and equations of state 2—10868
neutron, consititution of ground state of matter and its equation of state determ. in density region 4.3×10^{11}-5×10^{14}g/cm^3 2—4871
neutron, cooling, soft X-ray source, Monoceros Loop supernova remnant 2—23096
neutron, core, dense baryon matter 2—26708
neutron, effect of nuclear reactions on stability toward adiabatic radial perturbations 2—26678
neutron, equations of state 2—33659
neutron, evidence for presence in binary systems 2—10909
neutron, first and zero sound propagation 2—30481
neutron, formation or clustering as source of gravitational waves 2—16946
neutron, frictional heating model 2—7435
neutron, high-density nucleon localization 2—41103
neutron, magnetic, surface composition relative abundances of ^{4}He, ^{12}C, ^{16}O, ^{20}Ne, ^{24}Mg, ^{28}Si and ^{56}Fe 2—30477
neutron, magnetic properties 2—30482
neutron, mass formula and props. of matter at subnuclear densities 2—10889
neutron, or black holes, determining factors during gravitational collapse 2—10797
neutron, quasiradial pulsations in Newton's theory of gravity, central density 2—33657
neutron, rotating, considered as pulsars, maser emission mechanism 2—30518
neutron, rotating, e.m. models of pulsars 2—4939
neutron, rotating magnetized, structure and electrodynamics 2—4908
neutron, stability and radial pulsations 2—33656
neutron, superfluidity, BCS-bogoljubov-theory 2—30480
neutron matter, magnetic susceptibility 2—33660
neutron star model for the pulsed X-ray source Cen XR-3 2—13972
neutron-star matter and nuclear surface energy 2—34887
neutron-star matter microscopic investigation of isotropic proton superfluidity 2—20559
New Open Cluster, A and F star colour indices and reddening 2—4845
NGC6811 open cluster UBV photometry, colours excess, distance, age, and spectral classes det. 2—23082
NGC 1851 and 2808, BV photography 2—13916
NGC 2264, young cluster, circumstellar shells, i.r. and optical obs. 2—10896
NGC 2264, young cluster, obs. of CS, HCN, U89.2 and U90.7 lines 2—37313
NGC 2264 cluster, circumstellar gas shells 2—20596
NGC 2264 open cluster, Li abundance obs. 2—10900
NGC 2467, galactic cluster, membership obs., UBV and Hβ photometry 2—37285
NGC 6025 open cluster, distance and age estimates from photoelectric ubv meas. 2—20584
NGC 6171, studies of RR Lyrae stars in globular cluster 2—17009
NGC 6231, open cluster, four colour and Hβ photometry 2—4894
NGC 6304 and NGC 6401, globular clusters, photometric obs. 2—26734
NGC 6613 and 6716 open clusters, UBV photometry 2—13915
NGC 6811 open cluster, membership probabilities for 296 stars 2—13917
NGC 6838, globular cluster, bright membership obs. 2—7447
NGC 6940 and IC-1805, open clusters, membership probabilities 2—30494
Northern PZT Stars Observation program outline 2—20512
OB groupings in Puppis, UBV and Hβ photometry, relation of distributions to HI concentrations 2—4888
occultation by Moon, 1968-69 Gorky obs. 2—30437
occultations by Moon 2—1952
occultations by the Moon, in the year 1970 at Cracow Astronomical Observatory 2—26649
old cluster NGC 188, proper motions, membership and stellar content 2—26730
Oosterhoff period-groups of globular clusters 2—20582
opacities, effect of molecular line absorptions 2—4868
open clusters, Ca K-line photometry of A stars in population I clusters 2—7445
open clusters, elemental abundances 2—4893
open clusters, NGC 2360 and NGC 3680, colour excesses and metallicities of giant stars 2—20577
open clusters, obs. of Li abundances 2—10900
open clusters, Pleiades lower main sequence, gray extinction properties 2—10907
open clusters, young, as optical tracers of spiral structures in the galaxy 2—26616
open clusters rel. to blue filament in southern Milky way 2—26620
orbiting extreme Kerr black hole, optical appearance 2—37242
Orion population, second catalogue of emission line stars 2—37275
parallax simulation study, teaching demonstration 2—33848
parallaxes and proper motions 2—13888
XPer, as optical candidate for X-ray source 2—37340
phase space boundary integration of Vlasov eqn. for collisionless one-dimensional stellar systems 2—10849
photometry of 94 early type stars at 1450 angstroms 2—20544
photospheric angular velocity, effect of radiative equilibrium, von Zeipel currents 2—20519
planet detection by photometric colour indices 2—7405
plasma, phenomena 2—23083
plasma waves, longitudinal, contribution to transport processes 2—7411
Pleiades cluster, slow flare stars, comparison with objects in Orion 2—33674
Pleiades cluster, systematic errors in positions according to AGK3 catalogue 2—30438
Pleiades group and NGC 2516 cluster, UBV obs. 2—26726
Pleiades open cluster, Li abundance obs. 2—10900
polytropic masses, pulsations in rapid uniform rotation 2—4818
Population I in central areas of the elliptical galaxies NGC 185 and 205, near M31 2—13850
positions and proper motions of those between declinations −70° and −90° 2—20516
Praesepe open cluster, Li abundance obs. 2—10900
proper motions, derivation of solar apex, galactic rotation, precessional corrections 2—37253
proper motions for objects in the Bright Star Catalogue 2—4811
pulsating, constants for fundamental mode and first two harmonics 2—4873
Pup OB1 and Pup OB2 associations, UBV and Hβ photometry 2—37285

Stars continued
PZT systems as compared with the SAO catalog 2—7401
radial velocities of 528 7^m-10^m stars with photoelectric spectrometer 2—4814
radial velocity distributions of stars and gas in spiral arms 2—20485
radial velocity meas., photometer 2—7582
radial velocity spectrometer, rapid scanning, construction and testing 2—37428
radial velocity variations of HD226868 rel. to Cygnus X-1 flux variations 2—13890
random forces on star in stellar system, numerical det. 2—33628
red, in the 30 Doradus Nebula region 2—7392
red dwarf flare stars as sources of diffuse galactic X-rays 2—10884
red giant, population I, He burning obs. 2—7407
Red Giants, clump in luminosity distrib. in Draco dwarf Galaxy 2—20534
reduced proper motion diagrams, prediction of red degenerates 2—33623
reduction to absolute acceleration accuracy det. by long focus photographic astrometry 2—26658
relaxation processes enhancement by collective effects 2—10851
relaxation times in stellar dynamics 2—10847
rod and disk models of stellar systems, integration methods for smoothed gravitational field 2—20511
rotating, global dynamical stability 2—7410
rotating, relativistic, theory of level surfaces inside, Poincare's limit 2—26648
rotation, axial, effects on Schonberg- Chandrasekhar limit 2—1954
rotation speed, relativistic Poincare limitation 2—41082
s-process, nucleosynthesis of elements 2—10860
Schoneberg-Chandrasekhar limit, effects of axial rotation 2—1954
β Sco, faint companion from occultation by Io26835 2—26835
β Sco, occultation by Jupiter, light curves 2—26834
β Sco occultation by Io, photoelec. obs. 26835 2—26835
Sco X-1 and Tau X-1, nocturnal absorption of radiowaves due to ionization produced by emitted X-rays 2—26528
RR Scorpii, comparison stars 7406 2—7406
β Scorpii, occultation by Jupiter obs. 2—26836
β Scorpii, symmetry of flashes during Jovian occultation 37297 2—37297
α Scorpii (Antares), grazing lunar occultation 2—41091
β Scorpii C, estimates of distance and apparent angular diameter from duration of immersion during the occultation by Io4813 2—4813
Scorpio-Centaurus association, uvby and Hβ obs. of B-type stars in 2—16990
shell, differentially expanding atmospheres, line profiles 2—30509
shock wave propagation in interior of spherically symmetric stellar models 2—30448
solar type, rotation, thermally driven turbulence 2—10856
space motions from parallaxes, proper motions and radial velocities, K3-M2 dwarfs in solar neighbourhood 2—13887
spheroids, axially symmetric explosion 2—16984
stellar ring 274, bright stars distance 2—30495
super metal rich members of NGC 188, proper motion determinations 2—4889
superclustering of rich clusters re-examination of evidence 2—26740
superdense, cold, static, structure eqns. derivation and solution 2—33629
supergiant, α Ori, turbulence and thermal velocities in atmosphere 2—1953
supergiants, nonvariable in Cepheid instability strip 2—20562
supermassive stars, models, calculation 2—26659
systems, hose-pipe instabilities 2—41072
systems, pair correlations and thermodynamics, n-body calc. 2—41133
systems, two-phase-space-density collisionless one-dimensional, collective relaxation 2—41075
thermal stability of a He-burning shell in red supergiants of 15 solar masses 2—10867
turbulent velocity waves and kinematic dynamo activity in astrophysical objects 2—10792
uncertainties in observable properties of lower main sequence models 2—41078
W Virginis, model, using radiative transfer 2—20517
visual detection through spacecraft windows on illuminated side 2—26567
wake induced in field of stars, dynamical friction, polarization clouds 2—10846
white dwarf matter, phase transition, applic. of Tisza theory 2—10853
white dwarfs, electronographic obs. 2—10926
Wolf-Rayet, criteria for detection of new binaries 2—13918
Wolf-Rayet in M33 galaxy 2—20513
young cluster, NGC 2264, shell variability and pulsation 2—26721
young clusters in Galaxy, space velocities and z-motions 2—33685
ZC 3091, occultation by Moon during the total lunar eclipse of 6 Aug 1971 2—4815
C-burning, lower main sequence, equilibrium pulsational and secular stability properties 2—10855
Fe core collapse and propagation of shock waves in envelope, matter ejection 2—26663
H gas cloud, interstellar gas cloud, fragmentation and gravitational contraction in expanding universe, and stellar formation 2—33698
OH emission from i.r. sources 2—37296
Si burning in stellar explosions with various initial compositions 2—26673

composition
see also Elements/origin
Ap, magnetic review of anomalies and theories 2—26668
Ap type, Os-Pt-Hg abundance peaks and very heavy cosmic rays 2—33624
Ap-type, abundance peculiarities, evidence for restriction to surface layers 2—7409
B stars, He abundance det. 2—7408
changes during evolution, algorithms for calc. 2—41080
β CrB, rare earth abundances 4829 2—4829
exploding stars, neutron-proton ratio rel. to dense, high-temperature states 2—23070
exploding stars, postdetonation properties, equation of state, rates of beta processes and associated neutrino losses 2—26655
F, G, and early K-field type, Li isotope ratio 2—4816
F-type disk population, metal abundance indices 2—20553
giants, late-type, CN anomalies and space velocities 2—1956
globular cluster in M31, scanner abundance obs. 2—10897
globular clusters, det. from Q metallicity index 2—16979
Groombridge 1830 subdwarf, curve of growth and analysis and abundances of metals 2—41090
HD122563, metal poor red giant, analysis 2—30462
HD 4539, B-type subdwarf, chemical abundance analysis 2—33632

Stars continued
composition continued
Herbig Ar and Be types, H_2 line profiles and surface gravities 2—26650
L745-46A, white dwarfs, DF spectral type, element abundances 2—7414
late F dwarfs, Fe/H ratio, rel. to age and kinematics 2—26654
late type field stars, ^{6}Li/^{7}Li ratio 2—20522
late-type, heavy elements abundances by curve of growth method 2—1957
μ Leonis, supermetallicity test 2—30444
line-blanketed stellar atmospheres, artificial absorption edges 2—30446
M67 galactic cluster, metal content estimation 2—20539
metal abundances of 150 F and early G dwarf stars from colours 2—4877
neutron, magnetic relative abundances of ^{4}He, ^{12}C, ^{16}O, ^{20}Ne, ^{24}Mg, ^{28}Si and ^{56}Fe 2—30477
neutron, quantum crystal, solid ^{3}He, in interior 2—30478
neutron rich species, ^{54}Cr, ^{58}Fe, overabundances, weak s-process irradiations 2—33633
NGC 4833 globular cluster, metal deficiency and high He abundance from photometric obs. 2—30472
ε Peg, late type supergiant, abundance37284 2—37284
population II, contribution of cosmic ray nuclei to metallic elements 2—10852
29 Psc, He deficient photometric standard 20515 2—20515
29 Psc, photometric standard, abundance analysis 2—4817
rare earth elements, polynomial approx. of partition functions 2—20518
scanner abundance studies, strong CN and evolved stars 2—33646
Sgr A, fermaldehyde absorption at +40 km/sec 2—37277
space velocity, composition correlation, microphotometer measurements 2—20547
stellar models of white dwarfs, free electrons, Thomas-Fermi statistical model, rel. to densities 2—33631
supermetallicity test using central depth of Ca I and Mg I lines 2—30444
surface temperatures and curves of growth for Populations I and II stars 2—30442
o Vir, heavy metals obs. from spectra 20552 2—20552
vMa 2, DF spectral type, element abundances 2—7414
white dwarf matter, equation of state for a dense plasma, phase transition between liquid and solid 2—30441
white dwarfs, cool, element abundances 2—20540
white dwarfs, DF spectral type, element abundances 2—7414
C, type J subclass, rel. between strong ^{13}C and Li features 2—4858
CN and C_2 molecules in carbon stars, opacity probability distribution functions 2—5913
He, in hot stars, importance in spectral classification 2—37288
He, in hot, main sequence B-types, importance of non LTE 2—37287
^{3}He in photosphere of ρ Leonis 2—4857
Hg stars, relative isotopic abundances of Hg 2—4830
Li abundance in solar type stars 2—10856
Li abundances in open clusters 2—10900
Li depletion rel. to age in Pleiades, Hyades, Ursa Major and Sun 2—16986
^{6}Li/^{7}Li ratio in F and G field stars 2—4816
Mn, measurements in the Hyades and field giants with narrow-band photometry 2—16993
Na, measurements in the Hyades and field giants with narrow-band photometry 2—16993

evolution
5 $M_\odot$ type, model 2—30455
Altair, ancient records of colour differences 2—20555
angular momentum variations along the main sequence 2—20520
Ap stars, number density, possible origin of pulsars 2—33643
Ap type production, nuclear and non-nuclear processes 2—13891
B supergiants HD96248 and HD164402, comparison with mains sequence star τ Scorpii 2—23068
BD+16°516, Hyades member, eclipsing binary, mass loss obs. 2—37290
binaries, cluster models 2—10865
binaries, dynamically formed, properties 2—20581
binary systems, close, comparison of consequences of theories 2—4836
binary systems, theories, review 2—7419
U Cephei, close binary7455 2—7455
U Cephei, eclipsing binary7456 2—7456
Cepheid variables, evolutionary conditions allowing high mass stars to become variables 2—33670
classical Cepheids, appraent discrepancy between pulsation and evolution masses 2—26711
clusters, dynamical evolution, Monte Carlo models 2—41126
clusters, fluid-dynamical method, fundamental equations 2—41137
clusters, fluid-dynamical method 2—41127
clusters, spherical, collisionless phase, model of spherical concentric shells 2—41138
clusters, spherical, Monte Carlo models 2—10902
collective relaxation of two phase space density collisionless one dimensional self gravitating systems 2—10850
composition changes, algorithm for calc. 2—41080
core He burning at $5_\odot$ 2—7421
core He burning phase, semiconduction 2—10861
cores, up to C ignition, origin of pulsars? 2—16989
double radiosources, fluid dynamic stability 2—26796
in Draco dwarf Galaxy, anal. of colour-magnitude diagram 2—20534
dynamics of plane stellar systems, computer model 2—41065
early type, rapidly rotating, loss of angular momentum 2—20532
element nucleosynthesis, energy production 2—20464
extremely blue halo stars, horizontal branch 2—26676
final stages, gravitational collapse of spherical object 2—26683
final stages, X-ray source production 2—10862
formation by condensation models 2—30452
fragmentation of supermassive disks 2—7366
galactic clusters, rich, King type equil. models 2—13921
giants and subgiants, old disk, low mass, post main sequence 2—7417
globular cluster, stars, comparison of theory and obs. 2—20583
globular cluster type, oscillatory thermal instabilities at onset of He core burning 2—20531
globular clusters, age det. from Q metallicity index 2—16979
HD96248 and HD164402, composition 2—23068
heavy leptons and associated neutrinos, possible existence, consequences 2—2516
horizontal branch, with He core burning, occurrence of loops in H-R diagram 2—30454
hydrodynamics, time-dependent implicit code 2—20689
hydrostatic adjustment and mechanism of red giant development 2—26672

Stars continued
evolution continued
loops in H-R diagram during core He burning and effect of rotation 2—23071
luminous red giant, final stages, physical props. of static envelopes 2—26674
M5, M13 and M92 globular clusters, luminosity function evolutionary interpretation 2—30502
M5 and M13 globular clusters and luminosity function 2—33686
M67 rich galactic cluster, mass function 2—13920
10^3 $M_\odot$ type, relativistic, redshift, CNO composition and radiative equilibrium obs. 2—16980
magnetic field decoupling in dense interstellar clouds with angular momentum, formation of protostars 2—26671
massive main-sequence stars, formation of semi-convective zone, Gabriel's mechanism 2—30456
metal abundance effects on stellar models of 1.25 solar masses 2—33638
Monte Carlo scheme for dynamical evolution of spherical stellar systems 2—20510
multi-phase space density collisionless one-dimensional stellar system 2—30453
neutrino expts., effects on theory 2—26677
neutron, limiting mass 2—7436
neutron capture exp., element formation 2—41084
neutron emission in population II stars, Big- Bang cosmology 2—10863
nova outburst, white dwarf model at 1.00 $M_\odot$ 2—17002
nucleosynthesis theories 2—20461
one-dimensional stellar system, collisionless, multiple-phase space density, evolution 2—30453
oscillating polytrope, effect of poloidal mag. field 2—10864
planetary nebulae, pulsation of long period variables 2—26719
polytropes, supermassive rotating magnetic, Roche approximation 2—10859
Population I, core He burning phase semiconduction 2—10861
Population I, methods of age determination 2—20537
Population II, advanced, uncertainties in horizontal branch models 2—16977
population II, age determination 2—20538
Population II stars, blue field stars of galactic halo 2—26666
post detonation of dense cores, beta processes effects 2—26664
post main sequence, 20 $M_\odot$, semiconvective mixing 2—7416
post main sequence, low mass old disk giants and subgiants 2—7417
pre-white dwarf, effects of neutrino emission 2—20560
protostars, motion in a forming cluster 2—4777
pulsationally unstable stars evolving inhomogeneously, contribution to He content of Galaxy 2—23072
red giant evolution to He flash of super-metal-rich star 2—4835
red giants, envelope relaxation oscillations as possible mechanism for white dwarf formation 2—13912
red giants, population I He burning 2—7422
relativity parameter at high degeneracy 2—20529
rotating disks, initially balanced 2—16974
Schoneberg-Chandrasekhar limit, effects of axial rotation 2—1954
Sco OB_1, stellar form. stages 2—4834
secular stability, complex roots in secular spectra, 2.5, 5, 10, 15 solar masses 2—37281
secular stability onset of complex roots 2—7415
sequences for very low metal content types, computation using Paczynski code 2—26682
single stars, model nuclei of planetary nebulae 2—26687
spherical stellar systems, dynamical evolution, Monte Carlo method 2—41085
spherical systems, halo, random gravitational encounters 2—33639
in spiral systems, obs. using surface photometry 2—33640
stability properties for encounterless self-gravitational gas and plasma 2—10866
stellar, phase space boundary integration of Vlasov eqn. for collisionless one-dimensional stellar systems 2—10849
super He rich 2$M_\odot$ types 2—4838
supergiants, red, core He burning at $15_\odot$ 2—7420
supermassive objects, implosions and emplosions, static models 2—16982
supernovae, critical core mass for C detonation 2—33673
supernovae, rel. to r-process nuclides 2—37308
supernovae, theories, review 2—7419
theories, review 2—7419
upper mass limit, hydrodynamic calculations for protostars 2—26680
Urca neutrino processes, rate formulae 2—33641
URCA process in presence of positrons and large mag. fields 2—20535
white dwarfs, cooling sequences 2—13909
C, pitfalls of CNO bi-cycle theory 2—16978
C and O stars in their late stages and models of burnt-out cores 2—10868
H/He development study 2—20536
H_2-He type, in the Galaxy 2—16983
H_2 rich stellar envelopes, ejection from heavy element cores 2—26667
He, pure, 1.40 μ_θ, ^{12}C does not ignite 2—33642
O_2 stars, properties during hydrostatic O_2 burning 2—26675
^{16}O(p,α)^{13}N astrophysical importance of rate and cross section of reaction for nucleo-synthesis 2—24217

magnetism
see also Sun/magnetism
Ap-type, role in surface peculiarities 2—7409
α Boo, integrated longitudinal fields 30467 2—30467
53Camelopardalis, mean surface field meas., disagreement with decentered dipole rotator model 2—37276
Canopus, under investigation 2—7402
FOIb, under investigation 2—7402
HR2727, confirmation by Zeeman spectroscopy 2—7402
HR5049, HR5463, HR6870, discovery by Zeeman spectroscopy 2—7402
HR5303, HR2996, HR3185, under investigation 2—7402
hydromagnetic symmetrical terms for the zonal kinetic energy equation 2—24637
magnetic, surface characteristics 2—4826
magnetic, theoretical models 2—4827
models with nonlinear force free field 2—20521
neutron stars 2—23076
oblique rotator model and Ap stars, general theory of magnetic stars 2—30450
α Ori, integrated longitudinal30467 2—30467
β Ori, integrated longitudinal30467 2—30467
polytropic, axisymmetric multipole fields 2—16976

Stars continued
magnetism continued
rotating, v. large fields 2—16975
stationary rotating relativistic star, magnetic field generation 2—37282
supernovae remnants, field structure and polarimetric obs. 2—26718
α Tau, integrated longitudinal30467 2—30467
white dwarfs, field decay for dipolar and toroidal configurations 2—30443
radiation
see also Cosmic radiations, radiofrequency; Sun/radiation
A and F type stars, low-dispersion luminosity criteria, microturbulence in stellar atmospheres 2—13905
A stars in south galactic cap, UBV photometry 2—30475
AD-LEO flare star obs. 2—26699
CY Aquarii dwarf cepheid, three colour photometry41110 2—41110
Avrett-Krook temperature correction procedure, modification 2—33622
blue horizontal branch in ω Cen, colour 2—10873
3C461 flux density at 1440 MHz and rate of decrease 2—26693
contracting magnetized stars, generation of cosmic rays by emitted e.m. waves 2—20576
ε Coronae Austrinae, RI photoelectric photometry light and colour curves 2—33648
R Coronae Borealis, dust shell model 41081 2—41081
Crab, optical pulsations, absence of amplitude or pulsar-shape variations 2—20616
W Crucis, photometric observations of long period eclipsing binary41120 2—41120
CW Cephei, u.v. observations 2—7451
SS Cyg and N Del 1967 flares, brightness gradients 30466 2—30466
V1057 Cygni, UBVRI photometry and luminosity 10876 2—10876
energy transport in stellar winds hydromagnetics and heat conduction 2—20526
extragalactic radiosources; linearly polarized brightness distribution at 2695 MHz 2—20622
F-type disk population, luminosity 2—20553
far u.v. excess in M 31 central region possibly due to young main sequence stars 2—16960
G51-15, nearby red dwarf with low luminosity, photometric and astrometric obs. 2—41088
of galactic cluster Stock 2, UBV values 2—30474
globular clusters, luminosity functions 2—30473
gravity darkening effects in rapidly rotating, early B-type stars 2—37292
Haro 18, frequency of flare-ups 2—10872
intensity modulation at discrete radio frequencies 2—10885
interstellar polarization, general law 2—7428
invariable F and G stars, temp. scale from spectral scans in red and Hα profiles 2—30469
long-baseline time-delay measurements of rapidly varying X-ray stars 2—33720
luminosity function, det. using method of mean absolute magnitudes 2—26706
Magellanic Clouds, 4 colour and Hβ photometric of brightest stars 2—30426
Mira variables, near i.r. data, absolute magnitudes 2—20569
multichannel area photometry for stars of low apparent brightness 2—41269
neutron star, rapidly rot., gravitational rad. 2—13908
neutron stars, spinning, calc. of radiation from accelerated point magnetic dipoles in circular and Keplerian orbits 2—34235
NGC 4833 globular cluster, colour magnitude and two colour diagrams, metal and He abundance 2—30472
NGC 6231-92, highly reddened star of F5 Ia type, background supergiant 2—41089
OH microwave emission in i.r. stars, effects of i.r. radiation and collisions on vibrational and rotational states 2—30528
FU Orionis stars (fuors), energy source models rel. to rapid and slow flare stars33664 2—33664
DY Pegasi dwarf cepheid, three colour photometry 41109 2—41109
Perseus arm, luminosities Hγ compared to MK systems 2—10874
photoelectric obs. of stars near quasers, radio sources Seyfert and N-type galaxies 2—20554
polarized, extended electron scattering atmosphere 2—4820
primary minimum determination of the variable QS Aquilae 2—41112
rapid rotation, effect on weak absorption lines in sharp-lined stars in pole-on configuration 2—37280
RY Sagittarii, dust shell model 2—41081
VX Sagittarius, peculiar i.r. variations 20626 2—20626
λ and κ Scorpii, light variations, det. as new broad lined β Canis Majoris stars 2—33671
slow flare stars in Pleiades cluster, comparison with objects in Orion 2—33674
supergiants, photometric data and colour excesses 2—33647
two-dimensional photometric images using a Si- target vidicon photometer 2—41268
UBV photoelectric photometry of 500 southern stars 2—41092
u.v. stars, overlapping Stromgren spheres and H I clouds in interstellar medium 2—37318
Vega, absolute calibration of energy distribution 2—26652
α Virginis, short period light colour velocity and temp. variations 2—33655
BW Vulpeculae, intrinsic variable, spectral and photoelectric observations 2—41105
white dwarf Grw+70°8247, circular polarization, spectral depend. 2—10880
white dwarfs, spinning, calc. of radiation from accelerated point magnetic dipoles in circular and Keplerian orbits 2—34235
WOLF 424 flare star obs. 2—26699
X-ray background, universal, neutron stars as sources 2—20625
YZ-CMI flare star obs. 2—26699
OH, H$_2$O maser emission and radiative transport in envelope of infrared star 2—30447
spectra
19 Psc, cyanide and oxide band strengths meas. with rapid scanner 2—13907
125248, magnetic variable, eleven band photometry 2—26690
α Ori, cyanide and oxide band strengths meas. with rapid scanner 2—13907
A and F stars in the New Open Cluster, colour indices and reddening 2—4845
A and F type stars, low-dispersion spectral classification 2—13905
A type, electronic camera for metallic discontinuities in u.v. spectrum, rocket exprt. 2—10888

Stars continued
spectra continued
A-stars in Population I galactic clusters, Ca K-line strengths 2—20548
A-type, near south galactic pole, radial velocities and classification 2—4853
A-type, peculiar, with long periods, photometry 2—4867
A-type stars, BV photometry to detect interstellar absorption at the galactic poles 2—20602
A-type stars, determination of effective temperatures of stars with different effective gravities 2—30460
Altair, ancient records of colour differences 2—20555
Am -type cluster stars, microturbulence and abundance anomalies 2—13906
Ap, photometric variability 2—26688
Ap stars, effect at rare earths an opacities 2—26704
Arcturus, chromosphere, photoelectric scans 2—4831
Arcturus, identification of NdII in emission 2—16995
Arcturus, statistical description of line blanketing 2—30471
Arcturus, u.v., emission at 2800Å 2—16988
εAur, F-type supergiant, equivalent line widths 2—37298
RW Aur, in region 3080-6100 A, emission and absorption lines10870 2—10870
LY Aur, O-type eclipsing binary, photoelectric obs. 30498 2—30498
LY Aurigae, eclipsing binary, differential UBV photometry 41124 2—41124
AX Monocerotis, envelope spectrum 2—10883
B- and O-types, calibration of ubvyβ system in terms of intrinsic colour indices and absolute magnitude 2—4864
B-stars in δ and π Scorpii, vacuum ultraviolet region 2—1959
B-type, bright, in northern hemisphere, four colour, Hβ and UBV photometry 2—16991
B-type, in Scorpio-Centaurus association, uvby and Hβ obs. 2—16990
B-type, interstellar Ca II, H and K absorption lines, Orion region 2—4870
B-type, v.u.v., effect of corona problems 2—11166
band strengths, cyanide and oxide, cool stars with rapid scanner 2—4850
Bd + 40°4124 and two nearby stars Lk Hα 224 and 225, multiplier i.r. observations, 2 to 18 microns 2—33651
Be, B, Bp, O and A type between 7000 and 9000 Å 2—37291
Be, ultrarapid changes in Hα line profile 2—4842
Be type, emission obs. with narrow band photometry 2—30465
Be type, profiles of emission lines 2—16987
binaries exhibiting a single spectrum, mass ratio rederived 2—13893
blue horizontal branch in ω Cen, weak He lines 2—10873
blue-type, obs. in i.r., review 2—20557
α Boo, u.v., emission at 2800 Å 16988 2—16988
α Bootis (Arcturus), far u.v. emission spectrum 2—41086
brightest in Magellanic Clouds, strength of O I λ7774 line 2—10875
3C 273, circular polarization 2—26692
VY Canis Majoris, circular polarization 26692 2—26692
ρ Cas, R CrB variable, UBV obs. 17000 2—17000
central star of NGC 1514 planetary nebula 2—26684
δ Cephei, atmosphere study by high dispersion spectra 30476 2—30476
U Cephei, close binary, emission lines7455 2—7455
o Ceti, differential radial velocities, obs. of dynamical structure of atmosphere 4882 2—4882
o Ceti, Paschen beta emission line, variation of equivalent width 41096 2—41096
UV Ceti stars, infrared photometry, infrared excess in flare stars 2—33669
class determination using eight-colour intermediate band photometric system 2—37293
classification of brighter stars in open clusters NGC 6613 and NGC 6716 2—13915
classification schemes, calibration 2—4852
close binary systems, ring envelopes, absorption lines 2—26742
clouds in Large Magellanic Cloud colour magnetic diagrams 2—4866
VY CMa, in blue and i.r., photometry13894 2—13894
CN red system, synthesis assuming Milne-Eddington model atmosphere 2—4849
compact objects, optical classification 2—13860
computer processing of spectrograms with a digital microphotometer 2—13901
cool giant stars, mole. spectra effects, calc. using model atmospheres 2—16996
cool stars, scanner obs. 3400 to 11000 Å 2—30459
θ CrB, binary system, near i.r. photometry 2—23080
R CrB variable, UBV obs. 2—17000
V CVn, red variable, polarimetric obs. 2—30445
VI Cyg No. 12, interstellar SiO$_4$ absorption search 2—7467
CH Cygni, activity phase during 1967-1970 symbiosis 2—4840
χ Cygni, differential radial velocities, obs. of dynamical structure of atmosphere4882 2—4882
V1057 Cygni, interpretation of change in spectral type, K0 to A133667 2—33667
CH Cygni, semiregular variable, and relative monochromatic brightness10871 2—10871
V1057 Cygni, total absorption of O at λ7774 10876 2—10876
χ Cygni variable, forbidden emission lines of Mn I and Fe II 13895 2—13895
DB white dwarfs, absence of Balmer lines, accretion and convective envelopes 2—7418
digital processing using microphotometer and computer 2—4863
double, Fourier transform. applic. to reduction of meas. by photoelec. scanning 2—23074
double star photographs, interference figures 2—13903
double systems, UBV magnitudes and colour indices 2—4892
AI Draconis, eclipsing variable, photoelectric obs. 2—26713
early type in direction of association Perseus OB 2, interstellar absorption obs. 2—4856
early-type stars at high galactic latitudes, UBV photometry 2—13836
elements' abundance, critique of theory 2—26707
elliptical galaxies, line profile spectra from centre part 2—33608
F5 to K5 spectral classes, role of collisionally broadened wings or strong lines in blanketing problem 2—13900
F dwarfs in Coma open cluster Fe/H abundances 2—4893
F stars of intermediate luminosity spectral classification 2—26686
F-G supergiants in Large Magellanic Cloud, six colour photometry 2—7425
F-type supergiants, calibration of luminosity-sensitive O I λ7774 line 2—30457
F type supergiants, O I, Fe I and Fe II spectra, microturbulence 2—30458

Stars continued
- **spectra** continued
  - faint O-B2 stars in southern Milky Way, Carina spiral feature 2—41055
  - faint spectra using Lick Observatory image-dissector scanner 2—41270
  - forbidden emission lines and i.r. excesses in early type stars 2—33662
  - Fraunhofer lines, transfer eqn. system for nonscattering medium in magnetoactive atmosphere 2—16997
  - G5 III, velocity dispersion of absorption lines 2—7384
  - G8 III, velocity dispersion of absorption lines 2—7384
  - G and K dwarf stars, revised indices on the six colour system of Lick Observatory 2—13902
  - giants in old open clusters, color excesses and metallicities 2—20577
  - globular cluster in M31, scanner abundance obs. 2—10897
  - globular clusters, four-colour observations of blue horizontal branch stars 2—10906
  - Hα profiles, half widths, from spectrograms obtained with solar telescope 2—4859
  - HD122563, metal poor red giant, analysis 2—30462
  - HD45166, absorption and emission lines, possible binary, secondary star having quasi-WR type 2—7430
  - HD92207, HD100262, HD125835, HD161912, turbulent velocities for Fe I, Fe II, Cr II, abundance ratio of Ti/Fe 2—7403
  - HD, southern stars, two-dimensional calssification 2—13884
  - HD 187399, shell star, obs. before, during and after outburst 2—20551
  - HD 193516, suspected β Cephei type, photometry 2—4854
  - HD 226868, circular polarization 2—26692
  - HD 49798, O-subdwarf quantitative analysis 2—1961
  - HD 50138 and 51585 Be stars, continuous spectra in near i.r. 2—33717
  - HD 97671, in blue and i.r., photometry 2—13894
  - HDE 226868, BO Ib type, coincidence with X-ray source Cyg X-1 2—26698
  - g Her, red variable, polarimetric obs. 30445 2—30445
  - X Her, red variable, polarimetric obs.30445 2—30445
  - Herbig Ae and Be types associated with nebulosity 2—26656
  - Herbig Ar and Be types, H$_2$ line profiles and surface gravities 2—26650
  - HR 2902, spectral features in 1971, far u.v. observations, shell spectrum 2—30461
  - HR 2957, Cepheid variable of small amplitude, photoelectric obs. 2—37307
  - HR 465, Hg II line, shape changes (from 1961-1969) 2—10879
  - Hyades, Ca$^+$ emission decay, rotational braking and Li depletion rel. to age 2—16986
  - intensity modulation at discrete radio frequencies 2—10885
  - interstellar reddening law 3450 to 5800 Å structure 2—26751
  - IRC+10216, HCN and ^{12}C/^{13}C abundance ratio 2—4843
  - IRC type, narrow band and broadband i.r. photometry 2—4865
  - IV-59 in Arps catalogue, new CN strong star in cluster M5 2—13919
  - K2 III p Arcturus u.v. emissions from shock wave excited regions 2—26695
  - K4 III, velocity dispersion of absorption lines 2—7384
  - BL Lac, variable, phtoelectric obs. 2—30488
  - late F dwarfs, equivalent widths of spectral lines 2—41100
  - late type, effects of reddening on UBV colour transformation 2—30464
  - late-type stars, lines for curve of growth analysis 2—41101
  - light curves, synthetic, rectification, models 2—33652
  - line source fn. for two-level atom in inhomogeneous finite atmosphere 2—4851
  - lines of different metals and metal abundance effects on solar colours 2—33760
  - long period variables, fluorescent Fe I emission 2—37295
  - luminous late-type, survey in visual- red region 2—26689
  - S Lyr, unidentified bands in near i.r., possible molecular sources10878 2—10878
  - RRLyrae type, ΔS values 2—37299
  - M supergiant, α Ori, i.r., OH line formation 2—10877
  - M supergiants in Carina, spectroscopic and photometric obs. 2—13894
  - metal-deficient in the southern hemisphere 2—7431
  - metallic lines, photometry obs. 2—33654
  - Mira variables, analysis of light variation curves 2—26720
  - molecular line absorptions, effect on opacities 2—4868
  - TU Muscae, binary, light curve and minima20592 2—20592
  - neutron star crusts and the production of blackbody X-ray sources 2—20558
  - NGC 1068, circular polarization 2—26692
  - NGC 2264, polarization of pre-main sequence stars 2—26700
  - NGC 2516 and Pleiades group UBV observations 2—26726
  - NGC 4151, circular polarization 2—26692
  - NGC 6231, open cluster, four colour and Hβ photometry 2—4894
  - NGC 6231 open cluster, four colour and Hβ photometry 2—17005
  - NGC 7332, velocity dispersion of absorption lines 2—7384
  - nova Aquilae 1970, spectrogram 2—20571
  - nova Serpentis 1970, spectrscopic obs. of early decline 2—20571
  - O and Of type, line profiles, classification 2—4841
  - O and Of-type central stars of planetary nebulae, effective temperature calculations 2—10886
  - O type line broadening as evidence for macroturbulence in atmospheres 2—33649
  - O-B2 stars in Vela, Carina, and Centaurus, UBV photometry, distance determination 2—4846
  - O-subdwarf, HD 49798, quantitative analysis 2—1961
  - O-type, interstellar Ca II, H and K absorption lines, Orion region 2—4870
  - OB associations in Large Magellanic Cloud colour magnetic diagrams 2—4866
  - OB distribution in Puppis, UBV and Hβ photometry 2—37285
  - OB star groups, UBV and Hβ photometry of Monoceros 2—13837
  - OB stars, with C and N, anomalies, classification 2—26694
  - OB stars and absorption regions in NGC 185 and 205, the elliptical galaxies near M31 2—13850
  - opacities of astrophysical mixtures, new Los Alamos tables 2—26703
  - opacity of stellar mixtures, effects of autoionization 2—26702
  - ζ Oph, equivalent widths of interstellar CH and CH$^+$ lines 2—26749
  - ζOphiuchi, detection of interstellar CO and 3K background 2—20600
  - U Ophiuchi, minima obs. 2—20556
  - V 567 Ophiuchi, ultra short-period variable, five-colour photoelectric observations 2—26715
  - ζOphiuchi, ultraviolet lines 2—7429
  - VV Ori, eclipsing binary, UBV ground based obs., and u.v. OAO obs. 33683 2—33683
  - α Ori, M supergiant, i.r., OH line formation 2—10877
  - ζ Ori, P Cygni-type profile, stellar atmosphere models 2—13896
  - UX Ori, spectrophotometric temp and absolute energy distribution in continuum10869 2—10869
  - ε Ori, supergiant, radial velocities curve of growth analysis 30463 2—30463
  - ER Orionis, binary minimum 2—20591
  - θ^1 Orionis C, inverse P Cygni profile in He II line, accretion of infalling material 2—41087
  - Osborn's star 1018, new CN strong star in cluster M10 2—13919
  - peculiar early-types in Centaurus, colour and Balmer line widths 2—7426
  - ε Peg, late type supergiant, abundance analysis 2—37284
  - ζ Per, equivalent widths of interstellar CH and CH$^+$ lines 2—26749
  - αPer, normal composition supergiant, equivalent line widths 2—37298
  - KP Persei, β Cephei type variable, UBV photometry 2—26712
  - o Persei, spectroscopic binary, rel. to β Cephei stars and the II Perseus association 30493 2—30493
  - photometric observations, blanketed model atmospheres 2—26697
  - photometry centred on NGC 6522, red giants in nuclear bulge of the Galaxy 2—13838
  - Pleiades, Ca$^+$ emission decay, rotational braking and Li depletion rel. to age 2—16986
  - Polaris, colour excess from Hα profile and G-band strength 2—13897
  - populous and globular clusters in the two Magellanic Clouds, B, A, and F-stars 2—10910
  - Procyon, curve-of-growth analysis, comparison with Sun 2—16992
  - 29 Psc, Balmer and Paschen slopes, Balmer discontinuity 4817 2—4817
  - 29 Psc, He deficient photometric standard 20515 2—20515
  - pulsars, fluctuation spectra analysis, polarization of subpulse structure 2—26786
  - L$_2$ Pup, red variable, polarimetric obs. 2—30445
  - ζ Puppis, absorption and emission, effective temp. calc. 2—7424
  - ζ Puppis, visual line spectrum, static plane parallel models for atmosphere 2—23073
  - rapid rotation, effect on weak absorption lines in sharp-lined stars in pole-on configuration 2—37280
  - red giants in halo population clusters, UBVRI obs. 2—20542
  - red giants in nuclear bulge of Galaxy 2—30417
  - reddening of stars in the direction of RR Lyrae, BV photometry 2—20574
  - RR Lyrae short period variables, AE Boo, TV Lyn and RW Ari, UBV light curves 2—26725
  - RV Tauri, anomalous, i.r. radiation, broadband photometric measurements 2—30527
  - S Lyr, near i.r. spectrum at maximum and minimum light 2—20628
  - satellite, small astronomical design 2—7354
  - τ Sco, absorption profiles of He I lines with forbidden components, broadening 2—7427
  - ISco association, open cluster, four colour and Hβ photometry 2—17005
  - Sco X-1, low energy γ-ray spectrum, balloon altitude observation 2—20636
  - Sco X-1, rocket borne Bragg crystal spectrometer 2—10980
  - δ and π Scorpii, C 3 lines for v.u.v. region1959 2—1959
  - δScorpii, ultraviolet lines 2—7429
  - β Scorpii system, occultation of individual components by Jupiter and Io30497 2—30497
  - secular stability, complex roots in secular spectra, 2.5, 5, 10, 15 solar masses 2—37281
  - 60 Serpentis, radial velocity 2—4861
  - VX Sgr, in blue and i.r., photometry 13894 2—13894
  - shell type, early, i.r. obs. 2—4862
  - star rings 373 and 519, configurations of field stars 2—41093
  - supergiants, brightest in Magellanic Clouds, strength of O I λ7774 lines 2—10875
  - supergiants, early type, unusual absorption feature in far u.v. 2—4839
  - supergiants, F-G, in Large Magellanic Cloud, six colour photometry 2—7425
  - supergiants, UBVr colours, influence of radiation pressure and spherical effects 2—37294
  - supernova, type I, in NGC 5055 2—4883
  - supernova, Type I of 1954 in NGC 4214, intensity min. and blue shifted He I absorption 2—23077
  - supernovae, type I, absorption bands, laboratory simulation 2—7438
  - T Tau type stars, peculiarities 2—41099
  - T Tau types, absolute energy distribution in continuum 2—10869
  - 20 tau, equivalent widths of interstellar CH and CH$^+$ lines 2—26749
  - RW Tau, gradient and Balmer discontinuity variations during eclipse 17001 2—17001
  - ζ Tau, shell-type, unusual absorption feature in far u.v. 4839 2—4839
  - EU Tauri, classical Cepheid, UBVβ photometry41098 2—41098
  - thermal OH emission from interstellar dust clouds NGC 2264 young open cluster 2—26735
  - U Mon, circumstellar absorption components of Ca II H and K lines 2—26709
  - UBV equatorial-extinction star network 2—4855
  - Ursa Major, Ca$^+$ emission decay, rotational braking and Li depletion rel. to age 2—16986
  - 4 Ursae Minoris, binary, revised orbit from spectrographic data 2—20586
  - u.v., spectroscopy, using Cassegrain-echelle optics with image intensification, rocket payload 2—11163
  - u.v. emissions, obs. using stratospheric package 2—4869
  - u.v. line profiles, effects of broadening parameters 2—33650
  - u.v. observations from a stratospheric balloon, 2-5000Å 2—7433
  - u.v. spectrophotometer, for obs. of bright early stars 2—10887
  - van Maanen 2, cool white dwarf, velocity, redshift and pressure shift 2—26685
  - van Maanen 2, white dwarf, energy distrib. and line profiles 2—26691
  - variables, rapid irregular, absolute energy distribution in continuum 2—10869
  - variables in Large Magellanic Cloud 2—13910
  - variables in NGC 6304 and NGC 6401, globular clusters, photometric obs. 2—26734
  - Vega, absolute calibration of energy distribution 2—26652
  - γ^2 Vel system, spectral types and visual luminosity obs. 20578 2—20578
  - BU Velorum, eclipsing binary, light curve20590 2—20590
  - violet opacity in S and C-S stars, circumstellar SiC grains 2—4823
  - o Vir, elemental abundance obs. 2—20552
  - BW Vulpeculae, intrinsic variable, spectral and photoelectric observations 2—41105
  - white dwarf, Grw+70° 8247, interpretation of 4135 band 2—30468
  - white dwarf Grw+70°8247, Minkowski bands interpretation 2—10881

Stars continued
spectra continued
white dwarf R548, periodic variations, DA spectral type 2—20566
white dwarfs, cool, line profiles 2—20540
white dwarfs, rotating magnetic as X-ray sources 2—7500
white dwarfs and white dwarf suspects, UBVr photometry 2—41094
Wolf Rayet type in M33 Sc spiral galaxy, blue continuum magnitudes 2—20541
WR, upper excitation configurations of CIII, NIV and OV 2—41102
WUMa systems, rotationally broadened line profiles 2—20546
young stellar objects, 1 μ search in dark clouds and H II regions 2—26679
Zeeman triplet formation in magnetic field, isothermic atmosphere 2—33644
AIII, Av forbidden transitions in nebula of Nova Delphini 1967 increased stability of intensity 2—13911
BaII, mean absolute visual magnitudes, and identification of two types of spectra 2—4847
C, faint, at high galactic latitudes, coordinates and distances det. 2—41095
C, type J subclass, rel. between strong ^{13}C and Li features 2—4858
C 3 lines for vacuum ultraviolet region of B-stars 2—1959
C III, lines, equivalent widths in Wolf Rayet star envelopes 2—23075
C III excitation in Wolf-Rayet envelope, comparison with WC8 star 2—4848
C stars, with composite spectra, TU Tau, SZ Sgr 2—20545
CN, C_2 bands, oscillator strengths 2—5913
Ca II K-lines in 65 stars, interferometric study of interstellar gas 2—26746
Ca K-line photometry, southern A stars, temperature and abundance variations 2—7423
Ca^+ emission luminosity rel. to age, for Pleiades Ursa Major and Hyades stars 2—16986
CaII emission decay, Li depletion, rotational braking, time scales 2—26696
Fe I and II lines, Doppler broadening, curves of growth for Populations I and II stars 2—30442
FeII line weakening in nebula of Nova Delphini (1967) 2—13911
FeVII, FeX, FeXI, forbidden transitions in nebula of Nova Delphini 1967 increased stability of intensity 2—13911
H and He of O stars, non-LTE model atmospheres 2—20543
H lines, highly excited, $H\gamma$-H_{26} line splitting and shifts calc. 2—13899
$H\alpha$-emission stars in the vicinity of γ Cygni 2—33645
He, curves of growth and line profiles in early type stars 2—13904
He I λ4471 and Mg II λ4481 lines in rapidly rotating early β-type stars, effects of gravity darkening 2—37292
He lines of early type stars, departure from local thermodynamic equilibrium 2—16994
HeI line weakening in nebula of Nova Delphini (1967) 2—13911
Hg II line in HR 465 peculiar A type, shape changes (from 1961-1969) 2—10879
Hi line weakening in nebula of Nova Delphini (1967) 2—13911
$H\gamma$ line strengths in early-type stars, photoelectric measurements 2—4844
ρ Leonis, ^{3}He in photosphere 2—4857
Mg II doublet, from balloon born u.v. stellar spectrophotometer 2—30470
Mn, measurements in the Hyades and field giants with narrow-band photometry 2—16993
NII forbidden transitions in nebula of Nova Delphini 1967 increased stability of intensity 2—13911
Na, measurements in the Hyades and field giants with narrow-band photometry 2—16993
Ne ions, continuous absorption 2—15202
NiXV forbidden transitions in nebula of Nova Delphini 1967 increased stability of intensity 2—13911
O I total absorption measures, photoelectric photometry for 31 stars 2—33653
OH emission sources, search at 1665 MHz 2—7432
OI, OII forbidden transitions in nebula of Nova Delphini 1967 increased stability of intensity 2—13911
Oi line weakening in nebula of Nova Delphini (1967) 2—13911
γ^2Vel, C III lines, equivalent widths in envelopes 2—23075

structure
A- and F-type stars, convective envelopes rel. to mixing length theory 2—33630
adiabatic envelopes, stability problems, hard and compressible cores 2—37278
beta processes effects on post detonation evolution of dense cores 2—26664
β Cephei, nonlinear nuclear energized pulsations, computer simulation 20567 2—20567
VV Cephei, rotationally extended Be envelope17008 2—17008
circulation currents in differentially rotating stellar envelopes 2—41079
contact binary systems, models to explain lightcurves for W UMa systems 2—30492
convective mode, growth rate in convectively unstable self-gravitating gas sphere 2—37283
detonation in cores, effect of nuclear statistical equilibrium 2—20533
G55.7+3.4, possible supernova remnant, mapping at 11 and 21 cm wavelengths, to investigate possible relationship with CP1919 2—10961
G55.7+3.4, possible supernova remnant, non-thermal shell source close to the direction of CP1919 2—10960
IRC+10216, i.r. object, dust shell diameter determination from lunar occultations 2—33637
metal abundance effects on stellar models of 1.25 solar masses 2—33638
neutron, equation of state of matter at very high densities 2—10891
neutron star crusts and the production of blackbody X-ray sources 2—20558
neutron stars, microquakes and macroquakes, frequency jumps in radiation 2—30479
θ^1 Orionis C, accretion of infalling material, inverse P Cygni profile in He II spectral line 2—41087
planetary ellipsoids, MHD of liquids, exact solutions of equations 2—13889
Population II horizontal branch models, effects of semi-convection 2—26665
Population II stars of low mass, effect of composition gradients on convective core 2—23069
radial velocity det., internal probable errors 2—20528
rotating polytropes, perturbation theory using series-expansion method 2—30451
rotating with v. large mag. fields 2—16975

Stars (nuclear) *see Particle track visualisation*

Statistical analysis
see also Measurement/errors; Probability; Random processes
analytic approximation theory, representation of function inside its analytic domain 2—17274
binary and ternary fission, distribution of initial fragment kinetic energy 2—8367
counting distributions with complex exponential character, model for analysis 2—33964
data reduction, systematic error due to spacing of data points 2—7730
digital function generators and multipliers, variable geometry K-source detector system 2—5093
discrimination between models representing experimental results 2—28938
gaussian light of arbitrary spectral profile, generating function of photocounts 2—37941
Monte Carlo anal. of radiative transfer at atmosphere-ocean boundary 2—37157
Monte Carlo calc., bremsstrahlung spectral intensity 2—38227
Monte Carlo calc. of counting efficiency of coincidence spectrometer for positron annihilation radiation 2—11662
Monte Carlo method, emissivity of ceramic cylindrical cavity with circular baffles 2—37796
Monte Carlo method, particle beam optics 2—37893
Monte Carlo method for calc. of interaction of high energy radiation with matter 2—38766
Monte Carlo method for dynamical evolution of spherical stellar systems 2—41085
Monte Carlo models of star cluster dynamical evolution 2—10902
Monte Carlo simulation of motions of photoelectrons in ionosphere 2—16899
Monte Carlo simulation of propagation of cosmic rays in atmosphere 2—5567
Monte Carlo technique, gamma ray dose rate calc. through two layer slab shields 2—558
Monte Carlo techniques, effective temperature of emitting vapour in gold hollow-cathode lamps, large ejection velocity effects 2—15218
Monte Carlo techniques for simulation of light propagation in ocean water 2—37120
phase transitions of classical hard-ellipse system studied by Monte Carlo calcs., relation to nematic liquid crystal 2—37639
probability and statistics, undergraduate textbook 2—113
rain-scatter interference between terrestrial microwave and satellite comunication systems at 4 to 8 GHz 2—33488
sampling scheme, for wind measurement over ocean, with anemometers on buoys 2—1857
search, discrete theory 2—85
sequential analysis textbook 2—114
stellar dynamics and discontinuous Markov process 2—16972
three-body reactions, semiclassical Monte Carlo calc. of Coulomb effects in final state 2—35000
time-freq. dependent nonlinear radiation transport by Monte Carlo method 2—14143
H_2 glow discharge, Monte Carlo simulation 2—35617
Ne, liquid, statistical error due to finite time averaging in computer expts. on number density and kinetic energy-density autocorrelation 2—32220

applications
see also Counters/statistical analysis
acoustic noise analysis 2—34152
n-alkanes, configurational behaviour, computer simulation, Monte Carlo method 2—8727
amorphous solid, ion beam scatt., Monte Carlo simulations 2—17567
Apollo command Module, Monte Carlo simulation of land landing 2—20431
atmosphere boundary layer vertical two point longitudinal velocity fluctuation differences standard deviation 2—26488
atmospheric optics, inverse problems, comparison of techniques used 2—26500
atmospheric refractive index correlation with microwave fading 2—40971
atmospheric transmission of optical waves, statistics of optical intensity fluctuations 2—27590
atomic absorption spectroscopy, noise and detection limits 2—8042
Bayesian statistics, applications to physics 2—33963
b.c.c. lattice, blocking effect, Monte Carlo calc. 2—25699
beta-ray spectrometers, spherical electrostatic, calculation of form of spectral window by Monte Carlo method 2—31351
broadening of atomic spectral lines by perturber gas, unified theory including impact and statistical theories 2—38804
communication channels, tropospheric scatter propagation 2—17478
computer for processing of meas. results 2—26988
computing method for periods of cyclic phenomena 2—11317
condensation, homogeneous, upon moderate supersaturation, nucleation theory 2—32309
condensed media, multiquantum photocurrent 2—25977
curve fitting, experimentally determined function, numerical procedure for error computation 2—7729
dual resonance model, study of distribution of spins and effective trajectory 2—23817
ecology, interacting populations, volterra and other nonlinear models 2—2185
e.m. wave scattering, frequency cross correlation of wideband signals 2—23448
equilibrium, of viscous flow with random forcing by numerical integration 2—31909
equilibrium thermodynamics of nonideal reacting gases 2—18751
extensive Monte Carlo calculation, rel. to cosmic ray propagation in atmosphere and multiple meson production models 2—26552
fatigue limit scatter, rapid estimation method 2—25537
frequency response of a structure excited by transient or random forces 2—5170
geomagnetism, models for reversals 2—13801
geophysical obs. interpretation, statistical theory, physical aspects 2—40864
glass lenses, evaluation of reliability from mechanical strength data 2—27618
gravity data, based on minimum variance 2—26395
heat transfer, in rarefied gases, Monte Carlo solution of nonlinear Boltzmann equation 2—1035
information from noisy spectrum 2—38354
laser radiation energy stability 2—37948
lattice dynamics, insulators, anharmonic effects, Monte Carlo calcs. 2—4029

Statistical analysis continued
- **applications** continued
  - limiting distribution of end-to- end distances of chain mols., Monte Carlo simulation 2—860
  - liquid metal fast breeder reactor, hot channel analysis, statistical theory of extremes 2—28128
  - liquid scintillation spectrometry, coincidence detection efficiency 2—5577
  - liquid-gas equilibrium, semistatistical theory 2—9213
  - magneto-optical rotation and circular dichroism, dispersion curves distrib., least squares analysis 2—28253
  - Monte Carlo calc. for particle transmission through flat slab 2—23310
  - Monte Carlo calc. of characteristics of scintillation gamma spectrometer, in ring geometry 2—17998
  - Monte Carlo calc. of differential ranges of recoil product of $^{65}\mathrm{Cu}(\alpha,\alpha n)$ in 24-42 MeV range, comparison with expt. 2—35076
  - Monte Carlo calc. of errors in energy spectrum det. of cosmic particles 2—17985
  - Monte Carlo calc. of motions of flexible macromolecule in presence of obstacles 2—35365
  - Monte Carlo calc. of triplet correlation in liquid Ar 2—21952
  - Monte Carlo calcs. of excess thermodynamic props. of binary mixtures of Lennard-Jones 12-6 liquids 2—32223
  - Monte Carlo calcs. of small-angle plural scatt. 2_2145
  - Monte Carlo calculation of Helmholtz free energy for simple liquids 2—32222
  - Monte Carlo calculations, phase transitions of classical hard ellipse system rel. to nematic liquid crystal 2—37639
  - Monte Carlo evaluation of jacobian determinants, applic. to molecular scattering 2—24566
  - Monte Carlo intranuclear cascade simulation, effect of nuclear-pair correlation 2—11708
  - Monte Carlo method, det. of efficiency of detection of γ-rays using ^{10}B detector 2—27892
  - Monte Carlo method, passage of electrons and positrons through solids and liqs. 2—5502
  - Monte Carlo method, rel. to determination of harmonic potential constants 2—31739
  - Monte Carlo method appl. to nuclear reactors reactivity perturbations calc. 2—28120
  - Monte Carlo method for radiation transfer problems 2—23311
  - Monte Carlo methods, radiation shielding, comparison of expt. with calcs. 2_2879
  - Monte Carlo methods, simulation of H atom recombination, rate constant determination 2—715
  - Monte Carlo program for dE/dx systems to measure the charge and energy of relativistic particles 2—5573
  - Monte Carlo scheme for dynamical evolution of spherical stellar systems 2—20510
  - Monte Carlo simulation of ^{65}Cu spallation 2—28037
  - Monte Carlo simulation of EAS, on basis of aleph model of ultra high energy nuclear interactions 2—23981
  - Monte Carlo simulation of model ionosphere, calc. of photoionization yields of O, O_2 and N_2 2—4713
  - Monte Carlo simulation of nuclear-electromagnetic cascade for determ. energy losses not measured by ionization spectrometer 2—27794
  - 3d Monte Carlo simulation of nuclear-electromagnetic cascade in iron to determ. lateral spreading 27820 2—27820
  - Monte Carlo simulations,prediction of EAS properties 2—23977
  - Monte Carlo simulations of fluctuation phenomena in EAS cores 2—23976
  - Monte Carlo studies of thin film growth 2—9256
  - Monte-Carlo method for Heisenberg ferromagnet 2—16358
  - Monte-Carlo transport calcs. for semicond. 2—16206
  - neutron transport, stochastic 2—38686
  - neutron-produced single event spectra, Monte Carlo analysis 2—28106
  - nonlinearly vibrating structure, random pressure field, Monte Carlo soln. 2—27202
  - nuclear heavy ion reactions, predominance of proton stripping over proton pickup 2—28082
  - nuclear reactor concrete pressure vessels, failure analysis, Monte Carlo methods in finite element calculations 2—15070
  - nuclear reactor fuel, swelling models verification, use of microstructural data 2—21473
  - nuclear reactor fuel elements, probabilistic viscoelastic models 2—21463
  - nuclear reactors, neutron noise probability distrib. by maximum likelihood method 2—15102
  - ocean temperature response on atmospheric perturbations 2—33440
  - optical processing, non-uniform sampling 2—8017
  - orbits of comets, eccentricity charges in nearly parabolic orbits 2—20684
  - particle accelerator shields, mechanics of extra nuclear hadron cascades 2—5766
  - particulate mixture, anal. using social survey techniques 2—25607
  - particulate mixture, sampling 2—19276
  - photons, statistics of a composite formed of two fermions 2—38223
  - photonuclear yield curves 2—38566
  - plasma, Abel integration equation inversion 2—35456
  - plasticity of metals 2—3875
  - product reliability, random fatigue analysis 2—7734
  - quenched linear polymer chains, solutions of master equations and related random walks 2—37629
  - random coil polymer chains, Monte Carlo studies of relaxation of vector end-to-end length 2—24559
  - random medium, light wave propagation and irradiance distribution function 2—14445
  - Schrodinger equation, least squares solution by Monte Carlo method 2—30786
  - seismic records, method for evaluating correlational properties 2—30198
  - self gravitating systems, comparison of numerical exprts. with Lynden-Bell's statistics 2—10806
  - shock structure problem for gas used for statistical model evaluation 2—6143
  - smoothing of gamma-ray spectra, obs. of distortion caused 2—17991
  - solar radio bursts, time-dependent fine structure 2—14012
  - solar radio emission at 10.7 cm at Ottawa rel. to Zurich sunspot number 2—26895
  - spectra, iterative least squares procedure using digital computer 2—7731
  - spectroscopic binary systems, average mass ratio rederived 2—13893
  - speech evaluation method 2—37459
  - standard deviation evaluation in point recorded functions 2—5572
  - stellar dynamical systems, pair correlation effect 2—20474

Statistical analysis continued
- **applications** continued
  - stochastic analysis, fractured glass analytic technique, measurement method 2—1328
  - stochastic model for a fluid of hard cubes with attractive potential 2—17268
  - strain, theory of 2—27132
  - turbulence, weak homogeneous, statistical theory 2—39030
  - two particle coincidence meas. of four body break-up, kinematics, phase space and resonances 2—14772
  - urban radio noise model 2—34242
  - X-ray spectra correction, from scintillation spectrometery anal. of methods used 2—11652
  - α emission, 14 MeV neutron interactions with Ni 2—35055
  - Al, mechanical behaviour of coarse grained specimens in terms of microstructure 2—9682
  - $^{197}\mathrm{Au}(n,\gamma)^{198}\mathrm{Au}$ cross-section at 22.8 keV, Monte Carlo calculation of neutron energy spectrum 2—5704
  - H I absorption spectra at 21 cm, analysis of concentration in galactic disk 2—10967
  - HCl dissociation in Ar, Monte Carlo trajectory calculations 2—37029
  - ^{4}He, liquid, Monte Carlo ground-state energy calc. of pair potentials 2—12594
  - Nd laser, Q-switched 2—21084

Statistical mechanics
- *see also Heisenberg model; Lattices, theory and statistics; Quantum fluids*
- alloys, ternary, disordered, role of 3 body potentials 2—32715
- Ashkin-Teller model, critical props. 2—37643
- binary fluid, excitation spectrum calc., decoupling of Green functions 2—2157
- binary mixtures, one-chain approximation 2—2158
- binary rigid sphere mixture, Thorne's eqns. for transport coeffs. 2—7725
- biological motility, statistical mechanical nature 2—41275
- black body radiation spectrum, derivation 2—7702
- blackbody radiation, coherence props. 2—30828
- Bogoliubov inequality, derivation for classical systems 2—2168
- book, concepts and mathematical structure 2—30817
- book on statistical physics 2—37627
- canonical commutation relations, continuity for measure-space realization 2—2059
- canonical ensemble, long range correlations of the distrib. functions 2—30812
- charged hard spheres and sheets, structure function thermodynamic properties from mean spherical model integral eqn. 2—24586
- classical Coulomb systems under external field, thermodynamic limit 2—30811
- classical gas, linearized eqn. satisfied by one particle vel. distrib. function 2—27106
- classical lattice gases, use of small external fields in problem of symmetry breakdown 2—23294
- close-packed to b.c.c. transition, phase diagrams 2—22353
- commutator and anticommutatior functions, zero frequency poles and long time correlations 2—14129
- composites, linear anisotropic with periodic structure, variational principles of effective material consts. 2—29453
- continuum physics, linear heterogeneous dielectric, macroscopic description 2—16257
- continuum system with finite interactions, phase transitions 2—37641
- corrected Boltzmann statistics and Gibb's paradox 2—27074
- correlation functions, calculation from mol. dynamics data using fast fourier transform 2—20855
- correlation functions, long time space and time-dependent behaviour 2—35391
- correlation functions in closed system, relations 2—17270
- critical exponents, depend. on symmetry, dimensionality, pot. range and interaction strength 2—14127
- critical exponents for Heisenberg and Ising models calc. by Feynman graph expansion 2—23301
- critical phenomena, modifications in very small spin systems, Monte Carlo calc. 2—7705
- critical phenomena, scaling parameter and universality 2—27089
- critical pt. exponents, second neighbour interaction strength depend. 2—7707
- critical pt. exponents, universality rel. to lattice anisotropy 2—7708
- de Haas-van Alphen effect in metals, SCF approach in irreversible statistical mechanics framework 2—29609
- deformation of excited nuclei and disappearance of shell effects with excitation energy, statistical description 2—24133
- density matrices, entropy estimations 2—27091
- density variation through liquid- vapour interface, solution to Born-Green equation 2—14125
- disordered binary alloys, three-body potentials 2—15930
- dissipative nonstationary processes, general variational principle 2—37636
- dynamics of statistical phenomena, eqns. of motion 2—27088
- electrolyte solutions, primitive model calc. of thermodynamic properties compared with Debye model 2—28835
- electron transfer reactions, in simple fluids, statistical mechanical theory 2—26318
- entangled polymers 2_39018
- ergodic prop. of orthogonal ensemble of random matrices 2—11301
- fluctuation dissipation theorems in non-thermal equilibrium 2—37648
- fluid, thermodynamics in external field 2—12312
- fluids, two body statistical correlation function, invariant expansion 2—7700
- Fokker Planck coeffs. describing evolution of electron energy distrib. 2—17269
- gas of hard rods, determ. of pair distrib. function 2—7720
- Gibbs paradox appl. to particle physics 2—21211
- gravitational fields, covariant statistics 2—37584
- gravitational particle flow, stochastic theory 2—17272
- heat transfer analysis by collection of variables in dimensionless groups 2—27315
- high temperature system containing excited particles, statistical theory, abundance by S-matrix formalism 2—31179
- hydrodynamical equations for a system of particles interacting with nonadditive forces, determ. of stress tensor and heat current 2—30815
- infinite systems, bogoliubov inequalities, thermodynamic limits of physical systems 2—30810
- ionic solutions, primitive model 2—28799

Statistical mechanics continued
- irreversible processes, solid state, review 2—2169
- Jaynes's information-theoretic entropy and probability theory 2—2165
- kinetic equation for system of particles interacting with nonadditive intermolecular forces, determ. of transport coeff. 2—30816
- lattice gas, compressibility exponent 2—33939
- law of increase of entropy, proof from entropy definition as log. of no. of quantum states accessible to closed system 2—14128
- Liouville equation, approximate solutions and truncation scheme for distribution functions 2—14142
- Liouville equation, representation using dynamical correlation patterns 2—94
- Liouville equation for electron plasma with self-consistent field interaction 2—33958
- liquid microstructure, fluctuations in radial distribution function 2—28783
- liquid-solid transitions, lattice theory 2—39418
- Little model, off-diagonal long range order 2—14137
- low angle scattering curve, proportion of particles with specific radius of gyration 2—27094
- Lynden-Bell's, computer experiments 2—41049
- many-particle systems with Coulomb interactions, random walk model 2—37659
- mean field models 2—23297
- mean spherical model integral eqn. for charged hard spheres 2—24585
- memory function assoc. with phase space correlation function, classical derivatives 2—20880
- molecular fluids, perturbation theory for angular pair correlation function 2—32170
- Monte Carlo method, Doppler shift attenuation factor 2—34981
- most probable distribution, derivation by method of inequalities 2—27085
- multicomponent system, scaling approach to tricritical phase transitions 2—23304
- multicomponent systems with internal degress of freedom, density expansion of distribution functions 2—2166
- N-particle systems, necessary and sufficient conditions for rapid decay of correlations 2—99
- n.m.r. line shape governed by time dependent Hamiltonian, exact formula determ. 2—12093
- nonequilibrium statistical operator, extremal properties 2—33950
- nonlinear systems, critical energy for stochasticity 2—27090
- nonthermal equil. systems, fluctuation-dissipation theorems 2—17258
- one-dimensional fluid with long-range harmonic potential 2—20868
- Orlicz spaces in statistical mechanics 2—2163
- pair correl. functions, time-dependent, density hierarchy 2—11299
- particles accelerated by periodic forces, stochastic and adiabatic behaviour 2—30814
- partition function of the eight-vertex model 2—30798
- percolation transition 2—13072
- Percus-Yevick equation, modification 2—31889
- phase space mass distributions, approx. computation method 2—17264
- phase transitions and renormalization, scalar $\lambda_0\varphi^4$ theory, connection with quantum field theory 2—21187
- Planck-like distributions in solution of classical equations of motion for finite chain of particles with Lennard-Jones interaction 2—37646
- plasma, thermal, cut off criteria of electronic partition function and transport properties 2—28511
- plasma thermodynamics, thermodynamic potentials and plasma stability and equilibrium 2—39093
- plasma thermodynamics and stability of inhomogeneous Vlasov equilibria 2—39189
- polar fluid, dielectric polarization and alignment 2—1106
- quasi-equilibrium systems, possible metric description 2—30809
- quasistochastic model for motion of Brownian charge carrier in external electric field, absence of nonlinear response 2—23293
- response theory, integrodifferential equation 2—96
- rigid dipole liquids, statistical approach to Onsager and Kirkwood dielectric theory 2—6239
- rubber elasticity, applic. of modified description for systems with internal constraints 2—7699
- s-d exchange hamiltonian, decoupling schemes 2—11298
- scaling theory, critical indices 2—11300
- scaling theory of critical region of systems with long-range forces 2—17260
- scaling with a parameter in spin systems, near critical pt. 2—2167
- self consistent effective field theory 2—19757
- self-diffusion in dense fluids, applic. of BBGKY hierarchy 2—20881
- self-gravitating system, one dimensional, consisting of N uniform mass sheets 2—41047
- self-gravitating system of N-uniform mass sheets 2—14152
- solid solns., interstitial, thermodynamic prop. calc., entropy, enthalpy 2—6605
- solid solns., thermodynamic props., review 2—29414
- solid state irreversible processes 2—7703
- solid-vapour interface, props. calc. 2—35867
- solutions, quasi-chemical theory 2—89
- solutions, structure and statistical distributions 2—1081
- spectral theory of fluctuations, hypersonic relax. in light scatt. 2—27112
- spherical rotors, correlation functions, neutron scattering in spherical molecules 2—14117
- spin-temperature hypothesis, violation, Loschmidt paradox 2—7704
- spins, infinite order cumulant expansion 2—16389
- spontaneous self-regulating systems, spectral position 2—30808
- stability conditions for thermal process subject to finite disturbances 2—5160
- statistical thermodynamics, the most probable distribution, teaching paper 2—92
- stellar models of white dwarfs, free electrons, Thomas-Fermi statistical model, rel. to densities 2—33631
- stochastic Liouville method appl. to e.s.r. line shapes in slow motional region 2—18394
- stochastic processes, elements, review 2—86
- surface tension of liquid-vapour interface, fluctuation theory 2—39351
- thermodynamic scaling, comparison of various expansion, single comprehensive form suggested 2—11302
- time correlations, infinitely large systems, analysis by studying relaxation of spin-1/2 probe system 2—5159
- Ursell-Mayer virial expansion, renormalized for non-ideal reference system 2—33944
- Van Hove time-depend. correl. functions, generalization and functional relation 2—30807

Statistical mechanics continued
- water, bond lattice model, two-state thermodynamic props. 2—21954
- XY model, off diagonal time dependent spin correlation functions 2—95
- XY model, three dimensional, for study of dynamical critical properties 2—27086
- XY model, time dependent spin correlation functions 2—97
- NCl$_3$, isotopic species, atomic, bond, and mol. polarizabilities, root mean square amplitudes statistical thermodynamics 2—5937

quantum
- δ-function gases, cluster coefficient computation through U functions 2—2173
- 'gain of information' as equivalent to produced entropy 2—5162
- angular functions of definite perturbational symmetry for three-body problem, complete set calc. 2—101
- atoms, N two-level system, intensity fluctuation functions for spontaneous emission 2—24335
- Boltzmann density matrix, quantum corrections within the classical path approx. 2—27075
- book on statistical physics 2—37627
- Bose case, rel. between correlation function and Green's function 2—27101
- Bose statistics, parafield generalization 2—38194
- bose system, with condensate, bound states of excitations 2—37653
- causal description, using tachyon field 2—20822
- classical parastochastics and quantum mechanics 2—27087
- collision processes, effect of strong repulsion at short distances 2—23298
- convex function inequality, derivation of Peierls and Gibbs operators and coarse graining 2—33948
- correlation operators in many- particle physics 2—23305
- density matrix equation with separable interactions in Liouvillespace 2—17245
- dissipative and nondissipative systems, constants of motion 2—37645
- dissipative system, energy spectra, Darlington's group-theoretic method 2—30818
- equation of state for nonanalytic potential, quantum corrections 2—20873
- Fermi statistics, parafield generalization 2—38194
- fluctuation-dissipation theorem for stationary open systems, Liouville-space formalism 2—2170
- Friedrichs model, irreversible phenomena study, kinetic and ergodic problems 2—30813
- Kubo-Martin-Schwinger states, two systems in thermal contact 2—33946
- linear response function, Dyson eqn. 2—23299
- Liouville theory of nonequilibrium Fermi systems, Hartree-Fock resummation techniques 2—20876
- master equation, time-irreversible and generalized, derivation 2—2150
- off-diagonal long range order systems, canonical ensemble perturbation eval. 2—17265
- open systems, time evolution, harmonic oscillator model 2—20869
- partition function, classical limit, teaching paper 2—33942
- Planck radiation law, dimensional considerations in its development 2—14123
- position-momentum uncertainty relation 2—33927
- pressure, thermodynamic, review 2—5163
- product representation of exponential Hamiltonian operator, convergence of density matrix 2—14126
- quantum mechanical transport eqn. for atomic systems 2—20879
- quantum states, representation as ensembles of dispersion free states 2—27092
- quantum systems, statistical description 2—93
- Raman photon amplifier 2—31020
- response function, inequalities for derivatives of partition function 2—11297
- s-partial density matrices and chemical potential 2—14130
- Schrodinger eqn. derivation from Newtonian mechanics 2—30789
- statistical distrib. general dynamical model, analogy with Schrodinger eqn. 2—33945
- statistical semigroups, perturbation 2—2162
- superradiant laser, investigations using Fokker Planck equation 2—27458
- superradiant pulses, quantum statistics 2—27110
- third cluster coeff., low-temp. expansion, logarithmic term. 2—23300
- time-irreversible generalized master equation, derivation 2—2150
- transport coefficients and response functions, density expansion 2—33960
- transport coefficients and response functions, logarithmic term in density expansion 2—33961
- two-level system, excitation, damping by interaction with bosons 2—2160
- two-photon (different modes) amplifier 2—21039
- two-photon amplifier 2—21038
- two-time Green's function theory, projection operators 2—23296
- Wallace perturbation method applic. to uniaxial ferromagnets 2—6949
- Wallace perturbation method applic. to uniaxial ferromagnets 2—6950
- wave mechanics, statistical foundations and nonsymmetric binomial distribution, application of computer 2—27012

Statistical thermodynamics *see Statistical mechanics*

Steady-state theory *see Cosmology*

Steam
- condensation on laminar plane jet of liquid 2—28953
- corrosion of Zr and Zr-Cr alloys, 325-700°C, rate law 2—20191
- flow, steam-water, vertical annulus, dispersed upward flow, heat transfer coeff. 2—1042
- generator, sodium heated in fast reactor, estimation of tube wall temperatures in the evaporator region 2—5749
- heat transfer, annular flow, shear dominated, local condensing coeffs. 2—1147
- precipitation of drops onto wall liquid film, from dispersed steam-water flow 2—28695
- quick closing valve for use in power chemicals cooled by evaporating water 2—15176
- thermal cond., critical region obs. 2—18874
- viscosity, thermal conductivity and Prandtl number as function of temperature and pressure, correlation 2—32245

Steel
- ageing, effect of conditions on mech. props. 2—36118
- ageing and hardening phenomena, effect of alloying additions to 20% Ni steel 2—36214
- ageing mechanism, effect of quenching temp. and soln. hardening 2—36215
- annealed, cracking rel. to temp. and H_2 partial press. 2—36173
- austenite, $\delta\to\gamma$ transformation on quenching, martensite and ferrite content 2—15951

Steel continued
  austenite, C activity, effect of Cr, Mo and W 2—32787
  austenite, carbide precipitation kinetics 2—32772
  austenite, cyclic strength, effect of thermomechanical treatment 2—9688
  austenite, deform. texture, influence of form of stress state 2—36233
  austenite, diffusion of C, effect of annealing struct. defects 2—32561
  austenite, hot rolled, recrystallization 2—12943
  austenite, hot working, secondary recrystallization kinetics 2—15903
  austenite, plastic deform. rel. to martensitic transform. 2—32764
  austenite, recrystallization, grain orientation, metallography 2—9737
  austenite, solubility and precip. of NbN, effect of Mn, Si, Cr, or Ni 2—12968
  austenite, solubility of graphite and cementite, calc. 2—25597
  austenite, thermomechanical strengthening 2—9728
  austenite, X-ray analysis 2—1226
  austenite dispersion hardened system, martensite transition temp., excess phase particles depend. 2—6638
  austenite grain size, effect on hardness 2—36244
  austenite stainless, stress corrosion, effect of alloying elements 2—29326
  austenitic, carbide precipitation effect on grain boundary internal friction peal 2—29246
  austenitic, corrosion cracking in boiling soln. 2—1753
  austenitic, cracking in boiling sulphur studied 2—6576
  austenitic, effect of carbon on high temperature properties 2—1304
  austenitic, effect of welded joints of Si 2—3957
  austenitic, ferrite mag. props., comp. depend. 2—4366
  austenitic, form. of NbC inclusions, effect of hardening conditions 2—36234
  austenitic, hot working, struct. and strength 2—9729
  austenitic, intercryst. and corrosion cracking, dislocation arrays 2—33381
  austenitic, mass transfer and corrosion rate in liquid sodium 2—13583
  austenitic, precipitation-hardening, fatigue limit and durability 2—36152
  austenitic, stress corrosion cracking, fracture surface, electron microscope obs. 2—19212
  austenitic, superheater tubing failure 2—1313
  austenitic, unstable, det. of ε phase using density charge 2—19293
  austenitic, weldable structural, hot deformation, isothermal recrystallization kinetics 2—12942
  austenitic and austenitic-martensitic class, assessment of mechanical props. after subjection to thermomechanical treatment 2—22275
  austenitic Cr-Ni with B additive, solid soln. decomp. 2—36240
  austenitic grain boundares, heat treatments, etching 2—6397
  austenitic stainless, 20%Cr-25%Ni, localized melting 2—36301
  austenitic stainless, ferrite content mag. permeability meas. 2—27404
  austenitic stainless, hot ductility, effect of N_2 and Ni 2—9672
  austenitic stainless, N distrib. during solidification 2—9212
  austenitic stainless, Nb-stabilized, fatigue, 500-800°C 2—32629
  austenitic stainless, plastic flow deformation mathematical model 2—12858
  austenitic stainless, stress corrosion and design considerations for use in boiler plant 2—15115
  austenitic stainless, stress corrosion cracking, alloying effects 2—1325
  austenitics stainless, high strength, steel with dispersion of TiN 2—15932
  austenitization kinetics, form. from ferritic-pearlitic struct., at 1128K 2—32770
  austenitized, hardness-cooling rate curve 2—29336
  austeno-martensitic, martensite struct., hardening, martensite reversion, precip. 2—29399
  bainite, strengthening mechanism, rel. to microstructure 2—9686
  bainite formation kinetics 2—40005
  bearings, operational behaviour, structure effects 2—32653
  bending stress distributions, phase transformation effects 2—36125
  bimetal structure, cohesive strength, influence of thermal cycling on compatibility 2—1364
  bimetal structure, corrosion resistant effects of technol. processing 2—1365
  bimetal structure, steel nickel, tensile test, impact test 2—1363
  bimetal structures, diffusion of C and Ni 2—1270
  bimetals, optimum rolling temperature 2—1357
  blue brittleness, tensile testing study 2—36115
  borated, fatigue strength, residual stresses 2—39808
  brazed joints, effect of bond zones on mech. strength 2—19253
  brittle fracture, effect of cement-bound concrete, electrochemical investigation 2—6578
  brittle fracture, rel. to intercryst. cementite 2—29309
  brittle fracture, weld crack sensitivity, notch impact toughness testing 2—6580
  brittle fracture assessment 2—25567
  brittle fracture initiation 2—1338
  brittle fracture initiation in residual stress field 2—25522
  brittle fracture initiation of welded joints 2—25534
  brittle fracture propag., continuum aspects 2—15870
  brittle fracture strength for press. vessels 2—25526
  brittleness, effect of N content 2—36156
  building materials, frequency dependence of acoustic waves on complex elastic constants 2—17399
  cantilever beams, vibration attenuation, theory and recpirocal experiment 2—14237
  carbide form. during tempering 2—39984
  carbide layer build up by open arc 2—32739
  carbide precipitation, cold and hot plastic deformation effects 2—32771
  carbon, corrosive cracking 2—29312
  carbon, hot worked, fibrous fracture, rel. to ferrite grains and non-metallic inclusions 2—19198
  carbon steel, 0.7%, effect of heat treatment and decarbonization on fretting fatigue behaviour 2—3893
  carburisation process 2—1366
  carburization in carbon monoxide and methane 2—16678
  carburized, effect of mean stress on fatigue strength 2—32626
  case-hardening process, standardisation 2—3814
  casehardened, mech. props. B effect 2—12891
  cast, failure in shock loading, cracking rel. to inclusions 2—39813
  cast V, precipitation hardening 2—9749
  casting plants, continuous, operating techniques and utilization times 2—3944
  catalyst, CO decomp., inhibition, rel. to nuclear reactor coolant props. 2—4577
  cavitation resistance, effect of thermomechanical working 2—6597
  cermet, containing inclusions, optimum comp. for wear resist. 2—1334
  cermet, martensite transform. during cooling after sintering 2—12939

Steel continued
  chilled, hydrogen permeability and embrittlement, drawing temp. depend. 2—29219
  chrome aluminizing, joint diffusion of elements 2—3929
  COD test data applicability and determ. 2—25530
  cold extrusion, chemical surface treatment 2—3931
  cold forming fabrication 2—9760
  cold-rolled, hardened boiler tubes, e.m. inspection of microstructure and mechanical, electrical and magnetic properties 2—3934
  cold-rolled electrical, mag. characts. at different angles to rolling direction 2—6961
  composites, maraging/Armco iron, stress corrosion cracking 2—30069
  composition anal. using atomic fluorescence flame spectrometry 2—22898
  construction, high strength, elastic characts., ductile-brittle transition, rare earth additions effect 2—15797
  core, strain sensitivity reduction using glass coatings 2—39925
  corrosion, fracture, chemical activation by concrete 2—6560
  corrosion and exoemission, effect of friction reversal 2—9732
  corrosion fatigue cracking, stress corrosion cracking, environmental attack, fatigue loading effects 2—19218
  corrosion inhibitors, anion-cation types, for H_2SO_4 2—4594
  corrosion obs. in hot radioactive environment using laser beam 2—21467
  corrosion protection, in liq. Li by means of metallic diffused layers 2—4592
  crack arrest in transversely loaded elastic plates 2—36171
  crack corrosion resistance, effect of Si and Mn content 2—6579
  crack detection simulation, schlieren apparatus for ultrasound visualization 2—37765
  crack formation, fatigue cycling, fracture mechanics 2—9709
  cracking by H, cathode polarization in acid media 2—30070
  cracking resistance, effect of alloying and microalloying 2—3900
  creep and stress relaxation, low temp. 2—36129
  creep properties, Cr-Mn-Ni steel at 77K 2—36128
  creep properties of Cr-Mo-V steels, effect of enhanced purity 2—32617
  critical points, influence of original structure, exchange of experience 2—29469
  cyclic heating effects on mech. behaviour 2—25516
  cyclical strength during variations of local stress 2—19190
  cylinder, thick-walled, failure, fracture mechanics applic. 2—32643
  decarburization kinetics, in H_2 and H_2-steam mixture 2—36242
  deformation kinetics rel. to serrated yielding, impurity-dislocation reactions 2—22208
  deformation martensite formation by cold rolling 2—3995
  die, struct. and props., effect of C and V content 2—36237
  ductile, critical plane-strain stress intensity factor 2—19208
  ductility, in hot working, O content effects 2—39893
  ductility, inclusions effects 2—15853
  dynamic fracture strength, shock precompression effect 2—12889
  dynamic properties, obs. 2—29333
  dynamic strain-ageing embrittlement effect on press. vessel integrity 2—24294
  electron beam brazing, medical instruments components 2—1356
  embrittlement by H_2, cleavage cracking, kinetics 2—29318
  embrittlement by hydrogen, directionality in hot rolled plate 2—3896
  embrittlement criteria at low temps. 2—32632
  En 25, fracture toughness and Charpy impact data 2—25533
  erosion resist., vibr. cavitation obs. 2—39853
  eutectoid, transform., lower bainite, effect of austenitising conditions 2—29470
  exoelectron emission from sandblasted mild steel, influence of organic vapours 2—22653
  fatigue, low-cycle, correl. of effects of hold time and strain rate 2—39826
  fatigue and creep, cyclical meas., apparatus 2—25544
  fatigue at elevated temp., for superheater tube applic. 2—39933
  fatigue crack growth, high-temp. 2—15879
  fatigue crack growth, stress cycle asymmetry effects 2—39840
  fatigue crack propag., strength and stress history effects 2—36170
  fatigue cycled, propagation of surface cracks 2—32634
  fatigue fracture, electron microscope obs. 2—9707
  fatigue limit, effect of struct. and props. 2—36149
  fatigue limit, evaluation of Locati and Prot determ. methods 2—39816
  fatigue loading of notched specimens, crack development 2—29325
  fatigue strength, effect of heat treatment 2—36151
  fatigue strength, low-cycle, thermal effect 2—39827
  fatigue strength, notch dependency under superimposed h.f. stress 2—32631
  fatigue strength rel. to surface machining 2—29301
  fatigue strength under axial load, effect of surface hardening 2—36150
  fatigue testing apparatus, thermal and thermomechanical 2—22307
  fatigue tests, random load life prediction model 2—39865
  fault detection, X-ray obs. 2—3639
  ferrite austenite transformation, stability rel. to alloying elements 2—39985
  ferritic, mass transfer and corrosion rate in liquid sodium 2—13583
  forge-quenched, effect of tempering temp. on mech. props. 2—12898
  fracture, intergranular, propagation, temp. effect 2—6563
  fracture, low temp., microstruct. effects, meeting report 2—32646
  fracture, single-edge notch tension specimens, effect of crack angle 2—3906
  fracture control, arrest of propagating cracks 2—25531
  fracture damage, high temp., rest period effects 2—39841
  fracture of cementite particles, on room temp. deform. 2—39839
  fracture toughness, cracking, in corrosive conditions, review 2—6558
  fracture toughness, double cantilever beam test 2—25565
  fracture toughness, effect of specimen type and prep. 2—39864
  fracture toughness, rel. between standard samples and small samples 2—19199
  fracture toughness and structure, O content effects 2—36155
  fracture toughness variation prediction from small specimen tests 2—25524
  fractured wires, corrosion, surface defects, electron microscope obs. 2—6559
  friction and wear, low temp. 2—36178
  girders, fatigue strength, surface work hardening 2—1315
  ground surfaces, physical condition by electromagneic method 2—28990
  hardened, mech. of delayed propagation of cracks 2—32650
  hardness and structure, effect of explosive deform. 2—39930
  heat resistant, effect of alloying additions on creep rupture strength 2—9687
  heat resisting, microstructure and mech. props. rel. to heat treatment 2—3933

Steel continued
heat treated, fatigue life curve, 8 step programme tests, range $>10^7$ cycles 2—12894
heat treatment, applic. of diffusion laws 2—9741
heat treatment, brittle fracture and toughness rel. to serrated grain boundaries 2—19204
high C, cold drawn wire, ageing and recovery 2—9757
high C, containing Si, bainitic transform. 2—36300
high chrome steel, hot rolling, finegrained struct., plasticity 2—1362
high Cr, embrittlement, thermo-e.m.f. and galvanomagnetic obs. 2—3899
high stability deep tempered, mechanical properties, two industrial samples 2—1340
high strength, corrosion-resistant, transitional, phase comp., ht. treatment, Kh16N7M2Yu and Kh17N4MD 2—1361
high strength, fatigue failure, electron fractographical investigation 2—3894
high strength, tending to brittle rupture 2—39809
high strength Ti-structural type, recrystn. 2—29391
high-carbon, optimum continuous casting temp. 2—9762
high-speed, austenite decomp. and carbide precip. 2—36241
high-speed, cast, effect of Ti and V on struct. and props. 2—36176
high-speed, quench deform. due to complex carbide precip. 2—29392
high-speed, resist. to microplastic deform. and wear 2—36114
high-speed, W-Cr-V-Co, effect of C content on phase comp. 2—32726
high-strain fatigue life temp. depend. in parameter represent 2—39825
high-strength, fatigue crack growth, effect of purity 2—15880
high-strength KhGR steel under tension, mechanical characteristics 2—39877
hot rolling, semi-continuous mill 2—1362
hydrogenation, tensiometric investigation 2—3948
impact, axial on rods 2—9716
inclusion analyser, Quantimet 360, performance 2—6630
inclusion analyser, Quantimet 360 image analysing computer 2—6612
inclusions, nonmetallic, examination and determination techniques 2—1257
inclusions, nonmetallic, image analysing computer obs. of sampling errors associated with inclusion errors 2—6611
inclusions, quantitative electron microprobe anal. 2—36236
inclusions, significance of wetting on flotability of particles effect 2—3414
industrial sheet steel 25Kh17N4G15AF2 2—1360
laser beam stripping 2—39884
leaded, effect of comp. on Pb embrittlement 2—9652
liquid, destruction of TiB_2 or ZrB_2 rods by dissolved O_2 2—10625
liquid, nitrogen solubility, calc. 2—9771
liquid, transmission of ultrasound and measurement of ultrasonic attenuation during cooling 2—32685
low alloy, brittle fracture tendency, effect of alloying with molybdenum 2—1301
low alloy, brittle fracture tendency at liq. N temp., tests using notch fracture technique 2—1300
low alloy, brittle fracture tendency at low temperatures, effect of titanium additives 2—9680
low alloy, relation of strength to concentration and testing temperature 2—1305
low C, Al_2O_3, inclusion shape determ., scanning electron microscope obs. 2—29432
low C, brittleness transition temp. and fracture stress, effect of grain-boundary cementite 2—9708
low C, cold-rolled, surface fine struct. 2—1165
low C, grain size depend. of yield and fatigue strength 2—12855
low C, strain hardening, effect of type of stress 2—36212
low C, stress strain curve after cyclic plastic deform. 2—1285
low C, temper hardening, effect on creep elimination 2—9673
low C, texture control in rapid annealing 2—39892
low C Nb-structural type, electron diffr. study 2—32707
low carbon, effect of hydrostatic pressure on torsional deformation 2—3826
low carbon, relationship between brittle fracture and high strain fatigue behaviour 2—29294
low-C, AlN particle size at austenitic grain coarsening temp. 2—29433
low-C, dislocation struct. form. under static and cyclic loads 2—39783
magnetic, suitable for welded high speed bimetal rotary blades 2—9730
magnetic and mechanical properties of Cr-Ni-Mn steel as a function of carbon and vanadium 2—1318
magnetization meas. by contact eddy current probe 2—29819
magnets for high-energy physics 2—23516
maraging, austenite form. during ageing, X-ray obs. 2—32708
maraging, austenitic phase stabilization, thermal cycling 2—15909
maraging, Cr-Ni or high Ni type, hardening mechanism 2—36217
maraging, fatigue crack growth, fractographic study 2—32647
maraging, fatigue crack growth, fractographic study 2—32648
maraging, high-strength 2—36218
maraging, microstruct. and crack propagation 2—9710
maraging, optimum heat treatment 2—36204
maraging, stainless, struct. and mech. props. 2—36243
maraging, stress corrosion cracking, loading mode effects 2—19213
maraging, stress corrosion cracking 2—15881
martensite, χ-carbide formation and its transform. into cementite 2—39988
martensite, impact deformation strengthening 2—39901
martensite, newly heat-treated from Fe-Ni-C, peak in internal friction 2—39765
martensite, produced by plastic deform., struct. 2—39928
martensite, strain ageing mechanism 2—32700
martensite, X-ray diffr. study of two-phase decomp. 2—12967
martensite and residual austenite structures, in high Al steel 2—12724
martensite structure, in structural steels 2—36232
martensite transformation, dislocation mechanism 2—6637
martensitic, high C, carbide precipitate crystal structure and morphology 2—32725
martensitic phase diagrams, mech. and thermal treatment effects 2—9834
martensitic stainless, phase transforms., 400-650°C pulsed mag. field effects 2—36280
martensitic transform., lattice parameter anisotropy 2—32766
martensitic transformation in low C Mn type, rel. to damping effect 2—1395
mechanical properties at sub-zero temperatures 2—1406
mechanical props., hot working influence 2—1369
mechanical strength testing, reproducible static and dynamic loading procedures 2—1303

Steel continued
medium carbon, aluminized, effect of barrier layer on creep and resorption of Al layer 2—3876
melting, casting, working, heat treatment, defect origin 2—32690
metallurgy for non-destructive testing 2—29492
metastable austenitic, primary recrystn. texture development 2—25596
microalloyed, hot rolling, recrystallization 2—9735
microhardness, struct. changes, rel. to local pulse heating by laser beam 2—39846
microstructure exam. using electron microscope 2—39642
mild, ageing at 50°C 2—9750
mild, biaxial strength criterion at low endurance 2—15867
mild, crack opening displacement and fibrous fracture 2—32642
mild, fracture initiation, grain size effect 2—29327
mild, mechanical anisotropy 2—29255
mild, structure design for low endurance fatigue conditions 2—14187
mild Charpy specimen fracture toughness, crack opening displacement method 2—22285
nitrided, hard layer thickness determ. using combined microprobe analysis and colour etching 2—36227
nitrification, struct. and hardness changes 2—15962
normalizing, law of equivalence between duration and temperature 2—12941
notch ductility of irrad. 9Ni-4Co-0.20C weldment 2—15834
notch shape rel. to impact strength characteristics, 10GT steel at –20°C 2—39810
notched bar impact test for fracture toughness determ. 2—25564
notched fatigue strength, application of finite element elastic-plastic stress analysis 2—15819
nuclear reactor, hot box pressure dome and skirt, design and stress analysis 2—15052
nuclear reactor casing, oxidation by neutron activated UPu oxide fuel 2—13577
nuclear reactor pressure vessel models, fracture studies 2—15063
pearlite spheroidization, acceleration by thermochemical treatment 2—32695
permanent magnet materials characterization 2—40514
permeability of H, Pd addition effect 2—29217
phase analysis of low carbon steel for Nb 2—1741
phase transform. temp., meas. technique 2—19298
phase transformation, $\chi'\to\alpha_m$, onset temp., effect of C content 2—1392
phase transformation, χ'-martensite form., X-ray obs. 2—1393
phase transformation, austenite-martensite due to deformation, effect of Ni 2—3979
phase transformation on cooling, computer simulation of temp. distrib. 2—32689
pipe, work of fracture, effect of heat treatment 2—36207
pipelines, hoh pressure, induction heat treatment 2—29385
plasmic spraying, surface composition and structure 2—15900
plastic deformation, dynamic softening, differential equations 2—36116
plastic deformation, with and without u.s. vibr., second order residual stress 2—36117
plastic deformation and annealing, microcracking density meas. 2—32584
plastic flow velocity, stacking faults influence 2—3868
plastic properties, effect of Ni and S content 2—6538
plastic strain mech., alternating deform., substruct. 2—32610
plastic zone form. and fatigue crack extension during bending 2—19215
plastic zones in double cantilever beam specimens 2—19216
plasticity evaluation for thin sheet materials, method based on torsion testing, sheet stainless steel 2—39878
plate preparation, high strength, non-magnetic, 25Kh17N4G15AF2 2—1360
polyethylene steel composites, dynamic modulus changes under repeated plane bending 2—29236
porosity, elimination in nitrogen-containing stainless steels 2—1359
powder, X-ray line-broadening study 2—3706
pre-loaded, deform. kinetics during extension 2—39784
precipitate identification for Cr-Mo steels 2—9770
pressure melted, high N content, metallography 2—32686
pressure vessels, bulk and micro-flow fracture behaviour, neutron irrad. effects 2—25525
pressure vessels, equivalent energy procedure for fracture prediction 2—24290
pressure vessels, heat affected zone fracture toughness 2—25528
primary structure inhomogeneities of Co_2-weld metal 2—22200
quenched, aged, mech. props, weldability, rel. to alloy additions, heat treatment conditions 2—19239
quenched, low-temp. tempered, martensite decomp. compressive stresses relax. 2—15899
quenched, martensite transformation, C interactions, resist., temp. depend. 2—3927
quenched, recrystn. during rapid heating 2—29389
for reactor pressure vessels, high temp. damage functions for neutron embrittlement 2—11905
reactor pressure vessels, safety analysis, elastic fracture mechanics applic. 2—24296
recrystallisation, struct., during slow heating 2—15906
recrystallization, u.s. attenuation obs. 2—25572
recrystallization texture, effect of precip. hardening and martensitic transform. 2—3992
reinforced composite, steel/epoxy resin, multiple fracture 2—32649
reinforced concrete, strength 2—15868
residual stress distrib., surface layer, effect of thermomech. strengthening 2—39776
residual welding stresses in longitudinally welded beams, calculation of 2—22219
resistivity, temp. depend. in low C Mn type, rel. to phase transitions 2—1394
rhenium, quenching, martensitic transformation, X-ray, dilatometric and resist. obs. 2—3994
rimmed and Al-stabilized sheets, deformation constitutional diagram in axisymmetrical forming 2—6602
roll, hardening depth, grain size, u.s. sound meas. 6-20 MHz 2—12913
roll, hardening depth, u.s. meas. 2—1332
secondary electron emission coeff., reflection caracteristics for Pt blacked screened collector 2—22660
secondary recrystallization texture, effect of Ge content 2—36203
sheared edge bend test 2—39860
shock wave incidence onto wedge shaped cavity, processes 2—29250
SM50, low cycle fatigue tests 2—36146

Steel continued
smelting and hot working 2—1345
soft polycrystalline, stress/strain, temp., deformation rate and grain dia. depend. 2—12856
soldered rods, damping coeff. increase, compression and flexion vibr. obs. 2—29242
solidification, non-eutectic 2—28948
solidification of ingots, math. study, finite element method 2—32307
solidification process in ingot, differential mathematical model 2—3442
spectrochemical analysis for Co, interferences 2—10668
spectrographic analysis of extracted non metallic impurities 2—1770
spring characteristics of thin leaves of stainless steel 2—25476
stacking faults, spontaneous formation after deform. 2—36040
stainelss, austenitic, correlation between strain hardening parameters and dislocation substruct. 2—32703
stainless, 17-4 PH, behaviour of weld heat affected zones 2—29410
stainless, 18 Cr-8Ni, sheets, deformation constitutional diagram in axisymmetrical forming 2—6602
stainless, 18-8, tensile testing, −271°C-25°C 2—39785
stainless, 316, 20 MeV C^{2+} irradiation, void swelling, dose depend. 2—6468
stainless, adsorption of Ar, Kr, N_2 and methane, isotherm meas. at 77 to 90K and 10^{-9} to 10^{-4} torr 2—32390
stainless, AISI type 446, high. temp. embrittlement and corrosion resistance mechanism 2—29335
stainless, Al fibre reinforced composite, electron microscopy 2—9779
stainless, austenitic, for cryogenic appl. 2—12971
stainless, austenitic, mechanical anisotropy 2—29255
stainless, austenitic, quenching defects, precip., microstruct. 2—6483
stainless, austenitic, stress corrosion cracking, nitriding effects 2—1326
stainless, carburization in Na containing carbon impurities, effect on mech. props. 2—13569
stainless, containing Ti oxides, precip. morphology effect on creep at rupture 2—9674
stainless, corrosion by liquid Na 2—37045
stainless, corrosion cracking by thermal gradient stresses 2—6575
stainless, creep and creep rupture tests 2—3880
stainless, diffusion layer comp. determ. using combined microprobe analysis and colour etching 2—36227
stainless, eddy current diametral extensometer testing 2—39862
stainless, effect of cold working on creep properties 2—3879
stainless, elastic anisotropy, temp. depend. 2—12824
stainless, explosion welded, interface structure, electron microscopy obs. 2—3945
stainless, fast neutron damage, simulation by ion implantation 2—6475
stainless, fatigue ductility, under cyclic stressing 2—12905
stainless, fine wire, glow discharge deposition of B, Zr, graphite 2—3525
stainless, heavy ion bombardment, defect struct. 2—9517
stainless, high strength, cracking in sodium chloride 2—1324
stainless, high-strength, tempering temp. effects on struct. and mech. props. 2—32609
stainless, irrad. enhanced precip. 2—39931
stainless, mag. props. 2—40476
stainless, neutron irrad. induced He generation 2—12748
stainless, neutron irradiation, void formation, thermo-mechanical treatment effect 2—6469
stainless, nitrided layer formation, struct. and mechanism 2—12927
stainless, pitting corrosion after oxide film removal 2—13582
stainless, plating, diffusion of C, comparison of fabrication methods 2—9619
stainless, radiation-induced swelling 2—24283
stainless, rupture and creep, He environmental effects 2—12871
stainless, secondary defects formed on quench-ageing 2—1244
stainless, secondary electron emission, coeff. for metastable atoms, meas. by crossed beam method 2—6933
stainless, secondary electron emission, coeff. for metastable atoms, meas. by gas cell method 2—6932
stainless, secondary emission rel. to gas pressure dependence of prebreakdown conduction in high vacuum 2—6934
stainless, shock loading, recovery and recrystallisation 2—9657
stainless, sorption of CO and S, effect of Au coating 2—39558
stainless, stacking faults and $\gamma \rightarrow \varepsilon$ transform. 2—40003
stainless, stress corrosion cracking resist., comp. effects 2—15882
stainless, thermal cond., 100 to 600 K 2—19442
stainless, thermal insulation, prediction, optimization and meas. of thermal cond. 2—19437
stainless, type 304, creep rupture specimens, metallography 2—39800
stainless, type 304, elastic-plastic constitutive equations 2—15823
stainless, type 304, residual microstruct., explosive shock 2—9655
stainless, type 304, resistance to fatigue crack growth at high temps. due to cold working 2—15884
stainless, type 316, creep and creep-rupture testing rel. to cold-drawing 2—1292
stainless, types 304 and 316, fast reactor irrad. damage 2—1236
stainless, void formation rel. to neutron irrad. temp., 400-600 °C 2—19073
stainless, work function reduction by elec. fields 2—16325
stainless 304, creep analysis 2—15168
stainless austenitic, high strain fatigue resist., effect of carbides 2—9651
stainless bicrystals, high temp. intergranular creep 2—12876
stainless chrome-nickel, effect of vacuum thermochroming on mechanical properties 2—6587
stainless foil, deformed, quadrupole splitting, Mossbauer obs. 2—36840
stainless TRIP, mech. props. rel. to austenite formation temp. 2—12857
stainless type 304, martensite concentration det. by magnetometer for failure prediction at low temp. 2—39977
steel, ferritic, compatibility with liq. Na at high temp. 2—13570
steel, high strength, stress corrosion crack velocity 2—19214
steel/Cu sandwich sheet composite materials, mech. props., press-formability 2—12819
strain-ageing, dislocation model, stress-strain behaviour 2—22330
pre- strained, stressed, tensile and yield strength, ductility, permanent strain, cracks 2—12854
strength, brittle fracture, effect of V and N impurities 2—6517
strength, effect of nonmetallic inclusions 2—36139
strength and plastic flow, low temp. 2—36113
strength drop at cryogenic temperatures 2—36138
strength in ductile fracture 2—29276
strengthening using hydroextrusion 2—9745
stress corrosion crack velocity 2—36169

Steel continued
stress corrosion cracking, crystallography, morphology, kinetics, models 2—3909
stress corrosion cracking in water cooled reactors 2—11908
stress corrosion cracking rates in 300 M, 250 grade maraging, 9 Ni-4Co-0.45 C 2—3910
stressed, notched specimen, yield stress, tensile strength, area reduction, elongation at rupture 2—12890
structural, high strength, with Nb additive, precipitation study 2—9738
structural, relaxation after welding, heat treatment and residual stress 2—12944
structural, strength, effect of preliminary heat treatment 2—36206
structural damages effects on fracture toughness 2—15837
structural hardening and associated metallurgical phenomena 2—3959
structural recrystallisation, alloying effects 2—32696
structure, tensile properties, function of fast reactor irradiation temperature 2—1232
structures, strain-hardening effects on load-deformation relations 2—29397
super-high-density sintered, fatigue and fracture props. 2—6561
superplasticity, temp. cycling, creep and transformation strain 2—12853
surface, unlubricated, high speed sliding, surface temp. predictions 2—22302
surface hardening, mechanical polishing, Rehbinder effect 2—32704
surface hardening, u.s. and vibromagnetic methods 2—36196
surface layer, machined, with built-up edge, translational struct. analysis 2—29001
surface layer formation by diffusion and chemical reaction of Fe-Al-C 2—39927
surface structure and friction parameters, effect of Cu coating 2—3918
temper brittleness, internal friction obs. 2—32633
temper brittleness of single crysts. 2—39833
temper embrittlement, segregation, Auger spectroscopy 2—3897
tempering, carbide phase precip., effect of rate of heating 2—36216
tempering, fracture toughness, temp. depend. 2—3891
thermal expansion, cooperative measurement using pushrod dilatometers 2—16045
thermal fatigue under multiaxial thermal stresses 2—39820
three layered strip, nickel-steel-nickel, strength characteristics, bonding 2—9759
tool, heat treatment monitoring by mag. thickness meter 2—25549
torsional strength of keyed and shrink-fit assemblies 2—19197
transformation, martensitic, influence of thermomech. treatment and C conc. 2—15961
transformer, secondary recrystallization matrix, rel. to initial state 2—12936
TRIP-type, fracture toughness 2—36172
tubes, high-tensile, ultrasonic inspection 2—17390
twinning, discontinuous, during essentially elastic compression, 4.2 K 2—39787
two-layered corrosion resistant, technol. processing effects on structure 2—1365
viscosity under high velocity impact 2—6544
void concentrations, helium bubbles, function of fast reactor irradiation temperature 2—1232
wear characteristics, rel. to surface temp. 2—39849
wear resistance, effect of white layer formed due to cold working and ultrasound treatment 2—6586
weldable, heat treatment, structural transformations, hardenability rel. to comp. 2—12945
welded joint, heat affected zone hardness 2—32654
welding, technical strength comparison for CO_2-shielded and submerged arc process 2—12960
welding of austenitic steels to pearlitic steels, brittle crystallization of interlayers 2—15924
welds, short cycle fatigue, effects of heat treatment 2—3895
wire drawing, failure exam. 2—22286
work hardened carbon steel, fatigue 2—39824
X 15 N 9 Yu, strength, dynamic and static tensile and fatigue, effect of heat treatment 2—6554
Al-killed, C-Mn killed and Si alloy, continuous casting strand 2—1368
Al-stainless steel, thermal contact resistance by reflection of heat diffusion waves 2—1438
B, Li, N_2, Th, U determination using nuclear track technique 2—7200
C_1 thermoelectric measurement of thermochemically produced layers on 2—1177
^{252}Cf encapsulator compared to Zircaloy-2 2—549
Cr-C, martensite decomp. rel. to carbide formation during tempering 2—32727
Cr-Mn steels effect of Ti, C, Ni, N. 2—1359
Cr-Mo-V type, low-cycle fatigue, temp. depend. 2—39828
Cr-Mo martensitic, tensile strength, fracture toughness, quenching effect 2—12908
Cr-Ni-Mn type, mech. props., effect of nitrogen 2—9654
Cr-Ni-Ti, austenitic, creep resist., rel. to intercryst. rupture, diffusion, precip. 2—9675
Cr-Ni, spectral analysis of H 2—16700
Cr-Ni duplex and fully austenitic, hot cracking propensities 2—15920
Cr-V, effect of Mo content and yield pt. on creep rupture strength 2—29286
10CrMoNiNb910 coolant pipes, fracture behaviour investigations 2—19210
Fe-C alloy, precipitation, nonisothermal conditions 2—9811
Fe-Cr-Al, and Fe-Cr-Al-Si ductile-brittle transition, effects of added Cr and Si 2—25518
Fe-Cr-C, martensitic, tempering, internal frinction meas. 2—29393
Fe-Cr-Mn-Ni, hot rolled, ageing response, mech. props., embrittlement, stress corrosion cracking resist. 2—19248
Fe-Cr-Ni, austenitic, H embrittlement 2—29308
Fe-Cr-Ni, austenitic, magnetism and structural stability 2—26038
Fe-Cr-Ni, hardening process during ageing 2—32697
Fe-Cu-C, sintered, precip. process during ageing 2—25580
Fe-Cu steel, low C, ageing, stable lath substructure obs. 2—25629
Fe-Mn-C, martensite, aged, onset temp. of C redistrib. 2—15914
Fe-Mo-C, martensite, secondary hardening during ageing, rel. to Co, Al, Mn conditions 2—29398
Fe-3at.%Mo, phase transform. rel. to double Bragg scatt. 2—36279
Fe-N, martensitic, interstitial ordering, precip., microhardness, internal friction, Mossbauer obs. 293-353K 2—9543

Steel continued
Fe-Nb-C, segregation mech., phase struct., annealing tests, electron refr. obs. 2—32729
Fe-Ni-C, martensite, aged, onset temp. of C redistrib. 2—15914
Fe-Ni-Co-Mo, pre-precipitation and reversion 2—9809
Fe-Ni-Cr-Ti, austenitic, plastic deform. rel. to σ- phase form. 2—29471
Fe-Ni-Cr, austenitic, stainless, B solubility, solubility curve, solubility boundary 2—22340
Fe-Ni-Cr, austenitic, stainless, B solubility 2—22339
Fe-Ni-Cr alloy, inoxidizable, austenitic, metastable, level in elastic limit 2—25478
Fe-Ni austenitic phase stability, heat cycling effects 2—29436
Fe-Ni type, resist. change during maraging process 2—15915
Fe-Si thin tape, texture and mag. props., effect of heat treatment 2—36717
Fe-Ti, work hardened, annealed, recrystn., recovery, segregation, electron and optical microscope obs. 2—32698
Fe-W-Mo, tempered, precip., of carbide 2—29384
Fe-W, tempered, precip., of carbide 2—29384
Mn-Si, low C, influence of Nb on precipitate structure 2—9812
Mn, high-manganese steels for petrol engine exhaust valves 2—3958
N-Nb addition alloying, increased creep rupture strength 2—3880
N atom recombination on steel surface, effect of adsorbed gases 2—5802
Ni-Co-C, fatigue crack growth, compliance method meas. 550-634K 2—19217
Ni-Cr-Mo-V fracture toughness and Charpy impact data 2—25533
Pb coating, hot dip, adhesion mechanisms, grain boundary impregnation 2—3978
pressure vessels, overstressing technique for securing against brittle failure 2—24291
SiFe transformer steel, magnetostrictive strain 2—4381
UCV-Na-steel system, C transport, effects of V addition 2—9628

Stellar atmospheres
A and F type stars, microturbulence and low-dispersion luminosity criteria 2—13905
adiabatic envelopes, stability problems, hard and compressible cores 2—37278
Am type cluster stars, microturbulence, comparison with standard A stars 2—13906
Arcturus, chromosphere, photoelectric scans 2—4831
εAur, F-type supergiant, equivalent line widths 2—37298
Avrett-Krook temperature correction procedure, modification 2—33622
B supergiants HD96248 and HD164402, model atmosphere analysis and comparison with main sequence star τ Scorpii 2—23068
blanketed by H_2 and metallic lines, photometric observations 2—26697
δ Cephei, high dispersion spectral study 2—30476
o Ceti, dynamical structure obs. from differential radial velocities in spectra 2—4882
R Coronae Borealis, dust shell model 41081 2—41081
χ Cygni, dynamical structure obs. from differential radial velocities in spectra 2—4882
energy transport in stellar winds hydromagnetics and heat conduction 2—20526
expanding, shell stars and QSO's, line profiles 2—30509
extended electron scattering, transfer of linearly polarized radiation 2—4820
F-type supergiants, calibration of luminosity-sensitive O I λ7774 line 2—30457
F-type supergiants, OI, Fe I and Fe II spectra, microturbulence 2—30458
G and K giants, parameter obs. using photoelectric indices 2—4819
general structure, interpretation of solar chromosphere anomaly 2—23134
giant stars, theoretical models for cool atmospheres with carbon enrichment 2—20525
giants, cool, molecular opacity, model atmospheres 2—4824
gray, thermodynamics, entropy transfer and production 2—33634
HD96248 and HD164402, model atmospheres comparison with τ Scorpii 2—23068
HD 187399, detached shell, model 2—20551
HD 4539, B-type subdwarf, chemical abundance analysis 2—33632
Herbig Ae adn Be types, geometry of circumstellar shells 2—26656
hot extended atmospheres, continuous energy distributions from five models 2—20523
hydromagnetic stability of stratified atmosphere flowing over liquid 2—26657
late type stars, computer models of optically thin clouds 2—30445
line-blanketed model, artificial absorption edges 2—30446
luminous red giants, final stage of evolution, physical props. of static envelopes 2—26674
M supergiants, OH abundance obs. 2—10877
M-star, absorpt. coeff. calc. 2—13886
magnetoactive, transfer eqn. system for nonscattering medium, Fraunhofer lines 2—16997
massive F-type supergiants, mass loss in hydrostatic equilibrium 2—26651
microturbulence, reanalysis using new f-values, A and F stars 2—4825
microturbulent velocities in an atmosphere with convection 2—37397
non-LTE models, H and He spectra of O stars 2—20543
O type, macroturbulence, evidence from line broadening 2—33649
optically thin, isothermal, radiative relaxation of sound waves 2—37412
ζ Ori, spectra, P-Cygni type profile, models13896 2—13896
α Ori, turbulence and thermal velocities 2—1953
physical parameters det. from model atmosphere calculations 2—30449
Pleiades lower main sequence, circumstellar shells having gray extinction properties 2—10907
pulsar, magnetosphere structure, evaporation and accumulation of gas 2—26779
pulsar magnetosphere, model 2—30517
ζ Puppis, visual line spectrum, static plane parallel models 2—23073
radiative transfer, spherically symmetric boundary value problem 2—4821
radiative transfer by regional averaging method 2—1958
rapid differential rotation, turbulent flow 2—26705
RR Lyrae, calculations of shock waves 2—7439
RV Tauri, anomalous, i.r. radiation, extended cool dust thermospheres 2—30527
RY Sagittarii, dust shell model 2—41081
spectral line form., transfer eqn. soln. method 2—20550
static atmosphere, temp. governed by third-order non-linear ordinary differential equation 2—41068
supergiants, UBVr colours, influence of radiation pressure and spherical effects 2—37294
supernovae envelopes, p-process in explosive nucleosynthesis 2—4833

Stellar atmospheres continued
temperature correction, Poincare-Lighthill coordinate perturbation technique 2—4822
two-level scattering atom, line source fn. 2—4851
white dwarfs, nongray model 2—20540
white dwarfs, outer envelopes and cooling, structure and energy transport 2—26661
Wolf Rayet envelopes, excitation of C III 2—23075
CaII emission decay, Li depletion, rotational braking, time scales 2—26696
Fe I excitation temps. by curves of growth for late G- and K-giants 2—26660
H^- equilibrium, charge exchange reaction dominance over associative reaction for star classes A0 to F0 2—20524
H_2 rich stellar envelopes, ejection from heavy element cores 2—26667
ρ Leonis, ^{3}He in photosphere 2—4857
Ne ions, continuous absorption 2—15202
SiC grains, in S and C-S stars, cause of violet opacity 2—4823
Ti I excitation temps. by curves of growth for late G- and K-giants 2—26660
Stellar clusters *see Stars*
Stellar composition *see Stars/composition*
Stellar evolution *see Stars/evolution*
Stellar motion *see Celestial mechanics; Stars*
Stellar structure *see Stars/structure*
Stellarators
fast compression, low-β stellarators, plasma shift with finite electrical conductivity 2—24682
fusion reactors model design studies and economic feasibility 2—28141
high beta (l=1) experiments, shock wave heating 2—24738
injector divertor device, plasma stream capture length regulation 2—32024
injector-diverter apparatus, energy spectra of captured plasma 2—32040
injector-divertor device, trapped plasma density, microwave meas. 2—6088
J.I.P.P., dependence of plasma confinement on magnetic configuration and plasma properties 2—24762
JIPP, results using J×B gun and ECRH plasma 2—3219
L-1, quasistationary longitudinal ion streams 2—24827
plasma behaviour, large electron free-path lengths 2—28582
Proto-Cleo l=3, confinement times and unidirectional current 2—24761
SATURN-1 three turn stellarator-torsatron, plasma confinement and magnetic surfaces 2—24763
TOR-1, plasma confinement rel. to collision frequency, rotational transform angle and magnetic field intensity 2—28583
TOR-2, plasma confinement at rotational transform angle resonance values 2—28584
Torsatron SATURN-1, mag. field structure 2—12398
Uragan, high-shear stellarator, high temperature plasma under current heating 2—24674
Uragan, hot-electron collisionless plasma containment 2—15467
vintotron, motion of trapped particles 2—15468
Wendelstein II-a stellarator, particle confinement minima 2—24760
Stereoisomerism *see Isomerism*
Stereophonic sound *see Acoustics*
Steroscopy *see Vision*
Stimulated emission
see also Lasers; Luminescence, Masers
alkali metal atoms probability of microwave emission from Zeeman levels 2—31665
astronomical sources of maser action, review 2—30401
atom, rate of absorption near resonance 2—34372
collisions of two atoms of different species polarization of sensitized fluorescence 2—35171
dye, diaryl butadiene solns., pumped by ruby laser 2—6238
dyes, flashlamp pumped reviews 2—7926
fluorescein dyes, continuous laser action, triplet quenching argon-laser pumping 2—276
four photon parametric frequency selection in wide stimulated emission lines of dye laser 2—27487
gas, super radiance, crit. inversion density, line narrowing 2—5355
historical development, embodiment in first ruby laser 2—23563
laser, plane resonator, mode energy spatial distribution, radiation modulation 2—21056
laser, Raman and Brillouin emission in ultrashort pulses 2—37949
molecule, produced by d.c. discharge induced C_2H_2 oxidation 2—31787
polymethine dye, flashlamp excited, green to i.r. 2—37974
pulsars, maser emission mechanism 2—30518
pyrene complexes, irradiated by Q-switched ruby laser 2—1706
quantum electronics, atomic and molecular coherence, review 2—27445
Raman scattering, transient, exptl. investigation in linearly dispersionless medium 2—11454
Rhodamine 6G in ethanol, excitation threshold lowering by org. additives 2—21990
rhodamine 6G laser, rate equation model 2—17614
ruby, heavily doped, optical props., review 2—36868
ruby, multiple three level laser, transition dipole moment orientation depend. 2—4470
semiconductor, homogeneous with exponential band tail, laser generation threshold, theory 2—20090
semiconductor laser, spontaneous carrier lifetime meas. from emission delays 2—31053
two-level problems, spin 1/2 formalism 2—21557
$AgGaS(Se)_2$, obs. on scanning visible spectrum 2—10416
Al emission line obs., vac. u.v. 2—18305
(AlGa)As-GaAs heterojunction, lasing transitions investigated 2—23615
$Ba_2MgGe_2O_7$, exper. data 2—16617
CO, in 1800-2000 Å region observed following discharge in gas at 60 torr 2—267
CO_2, at pressure of 15 atm excitation by electric field and electron bombardment 2—27471
CdS lasers, of polaritons 2—34404
CuBr excitonic molecule, u.v. or ruby laser excitation 2—4473
$CuGaS_2$, $CuInS_2$, obs. on scanning visible spectrum 2—10416
D_2^- labile ion, 48 to 84 MHz 2—8637
DF, molecule, high gain i.r. transitions 2—15309
GaAs-AlAs injection laser, threshold dependence on duration of pumping current pulses 2—37997
GaAsP:N, indirect semiconductor, stimulated emission and laser operation (cw, 77K) associated with deep isoelectronic traps 2—17635

Stimulated emission continued
  $GaAs_{1-x}P_x$:N, on isoelectronic trap transitions 2—37995
  $GdAlO_3$:Er^{3+}, energy level diagram detn. 2—33313
  $Gd_2(MoO_4)_3$: Nd^{3+} due to $^4F_{3/2}\rightarrow{}^4I_{11/2}$ transition 2—1679
  $GdScO_3$;Nd, absorpt. and luminescence spectra 2—26235
  H_2, v.u.v. laser action in Werner bands 1161-1240 Å 2—34393
  H_2 Werner band, obs. of gain by stimulated emission of vacuum u.v. radiation 2—24469
  H_2 Werner bands, 1161-1240 Å, obs. of vacuum u.v. laser action 2—24470
  HF, in H_3-F_2 chemical laser, time resolved spectroscopy, vib.-rot. transitions 2—5364
  HF, molecule, high gain i.r. transitions 2—15309
  ^{2}HF molecules generated by chemical reactions in D_2+F_2, D_2+NF_3, $D_2+N_2F_4$ and D_2+FNO_2 mixtures 2—27481
  Mn:ZnS, population inversion, electrolum. excitation, impurity impact excitation 2—13524
  N_2, electron beam excited 2—23600
  Nd:glass fibre laser, regular pulsations of intensity 2—37987
  Nd^{3+}:glass, emission spectra asymmetry 2—1711
  Nd^{3+}:$KY(WO_4)_2$ crystals, laser props., transitions and luminescence line widths, absorption cross sections 2—27508
  Nd^{3+}:$POCl_3$-$ZrCl_4$, liquid laser system, emission cross section detn. 2—27497
  Nd^{3+}:$YAlO_3$, continuous laser action, losses 2—14427
  Nd^{3+}:$YAlO_3$, intensity parameters 2—4496
  Nd^{3+}, in $GdAlO_3$, room temp. and low temp. 2—20097
  Nd^{3+} in $POCl_3$, YAG, $CaWO_4$ and glass, cross sections 2—37985
  SnO_2, photoluminesc. 2—26243
  TlI, mechanism of pulsed lasing of green line in a vapour discharge 2—27486
  Xe, liquid, electron beam excited, vacuum u.v. region 2—28865
  ZnO, donor electron excited state obs. 2—4481
  ZnO, electron-beam-pumped, lasing action 2—16611
  ZnS:Cu luminophors, stimulated by varying energy photons, spectral props of stimulated emission 2—4497
Stimulated Raman scattering *see Lasers; Scattering/light, Raman spectra*
Stochastic processes *see Probability; Random processes; Statistical analysis*
Stokes flow *see Flow; Hydrodynamics*
Stokes law, fluids *see Flow; Viscosity*
Stokes law, optical *see Luminescence*
Stokes lines *see Luminescence; Scattering/light, Raman spectra; Spectra/molecules*
Stopping power *see Energy loss of particles*

Storage devices
  analog memory devices using ferroelec.-piezoelec. interactions for adaptive control voltage modules 2—40341
  beam-addressable memory, use of EuO:Fe, Eu films, chemical stability obs. 2—26049
  charge coupled device, with ion implanted barrier and two nonoverlapping electrodes per bit 2—19695
  charge coupled devices, fast interface state losses, simple model 2—33041
  ferroelectric memory, $Pb_{0.92}Bi_{0.07}La_{0.01}(Fe_{0.405})Nb_{0.325}Zr_{0.27})O_3$ film performance 2—40356
  ferroelectric memory array, piezoelec. response 2—40362
  ferroelectric-photoconductor, thin film, design and performance 2—40336
  ferroelectric-photoconductor memory, electrode requirements 2—40339
  ferroelectric-photoconductor memory, equiv. cct. analysis 2—40337
  ferroelectric-photoconductor optical storage medium 2—40349
  ferroelectrics in optical memories and display 2—40334
  hologram memory, high information storage density, randon phase shifter method 2—38013
  holographic memory, ferroelec. light value arrays 2—40335
  holographic memory device, substance identification from i.r. spectra 2—11493
  logic element, use of orthoferrites 2—16366
  memory elements, thin film structural and magnetic properties 2—19893
  memory using chalcogenide semiconductor 2—29716
  m.n.o.s. memory device, influence of charge storage mechanisms 2—36572
  plated wire memories, annealing effects 2—1348
  plated wire memories, annealing effects 2—1349
  plated wire memories, magnetic stress anisotropy field 2—1619
  scattering mode ferroelectric-photoconductor image storage and display devices 2—21172
  Al_2O_3-SiO_2-Si, in m.a.o.s. struct., charge storage 2—13293
  n-GaAs Schottky barrier, bistable switching and memory 2—33024
  GeTe film, amorphous, recording of optical information 2—40225
  InSb film, amorphous, recording of optical information 2—40225
  $LiNbO_3$, holographic storage, coupled wave analysis 2—23658
  $LiNbO_3$, solid state hologram 2—17663
  n-Si Schottky barrier, bistable switching and memory 2—33024
  $Te_{81}Ge_{15}Sb_2S_2$ film, light induced memory 2—19653
  VO_2, film, holographic storage, based on insulator-metal transition 2—7951
  ZnSe m.i.s. electroluminescent device, exhibiting switching and memory 2—33327
Storage rings
  Adone, magnetic field integral measurement, high sensitivity method 2—2657
  CERN intersecting storage rings for protons 2—38419
  CERN ISR, computer control system and interfaces 2—14890
  closed proton beam stability, effect of secondary charged particles 2—2652
  coherent beam break-up due to space charge 2—14901
  colliding beam system, proton-electron-position, high energy, performance 2—14867
  colliding proton-proton beams geometry, non-destructive obs. method 2—14889
  electron, for duty cycle smoothing of 40 MeV linac beam 2—14814
  electron, high intensity, effects of e.m. self forces 2—14900
  electron and positron, present state and future prospects 2—14860
  electron or positron, luminosity enhancement, beam enlargement with h.f. oscillating quadrupole 2—18055
  1.5 GeV electron positron, ADONE, status and two beam behaviour 2—14863
  electron pulse stretcher, inhalation injection 2—14862
  electron-positron, luminosity limit, beam-beam interaction 2—18056
  electron-positron VEPP-3, status report 2—14864

Storage rings continued
  intersecting, beam control and r.f. stacking 2—14894
  intersecting, beam dumping and scraping 2—14896
  intersecting, CERN, performance 2—14861
  intersecting, CERN development, for proton colliding beam expts. 2—38422
  intersecting, closed orbit manipulation and correction 2—14897
  intersecting, coherent space charge instabilities 2—14885
  intersecting, computer controlled system for forecast of beam parameters 2—14899
  intersecting, contribution of beam-gas collisions to pion filux at large angles 2—38418
  intersecting, incoherent space charge phenomena and beam lifetime 2—14792
  intersecting, observation of beam behaviour 2—14884
  intersecting, prevention of space charge neutralization of the beams 2—14886
  intersecting, proton-proton collisions at 15 GeV and other tests, parameters 2—449
  intersecting, working lines adjustment 2—14898
  intersecting damping of transverse oscillations 2—14895
  ISR, betatron frequencies, automatic digital meas. 2—14891
  luminosity measurement at Orsay 2—11668
  Orsay compensated colliding beam rings, main project features 2—14866
  phase motion stability of bunch, dependence on form of synchrotron frequency distribution function 2—14887
  Precetron, with offset target, calc. of particle orbits 2—5626
  proton beam instability due to electrons 2—5628
  proton intersecting, beam diagnostics and instrumentation 2—14785
  quantum electrodynamics, vector meson dominance and high energy studies 2—14783
  rectifiers, 14 MW stabilized, for magnet of CERN intersecting storage rings 2—11693
  SLAC positron-electron project, SPEAR, design and improvements 2—14865
  superconducting, for synchrotron, design 2—14784
  synchrotron, proton, 28 GeV, 95 MVA motor-generator set employment 2—14859
  synchrotron radiation, coherent, model 2—372
  synchrotron radiation as absolute standard in 1100 to 3000 Å range 2—7640
  transverse stability of bunched beam interacting with low Q-value systems 2—14791
Storms *see Atmosphere/movements; Magnetic storms; Thunderstorms*
Strain effects *see Deformation; Elastic deformation; Plastic deformation*
Strain gauges
  alloys, short-term stress relaxation creep strain measurement 2—29360
  characteristic strain meas., comparison with X-ray method 2—22264
  conducting paper design 2—20806
  creep measurements in bridges 2—3831
  diaphragm pressure transducer, strain gauge type, nonlinearity 2—20809
  diffraction grating, parallel incidence 2—12921
  eddy current diametral extensometer, for testing pressurized tubular specimens 2—39862
  fluids subject to large deformation apparatus for stress relaxation meas. 2—5190
  force and torque transducer, for meas. teaching 2—27009
  inertialess, surface impressed diffr. grating 2—36182
  installation technique for h.f., low amplitude strain obs. 2—3851
  longitudinal deformation in cylindrical samples 2—29349
  mechanical for obs. of strain distrib. at points close to one another 2—22309
  medical, resistance and piezoresistance, review 2—30663
  mounted on foil, to be bonded by contact welding high temp. measurements 2—27032
  nonlinear deformations, direct meas. method 2—25536
  pressure measurement, differential manometer 2—23230
  resistance, for study of fatigue failure of metals and alloys 2—29350
  resistance wire strain gauges working under rapid temperature fluctuations, thermal compensation technique 2—37564
  Reynolds shear stress in water by laser anemometry 2—15550
  sensitivity, effect of moistureproof coatings 2—29253
  thermal strain meas. system for turbine casings 2—39874
  transducer, fatigue testing, deform. testing 2—19229
  transducer temperature compensation using active transistor circuit 2—11415
  for vibratory strain obs., h.f., low amplitude 2—3851
  Se-CdSe heterojunction sensor, properties 2—2056
Strain hardening *see Work hardening*
Strange particles
  multiperipheral model, strange particle prod. cross-section 2—11599
  production, f′ and φ Regge trajectories, Pomeranchukon generation 2—14614
  production, in π^+p interactions in c.m. energy range 1820 to 2090 MeV 2—11615
  production, in π-p→ two charged final particles at 11.2 GeV/c 2—38304
  π^-p, 4 GeV/c, with strange particle production, phenomenological model 2—5541
Strangeness *see Elementary particles; Field theory, quantum*
Stratosphere *see Atmosphere*
Streamers *see Discharges, electric*
Strength *see Electric strength; Mechanical strength*
Stress analysis
  see also Bending; Photoelasticity; Strain gauges; Torsion
  Airy stress function visualization by hologram interferometry, analogue plate models 2—14202
  Almansi Michell's problem, solution for anisotropic beams 2—27156
  anelastic material in simple tension, failure 2—140
  anisotropic inhomogeneous media, elastic stresses of edge dislocation 2—25391
  anisotropic media, calc. using Green's function derivatives 2—22267
  anisotropic shells of revolution, rotationally symmetric stress and strain 2—27178
  annular plate, finite stretching 2—130
  arches, steep, compressible, nonlinear analysis of any shape 2—34003
  artificial earthquakes, response spectrum analysis with two ground predominant modes 2—16743
  aseismic design of nuclear reactor building, by finite element method 2—15081

Stress analysis continued
asperities in sliding interaction, junction deform. models 2—39851
axisymmetric circular membranes, large deflection response, nonlinear relaxation method 2—2203
axisymmetric external crack problems for media with cylindrical cavities 2—23331
axisymmetrical shells, analysis as beam 2—2205
beam/elastic half-space tensionless contact 2—11336
beams, continuous, minimum-weight design 2—27169
beams, nonlinear non-uniform torsion 2—27165
beams, nonlinear theory 2—27164
beams, segmentwise cross section, Foulkes mechanism in optimal plastic design for alternative loads 2—27144
beams resting on long elastic supports, effect of loading through elastic layer 2—37677
bimetallic cylindrical joint, explosively welded 2—14170
bimetallic media, dislocation densities and cracks 2—12760
bimetallic rectangular plate in nonuniform temperature field 2—14223
blood vessel hemorheology 2—14024
body with constrained rotations, couple stresses 2—17322
bonded dissimilar materials, stresses near flat inclusion 2—23326
bonded semi-infinite elastic media, cracks parallel to interface, plane problem 2—2196
box columns, thin walled, effects of residual stresses and geometrical imperfections on strength 2—27142
box of elastic orthotropic plates for various modes of failure 2—30839
brittle fracture, dynamics 2—29316
brittle fracture, unstable elastic-plastic, model under plane stress 2—15873
brittle materials, uniaxially compressed, tensile stress, influence of platen friction 2—19196
buckling analysis for structural sections and stiffened plates reinforced with laminated composites 2—17299
buckling analysis of rectangular plate by Kantorovich method 2—37678
buckling of strip on rigid half space with transverse pressure 2—14168
ceramic, brittle, thermal stress problem 2—19273
circular crack, surface of beam, pure bending 2—2197
circular crack, surface of semi-infinite solid 2—2197
circular cylinder with infinite row of penny-shaped cracks, biharmonic stress function 2—17314
circular cylindrical shells, buckling, effect of variation in creep exponent 2—2206
circular disc, use of Green's function 2—37676
circular hole, thermal stress conc., for elastic plastic strains 2—7738
circular plates, symmetrically loaded, flexure, also effect of transverse shear 2—34010
closed spherical shell, stability loss under critical compression 2—5184
composite, anisotropic plates, wave surfaces due to impact 2—36099
composite, fibrous, stress conc. factors near discontinuity 2—19173
composite beams under initial stress, equations of motion and boundary conditions 2—17300
composite laminates, cylindrical bending response 2—17320
composite rotating spheres, consideration of inertia forces only 2—11325
compounded rotating discs 2—7743
compressed rigid-plastic body, breaking stresses and deformation speeds along rupture 2—5201
computer program for complex structures in presence of creep, application to nuclear reactors 2—17306
computer programme for thermal stresses 2—37818
concrete end slabs in nuclear reactor pressure vessels 2—15069
concrete pressure vessels 2—15067
concrete reactor pressure vessel liners, prestressed 2—15154
concrete structures, thermodynamics of interacting continua with surfaces 2—14180
conforming displacement finite elements method for generating upper and lower bounds 2—14189
conical shells, asymptotic solution of nonlinear equations 2—27162
contact problems of solid bodies, finite element method 2—5179
continuous media, rigid, perfectly plastic, limit analysis 2—33989
coplanar Griffith cracks under surface traction, stress intensity factors 2—14199
corner flaw, stress intensity factor 2—39834
Cosserat medium, couple-stress effects on dynamic stress conc. around crack 2—34020
Cosserat medium, principle of virtual work 2—34015
crack, circumferential, in cylindrical shell under press. 2—27166
crack, circumferential, in cylindrical shell under torsion 2—27168
crack, penny-shaped, in plate of finite thickness 2—34019
crack, two-dimensional, isotropic elastic cylinder 2—27158
crack in plane orthotropic rectangular sheet 2—27167
crack nucleation, critical shear stress, conformed mapping 2—29313
crack propagation, elastic fields, stress function model, photoelastic investigation 2—2214
crack propagation rate under alternate stresses 2—39836
crack propagation under random loadings, simulation of random envelope processes 2—37685
crack tip, antiplane shear 2—11329
crack tip, stress intensity factors, elastic media, finite elements 2—2198
cracked plate, elastic-plastic analysis 2—14213
cracked structure, by optical interference method 2—15871
cracked three point loaded bend specimen, elastic work, stress intensity factor 2—2217
crackline-loaded edge-crack stress corrosion specimen 2—15872
cracks, cylindrical shells under internal pressure 2—14179
cracks, nonlinear effects, energy release rate, fracture toughness 2—2199
cracks, pressure vessels in nuclear reactors 2—15177
creep as constant stress in isotropic solids 2—33999
creep buckling of a curved column under a time- varying axial load 2—37680
creep buckling of tubes under external pressure 2—14165
cubic continuum, elastic interaction of point defects 2—22186
curved sandwich plates, finite element displacement method 2—12839
cylinder, non-uniformly heated deformable infinite circular effect of diffusion 2—33988
cylinder, two layered elastic, cracked, finite element solutions 2—2213
cylinders, oval, ring reinforced, computer program 2—2194
cylindrical shell loaded longitudinally 2—134
cylindrical shell under axial concentrated load 2—5187
cylindrical shell under circumferential concentrated load 2—7739
cylindrical shell with elliptical hole, stress concentration 2—23320
cylindrical shells, axially non-uniform, dynamic analysis 2—34022

Stress analysis continued
deformation energy in planar theory of elastic rods 2—27180
deformation of a multilayered half-space by stress dislocations and conc. forces 2—23322
direct flexibility finite element elastoplastic analysis for complementary energy solutions 2—14191
disc, inform of half band connected with quadrant, stretching 2—14160
disc shaped as a semi infinite strip connected with a semi plane, stresses at any arbitrary pt. 2—27138
disc shaped as a semi-plane, use of Green's function 2—37692
disc shaped as plane with excised semi infinite strip, stresses at any arbitrary pt. 2—27139
disc shaped as semi plane with skew edge slit, stresses at any arbitrary pt. 2—27140
disc under diametral compression, effects of couple stresses 2—17321
disclination wedge loop, elastic field and strain energy 2—32513
dislocation configurations 2—32516
domed structures composed of sandwich plates, finite element method analysis 2—11326
Dugdale model, variational methods for crack intensity factors and plastic regions 2—34037
dynamic stress distribution in vicinity of crack tip, three dimensional numerical analysis 2—142
Earth, model of a liquid-filled spherical shell in a radial gravity field 2—20261
edge crack interaction with other cracks or boundaries 2—29315
elastic, cylinder to cylinder shell models exprts. application to nozzles in cylindrical vessels 2—14178
elastic bodies in contact, relative approach in two dimensions 2—2204
elastic composites, determ. of thermal stress distrib. by shear lag methods 2—15816
elastic crack tip stress fields, stress intensity factor for symmetrical loads calc. 2—37679
elastic half-plane under concentrated load, nonradial stress distrib. 2—14201
elastic layer, indented, bounds on maximum contact stress 2—144
elastic layer, semi-infinite crack, antiplane strain state, crack propagation 2—20891
elastic layer/half space interface, penny-shaped crack problem 2—17312
elastic plane, crack interaction with inclusion stress intensity factor 2—17313
elastic plate, anisotropic, with arbitrary elliptical holes 2—17294
elastic relaxation phenomenon, thermodynamic theory 2—11366
elastic rod, semi-infinite, transient response to uniform pressure in terms of power series expansion 2—37684
elastic shallow structures subject to h.f. periodic loading, dynamic buckling 2—17318
elastic sheet, fibre reinforced, elastic consts., bond stress distrib. 2—36091
elastic slab, non-homogeneous infinite, under normal load on free surface, analysis using Hankel transforms 2—20898
elastic stiffener bonded to a half plane 2—34002
elastic structures, finite element method, FORTRAN program 2—37690
elastic-plastic, finite element method application to notched fatigue strength 2—15819
elastic-plastic, notched bar in plane strain bending 2—12838
elastic-plastic strain wave measurements, error bounds 2—30862
elastic-plastic wave motion in layered solids, numerical technique 2—17319
elastic-plastic-thermal solutions for solid structures 2—14171
elliptic hole in cylindrical shell 2—27131
elliptic hole in cylindrical shell under torsional loading 2—17325
fast high flux test reactor, residual stresses and design of loop pressure tubes 2—15050
fatigue limit, statistical scatter, rapid estimation method 2—25537
fibre composite, two elastic concentric cylinders, resilience rel. to fibre content 2—36106
fibre-reinforced beams on slabs, small deflections 2—37688
fibre-reinforced composite, load absorption by discontinuous filament 2—19284
fibre-reinforced composites, transversely isotropic, stress channelling 2—19285
fibre-reinforced materials, incompressible, plane deformations 2—132
finite element, three dimensional, of reactor pressure vessel nozzles 2—15057
finite element approach to thermal stress problems 2—37722
finite element formation for elastic structural deformation analysis 2—11339
finite plate, stress intensity factors of interior crack, numerical method 2—33997
fission reactor fuel elements subjected to internal heating shock effects, calculational techniques 2—38745
flexible macromolecule solutions, stress relaxation after shearing flow 2—24995
fluids, rotational, under rotationally symmetric loads, stress determ. by finite element method 2—7735
B 16.9 forged tees, by finite element method, computer program development 2—14173
fracture analysis, crack stability, rel. to energy and crack length 2—2200
fracture mechanics application of finite element method 2—15860
frames, segmentwise cross section, Foulkes mechanism in optimal plastic design for alternative loads 2—27144
fuel elements in nuclear reactor element analysis 2—15125
fuelled graphite bricks in nuclear reactors, finite element analysis 2—15127
glass, surface-treated, Rayleigh wave dispersion for stress profile obs. 2—39768
glass window, fracture studies 2—39844
granular medium. nonhomogeneous, plane strain, stress field construction, series method 2—2188
graphite components in nuclear reactors, strength rel. to design problems 2—15129
graphite fuel elements in a high temperature nuclear reactor, operational stresses 2—15131
graphite fuel elements in nuclear reactors, finite element method 2—15126
graphite nuclear reactor components, thermal and Wigner strain effects 2—15128
graphite reactor components, temperature and radiation induced stresses 2—15132
heterogeneous inclusion in infinite elastic plate under simple tension, stress distrib. 2—33985
heterogeneous solids, constitutive macro- variables at finite strain 2—7737

Stress analysis continued
high speed transient deformation, three dimensional Moire fringe technique 2—27187
high strength materials, safe stress equation 2—6528
holographic technique applications 2—11338
holography applications, conference (Los Angeles August 1971) 2—14147
hybrid finite element model for axisymmetric thick walled pressure vessel 2—14188
impact, selection of parameters for meas. device 2—22317
impact stress waves in composite structures 2—14231
impact-fatigue testing apparatus for low temp. obs. 2—29369
imperfection sensitivity of ring- stiffened shells of revolution, FORTRAN program 2—27150
impulsive loading of clamped beams, plastic deflection 2—37708
incompressible continuous medium, spatial plastic flows with instantaneously inextensible planes 2 20899
incompressible isotropic materials, boundary value problems for large deform. 2—6530
infinite elastic body with cylindrical hole, response to travelling load 2—30836
infinite plate with two rigid circular inclusions 2—23321
infinite wedge-shaped lamina loaded at edges, conformal mapping 2—2187
insulated flat plate moving at hypersonic speed, time dependent shear stress and temp. distrib. 2—6141
intensity factor, finite width corrections, centrally cracked sheet strip 2—2201
intersecting cylindrical shells by finite element method, application to nuclear piping 2—14177
isotropic, transversely inhomogeneous elastic material 2—34006
Kapradse potentials of a double layer, plane surface dislocation, plane crack 2—136
Lindemann law for setting of stress limits 2—14183
linear fracture mechanics, survey and evaluation of the finite element method 2—17305
linear plate and beam theory, class of admissible loads 2—33996
long hollow cylindrically aeolotropic cylinder with ends subjected to surface forces 2—30835
machined surface layer by grinding, struct., thermal residual stress, temp. distrib. 2—1284
in magnetoelastic medium, simple wave motion 2—27159
magnetoelasticity, geometrical treatment of propagation 2—27160
material interface, edge dislocation pile ups, stress conc. 2—32637
mechanically nonhomogeneous bodies, strain investigation using photosensitive coatings 2—29346
medium with anisotropic cohesion, failure stress and isotropic internal friction angle 2—141
membrane shells with edge beam supported by wall 2—37675
metal, ductile, critical plane-strain stress intensity factor 2—19208
micropolar continuum, analogy with grid frameworks under initial stress 2—17298
Mohr's circle for curvature and twist of a surface 2—27157
moire grid, thermostable, production and evaluation 2—34011
moire technique, practical improvements 2—27177
monopolar continuum, of grade n, thermodynamics 2—5205
multilayered cylindrical composites, uniaxially loaded, mechanical behaviour 2—33979
multilayered plate, residual stress by strain gauge method 2—30837
non random sedimentary fabrics, modification by strain 2—27149
non-axially symmetric shallow shells, singular solutions under normal surface loading 2—17350
nonlinear continuum, elastic field of screw dislocation dipole 2—22202
nonlinear deformations, direct meas. method 2—25536
notch at apex of infinite wedge, matrix components 2—14200
notch in round beam under cyclic impact bending, kinetics of plastic deformation 2—25498
nozzle-to-flat plate approach for stress concentration problem of nozzle to cylinder intersections 2—15056
nuclear equipment design, use of inelastic analysis 2—14215
nuclear fuel, coated particle, rel. to irradiation obs. 2—15119
nuclear fuel cladding, rupture 2—15826
nuclear fuel cladding tubes, strains due to cracked cylindrical fuel pellets expansion 2—21462
nuclear fuel element cladding, longitudinal distribution 2—14167
nuclear fuel elements, conference (Berlin 1971) 2—15035
nuclear fuels, coated particle, for consumption studies 2—15117
nuclear pressure vessel, prestressed concrete, stress analysis by the finite element method 2—15068
nuclear reactor, boiling water, finite element method for static and dynamic structural behaviour 2—15084
nuclear reactor, bolted core support structure, prediction of stresses and fatigue failure 2—15175
nuclear reactor, coolant gas circuit components, acoustically induced stress 2—15145
nuclear reactor, heat exchanger, tubesheets 2—15141
nuclear reactor, hot box pressure dome and skirt 2—15052
nuclear reactor, pressure tube type, loading due to channel rupture 2—15089
nuclear reactor circular end plate behaviour prediction using triangular thick plate bending elements 2—14190
nuclear reactor circulations pump 2—15036
nuclear reactor concrete pressure vessel, calculation and experimental verification 2—15077
nuclear reactor concrete pressure vessel, in Brazil 2—15074
nuclear reactor concrete pressure vessels, calculation by approximate method 2—15071
nuclear reactor concrete pressure vessels, design concept and analysis of structure with axial ribs 2—15075
nuclear reactor concrete pressure vessels, experimental and theoretical mode of behaviour when pressurized to failure hydraulically and pneumatically 2—15076
nuclear reactor core, pressure tubes type, internal supporting structures, analytical model for static analysis 2—15047
nuclear reactor core components, analysis of external loading stresses 2—15133
nuclear reactor cylindrical pressure vessels, plastic thermal stresses and strain det. 2—15054
nuclear reactor fuel cladding, under combined effect of creep and plasticity 2—21465
nuclear reactor fuel elements, nonuniform surface heat transfer 2—21464

Stress analysis continued
nuclear reactor fuel pins, bending strains in parallel flow induced vibrations 2—15136
nuclear reactor internals response under blowdown accident 2—15107
nuclear reactor pod boiler concrete pressure vessels 2—15073
nuclear reactor pressure vessels, thermal and mechanical stresses 2—15147
nuclear reactor pressure vessels, two-dimensional time-dependent analysis by the finite element method 2—15179
nuclear reactor pressure vessels 2—15146
nuclear reactor vessel, internal supporting flange, structural stresses and deformations 2—15046
nuclear reactors, fast breeder, design analysis for core restraint and support 2—15045
nuclear reactors, nonlinear creep analysis at elevated temps. 2—14184
nuclear reactors, pressure tubes and calandria tubes 2—15143
nuclear reactors, using BERSAFE finite element computer system 2—15083
nuclear steam generator head under internal pressure 2—15144
orthogonal cutting by photoelasto plasticity method 2—126
orthotropic plates, laminated, and shallow shells, finite element computer program 2—2212
parallelepiped, elastic deformation, under its own weight 2—33992
penny-shaped crack, 3-dimensional electrostriction, stress singularity 2—17333
photoelastic pressure vessel models 2—29238
photoelasticity, two- and three-dimensional analysis 2—37681
photothermoelastic analysis of a circular disc having a pair of holes 2—14227
pipe nozzle junctions with curved transitions three dimensional finite-element analysis, application to nuclear reactors 2—15058
pipework systems under creep conditions, stress relaxation 2—14228
plane with circular opening and radial cracks, stress field 2—33995
plastic materials, Prandtl-Reuss, generalized, equation for finite deformation 2—17339
of plastic rotationally symmetric flow zones, displacement velocity det., application to reactor structure 2—14175
plasticity theory 2—17356
plate, deep surface flaw, thickness effect 2_2197
plate, orthotropic, perfect plastic flow eqns., yield criterion 2—20902
plate, variable thickness, with circular hole, bending, moment conc. 2—17304
plate bending, by finite element method using decomposition of differential operator 2—27145
plate bending anal., rectangular finite element based on Hellinger-Reissner's variational principle 2—37683
plates, deflection meas., application to thermal stress problems 2—14161
plates, elastic, thick, in plane state of stress 2—20889
plates, of out of plane deformations by Moire method 2—33986
plates and shells, network method using finite difference eqns. 2—37687
polarimeter attachment, distribution measurement in transparent cubic crystals 2—23696
polycarbonate, glassy, strain limits for linear mechanical and optical behaviour 2—25495
polycrystalline bodies, determination of initial stress by ultrasonic method, theoretical justification 2—33978
polymer, failure surface in principle stress space 2—15815
polymer melts, flow, in entrance region of circular tube, wall normal stresses 2—25006
portable polarimeter, IG-86, using optically sensitive coatings 2—34501
pressure tube nuclear reactor, hot channels, allowable stresses 2—15051
pressurized shell, plastic growth through interaction of steady press. with thermal stresses 2—37723
prismatic shells, computer code for analysis of stress, buckling and vibration 2—20892
prismatic shells, transmission of concentrated forces 2—129
quarter-plane, stress at arbitrary point due to known stresses at edges, conformal mapping 2—2186
radial crack in finite elastic disc, stress intensity factor 2—23334
random loads, response of short cylindrical panels 2—14192
reactor materials finite element matrix displacement method 2—17307
reactor pressure vessels, equivalent energy procedure for fracture prediction 2—24290
reactor pressure vessels, simple finite method for stress concentration problems 2—15059
rectangular bars, elastic and elastoplastic bending, phase transformation effects 2—36125
rectangular plate, stress systems 2—30834
Reissner plate theory, error bound 2—30841
relaxation of stress concentration using supplementary curvature, photoelastic investigation 2—2218
residual stresses in metals, measurement by photoelastic gauges 2—17316
rigid-smooth boundary of quarter-space, dynamic stresses due to incident Rayleigh waves 2—34008
rod structure, statical and temp. loading, optimization, canonical equations solution 2—17303
rosette readings, principal stresses, strains and directions, FORTRAN program calc. 2—27147
rotating shells, perforated, applications to reactor pressure vessels 2—14176
seismology, frictional fault model, relation between apparent stress and stress drop 2—20246
semi-infinite cylindrical shells, pressing-in of sharp punches 2—5183
shear stress difference method for stress distrib. in curvilinear orthogonal system of coordinates 2—20887
shell, long cylindrical, upper critical load rel. to imperfections 2—20890
shell buckling eigenproblem, application of gradient minimization methods and higher order discrete elements 2—2211
shell theory, linear, rapid variation solns., Vlasof's theory generalization 2—33990
shell theory, violation of moment equilib. 2—34034
shell theory derivation based on thermodynamic considerations 2—11324
shell under internal press. 2—34024
shells, finite element analysis, basic computational problems 2—131
shells, hyperbolic paraboloid, obliquely angled, membrane theory 2—11323
shells, nonuniformly heated cylindrical and conical, computer analysis 2—27135
shells, programs BOSOR3 and STAGS, based on finite-difference energy method 2—2209

Stress analysis continued
shells of revolution, application to reactor primary vessels and containment shells 2—14174
short cylindrical shells, Koiter's buckling mode, critical stress determ. 2—27137
simultaneous post buckling at coincident branch points, multiple path generation 2—27163
slender cracked column, fixed ends, deflection, fracture load, stress intensity factor 2—2195
slender notch in uniform tensile field, shear stress distrib. 2—36159
slightly compressible rectangular rubberlike solids, instability under biaxial loadings 2—17295
solid continua, assumed stress hybrid finite element model 2—27133
sphere with surface conditions, axially symmetric problem solved using analytic complex functions 2—5199
spherical shell, loss of stability, external press effects 2—30843
star crack, static stress intensity factor 2—37704
star crack, static stress intensity factor 2—34036
statistical average response of bounded stochastic linearly elastic solid 2—14211
steel, high strength, crack-tip stress intensity rel. to corrosion crack velocity 2—19214
steel, high temp. fatigue crack growth 2—15879
steel, notched, fatigue loading, crack development 2—29325
steel, plastic zones in double cantilever beam specimens 2—19216
stiffness matrix, plate element, appl. of Hermite polynomials 2—17343
strain anisotropy, theoretical and expt'l calc. of effect 2—5185
strain fields, moire analysis 2—14194
strain hardening materials, stress concentrations at circular holes and inclusions 2—17296
strain obs., real-time, optical correlation techniques 2—14193
stress invariants, rel. to plasticity, teaching paper 2—27186
stress wave propagation and fracture in thin curved bars 2—5214
strip, dynamic stress analysis by finite element method 2—27146
strip, infinite row of parallel cracks, plane strain problem 2—17315
structural analysis using NASTRAN computer program 2—2210
structural cable arrays, internally redundant 2—37686
structural design of nuclear reactors, criteria from high temp. material properties 2—15110
structural elements subject to combining axial, shear force, and bending moment, interaction surfaces 2—14163
structural mechanics self correcting incremental approach 2—27136
structures undergoing creep deformations, quasilinearization and solution of nonlinear design problems 2—17297
system buildings, spatial stability against buckling 2—20888
thermal, clad nuclear fuel elements, cylindrical and spherical 2_14225
thermal, clad pellet stacks, interface stress states 2—14224
thermal buckling of square elastic plate exposed to random temperature field, probability of stability 2—37717
thermal stresses, conference, Berkeley, England (Sept. 1969) 2—39753
thermal stresses, quasi-static due to moving heat source in a circular disc closed form solution 2—20904
thermal stresses in a circular cylinder with a rectangular hole under heat generation 2—14226
thermal stresses in beams, limitations of elementary theory 2—23337
thermal stresses in nearly opaque materials exposed to continuous radiation 2—20897
thermal stresses in solid with parallel circular cracks 2—37712
thermal stresses in thin tube with circumferentially travelling heat load 2—37719
thermoelastic, generated in solid transparent dielectrics by focused laser beam 2—27192
thermoviscoelastic axisymmetric, finite element and finite difference computer techniques 2—17348
thick-walled cylinders, plane strain creep behaviour 2—30838
thickness reinforcement around circular hole in flat sheet under radial tension 2—14164
thin circular plate, thermal stresses due to transit temp. 2—37713
thin convex shell of revolution, axisymmetric moment state of stress, stability loss 2—23328
thin cylindrical rod, propagation and dispersion 2—133
thin elastic sheet, normal contact stresses, effect of friction 2—34009
thin elastic shells, first approximation in general linear theory 2—34021
thin elastic shells, post-buckling behaviour 2—30845
thin plates, development of simple shell elements 2—33983
thin rings, deformation produced by pulsed electron beam, numerical predictions 2—34046
thin shallow shell in form of paraboloid of revolution 2—33994
thin shell pressure vessels, finite element methods 2—15157
thin shell structures, curved finite elements analysis 2—15158
thin-walled circular cylindrical shells, first approximation theory, polynomial stress states 2—37674
thin-walled prismatic members, torsional-flexural behaviour 2—5181
thin-walled spherical shell in contact with rigid sphere, deformation and stress distribution 2—33993
toroidal shells, circular and elliptical cross sections, stress and deflexion distrib. 2—27143
transient response of elastic plastic strain rate sensitive shells, influence of finite duration pressure pulse 2—14172
Tresca material, effective plastic strain 2—34040
tubular specimen testing at high temp. under combined action of internal pressure and axial load 2—19225
turbine blade fastenings 2—5180
twisting deformation, transient response of a system 2—34013
two dimensional orthotropic bodies, photoelastic determ. of state of stress and strain 2—5186
two dimensional problems under simultaneous creep and plasticity 2—14186
ultrasonic method of determ. stresses 2—37761
ultrasound surface waves, estimation of elastic and plastic deformations 2—29378
unit composites, displacements, stresses, during impact loading, equilib. differential eqns. 2—34016
vibrating viscoelastic string, effect of stress relaxation 2—27208
vibration of curved bar caused by longitudinal impact 2—23346
viscoelastic cylinder, anisotropic, relaxation of temp. stresses 2—145
viscoelastic solid, moving crack problem 2—25519
waves in impacted frames meas. using strain gauges 2—161
weld seam joints, of reactor pressure vessel, use of fracture mechanism 2—12902

Stress analysis continued
welding, butt, transverse strains 2—3850
welds, temporary stresses during tempering 2—6534
wide sheet, effect of cold bending to circular profile 2—6529
X-ray diffr. determ. method for single crysts. 2—3610
X-ray diffr. line centroid shift due to geometrical factors 2—12706
X-ray diffr. meas., sample-curvature errors 2—22266
X-ray diffraction 2—25299
Al composites, control of thermal expansion coefficients 2—16046
Al sheet, calc. of Young's modulus 2—15860
Al_2O_3, bicryst. tensile specimens, stress distrib. across grain boundary 2—32598
BeO spherical fuel elements in nuclear reactors, three dimensional stresses 2—15130
Cu-In, base alloy, increase in critical resolved shear stress in temp. independent region 2—9766
Cu-In, base alloy, increase in critical resolved shear stress in temp. independent region 2—9766
Cu, stress distribution, residual, hydrostatically extruded rods 2—3883
SiO_2 film local stress meas. method 2—12664

Stress effects
aerospace materials and structure, shock sensitivity 2—9703
alloy, ferro- and antiferromagnetic, atomic ordering, spontaneous magnetization 2—4369
alloy stress and environmental effects in power plant 2—15116
anisotropic creep in fibre reinforced plate in plain stress state 2—37703
β- brass, single crystals, dynamic compressive behaviour, yield stresses 2—3853
α-brass, stress corrosion cracking, strain rate depend. 2—6573
cartilage, tensile properties, effect of strain rate 2—41283
corrosion cracking, mathematical simulation 2—19206
corrosion cracking, transgranular, solution treated and quenched Mg-8.6 Al alloy 2—1309
corrosion cracking rates, steel, in distilled water or NaCl soln. 2—3910
cracks in floating sea ice 2—10701
crazing phenomenon, apparatus to produce crazing, measurement of 2—1314
crystal growth by strain annealing 2—25270
cylindrical cantilever, response to axial air water flow 2—14245
diffusion, of point defect in strain gradient 2—1267
disc in diametral compression, couple stresses, effect on stress distributions 2—17321
dislocation creep, mechanical equations of state 2—3877
dislocation damping force, stress pulse disloc. velocity obs. 2—32509
elastic-plastic strain wave measurements, error bounds 2—30862
e.p.r., strain modulation using sample in composite oscillator 2—7801
F-centres in alkali halides, calc. of stress parameters in point-ion-lattice approx. 2—39713
fatigue crack growth, infrequent compressive cycles 2—25520
fatigue crack initiation, growth single edge notched specimen obs. 2—2202
fatigue crack propagation in reactor components due to acoustically induced stress, fracture mechanics approach 2—15171
Fe-Al(Cr)(Mn)(Ni)(Ti) alloys, stress corrosion cracking mechanism 2—6574
ferromagnetics, effect on mag., elastic magnetoelastic props. and magnetostriction sensitivity const 2—26043
film, strained, deform. of cross-linked domain boundaries 2—29821
film-substrate interface deadherance due to tensile stresses, model 2—29018
fluid saturated porous solid, wave propagation effects 2—22261
glass filaments, type E, stress corrosion cracking mechanism 2—39843
glass static fatigue, crack growth, water reaction 2—36161
graphite, static fatigue behaviour, applied stress rel. to fracture stress 2—32588
Inconel 600 heat exchanger tubing, stress assisted corrosion in high temp. water 2—11909
Inconel X750, intergranular stress corrosion cracking in pressurized water 2—11910
inert gas bubble growth on grain boundary 2—19067
ionic crystals, stress-induced diffusion 2—29173
magnetostrictive materials, sensitivity, theory 2—36718
metal, cause of fractures, tears or breaks 2—22281
metal, crack formation, dependence of trajectory on direction of stress application 2—3901
metal, stress corrosion cracking, capillary model 2—19205
metal, stress corrosion cracking mechanisms 2—32635
microstresses of dualistic composite material 2—15942
nylon, stress ageing, water content influence 2—3937
photoelastic pressure vessel models 2—29238
plastic, allowable amounts as basis for design 2—17344
point defects, diffusion in stress gradient 2—32496
polyethylene, drawn, morphology and molecular motion, n.m.r. obs. 2—15641
polyethylene, long term strengh characts. 2—39811
polymer, chem. equil. 2—4570
polymer fibre, irradiated, straining, crystalline region, radicals, e.p.r. obs. 2—15846
polymethylmethacrylate, crack growth, loading in liquid media 2—29332
polystyrene, isotactic stretched, crystal nucleation 2—22060
polyvinyl chloride, unplasticized, creep susceptibility 2—25511
pressure vessel, fatigue endurance, effect of prior and periodic overstressing 2—9695
quartz, stress corrosion cracking, static fatigue 2—1327
quartz phenolic, laser-induced stress waves 2—15814
quartz-phenolic composite under stress-wave loading in uniaxial strain, dynamic fracture 2—29279
reactor pressure vessels, overstressing technique for securing brittle failure 2—24291
rock from carboniferous strata, mechanical permeability 2—13603
seismology, frictional fault model, relation between apparent stress and stress drop 2—20246
semiconductor, Ge, piezothermoelec. power anisotropy 2—4292
semiconductors, opaque, Raman spectra, hydrostatic pressure effects 2—16539
solution, polyisobutylene in petroleum, rel. to deform. 2—28806
steel, alternating deform., plastic strain mech., substruct. 2—32610
steel, austenitic, stress corrosion cracking, fracture surface, electron microscope obs. 2—19212
steel, austenitic stainless, stress corrosion cracking, alloying effects 2—1325

Stress effects continued
  steel, austenitic stainless, stress corrosion cracking, effect of alloying elements 2—29326
  steel, austenitic stainless, stress corrosion testing for use in boiler plant 2—15115
  steel, corrosion fatigue cracking, stress corrosion cracking, environmental attack, fatigue loading effects 2—19218
  steel, high strength, stress corrosion crack velocity 2—19214
  steel, maraging, stress corrosion cracking, loading mode effects 2—19213
  steel, maraging, stress corrosion cracking 2—15881
  steel, notched, yield stress, tensile strength, area reduction, elongation at rupture 2—12890
  steel, pre-strained, ductility, yield and tensile strength, permanent strain, cracks 2—12854
  steel, stainless, austenitic, stress corrosion cracking, nitriding effects 2—1326
  steel, stainless, corrosion cracking by thermal gradient stresses 2—6575
  steel, stainless stress corrosion cracking resist., comp. effects 2—15882
  steel, stress corrosion crack velocity 2—36169
  steel, stress corrosion cracking in water cooled reactors 2—11908
  steel composites, maraging steel/Armco iron, s.c.c. 2—30069
  strain, statistical theory 2—27132
  stress corrosion cracking and fracture mechanics 2—1320
  stress corrosion cracking rel. to repassivation kinetics, tribo-ellipsometry technique obs. 2—36157
  stress wave propagation and fracture in thin curved bars 2—5214
  structural metals, mathematical model for elevated temperature deformation 2—15827
  styrene methacrylic acid copolymer ionomers, stress relaxation investigation 2—25491
  temperature and mechanical strain cycling, comparison with isothermal fatigue 2—15037
  transient shear stress on flat plate moving at hypersonic speed, exact numerical solution 2—21726
  void growth under applied stress, strain energy effects 2—22187
  wurtzite type crystal, piezospectroscopy of defects 2—33247
  Zircaloy, stress corrosion cracking in iodine vapour 2—15114
  Zircaloy tubing, stress oriented hydride orientation 2—15842
  Ag, strain coeffs. for electron mean free path and free electron density, thin film obs. 2—9954
  Al-Mg, alloy, Portevin-Le-Chatelier effect, rel. to Ag conc. at high temp. 2—25493
  Al-Zn-Mg, alloy, stress corrosion correl. with effect of Ag on precipitation 2—3951
  Al-Zn-Mg, alloy, stress corrosion resist., rel. to tensile props., microstruct., quenching conditions 2—12931
  Al, alloy, creep rupture props. 2—19187
  Al, exoemission and photoemission in ultrahigh vacuum 2—4315
  Al, impact loaded, deform. bands, secondary slip system 2—32621
  Al alloy, interaction with corrosion and fatigue 2—4595
  Al alloys, fatigue crack growth 2—36165
  Be-1%Fe, Mossbauer obs. 32722 2—32722
  Be, temp. depend. of cct. resolved shear stresses for basal and prismatic slip 2—32622
  C-SiC alloy, fracture stress 2—32447
  CaF_2, low temp irrad., F_3^- centre, zero-phonon line 2—19124
  CaF_2, zero-phonon line, F_3 centre 2—19123
  Cd, polycrystalline sample, in presence of adsorbing alloys, dependence of creep velocity on applied stress 2—6552
  CdS_xSe_{1-x}, directional stress effect on birefringence 2—29912
  Co-Ni-Cr alloys, ThO_2, dispersion strengthened, rupture testing, corrosion resist. 2—19266
  CoO crystal, creep, temp. and O_2 press. depend. 2—6553
  Cr-Zr-Nb-C alloy, stress rupture and ductility control by microstruct. modification 2—9692
  γ'-Cu-Al-Ni, alloy, martensitic, elastic twinning 2—15769
  γ'-Cu-Al, alloy, martensitic, elastic twinning 2—15769
  Cu, deform. strain, substruct. misorientation and hardness characts. 2—29334
  Cu alloys, stress corrosion cracking susceptibility, effect of post form. heat treatment 2—36168
  Fe-Cr-Mn-Ni, steel, hot rolled, stress corrosion cracking resist. 2—19248
  Fe, cast, crazing phenomenon testing apparatus 2—1314
  α-Fe, creep rate rel. to dislocation dynamics 2—25408
  Fe, hardness-flow stress-grain-size relationship 2—22289
  Fe, polycrystalline ferromag., remanent condition, domain struct. rel. to elastic deform. 2—19865
  Fe, work hardened by strain rate cyclic changes 2—19244
  Fe thin film, f.c.c.-b.c.c. transform. 2—9803
  GaP, G-value stress depend. corresponding to shallow acceptor band splitting 2—7119
  Ge, heteroepitaxial film on GaAs, orientation, thickness effects 2—3534
  Ge, piezothermoelec. power anisotropy 2—4292
  $Ge_2(MoO_4)_3$, ferroelec. ferroelastic and paraelec.-paraelastic phases, X-ray obs. 2—19052
  $KCl:In^+$, dichroism of u.v. absorp. bands 2—10386
  KCl:Li, paraelec reson., coupling between lattice strain and multiplet tunnelling levels 2—22619
  KCl crystal, dislocation motion, overcoming local obstructions 2—19100
  $KH_2PO_4:Cr^{3+}$, e.p.r., uniaxial stress effects 2—33340
  $KI:Tl^+$, dichroism of u.v. absorp. bands 2—10386
  LiF, acoustic emission, correl. with dislocation kinetics 2—4044
  Mg-(8.6wt.%)Al, transgranular stress corrosion fracture 2—1309
  NaCl, acoustic emission, correl. with dislocation kinetics 2—4044
  Nb single crystal, deformation twinning, pre-strain effects 2—32538
  Ni, film, amorphous, saturation magnetiz. 2—20129
  Ni, film, substrate stress rel. to magnetization 2—4392
  Ni, recrystallisation during hot deform., strain rate torsion tests, torque-twist curves 2—32699
  Ni alloy, superrefractory, creep during high-temp. fatigue rel. to stress 2—29271
  n-Si, hole cond., warm carrier energy relax. time, rel. to uniaxial stress at 90K 2—16242
  p-Si, thermo-e.m.f. under compression 2—4293
  SrF_2, low temp. irrad., F_3^- centre, zero-phonon line 2—19124
  SrF_2, zero-phonon line, F_3 centre 2—19123
  Ti-Al-Sn alloy, stress corrosion cracking, role of hydrogen diffusion 2—19147
  Ti-Al-V, alloy, creep, tensile and torsional loading effects 2—19188
  Ti alloy, resist. to stress corrosion in seawater 2—36174

Stress effects continued
  Ti alloy, s.c.c. arrest and initiation stress intensity correlation 2—1329
  Ti alloys, with metastable α-phase, reverse transform. 2—13000
  U-Mo alloy, corrosion cracking 2—12911
  U-Nb-Zr and U-Nb alloys, stress corrosion cracking, effect of Cl^- 2—29331
  U-5wt.%Nb alloy, γ-quenched, stress corrosion cracking, ageing conditions effects 2—36175
  Zn-Al, alloy, eutectoid, superplastic, extrusion speed and temp. rel. to extrusion stress and mech. props. 2—19255
  Zn, acoustic emission, correl. with dislocation kinetics 2—4044
  Zn, dislocation interactions as function of stress, at 298K and 84K 2—39703
  Zn, electron rad. induced stress relax. 2—25506
  Zn, polycrystalline sample, in presence of adsorbing alloys, dependence of creep velocity on applied stress 2—6552
  ZnO, acousto-electric oscillator, effect of uniaxial stress on modes 2—4058
  ZnO, Raman spectra, hydrostatic pressure effect 2—16574
  ZnO acoustoelectric single crystals, uniaxial pressure effects 2—1429
  ZnS, Raman spectra, hydrostatic pressure effect 2—16574
  ZnTe, stress induced splitting of exciton reflection spectra 2—16477
  Zr-Nb alloy, low cycle fatigue failure rel. to hydrogenation 2—29303
  α-Zr, stress induced diffusion of O, internal friction meas. 2—32567
  α-Zr, stress induced diffusion of O 2—32568
  Zr alloy, fracture in I_2 vapour, 250-510°C, annealing effect 2—6583
Stress measurement *see Strain gauges*
Stress/strain relations
  see also Elastic constants
  alloy, f.c.c., Portevin-Le Chatelier deform. bands 2—12849
  alloy, substitutional, Portevin-Le Chatelier effect, dislocation locking model 2—22263
  annular shear cell, failure plane rotation 2—19278
  artificial graphite, rate-independent continuum theory, experimental verification 2—39779
  β-brass, strain-rate depend. of yield stress 2—29258
  α-brass, stress corrosion cracking, strain rate depend. 2—6573
  composite, fibre reinforced metal matrix, repeated tensile load, fatigue 2—22282
  composite material, dualistic, microstress effects 2—15942
  concrete, under repeated compressive loads, effect of understressing 2—22345
  concrete reactor pressure vessels, prestressed 2—15153
  cracked plate, elastic-plastic analysis 2—14213
  deformations, three-dimensional theory rel. to treatment of moire fringes 2—34012
  elastic-plastic theory, artificial graphite 2—15831
  elastic/viscoplastic hollow sphere, wave propagation 2—27223
  fatigue crack propagation, strain hardening vs stress relaxaton effects 2—15876
  foam plastic, compressive strength, meas. apparatus 2—25542
  fracture mechanics, finite element method 2—23336
  fuel rod bundles, turbulent velocity distrib. and wall shear stress 2—15039
  graphite, deformed at high press. 2—32607
  graphite reactor components, temperature and radiation induced stresses 2—15132
  holography applications, conference (Los Angeles August 1971) 2—14147
  hysteresis, rel. to cumulative damage in low cycle fatigue 2—36146
  incompressible isotropic materials, boundary value problems for large deform. 2—6530
  incompressible rubberlike solids, isothermal strain-energy function 2—29254
  longitudinal strain during heating of plate edge by welding arc, device for obs. 2—22309
  low-cycle strength testing by bending with rotation 2—39856
  material with strong inclusions, primatic punching rel. to work hardening 2—22329
  measurement, dynamic incremental method to large strains 2—19171
  measurement technique 2—25496
  metal, fatigue failure prediction, complicated stress-strain history 2—39817
  metal, f.c.c. and b.c.c. conical flows in metal forming 2—36211
  metal oxide film, dielectric contact layer, Coulomb forces 2—25190
  metallic system, idealized dynamic stress/strain curve of uniaxial compression 2—32594
  metals, rel. to low temp. creep, exhaustion theory 2—39795
  microdynamics and slip initiation in tungsten and other metals 2—3885
  non-hookean materials, Ramberg-Osgood formula for matrix displacement analysis 2—17324
  nuclear fuel, coated particle, rel. to irradiation obs. 2—15119
  nuclear reactor, heat exchanger tubesheets, plastic strain analysis 2—15141
  nuclear reactors, rapidly heated fuel rods, viscous damping 2—15105
  optical correlation techniques, holography and image-image methods 2—14193
  planar bending of semi-infinite beam resting on a linear elastic support, derivation of exact solution 2—34026
  polycrystalline metal, anisotropic effect on deformation 2—36102
  polyethylene, high density, after cold rolling 2—39792
  polymer, glassy amorphous, yielding behaviour 2—3872
  polymer, isotropic, plastic flow 2—19185
  polymers, oriented, yield behaviour 2—6540
  quasistatic deform. of solids with press. 2—39773
  ring shaped specimens, program loading 2—25546
  sealing materials, laboratory testing device 2—22313
  serrated yielding, vacancy annihilation 2—32503
  steel, after strain ageing 2—22330
  steel, discontinuous twinning during essentially elastic compression, 4.2 K 2—39787
  steel, low C, yield point effect elimination by cyclic straining 2—1285
  steel, rel. to dynamic softening during plastic deformation 2—36116
  steel, soft polycrystalline, temp., deformation rate and grain dia. depend. 2—12856
  steel, stainless, type 304, multiaxial plastic relations 2—15823
  structural geology, strain ellipsoids and strain-charts of similar folds 2—7226
  superconductor, electron-dislocation interaction 2—13164
  temperature-time relationship, characterization in metals and alloys 2—15817
  tensile tests, determ. of stress- strain flow curve 2—36189
  thermal fatigue under multiaxial thermal stresses 2—39820

Stress/strain relations continued
ultimate tensile stress, structure sensitivity 2—25492
viscoplasticity, non-associated constitutive law 2—27183
welded beams, residual welding stresses and plastic contraction 2—6532
welding, effect of metal thickness on nature of stressed and strained states 2—19249
wide sheet, effect of cold bending to circular profile 2—6529
zircaloy-2, cold worked, 300-450°C, creep accel. mechanism 2—25510
Ag-O alloy, temp. and strain rate depend. of yield 2—32604
Ag alloy, tensile tests on different welded joints, MIG and TIG welding 2—3943
Al-Ga alloy, work hardening curves, Porteven-le Chatelier effect 2—32702
Al-Mg-Si alloy, inverse Portevin-Le Chatelier effect 2—32595
Al-Mg, alloy, Portevin-Le-Chatelier effect, rel. to Ag conc. at high temp. 2—25493
Al-Mg alloy, Portevin-LeChatelier effect, grain size influence 2—39774
Al-0.12-1.86 at.%Mg, alloy, single cryst., Portevin-Le Chatelier effect, influence of strain rate, modified Cottrell theory 2—6535
Al, under compressive loading, dependence on strain rate 2—29230
Al alloy, complicated stress-strain history, fatigue failure 2—39817
AlMg alloy, work hardening, Portevin Le Chatelier effect, vacancies 2—15818
Au-(14 at.%)Cu alloy, Portevin-Le Chatelier effect 2—22265
Au-Cu alloy, Portevin-Le Chatelier deform. bands 2—12849
BeO spherical fuel elements in nuclear reactors, three dimensional stresses 2_15130
C fibre, polyacrylonitrile-based, non-Hookean behaviour 2—3852
Cu-Al-Fe alloy, superplastic, high temp. tensile testing 2—15832
Cu-Co, work hardened, single crystals containing coherent precipitates, curves 2—3936
Cu-(1wt.%)Si, slip initiation and microstrain behaviour rel. to dislocation struct., single cryst. 2—3885
Cu, annealed, dynamic compressive test 2—39876
Cu, pressurized, effect of oxygen content 2—12851
Cu, sintered, stress-strain curve rel. to degree of deform. 2—19172
Cu, slip initiation and microstrain behaviour rel. to dislocation struct., single cryst. 2—3885
Cu, under compressive loading, dependence on strain rate 2—29230
Cu crystal, fatigue cracks 2—3908
Fe-(1.1 at%)Nb alloy, substitutional strain ageing, serrated flow6536 2—6536
Fe-Si alloy, rel. to edge and screw dislocation mobility, h.v. elec. microscope obs. 2—25407
Fe-(3 wt.%)Si alloy single crystals, stress-strain curves 2—22271
α-Fe, grain size dependence, dislocation model 2—3854
Fe, shear stress-shear strain curve 2—39696
Fe, sintered, stress-strain rel. to degree of deform. 2—19172
Fe crystal, tension deformation, elastic limit, yield stress 2—15835
LiF:Mg, Portevin-Le Chatelier effect, rel. to crit. resolved shear stress 2—32705
Mg-Ag alloy, plastically deformed, serrated yielding 2—29260
Nb Hall Petch parameters, extrapolation methods 2—15820
Ni-Cu, Ni-Cu-C alloys, at temperatures between 78 and 523 K 2—1278
Pb, etch pit disloc. density rel. to critical resolved shear stress 2—6549
α-Pu, extruded, elongation rel. to grain size 2—6550
Sn whiskers, deviation from linearity 2—19163
Ta, $\langle 100 \rangle$ and $\langle 110 \rangle$ single crysts., prestrain effects on micro- and macro-yielding 2—25496
Ti, curves, Pontevin-Le-Chatelier effect, rel. to dynamic strain ageing, 77-1026K 2—25581
α-Ti, dislocation dynamics, activation enthalpy 2—22211
TiH_x, yield and fracture stress, strain-rate depend. 2—19183
α-U, stress relaxation, apparent activation enthalpy 2—25494
W and other metals, slip initiation and microdynamics 2—3885
Zn, under compressive loading, dependence on strain rate 2—29230
α-Zr, aged, containing, O_2, Fe impurities, tensile stress-strain curve, yield point 2—12786

Stresses, internal
alkali feldspar, exsolution, elastic stresses, perioidic twins, electron microscopy 2—25414
alkali halides, deformed by ultrasound, elec. field effect 2—6537
alloy, f.c.c. cold worked, integral breadth, analysis X-ray line profile 2—22332
alloy, nimonic-type, aged, elastically strained by precipitates, X-ray diffr. intensity distrib. 2—15928
alloy crystal with dispersed precipitate, critical resolved shear stress 2—3861
alloys, short-term stress relaxation creep strain measurement 2—29360
anisotropic cubic cryst., mixed dislocation interaction with point defect stress fields 2—36024
anisotropic media, calc. using Green's function derivatives 2—22267
ceramic, phases with different coeffs. of expansion, thermal stresses 2—39775
ceramic composite, porous and filled, finite element analysis 2—32597
composite, C/PMMA, laser heating and stress generation 2—36103
composite, fibrous, stress conc. factors near discontinuity 2—19173
compounded rotating discs 2—7743
cracked transparent plate, stress intensity factor determ. method by projection into screen 2—17332
crystal dislocation, force acting upon 2—25395
crystal microstresses, distortions and block size determinations from shape of X-ray diffraction lines 2—29112
disc under diametral compression, effects of couple stresses 2—17321
dislocation strain distrib. function 2—12767
dynamic, in circular annulus of nonisotropic elastic material 2—34058
elastometric materials, meas. using radioactive implants 2—19226
electrodeposit, measurement method 2—3882
electrolytic coating, meas. using modified ribbon cathode device 2—39859
elliptic hole in cylindrical shell 2—27131
fatigue-cracked thin sheets, stress intensity factor determ. methods 2—9702
ferroelectric, displacive type, phenomenological theory 2—29751
ferroelectric ceramic, coarse grained, rel. to anomalous dielectric behaviour 2—16280
ferromagnet, approach to saturation, internal strain effect 2—1623
ferromagnet, polyaxial, domain dispersion 2—26028
ferromagnetic film, effect on perpendicular anisotropy 2—6982
ferromagnetics, obs. by mag. techniques 2—36023
film, dislocation stresses due to periodic distrib. 2—12763
film, grain growth and stress relief 2—39480

Stresses, internal continued
film, meas. using quartz resonators 2—35878
foil, strains due to nonuniform impurity distrib., theory 2—35877
fuel particles, coated, use of mathematical model 2—21472
garnet epitaxial film, misfit stress, influence on fracture 2—32350
glass-crystal composite, transition temp., dilation obs. 2—6629
grain boundary dislocation and deform. by cryst. glide dislocations 2—25390
graphite, relax. rel. to model for dimens. changes under neutron irrad. 2—12747
graphite, role in high press. deform. and recovery 2—32607
heterogeneous materials, bending moment meas. 2—12840
inclusions, elastic interaction with nearby dislocation 2—15756
infinite wedge-shaped lamina loaded at edges, conformal mapping 2—2187
intensity factors for Griffith crack, asymmetrical distrib. of body forces 2—3903
isotropic continuum, stresses produced by continuous distribution of moving dislocations 2—19097
in large elastic plate fixed at one free and subject to shearing force on alter 2—17310
laser materials, thermal stresses rel. to inclusions 2—23607
lattice strain in shocked stressed metals by impact test 2—19191
linear defects in sub-boundaries 2—3776
long hollow cylindrically aeolotropic cylinder with ends subjected to surface forces 2—30835
magnetic ordering, coexistence region, stress broadened 1st order transformation 2—10233
magnetic oxide heteroepitaxial film, model 2—22069
material with strong inclusions, primatic punching rel. to work hardening 2—22329
measuring device, for films 2—39508
metal, b.c.c., microstrain and dislocation relax. 2—12826
metal fibre, porous, pressing and sintering, deformation, residual stress relaxation 2—29257
metal microvolume decohesion, variable stress, dislocation density 2—36026
metal oxide, dielec. contact layer, stress/strain distrib. 2—25190
noble metal, H interstitial diffusion, lattice relaxation 2—9613
nuclear fuel rod bundles, due to temp. gradients 2—15120
nuclear fuels, coated particle, bonding and compact, irradiation behaviour 2—15118
perfect non-Bravais cryst., thermodynamics of internal strains 2—9883
Permalloy film, vacuum-deposited, struct. mechanism of stress form. 2—39516
polycrystal, distorted, with generalized strain distrib., apparent particle size and strain 2—22199
polyethylene melts, high density, molec. weight distribution effects 2—21929
polyvinyl chloride, oriented sheet, yielding behaviour 2—15847
quarter-plane, stress at arbitrary point due to known stresses at edges, conformal mapping 2—2186
rare earth metals, h.c.p., deform. struct. obs. from X-ray line broadening 2—3772
rectangular plate, stress systems 2—30834
residual stresses in metals, measurement by photoelastic gauges 2—17316
steel, borated, fatigue strength, residual stresses 2—39808
steel, brittle fracture initiation in residual stress field 2—25522
steel, Cr-Mn-Ni type, remanent strain under tensile load 2—36128
steel, cyclic heating effects 2—25516
steel, effect on fatigue limit 2—36149
steel, embrittlement by H_2, obs. 2—29318
steel, low temp. anomalies 2—36129
steel, on surface machining rel. to alternating fatigue strength 2—29301
steel, plastically deformed, with and without applied u.s. field 2—36117
steel, quenched, low-temp. tempered, martensite decomp. compressive stresses relax. 2—15899
steel, structural, relaxation after welding, heat treatment and residual stress 2—12944
steel, surface layer, machined, with built-up edge, plastic flow 2—29001
steel cores, glass coatings for strain sensitivity reduction in steel cores 2—39925
steel residual stress distrib., surface layer, effect of thermomech. strengthening 2—39776
thermal, in cylindrical body of finite height subject to convective heat losses 2—33998
thermal, in micropolar hollow cylinder 2—5206
due to thermal expansion, single phase ceramics and oxide single crystals 2—15821
thermoelastic, in thin semiinfinite plate due to time dependent temp. applied at point on its boundary 2—17349
two phase material, circular prismatic disloc. loop, elastic fields detn. 2—25393
as result of welding, calculation of 2—22219
welding, effect of metal thickness on nature of stressed and strained states 2—19249
X-ray diffr. determ. method for single crysts. 2—3610
X-ray diffr. meas., sample-curvature errors 2—22266
YAG active crystal elements, thermal stresses under continuous pumping 2—17621
Zircalloy-2, cold-rolled, X-ray and electron microscope obs. 2—29185
Al_2O_3, bicryst. tensile specimens, stress distrib. across grain boundary 2—32598
Al_2O_3, quenched, residual stress computation 2—36107
Bi, critical resolved shear stresses, slip planes, compression tests 2—32530
CaF_2:Eu, zero phonon line, strain broadening rel. to lattice imperfections 2—4456
CaO, e.p.r. of Ni^{2+} obs. 2—7116
Co, epitaxial, anomalously high elastic strains 2—32361
Co film, meas. device 2—39508
Cu/α-brass diffusion couple, stress due to vacancies, superposition with thermal stress 2—39739
Fe-Ni, film, electrodeposited on cylindrical substrate, disloc. theory 2—40506
Fe-Ni film, electrodeposited cylindrical, internal macrostresses 2—35889
Fe-Ni film, electrodeposited cylindrical internal macrostresses 2—35890
Fe-Ni film, electrodeposited, rel. to perpendicular anisotropy 2—36723
Fe-Ni martensite, transform. induced substructs., X-ray and elec. microscope obs. 2—22358
Fe, Armco, cyclic bending deformation, absorptional fatigue 2—29300
Fe, plastic zone around fatigue cracks 2—39782

Stresses, internal continued
Fe alloys, low temp. anomalies 2—36129
Fe alloys, rel. to mag. props. 2—26044
Fe film, electrodeposited, effect of S-containing cpds. 2—19895
Fe film, electrodeposited, effect of fine cryst. struct. 2—19894
Fe film, meas. device 2—39508
epitaxial GaAs, X-ray topographical measurement techniques 2—32364
KBr, elec. field gradient around point defects, continuum elasticity calc. 2—25385
KI, elec. field gradient around point defects, continuum elasticity calc. 2—25385
Mo, rel. to grain size depend. of elastic limit 2—12860
NaCl, due to dislocation motion 2—39700
NaCl, rel. to plastic deform. and strain hardening mechanisms 2—39789
Ni:ThO_2, rapid quenching effects, internal stresses, rel. to mech. props. 2—32599
Ni, magnetomech. damping, plastic deform. effect 2—19890
Ni alloy, on surface machining rel. to alternating fatigue strength 2—29301
Ni film, meas. device 2—39508
Ni film, vacuum-deposited, struct. mechanism of stress form. 2—39516
Ni powder compacts, verification of existence of oriented microstresses by X-ray examination 2—39960
Si, ion implantation damage, obs. 2—25379
Si epitaxial slices, plastic deform. in central regions 2—12865
Si ion implanted, internal and flexural resonance obs. 2—19166
SiO_2, SiO_xN_y evaporated films 2—8021
SiO_2 film local stress meas. method 2—12664
Ti-Pd-Au film, ageing effects 2—39534
TiO_2 evaporated film 2—8021
U-Nb-Zr alloy, stress generation during oxidation 2—10627
UO_2, deform. in compression, slip planes, shear stresses, dislocation structs. 2—32527
WO_3, non-stoichiometry, colour, micro-strain, Schottky defects, X-ray exam. 2—25246
YIG, epitaxial strains and fracture in Ga- substituted films 2—35897
YIG epitaxial film, verification of stress model 2—22069
Zr-Cr alloy, lattice strain, comp. depend. 2—22291

Striations *see Discharges, electric*

Stripping reactions
deuteron, calculations based on soluble two-channel model 2—38635
deuteron stripping on doubly even nuclei, theory using method of quantum Green functions 2—2799
deuteron-nucleus interaction, coupled eqns. 2—2797
heavy-ion reactions, predominance of proton stripping over proton pickup statistical theory 2—28082
isospin centroid energy calc. 2—34903
Mitra's three body model reexamination, formulation of a DWBA 2—2798
one nucleon reactions to unbound nuclear states 2—15001
singlet deuteron and trinucleon induced, normalization factor for zero and finite range DWBA calc. 2—15004
soft-pion theorems rel. to direct processes 2—24199
(d,p), to resonance state, peripheral model description, cross section calc. 2—21443
(d,p) Coulomb stripping reaction, cross-section and proton polarization 2—5708
(^{3}He,t) reactions, pickup-stripping mechanism 2—21442
(t,p) on deformed nuclei, finite range effects studied, cross-section determ. 2—11859
α-particle, structure factor for light nuclei 2—31575
d-, structure factor for light nuclei 2—31575
^{27}Al(α,t), 104 MeV, differential cross sections and normalization factors 2—21441
^{38}Ar(d,p)^{39}Ar, 10.064 MeV, determ. of level structure of ^{39}Ar, orbital angular momentum transfer to target nucleus 2—34934
^{9}Be(p,d_0)^{8}Be, BHMM theory of stripping reactions 2—31540
^{12}C(α,^{3}He), (α,t), 104 MeV, differential cross sections and normalization factors 2—21441
^{12}C(d,n)^{13}N* (p)^{12}C, sequential reaction, mechanism and symmetry axes determ. 2 28081
^{12}C(d,p) ^{13}C*, 2.6 and 2.8 MeV, importance of two-step processes determ. from identification of resonances 2—38558
^{40}Ca(α,^{3}He), (α,t), 104 MeV, differential cross sections and normalization factors 2—21441
^{40}Ca(d,n), neutron polarization meas., comparison with DWBA calc. 2—38614
^{24}Mg, deuteron stripping, coupled channel Born approx. description 2—15011
^{24}Mg(d,n), neutron polarization meas., comparison with DWBA calc. 2—38614
^{26}Mg(d,p)^{27}Mg, 2.0 to 3.0 MeV, angular distributions and excitation functions 2—35072
^{15}N (^{3}He,p) ^{17}O, 18 MeV, study of 2p-1h structure of ^{17}O 2—24150
^{15}N(d,p), leading to unbound states of ^{16}N, interference between resonant and continuum states 2—8361
^{58}Ni(d,p)^{59}Ni, Coulomb stripping, energy levels of residual nucleus 2—31584
^{62}Ni(d,p)^{63}Ni, Coulomb stripping, energy levels of residual nucleus 2—31584
^{64}Ni(d,p)^{65}Ni, Coulomb stripping, energy levels of residual nucleus 2—31584
^{28}Si(d,n), neutron polarization meas., comparison with DWBA calc. 2—38614
^{124}Sn(d,p)^{125}Sn, sub Coulomb stripping 2—18237
^{89}Y(d,n)^{90}Zr, Coulomb effects 2—28078
^{176}Yb, deuteron stripping, coupled channel Born approx. description 2—15011

Stroboscopes
basic principles, design criteria, technical features, accessories and applications 2—2455
with electronic shutter, for obs. of spectral dependence of luminescence kinetics 2—17722
holographic, based on ruby laser with passive shutter 2—17651
use in manometer, centrifugal, for meas. pressure differentials in rotating reference frame 2—37566
spectrometer, ultra-high speed, using image converter camera as signal sampling system 2—27653

Strong interactions *see Elementary particles/interactions, strong; Field theory, quantum/interactions, strong*

Strontium
atom, electron impact excited resonance transitions, minima in generalized oscillator strengths 2—5816
atom, electron impact ionization, cross section meas. from threshold to 200 eV 2—5819
atom, inelastic collisions with slow electrons, investigation of ionization and excitation using crossed beam technique 2—5818
atom, oscillator strengths and singlet triplet splittings, core polarization corrections 2—31662
clouds, artifical, resonance scattering of sunlight 2—30319
ionization constants for NO-acetylene flames 2—22897
mean residence times and atomic desorption as fn. of O_2 surface coverage 2—35904
oxidation studied by u.v. photoelectron spectroscopy 2—26349
shock melting and vaporization 2—39420
BaF_2:Sr, X-irrad., optical absorp., F_{ae} centres 2—33256
CaF_2:Sr, X-irrad., optical absorp., F_{ae} centres 2—33256
KCl:Ca, Sr, Ba, thermal electric alignment and Stark effect of Z_1-centres 2—20040
Sr III resonance-line spectrum in the vacuum u.v. 2—18312
Sr^+, optically pumped, spin depolarization in collisions with inert gas atoms 2—5846
Sr^{2+}, diffusion in MgO, short circuit mechanisms 2—3823
Sr^{2+} in KCl, Z_1-band resolution, numerical analysis method 2—3805
SrII lines at λ4077 and λ4215, means of classification of BaII stars 2—4847
^{85}Sr lung scan, diagnosis of pulmonary ossification 2—26954
^{85}Sr self-diffusion in water solutions 2—32253
$^{87}Sr^m$, scanning, optimum injection interval for spinal scans 2—2024
^{90}Sr, aerosol samples, ground level radioactivity 2—30305
^{90}Sr, radioactive fallout in atmospheric dust and rain during 1971, effect of Chinese and French nuclear tests 2—40973

Strontium compounds
borates, compounds and glasses, e.s.r. of Mn^{2+} 2—16648
dicalcium propionate, mol. motion p.m.r. obs. 2—10574
formate dihydrate, cryst. struct. 2—9514
SrO-Ir(Cr)O_2 system, high press. synthesis of $(ABX_3)(AX)_n$ compounds 2—18967
$SrWO_4$, flux growth forms 2—1212
(Ba,Sr)Si_2O_5:Eu^{2+} phosphor for fluorescent lamps 2—11524
BaF_2-SrF_2 system, liquidus and solidus, DTA, X-ray diffr. 2—1407
$Ba_xSr_{1-x}Nb_2O_6$, pyroelec. voltage response to rectangular i.r. signals 2—33064
$Ba_xSr_{1-x}Nb_2O_6$ solid solution cryst. growth, stability regions 2_25271
$CaSrGe_2O_6$ host lattice, luminescence of phosphors 2—4503
$Ca_xSr_{1-x}O$ solid solns., exposure to Ba vapour influence on elec. props. 2--6915
CdF_2-SrF_2, crystalline miscibility, X-ray obs. 2—22338
$1.8Cr_2O_3{\cdot}0.5SrO{\cdot}4.2Fe_2O_3$, paraprocess anisotropy at Curie pt., h.f. mag. field 2—6946
$KMnF_3$, phase transformations of displacement type, X-ray investigation thermodynamic description 2—1398
K,O-SrO-Nb_2O_5 system, ferroelec. characterization 2—40352
Sr-Cu, system, thermal and differential thermal analysis, phase diagram 2—3955
(Sr, Ba)TiO_3 ceramic with boundary layer struct. for h.f. applic. 2—40346
$SrAlF_5$, cryst. struct. 2—9452
$SrAl_2Si_2O_8$, metastable feldspar, displacive transformations, DTA obs. 2—22356
$Sr_2B_5O_9Cl(Br)$, crystal structure, preparation 2—9451
$SrBaGe_2O_6$ host lattice, luminescence of phosphors 2—4503
$Sr_{0.75}Ba_{0.25}Nb_2O_6$ temp. dependence of dielectric props., use for light modulation 2—4268
$Sr_{1-x}Ba_xNb_2O_6$, grown in Pt crucible, epitaxial Pt particle contamination 2—39579
$Sr_xBa_{1-x}Nb_2O_6$ ferroelec., spont. polariz. and coercive field, hysteresis obs. 2—33061
$SrCl_2$:Yb^{3+}, cryst. field levels, mag. susceptibility and optical absorpt. obs. 2—36888
SrCl and SrOH, dissociation energies and heats of reactions, spectrophotometric det. 2—12197
$SrCl_2$, alkali metal doped, colour centres obs. 2—3800
$SrCl_2$, Cl^- $L_{2,3}$ absorpt. spectra regularities 2—20032
$SrCl_2$, F-centres, e.s.r. and optical absorp. obs 2—33336
$SrCl_2$, $L_{2,3}$ absorpt. edge of Cl^- 2—33293
$SrCl_2$, spectrophotometric det. of molecular dissociation energies 2—38942
$SrCl_2$, vibronic spectra and electron-phonon coupling field 2—40026
$SrCl_2$ powder, X-ray struct. factors, Debye-Waller coeffs., unit cell consts., at 80 and 300 K 2—32473
$Sr(ClO_3)_2$, n.q.r., temp. depend. of freq. 2—8585
$Sr(ClO_3)_2$, n.q.r. of ^{35}Cl, and r.f. absorpt., 77-300K 2—40792
$SrCr_2S_4$ ferrimag. semicond., defects, electron microscope obs. 2—32507
SrF_2:Ca, Ba, X-irrad., optical absorp., F_{ae} centres 2—33256
SrF_2:Eu^{2+}, ENDOR meas. of hyperfine and transferred hyperfine interaction 2—40756
SrF_2:Eu^{2+}, ENDOR obs. of hyperfine interactions 2—30030
SrF_2:Eu^{2+}, temp. depend. of zero field splitting 2—19940
SrF_2:U^{3+}, ENDOR spectra of U^{3+}-F^- system, superhyperfine interaction constants 2—4565
SrF_2, anharmonicity, temp. and press. depend. 2—13022
SrF_2, channelling, MeV protons and He^+ ions 2—3754
SrF_2, critical point analysis of second- order Raman spectra 2—40691
SrF_2, far-u.v. reflectivity spectra, electronic struct. 2—13457
SrF , fluorescence and absorpt. spectra, F_3 centre, zero-phonon line 2—19122
SrF_2, hydrogenated, deuterated, containing Pr, i.r. local mode spectra vibronic splittings 2—10368
SrF_2, containing ion pairs of Gd, Ce, Pr with H, D, T, electron-phonon interactions, spectra 2—10499
SrF_2, ionic distortions of Tm^{2+} trigonal centres 2—40589
SrF_2, low temp. irrad., F_3^- centre, zero-phonon lines 2—19124
SrF_2, neutron diffr. data analysis in terms of thermal vibs. of atoms 2—4043
SrF_2, photoelastic consts. 2—29870
SrF_2, piezobirefr. coeff., energy band deform. pot. 2—26167
SrF_2, piezobirefringence in vac. u.v. 2—16470
SrF_2, pure and doped, thermoluminescence 2—4514
SrF_2, stress-induced g-shifts of Nd^{3+} and U^{3+}, freq. independ. 2—10524
SrF_2, zero-phonon line, F_3 centre, quadratic Stark effect 2—19123

Strontium compounds continued
SrF_2 crystal phosphors, exciton and electron-hole processes 2—26214
$SrFe_xMn_{1-x}O_{3-y}$, lattice parameters, oxygen deficiency determ., Fe valence states 2—9492
$SrFe_{12}O_{19}$, determination of complete temp. dependence of hyperfine fields at five Fe sites 2—22733
$Sr_4Fe_6O_{13}$, cryst. struct., Mossbauer effect and mag. props. 2—39652
$Sr_3Ge_3O_9$, vibr. spectrum interpretation 2—36908
$Sr_3Ge_3O_9$ and $Sr_3Si_{3-x}Ge_xO_9$, vibr. spectra, interpretation 2—36907
$Sr(IO_3)_2.H_2O$, cryst. struct. 2—35998
Sr_2IrH_5, crystal structure, prep. 2—3703
$SrIrO_3$ structure, properties, high and low pressure forms, phase transformations 2—3731
$SrMoO_4$:Er^{3+}, mag. props. and sp. ht., calc. from cryst. field parameters 2—40421
$SrMoO_4$:Gd^{3+}, e.p.r., tetragonal active centre obs. 2—10523
$SrMoO_4$, thermal expansion 2—9897
$Sr(NO_3)_2$, anharmonicity 2—19354
$Sr(NO_3)_2$, elastic and dynamic props. 2—32574
$Sr(NO_3)_2$, first and zero sound 2—19411
$Sr_2Ni_xAl_{1-x}SbO_6$, solid solns., mag. props. of Ni^{3+} 2—13378
$Sr^{2+}Ni_{2-y}Co_yFe_{16}O_{27}$, hexiferrite, mag. anisotropy energy, 75-750 K 2—36740
SrO:$^{55}Mn^{2+}$, e.p.r. and ENDOR obs., hyperfine struct. 2—26287
SrO-Gd_2O_3 system, phase diagram, high temp. DTA study 2—29472
SrO-SiO_2 glass, γ-irrad., e.p.r. and absorpt. spectra 2—30015
SrO-TeO_2-V_2O_5, glass system, formation and properties 2—12631
SrO-ThO_2 system, refractory, charact. using specially designed furnace 2—30719
SrO, elastic consts. and their press. derivatives, u.s. determ. 2—36093
SrO, elec. cond., thermal e.m.f. and thermionic emission 2—29659
SrO, evaporation of components during emission current take-off 2—33085
SrO, phonon dispersion curves 2—19350
SrO, positron lifetime correlations 2—4150
SrO, prod. by action of N_2O or NO_2 on metal crossed beam chemiluminescence studies 2—10457
SrO, transport number exam., rel. to oxygen pressure, low oxygen potential, 900 to 1180°C 2—4274
SrO powder, far-i.r. surface-activated band-mode absorpt. 2—7074
$Sr(OH)_2$, $Sr(OD)_2$, lattice vibration spectra, normal coordinate analysis of i.r. absorption spectra 2—40037
SrOHCl, spectrophotometric det. of molecular dissociation energies 2—38942
$SrO(S)$:Eu^{2+} dil. solid solns., e.p.r. linewidths 2—7118
$SrO.BaO.Nb_2O_5$ peak voltage of pyroelec. response to short i.r. laser pulses 2—19774
$SrO.4.1Fe_2O_3.1.9$ Al_2O_3, reversal processes in hysteresis loops of single particle domains 2—33128
$SrO.(6-x)Fe_2O_3.xAl_2O_3$, cryst. growth and bubble domain props. 2—22103
$Sr_2P_2O_7$:Eu^{2+} phosphor for photocopying lamps 2—11524
$Sr_{10}(PO_4)_6(OH)_2$, hydrothermally prepared, vibr. spectra 2—16527
$SrPbO_3$ structure, unit cell, space group, from powder diffraction data 2—3732
Sr_2RhH_5, crystal structure, prep. 2—3703
Sr_2RuH_6, crystal structure, prep. 2—3703
SrS:Zr, SrS:Cu, SrS:Cu, Zr phosphors, luminescence, effect of activator conc. variation 2—36934
SrS, charged evaluated by Wolfsberg-Helmholtz-crystal field semi-empirical method 2—29077
SrS, dynamic ionic charge determ. from i.r. spectra and static dielec. props. 2—22396
SrS(Cu) phosphors, spectral distrib. of luminescent emission, excitation spectra, decay and thermoluminescence 2—33310
$SrSO_4$, dislocation distrib. around indentation 2—3782
$SrSO_4$, single crystal growth by flux evaporation method, effect of cooling rate on morphology 2—3571
$SrSb_2O_6$, i.r. absorpt. spectra, cryst. chem. 2—26161
$SrSiO_3$-Nd_2SiO_5 amorphous system, apatite phase, i.r. spectra, comp. depend. 2—18894
$Sr_3Si_3O_9$ and $Sr_3Si_{3-x}Ge_xO_9$, vibr. spectra, interpretation 2—36907
Sr_2SiS_4:$Eu^{2+}(Ce^{3+})$, cathodoluminescence 2—10451
$SrThV_2O_8$, thermal expansion, rel. to cryst. chemistry 2—22430
$SrTiO_3$:Cr^{3+}, domain struct. effect on fluoresc. 2—4494
$SrTiO_3$:Mn, e.p.r., effect of annealing treatment 2—36992
$SrTiO_3$:Nb, free carrier optical absorpt. 2—36887
$SrTiO_3$-In barrier, tunnelling, rel. to polaron transitions 2—4139
$SrTiO_{3-x}$ and $Ca_ySr_{1-y}TiO_{3-x}$, soft mode supercond. 2—19598
$SrTiO_3$, band struct., from diffuse refl. spectra 2—1526
$SrTiO_3$, band structure determ. from X-ray photoelectron spectra 2—33092
$SrTiO_3$, critical behaviour near 105K 2—15974
$SrTiO_3$, cubic-tetragonal phase transition, soft modes, Raman scatt. obs. 2—16569
$SrTiO_3$, differential second order Raman spectroscopy 2—16568
$SrTiO_3$, displacive transition, u.s. vel., stress effects and interaction parameters 2—32780
$SrTiO_3$, displacive type transition, phonon freqs. 2—19305
$SrTiO_3$, e.p.r., Fe^{3+}-vacancy centre analysis 2—40766
$SrTiO_3$, energy storage capabilities 2—33049
$SrTiO_3$, fluctuations and correlations for $T \geqslant T_c$ 2—26266
$SrTiO_3$, force consts., temp. depend 2—16003
$SrTiO_3$, low temp. heat capacity 2—19427
$SrTiO_3$, paraelectric state, field-induced switching of tetragonal domains 2—19755
$SrTiO_3$, permittivity from zero to optic freqs. 2—40359
$SrTiO_3$, phase transitions, critical dynamics for $T \geqslant T_c$ 2—25932
$SrTiO_3$, top-seeded soln. growth 2—12696
$SrTiO_3$, u.s. attenuation and vel., temp. depend., 105 K transition, phonon modes 2—9879
$SrTiO_3$, u.s. props., anisotropy of phase transition 2—16022
$SrTiO_3$, wavelength-modulated absorption, reinterpretation not involving coexisting phases 2—20048
$SrTiO_3$ glass-ceramics, device applics. 2—40358
$SrTiO_3$ single crystals, Cr doped, e.s.r. of Cr^{5+} 2—20138
$SrVO_3$ structure, magnetic and electrical props. 2—3740
β $Sr_2V_2O_7$, cryst. struct. and refinement 2—19059
$SrWO_4$, e.p.r., radiative paramag. defects 2—13534
$SrWO_4$, elec. field induced g-shifts and hyperfine shifts for rare earth ions 2—36984

Strontium compounds continued
$Sr_3(XO_4)_2$, X=P, As, V, Cr, Mn, i.r. and Raman vibr. spectra, interpretation based on crystal structure 2—8586
$SrZrO_3$, band struct., from diffuse refl. spectra 2—1526

Structure factors *see Crystal structure, atomic; X-ray crystallography*

Structure of matter *see Crystal structure; Liquids/structure; Solids/structure*

SU(3) group theory *see SU(n) theory*

SU(n) theory
asymptotic SU(3) symmetry, boson nonet couplings and 9th pseudoscalar meson 2—363
broken *SU*(3) symmetry, composite model based on nonlinear realization of group 2—38248
broken SU(3)⊗SU(3) appl. to low energy πK scatt. 2—14650
C violating weak interaction, investigation in SU(3)′×SU(3)″ scheme of three-triplet model 2—38209
chain $U_n \supset R_m$, basis for irreducible representations of U_n 2—14530
chiral SW_3 model, generalization 2—21214
compact groups, applied problems of reduction 2—14069
hadron interactions, multiperipheral bootstrap model with SU(3) multiplets 2—21258
interactions, broken chiral SU(3)×SU(3) symmetry model, equivalence with tadpole model 2—2505
irreducible representation, SU(n-2)×SU(2)×u(1) bases 2—11251
light nuclei, sum rule for M1 transitions, validity of SU(4) symmetry 2—38449
n-body problem, hyperspherical functions of tree type 2—14136
pseudoscalar mesons, nonlinear realizations of broken SU(3)×SU(3) 2—21280
SU_3 representation of effective two-body interaction in 1f-2p shell 2—18064
SU_3xSU_3, breaking, weak PCAC study 2—5519
SU(1,1,) discrete series representations, connection with SU(2) matrix elements 2—33884
SU(1,1), spinor algebra and spin coefficients 2—5143
SU(1,1) coupling scheme for construction of dual vertices 2—17868
SU(1,3), rel. to calc. of total scattering cross sections in two-body strong interactions 2—31236
SU(2,2), principal series of unitary irreducible representations 2—30755
SU(2), application to gravitational radiation problems in general relativity 2—2099
SU(2), spinor algebra and spin coefficients 2—5143
SU(2), Thirring model, axial-vector currents anomalies 2—17777
SU(2), vanishing of exotic commutators, fixed symmetry breaking field theory 2—17779
SU(2)×SU(2) current algebra, restrictions of unitarity and analyticity 2—34586
SU(2)×U(1) symmetry renormalizable model for massive Yang Mills fields 2—5472
SU(2) breaking in renormalizable model for massive Yang Mills fields 2—5472
SU(2) symmetry breaking model in K^0 meson theory, Goldstone theorem 2—27733
SU(3), large violation due to short distance effect in non leptonic radiative decay 2—23809
SU(3), multiple particle production, unitary weights calc. 2—8093
SU(3), vanishing of exotic commutators, fixed symmetry breaking, field theory 2—17779
SU(3)×SU(3), anomalous Ward identities 2—388
SU(3)×SU(3), chiral, internal-symmetry groups 2—17804
SU(3)×SU(3), nonlinear realizations, symmetry-breakiing meson Lagrangian 2—8084
SU(3)×SU(3) broken chiral model used to calc. Kl_4 decay form factors 2—21284
SU(3)×SU(3) broken chiral symmetry and Cabibbo angle 2—387
SU(3)×SU(3) pole model for weak-electromagnetic K-meson decays 2—14634
SU(3) ×SU(3) rel. to Goldstone bosons, linear σ model 2—21216
SU(3)×SU(3) representations, broken chiral, scale invariance, symmetric algebra 2—14529
SU(3)×SU(3) symmetry and $K \rightarrow \pi\mu(e)\nu$ decay 2—17902
SU(3)×SU(3) symmetry breaking, field theoretic model 2—11561
SU(3)×SU(3) symmetry breaking, mesons and baryons, emphasis of Nambu Goldstone realisation 2—38309
SU(3)×SU(3) symmetry breaking in Lagrangian model, K_{l3} form factors description 2—27739
SU(3)⊗SU(3) chiral symmetry breaking, neutrino scatt. 2—380
SU(3) σ model, radius of convergence for perturbation expansions 2—8094
SU(3) comparison of φ and K(890) production 2—23877
SU(3) fractional parentage in 1p-shell, computer program 2—21348
SU(3) Gursey matrix, general form 2—31220
SU(3) invariance used in study of unitarity symmetry constraints on inclusive reaction 2—31318
SU(3) Lorentz invariance algebraization of hadron vertex function 2—14584
SU(3) multiplets, rel. to derivation of nonlinear hadron couplings from divergence conditions 2—17840
SU(3) orbits in E_8, parametrization 2—31221
SU(3) sigma model, (1,8)⊕(8,1) symmetry breaking and K_{l3} decay 2—21283
SU(3) symmetry breaking, generation of pseudoscalar and vector terms by 2nd class current 2—31185
SU(3) symmetry breaking, inclusion in calculation of $K_2^0 \rightarrow \gamma\gamma$ decay mode 2—11594
SU(3) symmetry model for determ. statistical weights of many-particle systems in unitary spin space 2—14534
SU(3) tests in hadron and photoproduction reactions 2—34635
SU(4) broken symmetry, quarter models based on fractionally charged urbaryons 2—31219
SU(6) symmetry, tensor meson photoproduction 2—5522
SU(n) Lie algebras, special bootstrapping property 2—31235
sum rule for Σ term from Bjorken limit and mass dispersion relations 2—11565
SU(2,2), decomposition of principal series of unitary irreducible representations restricted to subgroup SU(1,1)⊗SU(2) 2—11252

Sublimation
see also Heat of sublimation; Vaporization
α-brass, in vacuo, applic. of elec. analogy method 2—18888
ice nucleation, observed in cloud chamber, organic substances used as artificial nuclii 2—4660
monatomic elements, eqn. of state, l.p. 2—15632
vacuum pump, large volume using titanium 2—20784
As, speed and spatial distrib. of evaporated mols., retarded vaporization 2—35842
As_2Te_3, semiconducting chalcogenide glass 2—25156
Cd-Te, partial pressures, thermodynamic props. 2—12619
Cu-Pb system, in vacuo, applic. of elec. analogy method 2—18888
NaCl, cleaved, sublimation rate, activation energy estimation 2—32313
Na_2O, evaporation process, Na vapour pressure, torsion effusion determ. 2—22048
Ti, vacuum pumps 2—23195
Ti(s,β), standard enthalpy change, Knudsen n.p. determ., mass spectrometric analysis 2—18890
Zn-Te, partial pressures, thermodynamic props. 2—12619
ZnO, single cryst., anisotropic vaporization rates of opposite basal faces 2—18887
ZnO crystal, vaporization kinetics of opposite basal faces, temp. depend. 2—35841
Sudden commencement *see Magnetic storms*
Suhl effect *see Hall effect; Semiconductors*
Sulphur
absorption spectrum of S I in vac. u.v. 2—20691
adsorption on metal surfaces, distinction from sulphides by Auger spectroscopy 2—39557
adsorption on metal surfaces, LEED structural study 2—6359
amorphous, elec. cond., polaron formation, in review 2—10000
Andromeda galaxy, relative line strengths and abundances in emission regions in the nucleus and disk 2—13851
assaying by proton activation analysis using $^{32}C(p,n)^{32}Cl$ reaction and Cherenkov detection of emitted positron 2—37070
atom K_β spectra in SO_4^{2-} and SO_3^{2-}, comparison with intensity curves from CNDO/2 calcs. 2—35287
atom on wool fibre surface, oxidation, following subjection to discharge 2—37043
c O_2+S, surface reaction kinetics on Cu (110), Auger spectroscopy 2—9248
contamination of polycryst. Ag by adsorption from SO_2, Auger spectra and work function obs. 2—39552
diffusion in CdSe(Te), possible ternary cpd. prep. 2—3820
diffusion on (110) Ni face, Auger spectroscopy 2—3499
electrification in darkness and under illumination 2—25914
equilibrium charge state distributions of O and S ions in carbon stripper of tandem accelerator 2—27919
hydrocarbon-sulphur systems, high temp. laser- induced reactions 2—30096
impurities in GaSb, microanalysis by direct obs. of resonant nuclear reactions 2—10681
impurity, in calcite, effect on cryst., struct. 2—6422
impurity in Cu, spiral elongation test for annealability 2—3932
ions, photoionization cross sections for excited states, emission models for gaseous nebulae 2—20506
liquid, coherent scattering amplitude and total effective cross section to subthermal neutrons 2—18791
liquid, polymerization, chain dissociation, ring scission, elec. resist. 2—35785
in liquid binary alloys, quasichem. eqns. activity coeff., bonding 2—25584
molecular core-level binding-energy shifts calcs. from Mo theories 2—35195
orthorhombic, band struct., transport and optical props., comparison with monoclinic Se 2—40128
orthorhombic crystal, carrier generation by pulsed X-rays 2—29768
purple, Raman spectrum 2—29936
solar corona abundance, det. from e.u.v. spectra 2—20692
sorption on stainless steel, effect of Au coating 2—39558
steel impurity, effect on plastic properties 2—6538
X-ray $L_{II,III}$ emission spectra, ESCA technique 2—36919
X-ray $L_{II,III}$ photoemission spectra, fine structure study 2—36909
Ag surface incipient melting, in presence of O_2 2—1260
AgCl:S, paramag. centres, e.s.r. obs. 2—26271
CrO_2:S, mag. props. 2—36714
in Fe-Si alloy, effect on grain growth rate in primary recrystn. 2—39890
in Fe-Si alloy, effect on recrystn. texture 2—12937
in GaAs epitaxial layers, effect of $AsCl_3$ conc. on incorporation 2—9276
InSb:S, heavily doped, mobility, pressure depend. 2—10020
in rain meteorological interpretation of amount 2—1821
α-S, electron irrad. carrier generation, temp. and field depend. 2—36515
S II and O I line intensity ratios in nuclei of galaxies and gaseous nebulae 2—37266
S III photospheric lines of Delta Scorpii and Zeta Ophiuchi 2—7429
S IX, S X, S XI, S XII, calc. of energies of $1s^22s^22p^k$ to $1s^22s2p^{k+1}$ to $1s^22p_k^{+2}$ transitions 2—35144
S VII, extreme u.v., Hartree-Fock theoretical wavelengths, accuracy 2—24336
S XIV, XIII, solar flare, identification in the extreme u.v. 2—26915
S^+, in Si, LCAO MO treatment 2—10074
S_2- impurity centre in KI crystal, structure of phonon wing in spectra 2—26220
S_2^- excitation spectra in alkali halide crystals, vibrational structure 2—813
S_3, S_4, identification in unsaturated S spectrum at 300 to 650°C 2—15334
S_8, orthorhombic, phonon freqs. 2—19384
S_n, chain and ring conformation, predicted and observed spectral properties 2—15336
$^{33}S/^{32}S$, $^{34}S/^{32}S$, $^{36}S/^{32}S$ and concentrations in Apollo 12 samples 2—17027
$^{34}S/^{32}S$ in stratospheric aerosol 2—10720
$S(3^1D_2)+N_2O$, prod. of NS radicals, contrib. of this reaction channel to total cross section 2—4569
$S(3^3P_3)+O_2\rightarrow SO+O$, absolute rate meas. using kinetic spectroscopy in vacuum u.v. 2—33371
Sulphur compounds
alum, n.q.r., elec. field gradient determ. 2—33360
laser with premixed gases of He and H_2 or D_2, self pulsed high PRF to more than 100 kHz 2—23579
monohalides, mol. force field 2—8701
sulfoxide complexes, quasi-octahedral, coordinate bond, vibrational model 2—12280

Sulphur compounds continued
sulphates, double salts, crystal structure 2—29134
sulphides, refractory, metal-rich, cryst. chemistry, significance of Kasper polyhedra 2—9351
sulphides and sulphates, visible and near i.r. spectra of minerals and rocks 2—20010
sulphospinels, AB_2S_4-type, synthesis, high pressure phenomena 2—9342
Tutton salts, crystal structure 2—29134
As-S glass, hologram formation mechanism 2—23634
CS_2, susceptibility echos, short optical pulse 2—5908
CdS-S solid solution, photoelectret state formation and high photosensitivity and resistivity obs. 2—36603
Cu-Fe-S-O, phase equilibria, from 3-component phase diagrams 2—4012
Fe-S alloys precipitation of Fe sulfides during tempering 2—39891
Fe-S film, lattice parameter and magnetization, S conc. depend. 2—40479
Ge-S glass, thermal analysis rel. to structural model 2—12628
Ge-S system, fusibility diagram 2—1138
S-As, chalcogenide, glass transition 2—9225
S-Sn-P(As) system, glass and cpd. formation, n.m.r. study 2—37003
S-Te-As, chalcogenide, glass transition 2—9225
SCN- anion, Kβ X-ray emission spectrum calc. with all valence electron molecular orbital method 2—28267
SF_6/D_2O clathrate hydrate, powder, ^{19}F n.m.r. lineshapes, chemical shift and anisotropy, correlation times 2—28323
SF_6-He mixtures, stimulated concentration scattering 2—28860
SF_6-N_2 mixtures, surface discharges, obs. 2—15510
SF_6-NO system, laser irradiation, photochemistry 2—20200
SF_3, electron affinity 2—31826
SF_4, negative ion formation, autodetachment lifetimes, and attachment cross sections 2—31826
SF_6, arc constriction, negligible effect of negative ions 2—32139
SF_6, chemical shift of ^{19}F, press. and temp. depend. 2—5953
SF_6, dissociation and subsequent ionization, products formed at 1000-20,000°K and 1-10 atm. 2—6103
SF_6, electron drift velocity 2—35590
SF_6, electron drift velocity meas. 2—3252
SF_6, gaseous, depolarization of scattered Rayleigh radiation 2—35283
SF_6, gaseous, obs. of amplitude modulated train pulse 2—23665
SF_6, K-absorpt. structs. of S, 20-100 Å 2—18463
SF_6, molecule, absorpt. cross sections and ionization efficiencies, 300-1000 Å region 2—21639
SF_6, orbital determ., ESCA line intensities obs. 2—35219
SF_6, prebreakdown ionization current 2—6122
SF_6, Rayleigh linewidth measured near critical point 2—9038
SF_6, self-induced transparency, effect of resonant collisions 2—35383
SF_6, soft X-ray spectrum, effect of symmetry, photoionization of atoms 2—35285
SF_6, solid, dipolar and Zeeman spin-lattice relax., 300-4.2 K 2—26085
SF_6, spectrum and intensity of light scattered along critical isochore 2—12512
SF_6, spin-lattice relax. in liq.-vapour critical region 2—39426
SF_6, streamer propagation, preioniz. control 2—21898
SF_6, thermal conductivity 10^3 to 20×10^3 K and pressures 1 to 10 atm., calc. 2—12511
SF_6 and arcton 12, spark breakdown 2—9008
SF_6 conductance decay calculations of cylindrical arcs 2—24927
SF_6 decomposition products, calc. of electrical conductivity and viscosity at high temps. and pressures 2—39289
SF_6 gas, discharge characteristics, comparison with atmospheric air insulation 2—24898
SF_6 insulation breakdown characteristics, coaxial cylindrical electrodes 2—15516
SF_6 negative ion formation, autodetachment lifetimes, and attachment cross sections 2—31826
SF_6 surface discharges, obs. 2—15510
SF_6 wall stabilized arc, universal characteristic curves 2—24946
S_2F_2 ion molecule reactions, investigation using ion cyclotron resonance spectrometry 2—22871
SF_5Cl, quadrupole hyperfine effects in microwave spectrum 2—38939
SH, isotropic hyperfine coupling constants 2—31812
SO_2/O_2 mixtures, meas. of sound absorption due to vibrational relaxation, existence of vib.-vib. coupling 2—15338
SO, heat of formation in photodissociation of $OSCl_2$ in vacuum u.v. 2—33385
SO radical vibr. temp. in H_2S-O_2 flame 2—22874
SO_2, $^3B_1$ state, radiative and nonradiative lifetimes 2—8704
SO_2, collisions with Na atoms, 1 to 30 eV, electronic excitations 2—687
SO_2, fluorescence and predissociation 2—35286
SO_2, refractive index of liquid in temp. range 130-260 K 2—18825
SO_2, rot. anal. of O-O band, excited state consts., excited state r_0 structure 2—15333
SO_2, rotational analysis of $^3\beta_1\leftarrow{}^1A_1$ bands 2—12191
SO_2, single vibronic level lifetimes of first excited singlet state 2—8703
SO_2, thermal electron attachment in mixtures with N_2, CO_2, ethylene and methanol 2—21868
SO_2, vibrational amplitudes, electron diffraction study 2—822
SO_2, vibrational structure of 2348 Å system 2—15335
SO_2, vibronic effects in decay of fluorescence excited in first excited singlet state, lifetime 2—35284
SO_2 atmospheric pollutant, tunable i.r. laser techniques for det. 2—40923
SO_2 detection in air, by dual beam Fourier transform spectroscopy 2—10671
SO_2 dissoc. in d.c. He-SO_2 discharges, positive ion sampling 2—15506
SO_2 in atmosphere and its effect on corrosion 2—7266
SO_2 laser mechanism 2—23602
SO_2 neat crystals, optical detection of zero field splittings in phosphorescent triplet state 2—13512
SO_2 Raman, backscatt. cross sections 2—15542
SO_3, vibrational amplitudes, electron diffraction study 2—822
SO_3^{2}- anion, Kβ X-ray emission spectrum calc. with all valence electron molecular orbital method 2—28267
SO_3^{2-}, SK_β spectra, comparison with intensity curves from CNDO/2 calcs. 2—35287
SO_4 ions in sulphate solutions, viscosity independence of half width of $\nu_1(A_1)$ Raman line 2—1100
SO_4 radical, e.p.r. obs. 2—26375
SO_4^{2}- anion, Kβ X-ray emission spectrum calc. with all valence electron molecular orbital method 2—28267
SO_4^{2-}, bonding investigations using X-ray spectroscopy and ab initio SCF-MO calc. 2—31821

Sulphur compounds continued
- SO_4^{2-}, SK_β spectra, comparison with intensity curves from CNDO/2 calcs. 2—35287
- SO_2BrF, molecular force field calculation 2—28324
- $SO_2{}^{35}Cl^{35}Cl$ mol., ${}^6R$ type transitions identification 2—24486
- SO_2ClF, molecular force field calculation 2—28324
- $SO(^1\Delta)\rightarrow SO(^3\Sigma^-)$, mechanism of decay at reaction vessel walls, e.p.r. study 2—10612
- $SO(^3\Delta^-)$, transient species obs. using photoelectron and chemielectron spectroscopy 2—35163
- $SO(^3\Sigma^-)$, determ. of absolute conc. by gas phase e.p.r. using NO calibrant gas 2—10604
- $SO(^3\Sigma^-)+O_2(^1\Delta_g)\rightarrow SO(^1\Delta)+O_2(^3\Sigma_g^-)$, kinetic study by e.p.r., absolute rate constant 2—10612
- Sn-S-O-C system, phase diagrams, volatization of Sn 2—1150
- Sn-S system, Mossbauer study 2—1674

Sum rules
- Adler's for neutrino scattering rederived using light cone commutators 2—34612
- Casimir-Polder interactions, long-range, quantum- mechanical sum rules 2—21529
- charge renormalization constant in quantum electrodynamics 2—38199
- Chou Yang type for correlation functions in inclusive reactions 2—14591
- continuous-moment, analysis of $\pi\pi$ scattering for possible violation of exchange degeneracy 2—11621
- coupling constants of isoscalar vector mesons to nucleon and dispersion-theoretic sum rules 2—31311
- current algebra for πN scattering used to evaluate π— nucleus scattering lengths 2—14993
- current algebras for inclusive meas. of hadron collisions 2—5513
- derivation, requirement of smoothness near light cone and superconvergence 2—11560
- derivation, using equal-time commutators involving symmetric energy-momentum tensor 2—2499
- discontinuities of inelastic scatt. amplitudes 2—31244
- Drell-Hearn sum rule from equal-time commutators 2—21217
- duality finite energy, rel. to subtraction constant calc., applic. to $\eta\rightarrow\pi^0\gamma\gamma$ problem 2—2544
- duality type for difference in proton and neutron structure functions, deep inelastic scattering 2—27774
- finite energy, for inclusive processes 2—31225
- finite energy, for partial waves, formulation for N/D equations 2—34597
- finite energy, implications in $\pi\Lambda$ and $\pi\Sigma$ scattering 2—8171
- finite energy, on hyperbolas, rel. to πN scattering 2—17936
- finite energy, on hyperbolas, rel. to $N\bar{N}\rightarrow\pi\pi$ interaction 2—17958
- finite transform, duality considerations 2—34638
- fixed mass, corrections using light-cone commutators 2—8074
- form factors and derivatives at t=0, small distances 2—17775
- hadron interactions, local current algebra in rest frame 2—38267
- hadron scattering, inclusive cross sections, loop contributions 2—11585
- hadrons, coupling constant sum rules connected to compositeness test 2—27715
- halogenoethylene and halogenogermane molecules, sum rules for vibration 2—8782
- inclusive, construction of multiperipheral dynamical equations 2—38274
- inclusive, influence of s channel quantum numbers on inclusive distributions 2—8096
- KSFR sum rule, theorem giving validity conditions and connection to unitarity 2—11559
- light nuclei, sum rule for M1 transitions, validity of SU(4) symmetry 2—38449
- linear for inclusive type discontinuities, equivalence to unitarity 2—23776
- multiparticle, derivations by applying soft-pion theorems to dispersion relations 2—31278
- n-particle distributions, from energy momentum conservation 2—2500
- nondegenerate nuclear system, collective rotational motion 2—24128
- nuclear mass, violation rel. to empirical determination of characteristics 2—34889
- off-shell $\rho\pi$, in $\gamma\pi$ scattering, applic. to π and K em. mass differences 2—2512
- photonuclear reactions, consequences of isospin sum rules 2—31521
- photonuclear sum rules for (γ,n) reactions 2—38564
- plasma response theory, nonlinear 2—35452
- scalar three-point functions, matrix elements 2—2487
- scattering, Omnes equation with bounded state poles 2—38217
- scattering, spinless particles, rel. to multivariable expansion of n-body amplitude, crossing symmetry for partial waves 2—371
- slope of ion charge form factor used to calculate pion charge radius 2—21290
- spectral function, from current algebra, unitarity and analyticity 2—34586
- strong interactions, consistent continuous parameter sum rules, simple and general derivation 2—34594
- three-body interference, unitarity sum rules 2—21219
- van der Waals potentials, long-range, sum-rule moment bounds 2—21528
- vector and tensor trajectories 2—21228
- virtual Compton amplitudes, sum rules from analyticity in forward tube and complex scaling 2—21232
- Weinberg, determination of $\omega\varphi$ mixing angles 2—23871
- Weinberg, rel. to relationship between ρ and A_1 widths 2—23874
- Weinberg rules for chiral $SU_2\times SU_2$ current algebra, test using $e^-\bar{\nu}$ hadrons production 2—23794
- Weinberg-like resulting from closed linear-algebra of currents and baryon interpolating fields 2—17791
- (t,p) data, two-particle units in the analysis of two-neutron transfer reactions 2—31566
- ep scattering, asymptotic sum rule, derivation in perturbation theory 2—383
- ep scattering, consistency relation applicable to cross section data 2—14697
- ep scattering, finite energy sum rule 2—23799
- $\eta^0\eta^0$ scattering, finite-energy sum rules in Virasoro model 2—21282
- $K\rightarrow\pi\mu(e)\nu$, isovector spectral function 2—31265
- $K\rightarrow\pi\mu(e)\nu$, κ resonance and effective range approx. for $(K\pi)$ S-scattering 2—38286
- KN, forward scattering, from varus types of dispersion relations 2—2552
- $K^*\rightarrow K\pi$, $K_a\rightarrow K^*\pi$ vertices, calc. based on techniques of current algebra and dispersion relations 2—2570
- K^+p elastic scattering, finite-energy sum rules 2—17917
- ν scattering, high energy 2—21242
- νN-scattering current algebra sum rules and duality 2—377

Sum rules continued
- νN scattering, rules for virtual cross sections at $Q^2=0$ derived from Low Energy Theorems 2—21240
- pp scattering, consistency relation applicable to cross section data 2—14697
- π, electromagnetic form factor, π-π scattering 2—8180
- π photoproduction off nucleons, determination from dispersion relations 2—17924
- πK, scattering, unitarity sum rule 2—2561
- πN charge-exchange scattering, polarization and sum rules in complex-Regge-pole model 2—14662
- $\pi\pi$ scattering lengths, crossing symmetry restrictions on dispersion relations 2—416

Sun
- *see also Chromosphere; Photosphere; Solar activity; Sunspots*
- active regions, flare occurrence, association with photospheric motions 2—11101
- active regions, obs. of magnetic field changes 2—11119
- active regions, temp. meas. on 2 cm wavelength 2—26910
- age considerations 2—17044
- apex, galactic rotation, precessional corrections from proper motions by a maximum likelihood method 2—37253
- atlas from echelle rocket u.v. spectra 2—4997
- atmosphere, American Astronomical Society, Amherst, USA 1971, conference 2—26623
- atmosphere, dispersion of horizontal component of velocity field 2—41247
- atmosphere, optically thin, isothermal, radiative relaxation of sound waves 2—37412
- atmosphere, spectral line broadening by collisions, obs. of interatomic potentials 2—5824
- atmosphere, turbulent convection zone, depth dependence of physical parameters 2—7566
- bursts, complex, evolution of jet structure during late phase 2—7557
- circumsolar dust at 4 Ro, det. of vaporization temp. 2—26927
- conference (San Juan, December 1971) 2—26582
- convection, nonlinear, asymptotic methods 2—7547
- convection, nonlinear, with free boundaries at high Rayleigh number 2—7567
- convection nonlinear with hexagonal planform 2—7568
- convection zone, depth dependence on scale lengths in quasi-Vitense model 2—7565
- convection zone improved Vitense model 2—7563
- cosmic rays, charge composition and abundance of light heavy elements 2—26898
- cycle, 22 years, theory based on deeply penetrating magnetic field 2—7546
- cycle forecast 2—26872
- day, variations of period 40 days to 3 months 2—14717
- differential rotation law, systematic time variations and solar activity global distribution asymmetry 2—37405
- electron temperatures, relation with X-ray flare activity 2—26914
- EUV and soft X-ray images on March 11th 1971 2—11064
- extreme u.v. image from eclipse obs. of the ionospheric E-region 2—41229
- faculae, magnetic rope model 2—11096
- fluid motion, large-scale 2—20688
- force on Earth causing nutations in motion 2—10812
- gravitational deflection of microwave radiation 2—4991
- gravitational effect on e.m. waves 2—23250
- hydrodynamics, time-dependent implicit code 2—20689
- hydromagnetic structure at boundary of supergranule 2—7569
- instrumentation, review of equipment for optical observation 2—23140
- intensity meas., elimination of seeing effects 2—26879
- magnetic rotator model 2—11046
- magnetograph obs. of the 5-min. oscillations, interference effects 2—17073
- Mercury passage, position angles and contact instants 2—7534
- microturbulent velocities from stellar atmosphere models with convection 2—37397
- model atmosphere, acoustic natural modes rel. to 5 minute periodicity in gas vel. in photosphere and chromosphere 2—14018
- multichannel solar spectrometer, electronic systems 2—41221
- near stars, characteristics, position in Galaxy 2—4810
- Newcomb's Tables of the Sun and Improved Lunar Ephemeris, reference systems comparison 2—41189
- oblateness, combined effect of pole-equator difference and mechanical heating 2—26878
- orbit, spin stabilised orbit, attitude deviations 2—20444
- oscillation modes 2—26875
- plasma, partially ionized, electrical conductivity 2—30636
- plasma, phenomena 2—23083
- plasma rotation phenomena 2—41230
- primary nuclear processes, proton burning, deuteron structure 2—17047
- rare gases and astrophysical and cosmochemical problems 2—26874
- satellites orbiting earth, effect on motion 2—20442
- solar physics and gaseous nebulae, conference (Cambridge, USA, April 1971) 2—23122
- surges, rel. to spotgroups and flares 2—26921
- temp. fluctuations in convection zone, effects of thermal conductivity and viscosity 2—7564
- vacuum telescope and solar instrumentation 2—23141
- X-ray burst, impulsive, location and size, model for electric potential field generation 2—11125
- X-ray emission, Compton backscattering 2—11065
- B content, v.u.v. spectrum obs. 2—15213
- ${}^{12}C/{}^{13}C$ abundance ratio and neutrino emission process 2—11026
- Cr abundances, calc. from beam foil lifetime obs. 2—5785
- ${}^2H/H$ ratio in the primitive Sun, astrophysical implications of a new value 2—14010
- $H\alpha$ structures and small scale magnetic field configurations 2—11033
- Si abundance from forbidden spectral lines of Si I 2—4995

corona
- acoustic noise emission by convective turbulence, directional dependence 2—37422
- artificial satellite study, refinement of solar activity theories 2—17092
- bremsstrahlung X-ray generation in 1-100 Å range, determ. of flux reaching ionospheric heights 2—37420
- brightening, simultaneous obs., with white light coronameter and 80 MHz radioheliograph 2—7571
- brightness correlation with photospheric mag. field strength 2—41260
- brightness distribution, method of evaluation 2—30642
- chemical composition from spectral observations 2—23129

Sun continued
corona continued
chromosphere transition region, hydrodynamic model from radar obs. 2—37414
chromosphere transition region, structure and energy balance, model 2—26928
chromosphere transition region, theoretical and empirical models 2—30639
condensation of 10 Septermber 1970, electron density and velocity of macroscopic matter 2—26932
condensations, activity after long-enduring microwave events 2—41234
condensations, physical state from forbidden line emission 2—41231
diffuse external reinforcements obs. from March 7 total eclipse plates 2—30640
electron density at 1.5-10Ro, inferred from observations of corona 2—26870
electron density maps for 7 March 1970 derived from MgX λ625 spectroheliograms 2—41249
elemental abundance det. from e.u.v. spectra 2—20692
elemental abundances, forbidden line identifications 2—26929
emission line obs., effect of differential refraction and extinction 2—30641
emission lines 3400 to 9000 Å, linear polarization in inner corona 2—41258
enhancements, rel. to sector structure of photospheric magnetic field 2—11045
e.u.v. coronograph observations from OSO-7, comparison in white light 2—26881
e.u.v. emission lines of He II, Mg VIII and Mg IX, 300-second oscillation 2—41223
e.u.v. lines, observed heights 2—37384
expansion, large scale, theory 2—2004
extreme u.v. spectral lines identification 2—41228
forbidden line intensity 2—37382
gas-magnetic field interactions 2—11149
green line obs. during eclipse with electronic camera 2—30604
gyro-resonance absorption of plasma waves and the fine structure of radio bursts 2—11075
heating, rel. to small scale magnetic fields 2—11037
inner, fine structure obs. at 1970 eclipse 2—41226
inner, physical conditions from spectral data of solar eclipse (7 March 1970) 2—41250
instability associated with flare spray 2—11080
intensity at λ5303, correlation with galactic cosmic ray intensity 2—20473
ions, x-ray spectra calc. and relative abundance 2—37386
i.r. emission lines from high altitude obs. of 7 March 1970 solar eclipse 2—41252
i.r. observations, Thompson scattering from electrons, dust size >0.2μ 2—26871
K-corona, polarization-colour effect 2—41220
l.f. bursts, coronal density above active regions 2—26908
Lyman-α, brightness meas. 2—41253
Lyman-α line brightness during 1970, March 7 total solar eclipse 2—33771
mag. fields at time of solar eclipse of 7 March 1970 2—41248
mag. models related to connection between solar mag. field and interplanetary mag. field 2—2000
magnetic field contributions to effect 2—26581
magnetic field map, calculated from photospheric magnetic data 2—17095
magnetic field orientation from polarization meas. in green coronal line 2—11151
magnetic field patterns, large scale, det. from location of radioburst sources 2—11153
magnetic field structure 2—11152
magnetic fields, associated with expanding limb burst inferred form microwave obs. 2—11148
magnetic fields, structure and energy content rel. to differential rotation 2—37423
magnetic fields above active regions 2—11150
magnetic fields and 80 MHz obs. of moving type IV bursts 2—11154
MHD pulsations, radio-astronomical evidence 2—11155
motion detection, photography of eclipse of 7 March 1970 from 2 locations 2—41261
network, spectroheliograms of quiet regions 2—11144
neutron theory of coronal heating, observational test 2—11147
neutrons as an energy source 2—7570
observation by SEC vidicon camera system from satellite 2—11188
outer, polarization obs. from jet aircraft 2—41256
phase scintillations of signals from 3C273 and 3C279, observations with Haystack-Goldstone interferometer 2—26931
photometric intensity and polarization meas. 2—41257
physical state parameters from total spectral line intensities 2—35679
polarimetric K corona obs. and effects of polarization of skylight near sun 2—37418
quiet corona, recent progress in coronal physics 2—23135
rotation, det. from spectroscopy, and high latitude phenomena 2—11156
scattering, transfer characteristics of radiation 2—30614
solar wind velocity, correlation with 5303Å coronal intensity 2—17070
spectra, det. of K-corona intensity, and electron density 2—5019
spectral lines in interspicular regions of chromosphere 2—41246
spectrophotometry during 7 March 1970 total eclipse 2—41243
spike bursts, type III burst assocations 2—37388
stream instability, pulsating regime and the origin of 'rain' type radio bursts 2—11076
streamer, formation model based on two-dimens. plasma flow 2—6064
streamers, rocket-coronagraph photometry from 3 to 8.5 R_s 2—41255
temperature estimates from decay times of type III radio bursts 2—30612
thermal emission during solar cycle, 169 MHz 2—11145
total dielectronic recombination coefficient, rel. to Solar Corona 2—15502
U-type radio burst 2—20709
U-type radio burst 2—11077
upper, interaction between type III bursts and a collisionless shock wave 2—17055
visible lines, classification on basis of ionization potentials 2—37419
white light and XUV, relation on 7 March (1970) 2—41254
white light coronograph studies by OSO-7, streamers rel. to solar activity 2—26930
wind, expansion beyond heliosphere 2—41239
X ray emission, rel. to photospheric magnetic field 2—11067
X-ray features, electron temperature and density 3-60 Angstroms 2—26885

Sun continued
corona continued
X-ray spectrometer/monochromator rocket-borne system for mapping 2—11157
Fe X-XV coronal enhancements, temperature and electron density 2—37421
Fe XII emission line data, electron densities and temp. var. in an enhanced region 2—17094
Fe XIII, i.r. line intensities meas. 2—41251
Fe XIV spectral line, interferometric studies 2—41259
Fe XVII, transition probabilities in intermediate coupling and configuration mixing 2—5787
He and heavier ions, behaviour and abundances, models review 2—33770
He line ions, proton impact excitation 2—20708
Ne IX line emission and electron density in normal non-flare features 2—11146
Ni XV emission line data, electron densities and temp. var. in an enhanced region 2—17094
O VII line emission and electron density in normal non-flare features 2—11146
eclipses
7 March 1970, effect on geomagnetic activity during the storm period 6-10 March 2—7348
1965, May 30, polarimetry of daytime sky in visible region 2—33471
1966, November 12, ionosphere D-region electron loss coefficients measurements 2—33532
1966, November 12, ionospheric charged particle concentrations, rocket measurements 2—33521
1966, November 12, lower ionosphere positive ion composition measurements 2—33533
1966, November 12, polarimetry of daytime sky in visible region 2—33471
1968, September 22, effect on ionosphere F_2-layer 2—23032
1969, September 11, polarimetry of daytime sky in visible region 2—33471
1970, March 7, atmospheric electricity, turbulence and pseudo-sunrise effect 2—37160
1970, March 7, atmospheric electricity measurements 2—33475
1970, March 7, coronal and interplanetary mag. fields 2—41248
1970, March 7, international symposium (Seattle, 1971) 2—41222
1970, March 7, ionosphere D-region electron loss coefficients measurements 2—33532
1970, March 7, ionosphere D-region ledge, effect on electron density 2—33531
1970, March 7, lower ionosphere negative ion composition measurements 2—33533
1970, March 7, Lyman -α intensity distribution across solar disk and multiple scattering in atmosphere 2—33759
1970, March 7, Lyman-α line intensities for corona and chromosphere 2—33771
1970, March 7, naturally occurring v.l.f. radio signals from lower ionosphere 2—37199
1970, March 7, neutral particle response in upper atmosphere 2—33495
1970, March 7, obs. of green line during 2—30604
1970, March 7, OI forbidden line intensities in atmosphere and properties of shadow bands 2—33473
1970, March 7, shadow bands, visual and mechanical measurement 2—33472
1970, March 7, thermosphere electron heating rate and ion chemistry, rocket measurements 2—33522
1970, March 7, X-ray absorption profiles and residual fluxes 2—33763
atmospheric v.l.f. propagation at 12 to 24 kHz, phase behaviour effects 2—23015
comet searches during 4 major eclipses 2—41207
171 March 1970, obs. at wavelengths of 3.2 and 8.3 mm 2—41236
partial, 25 February 1971, meas. of limb brightening at 9 mm wavelength 2—17093
partial, February 25, 1971, photographic obs. 2—30602
phase variation of accurate time signal due to solar eclipse 2—17046
radio observations of filaments on September 11, 1969 and March 7, 1970 2—11095
September 11, 1969, synthesis of ionospheric data obtained during 2—33551
shadow bands, recording on magnetic tape 2—17045
short radio waves reflection from ionosphere, measurement during solar eclipse 2—13761
timings, use to compare reference systems of Improved Lunar Ephemeris and Newcomb's Tables of the Sun 2—41189
total, 7 March 1970, observations at the Maria Mitchell Observatory, Nantucket 2—7545
total, ionosonde and Faraday rotation of ionospheric effects 2—33545
Lα measurements on 12th November 1966 2—11053
flares
18 November 1968, energy spectrum of max. intensity particles, diffusion coeff. of generated particle 2—17067
21 Sep 1967, obs. of diurnal variation of cosmic rays 2—14724
28 August 1966, calc. of no. of electrons accelerated 2—17067
acceleration phase of high-energy particles on 7 July 1966 2—11127
and associated events, 1970 obs. 2—5017
associated solar wind disturbances and type II and type IVm radio bursts 2—30618
association with surges 2—26921
bursts at 3.3 mm, characteristics, association with flares 2—26888
chromospheric, as sources of directed corpuscular streams 2—30630
chromospheric, transfer of Lyman continuum radiation 2—26923
chromospheric component time development, magnetic deflection near sunspots 2—5014
composition of accelerated particles, enrichment of very heavy nuclei 2—11082
cosmic ray, 11-18 Apr. 1969, and assoc. polar cap absorption, effect in lower ionosphere 2—17066
cosmic ray decreases, interplanetary structure associated with active flare producing regions 2—17083
cosmic rays, registered in stratosphere Feb. to Apr. 1969 2—17065
cosmic-rays, sweeping and trapping by interplanetary shock waves 2—26901
D-region ion chemistry changes 2—41005
rel. to dashes, interpretation of dashes as eruptive instability of pinch effect 2—11134
electron acceleration in sunspot magnetic field 2—11125
electron density indicator using ratio of line intensities in He like ions 2—20710

- **Sun** continued
  - **flares** continued
    - energetic particle production, rel. to small scale magnetic fields 2—11037
    - energy storage in cylindrical mag. fields prior to flare 2—37416
    - EUV flashes observed via SFD 2—11126
    - e.u.v. spectroheliograms, 170-630 Å, of class 2N flare 2—26916
    - e.u.v. spectrometric obs. from OSO-5 2—26917
    - flash phase, upper limit on hardness of nonthermal electron spectra 2—2005
    - galactic cosmic ray intensity, effects of active solar regions 2—17081
    - gamma ray instrumentation for satellite experiment to meas. intensity and energy spectrum 2—11138
    - hard X-rays, angular distribution, bremsstrahlung emission of energetic electrons 2—17085
    - heating of flare plasma by high energy electrons 2—37409
    - heavy element enhanced abundances due to preferential acceleration, O/He, Si/He and Fe/He ratios 2—26897
    - impulsive, X-ray, relationship to type III radio bursts 2—26918
    - impulsive phase and X-ray, H_α and microwave emission 2—26919
    - ionospheric E- and F-region electron density enhancement 2—13782
    - ionospheric effects, sudden cosmic noise absorptions and SPA's at v.l.f. 2—13776
    - magnetic and gravitational energy release by resistive instabilities 2—982
    - magnetic channel, volume characteristics 2—11133
    - magnetic effects, digital Solar videomagnetograms 2—5010
    - magnetic field reconnection 2—26920
    - magnetic field-plasma relationship obs. 2—11135
    - magnetic fields 2—11130
    - magnetic fields and polarization of radio emission associated with 2—11120
    - Michigan OSO III ion chamber, soft X-ray photometer, detector response 2—26884
    - moving Type IV radio burst, synchrotron radiation in coronal magnetic field 2—17087
    - occurrence in active region, association with photospheric motions 2—11101
    - parallel drifting bands, associated with flares and bursts 2—5003
    - particle spectra in initial period of flare of 23 February (1956) 2—30633
    - plasma, cooling, energy input for flash phase, heating to produce optical and soft X-ray emission 2—30631
    - position regularities rel. to field maximum in sunspot groups 2—11132
    - prediction, prognosis function construction 2—5018
    - proton, associated electric currents 2—11131
    - proton, associated type iv bursts, centre-to-limb variation of peak flux spectra 2—11074
    - protons associated with 24th January 1969 2—11087
    - radio burst identification with S-type and P-type 2—20694
    - relativistic electrons, 0.3 to 12 MeV, rel. to proton intensity increases 2—37410
    - rel. to sector structure of photospheric magnetic field 2—11045
    - shock waves in interplanetary space after chromospheric flares 2—37375
    - spectra, Fe line emission 2—2001
    - spectrum below 10Å from satellite obs. 2—16904
    - spray, associated coronal instability and moving radio features 2—11080
    - u.v., extreme, correlation with $H\alpha$, X-ray, radio and SFD observations 2—5015
    - u.v. measurements 2—30634
    - X-ray, 30 January 1968, implications and ionospheric effects 2—13777
    - X-ray, activity rel. to source electron temp. 2—26914
    - X-ray, electron temp. and emission measure variations 2—26887
    - X-ray, ionospheric effects on v.l.f. propagation 2—4712
    - X-ray, obs. with X-ray telescope using modulation collimator 2—11139
    - X-ray, rel. to sudden ionospheric disturbances 2—16903
    - X-ray, rel. to sudden ionospheric disturbances and cosmic noise absorption 2—16905
    - X-ray burst, pulsed increase of intensity 2—41232
    - X-ray bursts, var. of temp. and emission measures with time 2—17053
    - X-ray decay rel. to electron loss in D-region 2—37207
    - x-ray emission, localization of source during 7 March 1970 eclipse 2—41244
    - X-ray emitting regions rel. to flare activity, results from OSO-IV 2—37385
    - X-ray instrument for OSO-H, monitoring of solar flares 2—30609
    - X-ray spectrum, polarization and anisotropy 2—17054
    - A XV, identification in the extreme u.v. 2—26915
    - Be, identification in the extreme u.v. 2—26915
    - CIII extreme u.v. observations at the limb, kinematics of flare surge 2—17086
    - CaXV, identification in the extreme u.v. 2—26915
    - Fe XIV, XV, XVI, identification in the extreme u.v. 2—26915
    - Fe XXIV line emission soft X-ray spectrum 2—30608
    - $H\alpha$, association with photospheric mag. field patterns, review 2—11129
    - Li, identification in the extreme u.v. 2—26915
    - Ni XVII, XVIII, identification in the extreme u.v. 2—26915
    - SXIV, XIII, identification in the extreme u.v. 2—26915
  - **magnetism**
    - absorption line formation, interpretation of magnetograph 2—11054
    - active region, evolution of configuration 2—11116
    - active regions, determination by circular polarization 2—11114
    - active regions, determination from chromospheric magnetograph 2—11115
    - active regions, obs. of field changes 2—11119
    - active regions of the atmosphere, magnetic fields at different levels 2—11112
    - arch filaments rooted in photospheric magnetic fields, new magnetic flux at surface 2—5009
    - bipolar sunspots, topology of force-free magnetic field 2—11102
    - chromosphere, field det. from obs. of active regions at mm. wavelengths 2—11143
    - chromosphere, trapped electrons and protons 2—30638
    - chromospheric flux ropes, kink instability suppresssion 2—37416
    - corona, and 80 MHz obs. of moving type IV bursts 2—11154
    - coronal, structure and energy content rel. to differential rotation 2—37423
    - coronal field orientation from polarization meas. in green coronal line 2—11151
    - coronal fields, associated with expanding limb burst inferred from microwave obs. 2—11148
    - coronal fields, interactions with gas 2—11149
    - coronal large scale field patterns det. from location of radioburst sources 2—11153
    - coronal mag. fields at time of solar eclipse of 7 March 1970 2—41248
- **Sun** continued
  - **magnetism** continued
    - coronal magnetic fields above active regions 2—11150
    - coupling of active chromosphere to solar interior 2—26924
    - dynamo model for large scale fields 2—11049
    - dynamo theory of general field using mean-field MHD 2—11048
    - dynamo theory of solar cycle and observational models 2—37404
    - energy flow in solar wind, effect of Sun's rotation 2—33765
    - faculae rel. to photospheric network 2—30624
    - field measuring methods, review 2—11028
    - field obs. using beam absorption filter 2—11180
    - field orientation in quiescent prominences 2—11136
    - field reconnection in flares 2—26920
    - field structure, association with photospheric motions 2—11101
    - field structure in active corona 2—11152
    - fields, extended, rel. to interplanetary mag. field 2—4994
    - fields, large scale activity, review 2—4993
    - fields, small scale structure, review 2—4992
    - fields and polarization of radio emission in active centre 2—11120
    - fields associated with flares 2—11130
    - filamentary fields 2—37378
    - fine structure, evidence for reality 2—11032
    - fine structure of magnetic fields from chromospheric structure 2—37396
    - forced diffusion of fields 2—20690
    - general magnetic field, nature and origin of time fluctuations 2—26876
    - horizontal magnetic stresses caused by differential rotation, effects on poleward migration of magnetic features 2—30601
    - hydromagnetic symmetrical terms for the zonal kinetic energy equation 2—24637
    - interference-polarizing filter for magnetic field studies, electrically controlled 2—27634
    - Joule dissipation in photosphere and sunspot layers, effect of anisotropy of electric conductivity 2—17077
    - large scale field, generation by convective currents in outer shell, model of oscillatory hydromagnetic dynamo 2—23121
    - large scale field distribution and effect of opposite polarities in development of regularities 2—11042
    - large scale fields, dynamics 2—11044
    - large scale fields and consequences 2—11039
    - large scale fields and magnetic activity cycle 2—11047
    - large-scale motions 2—30628
    - longitudinal fields, birefringent element to separate mag. polarity 2—26873
    - magnetic loop structure, multiple, of type IV solar radio outburst 2—7556
    - magnetic rotator, observations of sunspot groups 2—37402
    - magnetograms, analog video, in real time 2—11029
    - magnetograph, based on high resolution filter 2—11174
    - magnetograph, digitized filter, optics and electronics 2—11178
    - magnetograph, influence of miscentering spectral line on accuracy of complete field vector 2—11177
    - magnetograph, separate obs. of displacement of right and left circularly polarized lines 2—11176
    - magnetoplasma in active regions, statistical model of small scale discrete structure 2—11122
    - measurements and instrumentation, conference, Paris, August (1970) 2—11027
    - north-south component from Explorer and Mariner data 2—14009
    - origin in fine structure elements of photosphere and sunspots 2—11038
    - oscillations in field, 5-minute period 2—11036
    - oscillatory hydromagnetic dynamo, convective currents in outer shell of Sun 2—14017
    - photosphere, magnetograph measurements 2—17076
    - photosphere, model of fine structure 2—11097
    - photospheric, comparison with interplanetary field 2—37415
    - photospheric field, purely toroidal, time development and interaction with poloidal mag. field 2—30623
    - photospheric field, rel. to X-ray corona 2—11067
    - photospheric field strength correlation with coronal brightness 2—41260
    - photospheric fields, weak, detection using 40-channel magnetograph 2—14019
    - photospheric fields association with $H\alpha$ flares 2—11129
    - plage region, vertical velocities associated with mag. fields 2—11100
    - polar field, effect on interplanetary mag. field 2—2000
    - polar fields polarity and inversion line obs. 2—11043
    - polar prominences' magnetic fields 2—11137
    - prominences, fields from polarization meas. of scattered radiation 2—7908
    - and provinces 2—7562
    - quiescent prominences, observations with magnetograph 2—11128
    - regions of opposite polarity and circular polarization of active regions at 9 mm wavelength 2—26889
    - rotating dipole, obs. from effects on polar geomagnetic field and interplanetary magnetic field polarity 2—26877
    - sector magnetism, obs. and Babcock model compared 2—2003
    - sector structure and flares, coronal enhancements, plage structure and geomagnetic response 2—11045
    - small scale fields, theories, review 2—11037
    - solar general magnetic field, nature and origin of time fluctuations 2—26876
    - spectral line formation, effect of atomic collisions 2—11055
    - Stokes parameters, difficulties in simultaneous obs. 2—11030
    - sunspot fields, distribution of mag. force in surface layers 2—11123
    - sunspot fields, rel. to high energy electrons in flares 2—11125
    - sunspot fields and umbral dots 2—11121
    - sunspot groups field maximum rel. to position regularities of flares 2—11132
    - sunspot mag. fields associated with polarized solar radio emission at mm wavelengths 2—7553
    - sunspot magnetic fields, umbral atmospheres under similarity configuration 2—37408
    - sunspot umbral flux tubes, Alfven waves in 2—37417
    - sunspots, low frequency oscillations 2—20706
    - sunspots, observations of two-level structure 2—11113
    - sunspots, photoelectric measurements 2—11108
    - sunspots, precise determination of vector 2—17078
    - sunspots, rel. to turbulence 2—11107
    - sunspots, statics and dynamics of field structure developments 2—11109
    - sunspots and active regions, review 2—11106
    - supergranulation at the centre of the disc 2—11098
    - supergranule observations 2—11099
    - time dependence in the solar atmosphere, spectroheliogram movies 2—11031

Sun continued
magnetism continued
time evolution of general field, and polar fields 2—11041
time evolution of large scale field and surface harmonics 2—11040
time fluctuations of fields 2—11035
umbral spectrum, derivation of field strengths 2—11111
unipolar magnetic regions and 11 year activity cycle rel. to geomagnetic disturbances 2—30365
unipolar sunspots, structure of field 2—11110
variations, dynamo theory, contrib. to diurnal geomag. field variations 2—13795
videomagnetograms, during subflare, prior to major flare 2—5010
weakly active regions, magnetographic obs. 2—11118
CN λ3883 spectroheliograms to map weak fields in photosphere 2—11093
Hα fine structure at active region polarity boundaries in the solar chromosphere 2—17091
H_α structures and small scale field configurations 2—11033
HeI 10830 angstrom line measurements for chromospheric mag. field 2—11142
prominences
1956 September 10, kinetics 2—30632
eruptive loop, dash phenomena, physical nature and relation to flares 2—11134
erupture of 3 May 1971, obs. 2—26922
faculae rel. to photospheric network and magnetic fields 2—30624
facular models and the sunspot energy deficit 2—30625
filaments, radio observations during the eclipses of September 11, 1969 and March 7, 1970 2—11095
granulation patterns, intensity distribution, solar oblateness 2—5011
high dispersion spectroscopic study of line profile and velocity structure 2—17084
kinematics 10 September, 1956, solar prominence 2—30632
Kodaikanal Observatory, second half of 1967 obs. 2—41242
loop, thermal effects in formation 2—5016
magnetic fields 2—7562
magnetic fields by coherence properties of polarized radiation 2—7908
polar, magnetic fields 2—11137
quiescent, observations of magnetic fields 2—11128
quiescent, orientation of magnetic fields 2_11136
quiescent, spectrophotometry during 7 March 1970 total eclipse 2—41243
smoke ring formation from prominence, Hα observations of limb 2—37411
structure, rel. to small scale magnetic fields 2—11037
sudden disappearance, explanation 2—37414
radiation
see also Sunlight
absorption atmospheric det. of total water vapour content 2—16813
atmospheric depletion, model for building cooling load analysis by computer 2—30290
bremsstrahlung X-ray generation from corona in 1-100 Å range, determ. of flux reaching ionospheric heights 2—37420
corona brightening, simultaneous obs., with white light coronameter and 80 MHz radioheliograph 2—7571
Earth's shadowing effect on satellite orbital elements, solar radiation pressure 2—30392
earth's surface scattering, angular structure, statistical nature 2—20348
EUV flashes of solar flares observed via SFD 2—11126
flares, rel. to sudden ionospheric disturbances 2—16903
flux through model atmosphere, calc. 2—33466
gamma-ray emission 2—11090
line blanketing in solar model atmospheres, limb darkening 2—37380
Lyman-α intensity distribution across solar disk and multiple scattering in atmosphere during 1970, March 7 total eclipse 2—33759
Lyman-α line intensities for solar corona and chromosphere during 1970, March 7 eclipse 2—33771
microwave link interference 2—33481
moving Type IV radio burst, synchrotron radiation in coronal magnetic field 2—17087
penetration in Schumann-Runge bands of O_2 2—7299
sensing devices, for atmospheric monitoring 2—16799
solar concentrator with stationary plane mirrors 2—23674
sunlight, speckle patterns after scattering from blackened surface 2—14452
sunspot umbra, photometric obs. at 3.75 μ 2—26907
transmission through earth's atmosphere, investigation using transportable 16 GHz solar telescope 2—33772
u.v., rel. to mesospheric processes 2—7298
u.v., spectrometer calibration to meas. absolute intensity and centre-to-limb variation 2—11063
visible, from disk and corona, scanning photoelectric polarimeter for Stokes parameter obs. 2—11175
X-ray, control at ionization in E layer and sporadic E-layer 2—16910
X-ray apodised zone plates for solar image formation, construction 2—11070
X-ray burst, pulsed increase of intensity 2—41232
X-ray burst of 11 February 1970, observed at balloon altitude 2—33764
X-ray data normalization 2—37387
X-ray emission from active centres on solar disc 2—26886
X-ray events, 4 keV, correlation with type III radio bursts 2—26891
X-ray flux, from SPA and SES obs. 2—23128
X-ray impulsive bursts, decay phase 2—30607
X-ray instrument for OSO-H, monitoring of solar flares 2—30609
x-ray observations from Vela satellites 2—11066
X-rays, optical identification of activity assoc. with background fluctuations 2—30611
X-rays, type IV bursts and interrelation to solar-terrestrial phenomena 2—11072
X-rays 15-250 keV, meas. from 5^{th} Orbiting Solar Observatory 2—11091
X-rays from impulsive flares, relationship to type III radio bursts 2—26918
CIII extreme u.v. observations at the limb, kinematics of flare surge 2—17086
Fe XXIV soft X-ray line emission during flares 2—30608
H_α, X-ray and microwave emission during impulsive phase of flare 2—26919
NaI(Tl) γ-ray spectrometer, solar monitoring in OSO-7 spacecraft 2—30610
Si photocells for meas. 2—23499
radiation, corpuscular
1969. Feb. to Apr., cosmic ray/flares 2—17065
additional electron flux detection after magnetic perturbations 2—17072

Sun continued
radiation, corpuscular continued
azimuthally dependent solar wind, dynamics, hypervelocity approximation 2—37393
cosmic radiation fluctuations in stratosphere 2—26495
cosmic ray, analysis of semi-diurnal variation 2—33769
cosmic ray flare, 11-18 Apr. 1969 and assoc. polar cap absorption, effect in lower ionosphere 2—17066
cosmic ray flares, Feb. to Apr. 1969, registered in stratosphere 2—17065
cosmic rays, 27-day recurrence and long term modulation 2—11089
cosmic rays, energy spectrum and polar cap absorption 2—23126
cosmic rays, semi-diurnal anisotropy 2—33768
cosmic rays density distribution normal to solar equatorial plane and semi-diurnal anisotropy 2—38334
cosmic-ray bursts, propagation 2—11088
directed streams, chromospheric flares as sources 2—30630
energetic, low rigidity flare particles released from trapping field, plasma heated by flare process 2—17069
energetic particles access point to Earth's magnetosphere, magnetotail configuration 2—40982
energetic-particle events, composition, enrichment of very heavy nuclei 2—11082
flare of February 23, 1956, particle spectra in initial period 2—30633
heavy element enhanced abundances during flares, due to preferential acceleration, O/He, Si/He and Fe/He ratios 2—26897
interference and damage effects in charged particle expts. for deep space missions 2—20430
ionosphere absorption det. from data on solar cosmic-ray flux density and spectrum 2—33518
magnetopause, internal structure, review 2—16878
magnetopause and bow shock, average and unusual locations 2—13738
Martian bow wave, trajectory of Mariner 4 2—30576
multiple particle spectrometer, measurement of p, α and β solar particle events 2—30619
muons, diurnal variation, effect of atmosphere on observations 2—23127
neutrino radiation search in Brookhaven expt. 2—26896
neutrinos, energy transport by longitudinal plasma waves 2—33757
neutrinos discrepancy between calculated and observed flux 2—30617
neutron emission 2—11090
neutrons, near solar maximum, balloon borne plastic scintillator counter 2—17071
nuclei, charge >20, obs. of flux increases by 'Electron-4' satellite 2—17062
particle event, nuclear composition and energy spectra obs. 2—5006
particle generated in solar flare 18 Nov 1968, diffusion coeff. 2—17067
propagation in interplanetary space, study based on flare data 2—17065
proton flares, associated electric currents 2—11131
proton flux, low-energy, increases associated with interplanetary shock waves 2—26901
proton flux and energy spectra satellite measurement 2—5008
protons, associated with propagating interplanetary shock waves, directional and temporal properties 2—14015
protons, entry over polar caps 2—4704
protons, non-uniform entry into polar cap 2—30316
protons associated with the 24th January 1969 solar flare 2—11087
protons from flare events, entry from interplanetary space to magnetosphere 2—20375
solar wind, effect on occurrence of magnetospheric storms 2—13808
solar wind, shock-free deceleration 2—7558
solar wind, thermal anisotropy and cooling of protons under quiet conditions 2—5007
streaming of galactic cosmic rays in interplanetary magnetic field rel. to solar flare particles 2—37377
two-fluid models of solar wind, radial dependence of electron temperature 2—37394
wind, 11 yr cosmic ray modulation, mag. field study 2—17063
wind, as source of magnetospheric plasma, review 2—20365
wind, average proton properties from Pioneers 6 and 7 2—20698
wind, behaviour and abundances of He and heavier ions 2—33770
wind, collisionless, variable electron temp., model 2—20700
wind, cosmic ray modulation 2—11083
wind, dispersion relations for perpendicular magnetosonic waves in relativistic plasmas 2—8970
wind, effect of interplanetary magnetic field, analysed in magnetohydrodynamic approximation 2—14014
wind, effect or interplanetary scintillations, simultaneous observations of radio sources 2—26899
wind, electron density variations, responsible for interplanetary scintillation of small diameter radio sources 2—11024
wind, electron energy flux 2—17068
wind, expanding, solar modulation of galactic cosmic rays 2—30411
wind, expansion beyond heliosphere 2—41239
wind, galactic cosmic ray diffusion and stochastic variations 2—17064
wind, galactic cosmic ray modulation, primary spectrum from obs. of latitude effects 2—11084
wind, general survey of properties 2—30621
wind, heating of ion content near Earth's orbit 2—33766
wind, hydromagnetic waves and discontinuities 2—26903
wind, inducing mass loss from magnetic field free planets 2—4961
wind, interaction with comets, satellite observations and theories 2—30592
wind, interaction with interstellar He 2—14016
wind, interaction with lunar magnetic field 2—37348
wind, interaction with magneto-sheath 2—20370
wind, interaction with Venus, Venus probes data 2—37376
wind, interplanetary plasma phenomena 2—23083
wind, interplanetary scintillation of radiowaves 2—33756
wind, inviscid, supersonic solutions of equations, domains of existence of three types 2—17058
wind, kinetic models 2—20699
wind, lunar bombardment, crater population development 2—1975
wind, magnetic energy flow, effect of Sun's rotation 2—33765
wind, magnetic field contributions to effect 2—26581
wind, magnetic field generation in magnetopause, influence of Hall effect 2—26523
wind, magnetospheric storms, variation of magnetic activity with solar wind flux velocity 2—33502
wind, microscale fluctuations, theoretical constraints on characteristics 2—20704
wind, microstructure, effect of Alfven waves 2—37391
wind, motion of charged particles in spiral magnetic field and temp. anomalies 2—26900

Sun continued
radiation, corpuscular continued
wind, non-radial oscillations and energy transport 2—26902
wind, penetration into magnetosphere, perturbation obs. 2—33499
wind, plasma, higher moment equations and distribution function 2—20701
wind, plasma, velocity variation causing geomagnetic tail oscillations 2—33500
wind, plasma flow, ratio of specific heats through Earth's bow shock 2—16874
wind, protons, penetration of magnetosphere, through boundary of geomagnetic field 2—22988
wind, protons, temperature anisotropy and adiabatic cooling 2—11085
wind, rel. to outer radiation belt parameters 2—30334
wind, reverse and forward slow shocks 2—20703
wind, rotational discontiniuties in ansotropic plasma 2—11086
wind, satellite observations of interplanetary plasma and magnetic field 2—14008
wind, sensitivity of cometary tails to solar radiation 2—20685
wind, shock waves in space plasma 2—17059
wind, structure and electron temp. asymmetry 2—33767
wind, temperature profile, calc. from energy equation 2—20702
wind, termination theories 2—30620
wind, upstream from Earth, nonthermal electrons and l.f. waves 2—10800
wind, velocity, dependence of magnetospheric electric field 2—13744
wind, velocity determined from interplanetary scintillations 2—20696
wind contribution to lunar atmosphere 2—1982
wind disturbances, flare associated, and type II and IVm radio bursts 2—30618
wind model for magnetized solar wind with tensor plasma pressure 2—37392
wind plasma, shock waves in interplanetary space after chromospheric flares 2—37375
wind theory 2—2004
wind velocity, correlation with 5303Å coronal intensity 2—17070

radiation, radiofrequency
3.3 mm, enhanced emission during flares 2—11130
1969 activity at 600 and 151.5 MHz 2—26892
'rain' type bursts, origin in terms of a pulsating regime of stream instability 2—11076
active region associated with McMath plage 10 618, eclipse at 10 cm wavelength 2—41241
active regions at mm. wavelengths and chromospheric magnetic field det. 2—11143
activity in 1966, 600 MHz 2_7550
burst, moving features associated with flare spray 2—11080
burst activity index and burst incidence computed for 1968-69 period 2—41235
burst events, type III, meter wavelength, fine structure 2—5002
burst sources, for calc. of coronal mag. field patterns 2—11153
bursts, coronal density above active regions 2—26908
bursts, high time resolution spectral obs. 2—26890
bursts, identification with flare location 2—20694
bursts, impulsive rel. to gradual rise and fall types 2—20695
bursts, polarization observed at 17GHz 2—11078
bursts, space radioastronomy at all frequencies, the STEREO project 2—11081
bursts, time-dependent fine structure, statistical investigations 2—14012
bursts, type II and IVm, flare associated solar wind disturbances 2—30618
bursts, type III correlation with 4 keV X-ray events 2—26891
bursts, type III relationship to impulsive flare X-rays 2—26918
bursts, type IV, moving, obs. at 80 MHz and coronal magnetic field 2—11154
bursts at 3.3 mm, characteristics, association with flares 2—26888
bursts in the 19 GHz region from July 1967 to December 1969 2—11079
chromosphere, high resolution observations at mm and cm wavelengths 2—41237
circular polarization of active regions at 9 mm wavelength and magnetic regions 2—26889
circularly polarized emission at 7.8 GHz, two-dimensional maps 2—7554
coronal electron density variations effects on propagation 2—30614
emission at 10.7 cm at Ottawa rel. to Zurich sunspot number 2—26895
filament observations during the eclipses of September 11, 1969 and March 7, 1970 2—11095
gyro-resonance absorption of plasma waves in the corona and the fine structure of bursts 2—11075
limb brightening at 9 mm wavelength, obs. during a partial solar eclipse 2—17093
line splitting in drift pair solar bursts 2—7555
local sources, two groups 2—2002
magnetic loop structure, multiple, of type IV solar radio outburst 2—7556
microwave and extreme u.v. wavelengths, observations of solar bursts 2—17056
microwave burst, expansion of source, associated magnetic fields in corona 2—11148
microwave burst spectrographic radiometer 2—26893
microwave bursts, homologous events from different active centres 2—7552
microwave long-enduring events, activity of solar coronal condensations 2—41234
microwave outburst at 94.8 GHz, pencil beam antenna observations 2—37389
microwave radiometer for daily measurement of solar flux at 2800 MHz 2—30615
parallel drifting bands in meter wavelength emission 2—5003
polarization and total flux meas. of S-component at 81 and 250GHz 2—23125
polarization mapping at 7.8 GHz 2—5004
polarization of emission in active centre 2—11120
polarized emission at millimeter wavelengths in active regions 2—5005
polarized emission at mm wavelengths associated with sunspot mag. fields 2—7553
quiet and active regions at 1.2 mm wavelength 2—30616
quiet-Sun centre-limb observations at 6 and 11 cm. during cycle maximum 2—37399
radial brightness distribution at wavelengths of 3.2 and 8.3 mm 2—41236
radio emission, review 2—7492
radioelectric 600 MHz activity in 1967 2—7551
recombination lines, strengths 2—5001
spectral obs. of 7 March 1970 eclipse 2—41238

Sun continued
radiation, radiofrequency continued
spike bursts, spectral features 2—30613
spike bursts, type III burst assocations 2—37388
type III burst, interplanetary particles associated with 2—14013
type III bursts, high-resolution spectrographs, 310-340 MHz, 145-175 MHz 2—30612
type III bursts, interaction with a collisionless shock wave 2—17055
type III radio burst theories, comparison using electron flux meas. 2—26894
type IV bursts, associated with solar proton flares, centre-to-limb variation of peak flux spectra 2—11074
type IV bursts and interrelation to solar-terrestrial phenomena 2—11072
U-type burst from outer corona 2—20709
U-type burst originating in outer corona 2—11077

spectra
see also Sun/corona; Sun/flares; Sun/prominences
atomic interactions with polarized light 2—35128
atomic spectra and transition probabilities, experimental studies 2—21486
band absorption coefficient of diatomic molecules, rel. to u.v. opacity 2—4996
chromosphere, Hα and He 10830 Å line spectroheliograms, supergranules and fine structure 2—37413
coronal abundances, forbidden line identifications 2—26929
coronal condensation, Fe XIV, Ca XIII and Ca XV emission lines 2—26932
coronal condensations, physical state from forbidden line emission 2—41231
coronal emission line, effect of differential refraction and extinction 2—30641
coronal emission lines 3400 to 9000 Å, linear polarization in inner corona 2—41258
coronal emission lines from high altitude i.r. obs. of total eclipse 2—41252
coronal line classes, based on ionization potentials 2—37419
coronal lines, fine structure obs. at 1970 eclipse 2—41226
coronal lines in chromosphere at 1970 eclipse 2—41246
crossover and magneto-optical effects in sunspot spectra 2—37406
crossover and magneto-optical effects in sunspots 2—11105
curves of growth for Fe, Cr, Ni, revised gf-scale 2—33761
Doppler shifted observation of Si I lines, solar silicon abundance 2—4998
emission, for det. of ionospheric D-region extraionization of solar X-ray flux 2—23128
e.u.v., abundance det. in quiet and active regions 2—20692
e.u.v., identification of λ 417 line, collision strengths for Fe XV transitions 2—11050
e.u.v. emission lines of He II, Mg VIII and Mg IX, 300-second oscillation 2—41223
E.U.V. lines in transition zone and corona, observed heights 2—37384
Evershed effect, fine structure in sunspots from Fe I and Ca I lines and velocity measurements from Ti II, Fe II and CH lines 2—37407
extreme u.v., forbidden coronal lines, identification 2—41228
flare, class 2N, e.u.v. spectroheliograms from 170- 630 Å 2—26916
flares, e.u.v., obs. from OSO-5 2—26917
flares, X-ray, below 10 Å from satellite 2—16904
flares in the extreme u.v. 2—30634
forbidden line intensity, coronal 2—37382
Freundlich red shift, $\sigma_\odot$ for photon-photon interactions 2—17049
green line obs. during eclipse with electronic camera 2—30604
high dispersion spectroscopic study of line profile and velocity structure of quiescent prominences 2—17084
intensity variations of photospheric and chromospheric networks with time 2—17050
ir., brightness temp. obs. 2—11073
i.r. limb profile meas. 2—5000
line blanketing in solar model atmospheres, limb darkening 2—37380
line formation, effect of atomic collisions in magnetic regions 2—11055
line formation in inhomogeneous magnetic fields 2—11056
line intensities and physical state parameters 2—35679
line profile variations in transition region from photosphere to chromosphere 2—41225
lines of different metals, and metal abundance effects on solar colours 2—33760
lower chromosphere, meas. of non-thermal velocities from rare-earth emission lines in wings of H and K lines 2—17088
Lyman, rel. to chromosphere structure 2—41245
magnetic field spectroheliograms 2—11034
magnetograph results' interpretation, formation of absorption lines in a magnetic field 2—11054
optical, 2100 to 3200 Å, measured from Aerobee rocket 2—33758
Paschen-Back effect of the Li resonance doublet in sunspots 2—11104
photosphere, magnetic and velocity fields and brightness 2—17076
polarization of coronal green line, det. of magnetic field orientation 2—11151
radio recombination lines, strengths 2—5001
recording, photographic technique 2—11057
r.f. line splitting in drift pair solar bursts 2—7555
solar continuous spectrum intensities rel. to convergency of photospheric models 2—37398
spectroheliograph for u.v. 2—11062
spectroscopic equipment for use in rockets 2—41224
spectroscopy from space vehicles, techniques and discoveries 2—23123
time dependence of magnetic, velocity, and intensity fields in solar atmosphere, spectroheliogram movies 2—11031
type IV bursts and interrelation to solar-terrestrial phenomena 2—11072
umbral lines, derivation of magnetic field strengths 2—11111
u.v., 1970 to 1800 Å recorded by echelle spectrograph 2—26883
u.v., high resolution, echelle diffraction gratings in sounding rockets 2—11060
u.v., line blanketing in 2000-4000 Å regions 2—20693
u.v., missing opacity, band absorption coeff. of diatomic mols. in photosphere 2—4996
u.v., results from three balloon flights using a grating monochromator 2—11059
u.v., review of observational methods and results 2—11058
u.v. continuum, blocking effect of lines between 2000 and 3000 Å 2—30605
u.v flash spectrum, eclipse obs. 2—41227
weakly active regions, spectrographic obs. 2—11118
X-ray, as function of position on disk, rocket- borne study 2—11068
X-ray, Fe lines, Compton backscattering 2—11065

Sun continued
  spectra continued
    x-ray, from coronal ions, calc. 2—37386
    X-ray, satellite lines 2—7549
    X-ray, soft, optical system for spectrophotometry 2—11069
    X-ray absorption profiles and residual fluxes during 1970, March 7 eclipse 2—33763
    X-ray emission from active centres on solar disc 2—26886
    X-ray obs. with sinle crystal spectrometers 2—23124
    X-rays, polarization and anisotropy during flares 2—17054
    X-u.v. radiation obs. module 2—14471
    XUV lines of ions in Li isoelectronic sequence, relative intensities interpretation 2—37379
    Zeeman lines in sunspots and their temperature sensitivity 2—11103
    AXV, identifications in the extreme u.v. in a flare 2—26915
    Ag abundance from near u.v. studies, spectrum synthesis method, agreement with type I carbonaceous chondrites 2—26880
    Be, identifications in the extreme u.v. in a flare 2—26915
    C I emission line, 1993.6 Å 2—14011
    CH^+ line, search 2—11051
    CN λ3883 spectroheliograms to map weak magnetic fields in photosphere 2—11093
    CN spectroheliogram, intensity distribution of bright points 2—26906
    $^{12}C/^{13}C$ abundance ratio 2—17048
    $^{13}C^{16}O$ i.r., sunspots, det. of $^{12}C/^{13}C$ ratio 2—17048
    Ca II k line, chromospheric, multicomponent models 2—37383
    Ca^+ emission luminosity rel. to age 2—16986
    CaII emission lines from faculae, magnetic rope model of structure 2—11096
    CaII i.r. lines, inhomogeneities in the solar atmosphere 2—11052
    CaXV, identifications in the extreme u.v. in a flare 2—26915
    Fe, abundance, remarks on 1969 revision 2—4999
    Fe I, 5250.2 and 5225.5 angstroms, magnetic field and turbulence study in sunspots 2—11107
    Fe line emission during flares 2—2001
    Fe X-XV coronal enhancements, temperature and electron density 2—37421
    Fe XII emission line data, electron densities and temp. var. in an enhanced coronal region 2—17094
    Fe XIII in solar corona, i.r. lines, intensity meas. 2—41251
    Fe XIV, XV, XVI, identifications in the extreme u.v. in a flare 2—26915
    Fe XIV spectral line in corona, interferometric studies 2—41259
    FeI 5324 angstrom line for Hα structures and small scale magnetic field configurations 2—11033
    H ionization equilibrium, resonance line transfer, chromosphere 2—26925
    H_2O vibration-rotation bands, examined in umbra spectrum at 0.93 μ 2—17052
    Hα filaments, fibrils in middle chromosphere 2—17089
    Hα fine structure at active region polarity boundaries in the chromosphere 2—17091
    Hα fine structure in the chromosphere, interpretation of fibrils and threads 2—17090
    Hα line profiles, investigation of fine structure of chromosphere 2—11140
    Hα line wing, in solar limb, identification of spicular structure 2—17051
    Hα morphology, determination of magnetic field structure of active regions 2—11115
    Hα profile formation 2—37390
    He-like ion line emission in solar plasmas 2—37381
    HeI 10830 angstrom line measurement of magnetic fields 2—11142
    K absorption line at 7699 Å, red shift, atomic-beam resonance-scatt. meas. 2—33762
    Lα measurement during solar eclipse on 12th November 1966 2—11053
    Li, identifications in the extreme u.v. in a flare 2—26915
    Mg II u.v. lines, high resolution balloon- borne spectrograph with Cassegrain telescope 2—11061
    Mg X λ625 spectroheliograms on 7 March 1970, coronal electron density maps 2—41249
    MgII and CaII, comparison between spectroheliograms 2—30606
    Na D-line, broadening by H 2—7548
    Ne IX line emission and electron density in normal non-flare coronal features 2—11146
    Ni, identification of solar lines, 140-300 Å 2—21519
    Ni XV emission line data, electron densities and temp. var. in an enhanced coronal region 2—17094
    Ni XVII, XVIII, identifications in the extreme u.v. in a flare 2—26915
    O VII line emission and electron density in normal non-flare coronal features 2—11146
    S XIV, XIII, identifications in the extreme u.v. in a solar flare 2—26915
    Si I, forbidden lines, abundance calc. 2—4995
    Si I, lines in the extreme u.v. 2—26882
    Sr resonance line profiles in sunspot umbrae and penumbrae by atomic beam spectroscopy 2—11117
    TiO γ system (0,0) band in umbral spectrum and isotopic abundances of Ti 2—41233
Sunlight
  see also Sky brightness
    artificial sunlight illuminant, visual and biological aspects 2—38138
    baffle attenuation meas. in visible 2—5429
    circumsolar radiation calculated as function of aerosol type, field of view, wavelength and optical depth 2—4683
    daylight, photometric flux derivation from filtered meas. of global radiant energy 2—7296
    meas. and interpretation by new theoretical methods 2—33468
    natural illumination, eval. from pyrheliometric obs. 2—37150
    reflection from oil on water, airborne optical detection 2—26464
    resonance scattering by spherically symmetric optically thick Sr gas cloud 2—30319
    scattering by earth's surface, angular structure, statistical nature 2—20348
    spectral energy distribution, characteristic vector analysis for soil identification by spectral reflectance 2—16773
    transfer in atmosphere-ocean system, multiple scattering calculation 2—33467
    u.v. radiation rel. to mesospheric processes 2—7298
Sunspots
    active region associated with McMath plage 10 618, eclipse of radio emission at 10 cm wavelength 2—41241
    activity cycle models and numerical studies 2—11124
    bipolar, topology of force-free magnetic field 2—11102
    convective oscillations, low-frequency, in strong mag. fields 2—20706
Sunspots continued
    crossover and magneto-optical effects from magnetic splitting of spectral lines 2—37406
    crossover and magneto-optical effects in spectra 2—11105
    cycle, 1958/70, effect on ionospheric absorption and stratospheric temperature 2—4720
    80-year cycle, new representation 2—26913
    cycle 20, rel. to solar activity, predictions (1972) 2—37403
    cycle 21, probable behaviour 2—26911
    dynamics of a toroidal magnetic ring 2—17075
    Evershed effect, fine structure from Fe I and Ca I lines and velocity measurements from Ti II, Fe II and CH lines 2—37407
    facular models and the energy deficit 2—30625
    fine structure elements as origin of magnetic field 2—11038
    flares, S-type and P-type, association with radiobursts 2—20694
    formation, rel. to small scale magnetic fields 2—11037
    frequency, secularly smoothed maxima 2—17082
    geomagnetic activity, annual variation according to character figures and sunspot cycle 2—30374
    groups, field maximum, rel. to position regularities of flares 2—11132
    groups, indications of magnetic rotator 2—37402
    groups formed, number and average lifetime in solar activity cycle No. 19 2—30627
    effects on ionospheric characteristics 2—13767
    line profiles in umbrae and penumbrae by atomic beam spectroscopy 2—11117
    mag. fields associated with polarized solar radio emission at mm wavelengths 2—7553
    magnetic deflection of solar flares in the chromosphere 2—5014
    magnetic field and turbulence 2—11107
    magnetic field structure development, statics and dynamics 2—11109
    magnetic fields, Joule dissipation, effect of anisotropy of electric conductivity 2—17077
    magnetic fields, observations of two-level structure 2—11113
    magnetic fields, rel. to high energy electrons in fields 2—11125
    magnetic fields, review 2—11106
    magnetic fields, umbral atmospheres under similarity configuration 2—37408
    magnetic fields and umbral dots 2—11121
    magnetic vector, precise determination 2—17078
    magneto fluid mechanic turbulent damping theory 2—30626
    number, rel. to ionospheric absorption 2—30341
    Paschen-Back effect of the Li resonance doublet 2—11104
    penumbral and umbral areas ratio in 11 year solar activity cycle 2—26909
    photoelectric measurements of magnetic fields 2—11108
    photometric obs. of umbra at 3.75 μ 2—26907
    spotgroups associated with surges and flares 2—26921
    surface layers, distribution of magnetic force 2—11123
    umbra, effects of penumbral radiation on physical conditions 2—20697
    umbra intensity comparison with Mercury in Hα and white light 2—11010
    umbrae, filamentary structure during transit of Mercury 2—26912
    umbral flux tubes, Alfven waves 2—37417
    umbral spectrum, derivation of magnetic field strengths 2—11111
    unipolar, structure of magnetic field and electric currents 2—11110
    effect on VLF phase regression in ionosphere D region 2—7334
    Zeeman lines in spectra and their temperature sensitivity 2—11103
    $^{13}C^{16}O$ in i.r. spectrum, det. of $^{12}C/^{13}C$ 2—17048
    Fe I line, magneto-optical effects on circular polarization 2—17080
    Fe I line, magneto-optical effects on circular polarization 2—17080
    Li-abundance, influence of model on deduction 2—30629
    TiO γ system (0,0) band in umbral spectrum and isotopic abundances of Ti 2—41233
Superconducting devices
    bolometer automatic temp. control 2—27307
    bridge, Josephson effect and vortex motion 2—1487
    coaxial guide, cylindrical, plane e.m. wave propagation 2—2307
    coils, gas cooled, for Culham Levitron, design and test 2—37886
    composite conductors, current distrib., current sharing between supercond. and substrate 2—32956
    double point contact magnetometer, construction, with Cu filled hole 2—27408
    electron acceleration in circular cylindrical superconducting cavity 2—5615
    electron lens, axial field distribution det. using Faraday effect 2—34319
    films, thin, calorimetric obs. of a.c. losses 2—4182
    helical resonator, losses in Al_2O_3 rods from 130 to 450 MHz at low temp. 2—36577
    helical resonator for heavy ion accelerator, ponderomotive oscillations 2—34865
    helically loaded resonators in proton accelerator 2—14853
    Josephson current flow in SNS junction 2—9977
    Josephson current freq. depend. under microwave radiation 2—19608
    Josephson effect, use in l.f. field sensing 2—29647
    Josephson junction, analogue simulation 2—36478
    Josephson junction, anomalous d.c. singularities 2—13192
    Josephson junction, current fluctuations, power spectrum 2—13191
    Josephson junction, I-V characts. 2—32955
    Josephson junction, Nb/Al composite electrodes 2—36476
    Josephson junction, point contact, for use in mm and sub mm wavelength regions 2—4179
    Josephson junction, simple preparation method 2—16191
    Josephson junction, thermal fluctuations effect on IV characts. 2—13187
    Josephson junction 2—25797
    Josephson junction amplifier, positive feedback, current amplification 2—9976
    Josephson junction as freq. analyzer and mixer of submm. radiation sources 2—13185
    Josephson junction for voltage meas., patent 2—17524
    Josephson junction freq.-pulling effects, cavity detuning 2—13193
    Josephson junction magnetometer, magnetocardiography applic. 2—34305
    Josephson junction mixing at i.r. freqs. 2—38027
    Josephson junction transmission line, energy band struct., wave propag. 2—22512
    Josephson junctions, strongly coupled, noise effects 2—13186
    Josephson junctions, unbiased, microwave-induced d.c. voltages 2—22513
    Josephson oscillator, intrinsic fluctuations 2—29648
    Josephson point contact, self-pumped parametric amplification at 30 MHz 2—19604
    Josephson tunnelling barriers fabrication by r.f. sputter etching 2—6783

Superconducting devices continued
  Josephson tunnelling cryotron, effect of junction capacitance 2—9975
  Josephson weak-link junctions, cylindrical cavity modes 2—1499
  Josephson-junction voltmeters, resistive transition in Sn crystal whiskers 2—1491
  junction struct., microwave assisted tunnelling 2—40220
  Levitron, plasma production and heating 2—21829
  Levitron ring, negative feedback position control system 2—28567
  magnetic susceptibility meter, low temp. thermometry applic. 2—4178
  magnetometer, sensitive, 10^{-9} gauss 2—4176
  magnetometer, using superconducting quantum flux detectors 2—23507
  maser, critical re-examination rel. to threshold and crit. currents 2 21043
  microtron type accelerator, theoretical study of losses by Joules effect and energy limitations 2—34840
  microwave, cavities, high power less mechanism 2—6785
  modulator, high-stability, low power 2—17513
  narrow bridges, preparation by Pb and Sn deposition through masks onto uncoded glass substrate 2—22511
  point contact, harmonic generation by resistive feedback 2—40219
  point contact, temp. dependence of structure on I-V curves 2—19605
  point contact junction arrays, radiation generation and detection 2—13194
  point contact weak link as magnetometer 2—1500
  point contact with Josephson junction props. 2—19607
  power transmission cable, a.c., design features 2—13198
  power transmission cable, a.c. loss and flux instabilities in single and double component type II supercond. 2—22501
  pressure contacts, high critical current, applic. to relays and switches 2—25796
  quantum interferometer, point contact (SQUID) construction 2—4183
  resonators, in linear accelerators, energy storage processes 2—38399
  SQUID, broadband supercond. quantum magnetometer 2—40218
  SQUID, principles and applications 2—4180
  SQUID, r.f., with resistive section, noise currents 2—19609
  stabilized a.c. superconductor, patent 2—13199
  switch, mechanical, for low temp. instrumentation 2—26993
  thin film bridges, relax. oscillator model 2—19606
  transformers, power supplies for synchrotron 2—14832
  tunnel contact study of recomb. lifetime of quasiparticles 2—6710
  tunnel junction, anomalous temp. depend. of resist. 2—13189
  tunnel junction, as maintenance voltage standard 2—6784
  tunnel junction, I-V characts., rel. to density of states 2—6786
  tunnel junction, Josephson current as probe of fluctuations 2—13188
  tunnel junction, subharmonic struct. 2—13195
  tunnel junction, Ta-insulator-Al, zero-bias-conductance anomaly 2—19611
  tunnel junctions, subharmonic struct. 2—9978
  weak link, microwave radiation influence on IV charact. 2—36477
  weak link, thin film, T_c increase due to microwaves 2—13190
  weak links, absolute meas. of a.c. Josephson effect 2—16194
  weak links, SNS sandwich-type, I-V characts. 2—16192
  $Au-Al_2O_3-Al$ thin film sandwiches, electron-electron interaction parameter in Au films from proximity effect 2—36479
  $Nb-NbO_x-Pb$ junctions, sputtered, d.c. and a.c. Josephson effect 2—13184
  Nb cavities, coated with Nb_2O_5, r.f. losses 2—14882
  Nb cavities, effects of oxide films on surface resistance and peak fields 2—6787
  Nb cavities and structures, tests at S- and X-band frequencies, for accelerators 2—14875
  Nb cavities with high Q, r.f. beam separators and linear accelerators 2—14815
  Nb cavity, resistance ratio meas. for material evaluation 2—25800
  Nb deflecting cavities, experimental investigation of Q values and peak fields 2—14877
  Nb helices, obs. at high field strength, for accelerators 2—27921
  Nb test cavity, properties at 350 MHz 2—34866
  Nb vibrational circuits, resonant frequency dependence of temp. curves on position of Meissner plunger in induction coil 2—25799
  Pb-teflon-Nb miniature coaxial transmission line, time and frequency response 2—7792
  Pb Dayem bridges, I-V characts., negative resist. region 2—25795
  Pb plated on Cu substrate, r.f. separators, high field tests at 1.3 GHz 2—14876
  Sn-Sn-oxide-Sn Josephson tunnel junction, exptl. study of Riedel singularity 2—13196
  Sn-SnO-Sn, Josephson tunnel junction. rel. between normal resistance and barrier thickness 2—19610
  Sn diodes, emitted phonon spectrum and influence on detected signal 2—40222
  Te barrier, supercurrent tunnelling junction 2—13183
Superconducting magnets
  90 kG, description 2—37887
  accelerator systems, air-core, winding configurations 2—14874
  coil cooling channels, heat flow analysis 2—37885
  cooling system for use with MHD convertors 2—224
  cosmic ray nuclei, spectrometer 2—21317
  cryogenic system for magnet of large mass 2—1497
  design and operation 2—34307
  electron microscope objective lens 2—2364
  mechanical current switches for use in 1 kW MHD generators 2—225
  metallic and plastic, mechanical, thermal and mag. props at v. low temps. 2—14371
  n.m.r. spin echo measurements 2—35790
  for polarized nuclear bombardment targets 2—34759
  pulsed, dipole, construction and testing for 1000 GeV machine 2—14871
  pulsed, dipole, construction and testing for 1000 GeV synchrotron 2—14871
  pulsed, for 1000 GeV synchrotron 2—38420
  quadrupole, cryogenic partially stabilized 2—1498
  rectangular coil moving above cond. slab, lift and drag forces 2—30985
  removable current lead for power supply, applications to artificial satellites 2—34309
  research progress assessment 2—4177
  solenoid, characts. 1.6-5.2K and fields to 74000 Oe 2—30986
  solenoid in dewar for magnetic field investigation 2—21017
  spark chamber, design and manufacture 2—24105
  spark chamber, design features 2—27914
  synchrotron, circuit design and performance 2—14784
  synchrotron, dipole, pulsed, testing 2—14872
  synchrotron, irradiation effects 2—14372
  synchrotron, performance in closed circuit cryogenic system 2—14870
Superconducting magnets continued
  synchrotron, pulsed design 2—14873
  for synchrotrons, status 2—14846
  synchrotrons of more than 1000 GeV, characteristics 2—14869
  for Tokamak fusion reactor 24271 2—24271
  NbTi superconductors, enhancement of quench fields on cooling below 4.2 K, method for maintaining 2.17 K with He at constant 1 atm. 2—27410
Superconducting materials
  A15 type, linear chain model 2—19562
  A-15 cpds., strain depend. of T_c, struct. instability and anharmonicity 2—40201
  A-15 cpds., transverse acoustic phonons role 2—29633
  a-15 film prep. by co-sputtering, resist. ratio 2—29013
  actinide metal, carbides, phonon spectra and electron-phonon coupling const. 2—29644
  actinides, model obs. 2—29639
  actinides, review 2—13147
  alloy, analogy with precip. hardening 2—39912
  alloy, dil., critical temp. eqn. 2—40203
  alloy, dil., fluctuation-induced diamagnetism, pair propagator approach 2—19568
  alloy, layered materials, high superconducting transition temps. 2—13146
  alloy, localized spin fluctuations 2—16170
  alloy with mag. impurities, fluctuations 2—32933
  alloys, upper critical field, four-term Kubic expression 2—25779
  colloids calc. of multiple transition temperatures 2—19553
  composite, multiflamentary, design problems 2—1496
  dichalcogenide, layered transition metal intercalation complexes, lattice imperfections by electron microscopy and diffraction 2—36008
  dirty, gapless, relationship of 3rd order free energy term to incremental vortex entropy 2—4163
  dirty type II, thermodynamic fluctuation of order parameter in vortex state 2—16167
  dislocations, moving, energy losses, electronic component 2—25783
  electron microscope observation of magnetic effects 2—9405
  eutectic, critical temp. and field rel. to solidification rate 2—3437
  ferroelasticity, review 2—12988
  film, crit. temp., effect of dielectric coating 2—6767
  film, fluctuation-induced cond. above T_c, Maki contrib. 2—40202
  film, normal metal coated, tunnelling and energy spectrum, thermal cond. 2—9965
  film, sp. ht., effect of order parameter fluctuations 2—32935
  film, thick, e.m. wave transparency 2—13144
  film, transition temp. changes 2—13127
  fluctuation specific heat in a magnetic field, dimensionally change 2—36448
  Ginzburg-Landau parameter, spatial variation due to composition inhomogeneities 2—4162
  granular, bulk, Josephson effects 2—6774
  granular, fluctuation effects 2—19576
  granulated, exciton mechanism of supercond. 2—13115
  graphite intercalation cpds., comparison between ferromag. and supercond. 2—6959
  h.f. residual surface resistance rel. to sound wave generation by incident e.m. radiation 2—19554
  high field, microstruct., mats. design for commercial applic. 2—36463
  high-field, pulsed-field meas. rel. to metallurgical processes, comparative study 2—25790
  impurity bands and Kondo effect 2—32934
  inhomogeneous, density of states 2—6786
  intercalation cpds., NbS_2/pyridine complex, elec. field gradient 2—19947
  intermediate state, resonant u.s. absorpt. by nuclei 2—25782
  n.m.r. obs. 2—6768
  phonon spectra, neutron scatt. and tunnelling comparison 2—19395
  power transmission cable applic. 2—13197
  rare earth metals, press. depend. 2—29639
  semiconductor, low temp. heat capacity 2—19427
  small particles, transition temp. changes 2—13127
  small particles, tunnelling obs. of T_c 2—13145
  solid, lattice defects, flux lines and interactions 2—1489
  specific heat electronic and Debye temp., determ. method 2—16032
  strong-coupling, thermal cond., electronic contrib. and elastic electron scatt. 2—22503
  $Te_{0.81}Ge_{0.15}As_{0.04}$, memory state, transition temp., critical field 2—16168
  thin film, fluctuation heat capacity near T_c 2—9887
  transition metal, dirty, Hall effect near upper critical field 2—40213
  transition metal, exptl. survey 2—29641
  transition metal, grain size effect on T_c 2—19599
  transition metal, narrow d-band behaviour 2—13082
  transition metal, role of s-and d-band electrons 2—36455
  transition metal alloy, topologically close packed, band struct., mag. props. 2—35977
  transition metal alloys, 4d h.c.p. series, spin fluctuation effects on T_c 2—19600
  transition metal carbides, electron-phonon interactions, phonon spectra 2—19388
  transition metal carbides, nitrides and oxides, high T_c obs. 2—29645
  transition metal carbides, phonon spectra and electron- phonon coupling const. 2—29644
  transition metal carbides and nitrides, density of states 2—40215
  transition metal carbides and nitrides high T_c obs. 2—13182
  transition metal containing nonmag. impurities, thermal conductivity, low-band model 2—36472
  transition metal dichalcogenides, layered, high temp. cond. obs. 2—29643
  transition metal solid solns., transition temp., lattice instability, electron/atom ratio 2—40214
  transition metals, alloys and cpds., BCS theory 2—29642
  transition metals, conf., Rochester, USA, Oct. 1971 2—29632
  transition metals, electron-phonon coupling in tight-binding approx. 2—29591
  transition metals, electron-phonon coupling matrix elements 2—29600
  transition metals, electron-phonon interactions 2—16189
  transition metals, estimation of electron-phonon coupling constant, role of d-resonances 2—32931
  transition metals, Ettingshausen effect in mixed state 2—36474
  transition metals, high T_c systematics 2—16188
  transition metals, i.r. props., electron-phonon coupling 2—29646
  transition metals, Kohn anomaly in transition temp. 2—19492
  transition metals, lattice dynamics, electronic struct. depend. 2—32814
  transition metals, press. depend of T_c 2—29625

Superconducting materials continued
transition metals, symmetrized pair states in Wannier represent. 2—22510
transition metals, transition temp., energy band considerations 2—32953
transition metals, transition temp. order of magnitude 2—19491
transition metals and cpds., energy bands, review 2—29599
transition metals and cpds., press. depend. of T_c, theory 2—29624
transition temperature, effect of spin fluctuation 2—32924
transition-metal systems relation of anomalies in phonon dispersion curves to acoustical plasmons 2—25771
two-band, energy spectrum. Andersons theorem generalization 2—36451
type I, undergraduate expt. to determ. magnetic properties 2—16149
type-I, two-dimens. mixed state obs. 2—36457
u.s. absorption anisotropy, rel. to overlapping energy bands 2—32932
Al-Ag (Sn) systems, transition temp. 2—16171
Al-Au, solid soln., isothermal phase transformations, rel. to supercond. props. 2—9790
Al-Cr(Fe)(V) dil. alloys, transition temp. meas., conc. depend. 2—16175
Al-Ge film, normal and supercond. props. 2—32926
Al-Mn dil. alloys, T_c depression under press., localized spin fluctuations 2—1494
Al-Pb junctions, 9.3 GHz phonon interactions with electrons 2—4164
Al, critical mag. fields under press. 2—16173
Al, electron-phonon interaction, mixed-plane-wave effects 2—19489
Al, energy gap anisotropy 2—25784
Al, granular, density of states and resistive transitions in fluctuation regime 2—13151
Al, one-dimensional, meas. of excess fluctuation conductivity 2—13118
Al, penetration depth, mag. field and temp. depend. 2—16172
Al, supercooling and superheating, Ginzburg-Landau parameter 2—13155
Al, temperature variation in nuclear spin-lattice relaxation rate including anisotropy in energy gap 2—36450
Al, transition temperature, pressure depend., pseudopot. approach 2—36454
Al film, anomalous paracond. 2—16164
Al film, disordered, resistive transitions and critical fields 2—13149
Al film, Ginzburg-Landau parameter, mag. transitions and supercooling meas. discrepancy 2—9968
Al film, granular, momentum depairing in paracond. regime 2—13148
Al film, granular, supercond. enhancement mechanism 2—13154
Al film, paracond., elec. field depend. 2—13152
Al film, quasiparticle recomb. time, thickness depend. 2—13153
Al film, thickness depend. of transition temp. 2—13150
Al films, Knight shift, transition temp. obs. 2—16174
Al films and foils, critical fields, size effects 2—36464
Al films and small particles, T_c enhancement 2—9969
Al films with enhanced T_c, localized state effects 2—22504
Al strips, collective excitations 2—13156
$AuGa_2$, pressure induced electron transition near 6 kbar at liquid He temps. 2—40190
$(Au_{1-x}Pd_x)Te_2$ alloys, conc. depend. of T_c 2—19577
Ba, critical temperature, press. depend., 100-200 kbar 2—22508
Bi, critical temperature, press. depend., 100-200 kbar 2—22508
Bi film, thickness depend. of transition temp. 2—13150
Cd, intermediate isotope effect 2—16173
Cd, plastically deformed, transition temp., recovery 2—19559
Ce-La alloys, sp. ht., Fermi surface obs. 2—19578
$CeRu_2$, tunnelling using Ge-barriers 2—40204
$CeRu_2$ and mixed crysts., prep. and supercond. props. 2—19579
$CeRu_{2-x}Co_x$ dil. alloys, T_c depression and mag. susceptibility 2—1495
Cu film backed by Pb, induced supercond., tunnelling obs. 2—6775
film, anomalous paracond. 2—16164
Ga, critical mag. fields under press. 2—16173
Ga, gap determ. from u.s. attenuation 2—4174
Ga, length change anisotropy at T_c, magnetostriction obs. 2—19580
Ga, single crystal, evidence for selection rule for tunnelling presented 2—4161
Ga, u.s. absorpt. in intermediate state 2—13158
Ga film, thickness depend. of transition temp. 2—13150
H_2, high-temp. supercond. in metallic phase 2—16176
$(Hf,Ta)V_2$ and $(Hf,Zr)V_2$ alloys, transition temp. correl. with lattice instabilities 2—32937
HfC, electron-phonon interactions, phonon spectra 2—19388
Hg, electron-phonon mass enhancement, temp. depend. 2—25785
Hg, electronic thermal cond. 2—22507
Hg, in chrysotile asbestos., supercond. and semicond. transition 2—29634
In/Zn superimposed layers, mixed state props., critical phenomena 2—16177
In-Bi alloy, critical parameters, hydrostatic press. effect 2—29635
In-Bi metastable solid solution, transition temp. 2—16171
In-Mn dil. alloy films, electronic thermal cond., transition pt. phenomena 2—19582
In-Pb alloy, connected cylinders, mag. flux quantization 2—6769
In-Pb alloys, normal and flux-flow states, Hall effect 2—13162
In-Pb alloys, transport entropy of vortices 2—13161
In-Sn alloys, normal and flux- flow states, Hall effect 2—13162
In-Tl alloys, electron-phonon interaction 2—40205
In-2 to 4%Bi, multivalued critical current 2—13134
In, compression effects on T_c, role of pt. defects 2—25787
In, critical point fluctuations in thin films, and excess noise 2—40188
In, electron-dislocation interaction 2—13164
In, electronic thermal cond. 2—22507
In, excess diamag. susceptibility above T_c 2—13159
In, phonon spectra, neutron scatt. and tunnelling comparison 2—19395
In, plastically deformed, transition temp., recovery 2—19559
In, polycryst. bulk, supercond. energy gap, In-Al_2O_3-Pb tunnel junc. obs. 2—19574
In, thermally activated glide, comparison with normal In 2—22209
In cylinder, mag. field penetration pattern 2—19581
In dil. alloys, transition temp., depend. on solute conc. 2—25786
In film, Ginzburg-Landau parameter, mag. transitions and supercooling meas. discrepancy 2—9968
In film, mag. transitions 2—22506
In film, resist. peak at T_c 2—6776
In film between ferrites, transition temp. obs. 2—13163
In films, electromagnetic generation of transverse acoustic waves at 9 GHz 2—13119
In films, penetration depth and flux creep 2—40206
In whisker, critical current temp. depend. 2—13160
In_5Bi_3, mixed state, Hall effect 2—32938

Superconducting materials continued
InPb, alloys, magnetostriction and magnetization meas., Ginzburg Landau parameter 2—19823
K, transition temperature, pressure depend., pseudopot. approach 2—36454
La-Ce dilute system, temp. depend. of spin-flip scatt., determ. from H_{c2} 2—29620
La-Gd dilute system, temp. depend. of spin-flip scatt., determ. from H_{c2} 2—29620
La-actinide metal dil. alloys, impurity effects on supercond. T_c 2—19583
La, grain size effect on T_c 2—19599
La, tunnelling, surface contamination effects, electron-phonon coupling 2—29636
$LaAl_2$, Laves phase compound, low temp. specific heat 2—19425
$La_{3-x}Gd_xAl$, mag. impurity effect, gapless supercond., n.m.r. obs. 2—6777
$LaIn_3$, mag. interactions 2—16179
La_3In, thermal stability, paramag. impurity effects 2—16178
$LaSn_3$, electron energy levels, nonrel. modified OPW calc. 2—19510
$LaSn_3$, electron energy levels, relativistic corrections using perturb. theory 2—25733
Li, transition temperature, pressure depend., pseudopot. approach 2—36454
Mo-Re alloys, u.s. attenuation, energy gap anisotropy 2—16180
Mo, grain size effect on T_c 2—19599
Mo, hypersound attenuation 2—16181
MoS_2 intercalation cpds., transition obs. 2—32939
Na, transition temperature, pressure depend., pseudopot. approach 2—36454
Nb-Al-Ge film, high vac. annealed, supercond. props. 2—40200
Nb-Al-Ge films, critical parameters 2—32942
Nb-Ge-Al alloy, low temp. cubic- tetragonal transform. 2—9817
Nb-Mo alloy, flux-flow resist., Ettingshausen effect, thermal and mag. props. 2—13167
Nb-Mo alloys, transport entropy of vortices 2—13161
Nb-Ta-Ti, Nb-V-Ti system, T_c determ. from planned expt. method using simplex lattice concept 2—4175
Nb-Ta, magnetic behaviour at small Ginzburg-Landau parameters (χ) 2—19569
Nb-Ta alloy, critical current depend. on defect structure of flux line lattice 2—19556
Nb-Ta alloys, critical fields and strong coupling, conc. depend. 2—19588
Nb-(60 at.%)Ti alloy, critical supercurrents and pinning of vortices 19584 2—19584
Nb-Ti alloy, peak effect, rigidly pinned vortex model 2—13168
Nb-Ti system, electronic structure, heat capacity analysis 2—40195
Nb-50%Ti, crit, current density, neutron irrad. effects 2—29631
Nb-64%Ti alloy, cylindrical sample, magnetiz. and size effect36460 2—36460
Nb-(25 at.%)Zr, Joule-heating power dissipation in hollow tube 2—36461
Nb-Zr alloys, high-field, pulsed-field meas. rel. to metallurgical processes, comparative study 2—25790
Nb-25%Zr, crit. current density, neutron, irrad. effects 2—29631
Nb-25%Zr, low field critical current density from magnetiz. data 2—22502
Nb_3Al, high mag. field props. 2—19586
Nb_3Al, upper critical fields 2—32940
Nb_3Al film prep. by co-sputtering, resist. ratio 2—29013
$Nb_{0.75}(Al_{0.75}Ge_{0.25})_{0.25}$, upper critical fields 2—32940
$Nb_3Al_{0.75}Ge_{0.25}$ film prep. by co-sputtering, resist. ratio 2—29013
$Nb_3Al_xGe_{1-x}$, critical temp. conc. depend., cond. electron conc., phonon spectra 2—40207
$NbAs_2$-type compounds, transition temp. investigation 2—32927
Nb_3Ga, transition temp., phase diagram 2—32941
Nb_3Ga, upper critical fields 2—32940
Nb_xGa_{1-x} alloy, upper critical fields 2—25789
NbN, S-band state density at fermi energy 2—13089
NbN, stabilized, a.c. losses 2—9971
NbN film, reactively sputtered, supercond. props. rel. to substrate temp. and struct. 2—40199
NbN films, critical parameters 2—32942
NbN films, thickness depend. of T_c 2—19589
$NbSe_2$, layer structure, energy gap meas., temp. dependence 2—4165
$NbSe_2$, press. induced supercond. 2—16182
$NbSe_2$, ratio of effective masses, flux flow and pinning 2—19590
$NbSe_2$, ultrathin layers, superconducting resistive transition 2—19560
Nb_3Sn, normal and supercond. props. rel. to density of states 2—29637
Nb_3Sn, temp. dependent a.c. properties, calorimetric technique for obs. 2—4182
Nb_3Sn, uniaxial stress effect on T_c 2—19587
Nb_3Sn alloys, high-field, pulsed-field meas. rel. to metallurgical processes, comparative study 2—25790
Nb_3Sn films on Nb, deposition and critical temp. props. 2—12661
Nb_3Sn ribbon, prep., microstruct., doping, high field props. 2—32944
NbTa, flux line arrangements in hysteretic low-k samples 2—19570
$Nb_{0.73}Ta_{0.27}$, flux line lattice, neutron diffr. obs. 2—9967
$Nb_{75}Ta_{25}$, vortices, small-angle neutron scatt. obs. 2—19591
$Nb_{0.88}Ti_{0.12}N$ film, fluctuation rounding of resistive transition 2—13166
Pb-Bi, flux line-defect interaction distances 2—19555
Pb-Bi alloy in porous glass, spin-orbit effects, critical fields 2—19594
Pb-Bi alloy in porous glass, meas. of critical current density 2—4167
Pb-Bi amorphous alloys, tunnelling, energy gap, phonon spectra 2—13172
Pb-Bi type II system, flux line pinning by large normal particles 2—29628
Pb-In alloy, h.f. study of vortex pinning 2—32948
Pb-In alloys, Holstein process observed in far i.r. meas. of surface resistance, new sum rule 2—13120
Pb-In alloys, proximity effect and sp. ht. jumps 2—19593
Pb-In alloys, strong coupling, supercond. props., energy gap ratio 2—16184
Pb-In alloys, thermal cond. near upper critical field 2—25793
Pb-Tl alloy, bulk flux pinning, critical-state model 2—16183
Pb-Tl alloy system, hysteresis effects 2—6780
$Pb_{0.7}Bi_{0.3}$ alloy, strong coupling supercond., electron tunnelling obs. 2—4166
$Pb_{55}Bi_{45}$, amorphous and cryst. microwave surface resist. 2—13177
Re-Mo_2C solid solution, comp. depend. of crit. temp. 2—22498
ReC_x, high press. synthesis, struct. 2—19057
Sn:In, vortex transport entropy, tunnelling effect 2—16162
Sn-In alloy film, anomalous paracond. 2—16164
Sn-Pb alloy whiskers, fluctuation effects in resistive transition 2—13179
Sn, compression effects on T_c, role of pt. defects 2—25787
Sn, critical point fluctuations in thin films, and excess noise 2—40188

Superconducting materials continued
  Sn, dynamic intermediate state, regularity of domain motion 2—36469
  Sn, enhanced diamag. above T_c due to thermal fluctuations 2—13178
  Sn, IV charact., instabilities in transition curve 2—32950
  Sn, intermediate state, u.s. attenuation 2—36470
  Sn, intermediate state, u.s. absorpt. 2—36468
  Sn, phonon spectra, neutron scatt. and tunnelling comparison 2—19395
  Sn, plastically deformed, transition temp., recovery 2—19559
  Sn, spatial periodicity of moving domain structure, relation to predictions of Landau model 2—13117
  Sn cylinder, mag. field penetration pattern 2—19581
  Sn diodes, emitted phonon spectrum and influence on detected signal 2—40222
  Sn film, Ginzburg-Landau parameter, mag. transitions and supercooling meas. discrepancy 2—9968
  Sn film, mag. transitions 2—22506
  Sn films, cylindrical, stability of supercurrents 2—36471
  Sn one-dimens. wires, resist. ratios, electron mean free paths 2—13180
  Sn resist. peak at T_c 2—6776
  Sn small particles, h.f. mag. polarizability 2—9974
  Sn whisker, critical current temp. depend. 2—13160
  Sn whisker, fluctuation effects on T_c 2—19597
  Sn whisker crystals resistive transition, McCumber-Halperin modification of the Langer-Ambegaokar theory 2—1491
  Sn whiskers, fluctuation effects in resistive transition 2—13179
  SnTe, semicond., low temp. heat capacity 2—19427
  SnTe, transition temp. depend. on paramag. ion conc. 2—40210
  $SrTiO_{3-x}$ and $Ca_ySr_{1-y}TiO_{3-x}$, soft mode supercond. 2—19598
  $SrTiO_3$, supercond., low temp. heat capacity 2—19427
  Ta-N, magnetic behaviour at small Ginzburg-Landau parameters (χ) 2—19569
  Ta, mixed state, N_2 distrib. obs. using rot. hysteresis 2—32954
  Ta, phonon spectra, neutron scatt. and tunnelling comparison 2—19395
  Ta, surface impurity effects on supercond.-normal transition 2—36459
  Ta, surface impurity effects on supercond-normal transition 2—36458
  Ta, tunnelling, surface contamination effects, electron-phonon coupling 2—29636
  TaC, electron-phonon interactions, phonon spectra 2—19388
  TaC_x, lattice instability effects on supercond. 2—22509
  TaS_2, intercalation effect on electron transport 2—32951
  Ta_3Sn, nuclear quadrupole spin lattice relax. 2—4173
  Th-U, dil. alloys, T_c depression under press., localized spin fluctuations 2—1494
  Th-U dilute alloy, mag. props., sp. ht. study 2—29557
  Th, critical mag. fields under press. 2—16173
  Th, energy gap, tunnelling obs. 2—40211
  Th, transition temp. press. depend. 2—32952
  ThC/ThN system ternary cpds., transition temp. obs. 2—29640
  Th_4H_{15}, prep., elec. and supercond. props. 2—25772
  Ti-Mo alloy, fluctuation cond., mag. field quenching 2—13181
  Ti-Mo alloys, T_c enhancement on mech. deform. 2—6781
  Ti-Mo alloys, transition temp., lattice instability, electron/atom ratio 2—40214
  TiO, cubic and monoclinic, transition temp. obs. 2—40212
  TiO_x, transition temp. obs. 2—32992
  Tl:Cd, Hg, Zn transition temp., impurity effects 2—36473
  Tl-Pb alloy, phonon spectra, neutron scatt. and tunnelling comparison 2—19395
  Tl, electronic thermal cond. 2—22507
  Tl, excess diamag. susceptibility above T_c 2—13159
  Tl, phonon spectra, neutron scatt. and tunnelling comparison 2—19395
  α-U, transition temp. and mag. susceptibility under press. 2—25794
  V, flux line arrangements in hysteretic low-k samples 2—19570
  V, isothermal magnetiz. curves. critical parameters 2—19602
  V, mixed state, hysteresis, neutron depolarization obs., flux distrib. 2—6779
  V, mixed state, N_2 distrib. obs. using rot. hysteresis 2—32954
  V, mixed state, thermomag. props. 2—13165
  V, surface supercond., critical phenomena 2—13169
  V_3Au, annealing effects on transition temp. and upper critical field 2—19601
  V_3Ga alloys, high-field, pulsed-field meas. rel. to metallurgical processes, comparative study 2—25790
  V_3Ga solid solns., struct. influence on supercond. 2—9496
  $V_2Hf_xZr_{1-x}$, alloys, high-field, pulsed-field meas. rel. to metallurgical processes, comparative study 2—25790
  V_3Pt, spin-lattice relax. of ^{51}V near T_c 2—33183
  V_3Si, elastic softening arrest at T_c 2—9871
  V_3Si, mag. contrib. to low temp. sp. ht. in mixed state 2—16190
  V_3Si, single cryst., critical current peak effect 2—16169
  V_3Si film prep. by reactive diffusion 2—29013
  Zn, anisotropic length changes at T_c 2—19603
  Zn, supercooling and superheating, Ginzburg-Landau parameter 2—13155
  Zr, α and ω types, pressure dependence of transition temp. above 60 kb 2—32928
  ZrB_{12}, isotope effect due to optical phonon modes 2—6782
 lead
  amorphous, phonon spectra 2—13157
  amorphous and disordered, phonon enhanced cyclotron mass and electronic sp. ht. 2—16101
  Bernouilli effect, temp. depend. 2—13175
  creep strain jump, at supercond. transition 2—3881
  critical field curve 2—40217
  critical temperature, press. depend., 100-200 kbar 2—22508
  Dayem bridges, I-V characts., negative resist. region 2—25795
  electron-dislocation interaction 2—13164
  electron-phonon interaction, mixed-plane-wave effects 2—19489
  energy gap, photoelec. effect 2—9972
  energy gap anisotropy, tunnelling obs. 2—13173
  film, fluctuation effects in cond. 2—13171
  film, Ginzburg-Landau parameter, mag. transitions and supercooling meas. discrepancy 2—9968
  film, influence of film edge on resistance peak 2—4171
  film, intermediate state, resist., oscillating mag. fields influence 2—13176
  film, mag. flux penetration and eddy current damping 2—36467
  film, mag. relax. and eddy current damping 2—25792
  film, thick, backed by Fe, proximity effect, tunnelling obs. 2—16186
  film, thickness depend. of transition temp. 2—13150
  film, u.s attenuation, surface sheath effect 2—29638

Superconducting materials continued
 lead continued
  films, magneto-optical study of intermediate state, magnetic field and film thickness dependence 2—40196
  Ginzburg-Landau parameter determ. in thin films using acoustic surface waves 2—19596
  Holstein process observed in far i.r. meas. of surface resistance, new sum rule 2—13120
  intermediate state structures, magneto-optical obs. 2—6770
  Josephson junctions, unbiased, microwave-induced d.c. voltages 2—22513
  magnetization, effect of geometrical factors 2—32947
  narrow bridges, preparation by deposition through mask onto uncooled glass substrate 2—22511
  particles, size and surface effects on specific heat 2—32949
  peak critical current, degradation and reenhancement 2—25791
  penetration depth and e.m. absorpt. edge 2—16185
  phonon spectra, neutron scatt. and tunnelling comparison 2—19395
  plastically deformed, transition temp., recovery 2—19559
  plated on Cu substrate, r.f. separators, high field tests at 1.3 GHz 2—14876
  proximity effect, induced density of states in Cu 2—13174
  surface resist., far-i.r., absolute meas. 2—36466
  thermal cond., electronic contrib. 2—22507
  thermal cond., electronic contrib. and elastic electron scatt. 2—22503
  transition temperature, pressure depend., pseudopot. approach 2—36454
  tunnelling, splitting of phonon struct. 2—19595
  tunnelling in n-GaAs-Pb contact, press. depend. 2—40221
  vortex transport entropy, tunnelling effect 2—16162
  film, mag. transitions 2—22506
  $Nb-NbO_x-Pb$ junctions, sputtered, d.c. and a.c. Josephson effect 2—13184
  Pb/Cu double layer, crit. mag. fields detn. 2—25780
  Pb/Cu double layers, parallel critical mag. fields 2—16187
  Pb/Cu double layers, thickness depend. of critical mag. field 2—9973
  Pb-Cu-Pb sandwiches, supercurrent density 2—9961
  Pb-teflon-Nb miniature superconducting coaxial transmission line, time and frequency response 2—7792
  Pb and Pb-30%Bi disordered superconducting films, comparison of specific heat and tunnelling data 2—9979
 niobium
  a.c. magnetic field losses at 4.2 K of magnetic reversible Nb 2—40194
  cavities, coated with Nb_2O_5, r.f. losses 2—14882
  cavities, effects of oxide films on surface resistance and peak fields 2—6787
  cavities and structures, tests at S- and X-band frequencies, for accelerators 2—14875
  cavity, resistance ratio meas. for material evaluation 2—25800
  cavity, Te_{011} mode, with high critical mag. field and Q-value 2—25798
  charge transfer rel. to supercond., X-ray photoelectron spectroscopic obs. 2—22505
  creep strain jump, at supercond. transition 2—3881
  critical field temp. depend., non-local supercond. 2—13170
  deflecting cavities, experimental investigation of Q values and peak fields 2—14877
  film, critical current 2—32946
  film, flux line lattice and dislocations 2—19592
  film, r.f. sputtered, resist. ratio, transition temp., intrinsic mean free path 2—25788
  film, vacuum deposition parameters effect on transition temp. 2—9970
  flux line arrangements in hysteretic low-k samples 2—19570
  flux line lattice, neutron diffr. obs. 2—9967
  flux pinning mechanism 2—29630
  foil, ion bombarded, critical current increase 2—6778
  impurity effects on critical fields and strong coupling 2—19588
  magnetic behaviour at small Ginzburg-Landau parameters (χ) 2—19569
  magnetoelastic props., u.s. attenuation, vortices, dislocation dynamics 2—36465
  microtron type accelerator, theoretical study of losses by Joules effect and energy limitations 2—34840
  microwave cavities, with high Q, r.f. beam separators and linear accelerators 2—14815
  mixed state, flux line arrangement 2—13137
  mixed state, hysteresis, neutron depolarization obs., flux distrib. 2—6779
  mixed state, thermomag. props. 2—13165
  power transmission cable, a.c., design features 2—13198
  surface, control of morphology and purity during treatment, use in r.f. supercond. 2—39462
  surface electropolishing method and cavity resonator props. 2—4181
  surface struct., rel. to r.f. cavity design 2—32943
  surface supercond., critical phenomena 2—13169
  thermal cond. in mag. fields near H_{c2} 2—16071
  tunnelling, surface contamination effects, electron-phonon coupling 2—29636
  vibrational circuits, resonant frequency dependence of temp. curves on position of Meissner plunger in induction coil 2—25799
  vortex motion, atomic beam study 2—19585
  vortices, small-angle neutron scatt. obs. 2—19591
  $Nb:Al_2O_3$, sintered, cold worked, residual resist., mag. behaviour, critical current density 2—32945
  Nb/Al, composite electrode in Josephson junc. 2—36476
  $Nb-NbO_x-Pb$ junctions, sputtered, d.c. and a.c. Josephson effect 2—13184
  Nb-Zr alloy, supercond. wires critical current density control by dislocation substruct. 2—40209
  Pb-teflon-Nb miniature superconducting coaxial transmission line, time and frequency response 2—7792
Superconductivity
  see also BCS theory
  astrophysics, review 2—13820
  Bernouilli effect, temp. depend. 2—13175
  boson method, time-dependent theory 2—19567
  causes, rel. to movement of valency electrons 2—29619
  conference, Stanford, USA, Aug. 1969 2—13116
  Corbino discs, flux motion obs. 2—19571
  critical conductivity calcs. in consistent approx. containing fluctuations 2—16151
  critical point fluctuations in superconducting In and Sn thin films and excess noise 2—40188
  critical temp. calc. using McMillan eqn. 2—32936
  critical temp. variation and phonon model 2—6771
  current carrying cylinder, intermediate state 2—1490
  cylinder, current carrying, resistance ratio and mag. induction 2—16193

Superconductivity continued
cylinder, mag. field penetration pattern 2—19581
dislocation motion, supercond. and normal states, theory 2—12766
electric potentials near superconducting-normal boundary 2—36449
electron-dislocation interaction 2—13164
electron-electron interaction, mass and vol. depend. 2—16154
electron-electron interaction, retardation, s-state instabilities 2—16158
electron-electron interactions, effect on quasiparticle decay 2—19573
ferroelastic relationship 2—3828
and ferromagnetism, coexistence 2—19563
field theoretic treatment, collective modes, coupling constants and dynamical symmetry rearrangement 2—9962
filament, resistive transition 2—40193
film, flux flow, V-I plots 2—19561
film, paracond. due to fluctuations, mag. field effect 2—13129
fluctuation conductivity in thin films in mag. fields 2—19557
fluctuation effects above T_c, review 2—13121
fluctuation effects on smearing of phase transition 2—16160
fluctuation-induced diamagnetism, pair propagator approach 2—19568
fluctuation-induced diamagnetism above T_c 2—19566
fluctuations above T_c, mag. field effect 2—13128
flux lines with oscillating order parameter, interaction energy 2—6773
flux motion, time-dependent voltages 2—13131
flux motion and noise in dynamic intermediate state 2—13133
flux tubes motion, simulation by magnetic needles in $CuSO_4$ soln. 2—40187
gap states in small particles 2—29627
Ginzburg Landau eqn., time dependent and fluctuating pair propagator wave character 2—4160
Ginzburg-Landau eqns., oscillatory solns. at H_{c1} 2—9963
Ginzburg-Landau parameter, spatial variation due to composition inhomogeneities 2—4162
Ginzburg-Landau theory, time-dependent, charge conservation and chemical potential studied 2—9964
granulated superconductors, exciton mechanism of supercond. 2—13115
high field superconductor, influence of magnetic impurities 2—25781
high temperature, excitonic mechanism 2—13123
high temperature, review and anticorrels. 2—13124
high temperature problems due to metastability 2—29626
hollow cylinder, current carrying resistance 2—32925
hollow cylinder, fluctuation cond., oscillations in mag. field 2—6772
intermediate state, thermodynamics, transition fields, domain struct. 2—22500
Ising model of weakly coupled granular superconductor 2—16153
Josephson effect, d.c., technique for displaying magnetic field dependence 2—4159
Josephson effect 2—25797
Josephson effect 2—32955
Josephson effect analogue in superfluid 2—6275
Josephson phenomena, time dependent mechanical analogues 2—2049
Josephson tunnelling, pair breaking mechanisms 2—36456
Landau domain structure, exptl. realization of highly regular motion 2—13117
Landau-Ginzberg eqn. for small samples 2—16152
layered system, fluctuation-enhanced diamag., temp. depend. 2—19564
localized mag. moment form. 2—25774
low and ultralow research, at Sussex, Cambridge, and Birmingham Univs. 2—41362
magnetic impurity effects 2—13126
magnetization at T_c, universal law 2—16161
maximum transition temp. estimates 2—29622
McMillan equation, generalized form 2—16157
metal, critical temp. rel. to electronic struct. 2—40121
metal, plasticity 2—22499
metal, supercond. transition temp., pressure depend., pseudopot. approach 2—36454
metallo-organic layered media, exciton mechanism of high temp. supercond. 2—1683
narrow-band, press. depend of T_c, theory 2—29624
n.m.r. obs. 2—6768
non-degenerate system, undamped Cooper pairs 2—29594
non-transition metal, supercond. state parameters using various approx. for dielec. screening func. 2—36452
off-diagonal long range order systems, canonical ensemble perturbation eval. 2—17265
one-dimensional, critical behavior 2—32930
order parameter fluctuations, critical region 2—13122
oscillatory flux line profile near $T=T_c$ 2—19565
peak effect, rigidly pinned vortex model 2—13168
phase transitions, in exchange field 2—1642
phase transitions in magnetic fields, theory of nucleus formation 2—25773
phase transitions of first order at H_{c1} 2—40192
polyferrocene, phthalocyanines, polyvinyl pyridine and TCNQ complex, d.c. dark cond., Seebeck meas. 2—36475
proximity effect, BCS spectrum 2—16159
proximity effect in parallel mag. fields 2—25775
quantum fluctuation induced diamagnetiz. 2—32929
quantum phase fluctuations 2—13130
resistive states, electron refl., domain motion 2—16165
r.f., applications to particle accelerators 2—14789
rotating thin wall cylinder, quantum interference effects 2—6766
small structures, Josephson-like behaviour 2—13132
spin excitation effects, review 2—29623
strong coupling, derivation of explicit formula for critical temp. 2—4170
strong-coupling, penetration depth and e.m. absorpt. edge 2—16185
superconductor, two-band, energy spectrum, Andersons theorem generalization 2—36451
surface currents, contributary mechanisms 2—19572
surface impedance and anomalous microwave absorpt. 2—16156
surface impurity effects on supercond.-normal transition 2—36458
surface-sheath nucleation field, temp. depend. 2—1492
TCNQ charge-transfer complex, cond., Hall effect, Seebeck coeff. 2—40216
thermal fluctuation effects, review 2—4172
thin films, dirty, fluctuation of order parameter and Hall effect 2—6765
thin films, paraconductivity meas., effect of thermal phonon pair breaking on fluctuations 2—16150
transition metal, role of s-and d-band electrons 2—36455
transition metal carbides, rel. to phonon spectra obs. 2—6655

Superconductivity continued
transition temp. determ. from planned expt. method using simplex lattice concept 2—4175
transport phenomena, theory 2—13125
tunnelling, preferred direction, energy gaps and phonon struct. 2—16155
tunnelling, through barrier with paramagnetic interacting impurities 2—36453
tunnelling using Ge-barriers 2—40204
two band system, density of states determ. 2—29621
type I, destruction kinetics in wire by overcritical current 2—16163
type-I, two-dimens. mixed state obs. 2—36457
u.s. investigation 2—40189
valence electrons, energy operator, approx. diagonalization 2—19486
vortex lattice, elastic scattering of ultracold neutrons 2—19039
vortex transport entropy, tunnelling effect 2—16162
vortices, dynamic structure 2—4169
weak coupling superconductor, average gap critical temp. and gap anisotropy distribution 2—40191
$Nb:Al_2O_3$, sintered, cold worked, residual resist., mag. behaviour, critical current density 2—32945
Nb-Zr alloy, wire, critical current density control by dislocation substruct. 2—40209
Nb, rel to charge transfer, X-ray photoelectron spectroscopic obs. 2—22505
Pb/Cu double layer, crit. mag. fields detn. 2—25780
Pb-Bi alloy in porous glass, meas. of critical current density 2—4167
Pb-Cu-Pb sandwiches, supercurrent density 2—9961
$Pb_{0.7}Bi_{0.3}$ alloy, strong coupling, deviations from weak coupling BCS theory 2—4166
Sn-SnO-Sn, Josephson tunnel junction. rel. between normal resistance and barrier thickness 2—19610
Tl:Cd, Hg, Zn transition temp., impurity effects 2—36473
^{51}V in V_3Au, n.m.r. model proposed for normal and superconducting states 2—4564

type II
alloys, discontinuity of mag. moment, study using Ginzburg Landau parameters variation 2—4162
alloys, upper critical field, four-term Kubic expression 2—25779
bulk flux pinning, critical-state model 2—16183
Corbino discs, flux motion obs. 2—19571
critical current depend. on defect structure of flux line lattice 2—19556
critical state, new model, accounting for multivalued critical current 2—13134
current-voltage characts., nonlinearity 2—25777
dirty superconductors, thermodynamic fluctuation of order parameter in vortex state 2—16167
electron-dislocation interaction 2—13164
excitation spectrum, band structure 2—29629
film, flux flow, V-I plots 2—19561
fluctuation cond., mag. field quenching 2—13181
fluctuation-induced diamagnetism, paramag. effects 2—25778
flux line arrangements in hysteretic low-k samples 2—19570
flux line lattices, mixed state dependence on anisotropy of Fermi surface 2—9966
flux line lattices, stability 2—19575
flux line-defect interaction distances 2—19555
flux lines and pinning centres, interaction distance 2—13136
flux pinning mechanism 2—29630
flux quantization theories 2—1488
Ginzburg-Landau free energy function for isolated flux tube, variational solution 2—36462
hollow cylinder props., surface and bulk hysteresis contribs. 2—1493
Joule-heating power dissipation in hollow tube 2—36461
magnetic behaviour at small Ginzburg-Landau parameters (χ) 2—19569
magnetic impurity effect, n.m.r. obs. 2—6777
Meissner state, a.c. loss theory 2—13135
mixed state, fluctuation spectrum of flux motion 2—13140
mixed state, flux line arrangement 2—13137
mixed state, fluxoid interaction with phonons and electrons 2—13143
mixed state, oscillatory mag. field effect 2—40197
mixed state, u.s. absorpt. and thermal cond. 2—13138
resistive transition, fluctuation cond. 2—13142
single and double component systems, a.c. loss and flux instabilities 2—22501
superconductors, type-II, non-ideal, local model, generalised London eqn. 2—25776
surface currents, roughness effects 2—16166
surface impedance calc. method 2—13141
thermal stability, paramag. impurity effects 2—16178
transport entropy of vortices 2—13161
transport phenomena, theory 2—13125
u.s. investigation 2—40189
vortex lattice, Ginsburg-Landau theory 2—40198
vortex motion, theory 2—13139
vortices, small-angle neutron scatt. obs. 2—19591
Pb-Bi, flux line pinning by large normal particles 2—29628
Pb films, magneto-optical study of intermediate state, magnetic field and film thickness dependence 2—40196

Supercooling
amorphous deposits, transformation into supercooled liquids 2—32314
cholesteryl laurate, from dielec. const. temp. depend. on cycling 2—35781
liquids, viscoelastic relaxation 2—35710
polyethylene, amorphous surface layers, thickness, with rel. to supercooling, loops, cilia 2—18949
refractory oxide spheroidization times, droplet solidification 2—12613
superconducting film, Ginzburg-Landau parameter determ. 2—9968
Al, and superheating, Ginzburg-Landau parameter 2—13155
Zn, and superheating, Ginzburg-Landau parameter 2—13155

Superexchange *see Antiferromagnetism; Exchange interactions*

Superfluidity
see also Helium/liquid; Quantum fluids
astrophysics, review 2—13820
Bose condensation relation 2—5165
Bose liquid, critical indices calc. 2—17266
Bose-Einstein system, finite, density fluctuations and onset of superfluidity 2—7716
boson system, Gross Pitaevskii eqn. for order parameter 2—20875
cooling in vertical channels, high heat flux regime 2—25132
liquid, superfluid, vortices, quantum mech. form. 2—35808

Superfluidity continued
  metal, review 2—29256
  microscopic and phenomenological theory of He II connections 2—1128
  neutron matter, BCS-bogoljubov-theory 2—30480
  off-diagonal long range order systems, canonical ensemble perturbation eval. 2—17265
  phenomenological theory, Bose condensation, hydrodynamics 2—28929
  proton, in neutron star matter 2—20559
  pulsar interior, metastable flow states transition rel. to speedup 2—37324
  rotating neutron superfluid, electron velocity relaxation rel. to pulsar slow-down rate relaxation 2—7491
  surface elementary excitations 2—22028
  vapour-superfluid interface, temp. fluctuations associated with gravity waves 2—30819
  He, analogue of d.c. Josephson effect 2—32300
  He, bound roton pairs 2—12605
  He, consideration of Galilei invariance 2—39413
  He, criticism of single particle Green function approach to excitation spectrum 2—12602
  He, dynamics of atomic and molecular metastable states produced by electron bombardment 2—32299
  He, electron-bombarded, u.v. emission spectra 2—12604
  He, excitation spectrum near λ transition, Mossbauer obs. 2—12608
  He, liquid, review 2—1127
  He, liquid, second sound vel. decrease rel. to mutual friction force 2—18867
  He, low and ultralow research, at Sussex, Cambridge, and Birmingham Univs. 2—41362
  He, low temperature dependence of superfluid density in a restricted geometry 2—25131
  He, nonuniform states of an imperfect Bose gas 2—30820
  He, roton viscosity and roton roton interactions 2—32298
  He, superfluid density and critical velocity, persistent current meas. 2—12606
  He, theory based on roton-roton interaction developed for superfluid phase transition 2—9199
  He, vorticity 2—12607
  He construction of kinetic theory in agreement with hydrodynamics, determ. transport coeffs. in collision-time model 2—25133
  He films, two fluid model analysis of liquid vapour equilibrium 2—3424
  He II-He I transition temp. discrepancies 2—35811
  He II, analogous effect to Peltier effect in metals 2—28928
  He II, first sound, positive linear dispersions in velocity 2—12601
  He II, phonon lifetimes 2—6273
  He II, roton-limited mobility of ions 2—6271
  He II, uniformly rotating, coupling from second to first sound 2—35812
  He II, vortex core parameter, press. depend. 2—22023
  He II neutron scattering at large momentum transfer and condensate fraction 2—1133
  He in narrow bore, equations of motion 2—6275
  He vortex wave scattering by spherical impurity 2—1132
  ^{3}He-^{4}He dilute mixtures under pressure, supermobility and zero sound 2—32295
  ^{3}He-^{4}He mixtures, lattice model for superfluid phase transition and phase separation 2—25128
  ^{3}He-^{4}He mixtures, specific heat near junction of λ and phase separation curves 2—1129
  ^{4}He, heat capacity anomaly near λ transition, density depend. 2—25127
  ^{4}He, ion mobilities near superfluid transition and melting line 2—18866
  ^{4}He cryogenic bath with temp. gradient and coexistence of superfluid and normal phases 2—2045
  ^{4}He films, thick, sp. ht. maxima, superfluid phase transition phenomena 2—9196
  ^{4}He in dilute mixtures of ^{4}He in ^{3}He, superfluid film appearance and effects of molar concentration 2—22022
  ^{4}He kinematics of excitation pair contributions to dynamic structure 2—106

Superlattice structure *see Alloys; Crystal structure, atomic; Solid solutions*

Supernovae *see Novae*

Superparamagnetism
  alloy, dil.. linear low temp. sp. ht. due to clusters 2—29554
  glass, Fe_2O_3-rich, anomalous mag. behaviour 2—33132
  grains, size distribution determ. from magnetization-magnetic field curves 2—6263
  Au_4Mn, disordered, struct. 2—40462
  β-Co fine particles, ferromag.-superparamag. transition, relax. behaviour 2—1626
  Ni-Cu alloys, high field susceptibility, density of superparamag. clusters 2—26041
  Ni-Rh alloy, rel. to low temp. heat capacity anomaly 2—13045
  Ni-Rh alloys, giant moments 2—40486
  Ni granular films, magnetoresist. and Kerr rot. obs. 2—36727
  Ni powders, particle size depend. 2—40513

Supersonic flow
  see also Shock waves
  ablation phase duration of body in decelerated hypersonic flight 2—39252
  accelerated over notches, separation effects 2—28688
  aerodynamic decelerators, nonuniform freestreams in wake of primary vehicle 2—28724
  air, around spherical segment, radiation of shock layer 2—39250
  airflow over liquid film, film stability study 2—25028
  Alfvenic, second order Cowley-Imai analogy in UHD 2—24638
  axial compressor, flow visualization 2—18739
  axisymmetric cone, approx. analytic soln. for position and strength of shock waves 2—24969
  axisymmetric non-equilibrium flow, decay of weak shock waves 2—6131
  base, recirculaton zone, theoretical 2—9021
  base flow simulation, support design for wind-tunnel tests 2—18740
  base region, steady flow of monatomic rarefied gas over semi-infinite bar 2—39236
  boundary-layer, over a rearward facing step, study of separation 2—21733
  around circular cone, laminar boundary layer 2—3288
  circular cone, laminar Prandtl boundary layer 2—39253
  compressed layer in front of cylinder, Mach number distrib. 2—32164
  compressible boundary layer flow past a swept wavy wall with heat transfer and ablation 2—28708
  compressible turbulent boundary-layer heat transfer to rough surfaces 2—28690

Supersonic flow continued
  condensation augmented velocity 2—24950
  condensation of Zn vapour in supersonic carrier gas 2—32146
  contact discontinuity, effect on flow round a body 2—35646
  control-surface buzz, effect of Reynolds number and frequency parameters 2—18748
  delta wings, leeward surfaces, bow shock waves 2—6147
  delta wings, supersonic and hypersonic flow over lower surface, unified theory 2—3313
  delta-planform wing-body configurations, aerodynamic characteristics 2—12500
  drag measurement in a low-density supersonic gas stream 2—28723
  expanding jets, cluster formation, effect of press., temp., nozzle size and test gas 2—21904
  far from slender bodies, theory of characteristics, PLK method 2—18737
  flowfield about inclined circular cone, pressure formula for γ=1.4 2—35645
  gas, thermal meas., calorimetric probes 2—28721
  gas jets, self-oscillations 2—35677
  generation and propagation of shock waves from Apollo rockets at orbital altitudes 2—37178
  heat transfer downstream of a backstep in turbulent flow 2—39247
  heat transfer within resonant cavities 2—32175
  highly rarefied gas past sphere, ray model for reflecton of molecules 2—28706
  hypersonic, effects of mass transfer on turbulent boundary layer properties 2—35659
  hypersonic boundary layer transition in presence of wind tunnel noise 2—28719
  hypersonic He tunnel, hot wire meas. of freestream and shock layer disturbances 2—28717
  hypersonic near free molecules flow, sharp slender cones, drag meas. 2—28684
  hypersonic strong interaction boundary layer equations, numerical solutions for wide range of flow conditions 2—21732
  injection into supersonic stream, sweptback injection at angle of attack 2—18742
  integral relations method for flow past blunt body with detached shock wave 2—35642
  isentropic transonic flow, solution 2—39258
  jet, noise reduction 2—28713
  jets, axisymmetric, impingement on perpendicular flat plate 2—3306
  jets, subsonic flow, coexistence in a constant section duct 2—6139
  laminar boundary -layer/shock wave interactions on flared axisymmetric bodies under adiabatic conditions 2—18723
  laminar constant pressure boundary layers, hypersonic limits 2—24605
  leading edge wedge angle, flat plates 2—3301
  low density, abs. velocity determination 2—24951
  low density gas stream, flat plates 2—3301
  low shock wave for large angle cones, surface pressure distrib. and sonic point location 2—6148
  magneto-radiative, with variable specific heat 2—35651
  MHD, super Alfvenic, over cone in aligned fields 2—24960
  noise generation from supersonic shear layers, generalized convective wave theory 2—14276
  nonadiabatic flat plates, hypersonic turbulent skin-frinction and boundary-layer profiles 2—32158
  nozzle discharge coefficients in throat region at low Reynolds numbers 2—28683
  perfect gas, unsteady flows in two dimensional channel, constant specific heats 2—32151
  perturbed region struct. in front of cylinder 2—32163
  plane ionizing shock wave, stability in mag. field 2—18747
  planetary entry velocities, radiating laminar boundary layers 2—35664
  plasma, guiding centre, characteristic surfaces 2—28497
  plasma, possibility in collapsing post-sunset ionosphere 2—20418
  plasma streams high-energy, expts. with two flow-swallowing enthalpy probes 2—28587
  pressure oscillations in shallow cavities 2—1021
  radiation gas dynamics, plane phase method analysis 2—39256
  rarefied, laminar convective heat transfer rates on hemispheric cylinder 2—28689
  rarefied plasma, supersonic flow around plate and cylinder bodies 2—12377
  r.f. discharge, high speed gas flow, sparking potential 2—35629
  roughness effects on heat transfer in supersonic region of conical nozzle 2—18741
  shock capturing, finite difference approach, for aerodynamic wing-body configurations 2—32160
  shock wave alterations by alpha particle emissions 2—35676
  shock wave incidence on blunt body in supersonic flow 2—32165
  shock waves, formation and propagation from a concave boundary in simple and complex wave fields 2—11364
  slender body moving through air at supersonic and subsonic velocities 2—21903
  sonic boom generation theory and prediction methods 2—35667
  sonic boom minimization, modification of aircraft configuration 2—35668
  past steady and oscillating blunt bodies of revolution, theory using new method of series truncation 2—28687
  termination with weak shock at two-dimensional symmetric profile 2—917
  around thin cross shaped wing, current separation at edge 2—39255
  thin liquid films, stability of cross hatched wave patterns 2—32216
  three-dimensional hypersonic, alternating directional implicit numerical scheme 2—1020
  transition and mixing in the shear layer produced by tangential injection 2—32169
  transonic, with Mach numbers near unity, asymptotic method for solution of boundary value problems 2—39042
  transonic flow, linearization and equivalence rule 2—3316
  transonic flow about 2-dimensional airfoils, coordinate transformation 2—24952
  transonic flow about two-dimensional airfoils, relaxation procedures 2—28720
  transonic region of a supersonic boundary layer turning a sharp corner 2—35656
  turbulent boundary layers, compressible adverse pressure gradient, profile shape calc. 2—35663
  turbulent boundary layers, exptl. investigation of total temperature and Mach number distributions 2—18724

Supersonic flow continued

- turbulent boundary layers, jet interaction-induced separation, two dimensional problem 2—35660
- turbulent jets, schlieren obs. of density fluctuations 2—18729
- turbulent separating and reattaching flows in two dimensional compression corner 2—31910
- turbulent shock-boundary-layer interaction at wedge compression corner 2—39057
- two-dimensional wake behind heated slender flat plate, obs. on transition process 2—18722
- velocity measurement of gas stream in tube 2—35650
- viscous, about slender bodies, numerical computation 2—39264
- viscous slipstream, structure determ. downstream of centreline Mach reflection 2—21735
- wake of wedges transition and turbulence phenomena 2—21719
- past wedges and cones, perturbation analysis of shock shape and velocity 2—3303
- wind tunnels, compressible effects 2—18745
- wing, swept delta, boundary layer separation 2—2258
- Ar in arc plasmatron, optical meas. of electronic parameters 2—39113
- Ar plasma in transverse mag. field, discharge characteristics in induced electric field 2—12380
- CO_2, flow parameters behind shock waves 2—28693
- H_2-N_2, thermal recovery factors in gas mixtures 2—39232
- He-Ar, thermal recovery factors in gas mixtures 2—39232
- He, hypersonic tunnel, air condensation effects 2—6138
- N_2, flow parameters behind shock waves 2—28693
- Zn vapour in the carrier gas, with condensation, Pitot pressure 2—28707

Supersonics *see Ultrasonics*

Surface diffusion *see Diffusion in liquids; Diffusion in solids; Surface phenomena*

Surface energy

see also Crystal electron states/surface

- adsorbed ionic monolayers on metals 2—29067
- alkali feldspar, albite twinning, exsolution, elastic stress calc. 2—25414
- alkali halides, dislocation charge, u.s. obs. 2—29180
- bicrystal, rel. to boundary energy 2—6304
- calculation by broken bond method, pairwise-interaction theory 2—9243
- cubic crystal, surface energy of deformation, continuum theory 2—19150
- diamond structure crystal, mean square displacements of surface atoms 2—22389
- dipole potential, meas. method using asymmetric total reflection of polarized neutron beam 2—38347
- domain walls at antiferromagnetic-ferrimagnetic transition pt. 2—10230
- fracture, in dynamical cleavage analysis 2—9701
- liquid, local atomic anisotropy 2—6198
- liquid surfaces, curvature, rel. to new constant of matter, thermodynamics of surfaces 2—6185
- melt crystallization, interfacial energies of suspended particles 2—19014
- metal, intergranular force from free electron energy variation 2—29014
- metal, of adhesion from friction model rel. to compatibility determ. 2—29458
- nucleation theory, small clusters, vapour press. 2—12621
- polyethylene, friction meas. 2—12919
- polyethylene crystals, lateral surface energy from interatomic potentials 2—28993
- polymer fibre, strength rel. to mol. wt. and struct. 2—15643
- pyrographite, cleavage, crack development, water and aqueous ethanol effect 2—28998
- semiconductor device, potential gradient, scanning electron microscopy 2—10077
- solid, determ. from melting temp. of disperse particles 2—6318
- stress corrosion cracking and fracture mechanics 2—1320
- titanate ceramics, polarized, pot. distrib. obs., effects of adsorbed ions 2—16300
- Ag film, annealing, hole growth island formation 2—25194
- Al, surface state energies, band struct. matching method determ., Forstmann-Heine method 2—6732
- $BaTiO_3$, H_2O vapour effects on pot. 2—16285
- $Ca_{10}(PO_4)_6F_2$, fluorapatite, natural cryst. 2—6328
- Co film, chemisorption of oxygen, surface potential study 2—12683
- Cu-(1.9wt.%)Co, Cu-(2wt.%)-Co-(6wt.%)Zn, alloys, of precipitates rel. to ageing mechanism 2—3913
- Cu, adsorbed CO and Xe, surface potential study 2—12682
- Cu film, surface pot. due to physical adsorption of Xe 2—9315
- Fe film, chemisorption of oxygen, surface potential study 2—12683
- Fe film, surface pot. due to physical adsorption of Xe 2—9315
- Ge, ductility, brittleness and strength, rel. to molten metal contact 2—29310
- Ge, illumination induced stresses, surface pot. depend. 2—10314
- He, liquid, electron surface states inside and outside liquid meas. of lifetimes 2—39406
- Mn film, chemisorption of oxygen, surface potential study 2—12683
- Na film, surface pot. due to physical adsorption of Xe 2—9315
- Si-Al_2O_3, effects of heat treatment on Si surface potential 2—29736
- Si-SiO_2-Al_2O_3, effects of heat treatment on Si surface potential 2—29736
- Si diode, potential distrib. at surface of n-region 2—19709
- SiO_2 layer in m.o.s. system, relaxation polarization, surface potential stability 2—4269
- Sn, determ. from melting temp. of disperse particles 2—6318
- VC, cleavage fracture 2—22288
- W, field emission chemisorption of hydrocarbons, surface potential 2—25972
- W, ion irrad., atom displacement energy, surface damage 2—29010
- ZnO, chemisorbed oxygen, LEED study 2—18924
- ZrO_2, milled zirconia, rel. to monoclinic- tetragonal transformation 2—29484

Surface ionization *see Ionization, surface*

Surface measurement

see also Area measurement

- adsorbent surface area estimation, monolayer capacity determ. from adsorpt. isotherms 2—32387
- Auger electron spectroscopy, Auger electron energies from 0 to 2000 eV for atoms with $5\leqslant A\leqslant 103$ 2—31681
- Auger electron spectroscopy, surface chemical analysis, review 2—10670
- Auger spectroscopy of metals and semiconductors 2—1503
- backscattered ions analysis for surface composition 2—15653
- chemical profiles, normal to solid vacuum interface, Auger spectroscopy, inert gas sputtering 2—39452

Surface measurement continued

- composition analysis by ion scatt. spectrometry 2—39454
- composition with depth obs. using simultaneous electron and ion bombardment 2—16695
- curvilinear surfaces, operator and component errors 2—23217
- deformed, exo-emission testing 2—29778
- dipole potential, method using asymmetric total reflection of polarized neutron beam 2—38347
- electric potential, method using Auger electron spectroscopy, patent 2—34281
- electron energy distributions, photoelectron spectrometer for 2—4102
- by electron mirror microscope with guide field 2—17559
- electron spectroscopy, ionization and energy losses 2—6309
- ellipsometric method for det. of optical constants 2—11512
- filamentary crystals, adsorption rel. to optical microscope methods 2—19282
- glass. Vycor, porous, surface area, O_2 adsorpt., e.p.r. obs., 77K 2—35912
- ion microprobe mass analyser 2—20210
- ion microprobe mass analyzer applic. 2—20217
- ion scattering spectrometry, applic. 2—20216
- LEED examination 2—3656
- liquid and solid, analysis under polarized light based on Faraday effect 2—39450
- metal, electron structure, positron annihilation method 2—36419
- metal oxide powder, method of air permeability 2—1376
- metal with Na deposits, methods of determination 2—6366
- metals, adsorbed layers, i.r. spectroscopy 2—15673
- Mossbauer spectroscopy using conversion electron detection 2—16430
- powder, and porous bodies, specific surface, N_2 thermal desorp. 2—15938
- roughness by interference microscopes, comparison of types 2—23709
- roughness factor det., taking into account influence of surface relief on radiation props. 2—28984
- scanning electron microscopy 2—29127
- semiconductor, conductivity by field effect obs. 2—19676
- silica gels, specific surface areas, pore struct., adsorpt. and i.r. spectra obs. 2—35920
- silicas, porous and nonporous, adsorpt. of N_2, surface area calcs. by BET and α_s methods 2—35923
- specific surface area meas. of solid bodies by adsorption method 2—27021
- stress meas. using ultrasonic surface waves 2—29378
- substrate surfaces microstruct., scanning electron microscope obs. 2—39464
- surface finish and radii of curvature measurement, interference method 2—27024
- u.h. vacuum system for surface studies by ion backscatt. 2—41412
- vertical section geometry meas. by electron microscopy, method 2—28986
- X-ray topography, instantaneous video display 2—1161
- X-ray topography 2—25299
- zircaloy-2(-4), Auger spectroscopy 2—39472
- C fibre, wetted fibre area changes, electrochem. evaluation 2—12644
- Fe, LEED, Auger spectroscopy, microcontact studies obs. of friction, wear, lubrication, adhesion 2—39848
- Mo, photomicrographic study of temp. distribution in pulse heated specimen 2—25697
- Nb, morphology, purity, chem. analysis, X-ray diffr., electron microscopy, Auger surface analysis 2—39462
- SiO_2, glassy pyrogenic, area determ. by N_2 adsorption 2—39565
- W(100), LEED patterns, influence at O_2 adsorption on scattered electron intensity distribution 2—25175

Surface phenomena

see also Adsorption; Capillarity; Catalysis; Electron emission; Films; Interface phenomena; Ionization, surface; Liquid waves/surface; Sorption

- acoustic wave convolution, nonlinear material evaluation 2—19414
- alkali halide, anomalous d.c. polariz. current due to surface effects 2—10107
- alumina ceramic, compressive layer formation by chem. treatment in strengthening process 2—1331
- analysis techniques using Auger spectroscopy 2—6303
- atom-metal surface scatt., Debye-Waller factor 2—12635
- backscattering from rough surface, acoustic waves in water, surface spectrum dependence 2—14263
- bearing surfaces, wear mechanism, transfer of atoms from one surface to another 2—6588
- catalyst surface area rel. to crystallite size 2—26346
- cermet, polishing, diamond pastes evaluation 2—22064
- channelling of low energy ions on cryst. surfaces 2—36391
- clean surface preparation, by rupture in the melt 2—18911
- conducting crystal, new type of surface sound wave 2—32818
- contact of two nominally flat rough surfaces 2—3919
- crystal growth with surface diffusion, computer simulation model 2—32400
- crystal surface, low energy electron inelastic scatt. by one phonon processes, theory 2—25170
- crystallite Brownian migration, epitaxy relation 2—6339
- crystallite Brownian migration, epitaxy relation 2—6340
- deposit formation on heating surfaces, nonisothermal gas flow with suspended solid particles 2—12585
- dielectric, laser beam induced damage 2—29746
- diffusion, rel. to cryst. growth rates in impure soln. 2—29086
- diffusion processes, influence on kinetics of heterogeneous nucleation 2—1170
- disc, circular, pressure fluctuations near axisymmetric stagnation point 2—15529
- drill tube material, white layer formation on heat treatment 2—3892
- dynamic changes in morphology, laser reflection technique for obs. 2—35865
- exponential interatomic potentials, approx. for lattice sums 2—25168
- ferroelectric semiconductor, photocond. due to surface layers 2—4296
- field evaporation theory, models 2—28996
- field ion microscopy, surface processes 2—6301
- film, contamination analysis using vacuum u.v. reflectometer 2—18929
- films, metallic, surface polygonization, influence of light 2—15662
- gas-solid interaction, one-phonon inelastic scatt., continuum model appl. 2—32329
- gas-surface interaction calculation, summation of pairwise potential 2—39453
- gas-surface interaction theory, rate of attractive potential 2—9234
- gas-surface interactions, electron bombardment surface ion desorption obs. 2—29053

Surface phenomena continued
gas-surface scattering kernels, velocity and temp. slip coeffs. 2—39230
glass, cryst. growth due to electron bombardment 2—39437
glass, surface-treated, Rayleigh wave dispersion for stress profile obs. 2—39768
graphite, surface phonon entropy calc. 2—32335
Heisenberg ferromagnet, effect of a surface on low temp. properties 2—19839
insoluble film, rigorous thermodynamic formation 2—21946
insulator, elec. microscope obs. of electrical effects 2—9405
insulator, surface charging by ion irrad. 2—12633
ion reflection from solid surfaces, radiotracer technique meas. 2—7901
ion scatt. by cryst., surface semichannels influence 2—6306
ion-metal interaction, dynamics inclusion 2—6308
ion-neutralization spectroscopy, interrelation of physics and mathematics 2—3483
laser machining, math. model 2—15651
liquid, acoustic wave interaction, rupture and fountain effect 2—28847
liquid, acoustically induced instabilities 2—30044
liquid, mol. dynamics, stat. mech. calc. 2—6199
liquid system, binary, bulk-to-surface distrib. coeffs. and activity from surface tension 2—21967
mass spectrometry, field-ionization type, reviews 2—38785
metal, cracks, mag. field of eddy currents excited by contact inductor 2—29376
metal, H ion trapping, reflection and re-emission 2—39551
metal, residual polishing agent rel. to hardness, nucl. reaction reson. obs. 2—12634
metal, review 2—12637
metal, rough, photon interactions 2—4427
metal, self-diffusion, book 2—28989
metal, surface self-diffusion, elec. field effect 2—1162
metal particle, surface diffusion and sintering enhancement by addition of impurities decreasing surface m.p. 2—22326
metal surface, proximate atom and ion orbital splitting, surface field analysis 2—6317
metal system, hardened layer formation on electrospark alloying process 2—6608
microtopography, comparison of various microscopes 2—6307
m.i.s. structures, G/U charact. 2—19726
molecule interaction, free flow, drag and lift coeffs., model calc. 2—18912
nematic electrolyte systems, field induced surface charges 2—35782
optical surface deterioration by formation of intermetallic compounds 2—14460
phenol-formaldehyde polymer, study of fracture surface regularity 2—3485
phononlike surface modes in two-component plasmas and systems with short range interactions 2—40153
piezoelectric ceramic, surface wave scatter loss, optical measurement 2—36337
plasmon dispersion relation for metal, variational calculation 2—36425
point defect interaction with a surface layer 2—32495
point dipole near metal surface, Thomas-Fermi response, effective polarizability 2—15652
polyethylene, flashover in vacuum d.c., a.c., and surge voltages 2—22618
polymer film, surface electric discharge 2—6116
quartz, surface eastic waves, surface motion obs. 2—40056
resistance, superconducting Nb cavities, effects of oxide films 2—6787
rough surfaces, effect of depth on apparent plane of reflection for surfaces having centres of symmetry 2—23689
roughening, heterogeneous anodic dissolution, ellipsometry 2—25173
roughness, radiative properties studied by wave optics, solution of Maxwell's equations for scattering 2—17693
sealing wax, thermoelectret, effect of polarizing field 2—13330
semiconductor, band structure, surface curvature detn. 2—10060
sputtering, secondary emission and radiation damage, conference (Oxford, September 1971) 2—24828
sputtering, secondary emission and radiation damage, conference (Oxford, September 1971) 2—21860
steel, carbide layer formation by diffusion and chemical reaction of Fe-Al-C 2—39927
steel, surface hardening, u.s. and vibromagnetic methods 2—36196
steel, white layer formation, effect on wear resistance 2—6586
steel hardening, mechanical polishing, Rehbinder effect 2—32704
surface creation during phase transformations 2—32754
tetrafluoroethylene, flashover in vacuum d.c., a.c., and surge voltages 2—22618
textiles, polyacrylic acid grafting, by plasma generated free radical sites 2—3504
transition metal carbides, H surface recombination rel. to work function 2—29009
transparent dielectric subjected to laser light, surface photocurrent 2—19784
vacuum, ultra high, aspects of investigation 2—20790
vibrating crystal surface, LEED, temp. effects 2—6323
vibration mode, light scatt. 2—29505
X-ray photoelectron spectroscopy, use of electron flood gun to reduce surface charging 2—21030
zircaloy-2(-4), rel. to mech. and chem. props., Auger spectroscopy obs. 2—39472
Ag, polycrystalline, Na, K, Kr ion refl. coeffs., electronic stopping, surface effects 2—7902
Ag, single crystal, strain free prep. of thinned specimens 2—22126
Ag (111) surface, scatt. of Ar beams up to 20 eV 2—15657
Ag atoms on porous glass and silica gel surfaces, e.s.r. 2—1164
Ag atoms on porous glass and silica gel surfaces, e.s.r. 2—1163
Ag film, diffusion, hillock formation 2—25193
AgBr, self-diffusion of Ag^+, tracer technique 2—3491
Al, (100) and (110), LEED, inelastic collision model 2—6324
Al, single crystal, strain free prep. of thinned specimens 2—22126
Al_2O_3, alumina, fracture at surface flaws, thermal expansion anisotropy effect 2—12886
Au, polycrystalline, Na, K, Kr ion refl. coeffs., electronic stopping, surface effects 2—7902
Au, self-diffusion, contaminants effect, Auger spectra 2—32334
Au film, vacuum deposited, struct. rel. to substrate surface 2—25195
$BaSO_4$ substrate, charge voltage effects on photoelectron spectra of Au and Pd 2—13359
Be, ang. and energy distrib. of inelastically reflected electrons 2—9911
$Bi_{12}GeO_{20}$, Rayleigh wave propagation 2—19412

Surface phenomena continued
C, graphite, temp. and ablation characteristics 2—4060
CdS, semicond., surface recomb. centres, influence on recomb. luminesc. 2—22795
CdSe, single cryst., photocond., effects of HNO_3 etching 2—16312
CdTe, optical modulation of electron beam landing energy 2—22554
Cu, single crystal, strain free prep. of thinned specimens 2—22126
Cu, surface diffusion coeffs., vapour phase at transport rel. to meas. 2—32337
Cu (110), reaction kinetics of adsorbed O_2/S, Auger spectroscopy 2—9248
Cu crysal, Ar ion scattering mechanism 2—18922
Cu phthalocyanine, surface photoeffects 2—29765
CuFe dil. alloy, far-i.r. surface resist. 2—40172
D_2, oxid. on Pt surface reaction mechanism and rate 2—10629
α-Fe, Al-Fe layers formed by surface metal interaction with $AlCl_3$, HCl and H_2 gases 2—26320
Fe, cementation by C and N_2, and impurity influence 2—9274
α-Fe, diffusion layer form. by metal-gas interaction 2—39458
Fe, friction, wear, lubrication, adhesion, obs. by LEED, Auger spectroscopy, microcontact studies 2—39848
GaAs, passivation with Si_3N_4 2—35893
GaAs surface elastic waves, generation and detect., depletion layer transduction 2—13324
GaP, dispersion of surface polaritons 2—33233
Ge-electrolyte interface, surface recomb. states 2—22557
Ge, amorphous, Na, K, Kr ion refl. coeffs., electronic stopping, surface effects 2—7902
Ge, ion-electron emission, relaxation process 2—19815
Ge, sulphurization technique for stabilization 2—3488
H cold metallic, transition to molecular form involving 'evaporation' of surface atoms 2—25631
He, liquid, electron surface states inside and outside liquid meas. of lifetimes 2—39406
^3He, liquid, growth of layers from nearly saturated solutions in superfluid ^4He 2—12595
^4He, liquid, electron mobility, meas. from 0.9 to 3.2 K 2—3420
HgO, surface photoconductivity, spectral response 2—4304
InAs, ion-electron emission, relaxation process 2—19815
p-InSb, hyperfreq. surface waves, crossed mag. and elec. fields 2—6842
KBr single crystal, surface polarization capacitance 2—16270
LiF, reflection, diffr., selective adsorpt. of at. H 2—39461
$MgAl_2O_4$, crazing, etch rate, deterioration, in H_2 2—3497
MgF_2 film, surface potential, in presence of Malter emission 2—29777
MgO, immersed in N,N- dimethylformamide and dimethylsulphoxide, Rebinder effect 2—39699
Mo-C-O alloy, C and O atomic migration rel. to chemisorption and precipitation 2—9252
Mo, charact. electron energy loss spectra during oxidation 2—9250
Mo, permeability of H 2—29220
Mo, surface diffusion of Cu 2—28999
NaCl, surface reactions with alkali halides, ang. distribution of reaction and vaporization products 2—10609
Nb, migration of Zr, rel. to two dimensional crystal growth 2—18947
Nb, single crystal, strain free prep. of thinned specimens 2—22126
Nb alloy, Cb-132, surface scale formation rel. to oxidation 2—13578
Ni, diffusion of S on (110) face, Auger spectroscopy 2—3499
NiO, antiferromag., surface magnetization, exchange interaction temp. depend. electron scatt., $T_N \leqslant T \leqslant 295$K 2—6995
NiO, powder, degassing temp. rel. to sp. surface area and heat of wetting 2—6623
Pb, ang. and energy distrib. of inelastically reflected electrons 2—9911
Si-SiO_2-Al, m.o.s. diode, gamma irradiation effects 2—10105
Si, charge visualization, transition metal solution treatment, electron microscopy 2—4244
Si, Na contamination from water and alcohol 2—3501
Si, optical modulation of electron beam landing energy 2—22554
Si crystal, interaction of impinging O_2 supersonic beam 2—6314
SiO_2, on Si, Na contamination from water and alcohol 2—3501
Ti alloy, Si saturation of ground surface, following action of SiC 2—6604
W, (001), electron reflection, 1-10 eV, LEED 2—25185
W, diffusion of Si, in field emission microscope 2—12816
W, field ion microscopy, anomalous images, 78K 2—25184
W, migration of Zr and W, rel. to two dimensional crystal growth 2—18947
W(112) face, He atom scatt. 2—6334
Zn:O liq., evaporation kinetics, equilib., v.p., rel. to surface active impurities, 563-623K 2—28951
Zn single crystal deform. by sliding friction, surface film effects 2—15890
Zr-C alloy, chemisorption and precipitation, C atomic migration 2—9252

Surface structure
alkali halide crystals, effect on surface cleaning 2—1157
alkali halides, electron irrad. induced polygonization 2—39714
alkali halides, twist grain boundaries 2—9579
amorphous solids, sputtered, topography, computer simulation 2—39449
analysis by sputter ion mass spectrometer 2—565
anharmonicity, mol. dynamics method 2—18916
asperity heights, stat. distrib. 2—15655
atom scattering obs. technique 2—6298
Auger electron spectroscopy, chem. effects 2—35863
Auger electron spectroscopy, high-spatial-resolution 2—9242
brass, fatigue rupture, fracture morphology 2_12907
carbon blacks, methods of investigating 2—6302
chemical analysis, Auger electron spectroscopy and appearance potential spectroscopy comparison 2—9233
chemical profiles, normal to solid vacuum interface, Auger spectroscopy, inert gas sputtering 2—39452
cholesteric liq. crystals, texture, pitch contraction, d.c. elec. field induced 2—6209
colour etching, defects 2—32497
composition analysis by ion scatt. spectrometry 2—39454
conference, solid-state adsorption and related topics, Hannover, Germany, 1971 2—6299
crystallography, review, use of LEED 2—6298
defects, direct inspection, electron microscope obs. 2_3671
defects, steel wires, effect on fracture, electron microscope obs. 2—6559
deformation, resulting dislocations, electron microscope exam. 2—1250
diatomic linear lattice, surface modes, theory 2—22063
dielectric coatings, effect of heat treatment 2—39485
dynamics, vibr. modes, harmonic approx. 2—18914

Surface structure continued
electron probe analysis, performance limitations due to electron-electron interactions 2—37917
electron spectroscopy, applic. to glass research 2—22141
electron spectroscopy, conf., Pacific Grove, U.S.A., Sept. (1971) 2—31002
electron spectroscopy, review 2—31750
fatigue failure detection, coherent light reflection, optical correlation function 2—9725
flaw detection using oblique angle illumination 2—35868
frictional behaviour and microstructure of S-137 material 2—29341
glass, effect of mech. and chem. interaction with steam-water mixture 2—35870
glass, fractured, density function of surface area of particles 2—1328
glass, optical, polishing mechanism, effect of surface layer hardness on rate 2—6305
glass, sputter topographies, evolution, secondary processes 2—39466
glass, surface composition, Auger spectroscopy study 2—29003
HEED, glancing incidence, n-beam intensities 2—9238
HEED, glancing incidence n-beam dynamical diffr. 2—9237
ice, 100 keV proton channelling and backscatt. obs. 2—35871
impurity analysis, low energy ion refl. technique 2—32331
impurity analysis, low energy ion scatt. technique 2—32330
interface topography, atomic detail reconstruction using field ion microscopy 2—9239
ionic cryst., i.r. absorpt. due to surface modes 2—19340
ionization spectroscopy, principle and applications 2—36646
iridescent and specular, difference 2—1158
jet electrolytic polishing, preparation of electron-microscopic samples 2—37048
LEED, ion core scatt. model 2—6310
LEED, review 2—15650
LEED as a structure study method 2—6300
LEED determination 2—28987
LEED spectra in ion core scatt. model 2—6311
localized vibr. freqs. calc. method 2—18917
localized vibr. modes of free surfaces and systems with adsorbed layers 2—32323
machined layer by grinding, temp. distrib., cementite, thermal residual stress 2—1284
machining, metal surface layers, bulk vapour production by laser beam 2—28964
materials testing and quality control 2—19233
metal, effect on laser absorpt. characts. 2—25568
metal, polycrystalline, electron microscope obs. after ion bombardment at grazing incidence angles 2—39459
metal, rel. to work function calc. 2—39455
metal, replica technique for simultaneous obs. of surface and interior 2—19029
metal, surface quality rel. to LEED spectra 2—29000
metal, vacancy condensation pits, on quench annealing 2—6320
metal tips, b.c.c. and f.c.c. metals, field evaporated, shape 2—6322
metallographic apparatus for examining changes in temp. range 4.2-300 K due to deformation by stretching 2—39854
naphthalene, equilibrium form, nonsingular surfaces 2—18925
orthoferrites, bubble domain material, polishing rel. to surface struct., LEED obs. 2—32332
periodic terrace-ledge and spherical surfaces, calc. of reciprocal lattice by Fourier transformation of electron diffraction data 2—28988
phonon modes, inelastic slow electron scatt. 2—39451
polyethylene, amorphous surface layers, thickness, with rel. to supercooling, loops, cilia 2—18949
powder, and frost susceptibility 2—3971
relief, diffusion zones in thin layers, microscopy 2—32327
roughness, effect on optical spectra 2—22743
roughness design rel. to overcoming brightness handicap in birefringence meas. method 2—4433
roughness obs. using speckle patterns formed in broad band illumination 2—35869
scanning electron microscopy application 2—6295
scanning electron microscopy using absorbed current imagery 2—39619
secondary electron emission yield, fine struct. detection method 2—32322
self-imaging by field desorption 2—18918
semiconductor, boundary layers, surface states rel. to surface struct. 2—33005
semiconductor, p-n junc., elec. field distrib., electric mirror microscope 2—4227
semiconductor, Si film, chemically vapour deposited, smoothness 2—1536
silicas, highly dispersive, methods of investigating 2—6302
silicates, Auger spectra, Si peaks 2—25180
steel, austenitic, fatigue fracture microrelief, rel. to durability 2—36152
steel, effect of Cu coating 2—3918
steel, ground, electromagnetic monitoring 2—28990
steel, low C, cold-rolled, fine struct. 2—1165
steel, machining rel. to alternating fatigue strength 2—29301
steel, stainless, interface structure, explosion welded, electron microscopy obs. 2—3945
steel, surface layer, machined, with built-up edge, translational struct. analysis 2—29001
substrate surface defects, role in metal film nucleation 2—39486
substrate surfaces microstruct., scanning electron microscope obs. 2—39464
teflon coated polishers for precision optical flats 2—31107
tetrahedron form, etching pit, X-ray topograms, image calc. 2—32436
thin layers, elemental analysis, combination of r.f. glow-discharge sputtering and mass spectrometry 2—9232
transition metal, combined Auger and charact. loss spectra obs. 2—3484
transmission of struct. information by metallic polycryst. layers 2—6333
u.s. inspection, cracks and notch-shaped defects 2—1321
vertical section geometry meas. by electron microscopy, method 2—28986
water, absorbed layer, informational props. 2—29062
weld metal, effect of welding conditions 2—36222
Ag/Pd, pseudomorphic layer/substrate system, Rutherford scatt. study 2—40103
Ag, incipient melting, in presence of S and O_2 2—1260
Ag, interfacial layers, informational props. 2—39456
Ag film, thickness depend. 2—3522
Al, {110} surface, LEED and Auger spectroscopy 2—32333
Al, interface structure, explosion welded, electron microscopy obs. 2—3945
Al, LEED intensity profiles from (100), (110) and (111) faces 2—9245

Surface structure continued
Al, LEED rotation diagram, theory and expt. 2—3492
Al, roughness induced by dielectric layers, effects on reflectance obs. in surface plasmon excitation region 2—16464
Al, thermal pits, condensation cavities, obs. using liquid Ga embrittlement 2—9253
Al alloy, fatigue fracture, micropores, electron microscopy 2—3904
Al_2O_3, plasma arc sprayed, electron microscope obs. 2—15663
Al_2O_3, sapphire, chemical polishing 2—1201
Al_2O_3, sapphire, chemical polishing and etch pitting 2—9244
$Al(OH)_3$, surface topography during growth from seeded caustic aluminate soln. 2—18990
Au-Cu composite surface, Au layer struct., props., rel. to plated wire memory props. 2—22689
Au, defect obs. using field ion microscopy with noble gas imaging 2—6415
Au, interfacial layers, informational props. 2—39456
Au, vacancies, formation, migration, field ion microscope obs. 2—6326
$B_{12}C_3$, crystal morphology 2—9455
BPO_4, homogeneity obs. from Ar adsorption 2—22083
$BaFe_{12}O_9$, chemical polishing with H_3PO_4 2—1159
$BaTiO_3$, (001), LEED, temp. depend., 20—650°C 2—6321
$BaTiO_3$, (001) face, LEED, temp. depend. 2—6319
$BaTiO_3$, in para- and ferro-elec. phase, X-ray diffr. obs. 2—16275
Be, degree of oxidation, Auger electron spectroscopy 2—6327
C fibres and membranes, Kr adsorption 2—3494
CaF_2 (111) face, micromorphology and thermal vaporiz. 2—32336
CdS:Ag platelet crystal heated in Zn vapour, layer phase characterisation and fluorescence 2—16619
CdS, effect on oxygen chemisorption 2—29061
CdS, etched {00.1} faces, elec. microscope and diffr. obs. 2—9247
CdSe, thermally etched basal surfaces, electron microscope obs. 2—12645
Cr, soft X-ray appearance pot. spectra, effect of oxygen 2—35872
Cr film, evaporation deposited, surface, rel. to oxidizing and nitriding treatments 2—39503
Cu-(14.3 wt.%)Al alloy, equilib. surface segregation, Auger electron spectroscopy meas. 25625 2—25625
Cu-Al alloy, equilib. surface segregation, Auger electron spectroscopy meas. 2—25627
Cu-Al(Sn) alloys, surface segregation 2—22303
Cu-Ni alloy, comp. depend. of Auger spectra 2—12646
Cu, adsorbed CO and Xe, LEED obs. 2—12682
Cu, interface structure, explosion welded, electron microscopy obs. 2—3945
Cu, ion bombardment etching, scanning electron microscopy 2—18921
Cu, LEED spectra in ion core scatt. model 2—6311
Cu, oxidised, RHEED obs. 2—39457
Cu film, surface roughness rel. to physical adsorption of Xe 2—9315
Cu(100), rel. to adsorption of CO 2—25225
Fe-Al alloys, surface segregation 2—22303
Fe, effect of adhesion of metals, LEED and Auger spectroscopy study 2—39974
α—Fe (111), (100) and (110), LEED 2—6329
Fe film, surface roughness rel. to physical adsorption of Xe 2—9315
Fe_2Al_5 diffusion layer form. by metal-gas interaction 2—39458
Fe_2B diffusion layer form. by metal-gas interaction 2—39458
GaAs:Sn, Ge, Mg molecular-beam epitaxy, electrical and optical evaluation of layers thus grown 2—3553
GaAs, contamination due to org. solvents 2—32367
GaAs, correlation of heavy ion irradiation data 2—39469
GaAs, electron characteristic loss spectrum, fine struct. 2—6330
n-GaAs, film, epitaxial, photocond., influence of state of surface 2—22643
GaAs crystals, effect of etchants in the optical polishing suspension 2—6313
GaAs epitaxial layers, faceted surface defect formation 2—25200
n-GaP, chem. polishing by etching soln. 2—32340
GaP epitaxial layers, surface morphology, rel. to growth conditions 2—29032
Ge, ion bombardment induced disorder, sputtered atom ejection pattern studies 2—22370
Ge, ion scatt. study 2—25986
Ge, laser damage 2—12647
Ge (111) face disturbances 2—29002
Ge vacuum decoration, microtopography and physical properties of (111) face 2—12639
InAs crystals, effect of etchants in the optical polishing suspension 2—6313
InSb, abrasion-induced surface damage 2—12649
InSb crystals, effect of etchants in the optical polishing suspension 2—6313
KBr, twist grain boundaries 2—9579
LiF, surface dislocation struct. formed by scratching with needle 2—32522
$MgAl_2O_4$, spinel, chemical polishing 2—1201
$MgAl_2O_4$ single crystal, etch pit study 2—15691
MgO, cleaving in electron microscope 2—25309
MoS_2, etch pits struct. and growth 2—32341
Na film, surface roughness rel. to physical adsorption of Xe 2—9315
NaCl, plastically deformed, electron microscope obs. 2—9251
NaCl, twist grain boundaries 2—9579
Nb, electropolishing method 2—4181
Nb, morphology, purity, control during treatment, use in r.f. superconds. 2—39462
Nb, rel. to supercond. r.f. cavity design 2—32943
NbC, diamond grinding, surface work hardening, microstructure 2—3871
Ni/Na overlayer system, LEED obs. 2—28985
Ni, Auger spectra of C 2—3500
Ni, rel. to ferromag. reson. in deformed cryst. 2—36972
Ni, soft X-ray appearance pot. spectra, effect of oxygen 2—35872
Ni (111), characteristic energy loss of slow electrons scattered from surface, temperature dependence in Curie point region 2—28991
Ni alloy, machining rel. to alternating fatigue strength 2—29301
Ni alloys, He^+ ion injection effects, electron microscope obs. 2—3498
Ni(100), rel. to adsorption of CO 2—25227
Pt, of high Miller index surfaces, LEED obs. 2—35873
Pt, stepped surface, chemisorbed gases, LEED obs. 2—35918
Re, (0001) surface, C effects, LEED obs. 2—29004
Ru, electromech. polishing, etching, prep. for optical metallography 2—12650
Sb_2S_3, effect of grinding and polishing on reflectance 2—19965
Se, influence of organic solvents 2—28992
Si-Ge alloys, helical surface, etch pit obs. of impurity segregation 2—6331

Surface structure continued
Si, amorphization, bombardment induced, depth 2—1242
Si, correlation of heavy ion irradiation data 2—39469
Si, epitaxial layers, morphology, model derivation 2—3544
Si, ion scatt. study 2—25986
Si, microdefects, disloc. free float-zone cryst., annealing and etching obs. 2—3569
Si, passivation of surface with thermally grown silicon oxide films 2—4186
Si, secondary electron emission yield, fine struct. detection 2—32322
Si, sputtered, surface damage, depth of damage 2—39467
Si, thermally oxidized, cryst. orientation effect on fault form. 2—9570
Si (110), rel. to electron mobility anisotropy at low temp. 2—36548
Si film, chemically vapour deposited, smoothness 2—1536
Si lattice defects, surface layers, lapping 2—36270
Si transistor, bipolar, dislocation and stacking fault generation at surface heterogeneities 2—33035
Si wafers, stacking fault and dislocation loop generation 2—25181
SiC, polar surface identification, in alkaline soln. 2—18923
SiC, self-bonded, effect on fracture strength 2—29329
SiC, whiskers, ribbon-like, surface defects, tensile strength, etching 2—12673
Si(111), glancing incidence HEED obs. 2—9236
Si(111), glancing incidence HEED obs. 2—9238
Si(111), LEED, Auger spectroscopy 2—3502
Si(111) faces, LEED-AES obs. 2—39470
SnSe/NaCl film-substrate system, decoration processes 2—29008
SnSe/NaCl film-substrate system, decoration processes, elec. field effect 2—29007
Te, defects influence on carrier density and elec. cond. 2—10062
Ti-Al-V alloy, etching, O_2 effect, metallography 2—32735
Ti, H-ion microscopy, surface films 2—25182
Ti, soft X-ray appearance pot. spectra, effect of oxygen 2—35872
TiC, diamond grinding, surface work hardening, microstructure 2—3871
TiNi, martensitic transformation, surface relief 2—6640
W, ion irrad., atom displacement energy, surface damage 2—29010
W single crystal substrate, for epitaxial growth, prep. by electropolishing 2—25183
WC surface characterized by LEED, atomic and molecular diffraction and scattering 2—25174
WO_3, amorphization, bombardment induced, depth 2—1242
W(110) surface characterized by LEED, scattering of inert gases and deuterium 2—25176
Zn, defects leading to local evaporation of {0001} face 2_39471
Zn, technique for prep. of clean non-cleavage surface 2—22066
ZnO, electronic, LEED and Auger diagnostics 2—29012
ZnO, polar surfaces, LEED study 2—18924
ZrC, diamond grinding, surface work hardening, microstructure 2—3871

Surface tension
see also Capillarity
alcohols, binary mixtures, meas. at 25°C 2—32248
alkali metals, liq., calc. from structural data 2—21955
alkali molybdates and tungstates, vitreous and molten 2—35844
alkanes on alcohol-modified Al, contact angle meas. 2—22081
alveolar, thermodynamics, mathematical model 2—41282
amino acid aqueous solutions, applications of electrostatic theory of image potentials for multipoles embedded in a cavity 2—21002
binary liquid alloys, calc. from surrounded atom model 2—28816
binary liquid mixture and its vapour, surface tension at interface 2—39350
bubble, effect on growth on boiling via interfacial heat convection 2—25152
bubbles, spherical, behavior in vicinity of solid wall 2—6190
cohesive energy density, calc. from surface tension 2—32224
contact angles, dynamic, vel. relationship, surface roughening effect, θ_d-V relationship 2—32205
contact angles, on heterogeneous solid surfaces, thermodynamics 2—32204
damping of liquid metal drop oscillations in non-conducting fluid by transverse magnetic field 2—949
dielectric liquids, correlations with dielectric constant or refractive index 2—28815
drop, hollow, gas filled, surface tension, negative press. eqns. 2—32210
drop on surface, surface driving force causing spreading 2—35695
film, plane, magnetic field effects 2—1058
gas bubbles in deformable material containing dissolved gases, effect on stability 2—15560
n-hexane, superheated tensile strength by ultrasonic cavitation 2—9066
immiscible liqs., axisymmetric meniscus profiles 2—32203
interfacial tensions, determ. with Wilhelmy plate method 2—1087
in Ising model, difeined from surface of separation between two phases 23287 2—23287
liquid, local atomic anisotropy 2—6198
liquid, simple, rel. to liq. vapour density transition 2—15631
liquid metal, temp. behaviour, non-equilibrium, mathematical estimation 2—6223
liquid system, binary, and bulk-to-surface distrib. coeffs. and activity determ. 2—21967
liquid-vapour interface, fluctuation theory 2—39351
Marangoni films, effect of surface tension gradients on hydrodynamic stability 2—25027
Marangoni films, vertical surface, climbing under surface tension gradients 2—1067
menisci or cylinders, curative and height at contact 2—21969
meniscus elimination by container shape 2—35713
metal/electrolyte interphase, electrocapillary studies on Hg plated Au electrode in DMF/H_2O soln. 2—32247
molecular models, inhomogeneous fluids with interfacial layers 2—3159
n-octane film, on quartz, interaction press.-thickness isotherms 2—39352
organic liquids, correlation with isothermal compressibility determ. by ultracentrifugation 2—24991
organic pigments, surface free energy and polarity from contact angle meas. and s.t. eqn. 2—21968
phase transition effects, theory 2—22033
photoresist, adhesion 2—3518
polymer, liq., interfacial tension, polarity 2—18808
polyvinylacetate, at water/air interface, monolayer collapse 2—1089
polyvinylacetate, at water/air interface, monolayer collapse 2—1090
simple liquids, calc. using Kirkwood Buff theory 2—9117
solid, deformable, gas bubble growth and dynamics rel. to surface tension 2—9515
vapour bubble, wetting tension and boiling 2—35834

Surface tension continued
variation with time, multicomponent systems 2—1086
viscous drops, rel. to fusion, sintering mech. 2—36256
viscous liquids, method of determination 2—32246
wire coating, obs. of continuous free withdrawal of wires from Newtonian fluids 2—32219
$(AgPO_3)_m$, dehydration product from $(AgPO_3)_3.H_2O$ 2—30045
$Cd(PO_3)_4$, 900-1000°C 2—28817
Gd film, rel. to interatomic distance 2—29034
Hg, on glass, W and Mo substrates, sessile drop technique 2—21970
Li_2MoO_4-$Na_2(K_2)MoO_4$ molten systems, comp. depend. 2—28818
Pb, solid, creep characts. obs. 2—32619
Se, vitreous, detemination from obs. of thermal healing of scratches 2—39465
Yb, film, rel. to interatomic distance 2—29034

Surface tension measurement
alloys, sessile drop method, with alloying of drop during experiment 2—28814
contact angle meas., apparatus sensile drop method 2—18805
liquid-liquid, photographic technique 2—9118
at phase boundary, immiscible liquids or liquid/gas system 2—18806
polymer melts, pendent drop-sessile drop method 2—35746
polymers, liq., molten, and interfacial tension meas., Vonnegut's rot. drop procedure 2—18809
Wilhelmy method, automatic apparatus 2—1088
Hg, on glass, W and Mo substrates, sessile drop technique 2—21970
Pb-Sn, alloy, liq., max. bubble press. method 2—18807

Surface texture *see Surface structure*

Surveys *see Reviews*

Suspensions
see also Aerosols; Sedimentation; Sols
absorbing spheroids, electrooptic properties 2—9186
air-solids, turbulent flow, heat transfer 2—28902
biological cells, spherical, viscoelastic props. calc. 2—35804
blood, viscoelastic props. 2—14028
blood simulation, disk shaped particles in highly viscous Newtonian fluid 2—14025
Brownian motion effects on rheological properties 2—35798
buoyant liq. suspended in viscous liq., motion, deform., burst. 2—32209
colloidal, coagulated, plastic flow as repeptization phenomenon, viscous energy 2—15618
Compton and Rayleigh scattering of X-rays 2—7060
drops in water, coalescence of two colliding drops 2—9068
erythrocyte ghosts, light-beating spectrum, active transport processes in cell membrane 2—37433
flotation, wettability effects, glass sphere/water simulation of inclusion/steel system 2—3414
flow in vertical pipes, particle dynamics 2—25122
gas, solid particle conc. in flow, piezoelectric sensing technique 2—28912
gas-solid turbulence 2—32286
gases with solid-liquid suspensions, sound velocity 2—1037
glass beads in air, flow characteristics in turbulent flow pipe obs. 2—9188
graphite, polydisperse, flow, heat exchange, mag. field effect 2—39399
heat transfer, similarity variable test 2—25121
hydrodynamic interaction effects in rigid dumbbell suspensions, kinetic theory 2—35800
laminar, boundary layer, migration meas. by laser-Doppler anemometer 2—25120
levitation and counter-gravity motion of spheres by non-uniform hydrodynamic oscillations 2—9050
magnetic, viscosity rel. to field strength 2—22019
multispecies, slurry segregation, mech. interlocking process, critical conc. 2—18863
nylon-water, dielectric loss in microwave x-band 2—9189
oil-in-aqueous, dilute at high ionic strength, expt. in coalescence by flow through glass fibrous mats 2—32282
orientation distribs. of cylinders in shear and elec. fields 2—35435
photometer geometry effect on extinction efficiency of spherical scatterers 2—14456
Poiseuille flow, neutrally buoyant rigid particles in Newtonian liquid, interactions 2—22011
polystyrene latex, light scattering during coagulation 2—15619
pulsed electrical breakdown, polarization phenomena 2—39396
seawater, photoluminescence correlation with concentrations of yellow matter 2—1797
sediment transport, turbulent, averaging approach to two-phase flow theory application 2—35438
sedimentary pipe flow 2—35805
shear stress, rel. to velocity gradient, Casson equation 2—15614
shrimp egg suspensions, ultrasound scatt. 2—28922
solid particles in nonisothermal gas flow, deposit formation on surfaces, heat and mass transfer 2—12585
sound propagation, effect of particle viscosity 2—15616
spheres, slow flow through 2—15434
spherical particles in liquid, acoustic cavitation 2—35715
statistical hydromechanics, solution of kinetic equation 2—28905
thermal cond., particle size, shape and spatial distrib. effect 2—18864
in turbulent channel flow, entrainment mechanics 2—25124
in turbulent jets, diffusion rel. to small particle size 2—25123
u.s. scatt. in heterogeneous systems 2—28907
viscosity of spheres in conc. suspensions, statistical mechanical calcs. 2—35436
in water, instrumentation error in spectra obs. by small angles method 2—27018
wave eqn. for calc. of velocity of sound 2—35806
Fe in toluene, dispersion by electro- condensation, magnetic properties 2—28908
β-FeOOH, akaganeite, in H_2O, thermal props. 2—13038

Suzuki atmospheres *see Crystal imperfections/dislocations*

Switching time, ferroelectric *see Ferroelectric materials; Ferroelectric phenomena*

Switching time, ferromagnetic *see Ferromagnetism; Magnetic properties of substances/ferromagnetic*

Symbols *see Nomenclature and symbols*

Symmetry *see CPT conservation*

Synchrocyclotrons *see Particle accelerators/cyclotrons*

Synchrotron radiation
- absolute standard in 1100 to 3000 Å range, from electron storage ring 2—7640
- atomic fluorescence studies using synchrotron radiation 2—35132
- from auroral electrons, total power calculation 2—13758
- calibration of v.u.v. standard radiation sources 2—8023
- circular polarization in presence of hydromagnetic waves due to pitch angle anisotropies in relativistic electron gas 2—30909
- coherent, model, applied to pulsars, circular accelerators and storage rings 2—372
- Compton spectrum of γ-rays produced in Crab Nebula, calc. 2—26645
- cyclo-synchrotron, at small angles 2—16945
- electric field, pictures of electric lines of forces are presented 2—11409
- electron motion in a medium, spin effect, theory 2—7834
- gravitational radiation in the Schwarzschild geometry 2—33910
- gravitational waves, emission near Galactic centre 2—37237
- growth rate in system of relativistic electrons, linear theory of synchrotron instability 2—30514
- interstellar, effects of ionize medium and emissivity of cosmic electron 2—33688
- to ionize wall originated impurities in thermonuclear reactors 2—18253
- Jupiter, emission at 80 MHz 2—33734
- magnetic bremsstrahlung obs. of energy straggling and radiation reaction 2—17541
- quasars and single electron model 2—13943
- radio from relativistically expanding source 2—33715
- relativistic motion, with radiation reaction 2—37892
- statistical properties, effects of small phase perturbations of electron bunch 2—38406
- strength of the PTB 140 MeV electron facility 2—18045
- from ultra-anisotropic particle distributions application to pulsars 2—26790
- wave radiation zone formation, hyperbolically moving charge 2—37888

Synchrotrons *see Particle accelerators/synchrotrons*

Szilard-Chalmers reactions *see Radiochemistry*

Tables, mathematical
- No entries

Tables, physical *see Collections of physical data*

Tachometers *see Angular velocity measurement*

Tachyons
- gravitational field, Einstein's eqn. solution 2—30762
- instability and impossibility of free tachyons 2—2501
- neutral field implications 2—8066
- neutrino mass bounds considered from spacelike side 2—34608
- observability, implications of generalized Lorentz transformation 2—33900
- one dimension, theory consistent with special relativity and causality preservation 2—17199
- one dimension, theory preserving causality 2—17199
- signals, peculiar properties 2—5133
- tachyon field, rel. to causal description of quantum statistics 2—20822

Tandel *see Dielectric devices*

Tantalum
- adsorption of O_2, H_2, N_2, and H_2O vapour, RHEED obs. 2—12686
- atoms trapped in Ar matrices at 4.2K, absorption spectrum 2—36869
- cathode production, ribbon coated with LaB_6 2—18705
- diffusion of hydrogen, thermogravimetric study 2—36084
- diffusion of U, rate and temp. meas. 2—12795
- diffusion penetration plot of ^{233}U tracer; α-energy spectra 2—6516
- electrotransport of C, above 1900°C 2—22251
- emissivity meas., 1200-2400K 2—4083
- extraction, properties and applications 2—3925
- film, anodization, impurity distrib., ion microprobe mass spectrometric obs. 2—22879
- film, b.c.c. and β phases, X-ray diffr. study 2—32382
- film, sectioning by anodization and oxide stripping 2—9287
- film, self-induced sputtering during electron-beam evap. 2—12669
- film, sputtered, depth depend. of elec. props. 2—32922
- film, sputtered, elec. and struct. props., oxygen effect 2—9286
- film, sputtered, electrophys. props. and constitution 2—39530
- film, sputtered, purity, struct., elec. resist. 2—29042
- film, sputtered, struct. and elec. props. rel. to O_2 content 2—39533
- film, sputtered in Ar-H_2O mixture, resist. rel. to O_2 content 2—39532
- film, sputtered in Ar-O_2, struct. and props., oxygen content depend. 2—29044
- film, sputtered on Si, struct. and comp. 2—32381
- film, structure modification by ion bombardment during deposition 2—39482
- film, two layer model elec. conductivity 2—6764
- film preparation by double-cathode sputtering system 2—29043
- Frenkel defects prod., 4.5 K, rel. to spontaneous recombination processes, electron irradiation expts. 2—22195
- Frenkel pair prod. under irrad., threshold energy anisotropy 2—25388
- getter-ion pump, with cold cathode characteristics 2—33827
- lattice dynamics, frequency/wave vector dispersion relations for normal modes of vibration 2—22384
- lattice vibration spectra, determination of specific heats and Debye temp. 2—22405
- microstrain behaviour of $\langle 100\rangle$ and $\langle 110\rangle$ single crysts., plastic prestrain effects 2—25496
- oxidation kinetics, K_α X-ray emission study 2—32385
- phonon spectra, neutron scatt. and tunnelling comparison 2—19395
- resistivity, Bloch-Grueneisen parameters evaluation, program 2—32923
- solid, vibrational spectrum and specific heat calc. on basis of lattice dynamical model of Sharma and Joshi 2—4039
- superconducting mixed state, N_2 distrib. obs. using rot. hysteresis 2—32954
- superconducting-normal transition, surface impurity effects 2—36458
- superconducting-normal transition, surface impurity effects 2—36459
- superconductivity, tunnelling, surface contamination effects 2—29636
- surface ionization of fast K atoms 2—13364
- Ta:O films, thickness det. methods 2—18946
- β-Ta film, sputtered, elec. cond., struct., transform., X-ray diffr. obs. 2—18945
- thermal transport of N, conc. dependence 2—6512
- thermionic electron emission, surface barrier determ. 2—4322
- thermionic emission, temp. depend., effect of adsorbed Li atoms 2—19798
- tunnel junction, Ta-insulator-Al, zero-bias-conductance anomaly 2—19611

Tantalum continued
- Ta/W shadow casting, applic. to Au on NaCl nucleation and growth obs. 2—39495
- Ta-Hf mixtures in plasma spraying as sputtering source 2—5106
- β-Ta film, sputtered, O_2 and N_2 competitive diffusion at 828K 2—39531
- β-Ta film, very pure, sputtering conditions 2—1187
- ^{177}Ta half-life measurement using microsecond beam chopping by pulsing cyclotron deflector voltage 2—24118
- ^{182}Ta gamma spectra used in rel. intensities calibration of Ge(Li) spectrometer 2—443

Tantalum compounds
- columbite, phase transformation mechanism, cation displacements 2—3999
- oxide film on Ta substrate, quantitative X-ray emission analysis 2—12670
- Au-Ta_2O_3 cermets, secondary electron emission 2—10163
- Co-1 wt.% Be-7 wt.% Ta alloy, metastable struct. states in solid soln. decomp. 2—32450
- β-Co-γ-Co_2Ta, eutectic system, microstruct., precip., lateral diffusion of Ta 2—12720
- Hf,Ta)V_2 alloys, supercond. transition temp correl. with lattice instabilities 2—32937
- $Hf_yTa_{1-y}N_x$ film, prep. by reactive alloy sputtering 2—9277
- Nb-Ta alloy, type II superconductor, critical current depend. on defect structure of flux line lattice 2—19556
- Nb-Ta alloys, supercond. props. 2—19588
- NbTa, type II superconductor, flux line arrangements in hysteretic low-k samples 2—19570
- $Nb_{0.73}Ta_{0.27}$, supercond., flux line lattice, neutron diffr. obs. 2—9967
- $Nb_{75}Ta_{25}$, type II superconductor, small-angle neutron scatt. obs. of vortices 2—19591
- Ni-Ta alloy, hyperfine field at ^{181}Ta, temp. dependence 2—36799
- Ni-Ta alloy, Ni_8Ta nucleation 2—15970
- Ni-Ta alloy, solidified at fast cooling rates, metastable phases 2—36305
- Ni_8Ti alloy single crystal, partially ordered flow stress obs. 2—25504
- Pd-Ta system, diffusion investigation using electron probe 2—29205
- Ta/10W alloy, thermal expansion, cooperative measurements using pushrod dilatometers 2—16045
- Ta-Al alloy film, compositional control by d.c. biased a.c. sputtering 2—39478
- Ta-Al alloy films, anodic oxide form. 2—3548
- Ta-B system, phase diagram, from thermal and X-ray anal. 2—13015
- Ta-(1.53at.%)C, crystal struct., interstitial ordering, field ion microscope obs.9493 2—9493
- Ta-C, ζ phase, precip. in TaC, struct., electron microscope obs. 2—3733
- Ta-H system, ferroelasticity rel. to phase diagram determination 2—9694
- Ta-H system, p.m.r., 77-300 K 2—20165
- Ta-H(D) interstitial alloy, resist., comp. and temp. depend. 2—9960
- Ta-N, Nb-Ta, type II superconductor, magnetic behaviour at small Ginzburg-Landau parameters (χ) 2—19569
- Ta-Ni-Fe, alloy, mag. props., elec. resist., hardness 2—29812
- Ta-Ti, alloy, film, struct., composition rel. to sputtering conditions 2—12671
- Ta-V, alloy, dilate, mag. susceptibility, Knight shift 2—19836
- TaB_2, thermal expansion over temp. range 300-2500°K 2—6683
- $TaBF_9^-$ chem. shift, spin coupling, mag. resonance obs. 2—5927
- $TaBO_4$, thermal expansion, rel. to cryst. chemistry 2—22430
- TaC, indentation hardness, plastic flow and fracture 2—1294
- TaC, phonon dispersion calc. 2—19373
- TaC, phonon spectra, pseudopot. approach 2—19321
- TaC, phonon spectra and supercond. 2—19388
- TaC, sintered, polycryst. props. rel. to monocryst. props. 2—22254
- TaC_x, 0-3000°K, sp. ht. and thermodynamic props. 2—1436
- TaC_x, lattice instability effects on supercond. 2—22509
- Ta_2C, eutectoid decomposition, at 1400°C, obs. 2—4005
- $TaCo_2(Fe_2)$, Laves phases, temp. depend. of microhardness 2—22290
- Ta_2CrO_6-$TaCrO_4$ system, domain struct., Jahn-Teller effect 2—26095
- Ta_2MeO_6 (Me=Fe, Co, Ni, V, Cr), magnetic props obs. below 77 K 2—40566
- Ta_2N-TiPdAu film, adhesion to Al_2O_3 substrate rel. to substrate surface chem. 2—39474
- Ta_2N, temp. coeff. of resist. of bulk samples 2—22495
- $TaNF_{11}$, N=P, As, Sb, Nb, chem. shift, spin coupling, mag. resonance obs. 2—5927
- Ta_2O_5-GeO_2 system, X-ray and optical studies 2—1412
- Ta_2O_5-ZrO_2 system α-PbO_2 type phases, cation deficiencies and superstructure 2—9482
- Ta_2O_3, anodic films, mechanical properties 2—3857
- Ta_2O_5, amorphous film, dielec. polarization current, space charge contrib. 2—4271
- Ta_2O_5, film, current transport, effective dielec. const. 2—6872
- Ta_2O_5, film, formation kinetics on Ta(110) surface, X-ray emission study 2—32385
- Ta_2O_5, film, gaseous anodization, elec. and optical props. 2—13301
- Ta_2O_5, in m.i.s. struct., flat band shift, controlled charge injection 2—4260
- Ta_2O_5, in Ta-Ta_2O_5-Au diode, negative resistance and energetic electron processes 2—19725
- Ta_2O_5, O_2 self-diffusion, ionic cond. obs. 2—19148
- Ta_2O_5, positron lifetime correlations 2—4150
- Ta_2O crystal structure, constants, high temperature form, stabilised by doping with Sc_2O_3 2—3734
- Ta_2O_5 film, amorphous, complex dielec. const., thickness effects 2—40326
- Ta_2O_5 film, dielec. loss behaviour 2—40325
- Ta_2O_5 films rel. between thermal oxidation temp. and optical propagation 2—40608
- $TaOPO_4$, tetragonal high press. modification, prep. and struct. 2—22163
- Ta_3P, Knight shift, spin lattice relaxation, conduction process 2—4559
- TaS_2, intercalation effect on electron transport 2—32951
- Ta_2S imperfections, void channels 2—3723
- $TaS_2(Se_2)$, 1s-forms, diamag., semicond., spin-orbit coupling 2—16412
- Ta_3Sn, type II supercond., nuclear quadrupole spin lattice relax. 2—4173
- Ta_2VO_6-VO_2 system, evolution of crystallographic order 2—29153

Targets *see Nuclear bombardment targets*

Teaching
- astronomically determined dates and geometrical alignments, tutorial article 2—11236
- biophysics course 2—17150
- boundary layer theory, introduction 2—27013
- 'canned' computer lab, FORTRAN IV, use in introductory mechanics course 2—11318

Teaching continued
cellulose nitrate for α-particle track visualisation, use in undergraduate laboratory 2—33840
centripetal force, exptl. demonstration 2—17157
charge to mass ratio of electron meas. using magnetic field of a flat circular coil 2—14357
computational physics, undergraduate course 2—37545
computer, instructional uses, and quantum scattering theory 2—2051
computer augmented physics lab., analysis and simulation of expts. on wave propagation, sound, light 2—14059
computer program, DITRAN, for translating physics dialogues into templated conversational subprograms 2—7
concept formulation and exchange of knowledge in physics 2—17147
crystal orbital theory, descriptive 2—1448
crystal structure, bubble model 2—15693
crystals, arrangement of atoms, method for illustration 2—9372
degree course in physics for students embarking on non-science careers 2—6
dynamics, basic 2—7638
dynamics, initiating motion in child's swing 2—33855
dynamics of machines, use of vector notation and matrix methods 2—27011
eclipsing binaries, instructional uses of computer 2—33846
eigenvalue problem, square well in phase plane, film demonstration 2—27051
electrical analogue computer, construction of simple instrument to illustrate basic series and parallel laws in d.c. circuits 2—11238
electrometer for measurement of small currents in physics experiments 2—27006
electron creation and annihilation operators in solid state physics 2—16128
electron optics, suitable topic for computer applications course 2—17153
electronics course for the average child 2—37543
electronics for college science students, elementary practical course 2—37548
electrons, properties and applications, educational article 2—8116
electrostatic expt. using parallel plate capacitor, computer measurements 2—14353
elementary particles textbook 2—359
engineering syllabuses at GCE A level which have attempted to unite physics and technical studies 2—37544
external bremsstrahlung production by β particles in thin foils, Z dependence 2—27708
fluid oscillations in a U tube, undergraduate expt. 2—15440
Fresnel diffraction pattern of thin wire, intensity measurements 2—11514
Fresnel hologram of a square aperture 2—33853
functional analysis, review paper 2—28
functions of mathematical physics, graduate-level text 2—5121
Gauss's law, role of unenclosed charges 2—33852
general physics, teacher as organiser of learning conditions 2—37550
Green functions, classical statistical, using treatment of simple harmonic oscillator 2—17160
Griffith concept in fracture mechanics 2—23213
group theory, summary 2—34
heat, teaching the concept 2—37549
homework grading 2—14062
interference of elliptically polarized beams 2—34478
intermediate mechanics, computer assisted course 2—17149
invariants, theory, summary 2—27
kinematics, undergraduate assignment, study of results 2—27000
kinematics of machines, use of vector notation and matrix methods 2—27010
laboratory, organization for students in first 3 years 2—33839
lattice dynamics, illustration of critical points using a simple pendulum 2—17163
least-squares curve fitting, FORTRAN IV program 2—17159
light emitting diodes, operating parameters, laboratory investigation 2—29723
linear harmonic oscillator, derivation of generating function 2—17162
magnetic properties of superconductors, expt. for advanced undergraduate laboratory 2—16149
mean life of scintillation detctor crystal, use as analogue for radioactive deay 2—14757
mechanics, linear elastic and inelastic collisions between two or three objects 2—11322
Millikan oil-drop experiment, laser illuminations 2—17155
molecular spectroscopy and its interpretation, book for undergraduates 2—5898
neurophysiological wave-form generator 2—11193
neutron, properties and applications, educational article 2—8205
n.m.r. apparatus at low cost, use of earth's magnetic field and audio amplifiers 2—37863
nuclear lifetime meas. using Doppler effect, undergraduate expt. 2—11240
Nuffield advanced physics course, kit of modules for electronics option 2—37547
one-electron atomic wave functions, analysis in modern physics course 2—17221
open-ended cumulative physics expts. in advanced laboratory 2—14058
optical design and apparatus, lenses 2—23215
organic crystals, molecular interaction energy 2—1199
oscilloscope, self-instruction method for teaching usage 2—17151
photometer with small surface area used with He-Ne laser for studying diffraction phenomena 2—34503
physical chemistry course, introduction of laser to 1st year students 2—27001
physics, elementary schools, aid from univ. dept. 2—27003
physics, emphasis of context of inquiry 2—17146
physics, noncalculus derivation of Coulomb potential, nonscience students 2—27007
physics, pedagogical formation of teachers, discussion of learning process in schools 2—37542
physics, role for history of physics 2—37540
physics, strategy to develop skills early 2—14057
physics, theory, scientific value 2—26998
physics and philosophy for nonscience majors 2—17148
physics course for musicians 2—4
physics for freshman, team approach 2—14061
physics laboratory instruction, computer-aided, project CAPLIN 2—17152
physics teachers, relevance of history of physics 2—37541

Teaching continued
pinhole camera, understanding of physical optics 2—33854
Planck's constant determ. from Wien's displacement law 2—27005
probability and statistics, undergraduate textbook 2—113
properties and uses, educational article 2—8194
quantum mechanics, introductory course using a computer 2—11271
relativity, didactic approach 2—17165
Schrodinger equation, computer solutions 2—33844
Schrodinger equation, heuristic approach for elementary students 2—14100
science education in underdeveloped countries 2—2
science to nonscience majors 2—5
self-similar solution of partial differential equations, illustration with RC transmission line 2—17164
sequential analysis textbook 2—114
shock tube, high performance with air driver, design for undergraduate lab. 2—27290
slide rules and problem of three 2—3
spectral anal. using a camera, in introductory physics lab. 2—16698
speed of light meas. with laser and Pockels cell, undergraduate research project 2—11507
statistical mechanics, classical limit of partition function 2—33942
statistical thermodynamics, the most probable distribution 2—92
stochastic processes, elements, review 2—86
strain gauge force and torque transducer, for meas. teaching 2—27009
successive decay and related equilibria, computer simulation 2—30745
survey course with large entropy for appreciation of physics 2—26999
technology and modern social problems, new course for science students 2—11239
tensor, summary, educational paper 2—31
tensors, using coeff. of friction as example of second rank tensor 2—17161
thermodynamic exercise, apparent violation of second law 2—33857
thick lens theory, use of matrices for simple treatment at sixth form level 2—38040
vacuum u.v. spectroscopy, description of undergraduate laboratory and experiments 2—11242
vertical spring, mass distribution and frequencies 2—17158
visco-elastic liquids, linear and non-linear effects 2—25017
wave mechanics, statistical foundations and nonsymmetric binomial distribution, application of computer 2—27012
experiment on experiments in a senior laboratory 2—11241

demonstrations
acoustics for music majors, lab. course 2—27002
atomic physics and optics, exptl. demonstrations 2—7637
Brownian motion, simulation apparatus 2—33847
centrifugal reaction force 2—33851
cine films, use as a higher education aid 2—12
colour spectrum of white light, diffraction grating demonstration 2—10
deformation fronts, simple demonstration of pinning 2—29176
diffraction of laser light by u.s. waves in liquid, undergraduate demonstration 2—33842
dimensional display, space lattice presentation showing physical quantity relationships 2—23214
electric field distributions made visible by macroscopic charged particles 2—30970
electronic charge measurement, student view of Pasco-Millikan oil drop apparatus 2—33856
electropiano, acoustical output 2—34132
fatigue failure testing, small scale, oscillation in magnetic field 2—1311
film loops on electric fields of moving charges 2—11
Fourier-transform spectrometer based on Michelson interferometer, undergraduate expt. 2—14475
fringe visibility with Michelson interferometer, apparatus modification 2—27008
gyroscopic stabilization and destabilization 2—23317
Hall effect in flowing electrolyte, meas. in undergraduate lab. 2—15602
i.r. diffraction, technique and equipment 2—5417
laser beam optics 2—5382
light, interference and coherence 2—17154
light velocity, spark light source 2—33845
light velocity det, by rotating mirror method 2—9
linear accelerator, simulation apparatus 2—33847
liquid biprisms, determination of refr. index of liquids 2—33850
magnetic fields of current carrying wires, undergraduate laboratory experiment 2—33841
mechanical system, motion of mass centre 2—23316
microwave expts. for undergrads., yielding unexpected results 2—27004
momentum conservation principle, using bow, arrow and ballistic pendulum 2—17285
parallax, geocentric and heliocentric, demonstration devices 2—37427
Planck's constant expt., amplifier 2—2325
polarization of laser beam by scattering 2—8
relativistic mass increase, simple experiment 2—14080
resistor-capacitor line, demonstration of backward wave 2—33849
short access 8mm films 2—2050
stellar parallax simulation study 2—33848
vibration of monatomic and diatomic lattice, and lattice with defect, lab. demonstration using electrical analogues 2—15988
^{40}K, laboratory experiment for determining half-life for beta emission 2—33843

Technetium
magnetic anisotropy, temp. depend. 2—40420
^{99m}Tc-albumin, for placental scanning 2—20742
^{99m}Tc-pertechnetate brain scans, initial and delayed, comparison of accuracy 2—26953
^{99m}Tc feasibility of production on medical cyclotron 2—3009

Technetium compounds
TcO_4-, SCCC-MO calc. 2—18474
TcO_4^-, vibr. spectra, r.m.s. amplitude 2—3064

Tektites *see Meteorites*

Telescopes
16 in. Cassegrain, new method of alignment without long term drift 2—17703
catadioptric imaging systems, meniscus aberration correctors, book 2—27626
cosmic ray, contribution of scattered electrons to detected signal 2—27810
cosmic ray isotope and charge resolution using large area scintillation-Cherenkov-total energy telescopes 2—27811

Telescopes continued
  mirrors with random surface undulations, illumination distrib. in diffraction image 2—17677
  performance reciprocity for propagation in turbulent medium 2—34513
  quality evaluation, information theory criterion 2—38092
  radio, spectrograph, computer-run 2—23137
  solar, 16 GHz, transportable, for atmospheric transmissivity measurements 2—33772
  wave optical imaging performance for different wavefront deviations 2—2422
 astronomical
  see also Radioastronomy
  92 cm, with scanning spectrometer, for OAO 2—11172
  almucantar radio telescope, capabilities 2—26934
  Anglo-Australian 150 inch, progress 2—7578
  Arecibo radio-radar telescope, improvements 2—30645
  autocollimating, choice and use, practical aspects 2—5029
  Cassegrain, high resolution balloon-borne spectrograph, near solar u.v. 2—11061
  coma image at prime focus of OAN 2—26938
  computer controlled, for supernova search 2—26936
  cost-size relation as a polynomial expansion 2—7576
  drive and guidance using stepping motors 2—17098
  gamma ray, for satellite experiment to meas. intensity and energy spectrum of sun flares 2—11138
  gamma ray, for spectrometery of galactic sources 2—10821
  gamma ray, incorporating multiplate spark chamber, for obs. of Crab Nebula pulsar 0532 2—10989
  gamma ray, using gas Cerenkov detector for fine angular resolution for fine angular resolution of gamma astronomical sources 2—10988
  gamma-ray, digitized spark chamber type, satellite borne 2—33721
  gamma-ray, digitized spark chamber type, satellite borne 2—26811
  image tube-optical systems for far u.v. 2—11173
  interstellar communications techniques 2—17096
  i.r., designs and limitations 2—23138
  i.r., efficiency and choice for ground-based obs. 2—30651
  i.r. and submillimeter, 91.5 cm aperture for altitudes 12 to 14 km, design and operation 2—7575
  i.r. interferometer with 4 m Cassegrain 2—37430
  isochromatic mirror-lens system with spherical optics 2—30646
  large, design review 2—11170
  Large Space Telescope instrumentation, observing programme 2—41265
  mirrors, surface quality determination by the slit and wire method 2—7580
  motion picture photography 2—5023
  OAO Princeton expt., 80 cm diameter telescope with u.v. spectrometer 2—11164
  optical with rapid scanner, measurement of cyanide and oxide band strengths in cool stars 2—4850
  orbiting, u.v. spectroscopic with Fabry-Perot interferometer 2—11171
  orbiting large stellar telescopes, centrally obscured, figure of merit definition 2—7577
  photographic image sharpening laser process 2—20714
  primary mirror, paraboloidal, synthesis by spherical mirrors 2—34436
  radio, effects on amplitude scintillation spectrum 2—37167
  radio, paraboloidal, radiation pattern obs. using interfereometer 2—17097
  radio reflectors, deformation monitoring, experimental laser system 2—2009
  reflecting, pairs of spherical mirrors as field correctors for paraboloid mirrors 2—7579
  reflector, coude, 74″, echelle grating 2—7585
  solar vacuum telescope, observations of spicules 2—23141
  Steward Observatory 230-cm. and Optical Sciences Center 154-cm. primary mirrors, theoretical elastic deformations 2—27610
  Van Vleck 20-inch refractor, effect of coma on photographic astrometric measurements 2—5028
  X-ray, focusing, precision observation of location and spectra 2—10979
  X-ray, holographic production of zone plates 2—11185
  X-ray, paraboloid hyperboloid, design characteristics 2—23139
  X-ray and u.v. glancing incidence optics 2—11161
  X-ray with modulation collimator for solar flare obs. 2—11139
Tellurium
  acceptor states, Hall effect obs. 2—10053
  acoustic mode freq., dispersion curve 2—13031
  acoustoelectric amplification, studied using epitaxial Se transducers 2—10035
  adsorption, from soln., rel. to defective fuel location in reactors 2—12685
  atoms, scattering of I ions, 18-46 MeV, impact parameter dependence of X-ray production 2—38842
  conduction band obs., absorpt. spectrum, 30-246 eV 2—20050
  crystal, radioactive, 360-58 keV cascade of excited ^{127}I, angular γ quantum correlations 2—29854
  cyclotron reson. absorpt. struct. in valence band 2—33002
  dielectric constant anisotropy, 3-30 eV 2—22725
  diffusion, in CdS, vapour pressure method, concentration profiles detn. 2—9593
  diffusion in CdS(Se) possible ternary cpd. prep. 2—3820
  elastic limit and Peierls forces 2—3855
  electron energy in cryst. mag. field 2—36397
  electron-phonon interaction, rel. to temp. depend. of microwave absorpt. 2—25844
  electronic bands, Fourier expansion 2—22466
  film, deposition on glass substrate, crystallite orientation 2—1183
  film, on TGS substrate, ferroelec. field effect temp. dependence 2—36517
  film, struct., growth, orientation 2—3549
  films, electron microscope study of structure 2—25212
  films, obliquely deposited, transmittance and reflectivity determ. for 2-25 μ radiation 2—19963
  Hall coefficient and electrical conductivity, 1.4-77K 2—29676
  impurity in Cu, spiral elongation test for annealability 2—3932
  intervalence band transition, modulation by acoustoelec. domains 2—7075
  laser beams mixing, tunable coherent radiation source 2—7931
  liquid, Hall coeff. detn. 2—12581
  liquid, self-diffusion coeff., temp. depend. 2—39355
  liquid, struct. evolution, temp. depend., neutron diffr. obs. 2—12539
  long wave optical phonons, comparison with Se 2—22406
  molecular vapour condensation on epitaxial substrate 2—6337
  p-type, laser-excited, carrier relaxation times and recombination, optical obs. 2—16231
  Raman scatt., mode linewidths, polarization selection rules, wavevector shifts, second order struct. 2—16570
Tellurium continued
  resistance, pressure coeff., rel. to pressure sensor appl. 2—20780
  single crystal film, epitaxially grown on Se 2—35896
  supercurrent tunnelling junction 2—13183
  surface defects influence on carrier density and elec. cond. 2—10062
  surface layer on CdTe, detect. by Raman back scatt. 2—7082
  surface quantum states in accumulation layer 2—16232
  thermal expansion, negative, role of elastic consts. 2—25688
  thermal expansion of four single crystals, 6 to 200 K, behaviour in rel. to lattice structure 2—16061
  valence band, transform. under pressure, Shubnikov-de Haas effect obs. 2—10052
  valence band struct., impurity levels, chem. shifts, cond., Hall coeff., galvanomag. props. 2—29688
  Bi:Te, galvanomag. props., helicon standing wave resonance obs. 2—25749
  Bi:Te, hyperfine heat capacity and nucl. quadrupole interaction 2—16657
  Bi_2Te_3-BiI_3-Te, structure, phase composition and props. 2—3982
  CdS:Te, conc. depend. of emission intensity 2—4490
  CdSb:Te, Hg(In), influence of doping on elec. props. and band struct. 2—36499
  CdSb:Te layers, doping and elec. props. 2—36046
  in Fe-Si alloy, effect on grain growth rate in primary recrystn. 2—39890
  n-GaAs:Te, Dingle temp., cyclotron mass, Hall mobility, Dingle mobility, Shubnikov-de Haas effect, 1.9-4.2 K 2—22548
  GaAs:Te, radiative recomb. time characts. 2—33305
  GaAs;Te influence of dislocation densities on output characteristics of injection lasers 2—17641
  GaP:Te, Zn, epitaxial single cryst., Hall mobility and resistivity obs. 2—40255
  GaSb:Te, conduction band, Hall and conductivity obs. 2—4225
  GaSb:Te, Hall coeff., mobility, and resistivity, from thermal cond. data 2—22532
  GaSb:Te, phonon scatt. at low temp. 2—22533
  Ge:Te, precipitate form. on growth dislocations 2—12770
  in Ge(Li) detectors, preferential electron trapping 2—27882
  He-Te laser, new c.w. oscillation at 5708Å 2—31035
  InSb:Te, heavily doped, mobility, pressure depend. 2—10020
  InSb:Te, impurity solubility and distrib. coeff. 2—1254
  Te:Ag(Sb) layers, doping and elec. props. 2—36046
  Te:Sb, coupled plasmon-LO phonon modes, reflectivity obs. 2—32906
  Te:Sn, mobility and microhardness, impurity conc. depend. 2—13239
  Te, purification for CdTe crystal growth 2—35948
  Te_2 gas, $A0_u^+$, $B0_u^+$—$X0_g^+$ systems, rotational analysis 2—35292
  ^{203}Tl, spectral analysis by isotopic dilution method 2—37067
  ^{204}Tl, radioactive source preparation by electrodeposition on thin metallized plastic films 2—5673
Tellurium compounds
  tellurates, tellurites, in ionic crystals, inducement of i.r. absorption 2—16481
  Al-Te, liquid alloys, thermodynamic props. determ. using improved dew pt. method 2—39359
  As-Ge-Te, glassy system, elec. cond. variation with temperature 2—4151
  As_{20}-Te_{70}-Ge_{10}, amorphous semiconductor films, condition for memorization by laser light pulse 2—4188
  As-Te glass, switching processes 2—29658
  As-Te system, glass-forming ability vs. local order and covalency 2—39438
  Cd-Te, partial pressure, thermodynamic props., sublimation 2—12619
  $Cd_{0.1}Hg_{0.9}$ Te, film, Hall coeff. and mobility thickness depend. 2—10012
  CdTe, energy band pseudopotential model, optical, photoemissive props. 2—19666
  Co-Te system, phase relns. and thermodynamic props. 2—19311
  Co-Te system, stoichiometry, Mossbauer obs. 2—16433
  Cu-In-Te system, phase equilib. and hardness 2—1410
  Fe-Te system, stoichiometric or nearly stoichiometric compositions, quadrupole splitting and isomer shift, Mossbauer obs. 2—36841
  Ge-Se-Te glass, density, softening temp., hardness and elec. props. 2—35846
  Ge-Te alloy, amorphous, band struct. and transport props. 2—19646
  $GeSe_2$-Te system, stratification regions and glass formation 2—35847
  Ge_2SeTe_7, amorphous semicond., transient characteristics, filamentary plasma model 2—16248
  Hg_{1-x} Cd_xTe alloy, compositional dependence of energy bands and optical gap 2—9933
  MgO-$TeO_2V_2O_5$ and ZnO-TeO_2-V_2O_5 glasses, variation of physical props. and chemical stability with composition 2—6292
  Nb-Te system, phase study Nb_3Te_7 to Fe 2—9841
  $Pb_{1-x}Sn_xTe$, wavelength modulation derivative reflection spectra, assignment of obs. structures with band calcs. 2—4449
  Pd-Mn-Te, cryst. struct. and mag. props. 2—33134
  S-Te-As, chalcogenide, glass transition 2—9225
  $(Sb\text{-}Bi)_2$ $(Te\text{-}Se)_3$ quaternary solid solutions, thermoelectric properties 2—13335
  Se-Te-As, chalcogenide, glass transition 2—9225
  Se-Te alloy, dielec. tensors 2—1558
  Se-Te alloy, elastic stiffness consts., comp. depend. 2—25481
  Se-Te alloy, liquid, electrical switching 2—3407
  Se-Te single crystal alloy, piezoelec. and elastic props. 2—36600
  Si-As-Te and Si-Ge-As-Te glasses, glass-forming region and DTA study 2—15637
  Te-As-Ge-Si glass switching system, nature of ON-state 2—22577
  Te-As-Ge, amorphous to crystalline transition assoc. with elec. transition, review 2—13238
  Te-Ge-Se system, amorphous semiconductor, structure and elec. props. 2—29675
  Te-Se, liquid alloy, Hall coeff. detn. 2—12581
  Te-Se alloy, amorphous, microhardness, density, X-ray scatt. and heat capacity relax. effects 2—39772
  Te-U-C ternary system, phase equilibrium, solid state compatibility relationship 2—29482
  $Te_{40}As_{37}Ge_7Si_{18}$ films, ovonic threshold switching 2—10082
  $Te_{48}As_{30}Ge_{10}Si_{12}$, glass, switching and memory effects 2—16214
  $TeCl_2Br_2$, vapour phase, molecular structure study using data from $TeCl_4$ and $TeBr_4$ 2—24488
  TeGe-SnTe, alloy, film, plasmon energy, electron energy loss spectra, electron microscope obs. 2—4143
  $Te_{0.81}Ge_{0.15}As_{0.04}$, memory state, superconducting props. 2—16168
  $Te_{81}Ge_{15}As_4$, glass, switching and memory effects 2—16214
  $Te_{81}Ge_{15}Sb_2S_2$, amorphous film, light induced memory 2—19653

- **Tellurium compounds** continued
  - TeO_2-MO_2 system, M=Ti, Zr, Hf, Sn, V; structure of cpds. formed 2—9347
  - TeO_3-MTO_3 system (M=K, Rb, Cs, Tl; T=Nb, Ta), crystal chemistry 2—15682
  - TeO_2-SrO-V_2O_5, glass system, formation and properties 2—12631
  - TeO_2, optical props. 2—1658
  - TeO_2, paratellurite, second harmonic generation and Kleinman's symmetry relations 2—33193
  - TeO_2, Raman spectra, phonon modes 2—40695
  - TeO_2, second harmonic generation, Kleinman's symmetry condition violation 2—33194
  - TeO_2, single crystal growth from melt using Czochralski technique, for acousto-optic device applications 2—15692
  - TeO_2, thermal expansion, 30-461°C, X-ray determ. 2_32849
  - TeO_2 acoustic wave propagation in single crystal 2—16020
  - TlI, mechanism of pulsed lasing of green line in a vapour discharge 2—27486
  - V_2O_5-TeO_2 glass, between metal electrodes, I-V characts., —100-200°C 2—36519
  - Xe estimation in ores using gamma-ray analysis of ^{129}I 2—7193
  - Zn-Te, partial pressure, thermodynamic props., sublimation 2—12619
- **Temperature**
  - *see also High-temperature phenomena and effects; Low-temperature production*
  - control, hot wire changing conditions of cooling and evaporation, using power supply 2—34228
  - controller, for thermally stimulated conductivity and thermoluminescence obs. 2—27340
  - dynamic link between temperature and density of states 2—17257
  - international practical scale 2—37825
  - International Practical Temperature Scale of 1968, computation aids for 13.81 to 273.15 K range 2—23405
  - surface, nonlinearly radiating semi-infinite solid 2—30899
  - waves in plasma, meas. in connection with drift type instability 2—21856
  - ^3He-^4He mixtures, pressure-temp-density relations near liq.-vapour critical point 2_22025
- **Temperature control** *see Cryostats; Thermostats*
- **Temperature distribution**
  - air, inside heated premises, analysis 2—5280
  - axisymmetrical, deformation of thin cylindrical shell 2—27128
  - bubble surface during nucleate boiling, interferometric obs. 2—25153
  - bubble surface during nucleate boiling 2—25152
  - circular hollow cylinder, boundary conditions 2—37819
  - in Couette flow with and without additional pressure gradient 2—21741
  - near crack due to action of load and sudden temperature change, calc. of axially symmetric field 2—33991
  - crack in a plate, 3-D distribution, integral eqn. solution 2—5193
  - cylindrical body of finite height subject to convective heat losses, nonstationary quasi-static thermal displacements and stresses 2—33998
  - diffusion equation, composite medium, k sections, internal generation 2—11378
  - drilling, investigation in rock around a shaft 2—7235
  - Earth's crust and upper mantle, due to radioactive decay of U, Th and K isotopes 2—30216
  - filament lamp, interferometric method 2—27595
  - finite element method calculation 2—17353
  - finite element soln. 2—37722
  - finite element technique, computer programmes 2—17354
  - finite solid cylinder containing heat sources, conductive transfer 2—37815
  - flame, uniaxially symmetric, analysis, integral eqn. soln. method 2—27325
  - flash welding, temperature field in components being joined, automatic measurement 2—2280
  - in flat multilayer walls, analytical approx. methods for non-steady state problems 2—11372
  - flowing fluid, due to periodically varying heat source 2—14295
  - fluid, flowing in curved pipe 2—37808
  - fluids, laminar flow through circular tube 2—35406
  - furnace, high pressure, cylindrical, computation 2—27327
  - graphite arc electrodes, axial distrib. 2—32142
  - Gunn diode, Gauss-Seidel relaxation method 2—6868
  - Gyarmati theorem and variational principle 2—14141
  - ice sheet, polar, profile, computer analysis 2—7230
  - in solids with anisotropic non-constant thermal conductivity, functional solution 2—2276
  - infinite coaxial cylinders, tangential Newtonian flow, transpiration cooling 2—12325
  - infinite slab, plane source of finite duration 2—11382
  - isothermal wall, vertical, with natural turbulent condition 2—2278
  - lunar surface temp. at Tranquillity Base 2—23104
  - multiregional analysis of temp. fields in finite rod bundles cooled by liquid metals 2—15166
  - nonuniform thermal gradients in galvanothermomagnetic obs. using liquid crystals 2—34225
  - nuclear fuel rod assemblies, finite, theoretical predictions 2—38697
  - one-dimensional geometries, nonuniform heat generation, equal surface temps., max. internal temp. 2—17423
  - pipelines, hoh pressure, induction heat treatment 2—29385
  - for plane Couette flow of an incompressible non-Newtonian fluid 2—18556
  - plasma, circularly, symmetric, radial distrib. from lateral radiance ratio 2—28507
  - power reactor fuel element dynamic heat transfer analysis 2—15165
  - radial, in nuclear reactor mixed oxide fuel elements 2—38747
  - reactor core, determ. from thermal neutron capture γ spectra 2—38737
  - rotational, for underexpanded N_2 jet, rotational relaxation analysis 2—6140
  - steel ingot solidification, differential mathematical model 2—3442
  - substrate, during high-rate physical vapour deposition of materials 2—32347
  - insupersonic turbulent boundary layers, exptl. investigation in Mach. number range 1.75 to 4.5 2—18724
  - surface temperature, evaluation of specific heat flows, conduction 2—27328
  - thermal boundary layer of thin plate heated on reverse side by radiation 2—27305
  - thermal i.r. imaging devices, studying quasistationary thermal fields 2—37805
  - thermocline in lake, seasonal formation and movement 2—37116
  - thermocouples, effect of nonuniform distrib. 2—23411
  - thin-walled bodies of revolution with curvilinear anisotropy 2—27318
- **Temperature distribution** continued
  - vapour deposit, model for high rate physical vapour deposition process 2—32346
  - Ar long induction discharge, spectral method for meas. of radial temp. distribution 2—28661
  - He plasma fireball produced by CO_2 laser 2—6091
  - Mo, pulse-heated specimen, photomicrographic study 2—25697
  - Na vapour arc, high pressure 2—24945
  - UO_2 pellet, in-pile thermal gradient, out-of-pile simulation 2—28155
- **Temperature measurement**
  - *see also Pyrometers; Thermocouples; Thermometers*
  - absolute temperature from the noise thermometer method, 292 to 635 K 2—27335
  - cathode in Ar arc, technique 2—12373
  - chromel-alumel thermocouple, pressure corrections up to 7 kbar 2—5282
  - cold neutron source at reactor FRJ-2 2—24288
  - contactless, classification and terminology 2—23404
  - crescograph, magnetic, theory of operation 2—2053
  - d.c. thermistor thermometer, numerical method of linearizing 2—20963
  - deep ice, reinterpretation 2—7232
  - dew points and frost points down to —50°C, cooled mirror instruments 2—34227
  - by differential calorimeter, applic. to transition temp. and energy obs. 2—11384
  - rel. to dryout obs., combined photographic film thickness and temp. technique 2—24275
  - DTA, principle of regulation 2—11386
  - electronic thermometer employing Si diode 2—2283
  - exosphere, rocket and incoherent- scatter 2—13745
  - flame, enthalpy probe 2—27306
  - gas, high temperatures, calorimetry 2—27341
  - IPTS 68 realization 1064.43 to 2200°C using NSL photoelectric pyrometer 2—30898
  - Jimsonde, high resolution temperature sensor, comparative test results 2—16803
  - laser beam attenuation, application to molten glass 2—37827
  - liquidus temperature of multicomponent systems 2—1140
  - lunar surface, diurnal variation, Apollo 12 obs. 2—23111
  - metal crystals, plastic deformation, energy relations 2—19178
  - meter, narrow-range, measurement circuit 2—23408
  - nuclear fuel bundles, multielement, surface temp. meas. using thermocouples 2—5758
  - oceanographic applications of colour-enhanced satellite imageries 2—37118
  - Peake's microwave emission model 2—2282
  - physical metallurgy, tools and techniques, book 2—25560
  - pickup for local heat flux 2—37829
  - plasma, hot W-wire method 2—35549
  - plasma generator cooling water, use of resistor thermometers 2—34226
  - plasma in laser pulse induced air and He breakdown, soft X-ray continuum emission technique 2—32033
  - pyrometers performance 2—11370
  - quartz resonators as thermally sensitive elements of frequency transducers 2—37826
  - resistance thermometry, transformer cct. 2—27329
  - review of methods 2—23406
  - scale revision for solar furnace pyrometry 2—27330
  - sea, from space, effect of atmosphere 2—13665
  - sea surface, computer model for automated processing of i.r. satellite data 2—20296
  - sea surface, surface temperature mapping in west Atlantic 2—20298
  - in seawater, thermal probe for meas. vertical temp. profile 2—10717
  - small surfaces, attachment to radiation pyrometer 2—23395
  - solar active regions on 2 cm wavelength 2—26910
  - standards, organic reference substances, caloremetric evaluation 2—34224
  - steam water heater, exchanger tubes, thermocouple obs. 2—23403
  - steel, phase transform. temp., meas. technique 2—19298
  - surface temperature, evaluation of specific heat flows, conduction 2—27328
  - temperature electron and ion measurements of laser created plasma 2—24773
  - thermal probe by ref. to heat flow, for use in flame type furnaces 2—20961
  - thermistor, bridge circuits 2—193
  - thermogravimetric apparatus from standard units 2—20800
  - thermosphere, meas. technique using mol. beam sampler and metastable time-of-flight obs. 2—40978
  - transistor surface by means of a fluorescent phosphor 2—5281
  - u.s., temp. dependence of sound velocity 2—20962
  - VIPER pulsed reactor, temperature measurement using intrinsic junctions 2—38764
  - welded joint area produced by explosion using welding plates as thermocouples 2—27326
  - ^{161}Dy Mossbauer thermometer, low temp. calibration 2—37828
  - $Na_3[Ce(C_7H_3NO_4)_3]$.$15H_2O$ complex, low temperature production 2—13385
  - Pt/Pt-(10%wt)Rh thermocouple, pressure corrections up to 7 kbar 2—5282
  - **spectral methods**
    - A-type stars, determination of effective temperatures of stars with different effective gravities 2—30460
    - arc, Cu atomic spectrum lines obs. 2—30897
    - disappearing filament pyrometers, optics and residual aberrations 2—34197
    - flames, physical significance 2—14294
    - fluid boundary layer, laser interferometric holography applic. 2—17454
    - i.r. radiation rel. to earthquake activity associated with the volcanic eruption of Akita-komaga-take 2—10689
    - i.r. radiometer, error in measuring temperature of nonblack bodies 2—37803
    - Mossbauer effect, 10^{-3}K region 2—41363
    - nonvariable F and G stars, spectral scans in red and Hα profiles 2—30469
    - nonvariable F and G stars, temp. scale from spectral scans in red and Hα profiles 2—30469
    - O and Of-type central stars of planetary nebulae 2—10886
    - plasma, circularly symmetric, radial distrib. from lateral radiance ratio 2—28507
    - plasma diagnostics, field absorption method 2—35553
    - plasma diagnostics, theory of diffraction interferences 2—35552
    - rocket borne radiometer, low pass i.r. filter 2—34195

Temperature measurement continued
- **spectral methods** continued
  - semiautomatic spectrocomparator for temperature scale transmission 2—37801
  - H_2-F_2 flame, determ. of local temps., influence of autoabsorption and thermal gradients 2—7783
  - H_2S+O_2 flame, rot. temp. 2—11381
  - N_2 flames, using Raman scattering 2—37824
  - O_2 flames, using Raman scattering 2—37824

Tensile strength *see Mechanical strength/tensile*

Tensors
- analysis, summary, educational paper 2—31
- bivectorial and spinorial fields, energy- momentum tensor 2—27042
- bundles, b-boundary construction over space-time 2—2083
- Cartesian product expansions of spherical harmonics, distribution function of plasma 2—39092
- conformal stress tensor 2—17796
- energy, of relativistic perfect fluid 2—3161
- energy-momentum, condition for softness of trace 2—341
- energy-momentum tensor of system of charged particles 2—2346
- field theory, new invariance property of tensorial functions 2—7645
- fractional parentage coeffs. rel. to matrix elements of irreducible tensorial operators 2—24324
- Green's dyadics for elastic and electromagnetic waves in random media 2—2236
- irreducible operators, application of theory to molecular hyperfine structure 2—757
- magnetic susceptibility, of low-loss ferrites, in 2cm range, meas. 2—34283
- moving dispersive medium, symmetrized energy-momentum tensor 2—14307
- neo-geodesics in a Riemannian space, neo-tensor differentiation 2—14075
- second rank, teaching using coeff. of friction as example of second rank tensor 2—17161
- statistical tensors, bounds for linear combinations 2—8125
- uniformly rotating masses, energy momentum stress tensor and gravitational field 2—17206
- Weyl tensor, asymptotic form in empty space-time to ensure asymptotic flatness 2—5135

Terbium
- activated La and Gd oxyhalide, for X-ray image convertors, patent 2—20089
- deformation study by X-ray diffraction, stacking fault probability 2—3772
- ferromagnetic reson., mag. field rot. depend. 2—40746
- glass activation, borate, silicate and borosilicate, stability to flow of accelerated electrons 2—36957
- ions, energy transfer with Gd ions in borate glasses, luminescence quantum efficiency 2—16620
- lattice dynamics, SOE consts., calcs. using Keating's approach 2—19404
- magneto-elastic coupling, acoustic wave vel., magnon-phonon interactions 2—13393
- magnetoelastic interaction, static and dynamic effects 2—25999
- n.m.r., of ^{159}Tb, spin echo technique 2—16662
- X-ray excited optical fluorescence, in Gd_2O_3, La_2O_3, and Y_2O_3 2—22805
- Fe_3O_4, magnetostrictive excitation of sound 2—25675
- $LaBr_3$:Tb^{3+}, absorpt. and fluorescence. spectra, Tb^{3+} excited states determ., 77K 2—36946
- Mg_2SiO_4:Tb, OH, thermoluminesc., OH anion effects, illumination effects 2—29978
- Tb^{3+}, ferrimag. resonance in BiCaVI garnet 2—4534
- Tb^{3+}, in MBO_3, M=Sc, In, and Lu, calcite type cryst., 4f-5d transitions studied, luminescence obs. 2—29962
- Tb^{3+}, in oxygen dominated compounds, luminesc. and relax. props. 2—33318
- Tb^{3+}, in $TbAsO_4$, ground state crystal field comp., rel. to second order phase transition 2—10172
- Tb^{3+} emission in La_2O_2S, thermal quenching 2—1709
- Tb^{3+} in ZnS, electroluminesc. 2—16637
- TbI, spectrum, analysis of structure of sextet system of $4f^8(^7F)5$ of $6s^2$ 2—21523
- in ZnS thin film, implantation and luminesc. 2—19119

Terbium compounds
- $TbPd_3$, mag. props. 2—19829
- Cr-Tb alloy, phase diagram 2—40002
- Er-Tb alloy, mag. struct., neutron diffr., 4.2-293k 2—26024
- Fe-Tb alloy, film, mag. compensation 2—13405
- $Ho_xTb_{1-x}Fe_2$ cubic Laves compounds, magnetic anisotropy and spin rotations 2—19916
- $Sm_{0.55}Tb_{0.45}FeO_3$, annealing induced domain wall mobility changes 2—10199
- $Sm_{0.55}Tb_{0.45}FeO_3$, domain wall mobility enhancement through X-irrad. compared with annealing 2—26071
- $Sm_{0.55}Tb_{0.45}FeO_3$ platelets, bubble domain propag. 2—6967
- $(TB,Y)_3Co$, intrinsic coercivity 2—29840
- Tb-Mn-Al alloy, struct. and mag. props. 2—40553
- TbAl garnet, mag. phase diagram 2—40567
- $TbAsO_4$, second order phase transition, optical and mag. props. 2—10172
- $TbAu_2$, atomization energies by high temp. mass spectrometry 2—28302
- TbB_{12} thermal expansion, in range 78-1300°K 2—6684
- $TbCo_2$, mag. ordering temp., press. depend. 2—33142
- $TbCo_2$, strong field magnetiz. 2—33159
- $TbCo_3$, Curie temp., hydrostatic press. effect 2—26001
- $TbCo_3$, mag. structure, neutron diffr. obs. 2—36703
- $TbCo_3$, magnetostriction 2—40500
- Tb_3Co and $TbCo_3$, e.p.r., mag. behaviour 2—10518
- TbF_3, ^{160}Tb β-decay, search for atomic after-effects 2—18167
- TbF_3 in solid N_2 and on ZnS films, i.r. spectra 2—13455
- $TbFe_2$, and pseudo-binary systems, Mossbauer effect 2—4441
- $TbFe_2$, giant room temp. magnetostriction 2—36741
- $TbFe_{2(3)}$, magnetostriction 2—40500
- $Tb_3Ga_5O_{12}$, Czochralski growth 2—19003
- β-$Tb_2(MoO_4)_3$, cryst. struct., ferroelec. and ferroelastic props. 2—3735
- $Tb_2(MoO_4)_3$, precision lattice parameters, ferroelectric-paraelectric structural transition 2—9486
- $Tb_2(MoO_4)_3$, struct. and phase relns., ferroelectric transition 2—9340
- TbO_x, cryst. growth 2—9366
- Tb_2O_3 X-ray diffraction study of crystal structure near melting point 2—6451
- TbOOH, antiferromag., and metamag. props., Neel temp. obs. 2—19926
- $TbPO_4$, antiferromagnetic transitions, ^{31}P n.m.r. obs. 2—6992

Terbium compounds continued
- $TbPO_4$, mag. ordering, rel. to Jahn-Teller distortion 2—36779
- TbRh, ferromag., mag. moment compared with crystal field calc. 2—19884
- $TbRhO_3$, mag. ordering 2—1645
- $Tb_{1-x}Sm_xFeO_3$, growth from PbO-PbF_2-B_2O_3 melts 2—22114
- $TbVO_4$, crystallographic distortion at 32 K, second order transition 2—19306
- $TbVO_4$, Jahn-Teller induced phase transition, Raman scatt. obs. 2—16534
- $TbVO_4$, Jahn-Teller system, electron- phonon coupled modes, Raman theory 2—20066
- $TbZn_2$, study of ferromagnetic - antiferromagnetic transition below 60°K 2—36758
- Y-(10 wt.%) Tb alloy, spin wave dispersion relation 2—40569

Terrestrial electricity *see Earth/electricity*

Terrestrial heat *see Earth/heat*

Terrestrial magnetism *see Earth/magnetic field; Magnetic storms*

Tetraneutrons *see Neutrons and antineutrons*

Texture *see Crystal structure/microstructure; Surface structure*

Thallium
- activator, KBr, vac. u.v.-X-u.v. excited, photo- and electrophotoluminescence processes 2—16603
- atom, absorption spectrum in v.u.v. 2—18320
- atom, relative X-ray transition probs. to K-shell 2—21510
- atomic vapour, electronic stimulated Raman scatt. 2—35146
- atoms in flames, collisional ionization 2—38823
- cubic, thermo-and electrotransport of thermal lattice defects 2—36085
- diffusion in KCl, electron probe analysis 2—9607
- enthalpy of fusion determ. 2—28939
- enthalpy of transition, $\alpha\rightarrow\beta$ 2—28939
- ion implantation, in InSb and CdTe, lattice disorder and outdiffusion 2—25370
- lattice dynamics 2—6647
- lattice dynamics and elastic consts., 77 and 296K 2—36322
- liquid, structure factor and atomic distrib., X-ray diffr.obs. 2—18792
- liquid, thermoelec. and resist., temp. depend., calc. 2—3404
- liquid structure, X-ray obs., 290-450°C 2—21960
- muonic atom, L and K X-ray emission analysis in terms of ^{205}Tl nuclear excitation and resonance 2—18371
- phonon spectra, neutron scatt. and tunnelling comparison 2—19395
- pulsed gas laser, spatial and temporal coherence of superradiance 2—14420
- superconducting, electronic thermal cond. 2—22507
- superconductor, excess diamag. susceptibility above T_c 2—13159
- CsI:Tl^+, impurity-induced i.r. absorpt., lattice dynamical calc. 2—40661
- inIn, effect on Fermi surface topology 2—6724
- KX:Tl^+, X_Halogen, Tl^+ induced electron-phonon interactions rel. to Raman spectra 2—16086
- NaCl:Tl, x-irrad., thermoluminesc. glow peaks 2—29988
- NaI(Tl) γ-ray spectrometer, solar monitoring in OSO-7 spacecraft 2—30610
- Se:Tl, trigonal crystal grown by travelling solvent method, d.c. conductivity 2—40263
- Tl:Cd, Hg, Zn, supercond. transition temp., impurity effects 2—36473
- Tl I spectrum general relations of nf series with Al-I; Ga-I; In-I 2—8438
- Tl in KCl, phosphor, origin of 4750 Å emission 2—36931
- Tl^+, in KI, u.v. absorp. bands, uniaxial stress effects 2—10386
- Tl^{2+} centre interaction with F-centres, in alkali halide crystal, luminescence kinetics 2—40711
- ^{207}Tl, lifetime obs. of states excited by α-particle decay, microwave method 2—8222
- Tm^{2+} trigonal centres in alkaline earth fluorides, ionic distortions 2—40589

Thallium compounds
- aluminogermanate glass, polymerization, i.r. study 2—15638
- germanate glass, polymerization, i.r. study 2—15638
- halides, photoelectron spectra obs., use of cylindrical-mirror analyzer 2—35293
- lithium thallium tartrate, ferroelec. props. 2—29756
- In-Tl alloy, martensite transform., shape memory effect 2—9789
- In-Tl alloys, electron-phonon interaction and supercond. 2—40205
- In-Tl alloys, lattice stability near martensitic phase transformation, ultrasonic study 2—29474
- ^{39}K^{19}F, Stark effect, molec. beam resonance meas. 2—21646
- Pb-Tl alloy, band struct., elastic const. and mag. susceptibility obs. 2—6727
- Pb-Tl alloy, bulk flux pinning, critical-state model 2—16183
- Pb-Tl alloy system, supercond., hysteresis effects 2—6780
- Pb-Tl alloys, solid and liq., mag. props., n.m.r. 2—29796
- (80 at.%)Tl-In melt, struct., X-ray obs.21961 2—21961
- Tl-Pb alloy, phonon spectra, neutron scatt. and tunnelling comparison 2—19395
- $(Tl,Na,Li)NO_3$, $(Tl,Na,Rb)NO_3$, $(TlNa,Cs)NO_3$ systems, solid-liquid equilibria, polythermal projections 2—22035
- Tl complex, uranyl oxalate, cryst. struct. 2—22165
- TlAs, dissociation energy, exptl. investigation 2—15339
- $TlB^1{}_{1-x}B^{11}{}_xO_3$, $B^{11}=W^{6+}$ or Mo^{6+}, $B^1=$ various cations, pervoskite type ferroelectric crystals synthesis 2—1573
- TlBi gaseous molecule, determ. dissociation energy from thermodynamic treatment of Knudsen cell-mass spectrometric data 2—21644
- TlBr, and TlBr-TlCl(I) mixed cryst., dielec. props. 2—25933
- TlBr, derivation of electric dipole moments from Stark effect meas. on pure rotational transitions 2—8711
- TlBr, lattice dynamics, dispersion relations, three body force model 2—36332
- TlBr, photo-excited, Hall effect and magnetoresist., temp. depend. 2—40264
- TlBr, reson. Raman scatt., hot luminesc., exciton-optical phonon interaction 2—16588
- TlBr, second order Raman frequencies in terms of phonon frequencies 2—29935
- TlBr, static dielec. const., isochoric temp. depend., anharmonic interactions 2—19403
- TlBr antireflection coating for Si, in 2.5-50 μm region, transmittance obs. 2—8012
- TlBr(Cl), vacancy pair form. energies 2—22192
- TlBr—TlI solid solution, lattice constant dependence on composition, powder method 2—1372
- TlCl:P, luminesc., effect of i.r. irrad. 2—10430
- TlCl, and TlCl-TlBr mixed cryst., dielec. props. 2—25933

Thallium compounds continued
TlCl, Cl^- $L_{2,3}$ absorpt. spectra regularities 2—20032
TlCl, cyclotron reson. of photocarriers, circular polarization obs. 2—25752
TlCl, $L_{2,3}$ absorpt. edge of Cl^- 2—33293
TlCl, n.m.r. applic. to diffusion mechanism determ. 2—25458
TlCl, spin-lattice relax. in rot. frame, diffusion mechanism influence 2—10262
TlCl, TlBr, TlI photoelectron spectra, analysis 2—24490
TlCl antireflection coating for Si, in 2.5-50μm region, transmittance obs. 2—8012
TlCl isotopes, h.f.s. and Zeeman and Stark effect, molec. beam resonance meas. in different vibrational states 2—21645
TlCl(Be,I) scintillation spectrometer, response to high energy electrons 2—2632
TlCl(Br,I), for i.r. reflection and transmission meas. 2—4430
TlCl—TlBr solid solution, lattice constant dependence on composition, powder method 2—1372
TlF, dielec. props. 2—25933
$TlGaS_2$, synthesis, cryst. struct., and band gap 2—29498
$TlGaS_2(Se_2)$, elec. and photoelec. props. 2—29677
TlI-TlBr, KRS-5 ionic crystal, negative photocond. and thermostimulated current 2—13303
TlI, and TlI-TlBr(CsI) mixed cryst., dielec. props. 2—25933
TlI, derivation of electric dipole moments from Stark effect meas. on pure rotational transitions 2—8711
TlI, orthorhombic and cubic modifications, chem. shift and Van Vleck paramag. 2—4560
TlI, phase transform., elec cond. study 2—9826
TlI_3 plasma production in high pressure mercury lamps 2—3229
$Tl_3In_2Cl_9$, vibrational spectra and structure 2—31773
$TlInS_2$, elec. and photoelec. props. 2—29677
$Tl_2Ir(Os)(Ru)_2O_7$, electronic characterization, cryst. chem. considerations, elec. and mag. meas. 2—10076
$TlNO_3$, vibrational spectra of monomer and dimer, cation association effects 2—8610
$Tl_3NbS_4(Se_4)$ cathodoluminescence spectrum 2—26239
$TlNb(Ta)O_3$-$W(Te)O_3$ system, crystal chemistry 2—15682
Tl_2O_3-Ta_2O_5 mixture, sintering, tantalate prep. 2—29396
TlS-GaS system, phase diagram, and cpd. formation 2—29498
TlS, liq. and solid, thermal cond., heat transport mechanism 2—19468
Tl_2S, liq. and solid, thermal cond., heat transport mechanism 2—19468
Tl_2S binder layers, photocond. 2—33076
Tl_2Se-B_2Se_3 system, phase diagram determ. 2—36274
$TlTaGe_3O_9$, $Tl(Ta_{1-x}Nb_x)$ Ge_3O_9, $TlTa(Ge_{3-y}Si_y)O_9$, atomic positions 2—25334
$Tl_6Ta_4O_{19}$ and $Tl_6Ta_2O_{14}$, prep. by sintering of oxides, and props. 2—29396
$Tl_3TaS_4(Se_4)$, cathodoluminescence spectra 2—26239
Tl_2Te:Sn, liq., elec. cond., thermoelec. power, impurity effects, 750-950K 2—22003
Tl_xTe_{1-x}, liq., Hall mobility, temp. and comp. depend. 2—39387
$TlTiOPO_4$, space group, X-ray exam. 2—15723
Tl_3VS_4, cathodoluminescence spectra 2—26239
$^{205}Tl^{19}F$, Stark effect, molec. beam resonance meas. 2—21646
Thermal conductivity *see Conductivity, thermal*
Thermal decomposition *see Chemical reactions*
Thermal diffusion *see Diffusion in gases/thermal; Diffusion in liquids/thermal; Diffusion in solids/thermal*
Thermal diffusion columns *see Diffusion in gases/thermal; Isotope separation*
Thermal diffusivity *see Conductivity, thermal; Heat conduction*
Thermal expansion
see also Gruneisen relations
alkali halide 2—32877
alkali halide crystals, coefficient of volume expansion 2—9316
antiferromagnet, $CuCl_2.2H_2O$, low temp. mag. contribs. 2—19433
artificial graphites, dilatometric measurement 2—16047
atomic vacancies in crystalline solids, rel. to expansivity data 2—16042
rel. to atomic vibration amplitudes, theory 2—4072
azide crystals, exam. of anisotropic nature by a single crystal X-ray method 2—15734
bimetallic rectangular plate, stress analysis 2—14223
borates, dolomite type 2—9893
bowing of single rods, heat transfer surfaces 2—4071
$CdSiP_2$ crystal, high temps., coeffs. X-ray study 2—32844
ceramics, single phase, and oxide single crystals, localized stresses 2—15821
chlorinated polyethylenes, at glass-rubber transition, by temp, cycling rates 2—16065
coefficient of linear expansion, electrical method using stress coefficient of resistivity and resistance 2—14291
composites, control through design 2—32745
contact measurement, corrections for deform. and magnetostriction 2—1435
Corning crown glass, from 30 to 250°C 2—36353
crystal lattice, contrib. of bond length expansion and tilting 2—13049
Cu, rel. to electronic struct. temp. depend. by n.m.r. obs. through m.p 2—7136
cubic solid, negative expansion, role of elastic consts. 2—25688
cylindrical shells under internal pressure analysis 2—14185
deformation and melting in reactor rods and plates under internal heat generation 2—14293
dilatometric method for measuring thermal compressibility factor of metals with cubic crystalline lattices 2—29356
electron-phonon interaction factor in lattice expression for bulk thermal expansion 2—16044
Elinvar, Invar anomaly and ΔE-effect, rel. to elastic props. 2—12823
glass, discontinuities in temp. dependence of expansion coeff. 2—36357
glass pairs with different composition, fusion method 2—25687
glass ribbon reinforced plastics, verification of theoretical model 2—16060
graphite, effect of pre-stressing 2—39756
graphite, lattice consts. variation with temp. 2—9865
graphite, neutron irrad., effect of pitch-binder coke content 2—22175
graphite, neutron irrad., rel. to crystallite size 2—3756
graphite, neutron irrad. effects 2—3759
graphite, pseudoisotropic polycrystalline, control through composite design 2 32745
graphite, pyrolytic, neutron irrad. 250470°C, change in thermal expansion coeffs 2—19432

Thermal expansion continued
graphite, temp. depend., calc. 2—32846
graphite/Br intercalation cpd., anomalous behaviour, elec. resist. meas. 20-800°C 2—19536
halides, calc. using modified Born potential energy function 2—22094
inert gas crystal, and stabilizing calcs. 2—40082
inert gas solids, calc. by hard core intermol. pot. 2—40083
inert gases, solid, determ. at pressures to 20 kbar and temp. from 4 K to triple points 2—16057
instrument quality improving by raising precision in evaluating temp. coeffs. of linear expansion 2—27302
interatomic pot. anharmonicity calcs. 2—9842
Invar, 4.2-300K, effect of heat treatment conditions 2—36355
Invar effect origin 2—16379
keatite, significance of bridging oxygens 2—16062
low expansion materials, laser interferometry for measurement to 130°C 2 14290
measurement, theory and effects in metals, non-metals, composites and glasses, conference, New York, 1971 2—14287
measuring techniques 2—17452
metal, large vacancy thermal expansion effect on press. variation of activation enthalpy 2—39722
metallic system, volume change meas. and characts. 2—3862
methane, deuterated, Gruneisen relation between expansion coeff. and heat capacity 2—16064
p-nitroaniline, 290 to 380K 2—9898
noncubic crystal, dilatometric and X-ray obs., vacancy equilib. conc. and dislocation climb detn. 2—19431
perfect non-Bravais cryst. with internal strains 2—9883
phenanthrene, single cryst., dielectric and dilation anomalies, capacitance meas., 23- 75C 2—10111
polymethyl acrylate, from Brillouin spectra obs. of molecular relax. 2—26202
polystyrene in non-glassy liquid state, thermal expansion coeff. 2—1072
pushrod dilatometers, cooperative measurements of various materials up to 1000 degrees C 2—16045
pushrod type dilatometers, economy considerations 2—14292
pyrolytic graphite-Br_2 residual compound high temp. resistivity 2—6619
rare earth Laves phase compounds with Co and Ni, behavioural study 2—4073
rare earth zirconium oxides, $Ln_2O_3.2ZrO_2$ 2—36284
rocks of lunar type, for space mission mineral resources 2—17033
salund ceramics from borosilicate glasses 2—15935
scheelite-type compounds, ABO_4, rel. to cryst. chemistry 2—22430
semiconductor, amorphous, review 2—40224
solids, comparison of various lattice dynamical models 2—16043
spectroscopic applications at low temperatures 2—16041
β-spodumene, significance of bridging oxygens in thermal expansion 2—16062
steel, stainless, temp. depend. 2—12824
structural metals, mathematical model for elevated temperature deformation 2—15827
thermophysical properties of fluids 2—18813
thermophysical properties research, ASME meeting, Washington, D.C., USA, (1971) 2—19422
two phase textured composition, temp. and comp. depend. 2—40080
ultraprecise measurement using multiple beam optical interference, 0 to 300°C 2—14288
zircon-type compounds, ABO_4, rel. to cryst. chemistry 2—22430
Ag, anharmonic contrib., high temp. 2—32845
Ag, anharmonic contribs. at high temps. 2—40081
Ag, coeff. and lattice parameters determ. 30-180K, X-ray method 2—3694
Ag_2O, lattice expansion by annealing 2—29560
Al, anharmonic contrib., high temp. 2—32845
Al, anharmonic contribs. at high temps. 2—40081
Al, B-filament reinforced, control through composite design 2—32745
Al, coeff. and lattice parameters determ. 30-180K, X-ray method 2—3694
Al composites, control of expansion coefficients 2—16046
Al_2O_3 alumina, anisotropy, rel. to fracture at surface flaws 2—12886
Al_2TiO_5, cryst. struct., room temp. and 600°C 2—39630
Ar, solid, 1-35 K 2—13050
Ar, solid, low-temp. limit 2—32842
Ar solid, central force rigid at. model 2—40040
Au-In solid solution, lattice parameters, solubility limit, density, voids 2—19265
BaF_2, rel. to long wave optical mode freq. and self energy shift 2—19435
$Ba(NO_3)_2$, anharmonicity obs. 2—19354
$BaTiO_3$, and thermodynamic props. 473-1373K 2—32444
Be, anharmonic props., Gruneisen function temp. depend. 2—19355
C-C composites, measured as a function of temperature and orientation 2—16048
CO solid, linear coeff., 8-48K, orientational disordering effect 2—9894
$CaAl_2Si_2O_8$, metastable feldspar, displacive transformations, DTA obs. 2—22356
$CaCO_3$, calcite, from mode Gruneisen parameter calc. 2—40027
CaF_2, rel. to long wave optical mode freq. shift and self energy shift 2—19435
CaF_2 and BaF_2 polycrystalline material, from 10 to 300K 2—36356
$CaWO_4$, lattice parameters, X-ray obs., 28-347°C 2—22151
Cd, dilatometric and X-ray obs., vacancy equilib. conc. detn. 2—22428
Cd, vacancies 2—15752
$CdGeAs_2$ crystal, high temps., coeffs. X-ray study 2—32844
CdS microcrystalline hot pressed form, from 10 to 300K 2—36356
CdS polycrystalline, from 30 to 250°C 2—36353
CdSb, single cryst., X-ray obs. for Gruneisen parameter detn. 2—16067
CdTe microcrystalline hot pressed form, from 10 to 300K 2—36356
Co-Fe-Nb alloy, cold drawn annealed, hardness, coercive force, magnetization 2—1625
CoSi, 100-1000K 2—32847
Cr-Fe-Mn alloy, antiferromag. b.c.c. phase, Invar property 2—36354
Cr-Ni alloys containing B and Si 2—9892
Cr-Ti dilute alloys, linear temperature dependence of paramagnetic susceptibility caused by expansion effects 2—10237
Cr_2Fe_{17}, ferro-helimag. transition, lattice parameters obs. 2—26034
CrSi, 100-1000K 2—32847
$CrVO_4$, X-ray diffr. obs. 2—6681
CsI, thin layers, low- temp. 2—9798
Cs_2O-M_2O-SiO_2 glass, (M=Li, Na), rel. to struct. 2—28975
Cu, anharmonic contrib., high temp. 2—32845
Cu, anharmonic contribs. at high temps. 2—40081

Thermal expansion continued
- Cu, NBS sample, measurement of expansion coefficient below 30 K 2—16050
- Cu and alloys, expansion coefficients at 283 K 2—16049
- $CuCl_2.2H_2O$, low temp. mag. contribs. 2—19433
- CuS film, semiconductor, oscillations, 60-300K 2—40084
- DyB_{12}, in range 78-1300°K 2—6684
- $DyCo_2$, mag. transition obs. 2—26054
- ErB_{12}, in range 78-1300°K 2—6684
- Fe-Co alloy, low temp. anomaly, struct. change 2—13052
- Fe-Mn and Fe-Mn-Ni alloys, Invar anomaly 2—13051
- Fe-Ni-Co alloys, effect of Co invar characteristics 2—16051
- Fe-Ni-Co alloys, low temp. invar anomalies, magnetic field dependence 2—16052
- Fe-Ni alloys, invar anomalies, new model from expt. obs. of coarsening by electron diffr. 2—16053
- Fe-Ni alloys, magnetovol. effects 2—13402
- Fe, liquid, dilatometer method, 1833-2023K 2—28833
- $FeCl_2$, rel. to electronic charge density at nucleus 2—10323
- FeF_2, lattice expansion effects on ^{57}Fe quadrupole splitting 2—7057
- $FeF_{2(3)}$, rel. to electronic charge density at nucleus 2—10323
- FeSi, 100-1000K 2—32847
- GaAs, rel. to temp. depend. of energy gap 2—13258
- $GdNi_2$, mag. transition obs. 2—26054
- Ge-S glass, rel. to structural analysis 2—12628
- $Ge_{33}Se_{55}As_{12}$, chalcogenide glass 20, from 30 to 250°C 2—36353
- $Ge_{33}Se_{55}As_{12}$ non oxide chalcogenide glass, from 10 to 300K 2—36356
- $Ge_{33}Se_{55}As_{12}$ nonoxide chalcogenide glass, thermal expansion measurements from 10 to 300K 2—36356
- GeTe, near rhombohedral to f.c.c. transition 2—1396
- Hf oxycarbides and oxynitrides, temp. dependence of lattice parameters 2—29562
- HfB_2, over temp. range 300-2500°K 2—6683
- HoB_{12}, in range 78-1300°K 2—6684
- $HoCo_2$, mag. transition obs. 2—26054
- $KCl:Li^+$, below 30 K, temp. anomalies rel. to level splitting 2—16055
- KCl, calculation of free energy from the deformation dipole model 2—16054
- $KFeF_3$, rel. to electronic charge density at nucleus 2—10323
- Kr, solid, 1 to 45 K 2—13050
- Kr, solid, low-temp. limit 2—32842
- Kr, three-body force model obs. 2—32812
- Li, coeffs., lattice dynamics, screening effects 2—40046
- LiF, X-ray diffr. obs. 2—9895
- Li_2O-SiO_2 glass-ceramic, mech. props. rel. to crystallization 2—36140
- LuB_{12}, in range 78-1300°K 2—6684
- Lu_2Fe_{17}, ferro-helimag. transition, lattice parameters obs. 2—26034
- Mg, anharmonic props., Gruneisen function temp. depend. 2—19355
- Mn-Cu-Cr, alloy, nonmag., Elinvar-type, heat treated, cold worked, 123-673K 2—19160
- Mn-Cu-Fe, alloy, elinvar-type, nonmag., cold worked, heat treated 2—29233
- Mn-Cu alloys, Elinvar prop. 2—29438
- Mn-Cu alloys, temp. depend., Elinvar-type behaviour 2—13053
- MnSi, 100-1000K 2—32847
- Mo, coeff. and lattice parameters determ. 30-180K, X-ray method 2—3694
- Na-K liquid alloys, coefficients as function of temp. and compos. 2—25068
- Na, near melting pt. behaviour 2—16070
- NaCl, interpretations on the shell model 2—16056
- NaCl, pure and doped below 30 K, temperature anomalies 2—16055
- $Na_{0.88}Li_{0.12}NbO_3-Li_2O$, ceramic, cryst. symm., lattice parameters, 293-783K, X-ray and thermal expansion obs. 2—32470
- NbB_2, over temp. range 300-2500°K 2—6683
- $NdCo_2$, mag. transition obs. 2—26054
- Ni-Mn, alloy, nonmag., Elinvar-type, heat treated, cold worked 2—19162
- $Ni_3Al\ T_{1-x}$, x=0, 0.5, 1, lattice parameter mismatch, thermal expansion coeff. obs. 2—25345
- Nm-Cu-Ni, alloy, nonmag., Elinvar-type, heat treated, cold worked 2—19161
- Pb-Cd(Sn) alloys, two-phase region obs. 2—6682
- $Pb(NO_3)_2$, anharmonicity obs. 2—19354
- Pb_3O_4, high temp. X-ray diffr. obs. 2—13054
- $PbWO_4$, lattice parameter obs. 2—9896
- Pd-Ag-Au alloy system 2—4074
- Pr_7O_{12}, Pr_2O_2(C-form), measurements 2—4002
- Pt, determ. by X-ray diffraction 2—16059
- Pt, linear coeff., low temp. 2—32848
- Pt, using Fizeau interferometer and twin-microscope method, 293 to 1900 K 2—16058
- Se, hexagonal, anisotropic behaviour 2—15731
- Si, low temp. behaviour 2—19434
- SiO_2, fused, 80 to 1000 K, standard reference material 739 2—14289
- SiO_2 film thermally grown on Si, buckling rel. to thickness/window width ratio 2—9283
- Sn, double annealing, grain growth rel. to defects 2—32501
- SnF_2, monoclinic, meas. of elastic and thermoelastic consts. and thermal expansion 2—1277
- SnO_2, 283-1898K 2—36358
- $SrAl_2Si_2O_8$, metastable feldspar, displacive transformations, DTA obs. 2—22356
- $SrIrO_3$ coefficients, up to 1000°C 2—3731
- $SrMoO_4$, lattice coeffs. 2—9897
- $Sr(NO_3)_2$, anharmonicity obs. 2—19354
- TaB_2, over temp. range 300-2500°K 2—6683
- TbB_{12}, in range 78-1300°K 2—6684
- Te crystals, linear expansivities 6 to 200 K, behaviour in rel. to lattice structure 2—16061
- TeO_2, 30-461°C, X-ray determ. 2—32849
- Ti-Mo-Ni system, polythermal section 2—32788
- Ti and Ti-Al alloys, correl. with mag. susceptibility 2—4348
- TiB_2, over temp. range 300-2500°K 2—6683
- TiO_2-SiO_2 glasses and keatite and beta-spodumene, significance of bridging oxygens 2—16062
- TmB_{12}, in range 78-1300°K 2—6684
- UC-ZrC solid solns. cubic lattice parameter var. with temperature and composition 2—15733
- $UMoC_2$, anisotropic, 20-1100°C 2—36359
- UWC_2, anisotropic, 20-1100°C 2—36359

Thermal expansion continued
- VB_2, over temp. range 300-2500°K 2—6683
- V_2O_5, 0-685°C, X-ray diffr. study 2—40085
- Xe, solid, 1-105 K 2—13050
- Xe, solid, low-temp. limit 2—32842
- YB_{12}, in range 78-1300°K 2—6684
- YCo_2, mag. transition obs. 2—26054
- YbB_{12}, in range 78-1300°K 2—6684
- Zn, activated vacancy expansion coeff., self-diffusion 2—29561
- Zn, anharmonic props., Gruneisen function temp. depend. 2—19355
- Zn and a dilute ZnMn alloy, low temp., c/a effect on electronic density and Kondo effect 2—16063
- $ZnGeP_2$ crystal, high temps., coeffs. X-ray study 2—32844
- $ZnSnAs_2$ crystal, high temps., coeffs. X-ray study 2—32844
- $ZnSnP_2$ crystal, high temps., coeffs. X-ray study 2—32844
- $ZnSnSb_2$ crystal, high temps., coeffs. X-ray study 2—32844
- Zr oxycarbides and oxynitrides, temp. dependence of lattice parameters 2—29562
- ZrB_{12}, in range 78-1300°K 2—6684
- ZrB_2, over temp. range 300-2500°K 2—6683

Thermal measurement
- *see also Calorimeters; Calorimetry; Conductivity, thermal/measurement; Temperature measurement; Vapour pressure measurement; Entries describing measurement methods for specific thermal quantities and effects may also be found listed under the various headings for the subjects concerned*
- aqueous solutions of organic compounds, sp. ht. determ. by hydrocarbon mixing 2—25070
- Cp/Cv meas. for gases with steady oscillations new apparatus described for method of Ruchardt 2—32176
- differential thermal analysis of low weight samples, apparatus 2—20951
- glass, different compositions, thermal expansion determ., fusion method 2—25687
- heat transfer, precise measurement by holographic interferometer method 2—17417
- heat transfer coefficient in pool boiling measured by gas volumetric technique 2—6288
- metals, thermal diffusivity, temp. dependence, and true specific heat 2—29553
- radiation properties of solids 2—19474
- strain gauge for thermal strain meas. in turbine casings 2—39874
- stresses in this tube with circumferentially travelling heat load 2—37719
- thermal expansion techniques 2—17452
- thermograph optical system 2—2448
- thermophysical high temp. props., high speed meas. 2—19410
- thermophysical properties of fluids 2—18813
- thermophysical properties research, ASME meeting, Washington, D.C., USA, (1971) 2—19422

Thermal properties of substances
- *see also Conductivity, thermal; Equations of state; Heat conduction; Specific heat; Thermal expansion; Thermodynamic properties*
- alkaline earth oxides, analysis of anharmonic effects 2—40068
- anhydrite, exothermal effect rel. to hexagonal-orthorhombic transform 2—12992
- binary fluid mixture with solid phase, thermostatics 2—28437
- ceramics, thermal resist., brittle materials destruction theory 2—39949
- cholesteric liq. cryst., ambient temp. rel. to liq. cryst. tape system 2—9124
- dielectrics, application of periodic temp. oscillations to high temp. studies 2—6675
- gases, polyatomic, kinetic theory analysis of temp. jump and distribution at wall 2—12505
- injection laser, p-n junction, continuously operating, thermal resistance 2—11485
- metal systems, heat resist., superplasticity 2—36110
- metals for low temp. normal and superconducting magnets 2—14371
- nonconductors, propagation of elastic acceleration waves 2—27222
- plastic, water containing, heat shielding props. 2—36262
- quartz, fused, hypersonic phonons at low temp., stimulated Brillouin scatt. obs. 2—16587
- silicates, quantitative differential thermal analysis without standard for heat effects obs. 2—19430
- testing, application of liq. crysts. 2—32238
- thermophysical properties research, ASME meeting, Washington, D.C., USA, (1971) 2—19422
- thermophysics in space research and development 2—20432
- Ar, jets, freely expanding, perpendicular temp. meas. using mol. beams, translational freezing 2—28686
- As-Te-I glass, comp. depend. thermal, structural and elec. props., comp. depend. 2—22526
- $BaTiO_3$ experimental characterisation 2—39946
- C, graphite, temp. and ablation characteristics 2—4060
- CO_2-N_2, mixture, kinetic cooling, by CO_2 laser radiation absorp. 2—18757
- CO_2, jets, freely expanding, perpendicular temp. meas. using mol. beams, translational freezing 2—28686
- Cr single crystal, latent heat, hysteresis, superheating and supercooling observed by extension of ac calorimetric method 2—4402
- β-FeOOH, akaganeite, derivatograph obs. on sample in air and aq. suspension 2—13038
- N_2, jets, freely expanding, perpendicular temp. meas. using mol. beams, translational freezing 2—28686
- O_2, thermophysical props. from melting line to 600 R for pressures to 5000 psia 2—12558
- $SnS-Sb_2S_3$ system, phase diagram, DTA study 2—29496
- Ti-Mo-Zr-Al, alloy, thermal stability rel. to Al content 2—29411
- $Zn_5(OH)_8(NO_3)_2.2H(D)_2O$ thermal analysis 2—4460

Thermal radiation *see Radiation/heat*

Thermal spikes *see Crystal imperfections; Physical effects of radiations*

Thermal transformations *see Boiling; Condensation; Crystallization; Freezing; Heat of transformation; Melting; Phase transformations; Sublimation; Vaporization*

Thermionic emission *see Electron emission/thermionic; Ion emission/thermionic; Ionization, surface*

Thermionic generators *see Electricity, direct conversion/thermionic; Electron tubes*

Thermionic tubes *see Electron tubes*

Thermistors *see Semiconducting devices*

Thermo-optical effects
- *see also Thermoluminescence; Thermoreflectance*
- laser systems, optical distortion by heated windows 2—4152

Thermo-optical effects continued
lens objective thermal gradient effects on optical performance 2—299
polyurethane thermoplastic elastomers based on polybutylene adipinate 2—6522
HgS, thermomodulation of edge absorpt. 2—40666
Thermochemistry *see Heat of reaction, etc.*
Thermocouples
calibration of small gauge instruments 2—20967
characteristics, linearizer 2—23409
chromel-alumel, pressure corrections up to 7 kbar 2—5282
chromel-alumel, reactor rad. influence on thermo-e.m.f. 2—16305
correction of indications, effects of noise 2—20966
efficiency, calc. with respect to Thomson effect and temp. depend of resist. 2—14296
fine, for atmospheric vapour pressure and temp. obs. 2—20309
in heat exchanger water tubes, temp. meas. 2—23403
high-temperature stable, Ni thin-film, oxidation and diffusion problems 2—30900
homogeneity and interchangeability of wires, effects on spurious voltages, methods of assessment 2—27333
nonuniform temp. distrib. 2—23411
nuclear fuel bundles, multielement, surface temp. meas. 2—5758
nuclear reactor, insulation, boron nitride applic. 2—38742
pickup for local heat flux 2—37829
refractory metal, parameters needed for high performance 2—27334
temp. meas. of welded joint area produced by explosion using welding plates as thermocouples 2—27326
temperature meas. methods 2—23406
thermoelectric heat pump, patent 2—5314
thermopile, for c.w. and laser pulse obs. 2—2268
thin film thermocouple, obs. of phase transform. in films 2—39475
vacuum u.v. absolute intensity meas. by thermocouple recording of H arc spectrum 2—14490
Pt/Pt-(10%wt)Rh, pressure corrections up to 7 kbar 2—5282
Pt-10%Rh/Pt and Pt-13%Rh/Pt reference tables 2—37830
W/W-Re, high temperature characteristics 2—1290
W-Mo, calibration curve in 0-2000°C range 2—17455
W-Re, for oxidizing media at v. high temps. 2—27336
W-Re, reactor rad. influence on thermo-e.m.f. 2—16305
Thermodynamic properties
see also Critical constants, thermal; Entropy; Heat of reaction; Latent heat
alkali halide, ionic transport processes 2—33051
alkali halide, ionic transport processes 2—29745
alkali halide, thermodynamic funcs., phonon freq. moments and Blackman rule of sums 2—40067
alkali halide-alkaline earth halide fused systems, chem. potential, e.m.f. study 2—30074
alkali sulphates, ice calorimetry method, 273-1533K 2—4063
alloy, binary, liquid-liquid equilibr., Gibbs energy of mixing 2—32241
alloy melt, rel. to atomic struct. 2—25071
alloys, ternary, disordered, role of 3 body potentials 2—32715
o-, m- and p-aminophenol, thermodynamic functions calc. from vibrational spectroscopy data 2—15350
amorphous material, Raman scattering 2—20061
austenite, solubility of graphite and cementite, calc. 2—25597
benzene films, between differently polar fused silica surfaces 2—21947
binary liquid mixtures, rel. to viscosity 2—6221
binary mixtures, hydrodynamic correl. functions 2—3367
binary system, utility of first order Wagner interaction coeffs. in evaluation of thermodynamic data 2—29415
Bose fluid, variational model 2—14138
t-butyl chloride, calorimetric obs. of phase transitions 2—36352
butyric acid, enthalpy for u.s. absorption at 20 to 90°C 2—18819
chemical potential in fluids with high concentration gradients 2—3159
complex-formation in solution, enthalpy-entropy compensation 2—6214
composite, C/PMMA, laser heating and stress generation 2—36103
Coulomb gas, classical, nodal expansion of free energy 2—3195
critical phenomena, influence on ultrasonic wave attenuation and dispersion 2—36339
crystal, Helmholtz free energy calc. by diagrammatic method 2—29500
crystal-melt, interfacial free energy, from radial distrib. func. 2—18997
cubic cryst., free energy at finite temp. 2—9845
cyclopentane, critical region scale law, verification 2—25151
electrode processes, pressure and temp. coefficients 2—40822
electrolyte solutions comparison of treatment by Debye theory and primitive model of statistical mechanics 2—28835
electron gas, 1D with delta function interaction, finite temp. 2—7719
electron gas, in crossed electric and magnetic fields 2—2180
electron gas at metallic densities 2—19423
enthalpy difference on development of laminar free shear layer 2—12333
enthalpy profiles of shock heated air in explosively driven shock tube 2—12509
f.c.c. lattice, thermodynamics of strongly anharmonic crystals 2—25653
ferroelectric solid solution, dielec. permeability, thermodynamic theory 2—19767
ferroelectric solid solution, Ginzburg- Devonshire theory 2—19766
ferroelectrics of barium titanate type, book 2—13314
fluid system, multicomponent, correlation functions near crit. pt., thermodymamic struct. 2—15628
fluids, dielectric, molecular, Helmholtz free energy 2—8868
fluids, expressions in terms of invariant expansion of 2-body statistical correlation function 2—7700
fluids, inhomogeneous continuous, with anisotropic pressure and interfacial layers 2—3159
fluids, internal energy, gravity influence on behaviour near critical point 2—8874
free energy and electronic specific ht. due electron ion pseudopotential interaction 2—16092
fundamental derivative, negative, existence of real fluids 2—32157
gas, at high temps. and densities, theory 2—21911
gases, electronic excitation contribution at high temperature 2—21919
gases, microcrystalline clusters, calculation using single-configuration approximation 2—35683
Gibbs free energy of cavity formation, use in study of solvophobic interaction of gases and liquids 2—9102
glass, adsorbed water layer, adsorpt. of Ar 2—35913
group III-V systems, ternary, and phase diagram calcs. 2—22354
Heisenberg model for finite lattice 2—36681
hexafluorides, enthalpy, entropy, free energy and heat capacity 2—823
Thermodynamic properties continued
ideal gas, multiple ionization, thermodynamic functions and effective adiabatic index 2—12454
ideal gases and gas mixtures, heats of transport 2—1030
of interacting molecular system, effect of nonadditive interactions discussed 2—18540
interstitial solid solns., gas flow system design 2—32717
of ions in methanol solution calc. of partial modal volumes 2—15612
Ising antiferromag. mag tricritical pts. 2—19913
liquid, viscous, flow, nonisothermal theory 2—18773
liquid, work of isothermal compression 2—9113
liquid fluidized beds, heat transfer 2—2275
liquid surfaces, curvature, rel. to thermodynamics of surfaces, new constant of matter 2—6185
liquid system, binary, bulk-to-surface distrib. coeffs. and activity from surface tension 2—21967
liquids, high density, monatomic, generalization of cellular model 2—39324
metallic system, volume change meas. and characts. 2—3862
methane, liq., principle of corresponding states, validity 2—12535
methane-carbon tetrafluoride system, in neighbourhood of upper critical solution temp. 2—9111
neopentane-1-bromo-2,2-dimethylpropane liq. mixture, excess free enthalpy calc. 2—28840
neopentane-tetramethylsilane liq. mixture, excess free enthalpy calc. 2—28840
nucleation of solid from pure melts, free energy of fusion 2—18881
numerical methods for monatomic ionized gases 2—18758
n-octane film, on quartz, interaction press.-thickness isotherms 2—39352
optimized random phase approx. calc., role of attractive and repulsive forces 2—32221
oxide fuels, mixed, irrad., chem. effects of comp. changes 2—545
perfect non-Bravais cryst., internal strains influence 2—9883
perfluoroheptane iso-octane critical mixture, correl. lengths 2—3430
plasma, dense non-ideal, review 2—21768
polar liquids, use of Boltzmann factor in study of interaction potential between molecules 2—9125
polyethylene, linear, crystallized in bulk or from dilute solution 2—28969
polyethyleneterephthalate, enthalpy meas. rel. to crystallinity determination 2—6293
polymer, amorphous, PVT props. and transitions 2—3478
polymer solutions 2—15583
polymers, crystallized in bulk or from dilute solution 2—28969
polymethyl methacrylate, press. depend. 2—13048
polystyrene-cyclohexane system near upper critical segregation temperature, thermodynamic functions determ. from light scattering meas. 2—35772
$\text{pyrene}^+ + \text{pyrene} \rightleftharpoons (\text{pyrene})_2^+$, thermodynamic constants 2—16674
real gas flow in cylindrical pipe, isothermal permanent motion 2—39235
refractory borides, high temp. enthalpies 2—19274
saturated liquid volumes, corresponding states correlation 2—25069
solid solns., diffusional homogenisation during deform., energy stability, free energy 2—29413
solid solns., interstitial, statistical mech. calc., entropy, enthalpy 2—6605
solid solns., review 2—29414
solid solution, metallic binary f.c.c., free energy relations 2—25322
solid-liquid phase transformation, simulated molecular dynamic calc. 2—25137
spin-phonon system, coupled, free energy expansion 2—6676
steel, austenitic, C activity, effect of Cr, Mo and W 2—32787
steel, ferrite/austenite stabilising parameter of alloying elements 2—39985
stress-strain-temperature-time relationship, characterization in metals and alloys 2—15817
sub-cooled liquids with forced convection, boiling heat transfer 2—28958
superconductor, mag. impurity effects 2—13126
superconductor, very small size, from Landau-Ginzberg eqn. 2—16152
superconductors, dirty gapless, relationship of 3rd order free energy term to incremental vortex entropy 2—4163
symmetrical fundamental property relation 2—37789
ternary carbides, nonstoichiometric, thermodynamic model allowing for comp. depend. of parameters 2—25603
o-terphenyl, crystal, glass, liquid and heat capacity 2—9891
tetraalkylammonium molten salts, configurational thermodynamic properties, internal Coulomb field contributions 2—28841
tetraalkylborate molten salts, configurational thermodynamic properties, internal Coulomb field contributions 2—28841
tetraethyllead, vapour state chem. thermodynamic props. 2—24553
thermophysical high temp. props., high speed meas. 2—19410
thermophysical properties of fluids 2—18813
transition metal monocarbides, C self-diffusion 2—9622
transplutonium molecules, thermodynamic principles of systematics, extrapolation from rare earth and actinide series 2—22851
trypsin, enthalpies for fixation of competitive inhibitors proflavin and benzamidine 2—40798
two phase systems, finely dispersed state, thermodynamic stability 2—25583
two-dimensional system containing liquid theory of phase transition, applic. to surface tension calcs. 2—22033
water, bond lattice model, two-state thermodynamic props. 2—21954
water films, between entirely hydroxylated fused silica surfaces 2—21948
water-steam, out-of-pile subchannel meas. in nine-rod bundle for water at 1000 PSIA 2—25002
Ag-Cu, liq. binary, excess Gibbs energies mass spectrometric intensity ratio method determ., 1000-1250°C 2—18814
Ag-Ga system, 3/2 electron cpds. 2—39934
Ag-H(D) solid solution, calc. 2—3961
Ag-Sn system, solid and liquid phases 2—40000
AgBr-NaBr solid solutions, from miscibility gap meas. 2—22417
AgCl-NaCl solid solutions, from miscibility gap meas. 2—22417
AgF, B1-B2 phase change at high press. 2—36272
$AgNO_3$-$LiNO_3$, molten mixture, from liquidus curve 2—25138
$AgNO_3$ melts, from e.m.f. meas. 2_21980
Al-Au alloys, rel. to bonding 2—25591
Al-H(D) solid solution, calc. 2—3961
Al-Li liquid alloys, partial free energies, 957 and 987K 2—28836
Al-Te liquid alloys, determ. using improved dew pt. method 2—39359
Al-Zn liquid alloys, determ. using improved dew pt. method 2—39359
Al-Zn solid solution, activity meas., entropy, heat of formation 2—4059
α-Al_2O_3, NBS standard reference material, relative enthalpy 273-1173K 2—29555

Thermodynamic properties continued
Ar-methane, liq. mixt., excess Gibbs energy 2—35753
Ar, liq., principle of corresponding states, validity 2—12535
Ar+Kr liquid mixtures, excess properties 2—15579
Au-Ga liquid alloys, 1400K 2—28838
Au-Ga system, 3/2 electron cpds. 2—39934
Au-Sn alloy, liq., 380-1050°C 2—28837
Au-Sn liquid alloy, activity coeff., comp. depend. stirred H-cell study 2—28784
$BaTiO_3$, and expansion coeffs. 2—32444
Bi-Pb_2Bi, of Bi phase, analysis 2—3440
Bi_2O_3, free energy of formation, solid electrolyte technique 2—10606
COF_2, liquid, significant structure theory evaluation 2—28785
$CdGa_2S_4$, semiconductor, heat capacity, 14-300K 2—25684
$CdIn_2S_4$, semiconductor, heat capacity, 14-300K 2—25684
Co-H(D) solid solution, calc. 2—3961
Co-Te system, and phase relns. 2—19311
Cr-N system, partial and integral thermodynamic functions 2—22377
Cu-Ga system, 3/2 electron cpds. 2—39934
Cu-Ge alloy, liq., excess free enthalpy of mixing 2—32255
Cu-H(D) solid solution, calc. 2—3961
Cu-Sn alloy, liq., excess free enthalpy of mixing 2—32255
Cu-Zn, activity of Zn and heat of evaporation 2—16031
Cu, plastically deformed, stored energy, calorimetric determ. 2—9649
CuCl, rigid ion model calc. 2—9859
CuGa alloy, liq., excess free enthalpy of mixing 2—32255
CuP_2, temp. depend. of dissociation and thermodynamic parameters 2—30046
D_2O, enthalpy, 0.1-21 MN/m^2 absolute press., 20-640K, tables 2—35755
$ErB_{4(12)}$, high temp. enthalpies 2—19274
Er_2O_3, enthalpy obs. using method of mixtures, at high temp. 2—29556
Fe-Co alloy, mass spectrometric obs. 2—36351
Fe-Co(Cu)(Mn)-C system, austenite phase, C activity 2—40006
Fe-Cr-C alloy, austenitic, mass spectrometric investigation 2—29550
Fe-Cr alloy, austenitic, mass spectrometric investigation 2—29550
Fe-Cu alloy, mass spectrometric obs. 2—36351
Fe-H(D) solid solution, calc. 2—3961
Fe-Mo-O system 2—40008
Fe-Ni alloy, activity, entropy, heat of mixing, 750-1150°C 2—39929
Fe-Ni alloys, mass spectrometric obs. 2—36351
Fe-Ti alloy, mass spectrometric obs. 2—36351
Fe-V alloy, mass spectrometric obs. 2—36351
Fe-W-O system 2—40008
$Fe_{1-x}O$, Wustite, defect struct., stoichiometry, 685-1300°C, CO_2-H_2 atmos., thermogravimetry 2—1243
Fe—Cu—C alloy, activity coeff. of C, Cu content depend. 2—9768
Fe—Ni—C alloy, activity coeff. of C, Ni content depend. 2—9768
Fe—Zn—C alloy, activity of C, Zn content depend. 2—9768
Ga-M, M=Au,Ag,Cu, enthalpy of mixing for solid and liquid solutions 2—32730
GaAs, rel. to temp. depend. of energy gap 2—13258
β-$Gd_2(MoO_4)_3$, antiferromag., ferroelectric, entropy and enthalpy, 0.4-4.2K 2—10239
Ge-Li system, free energy of mixing 2—1370
H_2, at high temps. and densities, theory 2—21911
HCl solutions in formamide, relative partial molal enthalpy of HCl from e.m.f. meas. 2—28834
$H_3O^+(H_2O)_n$, n=0-4 2—24456
^3He in ^4He, superfluid solns., low temp. props. 2—1134
In-Ga system, thermodynamic interaction parameters 2—15984
KCl, free energy calc. using deformation dipole model 2—16054
KNO_3-$LiNO_3$, molten mixture, from liquidus curve 2—25138
Kr+Xe liquid mixtures, excess properties 2—15579
Li-Sn liquid alloys, 972 and 1123K 2—28839
LiF, Gibbs free energy, from stress dependence of activation energy 2—3869
$LiNO_3$-$AgNO_3$ melts, from e.m.f. meas. 2—21980
Mg-Cu-Al alloy, enthalpies of form., Laves phases binding conditions 2—29475
Mg-Cu-Sn alloy, enthalpies of form., Laves phases binding conditions 2—29475
Mg-Cu-Zn alloy, enthalpies of form., Laves phases binding conditions 2—29475
Mg_2Pb, semiconductor, lattice heat capacity, thermodynamic functions, temp. range 5-300K 2—4066
MgV_2O_4-Fe_3O_4, activity of components and free energy of mixing 2—1371
Mn_7C_3, standard free energy of formation e.m.f. measurements 2—3947
Mo, liq. and solid, enthalpy meas., heat of fusion calcs. 2—35819
N_2-Co liquid mixture, thermodynamic functions calc. 2—28840
NH, enthalpy of formation in $NH_3/O_2/N_2$ flames 2—22872
Na-O species, deduction from Hartree-Fock molec. orbital studies of neutral molecule and ions 2—37032
NaCl, ionic transport processes 2—29745
$NaNO_3$-$AgNO_3$ melts, from e.m.f. meas. 2—21980
$NaNO_3$-$LiNO_3$, molten mixture, from liquidus curve 2—25138
$NaNO_3$, enthalpy calculations, Frenkel defects, Schottky defects, formation 2—3767
Na_2SO_4, vaporization, study by transpiration method 2—28961
Nb-Mo-N system, α solid soln. 2—19313
Nb-Mo-N system, equilib. N_2 conc. and solubility 2—4020
Nb-Mo-N system, phase diagram 2—19314
NbC_x, 0-300 K, determ. from heat capacity 2—13044
Nb_4Si, Nb_5Si_3, enthalpy, 1200-2200 K 2—13039
NdH_2-NdH_3 system, thermodynamic functions and solution parameters 2—22379
Ni-H(D) solid solution, calc. 2—3961
NiO-MgO, solid soln. 2—4061
O_2, enthalpies of reaction, dissolution in Cu-Ni, Cu-Co, Cu-Fe melts, e.m.f. obs. 2—3956
$OH^-(H_2O)_n$, n=0-4 2—24456
PF_3 liquid, significant structure theory evaluation 2—28785
Pb-Bi eutectic alloy, heat of solidification 2—15630
$PbCl_4$, fundamental values determ. from Raman spectra of neat liquid and n-pentane solutions, force constants and thermodynamic properties calculated 2—12568
Pd-H(B), Pd-M-H(B) (M=metal), dissociation thermodynamics, d-band effects 2—36247
Pd-H(D) solid solution, calc. 2—3961
PrH_2 PrH_3 system, thermodynamic functions and solution parameters 2—22379

Thermodynamic properties continued
Sb_2O_3, Sb_2O_5, stability, rel. to nature of semiconductivity 2—40226
SeO_2, from i.r. spectral investigation of molec. vibrations 2—8705
Si film growth, open method, gas transport 2—3543
SiC, equation for enthalpy and specific heat in temp. range 273.15-2900K 2—40077
SmH_2-SmH_3 system, thermodynamic functions and solution parameters 2—22379
Sn-SiO system, rel. to tin extraction economics 2—1342
SnO, SnO_2, stability, rel. to nature of semiconductivity 2—40226
TaC_x, 0-3000°K, determ. from heat capacity 2—1436
$ThCl_4$-NaCl melt, complex ion formation, e.m.f. obs. 2—32256
Ti(s.,β), sublimation, standard enthalpy change, Knudsen n.p. determ., mass spectrometric analysis 2—18890
U-Nb alloys, γ-phase, 930-1900°C temp. range 2—29206
γ-U-Pb liquid alloy systems 2—39360
α-U, stress relaxation, apparent activation enthalpy 2—25494
UAl_4, UAl_3, UAl_2, liquid solutions, obs. by e.m.f. method 2—38739
UB_{12}, high temp. enthalpies 2—19274
UN, high temp. props. 2—40796
$UO_{2\pm x}$, composition changes, 1950 K 2—25637
$(U_{0.8}Pu_{0.2})O_{1.97}$, enthalpy, 2350 to 3000K 2—13040
V-O solid solution, e.m.f. study 2—25602
W halogen systems, free formation enthalpy of W halides 2—30055
W halogen systems, gas phase constitution and chemical transport reactions, thermodynamic aspects 2—30056
WSi_2, W_5Si_3, enthalpy, heat capacity, 1200-2200K 2—29559
$Y_{0.6}Zr_{0.4}B_{12}$, high temp. enthalpies 2—19274
Zn-Ge alloy, liq., excess free enthalpy of mixing 2—32255
Zn-Sn-Cd-Bi, liquid solutions, entropy, free energy, chemical potential 2—3382
ZnO, single crysts., enthalpies and entropies of vaporization reaction 2—18887
ZnO crystal, vaporization kinetics of opposite basal faces, temp. depend. 2—35841
Zr-Nb carbide, thermodynamic model allowing for comp. depend. of parameters 2—25603
ZrC-ZrO_2 system, oxycarbide stability 2—29499

Thermodynamics
see also Atmosphere/thermodynamics; Entropy; Equations of state; Statistical mechanics
adiabatic processes, local entropy 2—23392
adsorption in micropores, thermodynamics, generalized thermal eqn. 2—35901
alveolar surface tension, mathematical model 2—41282
Ashkin-Teller model, critical props. 2—37643
benzene, adsorbed on C black, thermodynamic evaluation of state 2—35907
binary mixture, free energy calc., one-chain approximation 2—2158
bipolymer growth, elementary biochemical explanation of instability of proteins and DNA 2—15411
bond graphs for thermal energy transport and entropy flow 2—7765
book on statistical physics 2—37627
Bose case, rel. between correlation function and Green's function 2—27101
caloric equation of state, for materials at high pressures, polytropic gas and Mie Gruneisen type material 2—14282
chemical equilibria, effects of gravitational field 2—4567
chemical fluid mechanics 2—28441
chemical reactions in metallurgical processes, theory of thermodynamic potentials 2—40799
classical Coulomb systems under external field, thermodynamic limit 2—30811
combustion cycle, of internal combustion turbine 2—2262
contact angles, on heterogeneous solid surfaces 2—32204
continuum system with finite interactions, phase transitions 2—37641
cosmological foundation and irreversibility of signal sending 2—2264
critical behaviour of model with coinciding phase transitions 2—14134
critical exponents, depend. on symmetry, dimensionality, pot. range and interaction strength 2—14127
critical fluctuations, coord. system elements 2—37642
critical phenomena, basic theoretical concepts and problems 2—7691
critical phenomena, perturbation theory, scaling and spherical model 2—37640
critical phenomena, scaling law corrections 2—37647
critical phenomena with infinite-range interactions, model Hamiltonian 2—17263
critical point, in one-component systems 2—7706
critical point exponents, universality hypothesis 2—23290
critical pt. exponents, second neighbour interaction strength depend. 2—7707
critical pt. exponents, universality rel. to lattice anisotropy 2—7708
crystals, anharmonic, free energy, sp. ht. at high temps. 2—40069
density matrices, entropy estimations 2—27091
efficiency definition, models 2—7766
EHD converter, efficiency 2—2333
electrolytes, 2 component fused mixtures, activity coeffs. 2—26353
electron gas, partially degenerate, semirelativistic, exchange contribution to thermodynamic potential 2—30825
energy conversion in electrochemical processes 2—40816
entropy, rel. to reversible process and second law 2—37793
entropy in Carnot's theorem and Shannon's fundamental inequality, analogies 2—5256
equation families, case of eight characteristic functions 2—34193
equations of state formulation for pure substances by statistical reduction of thermodynamic experimental data 2—28931
equilibrium, nonideal reacting gases 2—18751
equilibrium concepts 2—30882
ethanol, adsorbed on C black, thermodynamic evaluation of state 2—35907
exploding stars, postdetonation properties, equation of state, rates of beta processes and associated neutrino losses 2—26655
ferroelectric 'ice' models, analytic properties of free energy 2—33937
finite system, critical pts., and scaling laws 2—14133
fluid, in external field, statistical mechanical approach 2—12312
fluid mixtures, critical phenomena 2—8875
fluorescein and halo-fluorescein dyes, dimerization thermodynamics 2—22876
Fokker-Planck equations, generalization for a region containing moving boundary 2—37661

- **Thermodynamics** continued
  - force fluctuations in relaxing medium, calc. 2—5161
  - forces, nonlinear effects on transport coefficients of system 2—11315
  - free energy functional, nonlocal contributions, near critical point, applic. to two-dimensional Ising model 2—2159
  - Friedrichs model, irreversible phenomena study, kinetic and ergodic problems 2—30813
  - fundamental inequality, transformations 2—33949
  - fusion reactor blankets 2—31618
  - gaseous processes and heat exchange, general eqn. derivation 2—6155
  - gases, table of state functions, internal energy and enthalpy 2—6153
  - Gibbs' total entropy, rel. to H-theorem 2—33951
  - Gibbs Duhem relation, consisting of Hubbard's approx. 2—7701
  - global entropy production inequality 2—37792
  - gray atmospheres, entropy transfer and production 2—33634
  - Gyarmati theorem and variational principle 2—14141
  - Hagedorn theory applic. to proton-nucleus interactions 2—21430
  - Heisenberg-Ising ring, free energy, high temp. expansion 2—17254
  - Helmholtz free energy for system of particles acting through Lennard-Jones 12-6 potential 2—32222
  - Hubbard model, one-dimens. half-filled-band 2—22670
  - Hubbard model, partition functions calc. using functional integral method 2—26019
  - infinite system, locally perturbed equil., isothermal and adiabatic response 2—14132
  - interacting Fermi gas, one dimensional model, solution 2—37656
  - interacting particle homogeneous system, chem. pot. and energies per particle 2—37644
  - ionic fragmentation, quasi- equilibrium theory 2—38864
  - irreversibility, compatibility of astronomical and statistical observations 2—4765
  - isolated systems, space of states, topological props. 2—2261
  - isotropic spin system, critical behaviour 2—23288
  - lattice gas, compressibility exponent 2—33939
  - lattice gas models, one dimensional classical, discontinuity of pressure with density 2—30799
  - lattice models, three-dimens., with long range interactions, universality 2—17251
  - Lennard Jones fluid, analytical expressions for thermodynamic functions 2—21950
  - Lennard-Jones 12-6 liquids, binary mixtures, excess thermodynamic props., Monte Carlo calcs. 2—32223
  - Lennard-Jones system, crit. phenomena, mol. dynamical calcs. 2—15999
  - limits of physical systems, infinite volume states, Bogoliubov inequalities 2—30810
  - linear chain of classical spins, soluble model 2—20870
  - Little model, off-diagonal long range order 2—14137
  - magnetism, macroscopic and phenomenological props. 2—19821
  - molecules in fluid interacting via Stockmayer potential, thermodynamic perturbation theory 2—39024
  - monomer-dimer systems, partition function, Christoffell Darboux formulas 2—23295
  - monopolar continuum, of grade n 2—5205
  - multicomponent mixtures, one-chain, approx. 2—23303
  - nonequilibrium statistical operator, extremal properties 2—33950
  - nonhydrostatic, chemical potential in multiphase systems 2—6278
  - nonideal Bose gas, Green function treatment 2—37654
  - nonlinear problems, construction of dissipation potentials, Gyarmati principle 2—37649
  - nonstationary general relativistic, kinetic derivation from Chernikov thirteen moment approx. 2—33947
  - nonuniform solutions, baric interface theory, higher derivatives 2—32254
  - phase transitions, second-order, discussion of soft collective modes 2—23302
  - plasma, collisionless, relaxation of temp. anisotropy 2—28504
  - plasma, enthalpy conservation on magnetic surface for infinite conductivity MHD 2—12370
  - potentials, universal criteria of evolution for irreversible processes 2—27304
  - pressure, in quantum statistical mechanics, review 2—5163
  - relativistic, rest frames 2—17261
  - relativistic, rest frames 2—17262
  - relaxation amplitudes for systems of two coupled equilibria 2—40798
  - reversibility and irreversibility concepts in thermostatics 2—17407
  - rheological materials with internal changes, gradient theory 2—5178
  - scaling, dynamic and static, unified approach 2—37637
  - scaling hypothesis and critical exponents 2—14135
  - scaling theory, critical indices 2—11300
  - scaling theory of critical region of systems with long-range forces 2—17260
  - semiconductor electron gas in crossed fields 2—6745
  - solution, multicomponent, quaternary mixtures, activity coeffs. 2—22032
  - special relativity, inequalities 2—30770
  - stability criterion, statistical deduction near steady states 2—2171
  - static correl. functions, inequalities among critical pt. exponents 2—37638
  - statistical, of electrons in metals and semiconductors, undergraduate book 2—13068
  - statistical, of polymeric networks at large deformations 2—28980
  - statistical thermodynamics, the most probable distribution, teaching paper 2—92
  - systems, topological representation, bond graph rotation 2—2263
  - teaching exercise, apparent violation of second law 2—33857
  - universality hypothesis, next-nearest-neighbour-interactions 2—33938
  - Ursell-Mayer virial expansion, renormalized for non-ideal reference system 2—33944
  - white dwarf star matter, equation of state for a dense plasma, phase transition between liquid and solid 2—30441
  - zeroth and second law equivalence 2—181
  - $B_7O_{13}^{5-}$, cubic-orthorhombic phase transition, thermodynamic theory 2—9792
  - $D_2+2HCl=H_2+2DCl$ using dimethylformamide as solvent, electrochem. determination of equilibrium constants 2—22854
  - ^3He-^4He mixtures, scaling approach to superfluid and phase-separation transitions 2—23304
  - ^3He-^4He mixtures, thermodynamic relationships at tricritical point 2—28930
  - Li isotope exchange reactions, electrochemical investigations in diglyme and propylene carbonate, equilib. consts. 2—22855
  - TlBi gaseous molecule, determ. dissociation energy from thermodynamic treatment of Knudsen cell-mass spectrometric data 2—21644

- **Thermodynamics** continued
  - W-Br_2 (Cl_2)(F_2)(I_2), gas phase equilibr., simulation 2—20181
  - W-O_2 system, gas phase constitution and chemical transport reactions, thermodynamic aspects 2—30057
  - **applications**
    - acoustic relaxation phenomenon 2—11366
    - consolidation constitutive relations derivation of liquid filled porous media in elastic skeleton 2—21933
    - cyclopentane, critical region scale law, verification 2—25151
    - dielectric relaxation phenomenon 2—11366
    - drying processes, transport phenomena 2—37790
    - elastic relaxation phenomenon 2—11366
    - fluid system, multicomponent, correlation functions near crit. pt., thermodymamic struct. 2—15628
    - gas reaction, laminar boundary layer, integral solution 2—24958
    - interdiffusion, Kirkendall effect 2—22234
    - isenthalpic flow, Joule-Kelvin coefficients and mantle convection 2—4627
    - Ising double chain, zero field susceptibility 2—19838
    - magnetic relaxation phenomenon 2—11366
    - multiphase molecular system, phase transitions and equilibr., electronic photoexcitation effect 2—25136
    - phase transition, in small volume, deviation from Gibb's law 2—9201
    - plasma, statistical, and stability of inhomogeneous Vlasov equilibria 2—39189
    - plasma, statistical, thermodynamic potentials and plasma stability and equilibrium 2—39093
    - polystyrene, vitreous solidification 2—12625
    - solid solution, supersaturated, spinodal decomposition 2—3949
    - solutions, alternative derivation of Kirkwood-Buff theory 2—6215
    - surface film, insoluble, rigorous formalism 2—21946
    - ternary carbides, nonstoichiometric, thermodynamic model allowing for comp. depend. of parameters 2—25603
    - turbomachines theory, consistent mean values for compressible media 2—12484
    - water two-phase flow-boiling system, time-dependent diabatic flows prediction 2—24625
    - Ga-$AsCl_3$-H_2 system, dopant incorporation 2—3530
    - He, liquid, second sound vel. decrease and rel. to mutual friction force 2—18867
    - Zr-Nb carbide, thermodynamic model allowing for comp. depend. of parameters 2—25603

- **Thermoelasticity**
  - axial-symmetric problems, soln. using elastic potentials 2—2208
  - book 2—18892
  - buckling of square elastic plate exposed to random temperature field, probability of stability 2—37717
  - circular hole, thermal stress conc., for elastic plastic strains 2—7738
  - computer code TITUS for tridimensional structures 2—14229
  - computer programme for thermal stresses 2—37818
  - coupled, radiation conditions, Sommerfeld type 2—2222
  - crystal, phenomenological theory, closed system of eqns., long wavelength approx. 2—30852
  - cylindrical regions, thermomagnetoelasticity, dynamic problems 2—37714
  - cylindrical shell with infinite length, thermal stresses by axial temperature gradients 2—37716
  - cylindrical tube, thick-walled, graphical representation 2—27191
  - deformations, in hollow cylinder of finite length, Fortran program BAG—PIPE 2—2223
  - deformations in segment of hollow cylinder, Fortran program SEGPIPE 2—17352
  - dielectrics, transparent, stress generation by focused laser beam 2—27192
  - displacement functions 2—17351
  - Elinvar, influence of tempering 2—12823
  - finite element approach to thermal stress problems 2—37722
  - global entropy production inequality 2—37792
  - homogeneous isotropic elastic body, variational method description 2—27193
  - isothermal-isentropic changes of state in Mooney-Rivlin-Besseling material 2—37718
  - liquid crystal, cholesteric, thermo-mechanical coupling 2—9088
  - magnetothermoelasticity, dilatational waves 2—37744
  - micropolar, steady-state axisymmetric problem 2—11342
  - monopolar continuum, of grade n, thermodynamics 2—5205
  - non-axially symmetric shallow shells, singular solutions uner thermal loading 2—17350
  - nonlinear thermoviscoelasticity, formulation of constitutive eqn. 2—14222
  - nuclear containment vessels, steady state and transient thermoelastic behaviour, finite element analysis 2—15161
  - nuclear reactors, linear boundary problem solved by method of orthogonal projection in Hilbert space 2—14286
  - operational techniques and optimization of start-up procedures 2—37721
  - photothermoelastic analysis of a circular disc having a pair of holes 2—14227
  - plane multiply-connected regions soln. by boundary pt. least squares 2—37720
  - plane problems on doubly connected regions, use of analytic continuation in solutions 2—14230
  - plane waves, freq. eqn. soln. 2—37744
  - plates, deflection meas., application to thermal stress problems 2—14161
  - porous material, thermoelastic theory of consolidation 2—22352
  - pressurized shell, plastic growth through interaction of steady press. with thermal stresses 2—37723
  - propagation of thermoelastic waves in a homogeneous isotropic medium 2—23348
  - rectangular plate, simply supported, vibrations produced by temperatures prescribed on faces 2—37715
  - rod, nonlinear theory 2—33968
  - semi-infinite elastic solid, soln. of heated punch problems by point source methods 2—5207
  - shell under internal press. 2—34024
  - sliding contact, thermoelastic instability 2—22299
  - solids of revolution, analysis by finite element method, application to nuclear reactor technology 2—17355
  - stress, finite element method calculation 2—17353
  - stress analysis of a circular disc having a pair of holes 2—14227
  - stress field generated by moving heat source in a circular disc closed form solution 2—20904
  - stresses, in micropolar hollow cylinder 2—5206
  - stresses computation using finite element technique 2—17354

Thermoelasticity continued
stresses in thin semiinfinite plate due to time dependent temp. applied at point on its boundary 2—17349
thermal stresses and fatigue, conference, Berkeley, England (Sept. 1969) 2—39753
thermal stresses in a circular cylinder with a rectangular hole under heat generation 2—14226
thermal stresses in solid with parallel circular cracks 2—37712
thermal stresses in thin tube with circumferentially travelling heat load 2—37719
thermo-elastic, segment of hollow cylinder, Fortran program SEGPIPE 2—17352
thermoelastic waves in solids with thermal relaxation 2—27215
thin circular plate, thermal stresses due to transit temp. 2—37713
thin cylindrical shell, deformation due to axisymmetrical distrib. of temp. 2—27128
viscous nonlinear dynamic coupled, solution of problems by finite element method 2—11343
wedge shaped plate with linear heat source, temperature stresses 2—2220
YAG active crystal elements, internal stresses under continuous pumping 2—17621
BeO spherical fuel elements in nuclear reactors, three dimensional stresses 2—15130
SnF_2, monoclinic, meas. of elastic and thermoelastic consts. and thermal expansion 2—1277
UC, UO_2, rel. to fission spike props., electronic stopping power 2—36390
Thermoelectric conversion *see Electricity/direct conversion*
Thermoelectricity
see also Thermocouples
aerospace alloys, thermopower, 4-300K 2—25692
alkali method, liquid, Shaw's modified Heine-Abarenkov model potential 2—3359
alloy, Bi-Sb, transport phenomena 2—3954
alloy, dil., giant thermopower due to pair of interacting mag. impurities 2—25941
alloy, dil., low temp. thermopower due to phonon-drag induced electron diffusion 2—1579
alloys, thermoelectric power as research tool, review 2—33066
amorphous semiconductor, anomalous relative sign of Hall and Seebeck coeff. 2—22519
amorphous semiconductor, electrical props., review 2—13215
anisotropic parallelepiped, thermoelec. eddy currents in unsteady temp. field 2—40370
application to thickness meas. of thermochemically produced layers on steel 2—1177
chalcogenide glasses, thermoelectric power meas. rel. to investigation of small polaron hopping motion 2—32986
chromel-alumel thermocouple, reactor rad. influence on thermo-e.m.f. 2—16305
cooling, non-stationary, influence of commutation layer on characteristics 2—26989
copper phthalocyanine, thermo e.m.f. temp. depend. 2—36606
disordered systems, thermopower 2—10132
electric conversion, thermoelectric Peltier module, technique for determining operational characteristics 2—34295
ferromagnet, two-band, magnon drag contrib. to thermoelec. power 2—1580
film, polycrystalline, model, thermoelec. effect, Hall effect 2—25940
Ge-Se-In system, cryst. samples 2—25821
graphite, quantum oscills., minority carrier study 2—36497
graphite, thermopower temp. depend. doping influence 2—1510
heat pump, patent 2—5314
liquid metal, absolute thermoelectromotive force 2—21998
magnetic system, anomalies due to cond. electron scatt. by critical fluctuations 2—40122
measuring instrument for i.r. radiation power 2—17422
metal, alkali, liq., thermoelec. power, pseudopot. calc. 2—39384
metal, liq., inelastic electron scatt. influence on thermopower 2—12575
metal, low temp. thermopower, oscill. temp. dependence explained 2—16135
metal film, size effect 2—29612
metals, thermoelectric power as research tool, review 2—33066
metals, thermopower, diffusion term calc. without approximation 2—4289
Nordheim-Gorter rule for thermopower validity 2—29761
nuclear reaction radiation monitoring 2—8389
phenoxatiin, film, rel. to transport processes 2—16217
polyferrocene, phthalocyanines, polyvinyl pyridine and TCNQ complex, d.c. dark cond., Seebeck meas. 2—36475
Seebeck and Peltier effects, rel. to thermocouple efficiency calc. 2—14296
Seebeck coeff. meas. by guarded- longitudinal-heat-flow technique 2—17432
Seebeck effect for meas. of thermoelectric power of sintered semiconductors 2—17509
semiconductor, ferromag., thermopower, model calc. 2—13333
semiconductor, GaSb, p-n junc., thermal e.m.f. in p-region 2—1540
semiconductor, Ge, piezothermoelec. power anisotropy 2—4292
semiconductor, Ge, plastically deformed, dislocation effects, power obs. 2—4233
semiconductor, heavily doped, low temp. adiabatic effect, calc. 2—40269
semiconductor, heavily doped, low temp. thermoelec. effects, Green's function method 2—25942
semiconductor, heavily doped, weak mag. field depend., calc. 2—40268
semiconductor, inhomogeneous, thermally stimulated cond., rel. to trapping levels 2—6796
semiconductor, photoelectret state, non-isothermal relaxation, trapping levels, thermally stimulated currents 2—25950
semiconductor, Seebeck effect of paramag. polaron 2—10133
semiconductor, simultaneous meas. of thermally stimulated cond. and thermoluminesc. 2—13513
semiconductor thermoelectric solar heat transformer 2—34294
solar air conditioning with semiconductors 2—34297
solar cells, direct conversion to electricity, review of research 2—34296
solar generator with cylindrical receiver 2—23497
steel, high Cr, embrittlement, thermo-e.m.f. and galvanomagnetic obs. 2—3899
steel, high-Cr, effect of N content 2—36156
superconductor, mixed state, Peltier effect 2—13165
superionic conductor, transport model 2—25917
TCNQ charge-transfer complex, cond., Hall effect, Seebeck coeff. 2—40216

Thermoelectricity continued
TCNQ polymeric complex salts, Seebeck measurements 2—25837
TCNQ salts, compactions Seebeck effect 2—25833
thermal e.m.f. of epitaxial films, det. using probe 2—17508
thermocouple wires, methods of assessing homogeneity and interchangeability of wires and spurious voltages caused 2—27333
thermoelectret, thickness depend. of homo- and heterocharge density 2—6890
thermoelectret charge, law of formation 2—6891
thermopower and thermal cond., simultaneous meas. 2—19421
thin films, sensitivity meas. 2—13334
transducers using heat resistance semiconductors 2—11429
transition metal compounds, nonstoichiometric, Seebeck coeff. rel. to semiconductor-metal transition 2—4218
vacuum gauges, calibration from operation at constant temp. 2—30735
Vateria Indica, thermoelectret props. 2—40344
waves, propagation in a homogeneous isotropic medium 2—27218
Ag-R dil. alloys, R=rare earth metal, thermopower, electronic processes 2—13110
Ag alloys, phonon drag thermopower, 4-300K 2—40371
Al-M, M=Ag, Zn, Mg, thermopower, Nielsen-Taylor effect 2—22632
Al-Mg-Zn alloys, thermoelectric investigation of ageing kinetics 2—29400
As_2Se_3, amorphous, thermopower, 120 to 200 C 2—16303
As_2Se_3, vitreous, temp. depend., 180-225°C 2—22527
Au_3Cu, during ordering 2—15979
β-B, rhombohedral, thermoelec. power, determ. of density of states, carrier density 2—22458
BaBiO Seebeck coeff., 250-400K 2—4206
BaO, Fermi level determ. from thermal e.m.f. 2—29659
Bi-Sb alloy, transport phenomena 2—3954
Bi-Sb alloy, transport properties 2—29660
Bi-Sb alloys, thermopower, electron density depend. 2—9931
Bi-Sb alloys, thermopower, press. influence 2—32968
Bi, thermopower, electron density depend. 2—9931
BiOI crystal, adsorption of O_2, attachment levels, thermo-stimulated current 2—6805
p-$Bi_{0.5}Sb_{1.5}Te_{3-x}Se_x$ solid solutions, x=0 to 0.6, influence of internal conductivity on properties 2—29762
Bi_2Te_3-Bi_2Se_3 alloy, n-type semicond., Seebeck coeff. 2—36605
Bi_2Te_3-Sb_2Te_3-Sb_2Se_3 alloy, p-type semicond., Seebeck coeff. 2—36605
C, amorphous film, rel. cond. mechanisms 2—13221
C fibre, polyacrylonitrile-based, thermopower 2—13266
CaF_2:Ho^{3+},Nd^{3+}, thermal e.m.f. 2—10007
$Ca_xSr_{1-x}O$, solid solns. exposure to Ba vapour influence on thermopower 2—6915
Cd, liq., temp. depend., calc. 2—3404
Cd_3As_2, semicond. cryst., coeffs., calc. of effective mass from quantum oscills. 2—16226
$CdIn_2Se_4$-$CdInTe_4$ solid solution, electron effective mass determ. 2—19638
CdS, TSC obs. of electron traps 2—13339
CdS layers, photothermoelec. analysis, carrier density and mobility 2—16310
CdS platelets, thermally stimulated currents in range of unity gain factor, frozen-in current 2—19777
CdSb:Te, Hg(In), influence of double doping 2—36499
CdSb, temp. depend., rel. to band struct. 2—29662
CdTe, Seebeck effect, influence of optical phonons 2—25943
CdTe, thermo-e.m.f. of hot electrons, field depend. 2—19778
$Cd_{1-x}Zn_xSb$, temp. dependence thermoelectric power and resistivity 2—4210
CeN, Seebeck coefficients 2—18878
Co-Ni alloy, mag. field depend. 2—13403
Co, absolute thermopower, 90 to 1250K 2—19454
Co, thermopower anomaly at Curie pt. 2—1582
CoAl, resist., Hall effect 2_6760
$CoAl_2O_4$, force measurement, rel. to transport phenomena 2—25814
CoO, Seebeck coeff., high temp., rel. to defect struct. 2—36501
CoO, thermal e.m.f. rel. to hole mobility at high temp. 2—13226
Co_9S_8, metallic charact., mag. susceptibility, Pauli paramag., Mossbauer effect 2—25766
Co_2Si, e.m.f., physical props. 10-350K 2—40141
Cr-Mo alloy, Seebeck coeff. rel. to para-antiferromag. transition 2—13415
Cr-W alloy, Seebeck coeff. rel. to para-antiferromag. transition 2—13415
Cu-Cd ferrite, mag. transitions influence on thermopower 2—6983
Cu-Ni-Zn alloys, thermopower, 3d band filling 2—16304
Cu-Ni alloy films, thermopower, thickness depend. 2—6893
Cu, thermopower temp. depend., vacancy form. influence 2—10135
CuAlFe system, Kondo temp., thermoelec. power, temp. and comp. depend. 2—25946
$Cu_{0.75}Ni_{0.25}Fe_2O_4$, thermopower temp. depend. 2—1513
CuP_2, chemically deposited 2—29094
$Cu_{2-x}Se$, cubic, room temp. stable, composition depend. 2—36503
$(Fe,Ni)_9S_8$, metallic charact., mag. susceptibility, Pauli paramag., Mossbauer effect 2—25766
Fe, change in thermo e.m.f., following plastic deformation 2—3865
FeAl, resist., Hall effect 2—6760
$FeTiO_3$, thermo e.m.f. rel. to elec. cond. temp. variation 2—40249
GaAs, acceptor level study 2—10048
n-GaAs, Seebeck coeff., space-charge scatt. influence 2—13267
n-GaAs, thermoelec. force measurement 2—25944
GaAs seebeck coeff. rel. to dominant scatt. mechanisms, 300 to 700K obs. 2—6816
p-GaSb, doped, thermopower temp. depend. 2—16306
GaSb, p-n junc., thermal e.m.f. in p-region 2—1540
Gd, critical thermopower, Curie pt. 2—40372
Ge-Si, thermoelectric element, prep. by hot pressing 2—6857
Ge-Si solid soln., thermoelec. power, forbidden band width determ. 900-1200K 2—22559
Ge, amorphous film, rel. to transport mechanisms 2—10069
Ge, piezothermoelec. power anisotropy 2—4292
Ge, plastically deformed, dislocation effects, power obs. 2—4233
GeSe, liq., thermopower 2—9156
GeTe-$AgSbTe_2$, thermoelectric power meas. rel. to band gap width dependence on composition 2—32999
He II, analogous effect to Peltier effect in metals 2—28928
HfO_2, Seebeck coeff. rel. to electron hole mobility 2—10017
Hg, temp. depend., calc. 2—3404
Hg supercritical fluid, thermopower 2—25149
HgS_xSe_{1-x}, Seebeck coeff., temp. depend. 2—13233
p-HgTe, phonon drag contrib. to thermopower 2—32855

Thermoelectricity continued
- In-In_2S_3 liquid partial system, comp. and temp. depend. 2—1114
- In, liq., temp. depend., calc. 2—3404
- InSb, thermal e.m.f. rel. to impurity conc. 2—36509
- Ir, thermo-e.m.f. temp. depend. 2—40374
- K, thermopower meas. in liquid-gas critical region 2—9157
- KAg_4I_5, cationically disordered compound, thermoelec. power detn. 2—40332
- KAg_4I_5 solid electrolyte, thermopower 2—25947
- KBr (I), u.v. excitation, thermally stimulated cond. obs. 2—19074
- KH_2PO_4, X-ray irrad., light pulse emission accompanied current pulses 2—13515
- $LaSn_{3-x}In_x$, thermopower, 1.5 to 300 K, electronic struct. obs. 2—32919
- Li, thermopower, vol. depend. 2—1455
- $Li(NH_3)_4$, thermopower, 4.2-89K, calc. of mobilities and number densities using two-band model 2—19547
- $Mn_{1-x}Cr_x(Fe_x)Si_{1.7}$ solid solns., conc. depend. of thermopower 2—10024
- MnO, thermal e.m.f. rel. to hole mobility at high temp. 2—13226
- $MnSi_{2-x}$, x=0.25-0.28, cond. mechanism, thermoelec. power calc. 2—40261
- Mo electrode, effect of purity and high temp. on characteristics 2—29763
- MoO_3:Ni, temp. and oxygen press. depend. 2—10026
- MoS_2, molybdenite, thermopower 2—36513
- NaCl:M^{2+}, M=Ca, Cd, Mn, Mg, divalent impurity-vacancy complex reorientation obs. using thermocurrent method 2—12757
- $Na_4W_{14}O_{23}$, triclinic sodium tungsten bronze, Seebeck coeff. 2—9481
- Nb, mixed state, Peltier effect 2—13165
- $NbAs_2$-type compounds, Seebeck coeff., rel. to supercond. props. 2 -32927
- Nd-Bi alloy, temp. and comp. depend. 2—1413
- Ni-Fe invar alloys, absolute thermopower meas. in 1.5-125 K range, result, interpreted in weak ferromagnet band model 2—36440
- Ni, thickness dependence of the thermopower and temperature resistance coefficient 2—6892
- NiAl, resist., Hall effect 2—6760
- NiO, thermal e.m.f. rel. to hole mobility at high temp. 2—13226
- Ni_2Si, e.m.f., physical props. 10-350K 2—40141
- Os, thermo-e.m.f. temp. depend. 2—40374
- Pb, liq., temp. depend., calc. 2—3404
- $Pb_{1-x}Mn_xTe$ solid soln., density-of-states effective mass determ., 120K 2—22539
- PbSe-SnSe, thermal e.m.f., rel. to constitution diagram 2—1351
- PbTe, containing impurities, homogeneity study 2—36035
- $PbZrO_3$, rel. cond. temp. depend. and carrier activation 2—25948
- Pd-Ir alloy, thermoelec. power, 4-300K 2—40373
- Pd-Ni alloy, temp. and comp. effects 2—22494
- Pd-Ru alloy, thermoelec. power, 4-300K 2—40373
- Pd, absolute thermoelectric power meas. from 90-1300 K in two exptl. systems, result, analysed in simple two-band model 2—36367
- Pt-Os alloy, thermoelec. power, 4-300K 2—40373
- Pt, thermo-e.m.f. temp. depend. 2—40374
- Re, thermo-e.m.f. temp. depend. 2—40374
- Rh, pure, power meas., 4-300K 2—4290
- Rh_7B_3 and $RhB_{1.1}$, temp. depend. 2—1404
- $(Sb\text{-}Bi)_2$ $(Te\text{-}Se)_3$ quaternary solid solutions, thermoelectric properties 2—13335
- SbSI crystal, adsorption of O_2, attachment levels, thermo-stimulated current 2—6805
- Sb_2Se_3:Zn, In, liq., thermoelec. power, impurity effects, 950- 1200 K 2—22001
- Se:I, In, molten, impurity influence 2—3406
- Se, neutron irrad. effects on thermopower 2—6823
- -pSe, trigonal single cryst., power meas. rel. to barrier limited conduction mechanism 2—10030
- n-Si, phonon drag 2—6894
- n-Si, piezothermopower, in region of phonon drag 2—4239
- p-Si, thermo-e.m.f. under compression 2—4293
- SrO, Fermi level determ. from thermal e.m.f. 2_29659
- Ta film, sputtered, thermoelec. power rel. to O_2 content 2—39533
- Ta film, sputtered in Ar-O_2, effect of oxygen content 2—29044
- Te-Ge-Se system, amorphous semiconductor, thermopower 2—29675
- ThCe alloys, (2-8 at.%Ce), thermopower, impurity contribs. models 2—13113
- ThO_2, Seebeck coeff. rel. to electron hole mobility 2—10017
- TiO_x, Seebeck coeff. 2—32992
- Tl, liq., temp. depend., calc. 2—3404
- $TlGaS_2(Se_2)$, temp. depend. of thermostimaulated current 2—29677
- $TlInS_2$, temp. depend. of thermostimulated current 2—29677
- Tl_2Te:Sn, liq., thermoelec. power, impurity effects, 750-950K 2—22003
- U_3O_8, sintered, power, intrinisic semicond. behaviour 2—22541
- V, mixed state, Peltier effect 2—13165
- VO_2 film, thermoelec. power, struct. dependence 2—19654
- VO_x, polaron morphology, Seebeck coeff. obs. 2—10055
- VO_x, Seebeck coeff. 2—32992
- V_2O_5, thermopower sign 2—10036
- W-Re, thermocouple, reactor rad. influence on thermo-e.m.f. 2—16305
- $ZnGeP_2$, crysts., p-type, thermoelec. power, Hall effect, hole conc., hole effective mass 2—13245
- ZnSb, p- and n-type, thermoelectric power 2—1522
- ZnTe film, thermal e.m.f., stoichiometry depend. 2—25829
- ZrC, thermal e.m.f., composition and temp. depend. 2—1523
- ZrO_2, Seebeck coeff. rel. to electron hole mobility 2—10017

Thermoluminescence
- 3-methylpentane glass at 77K, γ-irradiated, thermoluminescence obs. 2—4516
- alkali halide, vacuum u.v. excited, glow peak processes 2—16629
- anthraquinone in solutions, delayed thermal fluorescence 2—28874
- Apollo 12 lunar samples 2—13986
- building materials characteristics for accident dosimetry 2—5767
- crystalline powder, effects of pressure and gaseous environment 2—16626
- diamond, semicond., and phosphoresc. 2—26245
- diamond, semicond., kinetic eqns., recomb., trapping 2—26246
- enamels, thermolum., dosimetric props. 2—29987
- fluorite, thermolum. response to γ-ray irrad. 2—27902
- frozen liquids, radiothermoluminescence studies of self absorption of emitted light 2—37058
- glass, fading, trap model 2—29972
- glass, laser damage obs. 2—1240
- glow curves, generalization of activation energy calc. 2—4507

Thermoluminescence continued
- halophosphate luminophores, exposure to mercury discharge lines (1849 and 2537 Å) 2—4511
- halophosphate luminophores, in temperature ranges 85-320°K and 293-573°K 2—4510
- heating rate controller for obs. 2—27340
- ionic cryst., KCl, X-ray coloured, relax. process parameters 2—4512
- luminescence dosimetry, conference, Risoe, Denmark, Oct (1971) 2—29948
- Luna 16 material 2—20660
- meteorite, Lost City, det. of temp. gradient induced by atmospheric friction 2—11021
- methylcyclohexane glass, biphenyl doped, isothermal deferred luminescence, electron tunnelling mechanism 2—4515
- methylcyclohexane glass containing biphenyl, peaks at 90 and 95 K, rel. to deferred luminescence at 4.2 K 2—7107
- minerals, abnormal fading characts. 2—29985
- model, application to thermoluminesc. dosimetry, traps, holes, glow curve 2—29969
- organic crystal, X-ray stimulated, dose depend. 2—16632
- phenyl acetylene, glassy soln., ascribed to fluoresc, of α-styryl radical 2—18528
- phosphors, weak, apparatus for studies over wide temp. range 2—4508
- quartz, fired, radiation-induced increase in sensitivity 2—13517
- quartz, press. and thermal effects, pot. as rad. dosimeter 2—29986
- sapphire crysts., glow peaks, storing carries, electron transfer, excitation 2—16628
- semiconductor, simultaneous meas. of thermally stimulated cond. and thermoluminesc. 2—13513
- silica gel γ-irradiated, with adsorbed gas molecules, luminescence and EPR spectra 2—6268
- smoky quartz, impurity colour centres, e.p.r. and thermoluminescence studies, trapped electron dating 2—22226
- squalane, rel. to competitive electron trapping 2—7101
- stone struck by ball lightning 2_7315
- tryptophan in ethylene glycol-water glass, due to deexcitation of triplet state 2—4517
- Al_2O_3, corundum, colour centre activation energies 2—29198
- Al_2O_3, fading, trap model 2—29972
- Al_2O_3, pulverized, active centres, e.p.r. 2—10522
- Al_2O_3 ceramic, thermolum. emission spectra, continuous determ. 2—29982
- BaF_2, radiation quality det. 2—38385
- BaO:OH, sensitivity, OH anion effects 2—29978
- BaS:Bi phosphors, trap depth evaluation from glow curves 2—36952
- $BaSO_4$, pulverized, active centres, e.p.r. 2—10522
- BeO:Li, Na, K, B, Al, Si, Ge, phosphors, thermolum. props. 2—29970
- BeO, glow curve, dosimetric props. 2—27904
- $CaCO_3$, oxygen adsorption influence 2—10450
- CaF_2:Dy phosphor batch characterization program for selected TLD properties 2—18023
- CaF_2:Ho^{3+},Nd^{3+}, form of complexes 2—10007
- CaF_2:Mn, thermolum. emission spectra, continuous determ. 2—29982
- CaF_2:Mn dosimeters, thermoluminesc. kinetics, glow curve analysis, 300-700K 2—29974
- CaF_2:OH, sensitivity, OH anion effects 2—29978
- CaF_2, continuous trapping model 2—29971
- CaF_2, dosimeter applic. 2—13514
- CaF_2, fading, trap model 2—29972
- CaF_2, glow curves, sensitivity, emission spectra, 300-823 K 2—29973
- CaS:Zr phosphors, decay studies by changing percentages of single fluxes 2—4509
- CaS:Zr(Na_2SO_4, NaF) phosphors, analysis of trap distribution and role of flux 2—22811
- $CaSO_4$:Tm, OH, sensitivity, OH anion effects 2—29978
- $CaSO_4$, fading, trap model 2—29972
- CdS:Cu, trap parameter determ. 2—19668
- CdS, comparison with i.r. stimulated luminesc. 2—10420
- GeO_2, pulverized, active centres, e.p.r. 2—10522
- KBr, annealing of X-ray induced defects at low temp. 2—3760
- KBr, X-irrad., glow peaks, F-centres, thermal trap depths 2—40728
- KCl:Cu, glow curves, trap parameters 2—36953
- KCl:KNO_3, electrolytically coloured, rel. to X-ray generation of stable centres 2—36067
- KCl, γ-irrad., F-centre obs. 2—16630
- KCl, X-ray coloured, relax. process parameters 2—4512
- KH_2PO_4, X-ray irrad., light pulse emission accompanied current pulses 2—13515
- KI, X-irradiated, role of Auger effect 2—33323
- $Li_2B_4O_7$, activation by Ag, Fe, Co, Mo 2—27900
- $Li_2B_4O_7$, supralinearity and sensitization props. 2—29980
- $Li_2B_4O_7$ glass, thermoluminesc. processes, trapping centres, e.s.r. obs. 2—29976
- LiF:Mg continuous trapping model 2—29971
- LiF:OH, OH ion impurity effects 2—29977
- LiF:OH, sensitivity, OH anion effects 2—29978
- LiF, activator doped, thermolum. glow curve struct., sensitivity 2—29983
- LiF, deep electron trap props., thermoluminesc. obs. 2—29981
- LiF, dose re-estimation, thermoluminesc. obs. 2—27895
- LiF, efficiency, rad. and thermal treatment effects 2—27894
- LiF, exposure response, glow curve, deep traps effects, trap models, 300-823K 2—29979
- LiF, fading, trap model 2—29972
- LiF, glow curve shapes interpretation, 100-500K 2—29975
- LiF, phosphor, prep. method, thermolum. prop. changes during prep. 2—27901
- LiF, radiothermolum., sensitivity, linearity, trap elimination, dosimeters 2—27903
- LiF, supralinearity and sensitization props 2—29980
- LiF, thermolum., props., applications 2—29984
- LiF, thermolum. emission spectra, continuous determ. 2—29982
- LiF dosimetry phosphor, radiation-induced increase of sensitivity 2—13516
- LiF phosphor, supralinearity and sensitization 2—4513
- Mg_2SiO_4:Tb, OH, sensitivity, OH anion effects 2—29978
- NaCl:Cu, glow curves, trap parameters 2—36953
- NaCl:Tl, x-irrad., glow peaks 2—29988
- (NaCl-KCl):Sn, mixed crysts., 300-500K 2—36954
- Pd-Pt alloys, low temp. thermopower 2—19551
- SiO_2 films, glow curve obs. of trapping centres 2—40729

Thermoluminescence continued
SnO$_2$, pulverized, active centres, e.p.r. 2—10522
SrF$_2$, dose dependence in pure and doped crystals 2—4514
SrS(Cu) phosphors, spectral distrib. of luminescent emission, excitation spectra, and decay 2—33310
YAG:Cr^{2+}, recombination excitation mechanism 2—40725
Zn$_x$Cd$_{-x}$S;Ag,Ni, due to trapping states, energy band model 2—4480
ZnS:AgAlS$_2$ 2—29958
ZnS:CdS:Ag:Ni:Co: phosphors 2—40730
ZnS:Co^{2+} phosphors, Cu and Ag activated 2—29989
ZnS:CuAlS$_2$ 2—29958
ZnS, trap centre properties study 2—20112
ZnS phosphors, effect of adding NaCl and preliminary heating in H on thermoluminescence 2—16631
Thermomagnetic effects *see Magnetothermal effects*
Thermometers
see also Pyrometers; Thermocouples
d.c. thermistor thermometer, numerical method of linearizing 2—20963
electronic, using Si diode 2—2283
i.r. radiation detectors for temperatures over 100°C 2—7772
low temperature, superconducting magnetic susceptibility meter applic. 2—4178
noise for temperature measurement in nuclear reactors 2—5761
noise thermometer method for measuring absolute temperature 2—27335
radiation thermometers at room temperatures 2—7773
scanning, radiometer, for black body temps. at rate of 15000 per second 2—2284
semiautomatic spectrocomparator for temperature scale transmission 2—37801
temperature meas. methods 2—23406
C, calibration and use in metal calorimetry 2—16032
Ce$_2$Mg$_3$(NO$_3$)$_{12}$.12H$_2$O thermometry scheme, calibration below 1 K 2—20774
^{161}Dy Mossbauer thermometer, low temp. calibration 2—37828
Si p-n junction diode, forward voltage-temp. characts. 2—40302
SrTiO$_3$ glass-ceramics applic. 2—40358
resistance
calibration, reproducible temp. obtained by controlled freezing of pure metals 2—17453
calibration with resistance box 2—23410
characteristics, linearizer 2—23409
liquid metal in quartz jacket 2—11383
low temperature, C resistors 2—27337
low-temp., high resolution four terminal a.c. resistance bridge 2—37872
for plasma generator cooling water temperature measurement 2—34226
Pt, accuracy improvements 2—20964
using stabilized zirconia, hot pt. localization and temp. detection 2—27331
system using elements of order of fraction of an ohm 2—27329
temperature meas. methods 2—23406
GaSb, for 2 to 100°K range 2—17456
ion implanted thermoresistive sensor, for cryogenic temperatures 2—25884
Pt, resistance meas., a.c. bridge 2—2281
Thermonuclear devices *see Plasma/devices*
Thermonuclear reactions *see Elements/origin; Nuclear fusion*
see also Elements/origin; Nuclear fusion
A-type stars, peculiar, production of anomalous abundances of elements 2—4837
collisionless high amplitude shock waves, plasma heating 2—24708
controlled fusion, application of laser produced dense plasmas 2—24783
controlled fusion research, microwave electron density measuring systems 2—28592
degenerate stars, effect on stability toward adiabatic radial perturbations 2—26678
neutron yield of fusion from solid D$_2$ irrad. by laser beam 2—32052
nucleosynthesis in the Galaxy, evolutionary models 2—20482
p-process synthesis in supernova envelopes 2—4833
in plasma, behind shockwaves due to absorption of laser radiation 2—6077
in plasma, bounded, cooling and damping of burning 2—28502
plasma, growth rate of magnetosonic waves 2—39171
in plasma, laser heating enhancement by addition of heavy impurities to target 2—18591
plasma heating by relativistic electron beams 2—24654
plasma studies, prospects for control 2—24260
prospects for energy production, Geneva 1971, conference 2—24257
radiation losses in plasma confinement systems, Tokamak and plasma focus 2—24729
rare neutron rich isotopes, thermonuclear synthesis 2—8368
S-process, nucleosynthesis of elements 2—10860
stars, loops in H-R diagram during core He burning and effect of rotation 2—23071
stars, red supergiants of 15$_\odot$, core He burning evolution 2—7420
stars of 5$_\odot$, core He burning evolution 2—7421
stellar cores, effect of nuclear statistical equilibrium on detonation 2—20533
superheavy element synthesis 2—31592
thermal explosion analogy, D-T plasma 2—509
Tokamak system, toroidal plasma column, maintenance of longitudinal current 2—24732
Urca neutrino processes, rate formulae 2—33641
white dwarfs, He rich, with H rich envelopes, hydronamic studies 2—26681
C burning in carbon-oxygen stars, late stages of evolution 2—10868
C burning in stellar environment corresp. to supernova explosion, abundance of major nuclei produced 2—16981
^{12}C+^{12}C carbon-burning in stars, reaction rate 2—13892
^{252}Cf synthesis in underground thermonuclear explosion 2—35094
^{250}Cm synthesis in underground thermonuclear explosion 2—35094
^{257}Fm synthesis in underground thermonuclear explosion 2—35094
^{2}H-^{3}H plasma, solid density, waves 2—18660
He-burning in red supergiant stars of 15 solar masses, theremal stability of shell source 2—10867
^{4}He,^{12}C,^{16}O,^{20}Ne,^{24}Mg,^{28}Si,^{56}Fe diffusing nuclear reaction chain in envelope of neutron star, investigation of cosmic ray production by pulsars 2—4929
^{14}N(α,γ)^{18}F rate obs., w.r.t. stellar evolution 2—20530
^{16}O+^{16}O, total reaction cross- section 2—37289
Si burning in stellar explosions with various initial compositions 2—26673
Thermopiles *see Thermocouples*
Thermoreflectance
Al, thermomodulation spectra interpret. 2—36855
Au, thermomodulation spectra interpret. 2—36855
CdSnP$_2$, single cryst., spectra 2—29900
Cu, thermomodulation spectra interpret. 2—36855
GaS(Se), temp. modulation of optical consts. 2—10346
GaSe(s) layer, 77K,, Kramers-Konig analysis 2—36858
Ge, E$_0$ region 2—10347
InAs, single cryst., spectra 2—29900
InP, single cryst., spectra 2—29900
PbS, film, spectra 2—29900
Thermosphere *see Atmosphere/upper; Ionosphere*
Thermostats
see also Cryostats
calorimeter baths, by toluene-Hg thermoregulator and i.r. heat lamp 2—2286
DTA, principle of temp. regulation 2—11386
electron microscope, heating device for temp. control, for metal whisker growth obs. 2—35972
high precision, bath temp. regulation using thermal rad. from elec. bulbs 2—27339
high vac. chamber, temp. control system 2_27338
n.m.r. meas., 95-475 K 2—14351
forn.m.r. pulse probe, doped-water type stat. 2—17504
temp. range −100 to +200°C using cooling and heating to desired temp. 2—2287
X-ray camera, suitable for sorption studies 2—3619
Theta pinch *see Plasma/confinement*
Thickness measurement
see also Particle size
dielectric layers, e.m. method with coil probe 2—32351
rel. to dryout obs., combined photographic film thickness and temp. technique 2—24275
epitaxial layers, i.r. technique, interpretation of phase shift at substrate layer interface 2—29039
fatty acids monolayers, by multiple beam interferometry 2—6357
film, light absorbing, ellipsometric meas. 2—6341
film, metallic, resist.-thickness data, Fuchs-Sondheimer theory fitting method 2—40164
film, Tolansky method, systematic errors 2—25191
films, by interferometry, bidirectional tilting table 2—38056
films, measurement during deposition using piezoelectric quartz crystals 2—35881
films, realizable precision with a quartz oscillator 2—35879
films, using Auger electron spectroscopy 2—29019
films using monoenergetic electron beam 2—37555
ice, mapping method using f.m. e.m. radiation, patent 2—37098
IOTA, computer controlled thin film meas. using scanning spectrophotometer 2—29713
liquid films, capacitance depth gauge 2—35716
metal film, Leonard-Ramey method 2—3508
metallic films, by means of absorption of coloured complexes 2—35880
nuclear fuel cladding, electrokinetic method, use of eddy currents 2—18263
opaque and transparent objects, twin microscope, thickness profiles of semiconductor counters 2—14063
optical films, multiple beam interferometry uniformity obs. 2—35883
radiometric, nuclear absorption measurement method and applications 2—37558
semiconductor detector rel. to scintillation electron detector 2—2635
separation of parallel plates using Michelson interferometers 2—8008
sputtered glass waveguides 2—38115
Ta:O films 2—18946
thermochemically produced layers on steel, thermoelec. meas. 2—1177
two-phase flow, skin-friction and film-thickness meas. in upward flow through annulus 2—24631
u.s. probe echo method, equipment appraisal 2—32668
very small particles, effect of scanning line width on error 2—27020
GaAs epitaxial layers 2—32364
He film, ellipsometric technique on gold substrate at 2.13 K and quartz substrate at 2.10 K 2—3419
KBrO$_3$, KClO$_3$ film, polycrystalline, and uniformity evaluation 2—9278
NaClO$_3$, NaBrO$_3$ film, polycrystalline, and uniformity evaluation 2—9278
Ni film, polarimetric compared with interferometric obs. 2—33199
Si epitaxial layer, far i.r. interference obs. 2—25207
Si film, polycryst., deposition in-process thickness monitor, i.r. interferometry method 2—22077
Si film, polycryst., determ. by i.r. interferometry 2—22076
SiO$_2$ film, on Si, using IOTA, computer controlled scanning spectrophotometer 2—29713
Thin film devices
d.c. conduction mechanism in insulating films, book 2—29732
ferroelectric memory, Pb$_{0.92}$Bi$_{0.07}$La$_{0.01}$(Fe$_{0.405}$)Nb$_{0.325}$Zr$_{0.27}$)O$_3$ film performance 2—40356
ferroelectric-photoconductor memory, electrode requirements 2—40339
ferroelectric-photoconductor storage device, design and performance 2—40336
group IV-VI compound semicond. films, device applications 2—40297
Josephson tunnelling barriers fabrication by r.f. sputter etching 2—6783
magnetic recording heads, efficiency analysis 2—7832
magnetometer, anisotropic ferromagnetic film employment, patent 2—17530
metal and dielec., microccts., passive and active, prod. by ion implantation 2—29189
metal-polyquinoline carboxylic acid-metal sandwich, I-V characteristics 2—19721
m.i.m. emitters, breakdown mechanism 2—13289
m.i.m. structs., current filament detect., a.c. detect. scheme, electron microscope obs. 2—40311
m.i.s.m., with CdS layer, electron emission 2—10098
nucleation imaging media, applications 2—23731
optical waveguide, laser mode conversion, gyrotropic and anisotropic material applics. 2—34425
piezoelectric transducer, efficiency and optimum thickness 2—29525
semiconductor, chalcogenide glass threshold switches, frequency dependence of negative capacitance effects obs. 2—6854
semiconductor switch, negative resist. and filamentary cond. 2—10079
superconducting bridges, relax. oscillator model 2_19606
superconducting calorimetric obs. of a.c. losses 2—4182

Thin film devices continued
- superconducting narrow bridges, preparation by Pb and Sn deposition through masks onto uncooled glass substrate 2—22511
- superconducting weak links, T_c increase due to microwaves 2—13190
- transducer, precip. under electron bombardment 2—4046
- tunnel diode, amplification of injected current from tunnel cathode in p-type amorphous layer 2—33034
- tunnel junction, superconducting, as maintenance voltage standard 2—6784
- AL-(Al_2O_3)-CdS-Al switching element, post-breakdown conduction mechanisms 2_19720
- Al, interconnections crossing Si-SiO_2 steps temperature cycling effects 2—1538
- Au-TiO_2-Si-TiO_2-Au structure, nonlinearity of capacitance 2—19729
- CdS transducer, precip. under electron bombardment 2—4046
- Ni high-temperature stable thermocouples, oxidation and diffusion problems 2—30900
- $Te_{40}As_{37}Ge_7Si_{18}$/Ge electrode, ovonic threshold switching 2—10082
- $Te_{40}As_{35}Ge_7Si_{18}$ threshold switch, nature of ON-state 2—22577
- ZnO u.s. transducers for longit. and shear modes, fabrication 2—29549

Thin films *see Films; Films, solid*

Thirring model *see Elementary particles; Field theory, quantum*

Thixotropy
- No entries

Thomas-Fermi method *see Atoms/structure*

Thomson effect *see Thermoelectricity*

Thorium
- Apollo 15 samples, primordial radioelements and cosmogenic radionuclides 2—41188
- atmosphere, vertical turbulent diffusivity, obtained from Tn profiles 2—37144
- corrosion and reactions with environment 2—20190
- detection in various matrices using nuclear track technique 2—7200
- e.s.r. of rare earth ions, linewidth temp. depend., exchange coupling 2—20152
- high temperature reactors, Th cycle compared with low enriched U cycle 2—38741
- ionic spectra, excited in interrupted vacuum arc, mag. enhancement 2—38799
- in lunar minerals by ion microprobe mass analysis 2—37344
- in minerals, content, nondestructive determ. by gamma ray spectrometry 2—4608
- radioactivity, in moon rock and terrestrial basalt, rel. Moon origin 2—30547
- Sea of Fertility, soil analysis 2—20668
- shock melting and vaporization 2—39420
- in soils, remote sensing by low altitude gamma spectrometric surveys 2—37096
- superconducting, critical mag. fields under press. 2—16173
- superconducting energy gap, tunnelling obs. 2—40211
- superconducting transition temp. press. depend. 2—32952
- superconductivity, review 2—13147
- in H_2SO_4 solutions, det. by gamma spectrometry simultaneously with U det. 2—40857

Thorium compounds
- alloys, corrosion and reactions with environment 2—20190
- hectoboride phase, lattice parameters and Knoop hardness 2—9833
- nuclear reactor fuel, phase diagrams 2—18262
- oxides, chemical deposition of u.v. wide- band reflectors 2—34515
- $Gd_{1-x}Th_xFe_3$, mag. props. 2—40527
- Ni:ThO_2, rapid quenching effects, internal stresses, rel. to mech. props. 2—32599
- TRO_2:$^{237}Np^{4+}$, e.p.r. studies on strained and unstrained crystals, electronic state of Np determ. 2—10486
- Th-C-N, alloy, cryst. struct. at temps. to 2250°C, X-ray diffr. obs. 2—19060
- Th-N-O system, phase diagram 2—36307
- Th-Ni, alloy, particle size, interparticle spacing, influence on mech. behaviour 2—3963
- Th-Ni, intermetallic compound, struct., disordered substitutions, X-ray obs. 2—6452
- Th-Os(Re) alloy, elec. and thermal cond., temp. depend. 2—29618
- Th-U dil. alloys, supercond. and localized spin fluctuations 2—1494
- Th-U dilute alloy, supercond. and normal states, sp. ht. study 2—29557
- $ThAl_2$, ^{27}Al n.m.r, dipolar doublet, quadrupole and anisotropic knight shift interactions 2—33347
- ThC/ThN system ternary cpds., supercond. 2—29640
- ThC, thermionic cathode, indirectly heated, high current density 2—37898
- ThC_2, vaporization and surface ionization 2—35840
- ThCe alloys, (2-8 at.%Ce), resistivity and thermopower, impurity contribs., models 2—13113
- $ThCl_4$-NaCl melt, complex ion formation, e.m.f. obs. 2—32256
- $ThCo_5$-$ThNi_5$, cryst. struct. and mag. props., comp. depend. 2—1634
- $ThCo_{5-5x}(Ni_{5-5x})Fe$, Mossbauer effect, magnetiz., cryst. struct. 2—25348
- ThF_4 film, in anti-reflection coating, one shot laser damage threshold 2—27637
- $ThGeO_4$, thermal expansion, rel. to cryst. chemistry 2—22430
- Th_4H_{15}, prep., elec. and supercond. props. 2—25772
- ThNiSn, atomic struct., Debye-Scherrer determ. 2—3736
- ThO_2-PaO_2-UO_2 solid soln. formation, exchange of Pa^{4+} in molten LiF-BeF_2-ThF_4 with U^{4+} and Th^{4+} 2—10593
- ThO_2-UO_2, measurement of temp. dependence of K_∞ for a high temperature gas-cooled reactor lattice 2—38744
- ThO_2-Y_2O_3 solid electrolyte, elec. cond. and operational limits 2—10634
- ThO_2, e.p.r. of $^{155}Gd^{3+}$, h.f.s. forbidden lines 2—13544
- ThO_2, e.p.r. of $^{155}Gd^{3+}$, h.f.s. 2—26288
- ThO_2, electron hole mobility, elec. cond., thermogravimetric and Seebeck coeff. obs. 2—10017
- ThO_2, in Ni, high temp.strength 2—9690
- ThO_2, porous, water vapour treated adsorpt. of Ar and N_2, pore struct. 2—35924
- ThO_2, sintered, polycryst. props. rel. to monocryst. props. 2—22254
- ThO_2, spin-lattice interaction for Gd^{3+}, temp. depend. 2—26277
- ThO_2 dispersion hardened Ni and alloys, role of microstruct. in strengthening 2—39936
- ThO_2 dispersion strengthening of Cu 2—9684
- ThO_2 dispersion strengthened cobalt alloys, stress-rupture and corrosion resist. 2—19266

Thorium compounds continued
- ThO_2 particle growth in dispersion strengthened Ni, electron microscopy 2—9734
- ThPdSn, atomic struct., Debye-Scherrer determ. 2—3736
- ThPtGe, atomic struct., Debye-Scherrer determ. 2—3736
- ThRhIn(Sn,Sb), atomic struct., Debye-Scherrer determ. 2—3736
- $Th(WO_4)_2$, decomposition temp. 2—36287
- Tho_2-SrO, ThO_2-BaO systems, charact. using specially designed furnace 2—30719
- Tho_2, reduction by C 2—30066
- TlO_2-base solid electrolytes, proton cond. 2—40819
- $(U,Th)O_2$ mixed cryst., thermal diffusivity 2—19467
- UO_2-$UO_{2.67}$-ThO_2 system, phase relations 2—1405

Thulium
- thermal conductivity, temp. range 0.5-4.5K 2—40097
- X-ray excited optical fluorescence, in Gd_2O_3, La_2O_3, and Y_2O_3 2—22805
- $CaSO_4$:Tm, OH, thermoluminesc., OH anion effects 2—29978
- Tm I spectrum, lifetimes of 14 levels meas. using technique of zero field level crossing 2—24351
- Tm^+, electronic wave functions by numerical Hartree-Fock SCF method 2—35141
- Tm^{2+}, accurate numerical Hartree Fock self consistent field wave functions 2—35134
- Tm^{2+}, in CaF_2, crystal field, ligand overlap effects 2—19941
- Tm^{2+}, in CaF_2, energy level splitting, covalency effects 2—19942
- Tm^{3+} emission in La_2O_2S, thermal quenching 2—1709
- Tm^{3+} in ZnS, cathodoluminesc. efficiency 2—1718
- YAG:Er, Ho, Tm, energy transfer process between Er^{3+} and Ho^{3+}, temp. and conc. effects, fluoresc. spectra obs. 2—26240
- Yb^{3+}-Tm^{3+}, stepwise energy transfer and i.r. to visible conversion 2—10427
- ZnSe:Tm, Li, luminesc., absorpt., and Zeeman effect 2—40721

Thulium compounds
- $TmAsO_4$, magnetically controllable cooperative Jahn-Teller distortion 2—4459
- TmB_{12} thermal expansion, in range 78-1300°K 2—6684
- TmB_2, cryst. growth and struct. 2—39591
- TmBi cryst. field splittings, neutron scatt. obs. 2—40592
- $TmFeO_3$, spin reorientation, ^{57}Fe, n.m.r. obs., 75-114 K 2—16663
- $TmFeO_3$, $TmCrO_3$, nonaxial antiferromag. axis, neutron diffr. 2—26064
- TmN, cryst. field splittings, neutron scatt. obs. 2—40592
- $TmPd_3$, mag. props. 2—19829
- $Tm_2(SO_4)_3.8H_2O$, mag. ordering, sp.ht. obs. 2—16399
- TmTe, mag. props. at press-induced electronic phase transition 2—40501
- TmTe, pressure induced electronic and structural transform., X-ray and resistivity obs. 2—36289
- $TmVO_4$, spectra, ground state doublet splitting, g-factor, mol. field effects. below T_d 2—22665

Thunderstorms
- *see also Lightning*
- attenuation meas., of radiowaves, in submillimetre range, experimental study 2—16828
- electrification, mechanisms by which electric charge is generated and separated to supply lightning flashes 2—40948
- explosive development, indication using vertically integrated liquid water content obs. 2—13707
- forecast technique from modelling considerations, severe storm development 2—13697
- forecasting, screening regression techniques, severe thunderstorms and tornadoes 2—13702
- formation and prediction, rel. to convective clouds and synoptic scale systems 2—13709
- freezing conditions and electrification due to melting precipitation, simulation in a cold vertical wind tunnel 2—7291
- gust fronts, characteristics 2—40953
- hail-producing, location and investigation by infrasound 2—13717
- h.f. radio noise studies, prediction of tornadoes 2—13705
- horizontal motion within, single Doppler radar obs. 2—13712
- ice pellets grown by accretion of supercooled drops, charge separation due to riming in an electric field 2—40956
- infrasound and subsonic disturbances 2—37124
- internal structure, revealed by θ_w surfaces 2—13713
- lee slope study, forecasting along front range of Rocky Mountains 2—13700
- lightning characteristics in N. Nigeria 2—40970
- locally severe, electrical characteristics 2—13706
- mechanism and power spectrum of thunder 2—22965
- mechanism and power structure of thunder 2—1856
- Oklahoma compared with Malaysia, aircraft obs. of turbulence, temp. variation and cloud top heights 2—40952
- potential energy transfer from sea to atmosphere by heating 2—26491
- prediction using instability energy index in combination with standard significators 2—13699
- severe, local, rel. to cirrus formations 2—13711
- severe, prediction, stability indices 2—13708
- severe local storms, detection, prediction, economics and structure, conference (Boston, USA, 1971) 2—13695
- severe storm prediction by screening regression using forecast predictors 2—13701
- snow, proximity soundings 2—13710
- surface pressure disturbance, rel. to sporadic E ionization 2—4726
- tornado forecasting, statistics of surface conditions after meso low of thunderstorm 2—13698
- tornado-producing, prediction by aerial photography 2—13703
- wind velocity measurement 2—20329

Thyratrons *see Gas-discharge tubes*

Tides *see Atmosphere/movements; Ionosphere; Oceanography*

Time interval measurement
- exponential clock producing output pulses with exponentially increasing intervals 2—30973
- perception mechanisms 2—17
- picosecond electron-optical chronography, electronically operated image tube streak camera 2—31153
- readout pulses in photoelectric systems, timing accuracy 2—27388
- ultrashort laser pulses, third-order correlation measurement 2—23621

Time measurement
- atomic beam tubes, power/linewidth relations 2—5120
- atomic clocks in spacecraft location 2—7358
- atomic frequency standards 2—571

Time measurement continued
clock paradox resolved 2—27043
Coordinated Universal Time scale, 1972 change 2—5117
Earth, variable rotation effect 2—7519
frequency stability, computation using discrete Fourier transform 2—5311
i.r. frequency synthesis using methane stabilized He-Ne laser 2—33863
leap second, review 2—7641
maser, hydrogen, wall shift variation with storage bulb diameter 2—5342
n.m.r. relaxation, by pulse method, apparatus 2—34268
optical correlation of real-time signals 2—7945
perception mechanisms 2—17
quantization error in repeated dependent transformations 2—37562
rapid processes, new optical methods 2—23223
review of present state of theory and practice, methods for comparing standards 2—37563
standards of frequency and time, atomic and molecular, review 2—30748
synchronization worldwide using NASA GEOS-11 2—33865
synchronization worldwide using TRANSIT satellite system 2—33864
Universal Time det. by lunar laser ranging 2—37074
Cs atomic frequency standard of Physikalisch-Technische Bundesanstalt 2—5119
Cs beam atomic frequency standards 2—571
Cs beam frequency standards, cavity phase dependent frequency shifts 2—30746
Cs clocks, diurnal freq. var. and refraction index 2—10738
Cs III atomic beam time scales, construction techniques and improvement suggesting 2—5118
H maser atomic frequency standards 2—571
He-Ne laser, cw at 88 THz, absolute frequency measurements 2—17174
Rb gas cell atomic frequency standards 2—571

Tin
acoustic waves velocity, meas. of quantum oscillations and e.m. excitation mechanism 2—5228
autoionization of high-temperature monatomic vapour 2—28201
crystal growth and grain boundary migration, optical obs. method 2—39590
dendrite growth, on free surface of supercooled melt, kinetics 2—12675
diamondlike lattice, dynamics and vibrational spectra, valence force pot. calcs 2—19357
diffusion g ^{110}Ag 2—22250
diffusion in α-Fe, Arrhenius law deviation, Curie pt. phenomena 2—39728
diffusion in Mg single cryst., diffusion constant, anisotropy, valence effect, activation energy 2—6515
diffusion in Zircaloy-2 2—12817
double anneal, grain growth rel. to defects 2—32501
enthalpy of fusion determ. 2—28939
film, electromigration direction 2—36075
film, evap. on Si and sapphire, growth by backscattering obs. 2—32379
film, films, cylindrical, stability of supercurrents 2—36471
film, Ginzburg-Landau parameter, mag. transitions and supercooling meas. discrepancy 2—9968
film, growth on SnTe, electron microscope obs. 2—32380
film, oxidation, electron microscopy study 2—12667
film, resist. peak at supercond. transition 2—6776
film, supercond., mag. transitions 2—22506
in glasses, temperature dependence of Mossbauer coeff. 2—10317
grain growth, secondary recrystallization, low temp. thermal cycling effect 2—32691
gray, Raman spectra, spectrum shape, polarization selection rules, rel. to mag. field 2—16567
grey, optical consts., band struct. 2—16475
grey, stress-induced band gap 2—36531
impurities in alkali metal solvents, struct. transition 2—18799
isotopes A=115, 117, 119, hyperfine structure anomalies 2—21527
lattice dynamics, optimum-model-potential obs. 2—32813
liquid, structure factor and atomic distrib., X-ray diffr.obs. 2—18792
liquid, thermal and natural convection 2—25005
molten bath for diffusion meas. of metals 2—9606
ohmic contact on n-GaAs, specific resistance 2—29715
oscillating magnetostriction, 1.4K 2—40151
phonon spectra, neutron scatt. and tunnelling comparison 2—19395
polycrystalline layer, on NaCl, transmission of struct. information 2—6333
polymorphous beta-alpha transformation kinetics 2—4004
positron annihilation in single crysts., temp. effects 2—25714
powder, in Cd-Pb-Sn mixture, sintering above the ternary eutectic temp. 2—29451
quantitative analysis in NBS SRM Cu-base alloys and ore concentrates by Mossbauer spectroscopy 2—16710
semiconductor-metal transition at high press. 2—15955
superconducting, dynamic intermediate state, regularity of domain motion 2—36469
superconducting, enhanced diamag. above T_c due to thermal fluctuations 2—13178
superconducting, IV charact., instabilities in transition curve 2—32950
superconducting, u.s. absorpt. in intermediate state 2—36468
superconducting cylinder, mag. field penetration pattern 2—19581
superconducting diodes, emitted phonon spectrum and influence on detected signal 2—40222
superconducting domain structure motion, spatial periodicity, relation to prediction of Landau model 2—13117
superconducting narrow bridges, preparation by deposition through mask onto uncooled glass substrate 2—22511
superconducting small particles, h.f. mag. polarizability 2—9974
superconducting thin films, critical point fluctuations and excess noise 2—40188
superconducting whisker crystals, resisitive transition, McCumber-Halperin modification of the Langer-Ambegaokar theory 2—1491
superconductor, compression effects on T_c, role of pt. defects 2—25787
surface, intensities of Auger lines excited by electron and X-ray irrad. 2—12638
surface energy, determ. from melting temp. of disperse particles 2—6318
surface reactions, O_2-H_2 radicals, low pressure discharges 2—35620
thermal and elec. cond., 4.5 to 77K 2—32857
thermal props. and i.r. absorbing power of thin layers 2—19448
u.s. attenuation, giant quantum oscillation 2—6667
u.s. attenuation in intermediate state 2—36470
whisker, fluctuation effects on supercond. T_c 2—19597
whisker, supercond., critical current temp. depend. 2—13160
whisker, supercond., fluctuation effects in resistive transition 2—13179

Tin continued
whiskers, third order elastic constants 2—19163
white, interpolation schemes, muffin tin zero 2—16099
white, pseudopot. form factors 2—13091
wire, one-dimens., supercond. 2—13180
Al-Sn multilayer, internal friction, yield point, thickness and defect depend 2—1287
GaAs:Sn, Zeeman spectra of principal bound exciton 2—33306
$NH_4Br(Cl)$:Sn phosphor, cryst. growth and spectra 2—1710
(NaCl-KCl):Sn, mixed crysts., thermolum., 300-500K 2—36954
Sn:In, vortex transport entropy, tunnelling effect 2—16162
Sn/GaAs, surface-barrier structures by chemical deposition 2—25892
Sn-Sn-oxide-Sn Josephson tunnel junction, exptl. study of Riedel singularity 2—13196
β-Sn, cryst. lattice geometry, lattice plane stacking, jogs, slip-forest dislocation elastic interaction 2—9491
β-Sn, Mossbauer recoilless fraction temp. variation 2—36326
α-Sn, RPA dielec. function in far-i.r. 2—10051
Sn IV, isotope shifts in resonance lines, size of specific mass shifts in alkali-like resonance lines 2—5784
Sn IV, optical isotope shifts, screening effects 2—586
Sn^{2+} in KI magnetic field dependence of radiative lifetime of A-band emission 2—36930
Sn(II), sensitizer deposit in Kapton film, Mossbauer obs. 2—13588
^{113}Sn, radioactive source preparation by electrodeposition on thin metallized plastic films 2—5673
^{119}Sn thin film, backscatter Mossbauer spectra obtained with internal conversion electrons 2—35895
Te:Sn, mobility and microhardness, impurity conc. depend. 2—13239
Tl_2Te:Sn, liq., elec. cond., thermoelec. power, impurity effects, 750-950K 2—22003

Tin compounds
alloy, homogenization, ageing solubility limits, residual resist. obs. 2—39940
alloy, liq., excess free enthalpy of mixing 2—32255
Ga-Cu liq., excess free enthalpy of mixing 2—32255
germanium acetate, lattice parameters and space groups 2—19063
lead-bronze, wear mechanism, dry state sliding 2—29340
Nd:$SnCl_4POCl_3$ circulation type, spatial and energy characteristics 2—273
ore concentrates, quantitative analysis by Mossbauer spectroscopy 2—16710
Ag-Sn alloy, solid and liq. phases, thermodynamic props. 2—40000
Al-Sn metastable solid solution, supercond. transition temp. 2—16171
Au-Sn liquid alloy, struct. and activity coeff., stirred H-cell study 2—28784
AuSn, sp. ht. low temp. meas. 2—4065
Bi-Sn alloy, metastable phase BiSn formation under pressure, kinetics, Mossbauer obs. 2—9794
Bi-Sn film, r.f. sputtered from two-phase sintered Bi-Sn cathodes 2—39497
Cd-Sn-Zn alloy system, liquidus temperature determ. 2—1140
CdS-SnS heterojunctions 2—33082
$Cr_xSn_{1-x}Te$ alloys, prep. and mag. props. 2—33131
Cu-Ni-Sn system, Cu corner, binary and ternary diffusion 2—19143
Cu-Sn alloy, elastic moduli, phase and composition depend. 2—39759
Cu-Sn alloys, surface segregation, adhesion, friction 2—22303
Cu-Sn system, liq., electronic struct. 2—9078
Cu_2MnSn alloy, Mossbauer effect study of hyperfine fields at Sn sites 2—36833
Fe-Sn, antiferromag. and paramag. states, hyperfine parameters, Mossbauer study 2—29884
Fe-Sn, C influence on equilib. diag., diffusion couple method 2—9835
Fe-Sn alloy, hyperfine field distrib., Mossbauer obs. 2—40627
Fe-Sn dilute alloy, hyperfine field at Fe atoms, temp. depend. 2—16435
Gd-Sn alloy, Mossbauer effect, nuclear Zeeman effect, mag. props. 2—13453
Ge-Sn solid soln., Mossbauer effect solid soln., of ^{119}Sn, quenching effect 2—29886
In-Sn alloy, change in ultrasonic velocity on melting 2—39421
In-Sn alloy, enthalpy of mixing anomalies due to Brillouin zone effects 2—22342
In-Sn alloys, normal and flux-flow states, Hall effect 2—13162
In-Sn alloys, thermal conductivity in solid and liquid states 2—13058
$LaSn_3$, electron energy levels, nonrel. modified OPW calc. 2—19510
$LaSn_3$, electron energy levels, relativistic corrections using perturb. theory 2—25733
Li-Sn liquid alloys, thermodynamic props., 973 and 1123K 2—28839
Nb_3Sn, high-field superconductor, pulsed-field meas. rel. to metallurgical processes 2—25790
Nb_3Sn film, cylindrical metallic substrate, fast rotation deposition technique 2—39515
Nb_3Sn ribbon, doped, prep., microstruct. and high field supercond. props. 2—32944
Ni_2MnSn alloy, Mossbauer effect study of hyperfine fields at Sn sites 2—36833
Pb-Cd-Zn-Sn system, phase diagram, computer calc. 2—13008
Pb-Sn alloys, thermal expansion 2—6682
Pb-Sn eutectic alloy, superplasticity 2—29263
Pb-Sn eutectic alloy system, elastic moduli, u.s. wedge method obs. 2—39760
Pb-Sn system, liq., electronic struct. 2—9078
PbSe-SnSe, constitution diagram 2—1351
PbSn eutectic alloy, extrusion in superplastic region 2—12864
$Pb_{0.918}Sn_{0.082}Se$ epitaxial growth on BaF_2 and CaF_2 substrates 2—25205
$Pb_{1-x}Sn_xSe$, elec. props., rel. to band struct. model 2—25825
$Pb_{1-x}Sn_xSe$, Shubnikov-de Haas effect, Fermi surface 2—25841
$Pb_{1-x}Sn_xSe$ diodes, laser emission and band crossing under press. 2—37998
$Pb_{1-x}Sn_xTe$, epitaxial growth, heat treatment and elec. props. 2—32375
$Pb_{1-x}Sn_xTe$, wavelength modulation derivative reflection spectra, assignment of obs. structures with band calcs. 2—4449
$Pb_{1-x}Sn_xTe$ epitaxial layers, bulklike photocond. 2—10139
$Pb_{1-x}Sn_xTe$ epitaxial layers, Hall mobilities and postgrowth annealing 2—4214
PbTe:Gd, mag. characts., localized moments 2—33141
Pd_2MnSn alloy, Mossbauer effect study of hyperfine fields at Sn sites 2—36833
Sn-Ag, ohmic contact on n-GaAs, specific resistance 2—29715
Sn-Ag alloy, elastic moduli, phase and composition depend. 2—39759
Sn-Au alloy, liq., thermodynamic props. 380-1050°C 2—28837
Sn-Bi-As system, constitution of Sn- and Bi-rich regions 2—22380

Tin compounds continued
Sn-Cd, alloy, evaporation rate vs. temp. curve 2—28952
Sn-Cd, Sn-Pb fusible alloys, effect on wear characteristics of thermoplastic polymers 2—6589
Sn-Cd alloy, Cd segregation during melting, neutron radiography obs. 2—15633
15 at.%Sn-Cu, alloy, b.c.c. to orthorhombic martensite transform. shape strain obs. 2—6634
Sn-Cu(Ag)(Au) alloys, liquid, Knight shift comp. depend. rel. to conduction electron density 2—9177
Sn-In, film, electromigration, void marker motion 2—6511
Sn-In alloy film, anomalous paracond. 2—16164
Sn-In dil. alloys, n.m.r. of ^{119}Sn, Knight shift anomalies 2—37014
Sn-In thin films, marker motion during electromigration 2—39747
Sn-Mg-Cu alloy, enthalpies of form., Laves phases binding conditions 2—29475
Sn-Mn-Ir alloy, cryst. struct., mag. props. 2—22160
Sn-Pb, alloy, composite struct., growth by zone melting 2—22112
Sn-Pb, alloy, liq., surface tension meas., max. bubble press. method 2—18807
Sn-Pb alloy, solidified at high cooling rate, struct. and props. 2—39941
Sn-Pb alloy whiskers, fluctuation effects in resistive transition 2—13179
Sn-Pb eutectic alloy, superplastically deformed, texture 2—12975
Sn-Pb eutectic alloy, unidirectional solidification, electronic microanalysis 2—12925
Sn-Pb exploding wire binary alloy, width of absorption lines 2—38812
Sn-S-As system, glass and cpd. formation, n.m.r. study 2—37003
Sn-S-O-C system, phase diagrams, volatization of Sn 2—1150
Sn-S system, Mossbauer study 2—1674
Sn-S(Se)-P system, glass and cpd. formation, n.m.r. study 2—37003
Sn-Sb-Cu alloy η phase segregation prevention, solidification depend. 2—3965
Sn-Sb alloy, elastic moduli, phase and composition depend. 2—39759
Sn-Sb dil. alloys, n.m.r. of ^{119}Sn, Knight shift anomalies 2—37014
Sn-Sb film, struct. and orientation, twinning 2—12668
Sn-Sb melt, interdiffusion coeffs., conc. depend. 2_9121
Sn-Se films, vacuum deposition 2—3547
Sn-Se system, Mossbauer study 2—1674
Sn-SiO_2 system, thermodynamics, rel. to tin extraction economics 2—1342
Sn-Zn, alloy, evaporation rate vs. temp. curve 2—28952
Sn-Zn eutectic alloy system, elastic moduli, u.s. wedge method obs. 2—39760
SnBr, u.v. absorption spectra 2—5928
SnCl, rotational analysis of visible band systems 2—31831
$SnCl_2$, matrix Raman spectra, 4.2K, Ar and N_2 matrices 2—12196
$SnCl_4$, depolarization ratios of isotope lines 2—38941
$SnCl_4$, vibratory spectra, intensities, electro-optical parameters 2—32267
SnD anomalous doublet splitting in $^2\Delta$ states 2—3063
SnF_2, monoclinic, meas. of elastic and thermoelastic consts. and thermal expansion 2—1277
SnH anomalous doublet splitting in $^2\Delta$ states 2—3063
SnH_4, analogue to ionized inert gas, mol. orbital determ. from vac. u.v. and photoelectron spectra 2—18409
SnH_4, photoelectron spectra 2—8795
SnH_3Br, microwave spectrum, molec. structure and constant determination 2—15337
SnH_3I, microwave spectrum, molec. structure and constant determination 2—15337
SnI_4, liq., mol. motion 2—15563
SnO_2:Fe^{3+}, superhyperfine interactions, ENDOR study 2—22847
SnO_2:Sb, resist., anomalous press. depend. 2—16213
SnO_2:Sb transparent conducting films on glass, surface hydrolysis of $SnCl_4$ 2—18943
SnO, SnO_2, nonstoichiometric and controlled valance n-type semicond. 2—40226
SnO, SnO_2 film, reactively sputtered, chemical aspects of oxide film formation 2—18944
α-SnO film, on Sn film substrate, morphology 2—12667
SnO_2, density of states effective mass 2—4226
SnO_2, electrotransmission spectra near fundamental threshold 2—40641
SnO_2, polycryst. semicond., prep. by precip. from soln. and props. 2—40227
SnO_2, pulverized, active centres, e.p.r., thermolum. 2—10522
SnO_2, stimulated photoluminesc. emission 2—26243
SnO_2, thermal expansion, 283-1898K 2—36358
SnO_2 layers, absorption spectra meas. in 3.1-5.2 eV region, obs. characteristic absorption 2—29921
SnS-Sb_2S_3 system, phase diagram, and intermediate cpd. props. 2—29496
SnS-Sb_2Se_3 system, phase diagram and intermediate cpd. props. 2—29497
SnS_2, layered, resist. changes due to decomp., switching effects 2—32991
$SnSO_4$, cryst. struct. 2—32472
$SnS_2(Se_2)$, electron energy band struct. 2—33001
SnSb films, vapour phase deposits, struct. 2—25211
SnSe/NaCl film-substrate system, decoration processes, elec. field effect 2—29007
SnSe/NaCl film-substrate system, decoration processes 2_29008
SnTe-GeTe, alloy, film, plasmon energy, electron energy loss spectra, electron microscope obs. 2—4143
SnTe-PbTe solid solution, thin film prep. and struct. 2—1180
SnTe, low temp. heat capacity 2—19427
SnTe, Mossbauer effect of ^{129}I isomer shift and effective charge 2—1673
SnTe, pressed powder, texture 2—1379
SnTe, supercond. transition temp. depend. on paramag. ion conc. 2—40210
p-SnTe, valence band struct., weak field magnetoresist. 2—25843
$SnWO_4$, α- and β-modifications, cryst. struct. 2—3730
Sn_xWO_3 orthorhombic bronzes, struct., X-ray and electron diffr. 2—25347
SnX_2, X=halide, electronic config. of α—Sn, Mossbauer effect method 2—4097
Ta_3Sn, type II supercond., nuclear quadrupole spin lattice relax. 2—4173
Ti-Al-Sn-Zr-Mo alloy, tensile props. rel. to microstruct. 2—39942
Ti-Al-Sn alloy, diffusion of H_2, rel. to stress corrosion cracking 2—19147
Ti-Al-Sn alloy, thermal cond., 90 to 600 K 2—19442
Zn-Sn-Cd-Bi, liquid solutions, thermodynamic properties 2—3382
Zr-Sn solid soln., substruct. strengthening 2—12953

Titanium
adsorption and reaction of Cl_2, field emission microscopy obs. 2—9307
atom, X-ray K-fluoresc. yields 2—8443
atoms, spectra Ti VI and VIII, meas. $3s^23p^k$—$3s3p^{k+1}$ transitions, determ. ground configuration intervals 2—28199

Titanium continued
band structure, self-consistent calc. 2—4126
in ceramic glazes, determ. by spectrophotometric method 2—40850
diffusion in TiO_2, rutile, rel. to high temp. compressive creep 2—29273
dispersion strengthening phases influence on plastic deform. resist. 2—9664
dynamic strain ageing, rel to impurity conc., stress strain relations, 77-1026K 2—25581
electron irrad., threshold energy for atomic displacements 2—25382
epitaxial growth on LiF and NaCl substrates 2—9272
extraction, properties and applications 2—3925
fatigue, slipless, scanning electron microscope obs. 2—36153
fatigue, use of high power ultrasonics 2—36185
fatigue mechanism at u.s. freq. 2—9696
fatigue resistance, rotating flexure test, heat treatment depend. 2—12895
film, elec. resist., resist.-temp. characts., thickness effects 2—40185
film, electrical resistivity, effects of bombardment with Ar^+ ions 2—22496
film, electron energy losses 2—6704
film, H_2 adsorption in vacuum, reaction rate detn. 2—39560
film, oxidation, in situ electron microscope obs. 2—18936
foil, N_2 adsorption at low pressure, ultrahigh vac. microbalance obs. 2—39566
getter-ion pump, with cold cathode characteristics 2—33827
heat of sublimation, mass spectrometric obs. 2—36351
in Inco 718, content change effect on precip. hardening9820 2—9820
isotopic abundances in sunspots det. from (0,0) band of TiO γ-system in umbral spectrum 2_41233
large volume titanium sublimation pump 2—20784
magnetic susceptibility, temp. depend. 2—4348
martensite transformation, shape memory effect 2—9789
nitriding by ionic bombardment, skin microstructure and corrosion resistance 2—12928
photoabsorption cross sections calcs. 2—22779
powder rolled metal, sintering 2—15926
pumping action, use in evaporation pump 2—41376
in Pyromet 860, effect on precip. 2—29394
sheet, deformation constitutional diagram in axisymmetrical forming 2—6602
shock propag. produced by planar impact 2—9637
spectral intensity increases due to presence of Na impurities in C arc 2—15524
in steel, austenitic stainless, effect on stress corrosion cracking 2—29326
in steel, cast high-speed, effect on struct. and props. 2—36176
steel, low alloy, brittle fracture tendency at low temperatures, effect of titanium additives 2—9680
sublimation, vacuum pumps 2—23195
sublimation pump, radiant heated, operating characs. 2—41388
surface, charact. electron energy loss spectra, plasma losses 2—19526
surface, soft X-ray appearance pot. spectra, effect of oxygen 2—35872
surface structure, H-ion microscopy 2—25182
thermal diffusivity, heat capacity, thermal and electrical conductivity and integral and monochromatic coeffs. or radiation blackness meas. in temp. range 1000-1700 K 2—29551
valence band structure from u.v. photoelectron spectra 2—36650
inAl film, distrib. and diffusion during Al deposition on Ti 2—12654
inAl film, distrib. and diffusion 2—12653
CdS:Ti^{3+}, e.p.r. study, 27 K 2—26275
CdTe:Ti, absorpt. spectra and crystal field parameters 2—22759
CoO:Ti, Hall mobility and defect struct., high temp. 2—36502
inFe-Al-Cr alloy, effect on oxidation resist. and mech. props. 2—29430
inNi-Cr alloy, effect of grain size and precip. on creep 2—12872
Ti/Au thin film couples, diffusion and compound formation 2—39749
Ti/Fe abundance ratio in HD92207, HD100262, HD125835, HD161912 2—7403
Ti/Pd thin film couples, diffusion and compound formation 2—39749
Ti/Pt thin film couples, diffusion and compound formation 2—39749
Ti-$TiC_{0.52}$ two-phase platelets, optical metallography, electron microfractography 2—6582
α-Ti, dislocation dynamics, activation enthalpy 2—22211
α-Ti, effect of β-stabilizer on mech. props. 2—36143
Ti, pitting and crevice corrosion, effect of anions and temperature 2—4596
Ti I, atomic g_J-values and lifetimes of z^3F- states 2—28200
Ti I excitation temp. by curve of growth in late G- and K-giants atmospheres 2—26660
Ti II lines in sunspots, velocity measurements at outer boundaries of dark filaments 2—37407
Ti XVII, carbon-like spectra in the range 16 to 22 Angstroms 2—15220
Ti XX spectrum in e.u.v. identification and classification of spectral lines 2—31666
Ti^{2+}, in CdS, $^3A_2(^3F) \to {}^3T_1(^3f)$ absorpt. band, Jahn-Teller struct. 2—10371
Ti^{2+} in CdS, e.p.r., spin echo 2—10500
Ti^{3+}, in AgBr(Cl), near i.r. absorpt., Jahn-Teller effect 2—40657
TiXI Mg I-like spectra, analysis and comparison with iso-electronic spectra of KVIII, CaIX, ScX 2—28198
Ti+Al complex additions to Ni-20wt.%Cr, effect on recrystallization 2—25573
Ti(s,β), sublimation, standard enthalpy change, Knudsen n.p. determ., mass spectrometric analysis 2—18890
VO_2:Ti, conduction band and impurity state electron lifetime, e.s.r. obs. 2—10037
VO_2:Ti, impurity conduction, microwave freq. cond. obs. 2—19655

Titanium compounds
aerospace alloy, Ti-A110AT, thermal conductivity, elec. resistivity and thermopower, 4-300K 2—25692
alloy, β-stabilized, ω phase formation kinetics 2—36288
alloy, deformation microstructure, fine subgrain struct. adjacent to fatigue cracks 2—32543
alloy, diffusion interaction with SiC abrasive under grinding and cutting conds. 2—6604
alloy, electron-beam welding to niobium alloys 2—19254
alloy, erosion rate, rel. to mech. props. 2—29339
alloy, etching behaviour, electron microscope obs. 2—32399
alloy, fracture characts. in air and seawater environment 2—36174
alloy, martensite transform., shape strains in deform. of lattices 2—29259
alloy, metastable phase decomp., volume changes 2—36308
alloy, stress corrosion cracking arrest and crack propag. 2—1329
alloy, with metastable α-phase, reverse transform. under applied tensile stresses 2—13000
alloys, ductile fracture equation 2—15878
alloys, effect of β-stabilizer on mech. props. 2—36143

Titanium compounds continued
- effect of grain structure on fatigue strength 2—6565
- goetzenite, cryst. struct. 2—9463
- rutile, crystallographic shear planes rel. to homogenous series formation in oxides 2—9549
- Ticonal, conjugation of metastable phases 2—12976
- titanate ceramics, O_2 self diffusion 2—12814
- titanates, alkali metal-rare earth, applic. of electron microscope to high temp. mats. exam. 2—9435
- titano-magnetite ores, spectral analysis in spark discharge of blast-formed disperse particles 2—4616
- trirutile, phase transformation mechanism, cation displacements 2—3999
- Al-Au, Al-Ti, vacuum u.v. spectra, comparison with sandwich structures 2—20021
- Al-Ti alloys, vac. u.v. spectra, comparison with sandwich structs. 2—20021
- Al-Ti dil. alloys, virtual bound state obs. from Al $L_{2,3}$ absorpt. spectra 2—20022
- Al_2O_3:TiO_2, MgO, point of zero of charge, doping effects 2—40828
- BN-TiB_2-Al powder, hot pressing, evaporating element prep. 2—39956
- BaO-TiO_2-Al_2O_3 system, ternary cpd. identification, X-ray anal. 2—29462
- CaO-Nb_2O_5-TiO_2-SiO , liquidus detn. in the 15% SiO_2 plane 2—9204
- Co-Ni-Ti alloy, decomposition, modulated structure 2—9467
- Co-Ti-X alloys, X=Cr, Fe, Ni, precip. of γ'-Co_3Ti 2—9797
- Co_3Ti, precipitation in Co-Ti-X alloy, X=Fe, Cr, Ni 2—9797
- Cr-Ti dilute alloys, determ. magnetic susceptibility and electrical resistivity 2—10237
- Cu-Ti alloy, supersaturated, decomp. and strengthening 2—39922
- Cu-Ti intermetallic phases, chemical bonding, X-ray absorpt. spectra 2—22763
- Fe-Ni-Cr-Ti steel, austenitic, plastic deform. rel. to σ-phase form. 2—29471
- Fe-Ti-C alloy, precip. rel. to formability and texture 2—32728
- Fe-Ti, steel, work hardened, annealed, recrystn., recovery, segregation, electron and optical microscope obs. 2—32698
- Fe-Ti alloy, stress corrosion cracking mechanism 2—6574
- Fe-Ti dilute alloy, hyperfine field at Fe atoms, temp. depend. 2—13449
- Fe-Ti oxides, rhombohedral, magnetic domain study 2—4341
- Fe-Ti oxides, rhombohedral, thermoremanence studies 2—4291
- $Fe_{36}Cr_{12}Ti_{10}$, χ-phase, dissociated anti- phase boundary 2—3791
- Mo-Ti-C alloy, deformed, subgrain growth during annealing 2—12946
- Na_2O-Fe_2O_3-TiO_2-SiO_2 glass, mag. susceptibility, temp. depend. 2—1598
- Nb-(60 at.%)Ti alloy, critical supercurrents and pinning of vortices 19584 2—19584
- Nb-Ti alloy, peak effect, rigidly pinned vortex model 2—13168
- Nb-Ti system, supercond., electronic struct., heat capacity analysis 2—40195
- Nb-50%Ti, type II supercond., crit. current density, neutron irrad. effects 2—29631
- Nb-64%Ti alloy, hard superconductor, cylindrical sample, magnetiz. and size effect 2—36460
- $Nb_{0.88}Ti_{0.12}N$ film, supercond. fluctuation rounding of resistive transition 2—13166
- Ni-Ti alloy, solidified at fast cooling rates, metastable phases 2—36305
- NiTi martensite, stacking faults 2—15768
- PbO+ZrO_2+TiO_2, high temp. reaction kinetics 2—13571
- SiC:Ti uniaxial metal matrix composite, subjected to axial and normal lateral loads 2—15851
- TIC-WC solid solution, short range order, X-ray obs. 2—9494
- Ti:O film, cermet, elec. resist., temp. and strain effects 2—40184
- Ti-(8 wt.%)Al-(1 wt.%)Mo-(1 wt.%)V alloy, sustained loud environmental crack growth 2—29330
- Ti-Al-Cr and Ti-Al-Cr-Mo alloys, strength and plasticity 2—36142
- Ti-Al-Ga, ordered phase formation, elec. microscope obs. 2—9774
- Ti-Al-Sn-Zr-Mo alloy, tensile props. rel. to microstruct. 2—39942
- Ti-Al-Sn alloy, diffusion of H_2, rel. to stress corrosion cracking 2—19147
- Ti-Al-Sn alloy, thermal cond., 90 to 600 K 2—19442
- Ti-Al-V, alloy, creep, tensile and torsional loading effects 2—19188
- Ti-Al-V, alloy, etching, O_2 effect, metallography 2—32735
- Ti-Al-V alloy, fracture toughness 2—22287
- Ti-Al, alloy, microsegregation of Al, rel. to cooling rate, comp., electron-probe analysis 2—29440
- Ti-Al alloys, mag. susceptibility, temp. depend. 2—4348
- Ti-Al alloys, mag. susceptibility, temp. depend. 2—4348
- Ti-Co, bonding and ordered state formation, X-ray spectral investigation of electronic energy spectrum 2—36920
- Ti-Co system, intermediate phases 2—40010
- Ti-Cu, alloy, electron struct., band struct. X-ray fluoresc. spectra obs. 2—16112
- Ti-Fe-Ni-Cr alloy, γ' hardened, strengthening mech., precip., γ_{apb} calcs. 2—32733
- Ti-Fe alloy, ductile-brittle transition, cold working effects 2—29307
- Ti-Fe alloy, elec. resist., magnetization, 4.2-300 K 2—22491
- Ti-Fe alloy, thermodynamic functions, activities, mass spectrometric obs. 2—36351
- β-Ti-Fe(Cr)(Mn)(Mo) alloys, isothermal phase transform. 2—12979
- Ti-H system, spin-lattice relax., electronic contrib., spin echo method 2—16405
- Ti-H system, spin echo investigation 2—16401
- Ti-M alloy, M=Cr, Mn, V, Mo, continuous cooling transform., rel. to ω phase precipitation 2—29481
- Ti-Mo-Ni system, polythermal section, microstructure, resistivity, dilatometry, X-ray analysis 2—32788
- Ti-Mo-Zr-Al, alloy, forming process behaviour, corrosion and oxidation resist. rel. to Al content 2—29411
- Ti-Mo, alloy, microsegregation, rel. to cooling rate, comp., electron probe analysis 2—29439
- Ti-Mo, bonding and ordered state formation, X-ray spectral investigation of electronic energy spectrum 2—36921
- Ti-Mo alloy, fluctuation supercond. 2—13181
- Ti-Mo alloys, supercond. T_c enhancement on mech. deform. 2—6781
- Ti-Mo alloys, supercond. transition temp., lattice instability, electron/atom ratio 2—40214
- Ti-(25 at.%)Nb alloy, omega phase formation, mechanism and kinetics, small angle X-ray scatt. 2—4006
- Ti-Nb alloy, Young's modulus temp. depend. 2—36095
- Ti-Ni, alloy, fractional determ. of TiO, TiN, TiC 2—30110
- Ti-O, interstitial mech. relax. and diffusion, internal friction obs. 2—36020
- Ti-O alloy, dil., comp. depend. of elastic const., u.s. velocity study 2—15802

Titanium compounds continued
- Ti-O system, absorpt. spectra 2—26174
- Ti-O system oxides, ionicity comp. depend. from structure factor determ. using electron diffraction 2—9348
- Ti-Pd-Au film, struct., and mech. props., ageing effects 2—39534
- Ti-Pd system, phase diagram 2—40011
- Ti-Si-C system, phase equilib., rel. to complex carbide deposition 2—25213
- Ti-Ta, alloy, film, struct., composition, rel. to sputtering conditions 2—12671
- Ti-$TiC_{0.52}$ two-phase platelets, optical metallography, electron microfractography 2—6582
- Ti-V-Al alloy, struct. and props., comp. depend. 2—36141
- Ti-V-O and Ti-V-Al-O alloys, effect of O content on mech. props. 2—36144
- Ti-V, alloy, microsegregation, rel. to cooling rate, comp., electron probe analysis 2—29439
- Ti-V alloy, struct. and props., comp. depend. 2—36141
- Ti-Zr-O alloys, phase characterisation 2—40009
- Ti-(6wt%)Al-(4wt%)V, alloy, texture analysis, colour metallography, colour anodizing technique 2—12735
- Ti-55 at.%Ni alloy, hardening, rel. to Ti_2Ni_3 precip.39903 2—39903
- Ti alloy, corrosion in hot saline water, elec. microscope obs. 2—10626
- Ti alloy, fatigue resistance, rotating flexure test, heat treatment depend. 2—12895
- Ti alloy, structural hardness, cold working and heat treatment 2—12949
- Ti alloys, heat treatment, equilibrium diagram, microstructure 2—1350
- Ti alloys, nitriding by ionic bombardment, skin microstructure and corrosion resistance 2—12928
- TiB_2/liquid steel system, destruction of TiB_2 by dissolved O_2 2—10625
- TiB_2, powder, supersonic grinding kinetics 2—15939
- TiB_2, sintered, polycryst. props. rel. to monocryst. props. 2—22254
- TiB_2, thermal expansion over temp. range 300-2500°K 2—6683
- TiB_2, ultra soft X-ray spectra 2—29943
- TiC-N alloy, sintered, wear resist. 2—9777
- TiC-NbC(ZrC), high porosity complex carbide prep. 2—39969
- TiC, diamond grinding, surface work hardening, microstructure 2—3871
- TiC, in Ni-Ti alloy, fractional determ. 2—30110
- TiC, powder, supersonic grinding kinetics 2—15939
- TiC, press forging, deformation, recrystallization, strength, fracture 2—36249
- TiC, sintered, polycryst. props. rel. to monocryst. props. 2—22254
- TiC, slip system determination by hardness anisotropy 2—9564
- TiC, stoichiometric, prep. and phys.- chem. charact. 2—22347
- TiC_x, shocked, microcrack form. and plastic deform. 2—29328
- $TiCl_4$, vibratory spectra, intensities, electro-optical parameters 2—32267
- $TiCl_6^{2-}$, force constants and mean amplitudes of vibration 2—3035
- $TiCl_nBr_{4-n}$, i.r. and Raman spectra, force constants 2—18471
- $TiCo_2$, Laves phase, polytypism, electron microscope obs. 2—19105
- $TiCr_2$, Laves phase, polytypism, electron microscope obs. 2—19105
- $TiFe_2Se_4$, mag. struct., neutron diffr., elec. cond., Mossbauer effect obs. 2—19908
- TiH_2, room temp. polymorphic transform 2—22366
- TiH_4, diffusion of H model, pulsed NMR technique 2—3813
- TiH_4 film injector by plasma cluster creation using induced discharge 2—21035
- TiH_x, plastic deform. characteristics 2—19183
- TiN, in Ni-Ti alloy, fractional determ. 2—30110
- TiN, pulsed compression, electron energy spectra 2—36532
- TiN dispersions in austenitic stainless steels to produce high creep strength 2—15932
- $Ti_2Nb_{10}O_{29}$, cryst. struct., high-resolution electron microscopy obs. 2—12734
- $Ti_2Nb_{10}O_{29}$ thin crystals, structure determ. by electron microscope image contrast technique 2—32427
- TiNi, martensite struct., rel. to premartensitic instability 2—9825
- TiNi, martensitic transform., cryst. struct. 2—13002
- TiNi, martensitic transformation, surface relief 2—6640
- TiNi, resistivity peak on thermal cycling, shape memory effect 2—29479
- TiO_2:Al, current noise measurements 2—40278
- TiO_2:Co^{2+}, rutile, ENDOR, hyperfine consts. detn. 2—26313
- TiO_2:Cr, rutile, travelling-wave maser 2—23561
- TiO_2:Fe^{3+}, photocond. spectra, Fe level 2—10141
- TiO_2:Mo^{5+}, Raman relax. time, temp. depend., theory 2—40578
- TiO_2:V^{4+}, microwave dielec. loss, low temp. 2—19748
- Ti_2O_3:V, low temp. sp. ht. anomaly, electronic origin 2—40078
- Ti_2O_3:V_2O_3, low temp. specific ht., contribution by one dimensional electron gas 2—4069
- TiO_2-CaO.Nb_2O_5-CaO.SiO_2, plane in quaternary CaO-Nb_2O_5-TiO_2-SiO_2 system, liquidus temp. determ. 2—3431
- TiO_2-Cr(Fe)TaO_4 solid solution, struct., elec. and mag. props. 2—1224
- Ti_2O_3-Cr_2O_3 solid solution, weak ferromag., 77-300K 2—19875
- TiO_2-Nb_2O_5, ceramic semiconductors, electrical properties, influence of Nb_2O_5 percentage 2—6793
- TiO_2-Nb_2O_5, high resoln. lattice imaging applic. of electron microscope to high temp. mats. exam. 2—9435
- TiO_2-SiO_2 glass, binary system, thermal expansion significance of bridging oxygens 2—16062
- TiO, $^1\Delta$ to $a^1\Delta$ transition, rotational analysis 2—31832
- TiO, cubic and monoclinic, supercond. 2—40212
- TiO, electronic struct. 2—13092
- TiO, electronic struct. 2—13093
- TiO, gaseous, dissociation energy derived from titanium-oxygen reactions studied with Knudsen effusion-mass spectrometer 2—28329
- TiO, in Ni-Ti alloy, fractional determ. 2—30110
- TiO, spectra of molecules in inert matrices at 4°K 2—24489
- TiO γ-system (0,0) band in umbral spectrum and isotopic abundances of Ti 2—41233
- TiO phases of variable composition, thermal conductivity in 100-1100°K range 2—6692
- TiO_2, ENDOR of V^{4+}, superhyperfine coupling 2—40767
- TiO_2, e.s.r. and molecular adsorption, simultaneous investigation 2—10487
- TiO_2, electrical ageing mechanism 2—36518
- TiO_2, film, gaseous anodization, elec. and optical props. 2—13301
- TiO_2, gaseous, dissociation energy derived from titanium-oxygen reactions studied with Knudsen effusion-mass spectrometer 2—28329
- TiO_2, growth by chem. transport, and stoichiometry 2—39584
- TiO_2, in m.i.s.i.m. structure, nonlinearity of capacitance 2—19729
- TiO_2, O_2 self-diffusion, ionic cond. obs. 2—19148
- TiO_2, opacified porcelain enamel, microstruct. 2—32474
- TiO_2, pressure induced polymorphism 2—15732

Titanium compounds continued

- TiO_2, reduced, electric charge transport, nonstoichiometry, defect ordering 2—29171
- TiO_2, reduced, O vacancy diffusion 2—39748
- TiO_2, reduced, point defect diffusion, contamination influence 2—29224
- TiO_2, rutile, antisymmetric suscept., Brillouin scatt. obs. 2—16423
- TiO_2, rutile, charge, discharge and optical absorpt. meas. 2—22778
- TiO_2, rutile, dielectric loss mechanism 2—22608
- TiO_2, rutile, e.s.r. of Co^{2+}, impurity-interstitial assoc. 2—16651
- TiO_2, rutile, e.s.r. of Co^{2+}, impurity- vacancy assoc. 2—16650
- TiO_2, rutile, elec. cond. 2—13240
- TiO_2, rutile, high temp. compressive creep 2—29273
- TiO_2, rutile, i.r. spectra of adsorbed HCl ·2—15678
- TiO_2, rutile, lattice dynamics, shell model 2—16013
- TiO_2, rutile, recovery of high temp. creep-resistant substruct. 2—29272
- TiO_2, rutile, X-ray spectra, mol. orbital energy level diagram 2—40707
- TiO_2, spectra of molecules in inert matrices at 4°K 2—24489
- TiO_2, surface electronic state, rel. to adsorbed p-benzoquinone molecules bonding 2—29058
- TiO_2, surface properties, i.r. study of H_2O and surface OH species 2—1197
- TiO_2, thin amorphous film, variation of dielectric constant with film thickness 2—4263
- TiO_2, tunable four photon parametric fluorescence 2—29866
- TiO_2 chemisorption probe for detection of H atoms 2—30106
- TiO_2 evaporated film, refractive index, absorptance i..r transmittance, stress, stability and structure 2—8021
- TiO_2 film, amorphous, dielec. const. freq. depend., Cole-Cole diagrams 2—40327
- TiO_2 film, sandwich, depth composition profile by ion scatt. spectroscopy 2—39454
- TiO_2 films, production by reactive evaporation in ionized gases 2—3505
- TiO_2 whiskers, growth, influence of $SiCl_4$ in vapour phase reaction 2—29051
- TiO_x, atomic vacancies influence on band struct. 2—32887
- TiO_x, elec. and mag. props., struct. characterization 2_32992
- TiO_x film, anodic, stripping from metal, a.c. procedure 2—40825
- Ti_xO_{2x-1}, system, e.p.r., mag. props. 2—36993
- Ti_xO_y film, ion implanted, cond. mechanisms 2—13111
- TiO(g), dissociation energy from vapour pressure obs. in equilibrium with Ti_2O_3(s) and Ti_3O_5(s,β) 2—37033
- Ti_3P, Knight shift, spin lattice relaxation, conduction process 2—4559
- TiPdAu-Ta_2N film, adhesion to Al_2O_3 substrate rel. to substrate surface chem. 2—39474
- TiRh(Pd)Si, cryst. chemistry 2—9349
- TiRhSi, TiPdSi, TiRuSi struct. relns. 2—18969
- TiS_2, layer-type crystal, non-polar, 2-10 eV spectra, plasmon processes 2—20005
- $TiSe_2$, layer-type crystal, non-polar, 2-10 eV spectra, plasmon processes 2—20005
- Ti_8Se_9, ordered struct. and epitaxy with Ti_3Se_4 2—22164
- $TiSi_2$, oxidation, complex surface and diffusion limited mechanism 2—13579
- $TiSi_2$, Si L-emission spectra 2—20086
- $Ti_{1-x}V(Cr)_xS_2$, prep. and characterization 2—9350
- Ti_2ZrO alloy, crystal structure of $\omega'(0)$ phase 2—39653
- U_2Ti, solid soln., neutron irradiation 2—3753
- V-Ti, V-Ti-Nb, Si/Ge alloying effects on creep and creep strength 2—1295
- V-Ti alloy, solid soln. strengthening and weakening 2—29441

Torquemeters *see Mechanical measurement*

Torsion

- *see also Elastic constants; Stress analysis*
- balance, with air bearings for obs. of mechanical props. of polymers 2—22310
- balances, factors determining quality in air and vacuum 2—27027
- bar, inhomogeneous anisotropic viscoelastic, transformations for modelling 2—123
- circumferentially grooved shafts, elastic torsion problems 2—27179
- composite material, fibre matrix adhesion, oscillation decay 2—9782
- disc bonded to dissimilar shaft 2—7741
- dynamometer for measuring small torques and axial forces during reaming 2—25558
- elastic medium, double layer, by annular punch 2—11331
- elliptic hole in cylindrical shell under torsional loading, stress analysis 2—17325
- frequency analysis, CDC 6600 computer code, application to nuclear reactors 2—5169
- hollow piecewise homogeneous beams 2—17281
- in large elastic plate fixed at one free and subject to shearing force on alter 2—17310
- magnetostrictive vibrator for u.s. applic. 2—30874
- meas. of vibrations in radio link antenna towers 2_6531
- nonlinear non-uniform torsion of thin-walled beams 2—27165
- oscillations of perfectly conducting elastic half-space 2—27219
- oscillator, long period and relaxation time 2—17289
- pendulum, oscillations, damping, magnetoelastic effects 2—149
- plasticity evaluation for thin sheet materials, method based on torsion testing 2—39878
- spring testing using general purpose recording instrument 2—25556
- steel, maraging, effect on stress corrosion cracking 2—19213
- strength of keyed and shrink-fit assemblies, comparison of torsional strengths using high tensile steel keys 2—19197
- testing machine, for hot workability study 2—39861
- thin-walled prismatic members, torsional-flexural behaviour 2—5181
- Al wires, mean shear strain, Kovacs-Nagy eqn. validity 2—9641

Total cross-sections *see under individual particles, no subheading*

Townsend coefficient *see Ionization/gases*

Transducers

- *see also Acoustic generators; Acoustic receivers; Microphones; Sound reproduction*
- acoustic coupling coefficients determined by time domain analyses 2—14270
- acoustic coupling through radiation between elements in an infinite array 2—14271
- acoustic decoupling, performance degradation of deep-ocean instruments using onionskin paper 2—14273
- acoustic elements in infinite array, radiation patterns 2—14272
- acoustic resonance matching in thin transition layers 2 37756
- acousto-optic light deflection, first order beam steering 2—5424

Transducers continued

- acoustoelectric, static field distrib. effect on mode behaviour 2—6672
- biomedical, future needs 2—14023
- capacitance, investigation of architectural acoustic, behaviour of thin plates, equivalent circuit 2—37768
- ceramic, effect of mechanical load on vibrations 2—20908
- contact type phonocardiographic transducer, problems 2—17112
- cylindrical, as optimum struct. for single acoustic beam convergence 2—9868
- design and array configuration improvements for underwater generation and reception 2—34121
- differential-transformer type pressure transducers, calculation of temperature errors 2—23228
- earphones, circumaural, artificial ear for quality control and acoustic tone obs. 2—17388
- elastic waveguide, coupling to volume waves 2—6658
- elastic waves, field reconstruction from components over single surface, transducer array 2—23350
- electret principle applic. 2—23372
- electroacoustical, complex impedance meas. in operational conditions 2—23376
- e.m., polarized shear wave testing in electrically conducting materials 2—2249
- flexural vibrating free edge plates with stepped thicknesses for generating high directional ultrasonic radiation 2—34117
- flexurally oscillating rectangular plate, analogue network 2—23373
- Hall effect, InSb, for mag. bubble domain detection 2—40445
- Hall e.m.f. for magnetic field meas. at liquid He temps. 2—234
- h.f. surface wave, fabrication by engraving 2—5240
- hollow piezoelectric ceramic sphere, vibrations 2—37738
- interdigital acoustic surface wave grid response 2—32819
- interdigital surface wave transducers, self- consistent theory 2—34123
- laser interferometer, photon-noise-limited, . for gravitational radiation antenna 2—2071
- long interdigital, distortion of central resonance, back-piezoelec. effects 2—40361
- magnetostrictive ferrite, magnetic annealing for increasing coupling constant 2—6979
- microments measuring device 2—20805
- for monitoring oscillations of circular membrane 2—17358
- particle velocity hydrophone, calibration 2—37767
- Pb(Zr.Ti)O_3, ceramic, mech. quality factor, impurity effects 2—13325
- photoelectric, for notched bar impact testing 2—121
- piezoceramic, fund. modes 2—29519
- piezoceramic, tuned, u.s. leakage detection 2—13323
- piezoelectric, as sound receiver, sensitivity det. 2—34129
- piezoelectric, effect of electrical and acoustic loading on basic characteristics 2—2248
- piezoelectric, freq. and transient response rel. to intermediate layers and matching ccts. 2—29520
- piezoelectric, mech. loaded, vibr. patterns 2—29521
- piezoelectric, review of definitions relating to conversion losses 2—5238
- piezoelectric, u.s. focussing with Gaussian vel. distrib. 2—27270
- piezoelectric ceramics, appl. in telecommunications 2—6887
- piezoelectric diffusion layer, losses due to inactive layer on working surface 2—7753
- piezoelectric field effect device, acoustic wave detection 2—20934
- piezoelectric for blood pressure meas. 2—14042
- piezoelectric thin film, efficiency and optimum thickness 2—29525
- for pressure differences in gas flow obs. 2—3294
- pressure fluctuations beneath turbulent boundary layer, in air, measured discrimination 2—15527
- quartz gauge, shock wave induced polarization 2—14356
- radiodefectoscope, microwave scanning of plastic tubing 2—2250
- resistance humidity sensing 2—13686
- rod-type resonant, geometrical designing for different resonant loads 2—23374
- Schottky barrier diode as press. transducer 2—29719
- seismic motion, response to nonharmonic input, analogue simulation 2—30187
- single crystal piezoelectric materials for surface acoustic waves 2—20933
- sound field excitation by transducer loaded on liquid wedge 2—5241
- strain gauge, fatigue testing, deform. testing 2—19229
- strain-type, solid-state microphone applic. 2—27268
- surface wave, X-cut quartz plate, impulse response calculations 2—5239
- Teflon cable applic. to strain transducers 2—25938
- temperature compensation for strain gauge transducer using active transistor circuit 2—11415
- ultrasonic, review 2—23359
- ultrasonic longitudinal energy, double mode conversion, antisymmetric Al trapezoid pair system 2—2247
- underwater, calibration at high u.s. frequencies 2—34124
- underwater line and disk, characteristics in near- to far-field transition region 2—34122
- u.s., cathodes in coaxial liq.-dielec. test cells 2—28809
- u.s., operation with different acoustical load 2—27269
- U.S. energy conc. of nonuniform amplitude distrib. 2—27267
- u.s. flowmeter, one-path, using electroacoustic feedback 2—31925
- u.s. vibr. directional convertors 2—27271
- vibration, absolute calibration, double frequency stroboscopic method 2—20912
- vibration mode convertor for u.s. power applic. 2—27272
- $Ba(Ti_{0.95}Zr_{0.05})O_3$ ceramic plates, surface wave propag. characts. 2—19408
- CdS, thin film, precip. under electron bombardment 2—4046
- CdS, wedge-shaped, for u.s surface waves 2—6660
- GaAs, interdigital pair, form. by Au deposition, Schottky barrier, surface elastic wave obs. 2—13324
- $PbNb_2O_6$-$BaNb_2O_6$ ceramic system. applic. to electromech. transducers 2—29739
- Pb(Zr,Ti)O_3 ferroceramic, electromechanical coupling coeffs. 2—13326
- Si Zener diode for high press. meas. in gaseous H_2 at 15000 atm. 2—20782
- ZnO, acoustic, r.f. diode sputtered 2—14269
- ZnO film, u.s., for longit. and shear modes, fabrication 2—29549

Transformations *see Phase transformations*

Transformations, mathematical

- Baktavatsalou operator. generalized expression 2—23231
- canonical, by computer 2—14146
- canonical, necessary and sufficient conditions 2—27034

Transformations, mathematical continued
Euler transforms, complex, single loop, analytic continuation of hypergeometric functions 2—14066
Hamiltonian by isolated fixed points, celestial mechanics 2—10814
of hypergeometric function allowing rapid convergence in free-free Gaunt factor calcs. 2—23
integral and Fourier, by fibre optics network 2—14462
Laplace, frequency response of a structure excited by transient or random forces using cross correlation 2—5170
Laplace transform inversion of rational fns., without calculation of roots 2—27037
Laplace transform. method for predicting radiation losses from laser-heated foil 2—17419
Lorentz, Bargmann-Hall-Wightman- Jost theorem, version using hyperfunctions 2—2076
numerical Fourier, for liquid state calculations 2—18788
optical fourier transformation of area-modulated spatial functions 2—2057
Patankar-Spalding, improved version for numerical solution of two-dimensional boundary layer flow 2—3167
scanning electron microscopy applic. of invariance under transformation concept 2—39615
similarity transformation of Schrodinger eqn. appl. to pseudopotential theory 2—20817
universal Noether's nature of infinitesimal transformations in Lorentz-covariant field theories 2—14504
z-transform method used to solve one dimensional wave eqn. 2—2062

Transistors *see Semiconducting devices/transistors*

Transition metal compounds
alloy, 4d h.c.p. series, spin fluctuation effects on supercond. 2—19600
alloy, dil., impurity resist. and spin fluctuation temp. 2—16146
alloy, dil., mag. susceptibility and low temp. sp. ht. 2—19827
alloy, dil., resist. minima 2—16147
alloy, dilute, with nonmag. impurity, two-band model 2—36472
alloy, disordered, spin fluctuations 2—10173
alloy, f.c.c., electronic sp. ht., interstitial carbon influence 2—16114
alloy, topologically close packed phases, band structure, elec. props. 2—35977
alloys and compounds, narrow d-band behaviour, review 2—13082
alloys with V, X-ray spectra and electron structure 2—29946
aluminides, L-emission bands, electronic struct. 2—20087
aluminium alloy films, electron energy losses 2—6704
antiferromagnetic fluorides, review of optical, neutron scattering, n.m.r. techniques for study of mixed crystals 2—40543
arsenides, struct. evolution 2—18968
arsenophosphides, struct. evolution 2—18968
bonding from multiplet splitting in X-ray photoelectron spectra 2—35291
borides, heat capacities in temp. range 1.5 to 15 K 2—22418
carbide, C self-diffusion 2—9622
carbides, high supercond. T_c obs. 2—13182
carbides, high temp. supercond. 2—29645
carbides, phonon spectra, chemical bonding, superconductivity 2—6655
carbides, phonon spectra, pseudopot. approach 2—19321
carbides, phonon spectra and electron-phonon coupling const. 2—29644
carbides, phonon spectra and supercond. 2—19388
carbides, stability, model 2—9330
carbides, struct. chemistry 2—9327
carbides, supercond. props. 2—40215
carbides, work function rel. to H surface recombination 2—29009
carboxylates, cryst. struct. 2—9513
chalcogenides, ternary, cryst. chemistry and mag. props. 2—9341
complex, two-dimensional layer system, struct., mag. props. 2—3692
complexes, aquo, spin density distrib., SCCC-DODS calcs. 2—12097
complexes, crystallizing in columnar structure, one-dimensional metallic properties from reflectance spectra 2—15681
complexes, solutions, e.s.r. spectral line exchange broadening 2—1117
complexes with PCl_3, ^{35}Cl nuclear quadrupole resonance 2—28317
complexes with phospine, P-P coupling constants 2—12098
diborides, ultra soft photoelectric and K-spectra 2—29943
dichalcogenide intercalation complex, elec. field gradient 2—19947
dichalcogenides, group IVA, band struct. 2—36417
dichalcogenides, group VIA, band struct. 2—32886
dichalcogenides, layered, supercond. 2—29643
dichalcogenides, semiempirical tight binding method for band struct. 2—32885
divalent complexes of cis chelating bidentate ligands, effect of d-orbital splitting on i.r. spectra 2—10363
energy bands, review 2—29599
group IV B octahedral haloanions, force constants and mean amplitudes 2—3035
halide complexes, effect of oxides on coloration of glass 2—36886
liquid alloy, resist., Faber-Ziman model 2—18847
metal-insulator transition 2—13241
monoborides, n.m.r. study, determ. ^{11}B nuclear electric quadrupole interaction parameters 2—16652
monoxides, electronic struct. 2—13092
monoxides, electronic struct. 2—13093
nickelides, MNi_5, sp. ht. obs., 1.6-4K 2—16037
niobates, i.r. absorpt. spectra, cryst. chem. 2—10396
nitrates, ethanol solutions, permittivity and loss factors at 28°C and 3.14 cm wavelength 2—35778
nitrides, high supercond. T_c obs. 2—13182
nitrides, high temp. supercond. 2—29645
nitrides, supercond. props. 2—40215
nitroxide radical complexes, e.p.r. and n.m.r. obs. 2—26376
nonstoichiometric, semiconductor- metal transition, magnetic and electrical properties 2—4218
oxide, band theory, Bloch and Heitler- London approach 2—13083
oxide, charge transport, interpretation of d.c. and optical props., review 2—9999
oxide, metallic transition orders very high press. 2—30729
oxides, atomic vacancies influence on band struct. 2—32887
oxides, formation of non-stoichiometric compounds, crystal chemistry 2—6394
oxides, free and bound charge carriers 2—10028
oxides, high temp. supercond. 2—29645
oxides, mixed, phase diagram 2—36533
oxides, powder, hot pressing, densification mech. props. 2—39954
paramagnetic to ferromagnetic transition region 2—33129
phonon spectra anomalies, resonances electronic polarization 2—25657

Transition metal compounds continued
phosphides, iron containing, structure, magnetic behaviour, Mossbauer obs. 2—4444
phosphides, struct. evolution 2—18968
phosphides, Ti_3P structure type, Knight shift, spin lattice relaxation, conduction process 2—4559
refractory, with high coord., valence bonding 2—9328
solid solns., supercond. transition temp., lattice instability, electron/atom ratio 2—40214
spinels, cryst. distortion, temp. depend. 2—3988
sulphides, magnetic and crystal structures 2—3722
sulphides, refractory, metal-rich, cryst. chemistry, significance of Kasper polyhedra 2—9351
sulphospinels, AB_2S_4-type, synthesis, high pressure phenomena 2—9342
superconducting transition temp., press. depend., theory 2—29624
superconductivity, BCS theory 2—29642
tetrathio and tetraselenometallates, i.r. and Raman spectra, normal coordinate analysis 2—15340
Al-transition metal alloy, localized spin fluctuations 2—19822
Al-transition metal solid solns., dil., mag. susceptibility 2—13373
Al alloy, residual resistivity 2—25764
Ni-transition metal dil. alloys, electronic sp. ht. 2—16039

Transition metals
$3d^9$ ions at tetrahedral sites, field models modification, Jahn-Teller interaction 2—7013
adatoms on W, binding energies 2—29071
atom, spin exchange splitting in Auger spectra 2—11983
atoms, one-centre quantities for semi-empirical MO calc. 2—3019
band struct., H-NFE-TB represent., basis functions and matrix elements 2—16113
band struct., renormalized atom approach 2—40145
cohesive energies and virial theorem 2—1200
cohesive prop. variations within series 2—18962
cohesive props. variation across series on d-band filling 2—22089
corrosion by liquid Na 2—37045
cubic, shear distortion interaction with nucl. spins 2—25997
density of states in conduction band, photoelectron spectroscopy obs. 2—9929
diffusion of ^3H, study using time lag methods 2—19136
dynamic spin susceptibility 2—6948
electrical resistance, high temp., deviation from linear law 2—1480
electron energy loss spectra, theory 2—6743
electron-phonon coupling constant, estimation using d-resonances rel. to superconducting transition temp. calc. 2—32931
electron-phonon coupling in tight-binding approx. 2—29591
electron-phonon interactions 2—16189
elelctron-phonon coupling matrix elements 2—29600
energy bands, review 2—29599
ferromagnetic, density of states of majority spin bands 2—40443
ferromagnetic, lifetime of resonance spin wave 2—40739
ferromagnetism, s-d hybridization 2—6955
film, amorphous, resist., annealing 2—15667
first group elements and ions, form factor calcs. 2—3595
groups IVA to VIIA, solubility of elements in groups IIIA to IB 2_22335
impurity centres in semiconductors, ground states and photoioniz. 2—19672
impurity interaction energies and d-band filling 2—1458
ion in cryst. environment, cluster model, bonding 2—18961
ions, dopant in glass, space charge limited hopping cond. 2—40239
ions, e.p.r. in BeF_2 glasses 2—10496
ions, in crysts., energy levels, intermediate coupling scheme 2—40588
ions, in crysts. effective mag. moment, derivation from cryst. elec. field 2—40587
ions, use as probes in study of interactions in solids 2—20012
lattice dynamics, electronic struct. depend. 2_32814
liquid, electronic props. 2—15564
magnetism, Hubbard model, tenfold d-electron degeneracy, para-ferromag. transition 2—36676
narrow d-band behaviour, review 2—13082
paramagnetic to ferromagnetic transition region 2—33129
phonons, modified shell model treatment 2—19347
photoemission, band struct. 2—19810
superconducting, Ettingshausen effect in mixed state 2—36474
superconducting, high T_c systematics 2—16188
superconducting, Kohn anomaly in transition temp. 2—19492
superconducting pair states in Wannier represent. 2—22510
superconducting relation of anomalies in phonon dispersion curves to acoustical plasmons 2—25771
superconducting T_c, grain size effect 2—19599
superconducting transition temp., energy band considerations 2—32953
superconducting transition temp., press. depend., theory 2—29624
superconducting transition temp., press. depend. 2—29625
superconducting transition temp. order of magnitude 2—19491
superconductivity, BCS theory 2—29642
superconductivity, conf., Rochester, USA, Oct. 1971 2—29632
superconductivity, i.r. props. electron-phonon coupling 2—29646
superconductivity, role of s-and d-band electrons 2—36455
superconductor, dirty, Hall effect near upper critical field 2—40213
superconductors, exptl. survey 2—29641
surface studies, combined Auger and charact. loss spectra obs. 2—3484
X-ray emission spectra in the supersoft band 2—29941
X-ray L-absorpt. of ^{72}Hf to ^{79}Au, white line obs. 2—16600
X-ray spectra, absorpt. in X-u.v. range 2—1702
X-ray spectra, influence of conduction electron excitation 2—36910

Transmission
coefficients, random medium 2—38
e.m. waves, ionosphere E_s region, numerical calc. of coeff. 2—4723
i.r., metal cryostat for obs. 2—41372
Lorentz absorption lines, new analysis procedures 2—8030
SH-waves, propagation in linear viscoelastic solids 2—26429
thermal radiation props. of solids 2—19474

acoustic waves
see also Acoustic wave propagation
air bubbles in water, coherence of sound 2—17384
cylinder walls, resonant sound transmission using statistical considerations 2—2241
dilute polyatomic gases, sound propagation from point of view of Waldmann-Snider eqn. 2—39286
double leaf wall, low frequency approximation 2—27251
duct walls of cylindrical pipe, internally propagated mode obs.' 2—34107

Transmission continued
acoustic waves continued
through elastic shell, h.f. asymptotic behaviour of sound field generated 2—5220
fish tag, transmitter-receiver 2—5248
glass, sheet, acoustic insulation 2—29522
Lamb waves in atmosphere, apparent violation of conservation of energy 2—37122
layer with space dependent velocity 2—14259
loss, rel. to normalized impact sound level 2—7759
noise, through thin walled spherical shell, ratio of sound pressures inside and out 2—27287
ocean, sound field analysis 2—30254
seawater, shallow, multiple frequency studies of fluctuations 2—1804
shock wave, at boundary, wave form 2—27257
sound insulation of heavy wall, brick wall experiment 2—17402
sound transmission loss, measurement by combining correlation and Fourier techniques 2—34115
through statistically rough plane interface between dissimilar fluids, Helmholtz-Kirchhoff theory 2—34109
vacuum sound barrier, normal incidence transmission loss, simple double panel 2—17404
vegetation, rel. to leaf area density, leaf width, breadth and canopy 2—14280
viscoelastic plate transparency 2—30864
vocal tract, parametric represent. of transfer function 2—30688
waveguide, reson. reflectors 2—27256
wavevector filters for press. field induced on surface by turbulent layer 2—23379
LiF, acoustic emission, correl. with dislocation motion 2—4044
NaCl, acoustic emission, correl. with dislocation motion 2—4044
Zn, acoustic emission, correl. with dislocation motion 2—4044
acoustic waves, ultrasonic
liquid steel, measurement of ultrasonic attenuation during cooling 2—32685
optical sensor, noncontacting 2—34528
anisotropic stress determination by ultrasound method 2—37761
vibration directional convertors 2—27271
electromagnetic waves *see Electromagnetic wave propagation*
light
see also Absorption/light; Filters, optical
alkaline earth metal film, optical consts. detn. 2—20017
alumina, high density, i.r. meas. rel. to mat. characts. 2—33204
atmosphere transmittance determination from sky brightness distribution 2—30295
atmospheric propagation, obs. by laser-radar techniques 2—16841
atmospheric transmission of optical waves, statistics of optical intensity fluctuations 2—27590
beryl, spectra measured in the i.r. with polarized light 2—10365
bimagnetic rotation of colloidal graphite, measurement of magnetic fields 2—7996
circumsolar radiation calculated as function of aerosol type, field of view, wavelength and optical depth 2—4683
clouds, visible light scattering, angular transmittance 2—22967
critical opalescence, height asymmetry 2—7989
datolite, spectra measured in the i.r. with polarized light 2—10365
density-log exposure curve and MTF curve from optical path variation of sinusoidally exposed images for bleached photographic materials 2—14493
deposited films, equilibrium point method for monitoring optical thicknesses 2—34470
discharge lamps, coolant liquid spectral characteristics 2—14469
fibre collector and channel transmission capacity 2—38107
fibre optics elements, contrast transmission coeff., main groups of factors in determination 2—17716
film, double layer formulae, rel. to optical consts. determ. 2—33202
film, normal incidence, optical consts. determ. 2—33203
gases, i.r., accurate formula 2—15539
incoherent, between Ronchi grids, det. of small angular changes 2—34465
inhomogeneity and surface roughness effects 2—22743
InSb:Te at 10.6 μ 2—29873
integrating sphere at diffused illumination, general theory for measurement of 2—27589
i.r., coeffs. for multigrid interference filters 2—17718
i.r., cryostat with pneumatic device, semiconductor specimens 2—20778
for i.r. external transmittance of Kel-F, Teflon, Ge, Millipore filters, Kodak Wratten filter 2—4430
laser beams in absorbing medium, effect of photochemical reaction 2—20196
light source shutter, with magnetic control of transmission 2—38088
liquid-vapour critical point 2—22038
loss meas. for liquid core, hollow glass fibre clad waveguides 2—38123
losses in liquid core quartz fibre 2—31120
metals, thin films, reflectance and transmittance from oblique incidence measurements 2—31088
mica, vacuum u.v. props. 2—40648
microcrystals, obs. at low temps. using casting resin 2—4429
mode dispersion in low loss multimode fibres meas. 2—38125
nematic liq. cryst., cholesteric additives effect 2—12540
nonlinear filters, broadening of laser radiation spectrum due to increase in transmission 2—27530
optical waveguide, transmission bandwidth, calc. 2—34461
plasma, nonequilibrium inhomogeneous 2—28565
polarized, by imbedded optical films 2—7974
polarized, determination of optical constants of partially transmitting sample 2—23708
polyacrylonitrile, evaporated film, band structure 2—29650
polyethylene terephthalate, film, transmittance meas., i.r. data 2—40604
polyimide film, transmittance meas., i.r. data 2—40604
rectangular multimode waveguide of visible coherent light images 2—27584
resonant interaction between ultrashort coherent light pulse and semiconductor 2—38051
rough interface, generation and development of straight regular beam, cooperative effects 2—17680
scattering absorbing medium, optical properties det. from transmittance 2—4420
screen, diffusing, with small angle light scatt. 2—320
self focusing medium, wave field struct. near foci 2—11503
selfoc fibres 2—8011

Transmission continued
light continued
semiconductor, layered inhomogeneous structures, transmission and reflection spectra, layer thickness detn. 2—40643
semiconductor glass filter, nonlinear radioscopy 2—22757
solarisation of glass transmitting u.v. light 2—11525
spectral transmissivity of real gas, exponential model 2—21921
spherical scatterers, dependence of extinction efficiency on photometer geometry 2—14456
sputtered glass waveguides losses 2—38115
stacked glass plates, calibration of spectrophotometer for specular light 2—17734
surfactant+additive+water systems 2—9095
suspensions of absorbing spheroids, electrooptic properties 2—9186
topaz, spectra measured in the i.r. with polarized light 2—10365
transparent condensed media, surface wave excitation 2—21943
turbulent atmosphere, 2/3 law for spherical wave propagation 2—33480
at uniaxial crystal and isotropic medium boundary 2—1660
vector representation 2—34467
vortices in liquids, visualization using Al powder 2—28759
zoisite, spectra measured in the i.r. with polarized light 2—10365
Ag and Ag alloy films, 2.4 to 4.4 eV, optical consts. detn. 2—22749
AgCl antireflection coating for Si, 2.5-50μm region 2—8012
Al, thermomodulation spectra interpret. 2—36855
Au, thermomodulation spectra interpret. 2—36855
Au and Au alloy films, 2.4 to 4.4 eV, optical consts. detn. 2—22749
Au black, theory at i.r. optical properties 2—26111
Au film, laser modification of transmittance 2—36813
Au thin films, 0.3-1 μ, optical constants determ. from reflection and transmission meas. 2—29871
CO_2, i.r. 2—5925
$Cd_3(As_xP_{1-x})_2$ alloys, optical transmission edge, temp. depend. 2—10336
$CdCr_2S_4$, hot pressed polycryst., near i.r. at liq. N_2 temp., rel. to magneto-optic applic. 2—19970
$CdIn_2Se_4$, spectra, band gap determ. 2—20031
CdS, modulation by acoustoelec. domains 2—7062
Cl_2, anomalous transparency in bound-free transitions, pure Cl_2 and Cl_2-He and Cl_2-Ar mixtures considered 2—18414
CsI antireflection coating for Si, 2.5-50μm region 2—8012
Cu, thermomodulation spectra interpret. 2—36855
Cu film, partially oxidised, rel. to parallel layer oxidation model 2—40812
$CuCl_2.2H_2O$, at elevated temps., passband characteristics 2—31145
Cu_2O, powder, i.r. region, optical phonons 2—36878
$FeCO_3$, far-i.r. spectra, Neel pt. phenomena 2—40638
GaP(Zn, O), rel. to impurity absorpt. and excitation processes 2—22797
$HgCr_2Se_4$, semicond. spinel, i.r. spectra, lattice vibrations 2—19374
$KClO_3$,$KBrO_3$ polycrystalline film, i.r. transmission 2—9278
KI, far-i.r. consts. and phonon freqs. 2—1681
KI, i.r. transmission spectra, multiphonon absorpt. bands 2—36883
LiF-O_2 fliter for Lyman-α radiation from electron impact on H_2 2—23728
α-$LiIO_3$, optical inhomogeneity, rel. to growth conditions 2—22724
MgF_2, extreme u.v. spectra, extinction coeffs. 2—33242
MgO, extreme u.v. spectra, extinction coeffs. 2—33242
N_2O i.r. 2—5925
NaCl, elec. field influence 2—1695
$NaClO_3$, $NaBrO_3$ polycrystalline film, i.r. transmission 2—9278
NaI, i.r. transmission spectra, multiphonon absorpt. bands 2—36883
Rb thin films, meas. as a function of thickness for polarised monochromatic radiation in 3000-6000Å range 2—16472
Si, plasma, optical transmission, absorpt. cross-section, recombination behaviour 2—29876
SiO_2, SiO_xN_y evaporated films, i.r. 2—8021
SrO powder, far-i.r. surface-activated band-mode absorpt. 2—7074
Ta_2O_5 films, rel. between thermal oxidation temp. and optical propagation 2—40608
Te films, obliquely deposited transmittance determ. for 2-25 μ radiation, electromag. treatment of passage through succession of thin films 2—19963
TiO_2 evaporated film, i.r. 2—8021
TlCl, TlBr antireflection coating for Si, 2.5-50μm region 2—8012
ZnS, thick epitaxial layer 2—9290
ZnSe, thick epitaxial layer 2—9290

Transmission lines, r.f. *see Electromagnetic wave propagation/guided waves*

Transparency
see also Optical constants; Transmission/light
cholesteric esters, spectrophotometric meas., solid to isotrope liq. phase 2—9132
molecular gas, induced due to electronic vibrational transitions 2—743
optical filters, interference, effect of thermal treatment on the position of maximum 2—38132
ruby:Cr^{3+}, area theorem of self-induced transparency, photon echo applic. 2—7031
semi-transparent materials, solidification by conduction and radiation 2—6282
snow rel. to density and air permeability in natural snow cover 2—16831
superconductor thick film, e.m. wave transparency 2—13144
viscoelastic plate, to sound 2—30864
BCl_3, CO_2 laser beam propag., self-induced transparency 2—5911
$CaCO_3$, electrolysis and cryst. effects 2—33255
Cl_2, anomalous transparency in bound-free transitions, pure Cl_2 and Cl_2-He and Cl_2-Ar mixtures considered 2—18414
CuBr characterization 2—39581
$Cu_{0.88}Ga_{1.04}S_2$, to beyond 10μ 2—9364
$CuInS_2$, to beyond 10μ 2—9364
PbTe film, deposition parameter effects rel. to i.v. multilayer filters 2—40602
SF_6, effect of resonant collisions on a self-induced transparency pulse 2—35383

Transport processes
see also Boltzmann equation; Diffusion; Kinetic theory; Liquids/theory; Mass transfer; Radiative transfer; Solids/theory; Statistical mechanics
alkali, metal monatomic vapours, transport coeffs, and interaction potential calc. 2—28743
atmosphere, vertical, of mean zonal kinetic energy in northern hemisphere 2—13688
binary liquids, near critical point, review of exptl. situation 2—9042
binary rigid sphere mixture, Thorne's eqns. 2—7725
biomedical model of active transport 2—41284

Transport processes continued
- boundary layers with suction or injection, turbulent transport processes modelling 2—28709
- coefficients for system of particles interacting with nonadditive intermolecular forces, statistical mechanics 2—30816
- condensation phenomenon near limit of inifinite dilution based on Poisson-Boltzmann eqn. 2—9101
- cosmic rays in random magnetic fields 2—4780
- dilute gases, contribution of orientational polarizations, collisionally uncoupled model 2—21923
- dilute gases, contribution of orientational polarizations in collisionally uncoupled model 2—21924
- electrolyte solutions, theory of Onsager coeffs. l_{ij} and R_{ij} 2—6219
- equations in transfer coordinates 2—7722
- extrapolation distance calc. for one-group transport with anisotropic scattering 2—23308
- fluid, Boltzmann eqn., boundary layer type soln. by Chapman-Enskog method 2—31918
- Fokker Planck coeffs. describing evolution of electron energy distrib. 2—17269
- Fokker Planck eqn., Cartesian tensor scalar product expansion 2—37660
- Fokker-Planck and random walk models, interrelation, with application to Coulomb interactions 2—37659
- Fokker-Planck equation applied to Brownian motion theory 2—23292
- Fokker-Planck equation in detailed balance, solutions 2—27109
- Fokker-Planck equations, generalization for a region containing moving boundary 2—37661
- Fokker-Planck model for determ. structure of strong shock waves in monatomic gas 2—28726
- friction coefficient formalism in statistical mechanics of transport processes 2—30806
- gas, binary, disparate mass, boltzmann eqn. soln. method 2—18754
- gas, coeffs. calc. by Enskog method, relativistic extension 2—9027
- gas, dil., coeffs. calc. using Boltzmann eqn. iterative soln. 2—18753
- gas dynamics, generalized master eqn., unimolecular decay and scattered field 2—24973
- gas in capillaries and porous solids, self diffusion and flow 2—18726
- gases, dilute diatomic, derivation of master eqn. for vibrational relaxation 2—9024
- gases, near critical point, review of exptl. situation 2—9042
- gravitational particles, stochastic theory 2—17272
- Green function theory, general kinetic equations 2—7724
- Gyarmati theorem and variational principle 2—14141
- hard-sphere test particle, correlation functions, molec. dynamic technique 2—7723
- heats of transport of low pressure gas flow through steel capillaries 2—18731
- ionized gases, determ. of dispersive transport coefficients 2—1038
- ionosphere, sporadic E-region, enhancement of the ion density by gravity waves 2—4740
- ions across biological membrane, electric field and impedance problems 2—11198
- Liouville equation, approximate solutions and truncation scheme for distribution functions 2—14142
- liquid, atomic transport coeff., rel. to neutron scatt. function 2—3360
- liquid surface, non-Ohmic electron transport 2—12574
- lower thermosphere, minor neutral constituents transport and photochemistry 2—33450
- master eqn. s-dimensional, time dependent Green's function 2—27076
- master eqns. derivation. from eqns. of motion of open systems 2—20858
- master equation, expansion for one-dimensional random walks 2—33934
- master equation for dissociation of dilute diatomic gas 2—30038
- master equation for intramolecular relaxation derived using projection operator techniques in Liouville space 2—33933
- Master equation for open systems, interference of coherent and incoherent interactions 2—27078
- master equations, asymptotic, equivalence of Balescu and Zwanzig equations 2—2149
- master equations with canonical invariance 2—11274
- memory function assoc. with phase space correlation function, classical derivatives 2—20880
- mesosphere, minor neutral constituents transport and photochemistry 2—33450
- mesospheric models, slantwise convection 2—7285
- metal, liquid, transport props., viscosity and self-diffusivity data 2—28807
- migration kinetics, solid-liquid interfaces, camphene and salol systems 2—3486
- molecular fluids, point-dipole and -quadrupole, collective motions, method of redundant variables 2—27096
- multigroup transport equation, degenerate kernel 2—21460
- nonlinear polyatomic molecules, rigid models, tetrahedral symmetry, classical collision integrals 2—35687
- nonlinear transport coefficients, general theory 2—11315
- order-of-scattering theory 2—37663
- particle, in spherical media with central black cavity 2—11314
- perfluorocyclobutene and perfluorobutene, electron transport, attachment and ioniz. coeffs. 2—35588
- in periodic media, numerical solution to matrix case 2—37662
- Poisson Boltzmann equation near limit of infinite dilution, upper bounds on solutions 2—9114
- polyatomic gases, resonant transport props. in oscillating mag fields 2—9040
- quantum coefficients and response functions, density expansion 2—33960
- quantum coefficients and response functions, logarithmic term in density expansion 2—33961
- quantum mechanical transport eqn. for atomic systems 2—20879
- radiating gas stream, limiting conditions of motion 2—35681
- radiation, relation between transfer matrix method and Case's method 2—109
- seawater, turbulent thermohaline convection, upper bound 2—10712
- in stars, contribution of longitudinal plasma waves 2—7411
- stochastic master equations, perturbative approach 2—20856
- thermal transport coeffs. calc. of self-diffusion coeff. using high temperature perturbation theory in Kubs-Green method shown to be invalid 2—30826
- thermal transport properties, thermal transpiration meas. dusty gas eqn. 2—32174
- transport equation, applic. of Noether's theorem 2—21461
- turbulence, isotropic, local energy transport eqn. 2—2181
- turbulent transfer in velocity space, analogy with plasma collisional transport in real space 2—15449

Transport processes continued
- two-group transport equation with a separable kernel 2—110
- van der Waals fluid, three-dimensional transport properties 2—31894
- water, bond lattice model 2—21954
- Ar arc, high pressure, radiation transport mechanism and transport properties 2—3275
- He, solid, charge-carrier mobilities 2—39411
- He superfluid, construction of theory in agreement with hydrodynamics, determ. transport coeffs. in collision-time model 2—25133
- NO, Senftleben-Beenakker effects and thermomag. torque in varying fields 2—9041
- Na in liver fragments, rate constants, kinetic basis of computer simulation 2—41281
- SiO_2 thermally grown, conduction mechanisms 2—10034

Transport theory, neutron *see Neutron transport theory*

Trapped free radicals *see Free radicals*

Traps *see Crystal electron states/impurity states and effects; Crystal imperfections; Semiconductors*

Travelling wave tubes *see Electron tubes*

Triboelectric emission *see Electron emission*

Triboelectricity
- No entries

Triboluminescence *see Luminescence*

Trions (^{3}He, ^{3}H) *see Helium-3; Tritons*

Triple point *see Critical constants, thermal*

Tritium
- detection, determination of efficiency of NTB nuclear track emulsions 2—5603
- detection, liquid scintillation emulsions, using electrolytic enrichment 2—38366
- in biological tissues, radioassay by modified plastic bag combustion technique 2—14040
- induced radioactivity in ground water system near proposed 300 GeV accelerator 2—5622
- ioization chamber for high conc. obs. 2—31360
- nuclear reactor effluent, monitoring problems and possibilities 2—11918
- scintillation counter, calibration and efficiency det. 2—34791
- target for 14 MeV neutron source 2—24065
- target for neutron production for therapy and activation analysis 2—34755
- thermal release from cryogenic surfaces 2—1193
- D-T, laser channelled gas embedded z pinch, theoretical estimate of structure 2—18646
- ^{2}H-^{3}H and ^{2}H-^{3}He mirror reactors, multi-species Fokker-Planck calculations 2—28579
- ^{2}H-^{3}H plasma, combined cumulation and laser heating average value model description for cylindrical wave 2—24652
- ^{2}H-^{3}H plasma, nuclear microfusion during laser heating process, methods for raising the energy recovery 2—24653
- ^{3}H-^{2}H fusion, laser triggered, maximum energy release calc. 2—6077

Tritium compounds *see Hydrogen compounds*

Tritons
- *see also Nuclear reactions and scattering due to/tritons*
- binding energy sensitivity to off-shell behaviour of the 2 body T-matrix 2—38472
- production with hypernucleus by K^- reaction at 1.5 GeV/c studied 2—38621
- Schrodinger wave eqn. for 3 nucleon system 2—38470

interactions
- No entries

scattering
- No entries

Troposphere *see Atmosphere*

Tungsten
- (112) crystal planes, diffraction of He atoms 2—6406
- acoustic cyclotron resonance, Doppler-shifted, Fermi surface obs. 2—22478
- adsorbed hydrogen, RHEED obs. of superstructure 2—29073
- with adsorbed layers of Nd and Yb, elec. field effect on coverage 2—9314
- adsorption and displacement of methane, H_2 and O_2 on (111) surface 2—25235
- adsorption of CO and NO-H_2 mixtures 2—32396
- adsorption of H_2, saturated state, FEM patterns 2—25236
- adsorption of hydrogen, kinetic isotope effect 2—12688
- adsorption of methane, flash desorption and work function study 2—12687
- adsorption of N_2, sticking probabilities, surface coverage, molecular beam technique 2—25234
- adsorption of O_2, LEED and Auger spectroscopy 2—35926
- adsorption of O_2, sticking coeffs., electron desorpt. 2—35925
- adsorption structure of CO, N_2, O_2 and H_2 obs. 2—6375
- atomic oscillator, collisions with He, semiclassical calc. of transition probabilities 2—8500
- b.c.c., point defect prod. on irrad., recovery 2—15745
- binding energies of transition metal adatoms on different cryst. planes 2—29071
- cathode, field electron currents numerical treatment 2—37919
- cathode, thoriated, erosion in N_2 2—24757
- in cemented carbides, X-ray analysis in scanning electron microscopes 2—4620
- channelling of low-energy alkali ions 2—36391
- chemical deposition, reactions in high temp. region of W-Cl system 2—25214
- chemisorption, O_2 and CO_2 contiguous layer prep. 2—30062
- chemisorption of H, surface short range interaction investigated 2—7175
- chemisorption of hydrocarbons, surface potential, field emission 2—25972
- composite, heat resist. alloy coated, creep rupture strength 2—12885
- crystal etching, dislocation pits, light figures 2—12765
- crystal growth, thermal dissociation method 2—32402
- dechannelling of MeV protons, 77-873K 2—36392
- dechannelling of protons, channelled fraction rel. to penetration depth calcs. 2—36389
- deformed, domain size, X-ray diffr. broadening shape analysis 2—3689
- desorption of H_2 and CO by electron and photon impact, primary excitation process 2—39567
- diffusion, of ^{14}C, carbide layer source, temp. range 1500-1800°C 2—9629
- diffusion, of Si, in field emission microscope 2—12816
- diffusion of U, rate and temp. meas. 2—12795

Tungsten continued
direct conversion, diffusion behavior of tungsten layers on molybdenum emitters, thermionic reactor 2—14363
dislocation interaction with C atoms, tensile tests, internal friction meas. 2—29184
dispersion hardening by ZrO_2 ThO_2, HfO_2 2—32747
dispersion strengthening, by chemical covapour deposition of W and HfN 2—22351
electrical cond., high field obs. 2—13060
electrical resist., 1100 to 2500 K 2—19552
electron emission, secondary, coeff for metastable atoms, meas. by gas cell method 2—6932
emissivity meas., 1200-2400K 2—4083
emitter surface, Cs- or Ba-covered, work function calc. 2—19794
emitter tip, thermal dissociation of methane, field emission microscopy 2—30059
extraction, properties and applications 2—3925
fast io dechannelling, theory and expt. 2—40099
Fermi surface, radiofrequency size effect 2—22497
fibre reinforced composite, W/Cu, dislocation distrib. 2—15946
field emission, effect of Au single crystal growth 2—9271
field emission from monocrystals, nanosecond region, patterns in prebreakdown stage 2—4320
field emission source prod. by oxygen-enhanced thermal- field shaping method 2—30994
field emitter, remoulding of the [031] tip 2—36624
field ion microscopy, anomalous images, 78 K 2—25184
field ionization characts. of individual atomic planes 2—3503
film, chemical vapour-deposition, FIM study 2—22073
film, Hall effect, H_2 chemisorpt. effects 2—40186
film, oxidation, in situ electron microscope obs. 2—18936
film, reactively sputtered, influence of surface adsorp. characts. 2—22068
films, sputtered from hot pressed targets, contamination levels 2—32383
fine wire, glow discharge deposition of B, Zr, graphite 2—3525
flash desorption of H_2 from (211) 2—6389
foil, ion irradiated, black-white contrast figures from small disloc. loops 2—32528
grain boundaries, atomic struct., FIM study 2—12736
heat capacity, elec. resistivity and thermal radiation props., 2000 to 3600K 2—25682
ion irrad., atom displacement energy, surface damage 2—29010
ion irradiated, defect struct., field ion microscope obs. 2—9528
K-radiation in target, attenuation of X-radiation 2—376
lamp, with halogens, thermochem. calcs. 2—13574
lattice dynamics, frequency/wave vector dispersion relations for normal modes of vibration 2—22384
LEED, inelastic energy losses, plasmons 2—25186
magnetoresistance, anomalous longit. 2—13108
Mossbauer effect, temp. variation of recoilless fraction and thermal shift for ^{183}W 2—36327
as neutron flux monitor, thermal, at v. high temps. 2—8239
neutron irrad. under stress., induced growth 2—32492
neutron radiation damage annealing, electron microscopy 2—9758
optical coating, characterization in 500-2000 Å region, extreme u.v. reflectance spectrum 2—17719
orientated bicrystal, intergranular fragility 2—12896
penetration and backscattering of Kr^+, computer simulation 2—29581
photoemission, band struct. 2—19810
photoemission obs. of surface states, u.v. region 2—22657
photon induced desorption of residual gas by synchrotron radiation 2—6387
powder, supersonic grinding kinetics 2—15939
radiation damage by low energy Ar ions, field ion microscopy investigation 2—39676
rolling workability in single crystals with (110)[001] and (001)[110] orientations 2—3451
scattering of He atoms at (112) surface 2—6334
self-diffusion, 1935-2500°C 2—36086
single crystal substrate, for epitaxial growth, prep. by electropolishing 2—25183
sintered, thermal expansion, cooperative measurement using pushrod dilatometers 2—16045
sintering kinetics of Ni activated W 2—6625
slip initiation and microdynamics 2—3885
solid, angular distribution of backscattered inelastic electrons in X-ray spectral microanalysis 3-30 keV 2—26384
solid surface energy accommodation coeff. of He calc. using simple model of surface 2—28994
specific heat, temp. modulation method 2—4070
specific heat, temperatue coefficient, direct measurement 2—25683
sputtering, 150 keV ion bombardment, cluster yield 2—40112
in steel, austenitic, interaction with C 2—32787
surface, cleaning, gas adsorption, LEED and Auger electron spectra obs. 2—29011
surface, electron reflection, 1-10 eV, LEED 2—25185
surface adatoms, ionization by electron impact 2—29072
surface electromigration of adsorbed Ce layer 2—6388
surface ionization of fast K atoms 2—13364
surface microstruct., scanning electron microscope obs. 2—39464
surface migration of adsorbed Y atoms, elec. field effect 2—9313
surface scattering of inert gases and deuterium 2—25176
thermal cond., lattice contrib. 2—13060
thermal desorption of N, kinetics 2—29056
thermal diffusivity, 20 to 2000°C 2—19462
thermionic cathode anomalously high emission in arc discharge in inert gas media 2—28676
thermionic emission, temp. depend., effect of adsorbed Li atoms 2—19798
thermophysical props., 2800K 2—19470
tip, exploding emission accompanying transition from field emission to vacuum breakdown 2—4321
two dimensional crystal, growth and surface migration on W 2—18947
vacancy formation, and clustering, quenching and elec. beam irrad. 2—3764
vortex plate, cracking in gas combustion metallography 2—32641
wire, annealed, internal cavities in fibre boundaries 2—9582
work function of alkaline earth metal adsorbed, cryst. 2—6916
work hardening, effect of deformation degree and temp. 2—9746
Ba adsorption, optimal coverage 2—3557
CaF_2-BaF_2 eutectic-impregnated, friction and wear obs. 2—12917
with Cs absorbing layer, ellipsometry 2—15670

Tungsten continued
H isosteric heat of adsorption, improved determ. 2—6376
Na^+ scattering peculiarities of secondary emission 2—36652
Ta/W shadow casting, applic. to Au on NaCl nucleation and growth obs. 2—39495
W:B, channelling, interstitial impurity location technique 2—36051
W/Br lamps, direction of chem. W transport 2—40797
W/Ge coated, field emission, adsorbed layer thickness depend. 2—19796
W-Br_2(Cl_2)(F_2)(I_2), gas phase equilibr., simulation 2—20181
W-Mo thermocouple, calibration curve in 0-2000°C temp. range 2—17455
W-O_2 system, gas phase constitution and chemical transport reactions, thermodynamic aspects 2—30057
W-Re thermocouple, for oxidizing media at v. high temps. 2—27336
W-ZrB_2, powder mixture, sintering, solid solution formation, phases 2—6626
W-ZrC composite with covering of vacuum deposite W, rate of evaporation from open surface 2—32748
W, black body radiators, calculated with new valves of Planck's radiation constants 2—14283
W halogen systems, free formation enthalpy of W halides 2—30055
W halogen systems, gas phase constitution and chemical transport reactions, thermodynamic aspects 2—30056
W implanted in single crystals, γ spectra obs. electric quadrupole perturbations 2—7026
W surface, ion emission intermittent enhancement using field-ion microscope 2—13362
W^{5+}, e.p.r. in Cs_2ZrCl_6, 4.2-77 K 2—4539
W(100) surface, LEED patterns, influence of O_2 adsorption on scattered electron intensity distribution 2—25175

Tungsten compounds
alloy, for incandescent lamp filaments 2—39914
oxide bronzes, single cryst. prod. by potentiostatic deposition 2—19007
tungstates, normal I-VI spinels, i.r. spectrum, vibrational assignment 2—10382
tungstates, trivalent metal, struct. and phase relns. 2—9340
Al-W alloy, rapidly quenched from the melt, phase transformations 2—25617
Co-W, alloy, liquid state, density meas. 2—3374
Co-W, supersaturated solid solution, decomposition, thermomagnetic obs. 2—3986
Cr-W alloy, Seebeck coeff. rel. to para-antiferromag. transition 2—13415
Cr-W system, grain boundary diffusion and interface reaction, Kirkendall effect 2—22246
Fe-W-O system, phase equilib. and thermodynamics 2—40008
Fe-W alloy, magnetic field at W nuclei, from obs. of Larmor precession of first 2+ states 2—40594
Fe-W dilute alloy, hyperfine field at Fe atoms, temp. depend. 2—16436
(Fe,Mn)WO_4, natural crystals, magnetic anisotropy and susceptibility meas. between 10 and 700K 2—6945
Mo-W-O system, ternary phase formation 2—22378
Nb-W system, phase diagram 2—39968
Ni-Al-W-Mo-Co alloy, dispersion-hardened, thermomechanical treatment 2—9733
Ni-Fe-W system, atom ordering 2—39650
Pd-W, system, X-ray diffraction study of phase diagram below 1100C 2—4022
Sn_xWO_3 orthorhombic bronzes, struct., X-ray and electron diffr. 2—25347
Ta/10W alloy, thermal expansion, cooperative measurement using pushrod dilatometers 2—16045
W-Cr alloy, resonant mode, electron-phonon interaction and exchange enhanced scatt. effects 2—40127
W-Mn-C system, phase equilib., X-ray study 2—13013
W-O system, absorpt. spectra 2—26174
W-Os alloy, work function of (111) and (100) faces, temp. depend. 2—19793
α-W-Pd, alloy, homogeneous mag. behaviour 2—6939
W-Re, alloy, thermocouple, reactor rad. influence on thermo-e.m.f. 2—16305
W-Re, physical properties, thermocouple 2—1290
W-Re alloy, annealed, plastic deformation, electronic struct., positron annihilation 2—22483
W-Re alloy, diffusion of ^{14}C, carbide layer source, temp. range 1500-1800°C 2—9629
W-Re alloy, elec. resist. and Hall effect, conc. depend. 2—36447
W-Re alloys, electrical resistivity 1200 to 2800°K 2—13114
W-Re alloys, self-diffusion, 1935-2500°C 2—36086
W-Re solid solution, Hall coeff. and resist., rel. to struct. 2—39944
W-V, alloy, dilate, mag. susceptibility, Knight shift 2—19836
W complex tetrachloro(trichloroacetonitrile)pentachloroethylnitrido- tungsten(VI), crystal structure 2—12737
WAs_2, supercond. props. 2—32927
WC/Co two-phase material, elastic consts. determ., finite element method 2—39762
WC-Co, cemented carbide, compressive deformation, microstruct. and mech. props. obs. 2—39791
WC-Co, hard alloy cermet, Co melt redistribution process 2—32736
WC-Co alloy, slip lines, deform. mech., electron microscope obs. 2—32531
WC-TiC solid solution, short range order, X-ray obs. 2—9494
WC, Co bonded, fracture energy 2—1323
WC, deform. characts., rel. to chem. bonding, X-ray line broadening obs. 2—32493
α-WC, low temp. resist. and Hall effect 2—1521
WC, powder, sintering, rel. to milling, dislocation density effects 2—22348
WC, valence bonding 2—9328
WC cemented, scanning electron microscope obs. of W content 2—4620
WC cermets, Co bonded, cavitation erosion resist. 2—22298
WC surface, atomic and molecular diffraction and scattering 2—25174
WC_x, powder prep. by freeze drying 2—29447
$W(CO)_6$, ^{182}W Mossbauer spectra 2—13452
$W(CO)_6$, liquid, Raman spectra, automatic assignment of observed frequencies and combinations 2—39369
WF_6, molecular force fields 2—38943
WO_3:Nb_2O_5, crystallographic shear, electron microscopy and diffr. 2—25412
WO_3-MTO_3 system (M=K, Rb, Cs, Tl; T=Nb, Ta), crystal chemistry 2—15682
WO_3-Nb_2O_5 Wadsley defects, effect of annealing 2—3792
WO_2, film, gaseous anodization, elec. and optical props. 2—13301

Tungsten compounds continued
WO_{3-y}, WO_{3-y}.Nb_2O_5, applic. of electron microscope to high temp. mats. exam. 2—9435
WO_3, ^{182}W Mossbauer spectra 2—13452
WO_3, amorphization, bombardment induced, by Ar, As, B, Ne, Pb, Sb, Si, Kr ions 2—1242
WO_3, prep., colour, non-stoichiometry, X-ray exam. 2—25246
WO_3 film, in m.i.m. struct., a.c. and d.c. characs., negative resistance obs. 2—36567
WO_3^-, $(WO_3)_2^-$, $(WO_3)_3^-$ ion source, using thermionic emission and hot cathode arc discharges 2—23551
WO_4^{2-}, vibr. spectra, r.m.s. amplitude 2—3064
WOI_2, synthesis, cryst. struct., and mag. props. 2—25254
$(WO_3)^-_{n=1,2,3}+Cl_2$, rate const. meas. in drift tube/mass spectrometer apparatus 2—10613
$(WO_3)^-_{n=1,2,3}+NO_2$, rate const. meas. in drift tube/mass spectrometer apparatus 2—10613
$WS_2(Se_2)$, band struct. 2—32886
WSe_2, energy gap, effect of dislocation struct. 2—36534
WSi_2, W_5Si_3, enthalpy, heat capacity, 1200-2200K 2—29559
WV_2O_6-VO_2 system, evolution of crystallographic order 2—29153
Yb-W, direct meas. of $N_{IV,V}$ X-ray emission spectra 2—36922
ZrB_2-W alloy, struct. and props. after sintering 2—12950
Tuning forks *see Vibrating bodies*
Tunnel diodes *see Semiconducting devices/tunnel and interface devices*
Tunnelling
beam-splitter based on tunnel effect, use in Michelson inteferometer for far infrared 2—14476
classical trajectory contributions, semiclassical limit of Feynman path integrals 2—7668
dislocation through Peierls barriers 2—38251
fatty acid salt monolayers between metal electrodes 2—1547
film, thickness depend. of resonant tunnelling 2—13081
in film insulators, mechanism, book 2—29732
glass, org., γ-irradiated, scavenging kinetics of electrons 2—40831
impurity assisted tunnelling theory with expression for conductance 2—40126
Josephson barriers fabrication by r.f. sputter etching 2—6783
Josephson cryotron, effect of junction capacitance 2—9975
Josephson effect, pair breaking mechanisms 2—36456
Josephson junction, Nb/Al composite electrodes 2—36476
Langmuir film, monomolecular layers 2—4273
metal film, discontinuous, elec. cond. by substrate assisted tunnelling 2—19540
metal film on dielec. substrate, pot. barrier height and tunnelling electron mass 2—1452
metals, density of states determ. from tunnelling conductance meas. 2—1459
metals, granular voltage induced tunnelling conduction 2—16133
methyl malonic acid cryst., γ-irrad., methyl group tunnelling rot. freq. 2—22848
methylcyclohexane glass, biphenyl doped, electron tunnelling mechanism for isothermal deferred luminescence 2—4515
m.i.m. junction, current response time limit 2—1545
m.i.m. junction, electron-phonon interaction effects 2—19722
m.i.m. junction, free electron description 2—6870
m.i.m. junction, localized impurity states influence 2—6871
m.i.m. junction, temp. depend. of tunnel current, insulator prop. effects 2—40308
m.i.m. structure, low energy barrier detn. 2—22597
m.i.s. memory transistor, charge transport time depend., direct tunnelling model 2—22598
m.i.s. structure, influence of band bending 2—19727
m.i.s. structure, tunnelling into amorphous Ge and Si 2—13298
molecular cryst., tunnelling rot. of kindered methyl groups 2—26291
nucleon, differential cross sections for ^{16}O reactions with ^{208}Pb, DWBA calc. 2—5714
potential barrier with pot. holes, tunneling probabilities eval. method 2—19487
probability of electron due to mag. breakdown, uncertainty principle derivation 2—19493
quantum mechanical, in methyl group n.m.r. line shape 2—10569
semiconductor, Meyer- Neldel rule, thermally assisted tunnelling and pseudointrinsic cond. 2—13211
superconducting barrier, containing paramagnetic interacting impurities 2—36453
superconducting film, normal metal coated, thickness depend. 2—9965
superconducting junction, Josephson current as probe of fluctuations 2—13188
superconducting junction struct., microwave assisted tunnelling 2—40220
superconducting small particles, T_c obs. 2—13145
superconductor, amorphous, phonon spectra obs. 2—13157
superconductor, generalized McMillan eqn. 2—16157
superconductor, mag. impurity effects 2—13126
superconductor, phonon spectra obs. 2—19395
superconductor, preferred direction tunnelling, energy gaps and phonon struct. 2—16155
superconductor, type-I, effect on vortex transport entropy 2—16162
superconductor, type-I, electron-electron interactions effect on density of states 2—19573
superconductor, using Ge-barriers 2—40204
surface plasmon excitation by electron tunnelling 2—1469
thin film tunnel triode, amplification of injected current from tunnel cathode in p-type amorphous layer 2—33034
two proton system, spin-lattice relaxation 2—10256
Al-Al_2O_3-Al junctions, tunnel thickness 2—40309
Al-Al_2O_3-Al structure, energy-momentum relation 2—19724
Al-Al_2O_3-Au m.i.m. struct., Fowler-Nordheim, I-V characts., electron emission 2—13290
Al, granular, density of states and resistive transitions in fluctuation regime 2—13151
Al film, granular, supercond. enhancement mechanism 2—13154
Al superconducting base electrodes, tunneling into both sides of weakly coupled Pb-Cu proximity sandwiches 2—19558
Au-Al_2O_3-Al thin film sandwiches, electron-electron interaction parameter in Au films from proximity effect 2—36479
Bi, supercond., amorphous, phonon spectra obs. 2—13157
C, amorphous film, between localized states 2—13222
CdTe-Au diode, reverse characts. 2—29733
CdTe, electroabsorpt., Franz-Keldysh effect, internal microfields 2—36873
Tunnelling continued
Cu/Pb interface, proximity effect 2—13174
Cu film backed by Pb, induced supercond. 2—6775
EuS, magnetiz. obs. 2—36709
Ga, supercond., amorphous, phonon spectra obs. 2—13157
Ga single-crystal superconductor, evidence for selection rules presented 2—4161
n-GaAs-Pb contacts, press. depend. 2—40221
GaSb amorphous film, effect of temp. and doping 2—19647
n-Ge, self energy effects 2—40290
$HCrO_2$, magnetically ordered system with superexchange through H bond, proton tunnelling 2—1603
He II, from electronic bubble states through liquid-vapour interface 2—12600
In-Al_2O_3-Pb, supercond. energy gap detn. for polycryst. bulk In 2—19574
In-$SrTiO_3$, rel. to polaron transitions 2—4139
InAs quantized surface accumulation layer 2—13265
InSb amorphous film, effect of temp. and doping 2—19647
KCl:Li, nonlinear susceptibility of tunnelling ions 2—29738
KCl, F_A(Li) centre spin lattice relaxation, e.p.r. obs., 4.2K 2—10507
KD_2PO_4, proton tunnelling modes, statistical perturbation theory, order-disorder ferroelec. 2—10124
KH_2PO_4, $KD_{2x}H_{2(1-x)}PO_4$, KH_2AsO_4, proton tunnelling, Raman spectra 2—16551
KI:KOH, microwave absorption study of OH- tunnelling 2—13479
La, supercond. and surface contamination effects 2—29636
Mg, film, electron standing wave states, group rel., tunnelling meas. 2—22459
$(NH_4)_2SnCl_6$, rel. to proton spin-lattice relax. of NH_4^+, 20-125 K 2—26083
NaBr:F-, impurity tunnelling, thermal and dielec. props. 2—33052
NaOH, vitrified aqueous solution, irradiated, reaction kinetics, 77 K 2—30093
Nb, supercond. and surface contamination effects 2—29636
Nb_2O_5, in m.i.m. struct., rel. to metallic impurities 2—10099
Ni, diffusion, quantum, of H, pot. barrier, transfer mechanism, migration energy 2—12813
NiO, antiferromag, magnon excitation by electron tunnelling through Ni-NiO-Pb junctions 2—10240
Pb-Bi amorphous alloys, supercond., energy gap, phonon spectra 2—13172
Pb, energy gap anisotropy obs. 2—13173
Pb, supercond., amorphous, phonon spectra obs. 2—13157
Pb, thick films backed by Fe, proximity effect 2—16186
Pb and Pb-30% Bi disordered superconducting films, rel. to determination of electronic props., comparison with specific heat data 2—9979
p^+-n Si-Ge, heterojunction, alloyed, transport mechanism 2—19702
Si-SiO_2 interface states, model for generation and distrib. 2—29737
n- Si, m.o.s. structure, phonon structure 2—16255
Sn-Sn-oxide-Sn Josephson tunnel junction, exptl. study of Riedel singularity 2—13196
Sn-SnO-Sn, Josephson tunnel junction. rel. between normal resistance and barrier thickness 2—19610
Ta, supercond. and surface contamination effects 2—29636
TaC_x, lattice instability effects on supercond. 2—22509
Te-TeO_2-Pb, tunnelling junction, phonon assisted tunnelling effect 2—29688
Te, supercurrent junction 2—13183
Th, supercond. energy gap obs. 2—40211
Turbidimetry *see Chemical analysis*
Turbidity *see Scattering/light; Suspensions*
Turbulence
see also Cavitation; Flow; Vortices
acoustic, near sound absorbent liners 2—20925
additive solutions, expt. on turbulent diffusion 2—32249
aerofoil, aerodynamic noise 2—28722
air, flow in concentric annuli, analysis, expt. obs. 2—3174
air, flow in pipes, vel. and temp. fluctuations 2—35647
air, transformation due to change of surface roughness 2—13694
air above simple water waves, momentum transfer 2—15553
air jet, axisymmetric, local entrainment rate in initial region 2—24959
air motions, obs. with Doppler radar 2—16829
air stream under transverse flow conditions, equations for diffusional electrically charged particles 2—32187
air-sea interaction and the boundary layer, turbulent exchange processes 2—40930
anemometry, laser Doppler, frequency tracker design 2—35440
asymmetric turbulent velocity profiles, negative eddy diffusivities 2—31904
Atlantic Ocean, characteristics of thermal inhomogeneities near Brazil current 2—33438
atmosphere, effects on angular scintillations in laser return from retroreflector 2—22973
atmosphere, extreme mechanical, obs. during low level aircraft flights 2—40935
atmosphere, gravity centre displacement of light beam, meas. 2—16839
atmosphere, heat and vapour transfer between water surface and atmosphere 2—7255
atmosphere, inner scale meas. 2—30292
atmosphere, light beam spatial structure 2—16838
atmosphere, mountain wave propagation 2—1851
atmosphere, power spectral response of aircraft and effects of non-linear longitudinal aerodynamic characteristics 2—35678
atmosphere, radiowaves propagation, submillimetre, fluctuations obs. 2—16863
atmosphere, remote laser sensing 2—40963
atmosphere, space-time relationships 2—40933
atmosphere, spot dancing of laser beam propagation 2—4685
atmosphere, two layer baroclinic model, nonlinear interaction of waves and zonal current 2—37143
atmosphere, unified discrete gust and power spectrum treatment 2—40947
atmosphere, upper, planetary, temp. fluctuations, radiative damping rate 2—4960
atmosphere boundary layer due to unstable stratification, temporal and spatial variability 2—1846
atmosphere boundary layer vertical two point longitudinal velocity fluctuation differences standard deviation 2—26488
atmosphere clear air, theoretical study of generation 2—37139
atmospheric, clear air and otherwise 2—40944
atmospheric, conference London (May 1971) 2—40931

Turbulence continued
atmospheric, errors caused by, measurement of angular position of radiation sources by optical electron monopulse method 2—23136
atmospheric, generalizations of Richardson criterion, for onset 2—1848
atmospheric, generation in boundary layer 2—40937
atmospheric, inducing laser beam spread 2—31057
atmospheric, Kelvin-Helmholtz instability 2—40938
atmospheric, macroturbulence and mean winds from radar observations of meteor trails 2—33497
atmospheric, over open sea, structure and intensity 2—20327
atmospheric, recorded by Civil Aircraft Airworthiness Data Recording Programme 2—40946
atmospheric, speed of dissipation, radar meas. 2—20322
atmospheric, statistically self similar, group theoretic implication 2—13669
atmospheric, temporal frequency spectra of multifrequency waves in 2—33479
atmospheric, vertical scan technique in infrared radiometric detection 2—15530
atmospheric boundary layer stratification and friction layer of sea, effect on vertical profile 2—30277
atmospheric flow over water, comparison of acoustic anemometers 2—26490
atmospheric heat flux, free convection 2—13676
atmospheric instability, within stable layers, f.m./c.w. radar obs. 2—33458
atmospheric propagation, multifrequency waves, temporal frequency spectra 2—16853
atmospheric spectroscopy, remote sensing 2—16840
atmospheric spectrum indissipation range from meas. of laser radiation fluctuations 2—20323
atmospheric structure from line-of-sight propagation expts. 2—1855
atmospheric surface layer, transfer mechanisms 2—40927
atmospheric turbulence and electricity during solar eclipse of 7 March 1970 2—37160
axial supersonic compressor, flow visualization 2—18739
azimuthal dissipative flow set up by rotating magnetic field 2—28491
baroclinic planetary boundary layers, parametrization of turbulent fluxes of momentum, heat and moisture 2—37123
blood flow in arteries, hot film probe for obs. of velocity distrib. and transition to turbulence 2—26945
boundary layer, accelerated, blown, sucked, unblown, hydrodynamics, mean vel. profile 2—18774
boundary layer, adiabatic compressible, wind tunnel model for obs. in adverse and favourable pressure gradients 2—21900
boundary layer, heat transfer, meas., flow along convergent-divergent nozzle 2—18760
boundary layer, heat transfer during kinetic burning on porous surface 2—27317
boundary layer, in free surface channel flow, different surface roughness conditions 2—6172
boundary layer, incompressible, over infinite yawed wing 2—3304
boundary layer development numerical calculation 2 18552
boundary layer excitation of airplane fuselage and interior noise radiated 2—174
boundary layer large scale motions during relaminarization 2—39056
boundary layer model near walls 2—12342
boundary layer on a porous plate, heat transfer with uniform blowing and suction 2—39068
boundary layer on helical blade rotating in fluid otherwise at rest 2—18561
boundary layer on rotating nose-body, soln. by converging iterative method 2—3305
boundary layers, effect of normal shock 2—32167
boundary layers, effects of mass transfer on hypersonic flow 2—35659
boundary layers, incompressible, effect on flow of discontinuity in wall blowing 2—6028
boundary layers, Reynolds stress fluctuations 2—39061
boundary layers, similitude solutionns in two- and three-dimensional flows 2—39262
boundary layers, solution of equations using implicit fine difference technique 2—28436
boundary layers with suction or injection, turbulent transport processes modelling 2—28709
boundary-layer shock interaction with and without injection 2—28710
Burgers, forced equation solution 2—18565
Burgers model, with two velocity components 2—24634
di-n-butylphthalate-water system, optical study of interfacial turbulence 2—6177
cavitation hydrodynamic noise, approx. theory 2—28760
characteristic functionals of random fields, turbulent diffusion 2—3155
circular cylinder in cross flow, effect of free-stream turbulence on mass transfer 2—35708
clear air, airborne remote detection equipment, development 2—40917
clear air, aircraft obs. 2—40932
clear air, aviation and atmospheric science, meas. program 2—4673
clear air, development by synoptic scale processes 2—40940
clear air, mechanics 2—40936
clear air, operational forecasting for aircraft safety 2—40942
clear air, over and downwind of mountain regions 2—40934
clear air, shear induced, radar, aircraft and meteorological obs. 2—40939
clear air, stable layers associated with 2—40945
clear air turbulence associated with large temperature change 2—30278
in closed conduits, Brettling's design formulae 2—21749
clouds, coalescence obs. of small droplets 2—20344
clouds, effect on distrib. of sizes of droplets growing by condensation 2—20345
coaxial jets, turbulent mixing coefficient correlation, with and without secondary flows 2—28699
compressible flow, turbulent boundary layers with pressure gradients, similitude solns. 2—28470
convection, in rotating radial circular pipe 2—191
convection heat transfer in vertical pipe 2—34222
cool electron θ-pinches, heating 2—39139
cylindrical wall jets, flow and heat transfer predictions 2—25023
deflecting flow-heated jet interaction, intensity profile 2—18734
density profile and instability in turbulent flow in stratified ocean 2—37107
depolarization of laser beam in a turbulent medium, gaussian and Kolmogorov spectra 2—31058
diffuser flow, measurement of intermittency factor 2—8879
diffusion in atmosphere from point-source, effect of observation time 2—10728
diffusion in Lake Michigan 2—10708

Turbulence continued
discharge lamps, coolant liquid spectral characteristics 2—14469
disperse system, fluid-particle, effective viscosity 2—3416
dispersion of matter in turbulent pipe flows 2—32193
drag reduction in liquids by polymer additives, nonuniform concentration as mechanism 2—32218
dynamic calibration of inclined and crossed hot wires 2—31912
dynamo action brought about by velocity turbulence, statistically exact equations 2—6057
Earth's atmosphere, backscattering of e.m. waves by irregularities 2—20355
eddy viscosity, Phillips' hypothesis, comparison with expt. 2—1040
eddy viscosity models for turbulent free shear flows 2—35672
eddy-viscosity model for turbulent-wake calculations 2—32159
effects on electrical conductivity of plasma combustion products under channel flow 2—28533
electrostatic, effects on trapped particles in toroidal plasmas 2—12429
e.m. processes in MHD channels, boundary discontinuity problem 2—28492
e.m. wave propagation, coherent Green's function, comparison of selective summation techniques 2—20980
energy transport eqn. 2—2181
entrainment interface in fluids 2—12335
ethylene glycol, pipe flow, low Reynolds no., turbulent vel. and temp. fields 2—9051
final period, two-species reactions, numerical examination 2—31896
flow, axial flow fans running in, and sound radiation 2—167
flow, Brownian particle motion, statistical description 2—91
flow, dispersion of starting points, 'backward diffusion' 2—39075
flow, gas in round tube, dissociating, heat transfer obs. 2—6127
flow, in smooth tubes, heat transfer, mass transfer, Reynolds analogy 2—18735
flow, internal intermittency and fine-structure distribution functions 2_6038
flow, over wavy boundary, prediction 2—28463
flow, passive scalar diffusion 2—28469
flow, pipe, physical model for drag reduction 2—6167
flow, turbulent, steady, in circular pipe downstream from sudden enlargement 2—35432
flow, two-dimens. vortex motion and negative temps. 2—35417
flow at low Reynolds number, von Karman's constant 2—39055
flow in tube, longitudinal turbulent diffusion studies by n.m.r. method 2—28455
flow meas. by hot-wire anemometers 2—3297
flow of incompressible viscous fluid between two parallel discs 2—28444
flow of power law fluids in circular tubes, heat, mass and momentum transfer analogies 2—24598
fluid, nearly Gaussian turbulent motion, time- dependent Wiener-Hermite expansion in Burgers' system 2—24622
fluid, turbulent flow, with high Reynolds number in tubes, Hamiltons principle 2—35433
fluid flow, aerodynamic sound due to source near half- plane 2—39259
fluid-solid dilute system, heat transfer, similarity variable test 2—25121
fluids, constituent equations 2—39067
fluids, derivation of Kubo type formulae for turbulent transport coeffs. 2—6047
fluids, speed and inclination of eddies near walls 2—8889
fluids, stationary homogeneous turbulence, perturbation theory 2—15433
free convection boundary layer, interaction with downward forced flow 2—34211
free convection in water near maximum density temperature 2—21936
free streams, eddy shedding from a sphere 2—921
free-stream effects of local heat transfer from a sphere 2—39245
fully developed turbulent flow, in annulus, radius of mass velocity 2—35430
gas, boundary layer, Schmidt and Lewis nos. 2—12486
gas, nonequilibrium dissociating, flow in circular tube, heat transfer 2—12485
gas flow, dark field laser schlieren technique for study of gas mixing 2—21901
gas flow, due to rotating disc 2—3292
gas flow, laser induced 2—32147
gas flow, weakly ionised, laser probing and comparison of neutral and plasma fluctuations 2—3291
gas jet, ionized, high temp., in longitudinal magnetic field 2—970
gas-solid suspension 2—32286
gases, highly turbulent flows, shielded hot-wire probe 2—28698
geophysics, numerical simulation of turbulent flows 2—39090
glass beads in air, flow characteristics in turbulent flow pipe obs. 2—9188
gun plasma, optical meas. of degree of turbulence from He I and II spectral lines 2—39170
heat and mass transfer in an incompressible turbulent boundary layer 2—39246
heat transfer, meas. on blunt cone at various angles of attack 2—24966
heat transfer downstream of a backstep in supersonic flow 2_39247
heat transfer for boundary layer flow 2—31903
heating in modified plasma two-stream instability, computer simulations 2—12371
holographic system for time varying random media compensation 2—23653
homogeneous, incompressible fluid flow, diffusion of a scalar 2—6042
hot jets, turbulence strength and characteristic parameters determ. from i.r. emission spectrum 2—39263
hypersonic flow, shock-boundary layer interaction at wedge compression corner 2—39057
incompressible elastically viscous fluids, attenuation of turbulent motion 2—39032
incompressible turbulent boundary layers, computation at low Reynolds numbers 2—24604
instability for viscous shear layer at low Prandtl number with Richardson number >0.25 2—35418
intense, effects on aerodynamics of circular cylinder at subcritical Reynolds numbers 2—32161
inviscid fluid flow between rotating cylinders under axial and transverse magnetic fields, stability of nonrotationally symmetric disturbances 2—39088
ion acoustic turbulence, turbulent heating theory 2—28616
ionosonic in a plasma, anisotropy of the electric fields in a powerful h.p. discharge 2—8988

Turbulence continued
isotropic, fluids, velocity spectrum in the inertial and dissipation ranges 2—12317
isotropic turbulence, spectrum 2—18570
jet, hot air, heat transfer to flat plate, normal impingement 2—3298
jet, supersonic, schlieren obs. of density fluctuations 2—18729
jet aircraft, dynamic response to turbulent air, accident prevention 2—39254
jet flows discharging into uniform crosswind, eptl. investigation 2—35654
jets, in transversal stream, trajectory and velocity calc. 2—12318
jets, in uniform streaming flow 2—3285
jets of liquids in gases, damping, inelasticity of collisions 2—24627
kinematic, in random function theory, growing modes eliminated by physical causality 2—37235
layer in ideal two dimensional fluid flow 2—12339
liquid film, falling, turbulent flow 2—39320
liquid flow, obs. in cylindrical pipe using real-time hologram-moire interferometry 2—31091
liquid fluctuations, laser beam attenuation 2—18823
liquid streams, exptl. meas. of rate of dissolution of solids 2—28757
macroturbulent exchange coefficient in different parts of atmospheric motion spectrum, calculation method 2—33457
magnetohydrodynamic flow, two-dimensional turbulence in strong mag. field 2—975
magnetohydrodynamic turbulence experiments in a transverse magnetic field, random fluctuations 2—39089
magnetohydrodynamics, transition, Reynold's number increase 2—974
magnetohydrodynamics, turbulent boundary layers with electron thermal nonequilib. and finite rate ionization 2—31935
magnetron, smooth-bore, turbulent diffusion study by Brownian motion 2—37925
mass transfer cylinder to air, rel. to turbulence and Reynolds number 2—18732
MHD, transition to laminar flow obs. 2—18582
MHD device with non-uniform distribution of forces, pressure calc. from internal hydraulics 2—971
micropolar fluid flow 2—18553
microturbulence, A and F stars, reanalysis using new f-values 2—4825
natural convection, on vertical isothermal wall, laws of velocity and temp. distribution 2—2278
natural convection adjacent to inclined and vertical surfaces 2—31905
natural convection boundary layer, laminar- to-turbulent transition 2—39301
natural convection boundary layer, study of hydrodynamics on a vertical plate and in a vertical layer 2—21935
nematic liquid, magnetic stabilization 2—18780
non-Newtonian pipe flows, laser anemometer obs. of structure 2—28758
non-Newtonian power law fluids, mixing length formulation 2—24616
O stars atmospheres, evidence from line broadening 2—33649
ocean, small scale, digital data recording and processing 2—20288
ocean surface wave dynamics with turbulent character of motion 2—20287
oceanographic, off-shore zone, peculiarities of horizontal turbulence 2—33439
photosphere microturbulent vel., analysis of Goldberg-Unno method 2—17074
pipe flow, eddy viscosity model 2—24603
pipe flow, laminarization by fluid injection 2—31911
pipe flow, swirling 2—12523
pipe flow, transition for water and dilute solutions of polyethylene oxide 2—12522
plain tube, non-symmetric turbulent diffusion, effect of tangential eddy diffusivity 2—35402
plasma, collisionless shock wave, laser scatt. meas. 2—39122
plasma, current driven, heating by dissipation 2—24657
plasma, depolarization of singly scattered radiation 2—39129
plasma, energy density spectrum of elec. field 2—31963
plasma, generated by instabilities in shock waves 2—3206
plasma, ion-sound, anomalous resistivity calc., inconsistency 2—18654
plasma, magnetically confined at high electric fields 2—24807
plasma, reflex-arc, spectral characts. 2—12423
plasma, shift and broadening of resonance 2—31937
plasma, studied by external ion beam 2—32041
plasma, validity of quasi linear approx. for bump-in-tail and two stream instabilities 2—18681
plasma bremsstrahlung emissivity 2—31996
plasma coaxial accelerator, filamentary structure of shock driving current sheath 2—35514
plasma electric microfield distribution 2—35451
plasma electron pitch angle diffusion driven by oblique whistler mode turbulence 2—8916
plasma flows, probe geometry effects on plasma diagnostics 2—21816
plasma heating 2—24655
plasma heating and electron cyclotron and ion acoustic instabilities in Tokamak devices 2—24821
plasma heating by intense pulsed discharges in OGRA-2T device and ion acoustic and beam instabilities 2—24816
plasma ion acoustic microinstability, strong current Z discharge 2—24817
plasma phase space density granulation 2—12366
plasma pinch heating and electron cyclotron drift instability 2—24667
plasma slab, scattering of e.m. waves 2—35484
polumer solution pipe flow, velocity obs. with laser dopplermeter 2—25007
polyacrylamide solution, non-Newtonian pipe flows, laser anemometer obs. of structure 2—28758
polyethylene oxide solution, non-Newtonian pipe flows, laser anemometer obs. of structure 2—28758
Prandtl layer spectra 2—4681
pressure fluctuations on smooth and rough walls 2—39303
propagation of weak nonlinear shock waves 2—30877
random atmospheric, optical wave propagation 2—22977
Reynolds stress model, application to thin shear flows 2—35410
sea, off-shore zone, rel. to horiz. conversion coeffs. detn. 2—30252
seawater, optical methods of observations in oceanographic research 2—13663
seawater, thermohaline convection, upper bound to transport processes 2—10712
separating and reattaching supersonic flows in two dimensional compression corner 2—31910
shear flow, general method for solving problem of longitudinal dispersion of matter 2—6030

Turbulence continued
shear flow, mean velocity profile of fluids 2—24617
shear flow, micropolar fluid model applic. 2—12327
shear flow response to stepwise change in wall roughness 2—936
shear layer in low speed flow downstream of steps, reattachment and relaxation 2—24615
similarity laws for unstably stratified fluid 2—12328
solar atmosphere, convective turbulence, emission of acoustic noise, directional dependence 2—37422
solar photosphere, microturbulent velocities from stellar atmosphere models with convection 2—37397
solar wind, effect of interplanetary magnetic field, analysed in magnetohydrodynamic approximation 2—14014
solid-gas flow in vertical pipes, particle dynamics 2—25122
sonic boom in turbulence, statistics of random overpressure peaks 2—9023
sound radiation production in axial flow fans 2—3310
spectra of thermally stratified turbulent flow with no shear 2—24963
stability det. of laminar flow with MHD-rotation 2—24641
statistical theory for weak homogeneous turbulence 2—39030
steady flow electric arcs, equations of motion and energy 2—24923
stellar atmosphere, α Ori, from spectral analysis 2—1953
stellar envelopes, rapid differential rotation, turbulent flow 2—26705
stratified flows, maintenance of turbulence in stratified atmosphere 2—40925
stratospheric, rel. to mesoscale horizontal temp. gradients, Project Coldscan 2—40943
structure in fully developed asymmetric flow in plane channel 2—15435
subsonic jet shear layer, optical crossed-beam meas. of turbulence intensities 2—18721
sun convection zone, eddy viscosity and depth dependence of physical parameters 2—7566
sunspots, magneto fluid mechanic turbulent damping theory 2—30626
sunspots, rel. to magnetic field 2—11107
supersonic, boundary layer, exptl. investigation of total temperature and Mach. number distributions 2—18724
supersonic boundary layers, jet interaction-induced separation, two dimensional problem 2—35660
supersonic flow, compressible boundary-layer heat transfer to rough surfaces 2—28690
suspension in turbulent jets, diffusion rel. to small particle size 2—25123
suspensions, air-solids, heat transfer 2—28902
swirling flow, accompanied by helical cavity core in circular pipe 2—6045
tangential stresses in liquid flow 2—39322
temperature boundary layers with constant wall temperature, momentum transfer 2—35707
temperature fluctuations in wake behind heated cylinder 2—3290
theory, asymmetric mechanics applic. 2—39036
three-dimensional homogeneous isotropic numerical simulation 2—12344
thunderstorms, Oklahoma compared with Malaysia, aircraft obs. of turbulence, temp. variation and cloud top heights 2—40952
time-dependent turbulent boundary layer eqns., analysis and appl. 2—24965
time-dependent Wiener-Hermite base 2—8894
toroidal discharge, high voltage, early departure from free acceleration and turbulent heating of electrons 2—39209
transfers inside vegetative canopy, use of Rn for meas. of diffusivity profiles 2—22963
transition, electrokinetic determination 2—21750
transitional flow in isosceles triangular ducts, study of mean velocity distribs. and turbulence intensity meas. 2—31907
tropospheric velocity meas. by radio links and pulsed radar 2—7289
turbon as discrete package of turbulent energy in specification of acoustic noise 2—20941
turbulent boundary layers, compressible adverse pressure gradient, profile shape calc. 2—35663
turbulent diffusion, concentration distrib. rel. to velocity field, characteristic functionals 2—6014
turbulent diffusion, Hopf eqn. based on Oseen eqn. 2—3156
two phase cylindrical type flows, comments and author's reply 2—39063
two-dimensional, stationary states 2—12345
two-dimensional supersonic wake, study of flow properties 2—18722
two-dimensional wall jet in moving stream with arbitrary pressure gradient, determ. flow and shear parameters 2—18725
two-equation model, prediction of laminarization 2—21740
velocity distribution and wall shear stress calc. for array of parallel rods 2—916
velocity waves and kinematic dynamo activity in astrophysical objects 2—10792
vibrating anemometer filaments in turbulent flow fields and errors in meas. of velocity fluctuations 2—12487
viscous sublayer, spatial structure 2—8877
and vortex motion 2—937
wake of flat plate, rotated hot wire anemometer for obs. 2—3295
wake of wedges, supersonic, study of axial development of frequency spectra of fluctuations 2—21719
wake visualization of hypersonic projectiles, holography 2—3284
wakes, entrainment mechanism 2—28756
water, spatial and temporal correlations by laser anemometry 2—15549
water flow, measurement using drag force on spheres 2—25012
wave mechanics theory of heat cond. 2—17437
weak, drift stationary solutions 2—12338
weakly interacting waves, Langevin eqn. 2—8893
wind turbulence spectra in Prandtl-layer 2—30280
Ar jet, high temp. coaxial, flowing into air wake, turbulent mixing 2—18720
Cs plasma, diffusion, heating and resistivity 2—24665
H plasma, heating of column in linear arc discharge 2—24658
H_2O, film, laminar and turbulent flow along vertical tube, heat transfer coeff. of evap. 2—18883
H_2O, production near a smooth wall in a turbulent boundary layer 2—1050
^{2}H hot high density plasma, heating and confinement in magnetic mirror trap 2—24747
He jet meas., hot-wire anemometry and digital techniques appl. 2—24971
Hg flow in travelling magnetic field, transitory reversed and turbulent motion 2—28493

Turbulent flow *see Flow*

Twilight
see also Atmospheric spectra; Zodiacal light
airglow, vacuum u.v. spectra, sounding rocket spectra 2—16883

Twilight continued
aureole, visual and spectral investigations from Soyuz-5 spacecraft 2—4705
brightness, influence of Quadrantids shower 2—4986
morning and evening, spectrum of airglow meas. between 3 and 4 microns, OH intensity variation 2—37194
noctilucent clouds, twilight probing with electrophotometers 2—7326
optical methods obs., review 2—7301
spectral degree of polarization of the sky radiation 2—20335
Na, Li and K airglow observations, vertical abundance characteristics 2—30321
O absorption bands to investigate upper layers 2—20381

Twinning *see Crystals, twinning*

Twistors *see Calculating apparatus; Magnetic devices*

Two-phase flow *see Flow/two-phase*

Type II superconductors *see Superconductivity/type II*

Ultracentrifuges *see Centrifuges*

Ultrasonics
see also separate headings, e.g. Absorption/acoustic waves, ultrasonic
absorption in concentrated polymer solns. in toluene and methyl ketone 2—27253
acousto-optic light deflection, first order beam steering transducers, design considerations 2—5424
amplifer gain control for pulse echo meas. 2—34116
amplitude and phase recording and visualisation in liquids by double interaction with light 2—37762
attenuation factor of ultrasonic vibrations using the echo-pulse contact method, measurement accuracy 2—27195
B-scan obs. of head and eye 2—20735
biological effects on fine structure of cells 2—20737
biomedicine, ultrasonic contrast increasing in human tissue 2—23145
biopsy specimens by percutaneous puncture, u.s. guide 2—41278
blood flow obs. instantaneous 2—5036
bonding of fine Al wire, deformation characteristics 2—15830
brains of man and animals, possibility of local action through skulls 2—17101
bubble chambers, dynamics of vapour bubbles in liquid H_2 2—28771
cavitation in liquid O_2, erosion intensity dependence on static pressure and frequency 2—39306
clinical diagnosis, fibre optical device for A- to B-scan conversion 2—41308
clinical scans, two dimensional, digital storage and display 2—17103
composite materials, nondestructive testing 2—29452
1971 conference. London 2—37764
crack detection simulation, schlieren apparatus for ultrasound visualization 2—37765
creep, metals, testing in ultrasonic field over wide temp. range 2—29363
crystal filters, application to communications, monolithic IC's 2—20938
defect detector, correlating, for rock material macrostructure 2—2253
defectoscopy, velocimetric method, both-sides variant 2—29161
delay line bonding layers, transverse wave attenuation, acousto-optical meas. 2—40060
delay lines, zero temperature coeff., synthetic quartz crystals 2—5231
delay-lines, surface-wave matched filters, sensor number minimization 2—5242
diagnosis, pulse echo method, sound head sensitivity 2—37446
diagnostic pulse methods, dosage problem, acoustic output and overall sensitivity 2—23382
diffraction grating, noninterference sampling method, CO_2 laser 2—7919
diffraction of light, visible images of acoustic sources 2—7959
Doppler technique, for transcutaneous aorotovelography 2—20734
dynamic viscosities in superposed oscillatory shear 2—35398
electroacoustic channel, mathematical modelling 2—25935
electroacoustic feedback for obs. of fluid flow velocity 2—21728
electrochemical processes, review of applications 2—40818
energy conversion, double mode, antisymmetric Al trapezoid pair system 2—2247
finite amplitude waves in free field in air 2—27242
flexural vibrating free edge plates with stepped thicknesses for generating high directional ultrasonic radiation 2—34117
flowmeter calibration 2—25011
focal field, flat, vel. potential calc. 2—2239
focused, high intensity, for local treatment of biological tissue 2—30666
foetus, effects 2—5245
n-hexane, superheated tensile strength by ultrasonic cavitation 2—9066
high power use for study of fatigue in metals 2—36185
holographic three-dimens. represent. of data 2—27277
holography, real time, using acousto-optical transducer 2—27556
imaging in solids 2—15891
imaging system using optical pulse compression 2—38010
industrial application, review of current and future status 2—20937
inhomogeneous field, spectroscopic visualization of progressive beam 2—17379
inspection of high-tensile petroleum tubes 2—17390
interference effect in multifrequency pulse echo and application to flaw characterisation in metals 2—34139
isometric imaging system for nondestructive testing 2—32671
laser beam modulation, ultrasonic vibrations of one mirror in optical cavity 2—27560
lesion development in brain and plastics 2—37441
light diffraction spectrum, intensity distribution, calculation by method of successive diffraction 2—17690
light modulation 2—295
liver scanning, quantitative analysis of normal A-scan 2—41303
materials testing and quality control, u.s. cyclic stressing method 2—19233
materials testing using reflection of waves from targets of simple geometry 2—30873
medical diagnosis, data preparation and processing 2—37445
medical diagnosis of liver malignancy, compared to isotope scanning 2—17115
medical diagnosis of pericardial effusion 2—17116
medical diagnostics, electronic sector scanning 2—26962
metallurgical treatment process, applic. to steel, white layer formation effects on wear resistance 2—6586
metals, diffusion, phase growth under influence of ultrasound 2—25460
method for det. initial stress in polycrystalline bodies, theory 2—33978
microsound, assessment for signal processing 2—20939
mitral echogram, criteria for acceptability 2—17102
non-destructive techniques for flaw size determination, review 2—32571

Ultrasonics continued
nondestructive testing, data analysis using computer 2—32669
nondestructive testing, fatigue crack growth, in gaseous environment 2—39835
nondestructive testing, notches and edges as reference flaws 2—39866
nondestructive testing, signal display, information extraction through probe manipulation 2—32667
nondestructive testing development trends, review of published material 2—2251
nondestructive testing of welds, ASME and AWS procedures comparison 2—32662
optical blank demounting 2—27578
parametric amplifier, theory and equivalent circuits 2—5234
polarimetry, vibrs. generation 2—29523
high polymer solution degradation 2—39020
pulse echo instrument, device for obs. of swept gain performance 2—17391
renal disease diagnosis 2—2022
resonance technique for NDT of fibre reinforced plastics 2—32658
scanner, three-dimensional images using fibre optics 2—17111
scanner and cathetertip echo technique for cardiology 2—17118
scanning, constant depth, clinical applic. 2—17120
scanning, multiple image store 2—17104
sonar, medical diagnosis of blighted ovum 2—17114
sonar applications in medic diagnosis conference (Glasgow, December 1971) 2—17113
spectrometer, continuous wave, for simultaneous obs. of sound velocity and attenuation variations 2—23378
spectroscopy of liquids, piezotransducer applics. 2—29520
standing wave density and press. distrib. plotting 2—27250
steel roll, hardening depth meas. 2—1332
anisotropic stress determination by ultrasound method 2—37761
surface inspection, crack and flaw detection 2—1321
surface waves, estimation of elastic and plastic deformations 2—29378
technique for studying rate of solidification 2—39423
temperature measurement, temp. dependence of sound velocity 2—20962
testing, Cagniard method for spherical elastic waves 2—20922
testing, communications, thermometry, conference (San Francisco, Oct 1970) 2—20936
testing, half-value depth of reflecting zones 2—11356
thickness meas. method, equipment appraisal 2—32668
time position and B-scanning of heart 2—17117
tomographic examination of blunt abdominal injuries 2—20723
transducer, u.s. focussing, with Gaussian vel. distrib. 2—27270
transducers, review 2—23359
underwater transducers, calibration at high u.s. frequencies 2—34124
v.h.f. quartz filter crystals, mode control 2—5235
visualisation of objects in ultrasonic fields by ultrasonic Raman light diffraction 2—27275
visualization, medical diagnosis, limitations and possible improvements 2—17119
visualization of pulse propagation and reflection in solids and liquids, schlieren apparatus 2—37765
In-Tl alloys, lattice stability near martensitic phase transformation, ultrasonic study 2—29474
KD_2PO_4, u.s. waves, diffraction of polarized light 2—19974

Ultraviolet detectors *see Radiation detectors*

Ultraviolet sources *see Light sources*

Umklapp process *see Crystals/lattice mechanics*

Uncertainty *see Indeterminacy; Probability*

Undor *see Electron theory; Field theory, quantum*

Unified field theory *see Relativity/unified field theories*

Unimolecular layers *see Adsorbed layers*

Units
see also Constants; Dimensions. Nomenclature and symbols
angular and linear momentum, proposal for names planck and galileo respectively 2—33858
electromagnetism, MKSA-formulation, general form of Maxwell's equations 2—27344
force, definitions and symbols 2—22
kilomole definition, and use as unit of quantity of matter 2—27016
mass and weight standard meas. 2—23219
photometry, new British standard, review 2—34504
SI, developments in changeover and modification to metric system 2—2052
temperature, international practical scale 2—37825
visual dimensional display system space lattice presentation showing physical quantity relationships 2—23214

Upper atmosphere *see Atmosphere/upper; Ionosphere*

Uranium
see also Nuclear fission/uranium
Apollo 15 samples, primordial radioelements and cosmogenic radionuclides 2—41188
Ariel, motion, calc. of dynamical oblateness factor for Uranus 2—4979
atmosphere, thermal opacity due to methane-H_2 collisions 2—26823
atom, L_{II} subshell fluorescence, Auger and Costner Kronig yields 2—18321
atom, relative X-ray transition probs. to K-shell 2—21510
atom, visualization, dark field electron microscopy, scattering cross sections 2—21521
chemical composition, spectroscopic obs. 2—30581
detection in various matrices using nuclear track technique 2—7200
diffusion in Ta crystal, ^{233}U tracer, α-energy spectra 2—6516
diffusion in V, Nb, Mo, Ta and W, rate and temp. meas. 2—12795
enrichment of isotopes, review of present trends and techniques 2—3010
fission track mapping, location of minute grains by precise coordinate control 2—11685
fuel, irrad., cutting techniques 2—38752
geometric albedo in 3400-8500Å spectral range 2—30554
ions, traversing He, Ar, Kr, Xe, H_2, N_2, O_2 gases and C and Au foils, 2-15 MeV, equilibrium charge state distribution determ. 2—675
i.r. spectral albedo from spectrophotometric data 2—11000
in lunar minerals by ion microprobe mass analysis 2—37344
mass determination from obs. of 5 outer planets and 7 minor planets 2—11002
in minerals, content, nondestructive determ. by gamma ray spectrometry 2—4608
Miranda, daily sidereal mean motion 2—4979
nuclear fuel, highly enriched, depletion and isotopic composition relation, empirical expressions 2—28152

Uranium continued
- oceanic upper mantle, fission track determinations and distribution 2—16748
- photometry, multicolour photoelectric wavelengths 0.315 to 1.06 μ 2—4978
- plasma, continuum source applic. 2—14487
- plasma production by single-ended operation of Q-device BARBARA 2—12421
- position, meridian obs. for 1963-67 2—1989
- potentiometric determination in mixed oxides 2—30104
- quantitative determ. in ore samples by radioisotope excited X-ray fluorescence 2—7198
- recovery, precipitation of UN from liquid U-Sn alloy 2—8405
- satellites, motion obs. 2—4979
- satellites, physical and chemical nature 2—7535
- Sea of Fertility, soil analysis 2—20668
- shock melting and vaporization 2—39420
- in soils, remote sensing by low altitude gamma spectrometric surveys 2—37096
- in steel, austenitic stainless, effect on stress corrosion cracking 2—29326
- superconductivity, review 2—13147
- in H_2SO_4 solutions, det. by gamma spectrometry simultaneously with Th det. 2—40857
- KCl:U, γ-irradiated, colouring and hardening due to secondary interstitial processes 2—36060
- α-U, stress relaxation, apparent activation enthalpy 2—25494
- α-U, supercond. transition temp. and mag. susceptibility under press. 2—25794
- U^{11+} UNILAC ion source and injection system 2—34842
- U^{3+}, e.s.r. in CaF_2, discrete saturation spectrum, hyperfine interactions 2—30008
- U^{3+} e.p.r. in SrF_2, stress-induced g-shifts 2—10524
- U^{3+} energy level scheme, from low-temp. absorption of U(HCOO) 2—10402
- in U_3O_8, det. by X-ray emission spectroscopy 2—30116
- ^{235}U-Al fuel forms, static and pulsed reactivity measurements in water 2—548
- ^{235}U, design and development of packaging for low enriched bundles 2—5755
- ^{235}U, det. of content in spent MTR type fuel elements, using delayed neutron yield technique 2—38748
- ^{235}U, new values of neutron nuclear data 2—28039
- ^{235}U diffusion in γ-phase of U-Nb alloys 2—29206
- ^{235}U minimum critical mass reflected by natural uranium in water 2—547
- $^{236}U/^{238}U$ in terrestrial minerals and processed ore 2—40900
- $U+O \rightarrow UO^{+}+e$, $U+O_2 \rightarrow UO_2^{+}+e$, collisional chemi-ionization processes, effective cross sections 2—33372

Uranium compounds
- nuclear fuel compositions, properties and irradiation behaviour 2—15112
- uranyl compounds, mechanism for appearance of internal vibrations of the ligands in luminescence spectra 2—24491
- uranyl compounds of type $MUO_2(C_2H_5COO)_3$, M = C_s, Rb, K, NH_4, luminescence 2—4495
- uranyl salts, frozen solns., energy transfer distances 2—3153
- Co-U-O system, $CoUO_4$ stability, $Co_3U_2O_8$ phase 2—15958
- $M^{II}U_2^{V}F_{12}.4H_2O$ (M=Co,Ni, or Cu), optical absorption spectra and magnetic susceptibilities 2—33275
- PuO_2-UO_2 fuel mixtures, neutron radiography testing with TiO_2, Eu_2O_3, RhO_2 mixtures as analogues 2—550
- Th-U dil. alloys, supercond. and localized spin fluctuations 2—1494
- Th-U dilute alloy, supercond. and normal states, sp. ht. study 2—29557
- U-7.5 wt.%Nb-2.5 wt.%Zr alloy, elastic consts. rel. to press., 1 bar-18 kbar 2—32580
- U-C-O system, phase diagrams 2—12611
- U-C-X, X=Ce, Nd, La, phase diagrams 2—9838
- U-Mo-Nb-Zr alloys, phase transformations, carbide inclusions effect 2—13004
- U-Mo alloy, stress corrosion cracking 2—12911
- U-Nb-Zr alloy, γ^0 phase domain struct. 2—9495
- U-Nb-Zr alloy, oxidation and temp. cycling, flexure study 2—10627
- U-Nb-Zr and U-Nb alloys, stress corrosion cracking, effect of Cl^- 2—29331
- U-Nb-Zr(Mo) system, kinetics of transform. of γ phase 2—36309
- U-Nb alloys ^{235}U and ^{95}Nb diffusion, in 930-1900°C temp. range 2—29206
- U-5wt.%Nb alloy, γ-quenched, stress corrosion cracking, ageing conditions effects 2—36175
- γ-U-Pb liquid alloy systems thermodynamic properties 2—39360
- U-Pu-C-O system, phase diagrams 2—12611
- U-Se-C ternary system, phase equilibria, solid state compatibility relationship 2—29482
- U-Si-Be system, phase relations 2—13016
- U-Si system, phase diagram 2—40012
- U-Te-C ternary system, phase equilibria, solid state compatibility relationship 2—29482
- U-V-C system, phase transform., C content effects 2—36310
- U-V alloy, phase transformations, C content effect 2—13003
- $(U, Pu)O_2$ fuel, creep, irrad. effect 2—11902
- $(U, Pu)O_2$ fuel, in-pile thermal cond. meas. 2—18266
- $(U, Pu)O_2$ mixed oxides, thermal cond., high temp. 2—19465
- $(U,Na)_{2-x}Nb_2O_{7-y}$, cryst. struct., order-disorder transform. X-ray obs. 2—32782
- $(U,Th)O_2$ mixed cryst., thermal diffusivity 2—19467
- U complexes, mono and tri-fluoro-oxalate, luminescence and i.r. absorption spectra 2—28330
- $UAl_{2(3)(4)}$, elec. and mag. props., temp. depend. 2—40405
- UAl_4, UAl_3, UAl_2, liquid solutions, thermodynamic props. obs. by e.m.f. method 2—38739
- UAs-USe system, mag. phase transitions 2—4380
- UAsS(Se)(Te), mag. props., struct., 77-1000K 2—26026
- UB_{12}, high temp. enthalpies 2—19274
- UC_2-C system, C thermal diffusion, model 2—29226
- UC-UC_2, UC-UN alloys, lattice dimensions, X-ray diffr., 760-2250°C 2—19307
- UC-ZrC solid solns. cubic lattice parameter var. with temperature and composition 2—15733
- UC, electronic stopping power, fission spike props., elec. microscope obs. 2—36390
- UC, low energy neutron scattering 2—28113
- UC, nuclear fuel, creep, neutron irrad. effects 2—29274

Uranium compounds continued
- UC, nuclear fuel, operational and design experience for fast reactors in USSR 2—15099
- UC, phonon spectra, pseudopot. approach 2—19321
- UC, sintered, polycryst. props. rel. to monocryst. props. 2—22254
- UC spheres preparation by carbothermic reduction of sol-gel UO_2-C spheres 2—7189
- UC_2, granulated, thermal decomp., reaction kinetics, grinding energy 2—4579
- UC_2, vaporization and surface ionization 2—35840
- $UC_{1-x}N_x$, mag. suscept. meas., 4-1100K 2—40422
- UCV-Na-steel system, C transport, effects of V addition 2—9628
- UCl_3-UCl_4-NaCl-KCl-$CaCl_2$ solid systems, phase diagrams 2—39998
- UCl_6, Raman spectrum, assignment 2—29937
- UF_6, ^{19}F rotating frame spin- lattice relaxation, obs. via anisotropic chemical shift 2—4561
- UF_6, continuous gas analysis using far i.r. Michelson interferometer 2—37064
- UF_6, molecular force fields 2—38943
- UF_6 H_2 reduction mechanism 2—30063
- $UGa_{2(3)}$, elec. and mag. props., temp. depend. 2—40405
- UGe_3, elec. and mag. props., temp. depend. 2—40405
- UIn_3, elec. and mag. props., temp. depend. 2—40405
- $UMoC_2$, anisotropic thermal expansion, 20-1100°C 2—36359
- UN-UC-Fe system, phase equil. 2—1416
- UN, heat capacity, 386.8-701.3K 2—19428
- UN, high temp. thermodynamic props. 2—40796
- UN, nuclear fuel, creep, neutron irrad. effects 2—29274
- UN, $UN_{1.572}$ and unsintered powder chemical analysis 2—26381
- U_2N_3, equilib. N_2 press., thermodynamic props. 2—7164
- β-U_2N_3, mag. props., 77 to 300 K 2—19885
- UO_2/PuO_2 fast nuclear reactor fuel, fluoridation method for reprocessing 2—15111
- $UO_{2\|x}$-NpO_2 system, phase relations 2—1405
- UO_2-PaO_2-ThO_2 solid soln. formation, exchange of Pa^{4+} in molten LiF-BeF_2-ThF_4 with U^{4+} and Th^{4+} 2—10593
- UO_2-PuO_2 fuel, O_2:metal ratio effects 2—2862
- UO_2-PuO_2 fuels, melting heat rating 2—2860
- UO_2-PuO_2 microlattice, expts. in LWR for design of fuel elements 2—24270
- UO_2-PuO_2 nuclear reactor fuels, det. of ^{238}U capture rates rel. to ^{239}Pu fission 2—35103
- UO_2-ThO_2, measurement of temp. dependence of K_∞ for a high temperature gas-cooled reactor lattice 2—38744
- UO_2-UO_3-$LaO_{1.5}$, phase transformations, phase diagrams, single phase regions 2—4023
- UO_2-$UO_{2.67}$-ThO_2 system, phase relations 2—1405
- UO, matrix isolated, i.r. spectrum 2—825
- UO_2, deform. in compression, slip planes, shear stresses, dislocation structs. 2—32527
- UO_2, electronic stopping power, fission spike props., elec. microscope obs. 2—36390
- UO_2, fission induced creep, instrumented capsule for meas. 2—11917
- UO_2, helix fabrication for irrad. creep meas. 2—36254
- UO_2, in H_2 atmosphere, thermal etch figure 2—28997
- UO_2, molten, pressure of vaporizing U-bearing species 2—28150
- UO_2, nuclear fuel, creep, neutron irrad. effects 2—29274
- UO_2, powders, cold pressing, energetic study 2—6624
- UO_2, sintered, polycryst. props. rel. to monocryst. props. 2—22254
- UO_2, stretching mode 2—825
- UO_2, thermal cond., 1473K to melting point 2—36368
- UO_2, thermal conductivity 500°C to melting point, temperature dependence, mechanisms 2—32858
- UO_2, Xe diffusion, effect of stoichiometry 2—29225
- UO_2 epitaxial film, growth and neutron irrad. effects 2—29045
- UO_2 fuel, in-pile thermal cond. meas. 2—18266
- UO_2 fuel, irrad., cutting techniques 2—38752
- UO_2 fuel elements for thermal water reactors 2—8404
- UO_2 fuel rods, Zircaloy clad failure characteristics under loss-of-coolant condits. 2—15086
- UO_2 ion, coordination geometry, correlation with vibronic spectra 2—15341
- UO_2 pellet, in-pile thermal gradient, out-of-pile simulation 2—28155
- UO_2 reactor fuel pin, elongation under radiation 2—5750
- $UO_{2\|x}$, self-diffusion of oxygen 2—12815
- $UO_{2\pm}$, composition changes, 1950 K 2—25637
- UO_2^{2+}, characteristic freq. of valency oscillations 2—35295
- UO_2^{2+}, new absorption bands, assignment rel. to vibr. levels of ground state 2—35294
- U_3O_8, det. of U content by X-ray emission spectroscopy 2—30116
- U_3O_8, sintered, elec. cond. and thermopower intrinsic-semicond. obs. 2—22541
- U_4O_9, superlattice struct., neutron diffr. obs. 2—32475
- $UO_2C_2O_4.3H_2O$, cryst. struct. 2—22165
- UP powder, sintering and porosity, 1500-2000°C 2—3935
- U_3P_4, magnetization, 77-300K 2—26030
- $(U_{0.8}Pu_{0.2})O_{1.97}$, enthalpy, 2350 to 3000K 2—13040
- $U_{0.8}Pu_{0.2}O_{2-x}$ thermal cond., 1473K to melting point 2—36368
- β-US_2 semiconductor, mag. moment, cryst. struct. refinement 2—25828
- USSe, magnetic props. studied including susceptibility 2—10217
- USTe magnetic props. studied including susceptibility 2—10217
- USe, low temp. mag. props., 2.8-300K 2—26072
- USi_3, elec. and mag. props., temp. depend. 2—40405
- U_3Si fuel elements, burnup and swelling temp. depend. 2—546
- U_3Si phase, X-ray diffr. pattern of U_3Si_2, rel. to microstruct. 2—32476
- USn_3, elec. and mag. props., temp. depend. 2—40405
- $(U_yTh_{1-y})O_{2\|x}$ solid solution, elec. cond., O_2 press. depend. 2—40265
- U_2Ti, solid soln., neutron irradiation 2—3753
- UWC_2, anisotropic thermal expansion. 20-1100°C 2—36359
- $U_{1-x}Y_xAl_2(Ga_2)$, elec. and mag. props., temp. depend. 2—40405

Uranus
- No entries

Urey-Bradley forces *see Molecules/internal mechanics*

V-centres *see Colour centres*

V-particles *see Hyperons; Mesons*

Vacancies *see Crystal imperfections/vacancies*

Vacancy breakdown *see Diffusion in solids*

Vacuum apparatus
see also Seals
5th international vacuum conference, Boston, Mass., USA, Oct. (1971) 2—41374
automatic, function of control unit 2—5103
CERN intersecting storage ring, dual seal bakeable sector valves 2—23202
CERN intersecting storage rings for protons 2—38419
chamber for conductivity obs. on ion bombarded CdS thin films 2—23204
chamber for hot pressing apparatus 2—29408
channelling target chamber 2—36378
cold traps, design and characteristics 2—33835
drive screw, self lubricating with solid Teflon insert 2—30737
electron beam welding 2—7630
for electron microscope, scanning 2—6412
electron synchrotron, 5 GeV, vacuum system problems 2—38405
for environmental friction-adhesion obs. 2—30736
evaporator, construction and performance 2—33833
furnace, miniature, for Mossbauer spectroscopy 2—5096
gas flows, eqns. 2—39238
gauge calibration, significance of H_2 condensation 2—39430
high temp. chamber for low cycle tension- compression test machine 2—29352
joints, demountable, thermoelastic 2—33824
mass spectrometer, secondary ion, u.h.v. prod. 2—38786
material desorption obs. using EID 2—39544
materials selection for device construction 2—41407
microbalance, factors causing readings fluctuations and their elimination 2—16
mobile multistage 3000-cfm pumping system 2—41377
molecular-flow network based, elec. circuit analogies 2—39241
proton supercond. linac, at Karlsruhe, vacuum system 2—38398
pumpable pressure relief valve and seal combined, low temp. use 2—23201
residual gas composition in vacuum system for optical coating deposition 2—37535
sample handling system for powders 2—5107
seal tests using halide leakage detector 2—30730
specimen chamber for electron microscope 2—23205
spectrometer, photoelectron windowless for obs. of solids and surfaces 2—4102
sputtering equipment for deposition of optical coatings 2—32352
switches, dynamic sheath obs. after arc extinction 2—24884
system for in-pile irradiation studies 2—41411
TOR-1 apparatus, for obs. of materials under lunar conditions 2—33825
torsion balances, factors affecting quality, energy scattering 2—27027
u.h. vacuum system for surface studies by ion backscatt. 2—41412
ultrahigh valve with In seal 2—20786
variable conductance apparatus for absolute calibration 2—41402
H_2-air mixture, ignition characteristics 2—23194

Vacuum gauges
Bayard Alpert gauge, extractor gauge, press. indication, comparative meas. 2—41397
Bayard-Alpert gauge, influence of grid and ion collector diameters on sensitivity and measuring range 2—30733
Bayard-Alpert gauge, ion current modulation by cage modulator operating without electron current 2—41396
Bayard-Alpert gauges, ion collection, press. meas., ion vel. spectrometry 2—41395
calibration, piston manometer as an absolute standard 2—41400
calibration, ultra-high vacuum applic., design and construction of small conductances 2—33834
capacitor manometer, variant, to meas. absolute pressures 2—23197
charged particle oscillator, use as a u.h. vacuum gauge 2—41403
electron orbit ion, u.h. 2—23200
field electron emitter as press. indicator 2—41394
floating vacuum gauges, optical readout 2—26996
gas friction manometer, spinning rotor press. gauge 2—41393
hot-cathode ionization, for u.h. pressure 10^{-1} to 10^{-13} torr, meas. 2—23199
ionization, MRO4, as secondary standard in range 10^{-3} to 10^{-7} torr 2—37534
ionization gauge, with collector mounted external to grid space 2—41398
ionization manometer combined with mass spectrometer, patent 2—8419
magnetic sector mass spectrometer with reduced mass discrimination, residual gas analyzer 2—38784
mass spectrometer, gas scatt. as partial press. sensitivity limit 2—41404
measurement accuracy, standards 2—41399
micromanometer using photomultiplier 2—30734
molecular, torsional suspension, for use with fluorocarbon gases 2—7634
for moon surface atmos. obs. on Apollo-14 mission 2—41175
Moser-Poltz McLeod gauges, design and operation modifications for greater repeatability 2—41401
Penning cold-cathode gauge, measurement of effective yield of electrons by ions from cathode 2—5104
Penning discharge, low pressure, mode changes in r.f. oscillations obs. during calibration 2—23198
pressure meas. techniques, ionization gauges, review 2—41392
quartz fibre manometer, bakeable to 520°C, for 10^{-1} to 10^{-6} torr 2—20785
residual gas analyser, analysis computer program 2—41405
residual gas analyzer, automation on time-shared computer 2—38790
residual gas analyzer, double chamber partial press. gauge 2—38789
thermoelectric, calibration for operation at constant temp. 2—30735
variable conductance apparatus for absolute calibration 2—41402

Vacuum polarization *see Quantum electrodynamics*

Vacuum pumps
accommodation, effects of surface factors 2—41378
adsorption, in ^{3}He cryostat for thermal and elec. conductivity meas. in range 0.4 to 4.2 K 2—41369
contamination suppression by activated Al_2O_3 foreline trap 2—17137
cryogenic pumping system for mass spectrometric ion source 2—10655
cryogenic vessels, multi-layered insulated, techniques 2—17138
cryosorption pumping speed in pressure range 10^{-6} to 10^{-3} torr for H_2, CH_4, CO, CO_2 and air 2—41390
cryostats, u.h. vac., investigation of surface properties of semiconductors 2—26990
diffusion, design 2—33830
diffusion, four-stage system, performance 2—33832
diffusion, pumping fluid condensation 2—41387
diffusion, theoretical pumping speed 2—41386
diffusion, v.p. and oil backstreaming, mass spectrometer obs. 2—41385
diffusion and rotary, parameters meas., methods and apparatus 2—33831

Vacuum pumps continued
evaporator, construction and performance 2—33833
getter, nonevaporable, possibilities and limitations 2—41389
getter, zeolite traps, characteristics 2—33828
getter-ion, with cold cathode, characteristics 2—33827
ion, H_2 backstreaming when pumping hydrocarbons 2—39545
ion, quadrupole, performance characs. 2—41379
ionic, use in preparation of Ge(Li) detectors 2—24087
large volume titanium sublimation pump 2—20784
mechanical, sorption trap 2—26995
mobile multistage 3000-cfm pumping system 2—41377
orbitron, 10 cm diameter, speed meas. of inert gas ion trapping 2—41391
orbitron getter-ion, characteristics and performance 2—33826
Penning, diode, inert gas pumping mechanism 2—41380
Penning-type ion pump, patent 2—11232
perfluoroalkyl polyether fluids lubricants 2—23196
pump oils, torpidity phenomena 2—41409
rotary, oil sealed, elimination of oil mols. from vacuum system 2—41384
sorption trap using $Fe_2O_3.Fe_3O_4$ for N-5S pump 2—20783
with sputter ion and Ti sublimation 2—23195
trochoid, development and application 2—41381
turbo-molecular pumps, improved performance 2—30732
turbomolecular, construction and performance characts. 2—41382
turbomolecular, of vertical design, design and props. 2—41383
zeolite getter, ion and sublimating, for ultra-high vacuum 2—33829
H_2 condensation significance to design 2—39430
Ti evaporation pump, use in nuclear fusion expts. and space simulation 2—41376
Ti getter pumps, use for preparation of Ge(Li) diodes, effect of introducing gases 2—24088
Ti sublimator, radiant heated, operating characs. 2—41388

Vacuum technique
see also Getters
5th international vacuum conference, Boston, Mass., USA, Oct. (1971) 2—41374
adsorption of mixed gases at very low press., Pyrex glass adsorbent 2—39564
atmosphere actuated linear motion device, preparation of samples free from surface contamination 2—41410
breakdown, role of fast processes 2—21886
deposition of antireflection coatings for Si 2—8012
deposition of polymers for encapsulation of electronic circuitry 2—14054
deposition of thin films, apparatus allowing visual obs. 2—23206
deposition of thin films, automatic control instrumentation 2—30739
electron-interferometer with field emission cathode for contact potential differences meas. at ultra-high vacuum 2—21031
evacuation of electron microscopes using adsorption pumps 2—20789
evaporator, ultra-high use of zeolite getter, ion and sublimating pumps 2—33829
film deposition, rotating substrate, thickness distrib. and step coverage 2—39479
freeze-drying, microwave, gas breakdown theory 2—7596
gas incorporation in sputtered and evaporated Au films 2—35882
graphite, uses in high and ultrahigh vacuum, review 2—5102
interface contact vacuum sealing processes, phenomena affecting leak rate 2—41408
intermetallic compound film deposition, cylindrical metallic substrate, fast rotation technique 2—39515
mass spectrometer, residual gas analysis 2—21482
maximum rate obtainable in sorption and degassing processes in vacuum metallurgical treatments 2—41415
oil backstreaming, v.p., detect. by mass spectrometric obs. 2—41385
outgassing, meas. using quartz crystal microbalance 2—41413
outgassing rate measurement by the variable conductance method 2—20788
outgassing rate measurements, variable conductance method, limitations 2—37533
pumping in multi-layered cryogenic vessels 2—17138
pumps, diffusion and rotary, parameter meas. 2—33831
purity processes for gas filled radiation detectors for nuclear reactors 2—30738
quadrupole mass spectrometer use 2—15190
surface phenomena, investigation in ultra high vacuum 2—20790
temp. control system in high vac. chamber 2—27338
vacuum arcs as vapour sources 2—39223
vacuum metallurgy, conf, New York (1971) 2—33836
wavelength standard, gas laser theory 2—31029
He leak detection, with better sensitivity than mass spectrometer leak detector 2—30740

Vacuum tubes *see Electron tubes*

Valence bands *see Crystal electron states/band structure*

Valency
covalency reduction factors in D_{4h} symmetry 2—3025
electronic structure in molecular ions and covalent solids studied by photoelectron spectroscopy 2—35225
oxide fuels, mixed, irrad., chem. effects of comp. changes 2—545
refractory transition metal cpds. with high coord., valence bonding 2—9328
sapphire, Fe, Ti doubly doped, redox reaction, e.s.r. and optical spectra, biparticle formation, valency states 2—25241
Yb, divalency in alloys from mag. susceptibility meas. 2—4024

Valves, thermionic *see Electron tubes*

Van Allen radiation *see Atmosphere/radiation belts*

Van de Graaff generators *see High voltage techniques; Particle accelerators/linear*

van der Waals forces *see Atoms; Kinetic theory; Molecules/intermolecular mechanics; Solids*

Vanadium
anelasticity, deuterium impurity effects 2—29247
atom, photoionization cross sections calcs. using plane-wave method allowing orthogonality 2—31684
atom, X-ray K-fluoresc. yields 2—8443
band structure self consistent calc., APW method, at normal and reduced lattice spacings 2—19516
crystal, atomic band estimation from X-ray charact. temp 2—18963
diffusion of C, nitrogen and oxygen, 60-1825°C 2—22252
diffusion of U, meas. 2—12795
epitaxial growth on LiF and NaCl substrates 2—9272
extraction, properties and applications 2—3925

Vanadium continued
film, electron energy losses 2—6704
film, in multilayer struct., ion back scattering analysis 2—15659
film, optical absorpt., interband transitions 2—7076
heat of fusion, determ. using induction heating 2—28940
heat of sublimation, mass spectrometric obs. 2—36351
ions in ZnO single crystals, e.s.r. spectrum meas. at low temps. 2—25415
neutron irrad., annealing, effect of interstitial impurities, 375-575K 2—25443
phonon freq. distrib. functions determ. 2—13023
photoabsorption cross sections calcs. 2—22779
positron annihilation radiation, angular correl., calc. 2—36433
precipitation, of $V_{16}N$, elec. microscope and X-ray diffr. obs. 2—15975
secondary ion emission on Ar bombardment, mass spectra 2—4330
in steel, austenitic stainless, effect on stress corrosion cracking 2—29326
in steel, cast high-speed, effect on struct. and props. 2—36176
in steel, effect on struct. and mech. props. 2—36237
steel impurity, effect on strength to brittle fracture relation 2—6517
superconducting, isothermal magnetiz. curves, critical parameters 2—19602
superconducting mixed state, N_2 distrib. obs. using rot. hysteresis 2—32954
superconductor, hysteretic low-k type II, flux line arrangement 2—19570
superconductor, mixed state, hysteresis, neutron depolarization obs., flux distrib. 2—6779
superconductor, mixed state, thermomag. props. 2—13165
surface, charact. electron energy loss spectra, plasma losses 2—19526
surface studies, combined Auger and charact. loss. spectra obs. 2—3484
surface supercond., critical phenomena 2—13169
thermal conductivity, elec. resist., emissivity, specific heat, 1200-1800 K 2—19469
CdTe:V, absorpt. spectra and crystal field parameters 2—22759
V-H system, ferroelasticity rel. to phase diagram determination 2—9694
V IX,X, classification of emission lines from $3s^2\ 3p^n$-$3s\ 3p^{n+1}$ and $3p^n$-$3p^{n-1}3d$ transitions 2—2936
V XVIII, carbon-like spectra in the range 16 to 22 Angstroms 2—15220
V^{2+} in $KMgF_3$, covalent spin transfer, e.p.r. and ENDOR obs. 2—20143
V^{3+}, octahedral complex in ionic cryst., overlapping and covalency effects on optical spectra 2—19990
V^{3+} in MgO, dynamical Jahn-Teller effects 2—20147
V^{4+}, in V_2O_5-P_2O_5 glass, e.p.r. obs. rel. to polar cond. and i.r. absorp. 2—10039
V^{4+} a.p.r. in Al_2O_3 2—36983
V^{4+} ENDOR in TiO_2, superhyperfine coupling 2—40767
V^{4+} in TiO_2, microwave dielec. loss, low temp. 2—19748
Va XXI spectrum in e.u.v. identification and classification of spectral lines 2—31666

Vanadium compounds
alloy cladding behaviour in helium cooled reactors 2—11912
alloy for sodium-cooled fast breeder reactors 2—18259
oxides, bonding rel. to structure 2—9318
V_2O_3, flux growth by reduction of V_2O_5 in graphite crucible 2—19006
vanadates, normal I-III-V spinels, i.r. spectrum, vibrational assignment 2—10382
Vicalloy, domain struct. change during partial hysteresis cycle 2—13388
X-ray spectra and electron structure of binary alloys with transition elements 2—29946
$[V(H_2O)_6]^{3+}$, $[V(H_2O)_5Br]^{2+}$, magnetic resonance obs. 2—7146
Al-V, X-ray emission spectrum study of band structure 2—36911
Al-V alloy, ordering, X-ray and neutron diffr. obs. 2—39994
Al-V dil. alloys, supercond. transition temp., conc. depend. 2—16175
Al-V dil. alloys, virtual bound state obs. from Al $L_{2,3}$ absorpt. spectra 2—20022
Au-V, dilute, low temp. resistivity rel. to simple powers of T in Kondo effect 2—29613
Au-V dil. alloys, electronic sp. ht., impurity effects 2—16034
Au-V dil. alloys, impurity susceptibility, ^{51}V n.m.r. obs. 2—33114
Au-V dil. alloys, T^2 temp. depend. of ^{51}V Knight shift 2—33350
$Bi_{3-x}Ca_{2x}Fe_{5-x}V_xO_{12}$ Mossbauer study of Fe^{3+} 2—13445
$Bi_{3-2x}Ca_{2x}V_xFe_{5-x}O_{12}$, magneto-optical effects 2—40611
Cr-V dilute alloy, magnetoelastic props. 2—13416
Cr-V steel, effect of Mo content and yield pt. on creep rupture strength 2—29286
Fe-Co-V, hot drawing, dislocation movement, electron microscopy 2—9780
Fe-Co-V alloy, effect of original Fe purity on mag. props. 2—36238
Fe-Co-V system, plastic deformation, $\gamma \rightarrow \alpha$ phase transformation, omnidirectional press. effect 2—9806
Fe-V-Nb-C alloy, VC_x precip., electron microscope obs. 2—9769
Fe-V alloy, yield strength, 77-400K, comp. depend. 2—39786
Fe-V dilute alloy, hyperfine field at Fe atoms, temp. depend. 2—13449
Fe-V dilute alloy, spin-lattice relax. time 2—19932
Fe—Ni—V—C alloy, martensite transform. twinning 2—9807
$Li_xV_{2-y}Mo_y(W_y)O_5$ bronzes, cryst. struct. 2—9474
MgO-$TeO_2V_2O_5$ and ZnO-TeO_2-V_2O_5 glasses, variation of physical props. and chemical stability with composition 2—6292
Mn-V dil. alloys, complex mag. interactions, resist. obs. 2—40561
β-$Na_xV_{2-x}Mo_xO_5$ bronzes, cryst. struct. 2—3714
Ni-Fe-V system, ordering 2—39938
Ni—V—C alloy, VC_x precip., electron microscope obs. 2—9769
Pd-V dilute alloy, n.m.r. 2—40782
Ti-(8 wt.%)Al-(1 wt.%)Mo-(1 wt.%)V alloy, sustained loud environmental crack growth 2—29330
Ti-Al-V, alloy, etching, O_2 effect, metallography 2—32735
Ti-Al-V alloy, fracture toughness 2—22287
Ti-V-Al alloy, struct. and props., comp. depend. 2—36141
Ti-V-O and Ti-V-Al-O alloys, effect of O content on mech. props. 2—36144
Ti-V alloy, continuous cooling transform., rel. to ω phase precipitation 2—29481
Ti-V alloy, struct. and props., comp. depend. 2—36141
Ti-(6wt%)Al-(4wt%)V, alloy, texture analysis, colour metallography, colour anodizing technique 2—12735
U-V-C system, phase transform., C content effects 2—36310
U-V alloy, phase transformations, C content effect 2—13003
V-Al-Ti, alloy, creep, tensile and torsional loading effects 2—19188
V-Bi-Ca ferrite garnet, indirect exchange interact., V participation, neutron diffr. obs. 2—36739
V-Co alloys, n.m.r. of ^{51}V and ^{59}Co, mag. props. 2—10566
V-D system, phase diagram 2—29247

Vanadium compounds continued
V-Fe-Co alloy, order-disorder, long range ordering kinetics 2—29487
V-Fe alloy, Mossbauer effect, 80-1100 K 2—39943
V-Fe alloy, thermodynamic functions, activities, mass spectrometric obs. 2—36351
V-Fe alloys, elec. and mag. props., defect struct. 2—33117
V-Fe alloys, mag. props. 2—16350
V-H system, H ordering in β-V_2H 2—32783
V-M alloy, M=Fe, Os, Ru, $VK\beta_5$ emission, electronic struct. 2—6728
V-N alloy, phase transformation, banded microstructure 2—22367
V-N(O) dil. solid solns., ^{51}V quadrupolar effects 2—26308
V-O solid solution, thermodynamic props., e.m.f. study 2—25602
V-O system, absorpt. spectra 2—26174
V-Pd alloy, X-ray spectral investigation 2—33301
V-Ru alloy, high pressure resistivity obs. rel. to anomaly in electronic props. 2—36290
V-Ti, alloy, microsegregation, rel. to cooling rate, comp., electron probe analysis 2—29439
V-Ti, V-Ti-Nb, Si/Ge alloying effects on creep and creep strength 2—1295
V-Ti alloy, solid soln. strengthening and weakening 2—29441
V-X, alloy, dilate, X=Mo,Rh,Ta,W,Re,Os,Ir, mag. susceptibility, Knight shift 2—19836
V-transition metal alloys, ^{51}V quadrupolar effects 2—26308
V-transition metal cpds., X-ray emission spectra, electronic struct. 2—40708
V complex, $[V(urea)_6]^{3+}$, ligand field analysis of optical and mag. props. 2—13374
V complex vanadyl porphyrins, e.s.r. study of metal ion separation 2—18418
V^{2+} complexes, orthorhombic crystalline field theory 2—40593
V_3Al-$Nb_3Al(Ta_3Al)$ system, annealing, solid solubility 2—9775
VAu_4, order-disorder transformation, magnetiz. and susceptibility study 2—19886
V_3Au,^{51}V n.m.r. model proposed for normal and superconducting states 2—4564
V_3Au annealing effects on supercond. props. 2—19601
VB_2, thermal expansion over temp. range 300-2500°K 2—6683
VB_2, ultra soft X-ray spectra 2—29943
VBO_3, phonon Raman scatt. temp. depend., mag. contrib. to intensities 2—40692
VC, band structure, tight binding method 2—4124
VC, cleavage fracture 2—22288
VC, slip system determination by hardness anisotropy 2—9564
VC, X-ray spectra, energy band struct. 2—40706
$VC_{0.84}$, ordered, effect of domain size on hardness 2—6585
$VC_{7/8}$, cryst. struct. and interatomic interaction 2—6453
VC_x, precipitate identity in Fe-V-Nb-C and Ni-V-C alloys 2—9769
V_6C_5, electron scatt. by vacancies, residual resist. 2—4219
V_8C_7, cryst. struct. 2—29154
$V_{1-x}Co_x$, alloy $0<x<0.75$, mag. susceptibility, Knight shift 2—19836
$V_{1-x}Cr_xB_2$, antiferromagnetic, spin fluctuation effects 2—19927
$V_xCr_{1-x}B_2$, n.m.r., antiferromag. transition obs. 2—36781
VF_3, mag. ordering obs. 2—36780
VFe_2Se_4, mag. struct., neutron diffr., elec. cond., Mossbauer obs. 2—19908
VFe_2Se_4, thermal cond., 100 to 500 K 2—19459
V_2Ga_5-Mn_2Ga_3 system, cryst. struct., X-ray diffr. obs. 2—39655
V_3Ga, 3d band structure, calc. in tight binding approximation 2—4127
V_3Ga, high-field superconductor, pulsed-field meas. rel. to metallurgical processes 2—25790
V_3Ga, tight binding integrals, calculation and parametrisation, simplified procedure 2—22468
V_3Ga solid solns., atomic struct. and supercond. 2—9496
α-VH_x ($x=0.198$, 0.57), quasielastic thermal neutron scatt. investigation of H diffusion 2—36073
$V_2Hf_xZr_{1-x}$ alloy, high-field superconductor, pulsed-field meas. rel. to metallurgical processes 2—25790
V(III) complex, trisacetylacetonate, lattice-ion interactions, calc. 2—36793
VN_x, n.m.r. spectra, Knight shifts, influence of mag. fields and composition 2—20166
$V_{16}N$, precipitation in V, elec. microscope and X-ray diffr. obs. 2—15975
VN_xO_y, region of existence, cubic phase 2—1417
V_xNbS_2 magnetic and crystal structure 2—3722
VO_2:Cr, struct. aspects of metal - insulator transition 2—25638
V_2O_3:Cr electronic phase transitions with symmetry change 2—15955
V_2O_5:Cr^{3+}, e.s.r., spin Hamiltonian parameter detn. 2—4545
β-V_2O_5:M^+, small polaron ground state orbitals 2—10055
VO_2:Ti, conduction band and impurity state electron lifetime, e.s.r. obs. 2—10037
VO_2:Ti, impurity conduction, microwave freq. cond. obs. 2—19655
V_2O_5-P_2O_5 glass, antiferromag. transition 2—32967
V_2O_5-P_2O_5 glass, dielec. const., conductivity, 80-350 K 2—19749
V_2O_5-P_2O_5 glass, in m-i-m struct., high resistance, negative resistance and high conductivity obs. 2—40314
V_2O_5-P_2O_5 glass, polar conductivity and i.r. absorp. 2—10039
V_2O_5-SrO-TeO_2, glass system formation and properties 2—12631
VO_2-Ta_2VO_6, VO_2-WV_2O_6 systems, evolution of crystallographic charact. 2—29153
V_2O_5-TeO_2 glass, between metal electrodes, I-V characts., —100-200°C 2—36519
VO, band structure, APW method calc. 2—36418
VO, electronic struct. 2—13092
VO, electronic struct. 2—13093
VO, non-stoichiometric vacancy order 2—4011
VO complexes in soln., hyperfine coupling consts. and g-factor temp. depend. 2—25112
$VO_{1\|x}$, mag. susceptibility, rel. to electron states 2—36782
VO_2, band struct., LCOAO approach 2—6834
VO_2, film, fast metal-insulator transition, laser beam induced 2—10054
VO_2, film, holographic storage, based on insulator-metal transition 2—7951
VO_2, metal-insulator transition 2—29679
VO_2, microhardness and cond. in semicond.-metal transition region 2—29678
VO_2, optical props., band struct. 2—33245
VO_2, semiconductor-metal transition, Raman scatt. obs. 2—16571
VO_2, semiconductor-metal transition 2—10055
VO_2, structure, conduction, bonding, transitions 2—4007
VO_2, susceptibility, correl. with Knight shift, rel. to band struct. 2—33118
VO_2 coplanar devices, thermal breakdown analysis 2—4243
VO_2 film, transport properties, struct. dependence 2—19654

Vanadium compounds continued
- VO^{2+} ion, in alkali borate glass, e.p.r. and optical spectra 2—40763
- VO_2^{2+} complexes with diethyldithiocarbamate and diethyldithiophosphate, ligand props., e.s.r. obs. 2—24450
- VO_4^{3-}, vibr. spectra, r.m.s. amplitude 2—3064
- VO_x, atomic vacancies influence on band struct. 2—32887
- VO_x, highly correlated electron gas props. 2—19633
- VO_x, polaron morphology 2—10055
- VO_x morphology and substruct. of b.c.c. to b.c.t. transform. induced by impurities 2—15976
- V_2O_3, antiferromag., n.m.r. of ^{51}V 2—10564
- V_2O_3, n.m.r. of ^{51}V 2—10565
- $V_2O_{3\|\delta}$, mag. susceptibility, rel. to metal-semicond. transition 2—10167
- V_2O_4, semiconductor-metal transition 2—29680
- V_2O_5, doped, e.s.r. spectrum, motional narrowing 2—22828
- V_2O_5, film, gaseous anodization, elec. and optical props. 2—13301
- V_2O_5, Hall and drift mobilities 2—10036
- V_2O_5, single crystal, elec. cond. and dielectric props. 2—10038
- V_2O_5, thermal expansion, 0-685°C, X-ray diffr. study 2—40085
- V_2O_5 electrical conductivity, catalysis, dislocation model 2—4220
- V_2O_5 powder, diffuse reflectance spectra 2—29901
- V_6O_{13}, semiconductor-semiconductor transition 2—10055
- $VOCl_25NH_3$ absorption spectra corresponding to deformation oscillations of coordinated molecule 2—15342
- $VO_{2-x}F_x$, 0<x<0.2, structure, properties, preparation 2—3739
- $V_2O_{5-x}F_x$, 0<x<0.025, structure, properties, preparation 2—3739
- V_3P, Knight shift, spin lattice relaxation, conduction process 2—4559
- V_3Pt, spin-lattice relax. of ^{51}V, near supercond. transition 2—33183
- VSi_2, Si L-emission spectra 2—20086
- V_3Si, elastic softening arrest at supercond. T_c 2—9871
- V_3Si, mag. contrib. to low temp. sp. ht. in mixed supercond. state 2—16190
- V_3Si, single cryst., supercond. critical current peak effect 2—16169
- V_3Si film prep., resist. ratio 2—29013
- $Y_{3-2x-a}Ca_{2x}Gd_aFe_{5-x-z}V_xIn_zO_{12}$, mag. props. and reson. linewidths, comp. depend., for microwave applics. 2—40519
- $Y_{3-2x}Ca_{2x}V_xFe_{5-x}O_{12}$, magneto-optical effects 2—40611

Vaporization
- *see also Boiling; Condensation; Distillation; Evaporation; Heat of vaporization; Vapour pressure*
- atomic spectroscopy samples 2—20218
- circumsolar dust at 4 Ro, temp. det. 2—26927
- laser induces, material removal from front surface 2—12412
- liquid characts., surface thermal anisotropy influence 2—28955
- liquid droplet, unsteady vaporization 2—22045
- metal, shock induced vaporiz. 2—39420
- metal surface layers, bulk vapour production by laser beam 2—28964
- metals, shock vaporization, rel. to equation of state determ. above 200 kbar 2—22044
- multicomponent mixtures, efficiency prediction from existing correlations for vapour and liq. film coeffs. 2—3447
- rare earth oxides.dielectric film formation with electron beam 2—29017
- refractories, determined in solar and arc furnaces 2—35831
- transparent media, by focused laser beam 2—12413
- volcanism, expansion waves causing explosion 2—13621
- Al and Ni alternate films, apparatus and techniques 2—18932
- As, residence lifetimes of As_4 molecules on (111) surface 2—25157
- As_2Te_3, semiconducting chalcogenide glass 2—25156
- CaF_2(111) face, micromorphology and thermal vaporiz. 2—32336
- CeC_2 2—35840
- CsCl single crystals in phase transition region, relation to bulk diffusion rate of Cs^+ ion discussed 2—12620
- Eu_2O_3, in presence of W at 2192K 2—28967
- H_2O, liq. inclusion in NaCl and KCl single crystals 2—3762
- K, liquid, vaporization entropy as function of temp. determ. from vapour pressure curves 2—28963
- KCl:Ca, rate meas., 430-550°C 2—9218
- LaC_2 2—35840
- N_2, bubble growth rate, on metallic heating surfaces 2—28772
- NaCl, on bombardment with alkali halide beams, ang. distribution of vaporization products 2—10609
- Na_2SO_4, thermodynamics, study by transpiration method 2—28961
- NdC_2 2—35840
- PrC_2 2—35840
- Sn-S-O-C system, phase diagrams, volatization of Sn 2—1150
- ThC_2 2—35840
- UC_2 2—35840
- UO_2, molten, pressure of vaporizing U-bearing species 2—28150
- ZnO, single crysts., anisotropic vaporization rates of opposite basal faces 2—18887
- ZnO crystal, kinetics of opposite basal faces, temp. depend. 2—35841

Vapour density *see Density/gases*

Vapour pressure
- *see also Humidity; Vaporization*
- atmospheric, obs. using fine thermocouples 2—20309
- over curved surfaces, exponential form of Kelvin equation, verification 2—1153
- isotope effects, near triple point 2—9202
- methane-argon liquid mixture, obs. 2—35753
- nucleation theory, small clusters, surface energy 2—12621
- toulene, in microscopic capillaries, liq.-vapour equilib., concave surface effect on v.p. 2—35829
- Ag-(5 at.%) Ir alloy, evaporation, beta irradiation effect 2—28965
- AmO_x, oxygen dissoc. press. and phase behaviour 2—9217
- As-I system, 100-800°C 2—28934
- BaO, nonstoichiometric, p-T-x diagram construction 2—35843
- BkO_x, oxygen dissoc. press. and phase behaviour 2—9217
- CO_2, in critical region 2—9203
- Cd-Te, sublimation and thermodynamic props. 2—12619
- Cd, effect on CdTe crystallization rel. to γ-ray spectrometer material props. 2—34809
- Cd, rel. to heat of sublimation determ. 2—25158
- CdS, determ. by torsion-effusion method 2—28966
- CmO_x, oxygen dissoc. press. and phase behaviour 2—9217
- Cu, rel. to surface diffusion coeffs. 2—32337
- H_2, D_2, condensation obs., 1.6-5.2K, significance in astrophysics and vac. technol. 2—39430
- H_2O, equation for 0 to 100°C temp. range 2—22046
- Hg, calc. from thermodynamic data 2—18756
- I, solid and liquid, thermodynamic equations 2—6226

Vapour pressure continued
- Kr isotopic mixtures, liquid and solid state, rel. to derivation of intermolecular forces 2—35839
- NH_4Cl, critical temp. and pressure determination from vapour pressure curves 2—9216
- NH_4HF_2, critical temp. and pressure determination from vapour pressure curves 2—9216
- Na, over Na_2O, torsion effusion determ. 2—22048
- NaCl aqueous solution, rel. to osmotic coeff. calc. 2—39433
- Na_2SO_4, study by transpiration method 2—28961
- Rb, saturated, 707 to 1541°K 2—12622
- TiO(g), in equilibrium with Ti_2O_3(s) and Ti_3O_5(s,β), derivation of dissociation energy 2—37033
- Ti(s,β), sublimation, standard enthalpy change, Knudsen n.p. determ., mass spectrometric analysis 2—18890
- UO_2, molten, pressure of vaporizing U-bearing species 2—28150
- Zn:O liq., equilib. v.p., rel. to surface active impurities, 563-623K 2—28951
- Zn-Te, sublimation and thermodynamic props. 2—12619

Vapour pressure measurement
- apparatus, meas. in 400-700 K range 2—25154
- methane, meas. from triple point to critical point 2—25142
- thermophysical properties of fluids 2—18813
- vacuum systems, oil backstreaming v.p., detect. by mass spectrometric obs. 2—41385
- Ag, 800-1600°K, low pressure 2—3450
- Cd, 350-594°K, low pressure 2—3450
- Hg, boiling point method 2—28962
- K, liquid meas. of curve up to critical point, determ. vaporization entropy as function of temp. 2—28963
- Ne, natural and isotopes ^{20}Ne, ^{22}Ne, from triple point to normal boiling point 2—30750
- O_2, equation 2—30749

Variable stars
- A-type, peculiar, with long periods, photometry 2—4867
- American Astronomical Society, Amherst, USA 1971, conference 2—26623
- ST Aquarii, eclipsing binary, variations of colour 2—30501
- CY Aquarii, overtones in lightcurve, harmonic analysis 2—30486
- CY Aquarii dwarf cepheid, three colour photometry41110 2—41110
- QS Aquilae, determination of primary minimum, increasing residual41112 2—41112
- BD+54°2698, VV Cephei type, emission lines and absolute magnitude1960 2—1960
- BD+61°219, VV Cephei type, emission lines and absolute magnitude 1960 2—1960
- BD+63°3, VV Cephei type, emission lines and absolute magnitude 2—1960
- Be, ultrarapid changes in Hα line profile 2—4842
- 44i Bootis, eclipsing contact binary, sudden period changes37310 2—37310
- TY Bootis eclipsing variable, orbital solution from UBV photometry33678 2—33678
- BW Vulpeculae, rate of change of period 2—1963
- β Canis Majoris type, non-radial oscillations4881 2—4881
- ρ Cas, R CrB variable, UBV obs. 17000 2—17000
- Cent X-3, X-ray pulsation due to occulting binary system 2—26799
- β Cephei, nonlinear nuclear energized pulsations, computer simulation 20567 2—20567
- VV Cephei type, emission lines and absolute magnitude1960 2—1960
- Cepheid loops, envelope opacities at 5 $M_\odot$ 2—33676
- Cepheids, classical, pulsation constants for fundamental mode and first two harmonics 2—4873
- Cepheids, evolutionary, conditions allowing high mass stars to become variables 2—33670
- Cepheids, mass from pulsation and evolution computations 2—16999
- Cepheids, radial velocities 2—33635
- Cepheids, secondary bumps, Robertson and Christie- Stobie models 2—7444
- cepheids, ultrashort periods, amongst blue stragglers in old disk population 2—20570
- *o* Ceti, differential radial velocities in spectra 4882 2—4882
- o Ceti, Paschen beta emission line, variation of equivalent width 41096 2—41096
- UV Ceti stars, infrared photometry, infrared excess in flare stars 2—33669
- classical Cepheids, appraent discrepancy between pulsation and evolution masses 2—26711
- classical Cepheids, conversion factor from radial to pulsational velocity, and radii 2—33665
- RW Coronae Borealis, eclipsing binary, light curve and orbital elements 41118 2—41118
- R CrB type, UBV obs. 2—17000
- W Crucis, photometric observations of long period eclipsing binary41120 2—41120
- 35 Crucis (BV 476), cepheid, amplitude and period7442 2—7442
- V CVn, polarimetric obs. and model 2—30445
- DT Cyg, Cepheid, light curves and period variations 7437 2—7437
- χ Cygni, differential radial velocities in spectra4882 2—4882
- CH Cygni, evidence for hot companion 30487 2—30487
- χ Cygni, forbidden emission lines of Mn I and Fe II in spectra 2—13895
- V1057 Cygni, interpretation of change in spectral type, K0 to A133667 2—33667
- V1057 Cygni, JHKL photometry in infrared 2—33668
- V 453 Cygni, minima and light elements4879 2—4879
- V 1057 Cygni, photometry and polarimetry 2—41113
- CH Cygni, semiregular spectra and relative monochromatic brightness 2—10871
- AI Draconis, eclipsing, photoelectric obs. 2—26713
- eclipsing binary KZ Pavonis as member of visual multiple h5231 2—7453
- envelope models for long-period stars 2—17003
- in globular cluster NCG 6171, periods and period changes 2—20568
- HD 105507, determination of period 2—7443
- HD 111133, peculiar A-type period 2—4880
- HD 125248, magnetic, eleven band photometry 2—26690
- X Her, polarimetric obs. and model30445 2—30445
- g Her, polarimetric obs. and model 30445 2—30445
- θHerculis, radial velocity measurements rel. to possible binary properties 2—41104
- HL Tau-76, rapid blue variable, high speed photometric observations 2—26724

Variable stars continued
- HR5491, pulsating metallic line 2—41114
- HR6773, possible eclipsing binary 2—20585
- HR 2957, Cepheid of small amplitude, photoelectric obs. 2—37307
- HR 5329, light curves from photoelectric observations 2—20575
- IRC+10216, i.r. object, dust shell diameter determination from lunar occultations 2—33637
- BL Lac, photoelectric obs. 2—30488
- in Large Magellanic Cloud, two colour photometry, extinction obs.13910 2—13910
- late M-type and Mira, OH emission sources associated with 2—37296
- UZ Leonis, eclipsing binary, photoelectric observations, light curve 41119 2—41119
- long period, ejection of stellar envelope to form planetary nebulae 2—26719
- long period, post maximum spectra, fluorescent Fe I 2—37295
- LR Cen, optical counterpart to Cen X-3 2—41161
- LY Aurigae, UBV meas. 2—26723
- RR Lyrae, BV photometry, reddening of stars in the same direction 2—20574
- RR Lyrae, period luminosity relations, physical interpretation 2—20561
- RR Lyrae types, masses, radii and luminosities 2—41116
- in M5, light curves and epochs of maximum light17010 2—17010
- M type Mira variables coincidence with OH 1612 MHz sources from i.r. obs. 2—23094
- magnetic, γ source search at 10^{11}-10^{12} eV, null result 2—33722
- magnetic, effect of line absorption on light flux 2—16998
- microwave and i.r. flux, OH/i.r. emission sources, time variations monitoring 2—4933
- Mira, analysis of light variation curves 2—26720
- Mira, forbidden emission lines of Mn I and Fe II 2—13895
- Mira, near i.r. data, absolute magnitudes 2—20569
- Mira type, kinematics, solar motion, galactic rotation and velocity ellipsoid parameters as function of period 2—26722
- N-type, red, intrinsic classification, UBVRI obs. 2—37301
- new, positions and characteristics 2—30489
- in NGC 2264, young cluster, pre-main-sequence10899 2—10899
- in NGC 2264, young cluster 2—26721
- NGC 6171, studies of RR Lyrae stars in globular cluster 2—17009
- in NGC 6304 and NGC 6401, globular clusters, photometric obs. 26734 2—26734
- V567 Ophiuchi, ultra short-period variable, five-colour photoelectric observations26715 2—26715
- FU Orionis stars (fuors), energy source models rel. to rapid and slow flare stars33664 2—33664
- DY Pegasi dwarf cepheid, three colour photometry 41109 2—41109
- X Per, Peculiar, connection with 2ASE 0352+30 X-ray source 2—23099
- period det., comparison of methods 2—20564
- KP Persei, β Cephei type, UBV photometry26712 2—26712
- X Persei identification with X-ray source23100 2—23100
- ζ Phoenicis, primary minimum of eclipsing binary system 2—30500
- pulsating globular cluster stars, comparison of theory and obs. 2—20583
- L_2 Pup, polarimetric obs. and model 2—30445
- RSPuppis galactic cepheid, spatial and time variations in reflection ring nebula's structure and light intenstiy 2—23078
- VV Puppis rapid blue variable, eclipses and qualitative model41108 2—41108
- R Coronae Borealis, visible and infrared radiation fluctuations, change in shape of spectrum, summary of observations 1968-71 2—1969
- R Coronae Borealis type stars, observational facts 2—41115
- rapid irregular, absolute energy distribution in continuum 2—10869
- red, in Camelopardalis, obs. 2—37304
- RR Lyrae, calculations of shock waves in atmosphere 2—7439
- RR Lyrae, proper motions 2—4884
- RR Lyrae short period variables, AE Boo, TV Lyn and RW Ari, UBV light curves 2—26725
- RR Lyrae stars in NGC 6171 2—17009
- VX Sagittarius, peculiar i.r. variations 20626 2—20626
- Sco X-1, short period oscillations in X-ray and optical flux 2—26806
- λ and κ Scorpii, new broad lined β Canis Majoris stars33671 2—33671
- δ Scuti stars, period determinations of 34 objects from photometric data 2—30483
- δ Scuti types, in lower part of Cepheid instability strip, pulsation properties of models37305 2—37305
- semidetached binary systems, time-dependent studies of dynamical instabilities 2—26727
- WZ Sge rapid blue variable, light curves, flickering and bright spot 41107 2—41107
- slow flare stars in Pleiades cluster, comparison with objects in Orion 2—33674
- RW Tau, gradient and Balmer discontinuity variations during eclipse 17001 2—17001
- EU Tauri, classical Cepheid, UBVβ photometry41098 2—41098
- RRTauri, power spectrum analysis applied to light curve 2—10893
- U Gem cataclysmic variables, ultra short-period binary, gravitation radiation and mass transfer 2—26741
- U Geminorum, light curves 1856-1964 2—4876
- UBV magnitudes, brightness gradients 2—30466
- W Ursae Majoris, eclipsing binary, photoelectric observations, variations in light curve 41117 2—41117
- V642 Orionis, eclipsing binary system, UBVRI photometry 2—20588
- velocity variable, HD 226868, possible connection with Cygnus X-1 X-ray flux variations 2—13890
- AI Velorum, in lower part of Cepheid instability strip, pulsation properties of models 2—37305
- T Vul, Cepheid, light curves and period variations 2—7437
- BW Vulpeculae, spectral and photoelectric observations 2—41105
- LV Vulpeculae = Nova Vulpeculae 1968 (1), photoelectric observations 2—41106
- W 90, shell variability and pulsation 2—26721
- W Ursae Majoris systems, common envelope models for V566 Ophiuchi, RR Centauri, RZ Tauri, FG Hydrae and DK Cygni 2—33684
- white dwarf R548, spectral type observations of period 2—20566
- χ Cygni, emission line intensities of Mn I and [Mn I] 2—20549

Variational calculus *see Mathematics*

Variational method *see Quantum theory/application methods*

Vavilov-Cherenkov radiation *see Cherenkov radiation*

Vectons (vector mesons) *see Mesons*

Vectors
- canonical transformation by computer for analysis 2—14146
- differentiation, direct method in orthogonal curvilinear coordinates 2-11246
- dynamics of machines, use of vectors in teaching 2—27011
- electromagnetic potentials in radially stratified spheres, solution 2—34234
- kinematics of machines, use of position vectors in teaching 2—27010
- magnetization, vector and scalar, relationship in magnetic recording theory 2—6972
- meteorology, finite difference estimates of derivatives for an irregular pattern of points 2—5168
- Poynting's method for equivalent circuit of electric induction machine 2—5313
- prediction filtering by matrix algebra using minimum variance principle 2—37572
- unit, testing for correlation 2—23043
- vector bundles in mathematical physics 2—33

Velocity
- elastic waves in crystals 2—1282
- laminar suspension boundary layer, migration meas. by laser-Doppler anemometer 2—25120
- plasma ions, electrostatic energy analyser 2—18639
- seismic waves, anisotropy in upper mantle in Pacific Ocean 2—22930
- solar wind, determined from interplanetary scintillations 2—20696
- solid-gas flow in vertical pipes, particle dynamics 2—25122
- waves propagating in uniaxially stressed elastic media 2—34080
- **acoustic waves**
  - *see also Dispersion, acoustic; Helium/liquid, sound propagation; Shock waves*
  - borosilicate optical crown glass, det. using vibration transducer 2—25672
  - concrete simulating system, vib. meas. testing 2—36190
  - dielectric crystal, acoustic propagation theory 2—16021
  - Dow Corning 200 fluids, anomalous behaviour 2—32830
  - electrolyte aqueous solns., rel. to water struct. 2—28853
  - in emulsions and suspensions, effect of particle viscosity 2—15616
  - in flow, two phase, propagation speed of small pressure disturbance, critical flow 2—18568
  - gas mixtures, mode coupling effects 2—35685
  - in gases with solid-liquid suspensions 2—1037
  - liquid binary mixtures near critical pt. 2—28855
  - liquid ethane under saturated vapour, law of corresponding states 2—35760
  - liquids, relation with density 2—35756
  - marine muds, dependence on mud elasticity 2—37099
  - molecular diameter meas. method 2—35217
  - molten salts, sonic vel. rel. to entropy 2—25074
  - multimode propagation in liquid cylinders 2—17380
  - nitrobenzene-n-hexane binary mixtures near critical pt. 2—28855
  - nonlinear elastic medium, surface wave vel. and second harmonic generation 2—25671
  - in progressive wave, meas. by means of Lissajous figures 2—34108
  - propagation speed from theory of sound based on relativistic kinetic gas theory 2—28730
  - quartz, fused, surface wave vel. and second harmonic generation 2—25671
  - Rao's rule discussion 2—15587
  - in rocks, dependence on hydrostatic pressure 2—26391
  - in rocks under hydrostatic pressure, equipment for obs. 2—20221
  - sedimentary rocks, effect of depth on propagation of seismic waves 2—30195
  - solids, elastic wave measurement 2—27224
  - sound field in media having pathwise variable vertical sound velocity profile 2—5222
  - suspensions, wave eqn. for calc. 2—35806
  - two phase fluid, single component, theory and expt. 2—32288
  - two-phase one-component media, effect of heat, mass and momentum transfer 2—11355
  - underwater velocimeter, using h.f. CW resonance technique 2—27274
  - vibrational relaxation times of methane and O_2 at increased pressure 2—14258
  - water, rel. to molecular model 2—35723
  - BaO-B_2O_3 glass, effect of liquation 2—35848
  - inCO_2 at temperatures <100°C, noise effects on reactor circuits components 2—3328
  - CdS, Brillouin scatt. obs. 2—26200
  - CoF_2, Mandelstam-Brillouin scatt. obs. 2—16580
  - Cs, liquid, velocity of sound, 301.5-655 K 2—28850
  - Cs vapour, saturated and superheated, up to 1280°C 2—6157
  - $DyVO_4$, elastic props. of mag. controllable Jahn-Teller distortion 2—9802
  - FeF_2, Ising behaviour 2—40072
  - Gd, ferromagnet, magnetoelastic anomaly 2—25490
  - ^4He, solid, sound vel., stimulated Brillouin scatt. obs. 2—16585
  - ^4He, superfluid, calc. using kinetic and Boltzmann eqns. 2—18868
  - Hg, vapour, condensation, sound vel. limitation of heat flux to cooling surface 2—18889
  - $KMnF_2$, Mandelstam-Brillouin scatt. obs. 2—16580
  - $LiNbO_3$, ferroelec., piezoelec. leaky surface wave propagation and amplification 2—22412
  - MnF_2, Mandelstam-Brillouin scatt. obs. 2—16580
  - Na, liq., 1000 to 1500C 2—15588
  - Na_2O-B_2O_3 glass, effect of liquation 2—35848
  - $PbTiO_3$-$PbZrO_3$-$Pb(Zn_{1/3}Nb_{2/3})O_3$ system, near morphotropic phase boundary 2—33058
  - $RbMnF_2$, Mandelstam-Brillouin scatt. obs. 2—16580
  - Tb, magneto-elastic coupling, magnon- phonon interactions 2—13393
  - in TeO_2, phase velocity surfaces and ray directions, existence of transverse mode 2—16020
  - V_3Si, elastic softening arrest at supercond. T_c 2—9871
- **acoustic waves, ultrasonic**
  - *see also Dispersion, acoustic/ultrasonic*
  - alkali halides, molten, temp. depend. 2—9128
  - alkali halides, photomech. effect 2—29529
  - alkali metal binary mixtures, liq., mol. assoc. 2—28851
  - alkaline-earth metal chlorides in solution, diffraction method, variaons in velocity relative to these in water presented 2—15585
  - alkyl acetates, pressure and temp. dependences 2—25078
  - aniline-nitrobenzene mixtures, relax. processes 2—32260
  - associated liquids, mol. vel. 2—32258
  - benzene shear waves, near melting point 2—29536
  - binary liquid mixtures, compressibility determ. 2—28803
  - bitumens, of transverse waves 2—32829

Velocity continued
acoustic waves, ultrasonic continued
bubbly mixture, varying void fractions 2—35799
cholesteryl acetate liquid crystal, meas. near cholesteric-isotropic transition point 2—21983
cholesteryl benzoate liquid crystal, meas. near cholesteric-isotropic transition point 2—21983
cholesteryl formate liquid crystal, meas. near cholesteric-isotropic transition point 2—21983
composite, laminated, elastic moduli obs. 2—19164
cyclohexane shear waves, near melting point 2—29536
diamond, elastic stiffness moduli 2—25477
dynamic critical phenomena, rel. to time depend. fluctuations above order-disorder T_c 2—19818
electrolyte, temp. depend., computer calc. 2—15586
electrolyte solutions, hypersonic vel. meas. 2—28862
epoxy resins, polarized 10 MHz waves, 4-100 K, calc. of specific heat and elastic moduli 2—40058
ferroelectric, KH_2PO_4 and KD_2PO_4. dielec. susceptibility and polarization obs. 2—4279
focal field axis, velocity potential calc. 2—2239
glass:La, flint, as function of frequency 2—6665
heneicosane shear waves, near melting point 2—29536
n-hexoic acid, 3 to 21 MHz and at 15 to 40°C 2—39362
h.f., in Canada, fir and cedar balsams 2—28842
liquid mixtures, temp. variation 2—35757
liquids, diffraction of laser beam, undergraduate demonstration 2—33842
liquids, meas. using piezoelectric lead zirconate titanate ceramic interferometer 2—23385
in liquids, semiautomatic pulse technique for velocity and absorption 2—17382
liquids, temp. coeff. determination 2—3385
metal, molten, temp. depend., computer calc. 2—15586
p-methoxy-benzylidine, p-n-butyl-aniline, nematic liquid crystal, dispersion and anisotropy obs. 2—32261
minerals and rocks, electronic computing method of obs. 2—33427
nonelectrolyte-water mixtures 2—1095
nylon, polarized 10 MHz waves, 4-100 K, calc. of specific heat and elastic moduli 2—40058
paraxylene shear waves, near melting point 2—29536
pentaerythritol, elastic consts. determ. 2—25483
PMMA, eqn. of state obs. 2—25479
polystyrene, eqn. of state obs. 2—25479
propane, critical region phenomena 2—6283
propylene oxide aqueous solutions 2—1095
quartz, fused, stimulated Brillouin scatt. obs. 2—16587
rare earth cryst., critical phenomena, spin diffusion coeff. 2—29530
rock material macrostructure, defect detection 2—2253
salicylic acid esters, temp. variation 2—3388
salol shear waves, near melting point 2—29536
teflon, polarized 10 MHz waves, 4-100 K, calc. of specific heat and elastic moduli 2—40058
temperature measurement, temp. dependence of sound velocity 2—20962
tert-butyl alcohol aqueous solutions 2—1095
tetrahydrofuran aqueous solutions 2—1095
n-tricosane shear waves, near melting point 2—29536
Ag, Bordoni peak height, meas. freq. depend. 2—15803
Al-Zn alloys, dependence on rel. concentrations 2—6661
Al, neutron irrad., elastic consts. detn. rel. to anharmonicity 2—40025
Ar, solid, calc. 2—32827
$Ba(NO_3)_2$, first and zero sound 2—19411
Bi-Cd alloy change in velocity on melting 2—39421
Bi-Sb alloy change in velocity on melting 2—39421
$Bi_{12}GeO_{20}$ surface wave velocities, electromechanical coupling 2—29539
$Bi_{1.6}Sb_{0.4}Te_3$ and Bi_2Te_3, elastic consts. determ. 2—32576
$CdBr_2$/KBr(Cl), molten mixture 2—25076
$CdCl_2$/KBr(Cl), molten mixture 2—25076
CdS, thermal Brillouin scatt. obs. 2—33289
Cu-Al alloys, α-phase, elastic consts. 2—3833
EuO(S)(Se)(Te), elastic consts., compressibility, Debye temp. 2—32577
EuTe, rel. to mag. ordering 2—25673
Fe-Ni -C, martensites, elastic moduli determ. by u.s. interferometric obs. 2—3829
GaAs, photoconductive, illumination depend. 2—19413
Gd, Curie pt. anomalous, elastic const. determ. 2—9870
$Gd_2(MoO_4)_3$, elastic props. at ferroelastic transition 2—16009
Ge, hypersonic vel. meas., low temp. 2—4047
H_2, translational dispersion for frequencies to 4.10^4 MHz/atm. 2—28742
Ho, critical effects near Neel pt. 2—29838
Ho, critical phenomena, spin diffusion coeff. 2—29530
In-Sn alloy change in velocity on melting 2—39421
In, elastic consts. press. depend. 2—29237
KCl/XCl fused mixture, (X=Rb,Cs) 2—25077
KF, aqueous solution, rel. to temp. and conc. 2—21982
KH_2PO_4, KD_2PO_4, dielec. susceptibility and polarization obs. 2—4279
Kr, solid elastic consts. 2—6519
LiBr/KBr(Cl), molten mixture 2—25076
LiBr/LiCl, molten mixture 2—25076
LiCl/KBr, molten mixture 2—25076
LiCl/XCl fused mixture, (X=K,Rb,Cs) 2—25077
LiCl aqueous and org. solns 2—28852
LiF, deformation effects, 78-350K 2—12859
LiF, deformed, dislocation loop density and length meas. 2—36033
$LiNbO_3$, piezoelec. leaky surface wave 2—29526
Mg, elastic consts., third-order 2—3836
NH_4Br, disordered cubic phase, Brillouin scatt. obs. 2—26201
NH_4Cl, order-disorder transform. effect 2—29528
NaF, aqueous solution, rel. to temp. and conc. 2—21982
$Pb(NO_3)_2$, first and zero sound 2—19411
RbBr/XBr fused mixture, (X=Li,Na) 2—25077
RbCl/CsCl fused mixture 2—25077
$RbCoF_3$, Neel pt. phenomena, elastic consts. 2—32828
RbI/NaI fused mixture 2—25077
α-Si_3N_4 filamentous crystals, elastic consts. determ. 2—39761
$Sr(NO_3)_2$. first and zero sound 2—19411
$SrTiO_3$, anisotropy at phase transition 2—16022
$SrTiO_3$, anomaly rel. to crit. dynamics for $T \geqslant T_c$ 2—25932
$SrTiO_3$, attenuation, temp. depend., 105 K transition, phonon modes 2—9879
$SrTiO_3$, displacive transition obs. 2—32780

Velocity continued
acoustic waves, ultrasonic continued
Ti-O alloy, dil. determ. of comp. depend. of elastic const. 2—15802
$ZnCl_2$, molten, temp. depend. 2—9128
light
frequency dependence of speed of light in space 2—31087
in gravitational field, vacuum dispersion and photon rest mass 2—37589
interferometer arrangement using laser beam mod. by 21.3 MHz signal applied to Pockels cell 2—11507
QSO PKS 2134+004, speed of light received greater than 440,000 km/sec 2—23085
rotating mirror method, suitable for undergraduate laboratories 2—9
sputtered glass waveguides 2—38115
super light velocities in quasars 2—30513
Velocity analysis, particles *see Particle velocity analysis*
Velocity measurement
see also Angular velocity measurement; Stroboscopes
air-water mixture, slip distrib. and ave. void fraction meas. techniques 2—24628
anemometer, variable density flow, checking of consistency 2—20799
anemometry, laser Doppler, frequency tracker design 2—35440
ear structures by Mossbauer effect 2—7608
elastic waves, acoustic anisotropy in metal plates 2—2238
electrical probes for two-phase flow obs. 2—24630
flow, and visualisation by Doppler holographic technique 2—6021
flow obs. using electroacoustic feedback 2—21728
flow-rate measurements, straight piping lengths for flowmeters 2—39260
fluid, coherent and noncoherent methods in optical beating of Doppler shifted light 2—21747
fluid, spectrum of locally isotropic turbulence in the inertial and dissipation ranges 2—12317
fluids, traversing laser velocimeter and signal analysing system 2—928
galaxies near NGC 7331, radial 2—13873
gas, using surface contact breaks 2—12494
gas flow, low velocity meas. 2—12489
gas flow in shock tube with hot wire anemometer 2—3287
gas-liquid high velocity flows, local velocity and void fraction meas. technique 2—24633
inexpensive velocity meter for airtrack 2—17175
laminar pipe flow, by single channel optical anemometer 2—15525
laser Doppler radar, for remote wind sensing 2—37126
laser doppler velocimeter, signal broadening effects 2—23224
laser dopplermeter for obs. of turbulent pipe flow of drag reducing polymer solution 2—25007
laser velocimeter, for process control 2—1337
laser velocimeter 2—21
laser velocimetry, monograph 2—20
liquid flow, device for contactless obs. 2—18779
liquid metals, by MHD meter with cylindrical magnet, potential distributions 2—947
photochromic liquids, optical tagging 2—28754
plasma flow in T-tube 2—24769
plasmatron jet, weakly ionized gas stream meas. using MHD pickup 2—15470
supersonic gas stream in tube 2—35650
third orthogonal velocity component det. using two rotationally displaced laser Doppler velocimeter systems 2—33866
underwater acoustic velocimeter, using h.f. CW resonance technique 2—27274
water drops in air flow, velocity determination by Doppler effect with laser light 2—28696
winds during thunderstorms 2—20329
acoustic waves
air-water mixture, and void fraction determ. from transport time of wave 2—24628
spectrometer, ultrasonic, for variation det. 2—23378
He phase velocity, up to 5.10^4 MHz/atm. 2—6159
Sn, quantum oscillation meas., and e.m. excitation 2—5228
acoustic waves, ultrasonic
digital interferometer for testing liquids 2—27282
Doppler vel. meter, M-sequence modulated, for cardiography 2—30679
waveguide effect on meas. using cylindrical interferometer 2—5227
light
spark light source for teaching demonstration 2—33845
vacuum, after Compton scatt. on fast electrons, exptl. feasibility 2—23667
Veneziano model
amplitude, calc. from lattice dual resonance model 2—8141
amplitudes, inverse amplitude (K-matrix) method for unitarization 2—398
dual crossing-symmetric representations with finite- width resonances reducing to Veneziano B-function in limit of zero resonance width 2—21274
dual vector current, non-existence suggested by analysis of new class of dual vertices 2—17868
eight-point amplitude used to investigate dual resonance model implications for inclusive two-particle spectra 2—17876
electromagnetic form factors, vector meson dominance, implications of Veneziano model 2—14619
final vector mesons, density matrix predictions 2—422
kaon nonleptonic decay investigation, satisfaction of current algebra rules 2—8157
low energy dip structure, phenomenological exploration from hadronic two-body processes 2—23822
Mandelstam-Veneziano model, partial widths rel. to Regge residues 2—8139
meson-meson scattering, pseudoscalar, multiperipheral model with Veneziano type production amplitudes, exchange degenerate and exotic trajectories 2—38279
missing mass experiments, study of production cross section of high-spin resonances 2—14620
N-point amplitude, factorization, cluster decomposition 2—27727
N-Reggeon vertex derivation from n-particle amplitude 2—27728
off-mass-shell continuation 2—23820
partial widths rel. to Regge residues 2—8139
partial-wave amplitudes, profile function controlled by spin distribution of resonances in dual model 2—17869
pion scattering off isovector currents and scaling limit, generalized model 2—31276
scattering amplitude, unitarization. vacuum singularity of nondual part 2—27730

Veneziano model continued
  - $\eta\to3\pi$ decay calc. by Lovelace-Veneziano pole model, systematics provided by electromagnetic tadpole 2—38284
  - $\gamma\pi\to\pi\pi$, amplitude 2—14555
  - $\bar{K}N$, charge exchange, Veneziano model with cuts 2—38291
  - KN, charge exchange, Veneziano model with cuts 2—38291
  - KN and $\bar{K}N$ scatt., exotic trajectories and pomeranchukon 2—11601
  - $\bar{K}N\bar{\Lambda}\pi\pi$, dual amplitude with spin 2—17890
  - $K^-p\to\bar{K}^0\pi^-p$, inclusion of spin 2—17912
  - $K^-p\to K^{*-}p$, inclusion of spin 2—17912
  - $K^+p\to K^0\Delta^{++}$, higher spin production processes, Veneziano model with absorptive corrections applied 2—38288
  - $K^+p\to\pi^+pK^0$, 12 GeV/c, detailed fits to data using generalized model 2—17910
  - $K^+p\Sigma K^{*+}p$, higher spin production processes, Veneziano model with absorptive corrections applied 2—38288
  - $\bar{p}N\to\pi^-\pi^+\pi^+$, Dalitz plot analysis 2—5558
  - $pn\to\pi^+\pi^-\pi^-$, comparison of analyses by rising-shift model and Veneziano model 2—34730
  - πN, scattering, short range potential, Reggeization using Veneziano amplitude 2—8175
  - πN scattering, construction from isospin degeneracy patterns 2—23860
  - πN scattering, off mass shell Veneziano type amplitude, rel. to estimation of σ term 2—34687
  - $\pi N\to K\Lambda$, dual amplitude and strange form factors 2—17930
  - $\pi\pi$, normalization using multiperipheral model with π, K and ω exchange 2—38299
  - $\pi\pi$, scattering, search for complex poles in unitarized model 2—14668
  - $\pi\pi$ amplitudes, K-matrix unitarization, positivity and crossing symmetry constraints 2—14670
  - $\pi\pi$ low energy scattering and model with subtraction constant 2—31296
  - $\pi\pi$ scattering, dispersive approximations for partial waves with essential singularities 2—418
  - $\pi\pi$ scattering, partial waves, asymptotic behaviour and complex zeros 2—417
  - $\pi\pi$ scattering, unitarized partial wave amplitudes, unique solution of dispersion relations found 2—14666

Venus
  - American and Soviet space research studies, review 2—17028
  - astronomical constants from Earth-Venus radar data 2—33748
  - atmosphere, American Astronomical Society, Amherst, USA 1971, conference 2—26623
  - atmosphere, clouds and surface, geochemical and meteorological perspectives 2—26853
  - atmosphere, height dependence of radiowave refractive index using results of direct measurements 2—41198
  - atmosphere, interpretation of CO_2 band and H_2O line 2—33747
  - atmosphere, i.r. and microwave transmission 2—41200
  - atmosphere, numerical experiments on general circulation 2—26855
  - atmosphere, radiative heat transfer below clouds 2—26858
  - atmosphere, review of data obtained by space probes and earth based investigations 2—26854
  - atmosphere, spectral composition emissivity and absorptivity of 91% CO_2 9% N_2 mixtures at 8500-11500 K 2—30584
  - atmosphere, spectroscopic evidence for structure of visible clouds 2—23114
  - atmosphere, thermal diffusion 2—1988
  - atmospheric circulation problems 2—4990
  - chemical composition and origin 2—20640
  - cloud tops, chemical composition, aqueous HCl 2—11012
  - clouds, occurrence of $FeCl_2.2H_2O$ 2—26859
  - clouds, presence of $FeCl_2$ 2—26860
  - clouds, variation with height 2—7536
  - cloudy atmosphere, theory of formation of spectral lines 2—23117
  - comet-like interaction with solar wind, characteristics of atmosphere 2—37376
  - equatorial swath topography from wavelength dependence of radar cross section 2—26852
  - exospheric temperature variations rel. to solar cycle 2—7520
  - imaging from a flyby 2—7524
  - ionosphere rate constants for CO_2^++H and CO_2+H^+, measurements in flowing afterglow system 2—17038
  - i.r. obs. at 345μ 2—10969
  - mass, from anal. of optical, radar and radio tracking data 2—13994
  - microwave brightness temp. and interpretations of radio and radar spectra 2—30582
  - position, meridian obs. for 1963-67 2—1989
  - present state of research, outline of future projects 2—7529
  - radar image, with 75 km resolution of $^1/_4$ surface 2—33749
  - radio source, 15.5 and 31.6 GHz, propagation test for satellite communications 2—16864
  - radiowaves, decimetre, atm. propagation, obs. 2—17039
  - seismic experiment at end of decade 2—26826
  - spectrum, CO_2 absorption lines, double-cloud model 2—26851
  - surface obs. 2—30558
  - topography, interplanetary radar echo delay obs. 2—30583
  - topside ionosphere, existence of thermal protons 2—17143
  - upper atmosphere, atomic carbon by photodissociation of CO and CO_2 2—11004
  - upper atmosphere, retrograde motion 2—26856
  - upper clouds, composition from occultation, transit and spectral data 2—41199
  - u.v. photometry from the Orbiting Astronomical Observatory 2—20675
  - u.v. region studies, upper atmosphere examination by near fly by 2—11009
  - H I emission from upper atmosphere 2—11011
  - O I emission from upper atmosphere 2—11011

Verdet constant *see Magneto-optical effects*

Verneuil process *see Crystals/growth*

Vertex functions *see Elementary particles; Field theory, quantum; Functions*

Vibrating bodies
  - *see also Crystals/lattice mechanics; Elastic waves; Pendulums; Piezoelectric oscillations*
  - analysis by moire contour-sum contour-difference 2—8054
  - anemometer filaments in turbulent flow fields and errors in meas. of velocity fluctuations 2—12487
  - atomic vibration amplitudes rel. to thermal expansion, theory 2—4072
  - autoparametric interactions in harmonic forcing of structure near internal resonance 2—34074

Vibrating bodies continued
  - axisymmetric vibrations of free finite length rod, orthogonalization procedure 2—14236
  - baffled beam, radiation resistance 2—34100
  - bar, designed to have specified end reactance in a certain frequency range 2—2230
  - beam carrying moving masses, dynamic stability, investigation including damping effects 2—34062
  - beams, fundamental frequency by integral equation approach 2—17365
  - beams and plates, scaling law obs. inc. shear and rotatory inertia 2—20914
  - box structure, response to travelling pressure waves and sonic booms 2—153
  - ceramic transducer, effect of mechanical load 2—20908
  - circular annulus of nonisotropic elastic material, dynamic vibrations and stresses 2—34058
  - circular arches, geometrically nonlinear, large amplitude free vibration and amplitude frequency relationship 2—34071
  - circular cylinder, micropolar vibrs., dispersion eqns. 2—11344
  - circular cylindrical shell, perturbation analysis of nonlinear free flexural vibrations 2—23341
  - circular cylindrical shells, nonlinear vibrations with arbitrary loading and boundary conditions 2—34072
  - circular disk, forced and free vibrations 2—34050
  - circular plate, modes of vibration with three simple support points 2—30854
  - composite cylinder, forced torsional vibrations produced by periodic shearing force along ring on outer boundary 2—17363
  - composite plates and shells, coupling and stacking effects 2—17338
  - conical shell, free vibrations under various boundary conditions 2—37736
  - control systems, buyer's guide 2—14278
  - coupled multimodal systems, exact solutions for response to excitation 2—14238
  - curved bar, analysis of vibrations caused by longitudinal impact 2—23346
  - curved sandwich beams, natural frequencies 2—5213
  - curved sandwich plates, effect of in-plane static stresses on vibration characteristics 2—37741
  - curvilinear plate bending elements, new nonconforming family 2—27209
  - cylindrical membranes, nonlinear theory 2—30846
  - cylindrical shells, fluid-filled, flexural vibrations 2—17359
  - cylindrical shells, with initial stress subjected to general three-dimensional surface loads, dynamic response 2—34061
  - damping additions for plates using constrained viscoelastic layers 2—34054
  - damping with sound frequency antivibrators, vibro-isolating properties 2—23347
  - driven nonlinear oscillations of string and instabilities 2—34051
  - dynamic contact problem of rigid block stamp on elastic half-space 2—37737
  - ear, pattern of round window in cats 2—11216
  - elastic wave propagation in cylinder, experimental and theoretical investigation of modes 2—14251
  - finite element method, minimization procedure for general eigenvalue problem 2—7749
  - flat plate subject to excitation by vortex shedding in airstream, effect of acoustic props of environment 2—20918
  - flexural vibrating free edge plates with stepped thicknesses for generating high directional ultrasonic radiation 2—34117
  - flexural vibrators, l.f., quarter or half wavelength mounting 2—23345
  - flutter of a thin panel, effect of a rigid boundary 2—2232
  - force method for free vibration of one-way continuous rectangular plates 2—34065
  - forced sinusoidal vibration of damped circular and annular membranes, impedance and transmissibility frequency dependence 2—34066
  - forced vibrations of rigid body on three-parameter foundation 2—5210
  - found motion problems in viscoelasticity 2—2221
  - frequency response excited by transient or random forces using cross correlation and its Laplace transform 2—5170
  - frictional daming effects on vibration of elastically supoorted beam 2—34076
  - glass-epoxy and boron-epoxy beams, stress waves, propagation study 2—25474
  - grid-stiffened simply supported plate, closed functional solution 2—14243
  - helicopter rotor blades, scale effects in bending vibrations 2—37734
  - hollow piezoelectric ceramic sphere, vibrations 2—37738
  - infinite beam on elastic foundation with randomly moving load, asymptotic dynamic response 2—27207
  - infinite plane periodic structure ruled with rectangular slots, sound radiation 2—27247
  - infinite thin elastic plate immersed in compressible fluid 2—23344
  - kettledrum, effect on frequency of applic. of mass load point 2—20913
  - large deflections of impacted helical springs 2—34052
  - linear viscoelastic beam, asymptotic stability of solutions 2—37733
  - mechanical structure elements, laser apparatus for amplitudes and resonance frequency obs. 2—27211
  - membrane shells on bases bounded by curves, conditions of freedom from lateral thrust 2—20906
  - metal disc, attenuation of Rayleigh waves on edge 2—17371
  - micro tubing forks 2—34049
  - mode coupling due to nonlinearity in vibration of thin panels 2—34077
  - motion and velocity of machine parts transported with jumping 2—2235
  - multiconductor overhead transmission lines, det. of natural frequencies 2—34055
  - multipolar elastic plate, equivoluminal vibration modes 2—23343
  - NASTRAN computer program for analysis 2—2210
  - natural frequencies of multispan circular curved frames 2—37730
  - nonhomogeneous spherical and cylindrical shells, radial vibrations 2—27203
  - nonlinear structure, random pressure field, Monte Carlo soln. 2—27202
  - nonprismatic thin space beams, generalized formulation of vectorial equations of motion 2—34060
  - nuclear reactor fuel rods, induced by coolant flow 2—15135
  - nuclear reactor internals, expts. rel. to calcs. 2—15174
  - orthotropic laminae, thick, exact natural freqs. and modal functions 2—17367
  - oval cylindrical shells, freely supported, free vibrations 2—27200
  - parametric instability of flat plates with sinusoidal direct and shear loading 2—34075
  - pellets in plastic medium, shock-no shock conditions at boundaries of sliding regions 2—5212

Vibrating bodies continued
- perfectly conducting viscoelastic infinite plate in mag. field, displacement obs. 2—34057
- plate, infinite with elastic foundation and damping, dynamic response 2—27210
- plate containing random inhomogeneities, flexural and longitudinal waves 2—27225
- plates, non-homogeneous, asymptotic theory 2—27198
- plates, orthotropic, skew, frequency analysis by finite strip method 2—152
- plates, rectangular, cracked, vibration and stability 2—7747
- polygonal plates natural frequencies applic. of conformal mapping and variational method to obs. 2—11345
- power flow between two coupled beams 2—14239
- prestressed concrete containment vessels, natural frequency and damping by dynamic analysis 2—15163
- prolate spheroids, local sound radiation impedance 2—34118
- radially polarized piezoelectric ceramic rings, axisymmetric modes and electrical impedance 2—27231
- radiation resistance of vibrating rectangular panel 2—34508
- random vibration with nonlinear damping, applications to aircraft 2—34073
- reactor control rod, rel. to neutron noise production 2—15101
- rectangular body on elastic stratum, harmonic rocking 2—37729
- rectangular plates, chordwise bending vibrations and flutter 2—2234
- response of plate bonded to randomly vibrating viscoelastic half-space 2—34053
- rigid circular body, vertical vibration 2—37729
- ring, using finite element shape functions as method of analysis 2—154
- shallow arches, discrete element displacement method of obs. of fundamental extensional frequency 2—5211
- shallow spherical shell, loaded, axisymmetric vibrations 2—37732
- shell, cylindrical, with variable curvature, comparison of various solution methods 2—2231
- shell cylindrical, partially filled with liquid, free vibration theory 2—2229
- shells, programs BOSOR3 and STAGS, based on finite-difference energy method, for analysis 2—2209
- shells with a doubly curved triangular finite element, dynamic analysis 2—11346
- short cylinders, longitudinal mode resonances 2—17361
- simple pendulum suspended from vibrator, Melde experiment to measure tension in cord 2—14148
- slightly curved beams of transversely isotropic composite materials 2—23340
- sound radiation by interacting elastic shells 2—37759
- spacer distributed masses, bundle vibration 2—37728
- spherical shells, fluid-filled and fibre-reinforced 2—2233
- stepped bar, free-free, resonant frequency and vibration mode anal. 2—17366
- structural system response, randomly excited, discrete time series synthesis 2—14240
- $^1/_2$-subharmonic oscillations, study by harmonic balance methods for single degree of freedom systems with nonlinear spring characteristics 2—34070
- symmetrically, pulsating segment in tank, wave radiation 2—27226
- thin convex shell of revolution, axisymmetric moment state of stress, stability loss 2—23328
- thin cylindrical shells conveying fluid, flutter 2—20911
- thin elastic beams, finite deflection dynamics 2—34087
- thin elastic circular plate diaphragm, acoustic impedance 2—34067
- thin plates, calculation by finite element method 2—37724
- Timoshenko beams, continuous, natural frequencies 2—11348
- trapezodial plates, symmetric, simply supported, numerical analysis 2—17364
- tuning fork of electronic watch, vibration analysis by holographic and photographic methods 2—14234
- tuning forks as inertial rotation sensors 2—5175
- ultrasonic vibrations of one mirror in optical cavity, laser beam modulation 2—27560
- uniform beam supported at ends, transversely impinging load at midspan, dynamic response 2—2190
- uniformly curved tube conveying fluid, stability 2—14235
- unsymmetric trapezoidal plates, simple supported 2—23342
- vertical spring, mass distribution and frequencies 2—17158
- vibrators in photoelectric devices effects of resonance on distortion and sensitivity threshold 2—23480
- vibrohammer with spring mounted driving motors, stability of motion 2—30829
- violin body vibrs. at eigenfreqs. 2—34136
- viscoelastic rectangular plates, simply- supported, exact three-dimensional analysis 2—7748
- viscoelastic reed, Fourier transform method in linear viscoelastic analysis 2—34044
- viscoelastic string, effect of stress relaxation 2—27208
- weak coupling effects on assembly of damped oscillators, application to ionic oscillations of unbounded plasma 2—28614
- wide band stabilizer for motion vibration reduction of instrument in aircraft 2—30857
- wood structures, damping sources in material and joints 2—14241
- wood structures, predictions of damping in nailed and glued joints 2—14242
- Al and steel cantilever beams, attenuation, theory and reciprocal experiment 2—14237

Vibration, molecular *see Molecules/vibration*

Vibrations
- *see also Acoustics; Damping; Oscillations; Vibrating bodies; Waves*
- bending, helicopter rotor blades, scale effects 2—37734
- biodynamic models of injury mechanisms 2—11191
- ceramic transducer, effect of mechanical load 2—20908
- convertor for u.s. power applic. 2—27272
- curved u.s. transmission lines, vibrations and wave characteristics 2—37754
- cylindrical cantilever, response to axial air water flow 2—14245
- cylindrical shell, free flexural vibr. characts. hybrid finite element theory 2—34022
- damped linear systems, local modifications, procedure for determ. eigenvalues and eigenvectors 2—17362
- deflection of elastic plate on viscoelastic foundation under moving load 2—34056
- dynamic, in circular annulus of nonisotropic elastic material 2—34058
- elastic bar, damping of flexural bars 2—30859
- elastic medium, layer pot. method applic. 2—30858

Vibrations continued
- elastic plane and half plane due to sudden appearance of crack 2—27220
- elastic plates, high frequency, approximate theory 2—30855
- elastic sphere, anisotropic, forced vibrs. 2—37727
- elastic thin plate, response to impulsive distribution 2—5191
- effect on elasto-plastic system with one degree of freedom 2—27199
- energy method of solving vibration problems 2—27204
- finite element eigenproblems, optimal gradient minimization 2—27194
- flat plate subject to excitation by vortex shedding in airstream, effect of acoustic props of environment 2—20918
- flexural, of rectangular orthotropic plates subject to in-plane forces 2—156
- flutter, thin cylindrical shells conveying fluid 2—20911
- free, doubly curved sandwich plates, effect of in-plane static stresses 2—37741
- heat exchanger, ring portion of U-bend segment, pinned and clamped conditions 2—5208
- h.f., holographic interferometry obs. using stroboscope based on ruby laser with passive shutter 2—17651
- holographic anal., time-average, envelope factors due to laser modulation 2—38011
- holographic analysis, use of normal mode theory, applic. to asymmetrical circular disc 2—2228
- holographic set-up for white light holograms, method of checking stability 2—5387
- kettledrum, effect on frequency of applic. of mass load point 2—20913
- kinematically forced, damping 2—34091
- lattice, effect of pressure on simple cubic crystals 2—15994
- linear conversative system, loading-frequency relationship in multiple eigenvalue problems 2—34063
- liquid-liquid interface, effect on ionic mass transfer 2—3376
- mechanical structure elements, laser apparatus for amplitudes and resonance frequency obs. 2—27211
- natural frequencies of polygonal plates, applic. of conformal mapping and variational method to obs. 2—11345
- nonlinear damper in stochastic approach 2—37726
- nonlinear reson. in systems with multiple degrees of freedom 2—34048
- nonlinear systems, entropy and self-oscillations 2—30856
- nonlinear transverse, at resonance in elastic layer and in layer of an ideally conducting fluid 2—37735
- nonstationary random process, definition of spectrum 2—27214
- nuclear reactor, boiling water, finite element method for analysis 2—15084
- nuclear reactor fuel pins, parallel flow induced 2—15136
- nuclear reactor fuel rods, induced by coolant flow 2—15135
- nuclear reactor internals, program system for anal. of long time series of signals 2—14246
- nuclear reactor power channels, two phase coolant flow induced 2—14247
- pipe containing flowing fluid, integral equation methods for investigating transverse vibrations 2—20915
- plane stress waves in membranes caused by arbitrary pressure wave 2—17375
- plate, coupling with acoustic field 2—30863
- plate, rectangular orthotropic, subject to in-plane forces, flexural vibrations 2—156
- plate-bending, rectangular and triangular finite elements 2—11347
- polygenic systems, one dimensional continuous, stability 2—27212
- power sources, amplitude and frequency, resonance 2—17368
- pressure loaded paraboloidal shells, free vibration analysis by finite element method 2—27201
- prismatic shells, computer code analysis 2—20892
- quartz cryst., neutron time spectrum 2—9430
- radial, cylinder and sphere bonded to thin nonhomogeneous casings 2—20907
- rapid loading testing machines, electrical correction of dynamometric systems 2—29364
- reactor containment, determination of damping matrix in dynamic structural analysis 2—14249
- rectangular cantilever plates with stepped cross-section, analysis by finite element method 2—27213
- rectangular plate, simply supported, thermoelastic vibrations produced by temperatures prescribed on faces 2—37715
- ring, symmetrical cross section, flexural vibrations study 2—147
- rods in parallel flow, self sustained 2—14244
- rotating cylindrical container, hydroelastic vibrations of liquid 2—18783
- rotating symmetrical shaft, 'Timoshenko beam' theory 2—151
- SH type, surface displacement due to propagating circular fracture 2—20260
- shallow spherical shell, loaded, axisymmetric vibrations 2—37732
- shells, initially stressed, stability and vibration 2—15159
- sine vibration testing using narrowband tracking filters 2—37740
- space, proper vibration 2—17179
- string vibr. nonlinearities 2—34068
- structural, use of digital computers in exptal. anal. 2—14248
- tapered skew plates, variable thickness, natural frequencies and modes 2—27206
- causing temporary hearing loss 2—37471
- thin elastic circular plate diaphragm, acoustic impedance 2—34067
- torsional, forced, of composite cylinder, produced by periodic shearing force along ring on outer boundary 2—17363
- torsional, in circular rods, damping 2—37739
- torsional loadings of perfectly conducting elastic half-space 2—27219
- transverse, of shallow arches using discrete element displacement method 2—5211
- transverse, perfectly conducting viscoelastic infinite plate in mag. field 2—34057
- transverse, pianoforte string struck by hammer, dynamics 2—20910
- viscoelastic beam, nonlinear constitutional equation 2—17360
- Whittaker's eqn., stability of a soln. 2—34059

excitation
- through bubble formation within water filled tubes 2—17394
- elastic, by gravitational wave 2—30853
- impulsive loading or ring structures 2—37731
- parallel-flow-induced, of flexible rod, mathematical model 2—38733
- in Phenix, Na cooled fast reactor due to turbulence in liquid Na flow38711 2—38711
- power sources, amplitude and frequency, resonance 2—17368

measurement
- *see also Seismology*
- accelerations and parameters of oscillatory processes, tolerances 2—27196
- amplitude det., stroboscopic technique, for calibration of vibration transducer 2—20912

Vibrations continued
- **measurement** continued
  - annular diffuser flow, factors affecting instability 2—39074
  - attenuation factor of ultrasonic vibrations using the echo-pulse contact method, measurement accuracy 2—27195
  - circular membrane, transducer for monitoring oscillations 2—17358
  - force method for free vibration of one-way continuous rectangular plates 2—34065
  - holographic and photographic methods, tuning fork of electronic watch 2—14234
  - holographic interferometry, real- time analysis of engineering structural components 2—23339
  - holographic method with phase modulated reference beam, for nonuniformity quasipiston vibrations 2—27197
  - in-plane, of structures, using laser- photocell combination 2—2227
  - by laser beam Doppler shift method 2—155
  - laser beams application 2—2225
  - laser speckle method real time 2—5209
  - laser-Doppler interferometer employment 2—2428
  - mechanical impedance by transient loading technique accuracy 2—37725
  - moire method of amplitude det. 2—20909
  - Philco TV receiver testing 2—2224
  - power spectral density functions calc., digital computer programs 2—23314
  - precision instruments for linear measurements, tests 2—23338
  - small, laser instrument 2—2226
  - speckling, in-plane analysis with lasers 2—7942
  - test techniques, industrial and commercial applications 2—150
  - torsion vibration meas. of radio link antenna towers 2—6531

Vibronic states *see Molecules/electronic structure; Molecules/vibration*

Vidicons *see Electron tubes*

Virial coefficients *see Equations of state*

Virtuons (virtual phonons) *see Crystals/lattice mechanics*

Viscoelasticity
- *see also Plasticity*
- anisotropic shells, analysis of viscoelasto- plastic structural behaviour by finite element method 2—14220
- axially symmetric stretching of nonlinear viscoelastic membrane 2—37710
- bil(m-(m-phenoxy phenoxy)phenyl)ether, at pressures up to 300 MN/m^2 2—39307
- biological cells, suspension, props. calc. 2—35804
- biological specimens, wave propagation in, apparatus for study 2—33779
- blood, considered as suspension 2—14028
- boundary value problems, establishment of Volterra principle 2—5203
- butadiene-styrene block copolymers, branched, behaviour governed by length of terminal blocks 2—6179
- cantilever, instability under follower load 2—34043
- compressed rod, critical stability under compressing force 2—34042
- creep kinetics rel. to dislocation viscous bowing 2—32613
- cylinder, anisotropic, relaxation of temp. stresses 2—145
- cylindrical shells under internal pressure analysis 2—14185
- deformation of nuclear reactor fuel elements, probabilistic models 2—21463
- di(2-ethylhexyl)phthalate, at pressures up to 1400 MN/m^2 2—39307
- dynamic moduli in superposed oscillatory shear, asymptotic relations 2—24594
- empirical equations for viscoelastic functions 2—14218
- epoxy resin, linear viscoelastic range from uniaxial tension tests 2—1279
- fission reactor fuel elements, analysis of internal heating shock effects, expansions, stresses in specific element geometry 2—38745
- flow of a viscoelastic fluid in a hydrodynamic wedge 2—21736
- fluids subject to large deformation apparatus for stress relaxation meas. 2—5190
- folding deformation of layered medium in compression, dynamic effect 2—34045
- forced motion problems, solution method 2—2221
- ground waves, separation from elastic waves 2—4634
- linear, analytical form of the dynamical functions 2—32585
- linear, correspondence principle appl. 2—17347
- linear analysis of vibrating reed by Fourier transform method 2—34044
- linear programming application to interconversion of viscoelastic functions 2—14217
- linear relaxation functions restrictions 2—14219
- linear theory appl. to dissipation in anelastic solids 2—2191
- liquid, u.s. attenuation meas. of relax. 2—28810
- liquid jets, effect on capillary breakup 2—25024
- liquids, effect of high pressure 2—39307
- liquids, gas bubble terminal velocity versus volume discontinuity 2—28768
- liquids, linear and non-linear effects, teaching 2—25017
- liquids of arbitrary memory, stability eqn. for flow 2—3347
- loudspeaker diaphragm papers, dynamic modulus of elasticity 2—30869
- macromolecular solutions, computerized measurement, frequency dependence over extended viscosity range 2—25015
- matrix differential equation and numerical solution 2—17301
- memory effects and internal changes of a material 2—27141
- multilayered orthotropic viscoelastic plates, simplified treatment of dynamics 2—23325
- nonlinear thermoviscoelasticity, formulation of constitutive eqn. 2—14222
- nonlinear vibrations of beam, constitutional equations 2—17360
- nonlinear viscoelastic bodies, generalised energy forms 2—20903
- nuclear reactors, linear boundary problem solved by method of orthogonal projection in Hilbert space 2—14286
- nylon 6, fatigued fibres temp. dependence of dynamic viscoelasticities 2—3846
- nylon 6, glass fibre reinforced effect of glass fibre content on temp. dependence of dynamic viscoelasticity 2—25486
- organic solvent, rel. to viscosity effect on dielec. props. of haloalkane solns. 2—18846
- orthotropic cylindrical shells, large deflections 2—14221
- plane viscoelastic problem in polar co-ordinate system 2—37711
- plate transparency to sound 2—30864
- polar solutes, variation of relaxation time with viscosity 2—32198
- poly(2-hydroxymethyl methacrylate) crosslinked solutions in diethylene glycol, comparison with polyethylene methacrylate and polybutyl acrylate with low crosslinking 2—35711
- polyacrylonitrile, mechanical relaxation properties 2—35859
- polyacrylonitrile, mechanical relaxation props. of drawn samples 2—35858

Viscoelasticity continued
- polyester-styrene copolymers, effect of three-dimensional network density 2—25485
- polyethylene, low density, uniaxially orientated, hot- and cold-drawn, tensile creep behaviour 2—12877
- polyethylene melt, flow behaviour, influence of dissolved gases 2—18778
- polyethylene melt, shear rate dependent relax. spectrum 2—15552
- polymer, conf., Los Angeles, USA, March (1971) 2—15808
- polymer, liq. or soft solid, shear mode strip delay line study 2—15811
- polymer, two-phase, time-temp. superposition 2—15809
- polymer, undergoing crosslinking reactions, response prediction 2—15810
- polymer, yield behaviour 2—15843
- polymer coating, role in application and drying 2—15668
- polymer solns., dilute, limiting stretch rate 2—3346
- polymers, oriented, yield behaviour 2—6540
- polymethyl methacrylate (perspex), linear viscoelastic range from uniaxial tension tests 2—1279
- polyvinyl chloride, filled plasticized 2—6524
- polyvinyl fluoride, rel. to thermal molecular motion 2—22061
- Rayleigh surface waves 2—162
- reinforced cylinders and spheres, dynamic problems when subjected to internal uniform pressures 2—34041
- response of viscoelastic sphere to a pulse from a point source at the centre 2—17345
- rheometer, concentric cylindrical design for high pressure applic. 2—24990
- rubber, crosslinked by S, meas. of width and time position of retardation spectrum 2—9635
- spherical wave propagation in Maxwell and Voigt type media 2—17346
- effects on stability of parallel flows of second order liquids, effects of viscoelasticity 2—9056
- supercooled liqs., retardation 2—35710
- Teflon, shock compression behaviour 2—9640
- thermal axisymmetric stress analysis, finite element and finite difference computer techniques 2—17348
- thermal nonlinear dynamic coupled, solution of problems by finite element method 2—11343
- thermoviscoelasticity, nonlinear, exact solution of problems 2—5204
- torsion bar, inhomogeneous anisotropic, transformations for modelling 2—123
- ultrasonic dynamic viscosities in superposed oscillatory shear 2—35398
- viscoplastic rod, nonlinear, subjected to constant velocity impact, similarity solution 2—27190
- wave propagation in elastic/viscoplastic hollow sphere 2—27223
- $Ca(NO_3)_2.xH_2O,(x=3.2,4)$, melts, u.s. relax. rel. to mol. rearrangements 2—35762
- Pd-Si based metallic glasses, anomalous behaviour 2—32590

Viscometers
- automatic Zimm-Crothers type, for measuring low shear stress 2—39293
- calibration of liquid viscometers, accuracy of measurements 2—39345
- capillary, development for low-viscosity molten salt meas. 2—28811
- capillary, kinetic energy and end corrections 2—32244
- capillary, obs. of kinetic energy correction 2—21727
- capillary, variable shear rate, for outflow viscometry in dogs 2—14030
- capillary tube type, estimation of errors when using deformed tube 2—28808
- channel flow, for absolute measurements 2—39347
- circular disk viscometer and related electrostatic problems-comments 2—25054
- discharge time, automatic measurement 2—28443
- extensional, historical survey 2—28442
- falling cylindrical shell, force centers shell in fall tube 2—35693
- falling-cylinder, nonvertical alignment effect on performance 2—12526
- gas, four capillary differential 2—32183
- for glass in temp. interval of softening and annealing 2—21938
- high-pressure for gas-liquid solutions, combination of falling body and capillary viscometer 2—39349
- hose type, design and theory 2—28442
- open-end type hose viscometer, combined extensional and squeezing motions 2—18782
- oscillating, with torus shaped crucible 2—3379
- oscillating-disc; determination of reference values of viscosity for twelve gases at 25°C 2—3330
- plunger type, digital readout 2—18800
- rheometer designs for elastico-viscous liquid 2—3344
- for solutions with solid components, modified Ubbelohde viscometer 2—21966
- surface, based on large amplitude oscillations, design and performance 2—35712
- torsional pendulum, calibration and errors 2—39346

Viscoplasticity *see Plasticity*

Viscosity
- bis(m-(m-phenoxy phenoxy)phenyl)ether, at pressures up to 300 MN/m^2 2—39307
- capillary rheometer obs., effect of viscous dissipation 2—21754
- cholesteric liquid cryst., u.s. propag. obs. 2—12559
- colloidal suspension, coagulated, plastic flow, viscous energy 2—15618
- compressible viscous flow, generalized finite-element method 2—24607
- di(2-ethylhexyl)phthalate, at pressures up to 1400 $MN/^2$ 2—39307
- disperse system, fluid-particle, turbulently suspended 2—3416
- disperse systems, low Reynolds numbers, relative velocities and pressure drops 2—3412
- drag coeff. determ. for particles in rarefied, low-Mach number flows 2—24629
- drag on neutral and charged spherical aerosol particles 2—28918
- Earth's core, kinematical viscosity 2—7223
- fluids, eddy viscosity, derivation of Kubo type formulae 2—6047
- fluids, effects of inertia on Brownian motion of rigid particles 2—24595
- friction viscous, effect on dislocation speed 2—6492
- gases, ionisation of shock thickness of shock waves with viscosity 2—28726
- glass fibre, torsional meas. 2—1291
- incompressible elastically viscous fluids, attenuation of turbulent motion 2—39032
- incompressible fluid, unsteady plane Poiseuille flow between two parallel plates 2—6043
- incompressible fluid stream, flow, from finite radius sphere, past rotating sphere 2—39047
- internal in linear macromolecules, origin 2—39013
- isotropic asymmetric non-gyrotropic medium 2—7745

- **Viscosity** continued
  - liquid containing gas bubbles, weak shock waves, viscosity effects 2—25016
  - liquid crystal, p-azoxyanisole, rel. to drift mobility 2—39341
  - Lorentz plasma in strong magnetic field, corrections calc. from electron distribution function 2—12369
  - nematic liquid cryst., thermal depend. of twist viscosity coeff. 2—32232
  - particular slow flow in channels and tubes, use of finite-element method application to biomechanics 2—35424
  - phenyl alkyl ketones in glassy matrices, viscosity dependent dual phosphorescence 2—36950
  - plasma thermal, effects of cut off criteria of electronic partition function and transport properties 2—28511
  - Poiseuille flow, power-law fluid, viscous heating 2—3165
  - pressure, deform. profile, between two colliding lubricated cylinders, composite pressure viscosity coeff. effects 2—31899
  - shear flow past semi-infinite flat plate, diffusion and viscous effects 2—28445
  - slipstream flow, structure determ. downstream of centre line Mach reflection 2—21735
  - solar convection zone, effects on temp. fluctuations 2—7564
  - solid-gas flow in vertical pipes, particle dynamics 2—25122
  - spheres in conc. suspensions, statistical mechanical calcs. 2—35436
  - steel, under high velocity impact 2—6544
  - Stokes problem in kinetic theory, linearized Boltzmann eqn. 2—31915
  - suspension in turbulent channel flow, entrainment mechanics 2—25124
  - turbulent pipe flow, eddy viscosity model 2—24603
  - two-phase flow, skin-friction and film-thickness meas. in upward flow through annulus 2—24631
  - ultrasonic dynamic viscosities in superposed oscillatory shear 2—35398
  - viscous flow through rigid porous medium, equation of motion 2—39049
  - effects on wave reflection nearly parallel to boundary in rotating fluid 2—3180
  - Al metal, under high velocity impact 2—6544
  - Ar plasma, meas. 2—3228
  - BaO-B$_2$O$_3$ glass, effect of liquation 2—35848
  - Cu metal, under high velocity impact 2—6544
  - N$_2$ plasma, meas. 2—3228
  - Na$_2$O-B$_2$O$_3$ glass, effect of liquation 2—35848
  - Pb, solid, creep characts. obs. 2—32619
  - **gases**
    - axisymmetric jets, quiescent and coflowing, eddy viscosity 2—24953
    - bulk viscosities, computer program for extraction from sound absorption data 2—32182
    - carbon tetrafluoride, shear viscosity in static mag. field and field free space, calc. using rigid model with tetrahedral symmetry 2—35687
    - delta wing, viscous layer interaction with external flow 2—6146
    - dilute gases, shear viscosity, contribution of orientational polarizations in collisionally uncoupled model 2—21924
    - drop motion in a viscous gas stream 2—39244
    - eddy models for turbulent free shear flows 2—35672
    - Enskog method, relativistic extension 2—9027
    - expansion, three-dimensional study radial, viscous gas from sonic source into a vacuum 2—32166
    - fluoroform, shear viscosity, room temp. mag. field effects 2—21925
    - inert, 270-2000°K 2—18769
    - interfacial shear viscosity at liquid-gas interfaces, theoretical analysis 2—25053
    - jets, turbulent and wall, in uniform streaming flow 2—3285
    - methane, shear viscosity, in static mag. field and field free space, calc. using rigid model with tetrahedral symmetry 2—35687
    - methane, shear viscosity, room temp. mag field effects 2—21925
    - methane combustion products 2—6165
    - mixtures, binary polar-nonpolar, normal pressures 2—1039
    - mono- and tri-methylamine vapours, variation with temperature 2—32183
    - Navier Stokes theory for flow between relatively rotating coaxial cylinders 2—3337
    - perdeuteromethane, shear viscosity, in static mag. field and field free space, calc. using rigid model with tetrahedral symmetry 2—35687
    - rare, dil., coeffs. determ., atm. press., 270 to 2000K 2—18764
    - reference values for twelve organic and inorganic gases at 25°C 2—3330
    - steam, correlation of viscosity, thermal conductivity and Prandtl number as function of temperature and pressure 2—32245
    - turbulent shear flow, Phillips' hypothesis comparison with expt. 2—1040
    - Ar, calc. 2×10^3 to 12×10^3 K and 10^{-4} to 1 atm. press. 2—12514
    - Ar, high temp. calc. 2—18770
    - Ar, meas. at atmospheric pressure, 25-700°C, using oscillating disc viscometer 2—35688
    - Ar, new relative meas. in 25-700°C range, analysis of long term reproductibility of oscillating disc viscomter 2—32186
    - CO, shear viscosity, room temp. mag. field effects 2—21925
    - CO$_2$, new relative meas. in 25-700°C range, rotational collision number computed using kinetic theory 2—32184
    - H, from study of H+H$_2$ mixture 2—9043
    - H$_2$, high temp. calc. 2—18770
    - H$_2$ isotopes, collision cross sections, interrelationships with other transport and relaxation phenomena 2—39026
    - HD, shear viscosity, room temp. mag. field effects 2—21925
    - He-N$_2$ binary mixture, relative meas., 25-700°C 2—32185
    - He, high temp. calc. 2—18770
    - Kr, high temp. calc. 2—18770
    - Kr meas. at atmospheric pressure, 25-700°C, using oscillating viscometer 2—35688
    - N$_2$, along saturation line in liquid and vapour phase and under pressure 2—39348
    - N$_2$, high temp. calc. 2—18770
    - N$_2$ shear viscosity, room temp. mag. field effects 2—21925
    - Ne-Kr binary mixtures, meas. at atmospheric pressure, 25-700°C, using oscillating viscometer 2—35688
    - Ne, high temp. calc. 2—18770
    - Ne meas. at atmospheric pressure, 25-70°C, using oscillating viscometer 2—35688
    - O$_2$, shear viscosity, room temp. mag. field effects 2—21925
    - SF$_6$ decomposition products, calc. at high temps. and pressures 2—39289
    - Xe, high temp. calc. 2—18770
    - Xe, new relative meas. in 25-700°C range, analysis of long term reproducibility of oscillating disc viscometer 2—32186
  - **liquids**
    - *see also Lubrication; Superfluidity*
    - absolute determination using channel flow 2—39347

- **Viscosity** continued
  - **liquids** continued
    - absolute determination using torsional pendulum 2—39346
    - accuracy of measurements, absolute measurements and uncertainty 2—39345
    - air bubbles-liquid two phase flow, apparent 2—8878
    - alcohols, volume viscosities, acoustical study 2—12553
    - alkali metals, calc. from structural data 2—21955
    - alkali metals, viscosity prediction 2—28788
    - alkali molybdates and tungstates, molten 2—35844
    - n-alkanes, short chain, intrinsic viscosity 2—6222
    - alloy melt, rel. to atomic struct. 2—25071
    - p-azoxyanisole crystal ultrasonic determ. of anisotropic shear and bulk viscosities 2—12552
    - p-azoxyphenetole crystal ultrasonic determ. of anisotropic shear and bulk viscosities 2—12552
    - benzaldehydes in benzene, substituted, mutual viscosity 2—39383
    - binary mixtures, prediction from thermodynamic properties 2—6221
    - blood, non Newtonian behavior, anomalies 2—14025
    - blood and blood plasma, discrepancies for different instruments 2—14029
    - butadiene-styrene block copolymers, branched dynamic viscosity studied above upper glass temperature 2—6179
    - chloroform-carbon tetrachloride system at 25°C 2—25065
    - cholesteric liquid crystals, compensated, flow behaviour 2—39338
    - cryolity-alumina mixtures, 980, 1000, 1020, 1050°C 2—28812
    - cyclohexane-aniline binary liquid system near critical mixing temp., 2—1085
    - di(2-ethylhexyl) sebacate, absolute measurement using channel flow 2—39347
    - di(2-ethylhexyl) sebacate, absolute measurement with torsional pendulum 2—39346
    - dye solution, fluorescence decay time 2—18837
    - elastico-viscous, limiting zero shear rate viscosity 2—12518
    - ethanol, ultrasonic meas. of temp. dependence of adiabatic volume viscosities in antiparallel dipole state 2—25056
    - falling ball viscometer for samples less than 1 ml 2—18801
    - falling cylindrical shell viscometer, force centers shell in fall tube 2—35693
    - film boiling on hemisphere, stagnation-point free-convection, viscous effects 2—25001
    - from Fourier transform. of density-density correl. function3378 2—3378
    - glycerine/dye solution, fluorescence, concentration depolarization 2—18840
    - high polymer solns., dilute, rel. to conc. 2—3377
    - hydrocarbons, press. depend. 2—35743
    - interfacial shear viscosity at liquid-liquid and liquid-gas interfaces, theoretical analysis 2—25053
    - magnetic silicate liquids, SiO$_2$ concentrations rel. to viscosity, model for calculation 2—40889
    - measurement using deformed capillary, error estimation 2—28808
    - metal, viscosity data, transport props. 2—28807
    - molecular motion study 2—35742
    - monosubstituted benzenes, high pressure measurement at 30°C 2—39392
    - non-Newtonian, laminar motion 2—35700
    - organic solvent, effect on dielec. props. of haloalkane solns. 2—18846
    - using oscillating toroidal crucible viscometer and obs. of damping coefficient 2—3380
    - perfluoroheptane iso-octane critical mixture 2—3430
    - polar, elec. field effects, field-induced rigidity 2—28809
    - polar solutes, variation of relaxation time, microwave frequencies, elastic behaviour 2—32198
    - polmers, dilute solutions, Mark-Houwink equation and Flory constant 2—15580
    - polydimethylsiloxane melts, high pressure, molec. weight dependence 2—25059
    - polyelectrolyte solutions, conc. dependence of reduced viscosity 2—25058
    - polyethylene in soln., determ. of molec. wt. distrib. and long-chain branching 2—8848
    - polyethylene melts, high density, molec. weight distribution effects 2—21929
    - polyethylenephthalate and solutions in anisole and nitrobenzene, over various concentrations and temperatures 2—9116
    - polyisobutylene, dil. soln., intrinsic viscosity, excluded volume effects 2—25033
    - polyisobutylene in ethyl heptanoate, meas. of intrinsic viscosity near θ-point 2—39395
    - polyisobutylene solution, falling sphere viscometry for det. of zero shear viscosity 2—35745
    - polymer, dilute soln., normal stress effects, Fixman's viscosity theory 2—25057
    - polymer solns., dilute 2—3346
    - polymer solution, moderately conc., solvent effects 2—18803
    - polystyrene in cyclohexane, meas. of intrinsic viscosity near θ-point 2—39395
    - polyvinyl chloride melt, high press. capillary viscosimetry 2—25060
    - polyvinyl chloride paste rheology 2—15894
    - polyvinyl chloride solutions, gamma irradiation induced branching effect 2—18804
    - rheometer, concentric cylindrical design for high pressure applic. 2—24990
    - solutions, effect of particle charge on radiationless energy transfer 2—28871
    - solutions with solid components, modified Ubbelohde viscometer 2—21966
    - squalane-gas solutions, viscosity-pressure dependence 2—9115
    - squalene with gases in solution, isotherms meas. in saturated and unsaturated state using high pressure viscometer 2—39349
    - squalene-gas solutions, viscosity-pressure dependence 2—9115
    - styrene-α-methylstyrene block copolymers in dilute solution 2—35371
    - supercooled liqs., viscoelastic retardation 2—35710
    - suspension, magnetic field effect 2—22019
    - tetraalkylammonium iodide/glycerol solutions 2—28813
    - u.s. attenuation meas. of relax. 2—28810
    - water, as basis of calibration of viscometers 2—39345
    - water, correlation of viscosity, thermal conductivity and Prandtl number as function of temperature and pressure 2—32245
    - water, supercooled, computation from self diffusion coeff., +30 to −25°C 2—9120
    - water at 250° to 370°C and up to 500 bar 2—1084
    - Au-Ge-Si alloy, near eutectic rel. to glass formation 2—32721
    - Ca(NO$_3$)$_2$, conc., aqueous soln., temp. dependence rel. to Fulcher eqn. and glass transition temp. 2—25055

Viscosity continued
- **liquids** continued
  - Fe, anomalous change, 1580-1640°C, oscill. crucible obs. 2—28805
  - p- H_2, pressure-temp.-viscosity diag., near critical temp., eqns. 2—18802
  - H_2O, pressure-temp.-viscosity diag., near critical temp., eqns. 2—18802
  - ^3He-^4He solutions, dilute, effective viscosity between 20 mK and 1K 2—22020
  - ^4He, ^3He-^4He mixtures, lambda point meas. of $\eta\rho_n$ 2—32294
  - Hg, thermal hysteresis rel. to metastable struct. near melting point, X-ray diffr. obs. 2—21959
  - LiCl-KCl, eutectic melt, viscosity, 400-500°C 2—28811
  - N_2, along saturation line in liquid and vapour phase and under pressure 2—39348
  - NaCl, solution in glycerol, rel. to ionic radii determination 2—15610
  - Ni, oscill. crucible obs. 2—28805
  - Se:I, In, impurity influence 2—3406
  - $ZnCl_2$, molten, viscosity and supercritical behaviour in binary solutions 2—35744

Visibility *see Atmospheric optics*

Vision
- *see also Colour vision; Eye*
- abstract visual perspective, dynamic display using fibre optic material as light-emitting line elements 2—31125
- acuity, vibrating objects, reading difficulty in relation to amplitude and frequency 2—5088
- adaptation, sensitization and masking, annular surrounds 2—7618
- adaptation effects, sinusoidal photopic amplitude threshold 2—20750
- adaptation threshold of photoreceptors, nonlinear summation 2—20760
- after images, negative brightness and full blackness solution to paradox of ceiling of blackness 2—14048
- after-image transfer, therapeutic procedure for amblyopia 2—41337
- after-images, fragmentation and closure in different eyes 2—7619
- alpha rhythm and uniform visual field in man 2—41272
- apparatus for the presentation of moving visual stimuli 2—26973
- area and visual threshold, relationship between area of visual stimulation and threshold luminance 2—37516
- artificial sunlight illuminant, visual and biological aspects 2—38138
- binocular addition of the response evoked by dichoptic patterned stimuli 2—5085
- binocular depth perception without geometrical cues 2—5086
- brightness contrast, low luminants, rod and cone system interaction 2—7622
- brightness perception constancy rel. to contrasts, implications for display lighting 2—14046
- cat, rate of dark adaptation 2—20762
- cats, average evoked potential correlates of two flash perceptual discrimination 2—41351
- cats, periphery effect, perceptual concept 2—30712
- contact lenses, use of hydrogel polymers, bibliography 2—11222
- contact lenses bifocal, retinal image effect, modulation transfer function 2—23706
- contrast difference thresholds with sinusoidal gratings, m.t.f. relationship 2—37510
- contrast enhancement and negative afterimage 2—41338
- contrast sensitivities, single bar detection, spatial frequency selection 2—33812
- contrast sensitivity, effect of exposure to glow 2—30701
- critical bands, analogy with auditory perception 2—33815
- dark adaptation in waning background luminescence 2—17130
- dark adaption in turtle, temporal course using behavioral avoidance paradigm 2—41352
- darkness enhancement during intermittent photic stimulation, subjective effect 2—20755
- definition problems 2—8004
- depth perception of adult and infant rats, effects of visual deprivation 2—41349
- detection of objects as function of angular size, contrast and search time 2—33811
- dynamic visual acuity, eye movements and peripheral acuity for moving targets 2—26980
- edge orientation discrimination by frogs 2—5091
- elasmobranch pupillary response, dilation and constriction in response to light and dark 2—7614
- electroretinographic responses of insects, variation with stimulation 2—20758
- entoptic diffraction halos and glare from bright monochromatic lights 2—20751
- equivalent luminance and spectral luminous efficiency in mesopic range 2—14047
- e.r.g. response to double flashes of light during dark adaptation, Fourier anal. of oscillatory potentials 2—26976
- flicker adaption, effect on apparent brightness of intermittent lights 2—41340
- flicker and flash thresholds, experimental relationship 2—26978
- flicker and flash thresholds, theoretical relationships 2—26979
- flicker and pattern detection thresholds, effects of frequency of variations 2—30698
- flicker fusion scotometry with solid state light sources 2—14045
- frog's brain, single-unit visual responses 2—41348
- frogs, retinal rods examined by polarizing microscope, measurement of linear dichroism 2—11219
- glare, luminaires with asymmetric light distributions, conversion tables for non-cosine axial distribution 2—41345
- Hering illusion, oblong shaped fields in visual system 2—41335
- horseshoe crab, effect of cyclic AMP on lateral eye retinular cells 2—7627
- human, reversibility of perceived motion, selective adaptation to speed, size and orientation 2—20753
- human, use of critical fusion frequency as measure of brightness 2—26982
- human visual system, spatial frequency channels, luminance and pattern drift rate effects 2—20752
- increment threshold for two identical flashes on steady background 2—11221
- increment thresholds for two nonidentical flashes 2—37511
- infant looking patterns, head and eye movements 2—7620
- inhibitory effects of orientational adaptation 2—2042
- interocular sustained suppression, evoked potential amplitude and distribution 2—30704
- involuntary eye movements, effects on visual image 2—11220
- lateral light adaptation effect in humans 2—26981

Vision continued
- light flashes, detection of Cherenkov radiation produced in the eye 2—5084
- lighting evaluation, sensory performance of eye 2—2043
- under lighting using Na lamps, relation of visibility to changes in coloured visual objects 2—37517
- line spread, point spread, and spatial modulation transfer functions 2—7612
- luminance time relationship, for partial time summation 2—41342
- luminosity magnitude estimation validity, preadaption and contrast effects 2—41344
- masking by interrupted gratings, orientation specificity, depth cues and absence of short duration spread 2—37515
- metacontrast, spatial characteristics 2—41339
- myopic, hypermetropic, emmetropic and astigmatic vision testing using laser speckle 2—37512
- neuronal connections in visual cortex, intercellular microelectrode recording 2—7616
- night myopia, relation to nycthemeral corneal rhythm 2—20754
- oblique-ray astigmatism, absolute threshold before and after correction 2—2041
- perception expts., applic. of fast computer displays 2—37513
- perceptual effects and reliability of ball lightning reports 2—5083
- performance data for 156 normal observers of various ages 2—41343
- photically evoked cortical potentials, intermittent background stimulation 2—33813
- pigeon eye, photopic spectral sensitivity, determined electroretinographically 2—30710
- rabbit, schematic eye, extent of monocular and binocular vision 2—20761
- real and apparent visual motion of a rotating object on a frontoparallel plane 2—17131
- receptor potential of honeybee drone, depolarizing aftereffect of intense light 2—20759
- resolution thresholds for moving targets at the fovea and in the peripheral retina 2—30694
- responsiveness, repeat variability over morning and afternoon sessions 2—41332
- retina, vision mechanism 2—33808
- retina models, picture processing 2—7621
- retinal, stabilised, dependent variable 2—11223
- retinal receptors and isolated retina, optical modulation 2—26977
- retinal responsiveness lack of symmetry shown by J_o stimulus pattern 2—7615
- rhesus monkey, effects of real and dark light on single unit activity 2—33819
- rod and core reception, effect of a flickering light 2—17132
- rod birefringence, measurement of retardance of single unbleached rods 2—7613
- rod saturation in cats 2—5090
- rod sensitization by annular surrounds, temporal properties 2—5087
- sinusoidal current and perceived brightness 2—26983
- small targets, influence of eye version, threshold luminance 2—41333
- space, size-distance relation and intrinsic geometry, implications for processing 2—30702
- spectacle lenses, high refraction negative, design parameters 2—17676
- stabilized images, influence of peripheral and central factors on disappearance 2—7617
- stereoacuity measurements, variations in size or orientation of small line segments 2—30703
- stereoperimetry, anal. of visual function 2—37514
- stereopsis, threshold rel. to monocular retinal illuminance 2—41336
- stereoscopic, mechanism binocular vision, simultaneous vision, fusion 2—30700
- straightness of dot and line stimuli, deviations 2—41341
- subnormal, historical survey of optical magnifiers 2—17127
- suppression-recovery effect, visual adaptation, in cats 2—7626
- telescopic low vision lenses, clinical method of field of view det. 2—26975
- temporal summation during dark adaptation 2—30705
- vertebrate retina and first layer in lateral geniculate nucleus, simulation 2—7611
- visibility meter, portable version, disability glare factor 2—41334
- Xenopus laevis, responses in optic tectum following visual stimulation 2—33818

Vitreous state
- *see also Glass*
- aromatic compounds, vitreous solutions, role of molec. association in temp. induced increase of delayed fluorescence 2—36947
- cellulose derivatives, glass transition temp. determ. 2—7047
- characteristic parameters, repeatability no., Deborah no. and critical cooling rates 2—18893
- fundamental liquids, at cryogenic temps., book 2—39323
- glasses, cation mobility determ. by direct meas. of drift velocities 2—1268
- metallic glassy alloy, structural model 2—32713
- polystyrene, thermodymamics of solidification process 2—12625
- semiconductor, chemical bonding, theory 2—19613
- silicate glasses, Raman spectra, phonon densities of states 2—19386
- structure study by X-ray emission spectroscopy 2—39436
- As-S-Sn system, glass formation, n.m.r. study 2—37003
- $As_2(Se,Te)_3$, semicond., elec. cond., Hall coeff., annealing effects 2—40243
- As_2Se_3, acousto-optical props., applic. to i.r. modulator 2—33214
- As_2Se_3 elec. cond. and Hall coeff., 180-225°C 2—22527
- AsSeI, semiconducting, preparation and obs. of thermal and optical props. 2—3456
- Au-Ge-Si alloy, viscosity and glass formation 2—32721
- B_2Se-Tl_2Se system, phase diagram, vitrification temp. 2—36274
- BeF_2, optically active vibrational modes calc. using β-quartz models determ. from X-ray diffraction 2—22382
- BeF_2, struct., neutron and X-ray diffr. obs. 2—25160
- C electron microscope study of structure 2—6290
- Cd-Ge-As, ternary system, glass forming region, phase transition temps. 2—15636
- $CdTl_{0.8}As_2$, elec. cond. and band gap 2—19637
- $FeCl_2$ amorphous frozen soln., glass transition 2—9220
- Ga-Sb-Se system, stratification region 2—35845
- GeO_2, diffusion and solubility coeffs. of He, Ne, Ar 2—39730
- GeO_2, ionic conduction, freq. and temp. depend. 2—25919
- GeO_2, photocond., rel. to band struct. model 2—22644
- GeO_2, pile irradiation, struct., X-ray and neutron diffr. 2—22056
- MgO-$TeO_2V_2O_5$, variation of physical props. and chemical stability with composition 2—6292

Vitreous state continued
- NaOH, aqueous solution, irradiated 77 K, reaction kinetics, electron tunnelling 2—30093
- P-S(Se)-Sn system, glass formation, n.m.r. study 2—37003
- Se, surface tension determination from obs. of thermal healing of scratches 2—39465
- SiO_2, migration and solubility of He 2—36083
- SiO_2, optically active vibrational modes calc. using β-quartz models determ. from X-ray diffraction 2—22382
- SiO_2, press. induced conformational changes, bond polarizability 2—18903
- $SrO-TeO_3-V_2O_5$ system, glass formation and properties 2—12631
- $ZnO-TeO_2-V_2O_5$, variation of physical props. and chemical stability with composition 2—6292

Vlasov equation *see Plasma*

Vocoders *see Speech*

Voigt effect *see Magneto-optical effects*

Volta effect *see Contacts, electrical*

Volume measurement
- metallic system, dilatometry, X-ray meas. 2—3862
- mixed material components, gamma ray albedo 2—27029
- steel, high-speed, quench deform., dimens. change, dilatometric alaysis 2—29392
- steel, rhenium, quenching, martensitic transformation 2—3994
- underground storage reservoirs, determination of shape and volume by hydroacoustic survey, errors 2—37760
- vacancies, dilatometric study using electrical transducer techniques 2—19228
- vacuum dilatometer, mechanotron sensing element for expansion of metal in welds 2—2054
- Fe, liq., thermal expansion, dilatometer method, 1833-2023K 2—28833

Vortices
- *see also Cavitation; Turbulence*
- acoustic interferences in vortex shedding from circular cylinder 2—1051
- air, effects of acoustic disturbances on velocity fluctuation and vortex shedding in shear layer behind circular cylinder 2—35648
- anticyclonic vortex trapped above seamount 2—16782
- atmospheric flow around the island of Madeira, Karman vortex streets, satellite observations 2—20319
- axisymmetric flow, mixing with coaxial jet 2—15557
- breakdown of double-helix, spiral and axisymmetric forms in swirling conical flows 2—28448
- chamber, with symmetric air inlet, aerodynamic study 2—18744
- concentrated, solitary waves in 2—21758
- Couette flow, Taylor vortices, stability problem, finite difference approach 2—35415
- decaying vortex rings with non-similar vorticity distributions, motion study 2—21743
- delta wing leading edge, oscillatory deformation in low-speed wind tunnel 2—6145
- diabatic gas flow, complex lamellar, vortexline geometry 2—6126
- distribution in field of random 2D vorticity, discontinuities, spectrum and decay 2—28472
- elastic filament analogy to vortex lines and waves 2—906
- elliptic wing, vortex interaction 2—35662
- filament containing axial flow, motion and stability slender-body analysis 2—6130
- filament motion near half plane, low Mach no. sound field from 2—14261
- flow, over flat surface with suction 2—24606
- flow through three-dimensional axially symmetric channels, numerical solution 2—1024
- formation by an elevated electrical heat source 2—6134
- frontal collision of two pairs, sound generation 2—18738
- gas vortex stabilised arc discharge as pumping source for c.w. Nd:YAG laser, comparative study of Ar, Xe, and Kr 2—27448
- generalized, boundary layers 2—35412
- ghost wakes on water surfaces caused by aerial votices 2—40950
- induced velocity computation of bilaterally symmetric vortex rings 2—12348
- infinite vortex line interaction with plane perpendicular boundary surface 2—12488
- injection into supersonic stream, sweptback injection at angle of attack 2—18742
- Karman vortex street, development flow past circle 2—18564
- laminar boundary layers, unstable, longitudinal vortices 2—12321
- liquid, superfluid, quantum mech. form. 2—35808
- longitudinal, onset in forced convection, secondary flow, critical Rayleigh number 2—18733
- longitudinal instability of boundary layer on concave wall to the onset 2—28461
- MHD flow in cone 2—969
- motion, and turbulence 2—937
- oceans, wind-driven equatorial currents 2—10709
- plane hollow, calc. of neutral stability, applicability of method of conformal transformations 2—39064
- plane Poiseuille flow, finite amplitude convection with longitudinal vortices, effect of uniform axial temp. gradient 2—39048
- rings, structure and stability 2—12524
- rings of small cross-section in ideal fluid 2—12336
- rotating fluid, finite amplitude disturbances 2—908
- rotationally symmetric quasi-cylindrical viscous incompressible vortex flow, computation by weighted residuals using exponentials 2—21731
- smoke ring formation from solar prominence, Hα observations of limb 2—37411
- in superconductors, dynamic structure 2—4169
- supersonic base flow, jet line 2—9021
- thin filament, incompressible inviscid fluid, soliton 2—18559
- tornado, nonstationary model 2—20333
- turbulent flow, two-dimens. vortex motion and negative temps. 2—35417
- turbulent shear flows, calc. methods 2—32148
- two vortices interaction between concentric rotating cylinders 2—31890
- two-dimensional turbulence, stationary states 2—12345
- unsteady wake of an oscillating cylinder at low Reynolds number hot wire anemometer meas. 2—35653
- viscous compressible vortex, dynamics and stability 2—6017
- visualization of Gortler-Taylor vortices in liquids using Al powder 2—28759
- vortex drag of lifting surface 2—3320

Vortices continued
- vortex regions in potential flow with Bernoulli const. discontinuity at boundary 2—6044
- wake interaction of accelerating sphere in free fall 2—21720
- in wake of slender cylindrical bodies, spacing position and strength at large incidence 2—8887
- water, motion of vortex rings from circular and lenticular orifices 2—32197
- He, nonuniform states of an imperfect Bose gas 2—30820
- He, report on superfluidity 2—12607
- He, superfluid, stochastic theory of nucleation of quantized vortices 2—6272
- He II, rotating, vortex wave creation theory 2—22024
- He II, temp. dependence of vortex-core parameter 2—22027
- He II, thermally assisted escape of ions 2—25129
- He superfluid, vortex wave scattering by spherical impurity 2—1132

Water
- *see also Ice; Seawater; Steam*
- acoustically excited vibrations in a cylindrical tank 2—3386
- adsorbate in presence of paramag. impurities, mol. mobility from n.m.r. obs. 2—25221
- adsorbed layer, controlling effect on elec. active struct. of cryst. surfaces, informational props. 2—29062
- adsorbed molecules, p.m.r., hydrogen bond and intermol. interactions 2—10618
- adsorbed on Al film, nucleation and growth model 2—39553
- adsorbed on $BaTiO_3$ powder, effect on dielec. props. 2—16282
- adsorbed on dispersed silica, forms of adsorbed and struct. water 2—29064
- adsorbed on GaAs, effect on surface photovoltage 2—13346
- adsorbed on silica, phase transitions 2—25233
- adsorption by hydrated portland cement pastes, pore struct. analysis 2—36269
- adsorption on α-Cr_2O_3, i.r. study 2—6379
- adsorption on alkali halide films, H-bond vibration, i.r. spectra 2—9305
- aerosol drop, light reactive motion due to evap. by radiational heating 2—39405
- air-H_2O interfaces, point charge and dipole image potentials 2—34278
- air-water flow, forced convection heat and mass transfer from moving interface 2—21752
- air-water system, pressure wave propagation 2—35442
- air-water two-phase system, pressure wave propagation 2—39285
- amorphous solid, preparation, demonstration of absence of crystalline ice 2—28971
- anomalous, adsorption of H_2O on hydroxylic silica surfaces as mechanism of formation 2—9074
- anomalous, impurity content, neutron activation analysis 2—28787
- anomalous, mass spectrometric study of pseudo-polywater shows polydimethylsiloxane as main constituent 2—28801
- anomalous, review 2—25031
- anomalous 2—6195
- atmospheric, raman spectra, obs. using remote spectrometer 2—34553
- atmospheric absorption at 10.6 μm, for field irradiance distrib. 2—26502
- atmospheric vapour meas. by Raman lidar 2—33454
- in Beaufort Sea, wind stress meas.16827 2—16827
- boiling, nucleate, saturated and subcooled, superheat layer thickness meas. 2—18885
- boiling, reactor containments, protection in case of accidents 2—15162
- boiling curve meas., heat transfer process, nucleate, transition, film boiling regions 2—18886
- brine to ice salinity ratio meas. in temp. gradient, up to 1.3°C/cm, comparison with computed salinity profiles 2—35826
- bubbles, spherical cap, shape, rise speed and wake 2—1066
- di-n-butylphthalate-water system, optical study of interfacial turbulence 2—6177
- capillary-gravity waves absorption in shallow water 2—3348
- cavitation threshold dependence on volume 2—21937
- cetane-water interface, meas. of interfacial velocities 2—25053
- chemisorption, on oxide surface, role in exo-emission 2—4314
- as Cherenkov counter radiator, threshold properties31366 2—31366
- cluster ions, detection in high summer mesopause 2—16814
- comet atmospheres, hydrodynamic description 2—33751
- convection flows resulting from combined buoyancy effects of thermal and mass diffusion 2—6027
- critical heat flux scaling from CHF data for Freon 11 flow 2—25003
- c.w. laser, correl. between 28 μ and 119 μ lines, 119 μm line pressure effect 2—17600
- density at atmospheric pressure, 0° to 100°C, revision of USSR standard tables 2—3375
- dielectric constant, complex, obs. using resonant cavity technique 2—9189
- dielectric relaxation, structural model 2—12572
- dielectric relaxation studied by new methods of complex permittivity up to 13 GHz 2—9150
- diffusion and association in polyalkylmethacrylates 2—15794
- diffusion coefficients of H_3PO_4 at 35°C 2—28826
- diffusion of O_2, applicability of Stokes-Einstein equation 2—32251
- dimer, hydrogen bond, effect of electron correl. 2—5930
- displacement of gas, without use of pistons, assuming capillarity 2—39231
- distilled, electrical stability under action of powerful high voltage impulses 2—21995
- drop-surface wave interaction 2—1060
- droplet generator for controlled pairs of equal and unequal size 2—18862
- droplets, decelerating in air, drag coefficients 2—1865
- droplets, effect of AgI as a result of multiple freezing 2—39425
- drops, condensation growth passivation by cetyl alcohol 2—1061
- drops, deformation when subjected to strong electrical forces 2—3355
- drops, explosive evaporation in field of optical radiation, dynamics 2—28957
- drops, holographic, visualisation and counting 2—287
- drops, in air flow, velocity determination by Doppler effect with laser light 2—28696
- drops, nucleation by Brownian contact with AgI and other aerosols 2—18859
- drops, stability of oscillations in electric field 2—9065
- electron impact excitation, 3 to 6 eV 2—8617
- electronic correlation effects, computer prog. for generalized Bethe Goldstone calcs. 2—35211
- emission at 22.23508 GHz associated with OH emission in southern Milky Way 2—33597
- emission spectrum of oxy-hydrogen flame, rotational analysis 2—12152

Water continued
- emissivity calc. at high temps. and pressures by just overlapping spectral line model 2—39282
- emulsion, dipolar type Debye relax. 2—28923
- environmental pollutants, nonflame atomic absorption techniques 2—22892
- evaporation and condensation in enclosure in presence of noncondensable gas 2—22043
- evaporation from free surface, nomogram 2—3449
- excitation of resonant triads by single internal waves 2—39310
- falling drops, interactions and coalescence 2—9067
- falling sheet, stability 2—9063
- film, electron diffr. obs. 2—9079
- film, laminar and turbulent flow along vertical tube, heat transfer coeff. of evap. 2—18883
- film, on Plexiglas, effect on oil drop spreading 2—1166
- films, between entirely hydroxylated fused silica surfaces, thermodynamic properties and molecular long range orientation 2—21948
- films condensed on cryogenic surfaces, refractive indices and densities 2—7039
- flow, low velocity, pressure obs. 2—20807
- flow, plane Poiseuille, influence of heat transfer on stability 2—18777
- flow, steam-water, vertical annulus, dispersed upward flow, heat transfer coeff. 2—1042
- flow in closed conduit, visualization technique by hydrogen bubble method 2—15547
- flowing, surface wave stability 2—15555
- flowing through tube with and without boiling, forced convection heat transfer at elevated flux 2—34199
- free convection heat transfer from isothermal spheres in water 2—20953
- free convection near maximum density temperature, fluid flow 2—21936
- freezing and melting, periodic, theoretical study 2—1135
- fresh and salt water jets in stably stratified salt water environment, shroud production studied 2—6184
- freshwater, radionuclides, particulate and dissolved, concentration, with sampler 2—4653
- freshwater lakes, thermal conductivity obs. at various depths, thermocline formation 2—37117
- galactic emission sources associated with H II regions 2—4809
- galactic radio sources, very long baseline interferometry of W49 2—30523
- in gases, traces, continuous det. with electrolytic measuring cell 2—1766
- glass adsorbed water layer, Ar adsorpt., thermodynamic props. 2—35913
- glass diaphragm, sintered, plugging by distilled water 2—25611
- glass-water system, phase transition, heat effects, dimens. changes in temp. cycles, 237-278K 2—35922
- graphite-H_2O system, neutron thermalization expts. 2_11888
- heat and moisture transfer in wet sand during freezing 2—20956
- heat transfer coeff. in supercritical pressure range 2—6169
- heavy, Canadian technology for producing and handling it 2—5759
- heavy, slowing down times 2—2838
- hydrated electrons, theoretical study using ab initio SCF MO calcs. on small clusters of water molecules 2—12153
- hydrogen bonded solvent, effect of solute on hydrogen bond formation 2—32240
- impact of conical shell 2—1052
- induced radioactivity in ground water system near proposed 300 GeV accelerator 2—5622
- internal gravity waves, instability 2—28762
- interstellar, photochemistry and lifetimes 2—4898
- interstellar masers, H_2O and OH, emission profiles, shapes and polarization 2—7460
- i.r. spectra of deformation vibration in micas 2—15304
- i.r. spectra of vapour, intensity-half-width products in 6.3 μm absorption band 2—32179
- jets, liquid-in-liquid, mass transfer, conc. driving force 2—3350
- laminar flow in horizontal tubes with uniform heat flux, combined forced and free convection effects 2—9054
- laser, gas, wavelength of 27.9 microns 2—17602
- leak rate through thin polycarbonate films 2—3816
- limiting shear strength, dependence of rate of motion of float on temp. 2—21939
- line emission from Orion A, VY C Ma and W49 2—4807
- liquid, mixture-model approach 2—24583
- localized excess electrons, ice cavity model 2—29078
- lower atmosphere, effect of water vapour on phase retardation of e.m. waves near 1.35 cm. absorption line 2—10719
- on Mars, explanation of white spots in Hellas area7530 2—7530
- Martian surface and atmosphere, proposed mass spectrometric anal. 2—30568
- metal-H_2O interfaces, point charge and dipole image potentials 2—34278
- in mica, quantitative determ. by i.r. spectroscopy 2—30114
- microwave complex permittivity measurement 2—21994
- microwave sources associated with H II regions, laser pumping, OH masering 2—30526
- mixtures with hydrocarbons, phase behaviour and critical phenomena 2—9109
- mixtures with inert gases, gas-liquid equilibria and critical curves 2—9107
- moderator, static and pulsed reactivity measurements on large ^{235}U fuel forms 2—548
- moisture content meas. during drying using gamma radiation 2—14050
- molecular beam, condensation coeff. on impinging Cu block 2—39429
- molecular model 2—35723
- molecular model for prenucleation clusters 2—35378
- molecule, analogue to ionized inert gas, mol. orbital determ. from vac. u.v. and photoelectron spectra 2—18409
- molecule, and isotopic species, submillimeter wave spectra, rotational transition assignment 2—12146
- molecule, anharmonic force constants, calc. in general quartic force field 2—21607
- molecule, comparative study of random phase approx. Hartree Fock of single excited configuration interaction methods of computing excitation energies 2—15277
- molecule, electronic struct. rel. to band struct. of cubic ice 2—16106
- molecule, energies and properties of excited states, ab initio calcs. 2—8640
- molecule, high resolution photoelectron spectrum meas. rotational structure partially resolved 2—12151
- molecule, in OH stretching region, contours of Raman bands 2—18433
- molecule, intermolecular motions in liquid state, normal coordinate analysis 2—39331
- molecule, intramolecular vibrations in liquid state 2—39330

Water continued
- molecule, optical and electron scatt. spectra, theoretical interpretation 2—12138
- molecule, photoionization total and differential cross sections, X- and u.v. excitation, calcs. 2—18458
- molecule, rot. transition by electron collision 2—18437
- molecule, rotation bending energy levels calc. 2—31754
- molecule, rovibrational energy levels, calc. using rigidly bending rigid-rotor Hamiltonian 2—15306
- molecule, SCF MO P(LCGO) computations 2—3045
- molecule, study of nonadiabatic coupling and transitions between electronic states 2—8559
- molecule, transcorrelated method for accurate correlation energies using gaussian-type functions 2—35105
- molecule, triplet excitation by low energy electron impact spectra 2—24453
- molecule, vacuum u.v. spectra below 1200 Å 2—18378
- molecule, zero pt. vibr. motion, near Hartree Fock limit, one-electron props., force constants 2—8642
- natural, optical characteristics 2—13632
- neutron inelastic scattering, temperature dependence 2—519
- neutron slowing down times 2—2838
- neutron thermalization at 318°K 2—28099
- nuclear coupling const. calc. by SCF LCGO MO methods, Fermi contact contrib. 2—8620
- nucleate boiling at high Jakob numbers, bubble growth rates 2—35838
- andoil flow in rectangular channel, stability 2—35709
- oil on, airborne optical detection 2—26464
- oil-in-aqueous suspensions, dilute at high ionic strength, expt. in coalescence by flow through glass fibrous mats 2—32282
- oil-in-water dispersion, coalescence by flow through porous media 2—32281
- optical properties as function of wavelength prediction for clean, naturally occurring water 2—13633
- oscillation of two spherical bubbles in water, natural frequencies 2—1065
- phantom, effect of lateral scattering on absorption of 400 MeV neutrons and protons 2—5070
- phase velocity of surface capillary gravity waves 2—12530
- physical properties, temp. depend., general expression, two-state theory 2—35724
- physisorption on ZnO surface 2—29074
- pipe flow, motion caused by piston 2—12347
- pollution, Raman spectra of organic and inorganic Hg compounds 2—12150
- polyheavywater, chem. comp. determ. 2—35737
- polystyrene in water sols, effect of dispersing agents on angular dependence of light scattering 2—6267
- polystyrene sphere-water sols, effects of dispersing agents on angular dependence of scattered light 2—28921
- polywater, ESCA spectra and distillation at 360 and 800°C 2—35738
- polywater, interpretation of i.r. spectra of clay adsorbed water 2—3393
- pore struct. analysis by water vapour adsorpt. 2—35910
- precipitable, in atmosphere, 4 to 6 wavelength band absorption 2—33476
- precipitation of drops onto wall liquid film, from dispersed steam-water flow 2—28695
- progressive waves, mass transport, drift profiles obs. 2—28763
- proton affinity studied using elevated pressures in ion source of quadrupole mass filter 2—22863
- proton transfer reactions, elec. field and chemisorbed ion induced 2—4573
- quick closing valve for use in power chemicals cooled by evaporating water 2—15176
- radiation of vapour calculation technique for use in computer programs 2—3041
- radiolysis, γ-rays, evidence that major fraction of residual hydrogen is not H atoms 2—7186
- Reynolds shear stress meas. by laser anemometry 2—15550
- shock waves due to explosion, effects of bottom coverings 2—6180
- solubility of gases, temp. dependence 2—25052
- solutions of propanol, determ. intensity of concentration scattering of light 2—15590
- sorption of Al_2O_3 surface, effect on loss factor 2—16263
- Southeastern Saskatchewan, groundwater studies, geophysical logging 2—30161
- in space, released from Apollo missions, interference with scientific observations 2—30600
- specific volumes of severely superheated water 2—39358
- spectra, using far i.r. spectrometer 2—8634
- spectral transmissivity of real gas, exponential model 2—21921
- steam, condensation in low pressure flows through tube banks, determ. heat transfer and flow resistance 2—22041
- steam-water condensation, boundary-layer theory investigation 2—39427
- structural absorption of u.s.waves, study based on structural relaxation theory 2—25075
- structurally anomalous, formed by condensation in quartz capillaries 2—1148
- structure, bond lattice model, thermodynamic and transport props. 2—21954
- structure, existence of free OH groups 2—28786
- structure, lattice model with directed bonding 2—39329
- structure, least-squares det. from gaseous electron- diffraction data 2—18391
- structure 2—35730
- supercooled, ice nucleation by coprecipitated AgI and AgBr 2—25144
- supercooled, self diffusion coeff. meas., +30 to −25°C, computation of viscosity and dielectric relaxation time 2—9120
- supercooled droplets, effect of CuS on freezing 2—39424
- surface oscillations in shallow two-dimensional basin 2—28476
- surface waves, capacitive probe for studying time dependence of individual Fourier components 2—28761
- surface waves effects on thermal boundary layers 2—6181
- suspensions, coalescence of two colliding drops 2—9068
- table, flow patterns in 2 dimensional diffusers with laminar boundary layer entry 2—6174
- thermal discharges, intermediate mixing into uniform current 2—10703
- thermal emissivity, cm wavelength, variations with temperature 2—1783
- thermal radiation during ultrasonic cavitation, obs. 2—18781
- triplet excitation by low energy electron impact spectroscopy, cross section determ. 2—15311
- turbidity, correlation of optical models and aircraft data 2—1815
- turbulence, holographic compensation 2—23653

Water continued
turbulence. spatial and temporal correlations by laser anemometry 2—15549
turbulence production near a smooth wall in a turbulent boundary layer 2—1050
two phase flow system, time-dependent diabatic flows prediction 2—24625
two-phase fluid system with Freon, modelling of critical heat flux in uniformly heated annuli 2—24996
ultrasonic absorption in 30-100 MHz region, effect of presence of alkali halides studied by pulse technique 2—35758
u.s. propagation, mag. field effects 2—18820
u.s. wave amplitude and phase modulation, turbulence effects 2—28849
u.s. wave amplitude modulation and turbulence effects 2—28848
vapor pressure equation for 0 to 100°C temp. range 2—22046
vapour, absorption coefficients, laser spectrometer 2—2464
vapour, adsorption on quartz crystal piezogravimetric method of obs. 2—25223
vapour, adsorption on Saran charcoal, vol. change 2—3559
vapour, adsorption on solids, effect on surface cond. 2—39547
vapour, adsorption on Ta, RHEED obs. 2—12686
vapour, adsorption on ZnS, cryolite or MgF_2 film 2—9291
vapour, atmospheric, absorpt. coeff., velocity laser spectroscopy determ. 2—11542
vapour, atmospheric, pole-to-pole eddy transport during IGY 2—20328
vapour, atmospheric, vertical exchange coeff., numerical det. 2—16815
vapour, effect on B doping in epitaxial Si 2—12665
vapour, effect on epitaxial growth of Cu films on NaCl 2—12657
vapour, electron attachment studies 2—21870
vapour, Martian atmosphere, proposed detection and mapping during Viking Mission 2—30564
vapour, measurement and interpretation of near i.r. bands 2—8659
vapour, photolysis between 1500 and 1700 angstroms, micrometer-sized particle formation 2—26359
vapour, pulsed laser, excitation processes and relaxation rates obs. 2—34398
vapour, resolution of anomalies in resonance dispersion of pressure broadened line at 22 GHz 2—8633
vapour, role in obs. of electron densities of D-region 2—7338
vapour, sorption by ball-milled calcite 2—35911
vapour, spectral isotopic analysis of small amounts based on compression of sample into discharge tube 2—30108
vapour, stratospheric emission, radiometer sonde for obs. 2—20308
vapour, total atmos. content, from obs. of solar radiation absorption 2—16813
vapour, trace impurity in H_2 gas, det. using solid electrolyte O_2 gauge 2—33390
vapour dimens., spectroscopic effects 2—7274
vapour in atmosphere, i.r. absorption of 0.5 to 3.0 mm and line shape 2—37155
vapour laser, excitation mechanism, direct electron impact 2—17598
vapour sorption hysteresis on activated C, mathematical model 2—25229
Venus, upper clouds, composition from occultation, transit and spectral data 2—41199
vibrational spectrum in organic solvents, possible motional effects in fundamental stretching region 2—39370
viscosity, as basis of calibration of viscometers 2—39345
viscosity, pressure-temp.-viscosity diag., near critical temp., eqns. 2—18802
viscosity, thermal conductivity and Prandtl number as function of temperature and pressure, correlation 2—32245
viscosity at 250° to 370°C and up to 500 bar 2—1084
volume mass, absolute value 2—23220
vortex ring motion, on ejection from circular and lenticular orifices 2—32197
W49 and Orion A radiosources, H_2O line emission very long baseline interferometry 2—33712
wake development of thin airfoil and wave characteristics 2—15556
light water thermalization parameters, meas. using pulsed neutron technique 2—2854
water-ice system, partitioning of HCl 2—25143
waves, acoustic model for experimental study 2—9060
waves, generalized function method applic. 2—39308
waves, transmission over shelf of arbitrary profile, new source potential 2—25021
wind disturbed surface waves, curvature distrib. at different viewing angles 2—25020
xylene-water interface, meas. of interfacial velocities 2—25053
$Ar.H_2O$ admixture, cylindrical hollow cathode discharge, mass spectrometric study of positive ions extracted from negative glow 2—39212
Cytherean atmosphere, absorption and scattering of clouds 2—33747
D_2O-potassium laurate, mesophases, mol. motion obs., n.m.r. obs. 2—6212
D_2O, enthalpy and sp. ht. 0.1-21 MN/M^2 absolute press., 20-640K, tables 2—35755
D_2O, high resolution photoelectron spectrum meas. rotational structure partially resolved 2—12151
D_2O adsorption on α-Cr_2O_3, i.r. study 2—6379
H-O stretching frequencies in salt hydrates 2—20016
H_2O-D_2O binary mixtures, exptl. study of ultrasonic absorption in 10-50°C range 2—35759
H_2O-D_2O mixtures, isotopic analysis with spectrophotometer 2—16692
H_2O-D_2O mixtures, pulsed-neutron diffusion parameters, near freezing point 2—518
H_2O-H_2O^+ collisions, comparison of integrated capture cross sections with reaction cross sections 2—31882
H_2O, HDO, D_2O, isotopic species, microwave spectrum 2—12148
H_2O and D_2O, spin echo n.m.r. 2—35790
H_2O line emission regions in Orion A study by very long baseline interferometry 2—41154
H_2O vapour, anomalous composition 2—6149
$H_2{}^{16}O$, submillimeter microwave spectrum, rotational transition meas. 2—18400
$H_2{}^{18}O$, anomalous proton chemical shift, mag. resonance obs. 2—6245
$H_2{}^{18}O$, i.r. spectra of vapour, rotational structure of ν_2 band, vals. of energy levels of 1st excited state 2—12132
HOD in OH stretching region, contours of Raman bands 2—18433
H_2O+Na reaction, research review rel. to nuclear reactor applic. 2—40801
HTO in troposphere, vertical profiles and transport 2—22981
${}^2H_2O$ and ${}^2H_2O$-H_2O mixtures, stimulated and spontaneous Raman scattering 2—21989

Water continued
${}^2H_2O$ thermal column, thermal neutron flux generation in nuclear reactor 2—38716
${}^2H$ enrichment by electrolysis, cell design and mean current density calc. 2—26354
Mars, H_2O lines in the 8200 Å region and their application to high dispersion spectra 2—7525
NaCl-water-ice, interfacial free energy detn. 2—18971

Wave equations, quantum theory *see Quantum theory/wave equations*

Wave functions *see Quantum theory/wave equations*

Wave mechanics *see Quantum theory*

Wavefront-reconstruction imaging *see Diffraction/light; Holography; Optical images*

Waveguides *see Electromagnetic wave propagation/guided waves*

Waves
see also Acoustic waves; Elastic waves; Electromagnetic waves; Liquid waves; Magnetohydrodynamics; Seismic waves; Shock waves
acoustic-gravity, in atmos., short period, anal. of spatial coherence 2—37182
air-sea interactions, wave follower for field study 2—20283
in atmosphere, long, transient motion of vertical modes by beta plane approx. 2—1850
atmosphere, partially trapped, models 2—40941
atmospheric, co-phase analysis technique for detection and parameter est. 2—37140
atmospheric, ultra-long, baroclinic instability 2—16825
baroclinic waves, study using three-level streak photography 2—39076
barotropic Rossby waves and resonant amplification for fluid in rotating cylindrical annulus 2—6050
book, waves in physical systems 2—33887
charge density, resonant excitation for coherent acceleration of ions 2—14810
cylindrical, having finite amplitude and slope on gentle-sloped depths, energy characteristics 2—18571
density, interaction with stars at Lindblad resonances in disc like collisionless system, energy and angular momentum exchanges 2—4832
diffraction, multilayer pot. method 2—33888
diffraction by reflecting screen of arbitrary shape 2—30759
dispersion relations for bounded systems, application to plasma 2—28612
fluid, weak turbulence, Langevin eqn. 2—8893
in fluid dynamics, soln. by perturbation techniques 2—8892
fluid surface oscillations in shallow two-dimensional basin 2—28476
galactic density waves, oscillation and overstability in rotating disc like star-gas system 2—33611
ghost wakes on water surfaces caused by aerial votices 2—40950
gravity, internal, longshore current generation 2—7239
gravity, internal, propagation in conducting fluid with shear flow, rotation and magnetic field 2—24639
gravity, internal and acoustic, in atmosphere, effects of moisture on propagation 2—33449
gravity, long internal, generation in waveguides, by rising buoyant air masses 2—37141
gravity, nonlinear, interaction with non-uniform currents 2—37115
gravity, nonlinear propagation in isothermal atmosphere 2—13730
gravity, propagation in realistic thermospheric model 2—40975
gravity obs. in night time F-region 2—41010
group velocity, relationship to phase velocities 2—17185
growth criteria, stability of dynamic systems with distributed parameters 2—23245
impact stress waves in composite structures 2—14231
incompressible fluids, finite three-dimensional surface waves in circular channels 2—31926
inertial, sideband instabilities in unbounded inviscid fluid 2—35444
Korteweg-de Vries equation, discrete models with damping 2—27035
long, generation by piston-type wave maker, linear theory 2—14072
long, model equations in nonlinear disperse systems 2—37576
magnetoacoustic, mutual transformation at plasma inhomogeneities 2—39115
matter, the Goos-Haenchen effect for grazing incidence 2—78
non-sinusoidal, averaging method and general variational principle 2—37577
nonhomogeneous fluid, effect of thin elastic plate 2—39072
nonlinear, dispersion, slight dissipation, average variational principle, asymptotic character 2—37
nonlinear dissipative, in inhomogeneous media 2—14071
nonlinear in rotating fluid, dissipative effects 2—3179
one-dimensional non uniform wave equation, soln. for movable boundaries 2—36
phase velocities, errors from frequency wavenumber spectral sections 2—37083
plane, propagation in linear homogeneous media, theory of holomorphic matrices 2—37578
planetary, solitary and cnoidal 2—7237
plastic wave propagation, effect of Young's modulus variation with plastic strain of temp. 2—14254
plastic wave theory of impacting rods 2—37707
pressure, travelling, response of box structure 2—153
pressure wave propagation in air-water two-phase system 2—35442
prolate spheroidal wave functions, review 2—35
propagation, stability characteristics of finite- difference numerical solution 2—11255
propagation expts. in undergraduate physics lab., use of computer for analysis and simulation 2—14059
propagation in arbitrary linear media 2—37575
propagation in inhomogeneous media, relations between phase and group velocity 2—23244
propagation in one-dimensional random media 2—5167
recombination, in Ge, exam. by electron mirror microscope 2—4236
reflection nearly parallel to boundary in rotating fluid, viscous effects 2—3180
rippling on small progressive gravity waves due to harmonic nonlinear nearly resonant interaction 2—35443
scalar, eigenvalue distribs., edge and corner contribs. 2—33886
scalar, propagation in a one dimensional random medium 2—38
scattering, from thin comb with hard boundaries 2—20819
solitary, in concentrated vortices 2—21758
solitary, in rotating fluid, damping 2—3179
soliton propagation, inhomogeneous media, equations 2—17248

Waves continued
- solitons, gradient-induced fission in inhomogeneous media studied 2—12350
- Southern Hemisphere, half-yearly variation of circumpolar surface drift 2—26492
- spheroidal functions, calculation with FORTRAN 2—14070
- stress wave propagation and fracture in thin curved bars 2—5214
- temperatures, in semiinfinite space with radiative heat transfer 2—27316
- thin film fluids, undulating flow in a gas stream 2—39321
- time-dependent waveforms, extrapolation along path of propagation 2—37084
- torsional and nonaxisymmetric end problem in solid circular cylinder 2—37745
- transverse, self sustaining on propagating detonation front 2—11365
- ultrasubharmonic resonances in Duffing system 2—148
- vapour-superfluid interface, temp. fluctuations associated with gravity waves 2—30819
- variational principle for propagation in random media 2—30758
- velocity, turbulent, and kinematic dynamo activity in astrophysical objects 2—10792
- wave eqn., application of z-transform method to solution 2—2062
- wind fluctuation induction over sea 2—22966

Waxes
- sealing, electret formation mechanism 2—4284
- sealing wax, thermoelectret, effect of polarizing field 2—13330
- shellac, magnetoelectret effect 2—1578
- shellac, water vapor effects on thermoelectret behaviour 2—36602
- sisal, elec. conductivity rel. to suitability for electret preparation 2—29759
- wax and gelatin film, i.r. holograms 2—7952

Weak interactions *see Elementary particles/interactions, weak; Field theory, quantum/interactions, weak*

Wear
- adhesive and abrasive, quantitative study 2—29338
- asperity load sharing in lubricated contacts, model 2—22295
- bearing surfaces, subatomic mechanism of wear 2—6588
- electrode erosion, on high current, high pressure sparking 2—12476
- frictional behaviour and surface struct. of S-137 material 2—29341
- graphite nuclear reactor components, strength and durability rel. to construction problems of a THTR 2—18265
- impact wear testing machine 2—22320
- lead-bronze, wear mechanism, dry state sliding 2—29340
- low temperature meas. apparatus 2—25547
- measurement, normal range, eddy-current method 2—25539
- metal, ductile, erosion 2—9719
- metal compatibility effects on tribological characts. 2—29343
- metal component failure, heat treatment effect 2—32627
- metals, cavitating effect of cryogenic liqs. 2—39915
- micropolar fluid lubricated squeeze film and externally pressurized bearings 2—22293
- Nimonic 75, high temp. props. 2—22297
- nimonic 75 alloy, rel. to surface temp. 2—39849
- plastic bearings, operational behaviour, structure effects 2—32653
- poly (amide-imide) in dry air at 260°C, obs. 2—12918
- polyimide in dry air at 260°C, obs. 2—12918
- pyrrone in dry air at 260°C, obs. 2—12918
- rails under rolling load, endurance model tests 2—22306
- resistance det., testing machine 2—22312
- ruby bearings, operational behaviour, structure effects 2—32653
- sliding and rolling, methods and results of research 2—3915
- sprayed coating, resistence improvement on press-sintering 2—1339
- stainless chrome nickel steel, effect of vacuum thermochroming 2—6587
- steel, cermet, containing inclusions, optimum comp. for wear resist. 2—1334
- steel, erosion resist., vibr. cavitation obs. 2—39853
- steel, high-speed, wear resistance 2—36114
- steel, in high vacuum and in air, low temp. 2—36178
- steel, rel. to surface temp. 2—39849
- steel, resistance, after coating with Cu, comparison with bronze 2—3918
- steel, wear resistance, effect of white layer formed due to cold working and ultrasound treatment 2—6586
- steel, wear-resistant, effect of C and V content on props. 2—36237
- steel bearings, operational behaviour, structure effects 2—32653
- steel reinforced phenolic resin 2—3916
- test apparatus for high temp. investigation in vacuum and gaseous media 2—6594
- testing under current, sliding electrical contacts 2—29365
- thermoplastic, C-fibre reinforced, tribological characteristics 2—1336
- thermoplastic polymers, effect of fusible alloy fillers 2—6589
- track, electron microscopy 2—9720
- Ag, fretting, spherical particle form. 2—39852
- AgCuO contact wear resistance testing 2—32677
- Al alloy, erosion rate, rel. to mech. props. 2—29339
- Al_2O_3, sapphire bearings, operational behaviour, structure effects 2—32653
- Al_2O_3, sapphire jewel bearings: tribological props. 2—9721
- Co-25wt.%Mo impregnated with CaF_2-BaF_2 eutectic, obs. 2—12917
- Cu alloy, erosion rate, rel. to mech. props. 2—29339
- Fe-Al alloys, dry and lubricated, influence of Al 2—12916
- Fe-Cr base alloy, austenitic, abrasive wear resist. 2—36177
- Fe, cast, effect of sulphurized surface layer on wear resist. 2—12915
- Fe, cast, spheroidal graphite, wear mechanism in dry sliding 2—22296
- Fe, LEED, Auger spectroscopy and microcontact obs. 2—39848
- Mo impregnated with CaF_2-BaF_2 eutectic, obs. 2—12917
- MoS_2 in epoxy resin, wear life coeffs. 2—22294
- Ni alloy, erosion rate, rel. to mech. props. 2—29339
- Ti alloy, erosion rate, rel. to mech. props. 2—29339
- TiC-N alloy, sintered, wear resist. 2—9777
- W impregnated with CaF_2-BaF_2 eutectic, obs. 2—12917
- WC cermets, Co bonded, cavitation erosion resist. 2—22298
- Zn, photopolymers, based on polyamides, wear resistance 2—3917
- ZrB_2-W alloy, durability after sintering 2—12950

Weather *see Meteorology*

Weighing *see Balances; Mechanical measurement*

Weissenberg cameras *see Cameras; X-ray crystallography/apparatus*

Welding *see Forming processes*

Wentzel-Kramers-Brillouin method *see Quantum theory*

Wertheim effect *see Magnetomechanical effects*

Wetting
- *see also Capillarity*
- alloys, sessile drop method, with alloying of drop during experiment 2—28814
- ceramic, by liq., contact angle meas., apparatus, sensile drop method 2—18805
- ceramic, wetting angle, determ. by drop method 2—39318
- contact angles, dynamic, vel. relationship, surface roughening effect, θ_d-V relationship 2—32205
- contact angles, on heterogeneous solid surfaces, thermodynamics 2—32204
- contact angles, static and kinetic, det., equipment 2—18787
- drop on surface, surface driving force causing spreading 2—35695
- glass, spreading kinetics of polydimethylsiloxanes 2—25177
- glass spheres, hollow, in water, flotability of wetting and non wetting particles 2—3414
- metal compatibility determ. by static friction tests 2—29458
- metal compatibility effects on tribological characts. 2—29343
- oxide-metal, carbide-metal, liq.-solid systems, rel. to sintering 2—6316
- Plexiglas, with water film, spreading of partially submerged oil drop 2—1166
- polymer melts, pendent drop-sessile drop method 2—35746
- porous body melting, initial stage 2—3434
- solid, spreading kinetics of polymers 2—25177
- vapour bubble, wetting tension and boiling 2—35834
- Al_2O_3 plate, by molten Fe 2—3496
- C black, interaction between active H and water 2—3495
- MgO plate, by molten Fe 2—3496
- mica, spreading kinetics of polydimethylsiloxanes 2—25177
- NiO, powder, heat of, rel. to degassing temp. 2—6623
- SiO_2 plate, by molten Fe 2—3496

Whiskers *see Crystals/whiskers*

Whistlers *see Atmospherics; Ionosphere*

White dwarfs
- BD+16°516, white dwarf elipsing binary 2—37309
- BD+16°516B, limb darkening obs. 2—1964
- BD+16°516B, limb darkening obs. 2—4895
- DA models, vibrational stability, radial pulsations 2—10858
- DF spectral type, element abundances 2—7414
- DG, metal abundances and internal temps. 2—33661
- evolution of close binary system, mass loss evidence 2—37290
- free electrons, Thomas-Fermi statistical model, rel. to densities 2—33631
- Grw+70° 8247, spectrum, interpretation of 4135 band 2—30468
- HL Tau-76, high speed photometric observations of rapid variations 2—26724
- L745-46A, DF spectral type, element abundances 2—7414
- magnetic, radio obs. at 10.63 GHz 2—4872
- mass-luminosity relation 2—1955
- masses and radii, calc. from model atmospheres and multichannel photoelectric scans 2—7413
- model for pulsating X-ray stars 2—7497
- nova outbursts, evolution at 1.00 $M_\odot$ 2—17002
- order envelopes and cooling, structure and energy transport 2—26661
- quasiradial pulsations in Newton's theory of gravity, central density 2—33657
- R548, X-ray emission, soft background obs. 2—37336
- R640, DF spectral type, element abundances 2—7414
- radial pulsations of pre-white dwarf stars, linear quasi-adiabatic analysis 2—20560
- rotating, integral parameters, general relativity 2—10844
- spectra and element abundances 2—20540
- stability toward adiabatic radial perturbations, effect of nuclear reactions 2—26678
- UBVr photometry, colour indices 2—41094
- uvby photometry, magnitudes and colours 2—33663
- van Maanen 2, spectra, energy distrib. and line profiles 2—26691
- van Maanen 2, velocity, redshift and pressure shift 2—26685
- vMa 2, DF spectral type, element abundances 2—7414
- X-ray emission, soft background obs. 2—37336
- He rich, cooling sequence 2—13909
- He rich, with H rich envelopes, hydronamic studies 2—26681

Wiedemann effect *see Magnetomechanical effects; Magnetostriction*

Wiedemann-Franz law *see Conductivity, electrical/solids; Conductivity, thermal/solids*

Wien effect *see Conductivity, electrical/liquids, electrolytic*

Wigner coefficients *see Quantum theory*

Wigner effect *see Physical effects of radiations*

Wilson cloud chambers *see Cloud chambers*

Wind
- 75-95 km, sensor for meas. and obs. 2—26511
- 80-150 km luminous cloud obs. over Volgograd 2—26521
- 110-174 km, obs. over Heiss Island using artificial luminous cloud technique 2—26515
- acoustic anemometers comparison in turbulent flow over water 2—26490
- acoustic radar design and operation for measurement 2—20312
- acoustic wave refraction and attenuation 2—13731
- ageostrophic wind determ. from satellite data for cloudiness 2—7276
- Antarctica, extreme winds, measurements and recordings 2—40951
- atmospheric flow around the island of Madeira, satellite observations 2—20319
- atmospheric spectroscopy, remote sensing 2—16840
- auroral zone wind and temp. correlation with geomagnetic activity 2—26514
- backscatter from sea surfaces at 2.25 cm 2—20282
- balance equations, modification with orographic effects 2—20320
- convective storms, Doppler radar identification by plan shear indicator 2—13704
- correlation with production of infrasonic signals in atmosphere 2—37181
- cyclone extratropical, development 2—1858
- D-region meas. 2—33542
- diffusion processes, water surface, quasi-periodic current structures 2—10713
- direction and speed, effect on rainfall, at coastal sites 2—1854
- direction and speed in upper atmosphere, seasonal and latitude variations 2—30306
- Earth motion caused by local atmospheric pressure changes 2—37080
- Ekman boundary layer stress due to flow over hills 2—10724
- e.m. wave propagation effect, refractive index structure function constant over 28 im at 35 GHz 2—37169

Wind continued
F-region horizontal neutral winds, from incoherent scatter observations 2—23033
field, statistical methods in obs. of structure 2—1827
field structure regularities for different scales of motion 2—13693
flow characteristics and turbulence, transformation due to change of surface roughness 2—13694
fluctuation over sea, wave induced 2—22966
geostrophic, rel. to ground wind 2—4679
ghost wakes on water surfaces caused by aerial votices 2—40950
Greenland ice cap, vertical variation of wind spirals through friction layer 2—37147
hodographs, steady state, in baroclinic boundary layer 2—26489
hot wire anemometers, constant temperature, feedback control theory 2—40915
hurricane Celia, August 1970, information received from NOMAD weather buoy 2—16830
hypersonic He tunnel, hot wire meas. of freestream and shock layer disturbances 2—28717
indirect meas. using aerial swing expts. 2—7290
ionosphere, F_2 ionization, intertropical, dynamic aspects 2—23031
ionosphere, prevailing and semi-diurnal components 2—26535
ionosphere, sporadic E-region, horizontal neutral wind shears and altitude profile of the vertical wind 2—4737
ionosphere, sporadic E-region, influence of tidal wind system, semidiurnal effect 2—4742
ionosphere, sporadic E-region, relation to effect of tidal winds 2—4741
ionosphere, sporadic E-region, rocket measurements of wind shear and electron density 2—4727
ionosphere, sporadic E-region, tidal winds acting through the wind shear mechanism 2—4740
ionosphere, sporadic E-region, wind profiles and relation between wind shear and fbEs 2—4733
ionosphere, sporadic E-region, wind shear amplitudes from horizontal wind profiles, relation to energy 2—4738
ionospheric, analysis of frequency distribution of vertical shear 2—37202
ionospheric, direction rel. to sporadic E layer 2—23019
ionospheric, E-region, transport processes, regular tidal winds, irregular gravity waves 2—37221
ionospheric D-region, speeds, density changes, radio wave absorption, correlation determ. 2—26536
jet aircraft, dynamic response to turbulent air, accident prevention 2—39254
Lake Michigan, normalized and equilibrium spectra of wind waves 2—30241
laser beam in crosswind, effect of diffraction on self induced thermal distortion 2—22962
low-level cross-equatorial current over eastern Africa 2—40949
Mars, explanation of surface roughness of Hellas 2—13995
measurement techniques, problems and instrument assessment 2—1831
Mediterranean summer storm of Sept. 1969, rapid cyclonic developments 2—33460
mesosphere, seasonal and latitudinal variations 2—7258
mesospheric temperatures and winds during a stratospheric warming 2—26513
meteor radar obs. of wind 100 km over Heiss Island 2—26519
meteor wind obs. of upper atmos., 35 and 72 hr periodicity 2—26517
monsoon field vertical velocity and circulation structure 2—1860
mountain station wind measurements, vertical gradients 2—30281
mountain wave front, upwind tilt and asymmetry 2—33461
neutral, influence on NO^+ and O_2^+ densities in lower nighttime ionosphere 2—23008
noise protection at microphones 2—23361
over ocean, velocity, temp. adn humidity fluctuations, Kolmogoroff constants det. 2—7288
ocean surface, det. by remote passive microwave technique 2_16786
ocean surface, effect on radar return 2—30939
ocean surface rel. to radar scatt. coefficient, expts. (1969-1971) 2—34255
radar continuous wind meas. over France 2—30279
radar detection of meteor trails, effect of antenna radiation pattern and wind velocity 2—22964
resonance in ionosphere, pressure fluctuations and turbulent friction 2—13771
sampling scheme, measurement over ocean with anemometers on buoys 2—1857
satisfying balance equation, dynamic meteorology 2—20334
scintillation patterns of laser beam to measure transverse component of wind blowing across beam 2—22961
Scotland, stratospheric, spring and autumn reversals 2—33459
at sea, diffusion sublayer thickness over disturbed surfaces 2—4651
sea noise spectrum level, surface generated ambient, logarithmic dependence on wind speed, effects of distant shipping 2—37111
sea roughness, variation of the normalized radar cross section with different windspeeds, North Atlantic Ocean, Beaufort Force 0 to 8 2—1802
effects on sea state and phase speed of waves, drag coeff. of air-sea interface relation to apparent roughness 2—26465
sea state and radar backscattering cross section correlation, model for relationship 2—16788
sea surface slope and equilibrium wind wave spectra, wind induced growth of small waves 2—33441
semi diurnal tide, 100-130 km. up, from incoherent scatt. obs. 2—26520
severe local storms, detection, prediction, economics and structure, conference (Boston, USA, 1971) 2—13695
severe thunderstorms and tornadoes forecasting, screening regression techniques 2—13702
severe weather forecasting, use of computers, SWEAT index 2—13696
shear, instruments for probing up to 1 km 2—1833
small scale wind shears, effects on radio meteor trails 2—30596
solar streamline analysis test using terrestrial data 2—11094
sound propagation through model cylindrical vortex, with viscous core, synoptic weather conditions 2—17381
Southern Hemisphere, half-yearly variation of circumpolar surface drift 2—26492
speed and direction, telemetering system with central monitoring and control of land and buoy telemeters 2—16802
speed dependence of undersea noise level 2—10716
speed dependences in microwave scatt. at 9.4, 24, 70 GHz 2—34254
speed derivatives in precipitation, radar method 2—1861
speeds in and above a pine forest 2—1859

Wind continued
stratosphere winter anomaly, height-time profiles of temp. and zonal wind, mechanism 2—16806
strength, past data from isotope studies 2—10727
stress discontinuity rel. to sea spray 2—20281
stress over ice and water in Beaufort Sea 2—16827
stress spectra rel. to non-regular sea level variations spectrum by hydrodynamical theory 2—20289
telemetry systems for obs. rel. to pressure as function of altitude 2—20317
thermal blooming in gases, wind transverse to beam propagation 2—27581
thermospheric, in F-region, equations of motion 2—10770
thermospheric, magnetic storm effects in neutral composition 2—30373
thunderstorm gust fronts, characteristics 2—40953
thunderstorms, velocity measurement 2—20329
tidal, influence on frequency of sporadic-E occurrence 2—37211
tornado forecasting, statistics of surface conditions after meso low of thunderstorm 2—13698
tornado generation and generalisation of rotating flame effect 2—4664
tornado-producing thunderstorms, prediction by aerial photography 2—13703
tornadoes, prediction from h.f. radio noise from thunderstorms 2—13705
tornadoes, stability indices in prediction 2—13708
tornadoes and water spouts, theoretical model 2—12488
transponder rocketsonde, miniaturised, for obtaining data 2—16801
tropical cyclone behaviour, cloud seeding and variations of sea surface temperature 2—37146
tropospheric velocity meas. by radio links and pulsed radar 2—7289
turbulence spectra in Prandtl-layer 2—30280
turbulent transfers inside vegetative canopy, use of Rn for meas. of diffusivity profiles 2—22963
two layer baroclinic model, nonlinear interaction of waves and zonal current 2—37143
upper anticyclones formation and blocking activity during Asia 2—20330
upper atmosphere, vertical velocity components of regular wind in meteor zone 2—22985
in valleys, morning dissipation, one dimensional model 2—7287
velocity and turbulence obs. using laser velocimeter 2—37126
velocity determination by sun glitter from a synchronous satellite 2—4650
velocity above seawater, oceanographic survey 2—37131
vertical neutral gas motions and deviations from barometric law in lower thermosphere 2—30312
vertical profile, effect of boundary layer and friction layer of sea stratification 2—30277
vertical profile rel. to turbulence spectrum 2—4680
vertical two point longitudinal velocity fluctuation differences in boundary layer, standard deviation 2—26488
vertical velocity spectra and variances just above surface layer 2—7286
water surface waves, curvature distrib. at different viewing angles 2—25020
wave driven, on liquid surface, kinematics of air layer motion 2—20331
wave follower for field study, of air-sea interactions 2—20283
wave generation, electro-hydraulic wave follower for wind field studies 2—16793
waves, in zonal wind meas. over Garchy, 80-105 km 2—26518

WKB method *see Quantum theory*

Wolfram *see Tungsten*

Wood
balsa, metal facings, mechanical strength of sandwich panels 2—1299
damping in nailed and glued joints in wood structures 2—14242
damping sources in material and joints of wood structures 2—14241

Work function
see also Electron emission
alkali earth metal oxide, cathode emission capacity mech. 2—40387
alkali metals, surface dipole contribution 2—16324
alkaline earth metals, surface dipole contribution 2—16324
aromatic hydrocarbon crystals 2—25849
hot-hole electron cascades in field emission 2—19795
metal, calc. using Shaw model potential 2—39455
metal, changes due to alkali adsorption, jellium model 2—4313
metal, negative work function of thermal positrons 2—25969
metal, of electron, relationship to electronic structure 2—6914
metal, polyvalent, surface dipole contribution 2—16324
metal, rel. to electronic struct. 2—40121
metals, determ. by charge accumulatoion method, meas. apparatus 2—36621
steel, stainless, reduction by elec. fields 2—16325
transition metal carbides, rel. to H surface recombination 2—29009
Ag, polycrystalline, meas. of contamination by S adsorption from SO_2 2—39552
Al_2O_3 films on Al, 30 to 600Å, obs and theory of oxide localized states 2—6913
Au, positron emission, negative work function 2—25970
Ba-W system, optimal coverage adsorption 2—3557
BaO-W system, temp. depend., 700-1400K 2—1586
BaO, thermionic emission 2—29659
CaO, thermionic emission, effect of adsorbed Ba layers 2—29784
$Ca_xSr_{1-x}O$ solid solns., exposure to Ba vapour influence 2—6915
CdS, single crystal, symmetrical surfaces, field emission 2—6918
Cs diode, emitter and collector, contact potential difference and effect of inert gas addition 2—23545
Cu single crystal, electron work function for (100), (110), (111) and (112) faces 2—33083
Fe, changes in α-γ transform. region 2—1587
GaAs, temp. and illumination depend., contact potential study 2—33006
p-Ge field emitter, O_2 adsorption, I-V characts. 2—25230
Ir(III)-C, dependence on degree of C coverage 2—9297
Mo-Nb monocrystalline alloys, additive character of variation, anisotropy 2—13352
Ni, variation with acetylene and ethane adsorption 2—1196
Pb, reduction by Cs coating 2—19809
Sb film on W(100) face 2—9281
SrO, thermionic emission 2—29659
Ta, thermionic emission, temp. depend., effect of adsorbed Li atoms 2—19798
Ti, field emission, change on adsorption of Cl_2 2—9307
W-Os alloy, (111) and (100) faces, temp. depend. 2—19793
W, adsorption of methane, binding energy determ. 2—12687
W, alkaline earth metal adsorbed, degree of coverage depend. 2—6916
W, Cs- or Ba-covered, electron emission, calc. 2—19794

Work function continued
W, field emission chemisorption of hydrocarbons, surface potential 2—25972
W, thermionic emission, temp. depend., effect of adsorbed Li atoms 2—19798

Work hardening
see also Cold working; Surface structure
computer model 2—15757
creep, recovery-work hardening model 2—9669
dislocation creep, work hardening/recovery model, mech. eqns. of state 2—39691
elastic-plastic materials with, model of, based on elastic model of materials with microstructure 2—29248
f.c.c. crystal, rate determ. from obstacle radius of screw dislocation pile-up 2—19098
f.c.c. crystal, stage III hardening, hydrostatic press. effects 2—19179
frictional behaviour and surface microstructure of S-137 material 2—29341
girders, steel, increased durability for cranes 2—1315
graphite, strain hardening parameter, creep study 2—32615
material with strong inclusions, primatic punching effect 2—22329
metal, alloy, at phase transform. rel. to double Bragg scatt. 2—36279
metal, b.c.c., ultimate tensile stress, structure sensitivity 2—25492
metal, dispersion hardening, strain hardening due to dispersed second phase 2—25574
metal, f.c.c. and b.c.c., in conical flows in metal forming 2—36211
metal, plastic deformation, strengthening coeff. 2—12951
pinning model, simple demonstration 2—29176
stage I, temp. depend. due to jog dragging 2—9743
steel, austenitic stainless, correlation between strain hardening parameters and dislocation substruct. 2—32703
steel, austeno-martensitic, hardening phenomena struct. analysis 2—29399
steel, computer simulation 2—32689
steel, high-Mn, resistance rel. to valve mat. development 2—3958
steel, impurity-dislocation reactions 2—22208
steel, low C, effect of type of stress 2—36212
steel, low C, temper hardening, effect on creep elimination 2—9673
steel, martensite, impact deformation strengthening 2—39901
steel, mechanical polishing, Rehbinder effect 2—32704
steel, metallurgical phenomena accompanying structural hardening 2—3959
steel, strengthening using hydroextrusion 2—9745
steel, thermomechanical strengthening 2—9728
steel austenitic, form. of NbC inclusions, effect of hardening conditions 2—36234
steel structures, strain-hardening effects on load-deformation relations 2—29397
Al-Ga alloy, curves, Ga influence 2—32702
Al, exoelectron energy and intensity meas. rel. to low temp. working 2—29779
AlMg alloy, Portevin Le Chatelier effect, vacancies 2—15818
Cu-Be alloys, ageing characts., under neutron irradiation, 100-160°C 2—39905
Cu-Cd, base alloy, increase in critical resolved shear stress in temp. independent region 2—9766
Cu-2at.%(10at.%Al, stage II, dislocation arrangements, electron microscope obs. 2—3788
Cu-Co, single crystals, containing coherent precipitates, plastic behaviour, dislocation arrangements 2—3936
Cu-Co alloy, single cryst. with coherent precip., dislocation arrangement 2—19243
Cu-In, base alloy, increase in critical resolved shear stress in temp. independent region 2—9766
59wt.%Cu-12wt.%Ni29wt.%Zn alloy, superposition of strengthening mech. by thermomech. treatment 2—32688
Cu, single crysts., fatigue life, fatigue hardening, cyclic deform., fracture 2—6568
CuAlZn alloy, extended dislocation clusters, energy obs. 2—15762
Fe-Mn alloy, shock loaded, twins, electron microscopy 2—9744
Fe-Mo-C, steel, martensite, secondary hardening during ageing, rel. to Co, Al, Mn additions 2—29398
Fe-(1.1 at%)Nb alloy, substitutional strain ageing, serrated flow 2—6536
Fe-Ni-Mo alloy, effect on martensitic transform. 2—29467
Fe-Ti, steel, work hardened, annealed, recrystn., recovery, segregation, electron and optical microscope obs. 2—32698
Fe, by cyclic changes of strain rate 2—19244
Fe polycrystal, pure, hydrostatic pressure effects on flow stress 2—39801
LiF(:Mg), temp., glide vel., Mg conc. effects, Frank's theory 2—36208
LiF, LiF:Mg, precip. hardening, crit. resolved shear stress 2—32705
Mg-Zn alloys, age-hardened, Ashby second slip theory applic. 2—6599
Mo polycrystal, pure, hydrostatic pressure effects on flow stress 2—39801
NaCl, strain hardening mechanism 2—39789
NbC, diamond grinding, surface deformation, microstructure 2—3871
Ni/ZrO$_2$ composite 2—12874
Ni-Al$_2$O$_3$, alloy, electrolytically deposited, dispersion hardening, tensile tests 2—19236
Ti-55 at.%Ni alloy, hardening, rel. to Ti$_2$Ni$_3$ precip. 2—39903
Ti, rel. to dynamic strain ageing, 77-1028K 2—25581
Ti alloy, structural hardness, cold working and heat treatment 2—12949
TiC, diamond grinding, surface deformation, microstructure 2—3871
W, hardening coeff., deformation degree and temp. depend. 2—9746
W alloy, for incandescent lamp filaments 2—39914
Zn polycrystal, hydrostatic pressure effects on flow stress 2—39802
Zr polycrystal, hydrostatic pressure effects on flow stress 2—39802
ZrC, diamond grinding, surface deformation, microstructure 2—3871

X and gamma-ray astronomy
γ absorption by photons in QSO's, pulsars and other source objects 2—26771
γ sources search at 10^{11}-10^{12}eV, null result 2—33722
γ-quanta, high energy, search for point sources from pulsars and radiogalaxy 2—17025
γ-rays spectral analysis techniques in COS-B satellite 2—11182
absorption of Crab Nebula X-rays by interstellar medium 2—37270
all sky X-ray monitor for UK-5, using pin-hole camera 2—30649
atmospheric v.l.f. signals, effects of stellar X-rays on phase 2—10757
balloon-borne experiments, use of magnetometers for plotting azimuth 2—30644
Bragg crystal spectrometer, rocket borne survey of Sco X-1 2—10980
3C 273, X-ray spectrum, determ. heavy element abundance in intergalactic medium 2—26612

X and gamma-ray astronomy continued
Cas A, precise location 2—20632
Cen A, X-ray emission spectrum 2—26803
Cen X-3, optical counterpart in LR Cen 2—41161
Cen X-3, pulsations due to occulting binary system 2—26799
Cen XR-3, wobbling neutron star model 2—13972
Cen XR-4, precursor to X-ray nova 2—26810
Centaurus X-3, limiting mass 2—41156
Centaurus X-3, model to explain luminosity, pulsation period and spectrum 2—26798
Centaurus X-3, neutron star component 2—41157
Centaurus X-3, reconsiders the white dwarf model 2—7501
Centaurus XR-4, X-ray burst before reported nova observations 2—13971
Cetus X-2 variable source, rocket obs. 2-10 keV 2—10977
collimation device, large area, construction and testing 2—5030
Coma Cluster, extended X-ray source, origin of mag. field 2—37335
compact objects, X-ray emission 2—13866
COS-B satellite instrumentation for galactic γ meas. 2—30398
cosmic x-ray sources, spectroscopy 2—23101
Crab nebula, search for polarized X-rays using focusing graphite crystal polarimeter 2—7388
Crab nebula, search for polarized X-rays using incoherent scattering polarimeter 2—7389
Crab Nebula, X-ray polarization det. 2—41155
Cyg X-1, coincidence with BO Ib star HDE 226868, spectral obs. 2—26698
Cyg X-1, hard X-ray pulsations, upper limits 2—7484
Cyg X-1, pulsating, UHURU obs. 2—7496
Cyg X-1, X-ray pulsations, mechanism 2—13973
Cygni X-2, obs. of λ4650 emission line 2—41162
Cygnus discrete sources, X-ray spectra 2—4943
Cygnus region, Cyg X-1, X-2, X-3, X-4 spectra, Cygnus Loop and Cygnus A obs. 2—26804
cygnus region, obs. of high energy γ-rays 2—10986
Cygnus X-1, dynamic spectrum analysis, oscillatory structure 2—23097
Cygnus X-1, flux var. rel. to radial velocity variations of the star HD 226868 2—13890
Cygnus X-1, further observations from UHURU, energy spectrum and pulsating nature 2—1970
Cygnus X-1, identification with HDE 226868 2—23098
Cygnus X-1, precise location 2—20632
Cygnus X-1 pulsations, shot-noise character 2—41158
Cygnus X-2, precise location 2—20632
data reduction using apodizing technique 2—26805
detector systems for gamma rays 2—11181
diffuse cosmic x-rays, autocorrelation function, inconsistent with superclustering 2—10976
diffuse cosmic X-rays, characteristic line spectra, mode of excitation 2—7370
diffuse cosmic X-rays, Galactic formed by bremsstrahlung and inverse Compton radiation 2—26605
diffuse galactic X-rays, red dwarf flare stars as possible source 2—10884
direction and energy spectrum meas. in energy range 1-10 MeV 2—11183
discrete X-ray sources and diffuse background in the Galaxy 2—10978
extended region near South Galactic Pole, diffuse X-ray background, no enhancement near 7 keV 2—20630
extended X-ray source centred on M87 in Virgo cluster 2—41058
extragalactic origin of low energy, diffuse, gamma rays 2—30532
focusing collector using a parabolic mirror, for long wavelength X-ray astronomy 2—11184
Galactic centre, γ-ray obs. 2—4948
galactic centre, spectrum and isotropy 2—7502
galactic centre obs. with gamma telescope 2—13842
galactic centre region sources 2—4790
galactic disk, diffuse component of X-ray emission, emission models 2—41056
galactic soft X-rays, role in alignment of interstellar grains, effect of interstellar absorption 2—10919
galactic sources, 30-200 keV X-rays directional detection unit 2—10983
galactic sources 2—33609
galactic sources seen from the southern hemisphere 2—13974
galactic X-ray sources in southern sky, positions, energy fluxes and models 2—26802
gamma ray spectra of celestial large energy sources 2—17026
gamma ray telescope, digitized spark chamber type, satellite borne 2—26811
gamma ray telescope using multiplate spark chamber for obs. of Crab Nebula pulsar 0532 2—10989
gamma spectrometry of galaxy, 0.5-5 MeV, using stilbene scintillator detector 2—10822
gamma telescope, for spectrometery of galactic sources 2—10821
gas proportional chamber for use in cosmic X-ray research 2—11186
gas-Cerenkov detector for 10 to 100 MeV gamma rays 2—8214
GX3+1, indentification from lunar occultations 2—17024
GX5-1 X-ray source, possible identification 2—37341
GX 340+0 location and X-ray pulsation limits 2—10973
GX 349+2, hard X-ray obs. 2—26809
GX 349+2 location and X-ray pulsation limits 2—10973
hard X-ray pulsations from Vela supernova remnant 2—26800
hard X-ray sources in southern sky, near galactic equator 2—26801
hard X-ray sources near galactic equator, l 335° to 350°, balloon flight 2—37338
intergalactic medium, X-ray observations, interpretations, review 2—26610
interstellar medium investigations 2—20606
isotropy between 1 and 6 MeV and implications for future observations 2—13829
line emission in diffuse X-ray background, upper limit 2—26606
long-baseline time-delay measurements of rapidly varying X-ray stars 2—33720
low energy γ radiation from galactic centre region, balloon altitude observation 2—23057
near M82, weak source data on location and spectrum7498 2—7498
M87, X-ray flux variations 2—23095
M87 region, X-ray emission obs., and structure of source 2—20634
Magallenic Clouds X-ray emission, 2-7 keV, obs. by Uhuru 2—4806
Magellanic cloud sources 2—7382
metagalactic gamma rays from relativistic electron interactions bremsstrahlung 2—10787
Michigan OSO III ion chamber, soft X-ray photometer 2—26884

X and gamma-ray astronomy continued
Michigan OSO III soft X-ray ion chamber, energy scale 2—37429
Monoceros Loop supernova remnant soft X-ray source of cooling neutron star 2—23096
neutron star crusts and the production of blackbody sources 2—20558
NGC 1068, Seyfert galaxy, satellite scan for X-ray emission 2—20633
NGC 1275, Seyfert galaxy, satellite scan for X-ray emission 2—20633
NGC 4151, Seyfert galaxy, satellite scan for X-ray emission 2—20633
NGC 5128, X-ray observations from Uhuru 2—26635
NGC 5128, X-ray spectrum 2—10950
Norma X-2, variable source, rocket obs. 2 to 10 keV 2—10977
North Polar Spur, soft X-rays detected 2—20483
NP0532, search for pulsed γ-ray emission above 50 MeV 2—7485
NP 0532, hard X-ray spectrum 2—7503
NP 0532, pulsed gamma radiation from the Crab Nebula, balloon observations at 50 MeV 2—10952
NP 0532, pulsed X-ray emission in 20 to 200 keV range 2—7481
NP 0532, X-ray observations, 30-100 keV 2—7482
paraboloid hyperboloid X-ray telescope, design characteristics 2—23139
X Per, connection with 2ASE 0352+30 X-ray source 23099 2—23099
X Persei identification with X-ray source23100 2—23100
Perseus and Coma clusters, extended X-ray sources, comparison with optical and radio emission 2—30499
planetary system, characteristic radiation 2—41192
pulsar near NP 0527, search for emission over 100 keV 2—41160
pulsed γ-ray emission above 50 MeV, search in Crab Nebula pulsar 2—26812
pulsed γ-rays of 10^{12} eV from Crab Nebula pulsar 2—41163
pulsed gamma rays from NP 0532 at about 10^{12} eV 2—10987
pulsed X-ray source near the Crab Nebula 2—20635
Puppis A, soft X-rays, rocket obs. 2—7495
satellite instrumentation, high sensitivity survey for X- and γ-ray sources 2—10985
Sco X-1, circular polarization 2—4944
Sco X-1, circular polarization obs. 2—37334
Sco X-1, Japanese photometric observations in 1970-1 period 2—30531
Sco X-1, long term obs. by OSO III 2—26808
Sco X-1, low energy γ-ray spectrum, balloon altitude observation 2—20636
Sco X-1, observations at 80 MHz to show existence of radio flares 2—4945
Sco X-1, precise location 2—20632
Sco X-1, short period oscillations in X-ray and optical flux 2—26806
Sco X-1, UHURU obs., intensity and temp., rel. with optical brightness 2—26807
Sco X-1, variable circular polarization in visible region, periods and amplitudes 2—33718
Sco X-1, wavelength and time dependence of optical polarization 2—20629
Sco X-1 search for pulsed radio emission 2—7493
Sco X-1 source, optical emission, variable circular polarization, (June-July 1971) 2—17023
Sco XR-1, differential X-ray energy spectrum, SHIRX X-ray spectrometer 2—30530
SCO-X1, time variation of X-ray spectrum and optical luminosity 2—10975
Scorpius X-1 spectra and model of continuum radiative transfer in hot plasma 2—37337
Seyfert galaxies, satellite scan for X-ray emission 2—20633
Seyfert Galaxies NGC 1275 and NGC 4151, X-ray source 2—7499
soft X-ray survey from Sagittarius to Vela 2—10972
soft X-rays, automatic stabilized detection system 2—11162
solar activity, X-ray emitting regions, temporal behaviour, results from OSO-IV 2—37385
solar and celestial X-rays 15-250 keV from 5th Orbiting Solar Observatory 2—11091
solar burst of 11 February 1970, observed at balloon altitude 2—33764
solar coronal X-ray features, electron temperature and density, 3-60 Angstroms 2—26885
solar flare plasma, X-ray emission from high energy electron heating 2—37409
solar hard X-radiation during flares, bremsstrahlung emission of energetic electrons 2—17085
solar soft X-ray spectrum, grating with parallel grazing incidence 2—11069
solar spectrum, satellite lines 2—7549
solar spectrum as function of position on disk, rocket-borne study 2—11068
solar X-radiation, polarization and anisotropy during flares 2—17054
solar X-ray absorption profiles and residual fluxes during 1970, March 7 eclipse 2—33763
solar X-ray flares, electron temp. and emission measure variations 2—26887
solar X-ray instrument for OSO-H, monitoring of solar flares 2—30609
spark chamber resolution for γ astronomy 2—8242
stars, visible, corresponding to X-ray sources 2—16949
status of γ-ray astronomy 2—11160
Sun, optical identification of activity assoc. with background fluctuations 2—30611
supernova remnants in Aquila, high-sensitivity X- ray search 2—33719
supernovae, extragalactic optical objects, upper limits to X-ray luminosities 2—26797
supernovae, upper limits to X-ray luminosity 2—4947
techniques and instrumentation, satellites and focusing X-ray telescopes 2—10979
telescope for satellite experiment to meas. intensity and energy spectrum of sun flares 2—11138
telescope using gas Cerenkov detector for fine angular resolution of gamma astronomical sources 2—10988
thermal cosmic X-ray sources electron density det. from ratio of lines in He like ions 2—20710
thermal X-ray emission from neutron stars due to frictional heating 2—7435
UHURU satellite borne X-ray observatory, all sky survey 2—30648
universal X-ray background, neutron stars as sources 2—20625
Vela X, soft X-rays, rocket obs. 2—7495
Virgo cluster, soft X-ray sources, upper limit to emission 2—20489
white dwarfs, rotating magnetic as X-ray sources 2—7500
X-ray, glancing incidence optics 2—11161

X and gamma-ray astronomy continued
X-ray astronomy experiments, use of magnetometers for plotting azimuth 2—30644
X-ray emission from degenerate stars 2—4946
X-ray emission from rich clusters of galaxies 2—37339
X-ray emission from supernova remnants 2—7473
X-ray emission from white dwarfs, soft background obs. 2—37336
X-ray optical system for surveying and locating cosmic X-ray sources 2—10984
X-ray polarimeter, incoherent Thomson scatter in Li metal 2—10981
X-ray pulsar, NP 0532, near Crab nebula 2—30529
X-ray solar flares, var. of temp. and emission measures with time 2—17053
x-ray source obs. by Uhuru satellite 2—41159
X-ray source production in final stages of stellar evolution 2—10862
X-ray sources, optical candidates X Per and HD 77581 for 2U 0352+30 and 2U 0900-40 2—37340
X-ray sources, polarisation, spectra, accurate locations 2—10982
X-ray sources along galactic equator, satellite obs. 2—20631
X-ray sources near galactic centre, diffuse and discrete, obs. by Uhuru satellite 2—10974
X-ray stars, pulsating, white dwarf model 2—7497
X-ray telescope with modulation collimator for solar flare obs. 2—11139
^{60}Fe flux det. by satellite 2—7504
NaI(Tl) γ-ray spectrometer, solar monitoring in OSO-7 spacecraft 2—30610

X-ray absorption
see also X-ray spectra/absorption
cylindrical sample, absorpt. and vol. corrections 2—32413
cylindrical sample, analytical soln. for absorpt. factor at Bragg angles 2—22131
distorted crystal interaction, dynamic theory 2—6695
galactic centre sources, at low energy 2—10974
transmission, three dimens., statistical 2—32414

X-ray analysis *see Chemical analysis/X-ray; Crystal structure, atomic; X-ray crystallography*

X-ray astronomy *see X and gamm-ray astronomy*

X-ray characteristic temperature *see Specific heat*

X-ray crystallography
see also Debye-Waller factors
For results of structure analysis see Crystal structure, atomic
absolute intensity calibration 2—3649
absolute scale of scatt. intensity 2—15701
absorption effects in anomalous transmission through perfect Ge crystals 2—3711
absorption in three-dimens. transmission, statistical evaluation 2—32414
atomic parameters, expressed by 5 scalar invariant quantities 2—3598
atomic scatt. factors, incoherent scatt. intensities, elements of at. number 2-36 2—35960
Borrmann effect, multiple beam, in perfect Ge and Si crystals 2—39602
Bragg diffr., dynamical, theory 2—9390
Bragg reflection, influence of strong elec. fields on intensity and location 2—32418
centroid and peak shifts due to dispersion 2—19026
centroid shift of diffr. line due to diffractometer geometrical factors 2—12706
cylindrical sample, absorpt. and vol. corrections 2—32413
defect structure, lattice dilation and attenuation factors in diffuse scatt. calcs. 2—12708
defocusing criterion, diffr. line profile variance 2—25296
diffraction enhancement of symmetry 2—35961
diffraction profile and moments, particle size broadening 2—3629
dislocations, theory of Borrmann contrast 2—22205
distorted crysts., location of diffuse maxima in scatt. patterns 2—3613
dynamic origin of diffr. maxima 2—9387
dynamical diffraction applied to spectral characterization of quartz 2—33292
dynamical diffraction characteristics at a Bragg angle of about $\pi/2$ 2—35966
dynamical scatt., Laue case, integral values of refl. and transmission 2—9391
dynamical theory, correspondence with electron diffr. dynamical theory via Schrodinger wave eqn. 2—3617
finite polyhedral cryst., Laue-(Bragg)^m diffr. theory 2—22140
finite polyhedral cryst., Laue-Bragg diffr. theory 2—22139
form factors, consistency expression 2—12709
Fresnel formulae, friction and slip considerations 2—35963
glass structure, quasicrystalline model 2—18897
grazing-angle scatt. by thin crysts. 2—35968
grazing-angle scatt. by thin crysts. 2—35967
instrumentation and analysis, a review 2—25299
ion spin-lattice-coupling, phonon damping and magnetic order 2—19848
ionic crystal with complete electron shells, scattering factor calc. 2—32435
lattice planes, parallel excited, Bragg reflexions 2—32415
light atom refinement in heavy atom structures 2—9395
maximum crystallite size obtainable by line broadening 2—3635
multiple small angle scattering theory 2—32420
multiple-diffraction effects in intensity obs. on single crysts. 2—3609
organic reaction obs. 2—35933
polytypic crysts., platelet-shaped, streaking of diffraction spots 2—3608
powder diffraction profile moments in kinematic tangent-plane approx. 2—3612
powder diffractometry, automatic, review 2—15707
quantum theory of scattering, absorpt. coeff., temp. depend. 2—19019
Seemann-Bohlin diffractometry, axial divergence error 2—3633
shear structure, diffr. effects 2—25297
small angle scattering, absolute intensity meas. 2—3627
small angle scattering, collimation corrections verification 2—15703
small angle scattering, inhomogeneities effect 2—3622
small angle scattering, interparticle interferences in close packed systems 2—15697
small angle scattering, theory 2—3630
small angle scattering apparatus, high temp. meas. 2—15700
small angle scattering in radial distribution function calculation 2—3648
thin crystal, Laue-case diffr., interference fringe obs. 2—6449
topography, use in determining sign of fault vectors 2—32534
transmission topographs, shadow images of absorbing wire using dislocation-free Si single crystal 2—15705
twin identification using intensity statistics 2—3655

- **X-ray crystallography** continued
  - twinned crysts., twins with superimposed reciprocal lattices, twinning parameter estimation 2—35962
  - X-ray topography, instantaneous video display 2—1161
  - Na, Debye parameter and vibration amplitude from Bragg intensity data 2—9862
  - **apparatus**
    - *see also X-ray monochromators; X-ray spectrometers*
    - automatic film reader, accuracy estimation 2—3652
    - bent spectrograph, 1 m radius, design, construction and performance 2—3592
    - camera, high temp. heater 2—9396
    - camera, h.p., two-film cassette 2—25301
    - camera, vapour thermostatted for diffraction pattern and sorption obs. 2—3619
    - camera with sample coding by mechanical refrigerator, 30-180K meas. 2—3694
    - cameras, Debye, high temp., design 2—3638
    - chamber for obs. of highly dispersive powders in temp. range from —175 to +400°C 2—19023
    - computer controlled diffractometer, loop closing program 2—3645
    - conference, Karlsruhe, Germany, Sept. 1971 2—25279
    - controlled temperature dewar for intensity meas. 2—3650
    - cryogenic attachment for single cryst. studies 2—25294
    - cryostat, for single cryst. studies, construction and operation 2—25284
    - detectors, solid state, diffr. powder work, fluorescence information 2—3607
    - diffractometer, computer control system 2—3634
    - diffractometer, programmed control 2—25298
    - diffractometer attachment, for precision meas. up to 2100°C 2—12710
    - diffractometer for polycryst., line intensity, position and width, specimen position influence 2—9392
    - diffractometer-multichannel analyzer interface, allowing X-ray diffraction data storage 2—41355
    - flash X-ray tube and image intensifier for pattern recording 2—12707
    - furnace, carbon resistor, adaptable to Philips goniometer, for high temp. reactive processes obs. 2—3636
    - goniometer adaptation for Manenc set-up 2—6407
    - goniometer for Berg-Barrett X-ray technique 2—39604
    - Guinier chamber, for single cryst. studies 2—29114
    - high-pressure camera powder patterns, compression up to 200 Kbar 2—19028
    - instrumentation problems in Lang topography for process control 2—25303
    - kappa geometry diffractometer system 2—3651
    - Kratky small angle collimation, camera parameter optimization 2—3647
    - Lang camera modification for defect distrib. in single crysts. 2—25302
    - local convergent beam set-up for single cryst. 2—19020
    - microanalysis combined with high resolution electron microscopy 2—9410
    - microfocus unit, construction and appl. 2—15706
    - monochromator, high resolution focussing, using Si and Ge plates 2—25285
    - premonochromator for Picker vertical axis diffractometer 2—32417
    - quarter circle goniostat, motorized rotation about polar axis 2—15704
    - rotating drum film scanner, computer controlled 2—35965
    - safety systems for use with Philips PW 1016 and PW 1316 tube shields 2—19024
    - slit subassembly, for crystals with small angle boundaries 2—29109
    - small angle scattering, rotatable Kratky camera, specimen orientation 2—3624
    - small angle scattering chamber with total reflection monochromator 2—15698
    - sources, detectors, chambers, diffractometers, densitometers, review 2—19022
    - Weissenberg goniometer design and use of integrating mechanism for producing one-dimensional spots 2—35964
  - **calculation apparatus**
    - intensity measurement, Weissenberg photograph, using TV cameras 2—9388
  - **calculation methods**
    - a priori phase information, application to noncentrosymmetric phase problems 2—3641
    - absorption correction for intensity data from poorly defined single crystal 2—3614
    - alloy scatt. factors calc. for Guinier-Preston zones precise determ. 2—6408
    - analytic approximations to form factors 2—3595
    - anti-phase domain structures, 1-dimens., classification and Patterson method applic. 2—3686
    - Bragg reflexion, Renninger formulae, correction 2—32416
    - Cartesian displacement coordinates, mass-weighted, use in kinematics of rigid body motion 2—4031
    - computer applications, review 2—25282
    - computer indexing of powder patterns, monoclinic case 2—3646
    - computer program, construction of pole figures from Schulz goniometer data 2—3632
    - computer program for choosing starting sets for use in tangent formula struct. soln. method 2—3687
    - computer program for Fourier synthesis 2—22147
    - computer program for stereographic projections 2—25319
    - computer programs for routine solns. of complex structures 2—25320
    - computing by time sharing system 2—3643
    - conference, Karlsruhe, Germany, Sept. 1971 2—25279
    - crystal, atomic bond estimation from X-ray charact. temp. 2—18963
    - diffraction peak broadening analysis, for h.c.p. metals, computer program 2—35974
    - diffractometer measurements, refl. symmetry and meas. errors, anal. using χ^2 test 2—32438
    - discrepancy factor for struct. analysis 2—22138
    - distortions and block size determinations from shape of diffraction lines 2—29112
    - doublet line profile in polycryst. analysis, charact. points 2—25293
    - electron density function calc., anomalous dispersion effects 2—9383
    - fibrous systems, small-angle equatorial scatt., direct analysis, Patterson function and intensity 2—3611
    - FIGATOM, graphic program for stereoscopic cryst. struct. illustrations 2—25318
    - FORTRAN IV computer program, scatt. by liquid, amorphous and microcrystallized substances 2—19041
    - Fourier coeffs. in $K\alpha_1$ component, direct evaluation from profile analysis 2—3685

- **X-ray crystallography** continued
  - **calculation methods** continued
    - Fourier coeffs. of paracrystalline diffraction 2—3616
    - Fourier synthesis, mean figure-of-merit 2—22132
    - Fourier transformation of intensity data, limitations for polyatomic glasses 2—22055
    - group refinement program, ORION 2—9510
    - intensity statistics, atomic scatt. factors determ., cubic crystals 2—3690
    - intrinsic ang. scatt. intensity distrib. curve, formula derivation 2—25292
    - Kossel projections, computer generation and identification 2—32425
    - lattice parameter meas. using divergent beam X-ray technique, computation by iterative process 2—12705
    - least squares refinement by polarized H atom 2—6418
    - least-squares refinement derivatives, constraints applic. 2—22128
    - least-squares refinement program, CELPAR 2—25300
    - matrix inversion for slit correction in small angle scattering 2—3623
    - modified tangent procedure applied to 9-t-butyl-9,10-dihydroanthracene struct. 2—3745
    - molecular charge densities from theoretical X-ray scatt. factors 2—6419
    - multiorigin method for struct. factor phase determ. 2—22133
    - multiorigin procedure applic. to steroid cryst. 2—25353
    - non-centrosymmetric cryst., Bijvoet differences, anomalous scatt. applic. 2—22135
    - normal probability plot analysis of small samples 2—22130
    - optimal algorithm for refinement 2—22146
    - Patterson and difference Fourier maps, improvement 2—22137
    - Patterson function, probability approach, key peaks display 2—9393
    - Patterson vectors of lattice complexes 2—9381
    - phase determ. using anomalous dispersion data for two wavelengths 2—22136
    - phase determination, direct method 2—25321
    - phase determination, multi-formula procedure 2—3642
    - phase determination from glycera haemoglobin, tangent formula combined with isomorphous replacement 2—3743
    - phase expansion limits in direct methods 2—32433
    - phase problem, pictorial pattern recognition 2—15694
    - powder diagrams, automatic treatment 2—39600
    - programming techniques for phase determ. 2—9431
    - rotation function, optimal sampling 2—39625
    - secondary scatt. intensity calc. for noncryst. materials, transmission geometry 2—22052
    - single crystal diffractometer meas., dispersion analysis 2—1222
    - single-crystal diffractometer meas., dispersion analysis 2—1221
    - small angle scattering curve analysis and simulation 2—3654
    - small angle scattering data desmearing by computer program 2—3628
    - small-angle scatt., structural parameter, multiple scatt. effect 2—19025
    - stress determination in single crysts. using diffr. 2—3610
    - structure analysis using PDP-8 computer programming 2—3644
    - structure definition by Fourier method, computer program 2—32439
    - structure factor determination, reflection intensity pattern 2—35975
    - structure factor equation, anomalous scattering 2—9397
    - structure-factor least-squares refinement, method for applying constraints 2—3688
    - superposition method of refinement, realization using computer programs 2—9432
    - symbolic addition method for phase determ. 2—22134
    - β-synthesis, rel. to holographic image deblurring techniques 2—34424
    - tetrahedron form, etching pit, X-ray topograms, image calc. 2—32436
    - truncated integrated intensity applic. to broadened diffr. line analysis 2—25290
    - vector space search methods applic. to Patterson function of myoglobin 2—22172
    - W, deformed, diffr. broadening shape analysis 2—3689
  - **structures** *see Crystal structure, atomic*
  - **technique**
    - anomalous transmission characteristics by varying effective thickness of crystals 2—25288
    - atomic mismatch on closure of controlled partial splits, shear displacement 2—19095
    - bent cryst., area contrast images 2—15755
    - Bijvoet intensity ratios, accurate measurement using CuK_α radiation 2—9394
    - Bonse-Hart system comparison with block collimation system 2—3626
    - compressibility, linear isothermal, high press. 2—3859
    - difference Patterson function, phase problem soln. 2—6455
    - diffraction method, for valence electron charge density determ. in covalent cpds. 2—19021
    - extended X-ray absorpt. fine struct. technique, obs. on non crystalline materials 2—3640
    - feedback control scheme for scanning topography 2—15696
    - film microdensitometer meas. of integrated reflexions 2—15702
    - globe and cap method for orienting cubic crysts. using Laue photographs 2—25291
    - intensity correction for thermal diffuse scatt. 2—12704
    - intensity meas. project, type I 2—25286
    - lattice parameter of small single crystal, scanning methods 2—3653
    - Laue diffraction, rocking-curves rel. to cryst. perfection, obs. on Ge 2—9398
    - least-squares method for refinement of phases of struct. factors 2—25287
    - line profiles, corrections for thermal diffuse scatt., secondary extinction and crystallite size 2—9385
    - optical diffr. masks representing static disorder, prod. method 2—25315
    - optimum scans in diffr. expts. 2—22127
    - powder photograph densitometry, double scan method 2—19027
    - protein, phase determ., anomalous dispersion method 2—32419
    - protein crystallography, contemporary developments 2—15735
    - pseudocubic lattices, precise meas. of lattice parameters 2—22129
    - pulse recording, K_β component determination, scatter curve correction 2—15699
    - sample preparation, small single cryst. sphere growth 2—22100
    - scanning counter, for defect distrib. in single crystals 2—25302
    - scanning oscillator technique, for semiconductor materials 2—39601
    - scanning topography with chromatic-aberration technique 2—3618
    - Schulz reflection method, defocussing phenomena 2—3631
    - screenless precession photography for all refl. intensity meas. 2—9386
    - setting of crystals on precession camera 2—39597
    - small angle scattering, comparison of Kratky and Beeman collimation system 2—3625
    - small-angle scatt. intensity normalization using glassy carbon standard 2—25295

X-ray crystallography continued
 technique continued
  stress determination in single crysts. using diffr. 2—3610
  symmetrical back-reflection for low temp. (30-180K) meas. 2—3694
  three-dimensional reconstruction from radiographs and electron micrographs by convolution method 2—29108
  wide-angle and lattice interference methods 2—39603

X-ray diffraction
  see also X-ray crystallography; X-ray scattering
  alkaline earth chlorides, aqueous solns., electron radial distrib. functions 2—32225
  atomic scatt. factors, incoherent scatt. intensities, elements of at. number 2-36 2—35960
  Bragg diffr., dynamical, theory 2—9390
  Bragg reflexion, Renninger formulae, correction 2—32416
  camera, vapour thermostatted 2—3619
  crystals, hyperextinction rules and hyperdiffraction symmetry 2—1218
  cylindrical sample, absorpt. and vol. corrections 2—32413
  diffraction enhancement of symmetry 2—35961
  dynamic origin of diffr. maxima 2—9387
  finite polyhedral cryst., Laue-(Bragg)^m diffr. theory 2—22140
  finite polyhedral cryst., Laue-Bragg diffr. theory 2—22139
  geometrical optics rel. to ideal and distorted crysts. 2—9389
  ionic state of crystals, methods of determ. 2—6392
  Kossel patterns, back reflection, reproduction 2—3620
  lattice planes, parallel excited, Bragg reflexions 2—32415
  Laue case, rocking-curves rel. to cryst. perfection, obs. on Ge 2—9398
  powder diagrams, automatic treatment 2—39600
  spectrometer, double crystal, simultaneous diffraction 2—38357
  symmetry, diffr. enhancement 2—32410
  texture rel. to background X-ray scatt. 2—29111
  Mg-Co-Ni 9-layer Laves phase, composition and lattice constants determ. by single crystal and powder X-ray diffraction 2—39645
  Mg-Cu-Zn 9-layer Laves phase, composition and lattice constants determ. by single crystal and powder X-ray diffraction 2—39645
  Mg-Li-Zn 9-layer Laves phase, composition and lattice constants determ. by single crystal and powder X-ray diffraction 2—39645

X-ray diffractometers *see X-ray crystallography/apparatus*

X-ray examination of materials
  see also Chemical analysis/X-ray; Radiography
  ablative material, response to simulated re-entry conditions, flash X-ray techniques 2—36184
  alkali halide, single phonon X-ray scatt., eigenvector influence 2—9855
  alloy, binary static displacement of atoms, determ. using anomalous scattering 2—3691
  alloy, disordered, diffuse scatt. obs. 2—9375
  alloy, disordered, multi-atom interaction energies 2—15931
  alloy, disordered binary substitutional, Debye charact. temp. 2—22422
  alloy, nimonic-type aged, elastically strained by precipitates, line intensity distrib. 2—15928
  alloy, quaternary, phase transformation 2—3654
  amino acids, γ-radiolysis study 2—7187
  ammonium hydrogen di-chloroacetate, paraelect. phase, cryst. struct. 2—36002
  ammonium oxalate monoperhydrate, cryst. struct. 2—36003
  ammonium Rochelle salt, ferroelectric phase superstructure 2—10119
  amorphous system, partial struct. factors separation using anomalous scatt. 2—12536
  anharmonic contribs. to diffuse scatt. 2—19330
  anisotropic lattice, fluctuations and Bragg peaks 2—19331
  Apollo 15 geochemical x-ray fluorescence experiment 2—41187
  apparatus for determ. the best conditions for photographing the image 2—30120
  azide crystals, anisotropic thermal expansion by single crystal method 2—15734
  $BaFe_2O_4$, polymorphism 2—39980
  β-brass, long-range order 2—36231
  brass, ordering parameter 2—25595
  bromoform, cryst. struct., 253K 2—32479
  4- butyloxybenzal-4′-ethylaniline, liquid crystal smectic phase detn. 2—32234
  calcite, crystal, struct., effect of S impurity 2—6422
  carbon, refractory oxide reactions, parameter meas., temps. to 2400°C 2—3636
  catalyst surface area rel. to crystallite size 2—26346
  cellulose, paracryst. lattice disorder 2—25165
  characteristic strain meas., comparison with strain gauge meas. 2—22264
  cholesterol esters, polymorphic and mesomorphic behaviour 2—25039
  coke structure 2—1385
  critical opalescence of one component fluid, gravitational effects in small angle X-ray scattering expts. 2—22036
  cubic crystal, double-force tensor of point defects, scatt. determ. 2—40019
  trans-cyclohexane-1,4-dicarboxylic acid, K salt, struct., bond lengths 2—36000
  cyclotrimethylene trinitramine, dislocations correl. with etch pits 2—3783
  diamond, F_{222} obs., bonding electron density meas. 2—3702
  diamond, inhomogeneous, impurity platelet distrib. and size 2—9588
  dibenzyl disulphide, space group ambiguity 2—22171
  1,1′-diethyl-4,4′-cyanine bromide, crystal structure determination using diffraction 2—3746
  1,1′-diethyl- 2,2′-cyanine bromide, crystal structure determination using diffraction 2—3746
  diffraction, ion source applications 2—7890
  dinaphtho[2,1-2′,3′]furan-8,13-dione, polymorphism 2—25356
  dipeptides, γ-radiolysis study 2—7187
  1,1-diphenylethylene: diphenyldiazomethane, photolysis and struct. obs. 2—37055
  dislocation strain fields analysis 2—1252
  disperse systems, molecular association 2—3417
  distorted crysts., location of diffuse maxima in scatt. patterns 2—3613
  distorted polycrystal with generalized strain distrib., apparent particle size and strain 2—22199
  $ErNaO_2$, cryst. struct. 2—35987
  eyes of frog, diffraction pattern from outer segments of visual cells 2—14049
  ferromagnet, diffractometer attachment appl. 2—12710
  fluidized bed bubble observation 2—28438
  fluidized beds bubble size and number in unrestrained growth 2—31895
  fluidized beds bubble transition from two to three dimensions 2—28439

X-ray examination of materials continued
  fluorescence analyser, non-dispersive, isotope source fluoresc. X-ray excitation 2—10674
  fluorescence analysis of powders, semiconductor detectors 2—34807
  fluorocarbon film, struct. determ. 2—9228
  glass, crystals in bubbles, method for analysis 2—32315
  glass, polyatomic, limitations of Fourier calc. 2—22055
  glass, silicate, decomposition, crystallization, small angle scatt. 2—3453
  glass, soda, rare earth doped, sensitivity to crystalline environment or included impurity ions obs. 2—9223
  glass systems, phase separation 2—32316
  greenschist facies meta-volcanic rocks, X-ray powder diffraction obs. 2—30129
  ice, dislocation density, increase due to diffused HF 2—39698
  inorganic substances, powder diffr. data for 63 materials 2—39629
  interference patterns, dependence on degree of chemical polishing, annealing, wavelength of X-rays and presence of wedge 2—25289
  Lang topography, electromechanical feedback control for camera to keep crystals in Bragg condition 2—3605
  liquid cryst., disordered, diffuse scatt. obs. 2—9375
  liquid crystal, nematic p-azoxyanisole, orientation, effect of flow 2—1077
  liquid crystals, calculation of the molecular cylindrical distribution function and the order parameter 2—35741
  lunar soil, Sea of Fertility, basaltic and monomineralic fragments 2—20647
  medical stereoscopic X-ray TV system 2—7635
  metal, defect clustering, anomalous transmission, theory 2—15746
  metal, f.c.c., scatt. by dumbbell interstitials 2—9540
  metal, liquid, structure factor and atomic distrib. detn. 2—18792
  metallic systems, volume changes, thermodynamic characts. 2—3862
  molecular cryst., disordered, diffuse scatt. obs. 2—9375
  myoglobin, Patterson function, vector space search methods applic. 2—22172
  myoglobin, vibration and defect contribs. to temp. factors, Mossbauer and X-ray obs. 2—4041
  nematic liquid cryst., scatt. intensity, mol. orientation distrib. function 2—21962
  p-nitroaniline, thermal expansion, 290 to 380K 2—9898
  non-crystalline two phase system, density fluctuations 2—3466
  nylon 12, polymorphism, X-ray diffraction study 2—25167
  pentaerythritol, hydrogen bonding, dispersion relations, from diffuse scatt. obs. 2—3749
  2-(4-n-pentylphenyl)-5-(4-pentyloxyphenyl)- pyrimidine, smectic modifications detn. 2—25042
  physical metallurgy, tools and techniques, book 2—25560
  piezoelectric, strain detn. for piezoelectric consts. 2—4282
  plagioclase satellite refls. origin 2—6420
  poly(ethylene oxide) of low molecular weight, melting behaviour studied by low angle X-ray scattering 2—39422
  poly(tetramethylene oxide), crystallization, small angle scatt. obs. 2—3469
  poly-γ-benzyl-L-glutamate, electrically induced molecular orientation 2—15577
  poly-P2VB, solid-state photopolymerization 2—3477
  polyamide, lamellar crystals, low and wide angle pattern interpretation 2—3464
  polyamides, chain folding 2—3465
  polyamides, doubly-oriented, small angle diffr. diagrams 2—18909
  polybutene-1, isotactic, and polyethylene glass transition temp., small angle diffr. 2—3463
  polyethylene, irrad., small-angle scatt. obs., ordered and disordered regions 2—25384
  polyethylene with simple orientation texture, small-angle diffr. diagrams 2—18910
  polyethyleneterephthalate, small angle scatt., absolute intensity, correlation function 2—3467
  polymer, plastic deformation, morphology, small angle scatt., electron microscopy 2—3462
  polymer characterization, small angle scatt, state-of-the-art 2—35852
  polymer characterization, wide-angle diffr., state-of-the-art 2—35856
  polypropylene, isotactic, small- and wide-angle obs., solid-solid transition 2—3468
  polytypic crysts., platelet-shaped, streaking of diffraction spots 2—3608
  potassium homophthalate, crystal structure 2—3750
  potassium hydrogen meso-tartrate, H-bonding 2—36001
  powders, integrated intensity changes, effective temp. factor, rel. to powder cryst. state 2—12714
  protein, phase determ., anomalous dispersion method 2—32419
  pyreno-(1′,2′:1,2)-pyrene, mol. struct. and cryst. struct. 2—32480
  quartz, determ. sign of fault vectors by X-ray topography 2—32534
  quartz powder, extrapolation method for grain size determ. 2—32744
  radiographic inspection of welds image quality 2—14056
  rare earth niobates, $RENbO_4$ type, cryst. struct. 2—6448
  rare earth sequisulphide, struct., density, reflection spectra 2—40671
  rare earth silicates, of type $RE_2[SiO_4]O$, cryst. struct. 2—6450
  smectic liquid crystal, A, B and C modifications, polymorphism 2—18794
  steel, $\chi' \rightarrow \alpha_m$ transform., effect of C 2—1392
  steel, χ'-martensite form. obs. 2—1393
  steel, maraging, austenite form. during ageing 2—32708
  steel, martensitic, two-phase decomp. study 2—12967
  steel, martensitic transform rel. to C conc. and thermomech. treatment. 2—15961
  steel, quenched, low-temp. tempered, martensite decomp. compressive stresses relax. 2—15899
  steel, quenched, recrystn. during rapid heating 2—29389
  steel, recrystallisation, struct., during slow heating 2—15906
  steel, recrystallization, u.s. attenuation obs. 2—25572
  steel, retained austenite 2—1226
  steel, rhenium, quenching, martensitic transformation 2—3994
  steel, structural, martensite struct. 2—36232
  steel powder, lattice parameter, cryst. size and lattice strain 2—3706
  steel reactor casing, oxidation by neutron activated UPu oxide fuel 2—13577
  stress meas., sample-curvature errors 2—22266
  stress measurement, lattice deformation, topography 2—25299
  sulphur phase ternaries, M Mo_nS_{n+1}, M=Ag, Sn, Ca, Sr, Pb, Ba, Ni, Co, Fe, Cr, Mn, Cu, Mg, Zn, Cd 2—9478
  ternary systems {Y, La, Ce}— {Al, Si}—B, X-ray analysis, isothermal sections determ. 2—39657
  thiogallate phosphor, MGa_2S_4:Ce^{3+}, Eu^{2+}, struct. 2—26234
  thiourea, satellite scatt., structural modulation 2—13320

X-ray examination of materials continued
tin (II) formate, difficulty in assigning unique unit cell to X-ray powder spectrum demonstrated 2—36005
transition metal, corrosion by liquid Na, ternary oxide formation 2—37045
X-ray intensifying screen using Gd_2O_2S:Tb phosphor 2—30672
X-ray topography, instantaneous video display 2—1161
zeolite lattices with Hg filled channels, struct. behaviour 2—6444
$[Co(NH_3)_5Cl]Cl_2$, structure, lattice dynamics meas. 2—3704
$[Co(NH_3)_5H_2O](ClO_4)_3$, structure, lattice dynamics meas. 2—3704
$[Co(NH_3)_5NCS](NO_3)_2$, structure, lattice dynamics meas. 2—3704
$[Co(NH_3)_6](NO_3)_3$, structure, lattice dynamics meas. 2—3704
Ag-23 at.%Ge alloy, metastable h.c.p. phase decomp., metallographic techniques obs. 2—39978
Ag-Cd alloy, plastically deformed 2—15829
Ag, thermal expansion coeff. and lattice parameters determ., 30-180K, special method 2—3694
Al-Ag alloys, Laue intensity 2—9444
Al-Mn, alloy, dilute, quenched, solute dispersion, X-ray diffr. obs. 2—25587
Al-Ni, alloy, dilute, quenched, solute dispersion, X-ray diffr. obs. 2—25587
Al-V alloy, disorder-order transform. obs. 2—39994
Al-Zn-Mg alloy, ageing, transition phase obs. 2—9753
Al-Zn-Mg alloy, quenched, aged, metastable miscibility gap, small angle scatt. 2—3981
Al-Zn, alloy, dilute, quenched, solute dispersion, X-ray diffr. obs. 2—25587
Al-Zn, alloy, precip., decomp., intermediate phase, ageing, X-ray diffr. obs. 2—19263
Al-(15 at.%)Zn alloy, quenched, coherent phase separation, small angle scatt. 2—3980
Al-Zn alloy, decomp. second stage, diffuse effects, X-ray scatt. obs. 2—25588
Al-Zn alloy, pre-precipitation, small-angle scatt. obs. 2—3939
Al, cold worked and annealed, small angle scatt. obs. 2—25592
Al, Debye temp. 2—9856
Al, mosaic. struct. in creep 2—29187
Al, scatt. from phonons 2—16002
Al, thermal expansion coeff. and lattice parameters determ., 30-180K, special method 2—3694
Al, thermal vibration freqs. 2—1421
Al wire, texture, obs. using Debye-Scherrer photography 2—22322
α-Al_2O_3, alumina ceramic, interatomic spacings obs. 2—29135
Al_2O_3, γ-α, phase transition, rel. to exoelectron emission 2—4316
Al_2O_3 film, phase transformations 2—1389
$AlPO_4.2H_2O$, high temp. phase transform., obs. 2—39979
Ar, critical opalescence, compressibility, small angle scatt. 2—3429
Au-Si alloy, on Si substrate, rel. to Au-Si phase transformations 2—39991
Au film, (111) surface relax. 2—29027
B-C-Si system, phase equilib. 2—32785
$B_{12}C_3$, crystal struct., pseudo-hexagonal representation 2—9455
BP, single cryst., refractory semicond., grown from B-Ni-P soln. 2—9358
BaO-Ni(Co)O-O-CO_2 systems, aragonite and 2H $BaNiO_3$ type phases structural relations 2—9454
BaO-TiO_2-Al_2O_3 system, ternary cpd. identification 2—29462
$BaTiO_3$, cryst. struct. lattice parameters 2—32444
$BaTiO_3$, surface layer in para- and ferro-elec. phase 2—16275
γ-$Ba[AlO(OH)_2]_2$, cryst. struct. 2—35979
BeF_2, noncrystalline, diffraction patterns and structure determ. at 25°C 2—22054
BeF_2, vitreous, struct. determ. 2—25160
$BiCl_3$, cryst. and mol. struct. 2—9457
$BiFe_{1.35}Al_{1.65}(BO_3)_4$ huntite, bismuth containing, diffraction pattern, cell parameters 2—3697
Bi_3TiNbO_9, ferroelec., crystal structure 2—32445
$Bi_4Ti_3O_{12}$, crystal struct. 2—32446
C-metal system, graphite-diamond transformation, X-ray obs. of ballas type synthetic diamond 2—32760
C, pyrolytic, neutron irrad., effect of annealing 2—3757
C, turbostratic, disordered regions, small angle scatt. obs. 2—3976
C black, graphitization process, heat treatment, 1673-2073K, at 5 kbar 2—36200
C fibre, K intercalation, multiple small angle scatt. obs. 2—3700
C_xBr, lamellar cpds., cryst. struct. 2—22149
CO_2, compressibility, critical point, small angle scatt. 2—3427
$CaCO_3$, vaterite and calcite crysts. grown in gels 2—15684
$CaCrO_3$, crystal structure 2—4407
CaF_2, anharmonic vibrs. 2—25660
$Ca_4Fe_9O_{17}$, $CaFe_3O_5$, $CaFe_5O_7$, lattice dimensions determ. by X-ray methods 2—39634
$Ca(H_2AsO_4)_2$, crystal structure, diffraction analysis 2—6423
$CaHPO_4$, synthetic monetite, cryst. struct. refinement 2—32448
Ca_2IrH_5, crystal structure 2—3703
CaO-Al_2O_3-CaF_2 system phase equilib. diagram 2—15982
CaO-MgO-Al_2O_3-SiO_2 system, phase equilibria at akermanite-anorthite-forsterite join 2—39416
CaO-ZnO-B_2O_3 system, phase equilib. 2—22376
Ca_2RhH_5, crystal structure 2—3703
Ca_2RuH_6, crystal structure 2—3703
$CaWO_4$, lattice parameters, thermal expansion, 28-347°C 2—22151
Cd_3-As_2-Zn_3P_2 solid solution, semiconducting props., 300-800K 2—19656
Cd, lattice dynamics, 88K 2—19363
CdF_2-MF_2, F=Ca, Sr, Pb, crystalline miscibility, X-ray obs. 2—22338
$CdGeAs_2$ crystal, high temps., thermal expansion coeffs. study 2—32844
CdI_2, polytypes, structural transformations, X-ray diffr. 2—25621
CdM_2F_6S, (M^{II}=Mn, Fe, Co, Ni, Cu, Zn), cryst. struct. 2—22153
CdS-MnS powder, particle size distrib., small angle obs. 2—3970
CdS, sintered layer, microstructure detn. 2—19046
CdSb, anisotropy of Debye- Waller factors, diffr. obs. 2—16006
CdSb, single cryst., thermal expansion detn. for Gruneisen parameter 2—16067
$CdSiP_2$ crystal, high temps., thermal expansion coeffs. study 2—32844
Ce-Fe-B system, phase diagram 2—29491
Ce-Mg, intermetallic compound, disordered substitutions struct 2—6452
$CeCo_5$-H, press.-comp. isotherms 2—32774
$Ce_2O_3.2TeO_3.10H_2O$, thermal stability study 2—29079
Co-8.8 wt.%Cu alloy, precip., complex form. 2—25593
Co, phase transform. rel. to double Bragg scatt. 2—36279
CoMnSb, Heusler alloy, atomic struct. determ. 2—19862
$Co(NO_3)_2.4CO(NH_2)_2.2H_2O$, cryst. struct. 2—35982
$Co_3U_2O_8$ phase in Co-U-O system 2—15958

X-ray examination of materials continued
Cr-Tb system, phase diagram determ. 2—40002
$(Cr,Fe)_2Ti_{n-2}O_{2n-1}$, crystallographic shear, lattice parameters 2—25243
Cr, atomic scatt. factor 2—35983
CrO_2, crystal structure and lattice parameters 2—25253
$CrTaO_4$-TiO_2 solid solutions 2—1224
$CrVO_4$, thermal expansion characts. 2—6681
$CsTl^{III}(SO_4)_2.2H_2O$, cryst. struct., X-ray obs. 2—35984
γ'-Cu-Al-Ni, alloy, martensitic, elastic twinning, stress effects 2—15769
γ'-Cu-Al, alloy, martensitic, elastic twinning, stress effects 2—15769
Cu-Al alloy, quasi-elastic force coeff. and anharmonic coeff. determ. 2—13024
Cu-Al alloys, cold worked and annealed, small angle scatt. obs. 2—25592
Cu-Mn-Al, Heusler alloy, precipitation and phase transformations 2—9801
Cu-Mn alloy, short-range order, MnO_2 contrib. to diffr. pattern 2—19267
Cu-Ni alloy, Debye temp., effect of lattice defects, obs. 2—19383
Cu-Ni alloys, disordered binary substitutional, Debye charact. temp. 2—22422
Cu-Pt alloys, ordering 2—15980
Cu, cold worked and annealed, small angle scatt. obs. 2—25592
Cu, Debye temp., effect of lattice defects, obs. 2—19383
Cu binary alloy, diffr. peak due to coherent scatt. by superlattices 2—12722
Cu complexes, $M_2[M'Cu](NO_2)_6$ type, cooperative Jahn-Teller effect obs. 2—19943
Cu_9Al_4—X, X=Mn, Fe, Ni, ternary mixed powder compacts, Kirkendall diffusion, sintering behavior 2—19279
CuB_2O_4 and $Cu_3B_2O_6$ pellets characterization 2—13568
$CuFeS_2$ single crystal, struct. detn. 2—25272
CuI, polymorphism at high pressure 2—3989
Cu(II) complex, crystal structure determ. by X-ray diffraction 2—35986
$Cu_2In_4Te_7$, defect phase semiconductor, sphalerite struct. 2—25807
$Cu(OH)_2$ temperature range 20-100°C 2—3991
Cu_3Pd alloy, long period ordered, phase transition 2—9799
Cu_2S, low chalcocite and relation to monoclinic system 2—6432
$DyNaO_2$, cryst. struct. 2—35987
Er-Co, intermetallic compound, disordered substitutions struct. 2—6452
Eu(III) complex, structure determ. by single crystal X-ray diffraction techniques 2—35988
Fe-Al-Si alloy, fine struct. 2—9470
Fe-Al solid solution, tempering, short range order 2—22324
Fe-Cr-Ni steel, austenitic, H embrittlement 2—29308
Fe-3at.%Mo, steel phase transform. rel. to double Bragg scatt. 2—36279
Fe-Ni-Cr, austenitic, carbide nucleation and precipitation, B effect 2—9810
Fe-Ni-Mo alloy, lattice distortion due to deformation 2—15721
Fe-Ni-graphite alloy, struct. and phase comp. 2—12938
Fe-Ni film, electrodeposited, struct. and anisotropy, lack of correl. 2—36723
Fe-Si, dislocation- ferromag. domain interaction 2—10198
Fe-Si alloy, magnetostrictive deform., diffr. obs. 2—19889
Fe, zone melted crystals, domain wall obs. 2—10197
Fe powder, lattice parameter, cryst. size and lattice strain 2—3706
Fe whisker, lattice distortion around edges, X-ray topographic obs. 2—18951
$Fe_3B_7O_{13}I$, ferroelec., low temp. phase transitions obs. 2—36592
Fe_3C, ferromag., spin orientation detn. from Mossbauer line intensity and X-ray textures 2—36702
$Fe_{1+x}Cr_{2-x}O_4$, cryst. struct., comp. depend. 2—22361
$FeFe_2O_4$-$MgFe_2O_4$-$NiFe_2O_4$ diffraction obs. 2—1595
Fe(N) sheets and foils, phase relations and epitaxy 2—39539
Fe_2O_3, magnetite, stacking faults, X-ray diffr. obs. 2—15767
Fe_3O_4, magnetite, Al^{3+}, Ga^{3+}, or In^{3+} substituted, cation distributions 2—19049
FeS, $Fe_{0.94}S$, defect structure, cryst. struct. and space group 2—35989
$FeTaO_4$-TiO_2 solid solutions 2—1224
Fe.5-13 at.%Si alloy, ordering, struct. singularities 2—29429
GaAs, and neutron scattering, by non-thermal phonon groups 2—4034
GaAs heteroepitaxial films on spinel, crystalline nature characterization 2—32368
GaP heteroepitaxial films on sapphire, crystalline nature characterization 2—32368
$Ga_{1-x}Se_x$, structural investigation, Ga_3Se_2 found 2—35973
Gd_5Si_4, crystal structure 2—9472
$Gd_2Si_2O_7$, crystallization from molten soln. in Bi_2O_3 2—1208
Ge-S glass, rel. to thermal analysis 2—12628
Ge, amorphous, extended X-ray absorpt. fine struct. obs. 2—3640
Ge, amorphous film, structure rel. to transport and optical props. 2—13273
Ge, F_{222} obs., bonding electron density meas. 2—3702
Ge, nearly perfect crystals, Laue case 2—9398
Ge, perfect crystal, multiple beam Borrmann effect 2—39602
Ge, precip. of Li, anomalous transmission obs. 2—15778
Ge, precip. of Li 2—9813
Ge epitaxial layers, grown in gas phase, dislocation struct. 2—6496
Ge perfect crystal, anomalous transmission, absorpt. effects 2—3711
GeO_2, amorphous, extended X-ray absorpt. fine struct. obs. 2—3640
GeO_2, vitreous, struct. 2—22056
HCl single crystal, structure and phase transition 2—32457
He, h.c.p., Bragg refls., anharmonicity 2—16017
^4He, liquid, structure factor from X-ray scattering data 2—12593
HfO_2-Y_2SiO_5 solid solutions 2—1411
Hg, liquid, metastable struct. near melting point, X-ray diffr. obs. 2—21959
Hg complex, $[(NH_2)_2CS]_2.Hg(CN)_2$, cryst. structure determ. 2—32458
α-HgS, film, cubic and hexagonal species detn. 2—3535
$HoNaO_2$, cryst. struct. 2—35987
$In_xGa_{1-x}As$, epitaxial, rel. to band struct. detn. 2—19004
InSb, abrasion-induced surface damage 2—12649
K, Debye-Waller factor 2—1422
KAg_4I_5, single cryst., crystal structure detn. 2—12698
$KAl(NH_2)_4$, crystal structure determ. 2—39643
$KAlO_2$-TiO_2; $KAlO_2$-SiO_2, crystal structure 2—3719
K_2CO_3-SiO_2 glass system, i.r. and X-ray spectra study 2—28973
$K_2CO_3.CCO_3.SiO_2$ glasses. structural changes 2—1154
$KFeO_2$-TiO_2, crystal structure 2—3719
KH_2PO_4 type crystal, pressure effects on lattice parameters and structure 2—32459
$KNbO_3$, orthorhombic, elastic consts., X-ray diffuse scatt. obs. 2—32578

X-ray examination of materials continued
K_2PtS_2, cryst. struct. 2—32462
La-Fe, intermetallic compound, disordered substitutions, struct. 2—6452
$LaCo_5$-H, press.-comp. isotherms 2—32774
La_2O_3-GeO_2 system, crystallization, X-ray and optical obs. 2—1209
Li_2CdGeO_4, crystalliz. in LiO_2-CdO-GeO_2-H_2O system, structure data 2—35943
$LiCrS_2$, cryst. struct. 2—3713
LiF, thermal expansion and freq. spectrum temp. depend. 2—9895
LiF crystal, γ-irrad., defect clusters, interstitials, small angle scatt. 2—3761
LiF crystal, γ-irrad., Frenkel defects, small angle scatt. 2—3770
$LiVS_2$, cryst. struct. 2—3713
MfC, deform. characts., rel. to chem. bonding, X-ray line broadening obs. 2—32493
$MgAl_2O_4$ single crystals 2—15691
$Mg_{0.7}Mn_{0.8}Fe_{1.6}O_4$ ferrite, square-loop 2—29147
$Mg(NH_4)_2(PO_3OH)_2.4H_2O$, cryst. struct. 2—35993
MgO, thermal vibration amplitude obs. at 2100C 2—36320
Mg_6Pd, cryst. struct. 2—32463
Mn-P-C alloy, amorphous, atomic and radial distrib. functions 2—15933
Mn complex. methyltetracarbonyltriphenylphosphine-manganese(I) evidence for cis and trans isomers 2—35991
$MnAl_2S_4$, pressure to 95 kb, temp. to 1000°C 2—3998
$MnGa_2S_4$, pressure to 95 kb, temp. to 1000°C 2—3998
Mn_2GeO_4, polymorphs, high-pressure, cryst. structs. 2—25337
$MnNi_2$-$MnCu_2$, phase cpd., cryst. struct. of Friauf-Laves phase 2—35990
x $Mn_3O_4+(1-x)Cu(Fe,Cr)_2O_4$, cation distrib. rel. to lattice distortion, X-ray and neutron scatt. obs. 2—22720
Mo-Mn-C system, phase equilib. 2—13013
Mo-W-O system, ternary phase obs. 2—22378
Mo, plastic deform., fine struct. changes during rolling 2—32508
Mo, thermal expansion coeff. and lattice parameters determ. 30-180K, special method 2—3694
Mo(II) complex, structure study using X-ray crystallography, determ. of MoCl bond lengths 2—39647
Mo(II) complex, X-ray determ. of structure and comparison with related compounds 2—35992
MoS_2 intercalation cpds., unit cell expansion upon intercalation 2—32939
$(NH_3CH_3)^+$, in methylammonium alum, scatt. curve, atomic scatt. factors 2—3690
$NH_{-}g_4I_5$, single cryst., crystal structure detn. 2—12698
$NaBa_3[Si_2O_7](OH)$, linear diortho group Si_2O_7, structure detn. 2—35995
$NaClO_3$, γ-irradiated, real structure 2—36013
$NaFeO_2$-TiO_2, crystal structure 2—3719
$NaNH_4CrO_4.2H_2O$, cryst. struct. 2—35993
$NaNO_2$, polarization reversal mechanism, obs. 2—40353
$NaNbO_3$, ferro- and antiferroelec., diffuse scatt., static model of one dimensional disorder 2—32469
T_2-$NaNbO_3$, struct., at 600°C 2—39648
NaOH, orthorhombic to monoclinic transition, obs. of diffuse X-ray scattering, change of lattice prameters 2—1400
Na_6Tl, cryst. struct. 2—32468
Nb, surface, morphology, purity meas. 2—39462
Nb_3Se_4 crystal structure, refinement 2—3723
Nb_3Sn, lattice transform. obs. 2—22364
Nd_2O_3-ZrO_2 system, solid soln. and compound formation 2—29495
Ni-P layers, imperfectly crystallized quasi-amorphous, struct. 2—22074
Ni-22.7-38 at.%Mn alloy, phase transform., 673-908 K 2—25635
Ni, electroless deposits on glass, interfacial props. 2—32372
Ni, recovery, recrystallization and polygonisation after high strain rate deformation 2—9748
Ni, single crystal, mechanical twinning, compression 2—9665
Ni, substruct changes rel. to high temp. creep 2—12730
Ni complex, $[TMPD^+]_2[Ni(mnt)_2]^{2-}$ cryst. structure 2—30005
Ni complexes, $M_2[N'Ni](NO_2)_6$ type, cooperative Jahn-Teller effect obs. 2—19943
Ni powder compacts, verification of existence of oriented microstresses 2—39960
Ni solid solns., non-equil., short-range order estab. 2—9772
$NiAs_2$, pararammelsbergite, crsyt. struct. 2—25342
$NiCr_2O_4$, Jahn-Teller phase transition, crit. scatt. obs. 2—32777
$NiFe_xCr_{2-x}O_4$, ferrite, oxide parameter, treatment grade, cation radii 2—40635
β-$Ni(IO_3)_2.2D_2O$, atomic crystal structure and magnetic structure 2—9484
NiMnSb, Heusler alloy, mag. struct. determ. 2—19862
NiO-α-Fe_2O_3, fired mixtures, quantitative phase anal. 2—13014
NiO-ZnO, lattice parameters, limits of solubility 2—3962
P_2O_5 orthorhombic form, powder diffraction, and i.r. absorption spectra 2—15729
PbO-B_2O_3-Al_2O_3 glass system, decomposition, small angle scatt. 2—3455
$PbO_{1.57}$, cryst. struct., superstruct.-cell, cell parameters, space group 2—15728
β-PbO_2, thermal decomp., intermediate structs. 2—22870
Pb_3O_4, thermal expansion 2—13054
Pd-Ag-Au alloy system, Debye temp. and thermal expansion 2—4074
$Pd_3(PS_4)_2$, crystal structure 2—3725
$PrO_{1.5}$-$PrO_{1.71}$ phase relationships, quenched samples and high temps. 2—4002
Pt-Pd-Fe, alloys, mag. hardening and props. 2—29813
Pt foil, determ. of linear thermal expansion 2—16059
$RbAg_4I_5$, single cryst., crystal structure detn. 2—12698
Rb_2PtS_2, cryst. struct. 2—32462
Se, amorphous, crystn. obs. 2—39434
Se, hexagonal, compressibility 2—32600
Se, hexagonal, determ. of anisotropic compressibility and thermal expansion 2—15731
Si:B diffused, surface layer conc. of boron 2—9589
Si, anharmonicity and temp. depend. of forbidden (222) refl. 2—13028
Si, autoepitaxial, dislocations at film-substrate interface 2—1184
Si, F_{222} obs., bonding electron density meas. 2—3702
Si, ion-bombarded, lattice strain 2—36021
Si, ion implanted, localized surface defects 2—9527
Si, ion implanted, precision lattice parameter obs. 2—3763
Si, perfect crystal, multiple beam Borrmann effect 2—39602
Si, struct. factors meas. using Pendellosung and interferometry fringes 2—9487
Si, thermal expansion, low temp. behaviour 2—19434
Si thin crystal, equal inclination interference fringes 2—6449
SiO_2, amorphous, structure detn. 2—22050

X-ray examination of materials continued
SiO_2, noncrystalline, diffraction patterns and structure determ. at 25°C 2—22054
SiO_2, quartz, diffuse X-ray scatt., near α-β transition 2—4038
Sn-Bi-As system, constitution of Sn- and Bi-rich regions 2—22380
SnO_2, polycryst. semicond., prep. by precip. from soln. 2—40227
SnS-Sb_2S_3 system, phase diagram determ. 2—29496
$SrCl_2$ powder, X-ray struct. factors, Debye-Waller coeffs., unit cell consts., at 80 and 300 K 2—32473
Sr_2IrH_5, crystal structure 2—3703
$SrMoO_4$, thermal expansion 2—9897
Sr_2RhH_5, crystal structure 2—3703
Sr_2RuH_6, crystal structure 2—3703
Ta-B system, phase diagram determ. 2—13015
Ta, b.c.c. and β phases, diffr. obs. 2—32382
β-Ta film sputtered, elec. cond., struct., transform., X-ray diffr. obs. 2—18945
Ta_2O_5-GeO_2 solid solutions 2—1412
$TaOPO_4$, tetragonal high press. modification 2—22163
$TbVO_4$, crystallographic distortion at 32 K, second order transition 2—19306
Te, acoustic mode freq., dispersion curve 2—13031
Th-C-N, alloy, cryst. struct., at temps. to 2250°C 2—19060
Ti-Mo-Ni system, polythermal section 2—32788
Ti-(25 at.%)Nb alloy, omega phase formation, mechanism and kinetics, small angle scatt. obs. 4006 2—4006
Ti-Pd-Au film, ageing effects 2—39534
Ti-Pd system, phase diagram determ. 2—40011
α-Ti and alloys, diffr. peak assignment 2—39654
TiC, stoichiometric, crystallinity, purity and particle morphology obs. 2—22347
TiNi, martensite struct., rel. to premartensitic instability 2—9825
TiO_2, prep by chem. transport reaction 2—39584
Tl-Ni, intermetallic compound, disordered substitutions, struct. 2—6452
TmTe, pressure induced structural transformation 2—36289
U-Se-C ternary system, phase equilibrium, solid state compatibility relationship 2—29482
U-Te-C ternary system, phase equilibrium, solid state compatibility relationship 2—29482
$(U,Na)_{2-x}Nb_2O_{7-y}$, cryst. struct., order-disorder transform. X-ray obs. 2—32782
U_3Si phase, diffr. pattern of U_3Si_2, rel. to microstruct. 2—32476
$VC_{7/8}$, cryst. struct. and interatomic interaction 2—6453
V_8C_7, cryst. struct. 2—29154
VO_2:Cr, struct. aspects of metal - insulator transition 2—25638
V_2O_5, thermal expansion, 0-685°C 2—40085
$VO_{2-x}F_x$, $0<x<0.2$, crystal structure 2—3739
$V_2O_{5-x}F_x$, $0<x<0.025$, crystal structure 2—3739
W-Mn-C system, phase equilib. 2—13013
WC, deform. characts., rel. to chem. bonding, X-ray line broadening obs. 2—32493
WC, powder, sintering, rel. to milling, dislocation density effects 2—22348
WO_3, prep., colour, non-stoichiometry, defects, microstrain 2—25246
Y-Ni, intermetallic compound, disordered substitutions, struct. 2—6452
$YNaO_2$, cryst. struct. 2—35987
Yb, martensitic transformation 2—6641
Yb film, h.c.p.⇌f.c.c. martensitic transform., phase stability 2—39992
YbTe, 4f-5d electron collapse, pressure induced 2—10056
$(Zn,M)_5(OH)_8Cl_2.H_2O$, pseudomorphs, M=Co, Ni, Mn, Cu, Zn, Na, cryst. struct. 2—3579
Zn complex, dichlorobis(4-methylpyridine)zinc(II, X-ray obs. 2—12738
Zn single crystal, annealed Berg-Barrett X-ray micrograph 2—39604
$ZnGeP_2$ crystal, high temps., thermal expansion coeffs. study 2—32844
ZnO-B_2O_3 system, borate stability, temp. depend. 2—22368
ZnO-Nb_2O_5 system, phase relations study 2—25644
$Zn_5(OH)_8(NO_3)_2$ indexing of diffr. diagram 2—4460
ZnS, Debye temp. detn. 2—22426
ZnS, phase transformation, effect of polytypism 2—25351
ZnS, polytypism and phase transformations, Cu doping effects 2—25350
ZnS polytypes, disordered, probability of layer superposition 2—9498
$ZnSnAs_2$ crystal, high temps., thermal expansion coeffs. study 2—32844
$ZnSnP_2$ crystal, high temps., thermal expansion coeffs. study 2—32844
$ZnSnSb_2$ crystal, high temps., thermal expansion coeffs. study 2—32844
ZnTe, Debye temp. detn. 2—22426
Zr-Cr alloy, lattice strain and crystallite size determ. 2—22291
Zr-Nb alloy, β→ω transform., obs. 2—40014
$Zr_xAs_yO_z$, lattice consts. and chem. formula 2—22169
$Zr_xAs_2S(Se)$, lattice consts. 2—22168
ZrO_2-Gd_2O_3 system, rel. to phase transformations 2—9840
ZrO_2-Ln_2O_3, and thermal analysis 2—4008
ZrO_2, deform. characts., rel. to chem. bonding, X-ray line broadening obs. 2—32493
ZrO_2, metastable cubic phase, powder pattern 2—12739
$ZrO_2.12Nb_2O_5$, polymorph characterization, structure and intergrowth obs. 2—9500

liquids
alloy, molten, small angle scatt. 2—15700
cholesteryl bromide and p-azoxyanisole, liquid crystals, phase transitions, small angle scatt. 2—3364
dye associates in solution, small angle scatt. 2—15567
hard sphere fluid model, random packing, small angle scatt. 2—3411
macromolecular solns., mol. shape determ. 2—35361
metals, inelastic scattering correction to neutron diffraction data, test 2—3362
nematic, (EAAA) cylindrical function of interatomic distances 2—18797
overviewed samples, diffraction techniques 2—21957
partial struct. factors separation using anomalous scatt. 2—12536
polymer solution, worm like chains, end-to-end distance calc., small-angle scatt. 2—3371
polysaccharide solution, stiff chain parameters, small angle scatt. 2—3369
polystyrene solution, small angle and wide angle obs. 2—3370
small angle scattering, structure theory 2—3363
Au, struct. 2—6201
Fe-Si alloys, struct. 2—6202
Ga at 20°C, determ. structure functions, comparison with neutron diffraction data 2—15565
HCl aqueous solns., radial distribution functions, X-ray diffraction study 2—21958
Hg, struct. factor, elec. resist. 2—35727
Mg-Cd molten alloys, structure, X-ray diffraction study 2—28789

X-ray examination of materials continued
liquids continued
Na-Li system, critical opalescence, small angle scatt. 2—3428
(80 at.%)Tl-In melt, struct. 2—21961
Tl, struct., 290-450°C 2—21960

microstructures
see also Crystal structure/microstructure
acrylic fibres, heat treated, meridional peaks in small angle scatter pattern 2—9221
alloy, f.c.c. cold worked, integral breadth analysis, particle size and strain detns. 2—22332
alloy, Guinier- Preston zones 2—6408
anomalous transmission characteristics by varying effective thickness of crystals 2—25288
trans-cyclohexane-1,4-dicarboxylic acid, cryst. struct. 2—35999
cyclotrimethylene trinitramine, defect struct. determ. 2—9563
graphite, pyrolytic, scroll-like struct. obs. 2—22150
hexamethylene, tetramine, dislocation structure, Lang technique obs. 2—36037
$L1_0$ superlattice, effect of twinning on particle size 2—3950
perfluoromethylcyclohexane, solid, phase transitions 2—1380
polyethylene, hot stretched, recrystallization, x-ray small angle scatt. 2—15893
polyethylene, low density, cold rolled, superstruct. 2—12632
polyethylene, single crystal, mosaic struct. 2—15647
polyethylene terephthalate, effect of sorbed I on small angle X-ray diffraction 2—35860
polymeric and oligomeric systems' phase transitions, small angle X-ray scattering 2—18907
radiography, single shot contact 2—6409
rare earth metals, h.c.p., deformation struct. obs. from X-ray line broadening 2—3772
steel, austenitic, deform. texture, influence of form of stress state 2—36233
steel, Fe-Cr-Ni, martensite charact. rel. to hardening process during ageing 2—32697
steel, high C, containing Si, bainitic transform. 2—36300
steel, martensite produced by plastic deform. 2—39928
steel sheet, fault detection, closed circuit TV display 2—3639
thin crystal, dislocation contrast in topographs 2—36027
Ticonal, conjugation of metastable phases 2—12976
weld metals deposited by pulsed-arc process 2—12958
Zircalloy-2, cold- rolled, particle size, microstrains, dislocations 2—29185
Ag powder, substructure data 2—15940
Al-Ag, alloy, particle size distrib., Guiner Preston zone shape distrib., X-ray scatt. profile analysis 2—19042
Al-Ag alloy, quenched, GP zones, Perod's law, X-ray Laue scatt. 2—32441
Al-Ag alloy, quenched from liquid state, X-ray diffraction obs. 2—25577
Al-Cu alloy, decomposition, Guinier-Preston zone 2—9445
Al-Cu alloys, G.P.(1) zone size determination by X-ray small-angle scattering 2—3940
Al-Mg alloy, Guinier-Preston zones 2—9752
Al-5.0 at%Ag-5.0 at%Zn, alloy, neutron irrad. rel. to precip and G.P.zones 2—29418
Al-2.8 at%Zn-1.4 at%Mg, alloy, neutron irrad. rel. to precip. and G.P.zones 2—29418
Al-Zn alloy, Guinier Preston zone formation 2—9448
Al-Zu alloy, size effects, Guinier-Preston zones 2—9449
Al, dislocation distrib. difference for crysts. prepared by hardening-annealing and recrystn. 2—25402
Al, quenched, dislocation density 2—15822
β-AlNi, stacking fault broadening and separation of strain and fault effects 2—32535
Al_2O_3, sapphire, Burgers vectors of basal dislocations 2—9557
As, atomic positional parameter pressure depend., linear compressibility 2—22268
C-SiC alloy, codeposited 2—32447
Co-1.7 wt.% Be alloy, metastable struct. states in solid state decomp. 2—32450
Co-1 wt.% Be-7 wt.% Ta alloy, metastable struct. states in solid state decomp. 2—32450
Cu-Co, work hardened, single crystals containing coherent precipitates, dislocation arrangement 2—3936
Cu, electrodeposition, o-phenanthroline impurity distrib., small-angle scatt obs. 2—19114
Cu film, electroplated and vapour deposited 2—22072
CuAu, effect of twinning on particle size 2—3950
$CuFe_5O_8$, eutectoid decomp. study 2—15959
β-CuPd, $a/8[110](1\bar{1}0)$ faulting in prestrain induced transform. stage 2—32763
Fe-Cr-Ni, alloy, transitional ferrite phase form. 2—29435
Fe-Cr-Ni alloy, transitional ferrite phase form. 2—29434
Fe-Ni martensite, transform. induced substructs. obs. rel. to mech. props. 2—22358
Fe-Si single crystal, mag. domain structure obs. 2—29814
Fe, Armco, cyclic bending deformation, absorptional fatigue 2—29300
Ge:Te, precipitate form. on growth dislocations 2—12770
Ge crystals investigation of Li precipitates 2—19093
LiF, neutron irrad., defects, struct., effect of annealing 2—32487
LiF, undergoing shock wave compression 2—3715
Mg-Cd alloy, rel. to plastic deform. mechanism 2—9679
Mg, rel. to plastic deform. mechanism 2—9679
MgIn, effect of twinning on particle size 2—3950
Mo, film, on thermally oxidized Si 2—12660
Mo, single cryst., slip bands 2—15726
MoS_2, natural molybdenite, cold working, stacking faults 2—25409
$Na_{0.88}Li_{0.12}NbO_3$-Li_2O, ceramic, cryst. symm., lattice parameters, 293-783K, X-ray and thermal expansion obs. 2—32470
Ni, tensional deformation, twin growth 2—12862
PbS film, rel. to mechanisms of photosensitivity 2—36613
Pt/Al_2O_3 disperse catalyst, metal particle size distrib., small angle scatt. 2—3973
$^{238}PuO_2$, temperature effects and long exposure effects of lattice parameters meas. 2—39651
Si:Li, precipitation, on dislocations and vacancy clusters 2—19115
Si, atomic mismatch on closure of controlled partial splits, shear displacement 2—19095
Si, oxidized, floating-zoned, dislocation free, spotty defects 2—19104
Sn-Pb alloy, solidified at high cooling rate 2—39941
Ta-B system, phase diagram determ. 2—13015

X-ray examination of materials continued
microstructures continued
V, precipitation of $V_{16}N$ 2—15975
W, deformed, domain size, strain values, diffr. broadening shape analysis 2—3689
Zn, annealing behaviour and laser induced damage, Berg Barrett contrast technique 2—22184
ZnO, ribbon cryst., orientation, whisker growth obs., X-ray etching obs. 2—12693

molecular structure
carboxylic acid salts, H atom position in A-type H-bands 2—8747
1-chlorobenz[α]phenazine-7N-oxide 2—12740
complex, dichlorobis(4-methylpyridine)zinc(II) 2—12738
cyclic phosphonium iodide 2—6465
dibenzene chromium TCQM complex, cryst. and molecular struct. 2—19066
diborane, molecular charge densities from theoretical X-ray scatt. factors 2—6419
polyethylene terephthalate fibre, annealed chain folding, i.r. absorpt. spectra obs. 2—15642
spectrograph, vertically oriented double-crystal attachment 2—21580
tris-(1,2-dimethylhydrazino)-diphosphine 2—6467
virus structures, diffraction examination 2—15412
Au complex, $Au[S_2CN(C_4H_9)_2]_2Au[S_2C_2(CN)_2]_2$ 2—12716
NH_4Cl, powder sample, X-ray structure factors of first twenty reflections 2—29148

X-ray fluorescence
see also Fluorescence, X-ray spectra/emission
No entries

see also Fluorescence; X-ray spectra/emission
conference (Toronto, October 1971) 2—13597
Coster-Kronig probability f_{23}, $Z \geqslant 90$ 2—24320
glass, structure obs. 2—9222
haemoglobin and derivatives electronic state of Fe determ. from X-ray fluorescence spectra 2—24558
intensity, effect of scatt. 2—30121
iron ore, spectrometry analysis 2—10675
isotope excited, use in heavy element analysis 2—13602
L_1 yields, for $33 \leqslant Z \leqslant 85$ calc. from X-ray emission rates 2—2930
myoglobin and derivatives electronic state of Fe determ. from X-ray fluorescence spectra 2—24558
naphthalene-d_8 in solid soln., triplet molecule formation 2—26364
non-dispersive, in analysis of plastics compositions 2—39971
phenanthrene, spectra compared with U.V. induced fluorescence 2—36951
photographic dosimetry, applic. of radioisotope X-ray fluorescence spectrometry 2—330
quantitative analysis, tertiary excitation 2—30123
spectrochemical analysis, data handling by computer 2—10677
spectroscopy, conference, Clayton, Australia (1971) 2—8509
thin films, characteristic radiation excitation by radiation from substrate 2—30122
Z=96, L_1 subshell fluorescence and Coster-Kronig yields 2—21496
^{195}Au decay, precision determ. of high-Z K-shell fluorescence yields 2—15205
^{207}Bi decay, precision determ. of high-Z K-shell fluorescence yields 2—15205
^{249}Cf, L_2 and L_3 subshell fluorescence and Coster-Kronig yields for Z=96 2—2933
Co, K-shell atomic yields 2—8443
Cr, K-shell atomic yields 2—8443
Cu-Ti, alloy electron struct. band struct., X-ray fluoresc., spectra obs. 2—16112
Cu, K-shell atomic yields 2—8443
Fe, K-shell atomic yields 2—8443
$Ga_{1-x}Al_xAs$, solution grown 2—18939
Ge, K-shell atomic yields 2—8443
Mn, K-shell atomic yields 2—8443
Ni, K-shell atomic yields 2—8443
^{235}Np decay, precision determ. of high-Z K-shell fluorescence yields 2—15205
$PbCl_2$, low temp. peak obs. 2—29954
Si cpds, K-spectrum of Si 2—33312
Ti, K-shell atomic yields 2—8443
U_3O_8 quantitative determ. in ore samples, ^{57}Co source and Ge(Li) detector for K X-rays 2—7198
V, K-shell atomic yields 2—8443
YAG:Cr^{2+}, recombination excitation mechanism 2—40725
Zn, K-shell atomic yields 2—8443
ZnS-Mn-phosphors, temp. depend. of X-ray luminescence obs. 2—29968

X-ray measurement
see also Dosimetry
calorimetric method 2—11680
camera, topographic, for one crystal rotation 2—3606
charge and light peak shifts from a proportional scintillation counter 2—11665
detector with bandpass response characteristics 2—18021
directional detection, 30-200 keV, Galactic sources 2—10983
flash burst time obs. with scintillation crystals 2—2630
industrial, conference, London, England (1972) 2—37536
intensitometer, VA-G-92, used with Soviet photographic materials 2—17758
Lang topography, electromechanical feedback control for camera to keep crystals in Bragg condition 2—3605
m.o.s. device for detecting low-energy X-rays 2—27887
particle size determination 2—37537
roentgenography with high-energy X-rays, luminescence yield 2—27687
scintillation block detectors 2—24080
soft X-rays, automatic stabilized detection system 2—11162
Ge(Li) semiconductor detectors, analysis of K-spectra of elements 2—24089
Si detectors, temperature dependence of photocurrents 2—38383
Si p-n junction detector, ion implantation fabrication 2—25896

X-ray microscopes *see Microscopes*

X-ray monochromators
crystal, misorientation produced during bending 2—3621
focusing, high resolution, precision support 2—29113
high resolution, using Si and Ge plates 2—25285
sources, monoenergetic of known absolute intensity 2—23784

X-ray monochromators continued
  for synchrotron orbital radiation, 0-1200 Å, construction and performance testing 2—17720
  total reflection for small angle scattering chamber 2—15698

X-ray photoeffect *see Electron emission/photoelectric*

X-ray reflection
  crystal, non-absorbing, dynamical theory of interference with extinction of primary waves 2—3637
  focusing collector using a parabolic mirror, for long wavelength X-ray astronomy 2—11184
  line grating, periodic intensity changes with incident beam direction 2—38066

X-ray scattering
  see also Compton effect; X-ray diffraction
  alloy, binary static displacement of atoms, determ. using anomalous scattering 2—3691
  atomic parameters, expressed by 5 scalar invariant quantities 2—3598
  atoms, incoherent scatt. factors, Thomas-Fermi-Dirac calcs. 2—18295
  CC HF, molecular scattering factors calc. 2—8865
  Compton and Rayleigh from heterogeneous materials scattering of X-rays 2—7060
  critical opalescence of one component fluid, gravitational effects in small angle X-ray scattering expts. 2—22036
  crystal, ion spin-lattice-coupling, phonon damping and magnetic order 2—19848
  distorted crysts., location of diffuse maxima in scatt. patterns 2—3613
  dynamical, Laue case, integral values of refl. and transmission 2—9391
  ethylene-acrylic acid copolymer, small angle X-ray scattering invariant 2—25163
  ethylene-vinyl acetate copolymer, small angle X-ray scattering invariant 2_25163
  fibrous systems, small-angle equatorial scatt., direct analysis, Patterson function and intensity 2—3611
  fluids, eqns. in terms of invariant expansion of 2-body statistical correlation function 2—7700
  fluorescence intensities, effect of scatt. 2—30121
  hydrocarbons, C_3H_6, C_6H_{12}, C_6H_6, C_6H_{14} and C_8H_{10}, identification of localized bonds from Compton profiles 2—3103
  incoherent Thomson scatter in Li metal, astronomical polarimeter 2—10981
  inelastic, by electrons in solids 2—16591
  inelastic, co-existence of Compton and Raman scatt. 2—3615
  by interstellar matter 2—20606
  liquid, amorphous and microcrystallized substances, FORTRAN IV computer program 2—19041
  macromolecule shape determ., X-ray scatt. in two dimens. from shapes with inclusions 2—35361
  polydisperse systems, distribution function 2—3413
  polymeric and oligomeric systems, small angle studies of phase transitions in 2—18907
  pulse recording, K_β component determination, scatter curve correction 2—15699
  quantum theory, temp. depend. absorpt. coeff. in crystals 2—19019
  rock powders, determ. of average atomic number 2—33838
  small angle, absolute intensity meas. 2—3627
  small angle, chamber with total reflection monochromator 2—15698
  small angle, collimation corrections verification 2—15703
  small angle, interparticle interferences in close packed systems 2—15697
  small angle, liquid structure theory 2—3363
  small angle, slit correction, matrix inversion method 2—3623
  small angle, theory 2—3630
  small angle apparatus, high temp. meas. 2—15700
  small-angle, structural parameter, multiple scatt. effect 2—19025
  solar emission, Compton backscattering 2—11065
  statistical atoms, functional of density for form factor incoherent scattering 2—18294
  texture rel. to background X-ray scatt. 2—29111
  Al-Zn alloy, critical composition, small angle scatt. near critical temp. of demixture 2—9447
  H_2, molecular scattering factors calc. 2—8865
  H_2S gas, coherent scattering factor calculation using SCF wavefunction 2—786
  LiF, molecular scattering factors calc. 2—8865
  N_2, molecular scattering factors calc. 2—8865
  $NaNbO_3$, ferro and antiferroelec., static model of one dimensional disorder 2—32469
  Se-Te alloy, amorphous, relax. effects 2—39772

X-ray spectra
  see also Atmospheric spectra; Chemical analysis/X-ray
  atoms, K X-ray intensity ratios 2—18277
  atoms, X-ray ratios for 2p shell 2—584
  auroral-zone X-ray spectra, energies opto 200 keV, balloon measurements 2—22996
  Compton profile, by use of solid state detector 2—34800
  Compton scattering and electron momentum distribution 2—1676
  Compton-Raman scattering 2—3615
  correction and smoothing, anal. of methods used 2—11652
  Cygnus discrete sources 2—4943
  elements from Z=92 to 126, calc. of K X-ray intensities, meons of identifying elements 2—2928
  hard, weakly relativistic plasma, produced by bremsstrahlung 2—24650
  heavy elements, chem. shifts of $K_{\alpha 1,2}$, $K_{\beta 1,3}$ and $K_{\beta 2,4}$ lines due to valency electrons 2—7086
  K-mesic atoms, $\bar{K}N$ scatt. length calc. from X-ray transitions 2—34672
  metals, many-electron effects 2—29942
  molecular ionic solids, P, S and Cl bearing, bonding concept interpretation 2—16590
  molecules and complexes with tetrahedral or octahedral symmetry 2—31767
  nonlinear response of bound electrons at X-ray freqs. 2—40698
  oxyfluorides and complex fluorides of group iv to vi elements, electron investigation 2—33295
  plasmon excitation in Compton scatt., process 2—6746
  quartz, refractive characts. from dynamical diffr. theory 2—33292
  rare earth oxides, $L_{\gamma 2,3}$ spectrum 2—33298
  rates and $K\alpha$ linewidths for 2p shells of Z=12—55 and 60, 65, 70, 75, 80, 85 atoms 2—578
  satellite emission by single electron jump 2—28172
  satellite spectra, study of screening doublets 2—21490

X-ray spectra continued
  secondary electron emission spectral dependence of fine structure study 2—35120
  solar, satellite lines 2_7549
  solar obs. with single crystal spectrometers 2—23124
  Sun, soft X-rays, grating with parallel grazing incidence 2—11069
  transition metals, influence of conduction electron excitation 2—36910
  Ag, 2 to 30 MeV proton bombardment, K and L X-ray yields 2—38808
  Al, Compton profile, electron momentum distrib. 2—16592
  Al, impulse approx. in Compton scatt. core contribs. 2—4114
  Al, $L_{2,3}$ edge energy 2—36912
  Ar-C collisions, 80 and 90 keV, differences in inner shell vacancy production for gas versus solid targets 2—12003
  Bk, K X-ray energies and intensities, binding energies 2—18302
  Br, collision induced by I^- bombardment inner shell vacancy prod. 2—15226
  C, impulse approx. in Compton scatt., core contribs. 2—4114
  CO_3^{2-}, rel. to bonding investigation 2—31821
  Cf, K X-ray energies and intensities, binding energies 2—18302
  ClO_3^-, rel. to bonding investigation 2—31821
  ClO_4^-, rel. to bonding investigation 2—31821
  Cm, K X-ray energies and intensities, binding energies 2—18302
  ^{246}Cm, rel. to electron binding energy calc. 2—11784
  Cr, fine struct. in K lines 2—4467
  CrB, obs. density of states in conduction band and energy losses 2—40702
  CrSb, obs. density of states in conduction band and energy losses 2—40702
  Cr_2Te_3, obs. density of states in conduction band and energy losses 2—40702
  Dy ion, analysis on basis of SCF calcs. 2—35135
  Es, K X-ray energies and intensities, binding energies 2—18302
  Fe-Co, electronic energy spectrum investigation rel. to bonding and ordered state formation 2—36920
  Fe, Fine struct. in K-lines 2—4467
  H(1s), Glauber calcs. polarization fraction of Lyman-α radiation emitted in collisions with e- 2—21540
  KBr(Cl)(I), KKR energy bands and optical consts. 2—40703
  Kr, collision induced by I^- bombardment, inner shell vacancy prod. 2—15226
  Li, Compton profile of interacting cond. electrons 2—19513
  Li, energy loss spectrum in intermediate momentum transfer region 2—16597
  Li, impulse approx. in Compton scatt. core contribs. 2—4114
  Li, plasmon scatt., dispersion relation 2—16596
  Li, polycryst., Compton profile 2—13497
  Li metal, lattice relaxation, effect on soft X-ray spectra near Fermi edge 2—20083
  LiCl, Compton profile, electron momentum distrib. 2—13496
  Mn nitrides with different magnetic properties, fine structure of emission and absorption of K-series 2—40704
  Na, Compton profile of interacting cond. electrons 2—19513
  Na metal, lattice relaxation, effect on soft X-ray spectra near Fermi edge 2—20083
  NbC, intensity maxima of subbands, energy band struct. 2—40706
  $NiFe_{2-x}Cr\ O_4$, investigation of crystal and band structure 2—35996
  PO_4^{3-}, bonding investigation 2—31821
  Pb L_2-L_3 Coster-Kronig transitions probability meas. 2—11961
  Pd-Ag, band structure investigation 2—36918
  Pd-Au, band structure investigation 2—36918
  Pd-Cu, band structure investigation 2—36918
  Pd-Ni, band structure investigation 2—36918
  PrF_3, energy shift of K-lines 2—16599
  PrO_2 and Pr_2O_3, energy shifts of K-line 2—16599
  Pt complexes of types K_2PtX_4, K_2PtX_6 and $(PPh_3)_2PtX_2$ 2—33300
  SF_6, soft X-ray spectrum, effect of symmetry, photoionization of atoms 2—35285
  SO_4^{2-}, rel. to bonding investigation 2—31821
  Sc, Compton profile, band struct. 2—1704
  Se; collision induced by I^- bombardment, inner shell vacancy prod. 2—15226
  Si:B ion implanted, ion produced, conc. distrib. and atom location 2—25436
  Si, $K\alpha$-X-ray spectra produced by 30 MeV oxygen bombardment 2—24350
  SiF_4, soft X-ray spectrum, effect of symmetry, photoionization of atoms 2—35285
  SiO_2, quartz, optical interband transitions detn. 2—20085
  Ti-Co, electronic energy spectrum investigation rel. to bonding and ordered state formation 2—36920
  Ti-Mo, electronic energy spectrum investigation rel. to bonding and ordered state formation 2—36921
  VC, intensity maxima of subbands, energy band struct. 2—40706
  Xe^{2+} ion-atom collisions, M spectra 2—5847
  Zn compounds, chemical shift of $K\alpha$ lines 2—33302
  Zr-Co, electronic energy spectrum investigation rel. to bonding and ordered state formation 2—36920
  ZrC, intensity maxima of subbands, energy band struct. 2—40706

  absorption
    chlorides, $L_{2,3}$ absorpt. edge of Cl^- 2—33293
    chloroform, gaseous and solid, K-spectra 2—3036
    cluster model applic. 2_19505
    electron gas, edge problem with finite hole mass 2—7084
    metal, electron gas correls. and core hole effects 2—1701
    metal, i.r. catastrophy and excitons 2—33291
    metal, threshold absorpt., theory 2—29940
    metals, soft X-ray range 2—1702
    molecular, semiquantitative interpretation 2—31766
    polar molecules, evidence of effective potential barrier 2—35193
    transition metals, L-absorpt. of ^{72}Hf to ^{79}Au, white line obs. 2—16600
    Ag, relations between L_{III} absorp. limit and $L\beta_{2,15}$ lines 2—26206
    Al-M dil. alloys, (M=Ti, V, Mn, Ni), virtual bound state obs. from Al $L_{2,3}$ absorption spectra 2—20022
    As, chem. shifts in L-absorpt. edge 2—40700
    CCl_4 gaseous and solid, K-spectra 2—3036
    Ca, K absorp., band struct. assignments 2—33294
    Cd sulphide and sulphate, L_{23} spectra, meas. quantum efficiency of S photoemission 2—26204
    CdS, band struct. 2—16595
    CdS, $L_{II,III}$ photoemission spectra, fine structure study 2—36909
    Ce, electronic energy states obs. 2—22791

X-ray spectra continued
absorption continued
Cl in gases and molecular crystals, K-spectra 2—3036
Co, K-absorption spectra, comparison with results for Co complexes 2—36913
Co complexes, diphenyl-dithiophosphinates of Co(ii) and tris-(isonitrosoacetophenonato) Co(iii), K-absorption spectra, comparison with results for the Co metal 2—36913
Cu-Ti intermetallic phases, chemical bonding 2—22763
$Cu_3(AsO_4)_2.4H_2O$ chemical shifts of K-absorption edges of Cu and As 2—1703
$CuHAsO_3$, chemical shifts of K-absorption edges of Cu and As 2—1703
Fe_2O_3 monocrystals, K-spectra interpretation based on crystal field theory 2—36914
GaSe, semiconductor, shift of X-ray K absorption edges 2—29944
HCl gaseous and solid, K-spectra 2—3036
Hg sulphide and sulphate, L_{23} spectra, meas. quantum efficiency of S photoemission 2—26204
HgS, $L_{II,III}$ photoemission spectra, fine structure study 2—36909
Ir, white line at L_{II} absorpt. edge 2—33297
La, electronic energy states obs. 2—22791
Mg-Mn ferrite, White Line obs. at K-absorp. edge of Mn 2—40705
Mg, anisotropy in Compton profile 2—4468
Mo, relations between L_{III} absorp. limit and $L\beta_{2,15}$ lines 2—26206
Na, electron gas correls. and core hole effects 2—1701
Ni-Co ferrite, rel. to thermomagnetic processing 2—40528
Ni ferrite, Co-containing, thermomagnetic effects on K-spectra 2—36917
PbS, K and $L_{II,III}$, band struct. determ. 2—29945
Pd, relations between L_{III} absorp. limit and $L\beta_{2,15}$ lines 2—26206
Rh, relations between L_{III} absorp. limit and $L\beta_{2,15}$ lines 2—26206
S, $L_{II,III}$ photoemission spectra, fine structure study 2—36909
Si, energy band obs. 2—40144
SiF_4, ultrasoft spectra of Si and F 2—31830
Sn chalcohalides, chem. shift, Mossbauer spectra and $K_{\alpha1}$ line 2—10329
TiO_2, rutile, band spectra, mol. orbital energy level diagram 2—40707
Y, electronic energy states obs. 2—22791
Zn sulphide and sulphate, L_{23} spectra, meas. quantum efficiency of S photoemission 2—26204
ZnS, $L_{II,II}$ photoemission spectra, fine structure study 2—36909
emission
see also X-ray fluorescence
alcohols, solid, O_2 K-emission spectra obs. 2—16598
atoms, inner-shell ionization by α particles and deuterons, projectile z dependence of K X-ray emission 2—31676
band emission, electron transition processes, metals, alloys, metal compounds 2—4465
boron suboxide, rel. to cryst. chemistry 2—9331
Cen A radiosource, model 2—26803
dichloroethylene, and photoelectron spectra, mol. orbital interpret. 2—35328
elements $18 \leqslant Z \leqslant 39$, $k\beta/K\alpha$ transition probability ratios 2—31657
elements between Z=58 and 94, L fluorescent X-ray relative intensities 2—31660
fluorides, K spectrum from F, chemical bonding obs. 2—13495
glass structure, applic. of X-ray emission spectroscopy 2—39436
graphite, strong plasmon coupling in appearance pot. spectrum 2—16594
heavy ion X-ray production cross sections from thick target yields 2—24384
ice, O_2 K-emission spectra obs. 2—16598
K-shell ionization cross sections meas. for elements with Z=26-92 using 160 MeV protons 2—28217
kaonic atoms, light, strong interaction shifts and widths 2—21556
light elements, relative intensities of satellite bands, assuming multiple ionization 2—35119
metal, electron gas correls. and core hole effects 2—1701
metal, electron interaction effects, first-order theory 2—26205
metal, i.r. catastrophy and excitons 2—33291
molecules, effect of symmetry of emitting atom on line shape and position 2—35192
muonic ^{209}Bi, hyperfine spectra of L and K X-rays, analysis in terms of nuclear excitation 2—18370
noble metal aluminides, L-emission bands, electronic struct. 2—20087
oxides, K spectrum from O, chemical bonding obs. 2—13495
photoelectron spectra of DPPH and diphenylpicrylhydrazine 2—7085
photoionization of gas clouds by non-thermal radiation spectra 2—10842
plasmon emission in appearance pot. spectroscopy 2—16593
rare earth metals and oxides, M_{IV}, M_V spectra 2—14471
in scanning electron microscopy, utilization of emitted X-ray signal 2—39618
superheavy elements, identification by in- flight X-ray measurements following heavy-ion-atom collisions 2—11993
thin films, characteristic radiation excitation by radiation from substrate 2—30122
transition metal aluminides, L-emission bands, electronic struct. 2—20087
transition metal diborides, ultra soft photolectric and K-spectra 2—29943
transition metals, in the supersoft band 2—29941
vacuum, 10^{-6} and 10^{-10} torr, rel. to prebreakdown currents 2—21885
Al-Co, band structure investigation 2—36911
Al-Mg alloys, electronic struct. 2—26207
Al-Nb, band structure investigation 2—36911
Al-Pd, band structure investigation 2—36911
Al-V, band structure investigation 2—36911
Al, high-energy satellites of $L_{2,3}$ emission bands 2—33299
Au, L_{II} and L_{III} ioniz. cross sections 2—4466
Au, N-band profiles, band struct. 2—7087
B, ultra soft photoelectric and K-spectra 2—29943
C heavy ion K X-ray production cross sections from thick target yields 2—24384
CO_2, solid O_2 K-emission spectra obs. 2—16598
Ca, $K\beta$ emission, band struct. assignments 2—33294
Ca to Th, atoms, M-shell Coster-Kronig yields 2—24311
$CaCrO_4$, intensity distribution of $K\alpha$ doublet 2—20056
CdS, band struct. 2—16595
CdS, $L_{II,III}$ spectra, ESCA technique 2—36919
^{252}Cf, spontaneous fission, fragment K X-ray emission 2—11882
^{252}Cf fragments of specified atomic numbers, study of multiplicities of K X-rays 2—11883
Cl $K\beta$ spectra of inorganic anions calc. using all-valence-electron molecular orbital methods 2—28267
Cm, relative transition probs. to K-shell 2—21510

X-ray spectra continued
emission continued
Co, Lorentzian representation of line shape 2—40699
Co, soft X-ray spectra, classification 2—5786
Cr, intensity distribution of $K\alpha$ doublet 2—20056
Cr, K, L_{III}, M_{III} spectra, zone structure, electron energies, density of states 2—36415
Cr, K_β spectrum, conduction electrons study 2—40701
Cr, soft X-ray appearance pot. spectra, effect of oxygen 2—35872
Cr, soft X-ray spectra, classification 2—5786
CrB, intensity distribution of $K\alpha$ doublet 2—20056
CrSb, intensity distribution of $K\alpha$ doublet 2—20056
Cr_2Te_3, intensity distribution of $K\alpha$ doublet 2—20056
Cu, compton profile due to 1s electrons 2—24340
Cu, heavy ion channelling, critical angle determ. using charact. X-ray generation 2—29575
Cu, Lorentzian representation of line shape 2—40699
Cu, proton dechannelling obs. 2—40106
Cu, soft X-ray spectra, classification 2—5786
Fe, changes due to inc. in defect conc. following plastic deformation 2—3865
Fe, Compton profile due to 1s electrons 2—24340
Fe, K_α spectrum, from multiple inner shell ionization in collisions with 30 MeV O^{5+} 2—665
Fe, L_{III} spectra, density of states of outer levels, line intensities 2—36915
Fe, soft X-ray spectra, classification 2—5786
Fe minerals and compounds, $K_{\alpha1,\alpha2}$ and $K_{\beta1},\beta'$ spectra 2—33296
H, pionic, X-ray yields 2—742
HgS, $L_{II,III}$ spectra, ESCA technique, position of 5d state 2—36919
K_2CrO_4, intensity distribution of $K\alpha$ doublet 2—20056
La, L_I and L_{II} emission edges 2—36916
La (L_I and L_{II} emission edges 2—36916
LaF_3, L_I and L_{II} emission edges 2—36916
LaH_x $(2 \leqslant x \leqslant 3)$, L_I and L_{II} emission edges 2—36916
La_2O_3, L_I and l_{II} emission edges 2—36916
Li, K-emission, band struct., b.c.c. and h.c.p. phase obs. 2—10415
Mg, high-energy satellites of $L_{2,3}$ emission bands 2—33299
Mn, soft X-ray spectra, classification 2—5786
N_2 gas, K_α emission spectrum 2—21628
Na, electron gas correls. and core hole effects 2—1701
Na, high-energy satellites of $L_{2,3}$ emission bands 2—33299
Nb, and Nb compounds, K-emission, ionicity and valence 2—20084
Ni, Compton profile due to 1s electrons 2—24340
Ni, Lorentzian representation of line shape 2—40699
Ni, piezo soft X-ray effect, band struct. 2—22792
Ni, soft X-ray appearance pot. spectra, effect of oxygen 2—35872
Ni, soft X-ray spectra, classification 2—5786
PbS, $K\beta$, band struct. determ. 2—29945
PbS, $L_{II,III}$ spectra, ESCA technique, position of 5d state 2—36919
Pd alloys, electronic structure, comparison with results from ESCA spectra 2—32884
Pt, N-band profiles, band struct. 2—7087
Pu, relative transition probs. to K-shell 2—21510
^{239}Pu, thermal neutron fission, fragment K X-ray emission 2—11882
Ra, L_{II} subshell fluorescence, Auger and Costner Kronig yields 2—18321
S, K_β spectra in SO_4^{2-} and SO_3^{2-}, comparison with intensity curves from CNDO/2 calcs. 2—35287
S, $L_{II,III}$ spectra, ESCA technique 2—36919
S $K\beta$ spectra of inorganic anions calc. using all-valence-electron molecular orbital methods 2—28267
Si, high-energy satellites of $L_{2,3}$ emission bands 2—33299
Si L-emission in Si, SiC, Si_3N_4, SiO_2 and silicides 2—20086
Ta(110) surface, oxidation kinetics study 2—32385
Te thin targets, scattering of I ions, 18-46 MeV, impact parameter dependence of X-ray production 2—38842
Ti, soft X-ray appearance pot. spectra, effect of oxygen 2—35872
TiO_2, rutile, band spectra, mol. orbital energy level diagram 2—40707
Tl, relative transition probs. to K-shell 2—21510
^{205}Tl, muonic, resonance processes and nuclear excitation rel. to L and K X-rays 2—18371
U, L_{II} subshell fluorescence, Auger and Costner Kronig yields 2—18321
U, relative transition probs. to K-shell 2—21510
^{233}U, thermal neutron fission, fragment K X-ray emission 2—11882
^{235}U, thermal neutron fission, fragment K X-ray emission 2—11882
V-M alloy, M=Fe, Os, Ru, V$K\beta_5$ emission, electronic struct. 2—6728
V-Pd alloy, investigation of $K\beta_5$ V and L_{III} band of Pd 2—33301
V-transition metal binary cpds., electronic struct. 2—40708
V binary alloys with transition elements 2—29946
Yb-W, direct meas. of $N_{IV,V}$ emission spectra 2—36922
ZnS, $L_{II,III}$ spectra, ESCA technique 2—36919
ZrN_x, $NK\alpha$ band, band struct. and bonding 2—20088
X-ray spectrometers
see also Gamma-ray spectrometers; X-ray crystallography/apparatus
absorption measurement device 2—14471
astronomical examination, satellites, and polarimeters 2—10982
automatic, applic. of small digital computer 2—17142
bent spectrograph, 1 m radius, design, construction and performance 2—3592
Bragg crystal, for stellar X-ray astronomy 2—10980
double crystal spectrometry, simultaneous diffraction 2—38357
double-crystal, spectrochemical analysis, detection limits 2—4612
frequency selector with adjustable mirrors, automated 2—14471
high resolution, with Si(LI) detector, energy resolution and analytical applics. 2—41420
module for sun's surface obs. 2—14471
PW 1410, applic to det. of low and high atomic numbered elements 2—17141
rocket-borne spectrometer/monochromator system for solar corona mapping 2—11157
with scanning electron microscope combination computer program 2—22900
SHIRX, rocket borne, differential X-ray energy spectrum of Sco XR-1 2—30530
space simulator for testing in rocket and satellite-borne installations 2—14471
spectrochemical analysis, detection limits rel. to spectrometer parameters 2—4610
spectrochemical analysis, optimum parameters rel. to detection limits 2—4611

X-ray spectrometers continued
two grating grazing incidence spectrograph for X-u.v. region 2—14471
Cd-Te, for low energy obs., fabrication and performance 2—24069
Cd-Te, for low energy obs., fabrication and performance 2—31350
CdTe, device and mat. evaluation, trapping obs. 2—34812
Ge radiation counter application 2—34819
n-Si guarded contact surface barrier device, detector for rapid evaluation of ore samples 2—38371
Si(Li) and Ge(Li) X-ray detectors, efficiency curves, and X/γ ratio for calibration sources 2—24068
Si(Li) Detector in a single cryostat 2—20791

X-ray spectroscopy
see also X-ray crystallography; X-ray diffraction
chemical profiles created by fluorescent analyses using energy, dispersive X-ray spectroscopy 2—22901
conference (Toronto, October 1971) 2—13597
cosmic sources 2—23101
ion beam profiles, static measurement technique 2—14395
ion excitation, for trace elemental anal. 2—15216
on-line computer systems applic. 2—23184
photographic dosimetry, applic. of radioisotope X-ray fluorescence spectrometry 2—330
proportional counters applic., positive pressure sealed type 2—14755
soft and u.v., research means at Univ. Paris, France 2—14471
in Z-pinch plasma focus devices time resolved Ross filter system 2—18624
U in U_3O_8, det. by emission 2—30116

X-ray topography *see X-ray crystallography; X-ray examination of materials*

X-ray tubes
characteristics for X-ray structural research 2—19022
cold cathode, soft X-ray source for radiography 2—25552
for electron spectrometer, cylindrical mirror type, design 2—31005
flying spot imaging system 2—32675
gravitational collapse, setting of flux limits for pulses accompanying Weber's pulses 2—5129
high power, review 2—11233
image convertor with d.c. voltage control 2—7636
image convertors utilizing La and Gd oxyhalide activated with Tb, patent 2—20089
loud characteristic, algebraic approximation 2—17140
microfocus, permitted load given as function of physical properties for continuous loads and loads of short duration 2—33837
mirrors of low-alloy Cr for anodes 2—30743
optically switched pulsed generator 2—23208
Philips PW 1016 and 1316 tube shields, safety systems 2—19024
portable TV X-ray introscope, with autonomic biological safeguard 2—30744
pulsed radiography, 2.5. MV accelerating voltage, rotating target 2—11234
rating considerations for maximum life 2—41417
selecting correct tube for X-ray generator 2—41416
shield, mechanical lock-on safety shutter 2—41419
source, soft X-rays, use in photoelectron spectrometer, design 2—11235
variable-focus, for aerospace component inspection 2—32665
with watercooled target, patent 2—20793

X-rays
see also Cosmic rays/X-rays; Gamma-rays
aurora, meas. in midnight sector during March 8, 1970 storm 2—30323
collimation device, use in astronomy 2—5030
films, processing and manufacturing rel. to grain size distribution 2—41418
filter pairs, Ni-Co and Zr-Sr, efficiency 2—29110
generation, high power sources, review 2—11233
image intensifier using channel plate with high time and space resolution 2—20792
intense, monochromatic, production using fluorescence 2—34753
multiple pinhole camera image synthesis by extended source Fourier transform holography 2—33774
plasma emission, laser produced plasma 2—21814
production using laser-heated dense plasma focus 2—14055
solar, burst, impulsive, location and size, model for electric potential field generation 2—11125
solar bursts, impulsive, decay phase 2—30607
solar emission, rel. to photospheric magnetic field 2—11067
solar flux, from SPA and SES obs. 2—23128
sources, monoenergetic of known absolute intensity 2—23784
transition radiation, application to detection of super high energy particles 2—27800
transition radiation generated by traversal of electrons through radiator, detection with multiwire proportional chambers 2—8231
zone plates, apodised, for solar X-ray image formation, construction 2—11070
zone plates, holographic production, for X-ray telescopes 2—11185
CdTe:Cu(Ga)(In), channelling obs. rel. to detector mat. evaluation 2—36539
CsI satellite detector, contribution to background rate by spallation products in crystal 2—17984
Fe XXIV line emission during solar flares 2—30608

effects
see also Nuclear reactions and scattering due to/photons
alkali borate glass, trapped electron centre, e.s.r. and optical obs. 2—20137
alkali metal compounds, effects on crystal structure 2—36375
alkaline earth fluorides, irrad., trigonal Gd^{3+} centres, e.s.r. 2—13530
anthracene, X-ray excited electron-hole pairs, geminate recombination 2—10040
chromosome rupture 2—2021
1-decanol-urea X-irrad. inclusion crystals, e.s.r. of free radicals 2—20153
ionization chamber liquid filled, X-ray and γ-ray induced photovoltaic effect 2—38360
on logic circuits, TTL, radiation hardened response 2—18019
molecules, gaseous, X-ray photoionization, relative abundances and recoil energies of fragment ions 2—28310
m.o.s.f.e.t., drain current and transfer characts., irrad. effects 2—13296
organic crystal, thermoluminescence, dose depend. 2—16632
piezoelectric quartz vibrators, resonance frequency and elastic properties 2—25934
poly-n-vinylcarbazole, thin film, induced conductivity 2—19535
polyethylene, irrad., small-angle scatt. obs., ordered and disordered regions 2—25384

X-rays continued
effects continued
α-quartz, Ti^{3+} centre production, e.p.r. investigation 2—4543
rats, isolated perfused liver, 5-hydroxytryptophan metabolism 2—30667
rats, wild and laboratory, survival time and mortality rate obs. 2—20720
reproductive survival of mammalian cells after irradiation at ultra-high dose-rates 2—37439
spark chambers, narrow-gap, measurement of characteristics 2—24112
surface effects of high energy X-rays at oblique incidence 2—41293
triglycine sulphate, on permittivity and losses 2—1560
triglycine sulphate, X-ray damaged, free radicals, e.p.r. study 2—5977
6-undecanol-urea X-irrad. inclusion crystals, e.s.r. of free radicals 2—20153
$BaYb_2F_8$:Er, up converting phosphor, X-ray induced variation of Yb^{3+} sensitizer time const. 2—20101
CaF_2:Ce irradiation, production of photochromic bands from dipole centres 2—3804
CaF_2, $CaF_2:Dy^{3+}$, $CaF_2:Na^+$, colour centre formation, dopant effects 2—36063
p-InSb, irrad. defects, cond. changes 2—6819
KBr, irrad. defects, thermal annealing 2—3760
KCL:NKO_3, electrolytically coloured, generation of stable centres 2—36067
KCl:Ca, colouring mechanism investigations at room temp. and 195K 2—29202
KCl:Co(Ba)(Cd), X-irrad., F-light bleaching and F- to M-centre conversion 2—22231
KCl, hole centre obs. 2—1262
KCl, irrad., conversion and equilibrium between F- and F_2-centres during warming 2—22228
KCl, irrad., D_3-centre studies 2—36065
KCl, pure and I^- doped, F- and V-centre form., irrad. intensity effects 2—22230
KCl, pure and Pb-doped, irrad., F-centre, accumulation kinetics 2—36070
KCl, pure and Pb-doped, irrad., F-centre accumulation kinetics 2—36069
KCl, X-ray irrad., F-, F_2-centres, dynamic equil., temp. depend. 2—25452
KCl single crystals, F-centre luminescence during X-ray iradiation at low temperatures 2—29953
KH_2PO_4, irrad., light pulse emission accompanied current pulses 2—13515
KI, colour centre formation rel. to role of Auger effect in thermostimulated phenomena 2—33323
LiF, F- and M-centre form., rel. to density decrease 2—19127
LiF, impure, irrad. induced lattice const. changes 2—9525
NaBr(Cl):M^{2+}, (M=Ba, Ca, Sr), irrad. type effects on symmetry of paramagnetic centres 2—26285
NaCl-AgCl solid solution, decomp., irrad. effects 2—36246
NaCl, F-centre formation, optical bleaching, room temperature 2—9597
NaCl, irrad., local defects, e.s.r. study 2—16649
NaCl, on self-diffusion of Na 2—32559
$^{238}PuO_2$, long exposure effects on lattice parameters meas. 2—39651
RbN_3, irrad., e.s.r. study of trapped N atom 2—22834
S, orthorhombic crystal, carrier generation, mobility and conc. detn. 2—29768
Si photodetector, for satellite appl., radiation damage 2—25967
SiO_2 films, sputtered, thermoluminesc., colour centres 2—40729
$Sm_{0.55}Tb_{0.45}FeO_3$, domain wall mobility enhancement 2—26071
ZnS phosphors, double-band, enhancement of electroluminescence 2—36965

protection *see Radiation protection*

Xenon
adsorbed on Cu, LEED and surface potential study 2—12682
adsorption, on graphite, two dimensional phase change, LEED obs. 2—25224
adsorption, physical, on Fe, Cu, Na films, surface pot., surface roughness effect 2—9315
adsorption of He and Ne, quantum mechanical states 2—25228
adsorption on layer-like halides, first layer formation by 2D condensation 2—22087
afterglow, decay of excited atoms and molecules 2—24359
arc lamp, current stabilization 2—38165
atom, collision with H_2, anisotropy of total collision cross section 2—3146
atom, collision with Ne*, Penning ionization electron energy spectra 2—12055
atom, collisions with He^+, He, analysis of ejected electrons 2—3003
atom, collisions with $Ne(^3P_{2,0})$, two state semiclassical model for Penning and associative ionization 2—11974
atom, collisions with $Ne(^3P_{2,0})$, velocity dependence of ionization cross section 2—11966
atom, g_J values of various 5d states, mag. resonance technique, hyperfine structure ^{129}Xe 2—18322
atom, Hartree-Fock-Slater theory, Herman-Skillman modification 2—5775
atom, ionization by ejection of outer shell s electron following electron impact, cross section for electrons up to 20 keV 2—5821
atom, ionization cross sections following collisions with H^+, He^+ and Ne^+ at energies below 100 eV 2—24382
atom, photoelectron ang. distrib., variation with energy obs. 2—38825
atom, structure obs. in total electron impact cross section using transmission spectroscopy 2—31689
atomic, collective reson. in $4d^{10}$ shell 2—11963
atoms, charge transfer collisions with 15 eV protons, producing spin polarized H atoms 2—5867
atoms, collisions with Li, differential cross sections and intermolecular potentials 2—892
atoms, photoabsorption spectrum of $5p^6$ shell, collective effects and screening 2—595
autoionizing and negative ion states below $^2P_{1/2}$ observed using electron impact apparatus 2—28205
BWR, axial transients in xenon, calc., computer program 2—38724
in chondrites, mass fractionation and isotropic anomalies 2—17042
condensation coefficient, measured with quartz crystal microbalance 2—3445
correlation range and compressibility near critical point 2—9034
crystal, compressive metallization 2—19498
cw amplified spontaneous emission, spectral profile meas. by heterodyne method 2—21062
diffusion in CaF_2, 750-1000°C, radiation defect trapping 2—22245
diffusion in UO_2, effect of stoichiometry 2—29225
discharge, saturable absorption effects, YAG:Nd^{3+} radiation 2—18619

Xenon continued
- discharge lamps, long linear, with metallic halide additives continuous emission spectra 2—3254
- flash lamp for e.p.r. kinetic studies, pulse transmitted by silica light pipe 2—23716
- glow discharge containing O_2, clear emission of OIλ5577 2—15514
- h.f. in source, photometric study of cross-over image 2—34847
- impulse discharges, emission studied in 1000-2000 Å region by photography 2—28667
- impurity in solid methane, effect on low temp. sp. ht. 2—9890
- ion source, magnetron with axial extraction, multicharged production 2—11445
- ionization by impact of metastable Ne atoms, velocity dependence of total cross section 2—8462
- i.r. spectra of ν_3 and ν_4 modes of deuterons methane in Xe matrix 2—40668
- lamps, emission spectrum 2—27641
- laser, high repetition rate, using He-Xe discharge 2—21078
- laser multicolour, visible 2—21065
- laser relaxation oscillations, time behaviour and spectra 2—14421
- laser spectral narrowing dependence on line broadening mechanism, saturation and distributed loss effects 2—14398
- liquid, stimulated emission, electron beam excited, vacuum u.v. region 2—28865
- liquid, Wannier excitons, reflection spectra obs. 2—10351
- Luna-16-G-7 fines, low fission solar wind production 2—20656
- lunar, solar flare proton effects 2—10994
- in meteorites, from ^{244}Pu fission 2—1997
- multiply charged ions, by hot cathode source 2—34860
- photoabsorption spectra, collective effects, study of $5p^6$ shell, ectation into $5p\text{-}nd^1P$ channel 2—11962
- photoionization, resonances in continuum 2—596
- photoionization cross section profiles of resonances in continuum 2—597
- photoionization of atoms, variation of angular distribution of ejected photoelectrons 2—607
- plasma, continuum absorption coefficient det. 2—35475
- plasma, laser produced, schlieren cinematographic and holographic diagnostics 2—21825
- plasma, pulsed discharge, dependence of frequency of oscillations on conditions 2—28627
- plasma, radiating plasma flow produced by shock waves, conductivity probe obs. 2—32050
- plasma, r.f. wave negative absorpt. near electron cyclotron harmonics 2—8936
- plasma discharge, initial stages at high pressure, current growth and broadening of current carrying channel 2—31966
- plasma produced in cascaded arc 2—21761
- positive corona breakdown, mechanism between coaxial cylindrical electrodes 2—24907
- post shutdown surge in activity, decay of I_2 extruded into primary coolant 2—8393
- pulse discharges, 50-100 μsec, emission characteristics, for u.v. lamps for pumping dye lasers 2—28670
- pulsed discharge lamp, for kinetic spectrophotometry, optical and electrical characteristics 2—34559
- shutdown problems in boron controlled reactor, optimal controls 2—5745
- single crystal, elastic constants, Brillouin spectra obs. 2—16586
- singly and multiply ionized, excited by electron collision, vacuum u.v. spectra observed 2—8465
- solid, absorpt. and luminesc. of Li, Na, K and Cs atoms 2—24387
- solid, determ. of thermal expansion at pressures to 20 kbar 2—16057
- solid, effect of zero point anharmonicity on the vibrational properties 2—4032
- solid, elastic consts., Brillouin spectra 2—3838
- solid, thermal and elastic props., low-temp. limit 2—32842
- solid, thermal eqn. of state, thermal expansion and stability calcs. 2—40082
- solid, thermal expansion above 1K 2—13050
- solid, Wannier excitons, reflection spectra obs. 2—10351
- transversely excited laser, high pulse repetition rate 2—11472
- u.s. absorption and dispersion along critical isochore 2—31893
- viscosity, new relative meas. in 25-700°C range, analysis of long term reproducibility of oscillating viscometer 2—32186
- viscosity and thermal cond., high temp. calc. 2_18770
- vortex discharge as pumping source for c.w. Nd:YAG laser, comparative study with Ar and Kr 2—27448
- Ar^+, collisions with methane, charge transfer mechanism 2—659
- He-Xe laser, amplitude characteristics 2—23599
- Kr^+, collisions with methane, charge transfer mechanism 2—659
- Rb-Xe vapour, third harmonic generation 1.06 μ radiation 2—6161
- Xe:Cs solid, optical absorpt. spectra, dynamical Jahn-Teller effect 2—10392
- Xe:Li solid, luminesc. and absorpt. spectra, 4-80 K 2—29963
- Xe-Ar solid solns., absorpt. spectra, 8-11 eV, exciton effects 2—20025
- Xe-H elastic scattering high energy, potential energy function determination 2—31707
- Xe-He gas mixtures, optical breakdown threshold 2—35626
- Xe-He laser, high pressure, high repetition rate 2—17582
- Xe-He mixtures, stimulated concentration scattering 2—28860
- Xe-Kr, mixed glass adsorpt. on Pyrex glass at very low press. 2—39564
- Xe^+-Xe, charge transfer efficiencies, $^2P_{3/2}$ and $^2P_{1/2}$ states 2—18342
- Xe^+-Xe, charge transfer reaction, relative cross sections for $^2P_{1/2}$ and $^2P_{3/2}$ ions 2—8480
- Xe I i.r. laser lines, h.f.s. 2—31672
- Xe II, transition probabilities of ionic lines 2—5788
- Xe^+, channelling in Cu, critical angle determ. using charact. X-ray generation 2—29575
- Xe^+, collisions with methane, charge transfer mechanism 2—659
- Xe^+ ion, sputtering of KBr, mass spectrometry obs. 2—22447
- Xe^{13+} cold cathode Penning source, low energy isotope separation of high charge states 2—34334
- Xe_2, absorption coeff. in u.v. near 147-nm resonance line 2—8713
- Xe_2, absorption spectrum, vacuum u.v. region, evidence for molecule formation 2—24492
- Xe^{2+} ion-atom collisions, M X-ray spectra 2—5847
- ^{129}Xe arc spectrum hyperfine structure 2—31651
- ^{129}Xe estimation in Te ores using gamma-ray analysis of ^{129}I 2—7193
- ^{129}Xe n.m.r., chemical shift induced by O_2 and NO admixtures 2—31833
- ^{131}Xe excess in lunar rocks 2—7506
- ^{136}Xe gas discharge, gain at 3.51-μm and 5.57-μm lines meas. under various discharge conditions 2—24863
- Xe+$Xe^+(^2P_j)$, collisions, cross sections for charge transfer and fine structure transitions 2—683

Xenon compounds
- XeF_6, Raman spectra and i.r., visible, u.v. absorption spectra in vapour and matrix isolation 2—38944
- XeHCl, dipole moment obs. 2—8645

Xerography *see Photography*

Y-particles *see Hyperons/resonances*

Yield *see Elastic limit; Plastic deformation; Plastic flow*

Young's modulus *see Elastic constants*

Ytterbium
- adsorbed layer, on W(111) face, elec. field influence on coverage 2—9314
- band structure, determ. by X-ray photoemission 2—22464
- e.p.r. of Eu^{2+}, dynamical effects, Ca impurity effect 2—22836
- e.s.r. in Au, hyperfine splitting parameter 2—26273
- film, h.c.p.$\rightleftharpoons$f.c.c. martensitic transform., phase stability 2—39992
- film, interatomic distance, grain size and surface tension effects 2—29034
- martensitic transformation, X-ray diffraction obs. 2—6641
- GdF_3:Er, Yb, luminesc. props., effect of preparation conditions 2—26216
- Si:Yb, ion backscatt., channelling, flux peaking, energy and depth depend. 2—36054
- Si:Yb ion implanted, atom location, flux peaking 2—25435
- YF_3:Er, Yb, luminesc. props., effect of preparation conditions 2—26216
- Y_2O_3:Yb:Er, red-emitting i.r.-excited phosphor, energy transfer processes 2—26224
- Yb:Eu^{2+}, e.p.r., 5-30K, 35 GHz and 9 GHz 2—30003
- Yb^{3+}-Tm^{3+}, stepwise energy transfer and i.r. to visible conversion 2—10427
- Yb^{3+}-sensitized rare earth phosphors, i.r.-visible conversion processes 2—33308
- Yb^+, electronic wave function by numerical Hartree-Fock SCF method 2—35141
- Yb^{3+}, in CdS, interstitial site, g-actor calc. 2—10287
- Yb^{3+}, in fluorides, luminesc., emission spectra, excitation mechanism 2—26217
- Yb^{3+}, in oxidic lattices, luminesc., i.r.-visible conversion efficiency 2—26225
- Yb^{3+}, in Yb_2O_2S, crystalline field, specific heat and mag. obs. 2—19928
- Yb^{3+}, paramagnetic impurity in yttrium ethyl sulphate, obs. from n.m.r. of proximate nuclei 2—37015
- Yb^{3+}, Yb^{2+}, accurate numerical Hartree Fock self consistent field wave functions 2—35134
- Yb^{3+} in CaF_2, anisotropic spin-orbit coupling in cryst. fields 2—29851
- Yb^{3+} in LaF_3, nonresonant energy transfer from Er^{3+} to Yb^{3+} 2—40718
- Yb^{3+} in LaF_3, nonresonant energy transfer from Er^{3+} 2—40717
- Yb^{3+} in $SrCl_2$, cryst. field energies 2—36888
- Yb^{3+} in yttrium ethyl sulphate, spin-bath relax. 2—19935
- Yb^{3+} in ZnSe, defect config. 2—7019
- Yb^{3+} sensitizer, in $BaYb_2F_8$:Er phosphor, X-ray induced variation of time constant 2—20101
- Yb^{3+} spin-phonon relax. in ytterbium ethyl sulphate 2—7011
- Yb(II), formation spectrum and chem. props. from pulse radiolysis of tervalent ion 2—30094
- Yb(III), aqueous soln., pulse radiolysis, formation spectrum and chem. props. of divalent ion formed 2—30094

Ytterbium compounds
- aluminium garnet, electronic Raman scatt. theory 2—29938
- gallium garnet, electronic Raman scatt. theory 2—29938
- garnet, YAG-YbAG mixed cryst., optical centres 2—20051
- iron garnet, ferrimagnetic, anisotropy effects on field induced phase transitions 2—16387
- ytterbium ethyl sulphate, spin-orbital phonon relax. of Yb^{3+} 2—7011
- ytterbium ethylsulphate, crystal field study 2—36794
- La_2O_3-Yb_2O_3 system, high temp. phase diagram 2—25642
- Yb-Cd, system, phase diagram from differential thermal, microscopic and X-ray analysis 2—4024
- Yb-Co system, cpd. formation, X-ray diffr. study 2—25349
- Yb-Fe system, cpd. formation, X-ray diffr. study 2—25349
- Yb-Ni system, cpd. formation, X-ray diffr. study 2—25349
- Yb-W, direct meas. of $N_{IV,V}$ X-ray emission spectra 2—36922
- YbB_{12} thermal expansion, in range 78-1300°K 2—6684
- $YbCl_2$ molecule, in Ar, Kr or N_2 matrix, i.r. absorpt. studies 2—28327
- $YbCl_3.6H_2O$, paramag. relax. temp. depend., Mossbauer obs. 2—10273
- YbF_2 molecule, in Ar, Kr or N_2 matrix, i.r. absorpt. studies 2—28327
- YbFe garnet, anisotropic, spin reorientations 2—40535
- YbFe garnet, sp. ht., mag. phase transitions 2—33160
- YbFe garnet, spin waves near mag. reorientation transition 2—40570
- $YbFe_2$, Laves phase compound, synthesis method 2—22343
- $YbFeO_3$, growth from PbO-PbF_2-B_2O_3 melts 2—22114
- $YbFeO_3$, self-biased bubbles 2—36783
- $YbFeO_3$, $YbCrO_3$, nonaxial antiferromag. axis, neutron diffr. 2—26064
- Yb_2O_3, polycryst., elastic constants, sonic resonance technique 2—12822
- Yb_2O_2S, specific heat and mag. props. rel. to Yb^{3+} crystalline field 2—19928
- $Yb_2O_2S(Se)$, Mossbauer spectra, Neel pt. phenomena mag. moments, h.f.s. 2—26133
- $YbPd_3$, mag. props. 2—19829
- YbS, energy band struct. and bond ionicity, optical spectra obs. 2—16476
- $Yb_2(SO_4)_3.8H_2O$, paramag. relax. temp. depend., Mossbauer obs. 2—10273
- YbSe, energy band struct. and bond ionicity, optical spectra obs. 2—16476
- YbTe, 4f-5d electron collapse, pressure induced 2—10056
- YbTe, energy band struct. and bond ionicity, optical spectra obs. 2—16476

Yttrium
- ferrite single crystal shape anisotropy effect on nonlinear ferromagnetc resonance instability 2—4531
- lattice dynamics and elastic constants 2—22401
- in metal oxidation resistance enhancement, void formation suppression mechanism 2—22877
- migration of adsorbed atoms on W surface, elec. field effect 2—9313
- n.m.r. of ^{89}Y, h.f.s., Kondo effect role 2—13555
- soft x-ray absorpt. and photoemission obs. by electronic energy states 2—22791
- X-ray tubes, alloying elements in Cr-Cu mirrors 2—30743
- Si:Y, γ-irrad., and thermally processed, A-centre form. 2—1534

Yttrium continued

- Y:Gd, obs. of anisotropies in e.p.r. linewidth and resonance fields due to crystal field effects 2—4546
- Y IV resonance-line spectrum in the vacuum u.v. 2—18312
- YV, spectral anal. to give energy level structure and configuration 2—38817
- ^{90}Y rods, shielded assembly for handling 2—15181

Yttrium compounds

- ethyl sulphate, ^{3}Ho spin-lattice relax. 2—19936
- ethyl sulphate, phonon bottleneck of spin-bath relax. of Yb^{3+} 2—19935
- ethyl sulphate, ytterbium doped, proton polarizations 2—19948
- orthovanadate phosphors, dependence of luminescence intensity on rare earth ion concentration 2—16608
- YAG, spectral linewidth studies of Pr^{3+} 2—10339
- YAG active crystal elements internal stresses under continuous pumping 2—17621
- YAG laser, influence of resonator matching on output power 2—17644
- YAG laser doped with Nd, time characteristics of radiation 2—17630
- YIG:Sn, temp. dependence of hyperfine field acting on ^{119}Sn, Mossbauer effect meas. 2—4354
- YIG, domain struct. 2—6968
- YIG, hypersound absorption in mag. field, 4.2-300K 2—6669
- YIG, Mossbauer study of h.p. phase 2—10330
- YIG, spin echo decay, low temp. 2—10535
- yttrium ethyl sulphate:Yb^{3+}effect of paramagnetic impurity on n.m.r. of proximate nuclei 2—37015
- yttrium ethylsulphate: Dy(Yb), proton polarization by rot. cooling at T<1K 2—29846
- $Ce_xY_{1-x}Al_3$, n.m.r. and mag. susceptibility 2—16658
- $Eu_xY_{3-x}Fe_{5-y}Ga_yO_{12}$ epitaxial films, mag. props., domains 2—36743
- $(Eu_xY_{1-x})_2O_3$, mag. susceptibility orbitally anisotropic exchange and cryst. field effects 2—36658
- Gd-Y alloys, ^{165}Ho n.m.r., hyperfine interactions rel. to noncollinear magnetic order 2—7138
- Gd-Y alloys, Hall effect, magnetiz., elec. resist. 2—6975
- HfO_2-Y_2SiO_5, phase equilib. and solid soln. struct. 2—1411
- Nb-Al-Y alloy, hardness rel. to comp. and annealing 2—4021
- Nd:YAG laser, applic. in optical communication system 2—21091
- Nd:YAG laser, CW, second harmonic generation in $LiNbO_3$ crystals 2—37989
- Nd:YAG laser, mode locked states obs. 2—21092
- Nd:YAG laser, solar pumping 2—21090
- Nd:YAG laser, u.v. light generation by frequency doubling twice 2—11480
- Nd:YAG lasers, TEM_{00} output power, obs. 2—21094
- Nd^{3+}:YAG pulsed laser, influence of lamp filling on pumping conditions 2—27500
- Nd:YAlG laser, applic. in pulse optical communications 2—21093
- Nd^{3+}:$Y_3Al_5O_{12}$ crystal lasers, with pyrolamp illuminator 2—27514
- $(TB,Y)_3Co$, intrinsic coercivity 2—29840
- ThO_2-Y_2O_3 solid electrolyte, elec. cond. and operational limits 2—10634
- Y-Ce dil. alloys, of ^{89}Y, h.f.s., Kondo effect role 2—13555
- Y-Ce dilute alloys, Kondo effect, use of Coqblin- Schrieffer exchange interaction 2—1465
- Y-Cu solid solution, atomic struct. 2—19271
- Y-Ge system, phase relationships, thermal, microscopic, chemical and X-ray analyses 2—9839
- Y-H system, spin lattice relax., electronic contrib., spin echo method 2—16405
- Y-Ni, intermetallic compound, struct., disordered substitutions, X-ray obs. 2—6452
- Y-Rh alloys, Y_3Rh, Y_7Rh_3 and YRh_3 phases, cryst. struct. 2—22161
- Y-(10 wt.%) Tb alloy, spin wave dispersion relation 2—40569
- YAG:Cr^{2-}, X-ray and thermoluminesc., recomb. excitation mech. 2—40725
- YAG:Cr^{3+}, Er^{3+}, thermal dependence Cr^{3+} and Er^{3+} fluorescence line positions and widths 2—16621
- YAG:Cr^{3+}, excitation and fluorescence spectra 2—26241
- YAG:Cr^{3+}, hyperfine and transferred hyperfine interaction, ENDOR obs. 2—10582
- YAG:Cr^{3+}, vibronic spectrum and fluoresc. lifetime, temp. depend. 2—13507
- YAG:Er, Ho, Tm, energy transfer process between Er^{3+} and Ho^{3+}, temp. and conc. effects, fluoresc. spectra obs. 2—26240
- YAG:Er^{3+}, crystal field study 2—36794
- YAG:Ho^{3+}, sensitized, laser, lamp pumped, output and efficiency 2—17625
- YAG:Ho^{3+}, stimulated emission spectroscopic and laser props. 2—17624
- YAG:Lu, Nd, ion site distrib. and spectral line broadening 2—36853
- YAG:Nd, laser, variable threshold acousto- optic Q-switching 2—17629
- YAG:Nd laser, single longitudinal mode, elimination of multilongitudinal mode oscillation 2—17628
- YAG:Nd^{3+}, mechanism of solubilization of Nd by Gd or Lu 2—29092
- YAG:Nd^{3+} laser, stimulated emission cross section 2—37985
- YAG-YbAG, optical centres 2—20051
- YAl garnet:Nd laser using $Ba_2NaNb_5O_{15}$ for intracavity conversion 2—281
- $YAlO_3$:Cr^{3+}, e.s.r. obs., comparison with $EuAlO_3$:Cr^{3+}, exchange interactions 2—7125
- $YAlO_3$:Nd^{3+}, continuous laser action, losses 2—14427
- $YAlO_3$:Nd^{3+}, optical spectra and intensities 2—4496
- $Y_3Al_5O_{12}$:Nd^{3+},Lu^{3+}, Czochralski grown, impurity distrib. coeffs. 2—19118
- $YAsO_4$:Dy^{3+}, Er^{3+}, paramag. resonance and relaxation 2—10488
- $YAsO_4$:Dy^{3+}, low lying ground level doublets, e.p.r. and optical absorp. obs. 2—33337
- YB_{12} thermal expansion, in range 78-1300°K 2—6684
- YB_{66}, crystal growth from the melt, pedestal technique 2—19008
- YBO_3:Ce, cathodoluminescence props. rel. to Ce conc. 2—4518
- $Y_{3-2x}Ca_{2x}Fe_{5-x}V_xO_{12}$, dynamics of initial magnetiz. reversal processes 2—29820
- $Y_{3-2x-a}Ca_{2x}Gd_aFe_{5-x-z}V_xIn_zO_{12}$, mag. props. and reson. linewidths, comp. depend., for microwave applics. 2—40519
- $Y_{3-2x}Ca_{2x}V_xFe_{5-x}O_{12}$, garnet, growth induced noncubic anisotropy 2—10285
- $Y_{3-2x}Ca_{2x}V_xFe_{5-x}O_{12}$, magneto-optical effects 2—40611
- YCo_2, paramag. behaviour 2—25998
- YCo_2, thermal variation of lattice parameters, mag. transition 2—26054
- YCo_3 and Y_2Co_{17}, e.p.r., mag. behaviour 2—10518
- $Y_{2+x}Co_{17-2x}$, magnetocrystalline anisotropy, comp. depend. 2—40458
- Y_2Co_7, Curie temp., hydrostatic press. effect 2—26001

Yttrium compounds continued

- $Y_{3-x}Eu_x(Gd_x)Fe_{5-y}Ga_yO_{12}$ epitaxial film, suitability for bubble domain devices 2—22690
- $(Y_{1-x}Eu_x)_2O_3$:Eu^{3+}, phosphor, colour shift mechanism 2—1716
- $(Y_{1-x}Eu_x)_2O_2S$:Eu^{3+}, phosphor, colour shift mechanism 2—1716
- YF_3:Er, Yb, luminesc. props., effect of preparation conditions 2—26216
- YF_3, up-conversion phosphor, prep. method 2—33321
- YF_3 i.r. to visible converting phosphors, Er activated, ultimate efficiency 2—40720
- YF_3 phosphors, YB^{3+} sensitized, i.r. excitation of visible Er^{3+} luminescence 2—16627
- $Y_3Fe_{5-x}Ga_xO_{12}$ film magnetic, uniaxial, growth by chem. vap. deposition 2—9288
- $YFe_{1-x}Mn_xO_3$, critical conc. for spin reorientation 2—40568
- YFeO, magnetic domain wall, concave, light beam focusing 2—7969
- YFeO , annealing induced domain wall mobility changes 2—10199
- $YFeO_3^3$, Faraday effect 2—10309
- $YFeO_3$, growth from PbO-PbF_2-B_2O_3 melts 2—22114
- $YFeO_3$, torque curve obs. in pulsed mag. fields 2—6997
- $YFeO_3$, weak ferromag., ^{57}Fe n.m.r., domain boundary oscillations, 77-400K 2—22681
- $Y_3Fe_5O_{12}$ garnet, Raman spectra, stretching modes 2—4464
- $Y_3Ga_xFe_{5-x}O_{12}$, temp. compensation point, Faraday rot. obs. 2—29831
- YGdFe garnet, resonant motion of domain walls 2—40534
- $Y_2GdFe_{4.2}Al_{0.8}O_{12}$, growth-induced anisotropy, microscopic theory 2—40533
- YH_3 diffusion of H, n.m.r. study, spin lattice relaxation time, resonance line shapes 2—29207
- YH_x moderator, neutron thermalization 2—31613
- YIG:Ga, on GdGa garnet substrate, acoustic surface wave isolator 2—40065
- YIG:Ga films, rare earth substituted, domain wall motion 2—40531
- YIG:Si, polarization-depend. photoinduced effects 2—26116
- YIG:Si, spontaneous and photoinduced linear dichroism 2—22730
- YIG, application of theory of Mossbauer γ-ray diffraction 2—29881
- YIG, axially magnetized single cryst., magnetostatic reson. absorpt. modes 2—19909
- YIG, e.m. modes coupling to magnetostatic modes 2—26009
- YIG, excitons, spin wave sidebands and exchange interactions 2—40681
- YIG, ferromagnet, spin wave conductivity 2—19844
- YIG, fine struct. of spin wave instabilities 2—40748
- YIG, growth-induced mag. anisotropy 2—40532
- YIG, inelastic light scatt. and magneto-optical effects 2—20060
- YIG, magnetoelastic coupling, dynamic 2—26045
- YIG, shock-induced anisotropy, demagnetiz., mag. grain interaction 2—33130
- YIG, shock-induced anisotropy, demagnetiz., domain theory analysis 2—36706
- YIG, spin configs. induced by anisotropic ions 2—26073
- YIG, standing spin waves and mag. anisotropy 2—13387
- YIG, synthesis, primary crystn. fields in PbO-PbF_2-B_2O_3 2—29101
- YIG films, ferromag. reson., spin wave band, signal edge obs. 2—40747
- YIG films, Ga-substituted, annealing effects on mag. props. 2—36752
- YIG films, Ga-substituted, epitaxial strains and fracture 2—35897
- YIG heteroepitaxial film, verification of stress model 2—22069
- YIG magnetoelastic delay lines with linear dispersion 2—33147
- YIG;Si, a.c. hopping cond. 2—13242
- YLF:Ho^{3+}, stimulated emission, spectroscopic and laser props. 2—17624
- $YNaO_2$, cryst. struct., X-ray obs. 2—35987
- Y_2O_3:Eu^{3+}, energy transfer, fluorescence decay curves time-resolved study 2—22803
- Y_2O_3:Eu^{3+}, random substitution of Eu^{3+} for Y^{3+}, reflection spectra obs. 2—13464
- Y_2O_3:Eu^{3+} phosphor, brightness enhancement by Ga_2O_3 addition 2—22814
- Y_2O_3:R, R=Pr, Sm, Eu, Gd, Tb, Dy, Ho, Er, and Tm, X-ray excited fluorescence 2—22805
- Y_2O_3:Yb:Er, red-emitting i.r.-excited phosphor, energy transfer processes 2—26224
- Y_2O_3-Fe_2O_3-50PbO.40PbF_2.10B_2O_3 system, optimum comp. for ferrite and garnet crystn. 2—36291
- Y_2O_3-Fe_2O_3 powder mixture, ferrite form. at 1100°C 2—30058
- YO, electronic states, and energy of $^2\Delta$ state, high resolution analysis 2—12192
- YO, low-lying electronic states, interpretation 2—5950
- Y_2O_3, pt. defect obs. using thermoelectronic emission 2—29172
- Y_2O_3, rare earth impurity analysis, X-ray excited optical fluorescence 2—4506
- Y_2O_3, sintered, dielec. props. 2—16268
- Y_2O_3 stabilisation of ZrO_2 base electrodes, potential falls and resistance 2—28479
- Y_2O_2S-Gd_2O_2S, phosphor host material, subsolidus phase relations 2—13010
- Y_2O_2S-La_2O_2S, phosphor host material, subsolidus phase relations 2—13010
- YPO_4:Er^{3+}, mag. props. and sp. ht., calc. from cryst. field parameters 2—40421
- YPO_4, thermal expansion, rel. to cryst. chemistry 2—22430
- $Y_{1-x}Sm_xVO_4$, $0 \leqslant x \leqslant 1$, temperature, concentration and kinetic parameters of luminescence, energy transfer 2—29955
- $Y_{1-x}Th_xAl_3$, low temp. specific ht. meas., influence of Brillouin zones on electronic density of states 2—1432
- $Y(V,P)O_4$:Eu^{3+} phosphor for h.p. Hg vapour lamps 2—11524
- YVO_4:Dy^{3+}, Er^{3+}, paramag. resonance and relaxation 2—10488
- YVO_4:Er^{3+}, mag. props. and sp. ht., calc. from cryst. field parameters 2—40421
- YVO_4, thermal expansion, rel. to cryst. chemistry 2—22430
- YZn, elastic consts., anisotropy ratio, temp. depend. 2—3834
- $Y_2Zn_{\sim 9}$, cryst. struct. 2—39656
- $Y_{0.6}Zr_{0.4}B_{12}$, high temp. enthalpies 2—19274
- Yal_2, Laves phase compound, low temp. specific heat 2—19425

Yukawa potential *see Field theory, quantum/meson field; Nuclear forces; Scattering*

Zeeman effect

- alkali metal atoms, probability of stimulated microwave emission from Zeeman levels 2—31665
- anthracene-d_{10}-fluorene mixed crystals, e.s.r. study 2—20154
- antiferromagnet, high field spectra, exchange interactions 2—19922
- antiferromagnetic conductor, dielectric const., mag. field effect 2—40540

Zeeman effect continued

- atomic collisions, nonresonant, with transition between Zeeman sublevels 2—5825
- atoms, ground state energy sublevels perturbed by nonresonant light beams, Zeeman light shifts 2—24330
- benzene, obs. in $^{3}B_{1u}$ state, evidence for dynamic pseudo Jahn-Teller distortion 2—20109
- bicyclobutane, molecular g values 2—35313
- 2- cyclopentane-1-one 2—12231
- 2,4-dibromoanisole and 2,4,6-tribromoanisole, n.q.r. of ^{81}Br 2—8745
- 3,4-dichloronitrobenzene, n.q.r. of ^{35}Cl 2—13560
- diketene, at fields near 20000 G, determ. magnetic properties and electric moments 2—21675
- dimethylketene, rotational Zeeman effect in microwave spectrum, determ. of molecular g-tensor 2—38978
- 2-fluoropyridine, obs. in rotational spectrum 2—843
- formaldehyde, spin-vibronic perturbations in $^{1}A_2$ state 2—15377
- formaldehyde mol. beam, multiphoton transition, 106 kHz 2—31855
- formamide, molecular g values 2—38982
- ^{15}N formamide, parameters and molecular quadrupole moments determ. 2—12246
- furan, [2,5-D_2], rotational Zeeman effect in ground vibrational state 2—38984
- ionic cryst., freq. dispersion, theory 2—10358
- lanthanide fluorides, far-i.r. splitting of rare earth ions 2—40669
- lanthanide ions, splitting of cubic cryst. field levels, covalent and vibronic contributions 2—19944
- laser emission intensity modulation in variable magnetic field 2—17577
- methylene fluoride, high-resolution molecular measurements, ^{19}F chemical shift anisotropy 2—35339
- molecular, magnetic susceptibility meas. 2—8510
- molecular beam. Zeeman-Stark effect due to translational motion 2—28264
- phenazine-fluorene (anthracene) mixed crystals, e.s.r. study 2—20154
- β-propiolactone, at fields near 20000 G, determ. magnetic properties and electric moments 2—21675
- pyrene-d_{10}-fluorene mixed crystals, e.s.r. study 2—20154
- 4- pyrone, molecular Zeeman effect 2—12231
- 2- pyrone, molecular Zeeman effect 2—12231
- rare-earth ions in crystal field with C_{3h} symmetry 2—36863
- solar spectrum, mag. field strength obs. 2—11029
- spin system in solid, Zeeman and dipole temps. in rot. frame, prolonged irrad. effects 2—33348
- trimeric clusters. Heisenberg-Dirac-van Fleck Hamiltonian, Zeeman splitting 2—30017
- triplet formation in isothermic stellar atmosphere with magnetic field 2—33644
- Ar laser, 4880 Å line, rel. to increase in saturation parameters 2—34388
- Ar$^+$ ion beams, det. in optical spectra 2—34357
- As II spectrograms from electrodeless discharge tubes, 24025 Gauss 2—15217
- Ba plasma, use in ion temp. obs. 2—32046
- $BaCl_2.2H_2O$, n.q.r. study 2—13559
- $BaFe_{12-2x}Zn_xTi_xO_{19}$, Mossbauer effect, mag. hyperfine fields, Zeeman patterns 2—33216
- Bi i multipole line at 4615 Angstroms, total intensity 2—38810
- BrCN molecule. magnetic properties and electric quadrupole moments 2—24437
- BrF molecule, magnetic properties and electric quadrupole moments 2—24437
- C atom, $^3P_1$ and $^3P_2$ levels, Lande factors calc. 2—8450
- $CaWO_4$:Nd^{3+}, polarized Zeeman fluorescence spectra, energy and polarization meas. 2—16615
- Cd, Lande factors of 5s6s $^3S_1$ levels 2—24341
- ClCN molecule, magnetic properties and electric quadrupole moments 2—24437
- ClF, BrF, ClCN, BrCN, ICN, parameters determ. 2—12123
- ClF molecule, magnetic properties and electric quadrupole moments 2—24437
- CuCl-CuBr solid solns., exciton band obs. 2—16486
- $DyPO_4$, high field spectra, exchange interactions 2—19922
- ErFe garnet, far-i.r. spectra, exchange interactions 2—40637
- $Fe_{1-x}O$, non-stoichiometry, Mossbauer effect 2—26129
- GaAs:Sn, photoluminesc., emission, principal bound exciton obs. 2—33306
- GaAs, donor states splitting 2—16229
- Gd-Sn alloy, Mossbauer effect, nuclear Zeeman effect, mag. props. 2—13453
- Gd I, arc spectrum, line splittings, assignments 2—15214
- Gd II, spark spectrum, line splittings, assignments 2—11954
- H_2, metastable $c^3\Pi_u$ state, magnetic hyperfine and Zeeman interactions 2—38914
- HCl molecular beam electric resonance spectroscopy, Stark-Zeeman spectra obs. 2—12145
- HF molecular beam electric resonance spectroscopy, Stark-Zeeman spectra obs. 2—12145
- He, 4^3P and 5^3P states, transitions between Zeeman levels, diamag. Zeeman effect 2—18360
- He I, combined Zeeman and h.f. Stark effects, calcs. of various spectral lines 2—18359
- He$^+$, n=3 state, $P_{3/2}$-$D_{3/2}$ splitting and crossing signals detection 2—5877
- Hg, Lande factors of 6s7s $^3S_1$ levels 2—24341
- Hg traces in host material detected by new atomic absorption spectrometer from hyperfine structure lines in mag. field 2—8038
- I in CF_3 and C_2F_5I photodissociation lasers, Zeeman effect in hyperfine structure of emission 2—31038
- ICN molecule, magnetic properties and electric quadrupole moments 2—24437
- KCl:Sm^{2+} single crystal, theory of Zeeman anisotropy fluorescence spectroscopy, numerical fit of low-J transitions 2—22804
- $MnCl_2$, $2MgCl_2$, $12H_2O$, absorption spectrum in near u.v., Zeeman splitting of 12 sharp lines 2—20044
- MnO, ^{119}Sn Mossbauer spectra, Zeeman splitting of Sn^{4+} nucl. levels 2—13450
- NF_2 radical, microwave Zeeman spectra, electron spin-rotation interaction 2—8678
- NSF, triplet state at 5360 Å, Zeeman study and preliminary rotational analysis 2—3051
- $^{14}NH_3$, quadrupole tensor evaluated first and second order Zeeman effects obs. 2—8682

Zeeman effect continued

- Na, $3^2P_{3/2}$ state, crossings of Zeeman sublevels calc. using dipolar magnetic and quadripolar electric interaction constants as parameters 2—18316
- O II and O III multiplet levels with optical cascades, quantum beats in transitions 2—35143
- O^+ ion beams, det. in optical spectra 2—34357
- $Pr_2Mn_{3-x}Zn_x(NO_3)_{12}.24H_2O$, satellite structures 2—4458
- ^{87}RbF, molec. beam resonance meas. 2—21641
- SF_6, solid, spin-lattice relax., 300-4.2 K 2—26085
- SiC:N, 6H polytype, absorp. lines R_o and S_o 2—36885
- TlCl isotopes, molec. beam resonance meas. in different vibrational states 2—21645
- $YAsO_4$:Dy^{3+}, low lying ground level doublets, e.p.r. and optical absorp. obs. 2—33337
- ZnSe:Tm, Li, absorpt. lines 2—40721

Zener diodes *see Semiconducting devices/diodes*

Zener effect *see Metals; Semiconducting materials; Semiconductors*

Zero sound

- *see also Helium/liquid, sound propagation*
- ^{3}He-^{4}He dilute mixtures, possible existence of zero sound for mixtures under sufficiently high external pressure 2—32295

Zeta-potential *see Electrokinetic effects*

Zinc

- acoustic emission, correl. with dislocation motion 2—4044
- anharmonic properties, thermal expansion 2—19355
- atmospheric pollutant, nonflame atomic absorption analysis 2—22892
- atom, collisions with Cd, energy dependence of excited CdI resonance line 2—2968
- atom, level lifetimes meas. by delayed coincidence method 2—8459
- atom, X-ray K-fluoresc. yields 2—8443
- atom spectra, Perot-Fabry interferometry in vacuum u.v. 2—15208
- atomic weight, new determination 2—38844
- atomic weight det., coulometric method 2—21536
- autoionization of high-temperature monatomic vapour 2—28201
- band structure. Green's function calc. 2—29601
- basal faces, evaporation and defects 2—39471
- bicrystal, surface and boundary energies relationship 2—6304
- bicrystals, grain boundary migration 2—12779
- binding energy and lattice constants, pseudopotential calc. 2—40139
- in brine, atomic absorption spectroscopy obs. 2—10661
- cavitating effect of cryogenic liqs. 2—39915
- crystal growth, rounded crystals from vapour 2—18987
- crystal growth by Bridgeman technique, variation of growth rate and radial heat loss 2—3588
- diffusion, in n-Si, reactor irrad. enhanced 2—29193
- diffusion, in ZnSe 2—3825
- diffusion, intergranular in Al, struct. effect 2—12799
- diffusion in Al bicrystals bent about <001> axis 2—25462
- diffusion in Al-$CuAl_2$ eutectic, dislocation and boundary effects 2—3818
- diffusion in Cu, resulting dislocation arrangements 2—25404
- diffusion in $GaAs_{0.6}P_{0.4}$:Te, from Ga-P-Zn source, p-n junction formation 2—9586
- diffusion in GaAs, isoconcentration technique 2—15789
- diffusion in GaAs 2—22224
- diffusion in GaAs 2—32562
- diffusion in liq. Ga, 238.5-365 K 2—15582
- diffusion in Zn_2SiO_4 2—32566
- dislocation damping, dragging atom effects 2—9562
- dislocation loops and stacking faults 2—15764
- dislocation mobility, at 44K, torsion technique obs. 2—32519
- dislocations, basal and non-basal, interactions, function of stress, at 298K and 84K 2—39703
- electrodeposition, morphology, effect of pulsating potentials 2—13586
- electron rad. induced stress relax., yield point, deform. resist. 2—25506
- electroplastically deform. effects, shift in cold brittleness limit 2—32611
- Fermi surface, stress depend. of needle-shaped electron pockets 2—36429
- grain boundary shape expt. verification of calc. 2—19109
- h.c.p., point defect prod. on irrad., recovery 2—15745
- in human skin biopsies, nondestructive neutron activation analysis 2—41304
- hydrostatic extrusion rel. to struct., plasticity and strength 2—19184
- interstitial, in coloured ZnO, ion channelling and blocking obs. 2—19094
- ion implantation in GaAs 2—25423
- laser induced damage, and annealing behaviour, X-ray obs. 2—22184
- liquid, compressibility, pseudopot. formalism calc. 2—12550
- liquid, specific resist., short range order, pseudopotential calc. 2—1116
- liquid, struct., neutron diffr., data scaling by Krogh Moe-Norman-Vainshtein method 2—35731
- mechanical behaviour under compressive loading 2—29230
- optical props., band struct. 2—33276
- phonon dispersion, and lattice specific heat calc. 2—19391
- phonon dispersion relation, Debye temp., modified axially symm. model 2—40049
- phonon dispersion relations 2—32815
- phonon freqs., 80K 2—1423
- phonon mode temp. estimation 2—22393
- plastic deformation, electrically induced, before brittle fracture 2—36121
- plastic deformation, Peierls mechanism significance at low temps. 2—36122
- polycrystal, hydrostatic pressure effects on flow stress 2—39802
- polycrystalline layer, on NaCl, transmission of struct. information 2—6333
- polycrystalline sample, in presence of adsorbing alloys, dependence of creep velocity on applied stress 2—6552
- single boundary motion, mobility and activation energy 2—29227
- single cryst., Baushinger effect on individual twins, phenomenological parameters calc. 2—15840
- single crystal surface deform. by sliding friction, surface film effects 2—15890
- sputtering, anomalous behaviour under metal ion bombardment 2—13062
- stacking fault, twin and point defect energies, pair pot. calcs. 2—15747
- superconducting transition phenomena, anisotropic length changes 2—19603
- supercooling and superheating, Ginzburg-Landau parameter 2—13155
- surface deform. during sliding, surface films effect 2—22304
- surface preparation, technique for clean non-cleavage surface 2—22066
- thermal coeff. of expansion of activated vacancy, self-diffusion 2—29561
- thermal expansion at low temp., c/a effect on electronic density 2—16063
- twin boundary motion under repeated loading, hardening loss 2—19107

Zinc continued
vacancies, positron trapping, angular correlation data analysis 2–25386
vapour, atom conc. determ. by atomic absorpt. method 2–20212
vapour, condensation in supersonic carrier gas 2–32146
vapour, electron impact spectrum at 50 to 150 Ev and 0 to 11° range 2–28210
vapour in He carrier gas, hypersonic flow with condensation, Pitot pressure 2–28707
whiskers, growth, and straightening of kinked ones by annealing 2–1191
work function and surface structure, calc. 2–39455
Al-Zn multilayer, internal friction, yield point, thickness and defect depend 2–1287
Cd-Zn coating, on steel, copper and brass, testing at marine microclimate 2–1751
GaAs:Zn, impurity conc. determ. from Hall effect and hole mobility 2–6837
n-GaAs:Zn, ion bombarded, enhanced diffusion 2–25446
GaAs:Zn, radiative recomb. time characts. 2–33305
GaAs:Zn,Fe, impurity interactions at m.p., calc. 2–29667
GaAs:Zn electroluminescent diodes, high-efficiency, fabrication effects 2 -26250
GaAs:Zn film, heteroepitaxial, formation and elec. props. 2–22531
GaP:Zn, impurity-to-band activation energies, conc. and temp. depend. 2–10057
GaP:Zn, Te, epitaxial single cryst., Hall mobility and resistivity obs. 2 -40255
GaP:Zn,O, annealing effects on luminesc. props. 2–26233
GaP:Zn,O growth from nonstoichiometric melt, red photoluminesc. 2–7098
GaP-Zn,O, luminescence 2–10421
inGaP, zone melted, distrib. determ. 2–1258
GaSb:Zn, low temp. phonon thermal cond., role of density of states effective mass 2–40092
Ge:Zn, symmetries and deform. pot. consts. of singly ionized Zn 2–29890
Sb_2Se_3:Zn, liq., elec. cond., thermoelec. power, impurity effects, 950-1200 K 2–22001
n-Si:Zn, p-n junctions, impurities with deep energy levels, compensation of spectral characteristics 2–29772
p-Si:Zn, P, photodielec. effect, polarizability of neutral atoms 2–13343
Tl:Zn, supercond transition temp., impurity effects 2–36473
Zn:O liq., evaporation kinetics, equilib., v.p., rel. to surface active impurities, 563-623K 2–28951
Zn/GaAs, surface-barrier structures by chemical deposition 2–25892
Zn/In superimposed layers, mixed state props., critical phenomena 2–16177
Zn-Cd, vapour laser, continuous oscillation, hollow cathode discharge 2–34395
Zn-Fe diffusion couple, intermetallic phase form. 2–29390
Zn-air secondary cell, use of Pd catalysed porous Ni air cathodes 2–11418
Zn^- e.p.r. in Si;P 2–13543
Zn^+ e.p.r. in sodaborate glasses 2–26284
Zn^{2+}, reactions in KBr(I) lattices, coloration, spectra 2–19125
Zn^{2+} in MnF_2, far i.r. and Raman spectra in two-magnon region 2–7080
^{68}Zn, spectral analysis by isotopic dilution method 2–37067

Zinc compounds
alloy, effect of hydrostatic pressure on torsional deformation 2–3826
brass, 70-30 cartridge, indentation hardness, grain size 2–32652
β-brass, annealing, high temp. deformation, discontinuous yielding, superdislocation climb 2–39781
brass, annealing twins, form. mechanism 2–39889
β-brass, band struct., u.v. photoemission obs. 2–1589
α-brass, deformed, grain growth rates 2–39924
α- brass, density of states 2–4109
brass, development of improved etchants, electrochemical techniques 2–18920
α-brass, fatigue ductility, under cyclic stressing 2–12905
brass, fatigue rupture, fracture surface morphology 2–12907
β'-brass, Fermi surface, positron annihilation 2–16129
β-brass, long-range order 2–36231
brass, ordering parameter 2–25595
brass, phase transform., detect. by exoelectron emission method 2–36623
α-brass, stress corrosion cracking, strain rate depend. 2–6573
α-brass, texture transition, orientations, neutron diffr. 2–19047
α-brass, twin boundary free energy-grain boundary free energy average ratio 2–32537
brass, vacancy form. during recrystn. 2–39888
β-brass, yield stress, anomalous temp. depend. 2–29258
α-brass deformation, meas. by electrolytic sodium thiosulphate etch, detect. sensitivity 2–12852
chalcogenides, core electron level obs., x-ray induced electron emission obs. 2–19811
chemical shift of Kα lines, X-ray technique 2–33302
ferrites, polycrystalline, meas. of Young, rigidity and bulk moduli at room temp. 2–36097
ordering kinetics, role of vacancies 2–13005
photopolymers, based on polyamides, wear resistance 2–3917
phthalocyanine, photocond., light-intensity depend. 2–10143
sulphates, X-ray L_{23} spectra of quantum efficiency of S photoemission 2–26204
tutton salts, spin-lattice relax. of Cu^{2+} 2–10274
Ag-Zn, electron microscopic investigation of ordered β' and ζ phases 2–32440
β'-Ag-Zn alloy, martensite formation, electron microscopy 2–1387
Ag-Zn alloy, radiation enhanced diffusion 2–3817
Ag-Zn cold-worked alloy, electron irrad. enhanced diffusion 2–9614
$AgAuZn_2$, solid soln, first and second neighbour ordering, stability criterion 2–19257
Al/Al-Zn diffusion couple, solid-liq. diffusion 2–6513
Al-Ag-Zn alloy, precipitation phenomena 2–3938
Al-Mg-Zn alloy, fatigue fracture, electron microscope obs. 2–9707
Al-Mg, alloy, rapidly solidified structures, effect of deposited metals on mechanical properties 2–3888
Al-2.8 at%Zn-1.4 at%Mg, alloy, neutron irrad. rel. to precip. and G.P.zones 2–29418
Al-5.0 at%Ag-5.0 at%ZN, alloy, neutron irrad. rel. to precip. and G.P.zones 2–29418
Al-Zn-Mg alloy, ageing, transition phase, X-ray obs. 2–9753
Al-Zn-Mg alloy, crack initiation and growth subject to fatigue loading 2 -32628

Zinc compounds continued
Al Zn Mg alloy, extruded, rel. between grain struct. and quench sensitivity 2 25589
Al-Zn-Mg alloy, notch toughness, Fe, Si content effect 2–12903
Al-Zn-Mg alloy, quenched, aged, metastable miscibility gap, small angle X-ray obs. 2–3981
Al-Zn-Mg alloy weld, notch toughness, Fe and Si content effect 2–12904
Al-Zn, Al-Zn-M alloys, M=Be, Fe, Mn, Si, clustering and solute-vacancy interactions elec. resistivity obs. 2–32693
Al-Zn, deviations from Matthiessen's rule 2–16141
Al-Zn, liquid alloys, thermodynamic props. determ. using improved dew pt. method 2–39359
Al-(15 at.%)Zn alloy, quenched, coherent phase separation kinetics, small angle X-ray scatt. 2–3980
Al-Zn alloy, critical composition small angle X-ray scatt. near critical temp. of demixture 2–9447
Al-Zn alloy, effect of Cu on phase transformation and ageing 2–29461
Al-Zn alloy, Guinier Preston, X-ray scatt. obs. 2–9448
Al-Zn alloy, pre-precipitation, X-ray and neutron scatt. obs. 2–3939
Al-Zn alloy, quenched, pre-precipitate formation and reversion 2–25590
Al-Zn alloy, solvus curve of Guinier-Preston zones 2–29422
Al-Zn alloy, thermopower, Nielsen- Taylor effect 2–22632
Al-Zn alloy, vacancy-Zn atom pair binding energy 2–36017
Al-Zn alloys, influence of Zn on stacking fault energy, plastic deformation, phase transformation 2–29186
Al-Zn alloys, precip. of stable β-phase, Mg additive effects 2–39919
Al-Zn alloys ultrasonic velocity and attenuation dependence on rel. concentrations 2–6661
Al-Zn based alloy, solute-vacancy interactions and clustering kinetics 2–9754
Al-Zn solid solution, activity coeffs., e.m.f. meas., thermodynamic props. 2–4059
Al-(4.4 at.%)Zn alloys, ageing, clustering, solute-vacancy binding energies, ternary additions 2–6481
$AlCl_3$-$ZnCl_2$, molten system, Raman spectral study 2–28863
AlZn alloy, zinc vacancy formation by evaporation, Kirkendall effect 2–19088
Au-Zn alloys, electronic sp. ht. below 3K 2–4064
AuZn, quenching temp. influence on high temp. phase retention 2–25570
α-brass/Cu diffusion couple, substruct. of diffusion zone 2–39739
α-brass, sublimation in vacuo, applic. of elec. analogy method 2–18888
CaO-ZnO-B_2O_3 system, phase equilib., X-ray diffr. 2–22376
Cd-Sn-Zn alloy system, liquidus temperature determ. 2–1140
CdF_2-ZnF_2 system, phase equilibrium 2–15983
$CdSiP_2$, thermal oxidation 2–1750
Cu-Al-Zn alloy, stacking fault energy, electron microscope determ. 2–12773
Cu-Ni-Zn alloy, phase regions, elec. resist. study 2–25641
Cu-Ni-Zn alloys, thermopower, 3d band filling 2–16304
β-Cu-Zn, ordered, Fermi surface topology from positron annihilation ang. correl. meas. 2–16130
Cu-Zn alloy, dendritic precipitate growth kinetics 2–19262
Cu-Zn alloy, effect of stacking fault energy on solid state creep rate 2–15850
Cu-Zn alloys, Fe local moment behaviour 2–40416
Cu-Zn alloys, spectrochemical analysis in elec. discharge, role of controlled atmos. in suppressing 'third' element effect 2–4615
Cu-Zn dil. alloys, low field magnetoresistance 2–1474
Cu-Zn heat of evaporation and activity of Zn determ. 2–16031
CuAlZn alloy, work hardened, extended dislocation clusters, energy obs. 2–15762
α-CuZn, disordered, Fermi surface topology from positron annihilation ang. correl. meas. 2–16131
$Cu_{85}Zn_{15}$ alloy, positron annihilation, Fermi surface 2–1475
Fe–Zn–C alloy, activity of C, Zn content depend. 2–9768
p-GaAs-n-ZnSe diode, I-V characts., junction capacitance, optical collection efficiency 2–25894
Ge/ZnSe/GaAs(Cs), heterojunc. photocathode 2–6926
Mg-Cu-Zn 9-layer Laves phase, composition and lattice constants determ. by single crystal and powder X-ray diffraction 2–39645
Mg-Li-Zn 9-layer Laves phase, composition and lattice constants determ. by single crystal and powder X-ray diffraction 2–39645
Mg-Zn alloy, strength in various ageing states, mechanism of precipitation hardening 2–6599
Mn-Zn, alloy, age hardened, grain size, dependence of yield stress and flow stress 2–6546
Mn-Zn ferrite, recording head, grain size effect on noise 2–10224
Mn-$ZnSiO_4$, hydrothermal synthesis from Na_2N-ZnO-SiO_2 system 2–29087
NaOH-KOH-ZnO mixture, flux for tinning Al wire 2–41357
Ni-Cu-Zn alloy, reciprocal mag. susceptibility, antiparallel coupling 2–4347
Ni-Zn, ferromag. alloy, n.m.r. study, localization of excess electrons around solute atoms 2–4558
Ni-Zn ferrites, cryogenically crushed, prep. and props. 2–16384
$Ni_{0.5}Zn_{0.5}Fe_2O_4$, anisotropy and mag. losses, effect of CoO addition 2–29830
$Ni_xZn_yFe_2O_4$, optical consts., ellipsometric determ. 2–36816
Pb-Cd-Zn and Pb-Cd-Zn-Sn systems, phase diagram, computer calc. 2–13008
Pd-Zn-Ga system, distorted CuZn struct. 2–29465
$RuZn_6$, crystal structure of primitive cubic, non-centrosymmetric phase by X-ray phase determ. 2–29152
Sn-Zn eutectic alloy system, elastic moduli, u.s. wedge method obs. 2–39760
Zn-Al-Mg, alloy, precipitation, effect of Ag, correl. with stress corrosion behaviour 2–3951
Zn-Al-Mg, alloy, stress corrosion resistance, tensile props. microstruct. rel to quenching conditions 2–12931
Zn-Al, alloy, dilute, quenched, solute dispersion, X-ray diffr. obs. 2–25587
Zn-Al, alloy, eutectoid, superplastic, extrusion speed and temp. rel. to extrusion stress and mech. props. 2–19255
Zn-Al, alloy, eutectoid growth rates, interlamellar spacings, isothermal transform 2–12964
Zn-Al, alloy, evaporation rate vs. temp. curve 2–28952
Zn-Al, alloy, precip. decomp., intermediate phase. ageing, X-ray diffr. obs. 2–19263
Zn-Al, alloy, stacking fault energy, rel. to dislocation interactions 2–9566

Zinc compounds continued
- Zn-Al alloy, decomp.. second stage, diffuse effects, X-ray scatt. obs. 2—25588
- Zn-Al eutectoid alloy, superplasticity, effect of processing history 2—29265
- Zn-Cd alloy, crystal growth from stagnant or flowing melt 2—3582
- Zn-Cu-Mg system, phase diagram, DTA, electron microprobe analysis 2—40013
- Zn-Cu, alloy, dilute, charge density oscill. around impurities n.q.r. obs. 2—16666
- Zn-Fe(Ni) systems, reactive diffusion phase formation, press. depend. 2—12996
- Zn-M extremely dil. alloys, M=Cr, Mn, Fe, resist. 0.4-30 K, Kondo model 2—16148
- Zn-Mg-Al system, constitution, metallography, magnetothermal and X-ray obs. 2—4025
- Zn-Mg-Cu alloy, enthalpies of form., Laves phases binding conditions 2—29475
- Zn-Mg dilute alloy, ageing characteristics 2—29405
- Zn-Mn-Al alloy, solid and liq., Curie-Weiss law behaviour 2—19887
- Zn-Mn alloy, solid and liq., Curie-Weiss law behaviour 2—19887
- Zn-Pb, alloy, evaporation rate vs. temp. curve 2—28952
- Zn-Sb, alloy, evaporation rate vs. temp. curve 2—28952
- Zn-Sn-Cd-Bi, liquid solutions, thermodynamic properties 2—3382
- Zn-Sn, alloy, evaporation rate vs. temp. curve 2—28952
- Zn-Te, partial pressure, thermodynamic props., sublimation 2—12619
- $(Zn,M)_5(OH)_8Cl_2.H_2O$, pseudomorphs, M=Co, Ni, Mn, Cu, Zn, Na, cryst. struct. 2_3579
- Zn complex, $[(C_2H_5)_4N]_2ZnCl_4$:Co, e.p.r. study of g-tensor orientation 2—33107
- Zn complex, dichlorobis(4-methylpyridine)zinc(II), crystal and molecular structure 2—12738
- Zn complex, tetrabenzoporphine, quasilinear phosphorescence, fluorescence and absorption spectra 2—4486
- $ZnAl_2O_4$, natural Gahnite, n.m.r. of ^{27}Al, reson. lines, line shifts 2—26309
- $ZnAl_2O_4$, normal spinel polarized Raman and phonon spectra 2—10408
- Zn_3As_2, $Cd_xZn_{3-x}As_2$, reflectivity obs., i.r.-vac. u.v. 2—20000
- $Zn(BrO_3).6H_2O$, γ-irradiated, free radicals, e.p.r., g-factors 2—10517
- $Zn_{1-x}Cd_xCr_2Se_4$, B-site spinel, exchange integrals detn., Weiss molecular field theory 2—36679
- $Zn_xCd_{1-x}S$:Mn monocrystals, photoluminescence spectra, determ. position of maximum of Mn emission band 2—29999
- $Zn_xCd_{1-x}S$, $0\leqslant x\leqslant 1$, two-photon absorpt. coeff., forbidden band width 2—22780
- $ZnCl_2$, molten, u.s. vel., temp. depend. 2—9128
- $ZnCl_2$, molten, viscosity and supercritical behaviour in binary solutions 2—35744
- $ZnCr_2O_4$ exchange integral determ. from paramag. neutron scatt. obs. 2—22666
- 29wt.%Zn59wt.%Cu-12wt.%Ni alloy, thermomech. treated., strengthening mech. superposition 2—32688
- $Zn_xCu_{1-x}Cr_2O_4$, cryst. distortion, temp. depend. 2—3988
- $ZnF_2:Fe^{2+}$, e.p.r., mag. dipole active lines 2—40555
- $ZnFe_2O_4$, electric field gradients at ^{57}Fe deduced from Mossbauer spectrum in applied magnetic field 2—1671
- $ZnFe_2O_4$, spinel, relaxation of electrical conductivity 2—19533
- $Zn_xFe_{3-x}O_4$, oxygen nonstoichiometry and defect struct. 2—29174
- $Zn_xFe_{3-x}O_{4\|\gamma}$ ferrites, with and without Co impurity, evidence for anisotropy induced near 100°C 2—26053
- $Zn_xFe_{3-x}O_{4-x}F_x$, prep., mag. props. and elec. cond. 2—22695
- $ZnGa_2O_4$, e.s.r., zero-field splittings of Cr^{3+} 2—10501
- $ZnGeAs_2$, reflectivity spectra, energy band struct. correlation 2—10345
- $ZnGeP_2$, band struct., empirical pseudopotential calc. 2—13260
- $ZnGeP_2$, chalcopyrite semiconductor, linear and nonlinear optical properties 2—26100
- $ZnGeP_2$ crystal, thermal expansion coeffs., high temp. X-ray study 2—32844
- $ZnIn_2S_4$, photocond. quenching due to hot electron capture, electric field variation 2—36614
- $ZnIn_2S_4$ and $Zn_3In_2S_6$, thermal oxidation 2—1750
- $ZnIn_2S_4$ and $Zn_3In_2S_6$, refl. spectra, band struct. determ. 2—29898
- ZnMn dilute alloy, thermal expansion in rel. to Kondo effect 2—16063
- $ZnMn_{1.9}Fe_{0.1}O_4$, Jahn-Teller distortion, Mossbauer obs. 2—36829
- $Zn_{0.87}Mn_{0.13}Fe_2O_4$, mag. struct., neutron diffr. obs. 2—36784
- $Zn_xMn_{1-x}Re_2O_4$, antiferro-ferrimag. transition, neutron diffr. obs. 2—4399
- $ZnNb_2O_6$, i.r. absorpt. spectra, cryst. chem. 2—10396
- $Zn_xNi_{1-x}Fe_2O_4$, effect of Dy substitution on props. 2—13413
- ZnO:Li, thermal cond. 2—19471
- $ZnO_2:Nd^{3+}$, absorpt. spectra and emission of Nd^{3+} 2—33269
- $ZnO:V^+$, conversion of trivalent V to divalent ions by heating in Zn vapour, meas. e.s.r. spectra of V^{2+} at low temp. 2—25415
- $ZnO-B_2O_3$ system, borate stability, temp. depend. 2—22368
- $ZnO-Nb_2O_5$ system, phase relations 2—25644
- ZnO-Si, heterojunc., lifht detector, elec. and optical props. 2—10088
- $ZnO-TeO_2-V_2O_5$ glass, variation of physical props. and chemical stability with composition 2—6292
- ZnO, acousto-electric oscillator, effect of uniaxial stress on modes 2—4058
- ZnO, band model interpretation of surface in glow discharge 2—35621
- ZnO, chemisorption of molecular H_2 2—33375
- ZnO, coloured, interstitial Zn conc., ion channelling and blocking obs. 2—19094
- ZnO, crystal growth, by chemical vapour transport in closed system, evaluation of transport agents 2—3576
- ZnO, diffusion of photoelectrically excited electrons, d.c. effect coefficients 2—4294
- ZnO, e.p.r. of Mn^{2+}, elec. field effect, piezoelec. and axial distortions influence 2—22837
- ZnO, electron-beam-pumped, lasing action 2—16611
- ZnO, electrotransmission and Pockels effect 2—7051
- ZnO, F^+ centre, electronic struct. 2—1261
- ZnO, far-i.r. free carrier absorpt. 2—16500
- ZnO, growth of single crystal plates 2—25259
- ZnO, luminesc., band-band recomb. and cond. electron conc. 2—16613
- ZnO, off-axis acoustoelec. domains, Brillouin scatt. 2—4056
- ZnO, one-equivalent adsorbates, intergranular contact resist, surface energy states 2—6840
- ZnO, photoconductor, conductivity enhancement by energy transfer mechanism 2—16317
- ZnO, photoluminesc., mixed-mode excitons, reabsorpt. and exciton diffusion 2—16612

Zinc compounds continued
- ZnO, photon counting distrib. of Brillouin scattered light from amplified vibr. noise 2—13494
- ZnO, physisorption of water, mechanism 2—29074
- ZnO, piezoelectric, ion implantation, monolithic acoustic surface wave amplifier formation 2—29190
- ZnO, polar surfaces, LEED study 2—18924
- ZnO, positron lifetime correlations 2—4150
- ZnO, radiation damage processes 2—19076
- ZnO, Raman spectra, hydrostatic pressure effects, Gruneisen parameters 2—16574
- ZnO, ribbon cryst., orientation, whisker growth obs., X-ray, etching obs. 2—12693
- ZnO, single crysts., anisotropic vaporization rates of opposite basal faces 2—18887
- ZnO, solubility of NiO, X-ray studies, magnetic investigation 2—3962
- ZnO, stimulated emission and excited states of donor electron 2—4481
- ZnO, surface Fermi level anchoring by chemisorbed species e.p.r. study 2—4228
- ZnO, surface phonons, inelastic slow electron scatt. 2—39451
- ZnO, u.v. photoemission obs. of upper d levels 2—25979
- ZnO, zincite, cryst. growth by vapour phase hydrolysis of $ZnCl_2$ 2—35940
- ZnO, Zn 3d states location from u.v. photoelectron spectra 2—36641
- ZnO acoustic transducers, r.f. diode sputtered 2—14269
- ZnO acoustoelectric single crystals, uniaxial pressure effects 2—1429
- ZnO catalyst, chemisorption of CO oxidation reactants, a.c. cond. 2—25830
- ZnO crystal, vaporization kinetics of opposite basal faces, temp. depend. 2—35841
- ZnO electron-beam-pumped, temp.-induced wavelength shift 2—2403
- ZnO electrophotographic papers, sensitization by organic charge transfer complexes 2—40832
- ZnO epitaxy, low temp., of Au 2—9261
- ZnO film, d.c. and r.f. sputtered, struct., elec. and optical props. 2—39536
- ZnO film u.s. transducers for longit. and shear modes, fabrication 2—29549
- ZnO films, sputtered, c-axis orientation, substrate depend. 2—6356
- ZnO single crystal growth rate and morphology under hydrothermal conditions 2—29093
- ZnO surface, electronic, LEED and Auger diagnostics 2—29012
- ZnO whiskers, platelets and dendrites, growth mechanisms 2—12674
- $Zn_5(OH)_8(NO_3)_2$ indexing of X-ray diffr. diagram 2—4460
- $Zn_5(OH)_8(NO_3)_2.2H(D)_2O$ i.r. spectrum, thermal props., thermal analysis 2—4460
- $Zn_5(OH)_8(NO_3)_2.2H_2O$, topotactic reaction with metalchloride solns., prep. of pseudomorphs 2—3579
- $Zn_3P_2-Cd_3As_2$ solid solution, Hall coeff., resist., 300-800K, X-ray analysis, dilatometry 2—19656
- ZnP_2, cathodoluminesc., interband transitions and exciton behaviour 2—26227
- Zn_3P_2 powder, ^{31}P n.m.r. chemical shielding anisotropy at 99.4 MHz 2—10561
- ZnS:Ag,Cl phosphor, luminesc., long decay, trap depth 2—36936
- (ZnS, ZnO):Cu, Cl electroluminors, binderless electroluminescence, carrier injection mechanism 2—29995
- β-$Zn(SCN)_2$, pure and Pb-activated, absorption spectra 2—16501
- ZnSb, p- and n- type, electrical transport values 2—1522
- $ZnSe:Cu,Er^{3+}$, cryst. field at Er^{3+}, LCAO-MO calcs. 2—26096
- $ZnSe:Er^{3+}$, site sensitive excitation mechanisms, photoluminesc. 2—22801
- ZnSe:Ni, two-stage excitation of anti-Stokes luminesc. 2—33311
- ZnSe:Tm, Li, luminesc., absorpt., and Zeeman effect 2—40721
- ZnSe-GaP n-p heterojunction, prep. and I-V characts. 2—29720
- ZnSe-Ge heterojunctions, switching and memory characts. 2—6860
- ZnSe-Ni, absorption spectra, charge transfer band region, bound state formation 2—36889
- ZnSe-ZnCl:Eu, Tb melt, luminescence rel. to investigation of interactions in melt 2—39373
- ZnSe-ZnTe heterojunction, epitaxial growth, green electroluminesc. 2—40735
- ZnSe, band struct. determ. 2—40279
- ZnSe, crystal, photoeffect in electrooptic effect 2—10313
- ZnSe, defect config. for Yb^{3+} and Er^{3+} codoped with Li, Ag and Cu 2—7019
- ZnSe, e.p.r. of Mn^{2+}, elec. field effect, piezoelec. and axial distortions influence 2—22837
- ZnSe, electroluminescence in ZnSe-In junction, reverse biased 2—29996
- ZnSe, electronic structure, empirical pseudopotential method 2—16225
- ZnSe, irrad., wurtzite-zincblende transform. 2—9529
- ZnSe, light emission at n-i junction when forward biased 2—29997
- ZnSe, resonant Raman cancellation 2—16573
- ZnSe, self diffusion of Zn and Se 2—3825
- ZnSe, solubility of Cu_2Se, 700-1000°C 2—36248
- ZnSe, stress-induced shifts of Raman freqs. 2—20057
- ZnSe, u.v. photoemission obs. of upper d levels 2—25979
- ZnSe epitaxial layer, electrooptical quality, growth and props. 2—9290
- ZnSe film, epitaxial deposition on Ge substrate 2—18948
- ZnSe film, epitaxial growth, from vapour, struct., resist., cathodolum. 2—39535
- ZnSe film, twinning probability calc. 2—39525
- ZnSe m.i.s. electroluminescent device, exhibiting switching and memory 2—33327
- $ZnSeO_4.6H_2O:Cu^{2+}$, Co^{2+}, optical activity 2—19966
- $ZnSeO_4.6H_2O:Cu^{2+}$, Ni^{2+}, Co^{2+}, optical activity 2—16420
- $ZnSeO_4.6H_2O$, e.p.r. of hydrated Ni^{2+}, Co^{2+} and Cu^{2+} ions 2_10525
- ZnSe(Te), semiconductor, pulse excited cathodoluminescence, relaxation kinetics, non-radiative recombination 2—7102
- $ZnSiAs_2$, chalcopyrite semiconductor, linear and nonlinear optical properties 2—26100
- $ZnSiF_6:Mn^{2+}$, spin-Hamiltonian higher order parameters, from ENDOR, at 4.2K 2—30028
- $ZnSiF_6.6H_2O$, internal motions, n.m.r. obs., 90-400K 2—40780
- Zn_2SiO_4:Mn, saturated cathodoluminescence, noise and modulation expts. 2—22816
- Zn_2SiO_4, diffusion of Si and Zn 2—32566
- Zn_2SiO_4, willemite, intrinsic cathodoluminescence emission 2—13520
- $ZnSiP_2$, thermal oxidation 2—1750
- $ZnSnAs_2$, electrorefl. spectra, electron transitions 2—20006
- $ZnSnAs_2$ crystal, thermal expansion coeffs. high temp. X-ray study 2—32844

Zinc compounds continued
- $ZnSnP_2$ crystal. thermal expansion coeffs., high temp. X-ray study 2 32844
- $ZnSnSb_2$ crystal. thermal expansion coeffs., high temp. X-ray study 2–32844
- ZnTe:Al, defect levels assignment, elec. transport and photoelectronic props. 2–13244
- ZnTe:Ga, negative photocond., room temp. 2–33078
- ZnTe:In, O, luminesc., self-activated and isoelectronic O emission 2–20106
- ZnTe-CdTe solid solution, negative photocond., room temp. 2–33077
- ZnTe-GaSb, p-p heterojunc., elec. and optical props. 2–10087
- ZnTe, band struct. determ. 2–40279
- ZnTe, Debye temperature, X-ray obs. 2–22426
- ZnTe, electron trapping-detrapping effect in cond. band, hydrogenlike donor obs. 2–13263
- ZnTe, electronic structure, empirical pseudopotential method 2–16225
- ZnTe, exchange splitting in excitons, interatomic distance depend. 2–29903
- ZnTe, interband Faraday effect 2–13435
- ZnTe, interband Faraday effect 2–13436
- ZnTe, interband Faraday rot., low mag. field 2–7049
- ZnTe, stress induced splitting of exciton reflection spectra 2–16477
- ZnTe, u.v. photoemission obs. of upper d levels 2–25979
- ZnTe film, elec. and optical props., stoichiometry depend. 2–25829
- ZnTe film, gas phase deposition 2–35898
- ZnTe film, recrystallization rel. to struct., elec. and optical props. 2–29046
- ZnTe film, twinning probability calc. 2–39525
- α-$Zn_3(VO_4)_2$, crystal structure 2–1230
- $ZnWO_4$, e.p.r. of Co^{2+} pairs 2–1730
- $ZnWO_4$, e.p.r. of Cr^{3+} and Mn^{2+}, linewidth temp. depend., spin- phonon interaction 2–10493
- ZnX, x=chalcogen, d-levels location from u.v. photoemission obs. 2–22658
- $ZnX_2(SO_4)_2.6H_2O:Cu^{2+}$, X=$NH_4$, K, Rb and Cs, sistant ENDOR obs. 2–30031
- Zn_2Y hexaferrite, magnetocalorimetric effect in spherical specimen, 290-450 K 2–10227
- $Zn[AsO_4]OH.H_2O$, legrandite, cryst. struct. 2–19061
- $Zn[Hg(SCN)_4]$ tetragonal crystals, nonlinear freq. conversion with phase matching 2–7035

zinc sulphide
- a.c. electroluminescence, effect of u.v. light, non validity of Fischer model 2–16638
- blue luminescence, excitation and temp. dependence 2–7097
- cathodoluminescence, effect of temp. of u.v. spectra, nature of emissions 2–10453
- cathodoluminescence, thin films, study as function of substrate, temp. at which film deposited 2–13521
- core electron level obs., x-ray induced electron emission obs. 2–19811
- d-levels location from u.v. photoemission obs. 2–22658
- Debye temperature, X-ray obs. 2–22426
- deformed, exciton spectra and exchange interaction 2–29902
- dielectric layers, meas. of dispersion of refractive index by modified interference method 2–13432
- double-band phosphors, X-ray induced enhancement of electroluminescence 2–36965
- elastic and photoelastic consts. of α-phase crysts. 2–25482
- electroluminescence, polytypism effects 2–26253
- electroluminescent layers, vapour-deposited, prep. and props. 2–36963
- electroluminescent quantum yield, in m.i.s.i.m. struct. 2–20121
- electronic structure, empirical pseudopotential method 2–16225
- epitaxial film, prep. by r.f. sputtering 2–29047
- epitaxial film growth, GaAs substrate. gas transport method 2–9289
- epitaxial layer, electrooptical quality, growth and props. 2–9290
- e.p.r. of Cr^+, elec. field effect, piezoelec. and axial distortions influence 2–22837
- e.p.r. of Mn^{2+}. axial impurity site obs. 2–26289
- exciton reflection spectra, effect of stacking faults 2–22752
- F^+ centre, electronic struct. 2–1261
- F-centre stability in additively coloured crystals, e.p.r. study 2–19132
- film, epitaxial, on sapphire, orientation, deposition parameter depend. 2–1188
- film, epitaxial growth, from vapour, struct., resist., cathodolum. 2–39535
- film, evap. quarterwave coating, ruby laser damage threshold 2–27636
- film, monolayer on NaCl, laser irrad., effects rel. to physics of damage 2–29865
- film, on Si, triode r.f. sputtering system 2–32384
- film, rare earth doped, prep. by ion implantation, and luminesc. 2–19119
- film, struct., rel. to sorption behaviour 2–9291
- film, twinning probability calc. 2–39525
- Franz-Keldysh effect, internal fields 2–4438
- growth impurities, optical spectra studies 2–36055
- internal elec. field mapping 2–25965
- luminescence, effects of Zn displacement 2–33326
- nonlinear susceptibility to harmonic generation rel. to microstructure 2–1653
- phase transformation, effect of polytypism, X-ray oscill. obs. 2–25351
- phosphor, low temp. stimulation by elec. field 2–26252
- phosphor, photodielectric effect response 2–10144
- phosphors, effect of adding NaCl and preliminary heating in H on thermoluminescence 2–16631
- photoluminescence, elec. field quenching mechanism 2–36935
- polytypes, disordered, probability of layer superposition 2–9498
- polytypes, genesis and relative abundance 2–6454
- polytypes, with number 1 in their Zhdanov symbols 2–22166
- polytypes relative abundance 2–9497
- polytypism and phase transformations, Cu doping effects 2–25350
- population inversion, electrolum. excitation, impurity impact excitation 2–13524
- powder layer, rare-earth activated, d.c. electroluminesc. 2–10455
- Raman scattering, resonant cancellation 2–16573
- Raman spectra, hydrostatic pressure effects, Gruneisen parameters 2–16574
- Raman spectra at high press., phase transform. investig. in hexagonal phase 2–22781
- rare earth doped, electro- and photoluminesc. 2–40737
- resonant Raman scattering, by selected phonons in hexag. single cryst. 2–16572

Zinc compounds continued

zinc sulphide continued
- thermally stimulated voltaic effects and luminescence, role of traps and luminescence centres 2–16301
- thin section prep. by fracture-extraction technique 2–6414
- trap centre properties, conduction and thermoluminescence study 2–20112
- X-ray L_{23} spectra of quantum efficiency of S photoemission 2–26204
- X-ray $L_{II,III}$ emission spectra, ESCA technique 2–36919
- X-ray $L_{II,III}$ photoemission spectra, fine structure study 2–36909
- Cu activated, photoelectret properties, surface charge and depolarization current studies 2–36604
- (Zn,Cd,Hg)S:Cu,In electroluminor, electrolum., radiation enhancement 2–36968
- $Zn_xCd_{1-x}S$:Ag,Ni, photoluminescence mechanism, energy band model 2–4480
- ZnS: $AgAlS_2$ luminescence, thermal and i.r. stimulation 2–29958
- ZnS: $CuAlS_2$ luminescence, thermal and i.r. stimulation 2–29958
- ZnS:Ag, luminescence from donor-acceptor transitions, noise and modulation 2–22815
- ZnS:CdS;Ag:Ni:Co phosphors, beta-ray irradiation, radiothermoluminescence 2–40730
- ZnS:Co^{2+} phosphors, Cu and Ag activated, thermoluminescence 2–29989
- ZnS:Cu, Cl film, l.v. electroluminesc. 2–40726
- ZnS:Cu, Cl film, optical and elec. switching of dark cond., and photocond. at 77K 2–40380
- ZnS:Cu, electrolum., impurity conc. and firing temp. effects 2–36964
- ZnS:Cu, electroluminesc., nature of luminous regions, dislocation theory 2–40736
- ZnS:Cu, phosphoresc. mechanisms 2–33322
- ZnS:Cu, photoluminesc. quenching by secondary rad., dynamic theory 2 26226
- ZnS:Cu, ruby laser induced luminescence flash 2–7096
- ZnS:Cu, temp. effect on electrolum. decay 2–20120
- ZnS:Cu,Cl phosphor electrolum., charged imperfections effects 2–36967
- ZnS:Cu luminescence decay, study by ion pulse excitation 2–22802
- ZnS:Cu luminophors, stimulated by varying energy photons, spectral props of stimulated emission 2–4497
- ZnS:Ga, luminescence and photoconductivity, description by donor-acceptor pair model 2–29957
- ZnS:I, low voltage electrolum., due to acoustoelectric instability 2–36966
- ZnS:Mn, elec. cond., temp. depend. and impurity effects 2–13243
- ZnS:Mn, high symmetry pts. in Brillouin zone 2–19361
- ZnS:Mn^{2+}, effect of spin-orbit and spin-spin interaction on Mn^{2+} $^4E(G)$ level 2–29853
- ZnS:Ni, ion-hole complexes formed in charge exchange between impurities 2–29956
- ZnS:Ni^+, e.p.r., g-factor and hyperfine struct. 2–30016
- ZnS:Tb^{3+} films, hot- electron impact excitation of electroluminesc. 2–16637
- ZnS:TbF_3 films, electroluminesc. 2–13455
- ZnS:Tm^{3+}, cathodoluminesc. efficiency 2–1718
- ZnS-GaP n-p heterojunction, prep. and I-V characts. 2–29720
- ZnS-Mn-phosphors, temp. depend. of X-ray luminescence obs. 2–29968
- ZnS-Ni, absorption spectra, charge transfer band region, bound state formation 2–36889
- ZnS layers, absorption spectra meas. in 3.1-5.2 eV region, obs. characteristic absorption 2–29921

Zirconium
- α and ω types, pressure dependence of superconducting transition temp. above 60 kb 2–32928
- arc emission spectroscopic obs. of content in Pb-Bi eutectics used as liquid metal coolants 2–16703
- corrosion in steam, 325-700°C, rate law 2–20191
- deformation of notched bend specimens, comparison of finite element and experimental studies 2–9666
- deformed, resistometric recovery above room temp. 2–36219
- electron diffraction analysis using four axis hexagonal reciprocal lattice 2–3741
- embrittlement by hydrogen, effect of plastic props. 2–29311
- glow discharge deposition, on steel and W fine wires 2–3525
- martensite transformation, shape memory effect 2–9789
- neutron irradiation, rel. to void formation 2–32494
- phonon spectra and heat capacity 2–32816
- plastic deformation, role of dislocations with (c+a) type Burgers vectors 2–36123
- polycrystal, hydrostatic pressure effects on flow stress 2–39802
- polygonization of cold rolled material, recrystallization and recovery, electron microscopy 2–6502
- precipitation of zirconium hydride, struct. rel. to heat treatment 2–22369
- recovery after deformation at 78 K, resist. obs. 2–15911
- in steel, austenitic stainless, effect on stress corrosion cracking 2–29326
- stressed, age hardening, rel. to O_2 diffusion, Fe impurity 2–12786
- texture and anisotropy rel. to plastic deformation 2–15892
- two dimensional crystal, growth and surface migration on Nb and W 2–18947
- CaS:Zr, Mn phosphor, luminesc. emission spectra, luminesc. mech. 2–36925
- Cu alloys, effect of Zr on rolling and annealing texture 2–3946
- inCu alloys, effect on struct., elec. cond. and hardness 2–9715
- α-Zr, diffusion, stress induced, of O, internal friction meas. 2–32567
- α-Zr, diffusion, stress induced, of O 2–32568
- α-Zr, internal friction, deform. peaks 2–1281
- α-Zr, post-deform. ageing kinetics, rel. to oxygen diffusion 2–9747
- α-Zr, substruct. strengthening 2–12953
- α-Zr, thermally oxidised, autodiffusion of O, meas. by obs. nuclear reaction $^{18}O(p,\alpha)^{15}N$ 2–12818
- Zr V, ionization pot. and Rydberg series 2–15219
- Zr V resonance-line spectrum in the vacuum u.v. 2–18312

Zirconium compounds
- alloy, fracture in I_2 vapour, 250-510 C, annealing effect 2–6583
- alloy, high temp. diffusion, rel. to creep deform. 2–12875
- alloy, high-strength, for reactor press. tube appl. 2–39945
- alloy, radiation enhancement of oxidation 2–13580
- alloy, rate of deposition of corrosion products on surface as function of coolant compos., temp., irradiation and exposure time 2–31625
- anodic oxide film, Zircaloy 2 substrate, elec. breakdown 2–10113
- Luna 16 fines, conc. 2–20662

Zirconium compounds continued
- alkyl orthozirconates, magnetic susceptibility, magneto-optical dispersion and rotation determ. 2—6940
- oxides, $Ln_2O_3.2ZrO_2$, synthesis and cryst. struct. 2—36284
- oxycarbides and oxynitrides, temp. dependence of lattice parameters, thermal expansion 2—29562
- Zircalloy-2, cold-rolled, microstruct. 2—29185
- zircalloy-2 reactor pressure tubes, creep limit in design 2—5751
- Zircaloy, fuel claddings and pressure tubes in water cooled reactors 2—18257
- Zircaloy, stress corrosion cracking in iodine vapour 2—15114
- Zircaloy, tetraongal hydride precipitation, elec. diffr. obs. 2—9828
- Zircaloy tubing, hydride platelets orientation and effect on mech. props. 2—15842
- Zircaloy tubing, in-pile corrosion and hydrogen pick-up 2—11907
- Zircaloy tubing, influence of reduction values on texture formation 2—25569
- zircaloy-2, cold worked, 300-450°C, creep accel. mechanism 2—25510
- Zircaloy-2, corrosion and hydriding in BWRs 2—15113
- Zircaloy-2, diffusion of Ni and Sn 2—12817
- zircaloy-2, effect of neutron irradiation on tangential and axial elastic limits 2—11900
- Zircaloy-2, embrittlement by hydrogen, effect of plastic props. 2—29311
- Zircaloy-2, encapsulator for ^{252}Cf compared to stainless steel 2—549
- zircaloy-2, precipitation of zirconium hydride, struct. rel. to heat treatment 2—22369
- Zircaloy-2, radiation enhancement of oxidation 2—13580
- zircaloy-2(-4), surface phenomena, rel. to mech. and chem. props., Auger spectroscopy obs. 2—39472
- zirconia, solid electrolyte, n-type cond. 2—22542
- zirconia, stabilized, applic. to thermal probe construction 2—27331
- zirconia ceramics, porous, impregnation by Pt-Au resinate coatings in prep. Pt-Au films 2—1182
- Al-Zr, precipitation of cubic Al_3Zr phase 2—36273
- Al-Zr alloy, recovery and recrystallization after cold working at liq. N_2 temp. 2—15912
- Cr-Zr-Nb-C alloy, stress rupture and ductility control by microstruct. modification 2—9692
- Cu-Zr-Cr alloys, role of Cr and Zr on rolling and annealing texture 2—3946
- Fe-Cr-Zr system, α-γ-δ type polymorphism 2—4018
- Hf-2.1%Zr, bulk self diffusion of ^{181}Hf 2—32563
- Hf,Zr)V_2 alloys, supercond. transition temp. correl. with lattice instabilities 2—32937
- MnO-FeO-ZrO_2-SiO_2 phase equilibria, liquidus temp. region, quenching technique 2—13012
- Nb-(25 at.%)Zr, Joule-heating power dissipation in hollow tube 2—36461
- Nb-Zr alloy, high-field superconductor, pulsed- field meas. rel. to metallurgical processes 2—25790
- Nb-25%Zr, supercond., low field critical current density from magnetiz. data 2—22502
- Nb-25%Zr, type II supercond., crit. current density, neutron irrad. effects 2—29631
- Nd^{3+}:$POCl_3$:$ZrCl_4$ liq. laser, Q-switched, output characts. 2—7928
- Ni/ZrO_2 composite, dispersion strengthening 2—12874
- Ni-Zr alloy, solidified at fast cooling rates, metastable phases 2—36305
- $POCL_3$—$ZrCl_4$:Nd^{3+}, liquid laser system 2—27497
- (Pb,Zr)TiO_3 transducers, fund. modes 2—29519
- $PbO+ZrO_2+TiO_2$, high temp. reaction kinetics 2—13571
- Pt-Rh-Zr alloys, internal oxidation and hardness 2—4591
- Ti-Al-Sn-Zr-Mo alloy, tensile props. rel. to microstruct. 2—39942
- Ti-Zr-O alloys, phase characterisation 2—40009
- Ti_2ZrO alloy, crystal structure of $\omega'(0)$ phase 2—39653
- U-Mo-Nb-Zr alloys, phase transformations, carbide inclusions effect 2—13004
- U-Nb-Zr alloy, γ^0 phase domain struct. 2—9495
- U-Nb-Zr alloy, oxidation and temp. cycling, flexure study 2—10627
- U-Nb-Zr alloy, stress corrosion cracking, effect of Cl^- 2—29331
- U-Nb-Zr system, kinetics of transform. of γ phase 2—36309
- UC-ZrC solid solns. cubic lattice parameter var. with temperature and composition 2—15733
- $Y_{0.16}Zr_{0.4}B_{12}$, high temp. enthalpies 2—19274
- Zn-Nb alloy, $\beta \to \omega$ transform., u.s., elastic consts., and X-ray studies 2—40014
- Zr-Al solid soln., supersatured, fan-shaped precip. form. during decomposition 2—32719
- Zr-C alloy, C surface migration rel. to chemisorption and precipitation 2—9252
- Zr-Co, bonding and ordered state formation, X-ray spectral investigation of electronic energy spectrum 2—36920
- Zr-Cr alloy, corrosion in steam, 325-700°C, rate law 2—20191
- Zr-Cr alloy, lattice strain, crystallite size and hardness 2—22291
- Zr-H system, spin-lattice relax., electronic contrib., spin echo method 2—16405
- Zr-(3 wt.%)Mo-(1 wt.%)Al alloy, thermal decomposition, Al effect 2—25640
- Zr-Nb alloy, hydrogenation and fatigue failure 2—29303
- Zr-Nb alloy, martensitic transform. 2—9827
- Zr-Nb alloy, supercond. wires, critical current density control by dislocation substruct. 2—40209
- Zr-Nb carbides, nonstoichiometric, thermodynamic model allowing for comp. depend. of parameters 2—25603
- Zr-(2.5 wt.%)Nb alloy, age hardening 2—12952
- Zr-Pu dilute alloy, $\beta \to \alpha$ transform., crystallographic study 2—29483
- Zr-Sn solid soln., substruct. strengthening 2—12953
- Zr-Ti-Mo, alloy, forming process behaviour, corrosion and oxidation resist. rel. to Al content 2—29411
- 2.5 wt.%Zr-7.5 wt.%Nb-U alloy, elastic consts. rel. to press. 1 bar-18 kbar 2—32580
- $Zr(As,P)_2O_7$ solid solns., As and P distrib. obs. 2—9499
- $Zr_xAs_yO_z$, density, chem. formula and lattice consts. 2—22169
- $Zr_xAs_2S(Se)$, density and lattice consts. 2—22168
- ZrB_2/liquid steel system, destruction of ZrB_2 2—10625
- ZrB_2-W, powder mixture, sintering, solid solution formation, phases 2—6626
- ZrB_2-W alloy, struct. and props. after sintering 2—12950
- ZrB_{12}, supercond. isotope effect due to optical phonon modes 2—6782
- ZrB_{12}, thermal expansion, in range 78-1300°K 2—6684
- ZrB_2, powder, supersonic grinding kinetics 2—15939
- ZrB_2, thermal expansion over temp. range 300-2500°K 2—6683

Zirconium compounds continued
- ZrB_2 single crystal, plastic deform. 2—15841
- ZrC-NbC, high porosity complex carbide prep. 2—39969
- ZrC-W composite with covering of vacuum deposite W, rate of evaporation from open surface 2—32748
- ZrC-ZrO_2 system, oxycarbide crystal struct. 2—29155
- ZrC-ZrO_2 system, oxycarbide stability 2—29499
- ZrC-graphite alloy, prep. and thermoemissive props. 2—1343
- ZrC, band structure, tight binding method 2—4124
- ZrC, diamond grinding, surface work hardening, microstructure 2—3871
- ZrC, elec. and mag. props. rel. to electronic structure 2—1523
- ZrC, emissivity at high temps. 2—6694
- ZrC, powder, supersonic grinding kinetics 2—15939
- ZrC, sintered, polycryst. props. rel. to monocryst. props. 2—22254
- ZrC, slip system determination by hardness anisotropy 2—9564
- ZrC, X-ray spectra, energy band struct. 2—40706
- ZrC_x, shocked, microcrack form. and plastic deform. 2—29328
- $ZrCl_6^{2-}$, force constants and mean amplitudes of vibration 2—3035
- $ZrCr_2$, wave dispersive electron beam microanalysis and energy dispersive scanning microscopy 2—22167
- ZrF_4-LiF-BeF_2, molten, diffusion of Ni, coeff. determ. by linear sweep voltammetry and chronopotentiometry 2—18810
- ZrFeGe, ZrRhGe, ZrPdGe, ZrRuSi, struct. relns. 2—18969
- $ZrGeO_4$, thermal expansion, rel. to cryst. chemistry 2—22430
- ZrH, magnetoresistance, Hall effect, field and H content depend. 2—6824
- ZrH_n, n=1.0-1.9, spin-spin, spin-lattice relax. times temp. depend., H self-diffusion, spin echo obs. 2—16402
- ZrH_x, fast neutron irrad. induced swelling 2—36014
- ZrMGe, M=Fe, Rh, Pd, cryst. chemistry 2—9349
- ZrN, diffusion of C, temp. depend. 2—39750
- ZrN_x, $NK\alpha$ X-ray emission band, band struct. and bonding 2—20088
- Zr-25%Nb fuel claddings and pressure tubes in water cooled reactors 2—18257
- ZrO_2:Er^{3+}, Y_2O_3 stabilized, oxygen ion co-ordination, absorp. spectra obs. 2—33277
- ZrO_2-CaO solid-electrolyte fuel cells, overpotential 2—11419
- ZrO_2-Cr_2O_3(-CaO), electrodiffusion, electronic defect model, point defects. colour centres, elec. cond. meas. 773-1273K 2—9630
- ZrO_2-Gd_2O_3, phase transformations, d.t.a. and X-ray diffr. obs. 2—9840
- ZrO_2-Ln_2O_3, phase transformations, phase diagrams, structure, thermal analysis, X-ray obs. 2—4008
- ZrO-Nb_2O_5, ceramic semiconductor, electrical properties, influence of Nb_2O_5 percentage 2—6793
- ZrO_2-Nd_2O_3 system, solid soln. and compound formation 2—29495
- ZrO_2, anodic layers, photoluminesc. 2—26228
- ZrO_2, CaO stabilized, ionic cond., lower P_{o2} limit, temp. range 1000-1400C 2—33053
- ZrO_2, cathode, in fuel cell coated with SnO_2/Sb_2O_3, voltage current characteristics 2—23493
- ZrO_2, deform. characts., rel. to chem. bonding, X-ray line broadening obs. 2—32493
- ZrO_2, dispersion strengthening of Ni 2—39902
- ZrO_2, electron hole mobility, elec. cond., thermogravimetric and Seebeck coeff. obs. 2—10017
- ZrO_2, film, gaseous anodization, elec. and optical props. 2—13301
- ZrO_2, growth from gel, positron lifetime spectra study 2—39580
- ZrO_2, metastable cubic phase, X-ray diffr. powder pattern 2—12739
- ZrO_2, milled zirconia, monoclinic-tetragonal transformation, particle size effects 2—29484
- ZrO_2, nonstoichiometric, thermogravimetric data, rel. to carrier conc. 2—29448
- ZrO_2, positron lifetime correlations 2—4150
- ZrO_2, solid state electrolyte cells, applications 2—40820
- ZrO_2 dispersion reinforced Cu, mech. props., prod. technique depend. 2—1341
- ZrO_2 electrodes stabilised with Y_2O_3, electrode potential falls and resistance in flow of ionized gas 2—28479
- ZrO_2 rare earth neutron poisons, X-ray excited optical fluorescence 2—4506
- $ZrO_2.12Nb_2O_5$, polymorph characterization, structure and intergrowth obs. 2—9500
- Zr_3P, Knight shift, spin lattice relaxation, conduction process 2—4559
- Zr_7Pt_{10} and Zr_9Pt_{11}, cryst. struct. 2—25352
- Zr_9S_2, and other metal-rich refractory sulphides, significance of Kasper polyhedra 2—9351
- $ZrS_2(Se_2)$, band struct. 2—36417
- $ZrSiO_4$, thermal expansion, rel. to cryst. chemistry 2—22430
- $ZrZn_2$, cubic Laves phases, electronic struct. 2—6729
- $ZrZn_2$, electronic struct., reflectivity spectra 2—40650
- $ZrZn_2$, ferromag., variation of Curie temp. as function of hydrostatic pressure 2—10192
- $ZrZn_2$, low temp. heat capacity anomaly 2—40079
- Zr—Cu, Zr-Cu—M alloys, (M=Mo, Ni, Cr), structural transforms. on continuous cooling 2—1391
- Zr—(3 wt.%)Mo-(1 wt.%)Al, tempering of strain induced martensitic phase. struct. and morphology 2—25639

Zodiacal light
- Gegenschein, optical methods obs., review 2—7301
- optical methods obs., review 2—7301

Zonal heating *see Atmosphere/thermodynamics*

Zone melting and refining
- heating arrangement, electrical induction 2—22325
- ingot, temp. field calc. 2—9361
- liquid inclusion movement in crystals under temperature gradient, theory 2—18996
- rare earth orthoferrites, growth by floating zone method 2—22113
- refractory compounds, review 2—39576
- AlMg alloy, crystallization, liquid zone velocity 2—18882
- Cd, purification for CdTe crystal growth 2—35948
- CdTe, purification by vertical zone melting after synthesis in Bridgman furnace 2—35950
- GaP, Zn impurity distrib. 2—1258
- GaSb, Fe and Co impurity distrib. 2—25274
- Ge, temp. field determ., comparison with theory 2—9361
- InSb, Fe and Co impurity distrib. 2—25274
- PbSn, alloy, composite struct., growth by zone melting 2—22112
- Sb, and Sb-Bi alloys, growth and dislocation etching 2—39589
- Te, purification for CdTe crystal growth 2—35948

Zone plates *see Diffraction/light*

Zoology
biological cells model, light scattering from coated spheres 2—30654

CLASSIFIED LIST OF SUBJECT INDEX HEADINGS

The headings are grouped into sections on the same basis as the arrangement of the abstracts in the fortnightly issues of Physics Abstracts. A summary of the layout of these sections (these are actually further subdivided), is given below. Each section lists the headings which concern its subject and it follows that many of the headings are listed in several places.

SUBJECT SECTIONS

01.00	GENERAL
02.00	MATHEMATICAL PHYSICS
03.00	MECHANICS. ELASTICITY. VIBRATION. ACOUSTICS
04.00	HEAT. THERMODYNAMICS
05.00	ELECTROMAGNETISM
06.00	ELECTRODYNAMICS & PARTICLE OPTICS
07.00	QUANTUM ELECTRONICS. QUANTUM OPTICS
08.00	OPTICS
09.00	QUANTUM FIELD THEORY
10.00	ELEMENTARY PARTICLES
11.00	ELEMENTARY PARTICLE & NUCLEAR MEASUREMENT
12.00	NUCLEAR PHYSICS
13.00	ATOMIC & MOLECULAR PHYSICS
14.00	FLUIDS
15.00	CHANGE OF STATE
16.00	SOLID-STATE STRUCTURE & MECHANICAL PROPERTIES
17.00	SOLID-STATE ELECTRICAL & MAGNETIC PROPERTIES
18.00	SOLID-STATE SPECTROSCOPY & OPTICAL PROPERTIES
19.00	PHYSICAL CHEMISTRY
20.00	GEOPHYSICS
21.00	ASTROPHYSICS
22.00	BIOPHYSICS
23.00	LABORATORY & EXPERIMENTAL TECHNIQUES

01.00 GENERAL

- Biographies
- Collections of physical data
- History
- Laboratories
- Laboratory apparatus and technique
- Nomenclature and symbols
- Physics
- Physics fundamentals
- Reviews

01.10 EDUCATION

- Biographies
- History
- Laboratories
- Laboratory apparatus and technique
- Physics
- Physics fundamentals
- Reviews
- Teaching demonstrations

01.20 UNITS. MEASUREMENT AND METROLOGY

- Acceleration measurement
- Anemometers
- Angle measurement
- Angular velocity measurement
- Area measurement
- Balances
- Constants
- Density measurement
- Dimensions
- Force measurement
- Instruments
- Interferometry
- Length measurement
- Manometers
- Measurement errors
- Mechanical measurement
- Micrometry
- Nomenclature and symbols
- Particle size
- Pressure measurement
- Recording
- Standards
- Strain gauges
- Stroboscopes
- Surface measurement
- Thickness measurement
- Time interval measurement
- Time measurement
- Units
- Vapour pressure measurement
- Velocity measurement
- Volume measurement

02.00 MATHEMATICAL PHYSICS

- Algebra
- Differential equations
- Equations
- Field theory, classical
- Fluctuations
- Fourier analysis
- Functions
- Geometry
- Green's function methods
- Group theory
- Hysteresis
- Information theory
- Integral equations
- Integrals
- Mathematics
- Matrices
- Probability
- Radiation
- Relaxation
- Series
- Space-time configurations
- Statistical analysis/applications
- Tensors
- Transformations, mathematical
- Vectors
- Waves

02.10 GRAVITATION AND RELATIVITY

- Gravitation
- Gravitational collapse
- Gravitational waves
- Red shift
- Relativity/
  - general
  - special
  - unified field theories
- Space-time configurations
- Tachyons

02.20 QUANTUM THEORY

- Collision processes
- Dispersion relations
- Indeterminacy
- Parity
- Perturbation theory
- Quantum electrodynamics
- Quantum theory/
  - application methods
  - quantisation
  - wave equations
- Scattering

02.30 STATISTICAL PHYSICS

- Boltzmann equation
- Brownian motion
- Electron gas
- Fluctuations
- Hysteresis
- Information theory
- Ising lattices and models
- Kinetic theory
- Lattices, theory and statistics
- Many-body problems
- Mass transfer
- Probability
- Quantum fluids/
  - boson systems
  - fermion systems
- Quantum theory
- Quasi-particles
- Radiation
- Radiative transfer
- Random processes
- Relaxation
- Statistical analysis/
  - applications
- Statistical mechanics/
  - quantum
- Thermodynamics
- Transport processes

02.40 MATHEMATICAL AND COMPUTATIONAL METHODS

- Calculation
- Computer applications
- Graphs
- Nomograms
- Statistical analysis/
  - applications
- Tables, mathematical

03.00 MECHANICS. ELASTICITY. VIBRATION. ACOUSTICS

- Oscillations
- Vibrations
- Waves

03.10 MECHANICS

- Ballistics
- Centrifuges
- Dynamics
- Friction
- Gravitation
- Gyroscopes
- Impact
- Kinematics
- Mechanics
- Pendulums
- Pressure
- Rockets
- Rotating bodies
- Torsion
- Velocity

03.15 RHEOLOGY, ELASTICITY AND PLASTICITY

- Bending
- Compressibility
- Damping
- Deformation
- Elastic deformation
- Elasticity
- Photoelasticity
- Plastic deformation
- Plasticity
- Relaxation
- Rheology
- Stress analysis
- Stresses, internal
- Thermoelasticity
- Viscoelasticity

03.30 VIBRATIONS AND ELASTIC WAVES

- Damping
- Elastic waves
- Magnetoelastic waves
- Membranes
- Oscillations
- Piezoelectric oscillations
- Relaxation
- Resonators
- Seismic waves
- Shock waves/
  - effects
- Vibrating bodies
- Vibrations/
  - excitation
  - measurement
- Waves

03.40 ACOUSTICS

- Absorption/
  - acoustic waves
  - acoustic waves, ultrasonic
- Acoustic analysis
- Acoustic generators
- Acoustic impedance
- Acoustic radiators
- Acoustic receivers
- Acoustic resonators
- Acoustic streaming
- Acoustic wave amplification
- Acoustic wave propagation/
  - ultrasonic
- Acoustic waves/
  - effects
- Acoustical laboratories
- Acoustical measurement
- Acoustics/
  - musical
- Acoustoelectric effects
- Architectural acoustics
- Atmospheric acoustics
- Biological effects of radiations
- Chemical effects of radiations/
  - acoustic waves
- Diffraction/
  - acoustic waves
  - acoustic waves, ultrasonic
- Diffusion/
  - acoustic waves
- Dispersion, acoustic/
  - ultrasonic
- Doppler effect
- Echo
- Helium/
  - liquid, sound propagation
- Holography
- Intensity measurement/
  - acoustics
- Interference/
  - acoustic waves
- Interferometers/
  - acoustic waves
- Interferometry/
  - acoustic waves
- Magnetoacoustic effects
- Microphones
- Musical instruments
- Noise/
  - acoustic
- Noise abatement
- Physical effects of radiations
- Radiation pressure
- Recording
- Reflection/
  - acoustic waves
  - acoustic waves, ultrasonic
- Refraction/
  - acoustic waves
  - acoustic waves, ultrasonic
- Refractories
- Reverberation
- Scattering/
  - acoustic waves
  - acoustic waves, ultrasonic
- Schlieren systems
- Sound ranging
- Sound reproduction
- Speech
- Stroboscopes
- Transducers
- Transmission/
  - acoustic waves
  - acoustic waves, ultrasonic
- Ultrasonics
- Velocity/
  - acoustic waves
  - acoustic waves, ultrasonic
- Velocity measurement/
  - acoustic waves
  - acoustic waves, ultrasonic

03.50 SHOCK WAVES

- Detonation
- Exploding wires
- Explosions/
  - nuclear
- Schlieren systems
- Shock tubes
- Shock waves/
  - effects
- Supersonic flow

04.00 HEAT. THERMODYNAMICS

- Annealing
- Bolometers
- Calorimeters
- Calorimetry
- Combustion
- Conductivity, thermal
- Convection
- Cooling
- Emissivity
- Entropy/
  - properties of substances
- Equations of state/
  - gases
  - liquids
  - solids
- Flames
- Heat
- Heat conduction
- Heat transfer
- Heat treatment
- Heating
- High-temperature phenomena and effects
- Joule-Thomson effect
- Latent heat
- Pyrometers
- Radiation/
  - heat
- Radiation detectors
- Radiation pressure
- Radiation transfer
- Specific heat
- Temperature
- Temperature distribution
- Temperature measurement/
  - spectral methods
- Thermal expansion
- Thermal measurement
- Thermocouples
- Thermodynamic properties
- Thermodynamics/
  - applications
- Thermometers/
  - resistance
- Thermostats

05.00 ELECTROMAGNETISM

- Eddy-currents
- Electromagnetism
- Electromagnetic fields
- Electromotive force
- Inductance

05.10 ELECTROMAGNETIC WAVES AND OSCILLATIONS

- Absorption/
  - electromagnetic waves
- Amplifiers
- Diffraction/
  - electromagnetic waves
- Diffusion/
  - electromagnetic waves
- Doppler effect
- Electromagnetic oscillations
- Electromagnetic wave propagation/
  - atmosphere
  - ionosphere
  - guided waves
- Electromagnetic waves/
  - radiators
- Interference/
  - electromagnetic waves
- Interferometers/
  - electromagnetic waves
- Interferometry/
  - electromagnetic waves
- Light/
  - electromagnetic theory
- Microwave techniques and devices
- Plasma/
  - electromagnetic wave propagation
- Radiation
- Reflection/
  - electromagnetic waves
- Refraction/
  - electromagnetic waves
- Scattering/
  - electromagnetic waves

05.20 RADIOFREQUENCY SPECTROSCOPY. MAGNETIC RESONANCES

- Acoustic paramagnetic resonance
- Antiferromagnetic resonance
- Cyclotron resonance
- ENDOR
- Ferrimagnetic resonance
- Ferroacoustic resonance
- Ferromagnetic relaxation
- Ferromagnetic resonance
- Magnetic resonance and relaxation
- Nuclear magnetic resonance and relaxation/
  - measurement
- Nuclear quadrupole resonance
- Paramagnetic resonance and relaxation/
  - measurement
- Spectra
- Spectrometers, radio frequency
- Spectroscopy, radio frequency

05.30 ELECTRICAL QUANTITIES AND THEIR MEASUREMENT. CIRCUITS

- Acoustoelectric effects
- Amplifiers
- Breakdown, electric
- Circuits
- Conductivity, electrical/
  - measurement
- Contacts, electrical
- Counting circuits
- Current, electrical
- Dielectric devices
- Dielectric measurement
- Dielectric phenomena
- Eddy-currents
- Electrets
- Electric charge
- Electric fields/
  - effects
- Electric strength
- Electrical machines
- Electrical measurement
- Electrical properties of substances
- Electrokinetic effects
- Electroluminescence
- Electromotive force
- Electron density
- Electron gas
- Electrons
- Electro-optical effects
- Electrophoresis
- Electrostatics
- Electrostriction
- Ferroelectric phenomena
- Fluctuations
- Hall effect
- High-voltage techniques
- Hysteresis
- Image convertors and amplifiers
- Inductance
- Magnetoelectric effects
- Magnetoresistance
- Noise, electrical
- Oscillators
- Permittivity
- Photoconductivity
- Photoelectricity
- Photoelectromagnetic effects
- Photovoltaic effects
- Piezoelectric oscillations
- Piezoelectricity
- Piezoresistance
- Plasma/
  - diagnostics
- Pyroelectricity
- Rectifiers
- Relaxation
- Semiconductors
- Skin effect
- Space charge
- Superconductivity
- Thermocouples
- Thermoelectricity
- Triboelectricity

05.35 DIRECT CONVERSION

- Electricity, direct conversion/
  - fuel cells
  - magnetohydrodynamics
  - solar cells
  - thermionic

05.40 MAGNETISM

- Antiferromagnetism
- Compasses
- de Haas-van Alphen effect
- Demagnetisation
- Diamagnetism
- Ferrimagnetism
- Ferromagnetism/
  - spin-wave theory
- Films, solid/
  - magnetic properties
- Gyromagnetic effect
- Gyromagnetic ratio
- Hall effect
- Magnetic devices
- Magnetic field measurement
- Magnetic fields/
  - effects
- Magnetic measurement
- Magnetic permeability
- Magnetic resonance and relaxation
- Magnetism
- Magnetisation process
- Magnetisation state
- Magnetoacoustic effects
- Magnetoelectric effects
- Magnetomechanical effects
- Magneto-optical effects
- Magnetoresistance
- Magnetostriction
- Magnetothermal effects
- Magnets
- Paramagnetism
- Storage devices

06.00 ELECTRODYNAMICS AND PARTICLE OPTICS

- Electrodynamics
- Electrohydrodynamics
- Energy loss of particles
- Particle beams
- Particle optics
- Particle velocity analysis
- Scattering, particles

06.10 ELECTRON BEAMS, ELECTRON OPTICS AND TUBES

- Anodes
- Electrodes
- Electron beams/
  - effects
- Electron density
- Electron diffraction
- Electron gas
- Electron lenses/
  - electrostatic
  - magnetic
- Electron microscopes
- Electron microscopy
- Electron optics
- Electron tubes
- Electrons/
  - absorption
  - ionisation
  - radiation
  - scattering
- Fluctuations
- Gas-discharge tubes
- Image convertors and amplifiers
- Noise, electrical
- Photomultipliers
- Space charge

06.20 ION BEAMS, ION OPTICS AND SOURCES

- Field ion microscopy
- Ion beams/
  - effects
- Ion microscopes
- Ion optics
- Ion sources
- Ion velocity
- Ions/
  - recombination
  - scattering
- Sputtering

07.00 QUANTUM ELECTRONICS. QUANTUM OPTICS

- Light/
  - coherence
- Optical pumping
- Photons
- Q-switching
- Quantum optics

07.10 MASERS

- Amplifiers
- Masers
- Optical pumping
- Q-switching

07.20 LASERS

- Amplifiers
- Lasers
- Light/
  - coherence
- Optical pumping
- Q-switching
- Resonators

07.23 Gas and Liquid Lasers

- Amplifiers
- Lasers/
  - gaseous
  - liquid
- Light/
  - coherence
- Optical pumping
- Q-switching

07.25 Solid Lasers

- Amplifiers
- Lasers/
  - semiconductor
  - solid
- Light/
  - coherence
- Optical pumping
- Q-switching

07.27 Laser Beam Optics. Holography

- Holography
- Laser beams/
  - applications
  - effects
- Light/
  - coherence
  - modulation
- Q-switching

08.00 OPTICS

- Doppler effect
- Electro-optical effects
- Light/
  - electromagnetic theory
  - modulation
- Light sources
- Nonlinear optics
- Optics
- Photons
- Photophoresis
- Radiation
- Radiation pressure
- Velocity/
  - light
- Velocity measurement/
  - light

08.10 GEOMETRICAL OPTICS

- Aberrations, optical
- Dispersion, optical
- Lenses/
  - aspherical
  - photographic
- Mirrors
- Optical images
- Optical systems
- Optics/
  - geometrical
- Prisms, optical
- Reflection/
  - light
- Refraction/
  - light
- Refractive index/
  - light
- Resolving power, optics
- Schlieren systems

08.20 PHYSICAL OPTICS

- Absorption/
  - light
- Diffraction/
  - light
- Diffraction gratings
- Diffusion/
  - light
- Dispersion, optical
- Doppler effect
- Double refraction/
  - flow
  - mechanical
- Electro-optical effects
- Ellipsometry
- Filters, optical
- Holography
- Interference/
  - light
- Interferometers/
  - light
- Interferometry/
  - light
- Magneto-optical effects
- Optical constants
- Optical films
- Optical pumping
- Optical rotation
- Photoelasticity
- Pleochroism
- Polarimeters
- Polarisation/
  - light
- Reflection/
  - light
- Reflectivity
- Refraction/
  - light
- Refractive index/
  - light
- Scattering/
  - light
- Thermo-optical effects
- Transmission/
  - light
- Transparency

08.30 PHOTOMETRY. CALORIMETRY

- Bolometers
- Brightness
- Colorimetry
- Colour
- Densitometry
- Emissivity
- Illumination
- Photometers
- Photometry/
  - light sources
- Pyrometers
- Radiation detectors

08.40 INSTRUMENTAL OPTICS

- Abberations, optical
- Dispersion, optical
- Fibres/
  - optical
- Films/
  - liquid
- Films, solid/
  - optical properties
- Filters, optical
- Glass
- Image convertors and amplifiers
- Lasers/
  - gaseous
  - solid
- Lenses/
  - aspherical
  - photographic
- Light sources
- Luminescent devices
- Microscopes
- Microscopy
- Mirrors
- Optical constants
- Optical images
- Optical instrument testing
- Optical instruments
- Optical materials
- Optical systems
- Prisms, optical
- Projectors, optical
- Quartz
- Reflection/
  - light
- Refraction/
  - light
- Refractive index/
  - light
- Refractive index measurement
- Refractometers
- Resolving power, optics
- Schlieren systems
- Stroboscopes
- Telescopes

08.45 Spectroscopy

- Astronomical spectra
- Atmospheric spectra
- Exploding wires
- Modulation spectroscopy
- Monochromators
- Spectral line breadth
- Spectrochemical analysis
- Spectrometers/
  - accessories
- Spectrophotometers
- Spectrophotometry
- Spectroscopy/
  - light sources
- Stark effect
- Temperature measurement/
  - spectral methods
- Zeeman effect

08.50 PHOTOGRAPHY

- Cameras
- Cinematography
- Densitometry
- Lenses/
  - photographic
- Light sources
- Nuclear track emulsions
- Photographic materials/
  - sensitivity
- Photographic process/
  - development
- Photography/
  - applications
  - colour
  - high-speed
- Radiography

09.00 QUANTUM FIELD THEORY

Bethe-Salpeter equation
Current algebra
Dispersion relations
Dual resonance model
Field theory, quantum/
  interactions
  interactions, strong
  interactions, weak
  meson field
  quantisation
  scattering

Lee model
Nuclear forces
Parity
Quantum electrodynamics
Quantum theory/
  application methods
  quantisation
  wave equations
S-matrix theory
Scattering

10.00 ELEMENTARY PARTICLES

Bosons
Elementary particles
Fermions

Gravitons
Parity
Energy loss of particles

Particle velocity analysis
Quarks

Strange particles
Synchrotron radiation

10.10 ELEMENTARY PARTICLE THEORY

Bootstrapping
Bosons
Chirality
CPT conservation
Current algebra
Dirac equation
Dispersion relations

Elementary particles/
  interactions
  interactions, electromagnetic
  interactions, strong
  interactions, weak
  scattering
  symmetry
  theory

Fermions
Form factors
Magnetic monopoles
Mass differences
Mass formulae
Nuclear forces

Parity
S-matrix theory
Strange particles
SU(n) theory
Sum rules
Tachyons

10.20 PHOTONS. GAMMA-RAYS. X-RAYS

Bremsstrahlung
Cherenkov radiation
Compton effect
Gamma-ray spectrometers

Gamma-rays/
  absorption
  angular distribution
  detection, measurement
  effects
  scattering

Mössbauer effect
Photons/
  interactions
  polarisation
  scattering
Synchrotron radiation

X-ray absorption
X-ray diffraction
X-ray measurement
X-ray reflection
X-ray scattering
X-rays/
  effects

10.30 LEPTONS

Leptons

10.35 Electrons

Beta-ray spectra/
  conversion electrons
Beta-ray spectrometers
Beta-rays/
  absorption
  angular distribution
  detection, measurement
  effects
  polarisation
  scattering
Dirac equation
Electron pairs/
  annihilation
  production

Electron theory
Electrons/
  absorption
  interactions
  ionisation
  radiation
  scattering
  scattering, electron-proton
Positronium
Positrons
Synchrotron radiation

10.37 Muons

Muons/
  capture
  decay
  detection, measurement

Muons/
  interactions
  production
  scattering
Muonium

10.33 Neutrinos

Neutrinos and antineutrinos

10.40 HADRONS

Hadrons/
  current
  decay
Quarks

10.41 Hadron interactions

Hadrons/
  interactions

10.42 Hadron scattering

Bootstrapping
Dual resonance model
Hadrons/
  scattering
Pomeranchuk poles and
  trajectories

Regge poles and trajectories
Veneziano model

10.45 Mesons

Mesons/
  absorption
  capture
  decay
  detection, measurement
  effects

Mesons/
  interactions
  magnetic moment
  mass
  production
  scattering
  spin and parity

10.46 Kaons

Kaons/
  decay
  interactions

Kaons/
  production
  scattering

10.47 Pions

Pions/
  decay
  interactions
  interactions, pion-nucleon
  interactions, pion-pion
  interactions, pion-proton

Pions/
  production
  scattering
  scattering, pion-nucleon
  scattering, pion-pion
  scattering, pion-proton

10.48 Meson Resonances

Intermediate bosons
Mesons/
  resonances

10.51 Baryons

Baryons/
  interactions
  scattering

10.52 Nucleons

Nuclear forces
Nucleons and antinucleons/
  antinucleons
  interactions
  interactions, nucleon-nucleon
  scattering
  scattering, nucleon-nucleon

10.53 Protons

- Proton spectra
- Protons and antiprotons/
  - absorption
  - angular distribution
  - antiprotons
  - detection, measurement
  - effects
  - interactions
  - interactions, proton-proton
  - magnetic moment
  - polarisation
  - production
  - scattering
  - scattering, proton-deuteron
  - scattering, proton-proton

10.54 Neutrons

- Neutron diffraction
- Neutron spectra
- Neutron spectrometers
- Neutrons and antineutrons/
  - absorption
  - angular distribution
  - detection, measurement
  - diffusion
  - effects
  - interactions
  - moderation
  - polarisation
  - production
  - reflection
  - scattering
  - scattering, neutron-proton

10.56 Hyperons

- Hypernuclei
- Hyperons/
  - absorption
  - capture
  - decay
  - detection, measurement
  - effects
  - interactions
  - magnetic moment
  - mass
  - production
  - resonances
  - scattering
  - spin and parity
- Strange particles

10.58 Baryon Resonances

- Baryons/
  - resonances
- Hyperons/
  - resonances
- Nucleons

10.60 COMPOSITE PARTICLES

Composite particles

10.63 Deuterons

- Deuterons/
  - effects
  - interactions
  - photodisintegration
  - polarisation
  - scattering

10.65 Tritons

- Tritons/
  - interactions
  - scattering

10.67 Alpha-particles and He^3

- Alpha-particle spectrometers
- Alpha-particles/
  - absorption
  - angular distribution
  - detection, measurement
  - effects
  - interactions
  - scattering
- Helium-3
  - interactions
  - scattering

10.70 COSMIC RAYS

- Cosmic rays/
  - absorption
  - apparatus
  - alpha-particles and helium nuclei
  - composition
  - deuterons
  - effects and interactions
  - electrons
  - mesons
  - muons
  - neutrinos
  - neutrons
  - nucleons
  - origin
  - photons
  - primary
  - protons
  - showers and bursts
  - variations
  - X-rays

11.00 ELEMENTARY PARTICLE AND NUCLEAR MEASUREMENT

11.10 APPARATUS. DETECTORS AND DETECTOR CIRCUITS

- Alpha-particle spectrometers
- Amplifiers
- Beta-ray spectrometers
- Counters/
  - accessories
  - Cherenkov
  - crystal
  - Geiger
  - operation technique
  - proportional
  - scintillation
  - semiconductor
  - spark
  - statistical analysis
- Counting circuits
- Dosimetry
- Gamma-ray spectrometers
- Ionisation chambers
- Neutron spectrometers
- Nuclear bombardment targets
- Particle accelerators
- Particle detectors
- Particle optics
- Particle spectrometers
- Particle velocity analysis
- Photomultipliers
- Radioactivity measurement/
  - apparatus

11.15 Track Visualisation

- Bubble chambers
- Cloud chambers
- Energy loss of particles
- Luminescence chambers
- Nuclear track emulsions
- Particle tracks
- Particle track visualisation
- Spark chambers

11.20 PARTICLE ACCELERATORS

- High-voltage techniques
- Ion sources
- Particle accelerators/
  - accessories
  - betatrons
  - cyclotrons
  - linear
  - synchrotrons
- Storage rings

12.00 NUCLEAR PHYSICS

Nuclear physics

12.10 NUCLEAR STRUCTURE AND ENERGY LEVELS

- BCS theory
- Beta-ray spectra/
  - conversion electrons
- Gamma-ray spectra
- Gamma-rays/
  - angular distribution
  - internal conversion
- Gyromagnetic ratio
- Hypernuclei
- Isobaric analog states
- Mössbauer effect
- Nuclear excitation
- Nuclear forces
- Nuclear isomerism
- Nuclear magnetic resonance and relaxation
- Nuclear polarisation
- Nuclear structure
- Nuclei with $A \leq 5$
- Nuclei with $6 \leq A \leq 19$
- Nuclei with $20 \leq A \leq 49$
- Nuclei with $50 \leq A \leq 89$
- Nuclei with $90 \leq A \leq 149$
- Nuclei with $150 \leq A$
- Nucleus/
  - electric moment
  - energy level transitions
  - energy levels
  - magnetic moment
  - models
  - size
  - spin and parity
  - theory

12.20 NUCLEAR DECAY AND RADIOACTIVITY

- Alpha-particles
- Alpha-particle spectra
- Alpha-particle spectrometers
- Alpha-particles/
  - absorption
  - angular distribution
  - detection, measurement
  - effects
  - scattering
- Beta-decay theory
- Beta-ray spectra/
  - conversion electrons
- Beta-ray spectrometers
- Beta-rays/
  - absorption
  - angular distribution
  - detection, measurement
  - effects
  - polarisation
  - scattering
- Biological effects of radiations
- Chemical effects of radiations/
  - ionising radiations
- Dosimetry
- Fallout
- Gamma-ray spectra
- Gamma-ray spectrometers
- Gamma-rays/
  - absorption
  - angular distribution
  - detection, measurement
  - effects
  - internal conversion
  - scattering
- Nuclear decay theory
- Nuclear bombardment targets
- Physical effects of radiations
- Radiation monitoring
- Radiation protection
- Radioactive dating
- Radioactive tracers
- Radioactivity/
  - decay periods
  - decay schemes
  - electron capture
- Radioactivity measurement/
  - apparatus
- Radiochemistry

12.30 NUCLEAR REACTIONS AND SCATTERING

- Chemical analysis/
  - by nuclear reactions
- Collision processes
- Nuclear bombardment targets
- Nuclear excitation
- Nuclear forces
- Nuclear reactions and scattering/
  - chemical effects
  - high energy $\geq$ 1GeV
- Nuclear reactions and scattering due to/
  - alpha-particles
  - cosmic rays
  - deuterons
  - electrons
  - helium-3
  - hyperons
  - mesons
  - muons
  - neutrinos
  - neutrons
  - nuclei of $Z > 2$
  - nucleons
  - photons
  - protons
  - tritons
- Nuclear spallation
- Nuclei with $A \leq 5$
- Nuclei with $6 \leq A \leq 19$
- Nuclei with $20 \leq A \leq 49$
- Nuclei with $50 \leq A \leq 89$
- Nuclei with $90 \leq A \leq 149$
- Nuclei with $150 \leq A$
- Radiation monitoring
- Radiation protection
- Scattering, particles
- Stripping reactions

12.39 Nuclear fission and fusion

- Explosions/
  - nuclear
- Nuclear fission/
  - products
  - uranium
- Nuclear fusion
- Nucleons and antinucleons
- Photo fission
- Plasma
- Thermonuclear reactions

12.40 NUCLEAR POWER STUDIES

12.43 Neutron Physics

- Neutron transport theory
- Neutrons and antineutrons/
  - absorption
  - angular distribution
  - detection measurement
  - diffusion
  - effects
  - interactions
  - moderation
  - polarisation
  - production
  - reflection
  - scattering
- Nuclear fission/
  - products
  - uranium
- Nuclear fusion
- Nuclear reactions and scattering
- Thermonuclear reactions

12.47 Nuclear Reactors

- Biological effects of radiations
- Chemical analysis/
  - by nuclear reactions
- Chemical effects of radiations/
  - ionising radiations
- Dosimetry
- Nuclear fission/
  - products
  - uranium
- Nuclear fusion
- Nuclear reactions and scattering/
  - chemical effects
- Nuclear reactors, fission/
  - materials
  - operation
  - theory
- Nuclear reactors, fusion
- Physical effects of radiations
- Plasma/
  - devices
- Radiation monitoring
- Radiation protection
- Radiochemistry
- Thermonuclear reactions

12.50 RADIATION TECHNOLOGY

- Dosimetry
- Neutron transport theory
- Physical effects of radiation
- Radiation protection
- Nuclear reactors, fission/
  - operation
- Biological effects of radiation
- Particle accelerators/
  - betatrons
  - cyclotrons
  - linear
  - synchrotrons

13.00 ATOMIC AND MOLECULAR PHYSICS

- Collision processes
- Orbital calculation methods
- Quantum theory

13.10 MASS SPECTROMETERS

- Mass spectra
- Mass spectrometers/
    - accessories
    - applications

13.20 ATOMS

- Atomic beams
- Atomic mass and weight
- Atoms
    - electron scattering
    - excitation
    - magnetic moment
    - structure
- Auger effect
- Binding energy
- Charge exchange
- Collision processes/
    - atoms
- Electron emission
    - photoelectric
- Elements
    - origin
    - relative abundances
- Exchange interactions
- Gyromagnetic ratio
- Hartree-Fock method
- Helium/
    - gas
- Hydrogen/
    - ions
    - neutral atoms
- Ionisation potential
- Isotope shifts
- Luminescence
    - gases
- Optical pumping
- Orbital calculation methods
- Periodic system
- Polarisability
- Rayleigh scattering
- Red shift
- Russell-Saunders coupling
- Spectra
    - atoms
- Spectral line breadth
- Stark effect
- Stimulated emission
- X-ray spectra
    - absorption
    - emission
- Zeeman effect

13.25 Isotopes

- Isotope effects
- Isotope exchanges
- Isotope separation
- Isotopes
    - detection
    - relative abundances
- Mass spectra
- Mass spectrometers/
    - applications
- Radioactive dating
- Radioactive tracers
- Radiochemistry
- Tracers

13.27 Mesic and Muonic Atoms

- Atoms, mesic and muonic

13.30 MOLECULES

- Binding energy
- Bonds
- Chemical shift
- Chemical structure
- Exchange interactions
- Isomerism
- Jahn-Teller effect
- Luminescence/
    - gases
- LCAO calculations
- Magnetic resonance and relaxation
- Molecular weight
- Molecules/
    - configuration and dimensions
        - inorganic
        - organic
    - dissociation
    - dissociation energies
    - excitation
    - electron scattering
    - internal mechanics
    - electronic structure
    - electronic structure, inorganic
    - electronic structure, organic
    - excitation
    - intermolecular mechanics
    - internal mechanics
    - moments
    - nuclear coupling
    - relaxation
    - rotation
    - vibration
- Nuclear magnetic resonance and relaxation
- Nuclear quadrupole resonance
- Optical pumping
- Orbital calculation methods
- Paramagnetic resonance and relaxation
- Polarisability
- Rayleigh scattering
- Red shift
- Scattering/
    - light
    - light, Brillouin spectra
    - light, Raman spectra
    - light, Raman spectra, inorganic
    - light, Raman spectra, organic
- Spectra/
    - inorganic molecules
        - diatomic
        - diatomic, radiofrequency
        - polyatomic
        - polyatomic, radio-frequency
    - inorganic liquids and solutions
    - inorganic solids
        - radiofrequency
    - molecules
    - organic molecules and substances
        - infrared
        - radiofrequency
- Spectral line breadth
- Stark effect
- Stimulated emission
- Valency
- Zeeman effect

13.35 Macromolecules

- Association
- Heat of formation
- Isomerism
- Macromolecules
- Molecules/
    - configuration and dimensions, macromolecules
- Polymers
- Proteins

13.36 Mesic and Muonic Molecules

- Molecules, mesic and muonic

13.37 Intermolecular mechanics

- Charge exchange
- Collision processes/
    - molecules
- Molecular beams
- Molecules/
    - intermolecular mechanics

14.00 FLUIDS

- Boundary layers
- Flow/
    - two-phase
- Fluidised beds
- Fluids
- Hydrodynamics
- Hydrostatics
- Non-Newtonian fluids
- Oscillations
- Turbulence
- Viscosity
- Vortices
- Waves

14.10 MAGNETOHYDRODYNAMICS

- Magnetohydrodynamics
- Shock waves/
  - effects
- Turbulence

14.20 PLASMA

- Discharges, electric/
  - glows
  - high-frequency
- Electrohydrodynamics
- Electrode density
- Exploding wires
- Nuclear fusion
- Nuclear reactors, fusion
- Plasma/
  - collison processes
  - electromagnetic waves
  - magnetohydrodynamics
  - production
  - shock waves
  - transport processes
- Shock waves/
  - effects
- Space charge/
  - gas
- Thermonuclear reactions

14.24 Plasma Confinement, Devices and Measurements

- Plasma/
  - confinement
  - devices
  - diagnostics
- Probes
- Stellarators

14.26 Plasma Oscillations and Stability

- Plasma/
  - magnetohydrodynamics
  - oscillations
  - stability

14.30 IONISATION

- Charge exchange
- Dissociation
- Ion velocity
- Ionisation/
  - gases
- Ionisation potential
- Ionisation, surface
- Ions/
  - recombination
  - scattering
- Magnetohydrodynamic waves
- Photoionisation/
  - gases
- Shock waves/
  - effects
- Space charge/
  - gas

14.40 ELECTRIC DISCHARGES

- Arcs, electric
- Breakdown, electric/
  - gases
- Corona, electric discharge
- Discharges, electric/
  - glows
  - high frequency
- Electron density
- Gas-discharge tubes
- Lightning
- Sparks, electric
- Sputtering

14.50 MECHANICS OF GASES

- Acoustic streaming
- Aerodynamics
- Anemometers
- Compressibility/
  - gases
- Condensation
- Density/
  - gases
- Diffusion in gases/
  - thermal
- Flow/
  - gases
  - two-phase
- Flowmeters
- Gases
- Humidity
- Hygrometers
- Jets
- Manometers
- Moisture
- Pressure
- Pumps
- Radiation pressure
- Supersonic flow
- Turbulence
- Viscometers
- Viscosity/
  - gases
- Vortices
- Waves

14.60 GASEOUS STATE

- Absorption/
  - acoustic waves
  - acoustic waves, ultrasonic
  - electromagnetic waves
  - light
- Acoustic wave amplification
- Association/
  - gases
- Breakdown, electric/
  - gases
- Conductivity, electrical/
  - gases
  - measurement
- Conductivity, thermal/
  - gases
  - measurement
- Dielectric properties of substances/
  - gases
- Diffraction/
  - acoustic waves
  - acoustic waves, ultrasonic
  - electromagnetic waves
  - light
- Diffusion/
  - acoustic waves
  - electromagnetic waves
  - light
- Electrical properties of substances
- Electroluminescence
- Equations of state/
  - gases
- Fluorescence
- Gases
- Helium/
  - gas
- Interference/
  - acoustic waves
- Joule-Thomson effect
- Kinetic theory/
  - gases
- Lasers/
  - gaseous
- Luminescence/
  - gases
- Magnetic resonance and relaxation
- Molecules/
  - intermolecular mechanics
- Nuclear magnetic resonance and relaxation
- Nuclear quadrupole resonance
- Optical properties of substances
- Paramagnetic resonance and relaxation
- Permittivity
- Phosphorescence
- Rayleigh scattering
- Reflection/
  - acoustic waves
  - acoustic waves, ultrasonic
  - electromagnetic waves
  - light
- Refraction/
  - acoustic waves
  - acoustic waves, ultrasonic
  - electromagnetic waves
  - light
- Scattering/
  - acoustic waves
  - acoustic waves, ultrasonic
  - electromagnetic waves
  - light
- Sorption
- Specific heat/
  - gases
- Spectra
- Statistical mechanics
- Thermoluminescence
- Transmission/
  - acoustic waves
  - acoustic waves, ultrasonic
  - light
- Velocity/
  - acoustic waves
  - acoustic waves, ultrasonic
- X-ray fluorescence

14.65 Viscosity and Diffusion of Gases

- Diffusion in gases/
  - thermal
- Transport processes
- Viscosity/
  - gases

14.70 MECHANICS OF LIQUIDS

- Acoustic streaming
- Bubbles
- Capillarity
- Cavitation
- Compressibility/
  - liquids
- Density/
  - liquids
- Diffusion in liquids
  - thermal
- Double refraction/
  - flow
- Drops
- Elasticity/
  - liquids
- Emulsions
- Films/
  - liquid
- Filters
- Flow/
  - liquids
  - two-phase
- Flowmeters
- Foams
- Hydrodynamics
- Hydrostatics
- Jets
- Liquid oscillations
- Liquid waves/
  - surface
- Lubrication
- Moisture
- Pressure
- Pumps
- Radiation pressure
- Rheology
- Schlieren systems
- Sprays
- Surface energy
- Surface tension
- Surface tension measurement
- Thixotropy
- Turbulence
- Viscometers
- Viscosity/
  - liquids
- Vortices
- Wetting

14.80 LIQUID STATE

- Liquids
- Liquid metals

14.82 Theory and Structure of Liquids and Solutions

- Association/
  - liquids
- Electron diffraction examination of materials
- Equations of state/
  - liquids
- Films/
  - liquid
- Heat of solution
- Liquid crystals
- Liquids/
  - structure
  - theory
- Neutron diffraction examination of materials
- Neutrons and antineutrons/
  - scattering
- Polymers
- Solubility
- Solutions
- X-ray examination of materials/
  - liquids

14.83 Viscosity, Surface tension and Diffusion

- Diffusion in liquids/
  - thermal
- Filters
- Membranes
- Osmosis
- Sorption
- Surface tension
- Surface tension measurement
- Transport processes
- Viscosity/
  - liquids

14.85 Thermal Properties of Liquids

- Conductivity, thermal/
  - liquids
  - measurement
- Heat of solution
- Specific heat/
  - liquids
- Thermal expansion
- Thermodynamic properties

14.86 Acoustical Properties of Liquids

- Absorption/
  - acoustic waves
  - acoustic waves, ultrasonic
- Acoustic wave amplification
- Acoustic wave propagation/
  - ultrasonic
- Diffraction/
  - acoustic waves
  - acoustic waves, ultrasonic
- Diffusion/
  - acoustic waves
- Interference/
  - acoustic waves
- Reflection/
  - acoustic waves
  - acoustic waves, ultrasonic
- Refraction/
  - acoustic waves
  - acoustic waves, ultrasonic
- Scattering/
  - acoustic waves
  - acoustic waves, ultrasonic
- Transmission/
  - acoustic waves
  - acoustic waves, ultrasonic
- Velocity/
  - acoustic waves
  - acoustic waves, ultrasonic

14.87 Optical Properties of Liquids

- Absorption/
  - electromagnetic waves
  - light
- Chemical shift
- Chemiluminescence
- Diffraction/
  - electromagnetic waves
  - light
- Diffusion/
  - electromagnetic waves
  - light
- Double refraction/
  - flow
- Electroluminescence
- Fluorescence
- Luminescence/
  - liquids and solutions
- Optical pumping
- Optical properties of substs.
- Phosphorescence
- Rayleigh scattering
- Reflection/
  - electromagnetic waves
  - light
- Refraction/
  - electromagnetic waves
  - light
- Scattering/
  - electromagnetic waves
  - light
  - light, Brillouin spectra
  - light, Raman spectra
  - light, Raman spectra, inorganic
  - light, Raman spectra, organic
- Spectra/
  - inorganic liquids and solutions
- Stimulated emission
- Thermoluminescence
- Transmission/
  - light
- X-ray fluorescence

14.88 Electrical and Magnetic Properties of Liquids

Absorption/
  electromagnetic waves
Acoustic paramagnetic resonance
Breakdown, electric/
  liquids

Conductivity, electrical/
  liquids
  liquids, electrolytic
  measurement
Dielectric properties of substs./
  liquids and solutions
Electrical properties of substs.
ENDOR
Ferroacoustic resonance

Ionisation, liquids
Liquid metals
Magnetic properties of substs.
Magnetic resonance and relaxation
Metals
Nuclear acoustic resonance
Nuclear magnetic resonance and relaxation

Nuclear quadrupole resonance
Paramagnetic resonance and relaxation
Permittivity
Proton magnetic resonance
Semiconducting materials
Semiconductors

14.90 DISPERSIONS AND COLLOIDS

Aerosols
Centrifuges
Colloids
Disperse systems
Electrophoresis

Emulsions
Filters
Foams
Gels
Heat of solution

Membranes
Osmosis
Particle size
Precipitation
Sedimentation

Sols
Solubility
Solutions
Surface phenomena
Suspensions
Thixotropy

14.95 Liquid and solid helium

Helium/
  liquid
  liquid, sound propagation
  solid

Quantum fluids/
  boson systems
  fermion systems

Second sound
Superfluidity
Zero sound

15.00 CHANGE OF STATE

Boiling
Boiling point
Condensation
Critical constants, thermal
Distillation
Drying

Equations of state
  gases
  liquids
  solids
Evaporation
Freezing
Heat of fusion

Heat of sublimation
Heat of transformation
Heat of vaporisation
Humidity
Liquefaction, gases
Melting
Melting point

Phase equilibrium
Phase transformations
Sublimation
Supercooling
Vapour pressure
Vapour pressure measurement
Vaporisation

16.00 SOLID STATE STRUCTURE AND MECHANICAL PROPERTIES

Crystal properties
Equations of state/
  solids

Solids/
  structure
  theory

16.10 NON-CRYSTALLINE STATE

Amorphous state
Glass

Plastics
Polymers

Rubber
Vitreous state

Waxes

16.20 SURFACE AND INTERFACE PHENOMENA

Ellipsometry
Interface phenomena
LEED

Metallography
Surface energy
Surface measurement

Surface phenomena
Surface structure

16.23 Films. Whiskers. Dendrites

Crystals/
  growth
Epitaxy
Evaporation

Films, solid/
  electrical properties
  magnetic properties
  optical properties
Sputtering
Sublimation

16.25 Adsorption

Adsorbed layers
Adsorption
Chemisorption
Composite materials

Desorption
Heat of adsorption
Sorption

16.30 CRYSTALLOGRAPHY

Binding energy
Bonds
Charge compensation
Cleavage
Crystal chemistry
Crystal morphology
Crystal properties

Crystallography
Crystals/
  etching
  faces
  orientation
  twinning

Debye-Waller factors
Field ion microscopy
Isomorphism
Lattice energy
Minerals

Polymorphism
Solids/
  structure
Surface structure

16.33 Crystal growth

Crystal morphology
Crystallisation
Crystals/
  growth
  whiskers

Dendrites
Epitaxy

Nucleation
Zone melting and refining

16.35 Crystal Structures, Techniques and Apparatus

- Alloys
- Amorphous state
- Computer applications
- Crystal morphology
- Crystal structure/
  - microstructure
- Crystal structure, atomic/
  - alloys
  - elements
  - inorganic compounds
  - organic compounds
- Debye-Waller factors
- Density/
  - solids
- Electron diffraction crystallography
- Electron diffraction examination of materials
- Electron microscope examination of materials
- Electron microscopy
- Fibres
- Field ion microscopy
- Grain boundaries
- Granular structure
- Ion microscopes
- Metallography
- Metallurgy
- Microscopy
- Neutron diffraction crystallography
- Neutron diffraction examination of materials
- Particle size
- Polymers
- Porous materials
- Powders
- Radiography
- Space groups
- Surface structure
- X-ray absorption
- X-ray crystallography/
  - apparatus
  - calculation apparatus
  - calculation methods
  - technique
- X-ray diffraction
- X-ray examination of materials
  - microstructure
  - molecular structure
- X-ray measurement
- X-ray monochromators
- X-ray reflection
- X-ray scattering
- X-ray tubes

16.40 DEFECT PROPERTIES OF SOLIDS

- Cold working
- Creep
- Crystal imperfections
  - dislocations
  - impurities
  - interstitials
  - vacancies
- Crystal structure
- Crystals
  - etching
  - twinning
- Deformation
- Elastic deformation
- Electron diffraction examination of materials
- Electron microscope examination of materials
- Grain boundaries
- Heat treatment
  - alloys
- Internal friction
- Neutron diffraction examination of materials
- Plastic deformation
- Plastic flow
- Slip
- Stacking fault
- Stresses, internal
- Work hardening
- X-ray examination of materials/
  - microstructure

16.43 Crystal Impurities

- Crystal imperfections/
  - impurities
  - interstitials
- Ion implantation
- Physical effects of radiation

16.45 Colour centres

- Absorption/
  - light
- Colour centres
- F-centres
- X-rays/
  - effects

16.50 DIFFUSION IN SOLIDS

- Diffusion in solids/
  - thermal
- Permeability, mechanical

16.60 MECHANICAL PROPERTIES OF SOLIDS

- Abrasion
- Bending
- Brittleness
- Compressibility
- Cracks
- Creep
- Deformation
- Densification
- Density/
  - solids
- Elastic constants/
  - measurement
- Elastic deformation
- Elastic limit
- Elastic relaxation
- Elastic waves
- Elasticity/
  - fatigue
- Fracture
- Friction
- Hardness
- High-pressure phenomena and effects
- Hysteresis
- Impact
- Internal friction
- Lubrication
- Magnetoelastic waves
- Magnetomechanical effects
- Mechanical properties of substances
- Mechanical strength/
  - compressive
  - shear
  - tensile
- Photoelasticity
- Plastic deformation
- Plastic flow
- Plasticity
- Rheology
- Slip
- Strain gauges
- Stress analysis
- Stress effects
- Stress/strain relations
- Stresses, internal
- Thermoelasticity
- Thixotropy
- Torsion
- Viscoelasticity
- Wear

16.65 Metallurgy. Materials Science. Phase Transformations

- Adhesion
- Aging
- Alloys
- Annealing
- Cold working
- Corrosion
- Densification
- Forming processes
- Granular structure
- Heat treatment/
  - alloys
- Metallurgy
- Order-disorder changes
- Phase equilibrium
- Particle size
- Phase transformations/
  - solid-state
- Physical effects of radiations
- Polymorphism
- Powders
- Precipitation
- Recovery
- Refractories
- Sintering
- Solid solutions
- Solubility
- Work hardening

16.70 LATTICE MECHANICS

- Crystals/
  - lattice mechanics
- Debye temperature
- Debye-Waller factors
- Mössbauer effect
- Phonons

16.80 ACOUSTICAL PROPERTIES OF SOLIDS

- Absorption/
  - acoustic waves
  - acoustic waves, ultrasonic
- Acoustic wave amplification
- Acoustic wave propagation/
  - ultrasonic
- Acoustoelectric effects
- Acousto-optical effects
- Diffraction/
  - acoustic waves
  - acoustic waves, ultrasonic
- Dispersion, acoustic/
  - ultrasonic
- Magnetoacoustic effects
- Reflection/
  - acoustic waves
  - acoustic waves, ultrasonic
- Refraction/
  - acoustic waves
  - acoustic waves, ultrasonic
- Scattering/
  - acoustic waves
  - acoustic waves, ultrasonic
- Transducers
- Transmission/
  - acoustic waves
  - acoustic waves, ultrasonic
- Velocity/
  - acoustic waves
  - acoustic waves, ultrasonic

16.90 THERMAL PROPERTIES OF SOLIDS

- Conductivity thermal/
    - measurement
    - solids
- Debye temperature
- Entropy/
    - properties of substances
- Equations of state/
    - solids
- Gruneisen relation
- Heat conduction
- Specific heat/
    - solids
- Thermal expansion
- Thermal properties of substances
- Thermodynamic properties

16.95 RADIATION INTERACTION WITH SOLIDS

- Acoustic waves/
    - effects
- Alpha-particles/
    - effects
- Beta-rays/
    - effects
- Channelling
- Deuterons/
    - effects
- Electron beams/
    - effects
- Energy loss of particles
- Gamma-rays/
    - effects
- Hyperons/
    - effects
- Ion beams/
    - effects
- Mesons/
    - effects
- Neutrons and antineutrons/
    - effects
- Physical effects of radiations
- Protons and antiprotons/
    - effects
- Sputtering
- X-rays/
    - effects

17.00 SOLID STATE ELECTRICAL AND MAGNETIC PROPERTIES

- Crystals/
    - internal fields

17.10 ELECTRON STATES IN SOLIDS

- Brillouin zones
- Crystal electron states
    - band structure
    - excitons
    - Fermi level
    - Fermi surface
    - impurity states and effects
    - plasma
    - polarons
    - surface
    - transport processes
- Crystal properties
- Cyclotron resonance
- de Haas-van Alphen effect
- Electron beams/
    - effects
- Electron density
- Electron gas
- Electron pairs/
    - annihilation
- Electron-phonon interactions
- Electron traps
- Electrons
    - absorption
    - radiation
    - scattering
- Hall effect
- Helicons
- Kondo effect
- Magnetoacoustic effects
- Magnetoresistance
- Metals/
    - theory
- Piezoresistance
- Pseudopotential methods
- Quasi-particles
- Skin effect
- Solids/
    - theory
- Surface phenomena
- Tunnelling
- Zero sound

17.20 ELECTRICAL PROPERTIES OF SOLIDS

- Acoustoelectric effects
- Conductivity, electrical/
    - measurement
    - solids
- Contacts, electrical
- Crystal electron states
- Eddy-currents
- Electrical properties of substs.
- Electron density
- Electron gas
- Electro-optical effects
- Films, solid/
    - electrical properties
- Fluctuations
- Hall effect
- Magnetoelectric effects
- Magnetoresistance
- Magnetothermal effects
- Noise, electrical
- Piezoelectricity
- Piezoresistance
- Space charge/
    - solid
- Thin film devices
- Tunnelling

17.22 Metallic Conducting Properties

- Electron gas
- Hall effect
- Magnetoelectric effects
- Magnetoresistance
- Metals/
    - theory
- Piezoresistance
- Semimetals
- Skin effect
- Thin film devices

17.24 Superconducting Properties

- BSC theory
- Galvanothermomagnetic effects
- Storage devices
- Superconducting devices
- Superconducting magnets
- Superconducting materials/
    - lead
    - niobium
- Superconductivity/
    - type II
- Thin film devices
- Tunnelling

17.26 Semiconducting Properties

- Acoustoelectric effects
- Contacts, electrical
- Electron gas
- Electro-optical effects
- Fluctuations
- Gunn effect
- Hall effect
- Ion implantation
- Magnetoelectric effects
- Magnetoresistance
- Magnetothermal effects
- Noise, electrical
- Piezoelectricity
- Piezoresistance
- Semiconductors
- Space charge/
    - solid
- Semiconducting materials/
    - gallium arsenide
    - germanium
    - indium antimonide
    - silicon
- Tunnelling

17.28 Semiconductor and Interface devices

- Gunn effect
- Ion implantation
- Metal-insulator-metal structures and devices
- Metal-insulator-semiconductor structures and devices
- Microwave techniques and devices
- Rectifiers
- Semiconductor devices/
    - diodes
    - junctions
    - transistors
    - tunnel and interface devices
- Semiconductor-metal boundaries
- Storage devices
- Thin film devices
- Tunnelling

17.29 Dielectric Properties

- Antiferroelectric materials
- Breakdown, electric/
    - solids
- Contacts, electrical
- Dielectric devices
- Dielectric measurement
- Dielectric phenomena
- Dielectric properties of substs./
    - solids
- Dielectric relaxation
- Domains
- Electrets
- Electric charge
- Electric fields
- Electric strength
- Electrostriction
- Ferroelectric materials/
    - barium titanate
- Ferroelectric phenomena
- Hysteresis
- Ionic conduction, solids
- Paraelectric resonance
- Permittivity
- Piezo-optical effects
- Piezoelectric oscillations
- Piezoelectricity
- Pyroelectricity
- Relaxation
- Rochelle salt
- Space charge/
    - solid
- Triboelectricity
- Tunnelling

17.40 THERMOELECTROMAGNETIC PROPERTIES

Magnetoelectric effects
Magnetothermal effects
Thermocouples
Thermoelectricity

17.50 PHOTOELECTRIC PROPERTIES

Photoconducting devices
Photoconductivity
Photoelectricity
Photoelectromagnetic effects
Photovoltaic effects

17.52 ELECTRON AND ION EMISSION BY SOLIDS

Cathodes/
  oxide
Electron emission
  field emission
  photoelectric
  secondary
  thermionic
Ion emission/
  secondary
  thermionic
Ionisation/
  solids
Ionisation, surface
Work function

17.60 MAGNETIC PROPERTIES OF SOLIDS

Antiferromagnetism
de Haas-van Alphen effect
Diamagnetism
Demagnetisation
Domains
Electron diffraction examination
    of materials
Electron microscope examination
    of materials
Exchange interactions
Ferrimagnetism
Ferrites
Ferromagnetism/
  spin-wave theory
Films, solid/
  magnetic properties
Gyromagnetic ratio
Hall effect
Hysteresis
Kondo effect
Magnetic devices
Magnetic fields/
  effects
Magnetic anisotropy
Magnetic permeability
Magnetic properties of dilute
  systems
Magnetic properties of substs.
  antiferromagnetic
  diamagnetic
  ferrimagnetic
  ferromagnetic
  paramagnetic
  transitions
Magnetic structure
Magnetism
Magnetisation process
Magnetoacoustic effects
Magnetoelastic waves
Magnetoelectric effects
Magneto-optical effects
Magnetoresistance
Magnetostriction
Magnetothermal effects
Neutron diffraction examination
    of materials
Paramagnetism
Zeeman effect

17.62 Paramagnetic Properties

Magnetic anisotropy
Magnetic properties of substances/
  paramagnetic
Magnetic structure
Paramagnetism

17.64 Ferromagnetic Properties

Domains
Exchange interactions
Ferromagnetism/
  spin-wave theory
Films, solid/
  magnetic properties
Heisenberg model
Helicons
Hysteresis
Ising lattices and models
Magnetic anisotropy
Magnetic devices
Magnetic properties of substances/
  ferromagnetic
Magnetisation process
Magnetic structure
Metamagnetism
Storage devices
Superparamagnetism
Spin waves
Thin film devices

17.66 Ferrimagnetic Properties

Domains
Exchange interactions
Ferrimagnetism
Ferrites
Films, solid/
  magnetic properties
Helicons
Hysteresis
Magnetic anisotropy
Magnetic devices
Magnetic properties of substances/
  ferrimagnetic
Magnetic structure
Thin film devices
Spin waves
Storage devices

17.68 Antiferromagnetic Properties

Antiferromagnetism
Domains
Exchange interactions
Heisenberg model
Magnetic anisotropy
Magnetic properties of substances/
  antiferromagnetic
Magnetic structure
Metamagnetism
Spin waves

17.69 Magnetic Relaxation Phenomena

Ferromagnetic relaxation
Magnetic resonance and relaxation
Nuclear magnetic resonance and
    relaxation
Paramagnetic resonance and
    relaxation
Spin lattice relaxation
Spin-spin relaxation

18.00 SOLID STATE SPECTROSCOPY AND OPTICAL PROPERTIES

Chemical shift
Crystal field theory
Crystals/
  hyperfine field interactions
Jahn-Teller effect
Isomer shift
Nuclear polarisation

18.10 OPTICAL PROPERTIES OF SOLIDS

Absorption/
  electromagnetic waves
  light
Acousto-optical effects
Diffraction/
  electromagnetic waves
  light
Diffusion/
  electromagnetic waves
  light
Dispersion, optical
Double refraction/
  mechanical
Electromagnetic wave propagation
Electro-optical effects
Electroreflectance
Ellipsometry
Emissivity
Faraday effect
Films, solid/
  optical properties
Interference/
  light
Isomer shift
Lasers/
  solid
Magneto-optical effects
Magnetoreflectance
Nonlinear optics
Optical constants
Optical materials
Optical properties of substances
Optical pumping
Optical rotation
Photoelasticity
Piezo-optical effects
Piezoreflectance
Pleochroism
Polarisation/
  light
Reflection/
  electromagnetic waves
  light
Reflectivity
Refraction/
  electromagnetic waves
  light
Refractive index/
  light
Scattering/
  electromagnetic waves
  light
Thermo-optical effects
Thermoreflectance
Transmission/
  light
Transparency
Velocity/
  light

18.20 RESONANT GAMMA RAY INTERACTIONS. MÖSSBAUER EFFECT

- Chemical shift
- Crystals/
  - hyperfine field interactions
  - internal fields
- Isomer shift
- Magnetoreflectance
- Mössbauer effect

18.30 OPTICAL SPECTRA OF SOLIDS

- Crystals/
  - hyperfine field interactions
- Electroreflectance
- Isomer shift
- Magnetoreflectance
- Piezoreflectance
- Reflection/
  - electromagnetic waves
  - light
- Reflectivity
- Scattering/
  - electromagnetic waves
  - light
  - light, Brillouin spectra
  - light, Raman spectra
  - light, Raman spectra, inorganic
  - light, Raman spectra, organic
- Spectra/
  - inorganic solids
  - inorganic solids, radio frequency
  - organic molecules and substances
  - organic molecules and substances, infrared
  - organic molecules and substances, radio frequency
- Spectral line breadth
- Stark effect
- Stimulated emission
- Thermoreflectance
- X-ray spectra/
  - absorption
  - emission
- Zeeman effect

18.40 LUMINESCENCE SPECTRA OF SOLIDS

- Cathodoluminescence
- Chemiluminescence
- Colour centres
- Counters/
  - scintillation
- Electroluminescence
- Fluorescence
- Luminescence/
  - solids, inorganic
  - solids, organic
- Luminescent devices
- Phosphorescence
- Stimulated emission
- Thermoluminescence
- X-ray fluorescence

18.50 MAGNETIC RESONANCES IN SOLIDS

- Crystals/
  - hyperfine field interactions
- Antiferromagnetic resonance
- Cyclotron resonance
- Ferrimagnetic resonance
- Ferroacoustic resonance
- Ferromagnetic relaxation
- Ferromagnetic resonance
- Gyromagnetic ratio
- Magnetic resonance and relaxation
- Magnetoelastic waves
- Magnetomechanical effects
- Optical pumping

18.52 Paramagnetic Resonances and Relaxation

- Acoustic paramagnetic resonance
- Crystals/
  - hyperfine field interactions
- Gyromagnetic ratio
- Paramagnetic resonance and relaxation/
  - measurement

18.54 Nuclear Magnetic Resonance and Relaxation

- Chemical shift
- Crystals/
  - hyperfine field interactions
- ENDOR
- INDOR
- Knight shift
- Nuclear acoustic resonance
- Nuclear magnetic resonance and relaxation/
  - measurement
- Nuclear quadrupole resonance
- Proton magnetic resonance

19.00 PHYSICAL CHEMISTRY

- Atomic mass and weight
- Balances
- Bonds
- Centrifuges
- Chemical structure
- Chemical technology
- Distillation
- Elements/
  - origin
  - relative abundances
- Filters
- Isomerism
- Laboratory app. and technique
- Macromolecules
- Molecular weight
- Molecular weight determination
- Periodic system
- Physical chemistry
- Precipitation
- Pumps
- Quantum chemistry
- Sedimentation
- Valency

19.10 THERMOCHEMISTRY AND REACTIONS

- Association
  - gases
  - liquids
- Catalysis
- Chemical reactions
- Combustion
- Crystal chemistry
- Detonation
- Dissociation
- Exchanges, chemical
- Explosions
- Flames
- Heat of adsorption
- Heat of combination
- Heat of dissociation
- Heat of formation
- Heat of reaction
- Isotope exchanges
- Phase equilibrium
- Phase transformations
- Polymerisation
- Polymers
- Reaction kinetics
- Sorption

19.15 Oxidation and Corrosion

- Corrosion
- Oxidation

19.20 ELECTROCHEMISTRY

- Anodes
- Conductivity, electrical/
  - liquids, electrolytic
- Dissociation/
  - electrolytic
- Electric cells
- Electrochemistry
  - electrodes
- Electrokinetic effects
- Electrolysis
- Electrolytic deposition
- Electrophoresis
- Ion velocity/
  - electrolytic
- Ions, electrolytic

19.30 PHOTOCHEMISTRY AND RADIOCHEMISTRY

Chemical effects of radiations/
    acoustic waves
    ionising radiations
Nuclear reactions and scattering/
    chemical effects
Photochemistry.
Photochromism
Radiochemistry

19.40 PHYSICAL METHODS OF CHEMICAL ANALYSIS

Chemical analysis/
    adsorption
    by mass spectrometry
    by nuclear reactions
    electrochemical
    radioactive
    X-ray
Chromatography
Electron-pole analysis
Probes
Radioactive tracers
Spectrochemical analysis
Tracers

20.00 GEOPHYSICS

Earth/
    age
    composition
    electricity
    heat
    rotation
Geodesy
Geophysical prospecting
Geophysics
Glaciers
Gravity
Minerals
Oceanography
Radioactive dating
Radioactivity
Seawater
Seismic waves
Seismology
Soil

20.10 ATMOSPHERE

Anemometers
Atmosphere/
    composition
    humidity
    movements
    precipitation
    radioactivity
    structure
    temperature
    thermodynamics
Atmospheric acoustics
Atmospheric electricity
Atmospheric optics
Atmospheric pressure and density
Atmospheric spectra
Atmospherics
Clouds
Condensation
Electromagnetic wave propagation/
    atmosphere
Evaporation
Fallout
Fog
Humidity
Hygrometers
Ice
Lightning
Meteorological instruments
Meteorology
Rain
Rockets
Satellites, artificial
Sky brightness
Snow
Sunlight
Thunderstorms
Twilight
Wind

20.20 UPPER ATMOSPHERE

Airglow
Atmosphere/
    composition
    movements
    radiation belts
    radioactivity
    structure
    temperature
    thermodynamics
    upper
Atmospheric electricity
Atmospheric optics
Atmospheric pressure and density
Atmospheric spectra
Atmospherics
Aurora
Fallout
Ionisation, atmosphere
Magnetosphere
Meteors
Rockets
Satellites, artificial
Sky brightness
Sunlight
Twilight
Zodiacal light

20.30 IONOSPHERE

Atmospherics
Aurora
Electromagnetic wave propagation/
    ionosphere
Ionisation, atmosphere
Ionosphere
Ionosphere measuring apparatus

20.35 D, E and F-regions

Ionosphere/
    D-region
    E-region
    F-region

20.40 GEOMAGNETISM

Compasses
Earth/
    magnetic field
    magnetic field, variations
Magnetic storms
Micropulsations
Rock magnetism

20.50 SPACE RESEARCH TECHNIQUES

Rockets
Satellites, artificial
Space research
Space vehicles/
    instrumentation

21.00 ASTROPHYSICS

Astronomical observations
Astronomical spectra
Astronomy and astrophysics
Celestial mechanics
Cosmic rays
Cosmology
Elements/
    origin
    relative abundances
Gravitation
Infrared astronomy
Interstellar matter

21.10 GALAXIES

- Cosmic radiations, r.f.
- Galaxies/
    - the Galaxy
- H I regions
- H II regions
- Intergalactic matter
- Magnetohydrodynamics
- Nebulae
- Planetary nebulae

21.20 STARS

- Gravitational collapse
- Interstellar magnetic field
- Interstellar matter
- Magnetohydrodynamics
- Multiple stars
- Novae
- Stars/
    - composition
    - evolution
    - magnetism
    - radiation
    - spectra
    - structure
- Stellar atmospheres
- Thermonuclear reactions
- White dwarfs
- Variable stars

21.30 RADIOSOURCES, X-RAY AND GAMMA-RAY SOURCES

- Cosmic radiation, r.f.
- Pulsars
- Quasars
- Radio sources
- X- and gamma-ray astronomy

21.40 SOLAR SYSTEM

- Asteroids
- Comets
- Cosmic rays
- Earth/
    - rotation
- Gravitation
- Interplanetary magnetic field
- Interplanetary matter
- Jupiter
- Mars
- Mercury, planet
- Meteorites
- Meteors
- Moon
- Neptune
- Planetary atmospheres
- Planets
- Pluto
- Saturn
- Solar system
- Uranus
- Venus

21.45 Sun

- Chromosphere
- Cosmic rays
- Photosphere
- Solar activity
- Sun/
    - corona
    - eclipses
    - flares
    - magnetism
    - prominences
    - radiation
    - radiation, corpuscular
    - radiation, r.f.
    - spectra
- Sunspots
- Zodiacal light

21.60 ASTRONOMICAL TECHNIQUES

- Astronomical instruments
- Astronomical observations
- Astronomy and astrophysics
- Radioastronomy
- Telescopes/
    - astronomical

22.00 BIOPHYSICS

Biophysics

22.10 HEALTH AND MEDICAL PHYSICS

- Biological effects of radiations
- Biological technique and instruments
- Blood
- Dosimetry
- Medical science
- Physiology
- Proteins
- Radiation protection
- Radiography
- Zoology

22.20 HEARING AND SPEECH

- Ear
- Hearing
- Noise/
    - acoustic
- Speech

22.30 VISION

- Eye
- Colour vision
- Vision

23.00 LABORATORY AND EXPERIMENTAL TECHNIQUES

- Biological technique and instruments
- Calculating apparatus/
    - analogue apparatus
    - digital computers
    - digital computer programmes
- Chemical technology
- Heat treatment/
    - alloys
- Laboratory apparatus and technique
- Leak detection
- Materials
- Metallurgy
- Zone melting and refining

23.10 HIGH AND LOW TEMPERATURE TECHNIQUES

- Cryostats
- High-temperature phenomena and effects
- High-temperature techniques
- Joule-Thomson effect
- Liquefaction, gases
- Low-temperature phenomena
- Low-temperature production
- Low-temperature technique
- Magnetic cooling
- Refractories

23.20 HIGH PRESSURE TECHNIQUES

- Getters
- High-pressure phenomena and effects
- High-pressure techniques

23.30 VACUUM TECHNIQUES

- Leak detection
- Manometers
- Seals
- Sputtering
- Vacuum apparatus
- Vacuum gauges
- Vacuum pumps
- Vacuum technique

23.40 X-RAY TUBES AND TECHNIQUES

- Dosimetry
- High-voltage techniques
- Radiation monitoring
- Radiation protection
- Radiography
- X-ray absorption
- X-ray diffraction
- X-ray examination of materials
- X-ray measurement
- X-ray monochromators
- X-ray reflection
- X-ray scattering
- X-ray spectra/
    - absorption
    - emission
- X-ray spectrometers
- X-ray spectroscopy
- X-ray tubes
- X-rays/
    - effects

SUBSTANCES

Chemical elements and inorganic compounds

All the chemical elements are listed by name, followed by their compounds, e.g. "Cadmium, Cadmium compounds".

"Hydrogen" is subdivided by the subheadings "neutral atoms", "neutral molecules" and "ions". "Deuterium" and "Tritium" are independent headings. "Hydrogen compounds" is supplemented by "Ice", "Steam" and "Water".

"Oxygen" is supplemented by "Ozone" and "Carbon" is supplemented by "Diamonds" and "Graphite".

The following inorganic compounds are further subdivided by subheadings as shown:-

- Barium compounds/
    - barium titanate*
- Cadmium compounds/
    - cadmium sulphide
- Calcium compounds/
    - calcium fluoride
- Gallium compounds/
    - gallium arsenide†
- Indium compounds/
    - indium antimonide†
- Lithium compounds/
    - lithium fluoride
- Nitrogen compounds/
    - ammonia
    - ammonium compounds
- Potassium compounds/
    - potassium bromide
    - potassium chloride
- Sodium compounds/
    - sodium chloride
- Zinc compounds/
    - zinc sulphide

* Ferroelectric properties are listed under "Ferroelectric materials/barium titanate"

† Semiconducting properties are listed under the corresponding subheadings of "Semiconducting materials"

Organic compounds

Organic compounds are grouped under headings "Organic compounds", "Polymers", "Plastics", "Proteins". "Rochelle salt" is an independent heading.

Co-ordination compounds

Metallic co-ordination compounds are regarded as inorganic with a few exceptions and are indexed under the appropriate metallic compound heading (not under organic compounds), e.g. Ni complex, bis (dimethylglyoximato) nickel (II) under Nickel compounds.

Substance groups

In addition there are the following headings for groups of elements, compounds or substances:-

- Actinides
- Actinide compounds
- Alkali metals
- Alkali-metal compounds/
    - halides
- Alkaline-earth metals
- Alkaline-earth compounds
- Ferrites
- Ferroelectric materials/
    - barium titanate‡
- Garnets
- Halogens
- Inert gases
- Metals
- Minerals
- Rare-earth metals
- Rare-earth compounds
- Semiconductors
- Semiconducting materials/
    - gallium arsenide§
    - germanium§
    - indium antimonide§
    - silicon§
- Superconducting materials/
    - lead‖
    - niobium‖
- Transition metals
- Transition-metal compounds

‡ Used for ferroelectric properties only

§ Used for semiconducting properties only

‖ Used for superconducting properties only

Alloys

General papers on alloys are indexed under "Alloys". Alloys of specified composition are listed under, either

(i) special alloy headings (there are five of them: "Aluminium alloys", "Copper alloys", "Iron alloys", "Nickel alloys", "Steel"), e.g. Al-Ni alloys under "Aluminium alloys" and "Nickel alloys".

(ii) compounds of the named elements, e.g. Mn-Zn alloys under "Manganese compounds" and "Zinc compounds". Silicon-iron under "Iron alloys" and "Silicon compounds".

Special substances and materials

There are also the following special headings for certain common substances:-

- Air
- Blood
- Ceramics
- Clay
- Coal
- Concrete
- Fibres
- Gelatin
- Glass
- Mica
- Optical materials
- Paper
- Porous materials
- Powders
- Quartz
- Rubber
- Ruby
- Sand
- Seawater
- Soil
- Waxes
- Wood

ABSTRACTS AND CURRENT PAPERS JOURNALS

Three main subject areas are covered by INSPEC abstracts and current papers journals: physics, electrical and electronics engineering, and computer and control engineering. For each field an abstracts journal and a companion titles journal are published. The abstracts journals are intended as library tools for retrospective information retrieval, whereas the companion titles journals, which omit the abstracts and associated indexes, are intended as low-cost current-awareness tools for the individual.

SUBSCRIPTION PRICES

ABSTRACTS JOURNALS	Annual subscription Paper or microfiche	Annual subscription Combined paper and microfiche
Physics Abstracts (PA) Published every two weeks in conjunction with the American Institute of Physics, New York, and the Institute of Physics, London	£120	£180
Electrical & Electronics Abstracts (EEA) Published monthly jointly with the Institute of Electrical & Electronics Engineers Inc., New York	£100	£150
Computer & Control Abstracts (CCA) Published monthly jointly with the Institute of Electrical & Electronics Engineers Inc., New York	£50	£75
Combined Subscription to Electrical & Electronics Abstracts and Computer & Control Abstracts (EEA/CCA)	£120	£180

CURRENT PAPERS JOURNALS	Annual subscription IEE, AIP, IEEE, IOP, IERE members	Annual subscription Non-members
Current Papers in Physics (CPP) Published every two weeks in conjunction with the American Institute of Physics, New York, and the Institute of Physics, London	£7	£14
Current Papers in Electrical & Electronics Engineering (CPE) Published monthly jointly with the Institute of Electrical & Electronics Engineers Inc., New York	£7	£14
Current Papers on Computers & Control (CPC) Published monthly jointly with the Institute of Electrical & Electronics Engineers Inc., New York	£6	£12

CUMULATIVE INDEXES

Cumulative indexes are available for *Physics Abstracts*, *Electrical & Electronics Abstracts*, and *Computer & Control Abstracts*, for both authors and subjects. These cumulations generally cover a period of four years, with the exception of *Computer & Control Abstracts* where the initial volume covered the period 1966–68. The table below shows the prices and periods for the two types of cumulative index.

	Physics Abstracts		Electrical & Electronics Abstracts		Computer & Control Abstracts	
	Subject	Author	Subject	Author	Subject	Author
1955–59	£20	£20	£15	£20	—	—
1960–64	£40	£17	£20	£12	—	—
1965–68	£60	£25	£35	£20	—	—
1966–68	—	—	—	—	£15 (combined)	

ORDERING PROCEDURE

AMERICAN SUBSCRIPTIONS

Physics Abstracts
Current Papers in Physics

For AIP members, wherever they reside, and from the public in the Americas, to the Subscription Department, American Institute of Physics, 335 East 45th Street, New York, NY 10017, USA. Please allow six weeks' notice for change of address, send both old and new addresses and include an address label from a recent issue.

Electrical & Electronics Abstracts
Computer & Control Abstracts and associated current papers journals in these fields

For IEEE members wherever they reside, and from the public in the Americas, to the Fulfillment Manager, Institute of Electrical & Electronics Engineers Inc., 345 East 47th Street, New York, NY 10017, USA.

REMAINDER OF THE WORLD

Abstracts Journals
Current Papers
Cumulative Indexes

For all remaining subscriptions, and for all cumulative indexes, to IEE, Savoy Place, London WC2R 0BL, England. Telephone 01-240 1871, Telex 261176, Telegrams Voltampere London WC2.

OTHER INSPEC SERVICES

SDI

(Selective Dissemination of Information.) This is a service individually tailored to the requirements and interests of the engineer or research worker. Details of information relevant to the interest profile of the individual subscriber are selected from the data being processed for the INSPEC database. Information is dispatched weekly on 150 mm × 100 mm (6″ × 4″) cards.

TOPICS

This is an SDI service based on standard profiles. There are 48 subjects covering high-activity areas of research and development. This is an inexpensive card service designed to alert engineers and researchers to the availability of literature within their subject area.

MAGNETIC TAPES

These are produced, containing all the information included in the INSPEC publications. They enable the larger research and development organisations to produce their own internal information and current-awareness services.

For more details of any of these services please write to:
INSPEC Marketing Department, The Institution of Electrical Engineers, Savoy Place, London WC2R 0BL, England

Cables Voltampere London WC2
Grams Voltampere London Telex

Telephone 01-240 1871
Telex 261176

INSPEC
The Institution of Electrical Engineers

All things being relative...

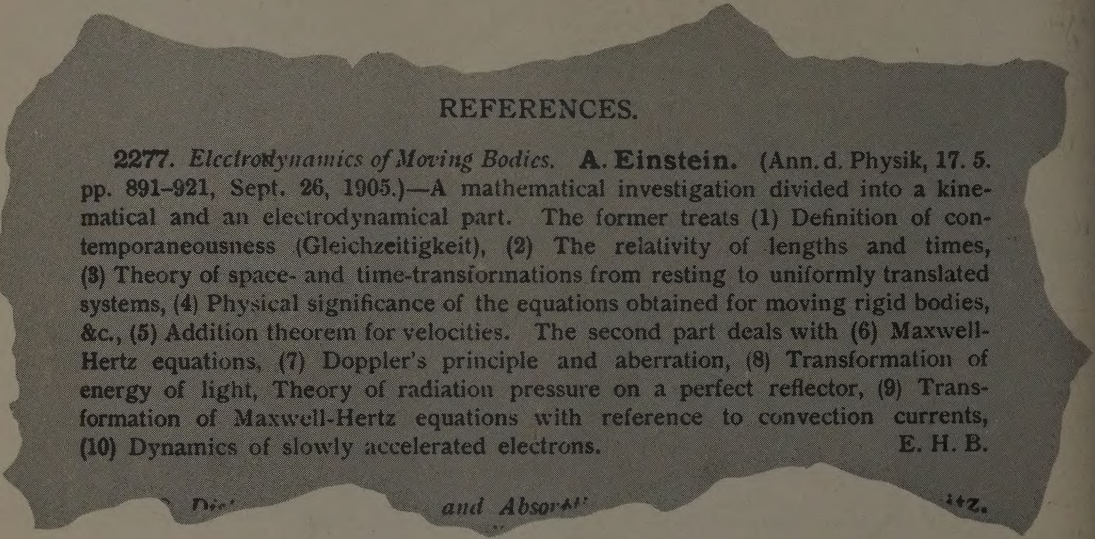

REFERENCES.

2277. *Electrodynamics of Moving Bodies.* **A. Einstein.** (Ann. d. Physik, **17.** 5. pp. 891–921, Sept. 26, 1905.)—A mathematical investigation divided into a kinematical and an electrodynamical part. The former treats (1) Definition of contemporaneousness (Gleichzeitigkeit), (2) The relativity of lengths and times, (3) Theory of space- and time-transformations from resting to uniformly translated systems, (4) Physical significance of the equations obtained for moving rigid bodies, &c., (5) Addition theorem for velocities. The second part deals with (6) Maxwell-Hertz equations, (7) Doppler's principle and aberration, (8) Transformation of energy of light, Theory of radiation pressure on a perfect reflector, (9) Transformation of Maxwell-Hertz equations with reference to convection currents, (10) Dynamics of slowly accelerated electrons. E. H. B.

and Absor

...you probably missed this Science Abstract

Einstein's paper on the special theory of relativity, published in September 1905, is only one of the many vital papers which have appeared in Science Abstracts since they began publication in 1898.

You can forgive yourself for missing that one, but are you sure there are no other knowledge gaps in your literature searches?

If there are, back issues of Science Abstracts will fill those gaps.

Abstracts journals, containing titles, authors, abstracts, together with information necessary to locate the source of the original document, are produced in three separate publications: Physics, Electrical & Electronics and Computer & Control Abstracts. They are also published in concurrent microfiche form.

Back issues of Science Abstracts can do for you what the apple did for Newton!

To obtain a quotation for supplying your missing issues, please write to:

INSPEC Marketing Department The Institution of Electrical Engineers
Savoy Place London WC2R 0BL England
Telephone 01-240 1871

INSPEC
The Institution of Electrical Engineers